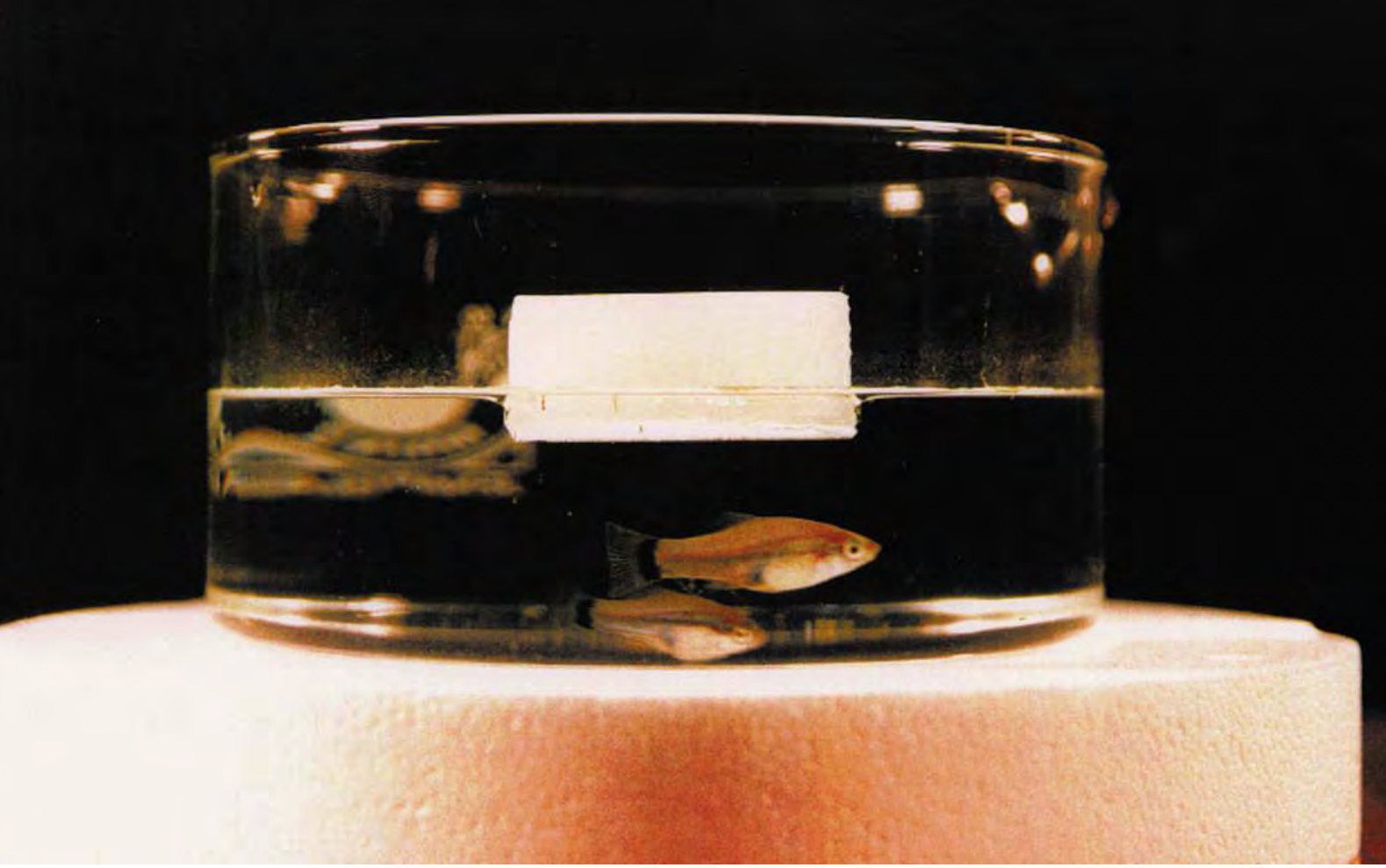


Two of the fascinating characteristics of aerogels—highly porous materials made, for example, from SiO_2 and air—are demonstrated by these pictures: In their hydrophobic form the aerogels float on water for months, and under suitable conditions one obtains plates that are translucent even with a thickness of about 2 cm.



ANGEWANDTE CHEMIE © WILEY-VCH

Aerogels—Airy Materials: Chemistry, Structure, and Properties

Nicola Hüsing* and Ulrich Schubert*

Aerogels are unique among solid materials. They have extremely low densities (up to 95% of their volume is air), large open pores, and a high inner surface area. This results in interesting physical properties, for example extremely low thermal conductivity and low sound velocity combined with high optical transparency. They are prepared from molecular precursors by sol–gel processing. The initially formed gels have a spongelike solid network filled with liquid. Special drying techniques must be applied to exchange the pore liquid with air while maintaining the filigrane solid network. Supercritical drying is most common. However, recently developed methods allow removal of the liquid in a classical way after chemical modification of the inner surface of the gels. The structure of the gel network, and thus the physical properties of aerogels, decisively depend on the choice of the precursors and the chemical reaction parameters for preparing the gels. Therefore, the later material properties are predetermined at the beginning of the preparation process. In this review, connections between the underlying sol–gel chemistry, the structure of the gels, and the resulting properties of the materials will be shown, which are the basis for a chemical "design" of aerogel properties.

Keywords: aerogels · materials science · mesoporosity · nanostructures · sol–gel processes

1. Introduction

Whipped egg whites or solid bubble bath are closest in appearance to aerogels. In principle, the name says everything: the main component of this material is air which is surrounded by a very filigrane, solid network. This network can be constructed in a way that the resulting aerogels have a density that is only three times that of air.

If an aerogel is given to a chemist, a physicist, or a materials scientist, each of them would discover interesting properties which individually are also observed in other materials. For example, SiO_2 aerogels have a high transparency that is close to that of glass, a thermal conductivity corresponding to that of polystyrene or polyurethane foams, or very high specific surface areas, which are also found in charcoal. The unique feature of aerogels is the combination of these physical properties in one material which can have different chemical compositions. Important aspects for various applications are thus combined, for example, for heat insulation (Figure 1), optical applications, sensors, catalysts, or catalyst carriers.

What exactly is an aerogel? The term aerogel is not uniformly used in the literature, and there are two different definitions:

1) First, all materials prepared from wet gels (see below) by a special drying process, the supercritical drying technique, were called aerogels irrespective of their structural properties. With the development of new drying techniques (e.g., the possibility of drying under conventional conditions, see Section 3.3), this definition no longer appears appropriate.
2) According to the alternative definition, materials in which the typical structure of the pores and the network is largely maintained (which is not always the case for supercritical drying) while the pore liquid of a gel is replaced by air are called aerogels. However, it is not always clear to what extent the structure was maintained. Rearrangement and shrinkage in the gel body during drying are normal phenomena! In many publications attention is not paid to this issue.

In this review we will mainly follow the second definition, which better applies to the special properties of this class of materials. However, we do not generally exclude materials which correspond only to the first definition.

There are already some excellent reviews on aerogels,[1] most of which focus on physical properties or applications. Here, we want to present these fascinating materials from a more chemical point of view. Aerogels are an excellent example for how important chemistry is for the development of new materials. We want to use aerogels as an example to demonstrate that the intimate knowledge and understanding of the chemistry of precursors and the chemistry of the formation of the solid are indispensible for the deliberate optimization and tailoring of materials properties.

[*] Dr. N. Hüsing, Prof. Dr. U. Schubert
Institut für Anorganische Chemie der Technischen Universität
Getreidemarkt 9, A-1060 Wien (Austria)
Fax: Int. code + (43) 1-581 6668
e-mail: nhuesing@fbch.tuwien.ac.at
uschuber@fbch.tuwien.ac.at

 © WILEY-VCH Verlag GmbH, D-69451 Weinheim, 1998 1433-7851/98/3701-0023 $ 17.50+.50/0

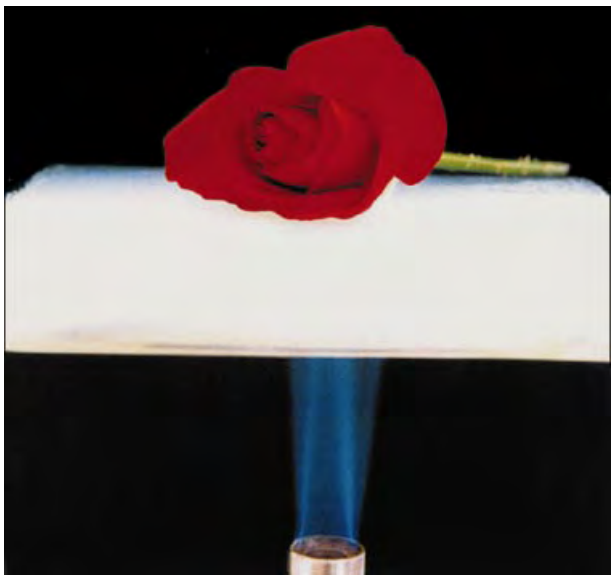


Figure 1. Aerogels have excellent insulating properties, as shown here for a silica aerogel tile.

Until recently, the chemical approach for developing materials with novel properties mainly consisted of preparing substances with a new chemical composition, that is, in an attempt to correlate the macroscopic properties and the chemical building blocks. The importance of the controlled synthesis of pore structures was only recently realized. A topical example is the family of mesoporous molecular sieves with regular channel systems (the M41S family).[2] Several emerging technologies depend on the development of engineered porous materials.[3] Nevertheless, deliberate tailoring of pores is still a major challenge in materials chemistry.

Materials are porous if they contain cavities, channels, or interstices that are deeper than they are wide.[4] The pores may be regularly arranged, as in molecular sieves. However, the more common situation is an irregular pore structure, as obtained by cross-linking of polymer chains, aggregation or agglomeration of small particles, or selective removal of elements of a solid (e.g. by etching or pyrolysis). The physical properties of a porous solid and its reactivity are effectively influenced by the kind, shape, and size of the pores. Some technical terms are defined in Table 1. The unique materials properties of aerogels result from the special arrangement of their solid network, which is schematically shown in Figure 2 for a SiO_2 aerogel.[6]

The structures of aerogels are characterized by well-accessible, cylindrical, branched mesopores. Other mesoporous materials are fumed silica, Vycor glass, carbon soot, or mesoporous molecular sieves. Among them, aerogels are

Table 1. Definition of terms used to characterize porous solids.

Term	Explanation
porosity	ratio of the pore volume to the volume occupied by the particles or powder
pore shape	ink-bottle, cylindrical, funnel, or slit-shaped
accessibility of the pores	closed, blind, or through pores
pore size,[5] dominating transport mechanisms	*micropores*: <2 nm, activated transport *mesopores*: 2–50 nm, Knudsen diffusion, surface diffusion along the pore walls, capillary transport *macropores*: >50 nm, molecular diffusion
density	skeletal density: density of the solid network bulk density: mass per total volume (volume = solid phase + closed pores + open pores)



N. Hüsing U. Schubert

Nicola Hüsing, born in Rheda-Wiedenbrück (Germany), received her Diplom in chemistry and in 1997 her Ph.D. at the Universität Würzburg (Germany). Her dissertaion was on the chemical modification of aerogels. Since 1994 she has been working as a research and teaching assistant at the Institut für Anorganische Chemie der Technischen Universität Wien (Austria). A research scholarship from the Deutschen Akademischen Austauschdienst allowed her to stay with Professor J. Zink at the University of California in Los Angeles (USA) for six months in 1996 to investigate enzymes trapped in inorganic gels. She was awarded an Erwin–Schrödinger scholarship of the Fonds zur Förderung der wissenschaftlichen Forschung for postdoctoral research in 1997/98 with Dr. J. Brinker at the Advanced Materials Laboratory in Albuquerque (USA) in the area of novel porous materials. In 1997 she received the Harry Kloepfer Aerosil Award, which was sponsored by the Degussa AG and awarded by the Gesellschaft Deutscher Chemiker. Her research interests are porous sol–gel materials.

Ulrich Schubert, born in Regensburg (Germany), studied chemistry at the Technische Hochschule München (Germany), and received his Ph.D. in 1974. His dissertation was on reactions of carbene complexes. After a postdoctoral year at Stanford University (USA) with Professor W. S. Johnson, he finished his Habilitation at the Technische Universität München in 1980 on the structural chemistry of metal complexes. From 1982 to 1994 he held the position of Associate Professor of Inorganic Chemistry at the Universität Würzburg. Since 1989 he also served in different positions at the Fraunhofer-Institut für Silikatforschung in Würzburg. In 1994 he was appointed ordinary Professor of Inorganic Chemistry at the Technische Universität Wien. The current research interests of his group center around applied fundamental research on sol–gel processes, the activation of silicon– and tin–element bonds by transition metal complexes, and the structural chemistry of molecular inorganic compounds.

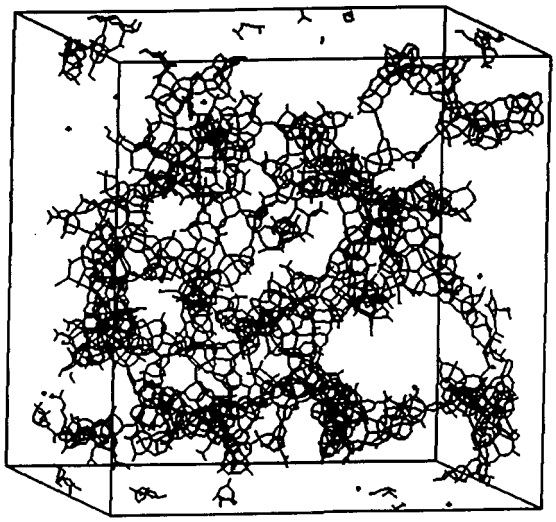


Figure 2. Schematic description of the structure of a silica aerogel (reproduced with friendly permission from ref. [6]).

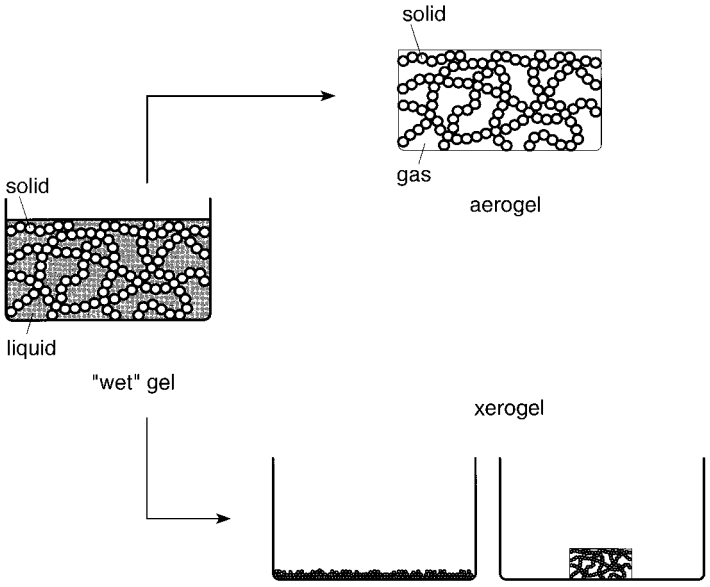


Figure 3. Shrinkage upon drying of a wet gel body to give an aerogel (top) and a xerogel (bottom) as a powder (left) and a monolith (right).

unique owing to their extremely high porosity (low density) and high specific surface area, and the possibility of making monoliths. Aerogels can also be obtained as granulates or powders. The bulk density of aerogels is in the range of 0.004 – 0.500 $g\,cm^{-3}$ owing to the high porosity (for comparison, the density of air is 0.00129 $g\,cm^{-3}$).

The pore structure of aerogels is formed by the controlled condensation of small (polymeric or colloidal) primary particles with a diameter of 1 – 3 nm, as discussed in detail in Section 2. Generation and aggregation of the particles is controlled by chemical processes, usually the sol – gel process, which has been extensively treated in books,[7, 8] conference proceedings,[9–11] and several reviews.[12, 13]

To begin, we want to explain some terms related to the sol – gel process which will be frequently used throughout this review. In a *sol* colloidal particles with diameters in the range of 1 – 1000 nm are dispersed in a liquid. A *gel* consists of a spongelike, three-dimensional solid network whose pores are filled with another substance (usually a liquid). When gels are prepared by hydrolysis and condensation of metal or semimetal alkoxides or other hydrolyzable metal compounds (through the sol stage), the pore liquid mainly consists of water and/or alcohols. The resulting ("wet") gels are therefore called *aquagels*, *hydrogels*, or *alcogels*. When the pore liquid is replaced by air without decisively altering the network structure or the volume of the gel body,[14] *aerogels* are obtained (or *cryogels* when the pore liquid is removed by freeze-drying). A *xerogel* is formed upon conventional drying of the wet gels, that is, by increase in temperature or decrease in pressure with concomitant large shrinkage (and mostly destruction) of the initially uniform gel body (Figure 3).

The large shrinkage of a gel body upon evaporation of the pore liquid is caused by capillary forces acting on the pore walls as the liquid retreats into the gel body. This results in the collapse of the filigrane, highly porous inorganic networks of the aquagels or alcogels. Therefore, other drying methods had to be developed to prepare aerogels (see Section 3). Kistler, who prepared the first aerogels in 1931, used the solvent in the supercritical state for drying.[15] The chemical composition of the gel networks included oxides of silicon, aluminum, tin, thorium, iron, and tungsten as well as organic compounds such as cellulose, cellulose nitrate, and gelatine. Therefore, the first publication on aerogels ended very optimistically: *"…and we see no reason why this list may not be extended indefinitely"*.

Despite the optimistic and encouraging prediction of Kistler, the application-oriented research and development of aerogels only started in the late 1960s, concomitant with the rapid development of the sol – gel process. They found their first application in particle detectors for high-energy physics (Çerenkov detectors). The continuing and steadily increasing interest, both in applied fundamental research and technical applications, is demonstrated by the increasing number of publications each year and the regular international symposia since 1985.[16]

2. Network Formation and Structure

Formation of the highly porous three-dimensional network is one of the key steps in the preparation of aerogels. It is remarkable that this can be achieved for inorganic, inorganic – organic, and purely organic systems under controlled conditions despite a typical solid content of only 1 – 15 vol %. Network formation is an excellent example for the influence of chemical parameters, in particular the kind of precursors and the reaction conditions, on the resulting microstructure. The microstructure, for their part, influences the macroscopic properties of the resulting solid. "Design" of the materials properties therefore requires mastering of the fundamental chemical processes. This is especially important for aerogels, because the network formed by wet chemical processes can be preserved nearly unchanged by the special drying techniques

(Section 3). Therefore, some possibilities for structural investigations should be mentioned at this point. In a simplifed manner we consider the structure of an aerogel, which is easier to investigate by physical methods, to be approximately equal to that of the corresponding wet gel. We thus want to link the chemical processes for the network formation with the structure of the (aero)gels.

The gathering of information on the structure of aerogels requires methods which cover the length scale from the lower nanometer (structure of the primary particles) to the micrometer range (linking of the particles).[17] No technique can provide the complete information, and a clearer picture only emerges by combining different methods. Some common methods for determining the structure of aerogels are listed in Table 2.

There are several other techniques for gaining structural information. For example, NMR spectroscopy was used to follow the evolution of the structure from the molecular precursors to the gel,[30] or to determine the pore diameters or fractal dimensions.[31] Mechanisms of the network formation can be derived from the fractality—that is, the self-similarity—of the structure.[32] Atomic force microscopy (AFM) was recently used to obtain information on the atomic structure at the surface.[33]

The irregular, branched three-dimensional gel network is usually formed by condensation of colloidal particles. There are two principal possibilities:

1. Solid gels are dissolved (peptized) and the obtained sols (colloids) then reaggregated under different conditions.
2. Sol particles are formed by chemical reactions from dissolved molecular precursors. Their condensation results in the formation of a gel. Most aerogel syntheses follow this route, with two variations:

a) Hydrolysis and subsequent condensation reactions are initiated starting from aqueous solutions of ionic precursors by changing the pH or the temperature.
b) Precursor molecules in an organic solvent are transformed into species capable of undergoing condensation. For example, the reaction of metal or semimetal alkoxide groups (E−OR) with water results in the formation of hydroxy groups (E−OH), which can then condense to form E-O-E units. Gel formation starting from multifunctional organic precursors proceeds similarly.

The production of inorganic and inorganic–organic aerogels is shown schematically in Figure 4. Some parameters are also listed with which the sol–gel process and therefore the properties of the resulting aerogels can be influenced and varied. Organic aerogels are produced similarly.

The solvent plays an important role in sol–gel processes. It not only serves to homogenize the precursors in the initial stage, but also influences the particle- and network-forming reactions to a very high degree due to its polarity and viscosity. In the preparation of aerogels it has an additional function, as shown in Figure 4. Since gelation results in only a marginal change in volume and the drying process during the aerogel production is performed (by definition) in a way that shrinking is minimal, the volume of the aerogel body (and thus its density) is determined by the volume of the reaction solution. Therefore, the density of aerogels is simply modified by varying the precursor concentration in the starting solution.

In principle, the structures of all covalently bonded gels are between those of colloidal and polymeric gels, which constitute the two extremes with regard to both the microstructure and the resulting properties (Figure 5). The three-dimensional network in both structural types is formed by connecting primary particles (clusters[34]). In colloidal gels, dense colloidal particles are interconnected like a string of pearls (Figure 5a). In polymer gels, linear or branched polymer chains are formed by condensation of small clusters (rings, cages) instead of dense particles (Figure 5b). There are several theoretical models for the aggregation of the clusters to three-dimensional networks.[7, 35]

Because the microstructure strongly depends on the preparation conditions, each aerogel has its own structural characteristics. It is difficult to compare different aerogels in spite of similar structural features. We therefore restrict ourselves in the following sections to discussing some basic concepts for network formation that are exemplarily for different chemical systems.

2.1. Inorganic Aerogels

Nearly all metal or semimetal oxides are known to form gels, and many served for the production of aerogels. A complete listing of all known inorganic aerogels would be beyond the scope of this review. For this reason, we restrict

Table 2. Typical methods for structurally characterizing aerogels and the structural information available from them.

Method	Structural information	Remarks/problems
N_2 adsorption and desorption according to Brunauer, Emmett and Teller (BET)[18]	specific surface area, distributions of pore radii,[19] interactions of adsorbents and adsorbates	only pores are detected which are accessible for N_2, structural changes by the N_2 pressure during the measurements results in falsification of the values for the pore radii[20]
helium pyknometry[21]	skeletal density	
mercury porosimetry[22]	pore volumina	compression of the network by the applied pressure instead of penetration of Hg into the matrix[23, 24]
electron microscopy [scanning, transmission, and scanning transmission electron microscopy (SEM, TEM, and STEM, respectively)]	particle sizes, form and arrangement of the particles (morphology)	sintering processes due to the high energy of the electron beam
light scattering (LS),[25] small-angle X-ray scattering (SAXS),[26, 27] small-angle neutron scattering (SANS)[28, 29]	particle and cluster sizes, fractal dimensions, surface area	inverse relation of the scattering vector and the structural dimension, information from the Angstroem to the micrometer range

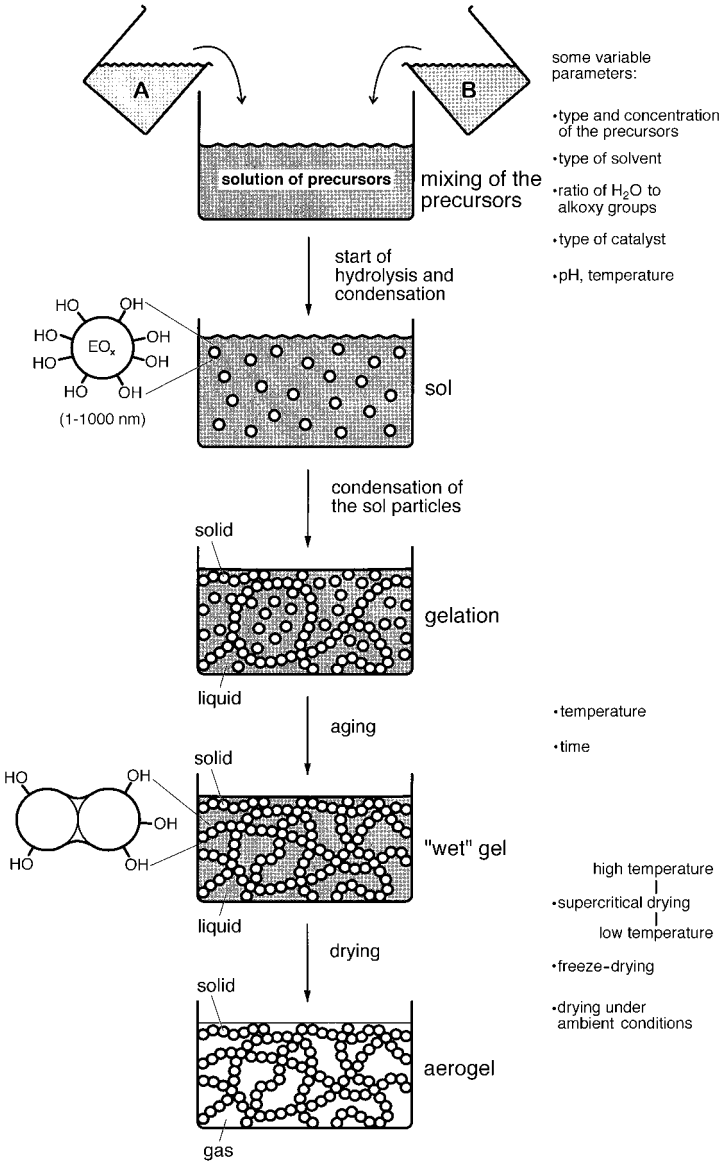


Figure 4. General scheme for preparing aerogels by sol–gel processing and some typical variable parameters.

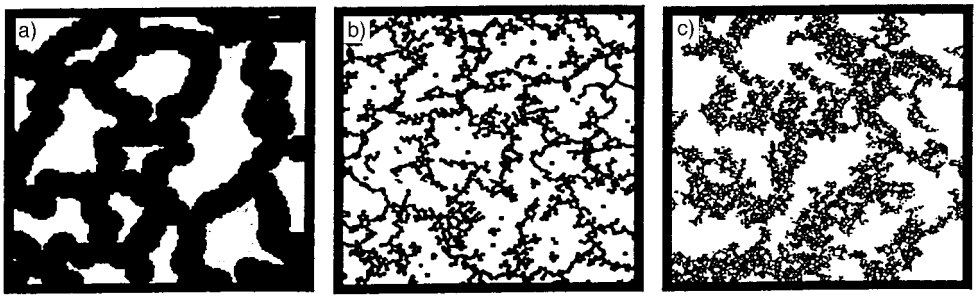


Figure 5. Two-dimensional structures of aerogels: a) colloidal, b) polymeric, and c) with a rough surface (see Section 2.1.1; reproduced with friendly permission from ref. [44]).

ourselves to some examples which we believe to be important or representative. A semantic aspect should be pointed out first. The term "SiO_2 gel" (correspondingly for other gels) is only used to characterize the type of inorganic skeleton. SiO_2 gels and aerogels often have the composition $SiO_x(OH)_y$ or, if they are prepared from alkoxides, $SiO_x(OH)_y(OR)_z$, where the values of y and z can be (but must not be) rather high. For example, in aerogels made from $Si(OMe)_4$ under basic conditions and then supercritically dried with methanol, 30% of the silicon atoms still carry a methoxy substituent ($z = 0.3$ in this case).[36]

2.1.1. SiO_2 Aerogels

Silica gels certainly belong to the best investigated materials in inorganic chemistry. Therefore, it is not surprising that Kistler used SiO_2 gels in 1931 for his first attempts to exchange the liquid in gels for air.[15] For this purpose he allowed water glass, an aqueous solution of sodium silicate, to react with hydrochloric acid [Eq. (1)].

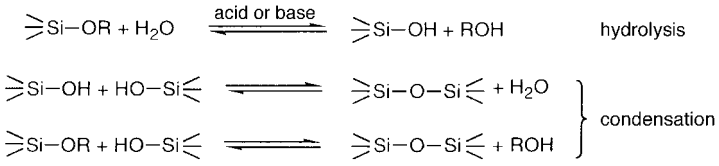
$$\text{“}Na_2SiO_3\text{”} + 2\,HCl \xrightarrow{H_2O} [SiO_2 \cdot x\,H_2O] + 2\,NaCl \quad (1)$$

To convert the aquagels into aerogels he first had to remove the formed NaCl by several washing cycles. Then the water had to be exchanged for another solvent, because supercritical drying of the aquagels resulted in their complete peptization. Kistler showed impressivly that the liquid of the gels can be removed without destroying the gel structure. One of the reasons why it took 30 years for the aerogels to become interesting for industrial applications was certainly the time-consuming preparation, which took more than a week.

A decisive simplification and acceleration of the synthesis was achieved by Teichner et al. in the 1960s.[37] They dissolved tetramethoxysilane (TMOS) in methanol and added a defined amount of water to start the hydrolysis and condensation reactions [Eq. (2)]. The pore liquid now mainly consisted of

$$Si(OCH_3)_4 + H_2O \xrightarrow{CH_3OH} [SiO_2 \cdot H_2O/CH_3OH] \quad (2)$$

alcohol, and therefore the wet alcogels could be dried supercritically without the awkward solvent exchange. The chemical reactions during sol–gel processing of alkoxysilanes can be formally described by three equations (Scheme 1). Condensation already occurs even if not all of the OR groups are hydrolyzed. Small oligomers (clusters) are initially formed by the condensation reactions and then the sol particles which eventually form the oxidic gel network. However, all intermediate species still contain Si–OR and/or Si–OH groups. Hydrolysis therefore takes place parallel to condensation during all steps of the sol–gel process.



Scheme 1. Chemical reactions for the sol – gel process of alkoxysilanes.

Parameters which influence the hydrolysis and condensation and whose deliberate variation are used for "materials design" are, inter alia, the kind and concentration of the precursors, the relative concentration of the components in the precursor mixtures, the kind of the solvent, the ratio of H_2O to alkoxy groups, the temperature, and the pH value.

A variety of physical-chemical measurements and also some computer simulations were performed to determine the influence of these parameters on the network formation of SiO_2 aerogels.[16, 38–42] For example, Schaefer et al. showed with in situ SAXS experiments that variation of the mentioned parameters strongly influences the silicate structures on a length scale of 1 – 20 nm.[43] Schaefer and Keefer postulated kinetic models for the growth of gel networks based on SAXS data.[44, 45] Although probably not universal, they are currently the only basis for a preparative design of aerogel structures in the nanometer range. Two of the most important models are shown in Figure 6.

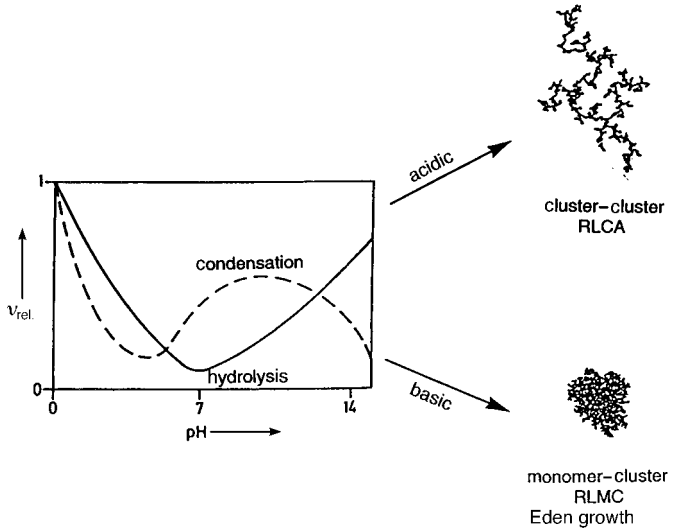


Figure 6. Dependency of the hydrolysis and condensation reaction on the pH, and derived models for kinetic growth of gel structures based on RLCA and RLMC growth (according to ref. [7, 35]). $v_{rel.}$ = relative rate of reaction.

The pH value is the decisive parameter for the relative rates of hydrolysis and condensation of tetraalkoxysilanes $Si(OR)_4$. Under acidic conditions (pH 2 – 5) hydrolysis is favored, and condensation is the rate-determining step. A great number of monomers or small oligomers with reactive Si–OH groups is simultaneously formed. Under these conditions, reactions at terminal silicon atoms are favored for electronic reasons. This results in polymerlike gels which are formed from chains with few branches; that is, small clusters condense to give a polymerlike network with small pores. This process is called reaction limited cluster aggregation (RLCA).

In contrast, hydrolysis is the rate-determining step under basic conditions. Due to a different mechanism, reaction at the central silicon atoms of an oligomer unit is favored. The resulting network is characterized by big particles and large pores ("colloidal" gels). Hydrolyzed species are immediately consumed because of the faster condensation. Condensation of clusters with each other is relatively unfavorable because it requires inversion of configuration at one of the silicon atoms involved in the reaction.[7] Therefore, the clusters grow mainly by condensation of monomers. This model is called reaction limited monomer cluster growth (RLMC) or Eden growth.[46, 47] It would ideally result in equally dense structures. However, for tetraalkoxysilanes this simple model must be slightly modified. Not all the four branching points are equal, because $Si(OR)_{4-x}(OH)_x$ is initially formed from $Si(OR)_4$ ("poisoned" Eden growth). Condensation is inhomogeneous owing to the presence of Si–OR groups at the growth front, and rough structures are obtained (see Figure 5c). Therefore, the kind of inorganic network formed upon condensation not only depends on the absolute rates of the individual reactions but also on the relative rates of hydrolysis and condensation.[48, 49]

The preparation of aerogels from polymeric gels is more difficult, because diffusion processes are strongly inhibited by the smaller pores. Complete removal of the pore liquid is therefore more difficult and results in greater shrinkage upon drying.[50] For this reason SiO_2 aerogels are usually prepared by base-catalyzed reaction of tetramethoxysilane (TMOS) or tetraethoxysilane (TEOS), usually with ammonia as the catalyst.

A modification of this procedure was developed by Brinker et al:[51] $Si(OR)_4$ is first prehydrolyzed with a small amount of water under acidic conditions. This results in the formation of small clusters of silicic acid. In a second step (which must not necessarily immediately follow the first) a defined amount of aqueous acid or base is added. Networks formed by this two-step procedure have a structure similar to that of the RLCA model; that is, they have polymeric character. The probable explanation is that the reactive clusters formed in the first step as structure-forming units are strongly responsible for the formation of the network, independent of the kind of catalyst used in the second step. The main difference caused by base or acid catalysis in the second step is the stiffness of the resulting network. The former results in a stiffening which stabilizes the gels. With this two-step procedure a more deliberate control of the microstructure and thus the particle and pore sizes of the SiO_2 gels is possible.

The group of Hrubesh used the two-step sol – gel process to vary the density of aerogels within a larger range.[52, 53] When aerogels are made by simple base- or acid-catalyzed reactions their density is restricted to 0.030 – 0.300 $g\,cm^{-3}$, because the alcohol formed during hydrolysis shifts the equilibrium towards species with alkoxy groups. This results in long gelation times. Tillotson and Hrubesh removed the alcohol by destillation after the first step and replaced it by an aprotic solvent (e.g. acetonitrile). Deliberate dilution, base-catalyzed hydrolysis of the remaining Si–OR groups, and condensation

of the SiO_2 particles resulted in the formation of a three-dimensional network and a solid with a density of only 0.004 g cm^{-3}.[53]

In principle, the work of Pajonk et al. is also based on a two-step procedure. They synthesized oligomeric polyethoxysiloxanes of a certain size from TEOS by adding an exact amount of water. These defined oligomers were then used as precursors for sol–gel processing to form the three-dimensional network.[54-56]

The preparative routes to SiO_2 aerogels described so far have one thing in common: an alkoxysilane was used as the precursor. For technical applications, in which large amounts of aerogels are needed, alkoxysilanes are too expensive. Therefore, BASF, Hoechst, and others use a procedure in which a solution of aqueous sodium silicate is ion-exchanged and then hydrolyzed under acidic conditions.[57, 58] For the production of Basogel, the aerogel product of BASF, a two step-procedure was applied. A solution of sodium silicate is mixed with sulfuric acid in the first step. Small hydrogel or aquagel droplets are formed by spraying. The metal salts are then extracted, and the water is exchanged for an organic solvent.[59] The gel droplets are then supercritically dried. The procedure of Hoechst and Nanopore, an American company, will be discussed with the drying methods.

Henkel patented a procedure in 1991 with which silicic acid is transfered into an organic solvent, and condensation is then performed under acidic, neutral or basic conditions. These wet gels are also potentially suited for producing aerogels.[60]

The transition from sol to gel is reached when a continuous network is formed (gel point). An extremely important aspect of the preparation of inorganic gels is that the chemical reactions are not finished with the formation of the gel network. First, the pore liquid is initially a sol. That is, it contains condensable particles or even monomers which slowly condense to the existing basic network. Second, there are structural rearrangements in the gel network for mainly two reasons. The gel network is originally still very flexible, and neighboring E–OH or E–OR groups can approach each other and undergo condensation ("aging"). Furthermore, hydrolysis and condensation are in principle reversible. Therefore, mass is dissolved from thermodynamically unfavorable regions, and the solutes condense to thermodynamically more favorable regions, in particular in pores, crevices, and particle necks ("Ostwald ripening"). This process results in the reduction of the net curvature, disappearance of small particles, and filling of small pores. Aging and ripening increase the stiffness of the gels (see Figure 4). This is an important aspect, particularly for aerogels, to which we will return when discussing the drying methods.

Because of the described differences in the structure of the primary particles and the network formation, which are caused by the different reaction mechanisms, the macroscopic properties of SiO_2 aerogels differ within a wide range. This is a very good example for the correlation between precursor chemistry and the properties of the final materials (see Section 5.1). "Typical" structural data therefore have only limited relevance. Nevertheless, some data for SiO_2 aerogels are listed in Table 3 to exemplify their properties.

Table 3. Important structural properties of SiO_2 aerogels

Property	Range	Typical value
bulk density [g cm^{-3}]	0.003 – 0.500	0.100
skeletal density [g cm^{-3}]	1.700 – 2.100	
porosity [%]	80 – 99.8	
mean pore diameter [nm]	20 – 150	
inner surface area [m^2 g^{-1}]	100 – 1600 [61]	600
refractive index	1.007 – 1.24	1.02
thermal conductivity λ (in air, 300 K) [W m^{-1} K^{-1}]	0.017 – 0.021	1.02
modulus of elasticity E [MPa]	0.002 – 100	1
sound velocity c_L [m s^{-1}]	< 20 to 800	100
acoustic impedance Z [kg m^{-2} s^{-1}]		10^4

2.1.2. Metal Oxide Aerogels

The principles for network formation of SiO_2 gels also hold for non-silicate inorganic gels. Aqueous solutions of salts or molecular precursors in organic solvents, again usually alkoxides, can be employed for sol–gel processing.

Metal alkoxides of, for example, titanium, zirconium, tin, or aluminum are much more reactive towards water than alkoxysilanes. This is due to the lower electronegativity and higher Lewis acidity as well as the possibility of increasing the coordination number. Table 4 lists some properties that are important for the reactivity of different tetravalent alkoxides. Reactivity in hydrolysis reactions decreases in the order $Si(OiPr)_4 <<< Sn(OiPr)_4$, $Ti(OiPr)_4 < Zr(OiPr)_4 < Ce(OiPr)_4$.

Table 4. Electronegativity EN, ionic radius r for the coordination number four, preferred coordination number CN, and the degree of coordinative unsaturation of the central atom (CN – N) for some tetravalent ($N = 4$) alkoxy compounds.[62]

Alkoxide	EN[a]	r [Å][63]	Preferred CN	CN – N
$Si(OiPr)_4$	1.74	0.40	4	0
$Sn(OiPr)_4$	1.72	0.69	6	2
$Ti(OiPr)_4$	1.32	0.56	6	2
$Zr(OiPr)_4$	1.22	0.73	7	3
$Ce(OiPr)_4$	1.08	1.02[b]	8	4

[a] Allred – Rochow electronegativities. [b] For the coordination number six.

The reactivity towards water is so high for many of these alkoxides that precipitates are spontaneously formed. Whereas the reactivity of alkoxysilanes has to be promoted by catalysts, the reaction rates of metal alkoxides must be moderated to obtain gels instead of precipitates. The most common method is the addition of acetic acid or acetylacetone to the precursor solution. This results in substitution of part of the alkoxy groups by acetate or acetylacetonate. Other chelating or bridging ligands can also be used. The new molecular compound $[M(OR)_y(L)_x]_n$ (L = bidentate anionic ligand, Figure 7) shows a different reactivity, structure, and functionality than the unsubstituted alkoxide $M(OR)_{y+x}$ as a function of the kind and number of the ligands.

Complexation allows the chemical design of the precursors, with which the properties of the sol–gel materials can be deliberately influenced. Not only are new building blocks introduced, but the average degree of condensation is also

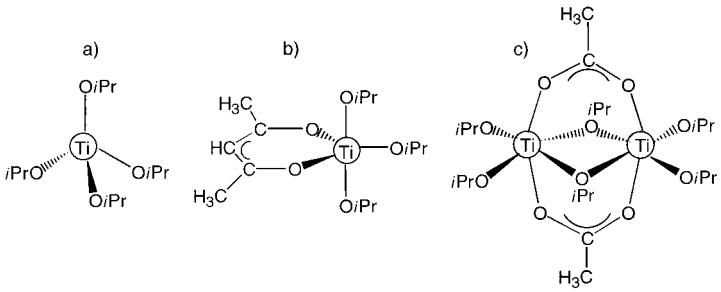


Figure 7. Molecular structure of a) $Ti(OiPr)_4$, b) the acetylacetonate derivative $[Ti(OiPr)_3(acac)]$, and c) the acetate derivative $[Ti(OiPr)_3(OAc)]_2$.

changed. Since the bidentate ligands are located at the surface of the oxo clusters, the size and structure of the primary particles can be engineered by deliberately varying the ratio of alkoxide to ligand.[64, 65]

Typical examples of metal oxide aerogels of some elements or combinations of elements will be discussed in the following. Compared to aerogels with a silicate network, only little work was done to elucidate their network formation and structure. One of the most important differences is the possibility of forming crystalline primary particles. As a general rule, the crystalline portion is favored by a large excess of water in the hydrolysis reaction.

Alumina

The preferred precursors for the synthesis of Al_2O_3 aerogels are $Al(OsBu)_3$ (ASB) and $Al(OtBu)_3$ (ATB). ASB has the advantage of being soluble in 2-butyl alcohol, whereas other aluminum alkoxides are insoluble in the corresponding alcohol. There are different possibilities for handling this problem.[66] The alkoxide can be dissolved in benzene followed by addition of pure water (two liquid phases are formed) or water dissolved in the corresponding alcohol. Alternatively, a dispersion of the alkoxide in the corresponding alcohol can be prepared, and water is added afterwards. Teichner et al investigated the basic chemistry of aluminum alkoxides in the context of preparing Al_2O_3 aerogels.[67–69] They found that one of the most important parameters is the relative amount of water, which allows control of the surface area, the pore volume, and the portion of crystalline (boehmite) and amorphous units in Al_2O_3 aerogels.

Mizushima and Hori prepared Al_2O_3 aerogels from ethylacetylacetonate-modified ASB.[70] They were able to interrupt the process at the sol stage owing to the better control of the hydrolysis and condensation reactions, to remove the solvent, and to modify the alumina particles. A hybrid network between alumina and organic units was prepared by cross-linking with, for example, hexamethylenediisocyanate (Figure 8), which has a lower density and a broader pore-radii distribution than an unmodified alumina aerogel.[71]

Markel et al. prepared Al_2O_3 aerogels by a different method.[72] They amalgamized the surface of metallic aluminum and then oxidized it with O_2. A layer of Al_2O_3 fibers oriented perpendicular to the metal surface was formed, which the authors called an aerogel.

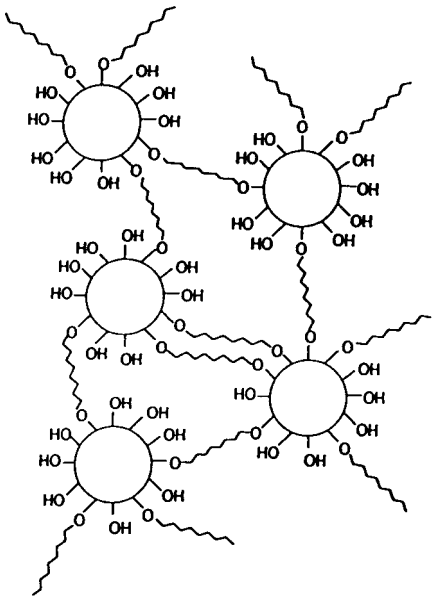


Figure 8. Schematic representation of an alumina gel cross-linked with hexamethylenediisocyanate (reproduced with friendly permission from ref. [71]). The large circles represent particles of hydroxylated alumina, and the snakelike lines $C(O)NH(CH_2)_6NHC(O)$ chains.

Titania and zirconia

The first TiO_2 and ZrO_2 aerogels were prepared by Teichner et al. as early as 1976.[67] Until today, the propoxides and butoxides of these metals are mainly used as precursors.[1f, 73–75]

TiO_2 aerogels can be prepared totally amorphous or with a network of anatase primary particles.[76] Zhu and Tomkiewicz were able to elucidate the microstructure and morphology over two length scales and three density regions by combining SAXS, SANS, N_2 sorption, and electron microscopy: the size and density of the nanoparticles (clusters) and the mesoparticles, and the bulk density of the whole network. Figure 9 schematically shows the network model derived from these measurements. Mesoparticles with a diameter of about 50 nm aggregate to give a three-dimensional network. They are formed by aggregation of the crystalline nanoparticles of about 5 nm in diameter.

As with the alumina gels, the amount of water added for hydrolysis is decisive for the structure of zirconia aerogel networks. Addition of substoichiometric amounts of water results in an amorphous network, whereas a structure composed of crystalline, monoclinic ZrO_2 particles is obtained with an excess of water.[1c, 67] Vesteghem et al. gelled $Zr(OnPr)_4$ in 1-propanol in the presence of acetic acid. The acetate ligand remained in the aerogel.[77]

Zeng et al. investigated the fractal dimension of amorphous and partially crystalline ZrO_2 aerogels.[78, 79] From the results of SAXS measurements (values for d_f [mass fractality] close to 2) they concluded that the aerogels have a branched, polymerlike fractal structure, which is analogous to that of the silicate systems investigated by Keefer and Schaefer,[45, 46] consisting of small primary particles with an average diameter of 5.2 nm (partially crystalline) or 2.5 nm (amorphous). Other one-component oxide aerogels are listed in Table 5.

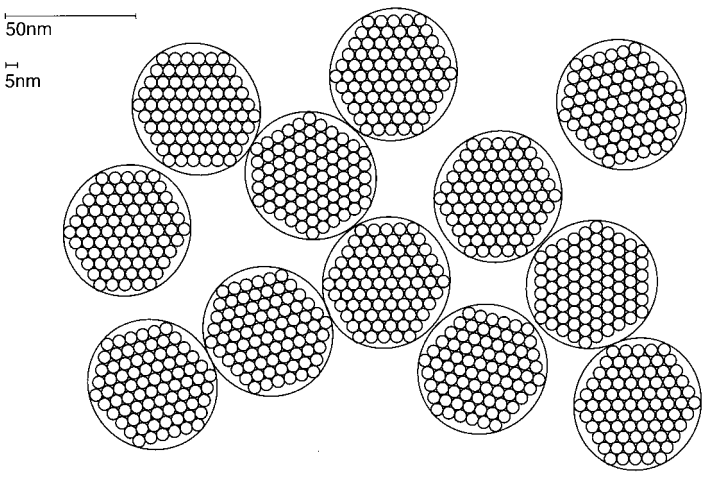


Figure 9. Schematic representation of the structure of partially crystalline TiO_2 aerogels (reproduced with friendly permission from ref. [76c]).

Table 5. Examples of purely inorganic aerogels, precursors for their preparation, and potential applications.

Aerogel	Precursor	Application
V_2O_5	$VO(OiPr)_3$,[80] $VO(OEt)_3$[81]	cathode in lithium batteries
Cr_2O_3	$Cr(NO_3)_3$,[82] $CrCl_3$,[83] $Cr(OAc)_3$[84, 85]	oxidizing properties, fluorination of hydrocarbons with HF
Fe_2O_3	$FeCl_3$,[82, 83] $[Fe(acac)_3]$[86–88]	
MoO_2	$[MoO_2(acac)_2]$[67, 89, 90]	electrocatalysis
Nb_2O_5	$Nb(OEt)_5$[91–94]	isomerizations, solid acids

Binary and ternary oxide aerogels

Compared to other methods for preparing multicomponent oxides, the sol–gel method offers the best control over the resulting properties of the materials by varying the processing parameters.[37, 89, 95, 96] When precursors that undergo hydrolysis and condensation at similar rates are combined, mixed metal oxides are obtained which are homogeneous at the molecular level. With increasing differences in the reaction rates, the microstructure of the product becomes more heterogeneous and phase separation may even occur. In particular, the "core-shell" phenomenon is observed. The faster reacting compound forms sol particles which are "coated" by the slower reacting component. There are several possibilities for avoiding this effect: The reaction rate of the faster reacting component can be moderated by the bidentate ligands discussed above. Alternatively, the slower reacting precursor can be prehydrolyzed, and the faster reacting component added afterwards.[97] The network in the thus prepared aerogels is analogous to that of the one-component oxide aerogels.

Typical binary or ternary systems consist of SiO_2, TiO_2, ZrO_2, or Al_2O_3 combined with NiO, CuO, ThO_2, PbO, or Fe_2O_3. A complete compilation is beyond the scope of this review. Some aerogels are exemplarily listed in Table 6. Mixed oxide aerogels for catalytic applications are summarized in reviews by Pajonk and Baiker.[1c, e]

The structural composition of Al_2O_3/SiO_2 (mullite) systems, prepared from the alkoxides in the presence of bidentate ligands, was thoroughly investigated by Heinrich et al.[101] The interpretation of the SAXS data again led to the postulation of a RLCA-related network. SiO_2 building blocks are partially incorporated into the alumina clusters and partially integrated onto the surface of these particles. The Si–OH groups at the surface of the clusters serve as condensation sites between the particles (Figure 10).

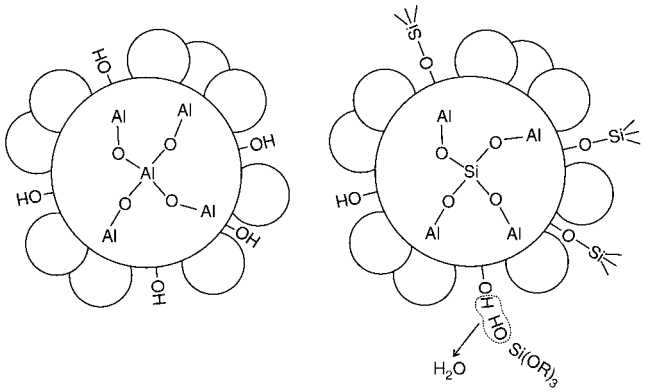


Figure 10. Schematic structure of alumina gel particles in the absence (left) and presence of alkoxysilanes (right). The circular segments at the outside of the particles represent the bidentate ligands (according to ref. [101]).

Several inorganic gels were investigated by X-ray diffraction (XRD). It was found that SiO_2 aerogels are always amorphous, whereas TiO_2, Al_2O_3, and ZrO_2 can also be partially crystalline as anatase, boehmite, or monoclinic ZrO_2.[67] In mixed oxide aerogels the SiO_2 and Al_2O_3 portions

Table 6. Examples of binary and ternary oxide aerogels.

Aerogel	Precursor	Application
TiO_2/SiO_2	$(Ti(OiPr)_4 + acac) + Si(OMe)_4$[98, 99]	epoxidation of olefins
Al_2O_3/SiO_2[100]	$(AlCl_3 +$ ethylene oxide$) + Si(OEt)_4$,[83] $Al(OAc)_3$, $[Al(acac)_3]$	catalyst support
$3\,Al_2O_3/2\,SiO_2$ (mullite)	$(ASB + \beta$-diketone$) + Si(OEt)_4$[101]	preparation of very pure ceramics
Fe_2O_3/SiO_2,[102] Fe_2O_3/Al_2O_3	$[Fe(acac)_3] + Si(OMe)_4$ and ASB	Fischer–Tropsch syntheses
V_2O_5/MgO	$[V(acac)_3] + Mg(OMe)_2$[103]	ammonia synthesis
PbO/Al_2O_3, PbO/ZrO_2	$Pb(OAc)_2 +$ ASB[104] and $Zr(OiPr)_4$[105]	nitroxidation of hydrocarbons to nitriles
BaO/Al_2O_3	$Ba[Al(OsBu)_4]_2 +$ ASB, Ba(1,3-butandiolate) + ASB[106]	car-exhaust catalysis
$x\,Li_2O/(1-x)\,B_2O_3$	$B(OBu)_3 + LiOMe$[107]	
$PbTiO_3$	$Pb(OAc)_2 + Ti(OiPr)_4$[108, 109]	model systems for piezoelectric lead zirconate/titanate (PZT) aerogels
$NiO/Al_2O_3/MgO$	$Ni(OAc)_2 +$ ASB $+ Mg(OMe)_2$	nitroxidation
$NiO/SiO_2/MgO$	$Ni(OAc)_2 + Si(OR)_4 + Mg(OMe)_2$[110]	
$2\,MgO/2\,Al_2O_3/5\,SiO_2$ (cordierite-like)	$Si(OEt)_4 +$ ASB $+ Mg(NO_3)_2$[77]	

are always amorphous.[87, 88, 110–112] However, crystalline aluminates are observed, for example $NiAl_2O_4$.

The structural data of some non-silicate aerogels are listed in Table 7. We want to emphasize again that this is only a selection, because particularly for these aerogels the structural parameters differ decisively with the preparation conditions.

Metals in Metal Oxide Aerogels

A second metal component in the gels must not necessarily yield a binary oxide aerogel. The use of alcohols for supercritical drying (see below) can, under the applied conditions, result in the conversion of easily reducible oxides into metals, because alcohols have reducing properties. Metal particles can also be generated by subsequently reducing the aerogels with hydrogen at high temperatures or by mixing hydrogen into the autoclave during supercritical drying.[118] Aerogels are particularly well suited as carriers for catalytically active metals because of their high porosity. Detailed discussions are found in reviews on aerogels as catalysts.[1c, e]

To incorporate metal components into the gel matrix, the formed aerogels can be impregnated with solutions of the corresponding metal salts (two-step process).[119, 120] Alternatively, suitable metal salts can be added to the precursor solution, which results in the incorporation of the metal compounds into the gel during sol–gel processing.[121] The first metal-containing aerogels, Pt/SiO_2 and Ni/SiO_2, were prepared by Foster and Keyes in this manner with water glass as the source of SiO_2.[82]

The number of examples of metal-doped aerogels and, correspondingly, the number of catalytic reactions in which these materials are employed increase every year. Table 8 gives a short selection.

2.2. Inorganic–Organic Hybrid Aerogels

Materials in which organic molecules or building blocks are combined with structural elements of ceramic materials have only been known for a short time. There are several reasons for modifying oxide aerogels with organic groups. Most importantly, the spectrum of properties of aerogels is widened or improved without influencing the existing positive properties, such as good heat insulation, transparency, and high surface area. For example, the hydrophobicity and the elastic properties of SiO_2 aerogels can be improved relative to unmodified SiO_2 aerogels by incorporating organic groups.[36, 129]

There are only limited possibilities for subsequently doping or modifying aerogels with organic compounds; they will be discussed in Section 4. A more general route is the integration of organic molecules or groups already during sol–gel processing. There are several options for doing this (Figure 11). Embedding molecules into gels without chemical bonding (Figure 11, top right) is achieved by dissolving the molecules in the precursor solution. The gel matrix is formed around them and traps them. Such doped wet gels can, in principle, be converted into aerogels, but the probability is very high that the organic groups are washed out during supercritical drying, which is usually used, and the associated rinsing processes. Bockhorst et al. were able to incorporate a fluorescent dye (POPOV) into the gel network. However, the extent of leaching during aging and drying was relatively high.[130] Although fullerenes C_{60} and C_{70} were also incorporated into SiO_2 aerogels, there is no information on how well the fullerenes are entrapped.[131]

Novak et al. investigated networks built analogously to those in Figure 11, top left (interpenetrating, but not con-

Table 7. Typical structural data of some non-silicate aerogels.

Aerogel	Density [g cm^{-3}]	Porosity [%]	Pore radii [nm]	BET surface area [m^2 g^{-1}]	Particle morphology [nm]
TiO_2[113]	0.3–1	78–90	1–25	316–690	
ZrO_2[67, 77, 81, 94]	0.2–0.3	84–96	10	81–480	2.5–5.2
Al_2O_3[67, 70, 114]	0.13–0.18		5	123–616	22–25 (platelike)
Al_2O_3/SiO_2[101, 115, 116]	0.06–0.21		12		1–5[a]
V_2O_5[81a, 117]	0.04–0.1	96		140–400	$<$ 10 nm (fibrous)
V_2O_5/GeO_2[81b]	0.08	96			
Cr_2O_3[111]	0.15–0.54			516–785	
PbO/TiO_2[108]	0.7	77	1–4	260	45 ± 10

[a] Controllable by the amount of added β-diketone.[116]

Table 8. Examples for metal-doped aerogels.

Aerogel	Precursor for the metal	Application
1. Impregnation		
Cu/SiO_2, Cu/MgO	$[Cu(NH_3)_4](OH)_2$ in alcohol[119]	
$Cu/ZnO/Al_2O_3$	$Cu(OAc)_2$[122]	hydrogenation
Pt/MoO_2	$H_2[PtCl_6]$ in MeOH[120]	hydrogenation
Pd/Al_2O_3, Pd/CeO_2, $Pd/BaO/Al_2O_3$	$PdCl_2$[123, 124]	car-exhaust catalysis
2. Sol–gel method		
Pt/TiO_2	$PtCl_2$, $[Pt(acac)_2]$, $(NH_4)_2[PtCl_6]$[125]	hydrogenation
Pd/Al_2O_3	$Pd(OAc)_2$[126]	car-exhaust catalysis
V/SiO_2	$V(OiPr)_3$	
Cu/SiO_2	$Cu(OAc)_2$[127]	
Pt/Al_2O_3	$H_2[PtCl_6]$[128]	dehydrocyclization

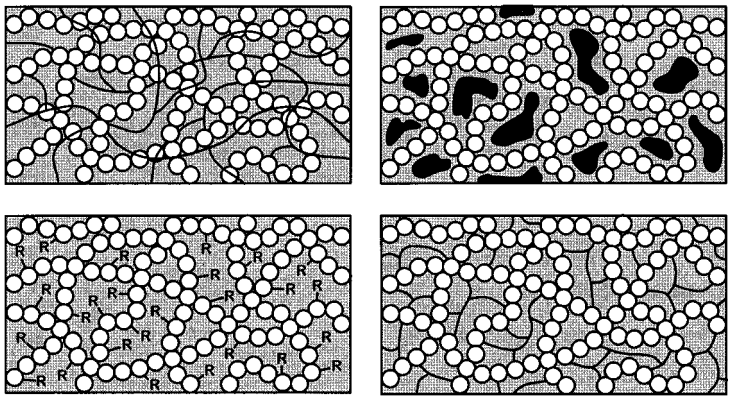


Figure 11. Inorganic–organic hybrid networks obtained by sol–gel processing. Top left: interpenetrating inorganic and organic networks; top right: incorporation of organic molecules (enzymes, dyes, etc.); bottom left: modification (functionalization) of oxidic materials with organic substituents; bottom right: dual networks.

nected networks). The organic polymer was generated in situ during the sol–gel reaction by radical polymerization of a vinyl monomer. The aerogel obtained by supercritical drying with CO_2 consists of interpenetrating inorganic and organic networks (Figure 12).

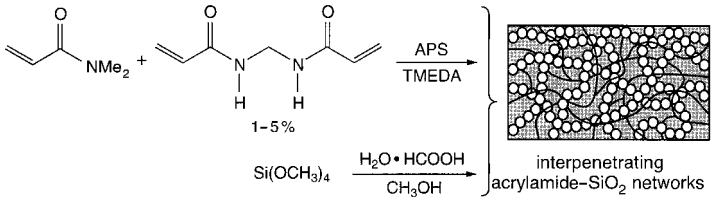


Figure 12. Formation of two interpenetrating networks (inorganic–organic) by simultaneous sol–gel reaction and polymerization of *N*,*N*-dimethylacrylamide (in the presence of *N*,*N*′-methylenebisacrylamide (APS = ammonium persulfate); according to ref. [132]).

Attempts to perform the sol–gel process in solutions of organic polymers usually failed, because the polymer was washed out during supercritical drying. The only success was observed with organic polymers capable of forming hydrogen bonds to the surface silanol groups of the inorganic matrix, such as poly(2-vinylpyridine).[132]

The more important modifications of aerogels are based on covalent bonding of the organic groups (Figure 11, bottom). In silicate systems precursors can be used in which the (functional) organic group is bonded through a hydrolytically stable Si–C link to the network-forming "inorganic" part of the molecule. Compounds of the type $R'Si(OR)_3$, in which R′ is the organic group modifying the inorganic gel, are usually employed. This kind of linkage is not possible for non-silicate systems because of the hydrolytic instability of M–C bonds. However, the organic groups can be introduced with bidentate ligands (Section 2.1.2). The preparation of organically modified xerogels is described in several reviews.[62, 133, 134]

In the remainder of this section we want to concentrate on organically modified SiO_2 aerogels, because these are best investigated. Schwertfeger et al. performed the sol–gel process with a mixture of a tetraalkoxysilane and an organically substituted trialkoxysilane $R'Si(OR)_3$ [Eq. (3)].[36, 129] The

$$x\,R'\text{–}Si(OR)_3 + (1-x)\,Si(OR)_4 + H_2O \xrightarrow{CH_3OH} [R'_x\text{–}SiO_{(2-0.5x)}\cdot H_2O/CH_3OH] \quad (3)$$

R′-substituted silanes (R′ = alkyl, aryl) condense in a kind of two-step process to the network formed from the tetraalkoxysilane under alkaline conditions, because the rate of hydrolysis and condensation of $R'Si(OR)_3$ is slower than that of the corresponding tetraalkoxysilane $Si(OR)_4$. Thus, they modify the inner surface without influencing the typical aerogel properties. The process is similar to the formation of the core-shell structures mentioned in Section 2.1.2. for the preparation of multicomponent oxide aerogels. This kind of network formation was verified by Hüsing et al. by Raman spectroscopy. The spectra clearly show that $Si(OR)_4$ hydrolyzes and condenses before $R'Si(OR)_3$. The R′-substituted silane units therefore condense to the then existing network much later (hours to days).[135, 136] These results are confirmed by NMR spectroscopic investigations, which additionally show the inverse trends for acid-catalyzed mixed sol–gel systems.

The integration of functional organic groups into the aerogel matrix allows further extension of the application spectrum of SiO_2 aerogels (for example, towards catalysts or sensors) because now the chemical properties can also be varied.[136–140] Figure 13 shows a selection of functional organic groups which were already

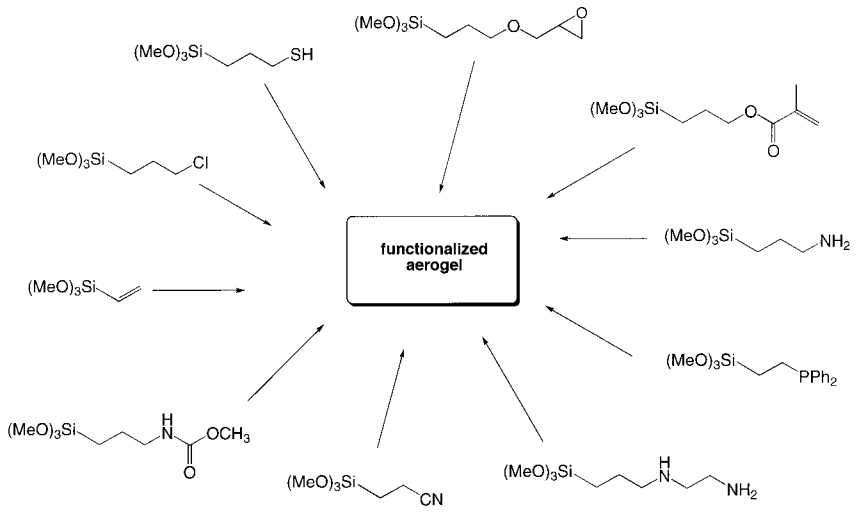


Figure 13. Silane precursors with organic substituents that were used for preparing functionalized aerogels.

successfully incorporated into aerogels. A two-step sol–gel mechanism was also established for most of these groups. Surprisingly, structural variations (porosity, inner surface area) in the functionalized aerogels are not induced as much by the properties of the functional group than by indirect influences on the sol–gel process. The trialkoxysilane basically acts as a co-solvent in the first phase of the reaction. Therefore, the tetraalkoxysilane is more diluted at this stage (resulting in a decrease in the network density), and a larger amount of water and catalyst is available for its reaction (resulting in larger particles).[140]

In another approach, the morphology (pore sizes, surface) of the aerogels is not tailored by the reaction conditions of sol–gel processing but instead by linking of the $Si(OR)_3$ groups in the precursors. Organic groups of variable length (for example saturated or unsaturated hydrocarbon chains, or polyaryls) substituted with $Si(OR)_3$ groups at both ends are used. An inorganic oxidic network in which the hydrocarbon chains bridge the inorganic building blocks is formed during sol–gel processing (Figure 14).

Loy et al. used precursors of the type $(RO)_3Si(CH_2)_n$-$Si(OR)_3$ with $n = 2$, 6, 8, 10, 14 without adding $Si(OR)_4$ for sol–gel processing under both basic and acidic conditions. They showed that the length of the spacer n decisively influences the later aerogel structure.[141] Ethylene- and hexamethylene-modified gels are highly porous and have high specific surface areas (about 700 $m^2 g^{-1}$). The specific surface area decreases with increasing length of the spacer. The tetradecylmethyl-

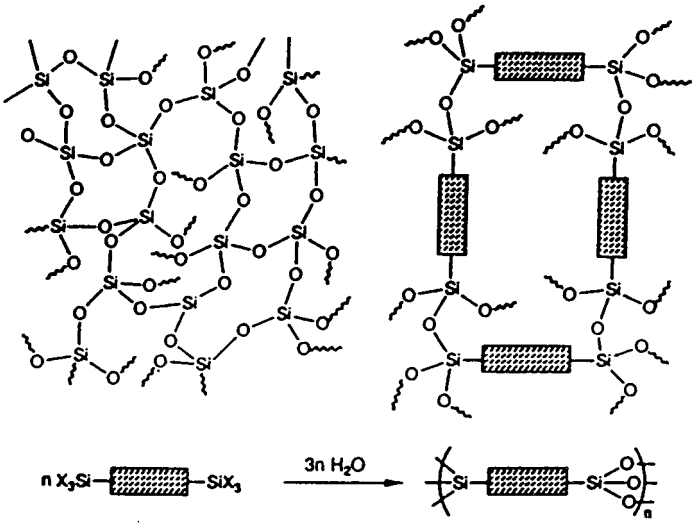


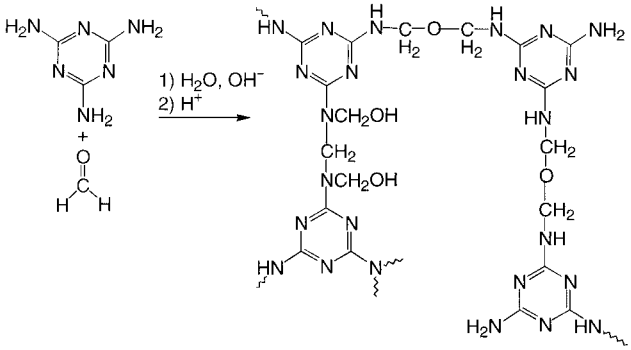
Figure 14. Schematic representation of silica gel (left) and inorganic–organic hybrid silsesquioxanes (right) as well as their syntheses (bottom, with drawings of the arenediyl, alkanediyl, and alkynediyl spacers; reproduced with friendly permission from ref. [141]).

ene-modified "aerogel" is nonporous, and SEM micrographs show a distinctly different morphology (whether this gel really is an aerogel is not discussed here, see Section 1).

2.3. Organic Aerogels

An interesting alternative to the inorganic aerogels was developed by Pekala et al. starting in 1987.[142] Purely organic aerogels were synthesized by polymerization of multifunctional organic monomers in dilute solution followed by supercritical drying.[143–145] Resorcinol/formaldehyde (RF) and melamine/formaldehyde (MF) were the first precursor mixtures for this organic sol–gel chemistry. Gelation was initiated by Na_2CO_3 or NaOH. The gels were then treated with dilute acid to increase the degree of cross-linking and, thus, to stabilize the network.

Resorcinol is a trifunctional monomer which can add up to three equivalents of formaldehyde. These substituted resorcinol derivatives then condense with formation of nanometer-sized clusters which then cross-link through groups at the surface (e.g. CH_2OH). For the polymerization of melamine with formaldehyde, either the monomers or MF polymers with low molecular mass can be used. Equation (4) shows the possible polymerization reactions.[146]



(4)

Topical developments in the area of organic aerogels are based on the polymerization of furfural with a phenolic Novolak resin (prepared by the reaction of phenol with formaldehyde) to give the "PF gels". A decisive advantage over RF or MF polymerization is that alcoholic solutions can be used, and the laborious solvent exchange before drying is avoided.[147]

The most important parameters for the synthesis of purely organic gels are the catalyst concentration and the pH of the solution. Their structure and properties—such as density, specific surface area, or particle and pore sizes—can be deliberately influenced by these variables.

Despite the structural differences originating from the different precursors, organic aerogels have some common properties. These include accessible pores with small diameters (≤ 50 nm), high specific surfaces (400–1000 $m^2 g^{-1}$), and a solid matrix which is formed from either connected colloidal particles or polymeric chains of about 10 nm in diameter.

RF and MF aerogels are built from linked colloidal particles formed during sol–gel processing. The size and number of the clusters strongly depends on the ratio of resorcinol to catalyst (R:C). Typical values are in the range of 50–300. High catalyst concentrations (for example R:C = 50) result in particles with diameters of 3–5 nm that are connected to each other through broad particle necks (polymeric gels). If the R:C ratio is increased, the particle are larger in diameter (11–14 nm) and cross-link like pearls on a string (colloidal gels). The structure of MF gels was investigated by Ruben by high-resolution transmission electron microscopy.[146] Table 9 shows some representative data for organic aerogels.

Table 9. Some typical structural data and properties of organic aerogels.

Parameter	RF aerogel	MF aerogel	PF aerogel[147]
density [g cm^{-3}]	0.03 – 0.06	0.10 – 0.80	0.10 – 0.25
surface area [m^2 g^{-1}]	350 – 900	875 – 1025	385
pore diameters [nm]	≤ 50	≤ 50	
particle morphology [nm]	3 – 20	2 – 10	irregular shape, ca. 10 nm
application	precursor for carbon aerogels	–	precursor for carbon aerogels
color	dark red, transparent	colorless, transparent	dark brown

Pekala and Schaefer tried to apply kinetic models for network formation, developed for inorganic gels, to organic RF aerogels.[148] However, no fractal character was found for these gels in SAXS experiments. Nanophase separation, both initiated and limited by the cross-linking, was discussed as an alternative explanation for the network formation.[3]

3. Drying Methods

Evaporation of the liquid from a wet gel is very complex, and different stages can be distinguished. At the first stage, the gel shrinks by the volume that was previously occupied by the liquid. The liquid flows from the interior of the gel body to its surface. If the network is compliant, as for gels derived from alkoxides, the gel deforms (Figure 15).

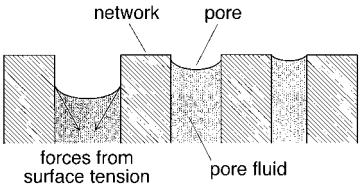


Figure 15. Representation of the contracting surface forces in pores of different size during drying. At the same pressure the curvature of all menisci in the pores is the same. For this reason the larger pores empty first (according to ref. [7]).

Upon shrinkage, OH groups at the inner surface approach and can react with each other. For example, new siloxane bridges are formed in SiO_2 gels. As drying proceeds the network becomes increasingly stiffer and the surface tension in the liquid rises correspondingly, because the pore radii become smaller. The second stage of the drying process begins when the surface tension is no longer capable of deforming the network and the gel body becomes too stiff for further shrinkage. This is the "critical point".[149] At this stage the tension in the gel becomes so large that the probability of cracking is at its highest. At the second stage of drying, the liquid/gas interface retreats into the gel body. Nevertheless, a contiguous funicular liquid film remains at the pore walls; that is, most of the liquid still evaporates from the exterior surface of the gel body. At the third stage of drying this film is raptured. Eventually only isolated pockets contain liquid, which can leave the network only by diffusion into the gas phase.[7, 150]

Two processes are important for the collapse of the network: First, the slower shrinkage of the network in the interior of the gel body results in a pressure gradient which causes cracks. Second, larger pores empty faster than smaller ones during drying; that is, if pores with different radii are present, the meniscus of the liquid drops faster in larger pores (see Figure 15). The walls between pores of different size are therefore subjected to uneven stress and crack.

The parameters influencing these capillary forces are well investigated, and strategies were developed to avoid cracking. Important options are, inter alia, the pore size (larger pores are more advantageous because the capillary force is inversely proportional to the pore radius),[151, 152] aging (the network becomes stiffer), or addition of tensides (reduction of the surface energy leads to a decrease in the capillary forces), organic templates, or drying-control chemical additives (DCCA).[153–157] Crack-free xerogels can be obtained by exact control of these parameters; however, large shrinkage cannot be avoided.

This situation is not sufficient for the production of aerogels. Methods have to be found to conserve the pore structure of the wet gels, that is, to avoid shrinkage. In the following sections possibilities are discussed with which the above-mentioned processes during drying and the occurrence of capillary forces can be avoided.

3.1. Supercritical Drying

In this procedure the solvent is put into the supercritical state, and therefore there are no liquid/gas interfaces in the pores during drying. The wet gel is placed in an autoclave and covered with additional solvent. Drying out of the samples (which would lead to the formation of cracks), is thus avoided, and the critical volume V_c is reached. After the autoclave is closed, the temperature is slowly raised resulting in an increase in pressure (pathway A in Figure 16). Both the

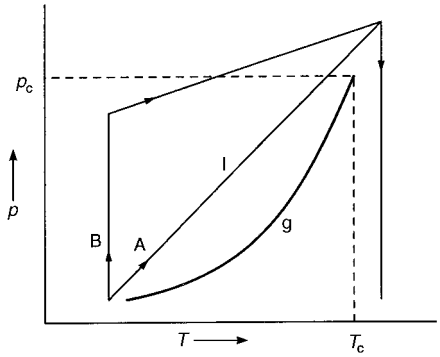


Figure 16. Schematic representation of the principle of supercritical drying. At the critical point (T_c, p_c) the densities of the liquid (l) and the gas (g) are equal. Supercritical drying can be performed along pathway A or B.

temperature and the pressure are adjusted to values above the critical point of the corresponding solvent (T_c, p_c) and kept there for a certain period of time. This ensures that the autoclave is completely filled with the supercritical fluid. The fluid is then slowly vented at constant temperature, which results in a drop in pressure. When ambient pressure is reached, the vessel is cooled to room temperature and then opened. Drying is often performed in a way that the vessel is prepressurized with nitrogen to avoid evaporation of the solvent (pathway B in Figure 16).[158] The phase boundary between the liquid and the gas must not be crossed during drying.

In principle, different organic solvents can be used for drying. The critical constants of the most common drying fluids are listed in Table 10. Supercritical drying is performed either "hot" (organic solvents) or "cold" (CO_2) depending on T_c.

Table 10. Critical constants for some solvents.

Solvent	T_c[°C]	p_c[Mpa]	V_c[cm^{3}mol^{-1}]
methanol	240	7.9	118
ethanol	243	6.3	167
acetone	235	4.7	209
2-propanol	235	4.7	
H_2O	374	22.1	56
CO_2	31	7.3	94
N_2O	37	7.3	97

3.1.1. Drying in Organic Solvents ("Hot")

The pore liquid, which is usually an alcohol or acetone owing to the preparation conditions, is used as the supercritical fluid. About 250 °C and 5–8 MPa are needed to put the solvent in the supercritical state. Problems arise from the combination of high temperatures and high pressure as well as the flammability of these solvents. In August 1984 the main gasket in the lid of a 3000-L pressure vessel for the production of 60×60 cm^2 aerogel tiles failed in a pilot plant in Lund (Sweden). More than 1000 liters of methanol were released, and a big explosion destroyed the whole building.[159]

In addition to the risks connected with supercritical drying in organic fluids, rearrangement reactions in the gel network are highly probable because of the high temperatures. For example, in SiO_2 aerogels a modification of the surface may occur upon conversion of Si–OH into Si–OR groups, or processes such as during aging and ripening of the gels are accelerated. Small pores are thus filled, and particle necks strengthened. As a consequence, the resulting aerogels have a lower specific surface area, a narrow pore-radii distribution (elimination of microporosity), and a stiffer network.[160–163] Organically modified aerogels are particularly sensitive to the high temperatures, and functional organic groups may be destroyed during drying.[164] Phase separation and loss of stoichiometry (SiO_2/B_2O_3, SiO_2/B_2O_5)[165] or crystallization (SiO_2/TiO_2)[166] may occur in multicomponent gels.[1e, 167]

3.1.2. Supercritical Drying with CO_2 ("Cold")

An alternative to drying in organic solvents is the use of liquid carbon dioxide.[168-170] This method was developed by biologists for electron microscopy[171] and has the advantage of a very low critical temperature at a moderate critical pressure. However, a time-consuming solvent exchange is necessary. The time required for exchanging the original pore liquid for liquid CO_2 is determined by the diffusion of carbon dioxide into the gel, and is therefore dependent on the dimensions of the gel body. Another requirement is the miscibility of the pore liquid with carbon dioxide. For example, water and CO_2 are immiscible, and therefore an intermediate solvent exchange (e.g. water for acetone) is necessary.[107]

Structural changes, as observed during supercritical drying with alcohols, take place to a minor extent with CO_2. Therefore, the network of the wet gel can be conserved almost unchanged.

A modification of this method and its application in a continuous plant in which CO_2 is recycled was described by van Bommel et al.[172, 173] Heating and cooling of the autoclave is avoided by exchanging the solvent with CO_2 that is already in the supercritical state.

Brodsky and Ko showed that deliberate structural changes can be induced in SiO_2/TiO_2, ZrO_2, and Nb_2O_5 aerogels by varying the temperature above T_c during supercritical drying with CO_2. For example, the ratio between crystalline and amorphous regions, which is important for catalytic applications, can thus be influenced.[174]

3.2. Freeze-Drying

Another possibility for avoiding phase boundaries between the liquid and gas phases during drying is freeze-drying. The pore liquid is frozen and then sublimed under vacuum.

Several attempts were made to use this method for producing aerogels.[175–177] However, aging periods have to be extended to stabilize the gel network, the solvent must be exchanged for another with a low expansion coefficient and a high pressure of sublimation, and low freezing temperatures should be achieved by addition of salts. Another disadvantage is that the network may be destroyed by crystallization of the solvent in the pores. Cryogels are therefore only obtained as powders.

3.3. Ambient-Pressure Drying

To make aerogels interesting for larger scale commercial applications, one must avoid the most expensive and risky part of the preparation: supercritical drying. Therefore, the interest in alternative ways for exchanging the pore liquid in the gels by air is very high. However, with the above-mentioned processes (Sections 3.1 and 3.2) during drying in mind, the intention already appears to face a contradiction.

The capillary forces exerted by the meniscus of the pore liquid and the pressure gradient upon the large shrinkage of the network are the main reasons for the collapse of the filigrane structure (see Section 3). To dry aerogels at ambient conditions (subcritical drying), one has to strengthen the network to avoid its collapse (irreversible shrinkage). Additionally or alternatively, the contact angle between the pore

liquid and the pore walls has to be influenced by deliberate modification of the inner surface and variation of the solvent to minimize the capillary forces.

Smith, Brinker, and Deshpande published the first synthesis of SiO_2 aerogels dried at ambient pressure in 1992.[178] In principle, their procedure involves a series of solvent-exchange processes and a modification of the inner surface.[179] The water/alcohol mixture in the pores of the gel is first exchanged for a water-free solvent, and the Si–OH groups at the surface are silylated (e.g. with chlorotrimethylsilane). The reactivity of the gel surface is thus reduced, and the surface hydrophobized. The actual drying process is performed after another solvent exchange. As expected, the gel shrinks strongly during evaporation of the solvent from the pores. However, no irreversible narrowing of the pores with formation of Si-O-Si bonds is possible because of the silylation. The gel therefore expands to nearly its original size after reaching the critical point. This is called the "spring-back effect". One of the prerequisites for this procedure is the strengthening of the network by exact control of the aging conditions. The network of the modified gels must be stable enough to tolerate a reversible shrinkage to 28% of its original volume![180]

Einarsrud et al. obtained similarly good results with another strategy.[181, 182] They increased the strength and stiffness of the network drastically by aging the wet gels in solutions of tetraalkoxysilanes in aqueous alcohols, and were thus able to avoid shrinkage during drying completely. The monomers added during aging mainly condense in the smallest pores and at the particle necks; the microporosity of the gels is thus lost. The gels can also be dried at ambient pressure between 20 and 180 °C because of the stiffer network.

The technique of ambient-pressure drying for preparing aerogels is still in its infancy, but is a highly topical area in which many research activities are concentrated. Since companies like Hoechst and Nanopore have taken over this method developed by Smith et al., a technically much simpler and therefore less expensive method is available. This makes the industrial application of aerogels economically interesting.[183]

4. Modification of Aerogels after Drying: Is There Chemistry after the Critical Point?

Chemical modifications are still possible even after drying. The intention of this section is to show some possibilities for improving or modifying the property profile of aerogels, in particular with respect to special applications. The examples show that this is another approach for chemically modifying aerogels which until now, however, was hardly used.

The subsequent doping of an aerogel host with active components appears attractive because of the high porosity of aerogels. However, follow-up treatment with a liquid phase is difficult because wet gels are formed again. As discussed in Section 2.1.2 aerogels can be doped with metals by impregnation with a suitable metal salt. The metal salt has to be introduced in alcoholic solution, and then the solvent has to be removed again in another supercritical drying step in order not to prevent destruction of the aerogel network.[122]

Another, more general possibility for subsequently modifying aerogels is their reaction with gaseous compounds. Early attempts were performed with gaseous dichlorodimethylsilane or other silylation reagents to remove the reactive silanol groups at the surface of the network and thus to hydrophobize the aerogel permanently.[184] There are now better possibilities for hydrophobation. However, doping with compounds from the gas phase is increasingly an attractive option. Even a homogeneous distribution in monoliths can be achieved.

Hunt et al. intensively investigated the reaction of aerogels with gaseous reactants, and called this method chemical vapor infiltration (CVI). Originally, the intention of this approach was to improve the thermal properties of aerogels by incorporation of carbon (see Section 5.2).[185–187] For this purpose, the aerogels were allowed to react with acetylene, methane, propane, xylol, or furfuryl alcohol in a stream of an inert gas at high temperatures. The temperatures necessary for pyrolysis depend on the gas and varied between 350 and 850 °C. The aerogels strongly favor decomposition of the organic compounds. Carbon is deposited as graphite on the inner surface of the aerogels, and even nanometer-sized carbon fibers, rings, and tubes were found.

The CVI method appears to be broadly applicable. Its potential is clearly visible for reactions in which new products are formed by chemical, thermal, or photolytic treatment. Cao et al. were able to prepare SiO_2/Si nanocomposites by decomposition of gaseous silanes (such as SiH_4 or $HSiCl_3$) in SiO_2 aerogels, which then showed photoluminescence upon irradiation with ultraviolet light.[188] Analogous reactions with ferrocene resulted in the deposition of iron particles in the aerogel matrix, which then displayed interesting magnetic properties.[188] Reaction of SiO_2 aerogels with $[W(CO)_6]$ and subsequent thermal decomposition of the metal carbonyl in the aerogel resulted in metallic tungsten particles. WN or WS_2 particles in aerogels were formed by follow-up treatment of the metal-doped aerogels with ammonia or sulfur. SiO_2 aerogels were analogously treated with gaseous $[Fe(CO)_5]$. Under an oxidizing atmosphere amorphous iron oxide/SiO_2 aerogels were formed, which were transformed into Fe_3O_4/SiO_2 (by reaction with additional $[Fe(CO)_5]$) or Fe_9S_{10}/SiO_2 aerogels (by reaction with H_2S).[189] Organic compounds can also be sublimed into the network through the gas phase as shown for a porphyrine derivative.[190]

Besides the treatment of aerogels with gaseous compounds, pyrolysis of organic groups which are part of the aerogel structure is another possibility for modifying aerogels. Schwertfeger et al. pyrolyzed the organic groups of inorganic–organic hybrid aerogels (see Section 2.2). They were thus able to coat the aerogel network with carbon nanostructures.[186a]

Pyrolysis reactions are most important for preparing carbon aerogels, which are of particular interest because they are the first electrically conducting aerogels.[191] They can be made by pyrolysis of resorcinol/formaldehyde or phenol/furfural aerogels under an inert atmosphere (1050 °C/N_2). Their structure and morphology basically corresponds to that of their precursors; that is, there are colloidal or polymeric gels (Table 11). The colloidal gels have spheric particles with

Table 11. Typical structural data of carbon aerogels.

skeletal density [g cm^{-3}]	2.06
density [g cm^{-3}]	0.05 – 0.80
specific surface area [m^2 g^{-1}]	600 – 800
pore size [nm]	< 50
particle morphology [nm]	3 – 20, amorphous
appearance	black, opaque

diameters of 12 – 15 nm which are loosely connected by graphitic ribbons. The polymeric gels have smaller particles (7 – 9 nm) connected by broad particle necks. Two factors mainly influence the properties of carbon aerogels: the ratio of precursor to catalyst during the preparation of the organic gels and the pyrolysis temperature.

5. Properties and Applications

SiO_2 aerogels are currently the aerogels with the highest potential for applications. They are not only the best investigated with regard to their preparation, structure, and properties, but can also be prepared with lower costs than other aerogels (cheaper precursors). There are already commercial applications. The development of the sol – gel process for non-silicate materials has recently boomed. One of the consequences is that the number of possibilities for varying aerogels becomes considerably larger. Non-silicate aerogels (see Section 2.1.2) increasingly play an important role, particularly in the search for new catalysts. In the case of organic aerogels, mainly their pyrolysis products (carbon aerogels) offer interesting new applications.

Since the main focus of this review is on the chemistry of aerogels, only a short overview on the properties of aerogels and the resulting applications will be given. Comprehensive information on these topics can be found in more physically oriented reviews.[1]

5.1. Optical Properties

The optical properties of SiO_2 aerogels and the derived inorganic – organic hybrid aerogels vary between transparent and translucent, depending on the preparation conditions. This means that the structure-forming units are smaller than the wavelength of visible light. However, inhomogeneities in the network in the nanometer range result in Rayleigh scattering. Therefore, aerogels appear yellowish under light and bluish against a dark background (see page 22). The portion of Rayleigh scattering correlates directly with the homogeneity of the gel network in the nanometer range. Objects that are viewed through an aerogel tile appear slightly blurred. Inhomogeneities in the micrometer range at the exterior surface of the aerogel body are responsible for this phenomenon.[192]

Numerous attempts were made to influence the optical properties of SiO_2 aerogels deliberately for their application in Çerenkov detectors (see below) or for transparent heat insulation. A transparency as high as possible is required for both applications. Initially, there were more physically oriented approaches to solving this problem, such as investigating the influence of the drying process, of water adsorbed to Si–OH groups, or of adsorbed organic components. It was found, for example, that supercritical drying with CO_2 results in more transparent materials than drying with organic fluids.[169, 193] Heating the aerogels also improves their transparency due to desorption of water and burning of organic components.[1d, 194]

However, these efforts are like putting the cart before the horse. Since scattering phenomena caused by inhomogeneities in the network are responsible for an insufficient transparency, it appears more logical to influence the transparency at its origin by optimizing the sol – gel parameters.[195, 196]

Russo and Hunt tried to quantify scattering in SiO_2 aerogels. They prepared aerogels from TMOS or TEOS under various conditions to determine the optimal precursor composition and gelation conditions.[196] They showed that transparency can be improved by lowering the concentration of water and the reaction temperature. Furthermore, base catalysis is more favorable, and aerogels prepared from TMOS show about nine times less scattering than the corresponding aerogels from TEOS. However, these are not necessarily general trends but instead specific statements for the investigated systems. The correlation of scattering measurements with other structural investigations (N_2 sorption according to Brunauer, Emmett, and Teller) was not successful.

Emmerling et al. investigated the pH dependence of the transparency of gels from TMOS. They showed that there are two distinct extinction minima (high transparency) at pH 1 and 13. They concluded from the correlation of these results with those from SAXS measurements that the particle diameter has to be kept small to improve the optical quality. Interestingly, the transparency was improved in this case when more than a stochiometric amount of water was used for hydrolysis and condensation.[197, 198] In subsequent work the same group correlated the transparencies of SiO_2 aerogels prepared in one step from TMOS, gels from water glass, and gels from the two-step synthesis with the nanostructure of their networks (SAXS, Ultra(U)-SAXS). Aerogels from water glass showed the lowest transparency because of the larger particles and the presence of sodium ions. The aerogels prepared in two steps were distinctly more transparent than gels prepared in one step, probably because smaller clusters are formed during the acid-catalyzed first step.[197]

The latter results were confirmed by Cao and Hunt.[199] They also showed that aerogels prepared by the two-step process (acid hydrolysis and subsequent base-catalyzed condensation) are more transparent than the corresponding aerogels prepared in one step (acid or base catalysis).

Çerenkov detectors

Çerenkov radiation is emitted by charged particles such as piones, muones, or protons if they move faster than light in a medium. A cone-shaped electromagnetic shock wave is formed, from which light is emitted. The velocity of the particles can be calculated from the cone angle. Since the speed of light depends on the refraction index of the medium,

media with different refraction indices were searched. SiO_2 aerogels with refraction indices between 1.007 and 1.024 offer a range not covered by the previously used compressed gases or liquids. Aerogels as solid materials additionally allow easier construction of the detectors and are therefore ideal materials for this application.[200, 201] They are now installed in several Çerenkov detectors worldwide, and the amount of aerogel tiles produced for this application is impressive. For example, 1000 liters of SiO_2 aerogels were produced by Henning for an experiment at the CERN in Geneva, and Poelz et al. equipped a detector (TASSO) at the German Electron Synchrotron (DESY) in Hamburg with 1700 liters of SiO_2 aerogel.[16a]

5.2. Thermal conductivity

The thermal conductivity of aerogels is extraordinarily low. It is made up of three components: thermal transportation by the gas phase, by the solid phase, and by radiation. Figure 17

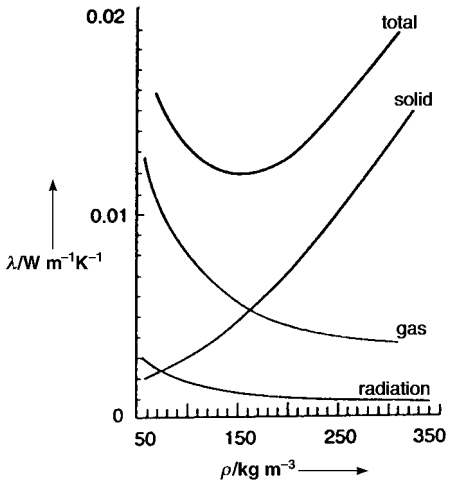


Figure 17. Composition of the thermal conductivity of aerogels: gas, solid, and radiation transport λ depending on the density ρ of the material (reproduced with friendly permission from ref. [200]).

schematically shows the contribution of these components depending on the bulk density. The solid conductivity clearly increases with increasing density, whereas the reverse is true for the gas and radiative transport. The minimum for the total thermal conductivity is at a density of about 0.150 $g\,cm^{-3}$.[200] Heat transport by the gas phase can be avoided by evacuation of the system. For example, an evacuated SiO_2 aerogel at about 300 K shows a thermal conductivity of only 0.010 $W\,m^{-1}\,K^{-1}$, compared to 0.020 $W\,m^{-1}\,K^{-1}$ in air.[202] This is not a special property of SiO_2 aerogels. Thermal conductivities as low as 0.012 $Wm^{-1}\,K^{-1}$ were measured for non-evacuated organic RF aerogels.[203]

Another possibility for reducing the thermal conductivity of SiO_2 aerogels is to reduce the radiative heat transport. This is more important at high temperatures, because the radiation maximum is then in a wavelength range in which SiO_2 does not sufficiently absorb (3–5 μm). Reduction of the thermal conductivity at these temperatures is possible by doping the aerogels with infrared opacifiers, such as carbon soot or TiO_2. These compounds can be mixed in a highly dispersed form to the precursor solution during sol–gel processing or to the sol.[203] Another possibility is the generation of carbon in the aerogel by pyrolysis of organic gases or covalently bonded organic groups of hybrid aerogels (see Section 4). The latter method leads to a particularly efficient decrease in the thermal conductivity (0.012 $W\,m^{-1}\,K^{-1}$ in air at 300 K), because the aerogel skeleton is partially covered with nanometer-sized carbon structures.[204] The improvement of heat-insulation properties is a continuing topic of intense research.[16]

Aerogels have the lowest thermal conductivities of all solids (Figure 18). There is no question that they belong to the best heat-insulation materials currently available. Additional ad-

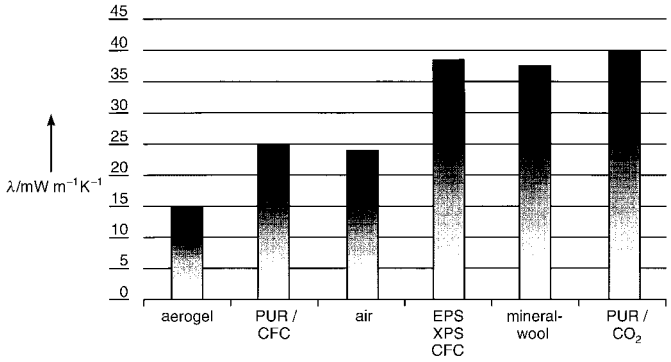


Figure 18. Comparison of the thermal insulation properties of some commercially available insulating materials. PUR: polyurethane foam, CFC: chlorofluorohydrocarbons; EPS, XPS: expanded and extruded polystyrene (reproduced with friendly permission from ref. [183]).

vantages are their nonflammability and transparency (see page 22 and Figure 1). However, a big problem for the insulation of windows is the production of large aerogel panels.[205] Conventional window systems cannot be equipped with the commonly prepared granulate, which is not transparent due to the roughness of its surface; they can only be used for "daylight windows" (for example bathroom, staircase, or ceiling windows). The scattering of the sunlight in the granulate layer is here rather advantageous, because a diffuse lighting of the rooms is achieved.

In addition to transparent thermal insulation, applications for a variety of other insulation problems are conceivable for which the transparency of the insulating material is not necessary, for example in cooling or heating systems and high-temperature batteries.[206, 207] Aerogels can also be utilized for the passive use of solar energy, for example for paneling house walls (Figure 19) or for coating solar-energy collectors.[208, 209] In the Cité Solaire in Ardon (Switzerland) a house was built using an aerogel granulate as a translucent insulating material. A layer of the transparent aerogel allows the penetration of the sun's radiation to the blackened wall, but not the escape of the heat generated there.[210]

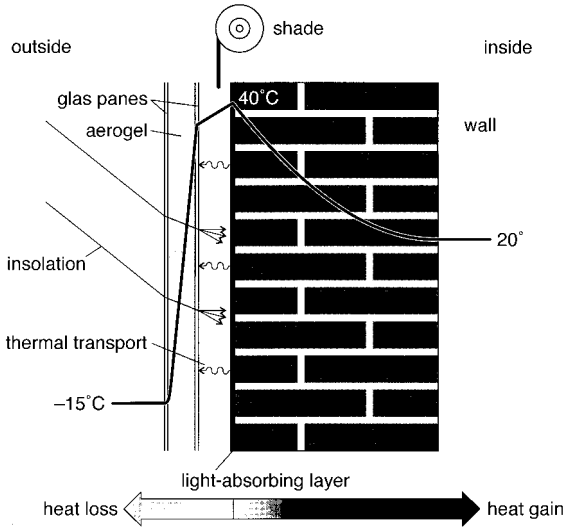


Figure 19. Concept for energy saving by passive use of the solar energy (reproduced with friendly permission from ref. [200]).

5.3. Hydrophobicity

One of the big problems of unmodified SiO_2 aerogels, in particular for technical use, is their long-term stability under a humid atmosphere. Owing to the large number of silanol groups on the inner surface of the material, adsorption and capillary condensation of water and eventually cracking of the gel body by the resulting capillary forces results. Approaches to hydrophobize aerogels permanently were therefore investigated quite early. The possibility of allowing an aerogel to react subsequently with a silylating reagent, such as chlorotrimethylsilane, has the disadvantage of a complicated processing procedure. This kind of modification is only possible by the gas phase (see Section 4).

Hydrophobation at the alkogel stage is time-consuming, since the diffusion rate of the silylating reagent into the pores is a limiting factor. However, this process is a key step in the prevailing ambient-pressure drying of aerogels (see Section 3.3); that is, aerogels prepared by this method are inherently hydrophobic.

Schwertfeger et al. prepared permanently hydrophobic aerogels with a one-step process using a mixture of a tetraalkoxysilane and an organically substituted trialkoxysilane for sol–gel processing (see Section 2.2).[36] They were able to prepare aerogels that floated on water for months (see full-page picture on page 22) while retaining the typical aerogel network.

5.4. Mechanical and Acoustic Properties

Mechanical properties have many aspects. Among others, rigidity, brittleness, and form stability as well as the method of investigation have to be considered. Although the rigidity of aerogels is low because of their structure and the brittleness of the SiO_2 particles, it is sufficient for most applications. The compressive strength of monolithic SiO_2 aerogels is between $0.15-0.30\ N\,mm^{-2}$, depending on the density, with an elastic compression of about 2–4%. The rigidity in vacuum is distinctly higher. The tensile strength is about $0.020\ N\,mm^{-2}$.[211]

One of the decisive parameters for the mechanical properties is the connection of the network in the nanometer range, which strongly depends on the preparation conditions. For example, aerogels prepared under acidic or neutral conditions are about twice as stiff as the corresponding samples prepared under base-catalyzed conditions.[212] Investigations of organically modified aerogels showed that the elastic properties of SiO_2 aerogels can also be improved by chemically modifying the precursors. Ultrasound measurements were used for these investigations. The longitudinal sound velocity is connected with one of the elastic constants (which correlates with the Youngs modulus), and the density of the aerogel. The reason for the improved elastic properties of hybrid aerogels is probably that the presence of alkyl or aryl groups at the surface of the secondary particles impairs stiffening of the particle necks by Ostwald ripening.[137]

Kramer et al. were able to prepare aerogels with very good elastic properties by cocondensation of flexible polydimethylsiloxanes (PDMS) with TEOS. An elastic compression of up to 30% was observed for aerogels into which 20 wt% of PDMS was incorporated.[213]

The particular network structure of aerogels results in impressive acoustic properties which, as mentioned above, correlate with the elastic properties.[214] The sound velocities in SiO_2 aerogels of $100-300\ m\,s^{-1}$ are among the lowest for inorganic solids (this is noteworthy when one considers that sound velocities of $5000\ m\,s^{-1}$ were measured in quartz glass).[215, 216]

The product of density and sound velocity is the acoustic impedance. Since both are low, SiO_2 aerogels have the lowest impedances of all solid materials ($Z = 10^4 - 10^5\ kg\,m^{-2}\,s^{-1}$). This allows interesting applications. For example, aerogels can be used as $\lambda/4$ layers for matching the high acoustic impedance of piezo ceramics to the low impedance of air. The efficiency of these devices is considerably increased by decreasing the reflexion losses at this interface.[217, 218]

5.5. Applications in Catalysis

All the advantages of sol–gel processing for preparing catalysts or catalyst supports—in particular the controllable dispersion of the active component and the possibility of deliberately influencing the microstructure—also apply for aerogels. Additionally, typical structural properties predestinate them for these applications: the extremely high inner surface (which is easily accessible because of the open porosity), the large pore volumes, the excellent temperature stability, and the high selectivities in catalytical processes. Nearly all oxides relevant for catalytical applications can be prepared as aerogels. This is also true for binary and ternary compositions, mixtures of metal oxides, or metal particles on oxide carriers. Furthermore, aerogels can be prepared as powders, granulates, or monolithes, either amorphous or with crystalline portions (see Section 2).

Despite these advantages, the use of aerogels in catalysis has only been increasingly investigated since 1974. The number of publications rises drastically every year. Considerable progress was achieved in solving problems originating from the low density and the low thermal conductivity, that is, pressure drops and bad heat dissipation in the catalyst bed. For example, heat-dissipating materials can be added, or the aerogels can be deposited already during their preparation (i.e. in the autoclave) on a carrier (such as Raschig rings, metal tubings, cordierite honeycombs, wire mesh screens, boiling stones, and others).[84]

It is impossible to list all the investigated systems here; they are summarized in more specialized reviews by Pajonk[1c] as well as Schneider and Baiker.[1e] The following incomplete selection is intended to give an impression of the numerous possibilities: nitroxidation of hydrocarbons to nitriles (NiO/Al_2O_3 with SiO_2 and MgO, PbO/ZrO_2),[105, 112] hydrogenation of nitrobenzene to aniline and of toluene to methylcyclohexane (Ni/SiO_2, Pd/Al_2O_3),[126] hydrogenation and hydrogenolysis after hydrogen "spillover" activation (ZrO_2, SiO_2, MgO, Al_2O_3),[219] isomerizations (Nb_2O_5, Nb_2O_5/SiO_2),[91, 92] Fischer–Tropsch syntheses (Fe_2O_3/Al_2O_3, Fe_2O_3/SiO_2),[102] polymerization of ethene or propene ($TiCl_4/Al_2O_3$),[220] deNO_x reactions ($Fe_2O_3/Cr_2O_3/Al_2O_3$, Pt/C),[143, 221] catalysis for combustion of car exhaust (Pd/Al_2O_3, Pt/Al_2O_3, $Pd/Al_2O_3/SiO_2$),[124, 222] and fluorinations (Cr_2O_3).[85]

5.6. Aerogel Films

Films (coatings) are one of the most important applications of sol–gel materials. Completely dense or partially densified films are prepared in most cases. However, there are numerous applications in which porous films are required. Aerogels with their high porosity and the resulting unique physical properties are highly interesting for such applications. Although aerogels can in principle also be prepared as films, supercritical drying is here a very delicate issue. Nevertheless, aerogel films were synthesized in some laboratories.[223, 224] The possibilities provided by ambient-pressure drying (see Section 3.3) eliminate the principal obstacles for preparing highly porous films.[225–227] The development and use of aerogel films is clearly just in its infancy.

Applications of aerogels as $\lambda/4$ layers for acoustic impedance matching or as catalytically active layers on carriers were already mentioned. Other examples for the application of aerogel films from the Lawrence Livermore National Laboratory in California are optical coatings for solar cells because of their low refractive index (aerogel films prepared for this purpose are subsequently fixed to the surface of the solar cell).[228] The currently used glass layers with high refractive indices can thereby be replaced by aerogels. More light reaches the active surface because of the lower Fresnel scattering losses. The efficiency of the solar cell is thus increased. Thermal applications are also interesting. For example, IR detectors can be coated to obtain a kind of shield against the heat radiating from the substrate.

Other applications for which aerogel films can compete with existing technologies are in microelectronics; here, the low dielectric constant of aerogels plays a particularly important role. With a value of lower than 2.0, they offer important progress in the velocity of electric curcuits. In addition, the dielectric constant is easily controlled because it is directly correlated with the porosity and thus the density of the materials.

This is only a short list of interesting possible applications for highly porous films. Many more will certainly emerge in the future.

5.7. Carbon Aerogels

Carbon aerogels are very well suited as electrode materials because of their low electric resistance ($< 40\ m\Omega\,cm$), their controllable pore-radii distribution (1–50 nm), and their high specific surface area. When a voltage is applied, a thin polarization layer with high capacity is formed on the large surface area. More charge can be stored than with conventional capacitors, because the surface area per volume is very high for aerogels. Compared with other materials (carbon powder or fibres), aerogels have the big advantage that they can be prepared as monoliths.[191]

5.8. Other Applications

Aerogels can be sintered at low temperatures and can therefore be processed to extremely pure and totally homogeneous glasses.[229, 230] The inner surface area and the porosity decrease during sintering. The pore structure can therefore be modified in a controlled way by partial sintering. This was used, for example, for producing gas filters with pores in the range of 20–100 nm.[231] Partially sintered aerogels can resist the tensions of a gas/liquid interface because their texture is strengthened during sintering. They can therefore be used for the storage, thickening, or transport of liquids, for example rocket fuels; in this case the low weight of aerogels is particularly advantageous.[1b]

There are no limits to the fantasy required to find other potential applications of aerogels. The concluding examples show that also exotic applications can be considered: SiO_2 aerogels are suitable as ecologically sound insecticides against pests in grain and seeds or on the ground, such as mites, ticks, cockroaches, or silver fish.[232,233] As a chemically inert dust with small particles and a high specific surface area, aerogels can remove the protecting lipide layer of insects by abrasion or adsorption. They are then killed by rapid loss of body liquid.

SiO_2 aerogels are currently one of the standard media for collecting cosmic dust,[234] and they are fixed on the outside of spacecrafts.[235] Aerogels have the advantage that they are extremely light with a unique mesostructure which is also transparent. This enables a "soft landing" of very fast extraterrestrial particles hitting with a velocity of more than $3\ km\,s^{-1}$, and also allows their later investigation by optical methods.

6. Final Remarks

The preparation of aerogels is "nanotechnology", because their unique optical, thermal, acoustic, and mechanical properties originate from the combination of a solid matrix (with a certain chemical composition) and nanometer-sized pores filled with air. We wanted to show in this review that there is a direct connection between the chemistry of the sol–gel process and the structure of the gels on one hand, and between the structure and the properties of the aerogels on the other. The choice of the precursors and the chemical reaction parameters already determines the physical properties of the final materials.

Physical research currently dominates the area of aerogels. The unique physical phenomena were and are intensively investigated, and are already well understood in many cases. In contrast, most aerogels are prepared empirically. Although the chemical principles are known, we are far away from a chemical "design" of aerogel properties and from an understanding of structure–property correlations. There is thus a wide field for applied chemical research. This is particularly true for the transfer of the physical effects investigated for simple systems, mostly SiO_2, to chemically more complex systems. Porous materials with totally new combinations of properties and applications can be expected by the combination of new chemical compositions with deliberately prepared micro- and nanostructures.

A big push forward can be expected in the next few years. The possibilities originating from ambient-pressure drying will provide strong impetus to preparative chemical research, because aerogels can now be prepared with standard laboratory equipment. The new drying methods have made the preparation process much "more chemical". There is now room for more extensive chemical modifications of the profile of properties of aerogels.

The new drying methods are also a big step forward from an economic point of view. Apart from special applications in which material costs only play a minor role, the rather high price of supercritically dried aerogels has hindered a broader range of applications. The most important area for the application of aerogels are all kinds of thermal and acoustic insulation. There is no doubt about the physical and ecological advantages (nontoxic, nonflammable, readily disposable) of SiO_2 aerogels over most other materials on the market. However, according to a study of the Austrian Academy of Science,[236] the period of amortization for aerogel insulation is relatively long when one considers the materials and energy streams over the whole preparation process (including the production of the precursors), even for favorable applications such as daylight elements. The new drying techniques will probably make the technical preparation much cheaper and will thus make aerogels more competitive.

Our own work was funded by the Bundesministerium für Wissenschaft und Forschung, Bonn (Germany), the Fonds zur Förderung der wissenschaftlichen Forschung, Vienna (Austria), and the Hoechst AG. We want to thank Professor J. Fricke (Physikalisches Institut der Universität Würzburg, Germany) and Professor P. Fratzl (Institut für Materialphysik der Universität Wien) and their co-workers as well as Professor W. Kiefer and Bernhard Riegel (Physicalisch-chemisches Institut der Universität Würzburg) for the very good cooperation and valuable discussions.

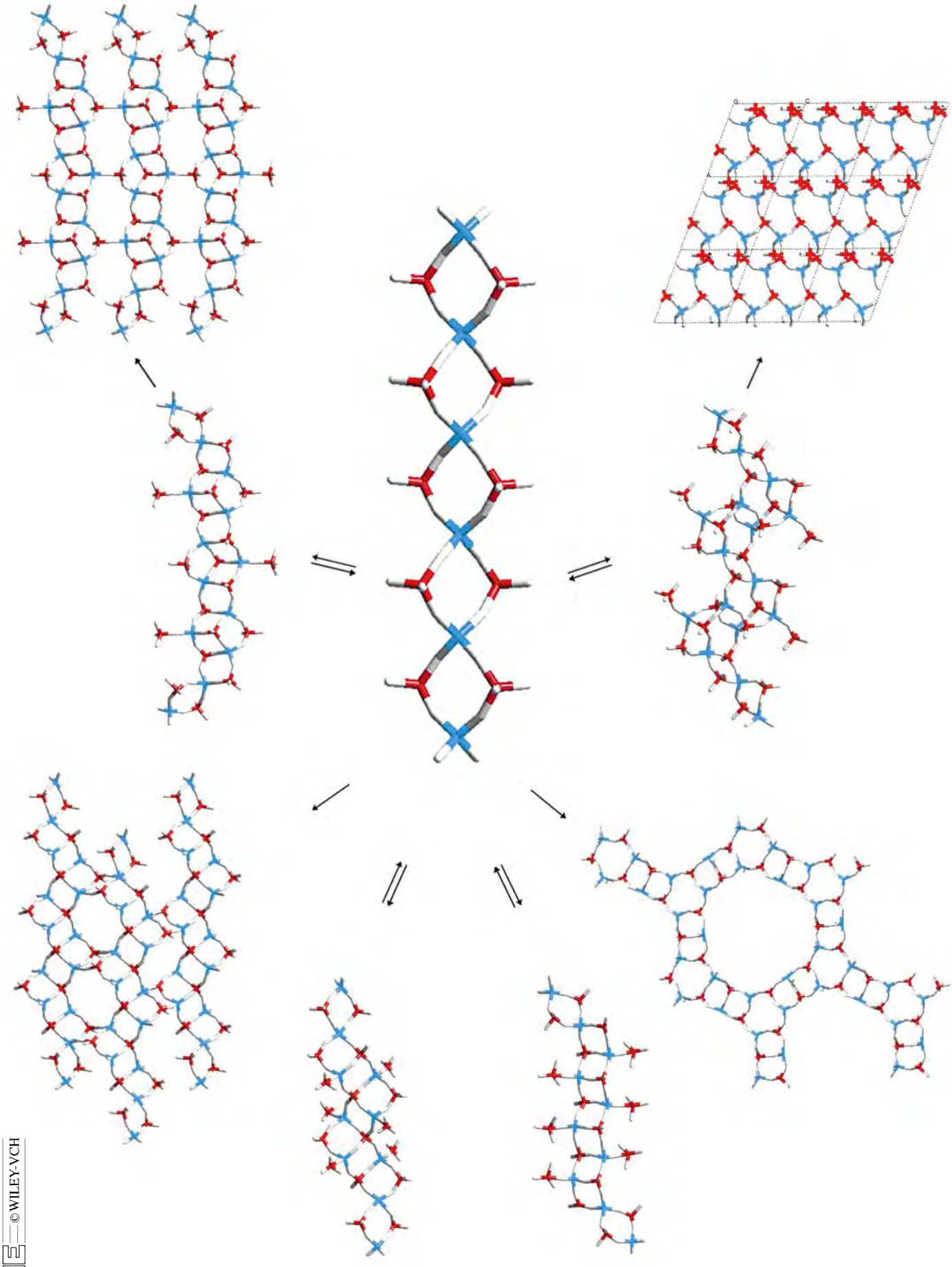
Received: February 5, 1997 [A 208 IE]
German version: *Angew. Chem.* **1998**, *110*, 22–47

[1] a) R. J. Ayen, P. A. Iacobucci, *Rev. Chem. Eng.* **1988**, *5*, 157; b) H. D. Gesser, P. C. Goswami, *Chem. Rev.* **1989**, *89*, 765; c) G. M. Pajonk, *Appl. Catal.* **1991**, *72*, 217; *Catal. Today* **1997**, *35*, 319; d) J. Fricke, A. Emmerling, *Struct. Bonding (Berlin)* **1992**, *77*, 37; e) M. Schneider, A. Baiker, *Catal. Rev. Sci. Eng.* **1995**, *37*, 515; *Catal. Today* **1997**, *35*, 339.
[2] N. K. Raman, M. T. Anderson, C. J. Brinker, *Chem. Mater.* **1996**, *8*, 1682.
[3] D. W. Schaefer, *MRS Bull.* **1994**, *19*(4), 14.
[4] J. Rouquerol, D. Avnir, C. W. Fairbridge, D. H. Everett, J. H. Haynes, N. Pernicone, J. D. F. Ramsay, K. S. W. Sing, F. K. Unger, *Pure Appl. Chem.* **1994**, *66*, 1739.
[5] K. S. W. Sing, D. H. Everett, R. A. W. Hanl, L. Moscau, R. A. Pierotti, J. Rouquerol, T. Siemieniewska, *Pure Appl. Chem.* **1985**, *57*, 603.
[6] D. W. Hua, J. Anderson, J. Di Gregorio, D. M. Smith, G. Beaucage, *J. Non-Cryst. Solids* **1995**, *186*, 141.
[7] C. J. Brinker, G. W. Scherer, *Sol–Gel Science*, Academic Press, New York, **1990**.
[8] R. K. Iler, *The Chemistry of Silica*, Wiley, New York, **1979**.
[9] a) "Better Ceramics Through Chemistry": *Mater. Res. Soc. Symp. Proc.* **1984**, *32*; b) "Better Ceramics Through Chemistry II": *ibid.* **1986**, *73*; c) "Better Ceramics Through Chemistry III": *ibid.* **1988**, *121*; d) "Better Ceramics Through Chemistry IV": *ibid.* **1990**, *180*.
[10] a) "Better Ceramics Through Chemistry V": *Mater. Res. Soc. Symp. Proc.* **1992**, *271*; b) "Better Ceramics Through Chemistry VI": *ibid.* **1994**, *346*; c) "Better Ceramics Through Chemistry VII": *ibid.* **1996**, *435*.
[11] a) *Ultrastructure Processing of Advanced Ceramics* (Eds.: J. D. Mackenzie, D. R. Ulrich), Wiley, New York, **1988**; b) *Ultrastructure Processing of Advanced Materials* (Eds.: D. R. Uhlmann, D. R. Ulrich), Wiley, New York, **1992**; c) *Chemical Processing of Advanced Materials* (Eds.: L. L. Hench, J. K. West), Wiley, New York, **1992**.
[12] H. Dislich in *Sol–Gel Technology of Thin Films, Fibers, Preforms, Electronic and Speciality Shapes* (Ed.: L. C. Klein), Noyes, Park Ridge, **1988**, p. 50.
[13] L. L. Hench, J. K. West, *Chem. Rev.* **1990**, *90*, 33.
[14] It should be pointed out again that some shrinkage (changes in volume) during drying cannot always be avoided. Therefore, it is sometimes a question of judgement whether the resulting gels are considered to be aerogels.
[15] S. S. Kistler, *Nature (London)* **1931**, *127*, 741; *J. Phys. Chem.* **1932**, *36*, 52.
[16] a) "Aerogels": *Springer Proc. Phys.* **1986**, *6*; b) *Rev. Phys. Appl.* **1989**, 24 (*Proc. 2nd Int. Symp. Aerogels*, Colloque C4, Les Editions de Physique, Les Ulis Cedex); c) *J. Non-Cryst. Solids* **1992**, *145* (*Proc. 3rd Int. Symp. Aerogels*); d) *ibid.* **1995**, *186* (*Proc. 4th Int. Symp. Aerogels*).
[17] D. M. Smith, D.-W. Hua, W. L. Earl, *MRS Bull.* **1994**, *19*(4), 44.
[18] S. Brunauer, P. H. Emmett, E. Teller, *J. Am. Chem. Soc.* **1938**, *60*, 309.
[19] S. J. Gregg, S. W. Sing, *Adsorption, Surface Area and Porosity*, Academic Press, New York, **1982**.
[20] G. W. Scherer, D. M. Smith, D. Stein in ref. [16 d], p. 309.
[21] T. Woignier, J. Phalippou, *J. Non-Cryst. Solids* **1987**, *93*, 17.
[22] E. W. Washburn, *Proc. Natl. Acad. Sci. USA* **1921**, *7*, 115.
[23] G. A. Nicolaon, S. J. Teichner, *Bull. Soc. Chim. Fr.* **1968**, 3555.
[24] J. Fricke, G. Reichenauer, *J. Non-Cryst. Solids* **1987**, *95/96*, 1135.
[25] M. Kerker, *The Scattering of Light*, Academic Press, New York, **1969**.
[26] A. Guinier, G. Fournet, *Small Angle Scattering of X-Rays*, Wiley, New York, **1955**.
[27] O. Glatter, G. Kratky, *Small Angle X-Ray Scattering*, Academic Press, London, **1982**.

[28] H. Dachs, *Neutron Diffraction*, Springer, Berlin, **1978**.
[29] G. Kostorz, *Neutron Scattering in Material Science*, Academic Press, New York, **1978**.
[30] a) R. A. Assink, B. D. Kay, *J. Non-Cryst. Solids* **1988**, *99*, 359; b) T. Ho, J. Fraissard, *J. Chem. Phys.* **1982**, *76*, 5225.
[31] F. Devreux, J. P. Boilot, F. Chaput, B. Savopal, *Phys. Rev. Lett.* **1990**, *65*, 614.
[32] D. W. Schaefer in ref. [16b], p. 121.
[33] A. Borne, B. Chevalier, J. L. Chevalier, D. Quenhard, E. Elaloui, J. Lambard, *J. Non-Cryst. Solids* **1995**, *188*, 235.
[34] In the sol–gel literature and in this review, the term cluster does not mean the usual metal clusters, but instead the primary oligomeric species (primary particles) formed during sol–gel processing. Their structure can be chainlike, cyclic, or three-dimensional.
[35] D. W. Schaefer, *Science* **1989**, *243*, 1023.
[36] F. Schwertfeger, W. Glaubitt, U. Schubert, *J. Non-Cryst. Solids* **1992**, *145*, 85.
[37] G. A. Nicolaon, S. J. Teichner, *Bull. Soc. Chim. Fr.* **1968**, 1900; *ibid.* **1968**, 1906.
[38] G. Orcel, R. W. Gould, L. L. Hench in ref. [9b], p. 289.
[39] T. Lours, *J. Non-Cryst. Solids* **1988**, *100*, 207.
[40] A. Hasmy, R. Jullien in ref. [16d], p. 442.
[41] P. I. Pohl, J.-L. Faulon, D. M. Smith in ref. [16d], p. 449.
[42] E. A. Chandler, D. F. Calef in ref. [16d], p. 456.
[43] D. W. Schaefer, K. D. Keefer in *Fractals in Physics* (Eds.: L. Pietronero, E. Toscatti), North-Holland, Amsterdam, **1986**, p. 39.
[44] D. W. Schaefer, *MRS Bull.* **1994**, *19*(4), 49.
[45] K. D. Keefer, D. W. Schaefer, *Phys. Rev. Lett.* **1984**, *53*, 1383.
[46] K. D. Keefer, D. W. Schaefer, *Phys. Rev. Lett.* **1986**, *56*, 2376.
[47] K. D. Keefer, D. W. Schaefer, *Phys. Rev. Lett.* **1986**, *56*, 2199.
[48] K. D. Keefer in ref. [9a], p. 1.
[49] J. Livage, M. Henry, C. Sanchez, *Prog. Solid State Chem.* **1988**, *18*, 259.
[50] T. Heinrich, U. Klett, J. Fricke, *J. Porous Mater.* **1995**, *1*, 7.
[51] C. J. Brinker, K. D. Keefer, D. W. Schaefer, C. S. Ashley, *J. Non-Cryst. Solids* **1982**, *48*, 47.
[52] T. M. Tillotson, L. W. Hrubesh, I. M. Thomas in ref. [9c], p. 658.
[53] T. M. Tillotson, L. W. Hrubesh in ref. [16c], p. 44.
[54] E. Elaloui, Dissertation, Lyon, **1994**.
[55] G. M. Pajonk, E. Elaloui, P. Archard, B. Chevalier, J.-L. Chevalier, M. Durant in ref. [16d], p. 1.
[56] G. M. Pajonk, E. Elaloui, M. Durant, B. Chevalier, J.-L. Chevalier, P. Archard in *Sol–Gel Processing and Applications* (Ed.: Y. A. Attia), Plenum, New York, **1994**, p. 275.
[57] R.-M. Jansen, B. Kessler, J. Wonner, A. Zimmermann (Hoechst AG), DE-A 431 6540 A1, **1993** [*Chem. Abstr.* **1995**, *122*, 65331r].
[58] R.-M. Jansen, A. Zimmermann (Hoechst AG), EP-A 690 023 A2, **1993** [*Chem. Abstr.* **1996**, *124*, 150025e].
[59] G. Herrmann, R. Iden, M. Mielke, F. Teich, B. Ziegler, *J. Non-Cryst. Solids* **1995**, *186*, 380.
[60] H. Dolhaine, J. Wolf-Leistekow (Henkel AG), EP-B 409 083, **1991** [*Chem. Abstr.* **1991**, *114*, 188475x].
[61] C. A. M. Mulder, J. G. van Lierop in ref. [16a], p. 68.
[62] C. Sanchez, F. Ribot, *New J. Chem.* **1994**, *18*, 1007.
[63] R. D. Shannon, *Acta. Crystallogr. Sect. A* **1976**, *32*, 751.
[64] J. Livage, C. Sanchez in ref. [16c], p. 11.
[65] G. Kickelbick, U. Schubert, *Chem. Ber.* **1997**, *130*, 473.
[66] M. A. Vicarini, G. A. Nicolaon, S. J. Teichner, *Bull. Soc. Chim. Fr.* **1969**, 1466; D. J. Suh, T.-J. Park, J.-H. Kim, K.-L. Kim, *Chem. Mater.* **1997**, *9*, 1903.
[67] S. J. Teichner, G. A. Nicolaon, M. A. Vicarini, G. E. E. Gardes, *Adv. Colloid Interface Sci.* **1976**, *5*, 245.
[68] S. J. Teichner in ref. [16a], p. 22.
[69] "Preparation of Catalysts": G. Tournier, M. Lacroix-Repellin, G. M. Pajonk, S. J. Teichner in *Studies in Surface Science and Catalysis*, *Vol. 31* (Eds.: B. Delmon, P. Grange, P. A. Jacobs, G. Poncelet), Elsevier, Amsterdam, **1987**, p. 333.
[70] Y. Mizushima, M. Hori, *J. Non-Cryst. Solids* **1994**, *167*, 1.
[71] Y. Mizushima, M. Hori, *J. Non-Cryst. Solids* **1994**, *170*, 215.
[72] E. J. Markel, E. Reddick, L. A. Napper, J. W. van Zee, *J. Non-Cryst. Solids* **1994**, *180*, 32.
[73] S. J. Teichner, *Rev. Phys. Appl.* **1989**, *24*, 1.
[74] a) C. J. Brodsky, E. I. Ko, *J. Mater. Chem.* **1994**, *4*, 651; b) L. K. Campbell, B. K. Na, E. I. Ko, *Chem. Mater.* **1992**, *4*, 1329; c) D. A. Ward, E. I. Ko, *ibid.* **1993**, *5*, 956.
[75] M. Schneider, A. Baiker, *J. Mater. Chem.* **1992**, *2*, 587.
[76] a) Z. Zhu, M. Tomkiewicz in ref. [10b], p. 751; b) Z. Zhu, Y. Tsung, M. Tomkiewicz, *J. Phys. Chem.* **1995**, *99*, 15 945; c) Z. Zhu, M. Lin, G. Dagan, M. Tomkiewicz, *ibid.* **1995**, *99*, 15 950.
[77] H. Vesteghem, T. Jacoon, A. Lecomte in ref. [16b], p. 59.
[78] A. Benedetti, G. Fagherazzi, P. Riello, Y. W. Zeng, F. Pinna, M. Signoretto, *J. Appl. Crystallogr.* **1993**, *26*, 717.
[79] Y. W. Zeng, P. Riello, A. Benedetti, G. Fagherazzi, *J. Non-Cryst. Solids* **1995**, *185*, 78.
[80] F. Chaput, B. Dunn, P. Fugua, K. Salloux, *J. Non-Cryst. Solids* **1995**, *188*, 11.
[81] a) H. Hiroshima, K. Sudoh in ref. [10a], p. 573; b) H. Hiroshima, K. Sudoh in ref. [16c], p. 51; c) K. Sudoh, H. Hiroshima, *J. Non-Cryst. Solids* **1992**, *147/148*, 386.
[82] H. D. Foster, D. B. Keyes, *Ind. Eng. Chem.* **1937**, *29*, 1254.
[83] K. Kearby, S. S. Kistler, S. Swann, *Ind. Eng. Chem.* **1938**, *30*, 1082.
[84] J. N. Armor, E. J. Carlson, *Appl. Catal.* **1985**, *19*, 327.
[85] E. J. Carlson, J. N. Armor, W. J. Cunningham, A. M. Smith (Allied-Signal Inc.), US-A 4 828 818, **1989** [*Chem. Abstr.* **1989**, *111*, 96640t].
[86] D. Bianchi, H. Batis-Landonsli, C. O. Bennett, G. M. Pajonk, P. Vergnon, S. J. Teichner, *Bull. Soc. Chim. Fr.* **1981**, 345.
[87] H. Zarouk, A. Ghorbel, G. M. Pajonk, S. J. Teichner, *Bull. Soc. Chim. Fr.* **1982**, 71.
[88] F. Blanchard, B. Pommier, J. P. Reymond, S. J. Teichner, *Stud. Surf. Sci. Catal.* **1983**, *16*, 395.
[89] M. Astier, A. Bertrand, D. Bianchi, A. Chenard, G. E. E. Gardes, G. M. Pajonk, M. B. Taghavi, S. J. Teichner, B. Villemin, *Stud. Surf. Sci. Catal.* **1976**, *1*, 315.
[90] M. Astier, A. Bertrand, S. J. Teichner, *Bull. Soc. Chim. Fr.* **1980**, 191.
[91] S. M. Maurer, E. I. Ko, *J. Catal.* **1992**, *135*, 125.
[92] S. M. Maurer, D. Ng, E. I. Ko, *Catal. Today* **1993**, *16*, 319.
[93] E. C. DeCanio, V. P. Nero, E. I. Ko, *J. Catal.* **1994**, *146*, 317.
[94] D. J. Suh, T.-J. Park, *Chem. Mater.* **1996**, *8*, 509.
[95] G. E. E. Gardes, G. M. Pajonk, S. J. Teichner, *Bull. Soc. Chim. Fr.* **1976**, 1321.
[96] G. E. E. Gardes, G. M. Pajonk, S. J. Teichner, *Bull. Soc. Chim. Fr.* **1976**, 1327.
[97] B. E. Yoldas, *J. Non-Cryst. Solids* **1980**, *38*, 81.
[98] D. C. Dutoit, M. Schneider, A. Baiker, *J. Catal.* **1995**, *153*, 165.
[99] R. Hutter, T. Mallat, A. Baiker, *J. Catal.* **1995**, *153*, 177.
[100] F. Chaput, A. Lecomte, A. Dauger, J. P. Boilot in ref. [16b], p. 137.
[101] T. Heinrich, F. Raether, H. Marsmann, *J. Non-Cryst. Solids* **1994**, *168*, 14.
[102] F. Blanchard, J. P. Reymond, B. Pommier, S. J. Teichner, *J. Mol. Catal.* **1982**, *17*, 171.
[103] R. Marinangelli, G. M. Pajonk, S. J. Teichner, *Proceedings of the 7th Simposio Iberoamericano de Catalisis* (La Plata, Argentina) **1980**, p. 126.
[104] S. Abouarnadasse, G. M. Pajonk, S. J. Teichner, *Actas Xe Simposio Iberoamericano de Catalisis*, *Vol. II* (Merida, Venezuela) **1986**, p. 615.
[105] G. M. Pajonk, T. Manzalji, *Catal. Lett.* **1993**, *21*, 361.
[106] Y. Mizushima, M. Hori, *J. Mater. Res.* **1994**, *9*, 2272.
[107] C. J. Brinker, K. J. Ward, K. D. Keefer, E. Holupka, P. J. Bray, R. K. Pearson in ref. [16a], p. 57.
[108] P. Löbmann, W. Glaubitt, J. Gross, J. Fricke, *J. Non-Cryst. Solids* **1995**, *186*, 59.
[109] P. Löbmann, J. Gross, W. Glaubitt, J. Fricke, *J. Non-Cryst. Solids* **1996**, *201*, 66.
[110] A. Sayari, A. Ghorbel, G. M. Pajonk, S. J. Teichner, *Bull. Soc. Chim. Fr.* **1981**, 220.
[111] J. N. Armor, E. J. Carlson, W. C. Conner, *React. Solids* **1987**, *3*, 155.
[112] G. M. Pajonk, *Stud. Surf. Sci. Catal.* **1990**, *55*, 229.
[113] G. Dagan, M. Tomkiewicz, *J. Non-Cryst. Solids* **1994**, *175*, 294.
[114] B. Himmel, T. Gerber, H. Bürger, G. Holzhüter, A. Olbertz in ref. [16d], p. 149.
[115] J. C. Pouxviel, J. P. Boilot in ref. [11a], p. 197.
[116] T. Heinrich, F. Raether, W. Tappert, J. Fricke in ref. [16c], p. 55.
[117] H. Hiroshima, M. Gengyo, C. Kojima, H. Imai in ref. [16d], p. 54.

[118] G. M. Pajonk, M. B. Taghavi, S. J. Teichner, *Bull. Soc. Chim. Fr.* **1975**, 983.
[119] M. B. Taghavi, G. M. Pajonk, S. J. Teichner, *J. Colloid Interface Sci.* **1979**, *71*, 451.
[120] M. Astier, A. Bertrand, S. J. Teichner, *Bull. Soc. Chim. Fr.* **1980**, 218.
[121] B. Heinrichs, J.-P. Pirard, R. Pirard (Solvay GmbH), EP-A 062 9442 A1 **1994** [*Chem. Abstr.* **1995**, *122*, 84259q].
[122] B. Pommier, S. J. Teichner, *Proc. Int. Congr. Catal. 9th* **1988**, *2*, 610.
[123] Y. Mizushima, M. Hori, *J. Mater. Res.* **1995**, *10*, 1424.
[124] C. Hoang-Van, B. Pommier, R. Harivololona, P. Pichat in ref. [16c], p. 250.
[125] M. Schneider, D. G. Duff, T. Mallat, M. Wildberger, A. Baiker, *J. Catal.* **1994**, *147*, 500.
[126] J. N. Armor, E. J. Carlson, P. M. Zambri, *Appl. Catal.* **1985**, *19*, 339.
[127] L. M. Hair, L. Owens, T. Tillotson, M. Fröba, J. Wong, G. J. Thomas, D. L. Medlin in ref. [16d], p. 168.
[128] K. Balakrishnan, R. D. Gonzales, *J. Catal.* **1993**, *144*, 395.
[129] F. Schwertfeger, N. Hüsing, U. Schubert, *J. Sol–gel Sci. Technol.* **1994**, *2*, 103.
[130] M. Bockhorst, K. Heinloth, G. M. Pajonk, R. Begag, E. Elaloui in ref. [16d], p. 388.
[131] L. Zhu, Y. Li, J. Wang, J. Shen, *Chem. Phys. Lett.* **1995**, *239*, 393.
[132] B. M. Novak, D. Auerbach, C. Verrier, *Chem. Mater.* **1994**, *6*, 282.
[133] U. Schubert, N. Hüsing, A. Lorenz, *Chem. Mater.* **1995**, *7*, 2010.
[134] B. M. Novak, *Adv. Mater.* **1993**, *5*, 422.
[135] B. Riegel, S. Plittersdorf, W. Kiefer, N. Hüsing, U. Schubert, *J. Mol. Struct.*, **1997**, *410/411*, 157.
[136] N. Hüsing, U. Schubert, B. Riegel, W. Kiefer in ref. [10c], p. 339.
[137] U. Schubert, F. Schwertfeger, N. Hüsing, E. Seyfried in ref. [10b], p. 151.
[138] N. Hüsing, U. Schubert, *J. Sol–Gel Sci. Technol.* **1997**, *8*, 807.
[139] W. Cao, A. J. Hunt in ref. [10b], p. 631.
[140] N. Hüsing, Dissertation, Universität Würzburg, **1997**; N. Hüsing, U. Schubert, K. Misof, P. Fratzl, *J. Am. Chem. Soc.*, submitted.
[141] D. A. Loy, G. M. Jamison, B. M. Baugher, E. M. Russick, R. A. Assink, S. Prabakar, K. J. Shea, *J. Non-Cryst. Solids* **1995**, *186*, 44.
[142] a) R. W. Pekala (U.S. Department of Energy), US-A 4 873 218, **1989** [*Chem. Abstr.* **1990**, *112*, 57435f]; R. W. Pekala, *J. Mater. Sci.* **1989**, *24*, 3221; c) R. W. Pekala (U.S. Department of Energy), US-A 4 997 804, **1991** [*Chem. Abstr.* **1991**, *115*, 94043j]; d) R. W. Pekala in ref. [11b], p. 711.
[143] R. W. Pekala, F. M. Kong in ref. [16b], p. 33.
[144] R. W. Pekala, F. M. Kong, *Polym. Prepr. (Am. Chem. Soc. Div. Polym. Chem.)* **1989**, *30*, 221.
[145] R. L. Ward, R. W. Pekala, *Polym. Prepr. (Am. Chem. Soc. Div. Polym. Chem.)* **1990**, *31*, 167.
[146] G. C. Ruben, R. W. Pekala in ref. [16d], p. 219.
[147] R. W. Pekala, C. T. Alviso, X. Lu, J. Gross, J. Fricke, *J. Non-Cryst. Solids* **1995**, *188*, 34.
[148] R. W. Pekala, D. W. Schaefer, *Macromolecules* **1993**, *26*, 5487.
[149] The "critical point" of the drying process should not be mistaken for the "critical point" at which a liquid changes into the supercritical state.
[150] C. J. Brinker, R. Sehgal, S. L. Hietala, R. Deshpande, D. M. Smith, D. Loy, C. S. Ashley, *J. Membr. Sci.* **1994**, *94*, 85.
[151] P. J. Davis, C. J. Brinker, D. M. Smith, *J. Non-Cryst. Solids* **1992**, *142*, 189.
[152] T. Mizuno, H. Nagata, S. Manabe, *J. Non-Cryst. Solids* **1988**, *100*, 236.
[153] H. Chen, E. Ruckenstein, *J. Colloid Interface Sci.* **1991**, *145*, 581.
[154] J. B. Chan, J. Jonas, *J. Non-Cryst. Solids* **1990**, *126*, 79.
[155] C. Roger, M. J. Hampden-Smith, *J. Mater. Chem.* **1992**, *2*, 1111.
[156] J. Zarzycki, M. Prassas, J. Phalippou, *J. Mater. Sci.* **1982**, *17*, 3371.
[157] L. L. Hench in *Science of Ceramic Chemical Processing* (Eds.: L. L. Hench, D. R. Ulrich), Wiley, New York, **1986**, p. 52.
[158] J. G. van Lierop, A. Huizing, W. C. P. M. Meermann, C. A. M. Mulder, *J. Non-Cryst. Solids* **1986**, *82*, 265.
[159] S. Henning in ref. [16a], p. 38.
[160] A. H. Boonstra, J. M. E. Baken, *J. Non-Cryst. Solids* **1989**, *109*, 1.
[161] P. Wang, A. Emmerling, W. Tappert, O. Spormann, J. Fricke, *J. Appl. Crystallogr.* **1991**, *24*, 777.
[162] T. Woignier, J. Phalippou, H. Hdach, G. W. Scherer in ref. [9d], p. 1087.
[163] K. Tajiri, K. Igarashi, T. Nishio, *J. Non-Cryst. Solids* **1995**, *186*, 83.
[164] N. Hüsing, F. Schwertfeger, W. Tappert, U. Schubert in ref. [16d], p. 37.
[165] T. Woignier, J. Phalippou in *Proceedings of the 1st International Workshop on Non-Crystalline Solids* (Eds.: M. D. Baro, N. Clavaguera) San Feliu de Guixols, World Scientific, Singapore, **1986**, p. 415.
[166] M. Prassas, L. L. Hench in *Ultrastructure Processing of Ceramics, Glasses and Composites* (Eds.: L. L. Hench, D. R. Ulrich), Wiley, New York, **1984**, p. 100.
[167] T. Woignier, J. Phalippou, J. F. Quinson, M. Pauthe, F. Laveissiere in ref. [16c], p. 25.
[168] P. H. Tewari, A. J. Hunt, K. D. Lofftus, *Mater. Lett.* **1985**, *3*, 363.
[169] P. H. Tewari, A. J. Hunt, K. D. Lofftus in ref. [16a], p. 31.
[170] P. H. Tewari, A. J. Hunt (U.S. Department of Energy), US-A 4 610 863, **1986** [*Chem. Abstr.* **1986**, *105*, 214727c].
[171] P. J. Lea, S. A. Ramjohn, *Microscop. Acta* **1980**, *83*, 291.
[172] M. J. van Bommel, A. B. de Haan, *J. Mater. Sci.* **1994**, *29*, 943.
[173] M. J. van Bommel, A. B. de Haan in ref. [16d], p. 78.
[174] C. J. Brodsky, E. I. Ko, *J. Non-Cryst. Solids* **1995**, *186*, 88.
[175] E. Degn Egeberg, J. Engell in ref. [16b], p. 23.
[176] D. Klvana, J. Chaouki, M. Repellin-Lacroix, G. M. Pajonk in ref. [16b], p. 29.
[177] G. M. Pajonk in ref. [16b], p. 13.
[178] D. M. Smith, R. Deshpande, C. J. Brinker in ref. [10a], p. 567.
[179] R. Deshpande, D. M. Smith, C. J. Brinker (University of New Mexico), WO-B 94/25149, **1994** [*Chem. Abstr.* **1995**, *122*, 171104d].
[180] D. M. Smith, D. Stein, J. M. Anderson, W. Ackerman in ref. [16d], p. 104.
[181] M. A. Einarsrud, S. Hæreid (Sinvent A/S), WO-B 92/20623, **1992** [*Chem. Abstr.* **1993**, *118*, 62629a].
[182] S. Hæreid, M. Dahle, S. Lima, M. A. Einarsrud in ref. [16d], p. 96.
[183] F. Schwertfeger (Hoechst AG), *Future Special Science* – the Hoechst magazine, **1997**, *2*, 28.
[184] M. Mielke (BASF AG), personal communication; ref. [1d].
[185] a) A. J. Hunt, W. Cao in ref. [10b], p. 451; b) W. Cao, X.-Y. Song, A. J. Hunt, *Mater. Res. Soc. Symp. Proc.* **1994**, *349*, 87; c) X.-Y. Song, W. Cao, A. J. Hunt, *ibid.* **1994**, *349*, 269; d) X.-Y. Song, W. Cao, M. R. Ayers, A. J. Hunt, *J. Mater. Res.* **1995**, *10*, 1995; e) A. J. Hunt, M. R. Ayers, W. Cao, *J. Non-Cryst. Solids* **1995**, *185*, 227; f) D. Lee, P. C. Stevens, S. Q. Zeng, A. J. Hunt in ref. [16d], p. 285.
[186] a) F. Schwertfeger, U. Schubert, *Chem. Mater.* **1995**, *7*, 1909; b) J. Kuhn, V. Bock, M. C. Arduini-Schuster, E. Seyfried, U. Schubert, J. Fricke, *Therm. Conduct.* **1994**, *22*, 589.
[187] a) J. Kuhn, T. Gleissner, M. C. Arduini-Schuster, S. Korder, J. Fricke in ref. [16d], p. 291; b) P. Wang, J. Kuhn, X. Lu in ref. [16d], p. 296.
[188] W. Cao, A. J. Hunt, *Appl. Phys. Lett.* **1994**, *64*, 2376.
[189] M. R. Ayers, X.-Y. Song, A. J. Hunt, *J. Mater. Sci.* **1996**, *31*, 6251.
[190] S. Reul, W. Richter, D. Haarer in ref. [16c], p. 149.
[191] a) R. W. Pekala, S. T. Mayer, J. L. Kaschmitter, F. M. Kong in *Sol–Gel Processing and Applications* (Ed.: Y. A. Attia), Plenum, New York, **1994**, p. 369; b) S. T. Mayer, R. W. Pekala, J. L. Kaschmitter, *J. Electrochem. Soc.* **1993**, *140*, 446; c) S. T. Mayer, J. L. Kaschmitter, R. W. Pekala, *ECS Symp. Proc.* **1993**, *93*, 38; d) "Novel Forms of Carbon II": R. W. Pekala, S. T. Mayer, J. F. Poco, J. L. Kaschmitter in ref. [10b], p. 79.
[192] P. Wang, W. Körner, A. Emmerling, A. Beck, J. Kuhn, J. Fricke in ref. [16c], p. 141.
[193] P. H. Tewari, A. J. Hunt, K. D. Lofftus, J. G. Lieber in ref. [9b], p. 195.
[194] G. Poeltz, R. Riethmüller, *Nucl. Instrum. Methods Phys. Res.* **1982**, *195*, 491.
[195] S. Henning, L. Svensson, *Phys. Scr.* **1981**, *23*, 697.
[196] R. E. Russo, A. J. Hunt, *J. Non-Cryst. Solids* **1986**, *86*, 219.
[197] A. Emmerling, R. Petricevic, A. Beck, P. Wang, H. Scheller, J. Fricke, *J. Non-Cryst. Solids* **1995**, *185*, 240.
[198] A. Emmerling, P. Wang, G. Popp, A. Beck, J. Fricke, *J. Phys. IV* **1993**, *3*, C8-360.
[199] W. Cao, A. J. Hunt, *J. Non-Cryst. Solids* **1994**, *176*, 18.
[200] J. Fricke, *Spektrum der Wissenschaft* **1988**, *7*, 60; *ibid.* **1992**, *11*, 14; *Sci. Am.* **1988**, *256*(5), 92.
[201] G. Poeltz in ref. [16a], p. 176.
[202] P. Scheuerpflug, R. Caps, D. Büttner, J. Fricke, *Int. J. Heat Mass Transfer* **1985**, *28*, 2299.

[203] X. Lu, P. Wang, M. C. Arduini-Schuster, J. Kuhn, D. Büttner, O. Nilsson, U. Heinemann, J. Fricke in ref. [16c], p. 207.
[204] J. Kuhn, F. Schwertfeger, M. C. Arduini-Schuster, J. Fricke, U. Schubert in ref. [16d], p. 184.
[205] V. Wittwer in ref. [16c], p. 233.
[206] J. Fricke, *Phys. Unserer Zeit* **1989**, *20*, 189.
[207] J. Fricke, M. C. Arduini-Schuster, D. Büttner, H.-P. Ebert, U. Heinemann, J. Hetfleisch, E. Hümmer, J. Kuhn, X. Lu, *Thermal Cond.* **1990**, *21*, 235.
[208] K. I. Jensen in ref. [16c], p. 237.
[209] a) J. Fricke, *J. Sol. Energy Mater.* **1987**, *16*, 267; b) L. F. Jesch, *Transparent Insulation Materials for Passive Solar Energy Utilization*, Franklin, Birmingham, **1987**; c) M. Rommel, V. Wittwer, A. Goetzberger, *Adv. Sol. Energy Technol.* **1988**, *4*, 1553; d) A. J. Hunt, K. D. Lofftus, *Adv. Sol. Energy Technol.* **1988**, *4*, 3146.
[210] B. Wolff, G. Seybold, F. E. Krueckau (BASF AG), EP-B 340 707, **1989** [*Chem. Abstr.* **1990**, *112*, 82924x].
[211] A. J. Hunt, K. D. Lofftus, *Mater. Res. Soc. Symp. Proc.* **1988**, *121*, 663.
[212] T. Woignier, J. Phalippou, R. Vacher, *J. Mater. Res.* **1989**, *4*, 688.
[213] S. J. Kramer, F. Rubio-Alonso, J. D. Mackenzie in ref. [10c], p. 295.
[214] M. Gronauer, J. Fricke, *Acustica* **1986**, *59*, 177.
[215] M. Gronauer, A. Kadur, J. Fricke in ref. [16a], p. 167.
[216] J. Gross, R. Goswin, R. Gerlach, J. Fricke in ref. [16b], p. 185.
[217] J. Gross, J. Fricke, L. W. Hrubesh, *J. Acoust. Soc. Am.* **1992**, *91*, 2004.
[218] V. Gibiat, O. Lefeuvre, T. Woignier, J. Pelous, J. Phalippou in ref. [16d], p. 244.
[219] W. C. Conner, G. M. Pajonk, S. J. Teichner, *Adv. Catal.* **1986**, *34*, 1.
[220] A. J. Fanelli, J. V. Burlew, G. B. Marsh, *J. Catal.* **1989**, *116*, 318.
[221] R. J. Willey, J. Olmstead, V. Djuhadi, S. J. Teichner, *Mater. Res. Soc. Symp. Proc.* **1988**, *111*, 359.
[222] Y. Mizushima, M. Hori, *Appl. Catal.* **1992**, *88*, 137.
[223] R. Sempere, D. Bourret, A. Sivade, R. Etienne, J. Bouaziz, *J. Non-Cryst. Solids* **1992**, *148*, 499.
[224] L. W. Hrubesh, J. F. Poco, *Mater. Res. Soc. Symp. Proc.* **1995**, *371*, 195.
[225] D. M. Smith, J. Anderson, C. C. Cho, B. E. Gnade, *Mater. Res. Soc. Symp. Proc.* **1995**, *371*, 261.
[226] S. S. Prakash, C. J. Brinker, A. J. Hurd, *J. Non-Cryst. Solids* **1995**, *190*, 264.
[227] S. S. Prakash, C. J. Brinker, A. J. Hurd, S. M. Rao, *Nature (London)* **1995**, *374*, 439.
[228] L. W. Hrubesh, J. F. Poco, *J. Non-Cryst. Solids* **1995**, *188*, 46.
[229] a) J. Phalippou, T. Woignier, J. Zarzycki in *Ultrastructure Processing of Advanced Ceramics*, *Glasses and Composites* (Eds.: L. L. Hench, D. R. Ulrich), Wiley, New York, **1984**, p. 70; b) M. Prassas, J. Phalippou, J. Zarzycki in *Science of Ceramic Chemical Processing* (Eds.: L. L. Hench, D. R. Ulrich), Wiley, New York, **1986**, p. 156; c) T. Woignier, J. Phalippou, M. Prassas, *J. Mater. Sci.* **1990**, *25*, 3118; d) C. A. M. Mulder, J. G. van Lierop, G. Frens, *J. Non-Cryst. Solids* **1986**, *82*, 92; e) E. Papanikolau, W. C. P. M. Meerman, R. Aerts, T. L. van Roy, J. G. van Lierop, T. P. M. Meeuwsen, *J. Non-Cryst. Solids* **1988**, *100*, 247.
[230] a) J. Iura, T. Kawaguchi in ref. [16b], p. 53; b) M. N. Rahaman, L. C. de Jonghe, S. L. Shinde, P. H. Tewari, *J. Am. Ceram. Soc.* **1988**, *71*, C338.
[231] A. Emmerling, J. Gross, R. Gerlach, R. Goswin, G. Reichenauer, J. Fricke, H.-G. Haubold, *J. Non-Cryst. Solids* **1990**, *125*, 230.
[232] a) W. Ebeling, D. A. Reierson, R. J. Pence, M. S. Viray, *Pestic. Biochem. Physiol.* **1975**, *5*, 81; b) P. K. Sen-Sarma, S. C. Mishra, *Indian J. Entomol.* **1976**, *38*, 77; c) C. H. Vrba, H. P. Arai, M. Nosal, *Can. J. Zool.* **1983**, *61*, 1481.
[233] a) S. R. Loschiavo, *J. Econ. Entomol.* **1987**, *81*, 1231; b) *ibid.* **1988**, *81*, 1237.
[234] P. Tsou, D. E. Brownlee, A. L. Albee, *LPSC* **1988**, *19*, 1205.
[235] P. Tsou in ref. [16d], p. 415.
[236] W.Schramm, *Technikbewertung von Aerogelen*, Austrian Academy of Science, Vienna, **1994**.



Starting from a chain aluminophosphate one-, two-, or three-dimensional structures can be formed by a hydrolysis-condensation self-assembly pathway (oxygen: white, phosphorus: red, aluminum: blue).

ANGEWANDTE CHEMIE © WILEY-VCH

A New Model for Aluminophosphate Formation: Transformation of a Linear Chain Aluminophosphate to Chain, Layer, and Framework Structures

Scott Oliver, Alex Kuperman, and Geoffrey A. Ozin*

Self-assembly pathways of inorganic compounds to form microporous framework materials continues to be a topic under intense debate. The current view of the mode of formation of this class of materials is constantly evolving, and is in many cases different for each framework composition, which now spans most of the periodic table. For aluminophosphates, several models have been proposed, some of which are closely related to those of the aluminosilicates. In this review we discuss the contemporary models for the formation of aluminophosphates and a new model, developed in our laboratory, which accounts for the formation and structures of a family of one-dimensional (1D) chain, two-dimensional (2D) porous layer, and three-dimensional (3D) open-framework aluminophosphate materials. The building block for this model is a linear chain aluminophosphate, which is the first species to crystallize from the synthesis system. Structural, stereochemical, charge, and chemical information present in the chain precursor can be transcribed, under a particular set of experimental conditions, to allow the formation of other chain types through a hydrolysis–condensation self-assembly pathway. The sibling aluminophosphate chains can be crystallized from the system or condense further to more complex porous layer or open-framework aluminophosphate structures. Other solute species, such as aluminum oxide double octahedra or fluorinated aluminum species, can be incorporated into the final structures by a chain-encapsulation process. This construction paradigm represents a new way of rationalizing aluminophosphate structures and their formation.

Keywords: aluminum · phosphorus · solid-state chemistry · zeolite analogues

1. Introduction

The large number of synthetic and naturally-occurring inorganic layered and open-framework materials constitutes an important area of materials chemistry.[1–3] Within the domain of aluminophosphate compositions, a large number of synthetic microporous framework materials have been documented since their initial discovery by Flanigen et al.[4, 5] A series of aluminofluorophosphate layers[6, 7] and frameworks[8–12] has also been discovered in the last several years.

Aluminophosphate frameworks are built of alternating, corner-sharing phosphorus(v) oxide and aluminum(iii) oxide tetrahedra. In some materials aluminum can be four-, five-, and/or six-coordinate. While a number of dense-phase and small-pore aluminophosphates occur as natural minerals, the majority of known structure types are synthetic. Their preparation typically entails hydrothermal treatment of an aqueous gel containing templating amine or quaternary ammonium species. Some structures can only be obtained with a specific template, such as JDF-20,[13] which can only be synthesized with triethylamine as template. In contrast, others such as $AlPO_4$-5[14] can be made in the presence of any of more than twenty-three amines ($AlPO_4$-n denotes a porous aluminum phosphate framework). Many of the frameworks contain a single channel system, in which the walls of the channel comprise six-rings of T atoms (T = alternating Al and P centers, bridged by oxygen), analogous to the double-pyroxene chains of $AlPO_4$-tridymite.

Recently the number of reports on new chain[15–20] and layer[19–29] aluminophosphate structures has increased steadily. Many of these materials, including those obtained in our laboratory, are prepared by nonaqueous synthesis procedures.[15, 17–19, 21–23, 27] The discovery of these new materials has been attributed to the drastically different properties of a nonaqueous system compared to an aqueous system.[24, 30, 31] In spite of the large number of organic templates that may be employed in the synthesis of these new chain and layer aluminophosphates, the only established compositions for

[*] Prof. G. A. Ozin, Dr. S. Oliver
Materials Chemistry Research Group
Lash Miller Chemical Laboratories
University of Toronto
80 St. George Street, Toronto, ON, M5S 3H6 (Canada)
Fax: Int. code + (1) 416 971-2011
e-mail: gozin@alchemy.chem.utoronto.ca
soliver@fas.harvard.edu
Dr. A. Kuperman
Catalysis Laboratory, The Dow Chemical Company
Midland, MI 48674 (USA)

 © WILEY-VCH Verlag GmbH, D-69451 Weinheim, 1998 1433-7851/98/3701-0047 $ 17.50+.50/0

layered structures to date are either $[Al_3P_4O_{16}]^{3-}$ or $Al_2P_3O_{12}H_x]^{(3-x)-}$ $(x = 1-2)$, where many of these inorganic layers possess the same architecture.

Similarly, there are only four known chain aluminophosphate structures containing tetrahedrally coordinated aluminum centers. Two are isostructural and of stoichiometry $[AlP_2O_8H_x]^{(3-x)-}$ $(x = 1, 2)$,[15,16] while the remaining two, UT-2[19] and UT-7[20] (University of Toronto, structure numbers 2 and 7), are isostructural and have the same formula, $[Al_3P_5O_{20}H]^{5-}$. The latter differ in their organic template species, namely cyclopentylammonium for UT-2 and cycloheptylammonium for UT-7. Two chain aluminophosphates are also known that contain exclusively octahedrally coordinated aluminum centers. The compound with a $[Al(H_2PO_4)_3]$ chain structure described by Kniep et al. was prepared by the evaporation of a concentrated, viscous solution,[17] while, more recently, Attfield et al. achieved the hydrothermal synthesis of an $[Al(PO_4)_2(OH)]^{4-}$ chain.[18]

A number of soluble aluminophosphate and aluminophosphonate monomeric complexes have also been reported; for instance, the tetramethylammonium salt of the trimeric diphosphatoaluminate complex was reported in 1969.[32] Cassidy et al. later isolated an $[Al_4(PO_4)_4]$ cubic complex from ethanol, in which each aluminum atom resides in an octahedral environment, connected to three phosphate ions of the cube corners and three ethoxy groups.[33] Kniep et al. also isolated a pentameric $[Al_2(H_2PO_4)_3](PO_4)$ cluster from a concentrated, viscous solution.[34] In 1996 Mason et al. prepared two different alkylaluminophosphate complexes, one of which contains a $Al_2O_4P_2$ four-ring. The other complex has a cubic $Al_4O_{12}P_4$ inorganic core, in which the nonbridging vertices of the aluminum and phosphorus tetrahedra are capped by *tert*-butyl and trimethylsiloxy groups, respectively.[35] Yang et al. also prepared a related cubic aluminophosphonate complex, in which the phosphorus centers carry terminal *tert*-butyl groups.[36] This research has also led to the discovery of related soluble phosphates and phosphonates containing boron[37,38] and gallium[39,40] centers.

In recent years significant progress has been made towards the development of mechanisms of formation of zeolites and aluminophosphate molecular sieves. Some models account for the final framework structures by postulating various building blocks, such as four-rings, six-rings, and other small secondary building units (SBUs; the primary building units are the simple monomeric polyhedra), similar to those believed to be involved in zeolite formation.[3a, 10] More recently, the role of the organic template has been discussed by Lewis et al.[41, 42] Their calculations were performed on aluminophosphate, metal-substituted aluminophosphate, and zeolite frameworks. Davis et al. have also made thermochemical calculations of both microporous and dense-phase aluminophosphates.[43] These results have led to a better understanding of the synthesis of aluminophosphate framework structures.

Other, older models are based on chain species that run through the structure parallel to the main channel system, such as the narsarsukite, double-crankshaft[44, 45] and triple-crankshaft chains.[46] Although these species can be identified in the frameworks, there is no direct evidence that they participate in the assembly process. Furthermore, double- or triple-crankshafts are rather complex and are difficult to envisage as stable species in solution. It has also been argued that pseudoboehmite is intercalated by polyphosphate, which forms an amorphous aluminophosphate layer either directly[47, 48] or via molecular species that are present in the aluminophosphate solution.[49, 50] The disordered layered material is proposed to undergo a solid-state transformation to give the crystalline framework. Chain tectons and models dealing with their transformation to give more complex chains or layers have not been reported. Only the mode of formation of 3D frameworks has been discussed previously.



S. Oliver



A. Kuperman



G. A. Ozin

Scott Oliver received his B.Sc. degree in chemistry from the University of Toronto in 1992 and recently completed his Ph.D. in inorganic materials chemistry in Professor Ozin's group. His thesis focussed on the solvothermal synthesis, characterization, and mode of formation of novel aluminophosphate materials. He is currently an NSERC postdoctoral fellow in Professor Whitesides' group at Harvard University.

Alex Kuperman graduated from the Moscow Institute of Fine Chemical Technology with an M.Sc. in Chemical Engineering. He received his Ph.D. in inorganic materials chemistry from the University of Toronto in Professor Ozin's group. He is now a Senior Specialist at the Dow Chemical Company in the Central R&D Catalysis Laboratory.

Geoffrey A. Ozin received his B.Sc. degree in chemistry from King's College, University of London in 1965 and his D. Phil. in inorganic chemistry from Oriel College, University of Oxford in 1967. From 1967 to 1969 he was an ICI Postdoctoral Fellow at Southampton University, before joining the chemistry faculty at the University of Toronto in 1969, where he is a full Professor. His field of specialization is interdisciplinary materials chemistry and his current research interests include nanochemistry chemistry, supramolecular chemistry, host–guest inclusion chemistry and biomimetic chemistry. He has published more than 400 articles in scientific journals and holds 10 patents.

The starting materials generally employed in the synthesis of aluminophosphates are phosphoric acid and an aluminum oxide in the form of pseudoboehmite or alkoxide.[3a] The mineralization of alumina by phosphoric acid is a well-documented process because of its relevance to soil science.[51, 52] Generally, phosphate ions form covalent bonds through bridging oxygen atoms to aluminum atoms by replacing hydroxide ions and breaking Al-O-Al linkages in the mineral. Through dissolution of the mineral structure, aluminophosphate molecular species are leached into the supernatant. Such species have been detected experimentally and their structure has been modeled.[53–58]

The next step in the formation of aluminophosphates is less clear. There is evidence that "aggregation polymers" exist for metal phosphates; the most studied are the aluminophosphate polymers in viscous gels.[59–63] These aggregation polymers are stable in acidic medium, and precipitate on rendering the medium alkaline.[60] The materials were found to be amorphous upon precipitation. The aggregation polymers have also been suggested as a "transition between the heteropoly acids and soluble complexes."[61] Chain species tend to form as the Al:P ratio of the solution is raised above 1:1;[61–63] for instance, Kniep et al. isolated large crystals of the $Al(H_2PO_4)_3$ chain structure by evaporation of a concentrated (Al:P = 1:5) solution.[17]

The stability of an unbranched chain aluminophosphate is also supported by the well-known fact that polyphosphates and ring metaphosphates avoid branching owing to the reduced negative charge of branching $PO_{2.5}$ groups over that of the negative PO_3^- groups of the chain, rendering branching points highly susceptible to removal by hydrolysis.[64] A similar tendency to avoid chain branching may occur for the aluminophosphates; thus, all higher molecular weight solution species may exist as nonbranched, 1D chains prior to their precipitation. This would also prevent the formation of condensed phosphates instead of aluminophosphate species. It is important to note that acidic starting conditions are also required for the synthesis of aluminophosphate molecular sieves; the pH value shifts into the range for alkaline compounds as the synthesis proceeds. Based on these observations, one can conclude that in the synthesis of aluminophosphates, it is initially necessary to build a concentration of aluminophosphate polymeric species in solution, which then self-assemble into various structures. Certainly, the work on aggregated aluminophosphate polymers clearly indicates that a polymeric aluminophosphate chain should be considered as the precursor in the formation of chain, layer, and framework aluminophosphates.

Here, we propose a new self-assembly model for the formation of aluminophosphates, in which a progenitor chain is introduced, which can account for the structures of 1D to 3D aluminophosphates and whose existence is supported by direct experimental evidence. Examples are given of the hydrolysis–condensation processes that can occur on the parent chain. These are only a few of the possible chain types that may be constructed in this way. We have also proposed a nomenclature scheme to denote a particular chain type, and it is hoped that this model will contribute to a greater understanding of the mode of formation of chain, layer, and framework aluminophosphates.

2. Discussion

2.1. The Parent Chain

The first structure that we obtained in our synthetic work using the tetraethylene glycol (TEG) solvent system was that of a 1D chain compound containing charge-balancing triethylammonium ions. This structure proved to be identical to that reported by Jones et al. when they used 2-butanol as solvent.[15] From the same TEG system we also obtained the anionic framework structure JDF-20, which contains triethylammonium ions in its channels; this had also been previously reported by Jones et al.[13] Inspection of the JDF-20 framework showed it to be composed of linear chains, which are linked to chains of a different type.[31] We proposed that the latter chain type was derived from hydrolysis and condensation of the linear aluminophosphate chain.[65] Arguably, the chain and JDF-20 structures co-crystallize and one phase grows in at the expense of the other.

Many other structures crystallize in the TEG–triethylamine system when water is used as an additive reagent.[24, 31] These new structures were also envisaged to be built of chain-building blocks derived from the parent chain. Structural studies of aluminophosphates prepared in other systems allow their architectures to be rationalized by similar chain-building blocks derived from the parent chain. We developed a scheme according to which many different types of chains can be formed by performing hydrolysis and condensation reactions on the parent chain.[65] However, the existence of this parent chain remained nebulous until one of the hypothetical crystal structures of this model was confirmed experimentally.[19, 20] Significantly, this 1D chain structure thermally transforms to give a 2D porous layer structure that we had previously isolated in the same synthesis system.[19] This appears to be one of the hitherto unrecognized assembly pathways for aluminophosphate layers and frameworks.

The parent chain is therefore the linear chain structure that crystallizes in the TEG–triethylamine system.[15] It consists of corner-sharing Al_2P_2 four-rings bridged at the aluminum(III) centers; two doubly bridging phosphates occur in each four-ring (Figure 1a). The parent chain only crystallizes for a specific set of templates, reagent concentrations, and reaction conditions, which explain its absence in other systems. The linear chain is likely the most stable polymeric aluminophosphate species. It has a simple structure, and contains only one type of aluminum(III) and phosphorus(V) site. The identical arrangement of orthogonally organized four-rings exists in other mixed oxides, such as the borosilicate chains of the mineral garrelsite,[3] and a zinc phosphate chain structure.[66] Importantly, the parent chain structure has also been isolated in an aqueous system, in which ethylenediamine was used as template.[16] This shows that the structure can also form in aqueous systems, which is an essential ingredient of the present model.

The tetrahedrally coordinated aluminum centers of the parent chain are fully coordinated to phosphate groups. This arrangement is similar to that found in homopolyoxo ions and heteropolyoxo ions. For example, the central aluminum atom in the Keggin ion is tetrahedrally coordinated, while the outer

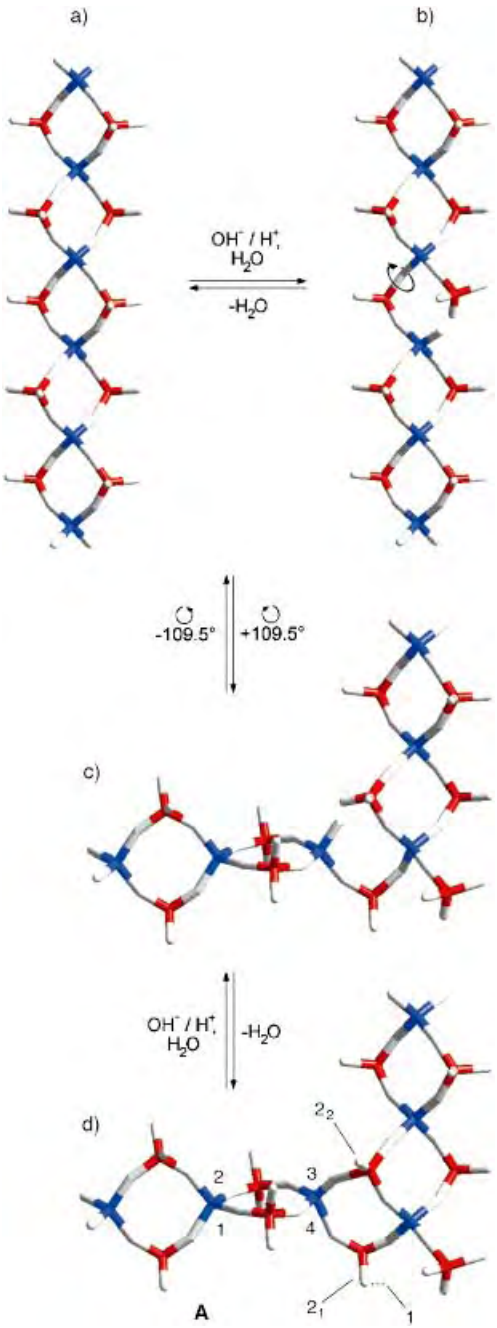


Figure 1. The transformation of the parent chain to give edge-sharing four-rings and terminal $P(O_{Al})(O)_3$ phosphate groups. All steps are reversible, as indicated by the equilibrium arrows. a) Parent chain. b) Ring-opening hydrolysis results in an AlOH group and a terminal phosphate group. c) Rotation about the remaining Al-O-P linkage of the chain brings the AlOH group in the vicinity of a POH group on the adjacent four-ring of the chain. d) Condensation and regeneration of the catalytic water molecule to define two edge-sharing four-rings (structure **A**; for numbering see text). Color scheme (same for all figures): Oxygen: white; phosphorus: red; aluminum: blue.

aluminum atoms are all octahedrally coordinated.[67] Similarly, phosphate groups display a tendency to doubly or triply bridge metal centers in inorganic chain structures, such as molybdenum phosphates[68–70] and vanadium phosphates[71] as well as in chain-building units of higher dimensionality structures.[72] The same is true for vanadium arsenates.[73] The preference of Al^{III} to be surrounded by four phosphate groups is also seen in molecular aluminophosphate complexes, in which one aluminum atom is coordinated to four phosphates groups.[74] It is possible that this type of monomeric unit is the precursor to the parent chain and is the species that is first mineralized from the starting materials.[74]

2.2. Chain-to-Chain Transformations

The parent linear chain is a metastable product that in solution can undergo dynamic hydrolysis of the Al–O and P–O bonds.[60–63] Even under predominantly nonaqueous conditions this will occur, as water will always be present in sufficient amounts. Depending on the pH, acid or base hydrolysis is expected to cleave the Al–O and P–O bonds, and terminal AlOH and POH groups are thereby formed (Figure 1b). Since polymeric aluminophosphate chains in solution are expected to be highly flexible, particularly at the elevated synthesis temperatures, rapid rotation and bending motions occur about the unhydrolyzed Al-O-P linkage (Figure 1b). Rotation would bring the AlOH and POH groups closer together (Figure 1c), allowing intra-chain condensation to occur with the loss of water (Figure 1d). In this way, two corner-sharing four-rings are transformed into two edge-sharing four-rings. Note that the reverse process is also likely, and is indicated by the equilibrium arrows for each step. A terminal phosphate group that is located at the aluminum atom common to the edge-sharing four-rings can remain on, or be cleaved off the chain by hydrolysis, allowing another degree of freedom for possible transformation pathways.

If the process shown in Figure 1 proceeds in the forward direction, the transformation is expected to continue down the chain backbone, for example, to the next four-ring of the parent chain. There are now several choices for the third four-ring to connect to the first two (Figure 2). Each Al-O-P linkage in the next four-ring, labeled 1 through 4 (see Figure 1d), has an equal chance of becoming hydrolyzed. Hydrolysis at sites 3 or 4 simply leads to an open-chain type (see below). If the ring is opened at site 1, rotation around the remaining oxygen bridge will bring the resulting AlOH group only within the proximity of the POH group also labeled 1. (Note that in Figure 1d, the POH group 1 is hidden behind the POH group 2_1.) The third four-ring thereby connects to form a new section in which the three edge-sharing four-rings define a "*cis*" conformation (Figure 2a).

Alternatively, for hydrolysis at site 2, rotation can bring the AlOH group close to one of two hydroxy groups, labeled 2_1 and 2_2 (Figure 2b and 2c, respectively). Rotation in one direction (i.e., $+109.5^\circ$) connects the chain onto phosphate group 2_1, and a section in which all the edge-sharing four-rings are "*trans*" to each other is formed (Figure 2b). Rotation in the other direction (i.e., -109.5°) results in condensation to phosphate group 2_2, and gives a "zigzag" chain section (Figure 2c). Subsequent four-ring "foldings" can be envisaged to continue down the chain, leading to an infinite chain with a new connectivity. For the "*trans*" chain, the process can continue down the chain without hindrance (Figure 3a). Similarly, the zigzag chain can readily be formed (Figure 3b). In the case of the "*cis*" chain, however, the chain must bend

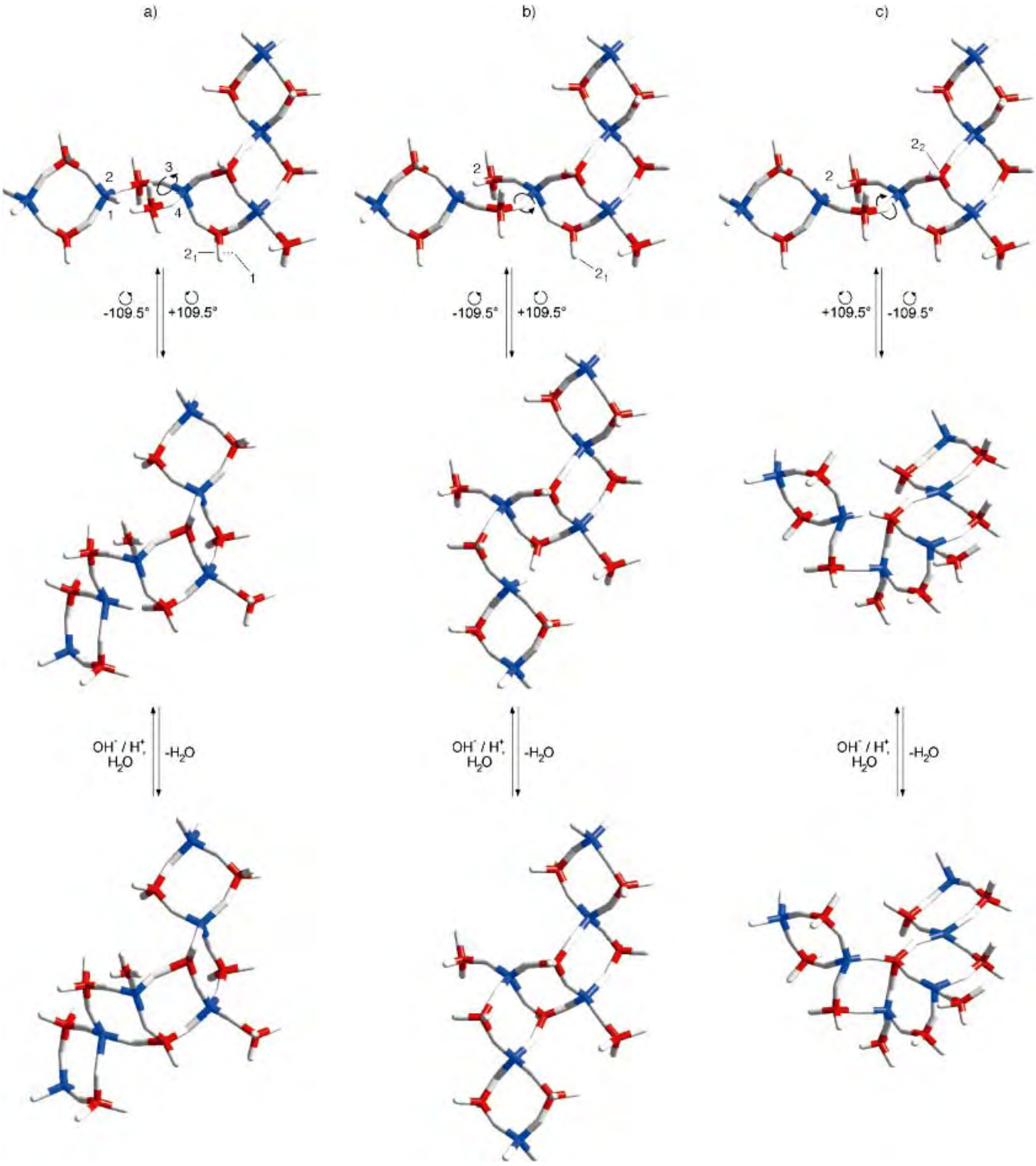


Figure 2. The next step in the transformation of the parent chain (after the formation of **A**) to form three edge-sharing four-rings. In each case the hydrolysis is followed by a rotation and a condensation. a) Formation of a "*cis*" section: ring-opening at position 1 and connection of the resulting AlOH group to the POH group 1. b) Formation of a "*trans*" section: ring-opening at position 2 and connection to the POH group 2_1. c) Formation of a "zigzag" section: ring-opening at position 2 and ring-closure at the POH group 2_2.

back in the opposite direction to avoid folding back onto itself. This leads to a chain with an alternating "*cis*–*trans*" arrangement (Figure 3c). An infinite connectivity scheme of this type would be equivalent to the double-crankshaft chain that has been previously described,[44, 45] except that in the present case, terminal phosphate groups are present on each aluminum atom. However, as will be seen, only small sections of the "*cis*–*trans*" chain type are necessary to rationalize aluminophosphate formation. With careful consideration of the means by which the ring-opening and ring-closing process propa-

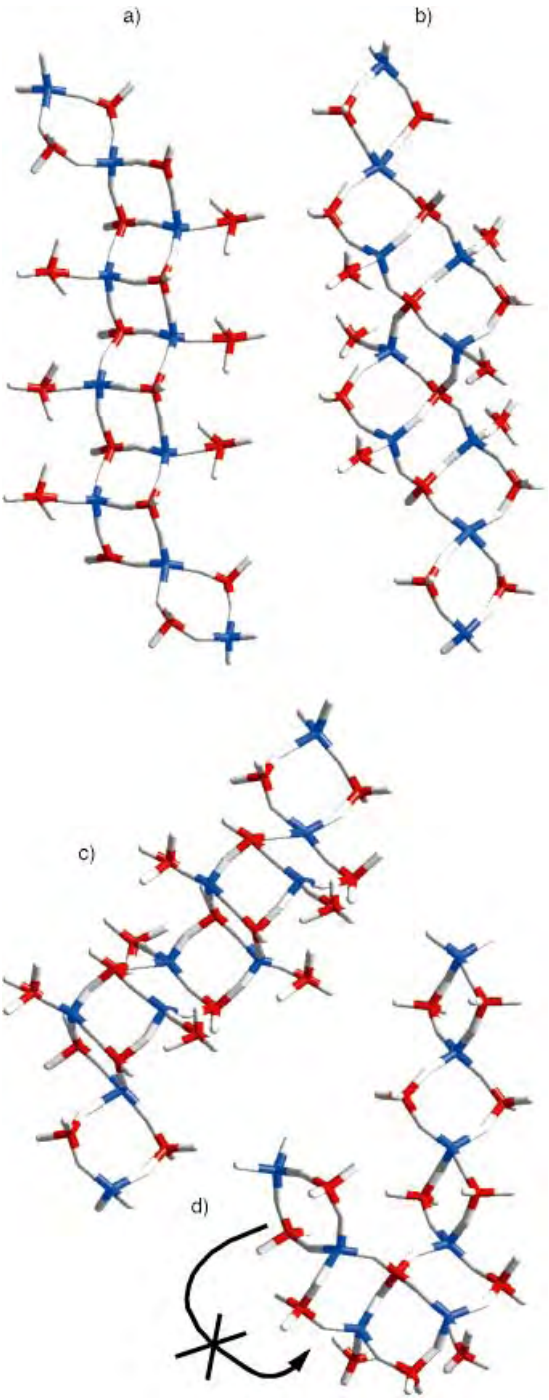


Figure 3. Extended sections of the chain types given in Figure 2. The terminal phosphate groups have been retained on each aluminum atom in these examples. The original connectivity on the end of the sections to the parent chain has also been shown for emphasis (as has been done for all the figures). a) A *trans* chain section, $(T_P)_7$; b) a zigzag chain section, $[Z(3,3)_P]_7$; c) an alternating *cis*–*trans* chain section, $(C_P)_7$; d) the zigzag chain given in Figure 2c. Hydrolysis of the next four-ring would not allow connection to the side necessary for a zigzag chain with two four-rings per leg. For nomenclature see Table 1.

gates down the axis of the parent chain, it becomes evident that for the zigzag chain, there must be an odd number of four-rings per leg (Figure 3d).

There are many other degrees of freedom for transformations of the parent chain by this process. For example, corner-sharing four-rings can be skipped in the process and remain intact (Figure 4a–e). Another example involves only ring-opening of the four-rings, resulting in an "open" chain intermediate as previously mentioned (Figure 4a). Further, each resulting chain type in principle represents an infinite family, since the different chain sections can be of any length, such as those shown in Figures 4b and 4c. Combinations of these processes can also occur on a single chain, allowing an unlimited number of mixed chain types; one example is shown in Figure 4e. The chains displayed in Figure 4 are but a few examples of the large number of possibilities. Additional intrachain condensation of a transformed chain can also occur, which results in, for example, phosphate-capped six-rings connected through four-rings (Figure 4f), or the connection of sections of five edge-sharing four-rings to sections of three corner-sharing four-rings (Figure 4g; this example will be important later). We will show that intrachain condensation and the formation of a chain with capped six-rings leads to many layer and framework aluminophosphates. Computer modeling studies show all chain types have high conformational stability. All tetrahedra remain only slightly distorted, as found in aluminophosphates, and bond angles and lengths need not be changed beyond their energetically accessible limits.[75]

With such a large number of possible chain types, we have introduced a nomenclature scheme, which is summarized in Table 1. Only the repeat unit of a particular chain need be described, and each section of the repeat unit is given a specific label for chain type, and a subscript for its length in terms of the number of aluminum atoms or four-rings. In this way, any chain type may be labeled. Examples of this nomenclature scheme are given throughout the figure captions.

Although the chain transformations can be viewed as a chain "zipping" process, it is more likely that they occur simultaneously or in short succession, along the entire length of the chain. It is possible that they happen during the short synthesis time scales that are sufficient for many aluminophosphate materials; for instance, the high-temperature or microwave synthesis of $AlPO_4$-5 only requires a few seconds.[76, 77] It should also be kept in mind that although chain transformations, such as those shown in Figures 1–4, seem complex, they only involve a very small number of operations per asymmetric unit.

The structure of polymeric UT-2, which we characterized in the TEG–cyclopentylamine system,[19] is in fact the chain structure shown in Figure 4g right. This is significant because we had previously hypothesized this chain to exist, and have now isolated what appears to be a "missing link" in the chain mechanism. As expected, the singly bridging, triply terminal $P(O_{Al})O_3$ phosphate groups reside on the edge-sharing four-rings of the *cis*–*trans* chain sections. The only other aluminophosphate crystal structure containing a singly bridging phosphate group is that of the monomeric $Al(PO_4)_4$ cluster previously mentioned.[74] It seems that a kinetic product has been trapped, in which the typically unstable terminal phosphate groups interact with those of other chains, thereby locking in the metastable structure. Even more surprising is that this structure, in which the chains are arranged into layers, undergoes a thermally induced solid-state transforma-

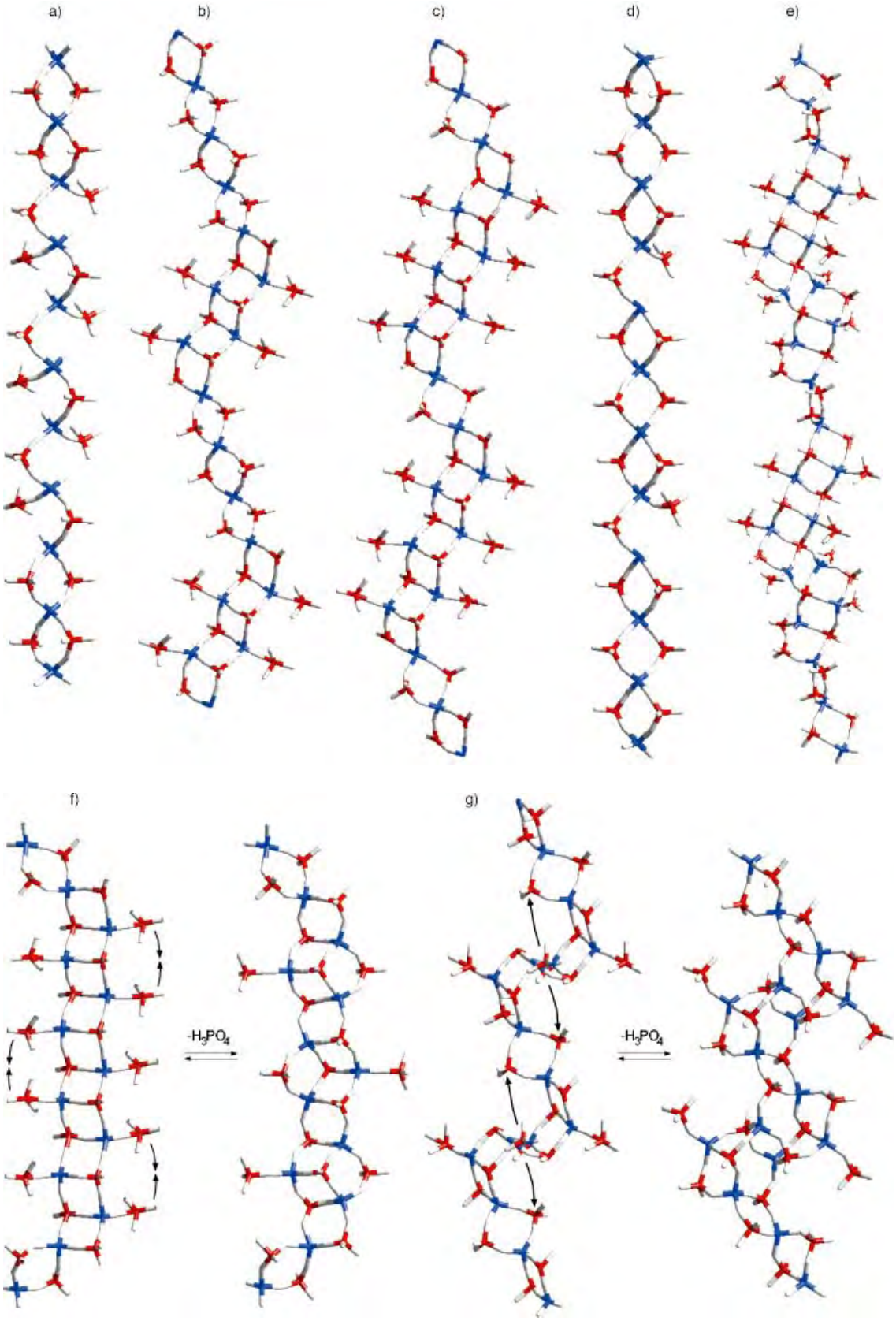


Figure 4. More examples of possible chain types; sections of varying length are displayed. a) A partially opened chain, $\diamond_2(O_P)_2$. b) A partial *trans* chain, $\diamond_5(T_P)_5$. c) Same as in b) but with sections of different length, $\diamond_3(T_P)_7$. d) Another partially opened chain, $\diamond_3(O_P)_1$. e) A chain containing three different sections, $\diamond_3(T_P)_5[Z(3,3)_P]_5$; f) Intrachain condensation of the *trans* chain ,$(T_P)_{10}$, results in a chain with edge-sharing four- and six-rings, in which the six-rings are capped by triply bridging phosphate groups alternating above and below the plane of the chain. g) Intrachain condensation of the C_p section of a partial *cis*–*trans* chain, $\diamond_3(C_P)_5$, with the parent chain section results in a new chain type, which we have characterized by X-ray crystallography.[19, 20] For nomenclature see Table 1.

Table 1. Nomenclature scheme for the description of the repeat units in aluminophosphate chains.

$\diamond_n$	Section of *n* corner-sharing four-rings of the unhydrolyzed parent chain
T_n	Section of *n* edge-sharing four-rings in a *trans* conformation
$(T_P)_n$	Section of *n* edge-sharing four-rings in a *trans* conformation, with terminal phosphate groups remaining on the aluminum centers
C_n	Section of *n* edge-sharing four-rings in a *cis*–*trans* conformation
$(C_P)_n$	Section of *n* edge-sharing four-rings in a *cis*–*trans* conformation, with terminal phosphates remaining on the aluminum centers
O_n	Section of *n* corner-sharing four-rings that have been ring-opened (and have lost their terminal phosphate groups)
$(O_P)_n$	Section of *n* corner-sharing four-rings that have been ring-opened, with terminal phosphate groups remaining on the aluminum centers
$[Z(a,b)]_n$	Section of *n* edge-sharing four-rings in a zigzag conformation; subsections of *a* and *b* four-rings per leg, respectively
$[Z(a,b)_P]_n$	Section of *n* edge-sharing four-rings in a zigzag conformation; subsections of *a* and *b* four-rings per leg, respectively, with terminal phosphate groups remaining on the aluminum centers

tion to the layered structure UT-3.[19] We had previously obtained UT-3 directly in the same synthetic system (i.e., in the presence of small amounts of water, which evidently catalyzed the transformation) and determined its structure by single-crystal X-ray diffraction.

We consider this unprecedented chain-to-layer transformation to be fundamentally important for comprehending the formation of aluminophosphates. The parent chain is initially hydrolyzed in solution, leading to the formation of other chain structure types. These chains are solvated and interact with alkylammonium ions, which keeps them apart in solution. The cationic templates reduce the chain–chain electrostatic repulsion, allowing them to crystallize from solution. Simple aggregation of the chains through ionic bonds to the template[15, 16, 18] or interchain hydrogen bonds[17, 19, 20] results in a chain structure, while chain condensation causes cross-linking and leads to a porous layer or open-framework structure. Rapid precipitation of the chains would result in an amorphous material that would appear to be layered by various experimental probes, but in reality contains layers of poorly arranged chains. Further heating of this phase would allow the chains to reconstruct, cross-link, and organize to form the final, crystalline structure. This would be consistent with, and account for, the various results and the typically fast precipitation rate of aluminophosphates that have been reported to date.[59–64] In the reconstruction process, the final structure is controlled by both the chain type and properties of the organic template. The templates are therefore only partly responsible for the resulting structure. This serves to elucidate the often unclear role of the template,[3a] and the template-dependent and template-independent trends that are observed for aluminophosphates.

The known solid-state transformations of aluminophosphate frameworks, such as that of VPI-5 to $AlPO_4$-8,[78, 79] $AlPO_4$-21 to $AlPO_4$-25,[44] and $AlPO_4$-C to $AlPO_4$-D,[45] as well as aluminophosphate minerals obtained through the solid-state transformation of other phases[80] provide supporting evidence for the present model. These transformations also involve hydrolysis–restructuring–condensation processes, and have been referred to as chain-to-chain transformations. Furthermore, they are chemically equivalent to the processes we propose, as well as to the UT-2 to UT-3 chain-to-layer transformation discussed above. In fact, solid-state transformations play a vital role in the formation of many chain, layered, and framework structures, as will be described in more detail below.

The chain model is also consistent with the P:Al ratios in aluminophosphates, which lie between 2.0 and 1.0 for most extended aluminophosphate structures. The largest value of 2 is only present in the parent linear chain. By hydrolytically cleaving the terminal phosphate groups from transformed chains (see Figures 4–10), the P:Al ratio is gradually reduced. The greater the degree of hydrolysis, the more phosphate groups that are removed, particularly in condensing to layers and frameworks. This accounts for the generally lower P:Al ratios in the higher dimensionality aluminophosphates.

Similarly, this accounts for the invariant, P:Al ratio of 1.0 for aluminophosphate frameworks. All aluminophosphates avoid direct Al-O-Al linkages between tetrahedral AlO_4 units; for zeolites this is known as Lowenstein's rule.[3] Recent calculations on the energy of formation of aluminophosphates show this rule to be both valid and strictly obeyed.[81] There are consequently no P-O-P linkages between the tetrahedral units in the nonmetal-substituted, aluminophosphate frameworks, and the P:Al ratio is 1.0. These rules are obeyed by the parent chain, which initiates the alternating Al and P centers. The maximum number of phosphate groups that may be removed from the chain by hydrolysis, while still maintaining an extended chain structure, is one of the two phosphate groups on each four-ring, thereby defining a minimum P:Al ratio of 1.0. Interestingly, in this respect the aggregation polymers of aluminophosphates prefer to form in solutions in which the P:Al ratio lies between 1 and 2.[61–63, 80] These also happen to be the ratios used for the synthesis of chain, layer, and framework aluminophosphates.

2.3. Chain-to-Layer and Chain-to-Layer-to-Framework Transformations

Having introduced the various chain types and the mode by which they form, we will now proceed to show structural examples of chain types and how they can account for the various architectures of aluminophosphate materials. The first example is that of the porous layer $AlPO_4$-5-like structure $[Al_3P_4O_{16}]^{3-} \cdot 3[R^+]$[22, 24, 27] (Figure 5). Intrachain condensation of $[Al_3P_4O_{16}]^{3-}$ chains of the type shown in Figure 5a forms a chain containing capped six-rings (Figure 5b), which snap together to create the two-dimensional net[82] (Figure 5c). The resemblance of the layer structure to $AlPO_4$-5 itself is not likely a coincidence. Removal of the caps and interlayer condensation would result in the $AlPO_4$-5 framework. However, the pathway given in Figure 5 does not necessarily have to be followed to obtain $AlPO_4$-5. Instead, the chains given in Figure 5a responsible for the $AlPO_4$-5 layer could bypass the layer "intermediate" and undergo

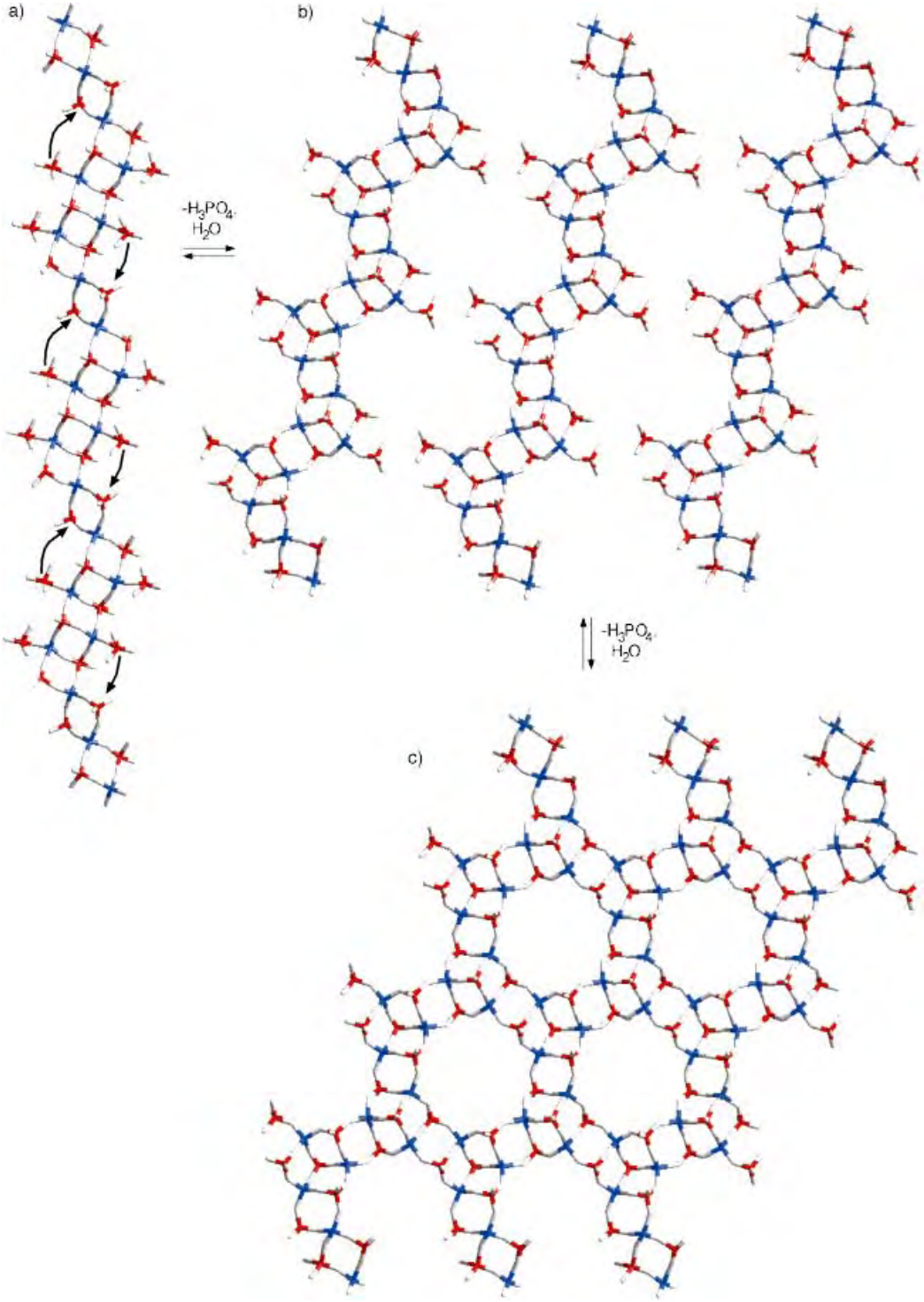


Figure 5. Formation of the capped $AlPO_4$-5-like layered structure. a) The partial *trans* chain, $\diamond_3(T_P)_7$. b) Intrachain condensation creates an array of edge-sharing four- and six-rings; phosphate caps on the six-rings alternate above and below the plane of the chain. c) Condensation of the chains to form the two-dimensional structure containing twelve-rings.

simultaneous chain-to-framework connection to create the framework, as will be shown for several frameworks below. The choice of the $AlPO_4$-5 layer or $AlPO_4$-5 framework as the end product is determined by parameters such as the synthesis conditions and template properties. Thermodynamically, the framework represents the more stable structure and is thus easy to isolate.[14] By contrast, the layer requires less vigorous reaction conditions to restrict hydrolysis and cross-linking processes.

In the context of the porous layer $AlPO_4$-5 structure (Figure 5c), two metal-substituted MAPO-*n* frameworks are worthy of mention.[14] The structure of MAPO-46 may be considered as two such capped layers arranged back-to-back, with the caps pointing in opposite directions. One layer is the

layered $AlPO_4$-5 structure, while the other contains six-rings in which, instead, the phosphorus centers of the six-rings are bound through their terminal oxygens to a capping metal atom. This "double-layer" in turn connects to its two neighboring double-layers through the respective phosphate and metal caps, to define the overall framework. The CoAPO-50 framework may also be considered to be constructed exclusively of layers with the $AlPO_4$-5 structure. In this case, the cobalt atoms cap the opposite side of the phosphate-capped six-rings, and connect to the phosphate caps of the next layer. While the predominance of the $AlPO_4$-5 framework architecture has been previously noted,[3, 41] it has not been pointed out that the capped $AlPO_4$-5 layer structure is also a predominant architecture among the $AlPO_4$-*n* structures. This underscores the importance of the chain shown in Figure 5a in the formation of $AlPO_4$-5 and related MAPO-*n* structures.

The result of another chain-to-layer transformation is the $[Al_3P_4O_{16}]^{3-}$ layer structure, which has been isolated in several nonaqueous systems.[20, 21, 25, 28] The $[Al_3P_4O_{16}]^{3-}$ chain, as was shown in Figure 4 f right, is formed from an "all-*trans*" chain by loss of terminal phosphate groups and intrachain condensation. Connection of the chains by further loss of phosphate groups forms the layered architecture, depicted in Figure 6. Interestingly, the layer arrangement of four-, six- and eight-rings is the same as that which occurs in the projection of the $AlPO_4$-12 structure along the *a* axis, with the exception that the the six-rings of the present layer are also capped by a triply bridging phosphate group.[14] As for the $AlPO_4$-5 layer, these layers can cross-link to form the $AlPO_4$-12 framework by removing the capping phosphate groups, or the starting chains (see Figure 4 f right) could by-pass the layer to directly form $AlPO_4$-12.

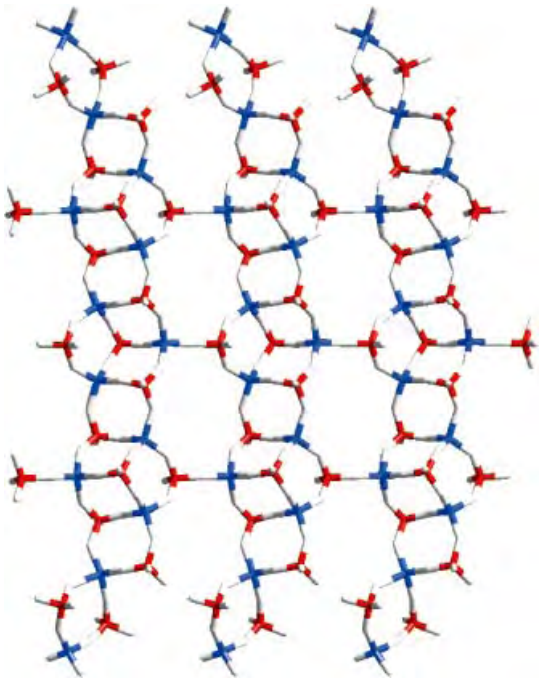


Figure 6. The $[Al_3P_4O_{16}]^{3-}$ layer from capped six-rings. Condensation of the chain given in Figure 4 f left with loss of terminal phosphate groups and water leads to the formation of a layer containing eight-rings.

2.4. Chain-to-Framework Transformations

An example of the connection of chains directly to a framework is shown in Figure 7. The formation of JDF-20 can be explained by the fusion of two simple types of chains,[31, 65] the parent chain (Figure 1 a), and the $[Al_4P_4O_{17}]^{2-}$ zigzag chain (Figure 3 b). The parent chain connects to two zigzag chains through six-rings (Figure 7 a). This building unit is arranged in a hexagonal array in the *ab* plane and thus defines the elliptical unidimensional channels of the framework, in which the units are connected through zigzag chains. Two sets of eight-ring channels perpendicular to the main channel are thereby created (Figure 7 b). The presence of parent and zigzag chains requires hydrolysis conditions that are less severe. This accounts for the fact that this material was only recently discovered in a predominantly nonaqueous triethylene glycol system. The ratio of parent $[AlP_2O_8H_2]^-$ chains to $[Al_2P_2O_{8.5}]^{2-}$ chains (the zigzag chains are one-half the length of the parent chain per asymmetric unit) in the structure is 1:2; their condensation affords a framework of the observed composition $[Al_5P_6O_{24}H]^{2-}$.

2.5. Chain Encapsulation

As two or more chain types can construct a new structure, it is expected that they can condense with other alumina or aluminophosphate solute species that coexist in the system. The coordination and aggregation state of aluminum(III) is known to be highly dependent on the pH value,[83, 84] as are those of the molecular aluminophosphates[57, 58] and aggregation polymers.[60–63] Such species might be incorporated between the chains under a particular set of synthesis conditions. This represents another degree of freedom for the chain model, and accounts for a number of other structure types.

One example is the aluminophosphate framework of tinsleyite (Figure 8 right). $AlPO_4$-tinsleyite[85] is exclusively built of octahedral AlO_6 and tetrahedral PO_4 units. Four vertices of the aluminum octahedra are occupied by the oxygen atoms of the neighboring phosphate groups. One third of the aluminum atoms have their coordination sphere completed by two terminal oxygen atoms (OH^-, H_2O), while the remaining two thirds achieve this as doubly oxygen-bridged pairs (Al-(μ_2-O)$_2$-Al). The structure of tinsleyite can be derived from the open chain given in Figure 8 left, which connects to aluminum(III)-based double octahedra (shown in the center of Figure 8) on either side of the chain. Octahedral coordination is favored for aluminum(III) under more acidic conditions.[83, 84] Thus, it is possible that under these conditions a chain aluminophosphate species contains octahedrally coordinated aluminum centers, as for the $[Al(H_2PO_4)_3]$ chain of Kniep et al.,[17] or that the aluminum coordination sphere changes from tetrahedral to octahedral by simply increasing its coordination with terminal water molecules. Aluminum(III) is known to partially exist as condensed oxo polyhedra, such as Al_2O_{10} dimers, in solution under acidic conditions.[83, 84] $AlPO_4$-tinsleyite therefore represents a chain-to-framework condensation in which a second species, in this case an alumina dimer, participates in the chain connection process.

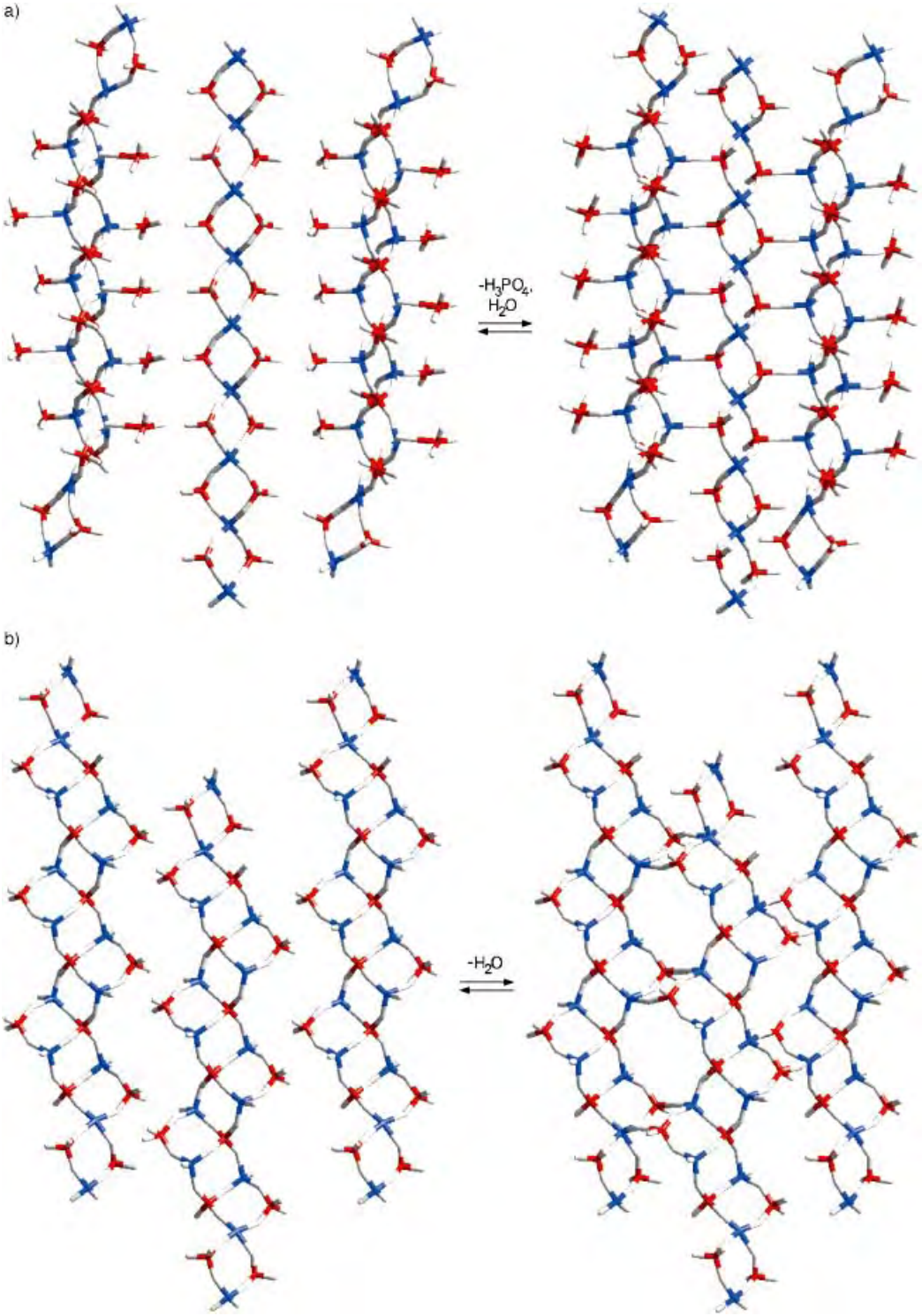


Figure 7. Chain condensation that leads to the framework topology of JDF-20. a) Two zigzag chains, $[Z(3,3)_P]_\infty$, connect to a parent chain, $\diamond_\infty$ and condense with formation of six-rings to give the building-block of the framework. Four such building blocks are arranged around the main channel of the structure: one on the top, one on the bottom, and one each side. b) The end-on view of three units from a), and the $[Z(3,3)]_\infty$ zigzag chains that reside on them; condensation of three of the zigzag chains leads to the formation of two independent eight-ring channels that intersect the main channels.

Another example of this kind of chain encapsulation is the recently reported framework of the aluminofluorophosphate UT-6.[12] This chabazite-like structure is related to $AlPO_4$-CHA (such as the $AlPO_4$-34, MAPO-34, MAPO-44 and MAPO-47 frameworks), in which one aluminum atom in each six-ring of the hexagonal prisms is replaced by an octahedrally coordinated aluminum atom, which connects to an octahedrally coordinated aluminum atom of an adjacent hexagonal prism through two bridging fluorine atoms. The UT-6 structure can be derived from the chain given in Figure 9a.

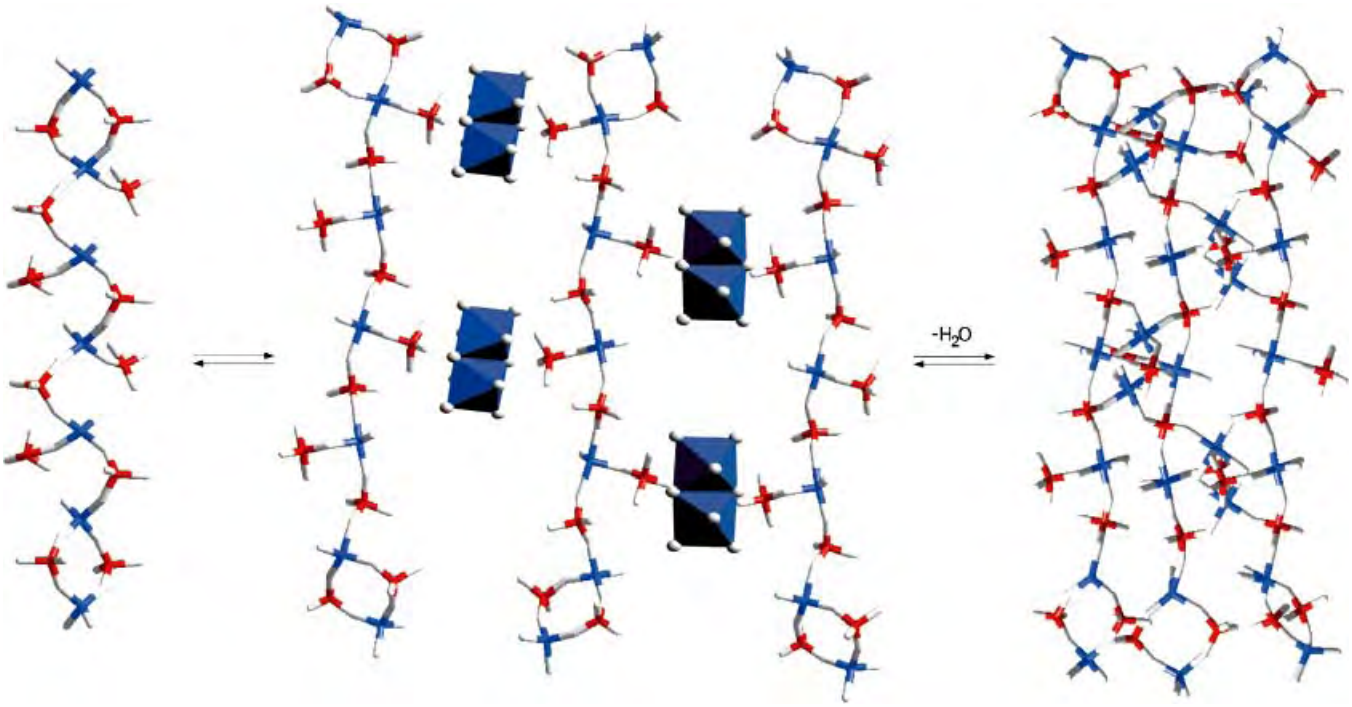


Figure 8. Model for the formation of the tinsleyite framework with its distorted eight-rings (right) from the open chain type, $(O_P)_\infty$ (left). The terminal phosphate groups extend outwards and reach above (center left) and below (center right) the Al_2O_{10} double-octahedra.

A plane of these chains surround one aluminum center of an adjacent plane of partially fluorinated (Al-(μ_2-F)$_2$-Al) double octahedra, to form the bottom six-ring of the hexagonal prism (depicted in yellow in Figure 9b). The other aluminum center of these double octahedra connects to the next layer of chains. Likewise, a plane of double octahedra above completes the upper six-ring of the hexagonal prism (not shown, but the second six-ring is depicted in pink, Figure 9c). In this way, a primitive array of hexagonal prisms is constructed that defines the framework of UT-6.

Significantly, the UT-6 structure thermally transforms in the solid state to $AlPO_4$-CHA, by removal of the bridging fluorine atoms and extra-framework template cations.[12] This is likely the mode by which the various polytypes of $AlPO_4$-CHA frameworks are formed. Initial condensation of the chains (Figure 9a) and Al_2O_{10} double-octahedra, followed by separation and dehydration of the double-octahedra to give tetrahedral centers, builds up the $AlPO_4$-CHA framework. Only with this knowledge of the UT-6 structure and its transformation is it possible to understand the origin of this framework. Similarly, it becomes possible to rationalize the formation of other aluminophosphate structures that would otherwise be very difficult to explain.

The final example, which also involves chain encapsulation of aluminum double-octahedra, is VPI-5. The chain proposed to be responsible for the formation of VPI-5 connects through aluminum double-octahedra to build up the structure of VPI-5, which contains 18-membered rings (Figure 10; the second octahedron of the dimer is not shown, but resides in the next layer). In this case, the alumina dimers separate but the octahedral coordination is retained; the fifth and sixth coordination sites of aluminum are occupied by terminal water molecules that reside in the main channel.[46] This mode of formation would account for the difficulty in synthesizing VPI-5,[49, 50] as one must first age the gel, and carefully control the pH. For the process given in Figure 10 to occur, one must first build up the more complex chain type given in Figure 10 left, as well as leach aluminum double-octahedra into the gel and encapsulate them with relatively labile terminal phosphate groups of the chain. Once this is achieved, nucleation of the material can begin.

The chain-assembly model has been developed by considering the relationships between crystal structures of various new aluminophosphate materials, which have been isolated by reaction profiling of nonaqueous synthesis systems. In many cases, the chain-to-layer and chain-to-framework transformations obscure the presence of the parent chain in the final structure of the product. This is evident in the UT-2 chain to UT-3 layer transformation.[19] Additionally, the chains responsible for the structures in most cases span the layer planes, which is also unique to the chain model. In this way, the complex arrangements of rings and channel systems of aluminophosphate frameworks can readily be understood. The dominance of particular chain precursors, such as that for $AlPO_4$-5 (Figure 5a), accounts for the large degree of template-independence observed for many aluminophosphate structures. The chain model only requires that the transformed sections of edge-sharing four-rings be three-to-five units long. This minimizes the number of chain hydrolysis steps of the parent linear chain.

2.6. Inorgano-Gene: The Progenitor Chain

Finally, it is interesting to consider that the paradigm shift presented in this review is in the same spirit as the emerging

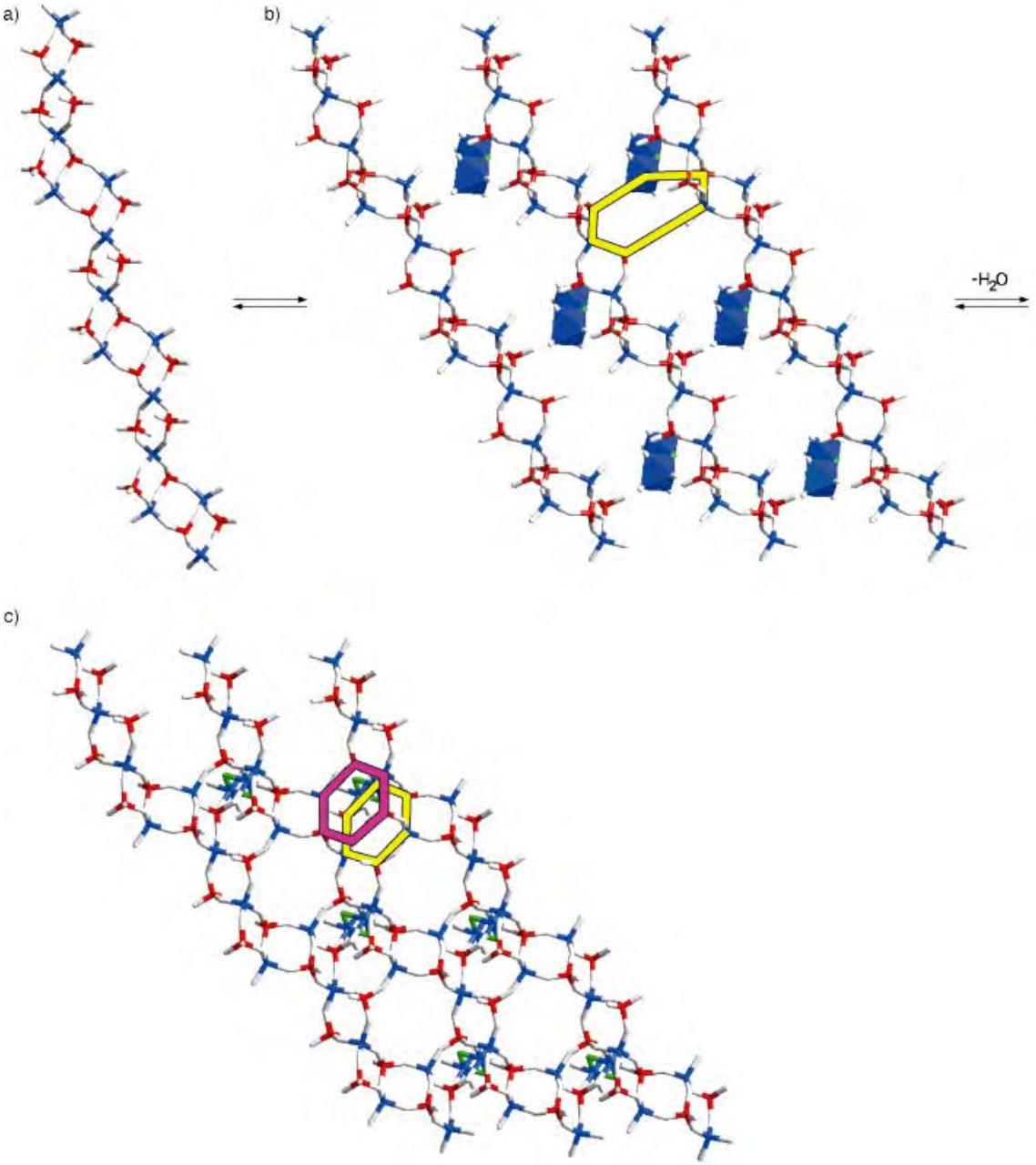


Figure 9. The build up of the UT-6 framework. a) $\diamond_3(T)_3$ chain. b) The chains surround the closer octahedron of the O_5Al-(μ_2-F)$_2$-AlO_5 dimeric units to form the bottom six-ring of the hexagonal prisms (yellow). (The $\diamond_3(T)_3$ chain has been slightly rotated to emphasize the shape that will become the hexagonal prisms). c) Condensation to the aluminum octahedra forms the bottom six-ring (yellow) and will connect in a like manner to the aluminum octahedra above the plane of the layer to form the other six-ring of the hexagonal prisms (pink). Fluorine atoms for UT-6 are shown in green.

biological view of materials chemistry and the description of inorganic materials with complex form.[86] The idea that inorganic materials have the capacity to store vast amounts of information is not new.[87] The thinking goes back to Schrödinger's aperiodic crystal description of the information-carrying genetic apparatus, and subsequently in another expression as the crystal abacus. In its more contemporary guise, the idea abounds in information storage materials found in, for example, records, tapes and discs. In the context of crystallography, Mackay first forwarded the proposal of an "inorganic gene" as a genetic algorithm in the search for the lowest energy configuration of a system of *N* atoms.[87]

In such a departure from the usual view of the aluminophosphate system, the structural, stereochemical, charge, and chemical information that is encoded in the chain can be transcribed to tectons based on an organic template and an aluminophosphate. In a synergistic co-assembly process these tectons will generate new and more complex structures, or "inorgano-phenotypes". Their survival in a particular synthesis is determined by the interplay of kinetic and thermodynamic factors, so that kinetic products are generated in local energy minima. Various hydrolysis "editing operations" of the parent linear chain can permute and alter the structure–directing information in the chain to produce

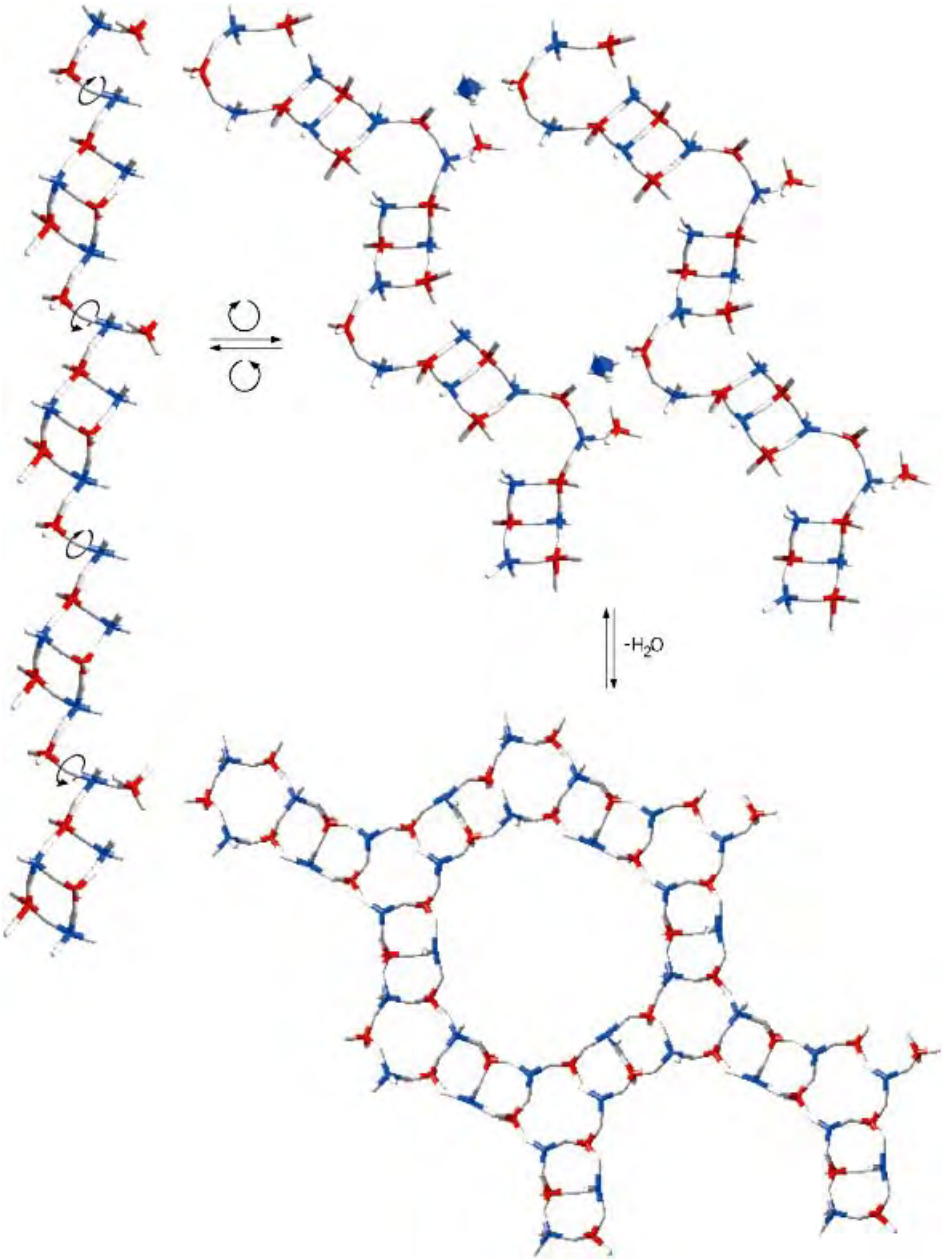


Figure 10. Direct formation of the VPI-5 framework, in which a capped VPI-5 layered "intermediate" of the type shown for $AlPO_4$-5 (Figure 5) is bypassed. Loss of phosphate groups from a chain type $(O_P)_2(T)_2$ gives the less symmetric chain type $(O)_2(T)_2(O)_1(O_P)_1(T)_2$ (left). Simple rotation around the linkages surround monomeric aluminum species with POH groups (center), and subsequent condensation leads to the framework topology.

condensed structures of varying dimensionality and degrees of "fitness."[87]

3. Summary and Outlook

The chain self-assembly model invokes a facile hydrolysis–condensation process of a metastable species that can be crystallized from the aluminophosphate synthesis system. Simple transformations of the parent chain can explain the wide variety of chain, porous layer, and open-framework structures found for aluminophosphates. Coupled hydrolysis and condensation reactions of the linear chain can produce a large number of other more complex chain structure types. Only a few selected examples of these are described herein. The amount of catalytic water in the system, which determines the amount of chain hydrolysis and thereby the resulting structure types. It should be possible to probe the aluminophosphate system and its structures in greater detail to further elucidate the chain self-assembly model. It is likely that new chain structures will be discovered that fit into the chain scheme presented. We hope that this chain model will allow for the rational design of new chain, layer, and framework structure types.

Financial assistance from the Natural Sciences and Engineering Research Council of Canada in support of this work is acknowledged. S. O. expresses his appreciation to the Ontario Graduate Scholarship program in partial support of his research. We thank Dr. Alan Lough of the Department of Chemistry, University of Toronto for single-crystal X-ray data collection and refinement of our series of aluminophosphate crystal structures and Dr. David Young for informative discussions.

Received: February 7, 1997 [A 209 IE]
German version: *Angew. Chem.* **1998**, *110*, 48 – 64

[1] D. W. Breck, *Zeolite Molecular Sieves*, Wiley, New York, **1974**.
[2] G. A. Ozin, *Adv. Mater.* **1992**, *4*, 612.
[3] a) R. Szostak, *Molecular Sieves: Principles of Synthesis and Identification*, Van Nostrand Reinhold, Toronto, **1989**; b) W. Loewenstein, *Am. Mineral.* **1954**, *39*, 92.
[4] S. T. Wilson, B. M. Lok, C. A. Messina, T. R. Cannan, E. M. Flanigen, *J. Am. Chem. Soc.* **1982**, *104*, 1146.
[5] S. T. Wilson, B. M. Lok, E. M. Flanigen, U. S. Pat. 4,310,440, **1982** [*Chem. Abstr.* **1982**, *96*, 130542w].
[6] D. Riou, T. Loiseau, G. Férey, *J. Solid State Chem.* **1993**, *102*, 4.
[7] J. Renaudin, G. Férey, *J. Solid State Chem.* **1995**, *120*, 197.
[8] a) *Proc. 9th Int. Zeolite Conf.* (Eds.: R. von Ballmoos, J. B. Higgins, M. M. J. Treacy), Butterworth-Heinemann, London, **1993**; b) J. L. Guth, H. Kessler, P. Caullet, J. Hazm, A. Merrouche, J. Patarin in ref. [8a], p. 215 ff.
[9] L. Yu, W. Pang, L. Li, *J. Solid State Chem.* **1990**, *87*, 241.
[10] G. Férey, *J. Fluorine Chem.* **1995**, *72*, 187.
[11] S. J. Kirkby, A. J. Lough, G. A. Ozin, *Z. Kristallogr.* **1995**, *210*, 956.
[12] S. Oliver, A. Kuperman, A. Lough, G. A. Ozin, *J. Mater. Chem.* **1997**, *7*, 807.
[13] a) Q. Huo, R. Xu, S. Li, Z. Ma, J. M. Thomas, R. H. Jones, A. M. Chippindale, *J. Chem. Soc. Chem. Commun.* **1992**, 875; b) R. H. Jones, J. M. Thomas, J. Chen, R. Xu, Q. Huo, S. Li, Z. Ma, A. M. Chippindale, *J. Solid State Chem.* **1993**, *102*, 204.
[14] R. Szostak, *Handbook of Molecular Sieves*, Van Nostrand Reinhold, New York, **1992**.
[15] R. H. Jones, J. M. Thomas, R. Xu, Q. Huo, Y. Xu, A. K. Cheetham, D. Bieber, *J. Chem. Soc. Chem. Commun.* **1990**, 1170.
[16] W. Tieli, Y. Long, P. Wengin, *J. Solid State Chem.* **1990**, *89*, 392.
[17] R. Kniep, M. Steffen, *Angew. Chem.* **1978**, *90*, 286; *Angew. Chem. Int. Ed. Engl.* **1978**, *17*, 272.
[18] M. P. Attfield, R. E. Morris, I. Burshtein, C. F. Campana, A. K. Cheetham, *J. Solid State Chem.* **1995**, *118*, 412.
[19] S. Oliver, A. Kuperman, A. Lough, G. A. Ozin, *Chem. Mater.* **1996**, *8*, 2391.
[20] S. Oliver, A. Kuperman, A. Lough, G. A. Ozin, *Inorg. Chem.* **1996**, *35*, 6373.
[21] R. H. Jones, J. M. Thomas, R. Xu, Q. Huo, A. K. Cheetham, A. V. Powell, *J. Chem. Soc. Chem. Commun.* **1991**, 1266.
[22] J. M. Thomas, R. H. Jones, R. Xu, J. Chen, A. M. Chippindale, S. Natarajan, A. K. Cheetham, *J. Chem. Soc. Chem. Commun.* **1992**, 929.
[23] A. M. Chippindale, A. V. Powell, L. M. Bull, R. H. Jones, A. K. Cheetham, J. M. Thomas, R. Xu, *J. Solid State Chem.* **1992**, *96*, 199.
[24] A. Kuperman, S. Nadimi, S. Oliver, G. A. Ozin, J. M. Garces, M. M. Olken, *Nature* **1993**, *365*, 239.
[25] a) R. H. Jones, A. M. Chippindale, S. Natarajan, J. M. Thomas, *J. Chem. Soc. Chem. Commun.* **1994**, 565; b) A. M. Chippindale, S. Natarajan, J. M. Thomas, R. H. Jones, *J. Solid State Chem.* **1994**, *111*, 18.
[26] K. Morgan, G. Gainsford, N. Milestone, *J. Chem. Soc. Chem. Commun.* **1995**, 425.
[27] P. A. Barrett, R. H. Jones, *J. Chem. Soc. Chem. Commun.* **1995**, 1979.
[28] D. A. Bruce, A. P. Wilkinson, M. G. White, J. A. Bertrand, *J. Chem. Soc. Chem. Commun.* **1995**, 2059.
[29] S. Oliver, A. Kuperman, A. Lough, G. A. Ozin, *Chem. Commun.* **1996**, 1761.
[30] R. Xu, Q. Huo, W. Pang in ref. [8a], p. 271 ff.
[31] S. Oliver, A. Kuperman, A. Lough, G. A. Ozin, J. M. Garces, M. M. Olken, P. Rudolf, *Stud. Surf. Sci. Catal. A* **1994**, *84*, 219.
[32] G. Kühl, *J. Inorg. Nucl. Chem.* **1969**, *31*, 1043.
[33] J. E. Cassidy, J. A. J. Jarvis, R. N. Rothon, *J. Chem. Soc. Dalton Trans.* **1975**, 1497.
[34] R. Kniep, A. Wilms, *Z. Naturforsch. B* **1979**, *34*, 750.
[35] M. R. Mason, R. M. Matthews, M. S. Mashuta, J. F. Richardson, *Inorg. Chem.* **1996**, *35*, 5756.
[36] Y. Yang, H.-G. Schmidt, M. Noltemeyer, J. Pinkas, H. W. Roesky, *J. Chem. Soc. Dalton Trans.* **1996**, 3609.
[37] M. G. Walawalkar, R. Murugavel, H. W. Roesky, H.-G. Schmidt, *Organometallics* **1997**, *16*, 516.
[38] K. Diemert, U. Englert, W. Kuchen, F. Sandt, *Angew. Chem.* **1997**, *109*, 251; *Angew. Chem. Int. Ed. Engl.* **1997**, *36*, 241.
[39] A. Keys, S. Bott, A. R. Barron, *Chem. Commun.* **1996**, 2339.
[40] M. R. Mason, M. S. Mashuta, J. F. Richardson, *Angew. Chem.* **1997**, *109*, 249; *Angew. Chem. Int. Ed. Engl.* **1997**, *36*, 239.
[41] D. W. Lewis, C. R. A. Catlow, J. M. Thomas, *Chem. Mater.* **1996**, *8*, 1112.
[42] D. W. Lewis, D. J. Willock, C. R. A. Catlow, J. M. Thomas, G. J. Hutchings, *Nature* **1996**, *382*, 604.
[43] Y. Hu, A. Navrotsky, C. Chen, M. E. Davis, *Chem. Mater.* **1995**, *7*, 1816.
[44] J. W. Richardson, Jr., J. V. Smith, J. J. Pluth, *J. Phys. Chem.* **1990**, *94*, 3365.
[45] E. B. Keller, W. M. Meier, R. M. Kirchner, *Solid State Ionics* **1990**, *43*, 93.
[46] H. Li, M. E. Davis, J. B. Higgins, R. M. Dessau, *J. Chem. Soc. Chem. Commun.* **1993**, 403.
[47] E. Jahn, D. Mueller, J. Richter-Mendau in *Synthesis of Microporous Materials, Vol. 1: Molecular Sieves* (Eds.: M. L. Occelli, H. E. Robson), Nelson Canada, Scarborough, **1992**, p. 248 ff.
[48] H. He, J. Klinowski, *J. Phys. Chem.* **1994**, *98*, 1192.
[49] M. E. Davis, D. Young, *Stud. Surf. Sci. Catal.* **1991**, *60*, 53.
[50] M. E. Davis, B. D. Murray, M. Narayana, *ACS Symp. Ser.* **1990**, *437*, 48.
[51] S. S. S. Rajan, K. W. Perrott, W. M. H. Saunders, *J. Soil Sci.* **1974**, *25*, 438.
[52] S. S. S. Rajan, *Nature* **1976**, *262*, 45.
[53] R. F. Jameson, J. E. Salmon, *J. Chem. Soc.* **1954**, 4013.
[54] A. Holroyd, J. E. Salmon, *J. Chem. Soc.* **1956**, 269.
[55] J. E. Salmon, J. G. L. Wall, *J. Chem. Soc.* **1958**, 1128.
[56] J. W. Akitt, N. N. Greenwood, G. D. Lester, *J. Chem. Soc. A* **1971**, 2450.
[57] R. F. Mortlock, A. T. Bell, C. J. Radke, *J. Phys. Chem.* **1993**, *97*, 767.
[58] R. F. Mortlock, A. T. Bell, C. J. Radke, *J. Phys. Chem.* **1993**, *97*, 775
[59] H. H. Greger, *Brick Clay Rec.* **1950**, *117*, 63.
[60] C. F. Callis, J. R. Van Wazer, P. G. Arvan, *Chem. Rev.* **1954**, *54*, 777.
[61] J. R. Van Wazer, *Phosphorus and Its Compounds: Vol. I*, Interscience, New York, **1958**, pp. 550 – 559.
[62] D. E. C. Corbridge, *The Structural Chemistry of Phosphorus*, Elsevier, New York, **1974**, pp. 124 – 126.
[63] J. H. Morris, P. G. Perkins, A. E. A. Rose, W. E. Smith, *Chem. Soc. Rev.* **1977**, *6*, 173.
[64] A. E. R. Westman in *Topics in Phosphorus Chemistry 9* (Eds.: E. J. Griffith, M. Grayson), Wiley, New York, **1977**, pp. 247 – 256.
[65] S. Oliver, A. Kuperman, A. Lough, G. A. Ozin, J. M. Garces, M. M. Olken, P. Rudolf, poster presentation at the 10th International Zeolite Conference, Garmisch-Partenkirchen, 1994.
[66] W. T. A. Harrison, T. M. Nenoff, T. E. Gier, G. D. Stucky, *Inorg. Chem.* **1992**, *31*, 5395.
[67] D. F. Shriver, P. Atkins, C. H. Langford, *Inorganic Chemistry,* 2nd ed., Freeman, New York, **1994**, p. 199.
[68] P. Kierkegaard, *Acta Chem. Scand.* **1958**, *12*, 1701.
[69] R. C. Haushalter, F. W. Lai, *Inorg. Chem.* **1989**, *28*, 2904.
[70] L. A. Mundi, R. C. Haushalter, *J. Am. Chem. Soc.* **1991**, *113*, 6340.
[71] M. E. Leonowicz, J. W. Johnson, J. F. Brody, H. F. Shannon, Jr., J. M. Newsam, *J. Solid State Chem.* **1985**, *56*, 370.
[72] K. Lii, T. Lee, S. Liu, S. Wang, *J. Chem. Soc. Dalton Trans.* **1993**, 1051.
[73] R. C. Haushalter, Z. Want, L. M. Meyer, S. S. Dhingra, M. E. Thompson, J. Zubieta, *Chem. Mater.* **1994**, *6*, 1463.
[74] D. Riou, T. Loiseau, G. Férey, *J. Solid State Chem.* **1992**, *99*, 414.

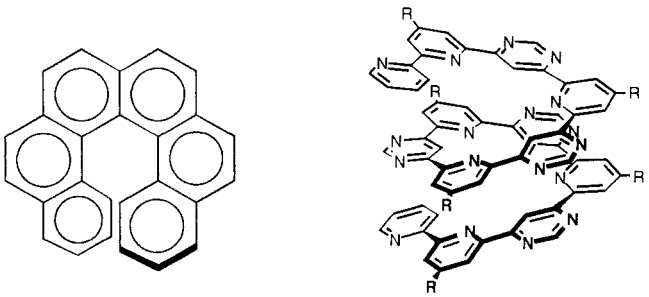
[75] R. Carson, E. M. Cooke, J. Dwyer, A. Hinchcliffe, P. J. O'Malley, *Stud. Surf. Sci. Catal.* **1989**, *46*, 39.
[76] Q. Huo, R. Xu, *J. Chem. Soc. Chem. Commun*. **1992**, 168.
[77] S. L. Cresswell, J. R. Parsonage, P. G. Riby, M. J. K. Thomas, *J. Chem. Soc. Dalton Trans*. **1995**, 2315.
[78] M. Stocker, D. Akporiaye, K. Lillerud, *Appl. Catal*. **1991**, *69*, L7.
[79] H. He, P. Barnes, J. Munn, X. Turrillas, J. Klinowski, *Chem. Phys. Lett*. **1992**, *196*, 267.
[80] R. Kniep, *Angew. Chem.* **1986**, *98*, 520; *Angew. Chem. Int. Ed. Engl*. **1986**, *25*, 525.
[81] C. R. A. Catlow, A. R. George, C. M. Freeman, *Chem. Commun.* **1996**, 1311.
[82] J. V. Smith, *Stud. Surf. Sci. Catal*. **1989**, *49*, 29.
[83] R. J. Moolenaar, J. C. Evans, L. D. McKeever, *J. Phys. Chem*. **1970**, *74*, 3629.
[84] J. W. Akitt, N. N. Greenwood, B. L. Khandelwal, G. D. Lester, *J. Chem. Soc. Dalton Trans*. **1972**, 604.
[85] J. B. Parise, *Acta Crystallogr. Sect. C* **1984**, *40*, 1641.
[86] S. Mann, G. A. Ozin, *Nature* **1996**, *382*, 313.
[87] A. L. Mackay, *THEOCHEM*. **1995**, *336*, 293.

Helical Molecular Programming

Alan E. Rowan and Roeland J. M. Nolte*

The self-organization of molecules into helical and multiple helical architectures can be found throughout nature: from simple α-helical polypeptides and double-helical nucleic acids to more complex helical protein structures, microtubules, and the protein coating of the tobacco mosaic virus.[1] The overall architectural plans required are encoded within the molecular building blocks. Understanding the "programming language" developed and utilized by nature to construct helical structures is of fundamental importance. This knowledge will not only lead to a greater understanding of life, but will also enable the design and construction of new functional helical architectures. The most relevant parameters for controlling the architecture are the molecular size, topology, stereochemistry, and shape. Through processes of self-organization these parameters can be expressed at several hierarchical levels—molecular, macromolecular, and nanomolecular.

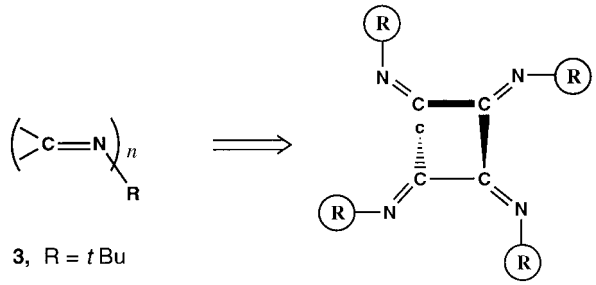
A simple example of molecular programming is the preorganized helical architecture of helicenes.[2] In hexahelicene **1** (Scheme 1) the structural information is encoded in the



1 **2**

Scheme 1. Helicity at a molecular level: Helicene **1** and the oligomeric heteroarene **2** both form helical architectures owing to specific information encoded within the molecules.

geometry of the covalent bonds linking adjacent moieties which, in combination with steric interactions, forces the molecule to adopt a helical geometry. This simple expression of supramolecular helicity was recently further developed by the group of Lehn, who synthesized an achiral polyheterocyclic strand **2** (Scheme 2) which spontaneously organizes to from a two-turn helical structure.[3] This architecture arises as



3, R = *t* Bu

Scheme 2. Polymeric isocyanides **3** form helical rigid rods because of N=C–C=N torsions and steric interactions between the side groups.

a result of several encoded features: an alternating pyridine–pyrimidine sequence, linkage at specific positions, and the preference for a s-*trans* conformation of the single bonds between the alternating units. The resulting helix is adopted both in the solid state and in solution, and is one of the clearest demonstrations of preprogrammed molecular self-organization through specific intramolecular nonbonding interactions. In an alternative approach Moore et al. synthesized oligomers of *m*-phenylacetylene which also spontaneously arrange to give a helical geometry. In this example the helical organization can be readily controlled by solvent and temperature.[4]

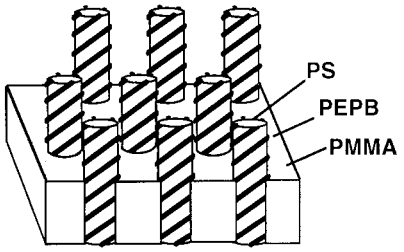
The direct linking of aromatic moieties in a *meta* geometry can also give rise to helicity in larger oligomers and polymers. The crystal structure of *m*-deciphenyl revealed an apparently infinite helical chain in which there are five aromatic rings for each turn of the helix.[5] The predicted X-ray powder pattern of this compound, although only a small oligomer, is virtually identical to that of poly(*m*-phenylene) prepared by nickel-catalyzed coupling of *m*-dichlorobenzene. This implies that the larger macromolecule also adopts a similar helical arrangement. Helical polymers are themselves of increasing interest because of their wide variety of possible applications—for example in optical devices, as chiral separation columns, and as components in organic/inorganic hybrid materials. In polymer chemistry the expression of helicity has long been observed since the early work of Natta, Pino, and others.[6] In fact, most isotatic polymers exist as short-range helices in solution. These, however, are dynamic in nature and

[*] Prof. R. J. M. Nolte, Dr. A. E. Rowan
Department of Organic Chemistry, NSR Center
University of Nijmegen
Toernooiveld, NL-6525 ED Nijmegen (The Netherlands)
Fax: Int. code + (31) 24-365 2929
e-mail: rowan@sci.kun.nl

 © WILEY-VCH Verlag GmbH, D-69451 Weinheim, 1998 1433-7851/98/3701-0063 $ 17.50+.50/0

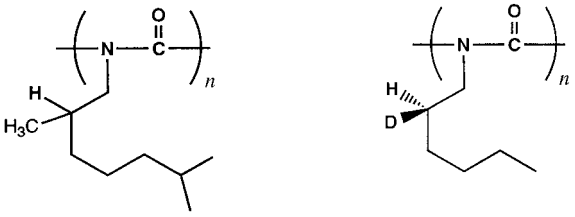
highly dependent on the solvent or slight changes in the polymer side chains. To date only a very limited number of stable, helical, synthetic macromolecules are known—for example polyisocyanides, poly(chloral), and poly(triphenylmethyl methacrylate). The helicity in polyisocyanides is determined by the torsional angle of the N=C–C=N bonds and the steric interactions of the side groups attached to the nitrogen atoms. Upon polymerization of *tert*-butyl isocyanide (**3**) two resolvable left- and right-handed helices were obtained (Scheme 2) with a turn at about every 3.9 units.[7] Unlike with helical biopolymers such as nucleic acids and proteins, the absence of chiral information in the basic building block leads in principle to an equal preference for either left- or right-handed helices. In practice, however, an enantiomeric excess of one helix can be obtained by using a chiral catalyst. The helical sense of the polymer can also be controlled by including chirality in the side group. Polymerization of homochiral isocyanides gives diasteroisomers in unequal amounts; polymerization of (*R*)-$(CH_3)_2CHCH_2CH(CH_3)NC$ preferentially gives a left-handed helix, whereas (*S*)-$CH_3CO_2CH_2$ $CH(CH_3)NC$ gives a right-handed helix. Takahashi et al. recently showed that by using a chiral isocyanide oligomer as an initiator subsequent polymerization with an achiral isocyanide monomeric unit gives a helical polymer with the same sense as the small oligomer.[8]

The subtlety of the parameters which induce chiral expression were clearly demonstrated by Green et al.[9] for polymeric isocyanates **4** (Scheme 3). These stiff helical polymers have no predetermined sense, and in long polymer chains helical reversals may occur. The cooperative stereochemistry of the side groups is so large that only a very small chiral bias in the monomeric unit is magnified and controls the helical sense of large portions of the macromolecule. Upon polymerization of a mixture of *R* and *S* enantiomers of **4a**—in which a 2% excess of the *R* enantiomer exists—the resulting polymer has similar chiral properties as the homochiral polymer made from enantiomerically pure (*R*)-**4a**. The chiral sense of the resulting polymer is determined by the major component. The reaction is so sensitive that even isotopic substitution of the side group results in a preference for one form (**4b**). This phenomenal positive cooperativity can be considered to be a form of molecular amplification. The two polymers discussed already possess a helical backbone whose helical preference can be modified by the size and stereochemistry of the side groups. The induction of helicity into nonhelical polymers is being studied in a very elegant way by Percec et al.[10] Inspired by the behavior of the tobacco mosaic virus, which induces a helical conformation in RNA, they synthesized a series of large, bulky "monodendron" side groups. When these large, tapered moieties are covalently attached to a polymer backbone, the conformation of the backbone is altered from a random coil to a helix. The size and shape encoded in the large side groups which pack on the outside of the polymer induce the chirality. The group of Stadler took one step further on the hierarchical ladder and synthesized a triblock copolymer: polystyrene(55)-*block*-polybutadiene(26)-*block*-poly(methyl methacrylate)(137) (**5**).[11] By a process of controlled phase separation this polymer forms an incredible self-organized system in which helices of polybutadiene microphases are wound around columns of polystyrene, which themselves are embedded in a matrix of poly(methyl methacrylate) (Scheme 4).



5

Scheme 4. Schematic representation of the self-organized architecture formed by phase separation of the triblock copolymer **5** (PS = polystyrene, PEPB = polybutadiene, PMMA = poly(methyl methacrylate)).



4a 4b

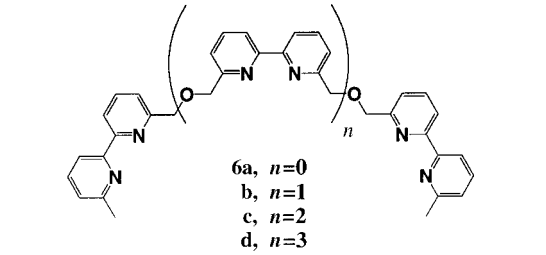
Scheme 3. The helical preference of polymeric isocyanates **4** can be controlled by isotopic substitution.

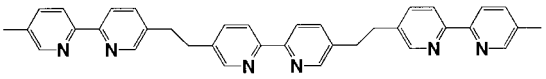
Intermolecular interactions between individual polymers chains can also lead to helical induction. Meijer and coworkers synthesized chiral, conjugated polythiophenes which show remarkable optical properties.[12] The helicity present in each polymer unit is only expressed upon cooling, when the polythiophene chains pack to form a helical aggregate. The helical sense of the assembled macromolecule can be easily controlled by varying the rate of cooling; rapid cooling gives one helical sense, and slow cooling the other. Another approach to the construction of chiral polymers was the elegant work by Ito et al., who prepared a variety of 2,3-quinoxalines from a chiral precursor.[13] The optical activity in these macromolecules could be easily tuned and results from the helicity in the backbone of the polymer and not the helical aggregated species.[14] An interesting recent development is the method for constructing double-helical polymer chains designed by Nozaki et al.[15] Condensation of (*S*)-1,1′-binapthyl-2,2′-dicarbonyl dichloride with biphenyl-2,2′,6,6′-tetrol generates oligomeric esters in which the chirality of the starting binapthyl is carried throughout the oligomer. Although only oligomers have been synthesized so far, polymeric chains can be expected to have interesting properties.

In nature numerous helical architectures result from self-assembly of small building blocks into larger molecular assemblages. This process of self-organization through noncovalent interactions is recognized as crucially important in the construction of biological systems. One approach to mimicking the helical arrays found in nature, in particular the double-stranded helix of DNA, has been the design and study

 © WILEY-VCH Verlag GmbH, D-69451 Weinheim, 1998 1433-7851/98/3701-0064 $ 17.50+.50/0

of metal–ligand complexes known as "helicates".[16] This area was investigated as early as the late 1970s by the group of Saenger, who constructed helical metal–polyether complexes,[17] but has rapidly expanded since the inspirational early work by Lehn and co-workers, who showed that oligobidentate ligands **6a** and **6b** (Scheme 5) form double-helical





7

Scheme 5. Oligopyridine ligands **6** and **7** self-assemble in the presence of metal ions to form a variety of helical arrays.

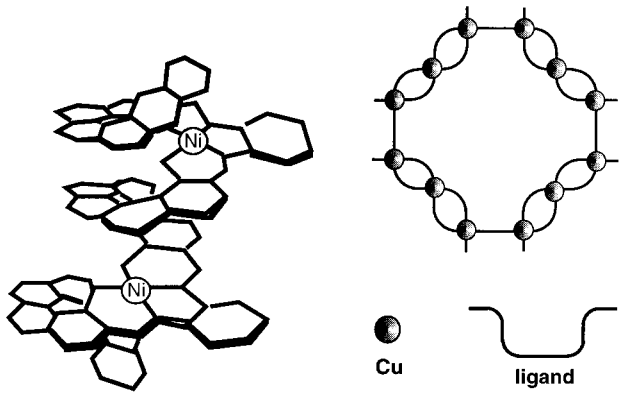
complexes.[18] These helicates possess many features seen for self-organizing biological systems. The binding of Cu^{I} ions is cooperative, and the oligoligands display self-selection. This means that for a mixture of ligands **6a**–**6d**, helical-forming species will only selectively bind a second ligand of the same size.[19] This phenomenon was described as "instructed system paradigm". Using this self-assembly to form a well-defined scaffold, Lehn et al. synthesized a helix with five copper ions and pendant nucleoside units, a "deoxyribonucleohelicate".[20] With possible applications as a complimentary ligand for the DNA double helix this nanometer-sized architecture highlights the possibilities for creating functional assemblies. The helical sense can also be controlled by a variety of means: introducing chirality in the oxymethylene linker,[21] using chiral bipyridine ligands,[22] or, as shown by Siegel et al., linking two strands of **6c** through a chiral spacer. The resulting helical sense of the copper–ligand helix is controlled by the chirality of the spacer at one end.[23]

The above-mentioned helical arrays can be considered as consisting of three basic components: a binding site, a metal, and a ligand linking this binding site to another. All three components can be programmed with specific information which spontaneously gives a defined final architecture upon mixing. The coordination preference of metal can be controlled by using the appropriate metal ions, and the ligand properties can be varied by altering the denticity (bidentate, tridentate). The spacer linking the ligand units must be sufficiently flexible to allow the molecule to wrap around but rigid enough to prevent the second binding site from coordinating to the first metal. The size and geometry of the spacer in part controls the pitch and also the sense of the resulting helix.

Using these structural parameters Williams et al. and Constable et al. demonstrated control over the resulting helical architectures by using different metal ions.[24] Upon adding Cu ions with a tetrahedral coordination geometry to a bidentate ligand a di-copper double helix is generated, whereas a triple helix is formed upon the addition of a metal ion with octahedral geometry. The latter, in which the metal centers are lanthanide ions, are currently being investigated as possible light-conversion devices.[25]

This process of spontaneous self-organization is also highly dependent on the data encoded within the ligand. Because of the 6,6′ linkage in ligands of type **6** (Scheme 5) octahedral metals cannot be accommodated due to steric hindrance if three strands were to bind to two metals; in the 4,4′ linkage in ligand **7** there would be no steric hindrance. When **6b** and **7** are mixed in the presence of Ni^{II} and Cu^{I} **6b** binds only to Cu and **7** only to Ni ions.[19] In the presence of Fe^{II} ions **7** forms an even more complex array. This bipyridine ligand self-assembles with the Fe^{II} ions around a chloride ion template to form a circular double-helicate architecture.[26]

Bell et al chose a slightly different approach to construct double-helical arrays.[27] Instead of using the coordination preference of the metal as a major driving force for assembly, a double helix was constructed by emphasizing the geometrical preference of the ligand. With a heterohelicene which already has a helical geometry enforced due to covalent bonds, it was demonstrated that with the correct ligand even Group 1 metal ions such as sodium may control the assembly of double-helical supermolecules. When sodium salts are added two types of double helices can be formed: one in which two helices wrap around one metal ion and one in which they wrap around two metal ions. Katz et al. took the combination of metals and helicene molecules a step further by constructing a helicene possessing a salicylaldehyde functionality at both ends. In combination with nickel acetate and a phenyldiamine ligand, a beautiful, helical, conjugated ladder polymer (**8**, Scheme 6) is formed.[28] The planarity of the "nickel salophene" connections not only results in a conjugated system but also induces the polymer to wind in just one direction.



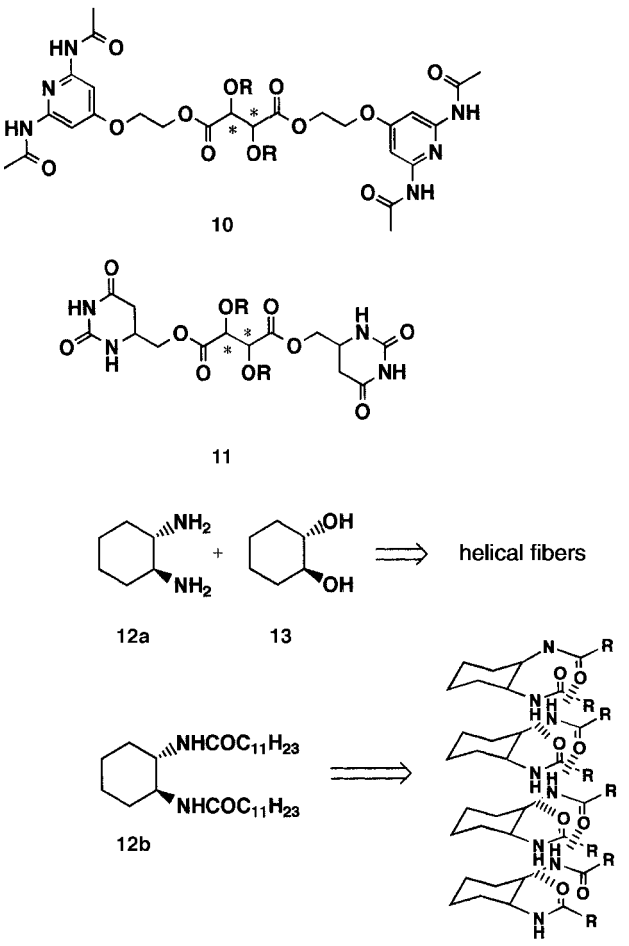
8 9

Scheme 6. Salicylaldehyde-functionalized helicenes complex nickel ions to form a helical polymeric assemblage (**8**). Schematic representation of the cyclic dodecacopper helicate from Lehn et al. which forms spontaneously in a preprogammed way.

 © WILEY-VCH Verlag GmbH, D-69451 Weinheim, 1998 1433-7851/98/3701-0065 $ 17.50+.50/0

Lehn et al. recently demonstrated that by using the molecular information encoded in the metal–ligand components it is possible to program the spontaneous assembly of even more highly complex, helical architectures. One of the most recent examples is the nanocyclic dodecanuclear Cu helicate **9**[29] (Scheme 6). In this assemblage twelve Cu ions and four multifunctional ligands spontaneously self-assembly in a two-step process to give a specific inorganic nanomolecule.

A variety of other approaches have also been investigated for the controlled construction of helical nanometer-sized architectures. The uracil and pyridine derivatives **10** and **11** based on tartaric acid assemble by complementarity of the base pairs to form helical superstructures. Species based on L-tartaric acid give right-handed helices, and those based on D-tartaric acid left-handed helices.[30] If a mixture of L-uracil and D-pyrimidine derivatives—or of D-uracil and L-pyrimidine derivatives—is used, no helicity is observed. Only configurationally compatible units assemble if all four possible species are mixed. This chiral resolution was also observed in the aggregation of chiral 1,2-diaminocyclohexanes by Hanessian et al.[31] When the (*R*,*R*) and (*S*,*S*) derivatives of **12a** were mixed with equimolar amounts of (*S*,*S*)-1,2-cyclohexanol **13**, two triple-helical supramolecular structures were generated (Scheme 7). The (*S*,*S*)-diamine of **12a** formed a homochiral left-handed helix with **13**, whereas **13** and the (*R*,*R*)-diamine of **12a** gave a heterochiral right-handed architecture. The group of Hanabusa modified the packing ability of *trans*-1,2-diaminocyclohexane by adding amide functionalities and long alkyl chains to give **12b**.[32] The (*R*,*R*) and (*S*,*S*) enantiomers of **12b** gelate in a variety of solvents to give right-and left-handed helical fibers, respectively, with a diameter of 40–70 nm. They result from cooperative, chiral self-organization.

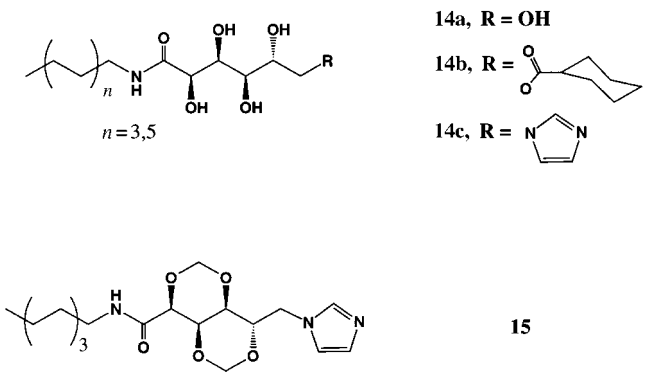


Scheme 7. Chiral tartaric acid derivatives **10** and **11** self-assemble to helical architectures. (*R*,*R*)- and (*S*,*S*)-diaminecyclohexanes **12a** assemble with **13** to give helical arrays. Cyclohexanediamides **12b** aggregate through a network of hydrogen bonds and packing to form gels consisting of helical fibers.

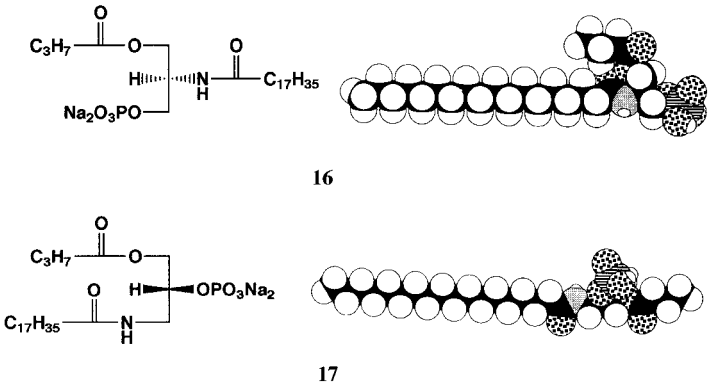
The expression of molecular information at the macroscopic level by self-organization is a topic of great interest since it may lead to a more thorough understanding of the construction processes used by nature. The assembly of surfactants and amphiphilic molecules is of particular interest, as chirality within the individual molecule can be expressed in the suprastructure by the formation of helices and twisted bilayers. A wide variety of chiral amphiphiles based on amino acids (glutamate,[33] alanine[34]), phospholipids,[35] and carbohydrates[36] form chiral architectures. In the case of the glutamate derivatives the sense of the resultant helix is related to the molecular chirality: An L derivative of glutamate gives a right-handed helix, whereas a D enantiomer yields a left-handed helix. The encoded molecular data is expressed at the macroscopic level. The groups of Fuhrhop,[36] Pfannemüller,[37] and O'Brien[38] studied the assembly behavior of chiral amphiphiles—in particular gluconamides—which assemble to create micellar helical and multihelical superstructures. *N*-*n*-Octyl-D-gluconamide (**14a**, Scheme 8) forms ropelike architectures with a length to width ratio of up to 104. These structures are believed to consist of a helix of six intertwined micellar strands.[39] As in the glutamates the pure enantiomers form helices with enantiomorphology (i. e., in the case of **14a** only right-handed helices are formed), whereas racemic mixtures crystallize. The expression of chirality at the macroscopic level is a result of strong hydrogen bonds between adjacent molecules and efficient packing of the alkyl chains. The group of Nolte has varied the head group of these gluconamides (e. g. **14b**, **14c**) and found that the molecules self-assemble even in organic solvents to form organogels. Closer examination of these gels showed that they consist of well-defined micrometer-sized helical fibers.[40]

The self-assembly process required to form such highly complex nanomolecular architectures consists of numerous processes which are hierarchical in nature. Modified gluconamide **15** (Scheme 8), which possesses an imidazole head group, has also been fully investigated by Nolte et al. Although the hydrogen-bonding OH groups are protected, this molecule still readily self-assembles. In the presence of Cu^{II} ions **15** forms a 4:1 ligand–copper complex, which in turn self-assembles to generate a bilayer; in a stepwise fashion this further organizes to yield a nanometer-sized "molecular braid" consisting of four strands.[40] The sensitivity of the resultant architecture to the molecular geometry is highlighted by the phospholipid analogues **16** and **17** (Scheme 9).[41] Although both have an *R* configuration they are structurally different and give dramatically different expressions of chirality. Phospholipid **16** gives platelike aggregates, whereas **17** forms left-handed helical strands with a diameter of 22 nm, which themselves further assembly to give large ropelike architectures (Figure 1). The helicity is the

 © WILEY-VCH Verlag GmbH, D-69451 Weinheim, 1998 1433-7851/98/3701-0066 $ 17.50+.50/0



Scheme 8. *N*-*n*-Octyl-D-gluconamides **14** self-assemble in a variety of solvents to form complex intertwined architectures in which the chirality of the simple building blocks is expressed at a macromolecular level. Protected imidazole gluconamide **15** assembles in the presence of copper ions in a hierarchical fashion to give nanometer-sized molecular braids.



Scheme 9. Phospholipids **16** and **17** (and their space-filling representations).

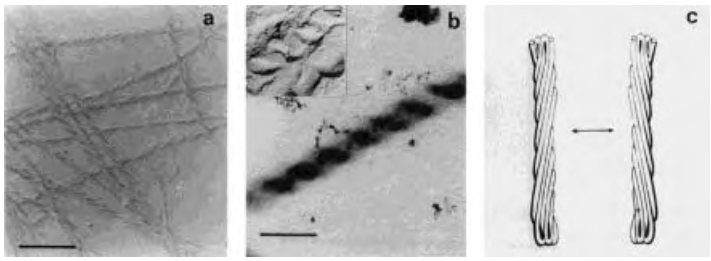


Figure 1. Electron micrographs of helices formed by **17** (2 wt %) in water (bar = 500 nm): a) left-handed helices (Pt shadowed), b) right-handed super helix (Pt shadowed; inset: image after freeze fracturing), c) schematic representation of supercoiled DNA.

result of the chirality within the molecular units and also the specific complementarity of intermolecular interactions, which carries this information through to the macroscopic level. Owing to its more linear shape **17** can pack more tightly, and hence the chiral molecular information is not lost upon self-assembly. The resultant nanomolecules themselves seem to be tunable by small changes in salt concentration or pH, which induces the left-handed helices to coil up and form large right-handed superhelices in a manner analogous to the formation of supercoiled DNA.[42]

Helicity in macromolecular and supramolecular systems can be obtained by a variety of methods. The principle of molecular programming is clearly demonstrated in the case of helicate structures resulting in the spontaneous self-assembly of, for example, large helical nanocycles. The rules governing the construction of helical nanosized arrays from amphiphlic building blocks are far more complex and are only now being elucidated. To mimic more closely the ability of nature to construct complex multicomponent helical architectures, a combination of many processes in a hierarchical assembly line will be required. The first steps in this direction are currently being taken. These helical assemblies and polymers are expected to have interesting physical and material properties, in particular as optical devices, that is, chiral light-emitting and nonlinear optical materials.[43] The ultimate goal is not just to mimic nature but to go a step further and be able to preprogram molecules to give not only specific architectures but also defined functionality.

German version: *Angew. Chem.* **1998**, *110*, 65 – 71

Keywords: helical structures · nanostructures · polymers · supramolecular chemistry

[1] a) J.-M. Lehn, *Angew. Chem.* **1990**, *14*, 1347 – 1362; *Angew. Chem. Int. Ed. Engl.* **1990**, *29*, 1304 – 1319; b) J. S. Moore, *Curr. Opin. Solid State Mater. Sci.* **1996**, *1*, 777 – 787; c) D. S. Lawrence, T. Jiang, M. Levett, *Chem. Rev.* **1995**, *95*, 2229 – 2260; d) D. B. Amabilino, J. F. Stoddart, *ibid.* **1995**, *95*, 2725 – 2828.

[2] a) W. H. Laarhoven, W. J. C. Prinsen, *Top. Curr. Chem.* **1984**, *125*, 63 – 130; b) K. P. Meurer, F. Vögtle, *ibid.* **1985**, *127*, 1 – 76; c) L. Owens, C. Thilgen, F. Diederich, C. B. Knobler, *Helv. Chim. Acta.* **1993,** *76*, 2757 – 2774.

[3] a) G. S. Hanan, J.-M. Lehn, N. Krytsakas, J. Fisher, *J. Chem. Soc. Chem. Commun.* **1995**, 765 – 766; b) D. M. Bassani, J.-M. Lehn, G. Baum, D. Fenske, *Angew. Chem.* **1997**, *109*, 1931 – 1933; *Angew. Chem. Int. Ed. Engl.* **1997**, *36*, 1845 – 1847.

[4] J. C. Nelson, J. G. Saven, J. S. Moore, P. G. Wolynes, *Science* **1997**, *277*, 1793.

[5] D. J. Williams, H. M. Colquhoun, C. A. O'Mahoney, *J. Chem. Soc. Chem. Commun.* **1994**, 1643 – 1644.

[6] G. Wulff, *Angew. Chemie.* **1989**, *101*, 22 – 38; *Angew. Chem. Int. Ed. Engl.* **1989**, *28*, 21 – 37, and references therein.

[7] R. J. M. Nolte, *Chem. Soc. Rev.* **1994**, 11 – 19.

[8] F. Takei, Y. Koichi, K. Onitsuka S. Takahashi, *Angew. Chem.* **1996**, *108*, 1634 – 1636; *Angew. Chem. Int. Ed. Engl.* **1996**, *35,* 1554 – 1556.

[9] a) M. M. Green, N. C. Peterson, T. Sato, A. Teramoto, R. Cook, S. Lifson, *Science* **1996**, *268*, 1861 – 1866; b) M. M. Green, B. A. Garetz, B. Munoz, H. Chang, *J. Am. Chem. Soc.* **1995**, *117*, 4181 – 4182.

[10] V. Percec, D. Schlüter, J. C. Ronda, G. Johansson, G. Ungar, J. P. Zhou, *Macromolecules* **1996**, *29*, 1464 – 1472.

[11] a) K. Jung, V. Abetz, R. Stadler, *Macromolecules* **1996**, *29*, 1076 – 1078; b) M. Moller, J. P. Spatz, *Curr. Opin. Coll. Interface Sci.* **1997**, *2*, 177 – 187.

[12] a) B. M. V. Langeveld-Voss, R. A. J. Janssen, M. P. T. Christiaans, S. C. J. Meskers, H. P. J. M. Dekkers, E. W. Meijer, *J. Am. Chem. Soc.* **1996**, *118*, 4908 – 4909; b) M. M. Bouman, E. W. Meijer, *Adv. Mater.* **1995**, *7*, 385 – 387.

[13] a) Y. Ito, E. Ihara, M. Murakami, *Angew. Chem* **1992**, *104*, 1508 – 1510; *Angew. Chem Int. Ed. Engl.* **1992**, *31*, 1509 – 11; b) Y. Ito, E. Ihara, M. Murakami, M. Sisido, *Macromolecules* **1992**, *25*, 6810 – 6813

[14] See also R. Fiesel, J. Huber, H. Scherf, *Angew. Chem* **1996**, 108, 2232 – 2234; *Angew. Chem. Int. Ed. Engl.* **1996**, *35*, 2111 – 2113.

[15] K. Nozaki, T. Terakawa, H. Takaya, T. Hiyama, *Angew. Chem.* **1998**, *110*, 138 – 140; *Angew. Chem. Int. Ed.* **1998**, *37*, 131 – 133.

 © WILEY-VCH Verlag GmbH, D-69451 Weinheim, 1998 1433-7851/98/3701-0067 $ 17.50+.50/0

[16] a) Recent review of helicates: A. Williams, *Chem. Eur. J.* **1997**, *3*, 16; b) E. C. Constable, *Angew. Chem.* **1991**, *103*, 1482 – 1483; *Angew. Chem. Int. Ed. Engl.* **1991**, *30*, 1450 – 1451.
[17] a) G. Weber, W. Saenger, F. Vögtle, H. Sieger, *Angew. Chem.* **1979**, *91*, 234 – 235; *Angew. Chem. Int. Ed. Engl.* **1979**, *18*; 226 – 227; b) G. Weber, W. Saenger, *ibid.* **1979**, *91*, 237 – 238 and **1979**, *18*, 227 – 228.
[18] J.-M. Lehn, A. Marquis-Rigault, *Angew. Chem.* **1988,** *100*, 1121 – 1122; *Angew. Chem. Int. Ed. Engl.* **1988**, *30*, 1095 – 1096.
[19] R. Kramer, J.-M. Lehn, A. Marquis-Rigault, *Proc. Natl. Acad. Sci. USA* **1993**, *90*, 5394 – 5398.
[20] a) U. Koert, M. M. Harding, J.-M. Lehn, *Nature* **1990**, *346*, 339 – 342; b) B. Schoentjies, J.-M. Lehn, *Helv. Chim. Acta* **1995**, *78*, 1 – 12.
[21] W. Zarges, J. Hall, J.-M. Lehn, C. Bolm, *Helv. Chim. Acta* **1991**, *74*, 1843 – 1852.
[22] N. C. Fletcher, F. R. Keene, H. Viebrock, A. von Zelewsky, *Inorg. Chem.* **1997**, *36*, 1113 – 1121.
[23] a) C. R. Woods, M. Benaglia, F. Cozzi, J. S. Siegel, *Angew. Chem.* **1996,** *108*, 1977 – 1980; *Angew. Chem. Int. Ed. Engl.* **1996**, *30*, 1830 – 1833; b) for control of the head-to-head/head-to-tail assembley, see E. C. Constable, F. R. Heirtzier, M. Neuburger, M. Zehnder, *Chem. Commun.* **1996**, 933 – 934.
[24] a) C. Piquet, G. Bernardinelli, B. Bocquet, A. Quattropani, A. F. Williams, *J. Am. Chem. Soc.* **1992**, *114*, 7440 – 7451; b) E. C. Constable, *Tetrahedron* **1992**, *48*, 10013 – 10059.
[25] C. Piquet, J.-C. Bunzli, G. Bernardinelli, G. Hopfgartner, A. F. Williams, *J. Am. Chem. Soc.* **1993**, *115*, 8197 – 8206.
[26] B. Hasenknopf, J-M. Lehn, B. O. Kneisel, G. Baum, D. Fenske *Angew. Chem.* **1996**, *108*, 1987 – 1890; *Angew. Chem. Int. Ed. Engl.* **1996**, *35*, 1838 – 1340.
[27] T. W. Bell, H. Jousselin, *Nature* **1994**, *367*, 441 – 444.
[28] Y. Dai, T. J. Katz, D. A. Nichols, *Angew. Chem.* **1996**, *108*, 2230 – 2232; *Angew. Chem. Int. Ed. Engl.* **1996**, *35*, 2109 – 2111.
[29] D. P. Funeriu, J.-M. Lehn, G. Baum, D. Fenske, *Chem. Eur. J.* **1997**, *3*, 99 – 104.
[30] T. Gulik-Krzywicki, C. Fouquey, J.-M. Lehn, *Proc. Natl. Acad. Sci. USA*, **1993**, *90*, 163 – 167.
[31] S. Hanessian, A. Gomtsyan, M. Simard, S. Roelens, *J. Am. Chem. Soc.* **1994**, *116*, 4495 – 4496.
[32] K. Hanabusa, M. Yamada, M. Kimura, H. Shirai, *Angew. Chem.* **1996**, *108*, 2086 – 2090; *Angew. Chem. Int. Ed. Engl.* **1996**, *35*, 1949 – 1951.
[33] a) T. Kunitake, N. Nakashima, S. Hayashida, K. Yonemuri, *Chem. Lett.* **1979**, 1413 – 1416; b) D. G. Rhodes, D. A. Frankel, T. Kuo, D. F. O'Brien, *Langmuir* **1994**, *10*, 267 – 75.
[34] T. Kunitake, N. Nakashima, K. Morimitsu, *Chem. Lett.* **1980**, 1347 – 1350.
[35] P. Yager, P. Schoen, *Mol. Cryst. Liq. Cryst.* **1984**, *106*, 371 – 381.
[36] J.-H. Fuhrhop, *Chem. Rev.* **1993**, *93*, 1565 – 1582.
[37] B. Pfannemüller, W. Welte, *Chem. Phys. Lipids* **1985**, *37*, 227 – 240.
[38] D. A. Frankel, D. F. O'Brien, *J. Am. Chem. Soc.* **1994**, *116*, 10057 – 10070.
[39] "Membranes and Molecular Assemblies: The Synkinetic Approach": J.-H. Fuhrhop, J. Koning, *Monographs in Supramolecular Chemistry* (Ed.: J. F. Stoddart), The Royal Society of Chemistry, Cambridge (UK), **1994**.
[40] a) R. J. H. Hafkamp, B. P. A. Kokke, I. M. Danke, H. P. M. Geurts, A. E. Rowan, M. C. Feiters, R. J. M. Nolte, *Chem. Commun.* **1997**, 545 – 546; b) R. J. H. Hafkamp, Dissertation, University of Nijmegen (The Netherlands), **1996**.
[41] a) A. E. Rowan, N. A. J. M. Sommerdijk, J. N. H. Reek, B. Zwanenburg, M. C. Feiters, R. J. M. Nolte, *Macromol. Symp.* **1997**, *117*, 291 – 304; b) N. A. J. M. Sommerdijk, P. J. J. A Buynsters, A. M. A. Pistorius, M. Wang, M. C. Feiters, R. J. M. Nolte, B. Zwanenburg, *J. Chem. Soc. Chem. Commun.* **1994**, 1941 – 1942; c) N. A. J. M. Sommerdijk, P. J. J. A Buynsters, H. Akdemir, D. G. Geurts, M. C. Feiters, R. J. M. Nolte, B. Zwanenburg, *Chem. Eur. J.* **1998**, *4*, 126.
[42] Z. Reich, L. Zaidman, S. B. Gutman, T. Arad, A. Minski, *Biochem.* **1994**, *33*, 14177 – 14184.
[43] M. Kauranen, T. Verbiest, C. Bouttoon, M. N. Teerenstra, K. Clays, A. J. Schouten, R. J. M. Nolte, A. Persoons, *Science* **1995**, *270*, 966 – 969

Conjugated π Systems with Heavy Main Group Elements— A Stable Neutral Silaarene and the First Tetrasilabutadiene**

Thomas Müller*

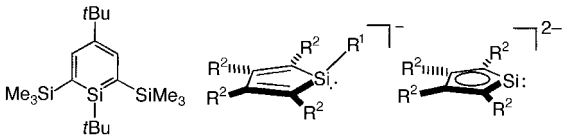
The question of conjugation and aromaticity in organosilicon compounds has recently attracted considerable interest. For instance, the influence of cyclic conjugation on the stability of aminosilylenes has aroused controversy.[1] However, even simple stable neutral silaarenes like derivatives of silabenzene have been elusive until very recently. This is in sharp contrast to the successful synthesis of kinetically stabilized silenes and 1-silaallenes.[2] In addition calculations predict for silabenzene a resonance stabilization of about 75% of that calculated for benzene.[3] Early fundamental investigations showed that silaarenes can be produced as short-lived intermediates in the gas phase or in the matrix at low temperatures and that they can be characterized by IR, UV, or PE spectroscopy.[4] None of these compounds could be however investigated in solution or even isolated in substance. Investigations by Märkl and co-workers[5] revealed the extraordinary reactivity of silaarenes. Even the with bulky groups substituted silabenzene **1** is at $-100^{\circ}C$ only of limited stability.

On the other hand the search for anionic silaarenes has been more successful during the last years. Almost simultaneously the groups of Boudjouk, Tilley, and West[6] reported the synthesis of silolyl anions **2**, analogues of the cyclopentadienyl anion, and silole dianions **3**. Surprisingly, the silicon in **2** is pyramidalized and the anions have localized C=C bonds. Cyclic conjugation with involvement of the silicon atom seems to play only a minor role in **2**. In contrast, silole dianions **3** as well as germole dianions[7] have delocalized π electron systems with almost identical CC bond lengths. The silicon atom in **3** is markedly deshielded relative to tetracoor-

[*] Dr. T. Müller
Fachinstitut für Anorganische und Allgemeine Chemie der Humboldt Universität
Hessische Strasse 1-2, D-10115 Berlin (Germany)
Fax: Int. code + (49) 30-2093 6966
e-mail: h0443afs@joker.rz.hu-berlin.de

[**] The author thanks the Deutschen Forschungsgemeinschaft for a scholarship.

 © WILEY-VCH Verlag GmbH, D-69451 Weinheim, 1998 1433-7851/98/3701-0068 $ 17.50+.50/0

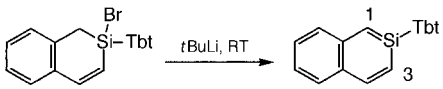


1 2 3

R^1 = alkyl, aryl, R_3Si; R^2 = Me, Et, Ph

dinated silicon atoms ($\delta(^{29}Si) = 64$, $R^2 = Ph$). Ab initio calculations for **3** ($R^2 = H$) and for its higher homologues suggest considerable resonance stabilization of the dianions, and the calculated magnetic properties give evidence for an aromatic ring current.[6c,d,7]

Another highlight of the experimental and theoretical studies in this area is the synthesis of a neutral silaarene stable at room temperature by the group of Tokitoh and Okazaki at Tokyo University. Like often in the chemistry of low-valent silicon, the sufficient protection from bimolecular reactions of the inherently stable target compound is also the key to success in this case. By taking advantage of the particular properties of the 2,4,6-tris[bis(trimethylsilyl)methyl]phenyl (Tbt) protecting group the Tokyo group synthesized the 2-Tbt-2-silanaphthalene **4** by a HBr eliminiation in 80% yield as a colorless crystalline powder.[8] An X-ray analysis of the compound established the molecular structure and proved the planar environment of the silicon atom; the severe disorder of the 2-silanaphthalene ring in the crystal, however, prevents any discussion of structural details. The reported spectroscopic data are certainly unambiguous. The ^{29}Si NMR chemical shift ($\delta(^{29}Si) = 87.4$) is characteristic for sp^2-hybridized silicon in silenes and is in good agreement with calculated NMR chemical shifts for substituted 2-silanaphthalenes (e.g., $\delta(^{29}Si) = 94.3$ for 2-phenyl-2-silanaphthalene in which the phenyl group is fixed in a perpendicular conformation to the plane of the silanaphthalene in analogy to the Tbt-residue in **4**). Unequivocally, **4** posseses a Si=C bond, a finding which is supported by the chemical reactivity of **4**, which is typical for silenes.

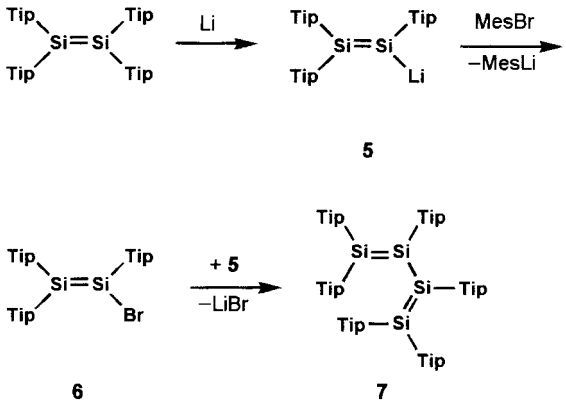


(a)

4

What can be learned about aromaticity in this compound? Is the Si=C bond localized, or is the π bond part of a delocalized system similar to naphthalene? An indication for a delocalized structure are the $^1J_{Si,C}$ coupling constants to both neighboring carbon atoms ($^1J_{Si,C1} = 92$ Hz and $^1J_{Si,C3} = 76$ Hz), which are both clearly larger than expected for a Si–C bond (about 50 Hz). The value of the coupling constant suggests double-bond character for both Si–C bonds, although the comparison with coupling constants in silenes is problematic due to the very limited number of comparative values ($^1J_{Si=C}$: 83–85 Hz in $(Me_3Si)_2Si{=}C(OSiMe_3)R$[2a] and 104 Hz in a 1-silaallene).[2b] A clear geometrical indication for the delocalized structure of 2-silanaphthalenes is provided by DFT calculations. The calculated SiC1 and SiC3 distances in 2-silanaphthalene are intermediate between the Si=C bond length in silene and the Si–C bond length in methylsilane. This implies a bond order between 1 and 2 for both SiC bonds in **4**. The calculation of the Nucleus Independent Chemical Shift (NICS)[9] for 2-silanaphthalene, a method invented by Schleyer and co-workers for the quantification of the aromaticity of a compound, support the experimental evidence for the aromaticity of 2-silanaphthalene. The NICS indicates the magnetic shielding in the center of a cyclic molecule. Characteristicly NICSs are negative for aromatic compounds: for benzene a shielding of −9.7 ppm is calculated. The NICS calculated for 2-silanaphthalene is only slightly larger than that for naphthalene (−8.9 ppm for 2-silanaphthalene and −9.9 ppm for naphthalene). The experimental and theoretical results show concurrently that the aromaticity of naphthalene is only marginally reduced by the replacement of a ring carbon by a silicon atom.

These results give rise to the next question: to what extent is conjugation between Si=Si bonds possible? Recent studies by Weidenbruch and co-workers give a preliminary answer. They synthesized in a fascinating, simple reaction sequence the first tetrasilabutadiene stable at room temperature (**7**)[10]. The key



5

(b)

6 7

step to the synthesis of **7** is the metathesis reaction between a transitory disilene bromide **6** and a disilenyllithium compound **5**.

Tetrasilabutadiene **7** is kinetically exceptionally stabilized by six bulky 2,4,6-triisopropylphenyl (Tip) substituents. In the absence of air the compound melts without decomposition, and only at 267°C it is destroyed irreversibly! In the crystal **7** adopts a twisted s-*cis* conformation (C_2 symmetry) with a dihedral angle of 51° between the planes of the planar Si=Si bonds. Of interest are the SiSi distances in the molecule. The Si=Si bond lengths (217.5 pm) are 2–3 pm longer than isolated Si=Si bonds,[11] and the central Si–Si bond (232.1 pm) is relatively short, especially in view of the bulky Tip substituents. Due the limited published data, however, it is hard to distinguish whether this short central Si–Si bond is an indication of conjugation, as suggested by Weidenbruch et al. or is a result of the sp^2 hybridization of the silicon atoms in **7**. SiSi separations for $Si(sp^2)–Si(sp^3)$ bonds in disilenes scatter between 233.4 and 241.1 pm.[11] The UV spectra of a solution of **7** provides more clear evidence. The bathochromic shift of about 100 nm of the characteristic band of the π–π*

 © WILEY-VCH Verlag GmbH, D-69451 Weinheim, 1998 1433-7851/98/3701-0069 $ 17.50+.50/0

transition in disilenes in **7** indicates the conjugation between the Si=Si bonds in **7** in solution. A similar red shift is also found by comparison of the UV absorption of ethene and of 1,3 dienes with s-*cis* conformation.[12] Further investigations of the bonding situation in **7** are, however, certainly desirable to determine more precisely the interaction between the two Si=Si bonds.

With the isolation and characterization of these two substances another two dream molecules of the organosilicon chemists became reality. What is next on the agenda? Certainly, the synthesis of other silaarenes up to hexasilabenzene and its valence isomers will give us further important insights in the nature of chemical bonding in main group chemistry. At the moment, however, the quest for compounds with dicoordinated silicon seems to be a hotter topic. While stable silylenes have already gained entry into text books, the evidence for molecules with triply bonded silicon is rather scarce. Possible synthetic approaches to silaalkynes, disilaalkynes, and also 2-silaallenes are currently under intensive investigation in several groups.[13–15] Theoretically oriented papers have been published, which suggest possible synthetic pathways to these also thermodynamically very unstable compounds.[13] Suitable precursors for the generation of 2-silaallenes have been recently synthesized,[14] and the doubly bridged isomer of the disilaalkyne has been indentified spectroscopically in the gas phase and in the matrix.[15] Further highlights from the chemistry of low-valent silicon might therefore be expected for the near future.

German version: *Angew. Chem.* **1998**, *110*, 71 – 73

Keywords: aromaticity · multiple bonds · pi interactions · silenes · silicon

[1] a) C. Heinemann, T. Müller, Y. Apeloig, H. Schwarz, *J. Am. Chem. Soc.* **1996**, *118*, 2023; b) C. Boehme, G. Frenking, *ibid.* **1996**, *118*, 2039, and references therein.
[2] Recent review: a) G. A. Brook, M. A. Brook, *Adv. Organomet. Chem.* **1995**, *39*, 71; b) M. Trommer, G. E. Miracle, D. R. Powell, R. West, *Organometallics* **1997**, in press; c) Y. Apeloig, M. Bendikov, M. Yuzefovich, M. Nakash, D. Bravo-Zhivotovskii, D. Blaeser, R. Boese, *J. Am. Chem. Soc.* **1996**, *118*, 12228.
[3] "Theoretical Aspects of Organosilicon Compounds": Y. Apeloig in *The Chemistry of Organic Silicon Compounds* (Eds: S. Patai, Z. Rappoport), Wiley, Chichester, **1989**, p. 57.
[4] "Multiple Bonds to Silicon": G. Raabe, J. Michl in *The Chemistry of Organic Silicon Compounds* (Ed: S. Rappoport, Z. Patai), Wiley, Chichester, **1989**, p. 1015.
[5] W. Schlosser, G. Märkl, *Angew. Chem.* **1988**, *100*, 1009; *Angew. Chem. Int. Ed. Engl.* **1988**, *27*, 963.
[6] a) P. Boudjouk, S. Castellino, J-H. Hong, *Organometallics* **1994**, *13*, 3387; b) T. Don Tilley, L. M. Liable-Sands, A. L. Rheingold, W. P. Freeman, *J. Am. Chem. Soc.* **1996,** *118*, 10457; c) H. Sohn, U. Bankwitz, J. Calabrese, Y. Apeloig, T. Müller, R. West, *ibid.* **1995**, *117*, 11608; d) R. West, H. Sohn, D. R. Powell, T. Müller, Y. Apeloig, *Angew. Chem.* **1996**, *108*, 1095; *Angew. Chem. Int. Ed. Engl.* **1996**, *35*, 1002.
[7] B. Goldfuss, P. v. R. Schleyer, *Organometallics* **1997**, *16*, 1543.
[8] N. Tokitoh, K. Wakita, R. Okazaki, S. Nagase, P. v. R. Schleyer, H. Jiao, *J. Am. Chem. Soc.* **1997**, *119*, 6951.
[9] P. v. R. Schleyer, C. Maerker, A. Dransfeld, H. Jiao, N. J. R. van Eikema Hommes, *J. Am. Chem. Soc.* **1997**, *118*, 6317.
[10] M. Weidenbruch, S. Willms, W. Saak, G. Henkel, *Angew. Chem*. **1997**, *109*, 2612 – 2613; *Angew. Chem. Int. Ed. Engl.* **1997**, *36*, 2503 – 2504.
[11] Recent review on the chemistry of disilenes: R. Okazaki, R. West, *Adv. Organomet. Chem.* **1995**, *39*, 232.
[12] M. Hesse, H. Meier, B. Zeeh, *Spektroskopische Methoden in der organischen Chemie*, 2nd ed., Thieme, Stuttgart, **1984**, p. 18.
[13] a) Y. Apeloig, M. Karni, *Organometallics* **1997**, *16*, 310; b) K. Kobayashi, S. Nagase *ibid.* **1997**, *16*, 2489.
[14] B. Goetze, B. Herrschaft, N. Auner, *Chem. Eur. J.* **1997**, *3*, 948.
[15] a) G. Maier, H. P. Reisenauer, A. Meudt, H. Egenolf, *Chem. Ber./ Recueil* **1997**, *130*, 1043; b) M. Bogey, H. Bolvin, M. Cardonnier, C. Demuynck, J.-L. Destombes, A. G. Csaszar, *J. Chem. Phys.* **1994**, *100*, 8614.

 © WILEY-VCH Verlag GmbH, D-69451 Weinheim, 1998 1433-7851/98/3701-0070 $ 17.50+.50/0

Crystal Structure Solution of Hydrated High-Alumina Cement from X-ray Powder Diffraction Data**

Francesc Guirado,* Salvador Galí, Servando Chinchón, and Jordi Rius

The use of high-alumina cement (HAC; a quickly binding cement with a high aluminum oxide content) in concrete, precast, prestressed elements became highly controversial after the roofs of three educational buildings collapsed in the United Kingdom in 1973 and 1974. There were further incidents in other countries, and in 1990 an apartment building fell down in Barcelona, Spain. The relevant technical characteristics of HAC are better resistance to sulfates than Portland cements, good refractory properties, and above all a rapid gain in concrete strength which allows quick manufacture. However, a subsequent, complex evolution of this material—which is still not well understood—leads to the collapses.

The main phase present in HAC is $CaAl_2O_4$; additional components are Ca_2FeAlO_5, $Ca_{12}Al_{14}O_{33}$, and minor amounts of Ca_2AlSiO_7 and Ca_2SiO_4. After binding the cement with water (hydraulic reaction), $CaAl_2O_4$ gives raise to a metastable hexagonal phase currently but erroneously labeled as $CaAl_2O_4 \cdot 10H_2O$ (or CAH_{10}). Furthermore, some $Ca_2Al_2O_5 \cdot 8H_2O$ and an amorphous phase are present. The dominant crystalline phase in the paste (which determines the valuable cementitious properties), CAH_{10} slowly transforms into a new cubic phase with the hydrogarnet structure plus gibbsite and water. This unavoidable conversion is completed within several years; the rate depends on the humidity and the temperature. The effect of this rather slow conversion is an increase in concrete porosity and loss of strength. Chemical reactions facilitated by the porosity probably cause the continuous loss of strength, even after full conversion. Since 1990 a great deal of work has been undertaken in Catalonia to throw light on the extent of HAC pathology in buildings. It became apparent that the phase CAH_{10} was poorly characterized, and that the solution of its crystal structure would be of much practical importance in understanding the behavior of this phase in concrete.

[*] F. Guirado i Gispert
Servei de Recursos Científics
Universitat Rovira i Virgili
Plaça Imperial Tàrraco, 1, 43005 Tarragona (Spain)
Fax: Int. code + (34) 77-55 95 97
e-mail: fgg@src.urv.es
Prof. Dr. S. Galí
Dept. Cristallografia i Mineralogia, Universitat de Barcelona (Spain)
Dr. S. Chinchón
Dept. Construccions Arquitectòniques, Universitat d'Alacant (Spain)
Dr. rer. nat. J. Rius
Institut de Ciència de Materials de Barcelona
Consell Superior d'Investigacions Científiques, Bellaterra (Spain)

[**] This work was supported by the Dirección General de Enseñanza (DGES) of the Spanish Goverment (project PB95-0115) and by the Direcció General de la Recerca (DGR) of the Catalan Goverment (grant SGR-00460, 1995). We thank Prof. J. Rodriguez-Carvajal for providing facilities for the neutron-diffraction measurements and the Serveis Científico Tècnics (SCT) of the Universitat de Barcelona for technical support.

The hydration of $CaAl_2O_4$ below 20 °C yields an undetachable mixture of an amorphous and a crystalline phase with an overall composition of $CaAl_2O_4 \cdot nH_2O$ ($n \approx 5-8$). All attempts to isolate the crystalline phase were unsuccessful, and the relative proportions of the phases in the mixture as well as their individual compositions and water content remained unknown. These uncertainties could not be cleared up until the structure was refined. The poor quality of the crystalline material was an additional drawback and accounted for the fact that the crystal structure remained unsolved since Assarsson reported the existence of this phase in 1933.[1]

Nevertheless, several works have given partial information on the structure by using different techniques (^{27}Al NMR, IR, thermogravimetry (TG), and X-ray diffraction (XRD)).[2–5] According to the NMR data, the coordination at aluminum should be a slightly distorted octahedron of OH^- groups, and, by mimetism with gibbsite, the structure was believed to include rings of edge-sharing $Al(OH)_6$ octahedra. IR spectra of CAH_{10} revealed the presence of both H_2O and OH^- groups in the structure. Accurate kinetic analyses of the loss of water with increasing temperature, based on thermogravimetric and thermodiffractometric measurements, showed that a small amount of crystalline water is lost at about 94 °C without appreciable changes in the structure. This water was thought to be interlaminar. A subsequent, more important loss at about 126 °C produces the collapse of the crystalline portion.[6]

Since the unit-cell parameters of CAH_{10} were already known,[4] the integrated intensities could be extracted from the X-ray powder pattern with a modified LeBail method[7] using the whole-profile fitting program AJUST.[8] Inspection of the list of integrated intensities showed that reflections of type (*00l*) with $l = 2n+1$ were systematically absent, and reflections of type ($h-h\,l$) and ($h-2h\,l$) with $l = 2n+1$ were present. Accordingly, the allowed space groups are $P6_322$ (182), $P6_3/m$ (176), and $P6_3$ (173). Whereas space group $P6_322$ has Laue symmetry 6/*mmm*, $P6_3$/m and $P6_3$ belong to the Laue group 6/*m*. This means that reflections of type (*hkl*) and (*khl*) systematically overlap in $P6_3/m$ and $P6_3$. A first attempt to solve the structure in $P6_322$ was unsuccessful. Consequently, the structure was solved assuming $P6_3$ symmetry. The whole-profile fitting procedure with use of 6/*m* Laue symmetry yielded 30 resolved integrated intensities from a total of 158 reflections ($2\theta_{max} = 51.3°$, $d_{min} = 1.78$ Å). For the systematically overlapped reflections, equipartioned intensities were assumed.[9]

The structure was solved with the SUMF tangent formula (SUMF-TF)[10] implemented in the program XLENS.[11] The electron-density map with the best figures of merit is shown in Figure 1; inspection of this map revealed the positions of Ca^{2+} and OH^- ions as well as the water molecule bound to Ca^{2+}. Surprisingly, Al^{3+} did not appear in this map, so its position was deduced from crystallochemical considerations. The fact that the electron-density map obtained assuming $P6_3$ symmetry possesses a center of symmetry indicated that the true space group is $P6_3/m$.

The model derived from the electron-density map was introduced as the starting structure for the Rietveld refinement with the program FULLPROF.[12] A Pearson-VII function was selected to describe individual line profiles,

 © WILEY-VCH Verlag GmbH, D-69451 Weinheim, 1998 1433-7851/98/3701-0072 $ 17.50+.50/0

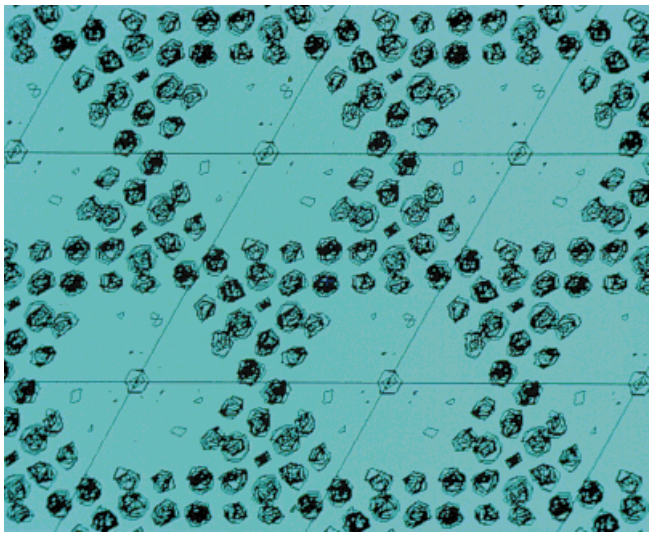


Figure 1. Electron-density map along [001] obtained by applying the SUMF-TF to the equipartioned intensities, which were extracted from the X-ray powder diffraction pattern with a resolution of up to 1.78 Å. One striking feature of this structure is the large channel parallel to the *c* axis, which can be seen clearly in this image. The graphic was produced with the FAN program.[20]

and possible angular variation of the mixing parameter was allowed. Peaks below 30° (2θ) were corrected for asymmetry following the model proposed by Berar and Baldinozzi.[13] The reflections with the 2θ intervals 5–9° and 70–100° were excluded from the refinement. Owing to the shortage of intensity data and the large number of atoms involved, geometrical restraints were applied to the cation–anion distances: $d_{Ca-O} = 2.468(7)$ Å (average distance for the coordination number eight) and $d_{Al-O} = 1.91(6)$ Å (average distance for coordination number six). The refinement converged to the conventional Rietveld residuals[14] $R_p = 16.7$, $R_{wp} = 18.0$, $R_B = 8.6$, and $\chi^2 = 3.5$. The result is shown in Figure 2. Table 1 gives the final atomic coordinates for CAH_{10}, which is better reformulated as $[CaAl_2(OH)_8(H_2O)_2] \cdot 1.84\,H_2O$.

The occupation parameters of the two "free" water molecules were refined after different isotropic temperature factors for groups of atoms were included in the refinement

The structure is based on ring-shaped units of three edge-sharing $Ca(OH)_6(H_2O)_2$ polyhedra at $z = 0.25$ which are laterally linked to the next units at $z = 0.75$ and $z = -0.25$ through two $Al(OH)_6$ octahedra. Each octahedron shares one edge with two Ca-containing polyhedra and one edge with two adjacent octahedra (Figure 3) to produce zig-zag chains of Al octahedra

Table 1. Refined atomic coordinates and isotropic temperature factors [Å^2] for $CaAl_2(OH)_8(H_2O)_2 \cdot 1.84\,H_2O$.

Atom	Wyckoff site	*x*	*y*	*z*	B_i	Occupation
Ca	6*h*	0.5185(7)	0.2791(8)	0.25	2.9(4)	1
Al	12*i*	0.5795(8)	0.4969(7)	0.068(1)	1.5(2)	1
O(1)	12*i*	0.623(1)	0.410(1)	0.072(2)	3.3(3)	1
O(2)	12*i*	0.403(1)	0.235(1)	0.039(2)	4.0(8)	1
O(3)	12*i*	0.521(1)	0.574(1)	0.072(2)	3.3(3)	1
O(4)	12*i*	0.330(1)	0.436(1)	0.090(2)	3.3(3)	1
O(5)	6*h*	0.663(1)	0.565(2)	0.25	3.3(3)	1
O(6)	6*h*	0.505(2)	0.428(2)	0.25	3.3(3)	1
O(7)	12*i*	0.000(3)	0.249(4)	0.921(3)	25(1)	0.71(7)
O(8)	6*h*	0.316(5)	0.567(3)	0.25	25(1)	0.42(4)

along the *c* axis. This peculiar atom connectivity gives rise to an extremely open structure with a large channel along *c* that is centered by the 6_3 screw axis. The balance of electrostatic valences for the oxygen centers of $CaAl_2(OH)_8(H_2O)_2$ estimated according to Allmann[15] is reproduced in Table 2. It allows recognition of the chemical role played by each oxygen atom. It can be seen that all oxygen atoms in the rigid part of the structure are in the form of hydroxy groups except for O(2), which belongs to a water molecule that is tightly bound to Ca^{2+}. The remainding water molecule in the structure is at partially occupied positions on the Ca units (O(8)) or inside the channel (O(7); see Table 1). The presence of water on the Ca units explains the slight shortening of the *c* axis by about 2% at 94 °C. The partial occupation as well as the abnormally high temperature factor of the water molecule in the channel suggest the possible existence of more disordered water molecules in the channel.

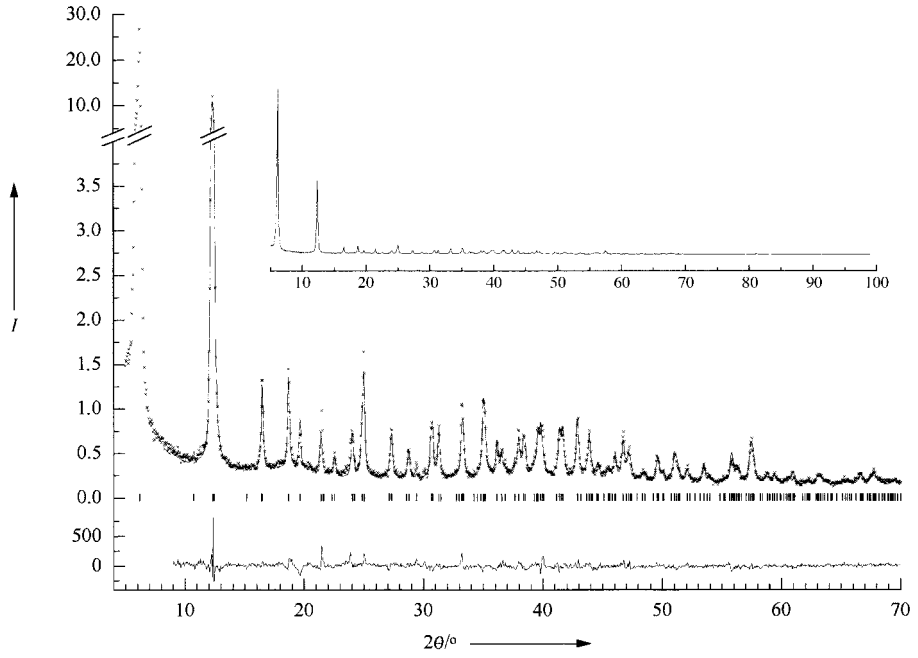


Figure 2. Calculated (inset) and experimentally observed (crosses) X-ray powder diffraction patterns of $[CaAl_2(OH)_8(H_2O)_2] \cdot 1.84\,H_2O$ as well as the difference profile (bottom). Intensity *I* is given in units of 10^{-3}. Measurement conditions: angle range 5–100° (2θ), step size 0.05° (2θ), counting time 15 s. An illumination correction was applied for reflections below 24° (2θ); the first diffraction line at very low angle could not be properly corrected and was excluded from the refinement. Reflections above 70° (2θ) were excluded as well. The short tick marks below the pattern give the positions of the Bragg reflections.

 © WILEY-VCH Verlag GmbH, D-69451 Weinheim, 1998 1433-7851/98/3701-0073 $ 17.50+.50/0

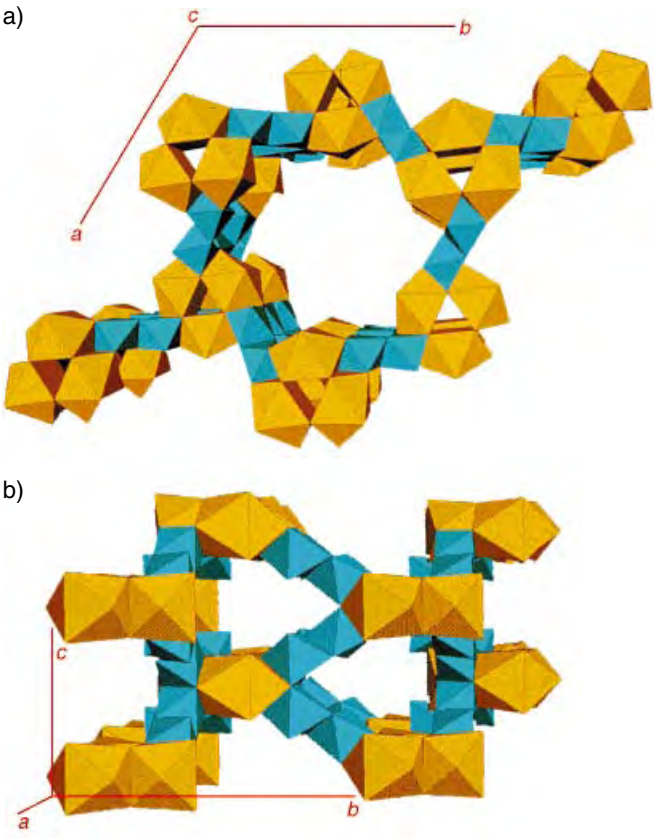


Figure 3. Structure of $[CaAl_2(OH)_8(H_2O)_2]\cdot 1.84\,H_2O$ as viewed a) along the *c* axis and b) along the *a* axis. Three-membered, ring-shaped units of polyhedra (yellow) with central Ca atoms are mutually connected to chains of octahedra (blue) with central Al atoms that run parallel to the *c* axis. The (free) water molecule not involved in the formation of the structure, which shows very high temperature factors, is located in three types of cavities. The most important is a tunnel parallel to the *c* axis, whose axis coincides with the symmetry axis 6_3 containing the O(7) water molecule (see Table 1). In b) the chains of Al-containing octahedra that are parallel to the *c* axis and the cavities parallel to the *a* axis can be observed. There are threefold intersecting tunnels at levels $z = 0.25$ and $z = 0.75$ (but rotated by 60°). The O(8) water molecule is inside these cavities.

The $Ca(OH)_6(H_2O)_2$ polyhedron is similar to the $Ca(OH)_8$ unit in hydrogarnet $(Ca_3Al_2(OH)_6)$[16, 17] and ettringite $(Ca_6(Al(OH)_6)_2(SO_4)_3\cdot 26\,H_2O)$.[18] The structure of the former is more compact, since each $Ca(OH)_8$ polyhedron shares four edges with four different $Ca(OH)_8$ and four more edges with four $Al(OH)_6$ polyhedra. These are in turn surrounded by six $Ca(OH)_8$ polyhedra. The slow conversion of the hexagonal phase into hydrogarnet and gibbsite (plus water) takes place with conservation of the first coordination shell—that is, without completely destroying the original structure. However, CAH_{10} is highly unstable in the presence of circulating water under atmospheric conditions, and quickly transforms into calcite and aluminum hydroxide.

The structural formula obtained from the refinement and given above can be converted into a conventional formula, namely $CaAl_2O_4\cdot 7.8\,H_2O$. This composition is very similar to the overall composition of the hydrated product (with crystalline and amorphous parts). Hence, the amorphous and crystalline portions have very similar compositions, a result that was not apparent when this work was initiated.

Table 2. Metal–oxygen bond lengths *L* [Å] and bond valences *v* (italics) of the oxygen atoms estimated according to Allmann;[15] $L(v) = L(1) - 2k \lg v$. The $L(1)$ and $2k$ values for Ca and Al are 1.896, 0.95 and 1.644, 0.88, respectively. The exchange of charge in the hydrogen bridges (Δe) is based on hydrogen-bond strengths according to Zachariasen.[18] The type of group that the oxygen atom belongs to is given in the last column. The coordination numbers for Al and Ca are 6 and 8, respectively.

Atom	Ca^{2+}	Al^{3+}	$\Sigma_c v$[a]	Δe	$\Sigma_c v_{corr}$	Type
O(1)	2.46[c], 2.44[c]	1.89	–	–	–	OH^-
		0.53	*1.05*	–	*1.05*	
	0.25, *0.27*					
O(2)	2.41[c]	–	–	–	--	H_2O
	0.29	–	*0.29*	*– 0.28*	*0.01*	
O(3)	–	1.93, 1.87	–	–	–	OH^-
	–	*0.47*, *0.55*	*1.02*	--	*1.02*	
O(4)	–	1.87	–	–	–	OH^-
	–	*0.55*	0.55	*+ 0.28*	*0.83*	
O(5)	2.57	1.97[d]	–	–	–	OH^-
	0.20	*0.43*	*1.06*	–	*1.06*	
O(6)	2.56	1.91[d]	–	–	–	OH^-
	0.20	*0.497*	*1.19*	–	*1.19*	
$\Sigma_A v$[e]	2.02	3.03				

[a] $\Sigma_c v$ = sum of bond valences for each anion. [b] $\Sigma_c v_{corr}$ = sum of bond valences for each anion after considering the H-bond charge exchange. [c] Two bonds per cation. [d] Two bonds per anion. [e] $\Sigma_A v$ = sum of bond valences for each cation. O(4)···O(2) 2.66(4) Å ≈ 0.28 valence units.

Experimental Section

The $CaAl_2O_4$ phase was obtained by heating an equimolar mixture of pure reactants Al_2O_3 and $CaCO_3$ at 1300 °C for 200 h. The progress of the reaction was periodically controlled by XRD. The final sintered product was finely ground and sieved through a 10-μ sieve. The optimal conditions were determined to be hydration of $CaAl_2O_4$ at 5 °C with excess water with periodic stirring. The final product was filtered, washed with acetone, and characterized by XRD. The X-ray powder diffraction pattern used for the structure solution and refinement was collected in reflection geometry on a high-resolution RIGAKU powder diffractometer equipped with a Cu rotating anode and a primary curved Ge(111) monochromator. Comparison with an additional pattern measured using a INEL X-ray PSD diffractometer with the sample enclosed in a glass capillary confirmed the absence of a preferred orientation in the flat sample.

To prepare a sample suitable for neutron diffraction, $CaAl_2O_4$ was hydrated with deuterated water as well. The results of neutron diffraction were very disappointing: Only few peaks emerged from an intense background, suggesting a high thermal and positional disorder of the deuterium atoms.

Received: July 21, 1997 [Z10715IE]
German version: *Angew. Chem.* **1998**, *110*, 76–79

Keywords: aluminum · cement · powder diffraction · solid-state structures · structure elucidation

[1] G. Assarsson, *Sveriges Geol. Undersonk. 27 Ser. C* **1933,** *379*, 22.
[2] V. W. Gessner, D. Müller, H. J.Behrens, G. Z. Scheler, *Z. Anorg. Allg. Chem.* **1982**, *486*, 193–199.
[3] X. Cong, R. J. Kirkpatrick, *J. Am. Ceram. Soc.* **1993**, *76*, 409–416.
[4] F. G. Buttler, H. F. W. Taylor, *Il cemento* **1978**, *75*, 147.
[5] J. Skibsted, E. Henderson, H. J. Jakobsen, *J. Inorg. Chem.* **1993**, *32*, 1013–1027.
[6] F. Guirado, S. Galí, S. Chinchón, *Cem. Concr. Res.*, submitted.
[7] J. Rius, J. Sañé, C. Miravitlles, J. M. Amigó, M. M. Reventós, D. Louër, *Anal. Quím. Int. Ed.* **1996**, *92*, 223–227.
[8] J. Rius, *AJUST: A whole-pattern profile-fitting program for extracting integrated intensities*, Institut de Ciència de Materials de Barcelona, CSIC, **1994**.
[9] Crystallographic data for $[CaAl_2(OH)_8(H_2O)_2]\cdot 1.84\,H_2O$: empirical formula $CaAl_2O_4\cdot 7.8\,H_2O$, M_r 299.2, hexagonal, space group $P6_3/m$,

 © WILEY-VCH Verlag GmbH, D-69451 Weinheim, 1998 1433-7851/98/3701-0074 $ 17.50+.50/0

$a = b = 16.387(2)$, $c = 8.279(1)$ Å, $Z = 6$, $V = 1925$ Å^3, $\rho_{calcd} = 1.548$ g cm^{-3}, white powder, $\lambda = 1.5406$ Å, T ≈ 25 °C, data range 5–100° (2θ), 1900 data points, 30 independent reflections, no absorption correction, Rietveld refinement with X-ray powder data with geometrical constraints; data range used 9–70° (2θ), $R_p = 16.7$, $R_{wp} = 18.0$, $R_B = 8.6$, $\chi^2 = 3.5$, $R_p = 100\Sigma|y_{oi} - y_{ci}|/\Sigma|y_{oi}|$, $R_{wp} = 100(\Sigma w|y_{oi} - y_{ci}|^2/\Sigma w|y_{oi}|^2)^{0.5}$, $R_B = 100\Sigma|I_k - I_{ck}|/\Sigma|I_k|^2 = (R_{wp}/R_{exp})^2$. Further details of the crystal structure investigation may be obtained from Fachinformationszentrum Karlsruhe, D-76344 Eggenstein-Leopoldshaften (Germany), on quoting the depository number CSD-407150.

[10] J. Rius, *Acta Crystallogr. Sect. A* **1993**, *49*, 406–409.
[11] J. Rius, *XLENS: A direct methods program based on the SUMF tangent formula*, Institut de Ciència de Materials de Barcelona, CSIC, **1992**.
[12] J. Rodriguez-Carvajal in *Abstracts of the Satellite Meeting on Powder Diffraction of the XV Congress of the IUCr,* Toulouse, Frankreich, **1990**, p. 127.
[13] J. F. Berar, G. Baldinozzi, *J. Appl. Crystallogr.* **1993**, *26*, 128–129.
[14] R. A. Young in *The Rietveld Method* (Ed.: R. A. Young), *IUCr Monographs on Crystallography, Vol. 5*, Oxford University Press, **1995**, pp. 1–39.
[15] R. Allmann, *Monatsh. Chem.* **1975**, *106*, 779–793.
[16] R. Weiss, D. Grandjean, *Acta Crystallogr.* **1964**, *17*, 1329–1330.
[17] G. A. Lager, T. Armbruster, J. Faber, *Am. Miner.* **1987**, *72*, 756–765.
[18] A. Moore, H. F. W. Taylor, *Acta Crystallogr. Sect. B* **1970,** *26*, 386–393.
[19] W. H. Zachariasen, *Acta Crystallogr.* **1963,** *16*, 385.
[20] E. A. Vernoslova, V. Lumin, *J. Appl. Crystallogr.* **1993**, *26*, 291–294.

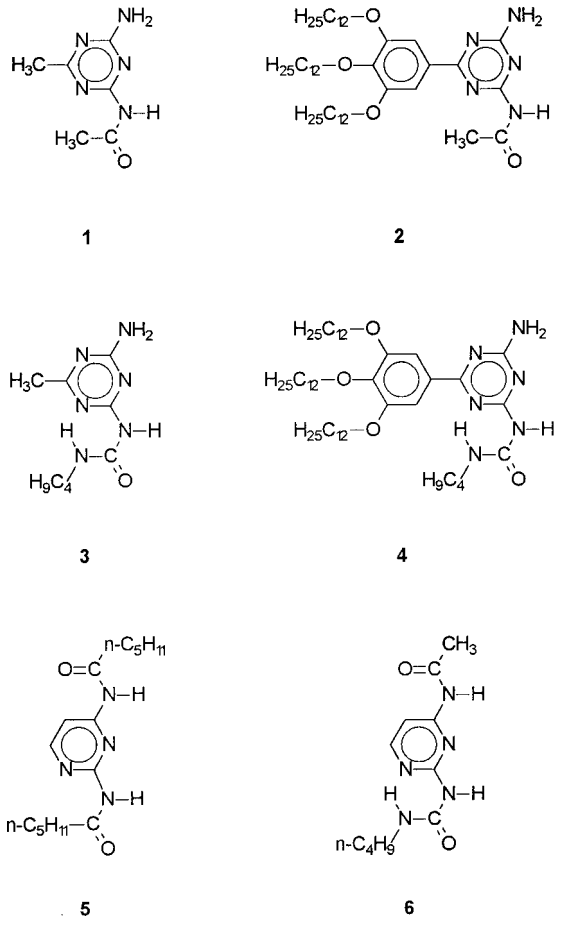
Self-Complementarity Achieved through Quadruple Hydrogen Bonding**

Felix H. Beijer, Huub Kooijman, Anthony L. Spek, Rint P. Sijbesma, and E. W. Meijer*

Hydrogen bonds are among the most useful interactions for encouraging molecules to self-assemble into well-defined aggregates.[1] The strength and selectivity of hydrogen bonds can be increased by introducing arrays of donor (D) and acceptor sites (A). Arrays of two and three hydrogen bonds have already been studied in detail, and their strength in $CHCl_3$ depends upon the particular arrangement of donor and acceptor sites. In triply hydrogen bonded complexes, for example, association constants vary from $K_a = 10^2 - 10^3$ M^{-1} for DAD–ADA pairs to $K_a = 10^5 - 10^6$ M^{-1} for DDD–AAA pairs.[2] Jorgensen[3] rationalized these differences as the result of secondary electrostatic interactions. Rules derived from this analysis are now widely used to design complementary host–guest systems characterized by high selectivity and recognition as well as strong binding.

However, for a number of applications ranging from container molecules[4] to supramolecular tubes,[5] self-complementarity is required. This is evidently found only in arrays with an even number of hydrogen bonds. Although examples exist of self-complementary arrays consisting of two hydrogen-bonding units,[6] arrays with four adjacent hydrogen-bonding sites are notably absent from the supramolecular literature.[7] Recently we reported the dimerization of a diacetyl diaminotriazine involving four hydrogen bonds with a dimerization constant K_{dim} of 35 M^{-1}.[8]

Here we show the generality of dimerization by way of the DADA sequence in readily available compounds, and present examples with unexpectedly high dimerization constants. Conceptually, the DADA arrays in compounds **1**–**6** are derived from DAD arrays in diaminotriazines or diaminopyrimidines that have been extended by an oxygen acceptor atom



from a *cis* amido or ureido group. The required *cis*-amide conformation in **1**, **2**, and **5** is favored by repulsion between the amide oxygen atom and nitrogen atoms in the heterocyclic ring, whereas an intramolecular hydrogen bond preorganizes the array in ureido derivatives **3**, **4**, and **6**.

[*] Prof. Dr. E. W. Meijer, F. H. Beijer, Dr. R. P. Sijbesma
Laboratory of Organic Chemistry
Eindhoven University of Technology
P.O. Box 513, 5600 MB, Eindhoven (The Netherlands)
Fax: Int. code + (31) 40-2451036
e-mail: tgtobm@chem.tue.nl
Dr. H. Kooijman, Dr. A. L. Spek[+]
Bijvoet Center for Biomolecular Research
Crystal and Structural Chemistry, Utrecht University (The Netherlands)
[+] Crystal structure analyses.

[**] The authors wish to thank H.-J. Luinge, B. Lutz, and J. van der Maas of Utrecht University for IR spectroscopic evaluation of the dimerization constant for **4**. This work was supported by the Netherlands Foundation for Chemical Research (SON) with financial assistance from the Netherlands Organisation for Scientific Research (NWO) and DSM Research

 © WILEY-VCH Verlag GmbH, D-69451 Weinheim, 1998 1433-7851/98/3701-0075 $ 17.50+.50/0

Compounds **1**–**6** were prepared by acylation of diaminotriazine and diaminopyrimidine derivatives. The structures of **1**, **3**, **5**, and **6** were determined by single-crystal X-ray diffraction (Figure 1).[9] All four compounds form centrosymmetric dimers in the solid state, which are held together by four hydrogen bonds between self-complementary DADA arrays. The dimers of triazines **1** and **3** form infinite chains by double hydrogen bonding of the remaining N–H group to a triazine-ring nitrogen atom. An additional intramolecular hydrogen bond is present in ureido derivatives **3** and **6** from the ureido nitrogen atom to a ring nitrogen atom. Distances between hydrogen-bonded atoms are listed in Table 1. The DADA arrays in all four crystal structures deviate significantly from linearity. Thus, the oxygen atom does not fall on the line joining the nitrogen atoms in the array. As a result, the inner N–H···N hydrogen bonds are 0.30–0.49 Å longer than the outer N–H···O hydrogen bonds. Apparently, the enforced differences in bond lengths between N–H···O and N–H···N hydrogen bonds (which have similar equilibrium lengths)[10] does not prevent the formation of stable dimers.

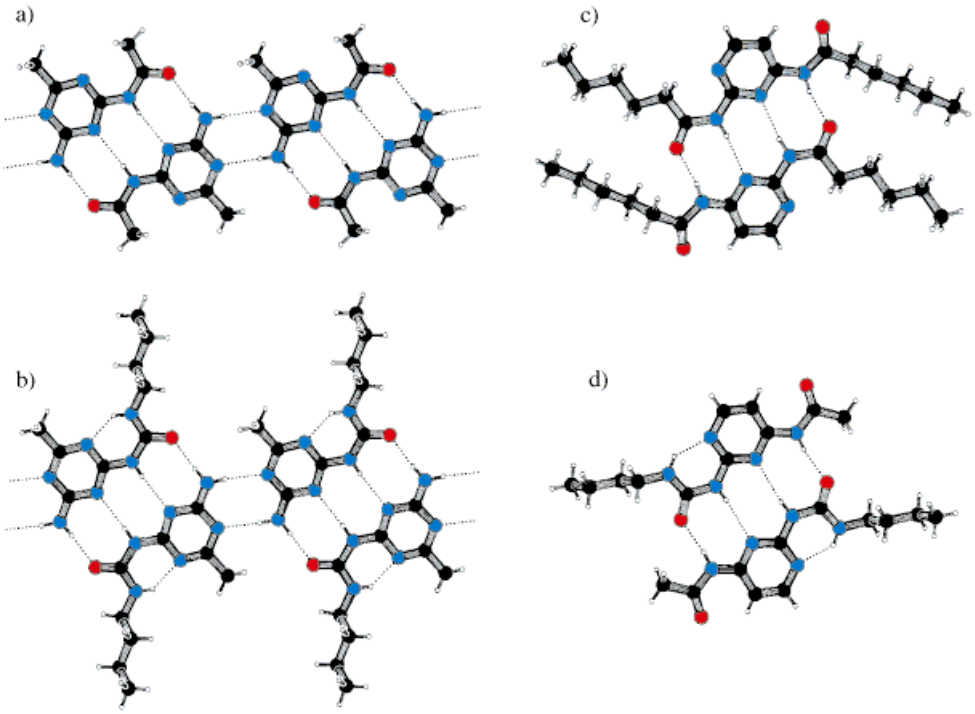


Figure 1. PLUTON representations of the structures of a) **1**, b) **3**, c) **5**, and d) **6**.

FT-IR spectra of solid samples and concentrated solutions of **2**, **4**, **5**, and **6** in chloroform are very similar both in the N–H region (3500–3170 cm^{-1}) and in the double-bond region (1750–1400 cm^{-1}), which indicates a similar complexation mode in the solid state and in solution. Dilution of the solutions in chloroform results in the appearance of the monomer IR spectrum. This permits derivation of both monomer and dimer absorptions, as well as the shifts that accompany complexation; all are typical for hydrogen bonding. Changes in the N–H stretching vibrations of **5** and **6** upon dimerization are very similar [$\Delta\nu = 167$ and 235 cm^{-1} (**5**) and 158 and 256 cm^{-1} (**6**)], which indicates that the hydrogen bonds themselves are similar.

^1H and ^{13}C NMR spectra taken both in chloroform and DMSO are in agreement only with the tautomeric form indicated in the structural formulas. In the ^1H NMR spectra of the soluble compounds **2**, **4**, **5**, and **6** the chemical shifts for the amide protons in chloroform are concentration-dependent. When the concentration is increased, the signals shift downfield, which indicates formation of a hydrogen-bonded complex. The concentration dependence of the N–H shifts can be simulated only with a model that assumes dimerization. Dimerization constants can be obtained from this model for **2**, **4**, and **5** (Table 2). The dimerization constant for **4** was determined to be $2.2 \times 10^4\,M^{-1}$ by evaluation of IR spectra at

Table 2. Dimerizaton constants for **2** and **4**–**6** in $CDCl_3$ at 298 K.

Compound	K_{dim} [M^{-1}][a]	$-\Delta G_{dim}$ [kJ mol^{-1}]
2	530	15.5 ± 0.5
4	2×10^4[b]	24.5 ± 0.3
5	170	12.7 ± 0.5
6	2×10^5	30.2 ± 0.5

[a] Estimated relative error <20%. [b] Average of values determined by IR and NMR spectroscopy.

Table 1. Hydrogen-bond distances [Å] and X-H-X angles [°], differences in length between inner and outer hydrogen bonds, as well as N···N···O angles in the DADA array.

	NH···N distance	NH···N angle	NH···O distance	NH···O angle	Difference in hydrogen-bond length	N···N···O angle
1	3.195(2)	175(2)	2.839(2)	175(2)	0.3556	169.60(6)
3	3.101(4)	176(3)	2.797(4)	176(3)	0.304	171.0(1)
5	3.245(2)	166(2)	2.789(2)	162(2)	0.456	167.71(7)
6	3.239(4)	171(2)	2.748(3)	169(2)	0.491	167.99(8)

 © WILEY-VCH Verlag GmbH, D-69451 Weinheim, 1998 1433-7851/98/3701-0076 $ 17.50+.50/0

various concentrations, whereas a value of $1.5 \times 10^4\,\text{M}^{-1}$ was obtained from NMR measurements. The dimerization constant of **6** is too high to be determined directly in $CDCl_3$. Limiting shift values for **6** in $CDCl_3$ containing 1, 2, 3, 4, and 5% methanol are identical, so these values can be used for extrapolation to pure $CDCl_3$. This results in an estimate for the dimerization constant in pure $CDCl_3$ of approximately $2 \times 10^5\,\text{M}^{-1}$.

The dimers of **2** and **4**–**6** in chloroform show remarkably different stabilities. Although all the dimers are stabilized by four intermolecular hydrogen bonds, the stabilities differ by as much as 17.5 kJ mol^{-1}. The most significant differences are observed between amide derivatives **2** and **5** on one hand, and ureido derivatives **4** and **6** on the other.

Sartorius and Schneider have recently proposed a simple free-energy relationship for the stability of multiply hydrogen bonded complexes in chloroform.[11] This is based on two increments: 7.9 kJ mol^{-1} for each hydrogen bond and $\pm$ 2.9 kJ mol^{-1} for each attractive or repulsive secondary electrostatic interaction. The increments were derived from association data for heterocyclic compounds with spatially fixed arrays. A dimerization constant of $310\,\text{M}^{-1}$ ($\Delta G^\circ_{\text{dim}} = -14.2$ kJ mol^{-1}) is predicted for a DADA array. The dimerization constants for amides **2** and **5** ($K_{\text{dim}} = 530$ and $170\,\text{M}^{-1}$, respectively) agree with the predictions, provided one takes into account the considerable degree of rotational freedom available. Most surprisingly, however, ureido derivatives **4** and **6** display stabilities that exceed the calculated values by 10.3 and 16.0 kJ mol^{-1}, respectively. The increased stability of the dimers from **4** and **6** relative to the dimers from **2** and **5** might be ascribed to preorganization of the DADA array provided by the intramolecular hydrogen bonds in these compounds, which fix the carbonyl groups in the plane of the ring. In both compounds a *cis* conformation for the amide groups and coplanarity with the aromatic ring are required for dimerization. Fixation of the amide in this conformation is unfavorable not only entropically, but also enthalpically.[12] Therefore, we propose that the higher stability of dimers of the ureido compounds compared to amido derivatives is caused by a combination of favorable entropic and enthalpic effects of the intramolecular hydrogen bonds of the ureido substituents. Although the difference in stability of dimers in the two series can indeed be explained this way, the argument does not account for the large deviations of the values for **4** and **6** from those calculated by Sartorius and Schneider;[11] this requires further investigation.

Self-complementary quadruply hydrogen bonded systems can be prepared very readily by acylation of DAD arrays, and the stabilities of the resulting dimers are anomalously high when the array is preorganized by intramolecular hydrogen bonds. Further elaboration of self-complementarity and preorganization by intramolecular hydrogen bonds, together with the application of four-point recognition in supramolecular chemistry, are the subjects of ongoing research.

Experimental Section

Dimerization studies in chloroform: Dimerization constants (K_{dim}) were obtained through ^{1}H NMR titrations, in which the shift of the N–H protons (as well as aromatic and CH_3 protons, where appropriate) was monitored as a function of concentration. At least ten data points in the 20–80% saturation range were measured, and dimerization constants were evaluated by nonlinear least-squares fitting of the data to the appropriate equation.[13] ^{1}H NMR titrations utilized $CDCl_3$ (Cambridge Isotope Laboratories, 99.8% D content, with TMS as internal reference). For the IR studies, freshly prepared anhydrous chloroform[8] was used.

1-6: Acetylaminotriazines **1** and **2** and ureidotriazines **3** and **4** were synthesized by heating the corresponding diaminotriazine in pyridine at reflux with excess acetic anhydride (15 min)[14] or excess butyl isocyanate (2 h). Cooling resulted in precipitation of pure **1** and **3**, and crystallization from DMF afforded crystals of sufficient quality for single-crystal X-ray analysis. Derivatives **2** and **4** were purified by precipitation in hexane or ethyl acetate and by column chromatography. Di(hexanoylamino)pyrimidine (**5**) was obtained by heating 2,4-diaminopyridine with hexanoic anhydride in pyridine at reflux for 2 h and crystallization from hexane/ethyl acetate. Crystals suitable for single-crystal X-ray analysis were obtained by evaporating a solution in hexane/dichloromethane under air. 2-Butylureido-4-acetylaminopyridine (**6**) was synthesized in two steps. Reaction of 2,4-diaminopyridine in warm THF with 1 equiv of butyl isocyanate afforded, after crystallization, pure 2-butylureido-4-aminopyridine. This was treated with 1 equiv of acetyl chloride in warm THF. Crystals suitable for single-crystal X-ray analysis were obtained by evaporating a solution in dichloromethane under air. All compounds provided satisfactory analyses. Full details regarding synthesis and characterization, together with a study of the observed association behavior, including bis-acylated derivatives, will be published elsewhere.

Received: June 10, 1997 [Z10538IE]
German version: *Angew. Chem.* **1998**, *110*, 79–82

Keywords: crystal engineering · hydrogen bonds · supramolecular chemistry

[1] J.-M. Lehn, *Makromol. Chem. Macromol. Symp.* **1993**, *69*, 1.
[2] a) T. J. Murray, S. C. Zimmerman, *J. Am. Chem. Soc.* **1992**, *114*, 4010; b) E. E. Fenlon, T. J. Murray, M. H. Baloga, S. C. Zimmerman, *J. Org. Chem.* **1993**, *58*, 6625; c) S. C. Zimmerman, T. J. Murray, *Tetrahedron Lett.* **1994**, *35*, 4077.
[3] a) W. L. Jorgensen, J. Pranata, *J. Am. Chem. Soc.* **1990**, *112*, 2008; b) J. Pranata, S. G. Wierschke, W. L. Jorgensen, *ibid.* **1991**, *113*, 2810.
[4] R. Wyler, J. de Mendoza, J. Rebek, Jr., *Angew. Chem.* **1993**, *105*, 1820; *Angew. Chem. Int. Ed. Engl.* **1993**, *32*, 1699.
[5] M. R. Ghadiri, J. R. Granja, R. A. Milligan, D. E. McRee, N. Khazanovich, *Nature* **1993**, *366*, 324.
[6] Y. Ducharme, J. D. Wuest, *J. Org. Chem.* **1988**, *53*, 5787.
[7] A crystal structure containing a DADA array has been reported: R. J. Griffin, P. R. Lowe, *J. Chem. Soc. Perkin Trans. 1* **1992**, 1811.
[8] F. H. Beijer, R. P. Sijbesma, J. A. J. M. Vekemans, E. W. Meijer, H. Kooijman, A. L. Spek, *J. Org. Chem.* **1996**, *61*, 6371.
[9] Crystal structure data for $\mathbf{1} \cdot C_6H_9N_5O$: $M_r = 167.17$, colorless needle-shaped crystal ($0.05 \times 0.10 \times 0.45$ mm^3), triclinic, space group $P\bar{1}$ (no. 2), $a = 4.0732(3)$, $b = 8.6054(9)$, $c = 11.1902(14)$ Å, $\alpha = 75.348(9)$, $\beta = 83.461(8)$, $\gamma = 78.752(8)^\circ$, $V = 371.33(7)$ Å^3, $Z = 2$, $\rho_{\text{calcd}} = 1.4951(3)$ g cm^{-3}, $F(000) = 176$, $\lambda(\text{Mo}_{\text{K}\alpha}) = 0.71073$ Å, graphite monochromator, ω scan, $T = 150$ K; of 3882 measured reflections ($1.9 < \theta < 27.5$), 1703 were independent ($R_{\text{int}} = 0.047$). Data were collected with an Enraf–Nonius CAD4 Turbo diffractometer with a rotating anode, and corrected for Lorentzian, polarization, and stability effects (three control reflections); there as no absorption correction. The structure was solved by automated direct methods (SHELXS-96) and refined on F^2 (SHELXL-96). Locations of hydrogen atoms were incorporated into the refinement; their initial values were obtained from a difference Fourier map. All non-hydrogen atoms were refined with anisotropic thermal parameters, and hydrogen atoms were refined with fixed isotropic thermal parameters established from the isotropic parameters of the atoms bearing the hydrogens (factor 1.5 for CH_3 and NH_2 hydrogen atoms, 1.2 for the others). $wR2 = [\Sigma\{\omega(F_o^2 - F_c^2)^2\}/\Sigma[\omega(F_c^2)^2]]^{0.5} = 0.1170$, $w = 1/[\sigma^2(F^2) + (0.0592\,P)^2 + 0.13\,P]$ with $P = (\max(F_o^2,0) + 2\,F_c^2)/3$, $R_1 = \Sigma\,||F_o| - |F_c||/|F_o| = 0.0426$ [for 1343 re-

 © WILEY-VCH Verlag GmbH, D-69451 Weinheim, 1998 1433-7851/98/3701-0077 $ 17.50+.50/0

flections with $I > 2\sigma(I)$], $S = 1.041$ for 136 parameters. A final difference Fourier map showed no residual density below -0.30 or above 0.28 e Å^{-3}. Crystal data for $\mathbf{3}\cdot C_9H_{16}N_6O$: $M_r = 224.27$, colorless needle-shaped crystal ($0.05 \times 0.10 \times 0.50$ mm^3), triclinic, space group $P\bar{1}$ (no. 2), $a = 4.703(2)$, $b = 7.924(6)$, $c = 15.833(18)$ Å, $\alpha = 78.69(9)$, $\beta = 86.18(6)$, $\gamma = 74.43(6)^\circ$, $V = 557.3(8)$ Å^3, $Z = 2$, $\rho_{calcd} = 1.3365(19)$ g cm^{-3}, $F(000) = 240$, $\mu(Mo_{K\alpha}) = 0.9$ cm^{-1}. Data collection and reduction as well as solution and refinement were conducted as described for **1**. Of 4350 measured reflections, 2567 were independent; $R_{int} = 0.059$, $(1.3 < \tau < 27.5)$. The refinement converged at $wR_2 = 0.1323$, $w = 1/[\sigma^2(F^2) + (0.0465P)^2 + 0.07P]$, $R_1 = 0.0553$ [for 1474 reflections with $I > 2\sigma(I)$], $S = 1.021$ for 193 parameters. A final difference Fourier map showed no residual density below -0.22 or above 0.27 e Å^{-3}. Crystal structure data for $\mathbf{5}\cdot C_{16}H_{26}N_4O_2$: $M_r = 306.41$, colorless block-shaped crystals ($0.2 \times 0.3 \times 0.5$ mm^3), triclinic, space group $P\bar{1}$ (no. 2), $a = 4.9675(11)$, $b = 8.1236(7)$, $c = 20.911(3)$ Å, $\alpha = 100.663(9)$, $\beta = 93.080(15)$, $\gamma = 91.680(12)^\circ$, $V = 827.4(2)$ Å^3, $Z = 2$, $\rho_{calcd} = 1.2299(3)$ g cm^{-3}, $F(000) = 332$, $\mu(Mo_{K\alpha}) = 0.8$ cm^{-1}. Data collection and reduction as well as solution and refinement were conducted as described for **1**. Of 4552 measured reflections, 3814 were independent, $R_{int} = 0.055$, $(1.0 < \tau < 27.5)$. The refinement converged at $wR_2 = 0.1567$, $w = 1/[\sigma^2(F^2) + (0.0880P)^2 + 0.31P]$, $R_1 = 0.0553$ [for 2963 reflections with $I > 2\sigma(I)$], $S = 1.015$ for 277 parameters. A final difference Fourier map showed no residual density below -0.27 or above 0.34 e Å^{-3}. Crystal structure data for $\mathbf{6}\cdot C_{11}H_{17}N_5O_2$: $M_r = 251.29$, colorless needle-shaped crystals ($0.1 \times 0.1 \times 0.7$ mm^3), monoclinic, space group $C2/c$ (no. 15), $a = 20.119(18)$, $b = 5.194(2)$, $c = 25.186(16)$ Å, $\beta = 94.55(4)^\circ$, $V = 2624(3)$ Å^3, $Z = 8$, $\rho_{calcd} = 1.2722(15)$ g cm^{-3}, $F(000) = 1072$, $\mu(MoK_\alpha) = 0.9$ cm^{-1}. Of 8860 measured reflections, 3007 were independent; $R_{int} = 0.075$, $(1.0 < \tau < 27.3, T = 293$ K) using an Enraf–Nonius FAST area detector on a rotating anode. Data collection and reduction as well as solution and refinement were conducted as described for **1**. The refinement converged at $wR_2 = 0.1332$, $w = 1/[\sigma^2(F^2) + (0.0300P)^2 + 4.33P]$, $R_1 = 0.0644$ [for 2305 reflections with $I > 2\sigma(I)$], $S = 1.160$ for 214 parameters. A final difference Fourier map showed no residual density below -0.25 or above 0.25 e Å^{-3}. Crystallographic data (excluding structure factors) for the structures reported in this paper have been deposited with the Cambridge Crystallographic Data Centre as supplementary publication no. CCDC-100480. Copies of the data can be obtained free of charge on application to CCDC, 12 Union Road, Cambridge CB2 1EZ, UK (fax: int. code + (44) 1223-336033; e-mail: deposit@ccdc.cam.ac.uk).

[10] The mean effective equilibrium bond length for a series of N–H···O= and N–H···N hydrogen bonds in crystal structures of purines and pyrimidines are 1.88 and 1.90 Å, respectively: G. A. Jeffrey, W. Saenger, *Hydrogen Bonding in Biological Structures*, Springer, Berlin, **1994**.

[11] J. Sartorius, H.-J. Schneider, *Chem. Eur. J.* **1996**, *2*, 1446.

[12] A. R. Katritzky, I. Ghiviraga, *J. Chem. Soc. Perkin Trans. 2* **1995**, 1651.

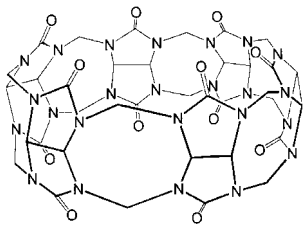
[13] K. A. Connors, *Binding Constants*, Wiley, New York, **1987**.

[14] a) A. Ostrogovich, G. Gheorghiu, *Gazz. Chim. Ital.* **1930**, *60*, 648; b) *ibid.* **1932**, *62*, 317.

A Molecular Bowl with Metal Ion as Bottom: Reversible Inclusion of Organic Molecules in Cesium Ion Complexed Cucurbituril**

Dongmok Whang, Jungseok Heo, Joo Hyun Park, and Kimoon Kim*

Molecular containers,[1] rigid molecules with large cavities in which small molecules can be encapsulated, are of much interest because of their potential applications in separations, catalysis, sensors, and drug delivery. Although a number of molecular container systems have been studied only a few of them have demonstrated reversible encapsulation and release of their guests at ambient temperatures.[2, 3] We recently reported[4] a novel molecular container assembly based on cucurbituril (**1**),[5, 6] a macrocyclic cavitand with a hollow core of ≈ 5.5 Å diameter, which is accessible through two portals laced with carbonyl groups. In aqueous solution containing sodium ions, two Na^+ ions and their coordinated water molecules cover each portal of cucurbituril like a lid on a barrel.[4, 7] The "Na^+-lidded" cucurbituril can encapsulate small organic molecules such as THF and benzene. Moreover, the encapsulation and release of the guest molecules can be controlled by complexation and decomplexation of the sodium ions at the portals. Extending this work to cucurbiturils complexed to other alkali metal ions, we thought cesium-complexed cucurbituril would be particularly interesting because Cs^+, whose ionic radius is 1.81–2.02 Å seems to fit the portal better. Indeed, Cs^+-complexed cucurbiturils are drastically different from the Na^+-complexed cucurbiturils.[4] Here we report the cesium-complexed cucurbiturils, which uniquely behave like a "metal-ion-bottomed" molecular bowl.



1

Although cucurbituril is sparingly soluble in water it dissolves appreciably in cesium chloride solution ($\approx 5.9 \times 10^{-2}$ mol in 1.0 L of 0.2 M CsCl solution at room temperature) as it does in aqueous solutions of other alkaline metal salts. Slow diffusion of ethanol into cucurbituril dissolved in 0.2 M CsCl solution results in the formation of crystals of **2**. The X-ray crystal structure of **2** (Figure 1)[8] reveals that a cesium ion is coordinated to each portal of cucurbituril, but the structure is in sharp contrast to the sodium-complexed cucurbituril in which two sodium ions are coordinated to each portal of cucurbituril.[4] The cesium ion leans toward one side of the portal, being coordinated to only four carbonyl oxygen atoms

[*] Prof. K. Kim, Dr. D. Whang, J. Heo, J. H. Park
Department of Chemistry, Center for Biofunctional Molecules and School of Environmental Engineering
Pohang University of Science and Technology
San 31 Hyojadong, Pohang 790–784 (South Korea)
Fax: Int. code + (82) 562-279 3399
e-mail: kkim@vision.postech.ac.kr

[**] This work was supported by Korea Science and Engineering Foundation. We thank Professors G. V. Smith and J. Chin for helpful comments.

 © WILEY-VCH Verlag GmbH, D-69451 Weinheim, 1998 1433-7851/98/3701-0078 $ 17.50+.50/0

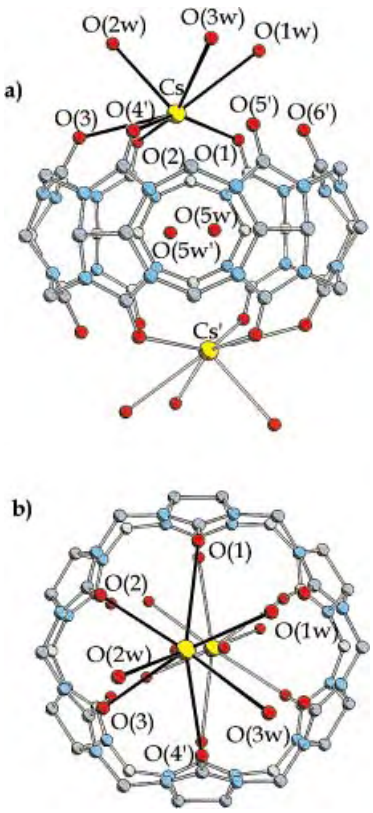


Figure 1. X-ray crystal structure of **2**: a) side view; b) top view. Color codes: Cs yellow, O red, N blue, C gray. Selected bond lengths [Å]: Cs–O(1) 3.378(6), Cs–O(2) 3.110(6), Cs–O(3) 3.100(6), Cs–O(4) 3.321(5), Cs–O(1w) 3.214(7), Cs–O(2w) 3.027(7), Cs–O(3w) 3.487(7).

at the portal with Cs–O distances of 3.100(6) – 3.378(6) Å. Three water molecules O(1w) – O(3w) are also bound to the metal ion from outside with distances of 3.027(7) – 3.487(7) Å. The cesium ion is 0.684(2) Å above the mean plane of the six carbonyl oxygen atoms of the portal. This value is much smaller than the average displacement of the sodium ions (1.577(4) Å) from the six-oxygen plane of the portal in the sodium-complexed cucurbituril. The smaller displacement from the portal and larger ionic radius of the cesium ion make the size of the cavity in **2** considerably smaller than that in the sodium-complexed cucurbituril. This is illustrated by the fact that only one disordered water molecule resides in the cavity of **2** whereas three water molecules exist in the Na^+-lidded cucurbituril. We therefore expected that the cavity of the Cs^+-complexed cucurbituril is not large enough to accommodate a tetrahydrofuran (THF) molecule which can be encapsulated in the Na^+-complexed cucurbituril.

To our surprise, however, when THF was added to the cucurbituril in 0.4 M CsCl solution two sets of signals for THF were observed in the ^1H NMR spectrum, the second of which is shifted upfield from that assigned to the free THF molecules. This NMR spectrum supports inclusion of a THF molecule inside the cucurbituril dissolved in CsCl solution. The formation constant of this inclusion complex **3** is estimated to be $(1.1 \pm 0.1) \times 10^3\,M^{-1}$ at room temperature,[9] which is even larger than that in the sodium-complexed cucurbituril ($(5.1 \pm 0.5) \times 10^2\,M^{-1}$).[4] Thermodynamic parameters[10] associated with the inclusion phenomenon are quite different from those for the Na^+ case: $\Delta H^\circ = -9.8 \pm 1.0$ kcal mol^{-1} and $\Delta S^\circ = -19 \pm 2$ cal mol^{-1} K^{-1} (Cs^+) and $\Delta H^\circ = -5.8 \pm 0.6$ kcal mol^{-1} and $\Delta S^\circ = -7.4 \pm 0.7$ cal mol^{-1} K^{-1} (Na^+).[4] The apparent conflict of this observation with our earlier expectation prompted us to study the X-ray structure of the crystal of **3**.[8] As we suspected, the X-ray structure reveals a THF molecule encapsulated in the cucurbituril cavity. The structure of **3** is, however, quite different from that of **2**; in particular, only one cesium ion is bound to cucurbituril in **3** (Figure 2). This is in contrast to the Na^+-lidded cucurbituril, in

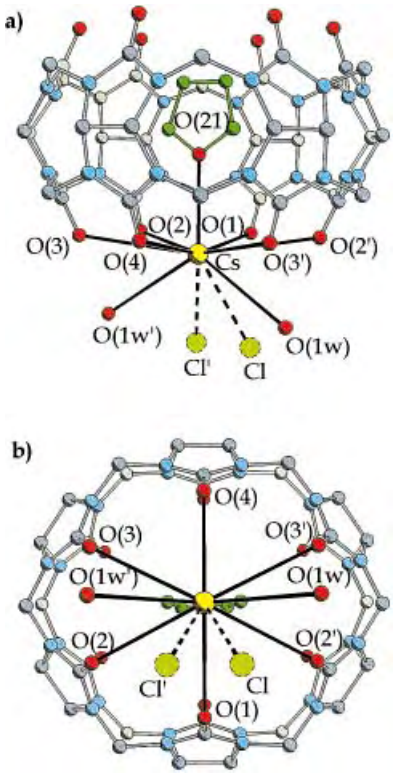


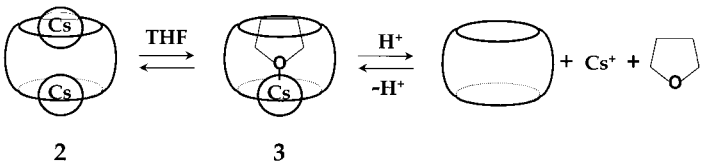
Figure 2. X-ray crystal structure of **3**: a) side view; b) top view. Color codes: Cs yellow, Cl greenish yellow, O red, N blue, C gray. The coordinated THF is highlighted in green. The coordinated Cl^- is disordered over two sites with half occupancy. Selected bond lengths [Å]: Cs–O(1) 3.250(7), Cs–O(2) 3.584(8), Cs–O(3) 3.574(6), Cs–O(4) 3.144(6), Cs–O(21) 2.934(10), Cs–O(1w) 3.591(10), Cs–Cl 3.365(3).

which the host structure of the complex that includes THF is nearly identical to that of the one free of the organic guest. In **3**, which is on a mirror plane in the crystal, the cesium ion is located at the center of the portal, which shows a severe ellipsoidal distortion. This distortion is manifested in the uneven distances between cesium and carbonyl oxygens at the portal: two of the six carbonyl oxygen atoms (O(1) and O(4)) are much closer to the metal center (Cs–O(1) = 3.250(7) Å, Cs(O(4) = 3.144(6) Å) than the four other carbonyl oxygens (Cs–O(2) = Cs–O(2′) = 3.584(8) Å; Cs–O(3) = Cs(O(3′) = 3.574(6) Å). The included THF molecule is coordinated to the metal ion (Cs–O(21) = 2.934(10) Å), and the molecular plane lies along the long axis of the ellipsoidal host molecule. Two water molecules and a disordered chloride ion are coordinated to the cesium ion from outside.[8]

 © WILEY-VCH Verlag GmbH, D-69451 Weinheim, 1998 1433-7851/98/3701-0079 $ 17.50+.50/0

The coordination of the guest THF to the cesium ion bottom of the molecular bowl may be responsible for the larger formation constant in the Cs^+-complexed cucurbituril than for the Na^+ analogue in which the encapsulated THF is not coordinated to the sodium ion lids. The larger enthalpy and entropy changes for the inclusion in the former than in the latter are also consistent with the coordination of the substrate. The fact that the inclusion complex formation constant for noncoordinating benzene in this Cs system is $2.1\,\text{M}^{-1}$, which is only 1/10 of that for the Na^+ case, also supports this explanation.

Reversible inclusion and release of the guest molecule in the cesium-complexed cucurbituril upon change in pH of the medium is observed as in the sodium-lidded cucurbituril.[4] Specifically, when trifluoroacetic acid is added to the solution containing the cesium-complexed cucurbituril and THF, the ^{1}H NMR signals for THF included in the cavity decrease, whereas those for free THF increase. Upon addition of about 300 equivalents of trifluoroacetic acid the signals for the bound THF essentially disappear. When the solution is neutralized again by adding Cs_2CO_3 the signals for the encapsulated THF are almost fully restored. A series of these observations suggests that the cesium ion coordinated to the portal is removed in strongly acidic solution due to the protonation of the carbonyl groups at the cucurbituril portals; consequently, the encapsulated THF molecule can escape from the cavity readily (Scheme 1). Neutralization of the



2 3

Scheme 1. Encapsulation and release of the THF guest molecule from the Cs-complexed cucrbituril host molecule.

solution restores the cesium ion bottom of the cucurbituril bowl and therefore also the ability to encapsulate THF.

In summary, we present a novel metal-ion-bottomed molecular bowl in which inclusion of a guest molecule can be reversibly controlled by the acidity of the medium. This work demonstrates the advantages of using metal ions as key control elements for reversible inclusion: 1) easy blocking and unblocking of portals and 2) coordination of encapsulated substrates. The latter provides additional guest selectivity of the inclusion process. Furthermore, the metal ion bottom may serve as a Lewis acid site for substrate activation and chemical catalysis. Work along this line is currently in progress.

Received: July 8, 1997 [Z10655IE]
German version: *Angew. Chem.* **1998**, *110*, 83 – 85

Keywords: cesium · host – guest chemistry · inclusion compounds · molecular recognition · supramolecular chemistry

[1] Reviews: a) D. J. Cram, *Nature* **1992**, *356*, 29; b) D. J. Cram, J. M. Cram, *Container Molecules and Their Guests*, Royal Society of Chemistry, Cambridge (UK), **1994**.

[2] a) R. Wyler, J. de Mendoza, J. Rebek, Jr., *Angew. Chem.* **1993**, *105*, 1820; *Angew. Chem. Int. Ed. Engl.* **1993**, *32*, 1699; b) N. Branda, R. Wyler, C. Valdes, J. Rebek, Jr., *Science* **1994**, *263*, 1267; c) N. Branda, R. D. Grotzfeld, C. Valdes, J. Rebek, Jr., *J. Am. Chem. Soc.* **1995**, *117*, 85; d) J. Kang, J. Rebek, Jr. *Nature*, **1996**, *382*, 239.

[3] R. G. Chapman, J. C. Sherman, *J. Am. Chem. Soc.* **1995**, *117*, 9081.

[4] Y.-M. Jeon, J. Kim, D. Whang, K. Kim, *J. Am. Chem. Soc.* **1996**, *118*, 9790.

[5] a) R. Behrend, E. Meyer, F. Rusche, *Liebigs Ann. Chem*. **1905**, *339*, 1; b) W. A. Freeman, W. L. Mock, N.-Y. Shih, *J. Am. Chem. Soc.* **1981**, *103*, 7367.

[6] Reviews: a) W. L. Mock in *Comprehensive Supramolecular Chemistry, Vol. 2* (Ed.: F. Vögtle), Pergamon, Oxford, **1996**, p. 477; b) W. L. Mock, *Top. Curr. Chem.* **1995**, *175*, 1; c) P. Cintas, *J. Incl. Phenom. Molec. Reco. Chem.* **1994**, *17*, 205.

[7] Complexation of alkali metal ions to cucurbituril was also studied by UV-visible spectroscopy. a) H.-J. Buschmann, E. Cleve, E. Schollmeyer, *Inorg. Chim. Acta* **1992**, *193*, 93; b) R. Hoffmann, W. Knoche, C. Fenn, H.-J. Buschmann, *J. Chem. Soc. Faraday Trans.* **1994**, *90*, 1507.

[8] Crystal data of **2**: $[(C_{36}H_{36}N_{24}O_{12})Cs_2(H_2O)_6\cdot(H_2O)](Cl)_2\cdot 2H_2O$, $M_r = 1495.75$, monoclinic, $P2_1/n$, $a = 14.277(2)$, $b = 11.887(1)$, $c = 15.901(3)$ Å, $\beta = 94.085(8)^\circ$, $V = 2691.8(7)$ Å^3, $Z = 2$, $\rho_{calcd} = 1.845\,\text{g cm}^{-3}$, $T = 296$ K, Enraf-Nonius CAD4 diffractometer, $Mo_{K\alpha}$ ($\lambda = 0.71073$ Å), $\mu = 15.54\,\text{cm}^{-1}$. Structure was solved by Patterson method (SHELXS-86). All non-hydrogen atoms were refined anisotropically (SHELXL-93). Final full-matrix least-squares refinement on F^2 with all 3288 reflections and 388 variables converged to *R1* ($I > 2\sigma(I)$) = 0.058, *wR*2 (all data) = 0.160 and GOF = 1.10. Crystal data of **3**: $[(C_{36}H_{36}N_{24}O_{12})CsCl(H_2O)_2\cdot C_4H_8O]\cdot 5H_2O$, $M_r = 1363.46$, orthorhombic, $Cmc2_1$, $a = 19.457(3)$, $b = 16.137(3)$, $c = 15.917(1)$ Å , $V = 4997(1)$ Å^3, $Z = 4$, $\rho_{calcd} = 1.812\,\text{g cm}^{-3}$, $T = 193$ K, Enraf-Nonius CAD4 diffractometer, $Mo_{K\alpha}$ ($\lambda = 0.71073$), $\mu = 9.02\,\text{cm}^{-1}$. Structure was solved by Patterson methods, and all non-hydrogen atoms were refined anisotropically. Final refinement on F^2 with all 2340 reflections and 431 variables converged to *R1* ($I > 2\sigma(I)$) = 0.035, *wR2* (all data) = 0.096 and *GOF* = 1.16. Crystallographic Data (excluding structure factors) for the structures reported in this paper have been deposited with the Cambridge Crystallographic Data Centre as supplementary publications no. CCDC-100615. Copies of the data can be obtained free of charge on application to CCDC, 12 Union Road, Cambridge CB2 1EZ, UK (fax: int. code + (44) 1223-336033; e-mail: deposit@ccdc.cam.ac.uk).

[9] The formation constant of the inclusion complex was estimated by the integration of the signals for the free and bound THF in ^{1}H NMR spectra of 0.4 M CsCl solutions (in D_2O) containing cucurbituril (2.6×10^{-2} M) and THF ($1.7 - 2.8 \times 10^{-2}$ M).

[10] The thermodynamic parameters were estimated from the temperature dependence of the formation constants between 20 and 60°C.

 © WILEY-VCH Verlag GmbH, D-69451 Weinheim, 1998 1433-7851/98/3701-0080 $ 17.50+.50/0

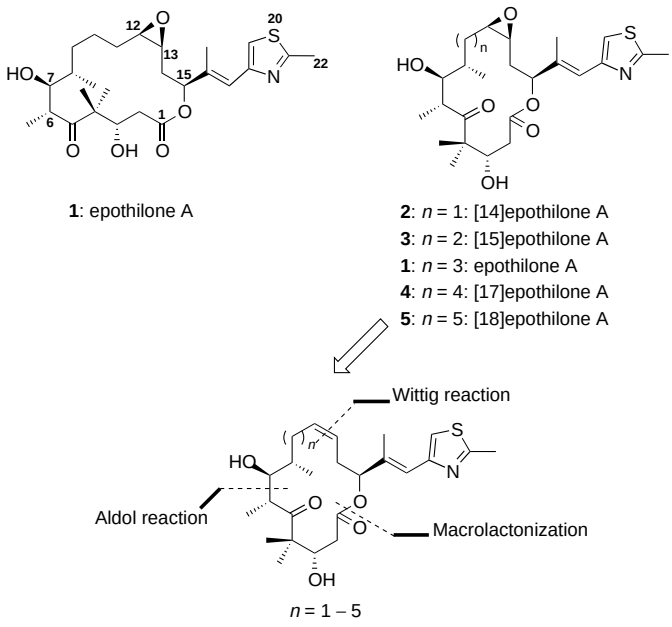
Probing the Ring Size of Epothilones: Total Synthesis of [14]-, [15]-, [17]-, and [18]Epothilones A**

K. C. Nicolaou,* Francisco Sarabia, Sacha Ninkovic, M. Ray V. Finlay, and Christopher N. C. Boddy

The discovery,[1] structural elucidation,[2] and biological activity[1–4] of the epothilones rapidly propelled them to the forefront of chemical[5] and biological research.[3, 4] Particularly exciting and stimulating was the recognition of their Taxol-like[6] mechanism of action[3] as antitumor agents and their ability to eradicate Taxol-resistant tumor cells.[4] Total syntheses of the 16-membered macrolactones epothilones A (**1**, Scheme 1),[7–11] B (**1** with a CH_3 group at C-12 instead of H),[10, 12, 13] and E (**1** with a CH_2OH group at C-21 instead of CH_3)[14] have been achieved, and many analogues[7–18] have already been synthesized and biologically investigated. From these studies, the epothilone pharmacophore has emerged as a well-defined and rather precise molecular structure tolerating only certain changes.[7–18] To probe the effect of the size of the macrocycle on its biological activity, we targeted the 14-, 15-, 17-, and 18-membered ring analogues of epothilone A (**1**), thus completing the [*n*]epothilone A series where $n = 1-5$ (Scheme 1). We report here on the successful total syntheses as well as the biological properties of these compounds (**2**–**5**).

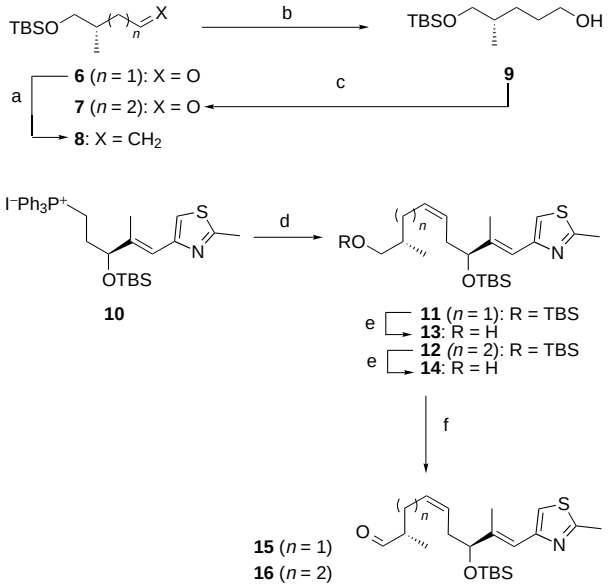
Molecular modeling and molecular dynamics of [14]-, [15]-, [17]-, and [18]epothilones A led to the minimized structures shown in Figure 1 (see p. 82). These models revealed considerable structural distortions for the 14-, 15-, and 17-membered ring epothilones. In contrast the overall shape of [18]epothilone A was very similar to that of natural epothilone A ([16]epothilone A), heightening expectations for biological activity of the latter compound, if not for the others.

The charted route projected epoxidation of the C12–C13 double bond of the macrocycle as the final step and a convergent assembly of the epothilone skeleton by means of a Wittig reaction, an aldol condensation, and a macrolactonization.[8b, 10, 13] This strategy required fragments **6**, **7**, and **10**[10, 13] for the construction of the key intermediates **15** and **16**, which were needed for the 14- and 15-membered rings, respectively (see Scheme 2). A slightly different strategy for the synthesis of key building blocks **33** and **35**, needed for the 17- and 18-membered rings, respectively, was adopted, which required fragments **19**, **21**, and **22**[13] (see Scheme 3).



Scheme 1. Structures and numbering of the epothilones A with $n = 1-5$.

Aldehyde **6** (Scheme 2) was prepared by a literature procedure[19] and served as a precursor for the second



Scheme 2. Synthesis of aldehydes **15** and **16**. a) 2.0 equiv $Ph_3P^+CH_3Br^-$, 1.98 equiv NaHMDS, THF, 0°C, 15 min; then 1.0 equiv **6** in THF, 0°C, 0.5 h, 95%; b) 1.5 equiv 9-BBN 0.5 M, THF, 25°C, 3 h; then 6 equiv 3 N NaOH and 6.0 equiv 30% H_2O_2, 0°C, 1 h, 85%; c) 2.0 equiv $(COCl)_2$, 4.0 equiv DMSO, 6.0 equiv Et_3N, CH_2Cl_2, $-78 \rightarrow 0$°C, 1.5 h, 98%; d) 1.2 equiv **10**, 1.2 equiv NaHMDS, THF, 0°C, 15 min; then 1.0 equiv **6** or **7**, 0°C, 15 min, 77% (*Z*:*E* ≈ 9:1) for **11** or 83% (*Z*:*E* ≈ 9:1) for **12**; e) 1.0 equiv CSA added portionwise over 1 h, CH_2Cl_2/MeOH (1/1), $0 \rightarrow 25$°C, 0.5 h, 81% for **13** and 61% for **14**; f) 2.0 equiv $SO_3 \cdot Py$, 10.0 equiv DMSO, 5.0 equiv Et_3N, CH_2Cl_2, 25°C, 0.5 h, 81% for **15** and 84% for **16**. NaHMDS = sodium bis(trimethylsilyl)amide; 9-BBN = 9-borabicyclo[3.3.1]nonane; DMSO = dimethylsulfoxide; CSA = 10-camphorsulfonic acid; TBS = *tert*-butyldimethylsilyl; Py = pyridine.

[*] Prof. Dr. K. C. Nicolaou, Dr. F. Sarabia, Dr. S. Ninkovic, Dr. M. R. V. Finlay, C. N. C. Boddy
Department of Chemistry and
The Skaggs Institute for Chemical Biology
The Scripps Research Institute
10550 North Torrey Pines Road, La Jolla, CA 92037 (USA)
and
Department of Chemistry and Biochemistry
University of California, San Diego
9500 Gilman Drive, La Jolla, CA 92093 (USA)
Fax: Int. code + (1) 619-784 2469

[**] We thank Dr. D. H. Huang and Dr. G. Siuzdak for assistance with recording NMR and mass spectra, respectively. This work was supported by Novartis, the National Institutes of Health (USA), The Skaggs Institute for Chemical Biology, and the CaP CURE Foundation. Fellowships from Fundación Ramón Areces (Spain) (F. S.) and the Fullbright Commission (M. R. V. F.), and grants from Merck, DuPont-Merck, Schering Plough, Hoffmann La Roche, and Amgen are acknowledged.

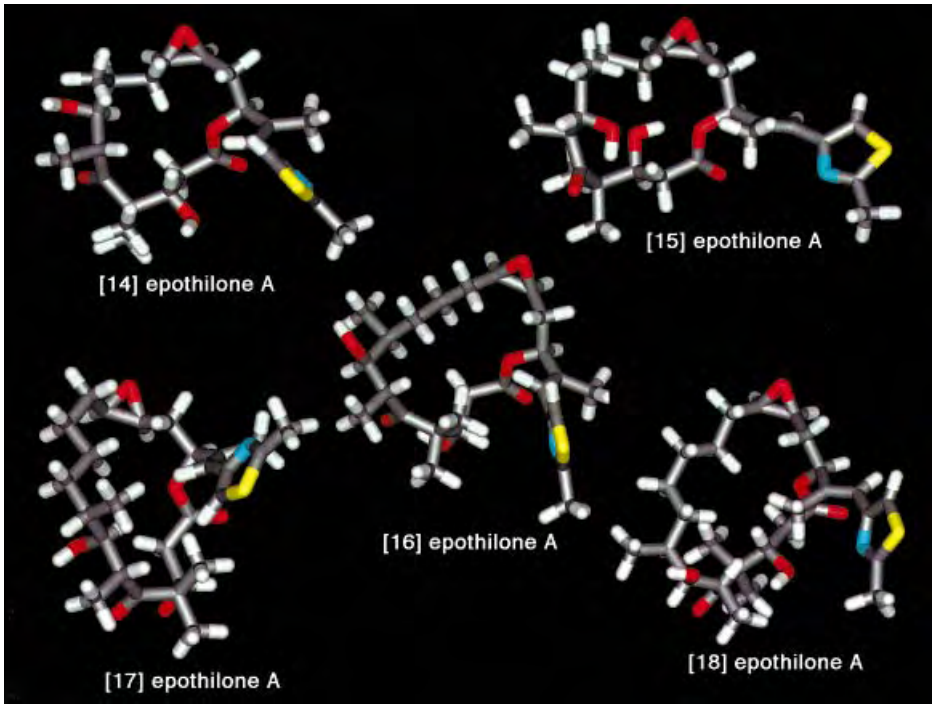
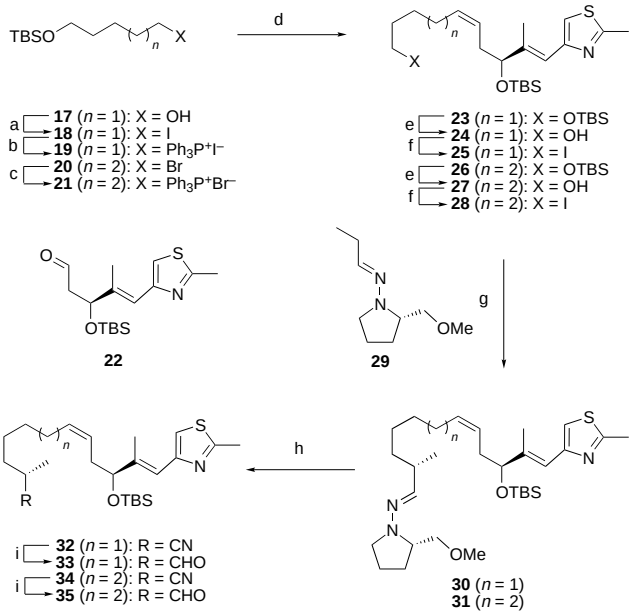


Figure 1. Computer-generated minimum-energy structures of [14]-, [15]-, [16]-, [17]-, and [18]epothilones A. Carbon = gray, hydrogen = white, oxygen = red, nitrogen = blue, sulfur = yellow. Molecular dynamics and minimization calculations (CV Force Field) were performed on a SGI Indigo-2 workstation using the program Insight II (Biosym Technologies Inc., San Diego, CA). Pictures were created with AVS software (AVS Inc., Waltham, MA) and locally developed modules running on a DEC Alpha 3000/500 with a Kubota Pacific Denali graphics card.

required aldehyde, **7**. Thus, olefination of **6**, hydroboration of the resulting olefin **8**, and oxidation of the formed primary alcohol **9** furnished the desired aldehyde **7** in excellent overall yield (Scheme 2). Each of these two aldehydes (**6** and **7**) was condensed separately with the ylide derived from phosphonium salt **10** (NaHMDS, THF) to afford the corresponding (*Z*) olefins (**11**, 77 % and **12**, 83 %) as the major geometrical isomer in each case (ca. 9:1 ratio). The silyl group was then selectively removed from the primary hydroxyl group by the action of CSA[20] leading to alcohols **13** (81 %) and **14** (61 %). Finally, oxidation of **13** and **14** with $SO_3 \cdot Py$ (DMSO/Et_3N) led to the targeted intermediates **15** and **16** in 81 and 84 % yield, respectively.

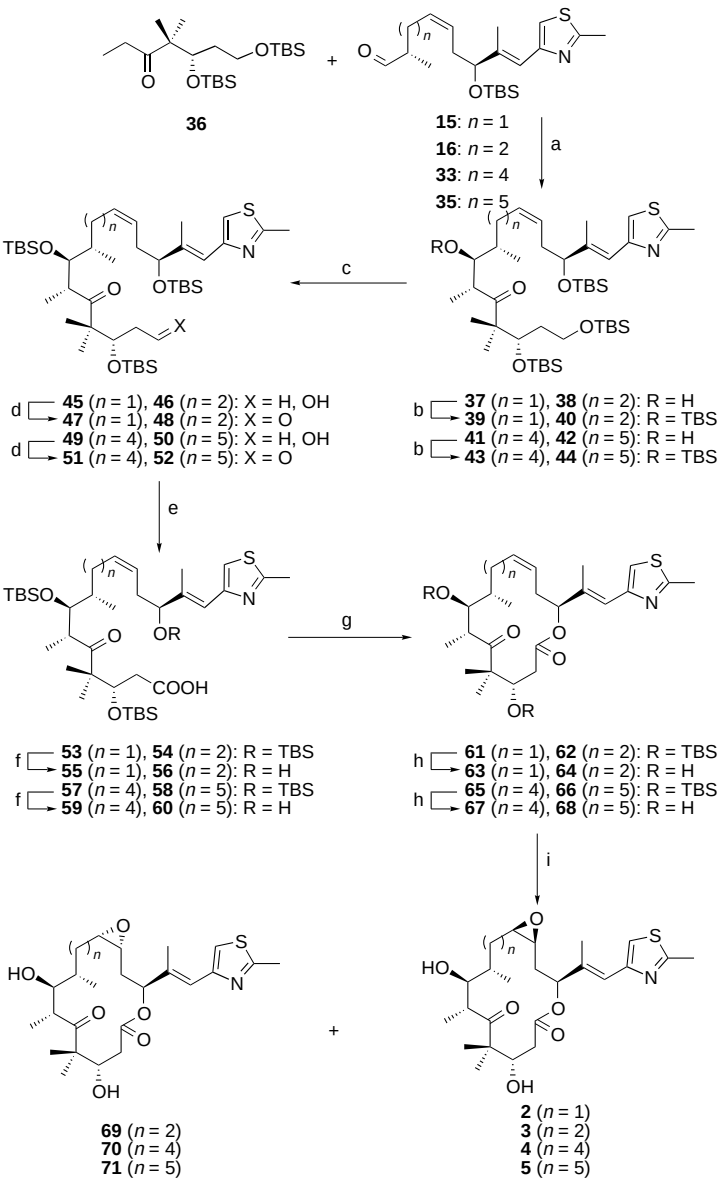
The reverse ylide – aldehyde condensation approach shown in Scheme 3 was utilized for the construction of advanced intermediates **33** and **35**. Thus, alcohol **17** was converted into iodide **18** by treatment with Ph_3P/I_2/imidazole (95 %) and thence to phosphonium salt **19** by heating with Ph_3P (neat, 100 °C, 97 %). A similar sequence was used to prepare phosphonium salt **21** from the bromide **20** as the intermediate. The ylides derived from **19** and **21** (NaHMDS, THF) were treated with aldehyde **22** to produce (*Z*) olefins **23** and **26** in 85 and 79 % yields, respectively, as the major isomers ($Z{:}E \approx$ 9:1). Each product, **23** and **26**, was selectively desilylated at the primary position with CSA, furnishing alcohols **24** (99 %) and **27** (95 %), respectively, and then converted into the corresponding iodides **25** (84 %) and **28** (98 %) by exposure to Ph_3P/I_2/imidazole. The iodides **25** and **28** were used to alkylate SAMP hydrazone **29** according to the method of Enders,[21] furnishing compounds **30** and **31** in 60 and 82 % yield, respectively. Each hydrazone (**30** and **31**) was converted into the corresponding nitrile[22] (**32**, 99 % and **34**, 96 %) by reaction with MMPP, and then into the desired aldehydes **33** (90 %) and **35** (81 %) by DIBAL reduction.



Scheme 3. Synthesis of aldehydes **33** and **35**. a) 1.5 equiv I_2, 3.0 equiv imidazole, 1.5 equiv Ph_3P, Et_2O/MeCN (3/1), 0 °C, 0.5 h, 95 %; b) 1.1 equiv Ph_3P, neat, 100 °C, 2 h, 97 %; c) 1.5 equiv Ph_3P, neat, 100 °C, 7 h, 99 %; d) 1.2 equiv **19** or **21**, 1.2 equiv NaHMDS, THF, 0 °C, 15 min; then 1.0 equiv **22**, 0 °C, 15 min, 85 % ($Z{:}E \approx$ 9:1) for **23**, 79 % ($Z{:}E \approx$ 9:1) for **26**; e) 1.0 equiv CSA added portionwise over 1 h, CH_2Cl_2/MeOH (1/1), 0 → 25 °C, 3 h, 99 % for **24**, 95 % for **27**; f) 1.5 equiv I_2, 3.0 equiv imidazole, 1.5 equiv Ph_3P, Et_2O/MeCN (3/1), 0 °C, 0.5 h, 84 % for **25**, 98 % for **28**; g) 1.5 equiv **29**, 1.5 equiv LDA, THF, 0 °C, 16 h; then 1.0 equiv **25** or **28** in THF, −100 → −20 °C, 10 h, 60 % for **30**, or 82 % for **31**; h) 2.5 equiv magnesium monoperoxyphthalate (MMPP), MeOH/phosphate buffer pH 7 (1/1), 0 °C, 1 h, 99 % for **32**, 96 % for **34**; i) 2.0 equiv DIBAL, toluene, −78 °C, 1 h, 90 % for **33**, 81 % for **35**. LDA = lithium diisopropylamide; DIBAL = diisobutylaluminum hydride.

Scheme 4 shows the coupling of the C1–C6 segment **36**[11] with fragments **15**, **16**, **33**, and **35**, and the elaboration of the products to the targeted epothilones. Thus, the (*Z*) enolate

 © WILEY-VCH Verlag GmbH, D-69451 Weinheim, 1998 1433-7851/98/3701-0082 $ 17.50+.50/0 *Angew. Chem. Int. Ed.* **1998**, *37*, No. 1/2



Scheme 4. Synthesis of epothilone A analogues **2**–**5**. a) 1.2 equiv LDA, THF, 0°C, 15 min; then 1.2 equiv **36** in THF, −78°C, 1 h; then 1.0 equiv aldehyde (**15**, **16**, **33**, or **35**) in THF at −78°C, 71% for **37** (single diastereoisomer), 72% for **38** and its (6*S*,7*R*) diastereoisomer (ca. 4:1 ratio), 77% for **41** and its (6*S*,7*R*) diastereoisomer (ca. 6:1 ratio), 60% for **42** and its (6*S*,7*R*) diastereoisomer (ca. 5:1 ratio); b) 1.5 equiv TBSOTf, 2.0 equiv 2,6-lutidine, CH_2Cl_2, 0°C, 1 h, 94% for **39**, 93% for **40**, 85% for **43**, 95% for **44**; c) 1.0 equiv CSA added portionwise over 1 h, CH_2Cl_2/MeOH (1/1), 0°C, 3 h, 77% for **45**, 82% for **46**, 91% for **49**, 83% for **50**; d) 2.0 equiv $(COCl)_2$, 4.0 equiv DMSO, 6.0 equiv Et_3N, CH_2Cl_2, −78 →0°C, 1.5 h, 93% for **47**, 85% for **48**, 99% for **51**, 95% for **52**; e) 5.0 equiv $NaClO_2$, 10.0 equiv 2-methyl-2-butene, 2.5 equiv NaH_2PO_4, *t*BuOH/H_2O (5/1), 0°C, 1 h, 99% for **53**, 95% for **54**, 99% for **57**, 98% for **58**; f) 6.0 equiv TBAF, THF, 25°C, 10 h, 92% for **55**, 77% for **56**, 85% for **59**, 85% for **60**; g) 2.5 equiv 2,4,6-trichlorobenzoyl chloride, 5.0 equiv Et_3N, THF, 0 →25°C, 1 h; then slow addition (1 mL h^{-1}) to a solution of 2.0 equiv 4-DMAP in toluene (0.005 M based on hydroxy acid), 70°C, 0.5–8 h, 70% for **61**, 82% for **62**, 73% for **65**, 75% for **66**; h) 20% HF · Py (by volume) in THF, 25°C, 24 h, 82% for **63**, 91% for **64**, 86% for **67**, 71% for **68**; i) methyl(trifluoromethyl)dioxirane, MeCN, 0°C, 54% for **2** (single diastereoisomer), 35% **3** and 35% **69** (ca. 1:1 ratio of diastereoisomers), 97% for **4** and **70** (ca. 6:1 ratio of diastereoisomers), 53% of **5** and 26% of **71** (ca. 2:1 ratio of diastereoisomers). Tf = triflate; TBAF = tetra-*n*-butylammonium fluoride; 4-DMAP = 4-dimethylaminopyridine.

generated from ketone **36** (LDA, THF, −78°C) reacted smoothly with aldehydes **15**, **16**, **33**, and **35** to afford compounds **37** (71%), **38** (72%), **41** (77%), and **42** (60%), respectively, together with their (6*S*,7*R*) diastereoisomers (see Scheme 4 for individual yields), which were removed by silica gel chromatography. These compounds were then silylated (TBSOTf/2,6-lutidine) leading to tetrasilyl ethers **39**, **40**, **43**, and **44** in 85–95% yield. Selective removal of the silyl group from the primary position with CSA led to alcohols **45**, **46**, **49**, and **50**, which were oxidized under Swern conditions [$(COCl)_2$/DMSO/Et_3N] to give the corresponding aldehydes (**47**, **48**, **51**, and **52**) in 85–99% yield. Further oxidation to the desired carboxylic acids (**53**, **54**, **57**, and **58**) was achieved by reaction with $NaClO_2$ (95–98% yield). The carboxylic acids were then selectively desilylated at C-15 by the action of TBAF[8b] producing hydroxy acids **55**, **56**, **59**, and **60** in 77–92% yield. Cyclization of **55**, **56**, **59**, and **60** was accomplished by the Yamaguchi method[23] as previously described for epothilones A and B[8b, 10, 13, 16] to furnish macrocyclic lactones **61**, **62**, **65**, and **66**, respectively, in yields ranging from 70 to 82% (Scheme 4). The silyl ethers were removed from **61**, **62**, **65**, and **66** by exposure to HF · Py in THF, leading to [14]-, [15]-, [17]- and [18]desoxyepothilones **63**, **64**, **67** and **68**, respectively (71–91% yield).

Epoxidation of [14]desoxyepothilone A (**63**) with methyl (trifluoromethyl)dioxirane[24] gave [14]epothilone A (**2**) essentially as a single product (52% yield), whereas epoxidation of the [15]desoxyepothilone A (**64**) under the same conditions led to a mixture of [15]epothilone A (**3**) and its diastereomeric epoxide **69** (70% yield, ca. 1:1 ratio). The [17]-membered macrolactone **67** furnished diastereomeric epoxides in a 6:1 ratio (97% combined yield) and the [18]-membered analogue provided products in a 2:1 ratio (79% total yield). In all cases the isomeric epoxides were separated by chromatography but their configurations have not yet been assigned.

Preliminary biological investigations with these compounds revealed significant tubulin polymerization activity for [18]desoxyepothilone A (**68**) (40% as compared to 72% for epothilone A and 53% for Taxol), but relatively weak activity for the two epimeric [18]epothilones A (**5** and **71**) and for all [14]-, [15]-, and [17]epothilones A (**63**, **64**, **67**, **2**–**4**, **69**, and **70**) in the filtration–colorimetric tubulin assay.[3] These results provide further support for the limited tolerance of the epothilone pharmacophore and its highly specific binding to the tubulin receptor. Further biological studies with **68** and related compounds are in progress.

Received: August 7, 1997 [Z10787IE]
German version: *Angew. Chem.* **1998**, *110*, 85–89

Keywords: epothilones · natural products · total synthesis · tubulin polymerization

[1] a) G. Höfle, N. Bedorf, K. Gerth, H. Reichenbach (GBF), DE-4138042, **1993** [*Chem. Abstr.* **1993**, *120*, 52841]; b) K. Gerth, N. Bedorf, G. Höfle, H. Irschik, H. Reichenbach, *J. Antibiot.* **1996**, *49*, 560–563.

[2] G. Höfle, N. Bedorf, H. Steinmetz, D. Schomburg, K. Gerth, H. Reichenbach, *Angew. Chem.* **1996**, *108*, 1671–1673; *Angew. Chem. Int. Ed. Engl.* **1996**, *35*, 1567–1569.

[3] D. M. Bollag, P. A. McQueney, J. Zhu, O. Hensens, L. Koupal, J. Liesch, M. Goetz, E. Lazarides, C. M. Woods, *Cancer Res.* **1995**, *55*, 2325–2333.

 © WILEY-VCH Verlag GmbH, D-69451 Weinheim, 1998 1433-7851/98/3701-0083 $ 17.50+.50/0

[4] R. J. Kowalski, P. Giannakakou, E. Hamel, *J. Biol. Chem.* **1997**, *272*, 2534 – 2541.

[5] a) K. C. Nicolaou, Y. He, D. Vourloumis, H. Vallberg, Z. Yang, *Angew. Chem.* **1996**, *108,* 2554 – 2556; *Angew. Chem. Int. Ed. Engl*. **1996**, *35,* 2399 – 2401; b) D. Meng, E. J. Sorensen, P. Bertinato, S. J. Danishefsky, *J. Org. Chem*. **1996**, *61*, 7998 – 7999; c) P. Bertinato, E. J. Sorensen, D. Meng, S. J. Danishefsky, *ibid.* **1996**, *61*, 8000 – 8001; d) D. Schinzer, A. Limberg, O. M. Böhm, *Chem. Eur. J.* **1996**, *2*, 1477 – 1482; e) J. Mulzer, A. Mantoulidis, *Tetrahedron Lett*. **1996**, *37*, 9179 – 9182; f) E. Claus, A. Pahl, P. G. Jones, H. M. Meyer, M. Kalesse, *ibid*. **1997**, *38*, 1359 – 1362; g) T. Gabriel, L. Wessjohann, *ibid.* **1997**, *38*, 1363 – 1366; R. E. Taylor, J. D. Haley, *ibid*. **1997**, *38*, 2061 – 2064.

[6] S. B. Horwitz, S. Fant, P. B. Schiff, *Nature* **1979**, *277*, 665 – 667.

[7] a) A. Balog, D. Meng, T. Kamenecka, P. Bertinato, D.-S. Su, E. J. Sorensen, S. J. Danishefsky, *Angew. Chem.* **1996**, *108,* 2976 – 2978; *Angew. Chem. Int. Ed. Engl.* **1996**, *35*, 2801 – 2803; b) D. Meng, D.-S. Su, A. Balog, P. Bertinato, E. J. Sorensen, S. J. Danishefsky, Y.-H. Zheng, T.-C. Chou, L. He, S. B. Horwitz, *J. Am. Chem. Soc.* **1997**, *119*, 2733 – 2734.

[8] a) Z. Yang, Y. He, D. Vourloumis, H. Vallberg, K. C. Nicolaou, *Angew. Chem.* **1997**, *109,* 170 – 172; *Angew. Chem. Int. Ed. Engl*. **1997**, *36*, 166 – 168; b) K. C. Nicolaou, F. Sarabia, S. Ninkovic, Z. Yang, *ibid*. **1997**, *109*, 539 – 540 and **1997**, *36*, 525 – 527.

[9] D. Schinzer, A. Limberg, A. Bauer, O. M. Böhm, M. Cordes, *Angew. Chem.* **1997**, *109,* 543 – 544; *Angew. Chem. Int. Ed. Engl*. **1997**, *36*, 523 – 524.

[10] K. C. Nicolaou, N. Winssinger, J. A. Pastor, S. Ninkovic, F. Sarabia, Y. He, D. Vourloumis, Z. Yang, T. Li, P. Giannakakou, E. Hamel, *Nature* **1997**, *387*, 268 – 272.

[11] K. C. Nicolaou, Y. He, D. Vourloumis, H. Vallberg, F. Roschangar, F. Sarabia, S. Ninkovic, Z. Yang, J. I. Trujillo, *J. Am. Chem. Soc.* **1997**, *119*, 7960 – 7973.

[12] D.-S. Su, D. Meng, P. Bertinato, A. Balog, E. J. Sorensen, S. J. Danishefsky, Y.-H. Zheng, T.-C. Chou, L. He, S. B. Horwitz, *Angew. Chem.* **1997**, *109*, 775 – 777; *Angew. Chem. Int. Ed. Engl*. **1997**, *36*, 757 – 759.

[13] K. C. Nicolaou, S. Ninkovic, F. Sarabia, D. Vourloumis, Y. He, H. Vallberg, M. R. V. Finlay, Z. Yang, *J. Am. Chem. Soc.* **1997**, *119*, 7974 – 7991.

[14] Isolation and structure elucidation: G. Höfle, personal communication. Total synthesis: K. C. Nicolaou, Y. He, F. Roschangar, N. P. King, D. Vourloumis, T. Li, *Angew. Chem.* **1998**, *110*, 89 – 92; *Angew. Chem. Int. Ed.* **1998**, *37*, 84 – 87.

[15] K. C. Nicolaou, H. Vallberg, N. P. King, F. Roschangar, Y. He, D. Vourloumis, C. G. Nicolaou, *Chem. Eur. J.* **1997**, *3*, 1957 – 1970.

[16] K. C. Nicolaou, F. Sarabia, M. R. V. Finlay, S. Ninkovic, N. P. King, D. Vourloumis, Y. He, *Chem. Eur. J.* **1997**, *3*, 1971 – 1986.

[17] A. Balog, P. Bertinato, D.-S. Su, D. Meng, E. J. Sorensen, S. J. Danishefsky, Y.-H. Zheng, T-C. Chou, L. He, S. B. Horwitz, *Tetrahedron Lett*. **1997**, *38*, 4529 – 4532.

[18] K. C. Nicolaou, D. Vourloumis, T. Li, J. Pastor, N. Winssinger, Y. He, S. Ninkovic, F. Sarabia, H. Vallberg, F. Roschangar, N. P. King, M. R. V. Finlay, P. Giannakakou, P. Verdier-Pinard, E. Hamel, *Angew. Chem.* **1997**, *109*, 2181 – 2187; *Angew. Chem. Int. Ed. Engl.* **1997**, *36*, 2097 – 2103.

[19] T. Eguchi, T. Terachi, K. Kakinuma, *J. Chem. Soc. Chem. Commun.* **1994**, 137 – 138.

[20] T. D. Nelson, R. D. Crouch, *Synthesis* **1996**, 1031 – 1069.

[21] a) D. Enders, *Asymmetric Synthesis Vol. 3*, Academic Press, **1984**, pp.275 – 339; b) D. Enders, M. Klatt, *Synthesis* **1996**, 1403 – 1418; c) D. Enders, H. Eichenauer, *Chem. Ber*. **1979**, *112*, 2933 – 2960; d) D. Enders, J. Tiebes, N. De Kimpe, M. Keppens, C. Stevens, G. Smagghe, O. Betz, *J. Org. Chem*. **1993**, *58*, 4881 – 4884; e) D. Enders, A. Plant, D. Backhaus, U. Reinhold, *Tetrahedron* **1995**, *51*, 10699 – 10714. We thank Prof. Enders for a generous gift of SAMP.

[22] D. Enders, D. Backhaus, J. Runsink, *Tetrahedron* **1996**, *52*, 1503 – 1528.

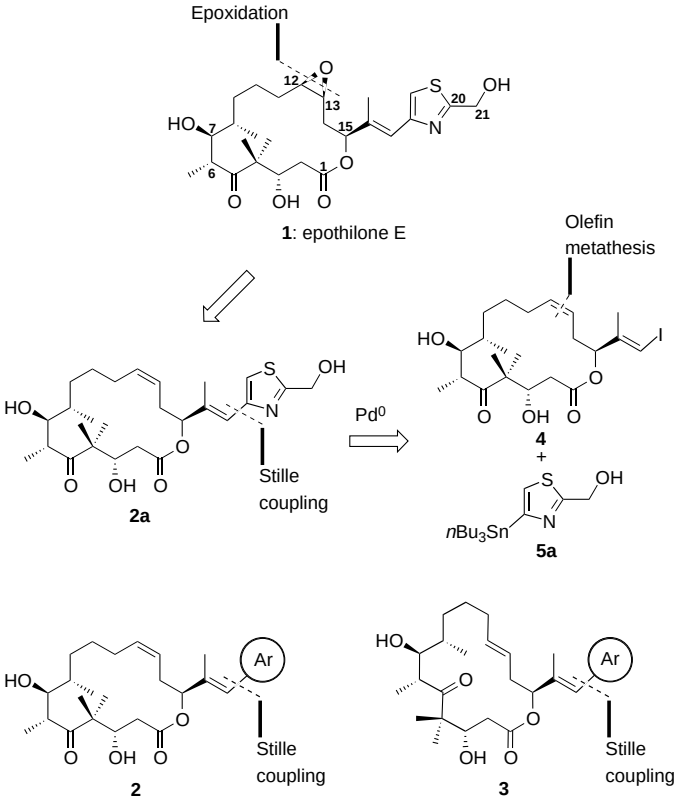
[23] a) J. Inanaga, K. Hirata, H. Saeki, T. Katsuki, M. Yamaguchi, *Bull. Chem. Soc. Jpn*. **1979**, *52*, 1989; b) J. Mulzer, P. A. Mareski, J. Buschmann, P. Luger, *Synthesis* **1992**, 215 – 228; c) K. C. Nicolaou, A. P. Patron, K. Ajito, P. K. Richter, H. Khatuya, P. Bertinato, R. A. Miller, M. J. Tomaszewski, *Chem. Eur. J.* **1996**, *2*, 847 – 868.

[24] D. Yang, M.-K. Wong, Y.-C. Yip, *J. Org. Chem.* **1995**, *60*, 3887 – 3889.

Total Synthesis of Epothilone E and Analogues with Modified Side Chains through the Stille Coupling Reaction**

K. C. Nicolaou,* Yun He, Frank Roschangar, N. Paul King, Dionisios Vourloumis, and Tianhu Li

The epothilones are a growing class of naturally occurring antitumor agents[1–3] whose importance is clearly reflected in the increasing number of publications reporting on their total synthesis,[4–11] analogue construction,[4–16] and biological activity.[1, 3, 4, 5b, 8, 9, 12, 15–17] Here we report the first total synthesis of the naturally occurring epothilone E (**1**, Scheme 1)[16] in



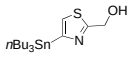
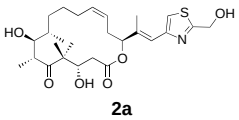
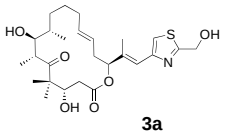
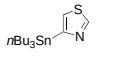
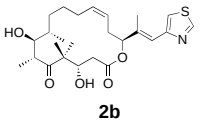
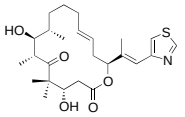
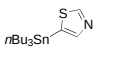
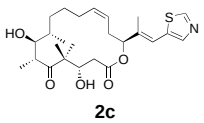
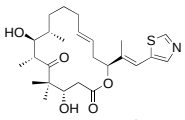
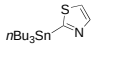
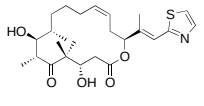
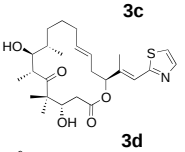
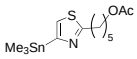
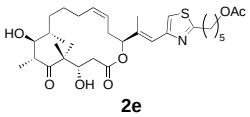
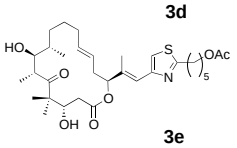
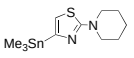
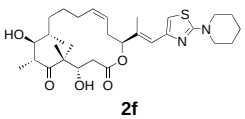
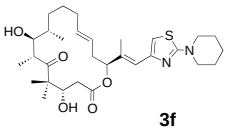
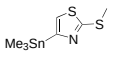
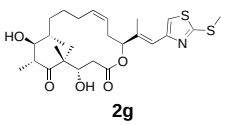
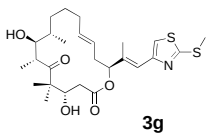
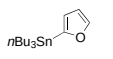
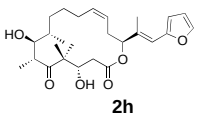
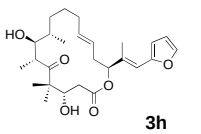
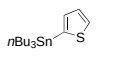
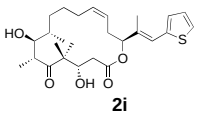
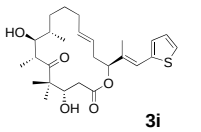
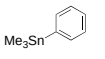
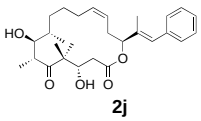
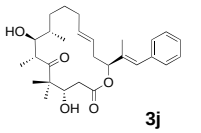
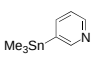
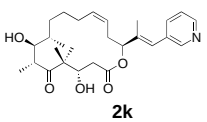
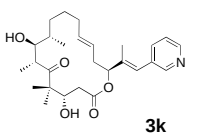
Scheme 1. Retrosynthetic analysis and strategy for the total synthesis of epothilone E (**1**) and analogues with modified side chains. (Ar) = aromatic moiety.

[*] Prof. Dr. K. C. Nicolaou, Y. He, Dr. F. Roschangar, Dr. N. P. King, Dr. D. Vourloumis, Dr. T. Li
Department of Chemistry and The Skaggs Institute for Chemical Biology
The Scripps Research Institute
10550 North Torrey Pines Road, La Jolla, CA 92037 (USA)
and
Department of Chemistry and Biochemistry
University of California, San Diego
9500 Gilman Drive, La Jolla, CA 92093 (USA)
Fax: Int. code + (1) 619-784 2469

[**] We thank Dr. D. H. Huang and Dr. G. Siuzdak for assistance with recording NMR and mass spectra, respectively. This work was supported by Novartis, the National Institutes of Health USA, The Skaggs Institute for Chemical Biology and the CaP CURE Foundation. Fellowships from the George E. Hewitt Foundation (N. P. K.), the Deutsche Forschungsgemeinschaft (F. R.), and Novartis (D. V.), and grants from Merck, DuPont-Merck, Schering Plough, Hoffmann La Roche, and Amgen are acknowledged.

 © WILEY-VCH Verlag GmbH, D-69451 Weinheim, 1998 1433-7851/98/3701-0084 $ 17.50+.50/0

Table 1. Epothilones synthesized according to Scheme 2.

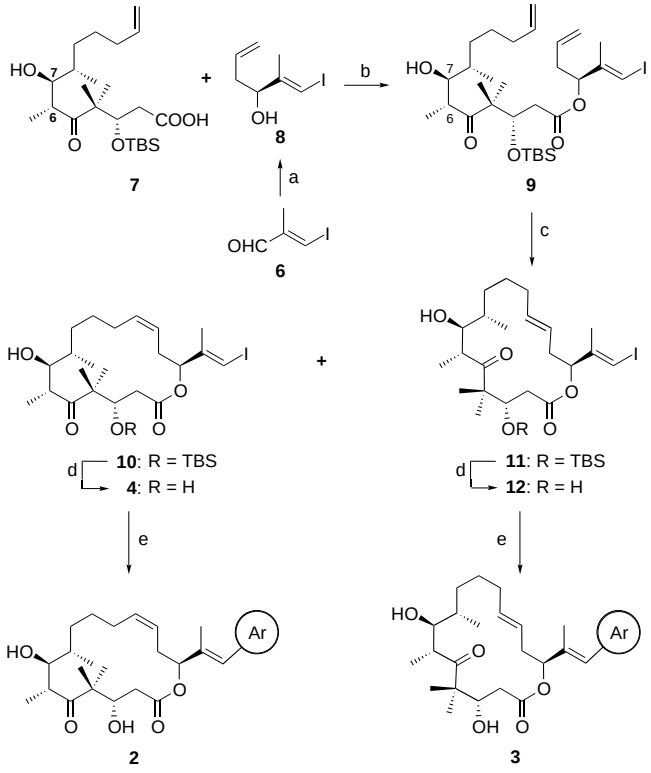
Entry	5	Procedure[a]	2	Yield [%]	3	Yield [%]
1	 **5a**	A	 **2a**	76	 **3a**	88
2	 **5b**	A	 **2b**	70	 **3b**	74
3	 **5c**	A	 **2c**	73	 **3c**	66
4	 **5d**	A	 **2d**	84	 **3d**	88
5	 **5e**	A	 **2e**	82	 **3e**	84
6	 **5f**	A	 **2f**	72	 **3f**	44
7	 **5g**	A	 **2g**	44	 **3g**	72
8	 **5h**	B	 **2h**	87	 **3h**	92
9	 **5i**	B	 **2i**	88	 **3i**	94
10	 **5j**	B	 **2j**	86	 **3j**	89
11	 **5k**	A	 **2k**	42	 **3k**	46

[a] See Scheme 2.

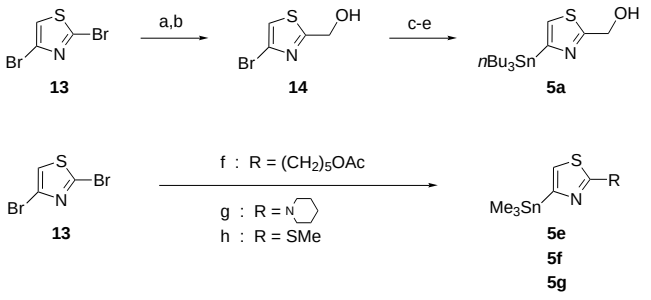
which an olefin metathesis reaction[4a, 5b, 6a, 7, 10, 13, 18, 19] is used to form the macrocycle and a Stille coupling[20] to construct the side chain. In addition, the developed strategy was applied to the synthesis of an analogue library containing a variety of aromatic systems in place of the 2-methylthiazole moiety of natural epothilone A (see Table 1). Scheme 1 outlines, in retrosynthetic format, the highly convergent metathesis/Stille coupling strategy towards epothilone E (**1**) and the new epothilones represented by structures **2** and **3**. The utilization of a common advanced intermediate (e.g. **4**) gives this Stille strategy a distinct advantage in delivering rapidly a plethora of side chain modified epothilone analogues for biological screening.

The epothilones shown in Table 1 were constructed as summarized in Scheme 2. Thus, alcohol **8**, prepared in 91% yield by addition of (+)-allyldiisopinocampheyl borane [(+)-Ipc_2B(allyl)] to the known aldehyde **6**,[21] was coupled with carboxylic acid **7**[10] (3:2 mixture with its C6,C7 diastereomer) with DCC and 4-DMAP to afford ester **9** (49% yield, after chromatographic separation from its C6,C7 diastereomer). Exposure of **9** to catalytic amounts of $[RuCl_2(=CHPh)(PCy_3)_2]$ in CH_2Cl_2 at ambient temperature resulted in a mixture of (*Z*) and (*E*) cycloolefins, which were chromatographically separated on silica gel (flash column, hexanes/ethyl acetate 9/1): **10** [R_f = 0.47, (hexanes/ethyl acetate 82/18), 35% yield]; **11** [R_f = 0.53, (hexanes/ethyl acetate 82/18), 30% yield]. Desilylation of **10** and **11** was then achieved with HF·Py in THF, leading to diols **4** (Table 2) (84%) and **12** (85%), respectively.

The required stannanes were either commercially available (**5h**, **i**), synthesized according to literature procedures (**5b–d**, **5j**, **k**),[22] or prepared by the sequences shown in Scheme 3. For the synthesis of epothilone E (**1**), dibromide **13**[23] was selectively metalated with *n*BuLi and then treated, in the presence of HMPA, with dimethylformamide (DMF); after reduction with $NaBH_4$ alcohol **14** was obtained in 63% overall yield. Protection of **14** as a silyl ether (TBSCl, imidazole, 96% yield) followed by a second metalation (*n*BuLi), exposure to nBu_3SnCl (85% yield), and desilylation with TBAF furnished stannane **5a** (95% yield). The synthesis of stannane **5e** required: 1) Sonogashira coupling of dibromide **13** with 4-pentyn-1-ol ($[Pd(PPh_3)_4]$/CuI, iPr_2NH, 70°C, 83% yield);[24] 2) chemoselective hydrogenation of the triple bond (cat. PtO_2/H_2, 100% yield); 3) acetate formation (Ac_2O, pyridine, 83% yield); and 4) reaction with $Me_3SnSnMe_3$/cat. $[Pd(PPh_3)_4]$ (toluene, 100°C, 93% yield). Stannane **5f** was prepared from dibromide **13** by reaction with piperidine (60°C, 100% yield), followed by palladium-catalyzed coupling with $Me_3SnSnMe_3$ ($[Pd(PPh_3)_4]$, toluene, 80°C, 100% yield). Similarly, **5g** was obtained from **13** by reaction with NaSMe (EtOH, 25°C, 94% yield) followed by the coupling (100% yield).



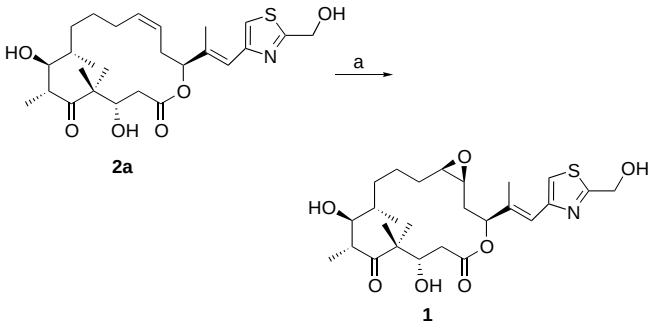
Scheme 2. Synthesis of intermediates **4** and **12** and desoxyepothilones **2** and **3**. a) 1.2 equiv (+)-Ipc$_2$B(allyl), Et$_2$O, −100°C, 0.5 h, 91%; b) 2.0 equiv **8**, 1.5 equiv DCC, 1.5 equiv 4-DMAP, toluene, 25°C, 12° h, 49% **9** and 33% of its (6*S*,7*R*) diastereomer; c) 10 mol% [RuCl$_2$(=CHPh)(PCy$_3$)$_2$], CH$_2$Cl$_2$, 25°C, 20 h, 35% **10** and 30% **11**; d) 10 equiv HF·Py, THF, 25°C, 30 h, **4** (84%); **12** (85%); e) procedure A: 1.5 equiv **5**, 10 mol% [Pd(PPh$_3$)$_4$], toluene, 100°C, 20 min; procedure B: 1.5 equiv **5**, 10 mol% [Pd(MeCN)$_2$Cl$_2$], DMF, 25°C, 10 h, see Table 1. TBS = *tert*-butyldimethylsilyl; DCC = dicyclohexylcarbodiimide; 4-DMAP = 4-dimethylaminopyridine; Py = pyridine.



Scheme 3. Preparation of stannanes **5a**, **5f**, **5g**, and **5e**. a) 1.1 equiv *n*BuLi, 1.2 equiv DMF, 1.1 equiv HMPA, −78→25°C, 2 h, 72%; b) 2.0 equiv NaBH$_4$, MeOH, 25°C, 20 min, 88%; c) 1.5 equiv TBSCl, 2.0 equiv imidazole, 25°C, 0.5 h, 96%; d) 1.2 equiv *n*BuLi, 1.2 equiv *n*Bu$_3$SnCl, −78→25°C, 2 h, 85%; e) 1.2 equiv TBAF, THF, 25°C, 20 min, 95%; f) 1. 2.0 equiv HCC(CH$_2$)$_3$OH, 0.05 equiv [Pd(PPh$_3$)$_4$], 0.1 equiv CuI, *i*Pr$_2$NH, 70°C, 2 h, 83%; 2. H$_2$, 0.1 equiv PtO$_2$, EtOH, 25°C, 4 h; 100%; 3. Ac$_2$O, pyridine, 25°C, 83%; 4. 10 equiv Me$_3$SnSnMe$_3$, 0.1 equiv [Pd(PPh$_3$)$_4$], toluene, 100°C, 3 h, 93%; g) 1. 10 equiv piperidine, 60°C, 6 h, 100%; 2. 10 equiv Me$_3$SnSnMe$_3$, 0.05 equiv [Pd(PPh$_3$)$_4$], toluene, 80°C, 3 h, 100%; h) 1. 3.0 equiv NaSMe, EtOH, 25°C, 2 h, 94%; 2. 10 equiv Me$_3$SnSnMe$_3$, 0.05 equiv [Pd(PPh$_3$)$_4$], toluene, 80°C, 3 h, 100%. HMPA = hexamethylphosphoramide; TBAF = tetra-*n*-butylammonium fluoride.

Attachment of the aromatic moieties onto the macrocyclic framework of vinyl iodides **4** and **12** was performed with the aromatic stannanes shown in Table 1 by means of palladium-catalyzed Stille couplings under conditions A ([Pd(PPh$_3$)$_4$], toluene, 100°C) or B ([Pd(MeCN)$_2$Cl$_2$], DMF, 25°C). Table 1 includes a selection of the synthesized epothilone A analogues, the coupling method, and the yields.

Epothilone E (**1**) (Table 2) was synthesized from its deoxy analogue **2a** (Table 2) by epoxidation with H$_2$O$_2$/KHCO$_3$/CH$_3$CN in methanol[13] as shown in Scheme 4 (65% yield, based on 50% conversion). Synthetic **1** exhibited identical ^{1}H and ^{13}C NMR spectra to those of the natural substance.[25] Epothilone E (**1**) exhibited 52% tubulin polymerization as compared to 76% for epothilone A, 98% for epothilone B, and 50% for Taxol in the filtration–colorimetric tubulin polymerization assay.[3]



Scheme 4. Synthesis of epothilone E (**1**). a) 33 equiv H$_2$O$_2$, 60 equiv CH$_3$CN, 9.0 equiv KHCO$_3$, MeOH, 25°C, 4 h, 65% (based on 50% conversion).

Table 2. Physical data for compounds **4**, **2a**, and **1**.

4: R_f = 0.21 (silica gel, EtOAc/hexanes, 1/3); $[\alpha]_{22}^{D} = -53.1$ (c = 1.37 in CHCl$_3$); IR (film): $\tilde{\nu}$ = 3499 (br), 2930, 1732, 1688, 1469, 1379, 1259, 1149, 1093, 1048, 1006, 732 cm^{-1}; ^{1}H NMR (500 MHz, CDCl$_3$): δ = 6.43 (s, 1H, IC*H*=C(CH$_3$)), 5.44 (ddd, J = 10.5, 10.5, 4.5 Hz, 1H, C*H*=CHCH$_2$), 5.34 (dd, J = 9.5, 2.0 Hz, 1H, CO$_2$CH), 5.32 (ddd, J = 10.5, 10.5, 5.5 Hz, 1H, C*H*=CHCH$_2$), 4.07 (ddd, J = 11.0, 6.0, 3.0 Hz, 1H, (CH$_3$)$_2$CC*H*(OH)), 3.73 (ddd, J = 2.5, 2.5, 2.5 Hz, 1H, C*H*OH(CHCH$_3$)), 3.10 (qd, J = 7.0, 2.5 Hz, 1H, CH$_3$C*H*(C=O)), 2.84 (d, J = 2.5 Hz, 1H, CH(CH$_3$)CHO*H*CH(CH$_3$)), 2.66 (ddd, J = 15.0, 9.5, 9.5 Hz, 1H, =CHC*H*$_2$CHO), 2.51 (dd, J = 15.5, 11.0 Hz, 1H, CH$_2$COO), 2.42 (dd, J = 15.5, 3.0 Hz, 1H, CH$_2$COO), 2.35 (d, J = 6.0 Hz, 1H, (CH$_3$)$_2$CHOH), 2.21–2.12 (m, 2H), 2.05–1.97 (m, 1H), 1.88 (s, 3H, ArCH=CC*H*$_3$), 1.76–1.70 (m, 1H), 1.70–1.62 (m, 1H), 1.32 (s, 3H, C(CH$_3$)$_2$), 1.18 (d, J = 7.0 Hz, 3H, C*H*$_3$CH(C=O)), 1.10 (s, 3H, C(CH$_3$)$_2$), 1.35–1.05 (m, 3H), 0.99 (d, J = 7.0 Hz, 3H, C*H*$_3$CHCH$_2$); ^{13}C NMR (125.7 MHz, CDCl$_3$): δ = 219.9, 170.0, 145.3, 133.8, 124.0, 80.2, 77.3, 74.1, 72.8, 52.7, 42.0, 38.8, 38.4, 32.5, 31.2, 27.5, 27.4, 22.2, 20.8, 19.7, 15.5, 13.6; HRMS (FAB): m/z calcd for C$_{22}$H$_{35}$CsIO$_5$ (M+Cs$^+$): 639.0584, found: 639.0604

2a: R_f = 0.29 (silica gel, EtOAc/hexanes, 1/1); $[\alpha]_{22}^{D} = -44.2$ (c = 0.60 in CHCl$_3$); IR (film): $\tilde{\nu}$ = 3387 (br), 2925, 2859, 1730, 1688, 1508, 1461, 1256, 1183, 1150, 1061, 980, 755 cm^{-1}; ^{1}H NMR (500 MHz, CDCl$_3$): δ = 7.12 (s, 1H, ArH), 6.61 (s, 1H, ArC*H*=C(CH$_3$)), 5.45 (ddd, J = 10.5, 10.5, 4.5 Hz, 1H, C*H*=CHCH$_2$), 5.38 (ddd, J = 10.5, 10.5, 5.0 Hz, 1H, C*H*=CHCH$_2$), 5.31 (d, J = 8.5 Hz, 1H, CO$_2$CH), 4.92 (d, J = 4.0 Hz, 2H, C*H*$_2$OH), 4.23 (ddd, J = 11.5, 5.5, 2.5 Hz, 1H, (CH$_3$)$_2$CC*H*(OH)), 3.75–3.71 (m, 1H, C*H*OH(CHCH$_3$)), 3.32 (d, J = 5.5 Hz, 1H, C(CH$_3$)$_2$CHOH), 3.25 (t, J = 4.0 Hz, 1H, CH$_2$OH), 3.13 (qd, J = 7.0, 2.0 Hz, 1H, CH$_3$C*H*(C=O)), 3.03 (d, J = 2.0 Hz, 1H, CH$_3$CHCH(O*H*)CHCH$_3$), 2.68 (ddd, J = 15.0, 9.5, 9.5 Hz, 1H, =CHC*H*$_2$CHO), 2.50 (dd, J = 15.0, 11.5 Hz, 1H, CH$_2$COO), 2.35 (dd, J = 15.0, 2.5 Hz, 1H, CH$_2$COO), 2.31–2.24 (m, 1H, =CHC*H*$_2$CHO), 2.24–2.16 (m, 1H), 2.09 (s, 3H, ArCH=CC*H*$_3$), 2.06–1.98 (m, 1H), 1.82–1.73 (m, 1H), 1.72–1.62 (m, 1H), 1.39–1.17 (m, 3H), 1.33 (s, 3H, C(CH$_3$)$_2$), 1.19 (d, J = 7.0 Hz, 3H, C*H*$_3$CH(C=O)), 1.08 (s, 3H, C(CH$_3$)$_2$), 1.00 (d, J =

 © WILEY-VCH Verlag GmbH, D-69451 Weinheim, 1998 1433-7851/98/3701-0086 $ 17.50+.50/0 *Angew. Chem. Int. Ed.* **1998**, *37*, No. 1/2

7.0 Hz, 3H, CH_3CHCH$_2$); ^{13}C NMR (125.7 MHz, $CDCl_3$): $\delta = 220.5$, 170.3, 169.9, 152.3, 139.0, 133.5, 124.9, 118.9, 116.5, 78.4, 74.2, 72.2, 61.8, 53.4, 41.7, 39.3, 38.6, 32.4, 31.7, 27.5, 27.4, 22.8, 18.4, 16.0, 15.5, 13.5; HRMS (FAB): *m/z* calcd for $C_{26}H_{39}CsNO_6S$ (M+Cs$^+$): 626.1552, found: 626.1530

1: $R_f = 0.56$ (silica gel, EtOAc/hexanes, 2/1); $[\alpha]_{22}^{D} = -27.5$ ($c = 0.20$ in $CHCl_3$); IR (film): $\tilde{\nu} = 3413$ (br), 2928, 2867, 1731, 1689, 1462, 1375, 1257, 1152, 1061, 978, 756 cm^{-1}; ^{1}H NMR (600 MHz, $CDCl_3$): $\delta = 7.13$ (s, 1H, ArH), 6.61 (s, 1H, ArC*H*=CCH$_3$), 5.46 (dd, 1H, $J = 8.1$, 2.4 Hz, CO$_2$CH), 4.94 (d, $J = 5.2$ Hz, 2H, CH_2OH), 4.16–4.12 (m, 1H, (CH$_3$)$_2$CC*H*(OH)), 3.82–3.78 (m, 1H, C*H*OH(CHCH$_3$)), 3.66 (br. s, 1H, OH), 3.23 (qd, $J = 6.8$, 5.2 Hz, 1H, CH$_3$C*H*(C=O)), 3.04 (ddd, $J = 8.1$, 4.5, 4.5 Hz, 1H, CH$_2$C*H*-O(epoxide)CH), 2.91 (ddd, $J = 7.3$, 4.5, 4.1 Hz, 1H, CH$_2$C*H*-O(epoxide)CH), 2.61 (t, $J = 5.2$ Hz, 1H, CH$_2$OH), 2.55 (dd, $J = 14.7$, 10.4 Hz, 1H, CH$_2$COO), 2.48 (br. s, 1H, OH), 2.45 (dd, $J = 14.7$, 3.2 Hz, 1H, CH$_2$COO), 2.14–2.07 (m, 1H, CH_2CH-O(epoxide)CH), 2.11 (s, 3H, ArCH=CCH_3), 1.91 (ddd, $J = 15.1$, 8.1, 8.1 Hz, 1H, CH_2CH-O(epoxide)CH), 1.78–1.66 (m, 2H, CH_2CH-O(epoxide)CH), 1.52–1.38 (m, 5H), 1.36 (s, 3H, C(CH$_3$)$_2$), 1.18 (d, 3H, $J = 6.8$ Hz, CH_3CH(C=O)), 1.10 (s, 3H, C(CH$_3$)$_2$), 1.01 (d, $J = 7.0$ Hz, 3H, CH_3CHCH$_2$); ^{13}C NMR (150.9 MHz, $CDCl_3$): $\delta = 220.0$, 170.6, 169.9, 152.3, 137.6, 119.8, 117.0, 76.7, 74.8, 73.6, 62.3, 57.5, 54.4, 52.7, 43.6, 38.9, 36.2, 31.4, 30.4, 27.0, 23.7, 21.3, 21.0, 17.2, 15.6, 14.3; HRMS (FAB): *m/z* calcd for $C_{26}H_{40}NO_7S$ (M+H$^+$): 510.2525, found: 510.2539

The described chemistry opens a convergent and convenient entry into a library of epothilones with varying side chains for biological screening. Further chemical and biological investigations with these and related compounds will be reported in due course.

Received: August 7, 1997 [Z 10788 IE]
German version: *Angew. Chem.* **1998**, *110*, 89–92

Keywords: epothilones · natural products · Stille coupling · total synthesis

[1] a) G. Höfle, N. Bedorf, K. Gerth, H. Reichenbach (GBF), DE-4138042, **1993** [*Chem. Abstr.* **1993**, *120*, 52841]; b) K. Gerth, N. Bedorf, G. Höfle, H. Irschik, H. Reichenbach, *J. Antibiot.* **1996**, *49*, 560–563.

[2] G. Höfle, N. Bedorf, H. Steinmetz, D. Schomburg, K. Gerth, H. Reichenbach, *Angew. Chem.* **1996**, *108*, 1671–1673; *Angew. Chem. Int. Ed. Engl.* **1996**, *35*, 1567–1569.

[3] D. M. Bollag, P. A. McQueney, J. Zhu, O. Hensens, L. Koupal, J. Liesch, M. Goetz, E. Lazarides, C. M. Woods, *Cancer Res.* **1995**, *55*, 2325–2333.

[4] a) K. C. Nicolaou, Y. He, D. Vourloumis, H. Vallberg, Z. Yang, *Angew. Chem.* **1996**, *108*, 2554–2556; *Angew. Chem. Int. Ed. Engl.* **1996**, *35*, 2399–2401; b) D. Meng, E. J. Sorensen, P. Bertinato, S. J. Danishefsky, *J. Org. Chem.* **1996**, *61*, 7998–7999; c) P. Bertinato, E. J. Sorensen, D. Meng, S. J. Danishefsky, *ibid.* **1996**, *61*, 8000–8001; d) D. Schinzer, A. Limberg, O. M. Böhm, *Chem. Eur. J.* **1996**, *2*, 1477–1482; e) J. Mulzer, A. Mantoulidis, *Tetrahedron Lett.* **1996**, *37*, 9179–9182; f) E. Claus, A. Pahl, P. G. Jones, H. M. Meyer, M. Kalesse, *ibid.* **1997**, *38*, 1359–1362; g) T. Gabriel, L. Wessjohann, *ibid.* **1997**, *38*, 1363–1366; R. E. Taylor, J. D. Haley, *ibid.* **1997**, *38*, 2061–2064.

[5] a) A. Balog, D. Meng, T. Kamenecka, P. Bertinato, D.-S. Su, E. J. Sorensen, S. J. Danishefsky, *Angew. Chem.* **1996**, *108*, 2976–2978; *Angew. Chem. Int. Ed. Engl.* **1996**, *35*, 2801–2803; b) D. Meng, D.-S. Su, A. Balog, P. Bertinato, E. J. Sorensen, S. J. Danishefsky, Y.-H. Zheng, T.-C. Chou, L. He, S. B. Horwitz, *J. Am. Chem. Soc.* **1997**, *119*, 2733–2734.

[6] a) Z. Yang, Y. He, D. Vourloumis, H. Vallberg, K. C. Nicolaou, *Angew. Chem.* **1997**, *109*, 170–172; *Angew. Chem. Int. Ed. Engl.* **1997**, *36*, 166–168; b) K. C. Nicolaou, F. Sarabia, S. Ninkovic, Z. Yang, *ibid.* **1997**, *109*, 539–540 and **1997**, *36*, 525–527.

[7] D. Schinzer, A. Limberg, A. Bauer, O. M. Böhm, M. Cordes, *Angew. Chem.* **1997**, *109*, 543–544; *Angew. Chem. Int. Ed. Engl.* **1997**, *36*, 523–524.

[8] K. C. Nicolaou, N. Winssinger, J. A. Pastor, S. Ninkovic, F. Sarabia, Y. He, D. Vourloumis, Z. Yang, T. Li, P. Giannakakou, E. Hamel, *Nature* **1997**, *387*, 268–272.

[9] D.-S. Su, D. Meng, P. Bertinato, A. Balog, E. J. Sorensen, S. J. Danishefsky, Y.-H. Zheng, T.-C. Chou, L. He, S. B. Horwitz, *Angew. Chem.* **1997**, *109*, 775–777; *Angew. Chem. Int. Ed. Engl.* **1997**, *36*, 757–759.

[10] K. C. Nicolaou, Y. He, D. Vourloumis, H. Vallberg, F. Roschangar, F. Sarabia, S. Ninkovic, Z. Yang, J. I. Trujillo, *J. Am. Chem. Soc.* **1997**, *119*, 7960–7973.

[11] K. C. Nicolaou, S. Ninkovic, F. Sarabia, D. Vourloumis, Y. He, H. Vallberg, M. R. V. Finlay, Z. Yang, *J. Am. Chem. Soc.* **1997**, *119*, 7974–7991.

[12] K. C. Nicolaou, D. Vourloumis, T. Li, J. Pastor, N. Winssinger, Y. He, S. Ninkovic, F. Sarabia, H. Vallberg, F. Roschangar, N. P. King, M. R. V. Finlay, P. Giannakakou, P. Verdier-Pinard, E. Hamel, *Angew. Chem.* **1997**, *109*, 2181–2187; *Angew. Chem. Int. Ed. Engl.* **1997**, *36*, 2097–2103..

[13] K. C. Nicolaou, H. Vallberg, N. P. King, F. Roschangar, Y. He, D. Vourloumis, C. G. Nicolaou, *Chem. Eur. J.* **1997**, *3*, 1957–1970.

[14] K. C. Nicolaou, F. Sarabia, M. R. V. Finlay, S. Ninkovic, N. P. King, D. Vourloumis, Y. He, *Chem. Eur. J.* **1997**, *3*, 1971–1986.

[15] A. Balog, P. Bertinato, D.-S. Su, D. Meng, E. J. Sorensen, S. J. Danishefsky, Y-H. Zheng, T-C. Chou, L. He, S. B. Horwitz, *Tetrahedron Lett.* **1997**, *38*, 4529–4532.

[16] G. Höfle, personal communication.

[17] R. J. Kowalski, P. Giannakakou, E. Hamel, *J. Biol. Chem.* **1997**, *272*, 2534–2541.

[18] For the development of the olefin metathesis as a ring-forming reaction, see: a) W. J. Zuercher, M. Hashimoto, R. H. Grubbs, *J. Am. Chem. Soc.* **1996**, *118*, 6634–6640; b) P. R. Schwab, H. Grubbs, J. W. Ziller, *ibid.* **1996**, *118*, 100–110; c) R. H. Grubbs, S. J. Miller, G. C. Fu, *Acc. Chem. Res.* **1995**, *28*, 446–452, and references therein; d) J. Tsuji, S. Hashiguchi, *Tetrahedron Lett.* **1980**, *21*, 2955–2959; For some earlier pioneering studies on this reaction, see: e) T. J. Katz, S. J. Lee, N. Acton, *ibid.* **1976**, 4247–4250; f) T. J. Katz, N. Acton, *ibid.* **1976**, 4241–4254; g) T. J. Katz, J. McGinnis, C. Altus, *J. Am. Chem. Soc.* **1976**, *98*, 606–608; h) T. J. Katz, *Adv. in Organomet. Chem.* **1977**, *16*, 283–317.

[19] For a number of applications of the olefin metathesis reaction in the synthesis of medium and large rings, see: a) B. C. Borer, S. Deerenberg, H. Bieräugel, U. K. Pandit, *Tetrahedron Lett.* **1994**, *35*, 3191–3194; b) T. D. Clark, M. R. Ghadiri, *J. Am. Chem. Soc.* **1995**, *117*, 12364–12365; c) A. F. Houri, Z. Xu, D. A. Cogan, A. H. Hoveyda, *ibid.* **1995**, *117*, 2943–2944; d) A. Fürstner, K. Langemann, *J. Org. Chem.* **1996**, *61*, 3942–3943; e) S. F. Martin, H.-J. Chen, A. K. Courtney, Y. Liao, M. Pätzel, M. N. Ramser, A. S. Wagman, *Tetrahedron* **1996**, *52*, 7251–7264; f) Z. Xu, C. W. Johannes, S. S. Salman, A. H. Hoveyda, *J. Am. Chem. Soc.* **1996**, *118*, 10926–10927.

[20] J. K. Stille, *Angew. Chem.* **1986**, *98*, 504–522; *Angew. Chem. Int. Ed. Engl.* **1986**, *25*, 508–524.

[21] R. Baker, J. L. Castro, *J. Chem. Soc. Perkin Trans I* **1990**, 47–65.

[22] A. Dondoni, A. R. Mastellari, A. Medici, E. Negrini, P. Pedrini, *Synthesis* **1986**, 757–760.

[23] P. Reynaud, M. Robba, R. C. Moreau, *Bull. Soc. Chim. Fr.* **1962**, 1735–1740.

[24] K. Sonogashira, Y. Tohda, N. Hagihara, *Tetrahedron Lett.* **1975**, *16*, 4467–4470.

[25] We thank G. Höfle for the ^{1}H and ^{13}C NMR spectra of natural epothilone E (**1**).

Novel, Highly Symmetrical Halogen-Centered Polynuclear Lanthanide Complexes: $[Cp_6Yb_6Cl_{13}]^-$ and $[Cp_{12}Sm_{12}Cl_{24}]$**

Winfried P. Kretschmer,* Jan H. Teuben, and Sergei I. Troyanov*

We recently discovered that numerous monocyclopentadienyllanthanide dihalides $[CpLnX_2(thf)_3]$ ($Cp = \eta^5$-C_5H_5) can be readily synthesized as very pure compounds in good yields by using trimethylsilylcyclopentadiene as the alkylating agent [Eq. (a)].[1] In contrast to the metathesis or synpropor-

$$Me_3SiCp + [LnX_3(thf)_n] \xrightarrow[2)\ thf]{1)\ toluene,\ -Me_3SiX,\ -thf} [CpLnX_2(thf)_3] \qquad (a)$$

Ln = La (X = Br, $n = 4$), Ce (Br, 4), Sm (Cl, 3), Yb (Cl, 3)]

tionation reactions reported to date, no coordination of a salt (LiCl, NaCl) nor the often observed multiple alkylation take place.[2,3]

The occurrence of distinct color changes during the synthesis (e.g. colorless →violet →orange in the case of ytterbium) indicated the presence of intermediates. Similar color changes were also observed earlier, in the synthesis of $[CpYbCl_2(thf)_3]$.[4] Recrystallization of the sparingly soluble residues, obtained after alkylation in toluene, led to compounds **1** and **2**, which contain very little or no THF, respectively. Single crystals of **1** and **2** could be reproducibly obtained by treating the THF adducts $[CpLnCl_2(thf)_3]$ (Ln = Sm, Yb) with hot toluene and simultaneous removal of the evolved tetrahydrofuran by distillation.

$[CpYbCl_2] \cdot {}^1/_3\,thf \cdot {}^2/_9\,toluene$ **1**

$[CpSmCl_2] \cdot {}^1/_6\,toluene$ **2**

Complex **1** exhibits an ionic structure, $[Cp_3Yb_3(\mu_3\text{-}Cl)_2(\mu\text{-}Cl)_3(thf)_3][Cp_6Yb_6(\mu_6\text{-}Cl)(\mu\text{-}Cl)_{12}] \cdot 2\,C_7H_8$, built up of trinuclear cations and hexanuclear anions (Figure 1).[5] The cation consists of an equilateral triangle of Yb atoms which are connected by doubly bridging Cl atoms over the edges ($\bar{d}$(Yb – Cl) 2.662 Å) and by triply bridging Cl atoms on either side of the triangular plane ($\bar{d}$(Yb – Cl) 2.764 Å). Three cyclopentadienyl ligands ($\bar{d}$(Yb – Cp_z) 2.29 Å) on one side of the plane and three THF ligands ($\bar{d}$(Yb – O) 2.25 Å) on the other side result in pseudooctahedral coordination for each Yb atom.[6] Thus, the cation can be assigned the quite common M_3X_{11} constitution.[7] The six Yb atoms of the anion in **1**

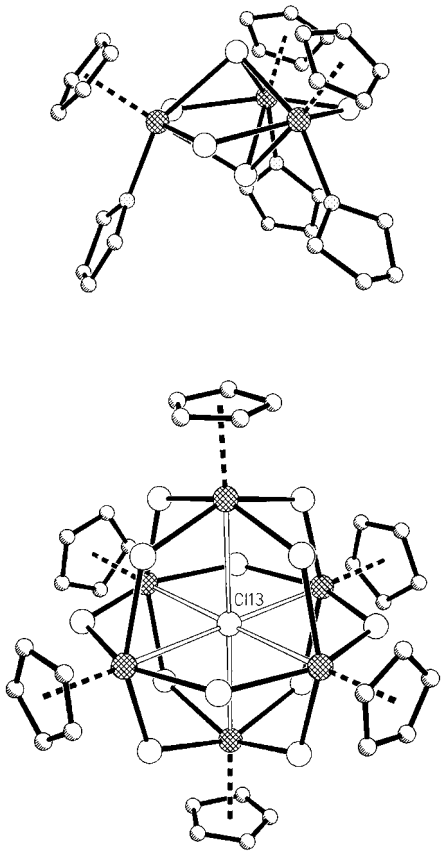


Figure 1. Crystal structure of the trinuclear cation $[Cp_3Yb_3Cl_5(thf)_3]^+$ (top) and the Cl-centered octahedral anion $[Cp_6Yb_6Cl_{13}]^-$ (bottom) of **1**.

delineate an almost regular octahedron, the edges of which are bridged by 12 Cl atoms with nearly equal Yb – Cl bond lengths of 2.61 – 2.67 Å. An additional Cl(13) atom with markedly longer Yb – Cl bond lengths of 3.14 – 3.28 Å lies at the center of the octahedron. The sixth coordination site of each Yb atom is occupied by a cyclopentadienyl ligand ($\bar{d}$(Yb – Cp_z) 2.29 Å). Thus, the anion exhibits uncommon high symmetry. In contrast, other hexanuclear complexes obtained from solutions, such as $[Cp^*_6Sm_6Se_{11}]$ ($Cp^* = \eta^5$-C_5Me_5) and $[\{Nd_3(\mu_3\text{-}OR)(\mu\text{-}OR)_3\}_2(OR)_3(\mu_6\text{-}Cl)]$ exhibit strongly distorted skeletons,[8,9] whereas the symmetrical octahedron in $[K(thf)_4]_2[Cp^s_6Yb_6I_8]$ ($Cp^s = \eta^5$-$C_5Me_4(SiMe_2$-tBu)) is not centered by a halogen and contains divalent Yb ions.[10]

An even greater degree of oligomerization than that attained in **1** is displayed by complex **2** $[Cp_{12}Sm_{12}(\mu_3\text{-}Cl)_{24}] \cdot 2\,C_7H_8$, which is built up from neutral molecules.[11] An X-ray crystal structure analysis showed that twelve $[CpSmCl_2]$ units are linked to produce the whole molecule, whereby the Sm atoms take up an icosahedral arrangement (Figure 2). The total molecular skeleton has 222 crystallographic symmetry with three twofold axes which intersect at the center of the molecule. As a result, only three Sm and six Cl atoms as well as three Cp ligands are crystallographically independent. Each Sm atom has a strongly distorted pentagonal-bipyramidal coordination sphere made up of six Cl atoms and one Cp ligand. Each Cl atom caps a triangle of samarium atoms, so that 20 Cl atoms form an "outer" pentagonal-dodecahedral

[*] Dr. W. P. Kretschmer, Prof. Dr. J. H. Teuben
Centre for Catalytic Olefin Polymerization
University of Groningen
Nijenborgh 4, NL-9747 AG Groningen (The Netherlands)
e-mail: teuben@chem.rug.nl
Dr. S. I. Troyanov
Chemistry Department
Moscow State University
119899 Moscow, Vorobyevy Gory (Russia)
Fax: Int. code + (7) 095-932 8846
e-mail: troyanov@thermo.chem.msu.su

[**] W.P.K. would like to thank the Deutsche Forschungsgemeinschaft for a post-doctorate grant.

 © WILEY-VCH Verlag GmbH, D-69451 Weinheim, 1998 1433-7851/98/3701-0088 $ 17.50+.50/0

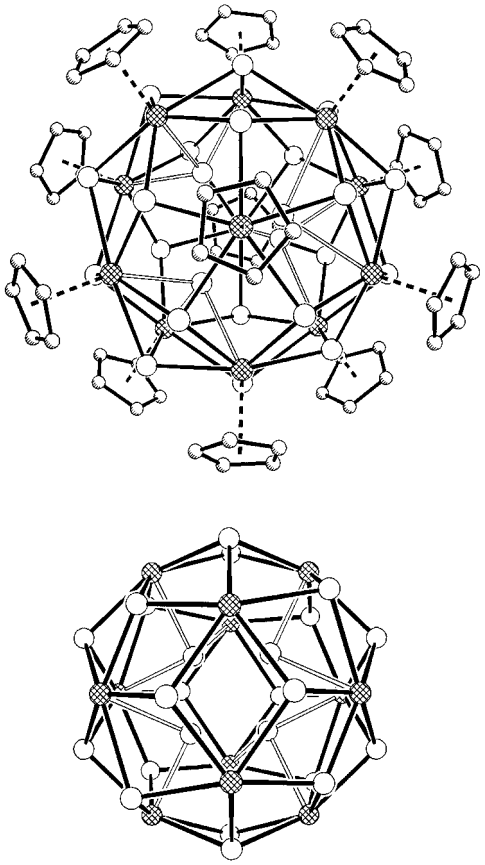


Figure 2. Top: Molecular structure of $[Cp_{12}Sm_{12}Cl_{24}]$ viewed along one of the six fivefold pseudoaxes. Bottom: Structure of the $Sm_{12}Cl_{24}^{-}$ skeleton of **2** with 20 outer and four inner Cl atoms viewed along one of the three twofold axes. The Sm atoms are represented as hatched circles, the Cl atoms as open circles, and the inner Sm–Cl bonds as double lines.

envelope (Sm–Cl_o distances in the range of 2.67–3.09 Å), and the other four Cl atoms form an "inner" tetrahedron(Cl_i–Cl_i 3.29 Å) at the center of the Sm icosahedron (Sm–Cl_i 2.95 Å). The arrangement of the 60 C atoms of the 12 Cp ligands ($\bar{d}$(Sm–Cp_z) 2.36 Å) corresponds to a truncated icosahedron, and is somewhat analogous to the C_{60} fullerene. The overall structure makes the Sm icosahedron unique—not only in lanthanide chemistry.

A comparison of the two complexes very effectively demonstrates the influence of the analogous reactivity of lanthanides with differing ionic radii on the structure. Thus, a pseudooctahedral environment (CN = 6) is a structural feature of monomeric $[CpLnCl_2(thf)_3]$ complexes, and is independent of the ionic radius.[12] If the bulky THF ligands are exchanged for the smaller μ-Cl atoms with a simultaneous elongation of the bond lengths, this leads to an increase in the coordination number from six to seven. This is the case in the analogous π-arene complexes $[(\eta^6\text{-arene})Ln(AlCl_4)_3]$, in all of which the Ln atom has a pentagonal-bipyramidal coordination sphere consisting of six μ-Cl atoms (between Ln and Al) and one arene ligand.[13] However, the coordination number seven can only be attained by the $[CpLnCl_2]$ complexes if each terminal Cl atom of the monomer becomes a μ_3-Cl atom in the oligomer. These conditions are excellently fulfilled in the Sm icosahedron, which, along with the pentagonal symmetry, also provides a cavity large enough to accommodate four Cl atoms. On the other hand, the smaller Yb ions ($r_{Yb} = 0.925$ Å, $r_{Sm} = 1.020$ Å for CN = 7)[14] prefer an octahedral Yb_6 arrangement with CN = 6.

The new compounds **1** and **2** prove very impressively, that in spite of analogous reactivity the lanthanides are capable of a rich and novel structural chemistry. It is expected that a systematic investigation of the removal of THF from the mononuclear monocyclopentadienyl compounds should lead to the isolation of new types of multinuclear complexes for the whole series of lanthanides.

Experimental Section

All the preparative work was carried out under an N_2 atmosphere.

1: A suspension of $[YbCl_3(thf)_3]$ (2.73 g, 5.5 mmol) and $C_5H_5SiMe_3$ (0.84 mL, 5 mmol) in toluene (50 mL) was heated at reflux for 24 h. After removal of the solvent under vacuum, the residue was washed with toluene until it was only slightly colored and then recrystallized from toluene. Slow cooling of the solution to room temperature gave violet prisms, which were filtered and dried under vacuum. Yield: 0.90 g (51 %). Elemental analysis $C_{71}H_{85}Cl_{18}O_3Yb_9$: calcd (found) C 26.80 (27.01), H 2.67 (2.78); IR (KBr, Nujol): $\tilde{\nu}$ [cm^{-1}] = 3097, 3081, 1688, 1681, 1673, 1651, 1038, 1012 (vs), 919, 854 (vs), 794 (vs), 788 (vs), 736, 694, 464.

2: A suspension of $[CpSmCl_2(thf)_3]$ (0.20 g, 0.4 mmol) in toluene (20 mL) was heated at reflux for 24 h with simultaneous removal of the solvent by distillation. The residue was repeatedly extracted with toluene (10 mL) at 80 °C until orange crystals formed. The liquid was decanted, and the crystals washed with a little toluene and dried under vacuum. Yield: 0.044 g (35 %).

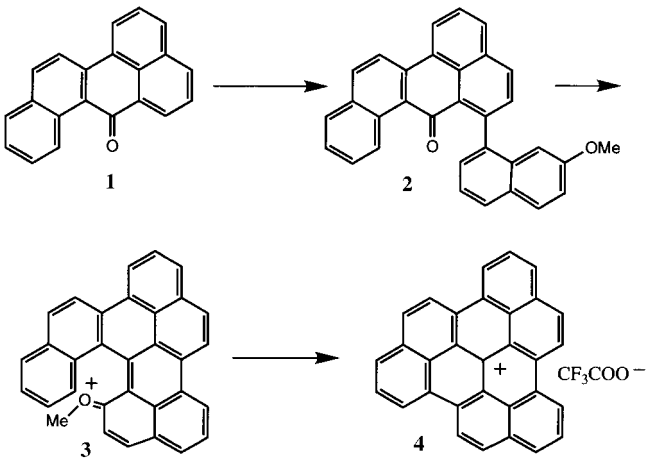
Received: August 26, 1997 [Z10761IE]
German version: *Angew. Chem.* **1998**, *110*, 92–94

Keywords: cyclopentadienyl complexes · polynuclear complexes · lanthanides · samarium · ytterbium

[1] W. P. Kretschmer, S. I. Troyanov, A. Meetsma, J. H. Teuben, *Proc. 31st Int. Conf. Coordination Chemistry, 18–23 Aug. 1996, Vancouver, Canada,* **1996**, abstr. p. 176.
[2] Review on lanthanide complexes: H. Schumann, J. A. Meese-Marktscheffel, L. Esser, *Chem. Rev.* **1995**, *95*, 865–986.
[3] Review on monocyclopentadienyl complexes: R. Poli, *Chem. Rev.* **1991**, *91*, 509–551.
[4] M. Adam, X.-F. Li, W. Oroschin, R. D. Fischer, *J. Organomet. Chem.* **1985**, *296*, C19–C22.
[5] Crystal data for **1**: monoclinic, $P2_1/c$, $a = 16.262(1)$, $b = 26.376(1)$, $c = 21.742(1)$ Å, $\beta = 101.027(5)^\circ$, $V = 9153.5(8)$ Å^3, $Z = 4$, $\rho_{calcd} = 2.309$ g cm^{-3}, $T = 295$ K, $1.5 < 2\theta < 48^\circ$ ($Mo_{K\alpha}$, $\lambda = 0.71073$ Å), CAD-4 (Enraf-Nonius); of 14655 reflections, 11333 were independent. The structure was solved by direct methods (SHELXS-86) and refined against $|F^2|$ (SHELXL-93) with 9563 reflections ($F_o^2 \geq 0$) and 912 parameters, wR_2(all) = 0.1070 and R_1(observed) = 0.0641.[11b]
[6] Here and throughout the definition of the coordination polyhedron refers to the arrangement of the σ ligands and the centers of the π ligands. See, for example, *Encyclopedia of Inorganic Chemistry, Vol. 2* (Ed.: R. B. King), Wiley, New York, **1994**, p. 819.
[7] Examples of M_3X_{11}: a) D. L. Clark, J. C. Gordon, J. C. Huffman, J. G. Watkin, B. D. Zwick, *New J. Chem.* **1995**, *19*, 495–502; b) W. J. Evans, M. S. Sollberger, T. P. Hanusa, *J. Am. Chem. Soc.* **1988**, *110*, 1841–1850.
[8] W. J. Evans, G. W. Rabe, M. A. Ansari, J. W. Ziller, *Angew. Chem.* **1994**, *106*, 2200–2201; *Angew. Chem. Int. Ed. Engl.* **1994**, *33*, 2110–2111.
[9] R. A Andersen, D. H. Templeton, A. Zalkin, *Inorg. Chem.* **1978**, *17*, 1962–1965.

 © WILEY-VCH Verlag GmbH, D-69451 Weinheim, 1998 1433-7851/98/3701-0089 $ 17.50+.50/0

[10] S. P. Constantine, G. M. De Lima, P. B. Hitchcock, J. M. Keates, G. A. Lawless, *Chem. Commun.* **1996**, 2421 – 2422.
[11] a) Crystal data for **2**: tetragonal, $I4_1/acd$, $a = 26.822(3)$, $c = 28.071(2)$, $V = 20195(4)$ Å^3, $Z = 8$, $\rho_{calcd} = 2.281$ g cm^{-3}, $T = 273$ K, $3.0 < 2\theta < 39.0^\circ$ ($Mo_{K\alpha}$, $\lambda = 0.71073$ Å), IPDS (Stoe); of 12239 reflections, 2160 were independent. The structure was solved by direct methods (SHELXS-86) and refined against $|F^2|$ (SHELXL-93) with 1568 reflections ($F_o^2 \geq 0$) and 160 parameters, wR_2(all) = 0.1233 and R_1(observed) = 0.0659. b) Crystallographic data (excluding structure factors) for the structures reported in this paper have been deposited with the Cambridge Crystallographic Data Centre as supplementary publication no. CCDC-100593. Copies of the data can be obtained free of charge on application to CCDC, 12 Union Road, Cambridge CB2 1EZ, UK (fax: int. code + (44)-1223 336-033; e-mail: deposit@ccdc.cam.ac.uk).
[12] X. Zhou, Z. Wu, H. Ma, Z. Xu, X. You, *Polyhedron* **1994**, *13*, 375 – 378.
[13] a) F. A. Cotton, W. Schwotzer, *J. Am. Chem. Soc.* **1986**, *108*, 4657 – 4658. b) Review: G. B. Deacon, Q. Shen, *J. Organomet. Chem.* **1996**, *506*, 1 – 17.
[14] R. D. Shannon, *Acta Crystallogr. Sect.A* **1976**, *32*, 751 – 767.



Scheme 1. Synthesis of **4** · CF_3COO.

Synthesis of the Trinaphthophenalenium Cation**

Masahiko Suenaga,* Yuji Miyahara, Nobujirou Shimizu, and Takahiko Inazu

The unique feature of odd-alternant hydrocarbons (i.e., polycyclic hydrocarbons with alternating double bonds and an odd number of carbon atoms), is the readily interconvertible redox triad (cation – radical – anion), which has been the subject of many experimental and theoretical studies. Recently we have disclosed a novel synthetic approach[1] to extended phenalenones as potential precursors of the corresponding odd-alternant hydrocarbons. Here we report the application of this method to the synthesis of the hitherto unknown trinaphthophenalenium cation **4**, a cation of a novel C_{3h}-symmetric odd-alternant hydrocarbon.

Treatment[2] of 7*H*-benzo[*hi*]chrysen-7-one (**1**)[3] with 7-methoxy-1-naphthyllithium (prepared from 7-methoxy-1-naphthyl iodide[4, 5] and *n*BuLi in ether at room temperature) and autooxidation of the resulting adduct in the usual workup afforded 6-(7-methoxy-1-naphthyl)-7*H*-benzo[*hi*]chrysen-7-one (**2**)[6] in 75% yield (Scheme 1). This molecule contains the necessary number of carbons for the construction of the desired trinaphthophenalene skeleton. The methoxy group was deliberately introduced to serve as an auxiliary in the following three key steps of the condensation to the target structure. First, it acts as an electron-donating group to make position 8 reactive enough to react with the central carbonyl group to give **3**. Second, it stabilizes the adjacent cationic center as shown in **3** to increase the chance for the ring-closing condensation with the facing benzene ring. Finally, it can leave as methanol to provide the trinaphthophenalenium cation **4**. Our system worked as beautifully as we had originally conceived.

The reaction proceeded in steps and we could isolate the intermediate **3** as a blue-violet solid after heating **2** in 30% HBr/HOAc at 95°C for 1 h. Although **3** was not fully characterized, the presence of 16 different aromatic protons and three methyl protons in the ^{1}H NMR spectrum supports the proposed structure. When the reaction temperature was increased to 110°C, the final transannular condensation occurred very smoothly to furnish trinaphthophenalenium trifluoroacetate **4** · CF_3COO as a dark violet solid (71% from **2**) after chromatographic purification (silica gel, CF_3COOH).

The characteristic absorption of **4** in acetonitrile ($\lambda_{max}(\varepsilon) =$ 568 (10400)) supports its extensively delocalized π system. The ^{1}H NMR spectrum[7] of **4** consists of four doublets at $\delta =$ 9.74, 9.42, 9.05, and 9.02 and one triplet at $\delta = 8.65$ in accord with the expected C_{3h} symmetry. The FAB mass spectrum (**4** in CF_3COOH/*m*-nitrobenzyl alcohol matrix) shows a peak for the trinaphthophenalenium cation at *m*/*z* 387.1172 (calcd for $C_{31}H_{15}$: 387.1174). As a measure of the thermodynamic stability of the trinaphthophenalenium cation, its pK_{R+} value was determined by spectrophotometric titration in buffered 50% aqueous acetonitrile. Although the titration curve was discontinuous[8] between pH 2.65 and 2.96, the preliminary pK_{R+} value was estimated to be roughly 4.2. Therefore, the stability of cation **4** is comparable to that of the tropylium ion ($pK_{R+} = 4.7$).

The electrochemical behavior of **4** was examined by cyclic voltammetry using a microelectrode (Table 1). Two quasi-reversible redox waves were observed. While the first reduction potential is much higher than that of phenalenium ion, the reverse is true with the second reduction potential. The electrochemical properties of the trinaphthophenalenium system are consistent with the results of semiempirical calculations.[11, 12] Thus, while the LUMO energy of cation **4** (−6.04 eV) is higher than that of phenalenium cation

[*] Dr. M. Suenaga, Dr. Y. Miyahara, Prof. Dr. N. Shimizu, Prof. Dr. T. Inazu
Department of Chemistry, Faculty of Science, Kyushu University
6-10-1 Hakozaki, Higashi-ku, Fukuora 812-81 (Japan)
Fax: Int. code + (81) 92-642 2607
e-mail: alohascc@mbox.nc.kyushu-u.ac.jp

[**] This work was supported by a Grant-in-Aid for Center of Excellence (COE) Research on the "Design and Control of Advanced Molecular Assembly Systems" from the Ministry of Education Science and Culture, Japan (grant no. 08CE2005).

 © WILEY-VCH Verlag GmbH, D-69451 Weinheim, 1998 1433-7851/98/3701-0090 $ 17.50+.50/0

Table 1. Results of cyclic voltammetric studies.[a]

Cation	E_{red1}	E_{red2}
4	−0.066	−0.762
phenalenium[b]	0.5 (0.7)	−1.1 (−0.9)

[a] Tetrabutylammonium tetrafluoroborate (4 mM) as the supporting electrolyte, scan rate 50 mV s^{-1}, 25°C; potential in volts vs. Ag/Ag$^+$, measured with a 25 μm Pt working microelectrode in MeCN; reduction peak potentials are for a quasi-reversible redox reaction; the observed potentials were corrected with reference to ferrocene/ferrocenium (Fc/Fc$^+$; $E_{1/2} = +0.089$ V) as an internal standard. [b] The originally reported[9] reduction potentials for phenalenium tetrafluoroborate (listed in parentheses) were given in volts vs. SCE. For comparison these data were converted into values vs. Ag/Ag$^+$ reference electrode according to Equation (a).[10]

$$E(\mathrm{Ag/Ag^+}) = E(\mathrm{SCE}) - 0.226\ \mathrm{V} \qquad \text{(a)}$$

(−6.76 eV), the SOMO energy of the trinaphthophenalenyl radical (−4.55 eV) is lower than that of phenalenyl radical (−4.43 eV).

Received: July 21, 1997 [Z 10705 IE]
German version: *Angew. Chem.* **1998**, *110*, 95–96

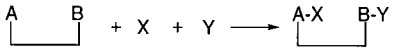
Keywords: arenes · cations · hydrocarbons · phenalenes · polycycles

[1] M. Suenaga, Y. Miyahara, T. Inazu, *J. Org. Chem.* **1993**, *58*, 5846–5848.
[2] C. F. H. Allen, *Can. J. Chem.* **1973**, *51*, 382–387.
[3] W. Bradley, F. K. Sutcliffe, *J. Chem. Soc.* **1952**, 1247–1251.
[4] J. A. LaBudde, C. Heidelberger, *J. Am. Chem. Soc.* **1958**, *80*, 1225–1236.
[5] F. Kehrmann, E. F. Engelke, *Ber.* **1909**, *42*, 350–353.
[6] Yellow needles (from $CHCl_3$/EtOH), m.p. 165–167°C; elemental analysis calcd for $C_{32}H_{20}O_2$: C 88.05, H 4.62; found: C 87.94, H 4.73.
[7] ^{1}H HMR (400 MHz, CF_3COOD, $\delta(CF_3COOH) = 11.5$) All signals were fully assigned with a COSY-45 experiment.
[8] The buffer had to be changed from the Clark–Lubs (W. M. Clark, H. A. Lubs, *J. Biol. Chem.* **1916**, *25*, 479–510) to the McIlvaine (T. C. McIlvaine, *J. Biol. Chem.* **1921**, *49*, 183–186) in the course of titration. With the Britton–Robinson buffer (H. T. S. Britton, R. A. Robinson, *J. Chem. Soc.* **1931**, 458–473 and 1456–1462), which can cover the required pH range, the sigmoid titration curve was not obtained.
[9] R. C. Haddon, F. Wudl, M. L. Kaplan, J. H. Marshall, R. E. Cais, F. B. Bramwell, *J. Am. Chem. Soc.* **1978**, *100*, 7629–7633.
[10] $E(\mathrm{SCE}) = E_{obsd}(\mathrm{ferrocene}) + 0.315$ V (W. E. Britton, J. P. Ferraris, R. L. Soulen, *J. Am. Chem. Soc.* **1982**, *104*, 5322–5325); $E(\mathrm{Ag/Ag^+}) = E_{obsd}(\mathrm{ferrocene}) + 0.089$ V (K. Komatsu, S. Aonuma, Y. Jinbu, R. Tsuji, C. Hirosawa, K. Takeuchi, *J. Org. Chem.* **1991**, *56*, 195–203). Therefore, $E(\mathrm{Ag/Ag^+}) = E(\mathrm{SCE}) - 0.226$ V.
[11] PM3 method: J. J. P. Stewart, *J. Comput. Chem.* **1989**, *10*, 209–220 and 221–264.
[12] MOPAC version 6: J. J. P. Stewart, QCPE No. 455. SYBYL version 6.1, TRIPOS Inc., 1699 S. Hanley Road, St. Louis, MO 63144-2913.

Parallel Differentiated Recognition of Ketones and Acetals**

Jian-xie Chen and Junzo Otera*

Integration of multistep chemical reactions into one-pot reactions is of great significance from both economical and ecological points of view. A number of one-pot processes, which are named tandem, cascade, domino reactions, etc., have received much attention.[1–3] In these protocols, similar or different types of reactions are performed in sequence without isolating intermediates. This strategy is particularly elegant in that the preceding reaction creates the necessary functionality for the subsequent one. Accordingly, the relevant reaction sites are inherited from one step to the next. In practical synthesis, however, we often need to carry out chemical transformations on separate reaction sites within a molecule. Conventionally, such transformations have been executed in a stepwise, not a one-pot, manner. If the manifold reactions could be performed simultaneously (that is, in parallel), the process would be efficient and expeditious [Eq. (1)]. Here we wish to advance a new concept based on



(1)

such parallel (or horizontal) treatment rather than the conventional series (or vertical) strategy.

To arrive at the ultimate goal of parallel recognition [Eq. (1)], we require a new concept of chemoselectivity in which a mixture of substrates A and B reacts with a mixture of reagents X and Y to furnish products A–X and B–Y exclusively or predominantly over other possible products [Eq. (2)]. The requirement would be satisfied if product AX could be formed predominantly over BX in the competition reaction of substrates A and B with reagent X [Eq. (3)] and

$$\mathrm{A + B + X + Y \longrightarrow A\text{–}X + B\text{–}Y} \qquad (2)$$

$$\mathrm{A + B + X \longrightarrow A\text{–}X\ (+B\text{–}X)} \qquad (3)$$

$$\mathrm{A + B + Y \longrightarrow B\text{–}Y\ (+A\text{–}Y)} \qquad (4)$$

BY in preference to AY in the reaction with reagent Y [Eq. (4)]. To our knowledge, no such treatment has been put forth intentionally, although the analogous selectivity might have incidentally resulted from unintentional performances on rare occasions.[4]

For reaction (2) to occur efficiently the substrates A and B should be similar to each other in chemical reactivity, so that reactions (3) and (4) can proceed under the identical reaction conditions. They should simultaneously undergo different reactions irrespective of the other. The reagents X and Y also

[*] Prof. Dr. J. Otera, Dr. J.-X. Chen
Department of Applied Chemistry
Okayama University of Science
Ridai-cho, Okayama 700 (Japan)
Fax: Int. code + (81) 86-252 6891
e-mail: otera@dac.ous.ac.jp

[**] This work was supported by the Japanese Society for the Promotion of Science under the "Research for the Future" Program (JSPS-PFTF96P00303)

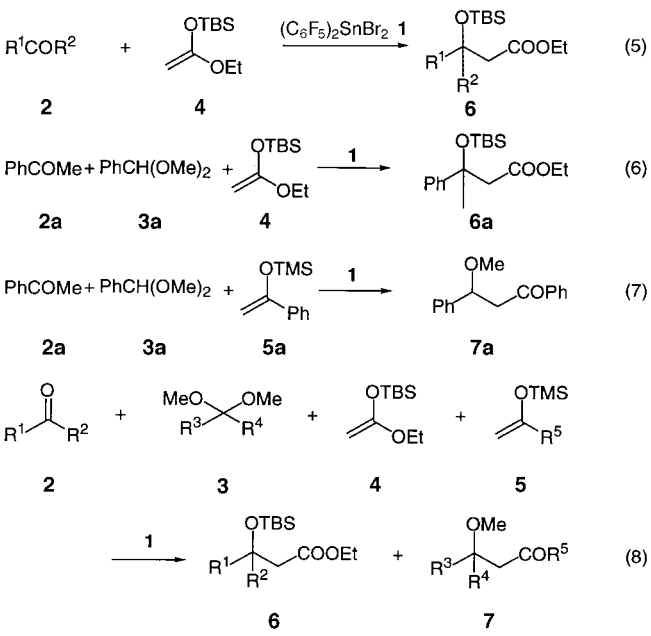
 © WILEY-VCH Verlag GmbH, D-69451 Weinheim, 1998 1433-7851/98/3701-0091 $ 17.50+.50/0

Table 1. Mukaiyama–aldol reaction of ketene silyl acetal **4** with ketone **2**, catalyzed by **1**.[a]

2		Reaction time [h]	Yield of **6** [%][b]
R^1	R^2		
Ph	CH_3	2	92
Ph	C_2H_5	5	85
C_2H_5	CH_3	1	87
n-C_6H_{13}	CH_3	2	95
t-C_4H_9	CH_3	4.5	78
$(CH_2)_5$		2	93

[a] Reaction conditions: 2:4:1 = 1.0:3:0.1, CH_2Cl_2, −78°C. [b] Yield of isolated product after column chromatography.

need to work in this way. In studies on synthetic applications of organotin Lewis acids we disclosed that bis(pentafluorophenyl)tin dibromide (**1**)[5] effects the Mukaiyama–aldol reaction of ketene silyl acetal **4** with ketones **2** quite smoothly [Eq. (5), TBS = *tert*-butyldimethylsilyl; Table 1]. These are the first examples, to our knowledge, in which ketones are successfully activated by an organotin Lewis acid. In addition, no reaction occurs with acetals **3** under the same reaction conditions. As a result, the competition reaction between acetophenone (**2a**) and benzaldehyde dimethyl acetal (**3a**) towards **4** furnishes ketone adduct **6a** exclusively (Eq. 6),[6] satisfying the condition for Equation (3). On the other hand, reaction of enol silyl ether **5a** derived from acetophenone led



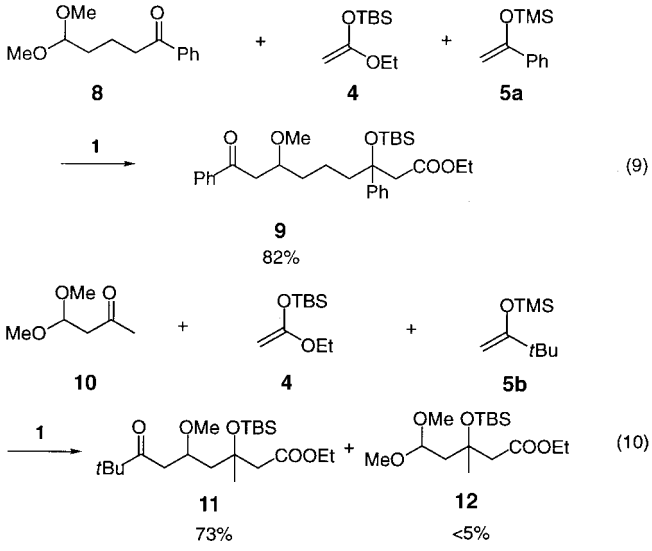
to the totally opposite outcome, giving acetal aldolate **7a** exclusively [Eq. (7), TMS = trimethylsilyl],[7] satisfying the condition for Equation (4). With these results in hand, we treated a mixture of **2** and **3** with a mixture of **4** and **5** [Eq. (8)].[8] A clean reaction took place, and the catalyst indeed fulfilled a double role. As shown in Table 2, only the doublet **6** and **7** emerged, and no products derived from other combinations were detected at all.

Table 2. Chemospecific parallel reactions (8).

2		**3**		**5**	Yield [%][a]	
R^1	R^2	R^3	R^4	R^5	**6**	**7**
Ph	CH_3	n-C_6H_{13}	CH_3	Ph	84[b]	83[c]
Ph	CH_3	n-C_7H_{15}	H	Ph	83	83
Ph	CH_3	Ph	H	tBu	89	73
4-$MeOC_6H_4$	CH_3	n-C_7H_{15}	H	Ph	83	65
n-C_6H_{13}	CH_3	n-C_6H_{13}	CH_3	Ph	83	83
n-C_6H_{13}	CH_3	n-C_7H_{15}	H	Ph	82	80
n-C_6H_{13}	CH_3	Ph	H	tBu	74	85
n-C_4H_9	CH_3	n-C_6H_{13}	CH_3	Ph	86	82
$(CH_2)_5$		Ph	H	tBu	74	80
$(CH_2)_5$		n-C_6H_{13}	CH_3	Ph	86	78

[a] Yields of **6** based on **4** and of **7** based on **3** were determined by gas chromatography. [b] 72% yield of isolated product. [c] 61% yield of isolated product.

This protocol was successfully applied to an intramolecular reaction. Keto acetals **8** and **10** were exposed to a mixture of enol silyl ethers **4** and **5** in the presence of **1** [Eqs. (9) and (10)].[9] As sole product **9**[10] was obtained in reaction (9), while reaction (10) provided a small amount of monoconverted product **12** in addition to major product **11**. Never-



theless, the complete parallel chemospecificity held in these cases as well.

We have already revealed the synthetic usefulness of weak Lewis acidity of organotin catalysts.[5, 11–13] It is the weak acidity of **1** that has enabled the parallel recognition. Its weak Lewis acidity is essential for detecting the subtle differences between ketone and acetal. Somewhat similar but actually different selectivity was found with a $Bu_2Sn(OTf)_2$ catalyst: Mukaiyama–aldol reaction of both **4** and **5** with acetal **3** took place smoothly but no reaction with ketone **2**.[11] Apparently, this catalyst succeeded in differentiating the substrates to some extent but failed to differentiate between reagents **4** and **5**. Moreover no preference for ketone over acetal was observed. This contrast well illuminates the unique activities of **1**.

 © WILEY-VCH Verlag GmbH, D-69451 Weinheim, 1998 1433-7851/98/3701-0092 $ 17.50+.50/0 *Angew. Chem. Int. Ed.* **1998**, *37*, No. 1/2

The intramolecular version is significant from a synthetic point of view, because it has potential as a new strategy for highly expeditious chemical processes. The following advantages are apparent for the parallel treatment: 1) No special elaboration on substrates is required. 2) Reactions that are commonly encountered in organic synthesis are employable. Needless to say, the carbonyl differentiation is not the only method suitable for this concept. 3) Conceivably, the scope will be expanded to a wider range where more than two parallel transformations are performed.

Promotion of multifold reactions by a single catalyst is of great importance. In some sequential reactions, catalysts work for more than one reaction,[14–18] yet each step involves a single reaction; hence, the catalysts are not required to promote several reactions simultaneously. On the other hand, the parallel recognition demands that the catalysts effect simultaneous reactions in a exclusive manner. Many catalysts, however, are available that can activate different types of reaction, and, accordingly, the concept of parallel recognition will find a variety of applications if the reaction conditions are suitably adjusted.

Experimental Section

General intermolecular parallel recognition: To a dichloromethane solution (3 mL) of **1** (31 mg, 0.05 mmol) was added a solution of ketone **2** (2.5 mmol) and acetal **3** (0.5 mmol) in dichloromethane (2 mL) at $-78^{\circ}C$. Then, a dichloromethane solution (2 mL) of **4** (0.5 mmol) and **5** (0.65 mmol) was added. The reaction mixture was stirred at this temperature for 4 h. Water (2 mL) was added to this solution. The reaction mixture was extracted with dichloromethane, and the extract washed with water and brine. The organic layer was dried (Na_2SO_4), and the solvent removed. The crude product thus obtained was analyzed by GLC.

Example of typical intramolecular parallel recognition: To a dichloromethane solution (5 mL) of **1** (122 mg, 0.2 mmol) and keto acetal **8** (122 mg, 0.55 mmol) was added a solution of **4** (101 mg, 0.5 mmol) and **5a** (384 mg, 2.0 mmol) in dichloromethane (2 mL) at $-78^{\circ}C$. The reaction mixture was stirred at this temperature for 7 h, after which water was added. The reaction mixture was extracted with dichloromethane, and the extract washed with water and brine. The organic layer was dried (Na_2SO_4), and the solvent removed. The residue was chromatographed on silica gel (eluent hexane/ethyl acetate 8/1) to give **9** (210 mg, 82 %). This compound was stirred in HF/CH_3CN solution at room temperature for 7 h. Usual workup and column chromatography quantitatively furnished the desilylated product (ethyl 8-benzoyl-3-hydroxy-7-methoxy-3-phenyloctanoate): ^1H NMR ($CDCl_3$): $\delta = 1.07$ (t, 3H, $J = 7.1$ Hz, CH_3), 1.42–1.82 (m, 6H, $3CH_2$), 2.77–3.24 (m, 4H, $2CH_2$), 3.25, 3.26 (1:1 mixture of diastereomers; s, 3H, OCH_3), 3.78 (m, 1H, CH), 4.00 (q, 2H, $J = 7.1$ Hz, CH_2), 4.40 (br., 1H, OH), 7.20–7.57 (m, $8H_{arom}$), 7.91 (m, $2H_{arom}$); ^{13}C NMR ($CDCl_3$): δ[19] = 13.85, 19.01 (19.07), 34.25 (34.35), 42.99 (43.06), 45.28 (45.33), 57.11, 60.62, 74.88, 77.28, 124.92, 126.67, 128.05 (128.08), 128.47, 132.98, 137.18, 145.15, 145.19, 172.77, 198.90; HRMS calcd for $C_{24}H_{31}O_5$ [$(M+1)^+$] 399.2171, found 399.2188; C,H analysis calcd. for $C_{24}H_{30}O_5$: C 72.34, H 7.59; found: C 72.39, H 7.34.

11: ^1H NMR[20] ($CDCl_3$): $\delta = 0.07$ (s, 3H, CH_3), 0.08 (s, 3H, CH_3), 0.83 (s, 9H, *t*Bu), 1.12 (s, 9H, *t*Bu), 1.24 (t, 3H, $J = 7.1$ Hz, CH_3), 1.43 (s, 3H, CH_3), 1.65–1.95 (m, 2H, CH_2), 2.51 (m, 2H, CH_2), 2.54–2.86 (m, 2H, CH_2), 3.24 (s, 3H, OCH_3), 3.89–3.93 (m, 1H, CH), 4.08 (q, 2H, $J = 7.1$ Hz, CH_2); ^{13}C NMR ($CDCl_3$): $\delta = -2.08$ (−1.96),[19] 14.16, 18.05, 25.75, 26.08, 27.40, 42.34, 44.30, 47.10, 48.57, 56.58, 60.08, 73.99, 74.46, 170.94, 214.16; HRMS: calcd for $C_{20}H_{39}O_5Si$ [$(M - CH_3)^+$] 387.2567, found 387.2558; C,H analysis calcd. for $C_{21}H_{42}O_5Si$: C 62.64, H 10.51; found: C62.87, H 10.68.

12: ^1H NMR ($CDCl_3$): $\delta = 0.09$ (s, 6H, CH_3), 0.84 (s, 9H, *t*Bu), 1.24 (t, 3H, $J = 7.1$ Hz, CH_3), 1.40 (s, 3H, CH_3), 1.87–2.01 (m, 2H, CH_2), 2.51 (m, 2H, CH_2), 3.28 (s, 6H, OCH_3), 4.09 (q, 2H, $J = 7.1$ Hz, CH_2), 4.61 (t, 1H, $J = 5.0$ Hz, CH); C,H analysis calcd. for $C_{16}H_{34}O_4Si$: C 57.45, H 10.24; found C 57.02, H, 9.89.

Received: June 24, 1997
Revised version: September 16, 1997 [Z10595/10596IE]
German version: *Angew. Chem.* **1998**, *110*, 96–98

Keywords: aldol reactions · carbonyl differentiation · chemoselectivity · one-pot reactions · tin

[1] G. H. Posner, *Chem Rev.* **1986**, *86*, 831.
[2] L. F. Tietze, U. Beifuss, *Angew. Chem.* **1993**, *105*, 137; *Angew. Chem. Int. Ed. Engl.* **1993**, *32*, 131.
[3] Special issues on this subject: *Chem. Rev.* **1996**, *96* (1); *Tetrahedron* **1996**, *52* (35).
[4] Mori et al. reported the analogous differentiation between aldehydes, but not different functional groups, by ketene silyl acetal and trimethylsilyl cyanide: A. Mori, H. Ohno, S. Inoue, *Chem. Lett.* **1992**, 631. Parallel kinetic resolution would be another relevant reaction if enantiomers are regarded as different substrates: J. Brandt, C. Jochum, I. Ugi, *Tetrahedron*, **1977**, *33*, 1353; E. Vedejs, X. Chen, *J. Am. Chem. Soc.* **1997**, *119*, 2584.
[5] J. Chen, K. Sakamoto, A. Orita, J. Otera, *Synlett* **1996**, 877.
[6] Reaction conditions: **2a**:**3a**:**4**:**1** = 1.0:1.0:1.3:0.1; CH_2Cl_2, $-78^{\circ}C$, 2 h; yield of isolated product: 91 %.
[7] Reaction conditions: **2a**:**3a**:**5a**:**1** = 1.0:1.0:1.3:0.1, CH_2Cl_2, $-78^{\circ}C$, 5 h; yield of isolated product: 63 %.
[8] Reaction conditions: **2**:**3**:**4**:**5**:**1** = 5.0:1.0:1.0:1.3:0.1, CH_2Cl_2, $-78^{\circ}C$, 5 h. It is crucial to use an excess of **2** to consume **4** as quickly as possible, otherwise the decomposition of the catalyst is inevitable during the reaction, resulting in low yields of **7**.
[9] Reaction conditions: **8**:**4**:**5**:**1** = 1.1:1.0:4.0:0.4 or **10**:**4**:**5**:**1** = 1.0:1.0:4.0:0.3; CH_2Cl_2, $-78^{\circ}C$, 7 h. Yields of isolated products were determined after column chromatography.
[10] Determined as the tertiary alcohol by cleavage of TBS (HF/CH_3CN).
[11] T. Sato, J. Otera, H. Nozaki, *J. Am. Chem. Soc.* **1990**, *112*, 901.
[12] J. Otera, N. Dan-oh, H. Nozaki, *J. Org. Chem.* **1991**, *56*, 5307.
[13] J. Otera, J. Chen. *Synlett* **1996**, 321.
[14] Review: A. Heumann, M. Réglier, *Tetrahedron* **1996**, *52*, 9289.
[15] R. Grigg, R. Rasul, J. Redpath, D. Wilson, *Tetrahedron Lett.* **1996**, *37*, 4609.
[16] L. F. Tietze, K. Heitmann, T. Raschke, *Synlett* **1997**, 35.
[17] K. Mikami, S. Matsukawa, M. Nagashima, H. Funabashi, H. Morishima, *Tetrahedron Lett.* **1997**, *38*, 579.
[18] A. Kojima, S. Honzawa, C. D. J. Boden, M. Shibasaki, *Tetrahedron Lett.* **1997**, *38*, 3455.
[19] Chemical shifts of the diastereomer are given in the parentheses.
[20] It is conceivable that there are diasteromers, yet no NMR evidence was obtained explicitly.

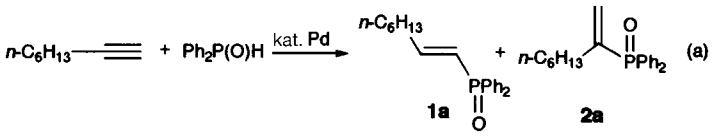
 © WILEY-VCH Verlag GmbH, D-69451 Weinheim, 1998 1433-7851/98/3701-0093 $ 17.50+.50/0

Phosphinic Acid Induced Reversal of Regioselectivity in Pd-Catalyzed Hydrophosphinylation of Alkynes with $Ph_2P(O)H$**

Li-Biao Han, Ruimao Hua, and Masato Tanaka*

One of the most attractive features of transition metal complex catalyzed addition to carbon–carbon multiple bonds is in the ease of fine-tuning the ligands for better regioselectivities. However, a sharp reversal of the selectivity by fine-tuning the ligand is not always an easy task, since the regioselectivity is usually inherent in the central metal of the catalyst.[1] We recently developed palladium-catalyzed additions of diphenylphosphane oxide to alkynes,[2] which allows efficient preparation of alkenylphosphane oxides of biological and synthetic value.[3] We now report a reversal of the regioselectivity: The selectivity of the addition of $Ph_2P(O)H$ to terminal alkynes, which normally forms (E)-β-adducts selectively,[2] switches in favor of α-adducts simply in the presence of just one drop of $Ph_2P(O)OH$ in the reaction mixture.

As previously reported,[2] when an equimolar mixture of diphenylphosphane oxide and 1-octyne in C_6D_6 was heated at 70 °C for 2 h in the presence of *cis*-$[Me_2Pd(PPhMe_2)_2]$ (5 mol% relative to the substrate), isomeric products **2a** and **1a** were formed in 75% total yield (NMR) in a ratio of 12:88 [Eq. (a)]. Surprisingly the regioselectivity was completely reversed when the same reaction was repeated in the presence of trace diphenylphosphinic acid. Therefore, the reaction in the presence of only 1 mol% of $Ph_2P(O)OH$ (relative to the substrate) resulted in 92% total yield and a **2a**:**1a** ratio of 79:21.[4] The regioselectivity for **2a** was further improved with an increased amount of $Ph_2P(O)OH$ to achieve nearly quantitative formation of the adducts in a ratio of 95:5 in the presence of 5 mol% of $Ph_2P(O)OH$. Besides the phosphinic acid, dibutyl phosphate (92%, **2a**:**1a** = 90:10) and phosphoric acid (89%, **2a**:**1a** = 85:15) also gave **2a** as the major product. However, a similar reversal did not result when hexamethyl phosphoramide (HMPA, 76%, **2a**:**1a** = 13:87), acetic acid (73%, **2a**:**1a** = 20:80), or benzoic acid (76%, **2a**:**1a** = 13:87) was employed.



As Table 1 suggests, the reactions catalyzed by palladium complexes with sterically less demanding and more basic phosphane ligands are more sensitively affected by $Ph_2P(O)OH$. In *cis*-$[PdMe_2(PPh_3)_2]$-catalyzed reactions, for instance, the **2a**:**1a** ratio of 9:91 in the absence of $Ph_2P(O)OH$ increased significantly, but without reversal of the regioselectivity, to 37:63 when 5 mol% of $Ph_2P(O)OH$ was added. On the other hand, as already described, addition of 5 mol% of $Ph_2P(O)OH$ to the *cis*-$[PdMe_2(PPhMe_2)_2]$-catalyzed reaction induced a reversal of the ratio from 12:88 to 95:5. In *cis*-$[PdMe_2(PPh_2Me)_2]$-catalyzed reactions neither decreasing the reaction temperature from 70 to 45 °C nor changing the solvent from benzene to THF affected the regioselectivity.

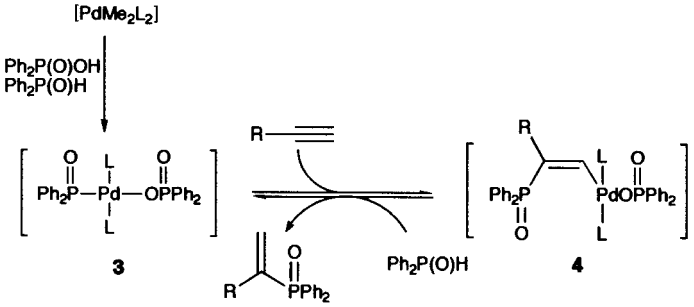
Table 1. Hydrophosphinylation of 1-octyne.[a]

Catalyst	Conditions	Yield [%] with $Ph_2P(O)OH$ (**2a**:**1a**)[b]	Yield [%] without $Ph_2P(O)OH$ (**2a**:**1a**)[b]
$[Pd(PPh_3)_4]$	70 °C, 3 h	89 (33:67)	54 (8:92)
cis-$[PdMe_2(PPh_3)_2]$	70 °C, 3 h	73 (37:63)	43 (9:91)
cis-$[PdMe_2(PPh_2Me)_2]$	70 °C, 3 h	100 (84:16)	56 (10:90)[c]
cis-$[PdMe_2(PPhMe_2)_2]$	70 °C, 2 h	93 (95:5)	75 (12:88)
$[PdMe_2(PEt_3)_2]$[d]	70 °C, 2 h	95 (91:9)	51 (13:87)
$[PdMe_2(dmpe)]$[e]	100 °C, 6 h	93 (92:8)	0

[a] All reactions were conducted in a sealed NMR tube with equimolar amounts of $Ph_2P(O)H$ and 1-octyne (0.25 mmol) dissolved in C_6D_6 (0.5 mL) in the presence of 5 mol% of Pd catalyst. [b] In the presence of 5 mol% of $Ph_2P(O)OH$. The yields for the reactions with and without $Ph_2P(O)OH$ were determined by NMR spectroscopy. [c] Reaction time = 2.5 h. [d] *cis*:*trans* = 1:1. [e] dmpe = 1,2-bis(dimethylphosphino)ethane.

$Ph_2P(O)OH$ also enhances the catalytic activity. For example $[PdMe_2(dmpe)]$, which was nearly inactive in the absence of $Ph_2P(O)OH$, catalyzed the addition at 100 °C. Activities of other palladium–phosphane complexes were also boosted (see Table 1). A seemingly puzzling aspect is that even 1% of $Ph_2P(O)OH$ was sufficient to reverse the regioselectivity, despite a larger quantity (5%) of *cis*-$[Me_2Pd(PPhMe_2)_2]$ in the reaction system (see above). This is presumably due to a new palladium species that is formed upon addition of the phosphinic acid and is more catalytically active.

The present results strongly indicate that the OH group plays a crucial role in inducing the intriguing effect of $Ph_2P(O)OH$ (and related compounds).[5] We believe that the process shown in Scheme 1 is occurring: 1) generation of a new reactive Pd species **3**, 2) insertion of a C≡C unit into the Pd–$P(O)Ph_2$ bond (phosphinylpalladation) with formation of an alkenylpalladium species **4**, and 3) subsequent protonol-



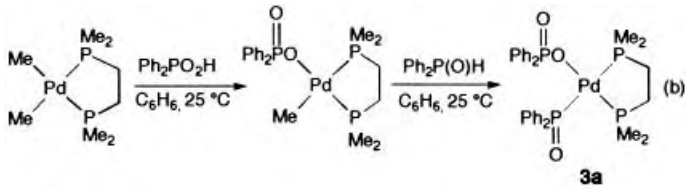
Scheme 1. Proposed mechanism for the Pd-catalyzed hydrophosphinylation (L = PR_3).

[*] Prof. Dr. M. Tanaka, Dr. L.-B. Han, Dr. R. Hua
National Institute of Materials and Chemical Research
Tsukuba, Ibaraki 305 (Japan)
Fax: Int. code + (81) 298-54 4474
e-mail: mtanaka@ccmail.nimc.go.jp

[**] We are grateful to the Japan Science and Technology Corporation (JST) for partial financial support through the Core Research for Evolutional Science and Technology (CREST) program and for a postdoctoral fellowship to R.H. We thank Dr. N. Choi for participation in the initial stage of this work.

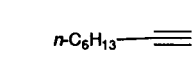
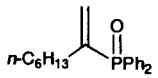
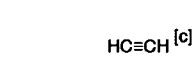
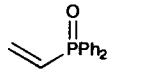
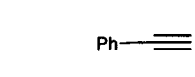
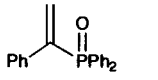
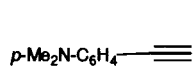
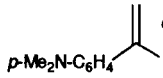
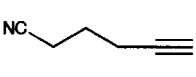
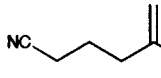
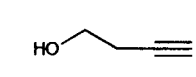
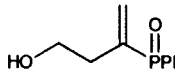
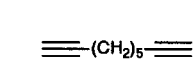
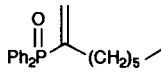
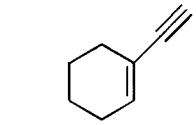
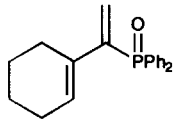
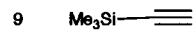
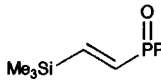
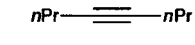
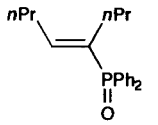
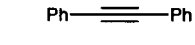
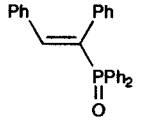
 © WILEY-VCH Verlag GmbH, D-69451 Weinheim, 1998 1433-7851/98/3701-0094 $ 17.50+.50/0

ysis of **4** with $Ph_2P(O)H$[6] leading to the α-adduct with concomitant regeneration of **3**.[7] Protonolysis of a C–Pd bond in the generation of **3** from $[PdMe_2L_2]$ and its regeneration from **4** appears reasonable, since similar protonolyses with various acidic reagents are known.[8] We were able to confirm such reactions with $Ph_2P(O)H$ and $Ph_2P(O)OH$. When $[PdMe_2(PEt_3)_2]$ and $[Ph_2P(O)H]$ (4 equiv) were mixed in C_6D_6 at 25 °C, methane gas immediately evolved, and the colorless solution became pale yellow. The starting material $[PdMe_2(PEt_3)_2]$ disappeared within 0.5 h, and the ^{31}P NMR spectrum displayed signals for a new Pd complex in addition to those for remaining $Ph_2P(O)H$ ($\delta = 17.2$) and free PEt_3 ($\delta = -19.6$). Although the complex could not be isolated, the structure was assigned as $[PdMe\{P(O)Ph_2\}(PPh_2OH)(PEt_3)]$ on the basis of NMR data; the oxygen atoms are linked through an O-H-O hydrogen bond. Likewise, when $Ph_2P(O)OH$ was added to *trans*-$[PdMe_2(PEt_3)_2]$ (1 equiv) in benzene at 25 °C, evolution of methane gas was immediately observed, and a colorless oil of *trans*-$[PdMe\{OP(O)Ph_2\}(PEt_3)_2]$ produced quantitatively.[9] A similar reaction with *cis*-$[PdMe_2(dmpe)]$ allowed isolation of analytically pure *cis*-$[PdMe[OP(O)Ph_2](dmpe)]$ as a white solid. The resulting complex did not react further with excess $Ph_2P(O)OH$, even at 70 °C. Very interestingly, however, protonolysis of the complex with one equivalent of $Ph_2P(O)H$ proceeded readily at room temperature and *cis*-$[Pd\{Ph_2P(O)\}\{OP(O)Ph_2\}(dmpe)]$ (**3a**) was obtained as a white solid in good yield with liberation of another molecule of methane [Eq. (b)].[10] We were unable to detect intermediates formed by insertion of a C≡C unit into the Pd–$P(O)Ph_2$ bond in reactions of **3a** with acetylenes. In strong support of the proposed mechanism shown in Scheme 1, however, **3a** catalyzed the addition of $Ph_2P(O)H$ to 1-octyne at 100 °C in the absence of $Ph_2P(O)OH$; the adducts were obtained in 95% yield (NMR) with a **2a**:**1a** ratio of 90:10 after 10 h, which was in good agreement with the value observed for $[PdMe_2(dmpe)]$-catalyzed addition in the presence of $Ph_2P(O)OH$ (Table 1).



As shown in Table 2, this new recipe for hydrophosphinylation could be generally applied to various aliphatic and aromatic terminal alkynes to afford a variety of 1-alken-2-ylphosphane oxides regioselectively and in good yields. Functionalities such as amino, cyano, and hydroxyl groups were tolerated under the reaction conditions. As exemplified by entry 7, two phosphinyl groups could be efficiently introduced to both C–C triple bonds. Under the reaction conditions an olefinic bond is unreactive with respect to hydrophosphinylation. Accordingly, 1-ethynylcyclohexene (entry 8) underwent selective addition at the triple bond. As for the regioselectivity, the reaction of (trimethylsilyl)acetylene is an exception: Only the terminal carbon atom was phosphinylated, presumably owing to the steric hindrance at the internal carbon atom. Acetylenes with internal C≡C units also reacted, albeit somewhat slowly, to afford the corresponding products selectively. Worth noting from another synthetic viewpoint is that the reaction run in the presence of the phosphinic acid is very clean. On the other hand, reactions carried out without the phosphinic acid resulted in unidentified by-products, in particular at higher temperatures.[2] Applications of the current finding to other transition metal complex catalyzed additions are now under extensive study.

Table 2. Hydrophosphinylation of alkynes.[a]

Entry	Alkyne	Adduct	Yield [%] (**2**:**1**)[b]
1			92 (95/5)
2			54
3			78 (98/2)
4			86 (97/3)
5			90 (94/6)
6			93 (93/7)
7			85 [d]
8			89 (98/2)
9			63 [e, f]
10			81 [g]
11			94 [h]

[a] Conditions: equimolar amounts of $Ph_2P(O)H$ and alkyne in benzene (≈ 0.5 M), 3–4 mol% of *cis*-$[PdMe_2(PPhMe_2)_2]$, ≈ 5 mol% of $Ph_2P(O)OH$, 70 °C, 2–4 h. [b] Yields refer to isolated amounts after column chromatography or preparative gel permeation chromatography (GPC). The ratios of isomers were determined by ^1H NMR spectroscopy of the crude reaction mixture. [c] 1 atm CH≡CH, 70 °C, 5 h. [d] Amount of $Ph_2P(O)H$ used = 2.2 equiv. Regioselectivity > 95%. [e] *cis*-$[PdMe_2(PPh_2Me)_2]$ was used as the catalyst. [f] Only the *trans* isomer was formed. [g] Heated for 36 h. [h] Heated for 12 h.

Experimental Section

Catalytic additions of $Ph_2P(O)H$: Diphenylphosphane oxide (202 mg, 1.0 mmol), 1-octyne (110 mg, 1.0 mmol), diphenylphosphinic acid (11 mg, 5 mol%), and *cis*-[$PdMe_2(PPhMe_2)_2$] (12 mg, 3 mol%) were dissolved in dry benzene (2 mL) under argon. The solution was heated at 70 °C for 4 h and evaporated in vacuo to leave a pale yellow oil, which was purified by column chromatography (SiO_2, EtOAc/hexane 1/1) to give the adducts as a colorless oil in 92% combined yield (287 mg, 0.92 mmol, **2a**:**1a** = 95:5). The two regioisomers (**2a** and **1a**) could be isolated by preparative thin layer chromatography (PTLC; silica gel, hexane/EtOAc 2/3; **2a**: 250 mg, 80% yield; **1a**: 11 mg, 4% yield).

2a: Colorless oil. ^{1}H NMR (300 MHz, C_6D_6): δ = 7.77 – 7.83 (m, 4H), 7.05 – 7.16 (m, 6H), 5.60 (d, 1H, J(H,P) = 42.1 Hz), 5.55 (d, 1H, J(H,P) = 20.4 Hz), 2.30 – 2.38 (m, 2H), 1.39 – 1.49 (m, 2H), 1.01 – 1.21 (m, 6H), 0.80 (t, 3H, J = 6.8 Hz); ^{13}C NMR (C_6D_6, 75.5 MHz): δ = 145.8 (J(C,P) = 90.8 Hz), 133.4 (J(C,P) = 99.8 Hz), 132.2 (J(C,P) = 9.3 Hz), 131.5 (J(C,P) = 2.7 Hz), 128.5 (J(C,P) = 11.6 Hz), 127.8 (J(C,P) = 9.6 Hz), 32.6 (J(C,P) = 15.0 Hz), 31.9, 29.2, 28.7 (J(C,P) = 4.9 Hz), 22.9, 14.2; ^{31}P NMR (C_6D_6, 121.5 MHz): δ = 27.9; IR (neat/NaCl): $\tilde{\nu}$ = 3058, 2930, 2860, 1437, 1191, 1120, 940, 727, 696 cm^{-1}. HRMS calcd for $C_{20}H_{25}OP$: 312.1642, found: 312.1624.

1a: White solid, m.p. 68 – 69 °C. ^{1}H NMR (300 MHz, C_6D_6): δ = 7.78 – 7.85 (m, 4H), 7.05 – 7.08 (m, 6H), 6.87 – 7.01 (m, 1H), 6.11 (dd, 1H, J = 16.9, J(H,P) = 25.1 Hz), 1.87 – 1.91 (m, 2H), 1.09 – 1.21 (m, 8H), 0.82 (t, 3H, J = 6.8 Hz); ^{13}C NMR (C_6D_6, 75.5 MHz): δ = 152.2 (J(C,P) = 1.7 Hz), 135.4 (J(C,P) = 92.9 Hz), 131.6 (J(C,P) = 9.5 Hz), 131.3 (J(C,P) = 2.7 Hz), 128.5 (J(C,P) = 11.7 Hz), 123.1 (J(C,P) = 101.8 Hz), 34.6 (J(C,P) = 16.6 Hz), 31.8, 29.1, 28.1, 22.9, 14.2; ^{31}P NMR (C_6D_6, 121.5 MHz): δ = 18.9; IR (KBr): $\tilde{\nu}$ = 2962, 2928, 2856, 1632, 1439, 1185, 1122, 1002, 814, 745 cm^{-1}. HRMS calcd for $C_{20}H_{25}OP$: 312.1642, found: 312.1603.

cis-[PdMe[OP(O)Ph_2](dmpe)]: To a solution of *cis*-[$PdMe_2$(dmpe)] (17.2 mg, 0.06 mmol) in toluene/CH_2Cl_2 (1/1, 6 mL) was added $Ph_2P(O)OH$ (13 mg, 0.06 mmol) at room temperature under nitrogen. As the solid $Ph_2P(O)OH$ gradually dissolved, gas evolution from the solution was observed. A transparent colorless solution was obtained after 1 h at room temperature. Concentration of the solution to about half its volume in vacuo afforded a white precipitate of *cis*-[PdMe[OP(O)Ph_2](dmpe)] (28.6 mg, 0.058 mmol, 97% yield); m.p. 164 °C (decomp). ^{1}H NMR (300 MHz, $CDCl_3$): δ = 7.26 – 7.94 (m, 10H), 1.74 (br s, 2H), 1.48 – 1.55 (m, 14H), 0.55 (dd, 3H, J(H,P) = 2.2, 8.2 Hz); ^{31}P NMR ($CDCl_3$, 121.5 MHz): δ = 37.2 (d, J(P,P) = 23.0 Hz), 22.6 (s), 21.4 (d, J(P,P) = 23.0 Hz); elemental analysis calcd for $C_{19}H_{29}O_2P_3Pd$: C 46.69, H 5.98; found: C 46.63, H 5.97.

3a: To a solution of *cis*-[$PdMe_2$(dmpe)] (116.4 mg, 0.406 mmol) in benzene (4 mL) was added $Ph_2P(O)OH$ (88.6 mg, 0.406 mmol) at room temperature under nitrogen. Gas evolution was observed immediately. After the mixture was stirred for 6 h at room temperature, a solution of $Ph_2P(O)H$ (82.1 mg, 0.406 mmol) in benzene (3 mL) was slowly added. The reaction mixture was stirred overnight to afford analytically pure **3a** as a white solid (255.1 mg, 0.378 mmol, 93%); m.p. 198 °C (decomp). ^{1}H NMR (300 MHz, $CDCl_3$): δ = 7.16 – 7.80 (m, 20H), 1.80 (dd, 6H, J(H,P) = 1.8, 12.0 Hz), 1.71 – 1.83 (m, 4H), 1.56 (dd, 6H, J(H,P) = 3.5, 10.2 Hz); ^{31}P NMR ($CDCl_3$, 121.5 MHz): δ = 66.8 (d, J(P,P) = 467.8 Hz), 42.7 (d, J(P,P) = 33.4 Hz), 26.1 (d, J(P,P) = 9.2 Hz), 20.6 (ddd, J(P,P) = 9.2, 33.4, 467.8 Hz); elemental analysis calcd for $C_{30}H_{36}O_3P_4Pd$: C 53.39, H 5.38; found: C 53.57, H 5.68.

Received: July 4, 1997 [Z 10638 IE]
German version: *Angew. Chem.* **1998**, *110*, 98 – 101

Keywords: alkynes · homogeneous catalysis · palladium · phosphorus · regioselectivity

[1] For partial reversal of the regioselectivity in hydrosilylation, see a) K. H. Pannell, J. Rozell, J. Lii, S.-Y. Tien-Mayr, *Organometallics* **1988**, *7*, 2524; b) M. Rivera-Claudio, J. Rozell, J. E. Ramirez-Oliva, J. Cervantes, K. H. Pannell, *J. Organomet. Chem.* **1996**, *521*, 267.

[2] L.-B. Han, N. Choi, M. Tanaka, *Organometallics* **1996**, *15*, 3259.

[3] a) *Handbook of Organophosphorus Chemistry* (Ed.: R. Engel), Marcel Dekker, New York, **1992**; b) C. R. Johnson, T. Imamoto, *J. Org. Chem.* **1987**, *52*, 2170; c) K. M. Pietrusiewicz, M. Zablocka, W. Wisniewski, *Phosphorus, Sulfur Silicon Relat. Elem.* **1990**, *49-50*, 263; d) K. M. Pietrusiewicz, W. Wisniewski, M. Zablocka, *Tetrahedron* **1989**, *45*, 337; e) K. M. Pietrusiewicz, M. Zablocka, *Tetrahedron Lett.* **1988**, *29*, 1991; f) H. Brunner, S. Limmer, *J. Organomet. Chem.* **1991**, *417*, 173; g) J. Berlan, J.-P. Battioni, K. Koosha, *Tetrahedron Lett.* **1976**, 3351; h) K. M. Pietrusiewicz, M. Zablocka, *ibid.* **1988**, *29*, 937; i) A. Brandi, S. Cicchi, A. Goti, *ibid.* **1991**, *32*, 3265.

[4] In the absence of the catalyst, neither **1a** nor **2a** was obtained under the same conditions.

[5] The possibility of isomerization of **1a** to **2a** catalyzed by $Ph_2P(O)OH$ as the origin of the reversal is readily ruled out, since **1a** did not isomerize to **2a** when heated with $Ph_2P(O)OH$ (13 mol% relative to **1a**) in C_6D_6 at 70 °C for 4 h. Isomerization was also not observed when pure **1a** was added to the solution of the *cis*-[$PdMe_2(PPhMe_2)_2$]-catalyzed reaction of $Ph_2P(O)H$ with 1-octyne in the presence of 5 mol% of $Ph_2P(O)OH$ (Table 1) and reheated at 70 °C for 2 h.

[6] Secondary phosphane oxides exist in two tautomeric forms, P(=O)H and P–OH; the former is dominant in the equilibrium: a) W. J. Bailey, R. B. Fox, *J. Org. Chem.* **1963**, *28*, 531; b) W. J. Bailey, R. B. Fox, *ibid.* **1964**, *29*, 1013; c) L. A. Hamilton, P. S. Landis in *Organic Phosphorus Compounds*, *Vol. 4* (Eds.: G. M. Kosolapoff, L. Maier), Wiley, New York, **1972**, chap. 11.

[7] Hydrophosphinylation of alkynes in the absence of $Ph_2P(O)OH$ proceeds by hydropalladation; see ref. [2].

[8] a) Y.-J. Kim, K. Osakada, A. Takenaka, A. Yamamoto, *J. Am. Chem. Soc.* **1990**, *112*, 1096; b) F. Kawataka, Y. Kayaki, I. Shimizu, A. Yamamoto, *Organometallics* **1994**, *13*, 3517.

[9] The reaction of *cis*-[$PdMe_2(PEt_3)_2$] gave the same product. The complex did not react further with excess $Ph_2P(O)OH$ even upon heating at 70 °C for 2 h.

[10] Complex **3a** was similarly obtained when $Ph_2P(O)H$ was added first to [$PdMe_2$(dmpe)] followed by treatment with $Ph_2P(O)OH$.

Molecular Aluminophosphonate: Model Compound for the Isoelectronic Double-Six-Ring (D6R) Secondary Building Unit of Zeolites**

Yu Yang, Mrinalini G. Walawalkar, Jiri Pinkas, Herbert W. Roesky,* and Hans-Georg Schmidt

Dedicated to Professor Herbert D. Kaesz on the occasion of his 65th birthday

One of the main thrusts in the area of advanced materials has been the synthesis of phosphate materials of Al and Ga,[1–5] which can potentially serve as highly organized matrices of tunable pore size and shape. Since the first successful synthesis of aluminophosphate materials in 1982,[1] several groups have synthesized alumino- and gallophosphate materials by hydrothermal routes in the presence of structure-directing agents.[2–5] To understand the local structures of these complex materials, a few soluble model compounds were prepared which can also serve as secondary building

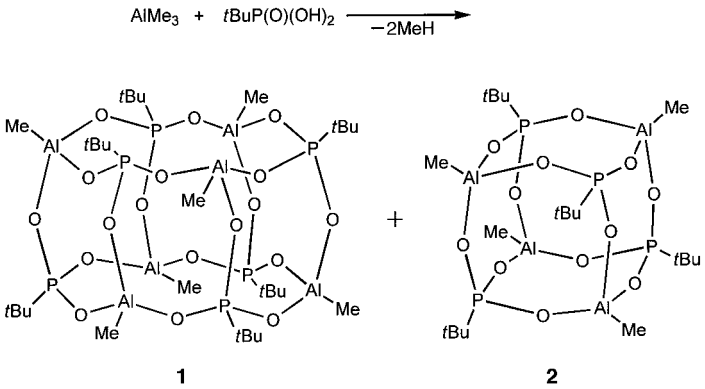
[*] Prof. Dr. H. W. Roesky, Y. Yang, M. G. Walawalkar, Dr. J. Pinkas, H.-G. Schmidt
Institut für Anorganische Chemie der Universität
Tammannstrasse 4, D-37077 Göttingen (Germany)
Fax: Int. code + (49) 551-393373
e-mail: hroesky@gwdg.de

[**] This work was supported by the Deutsche Forschungsgemeinschaft. J.P thanks the Alexander von Humboldt Foundation for a research fellowship. Y.Y wishes to thank Dr. Balaji Jagirdar for useful discussions.

 © WILEY-VCH Verlag GmbH, D-69451 Weinheim, 1998 1433-7851/98/3701-0096 $ 17.50+.50/0

units (SBUs). In particular, we[6–8] and others[9–12] synthesized Group 13 phosphonates as soluble molecular compounds with a) a double-four-ring (D4R or 4–4) core structure with a $M_4O_{12}P_4$ central unit (M = Al, Ga) or b) stable eight-membered ring structures, which are conceived as intermediates during the formation of D4R structures. However, it has not yet been possible to obtain other larger assemblies which resemble the higher SBUs of zeolites. Here we report the first successful synthesis and molecular structure of an aluminophosphonate that is soluble in organic solvents and has an $Al_6O_{18}P_6$ central core which is identical to the double-six-ring (D6R or 6–6) building units found in zeolites.[13]

The reaction of *tert*-butylphosphonic acid[14] with equimolar quantities of $AlMe_3$ in THF/*n*-hexane yields a mixture of $[MeAlO_3PtBu]_6$ (**1**) and $[MeAlO_3PtBu]_4$ (**2**; Scheme 1).



Scheme 1. Synthesis of aluminophosphonates **1** and **2**.

Hexamer **1** is obtained as hexagonal single crystals from the reaction mixture by fractional crystallization at 4 °C. After removal of **1**, tetramer **2** was obtained from the mother liquor as an analytically pure solid. All our previous attempts to prepare aluminophosphonates from alkyl aluminum compounds containing bulky substituents invariably resulted in the tetrameric compound of the general formula $[RAlO_3PR']$.[6–8] In the present case, the smaller methyl substituent on aluminum allows isolation of hexameric **1** along with tetrameric **2**.

The constitution of **1** and **2** can be ascertained unequivocally from their elemental analyses, EI mass spectra, and NMR data. The base peaks observed in the EI mass spectra for **1** ($m/z = 1053$) and **2** ($m/z = 697$) each correspond to the loss of one methyl group. The chemical shift in the ^{31}P NMR spectrum of **2** ($\delta = 17.5$) is consistent with the value for the tetrameric aluminophosphonate $[i\text{BuAlO}_3P t\text{Bu}]_4$ (**3**, $\delta = 16.9$), which could be characterized as a molecular tetramer by single-crystal structure analysis.[6] The ^{31}P NMR signal of **1** ($\delta = 13.4$) is shifted upfield by $\Delta\delta = 4.1$ with respect to that of **2**. Likewise, in the ^1H NMR spectra there are minor differences in the chemical shifts for the methyl and *tert*-butyl protons of **1** and **2**.

The X-ray structure analysis[15] showed that **1** crystallizes in the centrosymmetric triclinic space group with half of the hexamer in the asymmetric unit. The molecular structure (Figure 1) resembles the D6R building units found in

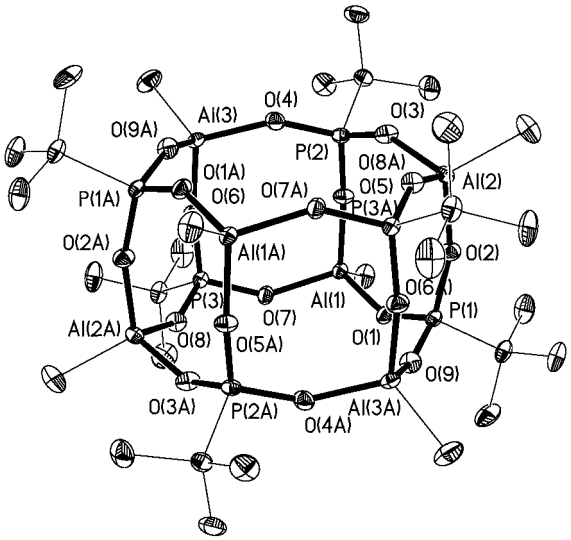


Figure 1. Molecular structure of **1** (thermal ellipsoids for the 20% probability level). Selected bond lengths [Å] and angles [°]: Al–O 1.747(2)–1.757(2) (av 1.752), P–O 1.511(2)–1.519(2) (av 1.515); P(1)-O(1)-Al(1) 149.3(1), P(1)-O(9)-Al(3A) 151.9(1), P(2)-O(3)-Al(2) 148.9(1), P(2)-O(4)-Al(3) 148.8(1), P(3)-O(7)-Al(1) 148.4(1), P(3)-O(8)-Al(2A) 151.2(1), P(1)-O(2)-Al(2) 162.5(1), P(2)-O(5)-Al(1) 166.4, P(3)-O(6)-Al(3) 163.0(1).

phosphate materials such as $AlPO_4$-5, CoAPO-5, CrAPO-5, and SAPO-5.[19]

The central core of the $Al_6O_{18}P_6$ polyhedron can be described as a cylindrical drum in the form of a hexagonal prism whose top and bottom faces are made up of twelve-membered $Al_3O_6P_3$ rings (including the oxygen atoms). The six remaining faces of this cylindrical drum are made up of $Al_2O_4P_2$ rings. All the twelve- and eight-membered rings exist in a crown conformation. The Al–O and P–O bonds within the molecule do not show any variation and are comparable to the corresponding values found for **3** (1.762 and 1.521 Å, respectively). All Al and P centers in the molecule largely have a tetrahedral geometry. The Al-O-P angles in the molecule fall into two different categories: The Al-O-P angles within the twelve-membered rings are much smaller (av 149.8°) than the six Al-O-P linkages that connect the two twelve-membered rings (av 164.0°).

Here we have shown that by tailoring the alkyl groups on aluminum and phosphorus, it is possible to generate bigger building units of aluminophosphate molecular sieves. By a proper balance of steric and electronic factors, it should be possible in the future to synthesize even larger SBUs such as D8R units. We plan to explore these possibilities.

Experimental Section

1 and **2**: A solution of *tert*-butylphosphonic acid (0.30 g, 2.17 mmol) in THF (20 mL) was added dropwise to an equimolar solution of $AlMe_3$ (2 M in hexane, 1.1 mL) in *n*-hexane (20 mL) at 0 °C. The reaction mixture was stirred at room temperature for 16 h and then concentrated to 20 mL in vacuo. The resulting solution was filtered and stored at 4 °C for two weeks to obtain hexagonal colorless crystals of **1** (0.041 g, 10.5%). The crystals, which were suitable for X-ray diffraction studies, were separated from the mother liquor by decantation. The mother liquor contained predominately **2** (0.185 g, 48.1%).

 © WILEY-VCH Verlag GmbH, D-69451 Weinheim, 1998 1433-7851/98/3701-0097 $ 17.50+.50/0

1: M.p. > 300 °C; IR (Nujol): $\tilde{\nu}$ = 1261, 1208, 1191, 1101, 1020, 974, 839, 800, 721, 686 cm^{-1}; ^{1}H NMR (400 MHz, C_6D_6): $\delta = -0.42$ (18 H, s, $AlCH_3$), 1.08 (54 H, d, J = 17.4 Hz, $C(CH_3)_3$); ^{31}P NMR (162 MHz, C_6D_6): δ = 13.4; MS (EI, 70 eV): m/z = 1053 ([M^+ − Me], 100 %); elemental analysis calcd for $C_{30}H_{72}Al_6O_{18}P_6$ (1068.6): C 33.74, H 6.80, P 17.40; found: C 33.64, H 6.74, P 17.86.

2: M.p. 192 – 195 °C; IR (Nujol): $\tilde{\nu}$ = 1261, 1208, 1190, 1097, 1021, 870, 801, 722, 688 cm^{-1}; ^{1}H NMR (200 MHz, C_6D_6): $\delta = -0.31$ (12 H, s, $AlCH_3$), 1.03 (36 H, d, J = 17.5 Hz, $C(CH_3)_3$); ^{31}P NMR (101 MHz, C_6D_6): δ = 17.5; MS (EI, 70 eV): m/z = 697 ([M^+ − Me], 100 %); elemental analysis calcd for $C_{20}H_{48}Al_4O_{12}P_4$ (712.4): C 33.74, H 6.80; found: C 33.42, H 6.88.

Received: July 18, 1997 [Z 10697 IE]
German version: *Angew. Chem.* **1998**, *110*, 101 – 103

Keywords: aluminum · phosphonates · structure elucidation · zeolite analogues

[1] S. T. Wilson, B. M. Lok, C. A. Messina, T. R. Cannan, E. M. Flanigen, *J. Am. Chem. Soc.* **1982,** *104*, 1146.
[2] M. Estermann, L. B. McCusker, C. Baerlocher, A. Merrouche, H. Kessler, *Nature* **1991**, *352*, 320.
[3] a) A. M. Chippindale, R. I. Walton, *J. Chem. Soc. Chem. Commun.* **1994**, 2453; b) R. H. Jones, A. M. Chippindale, S. Natarajan, J. M. Thomas, *ibid.* **1994**, 565.
[4] a) X. Yin, L. F. Nazar, *J. Chem. Soc. Chem. Commun.* **1994**, 2349; b) S. Oliver, A. Kuperman, A. Lough, G. A. Ozin, *Inorg. Chem.* **1996**, *35*, 6373.
[5] a) M. E. Davis, *Acc. Chem. Res.* **1993**, *26*, 111; b) *Ind. Eng. Chem. Res.* **1991**, *30*, 1675.
[6] Y. Yang, H.-G. Schmidt, M. Noltemeyer, J. Pinkas, H. W. Roesky, *J. Chem. Soc. Dalton. Trans.* **1996**, 3609.
[7] M. G. Walawalkar, R. Murugavel, A. Voigt, H. W. Roesky, H.-G. Schmidt, *J. Am. Chem. Soc.* **1997**, *119*, 4656.
[8] M. G. Walawalkar, R. Murugavel, A. Voigt, H. W. Roesky, H.-G. Schmidt, *Organometallics* **1997**, *16*, 516.
[9] K. Dimert, U. Englert, W. Kuchen, F. Sandt, *Angew. Chem.* **1997**, *109*, 251; *Angew. Chem. Int. Ed. Engl*. **1997**, *36*, 241.
[10] M. R. Mason, M. S. Mashuta, J. F. Richardson, *Angew. Chem.* **1997**, *109*, 239; *Angew. Chem. Int. Ed. Engl.* **1997**, *36*, 239.
[11] A. Keys, S. Bott, A. R. Barron, *Chem. Commun.* **1996**, 2339.
[12] M. R. Mason, R. M. Matthews, M. S. Mashuta, J. F. Richardson, *Inorg. Chem.* **1996**, *35*, 5756.
[13] W. M. Meier, D. H. Oslon, C. Baerlocher, *Atlas of Zeolite Structure Types*, 4th ed., Elsevier, London, **1996**.
[14] S. H. Metzger, O. H. Basedow, A. F. Isbell, *J. Org. Chem.* **1964**, *29*, 627.
[15] Crystal data for **1**: $C_{30}H_{72}Al_6O_{18}P_6$, M_r = 1068.58, triclinic, space group $P\bar{1}$, a = 9.780(3), b = 13.228(3), c = 13.692(3) Å, α = 117.56(3), β = 97.68(3), γ = 103.51(3)°, V = 1465.5(5) Å^3, Z = 1, ρ_{calcd} = 1.211 g cm^{-3}, 3846 independent reflections, $R1$ = 0.0342 for $I > 2\sigma(I)$, $wR2$ = 0.0897 for all data. The data were collected on a Stoe-Siemens-AED2 four-circle diffractometer equipped with graphite-monochromated $Mo_{K\alpha}$ radiation (λ = 0.71073 Å). The measurements were made with the Learnt Profile Method on a cooled crystal coated with a drop of oil.[16] The structures were solved by direct methods (SHELXS-90)[17] and refined with all data by full-matrix least squares on F^2.[18] All non-hydrogen atoms were refined anisotropically. Hydrogen atoms were added in idealized positions and included in the refinement. Crystallographic data (excluding structure factors) for the structure reported in this paper have been deposited with the Cambridge Crystallographic Data Centre as supplementary publication no. CCDC-100575. Copies of the data can be obtained free of charge on application to CCDC, 12 Union Road, Cambridge CB2 1EZ, UK (fax: int. code + (44)-1223 336-033; e-mail: deposit@ccdc.cam.ac.uk).
[16] W. Clegg, *Acta Crystallogr. Sect. A* **1981**, *37*, 22.
[17] G. M. Sheldrick, *Acta Crystallogr. Sect. A* **1990**, *46*, 467.
[18] G. M. Sheldrick, SHELXL-93, *Program for Crystal Structure Refinement*, Universität Göttingen, **1993**.
[19] a) A. Simmen, L. B. McCusker, C. Baerlocher, W. M. Meier, *Zeolites* **1991**, *11*, 654; b) N. K. Mcguire, C. A. Bateman, C. S. Blackwell, S. T. Wilson, R. M. Kirchner, *ibid.* **1995**, *15*, 460; c) B. M. Lok, C. A. Messina, R. L. Patton, R. T. Gajek, T. R. Cannan, E. M. Flanigen, *J. Am. Chem. Soc.* **1984**, *106*, 6092.

The Mechanism for Hydrogen Abstraction by n,π* Excited Singlet States: Evidence for Thermal Activation and Deactivation through a Conical Intersection**

Werner M. Nau,* Gerhard Greiner,* Julia Wall, Hermann Rau, Massimo Olivucci,* and Michael A. Robb

Salem's correlation diagram for hydrogen abstraction by n,π* excited chromophores,[1] most often depicted for the reaction between formaldehyde and methane, has become the classic textbook example for a theoretical rationalization of photochemical reactivity and for the contrast between the reactivity of singlet and triplet states. According to this diagram the hydrogen abstraction by triplet states proceeds smoothly and with unit efficiency, whereas for singlet states the system is predicted to "pause" at an avoided crossing and then to proceed either to the products or back to the reactants; this reduces the efficiency to below unity.[1,2] While the triplet reaction has received considerable experimental and theoretical attention, the distinct singlet mechanism has not been examined in detail.[3–6]

The intermolecular hydrogen abstraction of the n,π* excited singlet states of ketones is difficult to examine owing to short lifetimes and efficient intersystem crossing. This limitation warrants the choice of an alternative n,π* chromophore. The azoalkane 2,3-diazabicyclo[2.2.2]oct-2-ene (DBO) appeared to be the predestined experimental test case, since excited singlet DBO is very long-lived (up to 1 μs) and undergoes neither intersystem crossing[7] nor efficient photodecomposition (only about 2 %).[8] Moreover, excited singlet azoalkanes are efficiently quenched by C–H and O–H bonds of poor hydrogen donors such as chloroform or methanol.[9–11] This provides a fascinating case of a singlet hydrogen abstraction [Eq. (1)], which we have now elucidated in mechanistic detail. An unexpectedly low activation barrier and a large deuterium isotope effect are observed for chloroform as hydrogen donor. These findings are rationalized in terms of a thermally activated rather than a tunneling process.

[*] Dr. W. M. Nau
Institut für Physikalische Chemie der Universität Basel
Klingelbergstrasse 80, CH-4056 Basel (Switzerland)
Fax: Int. code + (41) 61-267 3855
e-mail: nau@ubaclu.unibas.ch

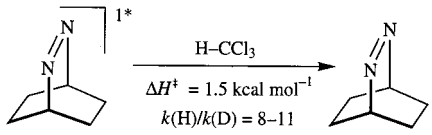
Priz.-Doz. G. Greiner, J. Wall, Prof. H. Rau
Institut für Chemie der Universität Hohenheim
Garbenstrasse 30, D-70599 Stuttgart (Germany)
Fax: Int. code + (49) 711-459 3881
e-mail: greiner@uni-hohenheim.de

Dr. M. Olivucci
Dipartimento di Chimica "G. Ciamician" dell'Università
Via Selmi 2, 40126 Bologna (Italy)
Fax: Int. code + (39) 51-259 456
e-mail: max@ciam.unibo.it

Prof. M. A. Robb
Department of Chemistry, King's College, London (UK)

[**] W.M.N. would like to thank the Fonds der Chemischen Industrie for a Liebig fellowship and Prof. J. C. Scaiano for helpful discussions. M.O. and M.A.R. are grateful to NATO for a travel grant and to Dr. Paolo Celani for help with the CAS computations.

 © WILEY-VCH Verlag GmbH, D-69451 Weinheim, 1998 1433-7851/98/3701-0098 $ 17.50+.50/0



(1)

Most importantly, the computed reaction pathway for hydrogen abstraction from C–H bonds by excited singlet azoalkanes involves decay at a conical intersection (i. e., a real surface crossing)[12,13] of the excited- and ground-state energy sheets (Figure 1) rather than the previously implicated

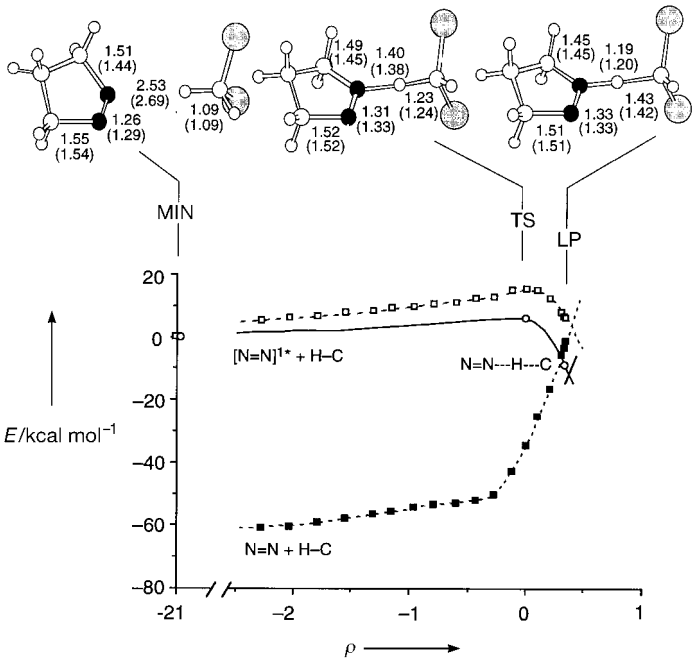


Figure 1. Energy profile along the S_1-(n,π*) reaction coordinate ρ [bohr (amu)$^{1/2}$] describing the hydrogen abstraction in the pyrazoline/CH_2Cl_2 system (see ref. [18] for computational details). Open and filled squares and the associated dashed lines indicate the relative CAS(8,7) energies of the S_1 and S_0 (CI values) states, respectively. Open circles and the solid line present the more accurate CAS(12,10)/PT2F energy profile for the S_1 state. The structures of MIN, TS, and LP [CAS(12,10) and (in parentheses) CAS(8,7) geometrical parameters in Å] document the geometrical progression along the reaction path. The LP point ($S_1 - S_0$ energy gap about 4 kcal mol^{-1}) is taken as representative of the conical intersection.

avoided crossing. The data lead us to propose a mechanism in which the deactivation of n,π* excited singlet azoalkanes is triggered by partial H abstraction from a solvent molecule loosely bound to a nitrogen center. In fact, the hydrogen abstraction on the excited-state surface is aborted at the conical intersection,[13] at which point the system must decay efficiently to the ground-state surface. The radiationless decay is experimentally manifested in low reaction quantum yields.

The decay rate of excited singlet DBO ($1/\tau$) can be analyzed as a composite of the rates of fluorescence (k_f), intramolecular radiationless deactivation (k_d), and intermolecular (solvent-induced) quenching (k_q)—that is, $1/\tau = k_f + k_d + k_q$. The gas-phase fluorescence lifetime[14,15] at ambient temperature (τ_0(DBO) = (930 ± 30) ns) is characteristic for conditions under which the latter process is absent ($1/\tau_0 = k_f + k_d$). In all common solvents, however, the fluorescence lifetime of DBO is shortened, whereas deuterated solvents display a smaller effect. Consequently, solvent-induced quenching (k_q) must be considered ($1/\tau = 1/\tau_0 + k_q$).

As previously corroborated by means of decomposition quantum yields,[9] most solvent-induced quenching of azoalkanes is chemically unproductive and results in radiationless deactivation; for DBO in nonprotic solvents the chemical reaction contributes less than 5%. Nevertheless, from the involvement of C–H bonds in the quenching process and the deuterium isotope effects we conclude that the solvent-induced deactivation must occur along the reaction coordinate for hydrogen abstraction, thus providing an example of an "aborted" hydrogen abstraction. This mechanistic interpretation of the experimental data is corroborated by our theoretical results (see Figure 1).

Chloroform as solvent was examined in experimental detail, since the observed quenching and isotope effects are amongst the largest (Table 1). The fluorescence lifetimes at ambient temperature (22–25 °C) were measured by three techniques (laser flash photolysis, single-photon counting, and streak camera detection) in different laboratories, and consistent results were obtained. The fluorescence quantum yields (Table 1) follow the same trend as the fluorescence lifetimes, and their ratio suggest a natural fluorescence lifetime (τ_n) of (1500 ± 300) ns, which is not significantly different from that in the gas phase (τ_n = (1700 ± 300) ns).[14] Most striking is that the fluorescence lifetime in chloroform is only (13 ± 1) ns, that is, nearly two orders of magnitude shorter than under conditions for which no intermolecular quenching applies (τ_0 = 930 ns). The use of the deuterated solvent ($CDCl_3$) increases the fluorescence lifetime by nearly one order of magnitude ((110 ± 5) ns). The calculated pseudo-unimolecular quenching rate constants k_q (Table 1) substantiate a deuterium isotope effect k_q(H)/k_q(D) of 8–11 at ambient temperature. This value exceeds the kinetic isotope effect expected from energy differences in C–H and C–D stretching vibrations alone (ca. 6), but lies at the upper limit when allowance for bending mode contributions is made (10).[16] This is the largest primary C–H/D isotope effect ever observed for an intermolecular photochemical hydrogen abstraction. For comparison, the isotope effects in the hydrogen abstraction by n,π* excited ketones range from 1–5.[3,4]

Table 1. Fluorescence lifetimes τ and quantum yields Φ for 2,3-diazabicyclo[2.2.2]oct-2-ene (DBO) as well as rate constants k_q and activation parameters for fluorescence quenching.

	Gas phase	$CHCl_3$	$CDCl_3$
τ/ns	930 ± 30 ($\equiv\tau_0$)	13 ± 1	110 ± 5
Φ	0.56 ± 0.10[a]	~0.01	0.075 ± 0.008
τ_n/ns[b]	1700 ± 300	~1300	1500 ± 250
$k_q/10^6$ s^{-1}		76 ± 6	8.0 ± 0.4
$A/10^9$ s^{-1}		2.3 ± 0.3	1.6 ± 0.3
E_A/kcal mol^{-1}		2.05 ± 0.07	3.15 ± 0.09
$\Delta S^{\neq}$/cal K^{-1} mol^{-1}		−17.6 ± 2.4	−18.3 ± 3.4
$\Delta H^{\neq}$/kcal mol^{-1}		1.50 ± 0.05	2.60 ± 0.07

[a] From ref. [14]. [b] Natural fluorescence lifetime ($\tau_n = \tau/\Phi$).

 © WILEY-VCH Verlag GmbH, D-69451 Weinheim, 1998 1433-7851/98/3701-0099 $ 17.50+.50/0

The fluorescence lifetimes of DBO in $CHCl_3$ and $CDCl_3$ increase at lower temperatures and decrease upon heating, indicating a thermally activated process. The temperature dependence of the solvent-induced quenching ($k_q = 1/\tau - 1/\tau_0$)[17] was measured from -30 to $+50\,^{\circ}C$ by single-photon counting. The corresponding Arrhenius (Figure 2) or Eyring

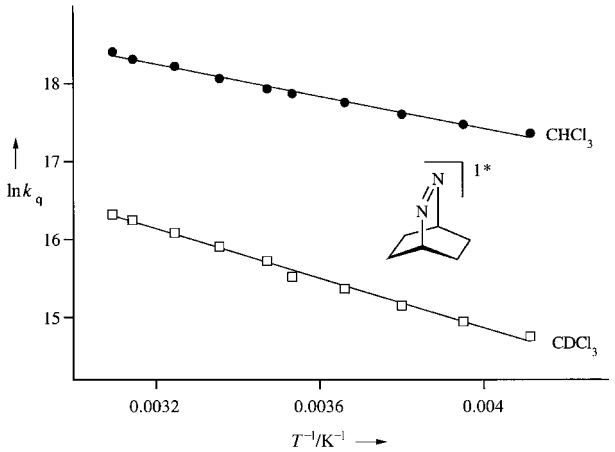


Figure 2. Arrhenius plots for the fluorescence quenching of DBO by $CHCl_3$ and $CDCl_3$ as solvents.

plots, which were linear in the examined temperature range ($r^2 > 0.99$), provide the activation parameters in Table 1. Most importantly, differences in the activation entropy ($\Delta S^{\neq}$) were insignificant, whereas the activation enthalpy ($\Delta H^{\neq}$) increased from 1.5 to 2.6 kcal mol^{-1} upon deuteration. This behavior suggests a classical kinetic isotope effect due to differences in the zero-point energy (ZPE).

The reaction pathway for the intermolecular hydrogen abstraction of an n,π* excited singlet azoalkane was established by ab initio methods.[18] A simpler model reaction, namely that between 1,2-diazacyclopent-1-ene (pyrazoline) and dichloromethane, was selected to allow the use of accurate but expensive computational methodology. It comprises the MCSCF calculation[19] and multireference Møller–Plesset perturbation theory (PT2F),[20] which provides excellent data when tested for other photochemical parameters of azoalkanes (Table 2), namely the 0–0 singlet excitation energy (GS MIN) and the activation energy for α-C–N bond cleavage (TS_α). The same level of theory successfully predicted virtually all experimental aspects of the solvent-induced deactivation of singlet excited azoalkanes, namely the low activation barriers, the isotope effects, and the high efficiency of radiationless deactivation at the expense of product formation.

The computed reaction pathway (see Figure 1) initiates at a loosely bound excited state complex (MIN) in which one of the two dichloromethane C–H bonds lies in the pyrazoline plane and points towards the nitrogen atom containing the "equatorial" unpaired electron; in this complex the geometry of pyrazoline corresponds to that of the isolated n,π* state. The reaction coordinate is initially dominated by the intermolecular distance. After shortening of the H–N distance from 2.5 to 1.6 Å the hydrogen transfer (i. e., simultaneous expansion of the C–H and contraction of the H–N distances) becomes important. Such motion is accompanied by expansion of the N–N bond and shortening of both C–N bonds of pyrazoline. After the transition state (TS) the energy decreases very rapidly. Remarkably, the reaction path does not end at a stationary point (as expected if the previously postulated avoided crossing took place)[1,9] but at a conical intersection (i.e., a singularity) between the excited- (S_1) and ground-state (S_0) potential energy surfaces. This intersection is located near the last calculated point (LP)[18] and about 6 kcal mol^{-1} below the initial complex and provides an extremely efficient channel for radiationless decay. Conceptually, the aborted hydrogen abstraction in Figure 1 presents an example of the minimum →transition state →conical intersection topology, which was documented for intramolecular photoreactions in polyenes and benzene.[13] In this particular topology, access to the radiationless decay channel is thermally controlled.

The energies (Table 2) and vibrational frequencies of the n,π* loosely bound complex and transition state provide a direct comparison of the computed (for the pyrazoline/CH_2Cl_2 model system) and experimentally measured (for DBO/$CHCl_3$) activation parameters. The computed activation enthalpy is 6.4 kcal mol^{-1} but becomes 2.9 kcal mol^{-1} when the ZPE correction is taken into account, and, thus, falls within 1.4 kcal mol^{-1} of the $\Delta H^{\neq}$ observed for the DBO/$CHCl_3$ system. The calculated activation enthalpy for monodeuterated dichloromethane is 0.95 kcal mol^{-1} higher as a consequence of ZPE differences, which is in good agreement with the experimental difference for chloroform (about 1.1 kcal mol^{-1}). Since the experimental and computed isotope effects are only manifested in enthalpic differences, tunneling does not seem to contribute significantly in the examined temperature range. Consequently, the photochemical hydrogen abstraction of excited singlet azoalkanes can be mecha-

Table 2. Calculated[a] and experimental energies for photochemical reactions of the S_1-(n,π*) state of pyrazoline/CH_2Cl_2, pyrazoline, and DBO.

System	Structure[b]	E [Hartree][c]	ΔE_{calcd}[d]	$\Delta E_{exp.}$[e]
pyrazoline/CH_2Cl_2	MIN (S_1)	−1184.97785 (0.73)	≡0.0	≡0.0
	TS (S_1)	−1184.96769 (0.73)	6.4 [2.9]	1.5–2.6[f]
	LP (S_1)[g]	−1184.98824 (0.73)	−6.5	
pyrazoline	GS MIN	−226.67300 (0.84)	−84.0 [−82.7]	−82[h]
	MIN (S_1)	−226.53910 (0.82)	≡0.0	≡0.0
	TS_α (S_1)	−226.52694 (0.82)	7.6 [6.4]	6–9[i]
DBO	GS MIN	−343.01729 (0.75)	−73.7	−76[h]
	MIN (S_1)	−342.89980 (0.74)	≡0.0	≡0.0
	TS_α (S_1)	−342.88167 (0.74)	11.4	8.6–10.2[j]

[a] The multireference Møller–Plesset (PT2F) level of theory was employed; see ref. [10] for details. [b] For the abbreviations MIN, TS, and LP see Figure 1; GS MIN: 0–0 singlet excitation energy, TS_α: activation energy for α-C–N bond cleavage. [c] Calculated absolute energy. The weight of the MCSCF reference function (zeroth-order function) in the first-order function is given in parentheses. [d] Calculated values in kcal mol^{-1}. ZPE-corrected values are given in square brackets. [e] Experimental values in kcal mol^{-1}. [f] Values for the DBO/$CHCl_3$ and DBO/$CDCl_3$ system determined in this work. [g] Last optimized point along the S_1 reaction coordinate. [h] From ref. [7]. [i] Value for a pyrazoline derivative.[22,23] [j] Values for DBO derivatives.[8,11]

 © WILEY-VCH Verlag GmbH, D-69451 Weinheim, 1998 1433-7851/98/3701-0100 $ 17.50+.50/0 *Angew. Chem. Int. Ed.* **1998**, *37*, No. 1/2

nistically viewed as a thermally activated process, as previously established for many triplet ketones.[4,21]

In conclusion, the combined experimental and theoretical data for the solvent-induced quenching of n,π* excited singlet azoalkanes support a hydrogen abstraction in which a transition state is followed by a conical intersection as the reaction coordinate. This photochemical reaction mechanism should be general for n,π* singlet excited chromophores and provides an important rationale for their reactivity and efficiency in hydrogen abstractions.

Received: June 11, 1997 [Z 10537 IE]
German version: *Angew. Chem.* **1998**, *110*, 103 – 107

Keywords: ab initio calculations · azo compounds · hydrogen transfer · isotope effects · photochemistry

[1] L. Salem, C. Leforestier, G. Segal, R. Wetmore, *J. Am. Chem. Soc.* **1975**, *97*, 479 – 487.
[2] N. J. Turro, J. McVey, V. Ramamurthy, P. Lechtken, *Angew. Chem.* **1979**, *91*, 597 – 612; *Angew. Chem. Int. Ed. Engl.* **1979**, *18*, 572 – 586.
[3] W. M. Nau, F. L. Cozens, J. C. Scaiano, *J. Am. Chem. Soc.* **1996**, *118*, 2275 – 2282, and references therein.
[4] M. A. Garcia-Garibay, A. Gamarnik, R. Bise, L. Pang, W. S. Jenks, *J. Am. Chem. Soc.* **1995**, *117*, 10264 – 10275.
[5] D. Severance, H. Morrison, *Chem. Phys. Lett.* **1989**, *163*, 545 – 548.
[6] A. E. Dorigo, M. A. McCarrick, R. J. Loncharich, K. N. Houk, *J. Am. Chem. Soc.* **1990**, *112*, 7508 – 7514.
[7] P. S. Engel, D. W. Horsey, J. N. Scholz, T. Karatsu, A. Kitamura, *J. Phys. Chem.* **1992**, *96*, 7524 – 7535.
[8] P. S. Engel, D. W. Horsey, D. E. Keys, C. J. Nalepa, L. R. Soltero, *J. Am. Chem. Soc.* **1983**, *105*, 7108 – 7114.
[9] W. M. Nau, W. Adam, J. C. Scaiano, *Chem. Phys. Lett.* **1996**, *253*, 92 – 96.
[10] M. J. Mirbach, M. F. Mirbach, W. R. Cherry, N. J. Turro, P. Engel, *Chem. Phys. Lett.* **1978**, *53*, 266 – 269.
[11] P. S. Engel, C. J. Nalepa, *Pure Appl. Chem.* **1980**, *52*, 2621 – 2632.
[12] M. Klessinger, *Angew. Chem.* **1995**, *107*, 597 – 599; *Angew. Chem. Int. Ed. Engl.* **1995**, *34*, 549 – 551, and references therein.
[13] F. Bernardi, M. Olivucci, M. A. Robb, *Chem. Soc. Rev.* **1996**, 321 – 328.
[14] B. S. Solomon, T. F. Thomas, C. Steel, *J. Am. Chem. Soc.* **1968**, *90*, 2249 – 2258.
[15] H. Rau, *Angew. Chem.* **1973**, *85*, 248 – 258; *Angew. Chem. Int. Ed. Engl.* **1973**, *12*, 224 – 239.
[16] R. P. Bell, *The Tunnel Effect in Chemistry*, Chapman und Hall, London, **1980**.
[17] For the calculation of k_q the ambient-temperature value of τ_0 ((930 ± 30) ns, gas phase) was employed for all temperatures. Inclusion of the much smaller temperature dependence of τ_0, which implicitly includes any temperature dependence of k_f and k_d and the possible contribution due to photodecomposition, does not affect the activation parameters within the limits of statistical regression error. For comparison, the gas-phase lifetimes are 950 and 885 ns at −20 and 65 °C, respectively; that is, they are within the limits of error of or very close to the ambient value.
[18] All MCSCF geometry optimizations were carried out with a complete active space (CAS) including 12 electrons in 10 orbitals (CAS(12,10)). The CAS orbitals comprise the π and π* N=N orbitals, the four σ and σ* C–N orbitals, the two nitrogen lone pair orbitals of the pyrazoline fragment, and the σ and σ* orbitals of the reactive C–H bond of CH_2Cl_2. To improve the description of the H transfer the standard 6-31G* basis set (double-ζ + d-type polarization function for atoms of the first and seconds rows of the periodic system) was augmented with p-type polarization and s-type diffuse functions on the CH_2Cl_2 hydrogen atoms and with sp-type diffuse functions (included in Gaussian 94)[19b] on the nitrogen centers. To improve the energetics by including the effect of dynamic electron correlation, the S_1 energies of MIN, TS, and LP were recomputed using multireference Møller–Plesset perturbation theory with the PT2F method included in MOLCAS.[20] To reduce the computational cost we used a CAS(8,7) with the 6-31G* basis set for the reaction coordinate and frequency computations. This reduced CAS does not include the σ and σ* orbitals of the "short" C–N bond and the lone-pair orbital on the alternative N atom. CAS(8,7) produces optimized geometries of MIN, TS, and LP which differ only slightly from that of CAS(12,10) (see Figure 1, top). The reaction coordinate was determined with the IRC method available in Gaussian 94. The conical intersection is easily located by computing the reaction coordinate until degeneracy of S_1 and S_0 is achieved. This manifests itself in failure of the MCSCF calculation to converge owing to $S_1 - S_0$ near-degeneracy. The last reaction coordinate point before degeneracy (LP) is taken as representative of the conical intersection.
[19] a) B. O. Roos, *Adv. Chem. Phys.* **1987**, *69*, 399 – 446; b) the MCSCF program used is implemented in Gaussian 94, Revision B.2: M. J. Frisch, G. W. Trucks, H. B. Schlegel, P. M. W. Gill, B. G. Johnson, M. A. Robb, J. R. Cheeseman, T. Keith, G. A. Petersson, J. A. Montgomery, K. Raghavachari, M. A. Al-Laham, V. G. Zakrzewski, J. V. Ortiz, J. B. Foresman, C. Y. Peng, P. Y. Ayala, W. Chen, M. W. Wong, J. L. Andres, E. S. Replogle, R. Gomperts, R. L. Martin, D. J. Fox, J. S. Binkley, D. J. Defrees, J. Baker, J. P. Stewart, M. Head-Gordon, C. Gonzalez, J. A. Pople, Gaussian, Inc., Pittsburgh, PA, USA, **1995**.
[20] a) K. Andersson, P.-A. Malmqvist, B. O. Ross, *J. Chem. Phys.* **1992**, *96*, 1218 – 1226; b) MOLCAS, Version 3: K. Andersson, M. R. A. Blomberg, M. Fülscher, V. Kellö, R. Lindh, P.-A. Malmqvist, J. Noga, J. Olsen, B. O. Roos, A. J. Sadlej, P. E. M. Siegbahn, M. Urban, P. O. Widmark, University of Lund, Sweden, **1994**.
[21] P. J. Wagner, Q. Cao, R. Pabon, *J. Am. Chem. Soc.* **1992**, *114*, 346 – 348.
[22] P. S. Engel, L. R. Soltero, S. A. Baughman, C. J. Nalepa, P. A. Cahill, R. B. Weisman, *J. Am. Chem. Soc.* **1982**, *104*, 1698 – 1700.
[23] M. F. Mirbach, M. J. Mirbach, K.–C. Liu, N. J. Turro, *J. Photochem.* **1978**, *8*, 299 – 306.

Catalytic, Highly Regio- and Chemoselective Generation of Radicals from Epoxides: Titanocene Dichloride as an Electron Transfer Catalyst in Transition Metal Catalyzed Radical Reactions**

Andreas Gansäuer,* Marianna Pierobon, and Harald Bluhm

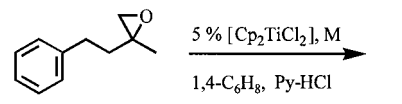
During the last two decades the development of efficient chain reactions has led to an explosive growth in free radical chemistry.[1] Although the understanding of how substrate control determines the stereo- and chemoselectivity of these reactions has reached a high level,[2] to the best of our knowledge little is known about reagent-controlled, catalytic transformations of radicals not proceeding as chain reactions.[3] The advantage of this type of reaction is broader application because the influence of the substrate on the chemo- and stereoselectivity can ideally be overruled and the course of the reaction determined solely by the reagent in catalytic amounts. Therefore a reagent-controlled catalytic reaction would extend the synthetic utility of free radicals even further.

[*] Dr. A. Gansäuer, M. Pierobon, H. Bluhm
Institut für Organische Chemie der Universität
Tammannstrasse 2, D-37077 Göttingen (Germany)
Fax: Int. code + (49) 551-392944
e-mail: agansae@gwdg.de

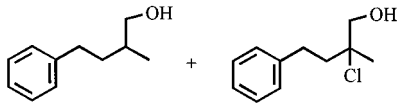
[**] This work was supported by the Fonds der Chemischen Industrie and the Socrates Program. We thank Prof. R. Brückner for constant support and encouragement.

An interesting alternative to radical chain reactions is the reductive opening of epoxides by single electron transfer (SET) from titanocene chloride dimers.[4] The β-titanoxy radical thus formed can undergo the typical radical reactions. Epoxides can be prepared conveniently from a number of functional groups, for example olefins[5] and carbonyl compounds,[6] and can thus serve as radical precursors. An attractive feature of this reaction is that an alcohol is formed after hydrolysis rather than a hydrocarbon, as in the reactions of halides with stannanes.[7] However, both the electron transfer reagent precursor, titanocene dichloride, and the reductant, usually zinc powder, are employed in at least stoichiometric quantities. This is clearly disadvantageous when more complex titanocenes are used.[8] If the reaction could be conducted with a catalytic amount of titanocene, this problem would be solved, and the way would be paved for transition metal catalyzed radical reactions with the potential for efficient reagent control. To achieve this goal the titanocene alkoxide formed must be converted into a derivative of the alcohol or the alcohol itself and titanocene dichloride, the catalyst precursor. In situ reduction by the stoichiometric reductant would yield the redox-active titanium(III) complex[9] and complete the catalytic cycle.

Recently Fürstner et al. have devised efficient catalytic McMurry[10] and Nozaki–Hiyama couplings[11] by adding chlorotrimethylsilane to the reaction mixture. The metal alkoxides and oxides formed in the couplings are thus silylated and the catalytically active metal species are regenerated. This method is, however, not applicable to epoxides because silylated chlorohydrins would form by Lewis acid initiated ring opening. We reasoned that protonation of the titanium-bound oxygen atom should also allow efficient regeneration of the catalyst. For this purpose the acid must be strong enough for the protonation, but neither may the metal powder be oxidized nor the catalyst deactivated by complexation of the resulting base. Pyridinium hydrochlorides (Py-HCl) seemed to be appropriate based on their pK_a values[12] and were therefore tested as acids in the reaction



1



2 **3**

of **1** with cyclohexadiene as the hydrogen atom donor, a stoichiometric reductant, and 5 mol% titanocene dichloride (Table 1).

All of the pyridine hydrochlorides tested, except the bulky 2,6-di-*tert*-butylpyridine hydrochloride, led to conversion. 2,4,6-Trimethylpyridine hydrochloride (collidine hydrochloride) was the most efficient. In addition to the milder reaction conditions required, there are two more general advantages to having protonation as the key step in the catalytic cycle: 1. Protonations are amongst the fastest reactions. 2. 2,4,6-Collidine can be recovered simply by acid–base extraction or distillation; treatment with HCl then provides the hydrochloride. Hydrolysis of the silylated alcohols yields hexamethyldisiloxane, which cannot be reconverted to chlorotrimethylsilane in a straightforward manner. These advantages should become especially important in large-scale applications.

Table 1. Optimization of the reductive opening of epoxide **1** with 5 mol% [Cp_2TiCl_2] and 1,4-cyclohexadiene.

Hydrochloride	M	t[h]	**1**:**2**:**3**[a]
Py-HCl	Zn	35	28:32:26
2,4-Me_2Py-HCl	Zn	36	30:43:22
2,4,6-Me_3Py-HCl	Zn	36	15:71[b]:12
2,4,6-Me_3Py-HCl	Mn	16	0:88[b]:0.5

[a] Determined from the ^{1}H NMR spectrum of the crude mixture. [b] Yield of the isolated product.

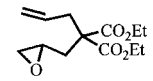
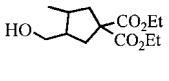
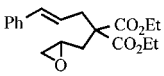
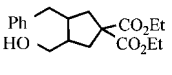
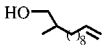
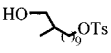
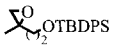
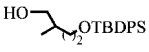
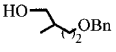
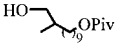
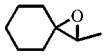
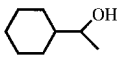
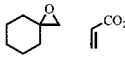
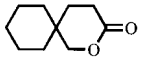
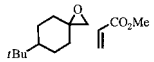
In hydrogen atom abstraction reactions with 1,4-cyclohexadiene, manganese is superior to zinc as the stoichiometric reductant in two respects. When manganese is used, no chlorohydrin **3** is formed by Lewis acid initiated ring opening of the epoxides, and the reaction proceeds significantly faster. Apparently the zinc chloride formed in the reaction complexes the epoxide, prevents complete conversion into product, and allows the slow chloride-mediated ring opening to compete. Gratifyingly the much less Lewis-acidic manganese dichloride[11] does not interfer with the catalytic reaction and thus the products are obtained cleanly in a reasonable time. It should be noted that other metals such as aluminum[13] do not lead to fast reduction of titanocene dichloride and are therefore not suitable as stoichiometric reductants.

To explore the generality of the optimized reaction conditions a number of epoxides were tested in inter- and intramolecular C–C bond forming reactions and reductions (Table 2). Terminal, 1,1- and 1,2-disubstituted (*cis* and *trans*, entry 3), and trisubstituted epoxides give the desired products in good yields. It should be noted that deoxygenation of the epoxide was not detected for any substrate. The regioselectivity of the epoxide opening is opposite to that of S_N2 reactions and seems to be governed only by the stability of the radical formed. Therefore the radical is produced only on the more substituted carbon atom of the epoxide. The observed diastereoselectivities of the cyclizations are typical for radical reactions and their well-known conformational effects.

For the intermolecular addition of the radical to methyl acrylate, zinc was used as the stoichiometric reductant (entries 12 and 13). The lactones were isolated in 75–80% yield after 40 h but the corresponding chlorohydrins (roughly 5%) were also detected. The reaction was much slower with manganese. After 40 h the conversion was estimated at 15%. This is presumably due to deactivation of the titanium catalyst by the MeOH generated. Zinc chloride seems to be Lewis-acidic enough to complex MeOH and thus prevent catalyst deactivation. When manganese was employed in combination with zinc chloride, essentially the same results were obtained

 © WILEY-VCH Verlag GmbH, D-69451 Weinheim, 1998 1433-7851/98/3701-0102 $ 17.50+.50/0 *Angew. Chem. Int. Ed.* **1998**, *37*, No. 1/2

Table 2. Titanocene-catalyzed reductive opening of epoxides under the optimized conditions.[a]

Entry	Substrate	t [h]	Yield [%]	Product
1		30	78[b]	
2		30	55[c]	
3		30	83[d]	
4		16	72	
5		18	58	
6		18	86	
7		12	67	
8		18	74	
9		18	69	
10	**1** 4-phenyl-2-butanone	60	70 95	**2** 4-phenyl-2-butanone
11		30	76[e]	
12		40	77[e]	
13		40	82[e,f]	

[a] See Experimental Section. [b] *cis*:*trans* = 88:12. [c] *cis*:*trans* = 85:15. [d] Substrate was a mixture of *cis* und *trans* isomers. [e] Zn was used as reductant. [f] *cis*:*trans* = 14:86.

as with zinc as reductant. This result supports the above-mentioned hypothesis of catalyst deactivation.

Since titanocene-mediated SET is the key step in the epoxide opening, a number of functional groups sensitive to electron transfer reagents such as samarium diiodide[14] were subjected to the optimized conditions. Gratifyingly benzyl ethers, chlorides, and even ketones (see Table 2, entry 10 for the competition experiment) are perfectly stable under the reaction conditions, and the corresponding products were isolated in good yields. Chlorides are not tolerated in radical chain reactions using tributylstannane (dehalogenation), and therefore the reaction described here allows a mild and highly chemoselective entry to radical chemistry.[7] Protecting groups that can migrate under basic conditions like pivalate (Piv), tosylate (Ts), and *tert*-butyldiphenylsilyl ether (OTBDPS) do not migrate even when it would be kinetically favorable, as in the case of the TBDPS ethers.[15] Also elimination of tosylate was not observed. Although these alcohols can also be obtained by hydroboration and oxidation, the method described here is superior because distant double bonds and ketones are not tolerated by the hydroboration protocol.[16] Also hydroboration of 2-methyl-1,11-dodecadiene takes place preferentially at the less substituted double bond and is therefore complementary to our reaction (entry 4).[17]

We have demonstrated that the reductive opening of epoxides with concommitant hydrogen atom abstraction and inter- or intramolecular C–C bond formation can be catalyzed efficiently and in a highly chemoselective manner by titanocene dichloride if manganese or zinc is used as the stoichiometric reductant and 2,4,6-collidine hydrochloride is used as an acid to protonate the titanium oxide and regenerate titanocene dichloride.

Experimental Section

All new compounds were characterized by the usual means. Preparation of cyclododecanol: A suspension of collidine hydrochloride (197 mg, 1.25 mmol), titanocene dichloride (12.4 mg, 0.05 mmol), manganese (60.0 mg, 1.1 mmol), 1,4-cyclohexadiene (0.425 mL, 4.5 mmol), and cyclododecene oxide (182 mg, 1.0 mmol) in THF (10 mL) was stirred at room temperature for 32 h. After extraction (5 mL 2 M HCl, 2×20 mL H_2O) and chromatography on silica gel (diethyl ether/petroleum ether 1/3) cyclododecanol (153 mg, 0.83 mmol) was obtained in 83 % yield.

Received: July 18, 1997 [Z 10701 IE]
German version: *Angew. Chem.* **1998**, *110*, 107–109

Keywords: chemoselectivity · epoxides · homogeneous catalysis · radical reactions · regioselectivity

[1] a) B. Giese, *Radicals in Organic Synthesis: Formation of Carbon-Carbon Bonds*, Pergamon, Oxford, **1986**; b) W. B. Motherwell, D. Crich, *Free Radical Chain Reactions in Organic Synthesis*, Academic Press, London, **1991**.
[2] a) A. L. J. Beckwith, C. J. Easton, A. K. Serelis, *J. Chem. Soc. Chem. Commun*. **1980**, 482; b) W. Smadja, *Synlett* **1994**, 1; D. P. Curran, N. A. Porter, B. Giese, *Stereochemistry of Radical Reactions*, VCH, Weinheim, **1996**.
[3] a) A. Gansäuer, *Chem. Commun*. **1997**, 457; b) *Synlett* **1997**, 363.
[4] a) W. A. Nugent, T. V. RajanBabu, *J. Am. Chem. Soc*. **1988**, *110*, 8561; b) T. V. RajanBabu, W. A. Nugent, *ibid*. **1989**, *111*, 4525; c) T. V. RajanBabu, W. A. Nugent, M. S. Beattie, *ibid*. **1990**, *112*, 6408; d) T. V. RajanBabu, W. A. Nugent, *ibid*. **1994**, *116*, 986.
[5] A. S. Rao in *Comprehensive Organic Synthesis*, *Vol. 7* (Eds.: B. M. Trost, I. Fleming, G. Pattenden), Pergamon, Oxford, **1991**, pp. 358–375.
[6] J. Aubé in *Comprehensive Organic Synthesis*, *Vol. 1* (Eds.: B. M. Trost, I. Fleming, G. Pattenden), Pergamon, Oxford, **1991**, pp. 819–834.
[7] J. O. Metzger, *Methoden Org. Chem. (Houben-Weyl) 4th ed. 1952–*, Vol. E19a/1, pp. 147–168.
[8] R. L. Halterman, *Chem. Rev*. **1992**, *92*, 965.
[9] M. L. H. Green, C. R. Lucas, *J. Chem. Soc. Dalton Trans*. **1972**, 1000.
[10] A. Fürstner, A. Hupperts, *J. Am. Chem. Soc*. **1995**, *117*, 4468.
[11] A. Fürstner, N. Shi, *J. Am. Chem. Soc*. **1996**, *118*, 2533, 12349.
[12] *Handbook of Chemistry and Physics*, 66th ed. (Ed.: R. C. Weast), CRC, Boca Raton, FL, **1985**, D159–D161.
[13] R. S. P. Coutts, P. C. Wailes, R. L. Martin, *J. Organomet. Chem*. **1973**, *47*, 375.
[14] G. A. Molander, *Chem. Rev*. **1992**, *92*, 29.
[15] T. W. Greene, P. G. M. Wuts, *Protective Groups in Organic Synthesis*, 2nd ed., Wiley, New York, **1991**, p. 83, p. 98.
[16] a) H. C. Brown, P. Heim, *J. Am. Chem. Soc*. **1970**, *92*, 1637; b) E.-I. Negishi in *Comprehensive Organometallic Chemistry*, *Vol. 7* (Eds.: G. Wilkinson, F. G. A. Stone, E. W. Abel), Pergamon, Oxford, **1982**, p. 255; c) H. Molin, B. G. Pring, *Tetrahedron Lett*. **1985**, *26*, 677.
[17] J. A. Soderquist in *Encyclopedia of Reagents for Organic Synthesis*, *Vol. 2* (Ed.: L. Paquette), Wiley, New York, **1995**, pp. 622–630.

 © WILEY-VCH Verlag GmbH, D-69451 Weinheim, 1998 1433-7851/98/3701-0103 $ 17.50+.50/0

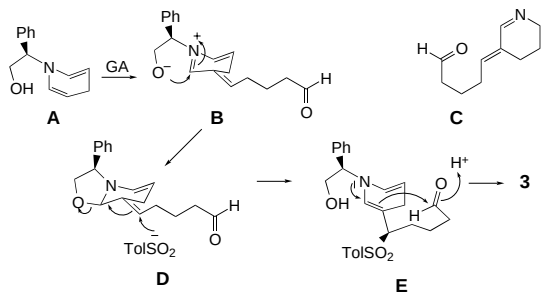
Expeditious Enantioselective Biomimetic Synthesis of the *Nitraria* Alkaloids (+)-Isonitramine and (−)-Sibirine

David François, Marie-Christine Lallemand, Mohamed Selkti, Alain Tomas, Nicole Kunesch,* and Henri-Philippe Husson*

Isonitramine **1** (Scheme 2) is a representative member of the *Nitraria* alkaloid family, for which considerable structural variety is encountered but in which a piperidine ring is an essential feature. We achieved the enantioselective syntheses of the spiropiperidine alkaloids (+)- and (−)-isonitramine,[1] and a number of other racemic[2] and asymmetric syntheses[3] have appeared. Some require numerous steps and have low overall yields. In a continuation of our work on the use of glutaraldehyde for constructing piperidine alkaloids,[4] we report here the most straightforward syntheses of natural sibirine (−)-**2** as well as isonitramines (+)-**1** and (−)-**1** from commercially available starting materials.

Despite the important achievements of Koomen et al.[2] in biomimetic approaches to synthesizing *Nitraria* alkaloids, some desirable objectives have not yet been attained. In particular, generation of a nonracemic chiral biogenetic intermediate with a suitable oxidation level remains an unsolved problem.

We previously showed[1] that the condensation of (*R*)-(−)-phenylglycinol with excess glutaraldehyde gives a tetracyclic compound containing the spiropiperidine skeleton of *Nitraria* alkaloids. However, six and eight additional steps are necessary to transform this precursor into (−)- and (+)-isonitramine, respectively. Such a reaction might form the basis of a biomimetic approach to synthesizing the title alkaloids. Since the first step of the reaction between (*R*)-(−)-phenylglycinol and glutaraldehyde is the formation of the enantiopure intermediate **A** (Scheme 1), we imagined that condensation of a second molecule of glutaraldehyde would afford aldehyde **B**, a chiral derivative of the piperideinoaldehyde **C** postulated by Koomen as a key intermediate in the biosynthesis of *Nitraria* alkaloids.[2]



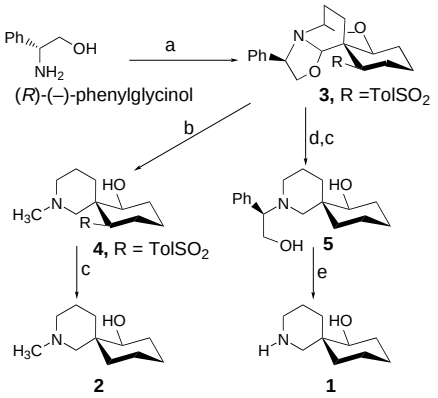
Scheme 1. Mechanism for the formation of spirocompound **3**.

[*] Dr. N. Kunesch, Prof. H.-P. Husson, D. François, Dr. M.-C. Lallemand
URA 1310 associée au CNRS
Faculté des Sciences Pharmaceutiques et Biologiques
Université René-Descartes
4, Avenue de l'Observatoire, F-75270 Paris Cedex 06 (France)
Fax: Int. code + (33) 1-43 29 14 03
e-mail: husson@pharmacie.univ-paris5.fr
Dr. M. Selkti, Prof. A. Tomas
Laboratoire de Biocristallographie, Université René-Descartes

According to this biogenetic hypothesis, the crucial step is the reduction of the conjugated iminium system of **C** to a simple enamine. We reasoned that a stereocontrolled Michael addition of a convenient nucleophile to **B** should a) create a new stereogenic center which would further control the spirocyclization and b) allow elimination of the nucleophile by reductive cleavage.

We chose sodium *p*-toluenesulfinate as the nucleophile in the expectation that 1,4-addition to the α,β-unsaturated oxazolidine system of **D** would generate the desired enamine. Whereas the 1,4-addition of phenylsulfinate ion to α,β-unsaturated ketones is well documented, there are few examples of reaction with iminium salts. As far as conjugated iminium ions are concerned, we observed the only known case for a rearrangement in which a 1,4-addition occurred.[5]

The first step of our synthetic sequence was accomplished by condensation of (*R*)-(−)-phenylglycinol and glutaraldehyde (2.5 equiv) followed by addition of sodium *p*-toluenesulfinate. This resulted in the formation of the spirocompound **3** (51 % yield) as the major diastereomer, which was isolated by simple crystallization (Scheme 2) and characterized by X-ray structure analysis.[6]



Scheme 2. a) Aqueous glutaraldehyde (2.5 equiv), pH 3.5, $NaSO_2Tol$ (2.2 equiv), $ZnBr_2$, 3 h (51 %); b) W-2 Raney Ni, MeOH (reflux), 2 h (91 %); c) Na(Hg), anhydrous MeOH, anhydrous Na_2HPO_4, 24 h, −20 °C (95 %); d) $LiAlH_4$, Et_2O (82 %); e) $H_2/Pd(OH)_2/C$ 20 %, MeOH, 24 h (85 %).

The outcome of this highly efficient reaction suggests that **3** is the most thermodynamically stable compound resulting from a series of equilibration reactions. The possible control elements include a) diastereoselective 1,4-nucleophilic addition of $TolSO_2^-$ to the α,β-unsaturated oxazolidine system of **D**[7] and b) addition of the substituted enamine goup of **E** to the aldehyde group via a chairlike transition state in which the sulfone and the developing secondary alcohol are in a diequatorial arrangement, which provides stereocontrolled spiroaldolization.

Finally, natural sibirine (−)-**2** was obtained in a two-step procedure from **3** by hydrogenolysis/alkylation with Raney nickel in MeOH[8] followed by sulfone elimination (yield 86 %).[9] The synthesis of isonitramine (−)-**1** required reduction with $LiAlH_4$, sulfone elimination, and hydrogenolysis of the chiral N substituent (yield for three steps from **3** 66 %).[10] Natural isonitramine (+)-**1** could be obtained starting from

 © WILEY-VCH Verlag GmbH, D-69451 Weinheim, 1998 1433-7851/98/3701-0104 $ 17.50+.50/0 *Angew. Chem. Int. Ed.* **1998**, *37*, No. 1/2

enantiomeric (*S*)-(+)-phenylglycinol. These results show the crucial role of the chiral phenylglycinol, which serves not only for the transfer of chirality but also for the stabilization of the intermediate iminium.

The nitramine alkaloids (derivatives of 2-azaspiro[5.5]undecan-7-ol) are structurally analogous to the neurotoxic histrionicotoxin alkaloids,[11] compounds which have a 1-azaspiro[5.5]undecan-8-ol skeleton with unsaturated lipophilic side chains. The introduction of such essential side chains on the nitramine skeleton is therefore of particular interest. Intermediate **3** opens the way to a variety of substitutions which can be made a) at the carbon atoms adjacent to the nitrogen of the piperidine ring by selective opening of the oxazolidine and/or 1,3-oxazine in an iminium ion and b) on the cyclohexane ring by the sulfone reactivity.

Experimental Section

All new compounds were characterized by 2D ^{1}H and ^{13}C NMR as well IR spectra, $[\alpha]_D$ values, simple and high-resolution mass spectrometry, or elemental analysis.

(*R*)-(−)-phenylglycinol (6.9 g, 50 mmol) was added to a solution of citric acid (24 g) in distilled water (200 mL). The mixture was stirred vigourously until complete dissolution of the phenylglycinol and then cooled to 0–5 °C in an ice/water bath. A 25% aqueous solution of glutaraldehyde (47 mL, 125 mmol) was added dropwise over 30 min, and then sodium *p*-toluenesulfinate (19.6 g, 110 mmol) was added simultaneously with CH_2Cl_2 (120 mL). The reaction mixture was stirred for 2 h at room temperature. The aqueous phase was neutralized with 5 N aqueous NaOH (80 mL) and extracted with CH_2Cl_2 (3 × 150 mL). The combined organic layers were concentrated under vacuum, diluted with MeOH (50 mL), and treated with $ZnBr_2$ (2 g, 8.9 mmol) over 12 h. Evaporation of the solvent gave an oily crude residue which crystallized from MeOH to give 11.19 g (51%) of **3** in two crops.

3: M.p. 222–223 °C; $[\alpha]_D$ −77 (c = 1 in $CHCl_3$); ^{1}H NMR (300 MHz, $CDCl_3$) δ = 1.12 (m, 1H, H-9), 1.50–2.10 (m, 6H, H-5, Hs-8, H-9, Hs-10), 1.95–2.10 (m, 1H, H-5), 2.15–2.35 (m, 2H, Hs-4), 2.44 (s, 3H, CH_3 Tol), 3.28 (dd, 1H, J = 13, 4 Hz, H-7), 3.66 (dd, 1H, J = 9.5, 8.5 Hz, H-13), 3.97 (dd, 1H, J = 11.5, 4.5 Hz, H-11), 4.30 (dd, 1H, J = 3.5, 1.5 Hz, H-6), 4.35 (dd, 1H, J = 8.5, 6.5 Hz, H-13), 4.60 (dd, 1H, J = 9.5, 6.5 Hz, H-12), 5.86 (s, 1H, H-2), 7.20–7.45 (m, 7H, Ar Hs), 7.78 (d, 1H, J = 8 Hz, Tol H); ^{13}C NMR (75.5 MHz, $CDCl_3$) δ = 16.4 (C-4), 21.4 (CH_3 Tol), 21.4 (C-9), 23.6 (C-10), 27.2 (C-5), 28.2 (C-8), 40.7 (C-3), 62.6 (C-7), 63.2 (C-12), 70.4 (C-11), 73.0 (C-13), 78.5 (C-6), 91.3 (C-2), 127.3, 128.2, 129.5 (Ar CH), 136.9 (Ar C), 139.9 (Ar C), 144.3 (Ar C).

4: M.p. 211–213 °C (MeOH); $[\alpha]_D$ −3 (c = 1 in $CHCl_3$); ^{1}H NMR (300 MHz, $CDCl_3$) δ = 1.1–1.2 (m, 1H), 1.3–2.0 (m, 8H), 2.0-2.2 (m, 4H), 2.30 (s, 3H, N-Me), 2.42 (s, 3H, CH_3 Tol), 2.5–2.9 (br m, 2H), 3.5–3.7 (m, 2H), 7.32 (d, 1H, J = 8 Hz, H Tol), 7.72 (d, 1H, J = 8 Hz, H Tol); ^{13}C NMR (75.5 MHz, $CDCl_3$) δ = 21.4 (CH_3 Tol), 21.7 (CH_2), 22.3 (CH_2), 23.2 (CH_2), 28.8 (CH_2), 43.0 (C-3), 46.0 (N-Me), 55.3 (C-6), 65.4 (C-2), 68.6 (C-7), 81.9 (C-11), 128.1 (CH Tol), 129.6 (CH Tol), 137.2 (C Tol), 144.3 (C Tol).

5: $[\alpha]_D$ −17 (c = 1 in $CHCl_3$); ^{1}H NMR (300 MHz, $CDCl_3$) δ = 0.7–1.0 (m, 2H), 1.0–1.8 (m, 8H), 1.85 (d, 1H, J = 11 hz, H-2), 2.0–2.1 (m, 2H), 2.25 (td, 1H, J = 10, 3 Hz, H-6), 2.67 (d, 1H, J = 11 Hz, H-2), 2.8–2.9 (m, 1H), 3.5–3.6 (m, 2H), 3.80 (dd, 1H, J = 11, 6 Hz), 4.08 (dd, 1H, J = 11, 8 Hz), 7.0–7.4 (m, 5H); ^{13}C NMR (75.5 MHz, $CDCl_3$) δ = 20.3 (CH_2), 22.8 (CH_2), 23.8 (CH_2), 28.1 (CH_2), 29.5 (CH_2), 35.9 (C-3), 51.8 (C-6), 62.1 (C-2), 62.7 (C-13), 71.0 (C-12), 79.0 (C-11), 127.8 (Ar CH), 128.4 (Ar CH), 128.6 (Ar CH), 147.5 (Ar C).

Received: July 25, 1997 [Z 10731 IE]
German version: *Angew. Chem.* **1998**, *110*, 112–114

Keywords: alkaloids · asymmetric synthesis · biomimetic synthesis · natural products · spiro compounds

[1] J.-C. Quirion, D. S. Grierson, J. Royer, H.-P. Husson, *Tetrahedron Lett.* **1988**, *29*, 3311–3314.
[2] M. J. Wanner, G.-J. Koomen in *Studies in Natural Products Chemistry: Stereoselectivity in Synthesis and Biosynthesis of Lupine and Nitraria Alkaloids*, *Vol. 14* (Ed.: Atta-ur-Rahman), Elsevier, Amsterdam, **1994**, pp. 731–768, and references therein.
[3] a) D. Kim, W. J. Choi, J. Y. Hong, I. Y. Park, Y. B. Kim, *Tetrahedron Lett.* **1996**, *37*, 1433–1434; b) T. Yamane, K. Ogasawara, *Synlett* **1996**, 925–926; c) M. Keppens, N. De Kimpe, *J. Org. Chem.* **1995**, *60*, 3916–3918, and references therein; d) B. Westermann, H. G. Scharmann, I. Kortmann, *Tetrahedron: Asymmetry* **1993**, *4*, 2119–2122; e) T. Imanishi, T. Kurumada, N. Maezaki, K. Sugiyama, C. Iwata, *J. Chem. Soc. Chem. Commun.* **1991**, 1409–1411; f) P. J. McCloskey, A. G. Schultz, *Heterocycles* **1987**, *25*, 437–447.
[4] a) C. Yue, I. Gauthier, J. Royer, H.-P. Husson, *J. Org. Chem.* **1996**, *61*, 4949–4954; b) H.-P. Husson, J. Royer in *Advances in the Use of Synthons in Organic Chemistry: Chemistry of Potential and Reversed Iminium Systems*, *Vol. 2* (Ed.: A. Dondoni), JAI Press, Greenwich, CT, USA, **1995**, pp. 1–68.
[5] D. S. Grierson, J.-L. Bettiol, I. Buck, H.-P. Husson, M. Rubiralta, A. Diez, *J. Org. Chem.* **1992**, *57*, 6414–6421.
[6] Crystallographic data (excluding structure factors) for the structure reported in this paper have been deposited with the Cambridge Crystallographic Data Centre as supplementary publication no. CCDC-100690. Copies of the data can be obtained free of charge on application to CCDC, 12 Union Road, Cambridge CB2 1EZ, UK (fax: int. code + (1223) 336-033; e-mail: deposit@ccdc.cam.ac.uk).
[7] a) P. Mangeney, A. Alexakis, J.-F. Normant, *Tetrahedron* **1984**, *40*, 1803–1808; b) M. Huche, J. Aubouet, G. Poncelot, J. Berlan, *Tetrahedron Lett.* **1983**, *24*, 585–586.
[8] a) X.-S. He, A. Brossi, *J. Heterocyclic Chem.* **1991**, *28*, 1741–1746; b) W. Meise, *Methoden Org. Chem. (Houben-Weyl)*, *4th ed. 1980-*, Vol. 4/1c, p. 257.
[9] B. M. Trost, H. C. Arndt, P. E. Strege, T. R. Verhoeven, *Tetrahedron Lett.* **1976**, 3477–3478.
[10] Isonitramine (−)-**1** could be obtained in a single step by treating **3** with Raney nickel at 80 °C and 25 bar in THF; however, the yield was modest (20%, not optimized).
[11] J. W. Daly, H. Martin Garraffo, T. F. Spande in *The Alkaloids: Amphibian Alkaloids*, *Vol. 43* (Ed.: G. A. Cordell), Academic Press, New York, **1993**, pp. 185–288.

Preparation of Lithium Oligosiloxane Aluminates and Acid Strength of Hydroxy Groups in a Molecular Aluminum Oligosiloxane

Michael Veith,* Maria Jarczyk, and Volker Huch

Dedicated to Professor Manfred Weidenbruch on the occasion of his 60th birthday

As we recently reported, the molecular aluminum oligosiloxane **1**, which contains four aluminum atoms that are connected through OH bridges to form a ring, can be readily prepared in a one-step synthesis.[1] We observed that the hydrogen atoms of the OH groups are available for coordination with Lewis bases. Compound **1** can therefore be isolated as an adduct with three molecules of diethyl ether (a fourth is incorporated within the crystal lattice and does not

[*] Prof. Dr. M. Veith, M. Jarczyk, Dr. V. Huch
Institut für Anorganische Chemie der Universität
Postfach 151150, D-66041 Saarbrücken (Germany)
Fax: Int. code + (681) 302-3995
e-mail: veith@rz.uni-sb.de

 © WILEY-VCH Verlag GmbH, D-69451 Weinheim, 1998 1433-7851/98/3701-0105 $ 17.50+.50/0

coordinate with a hydrogen atom). It can also be allowed to react with triethylamine to give a 2:1 adduct that may be described as an ion pair with the formula $[\{(Ph_2Si)_2O_3\}_4Al_4(OH)_2O_2]^{2-}(Et_3NH^+)_2$. It was a logical consequence for us to investigate the effect that various other Lewis bases with different steric requirements and basic strengths have on **1**. In addition, we wanted to study whether the Loewenstein rule (according to which the AlO_4 tetrahedra in such compounds are always separated by silicon atoms) is also applicable to molecular aluminum/silicon–oxygen compounds,[2] or whether the hydroxy compound **1** can be converted into a lithium derivative without rearrangement. Roesky et al. recently described a molecular sodium siloxoaluminate of the general formula $[\{Na(thf)\}_4][\{EtAlO_3SiR\}_4]$ in which the O_3R tetrahedra centered by aluminum and silicon atoms were indeed linked through oxygen vertices in an alternating fashion.[3]

Adduct $\mathbf{1}\cdot 4\,OEt_2$ reacts smoothly with pyridine (Py) under elimination of the diethyl ether molecule to give the pyridine adduct **2**[4] in almost quantitative yield (Scheme 1).The IR spectrum of crystalline **2** has a narrow band at 3630 cm^{-1}, and the ^{29}Si NMR spectrum has only one signal. Based on the integration of the ^1H NMR signals and the elemental analysis, **2** contains one pyridine molecule per OH group. A section of the structure of **2** as determined from the X-ray structure analysis[4] is shown in Figure 1. The molecule has $S_4(\bar{4})$ crystallographic symmetry with four pyridine molecules linked to the central $Al_4(OH)_4$ ring through bridging hydrogen bonds. The O–N distance of the linear N–H ··· O bridge is 2.548(3) Å; the adjacent Al atoms along with the N and O

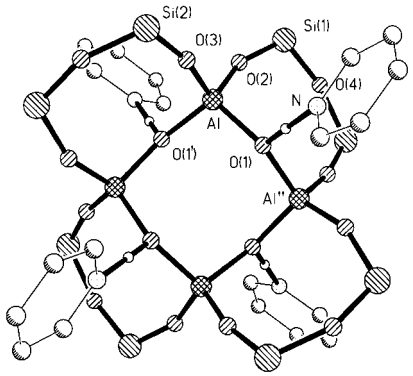
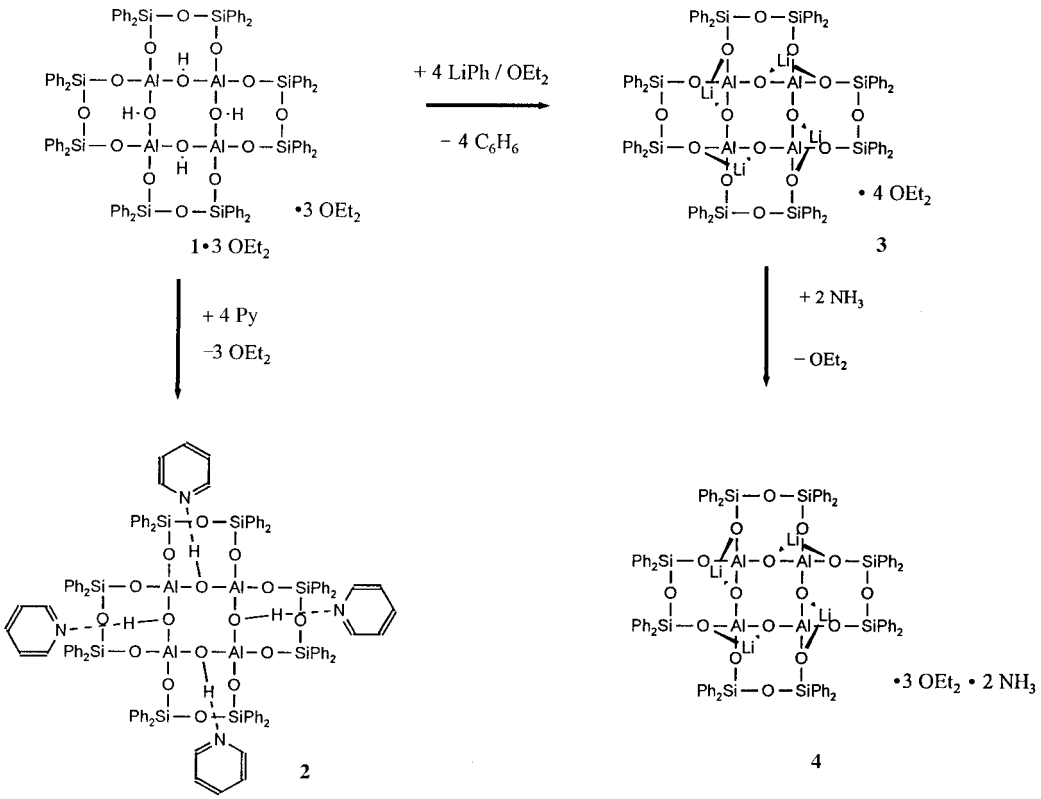


Figure 1. The framework of **2** in the crystal (for clarity the phenyl groups on the silicon atoms are not shown, see Figure 2). Selected bond lengths [Å] and angles [°]: Al–O(3) 1.703(2), Al–O(1) 1.768(2), Si(1)–O(2) 1.594(2), Si(2)–O(3) 1.586(2), Al–O(2) 1.714(2), Al–O(1′) 1.770(2), Si(1)–O(4) 1.633(2), Si(2)–O(4′) 1.632(2); O(3)-Al-O(2) 114.6(1), O(3)-Al-O(1) 106.6(1), O(2)-Al-O(1) 110.7(9), O(3)-Al-O(1′) 109.7(1), O(2)-Al-O(1′) 106.8(1), O(1)-Al-O(1′) 108.3(1), Al-O(1)-Al″ 132.4(1), Si(1)-O(2)-Al 154.4(1), Si(2)-O(3)-Al 166.5(1).[8]

atoms lie almost perfectly in a plane. In contrast to the triethylamine adduct (only two molecules per four OH groups) and the diethyl ether adduct (three molecules per four OH groups),[1] all OH groups in **2** are "coordinatively saturated". The fourfold incorporation of pyridine is attained in that half of the phenyl groups of the peripheral silyl groups are arranged parallel to each other and thus form a sandwich structure with the pyridine molecules (the average distance between the plane of the pyridine ring and the parallel phenyl



Scheme 1. Synthesis of compounds **2**–**4** from **1**.

 © WILEY-VCH Verlag GmbH, D-69451 Weinheim, 1998 1433-7851/98/3701-0106 $ 17.50+.50/0

groups is 3.6 Å, see Figure 2). The twofold symmetry of the $OSi(Ph)_2OSi(Ph)_2O$ handle is somewhat disturbed by the forced arrangement of the aryl groups. This manifests itself most clearly in the Si-O-Al angles of 154.4(1) and 166.6(1)°.

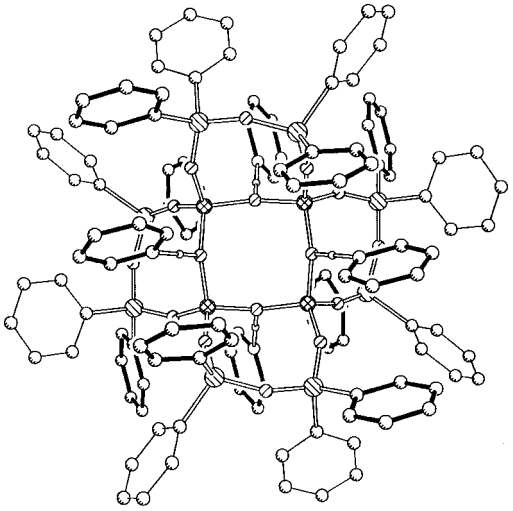


Figure 2. The parallel arrangement of the phenyl groups on the silicon atoms and the interstitial pyridine molecules in **2** (thick lines).

The Al–O(H) bond lengths are particularly informative with respect to the H···N interaction and the relative acidic strength of the OH groups. They are equal within the limits of the standard deviation (av 1.769(1) Å) and lie between the corresponding lengths in the adducts with diethyl ether (av 1.800 Å) and triethylamine (av 1.728 Å). In agreement with the pK_a values of diethyl ether (−3.0), pyridine (5.2), and triethylamine (10.8),[5] there is a correlation with the Al–O bond lengths; as expected, the strongest base effects the strongest attraction on the hydrogen atoms. This leads to a negative partial charge on the oxygen atoms and thus to a shortening of the Al–O bond. However, the lengths of the bridging hydrogen bonds (2.65 Å in $\mathbf{1}\cdot 4\,OEt_2$, 2.72 Å in the triethylamine adduct, and 2.55 Å in **2**) do not correlate with the base strengths. It appears that the steric requirements of the bases are reflected in these distances; pyridine clearly requires less space than diethyl ether or triethylamine. This is plausible when space-filling models of the molecules are considered.

With the reaction of $\mathbf{1}\cdot 4\,OEt_2$ with phenyllithium it is possible to replace all four hydrogen atoms of the hydroxy groups with lithium atoms[6] (Scheme 1). Product **3** reacts further with NH_3 in toluene; the formation of **4** is accompanied by the incorporation of two NH_3 molecules and the elimination of a diethyl ether molecule[7] (large molar amounts of NH_3 lead to mixtures of products, which could not yet be separated). The quantitative reaction can be inferred from the IR spectra of the reaction products: In the case of **3** no peaks between 3700 and 3150 cm^{-1} are found, and for **4** there is an intense peak at 3389 cm^{-1}, which can be attributed to the N–H vibrations of the NH_3 molecules coordinated to two lithium atoms (there is a signal at $\delta = -382.4$ in the ^{15}N NMR spectrum). X-ray structure analyses were performed on both compounds,[6, 7] the results of which are depicted in Figures 3 and 4.

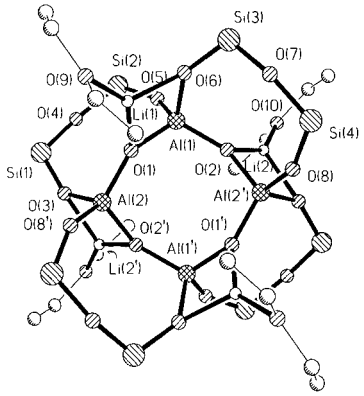


Figure 3. Section from the structure of **3** in the crystal (for clarity the phenyl groups on the silicon atoms are not shown). Selected bond lengths [Å] and angles [°]: Al(1)–O(2) 1.720(4), Al(1)–O(1) 1.729(4), Al(1)–O(5) 1.734(4), Al(1)–O(6) 1.799(4), Al(2)–O(1) 1.727(4), Al(2)–O(2′) 1.734(4), Al(2)–O(8′) 1.736(4), Al(2)–O(3) 1.786(4), Si(1)–O(3) 1.616(4), Si(1)–O(4) 1.618(5), Si(2)–O(5) 1.593(4), Si(2)–O(4) 1.631(5), Si(3)–O(6) 1.605(4), Si(3)–O(7) 1.617(5), Si(4)–O(8) 1.593(4), Si(4)–O(7) 1.630(5), O(1)–Li(1) 1.85(1), O(2)–Li(2) 1.84(1), O(3)–Li(2′) 2.03(1), O(6)–Li(1) 1.95(1), Li(1)–O(9) 1.91(1), Li(2)–O(10) 1.88(1); O(2)-Al(1)-O(1) 118.9(2), O(1)-Al(2)-O(2′) 116.4(2), Al(2)-O(1)-Al(1) 133.6(2), Al(1)-O(2)-Al(2′) 134.6(2).[8]

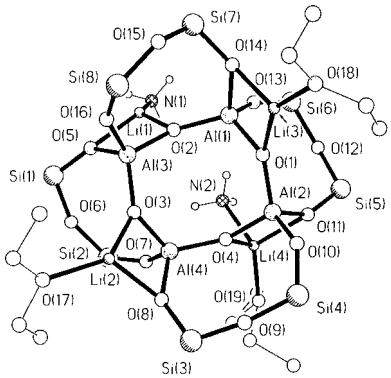


Figure 4. Section from the structure of **4** in the crystal that is analogous to that in Figure 3. Selected bond lengths [Å] and angles [°]: Al(1)–O(2) 1.715(3), Al(1)–O(13) 1.734(4), Al(1)–O(1) 1.746(3), Al(1)–O(14) 1.791(3), Al(2)–O(4) 1.733(3), Al(2)–O(1) 1.738(3), Al(2)–O(10) 1.748(3), Al(2)–O(11) 1.786(4), Al(3)–O(3) 1.727(3), Al(3)–O(2) 1.733(4), Al(3)–O(16) 1.743(4), Al(3)–O(5) 1.789(3), Al(4)–O(4) 1.714(3), Al(4)–O(3) 1.744(3), Al(4)–O(7) 1.757(3), Al(4)–O(8) 1.781(4), O(1)–Li(3) 1.85(1), O(2)–Li(1) 1.87(1), O(3)–Li(2) 1.85(1), O(4)–Li(4) 1.90(1), N(1)–Li(1) 2.00(1), N(2)–Li(4) 2.09(2); O(2)-Al(1)-O(1) 117.1(2), O(4)-Al(2)-O(1) 114.9(2), O(3)-Al(3)-O(2) 114.9(2), O(4)-Al(4)-O(3) 119.3(2), Al(2)-O(1)-Al(1) 127.1(2), Al(1)-O(2)-Al(3) 137.8(2), Al(3)-O(3)-Al(4) 128.5(2), Al(4)-O(4)-Al(2) 141.0(2).[8]

Compound **3** has the same central cyclic structural unit as **1**, but is supplemented by four annelated AlO_2Li rings. Each lithium atom is additionally connected to a diethyl ether ligand molecule, so that approximately trigonal-planar LiO_3 units are formed. Alternatively, the inner unit can also be described as consisting of four AlO_4 tetrahedra connected through common vertices with one edge of each tetrahedron being bridged by a lithium atom. The similarity to lithium aluminium silicates is also reflected by the formula $[\{Ph_2SiO\}_8][\{LiAlO_2\}_4]\cdot 4\,OEt_2$. The point symmetry of the molecule in the crystal is $C_2(2)$; however, the deviation from

 © WILEY-VCH Verlag GmbH, D-69451 Weinheim, 1998 1433-7851/98/3701-0107 $ 17.50+.50/0

$S_4(\bar{4})$ symmetry is only slight. Moreover, **3** crystallizes enantiomerically pure in a noncentrosymmetric space group. The Al–O bond lengths in the central Al_4O_4 ring alternate systematically according to whether the bond is situated within the AlO_2Li ring (av 1.732(3) Å) or outside it (av 1.723(3) Å). Otherwise, the distances are similar to those in the triethylamine adduct of **1**,[1] which suggests equivalent charge states on the oxygen atoms. Of all the Li–O distances, $Li–O(Al)_2$ is, as expected, the shortest (av 1.85(2) Å), followed by $Li–O(Et)_2$ (av 1.89(2) Å) and finally Li–O(Al,Si) (av 1.99(2) Å).

The fundamental structure of the framework of **4** is similar to that of **3**; the Al–O bond lengths of the central Al_4O_4 ring alternate also here. In contrast to the situation in **3**, the four lithium atoms are quite differently coordinated. Atoms Li(2) and Li(3) are coordinated by diethyl ether, which results in a slightly distorted trigonal-planar environment, whereas Li(1) is coordinated by an ammonia molecule, and Li(4) by both an ammonia and a diethyl ether molecule. Thus, Li(4) has the coordination number four. The asymmetrical ligand distribution leads to the point symmetry C_1 in the crystal. As in **3**, the shortest Li–O bond length is that between Li and O atoms of the central Al_4O_4 ring (1.846(9) – 1.865(9) Å). The $Li–O(Et_2)$ bond lengths (1.89(1) – 1.94(1) Å) are longer (as are Li–N bond lengths with 2.00(1) Å), and the Li–O(Al,Si) distances are the longest (2.01(1) – 2.03(1) Å). Due to the higher coordination number on Li(4), all bond lengths here are somewhat longer (e.g. Li(4)–N(2) 2.09(2) Å).

As shown unequivocally by the X-ray structure analyses of **3** and **4**, the fundamental framework is not altered by the incorporation of the lithium atoms into **1**. It thus appears that the Loewenstein rule does not apply for the molecular lithium oligosiloxane aluminates considered here. Their formation is apparently more "kinetically" than "thermodynamically controlled". Moreover, attack by bases occurs more readily than in the case of **1** (**3** contains four diethyl ether donors, and the corresponding adduct of **1** only three). The oxygen atoms of the $OSi(Ph)_2OSi(Ph)_2O$ handle readily coordinate to the lithium atoms, which leads to the observed cyclizations. It is expected that larger metal atoms would form coordinate bonds with even more oxygen atoms.

Received: July 23, 1997 [Z 10723 IE]
German version: *Angew. Chem.* **1998**, *110*, 109 – 112

Keywords: aluminum · N ligands · O ligands · polycycles · silicon

[1] M. Veith, M. Jarczyk, V. Huch, *Angew. Chem.* **1997**, *109*, 140; *Angew. Chem. Int. Ed. Engl.* **1997**, *36*, 117.
[2] W. Loewenstein, *Am. Mineral.* **1954**, *39*, 92.
[3] M. L. Montero, A. Voigt, M. Teichert, I. Usón, H. W. Roesky, *Angew. Chem.* **1995**, *107*, 2761; *Angew. Chem. Int. Ed. Engl.* **1995**, *34*, 2504.
[4] **2**: **1** · $4OEt_2$[1] (0.380 g, 0.18 mmol) in benzene (10 mL) was stirred with pyridine (0.056 g, 0.71 mmol) at room temperature for 2 h. The solvent was then removed under reduced pressure until crystals of **2** precipitated (0.366 g, 95 %). Correct elemental analysis. NMR: [D_6]benzene, 296 K, TMS; ^{1}H NMR (200 MHz): $\delta = 6.02$ (m, 8H, Py), 6.65 (m, 4H, Py), 7.03 (m, 48H, Ph), 7.53 (m, 16H, Ph), 7.85 (m, 8H, Py), 7.90 (m, 16H, Ph); ^{13}C NMR (50.3 MHz): $\delta = 123.87$ (s, Py), 127.39 – 128.11 (m, Ph), 134.89 (s, Ph), 135 (s, Ph/Py), 137.59 (s, Ph), 139.19 (s, Ph), 139.62 (s, Ph), 146.86 (s, Py); ^{29}Si NMR (39.7 MHz): $\delta = -45.98$ (s, $SiPh_2$). Crystal structure analysis:[8] $C_{116}H_{104}Al_4N_4O_{16}Si_8$, $M = 2142.73$ g mol^{-1}, tetragonal, space group $I\bar{4}$, $a = b = 1912.3(3)$, $c = 1561.7(3)$ pm, $V = 5711(2) \times 10^6$ pm^3, $Z = 2$, $\rho_{calcd} = 1.246$ Mg m^{-3}, $F(000)$ 2240, $T = 293$ K, $2 < 2\Theta < 48^\circ$; of 18188 reflections 4517 were independent ($R_{int} = 0.054$), and 4010 with $I > 2\sigma(I)$; $R_1 = 0.035$, $wR_2 = 0.081$.
[5] D. D. Perrin, B. Dempsey, E. P. Serjeant, *pK_a Prediction for Organic Acids and Bases*, Chapman & Hall, London, **1981**.
[6] **3**: Phenyllithium (2.63 mmol, 1.6 M in diethyl ether/cyclohexane) was added dropwise to **1** · $4OEt_2$[1] (1.398 g, 0.65 mmol) in diethyl ether (20 mL) and stirred for 30 min, and a clear solution formed. After a further 30 min a precipitate was formed, which was then recrystallized from diethyl ether. Yield: 0.989 g (70 %). Correct elemental analysis. ^{1}H NMR: $\delta = 0.70$ (t, 24H, OEt), 2.80 (q, 16H, OEt), 7.15 (m, 48H, Ph), 7.97 (m, 16H, Ph), 8.16 (m, 16H, Ph); ^{13}C NMR: $\delta = 14.34$ (s, OEt), 65.36 (s, OEt), 127.5 – 129.06 (m, Ph), 134.91 (s, Ph), 135.61 (s, Ph), 139.50 (s, Ph), 141.37 (s, Ph); ^{29}Si NMR: $\delta = -45.93$ (s, $SiPh_2$). Crystal structure analysis:[8] $C_{112}H_{120}Al_4Li_4O_{20}Si_8$, $M = 2146.48$ g mol^{-1}, monoclinic, space group $I2$, Flack parameter: 0.046, $a = 1812.2(4)$, $b = 1531.9(3)$, $c = 2244.1(4)$ pm, $\beta = 90.22^\circ$, $V = 6230(2) \times 10^6$ pm^3, $Z = 2$, $\rho_{calcd} = 1.144$ Mg m^{-3}, $F(000) = 2256$, $T = 293$ K, $2 < 2\Theta < 48^\circ$; of 14713 reflections 9565 were independent ($R_{int} = 0.041$), and 6036 with ($I > 2\sigma(I)$; $R_1 = 0.069$, $wR_2 = 0.164$.
[7] **4**: **3** (172 mg, 0.079 mmol) was stirred in toluene (5 mL) with NH_3 (0.2 mmol in toluene) for 30 min at room temperature. The solvent was then removed under reduced pressure and the residue recrystallized from a small amount of diethyl ether. Yield 135 mg (81 %). Correct elemental analysis. ^{1}H NMR: $\delta = -0.90$ (s, 6H, NH_3), 0.69 (t, 18H, OEt), 2.81 (q, 12H, OEt), 7.15 (m, 48H, Ph), 7.53 (m, 16H, Ph), 8.15 (m, 16H, Ph); ^{13}C NMR: $\delta = 14.84$ (s, OEt), 65.80 (s, OEt), 127.7 – 129.4 (m, Ph), 134.93 (s, Ph), 135.66 (s, Ph), 139.81 (s, Ph), 141.45(s, Ph); ^{29}Si NMR: $\delta = -45.83$ (s, $SiPh_2$); ^{15}N NMR (20.3 MHz): $\delta = -384.2$ (s, NH_3). Crystal structure analysis:[8] $C_{108}H_{116}Al_4Li_4N_2O_{19}Si_8$, $M = 2106.49$ g mol^{-1}, triclinic space group $P\bar{1}$, $a = 1564.1(3)$, $b = 1591.2(2)$, $c = 2689.2(7)$ pm, $\alpha = 91.93(2)$, $\beta = 92.12(3)$, $\gamma = 118.70(2)^\circ$, $V = 5857(2) \times 10^6$ pm^3, $Z = 2$, $\rho_{ber} = 1.194$ Mg m^{-3}, $F(000) = 2212$, $T = 293$ K, $1.7 < 2\Theta < 45^\circ$; of 37024 reflections 14208 were independent ($R_{int} = 0.066$), and 10208 with $I > 2\sigma(I)$; $R_1 = 0.070$, $wR_2 = 0.205$.
[8] General information regarding the crystal structure analyses: Stoe-IPDS-diffractometer. The structures were solved by direct methods (SHELXS-86) and refined (SHELXL-93) with anisotropic temperature factors for all non-hydrogen atoms; hydrogen atoms were in fixed geometrical positions. Further details concerning the crystal structure analyses can be obtained from the Fachinformationszentrum Karlsruhe, D-76344 Eggenstein-Leopoldshafen, on quoting the depository number CSD-407811 (**2**), 407812 (**3**), and 407813 (**4**).

 © WILEY-VCH Verlag GmbH, D-69451 Weinheim, 1998 1433-7851/98/3701-0108 $ 17.50+.50/0

RNA – Aminoglycoside Interactions: Design, Synthesis, and Binding of "Amino-aminoglycosides" to RNA**

Hai Wang and Yitzhak Tor*

At the frontiers of RNA chemistry and biology stands the intriguing and largely unexplored area of RNA recognition. Despite the central role RNA plays in numerous biological processes, little is known about the interactions between small organic molecules and RNA biomolecules.[1, 2] The discovery that aminoglycoside antibiotics interact specifically with diverse RNA molecules—such as 16S ribosomal RNA,[3, 4] introns of group I,[5] and the hammerhead ribozymes[6]—and block the binding of the Rev protein[7] and Tat peptide[8] to their viral RNA targets attracted considerable interest and stimulated studies attempting to identify the elements involved in these recognition phenomena.[9, 10] The elucidation of general "recognition rules" for RNA – ligand interactions is essential for developing RNA binders of low molecular weight that target pivotal bacterial and viral RNA sites.

As aminoglycosides are highly functionalized polycationic oligosaccharides, interactions between their polar residues (amino and hydroxyl groups) and the RNA backbone and/or heterocyclic bases are likely to occur.[11] Since the amino groups are predominantly protonated at pH 7.0,[12] the overall charge density presented by the aminoglycosides toward the RNA host is likely to be important for RNA binding. The reported structure – activity relationships for natural aminoglycosides support this general view. Hence, aminoglycosides containing four amino groups show very little ability to bind RNA, whereas the most active derivatives contain five or six amino groups.[5–8] Although rather general, this view does not explain marked differences in RNA binding among related aminoglycoside antibiotics.[5, 7]

Here we focus on the importance of electrostatic interactions for binding between RNA and aminoglycoside, and address the following questions: 1. Will the ability of poor RNA binders (e. g. kanamycin A) to bind RNA be increased by incorporating an additional amino group into their structures? 2 Will the ability of the most active antibiotics (tobramycin and neomycin) to bind RNA be further increased by adding more amino groups? 3. Can a common recognition pattern be identified? We report here the design, synthesis, and ribozyme inhibitory activity of novel "amino-aminoglycosides" derived from kanamycin A, tobramycin, and neomycin B. We provide experimental evidence for the critical role of the overall charge of aminoglycosides in RNA binding and propose a general recognition model emphasizing the stereochemical display of the charged ammonium groups.

[*] Prof. Dr. Y. Tor, H. Wang
Department of Chemistry and Biochemistry
University of California, San Diego
La Jolla, CA 92093-0358 (USA)
Fax: Int. code + (1) 619-5345383
e-mail: ytor@ucsd.edu

[**] This work was supported by the Universitywide AIDS Research Program, University of California (grant no. R96-SD-067) and by the Hellman Faculty Fellowship to Y.T.

In designing amino-aminoglycosides three major factors had to be considered: 1. the modification site, 2. the degree of substitution of the amine and its basicity, and 3. synthetic accessibility. We recently synthesized and studied a series of systematically deoxygenated analogues of tobramycin. Preliminary results indicated that 6″-deoxytobramycin is comparable, yet slightly inferior, to tobramycin in its affinity to the hammerhead ribozyme.[13] This observation suggests that while the primary 6″-OH group might not be essential for RNA binding it is likely to be involved in RNA contact. Regarding the basicity of the amino groups, the primary aminomethyl groups ($-CH_2NH_2$) in various aminoglycosides are more basic (pK_a 8.6 – 9.0) than the other primary amines (pK_a 6.2 – 8.1).[12] Taken together with the relative ease of derivatizing a primary alcohol, we selected position 6″ in kanamycin A and tobramycin, and position 5″ in neomycin B as the modification sites.

The derivatives studied (Figure 1) include kanamycin A (**1**), 6″-amino-6″-deoxykanamycin A (**2**), kanamycin B (**3**), tobramycin (**4**), 6″-amino-6″-deoxytobramycin (**5**), neomycin B (**6**), and 5″-amino-5″-deoxyneomycin B (**7**). These represent aminoglycoside derivatives in which a single primary hydroxyl group is replaced by a primary amine while all other functional groups remain intact. A representative synthesis is illustrated in Scheme 1 for **5**. Tobramycin (**4**) was first protected as its Cbz derivative **8** and then tosylated at the primary 6″-hydroxyl group. The fully Cbz-protected monotosylate **9** was treated with sodium azide to afford **10**, which was then reduced to amine **11** with triphenylphosphane and an aqueous solution of sodium hydroxide. Catalytic hydrogenation afforded **5**. Similar transformations were utilized for synthesizing **2**[14] and **7**.[15]

The aminoglycosides and their amino derivatives were tested for their ability to inhibit the hammerhead ribozyme, a well-studied, small RNA enzyme.[6, 16] The effect of aminoglycoside derivatives on the cleavage rate of the hammerhead ribozyme was investigated at pH 7.3 under single-turnover conditions in the presence of Mg^{2+} and ribozyme at subsaturating concentrations. Figure 2 illustrates the results of a typical experiment, and Table 1 summarizes the pseudo-first-order rate constants obtained at different aminoglycoside concentrations.

Under our conditions the ribozyme cleaves its substrate at a rate of 0.075 min^{-1}. At a concentration of 100 μM, kanamycin A (**1**) slows the ribozyme down to about 75 % of this rate, whereas at 10 μM **1** does not inhibit the ribozyme at all. In contrast, at a concentration of 100 μM 6″-amino-6″-deoxykanamycin A (**2**) decreases the cleavage rate fivefold, which is similar to the effect induced by kanamycin B (**3**). This observation indicates that adding an amino group can convert a very poor RNA binder into a reasonably strong one. Modifying a stronger RNA binder such as tobramycin further enhances its affinity to RNA. Thus, at a concentration of 10 μM 6″-amino-6″-deoxytobramycin (**5**) decreases the ribozyme-cleavage rate fivefold more effectively than the parent tobramycin (**4**).

Neomycin B (**6**) is one of the strongest RNA binders. At a concentratin of 10 μM it shows strong inhibitory activity that is comparable to that of **2** at 100 μM. Replacing the 5″- primary

 © WILEY-VCH Verlag GmbH, D-69451 Weinheim, 1998 1433-7851/98/3701-0109 $ 17.50+.50/0

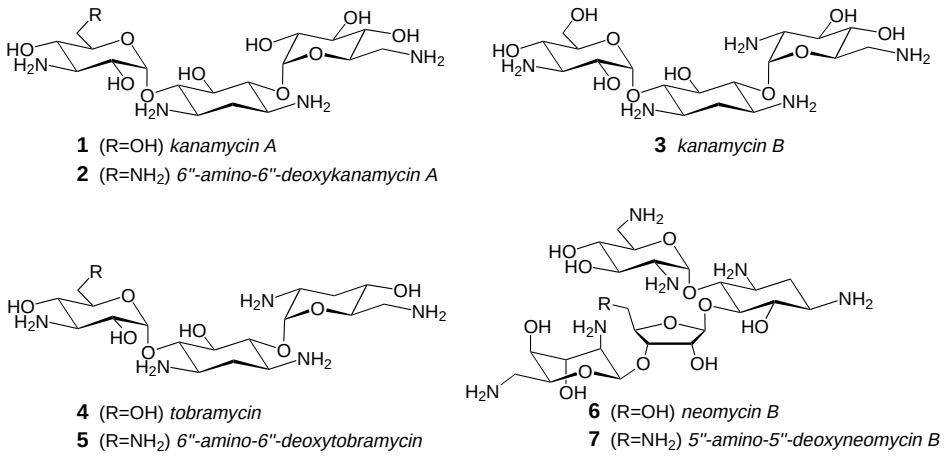
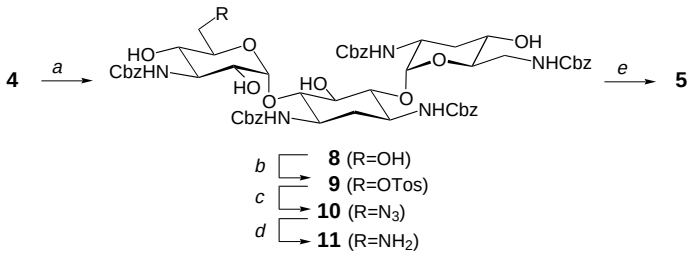


Figure 1. The structural formulas of the natural aminoglycosides and their amino derivatives studied in this work.

OH group with a primary NH_2 group leads to a novel aminoglycoside derivative **7** containing seven amino groups. At 10 μM **7** is an extremely potent inhibitor, and slows down the ribozyme by a factor of twenty-five. At 1 μM **7** slows down the hammerhead ribozyme twice as effectively as the parent neomycin B (**6**). These observations indicate that even the ability of the most active aminoglycosides to bind RNA can be further enhanced by increasing their overall charge.

The comparable ribozyme inhibitory activity of 6″-amino-6″-deoxykanamycin A (**2**) and kanamycin B (**3**) may not be coincidental. Both derivatives have five amino groups, albeit in different positions of the aminoglycosidic skeleton, and are likely to have a similar overall positive charge at a given pH. We propose that these aminoglycosides present a similar stereochemical array of positive charges. Thus, **2** is rotated around an imaginary pseudo-C_2 axis going through positions 2 and 5 in the central 2-deoxystreptamine ring so that the two central rings "overlap" (Figure 3). Amino groups 1 and 3 of **2** can overlap with amino groups 3 and 1 of **3**. The 3″-NH_2 group of **2** can take the position of the flexible 6′-NH_2 group in **3**, and the new 6″-NH_2 group in **2** can assume the position of the 2′-NH_2 group in **3**. In addition, 6′-NH_2 of **2** can occupy the position of 3″-NH_2 in **3**.[17] Taken together with the spherical shape of an ammonium group and its geometrical degeneracy, both derivatives can display a similar array of ammonium groups and charge densities toward the RNA skeleton (Figure 3).



Scheme 1. Synthesis of 6″-amino-6″-deoxytobramycin (**5**). Reagents and conditions: a) $PhCH_2OCOCl$, H_2O, Na_2CO_3, 90%; b) toluenesulfonyl chloride, pyridine, 4 °C, 52%; c) NaN_3, DMF, 80%; d) Ph_3P, THF, NaOH/H_2O; e) H_2, Pd/C, dioxane, H_2O, AcOH, 60% (for d+e).

Table 1. Inhibition of the hammerhead ribozyme by aminoglycoside derivatives.[a]

Derivative	k_2 [min^{-1}] 100 μM	10 μM	1 μM
none (control)		0.075	
kanamycin A (**1**)	0.058	–[b]	–[b]
6″-amino-6″-deoxykanamycin A (**2**)	0.018	0.050	–[b]
kanamycin B (**3**)	0.018	0.060	–[b]
tobramycin (**4**)	0.012	0.051	–[b]
6″-amino-6″-deoxytobramycin (**5**)	–[c]	0.011	–[b]
neomycin B (**6**)	–[c]	0.018	0.062
5″-amino-5″-deoxyneomycin B (**7**)	–[c]	0.003	0.030

[a] See Experimental Section for conditions. The values given are the average of three independent experiments, and the error is estimated to be 10%. [b] No inhibition is observed at this concentration. [c] Under these conditions the derivatives are too active, and complete inhibition is observed.

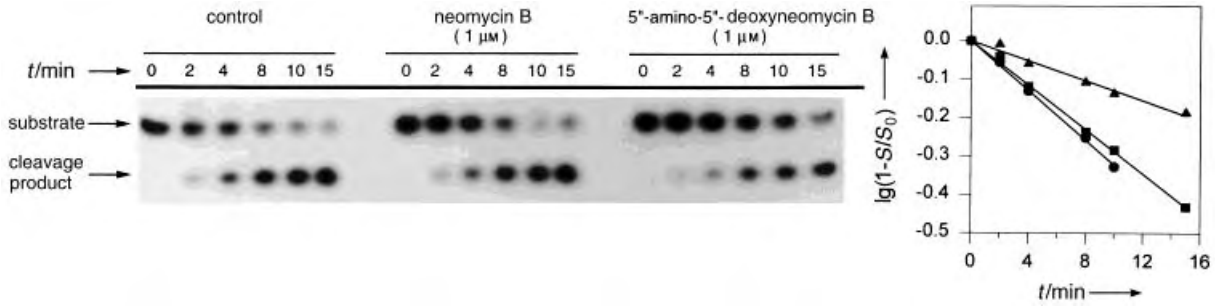
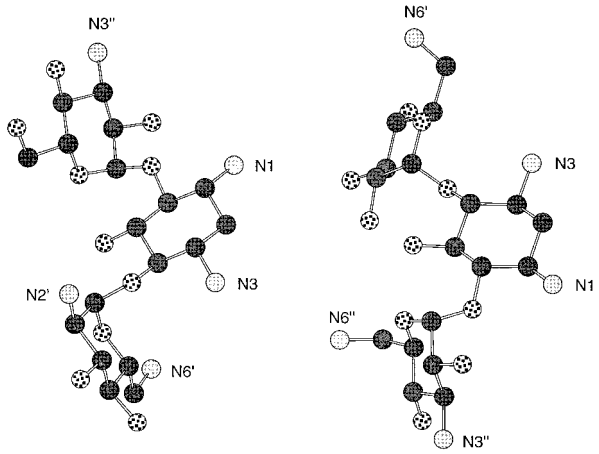


Figure 2. Left: autoradiograms of a 20% polyacrylamide gel used to separate the products of the time-dependent hammerhead ribozyme cleavage reactions in the absence (control) and the presence of **6** and **7**. Right: kinetic analysis of the quantified gel. Control (●), 1 μM **6** (■), and 1 μM **7** (▲).

 © WILEY-VCH Verlag GmbH, D-69451 Weinheim, 1998 1433-7851/98/3701-0110 $ 17.50+.50/0



2 *kanamycin B* **3** *6''-amino-6''-deoxykanamycin A*

Figure 3. Minimized conformations (Spartan program) of the fully protonated 6″-amino-6″-deoxykanamycin A (**2**) and the rotated kanamycin B (**3**) showing the similar position occupied by the ammonium groups in space. C: dark gray, N: light gray, O: dotted.

Previous studies showed that aminoglycoside antibiotics interact preferentially with the enzyme–substrate complex of the hammerhead ribozyme and inhibit the cleavage step.[6] The positively charged ammonium groups were suggested to displace critical Mg^{2+} ions.[18] Our results support this view and clearly demonstrate that the total number of amino groups in the aminoglycoside is correlated with inhibitory activity and RNA binding. Our aminoglycoside–RNA recognition model proposes a specific yet versatile three-dimensional projection of positively charged ammonium groups towards acceptor groups on the RNA binding site. This is in agreement with the results of recent NMR studies[10] and MD simulations[19] that suggest a three-dimensional electrostatic complementarity rather than highly specific contacts between aminoglycoside antibiotics and their RNA hosts.

Our studies have important implications for the design of RNA binders.[20] Such molecules will have to possess sufficient positive charges to bind electrostatically to the RNA target site. Competition with bound Mg^{2+} can be achieved by a strategic incorporation of ammonium groups with predetermined N–N distances and three-dimensional projection, and possibly by the incorporation of functional groups capable of coordinating Mg^{2+}. RNA binders of low molecular weight with higher efficacy and lower toxicity than aminoglycoside antibiotics may replace these drugs in clinical uses and may find novel applications as anti-viral agents.

Experimental Section

The syntheses of the aminoglycoside derivatives will be reported elsewhere.

The hammerhead ribozyme used was HH16, which contains the enzyme E16 and the ^{32}P-5′-labeled substrate S16.[6] Both E16 and S16 were prepared by in vitro transcription reactions of the corresponding synthetic DNA templates using T7 RNA polymerase. Ribozyme reaction conditions: 20 nM E16, trace ^{32}P-5′-labeled S16 ($\leq$ 1 nM), 7.5 mM $MgCl_2$, 50 mM Tris-HCl, and pH 7.3 with varying concentrations of aminoglycosides. The reactions were initiated by mixing equal volumes of preincubated solutions of the enzyme E16 and the labeled substrate S16. Aliquots were removed at various times and quenched by adding excess stop solution/loading buffer (8 M urea, 50 mM disodium ethylenediaminetetraactate (Na_2EDTA), pH 7.3, bromophenol blue, and xylene cyanol). The substrate and product were resolved on 20% polyacryamide/7 M urea gels, and the fraction cleaved was quantified using a Molecular Dynamics Phosphorimager with ImagQuant software. Plotting $\lg(1 - S/S_0)$ vs. time gives a straight line with a slope of $-k_2$ (Figure 2, right).

Received: July 8, 1997 [Z10657IE]
German version: *Angew. Chem.* **1998**, *110*, 117–120

Keywords: aminoglycosides · antibiotics · electrostatic interactions · ribozymes · RNA

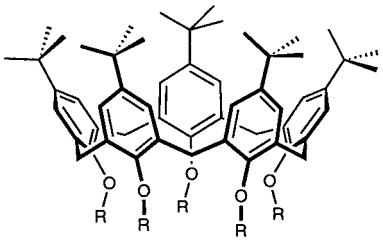
[1] C. S. Chow, F. M. Bogdan, *Chem. Rev.* **1997**, *97*, 1489–1513.
[2] W. D. Wilson, L. Ratmeyer, M. Zhao, L. Strekowski, D. Boykin, *Biochemistry* **1993**, *32*, 4089–4104; L. Ratmeyer, M. L. Zapp, M. R. Green, R. Vinayak, A. Kumar, D. W. Boykin, W. D. Wilson, *ibid.* **1996**, *35*, 13689–13696.
[3] D. Moazed, H. F. Noller, *Nature* **1987**, *327*, 389–394.
[4] P. Purohit, S. Stern, *Nature* **1994**, *370*, 659–662.
[5] U. von Ahsen, J. Davies, R. Schroeder, *Nature* **1991**, *353*, 368–370; U. von Ahsen, J. Davies, R. Schroeder, *J. Mol. Biol.* **1992**, *226,* 935–941; J. Davies, U. von Ahsen, R. Schroeder, *The RNA World* (Eds.: R. F. Gesteland, J. F. Atkins), Cold Spring Harbor Laboratory Press, New York, **1993**, pp. 185–204.
[6] T. K. Stage, K. J. Hertel, O. C. Uhlenbeck, *RNA* **1995**, *1*, 95–101.
[7] M. L. Zapp, S. Stern, M. R. Green, *Cell* **1993**, *74*, 969–978; G. Werstuck, M. L. Zapp, M. R. Green, *Chem. Biol.* **1996**, *3*, 129–137.
[8] H.-Y. Mei, A. A. Galan, N. S. Halim, D. P. Mack, D. W. Moreland, K. B. Sanders, H. N. Troung, A. W. Czarnik, *Bioorg. Med. Chem. Lett.* **1995**, *5*, 2755–2760.
[9] S. M. Lato, A. R. Boles, A. D. Ellington, *Chem. Biol.* **1995**, *2*, 291–303; M. G. Wallis, U. von Ahsen, R. Schroeder, M. Famulok, *ibid.* **1995**, *2*, 543–552; M. Famulok, A. Hüttenhofer, *Biochemistry* **1996**, *35*, 4265–4270; Y. Wang, J. Killian, K. Hamasaki, R. R. Rando, *ibid.* **1996**, *35*, 12338–12346; M. Hendrix, E. S. Priestley, G. F. Joyce, C.-H. Wong, *J. Am. Chem. Soc.* **1997**, *119*, 3641–3648; M. I. Pecht, D. Fourmy, S. C. Blanchard, K. D. Dahlquist, J. D. Puglisi, *J. Mol. Biol.* **1996**, *262*, 421–436. D. Fourmy, M. I. Pecht, S. C. Blanchard, J. D. Puglisi, *Science* **1996**, *274*, 1367–1371.
[10] L. Jiang, A. K. Suri, R. Fiala, D. J. Patel, *Chem. Biol.* **1997**,*4*, 35–50.
[11] M. Hendrix, P. B. Alper, E. S. Priestley, C.-H. Wong, *Angew. Chem.* **1997**, *109*, 119–122; *Angew. Chem. Int. Ed. Engl.* **1997**, *36*, 95–98.
[12] D. E. Dorman, J. W. Paschal, K. E. Merkel, *J. Am. Chem. Soc.* **1976**, *98*, 6885–6888; R. E. Botto, B. Coxon, *ibid.* **1983**, *105*, 1021–1028; L. Szilágyi, Z. Sz. Pusztahelyi, S. Jakab, I. Kovács, *Carbohyd. Res.* **1993**, *247*, 99–109.
[13] H. Wang, Y. Tor, *J. Am. Chem. Soc.* **1997**, *119*, 8734–8735.
[14] S. Inouye, *J. Antiobiot.* **1967**, *20*, 6–14.
[15] All new compounds showed satisfactory analytical and spectroscopic data.
[16] O. C. Uhlenbeck, *Nature*, **1987**, *328*, 596–600; M. J. Fedor, O. C. Uhlenbeck, *Biochemistry* **1992**, *31*, 12042–12054.
[17] Another approach is to compare the intramolecular $NH_3^+ \cdots NH_3^+$ distances in the minimized conformations of the two aminoglycoside derivatives. A similar set of distances (albeit for different pairs of ammonium groups) is obtained. This result supports the view that **2** and **3** display a comparable array of positive charges that are capable of competing with Mg^{2+} ions for binding to RNA.
[18] B. Clouet-d'Orval, T. K. Stage, O. C. Uhlenbeck, *Biochemistry* **1995**, *34*, 11186–11190.
[19] T. Hermann, E. Westhof, *J. Mol. Biol.*, in press.
[20] For a combinatorial approach to the synthesis of aminoglycoside mimetics, see W. K. C. Park, M. Auer, H. Jaksche, C.-H. Wong, *J. Am. Chem. Soc.* **1996**, *118*, 10150–10155.

 © WILEY-VCH Verlag GmbH, D-69451 Weinheim, 1998 1433-7851/98/3701-0111 $ 17.50+.50/0

Calix[5]arene-Based Molecular Vessels for Alkylammonium Ions**

Francoise Arnaud-Neu, Saowarux Fuangswasdi, Anna Notti, Sebastiano Pappalardo,* and Melchiorre F. Parisi

Dedicated to Professor Francesco Bottino on the occasion of his 70th birthday



	R
1a	H
1b	$(CH_2)_3CH(CH_3)_2$
1c	$(CH_2)_2OCH(CH_3)_2$
1d	$CH_2CO_2CH(CH_3)_2$
1e	$CH_2CO_2C(CH_3)_3$

Cation–π-electron interactions are known to play an important role in the recognition of positively charged guests by the electron-rich π-systems of natural[1] and synthetic hosts.[2] Calixarenes,[3] when suitably functionalized, can provide three-dimensional, rigid, π-rich cavities for the selective inclusion of organic cations in nonpolar media.[4] Recently we have shown that triether derivatives of (1,3)-*p*-*tert*-butylcalix[5]arene crown-6 are able to discriminate between linear and branched alkylammonium ions by means of *endo* complexation.[5] The low association constants (K_{ass} = 48–86 M^{-1}) observed for the selective inclusion of nBuNH$_3^+$ ions are probably related to the shape of the cavity of these host molecules (C_s symmetry) and their pronounced tendency to fill the cavity by canting a *tert*-butylphenyl residue inwards.[5]

To develop more powerful receptors, these calixarenes with distorted *cone* conformations should be replaced by compounds with an improved shape and preorganized, permanent *cone* conformations. Although the shape of the calix[5]arene cavity can, in principle, be tuned by changing the nature and bulkiness of substituents on both the upper and lower rims,[6] the presence of *tert*-butyl substituents on the upper rim is essential to keep the molecule in a *cone* conformation and ensure selective inclusion of RNH$_3^+$ ions. Therefore, structural modifications to the lower rim of *p*-*tert*-butylcalix[5]arene (**1a**) have been addressed. We have found that the attachment of long-chain pendant groups (bulkier than ethoxyethoxy)[7] on the lower rim of **1a**—by exhaustive alkylation with appropriate electrophiles—produces derivatives **1b**–**e**, which have a fixed and quite regular C_{5v} *cone* conformation. These receptors bind linear RNH$_3^+$ ions much more efficiently and selectively than the neutral synthetic host systems reported to date.

Host–guest binding affinities were investigated by ^{1}H NMR titration experiments of $CDCl_3/CD_3OD$ (9/1, v/v) solutions of **1b**–**e** with the four isomeric butylammonium picrate salts. Upon addition of increasing amounts of salts, the spectra consistently showed, from the first aliquot onwards, distinct sets of signals for the free and complexed species, indicating that exchange between the complexed and uncomplexed guests is slow on the NMR time scale. Consequently, the formation of 1:1 inclusion complexes was directly assessed by comparing the signal intensities of solutions containing equimolar amounts of host and guest. *endo* Complexation is unambiguously supported by the dramatic upfield shifts (complexation-induced shifts, CIS, up to $\Delta\delta$ = 4.1) of the resonances of the cavity-included alkyl chain of the guest. Due to the high preorganization of the host cavities prior to guest inclusion, the CIS of the receptors are lower ($\Delta\delta$ = 0.1–0.4).

The percentage of *endo* complexation for each butylammonium salt was determined by direct ^{1}H NMR analysis of equimolar solutions (5×10^{-3} M) of host and guest. Hosts **1b**–**e** show a remarkable affinity for the linear nBuNH$_3^+$ ion (68–95%) and a much lower affinity for the branched iBuNH$_3^+$ (6–38%) and sBuNH$_3^+$ (5–28%) ions. No interaction could be detected with the bulky tBuNH$_3^+$ ion, even when a large excess (10 equiv) of the salt was added under standard experimental conditions (15 min equilibration at 21°C before the spectrum was recorded). Furthermore, a direct NMR competition experiment has shown that when **1e** is mixed with equimolar mixtures of the four butylammonium picrates, only nBuNH$_3^+$ (95%) and iBuNH$_3^+$ (5%) ions undergo *endo* complexation. Owing to the high degree of *endo* complexation for the nBuNH$_3^+$ ion, relevant K_{ass} values could not be reliably assessed by ^{1}H NMR spectroscopy[8] and were determined in $CHCl_3$ saturated with water by using the picrate extraction method developed by Lein and Cram.[9]

The association constants of **1b**–**e** with the isomeric butylammonium picrates are summarized in Table 1. High lgK_{ass} values ($4.63 \le \lg K_{ass} \le 6.47$) are always found with the nBuNH$_3^+$ ion and receptors **1b**–**e**, while with the other branched cations and specifically with the tBuNH$_3^+$ ion they are significantly lower ($\lg K_{ass} \le 3.5$). For a given butylammonium picrate isomer, the stability of the complexes generally decreases in the following order: **1e** > **1b** > **1c** > **1d**. Accordingly, calix[5]arenes **1b** and **1e** appear to bind the nBuNH$_3^+$

Table 1. Association constants ($\lg K_{ass} \pm \sigma$) of isomeric BuNH$_3^+$ ions (picrate salts) with **1b**–**e**, obtained by UV spectroscopy.[a]

	nBuNH$_3^+$	iBuNH$_3^+$	sBuNH$_3^+$	tBuNH$_3^+$
1b	5.80 ± 0.02	3.72 ± 0.01	3.68 ± 0.01	3.16 ± 0.02
1c	4.68 ± 0.02	3.26 ± 0.06	3.24 ± 0.02	3.02 ± 0.03
1d	5.32 ± 0.01	3.69 ± 0.02	3.6 ± 0.1	3.5 ± 0.2
1e	6.47 ± 0.08	4.09 ± 0.01	3.8 ± 0.2	3.49 ± 0.02

[a] Measured in $CHCl_3$ at 25°C (σ: standard deviation of a minimum of three independent determinations).

[*] Prof. S. Pappalardo
Dipartimento di Scienze Chimiche
Università di Catania
Viale A. Doria 6, I-95125 Catania (Italy)
Fax: Int. code + (39) 95-580138
e-mail: spappalardo@dipchi.unict.it
Dr. F. Arnaud-Neu, S. Fuangswasdi
Laboratoire de Chimie-Physique de l'ECPM
Université Louis Pasteur, Strasbourg (France)
Dr. A. Notti, Dr. M. F. Parisi
Dipartimento di Chimica Organica e Biologica
Università di Messina, Messina (Italy)

[**] The Italian authors thank MURST for financial support of this work and Dr. M. Saitta for mass spectrometric measurements. S. F. acknowledges a scholarship from SFERE.

 © WILEY-VCH Verlag GmbH, D-69451 Weinheim, 1998 1433-7851/98/3701-0112 $ 17.50+.50/0

ion more selectively than the other isomeric cations. For instance, the selectivity of **1e** for nBuNH$_3^+$ over tBuNH$_3^+$, expressed as the ratio $K_{ass}(n\text{BuNH}_3^+)/K_{ass}(t\text{BuNH}_3^+)$ approaches 10^3. This is, to the best of our knowledge, the highest selectivity so far observed for this pair of isomers. It is higher than the values reported for [18]crown-6[10] and calix[6]arene hexaesters[11] by about three and two orders of magnitude, respectively. Kubo et al. have recently reported a reversed selectivity for tBuNH$_3^+$ ions [$K_{ass}(t\text{BuNH}_3^+)/K_{ass}(n\text{BuNH}_3^+ = 11$] by a chromogenic 1,1′-binaphthyl-derived calix[4]crown. In this case complexation is presumed to involve the crown ether moiety and a phenolate group.[12]

Since the structural motif of nBuNH$_3^+$ is present in biologically important amines, calix[5]arenes **1b**–**e** can also act as biomimetic host systems. A screening with a number of α-amino acid methyl esters (including Phe-OMe · HCl, Arg-OMe · 2 HCl, Val-OMe · HCl) and small peptides has shown that receptors **1b** and **1e** form specifically 1:1 inclusion complexes only with N^{α}-Ac-Lys-OMe · HCl and Lys-Gly-OMe · 2 HCl. Noteworthy, in the latter the ε-butylenammonium group is recognized by the cavity and complexed in the presence of an unprotected α-ammonium group. In addition, the methyl ester hydrochlorides of the neurotransmitter γ-aminobutyric acid (GABA)[13] and the plasmin inhibitor ε-aminocaproic acid (ε-Ahx)[14] are also strongly included with degrees of complexation up to 80 % (Figure 1).

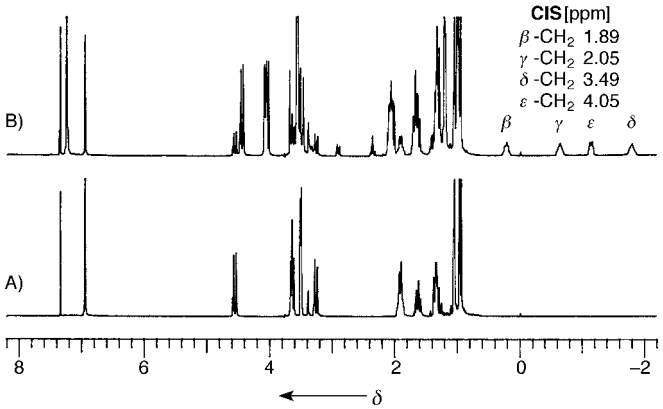


Figure 1. ^{1}H NMR spectra (300 MHz, $CDCl_3/CD_3OD$ 9/1, 21 °C) of receptor **1b** (A) and its 1:1 inclusion complex with ε-Ahx-OMe · HCl ([**1b**] = [ε-Ahx-OMe · HCl] = 5×10^{-3} M) showing characteristic CIS values for the included guest (B).

The calix[5]arene derivatives described here, which are frozen in a C_{5v}-symmetric *cone* conformation, are the most selective molecular receptors for linear alkylammonium ions reported to date. These receptors display an enzymelike selectivity[15] towards biologically important ammonium substrates. Enhancement of their efficacy as biomimetic host systems is currently in progress.

Experimental Section

1b: A stirred mixture of **1a**[16] (0.405 g, 0.50 mmol), isohexyl tosylate (1.923 g, 7.50 mmol), and anhydrous K_2CO_3 (1.037 g, 7.50 mmol) in dry CH_3CN (50 mL) was refluxed under N_2 for 16 h. After cooling, the precipitate was collected by filtration, washed with water, dried, and recrystallized from CH_3CN/CH_2Cl_2 to give **1b** in 72 % yield, m.p. 221–224 °C. ^{1}H NMR (300 MHz, $CDCl_3$): $\delta = 0.94$ (d, $J = 6.6$ Hz, CHMe_2, 30 H), 1.03 (s, tBu, 45 H), 1.32 (m, $OCH_2CH_2CH_2$, 10 H), 1.60 (septet, $J = 6.6$ Hz, CHMe$_2$, 5 H), 1.89 (m, $OCH_2CH_2CH_2$, 10 H), 3.25, 4.54 (d, $J = 13.8$ Hz, $ArCH_2Ar$, 10 H), 3.63 (t, $J = 7.2$ Hz, $OCH_2CH_2CH_2$, 10 H), 6.92 (s, Ar H, 10 H); FAB MS (positive ion): m/z (%) 1248 [100, $(M + NH_4)^+$].

Calixarene **1c** was obtained analogously from **1a** and 2-isopropoxyethyl tosylate in 84 % yield, m.p. 180–185 °C (EtOH). ^{1}H NMR (300 MHz, $CDCl_3$): $\delta = 1.02$ (s, tBu, 45 H), 1.19 (d, $J = 6.1$ Hz, CHMe_2, 30 H), 3.26, 4.56 (d, $J = 13.8$ Hz, $ArCH_2Ar$, 10 H), 3.70 (septet, $J = 6.1$ Hz, CHMe$_2$, 5 H), 3.78–3.89 (m, OCH_2CH_2, 20 H), 6.88 (s, Ar H, 10 H); FAB MS (positive ion): m/z (%) 1258 [100, $(M + NH_4)^+$].

Calixarenes **1d** and **1e**[17] were prepared similarly by treating **1a** with the appropriate alkyl bromoacetate. After the reaction mixture had been heated for 24 h at reflux, the inorganic salts were filtered off and washed with $CHCl_3$. The combined organic layers were concentrated to dryness, and the oily residue (mostly the K^+ complex)[17] was treated with petroleum ether. KBr was filtered off and the solvent removed to afford the free calixarenes. **1d**: 70 % yield, m.p. 184-186 °C (hexane/CH_2Cl_2); ^{1}H NMR (300 MHz, $CDCl_3$): $\delta = 1.01$ (s, tBu, 45 H), 1.27 (d, $J = 6.2$ Hz, CHMe_2, 30 H), 3.35, 4.84 (d, $J = 14.5$ Hz, $ArCH_2Ar$, 10 H), 4.62 (s, $OCH_2C{=}O$, 10 H), 5.08 (septet, $J = 6.2$ Hz, CHMe$_2$, 5 H), 6.87 (s, Ar H, 10 H); FAB MS (positive ion): m/z (%) 1333 [100, $(M + Na)^+$]. The physical and spectral data of **1e** were identical to those in the literature.[16]

Received: June 16, 1997 [Z 10551 IE]
German version: *Angew. Chem.* **1998**, *110*, 120–122

Keywords: amino acids · calixarenes · host–guest chemistry · inclusion compounds · molecular recognition

[1] J. L. Sussman, M. Harel, F. Frolow, C. Oefner, A. Goldman, L. Toker, I. Silman, *Science* **1991**, *253*, 872–879.
[2] a) F. Diederich in *Cyclophanes* (Ed.: J. F. Stoddart), The Royal Society of Chemistry, Cambridge, **1991**; b) P. C. Kearney, L. S. Mizoue, R. A. Kumpf, J. F. Forman, A. McCurdy, D. A. Dougherty, *J. Am. Chem. Soc.* **1993**, *115*, 9907–9919, and references therein.
[3] a) C. D. Gutsche, Calixarenes in *Monographs in Supramolecular Chemistry, Vol. 1* (Ed.: J. F. Stoddart), The Royal Society of Chemistry, Cambridge, **1989**; b) *Calixarenes, a Versatile Class of Macrocyclic Compounds* (Eds.: J. Vicens, V. Böhmer), Kluwer Academic, Dordrecht, **1991**; c) V. Böhmer, *Angew. Chem.* **1995**, *107*, 785–818; *Angew. Chem. Int. Ed. Engl.* **1995**, *34*, 713–745.
[4] a) K. Araki, H. Shimizu, S. Shinkai, *Chem. Lett.* **1993**, 205–208; b) G. De Iasi, B. Masci, *Tetrahedron Lett.* **1993**, *34*, 6635–6638; c) M. Takeshita, S. Nishio, S. Shinkai, *J. Org. Chem.* **1994**, *59*, 4032–4034; d) A. Casnati, P. Jacopozzi, A. Pochini, F. Ugozzoli, R. Cacciapaglia, L. Mandolini, R. Ungaro, *Tetrahedron* **1995**, *51*, 591–598; e) M. Takeshita, S. Shinkai, *Bull. Chem. Soc. Jpn.* **1995**, *68*, 1088–1097.
[5] S. Pappalardo, M. F. Parisi, *J. Org. Chem.* **1996**, *61*, 8724–8725.
[6] D. R. Stewart, M. Krawiec, R. P. Kashyap, W. H. Watson, C. D. Gutsche, *J. Am. Chem. Soc.* **1995**, *117*, 586–601.
[7] Pentakis(ethoxyethoxy)-*p*-*tert*-butylcalix[5]arene, synthesized by alkylation of **1a** with an excess of $EtOCH_2CH_2OTs$ and K_2CO_3, exists in $CDCl_3$ solution as a mixture of slowly interconverting *partial cone/cone* conformers in the ratio 19:1 at 21 °C.
[8] H.-J. Schneider, R. Kramer, S. Simova, U. Schneider, *J. Am. Chem. Soc.* **1988**, *110*, 6442–6448.
[9] G. M. Lein, D. J. Cram, *J. Am. Chem. Soc.* **1985**, *107*, 448–455.
[10] S.-K. Chang, M. J. Jang, S.-Y. Han, *Chem. Lett.* **1992**, 1937–1940.
[11] S.-Y. Han, M.-H. Kang, Y.-E. Jung, S.-K. Chang *J. Chem. Soc. Perkin Trans. 2* **1994**, 835–839.
[12] Y. Kubo, S. Maruyama, N. Ohhara, M. Nakamura, S. Tokita, *J. Chem. Soc. Chem. Commun.* **1995**, 1727–1728.
[13] E. Roberts, M. A. Sherman, *Neurochem. Res.* **1993**, *18*, 365–376.
[14] a) L. W. Steffen, B. W. Steffen, *Clin. Chem.* **1976**, *22*, 381–383; *Chem. Abstr.* **1976**, *84*, 132283p; b) J. L. Hoover-Plow, L. A. Miles, G. M.

 © WILEY-VCH Verlag GmbH, D-69451 Weinheim, 1998 1433-7851/98/3701-0113 $ 17.50+.50/0

Fless, A. M. Scanu, E. F. Plow, *Biochemistry* **1993,** *32*, 13681 – 13687; c) J. M. Marshall, A. J. Brown, C. P. Ponting, *ibid*. **1994**, *33*, 3599 – 3606.
[15] Plasminogen is a well-known example of an enzyme specific for lysine and lysine analogues (ω-amino acids): a) F. J. Castellino, J. R. Powell, *Methods Enzymol.* **1981**, *80*, 365 – 378; b) see also ref. [14].
[16] D. R. Stewart, C. D. Gutsche, *Org. Prep. Proc. Int*. **1993**, *25*, 137 – 139.
[17] G. Barrett, M. A. McKervey, J. F. Malone, A. Walker, F. Arnaud-Neu, L. Guerra, M.-J. Schwing-Weill, C. D. Gutsche, D. R. Stewart, *J. Chem. Soc. Perkin Trans. 2* **1993**, 1475 – 1479.

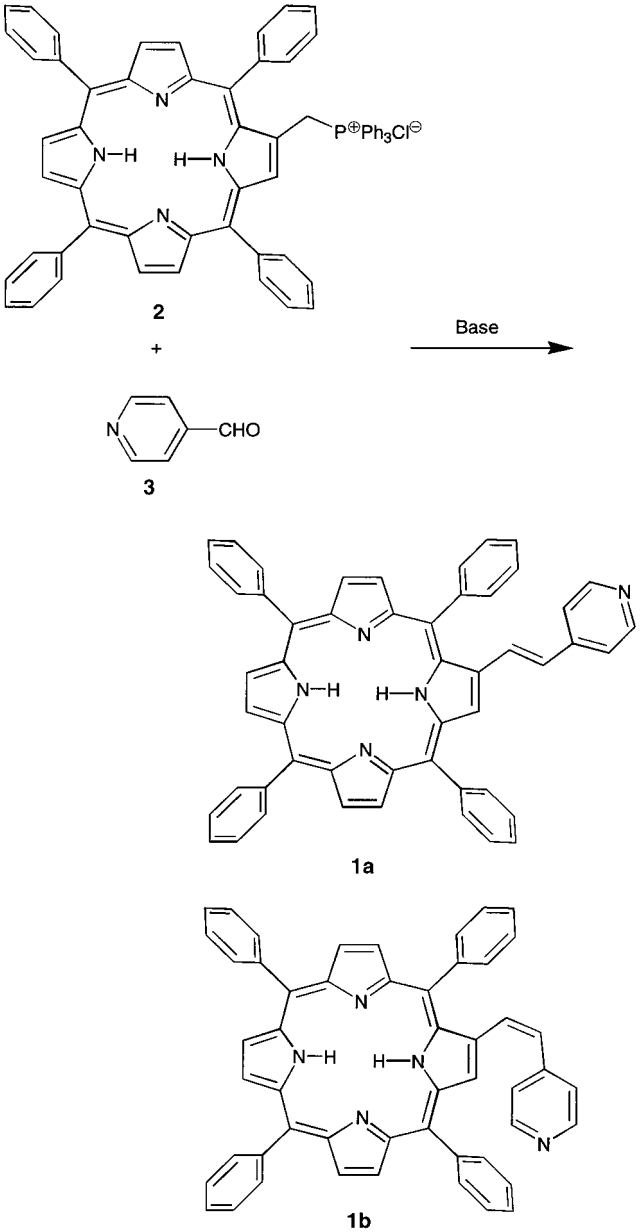
Controlling the Structure of Supramolecular Porphyrin Arrays**

Anthony K. Burrell,* David L. Officer,*
David C. W. Reid, and Kirstie Y. Wild

The importance of multichlorin assemblies in photosynthetic reaction centers and light-harvesting antenna complexes has inspired considerable interest in the synthesis of porphyrin arrays. Several synthetic strategies are employed for the assembly of multiporphyrin systems. A wide variety of porphyrin arrays of ever-increasing size have been constructed by the traditional methodology of covalently linking porphyrins.[1] More recently the incorporation of porphyrins into supramolecular assemblies has proven to be an attractive method for array formation. With careful choice of materials, the supramolecular structure of the array can be engineered. However, there is currently no porphyrin array system that can be "switched" from one ordered assembly to another. Here we report the first porphyrin system where the structure of the supramolecular assembly can be altered by a noninvasive technique such as photolysis.

With some notable exceptions,[2] the majority of the self-assembling porphyrin arrays are based upon metal – ligand interactions.[3] To a large extent this work has concentrated upon the coordination chemistry of *meso*-pyridyl porphyrins. Porphyrin assemblies prepared from *meso*-pyridyl porphyrins range from dimeric through to polymeric complexes.[3] Of particular interest are the ordered structures formed by a single component interacting with itself. The most common motif in this area is the use of pyridyl-functionalized metalloporphyrins; for example, the metal center of a zinc porphyrin will readily coordinate another ligand, such as pyridine. If the zinc porphyrin is also functionalized by a pyridine, the possibility for zinc – pyridine (inter-[4] or intramolecular[5]) interactions exist. The orientation of the pyridine functionality on the porphyrin macrocycle has a profound influence on the resulting superstructure, providing either dimeric[4f, 6] or oligomeric and polymeric[3j–l, 4] compounds. We have recently become interested in the formation of porphyrin arrays using coordination chemistry as a construction technique and the possibility that simple geometric changes, such as *cis/trans* alkene isomerization, would provide a method to control array superstructure.

As an introduction to this area we prepared the β-vinylpyridine functionalized porphyrin **1**. This compound can be obtained in 82% yield from the reaction of **2**[7] with 4-pyridinecarboxaldehyde (**3;** Scheme 1). The product isolated



Scheme 1. Synthesis of **1a** and **1b**.

is an isomeric mixture of *trans* **1a** (62%) and *cis* **1b** (20%) that can be separated by careful chromatography. The ^{1}H NMR spectra for both **1a** and **1b** are consistent with the structures reported. As expected **1a** is the more favored isomer, and solutions of **1b** convert into **1a** when heated in chloroform or if left exposed to light. Based on the X-ray

[*] Dr. A. K. Burrell, Dr. D. L. Officer, D. C. W. Reid, Dr. K. Y. Wild
Department of Chemistry, Massey University
Private Bag 11222, Palmerston North (New Zealand).
Fax : Int. code + (64) 6 350-5682.
e-mail: A.K.Burrell@massey.ac.nz

[**] We are grateful for support of this work from The Public Good Science Fund (MAU602), the Research Institute of Innovative Technology for the Earth, and the Massey University Research Fund. DCWR is grateful for assistance from a Massey University Postgraduate Scholarship, the William Georgetti Scholarship and the Freemasons Postgraduate Scholarship.

 © WILEY-VCH Verlag GmbH, D-69451 Weinheim, 1998 1433-7851/98/3701-0114 $ 17.50+.50/0

structure of a related compound,[1a] the porphyrin core, the olefin, and the pyridine ring of **1a** are presumed to be essentially planar, whereas simple molecular models indicate that it is not possible for the *cis* isomer **1b** to adopt a planar conformation. The effect the geometry of the alkene has on the reactivity of these porphyrins is most apparent when they are treated with Zn^{II}.

The reaction of **1a** with $Zn(OAc)_2$ results in the rapid insertion of Zn^{II} into the porphyrin core. Thin layer chromatography (TLC) of [Zn(**1a**)] did not yield a single spot as normally observed for metalloporphyrins. Instead [Zn(**1a**)] smears over a large portion of the TLC plate with almost every common eluent. The ^{1}H NMR spectrum of [Zn(**1a**)] is significantly changed from the spectrum observed for **1a**. The resonances of the pyridyl hydrogen atoms have shifted from $\delta = 7.11$ and 8.55 to 5.20 and 2.37, respectively, which is consistent with the coordination of the pyridine to a zinc porphyrin.[4] As it is not possible for this coordination to occur in an intramolecular fashion, the coordination must be intermolecular. This was confirmed by a single crystal X-ray analysis. The structure of [Zn(**1a**)] (Figure 1) consists of an

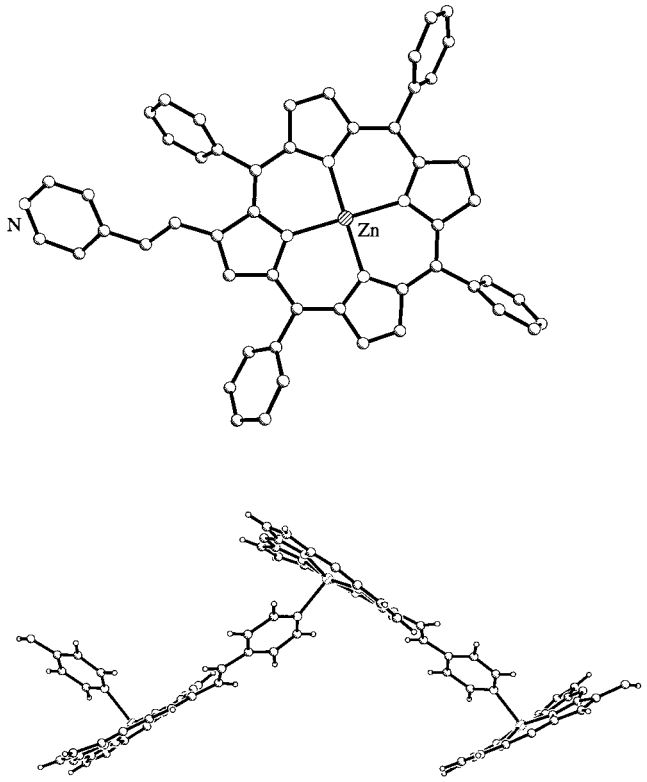


Figure 1. Molecular structure of a single molecule of [Zn(**1a**)] (top) and a section of the chain-like structure (bottom). The phenyl rings have been omitted from the second view for clarity.

infinite chain of porphyrins.[8] The pyridine is tilted 30.2(4)° from the plane of the zinc porphyrin core. The nitrogen atom of each pyridine group is coordinated, as an axial ligand, to the zinc in an adjacent molecule, resulting in an infinite solid-state polymer. The axial pyridine is not completely orthogonal to the plane of the zinc porphyrin, but tilted at 64.6(6)°. In the solid state, a second structural feature is also present. Each of the porphyrin chains is stacked on another at an average porphyrin–porphyrin distance of 3.8 Å, to give sheets of corrugated chains.

The reaction of **1b** with $Zn(OAc)_2$ also results in the insertion of Zn^{II} into the macrocycle, but the nature of [Zn(**1b**)] is completely different from that of [Zn(**1a**)]. [Zn(**1b**)] runs as a single spot on TLC and is significantly less polar than either **1b** or [Zn(**1a**)]. The ^{1}H NMR spectrum indicates that the pyridine group is coordinated to a porphyrin-bound zinc[4] as the pyridyl protons have shifted from $\delta = 7.07$ and 8.24 in **1b** to 5.18 and 2.06, respectively, in [Zn(**1b**)]. Once again these large chemical shift changes can only be explained by the coordination of the pyridine moiety to the zinc center in a porphyrin core. Fast atom bombardment (FAB) mass spectrometry provided a molecular ion peak corresponding to the dimeric complex $[\{Zn(\mathbf{1b})\}_2]$. X-ray diffraction grade crystals were difficult to obtain, but crystallizations that included small amounts of anthracene resulted in crystals suitable for analysis. The complex $[\{Zn(\mathbf{1b})\}_2]$ crystallizes in the space group $C2/c$[9] and the structure, shown in Figure 2, clearly illustrates the dimeric nature. Each

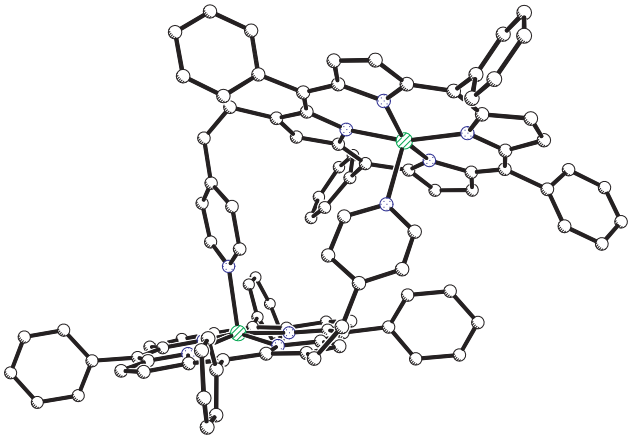


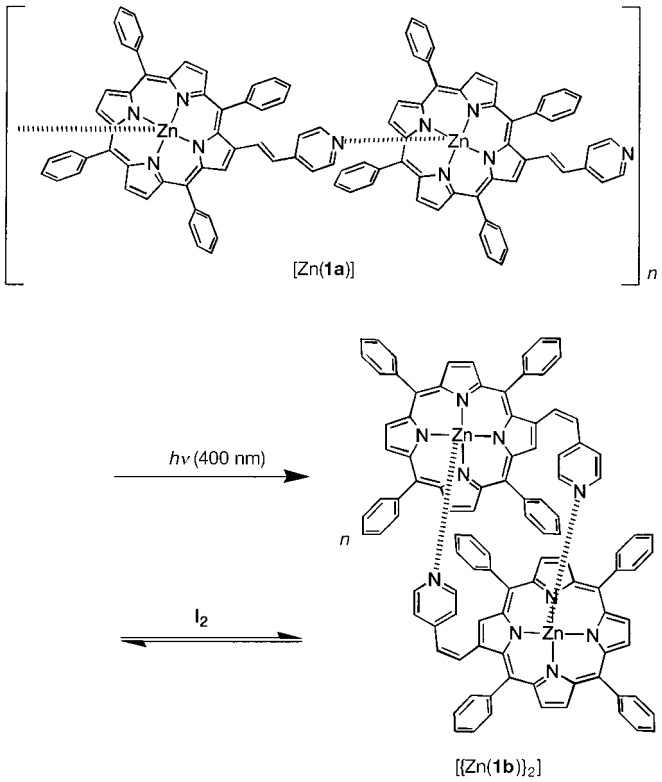
Figure 2. Molecular structure of $[\{Zn(\mathbf{1b})\}_2]$.

pyridine is coordinated to the zinc of the other porphyrin. The two porphyrin planes are tilted with respect to each other by 32(1)°. Presumably this distortion is to accommodate the geometrical requirements of the *cis* alkene linkage.

The chelation-like binding of the $[\{Zn(\mathbf{1b})\}_2]$ complex appears to result in a very stable complex, which is apparent from the strong molecular ion peak in the FAB mass spectrum. There is no evidence to indicate the presence of monomers. In contrast, the polymeric [Zn(**1a**)] appears to be quite dynamic in solution giving rise to an oligomeric mixture. The stability of the $[\{Zn(\mathbf{1b})\}_2]$ complex can be further demonstrated by the conversion of [Zn(**1a**)] (*trans*) into $[\{Zn(\mathbf{1b})\}_2]$ (*cis*) by irradiation with UV light, (Scheme 2). Other methods of isomerization have variable success. Thus, a mixture containing [Zn(**1a**)] and $[\{Zn(\mathbf{1b})\}_2]$ can be generated by treating pure solutions of either [Zn(**1a**)] or $[\{Zn(\mathbf{1b})\}_2]$ with iodine.

The alkene linkage in compounds **1a** and **1b** allows us to exert a control over the supramolecular structure of their derivatives. This is achieved by either beginning with the

 © WILEY-VCH Verlag GmbH, D-69451 Weinheim, 1998 1433-7851/98/3701-0115 $ 17.50+.50/0



Scheme 2. Conversion of [Zn(**1a**)] into [{Zn(**1b**)}$_2$].

appropriate *cis* or *trans* alkene as in traditional supramolecular chemistry or, more significantly, by converting the alkene, in the supramolecular complex, from *trans* to *cis* (or vice versa) and effectively switching from one supramolecular array to another. With this methodology it should be possible to control the molecular architecture of these supramolecular structures and thereby switch properties on or off as desired.

Experimental Section

1a and **1b**: A solution of **2** (135 mg, 0.146 mmol) and **3** (16 μL, 0.168 mmol) in CH_2Cl_2 (5 mL) was stirred at room temperature before 1,8-diazabicyclo[5.4.0]undec-7-ene (DBU) (67 μL, 0.448 mmol) was added. After 15 min, the reaction mixture was subjected to chromatography (silica, CH_2Cl_2/ethyl acetate 19/1) to give a *cis/trans* mixture (about 1:3 by ^{1}H NMR) of products. A second careful separation on a flash column with the same eluent gave two major fractions. The first fraction can be recrystallized from CH_2Cl_2/methanol to give **1b** as a purple solid (21 mg, 20 %): ^{1}H NMR (270 MHz, $CDCl_3$): $\delta = -2.70$ (br s, 2H; NH), 6.23 and 6.67 (2 d, both 1H, $^3J = 12.1$ Hz; H_{alkene}), 7.07 (d, 2H, $^3J = 5.8$ Hz; $H_{pyridyl}$), 7.58 – 7.82 (m, 12H; $H_{m,pPh}$), 8.09 (d, 2H, $^3J = 7.5$ Hz; H_{oPh}), 8.16 (d, 2H, $^3J = 7.5$ Hz; H_{oPh}), 8.21 – 8.27 (m, 6H; H_{oPh}, $H_{pyridyl}$), 8.47 (s, 1H; $H_{pyrrole}$), 8.77 – 8.85 (m, 6H; $H_{pyrrole}$); UV/Vis (CH_2Cl_2): $\lambda_{max} = 428$, 523, 563, 600, 657 nm. The second fraction contains **1a**, which is obtained as a purple solid after recrystallization from CH_2Cl_2/methanol (65 mg, 62 %): ^{1}H NMR (270 MHz, $CDCl_3$): $\delta = -2.59$ (br s, 2H; NH), 7.11 (d, 2H, $^3J = 6.1$ Hz; $H_{pyridyl}$), 7.19 (s, 2H, H_{alkene}), 7.74 – 7.85 (m, 12H; $H_{m,pPh}$), 8.19 – 8.28 (m, 8H; H_{oPh}), 8.55 (d, 2H, $^3J = 6.1$ Hz; $H_{pyridyl}$), 8.74 – 8.85 (m, 6H; $H_{pyrrole}$), 9.02 (s, 1H; $H_{pyrrole}$); UV/Vis (CH_2Cl_2): $\lambda_{max} = 428$, 523, 563, 600, 657 nm. HR-MS calcd for $C_{51}H_{36}N_5$ (MH^+): 718.2971; found: 718.2947.

[Zn(**1a**)]: ^{1}H NMR (270 MHz, $CDCl_3$): $\delta = 2.37$ (br s, 2H; $H_{pyridyl}$), 5.20 (br s, 2H; $H_{pyridyl}$), 6.09 and 6.31 (2 d, both 1H, $^3J = 16.1$ Hz; H_{alkene}), 7.21 – 7.27 (m, 3H; $H_{m,pPh}$), 7.68 – 7.79 (m, 11H; $H_{o,m,pPh}$), 8.08 – 8.24 (m, 6H; H_{oPh}), 8.57 – 8.60 (m, 2H; $H_{pyrrole}$), 8.79 – 8.83 (m, 5H; $H_{pyrrole}$); UV/Vis (CH_2Cl_2): $\lambda_{max} = 433$, 558, 563, 621, 758 nm; HR-MS: calcd for $C_{51}H_{34}N_5{}^{64}Zn$ ($M+H)^+$: 780.2106; found: 780.2095 (monomeric fragment).

[{Zn(**1b**)}$_2$]: ^{1}H NMR (270 MHz, $CDCl_3$): $\delta = 2.06$ (d, 2H, $^3J = 6.1$ Hz; $H_{pyridyl}$), 5.18 (d, 2H, $^3J = 6.1$ Hz; $H_{pyridyl}$), 5.28 and 6.28 (2 d, both 1H, $^3J = 11.8$ Hz; H_{alkene}), 7.31 – 7.43 (m, 6H; $H_{m,pPh}$), 7.71 – 7.93 (m, 10H; $H_{o,m,pPh}$), 8.10 – 8.36 (m, 4H; H_{oPh}), 8.44 (d, 1H; $^3J = 4.6$ Hz; $H_{pyrrole}$), 8.67 – 8.81 (m, 2H; $H_{pyrrole}$), 8.94 and 8.99 (m(AB), 4H, $^3J = 4.6$ Hz; $H_{pyrrole}$); UV/Vis (CH_2Cl_2): $\lambda_{max} = 429$, 527, 564, 603 nm. HR-MS calcd for $C_{102}H_{70}N_{10}{}^{64}Zn_2$ ($M+4H)^+$: 1562.4368; found: 1562.4329.

Received: August 15, 1997 [Z10822IE]
German version: *Angew. Chem.* **1998**, *110*, 122 – 125

Keywords: isomerizations · porphyrin array · porphyrinoids · supramolecular chemistry · zinc

[1] a) A. K. Burrell, D. L. Officer, D. C. W. Reid, *Angew. Chem.* **1995**, *107*, 986 – 988; *Angew. Chem. Int. Ed. Eng.* **1995**, *34*, 900 – 902; b) D. L. Officer, A. K. Burrell, D. C. W. Reid, *Chem. Commun.* **1996**, 1657 – 1658, and references therein; c) R. Gauler, N. Risch, *Tetrahedron Lett.* **1997**, *38*, 223 – 224.

[2] a) C. A. Hunter, R. K. Hyde, *Angew. Chem.* **1996**, *108*, 2064 – 2067; *Angew. Chem. Int. Ed. Eng.* **1996**, *35*, 1936 – 1939; b) J. L. Sessler, B. Wang, A. Harriman, *J. Am. Chem. Soc.* **1995**, *117*, 704-714; c) G. Steinberg-Yfrach, P. A. Liddell, S.-C. Hung, A. L. Moore, D. Gust, T. A. Moore, *Nature* **1997**, *385*, 239 – 241; d) C. M. Drain, K. C. Russell, J.-M. Lehn, *Commun.* **1996**, 337 – 338; e) J. L. Sessler, A. Andrievsky, P. A. Gale, V. Lynch, *Angew. Chem.* **1996**, *108*, 2954 – 2957; *Angew. Chem. Int. Ed. Eng.* **1996**, *35*, 2782 – 2785, and references therein.

[3] a) C. M. Drain, J.-M. Lehn, *J. Chem. Soc. Chem. Commun.* **1994**, 2313 – 2315; b) H. Yuan, L. Thomas, L. K. Woo, *Inorg. Chem.* **1996**, *35*, 2808 – 2817; c) N. Kariya, T. Imamura, Y. Sasaki, *ibid.* **1997**, *36*, 833 – 839; d) E. Alessio, M. Macchi, S. Heath, L. G. Marzilli, *Chem. Commun.* **1996**, 1411 – 1412; e) K. Funatsu, A. Kimura, T. Imamura, A. Ichimura, Y. Sasaki, *Inorg. Chem.* **1997**, *36*, 1625 – 1235; f) J. Wojaczynski, K. Latos-Grazynski, *ibid.* **1996**, *35*, 4812 – 4818; g) A. V. Chernook, U. Rempel, C. von Borczyskowski, A. M. Shulga, E. I. Zenkevich, *Chem. Phys. Lett.* **1996**, *254*, 229 – 241; h) G. M. Godziela, D. Tilotta, H. M. Goff, *Inorg. Chem.* **1986**, *25*, 2142 – 2146; i) J. Wojaczynski, K. Latos-Grazynski, *ibid.* **1995**, *34*, 1044 – 1053; j) B. F. Abrahams, B. F. Hoskins, D. M. Michail, R. Robson, *Nature* **1994**, *369*, 727 – 729; k) B. F. Abrahams, B. F. Hoskins, R. Robson, *J. Am. Chem. Soc.* **1991**, *113*, 3606 – 3607; l) M. O. Senge, K. M. Smith, *J. Chem. Soc. Chem. Commun.* **1994**, 923 – 924.

[4] a) E. B. Fleischer, A. M. Shachter, *Inorg. Chem.* **1991**, *30*, 3763 – 3769; b) H. Krupitsky, S. Stein, I Goldberg, C. E. Strouse, *J. Inclusion Phenom. Mol. Recognit. Chem.* **1994**, *18*, 177 – 192; c) X. L. Chi, A. J. Guerin, R. A. Haycock, C. A. Hunter, L. D. Sarson, *J. Chem. Soc. Chem. Commun.* **1995**, 2567 – 2569; d) A. M. Shachter, E. B. Fleischer, R. C. Halti-Wanger *ibid.* **1988**, 960 – 961; e) Y. Kuroda, Y. Kato, H. Ogoshi, *ibid.* **1997**, 469 – 470; f) R. T. Stibrany, J. Vasudevan, S. Knapp, J. A. Potenza, T. Emge, H. J. Schugar, *J. Am. Chem. Soc.* **1996**, *118*, 3980 – 3981; g) S. Anderson, H. Anderson, A. Bashall, M. McPartlin, J. K. M. Sanders, *Angew. Chem.* **1995**, *107*, 1196 – 1200; *Angew. Chem. Int. Ed. Engl.* **1995**, *34*, 1096 – 1099.

[5] M. A. Bobrik, F. A. Walker, *Inorg. Chem.* **1980**, *19*, 3383 – 3390.

[6] J. Vasudevan, R. T. Stibrany, J. Bumby, S. Knapp, J. A. Potenza, T. J. Emge, H. J. Schugar, *J. Am. Chem. Soc.* **1996**, *118*, 11676 – 11677.

[7] E. E. Bonfantini and D. L. Officer, *Tetrahedron Lett.* **1993**, *34*, 8531 – 8534.

[8] X-ray crystal structure analysis of [Zn(**1a**)] · 2MeOH · H_2O $C_{53}H_{43}N_5O_3Zn$: Red block, crystal size $0.23 \times 0.3 \times 0.25$ mm, monoclinic, space group $C2/c$, $a = 28.063(6)$, $b = 18.737(4)$, $c = 19.028(4)$ Å, $\beta = 118.65(3)^\circ$, $V = 8780(3)$ Å^3, $Z = 8$, $\rho_{calc} = 1.305$ g cm^{-3}, $\mu = 0.610$ mm^{-1}, $T = 293(2)$ K; Enraf-Nonius CAD4 diffractometer; $Mo_{K\alpha}$ radiation ($\lambda = 0.71073$ Å), scan method ω; 4191 data measured; 4083 independent reflections, R(int) = 0.0277. The structure was solved by direct methods and refined by a full-matrix least-squares procedure against F^2 (all non-hydrogen atoms anisotropic), with SHELXL-97.[10] $R = 0.0626$, $wR^2 = 0.1736$ for the 1942 reflections with $F_o > 4\sigma(F_o)$, GOF = 0.962. Max./min. residual electron densities 0.948/ – 0.282 e Å^{-3}. No absorption correction. See also [9b].

 © WILEY-VCH Verlag GmbH, D-69451 Weinheim, 1998 1433-7851/98/3701-0116 $ 17.50+.50/0

[9] a) X-ray crystal structure analysis of $[Zn(\mathbf{1b})]\cdot C_{14}H_{10}(C_{65}H_{43}N_5Zn)$: Red block, crystal size $0.23\times0.14\times0.12$ mm, monoclinic, space group $C2/c$, $a=25.410(5)$, $b=13.114(4)$, $c=28.920(6)$ Å, $\beta=107.54(4)^\circ$, $V=9189(4)$ Å^3, $Z=8$, $\rho_{calc}=1.378$ g cm^{-3}, $\mu=0.698$ mm^{-1}, $T=293(2)$ K; Enraf-Nonius CAD4 diffractometer; MoKα radiation ($\lambda=0.71073$ Å), scan method ω; 5761 data measured; 5607 independent reflections, $R(\mathrm{int})=0.2001$. The structure was solved by direct methods and refined by a full-matrix least-squares procedure against F^2 (all non-hydrogen atoms anisotropic), with SHELXL-97.[10] $R=0.0643$, $wR^2=0.1459$ for the 1218 reflections with $F_o>4\sigma(F_o)$, GOF = 0.867. Max./min. residual electron densities 0.323/ −0.618 e Å^{-3}. No absorption correction. b) Crystallographic data (excluding structure factors) for the structures reported in this paper have been deposited with the Cambridge Crystallographic Data Center, as supplementary publication CCDC-100641. Copies of the data can be obtained free of charge on application to CCDC, 12 Union Road, Cambridge CB2 1EZ, UK (fax: Int. code + (44) 1223 336033; e-mail: deposit@ccdc.cam.ac.uk).

[10] M. Sheldrick SHELXL-97, Universität Göttingen, Germany, **1997**.

Well-Defined Surface-Bonded Ruthenium Complexes with Molecular Nitrogen**

Hans Miessner* and Klaus Richter

Ruthenium is considered to possess great potential in the development of new catalysts for the ammonia synthesis. Indeed, recently a number of papers have reported the adsorption and the activation of nitrogen on ruthenium catalysts.[1]

The interaction of molecular nitrogen with supported transition metal catalysts is usually weak. By IR spectroscopy it was possible to confirm the adsorption of N_2 on ruthenium catalysts only at low temperatures (123 K),[2] or on certain supports (Al_2O_3, MgO).[3] Depending on the support, the promoter, and the pretreatment, the N_2 stretching vibrations were found in a wide range between 2214 and 1910 cm^{-1}.

Some reports have also covered the formation of dinitrogen–metal complexes in zeolites. For instance, monodinitrogen complexes with Cu^I ions have been identified in mordenite[4] and in ZSM-5.[5] We recently reported on the formation of well-defined surface-bonded rhodium complexes in dealuminated Y-zeolite (DAY),[6] which are stable up to 523 K in a nitrogen stream. The compounds were identified as the bis(dinitrogen) rhodium complex $[Rh^I(N_2)_2]^+$ and the mixed carbonyldinitrogen rhodium complex $[Rh^I(CO)N_2]^+$ and are probably located on cationic sites in the zeolite. In the present paper we show that ruthenium centers in zeolites also form defined surface-bonded compounds with molecular nitrogen. The chemistry of these compounds appears to be considerably more varied than that of the rhodium complexes.

The IR difference spectra obtained from a monocarbonyl ruthenium complex bonded to the DAY zeolite after treatment with a N_2/Ar gas mixture at 523 K are shown in Figure 1.

[*] Dr. H. Miessner, Prof. Dr. K. Richter
Gesellschaft zur Förderung der Naturwissenschaftlich-Technischen Forschung in Berlin-Adlershof e. V.
Rudower Chaussee 5, Geb. 2.6, D-12489 Berlin (Germany)
Fax: Int. code + (49) 30-6392 4831
e-mail: I.U.T.@t-online.de

[**] This work was supported by the Deutsche Forschungsgemeinschaft and the Fonds der Chemischen Industrie.

The complex was obtained by partial decarbonylation of a dicarbonyl ruthenium complex on the DAY zeolite, in a manner similar to that for the reactive monocarbonyl rhodium complex in Rh/DAY.[6] The negative band in the difference spectra at 2036 cm^{-1} and the positive bands in the carbonyl stretching region at 2083, 2023, 2016, 1997, and 1970 cm^{-1} clearly indicate that the monocarbonyl compound (2036 cm^{-1}) is replaced by other surface-bonded carbonyls, one of which is the starting dicarbonyl ruthenium reagent (2083 and 2016 cm^{-1}). At the same time, IR bands are clearly observed in the N_2 vibrational region at 2218, 2207, and 2173 cm^{-1}.

An analysis of the integrated band intensities from several experiments between 423 and 523 K and partial nitrogen pressures of 100–500 kPa indicated a correlation between the bands at 2218 and 2023 cm^{-1} on one hand, and between those at 2207 and 2173 cm^{-1} on the other (see Figure 1). Analogous

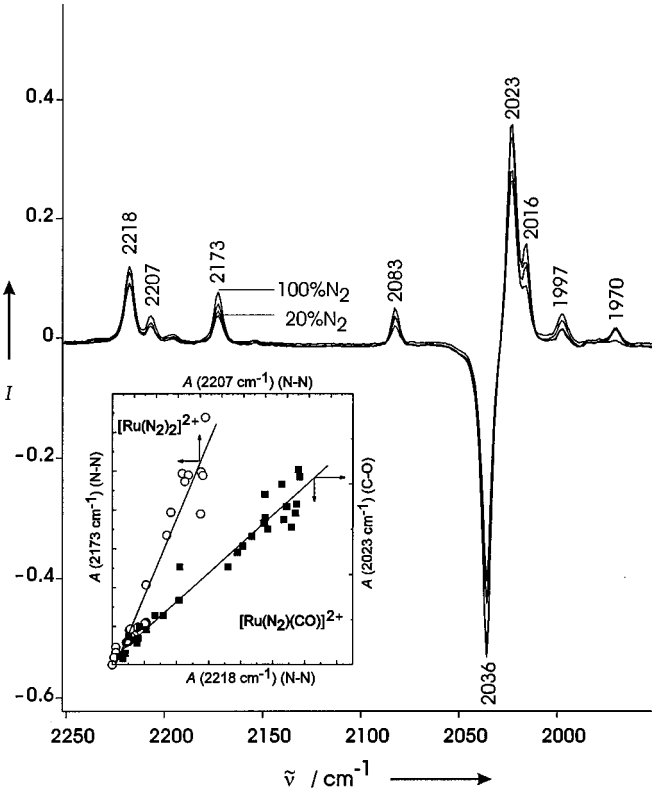


Figure 1. IR difference spectra (CO and N_2 vibration regions), recorded from the DAY-bonded monocarbonyl ruthenium complex after reaction with N_2/Ar at 523 K. The insert shows the correlation between the integrated intensities of the N_2 vibrations at 2207 and 2173 cm^{-1} (correlation coefficient $R^2=0.934$, $N=25$) and the N_2 vibration at 2218 cm^{-1} and the CO vibration at 2023 cm^{-1} ($R^2=0.957$, $N=30$). N = number of measurement values, A = absorption (arbitrary units).

to the results obtained with the Rh/DAY system,[6] the first band pair can be attributed to a carbonyldinitrogen ruthenium complex, and the second band pair to a bis(dinitrogen) ruthenium complex. The composition and the structure of the dinitrogen complexes were verified—similar to the manner employed in the Rh/DAY system[6]—from IR spectra recorded in the presence of ^{13}CO and $^{15}N_2$, and by force-field calculations. The formation of the dinitrogen complexes is reversible; the monocarbonyl is formed once again in the presence of hydrogen or in a pure argon stream at 523 K.

 © WILEY-VCH Verlag GmbH, D-69451 Weinheim, 1998 1433-7851/98/3701-0117 $ 17.50+.50/0

As is the case for the pure carbonyl complexes on Ru/DAY, the carbonyl and dinitrogen bands of the dinitrogen ruthenium complexes occur at lower wavenumbers than those of the corresponding rhodium complexes. This indicates that stronger bonds are formed between the ruthenium centers and the ligands as a result of stronger π back bonding, but also that the nitrogen molecules are more strongly activated.

In contrast to the dinitrogen rhodium complexes, the IR spectra of the ruthenium complexes change significantly at low temperatures. Below 400 K new bands are observed at 2257, 2239, 2231, and 2205 cm^{-1}. The intensities of these bands increase at the expense of the bands at 2218, 2207, and 2173 cm^{-1}. The band at 2257 cm^{-1} correlates with a new carbonyl band at 2039 cm^{-1}, and studies performed with ^{13}CO and $^{15}N_2$ confirm the formation of a further monocarbonyldinitrogen compound. The structure of the complex evidently changes with temperature, due to, for example, differences in the bonding to the zeolite framework.

An additional significant difference to the rhodium system may also be related to the higher stability of the ruthenium–nitrogen bond. The dinitrogen rhodium complexes are very sensitive to traces of CO in the gas stream and are irreversibly transformed into the stable dicarbonyl rhodium compounds.[6] In contrast, the dinitrogen ruthenium complexes react with CO in the gas phase at temperatures below 350 K to form a further stable dinitrogen compound with an intense N_2 vibration band at 2231 cm^{-1}. Figure 2 shows the changes in the IR spectra in the regions of the N_2 and CO vibrations. In addition to a broad band at approximately 2130 cm^{-1} from physisorbed CO and carbonyl bands at 2152, 2081, and 2049 cm^{-1}, which may be attributed to a tricarbonyl ruthenium complex, there is an intense band at 2061 cm^{-1} and a weak band at 2129 cm^{-1}. The intensities of these bands change with that of the N_2 band at 2231 cm^{-1}, and we assigned them to a *trans*-dicarbonyldinitrogen ruthenium complex. A ligand exchange reaction with $^{15}N_2$ and ^{13}CO confirmed this assignment.

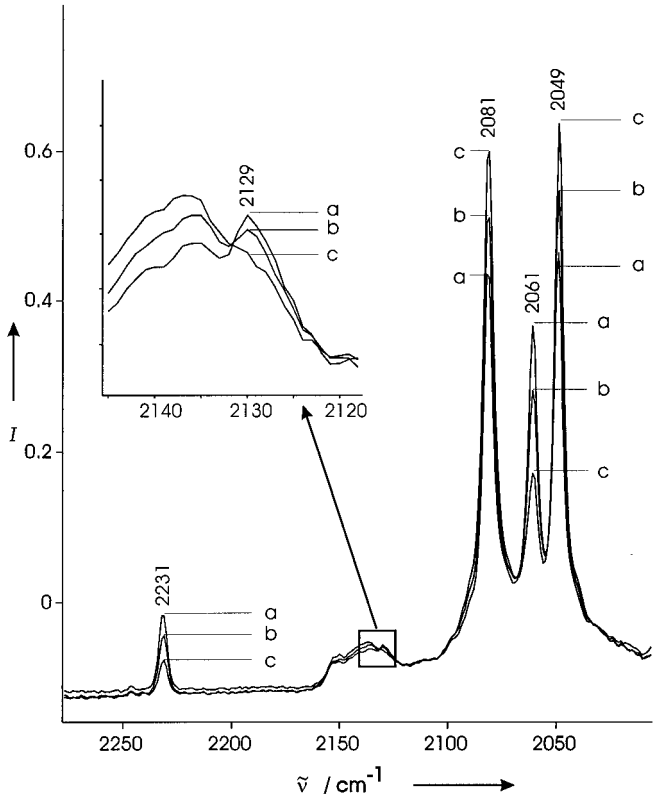


Figure 2. IR spectra in the CO and N_2 vibration regions in the presence of CO in the gas stream (5% CO/Ar:N_2 = 1:1) at 323 K (a), 343 K (b), and 363 K (c).

Table 1 provides an overview of the dinitrogen ruthenium complexes identified on the dealuminated DAY zeolite. As far as is presently known, the chemistry of molecular nitrogen and ruthenium compounds in dealuminated zeolites is considerably more diverse than that of rhodium compounds. Particularly remarkable is the higher bond strength of the molecular nitrogen to the ruthenium complexes compared to the rhodium complexes, and the associated weakening of the N≡N bond. Additional studies are required in order to show whether the nitrogen molecule can thus be sufficiently activated for further reactions such as, for example, protonation—the first step in a possible ammonia synthesis.

Table 1. N–N and C–O vibrational frequencies of the dinitrogen ruthenium complexes of the Ru/DAY system.

Species	T[K]	$\tilde{\nu}$[cm^{-1}] (N_2)	(CO)
$[Ru^{II}(N_2)(CO)]^{2+}$	523	2218	2023
$[Ru^{II}(N_2)_2]^{2+}$	523	2207	
		2173	
$[Ru^{II}(N_2)(CO)]^{2+}$	323	2257	2039
$[Ru^{II}(N_2)(CO)_2]^{2+}$	323	2231	2129
			2061

Experimental Section

The DAY support used (Degussa, Germany) is a dealuminated Y zeolite with a Si:Al ratio ≥ 100:1. The sample Ru/DAY (1 wt. % Ru) was prepared by impregnation of the support with the necessary amount of $RuCl_3$ in ethanolic solution and then dried in air at 353 K. The remaining pretreatment was carried out in the IR cell and involved a carbonylation in a CO/Ar stream (5% CO) at 523 K and a partial decarbonylation in a H_2 stream at 523 K.

In order to study the effect of the residual chlorine still present after this treatment, a control experiment was carried out with $Ru_3(CO)_{12}$ as the ruthenium source. Identical results were obtained with the dinitrogen ruthenium complexes obtained this way.

The IR transmission studies were carried out with pressed samples made from the pure substance (self-supported wafers) in a special steel cell in which in situ measurements up to 673 K and 5000 kPa are possible. The small dead volume coupled with a suitable gas supply and mass flow-rate controllers (MKS) allowed rapid changes in gas composition. The high purity gases used (AGA Gas GmbH) were additionally purified with OXYSORB (Messer Griesheim GmbH). ^{13}CO (99%; Linde AG) and $^{15}N_2$ (98%; Chemotrade) were used for the isotope exchange reactions.

The IR spectra were recorded on a Perkin–Elmer Paragon 1000 FTIR spectrometer at a resolution of 2 cm^{-1}.

Received August 1, 1997 [Z10765]
German version: *Angew. Chem.* **1998**, *110*, 125–127

Keywords: dinitrogen complexes · nitrogen fixation · surface chemistry · ruthenium · zeolites

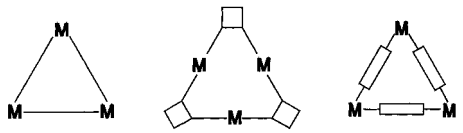
 © WILEY-VCH Verlag GmbH, D-69451 Weinheim, 1998 1433-7851/98/3701-0118 $ 17.50+.50/0

[1] a) Y. Kadowaki, K. Aika, *J. Catal.* **1996**, *161*, 178–185; b) C. T. Fishel, R. J. Davis, J. M. Garces, *ibid.* **1996**, *163*, 148–157; c) O. Hinrichsen, F. Rosowski, A. Hornung, M. Muhler, G. Ertl, *ibid.* **1997**, *165*, 33–44; d) F. Rosowski, A. Hornung, O. Hinrichsen, D. Herein, M. Muhler, G. Ertl, *Appl. Catal. A* **1997**, *151*, 443–460.
[2] V. S. Ljutov, Ju. G. Borodko, *Kinet. Katal.* **1971**, *12*, 1566.
[3] a) J. Kubota, K. Aika, *J. Chem. Soc. Chem. Commun.* **1991**, 1544–1545; b) J. Kubota, K. Aika, *J. Phys. Chem.* **1994**, *98*, 11293–11300.
[4] a) Y. Kuroda, S. Konno, K. Morimoto, Y. Yoshikawa, *J. Chem. Soc. Chem. Commun.* **1993**, 18–20; b) Y. Kuroda, Y. Yoshikawa, S. Konno, H. Hamano, H. Maeda, R. Kumashiro, M. Nagao, *J. Phys. Chem.* **1995**, *99*, 10621–10628; c) Y. Kuroda, H. Maeda, Y. Yoshikawa, R. Kumashiro, M. Nagao, *J. Phys. Chem. B* **1997**, *101*, 1312–1316.
[5] a) G. Spoto, S. Bordiga, G. Ricchiardi, D. Scarano, A. Zecchina, F. Geobaldo, *J. Chem. Soc. Faraday Trans.* **1995**, *91*, 3285–3290; b) C. Lamberti, S. Bordiga, M. Salvalaggio, G. Spoto, A. Zecchina, F. Geobaldo, G. Vlaic, M. Bellatreccia, *J. Phys. Chem. B* **1997**, *101*, 344–360.
[6] a) H. Miessner, *J. Chem. Soc. Chem. Commun.* **1994**, 927–928; b) H. Miessner, *J. Am. Chem. Soc.* **1994**, *116*, 11522–11530.

Molecular Triangle from enPt^{II} and 2,2′-Bipyrazine**

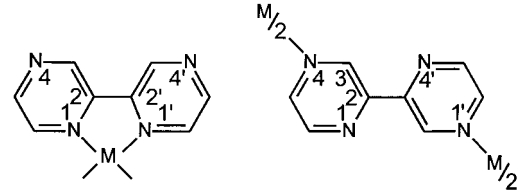
Ralf-Dieter Schnebeck, Lucio Randaccio,* Ennio Zangrando, and Bernhard Lippert*

Cyclic trimetallic complexes with metal–metal bonds[1] or bridging ligands[2,3] are known in large numbers (Scheme 1), but examples containing bridging heterocycles arranged approximately perpendicular to the metal triangle are relatively rare.[3] Here we report on a trinuclear Pt^{II} complex containing 2,2′-bipyrazine ligands (bpz) which fulfills the latter requirement and forms spontaneously in a self-assembly process. The compound is of interest with respect to the formation and stability of "molecular squares"[4] from 4,4′-bipyridine ligands and rectangular, square-planar metal units. However, the impression that combining these building blocks always leads to squares and rectangles is misleading. As first indicated by Fujita and co-workers,[5] *cis*-Pd^{II}en (en = ethylenediamine) can be used with 4,4′-bipy to form both molecular squares and triangles or both in a concentration-dependent equilibrium.



Scheme 1.

As demonstrated here, the heterocyclic ligand 2,2′-bipyrazine reacts with square-planar enM^{II} units (M = Pd or Pt) either with chelate or bridge formation (Scheme 2). In the first case bpz is practically coplanar with the coordination plane of M, whereas in the second case, following cyclization to the trinuclear complex, it is virtually perpendicular to the metal triangle. Compound **1** forms in 40% yield upon reaction of $[(en)Pd(H_2O)_2](NO_3)_2$ with bpz[6] and recrystallization of the crude product from water in the presence of $NaClO_4$. Figure 1 depicts the cation of **1**. The results of the X-ray structure determination[7–9] reveal that the N(1)-Pd-N(1′) angle of 80.7(1)° deviates markedly from 90° and is in the range found for related complexes containing 2,2′-bipyridine[10] or *o*-phenanthroline.[11] In the case of a Ru^{II} compound containing a chelating bpz ligand, this value is 78.92(6)°.[12] The geometry of the Pd(en) unit is normal.[13] Attempts to use cation **1** as a corner stone in the preparation of a molecular square in the true sense[14]—that is, cyclization through the 4 and 4′ positions via linear metal units—have been unsuccessful as yet. We assume that the low basicity[15] of these positions rather than the nonideal N(4)-Pd-N(4′) angle



Scheme 2.

Figure 1. Structure of cation of **1**. Selected bond lengths [Å] and angles [°]: Pd–N(1) 2.034(3), Pd–N(1′) 2.025(3), Pd–N(2) 2.026(3), Pd–N(3) 2.023(3); N(1)-Pd-N(1′) 80.7(1), N(1)-Pd-N(2) 98.8(1), N(1)-Pd-N(3) 178.2(1), N(1′)-Pd-N(2) 179.4(1), N(1′)-Pd-N(3) 97.6(1), N(2)-Pd-N(3) 83.0(1), N(4)-Pd-N(4′) 73.0(1).

$[(en)Pd(bpz)](ClO_4)_2$ **1**

$[(en)Pt(bpz)](NO_3)_2$ **1′**

[*] Prof. Dr. L. Randaccio, Dr. E. Zangrando
Dipartimento di Scienze Chimiche
Università di Trieste
via L. Giorgieri, I-34127 Trieste (Italy)
Fax: Int. code + (39) 40-676 3903
Prof. Dr. B. Lippert, Dipl.-Chem. R.-D. Schnebeck
Fachbereich Chemie der Universität
Otto-Hahn-Strasse 6, D-44227 Dortmund (Germany)
Fax: Int. code + (49) 231-755 3797

[**] This work was supported by the Deutsche Forschungsgemeinschaft, the Fonds der Chemischen Industrie, and MURST, Rome. It was part of a COST D1 project. en = ethylenediamine

 © WILEY-VCH Verlag GmbH, D-69451 Weinheim, 1998 1433-7851/98/3701-0119 $ 17.50+.50/0

(73.0(1)°) is responsible. However, we feel that metal units with a pronounced ability for π backdonation (e.g. Ru^{II})[16] might in principle be capable of forming such squares. There are many examples of complexes containing bridging pyrazine ligands[4e,f,17] for which similar criteria apply.

The Pt analogue of the cation in **1**, **1′**, was isolated as the nitrate salt and characterized by ^{1}H NMR spectroscopy. The sensitivity of crystals of **1′** has thus far prevented an X-ray crystal structure analysis.

A second Pt complex, which proved to be the cyclic species **2**, displays a markedly different ^{1}H NMR spectrum from **1′**. The cation of **2**[18] has C_2 symmetry (Figure 2). The three Pt

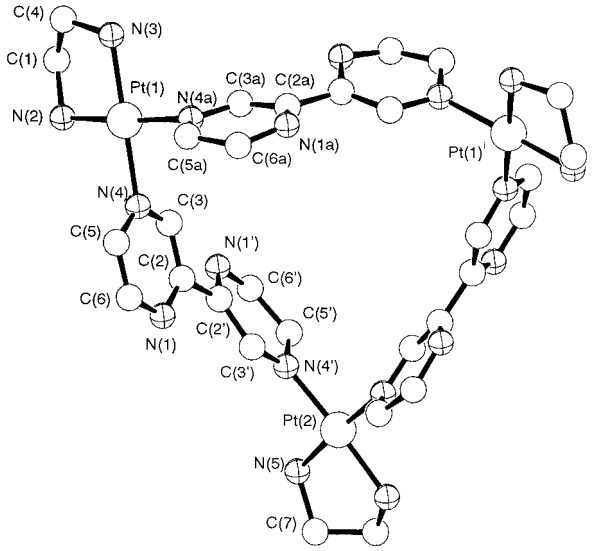


Figure 2. Structure of cation of **2**. Selected bond lengths [Å] and angles [°]: Pt(1)–N(4a) 2.017(13), Pt(1)–N(4) 2.075(14), Pt(1)–N(2) 1.97(2), Pt(1)–N(3) 2.043(13), Pt(2)–N(4′) 1.98(2), Pt(2)–N(5) 1.982(13); N(4a)-Pt(1)-N(4) 87.1(5), N(1)-Pt(1)-N(2) 175.5(5), N(4a)-Pt(1)-N(3) 93.8(5), N(4)-Pt(1)-N(2) 95.7(7), N(4)-Pt(1)-N(3) 178.6(7), N(2)-Pt(1)-N(3) 83.4(6), N(4′)-Pt(2)-N(4′)^i 93.3(9), N(5)-Pt-N(5)^i 84.6(7), N(4′)-Pt(2)-N(5) 91.1(6), N(4′)-Pt-N(5)^i 175.7(6).

atoms form an approximately equilateral triangle with Pt(1)–Pt(1)^i and Pt(1)–Pt(2) distances of 9.404(3) and 9.422(1) Å, respectively. The C_2 axis runs through Pt(2). In contrast to **1**, the bpz ligand in **2** is in a transoid orientation

$[\{(en)Pt(bpz)\}_3](NO_3)_6$ **2**

following rotation about the central C(2)–C(2′) bond. The three metal atoms are therefore linked through N(4) atoms. The N(4)-Pt-N(4′) angles at the Pt atoms are 87.1(5)° for Pt(1) and Pt(1)^i and 93.3(9)° for Pt(2).

The two pyrazine rings of each bpz ligand in **2** are markedly twisted with respect to each other (21 and 27°), which appears to be crucial for formation of the triangle. Considering the fact that similar twist angles have been observed for 2,2′-bipyridine in the gas phase and in solution,[19] it appears likely that formation of **2** and possibly even of the (en)Pd/4,4′-bipyridine triangle[5] is facilitated by this feature.

Formation of the chelate complex **1′** and of the molecular triangle **2** from $[(en)Pt(H_2O)_2]^{2+}$ and bpz apparently takes place from two different linkage isomers: bonding through N(1) for **1′** and through N(4) for **2**. Following the reactions with NMR spectroscopy (^{1}H, ^{195}Pt) confirms this assumption. In the ^{1}H NMR spectra the number of resonances decreases as the reactions proceed, as expected for formation of **1′** from $[(en)Pt(H_2O)(bpz\text{-}N(1))]^{2+}$ and of **2** from $[(en)Pt(H_2O)(bpz\text{-}N(4))]^{2+}$.

Based on model studies, it appears that the pyrazine rings of the bpz ligand in **2** can undergo rather facile rotation about the C(2)–C(2′) bond to produce different rotational isomers. The dynamics of this process and properties of the hydrophobic cavity of the cation of **2** with regard to possible host–guest interactions are subjects of ongoing work.

Experimental Section

1: (en)$PdCl_2$ (214 mg, 0.90 mmol) was suspended in water (30 mL) and stirred for 2 h at room temperature (RT) with $AgNO_3$ (297 mg, 1.75 mmol). After removal of AgCl by filtration and addition of bpz (138 mg, 0.87 mmol) to the filtrate, the mixture was stirred for 24 h at RT. The solution (pH 3.0) was then filtered and concentrated to 5 mL under vacuum. $NaClO_4$ (275 mg, 2.25 mmol) was then added to the yellow solution. Yellow **1** was obtained in 40% yield within two days at 4 °C. Satisfactory elemental analysis for $PdC_{10}H_{14}N_6O_8Cl_2$. ^{1}H NMR (200 MHz, D_2O, TSP): $\delta = 3.10$ (s, 4H, CH_2), 8.53 (dd, $^3J = 3.2$ Hz, $^5J = 1.1$ Hz, 2H, aromatic), 9.07 (d, $^3J = 3.2$ Hz, 2H, aromatic), 9.78 (d, $^5J = 0.9$ Hz, 2H, aromatic).

1′ and **2**: (en)$PtCl_2$ (325 mg, 0.99 mmol) was suspended in water (30 mL), $AgNO_3$ (323 mg, 1.90 mmol) added, and the mixture stirred for 1 h at 80 °C. After the mixture was cooled and AgCl removed by filtration, bpz (150 mg, 0.95 mmol) was added, and the mixture stirred for three days at 45 °C. The reaction mixture was filtered and concentrated to 5 mL under vacuum. $NaNO_3$ (170 mg, 2.0 mmol) was then added to the yellow solution (pH 4.5). Yellow $\mathbf{2} \cdot n\,H_2O$ was isolated in 35% yield after 6–10 d at 4 °C. Satisfactory elemental analysis for $Pt_3C_{30}H_{54}N_{24}O_{24}$) (for $n = 6$, the X-ray structure analysis gave $n = 4$). ^{1}H NMR (200 MHz, D_2O, TSP): $\delta = 2.85$ (s, 4H, CH_2), 8.84 (dd, $^3J = 3.2$ Hz, $^5J = 1.1$ Hz, 2H, aromatic), 9.10 (d, $^3J = 3.2$ Hz, 2H, aromatic), 9.33 (s, 2H, aromatic); ^{195}Pt NMR (43 MHz, D_2O): $\delta = -2753$ (PtN_4). Needles of **1′** are formed as a side product (5%) in the synthesis of **2** if the reaction time is shortened by two days and the reaction temperature kept at 25 °C. ^{1}H NMR (200 MHz, D_2O, TSP): $\delta = 2.88$ (s, 4H, CH_2), 8.90 (dd, $^3J = 3.2$ Hz, $^5J = 0.8$ Hz, 2H, aromatic), 9.15 (d, $^3J = 3.2$ Hz, 2H, aromatic), 9.79 (d, $^5J = 0.8$ Hz, 2H, aromatic); ^{195}Pt NMR (43 MHz, D_2O): $\delta = -2749$ (PtN_4).

Received: June 18, 1997 [Z10565IE]
German version: *Angew. Chem.* **1998**, *110*, 128–130

Keywords: metallacycles · N ligands · palladium · platinum · self-organization

[1] a) C. H. Wei, L. F. Dahl, *J. Am Chem. Soc.* **1969**, *91*, 1351; b) F. A. Cotton, J. M. Troup, *ibid.* **1974**, *96*, 4155; c) T. Yamaguchi, N. Nishimura, T. Ito, *ibid.* **1993**, *115*, 1612.

[2] a) W. Burger, J. Strähle, *Z. Anorg. Allg. Chem.* **1985**, *529*, 111; b) H. H. Murray, R. G. Raptis, J. P. Fackler, Jr., *Inorg. Chem.* **1988**, *27*, 26; c) R. G. Raptis, J. P. Fackler, Jr., *ibid.* **1990**, *29*, 5003.

[3] a) D. P. Smith, E. Baralt, B. Morales, M. M. Olmstead, M. F. Maestre, R. H. Fish, *J. Am. Chem. Soc.* **1992**, *114*, 10647; b) H. Chen, M. M. Olmstead, D. P. Smith, M. F. Maestre, R. H. Fish, *Angew. Chem.* **1995**, *107*, 1590; *Angew. Chem. Int. Ed. Engl.* **1995**, *34*, 1514; c) S. Rüttimann, G. Bernardinelli, A. F. Williams, *ibid.* **1993**, *105*, 432 and **1993**, *32*, 392; d) R. W. Saalfrank, S. Trummer, H. Krautscheid, V. Schünemann, A. X. Trautwein, S. Hien, C. Stadler, J. Daub, *ibid.* **1996**, *108*, 2350 and **1996**, *35*, 2206; e) L. Schenetti, G. Bandoli, A. Dolmella, G. Trovò, B. Longato, *Inorg. Chem.* **1994**, *33*, 3169.

 © WILEY-VCH Verlag GmbH, D-69451 Weinheim, 1998 1433-7851/98/3701-0120 $ 17.50+.50/0

[4] a) M. Fujita, K. Ogura, *Coord. Chem. Rev.* **1996**, *148*, 249, and references therein; b) P. J. Stang, D. H. Cao, S. Saito, A. M. Arif, *J. Am. Chem. Soc.* **1995**, *117*, 6273, and references therein; c) C. M. Drain, J.-M. Lehn, *J. Chem. Soc. Chem. Commun.* **1994**, 2313; d) H. Rauter, E. C. Hillgeris, A. Erxleben, B. Lippert, *J. Am. Chem. Soc.* **1994**, *116*, 616; e) J. Lu, T. Paliwala, S. C. Lim, C. Yu, T. Niu, A. J. Jacobson, *Inorg. Chem.* **1997**, *36*, 923, and references therein; f) R. V. Slone, J. T. Hupp, C. L. Stern, T. E. Albrecht-Schmitt, *ibid.* **1996**, *35*, 4096.

[5] M. Fujita, O. Sasaki, T. Mitsuhashi, T. Fujita, J. Yazaki, K. Yamaguchi, K. Ogura, *J. Chem. Soc. Chem. Commun.* **1996**, 1535.

[6] R. J. Crutchley, A. B. P. Lever, *Inorg. Chem.* **1982**, *21*, 2276.

[7] Crystal structure analysis of **1**: $C_{10}H_{14}N_6Cl_2O_8Pd$ ($M_r = 523.57$); orthorhombic, space group *Pbca*; $a = 13.612(1)$, $b = 14.899(1)$, $c = 17.258(1)$ Å, $V = 3500.0(3)$ Å^3, $Z = 8$, $\rho_{calcd} = 1.987$ g cm^{-3}, $F(000) = 2080$, $\mu = 1.42$ mm^{-1}, 3430 observed reflections with $F_o > 4\sigma(F_o)$, $R_1 = 0.0370$, $wR_2 = 0.0957$, $S = 1.079$, max./min. residual electron density 0.77/ − 0.73 e Å^{-3}, Enraf-Nonius-CAD4 diffractometer, $Mo_{K\alpha}$ radiation ($\lambda = 0.71069$ Å), graphite monochromator, absorption correction, Ψ scan, correction for Lorentzian and polarization effects. The structure was solved with the Patterson method[8] and refined with the least-squares method.[9] Oxygen atoms of ClO_4^- anions were disordered (occupancy factors 0.7 and 0.3).[18]

[8] SHELXS-86: G. M. Sheldrick, *Acta Crystallogr. Sect. A* **1990**, *46*, 467.

[9] SHELXS-93: G. M. Sheldrick, Universität Göttingen, **1993**.

[10] P. C. Chieh, *J. Chem. Soc. Dalton Trans. 2* **1972**, 1643.

[11] a) A. Hazell, O. Simonsen, O. Wernberg, *Acta Crystallogr. Sect. C* **1986**, *42*, 1707.

[12] A. Gerli, J. Reedijk, M. T. Lakin, A. L. Spek, *Inorg. Chem.* **1995**, *34*, 1836.

[13] For example, D. Holthenrich, E. Zangrando, E. Chiarparin, B. Lippert, L. Randaccio, *J. Chem. Soc. Dalton Trans.*, in press.

[14] H. Rauter, I. Mutikainen, M. Blomberg, C. L. Lock, P. Amo-Ochoa, E. Freisinger, L. Randaccio, E. Zangrando, E. Chiarparin, B. Lippert, *Angew. Chem.* **1997**, *109*, 1353; *Angew. Chem. Int. Ed. Engl.* **1997**, *36*, 1296.

[15] There is no indication for protonation of **1** at the N(4) and N(4′) positions from the pH*-dependent ^{1}H NMR spectra measured at different pH levels.

[16] P. Ford, F. P. DeRudd, R. Gaunder, H. Taube, *J. Am. Chem. Soc.* **1968**, *90*, 1187.

[17] L. Carlucci, G. Ciani, D. M. Proserpio, A. Sironi, *J. Am. Chem. Soc.* **1995**, *117*, 4562.

[18] Crystal structure analysis of **2**: $C_{30}H_{42}N_{24}O_{18}Pt_3 \cdot 4H_2O$ ($M_r = 1684.11$); monoclinic, space group *C*2/*c*; $a = 18.936(3)$, $b = 15.056(1)$, $c = 20.136(5)$ Å, $\beta = 107.84(2)^\circ$, $V = 5464.7(17)$ Å^3, $Z = 4$, $\rho_{calcd} = 2.047$ g cm^{-3}, $F(000) = 3232$, $\mu = 7.76$ mm^{-1}, 3272 observed reflections with $F_o > 4\sigma(F_o)$, $R_1 = 0.0610$, $wR_2 = 0.1878$, $S = 1.379$, max./min. residual electron density 1.29/ − 1.58 e Å^{-3}, Enraf-Nonius-CAD4 diffractometer, $Mo_{K\alpha}$ radiation ($\lambda = 0.71069$ Å), graphite monochromator, absorption correction, Ψ scan, correction for Lorentzian and polarization effects. The structure was solved with the Patterson method[8] and refined with the least-squares method.[9] The nitrate anions and water molecules were treated isotropically. It is possibe that there are still partially occupied water positions, but their refinement was impossible. Crystallographic data (excluding structure factors) for the structures reported in this paper have been deposited with the Cambridge Crystallographic Data Centre as supplementary publication no. CCDC-100386. Copies of the data can be obtained free of charge on application to CCDC, 12 Union Road, Cambridge CB2 1EZ, UK (fax: int. code + (44)1223-336-033; e-mail: deposit@ccdc.cam.ac.uk).

[19] a) C. L. Cheng, D. S. N. Murty, G. L. Retchie, *J. Chem. Soc. Faraday Trans. II* **1972**, *68*, 1679; b) S. T. Howard, *J. Am. Chem. Soc.* **1996**, *118*, 10269.

Supramolecular Arrays of 4,7-Phenanthroline Complexes: Self-Assembly of Molecular Pd_6 Hexagons**

Jeffrey R. Hall, Stephen J. Loeb,* George K. H. Shimizu, and Glenn P. A. Yap

The formation of supramolecular arrays of metal ions and ligands is favored by a metal-directed, self-assembly mechanism, which allows for high-yield synthesis under thermodynamic control.[1] Rigid complexes can be synthesized in which the overall structure is dictated by a combination of the binding constraints of the ligand and the geometrical requirements of the metal ions.[2] For example, tetranuclear squares were first prepared by combining the approximately 90° angles of a square-planar palladium complex with the linearly oriented donor atoms of 4,4′-bipyridine.[3] In a similar fashion, polypyridine ligands and metal ions have produced a fascinating variety of squares,[4] boxes,[3b, 5] helicates,[6] catenanes,[7] rotaxanes,[8] racks,[9] grids,[10] and ladders.[11]

To increase the scope of such assemblies, we have begun to explore the use of predesigned organometallic fragments as building blocks.[12] A similar strategy was recently employed to prepare dendrimers[13] as well as nanoscale squares[14] and hexagons.[15] Here we report the self-assembly of a rigid, cyclic structure that contains 4,7-phenanthroline (**1**) and the linear organopalladium complex fragments **2a** or **2b** as building blocks. Self-assembly of these complimentary molecular building blocks with angular requirements of 60 and 180° results in a six-component [3+3] cyclic array.

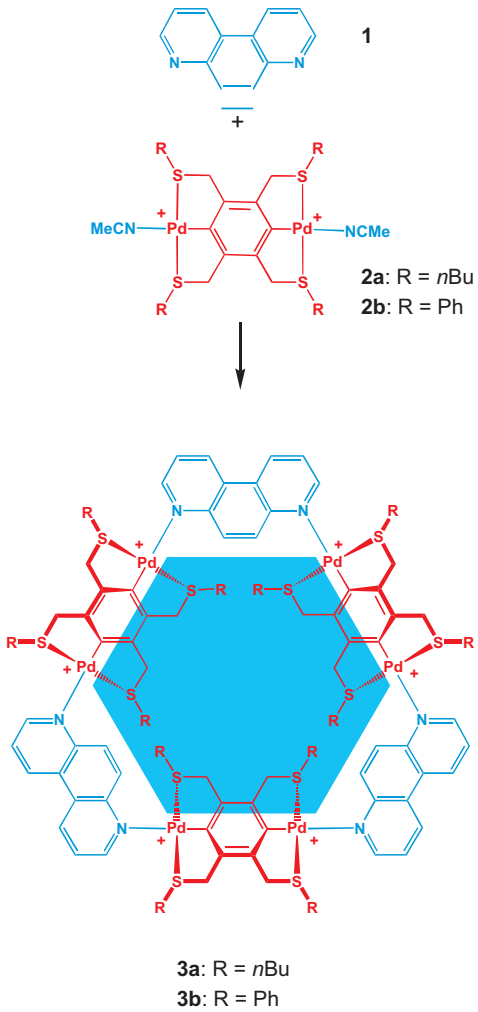
Complexes **2a** and **2b** are readily prepared by palladation of the thioether ligands 1,2,4,5-tetrakis(*n*-butylthiomethyl)benzene and 1,2,4,5-tetrakis(phenylthiomethyl)benzene, respectively, with two equivalents of $[Pd(MeCN)_4][BF_4]_2$ in acetonitrile. Combining equimolar amounts of **1** and **2a**$[BF_4]_2$ or **2b**$[BF_4]_2$ in an appropriate solvent (**2a**, CH_2Cl_2; **2b**, $(CH_3)_2CO$) resulted in quantitative formation of the hexanuclear complexes **3a** and **3b** (Scheme 1). These complexes can be isolated as BF_4^- salts in the form of air- and moisture-stable, pale yellow, microcrystalline solids; their solubility depends on the R group attached to the sulfur center.

The ^{1}H NMR spectra of **3a** and **3b** are consistent with highly symmetrical structures and show large coordination shifts for the phenanthroline ring protons, in the range from $\Delta\delta = 0.65$ for H1 and H10 to $\Delta\delta = 1.63$ for H5 and H6. Integration of the signals indicates a 1:1 ratio of organometallic complex fragment to 4,7-phenanthroline, and this is supported by elemental analyses. In attempts to observe intermediates in the self-assembly process, experiments involving stepwise addition of metal to ligand and ligand to metal were monitored by ^{1}H NMR spectroscopy. In no case were species other than the cyclic product and the component in excess

[*] Prof. Dr. S. J. Loeb, J. R. Hall, Dr. G. K. H. Shimizu, Dr. G. P. A. Yap
Department of Chemistry and Biochemistry
University of Windsor
Windsor, Ontario, N9B 3P4 (Canada)
Fax: Int. code + (1) 519-973 7098
e-mail: loeb@uwindsor.ca

[**] Financial support for this work was provided by the Natural Sciences and Engineering Research Council of Canada.

 © WILEY-VCH Verlag GmbH, D-69451 Weinheim, 1998 1433-7851/98/3701-0121 $ 17.50+.50/0



Scheme 1. Reaction of **1** with solvated **2a** and **2b** to give **3a** and **3b**, respectively (counterion BF_4^-).

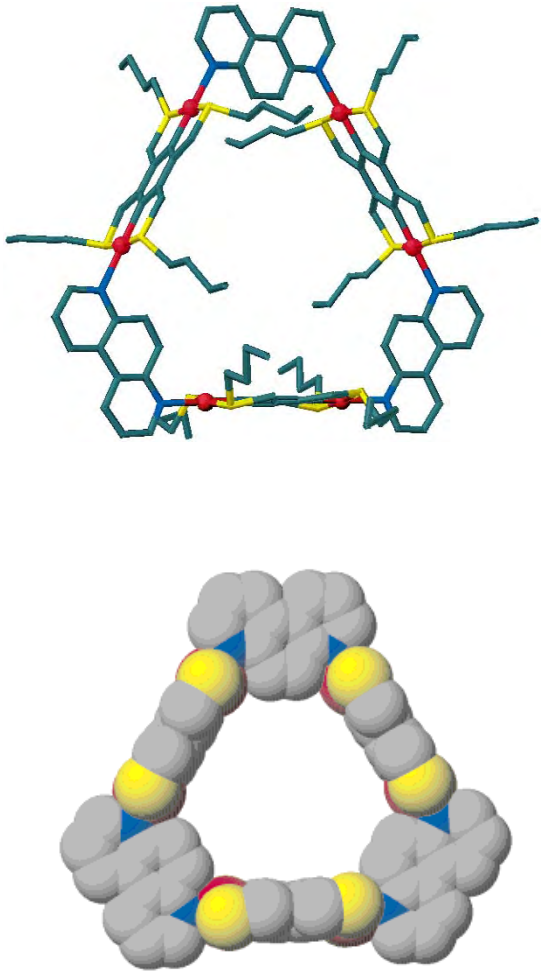


Figure 1. Crystal structure of **3a**. Top: Representation of the bonds in the framework (red = Pd, yellow = S, blue = N, gray = C). Bottom: space-filling representation (*n*Bu groups omitted for clarity).

observed. This is consistent with rapid formation of the thermodynamically favored cyclic product. An X-ray structural study of **3a** confirmed the postulated hexanuclear structure (Figure 1).[16]

As planned, the metalated aromatic units form three "walls" of the supramolecular array, and the 4,7-phenanthroline ligands form three corner pieces. The planes of the two different fragments are approximately perpendicular to each other. The Pd···Pd distances within the organopalladium unit average 6.83 Å, whereas the distance between two Pd atoms across the 4,7-phenanthroline ligand averages 7.80 Å. Since all six palladium atoms are constrained to lie in a single plane and the Pd-Pd-Pd angles are about 120° because of the geometrical requirements of the the phenanthroline bridges, the metal array approximates a Pd_6 hexagon. In overall dimensions, this rigid framework is about 2.0 nm in width, about 0.5 nm in depth (not including the *n*Bu groups), and contains a permanent cavity of approximately 1.2 nm in diameter.

In solution, two dynamic processes affect the line shape of the NMR signals of the benzylic protons: inversion at the sulfur center and rotation about the Pd–N bond. Variable-temperature ^{1}H NMR spectra of **3b** show that at elevated temperature (323 K, CD_2Cl_2) inversion at the sulfur center is rapid on the NMR time scale, but rotation about the Pd–N bond is restricted due to the steric requirements of the phenyl groups. This gives rise to an AB pattern at high temperature due to coupling of the benzylic protons which are constrained "inside" and "outside" of the cyclic structure. This is not observed for **3a**, which contains the smaller *n*Bu groups. The high-temperature spectrum of **3a** exhibits a single, sharp signal for the benzylic protons, which nonetheless provides evidence for the cyclic nature of this species in solution.

4,7-Phenanthroline is a simple, commercially available ligand that favors bridging over chelation and provides a rigid 60° corner for creating unique metal–ligand arrays. The self-assembly strategy allows the construction of large, rigid cavities, and this bodes well for the future development of metal-based receptors and nanoscale materials. An advantage of employing the organopalladium complex fragments described here is the readily variable substituent on the sulfur atom, which allows the physical properties to be modified. We are currently investigating the incorporation of R groups that make the product water-soluble so that solvophobic interactions inside the cavity become possible.

 © WILEY-VCH Verlag GmbH, D-69451 Weinheim, 1998 1433-7851/98/3701-0122 $ 17.50+.50/0

Experimental Section

3a: Equimolar solutions of 4,7-phenanthroline and **2a** were mixed in CH_2Cl_2 or acetone. The concentration range from 3.29 μM to 1.54 M was studied. The solvent was allowed to evaporate slowly. Pale yellow crystals were obtained from acetone, and microcrystalline powders from CH_2Cl_2. No further purification was required. In all cases, the yield of isolated product was greater than 90%. ^{1}H NMR (300 MHz, [D$_6$]acetone, 300 K): $\delta = 9.81$ (m, 12H, phen), 9.68 (m, 6H, phen), 8.28 (qt, 6H, phen), 4.69 (br s, 24H, Bz), 3.10 (br m, 24H, SCH_2), 1.63 (br m, 24H) 1.18 (br m, CH_2CH_3), 0.69 (br t, 36H, CH_3); FAB-MS: m/z = 965 $[M-3BF_4]^{3+}$; elemental analysis calcd for $C_{114}H_{156}B_6F_{24}N_6Pd_6S_{12}$: C 43.40, H 4.98, N 2.66; found: C 43.33, H 4.96, N 2.59.

3b: Equimolar solutions of 4,7-phenanthroline and **2b** were mixed in CH_2Cl_2, acetone, or MeOH. Neither the rate of addition nor the order of addition affected the product quality and yield. The concentration range from 3.17 μM to 1.54 M was studied. The solvent was allowed to evaporate slowly. Crystalline material was obtained from CH_2Cl_2, and microcrystalline powders from acetone and MeOH. No further purification was required. In all cases, the yield of isolated product was greater than 90%. ^{1}H NMR (300 MHz, CD_2Cl_2, 323 K): $\delta = 9.42$ (d, 6H, phen), 9.00 (br s, 6H, phen), 8.84 (br s, 6H, phen), 7.82 (qt, 6H, phen) 7.71 (m, 24H, SPh), 7.44 (m, 24H, SPh), 5.27 (dd, 24H, Bz); FAB-MS: $m/z = 1610$ $[M-2BF_4]^{2+}$. LSI-MS: $m/z = 1045$ $[M-3BF_4]^{3+}$; elemental analysis calcd for $C_{138}H_{108}B_6F_{24}N_6Pd_6S_{12}$: C 48.83, H 3.21, N 2.48; found: C 48.67, H 3.13, N 2.33.

Received: June 24, 1997 [Z 10593 IE]
German version: *Angew. Chem.* **1998**, *110*, 130 – 133

Keywords: N ligands · palladium · supramolecular chemistry

[1] J.-M. Lehn, *Supramolecular Chemistry—Concepts and Perspectives*, VCH, Weinheim **1995**, Chap. 9.

[2] a) *Comprehensive Supramolecular Chemistry, Vol. 9* (Eds.: J. -P. Sauvage, M. W. Hosseini), Pergamon, Oxford, **1996**; b) J.-P. Sauvage, C. Dietrich-Buchecker, J.-C. Chambron in ref. [2a], pp. 43 – 83; c) J. K. M. Sanders in ref. [2a], pp. 131 – 164; d) P. N. W. Baxter in ref. [2a], pp. 165 – 211; e) E. C. Constable in ref. [2a], pp. 213 – 252; f) M. Fujita, K. Ogura in ref. [2a], pp. 253 – 282.

[3] a) M. Fujita, J. Yazaki, K. Ogura, *J. Am. Chem. Soc.* **1990**, *112*, 5645; b) M. Fujita, K. Ogura, *Bull. Chem. Soc. Jpn.* **1996**, *69*, 1471, and references therein

[4] a) H. Rauter, I. Mutikainen, M. Blomberg, C. J. L. Lock, P. Omar-Ochoa, E. Freisinger, L. Randaccio, E. Chiarparin, B. Lippert, *Angew. Chem.* **1997**, *109*, 1353; *Angew. Chem. Int. Ed. Engl.* **1997**, *36*, 1296, and references therein; b) R. V. Slone, J. T. Hupp, C. L. Stern, T. E. Albrecht-Schmitt, *Inorg. Chem.* **1996**, *35*, 4096, and references therein; c) P. J. Stang, D. H. Cao, K. Chen, G. M. Gray, D. C. Muddiman, R. D. Smith, *J. Am. Chem. Soc.* **1997**, *119*, 5136, and references therein.

[5] a) P. N. W. Baxter, J.-M. Lehn, A. DeCian, *Angew. Chem.* **1993**, *105*, 74; *Angew. Chem. Int. Ed. Engl.* **1993**, *32*, 69; b) R. Kramer, J.-M. Lehn, *J. Chem. Soc. Chem Commun.* **1993**, 990.

[6] a) J.-M. Lehn, A. Rigault, J. Siegel, J. Harrowfield, B. Chevrier, D. Moras, *Proc. Natl. Acad. Sci. USA* **1987**, *84*, 2565; b) U. Koert, M. M. Harding, J.-M. Lehn, *Nature* **1994**, *346*, 339; c) E. C. Constable, *Tetrahedron* **1992**, *48*, 10013.

[7] a) J.-P. Sauvage, *Acc. Chem. Res.* **1990**, *23*, 319; b) M. Fujita, F. Ibukuro, H. Seki, O. Kamo, M. Imanuri, K. Ogura, *J. Am. Chem. Soc.* **1996**, *118*, 899, and references therein.

[8] a) H. Ogino, *J. Am. Chem. Soc.* **1981**, *103*, 1303; b) A. P. Lyon, D. H. Macartney, *Inorg. Chem.* **1997**, *36*, 729, and references therein.

[9] G. S. Hanan, C. R. Arana, J.-M. Lehn, G. Baum, D. Fenske, *Chem. Eur. J.* **1996**, *2*, 1292, and references therein.

[10] P. N. W. Baxter, J.-M. Lehn, J. Fischer, M.-T. Youinou, *Angew. Chem.* **1994**, *106*, 2432; *Angew. Chem. Int. Ed. Engl.* **1994**, *33*, 2284, and references therein.

[11] P. N. W. Baxter, G. S. Hanan, J.-M. Lehn, *Chem. Commun.* **1996**, 2019.

[12] S. J. Loeb, G. K. H. Shimizu, *J. Chem. Soc. Chem. Commun.* **1993**, 1395.

[13] a) W. T. S. Huck, F. C. J. M. van Veggel, D. N. Reinhoudt, *Angew. Chem.* **1996**, *108*, 1304; *Angew. Chem. Int. Ed. Engl.* **1996**, *35*, 1213; b) W. T. S. Huck, R. Hulst, P. Timmerman, F. C. J. M. van Veggel, D. N. Reinhoudt, *ibid.* **1997**, *109*, 1046; **1997**, *36*, 1006

[14] J. Manna, J. A. Whiteford, P. J. Stang, P. C. Muddiman, R. D. Smith, *J. Am. Chem. Soc.* **1996**, *118*, 8731.

[15] P. J. Stang, N. E. Persky, J. Manna, *J. Am. Chem. Soc.* **1997**, *119*, 4777.

[16] Crystal data[17] for **3b**$[BF_4]_6$: monoclinic, space group *C*2/*c*, $a = 26.8628(3)$, $b = 24.1205(2)$, $c = 28.4165(1)$ Å, $\beta = 113.504(1)^\circ$, $V = 16884.7(2)$ Å^3, $Z = 4$, $\rho_{calcd} = 1.241$ g cm^{-3}, $2\theta_{max} = 42.0^\circ$, $Mo_{K\alpha}$ radiation ($\lambda = 0.71073$ Å), $T = 296$ K. A pale yellow, crystal ($0.2 \times 0.2 \times 0.3$ mm^3), grown by slow evaporation of a saturated solution in acetone, was sealed with the mother liquor in a thin-walled glass capillary. Of 8710 reflections measured, 7422 were observed ($I > 2\sigma(I)$) and integrated from frame data obtained from programmed hemisphere scan routine on a Siemens SMART CCD diffractometer. Decay (< 1%) was monitored by 50 standard data frames measured at the beginning and end of data collection. Systematic absences in the diffraction data and determined unit-cell parameters were consistent with *Cc* and *C2/c*. Solution in the centrosymmetric space group yielded chemically reasonable and computationally stable refinement results. Lorentzian and polarization corrections and a semi-empirical absorption correction, based on redundant data at varying effective azimuthal angles, were applied to the data ($\mu = 0.837$ cm^{-1}, min/max transmission = 0.3516/0.4663). The structure was solved by direct methods, completed by subsequent Fourier syntheses, and refined with full-matrix least-squares methods against F^2 to $R(F) = 0.1277$, $wR(F^2) = 0.3627$, $N_o/N_v = 8704/456$. The cation is located on a twofold axis. One of three symmetry-unique BF_4^- counterions was located and refined as a geometrically idealized rigid group. Attempts to model nine peaks with substantial electron density, remote from the cation and the located counterion, as disordered BF_4^- counterions or as chemically reasonable solvent molecules were unsuccessful. These peaks were assigned arbitrary carbon identities but replaced in calculations for intrinsic properties by the expected number of anions. Remaining peaks in the final difference map (max. 1.7 e Å^{-3}) were associated with the heavy atoms and considered to be artifacts arising from nonideal absorption corrections. The non-carbon and non-hydrogen atoms. as well as the phenyl ring carbon atoms of the cation were refined with anisotropic displacement coefficients. All other non-hydrogen atoms were refined isotropically. Hydrogen atoms were treated as idealized contributions. Scattering factors and anomalous dispersion coefficients are contained in the SHELXTL 5.03 program library (G. M. Sheldrick, Madison, WI).

[17] Crystallographic data (excluding structure factors) for the structure reported in this paper have been deposited with the Cambridge Crystallographic Data Centre as supplementary publication no. CCDC-100501. Copies of the data can be obtained free of charge on application to CCDC, 12 Union Road, Cambridge CB2 1EZ, UK (fax: int. code + (44) 1223-336033; e-mail: deposit@ccdc.cam.ac.uk).

 © WILEY-VCH Verlag GmbH, D-69451 Weinheim, 1998 1433-7851/98/3701-0123 $ 17.50+.50/0

The Formation of Heteroleptic Carbene Homologues by Ligand Exchange—Synthesis of the First Plumbanediyl Dimer**

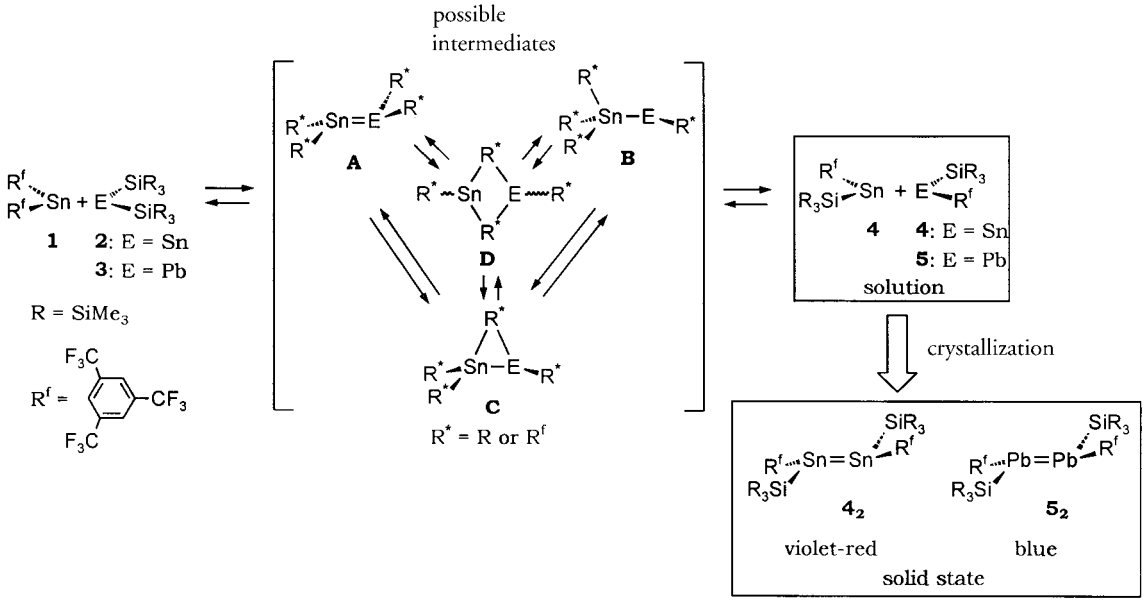
Karl W. Klinkhammer,* Thomas F. Fässler,* and Hansjörg Grützmacher*

Dedicated to Professor Manfred Weidenbruch on the occasion of his 60th birthday

Compounds of the heavier homologues of carbon containing double bonds ($R_2E{=}ER_2$, E = Si, Ge, Sn) differ strikingly from the corresponding alkenes, not only in their molecular structures but also in their chemical behavior. The type of bonding present in these molecules remains a very controversial subject.[1] The heaviest homologues, diplumbenes $R_2Pb{=}PbR_2$, were hitherto unknown. Plumbanediyls PbR_2 (also called plumbylenes), the constituent fragments homologous to carbenes, have, however, been isolated. They are monomeric even in the solid state, whereas the stannanediyls SnR_2 are known to dimerize in many cases, leading to the formation of distannenes $R_2Sn{=}SnR_2$.[2]

What happens if two carbene homologues, with differing dimerization tendencies, are mixed? Are mixed distannenes $R_2Sn{=}SnR'_2$ or even stannaplumbethenes $R_2Sn{=}PbR'_2$ accessible under such conditions? For our investigations we have chosen the stable monomeric stannanediyl [2,4,6-$(CF_3)_3C_6H_2]_2$Sn (**1**),[3] the distannene $[(Me_3Si)_3Si]_2Sn{=}Sn[Si(SiMe_3)_3]_2$ (**2_2**), and the plumbanediyl $[(Me_3Si)_3Si]_2$Pb (**3**).[4] In hydrocarbon solvents diyls **1**, **2**, and **3** exist as monomeric R_2E carbene analogues (E = Sn, Pb) in a singlet ground state. When equimolar solutions of **1** and **2** or **1** and **3** are mixed, the heteroleptic compounds **4** and **5**, respectively, are obtained (Scheme 1).

Fractional crystallization of the reaction mixtures in solution at $-60\,^{\circ}C$ led to thermochromic, needle-shaped crystals of the distannene **4_2**, which are violet-red at room temperature and brick-red at $-180\,^{\circ}C$, and blue prismatic crystals of the plumbanediyl dimer **5_2**. In both reactions a remarkable exchange of ligands has occurred with the result that each metal center E bears one 2,4,6-$(CF_3)_3C_6H_2$ and one $(Me_3Si)_3Si$ substituent. To our knowledge, a comparable rearrangement has been never observed in carbene or olefin chemistry but has been reported as a mechanism for the isomerization of disilenes, digermenes, and distannenes.[1] Although we have no spectroscopic evidence,[6] it is likely that the intermediates **A**–**D** play a crucial role in course of this rearrangement. Calculations showed that for R* = H and E = Sn or Pb, all E_2H_4 isomers correspond to local minima on the energy hypersurface following the order **A** < **B** < **C** < **D** of increasing stability within a narrow energy range.[6] In solution the dimers **4_2** and **5_2** dissociate into the monomers **4** and **5**. Note that no mixed Sn=Pb dimer was obtained from solutions containing **4** and **5** in accordance with calculated dimerization energies (Table 1) which show that the dismutation reaction as shown in Equation (a) is slightly exothermic.



Scheme 1.

$$2\,H_2Sn{=}PbH_2 \rightarrow H_2Sn{=}SnH_2 + H_2Pb{=}PbH_2 \qquad (a)$$

$$\Delta(\Delta E_{dim}) = -10\ kJ\,mol^{-1}$$

[*] Dr. K. W. Klinkhammer
Institut für Anorganische Chemie der Universität
Pfaffenwaldring 55, D-70550 Stuttgart (Germany)
Fax: Int. code + (49) 711 685-4241
E-mail: kw@anorg55.chemie.uni-stuttgart.de
Dr. T. F. Fässler, Prof. Dr. H. Grützmacher
Laboratorium für Anorganische Chemie, ETH-Zürich, Universitätstrasse 6, CH-8092 Zürich (Switzerland)
Fax: Int. code + (41) 1 632-1090
E-mail: gruetz@inorg.chem.ethz.ch

[**] This work was supported by the Deutsche Forschungsgemeinschaft and the Schweizerische Nationalfonds zur Förderung der wissenschaftlichen Forschung.

 © WILEY-VCH Verlag GmbH, D-69451 Weinheim, 1998 1433-7851/98/3701-0124 $ 17.50+.50/0

Table 1. Theoretical[a] and experimental data for various compounds of the type $R_2E{=}ER_2$ (E = C, Si, Ge, Sn, Pb).

	Theor. $d_{(E-E)}$ [pm]	Exp. $d_{(E-E)}$ [pm]	Theor. θ [°]	Exp. θ [°]	ΔE_{dim} [kJ mol^{-1}]	α [°]
C=C	135	134 – 137	0	0	739[c]	0
Si=Si	216	214 – 225	29.0	0 – 18	250[c]	9
Ge=Ge	234	221 – 235	43.7	12 – 36	180[c]	40
Sn=Sn	268	277 – 363	48.0	41.0, 41.5[b]	96	41
Pb=Pb	295	354	54.6	40.8	24	43
Sn=Pb	279	–	54.5(Sn) 49.3 (Pb)	–	55	–

[a] Calculation on Coupled-Cluster-Level.[9] [b] Data from very distorted distannenes were excluded.[1g] [c] Published data.[8]

Single-crystal X-ray diffraction experiments[7] performed at – 100 °C revealed that both compounds **4** and **5** crystallize as centrosymmetric *trans*-bent dimers $\mathbf{4}_2$ and $\mathbf{5}_2$ with idealized C_i symmetry (Figure 1). The experimentally determined tilt angles θ are 41.5° (E = Sn) and 40.8° (E = Pb). The Sn–Sn bond length in $\mathbf{4}_2$ [283.3(1) pm] is similar to the one in the distannene $\mathbf{2}_2$ [282 pm]. It is considerably longer, however, than the bond length in the distannene $R_2Sn{=}SnR_2$ [277 pm, $R = (Me_3Si)_2CH$, C_i symmetry][1f] and much shorter than the Sn–Sn distance in the stannanediyl dimer $R^f_2Sn{=}SnR^f_2$ [363 pm, R^f = 2,4,6-$(CF_3)_3C_6H_2$, C_i symmetry].[2b] The Pb–Pb bond length in $\mathbf{5}_2$ (353.7(1) pm) is long and exceeds the

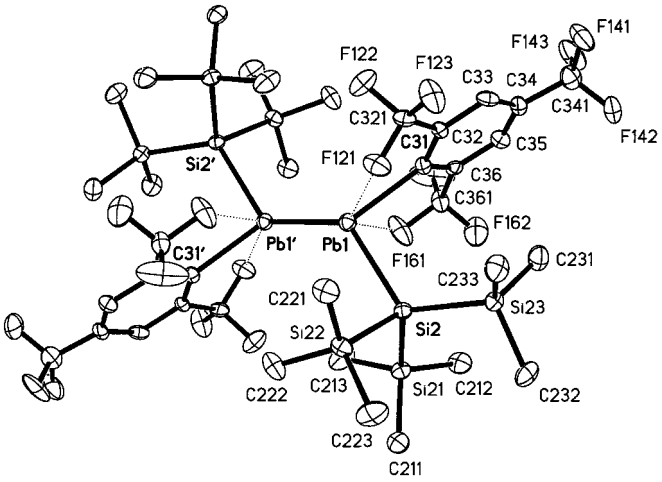


Figure 1. The structures of $\mathbf{4}_2$ and $\mathbf{5}_2$ in the crystal are very similar and only $\mathbf{5}_2$ is shown. Selected bond lengths [pm] and angles [°]: $\mathbf{4}_2$: Sn1–Sn1′ 283.3(1), Sn1–Si2 262.4(1), Sn1–C31 225.5(3); Si2-Sn1-Sn1′ 126.3(1), C31-Sn1-Sn1′ 107.8(1), Si2-Sn1-C31 103.8(1). $\mathbf{5}_2$: Pb1–Pb1′ 353.7(1), Pb1–Si2 270.5(2), Pb1–C31 236.9(7); Si2-Pb1-C31 96.7(2), Si2-Pb1-Pb1′ 124.82(5), C31-Pb1-Pb1′ 115.3(2).

calculated bond length in the parent compound $H_2Pb{=}PbH_2$ (295 pm) by about 50 pm. However, the potential curves for the tilt angles θ and the E–E distances in particular are very shallow.[8] In this case, the longer bonds and smaller tilt angles θ are a consequence of the steric demands of the substituents. The relatively short Pb–F contacts (276.7, 278.2 pm) in $\mathbf{5}_2$ also contribute to Pb–Pb bond elongation, an effect which is also present in $\mathbf{4}_2$ (Sn–F: 294.9, 295.6 pm) but to a lesser extent.[2b] The question arises whether the very long Pb–Pb distance is still consistent with the presence of a double bond.

In Table 1, theoretical[9] and experimental bonding parameters of the complete homologous series of unsaturated compounds of the type $R_2E{=}ER_2$ (E = C to Pb) are compared. While there is no acyclic olefin in which the carbon atoms deviate from planarity, and steric demands causes only slight bond elongation, the heavier homologues show increasing variations in bonds lengths and tilt angles θ with increasing main quantum number.

Frequently used indicators of the presence of double bonds such as *short bond lengths*, *planarity of the systems*, and *high dissociation energies* can be used to characterize "hard double bonds" like C=C bonds. According to these criteria no double bond is present in the plumbanediyl dimer $\mathbf{5}_2$. Several experimental results and extensive theoretical investigations in recent years,[1c] however, have shown that the application of these indicators to the (presumably) doubly-bonded dimers of the heavier carbene homologues is questionable. The presence of a double bond in compounds such as $\mathbf{5}_2$ cannot be confirmed with certainty until a more comprehensive and precise definition of a double bond than that given by the classical criteria becomes available.[10]

Received: March 28, 1997
Revised version: September 29, 1997 [Z 10289 IE]
German version: *Angew. Chem.* **1998**, *110*, 114 – 116

Keywords: carbene homologues · lead · main group elements · multiple bonds · tin

[1] For recent reviews, see a) G. Rabe, J. Michl, *Chem. Rev.* **1985**, *85*, 419 ; b) T. Tsumaraya, S. A. Batcheller, S. Masamune, *Angew. Chem.* **1991**, *103*, 916; *Angew. Chem. Int. Ed. Engl.* **1991**, *30*, 902; c) M. Driess, H. Grützmacher, *ibid.* **1996**, *108*, 900; and **1996**, *35*, 828; for the first structurally characterized Si=Si, Ge=Ge, and Sn=Sn double-bonded systems, see d) R. West, M. J. Fink, J. Michl, *Science* **1981**, *214*, 1343; e) P. B. Hitchcock, M. F. Lappert, S. J. Miles, A. J. Thorne, *J. Chem. Soc. Chem. Commun.* **1984**, 480; f) D. E. Goldberg, D. H. Harris, M. F. Lappert, K. M. Thomas, *ibid.* **1976**, 261; g) M. Weidenbruch, H. Killian, K. Peters, H. G. von Schnering, H. Marsmann, *Chem. Ber.* **1995**, *128*, 973.

[2] a) H. Grützmacher, H. Pritzkow, F. T. Edelmann, *Organometallics* **1991**, *10*, 23; b) U. Lay, H. Pritzkow, H. Grützmacher, *J. Chem. Soc. Chem. Commun.* **1992**, 260.

[3] K. W. Klinkhammer, W. Schwarz, *Angew. Chem.* **1995**, *107*, 1448; *Angew. Chem. Int. Ed. Engl.* **1995**, *34*, 1334.

[4] Selected physical data: **4**: m.p. (decomp.) 150 °C; ^{1}H NMR (250.133 MHz, C_6D_6, 300 K): δ = 0.15 (CH_3), 7.88 (H_{arom}); ^{29}Si NMR (39.761 MHz, C_6D_6, 300 K): δ = – 5.5 [*Si*($SiMe_3$)$_3$], – 69.6 [Me_3*Si*)$_3$Si]; ^{19}F NMR (235.36 MHz, C_6D_6, 300 K): δ = – 60.5 [*ortho*-CF_3, $J(^{109/107}Sn,^{19}F)$ = 102 Hz, $^1J(^{19}F,^{13}C)$ = 275.8 Hz]; – 63.0 [*para*-CF_3, $^1J(^{19}F,^{13}C)$ = 273.3 Hz]; ^{119}Sn{^{1}H} NMR (74.631 MHz, C_6D_6, 300 K):

$\delta = 168$ ($W_{1/2} = 800$ Hz); UV/Vis (*n*-pentane): λ_{max} 540 nm. **5**: m.p. (decomp) approximately 90 °C; ^{1}H NMR (250.133 MHz, C_6D_6, 300 K): $\delta = 0.25$ (CH_3), 8.04 (H_{arom}); ^{19}F NMR (235.36 MHz, C_6D_6, 300 K): $\delta = -66.6$ [*ortho*-CF_3, $J(^{207}Pb,^{19}F) = 374$ Hz, $^1J(^{19}F,^{13}C) = 275.4$ Hz]; -62.8 [*para*-CF_3, $^1J(^{19}F,^{13}C) = 272.5$ Hz]; UV/Vis (*n*-pentane): λ 586 nm; 1025 nm. Both compounds gave correct elemental analyses.

[5] Temperature-dependent ^{119}Sn NMR measurements, which would give valuable information about rearrangement processes or about the presence of a monomer/dimer equilibrium, could not be performed up to now for several reasons, such as very long aquisition times, the thermal lability of $\mathbf{4}_2$ at temperatures above room temperature, and the low solubility in inert solvents at low temperatures.

[6] G. Trinquier, *J. Am. Chem. Soc.* **1991**, *113*, 144.

[7] X-ray crystal structure analyses: P4 (Siemens), $\lambda(Mo_{K\alpha}) = 0.71073$ Å, ω scan mode, Lorenz and polarization correction, absorption correction (ψ scan, min/max. transmission: 0.73/0.99) for $\mathbf{5}_2$, solution by direct methods (SHELXS-86), refinement by a full-matrix least-squares procedure based on F_o^2 (SHELXL-93). $\mathbf{4}_2 \cdot C_5H_5$: monoclinic, space group $C2/c$ (no. 15), $a = 2213.3(4)$, $b = 1530.9(3)$, $c = 2057.1(4)$ pm, $\beta = 117.99(3)°$, $V = 6155(2)$ Å^3, $Z = 4$ (dimers), $\rho_{calcd} = 1.473$ Mgm^{-3}, $T = -100$ °C, $\mu = 1.049$ mm^{-1}, $3.4° < 2\theta < 55°$, 7264 measured reflections, 7080 independent, 332 parameters, 22 restraints, $R1$ [$F_o > 4\sigma(F_o)$] = 0.039, wR_2 [F_o^2; all data] = 0.110; $\mathbf{5}_2$: monoclinic, space group $I2/a$ (no. 15), $a = 2164.8(4)$, $b = 945.3(2)$, $c = 2864.2(6)$ pm, $\beta = 104.87(3)°$, $V = 5665(2)$ pm, $Z = 4$ (dimers), $\rho_{calcd} = 1.726$ Mgm^{-3}, $T = -100$ °C, $\mu = 6.190$ mm^{-1}, $3.9° < 2\theta < 48°$, 8675 measured reflections, 4419 independent, 289 parameters, $R1$ [$F_o > 4\sigma(F_o)$] = 0.038, wR_2 [F_o^2; all data] = 0.072. Crystallographic data (excluding structure factors) for the structures reported in this paper have been deposited with the Cambridge Crystallographic Data Centre as supplementary publication No. CCDC-100326. Copies of the data can be obtained free of charge on application to CCDC, 12 Union Road, Cambridge CB2 1EZ, UK (fax: int. code + (44) 1223 336033; e-mail: deposit@ccdc.cam.ac.uk).

[8] H. Jacobsen, T. Ziegler, *J. Am. Chem. Soc.* **1994**, *116*, 3667.

[9] Calculations: Equilibrium structures of E_2H_4 were determined by CCD (Sn) and CCSD (Pb) calculations (Gaussian 94) with Stuttgart quasi-relativistic pseudopotentials [W. Kuechle, M. Dolg, H. Stoll, H. Preuss, *J. Chem. Phys.* **1991**, *74*, 1245] and extended basis sets for Sn and Pb: (4s4p2d)/[5s5p2d]; basis sets for H: (3s2p)/[4s2p] [T. H. Dunning, *J. Chem. Phys.* **1970**, *19*, 553]. The dimerization energies were calculated at the CCSD level and have been corrected with respect to basis set superposition errors (full Counterpoise method) and zero-point vibrations. The identification of local minima on the hypersurface was verified by frequency calculations [NIMAG = 0].

[10] The definition of a double bond by means of quantum mechanics is based on the presence of two electron pairs shared by two nuclei. It is independent of the topology or the inherent bond energy. Thus—within the framework of LCAO-MO approximation (LCAO = *L*inear *C*ombination of *A*tomic *O*rbitals)—methods such as NBO (NBO = *N*atural *B*ond *O*rbitals) or NLMO analyses (NLMO = *N*aturally *L*ocalized *M*olecular *O*rbitals) can be used [J. E. Carpenter, F. Weinhold, *J. Mol. Struct. Theochem* **1988**, *169*, 41]. A further valuable method outside this framework is the Electron Localization Function (ELF), which is a function of the kinetic energy of the electrons [B. Silvi, A. Savin, *Nature* **1994**, *371*, 683]. We will present a detailed quantum chemical analysis of the bonding in compounds such as $\mathbf{5}_2$ using these methods elsewhere.

Dynamic Error Correction in Autocatalytic Peptide Networks**

Kay Severin, David H. Lee, Jose A. Martinez, Michael Vieth, and M. Reza Ghadiri*

Life operates precariously in between two extremes: evolution requires new information to be generated through mistakes during the self-reproduction step, but at the same time living systems need to preserve their information against excessive accumulation of errors.[1] Here we describe autocatalytic peptide networks that stabilize themselves against errors by subjugating the mutant population for the synthesis of the wild-type peptide. The systems are based on three or four peptide fragments that undergo competitive condensation reactions in neutral aqueous solutions to produce the native sequence of a peptide replicator along with its mutant products. The peptide self-replication process is shown to respond to the spontaneous formation of errors—experimentally simulated by the background coupling reactions that yield the mutant peptides—by employing the mutant product(s) as catalyst(s) for the synthesis of the native replicator sequence. Detailed analyses have revealed that this novel mode of sequence selection arises as the result of self-organization into networks composed of two or three interconnected (auto)catalytic cycles. These networks are among the first examples of biopolymer-based nonlinear chemical systems in which catalytic and autocatalytic processes are cooperatively coupled.[2]

The present study describes an unprecedented response of a self-replicating peptide system to the spontaneous generation of mutations by self-organizing into networks of cooperative autocatalytic and catalytic cycles that upregulates the production of the native sequence. The system is based on the recently reported sequence of a peptide replicator[3] and is composed of a maximum of four peptide fragments: the native electrophilic **E** and nucleophilic **N** fragments and their single alanine mutants $\mathbf{E_{9A}}$ and $\mathbf{N_{26A}}$, respectively (Figure 1). These peptides undergo competitive ligation reactions to produce four products: the native sequence **T** along with the single mutant peptides $\mathbf{T_{9A}}$ and $\mathbf{T_{26A}}$ and the double mutant peptide $\mathbf{T_{9/26A}}$. Thus addition of the mutant fragments to the initial mixture simulates the spontaneous formation of errors during the self-replication process. Furthermore, the mutations were chosen to be conservative replacements for the native amino acid residues (alanine in place of valine 9 or leucine 26) in order to simulate the production of a mutant population with a closely related informational content,[4] previously termed quasi-species.[5]

[*] Prof. Dr. M. R. Ghadiri, Dr. K. Severin, D. H. Lee
Dr. J. A. Martinez, Dr. M. Vieth
Departments of Chemistry and Molecular Biology, Skaggs Institute for Chemical Biology
The Scripps Research Institute
10550 North Torrey Pines Road, La Jolla, CA, 92037 (USA).
Fax: Int. code + (1) 619-784 2798
e-mail: ghadiri@scripps.edu

[**] We thank the Deutsche Forschungsgemeinschaft for a postdoctoral fellowship (K.S.), the Canadian Medical Research Council for a predoctoral fellowship (D.H.L.), and the Spanish Ministry of Education and Science for a postdoctoral fellowship (J.A.M.).

 © WILEY-VCH Verlag GmbH, D-69451 Weinheim, 1998 1433-7851/98/3701-0126 $ 17.50+.50/0

E: ArCONH-RMKQLEEKVYELLSKVA-COSBn
E_{9A}: ArCONH-RMKQLEEK**A**YELLSKVA-COSBn
N: H_2N-CLEYEVARLKKLVGE-$CONH_2$
N_{26A}: H_2N-CLEYEVAR**A**KKLVGE-$CONH_2$
T: ArCONH-RMKQLEEKVYELLSKVACLEYEVARLKKLVGE-$CONH_2$
T_{9A}: ArCONH-RMKQLEEK**A**YELLSKVACLEYEVARLKKLVGE-$CONH_2$
T_{26A}: ArCONH-RMKQLEEKVYELLSKVACLEYEVAR**A**KKLVGE-$CONH_2$
$T_{9/26A}$: ArCONH-RMKQLEEK**A**YELLSKVACLEYEVAR**A**KKLVGE-$CONH_2$

$$E + N_{26A} + N \longrightarrow T + T_{26A} \quad (1)$$
$$E + E_{9A} + N \longrightarrow T + T_{9A} \quad (2)$$
$$E + E_{9A} + N + N_{26A} \longrightarrow T + T_{9A} + T_{26A} + T_{9/26A} \quad (3)$$
$$E + N_{26A} \xrightarrow{[T_{26A}]} T_{26A} \quad (4)$$
$$E_{9A} + N \xrightarrow{[T_{9A}]} T_{9A} \quad (5)$$
$$E + N_{26A} \xrightarrow{[T]} T_{26A} \quad (6)$$
$$E_{9A} + N \xrightarrow{[T]} T_{9A} \quad (7)$$
$$E + N \xrightarrow{[T_{9A}]} T \quad (8)$$
$$E + N \xrightarrow{[T_{26A}]} T \quad (9)$$
$$E + N \xrightarrow{[T_{9/26A}]} T \quad (10)$$

Figure 1. Fragment condensation reactions performed in this study and the corresponding peptide sequences. For the design principles, synthesis, characterization, and kinetic analyses, see ref. [3].

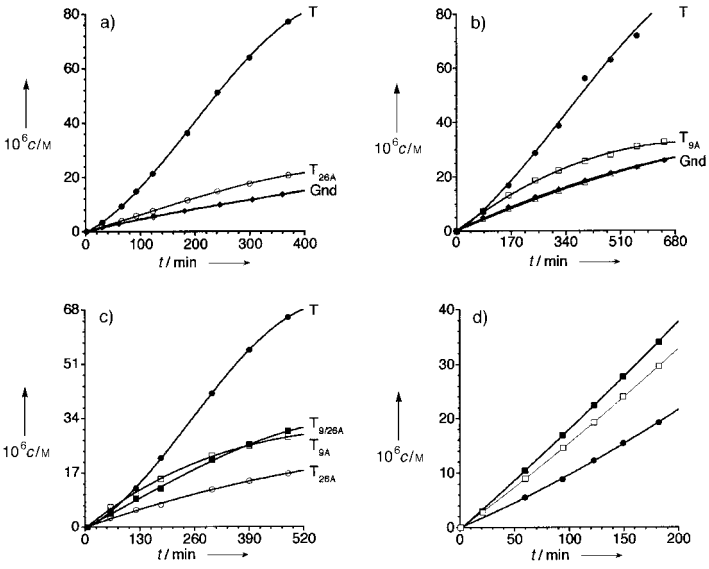


Figure 2. Product formation as a function of time. a) Reaction (1): **T** (●) and $\mathbf{T_{26A}}$ (○) and in the presence of 4 M Gnd **T** (◆) and $\mathbf{T_{26A}}$ (◇); b) reaction (2): **T** (●) and $\mathbf{T_{9A}}$ (□), and in the presence of 4 M Gnd **T** (◆) and $\mathbf{T_{9A}}$ (△); c) reaction (3): **T** (●), $\mathbf{T_{26A}}$ (○), $\mathbf{T_{9A}}$ (□), and $\mathbf{T_{9/26}}$ (■); d) reactions (8) and (9): **T** in the presence of 40 mM $\mathbf{T_{26A}}$ (□), 57 mM $\mathbf{T_{9A}}$ (■), or without any added template (●). It should be noted that the condensation of native fragments **N** and **E** is catalyzed by both single mutant products $\mathbf{T_{26A}}$ and $\mathbf{T_{9A}}$ [reactions (8) and (9) in d)], which leads to the pronounced selectivity for the native sequence **T** [reactions (1) – (3) in a) – c)].

Reaction mixtures composed of equimolar amounts of **E**, $\mathbf{N_{26A}}$, and **N** [Eq. (1)] or **E**, $\mathbf{E_{9A}}$, and **N** [Eq. (2)] in 4 M guanidinium (Gnd) solutions (pH 7.5) were shown to produce approximately equal amounts of the expected ligation products **T** and $\mathbf{T_{26A}}$ or **T** and $\mathbf{T_{9A}}$, respectively. This indicates a lack of kinetic preference for a specific ligation reaction under denaturing conditions. However, in the absence of denaturant, both reactions displayed pronounced preference for the production of the native peptide sequence **T** under neutral aqueous conditions (Figure 2a,b). A priori, the preferential production of the native peptide can be simply attributed to the known parabolic growth profile of the replicator sequence. Indeed, control experiments with equimolar amounts of **E** and $\mathbf{N_{26A}}$ [Eq. (4)] or $\mathbf{E_{9A}}$ and **N** [Eq. (5)] have shown that $\mathbf{T_{9A}}$ and $\mathbf{T_{26A}}$ are both incapable of catalyzing their own production. Therefore, the observed high selectivity in competitive ligation reactions can be attributed to a significant degree to the nonlinear growth profile of the peptide replicator[6] versus the linear background rate for the production of the mutants.

If one considers ternary complexes as the catalytically active intermediates,[3] for each reaction (1) and (2) there are two possible autocatalytic *and* two catalytic pathways that can lead to products formation (Figure 3). As suggested by the above experiments, pathways b and b′ for the autocatalytic production of the single mutant peptides $\mathbf{T_{9A}}$ and $\mathbf{T_{26A}}$ are not operative and the intermediate a is responsible for self-replication of the native sequence **T**. We therefore sought to examine the role of the remaining possible catalytic intermediates c, c′, d, and d′. Reactions composed of equimolar amounts of **E** and $\mathbf{N_{26A}}$ [Eq. (6)] or $\mathbf{E_{9A}}$ and **N** [Eq. (7)] do not

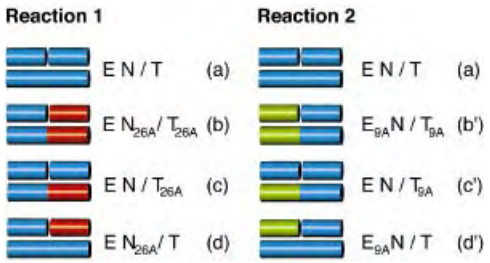


Figure 3. Schematic representation of plausible ternary intermediates for the autocatalytic (a, b, and b′) and catalytic (c, c′, d, and d′) production of ligation products in reactions (1) and (2). The ternary complexes are composed of an electrophilic peptide fragment (**E** or $\mathbf{E_{9A}}$), a nucleophilic peptide fragment (**N** or $\mathbf{N_{26A}}$), and the catalyst (**T**, $\mathbf{T_{9A}}$, or $\mathbf{T_{26A}}$). The different peptides are shown as colored cylinders to represent the α-helical configuration (native sequence: blue; E_{9A} and its corresponding T_{9A} segment: green; N_{26A} and its corresponding T_{26A} segment: red).

show any rate enhancements in the presence of added native peptide **T**. Therefore, the replicator sequence does not catalyze the formation of the mutant peptides, and pathways d and d′ are not operative. However, both single mutant peptides $\mathbf{T_{9A}}$ and $\mathbf{T_{26A}}$ catalyze the formation of the native sequence **T** [Eqs. (8) and (9), respectively; Figure 2d]. In fact, the catalytic efficiency of the mutant products for the production of the native sequence is approximately 75 % that of the native replicator sequence itself, as judged by the initial rate of product formation in the presence of similar amounts of added catalysts. The overall selectivity observed in reactions (1) and (2) is therefore the result of self-organized autocatlytic and catalytic cycles, which work in concert to favor the production of the native sequence **T** (Figure 4). It is

 © WILEY-VCH Verlag GmbH, D-69451 Weinheim, 1998 1433-7851/98/3701-0127 $ 17.50+.50/0

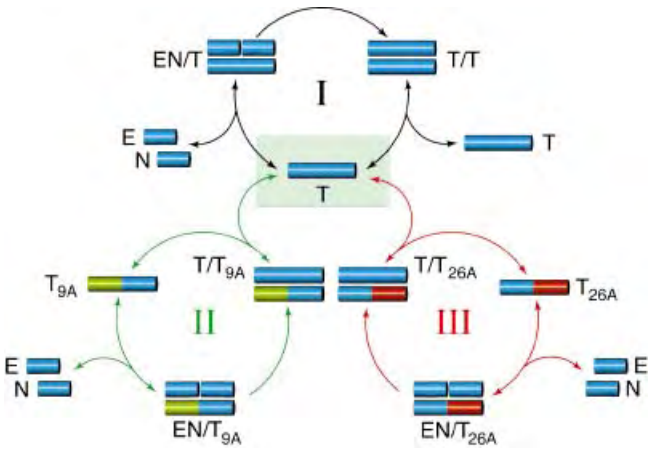


Figure 4. Peptide fragment condensations result in self-organized networks composed of two [cycles I and III or I and II for reactions (1) and (2), respectively] or three [reaction (3)] interconnected (auto)catalytic cycles with overall dynamic error-correcting properties. The mutant products $\mathbf{T_{9A}}$ (green-blue) and $\mathbf{T_{26A}}$ (red-blue) are infertile but catalyze the formation of the native replicator **T** (blue).

also interesting to note the asymmetry of the catalytic contribution: while the mutant peptides $\mathbf{T_{9A}}$ and $\mathbf{T_{26A}}$ are able to catalyze the formation of the native sequence **T**, **T** is "selfish" and does not accelerate the condensation of the mutant fragments. This unusual effect can be explained if one compares the stability of the intermediate ternary complex to the stability of the corresponding (self-inhibited) catalyst dimer. For reactions (6) and (7) the ternary complex is destabilized due to mutations in the hydrophobic core. Thus, the population of the intermediate is low, and no catalysis is observed. In Reactions (8) and (9), however, the mutation affects both the ternary complex and the catalyst dimer. The resulting increase in free catalyst concentration compensates for the reduced stability of the catalytic species.

The self-organized network persists also in reactions in which equimolar amounts of all four peptide fragments are employed [Eq. (3)]. In this case the double mutant product $\mathbf{T_{9/26A}}$ is not only infertile but also catalytically inactive [Eq. (10)]. Here the system is shown to self-organize into a network (*three* interconnected catalytic cycles), which displays a similar error-correction mechanism: each time a mutant product is formed, not only does it act as an efficient catalyst to generate several copies of the native sequence, but because these catalytic cycles are coupled to the native autocatalytic cycle, each new template produced in this way also serves to boost the production of the native sequence through the autocatalytic pathway (Figure 4). The net effect is significant upregulation in the production of the native peptide, leading to the selectivity observed in reactions (1) – (3) (Figure 2a – c).

The peptide-based systems described are the first examples of self-organized chemical networks that display characteristics essential for evolution: sequence-selective reproduction and dynamic error correction. Furthermore, these results suggest that short peptides are promising building blocks for complex nonlinear chemical systems, which may ultimately lead to the construction and understanding of molecular ecosystems.[7]

Experimental Section

All peptides were made by standard solid-phase peptide synthesis with *tert*-butyloxycarbonyl (Boc) chemistry. The electrophilic peptide fragments were synthesized as described previously.[3] The reactions were performed in 0.6 mL Eppendorf tubes. Temperature was maintained at 21.0($\pm$0.5)°C. A degassed, benzylthiol-saturated solution containing 3-(*N*-morpholino)-propane sulfonic acid (MOPS) buffer (pH 7.5), the nucleophilic peptide fragment(s) $\mathbf{N_x}$, and the internal standard 4-acetamidobenzoic acid (ABA) was incubated for 15 min. Reactions were initiated by adding a solution containing the electrophilic peptide fragment(s) $\mathbf{E_y}$ to give a total volume of 500 μL. Typically, the following final concentrations were employed: $\mathbf{N_x} = \mathbf{E_y} = 180 - 200\,\mu M$, MOPS = 140 μM, ABA = 100 μM. Peptide fragment condensations in the presence of Gnd ions (4 M) were performed as described above, except that MOPS buffer containing Gnd was used. Control experiments to probe (auto)catalytic contributions were performed with 15 – 40 mol % of the respective catalyst. All experiments were repeated twice. Samples (35 μL) were removed from the reaction vessel at various times, immediately quenched with 2% trifluoroacetic acid (70 μL), and stored at −78°C prior to HPLC analysis. Peptide concentrations were determined relative to the internal standard.

Received: June 6, 1997 [Z 10517 IE]
German version: *Angew. Chem.* **1998**, *110*, 133 – 135

Keywords: autocatalysis · error correction · networks · peptides · self-replication

[1] a) M. Eigen, P. Schuster, *Naturwissenschaften* **1971**, *58*, 465; b) B.-O. Küppers, *Information and the Origin of Life*, MIT Press, Cambridge, MA (USA) **1990**; c) S. A. Kauffman, *The Origins of Order*, Oxford Univ. Press, New York, **1993**.

[2] a) A hypercyclic peptide network that displays symbiosis among otherwise competitive peptide replicators: D. H. Lee, K. Severin, Y. Yokobayashi, M. R. Ghadiri, *Nature* **1997**, *390*, 591 – 594; b) nucleotide-based oligomers that display cross-catalytic behavior: D. Sievers, G. von Kiedrowski, *ibid.* **1994**, *369*, 221 – 224; c) synthetic structures that show cooperative behavior: J.-I. Hong, Q. Feng, V. Rotello, J. Rebek, Jr., *Science* **1992**, *255*, 848 – 850.

[3] a) D. H. Lee, J. R. Granja, J. A. Martinez, K. Severin, M. R. Ghadiri, *Nature* **1996**, *382*, 525 – 528; b) K. Severin, D. H. Lee, J. A. Martinez, M. R. Ghadiri, *Chem. Eur. J.* **1997**, 3, 1017 – 1024.

[4] Strong mutations such as placement of glutamic acid residues in the complementary hydrophobic interface have been shown previously to abolish template-directed catalysis.[3] Also see: J. C. Hu, E. K. O'Shea, P. S. Kim, R. T. Sauer, *Science* **1990**, *250*, 1400 – 1403.

[5] M. Eigen, P. Schuster, *The Hypercycle. A Principle of Natural Self-Organization*, Springer, Berlin, **1979**.

[6] A sigmoidal growth profile is a characteristic signature of efficient autocatalytic processes. This feature is clearly visible in reactions (1) – (3) (Figure 1).

[7] D. H. Lee, K. Severin, M. R. Ghadiri, *Curr. Opin. Chem. Biol.* **1997**, *1*, 491 – 496.

 © WILEY-VCH Verlag GmbH, D-69451 Weinheim, 1998 1433-7851/98/3701-0128 $ 17.50+.50/0

$(NH_4)_2Ge_7O_{15}$: A Microporous Material Containing GeO_4 and GeO_6 Polyhedra in Nine-Rings**

C. Cascales, E. Gutiérrez-Puebla, M. A. Monge,* and C. Ruíz-Valero

Crystalline microporous materials are widely used in the fields of catalysis, ion exchange, and adsorption. Since the first discovery of zeolites, many natural and synthetic zeolites,[1–7] silica polymorphs, aluminophosphate-based molecular sieves,[8–11] and microporous compounds built from MO_4 tetrahedra where the M centers are atoms other than aluminum or silicon[12] have been synthesized.

Like silicon, germanium atoms tend to be surrounded by a tetrahedron of oxygen atoms, which may join through shared corners to form larger units; in fact, some compounds of the two elements are isomorphous. However, in Ge zeotypes the structure of the framework can be formed by GeO_4 tetrahedra, GeO_6 octahedra, and sometimes even GeO_5 trigonal bipyramids.[13] For this reason it is surprising that few reports of microporous germanates exist in the literature. To our knowledge, the only fully characterized compounds are of the type $M_{3+x}H_{1-x}Ge_7O_{16}\cdot n\,H_2O$ (M = monovalent cation) with pharmacosiderite-type structure, obtained by ion exchange from the compounds $(NH_4)_3HGe_7O_{16}\cdot n\,H_2O$,[13–20] $[Ge_6O_{12}(OH)]^-[N(CH_3)_4]^+$[21] and $[Ge_{18}O_{38}(OH_4)]^{8-}[(C_2N_2H_{10})^{2+}]_4$.[22] All of them have the framework structure of zeolites and show many of their properties.

An extremely interesting question is whether different germanium dioxide frameworks can be obtained by changing the ratio of GeO_6 octahedra to GeO_4 tetrahedra while using the same template. In other words, can different phases be obtained inside the GeO_2/NH_4^+ system? In this paper we report the first results of our effort: the novel zeolite-like germanate, $(NH_4)_2Ge_7O_{15}$, containing octahedra and tetrahedra forming nine-rings, an arrangement that has never been observed before in microporous solids. Thus, this material could display new effects of shape selectivity in catalytic processes and offer unique properties as molecular sieves.

The title compound was synthesized hydrothermally from a reaction mixture containing GeO_2, $NH_4(OH)$, H_2O, and ethylene glycol in the molar ratio 1:0.6:30:12 on heating at 180°C for 14 days. The cubic and prismatic crystals observed in the resulting solid product were identified as $(NH_4)_3HGe_7O_{16}\cdot n\,H_2O$ and a new unknown phase, respectively. Figure 1 shows the X-ray diffraction patterns for both the cubic and the new microporous germanates.

A suitable single crystal of prismatic shape was selected and mounted in a diffractometer equipped with a CCD detector. The crystal structure (see Experimental Section) indicated that the composition is $(NH_4)_2Ge_7O_{15}$, in which six Ge atoms are tetrahedrally coordinated [range of Ge–O bond lengths 1.715(4)–1.782(4) Å; O-Ge-O bond angles 106.7(2)–116.1(2)°], and the remaining one is octahedrally coordinated to oxygen atoms [range Ge(4)–O bond lengths 1.863(4)–1.923(3) Å; bond angles between 86.2(2) and 93.8(2)°]. Therefore, in the unit cell there are 28 Ge atoms, 60 oxygen atoms, and 8 NH_4^+ ions.

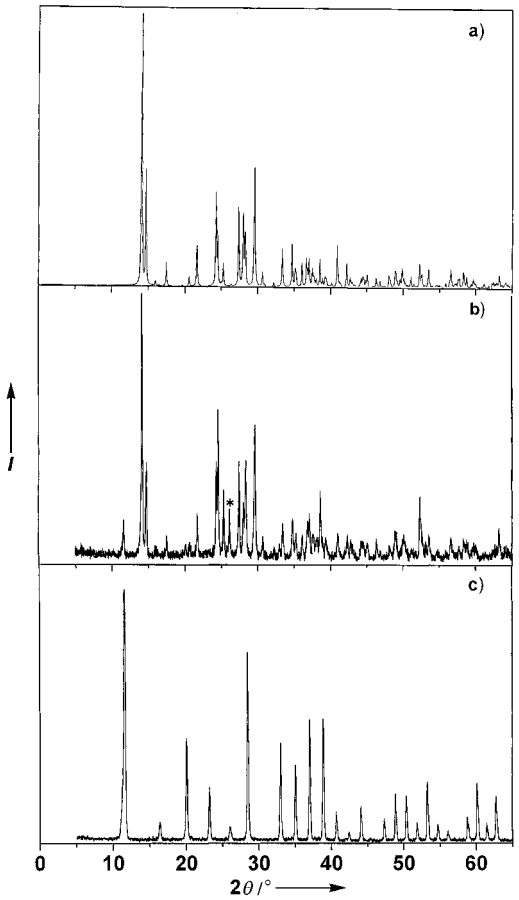


Figure 1. X-ray powder diagrams (XPD) a) calculated for $(NH_4)_2Ge_7O_{15}$ XPD from single-crystal structure data, b) recorded for the obtained material (* corresponds to the higher GeO_2 peak), and c) recorded for $(NH_4)_3HGe_7O_{16}\cdot 4\,H_2O$. I = intensity (arbitary units)

Tetrahedra and octahedra are linked by sharing corners in such a way that each tetrahedron is surrounded by one octahedron and three tetrahedra, and each octahedron is surrounded by six tetrahedra. The structure can be envisaged in terms of a two-dimensional sheet that is repeated to generate the full three-dimensional structure. This sheet is perpendicular to the c axes and is formed by nine-polyhedra rings (seven are tetrahedra and two are octahedra) in a 4Td-Oh-3Td-Oh sequence (Figure 2). This arrangement forces the formation of parallel double rings, which are held together through the octahedra and create some thickness to the layer. The shape of the ring is nearly a regular triangle.

This sheet, which is repeated by vertical translation along the stacking c direction, is bonded to the neighboring sheets located directly above and below through the only vertex of the tetrahedra not involved in connectivity inside the layer. As explained before, the octahedra are inside the sheet forming the double rings. This sort of packing gives rise to three types of channels, in all of which GeO_6 octahedra are

[*] Dr. M. A. Monge, Dr. C. Cascales, Dr. E. Gutiérrez Puebla, Dr. C. Ruíz-Valero
Instituto de Ciencia de Materiales de Madrid, CSIC
Cantoblanco, E-28049 Madrid (Spain)
Fax: Int. code + (34) 1-372 0623
e-mail: nines@immrx1.icmm.csic.es

 © WILEY-VCH Verlag GmbH, D-69451 Weinheim, 1998 1433-7851/98/3701-0129 $ 17.50+.50/0

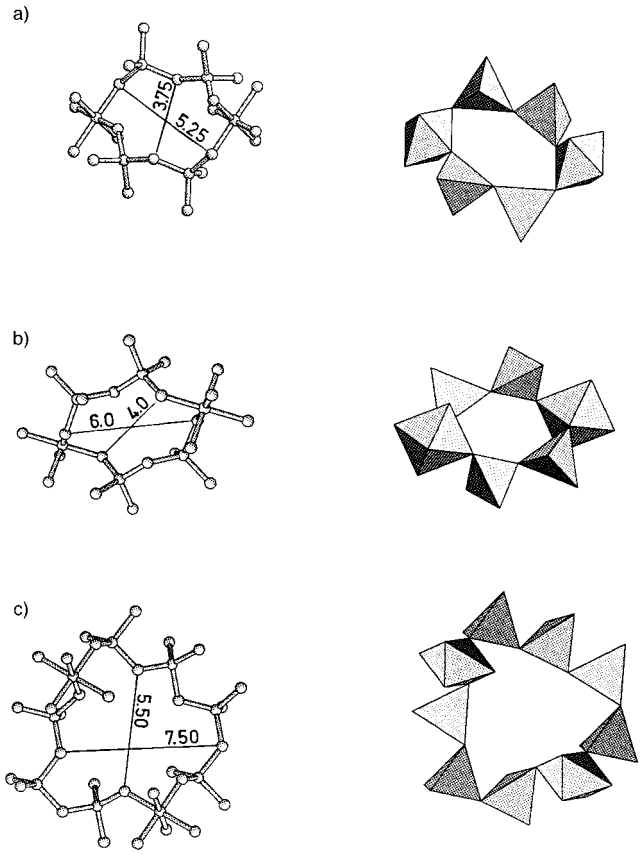


Figure 2. Ball-and-stick and polyhedral representations of the windows corresponding to the three different kinds of channels present in the structure of $(NH_4)_2Ge_7O_{15}$ along [110] (a), [010] (b), and [001] (c). Distances to the centers of atoms are given.

involved. The main channels are those that run in the *c* direction as a consequence of the stacking of the nine-rings. There are smaller hexagonal channels along [010] and [110] with a $2(GeO_4)$-(GeO_6)-$2(GeO_4)$-(GeO_6) sequence. Pore apertures and sizes are also shown in Figure 2.

Two NH_4^+ cations, whose positions are related by a inversion center, are guests in each cage along the main channels (Figure 3). Since every H atom was located in a difference synthesis and their coordinates refined with isotropic thermal parameters, the whole geometry around H bonds could be determined. The NH_4^+ cation is bonded to different oxygen atoms of the framework through the four hydrogen atoms; three of these atoms form bifurcated hydrogen bonds. The ranges of the N–H, N–O, and O–H bond lengths are 0.78(2)–1.05(1) Å, 2.631(5)–3.106(6) Å, and 1.82(1)–2.51(1) Å, respectively.

A comparison of the coordination polyhedra and their connectivities present in the cubic $(NH_4)_3HGe_7O_{16}\cdot n\,H_2O$ (structural type I), the $Ge_9O_{20}Na$ structure (structural type II),[23] and the new monoclinic $(NH_4)_2Ge_7O_{15}$ (structural type III) reveals a number of interesting features. Although the frameworks are always formed by GeO_4 tetrahedra and GeO_6 octahedra, the ratio GeO_4/GeO_6, which is 3/4 for I and 5/4 for II, is 6/1 in III. This composition avoids the formation of the Ge_4O_{16} cluster, which is present in I and II, and brings about the formation of tunnels of different sizes, creating a main

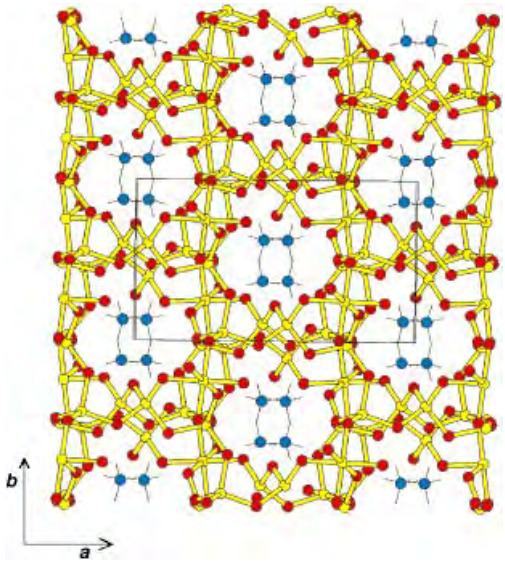


Figure 3. View along [001] of the structure of $(NH_4)_2Ge_7O_{15}$. The NH_4^+ ions are in blue.

channel and thus a preferential direction for ionic conductivity. In other tunnel-containing materials that are good ionic conductors[24] the amplitude of thermal vibration of the ions in the direction of the tunnels is associated with an unhindered motion of those cations and with high ionic conductivity. In this new germanate, although the NH_4^+ cations are involved in hydrogen bonds, the anisotropic thermal parameters of the N atom is especially large in the *c* direction (about twice as large: $U_{11} = 20(4)\times10^{-3}$, $U_{22} = 20(3)\times10^{-3}$, and $U_{33} = 44(4)\times10^{-3}$). Moreover, in the title compound the formal charge of the framework is compensated by two NH_4^+ cations per seven Ge atoms, which decreases the electrostatic interaction between the anion framework structure and the cations. In contrast, for the same number of Ge atoms in I, four cations are needed.

TGA-DTA (TGA = thermogravimetric analysis, DTA = differential thermal analysis) shows a 4% weight loss between 320 and 450°C, which is endothermic. This corresponds to the total decomposition of the $(NH_4)_2Ge_7O_{15}$ present in the sample (70% $(NH_4)_2Ge_7O_{15}$ and 30% GeO_2) by loss of one H_2O and two NH_3 molecules. Powder X-ray diffraction measurements show that the structure is maintained after heating to 312°C and collapses at 450°C to crystalline GeO_2.

As $(NH_4)_2Ge_7O_{15}$ is stable 100°C above the temperature limit for $(NH_4)_3HGe_7O_{16}\cdot n\,H_2O$,[16] we can obtain the monoclinic phase free of the cubic one by heating at 250°C for two hours. This material thus has an advantage for potential applications.

The charged framework of this material contains no Ge–OH group, which is present in analogous materials,[21–22] and therefore, besides potential use as a solid electrolyte, it might be possible to make this material acidic and thus catalytically active. Relative to silica molecular sieves and clathrates, this novel compound seems to have a unique structure: the interaction between GeO_4 and GeO_6 anion framework structure and the cations in the channels is weaker than the one between the tetrahedral anionic network of zeolites and their cations.

 © WILEY-VCH Verlag GmbH, D-69451 Weinheim, 1998 1433-7851/98/3701-0130 $ 17.50+.50/0

Experimental Section

X-ray structure analysis: Crystal dimensions $0.020 \times 0.015 \times 0.015$ mm. Monoclinic, space group $C2/c$, $a = 13.056(2)$, $b = 7.2941(9)$, $c = 15.162(2)$ Å, $\beta = 103.575(2)^\circ$, $V = 1403.6(3)$ Å^3, $Z = 4$, $M_w = 784.2$ g mol^{-1}, $\rho_{calcd} = 3.711$ g cm^{-3}, $F(000) = 1{,}464$. CCD Siemens diffractometer (sealed tube, 2.4 kW), $\lambda(Mo_{K\alpha}) = 0.71073$ Å, $\mu_{K\alpha} = 14.87$ mm^{-1}; of 2611 reflections measured, 1002 were independent ($R_{int} = 0.0547$), $2 < \theta < 23.5^\circ$. Structure determination and refinement software SHELXTL.[25] All the hydrogen atoms were located in the difference Fourier maps. The 114 variables were refined by full-matrix least-squares with anisotropic thermal parameters for all non-hydrogen atoms and isotropic for hydrogen atoms. The final residuals were $R_F = 0.024$ for $F > 4\sigma(F)$ and 0.027 for all data, GOF(F) = 1.167. Further details of crystal structure investigation may be obtained from the Fachinformationszentrum, Karlsruhe, D-76344, Eggenstein-Leopoldshargen (Germany), on quoting the depository number CSD-407222. Patent Registry No. $(NH_4)_2Ge_7O_{15}$ 9700705.

Received: July 4, 1997 [Z10637IE]
German version: *Angew. Chem.* **1998**, *110*, 135 – 138

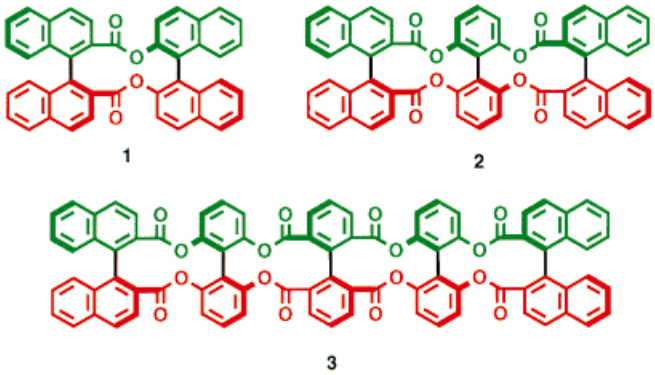
Keywords: germanium · solid-state structures · microporosity · zeolite analogues

[1] R. M. Barrer, *Hydrothermal Chemistry of Zeolites*, Academic Press, London, **1982**.
[2] *Adsorption and Ion Exchange with Synthetic Zeolites, Principle and Practice* (Ed.: W. H. Flank), ACS Symp. Ser. **1980**, 135).
[3] *Zeolites and Related Microporous Materials: State of the Art 1994, Proceedings of the 10th International Zeolite Conference, Vol. 84* (Eds.: J. Weitkamp, H. G. Karge, H. Pfeifer, W. Hölderich), Elsevier, Amsterdam, **1994**.
[4] A. Corma, *Chem. Rev.* **1995**, *95*, 559.
[5] G. D. Stucky, *Prog. Inorg. Chem.* **1992**, *40*.
[6] S. J. Weigel, J. C. Gabriel, E. Gutierrez Puebla, A. Monge Bravo, N. J. Henson, L. M. Bull, A. K. Cheetham, *J. Am. Chem. Soc.* **1996**, *118*, 2427.
[7] S. T. Wilson, B. M. Lok, C. A. Messina, T. R. Cannan, E. M. Flanigen, *J. Am. Chem. Soc.* **1982**, *108*, 1146.
[8] R. H. Jones, J. M. Thomas, R. Xu, Q. Huo, A. K. Cheetham, A. V. Powell, *J. Chem. Soc. Chem. Commun.* **1991**, 1266.
[9] Q. Gao, S. Li, R. Xu, *J. Chem. Soc. Chem. Commun.* **1994**, 1465.
[10] Q. Huo, R. Xu, *J. Chem. Soc. Chem. Commun.* **1992**, 1391.
[11] J. B. Parise, *J. Chem. Soc. Chem. Commun.* **1985**, 606.
[12] M. P. Attfield, R. E. Morris, E.Gutiérrez Puebla, A. Monge Bravo, A. K. Cheetham, *J. Chem. Soc. Chem. Commun.* **1995**, 843.
[13] M. A. Roberts, A. N. Fitch, *J. Phys. Chem. Solids* **1991**, *52*, 1209.
[14] J. Cheng, R. Xu, *J. Chem. Soc. Chem. Commun.* **1991**, 483.
[15] S. Feng, M. Greenblatt, *Chem. Mater.* **1992**, *4*, 462.
[16] S. Feng, M. Tsai, S. P. Szu, M. Greenblatt, *Chem. Mater.* **1992**, *4*, 468.
[17] S. Feng, M. Tsai, M. Greenblatt, *Chem. Mater.* **1992**, *4*, 388.
[18] B. Bialek, V. Gramlich, *Z. Kristallogr.* **1992**, *198*, 67.
[19] M. A. Roberts, A. N. Fitch, A. V. Chadwick, *J. Phys. Chem. Solids* **1995**, *56*, 1353.
[20] M. A. Roberts, A. N. Fitch, *Z. Kristallogr.* **1996**, *211*, 378.
[21] J. Cheng, R. Xu, G. Yang, *J. Chem. Soc. Dalton Trans.* **1991**, 1537.
[22] R. H. Jones, J. Chen, J. M. Thomas, A. George, M. B. Hurthouse, R. Xu, S. Li, Y. Lu, G. Yang, *Chem. Mater.* **1992**, *4*, 808.
[23] N. Ingri, G. Lundgren, *Acta Chem. Scand.* **1963**, *17*, 590.
[24] W. L. Roth, F. Reidinger, S. J. La Placa, *Superionic Conductors*, Plenum, New York, **1976**.
[25] SHELXTL, Siemens Energy & Automation Inc., Analytical Instrumentation, **1996**.

Double-Helical Oligo Esters: Chiral Twist of Two Aromatic Ester Chains

Kyoko Nozaki,* Takakiyo Terakawa, Hidemasa Takaya, and Tamejiro Hiyama

The double-helical structure is often found in nature, and artificial double-helical molecules are also of interest; for instance, in 1991 Lehn and co-workers prepared a double-helical structure by utilizing the coordination of nitrogen atoms of two chains to copper ions.[1] In another example, two chains are bound by hydrogen bonds of an oligopeptide.[2] However, in contrast to these approaches based on self-assembly, covalent bonds have been used less frequently in the synthesis of such molecules. Here we report the preparation of oligo esters **2** and **3**. In these molecules, biphenyl groups are sandwiched between two chiral binaphthyl groups. Through this "chiral twist", the originally achiral biphenyl groups are fixed in the same absolute configuration as the two binaphthyl groups on both ends. As a result, the two oligo ester chains in one molecule (green and red in **1** – **3**) are twisted to form a double-helical structure.[3]

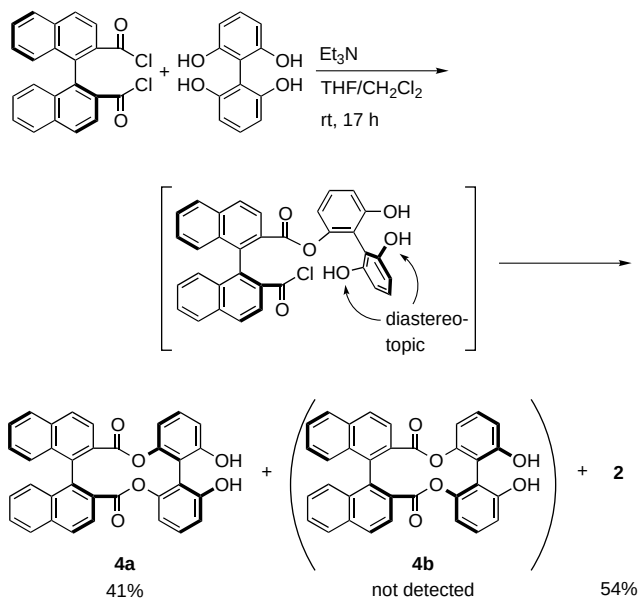


For the synthesis of these compounds (*S*)-1,1′-binaphthyl-2,2′-dicarbonyl dichloride was initially treated with biphenyl-2,2′,6,6′-tetrol (Scheme 1), which gave the 1:1 coupling product **4a** and the 2:1 product **2** in 41% and 54% yield, respectively. It is noteworthy that **4a** was obtained as a single diastereomer although two diastereomers **4a** and **4b** could have formed. Biphenyl-2,2′,6,6′-tetrol itself is an achiral molecule. After the first esterification of the 2-hydroxy group, the two hydroxy groups at the 2′- and 6′-positions are diastereotopic. Thus the second esterification step proceeds exclusively at one of these two hydroxy groups.

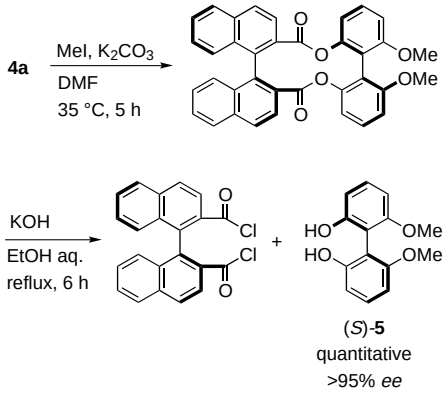
The absolute configuration of the biphenyl group was determined by the following method: The two hydroxy groups of **4a** were protected as methyl ethers, and then the compound was hydrolyzed to give the 2,2′-dimethoxybiphenyl-6,6′-diol (**5**) and 1,1′-binaphthyl-2,2′-dicarboxylic acid (Scheme 2). The

[*] Dr. K. Nozaki, T. Terakawa, Prof. Dr. H. Takaya,[+]
Prof. Dr. T. Hiyama
Department of Material Chemistry
Graduate School of Engineering, Kyoto University
Yoshida, Sakyo-ku, Kyoto, 606-01 (Japan)
Fax: Int. code + (81) 75 761-8846
e-mail: nozaki@npc05.kuic.kyoto-u.ac.jp
[+] Deceased October 4, 1997.

 © WILEY-VCH Verlag GmbH, D-69451 Weinheim, 1998 1433-7851/98/3701-0131 $ 17.50+.50/0



Scheme 1.



Scheme 2.

each other at their 2-positions to form a (*R*)-biphenyl group.[7, 8] In the 1:2 condensation product **2** (Scheme 1), one biphenyl group is sandwiched between the two binaphthyl groups. Only one diastereomer was formed. The absolute configuration of the central biphenyl group is assigned to be *S* on the basis of the above result. An optimized space-filling model of the oligo ester **2** is shown in Figure 1. In this model,

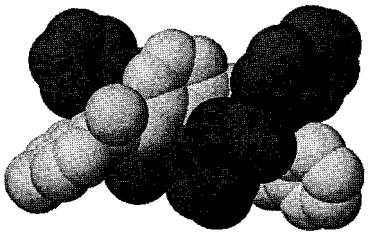
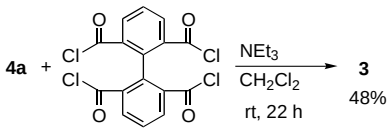


Figure 1. A model of **2** optimized with an MM2 force field (CAChe system). One ester chain, "naphthyl-C(=O)OC$_6$H$_3$OC(=O)C$_6$H$_3$-naphthyl", is depicted in light gray and the other in dark gray. The two chains form a double-helical structure.

two ester chains, whcih are depicted in light gray and dark gray in Figure 1, form the double-helical structure. The two chains are bound to each other by the covalent bond between the two benzene rings of each biaryl group.

The longer biphenyl ester **3** was synthesized from **4a** and biphenyl-2,2′,6,6′-tetracarbonyl tetrachloride (Scheme 3). Again, a single coupling product was obtained. The product



Scheme 3.

enantiomeic excess of **5** was determined to be $>95\,\%$ by HPLC on a chiral column. By comparison of the optical rotation value of **5** to that in the literature,[4] this compound was assigned the absolute configuration *S*. This indicates that the absolute configuration of the biphenyl group is controlled by that of the binaphthyl group. The 1,1′-binaphthyl-2,2′-dicarboxylic acid was recovered without racemization. Thus, the present method provides a novel synthetic route to optically active biphenyl compounds.[5]

The following experiments also suggest that the biphenyl group in such cyclic esters prefers to adopt the same absolute configuration as the binaphthyl group. The condensation of (*S*)-1,1′-binaphthyl-2,2′-diol with (*S*)-1,1′-binaphthyl-2,2′-dicarboxylic acid dichloride gave the cyclic ester **1** as a single product in 92 % yield, while a complex mixture of products was obtained from (*R*)-1,1′-binaphthyl-2,2′-diol and (*S*)-1,1′-binaphthyl-2,2′-dicarbonyl dichloride. In addition, Miyano and co-workers reported the asymmetric synthesis of a biphenyl group.[6] In their work, two benzoic acid derivatives were linked to (*R*)-1,1′-binaphthyl-2,2′-diol through ester bonds, and then the two phenyl groups were connected to was assigned as the aromatic oligo ester **3** with three *S* configured biphenyl groups and two binaphthyl groups.

The specific rotations of esters **1**–**3** $[\alpha]_D$ ($c = 1.00$ g 100 mL^{-1}) are shown in Table 1. The greater the number of biphenyl groups in the molecule, the more the specific rotation increases. This increase in specific rotation can be attributed to the double-helical structures of **1**–**3**. The CD absorption of the biaryl group at around 250–260 nm also increases in the series **1** → **2** → **3**. This is a further indication that all biphenyl groups in **3** are *S* configured. Unlike common

Table 1. Optical rotation and CD-spectroscopic data of the oligo esters **1**–**3**.

Ester	No. of biphenyl groups	$[\alpha]_D^{25}$	CD[c]	
			λ_{max}	ε_{max}
1	0	−553[a]	260	2
2	1	−589[a]	254	−131
3[d]	3	−821[b]	252	−286

[a] $c = 1.00$ in $CHCl_3$. [b] $c = 1.00$ in CH_2Cl_2. [c] 2.05×10^{-5} M in 1,4-dioxane. [d] Because of the low solubility of **3**, other solvents that were clear at <240 nm were not used.

 © WILEY-VCH Verlag GmbH, D-69451 Weinheim, 1998 1433-7851/98/3701-0132 $ 17.50+.50/0

macrocyclic compounds, the conformation of the cyclic oligo esters **2** and **3** is much more restricted because the binaphthyl groups are not allowed to rotate around the 1,1′ axis because of steric repulsion between the 8- and 8′-hydrogen atoms. Thus once the configuration of the biphenyl groups is regulated in **2** and **3**, the conformation of the whole molecule is restricted unequivocally except for the small changes in the torsion angles of the biaryl groups. Accordingly, a double-helical structure similar to that of **2** is suggested for **3**.

Experimental Section

2 and **4a**. A solution of biphenyl-2,2′,6,6′-tetrol (1.10 mmol) in THF[9] was added to a solution of the acid chloride derived from (*S*)-1,1′-binaphthyl-2,2′-dicarboxylic acid[10] (1.00 mmol) in CH_2Cl_2, and the resulting mixture was stirred at 20 °C for 22 h. Aqueous work-up followed by purification by silica-gel column chromatography (CH_2Cl_2/EtOAc, 9/1) gave **4a** (41 % yield) and **2** (54 % yield) as colorless solids. **4a**: Sublimed above 206.0 °C; ^{1}H NMR ($CDCl_3$): $\delta = 7.95-7.89$ (m, 4H), 7.81 (d, 2H, $J = 8.58$ Hz), 7.52 (t, 2H, $J = 6.93$ Hz), 7.30–7.03 (m, 6H), 6.79 (d, 2H, $J = 8.25$ Hz), 6.60 (d, 2H, $J = 8.25$ Hz); ^{13}C NMR ($CDCl_3$): $\delta = 166.76$, 154.16, 149.27, 136.95, 134.39, 133.01, 129.60, 129.49, 128.57, 128.17, 127.71, 127.53, 127.22, 124.56, 115.44, 113.98, 111.32. **2:** M.p. (CH_2Cl_2/hexane) 274.3–274.9 °C; ^{1}H NMR ($CDCl_3$): $\delta = 7.97-7.91$ (m, 8H), 7.81 (d, 4H, $J = 8.58$ Hz), 7.52 (t, 4H, $J = 6.93$ Hz), 7.31–7.24 (m, 4H), 7.05–6.99 (m, 6H), 6.75 (d, 4H, $J = 7.92$); ^{13}C NMR ($CDCl_3$): $\delta = 166.34$, 149.00, 136.35, 134.29, 132.96, 129.58, 128.57, 128.37, 128.18, 127.63, 127.42, 127.26, 124.56, 119.37, 116.17; HR-MS: *m*/*z* found for $[M+H]^+$: 831.1975; calcd.: 831.2017.

3: Biphenyl-2,2′,6,6′-tetracarboxylic acid[11] (0.21 mmol) was converted into the corresponding acid chloride and condensed with **4a** (0.41 mmol) in the presence of triethylamine (21 mmol). Work-up followed by purification by column chromatography (CH_2Cl_2) gave **3** (48 % yield) as fine needles: Sublimed above 470.0 °C. ^{1}H NMR (CD_2Cl_2): $\delta = 8.02-7.78$ (m, 16H), 7.58 (t, 4H, $J = 7.92$ Hz), 7.47 (t, 2H, $J = 8.24$ Hz), 7.32 (t, 4H, $J = 8.24$ Hz), 7.21–7.02 (m, 12H), 6.79 (d, 4H, $J = 8.25$ Hz); ^{13}C NMR (CD_2Cl_2): $\delta =$ 166.54, 165.35, 149.65, 149.14, 137.39, 136.80, 134.77, 133.46, 133.40, 131.75, 129.88, 129.04, 128.77, 128.68, 128.52, 128.21, 127.71, 127.65, 124.63, 120.39, 120.14, 116.33; HR-MS: *m*/*z* found for $[M+H]^+$: 1307.2607; calcd.: 1307.2548.

Received: June 3, 1997 [Z 10506 IE]
German version: *Angew. Chem.* **1998**, *110*, 138–140

Keywords: chirality · configuration determination · helical structures · oligomers

[1] W. Zarges, J. Hall, J.-M. Lehn, C. Bolm, *Helv. Chim. Acta* **1991**, *74*, 1843.
[2] M. Mascal, C. M. Moody, A. I. Morrell, A. M. Z. Slawin, D. J. Williams, *J. Am. Chem. Soc.* **1993**, *115*, 814.
[3] The construction of "single helical" polymers has been intensively studied by Pu et al. by utilizing the chirality of 1,1′-binaphthyl groups: a) L. Ma, Q.-S. Hu, D. Vitharana, C. Wu, C. M. S. Kwan, L. Pu, *Macromolecules* **1997**, *30*, 204; b) W.-S. Huang, Q.-S. Hu, X.-F. Zheng, J. Anderson, L. Pu, *J. Am. Chem. Soc.* **1997**, *119*, 4313; c) L. Ma, Q.-S. Hu, D. Vitharana, C. Wu, C. M. S. Kwan, L. Pu, *Macromolecules* **1997**, *30*, 204.
[4] $[\alpha]_D^{25} = -146$ ($c = 0.89$, $CHCl_3$) for the sample of > 95 % *ee* (determined by HPLC with CHIRALCEL OD). A value of $[\alpha]_D = -144$ ($c = 0.77$, $CHCl_3$) has been reported for (*S*)-**5**. H. Moorlag, A. I. Meyers, *Tetrahedron Lett.* **1993**, *34*, 6993.
[5] Asymmetric synthesis of **5** other than that given in ref. [3] see: a) T. Harada, T. Yoshida, A. Inoue, M. Takeuchi, A. Oku, *Synlett* **1995**, 283; b) G. Deglogu, D. Fabbri, *Tetrahedron: Asymmetry* **1997**, *8*, 759.
[6] S. Miyano, H. Fukushima, S. Handa, H. Ito, H. Hashimoto, *Bull. Chem. Soc. Jpn.* **1988**, *61*, 3249.
[7] A similar Ullmann coupling is used for the synthesis of **1**. S. Miyano, S. Handa, M. Tobita, H. Hashimoto, *Bull. Chem. Soc. Jpn.* **1986**, *59*, 235.
[8] T. Sugimura, H. Yamada, S. Inoue, A. Tai, *Tetrahedron: Asymmetry* **1997**, *8*, 649.
[9] G. Lindsten, O. Wennerström, R. Isaksson, *J. Org. Chem.* **1987**, *52*, 547.
[10] T. Ohta, M. Ito, K. Inagaki, H. Takaya, *Tetrahedron Lett.* **1993**, *34*, 1615.
[11] E. A. Coulson, *J. Chem. Soc.* **1937**, 1298.

From Molecular to One-Dimensional Polychalcogenides: Preparation, Structure, and Reactivity of $NaNbS_6$, the First Ternary Alkali Metal Niobium Polychalcogenide Exhibiting Infinite Anionic Chains**

Wolfgang Bensch,* Christian Näther, and Peter Dürichen

The preparation of multinary transition metal chalcogenides in reactive alkali polychalcogenide melts at temperatures between 250 and 500 °C is a fast-growing area of inorganic solid state chemistry.[1,2] Owing to the relatively low reaction temperatures, compounds containing large Q_x^{2-} ions ($x > 1$) are accessible which cannot be obtained with classical high-temperature syntheses.

Recently we investigated new polychalcogenide compounds of niobium. There are only a few examples of such compounds prepared by the reactive flux method.[3] Systematic variation of the preparation conditions yielded several novel niobium chalcogenides, all containing molecular $[Nb_2Q_{11}]^{4-}$ subunits (Figure 1).[4–7] These units occur as isolated anions, as in $K_4Nb_2S_{11}$,[4] or are connected through terminal sulfur ligands, as in $Rb_6Nb_4S_{22}$ or $Cs_6Nb_4S_{22}$.[5] Incorporation of additional S_3^{2-} fragments, which are present under the preparation conditions, can lead to an expansion of the $[Nb_2Q_{11}]^{4-}$ subunits. In $K_4Nb_2S_{14}$[6] the S_3^{2-} ion acts as a terminal ligand, and in $K_6Nb_4S_{25}$[7] it connects two units to form the novel complex $[Nb_4S_{25}]^{6-}$ ion.

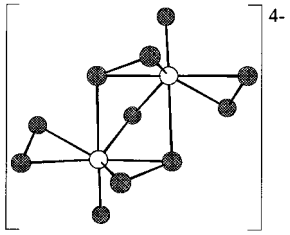


Figure 1. View of the $[Nb_2Q_{11}]^{4-}$ unit (Nb = ○, Q = ⊗).

By extending the synthetic conditions used for preparing the novel niobium compounds to sodium polysulfide melts, we succeeded in synthesizing transparent, orange-red needles.[8] All crystals investigated were grown together, and a twin refinement had to be performed.[9] Here we report on the synthesis, crystal structure, optical behavior, and reactivity of $NaNbS_6$, the first ternary niobium chalcogenide containing one-dimensional anionic polymeric chains.

[*] Prof. Dr. W. Bensch, Dr. C. Näther, Dipl.-Chem. P. Dürichen
Institut für Anorganische Chemie der Universität
Olshausenstrasse 40, D-24098 Kiel (Germany)
Fax: Int. code + (49) 431-880 1520
e-mail: wbensch@ac.uni-kiel.de

[**] This work was supported by the Deutsche Forschungsgemeinschaft (DFG).

 © WILEY-VCH Verlag GmbH, D-69451 Weinheim, 1998 1433-7851/98/3701-0133 $ 17.50+.50/0

The results of the structure determination revealed that a polymeric structure was formed, which is surprisingly not based on the above-mentioned $[Nb_2Q_{11}]^{4-}$ subunits. The structure of $NaNbS_6$ consists of $^1_\infty[NbS_6]^-$ chains running parallel to [001] (Figure 2a and b). These chains are separated by the Na^+ ions. The shortest interchain S–S contacts of 3.396(3) Å are only slightly shorter than the sum of the van der Waals radii (3.6 Å). Within the chains the Nb centers are ninefold coordinated by S atoms. The environment is best described as a pentagonal plane that contains one S_2 unit and three S atoms. Two S_2 units above and below this plane are twisted by about 90° to provide a $Nb(S_2)_3(S)_3$ polyhedron (Figure 2c). These polyhedra are condensed through three S atoms to one-dimensional chains. Every S_2^{2-} unit is coordinated to two Nb centers in a $\mu\eta^1\eta^2$ mode. The description of the title compound as $NaNb(S_2)_3$ leads to an assignment of the formal valences as Na^+, Nb^{5+}, and $(S_2)^{2-}$.

Alternatively, the environment at the Nb centers can be described as distorted trigonal prisms in which the basal planes are formed by the condensation of three S atoms. These prisms are joined through the trigonal faces to give rise to infinite columns parallel to [001]. Every corner of the prisms is occupied by a S atom of a S_2^{2-} ion. The environment of the Nb centers is completed by three S atoms of the S_2 dumbells, which are in turn directed towards the rectangular faces of the distorted prisms (Figure 2d). The Nb–S distances range from 2.501(2) to 2.713(2) Å (av 2.573(2) Å).

Bond-valence calculations according to Equation (1) developed by Pauling give Nb–S bond valences between 0.65 and 0.36, which are smaller than for a Nb–S single bond.

$$S_{ij} = \exp((r_0 - D_{ij})/b) \quad (1)$$

The chains are not strictly linear but slightly bent, as evidenced by the angle between three successive Nb atoms of 169.9°, and are better described as zigzag chains. The distance of 3.589(4) Å between adjacent Nb centers is about 0.7 Å larger than in metallic niobium and too long for Nb–Nb interactions. The S–S distances of 2.056(2) Å within the S_2^{2-} units are in the usual range. The Na centers are ninefold coordinated by S atoms with a mean Na–S distance of 3.090(4) Å. These values correspond to the sum of the ionic radii for Na^+ (1.24 Å) and S^{2-} ions (1.84 Å).[10]

The optical properties of $NaNbS_6$ were investigated with UV/Vis diffuse reflectance measurements.[11,12] The spectra showed a steep absorption edge, from which an optical band gap of about 2.3 eV is estimated (Figure 3). The orange-red color of the material as well as the value for the band gap corroborate the semiconducting nature. These findings are also in agreement with the oxidation states mentioned above.

The thermal behavior was studied by differential thermal analysis/thermogravimetry (DTA/TG) measurements.[13] The title compound is stable up to 400 °C. At 407 °C the onset of an endothermic peak together with a weight loss of 41 % indicates decomposition of the material**.** The weight loss can be attributed to the loss of four equivalents of sulfur.[14] The X-ray powder pattern of a decomposed sample obtained at 600 °C under vacuum could be indexed on the basis of a hexagonal cell of the intercalation compound Na_xNbS_2.[15] This result is also consistent with the atomic absorption spectrometry (AAS) analysis, which yields a composition of $NaNbS_2$ for the decomposed material. We note that the Nb centers in $NaNbS_2$ are in a trigonal-prismatic coordination of six S atoms. However, within the NbS_2 layers these prisms are joined by

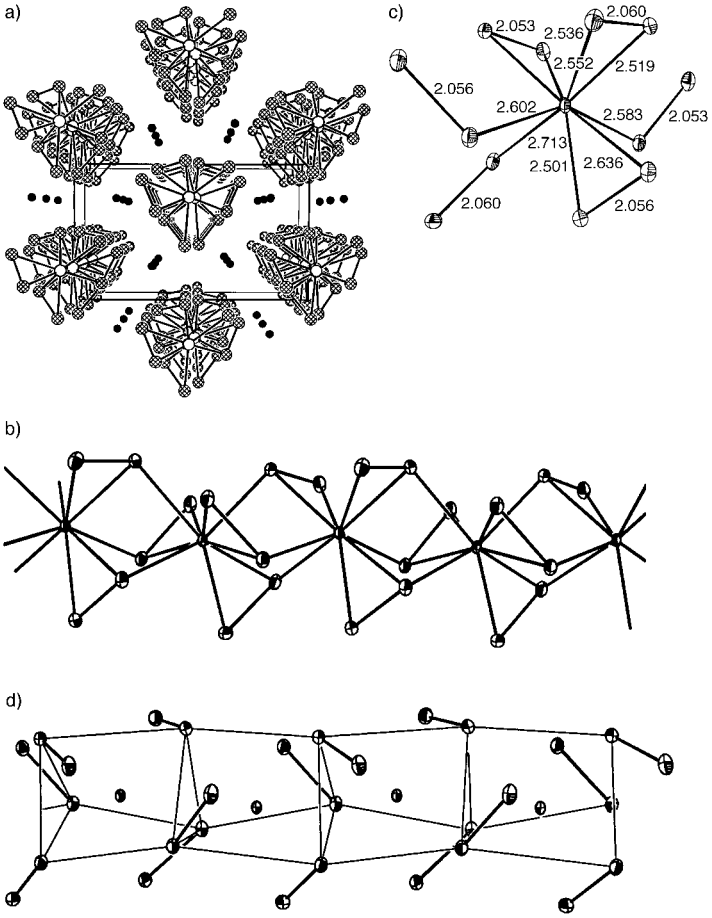


Figure 2. Crystal structure of $NaNbS_6$: a) view along the *c* axis (S = ⊗, Nb = ○, Na = ●); b) connection of the $NaNbS_6$ polyhedra; c) coordination sphere of the Nb centers with selected bond lengths [Å]; d) the NbS_6 trigonal prisms joined through common trigonal faces (thermal ellipsoids are drawn at the 50 % probability level).

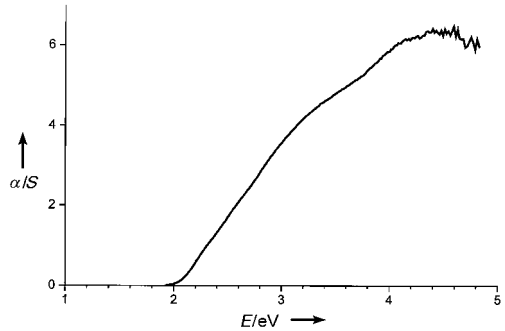


Figure 3. UV/Vis reflectance spectra of $NaNbS_6$ showing an optical band gap of 2.3 eV; α is the absorption coefficient, and S the scattering coefficient.

 © WILEY-VCH Verlag GmbH, D-69451 Weinheim, 1998 1433-7851/98/3701-0134 $ 17.50+.50/0

common edges. Hence, there is no simple relationship between the structures of the title compound and $NaNbS_2$.

The results presented clearly demonstrate the enormous synthetic potential of the reactive flux method. The mild reaction temperatures, at which the polychalcogenide building blocks are retained, together with a large pool of preparative data should enable the inorganic chemist to synthesize new compounds more predictably. This seems to be possible at least for the niobium compounds. In agreement with these assumptions we isolated the first chainlike niobium polyselenide using similar reaction conditions as for the sulfur compounds.[16] Again, its structure is based on $[Nb_2Q_{11}]^{4-}$ units connected through Se_2^{2-} and Se_3^{2-} ligands. It can be expected that many more new and interesting niobium compounds will be accessible by a systematic variation of the reaction conditions.

Received: April 25, 1997
Revised version: September 18, 1997 [Z 10383 IE]
German version: *Angew. Chem.* **1998**, *110*, 140 – 142

Keywords: chain compounds · chalcogens · low-dimensional materials · niobium · reactive melts

[1] S. A. Sunshine, D. Kang, J. A. Ibers, *J. Am. Chem. Soc.* **1987**, *109*, 6202 – 6204.
[2] Reviews: a) M. G. Kanatzidis, A. Sutorik, *Progr. Inorg. Chem.* **1995**, *43*, 151 – 265; b) J. A. Cody, M. F. Mansuetto, S. Chien, J. A. Ibers, *Material Science Forum, Vol. 152 – 153*, Trans Tech Publications, Switzerland, **1994**, 35 – 42.
[3] Selected examples for niobium chalcogenides prepared by the reactive flux method: a) KCu_2NbQ_4 (Q = S, Se): Y.-J. Lu, J. A. Ibers, *J. Solid State Chem.* **1991**, *94*, 381 – 385; b) $K_3Cu_3Nb_2Q_8$ (Q = S, Se): *ibid.* **1992**, *98*, 312 – 317; c) K_2CuNbS_4: W. Bensch, P. Dürichen, C. Weidlich, *Z. Kristallogr.* **1996**, 931; d) $Rb_2AgNbSe_4$: *ibid.* **1996**, 932; e) $K_3Nb_2Se_{11}$: S. Schreiner, L. E. Aleandri, D. Kang, J. A. Ibers, *Inorg. Chem.* **1989**, *28*, 392 – 393.
[4] W. Bensch, P. Dürichen, *Eur. J. Solid State Inorg. Chem.* **1996**, *33*, 527 – 536.
[5] W. Bensch, P. Dürichen, *Z. Anorg. Allg. Chem.* **1996**, *622*, 1963 – 1967.
[6] W. Bensch, P. Dürichen, *Inorg. Chim. Acta* **1997**, *261*, 103 – 107.
[7] W. Bensch, P. Dürichen, *Eur. J. Solid State Inorg. Chem.* **1996**, *33*, 1233 – 1240.
[8] Preparation of $NaNbS_6$: In a dry box Na_2S_3 (2.11 mmol) was mixed with niobium (1.06 mmol) and additional sulfur (4.22 mmol). Na_2S_3 was made by the reaction of stoichiometric amounts of sodium and sulfur in liquid ammonia under an argon atmosphere. The reactants were thoroughly ground together in a mortar and then transferred to a glass ampoule which was subsequently evacuated (10^{-3} mbar) and flame-sealed. The ampoule was heated to 350 °C within 5 h, held at this temperature for 6 d, and cooled to room temperature at a rate of 3 degrees per hour. By washing the resulting melt with DMF and diethyl ether, orange-red, transparent, fiberlike crystals of $NaNbS_6$ were isolated. The homogenity of the product was confirmed by powder X-ray diffraction. All reflections of the powder pattern could be indexed on the basis of $NaNbS_6$. $NaNbS_6$ is stable against air and water.
[9] Crystal structure determination of $NaNbS_6$ ($M_r = 308.26$), orange-red needles, crystal size: $0.05 \times 0.05 \times 1$ mm^3, $a = 7.451(2)$, $b = 12.743(2)$, $c = 7.151(2)$ Å, $\beta = 96.81(1)^\circ$, $V = 674.18$ Å^3 (RT), $\rho_{calcd} = 3.037$ g cm^{-3}, monoclinic, space group *Cc* (no. 15), $Z = 4$, STOE-AED-II four-circle diffractometer, $Mo_{K\alpha}$ radiation, $\mu = 3.58$ mm^{-1}, 1311 measured reflections in the range $3^\circ < 2\theta < 60^\circ$, 1249 independent reflections used for refinement, structure solution with direct methods (SHELXS-86), structure refinement against F^2 (SHELXL-93), 74 parameters, $w = 1/[\sigma^2(F_o^2) + (0.0235 \cdot P)^2 + 2.88P]$, R for 1224 $F_o > 4\sigma(F_o) = 0.0191$, w$R2$ for all 1249 data = 0.0547, GOF = 1.579, residual electron density: 0.56/ – 0.48 e Å^{-3}. Flack parameter: 0.08(7). All crystals investigated were grown together. For one crystal all 86 reflections found by searching the reciprocal space could be separated into two groups. The reflections in each of these two groups were successfully indexed on the basis of the same monoclinic *C*-centered cell. From the transformation matrix between both individuals, it was shown that all reflections *hk*0 as well as *hk*11 were overlapping. Therefore, a twin refinement with SHELXL-93 was performed. This led to a significantly improved model compared to those obtained only with the raw data (R for all reflections with $F_o > 4\sigma(F_o) = 0.0939$; w$R2 = 0.2887$; residual electron density: 11.60/ – 1.72 e Å^{-3}). Further details of the crystal structure investigation may be obtained from the Fachinformationszentrum Karlsruhe, D-76344 Eggenstein-Leopoldshafen (Germany), on quoting the depository number CSD-407 708.
[10] R. D. Shannon, *Acta Crystallogr. Sect. A* **1976**, *32*, 751 – 767.
[11] UV/Vis diffuse reflectance measurements were carried out on a Leica Orthoplan microscope equipped with a Leica MPV-SP, an ICS quartz UV optic, and a xenon lamp as light source. The resolution was 1 nm, and $BaSO_4$ was used as standard for 100 % reflectance. Absorption data were calculated from the reflectance data using the Kubelka – Munk function.[12] The approximate band gap was determined as the intersection point between the energy axis and the line extrapolated from the linear part of the absorption edge in a $(F(R))^2$ plot.
[12] G. Kortüm, *Reflectance spectroscopy*, Springer, New York, **1969**.
[13] TG/DTA measurements were performed on a SETARAM 92-16 device under N_2.
[14] Additional tempering experiments in glass ampoules produced a yellow solid at the colder end of the ampoule, which was identified as sulfur by X-ray fluorescence analysis (RFA).
[15] W. Omloo, F. Jellinek, *J. Less Common Met.* **1970**, *20*, 121 – 129.
[16] P. Dürichen, M. Bolte, W.Bensch, unpublished results.

Spin Polarization and Ferromagnetism in Two-Dimensional Sheetlike Cobalt(II) Polymers: $[Co(L)_2(NCS)_2]$ (L = Pyrimidine or Pyrazine)**

Francesc Lloret,* Giovanni De Munno,* Miguel Julve, Juan Cano, Rafael Ruiz, and Andrea Caneschi

The spin-polarization mechanism[1] describes how an unpaired electron on one atom polarizes the electron cloud on the adjacent atom in the opposite sense. This would result in an alternation of the spin density at atoms in a bridging unit, and consequently the sign of the magnetic exchange parameter J should alternate at each atom in the bridging unit. In this way, oligocarbenes or radicals linked through *m*-phenyl-

[*] Prof. F. Lloret, Prof. M. Julve, Dr. J. Cano, Dr. R. Ruiz
Departament de Química Inorgànica
Facultat de Química de la Universitat de València
Dr. Moliner 50, E-46100 Burjassot, València (Spain)
Fax: Int. code + (34) 6-386 4322
e-mail: lloret@uv.es

Prof. G. De Munno
Dipartimento di Chimica
Università degli Studi della Calabria
87030 Arcavacata di Rende, Cosenza (Italy)

Dr. A. Caneschi
Dipartimento di Chimica
Università degli Studi di Firenze
75/77 Via Maragliano, I-50144 Firenze (Italy)

[**] This work was supported by the Spanish Dirección General de Investigación Científica y Técnica (DGICYT) (project PB94-1002) and the Italian Ministero dell'Università et della Ricerca Scientifica et Tecnologica. R.R. acknowledges the Spanish Ministery of Education and Science for a postdoctoral fellowship.

 © WILEY-VCH Verlag GmbH, D-69451 Weinheim, 1998 1433-7851/98/3701-0135 $ 17.50+.50/0

enes have been designed with a high-spin ground state and prepared.[2] However, since unpaired electrons have a strong tendency to react and to form covalent bonds, stable high-spin organic materials can be expected to be hard to prepare. In contrast, transition metal ions are very stable spin carriers, and in principle, they would be the best candidates for this purpose. Although the spin polarization was shown to be valid for some oxygen- or nitrogen-containing organic systems[3] as well as for some systems comprising paramagnetic transition metal ions and organic radicals,[4] the limits of its application are unclear, especially for coordination compounds containing transition metal ions as the only spin sources. In fact, the first reports on this topic are not conclusive because the magnetic interactions are weak, and a structural determination is lacking.[5]

In an attempt to verify the validity of the spin-polarization mechanism for these systems, we have prepared the sheetlike polymeric compounds $[CoL_2(NCS)_2]_n$ (**1**, L = pyrazine (pyz); **2**, L = pyrimidine (pym); Figure 1) and studied their variable-

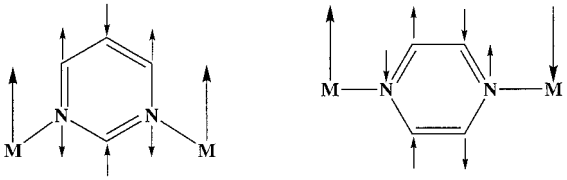


Figure 1. Representation of the spin polarization in pyrimidine (left) and pyrazine ligands (right) bound between two transition metal centers.

temperature magnetic properties. The monomeric complex $[Co(pyd)_4(NCS)_2]$ (**3**, pyd = pyridazine) has been also prepared, and its magnetic properties have been used as a reference for the magnetic behavior of the orbitally degenerate Co^{II} octahedral complex.

The crystal structure of **1**[6] and **2** consists of parallel sheets of square arrays of cobalt atoms bridged by bismonodentate pyz (**1**) or pym (**2**) groups (see Figure 1). A section of the sheetlike structure of **2** is shown in Figure 2. The thiocyanate groups occupy the axial positions. Cobalt is in a compressed octahedral environment with four long Co–N(L) bonds [2.210(1) and 2.261(2) Å for **1** and **2**, respectively] and two short Co–N(NCS) bonds [2.047(2) (**1**) and 2.026(3) Å (**2**)]. The metal atoms in **1** and **2** are on a 2/*m* site; that is, they lie on the inversion center at the intersection of a reflection plane and on a twofold axis perpendicular to it. Within each square of a layer the cobalt atoms lying diagonally opposite each other—Co(1)/Co(1g) and Co(1e)/Co(1f) [for **1** (g) at $x, 1+y, z$, (e) at $-0.5+x, 0.5+y, z$, and (f) at $0.5+x, 0.5+y, z$; for **2** (g) at $1+x, y, z$, (e) at $0.5+x, y, 0.5+z$, and (f) at $0.5+x, y, -0.5+z$]—are generated by a unit cell translation along the *x* and *z* axis for **2** (*x* and *y* axis for **1**). Therefore, the Co(1)···Co(1g) and Co(1e)···Co(1f) distances in **2** are the unit cell values of *a* (9.477(2) Å) and *c* (8.487(2) Å) [*b* (10.383(2) Å and *a* (10.049(2) Å in **1**]. The metal–metal separation through pym in **2** (6.361 Å) is significantly shorter

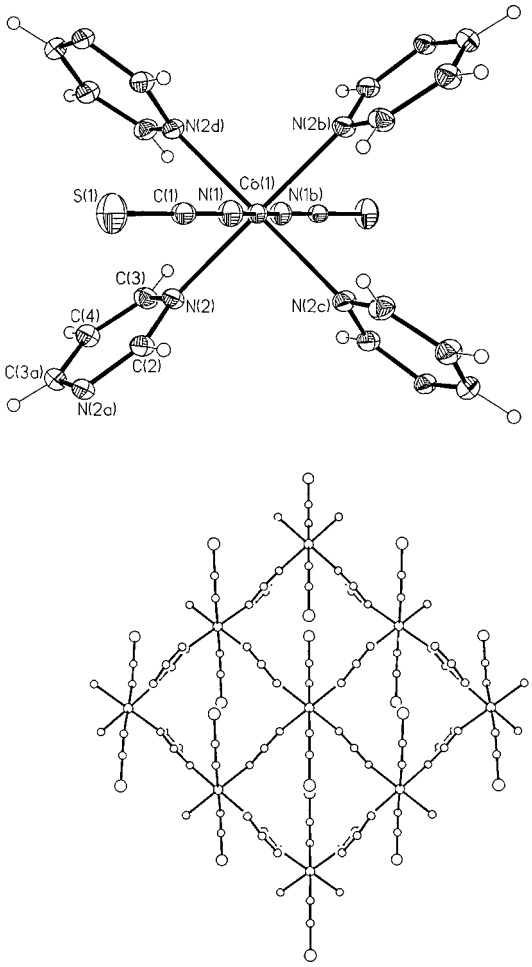


Figure 2. Section of the crystal structure of **2**. Top: Perspective view of the local coordination of the cobalt center (ellipsoids at the 30% probability level). Bottom: View of a sheet along the *xz* plane (hydrogen atoms have been omitted for clarity). Selected bond lengths [Å] and angles [°] with standard deviations in parentheses: Co(1)–N(1) 2.026(3), Co(1)–N(2) 2.261(2); N(1)-Co(1)-N(2) 89.9(1), N(2)-Co(1)-N(1b) 90.1(1), N(2)-Co(1)-N(2c) 91.6(1), N(2)-Co(1)-N(2d) 88.4(1) (generated by symmetry: (b) $-x, -y, -z$; (c) $x, -y, -z$; (d) $-x, y, z$).

than that through pyz in **1** (7.225 Å). Within a square unit of metal atoms in a sheet of **2**, the equatorial planes of opposite Co^{II} ions (constituted by four pyrimidine-nitrogen atoms) are coplanar, whereas the planes of neighboring metal ions form a dihedral angle of 80.7(1)°. The *xz* plane (sheet plane) forms dihedral angles of 40.4(1) and 90.0(1)° with these equatorial planes and with the mean plane of the pym ring, respectively. However, in the case of the related compound **1**, all the equatorial planes of the square unit (ligating atoms are pyrazine-N atoms) are coplanar, and the values of the dihedral angles between the sheet plane (*xy* plane) and the equatorial and mean pyz planes are much reduced [1.5(1) and 65.4(1)°, respectively]. Two adjacent sheets in **2** are separated by 8.487(2) Å (that is, a *b*/2 translation), and they are shifted with respect to the other in such a way that the cobalt atoms of one sheet are located above the centers of the square units of the next sheet. The distance between adjacent layers in **1** is 6.307 Å, and they are related by a translation of *a*/3 along the *x* axis. The shorter interlayer separation in **1** is due to the

 © WILEY-VCH Verlag GmbH, D-69451 Weinheim, 1998 1433-7851/98/3701-0136 $ 17.50+.50/0 *Angew. Chem. Int. Ed.* **1998**, *37*, No. 1/2

greater interpenetration of the axial NCS groups between the sheets that it exhibits. This is impossible in the case of **2**, in which the square units are more puckered and the pym rings are perpendicular to the sheet plane.

The structure of **3** is made up of neutral $[Co(pyd)_4(SCN)_2]$ units (Figure 3). The cobalt is in a compressed octahedral

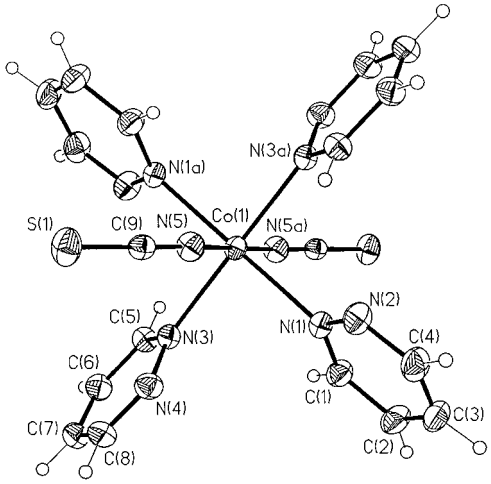


Figure 3. Perspective view of the structure of **3** with thermal ellipsoids at the 30% probability level. Selected bond lengths [Å] and angles [°] with standard deviations in parentheses: Co(1)–N(1) 2.199(2), Co(1)–N(3) 2.208(2), Co(1)–N(5) 2.057(2); N(1)-Co(1)-N(5) 92.9(1), N(1)-Co(1)-N(3) 89.0(1), N(5)-Co(1)-N(3) 90.1(1), N(5)-Co(1)-N(1a) 87.1(1), N(3)-Co(1)-N(1a) 91.0(1), N(3)-Co(1)-N(5a) 89.9(1) (generated by symmetry: (a) $0.5-x, 0.5-y, -z$).

environment with four long Co–N(pyd) bonds [2.199(2)–2.261(2) Å] in the equatorial plane and two short axial Co–(NCS) bonds [2.057(2) Å], as in **1** and **2**. The pyd ligands are planar, and the dihedral angle between the equatorial CoN_4 plane and the pyd ring planes are 50.3(1)° and 120.3(1)°. The shortest intermolecular metal–metal separation is 7.769(3) Å.

The magnetic behavior of **1**–**3** is shown in Figure 4. At room temperature, the $\chi_M T$ value (χ_M is the molar magnetic susceptibility per cobalt atom) is similar for all these

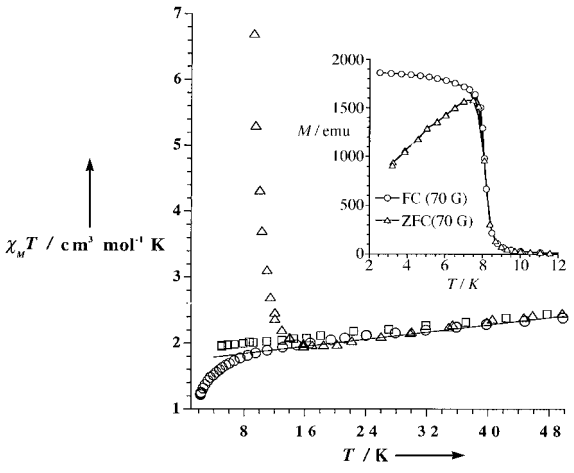


Figure 4. Dependence of the magnetic susceptibility $\chi_M T$ on temperature T for complexes **1** (○), **2** (△), and **3** (□). The inset shows the thermal dependence of the magnetization M in a field of 70 G for **2** after being cooled in an applied field (FC) or in zero field (ZFC).

compounds ($\chi_M T \approx 3.3$ cm³ K mol^{-1}), and it decreases upon cooling. This decrease is related to a spin–orbit coupling effect. In fact, their magnetic behavior can be theoretically modeled, in the temperature range 20–300 K, as monomeric octahedral Co^{II} complexes with λ (spin–orbit coupling parameter) $= -126$ cm^{-1} and κ (orbital reduction parameter) $= 0.75$ (solid line in Figure 4). Complex **3** still follows this theoretical behavior at low temperatures, whereas in the other two cases $\chi_M T$ increases (**2**) or decreases (**1**) rapidly, indicating the presence of ferro- (**2**) and antiferromagnetic (**1**) interactions.

The temperature dependence of the molar magnetization M for **2** was investigated under an applied magnetic field of $H = 70$ G (inset of Figure 4). When the sample was cooled within the field, the field-cooled magnetization showed an abrupt break at 8.2 K. After cooling the sample in zero field and then warming it within the field, the zero-field-cooled magnetization had a maximum just below 8.2 K. All these features are characteristic of a magnetically ordered state below 8.2 K. The ordering temperature T_c was also confirmed by the measurement of both the in-phase (χ') and out-of-phase (χ'') components of the *ac* magnetic susceptibility. The magnetic hysteresis loop for **2** measured at 2.3 K was characteristic of a soft magnet with a small coercive field of 120 G and a remnant magnetization of $0.25\ N\beta$.

The crystal structures of **1** and **2** are thus two important examples of how pyz and pym diazine ligands can spontaneously organize metal ions into a two-dimensional structure and also control the sign of the magnetic interaction in full agreement with the spin-polarization mechanism.

Experimental Section

Synthesis of **1** and **2**: These polymers were prepared in methanol (50 mL) by reaction stoichiometric amounts of $Co(NCS)_2$ and the appropriate diazine (2 mmol). Polymer **1** separates immediately as a polycrystalline orange powder, whereas pink octahedral single crystals of **2** were formed after a few days at room temperature. Prismatic single crystals of **1** were grown by the slow diffusion technique in an H-shaped tube.

Synthesis of **3**: Octahedral orange single crystals of **3** were obtained by slow evaporation (room temperature) of solutions of $Co(NCS)_2$ (1 mmol) and pyd (6 mmol) in methanol (50 mL).

Satisfactory elemental analysis (C,H,N) were obtained for **1**–**3**. Yield about 60%. Crystal structure analyses of **2** and **3**: Siemens R3m/V automatic diffractometer, $Mo_{K\alpha}$, $\lambda = 0.71073$ Å, graphite monochromator, 295 K; data collection, solution, and refinement: $\omega - 2\theta$ scan, standard Patterson methods with subsequent Fourier recycling, SHELXTL-PLUS.[7] **2** ($C_{10}H_8CoN_6S_2$): orthorhombic, space group *Cmca*, $a = 9.477(2)$, $b = 16.284(2)$, $c = 8.487(2)$ Å, $V = 1309.7(4)$ Å^3, $Z = 4$, $\rho_{calcd} = 1.700$ g cm^{-3}, $3 < 2\theta < 55°$, crystal size $0.38 \times 0.21 \times 0.10$ mm; of 811 unique reflections, 661 were assumed observed with $I > 3\sigma(I)$; refinement of 51 variables with anisotropic thermal parameters for all non-hydrogen atoms gave $R = 0.028$, $R_w = 0.031$ and $S = 1.22$. **3** ($C_{18}H_{16}CoN_{10}S_2$): monoclinic, space group *C2c*, $a = 12.341(5)$, $b = 12.950(5)$, $c = 14.322(5)$ Å, $\beta = 109.21(3)°$, $V = 2161(1)$ Å^3, $Z = 4$, $\rho_{calcd} = 1.523$ g cm^{-3}, $3 < 2\theta < 54°$, crystal size $0.42 \times 0.37 \times 0.32$ mm; of 2380 unique reflections, 1924 were assumed observed with $I > 3\sigma(I)$; refinement of 142 variables with anisotropic thermal parameters for all non-hydrogen atoms gave $R = 0.031$, $R_w = 0.038$ and $S = 1.23$. Crystallographic data (excluding structure factors) for the structures reported in this paper have been deposited with the Cambridge Crystallographic Data centre as supplementary publication no. CCDC-100411. Copies of the data can be obtained free of charge on application to

CCDC, 12 Union Road, Cambridge CB21EZ, UK (fax: int. code + (44) 1223-336033; e-mail: deposit@chemcrys.cam.ac.uk).

Received: June 9, 1997
Supplemented version: September 26, 1997 [Z10521IE]
German version: *Angew. Chem.* **1998**, *110*, 143 – 145

Keywords: cobalt · layered compounds · magnetic properties · N ligands · spin polarization

[1] a) H. M. McConnell, *J. Chem. Phys.* **1963**, *39*, 1910; b) N. Mataga, *Theor. Chim. Acta* **1968**, *10*, 372; c) O. Kahn, *Molecular Magnetism*, VCH, New York, **1993**.
[2] H. Iwamura, *Adv. Phys. Org. Chem*. **1990**, *26*, 179.
[3] a) F. Kanno, K. Inoue, N. Koga, H. Iwamura, *J. Phys. Chem*. **1993**, *97*, 13267; b) M. Kitano, Y. Ishimaru, K. Inoue, N. Koga, H. Iwamura, *Inorg. Chem*. **1994**, *33*, 6012.
[4] N. Koga, H. Ishimanu, H: Iwamura, *Angew. Chem.* **1996**, *108*, 815; *Angew. Chem. Int. Ed. Engl.* **1996**, *35*, 755, and references therein.
[5] a) H. Oshio, *J. Chem. Soc. Chem. Commun*. **1991**, 240; b) A. M. W. Cargill Thompson, D. Gatteschi, J. A. McCleverty, J. A. Navas, E. Rentschler, M. D. Ward, *Inorg. Chem*. **1996**, *35*, 2701.
[6] During the preparation of this manuscript the structure of **1** was published (J. Lu, T. Paliwala, S. C. Lim, C. Yu, T. Niu, A. J. Jacobson, *Inorg. Chem.* **1997**, *36*, 923). Because our structural data of **1** fully agree with that reported, we have quoted only a few pertinent structural data of **1** for comparison with that of **2**.
[7] SHELXTL-PLUS Version 4.21/V: Siemens Analytical X-Ray Instruments Inc., Madison, WI (USA), **1990**.

Synthetic *Shigella* Vaccines: A Carbohydrate – Protein Conjugate with Totally Synthetic Hexadecasaccharide Haptens**

Vince Pozsgay*

Carbohydrate-based antibacterial vaccines are among the most successful carbohydrate pharmaceuticals.[1] The basis of using carbohydrates as vaccine components is that the capsular polysaccharides (CPs) and the O-specific polysaccharides (O-SPs) on the surface of pathogenic bacteria are both essential virulence factors and protective antigens, and that serum antibodies raised against these polysaccharides may provide immunity by killing the inoculum.[1] This principle led to the development of CP vaccines against Pneumococci and other Gram-positive bacteria. The inability of polysaccharides to elicit protective levels of anti-carbohydrate antibodies in infants could be overcome by their covalent attachment to proteins that conferred T-cell dependent properties.[2] This principle led to the construction of vaccines against *Haemophilus influenzae* b (Hib),[3] and in countries where these vaccines are routinely used, meningitis and other diseases caused by Hib have been virtually eliminated.[4] Extension of the conjugate technology to the O-SPs of Gram-negative bacteria provided a new generation of glycoconjugate vaccines that are undergoing various phases of clinical trials.[5]

While the immunogenicity and the efficacy of the glycoconjugate vaccines are established, their structural requirements are not well defined. Further improvement of the immunologic properties of conjugate vaccines requires the knowledge of the optimal size of the saccharide, the preferred method of its attachment to the protein, and the saccharide/protein ratio necessary for optimal immunogenicity. Success in this area will depend on the availability of well-defined saccharides that are representative of the native polysaccharides.[6]

Here we describe our approach to a hexadecasaccharide fragment[7] of the O-SP (**A**) of *Shigella dysenteriae* type 1,[8] a human pathogen that is a major causative organism of endemic and epidemic dysentery worldwide.[9]

→3)-α-L-Rha*p*-(1→2)-α-D-Gal*p*-(1→3)-α-D-Glc*p*NAc-(1→3)-α-L-Rha*p*-(1→
A

The target saccharide is equipped with a spacer as the aglycon portion. A heterobifunctional linker unit was appended to this end of the saccharide assembly for covalent attachment to human serum albumin (HSA) as a model carrier protein. The single-point attachment leaves the entire saccharide chain available for interaction with B cell receptors. The average number of saccharide chains attached to HSA is defined by matrix-assisted laser desorption ionization time of flight (MALDI-TOF) mass spectrometry.

The overall strategy to the target **21** (see below) called for the assembly of a tetrasaccharide repeating unit (**12**, **14,** see Scheme 1) in a form that may be used in an iterative fashion for blockwise construction of higher oligosaccharides.[10] In this endeavor we relied on our previous experience in synthesizing related compounds.[7, 11] Of particular importance was the realization that for the iterative building of a saccharide of this size, the tetrasaccharide frame along the polysaccharide chain should correspond to that shown by formula **A**. We also found that

1) the tetrasaccharide block can be most conveniently assembled in a stepwise fashion,
2) the Gal and the Rha synthons should be installed in a prefabricated form which allows the attachment of the subsequent residue after only one deprotecting step, and that
3) the use of a prefabricated synthon for the GlcN unit has no advantage on the overall yield.

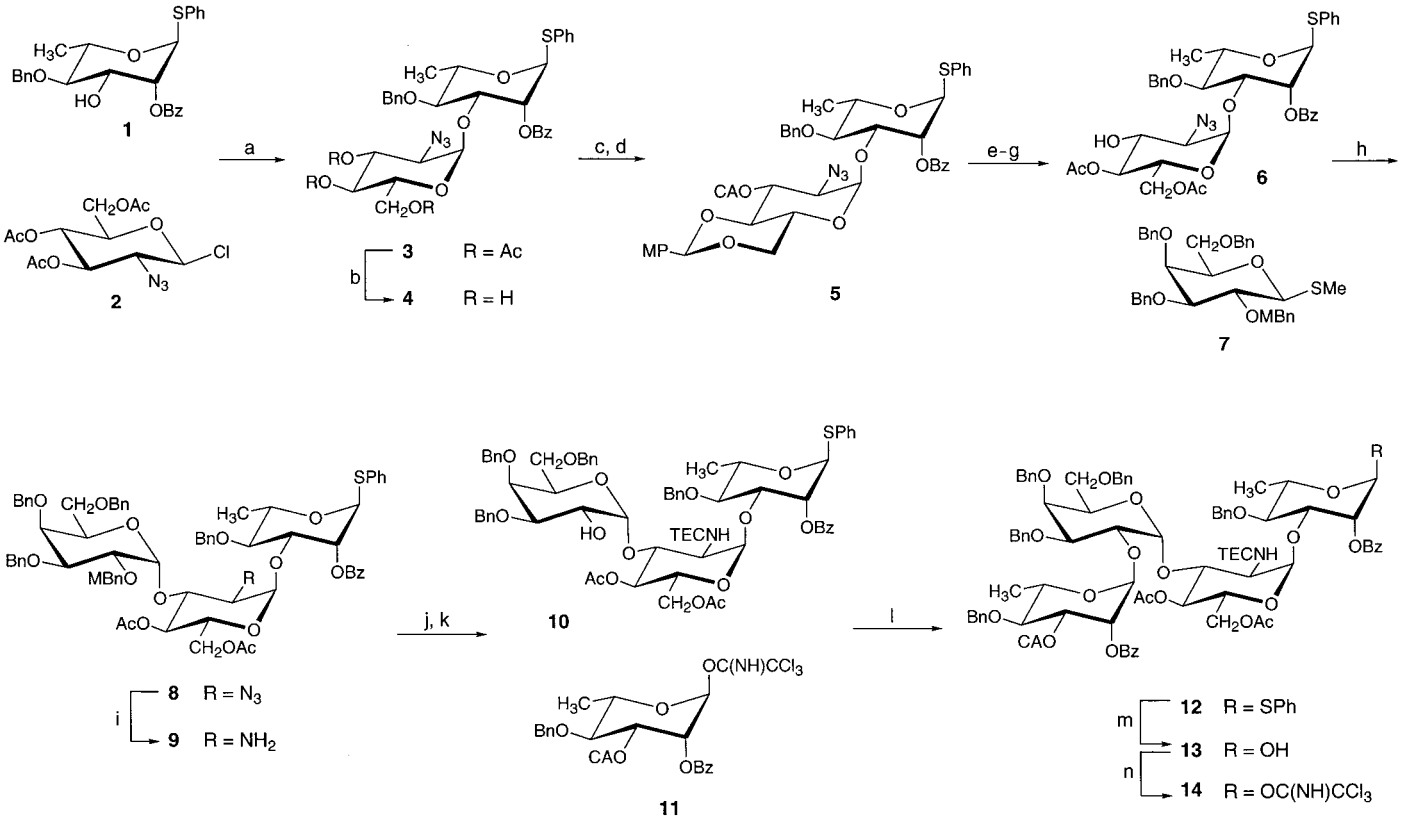
Furthermore, we concluded that intermediates with multiple azide groups should be avoided because of the difficulties that may arise in their conversion to acetamido functions.[12]

The principles established in previous studies led to the selection of four monosaccharide building blocks **1**, **2**, **7**, and **11** that were prepared as reported for related synthons.[7, 11, 13] The assembly of the tetrasaccharide **12** started with the condensation of the rhamnose derivative **1** with the chloride **2** (Scheme 1, Table 1). The nonparticipating azido group of **2**

[*] Dr. V. Pozsgay
Laboratory of Developmental and Molecular Immunity
National Institute of Child Health and Human Development
National Institutes of Health
6 Center Drive MSC 2720, Bethesda, MD 20892-2720 (USA)
Fax: Int. code + (1) 301 402-9108
e-mail: vipo@helix.nih.gov

[**] The author thanks Dr. John B. Robbins and Dr. Rachel Schneerson for many stimulating discussions. Dr. Lewis Pannell and Noel Whittaker are thanked for recording the mass spectra.

 © WILEY-VCH Verlag GmbH, D-69451 Weinheim, 1998 1433-7851/98/3701-0138 $ 17.50+.50/0



Scheme 1. a) **1** (1.6 equiv) CF_3SO_2OAg (1.5 equiv), 2,6-di-*tert*-butyl-4-methylpyridine (0.9 equiv), CH_2Cl_2, 0 °C, 2 h, 64 %; b) $HBF_4 \cdot Et_2O$, MeOH, 23 °C, 72 h, 79 %; c) 4-methoxybenzaldehyde dimethylacetal (5.4 equiv), 10-camphorsulfonic acid (CSA) (cat), CH_2Cl_2, 23 °C, 20 min; d) $(ClCH_2CO)_2O$ (2.2 equiv), C_5H_5N, 0 °C, 10 min, 92 % for two steps; e) $HBF_4 \cdot Et_2O$, MeOH/CH_2Cl_2, 0 → 23 °C, 30 min; f) Ac_2O, C_5H_5N, 4-dimethylaminopyridine (cat), 0 → 23 °C, 1 h; g) thiourea (5.5 equiv), DMF/C_5H_5N, 23 °C, 24 h, 71 % for three steps; h) **7** (1.4 equiv), CF_3SO_2OMe (1.7 equiv), 2,6-di-*tert*-butyl-4-methylpyridine (2.9 equiv), Et_2O, 23 °C, 66 h; i) PPh_3 (2.2 equiv), CH_2Cl_2, 35 – 40 °C, 48 h, then H_2O, 35 – 40 °C, 24 h, 58 % for three steps; j) $CCl_3CH_2OC(O)Cl$ (5.8 equiv), $NaHCO_3$, acetone/H_2O, 0 °C, 3 min; k) 2,3-dichloro-5,6-dicyano-1,4-benzoquinone (2.0 equiv), CH_2Cl_2/H_2O, 23 °C, 3 h, 82 % for two steps; l) **11** (3.5 equiv), $BF_3 \cdot Et_2O$ (0.33 equiv), CH_2Cl_2, 0 °C, 2 h, 89 %; m) $Hg(OCOCF_3)_2$ (2.0 equiv), CH_2Cl_2/H_2O, 30 min, 93 %; n) CCl_3CN (9.7 equiv), DBU (0.5 equiv), CH_2Cl_2, 23 °C, 1 h, 85 %. Bn = benzyl, Bz = benzoyl, CA = monochloroacetyl, MBn = 4-methoxybenzyl, MP = 4-methoxyphenyl.

assured sufficient stereocontrol to provide the disaccharide **3** in an acceptable yield. Treatment[11c] of **3** with HBF_4 chemoselectively removed the acetyl groups (→**4**), while the benzoate at O-2 of the rhamnose moiety survived this treatment. Next, the triol **4** was transformed to the diacetate **6**. First the 4-OH and 6-OH groups of the GlcN unit were temporarily protected to allow a monochloroacetyl group to be installed at O-3 of this residue (→**5**). Subsequent mild acid hydrolysis followed by O-acetylation and selective removal of the chloroacetyl group afforded **6** (71 % overall yield from **5**). The Gal-GlcN-Rha trisaccharide was prepared by selective activation of the methylthio galactoside[11c, d] **7** with MeOTf[14] (Tf = F_3CSO_2) in the presence of the phenylthio glycoside **6** to provide **8** in a highly stereoselective reaction. The latter was converted to the amino derivative **9** by the Staudinger reaction using PPh_3 and subsequent hydrolysis providing a 58 % overall yield for three steps. Next, the free amino group in **9** was protected with a 2,2,2-trichloroethoxycarbonyl (TEC) group[15] followed by oxidative removal[16] of the 4-methoxybenzyl group to afford the trisaccharide **10** in 82 % overall yield for two steps. The synthesis of the fully protected tetrasaccharide repeating unit was completed by reaction of **10** with the rhamnose donor **11** under $BF_3 \cdot Et_2O$ activation to afford **12** in 89 % yield.

Experience gained with a tetrasaccharide donor similar to **12** having an anomeric phenylthio group as the leaving group indicated that while such a compound can be successfully coupled with a reactive primary alcohol under I_2/TfOH activation,[17] the method is unsatisfactory for the planned iterative chain elongation. More favorable observations were arrived at with the imidate method.[18] Therefore, the phenylthio glycoside **12** was hydrolyzed with $Hg(OCOCF_3)_2$[19] to afford the hemiacetal **13** as a mixture of the α and β anomers in 93 % yield, which was converted to the imidate **14** as the α anomer, by using CCl_3CN and a catalytic amount of 1,8-diazabicyclo-[5.4.0]undec-7-ene (DBU)[18b] in 85 % yield.

As the first step in the iterative condensation sequence, the tetrasaccharide donor **14** was treated with an excess of the aglycon moiety **15** under Schmidt conditions[18] to provide the tetrasaccharide glycoside **16** in 68 % yield (Scheme 2, Table 1). The subsequent step involved the removal of the chloroacetyl group under essentially neutral conditions to afford the acceptor **17** in 96 % yield for the subsequent iterations. Three repetitive cycles involving glycosylation with the tetrasaccharide donor **14** and dechloroacetylation gave the desired target compound **19** in a protected form. Sequential deblocking that involved replacement of the TEC groups by acetyl groups (Cd/AcOH, then Ac_2O),

 © WILEY-VCH Verlag GmbH, D-69451 Weinheim, 1998 1433-7851/98/3701-0139 $ 17.50+.50/0

Table 1. Selected ^{1}H (300 MHz) and ^{13}C NMR data (75 MHz) of **1**, **3**–**6**, **9**–**14**, **16**–**19** (in $CDCl_3$), and **21** (in D_2O).

1: ^{1}H NMR: $\delta = 5.60$ (d, 1H, $J = 3.4$ Hz), 5.54 (d, 1H, $J = 1.7$ Hz), 4.88, 4.75 (2d, 2H, $J \approx 11$ Hz), 4.29 (dq, 1H), 4.20 (ddd, 1H), 3.56 (t, 1H, $J = 9.4$ Hz), 1.40 (d, 3H, $J = 6.2$ Hz); ^{13}C NMR: $\delta = 85.8$, 81.6, 75.1, 74.8, 70.9, 68.7, 18.0

3: ^{1}H NMR: $\delta = 5.88$ (dd, 1H), 5.57 (d, 1H, $J = 1.6$ Hz), 5.44 (dd, 1H, $J = 10.5$, $J = 9.3$ Hz), 5.36 (d, 1H, $J = 3.6$ Hz), 5.00 (dd, 1H, $J = 9.6$), 4.93, 4.81 (2d, 2H), 4.37 (dq, 1H), 3.72 (t, 1H, $J = 9.6$), 3.31 (dd, 1H), 2.10, 2.02, 1.89 (3s, 9H), 1.45 (d, 1H); ^{13}C NMR: $\delta = 93.1$, 86.1, 79.6, 75.9, 70.1, 69.3, 68.9, 68.0, 67.5, 61.6, 60.5, 20.7, 20.6, 20.5, 17.9

4: ^{1}H NMR: $\delta = 5.84$ (d, 1H, $J = 3.1$ Hz), 5.53 (d, 1H, $J = 1.6$ Hz), 5.20 (d, 1H, $J = 3.8$ Hz), 4.81, 4.62 (2d, 2H, $J \approx 11$ Hz), 4.30 (dq, 1H), 4.20 (dd, 1H), 3.12 (dd, 1H, $J = 10.3$ Hz), 1.32 (d, 1H, $J = 6.2$ Hz); ^{13}C NMR: $\delta =$ 93.7, 85.8, 79.5, 75.8, 73.2, 71.3 (2C), 69.9, 69.3, 69.0, 62.2, 61.0, 17.8

5: ^{1}H NMR: $\delta = 5.90$ (d, 1H, $J = 3.2$ Hz), 5.63 (t, 1H, $J = 10.0$ Hz), 5.56 (d, 1H, J = 1.6 Hz), 5.43 (s, 1H), 5.38 (d, 1H, $J = 3.6$ Hz), 4.97, 4.70 (2d, 2H, $J \approx 11$ Hz), 4.37 (dq, 1H), 3.22 (dd, 1H, $J = 10.3$ Hz), 1.30 (d, 1H, $J =$ 6.2 Hz); ^{13}C NMR: $\delta = 101.6$, 93.9, 85.9, 79.8, 78.7, 76.6, 73.0, 70.6, 69.3, 68.8, 68.4, 62.9, 61.0, 55.3, 40.5, 17.8

6: ^{1}H NMR: $\delta = 5.87$ (dd, 1H), 5.56 (d, 1H, $J = 1.6$ Hz), 5.29 (d, 1H, $J =$ 3.9 Hz), 4.84 (dd, 1H, $J = 9.3$ Hz), 4.83, 4.75 (2d, 2H), 4.35 (dq, 1H), 4.26 (dd, 1H, $J = 3.2$, 9.5 Hz), 4.18–3.93 (m, 4H), 3.69 (t, 1H), 3.24 (dd, 1H, $J =$ 10.2 Hz), 2.11, 1.99 (2s, 6H), 1.41 (d, 1H, $J = 6.2$ Hz); ^{13}C NMR: $\delta = 93.0$, 86.0, 79.7, 75.5, 73.0, 70.8, 70.2, 69.2, 69.0, 67.5, 63.0, 61.7, 20.8, 20.7, 17.9

9: ^{1}H NMR: $\delta = 5.83$ (dd, 1H), 5.55 (d, 1H, $J = 1.4$ Hz), 5.13 (d, 1H, $J =$ 3.7 Hz), 5.06 (dd, 1H, $J = 9.1$, 9.4 Hz), 4.88 (2H), 4.75, 4.70, 4.65, 4.58, 4.53, 4.48 (7d, 8H), 3.72 (s, 3H), 2.93 (dd, 1H, $J = 9.5$ Hz), 2.10, 1.74 (2s, 6H), 1.44 (d, 1H, $J = 6.2$ Hz); ^{13}C NMR: $\delta = 99.2$, 95.5, 86.1, 83.0, 79.8, 78.7, 76.3, 75.7, 75.3, 74.6, 73.3 (3C), 72.8, 70.3, 69.8, 69.2, 68.9, 68.8, 67.7, 62.0, 55.5, 55.2, 20.8, 18.0

10: ^{1}H NMR: $\delta = 6.05$ (m, 1H), 5.80 (dd, 1H, $J = 3.2$ Hz), 5.46 (d, 1H, $J =$ 1.6 Hz), 5.30 (d, 1H, $J = 3.2$ Hz), 5.11 (dd, 1H, $J \approx 9.2$ Hz), 4.34 (dq, 1H), 2.92 (dd, 1H, $J = 9.8$ Hz), 2.11, 1.92 (2s, 6H), 1.43 (d, 1H, $J = 6.1$ Hz); ^{13}C NMR: $\delta = 99.4$, 95.8, 92.9, 86.2, 79.8, 79.5, 75.4, 74.2, 73.9, 73.5, 73.2, 73.1, 73.0, 72.4, 70.6, 69.8, 69.4, 69.3, 68.9, 68.1, 61.6, 54.2, 20.8, 20.7, 17.9

11: ^{1}H NMR: $\delta = 6.32$ (d, 1H, $J = 1.4$ Hz), 5.72 (dd, 1H), 5.52 (dd, 1H, $J =$ 3.1, 9.7 Hz), 4.74, 4.68 (2d, 2H, $J \approx 11$ Hz), 4.13 (dq, 1H), 3.94, 3.85 (2d, 2H, $J \approx 15$ Hz), 3.73 (t, 1H), 1.45 (d, 3H); ^{13}C NMR: $\delta = 94.8$, 77.8, 75.5, 73.6, 70.7, 68.7, 40.6, 18.0

12: ^{13}C NMR: $\delta = 170.8$, 168.9, 165.8, 165.2, 165.0, 153.6, 98.1, 97.4, 95.9, 92.2, 86.1, 79.8, 79.6, 78.5, 75.5, 74.9, 74.1, 73.7, 73.5, 73.3, 72.9, 72.5, 72.3, 71.6, 71.3, 71.0, 70.3, 70.2, 69.4, 69.3, 68.0, 67.9, 62.0, 53.8, 40.6, 20.8, 17.9

13: ^{1}H NMR: $\delta = 5.94$ (d, 1H, $J \approx 10$ Hz), 5.62, 5.58 (2dd, 2H), 5.47 (dd, 1H, $J = 3.2$ Hz, $J = 9.6$ Hz), 5.42 (br. s, 1H), 5.28, 5.13 (2br. d, 2H), 5.24 (t, 1H), 2.06, 1.82 (2s, 6H), 1.41, 1.27 (2d, 2H, $J \approx 6.3$ Hz)

14: ^{1}H NMR: $\delta = 6.26$ (d, 1H, $J =$ 2.0 Hz), 5.99 (d, 1H, $J \approx 9.9$ Hz), 5.74, 5.63 (2dd, 2H), 5.50 (dd, 1H, $J = 3.3$, 9.7 Hz), 5.43 (d, 1H, $J = 1.5$ Hz), 5.32 (t, 1H, $J \approx 9$ Hz), 5.29, 5.14 (2d, 2H, $J \approx 3.5$ Hz), 2.06, 1.82 (2s, 6H), 1.41, 1.27 (2d, 2H, $J \approx 6.3$ Hz)

16: ^{1}H NMR: $\delta = 5.90$ (d, 1H, $J \approx 9$ Hz), 5.62 (dd, 1H, $J = 1.8$, 3.3 Hz), 5.52 (dd, 1H), 5.48 (dd, 1H, $J = 9.6$ Hz), 5.41 (d, 1H), 5.29 (t, 1H, $J \approx 9$ Hz), 5.23, 5.12 (2d, 2H, $J \approx 3.5$ Hz), 4.99, 4.75, 4.70, 4.62, 4.55, 4.49 (6d, 6H), 4.77 (br. s, 1H), 2.32 (t, 2H), 2.06, 1.81 (2s, 6H), 1.36, 1.26 (2d, 6H); ^{13}C NMR: $\delta = 174.0$, 170.7, 168.7, 165.7, 165.2, 153.6, 98.1, 97.5, 97.4, 95.8, 92.5, 79.8, 79.6, 78.5, 75.4, 74.81, 74.0, 73.7, 73.5, 73.2, 72.9, 72.4, 72.2, 71.9, 71.4, 70.7, 70.3, 69.9, 69.3, 68.0, 67.9, 67.8, 67.6, 61.6, 54.0, 51.5, 40.5, 33.8, 28.9, 25.5, 24.5, 20.7, 20.6, 17.9, 17.8

17: ^{1}H NMR: $\delta = 5.89$ (d, 1H, $J \approx 9$ Hz), 3.66 (s, 3H), 2.31 (t, 2H), 2.05, 1.82 (2s, 6H), 1.36, 1.29 (2d, 6H); ^{13}C NMR: $\delta = 97.94$, 97.86, 97.6, 95.8, 92.5, 81.2, 79.8 (2C), 75.5, 75.1, 74.1, 73.7, 73.3, 73.0, 72.9, 72.6, 72.1, 71.8, 70.9, 70.3, 70.1, 70.0, 69.4, 68.1, 67.9 (3C), 67.7, 61.6, 54.0, 51.5, 33.9, 29.0, 25.6, 24.6, 20.9, 20.8, 18.1, 18.0

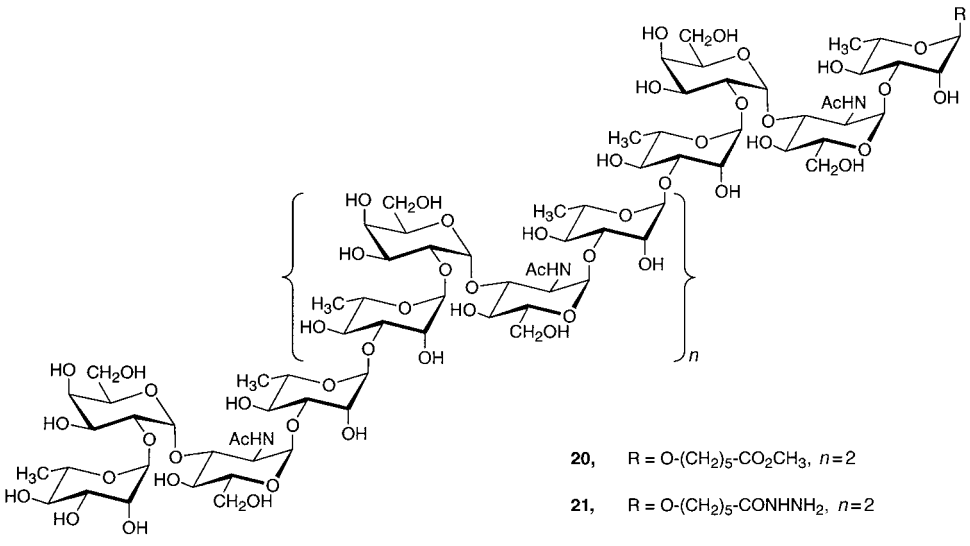
18: ^{13}C NMR: $\delta = 170.7$, 170.5 (2C), 170.43, 170.40, 169.83, 169.80, 169.6, 169.4, 168.87, 168.83 (2C), 165.8, 165.5, 165.4, 165.3, 165.2, 165.1, 164.81, 164.77, 99.5, 99.3 (3C), 98.1, 98.0 (5C), 97.4, 96.1, 94.32, 94.27, 93.9, 61.0, 60.8, 60.7 (2C), 51.6, 51.3, 51.1 (2C), 40.4, 33.8, 28.9, 25.5, 24.5, 23.1, 22.8 (2C), 22.6, 20.92, 20.86 (3C), 20.7, 20.4 (3C)

19: ^{1}H NMR: $\delta = 5.77$, 5.75 (2H), 5.74 (3d, 4H, $J \approx 9$ Hz), 2.32 (t, 2H, $J \approx$ 7.5 Hz), 1.98, 1.84, 1.81, 1.79, 1.72 (9H), 1.71 (6H), 1.59, 1.58, 1.47 (9s, 36H); ^{13}C NMR: $\delta = 174.0$, 170.7, 170.53 (2C), 170.50, 170.3, 169.9, 169.8, 169.7, 169.0, 168.9 (3C), 166.1, 165.5, 165.46, 165.4, 165.3, 165.1, 164.9, 164.8, 99.3 (4C), 98.4, 98.2, 98.1 (5C), 97.5, 95.4, 94.4, 94.3, 94.0, 61.1, 60.7, 60.0 (2C), 51.5, 51.3, 51.2 (2C), 33.9, 29.7, 25.6, 24.6, 23.1, 22.9 (2C), 22.7, 20.98, 20.94, 20.93 (2C), 20.8, 20.4 (3C), 18.1, 18.0 (2C), 17.95, 17.90, 17.74 (2C), 17.7

21: ^{1}H NMR: $\delta = 5.59$ (d, 4H, $J \approx 3.4$ Hz), 5.11 (d, 3H, $J \approx 1.6$ Hz), 5.08 (d, 1H, $J \approx 1.7$ Hz), 5.06 (d, 3H, $J \approx 1.6$ Hz), 5.04 (d, 3H, $J \approx 3.6$ Hz), 5.00 (d, 1H, $J \approx 3.5$ Hz), 4.80 (d, 1H, $J \approx 1.7$ Hz), 2.06 (s, 9H), 2.05 (s, 3H), 1.34 (d, 9H, $J \approx 6.1$ Hz), 1.31 (d, 3H, $J \approx 6.3$ Hz), 1.30 (d, 12H, $J \approx 6.1$ Hz); ^{13}C NMR: $\delta = 102.6$ (3C), 102.2, 102.1 (3C), 98.4 (4C), 94.9 (4C), 61.4 (4C), 61.0 (3C), 60.9, 52.7 (4C), 28.8, 26.1, 25.6, 25.5, 22.8 (4C), 17.6 (3C), 17.4 (4C), 17.3

removal of the acyl protecting groups under Zemplén conditions, and hydrogenolytic cleavage of the benzyl groups afforded the target hexadecasaccharide as the methyl ester **20** from which the hydrazide **21** (Table 1) was obtained by treatment with hydrazine in a combined yield of 26% for four steps from **19**.

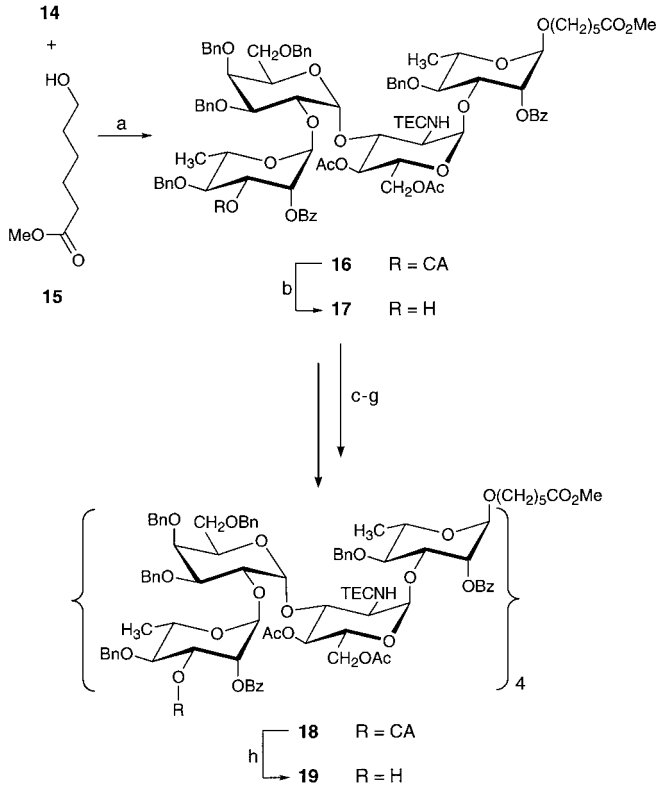
The acylation of the saccharide hydrazide **21** with the linker moiety[20] **22** was promoted by 1,2-dicyclohexylcarbodiimide (DCC), furnishing the intermediate acetal **23** that was deprotected with AcOH under mild conditions to afford the aldehyde **24**[21] (Scheme 3). Exposure of a solution of the linker-armed hexadecasaccharide and human serum albumin to $NaCNBH_3$ at pH 7[22] afforded the glycoconjugate **25** that was determined by MALDI-TOF mass spectrometry to have



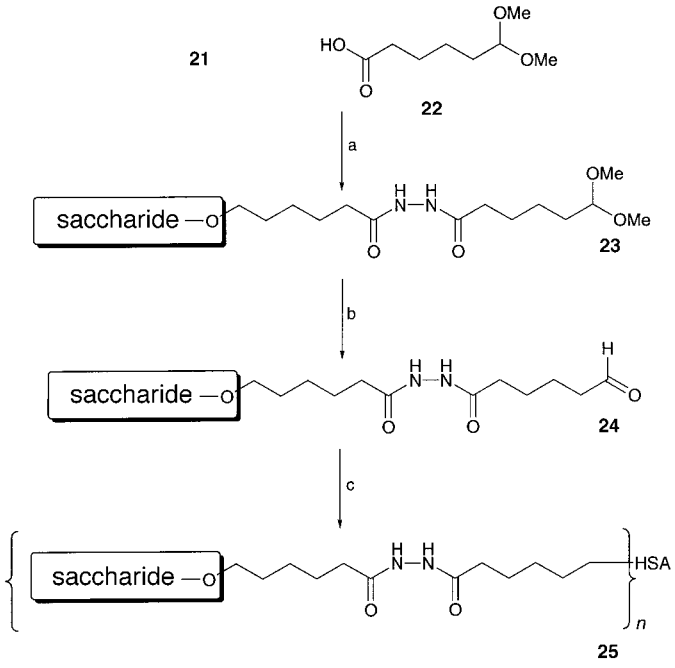
20, R = O-$(CH_2)_5$-CO_2CH_3, $n = 2$

21, R = O-$(CH_2)_5$-$CONHNH_2$, $n = 2$

 © WILEY-VCH Verlag GmbH, D-69451 Weinheim, 1998 1433-7851/98/3701-0140 $ 17.50+.50/0 *Angew. Chem. Int. Ed.* **1998**, *37*, No. 1/2



Scheme 2. a) **15** (3.5 equiv), $BF_3 \cdot Et_2O$ (1.4 equiv), CH_2Cl_2, 0 °C, 2 h, 68 %; b) thiourea (45 equiv), DMF/C_5H_5N, 23 °C, 24 h, 96 %; c) **14** (1.5 equiv), $BF_3 \cdot Et_2O$ (3.1 equiv), CH_2Cl_2, 0 °C, 15 min, 91 %; d) thiourea (24 equiv), DMF/C_5H_5N, 23 °C, 24 h, 82 %; e) **14** (2 equiv), $BF_3 \cdot Et_2O$ (4 equiv), CH_2Cl_2, 0 °C, 3 h; f) thiourea (33 equiv), DMF/C_5H_5N, 23 °C, 24 h, 62 % for two steps; g) **14** (3 equiv), $BF_3 \cdot Et_2O$ (10 equiv), CH_2Cl_2, 0 °C, 3 h, 48 %; h) thiourea (120 equiv), DMF/C_5H_5N, 23 °C, 24 h, 82 %.



Scheme 3. a) **22** (50 equiv), 1,3-dicyclohexylcarbodiimide (50 equiv), MeOH, 23 °C, 24 h; b) AcOH/H_2O, pH 2.7, 23 °C, 4 h; c) human serum albumin, pH 7 borate-phosphate buffer, $NaCNBH_3$ (15 equiv), 23 °C, 3 d, 32 % for three steps.

an average molecular weight of 93 kDa, and a molecular weight range of 83 – 103 kDa.[23] This corresponds to an average incorporation level of 11 saccharide chains per albumin molecule and an overall coupling efficiency of 32 %. We note that the tetra-, octa-, and the dodecasaccharide intermediates were likewise deprotected, equipped with the linker unit, and coupled to HSA, thus affording a series of compositionally related glycoconjugates for immunological studies.

In summary we have prepared the most complex, structurally defined synthetic carbohydrate – protein conjugate yet reported. The syntheses relied mostly on the Schmidt glycosylation, which proved to be highly efficient. This method as tested here offers a challenge against which new glycosylation methods should be evaluated as part of their performance test. Further improvements in the conjugation technology and preclinical evaluation of the synthetic glycoconjugates are in progress.

Received: June 9, 1997 [Z10526IE]
German version: *Angew. Chem.* **1998**, *110*, 145 – 149

Keywords: antigens · carbohydrates · oligosaccharides · protecting groups · vaccines

[1] Reviews: a) J. B. Robbins, R. Schneerson, S. Szu, V. Pozsgay in *Vaccinia, Vaccination and Vaccinology: Jenner, Pasteur and their Successors* (Eds.: S. Plotkin, B. Fantini), Elsevier, Paris, **1996**, pp. 135 – 143; b) R. K. Sood, A. Fattom, V. Pavliak, R. B. Naso, *Drug Discovery Today* **1996**, *1*, 381 – 387; c) A. Fattom, *Adv. Expt. Med. Biol.* **1995**, *383*, 131 – 139; d) U. B. S. Sørensen, *Danish Med. Bull.* **1995**, *42*, 47 – 53; e) H. J. Jennings, R. K. Sood in *Neoglycoconjugates. Preparation and Applications* (Eds.: Y. C. Lee, R. T. Lee), Academic Press, New York, **1994**, pp. 325 – 371; f) W. Egan, *Ann. Rep. Med. Chem.* **1993**, *28*, 257 – 265; g) P. R. Paradiso, K. Dermody, S. Pillai, *Vaccine Res.* **1993**, *2*, 239 – 248; h) H. J. Jennings, *Curr. Top. Microbiol. Immunol.* **1990**, *150*, 97 – 127.

[2] For the development of this concept, see: a) K. Landsteiner, *The specificity of serological reactions*, Harvard University Press, Cambridge, **1970**; b) W. F. Goebel, O. T. Avery, *J. Exp. Med.* **1929**, *50*, 521 – 531.

[3] R. Schneerson, O. Barrera, A. Sutton, J. B. Robbins, *J. Exp. Med.* **1980**, *152*, 361 – 376.

[4] J. B. Robbins, R. Schneerson, P. Anderson, D. H. Smith, *J. Am. Med. Assoc.* **1996**, *276*, 1181 – 1185.

[5] See for example: a) D. Cohen, S. Ashkenazi, M. S. Green, M. Gdalevich, G. Robin, R. Slepon, M. Yavzori, N. Orr, C. Block, Y. Ashkenazi, J. Shemer, D. N. Taylor, T. L. Hale, J. D. Sadoff, D. Pavliakova, R. Schneerson, J. B. Robbins, *Lancet* **1997**, *349*, 155 – 159; b) D. Cohen, S. Ashkenazi, M. S. Green, Y. Lerman, R. Slepon, G. Robin, N. Orr, D. N. Taylor, J. C. Sadoff, C. Chu, J. Shiloach, R. Schneerson, J. B. Robbins, *Infect. Immun.* **1997**, *64*, 4074 – 4077.

[6] For previous approaches to glycoconjugate vaccines against human pathogenic bacteria, see: a) E. Alonso de Velasco, A. F. M. Verheul, A. M. P. van Stein, H. A. T. Dekker, R. G. Feldman, I. M. Fernández, J. P. Kamerling, J. F. G. Vliegenthart, J. Verhoef, H. Snippe, *Infect. Immun.* **1994**, *62*, 799 – 808; b) C. C. A. M. Peeters, D. Evenberg, P. Hoogerhout, H. Käyhty, L. Saarinen, C. A. A. van Boeckel, G. A. van der Marel, J. H. van Boom, J. T. Poolman, *ibid.* **1992**, *60*, 1826 – 1833; c) A. F. M. Verheul, G. J. P. H. Boons, G. A. van der Marel, J. H. van Boom, H. J. Jennings, H. Snippe, J. Verhoef, P. Hoogerhout, J. T. Poolman, *ibid.* **1991**, *59*, 3566 – 3573; d) H. J. A. Jörbeck, S. B. Svenson, A. A. Lindberg, *ibid.* **1981**, *32*, 497 – 502.

[7] V. Pozsgay, *J. Am. Chem. Soc.* **1995**, *117*, 6673 – 6681.

[8] B. A. Dmitriev, Y. A. Knirel, N. K. Kochetkov, I. Hofman, *Eur. J. Biochem.* **1976**, *66*, 559 – 566.

 © WILEY-VCH Verlag GmbH, D-69451 Weinheim, 1998 1433-7851/98/3701-0141 $ 17.50+.50/0

[9] *New Vaccine Development: Establishing Priorities. Vol. 2. Diseases of Importance in Developing Countries*, National Academy Press, Washington, DC, **1986**, pp. 329 – 337.

[10] The term "oligosaccharide" is used in a liberal manner to denote the saccharides described here, while cognizant of the fact that by definition (Joint Commission on Biological Nomenclature, *Eur. J. Biochem*. **1982**, *126*, 433 – 437.) oligosaccharides contain up to and including ten monosaccharide units.

[11] a) V. Pozsgay, B. Coxon, *Carbohydr. Res.* **1995**, *277*, 171 – 178; b) V. Pozsgay, L. Pannell, *ibid.* **1994**, *258*, 105 – 122; c) V. Pozsgay, B. Coxon, *Carbohydr. Res.* **1994**, *257*, 189 – 215; d) V. Pozsgay, B. Coxon, H. Yeh, *Bioorg. Med. Chem.* **1993**, *1*, 237 – 257; e) V. Pozsgay, C. P. J. Glaudemans, J. B. Robbins, R. Schneerson, *Carbohydr. Res.* **1993**, *244*, 259 – 273; f) V. Pozsgay, C. P. J. Glaudemans, J. B. Robbins, R. Schneerson, *Tetrahedron* **1992**, *48*, 10249 – 10264.

[12] In one unpublished approach, a pentamer of a tetrasaccharide, similar to **14** was constructed, except that it contained an azido function at C-2 of the glucose unit. Various attempts to convert that protected eicosasaccharide to the corresponding acetamido derivative led to inseparable, complex mixtures.

[13] All new compounds gave satisfactory elemental analytical and mass spectral data. Yields refer to chromatographically homogeneous material.

[14] H. Lönn, *Carbohydr. Res.* **1985**, *139*, 105 – 113.

[15] a) V. Pozsgay in *Carbohydrates, Synthetic Methods and Applications in Medicinal Chemistry* (Eds.: H. Ogura, A. Hasegawa, T. Suami), Kodansha-VCH, Tokyo, Weinheim, **1992**, pp. 188 – 227; b) H. Paulsen, C. Krogmann, *Liebigs Ann. Chem.* **1989**, 1203 – 1213; c) M. Imoto, H. Yoshimura, T. Shimamoto, N. Sakaguchi, T. Shiba, *Bull. Chem. Soc. Jpn.* **1987**, *60*, 2205 – 2214; d) T. B. Windholz, D. B. R. Johnston, *Tetrahedron Lett.* **1967**, 2555 – 2557.

[16] Y. Oikawa, T. Yoshioko, O. Yonemitsu, *Tetrahedron Lett.* **1982**, *23*, 885 – 888.

[17] a) P. Konradsson, U. E. Udodong, B. Fraser-Reid, *Tetrahedron Lett.* **1990**, *31*, 4313 – 4316; b) G. H. Veeneman, S. H. van Leeuwen, J. H. van Boom, *ibid.* **1990**, *31*, 1331 – 1334.

[18] a) R. R. Schmidt, J. Michel, *Angew. Chem.* **1980**, *92*, 763 – 764; *Angew. Chem. Int. Ed. Engl.* **1980**, *19*, 731 – 732; b) M. Numata, M. Sugimoto, K. Koike, T. Ogawa, *Carbohydr. Res.* **1987**, *163*, 209 – 225; c) review: R. R. Schmidt, W. Kinzy, *Adv. Carbohydr. Chem. Biochem.* **1994**, *50*, 21 – 123.

[19] L. Yan, D. Kahne, *J. Am. Chem. Soc.* **1996**, *118*, 9239 – 9248.

[20] Compound **22** was obtained from **15** (S. Sabesan, J. C. Paulson, *J. Am. Chem. Soc.* **1986**, *108*, 2068 – 2080.) through a sequence involving oxidation (A. J. Mancuso, S. L. Huang, D. Swern, *J. Org. Chem.* **1978**, *43*, 2480 – 2482.), acetalization [$(MeO)_2CMe_2$, CSA], ester hydrolysis (LiOH), and acidification (citric acid) in 78% overall yield.

[21] For our earlier approaches for the introduction of a terminal, aldehydo group-containing linker moiety, see a) V. Pozsgay, L. Trinh, J. Shiloach, J. B. Robbins, A. Donahue Rolfe, S. B. Calderwood, *Bioconj. Chem.* **1996**, *7*, 45 – 55. b) V. Pozsgay, *Glycoconj. J.* **1993**, *10*, 133 – 141.

[22] G. R. Gray, *Arch. Biochem. Biophys.* **1974**, *163*, 426 – 428. Reductive amination attaches the ω-aldehydoalkyl moiety to the ε-amino group of the lysine residues of proteins resulting in an ε-N-alkylated construct that preserves the original net charge of the protein (C. P. Stowell, Y. C. Lee, *Adv. Carbohydr. Chem. Biochem.* **1981**, *37*, 225 – 281).

[23] The MALDI-TOF mass spectra were recorded on a KRATOS MALDI III instrument operated at an accelerating voltage of 22 kV. The sample was dissolved in 0.1% trifluoroacetic acid and 50% acetonitrile and applied to the target sample in a sinapinic acid matrix. The molecular weight of HSA was measured as 66350 Da.

Correlation between ^{51}V NMR Chemical Shift and Reactivity of Oxovanadium(v) Catalysts for Ethylene Polymerization**

Michael Bühl*

Olefin polymerization is one of the most important industrial applications of organometallic catalysts.[1] The most widely used catalysts in both homo- and heterogeneous reactions are of the Ziegler type, that is, based on Ti and Zr species along with certain cocatalysts.[2–4] The key step (not necessarily the rate-determining one) is the insertion of the olefin into a metal – carbon bond. Several such reactions and thus many potential catalysts for olefin polymerization are known. Silica-supported vanadium catalysts have attracted some attention in this context.[5] The oxidation state of the active vanadium species is still being debated;[5] low-valent species have been typically assumed, but studies on a soluble model compound have indicated that vanadium in the oxidation state v can also be catalytically active.[6] Upon addition of alkylaluminum reagents the simpler model compound **1** also shows mild catalytic activity for ethylene polymerization.[7] From multinuclear NMR spectroscopy it has been concluded that in the active catalyst, the organoaluminum compound is coordinated to the terminal oxygen atom of **1**.[7]

$[VO(CH_2SiMe_3)_3]$ **1** $[VOMe_3]$ **2** $[V(O\cdots AlH_3)Me_3]$ **3**

Recent calculations for model systems **2** and **3**, employing gradient-corrected levels of density functional theory (DFT), have corroborated this conclusion and have outlined a plausible mechanism for ethylene polymerization by **3** [Eq. (1)].[8] The rate-determining step is ethylene insertion into a V – C bond

$$[V(O\cdots AlH_3)Me_3] + H_2C{=}CH_2 \xrightarrow{\mathbf{3(TS)}} [V(O\cdots AlH_3)(CH_2CH_2Me)Me_2] \quad (1)$$

3

via the transition structure **3(TS)**, which has approximate square – pyramidal coordination about the vanadium center.

The role of the cocatalyst is addressed here in more detail, and the dependence of the computed insertion barrier on the specific Lewis acid is examined. As the latter is also found to affect the chemical shifts of the reactant complex substantially, it is suggested that prospective cocatalysts may be identified by ^{51}V NMR spectra of their adducts with, for example, **1**.

Apart from **3**, model catalysts $[V(O\cdots X)Me_3]$ derived by addition of Lewis acids X have been investigated: none (**2**), Li^+ (**4**), SbF_5 (**5**), and H^+ (**6**). Absolute and zero-point energies[9,10] of reactant minima and transition states, as well as the resulting barriers are collected in Table 1, and the transition structures are displayed in Figure 1. As expected,

[*] Dr. M. Bühl
Organisch-chemisches Institut der Universität
Winterthurerstrasse 190, CH-8057 Zürich (Switzerland)
Fax: Int. code + (41) 1-635 6812
e-mail: buehl@oci.unizh.ch

[**] I thank Prof. W. Thiel for his continuous support. Calculations were performed on a Silicon Graphics PowerChallenge at the Organisch-chemisches Institut, on IBM RS/6000 workstations at the ETH Zürich (C4 cluster), and on a NEC-SX4 supercomputer at the CSCS in Manno (Switzerland).

 © WILEY-VCH Verlag GmbH, D-69451 Weinheim, 1998 1433-7851/98/3701-0142 $ 17.50+.50/0

Table 1. Absolute energies E_{tot} and and zero-point energies (in square brackets) of reactants and transition states for the system $[V(O\cdots X)Me_3]+C_2H_4$, insertion barriers ΔE_a (including BP86/AE1 zero-point corrections), and chemical shifts $\delta(^{51}V)$ (with respect to $[VOCl_3]$) of the reactants.

Molecule	X	E_{tot} (minima)[a,b]	E_{tot} **(TS)**[a]	ΔE_a[c]	$\delta(^{51}V)$[d]
2	–	– 1139.12352 [66.0]	– 1217.67283 [101.5]	22.2	1062
3	AlH_3	– 1383.34929 [78.5]	– 1461.90418 [114.6]	19.1	1407
4	Li^+	– 1146.46946 [66.7]	– 1225.02605 [102.4]	17.8	1557
5	SbF_5	– 1643.87993 [74.3]	– 1722.43720 [109.6]	16.9	1766
6	H^+	– 1139.44031 [70.8]	– 1218.00770 [107.3]	11.9	1911

[a] BP86/I level; absolute energies in Hartree; ZPE in kcal mol^{-1}; each minimum has no imaginary frequency, each transition state has one imaginary frequency. [b] Values for ethylene at the same level are – 78.57773 [31.2]. [c] (BP86/I + ZPE) level; in kcal mol^{-1}. [d] GIAO-B3LYP/I level for BP86/I geometries.

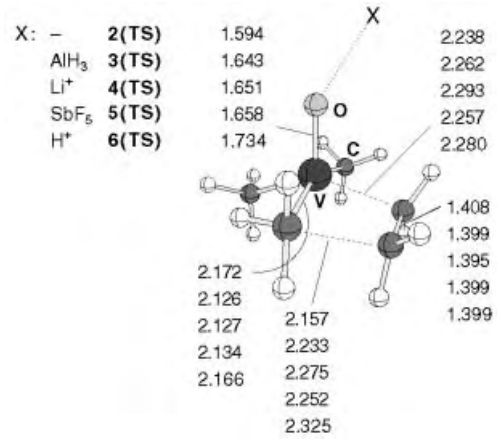


Figure 1. Transition structure for ethylene insertion into a V – C bond of **2** and Lewis adducts thereof; key distances are given in Å (BP86/I-optimized structures).

the uncatalyzed reaction (i.e. starting from **2**) has the highest computed insertion barrier, 22.2 kcal mol^{-1}. Addition of AlH_3 lowers the barrier by roughly 3 kcal mol^{-1}. Inspection of the natural charges[11] and Wiberg bond indices[12] in Figure 2 gives some information on the reason for this barrier reduction. As the coordination number at the vanadium atom is increased, in other words on going from the reactant **2** to the transition state **2(TS)**, the V – O bond order decreases and the negative charge on the oxygen atom increases. Both effects appear to be quite small, but they are somewhat more pronounced in the corresponding AlH_3 adducts. On going from **3** to **3(TS)** the negative charge on the oxygen atom increases by 13 % and the V – O bond order decreases by 7 % (Figure 2). Apparently, the Lewis acid stablilizes the negative charge on the oxygen atom more efficiently in the transition state than in the reactant complex, thereby lowering the overall barrier.

As a consequence, stronger Lewis acids should stabilize the transition structure even more effectively and should thus further reduce the barrier. For instance, with Li^+ as cocatalyst, a barrier of 17.8 kcal mol^{-1} is computed, more than 1 kcal mol^{-1} lower than that with AlH_3 (Table 1). Similar "electrostatic accelerations" have been predicted computationally for pericyclic reactions[13] and are known experimentally (for instance, the rates of Diels – Alder and ene reactions

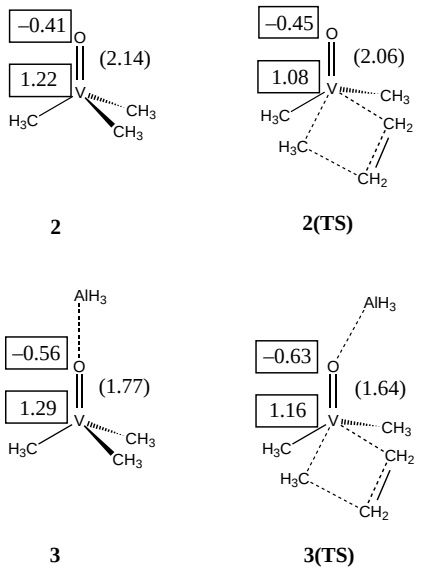


Figure 2. Natural charges (in boxes) and Wiberg bond orders (in parentheses) for **2**, **3**, and the corresponding transition structures for ethylene insertion (obtained from natural population analysis at the BP86/I level).

are enhanced by inorganic lithium salts[14]). A further reduction of the barrier to 16.9 kcal mol^{-1} is predicted when SbF_5 is the cocatalyst. Finally, with one of the strongest acids conceivable, unsolvated H^+, the computed barrier is only 11.9 kcal mol^{-1}. This result may be of little immediate relevance for chemistry in solution, but may serve as a rough estimate for the lower limit for the barrier that can be reached with this type of system. (Note that the theoretical numbers are not necessarily of quantitative accuracy; the computed trends, however, should be reliable.)

Complexation of the Lewis acid at the terminal oxygen atom affects not only the barrier, but also the chemical shifts of the oxovanadium(v) reactants. For instance, the ^{51}V signal of **1** is shifted to higher frequency by $\Delta\delta = 370$ upon coordination of $Al(CH_2SiMe_3)_3$.[7] Similar deshielding, $\Delta\delta = 345$, is obtained on going from model system **2** to its AlH_3 adduct **3** (see Table 1). Moreover, successive deshielding of the ^{51}V nucleus is computed on proceeding from **2** to compounds **4**, **5**, and **6**, with a value of up to $\Delta\delta = 851$ for the latter (Table 1). This deshielding can be understood in terms of paramagnetic contributions due to magnetically induced coupling[15] between the occupied V – C bonding MOs (one "σ_{VC}" and two "π_{VC}") and the virtual, antibonding orbital, "σ^*_{VO}". The latter is strongly stabilized upon protonation (on going from **2** to **6**), much more than the former. Hence, the energetic separation between both is reduced and the resulting paramagnetic contributions are enhanced.

As illustrated in Figure 3, the Lewis acid X affects both $\delta(^{51}V)$ of the reactants and the insertion barrier in a similar way. While there is no strictly linear relationship between these two properties, the general trend is obvious: enhanced deshielding of the ^{51}V nucleus is paralleled by a decrease of the insertion barrier.

There are several reports of empirical correlations of transition metal chemical shifts with kinetic parameters[16] and, in some cases, even with catalytic activities.[17,18] Such

 © WILEY-VCH Verlag GmbH, D-69451 Weinheim, 1998 1433-7851/98/3701-0143 $ 17.50+.50/0

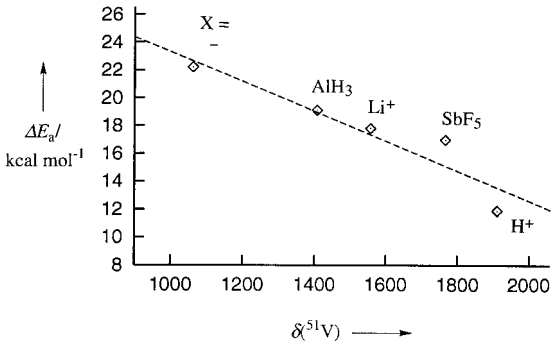


Figure 3. Correlation of DFT-derived barriers to ethylene insertion ΔE_a (BP86/I + ZPE) and chemical shifts $\delta(^{51}V)$(GIAO-B3LYP/I) for the Lewis acid adducts $[V(O\cdots X)Me_3]$.

correlations are potentially very useful because reactivities of new compounds can be estimated from the NMR spectra alone. In some cases, DFT calculations have reproduced and rationalized the experimental findings.[19] The results summarized in Figure 3 constitute the first theoretical prediction of such a NMR – reactivity correlation. When applied to the experimental system **1**, these data indicate that the polymerization activity towards ethylene may be increased by Lewis acids stronger than the alkylaluminum reagents employed so far.[7] Most significantly, it should be possible to screen suitable cocatalysts by recording ^{51}V NMR spectra of the complexes formed initially with **1**:[20] the complexes with the most deshielded $\delta(^{51}V)$ resonance should also be the most reactive ones. If the lower limit of the ethylene insertion barrier is around 12 kcal mol^{-1} as computed for **6** (with H^+ as cocatalyst), catalysts derived from **1** can most likely not match the high activity of the Kaminsky-type zirconocenes, for which propagation barriers on the order of 7 kcal mol^{-1} have been estimated.[21] Nevertheless, it would be very interesting to test experimentally whether the catalytic activity of **1** can be significantly increased by suitable cocatalysts, and whether the predicted NMR – reactivity correlation of Figure 3 can be verified (provided possible problems with the solubility and stability of potential catalysts can be overcome).

Received: July 9, 1997 [Z 10658 IE]
German version: *Angew. Chem.* **1998**, *110*, 153 – 155

Keywords: density functional calculations · homogeneous catalysis · NMR spectroscopy · polymerization · vanadium

[1] a) *Applied Homogeneous Catalysis with Organometallic Compounds, Vol. 1,2* (Eds.: B. Cornils, W. A. Herrmann), VCH, Weinheim, **1996**; b) W. A. Herrmann, B. Cornils, *Angew. Chem.* **1997**, *109*, 1074 – 1095; *Angew. Chem. Int. Ed. Engl.* **1997**, *36*, 1049 – 1067.
[2] K. Ziegler, *Angew. Chem.* **1964**, *76*, 545 – 566.
[3] J. Boor Jr., *Ziegler – Natta Catalysts and Polymerizations*, Academic Press, New York, **1979**.
[4] H. H. Brintzinger, D. Fischer, R. Mühlhaupt, B. Rieger, R. Waymouth, *Angew. Chem.* **1995**, *107*, 1255 – 1283; *Angew. Chem. Int. Ed. Engl.* **1995**, *34*, 1143.
[5] See for example: F. J. Karol, K. J. Cann, B. E. Wagner in *Transition Metals and Organometallics as Catalysts for Olefin Polymerization* (Eds.: W. Kaminsky, H. Sinn), Springer, New York, **1988**, p. 149.
[6] F. J. Feher, R. L. Blanski, *J. Am. Chem. Soc.* **1992**, *114*, 5886 – 5887.
[7] F. J. Feher, R. L. Blanski, *Organometallics* **1993**, *12*, 958 – 963.
[8] M. Bühl, F. A. Hamprecht, *J. Comput. Chem.*, in press.
[9] Method for geometry optimization: gradient-corrected exchange-correlation functionals of Becke (A. D. Becke, *Phys. Rev. A* **1988**, *38*, 3098 – 3100) and Perdew (J. P. Perdew, *Phys. Rev. B* **1986**, *33*, 8822 – 8824; *ibid.* **1986**, *34*, 7406), denoted BP86, and Basis I, which is Wachters's (14s11p6d)/[8s7p4d] all-electron basis augmented with one additional diffuse d function and two 4p functions for V (A. J. H. Wachters, *J. Chem. Phys.* **1970**, *52*, 1033 – 1036; P. J. Hay, *J. Chem. Phys.*, **1977**, *66*, 4377 – 4384), a relativistic 64-electron multi-electron-fit effective core potential together with the (4s4p)/[2s2p] valence double-zeta basis set for Sb (A. Bergner, M. Dolg, W. Küchle, H. Stoll, H. Preuss, *Mol. Phys.* **1993**, *80*, 1431 – 1441; augmented with one d-polarization function, exponent 0.211), and standard 6-31G* basis for all other elements (e.g. W. Hehre, L. Radom, P. von R. Schleyer, J. A. Pople, *Ab Initio Molecular Orbital Theory*, Wiley, New York, **1986**). Zero-point corrections have been computed with harmonic frequencies from analytical or numerical second derivatives. It is known that these types of density functionals afford reliable descriptions of geometries, vibrations, and energetics for transition metal complexes (see, for example, T. Ziegler, *Can. J. Chem.* **1995**, *73*, 743 – 761).
[10] Magnetic shieldings have been computed with the GIAO (Gauge-Including Atomic Orbitals) DFT method as implemented (J. R. Cheeseman, G. W. Trucks, T. A. Keith, M. J. Frisch, *J. Chem. Phys.* **1996**, *104*, 5497 – 5509) in the Gaussian 94 program (M. J. Frisch, G. W. Trucks, H. B. Schlegel, P. M. W. Gill, B. G. Johnson, M. A. Robb, J. R. Cheeseman, T. Keith, G. A. Petersson, J. A. Montgomery, K. Raghavachari, M. A. Al-Laham, V. G. Zakrzewski, J. V. Ortiz, J. B. Foresman, C. Y. Peng, P. Y. Ayala, W. Chen, M. W. Wong, J. L. Andres, E. S. Replogle, R. Gomperts, R. L. Martin, D. J. Fox, J. S. Binkley, D. J. DeFrees, J. Baker, J. J. P. Stewart, M. Head-Gordon, C. Gonzales, J. A. Pople, Gaussian 94, Pittsburgh PA, 1995), employing Basis I and Becke's three-parameter exchange DFT/Hartree – Fock hybrid functional (A. D. Becke, *J. Chem. Phys.* **1993**, *98*, 5648 – 5642) together with the correlation functional of Lee, Yang, and Parr (C. Lee, W. Yang, R. G. Parr, *Phys. Rev. B* **1988**, *37*, 785 – 789), denoted B3LYP, for the BP86/I-optimized geometries. Chemical shifts are reported relative to $[VOCl_3]$, the experimental standard, with a computed absolute shielding of $\sigma = -2317$ at the same level.[8] It is not mandatory that geometry optimizations and chemical shift calculations be performed at the same level. For the computation of some transition metal chemical shifts, the B3LYP functional has proven superior to others (M. Bühl, *Chem. Phys. Lett.* **1997**, *267*, 251 – 257); see also ref.[8]
[11] From natural population analysis; review: A. E. Reed, L. A. Curtiss, F. Weinhold, *Chem. Rev.* **1988**, *88*, 899 – 926.
[12] K. Wiberg, *Tetrahedron* **1968**, *24*, 1083 – 1096.
[13] a) H. Jiao, P. von R. Schleyer, *Angew. Chem.* **1993**, *105*, 1830 – 1833; *Angew. Chem. Int. Ed. Engl.* **1993**, *32*, 1760 – 1763; b) H. Jiao, P. von R. Schleyer, *J. Am. Chem. Soc.* **1995**, *117*, 11529 – 11535.
[14] See for example: G. Facita, P. Righetti, *Tetrahedron* **1995**, *51*, 9091 – 9102.
[15] For the origin of paramagnetic contributions see, for example: W. Kutzelnigg, U. Fleischer, M. Schindler, in *NMR Basic Princ. Prog.* **1990**, *23*, 165 – 262; an illustration for transition metal complexes can be found in, for example, Y. Ruiz-Morales, G. Schreckenbach, T. Ziegler, *J. Phys. Chem.* **1996**, *100*, 3359 – 3367.
[16] See for example: a) P. DeShong, D. R. Sidler, P. J. Rybczynski, A. A. Ogilvie, W. von Philipsborn, *J. Org. Chem.* **1989**, *54*, 5432 – 5437; b) M. Koller, W. von Philipsborn, *Organometallics* **1992**, *11*, 467 – 468; c) M. Koller, Ph.D. Thesis, Universität Zurich, **1993**; d) E. J. Meier, W. Kozminski, A. Linden, P. Lustenberger, W. von Philipsborn, *Organometallics* **1996**, *15*, 2469 – 2477.
[17] H. Bönnemann, W. Brijoux, R. Brinkmann, W. Meurers, R. Mynott, W. von Philipsborn, T. Egolf, *J. Organomet. Chem.* **1984**, *272*, 231 – 249.
[18] R. Fornika, H. Görls, B. Seeman, W. Leitner, *J. Chem. Soc. Chem. Commun.* **1995**, 1479 – 1480.
[19] a) M. Bühl, O. L. Malkina, V. G. Malkin, *Helv. Chim. Acta* **1996**, *79*, 742 – 754; b) M. Bühl, *Organometallics* **1997**, *16*, 261 – 267.
[20] No NMR spectra are necessary to order possible cocatalysts according to their Lewis acid strength, but rather to ensure that stable complexes are formed in each case.
[21] J. C. W. Chien, A. Razavi, *J. Polym. Sci. A* **1988**, *26*, 2369 – 2380.

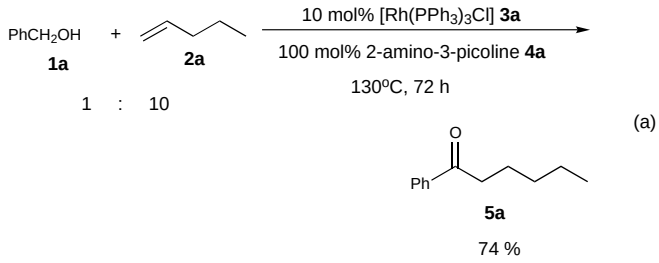
 © WILEY-VCH Verlag GmbH, D-69451 Weinheim, 1998 1433-7851/98/3701-0144 $ 17.50+.50/0

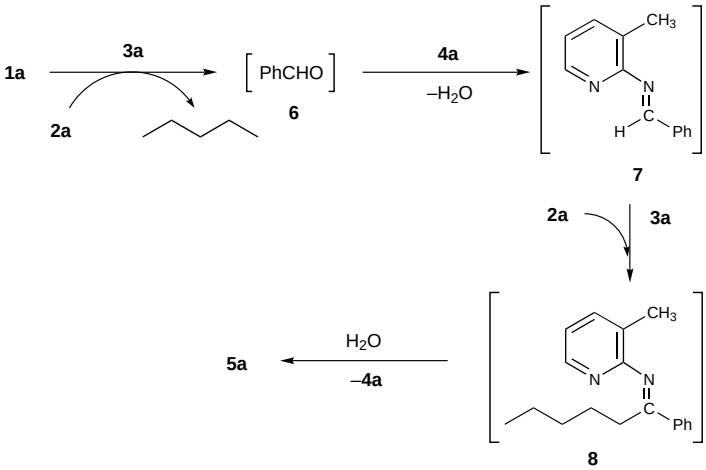
Direct Synthesis of Ketones from Primary Alcohols and 1-Alkenes**

Chul-Ho Jun,* Chan-Woo Huh, and Sang-Jin Na

Activation of the aldehydic carbon–hydrogen bond by transition metal complexes has received much attention in organic synthesis because of its potential to convert aldehydes into ketones by hydroacylation.[1] Although intramolecular hydroacylation has been studied in detail,[2] only a few methods have been reported for transition metal catalyzed intermolecular hydroacylation.[3] Recently, we developed a direct chelation-assisted intermolecular hydroacylation.[4] Primary and secondary alcohols can be oxidized to aldehydes and ketones through hydrogen transfer by a transition metal catalyst. In the course of this oxidation, hydrogen atoms are transferred to hydrogen acceptors such as ketones or alkenes to produce alcohols and alkanes, respectively.[5,6] If oxidation by transition metal mediated hydrogen transfer and hydroacylation occur consecutively with the aid of identical catalysts and olefins, it should be possible to prepare ketones directly from primary alcohols and alkenes. We describe here a one-pot synthesis of a ketone from a primary alcohol and a 1-alkene using a transition metal catalyst together with 2-aminopyridine derivatives. To the best of our knowledge, this is the first example of a direct ketone synthesis from a primary alcohol and a 1-alkene.

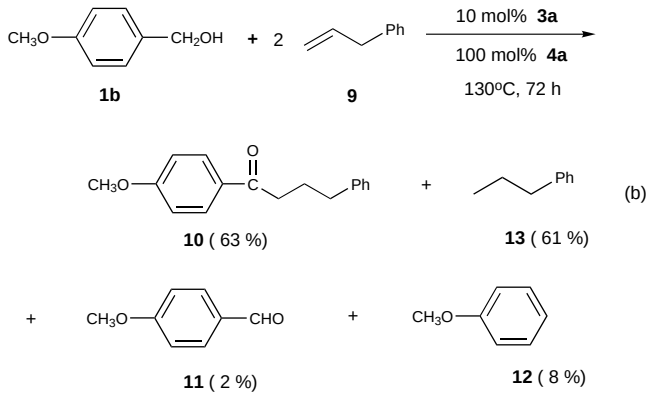
Benzyl alcohol (**1a**) was treated with 1-pentene (**2a**) at 130 °C for 72 h using as catalyst a mixture of [chlorotris(triphenylphosphane)rhodium(I)] (**3a**, 10 mol % based upon **1a**) and 2-amino-3-picoline [**4a**, 100 mol %; Eq. (a)]. Hexanophenone (**5a**) was isolated in 74 % yield after chromatography. The reaction proceeded quite well without a solvent. A possible mechanism for this one-pot synthesis of **5a** from **1a** and **2a** is illustrated in Scheme 1. The first step must be oxidation by hydrogen transfer, in which primary alcohol **1a** is converted into aldehyde **6** via complex **3a**. Hydrogen atoms generated from **1a** must be transferred to **2a** to afford pentane.[6] The aldehyde then reacts with **4a** to form aldimine **7** and H_2O. Formation of an aldimine from a primary alcohol and a primary amine in the presence of a transition metal catalyst is presumed to be the key step in N-alkylation of primary amines with primary alcohols.[7] Subsequent hydroiminoacylation of **2a** with **7** leads to ketimine **8**, as reported earlier.[8] Hydrolysis of **8** by H_2O, formed through the reaction of **4a** with **6**, affords ketone **5a** as the final product. Direct synthesis of **5a** from **2a** and **6** by chelation-assisted hydroacylation has already been reported.[4] Since **2a** must serve both as a hydrogen acceptor in the first step and as a hydroacylation substrate in the second step, the amount of **2a** should be at least twice that of **1a**.[9]





Scheme 1. Mechanism for the direct synthesis of ketones from primary alcohols and 1-alkenes by oxidation and hydroacylation.

To determine the intermediates, *p*-methoxybenzyl alcohol (**1b**) was allowed to react at 130 °C for 72 h with allylbenzene (**9**) under cocatalysis with **3a** (10 mol %) and **4a** (100 mol %). This resulted in a mixture of *p*-methoxy-γ-phenylbutanophenone (**10**), anisaldehyde (**11**), anisole (**12**), and propylbenzene (**13**) in 63, 2, 8, and 61 % yield, respectively, based upon **1b** [Eq. (b)].[10] Compound **13** is the hydrogenation product of **9**, while **11** is an oxidation product of **1b** and **12** the decarbonylation product of **11**. Establishment of the presence of **11** and **13** confirms that hydrogen transfer occurs from the primary alcohol to the 1-alkene.



[*] Prof. Dr. C.-H. Jun, C.-W. Huh, S.-J. Na
Department of Chemistry
Yonsei University
Seoul 120-749 (Korea)
Fax: Int. code + (82) 2-364-7050
e-mail: junch@alchemy.yonsei.ac.kr

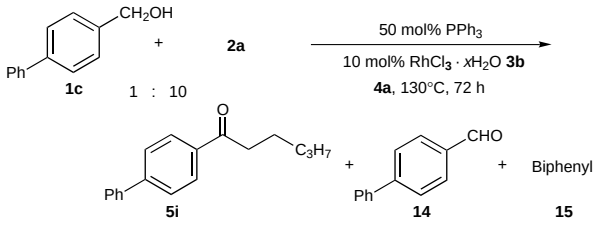
[**] This work was supported by the Korean Science and Engineering Foundation (grant-in-aid 961-0306-054-2) and the Korean Ministry of Education (project no. BSRI-96-3422). The authors wish also to thank IBRD (the International Bank for Reconstruction and Development) for the purchase of a 250-MHz NMR spectrometer.

 © WILEY-VCH Verlag GmbH, D-69451 Weinheim, 1998 1433-7851/98/3701-0145 $ 17.50+.50/0

In the catalytic reaction of **1a** and **2b** with $RhCl_3 \cdot H_2O$ (**3b**) and PPh_3 under the same reaction conditions as above, heptanophenone (**5b**) was obtained in much higher yield (84%) than in the reaction with **3a**. The reason is not clear, but the active catalyst **3a** might be freshly generated in situ by the reaction of **3b** with PPh_3.[11]

To clarify the influence of **4a**, this substance was introduced in various concentrations into the hydroacylation of **2a** with 4-biphenylmethanol (**1c**). Reaction occurred at 130 °C in the course of 72 h with the catalytic system composed of **3b** (10 mol%) and PPh_3 (Table 1). No ketone was obtained in the absence of **4a**, as expected. The yield of decarbonylation product **15** decreased with increasing concentration of **4a**. This suggests that a high concentration of **4a** retards the decarbonylation of aldehyde generated from alcohol by increasing the probability of carbon–hydrogen bond cleavage of carboxaldimine, which is present in higher concentration.

Table 1. Influence of the concentration of 2-amino-3-picoline (**4a**) on the reaction of 4-biphenylmethanol (**1c**) with 1-pentene (**2a**).[a]

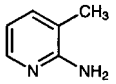
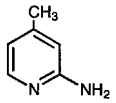
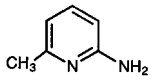
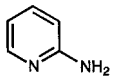
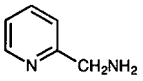
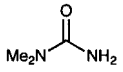


Entry	**4a** [mol%]	Yield (**5i**) [%]	**5i**[b]	**14**[b]	**15**[b]
1	20	21	55	9	36
2	50	55	86	4	10
3	100	67	92	0	8
4	200	88	100	0	0

[a] A mixture of **1c** (0.48 mmol), **2a** (4.8 mmol), **3b** (0.048 mmol), PPh_3 (0.24 mmol), and various amounts of **4a** was heated for 72 h at 130 °C. [b] Relative amounts determined by gas chromatography.

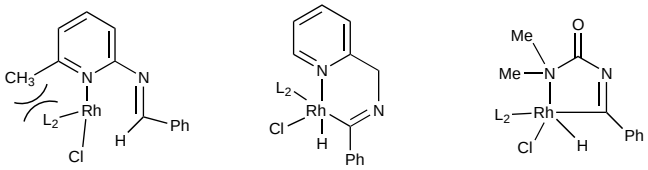
Various types of amine derivatives were examined with the catalytic system consisting of **3b** and PPh_3 (Table 2). Among 2-aminopyridine derivatives, 2-amino-4-picoline (**4b**) showed the greatest catalytic activity, and 2-amino-6-picoline (**4c**) the least. This may be because of steric hindrance by the 6-methyl group (see **16**). The nitrogen atom in the pyridinyl group would coordinate to the metallic center with difficulty in this case, so that the metal and carbon–hydrogen bonds in the aldimine would not be brought into sufficiently close proximity. 2-Aminomethylpyridine (**4e**) showed no catalytic activity, perhaps due to the formation of a less-favored six-membered ring metallacyclic complex such as **17**, or to the instability of the *N*-alkylaldimine compared with the more conjugated *N*-arylaldimine. Even *N*,*N*-dimethylurea (**4f**), which lacks the 2-aminopyridine moiety, provided a hydroacylated product in 3% yield, possibly via intermediate **18**. This clearly demonstrates that formation of the five-membered metallacyclic intermediate is a prerequisite for this reaction. No hydroacylated product was detected with triethylamine (**4g**).

Table 2. Results of the hydroacylation of 1-pentene (**2a**) with benzyl alcohol (**1a**) to give hexanophenone (**5a**) in the presence of $RhCl_3 \cdot xH_2O$ and PPh_3 as catalyst system, as well as various amines (100 mol%).[a]

Entry	Amine		Yield [%][b]
1		**4a**	54
2		**4b**	91
3		**4c**	9
4		**4d**	63
5		**4e**	0
6		**4f**	3
7	NEt_3	**4g**	0

[a] A mixture of **1a** (0.48 mmol), **2a** (4.8 mmol), **3b** (0.048 mmol), PPh_3 (0.24 mmol), and an amine (0.48 mmol) was heated for 40 h at 130 °C. [b] Isolated **5a**.

Catalytic reactions of various primary alcohols and 1-alkenes with **3b** (3.3 mol% based upon alcohol) and PPh_3 (16.5 mol%) as well as **4b** (100 mol%) at 130 °C for 12 h were also examined (Table 3). The resulting hydroacylated ketones

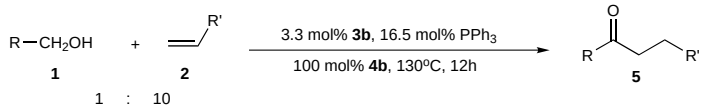


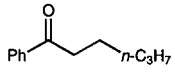
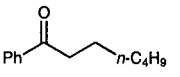
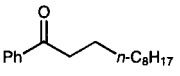
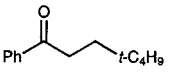
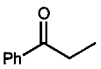
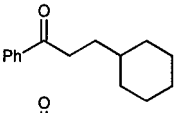
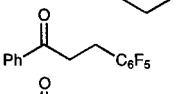
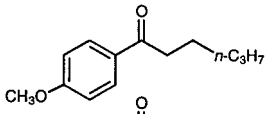
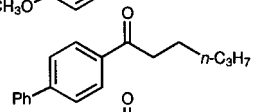
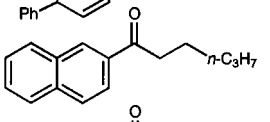
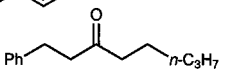
were linear, not branched systems.[12] There appear to be no limitations with respect to the 1-alkene component. Even the sterically hindered 1-alkene 3,3-dimethyl-1-butene (**2d**) provided **5d** in fairly good yield (85%). All the benzylic alcohols **1a**–**1d** provided good results, although yields with aliphatic primary alcohols like **1e** were low (22%).

We thus present a general synthesis for ketones starting from 1-alkenes and primary alcohols with the catalytic assistance of 2-aminopyridine derivatives and transition metal complexes. This newly developed synthesis achieves the generality required for a practical organic synthetic procedure.

 © WILEY-VCH Verlag GmbH, D-69451 Weinheim, 1998 1433-7851/98/3701-0146 $ 17.50+.50/0 *Angew. Chem. Int. Ed.* **1998**, *37*, No. 1/2

Table 3. Ligand-supported intermolecular hydroacylation of 1-alkenes **2** with primary alcohols **1**.[a]



Entry	Alcohol R (**1**)	1-Alkene R′ (**2**)	Hydroacylated product **5**		Yield [%][b]
1	Ph (**1a**)	n-C_3H_7 (**2a**)		**5a**	86
2	Ph (**1a**)	n-C_4H_9 (**2b**)		**5b**	84
3	Ph (**1a**)	n-C_8H_{17} (**2c**)		**5c**	66
4	Ph (**1a**)	t-C_4H_9 (**2d**)		**5d**	85
5[c]	Ph (**1a**)	H (**2e**)		**5e**	43
6	Ph (**1a**)	Cyclohexyl (**2f**)		**5f**	76
7[d]	Ph (**1a**)	C_6F_5 (**2g**)		**5g**	69
8	4-$MeOC_6H_4$ (**1b**)	n-C_3H_7 (**2a**)		**5h**	77
9	4-PhC_6H_4 (**1c**)	n-C_3H_7 (**2a**)		**5i**	84
10	2-Naphthyl (**1d**)	n-C_3H_7 (**2a**)		**5j**	78
11	$PhCH_2CH_2$ (**1e**)	n-C_3H_7 (**2a**)		**5k**	22[e]

[a] A mixture of **1** (1.435 mmol), **4b** (1.435 mmol), **3b** (0.048 mmol), PPh_3 (0.239 mmol), and **2** (14.300 mmol) was heated for 12 h at 130 °C. [b] Yield of hydroacylated product isolated by column chromatography (SiO_2, hexane/EtOAc, 5/2). [c] Benzene was used as solvent. [d] Toluene (200 mg) was added as a solvent. [e] With **3a** as catalyst. Use of the same molar quantity of **3b** and PPh_3 instead of **3a** led to the isolation of **5k** (10%).

Experimental Section

In a typical experiment, a mixture of **1a** (155 mg, 1.44 mmol), **4b** (155 mg, 1.44 mmol), and PPh_3 (62.6 mg, 0.239 mmol) was dissolved in **2a** (1000 mg, 14.3 mmol) in a 2.5-mL screw-capped vial. After the mixture had been stirred for several minutes, complex **3b** (10.0 mg, 0.048 mmol) was added, and the resulting mixture was stirred for 12 h at 130 °C. The solution was concentrated, and the residue obtained was purified by column chromatography (hexane/EtOAc, 5/2) to give 218 mg of **5a** (86% yield).

Received: July 2, 1997 [Z10629IE]
German version: *Angew. Chem.* **1998**, *110*, 150–152

Keywords: C–H activation · homogeneous catalysis · hydroacylations · hydrogen transfer · metallacycles

[1] a) J. Schwartz, J. B. Cannon, *J. Am. Chem. Soc.* **1974**, *96*, 4721; b) C. F. Lochow, R. G. Miller, *ibid*. **1976**, *98*, 1281; c) P. Isnard, B. Denise, R. P. A. Sneeden, *J. Organomet. Chem.* **1982**, *240*, 285.

[2] a) R. W. Barnhart, B. Bosnich, *Organometallics* **1995**, *14*, 4343; b) R. W. Barnhart, X. Wang, P. Noheda, S. H. Bergens, J. Whelan, B. Bosnich, *J. Am. Chem. Soc.* **1994**, *116*, 1821; c) Y. Taura, M. Tanaka, K. Funakoshi, K. Sakai, *Tetrahedron Lett.* **1989**, *30*, 6349; d) D. P. Fairlie, B. Bosnich, *Organometallics* **1988**, *7*, 946; e) D. P. Fairlie, B. Bosnich, *ibid.* **1988**, *7*, 936; f) B. R. James, C. G. Young, *J. Chem. Soc. Chem. Commun.* **1983**, 1215; g) D. Milstein, *ibid.* **1982**, 1357; h) R. C. Larock, K. Oertle, G. F. Potter, *J. Am. Chem. Soc.* **1980**, *102*, 190; i) R. E. Campbell, Jr., C. F. Lochow, R. G. Miller, *ibid.* **1980**, *102*, 5824; j) K. Sakai, J. Ide, O. Oda, N. Nakamura, *Tetrahedron Lett.* **1972**, *13*, 1287.

[3] a) T. Kondo, M. Akazome, Y. Tsuji, Y. Watanabe, *J. Org. Chem.* **1990**, *55*, 1286; b) Y. Tsuji, S. Yoshii, T. Ohsumi, T. Kondo, Y. Watanabe, *J. Organomet. Chem.* **1987**, *331*, 379; c) T. B. Marder, D. C. Roe, D. Milstein, *Organometallics* **1988**, *7*, 1451; d) K. P. Vora, C. F. Lochow, R. G. Miller, *J. Organomet. Chem.* **1980**, *192*, 257.

[4] C.-H. Jun, H. Lee, J.-B. Hong, *J. Org. Chem.* **1997**, *62*, 1200.

[5] a) R. Noyori, S. Hashiguichi, *Acc. Chem. Res.* **1997**, *30*, 97; b) G. Zassinovich, G. Mestroni, *Chem. Rev.* **1992**, *92*, 1051; c) R. A. W. Johnstone, A. H. Wilby, *ibid.* **1985**, *85*, 129; d) G. Brieger, T. J. Nestrick, *ibid.* **1974**, *74*, 567.

[6] R. Spogliarich, A. Tencich, J. Kaspar, M. Graziani, *J. Organomet. Chem.* **1982**, 453.

[7] a) Y. Watanabe, Y. Morisaki, T. Kondo, T. Mitsudo, *J. Org. Chem.* **1996**, *61*, 4214; b) S. I. Murahashi, K. Kondo, T. Hakada, *Tetrahedron Lett.* **1982**, *23*, 229.

[8] a) J. W. Suggs, *J. Am. Chem. Soc.* **1979**, *101*, 489; b) C.-H. Jun, J.-S. Han, J.-B. Kang, S.-I. Kim, *J. Organomet. Chem.* **1994**, *474*, 183; c) C.-H. Jun, J.-B. Kang, J.-Y. Kim, *ibid.* **1993**, *458*, 193; d) *Tetrahedron Lett.* **1993**, *34*, 6431.

[9] By increasing the ratio of **1a** to **2a** from 1:1 to 1:2, 1:5, and 1:10, the yield of **5a** was also increased by 44, 68, and 74%, respectively. We therefore chose a ratio of 1:10 for the concentrations of **1a** to **2a**.

[10] The yield of **10** is calculated on the basis of hydrogen atoms released from **1b**.

[11] J. A. Osborn, G. Wilkinson, *Inorg. Syn.* **1967**, *10*, 67.

[12] Under these reaction conditions, no decarbonylation product was detected from **1b–e**.

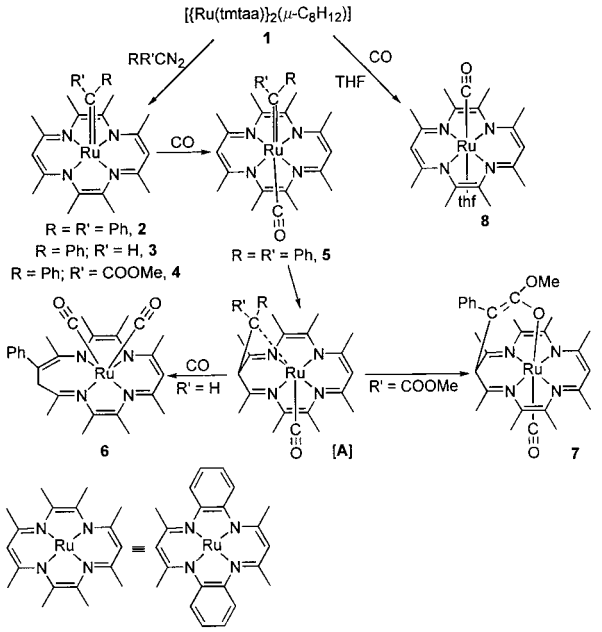
 © WILEY-VCH Verlag GmbH, D-69451 Weinheim, 1998 1433-7851/98/3701-0147 $ 17.50+.50/0

Ruthenium Carbenes Bonded to a Macrocycle: Carbon Monoxide Induced Carbene Migration Pathways from the Metal to the Ligand**

Alain Klose, Euro Solari, Carlo Floriani,* Silvano Geremia, and Lucio Randaccio

The potential of the metal–carbene functionality[1] bonded to a macrocyclic structure is still largely unexplored, except for some remarkable exceptions in metal–porphyrin chemistry, particularly in the case of the iron[2] and ruthenium[3] couple. This fact is rather surprising in the case of ruthenium, because recently the ruthenium–carbene functionality bonded to conventional ancillary ligands has had a large impact in catalysis of metathesis reactions.[4]

The present paper shows some aspects of the ruthenium–carbene unit when bonded to the easily accessible tetramethyldibenzotetraazaannulene [tmtaaH$_2$].[5] The chemistry of [Ru(tmtaa)] has so far been almost unexplored. Our starting material is not the stable [Ru(tmtaa)(PR$_3$)$_2$],[6] but the labile olefin complex **1** (Scheme 1).



Scheme 1. Synthesis of **2**–**8**. In the routes to **6** and **7** a ruthenium-to-macrocycle migration of the carbene functionality is indicated.

Reaction of **1** with diazoalkanes led to the corresponding carbene derivatives **2**–**4**,[7] which have been fully characterized. The X-ray analysis on **2**[8] is the first X-ray structure of a Ru–carbene bonded to a macrocyclic structure.

[*] Prof. Dr. C. Floriani, A. Klose, Dr. E. Solari
Institut de Chimie Minérale et Analytique
Université de Lausanne
BCH, CH-1015 Lausanne (Switzerland)
Fax: Int. code + (41) 21-692 3905
e-mail: carlo.floriani@icma.unil.ch
Dr. S. Geremia, Prof. Dr. L. Randaccio
Dipartimento di Scienze Chimiche, Università di Trieste (Italy)

[**] This work was supported by the "Fonds National Suisse de la Recherche Scientifique" (Grant No. 20-46′590.96) and Ciba Specialty Chemicals (Basel, Switzerland).

The coordination environment of the ruthenium center is a distorted tetragonal pyramid, unlike in carbene–Fe[2a] and carbene–Os porphyrins,[9] where the metal is always hexacoordinate. The metal is displaced by 0.374(3) Å from the average N$_4$ plane towards the carbene carbon. The Ru–C23 vector is perpendicular to the N$_4$ core. The carbene C23,C24,C30 plane is almost parallel to the N1–N3 vector (torsional angles: C30,C23,Ru,N3 −6.6(6) and C24,C23,Ru,N2 −91.0(6)°). The Ru=C bond length [1.874(8) Å], which does not have any counterpart in Ru–porphyrin or macrocyclic chemistry, is rather close to those found in Ru–phosphane derivatives.[4a, e, f] The question

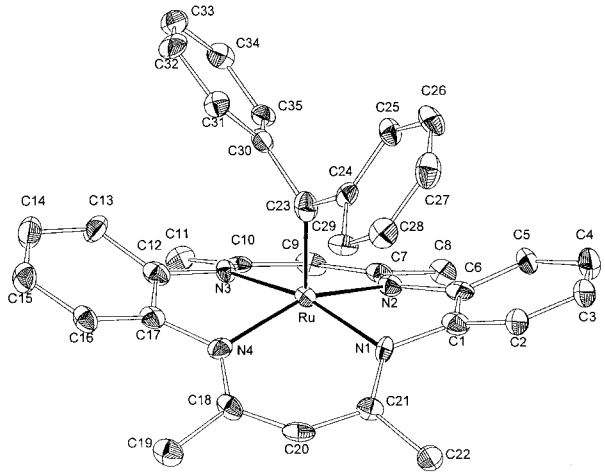


Figure 1. ORTEP drawing of **2** (thermal ellipsoids at 50% probability). Selected bond lengths [Å]: Ru–C23, 1.874(3); Ru–N1, 2.044(6); Ru–N2, 2.024(6); Ru–N3, 2.034(6); Ru–N4, 2.028(7). Bond angles [°]: Ru-C23-C24, 122.5(5); Ru-C23-C30, 122.3(5); C24-C23-C30, 116.4(6).

whether the oxidation state of Ru in **2** is II or IV can be reasonably answered by considering the Ru distance from the N$_4$ plane.[10] The value found in the present case [0.347(3) Å)] is expected for a low-spin diamagnetic d^6 center [compare with 0.216(5) Å in [Ru(tmtaa)(CO)(thf)] (**8**)].[7, 11] A much longer distance would be expected for a d^4 configuration. The tmtaa ligand has the usual saddle-shaped conformation.[5]

The carbene derivatives **2**–**4** are remarkably stable. However, when THF solutions of **2**–**4** are treated with carbon monoxide (1 atm), depending on the substituents at the carbene carbon, three different reaction pathways are observed. In the case of **2** we isolated **5**, which corresponds to the first common step of the reaction with the simple coordination of carbon monoxide *trans* to the diphenylcarbene fragment. In the case of **3** and **4**, carbon monoxide labilizes the carbene causing its migration to the *meso* carbon of the macrocycle.[5f] The reaction of the resulting free radical (intermediate A in Scheme 1) depends on the substituent R′. If R′ = H, the free radical causes the enlargement of the macrocycle to form the bent *cis*-dicarbonyl derivative **6**, whose structure has been confirmed by an X-ray analysis.[11] For R′ = COOMe (**4**), the free radical intermediate **A** delocalizes the free radical center on the COOMe substituent, which then undergoes a one-electron reduction and rearranges to form a Ru–O alkoxo bond (**7**, Figure 2).[8] The transfer of the carbene carbon to C9

 © WILEY-VCH Verlag GmbH, D-69451 Weinheim, 1998 1433-7851/98/3701-0148 $ 17.50+.50/0

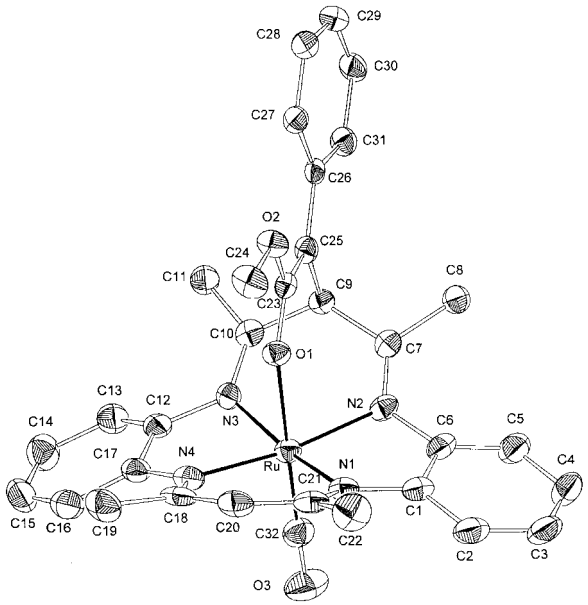


Figure 2. ORTEP drawing of **7** (thermal ellipsoids at 50% probability). Selected bond lengths [Å]: Ru–O1, 2.134(3); Ru–N1, 2.011(3); Ru–N2, 2.024(3); Ru–N3, 2.006(6); Ru–N4, 2.027(3); C7–C9, 1.518(5); C9–C10, 1.529(6); C9–C25, 1.538(5); C23–C25, 1.387(5); C23–O1, 1.260(4); C23–O2, 1.368(4).

removes the aromaticity and the planarity of the six-membered metallacycle Ru,N2,C7,C9,C10,N3; C9 is displaced 0.315(4) Å out of the N2,C7,C10,N3 plane. Consequently, C7–N2 [1.270(5) Å] and C10–N3 [1.278(5) Å] become imino groups, and the *meso*-alkylated tmtaa functions now as a monoanionic ligand. The assumption that C9 and Ru are bridged as shown in Scheme 1 is supported by a) the C23–C25 [1.390(5) Å] double bond character; b) the planarity of the bridge [torsional angle for C23-C25-C26-C27 is $-7.8(6)^\circ$]; c) some lengthening of the C23–O1 bond [1.260(4) Å], which is in agreement with a charge delocalization over the O1-C23-C25 fragment that functions as a monoanionic oxoallyl moiety.

The formation of **5**–**7**, on reaction of **2**–**4** with carbon monoxide, is extremely informative not only on the specific chemical behavior of the Ru–carbene in a macrocyclic environment, but in general on how such a functionality reacts. The Ru–carbene labilization by an incoming π acid is, in fact, the key step in the Ru–carbene assisted metathesis reaction,[4] though in the latter case the *cis*-geometrical proximity led to the reaction between the labilized carbene and the external substrate. The present investigation can serve as a model for the migration of carbene from the metal to the porphyrin in the iron systems.[2] Further applications of the present results are the use of this unconventional carbene bonded to a metal–macrocycle as a potential metathesis catalyst or as a precursor to high-valent ruthenium complexes.

Experimental Section

2: To a suspension of **1**·THF (3.77 g, 7.06 mmol) in THF (150 mL) was added a solution of diphenyldiazomethane (1.38 g, 7.10 mmol) in THF (50 mL). The mixture was stirred for 36 h, during which time it slowly became soluble with the concomitant evolution of nitrogen gas, and then concentrated to 10 mL. *n*-Hexane (30 mL) was added, and the microcrystalline material filtered off and dried in vacuo (3.55 g, 74%). Crystals suitable for X-ray analysis were grown in THF/hexane. Elemental analysis calcd for **2** ($C_{39}H_{40}N_4ORu$) (found): C 68.70 (68.78), H 5.91 (5.99), N 8.22 (8.52). ^{1}H NMR ([D$_6$]benzene, 200 MHz, 298 K): $\delta = 6.92-6.88$ (m, 4H, Ar); 6.73–6.69 (m, 4H, Ar); 6.45 (m, 10H, Ph); 4.91 (s, 2H, CH); 3.56 (m, 4H, THF); 2.13 (s, 12H, CH_3); 1.40 (m, 4H, THF). ^{13}C NMR (C_6D_6, 50.3 MHz, 298 K): $\delta = 291.8$ (C carbene). Crystals contain a THF molecule of crystallization.

7: An orange solution of **4** (0.58 g, 0.98 mmol) in THF (100 mL) was cooled (0°C) and then saturated with CO. The solution immediately became red and was kept overnight under CO. The solvent was removed in vacuo, and the product treated with hexane (30 mL), filtered, and the resulting solid dried in vacuo (0.39 g, 64%). Crystals suitable for X-ray analysis were grown in toluene/hexane (1/1). Elemental analysis calcd for **7** ($C_{32}H_{30}N_4O_3Ru$) (found): C 62.02 (61.50), H 4.88 (5.10), N 9.04 (8.92). IR (nujol, $\tilde{\nu} = 1905$ (s, CO), 1732 (m, COO) cm^{-1}. ^{1}H NMR ([D$_6$]benzene, 400 MHz, 298 K): $\delta = 7.87-6.51$ (m, 13H, Ar); 4.65 (s, 1H, HC=C); 4.48 (s, 1H, CH); 3.59 (s, 3H, OCH_3); 2.01 (s, 6H, CH_3); 1.88 (s, 6H, CH_3). ^{13}C NMR (C_6D_6, 100.6 MHz, 298 K): $\delta = 211.9$ (CO), 164.6, 161.7, 157.2, 150.9, 145.7, 142.4, 128.8, 126.9, 125.2, 122.0, 121.0, 120.6, 120.3, 109.1, 71.4, 63.7, 50.4, 23.7, 20.2.

Received: July 10, 1997 [Z10673IE]
German version: *Angew. Chem.* **1998**, *110*, 155–158

Keywords: carbenes · macrocycles · metathesis · rearrangements · ruthenium

[1] U. Schubert, H. Fischer, P. Hofmann, K. Weiss, K. H. Dötz, F. R. Kreissl, *Transition Metal Carbene Complexes*, VCH, Weinheim, **1983**; W. D. Wulff in *Advances in Metal-Organic Chemistry*, *Vol. 1* (Ed.: L. S. Liebeskind), Jay, London, **1989**, pp. 209–393; J. W. Herndon, S. U. Tumer, L. A. McMullen, J. J. Matasi, W. F. K. Schnatter in *Advances in Metal-Organic Chemistry*, *Vol. 3* (Ed.: L. S. Liebeskind), Jay, London, **1994**, pp. 51–95; M. P. Doyle, W. D. Wulff, L. S. Hegedus, J. R. Stille in *Comprehensive Organometallic Chemistry II*, *Vol. 12*, (Eds.: G. Wilkinson, F. G. A. Stone, E. W. Abel), Pergamon, Oxford, **1995**, Chapters 5.1–5.5.

[2] a) D. Mansuy, M. Lange, J. C. Chottard, J. F. Bartoli, B. Chevrier, R. Weiss, *Angew. Chem.* **1978**, *90*, 828–829; *Angew. Chem. Int. Ed. Engl.* **1978**, *17*, 781–782; b) A. L. Balch, R.-J. Cheng, G. N. La Mar, L. Latos-Grazynski, *Inorg. Chem.* **1985**, *24*, 2651–2656; c) P. J. Brothers, J. P. Collman, *Acc. Chem. Res.* **1986**, *19*, 209–215; d) D. Mansuy, *Pure Appl. Chem.* **1987**, *59*, 759–770; e) I. Artaud, N. Gregoire, J.-P. Battioni, D. Dupre, D. Mansuy, *J. Am. Chem. Soc.* **1988**, *110*, 8714–8716; f) I. Artaud, N. Gregoire, P. Leduc, D. Mansuy, *ibid.* **1990**, *112*, 6899–6905; g) J. R. Wolf, C. G. Hamaker, J.-P. Djukic, T. Kodadek, L. K. Woo, *ibid.* **1995**, *117*, 9194–9199; h) C. J. Ziegler, K. S. Suslick, *ibid.* **1996**, *118*, 5306–5307; i) D. Mansuy, J. P. Mahy in *Metalloporphyrin Catalyzed Oxidations* (Eds.: F. Montanari, L. Casella), Kluwer, Dordrecht, The Netherlands, **1994**, pp. 175–206.

[3] J. P. Collman, P. J. Brothers, L. McElwee-White, E. Rose, L. J. Wright, *J. Am. Chem. Soc.* **1985**, *107*, 4570–4571; J. P. Collman, P. J. Brothers, L. McElwee-White, E. Rose, *ibid.* **1985**, *107*, 6110–6111.

[4] a) P. Schwab, R. H. Grubbs, J. W. Ziller, *J. Am. Chem. Soc.* **1996**, *118*, 100–110; b) S. J. Miller, H. E. Blackwell, R. H. Grubbs, *ibid.* **1996**, *118*, 9606–9614; c) B. Mohr, D. M. Lynn, R. H. Grubbs, *Organometallics* **1996**, *15*, 4317–4325. d) R. H. Grubbs, S. J. Miller, G. C. Fu, *Acc. Chem. Res.* **1995**, *28*, 446–452; e) S. T. Nguyen, R. H. Grubbs, J. W. Ziller, *J. Am. Chem. Soc.* **1993**, *115*, 9858–9859; f) M. A. Esteruelas, F. J. Lahoz, E. Oñate, L. A. Oro, B. Zeier, *Organometallics* **1994**, *13*, 4258–4265.

[5] Leading references on the use of [tmtaa]$^{2-}$ as ancillary ligand in the organometallic chemistry of the early transition metals: a) V. L. Goedken, J. A. Ladd, *J. Chem. Soc. Chem. Commun.* **1981**, 910–911; *ibid.* **1982**, 142–144; b) C. Floriani, S. Ciurli, A. Chiesi-Villa, C. Guastini, *Angew. Chem.* **1987**, *99*, 86–88; *Angew. Chem. Int. Ed. Engl.* **1987**, *26*, 70–72; c) E. Solari, S. De Angelis, C. Floriani, A. Chiesi-Villa, C. Rizzoli, *Inorg. Chem.* **1992**, *31*, 96–101; d) S. De Angelis, E. Solari, E. Gallo, C. Floriani, A. Chiesi-Villa, C. Rizzoli, *ibid.* **1992**, *31*, 2520–2527; e) L. Giannini, E. Solari, C. Floriani, A. Chiesi-Villa, C.

 © WILEY-VCH Verlag GmbH, D-69451 Weinheim, 1998 1433-7851/98/3701-0149 $ 17.50+.50/0

Rizzoli, *Angew. Chem.* **1994**, *106*, 2279 – 2281; *Angew. Chem. Int. Ed. Engl.* **1994**, *33*, 2204 – 2206; f) L. Giannini, E. Solari, S. De Angelis, T. R. Ward, C. Floriani, A. Chiesi-Villa, C. Rizzoli, *J. Am. Chem. Soc.* **1995**, *117*, 5801 – 5811; g) D. G. Black, D. C. Swenson, R. F. Jordan, *Organometallics* **1995**, *14*, 3539 – 3550; h) A. J. Blake, P. Mountford, G. I. Nikonov, D. Swallow, *Chem. Commun.* **1996**, 1835 – 1836; i) H. Schumann, *Inorg. Chem.* **1996**, *35*, 1808 – 1813; j) G. I. Nikonov, A. J. Blake, P. Mountford, *ibid*. **1997**, *36*, 1107 – 1112.

[6] a) F. A. Cotton, J. Czuchajowska, *Polyhedron* **1990**, *9*, 1221 – 1224; b) L. Luo, E. D. Stevens, S. P. Nolan, *Inorg. Chem.* **1996**, *35*, 252 – 254.

[7] Correct analytical data are available for **3** – **6** and **8**.

[8] Crystal data for **2**: $C_{35}H_{32}N_4Ru \cdot C_4H_8O$, $M_r = 681.82$, triclinic, space group $P\bar{1}$, $a = 11.414(14)$ Å, $b = 14.297(12)$ Å, $c = 11.332(8)$ Å, $\alpha = 108.77(6)$, $\beta = 104.29(10)$, $\gamma = 105.25(11)^\circ$, $Z = 2$, $V = 1574(3)$ Å^3, $\rho_{calcd} = 1.439$ g cm^3, $\mu(Mo_{K\alpha}) = 5.37$ cm^{-1}, final $R1$, $wR2$, and S are 0.0878, 0.2225, and 1.030 for 410 parameters and 5831 unique observed reflections with $I > 2\sigma(I)$. **7**: $C_{32}H_{30}N_4O_3Ru \cdot 1.5\,C_7H_8$, $M_r = 757.37$, monoclinic, space group $P2_1/c$, $a = 11.269(4)$ Å, $b = 9.445(2)$ Å, $c = 33.854(12)$ Å, $\beta = 91.63(3)^\circ$, $Z = 4$, $V = 3602(2)$ Å^3, $\rho_{calcd} = 1.397$ g cm^3, $\mu(Mo_{K\alpha}) = 0.481$ mm^{-1}, final $R1$, $wR2$, and S are 0.0365, 0.1117, and 1.896 for 467 parameters and 4986 unique observed reflections with $I > 2\sigma(I)$. Crystallographic data (excluding structure factors) for the structures reported in this paper have been deposited with the Cambridge Crystallographic Data Centre as supplementary publication no. CCDC-179-177. Copies of the data can be obtained free of charge on application to CCDC, 12 Union Road, Cambridge CB2 1EZ, UK (fax: int. code + (44) 1223-336 033; e-mail: deposit@CCDC.cam.ac.uk).

[9] J.-P. Djukic, D. A. Smith, V. G. Young, Jr., L. K. Woo, *Organometallics* **1994**, *13*, 3020 – 3026.

[10] A correlation in tmtaa complexes has been established between the out of plane of the metal and its d^n configuration.[5d]

[11] C. Floriani, unpublished results.

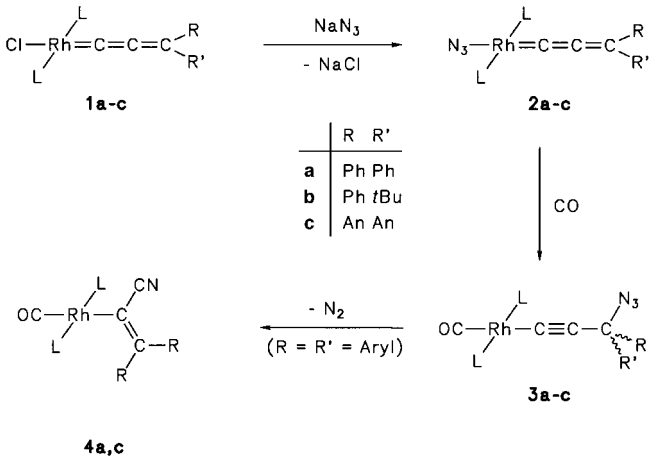
Unprecedented C–N Coupling Following Migration of an Azido Ligand to a C=C=CRR′ Unit**

Matthias Laubender and Helmut Werner*

Dedicated to Professor Lord Lewis on the occasion of his 70th birthday

Migratory insertion of CO into metal – carbon bonds represents one of the most important reactions in organometallic chemistry and homogeneous catalysis.[1, 2] In the course of our investigations on the reactivity of metallaallenes [L_nM=C=CRR′] and metallabutatrienes [L_nM=C=C=CRR′],[3] we found that not only compounds such as *trans*-[Rh(CH=CH$_2$)(=C=C=CPh$_2$)(P*i*Pr$_3$)$_2$]—generated in situ from **1a** and CH$_2$=CHMgBr—but also those of the general composition *trans*-[Rh(OR)(=C=C=CPh$_2$)(P*i*Pr$_3$)$_2$] (R = Ph, COCH$_3$) easily undergo insertion of the C$_3$Ph$_2$ unit into the Rh–C or Rh–O bond on treatment with CO.[4] This prompted us to prepare the structurally related complexes *trans*-[Rh(X)(=C=C=CRR′)(P*i*Pr$_3$)$_2$], where X is a N-bonded ligand, to find out whether a formal insertion of the allenylidene unit into the Rh–N bond also takes place in the presence of CO. Here we report that for X = N$_3$ such a reaction occurs and, more noteworthy, that the migration of the azide is followed by an unprecedented C–N coupling to generate a substituted acrylonitrile ligand.

The chlororhodium(I) complexes **1a** – **c** react with excess NaN$_3$ in acetone/THF (1/1) at room temperature to give, after recrystallization from acetone, deeply colored **2a** – **c** as crystalline solids in practically quantitative yields (Scheme 1;



Scheme 1. L = P*i*Pr$_3$, An = *p*-C$_6$H$_4$OMe.

2a: red, **2b**: green, **2c**: violet). The most characteristic features of the spectroscopic data of **2a** – **c** (Table 1) are the three low-field signals between $\delta = 255$ and 140 for the allenylidene

Table 1. Selected spectroscopic data for **2a** – **c**, **3b**, **4a**, **c**, and **5** (without data for phosphane ligands or *tert*-butyl and aryl groups).

2a: IR (C_6H_6): $\tilde{\nu} = 2060$ (N=N=N), 1870 cm^{-1} (C=C=C); ^{13}C NMR (100.6 MHz, CD_2Cl_2): $\delta = 244.6$ (dt, ^2J(Rh,C) = 15.1, ^3J(P,C) = 6.0 Hz, Rh=C=*C*=C), 233.7 (dt, ^1J(Rh,C) = 62.4, ^2J(P,C) = 17.1 Hz, Rh=*C*=C=C), 140.5 (s, Rh=C=C=*C*)

2b: IR (C_6H_6): $\tilde{\nu} = 2050$ (N=N=N), 1885 cm^{-1} (C=C=C); ^{13}C NMR (100.6 MHz, CD_2Cl_2): $\delta = 255.0$ (dt, ^1J(Rh,C) = 62.4, ^2J(P,C) = 17.1 Hz, Rh=*C*=C=C), 230.3 (dt, ^2J(Rh,C) = 16.1, ^3J(P,C) = 6.0 Hz, Rh=C=*C*=C), 162.0 (br s, Rh=C=C=*C*)

2c: IR (C_6H_6): $\tilde{\nu} = 2050$ (N=N=N), 1885 cm^{-1} (C=C=C); ^{13}C NMR (100.6 MHz, CD_2Cl_2): $\delta = 235.0$ (dt, ^1J(Rh,C) = 61.4, ^2J(P,C) = 17.1 Hz, Rh=*C*=C=C), 228.4 (dt, ^2J(Rh,C) = 15.1, ^3J(P,C) = 6.0 Hz, Rh=C=*C*=C), 142.0 (s, Rh=C=C=*C*)

3b: IR (C_6H_6): $\tilde{\nu} = 2100$ (N=N=N), 2065 (C≡C), 1945 cm^{-1} (CO); ^{13}C NMR (100.6 MHz, C_6D_6): $\delta = 195.4$ (m, RhCO), 121.5 (dt, ^1J(Rh,C) = 44.3, ^2J(P,C) = 19.1 Hz, Rh*C*≡C), 112.8 (dt, ^2J(Rh,C) = 12.1, ^3J(P,C) = 2.0 Hz, RhC≡*C*), 77.7 (br s, RhC≡C*C*)

4a: IR (C_6H_6): $\tilde{\nu} = 2145$ (C≡N), 1945 cm^{-1} (CO); ^{13}C NMR (100.6 MHz, C_6D_6): $\delta = 195.3$ (dt, ^1J(Rh,C) = 56.3, ^2J(P,C) = 15.6 Hz, RhCO), 160.3 (br t, ^3J(P,C) = 4.5 Hz, C=*C*Ph$_2$), 143.0 (dt, ^1J(Rh,C) = 31.2, ^2J(P,C) = 14.6 Hz, RhC), 125.2 (t, ^3J(P,C) = 2.0 Hz, C≡N)

4c: IR (C_6H_6): $\tilde{\nu} = 2145$ (C≡N), 1947 cm^{-1} (CO); ^{13}C NMR (100.6 MHz, C_6D_6): $\delta = 194.4$ (dt, ^1J(Rh,C) = 57.3, ^2J(P,C) = 15.1 Hz, RhCO), 160.4 (t, ^3J(P,C) = 5.0 Hz, C=*C*(*p*-MeOC$_6$H$_4$)$_2$), 136.9 (dt, ^1J(Rh,C) = 31.2, ^2J(P,C) = 15.1 Hz, RhC), 126.3 (br s, C≡N)

5: IR (C_6H_6): $\tilde{\nu} = 2213$ (NCO), 1892 cm^{-1} (C=C=C); ^{13}C NMR (100.6 MHz, C_6D_6): $\delta = 255.2$ (dt, ^1J(Rh,C) = 60.4, ^2J(P,C) = 17.1 Hz, Rh=*C*=C=C), 233.5 (dt, ^2J(Rh,C) = 15.1, ^3J(P,C) = 6.0 Hz, Rh=C=*C*=C), 159.9 (br s, Rh=C=C=*C*)

[*] Prof. Dr. H. Werner, Dipl.-Chem. M. Laubender
Institut für Anorganische Chemie der Universität
Am Hubland, D-97074 Würzburg (Germany)
Fax: Int. code + (49) 931-888 4605
e-mail: helmut.werner@mail.uni-wuerzburg.de

[**] This work was supported by the Deutsche Forschungsgemeinschaft (SFB 347), the Fonds der Chemischen Industrie, and BASF AG.

 © WILEY-VCH Verlag GmbH, D-69451 Weinheim, 1998 1433-7851/98/3701-0150 $ 17.50+.50/0

carbon atoms in the ^{13}C NMR spectra and the strong N=N=N stretching frequency at 2050–2060 cm^{-1} in the IR spectra. As the X-ray crystal structure analysis of **2b** (Figure 1) reveals,[5] the Rh-C1-C2-C3 chain is almost linear—as in the related chloro derivative *trans*-[RhCl{=C=C=C(*o*-Tol)Ph}-($PiPr_3$)$_2$][6]—whereas the *trans*-disposed Rh-N1-N2-N3 unit is bent. The bending of 143.7(5)° is more significant than in the analogous carbonyl compound *trans*-[Rh(N_3)(CO)(PPh_3)$_2$], in which the angle Rh-N1-N2 is 132(1)°.[7]

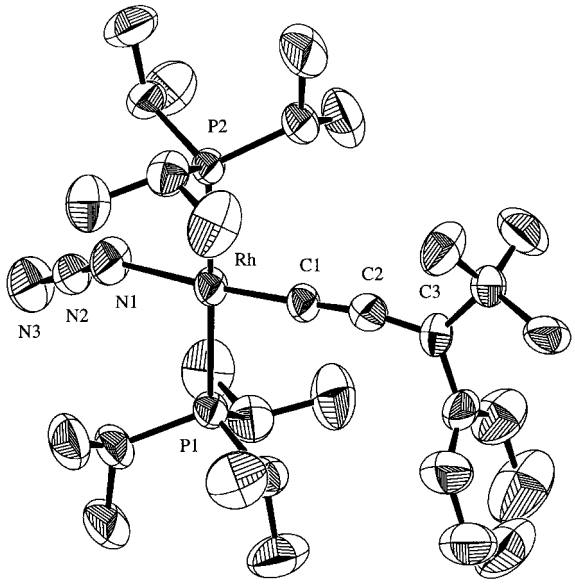


Figure 1. Molecular structure of **2b** (ORTEP plot) in the crystal. Selected bond lengths [Å] and angles [°]: Rh–P1 2.348(2), Rh–P2 2.347(1), Rh–C1 1.849(5), Rh–N1 2.057(5), N1–N2 1.177(7), N2–N3 1.161(7), C1–C2 1.269(7), C2–C3 1.348(7); P1-Rh-P2 175.59(6), C1-Rh-N1 175.7(2), P1-Rh-C1 89.4(2), P1-Rh-N1 93.5(2), P2-Rh-C1 89.9(2), P2-Rh-N1 87.4(2), Rh-C1-C2 177.6(5), Rh-N1-N2 143.7(5), N1-N2-N3 175.8(7), C1-C2-C3 169.1(6).

Like the phenolato- and acetatorhodium(I) derivatives *trans*-[Rh(OR)(=C=C=CPh_2)($PiPr_3$)$_2$], the azido complexes **2a–c** are highly reactive toward CO. When CO was passed through a solution of **2a–c** in toluene at −60 °C for 30 s and the temperature then slowly raised to 20 °C, yellow crystalline solids were obtained in yields of about 90 %. For R = Ph and R′ = *t*Bu the analytical composition of the isolated product corresponded to that of **3b** (see Scheme 1). In analogy to the related complexes *trans*-[Rh{C≡CC(OPh)Ph_2}-(CO)($PiPr_3$)$_2$],[4b] the ^{13}C NMR spectrum of **3b** displays two doublets of triplets at $\delta = 121.5$ and 112.8 for the carbon atoms of the C–C triple bond, and the IR spectrum two absorptions at 2100 and 2065 cm^{-1}, which are assigned to the N=N=N and C≡C stretching frequencies. Owing to these data, there is no doubt that treatment of **2b** with CO results in a migration of the N_3 ligand to the allenylidene unit and that the intact azido group in the product is linked to the γ-carbon atom of the C_3 chain.

Quite unexpectedly, the compounds obtained from **2a**, **c** and CO possess a different composition than **3b** (although they have the same color). The IR spectra display only *one* sharp absorption between 2000 and 2200 cm^{-1} (Table 1), and the ^{13}C NMR spectra *three* resonances at $\delta = 160–125$, which all show P–C coupling. These data, together with the stability of the solids toward air and moisture, indicate that the final products of the reaction of **2a** and **2c** with CO are the carbonyl(vinyl)rhodium complexes **4a** and **4c**, respectively. The assumption that they are formed via **3a** and **3c** as intermediates is consistent with the ^{31}P NMR ($\delta = 54.1$ (d, J(Rh,P) = 125.3 Hz)) and the ^{13}C NMR spectra of the species ($\delta = 127.4$ (dt, J(Rh,C) = 43.0, J(P,C) = 21.3 Hz, Rh–*C*≡C), 113.8 (br d, J(Rh,C) = 12.9 Hz, Rh–C≡*C*), 72.1 (s, C≡C–*C*)) generated by passing CO through a solution of **2a** in [D_8]THF at −55 °C. Upon warming to room temperature, this species is rapidly converted into **4a** by elimination of N_2. Theoretical work on the reactivity of unsaturated carbon chains C_n linked to a transition metal suggests that for $n = 3$ the α- and γ-carbon atoms are electron poor.[8] Therefore, it is conceivable that the supposed intermediates **3a** or **3c** rearrange to an isomer with a C(N_3)=C=CRR′ moiety. This would then eliminate N_2 to give the final product.

The X-ray crystal structure of **4c** is shown in Figure 2. The four-coordinated metal center possesses a slightly distorted square-planar configuration with Rh–C1, Rh–C3, Rh–P1, and

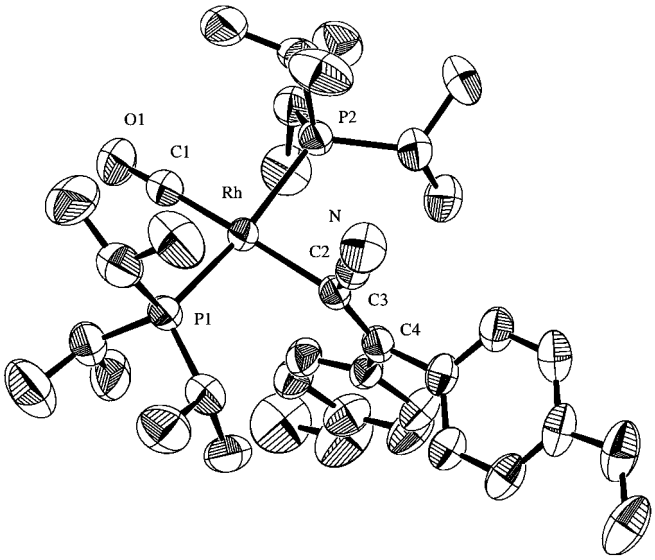


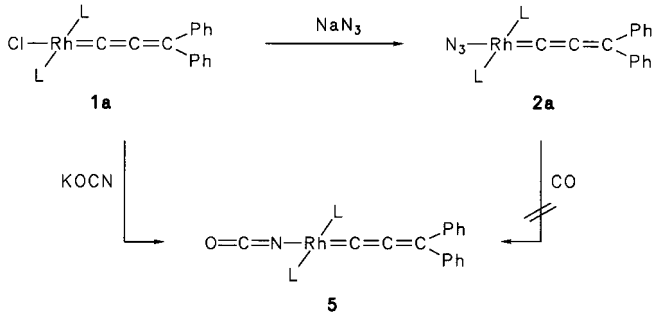
Figure 2. Molecular structure of **4c** (ORTEP plot) in the crystal. Selected bond lengths [Å] and angles [°]: Rh–P1 2.338(1), Rh–P2 2.340(1), Rh–C1 1.834(5), Rh–C3 2.106(4), C1–O1 1.146(5), C2–C3 1.428(6), C2–N 1.144(5), C3–C4 1.367(3); P1-Rh-P2 167.10(4), C1-Rh-C3 174.6(2), P1-Rh-C1 89.7(2), P1-Rh-C3 91.9(1), P2-Rh-C1 88.5(1), P2-Rh-C3 91.2(1), Rh-C1-O1 175.1(4), Rh-C3-C2 109.8(3), Rh-C3-C4 133.2(3), C3-C2-N 174.9(5), C2-C3-C4 117.0(4).

Rh–P2 distances that are quite similar to those of the butadienyl complex *trans*-[Rh{C(CH=CH_2)=CHPh}(CO)($PiPr_3$)$_2$].[9] The C1-Rh-C3 axis is nearly linear, whereas the P1-Rh-P2 axis is somewhat bent; the bending of 167.10(4)° is more pronounced than in **2b** (175.59(6)°). The plane including C2, C3, and C4 is almost perpendicular (86.8(1)°) to that formed by Rh, C1, C3, P1, and P2, which probably minimizes the repulsive interactions between the six isopropyl groups and the substituents at the C–C double bond.

In contrast to several azidometal complexes,[10] the allenylidene derivatives **2a–c** do not react with CO to give the corresponding isocyanato compounds *trans*-[Rh(NCO)-

 © WILEY-VCH Verlag GmbH, D-69451 Weinheim, 1998 1433-7851/98/3701-0151 $ 17.50+.50/0

(=C=C=CRR′)(P*i*Pr$_3$)$_2$]. Therefore, one representative of this type of species was prepared by a different route (Scheme 2). Treatment of **1a** with excess KOCN in acetone/THF (1/1) at room temperature gives complex **5** as a red solid in 95%



Scheme 2. L = P*i*Pr$_3$.

yield. Under the conditions used to form **3a**, **c** (in situ) and **3b**, **5** is completely inert toward CO. As far as N-bonded ligands are concerned, the reactivity of the Rh-bonded azido group in **2a**–**c** toward CO is unique. To the best of our knowledge, there is also no precedence for the type of C–N coupling which occurs during the conversion of **2a** and **2c** into **4a** and **4c**. With regard to the lability of the intermediate observed during the formation of **4a**, it is rather surprising that the related substituted alkynyl complex **3b** is completely inert and does not react either thermally or photochemically to afford *trans*-[Rh{C(CN)=C(Ph)*t*Bu}(CO)(P*i*Pr$_3$)$_2$]. Treatment of **4a** and **4c** with trifluoracetic acid results in cleavage of the Rh–C σ bond, leading to formation of the corresponding acrylonitrile derivatives R$_2$C=CHCN (R = Ph, An) in quantitative yields.

Received: July 29, 1997 [Z10748IE]
Publication delayed at authors' request
German version: *Angew. Chem.* **1998**, *110*, 158–160

Keywords: allenylidene complexes · azido complexes · C–N coupling · insertions · rhodium

[1] C. Elschenbroich, A. Salzer, *Organometallics*, VCH, Weinheim, **1992**, chap. 17; J. P. Collman, L. S. Hegedus, J. R. Norton, R. G. Finke, *Principles and Applications of Organotransition Metal Chemistry*, University Science Books, Mill Valley, CA, **1987**, chap. 6; A. Yamamoto, *Organotransition Metal Chemistry*, Wiley, New York, **1986**, chap. 6.3.

[2] Reviews: A. Wojcicki, *Adv. Organomet. Chem.* **1973**, *11*, 87–145; F. Calderazzo, *Angew. Chem.* **1977**, *89*, 305–317; *Angew. Chem. Int. Ed. Engl.* **1977**, *16*, 299–311; T. C. Flood, *Top. Stereochem.* **1981**, *12*, 37–117; J. J. Alexander in *The Chemistry of the Metal–Carbon Bond*, *Vol. 2* (Eds.: F. R. Hartley, S. Patai), Wiley, New York, **1985**, pp. 339–400.

[3] Reviews: H. Werner, *Nachr. Chem. Tech. Lab.* **1992**, *40*, 435–444; *J. Organomet. Chem.* **1994**, *475*, 45–55; *Chem. Commun.* **1997**, 903–910.

[4] a) R. Wiedemann, P. Steinert, O. Gevert, H. Werner, *J. Am. Chem. Soc.* **1996**, *118*, 2495–2496; b) H. Werner, R. Wiedemann, M. Laubender, J. Wolf, B. Windmüller, *Chem. Commun.* **1996**, 1413–1414.

[5] Data for the X-ray structure analyses: **2b**: crystals from pentane (−20 °C), $C_{31}H_{56}N_3P_2Rh$ (635.7); crystal dimensions 0.3 × 0.3 × 0.5 mm; triclinic; space group $P\bar{1}$ (no. 2); $a = 9.0808(6)$, $b = 11.7579(6)$, $c = 16.886(2)$ Å, $\alpha = 98.035(8)$, $\beta = 90.944(8)$, $\gamma = 102.408(5)°$, $Z = 2$, $V = 1741.5(3)$ Å^3, $\rho_{calcd} = 1.212$ g cm^{-3}; $T = 293(2)$ K; $2\Theta_{max.} = 46°$; of 4465 reflections measured, 4105 were unique ($R_{int.} = 0.0173$) and 3247 observed ($I > 2\sigma(I)$); Enraf-Nonius CAD4 diffractometer, $Mo_{K\alpha}$ radiation ($\lambda = 0.71073$ Å), graphite-monochromated, zirconium filter (factor 15.4); Lp and empirical absorption corrections (Ψ scan, min. transmission 96.83%). The structure was solved by direct methods and refined with the full matrix, least-squares method; $R_1 = 0.0399$, $wR_2 = 0.0839$ (for 3247 reflections with $I > 2\sigma(I)$), $R_1 = 0.0612$, $wR_2 = 0.1069$ (for all 4105 data); data-to-parameter ratio 10.98; residual electron density +0.753/−0.484 e Å^{-3}. **4c**: crystals from diethyl ether (−20 °C), $C_{36}H_{56}NO_3P_2Rh$ (715.7); crystal dimensions 0.3 × 0.3 × 0.4 mm; monoclinic; space group $P2_1/c$ (no. 14); $a = 11.560(1)$, $b = 16.790(1)$, $c = 19.253(1)$ Å, $\beta = 93.48(1)°$, $Z = 4$, $V = 3730.1(4)$ Å^3; $\rho_{calcd} = 1.274$ g cm^{-3}; $T = 293(2)$ K; $2\Theta_{max.} = 46°$; of 4984 reflections measured, 4238 were unique ($R_{int.} = 0.0174$) and 3431 observed ($I > 2\sigma(I)$); Enraf-Nonius CAD4 diffractometer, $Mo_{K\alpha}$ radiation ($\lambda = 0.71073$ Å), graphite-monochromated, zirconium filter (factor 15.4); Lp and empirical absorption corrections (Ψ scan, min. transmission 93.72%). The structure was solved by direct methods and refined with the full-matrix, least-squares method; $R_1 = 0.0340$, $wR_2 = 0.0703$ (for 3431 reflections with $I > 2\sigma(I)$), $R_1 = 0.0492$, $wR_2 = 0.0792$ (for all 4238 data); data-to-parameter ratio 10.53; residual electron density +0.343/−0.223 e Å^{-3}. Crystallographic data (excluding structure factors) for the structures reported in this paper have been deposited with the Cambridge Crystallographic Data Centre as supplementary publication no. CCDC-100601. Copies of the data can be obtained free of charge on application to CCDC, 12 Union Road, Cambridge CB2 1EZ, UK (fax: int. code + (1223) 336-033; e-mail: deposit@ccdc.cam.ac.uk).

[6] H. Werner, T. Rappert, R. Wiedemann, J. Wolf, N. Mahr, *Organometallics* **1994**, *13*, 2721–2727.

[7] Z. G. Aliev, L. O. Atovmyan, O. V. Golubeva, V. V. Karpov, G. I. Kozub, *Zh. Strukt. Khim.* **1977**, *18*, 336–340.

[8] a) B. E. R. Schilling, R. Hoffmann, D. L. Lichtenberger, *J. Am. Chem. Soc.* **1979**, *101*, 585–591; b) N. M. Kostic, R. F. Fenske, *Organometallics* **1982**, *1*, 974–982.

[9] R. Wiedemann, P. Steinert, M. Schäfer, H. Werner, *J. Am. Chem. Soc.* **1993**, *115*, 9864–9865.

[10] W. Beck, *J. Organomet. Chem.* **1990**, *383*, 143–160.

Three-Component Coupling Reactions of Alkyl Iodides, 1,3-Dienes, and Carbonyl Compounds by Sequential Generation of Radical and Anionic Species with $CrCl_2$**

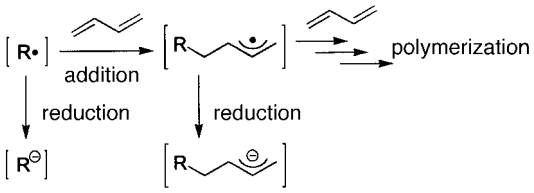
Kazuhiko Takai,* Naoto Matsukawa, Akira Takahashi, and Takafumi Fujii

Although conjugated dienes are good radical-trapping agents,[1] their use in organic synthesis is quite limited because further radical addition leading to polymerization occurs. Such radical chain reactions stem from the similar reactivity of the formed allylic radicals and the starting alkyl radicals. One way to prevent the undesirable side reactions is to reduce the allylic radicals to the corresponding anions (Scheme 1). However, a strong reductant such as samarium(II) readily reduces alkyl radicals, formed from alkyl halides, to furnish alkyl anions; the lifetime of the alkyl radicals is so short that intermolecular C–C bond formation cannot occur.[2, 3] We

[*] Prof. Dr. K. Takai, N. Matsukawa, A. Takahashi, T. Fujii
Department of Applied Chemistry, Faculty of Engineering
Okayama University
Tsushima, Okayama 700 (Japan)
Fax: Int. code + (81) 86-251-8021
e-mail: ktakai@cc.okayama-u.ac.jp

[**] Financial support by a Grant-in-Aid for Scientific Research on Priority Area No. 283 from the Ministry of Education, Science, Sports and Culture of Japan is gratefully acknowledged.

 © WILEY-VCH Verlag GmbH, D-69451 Weinheim, 1998 1433-7851/98/3701-0152 $ 17.50+.50/0

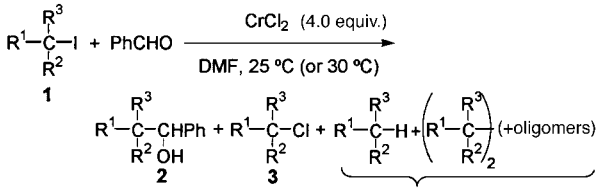


Scheme 1.

report here that chromium(II) chloride, a mild reductant, can discriminate between alkyl iodides, alkyl radicals, and allylic radicals. As a result, 1) an alkyl radical has a sufficient lifetime to undergo intermolecular addition to a 1,3-diene, and 2) radical polymerization of the 1,3-diene can be suppressed by fast one-electron reduction of the allylic radicals. The sequential process of addition and reduction[4, 5] provides an allylic chromium species[6, 7] which adds to an aldehyde to afford a three-component coupling product.

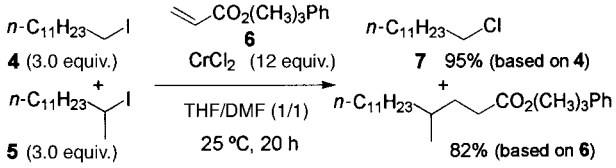
Chromium(II) salts are mild reducing agents, and reactive halides (such as allylic and benzylic halides) can be reduced to give the corresponding organochromium reagents.[8–10] However, it is more difficult to reduce simple alkyl halides in *aprotic* solvents. For example, treating a mixture of 1-iododododecane (**1a**, $R^1 = n\text{-}C_{11}H_{23}$, $R^2 = R^3 = H$) and benzaldehyde with $CrCl_2$ in DMF at 30 °C for 16 h afforded the Grignard adduct **2a** in only 7% yield, and most of the halide was recovered as 1-chlorododecane (**3a**).[4a] This result suggests that, in the case of primary alkyl iodides, the rate of substitution by the chloride ion is faster than that of one-electron reduction with a chromium(II) ion. In contrast, the reduction of secondary or tertiary alkyl iodides to form radical or anionic species proceeds smoothly under the same conditions.

Treating a mixture of the secondary alkyl iodide **1b** ($R^1 = n\text{-}C_{11}H_{23}$, $R^2 = Me$, $R^3 = H$) and benzaldehyde with $CrCl_2$ in DMF at 25 °C for 20 h gave the Grignard adduct **2b** and the alkyl chloride **3b** in 27 and 29% yield, respectively. Compounds derived from the alkyl radical (the dimer and the corresponding alkane) were also obtained in a combined yield



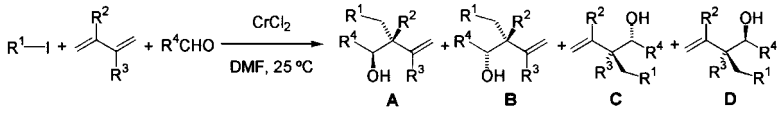
a) R^1 = alkyl; R^2, R^3 = H, 16 h	7%	88%	<2%	
b) R^1, R^2 = alkyl; R^3 = H, 20 h	27%	29%	44%	
c) R^1, R^2, R^3 = alkyl, 5 h	9%	<1%	84%	

of 44%. In the case of the tertiary alkyl iodide **1c** ($R^1 = n\text{-}C_{10}H_{21}$, $R^2 = R^3 = Me$), the Grignard adduct **2c** was produced in 9% yield, although most of the iodide was converted into the corresponding alkyl radicals. However, the formation of alkyl chloride **3c** was not observed. The intermediate alkyl radicals derived from the secondary iodide **5** could be trapped intermolecularly with the α,β-unsaturated ester **6** in 82% yield;[1,5,10b] the primary iodide **4** was recovered as the corresponding chloride **7** in 95% yield.



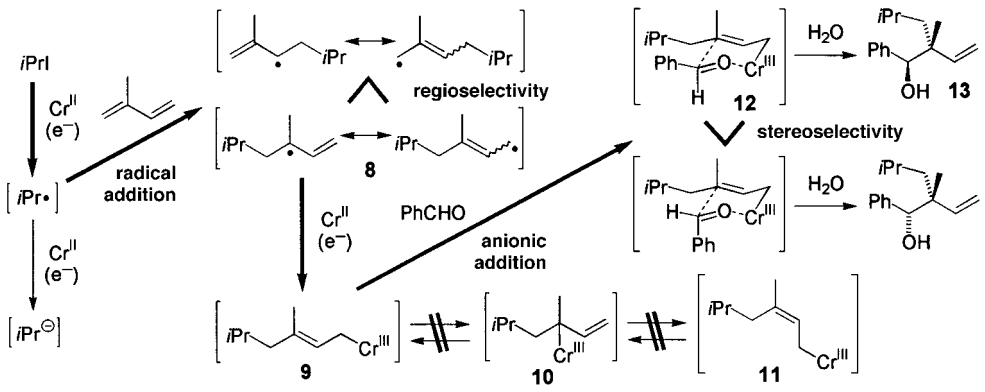
The secondary and tertiary alkyl radicals have a sufficient lifetime to undergo intermolecular addition to a 1,3-diene. Radical polymerization of the 1,3-diene did not occur, because fast one-electron reduction of the allylic radicals (leading to reactive allylic chromium species)[6, 7] took place smoothly. For example, treating a mixture of isopropyl iodide, isoprene, and benzaldehyde with $CrCl_2$ in DMF at 25 °C for 8 h produced two regioisomeric homoallylic alcohols in 53 and 13% yields, respectively (Table 1, entry 5). The major

Table 1. Three-component coupling of alkyl iodides, 1,3-dienes, and aldehydes.[a]



Entry	R^1	R^2	R^3	R^4	t [h]	Yield [%] **A**+**B**+**C**+**D**	Regioselectivity (**A**+**B**):(**C**+**D**)	d.r. **A**:**B**	**C**:**D**
1	*t*Bu	Me	H	Ph	0.1	71	78:22	>98:2	>98:2
2	*t*Bu	Me	H	$n\text{-}C_8H_{17}$	0.1	96	78:22	>98:2	96:4
3	*t*Bu	Me	Me	Ph	0.1	93	–	90:10	–
4	*t*Bu	Me	Me	$n\text{-}C_8H_{17}$	0.1	98	–	90:10	–
5	*i*Pr	Me	H	Ph	8	66	80:20	>98:2	69:31
6	*i*Pr	Me	H	$n\text{-}C_8H_{17}$	8	91	77:23	>98:2	67:33
7	*i*Pr	Me	H	$n\text{-}C_8H_{17}$	20	92[b]	68:32	79:21	68:32
8	*i*Pr	Me	H	$c\text{-}C_6H_{11}$	8	98	78:22	>98:2	62:38
9	*i*Pr	Me	Me	Ph	8	71	–	81:19	–
10	*i*Pr	Me	Me	$n\text{-}C_8H_{17}$	8	88	–	80:20	–
11	*i*Pr	Me	Me	$c\text{-}C_6H_{11}$	8	91	–	82:18	–

[a] The reactions were conducted on a 1.0-mmol scale. The ratios of the isomers were determined by isolation, gas chromatography, and/or NMR spectroscopy. [b] The following amounts were used per mole of nonanal: chromium(II) chloride: 0.2 mol, manganese: 2.6 mol, Me_3SiCl: 3.7 mol. The reaction was conducted in DMF/THF (1/1).

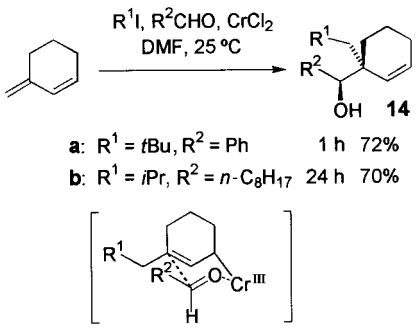


Scheme 2. Mechanism of the three-component coupling of alkyl iodides, 1,3-dienes, and aldehydes.

regioisomer contained one stereoisomer, which has isobutyl and hydroxyl groups in an *anti* geometry. The stereochemistry was determined by comparison with an authentic sample prepared by the Knochel procedure.[7] When *tert*-butyl iodide was used, the three-component addition proceeded within 10 min due to facile reduction of the iodide (entries 1–4). A catalytic system with chromium(II), manganese, and Me_3SiCl could also be employed for the three-component addition, although the regio- and stereoselectivities decreased slightly (entry 7).[11]

A mechanism which possibly explains the regio- and stereochemistry of the major isomer is shown in Scheme 2. An isopropyl radical preferentially adds to isoprene at the olefinic terminal on the side of the methyl group to form the most stable allylic radical **8**. Reduction of **8** produces the sterically favored extended allylic chromium reagent **9**. There is no fast equilibrium between the three allylic chromium compounds **9**, **10**, and **11** owing to the steric effect of γ,γ-disubstitution.[7] The chromium reagent **9** adds to benzaldehyde via the less sterically demanding six-membered transition state **12** to give homoallylic alcohol **13** selectively.[6, 7] This mechanism explains why diastereoselectivities for reactions with 2,3-dimethyl-1,3-butadiene (entries 3, 4, 9–11) are lower than for those with isoprene. Reduction of the steric difference by changing the β-substituent from H to Me decreases the selectivity of the extended allylic chromium reagents.

An example of the three-component addition to a cyclic compound is shown in Scheme 3. Because the stereochemistry of the allylic chromium reagent determines the configuration of an adduct with an aldehyde, fixation of a double bond by the cyclic system selectively produces only one of the stereoisomers **14**.



Scheme 3.

Experimental Section

Three-component coupling of isopropyl iodide, isoprene, and nonanal (Table 1, entry 6): To a mixture of $CrCl_2$ (0.74 g, 6.0 mmol)[12] in dry, oxygen-free DMF (12 mL) was added a solution of nonanal (0.14 g, 1.0 mmol), isoprene (0.20 g, 3.0 mmol), and isopropyl iodide (0.51 g, 3.0 mmol) in DMF (3 mL) at 25 °C. After the reaction mixture was stirred at 25 °C for 8 h it was poured into water (15 mL), and the mixture extracted with Et_2O (3×10 mL). The organic extracts were dried over anhydrous magnesium sulfate and concentrated. Purification by column chromatography on silica gel (hexane/Et_2O, 400/1) gave (3*R**,4*S**)-3-isobutyl-3-methyl-1-dodecen-4-ol in 70% yield (0.18 g) and 3-isobutyl-2-methyl-1-dodecen-4-ol in 21% yield (53 mg, *anti*:*syn* = 67:33).

14a: To a mixture of $CrCl_2$ (0.49 g, 4.0 mmol) in dry, oxygen-free DMF (7 mL) was added a solution of benzaldehyde (0.11 g, 1.0 mmol), 3-methylenecyclohexene (0.19 g, 2.0 mmol), and *tert*-butyl iodide (0.37 g, 2.0 mmol) in DMF (3 mL) at 25 °C. After the reaction mixture was stirred at 25 °C for 1 h it was poured into water (15 mL), and the mixture extracted with Et_2O (3×10 mL). The organic extracts were dried over anhydrous magnesium sulfate and concentrated. Purification by column chromatography on silica gel (hexane/Et_2O, 50/1) gave (1*R**,1′*R**)-(1-neopentyl-2-cyclohexenyl)(phenyl)methanol in 72% yield (0.19 g).

Received: July 7, 1997 [Z10646IE]
German version: *Angew. Chem.* **1998**, *110*, 160–163

Keywords: chromium · radical reactions · synthetic methods

[1] a) A. L. J. Beckwith, *Tetrahedron* **1981**, *37*, 3073–3100; b) G. Stork in *Current Trends in Organic Synthesis* (Ed.: H. Nozaki), Pergamon, Oxford, **1983**, pp. 359–370; c) Y. Ueno, *J. Synth. Org. Chem. Jpn.* **1984**, *42*, 1121–1131; d) B. Giese, *Angew. Chem.* **1985**, *97*, 555–567; *Angew. Chem. Int. Ed. Engl.* **1985**, *24*, 553–565; *Radicals in Organic Synthesis: Formation of Carbon-Carbon Bonds*, Pergamon, Oxford, **1986**; e) D. P. Curran, *Synthesis* **1988**, 417–439, 489–513; in *Comprehensive Organic Synthesis, Vol. 4* (Eds.: B. M. Trost, I. Fleming), Pergamon, Oxford, **1991**, pp. 715–777; f) J. M. Tedder, J. C. Walton, *Tetrahedron* **1980**, *36*, 701–707.

[2] G. A. Molander, C. Kenny, *J. Org. Chem.* **1991**, *56*, 1439–1445; G. A. Molander, J. A. McKie, *ibid.* **1995**, *60*, 872–882; D. P. Curran, M. J. Totleben, *J. Am. Chem. Soc.* **1992**, *114*, 6050–6058; D. P. Curran, T. L. Fevig, C. P. Jasperse, M. J. Totleben, *Synlett* **1992**, 943–961; G. A. Molander, C. R. Harris, *Chem. Rev.* **1996**, *96*, 307–338; T. Skrydstrup, *Angew. Chem.* **1997**, *109*, 355–358; *Angew. Chem. Int. Ed. Engl.* **1997**, *36*, 345–347.

[3] Coupling of a ketone and a 1,3-diene with SmI_2 under protic conditions: O. Ujikawa, J. Inanaga, M. Yamaguchi, *Tetrahedron Lett.* **1989**, *30*, 2837–2840.

[4] Intramolecular C–C bond formation with radicals followed by one-electron reduction and anionic addition: a) Cr^{II}/vitamin B_{12} or Cr^{II}: K. Takai, K. Nitta, O. Fujimura, K. Utimoto, *J. Org. Chem.* **1989**, *54*, 4732–4734; T. Lübbers, H. J. Schäfer, *Synlett* **1992**, 743–744; b) Et_2Zn/[$PdCl_2$(dppf)] or [Ni(acac)$_2$] (dppf = 1,1′-bis(diphenylphos-

 © WILEY-VCH Verlag GmbH, D-69451 Weinheim, 1998 1433-7851/98/3701-0154 $ 17.50+.50/0

phanyl)ferrocene; Hacac = acetylacetone): H. Stadtmüller, R. Lentz, C. E. Tucker, T. Stüdemann, W. Dörner, P. Knochel, *J. Am. Chem. Soc.* **1993**, *115*, 7027 – 7028; H. Stadtmüller, C. E. Tucker, A. Vaupel, P. Knochel, *Tetrahedron Lett.* **1993**, *34*, 7911 – 7914; A. Vaupel, P. Knochel, *ibid.* **1994**, *35*, 8349 – 8352; *J. Org. Chem.* **1996**, *61*, 5743 – 5753; c) Zn: B. S. Bronk, S. J. Lippard, R. L. Danheiser, *Organometallics* **1993**, *12*, 3340 – 3349.

[5] K. Takai, T. Ueda, N. Ikeda, T. Moriwake, *J. Org. Chem.* **1996**, *61*, 7990 – 7991.

[6] a) Y. Okude, T. Hiyama, H. Nozaki, *Tetrahedron Lett.* **1977**, 3829 – 3830; b) C. T. Buse, C. H. Heathcock, *ibid.* **1978**, 1685 – 1688; c) T. Hiyama, K. Kimura, H. Nozaki, *ibid.* **1981**, *22*, 1037 – 1040.

[7] C. Jubert, S. Nowotny, D. Kornemann, I. Antes, C. E. Tucker, P. Knochel, *J. Org. Chem.* **1992**, *57*, 6384 – 6386; S. Nowotny, C. E. Tucker, C. Jubert, P. Knochel, *ibid.* **1995**, *60*, 2762 – 2772.

[8] Reviews of organochromium reagents: a) K. Takai, K. Utimoto, *J. Synth. Org. Chem. Jpn.* **1988**, *46*, 66 – 77; b) N. A. Saccomano in *Comprehensive Organic Synthesis, Vol. 1* (Eds.: B. M. Trost, I. Fleming), Pergamon, Oxford, **1991**, pp. 173 – 209; c) P. Cintas, *Synthesis* **1992**, 248 – 257.

[9] Reduction of alkyl halides with chromium(II) in protic solvents: a) F. A. L. Anet, E. Isabelle, *Can. J. Chem.* **1958**, *36*, 589 – 590; b) J. K. Kochi, D. D. Davis, *J. Am. Chem. Soc.* **1964**, *86*, 5264 – 5271; c) J. K. Kochi, J. W. Powers, *ibid.* **1970**, *92*, 137 – 146; d) J. K. Crandall, W. J. Michaely, *J. Org. Chem.* **1984**, *49*, 4244 – 4248.

[10] The reducing power of chromium(II) is enhanced by complexation with ethylenediamine: a) J. K. Kochi, P. E. Mocadlo, *J. Am. Chem. Soc.* **1966**, *88*, 4094 – 4096; b) H. I. Tashtoush, R. Sustmann, *Chem. Ber.* **1992**, *125*, 287 – 289.

[11] A. Fürstner, N. Shi, *J. Am. Chem. Soc.* **1996**, *118*, 2533 – 2534, 12349 – 12357.

[12] Chromium(II) chloride (> 95% purity) was purchased from Aldrich Chemical Co.

First Isolation and Structural Characterization of Bis(Anthracene)Metal Complexes: $[Ti(\eta^6\text{-}C_{14}H_{10})(\eta^4\text{-}C_{14}H_{10})(\eta^2\text{-dmpe})]$ and $[Ti(\eta^4\text{-}C_{14}H_{10})(\eta^2\text{-}C_{14}H_{10})(\eta^5\text{-}C_5Me_5)]^-$**

John K. Seaburg, Paul J. Fischer, Victor G. Young, Jr., and John E. Ellis*

Dedicated to Professor Wolfgang Beck on the occasion of his 65th birthday

Reagents that function as storable sources of "naked" metal atoms or highly unsaturated organometallic groups offer exciting new possibilities in chemical syntheses owing to their facile reactions with a variety of small molecules and their strongly reducing nature.[1] Of particular significance in this regard are fused-ring arenemetal(0) complexes, which are of substantial interest as possible precursors for the general exploration of zerovalent transition metal chemistry by virtue of the remarkable lability of these arene ligands.[2] Outstanding among these are bis(naphthalene)metal(0) species,[3] for which conventional syntheses were recently reported for the first time.[4] Basolo has presented evidence to suggest that bis(anthracene)metal(0) complexes may be even more labile than their naphthalene counterparts.[5] The only previously known complex of this type, bis(anthracene)chromium(0), was obtained as an inseparable mixture of complex and excess free anthracene by the cocondensation of chromium atoms and anthracene vapor in a metal atom reactor.[6] To our knowledge, no ligand exchange reactions of this compound have been reported to date. The dearth of information on potentially interesting bis(anthracene)metal complexes prompted an investigation of their possible conventional syntheses by the interaction of main group metal anthracenes with transition metal halides. Previously, this approach yielded only mono(anthracene)metal complexes.[7] We now report on the syntheses and molecular structures of the first well-characterized metal complexes containing two coordinated anthracene ligands: $[Ti(C_{14}H_{10})_2(dmpe)]$ (**1**, dmpe = 1,2-bis(dimethylphosphino)ethane) and $[Ti(C_{14}H_{10})_2(C_5Me_5)]^-$ (**2**, counterion $[K(18\text{-crown-6})(thf)_2]^+$), THF = tetrahydrofuran). They are also of interest as the first structurally characterized Group 4 metal anthracene complexes.[8]

Reduction of $[TiCl_4(dmpe)]$ or $[TiCl_3(C_5Me_5)]$ by four equivalents of alkali metal anthracene (Na or K) in THF at −55 to −65°C gave deep red-brown or green-black solutions, from which **1** or $[K(18\text{-crown-6})(thf)_2]$-**2** were isolated in 54% or 28% yield, respectively, as satisfactorily pure, diamagnetic and deep purple or black microcrystalline substances (see Experimental Section). Reactions of pure **1** (in the presence of an additional equivalent of dmpe) or **2** in THF at −55 to −65°C with normal pressures of carbon monoxide, under the same conditions described for the corresponding alkali metal naphthalene mediated carbonylations,[9,10] provided the known $[Ti(CO)_3(dmpe)_2]$ (**3**)[11] or $[Ti(CO)_4(C_5Me_5)]^-$(**4**)[12] in 57% or 62% yields, respectively, of product isolated as the $[K(18\text{-crown-6})]^+$ salt. These syntheses, summarized in Equations 1 and 2, are very similar to previously reported

$$[TiCl_4(dmpe)] + 4\ NaC_{14}H_{10} \xrightarrow[-60\ ^\circ C]{THF} \mathbf{1} \xrightarrow[dmpe,\ -55 \rightarrow 20\ ^\circ C]{THF,\ CO} \mathbf{3} \quad (1)$$

$$[TiCl_3(C_5Me_5)] + 4\ KC_{14}H_{10} \xrightarrow[18\text{-C-}6,\ -60\ ^\circ C]{THF} \mathbf{2} \xrightarrow[-65 \rightarrow 20\ ^\circ C]{THF,\ CO} \mathbf{4} \quad (2)$$

naphthalene anion routes to these carbonyls and lend substantial credence to original suggestions that labile (naphthalene)metal complexes were involved in these and related carbonylation reactions.[13, 14] The anthracene complexes **1** and **2** appear to be substantially more stable in solution and the solid state than corresponding (naphthalene)titanium species, which could not be isolated as pure substances despite numerous attempts.[15] Nevertheless, at least in their reactions with carbon monoxide, **1** and **2** function as effective sources of

[*] Prof. J. E. Ellis, J. K. Seaburg, P. J. Fischer, Dr. V. G. Young, Jr.
Department of Chemistry
University of Minnesota
Minneapolis, MN 55455 (USA)
Fax: Int. code + (1) 612-626 7541
e-mail: ellis@chem.umn.edu

[**] Highly Reduced Organometallics, Part 44. This work was supported by the U.S. National Science Foundation and the Petroleum Research Fund administered by the American Chemical Society. We are grateful to Mikhail V. Barybin for carrying out the magnetic susceptibility measurements, a referee for helpful comments on the NMR spectra, and Christine Lundby for expert assistance in the preparation of the manuscript. Part 43: Ref. [4].

 © WILEY-VCH Verlag GmbH, D-69451 Weinheim, 1998 1433-7851/98/3701-0155 $ 17.50+.50/0

the highly unsaturated molecular fragments Ti(dmpe) and $[Ti(\eta^5\text{-}C_5Me_5)]^-$. Their reactions with similar small molecules are under investigation.

NMR solution spectra of **1** and **2** at or near room temperature established that their stoichiometries are identical to those observed in the solid state. HETCOR (i.e., ^1H,^{13}C-correlated) NMR spectra of **1** permitted identification of four equally intense quaternary ^{13}C signals at $\delta = 127.5$, 133.9, 135.3, and 148.6, which are indicative of two inequivalent ligated anthracenes. ^1H NMR spectra showed four equally intense AA′BB′ multiplets below $\delta = 5.4$, which are assigned to hydrogen atoms on two different bound anthracene rings. These spectra were temperature independent up to about 30°C, when broadening of peaks due to bound anthracenes began to occur. Unique assignments of ^1H or ^{13}C resonances to the different anthracene ligands were not possible in most cases. However, along with other supporting NMR data, the presence of a quaternary ^{13}C signal at $\delta =$ 148.6 is good evidence for the presence of one η^4-anthracene group,[16] but the hapticity of the other anthracene ligand in **1** in solution could not be definitely assigned with available data. In contrast, HETCOR NMR solution spectra of **2** at 25°C established that the anthracene ligands are equivalent: the ^1H and ^{13}C NMR spectra showed only five correlated resonances each. The absence of any anthracene ^1H resonances below $\delta = 5.4$ or quaternary ^{13}C resonances above $\delta =$ 133 effectively ruled out the possibility that **2** was an 18-electron species with two equivalent η^4-anthracene groups. Indeed, of all previously known fused-ring arene complexes of zerovalent transition metals, $[Ni(\eta^2\text{-naphthalene})(i\text{Pr}_2\text{PC}_2\text{H}_4\text{P}i\text{Pr}_2)]$ (**5**)[17] and $[Ni(\eta^2\text{-anthracene})(PEt_3)_2]$ **6**,[7f] have NMR spectral features that appear to most closely match those of **2**. These exhibit arene hydrogen resonances only above $\delta = 5.3$, and both are highly fluxional molecules, which exist predominantly as η^2-arene complexes in solution.[17] Based on the similarity of the NMR spectra of **2**, **5**, and **6**, along with the X-ray results for **2** (vide infra), it is possible that **2** may exist in solution as the 16-electron species $[Ti(\eta^4\text{-}C_{14}H_{10})(\eta^2\text{-}C_{14}H_{10})(\eta^5\text{-}C_5Me_5)]^-$, where each anthracene ligand becomes equivalent by rapid concerted η^2 to η^4 equilibria of bound terminal rings. However, available data do not rule out involvement of the 16 or 14 electron species $[Ti(\eta^6\text{-}C_{14}H_{10})(\eta^5\text{-}C_5Me_5)]^-$ (which would be closely related to $[Ti(\eta^6\text{-}C_{10}H_8)(\text{trmpsi})]$ (**7**, trmpsi = tBuSi$(CH_2PMe_2)_3$)[19]) or $[Ti(\eta^2\text{-}C_{14}H_{10})_2(\eta^5\text{-}C_5Me_5)]^-$, respectively. Clearly additional NMR studies are required to understand the solution behavior and structures of **1** and **2**.

Single crystal X-ray structural characterizations were carried out to provide detailed information on the nature of **1** and **2**.[18] Figures 1 and 2 depict their molecular structures and show that the complex $[Ti(\eta^6\text{-}C_{14}H_{10})(\eta^4\text{-}C_{14}H_{10})(\eta^2\text{-dmpe})]$ (**1**) is formally an 18 electron species, whereas $[Ti(\eta^4\text{-}C_{14}H_{10})(\eta^2\text{-}C_{14}H_{10})(\eta^5\text{-}C_5Me_5)]^-$ (**2**) is a 16-electron complex. All previous structurally characterized (arene)titanium(0) compounds, including compound **7**,[19] $[Ti(\eta^6\text{-arene})_2]$ (**8a**,**b**; arene = benzene, toluene),[20] and $[Ti(\eta^4\text{-}C_{10}H_8)_2(SnMe_3)_2]^{2-}$ (**9**),[21] are also 16-electron compounds. Compounds **1** and **2** represent rare examples of bis(arene)metal species containing identical arenes of different hapticities.[22a]

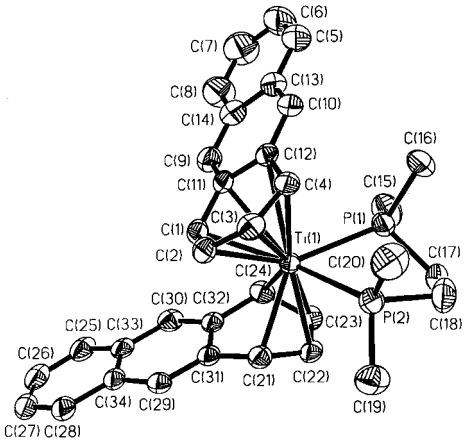


Figure 1. Molecular structure of **1** showing the labeling scheme. Thermal ellipsoids are drawn with 50 % probability boundaries, and hydrogen atoms are omitted for clarity. Selected bond lengths [Å] and angles [°]: Ti–C(1) 2.311(4), Ti–C(2) 2.356(4), Ti–C(3) 2.341(4), Ti–C(4) 2.322(4), Ti–C(11) 2.603(4), Ti–C(12) 2.656(4), Ti–C(21) 2.343(4), Ti–C(22) 2.320(4), Ti–C(23) 2.354(4), Ti–C(24) 2.424(4), Ti–P(1) 2.593(1), Ti–P(2) 2.626(1), C(1)–C(2) 1.399(6), C(2)–C(3) 1.398(6), C(3)–C(4) 1.419(6), C(1)–C(11) 1.447(6), C(11)–C(12) 1.459(5), C(4)–C(12) 1.431(6), C(21)–C(22) 1.433(6), C(22)–C(23) 1.375(6), C(23)–C(24) 1.427(6), C(24)–C(32), 1.463(6), C(21)–C(31) 1.464(5) C(31)–C(32) 1.443(5), C–$C_{avg.}$ for uncoordinated "exonaphthalene" carbons 1.40(3), P–$C_{avg.}$ 1.83(1); P(1)-Ti-P(2) 74.44(1).

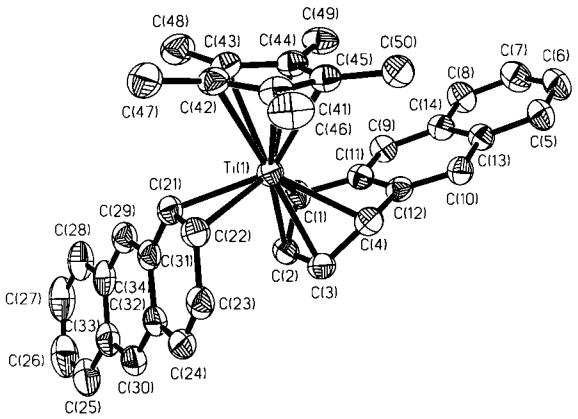


Figure 2. Molecular structure of **2** show the labeling scheme. Thermal ellipsoids are drawn with 50 % probability boundaries, and hydrogen atoms are omitted for clarity. Selected bond lengths [Å]: Ti–C(1) 2.306(3), Ti–C(2) 2.295(3), Ti–C(3) 2.305(3), Ti–C(4) 2.322(3), Ti–C(21) 2.264(3), Ti–C(22) 2.273(3), Ti–C(41) 2.444(3), Ti–C(42) 2.509(3), Ti–C(43) 2.451(3), Ti–C(44) 2.399(3), Ti–C(45) 2.407(3), C(1)–C(2) 1.452(4), C(2)–C(3) 1.386(5), C(3)–C(4) 1.430(4), C(1)–C(11) 1.469(4), C(11)–C(12) 1.444(4), C(4)–C(12) 1.473(4), C(21)–C(22) 1.476(4), C(22)–C(23) 1.441(4) C(23)–C(24) 1.352(5), C(24)–C(32) 1.448(5), C(21)–C(31) 1.453(4), C(31)–C(32) 1.450(4), C–$C_{avg.}$ of uncoordinated "exonaphthalene" carbons 1.41(3), ring C–$C_{avg.}$ of C_5Me_5 1.420(7), C–$Me_{avg.}$ of C_5Me_5 1.507(6).

Although several mono(arene)metal(0) compounds are known to contain η^2- or η^4-arene units,[7, 17, 23] **2** appears to be the first well-characterized η^2-arene complex of a low-valent early transition metal.[22b]

Distinctly nonplanar η^4-anthracene groups are present in **1** and **2**. They consist of planar coordinated diene and uncoordinated exonaphthalene components, which have normal dihedral angles of 35.5° and 31.5°, respectively, for η^4-

 © WILEY-VCH Verlag GmbH, D-69451 Weinheim, 1998 1433-7851/98/3701-0156 $ 17.50+.50/0 *Angew. Chem. Int. Ed.* **1998**, *37*, No. 1/2

anthracene complexes.[7e, 7i, 16] Coordinated diene portions of these anthracene groups have C–C distances that exhibit the usual long, short, long pattern characteristic of most early transition metal η^4-diene complexes and are indicative of the excellent acceptor ability of these ligands in **1** and **2**.[24] Little variation is seen in the Ti–C distances for the η^4-$C_{14}H_{10}$ group in **2**, and the average value of 2.31(1) Å is indistinguishable from the corresponding distance of 2.32(2) Å found in **9**, the only previously known (η^4-arene)titanium complex.[21] Analogous Ti–C distances in **1** are more variable and, except for Ti–C(22), are 0.02 to 0.13 Å longer than those in **2**. The longer Ti–C bonds in **1** relative to corresponding ones in **2** may be a result of a more crowded environment about the titanium center, since the titanium in **1** is formally seven coordinate (seven two-electron bonds), whilst that in **2** is six coordinate.

Another indication that the titanium center in **1** is relatively crowded is the fact that the Ti–C bonds to the η^6-anthracene unit are significantly longer in this complex than in **7**, which contains six-coordinate titanium.[19] Compounds **1** and **7** are otherwise closely related in that both contain fused-ring η^6-arenes, which are bent about C(1) and C(4) with dihedral angles of 15.1 and 12.4°, respectively. This folding results in three different sets of Ti–C distances, which for **1** have the following average values: Ti–C(1,4) 2.317(8), Ti–C(2,3) 2.35(1), and Ti–C(11,12) 2.63(3) Å. The Ti–C (quaternary) distances in **1** are about 0.27 Å longer than those in **7** and indicate that the formally η^6-anthracene unit is appreciably "ring-slipped" and has acquired a substantial degree of η^4-character.

The presence of the η^2-anthracene unit in **2** was unexpected. On the basis of the 18-electron formalism, both anthracenes should bind in a tetrahapto fashion, but the η^5-C_5Me_5 ligand may be sufficiently bulky to prevent this possibility. To our knowledge, the only other well-characterized (η^2-anthracene)-metal(0) compounds are the aforementioned nickel species of the formulation [Ni(η^2-$C_{14}H_{10}$)(PR_3)$_2$] (**6**, R = alkyl).[7b, f] As in the case of the nickel complexes, the η^2-anthracene group in **2** is nearly planar—the dihedral angle between the planes defined by C(21–23) and C(24–34) is only 6.2°. The C–C distances for the uncoordinated carbon atoms in the η^2-anthracene groups of **2** and the nickel complexes **6** are also similar and close to those reported for free anthracene.[25] However, the C–C distance of 1.476(4) Å of the two coordinated carbons in **2** is significantly longer than corresponding distances of 1.422(6) to 1.423(5) Å reported for **6**. This difference indicates that the 16-electron titanium(0) center more strongly participates in backbonding to the η^2-anthracene ligand than do the undoubtedly less strongly reducing 16-electron nickel(0) units. The average Ti–C distance of 2.268(5) Å for the η^2-anthracene group is longer than the Ti–C distances of 2.217–2.247(8) Å found for [Ti(η^6-C_6H_6)$_2$] (**8a**),[20a] but shorter than those for the η^4-anthracene group in **2**, vide supra. Other structural parameters for **1** and **2** are unexpectional, including those of the [K(18-crown-6)(THF)$_2$] cation, which is well separated from **2** in the crystalline lattice. Extension of this study to the synthesis of related anthracene complexes of the early transition metals is currently under examination in this laboratory.

Experimental Section

1: A solution of [$TiCl_4$(dmpe)] (1.75 g, 5.15 mmol) in THF (125 mL, −50°C) was added to a magnetically stirred slurry of $NaC_{14}H_{10}$ (21 mmol) in THF (100 mL, −60°C) and slowly warmed to 0°C over 4 h. The reaction mixture was then cooled to −60°C, filtered at −60°C, and warmed to 0°C. After removal of about 150 mL of THF in vacuo, excess pentane was added to precipitate a black microcrystalline powder. The latter was recrystallized from THF/pentane at 0°C to provide 1.54 g of **1** as sparkling black crystals. Correct C,H analysis, m.p. 194°C (with decomp.); ^{1}H NMR (300 MHz, [D_8]THF, 0°C, numbering as in Figure 1): δ = 0.92, 1.06 (m, each 6H, PCH_3), 1.62, 2.29 (m, each 2H, PCH_2), 3.18, 3.94, 4.38, 5.38 (m, each 2H, $H_{1-4,\ 21-24}$), 6.08, 6.38 (s, each 2H, $H_{9,\ 10,\ 29,\ 30}$), 6.76, 7.02 (m, each 2H, $H_{5-8,\ 25-28}$); ^{13}C{^{1}H}NMR (75.4 MHz, [D_8]THF, 0°C): δ = 13.8, 15.7 (br, PCH_3), 27.7 (t, PCH_2), 77.3, 93.8, 105.1, 105.8 (s, $C_{1-4,21-24}$), 111.1, 120.8 (s, $C_{9,\ 10,\ 29,\ 30}$), 122.6, 123.9, 125.5, 125.7 (s, $C_{5-8,\ 25-28}$), 127.5 (s, $C_{11,\ 12}$), 133.9, 135.3 (s, $C_{13,\ 14,\ 33,\ 34}$), 148.6 (s, $C_{31,\ 32}$); ^{31}P{^{1}H}NMR (121.4 MHz, [D_8]THF, 0°C): δ = 35.5 (s, dmpe). ^{1}H,^{13}C-correlated NMR spectra and trends previously established for monoanthracene or mononaphthalene metal(0) complexes,[7, 23] allowed resonances to be assigned to hydrogens and carbon on bound and unbound anthracene rings, but for quaternary carbon signals at δ = 148.6 and 127.5, the available data were insufficient to permit more detailed assignments. X-ray quality dark purple, nearly black needles of **1**·THF were grown from pentane/THF at −30°C for one week under an argon atmosphere.[18a]

2: A solution of [$TiCl_3(C_5Me_5)$] (1.43 g, 4.94 mmol) in THF (50 mL, 0°C) was added to a solution of $KC_{14}H_{10}$ (19.9 mmol) in THF (100 mL, 0°C). The reaction mixture was stirred at 0°C for 3 h. Following filtration at 0°C, 18-crown-6 (1.43 g, 5.4 mmol) was added and stirred with the filtrate for 3 h at 0°C. After removal of about 50 mL of solvent and filtration at −70°C, all but 25 mL of solvent was removed in vacuo. Addition of pentane (200 mL) caused precipitation of a black solid, which was recrystallized from THF/pentane and then THF/ether to give 1.36 g of microcrystalline black **2**. Correct C,H analysis, mp 165°C; ^{1}H NMR (300 MHz, [D_8]THF, 25°C, numbering as in Figure 2): δ = 1.65 (s, 15H, $C_5(CH_3)_5$), 3.45 (s, 24H, 18-crown-6), 5.43, 5.77 (m, each 4H, $H_{1-4,\ 21-24}$), 6.62, 6.80 (m, each 4H, $H_{5-8,\ 25-28}$), 6.91 (s, 4H, $H_{9,\ 10,\ 29,\ 30}$); ^{13}C{^{1}H}NMR (75.4 MHz, [D_8]THF, 25°C): δ = 15.9 (s, $C_5(CH_{3)5}$), 76.0 (s, 18-crown-6), 108.5, 113.4 (s, $C_{1-4,\ 21-24}$), 118.9 (s, $C_{9,\ 10,\ 29,\ 30}$), 119.1 (s, $C_5(CH_3)_5$), 121.2, 124.8 (s, $C_{5-8,\ 25-28}$), 133.3 (s, $C_{11-14,\ 31-34}$). As in the case of **1**, ^{1}H,^{13}C-correlated NMR spectra and trends previously established for similar complexes[7, 23] allowed resonances to be assigned to bound and unbound rings for the equivalent anthracene ligands in **2**. Black blocks of X-ray quality crystals of [K(10-crown-6)(THF)$_2$]·**2**·1/2 pentane were grown from pentane/THF at −30°C over a period of three weeks under an argon atmosphere.[18b]

Received: August 4, 1997 [Z 10774 IE]
German version: *Angew. Chem.* **1998**, *110*, 163–167

Keywords: arene complexes · carbonyl complexes · low-valent compounds · sandwich complexes · titanium

[1] a) K. Jonas, *Angew. Chem.* **1985,** *97*, 292; *Angew. Chem. Int. Ed. Engl.* **1985,** *24*, 295; b) G. Wilke, *ibid.* **1988**,*100*, 189 and **1988,** *27*, 186; c) K. Jonas, *Pure Appl. Chem.* **1990,** *62*, 1169. d) A. Fürstner, *Angew. Chem.* **1993,** *105*, 171; *Angew. Chem. Int. Ed. Engl.* **1993**, *32*, 164; e) H. Bönnemann, B. Bogdanovic, R. Brinkmann, B. Spliethoff, D.-W. He, *J. Organometal. Chem.* **1993**, *451*, 23, and references therein.

[2] a) T. A. Albright, P. Hofmann, R. Hoffmann, C. P. Lillya, P. A. Dobosh, *J. Am. Chem. Soc.* **1983**, *105*, 3396. b) E. P. Kündig, C. Perret, S. Sprichiger, G. Bernardinelli, *J. Organomet. Chem.* **1985**, *286*, 183.

[3] a) E. P. Kündig, P. L. Timms, *J. Chem. Soc. Chem. Commun.* **1977**, 912. b) C. Elschenbroich, R. Möckel, *Angew. Chem.* **1977**, *89*, 908; *Angew. Chem. Int. Ed. Engl* **1977**,*16*, 870.

[4] M. K. Pomije, C. J. Kurth, J. E. Ellis, M. V. Barybin, *Organometallics* **1997**, *16*, 3582.

[5] F. Basolo, *New J. Chem.* **1994**, *18*, 19.

[6] C. Elschenbroich, R. Möckel, L. Bilger, *Z. Naturforsch. B* **1984**, *39*, 375.

 © WILEY-VCH Verlag GmbH, D-69451 Weinheim, 1998 1433-7851/98/3701-0157 $ 17.50+.50/0

[7] a) K. Jonas, *J. Organomet. Chem.* **1974**, *78*, 273; b) D. J. Braun, C. Krüger, *Inorg. Chem.* **1977**, *16*, 884; c) H.-F. Klein, K. Ellrich, S. Lamac, G. Lull, L. Zsolnai, G. Huttner, *Z. Naturforsch. B* **1985**, *40*, 1377; d) J. Scholz, K.-H. Thiele, *J. Organometal. Chem.* **1986**, *314*, 7; e) J. D. Prostasiewicz, P. A. Bianconi, I. D. Williams, S. Liu, C. P. Rao, S. J. Lippard, *Inorg. Chem.* **1992**, *31*, 4132; f) A. Stanger, R. Boese, *J. Organomet. Chem.* **1992**, *430*, 235; g) A. Stanger, K. P. C. Vollhardt, *Organometallics* **1992**, *11*, 317; h) D. M. Roitershtein, L. F. Rybakova, E. S. Petrov, A. M. Ellern, M. Y. Antipin, Y. T. Struchkov, *J. Organomet. Chem.* **1993**, *460*, 39; i) R. Boese, A. Stanger, P. Stellberg, A. Shazar, *Angew. Chem.* **1993**, *105*, 1500; *Angew. Chem. Int. Ed. Engl.* **1993**, *32*, 1475; j) S. Lee, S. J. Geib, N. J. Cooper, *J. Am. Chem. Soc.* **1995**, *117*, 9572.

[8] Compounds of the formulation $[M(C_5H_5)_2(C_{14}H_{10})]$ (M = Ti, Zr) have been reported, but little is known in detail about the nature of their anthracene–metal interactions.[7d]

[9] K.-M. Chi, S. R. Frerichs, B. K. Stein, D. W. Blackburn, J. E. Ellis, *J. Am. Chem. Soc.* **1988**, *110*, 163.

[10] J. E. Ellis, S. R. Frerichs, B. K. Stein, *Organometallics* **1993**, *12*, 1048.

[11] P. J. Domailee, R. L. Warlow, S. S. Wreford, *Organometallics* **1982**, *1*, 935.

[12] B. A. Kelsey, J. E. Ellis, *J. Chem. Soc. Chem. Commun.* **1986**, 331.

[13] J. E. Ellis, *Polyhedron* **1989**, *8*, 1611.

[14] a) C. E. Dewey, J. E. Ellis, K. L. Fjare, K. M. Pfahl, G. R. Warnock, *Organometallics* **1983**, *2*, 388; b) K. Jonas, V. Wiskamp, *Z. Naturforsch. B* **1983**, *38*, 113.

[15] J. K. Seaburg, J. E. Ellis, unpublished results.

[16] This value lies in the quaternary carbon region characteristic of previously reported, structurally characterized η^4-polyarene transition metal complexes such as $[Ta(\eta^4\text{-}C_{14}H_{10})(dmpe)_2Cl]$ ($\delta_c = 151.8$)[7e] and [Fe(5-8-η^4-1,4-dimethylnaphthalene)$(P(OMe)_3)$] ($\delta_c = 144.9$): H. Schäufele, D. Hu, H. Pritzkow, U. Zenneck, *Organometallics* **1989**, *8*, 396.

[17] a) R. Benn, R. Mynott, I. Topalovic, F. Scott, *Organometallics* **1989**, *8*, 2299; b) F. Scott, C. Krüger, P. Betz, *J. Organomet. Chem.* **1990**, *387*, 113; c) A. Stanger, J. Weismann, *ibid.* **1996**, *515*, 183.

[18] a) Crystal data for **1**·THF: $C_{38}H_{44}OP_2Ti$, $M = 626.57$, monoclinic, $P2_{1/c}$, $a = 20.5789(1)$, $b = 9.6620(1)$, $c = 16.6477(2)$ Å, $\beta = 98.797(1)^\circ$, $V = 3271.18(5)$ Å^3, $Z = 4$, $\rho_{calcd} = 1.272$ g cm^{-3}, $F(000) = 1328$, $\mu(Mo_{K\alpha}) = 0.388$ mm^{-1}, $\lambda = 0.71073$ Å, $T = 173(2)$ K. The 16421 reflections measured on a Siemens SMART CCD area detector diffractometer yielded 5719 unique data ($2\theta_{max} = 50^\circ$, $R_{int} = 0.0525$, semi-empirical absorption corrections). The structure was solved by direct methods and refined by full-matrix least-squares method on F^2 with statistical weighting, anisotropic displacement parameters, constrained isotropic H atoms to give $wR2 = [\Sigma[w(F_o^2 - F_c^2)^2]/\Sigma[w(F_o^2)^2]]^{1/2} = 0.1581$ on all data, conventional $R = 0.0666$ on F values of 5720 reflections having $F_o^2 > 2\sigma(F_o^2)$, GOF = 1.095 for all F^2 values and 463 refined parameters. Largest difference peak and hole (e Å^{-3}): 0.690, −0.528. All calculations were performed with SGI INDY R4400-SC or pentium computers with SHEXTL-Plus program suite. b) Crystal data for $[K(18\text{-crown-6})(thf)_2]\cdot$**2**$\cdot 1/2$ pentane: $C_{60.5}H_{81}KO_8Ti$, $M = 1023.25$, triclinic, $P\bar{1}$, $a = 13.0974(2)$, $b = 15.6482(2)$, $c = 15.7479(2)$ Å, $\alpha = 96.170(1)$, $\beta = 107.993(1)$, $\gamma = 111.119(1)^\circ$, $V = 2775.09(7)$ Å^3, $Z = 2$, $\rho_{calcd} = 1.225$ g cm^{-3}, $F(000) = 1098$, $\mu(Mo_{K\alpha}) = 0.282$ mm^{-1}, $\lambda = 0.71073$ Å, $T = 173(2)$ K. The 14.304 reflections measured on a Siemens SMART CCD area detector diffractometer yielded 9364 unique data ($2\theta_{max} = 50^\circ$, $R_{int} = 0.0280$, semi-empirical absorption corrections). The structure was solved by direct methods and refined by the same procedure used for **1** to give $wR2 = 0.1711$ on all data, conventional $R = 0.0637$ on F values of 9368 reflections having $F_o^2 > 2\sigma(F_o^2)$, GOF = 1.075 for all F^2 values and 635 refined parameters. Largest difference peak and hole (e Å^{-3}): 1.771, −0.707. One molecule of pentane was located near an inversion center. It was ill-behaved until bond length constraints were employed for all 1,2 and 1,3 interatomic pairs after freeing C(3)S from placement on the inversion center. These atoms were refined isotropically with a common parameter for all carbon atoms. One large unidentified peak remains in the difference map near one of the THF oxygen atoms. Calculations were performed as detailed above for **1**. c) Crystallographic data (excluding structure factors) for the two structures reported in this paper have been deposited with the Cambridge Crystallographic Data Centre as supplementary publication no. CCDC-100606. Copies of the data can be obtained free of charge on application to CCDC, 12 Union Road, Cambridge CB2 1EZ, UK (fax: int. code + (44) 1223-336033; e-mail: deposit@ccdc.cam.ac.uk).

[19] T. G. Gardner, G. S. Girolami, *Angew. Chem.* **1988**, *100*, 1755; *Angew. Chem. Int. Ed. Engl* **1988**, *27*, 1693.

[20] a) G. G. Tairova, E. F. Krashina, O. N. Krasochka, G. A. Kichigina, Y. A. Schvetsov, E. M. Lisetsky, L. O. Atovmyan, Y. G. Borod'ko, *Nouv. J. Chim.* **1981**, *5*, 603; b) G. G. Tairova, O. N. Krasochka, V. I. Ponomaryov, V. J. Kvashina, Y. A. Shvetsov, E. M. Lisetsky, D. P. Kiryushkin, L. O. Atovmyan, Y. G. Borod'ko, *Trans. Met. Chem.* **1982**, *7*, 189.

[21] J. E. Ellis, D. W. Blackburn, P. Yuen, M. Jang, *J. Am. Chem. Soc.* **1993**, *115*, 11616.

[22] a) To our knowledge, the only previously well-established example is $[Ru(\eta^6\text{-}C_6Me_6)(\eta^4\text{-}C_6Me_6)]$; G. Huttner, S. Lange, *Acta Crystallogr. Sect. B* **1972**, *28*, 2049. b) An unusual high-valent tantalum η^2-benzene complex, $[\{Ta(silox)_3\}_2\{\mu\text{-}\eta^2\text{:}\eta^2\text{-}C_6H_6\}]$ (silox = $(tBu)_3SiO^-$) has been reported: D. R. Neithamer, L. Parkanyi, J. F. Mitchell, P. T. Wolczanski, *J. Am. Chem. Soc.* **1988**, *110*, 4421.

[23] a) J. O. Albright, S. Datta, B. Dezube, J. K. Kouba, D. S. Marynick, S. S. Wreford, B. M. Foxman, *J. Am. Chem. Soc.* **1979**, *101*, 611; b) W. L. Gladfelter, J. W. Hull, *Organometallics* **1984**, *3*, 605; c) R. L. Thompson, S. Lee, N. J. Cooper, *ibid.* **1991**, *10*, 1657; d) A. V. Protchenko, L. N. Zakharov, M. N. Bockharev, Y. T. Struchkov, *J. Organomet. Chem.* **1993**, *447*, 209; e) I. L. Fedushkin, M. N. Bochkarev, H. Schumann, L. Esser, G. Kociok-Köhn, *ibid.* **1995**, *489*, 145; f) S. Sun, C. A. Dullaghan, G. A. Carpenter, A. L. Rieger, P. H. Peiger, D. A. Sweigart, *Angew Chem.* **1995**, *107*, 2734; *Angew. Chem. Int. Ed. Engl.* **1995**, *34*, 2540.

[24] M. Jang, J. E. Ellis, *Angew Chem.* **1994**, *106*, 2036; *Angew. Chem. Int. Ed. Engl.* **1994**, *33*, 1973, and references therein.

[25] R. Mason, *Acta Crystallogr.* **1964**, *17*, 547.

Distance Dependence of Photoinduced Electron Transfer in DNA

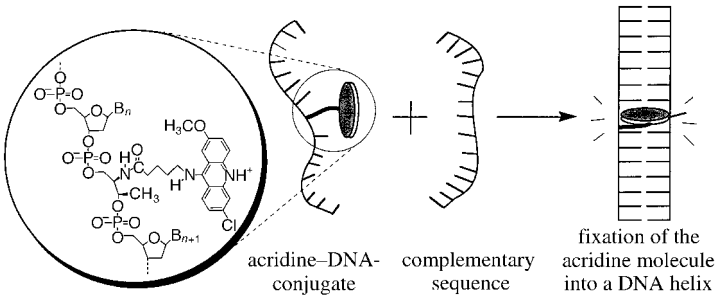
Keijiro Fukui and Kazuyoshi Tanaka*

The DNA helix is a useful molecular material for examining how the π stack mediates electron transfer. In recent years photoinduced electron transfers in DNA were investigated in many systems in which a donor and an acceptor randomly associate with DNA[1–6] or a donor and an acceptor are covalently linked at the terminus of DNA to avoid a multiplicity of the separation distance.[7, 8] The clearest evidence for mediation of electron transfer by the base pairs is the distance dependence; the efficiency of the reaction is represented by the β value. For a DNA–dye mixture, estimations of the β value have already been carried out.[3a,5b] Although a series of determinations of the β value is desirable, the lack of a method for introducing the dye precisely "into" the DNA helix makes it difficult to evaluate the distance dependence clearly. Here we report the distance dependence of electron transfer in a DNA helix using a novel system in which a chromophore is precisely fixed in DNA of defined sequence.

[*] Prof. Dr. K. Tanaka, Dr. K. Fukui
Department of Molecular Engineering
Graduate School of Engineering
Kyoto University
Sakyo-ku, Kyoto 606-01 (Japan)
Fax: Int. code + (81) 75-771 0172
e-mail: a51053@sakura.kudpc.kyoto-u.ac.jp

 © WILEY-VCH Verlag GmbH, D-69451 Weinheim, 1998 1433-7851/98/3701-0158 $ 17.50+.50/0

To anchor a chromophore at any desired site of a DNA and to suppress unfavorable thermal fluctuation around the chromophore, we adopted the strategy of introducing 9-amino-6-chloro-2-methoxyacridine (ACMA) at a defined internucleotide site of a DNA[9a, b] (Scheme 1). The thermal



Scheme 1. Schematic representation of the anchoring of ACMA at the desired site in a DNA helix.

stability of the helix and the fluorescence quantum yields from ACMA strongly depend on the chain length between the dye and the DNA as well as on the presence of a nucleobase at the opposite side of the acridine ring.[9c] A tetramethylene linker (Scheme 1) and adenosine at the opposite side of the ACMA unit are most suitable for fixing ACMA into a DNA helix. ACMA provides the strongest emission in the modified DNA, and the whole DNA structure shows particular thermal stability.[9c] The structure in which ACMA is intercalated between neighboring base pairs and the opposite adenosine is pushed out of the helix (extrahelical conformation) was confirmed with 2D-NMR spectroscopy.[10]

Using the corresponding acridine-phosphoramidite[9b] in a DNA synthesizer, we prepared the ACMA – DNA conjugate **I**, which consists of only adenosine and thymidine nucleotides, as well as conjugates **II** – **VIII**, which have a sequence similar to that of **I** and contain guanosine in the 5′ or 3′ directions at different distances (Table 1). To maintain the binding geometry between ACMA and the nucleobases, both sides of ACMA were fixed in purine bases (adenine or guanine). The absorption spectra of ACMA and the wavelengths of the fluorescence maxima (see below) were unchanged for a series of ACMA – DNA conjugates. Hence, the energy level of the ACMA units was identical for all ACMA – DNA conjugates.

We measured the fluorescence spectra of the ACMA units in duplexes **I** – **VIII** to investigate electron transfer through the DNA π stack under conditions in which all DNA molecules are sufficiently stable (0 °C).[9c] The fluorescence quantum yields of these duplexes are listed in Table 1, and the fluorescence spectra of **I** – **IV** are shown in Figure 1. Duplex **I**

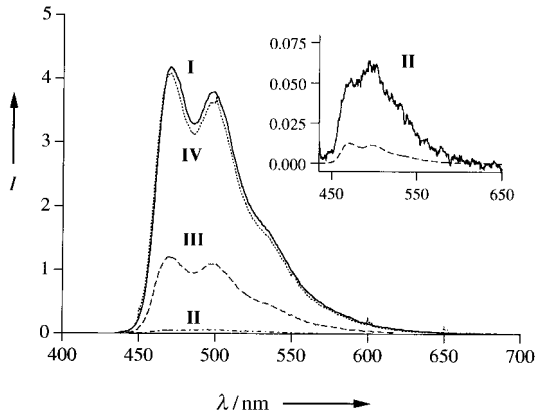


Figure 1. Fluorescence spectra of the ACMA – DNA conjugates **I** – **IV** (intensity *I* in arbitrary units). Inset: Enlarged section of the fluorescence spectrum of **II** (solid line). It can be divided into the SAS (dashed line) of the ACMA firmly fixed in a DNA helix and the nonintercalated (extrahelical) ACMA (see text and ref. [9c]).

Table 1. Fluorescence quantum yields Φ of the ACMA – DNA conjugates **I** – **VIII** and rates of electron transfer from guanine to an excited ACMA in a DNA helix.

Entry	Sample[a]	Direction (distance [Å])[b]	Φ[c]	k_{et} [s^{-1}][d]
I	5′-ATAATAA[Acr]AATTAAT-3′ 3′-TATTATT A TTAATTA-5′	–	0.655	–
II	5′-ATAATAA**G**[Acr]AATTAAT-3′ 3′-TATTATTC A TTAATTA-5′	5′ (3.4)	0.011 (0.002)[e]	1.4×10^{10}[e]
III	5′-ATAATAA**G**A[Acr]AATTAAT-3′ 3′-TATTATTCT A TTAATTA-5′	5′ (6.8)	0.195	1.0×10^{8}
IV	5′-ATAATAA**G**AA[Acr]AATTAAT-3′ 3′-TATTATTCTT A TTAATTA-5′	5′ (10.2)	0.622	2.3×10^{6}
V	5′-ATAATAA[Acr]**G**AATTAAT-3′ 3′-TATTATT A CTTAATTA-5′	3′ (3.4)	0.015 (0.003)[e]	9.5×10^{9}[e]
VI	5′-ATAATAA[Acr]A**G**AATTAAT-3′ 3′-TATTATT A TCTTAATTA-5′	3′ (6.8)	0.307	5.0×10^{7}
VII	5′-ATAATAA[Acr]AA**G**AATTAAT-3′ 3′-TATTATT A TTCTTAATTA-5′	3′ (10.2)	0.647	5.4×10^{5}
VIII	5′-ATAATAA**G**A[Acr]A**G**AATTAAT-3′ 3′-TATTATTCT A TCTTAATTA-5′	3′,5′ (6.8)	0.139	1.6×10^{8}

[a] Sample concentrations: 2.5 μM in 10 mM phosphate buffer (pH 7.2) with 150 mM NaCl. The samples were slowly annealed from 60 °C and kept overnight in the dark. [Acr] stands for the artificial base-free site connecting to ACMA through a tetramethylene linker (see Scheme 1). [b] Under the assumption that the distance between the base pairs is 3.4 Å (see ref. [24]). [c] Measured at 0 °C; excitation wavelength 427 nm. [d] Determined with Equation 2 (see text). [e] Calculated using only the emission from ACMA strictly fixed in a DNA helix (see text and inset of Figure 1).

 © WILEY-VCH Verlag GmbH, D-69451 Weinheim, 1998 1433-7851/98/3701-0159 $ 17.50+.50/0

showed strong emission bands at 475 and 500 nm, which are attributed to the species-associated spectrum (SAS) of ACMA and reflect its rigid microenvironment.[9c, 11] Indeed, the decay in intensity was monoexponential with a lifetime of 22.8 ns, as measured by single-photon counting.[12] These emission bands cannot be seen for free ACMA in water or for any other ACMA – DNA conjugates;[9c] fast relaxation of the environment around the excited ACMA only gave an emission band at 500 nm.[9c, 11] These results indicate that the ACMA was precisely fixed with unique conformation in a DNA helix, and that the origin of electron transfer can be evaluated without fail.

Since the fluorescence of an ACMA unit is not quenched by a d(AT) base pair,[9c, 13, 14] **I** acts as an "inert matrix" for the photoexcited ACMA. On the other hand, guanine can quench the ACMA fluorescence,[13, 14] and this mechanism is assigned as an electron transfer [Eq. (1)]. It is impossible for an energy

$$[\mathrm{Acr}]^{+}\cdots \mathrm{dG} \xrightarrow{h\nu} [\mathrm{Acr}]^{+*}\cdots \mathrm{dG} \xrightarrow{k_{et}} [\mathrm{Acr}]\cdots \mathrm{dG}^{+} \quad (1)$$

transfer to occur because of the lack of spectral overlap; nucleobases can absorb at $\lambda < 300$ nm. It is clear from electrochemical,[15] theoretical,[16a] and chemical aspects[16b, c] that guanine is the most readily oxidizable residue.

In general, when two dyes (e. g. donor and acceptor) intercalate into a DNA helix, at least two base pairs must exist between them. Furthermore, the loading of the two chromophores in this short distance is sufficient to cause local disruption of the DNA structure of a rod-shape.[17] However, since guanine is used as an electron donor in the present study, there is no such limitation. The fluorescence intensity of duplexes **II** – **VII** clearly decreased as a function of the distance between ACMA and guanine (see Table 1 and Figure 1). For **II** and **V**, in which guanine is adjacent to ACMA, the fluorescence was strongly suppressed to about 2 % of that for **I**. The fluorescence spectra of **II** and **V**, however, showed incomplete SAS of ACMA (inset of Figure 1). These spectra contain the emission from unfixed ACMA, presumably because a very small portion of ACMA can be in an extrahelical conformation.[9c, 18] Although it is rather small, the SAS can be clearly seen.

Since ACMA and guanine are connected through many bonds (alkyl chain, amide bond, and phosphate), it is difficult to imagine that the strong quenching is due to electron transfer through these long bonds.[19, 20] Therefore, it is rational to consider that direct electron transfer occurs through the π stack between ACMA and guanine.[21] The rates of intramolecular electron transfer were evaluated with Equation (2).

$$k_{et} = \frac{1}{\tau_0}\left(\frac{\Phi_0}{\Phi} - 1\right) \quad (2)$$

Here, τ_0 is the excited-state lifetime in the absence of the quencher guanine (that is, for **I**), and Φ_0 and Φ are the fluorescence quantum yields of the ACMA – DNA conjugates in the absence (**I**)[12] or presence of guanine, respectively (**II** – **VIII**; see Table 1). The rates of electron transfer for **II** and **V** were calculated from the quantum yields of the SAS. The rates of electron transfer decrease with increasing distance between ACMA and guanine (see Figure 2). The slopes of the

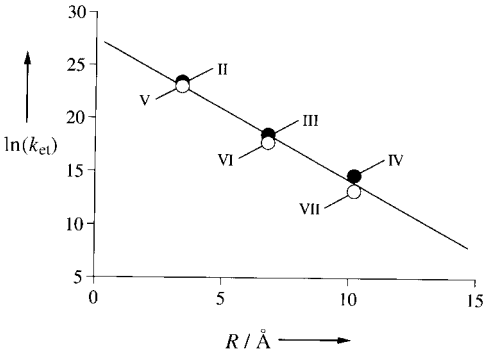


Figure 2. Correlation between the rate of electron transfer k_{et} and the separation distance R in a DNA helix for 5′ (●) and 3′ directions (○). The solid line represents the least-squares fit for the data points.

lines for the 5′ and 3′ directions are very similar, which indicates that the electronic coupling of these directions is practically identical.[26] It is noteworthy that the summation of the rates of electron transfer for **III** and **VI**, in which ACMA and guanine are separated with one d(AT) base pair, is $1.64 \times 10^8\ s^{-1}$. This value is almost identical to that of **VIII**, in which guanines exist in both sides of the ACMA with a separation of one d(AT) base pair. This result is consistent with selective intercalation of ACMA into the target position,[9c] and it can be concluded that the intercalation modes of ACMA – DNA conjugates are not perturbed by changes in base sequence near the ACMA unit.

The most common expression for the distance dependence of the rates of electron transfer can be derived from Equation (3).[19, 22] Here β stands for the effectiveness of the

$$k_{et} = A\, e^{-\beta R} \quad (3)$$

intervening base pairs between the coupling donor and acceptor, and R for the separation between them. When R is set equal to the distance along a B-DNA helix (i. e., 3.4 Å per base stacking;[17] see Figure 2), fitting the electron transfer data to Equation (3) gave a preexponential factor A of 1.20×10^{12} and a β value of 1.42 $Å^{-1}$. These values are comparable with those of protein matrices[19, 22, 23] and show that the π stack in DNA is a moderate mediator and not a special material for electron transfer. The β value is strikingly close to that recently predicted by theoretical calculations,[24] although the results of theoretical calculations are still in disagreement.[25] However, the β value for our system is larger than for electron transfer in other dye – DNA systems: 0.91 and 0.86 $Å^{-1}$ for transfer from photoexcited ethidium or acridine orange, respectively, to *N*,*N*′-dimethyl-2,7-diazapyrenium (DAP);[3a] 0.73 $Å^{-1}$ from Cu^{+} to oxidized ethidium.[5b] We account for the differences in these rates of electron transfer with the following: The donors of the systems are in an excited or high-energy state and are therefore better coupled to the corresponding high-energy bridging state in DNA.[26, 27] The electron transfer studied here occurs from the ground-state guanine with lower energy. This "hole transfer" is not well effectuated due to the high energy of the low-lying unoccupied orbital or LUMO of DNA that works as the transferring path. In fact, the reverse electron transfer for charge recombination from reduced DAP to oxidized ethidium gives

 © WILEY-VCH Verlag GmbH, D-69451 Weinheim, 1998 1433-7851/98/3701-0160 $ 17.50+.50/0

$\beta = 1.49$ Å^{-1}.[3a] This value is practically identical to that observed in the present study. However, our data is quite different from that of Murphy et al. ($\beta = 0.2$ Å^{-1}),[8a] although the same mediator was used. This large discrepancy could not be explained with the above description.

In conclusion, we measured the long-range electron transfer through a DNA helix and its distance dependence by introducing a dye precisely into a DNA helix. Since these modified DNA are readily prepared by a DNA synthesizer, it is easy to introduce the second or third dyes into the DNA structure and to change the base sequence. We are now in the position to use this system to delineate the reorganization energy, the reverse electron transfer, and the effect of base stacking[16] in a DNA π frame.

Received: July 21, 1997 [Z10708IE]
German version: *Angew. Chem.* **1998**, *110*, 167 – 170

Keywords: base stacking · DNA oxidation · electron transfer · oligonucleotides

[1] P. Fromherz, B. Rieger, *J. Am. Chem. Soc.* **1986**, *108*, 5361 – 5362.
[2] R. F. Pasternack, M. Caccam, B. Keoth, T. A. Stephenson, A. P. Williams, E. J. Gibbs, *J. Am. Chem. Soc.* **1991**, *113*, 6835 – 6840.
[3] a) A. M. Brun, A. Harriman, *J. Am. Chem. Soc.* **1992**, *114*, 3656 – 3660; b) **1994**, *116*, 10383 – 10393.
[4] a) M. D. Purugganan, C. V. Kumar, N. J. Turro, J. K. Barton, *Science* **1988**, *241*, 1645 – 1649; b) G. Orellana, A. Kirsch-De Mesmaeker, J. K. Barton, N. J. Turro, *Photochem. Photobiol.* **1991**, *54*, 499 – 509; c) C. J. Murphy, M. R. Arkin, N. D. Ghatlia, S. Bossmann, N. J. Turro, J. K. Barton, *Proc. Natl. Acad. Sci. USA* **1994**, *91*, 5315 – 5319; d) E. D. A. Stemp, M. R. Arkin, J. K. Barton, *J. Am. Chem. Soc.* **1995**, *117*, 2375 – 2376; e) R. E. Holmlin, E. D. A. Stemp, J . K. Barton, *ibid.* **1996**, *118*, 5236 – 5244; f) M. R. Arkin, E. D. A. Stemp, R. E. Holmlin, J. K. Barton, A. Hörmann, E. J. C. Olson, P. F. Barbara, *Science* **1996**, *273*, 475 – 479; g) E. D. A. Stemp, M. R. Arkin, J. K. Barton, *J. Am. Chem. Soc.* **1997**, *119*, 2921 – 2925; h) M. R. Arkin, E. D. A. Stemp, S. C. Pulver, J. K. Barton, *Chem. Biol.* **1997**, *4*, 389 – 400.
[5] a) S. J. Atherton, P. C. Beaumont, *J. Phys. Chem.* **1987**, *91*, 3993 – 3997; b) **1995**, *99*, 12025 – 12029.
[6] J.-P Lecomte, A. Kirsch-De Mesmaeker, J. M. Kelly, A. B. Tossi, G. Helmut, *Photochem. Photobiol.* **1992**, *55*, 681 – 689.
[7] a) T. J. Meade, J. F. Kayyem, *Angew. Chem.* **1995**, *107*, 358 – 340; *Angew. Chem. Int. Ed. Engl.* **1995**, *34*, 352 – 354.
[8] a) C. J. Murphy, M. R. Arkin, Y. Jenkins, N. D. Ghatlia, S. H. Bossmann, N. J. Turro, J. K. Barton, *Science* **1993**, *262*, 1025 – 1029; b) D. B. Hall, R. E. Holmlin, J. K. Barton, *Nature* **1996**, *382*, 731 – 735; c) P. J. Dandliker, R. E. Holmlin, J. K. Barton, *Science* **1997**, *275*, 1464 – 1468; R. E. Holmlin, P. J. Dandliker, J. K. Barton, *Angew. Chem.* **1997**, *109*, 2830 – 2848; *Angew. Chem. Int. Ed. Engl.* **1997**, *36*, 2714 – 2730.
[9] a) K. Fukui, M. Morimoto, H. Segawa, K. Tanaka, T. Shimidzu, *Bioconjugate Chem.* **1996**, *7*, 349 – 355; b) K. Fukui, K. Iwane, T. Shimidzu, K. Tanaka, *Tetrahedron Lett.* **1996**, *37*, 4983 – 4986; c) K. Fukui, K. Tanaka, *Nucleic Acids Res.* **1996**, *24*, 3962 – 3967.
[10] K. Fukui, K. Tanaka, unpublished results.
[11] J.-s. Sun, M. Rougée, M. Delarue, T. Montenay-Garestier, C. Hélène, *J. Phys. Chem.* **1990**, *94*, 968 – 977.
[12] **I**: $\tau = (22.8 \pm 0.1)$ ns (100%), $\chi^2 = 1.21$; **II**: 78 ps (86%); **III**: 5.55 ns (100%); **IV**: 22.6 ns (100%); **V**: 73 ps (91%); **VI** 9.84 ns (100%); **VII**: 22.3 ns (100%); **VIII**: 4.05 ns (100%). The measurements in Table 1 were carried out under the same conditions. We will report further detailed data for **II** – **VIII** in a forthcoming paper.
[13] U. Pachmann, R. Rigler, *Exp. Cell Res.* **1972**, *72*, 602 – 608.
[14] M. Nastasi, K. M. Morris, D. M. Rayner, V. L. Seligy, A. G. Szabo, D. F. Williams, R. E. Williams, R. W. Yip, *J. Am. Chem. Soc.* **1976**, *98*, 3979 – 3986.
[15] C. A. M. Seidel, A. Schulz, M. H. M. Sauer, *J. Phys. Chem.* **1996**, *100*, 5541 – 5553.
[16] a) H. Sugiyama, I. Saito, *J. Am. Chem. Soc.* **1996**, *118*, 7063 – 7068; b) I. Saito, M. Takayama, H. Sugiyama, K. Nakatani, *ibid.* **1995**, *117*, 6406 – 6407; c) S. Steenken, S. V. Javanovic, *ibid.* **1997**, *119*, 617 – 618.
[17] W. Saenger, *Principles of Nucleic Acid Structure*, Springer-Verlag, New York, **1984**.
[18] No degradation of the sample was observed during the photophysical experiments.
[19] B. A. Jacobs, M. R. Mauk, W. D. Funk, A. T. Ross, MacGillivray, A. G. Mauk, H. B. Gray, *J. Am. Chem. Soc.* **1991**, *113*, 4390 – 4394.
[20] P. Siddarth, R. A. Marcus, *J. Phys. Chem.* **1992**, *96*, 3213 – 3217.
[21] We tried to measure the transient absorption spectra by using a nanosecond transient absorption spectrophotometer. However, since 1) the absorption coefficient of the oxidized guanine is very small ($\varepsilon < 2000$ M^{-1}cm^{-1} at 450 – 650 nm), 2) the absorption spectrum is entirely dominated by the fluorescence of ACMA, and 3) the rate of the reverse electron transfer would be very fast (10^9 sec^{-1}, $t < 10^{-9}$ sec), this experiment was not successful.
[22] D. N. Beratan, J. N. Betts, J. N. Onuchic, *Science* **1991**, *252*, 1285 – 1288.
[23] C. C. Moser, J. M. Keske, K. Warncke, R. S. Farid, P. L. Dutton, *Nature* **1992**, *355*, 796 – 802.
[24] S. Priyadarshy, S. M. Risser, D. N. Beratan, *J. Phys. Chem.* **1996**, *100*, 17678 – 17682.
[25] a) A. K. Felts, W. T. Pollard, R. A. Friesner, *J. Phys. Chem.* **1995**, *99*, 2929 – 2940; b) E. J. C. Olson, D. H. Hörmann, P. F. Barbara, *J. Phys. Chem. B.* **1997**, *101*, 299 – 303.
[26] H. M. McConnell, *J. Chem. Phys.* **1961**, *35*, 508 – 515.
[27] C. A. Naleway, L. A. Curtiss, J. R. Miller, *J. Phys. Chem.* **1991**, *95*, 8434 – 8437.

Overcoming a Longstanding Challenge: X-Ray Structure of a $[Co_2(CO)_6]$-Complexed Propargyl Cation**

Gagik G. Melikyan,* Stephen Bright, Todd Monroe, Kenneth I. Hardcastle, and Joana Ciurash

The ability of mono- and polynuclear transition metal clusters to dramatically enhance the stability of neighboring carbocationic centers is well documented.[1–3] NMR spectroscopy has been widely used to structurally characterize homo- and heteronuclear metal complexes;[4] on the contrary, X-ray crystallography has been used to a lesser extent because of the thermal lability and low crystallinity of organometallic cations. Chronologically, ferrocenyl-[5] and bis(tricarbonylcyclobutadienyliron)-stabilized[6] methyl cations were characterized first, followed by a variety of organometallic species[7–11] with tetrahedral (or quasi tetrahedral) metal cores (Mo_2C_2,[7] $MoCoC_2$,[7a, 8, 11] W_2C_2,[9] and $CoFeC_2$[11]). The synthesis and structure of the propargyl cation stabilized by the $[Co_2(CO)_6]$ cluster have been thoroughly investigated.[12] NMR studies[13–15] revealed two modes of fluxionality, a low-energy *antara*-facial motion of the cationic center between metal atoms, and a high-energy rotation around the bond between the cationic center and the cluster (apical C – C

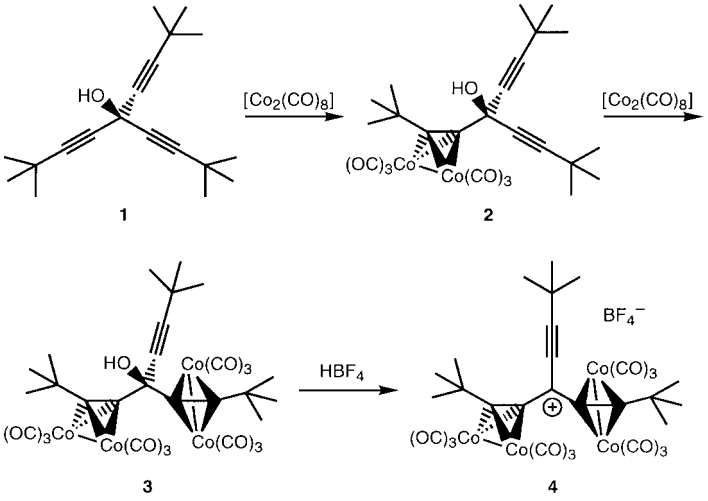
[*] Prof. G. G. Melikyan, S. Bright, T. Monroe, Prof. K. I. Hardcastle, J. Ciurash
Department of Chemistry, California State University Northridge
Northridge, CA 91330 (USA)
Fax: Int. code + (1) 818 677-2912
e-mail: hcchm025@csun.edu

[**] This work was supported by the Office of Graduate Studies and College of Science and Mathematics, California State University Northridge.

 © WILEY-VCH Verlag GmbH, D-69451 Weinheim, 1998 1433-7851/98/3701-0161 $ 17.50+.50/0

double bond).[14] Although a $[Co_2(CO)_6]$-complexed propargyl cation was isolated two decades ago,[13a] the X-ray crystal structure of such a cation was hitherto unknown.[2, 12]

As a part of a continuing study of the chemistry of π-bonded organometallic radicals and carbocations,[16] we report herein the synthesis and the first X-ray characterization of a doubly stabilized $[Co_2(CO)_6]$-complexed propargyl cation. The adopted strategy consists of introducing two charge-stabilizing metallaalkyne moieties in the α position to the cationic center to enhance the thermal stability and crystallinity of target species. The starting material **1** was synthesized by a modified literature procedure[17] in 55% yield (Scheme 1). Alkyne moieties of the latter were consecutively protected with $[Co_2(CO)_6]$ groups[18] to generate mono- and diclusters **2** and **3**[19] (Figure 1), respectively. Treatment of **3** with HBF_4 resulted in the salt **4** of the corresponding complex cation, a black solid stable at ambient temperature under aerobic conditions, which rapidly decomposes in solution (CH_2Cl_2, acetone).



Scheme 1. Synthesis of **4** from the triyne **1**.

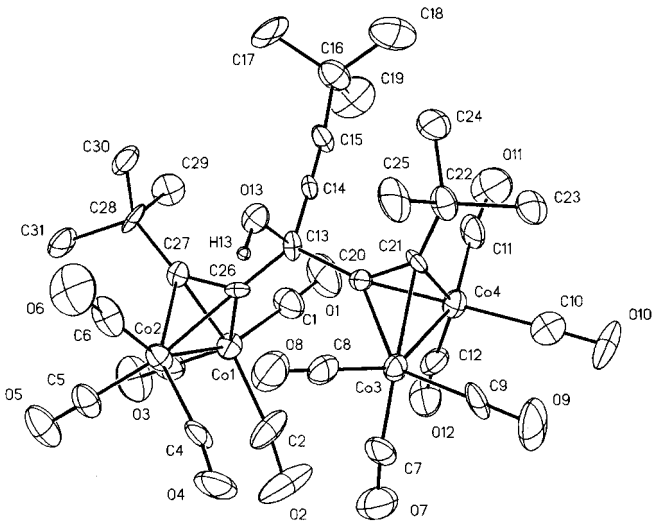


Figure 1. Molecular structure of **3** (30% probability ellipsoids). Selected interatomic distances [Å] and angles [°]: C13–C20 1.49(2), C13–C26 1.53(2), C13–C14 1.43(2), C13–Co1 3.29(1), C13–Co2 3.25(1), C13–Co3 3.26(1), C13–Co4 3.25(1); C14-C13-C20 108.9(11), C14-C13-C26 108.0(10), C20-C13-C26 119.5(12), C14-C13-O13 108.0(12), C20-C13-O13 106.0(10), C26-C13-O13 105.9(10), C27-C26-C13 133.6(12), C21-C20-C13 134.8(13), C28-C27-C26-C13 4.8(1), C22-C21-C20-C13 4.4(1); angle between the bonds C26–C27 and Co1–Co2 89.2(5), between C20–C21 and Co3–Co4 90.1(5), between Co1–Co2 and Co3–Co4 24.2(4).

The structure of **4** was characterized by low-temperature ^1H and ^{13}C NMR spectroscopy (−80 °C) and X-ray crystallography (−105 °C). In the ^1H NMR spectrum, the *tert*-butyl groups are deshielded compared to those in the neutral bis-cluster **3**. The absolute values of $\Delta\delta$ of 0.128 and 0.076 ppm for substituents at the uncomplexed and complexed triple bonds respectively, indicate a higher sensitivity of the former towards developing cationic center. Single crystals of **4** (Figure 2) were obtained by its slow precipitation from an

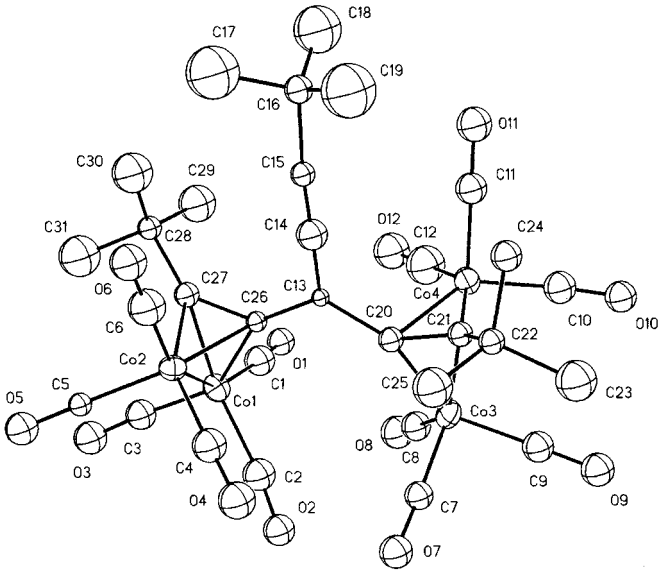


Figure 2. Molecular structure of **4** (30% probability ellipsoids; anisotropic refinement for Co atoms only).Selected interatomic distances [Å] and angles [°]: C13–C20 1.45(2), C13–C26 1.51(2), C13–C14 1.34(2), C13–Co1 3.07(1), C13-Co2 2.81(1), C13-Co3 3.27(1), C13-Co4 2.89(1), C14-C13-C20 120.5(11), C14-C13-C26 118.6(11), C20-C13-C26 120.9(10), C27-C26-C13 135.5(12), C21-C20-C13 135.9(12), C28-C27-C26-C13 55(1), C22-C21-C20-C13 43(1); angle between the bonds C26–C27 and Co1–Co2 82.3(6), between C20–C21 and Co3–Co4 89.7(6), between Co1–Co2 and Co3–Co4 88.0(5).

ethereal solution at −20 °C.[20] Generation of the cation leads to a rehybridization of the central carbon atom (C13) into sp^2, which is substantiated by its nearly flat geometry (out-of-plane $<0.5°$) and nearly ideal trigonal planar arrangement (119–121°). Covalent bonds around the cationic center are shortened slightly because of an increased s-character in hybridized orbitals; remarkably, the C13–C14 bond to the uncoordinated triple bond is more sensitive to the formation of the cation (1.43 Å in **3** vs. 1.34 Å in **4**) than the bonds to the coordinated triple bonds (C13–C20 1.49 vs. 1.45 Å; C13–C26 1.53 vs. 1.51 Å). Unexpectedly, the geometry of coordinated triple bonds (C27-C26-C13, C21-C20-C13) proved indifferent towards charge/hybridization changes of the central carbon atom (**3**: 134–135°, **4**: 136°). One of the important structural characteristics of binuclear metal complexes is the range of possible orientations of the C≡C and metal–metal bonds

 © WILEY-VCH Verlag GmbH, D-69451 Weinheim, 1998 1433-7851/98/3701-0162 $ 17.50+.50/0 *Angew. Chem. Int. Ed.* **1998**, *37*, No. 1/2

from perpendicular to each other to nearly parallel and σ-bonded.[3] In **3**, the corresponding angles are 89.2° and 90.1°. The development of positive charge at the central carbon atom makes the metal clusters nonequivalent (the angle between C26 – C27 and Co1 – Co2 is 82.3°, that between C20 – C21 and Co3 – Co4 is 89.7°) with one of them adopting a skew geometry, that is a twist from a perpendicular orientation by 7.7°. Among the configurational changes, attendant with generation of a cation in the α-position to the cobalt cluster, is a deviated linearity of the π-bonded ligand and a shift of the cationic center towards one of the vertices. The former is quantified by the magnitude of dihedral angles C28-C27-C26-C13 and C22-C21-C20-C13. In precursor **3** both values are small (4.8° and 4.4°, respectively), indicating a nearly undistorted linear arrangement. The build-up of positive charge at C13 results in preferential coordination of the cationic center with one of the metal atoms in each cluster, and consequently, a significant departure from linearity (55° and 43°, respectively). These findings are further confirmed by analysis of nonbonding distances between the cationic center C13 and all four cobalt atoms. In **3** the central carbon is equidistant from both metal atoms (differences in bond lengths are 0.04 Å for C13 – Co1 and C13 – Co2, and 0.01 Å for C13 – Co3 and C13 – Co4); in contrast, in **4** C13 is shifted 0.26 Å closer towards Co2 and, even more, 0.38 Å towards Co4; the shortest distances are 2.81 Å and 2.89 Å for C13 – Co2 and C13 – Co4, respectively.

Experimental Section

2: a) **1**: Synthesized according to protocol given in reference [17] in a yield of 54.6 %. R_f (TLC, petroleum ether/ether 10/1) = 0.40; m.p. 101 – 102 °C (sealed capillary) (in ref. [17] m.p. 102 – 103 °C); ^{1}H NMR (200 MHz, $CDCl_3$, 25 °C, TMS): δ = 1.24 (s, 27 H; *t*Bu), 2.64 (s, 1 H; OH).

b) Monocomplexation of **1**. A solution of $[Co_2(CO)_8]$ (376 mg, 1.1 mmol) in dry ether (15 mL) was added dropwise to a vigorously stirred solution of **1** (272 mg, 1 mmol) in dry ether (20 mL) at ambient temperature under an inert atmosphere. After the addition (55 min), the reaction mixture was stirred for 2 h (monitored by TLC). Ether was evaporated in vacuum, and the residue was chromatographed on silica gel to afford **2** (483 mg, 86.5 %) as dark red crystals. R_f (TLC, petroleum ether/ether 15/1) = 0.74; m.p. 110 – 122 °C (decomp; sealed capillary); ^{1}H NMR (200 MHz, $CDCl_3$, 25 °C, TMS): δ = 1.21 (s, 18 H; 2*t*Bu), 1.41 (s, 9 H; *t*Bu), 2.70 (s, 1 H; OH); MS-FAB: *m*/*z* (%): 557 (16) [M^+ – H], 530 (100) [M^+ – CO], 390 (15) [M^+ – 6 CO]; C,H analysis ($C_{25}H_{28}O_7Co_2$, 558.4): calcd. C 53.78, H 5.05; found C 53.89, H 5.09.

3: Analogously, treatment of **2** (407 mg, 0.73 mmol) in dry ether (20 mL) with $[Co_2(CO)_8]$ (250 mg, 0.73 mmol) in dry ether (15 mL) afforded **3** (439 mg, 71.3 %) as dark red crystals. R_f (TLC, petroleum ether) = 0.23; m.p. 84 – 101 °C (decomp; sealed capillary); ^{1}H NMR (500 MHz, CD_2Cl_2, – 80 °C, TMS): δ = 1.09 (s, 9 H; *t*Bu), 1.40 (s, 18 H; 2*t*Bu), 3.11 (s, 1 H; OH); ^{13}C NMR (125 MHz, CD_2Cl_2, – 70 °C, TMS): δ = 27.32, 29.00, 32.41, 36.26, 71.50, 84.34, 92.68, 100.41, 115.04, 200.25; MS-FAB: *m*/*z* (%): 843 (6) [M^+ – H], 788 (6) [M^+ – 2 CO], 508 (14) [M^+ – 12 CO]; C,H analysis ($C_{31}H_{28}O_{13}Co_4$, 844.3): calcd. C 44.10, H 3.34; found C 43.98, H 3.41. Single crystals suitable for X-ray structure analysis (Figure 1) were obtained by methanol vapor diffusion into a solution of **3** in pentane.

4: $HBF_4 \cdot Et_2O$ (58 mg, 0.36 mmol) was added dropwise (15 min) to a solution of **3** (101 mg, 0.12 mmol) in dry ether (30 mL) at – 20 °C under an inert atmosphere. The reaction mixture was allowed to warm to room temperature and stirred for 1 h. The ethereal layer was removed with a syringe, and the precipitate was thoroughly washed with dry ether (4 × 20 mL). The resulting complex **4** (96 mg, 88.1 %) was obtained as a black solid. ^{1}H NMR (500 MHz, CD_2Cl_2, – 80 °C, TMS): δ = 1.22 (s, *t*Bu), 1.48 (s, 2 *t*Bu); ^{13}C NMR (125 MHz, CD_2Cl_2, – 70 °C, TMS): δ = 12.25; 14.90; 32.00 (br.), 65.74; 83.58, 194 – 200 (br.). Single crystals suitable for X-ray structure analysis (Figure 2) were obtained by slow addition of HBF_4 to an ethereal solution of **3** at – 20 °C.

Received: June 9, 1997 [Z 10527 IE]
German version: *Angew. Chem.* **1998**, *110*, 170 – 172

Keywords: alkyne complexes · cations · cobalt · structure elucidation

[1] J. P. Collman, L. S. Hegedus, J. R. Norton, R. G. Finke, *Principles and Applications of Organotransition Metal Chemistry*, University Science Books, Mill Valley, CA, **1987**, Chapters 7 and 17 – 20; *Reactions of Coordinated Ligands*, *Vol. 1* (Ed.: P. S. Braterman), Plenum, New York, **1986**, Chapters 11, 14, and 16; see also: T. Laube in *Stable Carbocation Chemistry* (Eds.: G. K. S. Prakash, P. von R. Schleyer), Wiley, New York, **1996**, pp. 453 – 496.

[2] M. J. McGlinchey, L. Girard, R. Ruffolo, *Coord. Chem. Rev.* **1995**, *143*, 331 – 381.

[3] G. G. Melikyan, K. M. Nicholas in *Modern Acetylene Chemistry* (Eds.: P. J. Stang, F. Diederich), VCH, Weinheim, **1995**, pp. 99 – 138.

[4] M. F. D'Agostino, C. S. Frampton, M. J. McGlinchey, *J. Organomet. Chem.* **1990**, *394*, 145 – 166; P. A. Downton, B. G. Sayer, M. J. McGlinchey, *Organometallics* **1992**, *11*, 3281 – 3286; D. Seyferth, J. S. Merola, C. S. Eschbach, *J. Am. Chem. Soc.* **1978**, *100*, 4124 – 4131; M. Acampora, A. Ceccon, M. D. Farra, G. Giacometti, G. Rigatti, *J. Chem. Soc. Perkin Trans. 2* **1977**, 483 – 486; G. A. Olah, S. H. Yu, *J. Org. Chem.* **1976**, *41*, 1694 – 1697; N. M. Loim, L. A. Malutschenko, Z. N. Parnes, D. N. Kursanov, *J. Organomet. Chem.* **1976**, *108*, 363 – 369; L. L. Troitskaya, V. I. Sokolov, V. I. Bakhmutov, O. A. Reutov, M. Gruselle, C. Cordier, G. Joauen, *ibid.* **1989**, *364*, 195 – 206.

[5] S. Lupan, M. Kapon, M. Cais, F. H. Herbstein, *Angew. Chem.* **1972**, *84*, 1104 – 1106; *Angew. Chem. Int. Ed. Engl.* **1972**, *11*, 1025 – 1027; R. L. Sime, R. J. Sime, *J. Am. Chem. Soc.* **1974**, *96*, 892 – 896; U. Behrens, *J. Organomet. Chem.* **1979**, *182*, 89 – 98.

[6] R. E. Davis, H. D. Simpson, N. Grice, R. Pettit, *J. Am. Chem. Soc.* **1971**, *93*, 6688 – 6690.

[7] a) M. Gruselle, H. E. Hafa, M. Nikolski, G. Jaouen, J. Vaissermann, L. Li, M. McGlinchey, *Organometallics* **1993**, *12*, 4917 – 4925; b) A. Meyer, D. J. McCabe, M. D. Curtis, *ibid.* **1987**, *6*, 1491 – 1498; c) I. V. Barinov, O. A. Reutov, A. V. Polyakov, A. I. Yanovsky, Yu. T. Struchkov, V. I. Sokolov, *J. Organomet. Chem.* **1991**, *418*, C24 – C27.

[8] M. Kondratenko, H. Hafa, M. Gruselle, J. Vaissermann, G. Joauen, M. J. McGlinchey, *J. Am. Chem. Soc.* **1995**, *117*, 6907 – 6913.

[9] S. F. T. Froom, M. Green, K. R. Nagle, D. J. Williams, *J. Chem. Soc. Chem. Commun.* **1987**, 1305 – 1307.

[10] C. Cordier, M. Gruselle, J. Vaissermann, I. Bakhmutov, V. I. Sokolov, G. Joauen, *Organometallics* **1992**, *11*, 3825 – 3832.

[11] D. Osella, G. Dutto, G. Joauen, A. Vessieres, P. R. Raithby, L. Benedetto, M. J. McGlinchey, *Organometallics* **1993**, *12*, 4545 – 4552.

[12] K. M. Nicholas, *Acc. Chem. Res.* **1987**, *20*, 207 – 214; A. Caffyn, K. M. Nicholas in *Comprehensive Organomet. Chem., Vol. 12* (Ed.: G. Wilkinson), Pergamon, Oxford, **1995**, p. 685.

[13] a) R. E. Connor, K. M. Nicholas, *J. Organomet. Chem.* **1977**, *125*, C45 – C48; b) S. Padmanabhan, K. M. Nicholas, *ibid.* **1983**, *268*, C23 – C27.

[14] S. L. Schreiber, M. T. Klimas, T. Sammakia, *J. Am. Chem. Soc.* **1987**, *109*, 5749 – 5759.

[15] S. C. Benneth, M. A. Phipps, M. J. Went, *J. Chem. Soc. Chem. Commun.* **1994**, 225 – 226.

[16] G. G. Melikyan, V. M. Mkrtchyan, K. A. Atanesyan, G. Kh. Asaryan, Sh. O. Badanyan, *Bioorg. Khim.* **1990**, *16*, 1000 – 1001 [*Chem. Abstr.* **1992**, *113*, 230995j]; G. G. Melikyan, A. Mineif, O. Vostrowsky, H. J. Bestmann, *Synthesis* **1991**, 633 – 636; G. G. Melikyan, O. Vostrowsky, W. Bauer, H. J. Bestmann, *J. Organomet. Chem.* **1992**, *423*, C24 – C27; G. G. Melikyan, A. Deravakian, *ibid.* **1997**, *544*, 143 – 145.

[17] C. Tseng, K. Migliorese, S. I. Miller, *Tetrahedron* **1974**, *30*, 377 – 383.

[18] H. Greenfield, H. W. Sternberg, R. A. Friedel, J. H. Wotiz, R. Markby, I. Wender, *J. Am. Chem. Soc.* **1956**, *78*, 120 – 124.

 © WILEY-VCH Verlag GmbH, D-69451 Weinheim, 1998 1433-7851/98/3701-0163 $ 17.50+.50/0

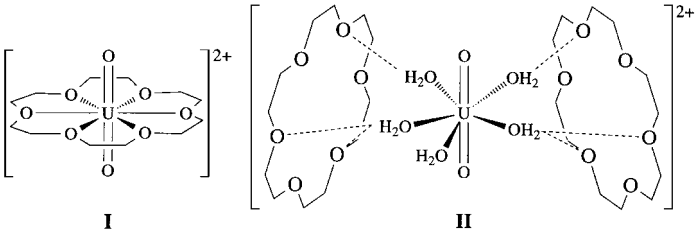
[19] a) Crystal data for **3**: crystal dimensions $0.12 \times 0.20 \times 0.37$ mm, orthorhombic space group *Pbca* (No. 61), $a = 17.277(5)$, $b = 19.393(7)$, $c = 21.190(8)$ Å, $V = 7100(4)$ Å^3, $Z = 8$, $\rho_{calcd} = 1.58$ g cm^{-3}, $\mu = 1.90$ mm^{-1}, $F(000) = 3408$; 10912 reflections with $3.7 < 2\theta < 40.0°$. Structure solution and refinement for 3316 independent reflections with $I > 2\sigma(I)$ and 433 parameters, max./min. empirical absorption correction 0.999/0.878; $R = 0.077$; $R_w = 0.168$; max./min. residual electron density 0.64/ − 1.13 e Å^{-3}. b) Nonius CAD4 diffractometer, $Mo_{K\alpha}$ radiation, graphite monochromator. Structure solution and refinement carried out on DEC 3000 and PC computers by using the programs Open MolEN and SHELXTL Version 5.0 and the Patterson–Fourier method. Hydrogen atoms were included in calculated positions (HFIX). Crystallographic data (excluding structure factors) for the structures reported in this paper have been deposited with the Cambridge Crystallographic Centre as supplementary publication no. CCDC-100541. Copies of the data can be obtained free of charge on application to CCDC, 12 Union Road, Cambridge CB2 1EZ (UK) (fax: int. code + (44) 1223 336-033; e-mail: deposit@ccdc.cam.ac.uk).

[20] Crystal data for **4**: crystal dimensions $0.07 \times 0.10 \times 0.23$ mm, tetragonal space group $P4_32_12$(No. 96), $a = 16.562(6)$, $c = 26.637(11)$ Å, $V = 7307(5)$ Å^3, $Z = 8$, $\rho_{calcd} = 1.66$ g cm^{-3}, $\mu = 1.86$ mm^{-1}, $F(000) = 3664$; 9927 reflections with $2.9 < 2\theta < 35.0°$. The crystal was mounted in Paratone oil and all measurements were performed at $-105\,°C$. Structure solution and isotropic refinement, except Co atoms, for 2469 independent reflections with $I > 2\sigma(I)$ and 227 parameters, no absorption correction, DAMP 1000, $R = 0.104$; $R_w = 0.175$; max./min. residual electron density 0.75/ − 0.59 e Å^{-3}.[19b]

Synthesis and Structure of the First Transuranium Crown Ether Inclusion Complex: $[NpO_2([18]Crown\text{-}6)]ClO_4$**

David L. Clark,* D. Webster Keogh, Phillip D. Palmer, Brian L. Scott, and C. Drew Tait

Crown ether ligands[1, 2] have been studied as potential actinide extractants for many years, and they have been shown to influence the partitioning of actinides in two-phase aqueous systems.[3–5] Although many examples of crown ether ligands that extract actinides in hydrocarbon/water systems are known,[6, 7] relatively few actinide crown ether complexes in which the actinide ion is coordinated by one or more donor atoms of the crown ether have been reported.[8] There are only two inclusion compounds of *trans*-dioxoactinide cations AnO_2^{n+} in which the actinide ion is completely encapsulated by a crown ether ligand and the counterions (perchlorate[9, 10] or triflate[11]) are uncoordinated in the crystal lattice: $[UO_2([18]crown\text{-}6)]^{2+}$ (**I**) and $[UO_2(dicyclohexano[18]\text{-}crown\text{-}6)]^{2+}$. It has been claimed that synthesis of inclusion complexes from uranyl ions UO_2^{2+} and crown ether ligands requires the use of weakly coordinating anions, nonaqueous conditions, and proper choice of cavity size.[8] Indeed, the majority of actinide crown ether complexes exhibit second-sphere hydrogen bonding between the oxygen atoms of the crown ether and water molecules coordinated to the actinide center.[12–19] Well-known examples include $[UO_2(H_2O)_5([18]crown\text{-}6)_2(H_2O)(CH_3CN)_2][ClO_4]_2$ (central unit: **II**)[15] and $[UO_2(H_2O)_5([18]crown\text{-}6)][CF_3SO_3]_2$.[17]



I **II**

Crown ether inclusion complexes of a transuranic ion in any oxidation state are unknown.

On attempting to employ this well-known ability of crown ether ligands to form second-sphere hydrogen-bonded complexes of *trans*-dioxometal ions (as in **II**), we were surprised to observe the complete encapsulation of the NpO_2^+ ion by the [18]crown-6 ligand. Addition of one equivalent of [18]crown-6 to a stirred solution of NpO_2^{2+} in 1 M HX ($X = ClO_4^-$, $CF_3SO_3^-$) resulted in reduction of Np^{VI} to Np^V and formation of large turquoise crystals of $[NpO_2([18]crown\text{-}6)][X]$ (**1**[X]) over 12–24 h. The presence of an absorption band at 980 nm ($\varepsilon = 395$ M^{-1} cm^{-1}), characteristic of the NpO_2^+ ion,[20] in the NIR spectra of the crystalline solids dissolved in 1 M $HClO_4$ confirms that reduction of Np^{VI} to Np^V has occurred. Even in the presence of O_3, the Np^{VI} was reduced to **1**[X] on addition of [18]crown-6. Finally, solutions of Np^V compounds in 1 M HX, which are present as hydrated NpO_2^+ ions, react smoothly with [18]crown-6 to give **1**[X] in almost quantitative yield.

A single-crystal X-ray diffraction study of **1**[ClO_4] revealed an NpO_2^+ ion completely encapsulated by a disordered [18]crown-6 ligand.[21] The Np center of the $[NpO_2([18]crown\text{-}6)]^+$ ion is coordinated by two *trans* oxo ligands and six approximately coplanar crown ether O atoms to give an approximate hexagonal bipyramidal coordination environment (Figure 1). In the crown ether ligand, all C-O-C-C units have an *anti* (a), and the O-C-C-O units a *gauche* conformation (g), and this results in a distorted $g^-g^+g^+g^-g^+g^+$ conformation,[22] similar to that reported for **I**.[11] The Np=O bond length of 1.800(5) Å is unusually short for an NpO_2^+ ion; 1.85 Å is usual.[23, 24] The average equatorial Np–O distance of 2.594(10) Å is unusually long for a neutral oxygen-donor ligand when compared with the U–OH_2 distance of 2.43 Å in $[UO_2(OH_2)_5]^{2+}$ complexes.[15, 17] Coordination of σ-donor ligands in the equatorial plane of an *trans*-dioxo actinide ion generally results in a slight lengthening of the An=O bond, accompanied by decreased intensity of the Raman-active ν_1 O=An=O stretching band.[25] However, in **1**[ClO_4] the Np=O bond is shorter, and presumably stronger, than in the uncomplexed cation. Similar structural changes are observed in the uranyl system, for which encapsulation by [18]crown-6 results in a significant shortening of the U=O bond from 1.758(2) to 1.64(4) Å.[15, 17]

[*] Dr. D. L. Clark, Dr. D. W. Keogh, P. D. Palmer, Dr. B. L. Scott, Dr. C. D. Tait
Chemical Science and Technology Division and
G. T. Seaborg Institute for Transactinium Science
Mail Stop G-739, Los Alamos National Laboratory
Los Alamos, NM 87545 (USA)
Fax: Int. code + (1) 505-665 4624
e-mail: dlclark@lanl.gov

[**] This work was supported by the Office of Basic Energy Sciences (U.S. DOE, contract no. W-7405-ENG-36 with the University of California) and by the Laboratory Directed Research and Development Program.

 © WILEY-VCH Verlag GmbH, D-69451 Weinheim, 1998 1433-7851/98/3701-0164 $ 17.50+.50/0

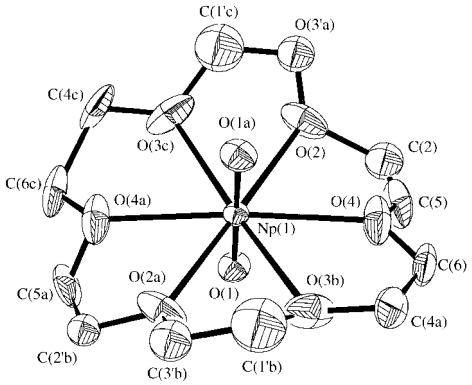


Figure 1. ORTEP plot of the molecular structure of **1** in crystals of **1**[ClO_4] (ellipsoids drawn at the 50 % probability level). Selected bond lengths [Å] and angles [°]: Np(1)–O(1) 1.800(5), Np(1)–O(2) 2.576(9), Np(1)–O(3) 2.604(10), Np(1)–O(4) 2.603(8); O(1)-Np(1)-O(2) 91.7(2), O(1)-Np(1)-O(4) 85.6(2), O(2)-Np(1)-O(4) 59.5(5), O(1)-Np(1)-O(3) 85.6(3).

For *trans*-dioxoactinide ions, the Raman-active ν_1 vibrational mode is a much better indicator of bond strength than bond length. For the $[NpO_2(H_2O)_5]^+$ ion[24] (Np=O 1.85 Å), the ν_1 vibrational mode occurs at 767 cm^{-1}.[26] Raman spectra of **1**[ClO_4] showed an intense band at 778 cm^{-1}, which is consistent with a stronger Np=O bond than in the aquo ion. To confirm this band assignment, ^{18}O was electrochemically incorporated into the Np=O unit [Eqs. (1)–(3); the asterisk

$$[NpO_2(OH_2)_n]^+ \xrightarrow[H_2^{*}O/HClO_4]{-0.2\,V\,(SCE)} [Np(^{*}OH_2)_n]^{3+}/[Np(^{*}OH_2)_n]^{4+} \quad (1)$$

$$[Np(^{*}OH_2)_n]^{3+}/[Np(^{*}OH_2)_n]^{4+} \xrightarrow[H_2^{*}O/HClO_4]{+1.22\,V\,(SCE)} [Np^{*}O_2(^{*}OH_2)_n]^{2+} \quad (2)$$

$$[Np^{*}O_2(^{*}OH_2)_n]^{2+} \xrightarrow[HClO_4]{[18]crown\text{-}6} [Np^{*}O_2([18]crown\text{-}6)][ClO_4] \quad (3)$$

indicates enrichment with ^{18}O]. Water enriched in ^{18}O (98 % ^{18}O) was added to 0.56 M NpO_2^+ (aq) in 1 M $HClO_4$ and reduced electrochemically at -0.2 V to a mixture of hydrated Np^{3+}/Np^{4+}[27] with removal of the oxo ligands. The potential was then reversed, and the mixture was oxidized to hydrated, ^{18}O-enriched $Np^{*}O_2^{2+}$ ions. The purity of the oxidized compounds was confirmed with NIR spectroscopy by monitoring the absorption band of hydrated NpO_2^{2+} at 1223 nm (ε = 45 $M^{-1}cm^{-1}$).[20] [18]Crown-6 was subsequently added, and turquoise crystals of ***1**[ClO_4] formed after cooling the mixture to 5 °C overnight. The Raman spectra of ***1**[ClO_4] crystals show ν_1 bands for all three isotopomers ^{18}O=Np=^{18}O, ^{18}O=Np=^{16}O, and ^{16}O=Np=^{16}O at 734, 751, and 780 cm^{-1}, respectively, confirming our original assignment.

The complete encapsulation of the NpO_2^+ ion by a crown ether ligand under any conditions is unprecedented, and **1**[ClO_4] represents the first structurally and spectroscopically characterized transuranium crown ether complex. The relative ease of encapsulation in aqueous solution contrasts with the related UO_2^{2+} ion, for which anhydrous conditions are necessary to ensure that the crown ether oxygen atoms bind directly to the metal center.[8] This difference attests to the ability of crown ether ligands to separate ions of almost identical chemical behavior, and the apparent preference for Np^V over Np^{VI} may be related to the differing ionic radii of these ions.[1] Although the mechanism is unknown, dicyclohexano-[18]crown-6 has been shown to separate Pu^{IV} from U^{VI} and fission products more effectively than tributyl phosphate,[3] the extractant used in the well-known Purex process.[20] The potential ability of crown ether ligands to extract actinide ions selectively from radioactive process streams or solutions of nuclear waste is particularly interesting due to its economic and environmental implications. The actinophilic nature of crown ether ligands towards other transuranic ions is under further investigation.

Received: May 26, 1997 [Z10472IE]
German version: *Angew. Chem.* **1998**, *110*, 173–175

Keywords: actinides · crown compounds · host–guest chemistry · neptunium

[1] G. Gokel, *Crown Ethers & Cryptands. Monographs in Supramolecular Chemistry*, The Royal Society of Chemistry, Cambridge, **1991**.
[2] S. R. Cooper, *Crown Ether Compounds: Toward Future Applications*, VCH, New York, **1992**.
[3] M. Lemaire, A. Guy, R. Chomel, J. Foos, *J. Chem. Soc. Chem. Commun.* **1991**, 1152.
[4] R. D. Rogers, C. B. Bauer, A. H. Bond, *J. Alloys Compd.* **1994**, *213/214*, 305.
[5] V. V. Proyaev, V. V. Romanovski, *Radiokhimiya* **1992**, *34*, 156.
[6] W.-J. Wang, Q. Sun, B. Chen, *J. Radioanal. Nucl. Chem.* **1986**, *98*, 11.
[7] C. M. Wai, H. S. Du, Y. Meguro, Z. Yoshida, *Anal. Sci. 7 (Suppl. Proc. Int. Congr. Anal. Sci. 1991, Pt. 1)* **1991**, 41.
[8] P. Thuéry, N. Keller, M. Lance, J. D. Vigner, M. Nierlich, *New J. Chem.* **1995**, *19*, 619.
[9] A. Dejean, P. Charpin, G. Folcher, P. Rigny, A. Navaza, G. Tsouaris, *Polyhedron* **1987**, *6*, 189.
[10] A. Navaza, F. Villain, P. Charpin, *Polyhedron* **1984**, *3*, 143.
[11] L. Deshayes, N. Keller, M. Lance, A. Navaza, M. Nierlich, J. D. Vigner, *Polyhedron* **1994**, *13*, 1725.
[12] R. D. Rogers, A. H. Bond, W. G. Hipple, A. N. Rollins, R. F. Henry, *Inorg. Chem.* **1991**, *30*, 2671.
[13] R. D. Rogers, M. M. Benning, *Acta Crystallogr. Sect. C* **1988**, *44*, 641.
[14] R. D. Rogers, L. K. Kurihara, M. M. Benning, *J. Chem. Soc. Dalton Trans.* **1988**, 13.
[15] R. D. Rogers, L. K. Kurihara, M. M. Benning, *J. Incl. Phenom.* **1987**, *5*, 645.
[16] R. D. Rogers, M. M. Benning, *J. Incl. Phenom. Mol. Recognit. Chem.* **1992**, *11*, 121.
[17] L. Deshayes, N. Keller, M. Lance, M. Nierlich, J. D. Vigner, *Acta Crystallogr. Sect. C* **1994**, *50*, 1541.
[18] P. G. Eller, R. A. Penneman, *Inorg. Chem.* **1976**, *15*, 2439.
[19] L. Deshayes, N. Keller, M. Lance, M. Nierlich, J. D. Vigner, *Acta Crystallogr. Sect. C* **1993**, *49*, 16.
[20] J. J. Katz, G. T. Seaborg, L. R. Morss, *The Chemistry of the Actinide Elements*, Chapman and Hall, London, **1986**.
[21] X-ray structure analysis of **1**[ClO_4]: Siemens P4/PC diffractometer, $Mo_{K\alpha}$ radiation (λ = 0.71073 Å), graphite monochromator, ω scan method, structure solved by Patterson und difference Fourier methods with the program SHELXS-86, space group $I4_1/a$, a = 10.686(1), b = 10.686(1), c = 16.771(1) Å, V = 1915.1(1) Å^3, ρ_{calcd} = 2.195 g cm^{-3}, Z = 4, T = 295 K. Least-squares refinement of the model based on 1383 independent reflections converged to $R1$ = 0.0261 and $wR2$ = 0.0682 with GOF = 1.111. The two crown ligands were offset by 30° to satisfy the $\bar{4}$ site symmetry, and each was refined with half occupancy. The carbon and oxygen atoms of the two disordered crown ligands were refined in a general position with site-occupancy factors of 0.5. All carbon and oxygen atomic coordinates were refined freely. Partially overlapping carbon atoms from different crown ligands were restrained to have the same U_{ij} values with a standard deviation of 0.05 Å^2 by using the SIMU command of SHELX-93. Crystallographic data (excluding structure factors) for the structure reported in this paper have been deposited with the Cambridge Crystallographic Data Centre as supplementary publication no. CCDC-100439. Copies of the data can be obtained free of charge on application to CCDC,

 © WILEY-VCH Verlag GmbH, D-69451 Weinheim, 1998 1433-7851/98/3701-0165 $ 17.50+.50/0

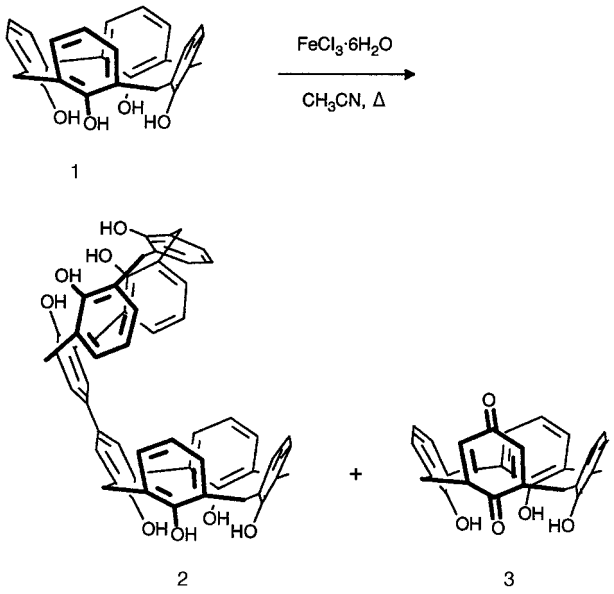
12 Union Road, Cambridge CB2 1EZ, UK (fax: int. code + (44) 1223-336033; e-mail: deposit@ccdc.cam.ac.uk).
[22] J. W. H. M. Uiterwijk, S. Harkema, B. W. van der Waal, F. Göbel, H. T. M. Nibbeling, *J. Chem. Soc. Perkin Trans. II.* **1983**, 1843.
[23] D. L. Clark, S. D. Conradson, S. A. Ekberg, N. J. Hess, M. P. Neu, P. D. Palmer, W. Runde, C. D. Tait, *J. Am. Chem. Soc.* **1996**, *118*, 2089.
[24] J.-M. Combes, C. J. Chisholm-Brause, G. E. Brown, Jr., G. A. Parks, S. D. Conradson, P. G. Eller, I. R. Triay, D. E. Hobart, A. Meijer, *Environ. Sci. Technol.* **1992**, *26*, 376.
[25] C. Nguyen-Trung, G. M. Begun, D. A. Palmer, *Inorg. Chem.* **1992**, *31*, 5280.
[26] C. Madic, G. M. Begun, D. E. Hobart, R. L. Hahn, *Inorg. Chem* **1984**, *23*, 1914.
[27] T. W. Newton, D. E. Hobart, P. D. Palmer, *The Preparation and Stability of Pure Oxidation States of Neptunium, Plutonium, and Americium*, Los Alamos National Laboratory, **1986**, LA-UR-86-967.

5,5′-Bicalix[4]arene: The Bridgeless Prototype of Double Calix[4]arenes of the "Head-to-Head" Type**

Placido Neri,* Alessandra Bottino, Francesca Cunsolo, Mario Piattelli, and Enrico Gavuzzo

In the past decade several double (or multiple) calixarenes[1] have been prepared as examples of higher order molecular architectures with new high-level host properties, such as allostery and cooperativity.[2] In these compounds, two (or more) calixarene units are linked at their upper or lower rims[3, 4] through one or more spacer elements. Various structural motifs have been used as spacers, including alkyl, alkenyl, and alkynyl chains, diesters, diamides, metallocenes, ethers and polyethers, sulfides, and diimines.[1, 2, 5] However, to the best of our knowledge, examples of the prototypal compounds with directly coupled (bridgeless) calixarene units have not been reported so far.[6] Here we describe the synthesis, X-ray crystal structure, and derivatization of the first double calixarene of the "head-to-head" type[7] with direct *para-para* linkage, 5,5′-bicalix[4]arene **2**.[8]

Linkage of the two calix[4]arene units was accomplished by oxidative coupling of the *p*-H-calix[4]arene **1**[9a] under conditions similar to those of Pummerer's classic binaphthol synthesis[10] (Scheme 1). A solution of **1** in hot CH_3CN was treated with solid $FeCl_3 \cdot 6H_2O$, and the suspension was heated at reflux for 4 h. Workup of the reaction mixture and column chromatography of the crude product afforded



Scheme 1. Synthesis of 5,5′-bicalix[4]arene **2** by oxidative coupling of *p*-H-calix[4]arene **1**.

bicalix[4]arene **2** (10%) and calix[4]monoquinone **3** (6%). The dimeric nature of **2** was indicated by a quasi-molecular ion at $m/z = 847$ in the positive-ion fast-atom-bombardment (FAB) mass spectrum. Correspondingly, the ^{13}C NMR spectrum contains two $ArCH_2Ar$ signals, six aromatic CH resonances, three C–OH singlets, and a diagnostic singlet at $\delta = 135.3$ attributable to quaternary carbon atoms involved in bonding of the two halves in **2**.

Both calixarene moieties are in the *cone* conformation because of the stabilizing cyclic hydrogen bond, as revealed by two broad AX systems for $ArCH_2Ar$ protons in the ^1H NMR spectrum.[1] These systems sharpen at low temperature, and a Gibbs free energy of activation $\Delta G^{\neq} = 14$ kcal mol^{-1} was estimated from the coalescence temperature for the *cone*–*cone* conformational interconversion, a value very similar to that reported for the parent monomer **1**.[9b] With respect to the biphenyl moiety, one can presume relatively free rotation around the Ar–Ar bond, with a slight deviation from coplanarity for the two aryl rings. This leads to a *syn* or *anti* orientation of the calix[4]arene units (Figure 1). Energy evaluations (MM2 and MM3) of the two geometries gave very similar values; the *anti* orientation is slightly lower in energy. Therefore, the *syn* and *anti* forms of bicalix[4]arene **2** are expected to be in equilibrium in solution (Figure 1).

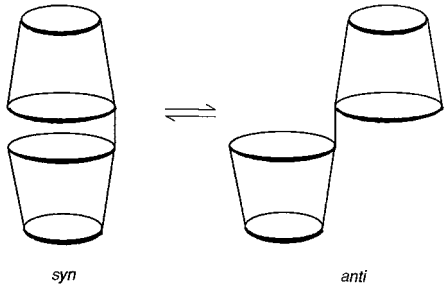


Figure 1. Schematic representation of the proposed equilibrium between the *syn* and *anti* conformations of 5,5′-bicalix[4]arene **2** in solution.

[*] Dr. P. Neri, Dr. A. Bottino, Dr. F. Cunsolo, Prof. Dr. M. Piattelli
Istituto per lo Studio delle Sostanze Naturali di Interesse Alimentare e Chimico-Farmaceutico
Consiglio Nazionale delle Ricerche
Via del Santuario 110, I-95028 Valverde, CT (Italy)
Fax: Int. code + (39) 95-721-2141
e-mail: neri@issn.ct.cnr.it
Dr. E. Gavuzzo
Istituto di Strutturistica Chimica "G. Giacomello"
C.N.R., Area della Ricerca di Roma, Montelibretti RM (Italy)
Area della Ricerca di Roma, Montelibretti, RM (Italy).

[**] We wish to thank Mr. R. Rapisardi (ICTMP-CNR, Catania) for FAB-MS measurements and Dr. G. Chessari (University of Sheffield) for evaluation of NMR titration data. The institutes cited are associated with the Istituto Nazionale di Coordinamento per la Chimica dei Sistemi Biologici.

 © WILEY-VCH Verlag GmbH, D-69451 Weinheim, 1998 1433-7851/98/3701-0166 $ 17.50+.50/0

Definitive proof of the structure of **2** was obtained through single-crystal X-ray structure analysis.[11] In the crystal the molecule resembles two bowls joined together by the Ar–Ar bond (1.50(1) Å; Figure 2), with the two concavities on

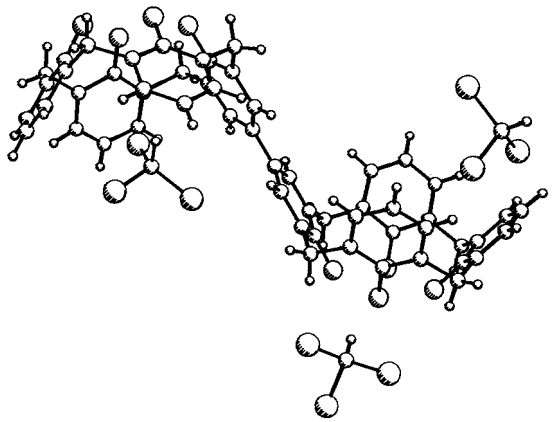


Figure 2. Crystal structure of **2** · 3 $CHCl_3$ (H, C, O, and Cl atoms are drawn as spheres of increasing size).

opposite sides. The bottom of each bowl is formed by four hydroxy groups. In each bowl an approximate square network of intramolecular hydrogen bonds is created by the four hydroxy groups, each acting once as donor and once as acceptor in two hydrogen bonds. The average length of the eight hydrogen bonds is 2.68 Å [minimum 2.66(1) Å, maximum 2.69(1) Å]. The angles C–O ··· O are all approximately 110°, and the hydroxy hydrogens and one of the two lone pairs from an oxygen atom presumably lie close to the plane formed by the four oxygens of each moiety. The angles O ··· O ··· O are all around 90°. The torsion angle between the Ar moieties is 35(2)°, a typical value for biphenyl systems in which there is very little conjugation between the two aromatic rings.[14] The canting angles between the mean plane of the four methylene carbons and the planes of the phenol rings vary from 51.6° to 61.4° in the two halves. The packing of the host molecules is governed mainly by van der Waals interactions, where the shortest contact is 2.96(1) Å between the O(1) atoms of two centrosymmetric molecules. The crystal contains chloroform, but only three chloroform molecules were identified because of disorder present in the solvent system. Two are included in the pseudocapsules formed by the two opposing bowls of facing centrosymmetric molecules (Figure 3), as a consequence of van der Waals interactions. The third chloroform molecule is outside the capsules, where its acidic hydrogen atom may form a possible hydrogen bond with an OH group (O ··· C = 3.30 Å, O ··· H–C = 166.3°).

Each phenol ring of bicalix[4]arene **2** can rotate freely through the 16-membered annulus, leading, in principle, to 21 extreme conformations (apart from enantiomers and *syn*/*anti* alternatives). Blocking this motion by alkylation with groups bulkier than ethyl[15] would then lead to as many atropisomers. Although this appears to be a considerable complication, it at the same time makes **2** a very appealing substrate, provided that conditions can be found for satisfactory stereochemical control of alkylation. To test this potentiality, **2** was treated

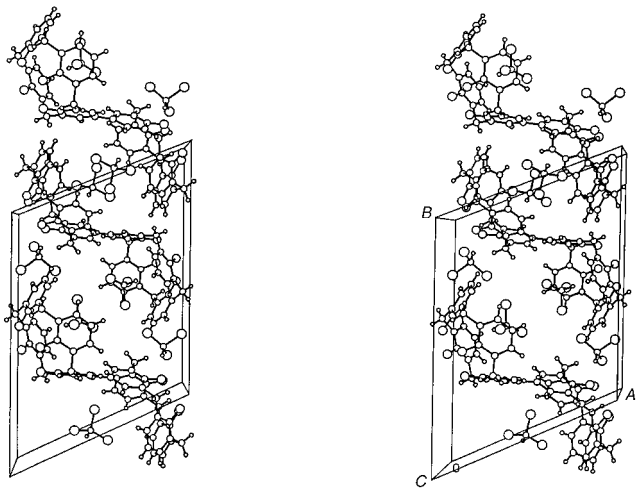
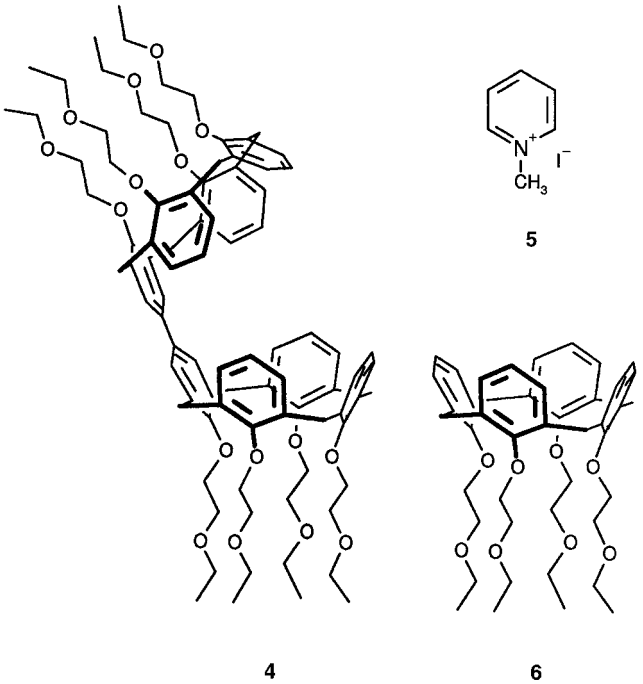


Figure 3. Crystal packing of **2** viewed along the *c* axis.

with 2-(ethoxy)ethyl bromide under conditions (NaH/DMF) known to favor alkylation products in the *cone* conformation.[16] Thus, the octakis[2-(ethoxy)ethoxy] derivative **4** fixed in a double-*cone* conformation was obtained in good yield (55 %) and high stereoselectivity. Further investigation in this direction might similarly lead to the selective preparation of other atropisomers.

The globular architecture of the *syn* conformation of **2** suggests the potential for cooperation between the two *cone* binding sites in the *endo*-calix complexation of suitable guests. A conformationally blocked double *cone* system like **4** of



5

4 **6**

course appears preferable to this end; indeed, preliminary ^1H NMR experiments (Figure 4) revealed the ability of **4** to include the *N*-methylpyridinium cation **5** (iodide counterion). A value of 153 M^{-1} was estimated for the association constant based on NMR titration,[17a] compared with 6 M^{-1} found for

 © WILEY-VCH Verlag GmbH, D-69451 Weinheim, 1998 1433-7851/98/3701-0167 $ 17.50+.50/0

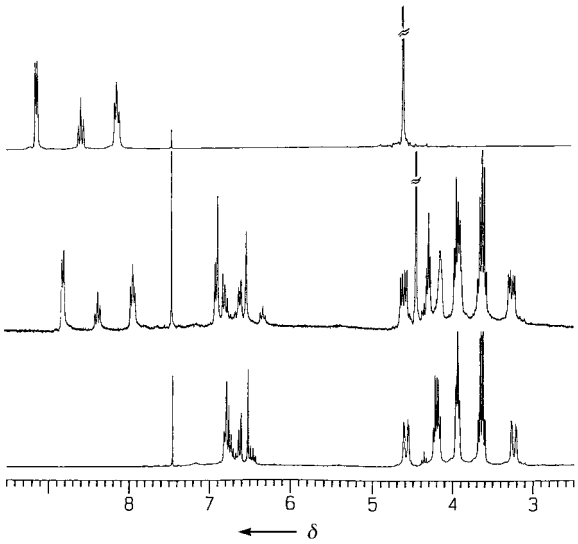
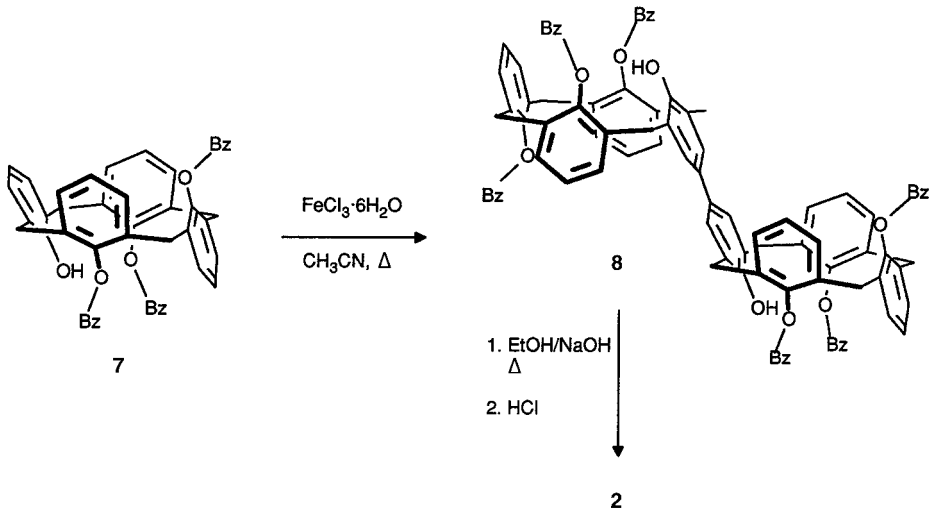


Figure 4. ^{1}H NMR spectra (250 MHz, 295 K, $CDCl_3/CD_3CN$ 5/1) of **4** (bottom), *N*-methylpyridinium iodide **5** (top), and a mixture of the two (middle).

the reference compound tetrakis[2-(ethoxy)-ethoxy]calix[4]-arene **6**.[16] This indicates the cooperative action of the two halves in cation inclusion.[17b]

The peculiar structural features of **2** and its high stereochemical potential make it an interesting new building block in host–guest and supramolecular chemistry. For this reason, the availability of larger amounts became imperative, which in turn required improvements in the synthesis. Because the main drawback to direct coupling of **1** seems to be competitive polymerization and/or polyoxidation, we were induced to try an indirect pathway for synthesizing **2** using as starting material a calix[4]arene with a single free phenolic OH group. Therefore, we subjected the readily available tribenzoate **7**, described by Gutsche et al.,[9a, 18] to oxidative coupling with $FeCl_3 \cdot 6H_2O$ (Scheme 2). This led to the dimeric hexabenzoate **8**, which upon alkaline hydrolysis gave 5,5′-bicalixarene **2** in 55–60% overall yield. With this latter procedure the way has become open for a full investigation into the potentialities of bicalixarene building blocks in supramolecular chemistry. An extension of this approach, using different coupling conditions,[20] may result in *para-para*-oligo-calixarenes with novel and interesting architectures. We are currently carrying out work in these directions.



Scheme 2. Improved synthesis of **2** through oxidative coupling of two molecules of **7**.

Experimental Section

2: A suspension of **7** (1.5 g, 2.04 mmol) and $FeCl_3 \cdot 6H_2O$ (1.10 g, 4.07 mmol) in CH_3CN (30 mL) was heated at reflux with stirring. After 1.5 h additional $FeCl_3 \cdot 6H_2O$ (1.10 g, 4.07 mmol) was added. The process was repeated several times until the starting material was completely consumed (based on TLC). The solvent was removed by evaporation in vacuo, 3 N HCl added to the residue, and the solid collected by filtration. This crude product was suspended in EtOH (85 mL), and after addition of 15% NaOH (13 mL) the mixture was heated at reflux with stirring for 7 h. Most of the EtOH was subsequently removed by evaporation in vacuo. The resulting suspension was neutralized with 1N HCl, and solid material collected by filtration. This was dissolved in CH_2Cl_2 and again filtered to remove small amounts of insoluble matter. Flash chromatography on silica gel (CH_2Cl_2/petroleum ether, 1/1) led to **2** (0.47 g, 55%). M.p. $>360\,^\circ$C; ^{1}H NMR (250.13 MHz, C_6D_6, 350 K) $\delta = 3.71, 3.76$ ($2 \times$ s, 8H each, $ArCH_2Ar$), 6.43 (t, $J = 7.8$ Hz, 2H, ArH), 6.47 (t, $J = 7.5$ Hz, 4H, ArH), 6.69–6.80 (m, 12H, ArH), 6.87 (s, 4H, Ar–ArH), 10.01 (br s, 8H, OH); ^{1}H NMR (250.13 MHz, C_6D_6, 295 K; partial spectrum): $\delta = 3.26$, 4.22 ($2 \times$ br, AX, each 8H, $ArCH_2Ar$); ^{1}H NMR (250.13 MHz, $CDCl_3$, 250 K; partial spectrum): $\delta = 3.55/4.26$ (AX, $J = 13.7$ Hz, 8H, $ArCH_2Ar$), 3.57/4.26 (AX, $J = 13.7$ Hz, 8H, $ArCH_2Ar$); ^{13}C NMR (62.9 MHz, $CDCl_3$, 295 K) $\delta = 31.7$, 31.8 (t, $ArCH_2Ar$), 122.2, 122.3, 127.8 (d, $C_{Ar}H$), 128.0, 128.1, 128.2 (s, $C_{Ar}CH_2$), 128.9($2 \times$ C), 129.1 (d, $C_{Ar}H$), 135.3 (s, C_{Ar}–C_{Ar}), 148.0, 148.7, 148.8 (s, $C_{Ar}OH$); positive-ion FAB-MS [*m*-nitrobenzylalcohol (NBA) matrix]: $m/z = 847$ [M^++H].

4: ^{1}H NMR (250.13 MHz, C_6D_6, 295 K) $\delta = 1.17$ (t, $J = 5.7$ Hz, 12H, CH_3), 1.18 (t, $J = 6.2$ Hz, 12H, CH_3), 3.18/4.71 (AX, $J = 13.3$ Hz, 8H, $ArCH_2Ar$), 3.25/4.75 (AX, $J = 13.5$ Hz, 8H, $ArCH_2Ar$), 3.37–3.49 (m, 16H, OCH_2), 3.79 (t, $J = 5.5$ Hz, 8H, CH_2CH_2), 3.88 (q, $J = 5.7$ Hz, 8H, CH_2CH_3), 4.15 (t, $J = 5.5$ Hz, 8H, $ArOCH_2$), 4.27 (t, $J = 5.6$ Hz, 4H, $ArOCH_2$), 4.28 (t, $J = 5.8$ Hz, 4H, $ArOCH_2$), 6.63–6.84 (m, 18H, ArH), 7.08 (s, 4H, Ar–ArH); ^{13}C NMR (62.9 MHz, $CDCl_3$, 295 K) $\delta = 15.3$ (q, OCH_2CH_3), 30.8, 31.0 (t, $ArCH_2Ar$), 66.4, 69.7, 73.0, 73.2 (t, OCH_2), 122.3, 126.7, 128.1 (d, $C_{Ar}H$), 134.8 (s, $C_{Ar}CH_2$), 135.1 (s, C_{Ar}–C_{Ar}), 155.5, 156.2, 156.4 (s, C_{Ar}–O); positive-ion FAB-MS (NBA): $m/z = 1425$ [M^++H].

Received: July 8, 1997 [Z10724IE]
German version: *Angew. Chem.* **1998**, *110*, 175–178

Keywords: biaryls · calixarenes · configuration determination · host–guest chemistry · macrocycles

[1] Review on calixarenes: V. Böhmer, *Angew. Chem.* **1995**, *107*, 785; *Angew. Chem. Int. Ed. Engl.* **1995**, *34*, 713.
[2] Review on double calixarenes: Z. Asfari, J. Weiss, J. Vicens, *Synlett* **1993**, 719.
[3] A few exceptions are the double calixarenes bridged at one $ArCH_2Ar$ group: a) O. Aleksiuk, S. E. Biali, *J. Org. Chem.* **1996**, *61*, 5670. b) *Calixarenes: A Versatile Class of Macrocyclic Compounds* (Eds.: J. Vicens, V. Böhmer), Kluwer, Dordrecht, **1991**, p. 60.
[4] Special cases of multiple calixarenes are Böhmer's "annelated"

calixarenes, in which the two macrocycles share two adjacent phenol rings: V. Böhmer, R. Dörrenbächer, M. Frings, M. Heydenreich, D. de Paoli, W. Vogt, G. Ferguson, I. Thondorf, *J. Org. Chem.* **1996**, *61*, 549.

[5] Recent examples not included in ref. [1, 2]: O. Struck, L. A. J. Chrisstoffels, R. J. W. Lugtenberg, W. Verboom, G. J. van Hummel, S. Harkema, D. N. Reinhoudt, *J. Org. Chem.* **1997**, *62*, 2487; J. A. Perez-Adelmar, H. Abraham, C. Sanchez, K. Rissanen, P. Prados, J. de Mendoza, *Angew. Chem.* **1996**, *108*, 1088; *Angew. Chem. Int. Ed. Engl.* **1996**, *35*, 1009; M. A. McKervey, M. Pitarch, *J. Chem. Soc. Chem. Commun.* **1996**, 1689; A. Siepen, A. Zett, F. Vögtle, *Liebigs Ann.* **1996**, 757; P. Lhotak, S. Shinkai, *Tetrahedron Lett.* **1996**, *37*, 645; P. Lhotak, M. Kawaguchi, A. Ikeda, S. Shinkai, *Tetrahedron* **1996**, *52*, 12399; A. Arduini, S. Fanni, G. Manfredi, A. Pochini, R. Ungaro, A. R. Sicuri, F. Ugozzoli, *J. Org. Chem.* **1995**, *60*, 1448; F. Ohseto, S. Shinkai, *J. Chem. Soc. Perkin Trans. 2* **1995**, 1103; H. Ross, U. Lüning, *Angew. Chem.* **1995**, *107*, 2723; *Angew. Chem. Int. Ed. Engl.* **1995**, *34*, 2555.

[6] The shortest spacer used so far is a single CH_2 group: K. Araki, K. Hisaichi, T. Kanai, S. Shinkai, *Chem. Lett.* **1995**, 569.

[7] The *para* positions (upper rim) of a calixarene system are commonly considered as the "head," while the OH groups (lower rim) represent the "tail": W. Wasikievicz, G. Rokicki, J. Kielkiewicz, V. Böhmer, *Angew. Chem.,* **1994**, *106*, 230; *Angew. Chem. Int. Ed. Engl.* **1994**, *33*, 214.

[8] The complete IUPAC name for this compound is 5,5′-bicalix[4]arene-25,25′,26,26′,27,27′,28,28′-octol.

[9] a) C. D. Gutsche, L.-G. Lin, *Tetrahedron* **1986**, *42*, 1633; b) C. D. Gutsche, L. J. Bauer, *J. Am. Chem. Soc.* **1985**, *107*, 6052.

[10] R. Pummerer, E. Prell, A. Rieche, *Ber. Dtsch. Chem. Ges. B* **1926**, *59*, 2159.

[11] Crystal structure analysis of **2**: $C_{56}H_{46}O_8 \cdot 3\,CHCl_3$, $M_r = 1205.11$, triclinic, space group $P\bar{1}$ (no. 2), $a = 15.389(3)$, $b = 19.630(4)$, $c = 10.790(2)$ Å, $\alpha = 90.45(2)$, $\beta = 108.78(1)$, $\gamma = 67.71(1)^\circ$, $V = 2831(1)$ Å^3, $Z = 2$, $\rho_{calcd} = 1.41$ g cm^{-3}, colorless crystals from $CHCl_3$/EtOH, crystal dimensions $0.25 \times 0.30 \times 0.45$ mm^3, θ-2θ scan ($2\theta_{max} = 124.2^\circ$), $F(000) = 1240$, room temperature. Of 9285 measured reflections, 8908 were independent ($R_{int} = 0.068$). Data were collected with a Rigaku AFC5R diffractometer with graphite-monochromated $Cu_{K\alpha}$ radiation and a 12 kW rotating anode generator. The data were corrected for Lorentzian and polarization effects, and an empirical absorption correction was applied to intensities based on azimuthal scans of several reflections; $\mu(Cu_{K\alpha}) = 45.27$ cm^{-1}, no decay correction. The structure was solved by direct methods with the program SIR 92.[12] Non-hydrogen atoms were refined anisotropically[13] except for one solvent molecule refined isotropically because of disorder. All hydrogen atoms (apart from OH) were positioned geometrically (riding model). Final refinements were carried out according to the full-matrix least-squares method based on 4189 observed reflections with $F_o > 10\,\sigma(F_o)$ and 665 variable parameters. $R = 0.117$, $R_w = 0.121$, $w = (\sin\theta/\lambda)^2$, $S = 1.38$. Maximum and minimum peaks of the final difference Fourier map: 2.20 and -1.03 e Å^{-3}; these residual electron densities could not be assigned to any chemically sensible moiety. Crystallographic data (excluding structure factors) for the structure reported in this paper have been deposited with the Cambridge Crystallographic Data Centre as supplementary publication no. CCDC-100536. Copies of the data can be obtained free of charge on application to CCDC, 12 Union Road, Cambridge CB2 1EZ, UK (fax: int. code + (44) 1223-336033; e-mail: deposit@chemcrys.cam.ac.uk).

[12] A. Altomare, G. Cascarano, C. Giacovazzo, A. Guagliardi, M. C. Burla, G. Polidori, M. Camalli, *J. Appl. Crystallogr.* **1994**, *27*, 435.

[13] M. Camalli, R. Spagna, *J. Appl. Crystallogr.* **1994**, *27*, 861.

[14] E. G. Boonstra, *Acta Crystallogr.* **1963**, *16*, 816.

[15] K. Iwamoto, K. Araki, S. Shinkai, *J. Org. Chem.* **1991**, *56*, 4955.

[16] J.-D. van Loon, J. F. Heida, W. Verboom, D. N. Reinhoudt, *Recl. Trav. Chim. Pays-Bas* **1992**, *111*, 353.

[17] a) NMR titrations (250 MHz, 295 K) were carried out in $CDCl_3$/CD_3CN (5/1). The association constants were determined with a nonlinear fitting program using the concentration-dependent shifts of the NMe group while the concentration of the host (**4** or **6**) was held constant. b) A similar cooperative action in the complexation of *N*-methylpyridinium iodide was found by Shinkai et al. for a CH_2-bridged double calix[4]arene.[6]

[18] For the "up-down-up" stereochemical assignment of **7**: C.-M. Shu, W.-C. Liu, M.-C. Ku, F.-S. Tang, M.-L. Yeh, L.-G. Lin, *J. Org. Chem.* **1994**, *59*, 3730.

[19] Further examples of biaryl coupling: M. Larsen, M. Jørgensen, *J. Org. Chem.* **1997**, *62*, 4171; S. Zhang, D. Zhang, L. S. Liebeskind, *ibid.* **1997**, *62*, 2312; N. G. Andersen, S. P. Maddaford, B. A. Keay, *ibid.* **1996**, *61*, 9556; N. Miyaura, A. Suzuki, *Chem. Rev.* **1995**, *95*, 2457; G. Sartori, R. Maggi, F. Bigi, M. Grandi, *J. Org. Chem.* **1994**, *59*, 3701; D. A. Whiting in *Comprehensive Organic Synthesis, Vol. 3* (Eds.: B. M. Trost, I. Fleming), Pergamon, New York, **1991**, p. 659; J. K. Stille, *Angew. Chem.* **1986**, *98*, 504; *Angew. Chem. Int. Ed. Engl.* **1986**, *25*, 508; E. Negishi, *Acc. Chem. Res.* **1982**, *15*, 340.

Lanthanide-Assisted Self-Assembly of an Inert, Metal-Containing Nonadentate Tripodal Receptor**

Stéphane Rigault, Claude Piguet,*
Gérald Bernardinelli, and Gérard Hopfgartner

Recent fascinating applications of lanthanide, Ln^{III}, complexes as contrast agents for medical resonance imagining (MRI), luminescent stains for fluoroimmunoassays, and catalysts for the selective cleavage of RNA and DNA require close and tunable control of the coordination sphere to enhance specific structural and electronic properties.[1] The development of tailored receptors for Ln^{III} remains a challenge for synthetic chemists, since Ln^{III} ions do not display pronounced stereochemical preferences for particular bonding modes.[2] Highly preorganized macrobicyclic cryptands allow only partial control of the coordination of Ln^{III} ions,[3] and their tedious preparation has encouraged the development of Ln^{III}-assisted template syntheses of macrocyclic Shiff base complexes.[4] However, the nondirectional Ln–ligand bonds and the high sensitivity of Ln^{III} to basic conditions severely limit their use as template ions in the preparation of macrobicycles[5] and self-assembled metal-containing supramolecular compounds.[6]

A recent approach uses the segmental ligands L^1 and L^2, which are predisposed for the selective recognition of f-block metal ions. The self-assembled homotopic triple-stranded helicates $[Ln_2(L^1)_3]^{6+}$ result from the reaction of L^1 with $Ln(ClO_4)_3$,[7] while equimolar mixtures of $Ln(ClO_4)_3$ and $M(ClO_4)_2$ (M = Zn, Fe) produce head-to-head heterotopic

[*] Dr. C. Piguet, S. Rigault
Department of Inorganic, Analytical and Applied Chemistry
University of Geneva
30 quai E. Ansermet, CH-1211 Geneva 48 (Switzerland)
Fax: Int. code + (41) 22-702 6069
e-mail: claude.piguet@chiam.unige.ch.
Dr. G. Bernardinelli
Laboratory of X-ray Crystallography, University of Geneva
Dr. G. Hopfgartner
Pharmaceuticals Division, Department of Drug Metabolism and Kinetics
F. Hoffmann-La Roche Ltd, Basel (Switzerland)

[**] This work was supported by the Swiss National Science Foundation and the Werner Foundation.

calixarenes, in which the two macrocycles share two adjacent phenol rings: V. Böhmer, R. Dörrenbächer, M. Frings, M. Heydenreich, D. de Paoli, W. Vogt, G. Ferguson, I. Thondorf, *J. Org. Chem.* **1996**, *61*, 549.

[5] Recent examples not included in ref. [1, 2]: O. Struck, L. A. J. Chrisstoffels, R. J. W. Lugtenberg, W. Verboom, G. J. van Hummel, S. Harkema, D. N. Reinhoudt, *J. Org. Chem.* **1997**, *62*, 2487; J. A. Perez-Adelmar, H. Abraham, C. Sanchez, K. Rissanen, P. Prados, J. de Mendoza, *Angew. Chem.* **1996**, *108*, 1088; *Angew. Chem. Int. Ed. Engl.* **1996**, *35*, 1009; M. A. McKervey, M. Pitarch, *J. Chem. Soc. Chem. Commun.* **1996**, 1689; A. Siepen, A. Zett, F. Vögtle, *Liebigs Ann.* **1996**, 757; P. Lhotak, S. Shinkai, *Tetrahedron Lett.* **1996**, *37*, 645; P. Lhotak, M. Kawaguchi, A. Ikeda, S. Shinkai, *Tetrahedron* **1996**, *52*, 12399; A. Arduini, S. Fanni, G. Manfredi, A. Pochini, R. Ungaro, A. R. Sicuri, F. Ugozzoli, *J. Org. Chem.* **1995**, *60*, 1448; F. Ohseto, S. Shinkai, *J. Chem. Soc. Perkin Trans. 2* **1995**, 1103; H. Ross, U. Lüning, *Angew. Chem.* **1995**, *107*, 2723; *Angew. Chem. Int. Ed. Engl.* **1995**, *34*, 2555.

[6] The shortest spacer used so far is a single CH_2 group: K. Araki, K. Hisaichi, T. Kanai, S. Shinkai, *Chem. Lett.* **1995**, 569.

[7] The *para* positions (upper rim) of a calixarene system are commonly considered as the "head," while the OH groups (lower rim) represent the "tail": W. Wasikievicz, G. Rokicki, J. Kielkiewicz, V. Böhmer, *Angew. Chem.,* **1994**, *106*, 230; *Angew. Chem. Int. Ed. Engl.* **1994**, *33*, 214.

[8] The complete IUPAC name for this compound is 5,5′-bicalix[4]arene-25,25′,26,26′,27,27′,28,28′-octol.

[9] a) C. D. Gutsche, L.-G. Lin, *Tetrahedron* **1986**, *42*, 1633; b) C. D. Gutsche, L. J. Bauer, *J. Am. Chem. Soc.* **1985**, *107*, 6052.

[10] R. Pummerer, E. Prell, A. Rieche, *Ber. Dtsch. Chem. Ges. B* **1926**, *59*, 2159.

[11] Crystal structure analysis of **2**: $C_{56}H_{46}O_8 \cdot 3\,CHCl_3$, $M_r = 1205.11$, triclinic, space group $P\bar{1}$ (no. 2), $a = 15.389(3)$, $b = 19.630(4)$, $c = 10.790(2)$ Å, $\alpha = 90.45(2)$, $\beta = 108.78(1)$, $\gamma = 67.71(1)^\circ$, $V = 2831(1)$ Å^3, $Z = 2$, $\rho_{calcd} = 1.41$ g cm^{-3}, colorless crystals from $CHCl_3$/EtOH, crystal dimensions $0.25 \times 0.30 \times 0.45$ mm^3, θ-2θ scan ($2\theta_{max} = 124.2^\circ$), $F(000) = 1240$, room temperature. Of 9285 measured reflections, 8908 were independent ($R_{int} = 0.068$). Data were collected with a Rigaku AFC5R diffractometer with graphite-monochromated $Cu_{K\alpha}$ radiation and a 12 kW rotating anode generator. The data were corrected for Lorentzian and polarization effects, and an empirical absorption correction was applied to intensities based on azimuthal scans of several reflections; $\mu(Cu_{K\alpha}) = 45.27$ cm^{-1}, no decay correction. The structure was solved by direct methods with the program SIR 92.[12] Non-hydrogen atoms were refined anisotropically[13] except for one solvent molecule refined isotropically because of disorder. All hydrogen atoms (apart from OH) were positioned geometrically (riding model). Final refinements were carried out according to the full-matrix least-squares method based on 4189 observed reflections with $F_o > 10\,\sigma(F_o)$ and 665 variable parameters. $R = 0.117$, $R_w = 0.121$, $w = (\sin\theta/\lambda)^2$, $S = 1.38$. Maximum and minimum peaks of the final difference Fourier map: 2.20 and -1.03 e Å^{-3}; these residual electron densities could not be assigned to any chemically sensible moiety. Crystallographic data (excluding structure factors) for the structure reported in this paper have been deposited with the Cambridge Crystallographic Data Centre as supplementary publication no. CCDC-100536. Copies of the data can be obtained free of charge on application to CCDC, 12 Union Road, Cambridge CB2 1EZ, UK (fax: int. code + (44) 1223-336033; e-mail: deposit@chemcrys.cam.ac.uk).

[12] A. Altomare, G. Cascarano, C. Giacovazzo, A. Guagliardi, M. C. Burla, G. Polidori, M. Camalli, *J. Appl. Crystallogr.* **1994**, *27*, 435.

[13] M. Camalli, R. Spagna, *J. Appl. Crystallogr.* **1994**, *27*, 861.

[14] E. G. Boonstra, *Acta Crystallogr.* **1963**, *16*, 816.

[15] K. Iwamoto, K. Araki, S. Shinkai, *J. Org. Chem.* **1991**, *56*, 4955.

[16] J.-D. van Loon, J. F. Heida, W. Verboom, D. N. Reinhoudt, *Recl. Trav. Chim. Pays-Bas* **1992**, *111*, 353.

[17] a) NMR titrations (250 MHz, 295 K) were carried out in $CDCl_3$/CD_3CN (5/1). The association constants were determined with a nonlinear fitting program using the concentration-dependent shifts of the NMe group while the concentration of the host (**4** or **6**) was held constant. b) A similar cooperative action in the complexation of *N*-methylpyridinium iodide was found by Shinkai et al. for a CH_2-bridged double calix[4]arene.[6]

[18] For the "up-down-up" stereochemical assignment of **7**: C.-M. Shu, W.-C. Liu, M.-C. Ku, F.-S. Tang, M.-L. Yeh, L.-G. Lin, *J. Org. Chem.* **1994**, *59*, 3730.

[19] Further examples of biaryl coupling: M. Larsen, M. Jørgensen, *J. Org. Chem.* **1997**, *62*, 4171; S. Zhang, D. Zhang, L. S. Liebeskind, *ibid.* **1997**, *62*, 2312; N. G. Andersen, S. P. Maddaford, B. A. Keay, *ibid.* **1996**, *61*, 9556; N. Miyaura, A. Suzuki, *Chem. Rev.* **1995**, *95*, 2457; G. Sartori, R. Maggi, F. Bigi, M. Grandi, *J. Org. Chem.* **1994**, *59*, 3701; D. A. Whiting in *Comprehensive Organic Synthesis, Vol. 3* (Eds.: B. M. Trost, I. Fleming), Pergamon, New York, **1991**, p. 659; J. K. Stille, *Angew. Chem.* **1986**, *98*, 504; *Angew. Chem. Int. Ed. Engl.* **1986**, *25*, 508; E. Negishi, *Acc. Chem. Res.* **1982**, *15*, 340.

Lanthanide-Assisted Self-Assembly of an Inert, Metal-Containing Nonadentate Tripodal Receptor**

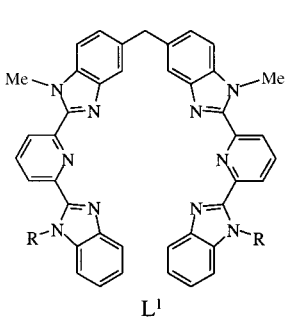
Stéphane Rigault, Claude Piguet,*
Gérald Bernardinelli, and Gérard Hopfgartner

Recent fascinating applications of lanthanide, Ln^{III}, complexes as contrast agents for medical resonance imagining (MRI), luminescent stains for fluoroimmunoassays, and catalysts for the selective cleavage of RNA and DNA require close and tunable control of the coordination sphere to enhance specific structural and electronic properties.[1] The development of tailored receptors for Ln^{III} remains a challenge for synthetic chemists, since Ln^{III} ions do not display pronounced stereochemical preferences for particular bonding modes.[2] Highly preorganized macrobicyclic cryptands allow only partial control of the coordination of Ln^{III} ions,[3] and their tedious preparation has encouraged the development of Ln^{III}-assisted template syntheses of macrocyclic Shiff base complexes.[4] However, the nondirectional Ln–ligand bonds and the high sensitivity of Ln^{III} to basic conditions severely limit their use as template ions in the preparation of macrobicycles[5] and self-assembled metal-containing supramolecular compounds.[6]

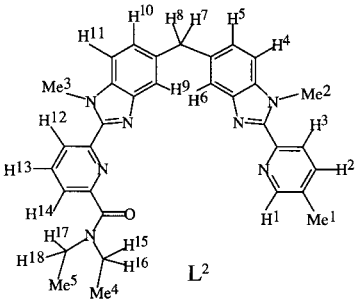
A recent approach uses the segmental ligands L^1 and L^2, which are predisposed for the selective recognition of f-block metal ions. The self-assembled homotopic triple-stranded helicates $[Ln_2(L^1)_3]^{6+}$ result from the reaction of L^1 with $Ln(ClO_4)_3$,[7] while equimolar mixtures of $Ln(ClO_4)_3$ and $M(ClO_4)_2$ (M = Zn, Fe) produce head-to-head heterotopic

[*] Dr. C. Piguet, S. Rigault
Department of Inorganic, Analytical and Applied Chemistry
University of Geneva
30 quai E. Ansermet, CH-1211 Geneva 48 (Switzerland)
Fax: Int. code + (41) 22-702 6069
e-mail: claude.piguet@chiam.unige.ch.
Dr. G. Bernardinelli
Laboratory of X-ray Crystallography, University of Geneva
Dr. G. Hopfgartner
Pharmaceuticals Division, Department of Drug Metabolism and Kinetics
F. Hoffmann-La Roche Ltd, Basel (Switzerland)

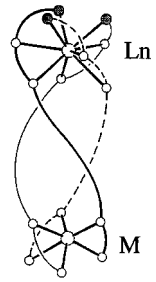
[**] This work was supported by the Swiss National Science Foundation and the Werner Foundation.



L^1



L^2



(HHH)-$[LnM(L^2)_3]^{5+}$

triple-stranded helicates (HHH)-$[LnM(L^2)_3]^{5+}$ (HHH = head-to-head helicate),[6] which are referred to as noncovalent lanthanide podates.[8] In the latter complexes, the facial pseudo-octahedral d-block and the pseudo-tricapped trigonal prismatic 4f-block ions display synergic structural and electronic effects that allow the design of supramolecular "devices" with predictable and tunable properties (luminescence, magnetism).[8] Here we report the selective formation of an inert, nine-coordinate metal-containing tripodal receptor by means of a related self-assembly process with Ln^{III} ions as template and subsequent modification[9] of the resulting helicate.

Cobalt is ideally suited to the preparation of inert d-block tripods since the pseudo-octahedral high spin d^7 Co^{II} ion coordinated to α,α'-diimine donors is expected to be labile. This allows the strict self-assembly of the supramolecular complex $[LnCo(L^2)_3]^{5+}$; its subsequent oxidation gives the inert low-spin d^6 Co^{III} complex with the cobalt ion in a similar pseudo-octahedral environment.[10] Electrospray (ES) MS titrations of L^2 with an equimolar mixture of $Ln(ClO_4)_3 \cdot n H_2O$ and $Co(ClO_4)_2 \cdot 6H_2O$ in acetonitrile show formation of the expected complexes $[LnCo(L^2)_3]^{5+}$ (Ln = La, Eu, Lu) together with traces of $[Co(L^2)_2]^{2+}$, as previously observed for $[LnM(L^2)_3]^{5+}$ (M = Zn, Fe).[8] Spectrophotometric titrations under the same conditions can be satisfactorily fitted to the equilibria of Equations (1) and (2) to give the stability constants $\lg(\beta_{113}^{LnCo}) = 21.7(6)$ (Ln = La), 23.2(9) (Ln = Eu), and 23.9(6) (Ln = Lu), which resemble those found for $[LnFe(L^2)_3]^{5+}$ ($\lg(\beta_{113}^{LnFe}) = 23.0(8)$, 24.6(9), and 23.6(7) for Ln = La, Eu, Lu, respectively).[8]

$$Co^{2+} + 2L^2 \rightleftharpoons [Co(L^2)_2]^{2+} \qquad \lg(\beta_{12}^{Co}) = 14.4(6) \qquad (1)$$

$$Ln^{3+} + Co^{2+} + 3L^2 \rightleftharpoons [LnCo(L^2)_3]^{5+} \qquad \lg(\beta_{113}^{LnCo}) \qquad (2)$$

At a complex concentration of 5 mM, $[LnCo(L^2)_3]^{5+}$ (Ln = La, Eu, Lu) is the only species present in acetonitrile, and the ^1H NMR spectrum displays 22 signals typical of a C_3-symmetrical head-to-head arrangement of the three strands. These are spread over a region of 100 ppm as a result of the paramagnetic Co^{II} center ($\mu_{eff} = 4.99(3)$ and 4.93(4) BM for $[LaCo(L^2)_3]^{5+}$ and $[LuCo(L^2)_3]^{5+}$, respectively, in CD_3CN at 298 K; Figure 1a).[11] Intra- and interstrand nuclear Overhauser effects (NOEs) clearly establish that (HHH)-$[LnCo(L^2)_3]^{5+}$ adopts the expected triple-helix structure[8] in which Co^{II} occupies the facial pseudo-octahedral site produced by the three wrapped bidentate binding units, and Ln^{III} the remaining nine-coordinate site. It is noteworthy that the reaction of L^2 (3 equiv) with $Co(ClO_4)_2 \cdot 6H_2O$ (1 equiv) in the absence of Ln^{III} provides mainly the 1:3 complex $[Co(L^2)_3]^{3+}$, in which the Co^{II} ion is coordinated by the three bidentate binding sites of the ligands. However, the latter complex exists in solution as a 4:1 mixture of the C_1-symmetrical *mer* and C_3-symmetrical *fac* isomers according to the integration of the ^1H NMR signals (expected statistical ratio 3:1).

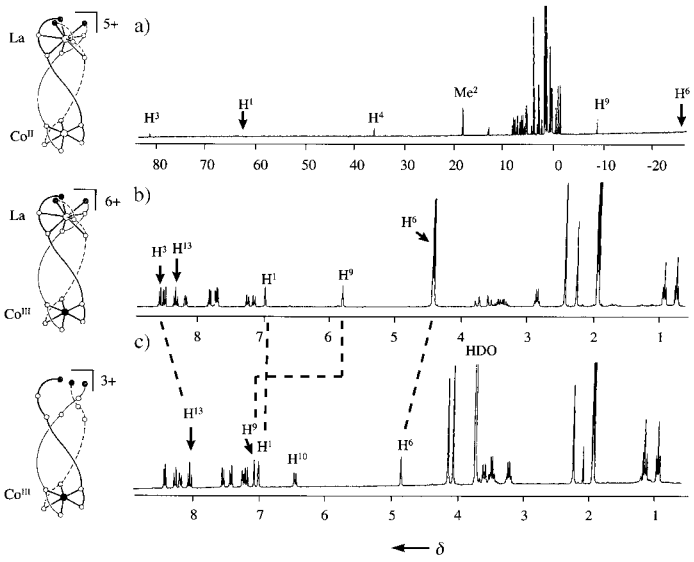


Figure 1. ^1H NMR spectra (CD_3CN) of a) (HHH)-$[LaCo(L^2)_3]^{5+}$, b) (HHH)-$[LaCo(L^2)_3]^{6+}$, and c) *fac*-$[Co(L^2)_3]^{3+}$ (12 M D_2O).

Cyclic voltammograms of (HHH)-$[LnCo(L^2)_3]^{5+}$ (Ln = La, Eu, Lu) show a quasi-reversible Co^{II}/Co^{III} oxidation wave at 0.42 V vs. SCE in acetonitrile/0.1 M NBu_4PF_6 in agreement with analogous Co^{II} complexes.[11] Oxidation with bromine in acetonitrile gives quantitatively the poorly soluble complexes (HHH)-$[LnCo(L^2)_3]^{6+}$ (Ln = La, Lu), whose ^1H NMR spectra exhibit 22 signals in the range $\delta = 0-10$, which is characteristic of diamagnetic Co^{III}. ES mass spectra confirm the exclusive formation of $[LnCo(L^2)_3]^{6+}$ (Ln = La, Eu, Lu) in solution, while specific NOEs (intrastrand: Me^2-H^3, Me^3-H^{12}, $H^{14}-H^{17,18}$; interstrand: Me^2-H^{10}, Me^3-H^5) imply that the head-to-head triple-helix structure is retained for (HHH)-$[LnCo^{III}(L^2)_3]^{6+}$. Precipitation with diethyl ether afforded the microcrystalline complex $[LaCo(L^2)_3](ClO_4)_5Br \cdot (H_2O)$. Recrystallization by slow diffusion of diisopropyl ether into a concentrated solution of the complex in acetonitrile/water (25/1) gave extremely fragile X-ray quality crystals of **1**.

$[LaCo(L^2)_3](ClO_4)_{5.5}(OH)_{0.5} \cdot 4CH_3CN \cdot 2H_2O$ **1**

The crystal structure determination of **1** confirms the presence of a head-to-head triple-helical cation (HHH)-$[LaCo(L^2)_3]^{6+}$ of approximate C_3 symmetry, together with disordered anions and solvent molecules (see Experimental Section). Figure 2 shows an ORTEP[12] stereoview of the cation perpendicular to the helical axis, and Table 1 lists the

 © WILEY-VCH Verlag GmbH, D-69451 Weinheim, 1998 1433-7851/98/3701-0170 $ 17.50+.50/0 *Angew. Chem. Int. Ed.* **1998**, *37*, No. 1/2

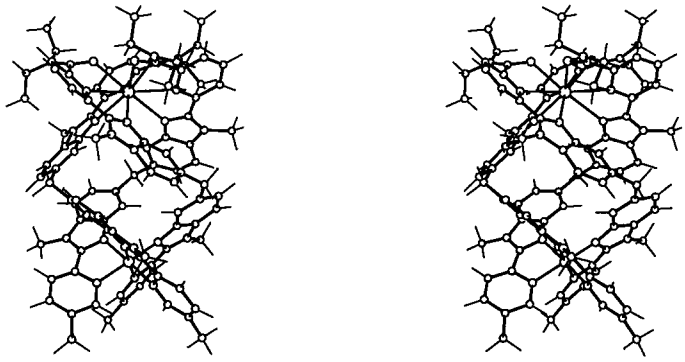


Figure 2. ORTEP[12] stereoview of the cation of **1** perpendicular to the helical axis.

Table 1. Distances [Å] and angles [°] in the coordination spheres of the Co^{III} and La^{III} atoms in **1**.

	Average[a]	Minimum	Maximum
Co – N(py)	2.03(2)	2.01(2)	2.04(2)
Co – N(bzim)	1.96(3)	1.94(2)	2.00(2)
N(py)-Co-N(bzim)[b]	80.9(11)	79.5(8)	82.4(9)
La – N(bzim)	2.67(4)	2.61(2)	2.70(2)
La – N(py)	2.74(3)	2.72(2)	2.78(2)
La – O(amide)	2.50(2)	2.48(2)	2.53(2)
N(bzim)-La-N(py)[b]	60.3(12)	58.8(7)	61.9(6)
N(py)-La-O(amide)[b]	62.1(12)	61.2(6)	63.7(6)

[a] Averaged for C_3 symmetry. [b] Chelate bite angles.

structural parameters obtained by averaging the distances and angles according to C_3 symmetry. The geometry around the Co^{III} center is best described as a slightly distorted octahedron flattened along the pseudo-C_3 axis as a result of chelate bite angles smaller than 90° (Table 1). The average Co – N(py) distance is slightly larger than the Co – N(bzim) distances, but both are in good agreement with the reported standard values of 2.034 and 1.946 Å, respectively.[12] Comparison with the Co – N(py) (1.96(3) Å) and Co – N(bzim) (1.92(3) Å) distances in an analogous homotopic triple-stranded helicate[13] suggests that the Co – N bonds in **1** are slightly stretched. This is also evident in the similar Fe – N(py) (2.00(3) Å) and Fe – N(bzim) (1.95(2) Å) distances in (HHH)-$[LnFe(L^2)_3]^{5+}$ [8] in spite of the about 12% larger ionic radius expected for low-spin d^6 Fe^{II}.[14] We attribute this distortion to steric constraints induced by the occupied pseudo-tricapped trigonal prismatic site. The La – Co distance is 8.865(4) Å, and detailed structural analysis of the complex indicates that (HHH)-$[LaCo(L^2)_3]^{6+}$ is structurally similar to (HHH)-$[LaFe(L^2)_3]^{5+}$, in which Fe^{II} also has the stereochemically demanding low-spin d^6 configuration.[15]

The addition of D_2O to a 5 mM solution of (HHH)-$[LnCo(L^2)_3]^{6+}$ (Ln = La, Lu) in CD_3CN (total D_2O concentration 10 M) results in decomplexation of Ln^{III}, which can be monitored by ESMS and ^1H NMR spectroscopy. The ESMS titration shows the exclusive formation of $[Co(L^2)_3]^{3+}$ (m/z 563.4), and the ^1H NMR spectrum still shows 22 signals corresponding to the quantitative formation of the C_3-symmetrical complex *fac*-$[Co(L^2)_3]^{3+}$. The ^1H NMR signals of the bidentate binding units are not significantly shifted (except for that of H^6, which is located between the Co^{III} and Ln^{III} centers in (HHH)-$[LnCo^{III}(L^2)_3]^{6+}$), whereas the signals of the tridentate units are strongly shifted—the signal for H^9 is shifted downfield by $\Delta\delta = 1.3$ owing to unfolding of the strands.[16] The signals for $H^{12} - H^{14}$ are shifted to high field by $\Delta\delta \approx 0.3$, since the associated pyridine ring is no longer coordinated to a metal ion.[8] Finally, the disappearance of the intrastrand NOEs $Me^3 - H^{12}$ and $H^{14} - H^{17,18}$ implies a *trans,trans* arrangement of the tridentate units, which is only compatible with the release of the Ln^{III} ion from the coordination site. This assumption is further supported by the use of Eu^{III} as a paramagnetic NMR probe in (HHH)-$[EuCo(L^2)_3]^{6+}$. Reaction of (HHH)-$[EuCo(L^2)_3]^{6+}$ with 12 M D_2O severely affects the signals of the protons and quantitatively produces the diamagnetic spectrum of *fac*-$[Co(L^2)_3]^{3+}$.

Treatment of (HHH)-$[LaCo^{III}(L^2)_3]^{6+}$ with a stoichiometric quantity of $(NBu)_4EDTA \cdot 6H_2O$ in acetonitrile/water (25/1) leads to formation of the insoluble salt $NBu_4[La(EDTA)]$, which can be separated by filtration. The desired inert, metal-containing tripodal receptor *fac*-$[Co(L^2)_3](ClO_4)_3(C_4H_{10}O)_{0.4} \cdot 6H_2O$ is obtained by fractional crystallization from diethyl ether as a red powder whose ^1H NMR spectrum is identical to that of the complex prepared in situ. This complex is a novel tailored helical nine-coordinate receptor which is currently being investigated in our laboratory for the selective complexation of Ln^{III}. This self-assembly with post-processing and release of the template Ln^{III} ion leads to the almost quantitative isolation of pure *fac*-$[Co(L^2)_3]^{3+}$, while direct bromine oxidation of the *mer*/*fac* mixture of $[Co(L^2)_3]^{2+}$ also gives a mixture containing only 20% of the desired *fac*-$[Co(L^2)_3]^{3+}$ and 80% of the *mer* isomer.

Experimental Section

$[LaCo(L^2)_3](ClO_4)_5Br \cdot H_2O$: Elemental analysis calcd for $LaCoC_{99}H_{101}N_{21}O_{24}Cl_5Br$: C 49.05, H 4.20, N 12.13, Br 3.30; found C 48.98, H 4.28, N 12.11, Br 3.00. ^1H NMR (300 MHz, CD_3CN, TMS, 298 K): $\delta = 0.73$ (t, J = 7 Hz, 9H), 0.91 (t, J = 7 Hz, 9H), 2.25 (s, 9H), 2.86 (q, J = 7 Hz, 6H), 3.35 (pseudo-sext., J = 15, 7 Hz, 3H), 3.42 (pseudo-sext., J = 15, 7 Hz, 3H), 3.55 (d, J = 16 Hz, 3H), 3.75 (d, J = 16 Hz, 3H), 4.41 (s, 9H), 4.44 (s, 3H), 4.44 (s, 9H), 5.78 (s, 3H), 6.97 (s, 3H), 7.15 (d, J = 8 Hz, 3H), 7.23 (d, J = 8 Hz, 3H), 7.69 (d, J = 8 Hz, 3H), 7.71 (d, J = 8 Hz, 3H), 7.80 (d, J = 8 Hz, 3H), 8.15 (d, J = 8 Hz, 3H), 8.31 (t, J = 8 Hz, 3H), 8.48 (d, J = 8 Hz, 3H), 8.55 (d, J = 8 Hz, 3H); ESMS (10^{-4} M, CH_3CN): $m/z = 304.8$ $[LaCo(L^2)_3]^{6+}$ (60%), 385.8 $[LaCo(L^2)_3(ClO_4)]^{5+}$ (100%), 506.7 $[LaCo(L^2)_3(ClO_4)_2]^{4+}$ (99%), 708.9 $([LaCo(L^2)_3(ClO_4)_3]^{3+}$ (43%), 1113.3 $([LaCo(L^2)_3(ClO_4)_4]^{2+}$ (5%).

$[Co(L^2)_3](ClO_4)_3 \cdot 0.4(C_4H_{10}O) \cdot H_2O$. Elemental analysis: calcd for $CoC_{100.6}H_{115}N_{21}O_18.4Cl_3$: C 56.84, H 5.45, N 13.84; found C 56.92, H 5.30, N 13.86. ^1H NMR (300 MHz, CD_3CN, TMS, 298 K): $\delta = 1.00$ (t, J = 7 Hz, 9H), 1.20 (t, J = 7 Hz, 9H), 2.35 (s, 9H), 3.28 (q, J = 7 Hz, 6H), 3.50 (q, J = 7 Hz, 6H), 3.55 (d, J = 16 Hz, 3H), 3.60 (d, J = 16 Hz, 3H), 4.13 (s, 9H), 4.15 (s, 9H), 4.98 (s, 3H), 6.59 (d, J = 8 Hz, 3H), 6.93 (s, 3H), 7.23 (d, J = 8 Hz, 3H), 7.30 (s, 3H), 7.32 (d, J = 8 Hz, 3H), 7.48 (d, J = 8 Hz, 3H), 7.52 (d, J = 8 Hz, 3H), 8.02 (t, J = 8 Hz, 3H), 8.17 (d, J = 8 Hz, 3H), 8.41 (d, J = 8 Hz, 3H), 8.44(d, J = 8 Hz, 3H). ESMS (10^{-4} M, CH_3CN): $m/z = 563.4$ $[Co(L^2)_3]^{3+}$ (95%), 894.2 $[Co(L^2)_3(ClO_4)]^{2+}$ (15%).

Crystal structure determination of **1**: A fragile red-orange crystal (0.18 × 0.30 × 0.32 mm) was mounted from the mother liquor on a quartz fiber with perfluoropolyether oil RS3000. $M_r = 2584.6$, monoclinic, $C2/c$, $a = 53.638(7)$, $b = 23.068(5)$, $c = 21.885(7)$ Å, $\beta = 92.78(1)°$, $V = 27047(11)$ Å^3 (by least-squares refinement of 20 reflections in the range $35 \le 2\theta \le 44°$), $Z = 8$, $\rho_{calcd} = 1.27$ g cm^{-3}, $F(000) = 10640$, $\mu(Cu_{K\alpha}) = 4.986$ mm^{-1}. *Data collection and processing:* Stoe STADI4 diffractometer, $T = 200$ K, $\omega - 2\theta$ scan, scan width 1.05+0.35 tanθ, scan speed 0.13° s^{-1}, $Cu_{K\alpha}$ radiation ($\lambda = 1.5418$ Å); 15658 measured reflections ($3 \le 2\theta \le 104°$, $-53 < h < 53$, $0 < k < 23$,

 © WILEY-VCH Verlag GmbH, D-69451 Weinheim, 1998 1433-7851/98/3701-0171 $ 17.50+.50/0

$0 < l < 22$), 15138 unique reflections ($R_{int} = 0.095$ for equivalent reflections) of which 8318 were observed [$|F_o| > 4\sigma(F_o)$]. Two reference reflections were measured every 45 min and showed a total decrease in intensity of 15.3%. All intensities were corrected for this drift. Data were corrected for Lorentzian, polarization, and absorption effects[17] ($A^*_{min} = 2.916$, $A^*_{max} = 5.163$). The structure was solved by direct methods with the program MULTAN 87;[18] all other calculations were performed with the XTAL[19] system and ORTEP II[12] programs. Full-matrix least-squares refinements on F with weights of $w = 1/(\sigma 2(\mathrm{Fo}) + 0.0005 F_o^2)$ gave final values $R = 0.125$ and $Rw = 0.128$ for 1460 variables and 8318 reflections. The five perchlorate ions and the four acetonitrile molecules were refined with 64 restraints on bond distances and angles. The remaining "half" perchlorate i was located in special position 4*c* and was fully disordered. Five atomic sites (of which two were in special position 4*e*) were observed for the water molecules and the half hydroxide anion. Two oxygen atoms of the perchlorate i, the carbon and nitrogen atoms of two acetonitrile molecules, and the five oxygen atoms of the water molecules were refined with isotropic displacement parameters (13 atoms), and all the other atoms (157) with anisotropic displacements parameters. The mean ratio of shift to error on the last cycle was 0.058. Hydrogen atoms were placed in calculated positions and included in F_c calculations. The final Fourier difference synthesis showed a maximum of $+1.44$ and a minimum of -2.06 e Å^{-3}. Complex **1** is isostructural with $[LaFe(L^2)_3](ClO_4)_{0.5}(CF_3SO_3)_{4.5} \cdot CH_3CN \cdot 4H_2O$ and $[EuZn(L^2)_3](ClO_4)(CF_3SO_3)_4 \cdot 4CH_3CN$.[8] Crystallographic data (excluding structure factors) for the structure reported in this paper have been deposited with the Cambridge Crystallographic Data Centre as supplementary publication no. CCDC-100482. Copies of the data can be obtained free of charge on application to CCDC, 12 Union Road, Cambridge CB21EZ, UK (fax: int. code + (44) 1223-336033; e-mail: deposit@ccdc.cam.ac.uk).

Received: June 16, 1997 [Z10549IE]
German version: *Angew. Chem.* **1998**, *110*, 178–181

Keywords: lanthanides · multidentate ligands · supramolecular chemistry · template synthesis

[1] D. Parker, J. A. Gareth Williams, *J. Chem. Soc. Dalton Trans.* **1996**, 3613; G. Mathis, *Clin. Chem.* **1995**, *41*, 1391; K. Kumar, M. F. Tweedle, *Pure Appl. Chem.* **1993**, *65*, 515.
[2] C. Piguet, *Chimia* **1996**, *50*, 144.
[3] N. Sabbatini, M. Guardigli, J.-M. Lehn, *Coord. Chem. Rev.* **1993**, *123*, 201; C. Galaup, C. Picard, L. Cazaux, P. Tisnès, D. Aspe, H. Autiero, *New J. Chem.* **1996**, *20*, 997; F. Bodar-Houillon, A. Marsura, *ibid.* **1996**, *20*, 1041.
[4] V. Alexander, *Chem. Rev.* **1995**, *95*, 273; P. Guerriero, S. Tamburini, P. A. Vigato, *Coord. Chem. Rev.* **1995**, *139*, 17.
[5] P. H. Smith, Z. E. Reyes, C. W. Lee, K. N. Raymond, *Inorg. Chem.* **1988**, *27*, 4154.
[6] D. S. Lawrence, T. Jiang, M. Levett, *Chem. Rev.* **1995**, *95*, 2229; D. B. Amabilino, J. F. Stoddart, *ibid.* **1995**, *95*, 2725; C. Piguet, G. Bernardinelli, G. Hopfgartner, *ibid*. **1997**, *97*, 2005
[7] C. Piguet, J.-C. G. Bünzli, G. Bernardinelli, G. Hopfgartner, A. F. Williams, *J. Am. Chem. Soc.* **1993**, *115*, 8197.
[8] C. Piguet, J.-C. G. Bünzli, G. Bernardinelli, G. Hopfgartner, S. Petoud, O. Schaad, *J. Am. Chem. Soc.* **1996**, *118*, 6681; C. Piguet, E. Rivara-Minten, G. Bernardinelli, J.-C. G. Bünzli, G. Hopfgartner, *J. Chem. Soc. Dalton Trans.* **1997**, 421.
[9] D. Philp, J. F. Stoddart, *Angew. Chem.* **1996**, *108*, 1242; *Angew. Chem. Int. Ed. Engl.* **1996**, *35*, 1154.
[10] R. G. Wilkins, *Kinetics and Mechanism of Reactions of Transition Metal Complexes*, 2. Aufl., VCH, Weinheim, **1991**, S. 265.
[11] C. Piguet, G. Bernardinelli, B. Bocquet, O. Schaad, A. F. Williams, *Inorg. Chem.* **1994**, *33*, 4112.
[12] C. K. Johnson, ORTEP II, Report ORNL-5138, Oak Ridge National Laboratory, Oak Ridge, TN, USA, **1976**.
[13] L. J. Charbonnière, G. Bernardinelli, C. Piguet, A. M. Sargeson, A. F. Williams, *J. Chem. Soc. Chem. Commun.* **1994**, 1419.
[14] R. D. Shannon, *Acta Crystallogr. Sect. A*. **1976**, *32*, 751.
[15] L. G. Vanquickenborne, K. Pierloot, *Inorg. Chem*. **1981**, *20*, 3673.
[16] C. Piguet, G. Hopfgartner, B. Bocquet, O. Schaad, A. F. Williams, *J. Am. Chem. Soc.* **1994**, *116*, 9092.
[17] E. Blanc, D. Schwarzenbach, H. D. Flack, *J. Appl. Crystallogr*. **1991**, *24*, 1035.
[18] P. Main, S. J. Fiske, S. E. Hull, L. Lessinger, D. Germain, J. P. Declercq, M. M. Woolfson, MULTAN 87, Universities of York, England, and Louvain-La-Neuve, Belgium, **1987**.
[19] S. R. Hall, J. M. Stewart, Eds. XTAL 3.2 User's Manual, Universities of Western Australia and Maryland, **1992**.

Crown Ethers, Double-Decker, and Sandwich Complexes: Cation-Mediated Formation of Metallatopomer Coronates**

Rolf W. Saalfrank,* Norbert Löw, Sabine Kareth, Verena Seitz, Frank Hampel, Dietmar Stalke, and Markus Teichert

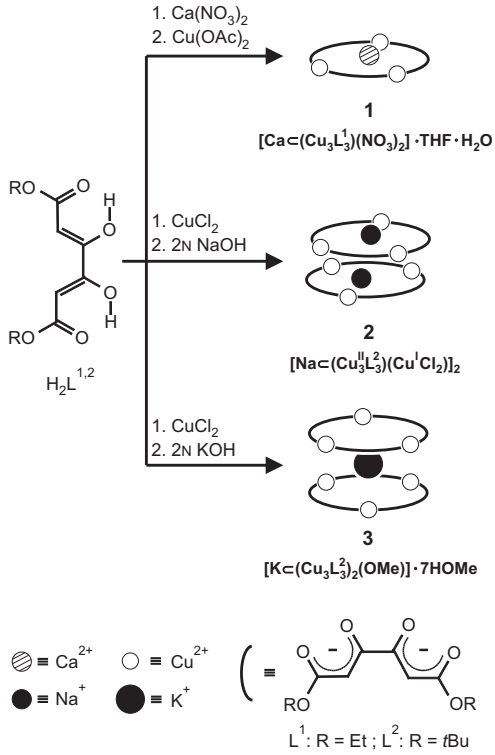
Crown ethers, [2]cryptands, and [3]cryptands selectively complex alkali metal ions.[1] This discovery led to the construction of novel supramolecular architectures[2] capable of recognizing neutral as well as cationic or anionic substrates with formation of well-defined host–guest compounds. Recently we pointed out the structural analogy between coronates and cryptates[3] and their topologically equivalent metallacoronates and metallacryptates.[4] If one applies the knowledge of crown ethers to the chemistry of metallacrown ethers (MC),[5] the complexation of differently sized cations by metallacrown ethers should lead to metallacoronates of varying structures. Since the ionic radii of alkaline and alkaline earth metal cations differ significantly (whereas the diameter of the metallacrowns essentially does not change) the inclusion of small cations such as Na^+ or Ca^{2+} should lead to a metallacoronate with 1:1 stoichiometry, and, in contrast, encapsulation of the larger K^+ ions to a metallacrown ether sandwich complex (K^+:MC = 1:2).

Reaction of diethyl ketipinate[6] H_2L^1 with copper(II) acetate in the presence of calcium nitrate leads to green microcrystals of **1** (Scheme 1) after crystallization from tetrahydrofuran/diethyl ether. According to elemental analysis and FAB-MS data (FAB = fast atom bombardment, $m/e = 977$) **1** is a metallacoronate. Compound **1** is a neutral, trinuclear metal cluster (Figure 1), as determined by X-ray

[*] Prof. Dr. R. W. Saalfrank, Dr. N. Löw, Dipl.-Chem. S. Kareth, Dipl.-Chem. V. Seitz, Dr. F. Hampel[+]
Institut für Organische Chemie der Universität Erlangen-Nürnberg
Henkestrasse 42, D-91054 Erlangen (Germany)
Fax: Int. code + (49) 9131-85 1165
Prof. Dr. D. Stalke[+]
Institut für Anorganische Chemie der Universität Würzburg (Germany)
Dipl.-Chem. M. Teichert[+]
Institut für Anorganische Chemie der Universität Göttingen (Germany)
[+] Single-crystal X-ray analyses.

[**] Chelate Complexes, part 10. This work was supported by the Deutschen Forschungsgemeinschaft, the Fonds der Chemischen Industrie, and the Volkswagen-Stiftung. We thank Prof. Dr. K.-P. Zeller, Universität Tübingen, for the FAB mass spectra. Part 9: ref. [4b].

 © WILEY-VCH Verlag GmbH, D-69451 Weinheim, 1998 1433-7851/98/3701-0172 $ 17.50+.50/0



Scheme 1.

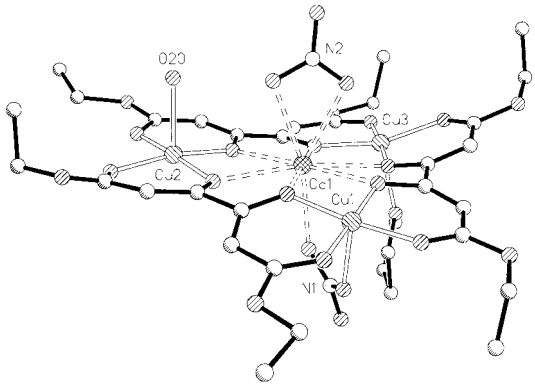


Figure 1. Molecular structure of **1**. Side view with counterion and coordinated solvent molecules; H atoms are omitted for clarity.

crystallographic analysis.[7] Formal replacement of the three copper(II) centers in the [15]metallacrown-6 system (15-MC-6) by ethylene bridges leads to the topologically equivalent crown ether [18]crown-6. The copper atoms are linked across the sides of the triangle through bis(bidentate) diethyl ketipinate dianions L^1, and each copper(II) ion is coordinated in a square-planar fashion to four oxygen atoms. Additional coordination of water, tetrahydrofuran, and nitrate leads to a square-pyramidal environment of O donors for each copper ion. The center of the resulting metallacoronand 15-MC-6 contains an encapsulated calcium ion, whose charge is compensated by two axially coordinated nitrate ions (Figure 1).

Double deprotonation of H_2L^2 by 2N sodium hydroxide and reaction of the formed dianion with copper(II) chloride dihydrate also yields the metallacoronate **2** (FAB-MS data, $m/e = 898$; see Scheme 1), whose molecular structure was determined by X-ray crystallographic analysis (Figure 2).[8]

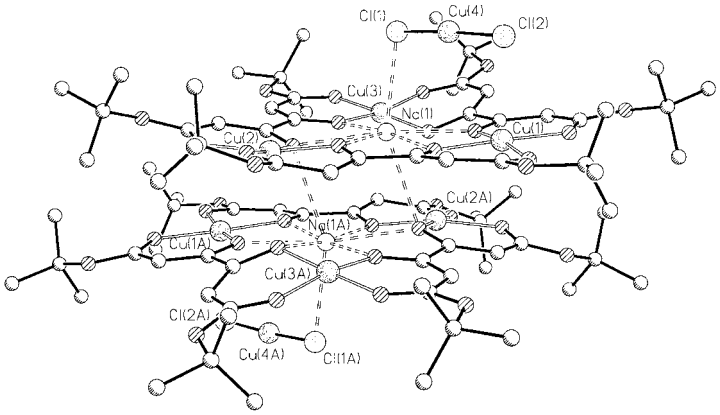


Figure 2. Molecular structure of dimer **2**. Side view; H atoms are omitted for clarity.

Metallacoronate **2** is a dimer of two $[Na \subset (Cu_3L^2_3)(CuCl_2)]$ building blocks. The monomer is composed of a $[Cu_3L^2_3]$ metallacrown with a sodium ion, which is η^6 coordinated to all oxygen atoms in the inner ring and located at the center. The counterion of the $[Na \subset (Cu_3L^2_3)]^+$ cation is a $(CuCl_2)^-$ ion[9] which coordinates to the encapsulated sodium ion through a chlorine atom. The tendency for eightfold coordination around Na^+ ions is the driving force for dimerization. The linkage of the coronates to give the dimer **2** is accomplished by coordination of one ring oxygen to the neighboring sodium center. This leads to a minor mutual deformation of the monomeric building blocks.

Whereas encapsulation of the small cations Na^+ and Ca^{2+} leads to host–guest systems of 1:1 stoichiometry, double deprotonation of di-*tert*-butyl ketipinate H_2L^2 with 2N potassium hydroxide and reaction with copper(II) chloride dihydrate affords the metallacrown ether sandwich complex **3** with 2:1 stoichiometry ($m/e = 2125$; see Scheme 1). X-ray crystallographic analysis[10] reveals that **3** is constructed of two neutral trimetallacrown-6 building blocks that are rotated relative to each other by 60° (Figure 3). The sandwichlike linkage results from a crystallographically disordered potassium ion between the two metallacrowns. The counterion of $[K \subset (Cu_3L^2_3)_2]^+$ of **3** is a methoxide ion which is bound to the encapsulated

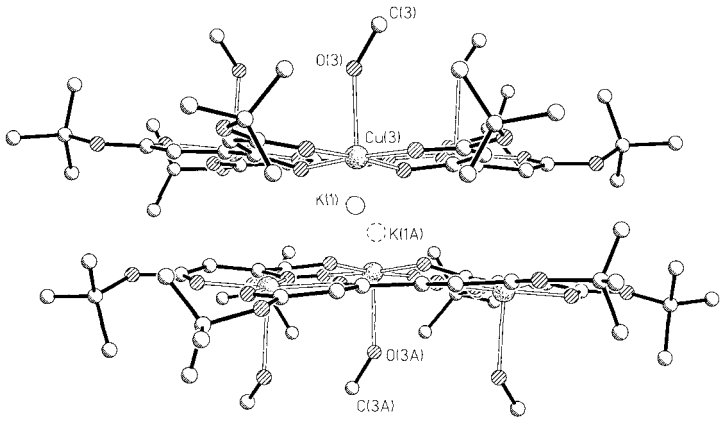


Figure 3. Molecular structure of the cation in **3**. Side view; H atoms as well as the methoxide and methanol molecules coordinated to potassium are omitted for clarity.

 © WILEY-VCH Verlag GmbH, D-69451 Weinheim, 1998 1433-7851/98/3701-0173 $ 17.50+.50/0

potassium ion; methanol is coordinated to the opposite sides (not shown). The coordination spheres of the six copper centers are saturated by methanol molecules, and, thus, each Cu^{2+} ion is surrounded by O donors in a tetragonal-pyramidal fashion.

As with organocrown ethers, the size of the cation (Na^+, Ca^{2+}, or K^+) determines whether metallacoronates (**1** and **2**) or a metallacrown ether sandwich complex (**3**) are formed in the case of metallacrown ethers $[Cu_3L_3]$ ($L = L^1$, L^2).

Experimental Section

1: A solution of copper(II) acetate monohydrate (200 mg, 1 mmol) in methanol (50 mL) was added dropwise to a mixture of H_2L^1 (230 mg, 1.0 mmol) and calcium nitrate tetrahydrate (475 mg, 2 mmol) in methanol (50 mL). The dark green solution was stirred for one hour and then concentrated to 10 mL. To achieve complete precipitation of the product, water (200 mL) was added. The product was filtered, washed with water, and dried under vacuum (oil pump). Yield of dark green crystals from tetrahydrofuran/diethyl ether: 320 mg (85%); decomp above 127 °C; IR ($CHBr_3$): $\tilde{\nu} = 2960$ (CH), 1614 (C⋯O), 1524 cm^{-1} (C=C); FAB-MS (3-nitrobenzyl alcohol (*m*-NBA) matrix): *m*/*z* (%) = 977 (100, $[Ca \subset (Cu_3L^1_3)NO_3]^+$); correct elemental analysis.

2 and **3**: General procedure: Aqueous sodium or potassium hydroxide (2 mL, 2 N) was added dropwise to a solution containing copper(II) chloride dihydrate (171 mg, 1.0 mmol) and H_2L^2 (286 mg, 1.0 mmol) in methanol (100 mL). To achieve complete precipitation of the products, water (200 mL) was added. The products were filtered, washed with water, and dried under vacuum (oil pump).

2: Yield of dark green crystals from chloroform/diethyl ether: 220 mg (55%); decomp above 230 °C; IR ($CHBr_3$): $\tilde{\nu} = 2950$ (CH), 1640, 1590 (C⋯O), 1540 cm^{-1} (C=C); FAB-MS (*m*-NBA): *m*/*z* (%) = 898 (100, $[Na \subset (Cu_3L^2_3)]^+$); correct elemental analysis.

3: Yield of dark green crystals from methanol: 280 mg (73%); decomp above 180 °C; IR ($CHBr_3$): $\tilde{\nu} = 3300$ (OH), 2970 (CH), 1655, 1600 (C⋯O), 15750 cm^{-1} (C=C); FAB-MS (*m*-NBA): *m*/*z* (%) = 2125 (30, $[K \subset (Cu_3L^2_3)_2]^+$), 1082 (95, $[K \subset (Cu_3L^2_3)_2]^+$); correct elemental analysis.

Received: July 2, 1997
Revised version: October 8, 1997 [Z 10623 IE]
German version: *Angew. Chem.* **1998**, *110*, 182 – 184

Keywords: copper · crown compounds · sandwich complexes · supramolecular chemistry

[1] C. J. Pedersen, *Angew. Chem.* **1988**, *100*, 1053 – 1059; *Angew. Chem. Int. Ed. Engl.* **1988**, *27*, 1021 – 1027; D. J. Cram, *ibid.* **1988**, *100*, 1041 – 1052 and **1988**, 27, 1009 – 1020; J.-M. Lehn, *ibid.* **1988**, *100*, 91 – 116 and **1988**, *27*, 89 – 112; F. Vögtle, *Supramolekulare Chemie*, Teubner, Stuttgart, **1992**, p. 45ff.

[2] D. Philp, J. F. Stoddart, *Angew. Chem.* **1996**, *108*, 1243 – 1286; *Angew. Chem. Int. Ed. Engl.* **1996**, *35*, 1154 – 1196; J.-M. Lehn, B. O. Kneisel, G. Baum, D. Fenske, *ibid.* **1996**, *108*, 1987 – 1990 and **1996**, *35*, 1838 – 1840; J.-M. Lehn, *ibid.* **1990**, *102*, 1347 – 1362 and **1990**, *29*, 1304 – 1319; I. Cragg-Hine, M. G. Davidson, O. Kocian, F. S. Mair, E. Pohl, P. R. Raithby, R. Snaith, N. Spencer, J. F. Stoddart, *ibid.* **1993**, *105*, 1254 – 1256 and **1993**, *32*, 1182 – 1184; M. Simard, D. Su, J. D. Wuest, *J. Am. Chem. Soc.* **1991**, *113*, 4696 – 4698.

[3] C. J. Pedersen, *J. Am. Chem. Soc.* **1967**, *89*, 2495 – 3496; J.-M. Lehn, *Supramolecular Chemistry*, VCH, Weinheim, **1995**, p. 17ff; "Crown Ethers and Cryptands": G. Gokel in *Monographs in Supramolecular Chemistry* (Ed.: J. F. Stoddart), Black Bear Press, Cambridge, **1991**, p. 64ff; "Crown-Type Compounds – An Introductory Overview": E. Weber, F. Vögtle, *Top. Curr. Chem.* **1981**, *98*, 1 – 41.

[4] a) R. W. Saalfrank, N. Löw, F. Hampel, H.-D. Stachel, *Angew. Chem.* **1996**, *108*, 2353 – 2354; *Angew. Chem. Int. Ed. Engl.* **1996**, *35*, 2009 – 2010; b) R. W. Saalfrank, I. Bernt, E. Uller, F. Hampel, *ibid.* **1997**, *109*, 2596 – 2599 and **1997**, *36*, 2482 – 2485; c) R. W. Saalfrank, R. Burak, S. Reihs, N. Löw, F. Hampel, H.-D. Stachel, J. Lentmaeier, K. Peters, E. M. Peters, H. G. von Schnering, *ibid.* **1995**, *107*, 1085 – 1087 and **1995**, *34*, 993 – 995.

[5] V. L. Pecoraro, A. J. Stemmler, B. R. Gibney, J. J. Bodwin, H. Wang, J. W. Kampf, A. Barwinski, *Prog. Inorg. Chem.* **1997**, *45*, 83 – 177; A. J. Stemmler, J. W. Kampf, V. L. Pecoraro, *Angew. Chem.* **1996**, *108*, 3011 – 3013; *Angew. Chem. Int. Ed. Engl.* **1996**, *35*, 2841 – 2843; A. J. Stemmler, A. Barwinski, M. J. Baldwin, V. Young, V. L. Pecoraro, *J. Am. Chem. Soc.* **1996**, *118*, 11962 – 11963; B. R. Gibney, D. P. Kessissoglou, J. W. Kampf, V. L. Pecoraro, *Inorg. Chem.* **1994**, *33*, 4840 – 4849; M. S. Lah, B. R. Gibney, D. L. Tierney, J. E. Penner-Hahn, V. L. Pecoraro, *J. Am. Chem. Soc.* **1993**, *115*, 5857 – 5858; I. Haiduc, R. B. King in *Large Ring Molecules* (Ed.: J. A. Semlyen), Wiley, New York, **1996**, p. 525ff; W. Hayes, J. F. Stoddart, in *Large Ring Molecules* (Ed.: J. A. Semlyen), Wiley, New York, **1996**, p. 433ff; A. J. Blake, R. O. Gould, C. M. Grand, P. E. Y. Milne, D. Reed, R. E. P. Winpenny, *Angew. Chem.* **1994**, *106*, 208 – 210; *Angew. Chem. Int. Ed. Engl.* **1994**, *33*, 195 – 197; A. J. Blake, R. O. Gould, P. E. Y. Milne, R. E. P. Winpenny, *J. Chem. Soc. Chem. Commun.* **1991**, 1453 – 1454; G. M. Gray, C. H. Duffey, *Organometallics* **1995**, *14*, 245 – 250; A. Caneschi, A. Cormia, S. J. Lippard, *Angew. Chem.* **1995**, *107*, 511 – 513; *Angew. Chem. Int. Ed. Engl.* **1995**, *34*, 467 – 469.

[6] H.-D. Stachel, *Arch. Pharm. Ber. Dtsch. Pharm. Ges.* **1962**, *295*, 735 – 744; H.-D. Stachel, M. Jungkenn, C. Koser-Gnoss, H. Poschenrieder, J. Redlin, *Liebigs Ann. Chem.* **1994**, 961 – 964.

[7] **1**: $C_{34}H_{46}CaCu_3N_2O_{26}$, $M = 1129.45$, triclinic, space group P, $a = 1204.9(2)$, $b = 1359.59(12)$, $c = 1449.58(8)$ pm, $\alpha = 92.057(6)$, $\beta = 105.35(9)$, $\gamma = 96.83(1)^\circ$, $V = 2268.1(4)$ Å^3, $\rho_{calcd} = 1.651$ g cm^{-3}, $Z = 2$, crystal dimensions $0.15 \times 0.2 \times 0.3$ mm^3. Enraf-Nonius Mach3 diffractometer, $Mo_{K\alpha}$ radiation ($\lambda = 71.073$ pm), $T = 200(2)$ K, graphite monochromator, scan range: $4.8 < 2\theta < 50.0^\circ$. Of 7982 measured reflections, 7982 were independent and 5777 with $I > 2\sigma(I)$. The structure was solved by direct methods using SHELXS-96 and refined with all data (356 parameters) by full-matrix least squares on F^2 using SHELXL93 (G. M. Sheldrick, Göttingen, **1993**). All non-hydrogen atoms were refined anisotropically, and hydrogen atoms were fixed in idealized positions with a riding model. Final R values: $R1 = \Sigma | F_o - F_c | / \Sigma F_o = 0.0377$ for $I > 2\sigma(I)$ and $wR2 = \Sigma w | (F_o^2 - F_c^2)^2 | / \Sigma w (F_o^2)^2)^{0.5} = 0.1040$ (all data); min./max. residual electron density: $-0.646/0.659$ e Å^{-3}.[15]

[8] **2**: $C_{84}H_{120}Cl_4Cu_8Na_2O_{36}$, $M = 2401.88$, triclinic, space group $P\bar{1}$, $a = 12.091(1)$, $b = 14.705(1)$, $c = 17.005(2)$ Å, $\alpha = 105.03(2)$, $\beta = 98.73(2)$, $\gamma = 92.52(2)^\circ$, $V = 2875.2(5)$ Å^3, $Z = 1$, $\rho_{calcd} = 1.525$ g cm^{-3}, $F(000) = 1350$, $\lambda = 0.71073$ Å, $T = 193$ K, $\mu(Mo_{K\alpha}) = 1.763$ mm^{-1}, min./max. transmission: 0.703/0.768, crystal dimensions $0.30 \times 0.30 \times 0.25$ mm^3, $3.88^\circ \le 2\theta \le 52.90^\circ$. Of 28414 measured reflections, 11697 were independent ($R_{int} = 0.0200$) and employed in the structure refinement of 695 parameters with 69 restraints. Final R values: $R1 = 0.0293$ ($I > 2\sigma(I)$) and $wR2 = 0.0709$ (all data); min./max. residual electron density: $-358/437$ e nm^{-3}. Crystallographic data for **2** and **3** were collected on a Stoe-Siemens-Huber four circle diffractometer with Siemens CCD area detector by using φ and ω scans on a shock-cooled crystal in an oil drop.[11] Data were integrated with the program SAINT. For all data a semiempirical absorption correction was applied. The structures were solved by direct methods[12] and refined on F^2 by the least-squares method.[13] All non-hydrogen atoms were refined anisotropically, and the hydrogen atoms were included with a riding model. All disordered components were refined anisotropically with the assistance of distance and ADP restraints.[14]

[9] The $[CuCl_2]^-$ counterion is presumably produced by reduction of $CuCl_2$ by the solvent methanol.

[10] **3**: $C_{92}H_{151}Cu_6KO_{44}$, $M = 2381.56$, triclinic, space group $P\bar{1}$, $a = 14.304(2)$, $b = 14.966(4)$, $c = 17.076(2)$ Å, $\alpha = 99.39(2)$, $\beta = 111.36(2)$, $\gamma = 104.56(2)^\circ$, $V = 3160.8(10)$ Å^3, $Z = 1$, $\rho_{calcd} = 1.336$ g cm^{-3}, $F(000) = 1338$, $\lambda = 0.71073$ Å, $T = 193$ K, $\mu(Mo_{K\alpha}) = 1.107$ mm^{-1}, min./max. transmission: 0.671/0.738, crystal dimensions $0.55 \times 0.50 \times 0.45$ mm^3, $5.32^\circ \le 2\theta \le 50.00^\circ$. Of 29889 measured reflections, 10442 were independent ($R_{int} = 0.0578$) and employed in the structure refinement of 770 parameters with 75 restraints. Final R values are $R1 = 0.0655$ ($I > 2\sigma(I)$) and $wR2 = 0.1755$ (all data); min./max. residual electron density: $-991/989$ e nm^{-3}. The potassium ion in **3** is disordered

 © WILEY-VCH Verlag GmbH, D-69451 Weinheim, 1998 1433-7851/98/3701-0174 $ 17.50+.50/0

around an inversion center with occupancies of 0.50. The carbon atom of one coordinated methanol molecule is disordered over two sites (0.74:0.26). The carbon atom of the methoxide ion is disordered over three sites (0.38:0.31:0.31). The asymmetric unit is occupied by one methanol solvent molecule and four partially occupied and one disordered water molecule (0.68:0.32). The hydrogen atoms of the hydroxyl groups and the methoxide ion could not be located in the difference fourier synthesis.[14]

[11] T. Kottke, D. Stalke, *J. Appl. Crystallogr.* **1993**, *26*, 615; T. Kottke, R. J. Lagow, D. Stalke, *ibid*. **1996**, *29*, 465.

[12] SHELXS-96, program for structure solution: G. M. Sheldrick, *Acta Crystallogr. Sect. A* **1990**, *46*, 467.

[13] SHELXL-96, program for structure refinement: G. M. Sheldrick, Universität Göttingen, **1996**.

[14] Crystallographic data (excluding structure factors) for the structures reported in this paper have been deposited with the Cambridge Crystallographic Data Centre as supplementary publication nos. CCDC-100739 (**1**) and 100744 (**2**, **3**). Copies of the data can be obtained free of charge on application to CCDC, 12 Union Road, Cambridge CB2 1EZ, UK (fax: int. code + (44)1223 336-033; e-mail: deposit@ccdc.cam.ac.uk). Red-green stereo presentations of **1**–**3** are available on the WWW under http://www.organik.uni-erlangen.de/saalfrank/index.html.

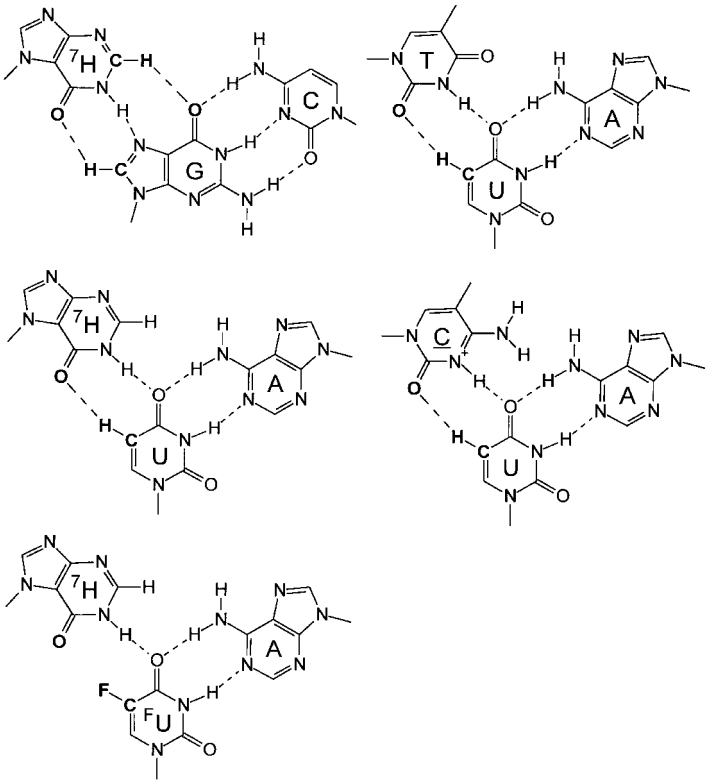


Figure 1. Experimentally investigated base triples in the parallel triple-helical binding motif.

Evidence for C–H···O Hydrogen Bond Assisted Recognition of a Pyrimidine Base in the Parallel DNA Triple-Helical Motif**

Judith Marfurt and Christian Leumann*

The structural and energetic influence of nonconventional C–H···O hydrogen bonds on molecular recognition has become a focus of interest. Whereas a large body of structural data evidences their importance in molecular recognition of small molecules in the crystalline state,[1] only limited experimental data is available on their contribution to biomolecular recognition in solution.[2] C–H···O hydrogen bonds have only recently begun to be used as design elements for directing intermolecular organization of small organic molecules (crystal engineering).[1, 3] Their use as a designer element for biomolecular complexation is virtually unexplored.

We recently reported on the selective recognition of G–C base pairs in DNA duplexes by parallel complementary oligodeoxynucleotides containing the unnatural nucleoside 7-(2′-deoxy-β-D-ribofuranosyl)hypoxanthine (^{7}H).[4] Although only one conventional N–H···N hydrogen bond between ^{7}H and G can be formed, the ^{7}H·G–C base triple (Figure 1) has the same stability as the canonical $\underline{C}^+$·G–C base triple ($\underline{C}$ = 5-methyl deoxycytidine) at pH 7.0, in which the base of the third strand is bound through two conventional hydrogen bonds to the purine base of the Watson–Crick duplex. Since precise structural data were lacking, we empirically attributed the extra stability to the presence of one or two C–H···O hydrogen bonds flanking the conventional hydrogen bond of the third-strand base.

To explore whether such weak electrostatic interactions can be further exploited for the recognition of DNA duplexes by oligonucleotides, we investigated the recognition of pyrimidine bases by considering such C–H···O hydrogen bonds. Specifically we investigated the interaction of a deoxyuridine unit in a DNA duplex with a ^{7}H unit in the third strand (Figure 1).

The DNA target duplexes **1** as well as the third-strand oligonucleotides **2** (Figure 2) were synthesized by standard phosphoramidite chemistry from commercially available and recently described DNA building blocks.[4] The binding efficiency of the third strands to the target duplex was

1 5′-GCTAAAAAGA**X**AGAGAGATCG
CGATTTTTCT**Y**TCTCTCTAGC-5′

2 5′-TTTTT$\underline{C}$T**Z**T$\underline{C}$T$\underline{C}$T$\underline{C}$T

Z	X Y	G C	dU A	^{F}U A	T A
$\underline{C}$		37.7 (-3.0)	24.2 (0)	18.5 (2.1)	17.9 (1.1)
^{7}H		40.0 (-3.4)	30.0 (-0.8)	24.0 (0.3)	18.2 (1.7)
T		---	27.7 (-0.7)	19.5 (1.9)	16.9 (2.0)

Figure 2. Top: Sequences of the target duplexes **1** and third strands **2**; bottom: T_m values [°C] for third-strand dissociation from UV melting curves (λ = 260 nm) and (in parentheses) ΔG values [kcal mol^{-1}] for triplex formation at 25 °C. Total single-strand concentration: 1.6 μM. Buffer: 10 mM sodium cacodylate, 100 mM NaCl, 0.25 mM spermine, pH 7.0.

[*] Prof. C. Leumann, Dr. J. Marfurt
Departement für Chemie & Biochemie der Universität
Freiestrasse 3, CH-3012 Bern (Switzerland)
Fax: Int. code + (41) 31-631 3422
e-mail: leumann@ioc.unibe.ch

[**] This work was supported by the Swiss National Science Foundation and by Ciba-Geigy AG, Basel.

 © WILEY-VCH Verlag GmbH, D-69451 Weinheim, 1998 1433-7851/98/3701-0175 $ 17.50+.50/0

around an inversion center with occupancies of 0.50. The carbon atom of one coordinated methanol molecule is disordered over two sites (0.74:0.26). The carbon atom of the methoxide ion is disordered over three sites (0.38:0.31:0.31). The asymmetric unit is occupied by one methanol solvent molecule and four partially occupied and one disordered water molecule (0.68:0.32). The hydrogen atoms of the hydroxyl groups and the methoxide ion could not be located in the difference fourier synthesis.[14]

[11] T. Kottke, D. Stalke, *J. Appl. Crystallogr.* **1993**, *26*, 615; T. Kottke, R. J. Lagow, D. Stalke, *ibid*. **1996**, *29*, 465.

[12] SHELXS-96, program for structure solution: G. M. Sheldrick, *Acta Crystallogr. Sect. A* **1990**, *46*, 467.

[13] SHELXL-96, program for structure refinement: G. M. Sheldrick, Universität Göttingen, **1996**.

[14] Crystallographic data (excluding structure factors) for the structures reported in this paper have been deposited with the Cambridge Crystallographic Data Centre as supplementary publication nos. CCDC-100739 (**1**) and 100744 (**2**, **3**). Copies of the data can be obtained free of charge on application to CCDC, 12 Union Road, Cambridge CB2 1EZ, UK (fax: int. code + (44)1223 336-033; e-mail: deposit@ccdc.cam.ac.uk). Red-green stereo presentations of **1**–**3** are available on the WWW under http://www.organik.uni-erlangen.de/saalfrank/index.html.

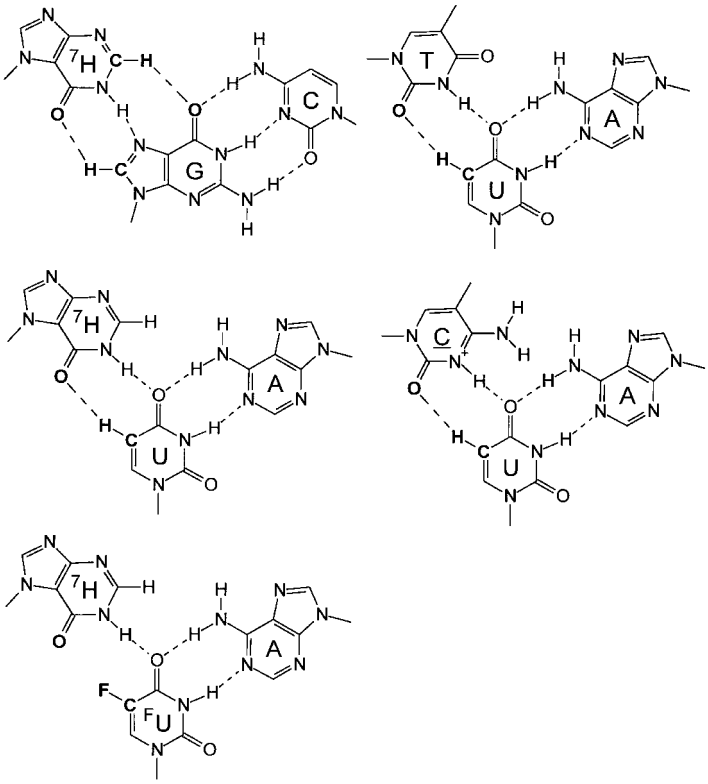


Figure 1. Experimentally investigated base triples in the parallel triple-helical binding motif.

Evidence for C–H···O Hydrogen Bond Assisted Recognition of a Pyrimidine Base in the Parallel DNA Triple-Helical Motif**

Judith Marfurt and Christian Leumann*

The structural and energetic influence of nonconventional C–H···O hydrogen bonds on molecular recognition has become a focus of interest. Whereas a large body of structural data evidences their importance in molecular recognition of small molecules in the crystalline state,[1] only limited experimental data is available on their contribution to biomolecular recognition in solution.[2] C–H···O hydrogen bonds have only recently begun to be used as design elements for directing intermolecular organization of small organic molecules (crystal engineering).[1, 3] Their use as a designer element for biomolecular complexation is virtually unexplored.

We recently reported on the selective recognition of G–C base pairs in DNA duplexes by parallel complementary oligodeoxynucleotides containing the unnatural nucleoside 7-(2′-deoxy-β-D-ribofuranosyl)hypoxanthine (^{7}H).[4] Although only one conventional N–H···N hydrogen bond between ^{7}H and G can be formed, the ^{7}H·G–C base triple (Figure 1) has the same stability as the canonical $\underline{C}^+$·G–C base triple ($\underline{C}$ = 5-methyl deoxycytidine) at pH 7.0, in which the base of the third strand is bound through two conventional hydrogen bonds to the purine base of the Watson–Crick duplex. Since precise structural data were lacking, we empirically attributed the extra stability to the presence of one or two C–H···O hydrogen bonds flanking the conventional hydrogen bond of the third-strand base.

To explore whether such weak electrostatic interactions can be further exploited for the recognition of DNA duplexes by oligonucleotides, we investigated the recognition of pyrimidine bases by considering such C–H···O hydrogen bonds. Specifically we investigated the interaction of a deoxyuridine unit in a DNA duplex with a ^{7}H unit in the third strand (Figure 1).

The DNA target duplexes **1** as well as the third-strand oligonucleotides **2** (Figure 2) were synthesized by standard phosphoramidite chemistry from commercially available and recently described DNA building blocks.[4] The binding efficiency of the third strands to the target duplex was

1 5′-GCTAAAAAGA**X**AGAGAGATCG
CGATTTTTCT**Y**TCTCTCTAGC-5′

2 5′-TTTTT$\underline{C}$T**Z**T$\underline{C}$T$\underline{C}$T$\underline{C}$T

Z	X Y	G C	dU A	^{F}U A	T A
$\underline{C}$		37.7 (-3.0)	24.2 (0)	18.5 (2.1)	17.9 (1.1)
^{7}H		40.0 (-3.4)	30.0 (-0.8)	24.0 (0.3)	18.2 (1.7)
T		---	27.7 (-0.7)	19.5 (1.9)	16.9 (2.0)

Figure 2. Top: Sequences of the target duplexes **1** and third strands **2**; bottom: T_m values [°C] for third-strand dissociation from UV melting curves (λ = 260 nm) and (in parentheses) ΔG values [kcal mol^{-1}] for triplex formation at 25 °C. Total single-strand concentration: 1.6 μM. Buffer: 10 mM sodium cacodylate, 100 mM NaCl, 0.25 mM spermine, pH 7.0.

[*] Prof. C. Leumann, Dr. J. Marfurt
Departement für Chemie & Biochemie der Universität
Freiestrasse 3, CH-3012 Bern (Switzerland)
Fax: Int. code + (41) 31-631 3422
e-mail: leumann@ioc.unibe.ch

[**] This work was supported by the Swiss National Science Foundation and by Ciba-Geigy AG, Basel.

 © WILEY-VCH Verlag GmbH, D-69451 Weinheim, 1998 1433-7851/98/3701-0175 $ 17.50+.50/0

assessed by an analysis of the UV melting curve in the buffers specified.[5] The melting temperatures (T_m) for dissociation of the third strand as well as the calculated Gibbs energies for triplex formation at 25 °C (ΔG) extracted from the melting curves[6] are summarized in Figure 2. A representative collection of melting curves are depicted in Figure 3.

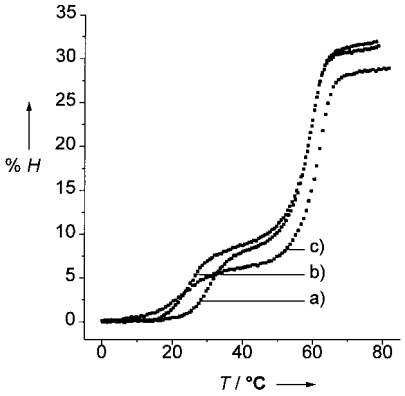


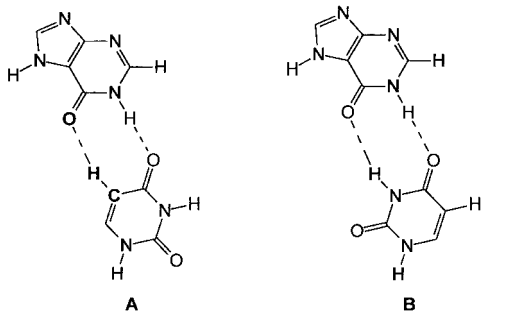
Figure 3. UV melting curves (%H = relative hyperchromicity, λ = 260 nm). a) **1·2** (**Z**·**X**–**Y** = ^{7}H·dU–A; b) **Z**·**X**–**Y** = ^{7}H·d^{F}U–A; c) **3·4**. Oligonucleotide concentration and buffer as in Figure 2 with the exception of pH 6.0 for c).

Inspection of the T_m data reveals that the oligonucleotide **2** (**Z** = ^{7}H) efficiently binds to the target duplex in which the base uracil is opposite to the ^{7}H residue (**1**; **X**, **Y** = dU, A) with formation of a ^{7}H·U–A base triple. This triplex is moderately less stable than the standard oligopurine/oligopyrimidine reference triplex displaying the conventional **Z**·**X**–**Y** = $\underline{C}^+$·G–C base triple ($\Delta T_m = -7.7$ K). If the ^{7}H residue of the third strand is placed opposite to a thymine unit (**Z**·**X**–**Y** = ^{7}H·T–A), a strong destabilization of the triplex relative to that containing the ^{7}H·U–A base triple is observed ($\Delta T_m = -11.8$ K). This corresponds to a typical mismatch situation and is due to the 5-methyl group of thymine, which completely obstructs the base-recognition process for steric reasons.

To investigate a possible energetic contribution of the C–H···O hydrogen bond to triplex stability, we replaced the 2′-deoxyuridine in the target duplex by 5-fluoro-2′-deoxyuridine (d^{F}U). The fluorine atom represents the closest non-isotopic isostere of hydrogen with an opposite electrostatic environment. As expected, this base is recognized by ^{7}H with distinctly lower affinity than uracil (ΔT_m of the corresponding triplexes = –6.0 K). This difference in T_m translates to a difference in binding enthalpy ($\Delta\Delta G$) of about –1.1 kcal mol^{-1} at 25 °C.

A similar hydrogen-bonding pattern between **X** and **Z** appears if ^{7}H in the third strand is replaced by either thymidine or 5-methyl-deoxycytidine (Figure 1, right). Indeed, replacement of ^{7}H by thymidine leads to a decrease in T_m of only 2.3 K. Thus, both nucleosides display almost equal efficiency in uracil recognition. Again, positioning the base thymine opposite to d^{F}U leads to a strong decrease in binding efficiency of the corresponding third strand ($\Delta T_m = -8.3$ K). Offering a thymidine unit in the duplex as the complexing partner for thymidine in the third strand results in a mismatch. Similar results were obtained for third strands containing 5-methyl-deoxycytidine, although on a lower affinity level. The overall lower T_m values most probably arise from the need for protonation of the base, an unfavorable process at pH 7.0.

We calculated the heat of formation (ΔH_f^0) of the base pairs **A** and **B** (Figure 4) in the gas phase with semi-empirical methods. Base pair **A** corresponds to the arrangement **Z**·**X** = ^{7}H·dU (Figure 2), whereas **B** represents an isomeric base pair



ΔH_f^0(PM3) = –5.29 kcal mol^{-1} ΔH_f^0(PM3) = –6.41 kcal mol^{-1}

Figure 4. Structures and standard heats of formation (ΔH_f^0) of base pairs **A** and **B** calculated with the semiempirical model PM3 for the gas phase as implemented in the program package Spartan V4.0 (Wavefunction Inc., USA).

between ^{7}H and uracil that is connected through two conventional hydrogen bonds. Interestingly, the heat of formation (ΔH_f^0) of base pair **A** displaying one conventional and one C–H···O hydrogen bond is only 1.12 kcal mol^{-1} less exothermic than **B**, which has two conventional hydrogen bonds. Thus, replacement of a conventional hydrogen bond by a C–H···O bridge is compromised by a loss of only about 1 kcal mol^{-1} in binding enthalpy. This is reasonably well reflected in the experimentally determined difference in stability between the triplex displaying a $\underline{C}^+$·G–C base triple and that displaying the ^{7}H·U–A base triple ($\Delta\Delta G \approx$ 2 kcal mol^{-1} at 25 °C). For comparison, typical $\Delta\Delta G$ values for the triplex containing $\underline{C}^+$·G–C and a true mismatch system are about 5 kcal mol^{-1} (e.g., T·T-A, Figure 2).

To explore the limitations of the C–H···O hydrogen bond assisted recognition of uracil with ^{7}H, we investigated the formation of the triple helix **3·4** (Figure 5), which is designed

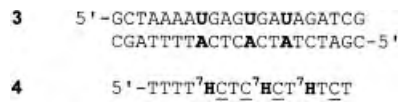


Figure 5. Sequence of the target duplex **3** and third strand **4**.

to incorporate three ^{7}H·dU interactions. This corresponds to a sequence context with a pyrimidine content of 20% in the triplex-recogniton region of the underlying duplex. As shown in Figure 3, binding at pH 6.0 is maintained even in this system with a T_m of 23.6 °C for third-strand dissociation. As expected, third-strand binding is less efficient in this case ($T_m \approx 1.5$ °C at pH 7.0) than for an all-purine target sequence under comparable conditions. We anticipate that in such systems the loss of affinity might be compensated by combining C–H···O hydrogen bond assisted recognition of pyrimidine bases with

 © WILEY-VCH Verlag GmbH, D-69451 Weinheim, 1998 1433-7851/98/3701-0176 $ 17.50+.50/0

further modifications to enhance triplex stability, for example replacing C by the 2-aminopyridine nucleoside **P** for recognition of guanine.[9, 10]

We can not definitely rule out the possibility of an energy-neutral contribution from the C–H···O arrangement in the corresponding base triples. Nevertheless, the experimental results described here are in good agreement with the general view that the energetic benefit of forming the C–H···O hydrogen bond is made up of a small, positive, direct electrostatic contribution[1] and a positive contribution due to the alleviation of a destabilizing interaction that arises if a hydrogen-bond acceptor (such as a carbonyl oxygen atom) is inactive or involved in secondary hydrogen bonding, for example, to solvent.[11] In any case, the final proof for the existence of a C–H···O hydrogen bond in the triplexes discussed here has to come from high-resolution structure analysis.

The efficient complexation of uracil by ^{7}H or T presented here is of direct relevance to the molecular recognition and folding of RNA. C–H···O hydrogen bonds in nucleic acids can compete with conventional hydrogen bonds under certain circumstances. This was shown by a recent X-ray structure analysis of an RNA duplex in which a U·U base pair built from one conventional and one C–H···O hydrogen bond was preferentially formed over an isomorphous base pair with two conventional hydrogen bonds.[12]

In applying this concept to triple-helical DNA recognition, the following restrictions have to be considered: 1. Uracil is not a DNA base, and there is no clear way to use the presented concept of C–H···O hydrogen bond assisted pyrimidine recognition for the complexation of the natural DNA base thymine. 2. Both thymidine and ^{7}H, as components of a third strand, have a primary binding preference for the purine bases adenine and guanine, respectively, which compromises the selectivity in the formation of DNA triple helices. This issue of selectivity, however, might be addressable by base design.

We have shown here that unconventional C–H···O hydrogen bonds may be advantageously used as a design element for enhancing the efficiency of weak base–base interactions in the complexation of nucleic acids. We are currently trying to expand this concept to triplex-mediated recognition of cytosine. Efficient and selective pyrimidine recognition definitely constitutes one way of extending the sequence range of triplex formation in nucleic acids, a widely sought but hitherto unsolved goal.[13]

Received: June 27, 1997 [Z 10607 IE]
German version: *Angew. Chem.* **1998**, *110*, 184–187

Keywords: antisense agents · hydrogen bonds · nucleic acids · pyrimidine recognition · triple helices

[1] G. R. Desiraju, *Acc. Chem. Res.* **1996,** *29*, 441–449.
[2] M. C. Wahl, M. Sundaralingam, *TIBS* **1997,** *22*, 97–102.
[3] G. R. Desiraju, *Angew. Chem.* **1995,** *107*, 2541–2558; *Angew. Chem. Int. Ed. Engl.* **1995**, *34*, 2311–2327.
[4] a) J. Marfurt, J. Hunziker, C. Leumann, *Bioorg. Med. Chem. Lett.* **1996**, *6*, 3021–3024; b) J. Marfurt, S. P. Parel, C. Leumann, *Nucleic Acids Res.* **1997,** *25*, 1875–1882.
[5] Melting curves were recorded with heating/cooling rates of 0.5 K min^{-1}. Under these conditions, melting and renaturation curves were superimposable in all cases and thus reflect equilibrium binding.
[6] The T_m data for third-strand binding in the triplexes **1·2** were independent of oligonucleotide concentration within the range 1–45 μM. The systems thus show pseudomonomolecular association, as reported previously for the parent canonical triplex.[7] Data for the Gibbs energy of formation for the triplexes (ΔG) were therefore calculated as described for a monomolecular two-state model from the experimentally determined association constant K_{ass} at 25 °C.[8]
[7] G. E. Plum, Y.-W. Park, S. F. Singleton, P. B. Dervan, K. J. Breslauer, *Proc. Natl. Acad. Sci. USA* **1990**, *87*, 9436–9440.
[8] L. A. Marky, K. J. Breslauer, *Biopolymers* **1987**, *26*, 1601–1620.
[9] S. Hildbrand, C. Leumann, *Angew. Chem.* **1996,** *108,* 2100–2102; *Angew. Chem. Int Ed. Engl.* **1996**, *35*, 1968–1970.
[10] S. Hildbrand, A. Blaser, S. P. Parel, C. Leumann, *J. Am. Chem. Soc.* **1997,** *119*, 5499–5511.
[11] G. A. Leonard, W. N. Hunter, *Acta Crystallogr. Sect. C* **1995,** *D51*, 136–139.
[12] M. C. Wahl, S. T. Rao, M. Sundaralingam, *Nature Struct. Biol.* **1996**, *3*, 24–31.
[13] J. Behr, S. O. Doronina, *Chem. Soc. Rev.* **1997,** 63–71.

Global and Local Aromaticity in Porphyrins: An Analysis Based on Molecular Geometries and Nucleus-Independent Chemical Shifts**

Michatl K. Cyrañski, Tadeusz M. Krygowski,* Marcin Wisiorowski, Nicolaas J. R. van Eikema Hommes, and Paul von Ragué Schleyer*

Dedicated to Professor Emanuel Vogel on the occasion of his 70th birthday

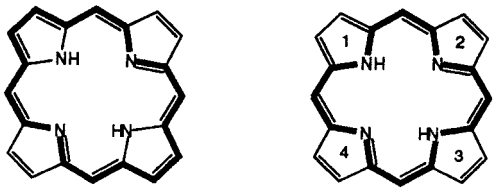
How and to what extent does aromaticity contribute to the geometric and electronic structure of porphyrins? Despite its widespread use for nearly two centuries, "aromaticity" is difficult to define.[1] Usually, this is done on the basis of energetic, geometric and magnetic criteria.[2] Molecular geometries are often the most accessible, and aromaticity indices have been derived from bond lengths.[3] Recently the nucleus-independent chemical shift (NICS) was proposed as a new magnetic criterion, based on MO calculations of the magnetic shieldings at the centers or other points of aromatic systems.[4] The aim of this paper is to deduce the electronic structure of porphyrins based both on a large number of geometries retrieved from the Cambridge Structural Database [5] and on computed NICS values.

[*] Prof. Dr. T. M. Krygowski, Dr. M. K. Cyrañski, Dr. M. Wisiorowski
Department of Chemistry, University of Warsaw
L. Pasteura 1, 02 093 Warsaw, (Poland)
Fax: Int. code + (48) 22-8222-892
e-mail: tmkryg@alfa.chem.uw.edu.pl
Prof. Dr. P. von R. Schleyer, Dr. N. J. R. van Eikema Hommes
Computer-Chemie-Centrum
Institut für Organische Chemie der Universität Erlangen-Nürnberg
Henkestrasse 42, D-91054 Erlangen (Germany)
Fax: Int. code + (49) 9131-85 9132
e-mail: pvrs@organik.uni-erlangen.de

[**] This work was supported by a BST-24/97 research grant (Warsaw) and by the Fonds der Chemischen Industrie (Erlangen). M.K.C. thanks the Foundation for Polish Science for a FNP Stipendium. We thank Dr. H. Jiao for valuable discussions.

 © WILEY-VCH Verlag GmbH, D-69451 Weinheim, 1998 1433-7851/98/3701-0177 $ 17.50+.50/0

The present analysis of the molecular geometry does not use the popular depiction of the porphyrin skeleton as a bridged [18]annulene derivative.[6] Instead, we divide the porphyrin moiety into the macrocyclic "internal cross"—an 18 π-electron system of 16 atoms—and the four peripheral pyrrole rings, as shown in Scheme 1.



Scheme 1. Two models of the π-electron system of porphyrin. Left: as bridged [18]annulene derivative; right: as macrocyclic internal cross (in bold) and four pyrrole rings (1–4).

The CC and CN bond lengths in porphyrins can be perturbed by exocyclic substitution and by coordination with a metal cation. Bond lengths can be analyzed by the harmonic oscillator model of aromaticity (HOMA),[3c] which in turn may be dissected into two components, EN and GEO [Eq. (1)]. Here, n is the number of bonds taken into the

$$\mathrm{HOMA} = 1 - \alpha(R_{\mathrm{opt}} - R_{\mathrm{av}})^2 - \frac{\alpha}{n}\Sigma\,(R_{\mathrm{av}} - R_{\mathrm{i}})^2 = 1 - \mathrm{EN} - \mathrm{GEO} \qquad (1)$$

summation, and α is an empirical constant fixed to give HOMA = 0 for the hypothetical Kekule structures of aromatic systems and 1 for the system with all bonds equal to the optimal value R_{opt}.[3c, d] R_{av} stands for the average bond length, while the individual bond lengths R_{i} are obtained[7] from the Pauling definition of bond number.[8] The EN term describes changes in aromatic character due to deviation of the average bond length from the optimal value, while the GEO term reflects the consequences of bond length alternation.[7]

Of the 456 porphyrin derivatives with the highest measurement precision (i.e., with AS = 1, 2[9]) that we retrieved from the Cambridge Structural Database,[5] 32 are exocyclically substituted species, while 424 are metal complexes. In free base porphyrin, two of the four pyrrole rings (rings 1 and 3 in Scheme 1) are protonated. Since it is difficult to localize the inner hydrogen positions accurately by X-ray diffraction,[10] the harmonic oscillator stabilization energy (HOSE) model[11] was used to assign the hydrogen atoms to the pyrrole rings. Note that N-H tautomerization[12] will tend to reduce the difference between the pyrrole rings. For comparison, we calculated the optimized structures of porphyrin, its dianion, and the Mg(II)-porphyrin complex at the B3LYP/6-31G* DFT level and computed the nucleus independent chemical shift (NICS) at characteristic points at GIAO-RHF/6-31+G*. All computations were performed with the Gaussian 94 program package.[13] Figure 1 presents the calculated[12, 14] and mean experimental geometries, which are in good agreement; the HOMA, EN, GEO and NICS values are given in Table 1.

The differences between the global HOMA values for the free base porphyrins and the metal complexes are insignificant. Decrease in aromaticity due to the bond length alternation (GEO term) is about twice as large as that due to the nonoptimal average bond length (EN term). Interestingly, both terms are somewhat smaller for the complexes containing trivalent metals (M = Mn^{III}, Fe^{III}, Tl^{III}) than for the divalent metal complexes (M = Mg^{II}, Fe^{II}, Co^{II}, Ni^{II}, Cu^{II}, Zn^{II}). Hence, the HOMA values for the complexes with trivalent metals are slightly higher.

Table 1. HOMA, EN, GEO, and NICS values for porphyrins and their metal complexes.

	HOMA[a]	HOMA[b]	EN[a]	GEO[a]	NICS [ppm][b]
Porphyrin	0.652	0.666	0.107	0.240	−16.5[c]
ring (1,3)	0.666	0.702	0.132	0.202	−15.2
ring (2,4)	0.452	0.381	0.175	0.373	−4.5
internal cross	0.880	0.932	0.075	0.045	−21.7
Porphyrin metal complex	0.656	0.671	0.094	0.249	
ring (1,3)	0.566	0.556	0.158	0.276	−10.0
;ring (2,4)	0.524	0.556	0.153	0.323	−10.0
internal cross	0.872	0.906	0.071	0.057	−21.0
Porphyrin dianion		0.448			−14.9[c]
ring (1,2,3,4)		0.287			−4.0
internal cross		0.908			−17.5
Porphyrin M^{II} complex	0.638		0.102	0.259	
Porphyrin M^{III} complex	0.682		0.084	0.233	

[a] Mean experimental geometries. [b] Calculated geometries. [c] Value at ring center, see Figure 2.

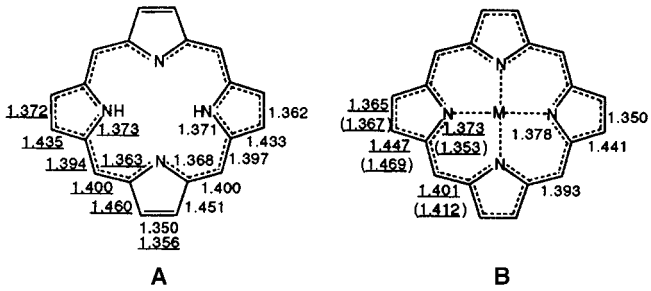


Figure 1. Mean experimental and calculated (underscored) bond lengths for porphyrin (**A**) and its metal complexes (**B**, calculated for M = Mg; values for the free anion in parentheses).

The pyrrole rings with NH groups (1 and 3) are clearly more aromatic[2d] than the other five-membered rings (2 and 4). The mean HOMA values are 0.666 and 0.452, respectively. The NICS values computed in the ring centers (Figure 2) show the difference more explicitly: the −15.2 NICS for rings 1 and 3 is identical with the pyrrole value (−15.1).[4] Thus, the NH groups are not inert bridging groups, as is suggested by the [18]annulene model, but instead are an integral part of the aromatic system. However, rings 2 and 4 have much lower NICS values (−4.5), implying that the C_2H_2 groups function as exocyclic "bridges".

Metal complexation strongly reduces the difference between the two types of pyrrole rings, but does not lead fully to D_{4h} symmetry for the porphyrin skeleton. Application of the HOSE model[11] reveals small residual differences. The HOMA values, as well as the contributing EN and GEO terms, approach the mean of the corresponding data for the free base porphyrin. This is reflected by the results of the DFT computations: The structure of the magnesium complex optimized to D_{4h} symmetry (Figure 1); the NICS at the centers of all the pyrrole rings is −10.0, the mean of the values

 © WILEY-VCH Verlag GmbH, D-69451 Weinheim, 1998 1433-7851/98/3701-0178 $ 17.50+.50/0 *Angew. Chem. Int. Ed.* **1998**, *37*, No. 1/2

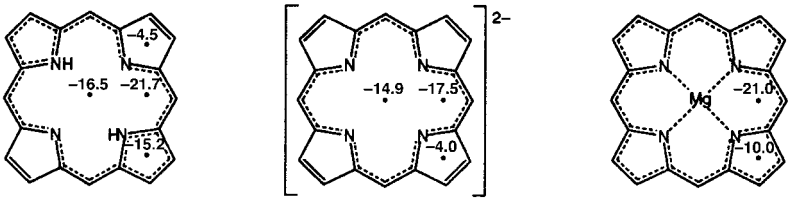


Figure 2. Computed NICS values for free porphyrin base, its dianion, and the Mg complex. The dashed lines indicate the delocalized π systems deduced from the NICS and HOMA analyses.

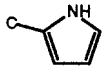
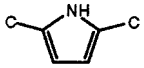
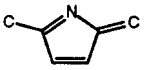
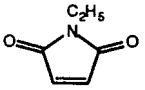
computed for uncomplexed porphyrin (Figure 2). Thus all four pyrrole rings are incorporated into the aromatic system. Interestingly, much lower NICS (only −4.0) are computed for all the pyrrole rings in the uncomplexed porphyrin dianion (Figure 2). Hence, the aromatic system of the dianion consists primarily of the *internal cross*, which must be considered to be an 18 π-electron species.

The mean HOMA values of the *internal cross* (Scheme 1) are significantly higher than those of the pyrrole rings for both the metallic and nonmetallic derivatives. The dearomatization contributions from the GEO and EN terms are comparable. The NICS values corroborate this finding. However, since computation of NICS in the center of the internal cross is impossible for the magnesium complex, we chose an additional point at the geometric mean of two adjacent C–N bonds (see Figure 2). NICS computed at this point for porphyrin is −21.7, slightly higher than the value of −21.0 computed for the Mg complex. The value for the porphyrin dianion is lower (−17.5) implying that the uncomplexed dianion is less aromatic than the Mg complex.

What is responsible for the decrease in aromaticity of the pyrrole rings, in particular rings 2 and 4, in the porphyrin macrocycle? Doubly bonded substituents are known to lead to strongly localized, quinonoid-like structures and hence to decrease the aromatic character of rings. For example, negative HOMA values and positive NICS are obtained for *para*-benzoquinone. Similar structural effects are observed for 2- and/or 5-substituted pyrroles (Table 2). The typical HOMA value for pyrroles of about 0.92 decreases substantially to 0.27, when a doubly bonded substituent is present. Similarly, the NICS value of −15.1 for pyrrole is reduced to −1.8 for 2-azafulvene. Maleimide has a negative HOMA and a positive NICS value (Table 2).

In conclusion, both the NICS values and the HOMA analyses (albeit attenuated due to the uncertainty in the hydrogen positions) agree: rings 1 and 3 in the porphyrin system can be considered to be true pyrrole rings. The π system consists of these rings and the internal cross. Rings 2 and 4 behave almost like pyrroles with doubly bonded substituents and have short, localized CC double bonds. While the dianion has four essentially localized double bonds, the corresponding metal derivatives involve all the π electrons in the aromatic system.

Table 2. HOMA, EN, GEO, and NICS values for four kinds of 2- and 5-substituted pyrrole derivatives and for *para*-benzoquinone.

Compound	HOMA	EN	GEO	NICS [ppm]
	0.907[a]	0.002	0.091	−15.1[d]
	0.932[b]	0.015	0.052	−15.1[d]
	0.274[c]	0.217	0.509	−1.8[e]
	−0.443	0.380	1.060	+0.9[f]
	−0.508	0.392	1.116	+7.9

[a] Mean of 15 geometries. [b] Mean of 6 geometries. [c] Mean of 5 geometries. [d] Computed for unsubstituted pyrrole. [e] Computed for 2-azafulvene. [f] Computed for maleimide.

Received: June 27, 1997 [Z10605IE]
German version: *Angew. Chem.* **1998**, *110*, 187–190

Keywords: annulenes · aromaticity · density functional calculations · porphyrinoids

[1] a) V. I. Minkin, M. N. Glukhovtsev, B. Ya. Simkin, *Aromaticity and Antiaromaticity—Electronic and Structural Aspects*, Wiley, New York, **1994**; b) P. von R. Schleyer, H. Jiao, *Pure Appl. Chem.* **1996**, *28*, 209–218.

[2] J. L. Eldridge, L. M. Jackman, *J. Chem. Soc.* **1961**, 859–866; b) H. J. Dauben, Jr., J. D. Wilson, J. L. Laity in *Non-benzenoid Aromatics, Vol. 2* (Ed.: J. Snyder), Academic Press, New York, **1971**, and references therein; c) A. R. Katritzky, P. Barczyñski, G. Musumarra, D. Pisano, M. Szafran, *J. Am. Chem. Soc.* **1989**, *111*, 7–15; K. Jug, A. Köster, *J. Phys. Org. Chem.* **1991**, *4*, 163–169; d) however, see P. von R. Schleyer, P. K. Freeman, H. Jiao, B. Goldfuss, *Angew. Chem.* **1995**, *107*, 332–335; *Angew. Chem. Int. Ed. Engl.* **1995**, *34*, 337–340, and ref. [1b]; e) U. Fleischer, W. Kutzelnigg, P. Lazzeretti, V. Müllenkamp, *J. Am. Chem. Soc.* **1994**, *116*, 5298–5306; f) H. Jiao, P. von R. Schleyer, M. N. Glukhovtsev, *J. Phys. Chem.* **1996**, *110*, 12299–12304.

[3] a) A. Julg, P. François, *Theor. Chim. Acta* **1967**, *8*, 249–259; b) C. W. Bird, *Tetrahedron* **1985**, *41*, 1409–1414; c) J. Kruszewski, T. M. Krygowski, *Tetrahedron Lett.* **1972**, 3839–3842; d) T. M. Krygowski, *J. Chem. Inf. Comput. Sci.* **1993**, *33*, 70–78; e) T. M. Krygowski, A. Ciesielski, C. W. Bird, A. Kotschy, *ibid.* **1995**, *35*, 203–210.

[4] a) P. von R. Schleyer, C. Maerker, A. Dransfeld, H. Jiao, N. J. R. van Eikema Hommes, *J. Am. Chem. Soc.* **1996**, *118*, 6317–6318; b) G. Subramanian, P. von R. Schleyer, H. Jiao, *Angew. Chem.* **1996**, *108*, 2824–2827; *Angew. Chem. Int. Ed. Engl.* **1996**, *35*, 2638–2641.

[5] Cambridge Structural Database, release October 1996; see: F. H. Allen, J. E. Davies, J. J. Galloy, O. Johnson, O. Kennard, C. F. MacRae, E. M. Mitchell, G. F. Mitchell, J. M. Smith, D. G. Watson, *J. Chem. Inf. Comput. Sci.* **1991**, *31*, 187–204.

[6] See, for example, E. Vogel, *J. Heterocycl. Chem.* **1996**, *33*, 1461–1487 and references therein.

[7] a) T. M. Krygowski, M. Cyrañski, *Tetrahedron* **1996**, *52*, 1713–1722; b) *ibid.* **1996**, *52*, 10255–10264.

[8] L. Pauling, *J.Am. Chem. Soc.* **1947**, *69*, 542–553.

[9] In the Cambridge Structural Database, AS refers to the precision of the crystal structure determination. For example, "AS = 1, 2" means that the mean estimated standard deviation for the bond lengths does not exceed 0.01 Å.

[10] See, for example, J. D. Dunitz, *X-Ray Analysis and the Structure of Organic Molecules*, Cornell University Press, Ithaca, **1979**.

[11] a) T. M. Krygowski, R. Anulewicz, J. Kruszewski, *Acta Crystallogr. Sect. B* **1983**, *39*, 732–739; b) T. M. Krygowski, R. Anulewicz, M. Wisiorowski, *Pol. J. Chem.* **1995**, *69*, 1579–1584. The HOSE model permits the estimation of the canonical structure weights directly from

 © WILEY-VCH Verlag GmbH, D-69451 Weinheim, 1998 1433-7851/98/3701-0179 $ 17.50+.50/0

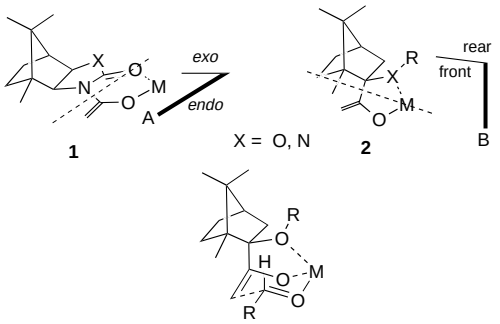
the bond lengths of the molecule containing π electrons or its fragment.
[12] See M. Boronat, E. Ortí, P. M. Viruela, F. Tomás, *J. Mol. Struct. Theochem* **1997**, *390*, 149–156.
[13] Gaussian 94: M. J. Frisch, G. W. Trucks, H. B. Schlegel, P. M. W. Gill, B. G. Johnson, M. A. Robb, J. R. Cheeseman, T. Keith, G. A. Petersson, J. A. Montgomery, K. Raghavachari, M. A. Al-Laham, V. G. Zakrzewski, J. V. Ortiz, J. B. Foresman, J. Cioslowski, B. B. Stefanov, A. Nanayakkara, M. Challacombe, C. Y. Peng, P. Y. Ayala, W. Chen, M. W. Wong, J. L. Andres, E. S. Replogle, R. Gomperts, R. L. Martin, D. J. Fox, J. S. Binkley, D. J. Defrees, J. Baker, J. P. Stewart, M. Head-Gordon, C. Gonzalez, J. A. Pople, Gaussian, Pittsburgh, PA, **1995**.
[14] For further calculations on the porphyrin system, see a) D. Lamoen, M. Parinello, *Chem. Phys. Lett.* **1996**, *248*, 309–315 and references therein; b) P. M. Kozlowski, A. A. Jarzecki, P. Pulay, *J. Phys. Chem.* **1996**, *100*, 7007–7013 and references therein.

Design and Evaluation of a Practical Camphor-Based Methyl Ketone Enolate for Highly Stereoselective "Acetate" Aldol Reactions**

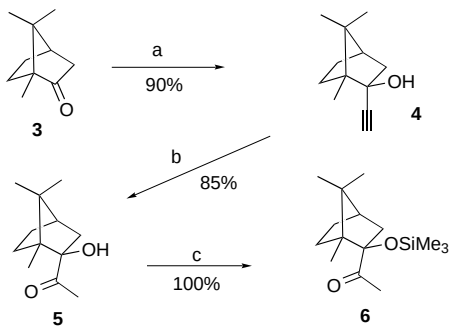
Claudio Palomo,* Alberto González, Jesús M. García, Cristina Landa, Mikel Oiarbide, Santiago Rodríguez, and Anthony Linden

Control of the configuration of newly forming stereogenic carbon atoms in aldol condensation processes has focused enormous efforts over the last two decades.[1] Special attention has been given to the use of chiral enolates derived from carboxylic acids[2] because of the easy final removal of the auxiliary to obtain either β-hydroxy carbonyl or 1,3-dihydroxylic compounds, which are frequently present in natural products.[3] A conceptually different, but in practice equivalent, strategy to access to these fragments lies in the use of enolates derived from chiral α-hydroxy ketones.[4] In this instance, the aldol products, upon oxidative cleavage of the α-ketol moiety, give the desired β-hydroxy carbonyl system.[5] The major drawbacks associated with this strategy are the destruction of the covalently bounded chiral adjuvant at the final stage, and the insufficient stereoselectivity generally attained with α-unsubstituted enolates.[6] Although considerable advances have been made in recent years to overcome this latter limitation by carrying out acetate aldol reactions mediated by both metal enolates bearing chiral ligands and external chiral catalysts,[7] the problem associated with enolates of chiral acetates still remains not well resolved;[8] in all but one case,[4j] the lack of stereoselection in aldol reactions with methyl ketone enolates is specially dramatic.[4b,g,h,i]

We have recently reported on the reaction of *N*-acetyl imide enolates **1** with aldehydes to give the corresponding adducts with modest levels of diastereoselectivity (Scheme 1).[9] In an attempt to take advantage of the stereodifferentiating power of the camphor skeleton more effectively, we designed the new camphor-derived enolate **2**. The conception of **2** has been guided by two major goals: a) to provoke the electrophilic aldehyde to follow a trajectory of approach closer to the camphor skeleton, and b) to force a facial discrimination between the rear side and the sterically more demanding front side of the camphor skeleton, depicted as the half-spaces defined by plane B in Scheme 1,[10] instead of the more commonly used *endo/exo* discrimination across opposite sides of plane A.[11] Accordingly, if one assumes that a chelating metal ion like lithium engages in three-point coordination, a very high diastereoselectivity should be expected through a Zimmerman–Traxler six-membered transition state.[12] From this design the methyl ketone **5**[13] (Scheme 2) is a primary candidate to evaluate the above



Scheme 1. Design of the new chiral methyl ketone enolate **2** by moving the acetyl moiety of **1** nearer to the camphor skeleton. Also shown is the transition state accounting for the aldol reaction of **2**.



Scheme 2. Synthesis of the chiral methyl ketone reagents **5** and **6**: a) HC≡CLi, THF, −78 →room temperature (RT) (*endo:exo* 97:3); b) HgO, H_2SO_4, Me_2CO, reflux; c) TMSO, TfOH cat., RT.

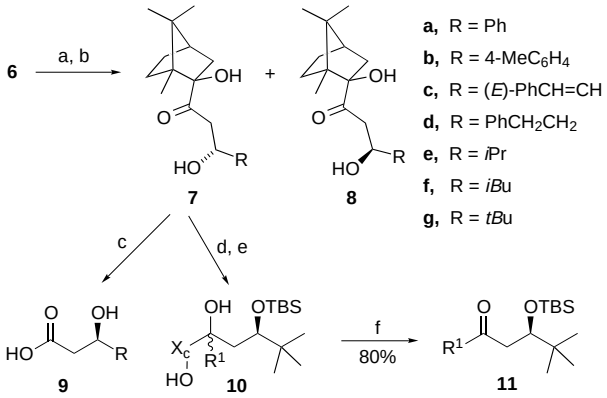
[*] Prof. Dr. C. Palomo, Dr. M. Oiarbide
Departamento de Química Orgánica
Universidad del País Vasco, Facultad de Química
Apdo 1072, E-20080 San Sebastián (Spain)
Fax: Int. code + (34) 43-212236
e-mail: qoboigaj@sc.ehu.es
Dr. A. González, Dr. J. M. García, C. Landa
Departamento de Química
Universidad Pública de Navarra
Campus de Arrosadía, E-31006 Pamplona (Spain)
Dr. A. Linden[+]
Organisch-chemisches Institut der Universität
Winterthurerstrasse 190, CH-8057 Zürich (Switzerland)
Dr. S. Rodríguez
Departamento de Química Inorgánica y Orgánica
Universidad Jaume I
E-12080 Castellón (Spain)
[+] X-ray structure analysis.

[**] This work was supported by the Government of Navarra (Project O.F. 68/1995) and in part by the Basque Government (Project PI 95/93). Grants to C.L. from the Government of Navarra and the Ministerio de Educación y Cultura (MEC) are acknowledged.

 © WILEY-VCH Verlag GmbH, D-69451 Weinheim, 1998 1433-7851/98/3701-0180 $ 17.50+.50/0

hypothesis. The crystalline **5** was prepared by addition of lithium acetylide to the commercially available (1*R*)-(+)-camphor (**3**) according to the procedure of Midland.[14] The addition proceeded in a 97:3 *endo:exo* ratio from which **4** was isolated in 90% yield after column chromatography. Standard hydration provided **5** [m.p.: 94–95°C, $[\alpha]_D^{25} = -65.6$ ($c = 1.0$ in CH_2Cl_2)] in 85% yield after crystallization from hexane.[15]

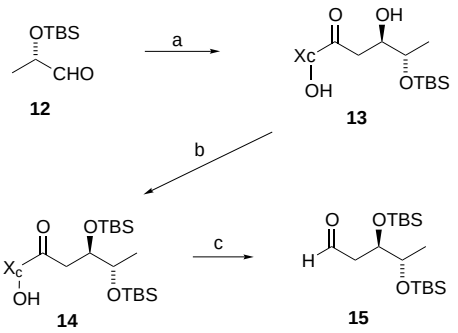
Concordant with our expectations, the corresponding aldol products obtained from the reaction of representative aldehydes with the lithium enolate of **6**, generated from **5** by silylation with *N*-trimethylsilyl-2-oxazolidinone (TMSO)[16] and subsequent treatment with lithium diisopropylamide (LDA), were indeed formed with remarkably high diastereoselectivity (Scheme 3). The diastereomeric ratio of the



Scheme 3. Diastereoselective synthesis of α-unsubstituted β-hydroxy carboxylic acids and ketones: a) LDA (1.2 equiv), THF, -78°C, 0.5 h then RCHO, 3–7 h; b) 1M HCl, MeOH or TBAF (2 equiv), THF, RT, 5 min; c) $NaIO_4$, MeOH/H_2O (2/1), RT or reflux, 12–48 h; d) $ClSiMe_2tBu$, imidazole, DMF, RT, 3 days, 86%; e) R^1MgBr, $CeCl_3$, THF or Et_2O, 0°C, 2 h; f) $Pb(OAc)_4$ (2 equiv), C_6H_6, 5°C, 2 h.

product was unchanged after desilylation to afford the adducts **7**/**8** (typically 95:5, Table 1). The stereochemical assignments for the major products **7** from the reaction with benzaldehyde, isobutyraldehyde, and pivalaldehyde were made by cleavage of the acyloin moiety[5] to afford the corresponding carboxylic acid **9** along with the recovery of the starting camphor (85–90%). The observed optical rotations of these β-hydroxy acids were then compared with published values.[17] In addition, a single-crystal X-ray analysis of the aldol **7g** corroborated the assigned configuration for the adducts. From the data in Table 1 it is evident that the reaction diastereoselectivity is independent of the nature of the aldehyde, showing generality for aromatic, α,β-unsaturated, and linear as well as branched chain aliphatic aldehydes. The excellent diastereoselectivity observed in these reactions is of particular interest in that it provides, through carbonyl addition and subsequent diol cleavage, the basis for an enantioselective synthesis of α-unsubstituted β-hydroxy ketones. For example, using organocerium reagents,[18] we could prepare the carbinols **10** [R^1 = Me, 85%; R^1 = Ph, 90%; R^1 = allyl, 80%],[19] which upon exposure to lead tetraacetate in benzene gave the α-unsubstituted β-silyoxy ketones **11** in good overall yields and essentially in optically pure form.

A further example that illustrates the efficiency of the present system is the reaction of the dianion of **5** with the α-oxy aldehyde **12** (Scheme 4), a chiral aldehyde that shows



Scheme 4. a) **5**, LDA (2.4 equiv), LiCl (6 equiv), THF, -78°C, 4 h, 75%. b) TBDMS-Cl, imidazole, DMF, RT, overnight, 90%. c) $BH_3 \cdot$THF, THF, 0°C, 7 h then $Pb(OAc)_4$ (2 equiv), C_6H_6, 5°C, 2 h, 70%.

essentially no diastereoselection with either methyl acetate or α-silyloxy methyl ketone enolates.[4b, 5b] When **12** was allowed to react with the dianion of **5** in the presence of LiCl, a mixture of diastereomeric aldols was obtained in the ratio 93:7. The major isomer **13** was isolated in 75% yield after column chromatography. A single crystal X-ray analysis of **13** confirmed the assigned configuration for the adduct.[20] Finally, diborane reduction of the keto group in the TBS-protected aldol **14** (TBS = *tert*-butyldimethylsilyl) followed by oxidative workup provided the α-unsubstituted β-silyloxy aldehyde **15** in 70% yield along with the recovery of the starting camphor.

The α-hydroxy methyl ketone enolate developed here helps to fill the existing gap with regard to the usual behavior of α-unsubstituted enolates in diastereoselective aldol reactions and, in addition, enables for the first time the recovery of the starting source of chiral information.

Table 1. Aldol condensation of the lithium enolate of **6** with representative aldehydes.[a]

Aldehyde	t [h]	**7**:**8**[b]	Yield (**7**) [%][c]
C_6H_5CHO	6	96:4	80
4-$CH_3C_6H_4CHO$	7	96:4	67
$C_6H_5CH{=}CHCHO$	6	92:8	80
$C_6H_5CH_2CH_2CHO$	2	95:5	81
i-C_3H_7CHO	3	97:3	67
$(CH_3)_2CHCH_2CHO$	6	96:4	75
$(CH_3)_3CCHO$	6	>98:2	70

[a] Reactions were carried out at -78°C on 0.5 mmol scale by adding a precooled (-78°C) solution of the aldehyde in THF to the lithium enolate of **6** in the same solvent at -78°C. [b] Ratios were determined by both ^{13}C NMR (area of *C*HOH signals of both diastereomers at $\delta = 65-75$) and HPLC analysis of the crude reaction mixture. Diastereomer **8** had the shorter retention time in all HPLC experiments. [c] Yields of **7** after purification of the crude product by column chromatography and separation of diastereomers by HPLC on a Merck LiChrosorb Si 60 column (7 μm) with mixtures of ethyl acetate and hexane as eluent.

Received: June 16, 1997 [Z10552IE]
German version: *Angew. Chem.* **1998**, *110*, 190–192

Keywords: acetylene · aldol reactions · asymmetric synthesis · camphor · methyl ketone

[1] Reviews on the asymmetric aldol condensation: a) D. A. Evans, J. V. Nelson, T. R. Taber, *Top. Stereochem*. **1982**, *13*, 1; b) S. Masamune, W. Choy, J. S. Petersen, L. R. Sita, *Angew. Chem.* **1985**, *97*, 1; *Angew. Chem. Int. Ed. Engl.* **1985**, *24*, 1; c) *Comprehensive Organic Chemistry*, *Vol. 2* (Eds.: B. M. Trost, I. Fleming, C. H. Heathcock), Pergamon, Oxford, **1991**; d) C. H. Heathcock in ref. [1c], p. 133; e) M. Kim. S. F. Williams, S. Masamune, in ref. [1c], p. 239; f) I. Paterson, in ref. [1c], p. 301; g) A. S. Franklin, I. Paterson, *Contemp. Org. Synth.* **1994**, *1*,317; h) M. Braun in *Stereoselective Synthesis. (Houben-Weyl)*, *Vol. E21/3* (Eds.: G. Helmchen, R. W. Hoffmann, J. Mulzer, E. Schaumann), Thieme, Stuttgart, **1996**, p. 1603.

[2] Extensive list of chiral auxiliaries: a) A.-ur Rahman, Z. Shah, *Stereoselective Synthesis in Organic Chemistry*, Springer, Berlin, **1993**; b) J.Seyden-Penne, *Chiral Auxiliaries and Ligands in Asymmetric Synthesis*, Wiley, New York, **1995**; c) D. J. Ager, I. Prakash, D. R. Schaad, *Chem Rev.* **1996**, *96*, 835.

[3] S. Hanessian, *Total Synthesis of Natural Products: The Chiron Approach*, Pergamon, Oxford, **1983**.

[4] a) C. H. Heathcock; M. C. Pirrung, C. T. Buse, J. P. Hagen, S. D. Young, J. E. Sohn, *J. Am. Chem. Soc.* **1979**, *101*, 7077; b) C. H. Heathcock, M. C. Pirrung, J. Lampe, C. T. Buse, S. D. Young, *J. Org. Chem.* **1981**, *46*, 2290; c) N. A. Van Draanen, S. Arseniyadis, M. T. Crimmins, C. H. Heathcock, *ibid.* **1991**, *56*, 2499; d) S. Masamune, SK. A. Ali, D. L. Snitman, D. S. Garvey, *Angew. Chem.* **1980**, *92*, 573; *Angew. Chem. Int. Ed. Engl.* **1980**, *19*, 557; e) S. Masamune, W. Choy, F. A. L. Kerdesky, B. Imperiali, *J. Am. Chem. Soc.* **1981**, *103*, 1566; f) C. Siegel, E. R. Thornton, *ibid.* **1989**, *111*, 5722; g) B. M. Trost, H. Urabe, *J. Org. Chem.* **1990**, *55*, 3982; h) C. H. Heathcock, C. T. White, J. J. Morrison, D. VanDerveer, *ibid.* **1981**, *46*, 1296; i) D. A. Evans, J. V. Nelson, E. Vogel, T. R. Taber, *J. Am. Chem. Soc.* **1981**, *103*, 3099; j) B. R. Lagu, H. M. Crane, D. C. Liotta, *J. Org. Chem.* **1993**, *58*, 4191; k) S. Figueras, R. Martín, P. Romea, F. Urpí, J. Vilarrasa, *Tetrahedron Lett.* **1997**, *38*, 1637.

[5] a) C. H. Heathcock, C. T. Buse, W. A. Kleschick, M. C. Pirrung, J. E. Sohn, J. Lampe, *J. Org. Chem.* **1980**, *45*, 1066; b) C. H. Heathcock, S. D. Young, J. P. Hagen, M. C. Pirrung, C. T. White, D. Vanderveer, *ibid.* **1980**, *45*, 3846.

[6] For a detailed information on this topic, see: a) M. Braun, *Angew. Chem.* **1987**, *99*, 24; *Angew. Chem. Int. Ed. Engl.* **1987**, *26*, 24; b) M. Braun in *Advances in Carbanion Chemistry, Vol. 1* (Ed.: V. Snieckus), Jai, London, **1992**, p. 177.

[7] Aldol reactions of achiral methyl ketones with achiral aldehydes on use of chiral boron reagents: a) I. Paterson, J. M. Goodman, *Tetrahedron Lett.* **1989**, *30*, 997; b) P. V. Ramachandran, W. Xu, H. C. Brown, *Tetrahedron Lett.* **1996**, *37*, 4911; c) A. Bernardi, C. Gennari, J. M. Goodman, I. Paterson, *Tetrahedron Asymmetry* **1995**, *6*, 2613; on use of chiral titanium reagents: d) R. O. Duthaler, P. Herold, W. Lottenbach, K. Oertle; M. Riediker, *Angew. Chem.* **1989**, *101*, 490; *Angew. Chem. Int. Ed. Engl.* **1989**, *28*, 495; on use of chiral palladium(II) reagents: e) M. Sodeoka, R. Tokunoh, F. Miyazaki, E. Hagiwara, M. Shibasaki, *Synlett* **1997**, 463; on use of external chiral catalysts: f) K. J. Hale, S. Manaviazar in *Advanced Asymmetric Synthesis*, *Vol. 2* (Ed.: G.-R. Stephenson), Chapman and Hall, London, **1996**, p. 27; g) T. Mukaiyama, *Aldrichimica Acta* **1996**, *29*, 59.

[8] Recent examples from chiral acetate imide enolates: a) K. Otsuka, T. Ishizuka, K. Kimura, T. Kunieda, *Chem. Pharm. Bull.* **1994**, *42*, 748; b) T.-H. Yan, A.-W. Hung, H.-C. Lee, C. S. Chang, W.-H. Liu, *J. Org. Chem.* **1995**, *60*, 3301; c) T. H. Yan, A.-W. Hung, H.-C. Lee, C. S. Chang, *ibid.* **1994**, *59*, 8187; from chiral *N*-acetyl sultam enolates: d) W. O. Oppolzer, C. Starkemmann, *Tetrahedron Lett.* **1992**, *33*, 2139; from Fisher carbene enolates: e) T. S. Powers, Y. Shi, K. J. Wilson, W. D. Wolff, *J. Org. Chem.* **1994**, *59*, 6882.

[9] a) C. Palomo, M. Oiarbide, A. Gonzalez, J. M. García, F. Berree, A. Linden, *Tetrahedron Lett.* **1996**, *37*, 6931; b) C. Palomo, F. Berree, A. Linden, J. M. Villalgordo, *J. Chem. Soc. Chem. Commun.* **1994**, 1961.

[10] For an earlier camphor-based ester acetate aldol approach exploiting this concept in another way, see G. Helmchen, U. Leikauf, I. Taufer-knöpfel, *Angew. Chem.* **1985**, *97*, 874; *Angew. Chem. Int. Ed. Engl.* **1985**, *24*, 874.

[11] Review on camphor-based chiral auxilaries: W. Oppolzer, *Tetrahedron* **1987**, *43*, 1969.

[12] H. E. Zimmerman, M. D. Traxler, *J. Am. Chem. Soc.* **1957**, *79*, 1920.

[13] M. Kagawa, *Chem. Pharm. Bull.* **1959**, *7*, 306

[14] a) M. M. Midland, *J. Org. Chem.* **1975**, *40*, 2250; b) M. M. Midland, J. I. McLoughlin, R. T. Werley, Jr., *Org. Synth. Coll.* **1993**, *Vol 8*, p 391.

[15] The addition of lithium acetylide to (1*R*)-(+)-camphor has been previously reported to give the *endo* adduct: a) M.-L. Capmau, W. Chodkiewicz, P. Cadiot, *Bull. Soc. Chim. Fr.* **1968**, 3233. Other authors, however, suggest that the *exo* adduct was produced instead: b) C. D. Johnson, S. Lane, P. N. Edwards, P. J. Taylor, *J. Org. Chem.* **1988**, *53*, 5130; c) P. Bovonsombat, E. McNelis, *Tetrahedron Lett.* **1993**, *34*, 4277. In our hands the procedure of Midland[14] gives reproducible results. Product **5** can also be obtained by direct hydration of the crude *endo*:*exo* mixture of **4** followed by a single crystallization from hexane (yield, 90%).[20]

[16] J. M. Aizpurua, C. Palomo, A. L. Palomo, *Can. J. Chem.* **1984**, *62*, 336.

[17] Observed values **9a**: +15.5 ($c = 0.9$ in EtOH) [Published value: +17.9 ($c = 2.3$ in EtOH 95%)[10]]; **9e**: +41.7 ($c = 1.0$ in $CHCl_3$) [Published value: +40.5 ($c = 0.6$ in $CHCl_3$)[10]]; **9g**: +53.0 ($c = 1.0$ in $CHCl_3$) [Published value: +53.2 ($c = 1.0$ in $CHCl_3$)[7d]].

[18] T. Imamoto, N. Takiyama, K. Nakamura, T. Hatajima, Y. Kamiya, *J. Am. Chem. Soc.* **1989**, *111*, 4392.

[19] Every attempt at attacking the carbonyl group of the corresponding aldols with both lithium and Grignard reagents led to unsatisfactory results.

[20] Crystallographic data (excluding structure factors) for the structures **5**, **7g**, and **13** have been deposited with the Cambridge Crystallographic Data Centre as supplementary publication no. CCDC-100315. Copies of the data can be obtained free of charge on application to: CCDC, 12 Union Road, Cambridge CB21EZ, UK (fax: int. code + (44) 1223-336033; e-mail: deposit@chemcrys.cam.ac.uk).

[{Pt(CN)($C_{10}H_{21}N_4$)}$_6$]: A Luminescent Hexanuclear Platinum(II) Macrocycle Containing Chelating Dicarbene and Bridging Cyanide Ligands**

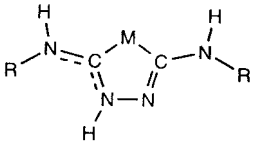
Siu-Wai Lai, Kung-Kai Cheung, Michael Chi-Wang Chan, and Chi-Ming Che*

Transition metal mediated self-assembly reactions are a versatile strategy for generating supermolecules with appealing structural and spectroscopic properties.[1–6] In this context we are interested in luminescent molecular hosts[7] composed of square-planar platinum(II) complexes as building blocks, since such materials could have applications in host–guest photochemistry and as novel luminescent sensors. Fujita et al.[1] and Stang et al.[5a, b] reported the preparation of tetranuclear platinum(II) compounds with pyridine-based ligands. Here we describe the crystal structure of a novel luminescent hexanuclear platinum(II) macrocycle bearing cyclic dicarbene and bridging cyanide ligands.

[*] Prof. C. M. Che, S. W. Lai, Dr. K.-K. Cheung, Dr. M. C.-W. Chan
Department of Chemistry
The University of Hong Kong
Pokfulam Road, Hong Kong (China)
Fax: Int. code + (852) 2857-1586
e-mail: cmche@hkucc.hku.hk

[**] We acknowledge financial support from The University of Hong Kong, the Hong Kong Research Grants Council, and the Croucher Foundation. M. C.-W. C. is grateful for a University Postdoctoral Fellowship from the University of Hong Kong.

 © WILEY-VCH Verlag GmbH, D-69451 Weinheim, 1998 1433-7851/98/3701-0182 $ 17.50+.50/0



1

The synthesis of a mononuclear platinum(II) complex with the chelating $C_4H_9N_4$ ligand (**1**, $R = CH_3$) by addition of methyl isocyanide and hydrazine to $K_2[PtCl_4]$ in water has long been known.[8] Subsequent investigations revealed the $[C_4H_9N_4]$ moiety to be a monoanionic planar "resonance-stabilized" dicarbene ligand.[9] In contrast, heating K_2PtCl_4, *tert*-butyl isocyanide, and hydrazine hydrate in water at reflux for one hour resulted in the formation of $[Pt(CN)(C_{10}H_{21}N_4)]_6$ (**2**), which was isolated as acetonitrile-solvated yellow crystals upon recrystallization from acetonitrile/diethyl ether.

The X-ray structure of **2** (Figure 1)[10] shows it to be a rare example of a Pt_6 macrocycle.[11] The core of **2** consists of six platinum atoms linked through crystallographically disordered[10] cyanide units and is puckered in a chairlike conformation. Alternatively, this 18-membered ring can be regarded as a open cubane-type structure in which a pair of opposite corners is missing. The other six corners are occupied by platinum atoms, and the bridging cyanide ligands form the sides. The angles within the core are in accordance with this geometry: the CN-Pt-CN angles at the corners are almost orthogonal (av 92.4°), while the Pt-C-N and Pt-N-C groups are nearly linear (av 174°).

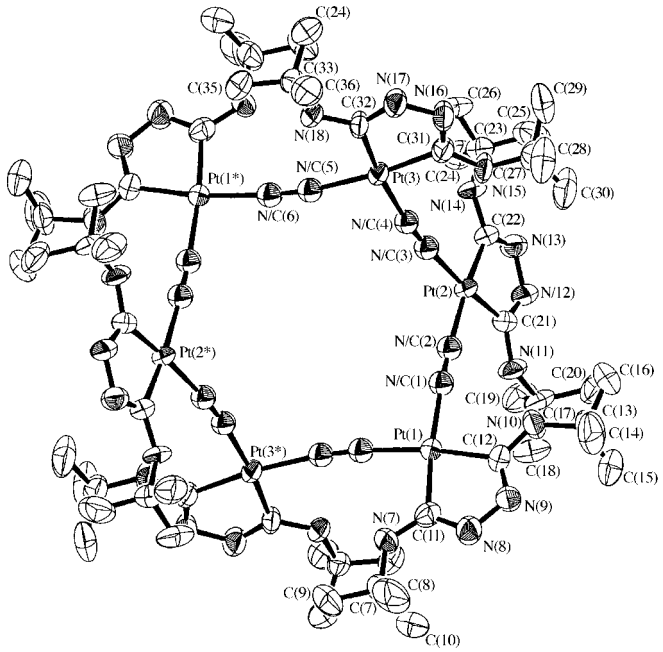


Figure 1. Crystal structure of **2** with atomic numbering scheme (40% probability ellipsoids). Hydrogen atoms and solvent molecules are omitted for clarity. Selected bond lengths [Å] and angles [°]: Pt(1)–N/C(1) 2.05(1), N/C(1)–N/C(2) 1.13(2), Pt(2)–N/C(2) 2.03(1), Pt(2)–N/C(3) 2.02(1), N/C(3)–N/C(4) 1.17(1), Pt(3)–N/C(4) 2.02(1), Pt(1)–C(11) 2.00(1), Pt(1)–C(12) 2.01(1), Pt(2)–C(21) 1.97(1), Pt(2)–C(22) 1.97(1), N(12)–C(21) 1.31(2), N(12)–N(13) 1.41(1), N(13)–C(22) 1.30(2), Pt(3)–C(31) 2.01(1), Pt(3)–C(32) 1.98(1); N/C(1)-Pt(1)-N/C(6) 92.2(5), N/C(2)-Pt(2)-N/C(3) 92.5(5), N/C(4)-Pt(3)-N/C(5) 92.4(5), Pt(1)-N/C(1)-N/C(2) 174(1), Pt(2)-N/C(2)-N/C(1) 175(1), Pt(2)-N/C(3)-N/C(4) 175(1), Pt(3)-N/C(4)-N/C(3) 174(1), C(11)-Pt(1)-C(12) 78.8(6), C(21)-Pt(2)-C(22) 78.2(6), C(31)-Pt(3)-C(32) 78.7(5), Pt(2)-C(22)-N(13) 117.5(10), Pt(2)-C(22)-N(14) 121(1), N(13)-C(22)-N(14) 120(1).

The $C_{10}H_{21}N_4$ motif (see **1**, R = *t*Bu) is analogous to the $C_4H_9N_4$ group in earlier work,[8, 9] and hence a planar PtC_2N_2 five-membered metallacycle is present. The Pt–carbene distances are in the range 1.97(1)–2.01(1) Å and are similar to those in the platinum(II) complexes *trans*-[Pt{C(NEt$_2$)(O-C(O)Ph)}(PPh$_3$)I$_2$] (1.969(7) Å),[12] [Pt(H)(CH$_2$CN)-{C(NC$_3$H$_6$)N(H)(*p*-MeOC$_6$H$_4$)}(PPh$_3$)] (2.069(4) Å),[13] and *trans*-[Pt(Me){C(NMe$_2$)Me}(PMe$_2$Ph)$_2$]PF$_6$ (2.079(13) Å).[14] Intriguingly, the Pt–C(sp^3) distance of 2.147(11) Å in the latter is only slightly longer, and this can be attributed to the *trans* influence of the carbene ligand. Nevertheless, the carbene description is vindicated by the sp^2-type hybridization of the respective carbon centers in **2**; the angles at C(21) are 122.8(10), 121(1), and 115.7(9)°. Formation of **2** can be explained as follows: two coordinated *t*BuNC ligands react with hydrazine to give the chelating dicarbene ligand, and platinum(II)-mediated dealkylation of *t*BuNC gives rise to the cyanide ligands. We note that heating a solution of $[PtCl_4]^{2-}$ and *t*BuNC in water for one hour similarly generated a partially dealkylated species, namely, $[Pt(CNtBu)_2(CN)_2]$.[15]

The absorption spectrum of **2** in methanol (Figure 2a) exhibits an intense band at 356 nm. The very high extinction coefficient of $\varepsilon_{max} = 18000\ dm^3mol^{-1}cm^{-1}$ indicates a spin-allowed charge-transfer (CT) transition, and we tentatively assign this to a Pt $\rightarrow\pi^*$(carbene) transition. Transitions within the chelating dicarbene groups are discounted, since they would occur at higher energy. The alternative assignment as a Pt $\rightarrow\pi^*(CN^-)$ transition is not favored, since mononuclear Pt^{II} cyanide derivatives bearing π-acid ligands such as phosphane or alkyl isocyanide do not absorb strongly at $\lambda > 300$ nm. For example, the lowest energy bands of [Pt(dppe)(CN)$_2$] (dppe = 1,2-bis(diphenylphosphanyl)ethane) and [Pt(CN*t*Bu)$_2$(CN)$_2$] appear at 294 and 282 nm respectively in methanol.[16] Furthermore, the Pt $\rightarrow\pi^*(CN^-)$ transition of $[Pt(CN)_4]^{2-}$ occurs at 280 nm.[17] The relatively low energy of the Pt $\rightarrow\pi^*$(carbene) transition means that the carbene ligand can readily be exploited in photochemical studies of metal-to-ligand charge transfer (MLCT) in platinum(II) derivatives.

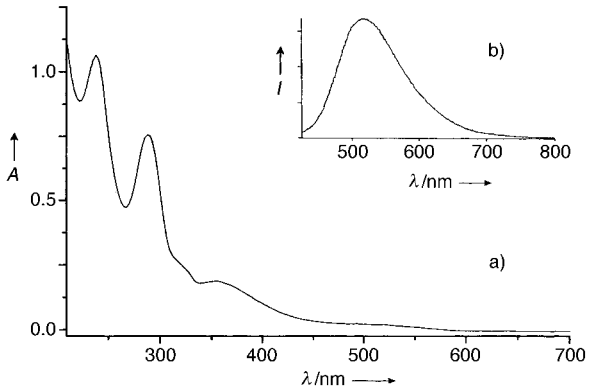


Figure 2. a) UV/Vis spectrum of **2** in methanol. b) Emission spectrum of **2** in CH_2Cl_2 (intensity *I* in arbitrary units).

 © WILEY-VCH Verlag GmbH, D-69451 Weinheim, 1998 1433-7851/98/3701-0183 $ 17.50+.50/0

Upon excitation at 350 nm at 301 K, crystalline **2** shows a structureless emission band centered at 514 nm, which at 77 K is blue-shifted to 507 nm. In a degassed solution in CH_2Cl_2 at 301 K, an emission band is observed at 519 nm with a lifetime of 0.22 μs (Figure 2b). The emission at $\lambda > 500$ nm provides further evidence for a Pt→π*(carbene) transition, since $[Pt(CN)_4]^{2-}$ displays an intense emission band at 408 nm only with a shoulder at 460 nm.[17] Despite previous studies,[18] we believe that this is the first observation of an emissive metal→π*(carbene) CT excited state in solution at room temperature. The long lifetime and high energy (ca. 2.8 eV, E_{0-0} taken as 450 nm) of the excited state imply that these platinum(II) species can undergo bimolecular photoreactions, and preliminary results confirm that the emission of **2** is quenched by *N*,*N*′-dimethyl-4,4′-bipyridinium hexafluorophosphate in dichloromethane. Future work will be directed towards probing the excited state reactivities of carbene complexes by utilizing the MLCT emission of the platinum(II) carbene moiety.

Experimental Section

2: A solution of $K_2[PtCl_4]$ (0.20 g, 0.48 mmol), *tert*-butyl isocyanide (0.20 mL, 1.93 mmol), and hydrazine hydrate (0.10 mL, 2.06 mmol) in water was heated to reflux for 1 h. The volatile components were removed in vacuo, and the residue was extracted with acetonitrile/diethyl ether. Slow evaporation of this solution at 5 °C yielded yellow crystals (yield 32 %). ^{1}H NMR (300 MHz, $CDCl_3$, 27 °C): $\delta = 1.40$ (s, *t*Bu); IR (Nujol): $\tilde{\nu} = 3453$, 3412 (N–H); 2141 (C≡N); 1562, 1535 cm^{-1} (C=N); UV/Vis (methanol): λ_{max} (ε) = 238 (95000), 288 (68000), 316 (22000), 356 nm (18000); FAB-MS: *m/z* (%) = 2510 (100) $[Pt(CN)(C_{10}H_{21}N_4)]_6^+$, 1255 (50) $[Pt(CN)(C_{10}H_{21}N_4)]_3^+$. Satisfactory elemental analysis.

Received: August 14, 1997 [Z10816IE]
German version: *Angew. Chem.* **1998**, *110*, 193–195

Keywords: carbene complexes · luminescence · macrocycles · platinum · self-assembly

[1] a) M. Fujita, K. Ogura, *Bull. Chem. Soc. Jpn.* **1996**, *69*, 1471–1482; b) M. Fujita, D. Oguro, M. Miyazawa, H. Oka, K. Yamaguchi, K. Ogura, *Nature* **1995**, *378*, 469–471.
[2] J. P. Sauvage, *Acc. Chem. Res.* **1990**, *23*, 319–327.
[3] J. M. Lehn, A. Rigault, *Angew. Chem.* **1988**, *100*, 1121–1122; *Angew. Chem. Int. Ed. Engl.* **1988**, *27*, 1095–1097.
[4] D. Philp, J. F. Stoddart, *Angew. Chem.* **1996**, *108*, 1242–1286; *Angew. Chem. Int. Ed. Engl.* **1996**, *35*, 1154–1196.
[5] a) P. J. Stang, D. H. Cao, S. Saito, A. M. Arif, *J. Am. Chem. Soc.* **1995**, *117*, 6273–6283; b) P. J. Stang, B. Olenyuk, *Angew. Chem.* **1996**, *108*, 798–802; *Angew. Chem. Int. Ed. Engl.* **1996**, *35*, 732–736; c) P. J. Stang, N. E. Persky, J. Manna, *J. Am. Chem. Soc.* **1997**, *119*, 4777–4778.
[6] C. K. Chan, K. K. Cheung, C. M. Che, *Chem. Commun.* **1996**, 227–228.
[7] a) R. V. Slone, J. T. Hupp, C. L. Stern, T. E. Albrecht-Schmitt, *Inorg. Chem.* **1996**, *35*, 4096–4097; b) B. C. Tzeng, W. C. Lo, C. M. Che, S. M. Peng, *J. Chem. Soc. Chem. Commun.* **1996**, 181–182.
[8] L. Tschugajeff, M. Skanavy-Grigorjewa, A. Posnjak, *Z. Anorg. Allg. Chem.* **1925**, *148*, 37–42.
[9] a) G. Rouschias, B. L. Shaw, *J. Chem. Soc. A* **1971**, 2097–2104; (b) W. M. Butler, J. H. Enemark, J. Parks, A. L. Balch, *Inorg. Chem.* **1973**, *12*, 451–457.
[10] Crystal data for **2**: $C_{66}H_{126}N_{30}Pt_6 \cdot 10\,CH_3CN$; M = 2920.94, triclinic, space group $P\bar{1}$ (no. 2), $a = 14.713(6)$, $b = 18.186(6)$, $c = 14.042(8)$ Å, $\alpha = 101.03(3)$, $\beta = 105.84(4)$, $\gamma = 113.83(3)°$, $V = 3106(2)$ Å^3, $Z = 1$, $\rho_{calcd} = 1.561$ g cm^{-3}, $\mu = 67.55$ cm^{-1}, $F(000) = 1420$, $T = 301$ K. A yellow crystal of dimensions $0.25 \times 0.20 \times 0.35$ mm^3 was used for data collection at 301 K on a Rigaku AFC7R diffractometer (graphite-monochromatized $Mo_{K\alpha}$ radiation; $\lambda = 0.71073$ Å), ω-2θ scan mode, ω-scan angle $(0.73+0.35 \tan\theta)°$, scan speed 16.0° min^{-1} (up to six scans for reflections with $I < 15\sigma(I)$). Measurement range: $2\theta_{max} = 46°$; *h*: 0 to 16; *k*: −19 to 19; *l*: −15 to 15. Three standard reflections were measured after every 300 reflections and showed a decay of 3.74 %. The intensity data were corrected for decay, Lorentz, and polarization effects, and empirical absorption corrections based on the ψ scan of six strong reflections (min./max. transmission factors 0.671/1.000) were made. Of 9041 reflections measured, 8644 were unique with $R_{int} = 0.026$. 5738 reflections with $I > 3\sigma(I)$ were considered observed and used in the structural analysis. The structure was solved by Patterson methods, expanded by Fourier methods (PATTY), and refined by full-matrix least squares with the software package TeXsan on a Silicon Graphics Indy computer. The crystallographic asymmetric unit consists of one half of the complex molecule and five molecules of acetonitrile. The six CN groups forming the 18-membered ring system were disordered; all the atomic sites were occupied half by N atoms and half by C atoms. Atoms N(1) to N(6) and C(1) to C(6) were refined isotropically with occupation numbers of 0.5, whereby the positions and thermal parameters of the C atoms were constrained to those of the corresponding N atoms (i.e. N/C(1) to N/C(6)). The C and N atoms of the five solvent molecules had large temperature factors and were also refined isotropically. The other non-hydrogen atoms of the complex were refined anisotropically. The hydrogen atoms bonded to the N atoms of the ligand molecules were not located in difference Fourier synthesis. The other 69 H atoms (including solvent) were introduced at calculated positions with thermal parameters equal to 1.3 times that of the attached C atoms and were not refined. Convergence for 490 variable parameters by least-squares refinement on *F* with $w = 4F_o^2/\sigma^2(F_o^2)$ ($\sigma^2(F_o^2) = [\sigma^2(I) + (0.035F_o^2)^2]$) for 5738 reflections with $I > 3\sigma(I)$ was reached at $R = 0.038$ and $wR = 0.056$ and GOF = 1.67. $(\Delta/\sigma)_{max.} = 0.04$ for atoms of the complex. The final difference Fourier map was featureless with maximum positive and negative peaks of 2.40 and −0.71 e Å^{-3}. Crystallographic data (excluding structure factors) for the structure reported in this paper have been deposited with the Cambridge Crystallographic Data Centre as supplementary publication no. CCDC-100633. Copies of the data can be obtained free of charge on application to CCDC, 12 Union Road, Cambridge CB2 1EZ, UK (fax: int. code + (44) 1223-336033; e-mail: deposit@ccdc.cam.ac.uk).
[11] a) J. Lorberth, W. Massa, M. E.-Essawi, L. Labib, *Angew. Chem.* **1988**, *100*, 1194–1195; *Angew. Chem. Int. Ed. Engl.* **1988**, *27*, 1160–1161; b) B. Longato, G. Bandoli, G. Trovó, E. Marasciulo, G. Valle, *Inorg. Chem.* **1995**, *34*, 1745–1750.
[12] J. T. Chen, W. H. Tzeng, F. Y. Tsai, M. C. Cheng, Y. Wang, *Organometallics* **1991**, *10*, 3954–3955.
[13] R. A. Michelin, R. Bertani, M. Mozzon, L. Zanotto, F. Benetollo, G. Bombieri, *Organometallics* **1990**, *9*, 1449–1459.
[14] R. F. Stepaniak, N. C. Payne, *Inorg. Chem.* **1974**, *13*, 797–801.
[15] L. Malatesta, F. Bonati, *Isocyanide Complexes of Metals*, Wiley, London, **1969**, p. 169.
[16] S. W. Lai, C. M. Che, unpublished results.
[17] J. W. Schindler, R. C. Fukuda, A. W. Adamson, *J. Am. Chem. Soc.* **1982**, *104*, 3596–3600.
[18] a) H. C. Foley, L. M. Strubinger, T. S. Targos, G. L. Geoffroy, *J. Am. Chem. Soc.* **1983**, *105*, 3064–3073; b) A. D. Rooney, J. J. McGarvey, K. C. Gordon, R.-A. McNicholl, U. Schubert, W. Hepp, *Organometallics* **1993**, *12*, 1277–1282; c) L. S. Hegedus, *Tetrahedron* **1997**, *53*, 4105–4128.

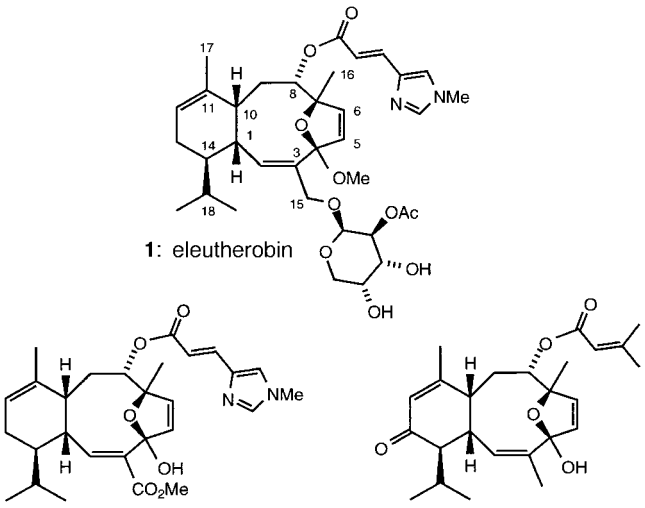
 © WILEY-VCH Verlag GmbH, D-69451 Weinheim, 1998 1433-7851/98/3701-0184 $ 17.50+.50/0

A Convergent Route for the Total Synthesis of the Eleuthesides**

Xiao-Tao Chen, Clare E. Gutteridge, Samit K. Bhattacharya, Bishan Zhou, Thomas R. R. Pettus, Tony Hascall, and Samuel J. Danishefsky*

The marine environment is taking its place beside plant sources and fermentation in providing access to biologically active substances.[1] From the standpoint of organic chemistry, the aquatic biomass warrants particularly close attention, due to the richly varied structures provided therein. Moreover, the reliability of marine feedstocks as a bulk source of natural products is often less than the case with their plant and microbially derived counterparts. Hence, marine-derived natural products may well furnish excellent opportunities for the subspecialty of synthesis.

Such an opportunity is presented by a group of structurally related natural products, which we loosely group under the term "eleuthesides" (e.g. eleutherobin (**1**),[2] sarcodictyin (**2**),[3] and valdivone (**3**)[4]). These are each isolated from different marine sources. Interest in the family was considerably heightened by the recent report by Fenical et al.[2] that eleutherobin displays excellent potency in a variety of tumor cell lines and that the mechanism of its cytotoxicity involves inhibition of microtubule disassembly. Thus, at least eleutherobin (**1**), manifests a taxol—epothilone—discodermolide mode of action.[5] In light of the very interesting structures of these closely related compounds, the high potency of **1,** and the difficult availability of all of the eleuthesides from their natural habitats, this family presents a challenging opportunity for creative chemistry.



Given the discussion above, we defined the criteria for success in our synthetic venture as going beyond the completion of a ceremonial level route to the natural products. Rather, the substantive goal is that of providing significant quantities of end products for thorough biological scrutiny in the context of a detailed SAR (structure – activity relationship) investigation. An account of the attainment of a flexible and convergent synthesis of the eleuthesides is provided herein.

The underlying logic of our scheme, in qualitative terms, is implicit in Scheme 1. Reference to this scheme will identify the stages of the synthesis subsequently documented in Scheme 2 (vide infra). The chiral matrix material selected for elaboration is the readily available *R*-(−)-α-phellandrene (**4**).[6] This compound undergoes cycloaddition with a ketene derivative (dichloroketene). A C1 fragment is then appended to the modified cyclobutanone cycloadduct, and the ring is fragmented to produce a system of the type **5** with differentiated arms for subsequent elaboration.

A furanoid building block (2,5-dibromofuran (**6**)[7]) provides system **7** as a nucleophile. The remaining furyl – bromine bond constitutes a latent form of carbon nucleophilicity, to be exploited later (vide infra). In the first coupling event, system **7** is delivered to the aldehyde function of **5**. Next, the "arm" extending from the C1 ester linkage is expanded by one carbon through a cyanation reaction. An eventual acetaldehyde appendage is coupled to the "bromofuryl" carbon (C4), producing a compound of type **8**, a highly strained 2,5-furano[6]phane. In this construction, the two benzylic oxygen functions at C8 and C3 in **8,** are presented in differentiated forms. The free hydroxyl group at C8 (R = H) accelerates oxidation of the proximal furan. Following bond reorganization (**9** → **10**), ring formation between the hydroxyl and appropriate keto group leads to a pyranose of the type **11**. In this system, the C7 keto group, destined for nucleophilic methylation, has been uniquely identified. Moreover, in **11**, the setting for entry of the methyl group in the desired stereochemical sense has been established, since reaction would be directed *anti* to the more sterically demanding five-membered carbon bridge. Following suitable manipulations, the pyranose ring in **11** is rearranged to a furanose, thereby exposing the two oxygen atoms projecting from C3 and C8 of the skeleton in differentiated form (see compound **12**).

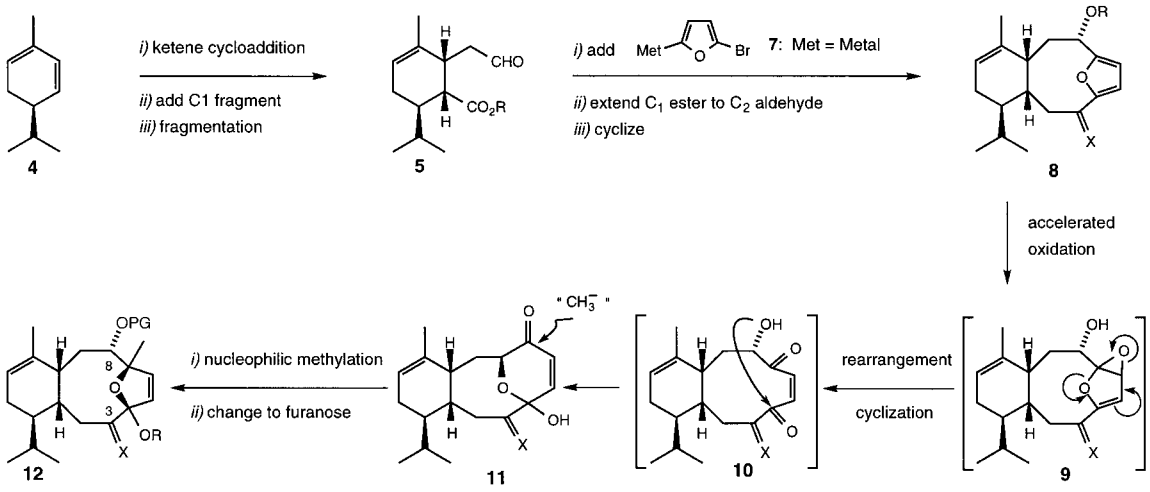
The actual steps employed for building the eleutheside are summarized in Scheme 2. To be noted here is the regiospecificity of the cycloaddition of dichloroketene to **4** (the stereoselectivity is 9:1 in favor of the shown isomer **13**).[8] The product (**14**) resulting from the dechlorination of the initial cycloadduct (**13**) is subjected to a Bredereck-type trans-

[*] Prof. S. J. Danishefsky,[+] X.-T. Chen, Dr. C. E. Gutteridge, Dr. S. K. Bhattacharya, B. Zhou, Dr. T. R. R. Pettus, T. Hascall
Department of Chemistry, Columbia University
Havemeyer Hall, New York, NY 10027 (USA)

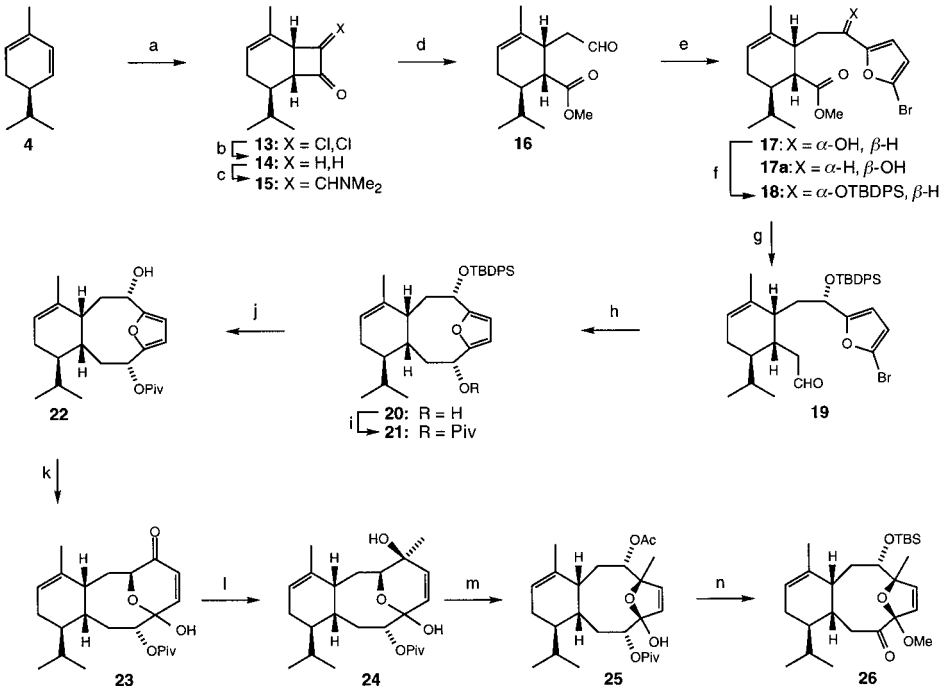
[+] Other address:
Laboratory for Bioorganic Chemistry
Sloan-Kettering Institute for Cancer Research
1275 York Avenue, New York, NY 10021 (USA)
Fax: Int. code + (1) 212 772-8691
e-mail: c-kandell@ski.mskcc.org

[**] This work was supported by the National Institutes of Health (grant HL 25848). Graduate Fellowships are gratefully acknowledged by X.T.C. (Kanagawa Academy of Science and Technology) and B.Z. (Pharmacia-Upjohn) and Postdoctoral Fellowships by C.E.G. (The Royal Commission for the Exhibition of 1851) and T.R.R.P. (The National Science Foundation). We are grateful to Vinka Parmakovich and Barbara Sporer of the Columbia University Mass Spectral Facility, and we thank Prof. G. Parkin for supervising Mr. T. Hascall in expeditiously solving the X-ray crystal structure.

 © WILEY-VCH Verlag GmbH, D-69451 Weinheim, 1998 1433-7851/98/3701-0185 $ 17.50+.50/0



Scheme 1. Underlying logic of the synthetic plan. PG = protecting group.



Scheme 2. Construction of the eleutheside skeleton. a) trichloroacetyl chloride, Zn, Et_2O, sonication, 0 °C, 65 %; b) Zn, MeOH, NH_4Cl, 87 %; c) *t*BuOCH(NMe_2)$_2$, 60 °C, 75 %; d) 1. *p*TsOH · H_2O, MeOH, 60 °C, 2. *p*TsOH · H_2O, Me_2CO, 60 % for the two steps; e) 2,5-dibromofuran (**6**) + *n*BuLi, THF, −78 °C, →**7** (Met = Li), **7**+**16** in THF →**17**, 57 %; f) TBDPSCl, imidazole, DMAP, 0 °C, 97 %; g) 1. DIBAL – toluene, toluene, −78 °C, >95 %; 2. MsCl, pyridine, DMAP, 0 °C, >95 %; 3. KCN, [18]crown-6, CH_3CN, 80 °C, 96 %; 4. DIBAL-hexanes, toluene, −78 °C to 0 °C, 84 %; h) $CrCl_2$/$NiCl_2$, DMF, 70 %; i) PivCl, CH_2Cl_2, Et_3N, DMAP, 0 °C, >95 %; j) TBAF, THF, 92 %; k) DMDO, $(CH_3)_2CO$, CH_2Cl_2, −78 °C; l) MeLi-Et_2O, THF, −78 °C, 42 % for k) and l); m) Ac_2O, DMAP, CH_2Cl_2, 0 °C, 73 %; n) 1. Ag_2O, MeI-MeCN, 94 %; 2. KCN, EtOH, 60 °C, >95 %; 3. TBSOTf, 2,6-lutidine, CH_2Cl_2, 0 °C, 91 %; 4. DIBAL-hexanes, CH_2Cl_2, −78 °C, 95 %; 5. cat. TPAP, NMO, CH_2Cl_2, >95 %. TBDPS = *tert*-butyldiphenylsilyl, DMAP = 4-dimethylaminopyridine, DIBAL = diisobutylaluminum hydride, Ms = mesyl, DMDO = dimethyldioxirane, Piv = pivaloyl (CO*t*Bu), TBAF = tetrabutylammonium fluoride, TBS = *tert*-butyldimethylsilyl, TPAP = tetra-*n*-propylammonium perruthenate, NMO = *N*-methylmorpholine-*N*-oxide.

formation, leading to **15**.[9] An elegant and little appreciated acid-catalyzed fragmentation of the cyclobutanone[8, 9] exposes a formyl group and a methyl ester; the carbonyl carbon atoms of the product **16** correspond to C2 and C8 of the eleutheside. We have found that 2,5-dibromofuran (**6**) can be monolithiated; the resulting, interesting organolithium compound **7** (Met = Li) can be appended to **16** to give compound **17** and its redeemable C8 epimer, **17a**. Following suitable protection of the hydroxyl group, **18** was obtained.[10] At this point, the one-carbon ester in **18** was expanded to a two-carbon aldehyde (see compound **19**), in which the formyl carbon corresponds to the eventual C3 of the eleuthesides. The critical step leading to the metacyclophane **20** was a remarkable and stereoselective Nozaki – Kishi[11] reaction. The hydroxyl group at the future C3 was protected as its pivaloate ester (cf. **21**).

The groundwork was now secure to move on to construction of the eleutheside skeleton. After removal of the silyl

 © WILEY-VCH Verlag GmbH, D-69451 Weinheim, 1998 1433-7851/98/3701-0186 $ 17.50+.50/0 *Angew. Chem. Int. Ed.* **1998**, *37*, No. 1/2

protecting group, treatment of **22** with dimethyldioxirane generates presumably an epoxide of type **9** (X = H, OPiv; see Scheme 1). Following suitable bond reorganizations, passing through presumed diketone type **10**, the pyranose derivative **23** was in hand. The predicted stereoselective nucleophilic methylation of the keto function was achieved with methyllithium, giving rise to **24**. On treatment of the latter compound with acetic anhydride, we took advantage of the fact that the masked secondary alcohol at C8 could be selectively acetylated. This paved the way for cyclization of the tertiary alcohol (corresponding to C7 of the future eleutheside) into the carbonyl group of the enone of the open form, leading to formation of compound **25**. All structural assignments asserted thus far, were corroborated by an X-ray crystallographic determination of **25** (Figure 1).[12] Compound **25** has been

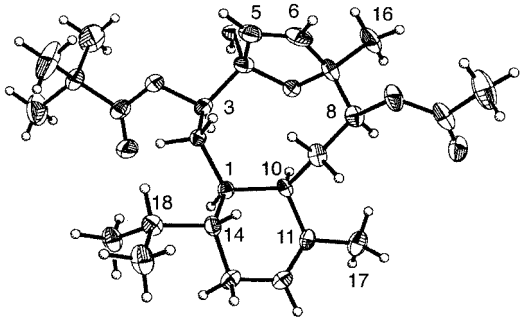


Figure 1. Crystal structure of **25**.

advanced in several directions, including the generation of the flexible platform compound, ketone **26**.

In summary, the novel chemical steps of particular interest are: 1. the elongation and fragmentation of cyclobutanone **14**, 2. the viability of 2-lithio-5-bromofuran as a readily available and functionally differentiated furano nucleophile **7**, 3. the Nozaki–Kishi reaction creating a highly strained cyclophane (**19** → **20**), and 4. the oxidative and ring–chain tautomerism manipulations leading to the differentiated eleutheside **25**. Preparations of the natural products and congeners for SAR purposes are well underway.[13,14]

Received: November 3, 1997 [Z11110IE]
German version: *Angew. Chem.* **1998**, *110*, 195–197

Keywords: antitumor agents · cyclophanes · eleuthesides · natural products · total synthesis

[1] D. J. Faulkner *Nat. Prod. Rep.* **1996**, *13*, 75.
[2] a) W. H. Fenical, P. R. Jensen, T. Lindel (UC), US Patent No. 5473057, **1995** [*Chem. Abstr.* **1996**, *102*, 194297z]; b) T. Lindel, W. H. Fenical, P. R. Jensen, B. H. Long, A. M. Casazza, J. Carboni, C. R. Fairchild, *J. Am. Chem. Soc.* **1997**, *119*, 8744.
[3] a) M. D'Ambrosio, A. Guerriero, F. Pietra, *Helv. Chim. Acta* **1987**, *70*, 2019; b) *ibid.* **1988**, *71*, 964.
[4] a) O. Kennard, D. G. Watson, *Tetrahedron Lett.* **1968**, 2879; b) Y. Lin, C. A. Bowley, D. J. Faulkner, *Tetrahedron* **1993**, *49*, 7977.
[5] D. T. Hung, T. F. Jamison, S. L. Schreiber, *Chem. Biol.* **1996**, *3*, 623.
[6] (*R*)-(−)-α-Phellandrene **4** is available from Fluka Chemical Corp.
[7] For preparation see: M. A. Keegstra, A. J. A. Klomp, L. Brandsma, *Synth. Commun.* **1990**, *20*, 3371. For use see: U. Wellmar, *J. Heterocycl. Chem.* **1995**, *32*, 1159. For 2-iodo-5-(iodomagnesium) furan see: H. Gilman, G. F. Wright, *J. Am. Chem. Soc.* **1933**, *55*, 3302. For 2-bromo-5-lithiothiophene see: M.-J. Shiao, L.-H. Shih, W.-L. Chia, T.-Y. Chau, *Heterocycles* **1991**, *32*, 2111.
[8] For a ketene cycloaddition with a cyclohexadiene see the following: a) M. L. Greenlee, *J. Am. Chem. Soc.* **1981**, *103*, 2425. For a diastereoselective ketene cycloaddition see: A. Kanazawa, P. Delair, M. Pourashraf, A. E. Greene, *J. Chem. Soc. Perkin Trans. 1* **1997**, 1911.
[9] B. M. Trost, M. Preckel, L. M. Leichter, *J. Am. Chem. Soc.* **1975**, *97*, 2224.
[10] Compound **17a** (in contrast to the desired **17**) undergoes partial lactonization during workup. This lactone can be converted back to **17a**. Epimer **17a** can be recycled to the synthetic mainstream by oxidation, followed by reduction of the common ketone. These adjustments to the main synthetic stream will be reported in the full paper.
[11] For a review of the Nozaki–Kishi reaction see: P. Cintas, *Synthesis* **1992**, 248. See also: M. Eckhardt, R. Brückner, *Liebigs Ann.* **1996**, 473.
[12] Crystallographic data (excluding structure factors) for the structures reported in this paper have been deposited with the Cambridge Crystallographic Data Center as supplementary publication no. CCDC-100974. Copies of the data can be obtained free of charge on application to CCDC, 12 Union Road, Cambridge CB2 1EZ (fax: int. code +(44) 1223 336-033; e-mail: deposit@ccdc.cam.ac.uk). No claims, regarding absolute stereochemistry, are based on this data.
[13] Sarcodictyin and eleutherobin were recently synthesized: K. C. Nicolaou, J.-Y. Xu, S. Kim, T. Ohshima, S. Hosokawa, J. Pfefferkorn, *J. Am. Chem. Soc.* **1997**, *119*, 11353; K. C. Nicolaou, F. van Delft, T. Ohshima, D. Vourloumis, J. Xu, S. Hosokawa, J. Pfefferkorn, S. Kim, T. Li, *Angew. Chem.* **1997**, *109*, 2630; *Angew. Chem. Int. Ed. Engl.* **1997**, *36*, 2520.
[14] Note added in proof: We have recently completed a synthesis of eleutherobin: X.-T. Chen, B. Zhou, S. K. Bhattacharya, C. E. Gutteridge, T. R. R. Pettus, S. J. Danishefsky, *Angew. Chem.* and *Angew. Chem. Int. Ed.*, in press.

Total Synthesis of Altohyrtin A (Spongistatin 1): Part 1**

Jiasheng Guo, Kevin J. Duffy, Kirk L. Stevens, Peter I. Dalko, Rebecca M. Roth, Matthew M. Hayward, and Yoshito Kishi*

In 1993 three groups independently reported the isolation and structural elucidation of a new class of macrolides (spongipyran) derived from marine sponges of the genus *Spongia*[1] and *Spirastrella*[2] (spongistatins 1 through 9), *Cinachyra*[3] (cinachyrolide A), and *Hyrtios*[4] (altohyrtins A–C). These compounds displayed extraordinarily potent cytotoxicity against a wide variety of cancer cell lines.[5, 6] Structurally, spongistatin 1 appeared to be identical to altohyrtin A and spongistatin 4 to cinachyrolide A, although no definitive proof had been previously presented. The Kitagawa group has proposed the complete structure of altohyrtin A[4c] to be that shown in structure **1**. However, this structure is in conflict with the relative configuration proposed by the Pettit[2b] and Fusetani[3] groups. In this and the following communication, we report the first total synthesis of altohyr-

[*] Prof. Y. Kishi, Dr. J. Guo, Dr. K. J. Duffy, Dr. K. L. Stevens, Dr. P. I. Dalko, R. M. Roth, Dr. M. M. Hayward
Department of Chemistry and Chemical Biology,
Harvard University
Cambridge, MA 02138 (USA)
Fax: Int. code +(1) 617 495-5150
e-mail: kishi@chemistry.harvard.edu

[**] Financial support from the National Institutes of Health (CA-22215) and Eisai Pharmaceutical Company is gratefully acknowledged, as are postodctoral fellowships from the American Cancer Society (K.L.S.; PF-4423), NATO (P.I.D.; 12B93FR), and the NIH (M.M.H.; 5 F32 CA66299). We thank Dr. Yuan Wang (Eisai Research Institute, Andover, MA, USA) for performing NMR experiments.

 © WILEY-VCH Verlag GmbH, D-69451 Weinheim, 1998 1433-7851/98/3701-0187 $ 17.50+.50/0

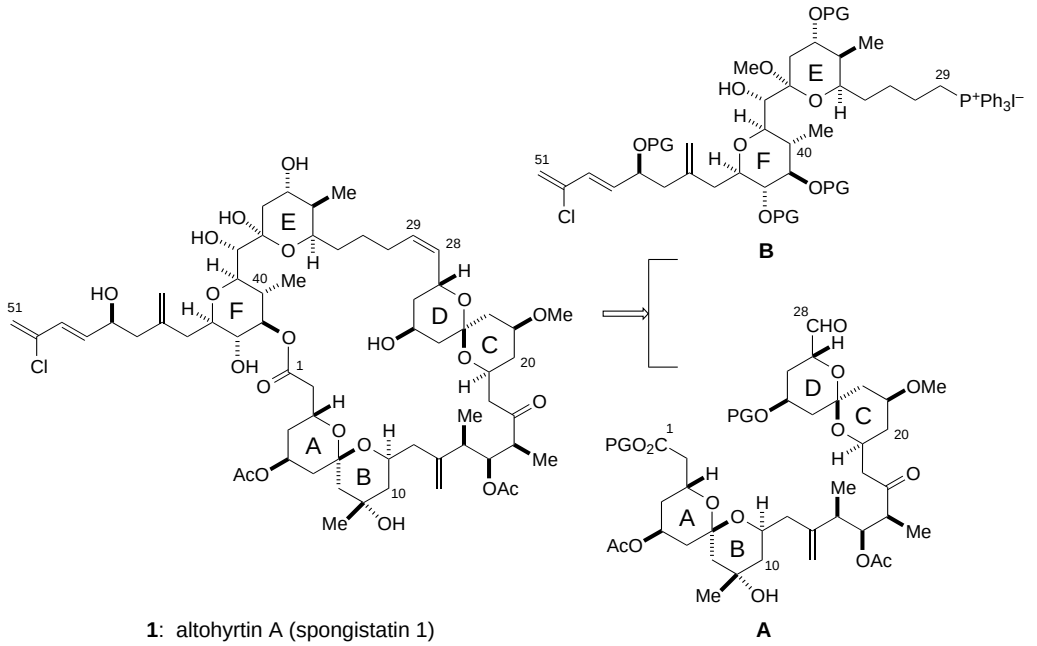


Figure 1. Retrosynthesis of altohyrtin A (spongistatin 1). PG = protecting group.

tin A (spongistatin 1), which firmly establishes the relative and absolute configuration proposed by Kitagawa.

All of the members in this class of natural products contain a 51-carbon chain, 6 pyran rings, and a 42-membered lactone ring. In addition, the most potent congeners (spongistatins 1, 4, 5, and 9)[5, 6] contain the novel chlorodiene functionality, which had neither been seen in a natural product nor synthesized before. We chose altohyrtin A (spongistatin 1) as our synthetic target, due to its historical position in this class of natural products, the availability of spectroscopic data from two independent research groups, and finally its position as the most cytotoxic congener. Several synthetic approaches to the spongipyran class of natural products have been reported,[7] and most recently a beautiful total synthesis of altohyrtin C (spongistatin 2) has been completed by Evans et al.[8]

Upon close examination of the spectroscopic data on spongipyrans disclosed by the three groups, it became evident that the correct relative and absolute configuration of altohyrtin A was most likely that proposed by Kitagawa,[4c] and thus we chose altohyrtin A (**1**) as the target for our total synthesis.[9] In the retrosynthetic analysis, **1** was dissected into the two segments **A** and **B** which could be joined by Wittig olefination of the C29 phosphonium salt with the C28 aldehyde and subsequent macrolactonization of the C1 carboxylic acid with the C41 alcohol (Figure 1). It might be expected that, to effect the proposed macrolactonization selectively, the C41 alcohol must be differentiated from the remaining alcohols, particularly the C42 alcohol. However, we recognized the possibility that such macrolactonization might take place preferentially at the C41 alcohol under controlled conditions. Therefore, we chose to leave the C41 and C42 alcohols undifferentiated for synthetic simplicity.

Based on the precedents gained in the halichondrins[10] and the polyether antibiotic (−)-A23187[11] syntheses, **A** was envisioned to arise from the intramolecular Michael addition of enone **C** (Figure 2). Enone **C** could be realized from the

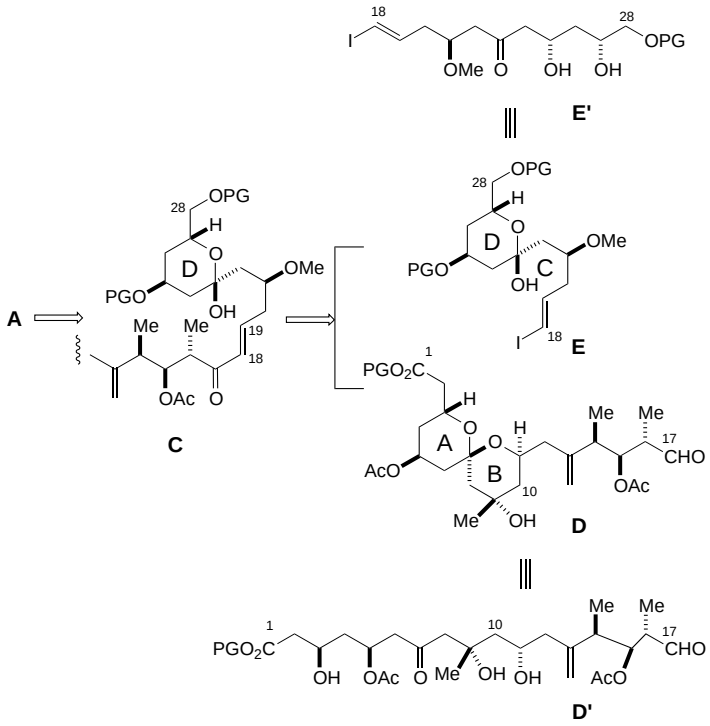


Figure 2. Retrosynthesis of the C1 – C28 fragment.

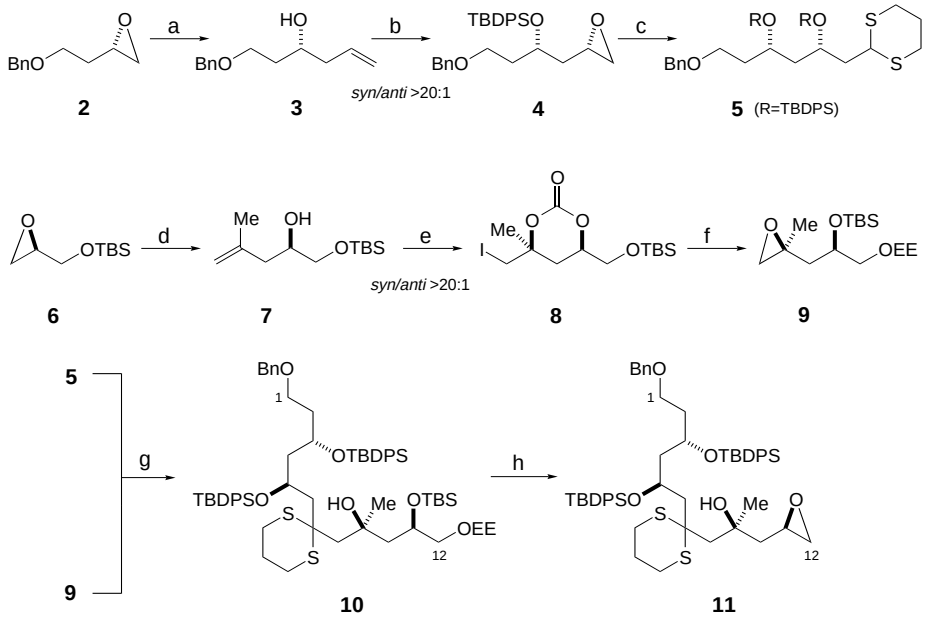
Ni^{II}/Cr^{II}-mediated coupling[12] between fragments **D** and **E**, followed by oxidation. The two building blocks **D** and **E** thus obtained should be synthetically equivalent to their open forms **D′** and **E′**. Two structural characteristics present in both **D′** and **E′** are noteworthy. A typical polypropionate structure is apparent in the C14 – C17 unit, while a 1,3-*syn*-diol structure is found repeatedly in the C3 – C5, C9 – C11, and C25 – C27 units. The synthesis of these functionalities has been studied extensively over the past few decades. We anticipated that, coupled with a well-precedented regioselective ring-opening

 © WILEY-VCH Verlag GmbH, D-69451 Weinheim, 1998 1433-7851/98/3701-0188 $ 17.50+.50/0 *Angew. Chem. Int. Ed.* **1998**, *37*, No. 1/2

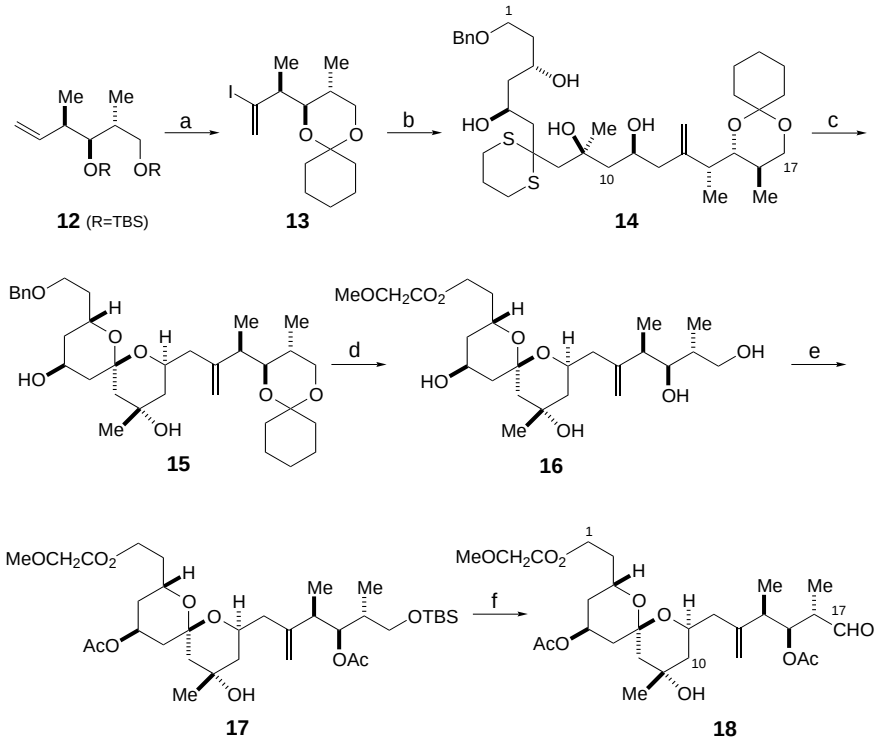
of terminal epoxides with nucleophiles, the synthesis of **D**′ and **E**′ could be achieved by a combination of these methods.

Along this line of analysis, the C1 – C12 segment was synthesized as summarized in Scheme 1.[13, 14] The two key reactions in this sequence were 1) regioselective ring-opening of terminal epoxides with vinyl cuprates and dithiane anions, and 2) stereoselective iodocarbonylation under the conditions developed by Smith et al.,[15] followed by base treatment to furnish the subsequent terminal epoxide.

The C13 – C17 segment **13** was prepared from the known alkene **12**[16] (Scheme 2). The C12 – C13 bond formation was realized by ring opening of **11** with the higher order 2-thienyl



Scheme 1. Synthesis of the C1 – C12 fragment: a) CuCN, vinyllithium, – 78°C, then **2**, – 30 →0°C, 90 %; b) *n*BuLi, Et_2O, – 78°C, BOC–ON, THF, 0 →20°C, 90 %; IBr, PhMe, – 78 →0°C; K_2CO_3, MeOH, 73 % over 2 steps; imidazole, TBDPSCl, CH_2Cl_2, 92 %; c) 1,3-dithiane, *n*BuLi, THF, – 20°C, then – 78°C, DMPU, **4**, THF, – 20°C, 97 %;[30] imidazole, TBDPSCl, CH_2Cl_2, 87 %; d) 2-bromopropene, *t*BuLi, Et_2O, – 78°C, then CuI, **6**, Et_2O, – 78 →0°C, quant.; e) *n*BuLi, Et_2O, – 78°C, BOC–ON, THF, 0 →20°C, 93 %; IBr, PhMe, – 78 →0°C, 93 %; f) HOAc/THF, 81 %; ethyl vinyl ether, CH_2Cl_2, PPTS, 96 %; K_2CO_3, 94 %; imidazole, TBSCl, 87 %; g) *t*BuONa, *n*BuLi, pentane, 0 →20°C,[31] then – 78°C, **5**, then **9**, – 78 → – 20°C, 59 %; h) PPTS, MeOH, 80 %; NaH, THF, 0°C, then Ts-im,[32] 0°C, 93 %.

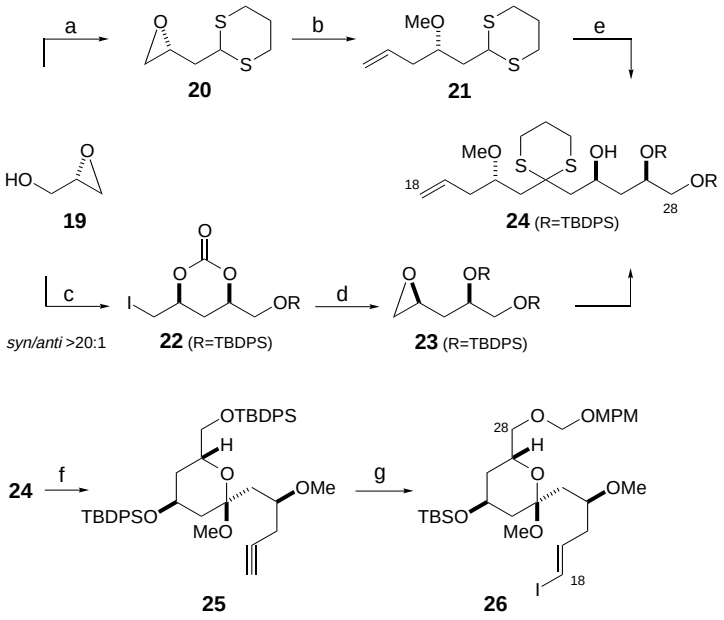


Scheme 2. Synthesis of the C1 – C17 fragment: a) NMO, OsO_4,[33] acetone/H_2O; $Pb(OAc)_4$, benzene, 81 % over 2 steps; DAMP,[34] *t*BuOK, THF, – 78°C, then aldehyde, 96 %; *B*-I-9-BBN,[35] pentane, – 20°C, 88 %; HF · py, CH_3CN, 91 %; 1,1-dimethoxycyclohexane, PPTS, 97 %; b) **13**, *t*BuLi, THF, – 78°C, then lithium 2-thienylcyanocuprate, then **11**, THF, – 78 →0°C, 72 %; TBAF, 0°C, quant.; c) $CaCO_3$, NIS, CH_3CN, 0°C, then PPTS, CH_3CN, 68 %; d) Li/NH_3, THF, – 78°C, quant.; methoxyacetyl chloride, CH_2Cl_2/py, 93 %; PPTS, MeOH, 50°C, 87 %; e) Et_3N, TBSCl, DMAP, CH_2Cl_2, 94 %; py, Ac_2O, DMAP, 96 %; f) HF · py, CH_3CN, 95 %; Dess – Martin periodinane, CH_2Cl_2, 91 %.

 © WILEY-VCH Verlag GmbH, D-69451 Weinheim, 1998 1433-7851/98/3701-0189 $ 17.50+.50/0

cyanocuprate[17] derived from **13**, to yield the diol. After cleavage of the silyl protecting groups, **14** was subjected to NIS-induced dithiane deprotection to form the single spiroketal **15** in good overall yield. Based on literature precedent,[18] we anticipated spiroketal formation to be stereoselective in the desired sense; indeed, NOE experiments (NOE = nuclear Overhauser enhancement) confirmed this configuration at the spirocenter. By routine synthetic operations the protecting groups of alcohols in **15** were then adjusted resulting in tetraol **16**. The protecting groups at the C1 and C17 primary alcohols were differentiated, and the C9 tertiary alcohol was left unprotected. Since the requisite C5 and C15 acetates were compatible with the remaining synthetic operations, they were installed at this juncture.[19] The C15 acetyl group was found to migrate readily to the C17 primary alcohol once the TBS protecting group was removed. Therefore, the C17 alcohol generated from **17** was immediately subjected without purification to Dess–Martin oxidation[20] to furnish aldehyde **18**.

Scheme 3 summarizes the synthesis of the *trans* vinyl iodide **26**.[21] The key reactions used in this sequence were fundamentally the same as those described for the synthesis of the C1–C17 segment. However, several comments are in order.



Scheme 3. Synthesis of the C18–C28 fragment: a) Et_3N, TBSCl, DMAP, CH_2Cl_2, 90%; 1,3-dithiane, *n*BuLi, THF, −20°C, then DMPU, then epoxide, THF, −78 → −20°C, 83%; TBAF, THF, quant.; NaH, THF, 0°C, Ts-im, 0°C, 79%; b) CuCN, vinyllithium, −78°C, then **20**, THF, −20 → 0°C, 85%; NaH, MeI, THF, 0°C, 90%; c) Et_3N, TBDPSCl, DMAP, CH_2Cl_2, 90%; CuCN, vinyllithium, −78°C, then epoxide, Et_2O, −30 → 0°C, 92%; *n*BuLi, Et_2O, BOC–ON, THF, −78 → 20°C, 96%; IBr, PhMe, −78 → 0°C, 78%; d) K_2CO_3, MeOH, 78%; imidazole, TBDPSCl, CH_2Cl_2, 91%; e) *t*BuONa, *n*BuLi, pentane, 0 → 20°C, then −78°C, **21**, THF, −78°C, then **23**, THF, −78 → −20°C, 54% and 44% recovered **23**; f) TBAF, THF, 0°C, 92%; Et_3N, TBDPSCl, DMAP, CH_2Cl_2, 72%; NIS, $CaCO_3$, MeOH, 0°C, 78%; imidazole, TBDPSCl, CH_2Cl_2, 86%; NMO, OsO_4, acetone/H_2O; $NaIO_4$, MeOH/(pH 7 phosphate buffer), 0 → 20°C; DAMP, *t*BuOK, THF, −78°C, then aldehyde, THF, −78°C, 79% over 3 steps; g) nBu_3SnH, AIBN, toluene, 105°C, 67%; $CaCO_3$, NIS, THF, quant.; TBAF, THF, 92%; iPr_2NEt, $MPMOCH_2Cl$,[36] CH_2Cl_2, 98%; TBAF, THF, quant.; imidazole, TBSCl, CH_2Cl_2, 99%.

First, while ring-opening of **20** was accomplished with the anion of TMS-acetylene allowing earlier incorporation of the alkyne moiety, clean lithiation of the resultant dithiane proved difficult. Second, deprotection of the dithiane group (step f) resulted in a single methyl ketal, whose configuration was tentatively assigned as indicated but was not established experimentally. Third, the hydrostannylation of **25**, followed by NIS treatment, yielded mainly the expected product, along with a small amount of its regio- and stereoisomers. Finally, the C25 TBDPS protecting group was required for efficient synthesis of **25** but the final deprotection to form altohyrtin A (**1**) necessitated substitution to the more labile TBS protecting group.

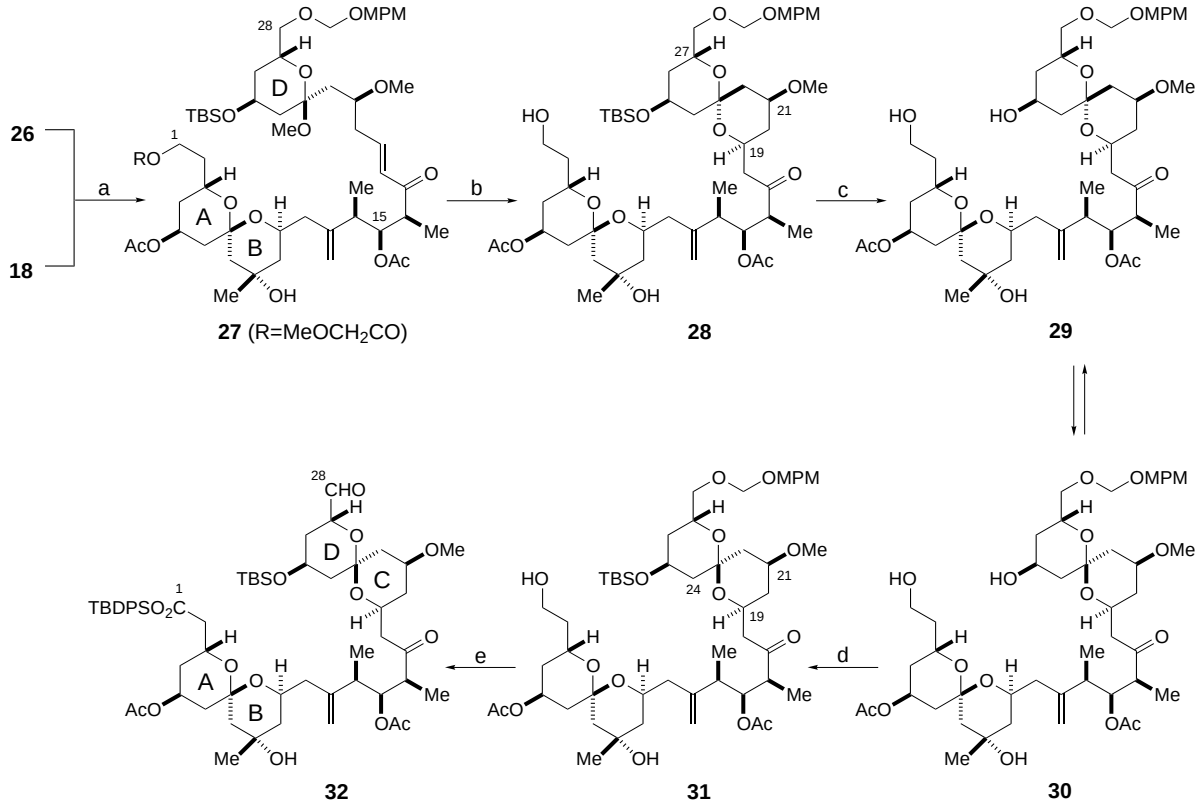
The completion of the synthesis of **32** is illustrated in Scheme 4. The Ni^{II}/Cr^{II}-mediated coupling[12] of **26** with **18** proceeded smoothly to yield the two expected allylic alcohols, which were oxidized to α,β-unsaturated ketone **27**. After hydrolysis to the C23 hemiketal, the crucial intramolecular Michael cyclization was effected with Triton-B to furnish spiroketal **28** with concomitant deprotection of the C1 methoxyacetate.[22] Out of four possible products, only one diastereomer was isolated. ROESY data on the C1 TBS ether of **28** clearly demonstrated the C19 stereocenter to be desired but the C23 spirostereocenter to be undesired.[23, 24] In light of recent work by Heathcock,[7b] the stereochemical outcome at this spirocenter was not surprising. This stereocenter was configurationally stable under acidic conditions with a protected C25 alcohol, but was expected to epimerize readily if the C25 alcohol was deprotected.[7b] Indeed, deprotection of **28** with HF · py in CH_3CN provided a separable 1:1 mixture of desired C23 diastereomer **30** and undesired **29**, which could be recycled efficiently under acidic conditions (HF · py/CH_3CN or CSA/CH_2Cl_2). Reprotection of the C1 and C25 alcohols with TBSOTf proceeded without compromising the integrity of C23 spiroketal stereocenter.

NMR (NOE) data on the C1 TBS-ether of **31** clearly demonstrated the desired configurations at C19 and C23.[23,24] Selective deprotection of the C1 TBS group, followed by TPAP[25] oxidation, $NaClO_2$[26] oxidation, TBDPSCl protection,[27] and finally cleavage of the C28 protecting group with DDQ[28] furnished the desired product. Interestingly, a small amount of the C23 epimeric spiroketal was isolated during the DDQ deprotection step. Finally, Dess–Martin oxidation of the C28 primary alcohol furnished **32**, the ABCD unit of the target.

Using the methods disclosed in the following communication, we completed the total synthesis of the C23 epimer of altohyrtin A from intermediate **28** with the hope that the C23 stereocenter might be equilibrated to the natural configuration. Although both altohyrtin A and its C23 epimer were relatively stable under acidic conditions (HF · py/THF, CSA/CH_2Cl_2, or HCl/$CHCl_3$), there was no evidence of inversion at the C23 stereocenter.[29] This experiment demonstrated that the macrolactone prevents epimerization at the C23 position, suggesting that the correct C23 configuration must be installed prior to macrolactonization.

Received: November 17, 1997 [Z11165IE]
German version: *Angew. Chem.* **1998**, *110*, 198–202

 © WILEY-VCH Verlag GmbH, D-69451 Weinheim, 1998 1433-7851/98/3701-0190 $ 17.50+.50/0



Scheme 4. Synthesis of the C1 – C28 fragment: a) $NiCl_2/CrCl_2$, (–)-bispyridinyl ligand,[12c] THF, 86 %; Dess – Martin periodinane, py, CH_2Cl_2, 83 %; b) PPTS, acetone/H_2O; Triton-B, MeOH/ MeOAc, 0 °C, 50 % over 2 steps; c) HF · py, CH_3CN, 25 % (an additional 25 % was obtained by equilibration of the C23 epimer **29** with CSA/CH_2Cl_2); d) 2,6-lutidine, TBSOTf, –78 °C, 79 %; HF · py/py/THF, 82 %; e) TPAP, NMO, 4 Å molecular sieves, CH_2Cl_2; $NaClO_2$, NaH_2PO_4, *t*BuOH/2-methyl-2-butene, 83 % over 2 steps; Et_3N, TBDPSCl, CH_2Cl_2, 82 %; DDQ, CH_2Cl_2/H_2O, 53 %; Dess – Martin periodinane, py, CH_2Cl_2, 81 %.

Keywords: altohyrtin · antitumor agents · natural products · spongistatin · total synthesis

[1] a) G. R. Pettit, Z. A. Cichacz, F. Gao, C. L. Herald, M. R. Boyd, J. M. Schmidt, J. N. A. Hooper, *J. Org. Chem.* **1993**, *58*, 1302 – 1304; b) G. R. Pettit, Z. A. Cichacz, F. Gao, C. L. Herald, M. R. Boyd, *J. Chem. Soc. Chem. Commun.* **1993**, 1166 – 1168.

[2] a) G. R. Pettit, C. L. Herald, Z. A. Cichacz, F. Gao, J. M. Schmidt, M. R. Boyd, N. D. Christie, F. E. Boettner, *J. Chem. Soc. Chem. Commun.* **1993**, 1805 – 1807; b) G. R. Pettit, C. L. Herald, Z. A. Cichacz, F. Gao, M. R. Boyd, N. D. Christie, J. M. Schmidt, *Nat. Prod. Lett.* **1993**, *3*, 239 – 244; c) G. R. Pettit, Z. A. Cichacz, C. L. Herald, F. Gao, M. R. Boyd, J. M. Schmidt, E. Hamel, R. Bai, *J. Chem. Soc. Chem. Commun.* **1994**, 1605 – 1606.

[3] N. Fusetani, K. Shinoda, S. Matsunaga, *J. Am. Chem. Soc.* **1993**, *115*, 3977 – 3981.

[4] a) M. Kobayashi, S. Aoki, H. Sakai, K. Kawazoe, N. Kihara, T. Sasaki, I. Kitagawa, *Tetrahedron Lett.* **1993**, *34*, 2795 – 2798; b) M. Kobayashi, S. Aoki, H. Sakai, N. Kihara, T. Sasaki, I. Kitagawa, *Chem. Pharm. Bull.* **1993**, *41*, 989 – 991; c) M. Kobayashi, S. Aoki, I. Kitagawa, *Tetrahedron Lett.* **1994**, *35,* 1243 – 1246; d) M. Kobayashi, S. Aoki, K. Gato, I. Kitagawa, *Chem. Pharm. Bull.* **1996**, *44*, 2142 – 2149.

[5] G. R. Pettit, *Pure Appl. Chem.* **1994**, *66*, 2271-2281.

[6] The spongistatins were shown to exhibit potent antimitotic activity resulting from strong tubulin binding: R. Bai, G. F. Taylor, Z. A. Cichacz, C. L. Herald, J. A. Kepler, G. R. Pettit, E. Hamel, *Biochemistry* **1995**, *34*, 9714 – 9721.

[7] a) M. M. Claffey, C. H. Heathcock, *J. Org. Chem.* **1996**, *61*, 7646 – 7647; b) C. J. Hayes, C. H. Heathcock, *ibid.* **1997**, *62*, 2678 – 2679; c) I. Paterson, R. M. Oballa, R. D. Norcross, *Tetrahedron Lett.* **1996**, *37*, 8581 – 8584; d) I. Paterson, L. E. Keown, *ibid.* **1997**, *38*, 5727 – 5730; e) L. Paterson, D. J. Wallace, K. R. Gibson, *ibid.* **1997**, *38*, 8911 – 8914; f) L. A. Paquette, D. Zuev, *ibid.* **1997**, *38*, 5115 – 5118; g) L. A. Paquette, A. Braun, *ibid.* **1997**, *38*, 5119 – 5122, h) A. B. Smith, Q. Lin, K. Nakayama, A. M. Boldi, C. S. Brook, M. D. McBriar, W. H. Moser, M. Sobukawa, L. Zhuang, *ibid.* **1997**, *38*, 8675 – 8678, and references therein.

[8] D. A. Evans, B. W. Trotter, B. Côté, P. J. Coleman, L. C. Dias, A. N. Tyler, *Angew. Chem.* **1997**, *109*, 2957 – 2961; *Angew. Chem. Int. Ed. Engl.* **1997**, *36*, 2744 – 2747.

[9] For this reason, we adopted the use of the name altohyrtin A in this paper. As discussed in the following paper, altohyrtin A is identical to spongistatin 1.

[10] T. D. Aicher, K. R. Buszek, F. G. Fang, C. J. Forsyth, S. H. Jung, Y. Kishi, M. C. Matelich, P. M. Scola, D. M. Spero, S. K. Yoon, *J. Am. Chem. Soc.* **1992**, *114*, 3162 – 3164.

[11] D. P. Negri, Y. Kishi, *Tetrahedron Lett.* **1987**, *28,* 1063-1066.

[12] a) H. Jin, J.-i. Uenishi, W. J. Christ, Y. Kishi, *J. Am. Chem. Soc.* **1986**, *108,* 5644 – 5646; b) K. Takai, M. Tagashira, T. Kuroda, K. Oshima, K. Utimoto, H. Nozaki, *ibid.* **1986**, *108,* 6048 – 6050; c) C. Chen, K. Tagami, Y. Kishi, *J. Org. Chem.* **1995**, *60*, 5386 – 5387, and references therein.

[13] Satisfactory spectroscopic data (^1H and ^{13}C NMR, MS, and others) were obtained for all new compounds.

[14] Abbreviations used: AIBN = 2,2′-azobisisobutyronitrile; BOC-ON = 2-(*tert*-butoxycarbonyloxyimino)-2-phenylacetonitrile; CSA = 10-camphorsulfonic acid; DAMP = dimethyl(diazomethyl)phosphonate; DDQ = 2,3-dichloro-5,6-dicyano-1,4-benzoquinone; diketene acetone adduct = 2,2,6-trimethyl-4*H*-1,3-dioxan-4-one; DMAP = 4-dimethylaminopyridine; DMDO = dimethyldioxirane; DMPU = 1,3-dimethyl-3,4,5,6-tetrahydro-2(1*H*)-pyrimidinone; HMPA = hexamethylphosphoramide; HF · py = hydrogen fluoride pyridine complex; *B*-I-9-BBN = *B*-iodo-9-borabicyclo[3.3.1]nonane; LDA = lithium diisopropylamide; MPM = *para*-methoxybenzyl; MsCl = methanesulfonyl

 © WILEY-VCH Verlag GmbH, D-69451 Weinheim, 1998 1433-7851/98/3701-0191 $ 17.50+.50/0

chloride; NCS = *N*-chlorosuccinimide; NIS = *N*-iodosuccinimide; NMO = *N*-methylmorpholine *N*-oxide; Piv = pivaloyl; PPTS = pyridinium *p*-toluenesulphonate; TBAF = tetrabutylammonium fluoride; TBAI = tetrabutylammonium iodide; TBDPS = *tert*-butyldiphenylsilyl; TBS = *tert*-butyldimethylsilyl; Tf = triflate; TIPS = triisopropylsilyl; TPAP = tetrapropylammonium perruthenate; Ts-im = *para*-toluenesulphonyl imidazole; Ts_2O = *para*-toluenesulfonic anhydride.

[15] J. J.-W. Duan, A. B. Smith III, *J. Org. Chem.* **1993**, *58*, 3703 – 3711.

[16] J. B. Nerenberg, D. T. Hung, P. K. Somers, S. L. Schreiber, *J. Am. Chem. Soc.* **1993**, *115*, 12621 – 12622.

[17] B. H. Lipshutz, M. Koerner, D. A. Parker, *Tetrahedron Lett.* **1987**, *28*, 945 – 948.

[18] P. Deslongchamps, *Stereoelectronic Effects in Organic Chemistry*, Pergamon, Oxford, **1983**, Chap. 1.

[19] Careful planning of the protecting group sequence allowed incorporation of an acetate on both the C5 and C15 alcohols (spongistatin 1) or only on the C5 alcohol (spongistatin 4). Protection of the C9 tertiary alcohol was also possible with silyl groups.

[20] D. B. Dess, J. C. Martin, *J. Org. Chem.* **1983**, *48*, 4155 – 4156.

[21] The *cis* vinyl iodide corresponding to **26** might be suitable for the following key Michael cyclization, though this was not tested.

[22] The yields (50% to 80%) for the hydrolysis and subsequent Michael addition depended on the protecting group arrangement. A substrate bearing TBS groups on the C5, C9, and C15 alcohols and TBDPS on the C25 alcohol gave the best result. One of the by-products isolated in the case of **27** was the α,β-unsaturated ketone resulting from elimination of the C15 acetate.

[23] These experiments were performed by Dr. Yuan Wang at Eisai Research Institute, Andover, Massachussetts.

[24] For the C1 TBS ether of **28**, distinct NOEs between the C19 and C21 protons and between the C27 and C22(eq) protons were observed. For the C1 TBS ether of **31**, distinct NOEs between the C19 and C21 protons and between the C19 and C24(eq) protons were observed.

[25] a) W. P. Griffith, S. V. Ley, G. P. Whitcombe, A. D. White, *J. Chem. Soc. Chem. Commun.* **1987**, 1625 – 1627; b) S. V. Ley, J. Norman, W. P. Griffith, S. P. Marsden, *Synthesis* **1994**, 639 – 666.

[26] G. A. Kraus, M. J. Taschner, *J. Org. Chem.* **1980**, *45*, 1175 – 1176.

[27] The Wittig reaction was also studied with the aldehyde bearing the unprotected carboxylic acid at C1; the olefination did yield the desired product but in much poorer yield.

[28] K. Horita, T. Yoshioka, T. Tanaka, Y. Oikawa, O. Yonemitsu, *Tetrahedron* **1986**, *42*, 3021 – 3028.

[29] The most diagnostic ^{1}H NMR signals to distinguish altohyrtin A and its C23 epimer were the C28 – C29 olefinic protons; these signals in altohyrtin A were observed at $\delta = 5.36$ and 5.35 ([D_6]DMSO), whereas those in the C23 epimer were at $\delta = 5.80$ and 5.37.

[30] a) T. Mukhopadhyay, D. Seebach, *Helv. Chim. Acta* **1982**, *65*, 385 – 391; b) B. H. Lipshutz, H. Kotsuki, W. Lew, *Tetrahedron Lett.* **1986**, *27*, 4825 – 4828.

[31] B. H. Lipshutz, E. Garcia, *Tetrahedron Lett.* **1990**, *31*, 7261 – 7264.

[32] D. R. Hicks, B. Fraser-Reid, *Synthesis* **1974**, 203.

[33] V. VanRheenen, R. C. Kelly, D. Y. Cha, *Tetrahedron Lett.* **1976**, *23*, 1973 – 1976.

[34] a) D. Seyferth, R. S. Marmor, P. Hilbert, *J. Org. Chem.* **1971**, *36*, 1379 – 1386; b) J. C. Gilbert, V. Weerasooriya, *ibid.* **1982**, *47*, 1837 – 1845; c) For a more convenient preparation of the DAMP reagent, see: D. G. Brown, E. J. Velthuisen, J. R. Commerford, R. G. Brisbois, T. R. Hoye, *ibid.* **1996**, *61*, 2540 – 2541.

[35] S. Hara, H. Dojo, S. Takinami, A. Suzuki, *Tetrahedron Lett.* **1983**, *24*, 731 – 734.

[36] A. P. Kozikowski, J.-P. Wu, *Tetrahedron Lett.* **1987**, *28*, 5125 – 5128.

Total Synthesis of Altohyrtin A (Spongistatin 1): Part 2**

Matthew M. Hayward, Rebecca M. Roth, Kevin J. Duffy, Peter I. Dalko, Kirk L. Stevens, Jiasheng Guo, and Yoshito Kishi*

In the preceding communication we reported the synthesis of the ABCD unit of altohyrtin A.[1] We will now present the synthesis of the EF unit and the completion of a total synthesis of altohyrtin A.

The first step in the retrosynthetic analysis of EF fragment **B** was the C37 – C38 bond disconnection. In the synthetic direction, it was expected that this bond formation could be realized by nucleophilic addition of glycal carbanion **F** to C38 aldehyde **G**, followed by acid-catalyzed methanolysis of the resultant glycal. Fragment **G** was then disconnected into carbanion **I** and glycal epoxide **H**, which should be available from the corresponding glycal **J**.[2] We were particularly interested in this disconnection strategy because of the obvious structural similarity between **F** and **J**; **F** and **J** might be synthesized with similar chemistry or even via a common intermediate. These glycals could be prepared from the corresponding acyclic precursors **F′** and **J′**, which contain a typical polypropionate/acetate arrangement of functional groups. Among the many synthetic methods known for the preparation of polypropionates/acetates, the chemistry developed by Roush et al.[3] and by Brown et al.[4] were chosen. The proposed carbanion **I**, or its synthetic precursor, contained the novel chlorodiene functionality which, to the best of our knowledge, had never been synthesized before. It was anticipated that the chlorodiene moiety could be incorporated by the addition of an organometallic species, derived from 2,3-dichloropropene, to aldehyde **L**, followed by dehydration.

As illustrated in Scheme 1, the E-ring building block was synthesized by utilizing sequential crotyl- and allyl-boronate chemistry.[5, 6] While both the Brown and Roush methods gave the desired adducts, the Brown methodology was superior in terms of stereoselectivity. After protection of the C35 alcohol of **5** and cleavage of the C33 benzyl protecting group, **6** was transformed into glycal **7** by means of a β-ketoester to facilitate the thermally induced elimination. Finally, glycal **7** was converted into iodoglycal **8** with the method developed by Freisen;[7] the TIPS protecting groups at C29 and C35 were required for clean lithiation of the glycal. Alternatively, **6** was

[*] Prof. Y. Kishi, Dr. M. M. Hayward, R. M. Roth, Dr. K. J. Duffy, Dr. P. I. Dalko, Dr. K. L. Stevens, Dr. J. Guo
Department of Chemistry and Chemical Biology
Harvard University
Cambridge, MA 02138 (USA)
Fax: Int. code + (1) 617 495-5150
e-mail: kishi@chemistry.harvard.edu

[**] Financial support from the National Institutes of Health (CA-22215) and Eisai Pharmaceutical Company is gratefully acknowledged. For postdoctoral fellowships we thank the NIH (MMH; 5 F32 CA66299), NATO (PID; 12B93FR) and the American Cancer Society (KLS; PF-4423). We would like to thank Professor Motomasa Kobayashi for providing an authentic sample of altohyrtin A. We thank Dr. Yuan Wang and Dr. Bruce A. Littlefield (Eisai Research Institute, Andover, MA, USA) for performing NMR experiments and bioassays, respectively.

 © WILEY-VCH Verlag GmbH, D-69451 Weinheim, 1998 1433-7851/98/3701-0192 $ 17.50+.50/0

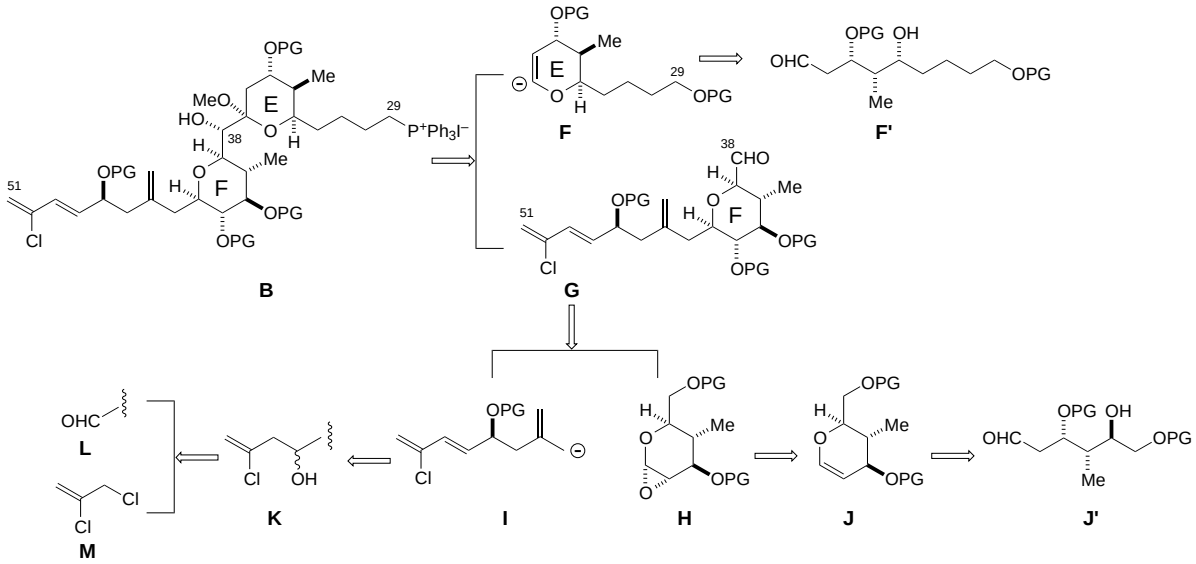
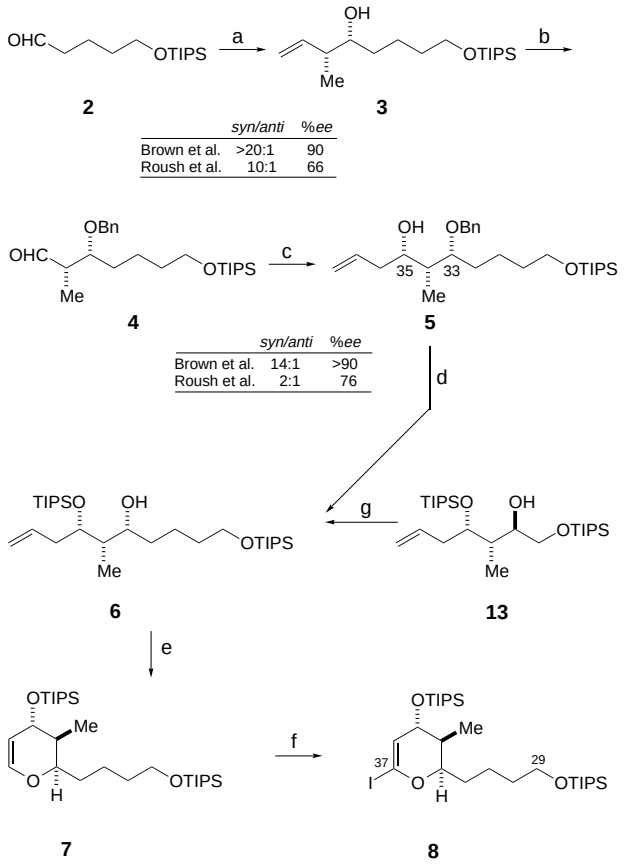


Figure. 1. Retrosynthesis of the C29 – C51 fragment (EF unit). PG = protecting group.



Scheme 1. Synthesis of the C29 – C37 fragment: a) (−)-Ipc$_2$-(*Z*)-crotyl boronate,[4b] THF, −78°C, 65%; b) NaH, BnBr, TBAI, THF, 0→20°C, 97%; NMO, OsO_4, THF/H_2O; $NaIO_4$, MeOH/H_2O, 0→20°C; c) (−)-Ipc$_2$-allyl boronate,[4a] PhMe, −78°C, 64% over 3 steps; d) 2,6-lutidine, TIPSOTf, CH_2Cl_2, 0→20°C; Li/NH_3, THF, −78°C, 81% over 2 steps; e) NMO, OsO_4, THF/H_2O; $NaIO_4$, MeOH/H_2O, 0→20°C; Et_3N, diketene acetone adduct, hexanes, 70°C; 125°C, 0.2 Torr, 54% over 4 steps; f) *t*BuLi, THF, −78→−30°C, then Bu_3SnCl, −78→20°C; K_2CO_3, NIS, THF, 0°C, 75% over 2 steps; g) Et_3N, MsCl, Et_2O; HF·py/py/THF, 61% over 2 steps (an additional 15% was obtained by recycling the bis-silylated starting material once); KOH, MeOH, 92%; sulfone,[30] *n*BuLi, −78→20°C, 87%; Li/NH_3, THF, −78°C, 85%.

also obtained from intermediate **13**, used in the F-ring synthesis (Scheme 2).

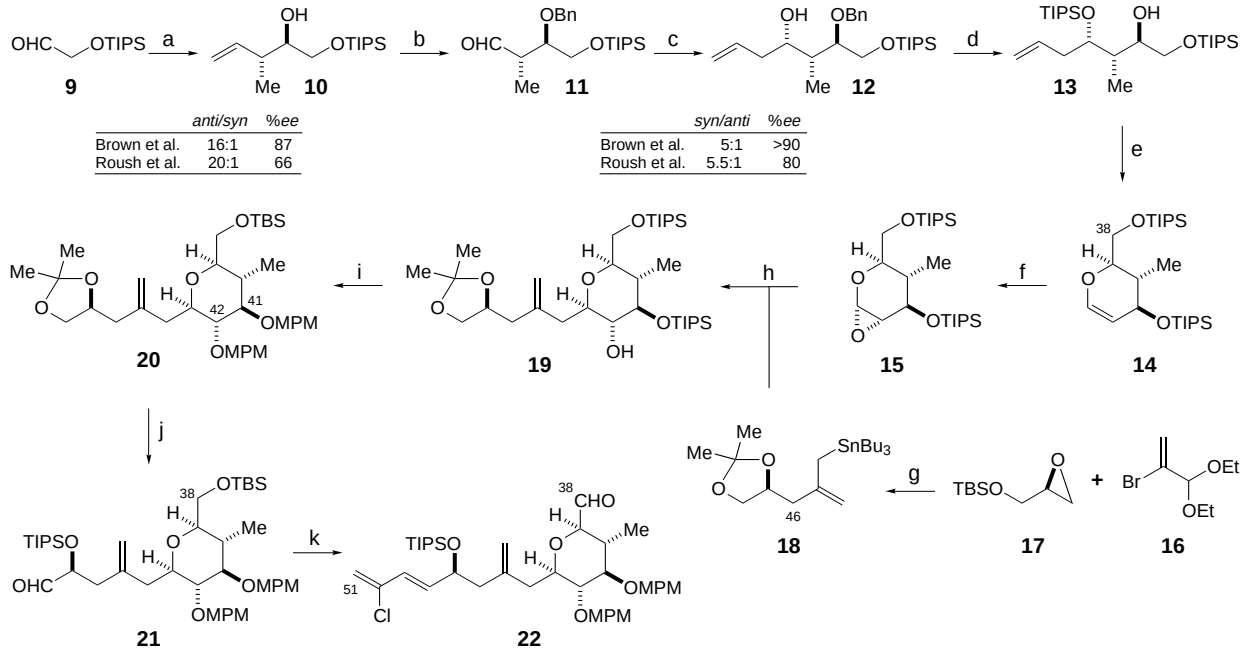
The same methods were used to construct the F-ring building block **14**. The TIPS protecting groups for the C38 and C41 alcohol in glycal **14** enhanced the stereoselectivity of epoxidation with DMDO;[2] only epoxide **15** was detected by ^{1}H NMR.

The synthesis of C44 – C48 segment **18** is also included in Scheme 2.[8] The C45 – C46 bond was formed by cuprate coupling between α-bromoacrolein diethyl ketal **16**[9] and (*R*)-TBS-glycidol **17** to afford the homoallylic alcohol. Acid treatment in acetone allowed concomitant deprotection of the TBS ether, formation of the acetonide, and hydrolysis of the acetal to form the α,β-unsaturated aldehyde, which was transformed into the allylstannane **18** in three steps.

Simple alkyl cuprate addition to a glycal epoxide was first reported by this group.[10] The present case required the addition of a highly functionalized allylic derivative. Although methallyl cuprates readily added to **15**, allyl cuprates bearing the C47 and C48 functionalities exhibited greatly diminished reactivity towards epoxide **15**. Among a variety of allylstannanes prepared and tested, only acetonide allylstannane **18** gave satisfactory results. While an excess of **18** was required to drive the reaction to completion, it was readily recovered from the crude reaction mixture. In this fashion, **19** was obtained in good yield with high stereoselectivity. As noted previously,[1] the C41 and C42 alcohols were masked with identical protecting groups followed by manipulation at C47 and C48 to allow for oxidation to aldehyde **21**.

Although no methodology existed to install the chlorodiene, it was known that allylindium species prepared from allylic halides react with aldehydes under mild conditions.[11] Coupling of the allylindium reagent derived from 2,3-dichloropropene[12] with aldehyde **21** cleanly afforded the two homoallylic alcohols, which were then dehydrated with Martin's sulfurane[13] to afford exclusively the *trans*-chlorodiene in high overall yield. Cleavage of the C38 TBS protecting group, followed by Swern oxidation of the primary alcohol, furnished aldehyde **22**.

 © WILEY-VCH Verlag GmbH, D-69451 Weinheim, 1998 1433-7851/98/3701-0193 $ 17.50+.50/0



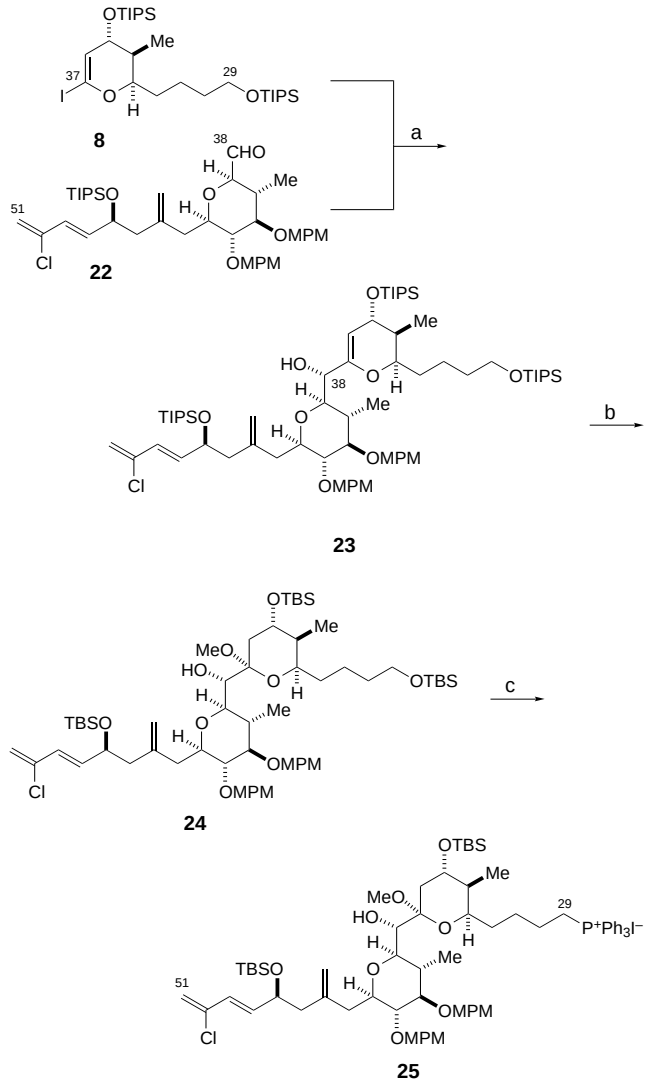
Scheme 2. Synthesis of the C38–C51 fragment: a) (*S*,*S*)-diisopropyl-(*E*)-crotyl boronate,[3b] PhMe, −78°C, 80%; b) NaH, BnBr, TBAI, THF, 0→20°C, 84%; NMO, OsO_4, THF/H_2O; $NaIO_4$, MeOH/H_2O, 0→20°C; c) (*R*,*R*)-diisopropyl-allyl boronate,[3a] PhMe, −78°C, 74% over 3 steps; d) 2,6-lutidine, TIPSOTf, CH_2Cl_2, 0→20°C; Li/NH_3, THF, −78°C, 80% over 2 steps; e) NMO, OsO_4, THF/H_2O; $NaIO_4$, MeOH/H_2O, 0→20°C; Et_3N, diketene acetone adduct, hexanes, 70°C; 125°C, 0.2 Torr, 61% over 4 steps; f) DMDO,[31] CH_2Cl_2/acetone, −10°C, quant.; g) **16**, *n*BuLi, Et_2O, −78°C, then CuI, Et_2O, −78°C, then **17**, −78→20°C, 65%; TsOH·H_2O, acetone, 64%; $CeCl_3 \cdot H_2O$, CH_2Cl_2/MeOH, then −78°C, $NaBH_4$, 83%; Ph_3P, NCS, CH_2Cl_2, 0°C, 95%; Bu_3SnLi,[32] THF, −78°C, 81%; h) $Me_2Cu(CN)Li_2$, **18**, 0°C, then **15**, −43→−15°C, 70%;[33] i) TBAF, THF, quant.; TBSCl, DMAP, CH_2Cl_2/Et_3N, 91%; KH, MPMCl, DMF/THF, 0→20°C, 81%; j) $ZnBr_2$, H_2O, CH_2Cl_2, 56% and an additonal 5% on resubmission of recovered starting material; PivCl, DMAP, CH_2Cl_2/py, 80%; 2,6-lutidine, TIPSOTf, CH_2Cl_2, 91%; LAH, THF, −78°C, 61% and an additonal 6% on resubmission of recovered starting material; oxalyl chloride, DMSO, CH_2Cl_2, −78°C, Et_3N, −78→0°C, 95%; k) In, 2,3-dichloropropene, NaI, DMF, then **21**; Martin's sulfurane, CH_2Cl_2, 85% over 2 steps; HF·py/py/THF, 76% and an additonal 10% on resubmission of recovered starting material; oxalyl chloride, DMSO, CH_2Cl_2, −78°C, 10 min, alcohol, Et_3N, −78→0°C, 89%.

The crucial coupling of the E- and F-ring building blocks (Scheme 3) was envisioned to arise from the addition of an E-ring nucleophile to the highly functionalized aldehyde **22**. Studies on model compounds suggested the importance of a chelation-controlled addition to obtain the desired configuration at C38.[14] Thus, the novel Grignard reagent was prepared by treatment of **8** with *tert*-butyllithium, followed by addition of magnesium dibromide, and was coupled with aldehyde **22** to furnish the desired alcohol **23** in excellent yield and with high stereoselectivity.[15] Attempts to form the methyl ketal directly from glycal **23** by addition of acidic methanol resulted in undesired Ferrier-type rearrangements. However, a two step procedure involving iodomethanolysis[16] and reductive dehalogenation gave a satisfactory result. Addition of bromobenzene allowed for selective reduction of the alkyl iodide in the presence of the chlorodiene. The configuration of the C38 alcohol was established by modified Mosher ester analysis on the methyl ketal of **23**.[17, 18] The TIPS protecting groups at C29, C35, C47 were switched to the more labile TBS groups at this stage.[19] After selective cleavage of the primary C29 TBS group, **24** was converted into phosphonium salt **25**. The methyl ketal present at C37 was prone to elimination to form the corresponding glycal under thermal and acidic conditions. This side reaction was significantly suppressed by addition of methanol.

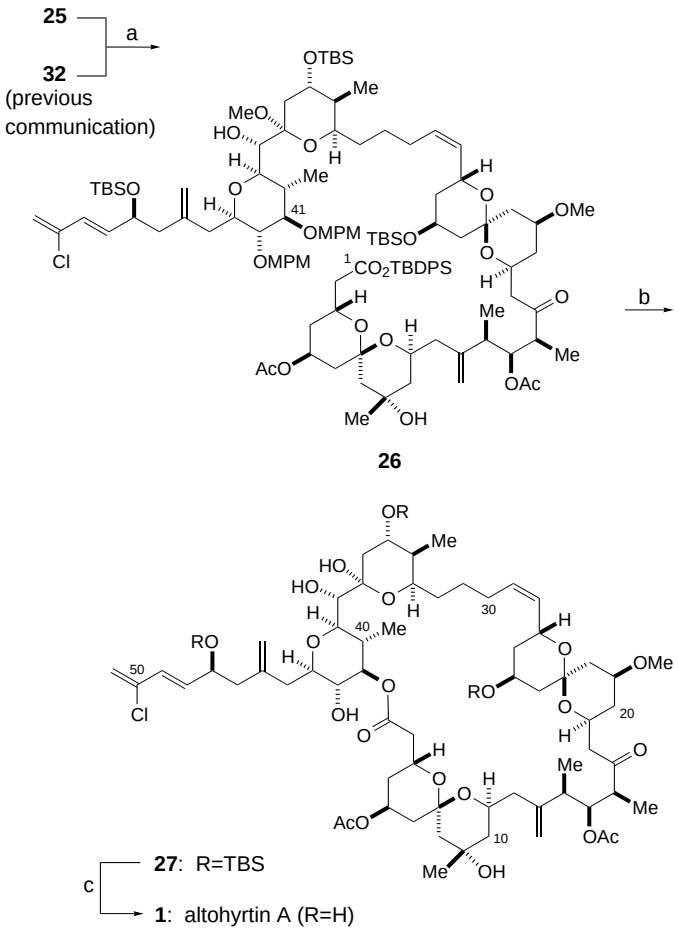
As shown in Scheme 4, **25** and **32** (synthesis described in the preceding communication) were coupled by utilizing a titration protocol[20] for Wittig olefination to afford the *cis*-olefin **26** ($J_{H28,H29} = 10.0$ Hz). DDQ cleavage[21] of the C41 and C42 MPM protecting groups occurred with concomitant, but incomplete, hydrolysis of the methyl ketal. Fluoride induced removal of the silyl ester and macrolactonization under the Yamaguchi conditions[22] proceeded smoothly to furnish the desired macrolactone **27**. As anticipated,[1] macrolactonization occurred selectively at the C41 alcohol.[23] At this stage the unhydrolyzed C37 methyl ketal could be separated from the lactol.[24] Finally, cleavage of the three TBS protecting groups in **27** furnished synthetic altohyrtin A (or spongistatin 1; **1**).[25] The synthetic material was found to be identical (^{1}H NMR in [D_6]DMSO and CD_3CN, MS, $[\alpha]_D$, TLC) with the authentic sample kindly provided by Professor Motomasa Kobayashi at Osaka University. In addition, the synthetic and natural materials exhibited the same biological activity.[26,27] It is exciting and intriguing to note that the C23 epimer of alothyrtin A[1] also exhibits potent cytotoxicty.[26, 27]

In summary, this synthesis has firmly established the relative and absolute configuration proposed for altohyrtin A by the Kitagawa group. To the best of our knowledge, there has been no direct comparison of altohyrtin A and spongistatin 1. However, comparison of the ^{1}H NMR spectra for both authentic and synthetic altohyrtin A with the spectrum (CD_3CN) of spongistatin 1 deposited in the supplementary material by Pettit[28] presents a convincing case that they are indeed the same compound. Thus, this work resolves the

 © WILEY-VCH Verlag GmbH, D-69451 Weinheim, 1998 1433-7851/98/3701-0194 $ 17.50+.50/0



Scheme 3. Synthesis of the C29–C51 fragment: a) **8**, *t*BuLi, Et_2O, −78°C, then $MgBr_2$, **22**, −78 → −50°C, 78%; b) NIS, $CaCO_3$, MeOH/THF/CH_3CN/HC$(OMe)_3$, 0 → 20°C, 81%; Bu_3SnH, AIBN, THF/PhBr, 80°C, 54% and an additional 16% on resubmission of recovered starting material; TBAF, THF, 76%; imidazole, TBSCl, DMF, 75%; c) HF · py/py/THF/MeOH, 78%; Ts_2O, DMAP, CH_2Cl_2/*i*Pr_2NEt, 75%; NaI, acetone/*i*Pr_2NEt, 85%; Ph_3P, CH_3CN/MeOH, 80°C, 75% and an additonal 10% on resubmission of recovered starting material.



Scheme 4. Synthesis of altohyrtin A (spongistatin 1): a) LDA, THF/HMPA, −5°C, 40%; b) DDQ, CH_2Cl_2/H_2O, 60% as a 3:2 mixture of hemiketal and methyl ketal; KF, MeOH; Et_3N, 2,4,6-trichlorobenzoyl chloride, PhMe, then DMAP, 50% as a 3:2 mixture of hemiketal and methyl ketal; c) HF · py/py/THF, 20–30%.[25]

discrepancies in the configuration between altohyrtin A and spongistatin 1, and we further speculate that configuration of all the members in the spongipyran class of natural products is represented by structure **1**.[29]

Received: November 17, 1997 [Z 11166 IE]
German version: *Angew. Chem.* **1998**, *110*, 202–206

Keywords: altohyrtin · antitumor agents · natural products · spongistatin · total synthesis

[1] J. Guo, K. J. Duffy, K. L. Stevens, P. I. Dalko, R. M. Roth, M. M. Hayward, and Y. Kishi, *Angew. Chem.* **1998**, *109*, 198–202; *Angew. Chem. Int. Ed. Engl.* **1998**, *37*, 187–192.

[2] R. L. Halcomb, S. J. Danishefsky, *J. Am. Chem. Soc.* **1989**, *111*, 6661–6666.

[3] a) W. R. Roush, A. E. Walts, L. K. Hoong, *J. Am. Chem. Soc.* **1985**, *107*, 8186–8190; b) W. R. Roush, K. Ando, D. B. Powers, A. D. Palkowitz, R. L. Halterman, *ibid.* **1990**, *112*, 6339–6348.

[4] a) H. C. Brown, K. S. Bhat, *J. Am. Chem. Soc.* **1986**, *108*, 5919–5923; b) P. K. Jadhav, K. S. Bhat, P. T. Perumal, H. C. Brown, *J. Org. Chem.* **1986**, *51*, 432–439.

[5] Satisfactory spectroscopic data (^1H and ^{13}C NMR, MS, and others) were obtained for all new compounds.

[6] For abbreviations used, see reference 14 in ref. [1] (preceding communication).

[7] a) R. W. Friesen, C. F. Sturino, A. K. Dalijeet, A. Kolaczewska, *J. Org. Chem.* **1991**, *56*, 1944–1947; b) R. W. Friesen, R. W. Loo, *ibid.* **1991**, *56,* 4821–4823.

[8] The allylstannane was also prepared by an alternative synthetic route: addition of the 1,3-dithiane anion to TBS-glycidol, followed by cleavage of the TBS protecting group and acetonide formation, yielded the functionalized 1,3-dithiane, which was further lithiated and trapped with DMF. Reduction of the resultant aldehyde, followed by TBS-protection, dithiane deprotection, Wittig-olefination, and TBS-deprotection, gave an allyl alcohol, which was converted into **18** by adopting the last two reactions of step g in Scheme 2).

[9] P. A. Grieco, C.-L. J. Wang, G. Majetich, *J. Org. Chem.* **1976**, *41*, 726–729.

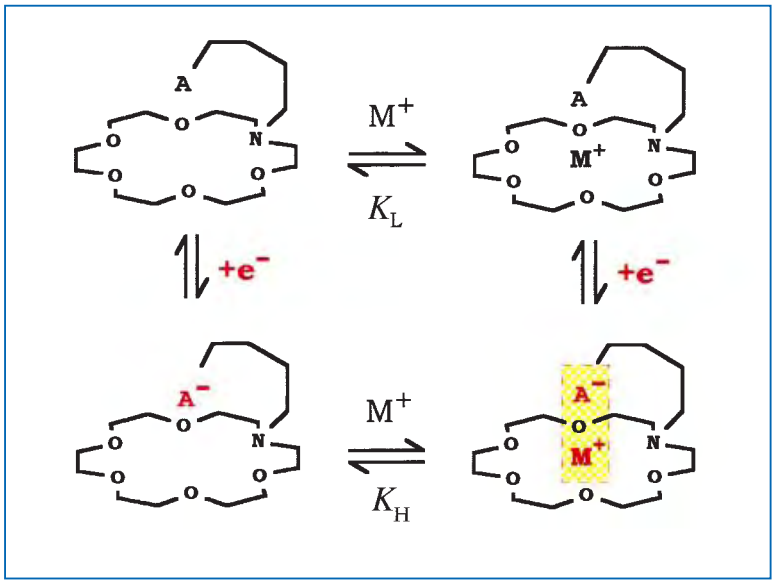
[10] L. L. Klein, W. W. McWhorter, Jr., S. S. Ko, K.-P. Pfaff, Y. Kishi, *J. Am. Chem. Soc.* **1982**, *104,* 7362–7364.

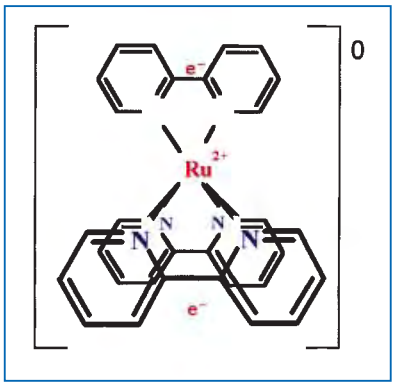
[11] a) S. Araki, H. Ito, Y. Butsugan, *J. Org. Chem.* **1988**, *53,* 1831–1833; b) S. Araki, T. Shimizu, P. S. Johar, S.-J. Jin, Y. Butsugan, *ibid.* **1991**, *56,* 2538–2542.

 © WILEY-VCH Verlag GmbH, D-69451 Weinheim, 1998 1433-7851/98/3701-0195 $ 17.50+.50/0

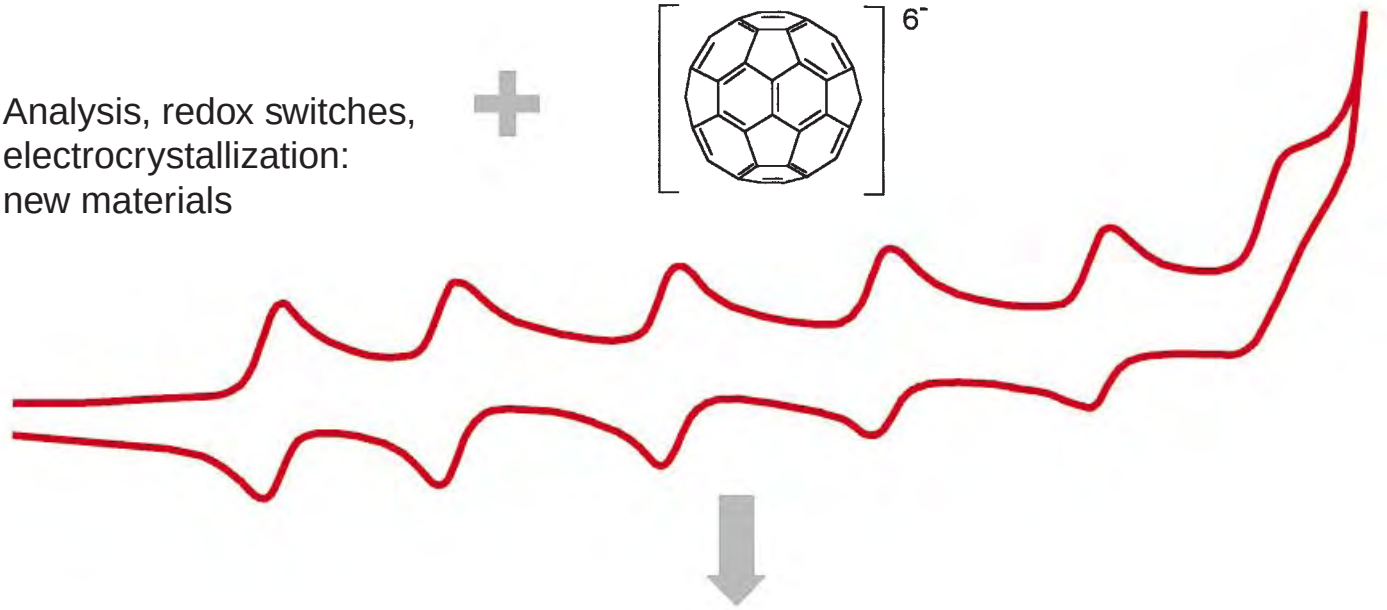
[12] Example of 2,3-dihalopropenes used in organoindium reactions: X.-H. Yi, Y. Meng, C.-J. Li, *Tetrahedron Lett.* **1997**, *38*, 4731 – 4734.
[13] R. J. Arhart, J. C. Martin, *J. Am. Chem. Soc.* **1972**, *94,* 5003 – 5010.
[14] Two alternative bond-forming reactions were examined on model compounds. First, the Ni^{II}/Cr^{II}-mediated couplings of iodoglucals with aldehydes proceeded smoothly to yield a diastereomeric mixture of allylic alcohols; the major product was the undesired stereoisomer. Second, addition of the 1,3-dithiane anion (THF, HMPA) of an acyclic E-ring precursor to a model aldehyde gave the undesired diastereomer as the major product.
[15] ^{1}H NMR analysis of the crude product showed the stereoselectivity of this coupling to be greater than 7:1. The minor undesired C38 diastereomer could be converted stereospecifically into the desired isomer by oxidation with TPAP/NMO followed by Luche reduction.
[16] R. U. Lemieux, S. Levine, *Can. J. Chem.* **1964**, *42*, 1473 – 1480.
[17] I. Ohtani, T. Kusumi, Y. Kashman, H. Kakisawa, *J. Am. Chem. Soc.* **1991**, *113,* 4092 – 4096.
[18] The chemical shift differences of the (*S*)- and (*R*)-Mosher esters at C38 were positive for the C33 – C36 region and negative for the C39 – C51 region, demonstrating the desired absolute configuration at C38.
[19] Preliminary studies on deprotection of silyl-protected altohyrtin A demonstrated that removal of the C35 TIPS group required prolonged and detrimental exposure to HF · py (5 days).
[20] R. W. Armstrong, J.-M. Beau, S. H. Cheon, W. J. Christ, H. Fujioka, W.-H. Ham, L. D. Hawkins, H. Jin, S. H. Kang, Y. Kishi, M. J. Martinelli, W. W. McWhorter, Jr., M. Mizuno, M. Nakata, A. E. Stutz, F. X. Talamas, M. Taniguchi, J. A. Tino, K. Ueda, J.-i. Uenishi, J. B. White, M. Yonaga, *J. Am. Chem. Soc.* **1989**, *111*, 7525 – 7530.
[21] K. Horita, T. Yoshioka, T. Tanaka, Y. Oikawa, O. Yonemitsu, *Tetrahedron* **1986**, *42*, 3021 – 3028.
[22] J. Inanaga, K. Hirata, H. Saeki, T. Katsuki, M. Yamaguchi, *Bull. Chem. Soc. Jpn.* **1979**, *52*, 1989 – 1993.
[23] COSY experiments demonstrated exclusive acylation of the C41 alcohol.
[24] While conversion of the C37 methyl ketal in the C37 lactol should be facile, this has not been tested experimentally.
[25] The deprotection under the specified condition in Scheme 4 was very clean (TLC analysis), but the yield of the isolated product was only in the range of 20 – 30 %. It is not yet established whether this low yield is due to a problem with isolation and/or with unidentified decomposition/side-reactions.
[26] The bioassays were performed by Dr. Bruce Littlefield at Eisai Research Institute, Andover, Massachussetts.
[27] The cytotoxicity was tested against DLD-1 human colon cancer, U937 human histiocytic lymphoma, and LOX human melanoma cells. Details of these experiments shall be reported elsewhere.
[28] G. R. Pettit, Z. A. Cichacz, F. Gao, C. L. Herald, M. R. Boyd, J. M. Schmidt, J. N. A. Hooper, *J. Org. Chem.* **1993**, *58*, 1302 – 1304.
[29] Through the total synthesis of altohyrtin C (spongistatin 2), Evans has reached the same conclusion: D. A. Evans, B. W. Trotter, B. Côté, P. J. Coleman, L. C. Dias, A. N. Tyler, *Angew. Chem.* **1997**, *109*, 2957 – 2961; *Angew. Chem. Int. Ed. Engl.* **1997**, *36*, 2744 – 2747.
[30] The sulfone was derived from the addition of sodium benzene sulfinate to the TIPS ether of 3-bromo-1-propanol.
[31] a) R. W. Murray, R. Jeyaraman, *J. Org. Chem.* **1985**, *50*, 2847 – 2853; b) W. Adam, J. Bialas, L. Hadjiarapoglou, *Chem. Ber.* **1991**, *124*, 2377.
[32] W. C. Still, *J. Am. Chem. Soc.* **1978**, *100,* 1481 – 1487.
[33] B. H. Lipshutz, R. Crow, S. H. Dimock, E. L. Ellsworth, R. A. J. Smith, J. R. Behling, *J. Am. Chem. Soc.* **1990**, *112,* 4063 – 4064.

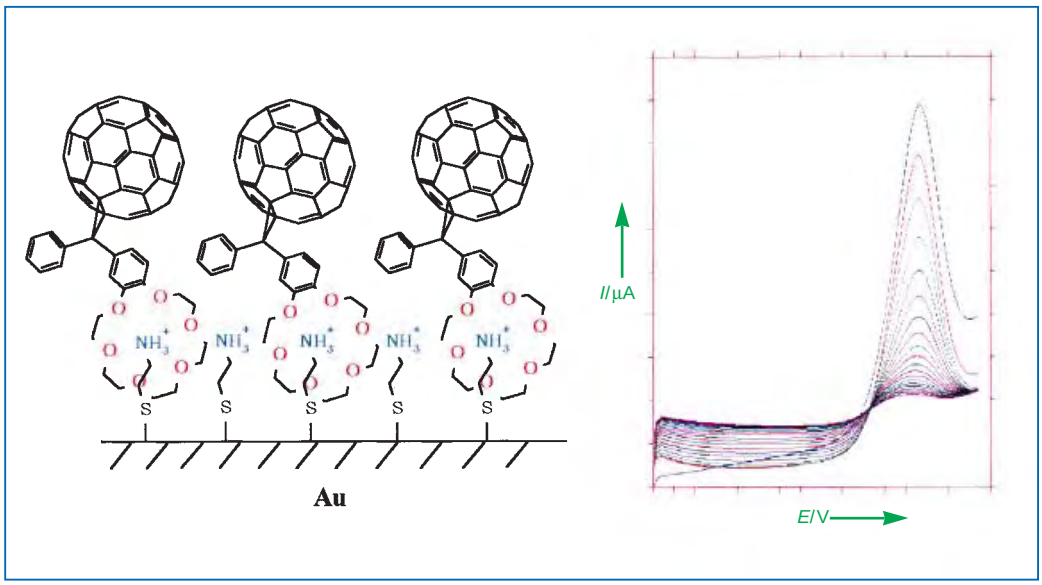
 © WILEY-VCH Verlag GmbH, D-69451 Weinheim, 1998 1433-7851/98/3701-0196 $ 17.50+.50/0





Analysis, redox switches, electrocrystallization: new materials





ANGEWANDTE CHEMIE © WILEY-VCH

Electrochemistry of Supramolecular Systems

Pierre L. Boulas, Marielle Gómez-Kaifer, and Luis Echegoyen*

Thirty years after the inception of the field of supramolecular chemistry, the volume of work in the area continues to expand at an ever-increasing rate. Biologists, chemists, and physicists continue to take strides in this well-established discipline and are beginning to make systems with serious potential applications. As the sizes of the molecular aggregates (prepared frequently by self-assembly) continue to increase, an unusual burden is being placed on existing analytical and physical characterization tools. The classical nuclear magnetic resonance (NMR) and mass spectral (MS) techniques sometimes fall short and thus are frequently unable to provide the necessary confirmation of structure and/or function of these aggregates. Although advances in these analytical areas have been remarkable (for example, matrix-assisted laser desorption ionization (MALDI) and electrospray mass spectroscopy (ES-MS), which allow the analysis of very large molecules and aggregates), other techniques are essential for complete structural and functional characterization of supramolecular ensembles. Additionally, as the aggregates are called upon to perform specific functions, as they are in the fields of biology and materials science, measurement of their electronic properties is of fundamental importance. Electrochemical techniques can fulfill many of these specific needs in the characterization and even in the preparation of some supramolecular aggregates. Developments in the field of electrochemistry, such as the implementation of potential pulsing techniques, have increased the sensitivity of the methods and offer relatively easy detection of dilute analyte solutions. Electrochemical techniques are particularly useful and informative for species confined to the surfaces of electrode materials. In addition to serving as sophisticated analytical tools, electrochemical techniques are also useful to produce electronic changes in host and guest molecules that induce (or inhibit) supramolecular aggregation. As such, they are switching controls that offer much promise in the field of supramolecular chemistry, since they offer the possibility to turn on or off a particular intermolecular interaction and thus to read/write information at the molecular level. These switching processes can also be used to effect directed translocation of molecular or ionic species, for example, across membranes. Be they as analytical tools or as powerful effectors to change the properties and binding of supramolecular aggregates, electrochemical techniques are of fundamental and practical importance in the rapidly growing field of supramolecular science. Here we provide examples of how these techniques have been applied to analyze and to influence the properties of guest–host complexes, aggregates, and other related structures.

Keywords: aggregation · cyclic voltammetry · electrochemistry · redox chemistry · supramolecular chemistry

1. Introduction: Electrochemistry and Supramolecular Chemistry

It seems appropriate to begin this review by asking: why should the supramolecular chemist be interested in electrochemistry?

While the usual goal of an electrochemical experiment is to determine redox potentials and to correlate these with intrinsic molecular properties, the method can offer much more to the supramolecular chemist.[1] Electrochemistry, a very powerful tool for monitoring supramolecular events such as self-aggregation on solid electrode materials, can also be used to "effect" structural and electronic changes, thus offering *control* over supramolecular processes. These latter applications are less known and thus often unappreciated by many who are not familiar with the field.

Redox changes can be used to enhance (or diminish) the binding affinity of ligands for guest molecules or ions. Such ligands can thus be viewed as redox switches (Section 2). Examples include the redox-active lariat ethers,[2a–c] and flavin cyclophanes or flavinophanes.[2d] Redox-switching has also been employed in molecular shuttles as described in Section 5.[3] Similarly, electrochemistry can also lead to pronounced structural changes in supramolecular systems. Work with the helicates, a topic of recent studies by Lehn,[4]

[*] Prof. L. Echegoyen, Dr. P. L. Boulas, Dr. M. Gómez-Kaifer
Department of Chemistry,
University of Miami
Coral Gables, FL 33124 (USA)
Fax: Int. code + (1) 305 284-4571

 © WILEY-VCH Verlag GmbH, D-69451 Weinheim, 1998 1433-7851/98/3703-0217 $ 17.50+.50/0

Abruña,[5] and Constable,[6] has demonstrated that as the chelating ligands in these systems are lengthened (a septipyridine system has been studied[5d]), the nuclearity of the complexes depends upon the redox state of the chelated ions. By controlling the redox state of these ions the electrochemist can switch between di-, tri- and tetranuclear complexes.

In addition to these examples in which redox chemistry can be used to control the different binding states and the structures of some aggregates, electrochemistry can also play an important role in redox-controlled self-assembly and in the generation of new materials by electrocrystallization. We have employed the latter to prepare single crystals of reduced complexes of ruthenium with pyridine-type ligands, which have interesting physical properties.[7] Electrocrystallization has also been used in the field of metalloporphyrins to generate molecular conductors with a stacked metal-over-metal structural motif.[8]

Thus, the dual utility of electrochemistry as an "effector" to direct and control supramolecular interactions, as well as a "detector" to monitor and measure the changes makes it uniquely powerful and useful in supramolecular studies. It is certainly one of the most important techniques in the field and one of the easiest to implement.

2. Switching and External Binding Control

The topic of redox switching has been of considerable interest in supramolecular chemistry for well over two decades and is one of the most important applications of electrochemistry in this field. A thorough discussion of the topic is beyond the scope of the present work, and thus the reader is referred to a number of excellent reviews for a more detailed discussion.[2c, 9]



P. L. Boulas



M. Gómez-Kaifer



L. Echegoyen

Pierre L. Boulas was born in Villefranche/Saone, France, and educated in Libreville, Gabon. He received a diploma from the Ecole Nationale Superieure de Chimie et Physique de Bordeaux, France in 1992. He joined Professor Kadish's group at the University of Houston, Texas, in 1992 and received his PhD in Analytical Chemistry in 1995. His graduate research work dealt with the electrochemistry and spectroelectrochemistry of fullerenes, fullerene derivatives, and novel metalloporphyrinoids. In August 1995 he joined Professor Echegoyen's research group at the University of Miami, Florida, as a PRF/NSF postdoctoral fellow. His research focuses on the electrochemical and spectroelectrochemical characterization of fullerene derivatives and supramolecular complexes, and on the electrosynthesis of novel fullerene-derived materials.

Marielle Gómez-Kaifer was born and educated in Miami, Florida. The daughter of a physician/biochemist and an artist, she obtained a Bachelor of Fine Arts degree in 1981 and then turned toward science, gaining a double Bachelor of Science degree in Chemistry and Microbiolgy/Immunology in 1991. After earning a National Science Foundation Graduate Fellowship in 1992 she spent one year at the University of Texas at Austin and then returned to the University of Miami, where she completed her Ph.D. thesis on redox-active calixarenes, employing electrochemical, ESR, and NMR techniques. She is presently pursuing post-doctoral studies on encapsulated redox centers.

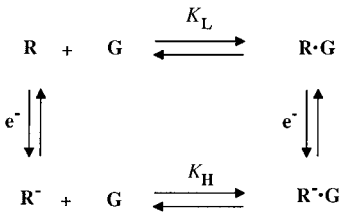
Luis Echegoyen was born in Habana, Cuba, and educated in Puerto Rico. He obtained both his B.S. and Ph.D. degrees from the University of Puerto Rico in Río Piedras in 1971 and 1974, respectively. After a one-year postdoctoral stay at the University of Wisconsin-Madison, he worked with Union Carbide Corporation for two years. He then returned to the University of Puerto Rico as assistant professor in 1977, where he was promoted to associate professor in 1980. In 1982 he took a leave of absence to work as a Program Officer in charge of Chemical Dynamics in the National Science Foundation in Washington, DC, while simultaneously holding an adjunct professorship at the University of Maryland-College Park. He then moved to the University of Miami-Coral Gables as associate professor and was promoted to professor in 1987. During calendar year 1990 he spent his sabbatical working with Prof. Jean-Marie Lehn at the Universitéˊ Louis Pasteur in Strasbourg, France. He received the Florida-American Chemical Society Award for 1996. Professor Echegoyen has published about 120 communications, papers, reviews, and monographs and his research interests have centered around supramolecular chemistry since the early eighties. His current work involves electrochemical and magnetic resonance spectroscopic studies of supramolecular systems, with a particular emphasis on their potential applications in materials science.

During the mid-1980s much interest centered on redox-switchable cation-binding systems as potential mimics of biological transport systems.[9c] At present redox switchable host–guest systems are frequently proposed as the chief components of potential molecular devices and sensor systems.[10] Regardless of the specific structures and their intended function, the basic principles behind electrochemical switching are the same.

2.1. The Concept of Redox Switching

The concept of an electrochemically switchable system is a simple one. The oxidized and reduced states of a switchable molecule must display differing degrees of affinity for a second species. Thus, the oxidation state determines the thermodynamic stability of the complex between the receptor and a guest species. The basis of the differential interaction in such a system is typically purely electrostatic. Either the receptor or the guest, or both, need to be redox active. The requirements of an electrochemically switchable receptor or guest are essentially the same. The redox-active component of such a system must exhibit reversible heterogeneous electron transfer kinetics and interact strongly with the binding component. When the binding interaction is strong, the complexed and the free forms will typically exhibit separate redox waves. This situation is ideal for analytical work, because the intensity of each wave is proportional to the concentration of the corresponding complexed or free molecule. In such a system there are two clearly defined binding states that are readily discerned by voltammetric techniques. These states are defined as "on–off" or more accurately, "high–low" states. Both of these forms of the switchable compound must have sufficiently high binding affinity if separate redox waves for the two states are to be observed by voltammetry.[11] This is an important consideration when trying to extract binding constant information from voltammetric data, especially if digital simulations are not performed.

An electrochemically switchable system is usually described by a simple square scheme (Scheme 1) in which the redox equilibrium is coupled with the reversible binding reaction. In this situation we assume that the receptor R is electroactive.



Scheme 1. Square scheme for a redox-switchable system.

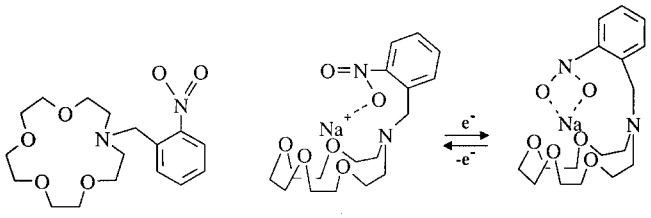
In Scheme 1, receptor R forms more stable complexes with guest G when it is reduced (R^-) than when it is oxidized (R). Therefore K_H is much larger than K_L. The magnitude K_H/K_L is defined as the binding enhancement.

The value of K_L determines whether R or R·G is reduced at the electrode surface. When K_L is large, the already formed complex R·G is electrochemically reduced to a higher affinity state, $R^-\cdot G$. In this situation the diffusion of the guest species is not a relevant factor. In contrast, if K_L is not large, the species undergoing reduction will be R, which will subsequently bind the guest to yield $R^-\cdot G$. In this instance, after reduction of the free receptor to the "high" binding state (R^-), the complexation process is essentially diffusion controlled, that is, determined by the diffusion of available guest to the reduced receptor. Generally, two separate voltammetric waves corresponding to the redox processes of the free (R) and complexed (R·G) species will *not* be observed for systems with a low K_L value ($\leq 10^3$‰M^{-1}) unless the rate constants for complexation and decomplexation are very fast. The typical electrochemical response of a system with a low K_L value is a shift of the half-wave potential for the free host species as guest is added to the solution.[12] If efficient transport of a guest species is of interest, K_L should not be so high as to prevent the eventual release of the bound guest. For a discussion of these points, see ref. [13].

2.2. Early Examples of Redox Switches

2.2.1. Lariat Ethers and Other Macrocyclic Hosts

The foregoing principles can be readily applied to lariat ether **1** (Scheme 2),[11b, 14] which represents a typical example of a redox-active guest whose affinity for a host can be greatly



1 [Na(**1**)]$^+$ [Na(**1**)]^0

Scheme 2. The free and Na^+-bound lariat ether **1**.

enhanced upon reduction. In **1** the optimal placement of the nitro substituent (ortho to the pivot attachment) allows for strong interaction with a macrocycle-bound cation. When Na^+ is bound by the macrocyclic crown ring, it can simultaneously interact strongly with the nitroaromatic group. At substoichiometric amounts of Na^+, two reduction waves are seen, one for the free and one for the Na^+-bound species of **1** (Figure 1).[11b]

The reduction potential of [Na(**1**)]$^+$ is anodically shifted by 260 mV relative to that of **1**, because the nitroaromatic anion radical is stabilized by Na^+. The cyclic voltammetric behavior of [Na(**1**)]$^+$ can be readily simulated, and this allows the determination of the binding enhancement (K_H/K_L) from Equation (1).[11a] In this equation $E_F^{o'}$ and $E_C^{o'}$ represent the

$$K_H = K_L \exp[-F(E_F^{o'} - E_C^{o'})/RT] \quad (1)$$

formal potentials, often estimated from the half-wave potentials, of the free and complexed species, respectively. The

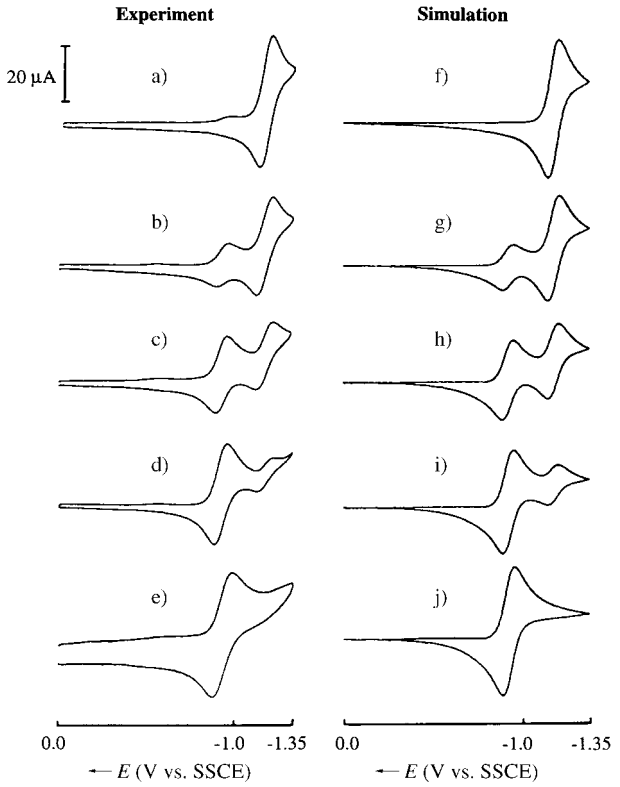
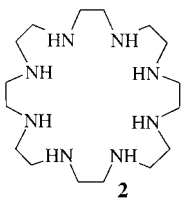


Figure 1. Cyclic voltammetry of a 1 mM solution of lariat ether **1** in the presence of increasing amounts of $NaClO_4$. a)–e): Voltammograms acquired by experiment: scan rate of 100 $mV s^{-1}$ in CH_3CN, 0.10 M NBu_4PF_6, 25°C, potentials vs. SSCE. f)–j) Simulated voltammograms. a) and f) 0.0 equiv $NaClO_4$, b) and g) 0.25 equiv $NaClO_4$, c) and h) 0.50 equiv $NaClO_4$, d) and i) 0.75 equiv $NaClO_4$, e) and j) 1.0 equiv $NaClO_4$ (reprinted with permission from ref. [11b]).

estimated binding enhancement for $[Na(\mathbf{1})]^+$ is 2.5×10^4. In many instances the potential for the wave corresponding to the reduction of the complex may shift as the cation concentration is increased. Since a change of only 10 or 20 mV results in an order of magnitude difference in the calculated binding enhancement, digital simulations of the voltammetric behavior across the full range of cation concentrations provide the best estimate of this factor. Additionally it should be noted that when $K_L \leq 10^4$ ‰M^{-1}, values of K_H may be significantly underestimated by Equation (1).[11b]

Occasionally lower peak currents are observed for the complexed species than for the free species. This effect is typically noted when a small guest, rather than the larger host (which is more common), is the redox active species. For a truly reversible process, the lower currents observed for the complexed species are really attributable to the smaller diffusion coefficient of the complex, rather than to electrochemical irreversibility or interfering chemical reactions. One such system was reported by Lehn and co-workers, who examined a polyamine macrocycle (**2**) that binds the comparatively small ferrocyanide ion.[15]



2

In this system the oxidation of ferrocyanide to ferricyanide is shifted to more positive potentials upon binding to **2**. At less than stoichiometric amounts of the polyamine ligand, two redox waves are seen. After addition of 1.2 equivalents of the macrocycle, a single wave is observed, which shows noticeably lower current intensity than the wave corresponding to the uncomplexed ferrocyanide (Figure 2).[15]

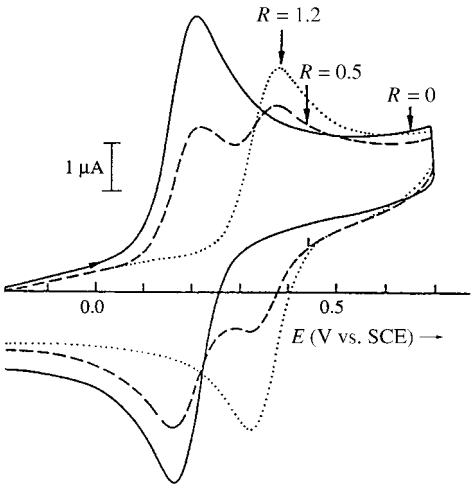
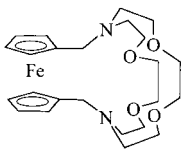


Figure 2. Cyclic voltammetry of ferrocyanide (0.9 mM in 0.1 M KCL, pH = 5.5) in the presence of increasing amounts of **2**. Platinum disk electrode, scan rate = 50 $mV s^{-1}$, potentials vs. SCE, $R = c(\mathbf{2})/c([Fe(CN)_6]^{4-})$ (reprinted with permission from ref. [15]).

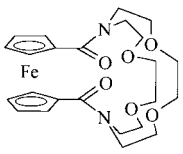
The lower current intensity is simply due to the difference in the diffusion coefficients between the free and the bound ferrocyanide species and not to a change in the overall reversibility of the system. Differences between the diffusion coefficients of the complexed and free species have been observed in the electrochemistry of other supramolecular systems such as cyclodextrin inclusion complexes.[16] For example, a decrease in the diffusion coefficient of ferrocyanide was detected upon complexation by an amino-substituted β-cyclodextrin.[16a] In these cases, simulations of the voltammetric behavior must take into account the difference in diffusion coefficients in order to accurately reproduce the observed behavior, which can include shifts in the observed redox potentials. Simulation may also be employed to extract binding constant information based on changes in the diffusion coefficient.[16a]

2.2.2. *Ferrocenyl Macrocycles and Cryptand Switches*

The development of more complex redox-switchable cation binding receptors continued at a rapid pace throughout the 1980s and early 1990s. Ferrocene-based systems were very prevalent in the literature, perhaps due to their ease of preparation and their well-behaved electrochemistry. Ferrocene undergoes a monoelectronic quasi-reversible oxidation to ferrocenium at easily attainable potentials and has the advantage of being rather insensitive to protic solvents and to the presence of molecular oxygen. Additionally, the ferrocene ligand acts as a redox antenna in that its oxidation potential is sensitive to binding with other molecules. For example, Gokel and co-workers designed structure **3** , a redox-switched system in which the ferrocene acts as the cap of a diazacryptand.[17]



3



4

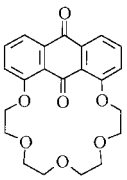
Complexation with alkali, alkaline earth, or silver ions was shown to shift the oxidation potential of the ferrocene moiety by as much as 290 mV, to more positive potentials. This is essentially a *negative* enhancement by a factor of 10^4 in favor of the neutral ferrocene ligand. (By negative enhancement we imply that oxidizing the ligand *disfavors* binding of the guest.) In this system, the binding of various cations resulted in characteristic half-wave potentials, a property with potential analytical applications.[10f] A related ferrocenyl macrocycle **4** also exhibited a "high – low" behavior with distinct oxidation waves (large K_L and $K_{H)}$ for both the free and bound forms of **4** in the presence of Be^{2+}.[18] However, differences in the cathodic and anodic current intensities suggested decomposition of the $\mathbf{4}\cdot Be^{2+}$ complex on the voltammetric time scale. In the presence of Mg^{2+}, Ca^{2+}, Sr^{2+} or Ba^{2+}, **4** exhibited voltammetric behavior typical of lower K_L systems: a single oxidation wave was observed for the free and bound ligand, at an $E_{1/2}$ shifted from that of the free ligand.[18]

Other significant results involving ferrocenyl macrocycles include the transport of cations by an electrochemically switchable ferrocenyl crown ether ligand across a bulk liquid membrane, which was achieved in 1986 by Saji and Kinoshita.[19] Transport across a CH_2Cl_2 liquid membrane was found to be enhanced upon oxidation of the ferrocene, since the Na^+ complex is destabilized in the oxidized state, favoring release of the Na^+ ion to the receiving phase.

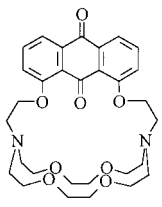
Interestingly, Fabrizzi et al. have prepared a novel ferrocene receptor that has an *increased* affinity for cations upon oxidation.[20] Beer and co-workers have synthesized and characterized a large number of ferrocenyl receptors, as well as a series of cobaltocene- and ruthenocene-based receptor systems.[21]

2.2.3. Quinone-Based Switches

Other compounds have relied on the presence of *p*-benzoquinone and anthraquinone redox-active moieties as the switching antennae for enhanced cation binding. The quinone moiety undergoes two successive monoelectronic reductions to the anion radical and then the dianion.[22] Echegoyen et al. developed anthraquinone-based crown ethers and cryptands such as **5** and **6**.[23, 24]



5



6

Compound **5** exhibits two reversible monoelectronic reduction waves in the absence of Na^+.[23] In the presence of 0.5 equivalents of Na^+ each of these waves is split into two waves, reflecting the redox processes of the free and the complexed ligand. Cryptand **6** displays even more dramatic behavior, exhibiting a 400 mV anodic shift for the reduction of the anthraquinone moiety upon binding with two Li^+ ions. Such a shift corresponds to a binding enhancement of 8×10^5.[24] Further reduction to the dianion leads to a total binding enhancement of 10^{11} relative to the neutral cryptand, a most impressive switching effect. Cryptand **6** has also shown the potential for lithium isotope discrimination.[25]

Cryptand **6** also binds Na^+ and K^+.[24] In its reduced state, **6** binds K^+ so strongly that it cannot be removed competitively by cryptand [2.2.2]. Use of anthraquinones as the redox-switchable component of cation binding compounds has continued with the work of Echegoyen and Torres, who have studied a series of anthraquinones bearing pendant diaza-crown ethers, and bis(anthraquinone) systems with diaza-crown ether spacers.[26] Na^+ binding enhancements obtained upon one-electron reduction in several of these systems have exceeded 10^5.

2.2.4. Other Switchable Systems

Various other cryptands such as azobenzene cryptands have also been studied.[27] These exhibited a greater degree of selectivity for K^+ than that of the cryptands mentioned above, which typically were selective for Na^+ or Li^+. True binding selectivity coupled with redox switching enhancement is an issue that has yet to be widely addressed and remains a challenge for future work.

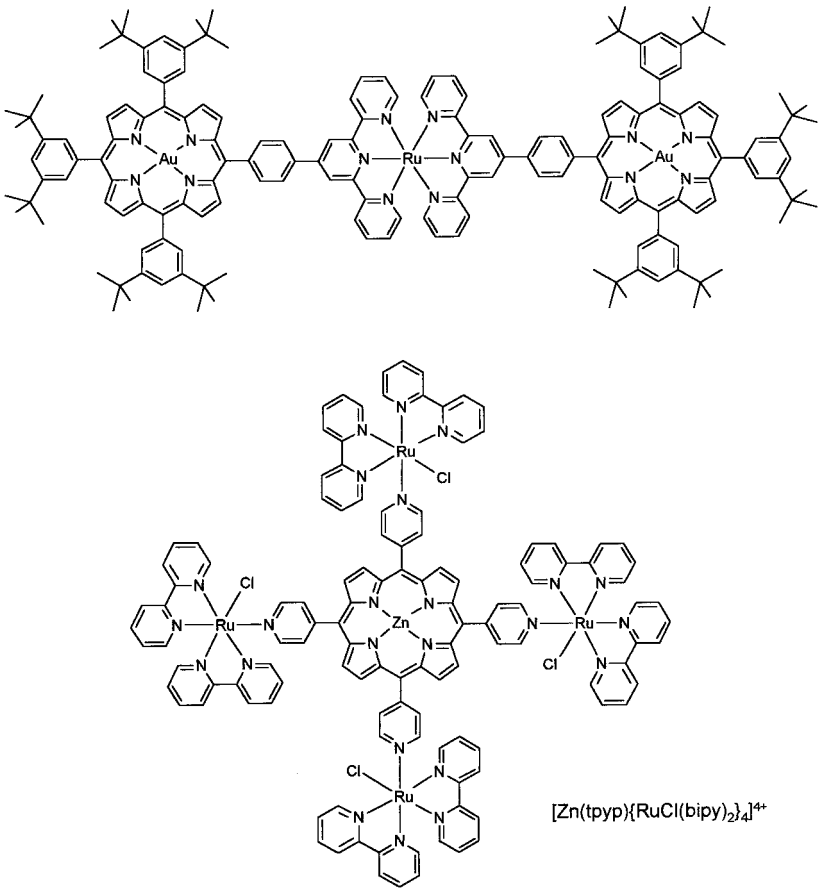
The area of anion binding enhancement by switching mechanisms has been less explored than that of cation binding. Most of the work in this area has been that of Beer and co-workers.[28] Their strategy has been to employ multiple positively charged redox moieties, which are then switched electrochemically to higher charge states. An excess of the anion guest must be added in order to see measurable changes. The effects of binding are rather modest, on the order of 50 mV or less, indicating very low binding enhancements. The reader is referred to reference [29] for further discussion of this work.

More recent work in the field of redox switching of ion binding involves the use of more complicated support frameworks. Related work will be discussed in the following sections.

3. Porphyrinoids

3.1. Porphyrins and Supramolecular Chemistry

The synthesis of porphyrinoids[28b, 30–37] is a very active field of research, and a great variety of porphyrin-like compounds with cavities of different sizes and shapes have been reported. Porphyrin-like compounds have been employed as the building blocks to form a number of supramolecular assemblies. Selected recent structural examples are shown in Scheme 3.[36]



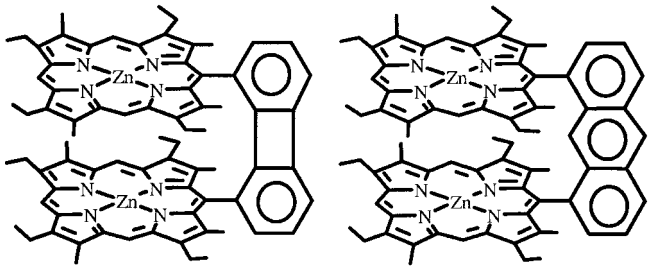
Scheme 3. Porphyrins as building blocks for supramolecular assemblies.

Considerable work has been reported in the field of the self-assembly of porphyrin oligomers and of the binding properties of these supramolecular receptors.[35] In addition to variation of the size and shape of the cavity, substitution of the porphyrinoid macrocycle is readily achieved. This allows for fine-tuning the physical and chemical properties of any given porphyrinoid ligand.[37] Some of these derivatized porphyrinoids have already revealed their potential as hosts for a variety of guest molecules.[28b, 37a–b] Thus, porphyrinoids are good precursors to supramolecular assemblies.

3.2. Cofacial Bis(metallo)porphyrinoids as Electrocatalysts

Cofacial bis(metallo)porphyrinoids (Scheme 4) were initially prepared to study the interaction between closely lying electroactive centers such as in the case of cytochromes,[38] to obtain multi-electron transfer,[39] or to find new catalysts for the reduction or oxidation of small substrate molecules such as O_2, H_2, or N_2.[40]

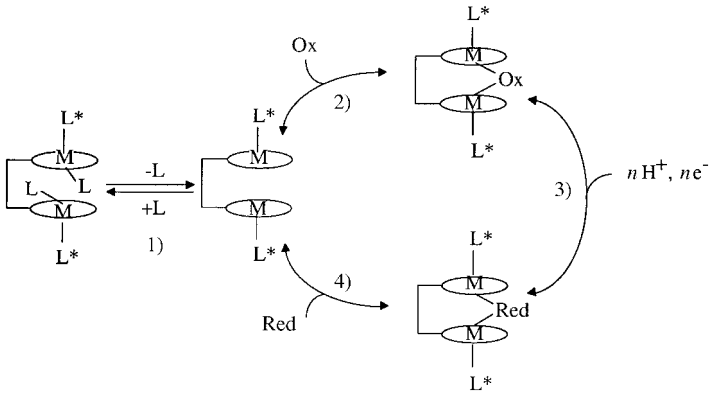
Catalytic activity in these systems can be easily detected with cyclic voltammetry (CV) or rotating disk electrode voltammetry (RDE).[41, 42] In the case of CV, a comparison of the current–voltage curves obtained for the substrate with a bare electrode and with an electrode modified with the cofacial bis(metallo)porphyrin will suffice to demonstrate catalytic activity. Higher current density and a decrease in the substrate overpotential when using the modified electrode are reliable indicators that the cofacial complex catalyzes the reduction or the oxidation of the substrate.[40] RDE is also very useful in that it provides more information about the kinetics of the catalytic process. In addition, rotating ring-disk electrode (RRDE) voltammetric experiments[42c] help to gain insight into the electrochemical nature of the intermediary and final products of the catalytic reaction.



[Zn_2(dpb)] [Zn_2(dpa)]

Scheme 4. Examples of cofacial bis(metallo)porphyrins.

Electrochemical studies of these porphyrins led to the conclusion that the rigidity and length of the spacer or linker between the two porphyrin units play a major role in how good a catalyst the cofacial complex is. If the spacer is too flexible, the two porphyrins do not adopt a face-to-face configuration.[43] Indeed, X-ray data revealed that the two units are laterally shifted with respect to each other to maximize $\pi-\pi$ overlap. If the two porphyrin units are too tightly linked to each other, the geometry of the cavity where the binding of the substrate occurs is not flexible enough to accommodate the structural changes that will take place during the catalytic process. If the linker is too long, communication between the two chromophores is absent. Anthracene and biphenylene linkers optimize this length/rigidity compromise.[44] A proposed overall catalytic process is schematically represented in Scheme 5.



Scheme 5. Cofacial bis(metallo)porphyrins as electrocatalysts.[40] 1) Formation of the active site; 2) and 4) substrate binding or product release; 3) multielectron transfer. L* = bulky ligand blocking the outer coordination sites (solvent molecule or imidazole, for example); L = smaller ligand that can be displaced by the substrate.

The latter case exemplifies the use of electrochemistry as an effector of supramolecular events and as a detection technique. The substrate binding, which allows for the catalytic activity is controlled by the redox state of the substrate. The release of the product, on the other hand, from the cofacial bis(metallo)porphyrin is also redox-controlled.

3.3. Dendritic Porphyrins

Research on dendrimers has been expanding for the last decade.[45–50] Dendritic porphyrins are a rather important class of dendrimers that present interesting properties with potential industrial applications. They were initially synthesized with the aim of mimicking the environment that surrounds a heme center such as that of cytochrome c.[46] The first one was prepared by Inoue et al.[47] The electrochemistry of dendritic porphyrins has been studied by Diederich et al.[49, 50] In this case, electrochemistry has been used solely to measure redox potentials and correlate them with electronic properties. Some examples of dendrimers studied are shown in Scheme 6.

The redox behavior of dendritic porphyrins is markedly different from that of "simple" metalloporphyrins because of the influence of the dendrimeric branching around the porphyrin core (Figure 3).[49]

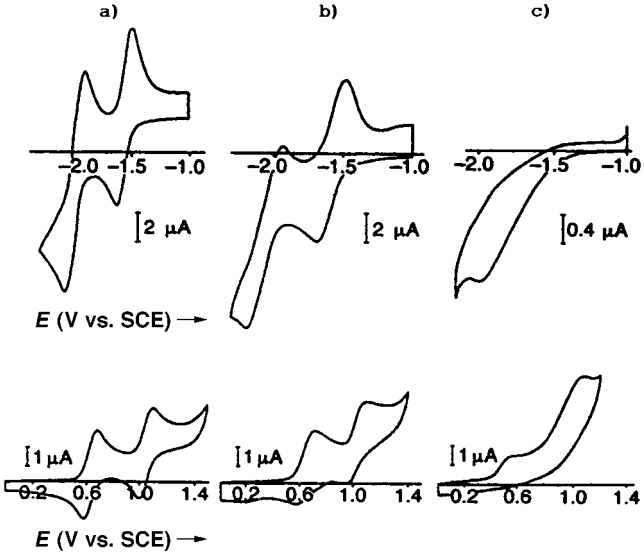
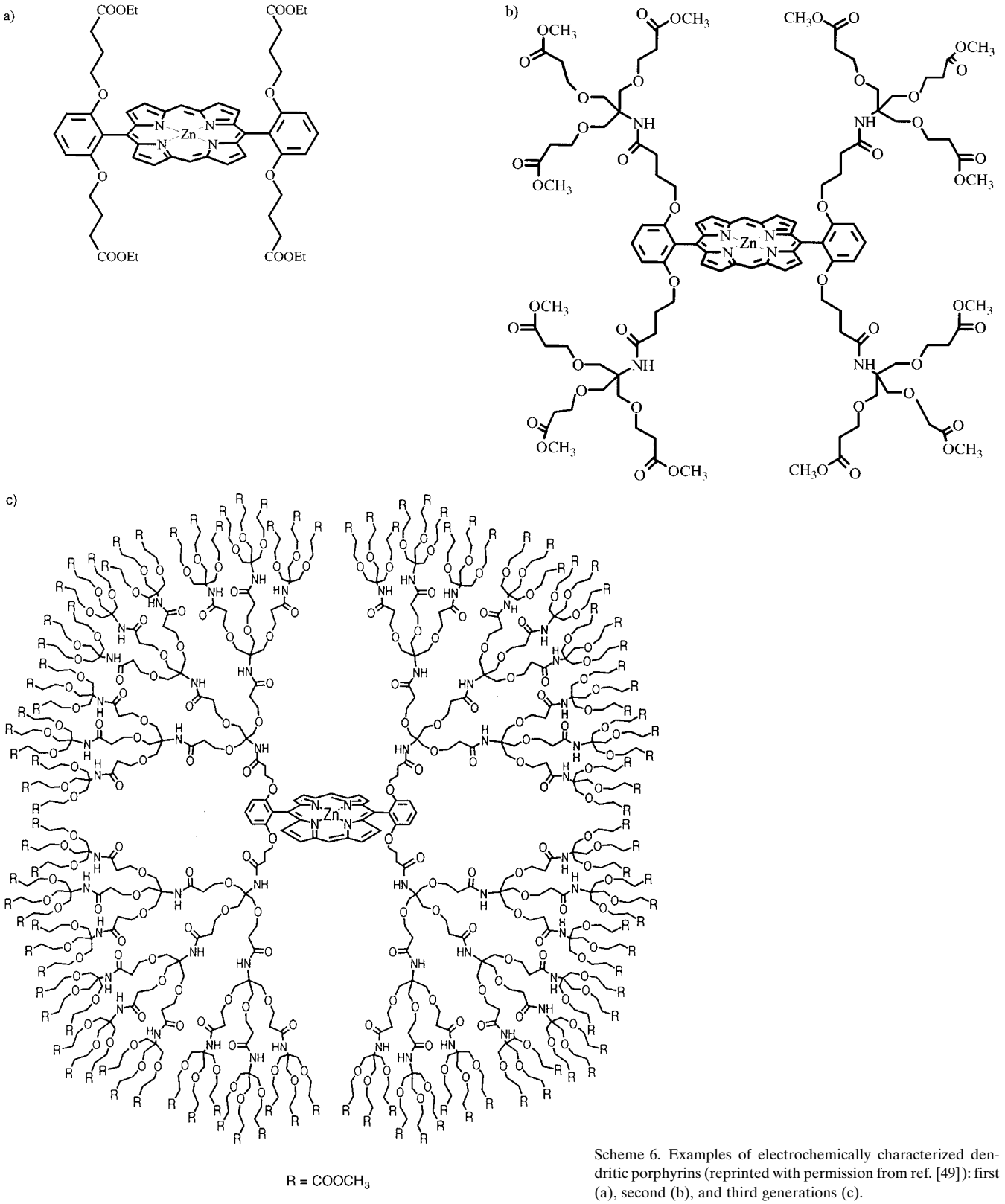


Figure 3. Cyclic voltammograms showing the reduction (top) and the oxidation (bottom) of dendritic porphyrins whose structures are represented in Scheme 6.[49] Dendrimers of a) the first, b) the second, and c) third generation. Conditions: top: THF, 0.1 M Bu_4NPF_6, Hg dropping electrode as working electrode, scan rate = 8 $V\,s^{-1}$, 25 °C; bottom: CH_2Cl_2, 0.1 M Bu_4NPF_6, platinum working electrode, scan rate = 0.1 $V\,s^{-1}$, 25 °C (reprinted with permission from ref. [49]).

As the dendrimer shell grows (Figure 3a to 3c), the porphyrin electrophore is more shielded by electron-rich dendritic branches, rendering the reductions more difficult and the oxidations easier. By the third generation, the zinc porphyrin dendrimer shows only ill-defined and mainly irreversible CV processes. The poor definition is due in part to the very small diffusion coefficient of the species, while the irreversibility results from the superimposition of redox processes involving the porphyrin core and the functional groups on the branches of the dendrimer. The dendrimeric branching not only affects the porphyrin ring-centered reactions but also the metal-centered ones. As reported by Diederich et al.[50] in the case of iron porphyrin dendrimers, the half-wave potentials for the metal-centered reductions ($Fe^{III} \rightarrow Fe^{II}$ and $Fe^{II} \rightarrow Fe^{I}$) were found to depend greatly on the size of the dendrimer surrounding the metalloporphyrin. The dendrimer was also found to shield the metal center from the external medium and particularly the solvent.[50]

3.4. Ruthenated Metalloporphyrins

Examples of such complexes are shown in Scheme 3.[36] Although several architectures have been designed and built that make use of the ability of pyridyl-type ligands to complex ruthenium(II), only one of them, to our knowledge, has been thoroughly characterized electrochemically (Scheme 3, bot-



Scheme 6. Examples of electrochemically characterized dendritic porphyrins (reprinted with permission from ref. [49]): first (a), second (b), and third generations (c).

tom structure).[36b] The CV recorded for the tetraruthenated zinc porphyrin $[Zn(tpyp)\{Ru(bpy)_2Cl\}_4]^{4+}$ shows a multitude of redox processes (Figure 4) in agreement with the fact that four sites of electron transfer can be envisaged: the metal center, the porphyrin ring, ruthenium(II), and the pyridyl ligands.

Two reversible oxidations can be discerned in the CV. The first one at 0.92 V has the intensity of a four-electron oxidation and corresponds to a $Ru^{II} \rightarrow Ru^{III}$ reaction for each $Ru(bpy)_2$ ligand. The fact that the four Ru^{II} centers are oxidized simultaneously indicates that only very weak coupling exists between the ruthenium centers. The second

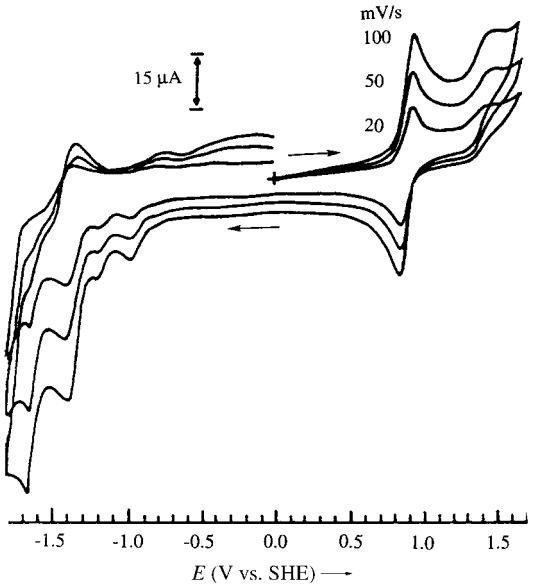
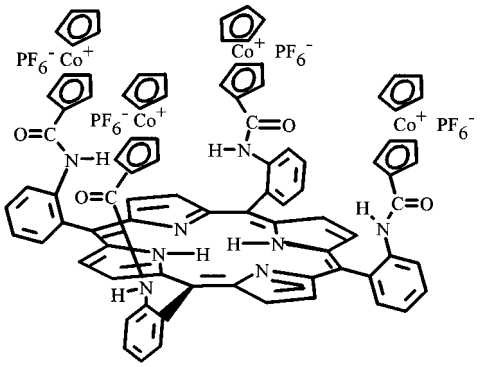


Figure 4. Cyclic voltammogram (DMF, 0.1M $TEAClO_4$, platinum disk working electrode) for the reduction and the oxidation of the $[Zn(tpyp)\{RuCl(bpy)_2\}_4]^{4+}$ (0.99mM) (reprinted with permission from ref. [36b]).

oxidation located at 1.5 V corresponds to the one-electron oxidation of the porphyrin ring. Interestingly, the first one-electron reversible reduction observed for the tetraruthenated porphyrin corresponds, as confirmed by spectroelectrochemistry, to a $Zn^{II} \rightarrow Zn^{I}$ reduction. This contrasts drastically with the electrochemistry of Zn(tpyp) for which the first reduction is ring-centered.[51] The second reduction (reversible when only the first two waves are scanned) at -1.2 V is a one-electron transfer and involves the porphyrin ring. The multi-electron process at -1.35 V is a superposition of the second porphyrin ring-centered reduction and the reduction of four bpy units, one on each $Ru(bpy)_2$ ligand. Finally, the reduction at -1.67 V is irreversible and involves the remaining four bpy ligands. The complexity of the electrochemistry of the ruthenated zinc porphyrin described above exemplifies the typical expectation when dealing with supramolecular assemblies that possess several available sites for electron transfer.

3.5. Sensing of Anions by a Porphyrin Receptor

As mentioned earlier, the porphyrin ring is amenable to chemical derivatization. A judicious choice of ligand led to the synthesis of a porphyrin (Scheme 7) with interesting anion recognition properties.[28b] This novel anion sensor presents a pronounced affinity for halides, $H_2PO_4^-$, and HSO_4^- over NO_3^-. The anion binding properties of the porphyrin sensor were monitored by NMR, UV/Vis spectroscopy, and electrochemistry. Interestingly, upon addition of anion guests to solutions containing the porphyrin host, only shifts in the oxidation potentials of the porphyrin ring and reduction potentials of the cobaltocenium ligand were detected. No influence due to anion binding was detected on the reduction potentials of the porphyrin ring.[28b]



Scheme 7. Example of a porphyrin-based anion sensor.

In two other examples a porphyrin-based system has been used for molecular recognition. The first one is the preparation of a porphyrin host for a guest analogous to ubiquinone,[52] while the second one is the synthesis of a sapphyrin–cytosine conjugate for selective through-membrane transport of guanosine 5′-monophosphate.[37a] Unfortunately none of these systems has been electrochemically characterized.

3.6. Electrochemically Induced Self-Assembling of Porphyrinoids

The porphyrin-like compounds are not only of interest because of their biological relevance but also because of their potential uses as materials, such as "molecular metals"[53] or catalysts.[40] Thus a great deal of effort has been devoted to designing and creating new conducting materials that incorporate porphyrin and its derivatives as molecular building blocks.[8, 54–56] Electrochemical[8, 55] or chemical[54, 56] oxidation of a series of metalloporphyrinoids [M(P)], where P is a phthalocyanine, a porphyrin, or a porphycene, leads to molecular conductors, which usually have the same stacked structural motif.[57] This motif is best characterized as an ABAB arrangement in which A and B are staggered by an angle that depends upon the nature of the macrocycle. Whereas the undoped materials crystallize with a stacking pattern in which the units are slipped with respect to each other, the doped materials most often crystallize in a metal-over-metal arrangement (Figure 5).[57]

The conductivity of these systems increases by several orders of magnitude from the undoped to the doped material.[54, 55] Examples of dopants include I^-, BF_4^-, PF_6^- and ReO_4^-. As mentioned earlier, these conducting materials can be prepared by chemical or electrochemical oxidation, but the latter pathway offers more alternatives than the former. Electrochemistry permits facile variation of the dopant and the ability to reach doping levels that are not accessible through chemical oxidation. Both of these factors, nature of the dopant and extent of oxidation of the metalloporphyrinoid, play a major role in the physical properties, such as conductivity, of the final product.[8, 54–57] The list of materials that have been prepared by partial oxidation of metalloporphyrinoids is vast and beyond the scope of this review. Thus we chose to describe one of the most recent examples, the

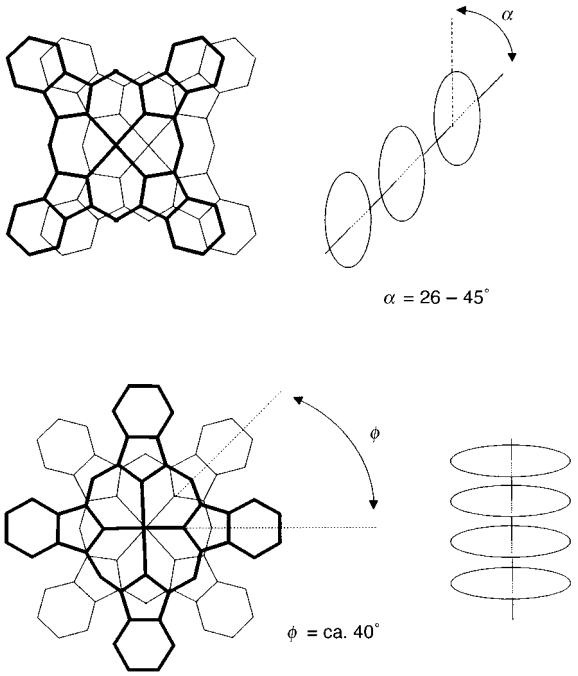


Figure 5. Schematic drawing of the strucutres of the undoped and doped crystallized metalloporphyrinoids (adapted from ref. [57]).

electrocrystallization of a new porphycene-based material, $[Ni(ompc)]_{2.5}(BF_4)_2 \cdot C_{10}H_7Cl$, where ompc stands for 2,3,6,7,12,13,16,17-octamethylporphycene.[8] Single crystals of $[Ni(ompc)]_{2.5}(BF_4)_2$ were harvested at the anode of a two-electrode system by using controlled current (5 μA) electrolysis. The unit cell consists of 10 macrocycles (Figure 6).

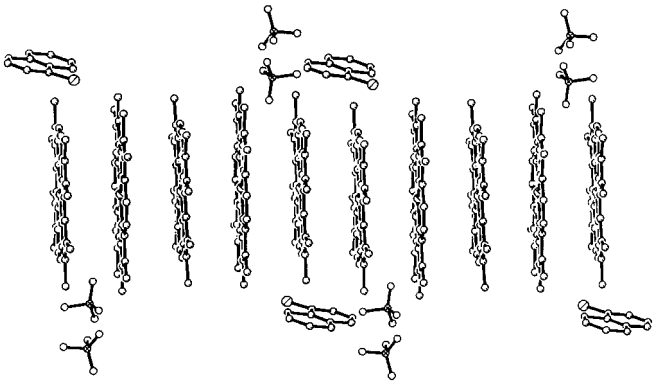


Figure 6. Stacking in the crystal of electrooxidized $[(OMPc)Ni]^+BF_4^-$ (reprinted with permission from ref. [8]).

The structural motif, as expected, consists of stacked macrocycles that are staggered by 90° (Figure 5). The stacks of metallomacrocycles are surrounded by channels, which are occupied by counter anions (BF_4^-) and solvent molecules (1-chloronaphtalene). Within the crystal unit, the 10 macrocycles are arranged as pentamers. The presence of four BF_4^- anions for each pentamer suggests four oxidation sites per pentamer. Within a pentamer, the distance between the elements is 3.33 – 3.38 Å, whereas the distance between two neighboring pentamers is 3.40 Å. The 90° staggering angle between successive units is postulated to minimize the steric hindrance between the Ni porphycenes. The conductivity of this electrocrystallized porphycene at room temperature is 0.06 Ω^{-1} cm^{-1} and was found to be thermally activated.[8]

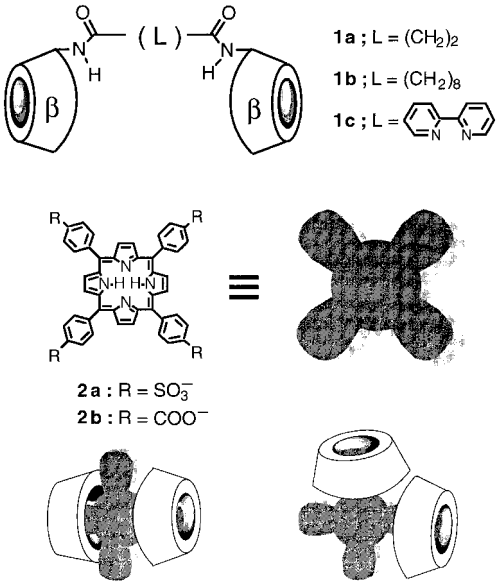
An important question for all of the conducting materials made out of metalloporphyrinoids like the one just described concerns the conduction pathway. Electrochemical studies of nickel porphycenes showed that the first reduction of these compounds is a reversible one-electron, ring-centered process.[58] Thus, it was expected that the conduction pathway in $[Ni(ompc)]_{2.5}(BF_4)_2$ was induced by intermolecular electon transfer from ring to ring. This was actually confirmed by ESR spectroscopy.[8] Modifying the central metal ion in this system, for example by replacing nickel(II) with cobalt(II), might induce another type of conductivity supported by the metal pathway of the material. Indeed, an example that displays metal-pathway conductivity, (phthalocyano)cobalt iodide, has been reported.[54d]

3.7. Outlook

Not a month goes by without a major scientific journal reporting the synthesis of a new porphyrin-based system. Thus it is an almost impossible task to follow the porphyrin literature. This last part of this section will be used to describe recently reported porphyrin-based systems that will probably play important roles in the future of supramolecular chemistry. The electrochemistry of these systems has yet to be explored and is, in our opinion, an area warranting immediate study.

First, electrochemical characterization of porphyrin oligomers is of obvious importance. Of special interest in this field are the iron and gallium porphyrin trimers recently reported by Wojaczynski et al.[59] The electrochemistry of the first binuclear $[Mn^{II}(bipy)-Fe^{III}(porphyrin)]$ could be crucial. Its potential as a biomimetic system for manganese peroxidase has already been suggested.[60] Recently porphyrin[2]catenanes, in which conformational control is exerted by simple acid – base chemistry, have been reported.[61] These systems might represent new types of supramolecular assemblies in which conformational control can be effected electrochemically or by acid–base chemistry. Finally, the self-assembly of cyclodextrins and porphyrins has already been investigated by several groups.[62, 63] Several types of porphyrin – cyclodextrin complexes have been synthesized (Scheme 8) with the aim of mimicking the hydrophobic environment around the heme center in heme proteins.[62a, b]

In addition, studies of porphyrin – cyclodextrin inclusion complexes have been justified by the search for new supramolecular catalytic systems,[62c] the inhibition of porphyrin aggregation[62d] or dimerization,[62e–g] as well as the enhancement of the spin-lattice relaxation of water protons by manganese porphyrin – cyclodextrin complexes.[62h] In spite of the interest in this area, the electrochemistry of the porphyrin – cyclodextrin inclusion compounds remains a relatively unexplored area.



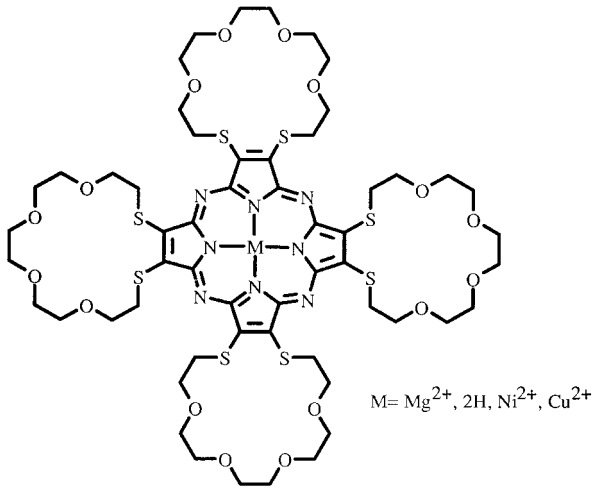
Scheme 8. Example of porphyrin–cyclodextrin inclusion complex (reproduced with permission from ref. [62].)

Since 1985 crown ethers and porphyrins have been intimately combined to generate species with multiple metal binding sites.[64] One recent example is the octathioporphyrazine crown ether,[65] the structure of which is shown in Scheme 9. Beautiful and sophisticated molecular architectures have been built from porphyrinoids and their metal complexes. As the fields of porphyrin and supramolecular chemistry merge, the tools and concepts used in both fields will surely help to create a very rich research area. Electrochemistry will, of course, play an important role in this exciting field because of the uniqueness of the information that it can provide about these systems.

4. Pyridine-Based Systems

Pyridines (py), including bipyridine (bpy), terpyridine (tpy), other extended pyridines, and biquinoline, have been among the most utilized ligands for the preparation of supramolecular structures. In this section we will consider coordination-based complexes of pyridine systems. The electrochemistry of the well-known bpy-based cyclophane systems is described in Section 5. The large number of reports in this area precludes an exhaustive review of the field. Our focus will be on the py-based cryptates, helicates, molecular wires, and the stacked and gridlike arrays that have recently dominated the supramolecular literature. We will also briefly describe the electrochemistry of dendrimer systems based on bipyridine complexes.

The majority of the complexes described here readily self-assemble, relying on the template effect provided by the transition metal ions. Since many of the metal ions are themselves electroactive, the electrochemistry of these systems is as rich and complex as that of the porphyrinoids described in Section 3. In a number of instances, changing the valence state of the transition metal ion has profound effects



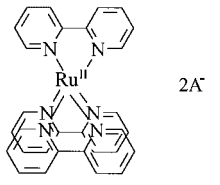
Scheme 9. Framework of the octathioporphyrazine crown ether.

on the type of coordination observed in a complex. This is especially true in the case of copper complexes, some of which are described below. Changes in the oxidation state of the metal ion can also result in changes of the nuclearity of the complexes (e.g. monometallic to di- or even trimetallic structures).

4.1. Pyridine-Based Complexes and Cryptates

Among the pyridine and polypyridine metal complexes, by far the most extensively studied ligand is bipyridine.[66] A large number of 2,2′-bipyridine (bpy) complexes with metal ions such as the tris(bipyridine) complexes are known, and most have been characterized electrochemically.[67, 68] The prototypical example of this class of complexes is $[Ru^{II}(bpy)_3]^{2+}$, which has been studied by a number of authors.[69]

Some of the most detailed work in this area was reported by DeArmond and co-workers, who studied the electrochemical and ESR behavior of $[Ru^{II}(bpy)_3]^{2+}$. This complex exhibits some characteristics that are important to describe since they are typical for this class of compound.



$[Ru^{II}(bpy)_3]A_2$ $A^- = Cl^-, PF_6^-$ etc.

In $[Ru^{II}(bpy)_3]^{2+}$ both metal- and ligand-based electron transfer processes can occur. Oxidation of $Ru^{II} \rightarrow Ru^{III}$ in the tris(bpy) complex occurs at 0.82 V vs. Fc^+/Fc in CH_3CN/TEAP (tetraethylammonium perchlorate).[70] For comparison, the Ru^{II}/Ru^{III} oxidation occurs at -0.46 V vs. Fc^+/Fc in the hexaaquo species.[71] Thus, Ru^{II} is stabilized by the chelating ligand. The free bpy ligand can accept two electrons.[72] The first electron transfers onto the bpy ligands in the $[Ru^{II}(bpy)_3]^{2+}$ complex occur (as monoelectronic reductions) at three successive potentials (Figure 7): -1.76, -1.92, and -2.14 V vs. Fc/Fc^+ in DMF/$TEAPF_6$ (tetraethylammonium hexafluorophosphate).[73a]

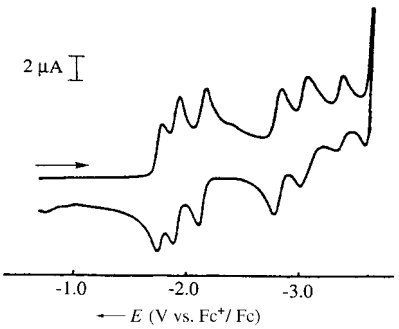
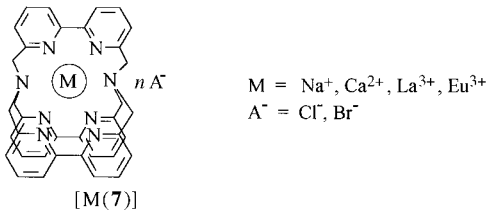


Figure 7. Cyclic voltammograms of $[Ru(bpy)_3]^{2+}$ (0.5 mM) in DMF, 0.1 M $TEAPF_6$; scan rate = 0.1 $V s^{-1}$, −54 °C (reprinted with permission from ref. [73b]).

These reductions are more facile than those of the *free* 2,2′-bpy ligand indicating that the binding to the metal ion lowers the energy of the ligand's π* orbital. The fact that these reductions occur at three different potentials, rather than at a single potential, indicates that there is electronic coupling between the bpy units in the $[Ru^{II}(bpy)_3]$ complex.[73b]

The ESR spectrum of the single-electron reduction product, $[Ru^{II}(bpy^-)(bpy)_2]^+$, shows a single broad line, the line width of which is temperature-dependent, suggesting a thermally activated delocalization (electron hopping).[74] In fact, a number of researchers have shown that the π orbitals of the bpy ligands in $[Ru^{II}(bpy)_3]^{2+}$ are isolated but that thermally activated electrons can hop from ligand to ligand.[74] Similar ESR behavior is noted for the doubly reduced (overall neutral) species.[74] After the third monoelectronic reduction step, which results in the formation of the $[Ru^{II}(bpy)_3]^-$ complex anion, some hyperfine structure emerges, indicating that the electrons are somewhat localized on the individual bpy ligands. The fourth to sixth electron reductions for this complex were observed at low temperature,[73b] and the potentials reported, −2.78, −3.00, and −3.30 V vs. Fc/Fc^+ in DMF/$TEAPF_6$, again indicate that electronic coupling exists between the ligands. The observation of six separate waves for the complex has been offered as confirmation of the so-called spatially isolated redox orbital model, in which the reduced species exhibit properties of the ligand alone.[75] Thus the presence of the metal ion simply provides a way to tune the potential at which the ligand reduction occurs. The electrochemical behavior of $[Ru^{II}(bpy)_3]^{2+}$ will be used as the standard for comparison with the other pyridine-based systems discussed below.

Tris(bipyrimidine)[70] and tris(biquinoline),[70b] tris(phenanthroline),[70b, 76] and terpyridine[77] complexes of transition metal ions have been characterized by a number of authors. A number of these complexes are of current interest in materials chemistry. We have successfully electrocrystallized several pyridine-based Ru^{2+} complexes.[7] These ligands have also been used as the framework for a series of cryptands and cryptates. Bpy cryptands can undergo electrochemical reduction, as can, in some instances, the cation bound in the corresponding cryptates (for example, a lanthanide such as Eu^{3+}). In these complexes the ligand surrounds and traps the metal in a cagelike coordination sphere (see Section 8). The electrochemistry of the cryptates $[M(\mathbf{7})]^+$ was studied by Echegoyen and co-workers.[78] For $[M(\mathbf{7})]^+$, where M = Na^+, Ca^{2+}, or La^{3+}, although six electrons may be transferred to the three bpy ligands overall, typically only the first three reductions are observed (Figure 8).



[M(**7**)]

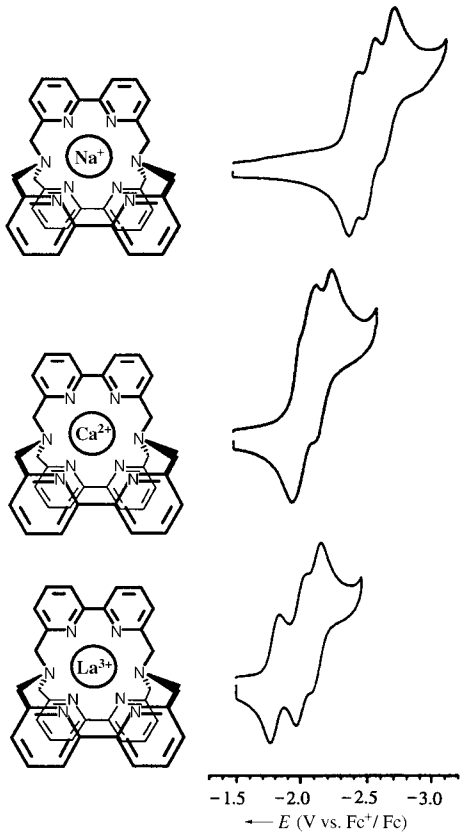


Figure 8. Cyclic voltammograms for $[Na(\mathbf{7})]^+$, $[Ca(\mathbf{7})]^{2+}$ and $[La(\mathbf{7})]^{3+}$, in DMF, 0.1 M $TBAPF_6$; Scan rate = 0.1 $V s^{-1}$ (reprinted with permission from ref. [78b]).

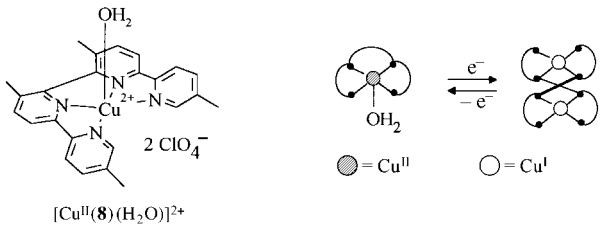
The potentials of these ligand-centered redox processes are strongly influenced by the nature of the metal ion. For example, the first reductions of $[Na(\mathbf{7})]^+$, $[Ca(\mathbf{7})]^{2+}$, and $[La(\mathbf{7})]^{3+}$ occur at −2.40, −1.98, and −1.76 V vs. Fc^+/Fc. The positive potential shift in the series Na^+, Ca^{2+}, and La^{3+} can be easily understood in terms of simple electrostatic considerations. Interestingly, $[La(\mathbf{7})]^{3+}$ showed a total of six one-electron reductions. The first three reductions correspond to the addition of one electron on each bpy unit. A noticeable gap between the third and fourth reductions reflects the electron–electron repulsion that needs to be overcome to generate the first dianionic bpy unit. Interest in the generation of new materials led to the successful electrocrystallization of $[Na(\mathbf{7})]^+$.[78a] This work is discussed in Section 8.

The electrochemistry of the $[Eu(\mathbf{7})]^{3+}$ complex has also been examined,[79] but it deviates considerably from the behavior of the systems described above. In this complex Eu^{III} undergoes reduction to Eu^{II} at -0.245 V vs. Fc/Fc^+ in DMF/$TBAPF_6$ (tetrabutylammonium hexafluorophosphate), and two pairs of poorly resolved, quasi-reversible reduction waves follow this redox couple. A number of other pyridine-based cryptates have been studied.[78b] However, for the sake of brevity they will not be described here.

4.2. Helicates

Another type of bpy-based architecture that has received considerable attention over the past decade are the helicates, which are complexes based on oligopyridine ligands that self-assemble in the presence of metal ions, to form helical structures.[80] This work was pioneered by Constable[6] and Lehn.[4] These complexes are prime examples of how redox switching can be used to control the molecular architecture.

The first reported example of a Cu^{II} system of this type was the Cu^{II}-tetramethylquaterpyridine complex $[Cu^{II}(\mathbf{8})(H_2O)]^{2+}$ [4a] (Scheme 10), prepared and characterized electrochemically



Scheme 10. Dimerization of $[Cu^{II}(\mathbf{8})(H_2O)]^{2+}$ after reduction to form a helicate.

by Lehn and co-workers. This complex can undergo monomer–dimer interconversion as a consequence of switching the oxidation state of the Cu ion. The cyclic voltammetry of $[Cu^{II}(\mathbf{8})(H_2O)]^{2+}$ shows one irreversible reduction at 0.1 V vs. SCE (Figure 9). When the potential scan is reversed after this reduction, two reversible oxidations are observed ($E_{1/2} = 0.53$ and 0.73 V vs. SCE). The reduction at 0.1 V generates $[Cu^{I}(\mathbf{8})(H_2O)]^{1+}$, which is unstable and dimerizes into $[\{Cu^{I}(\mathbf{8})\}_2]^{2+}$, a primitive helicate. The dimeric complex then undergoes two reversible oxidations (labeled $(Cu^{I})_2 \longrightarrow Cu^{II}-Cu^{I}$ and $Cu^{II}-Cu^{I} \longrightarrow (Cu^{II})_2$ in Figure 9), which lead to the mixed valence dimer $[Cu^{II}Cu^{I}(\mathbf{8})_2]^{3+}$ and the $[\{Cu^{II}(\mathbf{8})\}_2]^{4+}$ dimer, respectively. The latter eventually decomposes to regenerate the monomeric $[Cu^{II}(\mathbf{8})(H_2O)]^{2+}$ complex, albeit on a longer time scale. The monomeric Cu^{II} complex exists as a tetragonal pyramid with an apical water molecule, whereas the dimeric Cu^{I} complex exists as a dinuclear species with helical structure in which each metal center has a distorted tetrahedral environment. The difference in the half-wave potentials for the oxidation of the Cu^{I} ions in the $[\{Cu^{I}(\mathbf{8})\}_2]$ dimer indicates that the metallic centers are not electronically independent of one another. For a detailed discussion of this fascinating system the reader is referred to reference [4a].

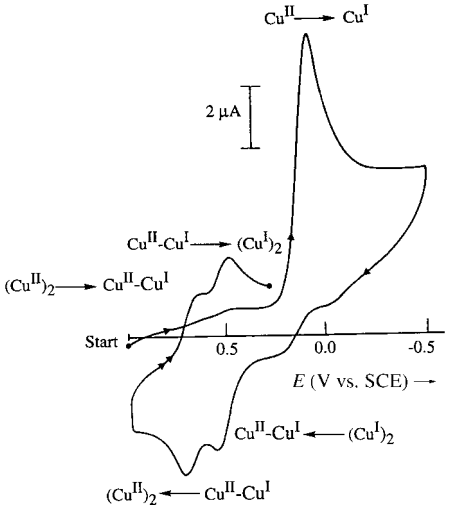
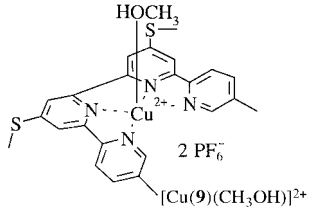


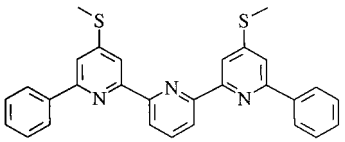
Figure 9. Cyclic voltammogram for $[Cu^{II}(\mathbf{8})(H_2O)]^{2+}$ in CH_3CN, 0.1 M NEt_4PF_6; scan rate = 0.1 $V s^{-1}$ (reprinted with permission from ref. [4a]).

Lehn and co-workers have extended their work on the design of oligobipyridine ligands to include from two to five bipyridine ligands bridged by 2-oxapropylene linkages.[4b–d] They have also prepared Cu^{II} complexes based on oligoterpyridine structures.[4e] Constable et al. have also examined a number of oligopyridine systems,[6] complexed with a variety of transition metal ions, including a quinquepyridine ligand bearing pendant "redox spectator" ferrocene moieties.[6b] Many of these systems have been characterized electrochemically. Additionally, the electrochemical behavior of an entire series of alkylthio-substituted 2,6-oligopyridines has been reported in detail by Abruña, Potts, and co-workers.[5a–d] These authors first reported the electrochemical behavior of Cu^{II} complexes of ligand **9**, a methylthioquaterpyridine.

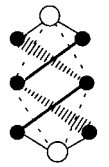


The voltammetric results obtained for $[Cu^{II}(\mathbf{9})(CH_3OH)]^{2+}$ differ somewhat from those reported for the analogous $[Cu^{II}(\mathbf{8})(H_2O)]^{2+}$. While both the Cu^{II} complexes of ligands **8** and **9** clearly dimerize upon reduction to the corresponding Cu^{I} complex, only a single wave for the oxidation to the Cu^{II} state is observed (in DMSO or DMF/TBAP) in the case of **9**; that is, no mixed valent state is apparent.[5a] Furthermore, the time scale for the regeneration of monomeric $[Cu^{II}(\mathbf{9})(CH_3OH)]^{2+}$ appears to be much shorter for the thio-substituted complex. Additionally, there is a notable difference in the $Cu^{II} \rightarrow Cu^{I}$ reduction potentials (+0.13 V vs. SSCE for $[Cu^{II}(\mathbf{8})(H_2O)]^{2+}$ and -0.07 V vs. the sodium-saturated calomel electrode (SSCE) for $[Cu^{II}(\mathbf{9})(CH_3OH)]^{2+}$) that cannot be accounted for by the negligible difference between the reference electrodes. It was proposed[5a] that such a difference might be due to the different solvents used in these studies: interaction of CH_3CN with the metal center might affect the reduction of $[Cu^{II}(\mathbf{8})(H_2O)]^{2+}$. $[\{Cu^{I}(\mathbf{9})\}_2]$ undergoes four reversible or quasi-reversible ligand-centered reductions at -1.38, -1.58, -1.83, and -2.02 V vs. SSCE. Spectroelectrochemistry of this system was also reported.[5a]

The electrochemical behavior of helical complexes based on oligopyridines from quater-, quinque-, sexi-, and septipyridine have been reported.[5a–c, 6] The structural variations observed for these helicates become more complicated as the length of the ligand increases. Cu^{II} complexes as well as Ni^{II}, Ag^{I}, Fe^{II}, Co^{II}, Zn^{II}, and Pd^{II} oligopyridine complexes have been electrochemically characterized.[5, 6] The potential difference between the redox processes that involve the metal centers of the helicates reflects the degree of interaction between the metal ions. For example, a 860 mV difference between the two successive Cu^{II}/Cu^{I} redox processes was observed for $[\{Cu^{I}(\mathbf{10})\}_2]$, where **10** is a methylthiodiphenyl-substituted terpyridine.[5c]



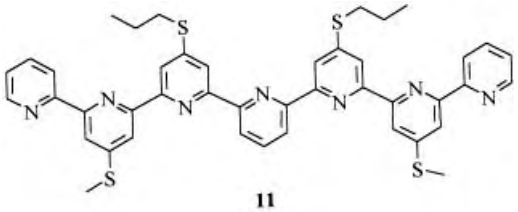
10



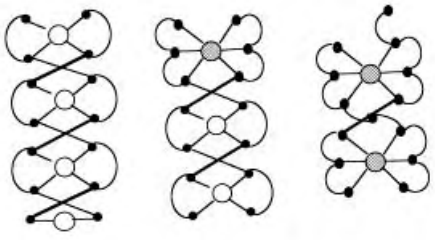
○ = Cu^{I}

The large potential difference for the reductions indicates a strong interaction between the two copper centers in the dimeric species. This agrees well with the solid-state structural data obtained on the dimeric complex which gives a $Cu^{I}-Cu^{I}$ distance of 2.6 Å.

The ultimate example of how electrochemistry can influence the structure of helicates is that of ligand **11** (Scheme 11).[5d] This ligand was used to generate bi-, tri-, and trametallic



11



○ = Cu^{I} ● = Cu^{II}

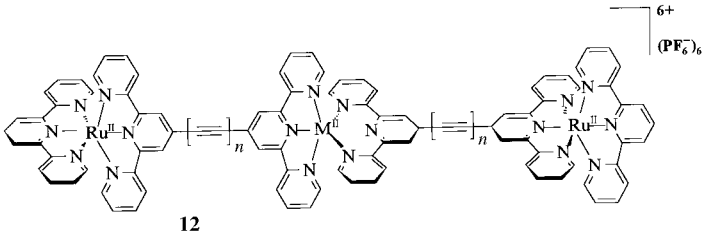
Scheme 11. Bi-, tri-, and tetranuclear complexes with ligand **11**.

species containing two Cu^{II} ions, two Cu^{I} and one Cu^{II}, or four Cu^{I} ions. In each complex, the Cu^{II} ions are expected to have an octahedral geometry and the Cu^{I} ions a tetrahedral geometry. However, whereas the dimetallic species was confirmed to have octahedral symmetry, the tetrametallic species shows evidence of a D_2-diamondlike symmetry.[5d] The Cu^{II}/Cu^{I} redox waves for $[\{Cu^{II}(\mathbf{11})\}_2]$ are quasi-reversible and located at 0.05 and 0.24 V vs. SSCE. For the trimetallic complex $[Cu^{I}(Cu^{II})_2(\mathbf{11})_2]$, the Cu-centered oxidations appear at 0.01, 0.43, and 0.82 V vs. SSCE and, as in the case of the bimetallic species, are quasi-reversible. The tetrametallic complex $[Cu^{I}_4(\mathbf{11})_2]$ undergoes four reversible one-electron oxidations involving the Cu centers at $E_{1/2} = 0.02$, 0.44, 0.84, and 1.08 V vs. SSCE. Thus, the bi-, tri-, and tetrametallic complexes all show interaction between the Cu centers. The reported ligand reductions in the tetra- and trimetallic complexes appear to differ markedly, a finding not noted in the smaller oligopyridine helicates. Reduction of the ligands were noted at -1.11, -1.27, and -1.49 V (the latter irreversible) vs. SSCE in the tetrametallic complex, while the same processes occur at -1.42, -1.62, and -1.83 V (the latter irreversible) vs. SSCE in the trimetallic complex. The transformation from the tetrametallic to the dimetallic complex was relatively slow, and spectroelectrochemical results suggested that multiple species are present and that a simple equilibrium does not exist.

One final report deserves to be mentioned in this section. Shanzer and co-workers recently prepared a triple helical system bearing bipyridine moieties.[81] This helical structure provides a coordination site for an Fe^{II} ion (bipyridine) or an Fe^{III} ion (hydroxamate). By switching the redox state of the Fe center, the ion reversibly translocates from one end of the helix to the other. Although the redox switching was accomplished chemically rather than electrochemically, this system provides a fine example of a self-assembled redox-switchable helical complex. The authors are pursuing anchoring these complexes onto conducting surfaces.

4.3. Pyridine-Based Molecular Wires

Molecular wires have been a topic of interest over the past several years.[82] We mention here a recently prepared alkyne-bridged, terpyridine-based system prepared by Harriman and Ziessel, who reported a mixed metallic wire structure **12**, containing two Ru^{II} ions and a different central ion (Zn^{II}, Fe^{II},



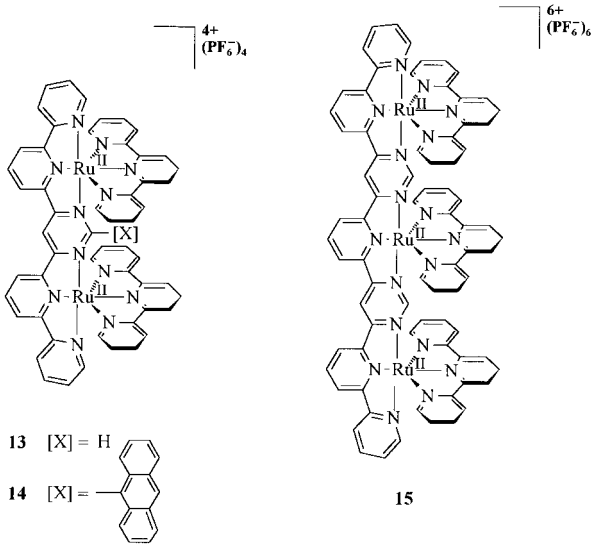
12

or Co^{II}).[83] The half-wave potentials for the oxidation of the Ru^{II} center in these complexes are similar to those of the parent terpy complexes, and the number of bridging alkyne units ($n = 1$ or 2) have only a small effect on the oxidation or reduction potentials of the Ru^{2+} metal centers.

4.4. Racks, Stacks, and Grids

Another very current topic is the preparation of rack molecules that self-assemble in the presence of transition

metal ions.[84] Several examples of these complexes have recently been published.[85] The electrochemistry of some of these[85b] (structures **13**–**15**) is described here.



13 [X] = H

14 [X] =

15

The crystal structure of **14** displays octahedral coordination geometry about the Ru^{II} centers. The CV of **13** reveals two Ru-centered reversible oxidations at 1.41 and 1.57 V vs. SCE, while the bipyrimidine units are reversibly reduced at -0.43 and -1.03 V vs. SCE, and the terpyridine units are irreversibly reduced at $E_{pc} = -1.50$ and -1.59 V vs. SCE. A stripping peak at -1.40 V indicates absorption of the neutral species. The electrochemical behavior of **14** is similar, indicating that the anthryl spacer does not perturb the electrochemical properties of the complex. The Ru–Ru distance in **14** is 6.40 Å, which suggests a rather weak interaction between the two metal centers. The voltammetry of the trimetallic rack **15** is different, since the oxidations of the Ru^{II} ions occur in two steps, a two-electron wave at $+1.47$ V and a single-electron wave at $+1.88$ V vs. SCE. The latter process is assigned to the central Ru^{II} ion, which is likely to be more difficult to oxidize when placed between the two centers of higher charge. The ligand-based reductions in this system occur at -0.33 and -1.28 V for the bipyrimidine centers, and at -1.62 V (vs. SCE) a single irreversible adsorption wave is noted for the terpyridine units.

Lehn and co-workers are presently working on more complex systems involving ladders and grids that self-assemble in the presence of various transition metal ions.[86] Based on the results obtained for the helicates and rack complexes, the electrochemistry of these new molecular structures should be quite interesting.

4.5. Pyridine Dendrimers

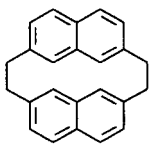
A final topic of current interest in the field of pyridine-based systems is the preparation of pyridine-bearing dendrimers.[45] The high molecular weight of these compounds and the limited availability of material renders their electrochemical characterization challenging. Balzani et al. were among the first to report a decanuclear structure complexed to Ru^{II} and/or Os^{II}, based on a bridging bis(pyridyl)pyrazine ligand and bipyridine or biquinoline ligands.[87] These authors reported the differential pulse voltammetry of these complexes. Puddephatt and co-workers reported a bipyridine-based ligand coordinated to Pt^{II} ions,[88] while Constable et al. reported a simple terpyridine-based ligand that can be used to construct Ru^{II}(terpy) arborols.[89] A common finding for these compounds is that the redox active sites are reduced at the same potential, that is, they are not coupled. Recent work of Echegoyen and Newkome confirm these results.[90] A terpyridine dendrimer that was expanded over several generations showed waves corresponding only to the two reductions of the terpy unit. As with the porphyrin dendrimers mentioned in Section 3, the reversibility of the redox processes suffers as the dendrimer becomes more sterically hindered over successive generations.

5. Cyclophane-Based Systems

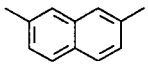
This class of compounds has been extensively studied over the last three decades, although electrochemical studies of redox-active cyclophane systems have been comparatively few. Much of the early work in this field was centered on metal complexes of simple cyclophane systems, while more recent work pursues redox-switchable binding with various guests. The electrochemical studies of cyclophane systems can be divided into three general areas: 1) electroactive cyclophanes, 2) systems involving metal coordination to cyclophanes (metallocyclophanes), and 3) cyclophanes as components of catenanes, rotaxanes, and shuttles. Calixarenes, which are a special class of cyclophane, are discussed in Section 6.

5.1. Early Studies with Cyclophanes

The early work on electroactive cyclophanes, such as the studies of Wasielewski and co-workers[91] or Sato et al.,[92, 93] aimed at investigating the electrochemistry of closely positioned redox-active centers. For example, in the naphthalene-based cyclophane **16** and its model compound 2,7-dimethylnaphthalene **17**, conformational isomerism was found to be an important determinant of the redox chemistry:[92] The oxida-



16



17

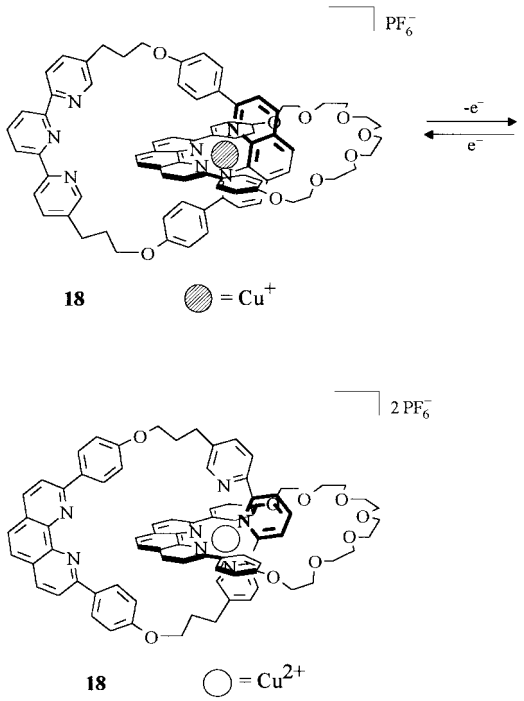
tion of the model compound **17** occurs in one step, as does that of the *cis* isomer of **16**, whereas the *trans* isomer of **16** is oxidized in two distinct steps.[92] This latter finding indicates electronic coupling between the two naphtalene units of *trans*-**16**. Some of the cyclophanes studied by these authors were

easier to oxidize than their model compounds by as much as 1 V. This is evidence for charge delocalization. A series of simple metacyclophanes with various substituents,[93] and of larger [2*n*]paracyclophane systems[94] were also characterized electrochemically in these early studies.

5.2. Metallocyclophanes

Interest in the iron and ruthenium complexes of [2*n*]cyclophanes and their electrochemistry began with the work of Boekelheide et al.,[95] but complexes with other transition metals have also been studied.[96] More recently, iron–sulfur clusters in a cyclophane cage[97] and a diamagnetic diiron–[2.2]paracyclophane complex[98] have been studied. Metal complexes of porhyrin-based cyclophanes are currently a topic of interest, studied by Staab, and co-workers[99] and Diederich et al.[100]

In the area of metal complexes of cyclophanes, an elegant example studied by electrochemistry was recently provided by Sauvage and co-workers: linkage isomerism in a catenane system **18** that contains an interlocking diphenylphenanthroline (dpp) and terpyridine (terpy) cyclophane and a dpp crown ether as metal binding ligands (Scheme 12).[101] As in

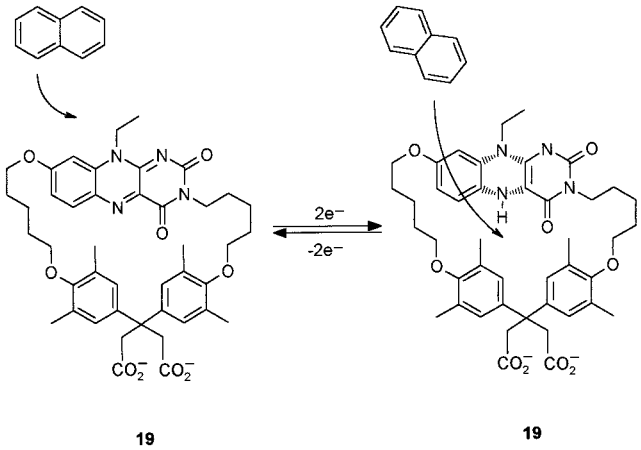


Scheme 12. The "swinging catenate" **18**: tetracoordination (top) and pentacoordination of the copper ion.

the case of the helicates, changes in the redox state of the coordinated copper ion provides redox-switchable binding to components of the catenane system. The cyclophane component of the "swinging catenate" structure **18** is capable of binding copper(I) or copper(II). Reduction of copper(II) to copper(I) results in a rearrangement from a five-coordinate (terpy/dpp, CN = 5) structure favored by copper(II) to a four-coordinate (dpp/dpp, CN = 4) copper(I) structure. The electrochemical processes are reversible in both the four-coordinate and five-coordinate species, with half-wave potentials of 0.63 V and −0.07 V vs. the saturated calomel electrode (SCE), respectively, in CH_3CN. The more negative reduction potential of the five-coordinate species reflects the greater stabilization of copper(II) in this complex. The time scale for the coordination processes was noted to be very different for the forward and reverse steps. While the oxidation $Cu^I \rightarrow Cu^{II}$ results in a slow (on the order of days) sliding of the cyclophane into the five-coordinate structure, the reverse process, reduction back to Cu^I, restores the four-coordinate geometry in a matter of seconds. The slower kinetics of the overall forward process has been attributed to other concomitant conformational changes.

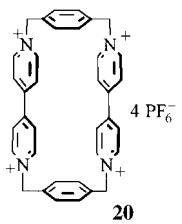
5.3. Switchable Cyclophanes, Catenanes, Rotaxanes, and Shuttles

Within the past decade, attention has centered on the molecular binding capabilities of redox-switchable cyclophanes. In 1990 Diederich and co-workers were the first to report a redox-switchable cyclophane system.[2d] A flavin cyclophane, or flavinophane (**19**, Scheme 13) as termed by the

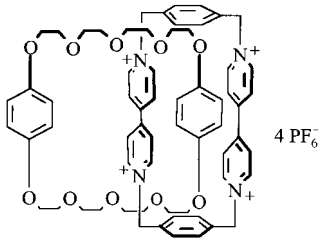


Scheme 13. Different binding modes of flavinophane **19**: the oxidized form (left) favors the binding of naphthalene at an external site, whereas the reduced form (right) forms inclusion complexes.

authors, displayed switchable binding ability due to a change in the geometry of the isoalloxazine unit from a planar to a "butterfly," or bent state, after a 2 e^- reduction. The reduced form of compound **19** formed inclusion complexes with naphthalene derivatives, while the oxidized form displayed external association. The association constants for these complexes are similar. The 2 e^- reduction of **19** is quasi-reversible and occurs at −0.581 V vs. Ag/AgCl in an aqueous borate buffer at pH 10.



The electrochemistry of **20** has been the subject of considerable attention.[102] This cyclophane has been elec-



21

trochemically characterized as a component of catenanes (**21**),[102c, 102e, 102f] rotaxanes (**22**),[103] and molecular shuttles (**23**).[3a] Thus, **20** can be used to exemplify effects on the redox properties of a cyclophane when it is embedded in more complicated architectures. In addition, **20** can also be used to demonstrate how electrochemistry can control the structure of a supramolecular assembly. The reversible redox processes are characteristic of the parent methylviologen unit;[102f] that is, each viologen unit can undergo two monoelectronic redox processes.

Figure 10 shows the cyclic voltammetric behavior of cyclophane **20** and that of the same cyclophane as a component of catenane **21**.[102e] The first wave in Figure 10a, a two-electron

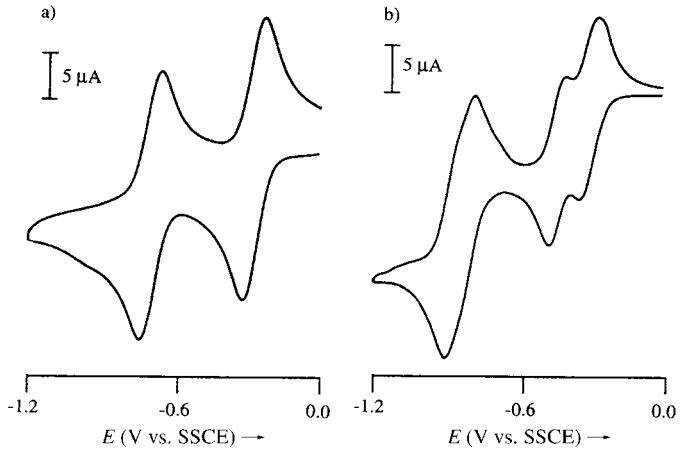


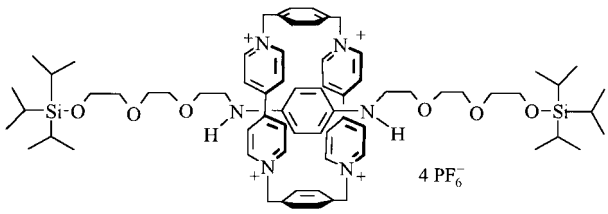
Figure 10. Cyclic voltammograms of 0.50 mM solutions of cyclophane **20** (a) and catenane **21** (b) in CH_3N, 0.1 M $TBAPF_6$; scan rate = 50 mV s^{-1}, 25°C (reprinted with permission from ref. [102e].).

process, corresponds to the reduction of the two viologen moieties (one electron each) of **20** to their corresponding cation radicals at −0.279 V vs. SSCE in $CH_3CN/TBAPF_6$, while the second wave (two electrons) corresponds to their subsequent reduction to the neutral viologens, which occurs at −0.703 V. Clearly no electronic coupling is evidenced by the voltammetry.[104] In contrast, catenane **21** exhibits three waves, the first two of which correspond to the separate monoelectronic reductions of the two viologen moieties (Figure 10b).

The reduction of the first viologen unit occurs at −0.307 V and the second at −0.438 V. The final two-electron reduction occurs as a single redox wave (reduction of both viologens to their neutral state) at −0.841 V. The fact that two separate reductions are observed for the first redox processes is attributed to the topological differences between the "inside" and "outside" viologen units in the catenane. The inner viologen is stabilized to a greater extent by the two-electron-rich hydroquinone units, while the "outside" viologen interacts with only one of these units. Interestingly, subsequent work on a related surface-attached catenane comprising **20** and a bis(thiol)-terminated poly(ether) hydroquinone thread does *not* show a splitting of the first reduction processes, but rather exhibits behavior similar to that of free **20** in which the first reduction of the two viologen moieties occurs as a single two-electron wave.[105]

Catenanes containing cyclic crown ethers with napthyl spacers in combination with **20** or cyclophanes with π-extended viologens have recently been examined by Stoddart and Balzani.[106] The electrochemistry of **20** in these naphthyl-bearing catenanes exhibits split waves for both the first and the second viologen reduction waves. Cyclophane **20** has also been used as a component of a series of novel [3]pseudocatenanes containing TTF-based macrocycles (TTF = tetrathiafulvalene).[107] The orientation of the cyclophane bead about the TTF moiety affected the electrochemical reversibility of the oxidation of the TTF moiety.

Cyclophane **20** has recently been used as the bead component in a rotaxane.[103] In structure **22**, both the cyclophane bead and the thread are electroactive and exhibit



22

reversible electrochemistry (Figure 11). Rotaxane **22** shows two redox waves for the first reduction of the viologen moieties at −0.272 V and −0.362 V vs. Ag/AgCl in CH_3CN/

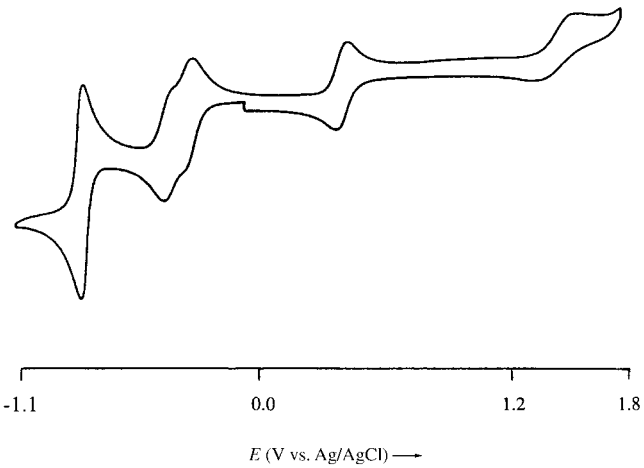
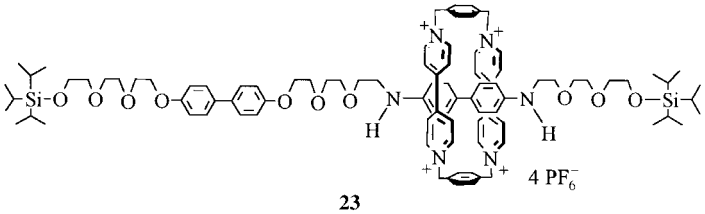


Figure 11. Cyclic voltammogram of rotaxane **22** in CH_3CN, 0.10 M $TBAPF_6$; scan rate = 200 mV s^{-1}; 25°C (reprinted with permission from ref. [103]).

$TBAPF_6$. The second electron transfer to the viologen moieties occurs in a single step at a half-wave potential of −0.780 V vs. Ag/AgCl. While the free thread exhibits two oxidation waves at 0.203 V and 0.732 V, the thread in the

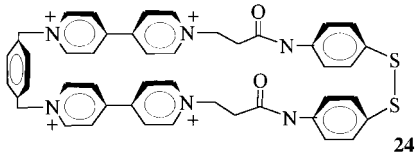
rotaxane undergoes oxidation at 0.463 V and 1.505 V (all potentials vs. Ag/AgCl). Electron transfer is thus slower, reflecting the unfavorable electrostatics.

In the molecular shuttle **23**, which contains cyclophane **20** and a thread with benzidine and biphenyl stations,[3a] the electrochemistry of **20** is similar to that of the *free* cyclophane, with two-electron reductions in single waves at -0.235 V and -0.755 V vs. Ag/AgCl in CH_3CN. Relative to that of the free benzidine thread, the first oxidation of the benzidine station in **23** occurs at a more positive potential (0.570 V vs. Ag/AgCl), whereas the second oxidation occurs at a comparable potential value (0.720 V). The difficulty of the first oxidation of the benzidine station is attributable to the stabilizing presence of the cyclophane **20** bead, while the ease of the second oxidation (comparable to that of the free elongated benzidine thread) indicates that **20** has shuttled off the benzidine station to the other portions of the thread, presumably to the second (weaker) donor biphenyl station.



23

Analytical applications for **20** have also been explored: this redox-switchable receptor binds both aromatic amino acids and neurotransmitters.[108, 10d] While the solubility of **20** in organic solvents is high even in its fully reduced neutral state, its solubility in aqueous solution in the reduced state is quite poor and results in precipitation on the electrode surface. Kaifer et al. conducted binding studies with Nafion-modified electrodes.[10d] Differential pulse voltammetry of **20** was useful in the detection of binding to catechol and indole and their related neurotransmitters in the micromolar concentration range. The half-wave potential shifts exhibited by the host–guest complex were modest (10–70 mV).[10d] This work was recently extended with the self-assembly of a surface-attached cyclophane capable of molecular recognition.[109] Compound **24** self-assembles through thiol bonds with the gold electrode surface. Binding of catechol and indole at an even lower concentration range has been achieved.



24

6. Calixarene Systems

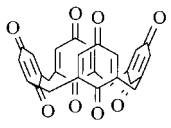
The calixarenes are a special class of cyclophanes capable of binding both neutral and charged guests. Electrochemical analyses of these systems may be divided into two broad areas: 1) electroactive calixarenes, in which the redox unit is an integral part of the σ-bonded framework, and 2) complexes of electroinactive calixarenes with electroactive guest species. The electroactive calixarenes may be further subdivided into two groups, those with the redox-active unit in the main cyclophane framework (e.g., where the phenolic groups are transformed into nitroaromatic or quinone units) and those containing electroactive pendant groups covalently attached as tethers.

6.1. Electroactive Calixarenes

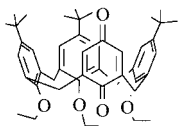
The interest in electroactive calixarenes revolves around the type, number, and location of the electroactive groups in the macrocycle. If the redox units are within the cyclophane framework, the overall size of the calixarene (as represented by the common nomenclature calix[4], calix[6], etc.) is important in understanding its redox behavior. In smaller calixarene systems, such as the calix[4]arenes, the constraints of distance and rotational flexibility are expected to influence the electrochemical behavior of the redox-active units in the basic framework dramatically. The close proximity of neighboring redox units in smaller calixarenes should have strong effects on the redox behavior. Identical neighboring redox units should reduce sequentially as opposed to simultaneously if electronic communication exists between proximal units.[104] On the other hand, the electrochemistry of pendant electroactive groups should be affected less by the size of the calixarene ring, although this may not always be the case.

6.1.1. Calixquinones

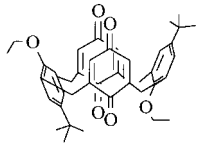
The calixquinone series **25**–**28** provides a prototypical example of electroactive calixarenes. The first compound of the series the calix[4]quinone (**25**) was synthesized and its electrochemistry reported in 1989.[110–112] Interest in the other calixquinones quickly followed.[113–117]



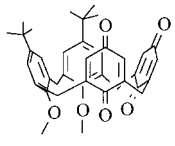
25



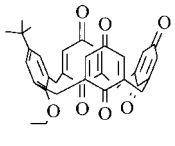
26



27a



27b



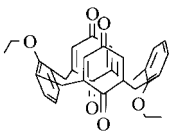
28

In general, compounds functionalized with quinones are capable of undergoing two-electron reductions for each quinone, the first of which is generally reversible, while the second is typically quasi-reversible.[22] The presence of protons complicates the electrochemical behavior of quinones.[22]

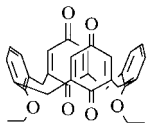
The redox potentials of quinones in the calix[4]quinone series **25**–**28** were found to be dependent upon the number of quinone units present as well as their respective locations[115]

and orientations.[114a] Successive quinone substitutions resulted in a greater ease of reduction, that is, a shift of the half-wave potentials to more positive values, due to electron withdrawing effects. For example, the first reduction potential of triethoxycalix[4]monoquinone (**26**) in $CH_3CN/TBAPF_6$ occurred at -0.823 V vs. Ag/AgCl, whereas for the related 1,3-diquinone **27a** the first electron reduction is -0.699 V.[115] The placement of the quinones is important for the contrasting electrochemical behavior in the isomeric diquinone compounds **27a** and **27b**,. The 1,2-substituted system **27b** is reduced more readily (by about 70 mV) than the related 1,3-substituted system **27a**. This behavior indicates that the adjacent quinone units in **27b** have a stronger electronic communication than those in the 1,3-isomer **27a**. The potential gap between successive reductions reflects the extent of this electronic communication between the neighboring redox sites. In **27a**, where the quinone moieties are opposite each other, the potential gap between the first reductions of the first quinone and second quinone units is 140 mV. In **27b** this gap increases to 300 mV. Conformations of the calix[4]quinones have been found to influence the potentials of the first and second electron reductions in the diquinones by as much as 45 mV.[114a]

The voltammetry in $CH_2Cl_2/TBAPF_6$ of chromatographically separated **29** and pure **30** revealed that the reduction of the first quinone was only slightly more positive (5 mV) in **29**



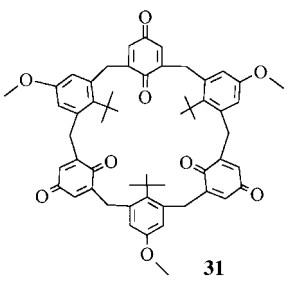
29



30

(-0.760 V vs. SCE) than reduction of the corresponding quinone unit in **30**.[114a] The effect on the *second* reduction is more pronounced, however: as the potential difference between the first and second reductions of the quinone units in **29** and **30** is 145 and 95 mV, respectively. Thus, it appears that electronic coupling between the quinone sites is stronger in the partial cone conformer **29** than in **30**.

As the calixquinone ring is enlarged on going from the calix[4] to the calix[6] and calix[8] series, the more conformational mobility leads to the electrochemical behavior typically observed for systems bearing multiple, noninteracting, identical redox units.[104] For instance, in a 1,3,5-triquinone calix[6]arene (**31**)[118] all three quinone units are reduced simultaneously at -0.587 V vs. Ag/AgCl. This contrasts with the behavior of calix[4]di- or triquinone systems, in which each quinone unit is reduced at a different potential (Figure 12).[115, 118]



31

Conceptually, the calix[6]triquinone **31** is a simple extension of the calix[4]diquinone **27**, with alternating quinone and arene units. Though the simultaneous quinone reduction

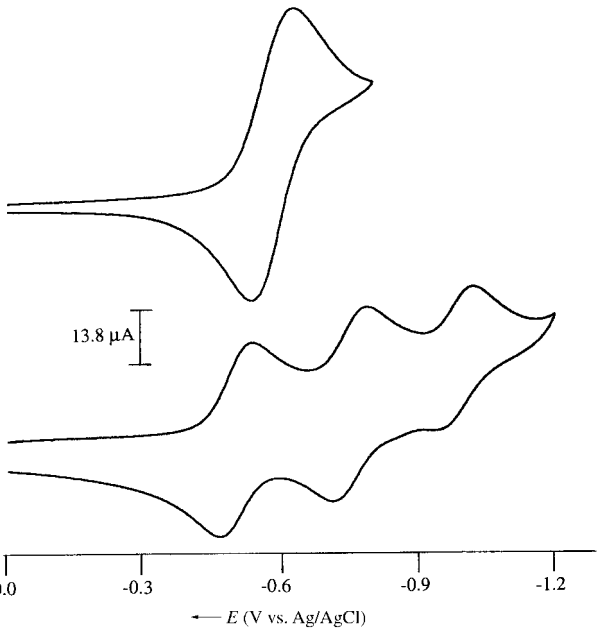


Figure 12. Cyclic voltammograms for the reduction of 1 mM solutions of calix[4]arenetriquinone (**28**)[115] (bottom) and calix[6]arenetriquinone (**31**)[118] (top) obtained on a glassy carbon electrode in CH_3CN, 0.10 M $TBAPF_6$; scan rate = 100 mV s^{-1}, 22°C.

observed in **31** would appear to be a consequence of the greater conformational mobility afforded by the larger framework, results with a series of calix[6]diquinones[119] suggest that this may not always be the case, vide infra.

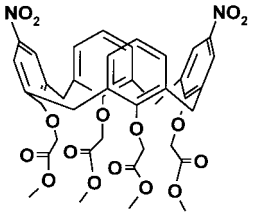
6.1.2. Cation Binding by Calixquinones

As expected, binding of calixarenes with alkali, alkaline earth, or transition metal ions, or with ammonium ions, has an effect on their electrochemistry.[115–117] The first electron reduction potentials of these compounds with binding constant on the order of those exhibited by the crown ethers shift anodically between 90–600 mV in the presence of a bound ion, corresponding to sizable binding enhancements.[115–117] Recent work has also suggested that binding to ions can affect the conformations of calixarenes.[120, 121] This point has not been directly noted as a significant factor when interpreting the electrochemistry of the free and bound calixarenes, but the finding that different conformations[114a] may well have (albeit slightly) different reduction potentials does make conformational change an important consideration when determining binding constants by electrochemical methods. Care must be exercised to assure that any potential shift used to estimate binding or binding enhancements does not include a component due to a concomitant change in the conformation of the calixarene.

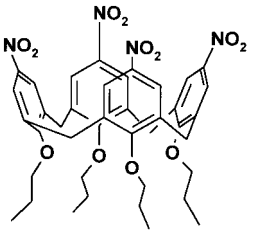
6.1.3. Nitroaromatic Calixarenes

Calixarenes with nitro groups in the *para* position of the phenol rings (nitroaromatic calixarenes) have been prepared,[122] and these exhibit slightly different electrochemical behavior. In contrast to results obtained for **26**, a symmetrically 1,3-

substituted calix[4]nitroarene tetramethylester **32** undergoes a quasi-reversible single-electron reduction at each nitroaromatic unit at -1.22 V vs. Ag/AgCl in CH_2Cl_2/TBAPF$_6$.[119]

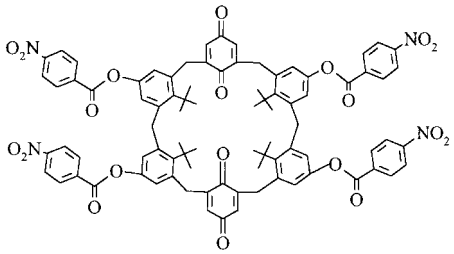


32



33

The cyclic voltammetry of a calixarene bearing four nitroaromatic groups (**33**) shows two two-electron reduction waves.[119] Each wave corresponds to the simultaneous reduction of diagonally opposite pairs of nitroaromatic units. A calix[6]diquinone bearing four pendant nitroaromatic esters (**34**) has also been examined.[119] In CH_2Cl_2/TBAPF$_6$ the



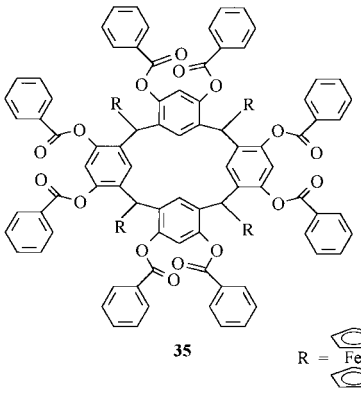
34

reversible first electron reduction for each of the quinones occurs at different potentials (-0.472 and -0.785 V vs. Ag/AgCl), reminiscent of the observations with **27a** and **27b**. The bulky lower rim substituents may introduce greater conformational rigidity than would normally be anticipated for the larger calix[6] system and permit greater electronic communication between the quinones than would be expected for this larger system. The second electron transfers, to the quinone radicals, occur simultaneously at -1.15 V vs. Ag/AgCl and are quasi-reversible. The four pendant nitroaromatic units are then reduced simultaneously at -1.50 V vs. Ag/AgCl in a quasi-reversible electron transfer process.

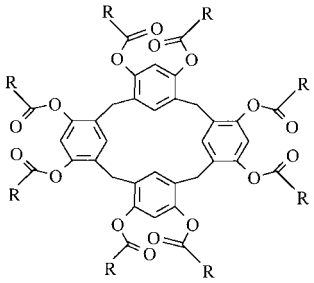
6.1.4. Calixarenes with Pendant Electroactive Groups

Attachment of pendant electroactive groups to the upper, lower, or methylene side-arm positions has been explored by several groups. Recently, Beer and co-workers utilized pendant lower rim pyrrole moieties to electropolymerize calix[4]arenes onto the surface of a glassy carbon electrode.[123] Other compounds that have been reported include calix[4]arenes and resorcinarenes with pendant metallocene units,[124] with a pendant $\{Ru(bpy)_3\}^{2+}$ group,[125] and a calix[8]arene with a pendant C_{60}.[126] The ferrocenyl resorcinarenes[124b] provide an interesting comparison between the electrochemical behavior of ferrocenyl substitution at the methylene bridge sites and that observed when the units are appended to the upper rim.

Compound **35**, a resorcinarene substituted at the methylene bridge positions, shows two separate cyclic voltammetric peaks (+0.60, +0.69 V vs. SCE) corresponding to two mono-



35



36

electronic processes.[124b] The two reversible waves have been ascribed to the two differing ferrocenyl environments detected in ^{1}H and ^{13}C NMR studies. In contrast, an upper rim substituted ferrocenyl resorcinarene analogue (**36**) demonstrated a single reversible oxidation wave in which the eight ferrocenyl units are independently oxidized at roughly the same potential (0.89 V vs. SCE).[124b] This result agrees with the fact that, in the latter case, the ferrocene units are farther apart from one another than they are in **35**.

6.2. Calixarene Complexes with Electroactive Guests

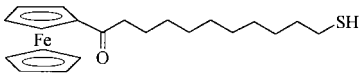
Another area where electrochemical studies have been useful is in the study of complexes of calixarenes with electroactive species. In complexes between sulfonic acid calix[6]arenes and surface-attached ferrocene units,[127] as well as dissolved viologen[128] and ferrocene,[129, 130] the presence of the calixarene has been shown to affect the electrochemistry of the included guest.[127–130]

A particularly striking example is the complex between the ferrocenethiol **37** and the sulfonated host calix[6]arene **38**.[127] Compound **37** self-assembles on the surface of smooth gold electrodes and exhibits surface-confined electrochemistry. It is oxidized at a half-wave potential of 0.51 V vs. SSCE. In the presence of submicromolar amounts of **38**, the single voltammetric wave observed for pure surface-confined **37** is split into two waves, corresponding to the oxidation of the free and bound ferrocene sites. At 2 μM, a single wave is observed for **38** at the formal potential of the bound ferrocene, which occurs 90 mV more positive than that of the unbound, surface-confined ferrocene.

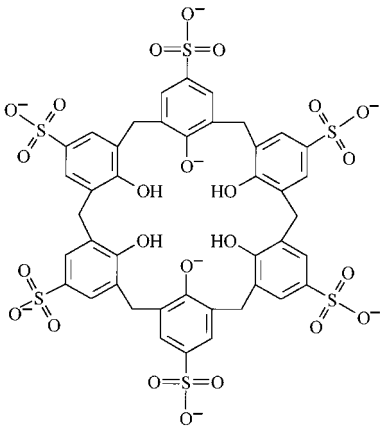
7. Fullerene-Based Systems

7.1. Fullerene Inclusion Complexes: Fullerenes as Hosts and as Guests

Complexes between calixarenes and fullerenes have also been of interest to a number of authors.[126, 131–135] Two types of

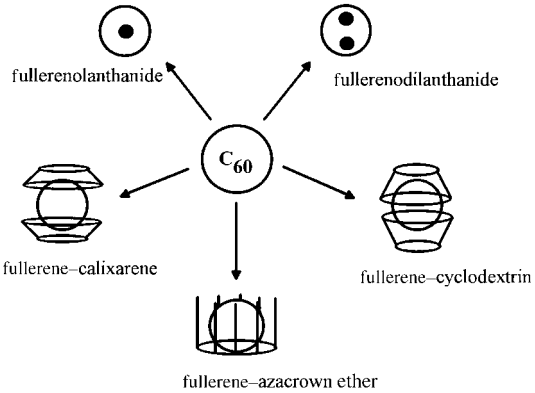


37



38

fullerene inclusion structures have been electrochemically characterized. In the first type, called endohedral fullerenes,[136] the fullerene is host to a small molecule or ion such as a lanthanide cation, while in the second type the fullerene is embedded in the cavity of a larger molecule such as a cyclodextrin,[137a–c, 137f] a calixarene,[126, 131–135, 137d] or a crown ether[137e] (Scheme 14).



Scheme 14. Supramolecular host–guest complexes with fullerenes.

7.1.1. Fullerenes as Hosts

Endohedral structures have been synthesized[136] with C_{82}, C_{84}, and C_{86} as hosts with lanthanide cations (La^{3+}, Y^{3+}, Sc^{3+}, Ce^{4+}…) as guests. These compounds are designated by the formula $M_m@C_{2n}$ where M is the lanthanide, C_{2n} the carbon cage, and $m = 1$, 2, or 3. These supramolecular structures are conceptually very intriguing, since they are formed from the ionic association between an anion (fulleride) of charge n^- and a cation (lanthanide) of charge n^+ which cannot escape from the anion. In the strictest sense of the word, these cannot be considered classical complexes, since the ion pairing interactions are not really the only ones holding together the complete structure. As a matter of fact, endohedral structures of C_{60} with noble gases are known,[138] and these are definitely not complexes, but more like "molecular rattles." In these, the noble gas molecule is incarcerated inside the fullerene but is not truly held by intermolecular electronic forces. In a way they are analogous to the catenanes, where two or more molecules are held together like the links of a chain.

The electrochemistry of fullerenolanthanides[139] is completely different from that of empty fullerenes, which usually displays equidistant one-electron reductions.[140, 141] Even though the fullerenolanthanides can be reduced by stepwise electrode processes, these reductions are not equally spaced on the potential scale, and they do not correspond always to one-electron processes. For example, $Y@C_{82}$ and $Gd@C_{82}$ undergo four reductions, but the second one is a two-electron process (Figure 13).

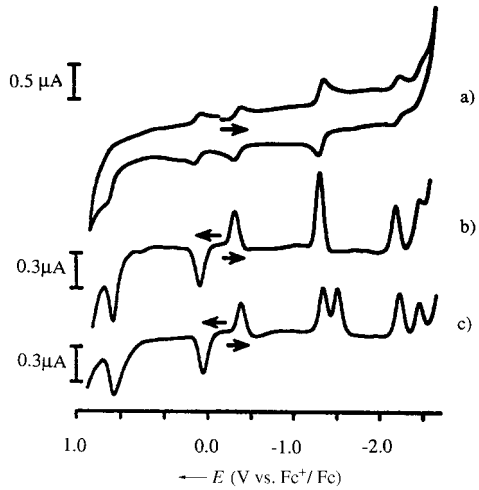
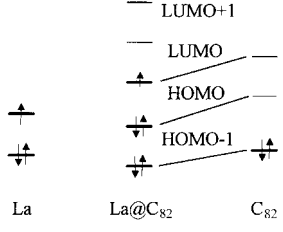


Figure 13. a) Cyclic voltammogram of $Y@C_{82}$; scan rate 20 mV s^{-1}. b) and c) Differential pulse voltammograms of $Y@C_{82}$ (b) and $La@C_{82}$ (c) in 1,2-dichlorobenzene, 0.1M $TBAPF_6$; scan rate 20 mV s^{-1} (reprinted with permission from ref. [139b]).

On the other hand, $La@C_{82}$ and $Ce@C_{82}$ undergo five distinct one-electron reductions (Figure 13). An explanation for such a peculiar electrochemical behavior for the fullerenolanthanides is still needed. Another noticeable characteristic of the electrochemistry of fullerenolanthanides is that all undergo a relatively easy reversible one-electron oxidation (see Figure 13). This might reflect the single occupancy of the HOMO for these complexes, where the metal ion is in its +3 oxidation state (Scheme 15). In other words, the ease of the first oxidation of fullerenolanthanides may be because removal of one electron in $M^{3+}@C_{82}$ leads to a closed-shell species.[139]



Scheme 15. Schematic MO diagrams of La, $La@C_{82}$, and C_{82}.

Changing the nature of the metal inside the cage affects the electrochemistry of the endohedral fullerenes only slightly. It was proposed[139b] that the 4f orbitals of the lanthanide cations do not play a significant role in the electrochemistry of fullerenolanthanides and that the first reduction and the first oxidation occur on the Singly Occupied Molecular Orbital (SOMO). The electron density of the latter is located mainly on the part of the fullerene cage closest to the lanthanide cation. Thus, the bigger the lanthanide, the closer it is to the cage and the more stabilized the negative charge on the cage. In other words, the larger the lanthanide, the easier the reduction and the more difficult the oxidation.

Very recently[139d,e] preliminary results on the physical and chemical properties of endohedral fullerene complexes containing two metal cations have appeared. Only very preliminary electrochemical data were listed, and no discussion of these data was provided in this article.

7.1.2. Fullerenes as Guests

Mainly three types of inclusion complexes in which a fullerene is the guest have been synthesized: C_{60}–cyclodextrin complexes (C_{60}/CD),[137a–c,f] C_{60}–calixarene complexes,[126, 131–134, 137d] and a C_{60}–azacrown complex.[137e]

Interestingly, the inclusion of the fullerene derivative $C_{61}(C_6H_5)_2$ inside the cavity of an HIV protease was studied by computer modeling with the hope of altering the reactivity of the protease.[142a,b] The results obtained are surprisingly promising, and several laboratories are now participating in the study of the biological activity of C_{60} and its derivatives.[142c]

The electrochemistry of C_{60}/γ-CD in DMF is very similar to that of C_{60}.[137c] However, in the case of C_{60}/γ-CD, the third reduction wave is followed by a chemical reaction that produces a species yet to be identified. C_{60}/γ-CD is only slightly soluble in water, but enough dissolves to allow recording its electrochemistry (Figure 14).

Cyclic voltammetry of C_{60}/γ-CD in water containing 0.15 M $LiClO_4$ at scan rates higher than 200 mV s^{-1} reveals two reversible one-electron reductions at $E_{1/2} = -0.62$ and -1.03 V vs. SCE, and one irreversible reduction at $E_{pc} = -1.34$ V vs. SCE. At slower scan rates (<200 mV s^{-1}), only the first reduction is reversible, and, as can be shown by differential pulse voltammetry (DPV), the second reduction is followed by a chemical reaction. The authors speculated that C_{60}^{-} is still embedded in γ-CD whereas C_{60}^{2-} is released and undergoes a chemical reaction with water.

As mentioned above, a second type of supramolecular complex where a fullerene is the guest has appeared in the literature: the C_{60}/calixarene complexes.[126, 131–135, 137d] Interestingly, the only calixarene to complex C_{60} and C_{70} efficiently is **39** (Scheme 16). The forces that induce formation of such a complex are probably of the CH–π and π–π type. To our knowledge, only one report that succinctly investigated the electrochemical behavior of C_{60} in the presence of calixarenes (the diethyl esters of *para-tert*-butylcalix[8]arene, *para-tert*-butylcalix[5]arene, and *para-tert*-butylcalix[4]arene) has been published.[134] The calixarenes, whatever their size, interact or react with C_{60} anions. The products of these reactions are more difficult to reduce than C_{60} itself. During the electrochemical experiments, addition of calixarene to a solution of C_{60} also caused adsorption on the working electrode at potentials more negative than the second reduction wave of C_{60}.

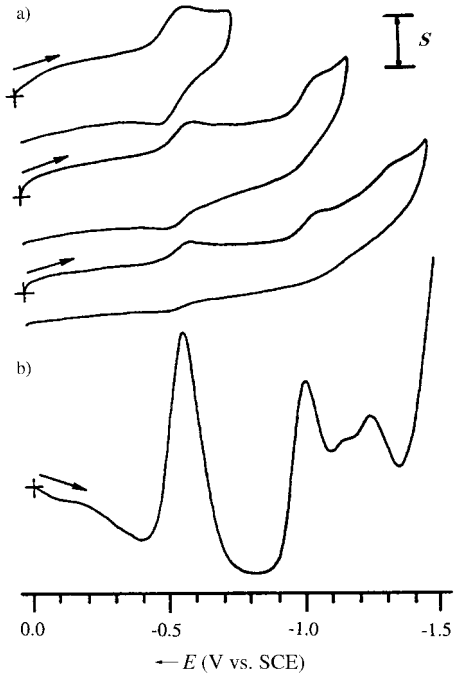
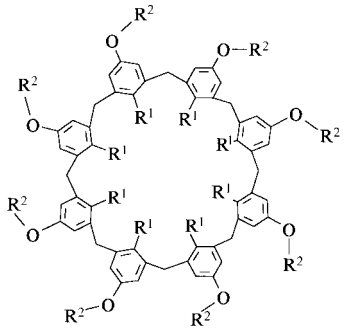


Figure 14. a) Cyclic voltammograms and b) differential pulse voltammograms of nearly saturated magenta γ-CD/C_{60} solution in water, 0.15 M $LiClO_4$; glassy carbon electrode. CV: potential scan rate 50 mV s^{-1}; DPV: potential scan rate 10 mV s^{-1}, pulse amplitude 20 mV, pulse width 50 ms. *S* is equal to 1.0, 1.5, 2.0, and 0.2 mA for the curves from top to bottom (reprinted with permission from ref. [137c]).



39 R^1 = *t*Bu, R^2 = H

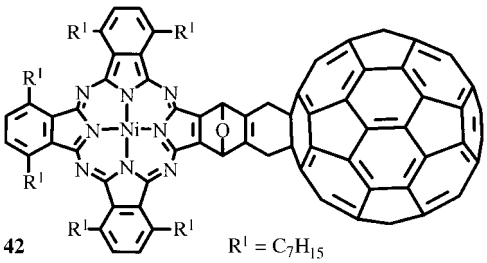
40 R^1 = H, R^2 = H

41 R^1 = *t*Bu, R^2 = CH_3

Scheme 16. Calixarenes investigated as hosts for complexation of C_{60}.

7.2. Latest Work on Fullerenes Related to Supramolecular Chemistry

Recently C_{60} was derivatized with the aim of building a starting block to form supramolecular complexes. Initially Hirsch et al. reported the synthesis and electrochemistry of **42**, the Diels–Alder adduct of C_{60} with a phthalocyanine.[143] The CV of the complex reveals five reversible one-electron reductions, which involve either the fullerene or the Ni



42 $R^1 = C_7H_{15}$

metallophthalocyanine center. Reduction potentials for two complexes in which a porphyrin is covalently bonded to C_{60} have been reported.[144, 145] In both cases redox processes centered on C_{60} and on the porphyrin ligand can be observed. In all of these studies, the electrochemical results suggested that the coupling between the carbon cage and the ligand is not very effective when both molecules are in the ground state. A second example of a C_{60} derivative for further supramolecular binding is a C_{60}–$[Ru^{II}(bpy)_3]$ complex.[146]

7.3. Electrocrystallization of Fulleride Salts

As already discussed, electrochemistry can be used as an effector to prepare novel materials mainly by electrocrystallization. The final electrogenerated products are crystalline supramolecular assemblies with unique properties. This is truly a field of research in which electrochemistry, supramolecular chemistry, and material science merge. The first electrochemical preparation of a fulleride salt was reported in 1991 by Wudl et al.[147] Attempts by these authors to prepare a bulk solution of C_{60}^- with tetraphenylphosphonium iodide (TPPI) as supporting electrolyte resulted in the precipitation of its salt, $C_{60}^-(TPP^+)_3(Cl^-)_2$. Because the sample precipitated as a powder, no structural information was obtained.

The first electrocrystallization of a fulleride salt was achieved by Moriyama et al. in 1993.[148] Needlelike single crystals of $C_{60}^-(PPN^+)$ ($PPN^+ = \{N[P(C_6H_5)_3]_2\}^+$) are air- and light-sensitive and showed no electrical conductivity at room temperature.[148] No detailed X-ray characterization of the crystal was provided in this article. Later the same year, Pénicaud et al. reported the X-ray characterization of electrocrystallized $[(C_6H_5)_4P]_2(C_{60})(I)_x$ ($x \ll 1$).[149] The black shiny single crystals that grew under controlled current electrocrystallization of C_{60} in a toluene/CH_2Cl_2 mixture with tetraphenylphosphonium iodide as supporting electrolyte revealed that the C_{60} monoanions were separated at least by 12.588 Å (center-to-center distance for C_{60}: $d = 10$ Å). This indicates that the C_{60} monoanions in $[(C_6H_5)_4P]_2(C_{60})(I)_x$ are isolated.[149] The tetraphenylphosphonium C_{60}^- salt was stable in air, and its conductivity at room temperature was $2-5 \times 10^{-5}\ \Omega^{-1}cm^{-1}$.[149] Interestingly, even though the C_{60} radical anions are well separated from each other, the magnetic susceptibility data did not follow a Curie–Weiss law.[149]

Controlled-potential electrocrystallization of $[(C_6H_5)_4P]$-$C_{60}\cdot[(C_6H_5)_4P]Cl$ in 1,2-dichlorobenzene was reported in 1994 by Bilow et al.[150] The black, air-stable, square-pyramidal crystals were characterized by X-ray.[150] As expected, this salt is isostructural with the one electrocrystallized by Pénicaud et al. Similarly, electrocrystallization of the tetraphenylarsonium salt of C_{60}^- was also reported.[151] It is important to note that both X-ray structures (Pénicaud's and Bilow's) showed disorder in the arrangement of the C_{60} monoanions and this precluded a clear picture of the distortions that the carbon cage undergoes upon addition of one electron. The first example of a highly ordered salt of C_{60}^- was reported in 1995.[152] $[Ni\{C_5(CH_3)_5\}_2]^+[C_{60}]^-$ was prepared by chemical reduction of C_{60} with one equivalent of decamethylnickelocene.[152] The X-ray characterization of the dark red parallelepiped crystals revealed structural evidence of a Jahn–Teller distortion of the C_{60} cage upon reduction.

In an attempt to generate new materials with interesting electrochemical and photochemical properties, Foss et al. electrocrystallized $[Ru(bpy)_3](C_{60})_2$.[153] The conductivity of powdered samples was $0.01\ \Omega^{-1}cm^{-1}$ at room temperature.[153] No photoconductivity was observed.[153] In 1994 Kobayashi et al. reported the first electrocrystallization of an alkali metal fulleride salt, $Na_{0.39}C_{60}(THF)_{2.2}$.[154] The room temperature conductivity of the sodium salt was $50\ \Omega^{-1}cm^{-1}$ and increased to $1000\ \Omega^{-1}cm^{-1}$ at 100 K.[154] This sodium salt was found to be isostructural with respect to other chemically prepared alkali metal fulleride salts, $M_xC_{60}(THF)_y$ (M = Li, Na, K).[154] The X-ray data for the electrocrystallized sodium salt indicate that there are direct interactions between the C_{60} monoanions (shortest distance of 9.93 Å), and this might explain the metallic character of the salt.[154] Only one fulleride salt made from a higher fullerene has been electrocrystallized to date.[155] Single crystals of $[(C_6H_5)_4P]_2(C_{70})[I]$ are air-stable, and their magnetic susceptibility follows a Curie-Weiss law, which suggests isolated C_{70} monoanions. This was confirmed by X-ray data, which revealed a shortest center-to-center C_{70} distance of 12.682 Å[155] ($d \approx 10$ Å for C_{70} itself, along its equatorial belt). However, as for the corresponding C_{60} salt, disorder in the crystals prevented any clear picture of how the C_{70} molecular structure is affected by the addition of one electron.

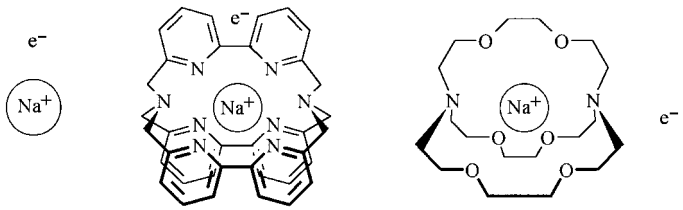
Finally, it is important to note that only salts of C_{60}^- and C_{70}^- have been electrocrystallized. No salts with higher charges have been prepared by electrocrystallization. However, chemical reduction of C_{60} to C_{60}^{2-} with either Na or cobaltocene as reducing agent has been reported.[156] Black shiny single crystals of $[PPN^+]_2C_{60}^{2-}$ are "somewhat air sensitive", and their magnetic characteristics led the authors to the conclusion that C_{60}^{2-} is paramagnetic at room temperature.[156b] The high precision of the X-ray structure obtained for the crystals of this C_{60}^{2-} salt allowed the observation that Jahn–Teller distortion in the dianion changed the icosahedral symmetry of the neutral molecule to C_i.[156a] These results reported by Boyd et al. suggests that the electrocrystallization of salts of C_{60}^{2-} and probably C_{70}^{2-} are possible and should be attempted.

8. Electrogeneration of Expanded Atomlike Structures

A conceptual link between reduced cryptates (cryptatia) and endohedral fullerene complexes exists, even though the two types of materials seem rather unrelated. A cryptatium is

obtained by reduction of a positively charged complex between cation and cryptand (cryptate)[78, 157] to its neutral form. In other words, a cryptatium can be visualized as an anionic armor surrounding a metallic heart. The analogy with endohedral fullerene structures containing metal ions[136] then becomes obvious. The endohedral fullerenes that contain metal ions inside are also made of a positively charged core surrounded by a negatively charged spherical shield. Both cryptatia and endohedral fullerene structures are neutral entities. However, if one was to approach either of these molecules on a nanometer scale, the first observation would be that of a negative electron density corresponding to the electrons located on the cryptate ligand or on the fullerene cage. Beyond this negatively charged shield, one would find the positively charged metal ion, the "nucleus" of such a "pseudo-atom." Thus both are classified as "expanded atoms."

Cryptatia and endohedral fullerene complexes thus can be considered as intermediate between a metal atom and an electride[158, 159] (Scheme 17). In the metal atom, for example



Scheme 17. The relationship between an alkali metal atom (left), a cryptatium (center), and an electride (right).

sodium, the loosely bound electron is confined to the 3s orbital. Because of the very strong affinity of the cryptand [2,2,2] for metal cations such as the sodium cation, the electron of the metal in the electride is expelled from its interaction with the cationic center into the cavities present in the crystal lattice.[158] In cryptatia and endohedral fullerene structures, the electron is not confined to the corresponding s orbital of the metal cation but neither is it completely expelled from its interaction with the metal cation.

It is not a simple task to establish that in a given cryptatium, the electrons balancing the metal ion charge are located on the cryptate ligand. This was accomplished in 1991 by X-ray characterization of single crystals of the first cryptatium, $[Na \subset (bpy_3)]^0$.[78] Single crystals of this sodio-cryptatium were grown at a platinum electrode by the electrocrystallization technique, which is probably the most efficient way to grow crystals of cryptatium species. $[Na \subset (bpy_3)]^0$ (bpy_3 is a cryptand constructed from three bpy units as shown in Scheme 17) is the only cryptatium for which a crystal structure has been determined successfully to date. Its crystal structure revealed that of the three bipyridine units that are covalently linked to form the cryptand ligand, only one was planar. In addition, the $Na^+ - N$ distance for the planar bpy unit was shorter than that for the other two (2.59 vs. 2.82 – 2.83 Å). This suggests that the electron added to the cryptate ligand during its reduction is located on the flat bpy unit. Thus, the sodio-cryptatium is more accurately described as $[Na^+ \subset (bpy^-)\text{-}(bpy)_2]$.

The conceptually related endohedral fullerene systrems still have to be structurally characterized. One striking result was recently reported by Takata and co-workers, who used synchrotron X-ray diffraction spectroscopy.[160] They were able to detect the encapsulated metal ion of $Y@C_{82}$ (Figure 15).[160]

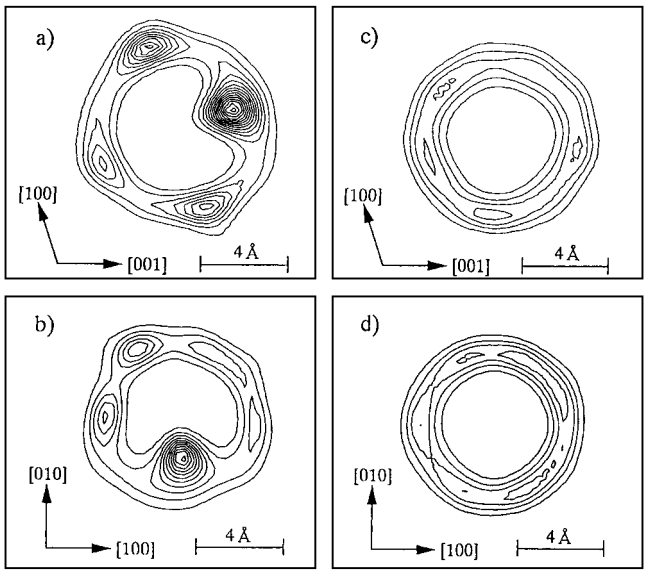


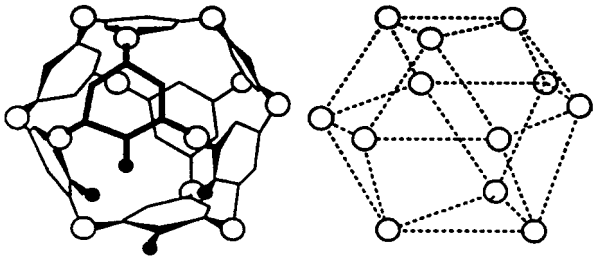
Figure 15. The maximum entropy model (MEM) electron density distribution of $Y@C_{82}$ for a) the (010) and b) the (001) sections, and of C_{82} for c) the (010) and d) the (001) sections. The contour lines are drawn from 0.0 e A^{-3} at 0.5 e A^{-3} intervals. The yttrium atom's seat inside C_{82} can be clearly seen in a) and b). (Reprinted with permission from ref. [160].)

The family of compounds $[M(bpy)_3]^0$ (M = Fe, Ru, or Os) is also another example of the general class of structures defined as "expanded atoms." Even though these cationic complexes have been studied for 30 years, only recently was their potential as novel "expanded atoms" revealed.[161, 162] In these complexes the three bpy units are not covalently linked to each other; nevertheless they surround the positively charged metal center in a similar fashion to the tris(bpy) cryptand ligand. The series of compounds, $[M(bpy)_3]^0$ (M = Fe, Ru, or Os) was successfully electrocrystallized at a platinum electrode from the corresponding precursor cations, $[M(bpy)_3]^{2+}$.[7, 161] The structures of these complexes have not yet been published, but they seem to retain the original octahedral symmetry of the unreduced complex. This surprising result is currently under intense investigation. Another intriguing result with the $[M(bpy)_3]^0$ single crystals is their lack of an ESR signal. This contrasts with results reported by DeArmond et al.,[74, 163] who described a 250 G wide ESR line centered at $g = 2.23$ for the same materials but studied as powders. This might indicate interesting conducting or semiconducting properties. Only the reduced ruthenium complex has been thoroughly characterized at the present time.[162]

Magnetic susceptibility measurements on electrochemically prepared single crystals revealed that $[Ru(bpy)_3]^0$ is best characterized by the spatially isolated redox orbital model.[162] The reduction electrons are located on two of the three bpy units of each molecule in the ligand's π^* orbitals. A comparison

of the magnetic properties of $[Ru(bpy)_3]^0$ in solution and in the solid state suggests that removal of the solvent leads to a decrease in the energy gap between the metal dσ* and the ligand π* orbitals. The best fit of the experimental magnetic data was obtained when $[Ru(bpy)_3]^0$ was considered as a one-dimensional chain structure in which each electron on a ligand is coupled intramolecularly to the electron on the other bpy ligand and intermolecularly to the closest bpy unit of the neighboring molecule. $[Ru(bpy)_3]^0$ is a semi-conductor, and the temperature dependence of its conductivity can be rationalized with a hopping conduction mechanism.

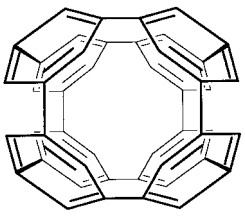
Four years ago Ross et al.[164] reported the theoretical calculations of the polarizabilities of a series of spherical molecules with encapsulated cations, the heterospherophanes (Scheme 18). These compounds, yet to be synthesized, are



Scheme 18. Schematic representation of heterospherophanes (reprinted with permission from ref. [164]). Open spheres = heteroatoms, solid spheres = selected hydrogen atoms to show steric crowding around cavity entrance.

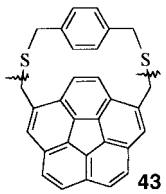
closely related to the cryptatia and the endohedral fullerene complexes. In the particular case of the thiaspherophanes, the sulfur atoms should allow the electrons that balance the charge of the embedded cation to be delocalized over the entire molecule and, in the crystalline state, should favor intermolecular electronic coupling. The cation would be shielded by the field generated by the delocalized charge, producing a true "expanded atom."

Two recent reports are also conceptually related to "expanded atoms". In 1995 Diederich et al.[165] reported the electrochemistry of the mono- through hexakis-adducts of C_{60}. One of their conclusions was that successive rupture of the C_{60} double bonds during six successive addition processes to the cage ultimately revealed the benzenoid "cubic" cyclophane structure enclosed in the fullerene framework (Scheme 19). Synthesis (or retrosynthesis from C_{60}) of such a "cubic" cyclophane would truly represent an important step toward the synthesis of a novel "expanded atom". Finally, Siegel and co-workers[166] recently reported the synthesis of the first corannulene cyclophane (**43**), which obviously is a well-suited candidate for the synthesis of "expanded atoms" given that the "organic skin" could allow for delocalization of the excess negative charge around a centrally located and bound cation.



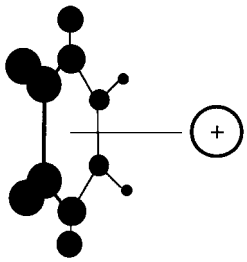
Scheme 19. Benzenoid "cubic" cyclophane structure contained in C_{60}.

In conclusion, the concept of an "expanded atom" is more than just an idea and its exploration could easily lead to the preparation of novel materials with unique properties. The most solid experimental evidence that "expanded atoms" can be made is the successful synthesis of endohedral fullerene structures. In fact, endohedral fullerenes containing more than one metal ion have been isolated and characterized.[139d, 139e] In those cases, in addition to the attractive interaction between the cations and the negatively charged fullerene sphere, one has to take into account the electrostatic repulsion between the two metal cations within the cage. In a way, the entire situation is reminiscent of charge repulsion in nuclei and their attractive interactions with the orbiting electrons in an atom.



43

In all of the previously mentioned examples of "expanded atoms", the metal cation is surrounded by a structure derived from the benzene ring. One can envisage then that cation–π interactions (Scheme 20)[167] will be omnipresent in these systems. These noncovalent bonds between cations and π-rings might be used as a driving force in the tethered synthesis of novel "expanded atoms".



Scheme 20. The cation–π interaction.

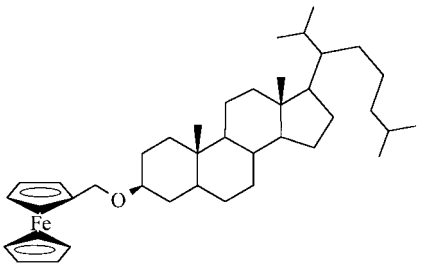
9. Potentially Functional Aggregates and Some Future Prospects

In the previous sections examples were presented of how electrochemical techniques have been used to characterize single molecules, complexes, and aggregates composed of a relatively small number of molecules. Instead of using this last section as a prophetic platform to try to preach about the future, two additional examples of work from our laboratory have been selected to illustrate how important electrochemistry is for the formation and detection of large aggregates of supramolecular assemblies. In one example, electrochemistry was used to induce the formation of liposomal aggregates,[168] while in the other it was the technique used to detect aggregate formation on a surface, which occurred spontaneously through molecular recognition.[169]

Typical natural bilayer membranes are formed from phospholipids derived from glycerol and fatty acids. The formation of these membranes primarily relies on the hydrophilic/hydrophobic balance that exists between the headgroup/tail portions of these compounds. It is this balance that confers the unusual stabilities associated with these highly organized supramolecular aggregates. Either polar or charged moieties in the headgroups interact strongly with the surrounding water medium, while the hydrophobic alkyl tails interact with each other inside the bilayer. A while back we showed that a crown ether, even uncomplexed, was suffi-

ciently hydrophilic to induce formation of nonionic liposomes (niosomes) when attached to a cholesterol group.[170]

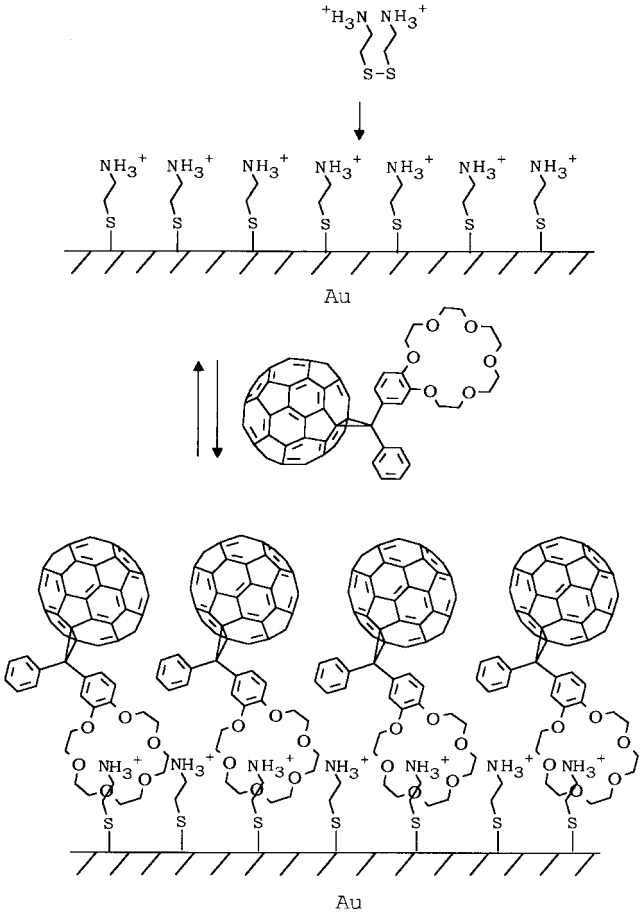
The concept of redox switching as applied to binding control was already discussed in Section 2. In those cases, electrochemistry was used to generate charge in part of a molecule, and this charge resulted in inter- or intramolecular electrostatic interactions with species of the opposite charge, thus leading to enhanced binding. In the present context of bilayer membrane formation, electrochemical switching was used to generate charged headgroups for enhanced hydrophilicity. The switchable headgroup that was selected originally was ferrocene, and the hydrophobic tail was either cholesterol or cholestanyl (Scheme 21).[168] Electrochemical



Scheme 21. Structure of steroidal ferrocene derivatives used to form liposomes after oxidation of the ferrocene head group to ferricinium.

oxidation of the ferrocene group to ferrocinium followed by sonication in water led to the formation of stable vesicles.[168] These vesicles constitute rather complex aggregates with potential applications as redox-active drug delivery systems. Reduction of the vesicles back to their neutral states, either chemically or electrochemically, resulted in their total disruption. An extension of this work was reported very recently.[171]

A striking example of how electrochemistry is uniquely useful in characterizing the formation of architecturally complex and dimensionally large assemblies was published very recently.[169] A self-assembled monolayer (SAM) of cystamine was first allowed to form on a gold [111] electrode by following well-established procedures.[172] This monolayer, which forms spontaneously, terminates in positively charged ammonium groups, as represented in Scheme 22. If this monolayer is now exposed to a solution of a crown ether-containing compound such as the methanofullerene shown in Scheme 22, hydrogen bonding between these two functional groups should induce the formation of a secondary SAM.[173] The overall process is described in Scheme 45. Although reflectance spectroscopic techniques can be applied to characterize the formation of such monolayers at the electrode–solution interface, electrochemistry offers an easy and convenient way to establish whether such supramolecular aggregates form. Since the fullerene group is electroactive, as described in Section 7, it is very easy to detect the current for the first reduction of the fullerene moiety to its monoanionic state. The current detected for the same solution of the methanofullerene in the absence of a cystamine monolayer can be easily subtracted from that observed in the presence of the monolayer to obtain the surface concentration effect. After simulation and appropriate calibration of the electrode surface area, a surface covarage of 1.4×10^{-10} mol cm^{-2} was



Scheme 22. Formation of a cystamine monolayer on gold followed by its interaction with a benzo[18]crown-6 methanofullerene. A secondary monolayer of fullerenes is formed by self-assembly due to molecular recognition between the ammonium groups and the crown ethers.

determined. Assuming an area per molecule of 100 Å^2 for the C_{60} group, a close-packed coverage of 1.9×10^{-10} mol cm^{-2} is calculated. This means that about 75% of the surface is covered by this double self-assembly process driven.

These two examples should give the reader some concrete ideas on how electrochemistry can be used to either induce or measure the formation of rather complex supramolecular aggregates. In the field of SAMs, electrochemistry is undoubtedly one of, if not the premier, technique used to characterize the aggregates. Future uses in this field, as well as in supramolecular science, in general are certain to continue to increase in view of the power and simplicity of the techniques involved.

Addendum

Since this article was initially accepted for publication, the application of electrochemical techniques to supramolecular structures has continued apace. Here we highlight but a few of the latest articles in the field. In the area of redox switching the group of Rotello has recently reported a novel, electrochemically controlled three-component molecular switch based on hydrogen bonding.[174] Kaifer, Morán and co-workers have reported the electrochemically switchable formation of inclusion complexes of β-cyclodextrins and multisite guests,

dendrimers bearing up to 16 ferrocenyl moieties.[175] Beer and co-workers have continued to make progress in the area of anion binding and have recently reported enhanced selectivity for $H_2PO_4^-$ anions employing a calix[4]arene derivative with a pendant $[Ru^{II}(bpy)_3]^{2-}$ group.[176] With respect to cyclophane chemistry, the work of Becher and co-workers on TTF-based systems has expanded rapidly and includes pseudocatenanes, catenanes, and rotaxanes, among others.[177] In the area of pyridine-based systems, the beautiful and intricate helicates reported within the past year[178] are sure to have attracted much attention among supramolecular electrochemists, though potential solubility problems and limited amounts of material appear to have curbed reports on the electrochemical behavior of these fascinating systems.

In the area of endohedral metallofullerenes, a recent report by Suzuki and co-workers reviews the electrochemistry of $La@C_{82}$, $Ce@C_{82}$, $Gd@C_{82}$, and $Y@C_{82}$.[179] Anderson and co-workers have reported very interesting results on the electrochemistry of the trinuclear endohedral complex, $Sc_3@C_{82}$.[180] These results indicate that the MOs of the trinuclear complex are very similar in energy to those of the mononuclear complexes. However, considering that more electrons are transferred to the cage by the trimetallic system, occupancy of the energy levels is different. Therefore, its second oxidation and first reduction occur at potentials close to where the first oxidation and second reduction occur for mononuclear endohedral complexes. These considerations, along with the fact that the neutral state is EPR silent, have led the authors to suggest that $Sc_3^{4+}@C_{82}^{4-}$ represents the formal charges of the complex. Further progress in the isolation and purification of endohedral complexes has been made by Dunsch and co-workers. They have successfully isolated three stable isomers of $Tm@C_{82}$, and preliminary electrochemical studies for all three isomers have been reported.[181]

The authors wish to express their gratitude to the many people who, in one way or another, contributed to the work presented here. Particular thanks go to Professors Javier de Mendoza (Madrid), David Gutsche (Fort Worth), David Reinhoudt (Enschede), and Rocco Ungaro (Parma) for their collaboration in the field of calixarenes. A very special acknowledgement goes to Professor Jean-Marie Lehn for his inspiration and collaboration, especially in the early stages of the cryptatium work. It is also a pleasure to acknowledge the National Science Foundation, Divisions of Chemistry and Materials Research (grants CHE-9313018 and DMR-9119986), and Graduate Fellowship Program (M.G.-K.) as well as the Petroleum Research Fund, administered by the American Chemical Society (grant 27827), for their generous financial support. Special thanks go to Ms. Soomi Pyo and Eduardo Pérez-Cordero for their help with some figures and to Dr. Lourdes E. Echegoyen for her invaluable help during the last stages of the work.

Received: September 19, 1997 [A 190 IE]
German version: *Angew. Chem.* **1998**, *110*, 226 – 258

[1] Selected references for this field: a) A. E. Kaifer in *Comprehensive Supramolecular Chemistry, Vol. 8* (Eds.: J. E. D. Davies, J. A. Ripmeester), Pergamon, Tarrytown (NY), **1996**; b) A. J. Bard, L. Faulkner, *Electrochemical Methods*, Wiley, New York, **1980**; c) *Laboratory Techniques in Electroanalytical Chemistry*, 2nd ed. (Eds.: P. T. Kissinger, W. R. Heineman), Dekker, New York, **1996**; d) *Physical Electrochemistry* (Ed.: I. Rubinstein), Dekker, New York, **1995**.

[2] a) A. E. Kaifer, S. Mendoza in *Comprehensive Supramolecular Chemistry, Vol. 1* (Ed.: G. W. Gokel), Pergamon, Tarrytown (NY), **1996**, p. 714; b) A. E. Kaifer, L. Echegoyen in *Cation Binding by Macrocycles* (Eds.: Y. Inoue, G. W. Gokel), Dekker, New York, **1990**, p. 373; c) P. D. Beer, *Chem. Soc. Rev.* **1989**, *18*, 409 – 450; d) E. M. Seward, R. B. Hopkins, W. Sauerer, S.-W. Tam, F. Diederich, *J. Am. Chem. Soc.* **1990**, *112*, 1783 – 1790.

[3] a) R. A. Bissell, E. Cordova, J. F. Stoddart, A. E. Kaifer, *Nature* **1994**, *369*, 133 – 137; b) A. C. Benniston, A. Harriman, V. M. Lynch, *J. Am. Chem. Soc.* **1995**, *117*, 5275 – 5291; c) A. C. Benniston, A. Harriman, *Angew. Chem.* **1993**, *105*, 1553 – 1555; *Angew. Chem. Int. Ed. Engl.* **1993**, *32*, 1459 – 1461.

[4] a) J.-P. Gisselbrecht, M. Gross, J.-M. Lehn, J.-P. Sauvage, R. Ziessel, C. Piccini-Leopardi, J. M. Arrieta, G. Germain, M. Van Meerssche, *Nouv. J. Chim.* **1984**, *8*, 661 – 667; b) J.-M. Lehn, A. Rigault, *Angew. Chem.* **1988**, *100*, 1121 – 1122; *Angew. Chem. Int. Ed. Engl.* **1988**, *27*, 1095 – 1097, c) R. Krämer, J.-M. Lehn, A. Marquis-Rigault, *Proc. Natl. Acad. Sci. USA* **1993**, *90*, 5394 – 5398; d) J.-M. Lehn, A. Rigault, J. Siegel, J. Harrowfield, B. Chevrier, D. Moras, *ibid.* **1987**, *84*, 2565 – 2569; e) B. Hasenknopf, J.-M. Lehn, G. Baum, D. Fenske, *ibid.* **1996**, *93*, 1397 – 1400.

[5] a) K. T. Potts, M. Keshavarz-K, F. S. Tham, H. D. Abruña, C. R. Arana, *Inorg. Chem.* **1993**, *32*, 4422 – 4435; b) K. T. Potts, M. Keshavarz-K, F. S. Tham, H. D. Abruña, C. R. Arana, *ibid.* **1993**, *32*, 4436 – 4449; c) K. T. Potts, M. Keshavarz-K, F. S. Tham, H. D. Abruña, C. R. Arana, *ibid.* **1993**, *32*, 4450 – 4456; d) K. T. Potts, M. Keshavarz-K, F. S. Tham, K. A. Gheyson Raiford, C. R. Arana, H. D. Abruña, *ibid.* **1993**, *32*, 5477 – 5484.

[6] a) E. C. Constable, M. J. Hannon, D. A. Tocher, *J. Chem. Soc. Dalton Trans.* **1993**, 1883 – 1890; b) E. C. Constable, R. Martínez-Mañèz, A. M. W. Cargill Thompson, *ibid.* **1994**, 1585 – 1594; c) E. C. Constable, M. G. B. Drew, M. D. Ward, *J. Chem. Soc. Chem. Commun.* **1987**, 1600 – 1602; d) M. Barley, E. C. Constable, S. A. Corr, M. G. B. Drew, C. S. McQueen, J. C. Nutkins, M. D. Ward, *J. Chem. Soc. Dalton Trans.* **1988**, 2655 – 2660; e) E. C. Constable, J. Lewis, M. Schröder, *Polyhedron* **1982**, *1*, 311 – 312.

[7] E. Pérez-Cordero, N. Brady, L. Echegoyen, R. Thummel, C.-Y. Hung, S.-G. Bott, *Chem. Eur. J.* **1996**, *2*, 781 – 788. My group has also successfully electrocrystallized tris(bipyridine) complexes of Ru^{2+}, Fe^{2+}, and Os^{2+}, as well as a Ru^{2+} terpyridine complex (work of E. Pérez-Cordero and Soomi Pyo). See Section 8 of this review and ref. [161, 162] for further information.

[8] See, for example, J.-M. Barbe, P. Richard, M. A. Aukauloo, C. Lecomte, P. Petit, R. Guilard, *J. Chem. Soc. Chem. Commun.* **1994**, 2757 – 2758.

[9] a) Ref. [2a], p. 701; b) ref. [2b], p. 363; c) M. A. Wilson, A. Pohorille, *J. Am. Chem. Soc.* **1996**, *118*, 6580 – 6587, and references therein.

[10] see for example a) A. P. de Silva, C. P. McCoy, *Chem. Ind. (London)* **1994**, 992 – 996; b) A. P. de Silva, H. Q. Gunaratne, C. P. McCoy, *Nature* **1993**, *364*, 42 – 44; c) P.-L. Agnelli, N. Spencer, J. F. Stoddart, *J. Am. Chem. Soc.* **1991**, *113*, 5131 – 5133; d) A. R. Bernardo, J. F. Stoddart, A. E. Kaifer, *ibid.* **1992**, *114*, 10624 – 10631; e) K. Leutwyler, *Sci. Am.* **1994**, (**8**), 87; f) M. T. Rojas, J. C. Medina, G. W. Gokel, A. E. Kaifer, *Supramol. Chem.* **1993**, *2*, 145 – 153.

[11] a) Ref. [2a], p. 707; b) S. R. Miller, D. A. Gustowski, Z.-H. Chen, G. W. Gokel, L. Echegoyen, A. E. Kaifer, *Anal. Chem.* **1988**, *60*, 2021 – 2024.

[12] Ref. [2a], p. 709.

[13] Ref. [2b], p. 382.

[14] a) D. A. Gustowski, L. Echegoyen, D. M. Goli, A. E. Kaifer, R. A. Schultz, G. W. Gokel, *J. Am. Chem. Soc.* **1984**, *106*, 1633 – 1635; b) A. E. Kaifer, D. A. Gustowski, L. Echegoyen, V. J. Gatto, R. A. Schultz, T. P. Cleary, C. R. Morgan, A. M. Rios, G. W. Gokel, *ibid.* **1985**, *107*, 1958 – 1965.

[15] F. Peter, M. Gross, M. W. Hosseini, J.-M. Lehn, *J. Electroanal. Chem.* **1983**, *144*, 279 – 292.

[16] See for example: a) L. A. Godínez, J. Lin, M. Muñoz, A. W. Coleman, A. E. Kaifer, *J. Chem. Soc. Faraday Trans.* **1996**, *92*, 645 –

650; b) P. M. Bersier, J. Bersier, B. Klingert, *Electroanalysis* **1991**, *3*, 443 – 455, and references therein.
[17] a) J. C. Medina, T. T. Goodnow, S. Bott, J. L. Atwood, A. E. Kaifer, G. W. Gokel, *J. Chem. Soc. Chem. Commun.* **1991**, 290 – 292; b) J. C. Medina, T. T. Goodnow, M. T. Rojas, J. L. Atwood, B. C. Lynn, A. E. Kaifer, G. W. Gokel, *J. Am. Chem. Soc.* **1992**, *114*, 10583 – 10595.
[18] C. D. Hall, N. W. Sharpe, I. P. Danks, Y. P. Sang, *J. Chem. Soc. Chem. Commun.* **1989**, 419 – 421.
[19] T. Saji, I. Kinoshita, *J. Chem. Soc. Chem. Commun.* **1986**, 716 – 717.
[20] G. De Santis, L. Fabrizzi, M. Licchelli, P. Pallavicini, A. Perotti, *J. Chem. Soc. Dalton Trans.* **1992**, 3283 – 3284.
[21] a) P. D. Beer, H. Sikanyika, C. Blackburn, J. F. McAleer, *J. Chem. Soc. Chem. Commun.* **1989**, 1831 – 1833; b) P. D. Beer, C. Blackburn, J. F. McAleer, H. Sikanyika, *Inorg. Chem*. **1990**, *29*, 378 – 381; c) P. D. Beer, A. D. Keefe, H. Sikanyika, C. Blackburn, J. F. McAleer, *J. Chem. Soc. Dalton Trans.* **1990**, 3289 – 3294, 3295 – 3300.
[22] See for example: J. Q. Chambers in *The Chemistry of Quinoids Compounds*, *Vol. 2*, *Part 1* (Ed.: S. Patai), Wiley, London, **1988**, Chap. 12.
[23] a) D. A. Gustowski, M. Delgado, V. J. Gatto, L. Echegoyen, G. W. Gokel, *J. Am. Chem. Soc.* **1986**, *108*, 7553 – 7560; b) M. Delgado, D. A. Gustowski, H. K. Yoo, V. J. Gatto, G. W. Gokel, L. Echegoyen, *ibid.* **1988**, *110*, 119 – 124.
[24] Z. Chen, O. F. Schall, M. Alcalá, Y. Li, G. W. Gokel, L. Echegoyen, *J. Am. Chem. Soc.* **1992**, *114*, 444 – 451.
[25] L. Echegoyen, R. C. Lawson in *Comprehensive Supramolecular Chemistry*, (Ed.: D. N. Reinhoudt), Pergamon, Tarrytown (NY), **1996**, p. 151.
[26] a) L. Echegoyen, Y. Hafez, R. C. Lawson, J. de Mendoza, T. Torres, *Tetrahedron Lett.* **1994**, *35*, 6383 – 6386; b) L. Echegoyen, R. C. Lawson, C. Lopez, J. de Mendoza, Y. Hafez, T. Torres, *J. Org. Chem.* **1994**, *59*, 3814 – 3820; c) L. Echegoyen, Y. Hafez, R. C. Lawson, J. de Mendoza, T. Torres, *ibid.* **1993**, *58*, 2009 – 2012.
[27] D. A. Gustowski, V. J. Gatto, A. E. Kaifer, L. Echegoyen, R. E. Godt, G. W. Gokel, *J. Chem. Soc. Chem. Commun.* **1984**, 923 – 925.
[28] a) P. D. Beer, S. E. Stokes, *Polyhedron* **1995**, *14*, 2631 – 2635; b) P. D. Beer, M. G. B. Drew, D. Hesek, R. Jagessar, *J. Chem. Soc. Chem. Commun.* **1995**, 1187 – 1189; c) P. D. Beer, M. G. Drew, C. Hazlewood, D. Hsek, J. Hodacova, S. E. Stokes, *ibid.* **1993**, 229 – 231.
[29] For a general discussion of anion recognition, see Ref. [2a], p. 724.
[30] B. Franck, A. Nonn, *Angew. Chem.* **1995**, *107*, 1941 – 1957; *Angew. Chem. Int. Ed. Engl*. **1995**, *34*, 1795 – 1811.
[31] a) H. Fisher, B. Walach, *Justus Liebigs Ann. Chem*. **1926**, *450*, 164 – 181; b) *Porphyins and Metalloporphyrins* (Ed.: K. M. Smith), Elsevier, New York, **1975**; c) *The Porphyrins*, *Vol. 1 – 4* (Ed.: D. Dolphin), Academic Press, New York, **1978**.
[32] A. W. Johnson, I. T. Kay, *J. Chem. Soc*. **1965**, 1620 – 1629.
[33] E. Vogel, M. Köcher, H. Schmickler, J. Lex, *Angew. Chem.* **1986**, *98*, 262 – 264; *Angew. Chem. Int. Ed. Engl*. **1986**, *25*, 257 – 259.
[34] G. Knübel, B. Franck, *Angew. Chem.* **1988**, *100*, 1203 – 1211; *Angew. Chem. Int. Ed. Engl*. **1988**, *27*, 1170 – 1172.
[35] a) X. Chi, A. J. Guerin, R. A. Haycock, C. A. Hunter, L. D. Sarson, *J. Chem. Soc. Chem. Commun.* **1995**, 2567 – 2569; b) C. A. Hunter, L. D. Sarson, *Angew. Chem.* **1994**, *106*, 2424; *Angew. Chem. Int. Ed. Engl*. **1994**, *33*, 2313 – 2316; c) H. L. Anderson, J. K. M. Sanders, *ibid.* **1990**, *102*, 1478 and **1990**, *29*, 1400 – 1403; d) H. L. Anderson, A. Bashall, K. Henrick, M. McPartlin, J. K. M. Sanders, *ibid.* **1994**, *106*, 445 and **1994**, *33*, 429 – 431; e) M. J. Crossley, T. W. Hambley, L. G. Mackay, A. C. Try, R. Walton, *J. Chem. Soc. Chem. Commun.* **1995**, 1077 – 1079; f) H. L. Anderson, J. K. M. Sanders, *ibid.* **1992**, 946 – 947.
[36] a) A. Harriman, F. Odobel, J.-P. Sauvage, *J. Am. Chem. Soc*. **1995**, *117*, 9461 – 9472; b) K. Araki, H. E. Toma, *J. Photochem. Photobiol. A: Chem*. **1994**, *83*, 245 – 250.
[37] a) V. Kral, J. L. Sessler, H. Furuta, *J. Am. Chem. Soc*. **1992**, *114*, 8704 – 8705; b) J. L. Sessler, M. J. Cyr, V. Lynch, E. McGhee, J. A. Ibers, *ibid.* **1990**, *112*, 2810 – 2813; c) see for example: T. Takeuchi, H. B. Gray, W. A. Goddard III, *ibid.* **1994**, *116*, 9730 – 9732.
[38] a) F. P. Shwartz, M. Gouterman, Z. Muljiani, D. Dolphin, *Bioinorg. Chem*. **1972**, *2*, 1 – 32; b) J. P. Collman, C. M. Elliott, T. R. Halbert, B. S. Tovrog, *Proc. Natl. Acad. Sci. USA* **1977**, *74*, 18 – 22; c) H. Ogoshi, H. Sugimoto, Z. I. Yoshida, *Tetrahedron Lett*. **1977**, *2*, 169 – 172; d) C. K. Chang, M.-S. Kuo, C.-B. Wang, *J. Heterocycl. Chem.* **1977**, *14*, 943 – 945.
[39] a) J. P. Collman, P. Denisevich, Y. Konai, M. Marrocco, C. Koval, F. C. Anson, *J. Am. Chem. Soc*. **1980**, *102*, 6027 – 6036; b) R. R. Durand, Jr., C. S. Bencosme, J. P. Collman, F. C. Anson, *ibid.* **1983**, *105*, 2710 – 2718.
[40] J.P Collman, P. S. Wagenknecht, J. E. Hutchison, *Angew. Chem.* **1994**, *106*, 1620 – 1639; *Angew. Chem. Int. Ed. Engl*. **1994**, *33*, 1537 – 1554.
[41] a) A typical example of the electrochemistry of cofacial bis(metallo)porphyrins in solution: Y. Le Mest, M. L'Her, N. H. Hendricks, K. Kim, J. P. Collman, *Inorg. Chem*. **1992**, *31*, 835 – 847; b) J. P. Collman, N. H. Hendricks, C. R. Leidner, E. Ngameni, M. L'Her, *ibid.* **1988**, *27*, 387 – 393.
[42] a) Ref. [1b], p. 283; b) ref. [1b], p. 298; c) H. R. Thirsk, J. A. Harrison in *Guide to the Study of Electrode Kinetics*, Academic Press, New York, **1972**.
[43] a) J. P. Fillers, K. G. Ravichandran, I. Abdalmuhdi, A. Tulinsky, C. K. Chang, *J. Am. Chem. Soc*. **1986**, *108*, 417 – 424; b) J. P. Collman, A. O. Chong, G. B. Jameson, R. T. Oakley, E. Rose, E. R. Schmittou, J. A. Ibers, *ibid.* **1981**, *103*, 516 – 533.
[44] a) W. R. Scheidt, Y. J. Lee, *Struct. Bonding (Berlin)* **1987**, *64*, 1; b) J. P. Collman, J. E. Hutchison, M. A. Lopez, R. Guilard, *J. Am. Chem. Soc*. **1992**, *114*, 8066 – 8073.
[45] J. Issberner, R. Moors, F. Vogtle, *Angew. Chem.* **1994**, *106*, 2507 – 2514; *Angew. Chem. Int. Ed. Engl*. **1994**, *33*, 2413 – 2420.
[46] G. R. Moore, G. W. Pettigrew, *Cytochromes c: Evolutionary, Structural, and Physicochemical Aspects*, Springer, Berlin, **1990**, p. 309.
[47] R. H. Jin, T. Aida, S. Inoue, *J. Chem. Soc. Chem. Commun.* **1993**, 1260 – 1262.
[48] T. Ema, M. O. Senge, N. Y. Nelson, H. Ogoshi, K. M. Smith, *Angew. Chem.* **1994**, *106*, 1951 – 1953; *Angew. Chem. Int. Ed. Engl*. **1994**, *33*, 1879 – 1881.
[49] P. J. Dandliker, F. Diederich, M. Gross, C. B. Knobler, A. Louati, E. M. Sanford, *Angew. Chem.* **1994**, *106*, 1821 – 1824; *Angew. Chem. Int. Ed. Engl*. **1994**, *33*, 1739 – 1742.
[50] P. J. Dandliker, F. Diederich, J.-P. Gisselbrecht, A. Louati, M. Gross, *Angew. Chem.* **1995**, *107*, 2906 – 2909; *Angew. Chem. Int. Ed. Engl*. **1995**, *34*, 2725 – 2728.
[51] K. M. Kadish, C. Auraullo, G. B. Maya, D. Sazou, J.-M. Barbe, R. Guilard, *Inorg. Chem*. **1989**, *28*, 2528 – 2533.
[52] a) T. Hayashi, T. Miyahara, Y. Aoyama, M. Nonoguchi, H. Ogoshi, *Chem. Lett.* **1994**, 1749 – 1752; b) T. Hayashi, T. Miyahara, N. Hashizume, H. Ogoshi, *J. Am. Chem. Soc.* **1993**, *115*, 2049 – 2051; c) T. Hayashi, T. Asai, H. Hokazono, H. Ogoshi, *ibid.* **1993**, *115*, 12210 – 12211; d) T. Hayashi, T. Miyahara, Y. Aoyama, M. Kobayashi, H. Ogoshi, *Pure Appl. Chem*. **1994**, *66*, 797 – 802.
[53] a) *Molecular Metals* (Ed.: W. Hatfield), Plenum, New York, **1979**; b) J. P. Collman, J. T. McDevitt, G. T. Yee, C. R. Leidner, L. G. McCullough, W. A. Little, J. B. Torrance, *Proc. Natl. Acad. Sci. USA* **1986**, *83*, 4581 – 4585; c) *Extended Linear Chain Compounds*, *Vol. 1 – 3* (Ed: J. S. Miller), Plenum, New York, **1982**; d) J. B. Torrance, *Acc. Chem. Res.* **1979**, *12*,79 – 86.
[54] a) J. L. Petersen, C. S. Schramm, D. R. Stojakovic, B. M. Hoffman, T. J. Marks, *J. Am. Chem. Soc*. **1977**, *99*, 286 – 288; b) T. E. Phillips, R. P. Scaringe, B. M. Hoffman, J. A. Ibers, *ibid.* **1980**, *102*, 3435 – 3444; c) C. J. Schramm, R. P. Scaringe, D. R. Stojakovic, B. M. Hoffman, J. A. Ibers, T. J. Marks, *ibid.* **1980**, *102*, 6702 – 6713; d) J. Martinsen, J. L. Stanton, R. L. Greene, J. Tanaka, B. M. Hoffman, J. A. Ibers, *ibid.* **1985**, *107*, 6915 – 6920; e) K. Liou, T. P. Newcomb, M. D. Heagy, J. A. Thompson, W. B. Heuer, R. L. Musselman, C. S. Jacobsen, B. M. Hoffman, J. A. Ibers, *Inorg. Chem*. **1992**, *31*, 4517 – 4523; f) D. E. Rende, M. D. Heagy, W. B. Heuer, K. Liou, J. A. Thompson, B. M. Hoffman, R. L. Musselman, *ibid.* **1992**, *31*, 352 – 358; g) M. R. Godfrey, T. P. Newcomb, B. M. Hoffman, J. A. Ibers, *J. Am. Chem. Soc*. **1990**, *112*, 7260 – 7269.
[55] a) R. Guilard, J.-M. Barbe, P. Richard, P. Petit, J. J. Andre, C. Lecomte, K. M. Kadish, *J. Am. Chem. Soc*. **1989**, *111*, 4684 – 4687; b) T. P. Newcomb, M. R. Godfrey, B. M. Hoffman, J. A. Ibers, *ibid.* **1989**, *111*, 7078 – 7084; c) *Inorg. Chem*. **1990**, *29*, 223 – 228; d) E. M. McGhee, M. R. Godfrey, B. M. Hoffman, J. A. Ibers, *ibid.* **1991**, *30*, 2162 – 2165; e) M. R. Godfrey, K. Liou, T. P. Newcomb, W. P. Halperin, B. M. Hoffman, J. A. Ibers, *Synth. Met*. **1989**, *29*, F51 –

F58; f) K. Yakushi, M. Sakuda, I. Hamada, H. Kuroda, A. Kawamoto, J. Tanaka, T. Sugano, M. Kinoshita, *ibid.* **1987**, *19*, 769 – 774; g) M. Almeida, M. G. Kanatzidis, L. M. Tonge, T. J. Marks, H. O. Marcy, W. J. McCarthy, C. R. Kannewurf, *Solid State Commun.* **1987**, *63*, 457 – 461; h) M. Mossoyan-Deneux, D. Benlian, M. Pierrot, A. Fournel, J. P. Sorbier, *Inorg. Chem.* **1985**, *24*, 1878 – 1882.

[56] D. C. Miller, J. C. Bollinger, B. M. Hoffman, J. A. Ibers, *Inorg. Chem.* **1994**, *33*, 3354 – 3357.

[57] A. Rosa, J. Baerends, *Inorg. Chem.* **1992**, *31*, 4717 – 4726.

[58] K. M. Kadish, E. Van Caemelbecke, P. Boulas, F. D'Souza, E. Vogel, M. Kisters, C. J. Medforth, K. M. Smith, *Inorg. Chem.* **1993**, *32*, 4177 – 4179.

[59] J. Wojaczynski, L. Latos-Grazynski, *Inorg. Chem.* **1995**, *34*, 1044 – 1053, 1054 – 1062.

[60] C. Policar, I. Artaud, D. Mansuy, *Inorg. Chem.* **1996**, *35*, 210 – 216.

[61] a) M. J. Gunter, D. C. R. Hockless, M. R. Johnston, B. W. Skelton, A. H.White, *J. Am. Chem. Soc.* **1994**, *116*, 4810 – 4823; b) M. J. Gunter, M. R. Johnston, *J. Chem. Soc. Chem. Commun.* **1992**, 1163 – 1165; c) M. J. Gunter, M. R. Johnston, *ibid.* **1994**, 829 – 830.

[62] a) T. Jiang, D. S. Lawrence, *J. Am. Chem. Soc.* **1995**, *117*, 1857 – 1858; b) D. L. Dick, T. V. S. Rao, D. Sukumaran, D. S. Lawrence, *ibid.* **1992**, *114*, 2664 – 2669; c) F. Venema, A. E. Rowan, R. J. M. Nolte, *ibid.* **1996**, *118*, 257 – 258; d) J. M. Ribo, J.-A. Farrera, M. L. Valero, A. Virgili, *Tetrahedron* **1995**, 51, 3705 – 3712; e) S. Mosseri, J. C. Mialocq, B. Perly, P. Hambright, *J. Phys. Chem.* **1991**, *95*, 2196 – 2203; f) J. S. Manka, D. S. Lawrence, *J. Am. Chem. Soc.* **1990**, *112*, 2440 – 2442; g) J. S. Manka, D. S. Lawrence, *ibid.* **1990**, *112*, 4659 – 4663; h) S. K. Sur, R. G. Bryant, *J. Phys. Chem.* **1995**, *99*, 4900 – 4905.

[63] a) J. S. Manka, D. S. Lawrence, *Tetrahedron Lett.* **1989**, *30*, 7341 – 7344; b) S. Matile, T. Hansen, A. Stocker, W.-D. Woggon, *Helv. Chim. Acta* **1994**, *77*, 1087 – 1098; c) S. Zao, J. H. T. Luong, *J. Chem. Soc. Chem. Commun.* **1994**, 2307 – 2308; d) I. Willner, E. Adar, Z. Goron, B. Steinberger, *New J. Chem.* **1987**, 11, 769; e) S. Zhao, J. H. T. Luong, *J. Chem. Soc. Chem. Commun.* **1995**, 663 – 664.

[64] J.-M. Lehn, *Angew. Chem.* **1988**, *100*, 91 – 116; *Angew. Chem. Int. Ed. Engl.* **1988**, *27*, 89 – 112.

[65] J. W. Sibert, S. J. Lange, C. L. Stern, A. G. M. Barrett, B. M. Hoffman, *Angew. Chem.* **1995**, *107*, 2173 – 2176; *Angew. Chem. Int. Ed. Engl.* **1995**, *34*, 2020 – 2022. For the same type of complex, see also a) L. Sun, J. von Gersdorff, D. Niethammer, P. Tian, H. Kurreck, *ibid.* **1994**, *106*, 2396 and **1994**, *33*, 2318 – 2320; b) T. Toupance, V. Ahsen, J. Simon, *J. Chem. Soc. Chem. Commun.* **1994**, 75 – 76.

[66] P. Tomasik, Z. Ratajewicz in *Heterocyclic Compounds*, *Vol. 14, Part. 6* (Eds.: G. R. Newkome, L. Strekowski), Wiley, New York, **1985**, p. 189.

[67] See, for example, A. A. Vlcek *Coord. Chem. Rev.* **1982**, *43*, 39 – 62.

[68] V. Balzani, A. Juris, M. Venturi, S. Campagna, S. Serroni *Chem. Rev.* **1996**, *96*, 759 – 833.

[69] A. Juris, V. Balzani, F. Barigelletti, S. Campagna, P. Belser, A. von Zelewsky, *Coord. Chem. Rev.* **1988**, *84*, 85 – 277.

[70] a) P. E. Rillema, G. Allen, T. J. Meyer, D. Conrad, *Inorg. Chem.* **1983**, *22*, 1617 – 1622, and references therein; b) F. Barigelletti, A. Juris, V. Balzani, P. Belser, A. von Zelewsky, *Chem. Phys. Lett.* **1982**, *89*, 101 – 104, and references therein.

[71] Based on conversion of the reduction potential (vs. SCE): W. P. Griffith, *The Chemistry of the Rarer Platinum Earth Metals (Os, Ru, Ir, and Rh)*, Interscience, New York, **1967**, p. 215.

[72] See, for example,: A. Rusina, A. A. Vlcek, S. Zális, *Z. Chem.* **1979**, *19*, 27.

[73] a) Y. Ohsawa, M.-H. Whangbo, K. W. Hanck, M. K. De Armond, *Inorg. Chem.* **1984**, *23*, 3426 – 3428; b) Y. Ohsawa, M. K. De Armond, K. W. Hanck, D. E. Morris, *J. Am. Chem. Soc.* **1983**, *105*, 6522 – 6524.

[74] D. E. Morris, K. W. Hanck, M. K. DeArmond, *J. Am. Chem. Soc.* **1983**, *105*, 3032 – 3038, and references therein.

[75] M. K. DeArmond, M. L. Myrick, *Acc. Chem. Res.* **1989**, *22*, 364 – 370.

[76] Example of the Ru^{II} complexes: Y. Kawanishi, N. Kitamura, Y. Kim, S. Tazuke, *Riken. Q.* **1984**, *78*, 212, and references therein.

[77] Review of terpyridine coordination: E. C. Constable, *Adv. Inorg. Radiochem.* **1986**, *30*, 69 – 121.

[78] a) L. Echegoyen, A. DeCian, J. Fischer, J.-M. Lehn, *Angew. Chem.* **1991**, *103*, 884 – 886; *Angew. Chem. Int. Ed. Engl.* **1991**, *30*, 838 – 840; b) L. Echegoyen, E. Pérez-Cordero, J.-B. Regnouf de Vains, C. Roth, J.-M. Lehn, *Inorg. Chem.* **1993**, *32*, 572 – 577.

[79] M. Gómez-Kaifer, unpublished results.

[80] a) E. Constable, *Tetrahedron* **1992**, *48*, 10013 – 10059; b) in *Progress in Inorganic Chemistry*, *Vol 42* (Ed.: K. D. Karlin), Wiley, New York, **1994**, p. 67.

[81] L. Zelikovich, J. Libman, A. Shanzer, *Nature* **1996**, *374*, 380 – 382.

[82] *Supramolecular Chemistry* (Ed.: J.-M. Lehn), VCH, New York, **1995**, p. 106.

[83] V. Grosshenny, A. Harriman, R. Ziessel, *Angew. Chem.* **1995**, *107*, 2921 – 2925; *Angew. Chem. Int. Ed. Engl.* **1995**, *34*, 2705 – 2708.

[84] Ref. [82], p. 157.

[85] a) H. Sleiman, P. Baxter, J.-M. Lehn, K. Rissanen, *J. Chem. Soc. Chem. Commun.* **1995**, 715 – 716; b) G. S. Hanan, C. R. Arana, J.-M. Lehn, D. Fenske, *Angew. Chem.* **1995**, *107*, 1191 – 1193; *Angew. Chem. Int. Ed. Engl.* **1995**, *34*, 1122 – 1124.

[86] See, for example, P. N. Baxter, J.-M. Lehn, J. Fischer, M.-T. Youinou, *Angew. Chem.* **1994**, *106*, 2432; *Angew. Chem. Int. Ed. Engl.* **1994**, *33*, 2284 – 2287.

[87] G. Denti, S. Campagna, S. Serroni, M. Ciano, V. Balzani, *J. Am. Chem. Soc.* **1992**, *114*, 2944 – 2950.

[88] A. Achar, R. J. Puddephatt, *Angew. Chem.* **1994**, *106*, 895 – 897; *Angew. Chem. Int. Ed. Engl.* **1994**, *33*, 847 – 849.

[89] E. C. Constable, A. M. W. Cargille Thompson, *J. Chem. Soc. Chem. Commun.* **1992**, 617 – 619.

[90] G. R. Newkome, R. Güther, C. N. Moorefield, F. Cardulla, L. Echegoyen, E. Pérez-Cordero, H. Luftmann, *Angew. Chem.* **1995**, *107*, 2159 – 2162; *Angew. Chem. Int. Ed. Engl.* **1995**, *34*, 2023 – 2026.

[91] R. Wasielewski, W. A. Svec, B. T. Cope, *J. Am. Chem. Soc.* **1978**, *100*, 1961 – 1962.

[92] T. Sato, K. Torizuka, *J. Chem. Soc. Perkin Trans. 2* **1978**, 1199 – 1204.

[93] T. Sato, K. Torizuka, R. Komaki, H. Atobe, *J. Chem. Soc. Perkin Trans. 2* **1980**, 561 – 568.

[94] B. Thulin, *J. Chem. Soc. Perkin Trans. 1* **1981**, 664 – 667.

[95] a) E. V. Laganis, R. H. Voegeli, R. T. Swann, R. G. Finke, H. Hopf, V. Boekelheide, *Organometallics* **1981**, *1*, 1415 – 1420; b) W. J. Bowyer, W. E. Geiger, V. Boekelheide, *ibid.* **1984**, *3*, 1079 – 1086.

[96] a) P. Jutzi, U. Siemeling, A. Mueller, H. Boegge, *Organometallics* **1989**, *8*, 1744 – 1750; b) C. Elschenbroich, J. Schneider, M. Wuensch, J. L. Pierre, P. Baret, P. Chautemps, *Chem. Ber.* **1988**, *121*, 177 – 183.

[97] T. Tomohiro, H. Y. Okuno, *Inorg. Chim. Acta* **1993**, *204*, 147 – 152.

[98] R. Hassan, M. Lacoste, M.-H. Delville-Desboise, J. Ruiz, B. Gloaguen, N. Ardoin, D. Astruc, A. L. Beuze, J.-Y. Saillard, *Organometallics* **1995**, *14*, 5078 – 5092.

[99] H. A. Staab, G. Voit, J. Weiser, M. Futscher, *Chem. Ber.* **1992**, *125*, 2303 – 2310.

[100] D. R. Benson, R. Valentekovich, S.-W. Tam, F. Diederich, *Helv. Chim. Acta* **1993**, *76*, 2034 – 2060.

[101] A. Livoreil, C. O.Dietrich-Buchecker, J. P. Sauvage, *J. Am. Chem. Soc.* **1994**, *116*, 9399 – 9400.

[102] a) R. R. Lilienthal, D. K. Smith, *Anal. Chem.* **1995**, *67*, 3733 – 3739; b) E. A. Smith, R. R. Lilienthal, R. J. Fonseca, D. K. Smith, *ibid.* **1994**, *66*, 3013 – 3020; c) P. R. Ashton, C. L. Brown, E. J. T. Chrystal, T T. Goodnow, A. E. Kaifer, K. P. Parry, D. Philp, A. M. Z. Slawin, N. Spencer, *J. Chem. Soc. Chem. Commun.* **1991**, 634 – 639; d) R. J. Fonseca, J. T. Colina, D. K. Smith, *J. Electroanal. Chem.* **1992**, *340*, 341 – 348; e) P. L. Anelli, P. R. Ashton, R. Ballardini, V. Balzani, M. Delgado, M. T. Gandolfi, T. T. Goodnow, A. E. Kaifer, D. Philips, M. Pietraszkiewicz, L. Prodi, M. V. Reddington, A. M. Z. Slawin, N. Spencer, J. F. Stoddart, C. Vicent, D. J. Williams, *J. Am. Chem. Soc.* **1992**, 114, 193 – 218; f) P. R. Ashton, T. T. Goodnow, A. E. Kaifer, M. V. Reddington, A. M. Z. Slawin, N. Spencer, J. F. Stoddart, *Angew. Chem.* **1989**, *101*, 1404 – 1408; *Angew. Chem. Int. Ed. Engl.* **1989**, *34*, 1396 – 1399.

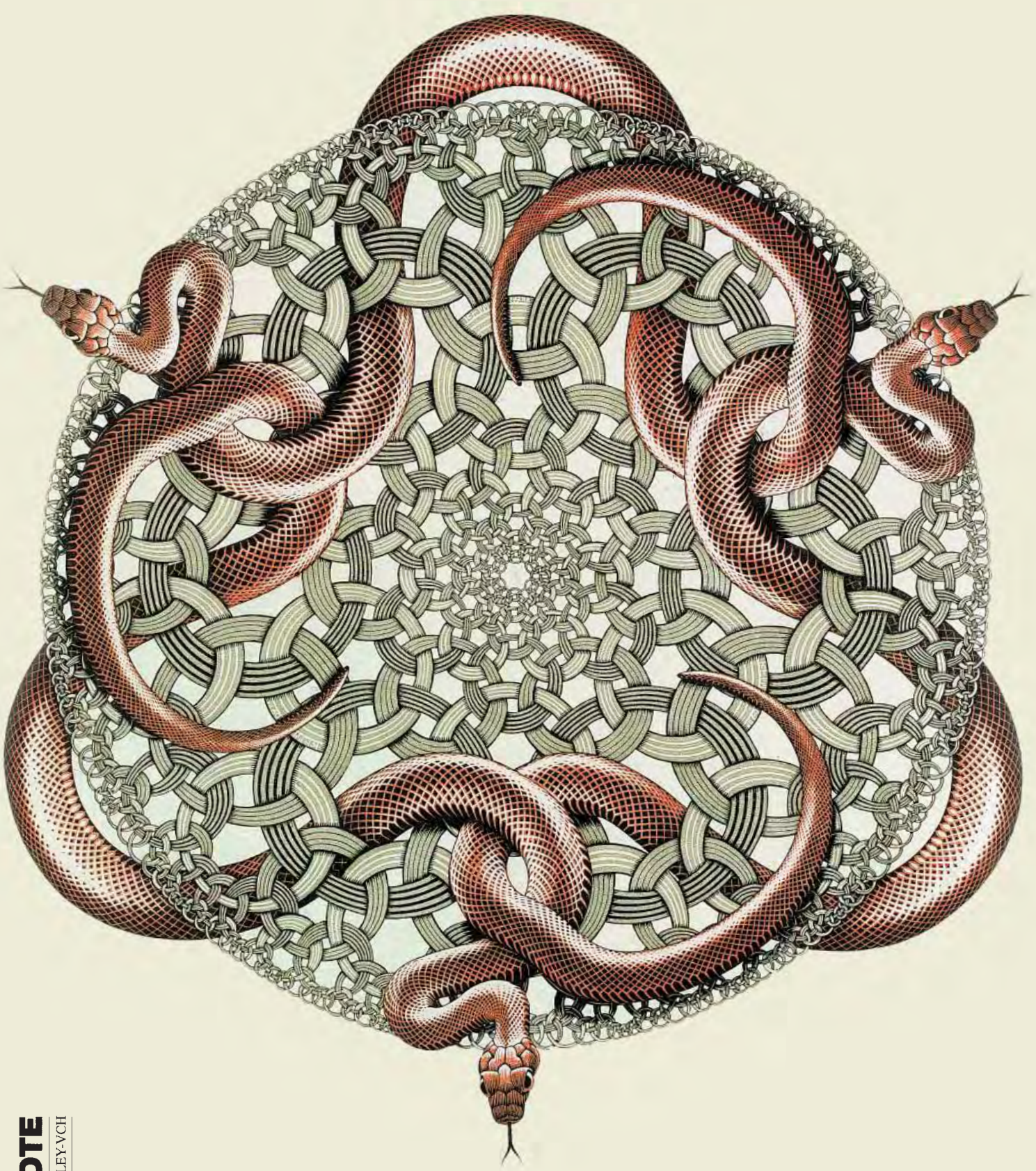
[103] R. A. Bissell, E. Cordova, A. E. Kaifer, *J. Org. Chem.* **1995**, *60*, 1033 – 1038.

[104] a) J. B. Flanagan, S. Margel, A. J. Bard, F. C. Anson, *J. Am. Chem. Soc.* **1978**, *100*, 4248 – 4254; b) A. El-Kasmi, D. Lexa, P. Maillard, M. Momenteau, J. M. Savéant, *J. Phys. Chem.* **1993**, *97*, 6090 – 6095, and references therein.

[105] T. Lu, L. Zhang, G. W. Gokel, A. E. Kaifer, *J. Am. Chem. Soc.* **1993**, *115*, 2542 – 2543.

[106] P. A. Ashton, R. Ballardini, V. Balzani, A. Credi, M. T. Gandolfi, S. Menzer, L. Pérez-Garcia, L. Prodi, J. F. Stoddart, M. Venturi, A. J. P. White, D. J. Williams, *J. Am. Chem. Soc.* **1995**, *117*, 11171 – 11197.
[107] a) Z.-T. Li, P. C. Stein, J. Becher, D. Jensen, P. Mørk, N. Svenstrup, *Chem. Eur. J.* **1996**, *2*, 624 – 633; b) Z.-T. Li, P. C. Stein, N. Svenstrup, K. H. Lund, J. Becher, *Angew. Chem.* **1995**, *107*, 2719 – 2723; *Angew. Chem. Int. Ed. Engl.* **1995**, *34*, 2524-2528.
[108] T. T. Goodnow, M. V. Reddington, J. F. Stoddart, A. E. Kaifer, *J. Am. Chem. Soc.* **1991**, *113*, 4335 – 4337.
[109] M. T. Rojas, A. E. Kaifer, *J. Am. Chem. Soc.* **1995**, 117, 5883 – 5884.
[110] Y. Morita, T. Agawa, Y. Kai, N. Kanehisa, N. Kasai, E. Nomura, H. Taniguchi, *Chem. Lett.* **1989**, 1349 – 1352.
[111] K. Suga, M. Fujihira, Y. Morita, T. Agawa, *J. Chem. Soc. Faraday Trans.* **1991**, *87*, 1575 – 1578.
[112] Y. Morita, T. Agawa, *J. Org. Chem.* **1992**, *57*, 3658 – 3662.
[113] P. A. Reddy, R. P. Kashyap, W. H. Watson, C. D. Gutsche, *Isr. J. Chem.* **1992**, *32*, 89 – 96.
[114] a) A.Casnati, E. Comelli, M. Fabbi, V. Bocchi, G. Mori, F. Ugozzoli, A. M. Manotti Lafredi, A. Pochini, R. Ungaro, *Recl. Trav. Chim. Pays-Bas* **1993**, *112*, 384 – 392; b) J.-D. van Loon, A. Arduini, L. Coppi, W. Verboom, A. Pochini, R. Ungaro, S. Harkema, D. N. Reinhoudt, *J. Org. Chem.* **1990**, *55*, 5639 – 5646.
[115] M. Gómez-Kaifer, P. A. Reddy, C. D. Gutsche, L. Echegoyen, *J. Am. Chem. Soc.* **1994**, *116*, 3580 – 3587.
[116] P. D. Beer, Z. Chen, P. A. Gale, *Tetrahedron* **1994**, *50*, 931 – 940.
[117] T. D. Chung, D. Choi, S. K. Kang, S. K. Lee, S.-K. Chang, H. Kim, *J. Electroanal. Chem.* **1995**, *396*, 431 – 439.
[118] M. Gómez-Kaifer, PhD thesis, University of Miami, (USA) **1997**. The sample of 1,3,5-triquinonecalix[6]arene was privided by the group of Rocco Ungaro.
[119] Ref. [118]; the calix[6]diquinone was provided by Javier de Mendoza and the nitrocalix[4]arenes from D. N. Reinhoudt.
[120] J. Blixt, C. Detellier, *J. Am. Chem. Soc.* **1995**, *117*, 8536 – 8540.
[121] M. Gómez-Kaifer, P. A. Reddy, C. D. Gutsche, L. Echegoyen, *J. Am. Chem. Soc.* **1997**, *119*, 5222 – 5229.
[122] W. Verboom, A. Durie, R. J. M. Egberink, A. Asafri, D. N. Reinhoudt, *J. Org. Chem.* **1992**, *57*, 1313 – 1316.
[123] P. D. Beer, Z. Chen, P. A. Gale, *J. Electroanal. Chem.* **1995**, *393*, 113 – 117.
[124] a)P. D. Beer, D. Hesek, J. E. Kingston, D. K. Smith, S. E. Stokes, M. G. B. Drew, *Organometallics* **1995**, *14*, 3288-3295; b) P. D. Beer, E. L. Tite, A Ibbotson, *J. Chem Soc. Dalton Trans.* **1991**, 1691 – 1698.
[125] P. D. Beer, Z. Chen, A. J. Goulden, A. Grieve, D. Hesek, F. Szemes, T. Wear, *J. Chem. Soc. Chem. Comm.* **1994**, 1269 – 1271.
[126] S. Shinkai, *J. Chem. Soc. Chem. Comm.* **1994**, *22*, 2587 – 2588.
[127] L. Zhang, L. A. Godinez, T. Lu, G. W. Gokel, A. E. Kaifer, *Angew. Chem.* **1995**, *107*, 236 – 239; *Angew. Chem. Int. Ed. Engl.* **1995**, *34*, 235 – 237.
[128] A. R. Bernardo, T. Lu, E. Córdova, L. Zhang, G. W. Gokel, A. E. Kaifer, *J. Chem. Soc. Chem. Commun.* **1994**, 829 – 830.
[129] L. Zhang, A. Macias, R. Isnin, T. Lu, G. W. Gokel, A. E. Kaifer, *J. Inclusion Phenom. Mol. Recognit. Chem.* **1994**, *19*, 361 – 370.
[130] L. Zhang, A. Macias, T. Lu, J. I. Gordon, G. W. Gokel, A. E. Kaifer, *J. Chem. Soc. Chem. Commun.* **1993**, 1017 – 1019.
[131] R. M. Williams, J. W. Verhoeven, *Recl. Trav. Chim. Pay-Bas* **1992**, *111*, 531 – 532.
[132] J. L. Atwood, G. A. Koustantonis, C. L. Raston, *Nature* **1994**, *368*, 229 – 231.
[133] T. Suzuki, K. Nakashima, S. Shinkai, *Chem. Lett.* **1994**, 699 – 702.
[134] Z. Chen, J. M. Fox, P. A. Gale, A. J. Pilgrim, P. D. Beer, M. J. Rosseinsky, *J. Electroanal. Chem.* **1995**, *392*, 101 – 105.
[135] R. Castillo, S. Ramos, R. Cruz, M. Martinez, F. Lara, J. Ruiz-Garcia, *J. Phys. Chem.* **1996**, *100*, 709 – 713.
[136] a) Recent review on fullerene endohedral complexes: D. S. Bethune, R. D. Johnson, J. R. Salem, M. S. de Vries, C. S. Yannoni, *Nature* **1993**, *366*, 123 – 128; b) Y. Chai, T. Guo, C. Jin, R. E. Haufler, L. P. F. Chibante, J. Fure, L. Wang, J. M. Alford, R. E. Smalley, *J. Phys. Chem.* **1991**, *95*, 7564 – 7568, and references therein.
[137] a) T. Andersson, K. Nilsson, M. Sundahl, G. Westman, O. Wennerström, *J. Chem. Soc. Chem. Commun.* **1992**, 604 – 606; b) Z.-I. Yoshida, H. Takekuma, S.-I. Takekuma, Y. Matsubara, *Angew. Chem.* **1994**, *106*, 1658 – 1660; *Angew. Chem. Int. Ed. Engl.* **1994**, *33*, 1597 – 1599; c) P. Boulas, W. Kutner, M. T. Jones, K. M. Kadish, *J. Phys. Chem.* **1994**, *98*, 1282 – 1287; d) R. M. Williams, J. M. Zwier, J. W. Verhoeven, G. H. Nachtegaal, A. P. M. Kentgens, *J. Am. Chem. Soc.* **1994**, *116*, 6965 – 6966; e) F. Diederich, J. Effing, U. Jonas, L. Jullien, T. Plesnivy, H. Ringsdorf, C. Thilgen, D. Weinstein, *Angew. Chem.* **1992**, *104*, 1683 – 1686; *Angew. Chem. Int. Ed. Engl.* **1992**, *31*, 1599 – 1602; f) D. M. Guldi, H. Hungerbuhler, K. D. Asmus, *J. Phys. Chem.* **1995**, *99*, 13487 – 13493.
[138] a) M. Saunders, H. A. Jiménez-Vázquez, R. J. Cross, R. J. Poreda, *Science* **1993**, *259*, 1428 – 1430; b) M. Saunders, H. A. Jiménez-Vázquez, R. J. Cross, W. E. Billups, C. Gesenberg, A. Gonzales, W. Luo, R. C. Haddon, F. Diederich, A. Herrmann, *J. Am. Chem. Soc.* **1995**, *117*, 9305 – 9308, and references therein.
[139] a) T. Suzuki, Y. Maruyama, T. Kato, K. Kikuchi, Y. Achiba, *J. Am. Chem. Soc.* **1993**, *115*, 11006 – 11007; b) K. Kikuchi, Y. Nakao, S. Suzuki, Y. Achiba, T. Suzuki, Y. Maruyama, *ibid.* **1994**, *116*, 9367 – 9368; c) T. Suzuki, K. Kikuchi, Y. Nakao, S. Suzuki, Y. Achiba, K. Yamamoto, H. Funasaka, T. Takahashi in *Fullerenes: The Physics and Chemistry of Fullerenes and Related Materials* (Eds.: K. M. Kadish, R. S. Ruoff), The Electrochemical Society, Pennington (NJ), **1995**, p. 259; d) S. Nagase, K. Kobayashi, T. Akasaka in *Fullerenes: The Physics and Chemistry of Fullerenes and Related Materials* (Eds.: K. M. Kadish, R. S. Ruoff), The Electrochemical Society, Pennington (NJ), **1995**, p. 747; e) T. Suzuki, Y. Maruyama, T. Kato, K. Kikuchi, Y. Nakao, Y. Achiba, K. Kobayashi, S. Nagase, *Angew. Chem.* **1995**, *107*, 1228 – 1230; *Angew. Chem. Int. Ed. Engl.* **1995**, *34*, 1094 – 1096; f) E. Yamamoto, M. Tansho, T. Tomiyama, H. Shinohara, H. Kawahara, Y. Kobayashi, *J. Am. Chem. Soc.* **1996**, *118*, 2293 – 2294, and references therein.
[140] Q. Xie, E. Pérez-Cordero, L. Echegoyen, *J. Am. Chem. Soc.* **1992**, *114*, 3978 – 3980.
[141] a) Y. Ohsawa, T. Saji, *J. Chem. Soc. Chem. Commun.* **1992**, 781 – 782; b) F. Zhou, C. Jehoulet, A. J. Bard, *J. Am. Chem. Soc.* **1992**, *114*, 11004 – 11006.
[142] a) S. H. Friedman, D. L. Decamp, R. P. Sijbesma, G. Srdanov, F. Wudl, G. L. Kenyon, *J. Am. Chem. Soc.* **1993**, *115*, 6506 – 6509; b) R. P. Sijbesma, G. Srdanov, F. Wudl, J. A. Castoro, C. Wilkins, S. H. Friedman, D. L. Decamp. G. L. Kenyon, *ibid.* **1993**, *115*, 6510 – 6512; c) A. W. Jensen, S. R. Wilson, D. I. Shuster, *Bioorg. Med. Chem.* **1996**, *4*, 767 – 779.
[143] T. G. Linssen, K. Dürr, M. Hanack, A. Hirsch, *J. Chem. Soc. Chem. Commun.* **1995**, 103 – 104.
[144] H. Imahori, K. Hagiwara, T. Akiyama, S. Taniguchi, T. Okada, Y. Sakata, *Chem. Lett.* **1995**, 265 – 266.
[145] P. A. Liddell, J. P. Sumida, A. N. MacPherson, L. Noss, G. R. Seely, K. N. Clark, A. L. Moore, T. A. Moore, D. Gust, *Photochem. Photobiol.* **1994**, *60*, 537 – 541.
[146] a) M. Maggini, A. Dono, G. Scorrano, M. Prato, *J. Chem. Soc. Chem. Commun.* **1995**, 845 – 856; b) N. S. Sariciftci, F. Wudl, A. J. Heeger, M.Maggini, G. Scorrano, M. Prato, J. Bourassa, P. C. Ford, *Chem. Phys. Lett.* **1995**, *247*, 510 – 514.
[147] P.-M. Allemand, G. Srdanov, A. Koch, K. Khemani, F. Wudl, Y. Rubin, F. Diederich, M. M. Alvarez, S. J. Anz, R. L. Whetten, *J. Am. Chem. Soc.* **1991**, *113*, 2780 – 2781.
[148] H. Moriyama, H. Kobayashi, A. Kobayashi, T. Watanabe, *J. Am. Chem. Soc.* **1993**, *115*, 1185 – 1187.
[149] A. Penicaud, A. Pérez-Benitez, R. Gleason V. E. Munoz P. R. Escudero, *J. Am. Chem. Soc.* **1993**, *115*, 10392 – 10393.
[150] U. Bilow, M. Jansen, *J. Chem. Soc. Chem. Commun.* **1994**, 403 – 404.
[151] B. Miller, J. M. Rosamilia, *J. Chem. Soc. Faraday Trans.* **1993**, *89*, 273 – 276.
[152] W. C. Wan, X. Liu, G. M. Sweeney, W. E. Broderick, *J. Am. Chem. Soc.* **1995**, *117*, 9580 – 9581.
[153] C. A. Foss, D. L. Feldheim, D. R. Lawson, P. K. Dorhout, C. M. Elliott, C. R. Martin, B. A. Parkinson, *J. Electrochem. Soc.* **1993**, *140*, L84 – L86.
[154] H. Kobayashi, H. Moriyama, A. Kobayashi, T. Watanabe, *J. Am. Chem. Soc.* **1994**, *116*, 3153 – 3154.
[155] A. Penicaud, A. Pérez-Benitez, R. Escudero, C. Coulon, *Solid State Commun.* **1995**, *96*, 147 – 150.
[156] a) P. Paul, Z. Xie, R. Bau, P. D. W. Boyd, C. A. Reed, *J. Am.Chem. Soc.* **1994**, *116*, 4145 – 4146; b) P. D. W. Boyd, P. Bhyrappa, P. Paul, J.

Stinchcombe, R. D. Bolskar, Y. Sun, C. A. Reed, *ibid.* **1995**, *117*, 2907 – 2914.
[157] a) J.-M. Lehn, *Acc. Chem. Res.* **1978**, *11*, 49 – 57; b) J.-M. Lehn, *Pure Appl. Chem*. **1980**, *52*, 2303 – 2319.
[158] a) R. H. Huang, M. K. Faber, K. J. Moeggenborg, D. L. Ward, J. L. Dye, *Nature* **1988**, *331*, 599 – 601; b) J. L. Dye, *Science* **1990**, *247*, 663 – 668; c) J. L. Dye, *Pure Appl. Chem*. **1989**, *61*, 1555 – 1562; c) J. L. Dye, M. J. Wagner, G. Overney, R. H. Huang, T. F. Nagy, D Tomanek, *J. Am. Chem. Soc*. **1996**, *118*, 7329 – 7336.
[159] a) N. Mammano, M. J. Sienko, *J. Am. Chem. Soc*. **1968**, *90*, 6322 – 6324; b) R. K. Quinn, J. J. Lagowski, *J. Phys. Chem*. **1968**, *72*, 1374; c) J. O. Littlehailes, B. J. Woodhall, *Discuss. Faraday Soc*. **1968**, *45*, 187.
[160] M. Takata, B. Umeda, E. Nishibori, M. Sakata, Y. Saito, M. Ohno, H. Shinohara, *Nature* **1995**, *377*, 46 – 49.
[161] a) L. Echegoyen, Q. Xie, E. Pérez-Cordero, *Pure Appl. Chem*. **1993**, *65*, 441 – 446; b) L. Echegoyen, E. Pérez-Cordero in *Transition Metals in Supramolecular Chemistry* (Eds.: L. Fabrizzi, A. Poggy), Kluwer, Dordrecht, **1994**, p. 115; c) E. Pérez-Cordero, R. Buigas, N. Brady, L. Echegoyen, C. Arana, J.-M. Lehn, *Helv. Chim. Acta* **1994**, *77*, 1222 – 1228.
[162] M. J. Wagner, J. L. Dye, E. Pérez-Cordero, R. Buigas, L. Echegoyen, *J. Am. Chem. Soc.* **1995**, *117*, 1318 – 1323.
[163] a) D. E. Morris, K. W. Hanck, M. K. DeArmond, *Inorg. Chem*. **1985**, *24*, 977 – 979; b) A. G. Motten, K. W. Hanck, M. K. DeArmond, *Chem. Phys. Lett*. **1981**, *79*, 541.
[164] R. S. Ross, P. Pincus, F. Wudl, *J. Phys. Chem*. **1992**, *96*, 6169 – 6172.
[165] C. Boudon, J.-P. Gisselbrecht, M. Gross, L. Isaacs, H. L. Anderson, R. Faust, F. Diederich, *Helv. Chim. Acta* **1995**, *78*, 1334 – 1344.
[166] T. J. Seiders, K. K. Baldridge, J. S. Siegel, *J. Am. Chem. Soc*. **1996**, *118*, 2754 – 2755.
[167] D. A. Dougherty, *Science* **1996**, *271*, 163 – 168.
[168] J. C. Medina, I. Gay, Z. Chen, L. Echegoyen, G. W. Gokel, *J. Am. Chem. Soc.* **1991**, *113*, 365 – 366.
[169] F. Arias, L. A. Godínez, S. R. Wilson, A. E. Kaifer, L. Echegoyen, *J. Am. Chem. Soc.* **1996**, *118*, 6086 – 6087.
[170] a) L. E. Echegoyen, J. C. Hernandez, A. E. Kaifer, G. W. Gokel, L. Echegoyen, *J. Chem. Soc. Chem. Comm.* **1988**, 836 – 837; b) L. E. Echegoyen, L. Portugal, S. R. Miller, J. C. Hernandez, L. Echegoyen, G. W. Gokel, *Tetrahedron Lett*. **1988**, 29, 4065 – 4068.
[171] K. Wang, S. Muñoz, L. Zhang, R. Castro, A. E. Kaifer, G. W. Gokel, *J. Am. Chem. Soc.* **1996**, *118*, 6707 – 6715.
[172] I. Willner, M. Lion-Dagan, S. Marx-Tibbon, E. Katz, *J. Am. Chem. Soc.* **1995**, *117*, 6581 – 6586.
[173] R. M. Izatt, K. Pawlak, J. S. Bradshaw, R. L. Bruening, *Chem. Rev.* **1991**, *91*, 1721 – 2085.
[174] R. Deans, A. Niemz, E. C. Breinlinger, V. M. Rotello, *J. Am. Chem. Soc.* **1997**, *119*, 10863 – 10864.
[175] R. Castro, I. Cuadrado, B. Alonso, C. M. Casado, M. Morán, A. E. Kaifer, *J. Am. Chem. Soc.* **1997**, *119*, 5760 – 5761.
[176] F. Szemes, D. Hesek, Z. Chen, S. W. Dent, M. G. B. Drew, A. J. Goulden, A. R. Graydon, A. Grieve, R. J. Mortimer, T. Wear, J. S. Weightman, P. D. Beer, *Inorg. Chem.* **1997**, *35*, 5868 – 5879.
[177] a) J. Lau, P. Blanchard, A. Riou, M. Jubault, M. P. Cava, J. Becher, *J. Org. Chem.* **1997**, *62*, 4936 – 4942; b) K. B. Simonsen, K. Zong, R. D. Rogers, M. P. Cava, J. Becher, *ibid.* **1997**, *62*, 679 – 686; c) Z.-T. Li, P. C. Stein, J. Becher, D. Jensen, P. Moerk, N. Svenstrup, *Chem. Eur. J.* **1996**, *2*, 624 – 633.
[178] a) B. Hasenkopf, J.-M. Lehn, N. Boumediene, A. Dupont-Gervais, A. Van Dorsselaer, B. Kneisel, D. Fenske, *J. Am. Chem. Soc.* **1997**, *119*, 10956 – 10962; b) Constable, E. C. F. Heirtzler, M. Neuberger, M. Zehnder, *ibid.* **1997**, *119*, 5606 – 5617; c) D.-P. Funeriu, Y.-B. He, H.-J. Bister, J.-M. Lehn, *Bull. Soc. Chim. Fr.* **1996**, *133*, 673 – 678; d) Constable, E. C. T. Kulke, M. Neuberger, M. Zehnder, *Chem. Commun.* **1997**, 489 – 490 and references therein.
[179] T. Suzuki, K. Kikuchi, F. Oguri, Y. Nakao, S. Suzuki, Y. Achiba, K. Yamamoto, H. Funasaka, T. Takahashi, *Tetrahedron* **1996**, *52*, 4973 – 4982.
[180] M. R. Anderson, H. C. Dorn, S. Stevenson, P. M. Burbank, J. R. Gibson, *J. Am. Chem. Soc.* **1997**, *119*, 437 – 438.
[181] U. Kirbach, L. Dunsch, *Angew. Chem.* **1996**, *108*, 2518 – 2521; *Angew. Chem. Int. Ed. Engl.* **1996**, *35*, 2380 – 2383.



ANGEWANDTE CHEMIE © WILEY-VCH

C_3 Symmetry is fascinating not only in the visual arts, as this picture by M. C. Escher demonstrates (Copyright © Cordon Art, Baarn, The Netherlands, 1997), but also in chemistry. Of particular interest are the potential advantages of chiral compounds of higher symmetry as ligands and catalysts.

C_3 Symmetry in Asymmetric Catalysis and Chiral Recognition

Christina Moberg*

Chiral recognition is a key process in all efforts aimed at obtaining enantiomerically pure chiral compounds, whether by synthetic procedures or by separation techniques. Several cooperating factors contribute to achieving high selectivity in the processes involving chiral recognition. A complete understanding of these factors is beyond the scope of today's knowledge. It is a great challenge, however, to gain a deeper understanding of the factors responsible for chiral discrimination by taking into account the important characteristics of the interacting species. These include primarily their steric and electronic properties, the various attractive intermolecular interactions, and the dynamics of the recognition process. A further factor that may be important is the symmetry properties of the interacting entities. This review highlights the role of rotational symmetry, with an emphasis on C_3 symmetry, in asymmetric catalysis and chiral recognition. The situations in which rotational symmetry is important are considered, methods for the preparation of molecules with threefold rotational symmetry are discussed, and the various types of compounds with threefold rotational symmetry and their applications in asymmetric catalysis and chiral recognition are surveyed.

Keywords: asymmetric catalysis · chirality · rotational symmetry

1. Introduction

Symmetry is a property of objects, systems, and states that is closely connected with beauty and the harmony of proportions. Symmetrical objects are often considered to be aesthetically appealing. Symmetry plays a fundamental role in such diverse disciplines as art, music, architecture, philosophy, mathematics, physics, and chemistry.[1] In problem solving the consideration of symmetry may help to simplify and systematize.[2] In chemistry molecules with symmetry exert a special attraction due to their beauty. In addition, symmetry may be advantageous in synthesis design,[3] in supramolecular self-assembly,[4] and for chemical selectivity.[5]

Chiral molecules containing symmetry elements are of special interest.[6] Among the symmetry elements, only proper rotational axes are compatible with chirality. In contrast to molecules that contain no element of symmetry and are therefore truly asymmetric (C_1-symmetric), molecules with rotational axes—and rotational axes *only*—are dissymmetric and belong to either the point groups C_n or D_n ($n>1$) or to one of the less common groups *T*, *I*, and *O*. Molecules with twofold rotational symmetry have been the subject of wide recent interest. Extensive original literature dealing with this topic and a review covering the subject have appeared.[7] The extension to threefold and higher rotational symmetries has been less noticed, although a few reviews covering the preparation of chiral molecules with high symmetry exist.[8, 9]

This survey deals with molecules having rotational symmetry and their role in asymmetric synthesis and in other processes involving chiral recognition. It mainly covers threefold symmetry, with emphasis on chiral molecules belonging to point groups C_3 and D_3. Selected compounds and their applications which have appeared in the literature or have been studied by our own group serve as examples. Some achiral ligands with threefold rotational axes that can be potentially transformed into C_3-symmetric compounds are included. Most of the results covered by previous reviews[8, 9] are not repeated here. Compounds with chiral conformations having low barriers of inversion and achiral compounds that crystallize in chiral space groups are not covered by this survey.

2. Topology

Topology, also known as "rubber band geometry", is a branch of modern mathematics that can be used for the description of molecules, conformational changes, and chemical reactions. It deals with the continuity of functions, with the connectivity of objects, and with shape, in other words, with those properties of objects that remain unchanged upon

[*] Prof. C. Moberg
Department of Chemistry, Organic Chemistry
Royal Institute of Technology
SE-10044 Stockholm (Sweden)
Fax: Int. code + (46) 8-791 2333
e-mail: kimo@kth.se

 © WILEY-VCH Verlag GmbH, D-69451 Weinheim, 1998 1433-7851/98/3703-0249 $ 17.50+.50/0

stretching, twisting etc.[10] An object that does not have a precisely defined geometry but preserves some topological features is classified as a topological object. Molecules should thus not be considered as geometrical but as topological objects.

A tridentate ligand or a trifunctional molecule with C_3 symmetry can have four principally different topologies (Figure 1). It may be acyclic (a), "exocyclic" (b), macrocyclic

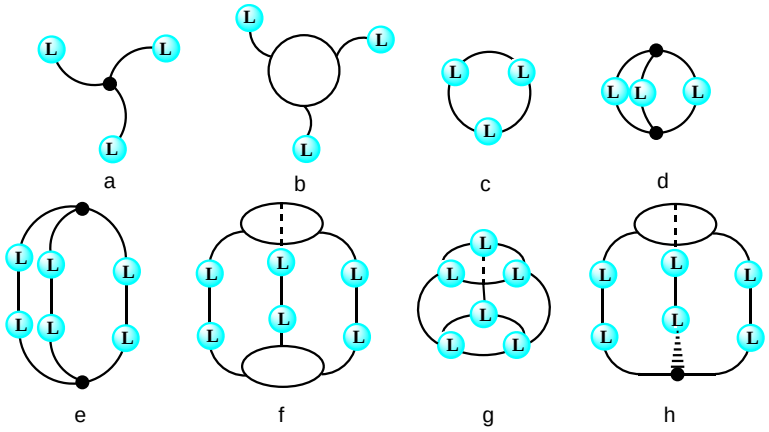


Figure 1. Topologies of structures with C_3 and D_3 symmetry.

(c), or bicyclic (d). If two twofold rotational axes perpendicular to the main axis are present, the molecule belongs to a point group of higher symmetry, D_3. Several examples of molecules are known for all of these forms. In addition, dimeric arrangements may be formed by combining any two of the structures a–d. When two equal halves are combined, the result is a species with D_3 symmetry (Figure 1e–g), whereas the combination of two unequal parts gives a molecule with C_3 symmetry (Figure 1h).

In all of these types of molecules the presence of a center of chirality (as in Figure 2a) is commonly a requirement for dissymmetry, although molecules are known in which axes of chirality cause dissymmetry. These include cyclic compounds in which the chirality originates from the direction of the array of substituents on the ring (Figure 2b).

Conformational preferences may also result in chiral species. Occasionally the barriers of inversion are sufficiently high to permit the isolation of nonsymmetric species. A

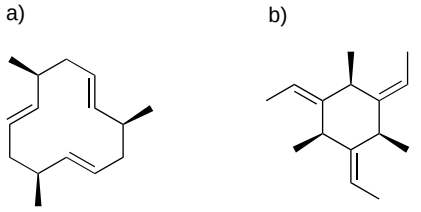


Figure 2. C_3-symmetric molecules with stereogenic centers (a) and axes (b).

further possible arrangement possessing C_3 symmetry is a triple helix.[11] Here the chirality is based on an axis of chirality. The asymmetric folding of the strands may be induced by stereogenic centers in the strands.[12]

3. Synthetic Routes: The Desymmetrization of Molecules with Higher Symmetry

Molecules belonging to point group C_3 or to a chiral group of higher order containing threefold axes can be obtained in two ways: by the proper assembly of homochiral or occasionally even achiral entities, and by the desymmetrization of molecules having improper rotational axes or mirror planes in addition to the C_3 axis. Such molecules belong to one of the following point groups: I_h, O_h, T_h, T_d, S_6, D_{6d}, D_{6h}, C_{6h}, C_{6v}, D_{3d}, D_{3h}, C_{3h}, C_{3v}.[13] The desired desymmetrization is brought about by destruction of all symmetry elements of the second kind (s, i, S_n), while symmetry elements of the first kind (C_n), at least one threefold axis, are maintained. The desymmetrization can be a change in conformation, but more important situations, in which configurationally stable species are formed, will be discussed here.

A simple illustration is given by methane (point group T_d), which, at least theoretically, can be desymmetrized in various ways. Substitution of three of the four hydrogen atoms by homochiral groups (of identical constitution) yields C_3-symmetric compounds (Figure 3a), whereas substitution of all four hydrogen atoms normally destroys the threefold rotational axes, leading to three different possible cases



Christina Moberg was born in 1947 in Gävle, Sweden and studied chemistry at the University of Stockholm (B.Sc. 1970). She then moved to the Royal Institute of Technology in Stockholm, where she earned her doctorate under the direction of Professor M. Nilsson. After a postdoctoral stay with Professor J. Normant at the Université Paris 6, she worked in the group led by Professor Åkermark at the Royal Institute of Technology before starting independent research. In 1989 she was granted a research position in organometallic chemistry by the Swedish Scientific Research Council, and she became a full professor in 1994.

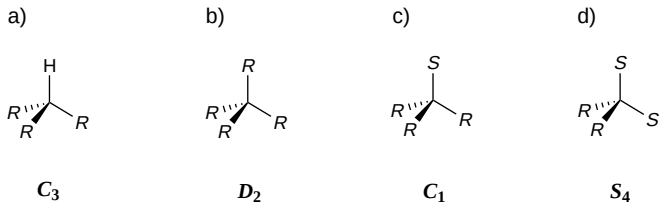


Figure 3. Symmetry of substituted methanes. *R* and *S* indicate the absolute configurations of isometric asymmetric ligands.

(Figure 3b–d). Complete substitution by homochiral groups with identical constitution yields a D_2-symmetric species; with one heterochiral substituent an asymmetric (C_1) species is obtained; and the third product is achiral since it has an S_4 symmetry axis. This topic was discussed by Mohr already at the beginning of this century,[14] and was experimentally verified half a century later by studies of esters prepared from pentaerythritol and chiral acids.[15]

The situation is different, though, when the desymmetrization is brought about by substituents with inherent C_3 symmetry. This operation is expected to yield a compound with *T* symmetry containing no less than four C_3 axes (in addition to two C_2 axes). This kind of operation has indeed been accomplished experimentally, not with methane[16] but instead with adamantane, which like methane has T_d symmetry (Figure 4).[17]

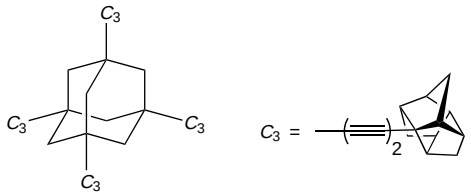


Figure 4. A *T*-symmetric adamantane derivative with four identical, C_3-symmetric substituents.

In regular polyhedra, symmetry elements of the second kind are generally destroyed while symmetry elements of the first kind are preserved by the attachment to each vertex of a chiral group having a rotational axis of the same order as and coinciding with that passing through the vertex.[9] In this manner, a chiral species having the same symmetry number as the regular polyhedron is obtained. Thus, when C_3-symmetric substituents are attached to each of the eight carbon atoms of cubane, [18] its symmetry is reduced from O_h to pure rotational *O* (with three C_4 axes and six C_2 axes in addition to the four C_3 axes). The analogous desymmetrization of an octahedral arrangement of atoms requires substituents with local C_4 symmetry, since fourfold instead of threefold axes pass through the atoms at the corners of a regular octahedron. The desymmetrization of molecules with I_h symmetry can also be achieved by a proper choice of substituents. For an icosahedral arrangement of atoms, substituents with a fivefold rotational axis at each of the twelve vertices result in *I* symmetry (with six C_5 axes and fifteen C_2 axes in addition to the ten C_3 axes). In dodecahedrane,[19] however, desymmetrization is achieved by twenty substituents with inherent threefold rotational symmetry. Since only C_1 axes pass through the vertices of a truncated icosahedron, any chiral substituent attached to each vertex would reduce its symmetry from I_h to *I*. Thus, if it were possible to add chiral groups to all of the 60 carbon atoms of buckminsterfullerene,[20] a species with *I* symmetry would be obtained.

The desymmetrization of molecules with polyhedral symmetry can also be achieved by introducing chiral groups at axes passing through the edges or faces of the polyhedra. The requirement is that the local symmetry of the group is equal to the order of the axis. C_2-Symmetric bridges would thus serve to reduce the T_d symmetry of methane to *T*.[21] Since twofold axes bisect the sides of the other regular polyhedra as well, the desymmetrization of molecules with cubic and icosahedric symmetries can be brought about analogously.

Experimentally, the simplest and probably the most common route to chiral molecules containing a threefold rotational axis is the desymmetrization of molecules containing mirror planes, inversion centers, and/or improper axes in addition to the threefold axis, but having lower symmetry than the special groups *T*, *I*, and *O*. Molecules of this type have C_{3v}, C_{3h}, D_{3h}, D_{3d} symmetry (or those having sixfold instead of threefold axes) or S_6 symmetry. A variety of simple starting materials that can serve as excellent precursors for C_3- and D_3-symmetric molecules are commercially available.

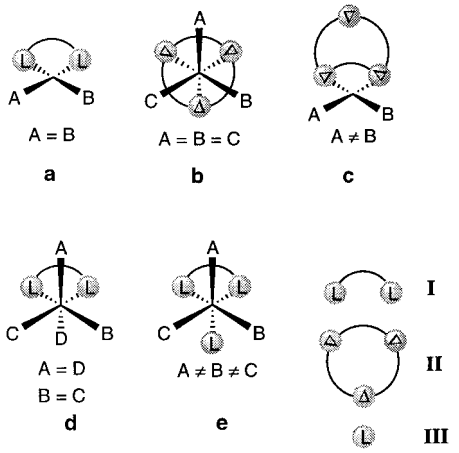
A desymmetrization procedure may also involve some asymmetric modification of a compound with higher symmetry leading to the formation of several diastereomers, which must be separated subsequently. The assembly of prochiral entities or of components in a racemic mixture is also expected to lead to a mixture of stereoisomers. This type of procedure as well as reactions performed on a prochiral, trifunctional compound with a threefold rotational axis should statistically lead to a 1:3:3:1 mixture of the *RRR*, *RRS*, *RSS*, and *SSS* isomers, although deviations may arise due to cooperative effects.

4. Metal-Binding Ligands

4.1. Metal Complexes: Molecular Equivalence Caused by Rotational Axes

The consideration of molecular symmetry is sometimes important, since symmetry can reduce the number of possible intermediates/transition states, thus increasing the probability of success in asymmetric reactions and other chiral recognition processes. By definition, C_2 symmetry is characterized by the fact that an identical situation is obtained upon rotation of the C_2-symmetric species 180° about the rotation axis. In an event involving chiral recognition this implies that two complexes that are identical in the C_2 case would be diastereomeric in the C_1 case. With threefold symmetry each rotation of 120° yields an identical situation, thereby reducing the number of different complexes. Examples of these situations will be given and analyzed.[22]

Let us consider a square-planar metal complex containing a bidentate, C_2-symmetric ligand (Scheme 1, **a**). This is a favorable situation, since the two remaining coordination



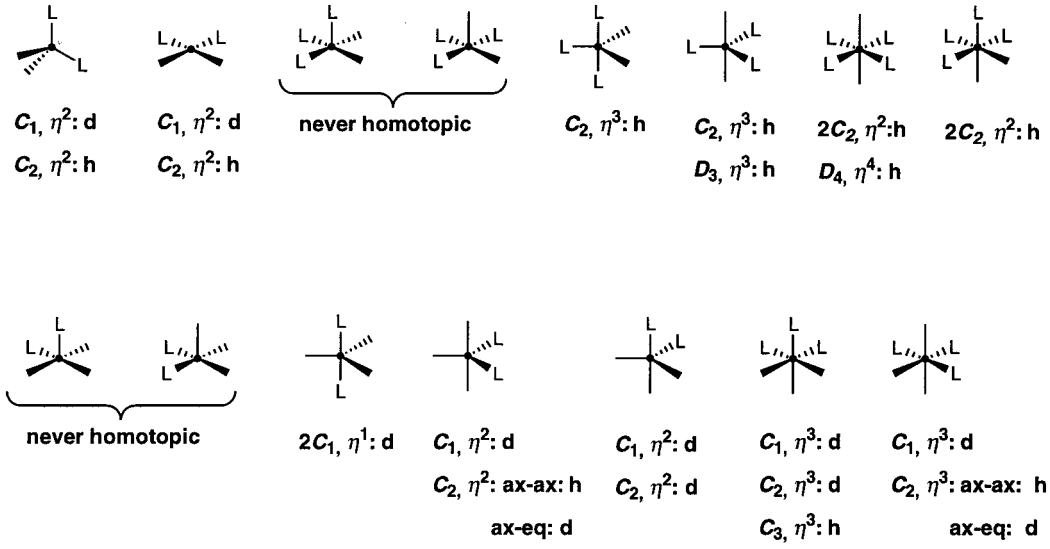
Scheme 1. Relationships between empty coordination sites (A – D) in complexes with C_2-symmetric, bidentate (**I**) and C_3-symmetric, tridentate ligands (**II**). **III**: achiral, monodentate ligand; h = homotopic, d = diastereotopic.

sites (A and B) are homotopic, in other words, identical. Another favorable situation is created by a tridentate, C_3-symmetric ligand in an octahedral environment (**b**), where the three remaining positions (A, B, and C) are identical (homotopic). On the other hand, this kind of ligand may yield an unfavorable situation in a square-planar arrangement where the ligand occupies two sites (**c**). Here the two remaining positions (A and B) are different (this may not be valid if the complex is dynamic and the positions are identical with time). In an octahedral environment the introduction of a bidentate, C_2-symmetric ligand results in a complex (**d**) with two sets of coordination sites, which are pairwise homotopic (A/D, B/C) but mutually diastereotopic (e.g. A/C). Addition of a monodentate ligand results in a complex with three different (diastereotopic) coordination sites (**e**). Thus, the conclusion is that C_2-symmetric ligands have favorable properties in square-planar geometries, whereas C_3-symmetric ligands are versatile in octahedral complexes.

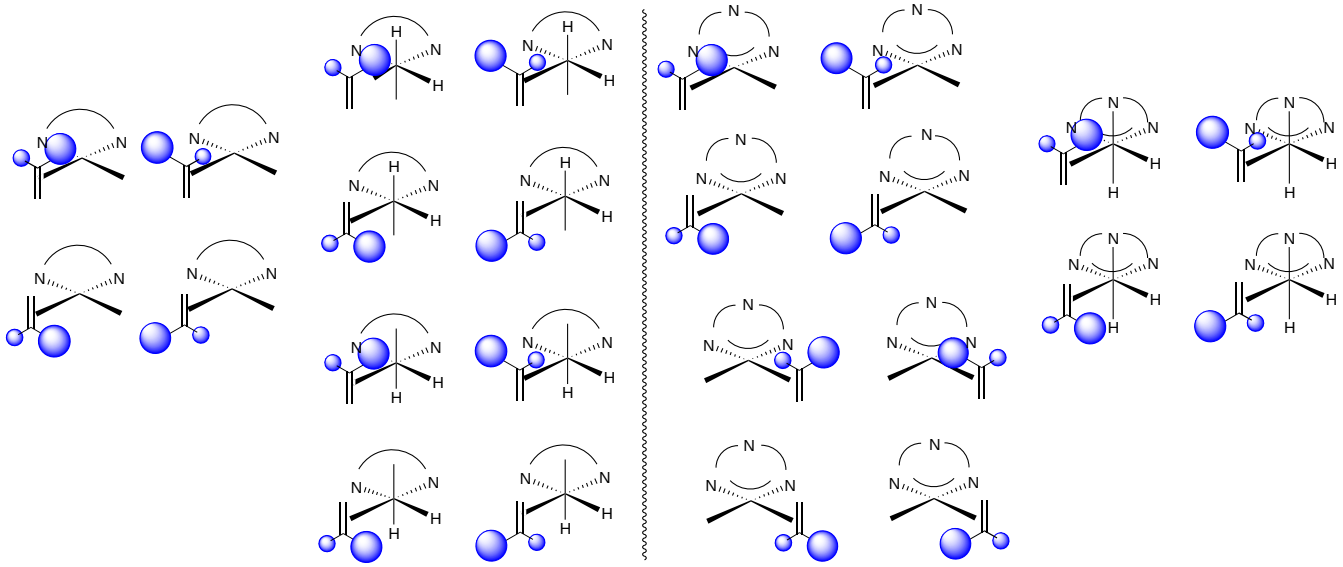
Scheme 2 shows a more complete analysis of situations arising from the coordination of mono-, bi-, and tridentate ligands with C_1, C_2, and C_3 symmetry, respectively, in their most common coordination geometries. Homotopic coordination sites are encountered with C_2-symmetric ligands under several conditions, whereas homotopicity with C_3-symmetric ligands is restricted to a few types of complexes. The following is evident in Scheme 2: 1) Two identical coordination sites remain in tetrahedral and square-planar environments upon coordination of one bidentate ligand with C_2 symmetry and in octahedral geometry upon coordination of two such ligands. 2) Homotopic sites also result from coordination of a tridentate, C_2-symmetric ligand in trigonal-bipyramidal complexes. 3) In the presence of a C_2-symmetric ligand three sites are never homotopic in any of the coordination environments shown in Scheme 2. 4) The only situation in which homotopic coordination sites are observed with a C_3-symmetric ligand is in octahedral geometry. 5) Ligands with threefold and fourfold dihedral symmetry result in homotopic sites in trigonal-pyramidal and octahedral complexes, respectively.

Let us analyze the special case that arises when a prochiral olefin is coordinated to a complex containing either a bidentate ligand with a twofold rotational axis or a tridentate ligand with a threefold rotational axis. These situations are encountered in common catalytic processes such as hydrogenations, hydroformylations, and hydrosilylations.[23] The specific example illustrated in Scheme 3 is a catalytic hydrogenation, where the coordination of the olefin is assumed to occur before the oxidative addition of hydrogen. This is the mechanism known for catalysts prepared from noncharged rhodium(I) complexes.[23]

With two homotopic sites in the square-planar complex containing a bidentate, C_2-symmetric ligand, four possibilities exist for the coordination of the prochiral olefin (provided that the presence of only two rotamers is considered likely),



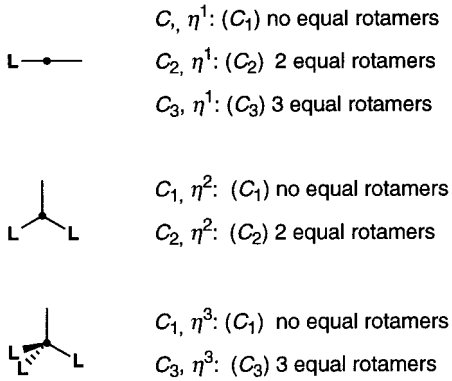
Scheme 2. Relationships between coordination sites in chiral complexes containing ligands of different denticities (η^n) and symmetries (C_n); h = homotopic, d = diastereotopic. Top: two free coordination sites; bottom: three free coordination sites; ax-ax describes the relationship between two axial coordiation sites, ax-eq that between an axial and an equatorial site.



Scheme 3. Square-planar metal–olefin complexes containing a bidentate, C_2-symmetric (left) or a tridentate, C_3-symmetric ligand (right), and isomeric complexes obtained through oxidative addition of H_2 to these complexes.

since coordination to the second site would yield a set of identical complexes due to the C_2 symmetry of the ligand. After addition of H_2 and formation of an octahedral complex, the two sites left for coordination of the olefin are no longer homotopic. Consequently, eight diastereomeric complexes are possible. In contrast, with a tridentate, C_3-symmetric ligand, only four different octahedral complexes arise due to the equivalence of the three sites. (If the olefin is equipped with an additional coordinating group, the number of isomeric complexes may be further reduced by a factor of two.) The conclusion from this analysis is that a C_2-symmetric ligand should be chosen if the selectivity is determined in a square-planar complex, whereas a C_3-symmetric ligand is the choice when the selectivity-determining step involves an octahedral complex. (If the square-planar complexes with C_3 symmetry equilibrate to render the two sites homotopic with time, a situation equivalent to that of a complex with a C_2-symmetric ligand may obviously be obtained.) As yet, this conclusion has not been unambiguously verified in practice, and it cannot be excluded that the mechanism of a particular reaction may change when a C_2-symmetric ligand is replaced by one having C_3 symmetry.

The olefin complexes in Scheme 3 are pairwise diastereomeric due to restricted rotation around the metal–olefin bond. In principle an infinite number of rotamers are possible, but only a limited number are usually observed. The symmetry properties of ligands can be exploited to reduce the number of structurally different rotamers in complexes having a single free coordination site. This is reflected by the site symmetry of that free site, as shown in Scheme 4.



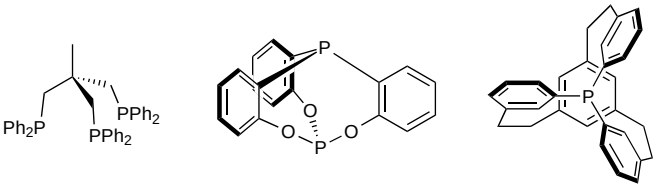
Scheme 4. The influence of the symmetry (C_n) and hapticity (η^n) of a ligand L in linear, trigonal, and tetrahedral complexes on the symmetry (C_n in parentheses) of the remaining free coordination site and the number of identical rotamers.

4.1.1. *Phosphanes and Phosphites with C_3* Symmetry

The most common method for preparing chiral metal complexes is the coordination of chiral ligands to the metal ion. A large variety of such ligands are known today and their metal complexes have proven highly useful in asymmetric synthesis.[24]

Phosphane ligands have been the most commonly studied ligands for application in homogeneous catalysis. A wide range of monodentate and bidentate phosphane ligands, chiral as well as achiral, are known and some of them are applied even in industrial processes.[25]

Achiral tripodal phosphanes with threefold rotational axes have been studied extensively over the last three decades mainly by the groups of Sacconi,[26] Meek,[27] Venanzi,[28] and Bianchini.[29] The most frequently studied ligands of this type are triphos (**1**) and analogues in which the central carbon



1 **2** **3**

atom has been replaced by a heteroatom (nitrogen or phosphorus). Such compounds have proven to be versatile ligands in coordination and organometallic chemistry. They have excellent bonding properties and form complexes with metal ions in various oxidation states.

It is not surprising, therefore, that the preparation of chiral analogues was soon attempted. C_3-Symmetric monophosphanes carrying three identical chiral groups on phosphorus were used in early investigations of enantioselective, nickel-catalyzed oligomerizations.[30] In contrast, monophosphanes **2** and **3**, in which the threefold rotational axis is a chirality axis, could not be resolved due to rapid racemization.[31]

More recently, a few enantiomerically pure tripodal phosphanes with C_3 symmetry have been reported. The first examples, **4** and **5**, were prepared from cyclic lithiophosphanes and the appropriate trichloro compounds.[32] Cationic rhodium(I) complexes of **4** and **5** were both shown by X-ray structural investigations to have trigonal-bipyramidal geometry. The use of the former as a catalyst precursor for the hydrogenation of methyl acetamidocinnamate resulted in 89% enantiomeric excess, a selectivity similar to that observed when the corresponding bidentate, C_2-symmetric ligand is used (85% *ee*). In the hydrogenation of dimethyl itachonate with **4**, 94% *ee* was obtained (90% with the C_2-symmetric ligand).[33] The tridentate ligand **4** was less reactive, however, requiring higher reaction temperature and longer reaction time. This was suggested to be due to the required dissociation of one ligand arm from a stable five-coordinate intermediate. Compound **6**, another C_3-symmetric, tripodal phosphane, has centers of asymmetry on phosphorus instead of carbon (as in **4** and **5**). This tridentate ligand was prepared by Venanzi and co-workers from (*R*)-(*tert*-butyl)(methyl)(phenyl)phosphane–borane by deprotonation, reaction with trichloromethylsilane, and finally deprotection.[34] The structure of the cationic Rh^I complex of **6** was determined and shown to have a distorted square-pyramidal geometry. No reports on its ability to induce chirality in asymmetric synthesis have appeared as yet.

The tripodal, tetradentate, C_3-symmetric ligand **7** was described in 1993.[35] With Pt^0 this ligand formed a tetrahedral complex, which could be protonated and methylated to yield trigonal-bipyramidal complexes, all with C_3 symmetry. A monodentate phosphite containing three identical sugar residues, tris(1,2:5,6-di-*O*-isopropylidene-α-D-glucofuranosido)phosphite, was also prepared recently and shown to form a tetrameric Cu^I complex with a cubane structure.[36]

4.1.2. C_3-Symmetric Compounds Containing Pyridine Rings

In recent years nitrogen-based ligands such as pyridine derivatives[37] have replaced those containing phosphorus in many reactions mainly due to their ease of preparation and their often higher stability.[38] However, since pyridine ligands do not exert the strong *trans* effect characteristic of phosphorus ligands,[22] they sometimes have different applications.

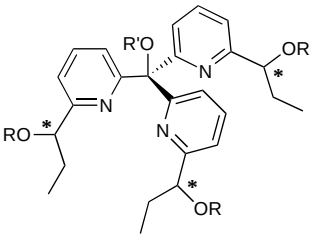
Three pyridine rings can be connected to form either acyclic, macrocyclic, or bicyclic arrangements. The first case is represented by tri(2-pyridyl)methane and derivatives such as **8**, R = H, Et, OAc.[39] This ligand was known already in the 1950s.[40] This type of compound has since been extensively studied because it can serve as a symmetric, tridentate ligand. It has thus been used to mimic the tetrahedral transition state in the reaction of carbonic anhydrase, the enzyme responsible for the fixation of carbon dioxide and its physiologically important reversible hydration to bicarbonate.[41] The active site in the enzyme is composed of a zinc ion coordinated to the imidazole side chains of three histidine residues and either a water molecule or a hydroxide ion. Mimicking this structure

with synthetic ligands is one way to gain knowledge about the mechanism of the enzymatic processes.[42]

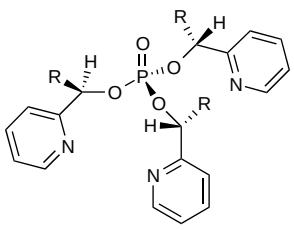
Tripyridylmethanol **8**, R = H, can give complexes with metal ions by either N,N,N-coordination or N,N,O-coordination, whereas O-alkylated derivatives undergo symmetric N,N,N-coordination only. Transition metal complexes of this type of ligand have also proven to be important in synthetic applications, for example for use as transition metal Lewis acids.[43, 44]

A macrocyclic arrangement of pyridine units is found in cyclophane **9**, which was prepared in four steps starting from 2,6-bis(6-bromopyridinoyl)pyridine.[45] Finally, the macrobicyclic pyridine derivative **10** was prepared by reaction of 2,6-dichloropyridine with the anion of triethanolamine.[46] Several cage compounds of this type with bipyridine incorporated in the chains have also been described.[47]

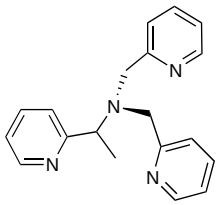
Chiral analogues, compounds lacking the vertical and/or horizontal mirror plane present in these symmetric parent compounds, can be constructed in a variety of ways. This has been realized for tripyridylmethanol **8**, R = H, by the introduction of keto substituents in the 6-positions of the pyridine nuclei and subsequent reduction of the keto groups using a chiral reagent to give compounds such as **11**.[48]



R = H, Me
R' = H, Me
11



R = Me, *t*-Bu, 2-neomenthyl
12



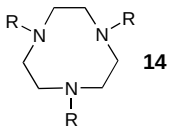
13

Although the chiral reagent was shown to afford roughly 90% *ee* upon reduction of an analogous monomer, essentially complete selectivity was observed with the trifunctional compound (instead of the expected 85.74:13.54:0.71:0.01 mixture). Another experimentally facile method is the reaction of phosphorus oxychloride with 2-(1-hydroxyalkyl)-pyridine to yield compounds of type **12**.[49] The reaction of racemic 2-(1-hydroxyethyl)pyridine with phosphorus oxychloride gave the expected 1:3 mixture of homochiral and heterochiral isomers. In contrast, reaction of the sterically more hindered 2-(1-hydroxy-2,2-dimethylpropyl)pyridine afforded a 1:1 mixture of isomers; in other words, the reaction proceeded in favor of the homochiral compound. Since enantiomerically pure 2-(1-hydroxyethyl)pyridines are available by a variety of procedures, enantiopure compounds with the structure **12** are easily accessible. Methods have also been developed that permit the grafting of the tripyridyl ligands onto various types of polystyrenes, thus allowing convenient handling.[44]

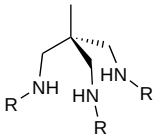
Tris[(2-pyridyl)methyl]amine adopts a helical conformation upon complexation to metal ions. The α-methyl-substituted analogue **13** was prepared in order to favor one enantiomeric conformation.[50] Although this compound has C_1 symmetry, metal complexes of the ligand probably fold in a manner similar to that expected with a trisubstituted C_3-symmetric ligand.

4.1.3. Aliphatic Amines

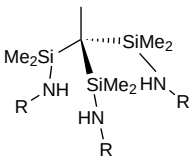
Several simple starting materials suitable for the preparation of amines with acyclic and cyclic topologies are commercially available. Numerous achiral 1,4,7-triazacyclononanes **14**[51] have been prepared and investigated, in particular in



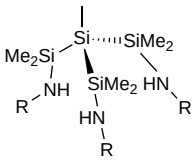
14



15



16



17

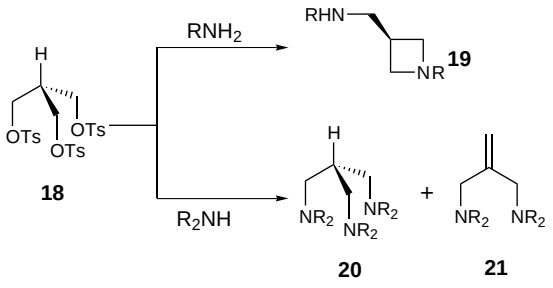
connection with studies of carbonic anhydrase mimics.[52] Compounds with three identical chiral R groups, thus with C_3 symmetry, have also been prepared.[53]

A variety of tridentate, acyclic, C_3-symmetric amines having a central carbon skeleton (**15**) or a skeleton containing silicon (**16**, **17**) have also been prepared, and some of their metal complexes have been studied.[54] The ligands with silicon atoms in their skeleton allow the complexation of larger metal ions than the ligands based on carbon only. The synthetic method used for preparing ligands **16** and **17**, the reaction of an alkylsilicon bromide with a primary amine, gives easy access to chiral analogues when a chiral primary amine is employed. A chiral analogue of **16** (R = (*S*)-CH(CH$_3$)Ph) was prepared with (*S*)-1-phenethylamine.[55]

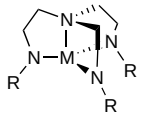
In the triamidostannate obtained by reaction of compound **16** (R = (*S*)-CH(CH$_3$)Ph) with butyllithium followed by $SnCl_2$ the metal ion was shown to bind to the three nitrogen atoms; however, the symmetry was reduced by a lithium ion bridging two nitrogen atoms. This bridging was dynamic and resulted in time-averaged threefold symmetry.[56] The complex served as a metal-centered nucleophile and reacted with some electrophiles to yield C_3-symmetric complexes. Ti^{IV},[57] Y^{III},[57] Zr^{IV},[58] Sn^{II},[58] and Pb^{II} complexes[59] with achiral analogues of ligand **16** have also been prepared and characterized.

Attempts to prepare ligands analogous to **15** starting from **18**, the tritosylate of 2-hydroxymethyl-1,3-propanediol, were

less successful. Reactions with primary amines resulted in the exclusive formation of 3-(aminomethyl)azetidines **19**. Secondary amines afforded the desired triamines **20**, but the



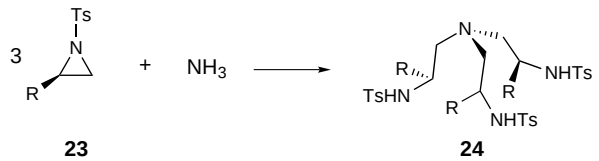
elimination of one ligand to form C_2-symmetric unsaturated amines **21** was a serious side reaction in that case (C_2:$C_3 \approx$ 1:4.4 when prolinol was used as the amine component).[60] The tritosylate of 2-hydroxymethyl-2-methyl-1,3-propanediol did not react with either primary or secondary amines.



22

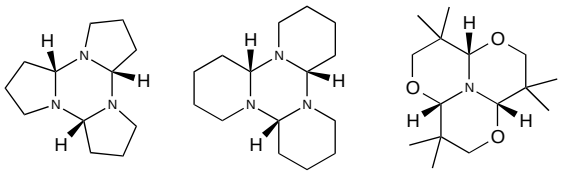
Tetradentate trisaminoamine ligands like that in **22** have been the subject of extensive studies.[61] The properties of these complexes are dependent on the nature of the substituents R, and on the extent to which the bridgehead nitrogen atom takes part in the complexation.[62] Several complexes with early transition metals were recently prepared.[63] Monomeric trigonal bipyramidal complexes with vacant apical positions were obtained with Ti^{III}, V^{III}, Cr^{III}, Mn^{III}, Fe^{III} and R = *tert*-butyldimethylsilyl,[64] with M = B and R = methyl, and with M = Al and R = trimethylsilyl.[65] The boron compound was shown to adopt a chiral conformation; interconversion between the enantiomers was slow on the NMR time scale at room temperature.

Tetradentate, tripodal, C_3-symmetric amines analogous to the ligand in **22** can probably be prepared easily by N-alkylation with chiral electrophiles. However, such ligands are expected to exert insufficient stereocontrol in catalytic reactions, since their conformation is most likely flexible. It would probably be more efficient to have the stereogenic center residing in the chelate framework. Chiral analogues such as **24** were, in fact, conveniently obtained in high yields by nucleophilic ring-opening of chiral aziridines **23** (in turn



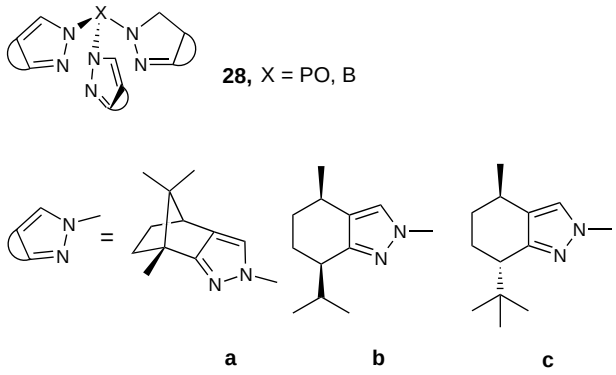
obtained from readily available chiral aminoalcohols[66]) using ammonia as the nucleophile.[67] The aziridines have to be activated by an electron-withdrawing substituent (for example a tosyl or mesityl group) attached to the nitrogen atom in order for ring-opening to occur.

Some C_3-symmetric amines with interesting structures have been known for a long time, although no applications to catalytic reactions have been reported. 1,2-Didehydropyrrolidine[68] and Δ^1-piperideine (3,4,5,6-tetrahydropyridine)[69] trimerize spontaneously to yield **25** and **26**, respectively. C_3-Symmetric, racemic monoamines like **27** have been prepared by some different methods.[70]



4.1.4. Dihydroborazoles and -oxazoles and Related Compounds

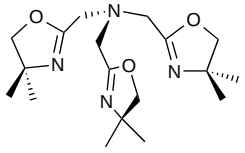
Like tripyridylmethane derivatives, tris(pyrazolyl)hydroborates have been employed in organometallic chemistry and in studies aimed at mimicking biological processes.[71] They are used as terminal ligands in the study of iron binding in proteins,[72] they are used to approximate the binding site typically found or suggested for copper(I) ions in metalloproteins, and they serve as models of carbonic anhydrase.[41] Successful results were obtained with 3-substituted tris(pyrazolyl)hydroborates, in that the desired monomeric complexes with threefold rotational axes were observed.[73] The logical extension, the preparation of C_3-symmetric chiral analogues such as **28a–c** (X = B), was readily achieved by



reaction of chiral pyrazoles with potassium tetrahydroborate.[74] Analogous ligands with a phosphorus atom joining the three heterocyclic moieties were obtained by reaction of the pyrazoles with phosphorus oxychloride. A Cu^I complex of one of these ligands was shown to catalyze the cyclopropanation of styrene with diazoesters with up to 60% *ee*.[75] The geometry around the metal ion heavily depends on the structure of the ligand: in the Tl^I complex of the tris(pyrazolyl)hydroborate prepared from **28b** the torsion angles Tl-N-N-C are close to 180°, and the Tl^I complex prepared from **28c** (X = B) has a distorted propellerlike structure.[76]

A little later three types of borate–[Rh^{I}LL] complexes (LL = 2 CO, norbornadiene, cyclooctadiene) were identified. In one type of complex the tris(pyrazolyl)borate ligand serves as an η^3 ligand, and in two other forms the ligand occupies only two coordination sites.[77] Upon irradiation the Rh^{I} carbonyl complexes of **28b** (X = B) underwent stereo- and regioselective C–H bond activation to give alkyl(hydrido)-rhodium complexes resulting from insertion of the metal in a C–H bond of a methyl substituent in the ligand isopropyl group.[78] No intermolecular C–H bond activation was observed; such processes are probably prevented by the steric bulk of the ligand.

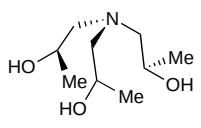
In contrast to the trispyrazolyl ligands **28**, the C_3-symmetric, tripodal trisdihydrooxazole ligand **29** forms a dimeric Cu^{I} complex, in which the metal ion is surrounded by two oxazolyl nitrogen atoms from one ligand and one from the second ligand.[79] Cu^{I} and Cu^{II} complexes of chiral analogues of **29** were shown to catalyze the oxidation of cyclopentene with *tert*-butyl perbenzoate in up to 84% *ee* (somewhat higher under conditions that gave low yields of products).[80] Tris(imidazolyl)phosphane ligands and their metal complexes have been prepared, although no chiral analogues have been reported.[81] In our group we have attempted to prepare chiral tris(dihydrooxazolyl)methanes without success.



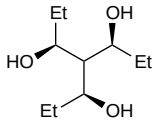
29

4.1.5. Alcohols

Atranes, triethanolamine derivatives in which silicon, phosphorus, tin, or other metal ions are bound to the three deprotonated hydroxy groups, have been extensively studied.[54] Examples are titanatranes, complexes with Ti^{IV}, which are monomers or dimers depending on the nature of the ligand occupying the fifth coordination site of the metal.[82] Analogous chiral metal complexes were obtained when triethanolamine was replaced by C_3-symmetric tris(2-hydroxypropyl)amine (**30**).[83] This ligand and its complexes have also been employed in asymmetric synthesis. Triol **30** has been used as a chiral auxiliary in reductions with lithium aluminum hydride,[84] and a boron compound having the same ligand has been prepared.[85] The Zr^{IV} complex of the chiral ligand has a complicated oligomeric structure but has proved to be an efficient catalyst for the ring-opening of *meso* epoxides under certain conditions; ring-opened products are obtained with high selectivity (up to 93% *ee*).[86] Mechanistic studies indicate that a dimer is the catalytically active species, and that the catalytic activity requires the cooperative action of two Zr^{IV} centers.[87] Interestingly, no stereoselectivity was observed when the *R*,*R*,*S* isomer was employed in the catalytic reaction. In contrast, the Ti^{IV} complex of **30** turned out to be a poor catalyst for this same reaction,[88] but was used for the enantioselective oxidation of sulfides to sulfoxides (up to 66% *ee*).[89] The C_3-symmetric, tridentate triol **31** has also been prepared,[90] but no reports of its use in asymmetric synthesis have appeared.

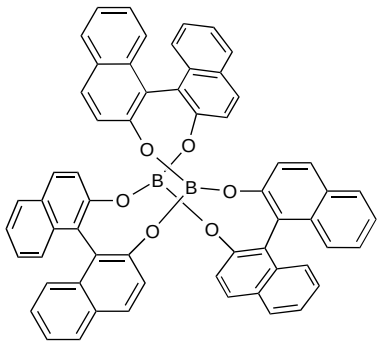


30



31

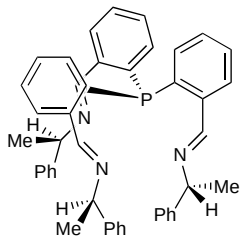
The C_3-symmetric diborate **32** was obtained from the reaction of (*S*)-(−)-1,1′-bi-2-naphthol with monobromoborane/dimethyl sulfide. This compound catalyzed the Diels–Alder reaction of cyclopentadiene and methacrolein in a highly enantioselective manner (90% *ee*, 97.4% *exo* selectivity).[91]



32

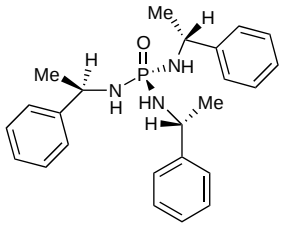
4.1.6. Other Ligands

The use of the Schiff's base **33**, obtained by condensation of tris(2-formylphenyl)phosphane with (*R*)-(+)-1-phenylethylamine, as a ligand in rhodium-catalyzed reductions was investigated.[92] A complex prepared in situ from **33** and [Rh(cod)Cl]$_2$ did not catalyze the hydrogenation of (*Z*)-α-(acetylamino)cinnamic acid at 50°C and 1 bar. Although a complex prepared in the same manner did catalyze the hydrosilylation of acetophenone, no enantioselectivity was observed. This disappointing result does not seem to be attributable to the threefold symmetry of the ligand, since an asymmetric, monodentate ligand, in which two of the chiral groups on phosphorus (in **33**) were replaced by phenyl rings, also showed poor selectivity under the same conditions.

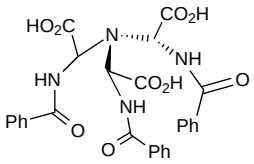


33

The reduction of acetophenone was also performed using **34** as a chiral catalyst, but with borane/dimethyl sulfide as the reducing agent instead of a hydrosilane.[93] The results were slightly inferior to those obtained when asymmetric analogues were employed in which one or two of the chiral substituents on phosphorus (in **34**) were replaced by phenyl groups (70% yield of (*S*)-1-phenylethanol with 20% *ee*).



34



35

The synthetic pseudotripeptide **35**, which is of potential interest both as an asymmetric ligand in catalytic applications and as a model for studies of metalloenzymes (vide infra), was described in 1995.[94] In the complex obtained from **35** and [$CpTiCl_3$] the C_3 symmetry was lost because one carbonyl group is also coordinated to the metal ion. This was evident in the ^1H NMR spectrum, in which separate signals were observed for the three amide chains. The advantage of a ligand with threefold symmetry is that only one complex is formed, no matter which of the three equivalent carbonyl groups takes part in the complexation.

4.2. Lack of Rotational Symmetry May Be Advantageous

It should be noted that the benefits achieved by using reagents with rotational symmetry may also be obtained by other means, which may occasionally even be more efficient. Consider, for example, a macrocyclic metal complex that in a particular reaction coordinates a substrate in one of the two axial positions, a situation encountered, for instance, in oxidative processes.[95] The approach of a C_2-symmetric reagent from below is identical to approach from above, and the number of different reaction paths is thus reduced by a factor of two. Alternatively, only one kind of approach is also possible if one face is blocked by a pendent arm of the ligand (Figure 5).[96]

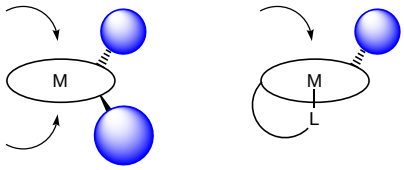


Figure 5. The approach of a substrate to macrocyclic complexes. Left: the complex is C_2-symmetric; right: the complex is C_1-symmetric and bears a blocking group. See text for details.

In certain situations truly asymmetric reagents offer clear advantages over reagents with rotational symmetry. In reactions where the asymmetric induction relies on the regiodifferentiating ability of the reagent, for example, the absence of rotational symmetry may likely be beneficial in given situations. Consider the attack of a nucleophile on a π-allylpalladium complex containing a prochiral (*meso*) allyl group derived, for example, from *rac*-1,3-diphenyl-2-propenyl acetate.[97] With an asymmetric ligand, two diastereomeric complexes (**A** and **B**, Figure 6) may form and both are usually

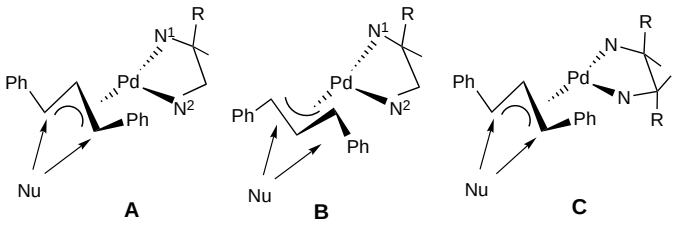
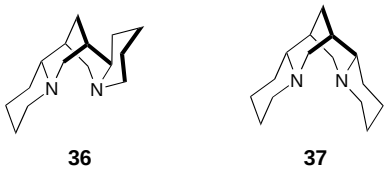


Figure 6. π-Allylpalladium complexes with C_1- (**A** and **B**) and C_2-symmetric ligands (**C**).

also obtained. The enantioselectivity in this case arises from regioselective attack on one of the complexes. The most abundant complex is usually the one being attacked, since the reactions are exothermic and therefore the transition states and the intermediates are close in energy.[98] With a C_2-symmetric ligand, only one complex (**C**) is obtained (rotation of the π-allyl ligand 180° yields an identical complex), and the selectivity depends on the regiodifferentiation of the reagent alone.

It is probably easier to achieve high regioselectivity when the complexing atoms in the ligand are different. Their *trans* effects are different and thus the reactivities at the two sites are different. When the coordinating atoms are different, the ligand is by definition C_1-symmetric. These arguments imply that regiodifferentiation could be an easier task in **A** and **B** (C_1-symmetric ligand) than in **C** (C_2-symmetric ligand). What is crucial in reactions employing C_1-symmetric ligands is that the diastereomeric complexes **A** and **B** have different reactivities. The advantage of using a ligand with C_2 symmetry is thus that only one complex is formed and the selectivity is determined solely by the regioselectivity. When the ligand has C_1 symmetry, however, regiodistinction may be a much simpler matter. As soon as the two complexes **A** and **B** have different properties, and one of them leads preferentially to product, the asymmetric ligand may be the more successful one.

Several ligands, C_1- as well as C_2-symmetric, are known for high asymmetric induction (>99% *ee*) in the palladium-catalyzed allylation.[97, 99] It is not possible to find two ligands that differ *only* in their symmetry properties, and thus to compare the efficiencies of the different types of ligands. It is interesting, however, to compare sparteine (**36**)[100] and α-isosparteine (**37**).[101] With 1,3-diphenyl-2-propenyl acetate as

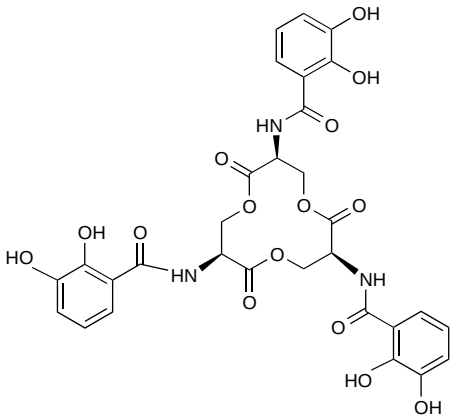


36 37

a substrate, higher selectivity was observed when the asymmetric ligand **36** was employed (92% *ee* vs 70% *ee* with **37**; both reactions in refluxing THF).[101] However, with aliphatic substrates, the C_2-symmetric ligand led to higher stereoselectivity and also turned out to be more reactive. This shows that ligands with rotational symmetry are not necessarily superior.

4.3. Natural Siderophores and Other Ionophores

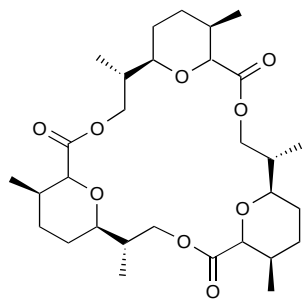
In nature strong complexing agents are required to keep trivalent iron ions in solution and to enable transport.[102] This is accomplished by siderophores, a class of compounds that transport cations and promote bacterial growth. Several compounds of this type have been found in nature, for example enterobactin (**38**), which was first described in



38

1970.[103] The molecule, the cyclic triester of 2,3-dihydroxybenzoyl-L-serine, possesses C_3 symmetry. This geometry is highly advantageous, since it allows extremely efficient binding to Fe^{III} ions in an octahedral arrangement, as shown by the resistance of its iron complex towards ligand exchange with EDTA.

A variety of C_3-symmetric molecules have been prepared in attempts to mimic the properties of the natural siderophores.[104] The synthetic models typically have catecholate or hydroxamate units as ligating groups in open or bicyclic arrangements, with six oxygen atoms serving as donors.[105] Most of the models are achiral, although they contain a threefold rotational axis.[106] Ionophores aimed at complexation with metals other than iron, some of them possessing C_3 symmetry, have also been prepared. Recent examples include ionophore **39**, whose binding to alkali metal ions has been examined,[107] and similar compounds studied in the context of transmembrane ion channels.[108]



39

4.4. Octahedral Metal Complexes

Metal complexes can be chiral and belong to point group C_n or D_n even when they contain only achiral ligands.[109] The simplest example is a tetrahedral complex with four different ligands, which like the analogous carbon-based compound has C_1 symmetry. Octahedral metal complexes may be chiral as a result of the arrangement of achiral ligands around the metal ion. Frequently encountered examples are complexes in which the metal ion is coordinated to three identical bidentate ligands (Figure 7).[110] The first thoroughly



Figure 7. Enantiomeric octahedral complexes with Λ and Δ configurations.

studied examples were complexes containing a metal ion surrounded by three 1,2-diaminoethane molecules. The ligands can arrange themselves in two different ways with a mirror image relationship, and thus with different absolute configurations (Λ and Δ). Such complexes have D_3 symmetry.[111]

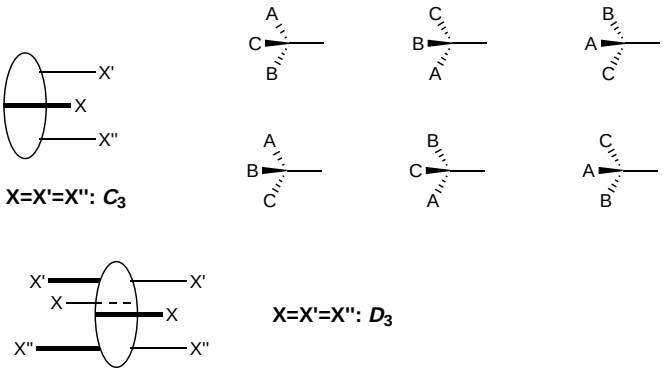
5. Receptors for Organic Molecules and Ions

5.1. Molecular Recognition

A common requirement for a chiral receptor is that it differentiate between the two enantiomers of a substrate. If the substrate is endowed with three sites that can interact with a receptor, the receptor should in turn contain three complementary groups for efficient complexation. Obviously, a receptor with threefold rotational symmetry should be advantageous for the complexation of a substrate with the same symmetry. This has also been unambiguously demonstrated in two sets of complexation reactions: 1) an alkylammonium ion was more strongly bound to calix[6]arenes than to calix[4]arenes (the latter lacks threefold symmetry),[112] and 2) the same ion formed a stronger complex with a hexahomotrioxacalix[3]arene having a C_3-symmetric conformation than with conformers lacking that symmetry.[113]

With this kind of three-point interaction, chiral discrimination is, in principle, possible. The situation is complicated by the fact that six different complexes may be formed by the interaction of the racemic substrate with the receptor (Scheme 5). With a C_3-symmetric receptor ($X = X' = X''$), each enantiomer gives rise to only one complex; in other words, there are only two possible modes of coordination, one for each enantiomer. The situation is thus simplified and the probability of chiral discrimination is increased.

If the substrate can approach the receptor from both faces, it is desirable that these faces be identical. This is the key to the favorable properties observed with many C_2-symmetric



Scheme 5. The six possible modes of binding a racemic substrate to a trifunctional receptor are reduced to only two when the receptor has C_3 symmetry. This is because for each enantiomer (top and bottom rows) the three possible binding modes lead to identical results.

compounds. If the threefold symmetry is to be kept, a receptor with D_3 symmetry, which by definition has two equal faces, is required. The general conclusion from these arguments is that when the substrate can be approached both from the front and from the back, D_3 symmetry is most efficient for decreasing the number of interactions, whereas with a bowl-shaped receptor, in which the interacting sites reside inside the cavity, C_3 symmetry is desirable.

A different solution to making the faces of a receptor homotopic was presented in 1996.[114] In this example a calixarene was trialkylated with two different electrophiles. The one used for monoalkylation was small enough to slip through the cavity, and the resulting methyl ether unit was thus able to take part in the binding at both faces (Figure 8).

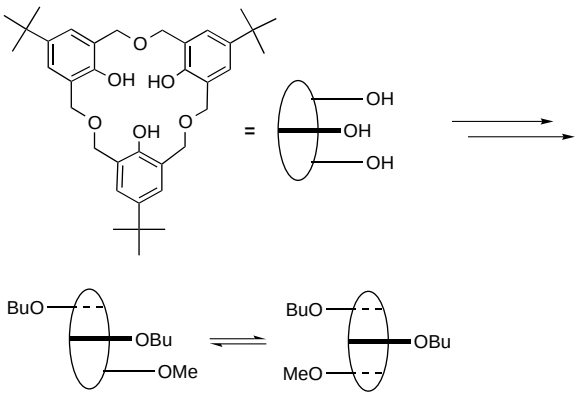


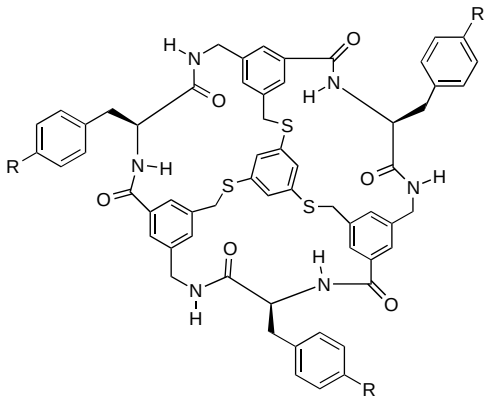
Figure 8. Alkylation transforms a C_{3v}-symmetric calixarene into a C_2-symmetric receptor, which exposes two identical faces to a reagent.

The result was that two equal faces were exposed by the receptor to an incoming substrate, and that the substrate could still be bound to three oxygen donors, two alkoxy oxygens, and one ether oxygen. A trivial case is provided by a substrate capable of being bound through a single one-point interaction. Obviously, the higher the order of the rotational axis, the higher the number of equal interactions.

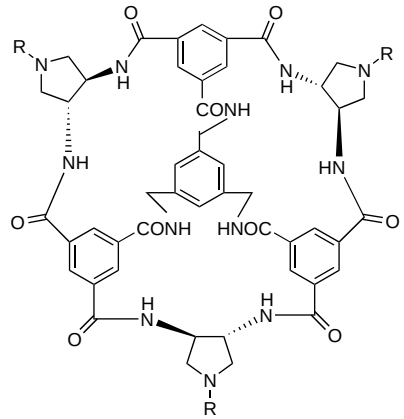
The next sections provide a survey of receptors that can bind organic molecules and ions. Several of the receptors may also form complexes with metal ions and may thus serve as ionophores as well.

5.1.1. Peptides and Pseudopeptides

In the design of synthetic model receptors, symmetric host molecules have the advantage of more selective binding because several modes of binding are equivalent. Numerous synthetic receptors that take advantage of this feature have been described.[115] High selectivity was reported by Still for the reversible binding of peptides to some C_3-symmetric, tricyclic receptors.[116] Receptor **40** (R = H, $OCH_2CH{=}CH_2$)



40

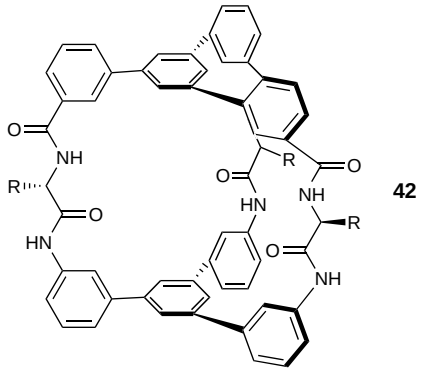


41

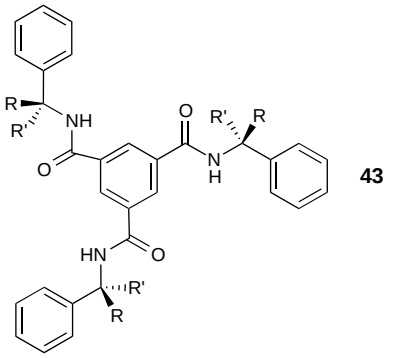
showed a high enantioselectivity in the complexation of amino acids.[117] Its potential as a resolving agent was elucidated by covalent attachment of the ligand to silica gel. Separation factors up to 21 were observed for neutral tripeptides.[118] The binding properties of an analogous receptor, **41**, in which the pyrrolidine units were linked to a dye (R = $CO(CH_2)_2CO_2$-dye), were established with a polymer-supported library of about 50 000 acylated tripeptides, where each polymer bead was coated with *one* of the tripeptides.[119]

Macrocyclic C_3-symmetric amides with structures resembling that of receptor **40** were also prepared. Hexacarboxylic acids were transformed into macrolactams by reaction with (*R*,*R*)-1,2-diaminocyclohexane. No binding studies with these new receptors were reported.[120]

The cage compound **42** (R = CH_2CHMe_2, CH_2Ph), in which short peptide chains join two triarylbenzene residues, was shown to bind N-protected amino acids.[121] Chiral recognition was demonstrated upon complexation of the enantiomers of N-Z-protected glutamic acid: the complex of **42** (CH_2Ph) with the L enantiomer was 1.0 kcal mol^{-1} more stable than that with the D enantiomer. The discrimination of enantiomers having a



42

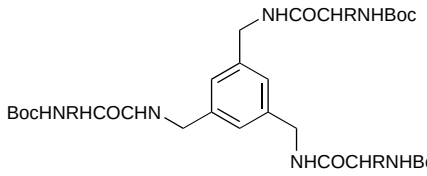


43

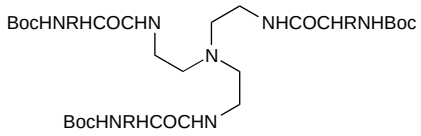
chiral center directly attached to an electron-rich aromatic ring was studied using **43**.[122]

C_3-Symmetric pseudopeptides containing three parallel peptide chains were also prepared by using the triacid **35** as a reactive template.[94, 123] $CpTi^{IV}$ complexes of pseudononapeptides were shown to have C_3 symmetry based on their NMR spectra, which exhibited only one set of signals for each peptide chain. This arrangement is stabilized by hydrogen bonds. The cavity formed by the cyclic arrangement in the metal complex was believed to be too small for a hypothetical guest molecule. Some pseudopentadecapeptides were prepared with the same template. An interesting pattern of interstrand hydrogen bonding, the nature of which was shown to depend on the structure of the amino acid incorporated in the peptide and on the solvent, was found during studies of tripeptides **44** and **45**.[124] Leucine-derived **44** (R = *i*Bu) was found to have a propellerlike conformation. Studies of the ability of metal ions to serve as regulatory elements in C_3-symmetric, tripodal tripeptides showed that Li^+ generates a chiral helical conformation in **46** ($n = 1$), whereas Ca^{2+} does so in the larger analogue ($n = 2$).[125]

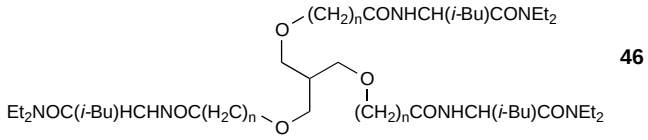
Some naturally occurring, C_3-symmetric or pseudo-C_3-symmetric, cyclic hexapeptides with cytotoxic activity were recently isolated. Compounds **47**[126] and **48**[127] were found in a



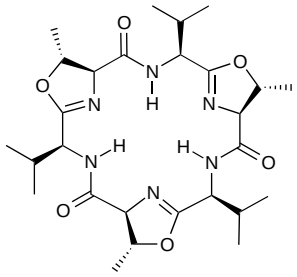
44



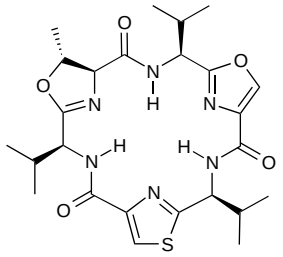
45



46



47

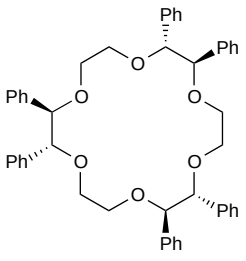


48

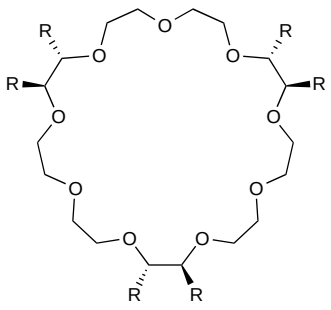
marine alga, and **47** also in a terrestrial cyanophyte.[128] The total synthesis of **47** relied on a cyclotrimerization, in which the desired trimer was formed along with a C_4-symmetric tetramer.[129]

5.1.2. Crown Ethers and Podands

The D_3-symmetric [18]crown-6 ether **49** was used as a catalyst in the Michael addition of methyl phenylacetate to methyl acrylate with potassium *tert*-butoxide as base.[130] The yield was low and the enantioselectivity moderate. Similar selectivity but considerably higher yields were obtained with tetraphenyl-substituted, D_2-symmetric analogues. The best results were obtained when a C_2-symmetric, dimethyl-substituted [18]crown-6 ether was used.



49

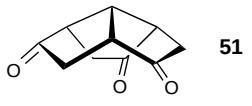


50

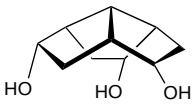
The larger [27]crown-9 ion **50** ($R = CO_2^-$) forms more stable complexes with guanidinium ion than with ammonium ion, while the reverse was found for a D_2-symmetric [18]crown-6 analogue.[131] The symmetric, uncomplexed, (*R*,*R*,*R*)*-trisbinaphthyl[18]crown-6 ether was shown to be slightly destabilized in relation to the (*R*,*R*,*S*)* diastereomer.[132] The reaction of D-diisopropylidenemannitol with diethylene glycol tosylate afforded a C_3-symmetric [27]crown-9 ether as a by-product.[133]

5.1.3. Cyclotriveratrylenes

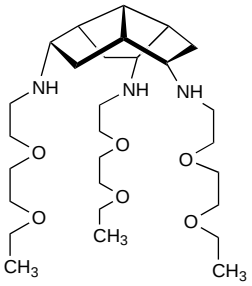
The C_3-symmetric perhydrotriquinacene ketone **51** serves as a useful precursor for the preparation of C_3-symmetric podands.[134] Catalytic hydrogenation afforded the tris(*endo* alcohol) **52**, which, however, turned out to be quite unreactive towards alkylation reagents. Instead, direct reductive amination of **51** with 1-aminooligoethers afforded aminopodands such as **53**.[135] Triketone **51** could also be used for the synthesis of cage compound **54** ($n = 2$, 3) and analogues.[136] Compound



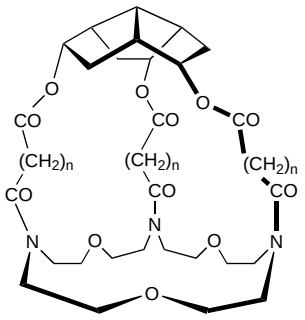
51



52



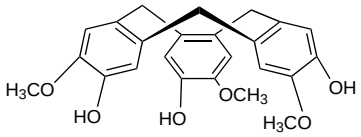
53



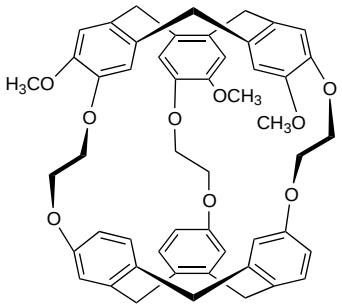
54

54 was shown to complex the methylammonium ion efficiently, although possibly to the external face of the polar subunit. No attempts to achieve chiral induction were reported.

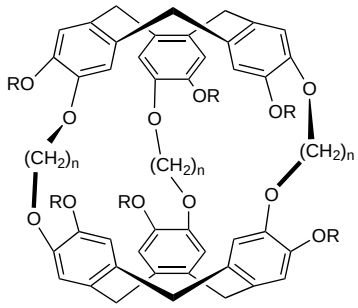
Ring inversion in cyclotriveratrylene takes place only around 200°C, and compounds of this type with two different substituents are therefore chiral under ordinary conditions. The C_3-symmetric cyclotriveratrylene **55** was described early on by Collet and Jacques.[137] The enantiomerically pure cryptophane **56** based on the same compound was shown to give an inclusion complex with racemic bromochlorofluoromethane.[138] Different ^{1}H NMR signals were observed for the guest molecules in the diastereomeric complexes formed. Interestingly, chiral recognition was achieved: one complex was favored over the other by about 1.1 kJ mol^{-1}. Analogous, D_3-symmetric compounds **57**[139] afford inclusion complexes with a variety of guest compounds such as methane ($n = 2$, R = Me),[140] isobutane ($n = 3$, R = Me),[141] tetramethylammonium ion ($n = 3$, R = Me, K = 225 000 M^{-1}), and acetylcholine ($n = 5$, $R = CH_2CO_2H$).[142] For larger members of this family of compounds ($n \geq 6$), equilibrating in–out and out–out topoisomers were observed.[143] Self-assembled, heterodimeric cyclotriveratrylenes, in which the two units are held together by hydrogen bonds, were also prepared and shown to form inclusion complexes.[144] Some new cyclotriveratrylenes bearing iodine substituents on the benzene rings are expected to serve as useful precursors for a variety of derivatives.[145]



55



56



57

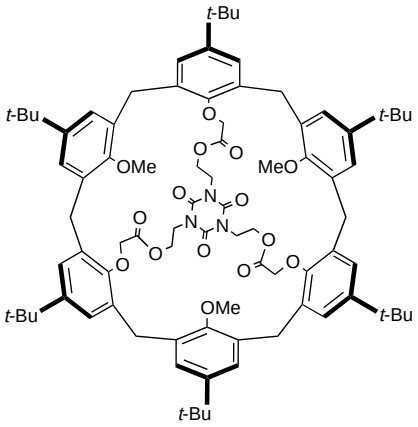
Cyclotriveratrylenes equipped with substituents suitable for complexation to metal ions have been prepared.[146] Studies of octahedral Fe^{II} complexes revealed that when complexed with a racemic host containing three bipyridine units, the absolute configuration at the metal center was determined by the absolute configuration at the cyclotriveratrylene unit: only the enantiomeric pair $M\Delta/P\Lambda$ was observed.[147]

5.1.4. Calixarenes

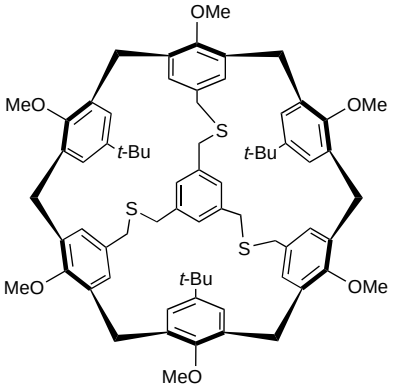
A variety of achiral calixarenes with threefold symmetry (C_{3v}-symmetric) have been prepared by proper substitution of calix[6]arenes.[148] To avoid conformational changes destroying the threefold symmetry and favorable complexing ability, the conformationally immobilized calix[6]arenes **58**[149] and **59**,[150] capped on the lower[151] and upper rim, respectively, were synthesized.

Some chiral, although not enantiomerically pure, calix[3]indols have been described.[152] Compound **60** (Ar = C_6H_5, *p*-BrC_6H_4, *p*-$MeOC_6H_4$) is achiral, however, as indicated by its ^{1}H NMR spectrum, which exhibits a singlet for the methylene protons. This is consistent with either a rapidly inverting *cone* conformer or a fluxional, flattened *partial cone* conformer. On the other hand, compound **61** (Ar = *p*-ClC_6H_4, R = Me, *t*Bu), which has substituents on the bridging methylene groups, is chiral. It was isolated as a mixture of two conformers, which could be separated for R = *tert*-butyl, Ar = *p*-ClC_6H_4.[153] The C_3-symmetric compound was obtained in 17% yield, and the stereoisomer in 45% yield.

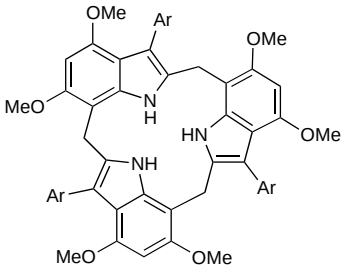
Calixarenes containing three dihydroxybiphenyl residues have been prepared.[154] Alkylation of the hydroxyl groups resulted in restricted rotation around the Ar–Ar bonds. The isomer with D_3 symmetry was, however, not observed among the atropisomers obtained.



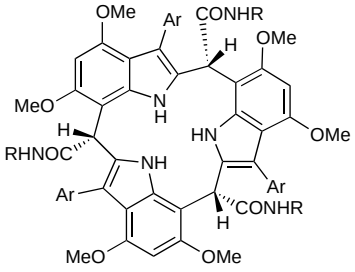
58



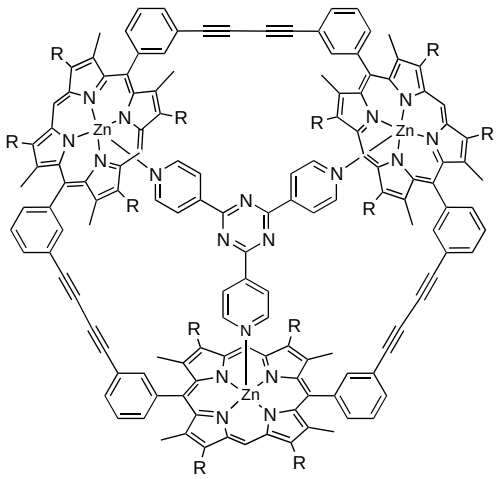
59



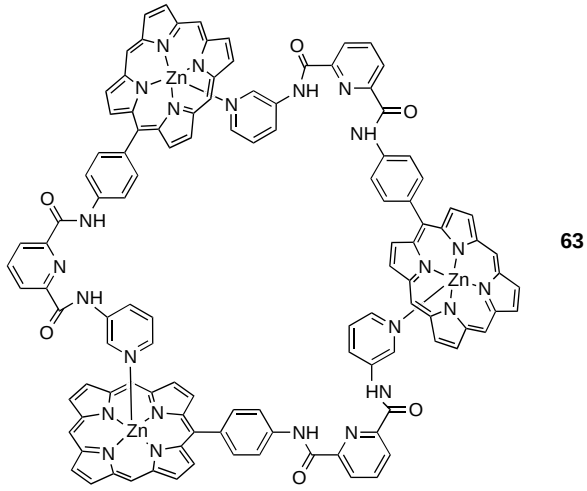
60



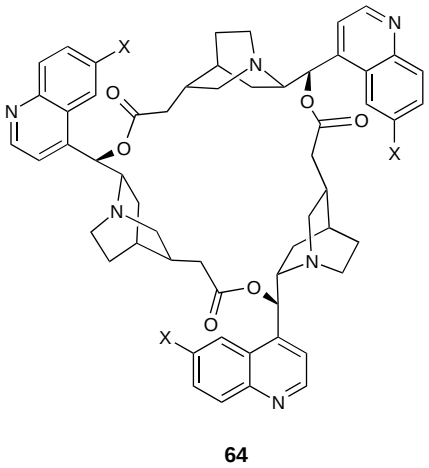
61



62



63



64

5.1.5. Porphyrins

The cyclic zinc porphyrin trimer **62** ($R = CH_2CH_2CO_2Me$), which has a cavity suitable for complexation of tris(4-pyridyl)-triazine, was obtained when this guest was used as a template.[155] By proper adjustment of the angle between the plane of the porphyrin ring and the pyridine ligand in the monomer, self-assembled trimers such as **63** were obtained.[156] Although the compounds described were achiral, desymmetrization to achieve C_3 symmetry can easily be imagined.

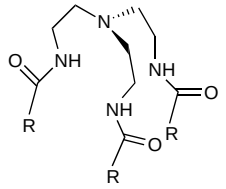
5.1.6. Other Receptors

Macrocyclic trimers of derivatives of the cinchona alkaloids quinine (**64**, X = OMe) and cinchonidine (**64**, X = H) were obtained in high yield from monomeric derivatives of the alkaloids.[157] The trimers were shown to be the thermodynamic products formed in a reversible process. A thermodynamic mixture of products consisting of dimers, trimers, and higher oligomers was also obtained by macrolactonization of cholic acid derivatives.[158]

Cyclodextrins are cyclic oligomers consisting of six, seven, or eight glycose units. The smallest member of the series, α-cyclodextrin, has been substituted symmetrically with three substituents to give C_3-symmetric receptors.[159] A trisammo-

nium derivative of α-cyclodextrin was used as a host for benzyl phosphate.[160] Recently, C_3- and C_4-symmetric cyclodextrin analogues were described which were made up of L-rhamnose and D-mannose units.[161]

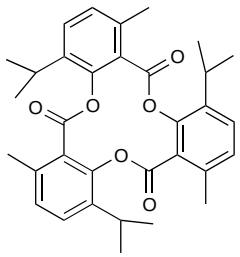
Interesting, although achiral amides **65** ($R = CH_2Cl$, $(CH_2)_4CH_3$, C_6H_5, 4-$MeOC_6H_4$), obtained from tris(2-aminoethyl)amine, were shown to serve as phosphate or sulfate receptors. The properties of the receptors depend on the structure and the substituents.[162] Examples of other achiral compounds serving as receptors for small organic molecules include macrocyclic cage compounds containing phosphane oxide units,[163] bowl-shaped or capped aryl thioethers,[164] macrocyclophanes,[165] and bridged triarylmethanes.[166] Some receptors with threefold symmetry were also included in recent reviews.[167]



65

5.1.7. Clathrands

Several important clathrands (compounds acting as hosts in the solid state) possess threefold symmetry.[8,9] Although many of the hosts are achiral, propellerlike conformations have been observed for the hosts as well as for their complexes.[168] Common examples are perhydrotriphenylene (C_3 symmetry), triphenylmethane, and tri-*o*-thymotide (**66**),[169] the last two of which adopt chiral conformations.



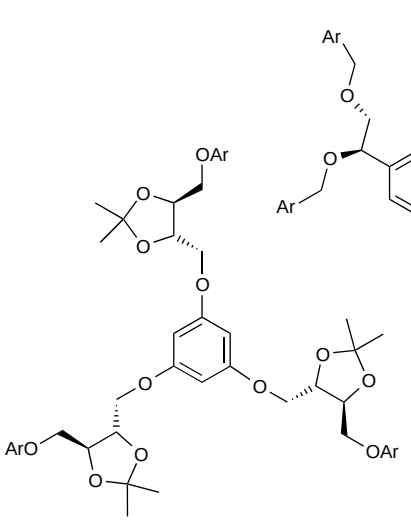
66

6. Other Compounds

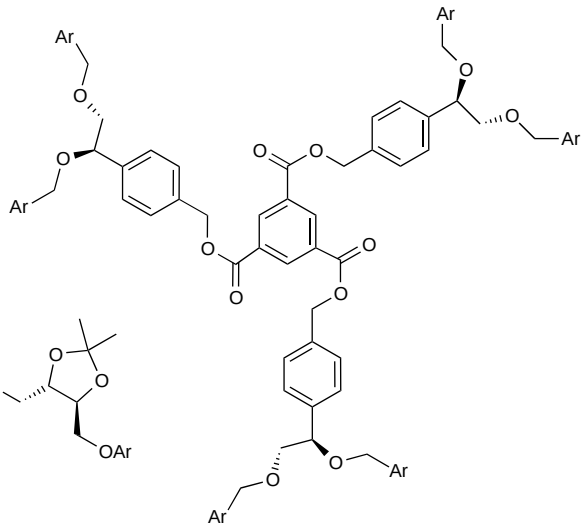
A variety of other compounds possessing threefold symmetry, hydrocarbons as well as compounds containing functional groups, have been prepared. Surveys of such compounds are given in the reviews by Nakazaki[9] and by Farina and Morandi.[8] Only a few recent examples will be given here.

Dendrimers are three-dimensional, branched, highly ordered macromolecules.[170] Although such compounds have been known for several decades, the first syntheses of chiral dendrimers have been undertaken only recently.[171] The chirality of dendrimers may be due either to a chiral nucleus, to which achiral building blocks are attached, or to the attachment of chiral substituents to the core, or, finally, to the use of chiral building blocks, resulting in a chiral interior domain. These kinds of chiral macromolecules are expected to become useful in chemical operations including asymmetric catalysis, chiral recognition, and resolution.

A few dendrimers with overall C_3 symmetry are known. Such dendrimers have been synthesized from 1,3,5-substituted benzene derivatives and tartaric acid derivatives (**67**; only the first generation of the dendrimers is shown)[172] or 3-hydroxybutanoic acid[173] as chiral units and by asymmetric synthesis, using the Sharpless dihydroxylation reaction (**68**).[174] It is doubtful, however, whether the overall C_3 symmetry of the macromolecule is of any importance in the microenvironment of a guest molecule or of a substrate bound to a catalytically active site.



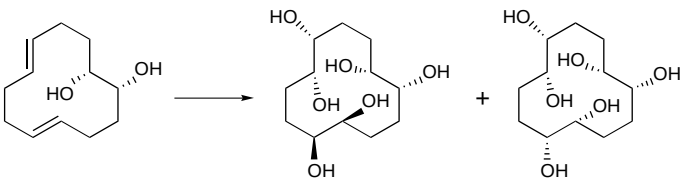
67



68

Fullerenes are carbon clusters having symmetries ranging from I_h to C_1. It is interesting to note that one of the C_{78} isomers possesses D_3 symmetry.[175]

It seems appropriate to close this survey of chiral compounds having threefold rotational symmetry with an example of a compound whose preparation relies on one of today's most potent asymmetric reactions, the Sharpless dihydroxylation.[176] Dihydroxylation of the three olefinic bonds of all-*trans*-1,5,9-cyclododecatriene is expected to yield a mixture of two compounds, **69** and **70**, which have C_2 and D_3 symmetry, respectively. Enantiomerically pure (*R*,*R*)-diol **71** afforded only small amounts of the hexol with threefold symmetry when quinuclidine or 2,5-diphenyl-4,6-bis(9-*O*-dihydroquinyl)pyrimidine, $(DHQ)_2$-PYR, was employed as the ligand in the reaction. 2,5-Diphenyl-4,6-bis(9-*O*-dihydroquinidyl)-pyrimidine, $(DHQD)_2$-PYR, gave the two compounds in a ratio of 2:1; the total yield of the D_3-symmetric compound **70** was as high as 32%.[177]



71 *(R,R)* **69** *(R,R,R,R,S,S)* **70** *(R,R,R,R,R,R)*

7. Molecules with Higher Symmetry

Some chiral compounds analogous to those described above but with higher symmetry have been reported. Examples of compounds with a single fourfold axis include some calixarenes,[178] a tetraphenylporphyrin capped with a calix[4]amide,[179] and a C_4-symmetric dendrimer.[180] C_5 through C_7 symmetries are represented by the cyclodextrins. Examples of high-symmetry compounds belonging to a dihedral group are a D_4-symmetric metallotetraphenylporphyrin,[181] a D_4-symmetric amine,[182] and a hexaamine with D_6 symmetry.[182] This last compound has symmetry number 12 and is, together with the *T*-symmetric adamantane shown in Figure 4,[17] the most symmetric chiral compound synthesized to date. Nature, however, has provided us with supramolecular assemblies of proteins[183] and viruses[184] having *O* and *I* symmetry, in other words, with symmetry numbers as high as 24 and 60, respectively.

8. Summary and Outlook

The justification for using rotational symmetry to achieve high symmetry has been discussed repeatedly, and symmetry is sometimes considered to be a more or less magic property. Symmetry is advantageous when it improves the selectivity by decreasing the number of different reaction paths and thereby the number of intermediates; what is achieved by symmetry is simply the reduction of competing alternatives. This may have a profound effect on the selectivity, as has been demonstrated repeatedly in recent years. Symmetry may also be helpful for the monofunctionalization of a compound containing several reactive sites; if the reactive groups are symmetry-related, the compound desired is obtained by functionalization at any site. Furthermore, the analysis of the observed enantioselectivity and thus the mechanistic interpretation may be simplified.

Rotational symmetry is often but not always the key to high stereoselectivity. What is always important is a thorough analysis of the symmetry and the number of possible intermediates in the reaction under study. The purpose of this survey was to present the known compounds with C_3 symmetry, which have been used or which may be useful in asymmetric synthesis or chiral recognition, and to show under which circumstances these compounds may be advantageous. Another purpose was to demonstrate that the key to high stereoselectivity is often found within the larger family of reagents with various types of rotational symmetry.

I am grateful to Professor Jean-Claude Fiaud and Professor John Osborn for encouraging me to write this review and to Dr. Hans Adolfsson, Dr. Gunhild Aulin-Erdtman, Professor Carsten Bolm, Professor Jan-Erling Bäckvall, Professor Torbjörn Norin, Dr. Tobias Rein, Professor Olof Wennerström, and Dr. Paul Wyatt for valuable criticism and comments on the manuscript. I would also like to thank one of the referees for many valuable suggestions.

Received: July 10, 1996
Revised version: July 2, 1997 [A 179 IE]
German version: *Angew. Chem.* **1998**, *110*, 260 – 281

[1] A. L. Loeb, *Color and Symmetry*, Wiley, New York, **1971**; J. Rosen, *Symmetry Discovered*, Cambridge University Press, Cambridge, **1975**; E. H. Lockwood, R. H. Macmillan, *Geometric Symmetry*, Cambridge University Press, Cambridge, **1978**; K. Mainzer, *Symmetrien der Natur. Ein Handbuch der Natur- und Wissenschaftsphilosophie*, DeGruyter, Berlin, **1988**; M. C. Escher, *Visions of Symmetry*, Freeman, New York, **1990**.
[2] E. Heilbronner, J. D. Dunitz, *Reflections on Symmetry*, VCH/Helvetica Chimica Acta, Weinheim/Basel, **1993**.
[3] T.-L. Ho, *Symmetry. A Basis for Synthesis Design*, Wiley, New York, **1995**.
[4] T. Beissel, R. E. Powers, K. N. Raymond, *Angew. Chem.* **1996**, *108*, 1166 – 1168; *Angew. Chem. Int. Ed. Engl.* **1996**, *35*, 1084 – 1086; A. Müller, C. Beugholt, *Nature* **1996**, *383*, 296 – 297.
[5] H. Weyl, *Symmetry*, Princeton University Press, Princeton, **1952**; I. Hargittai, M. Hargittai, *Symmetry through the Eyes of a Chemist*, Plenum, New York, **1995**.
[6] F. A. Cotton, *Chemical Applications of Group Theory*, Wiley, New York, **1971**.
[7] J. K. Whitesell, *Chem. Rev.* **1989**, *89*, 1581 – 1590.
[8] M. Farina, C. Morandi, *Tetrahedron* **1974**, *30*, 1819 – 1831.
[9] M. Nakazaki, *Top. Stereochem.* **1984**, *15*, 199 – 251.
[10] N. J. Turro, *Angew. Chem.* **1986**, *98*, 872 – 892; *Angew. Chem. Int. Ed. Engl.* **1986**, *25*, 882 – 901; P. G. Mezey, *Shape in Chemistry. An Introduction to Molecular Shape and Topology*, VCH, New York, **1993**; V. I. Sokolov, *Introduction to Theoretical Stereochemistry*, Gordon and Breach, New York, **1991**.
[11] R. Krämer, J.-M. Lehn, A. DeCian, J. Fischer, *Angew. Chem.* **1993**, *105*, 764 – 767; *Angew. Chem. Int. Ed. Engl.* **1993**, *32*, 703 – 705; L. J. Charbonniere, G. Bernardinelli, C. Piguet, A. M. Sargeson, A. F. Williams, *J. Chem. Soc. Chem. Commun.* **1994**, 1419 – 1420.
[12] J. Libman, Y. Tor, A. Shanzer, *J. Am. Chem. Soc.* **1987**, *109*, 5880 – 5881; E. J. Enemark, T. D. P. Stack, *Angew. Chem.* **1995**, *107*, 1082 – 1084; *Angew. Chem. Int. Ed. Engl.* **1995**, *34*, 996 – 998.
[13] E. E. Eliel, S. H. Wilen, *Stereochemistry of Organic Compounds*, Wiley, New York, **1994**.
[14] E. Mohr, *J. Prakt. Chem.* **1903**, *68*, 369 – 384.
[15] G. E. McCasland, R. Horvat, M. R. Roth, *J. Am. Chem. Soc.* **1959**, *81*, 2399 – 2402.
[16] According to calculations, tetra-*tert*-butyltetrahedrane has *T* symmetry in the ground state. However, since the chirality relies on the rotation around a single bond, the barrier to racemization is low (2.5 kcal mol^{-1}): W. D. Hounshell, K. Mislow, *Tetrahedron Lett.* **1979**, 1205 – 1208.
[17] M. Nakazaki, K. Naemura, *J. Chem. Soc. Chem. Commun.* **1980**, 911 – 912; M. Nakazaki, K. Naemura, Y. Hokura, *ibid.* **1982**, 1245 – 1246.
[18] P. E. Eaton, T. W. Cole, Jr., *J. Am. Chem. Soc.* **1964**, *86*, 3157 – 3158.
[19] R. J. Ternansky, D. W. Balogh, L. A. Paquette, *J. Am. Chem. Soc.* **1982**, *104*, 4503 – 4504.
[20] H. W. Kroto, J. R. Heath, S. C. O'Brien, R. F. Curl, R. E. Smalley, *Nature* **1985**, *318*, 162 – 163; R. F. Curl, R. E. Smalley, *Sci. Am.* **1991**, *265*, 32 – 41.
[21] R. S. Cahn, C. Ingold, V. Prelog, *Angew. Chem.* **1966**, *78*, 413 – 447; *Angew. Chem. Int. Ed. Engl.* **1966**, *5*, 385 – 415.
[22] The effect of symmetry on chiral recognition has previously been analyzed and applied to chromatographic separation: R. Isaksson, H. Wennerstr m, O. Wennerstr m, *Tetrahedron* **1988**, *44*, 1697 – 1705.

[23] J. P. Collman, L. S. Hegedus, J. R. Norton, R. G. Finke, *Principles and Applications of Organotransition Metal Chemistry*, University Science Books, Mill Valley, **1987**.

[24] R. Noyori, *Asymmetric Catalysis in Organic Synthesis*, Wiley, New York, **1994**; I. Ojima, *Catalytic Asymmetric Synthesis*, VCH, New York, **1993**.

[25] H. B. Kagan; K. E. Koenig; I. Ojima and K. Hirai; T. Hayashi and M. Kumada in *Asymmetric Synthesis, Vol. 5* (Ed.: J. D. Morrison), Academic Press, New York, **1985**, Chapters 1, 3, 4, and 5, respectively.

[26] L. Sacconi, F. Mani, *Transition Met. Chem*. **1982**, *8*, 179 – 252.

[27] W. H. Hohman, D. J. Kountz, D. W. Meek, *Inorg. Chem*. **1986**, *25*, 616 – 623.

[28] L. F. Rhodes, C. Sorato, L. M. Venanzi, F. Bachechi, *Inorg. Chem.* **1988**, *27*, 604 – 610.

[29] C. Bianchini, A. Meli, M. Peruzzini, F. Vizza, F. Zanobini, *Coord. Chem. Rev*. **1992**, *120*, 193 – 208.

[30] B. Bogdanović, B. Henc, B. Meister, H. Pauling, G. Wilke, *Angew. Chem.* **1972**, *21*, 1070 – 1071; *Angew. Chem. Int. Ed. Engl.* **1972**, *11*, 1023 – 1024; B. Bogdanoví, *ibid.* **1973**, *85*, 1013 – 1023 and **1973**, *12*, 954 – 964; E. Müller, H.-B. Bürgi, *Helv. Chim. Acta* **1987**, *70*, 1063 – 1069.

[31] C. Bolm, W. M. Davis, R. L. Halterman, K. B. Sharpless, *Angew. Chem.* **1988**, *100*, 882 – 883; *Angew. Chem. Int. Ed. Engl.* **1988**, *27*, 835 – 837; C. Bolm, K. B. Sharpless, *Tetrahedron Lett*. **1988**, *29*, 5101 – 5104.

[32] M. J. Burk, R. L. Harlow, *Angew. Chem.* **1990**, *102*, 1511 – 1513; *Angew. Chem. Int. Ed. Engl.* **1990**, *29*, 1462 – 1464.

[33] M. J. Burk, J. E. Feaster, R. L. Harlow, *Tetrahedron: Asymmetry* **1991**, *2*, 569 – 592.

[34] T. R. Ward, L. M. Venanzi, A. Albinati, F. Lianza, T. Gerfin, V. Gramlich, G. M. R. Tombo, *Helv. Chim. Acta* **1991**, *74*, 983 – 988.

[35] M. J. Baker, P. J. Pringle, *J. Chem. Soc. Chem. Commun*. **1993**, 314 – 316.

[36] M. Stolmár, C. Floriani, G. Gervasio, D. Viterbo, *J. Chem. Soc. Dalton Trans.* **1997**, 1119 – 1121.

[37] G. Chelucci, *Gazz. Chim. Ital.* **1992**, *122*, 89 – 98.

[38] K. Tomioka, *Synthesis* **1990**, 541 – 549; A. Togni, L. M. Venanzi, *Angew. Chem.* **1994**, *106*, 517 – 547; *Angew. Chem. Int. Ed. Engl*. **1994**, *33*, 497 – 526.

[39] D. L. White, J. W. Faller, *Inorg. Chem*. **1982**, *21*, 3119 – 3122.

[40] J. P. Wibaut, A. P. de Jonge, H. G. P. van der Voort, P. P. H. L. Otto, *Rec. Trav. Chim. Pays-Bas* **1951**, *70*, 1054 – 1066.

[41] J. S. Olson, R. E. McKinnie, M. P. Mims, D. K. White, *J. Am. Chem. Soc.* **1983**, *105*, 1522 – 1527.

[42] S. J. Lippard, J. M. Berg, *Principles of Bioinorganic Chemistry*, University Science Books, Mill Valley, **1994**.

[43] J. W. Faller, Y. Ma, *J. Am. Chem. Soc.* **1991**, *113*, 1579 – 1586; J. W. Faller, L.-L. Gundersen, *Tetrahedron Lett.* **1993**, *34*, 2275 – 2278.

[44] V. Levacher, H. Adolfsson, C. Moberg, *Acta Chem. Scand.* **1996**, *50*, 454 – 457.

[45] G. R. Newkome, Y. J. Joo, D. W. Evans, F. R. Fronczek, G. R. Baker, *J. Org. Chem*. **1990**, *55*, 5714 – 5719.

[46] G. R. Newkome, V. Majestic, F. Fronczek, J. L. Atwood, *J. Am. Chem. Soc*. **1979**, *101*, 1047 – 1048.

[47] K. E. Krakowiak, J. S. Bradshaw, *Isr. J. Chem*. **1992**, *32*, 3 – 13.

[48] H. Adolfsson, K. Wärnmark, C. Moberg, *J. Chem. Soc. Chem. Commun.* **1992**, 1054 – 1055.

[49] H. Adolfsson, K. Nordström, K. Wärnmark, C. Moberg, *Tetrahedron: Asymmetry* **1996**, *7*, 1967 – 1972.

[50] J. W. Canary, C. S. Allen, J. M. Castagnetto, Y. Wang, *J. Am. Chem. Soc.* **1995**, *117*, 8484 – 8485.

[51] J. E. Richman, T. J. Atkins, *J. Am. Chem. Soc*. **1974**, *96*, 2268 – 2270.

[52] E. Kimura, T. Shiota, T. Koike, M. Shiro, M. Kodama, *J. Am. Chem. Soc.* **1990**, *112*, 5805 – 5811.

[53] A. A. Belal, I. Fallis, L. J. Farrugia, N. M. Macdonald, R. D. Peacock, *J. Chem. Soc. Chem. Commun.* **1991**, 402 – 403; A. A. Belal, P. Chadhuri, I. Fallis, L. J. Farrugia, R. Hartung, N. M. Macdonald, B. Nuber, R. D. Peacock, J. Weiss, K. Wieghardt, *Inorg. Chem.* **1991**, *30*, 4397 – 4402.

[54] L. H. Gade, N. Mahr, *J. Chem. Soc. Dalton Trans.* **1993,** 489 – 494; L. H. Gade, C. Becker, J. W. Lauher, *Inorg. Chem*. **1993**, *32*, 2308 – 2314; M. Schubart, B. Findeis, L. H. Gade, W.-S. Li, M. McPartlin, *Chem. Ber.* **1995**, *128*, 329 – 334.

[55] H. Memmler, L. H. Gade, J. W. Lauher, *Inorg. Chem*. **1994**, *33*, 3064 – 3071.

[56] H. Memmler, U. Kauper, L. H. Gade, D. Stalke, *Organometallics* **1996**, *15*, 3637 – 3639.

[57] S. Friedrich, L. H. Gade, A. J. Edwards, M. McPartlin, *Chem. Ber.* **1993**, *126*, 1797 – 1805.

[58] H. Memmler, K. Walsh, L. H. Gade, J. W. Lauher, *Inorg. Chem*. **1995**, *34*, 4062 – 4068.

[59] K. W. Hellmann, L. H. Gade, O. Gevert, P. Steinert, J. W. Lauher, *Inorg. Chem*. **1995**, *34*, 4069 – 4078.

[60] M. Cernerud, C. Moberg, unpublished results.

[61] J. G. Verkade, *Acc. Chem. Res.* **1993**, *26*, 483 – 489; J. Pinkas, J. Tang, Y. Wan, J. G. Verkade, *Phosphorus Sulfur Silicon* **1994**, *87*, 193 – 207.

[62] A. A. Naiini, W. M. P. B. Menge, J. G. Verkade, *Inorg. Chem.* **1991,** *30*, 5009 – 5012; W. Plass, J. G. Verkade, *J. Am. Chem. Soc*. **1992**, *114*, 2275 – 2276; J. S. Freundlich, R. R. Schrock, C. C. Cummins, W. M. Davis, *ibid.* **1994**, *116*, 6476 – 6477; C. C. Cummins, R. R. Schrock, *Inorg. Chem*. **1994**, *33*, 395 – 396; C. C. Cummins, R. R. Schrock, W. M. Davis, *ibid*. **1994**, *33*, 1448 – 1457; V. Christou, J. Arnold, *Angew. Chem.* **1993**, *105*, 1551 – 1553; *Angew. Chem. Int. Ed. Engl.* **1993**, *32*, 1450 – 1452; R. R. Schrock, C. C. Cummins, T. Wilhelm, S. Lin, S. M. Reid, M. Kol, W. M. Davis, *Organometallics* **1996**, *15*, 1470 – 1476.

[63] Z. Duan, A. A. Naiini, J.-H. Lee, J. G. Verkade, *Inorg. Chem*. **1995**, *34*, 5477 – 5482.

[64] C. C. Cummins, J. Lee, R. R. Schrock, W. D. Davis, *Angew. Chem.* **1992**, *104*, 1510 – 1512; *Angew. Chem. Int. Ed. Engl.* **1992**, *31*, 1501 – 1503.

[65] J. Pinkas, B. Gaul, J. G. Verkade, *J. Am. Chem. Soc*. **1993,** *115*, 3925 – 3931.

[66] D. Tanner, *Angew. Chem.* **1994**, *106*, 625 – 646; *Angew. Chem. Int. Ed. Engl.* **1994**, *33*, 599 – 619.

[67] F. Bienewald, C. Bolm, unpublished results; M. Cernerud, H. Adolfsson, C. Moberg, *Tetrahedron: Asymmetry* **1997**, 8, 2655 – 2662.

[68] D. W. Fuhlhage, C. A. VanderWerf, *J. Am. Chem. Soc*. **1958**, *80*, 6249 – 6254; K. Ogawa, Y. Nomura, Y. Takeuchi, S. Tomoda, *J. Chem. Soc. Perkin Trans. 1* **1982**, 3031 – 3035; E. C. Ashby, B. Park, G. S. Patil, K. Gadru, R. Gurumurthy, *J. Org. Chem.* **1993**, *58*, 424 – 437.

[69] C. Schöpf, H. Arm, H. Krimm, *Chem. Ber*. **1951**, *84*, 690.

[70] J. W. Lynn, *J. Am. Chem. Soc*. **1955**, *77*, 6067 – 6068; J. F. Cavalla, *J. Chem. Soc*. **1956**, 4672 – 4673; R. H. Hasek, J. C. Martin, *J. Org. Chem*. **1961**, *26*, 4134 – 4135; H. P. Fritz, H. Gebauer, G. Huttner, A. Frank, H. Lorenz, *Chem. Ber*. **1976**, *109*, 650 – 658; K. Kehagia, A. Dömling, I. Ugi, W. Hiller, J. Riede, *Z. Naturforsch. B* **1995**, *50*, 667 – 670; K. Kehagia, A. Dömling, I. Ugi, *Tetrahedron* **1995**, *51*, 139 – 144.

[71] N. Kitajima, W. B. Tolman in *Prog. Inorg. Chem*. **1995**, *43*, 419 – 531.

[72] D. M. Kurtz, Jr., *Chem. Rev.* **1990**, *90*, 585 – 606.

[73] R. Alsfasser, A. K. Powell, H. Vahrenkamp, *Angew. Chem.* **1990**, *102*, 939 – 941; *Angew. Chem. Int. Ed. Engl.* **1990**, *29*, 898 – 899.

[74] D. D. LeCloux, W. B. Tolman, *J. Am. Chem. Soc.* **1993**, *115*, 1153 – 1154.

[75] C. J. Tokar, P. B. Kettler, W. B. Tolman, *Organometallics* **1992**, *11*, 2737 – 1039.

[76] D. D. LeCloux, C. J. Tokar, M. Osawa, R. P. Houser, M. C. Keyes, W. B. Tolman, *Organometallics* **1994**, *13*, 2855 – 2866.

[77] U. E. Bucher, A. Currao, R. Nesper, H. Rüegger, L. M. Venanzi, E. Younger, *Inorg. Chem*. **1995**, *34*, 66 – 74.

[78] M. C. Keyes, V. G. Young, Jr., W. B. Tolman, *Organometallics* **1996**, *15*, 4133 – 4140.

[79] T. N. Sorrell, F. C. Pigge, P. S. White, *Inorg. Chim. Acta* **1993**, *210*, 87 – 90.

[80] K. Kawasaki, S. Tsumura, T. Katsuki, *Synlett.* **1995**, 1245 – 1246.

[81] C. Kimblin, V. J. Murphy, G. Parkin, *Chem. Commun*, **1996**, 235 – 236.

[82] W. M. P. B. Menge, J. G. Verkade, *Inorg. Chem*. **1991**, *30*, 4628 – 4631.

[83] W. A. Nugent, R. L. Harlow, *J. Am. Chem. Soc.* **1994**, *116*, 6142 – 6148.

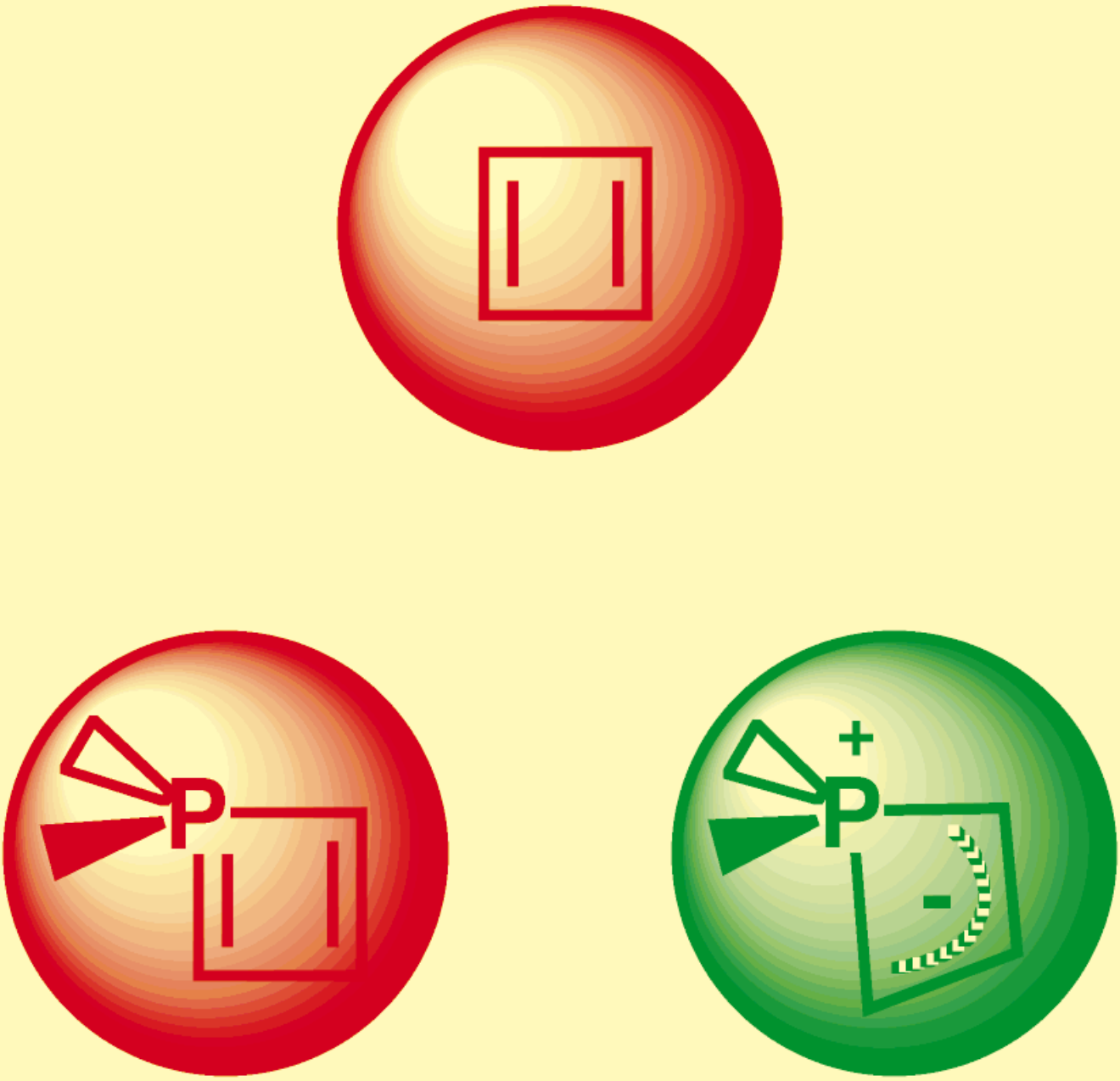
[84] J. D. Morrison, E. R. Grandbois, G. R. Weisman, in *Asymmetric Reactions and Processes in Chemistry* (*ACS Symp. Ser.* **1982**, *185*), pp. 278 – 279.

[85] M. Grassi, G. Di Silvestro, M. Farina, *Tetrahedron* **1985**, *41*, 177 – 181.

[86] W. A. Nugent, *J. Am. Chem. Soc.* **1992**, *114*, 2768 – 2769.
[87] B. W. McCleland, W. A. Nugent, M. G. Finn, personal communication.
[88] W. A. Nugent, T. V. RajanBabu, M. J. Burk, *Science* **1993**, *259*, 479 – 483.
[89] F. Di Furia, G. Licini, G. Modena, R. Motterle, W. A. Nugent, *J. Org. Chem.* **1996**, *61*, 5175 – 5177.
[90] H. Lütjens, P. Knochel, *Tetrahedron: Asymmetry* **1994**, *5*, 1161 – 1162.
[91] D. Kaufmann, R. Boese, *Angew. Chem.* **1990**, *102*, 568 – 569; *Angew. Chem. Int. Ed. Engl.* **1990**, *29*, 545 – 546.
[92] H. Brunner, A. F. M. M. Rahman, *Chem. Ber.* **1984**, *117*, 710 – 724.
[93] B. Burns, J. R. Studley, M. Wills, *Tetrahedron Lett.* **1993**, *34*, 7105 – 7106.
[94] K. Severin, W. Beck, G. Trojandt, K. Polborn, W. Steglich, *Angew. Chem.* **1995**, *107*, 1570 – 1572; *Angew. Chem. Int. Ed. Engl.* **1995**, *34*, 1449 – 1451.
[95] K. A. Jørgensen, *Chem. Rev.* **1989**, *89*, 431 – 458.
[96] H. Adolfsson, K. Wärnmark, C. Moberg, *J. Org. Chem.* **1994**, *59*, 2004 – 2009.
[97] C. G. Frost, J. Howarth, J. M. J. Williams, *Tetrahedron: Asymmetry* **1992**, *3*, 1089 – 1122; T. Hayashi in *Catalytic Asymmetric Synthesis* (Ed.: I. Ojima) VCH, New York, **1993**, pp. 325 – 365; B. M. Trost, D. L. Van Vranken, *Chem. Rev.* **1996**, *96*, 395 – 422.
[98] P. B. Mackenzie, J. Whelan, B. Bosnich, *J. Am. Chem. Soc.* **1985**, *107*, 2046 – 2054.
[99] K. Nordström, E. Macedo, C. Moberg, *J. Org. Chem.* **1997**, *62*, 1604 – 1609.
[100] A. Togni, *Tetrahedron: Asymmetry* **1991**, *2*, 683 – 690.
[101] J. Kang, W. O. Cho, H. G. Cho, *Tetrahedron: Asymmetry* **1994**, *5*, 1347 – 1352.
[102] F. Vögtle, *Supramolecular Chemistry*, Wiley, Chichester, **1991**.
[103] J. R. Pollack, J. B. Neilands, *Biochim. Biophys. Res. Commun.* **1970**, *38*, 989; I. G. O'Brien, F. Gibson, *Biochim. Biophys. Acta* **1970**, *215*, 393 – 402.
[104] Y. Tor, J. Libman, A. Shanzer, S. Lifson, *J. Am. Chem. Soc.* **1987**, *109*, 6517 – 6518; Y. Tor, J. Libman, A. Shanzer, C. E. Felder, S. Lifson, *ibid.* **1992**, *114*, 6661 – 6671; Y. Hisaeda, T. Ihara, T. Ohno, Y. Murakami, *Chem. Lett.* **1991**, 2139 – 2142; T. B. Karpishin, T. D. P. Stack, K. N. Raymond, *J. Am. Chem. Soc.* **1993**, *115*, 6115 – 6125; A. Shanzer, J. Libman, H. Weizman, B. Mester, Y. Hadar, Y. Chen, E. Jurkevitch, O. Ardon, *Pure Appl. Chem.* **1996**, *68*, 757 – 760.
[105] K. N. Raymond, G. Müller, B. F. Matzanke, *Top. Curr. Chem.* **1984**, *123*, 49 – 102.
[106] T. M. Garrett, T. J. McMurry, M. W. Hosseini, Z. E. Reyes, F. E. Hahn, K. N. Raymond, *J. Am. Chem. Soc.* **1991**, *113*, 2965 – 2977; T. B. Karpishin, M. S. Gebhard, E. I. Solomon, K. N. Raymond, *ibid.* **1991**, *113*, 2977 – 2984; T. D. P. Stack, T. B. Karpishin, K. N. Raymond, *ibid.* **1992**, *114*, 1512 – 1514; T. B. Karpishin, T. D. P. Stack, K. N. Raymond, *ibid.* **1993**, *115*, 182 – 192.
[107] S. D. Burke, W. J. Porter, J. Rancourt, R. F. Kaltenbach, *Tetrahedron Lett.* **1990**, *31*, 5285 – 5288; S. D. Burke, C. R. Heap, W. J. Porter, Y. Song, *ibid.* **1996**, *37*, 343 – 346.
[108] S. D. Burke, C. R. Heap, W. J. Porter, Y. Song, *Tetrahedron Lett.* **1996**, *37*, 343 – 346; C. R. Heap, S. D. Burke, *211th ACS National Meeting*, New Orleans **1996**, Abstract 83; C. W. Moon, S. D. Burke, *ibid.* Abstract 84; C. J. O'Donnell, S. D. Burke, ibid, Abstract 85; A. N. Raymond, S. D. Burke, *ibid.* Abstract 444.
[109] V. I. Sokolov, *Chirality and Optical Activity in Organometallic Compounds*, Gordon and Breach, New York, **1990**.
[110] A. von Zelewsky, *Stereochemistry of Coordination Compounds*, Wiley, Chichester, **1996**.
[111] H. P. Jensen, *Acta Chem. Scand. A* **1981**, *35*, 127 – 130.
[112] S.-K. Chang, M. J. Jang, S. Y. Han, J. H. Lee, M. H. Kang, K. T. No, *Chem. Lett.* **1992**, 1937 – 1940.
[113] K. Araki, N. Hashimoto, H. Otsuka, S. Shinkai, *J. Org. Chem.* **1993**, *58*, 5958 – 5963.
[114] K. Araki, K. Inada, S. Shinkai, *Angew. Chem.* **1996**, *108*, 92 – 94; *Angew. Chem. Int. Ed. Engl.* **1996**, *35*, 72 – 74.
[115] H.-J. Schneider, *Angew. Chem.* **1993**, *105*, 890 – 892; *Angew. Chem. Int. Ed. Engl.* **1993**, *32*, 848 – 850.
[116] W. C. Still, *Acc. Chem. Res.* **1996**, *29*, 155 – 163.
[117] J.-I. Hong, S. K. Namgoong, A. Bernardi, W. C. Still, *J. Am. Chem. Soc.* **1991**, *113*, 5111 – 5112; S. D. Erickson, J. A. Simon, W. C. Still, *J. Org. Chem.* **1993**, *58*, 1305 – 1308; R. Liu, W. C. Still, *Tetrahedron Lett.* **1993**, *34*, 2573 – 2576; D. Q. McDonald, W. C. Still, *J. Am. Chem. Soc.* **1996**, *118*, 2073 – 2077.
[118] F. Gasparrini, D. Misiti, C. Villani, A. Borchardt, M. T. Burger, W. C. Still, *J. Org. Chem.* **1995**, *60*, 4314 – 4315.
[119] S. S. Yoon, W. C. Still, *Angew. Chem.* **1994**, *106*, 2517 – 2520; *Angew. Chem. Int. Ed. Engl.* **1994**, *33*, 2458 – 2460.
[120] T. W. Kim, J.-I. Hong, *Bull. Korean Chem. Soc.* **1995**, *16*, 781 – 783.
[121] R. J. Pieters, F. Diederich, *Chem. Commun.* **1996**, 2255 – 2256.
[122] B. S. Jursic, *211th ACS National Meeting*, New Orleans **1996**, Abstract 337.
[123] G. Trojandt, K. Polborn, W. Steglich, M. Schmidt, H. Nöth, *Tetrahedron Lett.* **1995**, *36*, 857 – 860.
[124] Y. Tor, J. Libman, A. Shanzer, C. E. Felder, S. Lifson, *J. Am. Chem. Soc.* **1992**, *114*, 6653 – 6661.
[125] I. Dayan, Y. Tor, J. Libman, A. Shanzer, *J. Org. Chem.* **1992**, *57*, 6060 – 6063.
[126] T. W. Hambley, C. J. Hawkins, M. F. Lavin, A. van den Brenk, D. J. Watters, *Tetrahedron* **1992**, *48*, 341 – 348.
[127] M. P. Foster, G. P. Concepción, G. B. Caraan, C. M. Ireland, *J. Org. Chem.* **1992**, *57*, 6671 – 6675.
[128] M. R. Prinsep, R. E. Moore, I. A. Levine, G. M. L. Patterson, *J. Nat. Prod.* **1992**, *55*, 140.
[129] P. Wipf, C. P. Miller, *J. Am. Chem. Soc.* **1992**, *114*, 10975 – 10977.
[130] J. Crosby, J. F. Stoddart, X. Sun, M. R. W. Venner, *Synthesis* **1993**, 141 – 145.
[131] J. M. Lehn, P. Vierling, R. C. Hayward, *J. Chem. Soc. Chem. Commun.* **1979**, 296 – 298.
[132] E. P. Kyba, G. W. Gokel, F. de Jong, K. Koga, L. R. Sousa, M. G. Siegel, L. Kaplan, G. D. Y. Sogah, D. J. Cram, *J. Org. Chem.* **1977**, *42*, 4173 – 4184.
[133] W. D. Curtis, D. A. Laidler, J. F. Stoddart, G. H. Jones, *J. Chem. Soc. Perkin Trans 1* **1977**, 1756 – 1769.
[134] C. Almansa, A. Moyano, F. Serratosa, *Tetrahedron* **1988**, *44*, 2657 – 2662.
[135] C. Almansa, A. Moyano, F. Serratosa, *Tetrahedron* **1991**, *47*, 5867 – 5876.
[136] C. Almansa, A. Moyano, F. Serratosa, *Tetrahedron* **1992**, *48*, 1497 – 1506.
[137] A. Collet, J. Jacques, *Tetrahedron Lett.* **1978**, 1265 – 1268.
[138] J. Canceill, L. Lacombe, A. Collet, *J. Am. Chem. Soc.* **1985**, *107*, 6993 – 6996.
[139] J. Gabard, A. Collet, *J. Chem. Soc. Chem. Commun.* **1981**, 1137 – 1139.
[140] L. Garel, J.-P. Dutasta, A. Collet, *Angew. Chem.* **1993**, *105*, 1249 – 1251; *Angew. Chem. Int. Ed. Engl.* **1993**, *32*, 1169 – 1171.
[141] J. Canceill, M. Cesario, A. Collet, J. Guilhem, L. Lacombe, B. Lozach, C. Pascard, *Angew. Chem.* **1989**, *101*, 1249 – 1251; *Angew. Chem. Int. Ed. Engl.* **1989**, *28*, 1246 – 1248.
[142] L. Garel, B. Lozach, J.-P. Dutasta, A. Collet, *J. Am. Chem. Soc.* **1993**, *115*, 11652 – 11653.
[143] C. Garcia, A. Aubry, A. Collet, *Bull. Soc. Chim.* Fr. **1996**, *133*, 853 – 867.
[144] S. B. Lee, J.-I. Hong, *Tetrahedron Lett.* **1996**, *37*, 8501 – 8504.
[145] C. Garcia, A. Collet, *Bull. Soc. Chim. Fr.* **1995**, *132*, 52 – 58.
[146] J. A. Wytko, J. Weiss, *Tetrahedron Lett.* **1991**, *32*, 7261 – 7264; G. P. F. van Strijdonck, J. A. E. H. van Haare, J. G. M. van der Linden, J. J. Steggerda, R. J. M. Nolte, *Inorg. Chem.* **1994**, *33*, 999 – 1000.
[147] G. Matouzenko, G. Vériot, J.-P. Dutasta, A. Collet, J. Jordanov, F. Varret, M. Perrin, S. Lecocq, *New J. Chem.* **1995**, *19*, 881 – 885; G. Vériot, J.-P. Dutasta, G. Matouzenko, A. Collet, *Tetrahedron* **1995**, *51*, 389 – 400.
[148] D. J. Cram, J. Weiss, R. C. Helgeson, C. B. Knobler, A. E. Dorigo, K. N. Houk, *J. Chem. Soc. Chem. Commun.* **1988**, 407 – 409; J. de Mendoza, P. M. Nieto, P. Prados, C. Sánchez, *Tetrahedron* **1990**, *46*, 671 – 682; A. Casnati, P. Minari, A. Pochini, R. Ungaro, *J. Chem. Soc. Chem. Commun.* **1991**, 1413 – 1414; K. Araki, N. Hashimoto, H. Otsuka, T. Nagasaki, S. Shinkai, *Chem. Lett.* **1993**, 829 – 832; M. Takeshita, S. Shinkai, *ibid.* **1994**, 1349 – 1352.
[149] K. Araki, K. Akao, H. Otsuka, K. Nakashima, F. Inokuchi, S. Shinkai, *Chem. Lett.* **1994**, 1251 – 1254.
[150] M. Takeshita, S. Nishio, S. Shinkai, *J. Org. Chem.* **1994**, *59*, 4032 – 4034.

[151] For another example, see: M. Takeshita, F. Inokuchi, S. Shinkai, *Tetrahedron Lett*. **1995**, *36*, 3341 – 3344.
[152] D. St. C. Black, M. C. Bowyer, N. Kumar, P. S. R. Mitchell, *J. Chem. Soc. Chem. Commun.* **1993**, 819 – 821.
[153] D. St. C. Black, D. C. Craig, N. Kumar, D. B. McConnell, *Tetrahedron Lett*. **1996**, *37*, 241 – 244.
[154] P. O'Sullivan, V. Böhmer, W. Vogt, E. F. Paulus, R. A. Jakobi, *Chem. Ber*. **1994**, *127*, 427 – 432.
[155] H. L. Anderson, J. K. M. Sanders, *Angew. Chem.* **1990**, *102*, 1478 – 1480; *Angew. Chem. Int. Ed. Engl*. **1990**, *29*, 1400 – 1402.
[156] X. Chi, A. J. Guerin, R. A. Haycock, C. A. Hunter, L. D. Sarson, *J. Chem. Soc. Chem. Commun.* **1995**, 2563 – 2565; X. Chi, A. J. Guerin, R. A. Haycock, C. A. Hunter, L. D. Sarson, *ibid.* **1995**, 2567 – 2569.
[157] S. J. Rowan, P. A. Brady, J. K. M. Sanders, *Angew. Chem.* **1996**, *108*, 2283 – 2285; *Angew. Chem. Int. Ed. Engl.* **1996**, *35*, 2143 – 2145.
[158] P. A. Brady, R. P. Bonar-Law, S. J. Rowan, C. J. Suckling, J. K. M. Sanders, *Chem. Commun.* **1996**, 319 – 320.
[159] J. Boger, D. G. Brenner, J. R. Knowles, *J. Am. Chem. Soc*. **1979**, *101*, 7630 – 7631.
[160] J. Boger, J. R. Knowles, *J. Am. Chem. Soc*. **1979**, *101*, 7631 – 7633.
[161] P. R. Ashton, C. L. Brown, S. Menzer, S. A. Nepogodiev, J. F. Stoddart, D. J. Williams, *Chem. Eur. J.* **1996**, *2*, 580 – 591.
[162] S. Valiyaveettil, J. F. J. Engbersen, W. Verboom, D. N. Reinhoudt, *Angew. Chem.* **1993**, *105*, 942 – 944; *Angew. Chem. Int. Ed. Engl*. **1993**, *32*, 900 – 901; C. Raposo, M. Almaraz, M. Martin, V. Weinrich, M. L. Mussóns, V. Alcázar, M. C. Caballero, J. R. Morán, *Chem. Lett*. **1995**, 759 – 760.
[163] B. P. Friedrichsen, H. W. Whitlock, *J. Am. Chem. Soc*. **1989**, *111*, 9132 – 9134; B. P. Friedrichsen, D. R. Powell, H. W. Whitlock, *ibid*. **1990**, *112*, 8931 – 8941.
[164] A. P. West, Jr., D. van Engen, R. A. Pascal, Jr., *J. Am. Chem. Soc*. **1989**, *111*, 6846 – 6847; R. A. Pascal, Jr., M. L. Carter, M. R. Johnson, D. M. Ho, *Tetrahedron Lett*. **1996**, *37*, 8125 – 8128.
[165] M. Lofthagen, R. Chadha, J. S. Siegel, *J. Am. Chem. Soc*. **1991**, *113*, 8785 – 8790.
[166] R. Berscheid, M. Nieger, F. Vögtle, *Chem. Ber.* **1992**, *125*, 1687 – 1695.
[167] C. Seel, F. Vögtle, *Angew. Chem.* **1992**, *104*, 542 – 563; *Angew. Chem. Int. Ed. Engl.* **1992**, *31*, 528 – 549. F. Diederich, *ibid.* **1988**, *100*, 372 – 396 and **1988**, *27*, 362 – 386.
[168] D. D. MacNicol, J. J. McKendrick, D. R. Wilson, *Chem. Soc. Rev.* **1978**, *7*, 65 – 87.
[169] A. P. Downing, W. D. Ollis, I. O. Sutherland, J. Mason, S. F. Mason, *J. Chem. Soc. Chem. Commun.* **1968**, 329 – 332; D. J. Williams, D. Lawton, *Tetrahedron Lett*. **1975**, 111 – 114; R. Gerdil, J. Allemand, *ibid.* **1979**, 3499 – 3502.
[170] D. A. Tomalia, A. M. Naylor, W. A. Goddard III, *Angew. Chem.* **1990**, *102*, 119 – 157; *Angew. Chem. Int. Ed. Engl.* **1990**, *29*, 138 – 175.
[171] D. Seebach, J.-M. Lapierre, G. Greiveldinger, K. Skobridis, *Helv. Chim. Acta* **1994**, *77*, 1673 – 1688.
[172] H.-F. Chow, L. F. Fok, C. C. Mak, *Tetrahedron Lett*. **1994**, *35*, 3547 – 3550.
[173] D. Seebach, G. F. Herrmann, U. D. Lengweiler, B. M. Bachmann, W. Amrein, *Angew. Chem.* **1996**, *108*, 2969 – 2972; *Angew. Chem. Int. Ed. Engl.* **1996**, *35*, 2795 – 2797.
[174] H.-T. Chang, C.-T. Chen, T. Kondo, G. Siuzdak, K. B. Sharpless, *Angew. Chem.* **1995**, *107*, 202 – 206; *Angew. Chem. Int. Ed. Engl.* **1996**, *35*, 182 – 186.
[175] C. Thilgen, F. Diederich, R. L. Whetten in *Buckminsterfullerenes*, (Eds.: W. E. Billups, M. A. Ciufolini), VCH, New York, **1993**, pp. 59 – 81.
[176] H. C. Kolb, M. S. VanNieuwenhze, K. B. Sharpless, *Chem. Rev.* **1994**, *94*, 2483 – 2547.
[177] H. Becker, M. A. Soler, K. B. Sharpless, *Tetrahedron* **1995**, *51*, 1345 – 1376.
[178] P. Neri, C. Geraci, M. Piattelli, *Tetrahedron Lett*. **1993**, *34*, 3319 – 3322; G. D. Andreetti, V. Böhmer, J. G. Jordon, M. Tabatabai, F. Ugozzoli, W. Vogt, A. Wolff, *J. Org. Chem*. **1993**, *58*, 4023 – 4032; R. Arnecke, V. Böhmer, E. F. Paulus, W. Vogt, *J. Am. Chem. Soc*. **1995**, *117*, 3286 – 3287.
[179] T. Nagasaki, H. Fujishima, M. Takeuchi, S. Shinkai, *J. Chem. Soc. Perkin Trans. 1* **1995**, 1883 – 1888.
[180] G. R. Newkome, X. Lin, C. D. Weis, *Tetrahedron: Asymmetry* **1991**, *2*, 957 – 960.
[181] R. L. Halterman, S.-T. Jan, *J. Org. Chem*. **1991**, *56*, 5253 – 5254.
[182] K. Naemura, Y. Kanda, M. Yamanaka, H. Chikamatsu, *Chem. Lett.* **1989**, 283 – 284.
[183] J. Trikha, E. C. Theil, N. M. Allewell, *J. Mol. Biol*. **1995**, *248*, 949 – 967.
[184] E. Arnold, M. G. Rossmann, *Acta Crystallogr. Sect. A* **1988**, *44*, 270 – 282.

The escape from antiaromaticity in four π electron four-membered ring systems



ANGEWANDTE CHEMIE
© WILEY-VCH

Ylidic Four π Electron Four-Membered λ^5-Phosphorus Heterocycles: Electronical Isomers of Heterocyclobutadienes

Guy Bertrand*

The first inorganic heterocycle, $(Cl_2PN)_3$, was discovered in the last century. Nevertheless, up to the beginning of the 1980s it was claimed that cyclodiphosphazenes $(R_2PN)_2$ could not exist because of ring strain and contraction of the N-P-N bond angles below 115°, which would cause serious interpenetration of the van der Waals boundaries of the nitrogen atoms. In 1984 we reported the synthesis and single-crystal X-ray structure analysis of the smallest member of the well-known family of cyclopolyphosphazenes, namely, tetrakis(diisopropylamino)-1λ^5,3λ^5-diphosphete. The parallel to the history of benzene and cyclobutadiene is striking, but here the comparison has to stop: Cyclobutadienes that contain λ^5-phosphorus atoms are not antiaromatic; they feature a strong ylide character with a four π electron system that follows either an island model or presents an interrupted cyclic delocalization. Despite the lack of antiaromaticity, the preparation of these heterocycles remains a challenging example of non-natural-product synthesis because of the ring strain. "Heterocyclobutadienes" of this type are very reactive, which makes them attractive precursors to a variety of novel heterocycles; the synthesis by Karsch of a spirocyclic ten-electron cation featuring an unprecedented pseudo-trigonal-bipyramidal PP_4 fragment is a good illustration. They also act as +ligands for transition metals, and preliminary results indicate that they could be used as building blocks for coordination polymers.

Keywords: antiaromaticity · phosphorus heterocycles · phosphorus ylides · strained molecules

1. Introduction

For more than a century, the synthesis and bonding description of six π electron six-membered and four π electron four-membered rings have attracted considerable attention.[1] Although benzoic acid has been known since the 16th century and benzene was discovered in 1825 by Faraday,[2] it was only in 1965 that Pettit[3] prepared an organometallic complex featuring cyclobutadiene as a ligand, and in 1968 that Gompper and Seybold[4] isolated a free cyclobutadiene derivative stabilized by push–pull effects. Outside the coordination sphere of transition metals, the parent cyclobutadiene is only stable in matrices at low temperature[5a–d] or in a molecular container, as recently shown by Cram.[5e, f]

Even by the end of the 19th century, Kekulé tried to rationalize the very peculiar stability of benzene. He stated that it was due to the structure of the ring exhibiting an alternance of single and double bonds, and introduced the oscillation theory:[6] This was the premise of aromaticity. The only mistake was to think that, as vinylogues of benzene, cyclobutadiene and cyclooctatetraene should also be aromatic and very stable, although this idea was reinforced by the synthesis of cyclooctatetraene by Willstätter in 1911.[7] In 1930 Hückel tried to rationalize the "mysterious" difference in behavior between benzene on the one hand and cyclobutadiene and cyclooctatetraene on the other using molecular-orbital theory.[8] According to the Hückel rules, annulenes of the type $(C_2H_2)_n$ have to be divided into two groups: 1) Compounds which have $(4n+2)$ π electrons, such as benzene, are stabilized by delocalization and thus aromatic. 2) Compounds which have $(4n)$ π electrons, such as cyclobutadiene, have no particular stabilization. Only one element was missing: the destabilizing effect called "antiaromaticity" in 1965 by Breslow and Dewar. Nowadays antiaromaticity accounts for 60% of the excess energy of cyclobutadiene (estimated at 35 kcal mol^{-1}); the remaining 40% is attributed to ring strain.[9] Even in the most recent book published on aromaticity (and antiaromaticity),[1a] the authors concluded: "at any rate, up to this time nobody has been able to produce a physically sound explanation to this effect"!

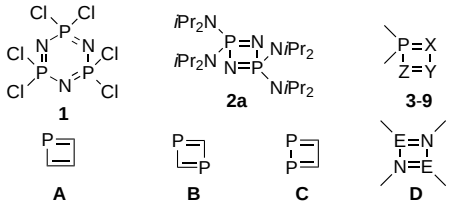
The aromatic and antiaromatic character is perturbed when one or more heteroatoms from the second row of the periodic system are present in the ring.[10] With an element from the third (or higher) row that possesses p orbitals for building the π system, the comparison is even more striking;[10] for

[*] Dr. G. Bertrand
Laboratoire de Chimie de Coordination du CNRS
205 route de Narbonne, F-31077 Toulouse Cédex (France)
Fax: Int. code + (33) 561-553 003
e-mail: gbertran@lcctoul.lcc-toulouse.fr

 © WILEY-VCH Verlag GmbH, D-69451 Weinheim, 1998 1433-7851/98/3703-0271 $ 17.50+.50/0

example, neither silabenzene[11] nor germabenzene[12] are stable. When the heteroatom has no p orbital available for the π system, the six-membered ring is no longer a Hückel aromatic system[13] and, consequently, the four-membered ring should not be antiaromatic.

Starting from this hypothesis, six π electron six-membered and four π electron four-membered rings featuring an element from the third row should not be particularly stable and unstable, respectively. However, it is amazing to realize that the first six-membered heterocycle of this type, the cyclotriphosphazene **1**,[14] was discovered in 1834, whereas the first vinylogue, the cyclodiphosphazene **2a** (Scheme 1), was reported by our group as recently as 1984![15]



3: X=Z: P, Y: PR_2 ;**4**: X=Z: CR, Y: PR'$_2$; **5**: X=Y=Z: CR;
6: X: N, Y=Z: CR; **7**: X: P, Y=Z: CR; **8**: X=Z: N, Y: CR;
9: X: P, Y:PR_2 , Z: CR'; **9'**: X: As, Y:PR_2 , Z: CR'.
E: B, Al, In.

Scheme 1. Cyclotriphosphazenes **1**, cyclodiphosphazenes **2**, and four π electron four-membered heterocycles containing phosphorus (**3**–**9**, **A**–**C**) or a Group 13 element (**D**).

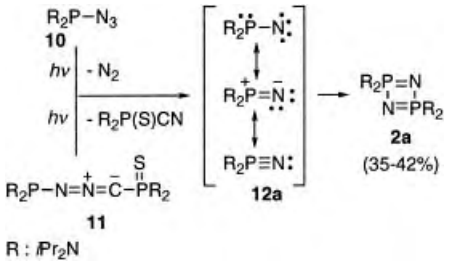
This review deals with the synthesis, bonding properties, and reactivity of four π electron four-membered rings **2**–**9**, which feature a λ^5-phosphorus atom.[16] So far, the related, but antiaromatic, λ^3-phosphete **A** and λ^3,λ^3-diphosphetes **B** and **C** (Scheme 1) are only known as transient species or as ligands for transition metal complexes; they are the subject of recent reviews.[17] On the other hand, there are very few four π electron four-membered rings featuring a main group element from the third (or higher) row. Indeed, to the best of our knowledge, there are no stable examples involving Group 14[18] or 16 elements (although some have been erroneously claimed for the latter),[19] and only a couple of compounds of type **D** involving Group 13 elements[20] (Scheme 1).

2. Synthesis

Several synthetic routes have been used to prepare the desired "λ^5-phosphacyclobutadiene" derivatives **2**–**9**. Although some routes can be used to prepare different classes of compound, none is general.

2.1. [2+2]Cycloadditions

This story begins with calculations by Trinquier,[21] which predicted that the singlet phosphanylnitrene **12** (R = H; Scheme 2) will exhibit a phosphorus–nitrogen multiple bond due to delocalization of the lone pairs n_π(P) into p_π(N) and, to some extent, n_π(N) into d_π(P). We confirmed this hypothesis



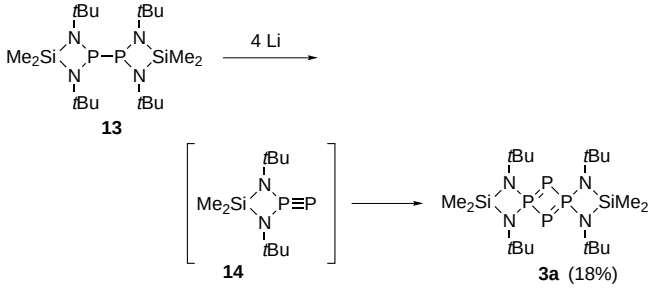
Scheme 2. Synthetic routes to the cyclodiphosphazene **2a**.

by irradiating bis(diisopropylamino)phosphanyl azide (**10**) in the presence of various trapping agents. As hoped, the products obtained resulted from simple addition across a formal phosphorus–nitrogen triple bond of the λ^5-phosphonitrile **12a**.[22] We then realized that irradiation of **10** in the absence of any trapping agent led to the head-to-tail cyclic dimer of **12a**, 2,2,4,4-tetrakis(diisopropylamino)-1,3,2λ^5,4λ^5-diazadiphosphete (**2a**, R = iPr$_2$N), in 42% yield.[15] We more recently found that photolysis of the stable nitrilimine **11** also led to the cyclodiphosphazene **2a** in 35% yield along with bis(diisopropylamino)thiophosphorylnitrile (Scheme 2).[23] Since phosphanyl azides are in general highly explosive materials,[24] the use of N-phosphorus-substituted nitrilimines seems more attractive. Unfortunately only very few nitrilimines are stable,[25] and most rearrange under irradiation into carbodiimides[26] rather than undergoing nitrogen–nitrogen bond cleavage to give a phosphonitrile.



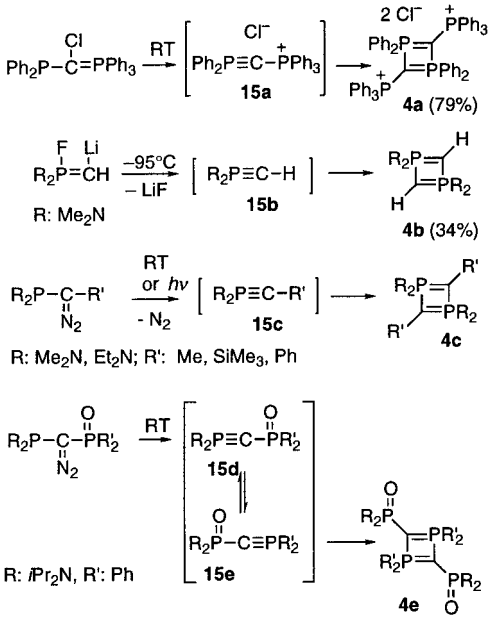
Guy Bertrand was born in Limoges (France) in 1952. He graduated from the University of Montpellier as ingénieur ENSCM and moved to Toulouse as an Attaché de Recherche CNRS in 1975. He defended his Thèse d'Etat at the University Paul Sabatier of Toulouse in 1979 and spent one year at Sanofi Recherche Company. Since 1988 he is Directeur de Recherche at the Laboratoire de Chimie de Coordination du CNRS at Toulouse. He has authored over 180 publications and patents, and his research spans a wide range of topics at the border between organic and inorganic chemistry. He received the International Council on Main Group Chemistry Award in 1993 and the Humbold Award in 1994, and was elected Membre Correspondant of the French Academy of Sciences in 1996.

The mixed-valent tetraphosphete **3**, which was recently obtained by Frank et al.,[27] formally results from dimerization of the phosphidophosphorane **14**. This transient species would be formed upon reduction of diphosphane **13** with lithium (Scheme 3).



Scheme 3. Synthesis of the mixed-valent tetraphosphete **3a**.

Head-to-tail dimerizations of transient λ^5-phosphalkynes **15** to 1λ^5,3λ^5-diphosphetes **4** were observed by Appel et al.,[28] Fluck et al.,[29] and Regitz et al[30] (Scheme 4). It is noteworthy



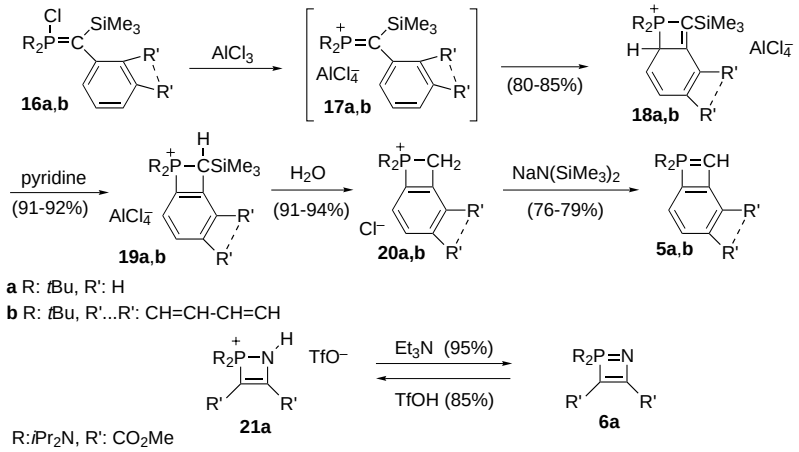
Scheme 4. Head-to-tail dimerization of transient λ^5-phosphalkynes.

that diphosphete **4e** does not originate from the dimerization of the initially generated **15d**, but from that of isomeric **15e**, which forms after a 1 →3 shift of the oxygen atom from one phosphorus atom to another.[30] This result suggests a possible equilibrium between the two isomeric *C*-phosphoryl-λ^5-phosphalkynes **15d** and **15e**; dimerization occurs with the least sterically hindered form. The very rare examples of compounds of type **15** which have been isolated do not dimerize even upon heating.[31]

So far, all attempts to prepare λ^5-phosphetes or λ^5-aza- or diazaphosphetes by [2+2]cycloaddition of λ^5-phosphalkynes **15** or λ^5-phosphonitriles **12** with alkynes or nitriles have failed.

2.2. 1,2-Eliminations

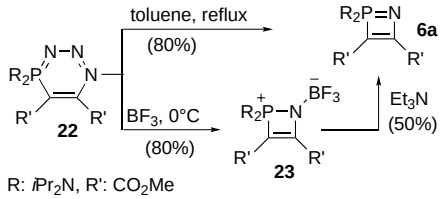
In 1968 Gompper and Seybold prepared the first stable cyclobutadiene by deprotonation of the corresponding cyclobutadienyl salt.[4] Similarly, addition of sodium bis(trimethylsilyl)amide to 1,2-dihydrophosphet-2-ylium salts **20a** and **20b** gives rise to benzo- and naphto-λ^5-phosphetes **5a** (76% yield) and **5b** (79% yield), respectively (Scheme 5).[32] The synthesis of derivatives **20a**, **b** deserves some comment, since it explains why non-benzo-λ^5-phosphetes are not available by this route. The key step in this synthesis is the generation of transient methylene phosphonium salts[33] **17a**, **b** from P-halogenated ylides[34] **16a**, **b**. Indeed, thanks to the high electrophilicity of the phosphorus atom in **17a**, **b**, an intramolecular ring closure leading to **18a**,**b** occurs. All attempts to generate the corresponding benzo-1λ^5-phosphetes from **18a**, **b** with a strong base failed. In the presence of pyridine an irreversible and quantitative isomerization to **19a**, **b** occurs. Deprotonation of **19a**, **b** was not clean in contrast to that of **20a**, **b**, which were generated by hydrolysis of the C–Si bond in **19a**, **b**. Deprotonation of **21a** with excess triethylamine affords 1,2λ^5-azaphosphete **6a** in 95% yield[32] (Scheme 5). However, this route is of no synthetic value, since **21a** is prepared by protonation of **6a**.



Scheme 5. Synthesis of benzo-λ^5-phosphetes **5a** and **5b**.

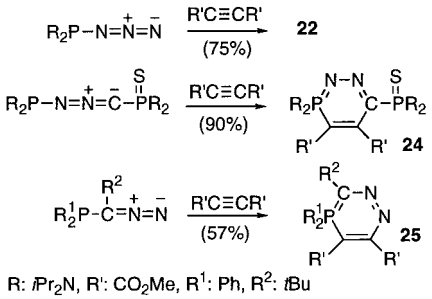
2.3. Ring Contractions

The thermal and photochemical elimination of dinitrogen from cyclic azoalkanes is an efficient method for preparing strained heterocycles,[35] including antiaromatic four-membered rings. Indeed, vapor flash pyrolysis of 1,2,3-triazines gives rise to azetes.[36] Similarly, heating 1,2,3,4λ^5-triazaphosphinine **22** in toluene under reflux for 14 h affords the 1,2λ^5-azaphosphete **6a** in 80% yield (Scheme 6).[37] Compound **6a** can also be obtained in a two-step one-pot reaction by first adding boron trifluoride to **22** at 0 °C, which initially leads to the zwitterionic heterocycle **23**, followed by decomplexation with excess triethylamine.[37b]



Scheme 6. Synthesis of the $1,2\lambda^5$-azaphosphete **6a** by ring contraction.

Like **22**, $1,2,3\lambda^5$- and $1,2,4\lambda^5$-diazaphosphinines **24**[38] and **25**[39] are readily available since phosphanyl-substituted 1,3-dipoles are able to react as formal 1,4-dipoles (Scheme 7).



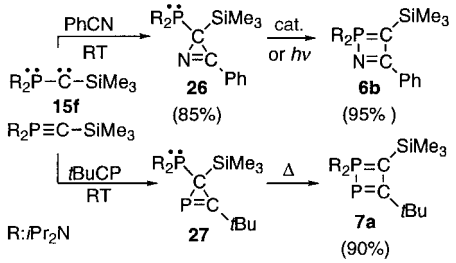
Scheme 7. Phosphanyl-substituted 1,3-dipoles react as formal 1,4-dipoles.

However, all attempts to eliminate dinitrogen from **24** and **25** failed. The reluctance of **24** to loose N_2 is consistent with the high stability of phosphazo derivatives. Indeed, **24** features the same $R_3P{=}N{-}N{=}C<$ sequence as Staudinger–Meyer adducts (phosphane+diazo derivative), which are not precursors of phosphorus ylides.[40] In contrast, **22** features a phosphazide skeleton in a *cis* configuration, which has been postulated to be the geometry of the transition state[41] in the Staudinger reaction (phosphane+azide $\rightarrow$phosphazene+N_2). The high stability of **25** is more difficult to rationalize. Therefore, the ring-contraction route is so far restricted to the synthesis of $1,2\lambda^5$-azaphosphetes.

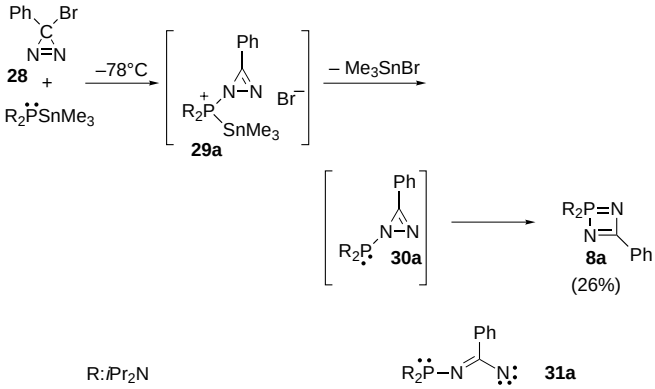
2.4. Ring Expansions

A few cyclobutadienes and azetes were prepared by ring expansions involving transient cyclopropenyl carbenes and nitrenes.[42] Similarly, 2-phosphanyl-2*H*-azirine **26** and 2-phosphanyl-2*H*-phosphirene **27** rearrange into $1,2\lambda^5$-azaphosphete **6b** (95% yield)[43] and $1\lambda^5,2\lambda^3$-diphosphete **7a** (90% yield),[44] respectively (Scheme 8). Both starting materials were prepared from our stable "carbene" **15f**.[31a–d] Although the only other example of a stable 2*H*-phosphirene was prepared using a transient carbene,[45] **26** is the first 2*H*-azirine prepared by a [1+2]cycloaddition.

The third example of a ring expansion leading to a four π electron four-membered heterocycle involves the transient 1-phosphanyl-1*H*-diazirine **30a**. This antiaromatic four π electron three-membered ring was prepared by adding bis(diisopropylamino)trimethylstannylphosphane to 3-bromo-3-phenyldiazirine (**28**) followed by elimination of bromotrimethylstannane (Scheme 9).[46]



Scheme 8. From the stable carbene **15f** to $1,2\lambda^5$-azaphosphete **6b** and $1\lambda^5,2\lambda^3$ diphosphete **7a** by ring expansions of unsaturated three-membered heterocycles **26** and **27**, respectively.

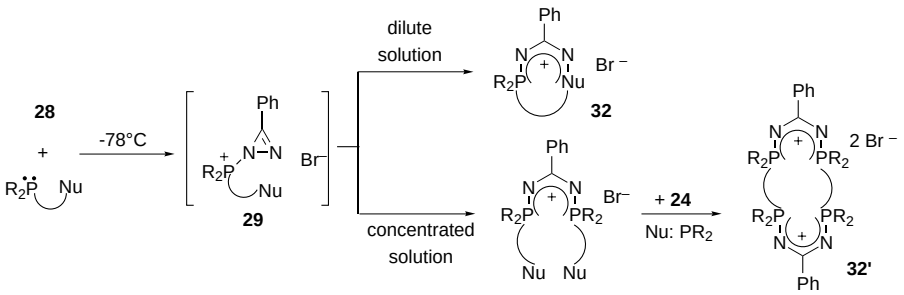


Scheme 9. Synthesis of the transient 1-phosphanyl-1*H*-diazirine **30a** and its ring expansion to the $1,3,2\lambda^5$-diazaphosphete **8a**.

We were able to prove that the first step of the reaction proceeds by an S_N2' mechanism and leads to *N*-phosphoniodiazirine **29a**; this is in agreement with independent works by Creary[47] and Dailey[48] with other nucleophiles. We also demonstrated experimentally and with ab initio calculations that the rearrangement of **30a** to **8a** involves nucleophilic attack by the phosphorus lone pair at the second nitrogen atom of the diazirine, and not the imidoylnitrene intermediate **31a** (Scheme 9).[46b] Indeed, the parent parent compound **31** (R = H) is an unstable species on the singlet hypersurface and rearranges without requiring any activation energy to the corresponding carbodiimide. On the other hand, diazaphosphete **8a** is over 23 kcal mol^{-1} more stable than the corresponding 1-phosphino-1*H*-diazirine **30a**, and the activation energy for the rearrangement of **30a** to **8a** is around 24 kcal mol^{-1}. Interestingly, *N*-phosphoniodiazirines **29** have a reasonable lifetime, probably due to the presence of the phosphonio group, which decreases the effect of the destabilizing antiaromatic energy through "negative hyperconjugation".[49] The relative stability of **29** allows inter and intramolecular S_N2 reactions to compete. This makes the reaction of bromodiazirine with phosphanes possessing a second nucleophilic center of synthetic interest, as proven by the high-yield synthesis of mono- and dicationic heterocycles **32** and **32'**[46b] (Scheme 10).

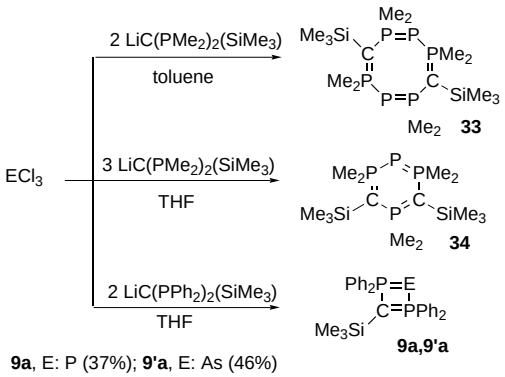
2.5. Use of Diphosphanylmethanides

Diphosphanylmethanides are suitable starting materials for synthesizing $n\,\pi$ electron *n*-membered phosphorus hetero-



Scheme 10. Transient *N*-phosphoniodiazirines **29** as precursors for cationic and dicationic heterocycles.

cycles.[50] It is particularly interesting that $Li[C(PMe_2)_2(SiMe_3)]$ reacts with PCl_3 in toluene to afford the eight-membered heterocycle **33**, whereas the six-membered ring **34** is formed in THF (Scheme 11).[50a] Heterocycle **34** is an



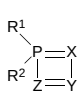
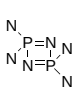
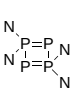
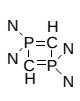
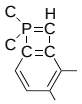
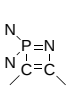
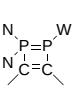
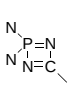
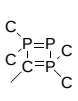
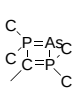
Scheme 11. Diphosphanylmethanides as precursors of $n\pi$ electron *n*-membered heterocycles.

analogue of cyclotriphosphazenes in which the three nitrogen atoms have been replaced by a phosphorus atom and two CR groups. With the more sterically crowded $Li[C(PPh_2)_2(SiMe_3)]$, the $1\lambda^5,2\lambda^3,3\lambda^5$-triphosphete **9a** was obtained in 37% yield.[50b] The same synthetic route allowed Karsch et al. to obtain the corresponding $2\lambda^3,1\lambda^5,3\lambda^5$-arsadiphosphete **9′a** in 46% yield.[50b]

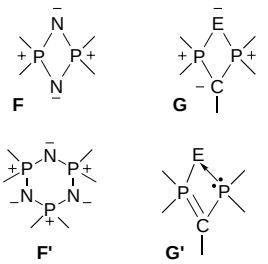
3. Structural and Spectroscopic Data

Single-crystal X-ray diffraction studies were performed on several λ^5-phosphacyclobutadienes. The most important geometric parameters of derivatives **2a**,[15a] **3**,[27] **4b**,[29a] **5b**,[32] **6a**,[37a] **7′a** (a $W(CO)_5$ complex of **7a**),[44] **8a**,[51] **9a**, and **9′a**[50b] are listed in Table 1. In $1\lambda^5,3\lambda^5$-diphosphetes **2**, **3**, and **4** of type P_2X_2, the four-membered ring is organized around a crystallographically imposed symmetry center, which highlights the absolute planarity of the ring. All endocyclic P–X bond lengths are equal and lie between those of single and double bonds. Of special interest is the pinching of the ring around the nitrogen atom of **2a**, which induces a P···P distance (2.22 Å) as short as that in diphosphines.[52] Ab initio calculations[53a, b] rationalized these experimental data. Cyclodiphosphazenes **2** can be conceptualized as a sequence of amide and phosphonium units in which the negative charge of nitrogen is carried by a pure p lone pair that is perpendicular to the mean plane of the ring. Formally, this charge is equal to -1, but is in fact reduced due to σ polarization and to a certain amount of conjugation with the phosphorus atoms. The electrostatic repulsion between the nitrogen atoms explains the acute angle at nitrogen and the short P···P distance; there is no transannular P···P bonding interaction, as shown by the strongly negative overlap population. In conclusion, the four π electron system of **2** and related P_2X_2 heterocycles **3** and **4** as well as the six π electron system of cyclotriphospha-

Table 1. Selected bond lengths [Å] and angles [°] determined from X-ray diffraction studies

										
	2a	**3a**	**4b**	**5b**	**6a**	**7′a**	**8a**	**9a**	**9′a**	
P-R[1]	1.645(8)		1.681(11)	1.840(6)	1.629(3)	1.664(6)	1.625(4)			
P-R[2]	1.644(9)		1.680(1)	1.852(6)	1.626(3)	1.651(6)	1.644(3)			
P-X	1.651(8)	2.139(1)	1.725(1)	1.772(8)	1.702(3)	2.176(3)	1.670(4)	2.1489(5)	2.2710(7)	
P-Z	1.648(8)	2.142(1)	1.725(1)	1.773(6)	1.764(4)	1.804(7)	1.675(4)	1.729(1)	1.741(2)	
X-Y	1.651(8)	2.139(1)	1.725(1)	1.401(8)	1.352(5)	1.842(7)	1.368(7)	2.1530(6)	2.2692(7)	
Y-Z	1.648(8)	2.142(1)	1.725(1)	1.406(7)	1.406(6)	1.391(10)	1.377(6)	1.738(1)	1.731(2)	
P-Y	2.22	2.736	2.410	2.206	2.109		1.987	2.548	2.601	
Z-P-X	95.0(6)	100.6(1)	91.4(1)	78.9(3)	81.2(2)	83.1(2)	86.0(2)	96.44(5)	96.21(8)	
P-X-Y	85.0(5)	79.4(1)	88.6(1)	87.2(5)	86.5(2)	71.9(3)	81.1(3)	72.65(2)	69.90(2)	
X-Y-Z	95.0(6)	100.6(1)	91.4(1)	106.7(6)	109.7(3)	109.6(5)	112.4(3)	96.03(5)	96.59(8)	
Y-Z-P	85.0(5)	79.4(1)	88.6(1)	87.1(5)	82.6(3)	95.1(5)	80.6(3)	96.64(7)	97.0(1)	
Abw.[a]	0	0	0	0.022	0.003	0.028	0.006	0.074	0.088	

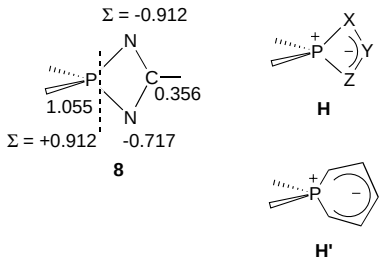
[a] Mean deviation from the best plane of the four-membered ring.



zenes **1** basically follow the island models **F** and **F′**,[13] respectively.

In the nonsymmetrical $1\lambda^5,3\lambda^5$-diphosphetes **9a** and **9′a**[50b] the four-membered rings are not completely planar: The dicoordinated phosphorus and arsenic atoms project out of the P-C-P plane, and once again there is a pinching of the ring at the σ^2-P* (or As) atom, which induces a relatively short nonbonding λ^5-P–λ^5-P distance. The structural parameters suggest a representation of **9a** and **9′a** as cyclic bis(ylides) **G**, very comparable to **F**, or alternatively as internally donor-stabilized phosphinidenes and arsinidenes **G′**, respectively.

The four π electron system of $1\lambda^5$-phosphetes **5**–**8** cannot follow the island model, and one should therefore find an alternative way to escape from the concept of antiaromaticity. Also these four-membered rings are nearly planar, as shown by the mean deviation from the best plane (Table 1). The exocyclic P–N bonds of **6a**, **7′a**, and **8** (as in **2a** and **4b**) are rather short and are comparable to those observed in bis(diisopropylamino)phosphenium salts (1.61 Å).[54] This indicates a positive charge located on the $(R_2N)_2P$ fragment, although according to calculations[51] a delocalization of this charge towards the exocyclic amino groups seems unpronounced. All the X–Y and Y–Z bond lengths are between those of single and double bonds, indicating that the XYZ part of the rings can be regarded as an anionic propenyl system. This zwitterionic formulation of **5**–**8** is illustrated by the calculated electron density Σ (Mulliken charges) for the parent compound **8**. The value of the inner ring angle at



phosphorus is small and that of the opposite angle is large, which induces a short P···Y distance across the diagonal. Since the P–X and P–Z bond distances are long in all the derivatives, these results as a whole demonstrate that λ^5-phosphetes **5**–**8** have a rhomboidal zwitterionic structure of type **H**.

[*] Editorial comment: If the bonding number of a ring atom deviates from its standard value, according to IUPAC rules the actual bonding number is expressed by an Arabic number cited as a superscript to the Greek letter lambda, which follows the corresponding locant. In contrast to this recommendation, the Greek letter sigma is used here to indicate the structural features. The exponent gives the number of σ bonds that originate at phosphorus ring atoms.

Interestingly, the related six π electron six-membered heterocycles can be almost planar, such as various λ^5-di- and triphosphinines,[55] or have a boat conformation, such as the $1\lambda^5,3\lambda^5,5\lambda^5,2\lambda^3$-tetraphosphinine **34** reported by Karsch (interplanar angle 127°).[50a] λ^5-Diaza- and triazaphosphinines such as **24**, **25**, and **22** have a zwitterionic structure of type **H′**.[37b, 39, 51] Clearly, all these heterocycles are not aromatic.

Ab initio SCF calculations were performed on the parent benzannulated derivatives **5** and **35**–**40**.[32] Apart from the geometric parameters, the anisotropy of magnetic susceptibilies Δχ (Table 2) gives an indication of the degree of aromatic or antiaromatic character.[56] For instance, the calculated value of Δχ is strongly negative in benzene (-63.4×10^{-6} cm^{3}mol^{-1}), while much larger anisotropies are observed for π systems possessing antiaromatic character; Δχ is even positive in cyclobutadiene. Annulation of a saturated four-membered cyclic system on a benzene ring (**37** and **40**) reduces the value of Δχ by about 15%, which signifies relatively little perturbation of the electronic properties of the aromatic moiety. The small negative values of Δχ for **35**, **38**, and **39** are indicative of antiaromatic π systems. Compounds **38** and **39** are formally derived from benzocyclobutadiene **35** by replacement of one CH unit by a P or PH^+ group; both groups are able to participate in the π-electron system by (p,p)-π interactions. On the other hand, the Δχ values for the cyclic hydrocarbon anion **36** and λ^5-benzophosphete **5** are similar; this confirms that four π electron four-membered heterocycles possessing one heteroatom that has no suitable p orbital show an interrupted cyclic π delocalization.

Table 2. Calculated anisotropy of magnetic susceptibilities, Δχ [10^{-6} cm^{3}mol^{-1}].[32]



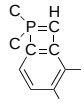
	35	**36**	**37**	**38**	**39**	**50**	**5**
A	CH	CH_2	CH_2	P	PH^+	PH_2^+	PH_2
B	CH	CH^-	CH_2	CH	CH	CH_2	CH
Δχ[a]	−11	−26	−55	−8	−2	−54	−29

[a] $\Delta\chi=\chi_{op}-\chi_{ip}$, where χ_{ip} is the average of the difference of the in-plane components of the susceptibility (op = out-of-plane; ip = in-plane).

Table 3 summarizes the most important NMR data for compounds **2**–**9**. There are some striking features. The ^{31}P NMR chemical shifts for the λ^5-phosphorus atom of all heterocycles bearing dialkylamino groups are similar; these atoms are more deshielded than those in analogous six-membered rings and linear systems. The ylid character of the P–X or P–Z bonds is indicated by the high-field chemical shifts of the corresponding nuclei, which are, however, less shielded in **5**–**7** than in **3**, **4**, and **9**; this supports the representations **F**, **G**, and **H** for **2**–**4**, **9**, and **5**–**8**, respectively. The very low field chemical shift of the signal for the carbon atom (Y) in **5**–**8** is typical of unsaturated small rings, including the antiaromatic cyclobutadienes and azetes.

The HOMO of the four-membered rings **2**–**9** is located at the X or Z atom. For example, in the parent compound **8** the

Table 3. Selected NMR data; coupling constants are given in Hz.

										
	2a	**3a**	**4b**	**5b**	**6a**	**6b**	**7a**	**8a**	**9a**	**9′a**
$\delta(^{31}P)$	+40.0	+102.4	+48.9	+73.0	+52.5	+52.3	+49.2	+54.2	+20.2	−0.5
δ(X)		+62.6	8.2	41.3			+58.4		−86.3	
J(PX)		372	97.3	77.6			201.2		261.0	
δ(Y)	+40.0	+102.4	+48.9	170.1	182.4	192.4	224.3	194.7	+20.2	−0.5
J(PY)				3.8	28.0	46.7	9.9	48.4		
δ(Z)		+62.6	8.2	106.0	91.9	84.9	105.7			
J(PZ)		372	97.3	76.9	81.6	42.9	36.8			

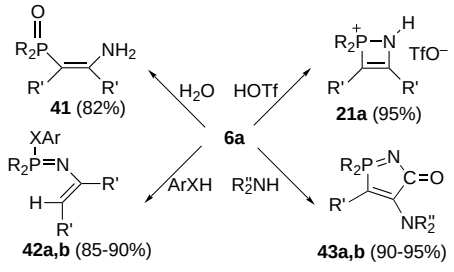
HOMO is a mixture of the nonbonding orbitals of the lone pair of the endocyclic nitrogen atoms and the nonbonding allylic π orbital of the ring (computed to be −8.7 eV).[51] Not surprisingly, the LUMO is at the carbon atom β to the λ^5-phosphorus atom. These theoretical results may serve as a good model for explaining the reactivity of **2**–**9**.

4. Reactivity

The λ^5-phosphacyclobutadienes **2**–**9** are quite reactive. It would take too long to provide a comprehensive review, and, therefore, only a few representative reactions will be presented here. They highlight the versatility of these heterocycles as well as their usefulness as starting materials in several fields.

4.1. Addition of Protic Reagents

All λ^5-phosphacyclobutadienes considered in this review are moisture-sensitive. For example, **6a** in dichloromethane reacts to give the phosphoranyl compound **41** (82% yield, Scheme 12) after contact with air for a few minutes.[37b] The



R:*i*Pr$_2$N; R': CO_2Me **42a**, X: O; **42b**, X: S

R"$_2$NH: piperidine, *c*-hexylamine

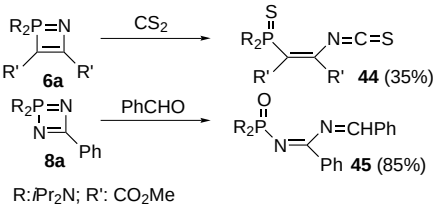
Ar: *p*-tolyl

Scheme 12. Reactivity of the 1,2λ^5-azaphosphete **6a** towards protic reagents. Tf = F_3CSO_2.

first step is certainly protonation at nitrogen. The ring opening is induced by the formation of a strong P=O bond, which converts the phosphonium center into a phosphorane. Indeed, with triflic acid, cyclic phosphonium salt **21a** was isolated in 95% yield.[32] The behavior of **6a** towards protic nucleophiles appears to depend dramatically on the nature of the nucleophiles. Although P–N bond cleavage occurs in the presence of water, P–C bond cleavage takes place upon adding *p*-cresol or *p*-thiocresol[57] to afford **42a**, **b** (85–90% yield). With primary or secondary amines a ring expansion is observed leading to five-membered heterocycles **43a**, **b** in excellent yields.[57] Derivatives of type **42** are starting materials for the synthesis of electron-poor 2-azadienes,[58] and five-membered cyclic phosphazenes **43** are not readily available by other routes.

4.2. Addition of Unsaturated Compounds

The Wittig reaction is one of the most famous and useful reactions in chemistry. Not surprisingly, classical aza-Wittig reactions were observed when azaphosphete **6a** or diazaphosphete **8a** was treated with carbon disulfide and benzaldehyde to afford thiophosphoryl and phosphoryl derivatives **44**[37b] and **45**[51] as single isomers in 35 and 85% yield, respectively (Scheme 13).

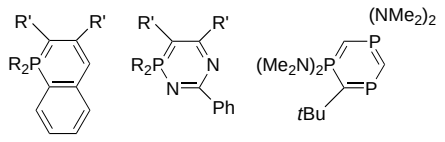


R:*i*Pr$_2$N; R': CO_2Me

Scheme 13. Two examples of classical aza-Wittig reactions.

Electron-poor alkynes are known to insert into P–C and P–N ylidic bonds.[40] Indeed, dimethylacetylene dicarboxylate cleanly inserts into the P–X bond of **5a** and **8a** at room temperature to lead to the expected benzophosphinine **46**[32] and diazaphosphinine **47**[51] in 76 and 70% yield, respectively (Scheme 14). Noteworthy is the reaction of diphosphete **4b** with *tert*-butylphosphaethyne, which provided the first triphosphabenzene **48** in 35% yield.[59]

In fact, **6a** and its congeners very often react as nonclassical Wittig reagents. For example, isocyanates and isothiocyanates

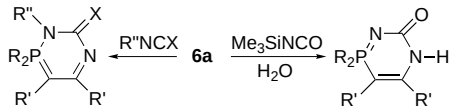


46 (76%) **47** (70%) **48** (35%)

R: *t*Bu, R': CO_2Me

Scheme 14. Some six π electron six-membered heterocycles available by addition of alkynes or phosphalkyne to four π electron four-membered phosphorus heterocycles.

have been widely employed in aza-Wittig reactions to give unsymmetrical carbodiimides and the corresponding phosphoryl and thiophosphoryl derivatives.[40] In marked contrast, phenyl isocyanate and methyl isothiocyanate react with **6a** to provide the corresponding ring insertion products **49a** (66% yield) and **49b** (90% yield), respectively;[37b] these results are reminiscent of the Dimroth rearrangement.[40b, 60] Compound **6a** also reacts with trimethylsilyl isocyanate to afford, after hydrolysis, heterocycle **50** (50% yield),[37b] which formally results from the insertion of the cumulene into the N–C bond (Scheme 15). However, insertion into the P–N bond of **6a**



49a (66%)
49b (90%)

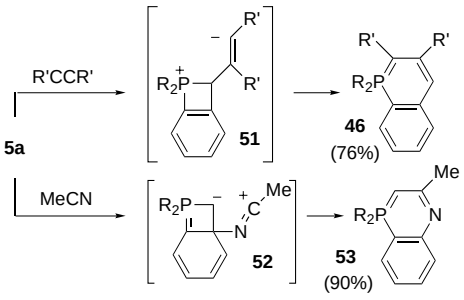
50 (50%)

R: *i*Pr2N; R': CO_2Me
a: R": Ph, X: O; **b**: R": Me, X: S

Scheme 15. Reactivity of 1,2λ^5-azaphosphete **6a** towards cumulenes.

followed by a 1,3-silyl or hydrogen shift is more likely. Intriguingly, **50** exists as a hydrogen-bonded dimer in the solid state and has a structure very similar to that of cytosine. The $C(NH_2)$ is replaced by a $P(NiPr_2)_2$ group; **50** could be considered as a "labeled" cytosine.

The only clear example for the expansion of a four-membered to a six-membered ring involving the X–Y and not the P–X or P–Z bonds is the reaction of λ^5-phosphete **5a** with acetonitrile, which leads to 1,4λ^5-azaphosphinine **53** (Scheme 16).[32] The striking difference in the behavior of **5a** towards dimethylacetylene dicarboxylate (insertion into the



R: *t*Bu, R': CO_2Me

Scheme 16. Versatile behavior of the naphto-λ^5-phosphete **5a** towards reagents with triple bonds.

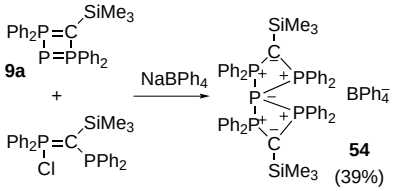
P–C bond to form **46**) and acetonitrile can be explained by considering that the HOMO of **5a** is located at the α-carbon atom, while the LUMO is at the carbon atom β to the phosphorus atom. Therefore, the electron-poor alkyne reacts with **5a** to give **51** as an intermediate, whereas the nitrogen end of the nitrile adds to the β-carbon atom to form **52** initially (Scheme 16).

In contrast to the other four-membered heterocycles discussed in this review, the 1λ^5,2λ^3-diphosphetes **3**, **7a**, and **9** seem reluctant to undergo any kind of insertion.

4.3. Reactions with Retention of the Four-Membered Ring

These reactions are surprisingly numerous, but the most striking results were obtained with the 1λ^5,2λ^3, 3λ^5-triphosphete **9a**[50b] and the 1λ^5,2λ^3-diphosphete **7a**.[61]

The reaction of **9a** with $[Ph_2PC(PPh_2)(SiMe_3)]^+BPh_4^-$ results in formation of the spirocyclic ten-electron cation **54** (Scheme 17), which features an unprecedented pseudo-

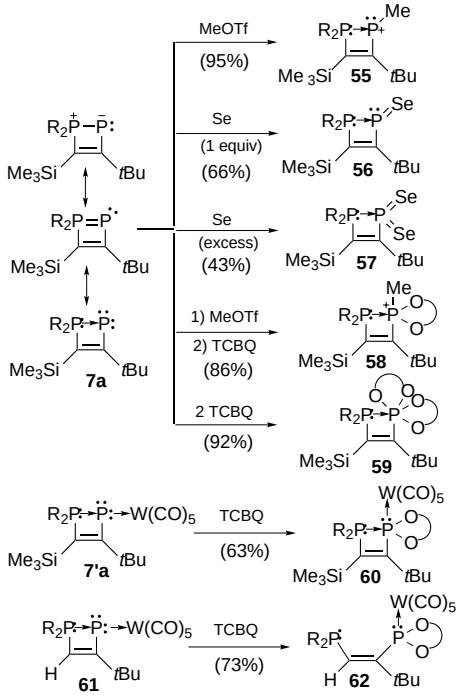


Scheme 17. Synthesis of a spirocyclic ten-electron cation with a pseudo-trigonal-bipyramidal PP_4 skeleton.

trigonal-bipyramidal PP_4 skeleton.[50b] Compound **54** can also be described as a tetraphosphonio-substituted phosphoranide[62] with partial charge compensation by two internal carbanion functionalities.

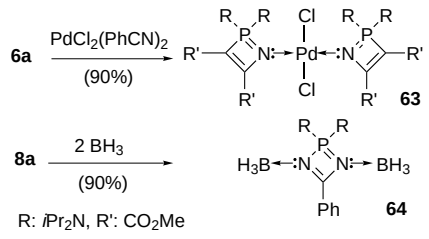
Methyltrifluoromethane sulfonate, a stoichiometric amount or two equivalents of elemental selenium, and two equivalents of tetrachloro-*o*-benzoquinone cleanly react with **7a** at its dicoordinate phosphorus atom to provide the corresponding heterocycles **55**, **56**, **57**, and **59** (Scheme 18), which can be regarded as phosphenium–, selenoxophosphane–, diselenoxophosphorane– and phosphorane–phosphane adducts, respectively.[61] The four-membered ring is also retained when tetrachloro-*o*-benzoquinone is added to **55**; the resulting derivative **58** is an example of a phosphonium–phosphane adduct. In other words, the σ^2-phosphorus atom of **7a** (a phosphanylidene-phosphane adduct) can extend its coordination number up to six without destroying the four-membered ring! The tendency of derivatives of **7a** and **55**–**57** to retain the ring structure can be explained by the presence of an electrophilic low-coordinate phosphorus center. It was only recently that the cyclic structure of derivatives **58** and **59**, which feature a high-coordinate phosphorus atom, was rationalized.[63] The presence of bulky substituents at the two carbon atoms of the ring induces small C-C-P angles, as proven by the formation of heterocycle **60** on the one hand and the linear adduct **62** on the other in the

reaction of diphosphetes **7′a** and **61**, respectively, with tetrachloro-*o*-benzoquinone (Scheme 18).



Scheme 18. The persistence of the P–P bond in $1\sigma^4,2\sigma^x$-diphosphetes.

In contrast to their organic analogues—in particular the azetes,[42c, 64] which give η^4-complexes—**2**–**8** usually[65] act as η^1-ligands towards transition metal complexes.[44, 66] For example, azaphosphete **6a** reacts at room temperature with half an equivalent of $[PdCl_2(PhCN)_2]$ to lead to the bis(η^1-azaphosphete)palladium(II) complex **63** in 90% yield (Scheme 19). Interestingly, two equivalents of a neutral Lewis



Scheme 19. λ^5-Aza- and -diazaphosphetes as η^1 ligands.

acid, such as BH_3, react with diazaphosphete **8a** to provide the bis-adduct **64** in 90% yield.[51] In both cases the geometric parameters and NMR data for the free and the coordinated ring are very similar, which suggests that the four π electron system is not perturbed upon complexation. From the results of both reactions presented in Scheme 19, it seems quite likely that mixed inorganic–organometallic polymers could be prepared with **8a**.

5. Summary and Outlook

These results as a whole clarify the bonding situation in four π electron four-membered heterocycles with a phosphorus atom that possesses no available p orbital for the π system. When two phosphorus atoms are present in the 1,3-positions, the four π electron system basically follows the island model. However, when there is only one phosphorus atom the negative charge is delocalized on an allylic fragment, and the positive charge is localized at the phosphorus center. In all cases there is an interrupted cyclic π delocalization, and, therefore, these compounds are not antiaromatic. Similarly, six π electron six-membered heterocycles with a λ^5-phosphorus atom are not aromatic.

Some of these four π electron four-membered heterocycles can be prepared on a multi-gram scale and are no longer laboratory curiosities. They are valuable precursors for highly functionalized neutral or cationic heterocycles and polycycles that exhibit unusual bonding situations; they are also interesting ligands for transition metals.

Most of the "λ^5-phosphacyclobutadiene derivatives" prepared so far bear bulky substituents at phosphorus atom with the exception of **9a** and **9′a**, which have phenyl substituents. Although all attempts[67] to prepare stable cyclodiphosphazenes **2** with other substituents failed, it is important to continue trying to prepare phosphacyclobutadienes bearing small substituents if one wants to use these compounds as starting materials for polymers. We have to keep in mind that phosphorus polymers (such as polyphosphazenes) have numerous peculiar and industrially important properties.

We have shown that the presence of a λ^5-phosphorus atom is sufficient to stabilize four π electron four-membered rings. Clearly other heteroatoms possessing no available p orbital should also allow the synthesis of analogous heterocycles.

At the end of this review I would like to make clear the main motivations of this work. We wanted to play tricks with the concept of antiaromaticity while seriously keeping in mind that the search for the physical reality in which this concept may be rooted is an important issue for future studies. To nonspecialists, natural-product synthesis appears to be just an intellectual game; this review deals with nonnatural-product synthesis. However, novel properties can only be discovered if new families of compounds are prepared, and history has demontrated that it is difficult to predict the impact and development of new materials or new reactions. Let us wait and see what the future of these heterocycles will be.

I would like to thank all my co-workers for their dedication, intellectual contribution, and hard work, and the CNRS for generous support of this work

Received: January 7, 1997 [A 201 IE]
German version: *Angew. Chem.* **1998**, *110*, 282–293

[1] a) V. L. Minkin, M. N. Glukhovtsev, B. Y. Simkin, *Aromaticity and Antiaromaticity*, Wiley, New York, **1994**; b) F. Toda, P. Garrat, *Chem. Rev.* **1992**, *92*, 1685; c) G. Maier, *Angew. Chem.* **1988**, *100*, 317; *Angew. Chem. Int. Ed. Engl.* **1988**, *27*, 309; d) P. Garrat, *Aromaticity*, Wiley, New York, **1986**; e) T. Bally, S. Masamune, *Tetrahedron* **1980**, *36*, 343;

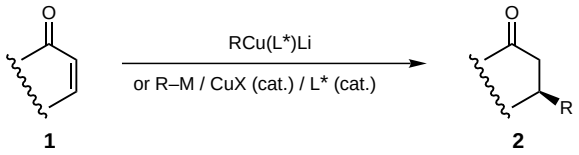
f) M. R. Cava, M. J. Mitchell, *Cyclobutadiene and Related Compounds*, Academic Press, New York **1967**.
[2] M. Faraday, *Phil. Trans. Roy. Soc.* **1825**, 440.
[3] a) G. F. Emerson, L. Watts, R. Pettit, *J. Am. Chem. Soc.* **1965**, *87*, 131; b) L. Watts, J. D. Fitzpatrick, R. Pettit, *ibid.* **1965**, *87*, 3253.
[4] R. Gompper, G. Seybold, *Angew. Chem.* **1968**, *80*, 804; *Angew. Chem. Int. Ed. Engl.* **1968**, *7*, 824.
[5] a) O. L. Chapman, C. L. McIntosh, J. Pacansky, *J. Am. Chem. Soc.* **1973**, *95*, 614; b) O. L. Chapman, D. De La Cruz, R. Roth, J. Pacansky, *ibid.* **1973**, *95*, 1337; c) A. Krantz, C. Y. Lin, M. D. Newton, *ibid.* **1973**, *95*, 2744; d) S. Masamune, M. Suda, H. Ona, L. M. Leichter, *J. Chem. Soc. Chem. Commun.* **1972**, 1268; e) D. J. Cram, *Nature* **1992**, *356*, 1992; f) D. J. Cram, M. E. Tanner, R. Thomas, *Angew. Chem.* **1991**, *103*, 1048; *Angew. Chem. Int. Ed. Engl.* **1991**, *30*, 1024.
[6] a) A. Kekulé, *Bull. Soc. Chim. Fr.* **1865**, *3*, 98; b) A. Kekulé, *Justus Liebigs Ann. Chem.* **1866**, *137*, 129; c) *ibid.* **1872**, *162*, 77.
[7] R. Willstätter, E. Waser, *Ber.* **1911**, *44*, 3423.
[8] E. Hückel, *Z. Phys.* **1931**, *70*, 204.
[9] M. J. S. Dewar, K. M., Merz, Jr., *J. Am. Chem. Soc.* **1985**, *107*, 6175.
[10] W. W. Schoeller, T. Busch, *Angew. Chem.* **1993**, *105*, 635; *Angew. Chem. Int. Ed. Engl.* **1993**, *32*, 617.
[11] a) B. Solouki, P. Rosmus, H. Bock, G. Maier, *Angew. Chem.* **1980**, *92*, 56; *Angew. Chem. Int. Ed. Engl.* **1980**, *19*, 51; b) G. Maier, G. Mihn, P. Reisenauer, *ibid.* **1980**, *92*, 58 and **1980**, *19*, 52.
[12] G. Märkl, D. Rudnick, R. Schulz, A. Schweig, *Angew. Chem.* **1982**, *94*, 222; *Angew. Chem. Int. Ed. Engl.* **1982**, *21*, 221.
[13] a) D. H. R. Barton, M. B. Hall, Z. Lin, S. I. Parekh, *J. Am. Chem. Soc.* **1993**, *115*, 955; b) M. J. S. Dewar, E. A. C. Lucken, M. A. Whitehead, *J. Chem. Soc.* **1960**, 2423.
[14] J. Liebig, *Ann. Chem.* **1834**, *11*, 139.
[15] a) A. Baceiredo, G. Bertrand, J.-P. Majoral, G. Sicard, J. Jaud, J. Galy, *J. Am. Chem. Soc.* **1984**, *106*, 6088; b) A. Baceiredo, G. Bertrand, J.-P. Majoral, F. El Anba, G. Manuel, *ibid.* **1985**, *107*, 3945.
[16] L. Weber, *Angew. Chem.* **1996**, *108*, 2779; *Angew. Chem. Int. Ed. Engl.* **1996**, *35*, 2618.
[17] a) R. Streubel, *Angew. Chem.* **1995**, *107*, 478; *Angew. Chem. Int. Ed. Engl.* **1995**, *34*, 436; b) J. F. Nixon, *Endeavour* **1991**, *15*, 49; c) M. Regitz, *Chem. Rev.* **1990**, *90*, 191; d) M. Regitz, P. Binger, *Angew. Chem.* **1988**, *100*, 1541; *Angew. Chem. Int. Ed. Engl.* **1988**, *27*, 1484; see also M. D. Francis, D. E. Hibbs, M. B. Hursthouse, C. Jones, K. M. A. Malik, *J. Chem. Soc. Chem. Commun.* **1996**, 631.
[18] J. R. Gee, W. A. Howard, G. L. McPherson, M. J. Fink. *J. Am. Chem. Soc.* **1991**, *113*, 5461.
[19] a) E. Benseler, A. Haas, *Chem. Ztg.* **1971**, *95*, 757; b) T. Chivers, *Main Group Chem. News* **1993**, *1*, 6.
[20] a) S. Schulz, L. Häming, R. Herbst-Irmer, H. W. Roesky, G. M. Sheldrick, *Angew. Chem.* **1994**, *106*, 1052; *Angew. Chem. Int. Ed. Engl.* **1994**, *33*, 969; b) P. Paetzold, A. Richter, T. Thijsen, S. Wurtenberg, *Chem. Ber.* **1979**, *112*, 3811; c) P. Paetzold, C. von Plotho, G. Schmid, R. Boese, B. Schrader, D. Bougeard, U. Pfeiffer, R. Gleiter, W. Schafer, *ibid.* **1984**, *117*, 1089; d) H. Nöth, M. Schwartz, S. Weber, *ibid.* **1985**, *118*, 4716.
[21] G. Trinquier, *J. Am. Chem. Soc.* **1982**, *104*, 6969.
[22] G. Sicard, A. Baceiredo, G. Bertrand, J.-P. Majoral, *Angew. Chem.* **1984**, *96*, 450; *Angew. Chem. Int. Ed. Engl.* **1984**, *23*, 459.
[23] M. Granier, A. Baceiredo, Y. Dartiguenave, M. Dartiguenave, M. J. Menu, G. Bertrand, *J. Am. Chem. Soc.* **1990**, *112*, 6277.
[24] a) K. L. Paciorek, R. Kratzer, *Inorg. Chem.* **1964**, *3*, 594; b) G. Tesi, C. P. Haber, C. M. Douglas, *Proc. Chem. Soc. (London)* **1960**, 219.
[25] G. Bertrand, C. Wentrup, *Angew. Chem.* **1994**, *106*, 549; *Angew. Chem. Int. Ed. Engl.* **1994**, *33*, 527.
[26] a) M. P. Arthur, H. Goodwin, A. Baceiredo, K. B. Dillon, G. Bertrand, *Organometallics* **1991**, *10*, 3205; b) F. Castan, A. Baceiredo, G. Bertrand, *Angew. Chem.* **1989**, *101*, 1253; *Angew. Chem. Int. Ed. Engl.* **1989**, *28*, 1250; c) F. Castan, A. Baceiredo, D. Bigg, G. Bertrand, *J. Org. Chem.* **1991**, *56*, 1801.
[27] W. Frank, V. Petry, E. Gerwalin, G. J. Reiss, *Angew. Chem.* **1996**, *108*, 1616; *Angew. Chem. Int. Ed. Engl.* **1996**, *35*, 1512.
[28] R. Appel, F. Knoll, H. D. Wihler, *Angew. Chem.* **1977**, *89*, 415; *Angew. Chem. Int. Ed. Engl.* **1977**, *16*, 402.
[29] a) J. Svara, E. Fluck, H. Z. Riffel, *Naturforsch. B* **1985**, *40*, 1258; b) B. Neumüller, E. Fluck, *Phosphorus and Sulfur* **1986**, *29*, 23.
[30] H. Keller, G. Maas, M. Regitz, *Tetrahedron Lett.* **1986**, *27*, 1903.
[31] a) A. Igau, H. Grützmacher, A. Baceiredo, G. Bertrand, *J. Am. Chem. Soc.* **1988**, *10*, 6463; b) A. Igau, A. Baceiredo, G. Trinquier, G. Bertrand, *Angew. Chem.* **1989**, *101*, 617; *Angew. Chem. Int. Ed. Engl.* **1989**, *28*, 621; c) G. Gillette, A. Igau, A. Baceiredo, G. Bertrand, *ibid.* **1990**, *102*, 1486 and **1990**, *29*, 1429; d) G. Alcaraz, R. Reed, A. Baceiredo, G. Bertrand, *J. Chem. Soc. Chem. Commun.* **1993**, 1354; e) M. Soleilhavoup, A. Baceiredo, O. Treutler, R. Ahlrichs, M. Nieger, G. Bertrand, *J. Am. Chem. Soc.* **1992**, *114*, 10959; f) M. Soleilhavoup, A. Baceiredo, G. Bertrand, *Angew. Chem.* **1993**, *105*, 1245; *Angew. Chem. Int. Ed. Engl.* **1993**, *32*, 1167; g) P. Dyer, A. Baceiredo, G. Bertrand, *Inorg. Chem.* **1996**, *35*, 46.
[32] U. Heim, H. Pritzkow, U. Fleischer, H. Grützmacher, M. Sanchez, R. Réau, G. Bertrand, *Chem. Eur. J.* **1996**, *2*, 68.
[33] a) A. Igau, A. Baceiredo, H. Grützmacher, H. Pritzkow, G. Bertrand, *J. Am. Chem. Soc.* **1989**, *111*, 6853; b) H. Grützmacher, H. Pritzkow, *Angew. Chem.* **1991**, *103*, 721; *Angew. Chem. Int. Ed. Engl.* **1991**, *30*, 709; c) U. Heim, H. Pritzkow, H. Schönberg, H. Grützmacher, *J. Chem. Soc. Chem. Commun.* **1993**, 673.
[34] O. I. Kolodyazhnyi, *Russ. Chem. Rev.* **1991**, *60*, 391.
[35] W. Adam, O. De Lucchi, *Angew. Chem.* **1980**, *92*, 815; *Angew. Chem. Int. Ed. Engl.* **1980**, *19*, 762.
[36] a) B. M. Adger, M. Keating, C. W. Rees, R. C. Storr, *J. Chem. Soc. Chem. Commun.* **1973**, 19; b) B. M. Adger, C. W. Rees, R. C. Storr, *J. Chem. Soc. Perkin. Trans. 1* **1975**, 45; c) G. Seybold, U. Jersak, R. Gompper, *Angew. Chem.* **1973**, *85*, 918; *Angew. Chem. Int. Ed. Engl.* **1973**, *10*, 847.
[37] a) J. Tejeda, R. Réau, F. Dahan, G. Bertrand, *J. Am. Chem. Soc.* **1993**, *115*, 7880; b) K. Bieger, J. Tejeda, R. Réau, F. Dahan, G. Bertrand, *ibid.* **1994**, *116*, 8087.
[38] a) M. Granier, A. Baceiredo, M. Nieger, G. Bertrand, *Angew. Chem.* **1990**, *102*, 1185; *Angew. Chem. Int. Ed. Engl.* **1990**, *29*, 1123; b) F. Castan, M. Granier, T. Straw, A. Baceiredo, K. B. Dillon, G. Bertrand, *Chem. Ber.* **1991**, *124*, 1739.
[39] T. Facklam, O. Wagner, H. Heydt, M. Regitz, *Angew. Chem.* **1990**, *102*, 316; *Angew. Chem. Int. Ed. Engl.* **1990**, *29*, 314.
[40] a) A. W. Johnson, *Ylides and Imines of Phosphorus*, Wiley, New York, **1993**; b) Y. G. Gololobov, L. F. Kasukhin, *Tetrahedron* **1992**, *48*, 1354.
[41] H. Bock, M. Schnöller, *Angew. Chem.* **1968**, *80*, 667; *Angew. Chem. Int. Ed. Engl.* **1968**, *87*, 636.
[42] a) G. Maier, R. Wolf, H. O. Kalinowski, *Chem. Ber.* **1994**, *127*, 201; b) G. Maier, D. Born, I. Bauer, R. Wolf, R. Boese, D. Cremer, *ibid.* **1994**, *127*, 173; c) M. Lederman, M. Regitz, K. Angermund, P. Binger, C. Krüger, R. Mynott, R. Gleiter, I. Hyla-Kryspin, *Angew. Chem.* **1988**, *100*, 1616; *Angew. Chem. Int. Ed. Engl.* **1988**, *27*, 1559; d) S. Masamune, N. Nakamura, M. Suda, H. Ona, *J. Am. Chem. Soc.* **1973**, *95*, 8481; e) P. Eisenbarth, M. Regitz, *Chem. Ber.* **1982**, *115*, 3796.
[43] G. Alcaraz, U. Wecker, A. Baceiredo, F. Dahan, G. Bertrand, *Angew. Chem.* **1995**, *107*, 1358; *Angew. Chem. Int. Ed. Engl.* **1995**, *34*, 1246.
[44] R. Armbrust, M. Sanchez, R. Réau, U. Bergsträsser, M. Regitz, G. Bertrand, *J. Am. Chem. Soc.* **1995**, *117*, 10785.
[45] O. Wagner, G. Maas, M. Regitz, *Angew. Chem.* **1987**, *99*, 1328; *Angew. Chem. Int. Ed. Engl.* **1987**, *26*, 1257.
[46] a) G. Alcaraz, A. Baceiredo, M. Nieger, G. Bertrand, *J. Am. Chem. Soc.* **1994**, *116*, 2159; b) G. Alcaraz, V. Piquet, A. Baceiredo, F. Dahan, W. W. Schoeller, G. Bertrand, *ibid.* **1996**, *118*, 1060.
[47] X. Creary, *Acc. Chem. Res.* **1992**, *25*, 31.
[48] a) K. E. Brainbridge, W. P. Dailey, *Tetrahedron Lett.* **1989**, *30*, 4901; b) W. P. Dailey, *ibid.* **1987**, *28*, 5801.
[49] a) D. G. Gilheany, *Chem. Rev.* **1994**, *94*, 1339; b) A. E. Reed, P. von R. Schleyer, *J. Am. Chem. Soc.* **1990**, *112*, 1434.
[50] a) H. H. Karsch, E. Witt, A. Schneider, E. Herdtweck, M. Heckel, *Angew. Chem.* **1995**, *107*, 628; *Angew. Chem. Int. Ed. Engl.* **1995**, *34*, 557; b) H. H. Karsch, E. Witt, F. E. Hahn, *ibid.* **1996**, *108*, 2380 and **1996**, *35*, 2242; see also A. Schmidpeter, F. Steinmüller, W. S. Sheldrick, *Z. Anorg. Allg. Chem.* **1989**, *579*, 158.
[51] G. Alcaraz, A. Baceiredo, M. Nieger, W. W. Schoeller, G. Bertrand, *Inorg. Chem.* **1996**, *35*, 2458.
[52] a) A. H. Cowley, *Chem. Rev.* **1965**, *65*, 617; b) L. Lamandé, K. B. Dillon, R. Wolf, *Phosphorus, Sulfur, Silicon Relat. Elem.* **1995**, *103*, 1.
[53] a) R. Ahlrichs, H. Schiffer, *J. Am. Chem. Soc.* **1985**, *107*, 6494; b) G. Trinquier, *ibid.* **1986**, *108*, 568.

[54] A. H. Cowley, M. C. Cushner, J. S. Szobota, *J. Am. Chem. Soc.* **1978**, *100*, 7784.
[55] a) E. Fluck, W. Plass, G. Heckmann, *Z. Anorg. Allg. Chem.* **1990**, *588*, 181; b) E. Fluck, G. Heckmann, W. Plass, M. Spahn, H. Borrmann, *J. Chem. Soc. Perkin Trans. 1* **1990**, 1223.
[56] a) P. von R. Schleyer, P. K. Freeman, H. Jiao, B. Goldfuss, *Angew. Chem.* **1995**, *107*, 332; *Angew. Chem. Int. Ed. Engl.* **1995**, *34*, 337; b) C. von Wüllen, W. Kutzelnigg, *Chem. Phys. Lett.* **1993**, *205*, 563; c) W. Kutzelnigg, U. Fleischer, M. Schindler, *NMR Basic Princ. Prog.* **1990**, *23*, 165.
[57] G. Bouhadir, K. Bieger, P. Livotto, R. Réau, H. Gornitzka, F. Dahan, G. Bertrand, *J. Organomet. Chem.* **1997**, *529*, 79.
[58] F. Palacios, I. P. de Heredia, G. Rubiales, *J. Org. Chem.* **1995**, *60*, 2384.
[59] E. Fluck, G. Becker, B. Neumüller, R. Knebl, G. Heckmann, H. Riffel, *Angew. Chem.* **1986**, *98*, 1018; *Angew. Chem. Int. Ed. Engl.* **1986**, *25*, 1002.
[60] P. Molina, A. Arques, M. V. Vinader, *J. Org. Chem.* **1988**, *53*, 4654.
[61] M. Sanchez, R. Réau, F. Dahan, M. Regitz, G. Bertrand, *Angew. Chem.* **1996**, *108*, 2386; *Angew. Chem. Int. Ed. Engl.* **1996**, *35*, 2228.
[62] K. B. Dillon, *Chem. Rev.* **1994**, *94*, 1441.
[63] M. Sanchez, R. Réau, H. Gornitzka, F. Dahan, M. Regitz, G. Bertrand, *J. Am. Chem. Soc.*, **1997**, *119*, 9720.
[64] O. J. Curnow, W. H. Hirpo, W. M. Mutler, M. D. Curtis, *Organometallics* **1993**, *12*, 4479.
[65] Ring opening occurred in rare cases: F. Rosche, G. Heckmann, E. Fluck, F. Weller, *Z. Anorg. Allg. Chem.* **1996**, *622*, 974.
[66] K. Bieger, G. Bouhadir, R. Réau, F. Dahan, G. Bertrand, *J. Am. Chem. Soc.* **1996**, *118*, 1038.
[67] a) J. Barendt, E. G. Bent, R. C. Haltivanger, A. D. Norman, *Inorg. Chem.* **1989**, *28*, 2334; b) R. Rolland, E. Ocando, P. Potin, J.-P. Majoral, G. Bertrand, *ibid.* **1991**, *30*, 4095; c) J. Böske, E. Niecke, E. Ocando, J.-P. Majoral, G. Bertrand, *ibid.* **1986**, *25*, 2695.

Copper-Catalyzed Enantioselective Michael Additions: Recent Progress with New Phosphorus Ligands

Norbert Krause*

Enantioselective Michael addition of a chiral organometallic reagent to a prochiral substrate is an attractive method for creating a center of chirality in an organic molecule.[1] For this purpose chirally modified organocopper compounds of composition RCu(L*)Li can be used; the chiral nontransferable ligand L* controls the stereochemical course of the transfer of group R to the substrate **1**. By using stoichiometric amounts of these "chiral cuprates", the groups of Bertz, Corey, Dieter, Rossiter, and Tanaka obtained the 1,4-adducts **2** with good



enantioselectivities (over 90% *ee* in some cases). Naturally occuring alcohols and amines were used as chiral ligands L* (e.g., ephedrine and proline derivatives).[1] However, these investigations also revealed two fundamental problems of enantioselective Michael additions:

1) In solution organocopper compounds show dynamic behavior with equilibria between several species. If this leads to the formation of achiral, but more reactive cuprates, a loss of enantioselectivity is unavoidable. Therefore, it is crucial to develop chiral reagents which react so rapidly with the substrate that undesired competing reactions are suppressed.
2) Many chiral organocopper reagents exhibit high substrate specificity; that is, they give good stereoselectivities with only one or very few Michael acceptors.

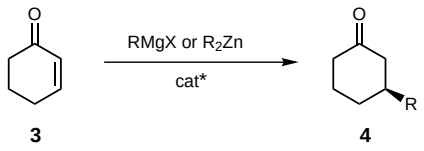
Both problems may be solved by taking advantage of the concept of *ligand-accelerated catalysis*,[2] which involves catalytic reactions characterized by dynamic ligand-exchange processes. The presence of a suitable ligand can lead to the formation of a highly reactive and selective catalyst by self-assembly. If a chiral ligand is used, a stereoselective reaction may be favored over a nonselective one. Other advantages of catalytic transformations compared to their stoichiometric counterparts are the more efficient use of the metal and the chiral ligand, as well as the minimization of waste production.

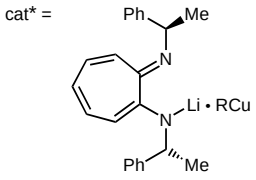
Michael additions of organolithium, Grignard, and diorganozinc reagents to enones and other α,β-unsaturated carbonyl compounds are catalyzed inter alia by copper, nickel, and cobalt salts. The best results are obtained with copper(I) catalysts, especially those in which copper is bound to a "soft", readily polarizable center (sulfur or phosphorus).

The first reaction of this type was reported by Lippard et al. in 1988: the reaction of 2-cyclohexenone (**3**) with Grignard reagents in the presence of the chiral aminotroponeimine copper complex **5** as catalyst gave the 1,4-adducts **4** with 4–14% *ee*.[3a] The selectivity was increased to 74% *ee* by addition of hexamethylphosphoric triamide (HMPA) and silyl halides.[3b] Spescha et al.[4] used the copper complex **6**, which was obtained from a thioglucofuranose derivative, as catalyst for 1,4-additions of Grignard reagents to **3**, and observed enantioselectivities of up to 60% *ee*. The dihydrooxazolylthiophenolato copper complex **7** was employed by Pfaltz et al.[5] for the enantioselective catalysis of Michael additions to cyclic enones; the best results were obtained with tetrahydrofuran as solvent and HMPA as additive. There was a pronounced dependence of the stereoselectivity on the ring size of the substrate: 16–37% *ee* for 2-cyclopentenone, 60–72% *ee* for **3**, and 83–87% *ee* for 2-cycloheptenone. Alexakis et al.[6] used the heterocycle **8**, which is readily accessible from ephedrine, as chiral ligand for the copper(I)-catalyzed addition of diethylzinc to **3**, and obtained ketone **4** (R = Et) with 32% *ee*. Another neutral phosphorus ligand is the proline derivative **9**, with which Kanai and Tomioka[7] obtained 67–90% *ee* in the Cu(I)-catalyzed 1,4-addition of Grignard reagents to 2-cyclohexenone (**3**). Recently, Feringa et al.[8] reported the use of phosphorus amidites of type **10** in Michael additions of diethylzinc to enones. These reactions are catalyzed by copper(I) salts and by copper(II) triflate; when **3** was used as substrate, stereoselectivities of 60% *ee* (with CuOTf) and 63% *ee* (with $Cu(OTf)_2$) were obtained (a much higher value of 81% *ee* resulted with 4,4-dimethyl-2-cyclohexenone in the presence of **10**. Even when $Cu(OTf)_2$ is employed, the actual chiral catalyst is probably a copper(I) species which is formed by in situ reduction of the copper(II) complex. In all these cases, the regioselectivities (1,4- vs. 1,2-addition) and chemical yields are acceptable or good.

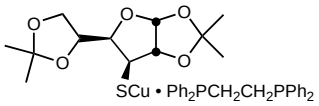
[*] Prof. Dr. N. Krause
Kekulé-Institut für Organische Chemie und Biochemie der Universität
Gerhard-Domagk-Strasse 1, D-53121 Bonn (Germany)
Fax: Int. code + (49) 228 73-5683
e-mail: krause@uni-bonn.de

 © WILEY-VCH Verlag GmbH, D-69451 Weinheim, 1998 1433-7851/98/3703-0283 $ 17.50+.50/0

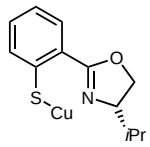




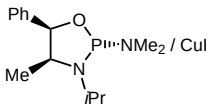
5 (4–14% *ee*[3a])
(max. 74% *ee*; + *t*Bu$_2$PhSiCl / HMPA[3b])



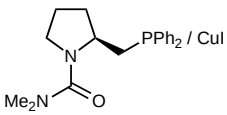
6 (max. 60% *ee*[4])



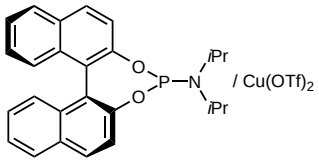
7 (60–72% *ee*; + HMPA[5])



8 (32% *ee*[6])

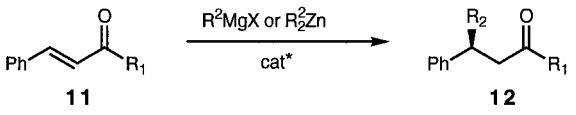


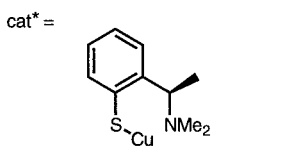
9 (67–90% *ee*[7])



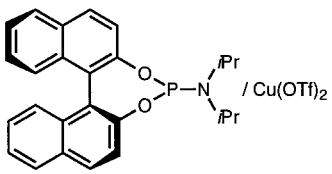
10 (63% *ee*[8])

As these examples show, cyclic enones are normally used as substrates for copper-catalyzed enantioselective Michael additions. In some cases, however, good stereoselectivities were also attained with acyclic enones of type **11**. Thus van Klaveren, van Koten et al.[9] employed the copper arenethiolate **13** as catalyst for the 1,4-addition of methylmagnesium iodide to benzylideneacetone and obtained adduct **12**





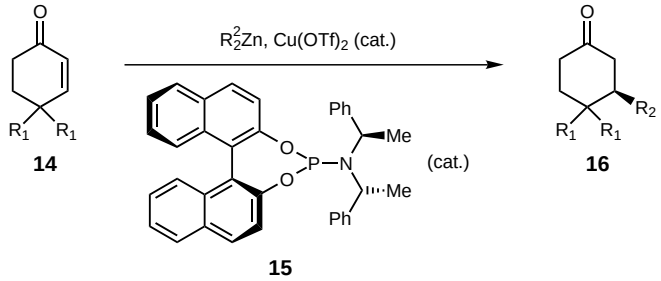
13 ($R^1 = R^2 =$ Me: 76% *ee*[5])

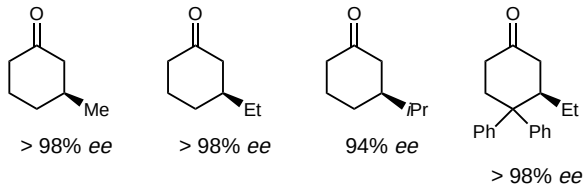


10 (R^1 = Ph, R^2 = Et: 87% *ee*[8])

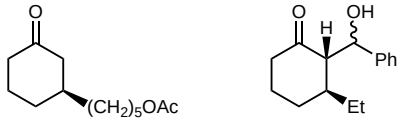
($R^1 = R^2 =$ Me) with 76% *ee*. Interestingly, this catalyst is not suitable for analogous additions to cyclic enones; similarly, the structurally related copper thiolate **7** does not catalyze enantioselective Michael additions of Grignard reagents to acyclic enones of type **11**. With **7** and **13**, complicated nonlinear relationships between the enantiomeric excesses of the catalyst and the product were observed, indicating that the product is formed via different organocopper intermediates in several reaction pathways. Progress with regard to this undesired substrate specificity was achieved with the phosphorous amidite **10**, which catalyzes not only Michael additions of organozinc reagents to cyclic enones but also to chalcone (**11**, $R^1 =$ Ph) and related acyclic substrates. In the case of the addition of diethylzinc to chalcone, a good stereoselectivity of 87% *ee* was observed.[8]

The last example shows that neutral binaphthol phosphorus ligands are particularly well suited for enantioselective Michael additions. On the basis of this structural feature, Feringa et al.[10] achieved a breakthrough. By combining C_2-symmetrical axially chiral binaphthol with C_2-symmetrical bis(1-phenylethyl)amine through a phosphorus center, they obtained the new ligand **15**, which can be used in highly enantioselective copper-catalyzed Michael additions of diorganozinc reagents to numerous cyclic enones. Here the steric properties of the substrate and the reagent are unimportant, since the transfer of methyl, ethyl, and isopropyl groups to 2-cyclohexenone takes place with high enantioselectivities ($\geq$94% *ee*) and good chemical yields (72–95%), as does the transfer of an ethyl group to 4,4-diphenyl-2-cyclohexenone. Additional functional groups can be introduced into the addition product in several ways without affecting the stereo-

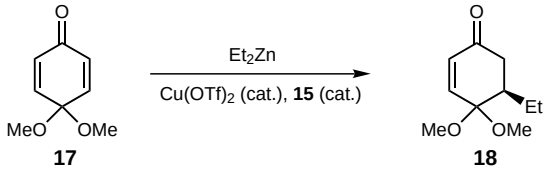




> 98% *ee* > 98% *ee* 94% *ee* > 98% *ee*



95% *ee* 95% *ee*

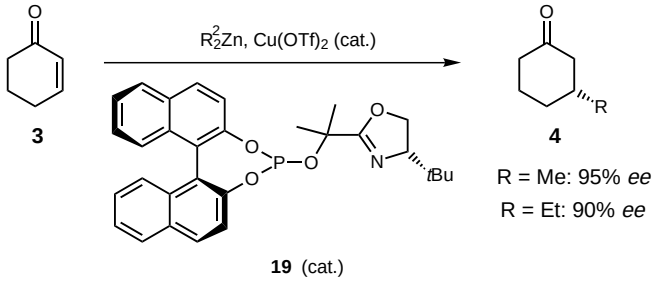


94% *ee*

 © WILEY-VCH Verlag GmbH, D-69451 Weinheim, 1998 1433-7851/98/3703-0284 $ 17.50+.50/0 *Angew. Chem. Int. Ed.* **1998**, *37*, No. 3

chemical course of the reaction. Thus the addition of diethylzinc to 4,4-dimethoxy-2,5-cyclohexadienone (**17**), catalyzed by **15** und $Cu(OTf)_2$, gives adduct **18** with 94% *ee*. The functionalized zinc reagent $[AcO(CH_2)_5]_2Zn$, prepared by hydroboration of the corresponding alkene and transmetalation according to Knochel's method, can be added to 2-cyclohexenone with excellent selectivity of 95% *ee*. Finally, the zinc enolates formed in these transformations can also be treated with more complex electrophiles instead of protons. For example, the three-component coupling of 2-cyclohexenone, diethylzinc, and benzaldehyde in the presence of **15** and $Cu(OTf)_2$ furnishes the expected hydroxyketone with 95% *ee*; however, the diastereoselectivities of these transformations are not yet satisfactory.[10]

With the combination of phosphorus amidite **15** and $Cu(OTf)_2$, a catalyst has been developed for the first time which can be applied with confidence to almost any combination of Michael acceptor and organozinc reagent. This system apparently exploits the pinciple of ligand-accelerated catalysis. However, an important limitation has to taken into account: Only enones with six-membered rings give high stereoselectivities (the analogous reactions of diethylzinc with 2-cyclopentenone and 2-cycloheptenone gave the adducts with 10 and 53% *ee*, respectively). Another recent report by Pfaltz et al.[11] underlines that the bridging of binaphthol and a chiral amine through a phosphorus center is a general feature of catalysts which are suitable for highly enantioselective Michael additions. In the presence of the phosphite **19** with oxazoline structure, the 1,4-additions of dimethyl- and diethylzinc to **3** also give stereoselectivities of 95 and 90% *ee*, respectively. Hopefully, this major progress will trigger further investigations leading to new chiral copper catalysts which can be applied even more generally to cyclic Michael acceptors with different ring sizes as well as to acyclic substrates.



German version: *Angew. Chem.* **1998**, *110*, 295 – 297

Keywords: asymmetric catalysis · biaryls · enantioselectivity · ligand-accelerated catalysis · Michael additions

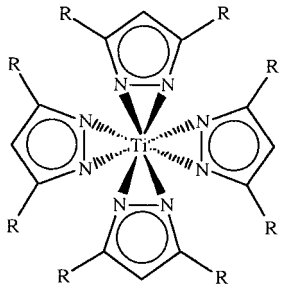
[1] Reviews: a) B. E. Rossiter, N. M. Swingle, *Chem. Rev.* **1992**, *92*, 771 – 806; b) N. Krause, *Kontakte (Darmstadt)* **1993** (1), 3 – 13; c) N. Krause, A. Gerold, *Angew. Chem.* **1997**, *109*, 194 – 213; *Angew. Chem. Int. Ed. Engl.* **1997**, *36*, 186 – 204.
[2] D. J. Berrisford, C. Bolm, K. B. Sharpless, *Angew. Chem.* **1995**, *107*, 1159 – 1171; *Angew. Chem. Int. Ed. Engl.* **1995**, *34*, 1050 – 1064.
[3] a) G. M. Villacorta, C. P. Rao, S. J. Lippard, *J. Am. Chem. Soc.* **1988**, *110*, 3175 – 3182; b) K. H. Ahn, R. B. Klassen, S. J. Lippard, *Organometallics* **1990**, *9*, 3178 – 3181.
[4] M. Spescha, G. Rihs, *Helv. Chim. Acta* **1993**, *76*, 1219 – 1230.
[5] a) Q.-L. Zhou, A. Pfaltz, *Tetrahedron Lett.* **1993**, *34*, 7725 – 7728; b) Q.-L. Zhou, A. Pfaltz, *Tetrahedron* **1994**, *50*, 4467 – 4478.
[6] A. Alexakis, J. Frutos, P. Mangeney, *Tetrahedron: Asymmetry* **1993**, *4*, 2427 – 2430.
[7] M. Kanai, K. Tomioka, *Tetrahedron Lett.* **1995**, *36*, 4275 – 4278.
[8] A. H. M. de Vries, A. Meetsma, B. L. Feringa, *Angew. Chem.* **1996**, *108*, 2526 – 2528; *Angew. Chem. Int. Ed. Engl.* **1996**, *35*, 2374 – 2376.
[9] a) F. Lambert, D. M. Knotter, M. D. Janssen, M. van Klaveren, J. Boersma, G. van Koten, *Tetrahedron: Asymmetry* **1991**, *2*, 1097 – 1100; b) G. van Koten, *Pure Appl. Chem.* **1994**, *66*, 1455 – 1462; c) M. van Klaveren, F. Lambert, D. J. F. M. Eijkelkamp, D. M. Grove, G. van Koten, *Tetrahedron Lett.* **1994**, *35*, 6135 – 6138.
[10] B. L. Feringa, M. Pineschi, L. A. Arnold, R. Imbos, A. H. M. de Vries, *Angew. Chem.* **1997**, *109*, 2733 – 2736; *Angew. Chem. Int. Ed. Engl.* **1997**, *36*, 2620 – 2623.
[11] A. K. H. Knöbel, I. H. Escher, A. Pfaltz, *Synlett*, submitted.

 © WILEY-VCH Verlag GmbH, D-69451 Weinheim, 1998 1433-7851/98/3703-0285 $ 17.50+.50/0

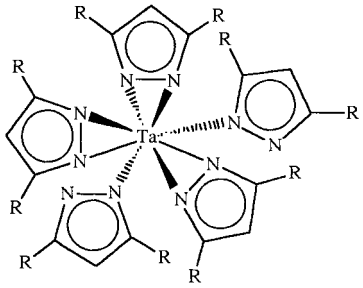
Another Surprise from Pyrazolate Ligands**

Joanna E. Cosgriff and Glen B. Deacon*

Winter et al.[1] recently synthesized two pyrazolatotitanium(IV) complexes $[Ti(\eta^2\text{-}R_2pz)_4]$ (**1**, pz = pyrazolate, R = Ph, Me) with four 3,5-disubstituted pyrazolate rings. These are the first homoleptic pyrazolato complexes, and contain exclusively η^2-pyrazolate ligands. This was followed by the synthesis of the homoleptic 3,5-disubstituted pyrazolatotantalum(V) complex $[Ta(\eta^2\text{-}Me_2pz)_3(\eta^1\text{-}Me_2pz)_2]$[2] (**2**), which has



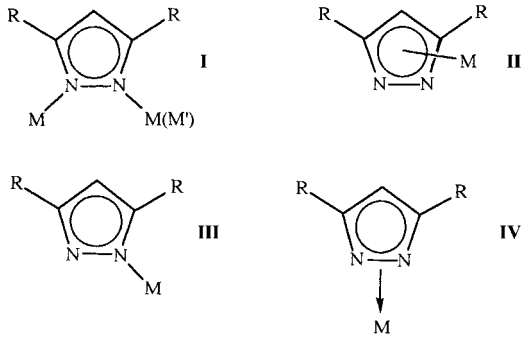
1



2

both η^1- and η^2-pyrazolate ligands. These complexes establish η^2-pyrazolate binding as a new feature in the chemistry of d-block transition metals. There is only one previous example of η^2-binding to a d-block element: $[ZrCp_2(\eta^2\text{-pz})(thf)](BPh_4)\cdot 0.5\,thf$,[3] in which there is just one ligand of this type. The preparation of homoleptic pyrazolato complexes and in particular homoleptic (η^2-pyrazolato)titanium(IV) complexes is the most significant development in the coordination chemistry of these ligands since the unexpected discovery of *endo* bidentate (η^2) coordination in $[UCp_3(\eta^2\text{-pz})]$.[4] The bonding in $[Ti(\eta^2\text{-}R_2pz)_4]$ contrasts the expected d-block bridging bidentate coordination seen in $[\{TiCp_2(\mu\text{-pz})\}_2]$.[5] The homoleptic complexes **1** and **2** are of considerable interest as molecular precursors for chemical vapor deposition (CVD).[1, 2]

In his seminal review of pyrazole and pyrazolate coordination, Trofimenko considered two possible types of bonding for the pyrazolate ion: bridging [that is, *exo*-bidentate (**I**)] or η^5 (the pyrazolate functions as 1,2-diazacyclopentadienide).[6] However, claims of π bonding were dismissed as unsubstantiated,[6] and this mode of coordination (**II**) remains to be established. Unidentate coordination as in **III**, which is formally present in pyrazolylborates $[R_nB(pz)_{4-n}]^-$,[6, 7] was first crystallographically observed for bis[3-phenyl-5-(2′-pyridyl)pyrazolato]nickel(II).[8] In this case the coordination of



I **II** **III** **IV**

the 2′-pyridyl nitrogen atom forces the metal to comply with unidentate rather than *exo* bidentate coordination. More latterly, several complexes with η^1-pyrazolate ligands have been prepared. In these cases unidentate coordination is generally dictated by the metal: Either only certain coordination sites are available, as in *cis*-chloro(η^1-3,5-diphenylpyrazolato)bis(triphenylphosphane)platinum(II),[9] or there are electronic requirements, as in bis(η^5-cyclopentadienyl)bis(η^1-pyrazolato)molybdenum(IV)[10] or $[Me_2Ga(pz)_2]^-$.[11]

The first observation of η^2-coordinated pyrazolate ligands (complexes of type **IV**) in $[UCp_3(\eta^2\text{-pz})]$ was unexpected; the authors anticipated $[UCp_3(\mu\text{-pz})]_2$.[4] This form of binding to an f-block metal was rationalized in terms of the highly ionic, nondirectional nature of the U–N bonds and binding to the more negative side of the pyrazolate ring. Other examples of η^2-coordinated pyrazolate ligands followed for uranium[12] and then for lanthanoids. This coordination mode was initially observed together with μ-pyrazolate binding.[13, 14] In an important subsequent development the first tris(η^2-pyrazolato)lanthanoid complexes $[Ln(R_2pz)_3(L)_n]$ (L = thf, dme, Ph_3PO) were prepared by using the bulky 3,5-diphenyl- and 3,5-di-*tert*-butylpyrazolate ligands.[15] These were the first complexes with η^2-pyrazolates as the sole anionic ligands. These studies also introduced metal-based redox transmetalation/ligand exchange [Eq. (a); R = *t*Bu, Ph, R′ = C_6F_5] as a synthetic method, in contrast to the commonly used metatheses or deprotonations.[6, 7] However, the ligands were not

$$2\,Ln + 6\,R_2pzH + HgR'_2 \longrightarrow 2\,[Ln(R_2pz)_3] + 3\,Hg + 6\,R'H \qquad (a)$$

bulky enough to produce homoleptic η^2-pyrazolato complexes for the large Ln^{3+} ions, but have now proven sufficiently bulky to give such complexes for the smaller (by ca. 15%)[16] titanium(IV).[1]

The failure to observe d-block transition metal complexes of η^2-coordinated pyrazolato ligands prior to $[ZrCp_2(\eta^2\text{-pz})(thf)](BPh_4)$[3] was attributed to a correlation between common *exo* bidentate binding and the directional properties of the nitrogen donor atoms.[4, 6, 15] Even the example of $[ZrCp_2(\eta^2\text{-pz})(thf)](BPh_4)$, in contrast to the numerous

[*] Prof. Dr. G. B. Deacon, Dr. J. E. Cosgriff
Chemistry Department
Monash University
Clayton, Victoria 3168 (Australia)
Fax: Int. code + (613) 99054597
e-mail: glen.deacon@sci.monash.edu.au

[**] We are grateful to the Australian Research Council for support.

 © WILEY-VCH Verlag GmbH, D-69451 Weinheim, 1998 1433-7851/98/3703-0286 $ 17.50+.50/0

d-block transition metal complexes of μ-pyrazolate ligands,[6, 7] can be viewed as an exceptional result of the need to achieve electronic saturation (18 electrons).

The syntheses of $[Ti(\eta^2\text{-}R_2pz)_4]$[1] and $[Ta(\eta^2\text{-}R_2pz)_3(\eta^1\text{-}R_2pz)_2]$[2] by protolytic transamination [Eq. (b)] have established η^2-bound pyrazolato ligands in d-block transition metal

$$[M(NMe_2)_n]+n\,R_2pzH \longrightarrow [M(R_2pz)_n]+n\,HNMe_2 \qquad (b)$$

complexes as a general feature. Moreover, their presence in compounds such as **1** and **2** cannot be related to the need for coordinative saturation, since these complexes are 16-electron systems. In addition, the formation of **2** indicates that **1** is not sterically saturated (eight-coordinate Ti^{4+} and Ta^{5+} have similar ionic radii[16]). The formation of homoleptic, coordinative, and sterically unsaturated tetrakis(η^2-pyrazolato)titanium(IV) complexes **1** (R = Me or Ph) can be attributed to the use of a noncoordinating solvent with an elevated boiling point (toluene). This discourages coordination of an additional ligand, for example the low-boiling dimethylamine product [Eq. (b)]. There is the possibility of coordination of R_2pzH (R = Me, Ph) to give $[Ti(R_2pz)_4(R_2pzH)]$, as in the synthesis of $[La(tBu_2pz)_3(tBu_2pzH)_2]$ (Ln = La, R = *t*Bu, R′ = Ph) in Equation (a) in low-boiling petroleum ether.[17] The higher boiling point of toluene obviates this in Equation (b).

Winter et al. provided a bonding model based on ab initio calculations[1] for the $[Ti(\eta^2\text{-}R_2pz)_4]$ complexes in which electron density from the nitrogen lone pairs is placed in molecular orbitals which interact with appropriate empty d orbitals on Ti. In the calculations η^1-coordination did not constitute a minimum, and it was proposed that the presence of empty d orbitals favors η^2-bonding over η^1-bonding.[1] On this basis, the formation of $[Ta(\eta^2\text{-}Me_2pz)_3(\eta^1\text{-}Me_2pz)_2]$ is surprising. The alternative formation of $[Ta(\eta^2\text{-}Me_2pz)_5]$ is unlikely, since it is a formal 20-electron system, but $[Ta(\eta^2\text{-}Me_2pz)_4(\eta^1\text{-}Me_2pz)]$ is plausible. The steric coordination number[18] of η^2-Me_2pz is 1.54,[14] whereas that of η^1-Me_2pz should be comparable with that of one end of a bridging Me_2pz group (1.37). Therefore, the sum of the steric coordination numbers of the ligands in $[Ta(\eta^2\text{-}Me_2pz)_5]$ (7.7) is high for an ion of the size[16] of Ta^{5+}, and it reduces to 7.4 in $[Ta(\eta^2\text{-}Me_2pz)_3(\eta^1\text{-}Me_2pz)_2]$, which evidently provides the most stable steric/electronic balance (formally 16 electrons). Based on the calculations it was predicted that η^2-binding will be observed in early to middle transition metal complexes.[1] For ions of the same charge, steric factors also favor a change from η^2 to η^1 over the series. It is of interest both to test this prediction and to establish whether steric or electronic factors are dominant in determining the bonding mode.

The biggest challenge now is to achieve η^5-pyrazolate coordination (type **II**). Azacyclopentadienes can form π bonds, since η^5-bonding of the 2,5-di-*tert*-butylpyrrolyl ligand is known for main group, d-block, and f-block metals,[19] but in this case binding of nitrogen to metals is substantially blocked. It will take more ingenuity to achieve this outcome for pyrazolate ligands.

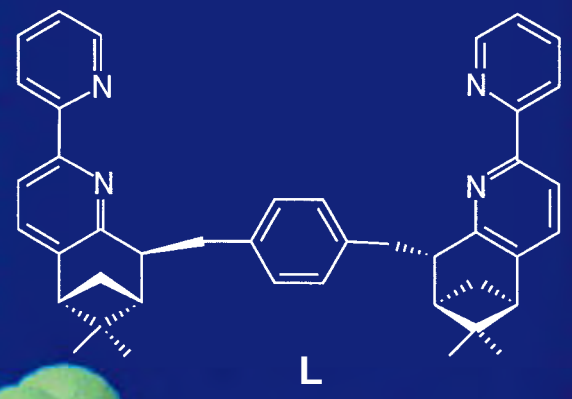
German version: *Angew. Chem.* **1998**, *110*, 298 – 299

Keywords: N ligands · pyrazolate complexes · tantalum · titanium · transition metals

[1] I. A. Guzei, A. G. Baboul, G. P. A. Yap, A. L. Rheingold, H. B. Schlegel, C. H. Winter, *J. Am. Chem. Soc.* **1997**, *119*, 3387 – 3388.
[2] I. A. Guzei, G. P. A. Yap, C. H. Winter, *Inorg. Chem.* **1997**, *36*, 1738 – 1739.
[3] D. Röttger, G. Erker, M. Grehl, R. Frölich, *Organometallics* **1994**, *13*, 3897 – 3902.
[4] C. W. Eigenbrot, K. N. Raymond, *Inorg. Chem.* **1981**, *20*, 1553 – 1556.
[5] B. F. Fieselmann, G. D. Stucky, *Inorg. Chem.* **1978**, *17*, 2074 – 2077.
[6] S. Trofimenko, *Chem. Rev.* **1972**, *72*, 497 – 509.
[7] S. Trofimenko, *Prog. Inorg. Chem.* **1986**, *34*, 115 – 210.
[8] J. Sieler, H. Hennig, *Z. Anorg. Allg. Chem.* **1971**, *381*, 219 – 225.
[9] J. P. Fackler, R. G. Raptis, H. H. Murray, *Inorg. Chim. Acta* **1992**, *193*, 173 – 183.
[10] M. A. A. F. C. D. T. Carrondo, A. M. T. S. Domingos, *J. Organomet. Chem.* **1983**, *253*, 53 – 63.
[11] K. R. Breakell, D. J. Patmore, A. Storr, *J. Chem. Soc. Dalton Trans.* **1975**, 749 – 754.
[12] C. W. Eigenbrot, K. N. Raymond, *Inorg. Chem.* **1982**, *21*, 2653 – 2660.
[13] H. Schumann, P. R. Lee, J. Loebel, *Angew. Chem.* **1989**, *101*, 1073 – 1074; *Angew. Chem. Int. Ed. Engl.* **1989**, *28*, 1033 – 1035.
[14] G. B. Deacon, B. M. Gatehouse, S. Nickel, S. N. Platts, *Aust. J. Chem.* **1991**, *44*, 613 – 621.
[15] J. E. Cosgriff, G. B. Deacon, B. M. Gatehouse, H. Hemling, H. Schumann, *Angew. Chem.* **1993**, *105*, 906 – 907; *Angew. Chem. Int. Ed. Engl.* **1993**, *32*, 874 – 875; *Aust. J. Chem.* **1994**, *47*, 1223 – 1235; J. E. Cosgriff, G. B. Deacon, B. M. Gatehouse, *ibid.* **1993**, *46*, 1881 – 1896; J. E. Cosgriff, G. B. Deacon, G. D. Fallon, B. M. Gatehouse, H. Schumann, R. Weiman, *Chem. Ber.* **1996**, *129*, 953 – 958; J. E. Cosgriff, G. B. Deacon, B. M. Gatehouse, P. R. Lee, H. Schumann, *Z. Anorg. Allg. Chem.* **1996**, *622*, 1399 – 1403.
[16] R. D. Shannon, *Acta Crystallogr. A* **1976**, *32*, 751 – 767.
[17] J. E. Cosgriff, G. B. Deacon, B. M. Gatehouse, unpublished results.
[18] J. Marçalo, A. P. De Matos, *Polyhedron* **1989**, *8*, 2431 – 2437.
[19] For example, H. Schumann, J. Winterfeld, H. Hemling, N. Kuhn, *Chem. Ber.* **1993**, *126*, 2657 – 2659; H. Schumann, E. C. E. Rosenthal, J. Winterfeld, G. Kociok-Köhn, *J. Organomet. Chem.* **1995**, *495*, C12 – C14; N. Kuhn, G. Henkel, S. Stubenrauch, *J. Chem. Soc. Chem. Commun.* **1992**, 760 – 761; N. Kuhn, M. Köckerling, S. Stubenrauch, D. Bläser, R. Boese, *ibid.* **1991**, 1368 – 1370.

 © WILEY-VCH Verlag GmbH, D-69451 Weinheim, 1998 1433-7851/98/3703-0287 $ 17.50+.50/0

Chiral derivatives of pyridine and bipyridines with fused pinene groups are interesting for several applications. For example helicates with predetermined chirality can be obtained: $[Ag_6L_6]^{6+}$



L



An esthetically highly pleasing structure, formed by a self-assembly process from Ag^+ ions and an enantiomerically pure bipyridine-type ligand, is described on the following pages.

 © WILEY-VCH Verlag GmbH, D-69451 Weinheim, 1998 1433-7851/98/3703-0289 $ 17.50+.50/0

Completely Stereospecific Self-Assembly of a Circular Helicate**

Olimpia Mamula, Alex von Zelewsky,* and Gérald Bernardinelli

Self-assembly of helicates with labile metal centers has been recently a subject of great interest in the field of supramolecular chemistry.[1, 2] The inherently chiral helicates are formed as racemates if nonchiral ligands are used. Various procedures for resolution have been successfully applied in order to obtain the pure enantiomers.[3–6] The enantioselective synthesis of chiral structures in general and of supramolecular assemblies in particular is a challenge. Chiral helicating ligands can induce stereoselectivity; that is, the chiral centers of the ligands influence the chirality of the resulting helix.[7–15]

So far most studies in the coordination chemistry of helicates were carried out on structures that are noncyclic. In few cases circular helical assemblies have been reported.[5, 16–20] However, with the exception of a recently reported trinuclear species,[19] in all such cases racemates were obtained. Here we present an example of a completely stereospecific, self-assembled, circular helical structure.

We have recently shown that a family of ligands, which now comprises several molecules, is easily accessible from natural terpene type compounds.[21] These pyridine and bipyridine (bipy) ligands can be used to synthesize configurationally stable coordination compounds in which the stereochemistry at the metal center is completely predetermined by the configuration of the ligands.[22, 23] Here we describe the application of a related ligand, which was designed for stereoselective self-assembly processes.

An important feature of the molecules of the pinene-2,2′-bipyridine series is their reactivity at one center of the pinene group. Ligand **L1** (Figure 1) obtained from (−)-α-pinene is deprotonated regioselectively by lithium diisopropyl amide (LDA) at the methylene group in α-position to the pyridine ring. The carbanion obtained reacts stereoselectively (in the less hindered position opposite to the methyl groups) with almost any alkyl bromide to give various derivatives. One possibility is to connect two bipy-type moieties with α,α'-dibromo-*para*-xylene to obtain the ligand **L2**.

In contrast to other similar ligands,[23] for instance **L4** (Figure 1), **L2** cannot coordinate in a tetradentate manner to *one* coordination center because of steric constraints. We therefore tested the behavior of **L2** with labile coordination centers in view of the formation of polynuclear self-assembled structures.

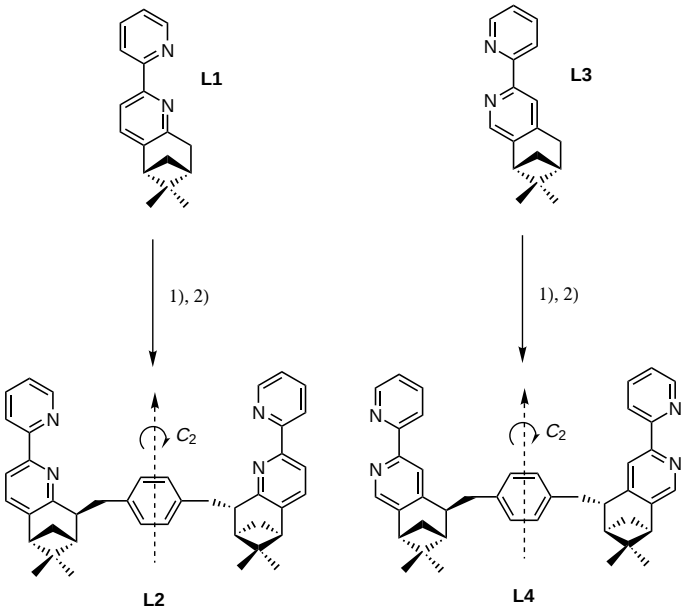


Figure 1. Synthetic pathways to chiral ligands **L2** and **L4**. 1) LDA; 2) α,α'-dibromo-*para*-xylene. The twofold axis is drawn in the structural formulas of **L2** and **L4**.

The ligand **L2** spontaneously forms a sixfold, circular single-stranded helicate with Ag^I ions (see Experimental Section), as indicated by X-ray diffraction in the solid state. NMR and circular dichroism (CD) spectroscopy in solution, as well as preliminary electrospray mass spectrometry (ES–MS) results, indicate that this species persists in the dissolved state, but detailed investigations have to be carried out to elucidate the exact behavior in solution. In addition, preliminary results with other metal ions like Cu^I show that helix formation with **L2** is a general phenomenon.

As indicated by the CD spectra of the solutions, complex formation leads to a chiral coordination unit with Ag^I. There is virtually no CD activity of **L2** in the $\pi-\pi^*$ region of the spectrum (230–320 nm). The CD activity ($\Delta\varepsilon_{314} = +16\,M^{-1}cm^{-1}$ for one metal center) of the helicate in this spectral region can be attributed to an exciton coupling.[24]

The ^1H NMR spectrum of ligand **L2** shows a half-set of protons due to its C_2-symmetry axis. The complex obtained by mixing **L2** and $AgPF_6$ at room temperature in acetonitrile in a 1:1 stoichiometric ratio shows a ^1H NMR spectrum containing the same number of lines as the free ligand (Figure 2). Two features of the ^1H NMR signals of the complex are worth special mention: a) The signals of all the aromatic protons are shifted relative to those of the free ligand. Most notably is an upfield displacement (1.45 ppm) of C20 and C24 in the xylylene bridge. This signal is broadened significantly. Spectra taken at lower temperatures (down to −40°C in CD_3CN) show a distinct sharpening of this line leading eventually to a splitting into two lines. This behavior indicates the existence of at least two rapidly exchanging species in solution. b) The lines of the methyl groups from the pinene moieties (not shown) shift to a lesser degree (about 0.5 ppm) relative to the signals of protons from the xylylene bridge, and a broadening at room temperature is observed again.

[*] Prof. Dr. A. von Zelewsky, O. Mamula
Institute of Inorganic Chemistry
University of Fribourg, Perolles
CH-1700 Fribourg (Switzerland)
Fax: Int. code + (41) 26 300-9738
E-mail: alexander.vonzelewsky@unifr.ch
Dr. G. Bernardinelli
Laboratory of X-Ray Crystallography
University of Geneva
24, quai E. Ansermet, CH-1211 Geneva (Switzerland)

[**] This work was supported by the Swiss National Science Foundation. We thank Dr. Gérard Hopfgartner for recording ES mass spectra.

 © WILEY-VCH Verlag GmbH, D-69451 Weinheim, 1998 1433-7851/98/3703-0290 $ 17.50+.50/0

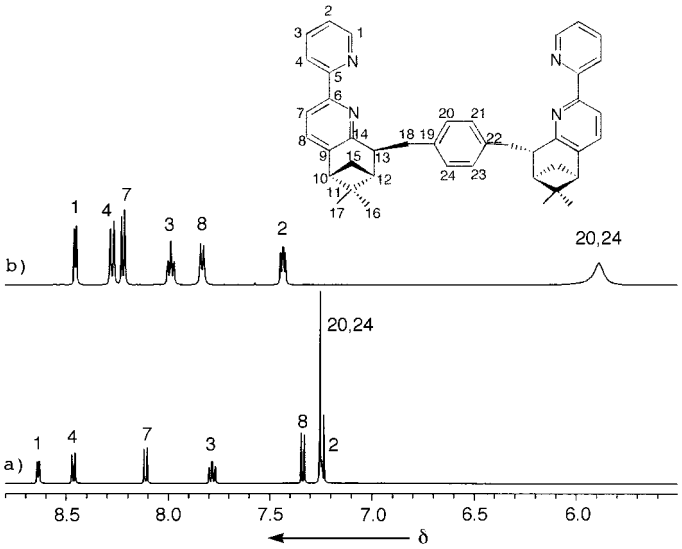


Figure 2. Partial ^{1}H NMR spectra (500 MHz, aromatic protons) of a) ligand **L2** (in $CDCl_3$ for solubility reasons; the displacements are the same in CD_3CN) and b) the Ag^{I} complex in CD_3CN. Assignment of the signals has been achieved with ^{13}C NMR, NOESY, COSY, HETCOR experimental data.

X-ray diffraction analysis of the salt of the silver complex shows the presence of a circular, hexameric, single-stranded helicate (Figure 3), which could be obtained by slow diffusion of diethyl ether into an acetonitrile solution containing **L2** and $AgPF_6$ in a 1:1 molar ratio. This structure represents a first example of a large self-assembled hexanuclear species, which is circular, helical, and predetermined in its absolute configuration. It can be considered a chiral macrocycle containing 78 atoms ($C_{60}N_{12}Ag_6$) in which one bisbidentate ligand forms a bridge between two adjacent Ag centers ($Ag\cdots Ag = 9.961(2)$ Å). The six Ag(**L2**) units making up the structure are related by a crystallographic C_6 axis (Figure 4). The silver ions are tetrahedrally coordinated by four almost equidistant (2.31 Å) nitrogen donor atoms located on two different ligands. The bite angles of the chelates are 72.0(4) and 72.7(5)°, and the dihedral angle between the two N-Ag-N chelate planes at one center is 66.8(2)°. Within each bipyridine unit of the ligand the two pyridine rings are twisted relative to each other (by 18.0(6) and 22.5(5)°). All chiral centers of the ligands, the pinene groups, are oriented towards the center of the circular structure making up two distinct layers, surrounding the chiral cavity.[25] The xylylene bridges are all nearly parallel (1.5°) to the C_6 axis and form the sides of the hexagonal skeleton (distance between two opposite xylene moieties ≈ 18.1 Å), whereas the terminal pyridines form the external shell of the circular complex. Both the absolute structure parameter (see Experimental Section) and the relation of the known chirality of the pinene group to that at the metal centers clearly indicate that the handedness of the helix is *P*. The same absolute configuration has been observed in helicates obtained with octahedral coordination centers with ligand **L4**,[26] as well as in mononuclear complexes[27] of Ru^{II}. The commercially available (+)-α-pinene yields **L1** in the other enantiomeric form, and the same sequence of reactions will afford the *M*-helical form of the circular helicate. Studies of chiral recognition when both isomers are present simultaneously in solution are in progress. The outside diameter of the hexagonal structure is about 3 nm and the cavity has a diameter of 0.84 nm. The thickness of a hexagonal disc is about 1.4 nm.

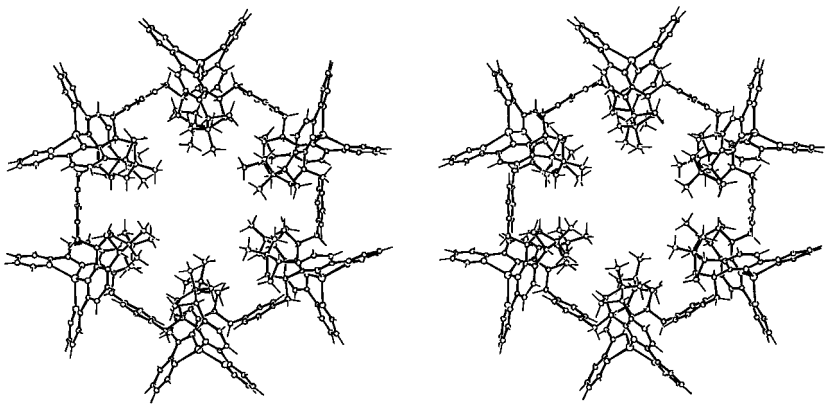


Figure 4. Stereoview of the $[Ag_6(L2)_6]^{6+}$ ion along its sixfold axis.

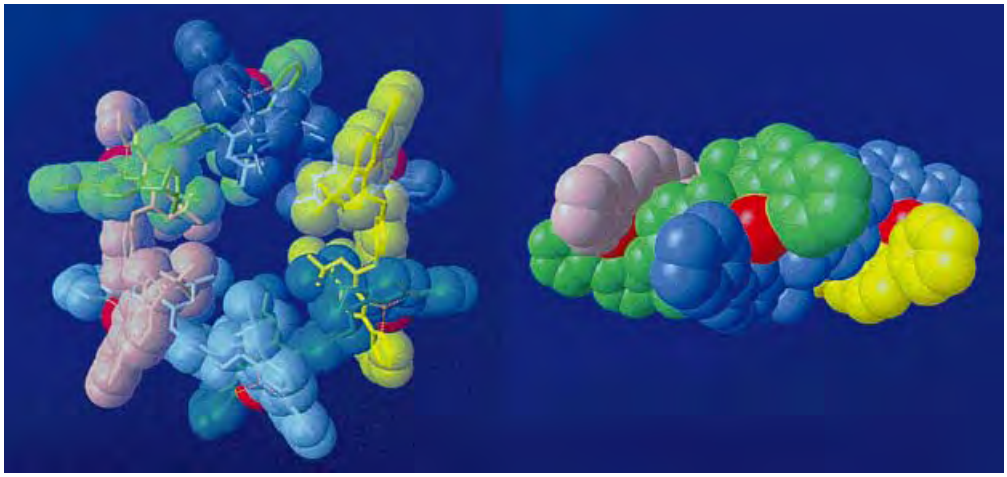


Figure 3. Crystal structure of **1** (hydrogen atoms are omitted for clarity). Left: Top view with superimposed stick model of the structure. Right: View from the side. The representation was generated by computer from X-ray diffraction data.

 © WILEY-VCH Verlag GmbH, D-69451 Weinheim, 1998 1433-7851/98/3703-0291 $ 17.50+.50/0

In contrast to other circular helical systems,[5, 17, 20] this structure self-assembles from the metal ion and the ligand alone. In this case there is no central element, for example an anion, which could act as a template for generating a circular structure. Thus it is demonstrated that careful design of the ligands can lead to large, highly organized systems, which is a prerequisite for the construction of molecular assemblies with well-defined functionalities. The facile ligand synthesis and the spontaneous formation of this new class of self-assembled structures makes them objects of great interest for investigations of hitherto not well understood phenomena in supramolecular chemistry. The chiral cavity of $[Ag_6(\mathbf{L2})_6]^{6+}$ looks promising for the study of stereospecific noncovalent interactions, chiral recognition, and possibly stereoselective catalytic processes.

Experimental Section

The ligand **L1** was synthesized according to published procedures.[21] Ligand **L2** was obtained from **L1** following the same procedure as for **L4**.[23]

L2 · H_2O (62.1 mg, 0.1 mmol) dissolved in 10 mL mixed solvent (acetonitrile/chloroform 5/1) was added rapidly under inert atmosphere (Ar) to a solution containing $AgPF_6$ (Fluka; 25.3 mg 0.1 mmol). The resulting colorless solution was stirred for few minutes, and after the removal of the solvents, the white powder was dried under high vacuum and analyzed. The complex can be obtained also by reaction between ligand and silver acetate in methanol followed by precipitation with NH_4PF_6.

L2: ^{1}H NMR (500 MHz, $CDCl_3$, 25°C): $\delta = 8.65$ (ddd, 2H, H(1), $^3J_{1,2} = 4.8$ Hz, $^4J_{1,3} = 1.8$ Hz, $^5J_{1,4} = 0.9$ Hz), 8.46 (ddd, 2H, H(4), $^3J_{4,3} = 8.0$ Hz, $^4J_{4,2} = 1.1$ Hz, $^5J_{4,1} = 0.9$ Hz), 8.12 (d, 2H, H(7), $^3J_{7,8} = 7.7$ Hz), 7.79 (ddd, 2H, H(3), $^3J_{3,4} = 8$ Hz, $^3J_{3,2} = 7.5$ Hz, $^4J_{3,1} = 1.8$ Hz), 7.34 (d, 2H, H(8), $^3J_{8,7} = 7.7$ Hz), 7.26 (s, 4H, H(20,24)), 7.25 (m, 2H, H(2)), 3.82 (dd, 2H, H(18b), $^2J_{18b,18a} = 13.7$ Hz, $^3J_{18b,13} = 3.8$ Hz), 3.42 (ddd, 2H, H(13), $^3J_{13,18b} = 3.8$ Hz, $^3J_{13,18a} = 11.0$ Hz, $^3J_{13,12} = 3$ Hz), 2.80 (dd, 2H, H(10), $^3J_{10,15b} = 5.5$ Hz, $^4J_{10,12} = 5.5$ Hz), 2.73 (dd, 2H, H(18a), $^2J_{18a,18b} = 13.7$ Hz, $^3J_{18a,13} = 11$ Hz), 2.58 (ddd, 2H, H(15b), $^3J_{15b,10} = 5.5$ Hz, $^3J_{15b,12} = 5.5$ Hz, $^2J_{15b,15a} = 9.8$ Hz), 2.16 (ddd, 2H, H(12), $^3J_{12,15b} = 5.5$ Hz, $^4J_{12,10} = 5.5$ Hz, $^3J_{12,13} = 3$ Hz), 1.43 (d, 2H, H(15a), $^2J_{15a,15b} = 9.8$ Hz), 1.36 (s, 6H, H(17)), 0.63 (s, 6H, H(16)). ^{13}C NMR (75.44 MHz, $CDCl_3$, 25°C): $\delta = 158.79$ (q), 156.89 (q), 153.29 (q), 149.05 (C(1)), 142.34 (q), 138.65 (q), 136.76 (C(13)), 133.73 (C(8)), 129.26 (C(20), C(21), C(23), C(24)), 123.10 (C(2)), 120.86 (C(4)), 118.00 (C(7)), 47.00 (C(10)), 46.26 (C(13)), 42.79 (C(12)), 41.25 (q, C(11)), 38.48 (C(18)), 28.40 (C(15)), 26.37 (C(17)), 20.97 (C(16)). $[\alpha]_D$ (25°C, 13.6 mg in 10 mL CH_2Cl_2) = −132. UV/Vis (CH_2Cl_2): λ_{max} (ε_{max}): 230 nm (2.4×10^4), 249 nm (2×10^4), 256 nm (2.1×10^4), 296 nm (3.9×10^4), 314 nm (2.9×10^4, sh). Elemental analysis calculated for $C_{42}H_{42}N_4 \cdot H_2O$: C 81.26, H 7.14, N 9.02%; found: C 81.26, H 7.02, N 9.03%. Thin-layer chromatography: Silica gel, hexane/ethyl acetate/triethylamine 2/1/0.1. $R_f = 0.39$.

$[Ag_6(L2)_6](PF_6)_6$: ^{1}H NMR (CD_3CN, 500 MHz, 25°C): $\delta = 8.44$ (d, 2H, H(1), $^3J_{1,2} = 5.1$ Hz), 8.27 (d, 2H, H(4), $^3J_{4,3} = 8.2$ Hz), 8.21 (d, 2H, H(7), $^3J_{7,8} = 8.0$ Hz), 7.98 (dd, 2H, H(3), $^3J_{3,4} = 8.2$ Hz, $^3J_{3,2} = 7.0$ Hz), 7.83 (d, 2H, H(8), $^3J_{8,7} = 8.0$ Hz), 7.43 (dd, 2H, H(2), $^3J_{2,1} = 5.1$ Hz, $^3J_{2,3} = 7.0$ Hz), 5.89 (s, 4H, H(20, 24)), 3.73 (d, 2H, H(18b), $^3J_{18b,18a} = 11.4$ Hz), 3.01 (dd, 2H, H(10), $^3J_{10,15b} = 5.6$ Hz, $^3J_{10,12} = 5.6$ Hz), 2.82 (d, 2H, H(13), $^3J_{13,18b} = 11.4$ Hz), 2.55 (ddd, 2H, H(15b), $^2J_{15b,15a} = 10.1$ Hz, $^3J_{15b,12} = 5.6$ Hz, $^3J_{15b,10} = 5.6$ Hz), 2.41 (dd, 2H, H(18a), $^2J_{18a,18b} = 11.4$ Hz, $^3J_{18a,13} = 11.4$ Hz), 1.57 (d, 2H, H(15a), $^2J_{15a,15b} = 10.1$ Hz), 1.39 (s, broad, 2H, H(12)), 1.17 (s, 6H, H(17)), 0.08 (s, 6H, H(16)). ^{13}C NMR (CD_3CN, 125.75 MHz, 25°C): $\delta = 159.95$ (q), 153.23 (q), 151.35 (C(1)), 151.14 (q), 146.19 (q), 140.23 (C(3)), 137.57 (q), 137.43 (C(8)), 129.29 (C(20), C(21), C(23), C(24)), 126.33 (C(2)), 123.50 (C(4)), 122.31 (C(7)), 50.36 (C(13)), 47.15 (C(10)), 42.99 (C(12)), 41.42 (q, C(11)), 38.20 (C(18)), 27.95 (C(15)), 26.44 (C(17)), 21.65 (C(16)). UV-Vis (CH_3CN, $c = 1.27 \times 10^{-5}$ M $[AgL]^+L^{-1}$): λ_{max} (ε_{max}): 249 nm (1.7×10^4), 254 nm (2.16×10^4), 294 nm (3.73×10^4), 304 nm (2.82×10^4). Elemental analysis calculated for $Ag_6C_{252}H_{252}N_{24}P_6F_{36}$: C 58.96, H 4.95, N 6.55%; found C 59.25, H 5.48, N 6.28%. Crystal structure determination of $[Ag(C_{42}H_{42}N_4)]_6(PF_6)_6(CH_3CN)_6(C_4H_{10}O)_3(H_2O)_{1.5}$: $M_r = 5630$; $\mu = 4.052$ mm^{-1}, $F(000) = 2901$, $\rho_{calcd} = 1.25$ g cm^{-3}, hexagonal, $P6$, $Z = 1$, $a = 26.521(3)$, $c = 12.236(2)$ Å, $V = 7453(2)$ Å^3, colorless hexagonal prism $0.26 \times 0.26 \times 0.26 \times 0.75$ mm^3; $T = 200$ K; Stoe Stadi4 diffractometer; $Cu_{K\alpha}$ radiation ($\lambda = 1.5418$ Å), 2θ range = 2–100°; $0 < h < 22$; $0 < k < 22$; $0 < l < 12$ and all antireflections; 5424 measured reflections, 5109 unique of which 4688 observables ($|F_o| > 4\sigma(F_o)$); analytical absorption corrections[28] (A* min/max = 2.295/3.215). Structure solved by direct methods,[29] all other calculations used XTAL[30] system and ORTEP[31] programs. Full-matrix least-squares refinement (on F), absolute structure parameter[32] $x = 0.00(1)$, $S = 1.73(3)$, $R = 0.046$, $\omega R = 0.063$ ($\omega = 1/[\sigma^2(F_o) + 0.002(F_o^2)]$), for 536 variables and 4688 reflections. Hydrogen atoms were placed in calculated positions. The diethyl ether and water molecules are disordered and refined with U_{iso} and population parameters of 0.5. The water molecules are located on sixfold axes with one of them at the center of the Ag_6L_6 complex. The molecular packing shows compact layers of cations with interstitial acetonitrile molecules separated by layers containing the anions, the diethyl ether molecule, and the remaining water molecules, explaining the easy cleavage of the crystals along the (110) planes. It should be noted that a large majority of crystals show important disorders or cleavages leading to a poor diffraction, very large overall displacement parameters, and enlarged or split diffraction profiles.[33]

Received: September 8, 1997 [Z 10897 IE]
German version: *Angew. Chem.* **1998**, *110*, 301 – 305

Keywords: bipyridine ligands · chirality · helical structures · silver · supramolecular chemistry

[1] J.-M. Lehn, *Supramolecular Chemistry—Concepts and Perspectives*, VCH, Weinheim, **1995**, Chap. 9.
[2] C. Piguet, G. Bernardinelli, G. Hopfgartner, *Chem. Rev.* **1997**, *97*, 2005.
[3] L. J. Charbonnière, G. Bernardinelli, C.Piguet, A. M. Sargerson, A. F. Williams, *J. Chem. Soc. Chem. Commun.* **1994**, 1419.
[4] B. Hasenknopf, J.-M. Lehn, *Helv. Chim. Acta* **1996**, *79*, 1643.
[5] B. Hasenknopf, J.-M. Lehn, B. O. Kneisel, G. Baum, D. Fenske, *Angew. Chem*. **1996**, *108*, 1987; *Angew. Chem*. *Int. Ed. Engl*. **1996**, *35*, 1838.
[6] R. Krämer, J.-M. Lehn, A. De Cian, J. Fischer, *Angew. Chem.* **1993**, *105*, 764; *Angew. Chem. Int. Ed. Engl.* **1993**, *32*, 703.
[7] W. Zarges, J. Hall, J.-M. Lehn, C. Bolm, *Helv. Chim. Acta* **1991**, *74*, 1843.
[8] J. Libman, Y. Tor, A. Shanzer, *J. Am. Chem. Soc*. **1987**, *109*, 5880.
[9] E. C. Constable, T. Kulke, M. Neuburger, M. Zehnder, *Chem. Commun.* **1997**, 489.
[10] M. Albrecht, *Synlett* **1996**, 565.
[11] E. J. Enemark, T. D. P. Stack, *Angew. Chem.* **1995**, *107*, 1082; *Angew. Chem. Int. Ed. Engl.* **1995**, *34*, 996.
[12] T. Suzuki, H. Kotsuki, K. Isobe, N. Moriya, Y. Nakagawa, M. Ochi, *Inorg. Chem.* **1995**, *34*, 530.
[13] C. R. Woods, M. Benaglia, F. Cozzi, J. S. Siegel, *Angew. Chem.* **1996,** *108,* 1977*; Angew. Chem. Int. Ed. Engl.* **1996**, *35*, 1830.
[14] A. L. Airey, G. F. Swiegers, A. C. Willis, S. B. Wild, *J. Chem. Soc. Chem. Commun.* **1995**, 695.
[15] P. J. Stang, B. Olenyuk, *Angew. Chem.* **1996**, *108*, 798; *Angew. Chem. Int. Ed. Engl.* **1996**, *35*, 732.
[16] G. Hopfgartner, C. Piguet, J. D. Henion, *J. Am. Soc. Mass Spectrom.* **1994**, *5,* 748.
[17] P. L. Jones, K. J. Byrom, J. C. Jeffery, J. A. McCleverty, M. D. Ward, *Chem. Commun*. **1997**, 1361.
[18] P. N. W. Baxter, J.-M. Lehn, K. Rissanen, *Chem. Commun*. **1997**, 1323.
[19] C. Provent, S. Hewage, G. Brand, G. Bernardinelli, L. J. Charbonnière, A. F. Williams, *Angew. Chem.* **1997**, *109*, 1346; *Angew. Chem. Int. Ed. Engl.* **1997**, *36*, 1287.
[20] M. A. Houghton, A. Bilyk, M. M. Harding, P. Turner, T. W. Hambley, *J. Chem. Soc. Dalton Trans.* **1997**, 2725.
[21] P. Hayoz, A. von Zelewsky, *Tetrahedron Lett.* **1992**, *33*, 5165; N. C. Fletcher, F. R. Keene, H. Viebrock, A. von Zelewsky, *Inorg. Chem.* **1997**, *36*, 1113; M. Gianini, A. von Zelewsky, *Synthesis* **1996**, *6*, 702; M.

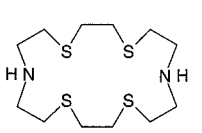
 © WILEY-VCH Verlag GmbH, D-69451 Weinheim, 1998 1433-7851/98/3703-0292 $ 17.50+.50/0

Gianini, A. Forster, P. Haag, A. von Zelewsky, H. Stoeckli-Evans, *Inorg. Chem.* **1996**, *35*, 4889.
[22] P. Hayoz, A. von Zelewsky, H. Stoeckli-Evans, *J. Am. Chem. Soc.* **1993**, *115*, 5111.
[23] H. Muerner, P. Belser, A. von Zelewsky, *J. Am. Chem. Soc.* **1996**, *118*, 7989.
[24] N. C. Fletcher, F. R. Keene, M. Ziegler, H. Stoeckli-Evans, H. Viebrock, A. von Zelewsky, *Helv. Chim. Acta* **1996**, *79*, 1192.
[25] This arrangement is a molecular analogue of the Francis turbine wheel (http://www.asc-corp.com/francis.html).
[26] H. Muerner, A. von Zelewsky, G. Hopfgartner, *Inorg. Chim. Acta* **1997**, in press.
[27] H. Muerner, A. von Zelewsky, H. Stoeckli-Evans, *Inorg. Chem.* **1996**, *35*, 3931.
[28] E. Blanc, D. Schwarzenbach, H. D. Flack, *J. Appl. Crystallogr.* **1991**, *24*, 1035.
[29] P. Main, S. J. Fiske, S. E. Hull, L. Lessinger, G. Germain, J.-P. Declercq, M. M. Woolfson, *A System of Computer Programs for the Automatic Solution of Crystal Structures from X-Ray Diffraction Data*, Universities of York, England, and Louvain-la-Neuve, Belgien, **1987**.
[30] S. R. Hall, H. D. Flack, J. M. Stewart, *XTAL3.2 User's Manual*, Universities of Western Australia and Maryland, **1992**.
[31] C. K. Johnson, *ORTEP II*, Report ORNL-5138, Oak Ridge National Laboratory, Oak Ridge, TN, **1976**.
[32] G. Bernardinelli, H. D. Flack, *Acta Crystallogr. Sect. A* **1985**, *41*, 500.
[33] Any disturbance of the equilibrium between the crystals and their mother liquor leads rapidly to the autocleavage of the crystals that become like pre-sliced salami.

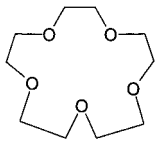
Template Assembly of Polyiodide Networks at Complexed Metal Cations: Synthesis and Structures of $[Pd_2Cl_2([18]aneN_2S_4)]_{1.5}I_5(I_3)_2$ and $[K([15]aneO_5)_2]I_9$**

Alexander J. Blake, Robert O. Gould, Wan-Sheung Li, Vito Lippolis, Simon Parsons, Christian Radek, and Martin Schröder*

Although crystal engineering has become an area of increasing activity over recent years,[1–4] most interest has centered upon the use of hydrogen-bonding between suitable organic molecules to generate three-dimensional arrays and networks.[1–3] The design of inorganic networks is much less well developed[4–8] but recent examples feature cationic three-dimensional networks based on linear bridging ligands bound to tetrahedral metal ions such as Cu^I and Ag^I.[5, 6, 9] Anionic, nonzeolitic inorganic supramolecular architectures are by contrast very rare, and the only examples known involve iodine-rich compounds.[10, 11] In this context we have been interested in ascertaining whether metal cations complexed by macrocycles can be used as templates in the synthesis of extended polyiodide arrays and to achieve control over the resulting three-dimensional architectures.[12] We report herein two unique inorganic matrices composed of polyiodide arrays assembled around a hydrogen-bonded $[Pd_2Cl_2([18]aneN_2S_4)]^{2+}$ cationic polymer and around the sandwich crown ether complex $[K([15]aneO_5)_2]^+$.



$[18]aneN_2S_4$



$[15]aneO_5$

Reaction of the binuclear complex $[Pd_2Cl_2([18]aneN_2S_4)](PF_6)_2$[13] with nBu_4NI and I_2 in a 1:2:4 molar ratio in acetonitrile, followed by several days of slow evaporation of the solvent, affords black prismatic crystals in 90% yield. X-ray diffraction studies were undertaken to determine their structure.[14] The asymmetric unit consists of one I_5^- and two I_3^- ions and one and a half binuclear $[Pd_2Cl_2([18]aneN_2S_4)]^{2+}$ dications. The Pd^{II} ions are each coordinated to one N- and two S-donor atoms, and a Cl^- ligand completes the square-planar coordination. The two coordination planes lie parallel to each other but the overall binuclear dication adopts a stepped conformation in order to minimize steric interactions. Significantly, unlike the structure of the corresponding PF_6^- salt,[13] the dications are linked pairwise by hydrogen bonds between the (N)H and Cl atoms to form infinite chains in the crystal lattice [Cl···N distances 3.254(14)–3.356(12) Å; (N)H···Cl 2.57 Å] (Figure 1). The intracation Pd···Pd distances are 4.055(2) and 4.155(2) Å, while the Pd···Pd distances between adjacent cations are significantly shorter

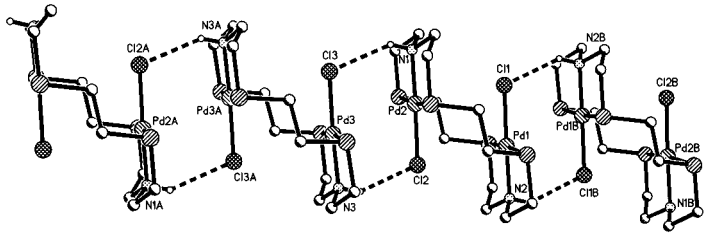


Figure 1. Structure of cation in $[Pd_2Cl_2([18]aneN_2S_4)]_{1.5}I_5(I_3)_2$.

[3.449(2), 3.463(2) Å]. The infinite chains of binuclear dications are embedded in a unique matrix of polyiodides whose fundamental units are one "L"-shaped I_5^- ion consisting of an asymmetric I_5^- ion [I(1)–I(2) 2.845(2), I(2)–I(3) 3.045(2) Å; I(1)-I(2)-I(3) = 179.69(9)°] interacting with a I_2 molecule [I(10)–I(11) 2.775(3), I(3)–I(10) 3.349(2) Å; I(2)-I(3)-I(10) = 90.00(6)°], and two slightly asymmetric I_3^- ions [I(4)–I(5) 2.904(2), I(5)–I(6) 2.959(2) Å; I(4)-I(5)-I(6) =

[*] Prof. Dr. M. Schröder, Dr. A. J. Blake, Dr. W-S. Li, Mr. V. Lippolis
Department of Chemistry, The University of Nottingham
University Park, Nottingham, NG7 2RD (UK)
Fax: Int. code + (44) 115 9513563
E-mail: m.schroder@nottingham.ac.uk
Dr. R. O. Gould, Dr. S. Parsons, Dr. C. Radek
Department of Chemistry, The University of Edinburgh
West Mains Road, Edinburgh EH9 3JJ (UK)

[**] This work was supported by the Engineering and Physical Sciences Research Council (UK). We thank the EPSRC National Mass Spectrometry Service, University of Swansea. ([18]aneN$_2$S$_4$ = 1,4,10,13-tetrathia-7,16-diazacyclooctadecane, [15]aneO$_5$ = 1,4,7,10,13-pentaoxacyclopentadecane).

176.47(6)°; I(7)–I(8) 2.948(2), I(8)–I(9) 2.929(2) Å; I(7)-I(8)-I(9) = 171.58(5)°]. The I_3^- ions, including those belonging to the I_5^- units, lie in parallel planes and form unprecedented continuous, planar two-dimensional layers. Each layer (Figure 2) may be visualized topologically as fused ribbons of 14-membered and 24-membered rings with cross-linking secondary interactions among the I_3^- ions ranging from 3.758(2) to 4.217(2) Å. Pairs of parallel and slightly interacting I_2 molecules [$I_2 \cdots I_2$ 4.257(2) Å, van der Waals diameter for

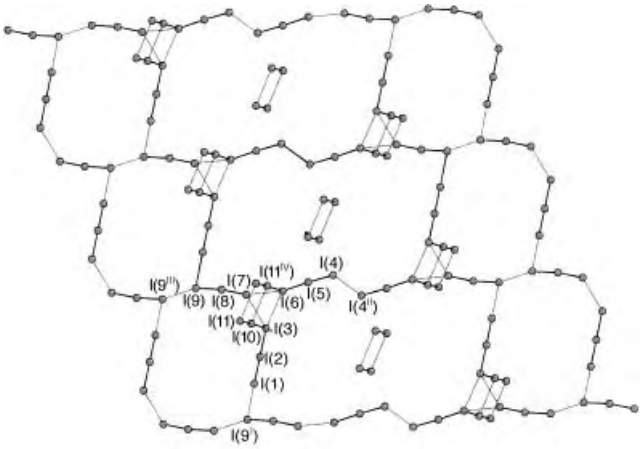


Figure 2. View of two-dimensional polyiodide layers in $[Pd_2Cl_2([18]aneN_2S_4)]_{1.5}I_5(I_3)_2$ comprising linked I_3^- ions and fused ribbons of 14-membered and 24-membered rings. Dications are omitted for clarity. Important distances [Å]: I(1)–I(2) 2.845(2), I(2)–I(3) 3.045(2), I(4)–I(5) 2.904(2), I(5)–I(6) 2.959(2), I(7)–I(8) 2.948(2), I(8)–I(9) 2.929(2), I(10)–I(11) 2.775(3), I(3)–I(10) 3.349(2), I(3)···I(6) 4.217(2), I(3)···I(7) 4.184(2), I(6)···I(7) 4.006(2), I(1)···I(9^{I}) 3.812(2), I(4)···I(4^{II}) 4.017(2), I(9)···I(9^{III}) 3.758(2), I(6)–I(11^{IV}) 3.579(2). Symmetry operation: I = $x-1, y-1, 1+z$; II = $1-x, 1-y, 1-z$; III = $2-x, 1-y, -z$, IV = $2-x, -y, 1-z$.

I = 4.3 Å[11, 12]] from two symmetry-related I_5^- ions lie orthogonal to the parallel layers and connect two of these by passing through the centers of the 24-membered rings of a third layer located between them (Figure 3). The connection of two alternating layers takes place through a reasonably short $I_5^- \cdots I_3^-$ interaction of 3.573(2) Å giving rise to an overall I_8^{2-} unit observable as an $I_2 \cdot 2I_3^-$ adduct (Figure 3), which can be

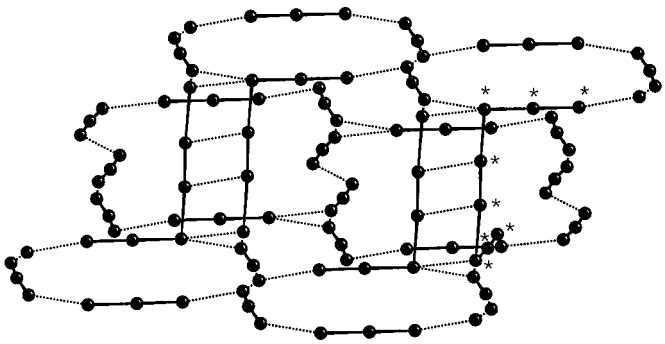


Figure 3. View of the poly-I_3^- layers linked by I_2 bridges, which connect two 14-membered rings through a 24-membered ring. Starred atoms identify one I_8^{2-} unit. Dications are omitted for clarity.

envisaged as the yarn interlocking the infinite two-dimensional poly-I_3^- sheets. The 24-membered rings of each layer measure about 25.31 × 13.31 Å: the dimensions of each half [ca. 12.65 × 13.31 Å] are similar to those of the 14-membered rings [ca. 12.18 × 14.73 Å], resulting in channels along the body diagonal of the unit cell. These channels are occupied by the chains of hydrogen-bonded binuclear complexes described above (Figure 4) and it appears that it is these chains rather than the individual dication that act as the template for the polyiodide architecture.

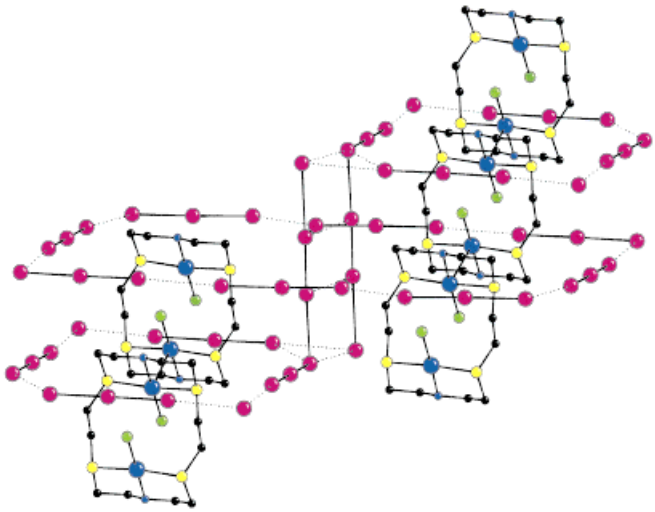


Figure 4. View of the structure of $[Pd_2Cl_2([18]aneN_2S_4)]_{1.5}I_5(I_3)_2$: chains of $[Pd_2Cl_2([18]aneN_2S_4)]^{2+}$ ions occupy channels in the three-dimensional polyiodide network.

In order to determine whether other macrocyclic complexes with different shape and charge can have the same templating effect on the self-assembly of extended polyiodide arrays, we treated $[K([15]aneO_5)_2]I$, prepared in situ by reaction of KI with two equivalents of $[15]aneO_5$, with an excess of I_2 in acetonitrile. After several days, dark red crystals were obtained by slow evaporation of the solvent. The crystal structure determination established the formulation $[K([15]aneO_5)_2]I_9$.[14] Within the cation, two crown ether ligands sandwich one K^+ ion within a ten-coordinate environment; the K–O bond lengths range between 2.62(2) and 3.21(2) Å.[20] Complex cations of this type are embedded in a three-dimensional polyiodide matrix made up of I_9^- units (Figure 5). Nonaiodides are very rare[21] and in this case each I_9^- ion can be described as an $[I_3^- \cdot (I_2)_3]$ charge-transfer complex; the three perturbed I_2 molecules have molecular distances ranging from 2.716(3) to 2.740(4) Å and interact with the slightly asymmetric I_3^- [I(7)–I(8) 2.874(3), I(8)–I(9) 2.978(3) Å; I(7)-I(8)-I(9) 178.2(2)°] through contacts of 3.396(4)–3.503(4) Å. Two of the three I_2 molecules [I(5)–I(6) and I(3)–I(4)] and the I_3^- ion [I(7)-I(8)-I(9)] lie approximately in the same plane, whereas the third I_2 molecule [I(1)–I(2)] is perpendicular to it [I(1)-I(9)-I(8) 92.4(5)°, I(1)-I(9)-I(3) 97.6(5)°]. This configuration for the I_9^- polyiodide units allows them to form a three-dimensional network of puckered cages through I···I secondary interactions of 3.732(4)–4.074(4) Å (Figure 6). Each cage measures

 © WILEY-VCH Verlag GmbH, D-69451 Weinheim, 1998 1433-7851/98/3703-0294 $ 17.50+.50/0

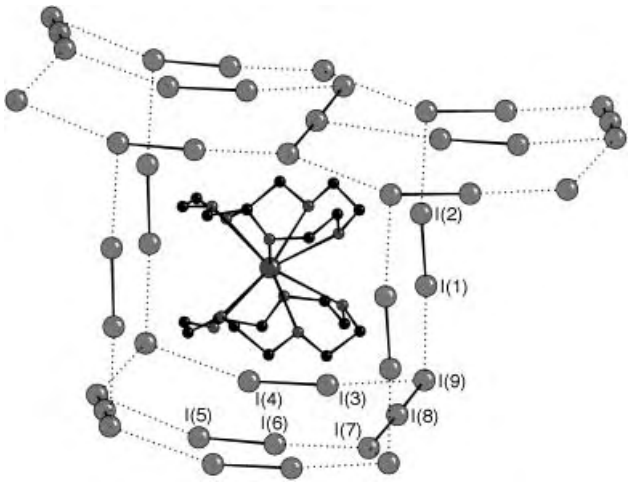


Figure 5. View of the puckered cage of I_9^- ions around the $[K([15]aneO_5)_2]^+$ cation template. Important distances [Å]: I(1)–I(2) 2.740(4), I(3)–I(4) 2.716(3), I(5)–I(6) 2.728(4), I(7)–I(8) 2.874(3), I(8)–I(9) 2.978(3), I(1)···I(9) 3.503(4), I(3)···I(9) 3.396(4), I(7)···I(6) 3.346(4).

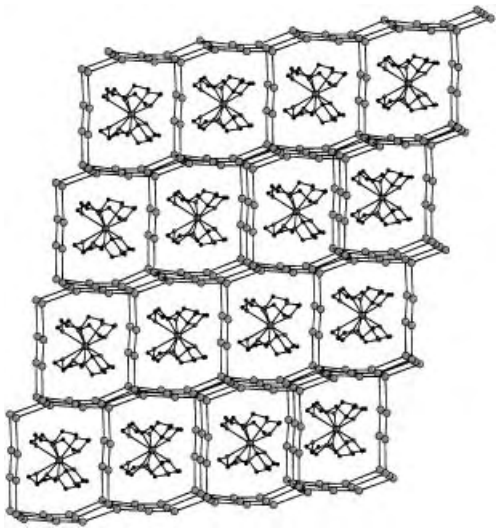


Figure 6. View of the structure of $[K([15]aneO_5)_2]I_9$ along the crystallographic *c* axis.

$9.658 \times 9.521 \times 9.959$ Å, with body diagonals of 17.371 and 17.393 Å, and the $[K([15]aneO_5)_2]^+$ ion lies nearly at the center of the cage. This polyiodide array is related to the ideal cube made up of I_7^- ions in $[Ag([18]aneS_6)]I_7$;[12] the main difference is an additional I_2 molecule in the I_9^- ion located in the middle of the lower face of each cage, which reflects the different topologies of the Ag^I and K^I complexes. There is therefore a clear link between the templating effect of I_7^-[12] and I_9^- ions. The puckered cages are arranged in a centered lattice and in projection along the crystallographic (100) axis each cage lies above the midpoint of four cages in the layer below.

Our results confirm the general principle of template condensation of three-dimensional polyiodide networks at metal cations complexed by macrocycles. The formation of polyiodide architectures may be regarded as a template reaction in the second coordination sphere of complex cations in which the unique topology of the resultant polyanionic networks depends upon the shape and charge of the template cations.

Received: August 18, 1997 [Z10825IE]
German version: *Angew. Chem.* **1998**, *110*, 305–308

Keywords: iodine · macrocycles · palladium · potassium · supramolecular chemistry

[1] G. R. Desiraju, *Crystal Engineering: Design of Organic Solids*, Elsevier, Amsterdam, **1989**.
[2] *The Crystal as a Supramolecular Entity*, (Ed.: G. R. Desiraju), Wiley, Chichester (UK), **1995**.
[3] G. R. Desiraju, *Angew. Chem.* **1995**, *107*, 2541; *Angew. Chem. Int. Ed. Engl.* **1995**, *34*, 2311.
[4] R. Robson, B. F. Abrahams, S. R. Batten, R. W. Gable, B. F. Hoskins, J. Liu, *Supramolecular Architecture*, ACS, Washington, DC, **1992,** chapter 19.
[5] L. R. MacGillivary, S. Subramaniam, M. J. Zaworotko, *J. Chem. Soc. Chem. Commun.* **1994**, 1325.
[6] L. Carlucci, G. Ciani, D. M. Proserpio, A. Sironi, *J. Chem. Soc. Chem. Commun.* **1994**, 2755.
[7] S. B. Copp, K. T. Holman, J. O. S. Sangster, S. Subramaniam, M. J. Zaworotko, *J. Chem. Soc. Dalton Trans.* **1995**, 223, and references therein.
[8] B. F. Abrahams, S. R. Batten, H. Hamit, B. F. Hoskins, R. Robson, *Angew. Chem.* **1996**, *108*, 1794; *Angew. Chem. Int. Ed. Engl.* **1996**, *35*, 1691; L. Carlucci, G. Ciani, D. M. Proserpio, A. Sironi, *J. Am. Chem. Soc.*, **1995**, *117*, 4562; O. M. Yaghi, H. Li, *ibid.* **1995**, *117*, 10401; B. F. Abrahams, S. R. Baten, H. Hamit, B. F. Hoskins, R. Robson, *Chem. Commun.* **1996**, 1313; L. Carlucci, G. Ciani, D. M. Proserpio, A. Sironi, *ibid.*, **1996**, 1393; J. R. Black, N. R. Champness, W. Levason, G. Reid, *Inorg. Chem.* **1996**, *35*, 4432.
[9] A. J. Blake, N. R. Champness, S. S. M. Chung, W.-S. Li, M. Schröder, *Chem. Commun.* **1997**, 1005; A. J. Blake, N. R. Champness, A. Khlobystov, D. A. Lemenovskii, W.-S. Li, M. Schröder, *ibid.* **1997**, 1339; M. A. Withersby, A. J. Blake, N. R. Champness, P. Hubberstey, W-S. Li, M. Schröder, *Angew. Chem.* **1997**, *109*, 2421; *Angew. Chem. Int. Ed. Engl.* **1997**, *36*, 2327; A. J. Blake, N. R. Champness, S. S. M. Chung, W.-S. Li, M. Schröder, *Chem. Commun.* **1997**, 1675.
[10] K.-F. Tebbe, T. Farida, *Z. Naturforsch. B* **1995**, *50*, 1685; K.-F. Tebbe, T. Gilles, *Z. Anorg. Allg. Chem.* **1996**, *622*, 138.
[11] K.-F. Tebbe, R. Buchem, *Angew. Chem.* **1997**, *109*, 1403; *Angew. Chem. Int. Ed. Engl.* **1997**, *37*, 1345.
[12] A. J. Blake, R. O. Gould, S. Parsons, C. Radek, M. Schröder, *Angew. Chem.* **1995**, *107*, 2563; *Angew. Chem. Int. Ed. Engl.* **1995**, *34*, 237; A. J. Blake, V. Lippolis, S. Parsons, M. Schröder, *Chem. Commun.* **1996**, 2207; see also A. J. Jircitano, M. C. Colton, K. Bowman Mertes, *Inorg. Chem.* **1981**, *20*, 890; A. J. Jircitano, K. B. Mertes, *ibid.* **1983**, *22*, 1828.
[13] A. J. Blake, G. Reid, M. Schröder, *J. Chem. Soc. Dalton Trans.* **1990**, 3363.
[14] Elemental analysis: found (calc. for $[Pd_2Cl_2([18]aneN_2S_4)]_{1.5}I_5(I_3)_2$): C 9.25 (9.35), H 1.75 (1.70), N 1.85 (1.82); found (calc. for $[K([15]aneO_5)_2]I_9$): C 14.90 (14.80); H 2.65 (2.49). Crystal structure analysis: Stoe Stadi-4 four-circle diffractometer, graphite-monochromated $Mo_{K\alpha}$ radiation, $T = 220$ K, $\theta_{max} = 25°$. Both structures were solved by using direct methods[15, 16] and all non-H atoms were located by using subsequent difference Fourier methods.[17, 18] Hydrogen atoms were placed in calculated positions and were allowed to ride on their parent atoms during refinement. $[Pd_2Cl_2([18]aneN_2S_4)]_{1.5}I_5(I_3)_2$: $C_{18}H_{39}Cl_3I_{11}N_3Pd_3S_6$, $M = 2311.34$, triclinic, space group $P\bar{1}$ (no. 2), $a = 11.667(3)$, $b = 13.422(3)$, $c = 16.998(4)$ Å, $\alpha = 97.145(15)$, $\beta = 91.721(14)$, $\gamma = 106.589(16)°$, $V = 2527.2(10)$ Å^3, $Z = 2$, $F(000) = 2072$, $\rho_{calcd} = 3.037$ g cm^{-3}, $\mu(Mo_{K\alpha}) = 8.201$ mm^{-1}, black facetted prism ($0.27 \times 0.19 \times 0.16$ mm^3). ψ scan absorption corrections ($T_{min} = 0.056$, $T_{max} = 0.141$), 8857 unique reflections [$R_{int} = 0.051$], of which 6470 had $I \geq 2\sigma(I)$. The weighting scheme $w^{-1} = [\sigma^2(F_o^2) + (0.052P)^2 + 48.0P]$, $P = [MAX(F_o^2, 0) + 2F_c^2]$, was applied. At final convergence R_1 [$I \geq 2\sigma(I)$] $= 0.0571$, wR_2 [all data] $= 0.1608$ for 393 refined parameters, $S = 1.11$, $(\Delta/\sigma)_{max} = 0.001$, $\Delta\rho_{max} = 1.73$ e Å^{-3} (near I^- atoms). $[K([15]aneO_5)_2]I_9$: $C_{20}H_{40}I_9KO_{10}$, $M = 1621.72$, monoclinic, Cc, $a = 24.348(5)$, $b = 9.521(2)$, $c = 19.244(7)$ Å, $\beta = 107.460(17)°$, $V = 4256$ Å^3 [from 2θ values for 41 reflections measured at $\pm\omega$ ($30 < 2\theta < 32°$),

 © WILEY-VCH Verlag GmbH, D-69451 Weinheim, 1998 1433-7851/98/3703-0295 $ 17.50+.50/0

$\lambda = 0.71073$ Å]. $Z = 4$, $\rho_{calcd} = 2.531\ g\,cm^{-3}$, $F(000) = 2944$, $T = 220$ K, $\mu(Mo_{K\alpha}) = 6.692\ mm^{-1}$. Dark red block, $0.27 \times 0.27 \times 0.19\ mm^3$. Absorption correction based on ψ-scans ($T_{min} = 0.051$, $T_{max} = 0.103$). Data collection and processing: The unit cell was obtained by using the program DIRAX[19] for 19 out of 25 reflections located during a random search. The two crystallographically unique macrocycles were restrained to be geometrically similar, while the displacement parameters of the C and O atoms were subject to rigid bond and body restraints. The refinement converged to a conventional R value of 0.069 with difference map extrema of $+2.61$ and $-1.66\ e\,Å^{-3}$ and a large number of poorly agreeing data with $l = 8n$. The matrix ($-1\ 0\ -0.75/0\ -1\ 0/0\ 0\ 1$) converts the cell into an equivalent cell. Reciprocal lattice points from these two cells will coincide only when l is a multiple of 4 and the sum of the transformed indices h and k is even (because of the lattice centering). Splitting the reflections in this way and proceeding with refinement with a scale factor relating the two twin components [0.147(4)] gave a final conventional R value of 0.0624 (based on F and 3839 data with $F > 4\sigma(F)$) and w$R2 = 0.1633$ (based on F^2 and all 4690 data used during refinement) for 362 parameters. The final difference map extrema were 1.44 and $-1.46\ e\,Å^{-3}$; the Flack absolute structure parameter was 0.16(13). Crystallographic data (excluding structure factors) for the structures reported in this paper have been deposited with the Cambridge Crystallographic Data Centre as supplementary publication no. CCDC-100768. Copies of the data can be obtained free of charge on application to CCDC, 12 Union Road, Cambridge CB2 1EZ, UK (fax: int. code + (44)1223336-033; E-mail: deposit@ccdc.cam.ac.uk).

[15] G. M. Sheldrick, SHELXS-86, *Acta Crystallogr. Sect. A* **1990**, *46*, 467 for $[Pd_2Cl_2([18]aneN_2S_4)]_{1.5}I_5(I_3)_2$.

[16] A. Altomare, M. C. Burla, M. Camelli, G. Giacovazzo, A. Guagliardi, G. Polidori, *J. Appl. Crystallogr.* **1994**, *27*, 435 for $[K([15]aneO_5)_2]I_9$.

[17] G. M. Sheldrick, SHELXL-93, Universität Göttingen, Germany, **1993** for $[Pd_2Cl_2([18]aneN_2S_4)]_{1.5}I_5(I_3)_2$.

[18] G. M. Sheldrick, SHELXL-96, Beta test version, Universität Göttingen, Germany, **1996** for $[K([15]aneO_5)_2]I_9$.

[19] A. J. M. Duisenberg, *J. Appl. Crystallogr.* **1992**, *25*, 92.

[20] B. Neumüller, F. Gahlmann, M. Schäfer, S. Magull, *J. Organomet. Chem.* **1992**, *440*, 263.

[21] W. J. James, R. J. Hach, D. French, R. E. Rundle, *Acta Crystallogr.* **1955**, *8*, 814; K.-F. Tebbe, *Z. Kristallogr. Suppl.* **1988**, *185*, 496.

Breaking the Mold of Discotic Liquid Crystals**

Joaquín Barberá, Oleg A. Rakitin, M. Blanca Ros,* and Tomás Torroba

Organic Chemistry is currently living its "supramolecular epoch". Innovative and fascinating research has been focused on the synthesis and study of "living" molecules in an interdisciplinary field.[1] Development of the chemistry of complex molecules such as crown ethers, cryptands, phthalocyanines, dendrimers, catenanes, rotaxanes, and a variety of related compounds could seem, at first sight, interesting only from an exotic or theoretical point of view. However, possibilities have turned into reality for many of these systems.[1] Researchers in Chemistry, Biology, Materials Science, and even Physics are looking at these supramolecules as unique tools for achieving the ultimate aim of miniaturization. Alternatively, chemists are also becoming increasingly interested in investigating chemistry beyond the covalent bond; a concept expressed by J. M. Lehn as "the chemistry beyond the molecule".[1b] In this case, the active supramolecular structures are obtained by simple interactions between suitable functional units.

Liquid crystals are well-known examples of supramolecular assemblies.[1, 2] Based on self-organization, they combine the properties of order and mobility, a combination which allows the broad range of applications already exploited for these systems. Calamitic liquid crystalline compounds have been known since the end of the last century. However, in 1977 a new type of liquid crystal emerged, the discotic liquid crystals (DLCs).[3] These compounds have enriched the research and the possibilities of the so-called fourth state of matter.

Discotic liquid crystals are characterized by their ability to self-organize into columns, giving rise to two-dimensional superlattices of different types.[1c, 2b, 4] Consequently, one of the main issues in relation to columnar liquid crystals is the possibility of generating one-dimensional molecular "pathways" for electron, photon, energy or ion migration.[5]

Many molecules, either of low molecular mass or polymeric, have been reported to arrange in columnar mesomorphic states.[2b, 4, 5b, 6] However, most of these systems follow common structural guidelines. In general, DLCs consist of a rigid central core (planar, conical, pyramidal, or other such geometry) surrounded by four or more flexible groups, which make up the "soft" region. In certain cases, individual molecules do not match these criteria, but they are capable of aggregating into units which do fulfill them.[6] Scarce variations to this general structure are the "carbonaceous" group of compounds,[7] which are large, disc-shaped, polycondensed aromatic molecules with high molecular mass or, in the field of the lyotropic mesophases, the chromonic liquid crystals. These latter compounds with no flexible hydrocarbon chains in their structure exhibit columnar phases in the presence of a solvent.[8] The role of the soft region is played by water or another suitable liquid.

This paper deals with a type of compound which constitutes the first exception to the above trends in the field of thermotropics. We report here the first examples of thermotropic DLCs which do not contain flexible groups, namely indenes **1**–**4** and pseudoazulene **5**.

Our interest in these organic compounds is twofold. Their synthesis has recently been reported[9] to proceed by a unified mechanism based on the initial abnormal Beckmann rearrangement of oximes to cyanides, followed by cyclization and/or exhaustive chlorination and dehydrochlorination. Furthermore, and surprisingly, when these small molecules were treated thermally and studied under polarized light, the

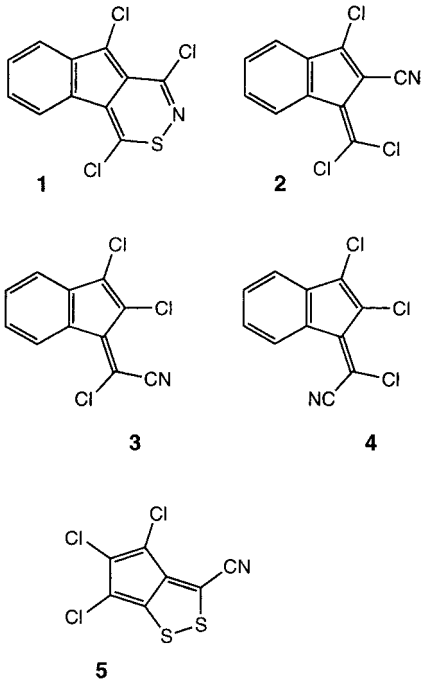
[*] Dr. M. B. Ros, Dr. J. Barberá
Química Orgánica, Facultad de Ciencias-ICMA
Universidad de Zaragoza-CSIC, 50009-Zaragoza (Spain)
Fax: Int. + (34) 976 76-1209
E-mail: bros@posta.unizar.es

Dr. O. A. Rakitin
N. D. Zelinsky Institute of Organic Chemistry, Academy of Sciences, Moscow B-334 (Russia)

Prof. T. Torroba
Química Orgánica, Facultad de Veterinaria, Universidad de Extremadura, Cáceres (Spain)

[**] This work was supported by the Comisión Interministerial de Ciencia y Tecnología (project MAT96-1073-CO2-02) and the Dirección General de Investigación Científica y Técnica (projects PB93-0414 and SAB94-0169) of Spain, and the Conserjería de Educación de la Junta de Extremadura y Fondo Social Europeo (ref. EIA94-93).

 © WILEY-VCH Verlag GmbH, D-69451 Weinheim, 1998 1433-7851/98/3703-0296 $ 17.50+.50/0



fluid samples exhibited birefringence. Such behavior suggested thermotropic transitions to a liquid crystalline state. Therefore we investigated the liquid crystal behavior of these compounds by polarizing optical microscopy, differential scanning calorimetry (DSC), and X-ray diffraction. The most important data obtained from these three techniques are summarized in Table 1 and Table 2.

Table 1. Optical and thermal properties of the compounds **1**–**5.**

Compound	Mesomorphic properties (T [ΔH])[a]
1	*K* (205.1 [12.2]) Col_h (230.0 [11.9]) *I*
2	*K* (183.9 [13.9]) Col_h (196.4 [12.0]) *I*
3	*K* (131.6 [9.9]) Col_h (152.3 [6.04]) *I*
4	*K* (97.3 [9.8]) *M*[b] (159.5 [1.1]) Col_h (184.8 [10.0]) *I*
5	*K* (144.0[c] [13.4]) *I I* (144.0 [0.81]) Col_h[d] (120)[e] *K*

[a] *K* = crystal, Col_h = hexagonal columnar phase, *I* = isotropic phase, *T* = temperature in °C; Δ*H* = transition enthalpy in kJ mol^{-1}. The temperatures given are for the onset of the first scan transitions. Heating and cooling scans at 10 K min^{-1}. [b] Unidentified phase. [c] Transition observed after successive cooling and heating scans. [d] Monotropic mesophase. [e] Optical data.

On examination by optical microscopy (OM) with polarized light (Figure 1) all the compounds display pseudo-focal-conic or mosaic textures on heating and form leaflike domains on cooling from the isotropic liquid (in most cases, the dendritic formations are seen more clearly without crossed polarizers). These textures strongly suggest columnar mesophases of hexagonal symmetry.[4b, 10] Likewise, on cooling some of the samples, large black areas lacking birefringence were observed. This indicates that the optical axis readily aligns normal to the glass microscope slides.

Analysis by DSC revealed melting and clearing endotherms of similar enthalpy in the range of 6–14 kJ mol^{-1}, which indicates a high degree of order within the mesophase (Figure 2). With the exception of **4**, all compounds exhibit a

Table 2. X-ray diffraction data for the mesophase of compounds **1**–**5**.

Compound	T [°C]	hkl	d_{obs} [Å]	d_{calcd} [Å]	Hexagonal lattice constants [Å]
1	210	100	8.49	8.52	$a = 9.84$
		110	4.93	4.92	
		200	4.27	4.26	
2	187	100	8.29	8.28	$a = 9.56$
		110	4.77	4.78	$c = 3.6$
		001	3.63		
3	145	100	8.36	8.37	$a = 9.66$
		110	4.81	4.83	$c = 3.6$
		200	4.20	4.18	
		001	3.60		
		210	3.17	3.16	
4	165	100	8.36	8.35	$a = 9.64$
		110	4.81	4.82	$c = 3.6$
		200	4.17	4.17	
		001	3.63		
		210	3.16	3.16	
5	135[a]	100	7.57	7.53	$a = 8.69$
		200	3.74	3.76	$c = 3.5$
		001	3.48		

[a] Monotropic mesophase obtained by cooling the isotropic liquid

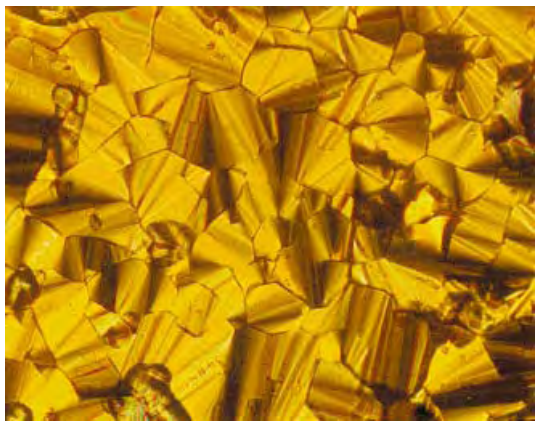


Figure 1. Pseudo-focal-conic texture of the Col_h phase of compound **2** viewed by optical microscopy through between crossed polarizers.

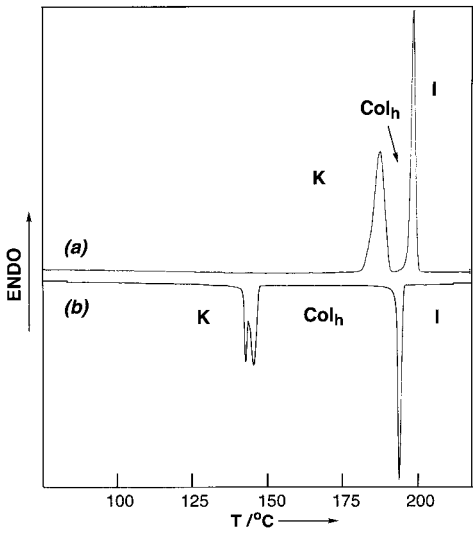


Figure 2. DSC traces corresponding to the first heating (a) and cooling (b) runs of compound **2** (scan rate = 10 K min^{-1}).

 © WILEY-VCH Verlag GmbH, D-69451 Weinheim, 1998 1433-7851/98/3703-0297 $ 17.50+.50/0

single mesophase that is either enantiotropic (**1**, **2**, and **3**) or monotropic (**5**) in nature. The *Z* isomer **4** displays one intermediate peak before the clearing endotherm, which can also be detected by OM as a smoothing of the broken pseudo-focal-conic texture. On cooling, an exotherm corresponding to the liquid–mesophase transition is observed for all the compounds. However, although a clear crystallization is observed by OM and DSC for indenes **1** and **2**, no such peak is observed in the thermograms of **3**, **4**, and **5**. This fact is consistent with the subtle texture changes detected for the latter compounds on cooling to room temperature.

To confirm the observations discussed above and to obtain more information on the structures of the liquid-crystalline arrangement exhibited by these compounds, their mesophases were studied by powder X-ray diffraction with a pinhole camera equipped with a high-temperature device. Typical of crystalline structures, the patterns taken at room temperature are, in all cases, characterized by the presence of numerous diffraction rings across the whole angular region, which can only be assigned to a three-dimensional arrangement. When the samples are heated above their melting temperature, the diffraction patterns contain fewer rings, which indicates a loss of order relative to the crystalline solid. The spacings measured experimentally for compounds **1**–**5** are collected in Table 2 together with the proposed indexation and the calculated spacings.

The high temperature patterns of all the compounds considered are qualitatively very similar, although the number of diffraction rings observed depends on the particular compound. The patterns of compounds **3** and **4** taken at 145°C and 165°C, respectively, have in common the existence of a set of four sharp maxima with a reciprocal spacing ratio $1:\sqrt{3}:\sqrt{4}:\sqrt{7}$ (Figure 3). This is characteristic of a hexagonal

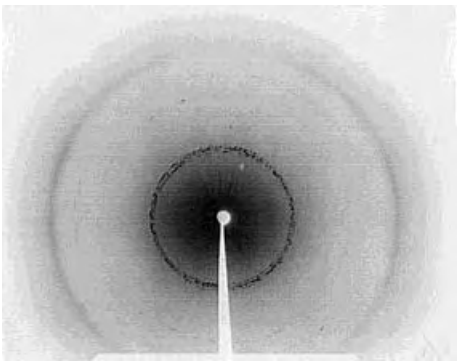


Figure 3. X-ray diffractogram of compound **4** at 165°C (Col_h mesophase).

lattice, and the four maxima can be assigned to the (100), (110), (200), and (210) reflections. The additional sharp ring observed at 3.6 Å is assigned to the (001) reflection and corresponds to the *c* parameter of the hexagonal network. The absence of reflections with Miller indices *h*, *k*, and *l* simultaneously different from zero, even on overexposed photographs, indicates that there is no three-dimensional order. All these features are characteristic of a columnar hexagonal mesophase. Moreover, when treated mechanically at the mesophase temperature range, a sample of compound **3** yielded an aligned pattern with the column axes oriented along the stretch direction. This confirms the columnar liquid-crystalline nature of the phase. The sharpness of all the diffraction rings indicates that there is long-range order not only in the plane of the hexagonal lattice, but also in the stacking direction, and thus the hexagonal columnar mesophase can be described as *ordered* (Col_{ho} mesophase). The X-ray patterns suggest that the phase exhibited by compound **4** between 97°C and 159°C (see Table 1) could be either a disordered solid or a very organized mesophase. However, we have not been able to assign its structure unequivocally.

As compounds **1** and **2** exhibit the mesomorphic state at very high temperatures, decomposition was detected after long exposure times. Furthermore, the mesophase of compound **5** is monotropic, that is, it is thermodynamically unstable and has a strong tendency to crystallize. Consequently, it was not possible to obtain long-exposure photographs for compounds **1**, **2**, and **5**, and therefore fewer maxima are observed on their X-ray photographs. Nevertheless, in spite of the absence of some reflections that were observed for compounds **3** and **4**, all the patterns are consistent with a columnar hexagonal mesophase (see Table 2).

For all the compounds except **1**, for which the extent of decomposition precludes the appearance of the corresponding reflection, the stacking distance (*c* axis of the hexagonal network) is 3.5–3.6 Å. In contrast, the hexagonal lattice constant (*a* axis) depends on the particular compound (see Table 2). On comparison of the experimental values for *a* (column diameter) with the molecular sizes estimated from Dreiding stereomodels, it can be deduced that the columns contain single molecules as stacking entities. This deduction leads to reasonable density values for the mesophases.

Discotic mesomorphism is the result of the balance between interactions of the central core and the peripheral flexible structure (soft part). The hard central core is responsible for the columnar stacking, while the flexible part acts as a lubricant and plays an active role in reducing correlation between neighboring columns. This role is usually played by conformationally disordered aliphatic chains, although in some short-chain ionic discotic materials, mesophase formation has been explained in terms of rotation of tetrafluoroborate anions which reduce correlation between the cationic columns.[11] In the compounds described in this paper, the aromatic structures constitute the hard part, while the polarizable chlorine and sulfur atoms, as well as the polar and polarizable cyano groups, behave as *unusual* soft parts through weaker molecular interactions.[12] In the solid these atoms and groups give rise to strong intermolecular attractions,[9] which become weaker as the temperature increases due to increasing thermal disorder. On melting, the weakening of the polar attractions relaxes the molecular packing, and thus the transition from the crystal to the mesophase is associated with the onset of molecular rotation.

It is worth noting the similar enthalpy changes measured for both the melting and the clearing processes for these compounds. Typical ordered hexagonal discotic liquid crystals exhibit Col_h-I enthalpies in the same range as those reported in this paper.[4, 10, 13] However, the transitions from the solid to

 © WILEY-VCH Verlag GmbH, D-69451 Weinheim, 1998 1433-7851/98/3703-0298 $ 17.50+.50/0

the Col_h state, which are attributed to the melting of the flexible chains, involve energies two to three times higher than the ones reported here.

The crystal structure of pseudoazulene **5** is hexagonal with cell constants $a = 15.57$ Å and $c = 6.815$ Å, and six molecules per unit cell.[9] The molecular packing corresponds to a pseudo-hexagonal arrangement in which the centers of close-neighboring molecules lie at $15.57/\sqrt{3} = 8.99$ Å (Figure 4a). In the solid the molecules are kept in a fixed orientation by strong intermolecular attractions. However, upon transition

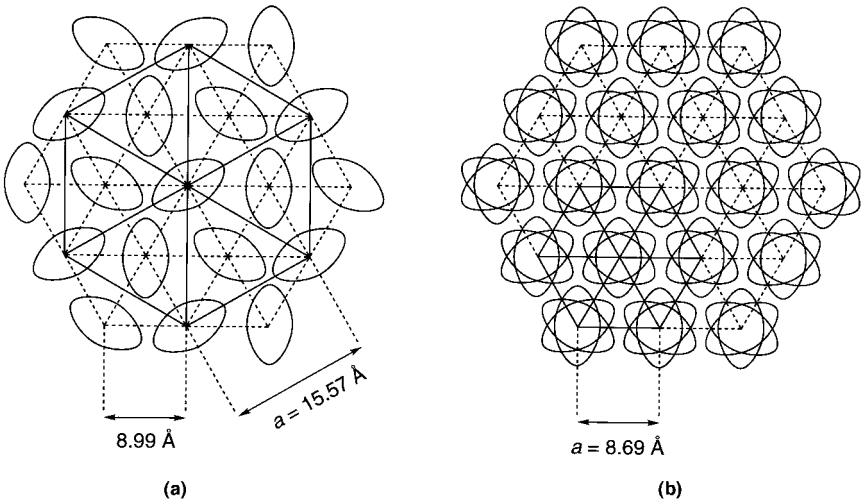


Figure 4. Schematic drawing of the structure of the crystalline phase (a), and of the Col_h mesophase (b) of compound **5** viewed along the *c* axis. The transition from the crystal to the mesophase is associated with the onset of molecular rotation: neighboring columns become less correlated.

to the mesophase these attractions become weaker, thus allowing rotation of the molecular planes around the *c* axis (Figure 4b) in such a way that the molecules project an averaged circular shape along the columnar axis (*c* axis). The transition to the liquid-crystalline state implies that neighboring columns become discorrelated, and a hexagonal columnar structure is obtained in which the interdisc interactions inside the columns are still maintained. In accordance with this, the intercolumnar parameter in the mesophase of 8.69 Å is similar to the intermolecular distance in the hexagonal crystal (8.99 Å).

In summary, we have described the first examples of thermotropic DLCs without long terminal substituents, which opens new and interesting possibilities for the study and the design of this type of material. Synthesis of other suitable compounds for the study of the relationship between structure and liquid crystal activity is currently in progress. The new scope for novel soft units within disclike systems, along with the study of the influence of their position and number on mesomorphic behavior and other physical properties (electrical, optical, etc.), provides a very promising direction for new areas of research.

Received: July 9, 1997 [Z 10664 IE]
German version: *Angew. Chem.* **1998**, *110*, 308 – 312

Keywords: liquid crystals · materials science · mesophases · supramolecular chemistry

[1] a) F. Vögtle, *Supramolecular Chemistry*, J. Wiley, Chichester, **1991**; b) J. M. Lehn, *Supramolecular Chemistry, Concepts and Properties*, VCH, Weinheim, **1995**; c) *Comprehensive Supramolecular Chemistry* (Eds.: J. L. Atwood, J. E. D. Davies, D. D. MacNicol, F. Vögtle, J. M. Lehn), Pergamon, Oxford, **1996**.

[2] a) J. M. Lehn, *Angew. Chem.* **1988**, *100*, 91 – 114; *Angew. Chem. Int. Ed. Engl.* **1988**, *27*, 89 – 112; b) *Liquid Crystals* (Ed.: H. Stegemeyer), Steinkopff Verlag, Darmstadt, **1994**.

[3] S. Chandrasekhar, B. K. Sadashiva, K. A. Suresh, *Pramana* **1977**, *7*, 471 – 480.

[4] Review on DLCs: a) S. Chandrasekhar in *Advances in Liquid Crystals*, *Vol. 5* (Ed.: G. H. Brown), Academic Press, New York, **1982,** pp. 47 – 78; b) C. Destrade, P. Foucher, H. Gasparoux, N-H. Tinh, A. M. Levelut, J. Malthête, *Mol. Cryst. Liq. Cryst.* **1984**, *106*, 121 – 146; c) S. Bauer, T. Plenivy, H. Ringsdorf, P. Schumacher, *Makromol. Chem. Macromol. Symp.* **1992**, *64*, 19 – 32; d) S. Chandrasekhar, *Liq. Cryst.* **1993**, *14*, 3 – 14.

[5] a) D. Adams, P. Schuhmacher, J. Simmerer, L. Häussling, K. Siemensmeyer, K. H. Etzbach, H. Ringsdorf, D. Haarer *Nature* **1994**, *371*, 141 – 143; b) E. Dalcanale in *Supramolecular Chemistry, Vol. 10* (Eds.: J. L. Atwood, J. E. D. Davies, D. D. MacNicol, F. Vögtle, J. M. Lehn), Pergamon, Oxford, **1996,** pp. 583 – 635; c) M. B. Ros in *Metallomesogens: Synthesis, Properties and Applications* (Ed.: J. L. Serrano), VCH, Weinheim, **1996**, pp. 419-480.

[6] J. Barberá in *Metallomesogens: Synthesis, Properties and Applications* (Ed.: J. L. Serrano), VCH, Weinheim, **1996**, pp. 131 – 192.

[7] a) J. E. Zimmer, J. L. White in *Advances in Liquid Crystals, Vol. 5* (Ed.: G. H. Brown), Academic Press, New York, **1982**, pp. 157 – 213; b) H. Honda, *Carbon* **1988**, *26*, 139 – 156.

[8] a) J. S.G. Cox, G. D. Woodard, W. C. McCrone, *J. Pharm. Sci.* **1971**, *60*, 1458 – 1465; b) N. H. Hartshorne, G. D. Woodard, *Mol. Cryst. Liq. Cryst.* **1973**, *23*, 343 – 368.

[9] O. A. Rakitin, C. W. Rees, D. J. Williams, T. Torroba, *J. Org. Chem.* **1996**, *61*, 9178 – 9185.

[10] a) E. Keinan, S. Kumar, S. P. Singh, R. Ghirlando, E. J. Wachtel, *Liq. Cryst.* **1992**, *11*, 157 – 173; b) S. Kumar, E. J. Wachtel, E. Keinan, *J. Org. Chem.* **1993**, *58*, 3821 – 3827; c) A. G. Serrette, C. K. Lai, T. M. Swager, *Chem. Mater.* **1994**, *6*, 2252 – 2268.

[11] M. Veber, P. Sotta, P. Davidson, A. M. Levelut, C. Jallabert, H. Strzelecka, *J. Phys. (Paris)* **1990**, *51*, 1283 – 1301.

[12] a) D. S. Reddy, K. Panneerselvam, T. Pilati, G. R. Desiraju, *J. Chem. Soc. Chem. Commun.* **1993**, 661 – 662; D. S. Reddy, B. S. Goud, K. Panneerselvam, G. R. Desiraju, *ibid.* **1993**, 663 – 664; b) J. J. Novoa, M. C. Rovira, C. Rovira, J. Veciana, J. Tarrés, *Adv. Mater.* **1995**, *7*, 232 – 233; c) O. Navon, J. Berstein, V. Khodorkovsky, *Angew. Chem.* **1997**, *36*, 640 – 642, *Angew. Chem. Int. Ed. Engl.* **1997**, *36*, 601 – 602.

[13] N-H. Tinh, M. C. Bernaud, G. Sigaud, C. Destrade, *Mol. Cryst. Liq. Cryst.* **1981**, *65*, 307 – 316.

 © WILEY-VCH Verlag GmbH, D-69451 Weinheim, 1998 1433-7851/98/3703-0299 $ 17.50+.50/0

Single-Molecule Magnets: Different Rates of Resonant Magnetization Tunneling in Mn_{12} Complexes**

Daniel Ruiz, Ziming Sun, Belen Albela, Kirsten Folting, Joan Ribas,* George Christou,* and David N. Hendrickson*

There is considerable and growing interest in single-molecule magnets.[1] A single-molecule magnet has a large-spin ground state with appreciable magnetic anisotropy, resulting in a barrier for reversal of the direction of magnetization. At low temperatures magnetization hysteresis loops are seen, as are out-of-phase ac susceptibility signals. The most thoroughly studied single-molecule magnet is **1**,[2–7] commonly called "Mn_{12}–acetate" or simply "Mn_{12}". In

$[Mn_{12}O_{12}(O_2CMe)_{16}(H_2O)_4]\cdot 2HO_2CMe\cdot 4H_2O$ **1**

addition to an application as a molecular memory device, interest in these molecular magnets stems from the possibility of observing macroscopic quantum tunneling (MQT).[8] Friedman et al.[9] reported for the first time the observation of resonant magnetization tunneling for Mn_{12}–acetate molecules in a crystal. Steps were observed at regular intervals of magnetic field in the magnetization hysteresis loop for oriented crystals. This has been confirmed by others.[10, 11] Herein we present magnetization hysteresis data for several $[Mn_{12}O_{12}(O_2CR)_{16}(H_2O)_4]$ complexes with different carboxylate ligands. Data are presented for oriented crystal samples. The hysteresis step heights are highly dependent on the substituent R. Thus, the rate of resonant magnetization tunneling varies appreciably from complex to complex.

Two new Mn_{12} complexes with the composition $[Mn_{12}O_{12}(O_2CR)_{16}(H_2O)_4]$, where R is either C_6H_4-2-Cl (**2**) or C_6H_4-2-Br (**3**), were prepared. As confirmed by the X-ray structure analysis,[12] complex $\mathbf{2}\cdot CH_2Cl_2\cdot 5H_2O$ possesses a $[Mn_{12}(\mu_3\text{-}O)_{12}]$ core comprising a central $[Mn^{IV}_4O_4]^{8+}$ cubane held within a nonplanar ring of eight Mn^{III} ions by eight μ_3-O^{2-} ions (Figure 1).

$[Mn_{12}O_{12}(O_2CC_6H_4\text{-}2\text{-}Cl)_{16}(H_2O)_4]$ **2**

$[Mn_{12}O_{12}(O_2CC_6H_4\text{-}2\text{-}Br)_{16}(H_2O)_4]$ **3**

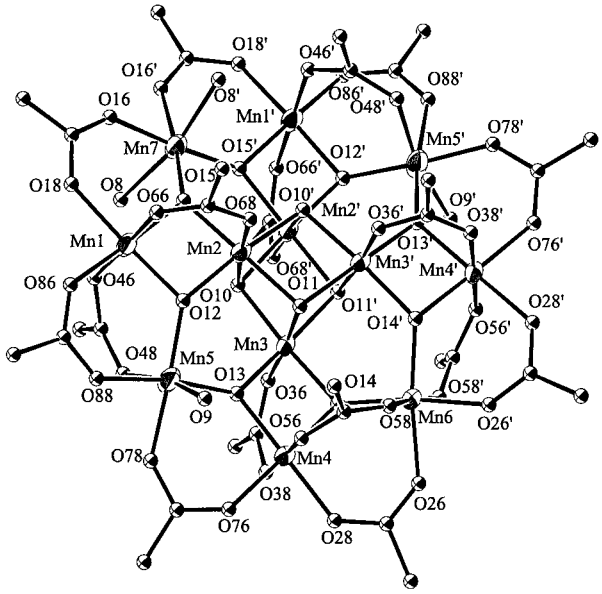


Figure 1. Structure of the core of $\mathbf{2}\cdot CH_2Cl_2\cdot 5H_2O$. The 2-chlorobenzoate rings are omitted for clarity.

Peripheral ligation of complex **2** is provided by sixteen η^2-μ-carboxylate groups and four H_2O ligands. Complex **2** is structurally similar to complex **1**. The most notable difference is the positioning of the four H_2O ligands: The acetate complex **1** has one H_2O ligand on each of four Mn^{III} ions. Complex **2** has one H_2O ligand [O9] on each of the two atoms labeled Mn5; the other two H_2O ligands [O8] are disordered together with the carboxylate oxygen atom that is shared by Mn1, Mn5, and Mn7. Complex **2** is located on a twofold axis, whereas complex **1** has a higher 2,2,2 crystal site symmetry. A variety of data, including variable-field magnetization, indicate complex **3** also has the same basic Mn_{12} core as **1** and **2**.

Magnetization hysteresis data obtained for oriented crystal samples of complexes **1**, **2,** and **3** at 2.0 K are shown in Figure 2. In each case, a few small crystals of a complex were suspended in eicosane held at 40 °C. This eicosane suspension was then introduced into a 5.5 T field, whereupon the crystals were oriented, each with their easy axis (i.e. the direction of the largest component of the crystal's magnetic susceptibility tensor) parallel to the field. The eicosane was then cooled to room temperature, which resulted in a solid wax cube with the crystals oriented with parallel easy axes. After thermal equilibration at 2.0 K, each sample was saturated in a field of +2.5 T. Then, the field was swept down to −2.5 T, and subsequently cycled back to +2.5 T. Each hysteresis loop was collected in a period of 1.5 h.

Steps are seen in the hysteresis loops for all three Mn_{12} complexes. The positions of the steps are highlighted by Figure 3, which shows the first derivative plots for the three hysteresis loops. Such steps in a hysteresis loop have been

[*] Prof. Dr. J. Ribas, Dr. B. Albela
Departament de Quimica Inorganica
Universitat de Barcelona
Diagonal, 647, E-08028-Barcelona (Spain)
Fax: Int. code + (34) 3490-7725
E-mail: jribas@kripto.qui.ub.es
Prof. Dr. G. Christou, Dr. K. Folting
Department of Chemistry
Indiana University
Bloomington, IN 47405-4001 (USA)
Fax: Int. code + (1) 812855-2399
E-mail: christou@indiana.edu
Prof. Dr. D.N. Hendrickson, Dr. D. Ruiz, Z. Sun
Department of Chemistry-0358
University of California at San Diego
La Jolla, CA 92093-0358 (USA)
Fax: Int. code + (1) 619534-5383
E-mail: dhendrickson@ucsd.edu

[**] This work was supported by the U.S. National Science Foundation. D.R. is grateful to the Spanish Ministry of Education for a postdoctoral fellowship. B.A. is grateful to the Spanish Ministry of Education for a doctoral fellowship. J.R. thanks the Dirección General de Investigación Científica y Técnica for financial support.

 © WILEY-VCH Verlag GmbH, D-69451 Weinheim, 1998 1433-7851/98/3703-0300 $ 17.50+.50/0

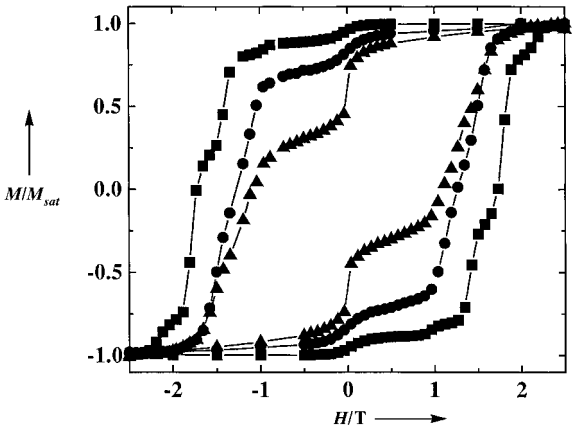


Figure 2. Magnetization hysteresis loops measured at 2.0 K for oriented crystals in eicosane matrix for three complexes: (■) acetate complex **1**; (●) 2-bromobenzoate complex **3**; (▲) 2-chlorobenzoate complex **2**. The magnetization data for each complex is plotted as a normalized value relative to the saturation magnetization M_{sat} for the complex.

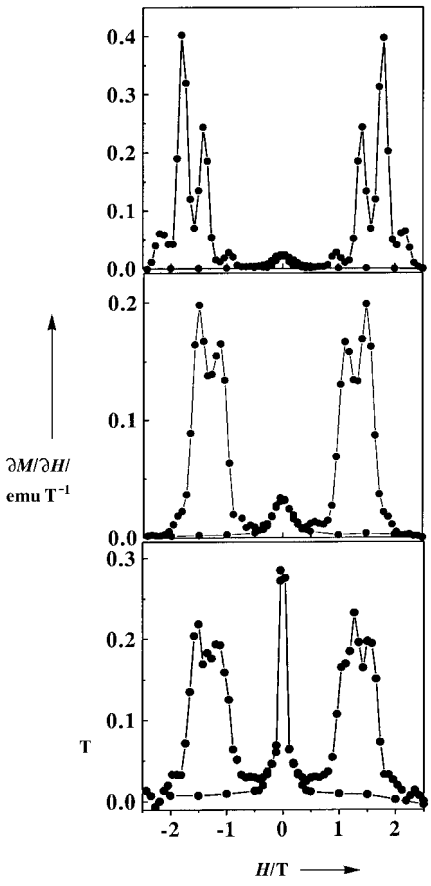


Figure 3. First derivative plots corresponding to the 2.0 K magnetization hysteresis loops shown in Figure 2. Top: acetate complex **1**; middle: Mn_{12}-2-bromobenzoate complex **3**; bottom: Mn_{12}-2-chlorobenzoate complex **2**.

shown[9–11] to be due to increases in the rate of change of the magnetization resulting from resonant magnetization tunneling. The relatively large ground-state spin of $S = 10$ together with considerable *negative* magnetic anisotropy for each molecule gives the double-well potential-energy diagram shown in Figure 4. The double well represents the change in

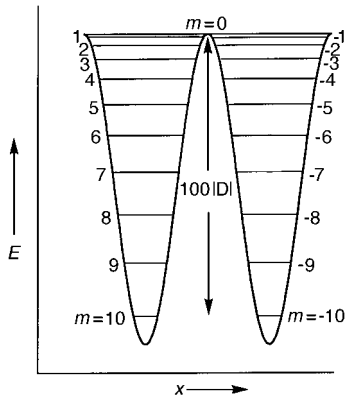


Figure 4. Plot of potential energy versus the magnetization direction for a single molecule with a $S = 10$ ground state. The axial zero-field interaction (DS_z^2) splits the $S = 10$ state into $m = \pm 10,\ \pm 9, \cdots \pm 1, 0$ levels. The barrier height U is equal to $|D|S^2 = 100\ |D|$ for the thermally activated process that involves converting the magnetic moment of the molecule from the "spin up" $m_s = 10$ level to the "spin down" $m_s = -10$ level. The diagram is drawn for zero applied field. x = Magnetization direction.

potential energy as a Mn_{12} molecule converts from the spin up to the spin down state. The application of a magnetic field stabilizes one state (e.g., $m_s = -10$) relative to the other. All of the Mn_{12} molecules populate the $m_s = -10$ when the sample is saturated in a large magnetic field. In sweeping out a hysteresis loop the first step occurs at zero field when there is an alignment of energy levels in the two parts of the double-well potential. At this point there is a resonant quantum mechanical tunneling. Additional steps are seen as the field is reversed and increased to give another alignment of levels in the two wells. Regularly spaced steps are seen[9–11] at temperatures lower than 2.0 K.

As can be seen in Figures 2 and 3, there are appreciable differences in the step heights between complexes **1**, **2,** and **3**. The scan rate and number of data points are the same for each of the three complexes. Thus, as the field is swept from +2.5 T to zero field, the first step seen for the acetate complex **1** is small. Complex **3** shows a steeper step at zero field. The steepest step is seen for complex **2**. Exactly what factors influence the rate of quantum tunneling of magnetization in these molecules is not known.[9–11] It is clear that a transverse (i.e., perpendicular to easy axis) magnetic anisotropy is needed, and this could arise from transverse quartic zero-field interactions[13] or from transverse magnetic fields caused by the nuclear spins.[14] Tunneling may not in fact occur between the lowest energy levels (e.g., $m_s = +10$ and -10 in zero field), but instead an Orbach process may be involved.[4] In this case, phonons are absorbed by a Mn_{12} molecule in a crystal exciting the molecule to a higher energy level from which it can tunnel through and/or be thermally excited over the barrier. The very appreciable differences seen in the zero-field steps for complexes **1**–**3** demonstrate a significant dependence of the observed tunneling behavior on the complex identity, and such studies should ultimately give insight about the mechanism of the tunneling; this information would be essential if the potential application of single-molecule magnets to, for example, memory devices is to be realized.

 © WILEY-VCH Verlag GmbH, D-69451 Weinheim, 1998 1433-7851/98/3703-0301 $ 17.50+.50/0

Experimental Section

Samples of complex **1** were synthesized as previously described.[15]

$[Mn_{12}(\mu_3\text{-}O)_{12}(\mu\text{-}RCOO)_{16}(H_2O)_4]$, R = C_6H_4-2-Cl, C_6H_4-2-Br: A slurry of $[Mn_{12}(\mu_3\text{-}O)_{12}(\mu\text{-}MeCOO)_{16}(H_2O)_4]$ (0.50 g, 0.25 mmol) in CH_2Cl_2 (50 mL) was treated with an excess of the corresponding carboxylic acid RCOOH (8.0 mmol). The mixture was stirred overnight in a closed flask and filtered to remove any undissolved solid. Hexanes were added to the filtrate until precipitation of a dark brown solid was observed. The resulting solid was collected by filtration and the above treatment was repeated. The resulting filtrate was layered with hexanes (100–150 mL) and stored at room temperature for several days. Since the acid was highly soluble in diethyl ether but the Mn_{12} complex was only partially soluble in this solvent, a diethyl ether/hexane(s) mixture (1:4) was used to wash the resulting solid, which was finally dried in air. Recrystallization from CH_2Cl_2/hexane(s) gave crystals of complex **2** suitable for X-ray structure analysis. Complex **2:** Elemental analysis calcd for $[Mn_{12}O_{12}(O_2CC_6H_4\text{-}2\text{-}Cl)_{16}(H_2O)_4]\cdot 4H_2O$, $C_{112}H_{80}O_{52}Cl_{16}Mn_{12}$: C 38.58, H 2.30, Cl 16.30; found: C 38.4, H 2.4, Cl 16.2%. FT-IR (KBr): $\tilde{\nu}$ = 1589, 1560, 1544, 1519, 1473, 1412, 1164, 1054, 750, 725, 702, 651, 614, 552, 522 cm^{-1}. Complex **3:** Elemental analysis calcd for $[Mn_{12}O_{12}(O_2CC_6H_4\text{-}2\text{-}Br)_{16}(H_2O)_4]\cdot 3H_2O$, $C_{112}H_{78}O_{51}Br_{46}Mn_{12}$: C 32.17, H 1.88, Br 30.64; found: C 32.1, H 1.9, Br 30.7%. FT-IR (KBr): $\tilde{\nu}$ = 1585, 1543, 1518, 1470, 1411, 1161, 1045, 1028, 747, 695, 644, 614, 552, 518 cm^{-1}.

Received: August 11, 1997 [Z 10800 IE]
German version: *Angew. Chem.* **1998**, *110*, 315–318

Keywords: magnetic properties · manganese · single-molecule magnets · tunneling

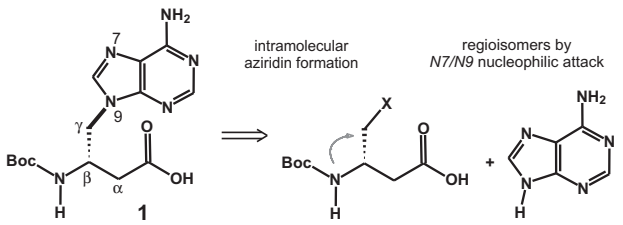
[1] B. Schwarzschild, *Physics Today* **1997**, January 17; E. M. Chudnovsky, *Science* **1996**, *274*, 938.
[2] H. J. Eppley, H.-L. Tsai, N. De Vries, K. Folting, G. Christou, D. N. Hendrickson, *J. Am. Chem. Soc.* **1995**, *117*, 301.
[3] R. Sessoli, D. Gatteschi, A. Caneschi, M. A. Novak, *Nature* **1993**, *365*, 141; D. Gatteschi, A. Caneschi, L. Pardi, R. Sessoli, *Science* **1994**, *265*, 1054.
[4] M. A. Novak, R. Sessoli in *Quantum Tunneling of Magnetization—QTM'94* (Eds: L. Gunther, B. Barbara), Kluwer, Dordrecht, **1995**, pp. 189–207.
[5] R. Sessoli, H.-L. Tsai, A. R. Schake, S. Wang, J. B. Vincent, K. Folting, D. Gatteschi, G. Christou, D. N. Hendrickson, *J. Am. Chem. Soc.* **1993**, *115*, 1804.
[6] A. L. Burion, N. V. Prokof'ev, P. C. E. Stamp, *Phys. Rev. Lett.* **1996**, *76*, 3040.
[7] F. Lionti, L. Thomas, R. Ballou, B. Barbara, A. Sulpice, R. Sessoli, D. Matteschi, *J. Appl. Phys.* **1997**, *81*, 4608.
[8] D. P. Di Vincenzo, *Physica B* **1994**, *197*, 109; D. Loss, D. P. Di Vincenzo, G. Grinstein, D. D. Awschalom, J. F. Smyth, *ibid.* **1993**, *189*, 189.
[9] J. R. Friedman, M. P. Sarachik, J. Tejada, R. Ziolo, *Phys. Rev. Lett.* **1996**, *76*, 3830.
[10] L. Thomas, F. Lionti, R. Ballou, D. Gatteschi, R. Sessoli, B. Barbara, *Nature* **1996**, *383*, 145.
[11] J. Tejada, R. F. Ziolo, X. X. Zhang, *Chem. Mater.* **1996**, *8*, 1784.
[12] Crystal data for $[Mn_{12}O_{12}(O_2CC_6H_4\text{-}o\text{-}Cl)_{16}(H_2O)_4]\cdot(CH_2Cl_2)\cdot 5(H_2O)$ (complex **2**): $C_{113}H_{82}Cl_{18}Mn_{12}O_{56}$, noncentrosymmetric space group *Pnn*2, $T = -175\,^{\circ}C$, $a = 18.033(3)$, $b = 22.752(4)$, $c = 17.319(3)$ Å, $V = 7105.62$, $Z = 2$, $6.0^{\circ} \le 2\theta \le 45^{\circ}$. There were 4197 unique reflections with 3702 unique reflections with $F > 2.33\sigma(F)$; $R(F) = 0.0880$; $R_w(F) = 0.0872$. Several of the 2-chlorobenzoate ligands exhibited disorder in the position of the chlorine atom. The CH_2Cl_2 and five H_2O solvate molecules were present at about 50% occupancy. Crystallographic data (excluding structure factors) for the structure reported in this paper have been deposited with the Cambridge Crystallographic Data Centre as supplementary publication no. CCDC-100605. Copies of the data can be obtained free of charge on application to CCDC, 12 Union Road, Cambridge CB2 1EZ, UK (Fax: int. code + (44) 1223 336-033; e-mail: deposit@ccdc.cam.ac.uk).
[13] A. L. Barra, D. Gatteschi, R. Sessoli, *Phys. Rev. B*, in press.
[14] P. Polito, A. Rettori, F. Hartmann-Boutron, J. Villain, *Phys. Rev. Lett.* **1995**, *75*, 537; A. Garg in *Quantum Tunneling of Magnetization—QTM'94* (Eds.: L. Gunther, B. Barbara); Kluwer, Dordrecht, **1995**, pp. 273–287. A. Garg, *Phys. Rev. B* **1995**, *51*, 15161.
[15] T. Lis, *Acta Crystallogr. Sect. B* **1980**, *36*, 2042.

β-Homoalanyl PNAs: Synthesis and Indication of Higher Ordered Structures**

Ulf Diederichsen* and Harald W. Schmitt

Peptide nucleic acids (PNAs) are oligomers possessing a polyamide backbone in which the nucleobases of DNA/RNA function as recognition units. The interaction of PNAs with DNA double strands or RNA have increased in importance because of their potential use in antigene or antisense therapy.[1] In contrast, helical[2] or linear PNA–PNA self-pairing complexes[3] are uncharged models that are appropriate for investigating interactions between nucleobases or between nucleobases and amino acids[4] and for examining intercalation.[5] The linearity of two complementary strands is an important structural feature of our previous investigations on α-alanyl and α-homoalanyl PNAs. It is based on the 3.6-Å distance between two consecutive amino acid side chains in the β-sheet conformation, which is similar to the stacking distance of base pairs in DNA. Here we describe the synthesis of Boc-β-homoalanyladenine (**1**) and its oligomerization to β-PNAs. UV and CD spectra suggest that the hexamer and pentamer are self-organized in higher ordered structures, which can be rationalized from model studies as being structurally inevitable.

Although there are many methods to synthesize β-amino acids[6], nucleo-β-amino acids have not been described to date. The following difficulties have to be considered in linking the nucleobase to the γ position of the side chain (Scheme 1): 1) Nucleobases are poorly soluble in most organic solvents. 2) The desired nucleophilic attack by the *N*9 nitrogen atom of



Scheme 1. Side reactions in the synthesis of nucleo-β-amino acid **1**.

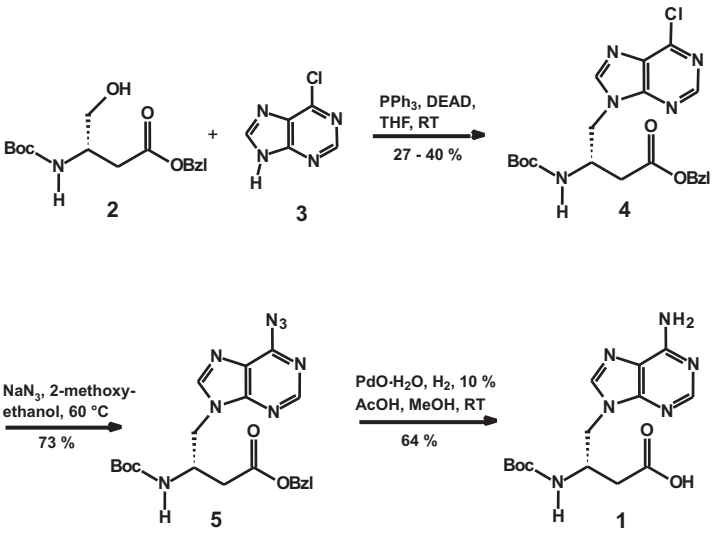
[*] Dr. U. Diederichsen, H. W. Schmitt
Institut für Organische Chemie und Biochemie der
Technischen Universität München
Lichtenbergstrasse 4, D-85747 Garching (Germany)
Fax: Int. code + (49) 89 2891-3210
E-mail: ud@linda.org.chemie.tu-muenchen.de

[**] This work was supported by the Hermann-Schlosser-Stiftung (Ph.D. fellowship for H.W.S.) and the Deutsche Forschungsgemeinschaft (Di 542 2-1). We are grateful to Professor H. Kessler, Garching, for generous support.

 © WILEY-VCH Verlag GmbH, D-69451 Weinheim, 1998

the purine competes with that by the *N*7 nitrogen atom and with intramolecular azridine formation. 3) In situ generation of the leaving group at the γ position of the amino acid appears significant. 4) Arndt–Eistert homologization of aromatic α-amino acids is expected to proceed with racemization.[6d]

The desired coupling to provide a purine attached through the *N*9 nitrogen atom to the γ position of the β-homoalanine was performed with the Mitsunobu reaction[7] (Scheme 2).



Scheme 2. Synthesis of nucleo-β-amino acid **1**: The key step is the attachment of amino acid **2** with **3** under Mitsunobu conditions (DEAD = diethyl azodicarboxylate).

At room temperature the β-homoserine derivative **2**[8] was added to 6-chloropurine (**3**) together with the Mitsunobu reagents. The direct use of adenine was not successful; the 6-chloropurine nucleo amino acid **4** could be converted into the azidopurine derivative **5**, which then was reduced and deprotected to yield **1**.[9] The presence of the *N*9 regioisomer was proven by HMQC and HMBC NMR experiments.[10] Nucleo amino acid **1** was oligomerized by solid-phase peptide synthesis (SPPS) on a 4-methylbenzhydrylamine (MBHA)–polystyrene support loaded with R-lysine(Z)-OH (Z = benzyloxycarbonyl; lysine was introduced at the C terminus for solubility reasons). The coupling was activated by *O*-(7-azabenzotriazol-1-yl)-1,1,3,3-tetramethyluronium hexafluorophosphate (HATU) and proceeded with at least 95% yield. After the oligomers were purified with HPLC (RP-C18), they were characterized with electrospray ionization mass spectrometry (ESI-MS) and ^{1}H NMR spectroscopy.

Although adenine–adenine pairing is not observed in DNA because of the helix topology, it is well established for oligomer pairing complexes[11] with a linear backbone. High stability of hexamer double strands based on A–A base pairs is known for the homo-DNA series (which contain 2′,3′-dideoxyglucopyranosyl sugar moieties, $T_m = 47\,^\circ$C)[12] as well as for α-alanyl PNA ($T_m = 31\,^\circ$C).[3] We investigated the pairing of β-homoalanyl PNAs by examining hexamer H-(β-HalA)$_6$-Lys-NH$_2$ (β-HalA = γ-(adenin-9-yl)-β-(*S*)-homoalanine, Lys-NH$_2$ = (*R*)-lysine amide). Cooperative depairing of a double strand can be recognized in UV melting curves by the sigmoidal increase in absorption upon raising the temperature. The extraordinary high stability of H-(β-HalA)$_6$-Lys-NH$_2$ was surprising; it was not possible to detect a melting point up to 95 °C (Figure 1). Furthermore, the unusual high hyperchromicity ($A_{rel.} > 40\%$) is striking. We also observed this effect with alternating G/C sequences in the alanyl PNA series for the formation of higher ordered structures.[13] The shorter oligomers H-(β-HalA)$_5$-Lys-NH$_2$ and H-(β-HalA)$_4$-Lys-NH$_2$ were synthesized to obtain UV melting curves within a measurable temperature range. Indeed, the pentamer melts at $T_m = 72\,^\circ$C ($A_{rel.} > 60\%$), and the tetramer at $T_m = 26\,^\circ$C ($A_{rel.} = 16\%$). The remarkable difference in stability and hyperchromicity of the two species (Figure 1) indicates that the structural organizations are not identical. The CD spectra of pentamer H-(β-HalA)$_5$-Lys-NH$_2$ measured at different temperatures confirm the UV melting curve. The nucleobases display a strong Cotton effect when conformationally restricted in a double strand, which begins to diminish at 40 °C when the number of flexible single strands increases. The high stabilities of adenine β-PNA oligomers is only partly the result of depairing of double strands, because the formation of higher ordered structures is indicated for the pentamer and hexamer. β-Homoalanyl PNA has a particular potential for

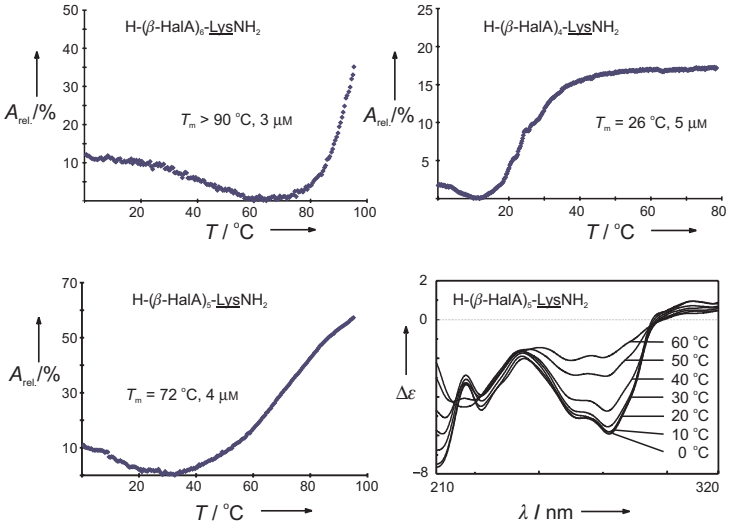


Figure 1. UV melting curves of β-PNA oligomers H-(β-HalA)$_n$-Lys-NH$_2$ ($n = 4-6$) and CD spectra of H-(β-HalA)$_5$-Lys-NH$_2$ (0.1 M NaCl, 0.01 M Na_2HPO_4/H_3PO_4, pH 7).

forming higher associations, as shown by a single-strand model (Figure 2): A homochiral β-homoalanyl PNA strand with an extended conformation provides a uniform orientation of all the side chains, and all adenine bases are aligned in the same way. This leads to pairing planes based on all Watson–Crick and Hoogsteen sites, respectively.

Adenine–adenine self-pairing can be achieved in three pairing modes: the symmetrical reverse Watson–Crick and reverse Hoogsteen modes as well as the Hoogsteen mode (Scheme 3). A chain of H-(β-HalA)$_n$-Lys-NH$_2$ oligomers based on adenine self-pairing with simultaneous participation

 © WILEY-VCH Verlag GmbH, D-69451 Weinheim, 1998 1433-7851/98/3703-0303 $ 17.50+.50/0

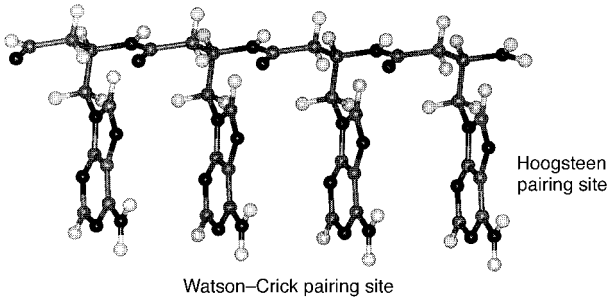
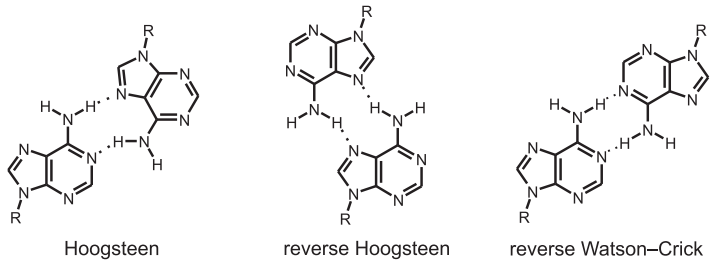


Figure 2. Model of a homochiral β-homoalanyl PNA single strand: In the extended backbone conformation, all nucleobases are uniformly aligned. This creates a pairing plane at the Watson – Crick and the Hoogsteen site.



Scheme 3. Possible adenine – adenine pairing modes.

of the Watson – Crick and Hoogsteen site is possibly responsible for the strong aggregation indicated by the melting curves.

We introduced nucleo amino acid **1** as a new building block for the synthesis of β-PNA oligomers. β-PNA is a special case of β-peptides.[14] Nevertheless, differences in structure are expected because the aggregates of β-PNA are defined by the β-peptide backbone and base-pair stabilization. The uniform alignment of all nucleobases in the extended conformation could be causal for the exceptional self-pairing of adenine oligomers in higher ordered structures. We are presently investigating the pairing possibilities and selectivities of the other canonical nucleobases as well as the influence of heterochiral base pairs.

Experimental Section

4: DEAD (1.69 g, 14.55 mmol) was added at room temperature under argon to PPh_3 (3.82 g, 14.55 mmol) in THF (18 mL) within 10 min. 6-Chloropurine (**3**, 1.45 g, 9.70 mmol) was added, and the suspension heated to 40 °C until a clear yellow solution was obtained. A solution of **2** (3.00 g, 9.70 mmol) in THF (10 mL) was added dropwise within 10 min at room temperature. After the reaction mixture was stirred for 2 d, it was heated for 4 h at 60 °C. The product was purified by consecutive flash chromatography with hexanes:ethyl acetate (1:3), hexanes:ethyl acetate (1:1), and hexanes:acetone (7:3); yield: 1.15 g (27 %). Further experiments improved the yield up to 40 %. M.p. 131 – 132 °C; $\alpha_D^{25} = 31$ ($c = 5$ in $CHCl_3$); $R_F = 0.27$ (hexanes:acetone 7:3); ^{1}H NMR (250 MHz, $CDCl_3$): $\delta = 1.21 - 1.45$ (m, 9H, *t*Bu), 2.70 (d, 2H, ^3J(H,H) = 6 Hz, α-CH_2), 4.33 – 4.43 (m, 1H, β-CH), 4.43 – 4.55 (m, 2H, γ-CH_2), 5.14 (s, 2H, CH_2–Ph), 5.30 (m, 1H, NH), 7.35 (m, 5H, Ph), 8.04 (s, 1H, H8), 8.68 (s, 1H, H2); ^{13}C NMR (62 MHz, $CDCl_3$): $\delta = 28.0$, 36.0, 46.5, 47.6, 66.8, 80.1, 128.3, 128.5, 128.6, 131.3, 135.0, 145.7, 150.9, 151.8, 152.0, 154.8, 170.4; MS: *m*/*z*: 446.3 (*M*H)$^+$; elemental analysis calcd for $C_{21}H_{24}N_5O_4Cl$: C 56.57, H 5.42, N 15.71; found: C 56.60, H 5.36, N 15.71.

5: A solution of **4** (690 mg, 1.547 mmol) and sodium azide (1.10 g, 16.92 mmol) in 2-methoxyethanol (8 mL) was heated for 5 h at 60 °C. The solvent was evaporated, and the residue suspended in ethyl acetate. After the salts were removed by filtration, the product was purified by flash chromatography with silica gel (110 g) and hexanes:ethyl acetate (3:1); yield: 512 mg (73 %); m.p. 76 – 78 °C, $[\alpha]_D^{25} = 40$ ($c = 1$ in $CHCl_3$); $R_F = 0.30$ (hexanes:ethyl acetate 1:3); ^{1}H NMR (250 MHz, [D$_6$]DMSO): $\delta = 1.15 - 1.23$ (m, 9H, *t*Bu), 2.54 – 2.86 (m, 2H α-CH_2), 4.28 – 4.42 (m, 2H, γ-CH_2), 4.44 – 4.68 (m, 1H, β-CH), 5.09 (s, 2H, CH_2–Ph), 7.00 (d, 1H, ^3J(H,H) = 8 Hz, NH), 7.33 (m, 5H, Ph), 8.48 (s, 1H, H8), 10.13 (s, 1H, H2); ^{13}C NMR (62 MHz, [D$_6$]DMSO): $\delta = 27.8$, 36.4, 47.5, 47.6, 65.7, 78.0, 119.5, 127.8, 127.9, 128.3, 135.4, 135.9, 142.7, 144.8, 145.4, 154.7, 170.1; MS: *m*/*z*: 904.8 (M_2H)$^+$, 453.2 (*M*H)$^+$; elemental analysis calcd for $C_{21}H_{24}N_8O_4$: C 55.75, H 5.35, N 24.76; found: C 55.60, H 5.52, N 24.53.

1: A solution of **5** (457 mg, 1.02 mmol) in methanol:acetic acid (9:1, 110 mL) was treated with palladium oxide hydrate (220 mg, 1.80 mmol) under argon and saturated with hydrogen. After 105 min the catalyst and the partially precipitated nucleo amino acid were separated by centrifugation, and the solid phase was extracted several times with ethyl acetate:acetic acid (9:1). Subsequent flash chromatography (ethyl acetate:methanol:water:acetic acid 40:7:3:1). Yield: 218 mg (64 %). M.p. 286 °C (decomp); $[\alpha]_D^{25} = 41$ ($c = 1$ in DMSO); $R_F = 0.36$ (ethyl acetate:methanol:water:acetic acid 10:1:1:0.5, NaCl saturated); ^{1}H NMR (500 MHz, [D$_6$]DMSO): $\delta = 0.95 - 1.03$ (m, 1.5H, *t*Bu), 1.15 – 1.30 (m, 7.5H, *t*Bu), 2.36 – 2.52 (m, 2H, α-CH_2), 4.05 – 4.20 (m, 2H, γ-CH_2), 4.21 – 4.30 (m, 1H, β-CH), 6.42 (m, 0.2H, NH), 6.90 (d, 0.8H, J = 7.1 Hz, NH), 7.13 (s, 2H, NH_2), 7.92 (s, 1H, H8), 8.12 (s, 1H, H2); ^{13}C NMR (125 MHz, [D$_6$]DMSO): $\delta = 27.6$ (*t*Bu), 37.1 (Cα), 45.8 (Cβ), 47.3 (Cγ), 77.5 (*t*Bu), 118.3 (C5), 140.6 (C8), 149.5 (C4), 152.0 (C2), 154.5 (CO of Boc), 156.0 (C6), 171.7 (COOH); the ^{13}C NMR signals were assigned with HMBC and HMQC experiments; MS: *m*/*z*: 337.1 (*M*H)$^+$; UV (H_2O): $\lambda_{max} = 263$ nm (14000).

H-(β-HalA)$_4$-Lys-NH_2: ^{1}H NMR (500 MHz, D_2O): $\delta = 1.29 - 1.35$ (m, 2H, Lys), 1.50 – 1.71 (m, 4H, Lys), 2.00 (m, 1H, Hα), 2.12 (m, 1H, Hα), 2.18 – 2.38 (m, 4H, Hα), 2.42 (m, 1H, Hα), 2.65 (m, 1H, Hα), 2.85 (m, 2H, Hε-Lys), 3.22 – 3.50 (m, 4H, Hβ, Hγ), 3.55 (m, 1H, Hβ, Hγ), 3.63 – 3.84 (m, 3H, Hβ, Hγ), 3.98 (m, 1H, Hβ, Hγ), 4.11 (m, 1H, Hα-Lys), 4.25 – 4.35 (m, 2H, Hβ, Hγ), 4.42 (m, 1H, Hβ, Hγ), 7.79 (s, 1H, H2, H8), 7.84 (s, 1H, H2, H8), 7.90 (s, 1H, H2, H8), 7.91 (s, 1H, H2, H8), 7.97 (s, 1H, H2, H8), 7.98 (s, 1H, H2, H8), 8.00 (s, 1H, H2, H8), 8.02 (s, 1H, H2, H8); MS: *m*/*z*: 1018.3 (*M*H)$^+$, 511.0 (MH$_2$)$^{2+}$.

H-(β-HalA)$_5$-Lys-NH_2: ^{1}H NMR (500 MHz, D_2O): $\delta = 1.21 - 1.40$ (m, 2H, Lys), 1.50 – 1.75 (m, 4H, Lys), 2.15 – 2.40 (m, 7H, Hα), 2.42 – 2.55 (m, 2H, Hα), 2.68 (m, 1H, Hα), 2.87 (m, 2H, Hε-Lys), 3.70 – 4.50 (m, 16H, Hβ, Hγ, Hα-Lys), 7.95 – 8.20 (m, 10H, H2, H8); MS: *m*/*z*: 1236.4 (*M*H)$^+$, 619.0 (MH$_2$)$^{2+}$.

H-(β-HalA)$_6$-Lys-NH_2: ^{1}H NMR (500 MHz, D_2O): $\delta = 1.25 - 1.38$ (m, 2H, Lys), 1.50 – 1.72 (m, 4H, Lys), 2.11 – 2.40 (m, 9H, Hα), 2.41 – 2.56 (m, 2H, Hα), 2.68 (m, 1H, Hα), 2.87 (m, 2H, Hε-Lys), 3.58 (m, 1H, Hβ, Hγ), 3.61 – 3.75 (m, 2H, Hβ, Hγ), 3.77 – 3.98 (m, 8H, Hβ, Hγ), 4.06 (m, 1H, Hα-Lys), 4.10 – 4.20 (m, 2H, Hβ, Hγ), 4.24 – 4.36 (m, 3H, Hβ, Hγ), 4.38 – 4.49 (m, 2H, Hβ, Hγ), 7.77 (s, 1H, H2, H8), 7.82 (s, 1H, H2, H8), 7.90 (m, 2H, H2, H8), 7.94 (s, 1H, H2, H8), 7.96 (s, 1H, H2, H8), 7.97 (s, 2H, H2, H8), 8.03 (s, 1H, H2, H8), 8.04 (s, 1H, H2, H8), 8.07 (s, 1H, H2, H8), 8.08 (s, 1H, H2, H8); MS: *m*/*z*: 1455.4 (*M*H)$^+$, 727.9 (MH$_2$)$^{2+}$.

Received: June 26, 1997
Revised version: August 7, 1997 [Z10603IE]
German version: *Angew. Chem.* **1998**, *110*, 312 – 315

Keywords: amino acids · Mitsunobu reaction · nucleic acids · peptide nucleic acids · supramolecular chemistsry

[1] a) M. Egholm, O. Buchardt, L. Christensen, C. Behrens, S. M. Freier, D. A. Driver, R. H. Berg, S. K. Kim, B. Nordén, P. E. Nielsen, *Nature* **1993**, *365*, 566; b) B. Hyrup, P. E. Nielsen, *Bioorg. Med. Chem.* **1996**, *4*, 5.

[2] P. Wittung, P. E. Nielsen, O. Buchardt, M. Egholm, B. Nordén, *Nature* **1994**, *368*, 561.

[3] a) U. Diederichsen, *Angew. Chem.* **1996**, *108*, 458; *Angew. Chem. Int. Ed. Engl.* **1996**, *35*, 445; b) U. Diederichsen, H. W. Schmitt, *Tetrahedron Lett.* **1996**, *37*, 475.

[4] U. Diederichsen, D. Weicherding, unpublished results.

 © WILEY-VCH Verlag GmbH, D-69451 Weinheim, 1998 1433-7851/98/3703-0304 $ 17.50+.50/0

[5] U. Diederichsen, *Bioorg. Med. Chem. Lett.* **1997**, *7*, 1743.
[6] a) E. Juaristi, D. Quintana, J. Escalante, *Aldrichim. Acta* **1994**, *27*, 3; b) D. C. Cole, *Tetrahedron* **1994**, *50*, 9517; c) J. Podlech, D. Seebach, *Angew. Chem.* **1995**, *107*, 507; *Angew. Chem. Int. Ed. Engl.* **1995**, *34*, 471; d) *Liebigs Ann. Chem.* **1995**, 1217; e) N. N. Romanova, A. G. Gravis, Y. G. Bundel, *Russ. Chem. Rev.* **1996**, *65*, 1083.
[7] a) T. F. Jenny, N. Previsani, S. A. Benner, *Tetrahedron Lett.* **1991**, *32*, 7029; b) M. L. Peterson, R. Vince, *J. Med. Chem.* **1991**, *34*, 2787; c) A. Toyota, N. Katagiri, C. Kaneko, *Synth. Commun.* **1993**, *23*, 1295; d) M. R. Harnden, A. Parkin, M. J. Parratt, R. M. Perkins, *J. Med. Chem.* **1993**, *36*, 1343; e) A. Bouali, D. F. Ewing, G. Mackenzie, *Nucleosides Nucleotides* **1994**, *13*, 491.
[8] Homoserine derivative **2** was obtained in 95% yield by reduction of the C-terminal carbonyl group of Boc-Asp(Bzl)OH in analogy to G. Kokotos, *Synthesis* **1990**, 299.
[9] a) Z. Kazimierczuk, H. B. Cottam, G. R. Revankar, R. K. Robins, *J. Am. Chem. Soc.* **1994**, *106*, 6379; b) F. R. Benson, T. W. Hartzel, E. A. Otten, *ibid.* **1954**, *76*, 1858.
[10] H. Kessler, S. Seip in *Two-Dimensional NMR Spectroscopy* (Eds.: W. R. Croasmun, R. M. K. Carlson), 2nd ed., VCH, Weinheim, **1994**, p. 619.
[11] a) W. Saenger, *Principles of Nucleic Acid Structure*, Springer, New York, **1983**; b) I. Berger, C. Kang, A. Fredian, R. Ratliff, R. Moyzis, A. Rich, *Nat. Struct. Biol.* **1995**, *2*, 416; c) K. J. Baejens, H. L. De Bondt, A. Pardi, S. R. Holbrook, *Proc. Natl. Acad. Sci. USA* **1996**, *93*, 12851.
[12] J. Hunziker, H.-J. Roth, M. Böhringer, A. Giger, U. Diederichsen, M. Göbel, R. Krishnan, B. Jaun, C. Leumann, A. Eschenmoser, *Helv. Chim. Acta* **1993**, *76*, 259.
[13] U. Diederichsen, *Angew. Chem.* **1997**, *109*, 1966; *Angew. Chem. Int. Ed. Engl.* **1997**, *36*, 1886.
[14] The preferred conformation of a β-peptide hexamer in pyridine is the 3_1 helix. For β-peptides, compare with a) D. Seebach, M. Overhand, F. N. M. Kühnle, B. Martinoni, L. Oberer, U. Hommel, H. Widmer, *Helv. Chim. Acta* **1996**, *79*, 913; b) D. Seebach, P. E. Ciceri, M. Overhand, B. Jaun, D. Rigo, L. Oberer, U. Hommel, R. Amstutz, H. Widmer, *ibid.* **1996**, *79*, 2043; c) D. H. Appella, L. A. Christianson, I. L. Karle, D. R. Powell, S. H. Gellman, *J. Am. Chem. Soc.* **1996**, *118*, 13071; d) D. H. Appella, L. A. Christianson, D. A. Klein, D. R. Powell, X. Huang, J. J. Barchi, Jr., S. H. Gellman, *Nature* **1997**, *387*, 381. The conformation of β-PNA should not be helical because of the base-pair distances of 5 Å and the maximum of two bases on top of each other, which leads to a substantial loss of stacking interactions.

Redox-Switched Exciton-Coupled Circular Dichroism: A Novel Strategy for Binary Molecular Switching**

Steffen Zahn and James W. Canary*

A recent and exciting prospect in the area of information technology lies in the development of molecular switches that operate with efficiency, reversibility, and resistance to fatigue.[1] The development of electrochemical switches has recently attracted much attention due to possible applications such as data storage.[2–8] Redox switches require a) components whose structures and physical properties can be turned on or off electrochemically,[3, 6–8] and b) sufficiently different optical spectra that allow the individual states to be addressed.[2, 4] Here we describe a method for generating a redox switch through redox control of the ligand conformation. This approach resulted in a novel molecular switch with reproducible redox-dependent optical properties; the switch should be easily adaptable to solid-state technology.

Our molecular redox switch is based on a) complexes in which a single metal center can exist in two different oxidation states, and b) chiral ligands having easily distinguishable optical properties. Copper(II) complexes are particularly suitable since they show fast ligand exchange, which potentiates fast signal interchange. The ligand (*S*)-*N*,*N*-bis[(2-quinolyl)methyl]-1-(2-quinolyl)ethylamine, (*S*)-α-MeTQA, was selected for this study because of the steric hindrance and strong chromophoric properties presented by the 2-quinolyl groups and the expected optimal chromophoric orientation provided by the propellerlike geometry of the complexes. Reduction of the sterically hindered Cu^{II} complex was anticipated to result in a change in the orientation of the 2-quinolyl arms with respect to the central axis (Scheme 1). Since the exciton-coupled circular dichroism (ECCD) signal generated from these complexes is critically dependent upon the distance and dihedral angle between the planar chromophores,[9] the magnitude of the ECCD spectrum was expected to vary with the oxidation state of the copper ion.

The preparation of the ligand (*S*)-α-MeTQA began with the asymmetric synthesis of (*S*)-2-(1-aminoethyl)quinoline from the 2-aminomethylquinoline imine of (+)-pinanone.[10] A single recrystallization of the L-(+)-tartrate salt of the chiral primary amine yielded the desired product with 99.7% *ee* in 19% overall yield. Alkylation of the enantiomerically pure amine with 2-bromomethylquinoline provided (*S*)-α-MeTQA in 81% yield. Copper complexes **1** and **2** were prepared by mixing homogeneous solutions of the ligand and the appropriate salt.[11, 12] The UV/Vis spectrum of **2** shows a

$[Cu^{I}\{(S)\text{-}\alpha\text{-MeTQA}\}](PF_6)$ **1**

$[Cu^{II}\{(S)\text{-}\alpha\text{-MeTQA}\}](ClO_4)(PF_6)$ **2**

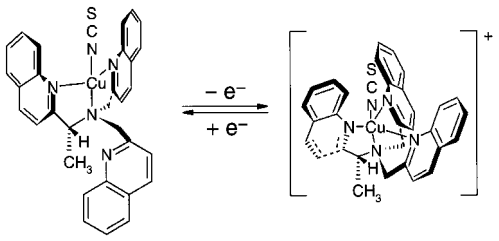
d–d transition at 691 nm ($\varepsilon = 202$), which is consistent with a coordination geometry for the Cu^{II} ion that is closer to a square pyramid than the desired trigonal bipyramid.[11, 13] However, addition of one equivalent of NH_4NCS (to yield **4**) resulted in two d–d bands (719 nm, $\varepsilon = 202$; 867 nm, $\varepsilon = 296$); this indicates trigonal-bipyramidal geometry.[13] The color change of **4** from turquoise to green-yellow is due to a ligand-to-metal charge transfer (LMCT) at 420 nm ($\varepsilon = 445$).[14] Cyclic voltammograms of the copper complexes in acetonitrile or dimethylformamide were well-behaved and displayed single quasi-reversible one-electron redox waves ($i_{pa}/i_{pc} \approx 1$).[15]

The CD spectra of **1** ($A = 174$) and **2** ($A = 455$) displayed bisignate curves with remarkably large amplitudes (that is, large positive and negative Cotton effects).[16] The split CD

[*] Prof. J. W. Canary, S. Zahn
Department of Chemistry
New York University
New York, NY 10003 (USA)
Fax: Int. code + (1) 212 260-7905
E-mail: james.canary@nyu.edu

[**] We thank the National Institutes of Health (GM 49170) for financial support of this work.

 © WILEY-VCH Verlag GmbH, D-69451 Weinheim, 1998 1433-7851/98/3703-0305 $ 17.50+.50/0



3 4

Scheme 1. The redox system [Cu^{I}{(*S*)-α-MeTQA}](NCS) (**3**)/[Cu^{II}{(*S*)-α-MeTQA}(NCS)]$^{+}$ (**4**). The structure of **3** was determined from ^{1}H NMR spectra at various temperatures, CD spectra, and comparison with structural data for analogous complexes.[13, 20] The geometrical arrangement of **4** is supported by CD and VIS spectroscopic data and comparison of structurally related Cu^{II} complexes.[15]

curve, the coincidence of the inflection point with the λ_{max} of the low-energy absorption band of the UV/Vis spectrum, and the large intensity of the signal are consistent with an exciton-coupling mechanism. Adding NH_4NCS to solutions of **1** and **2** resulted in a weaker signal for **3** ($A = 70$) and a stronger signal for **4** ($A = 670$, Figure 1). The intensity for **4** was such that it

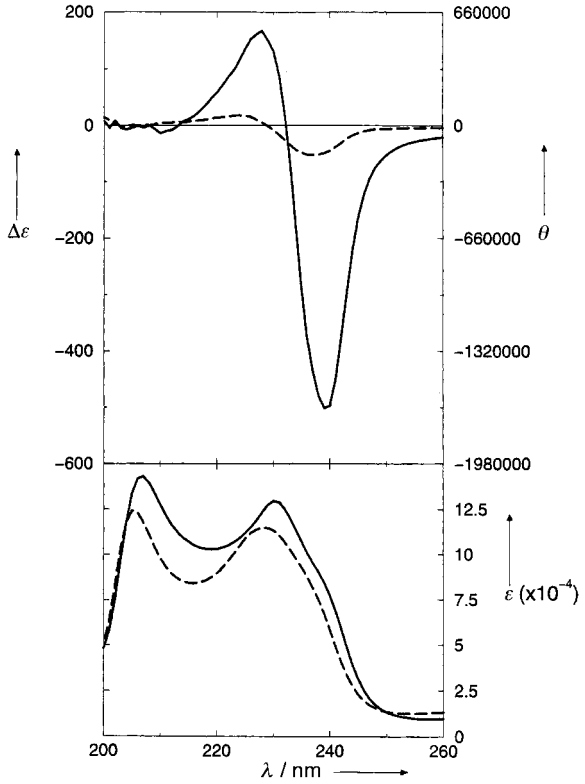


Figure 1. Circular dichroism (top) and UV/Vis spectra (bottom) of complexes **3** (dashed lines) and **4** (solid lines). UV/Vis (5 μM) and CD spectra (0.3 mM) were measured at room temperature in methanol. ε and $\Delta\varepsilon$ are given in L mol^{-1} cm^{-1}.

was possible to obtain good spectra at concentrations as low as 700 nM. Films of complex **4** prepared on quartz exhibited a CD curve that is similar in pattern and sign to that shown in Figure 1 but even more intense than that observed in methanol, as estimated by comparison with the isotropic absorption spectrum of the film. The large variation in intensity of the CD spectra of **3** and **4** was also maintained in the film.

Quantitative analysis of the CD spectra[17] of Cu^{I} complexes **1** and **3** suggest that addition of NCS^{-} displaces one quinoline arm of the ligand, which is similar to the behavior of other closely related tripodal Cu^{I} complexes.[11] Consequently, **3** provides one couplet, whereas **1** provides three couplets that together afford a much more intense spectrum. The substantially stronger intensities of **2** and **4**, compared with analogous bis(quinoline) ligands,[18] are also consistent with tetradentate coordination of the Cu^{II} ion.

To assess the ability of systems **1**/**2** and **3**/**4** to behave as reversable switches, redox cycling studies were conducted in solution and monitored by CD and UV/Vis spectroscopy. Reduction of **2** with ascorbic acid immediately gave CD and UV/Vis spectra identical to those of **1**. Reaction of **1** with ammonium persulfate was more sluggish and required 10 min at 50 °C in order to achieve the CD signal of **2**. This process was repeated three times; each cycle gave a less intense UV/Vis absorption band for **1**. However, in the presence of NCS^{-} much better results were obtained (Figure 2). Treatment of **4**

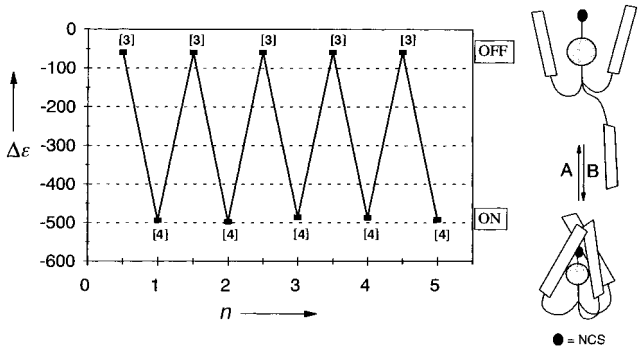


Figure 2. Left: Plot of $\Delta\varepsilon$ vs. the number of cycles n at 240 nm in methanol. The reduction of **4** to **3** proceeded with ascorbic acid, whereas **3** was oxidized back to **4** with ammonium persulfate. The average difference in signal intensity between **3** and **4** is $\Delta\Delta\varepsilon_{240} = 430$. $\Delta\Delta\varepsilon_{240}$ is the absolute difference in the $\Delta\varepsilon$ values for the binary system at 240 nm ($\Delta\Delta\varepsilon_{240} = |\Delta\varepsilon_{240(on)}| - |\Delta\varepsilon_{240(off)}|$). Right: Schematic representation of dynamic behavior of complexes **3** and **4** that leads to different arrangements of the chromophores and thus to distinct ECCD signal intensities representing the "on" and "off" states of the molecular switch. A = reduction, B = oxidation.

with ascorbic acid resulted in a CD spectrum that is identical to that of **3**, whereas oxidation of **3** with ammonium persulfate produced the CD signal of **4** immediately at room temperature.[19] Up to five cycles were carried out without a significant decrease in signal intensity; this demonstrates the superb reversibility and reproducibility of the chiroptical signal.

The magnitude of the changes in the chiroptical properties of the system **3**/**4** is quite remarkable ($\Delta\Delta\varepsilon_{240} = 430$). The low energetic barrier for the change in coordination geometry in the system **3**/**4**, its rapid response, its high signal intensities, and its stability on multiple cycling support the adaptability of

 © WILEY-VCH Verlag GmbH, D-69451 Weinheim, 1998 1433-7851/98/3703-0306 $ 17.50+.50/0

this type of coordination complex to real applications which depend on easily distinguished "on" and "off" signals. Studies on the immobilization of these complexes on appropriate conducting surfaces are underway.

Received: July 18, 1997 [Z 10703 IE]
German version: *Angew. Chem.* **1998**, *110*, 321 – 323

Keywords: chiral complexes · circular dichroism · copper · molecular switches

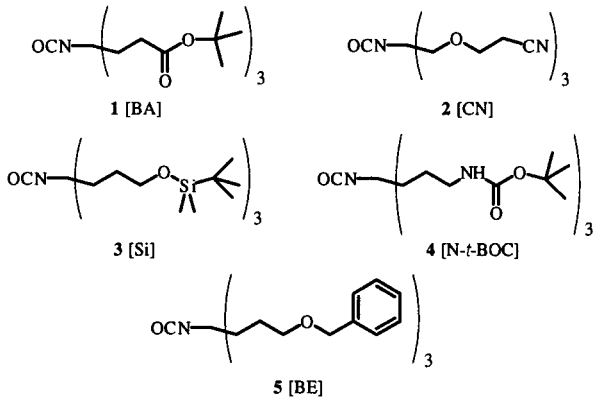
[1] J. M. Lehn, *Supramolecular Chemistry—Concepts and Perspectives*, VCH, Weinheim, **1995**.
[2] N. P. M. Huck, W. F. Jager, B. de Lange, B. L. Feringa, *Science* **1996**, *273*, 1686 – 1688.
[3] L. Fabbrizzi, A. Poggi, *Chem. Soc. Rev.* **1995**, 197 – 202.
[4] L. Zelikovich, J. Libman, A. Shanzer, *Nature* **1995**, *374*, 790 – 792.
[5] J. A. Wytko, C. Boudon, J. Weiss, M. Gross, *Inorg. Chem.* **1996**, *35*, 4469 – 4477.
[6] R. A. Bissell, E. Cordova, A. E. Kaifer, J. F. Stoddart, *Nature* **1994**, *369*, 133 – 137.
[7] A. Livoreil, C. O. Dietrich-Buchecker, J.-P. Sauvage, *J. Am. Chem. Soc.* **1994**, *116*, 9399 – 9400.
[8] S. H. Kawai, S. L. Gilet, R. Ponsinet, J. M. Lehn, *Chem. Eur. J.* **1995**, *1*, 285 – 293, and references therein.
[9] *Circular Dichroism: Principles and Applications* (Eds.: K. Nakanishi, N. Berova, R. W. Woody), VCH, New York, **1994**.
[10] A. Mi, X. Xiao, L. Wu, Y. Jiang, *Synthetic Commun.* **1991**, *21*, 2207 – 2212.
[11] N. Wei, N. N. Murthy, Q. Chen, J. Zubieta, K. D. Karlin, *Inorg. Chem.* **1994**, *33*, 1953 – 1965.
[12] Elemental analyses: **1** ($CuC_{31}H_{26}N_4PF_6$): calcd: C 56.15, H 3.95, N 8.45; found: C 55.91, H 3.75, N 8.35; **2**: ($CuC_{31}H_{26}N_4O_4PF_6Cl$): calcd: C 48.83, H 3.43, N 7.35; found: C 49.10, H 3.61, N 7.34. Complexes **3** and **4** were prepared in situ from **1** and **2**, respectively, and NH_4NCS.
[13] N. Wei, N. N. Murthy, K. D. Karlin, *Inorg. Chem.* **1994**, *33*, 6093 – 6100.
[14] M. Herve, A. Garnier, L. Tosi, M. Steinbuch, *Eur. J. Biochem.* **1981**, *116*, 177 – 183.
[15] For example, **1** is reduced in MeCN at $E_{1/2} = -49.9$ mV (reference: $Fc/Fc^+ = 45.6$ mV; Fc = ferrocene). The cyclic voltammogram was measured under N_2 with a standard three-electrode apparatus (glassy-carbon working electrode, Pt-wire auxiliary electrode, and 0.1M $AgNO_3$ in MeCN as reference electrode) with 0.1M $n Bu_4NPF_6$ as supporting electrolyte and a scan rate of 50 mV s^{-1}. Addition of SCN^- to the solution resulted in a shift in $E_{1/2}$ of -250 mV and afforded an improvement in the reversibility of the voltammograms. There was no indication of oxidation or reduction of SCN^- under the conditions of the experiment.
[16] Amplitude (A): difference in the $\Delta\varepsilon$ values for the two extrema of split CD curves ($A = |\Delta\varepsilon_{1C.E.}| + |\Delta\varepsilon_{2C.E.}|$).
[17] W. Kauzmann, F. B. Clough, I. Tobias, *Tetrahedron* **1961**, *13*, 57 – 105.
[18] J. W. Canary, C. S. Allen, J. M. Castagnetto, Y. Wang, *J. Am. Chem. Soc.* **1995**, *117*, 8484 – 8485.
[19] NH_4NCS was added after every oxidation to correct for loss of NCS^- through oxidation. Oxidation at a controlled potential avoided this problem.
[20] H. Nagao, N. Komeda, M. Mukaida, M. Suzuki, K. Tanaka, *Inorg. Chem.* **1996**, *35*, 6809 – 6815.

Isocyanate-Based Dendritic Building Blocks: Combinatorial Tier Construction and Macromolecular-Property Modification**

George R. Newkome,* Claus D. Weis, Charles N. Moorefield, Gregory R. Baker, Bradley J. Childs, and Jon Epperson

In the current development of dendritic chemistry[1] the application of iterative technology is being examined from many different perspectives. These areas include the use of dendrimers and related materials as unimolecular micelles,[2] ordered network building blocks,[3] chromatography additives,[4] cancer therapeutics,[5] and electrically conducting materials.[6] Central to the construction of these macromolecular assemblies is the design and tuning of properties such as solubility, viscosity, and reactivity for specific applications. Hence it is desirable to design synthetic methods for the ready introduction of functionally diverse terminal groups.

Recently we reported the synthesis of the stable isocyanate triester **1** and its use as a building block in the rapid "dendrimerization" of protic materials and surfaces.[7] In addition, we disclosed the syntheses of the related branched



monomers[8] **2** – **5**. Each of these monomers possesses a triad of protected functional groups, an sp^3 C-branching center and a reactive isocyanate moiety. We herein report on the concept of the rapid modification of properties through combinatorial synthesis analogous to that used for the discovery of novel solid-state materials,[9] biologically active substrates,[10] and artificial receptors.[11] While dendrimers have recently been employed[12] and touted[13,14] as vehicles for the generation of standard small-molecule libraries, our combinatorial method relies on mixtures of AB_3-type monomers having varying compositions of different, yet mutually compatible building

[*] Prof. Dr. G. R. Newkome, Dr. C. D. Weis, Prof. Dr. C. N. Moorefield, Prof. Dr. G. R. Baker, Dr. B. J. Childs, J. Epperson
Center for Molecular Design and Recognition
Department of Chemistry, University of South Florida
4202 East Fowler Avenue, Tampa, FL 33620-5250 (USA)
Fax: Int. code + (1) 813 974-4962

[**] Chemistry of Micelles, Part 74. Support for this work was provided by the National Science Foundation (DMR-96-22609) and the Army Office of Research (DAAHO4-93-0048). We gratefully acknowledge DSM for providing the poly(propylene imine) dendrimers. Part 73: G. R. Newkome, V. V. Narayanen, L. Echegoyen, E. Pérez-Cordero, H. Luftmann, *Macromolecules*, **1997**, *30*, 5187.

 © WILEY-VCH Verlag GmbH, D-69451 Weinheim, 1998 1433-7851/98/3703-0307 $ 17.50+.50/0

blocks for sequential formation of "tiers" and dendrimer construction.

Reaction of the isocyanate monomers **1**–**5** with a fourth-generation poly(propylene imine) dendrimer (DSM, 32-PPI)[15] bearing 32 NH_2 groups in refluxing *tert*-butyl alcohol or dichloromethane afforded (>90%) the corresponding 96-ester **6**, 96-cyanide **7**, 96-siloxane **8**, 96-*N*-*t*-BOC compound **9**, and 96-benzyl ether **10**. Formation of these compounds is supported by their ^{13}C NMR spectra (Figures 1 and 2, Table 1). Anticipated key absorptions corresponding to the

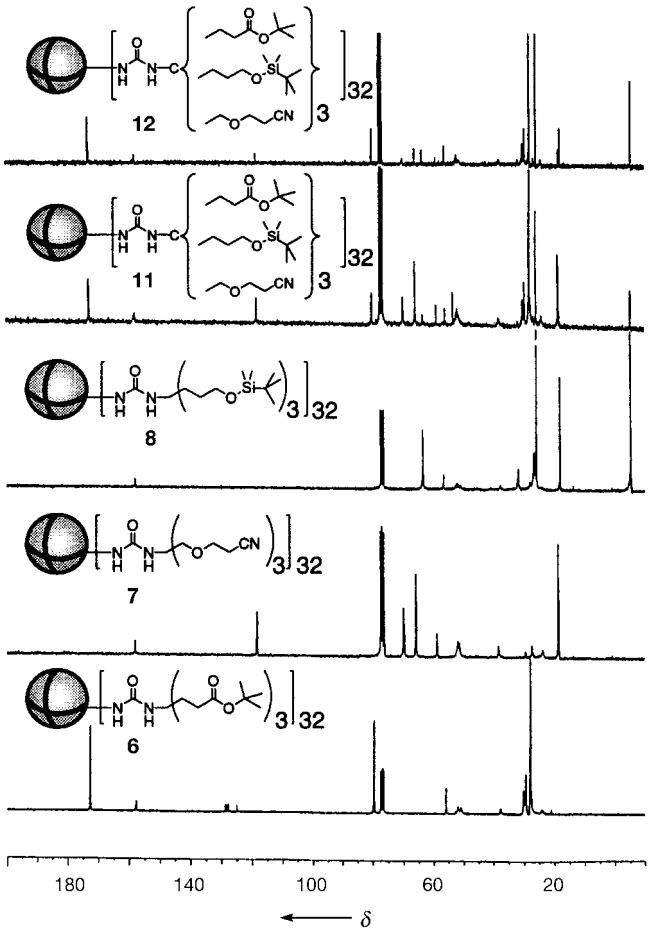


Figure 1. ^{13}C NMR spectra for the peripherally homogeneous ester, cyano, and siloxane dendrimers **6**, **7**, and **8**, respectively, and the peripherally heterogeneous dendrimers **11** (prepared from 0.5, 0.4, and 0.1 equivalents of monomers **1**, **2**, and **3**, respectively) and **12** (0.7, 0.15, and 0.15 equivalents of **1**, **2**, and **3**, respectively). Spheres represent the DSM-32-PPI dendritic core.

covalently attached 1 →3 branched monomers are observed in each spectrum (δ values): **6**: 172.7 (CO), 80.0 ($C(CH_3)$), 27.9 (CH_3); **7**: 118.4 (CN), 69.8, 65.9 (CH_2OCH_2), 18.8 (CH_2CN); **8**: 63.6 (CH_2O), 26.0 ($C(CH_3)_3$), 18.2 ($C(CH_3)_3$), −5.2 ($Si(CH_3)_2$); **9**: 156.5 (CO), 78.9 ($C(CH_3)_3$), 28.3 ($C(CH_3)_3$); **10**: 138.6, 128.4, 127.6, 127.4 (C-aryl), 72.8 ($CH_2C_6H_5$), 71.0 (CH_2CH_2O). As expected, signals attributed to the imine-based superstructure are broadened and less intense (δ values): **6**: 52.0 ($CH_2CH_2CH_2$, $CH_2CH_2CH_2CH_2$), 51.0 ($CH_2CH_2CH_2NHCONH$).

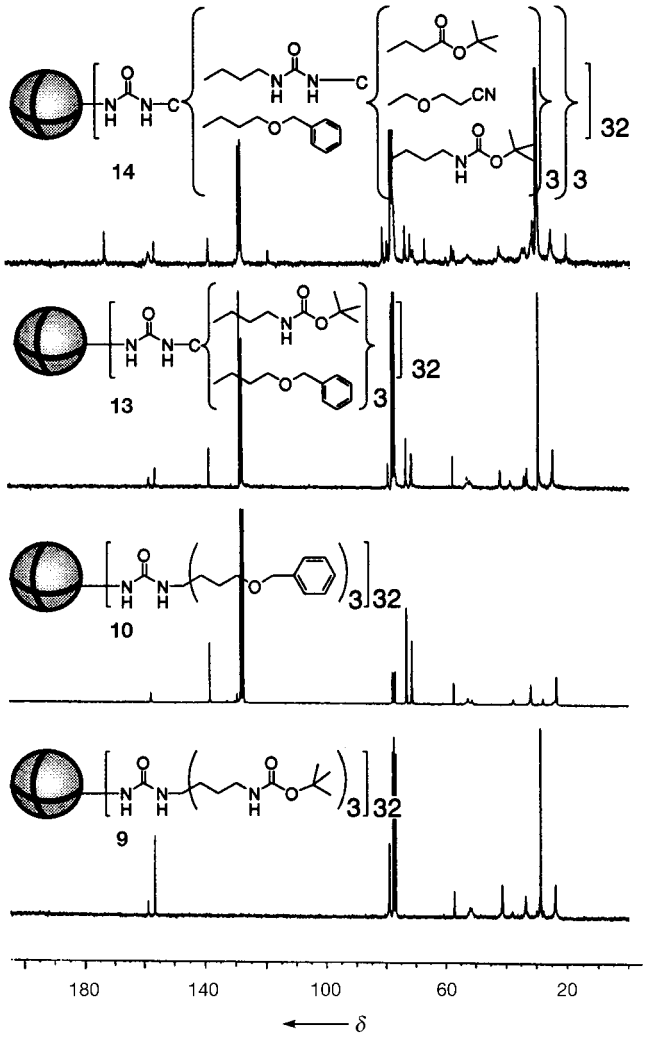


Figure 2. ^{13}C NMR spectra of dendrimers **9** and **10**, which have carbamate and benzyl ether terminal groups, respectively, and the peripherally heterogeneous dendrimers **13** (prepared from 0.5 equivalents each of monomers **4** and **5**) and **14** (prepared from **13**, see text).

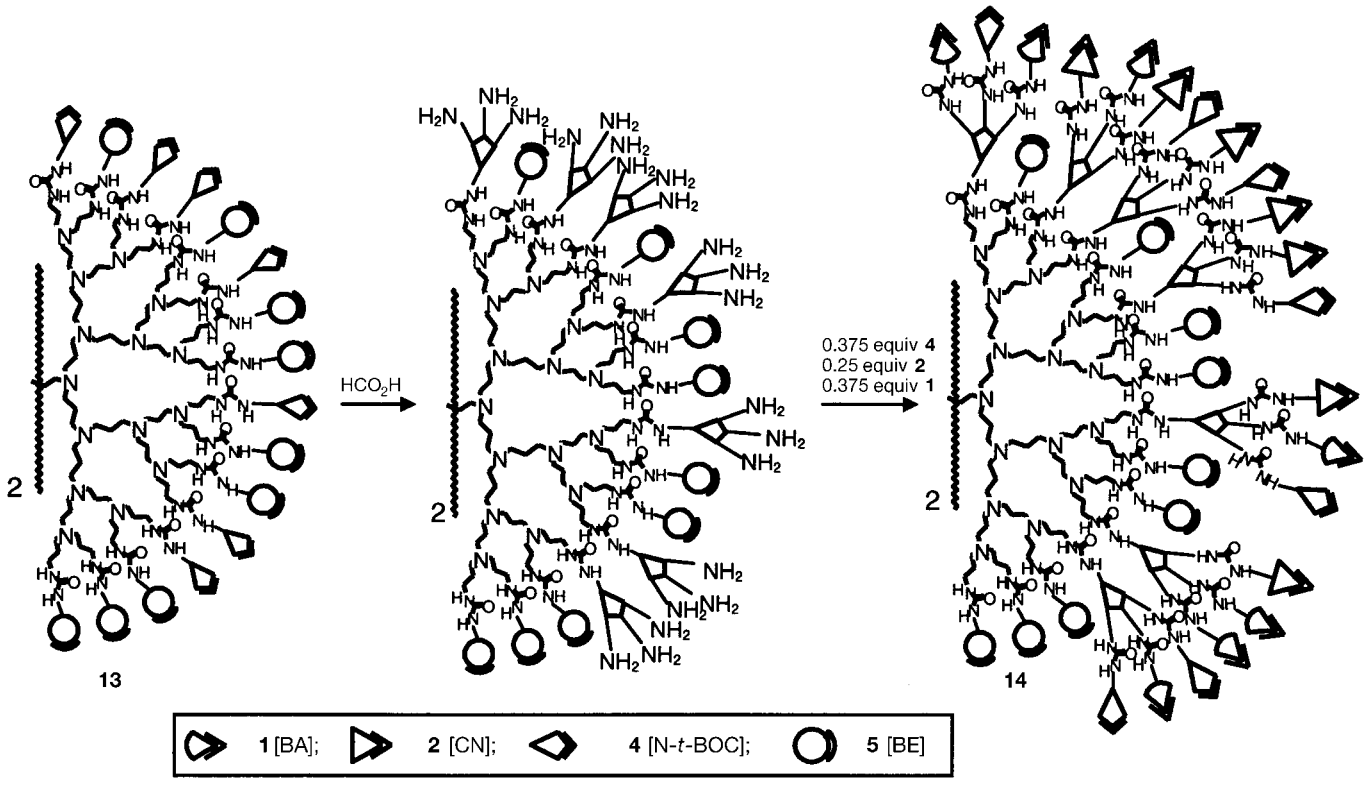
Further potential to exploit the connectivity of the isocyanate-based monomers was subsequently examined by treatment of the 32-PPI dendrimer with mixtures of monomers **1**–**3** (total of 32 equivalents). Specifically, mixtures of building blocks **1**, **2**, and **3** in various ratios [(0.5:0.1:0.4) and (0.7:0.15:0.15)] afforded the corresponding combinatorial-based dendrimers **11** and **12** (Figure 1). Evidence for the formation of these *peripherally heterogeneous* dendrimers includes the observation (after chromatographic purification) of all the pertinent ^{13}C NMR signals exhibited in the spectra of the analogous, peripherally homogeneous macromolecules **6**–**8**. More specifically, the spectrum of each peripherally heterogeneous dendrimer exhibits signals at $\delta = 172.8$, 118.3, 80.1, 63.5, 51.5, 18.7, and −5.3 (corresponding to $CO_{[BA]}$, CN, $C(CH_3)_{3[BA]}$, $CH_2O_{[Si]}$, $CH_2CH_{2[DSM]}$, CH_2CN, and $Si(CH_3)_2$, respectively). The observed low intensity and slightly broadened signals at $\delta = 157.8$ and 157.6 ($NHCONH_{[BA, Si, CN]}$) suggest that the surface is relatively rigid as a result of hydrogen bonding between the urea units and crowding of the terminal groups.

 © WILEY-VCH Verlag GmbH, D-69451 Weinheim, 1998 1433-7851/98/3703-0308 $ 17.50+.50/0 *Angew. Chem. Int. Ed.* **1998**, *37*, No. 3

Table 1. ^{13}C NMR data for compounds **6**–**14** (subscripts denote absorptions arising from specified units) (62.9 MHz, $CDCl_3$, 25 °C).

6: $\delta = 172.7$ (CO), 157.9 (NHCONH), 80.0 ($C(CH_3)_3$), 56.0 (*tert*-C), 52.1 ($CH_2CH_2CH_2CH_2$, $CH_2CH_2CH_2$), 51.0 ($CH_2CH_2CH_2NHCONH$), 37.8 ($CH_2NHCONH$), 30.2, 29.5 ($CH_2CH_2CO_2$, $CH_2CH_2NHCONH$), 27.9 ($C(CH_3)_3$), 24.2 ($CH_2CH_2CH_2CH_2$, $CH_2CH_2CH_2$)
7: $\delta = 158.2$ (NHCONH), 118.4 (CN), 69.8, 65.9 (CH_2OCH_2), 58.9 (*tert*-C), 52.0 ($CH_2CH_2CH_2$, $CH_2CH_2CH_2CH_2$), 51.0 ($CH_2CH_2CH_2NHCONH$), 38.3 ($CH_2NHCONH$), 29.6 ($CH_2CH_2CH_2CH_2$), 27.4 ($CH_2CH_2NHCONH$), 23.8 ($CH_2CH_2CH_2$), 18.8 (CH_2CN)
8: $\delta = 158.2$ (NHCONH), 63.6 (CH_2O), 56.7 (*tert*-C), 52.2 ($CH_2CH_2CH_2$, $CH_2CH_2CH_2CH_2$), 51.0 ($CH_2CH_2CH_2NHCONH$), 38.0 ($CH_2NHCONH$), 32.0 ($CH_2CH_2CH_2O$), 29.0 ($CH_2CH_2CH_2CH_2$), 26.9 (CH_2CH_2O), 26.0 ($C(CH_3)_3$), 25.0 ($CH_2CH_2NHCONH$), 24.2 ($CH_2CH_2CH_2$), 18.2 ($C(CH_3)_3$), -5.2 ($Si(CH_3)_2$)
9: $\delta = 158.7$ (NHCONH), 156.5 (CO), 78.9 ($C(CH_3)_3$), 57.0 (*tert*-C), 52.4 ($CH_2CH_2CH_2$, $CH_2CH_2CH_2CH_2$), 51.4 ($CH_2CH_2CH_2NHCONH$), 41.2 (CH_2CH_2NH), 37.9 ($CHNHCONH$), 33.3 ($CH_2CH_2CH_2$), 29.8 (CH_2CH_2-NHCONH), 28.7 ($C(CH_3)_3$), 23.9 ($CH_2CH_2CH_2$, $CH_2CH_2CH_2CH_2$)
10: $\delta = 158.2$ (NHCONH), 138.6 (C_1-Aryl), 128.4 (C_2-Aryl), 127.6 (C_3-Aryl), 127.4 (C_4-Aryl), 72.8 ($CH_2C_6H_5$), 71.0 (CH_2CH_2O), 56.9 (*tert*-C), 52.3 ($CH_2CH_2CH_2CH_2$, $CH_2CH_2CH_2$), 50.9 ($CH_2CH_2CH_2NHCONH$), 37.7 ($CH_2NHCONH$), 32.1 ($CH_2CH_2CH_2O$), 28.2 ($CH_2CH_2NHCONH$), 23.8 ($CH_2CH_2CH_2O$)
11/12: $\delta = 172.8$ ($CO_{[BA]}$), 157.8, 157.6 ($NHCONH_{[BA,\,Si,\,CN]}$), 118.3 (CN), 80.1 ($C(CH_3)_{3[BA]}$), 69.9, 65.8 ($CH_2OCH_{2[CN]}$), 63.5 ($CH_2O_{[Si]}$), 58.9 (*tert*-$C_{[CN]}$), 56.0 (*tert*-$C_{[BA]}$), 51.5 ($CH_2CH_2CH_{2[DSM]}$, $CH_2CH_2CH_2CH_{2[DSM]}$, $CH_2CH_2CH_2NHCONH_{[DSM]}$), 38.8 ($CH_2NHCONH_{[DSM]}$), 32.0 ($CH_2CH_2O_{[Si]}$), 30.3, 29.6, 28.0 ($CH_2CH_2CO_2$, $C(CH_3)_{3[BA]}$), 25.9 ($C(CH_3)_{3[Si]}$), 24.2 ($CH_2CH_2CH_{2[DSM]}$), 18.7 ($CH_2CN_{[CN]}$), 18.2 ($C(CH_3)_{3[Si]}$), -5.3 ($Si(CH_3)_2$)
13: $\delta = 158.5$ ($NHCONH_{[N\text{-}t\text{-}BOC,\,BE]}$), 156.4 ($CO_{[N\text{-}t\text{-}BOC]}$), 138.7 ($C_1$-$Aryl_{[BE]}$), 128.6 ($C_2$-$Aryl_{[BE]}$), 127.8 ($C_{3,4}$-$Aryl_{[BE]}$), 78.9 ($C(CH_3)_{3[N\text{-}t\text{-}BOC]}$), 72.9 ($CH_2C_6H_{5[BE]}$), 71.0 ($CH_2CHO_{[BE]}$), 57.0 (*tert*-$C_{[N\text{-}t\text{-}BOC,\,BE]}$), 52.4 ($CH_2CH_2$-$CH_2CH_{2[DSM]}$, $CH_2CH_2CH_{2[DSM]}$), 51.4 ($CH_2CH_2CH_2NHCONH_{[DSM]}$), 41.2 ($CH_2CH_2NH_{[N\text{-}t\text{-}BOC]}$), 37.9 ($CH_2NHCONH_{[DSM]}$), 33.2 ($CH_2CH_2CH_{2[N\text{-}t\text{-}BOC]}$), 32.3 ($CH_2CH_2CH_2O_{[BE]}$), 28.8 ($C(CH_3)_{3[N\text{-}t\text{-}BOC]}$), 23.9 ($CH_2CH_2CH_{2[N\text{-}t\text{-}BOC,\,BE]}$, $CH_2CH_2CH_2CH_{2[DSM]}$)
14: $\delta = 173.1$ ($CO_{[BA]}$), 158.2 ($NHCONH_{[BA,\,CN,\,N\text{-}t\text{-}BOC,\,BE]}$), 156.5 ($CO_{[N\text{-}t\text{-}BOC]}$), 138.7 ($C_1$-$Aryl_{[BE]}$), 128.5 ($C_2$-$Aryl_{[BE]}$), 127.7 ($C_{3,4}$-$Aryl_{[BE]}$), 118.7 ($CN_{[CN]}$), 80.5 ($C(CH_3)_{3[BA]}$), 78.9 ($C(CH_3)_{3[N\text{-}t\text{-}BOC]}$), 72.9 ($CH_2C_6H_{5[BE]}$), 71.1 ($CH_2CH_2$-$O_{[BE]}$), 70.1, 66.0 ($CH_2OCH_{2[CN]}$), 57.1, 56.2 (*tert*-$C_{[BA,\,CN,\,N\text{-}t\text{-}BOC,\,BE]}$), 51.4 ($CH_2CH_2CH_{2[DSM]}$, $CH_2CH_2CH_2CH_{2[DSM]}$, $CH_2CH_2CH_2NHCONH_{[DSM]}$), 41.1 ($CH_2CH_2CN_{[CN]}$), 38.3 ($CH_2NHCONH_{[DSM]}$), 33.2 ($CH_2CH_2CH_{2[N\text{-}t\text{-}BOC]}$, $CH_2CH_2CH_2O_{[BE]}$), 32.2, 29.9 ($CH_2CH_2CO_{2[BA]}$), 28.7, 28.3 ($C(CH_3)_{3[BA,\,N\text{-}t\text{-}BOC]}$), 23.8 ($CH_2CH_2CH_{2[N\text{-}t\text{-}BOC,\,BE]}$, $CH_2CH_2CH_2CH_{2[DSM]}$), 18.9 ($CH_2CN_{[CN]}$)

Scheme 1 illustrates the concept of combinatorial growth as it relates to the construction of dendrimers such as **14** having surfaces with multifarious functional groups. Thus, treatment of the DSM-32-PPI dendrimer with a mixture of monomers **4** and **5** (16 equivalents each) in refluxing dichloromethane afforded the heterogeneous macromolecule **13**. Following isolation and purification, the structure of the new *hetero*-dendrimer **13** was confirmed by its ^{13}C NMR spectrum (Figure 2, Table 1), which contains the relevant signals exhibited in the spectra of both the corresponding homogeneous macromolecules **9** and **10**. Principal signals are observed at $\delta = 138.7$, 128.6, 127.8 (C-aryl$_{[BE]}$), 78.9 ($C(CH_3)_{3[N\text{-}t\text{-}BOC]}$), 72.9 ($CH_2C_6H_{5[BE]}$), 71.1 ($CH_2CHO_{[BE]}$), 41.2 ($CH_2CH_2NH_{[N\text{-}t\text{-}BOC]}$), 28.8 ($C(CH_3)_{3[N\text{-}t\text{-}BOC]}$). Removal of the BOC groups by treatment with formic acid and subsequent reaction of the free amines with a mixture of isocyanate monomers **1**, **2**, and **4** (0.375, 0.25, 0.375 equivalents, respectively) yielded the peripherally hetereogeneous dendrimer **14**. Its structure was verified by its ^{13}C NMR spectrum (Figure 2), which displays the expected peaks at $\delta = 173.1$ ($CO_{[BA]}$), 156.5



Scheme 1. Combinatorial synthesis of dendrimer **14**, which is characterized by diversity in the surface functional groups.

 © WILEY-VCH Verlag GmbH, D-69451 Weinheim, 1998 1433-7851/98/3703-0309 $ 17.50+.50/0

($CO_{[N\text{-}t\text{-}BOC]}$), 138.7, 128.5, 127.7 (C-$aryl_{[BE]}$), 118.7 (CN), 80.5 ($C(CH_3)_{3[BA]}$), 78.9 ($C(CH_3)_{3[N\text{-}t\text{-}BOC]}$), 72.9 ($CH_2C_6H_{5[BE]}$), 28.7, 28.3 ($C(CH_3)_{3[N\text{-}t\text{-}BOC,\ BA]}$), 18.9 ($CH_2CN_{[CN]}$). Similar signals are observed in the spectra of the homogeneous macromolecules **6**, **7**, **9**, and **10**. Higher generation materials can easily be constructed by further selective deprotection of functional groups and subsequent treatment with any mixture of compatible isocyanate-based monomers.

A great advantage of this protocol is the potential to adjust dendritic properties by modifying the surface groups. The polyamine dendrimer afforded by liberation of the NH_2 moieties on dendrimer **13** (50:50 mixture of *N*-*t*-BOC and BE terminal groups) displays amphiphilic behavior. For example, it is highly soluble in MeOH as well as partially soluble in both H_2O and $CHCl_3$; this compound is thus reminiscent of a "universal micelle". Key ^{13}C NMR signals arising from the NH_2- and $PhCH_2O$-terminated arms collapse and broaden in the deuterated solvents $CDCl_3$ and D_2O, respectively. This can be rationalized by considering that surface groups with termini that favor solvation are extended and freely rotating, while groups with unfavorable solvent interactions are contracted and folded back into the molecular superstructure where less freedom of movement is afforded. Fréchet et al.[16] observed analogous behavior when dendritic wedges were attached to polyethylene glycol star polymers. This behavior can be modified by altering the ratio of the functional groups on the dendrimer surface. For example, a dendrimer with a 75:25 mixture of amino and benzyl ether moieties is completely miscible in H_2O and insoluble in $CHCl_3$.

Combinatorial construction of dendrimers is well suited to the rapid design and construction of nanoscale superstructures having a variety of forms and functions. The large-scale screening of vastly differing material properties should thus be possible. These dendritic materials are likely to have cavities and clefts within the framework, resulting in various degrees of local as well as overall asymmetry. As such, these materials can be viewed as being intermediate between dendrimers and classical polymers: a "polycelle". We are currently investigating their potential use as catalysts and phase-transfer agents.

July 7, 1997 [Z 10643 IE]
German version: *Angew. Chem.* **1998**, *110*, 318 – 321

Keywords: combinatorial synthesis · dendrimers · isocyanates

[1] G. R. Newkome, C. N. Moorefield, F. Vögtle, *Dendritic Molecules: Concepts, Syntheses, Perspectives*, VCH Weinheim, **1996**; C. N. Moorefield, G. R. Newkome, *Adv. Dendritic Macromol.* **1994**, *1*, 1; J. Issberner, R. Moors, F. Vögtle, *Angew. Chem.* **1994**, *106*, 2507; *Angew. Chem. Int. Ed. Engl.* **1994**, *33*, 2413; J. M. J. Fréchet, C. J. Hawker, K. L. Wooley, *J. Macromol. Sci. Part A* **1994**, *31*, 1627; J. M. J. Fréchet, *Science* **1994**, *263*, 1710; D. A. Tomalia, A. M. Naylor, W. A. Goddard, III, *Angew. Chem.* **1990**, *102*, 119; *Angew. Chem. Int. Ed. Engl.* **1990**, *29*, 138; B. I. Voit, *Acta Polymer* **1995**, *46*, 87; N. Ardoin, D. Astruc, *Bull. Soc. Chim. Fr.* **1996**, *132*, 875.

[2] S. Stevelmans, J. C. M. van Hest, J. F. G. A. Jansen, D. A. F. J. van Boxtel, E. M. M. de Brabander-van den Berg, E. W. Meijer, *J. Am. Chem. Soc.* **1996**, *118*, 7398; G. R. Newkome, Z.-q. Yao, G. R. Baker, V. K. Gupta, *J. Org. Chem.* **1985**, *50*, 2003.

[3] G. R. Newkome, R. Güther, C. N. Moorefield, F. Cardullo, L. Echegoyen, E. Pérez-Cordero, H. Luftmann, *Angew. Chem.* **1995**, *107*, 2159; *Angew. Chem. Int. Ed. Engl.* **1995**, *34*, 2023.

[4] S. A. Kuzdzal, C. A. Monnig, G. R. Newkome, C. N. Moorefield, *J. Chem. Soc. Chem. Commun.* **1994**, 2139; *J. Am. Chem. Soc.* **1997**, *119*, 2255.

[5] G. R. Newkome, C. N. Moorefield, J. M. Keith, G. R. Baker, G. H. Escamilla, *Angew. Chem.* **1994**, *106*, 701; *Angew. Chem. Int. Ed. Engl.* **1994**, *33*, 666; R. F. Barth, A. H. Soloway, *Mol. Chem. Neuropathol.* **1994**, *21*, 139; R. F. Barth, D. M. Adams, A. H. Soloway, F. Alam, M. V. Darby, *Bioconjugate Chem.* **1994**, *5*, 58.

[6] R. J. Duan, L. L. Miller, D. A. Tomalia, *J. Am. Chem. Soc.* **1995**, *117*, 10783.

[7] G. R. Newkome, C. D. Weis, C. N. Moorefield, F. R. Fronczek, *Tetrahedron Lett.* **1997**, *38*, 7053; G. R. Newkome, C. D. Weis, U.S. Patent 5 703 271 (December 30, 1997).

[8] G. R. Newkome, C. D. Weis, B. J. Childs, *Designed Monomers Polym.* **1997**, in press

[9] X.-D. Xiang, X. Sun, G. Briceño, Y. Lou, K.-A. Wang, H. Chang, W. G. Wallace-Freedman, S.-W. Chen, P. G. Schultz, *Science* **1995**, *268*, 1783.

[10] T. Carell, E. A. Wintner, A. J. Sutherland, J. Rebek, Jr., Y. M. Dunayevskiy, P. Vouros, *Chem. Biol.* **1995**, *2*, 171; L. Bourel, X. Willard, I. Pop, R. Bandelle, D. Horvath, B. Déprey, P. Melnyk, A. Tartar, *L'Actual. Chem.* **1995**(12), 33; M. Cardno, M. Bradley, *Tetrahedron Lett.* **1996**, *37*, 135.

[11] M. Goodman, V. Jubian, B. Linton, A. D. Hamilton, *J. Am. Chem. Soc.* **1995**, *117*, 11610.

[12] R. M. Kim, M. Manna, S. M. Hutchins, P. R. Griffin, N. A. Yates, A. M. Bernick, K. T. Chapman, *Proc. Natl. Acad. Sci. USA* **1996**, *93*, 10012.

[13] V. Swali, N. J. Wells, G. J. Langley, M. Bradley, *J. Org. Chem.* **1997**, *62*, 4902.

[14] D. Seebach, R. E. Marti, T. Hintermann, *Helv. Chim. Acta* **1996**, *79*, 1710.

[15] Commercially available poly(propylene imine) dendrimers were generously provided by DSM. The preparation and characterization was reported: E. M. M. de Brabander-van den Berg, E. W. Meijer, *Angew. Chem.* **1993**, *105*, 1370; *Angew. Chem. Int. Ed. Engl.* **1993**, *32*, 1308; C. Wörner, R. Mülhaupt, *Angew. Chem.* **1993**, *105*, 1367; *Angew. Chem. Int. Ed. Engl.* **1993**, *32*, 1306.

[16] I. Gitsov, J. M. J. Fréchet, *J. Am. Chem. Soc.* **1996**, *118*, 3785; *Macromolecules* **1993**, *26*, 6536.

Self-Assembly of Novel Polyrotaxanes: Main-Chain Pseudopolyrotaxanes with Poly(ester crown ether) Backbones**

Caiguo Gong and Harry W. Gibson*

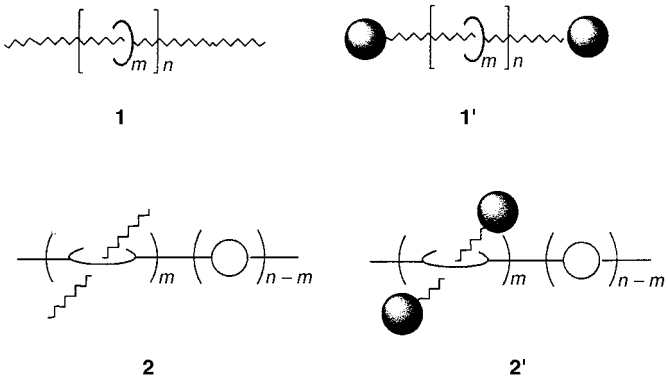
Physically linked molecules, rotaxanes and catenanes,[1] comprise a major research field of supramolecular chemistry[2] which has fascinated scientists in recent decades. Polyrotaxanes, in which a cyclic and a linear species (one of which is part of a macromolecule) are mechanically interlocked with each other, have also been extensively studied since their properties are different than those of conventional covalent polymers.[1, 3–10] The novel properties of these compounds often result from their unusual architectures. Therefore, designing

[*] Prof. H. W. Gibson, C. Gong
Department of Chemistry
Virginia Polytechnic Institute and State University
Blacksburg, VA 24061 (USA)
Fax: Int. code + (1) 540 231-5902
E-mail: hwgibson@vt.educgong@vt.edu

[**] This work was supported by the National Science Foundation through Individual Investigator Awards DMR-93-20196 and DMR-97-06909.

 © WILEY-VCH Verlag GmbH, D-69451 Weinheim, 1998 1433-7851/98/3703-0310 $ 17.50+.50/0

and synthesizing polyrotaxanes with new topologies is very important to polymer science. Two types of main-chain polyrotaxanes are proposed:[1a, 1d] types **1** and **1′** as well as types **2** and **2′** (Scheme 1). To our knowledge, however, only



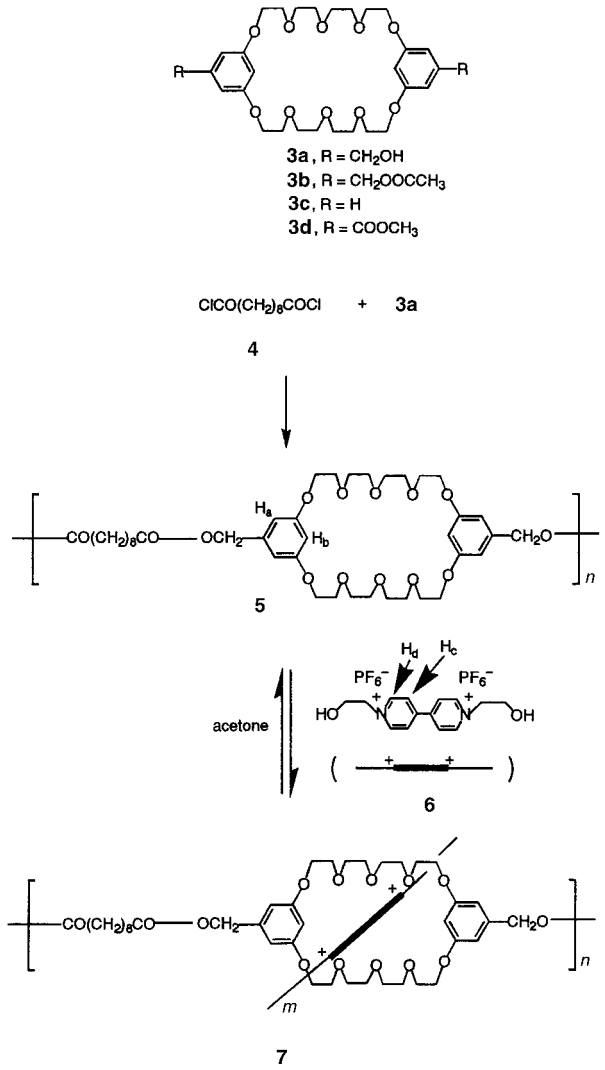
Scheme 1. Different types of main-chain polyrotaxanes: main-chain pseudopolyrotaxanes (**1**, **2**) and main-chain polyrotaxanes (**1′**, **2′**).

main-chain polyrotaxanes of types **1** and **1′** have been constructed by threading macrocycles onto polymeric backbones.[1, 3, 5–10] Here, we report an approach to polyrotaxanes of type **2** which self-assemble by threading linear components of low molar mass through the cavities of in-chain cyclic units of a preformed poly(ester crown ether).

The difunctional macrocycles bis(5-hydroxymethyl-*m*-phenylene)-[32]crown-10 (**3a**), bis(5-acetoxymethyl-*m*-phenylene)-[32]crown-10 (**3b**), and bis(*m*-phenylene)-[32]crown-10 (BMP32C10) derivatives **3c** and **3d** were prepared by a well-established procedure.[11] Polycondensation of **3a** with sebacoyl chloride (**4**) afforded poly(sebacate crown ether) **5** (see Scheme 2), which can serve as a backbone for constructing designed main-chain polyrotaxanes.

Stoddart et al. demonstrated that bis-phenylene-based crown ethers complex with bipyridinium salts under charge transfer accompanied by hydrogen bonding and dipole–dipole interactions.[1, 12] More specifically, they found that **3c** and *N*,*N*′-dimethyl-4,4′-bipyridinium hexafluorophosphate ("paraquat") formed a pseudorotaxane.[12a] Therefore, *N*,*N*′-bis(*β*-hydroxyethyl)-4,4′-bipyridinium hexafluorophosphate (**6**)[13] is expected to penetrate the cavity of the cyclic component of **5** to form the targeted main-chain pseudopolyrotaxane **7** (Scheme 2).

Indeed, a solution of **6** in acetone immediately turned orange upon addition of **5**, indicating the formation of **7**.[1, 8, 9, 12] ^{1}H NMR spectroscopy affords direct evidence. The signals for the aromatic protons H_a and H_b of the macrocyclic moiety in **7** (Figure 1 b, c) shifted upfield upon complexation with respect to those for **5** (Figure 1 a); this is consistent with the expected complexation, that is, the existence of through-space interactions owing to π stacking between these two components.[1, 8, 9, 12] All these signals are time-averaged; no peaks corresponding to threaded and unthreaded structures exist in the room-temperature spectra. Therefore, although the cyclic component was incorporated into the backbone, the complexation is still rapid on the ^{1}H NMR time scale.



Scheme 2. Preparation of poly(sebacate crown ether) **5** and polyrotaxane **7**.

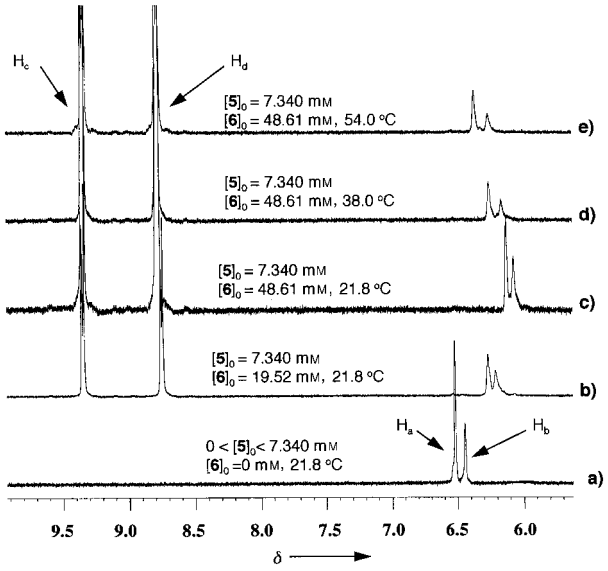


Figure 1. The expanded aromatic regions of the 400-MHz ^{1}H NMR spectra of a) **5** and b–e) solutions of **5**, **6**, and **7** of different compositions and at different temperatures in [D_6]acetone.

 © WILEY-VCH Verlag GmbH, D-69451 Weinheim, 1998 1433-7851/98/3703-0311 $ 17.50+.50/0

Since the complexation is rapid, the chemical shifts for the totally complexed form (e.g. H_a or H_b of the cyclic moiety in **7**) are necessary to calculate the equilibrium constant K.[2a] The continuous titration of a solution of **5** with **6** according to Benesi–Hildebrand method[14] gave the corresponding Δ values for proton H_b (Table 1). The plot of $1/\Delta$ versus $1/[\mathbf{6}]_0$ (Figure 2) afforded K and Δ_0, which are 39.6 M^{-1} and

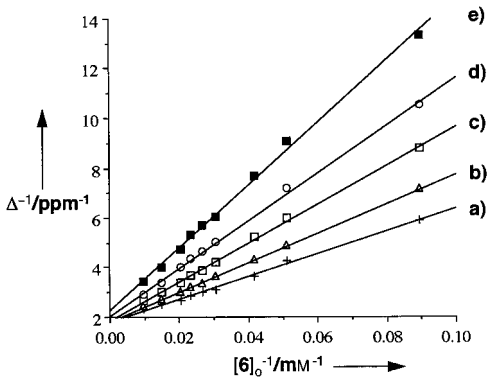


Figure 2. Benesi–Hildebrand plots for the formation of polyrotaxane **7** at a) 21.8, b) 30.0, c) 38.0, d) 46.0, and e) 54.0 °C in acetone.

0.556 ppm, respectively, for the formation of **7** in acetone at 21.8 °C (Table 2). For any other given stoichiometry the percentage of threaded macrocycle, that is, the threading efficiency [m/n value; fraction of cyclic repeat units threaded = [**7**]/([**5**] + [**7**])] can be derived (Table 1).

Table 1. The feed concentrations of **5** and **6**, the changes in chemical shift, and the threading effiencies of **7** in [D_6]acetone at 21.8 °C.

$[\mathbf{5}]_0$[a] [mM]	$[\mathbf{6}]_0$ [mM]	δ_0/Δ[b]	m/n for **7**[c]
0–7.340[d]	0	6.441/0.000	0
7.340	11.16	6.271/0.170	0.306
7.340	19.52	6.206/0.235	0.425
7.340	23.87	6.166/0.275	0.495
7.340	32.54	6.119/0.322	0.582
7.340	37.43	6.111/0.330	0.597
7.340	42.55	6.094/0.347	0.628
7.340	48.61	6.070/0.371	0.671
7.340	67.00	6.042/0.399	0.722
7.340	100.8	6.010/0.431	0.779

[a] Based on the cyclic units. [b] Based on the chemical shift of H_b (measured with ^{1}H NMR spectroscopy[14]). [c] Calculated according to ref. [14]. [d] Polymer **5** by itself is only partially soluble in acetone.

Because the complexation is exothermic, increasing the temperature disfavors rotaxane formation. This is indicated by the fact that the signals for H_a and H_b are shifted downfield at higher temperatures (Figure 1c–e). To quantitively understand the effect of temperature on the complexation, K values were measured at different temperatures according to the above-mentioned method (Figure 2b–e and Table 2); K indeed decreases with increasing temperature. From the van't Hoff plot (Figure 3a) ΔH was determined to be -1.93×10^4 J mol^{-1}, and ΔS -35.0 J K^{-1} mol^{-1}. Therefore, as shown

Table 2. Equilibrium constants and changes in free energy for the complexation of **5** and **6** at different temperatures in [D_6]acetone.

T [K][a]	Slope[b] [mM ppm^{-1}]	Intercept[b] [ppm^{-1}]	R^2[b]	Δ_0[b] [ppm]	K[b] [M^{-1}]	ΔG [kJ mol^{-1}]
295.0	45.6	1.80	0.996	0.556	39.6	–9.02
303.2	59.3	1.83	1.000	0.547	30.9	–8.65
311.2	78.0	1.87	0.998	0.535	23.9	–8.21
319.2	95.8	2.07	0.998	0.484	21.6	–8.15
327.2	126	2.28	0.996	0.439	18.0	–7.88

[a] ±0.1 K. [b] Based on the Benesi–Hildebrand plot (Figure 2).

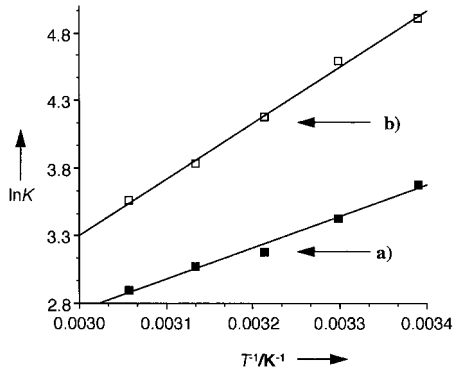


Figure 3. van't Hoff plots for a) the polymer system **5** + **6** and b) the model system **3b** + **6**. Curve a): intercept: -4.21; slope: 2.32×10^3 (K); $R^2 = 0.985$. Curve b): intercept: -9.17; slope: 4.16×10^3 (K); $R^2 = 0.997$.

in Figure 4, the threading efficiency m/n of polyrotaxane **7** can be controlled by simply varying the temperature and the concentration; that is, the m/n values for **7** increase for higher ratios of **6** to **5** at a given temperature as well as for a given concentration at lower temperatures.

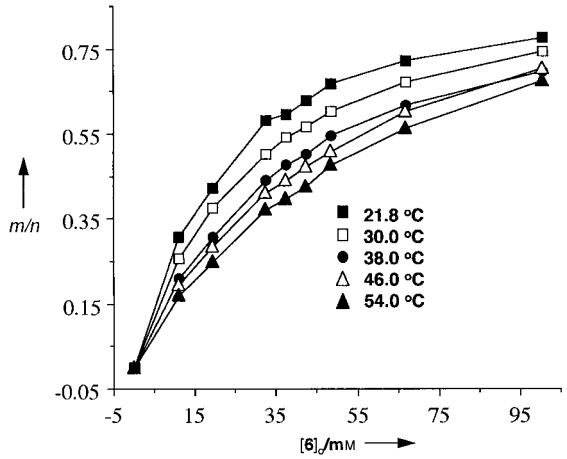


Figure 4. The relationship between the threading efficiency (m/n) of **7** and the feed concentration of **6** with $[\mathbf{5}]_0 = 7.340$ mM in [D_6]acetone at different temperatures.

The K value at room temperature for the polymeric system is much lower than that reported for the complexation of monomeric **3c** with **6** (760 M^{-1}, room temperature).[12a] To take into account the possible effect of the ester linkage in **5**, a

 © WILEY-VCH Verlag GmbH, D-69451 Weinheim, 1998 1433-7851/98/3703-0312 $ 17.50+.50/0 *Angew. Chem. Int. Ed.* **1998**, *37*, No. 3

model study was carried out with the diester derivative **3b** and **6**. The K value obtained ($135\,\text{M}^{-1}$ at 21.8 °C)[16] is also higher than that for the polymeric system ($39.6\,\text{M}^{-1}$ at 21.8 °C, Table 1). We believe that is the difference is due to the reduced flexibility of the cyclic units in **5**. For π stacking to occur, the phenylene rings of the macrocycle have to rotate towards each other relative to their parallel but nonoverlapping comformation in the uncomplexed state.[12a, 17] As soon as they are incorporated into the polymer backbone, rotation of these phenyl rings becomes much more difficult because it involves local or probably more extensive chain movement; this leads to enthalpic penalties and consequently a lower K value. Indeed, ΔH is more negative for the model system ($-3.46\times10^4\,\text{J mol}^{-1}$, Figure 3b). On the other hand, the ethyleneoxy units of the cyclic moiety in polymer **5** are restricted and expected to be less flexible than in the free macrocycle **3b**, whereas both will be rigidified upon complexation with **6**; this results in a more negative ΔS for the model system ($-76.2\,\text{J K}^{-1}\text{mol}^{-1}$)[16] than for polymeric **7**.

Because of its new topology polyrotaxane **7** had different physical properties than the starting polymer **5**. Polymer **5** is only partially soluble in acetone (Table 1), and paraquat **6** is insoluble in THF. Pseudopolyrotaxanes **7**, however, are soluble in both acetone and THF. Furthermore, the reduced viscosity of **7** prepared with reagent concentrations of $[\mathbf{5}]_0 = 7.427\,\text{mM}$ and $[\mathbf{6}]_0 = 22.28\,\text{mM}$ ($m/n = 0.430$[18]) is $0.215\,\text{dL g}^{-1}$, which is much higher than the value of $0.122\,\text{dL g}^{-1}$ for **7** prepared with $[\mathbf{5}]_0 = 7.427\,\text{mM}$ and $[\mathbf{6}]_0 = 1.857\,\text{mM}$ ($m/n = 0.0544$[18]) in acetone at 21.8 °C. The higher viscosity indicates a larger hydrodynamic volume for the pseudopolyrotaxane **7** with higher m/n.

Polymer **5** is a colorless elastomer with a glass-transition temperature T_g of −6.3 °C. Interestingly, **7** ($m/n = 0.69$)[19] obtained by freeze-drying a solution of **5** and **6** (molar ratio 1:0.75) is a glassy orange material with a T_g of 85.6 °C; the higher for **7** is attributed to its increased rigidity after complexation. The orange color proved that the rotaxane structure **7** in solution remained in the solid state after freeze-drying. This is very important, because use of these pseudopolyrotaxanes in the solid state becomes possible.

We have demonstrated an approach to novel main-chain polyrotaxanes of type **2** (Scheme 1) for the construction of pseudopolyrotaxane **7** by threading linear species **6** through the cavities of the cyclic repeat units of polymacrocycle **5**. Polyrotaxane **7** has a higher viscosity and higher T_g than its starting backbone **5**, and shows different solubility characteristics. The m/n value for the solution of the polyrotaxane increases with increasing amounts of bipyridinium salt **6** as well as with decreasing temperature. The values of K, ΔH, and ΔS provide the basis for predicting the threading efficiency for the preparation of analogous polyrotaxanes. Since bipyridinium guest **6** bears two hydroxy groups, **7** can further react, for example, with diisocyanates to form interesting networks. We are currently studying such systems.

Experimental Section

6: Macrocycle **3a** (150.0 mg, 0.6272 mmol) and **4** (374.3 mg, 0.6272 mmol) were dissolved in a mixture of diglyme and dimethyl sulfoxide (DMSO; 4 mL, 1/1 v/v) at 60 °C. Polymerization proceeded for 2 d at this temperature under N_2. The product was purified by precipitation into methanol (100 mL) to afford **6** (421.1 mg, 88 %), $M_n = 14.9\,\text{kg mol}^{-1}$, PDI = 1.97 (gel permeation chromatography with polystyrene standards).

Received: July 15, 1997
Revised version: October 21, 1997 [Z10685IE]
German version: *Angew. Chem.* **1998**, *110*, 323 – 327

Keywords: crown compounds · host – guest chemistry · polymers · rotaxanes · supramolecular chemistry

[1] Reviews: a) H. W. Gibson, M. C. Bheda, P. T. Engen, *Prog. Polym. Sci.* **1994**, *19*, 843 – 945; b) D. B. Amabilino, J. F. Stoddart, *Chem. Rev.* **1995**, *95*, 2725 – 2828; c) D. Philp, J. F. Stoddart, *Angew. Chem.* **1996**, *108*, 1242 – 1286; *Angew. Chem. Int. Ed. Engl.* **1996**, *35*, 1154 – 1196; d) H. W. Gibson in *Large Ring Molecules* (Ed.: J. A. Semlyen), Wiley, New York, **1996**, pp. 191 – 262.

[2] Reviews: a) *Comprehensive Supramolecular Chemistry*, *Vol. 6* (Eds.: J. L. Atwood, J. E. D. Davies, D. D. MacNicol, F. Vögtle), Pergamon, Oxford, **1996**; b) J.-M. Lehn, *Supramolecular Chemistry*, VCH, New York, **1995**; c) D. J. Cram, J. M. Cram, *Container Molecules and Their Guests*, Royal Society of Chemistry, Cambridge, **1994**; d) F. Vögtle, *Supramolecular Chemistry*, Wiley, New York, **1991**.

[3] M. B. Steinbrunn, G. Wenz, *Angew. Chem.* **1996**, *108*, 2274 – 2277; *Angew. Chem. Int. Ed. Engl.* **1996**, *35*, 2139 – 2142; W. Herrmann, B. Keller, G. Wenz, *Macromolecules*, **1997**, *30*, 4966 – 4972.

[4] a) M. Born, H. Ritter, *Adv. Mater.* **1996**, *8*, 149 – 151; b) M. Born, H. Ritter, *Macromol. Rapid Commun.* **1996**, *17*, 197 – 202; c) O. Noll, H. Ritter, *ibid.*, **1997**, *18*, 53 – 58.

[5] a) A. Harada, J. Li, M. Kamachi, *Macromolecules* **1994**, *27*, 4538 – 4543; b) A. Harada, M. Okada, J. Li, M. Kamachi, *ibid.* **1995**, *28*, 8406 – 8411; c) A. Harada, J. Li, M. Kamachi, *Chem. Commun.* **1997**, 1413 – 1414.

[6] Y. X. Shen, D. Xie, H. W. Gibson, *J. Am. Chem. Soc.* **1994**, *116*, 537 – 548; H. W. Gibson, S. Liu, P. Lecavalier, C. Wu, Y. X. Shen, *ibid.* **1995**, *117*, 852 – 874; H. W. Gibson, S. Liu, C. Gong, Q. Ji, E. Joseph, *Macromolecules*, **1997**, *30*, 3711 – 3727.

[7] C. Gong, H. W. Gibson, *Macromolecules* **1996**, *29*, 7029 – 7033; C. Gong, H. W. Gibson, *Macromol. Chem. Phys.* **1997**, *198*, 2321 – 2332; C. Gong, Q. Ji, T. E. Glass, H. W. Gibson, *Macromolecules* **1997**, *30*, 4807 – 4813.

[8] H. W. Gibson, S. Liu, Y. X. Shen, M. C. Bheda, S.-H. Lee, F. Wang, *NATO ASI Ser. Ser. C* **1995**, *456*, 41 – 58.

[9] P. E. Mason, I. W. Parsons, M. S. Tolley, *Angew. Chem.* **1996**, *108*, 2405 – 2408; *Angew. Chem. Int. Ed. Engl.* **1996**, *35*, 2238 – 2241; G. J. Owen, P. Hodge, *Chem. Commun.* **1997**, 11 – 12.

[10] a) C. Gong, H. W. Gibson, *J. Am. Chem. Soc.* **1996**, *119*, 5862 – 5866; b) *ibid.* **1996**, *119*, 8585 – 8591.

[11] H. W. Gibson, D. S. Nagvekar, *Can. J. Chem.* **1997**, *75*, 1375 – 1384.

[12] a) B. L. Allwood, N. Spencer, H. Shahriari-Zavareh, J. F. Stoddart, D. J. Williams, *J. Chem. Soc. Chem. Commun.* **1987**, 1058 – 1061; b) M. Asakawa, P. R. Ashton, R. Ballardini, V. Balzani, M. Belohradsky, M. T. Gandolfi, O. Kocian, L. Prodi, F. M. Raymo, J. F. Stoddart, M. Venturi, *J. Am. Chem. Soc.* **1997**, *119*, 302 – 310, and references therein.

[13] Y. X. Shen, P. T. Engen, M. A. G. Berg, J. S. Merola, H. W. Gibson, *Macromolecules* **1992**, *25*, 2786 – 2788.

[14] The association constant K is calculated according to the Benesi – Hildebrand method[15] as follows: For a given temperature and a given feed concentration of one component (e.g. $[\mathbf{5}]_0$), the feed concentration of another component (e.g. $[\mathbf{6}]_0$) is changed: $1/\Delta = 1/(\Delta_0 K[\mathbf{6}]_0) + 1/\Delta_0$, where $\Delta = \delta_f - \delta$, $\Delta_0 = \delta_f - \delta_c$, and δ, δ_c, and δ_f are the time-averaged chemical shifts of the partially complexed, totally complexed, and unthreaded forms, respectively (e.g. H_a and H_b of **5**). Therefore, K, Δ_0, and m/n (threading effiency $= \Delta/\Delta_0$) were calculated (Table 2) from the plot of $1/\Delta$ vs. $1/[\mathbf{6}]_0$ (Figure 2).

[15] H. A. Benesi, J. H. Hildebrand, *J. Am. Chem. Soc.* **1949**, *71*, 2703 – 2710; H. Tsukube, H. Furuta, A. Odani, Y. Takeda, Y. Kudo, Y. Inone, Y. Liu, H. Sakamoto, K. Kimura, *Comprehensive Supramolecular*

 © WILEY-VCH Verlag GmbH, D-69451 Weinheim, 1998 1433-7851/98/3703-0313 $ 17.50+.50/0

Chemistry, *Vol. 6* (Eds.: J. L. Atwood, J. E. D. Davies, D. D. MacNicol, F. Vögtle), Pergamon, Oxford, **1996**, pp. 425–482.

[16] The values for K, ΔH, and ΔS were also determined by the Benesi–Hildebrand method.[14, 15] K values in [D$_6$]acetone: 135 M^{-1} at 21.8 °C, 98.1 M^{-1} at 30.0 °C, 65.6 M^{-1} at 38.0 °C, 46.1 M^{-1} at 46.0 °C, 34.9 M^{-1} at 54.0 °C; $\Delta H = -34.6 \times 10^4$ J mol^{-1}; $\Delta S = -76.2$ J K^{-1} mol^{-1} (Figure 3b).

[17] The crystal structure of **3c** indicates an open cavity (4.9 × 7.8 Å) which undergoes a small conformational change when it complexes with paraquat.[12a] However, **3d** in the solid state has a collapsed cavity (0.75 × 7.8 Å), perhaps due to crystal packing forces and not intrinsic conformational preferences: Y. Delaviz, J. S. Merola, M. A. G. Berg, H. W. Gibson, *J. Org. Chem.* **1995**, *60*, 516–522.

[18] The values for m/n were calculated by the method specified in ref. [14].

[19] The solution of **5** and **6** in acetone was slowly cooled to −90 °C and then frozen with an acetone/dry ice bath. The solvent was removed under high vacuum to afford an orange solid, pseudopolyrotaxane **7**. The m/n value was calculated from K (4748 M^{-1}), which was estimated from the measured ΔH and ΔS values.

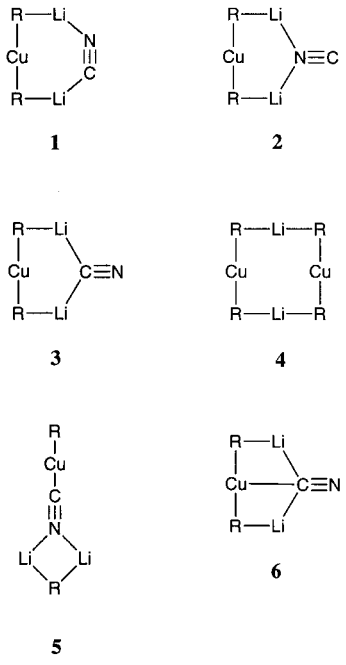
The Use of ^{15}N NMR Spectroscopy To Resolve the "Higher Order Cyanocuprate" Controversy: ^{15}N, ^{6}Li, and ^{13}C NMR Spectroscopic Investigations of CuCN-Derived Butyl Cuprates**

Steven H. Bertz,* Karolina Nilsson, Öjvind Davidsson, and James P. Snyder*

In the modern era of organocopper chemistry,[1] the first cyanocuprate experiments involved the addition of one equivalent of RLi to CuCN to prepare cyanocuprates RCu(CN)Li.[2] Two-bond ^{13}C-^{13}C coupling constants ^2J across copper proved that the R group and the CN group are both bonded to the same Cu in these 1:1 reagents.[3] In 1981 Lipshutz et al. added two equivalents of RLi to CuCN and claimed not only a new class of highly reactive reagents but a new *kind* of organocopper(I) species, the "higher order cyanocuprates."[4] Spectroscopic evidence was not presented, but NMR and IR data were reported later.[5]

Subsequently, Bertz showed that the ^{13}C NMR chemical shifts of the cuprates prepared from two equivalents of RLi and CuCN or CuI were the same and that the shift of the CN carbon atom was independent of the electronic nature of R.[6] In contrast, the chemical shifts of the CN carbon atoms in the "lower order" cyanocuprates RCu(CN)Li vary with R.[3, 6] These observations and the absence of ^2J in the 2:1 compounds cast grave doubt on the higher order formulation $R_2Cu(CN)Li_2$.[4, 7] Extended X-ray absorption fine structure (EXAFS)[8, 9] investigations by Penner-Hahn, Knochel, Frenking et al. and IR[10] studies by Penner-Hahn, Snyder et al. supported the conclusions of these NMR studies. Theoretical investigations by Snyder et al.[11] and Penner-Hahn, Knochel, Frenking et al.[9] indicated that higher order structures are 20–30 kcal mol^{-1} higher in energy than lower order alternatives.

Various lower order structures have been proposed for the 2:1 reagents, for example, **1**–**3**. They are related to the Gilman dimer **4** by the substitution of CN^- for R_2Cu^- in three archetypal ways: 1) one Li atom is attached to N and one to C, 2) both Li atoms are bonded to N, and 3) both Li atoms are bonded to C. While initial theoretical studies favored variants of **1**–**3**,[11] all of these cyano-Gilman reagents are close



enough in energy to be viable candidates. We have now prepared the 1:1 and 2:1 reagents, BuCu(C^{15}N)^{6}Li and Bu$_2$Cu^{6}Li · ^{6}LiC^{15}N, respectively, as well as intermediate stoichiometries from Bu^{6}Li and CuC^{15}N.[12] The results of this ^{15}N NMR study, coupled with theoretical calculations reported herein, strongly support structure **1** over the others.

Figure 1 shows the ^{15}N NMR spectra of solutions in [D$_8$]THF at −80 °C when a) 1.0, b) 1.3, or c) 2.0 equivalents of Bu^{6}Li is added to CuC^{15}N.[12] The 1:1 reagent BuCu(C^{15}N)-^{6}Li is characterized by a singlet at $\delta = -129.3$ (6 Hz width at

[*] Dr. S. H. Bertz
Complexity Study Center
Mendham, NJ 07945 (USA)
E-mail: sbertz@ispcorp. com
Dr. J. P. Snyder
Department of Chemistry
Emory University
Atlanta, GA 30322 (USA)
E-mail: snyder@euch4e.chem.emory.edu
Dr. K. Nilsson
Department of Organic Chemistry
Chalmers University of Technology (Sweden)
Dr. Ö. Davidsson
Department of Organic Chemistry
Göteborg University (Sweden)

[**] New Copper Chemistry, Part 28. The authors are grateful to Lars Baltzer and Thomas Andersson for technical assistance and to the Swedish Natural Science Research Council for partial support of this work. S.H.B. wishes to thank Christina Ullenius for arranging this collaboration and Mikael Håkansson for helpful discussions. J.P.S. wishes to thank Dennis Liotta for his hospitality. Part 27: S. H. Bertz, M. Eriksson, G. Miao, J. P. Snyder, *J. Am. Chem. Soc.* **1996**, *118*, 10906–10907.

 © WILEY-VCH Verlag GmbH, D-69451 Weinheim, 1998 1433-7851/98/3703-0314 $ 17.50+.50/0

Chemistry, *Vol. 6* (Eds.: J. L. Atwood, J. E. D. Davies, D. D. MacNicol, F. Vögtle), Pergamon, Oxford, **1996**, pp. 425–482.

[16] The values for K, ΔH, and ΔS were also determined by the Benesi–Hildebrand method.[14, 15] K values in [D$_6$]acetone: 135 M^{-1} at 21.8 °C, 98.1 M^{-1} at 30.0 °C, 65.6 M^{-1} at 38.0 °C, 46.1 M^{-1} at 46.0 °C, 34.9 M^{-1} at 54.0 °C; $\Delta H = -34.6 \times 10^4$ J mol^{-1}; $\Delta S = -76.2$ J K^{-1} mol^{-1} (Figure 3b).

[17] The crystal structure of **3c** indicates an open cavity (4.9 × 7.8 Å) which undergoes a small conformational change when it complexes with paraquat.[12a] However, **3d** in the solid state has a collapsed cavity (0.75 × 7.8 Å), perhaps due to crystal packing forces and not intrinsic conformational preferences: Y. Delaviz, J. S. Merola, M. A. G. Berg, H. W. Gibson, *J. Org. Chem.* **1995**, *60*, 516–522.

[18] The values for m/n were calculated by the method specified in ref. [14].

[19] The solution of **5** and **6** in acetone was slowly cooled to −90 °C and then frozen with an acetone/dry ice bath. The solvent was removed under high vacuum to afford an orange solid, pseudopolyrotaxane **7**. The m/n value was calculated from K (4748 M^{-1}), which was estimated from the measured ΔH and ΔS values.

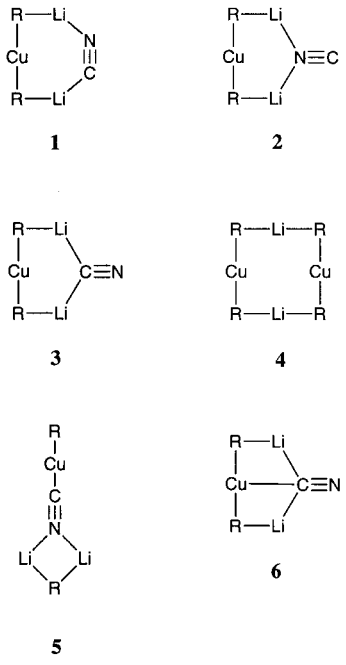
The Use of ^{15}N NMR Spectroscopy To Resolve the "Higher Order Cyanocuprate" Controversy: ^{15}N, ^{6}Li, and ^{13}C NMR Spectroscopic Investigations of CuCN-Derived Butyl Cuprates**

Steven H. Bertz,* Karolina Nilsson, Öjvind Davidsson, and James P. Snyder*

In the modern era of organocopper chemistry,[1] the first cyanocuprate experiments involved the addition of one equivalent of RLi to CuCN to prepare cyanocuprates RCu(CN)Li.[2] Two-bond ^{13}C-^{13}C coupling constants ^2J across copper proved that the R group and the CN group are both bonded to the same Cu in these 1:1 reagents.[3] In 1981 Lipshutz et al. added two equivalents of RLi to CuCN and claimed not only a new class of highly reactive reagents but a new *kind* of organocopper(I) species, the "higher order cyanocuprates."[4] Spectroscopic evidence was not presented, but NMR and IR data were reported later.[5]

Subsequently, Bertz showed that the ^{13}C NMR chemical shifts of the cuprates prepared from two equivalents of RLi and CuCN or CuI were the same and that the shift of the CN carbon atom was independent of the electronic nature of R.[6] In contrast, the chemical shifts of the CN carbon atoms in the "lower order" cyanocuprates RCu(CN)Li vary with R.[3, 6] These observations and the absence of ^2J in the 2:1 compounds cast grave doubt on the higher order formulation $R_2Cu(CN)Li_2$.[4, 7] Extended X-ray absorption fine structure (EXAFS)[8, 9] investigations by Penner-Hahn, Knochel, Frenking et al. and IR[10] studies by Penner-Hahn, Snyder et al. supported the conclusions of these NMR studies. Theoretical investigations by Snyder et al.[11] and Penner-Hahn, Knochel, Frenking et al.[9] indicated that higher order structures are 20–30 kcal mol^{-1} higher in energy than lower order alternatives.

Various lower order structures have been proposed for the 2:1 reagents, for example, **1**–**3**. They are related to the Gilman dimer **4** by the substitution of CN$^-$ for R$_2$Cu$^-$ in three archetypal ways: 1) one Li atom is attached to N and one to C, 2) both Li atoms are bonded to N, and 3) both Li atoms are bonded to C. While initial theoretical studies favored variants of **1**–**3**,[11] all of these cyano-Gilman reagents are close



enough in energy to be viable candidates. We have now prepared the 1:1 and 2:1 reagents, BuCu(C^{15}N)^{6}Li and Bu$_2$Cu^{6}Li · ^{6}LiC^{15}N, respectively, as well as intermediate stoichiometries from Bu^{6}Li and CuC^{15}N.[12] The results of this ^{15}N NMR study, coupled with theoretical calculations reported herein, strongly support structure **1** over the others.

Figure 1 shows the ^{15}N NMR spectra of solutions in [D$_8$]THF at −80 °C when a) 1.0, b) 1.3, or c) 2.0 equivalents of Bu^{6}Li is added to CuC^{15}N.[12] The 1:1 reagent BuCu(C^{15}N)-^{6}Li is characterized by a singlet at $\delta = -129.3$ (6 Hz width at

[*] Dr. S. H. Bertz
Complexity Study Center
Mendham, NJ 07945 (USA)
E-mail: sbertz@ispcorp. com
Dr. J. P. Snyder
Department of Chemistry
Emory University
Atlanta, GA 30322 (USA)
E-mail: snyder@euch4e.chem.emory.edu
Dr. K. Nilsson
Department of Organic Chemistry
Chalmers University of Technology (Sweden)
Dr. Ö. Davidsson
Department of Organic Chemistry
Göteborg University (Sweden)

[**] New Copper Chemistry, Part 28. The authors are grateful to Lars Baltzer and Thomas Andersson for technical assistance and to the Swedish Natural Science Research Council for partial support of this work. S.H.B. wishes to thank Christina Ullenius for arranging this collaboration and Mikael Håkansson for helpful discussions. J.P.S. wishes to thank Dennis Liotta for his hospitality. Part 27: S. H. Bertz, M. Eriksson, G. Miao, J. P. Snyder, *J. Am. Chem. Soc.* **1996**, *118*, 10906–10907.

 © WILEY-VCH Verlag GmbH, D-69451 Weinheim, 1998 1433-7851/98/3703-0314 $ 17.50+.50/0

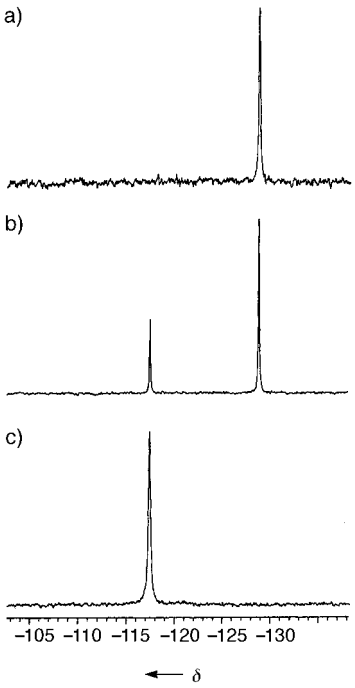


Figure 1. ^{15}N NMR spectra (50.65 MHz) in [D_8]THF at $-80\,^{\circ}$C of the cuprates prepared from various ratios of Bu^{6}Li:CuC^{15}N: a) 1:1, b) 1.3:1, and c) 2:1.

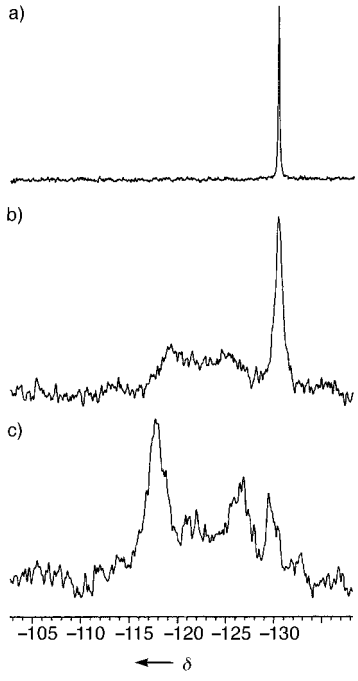


Figure 2. ^{15}N NMR spectra (50.65 MHz) in [D_{10}]diethyl ether at $-80\,^{\circ}$C of the cuprates prepared from various ratios of Bu^{6}Li:CuC^{15}N: a) 1:1, b) 1.4:1, and c) 2:1.

half-height, $\Delta\nu_{1/2}$), measured on a scale that assigns a value of $\delta = 0$ to neat nitromethane and $\delta = -77.7$ to trimethylsilylcyanide (TMSCN).[13] The spectrum of the 2:1 reagent $Bu_2Cu^6Li \cdot {}^6LiC^{15}N$ is a singlet at $\delta = -117.5$ ($\Delta\nu_{1/2} = 10$ Hz) under these conditions. The spectrum of a mixture with intermediate stoichiometry (Figure 1b) has both peaks at their characteristic chemical shifts in the expected ratio. No "free" ^{6}LiC^{15}N is observed in any of these spectra.

Figure 2a shows that the ^{15}N NMR spectrum of the 1:1 reagent in [D_{10}]ether at $-80\,^{\circ}$C is also a singlet ($\delta = -130.5$, $\Delta\nu_{1/2} = 6$ Hz). It is critical that the BuLi be added slowly with sonication if the BuCu(CN)Li is to be obtained as pure as in Figure 2a. In contrast, the spectrum of the 2:1 reagent (Figure 2c) is dramatically different in [D_{10}]diethyl ether: there is a relatively broad peak at $\delta = -118.0$ ($\Delta\nu_{1/2} = 120$ Hz), but there is also a plethora of peaks at chemical shifts between the values for the 2:1 and 1:1 species. The intermediate peaks are due to aggregates (see below). Upon warming the sample to $-50\,^{\circ}$C, all the ^{15}N peaks in this spectrum coalesce into a single broad peak ($\delta = -121.5$, $\Delta\nu_{1/2} = 55$ Hz).

With 1.4:1 stoichiometry in [D_{10}]diethyl ether (Figure 2b), there was little of the 2:1 reagent ($\delta = -118$, 5%) relative to the 1:1 reagent ($\delta = -130.5$, $\Delta\nu_{1/2} = 50$ Hz, 35%) or "intermediate" species. When the reactant ratio was reduced to 1.3:1, the $\delta = -118$ peak increased to 15% of the total area as the intermediate peaks decreased to 25%, and when this solution was cooled from $-80\,^{\circ}$C to $-100\,^{\circ}$C, it further increased to 25% as the intermediate area diminished to 10%. The addition of THF to the [D_{10}]diethyl ether solution also converts the intermediate peaks cleanly to the $\delta = -118$ and -130 peaks. The effects of solvent, concentration, and temperature are similar to those observed for RLi,[14] and it can be concluded that the intermediate peaks in this case correspond to aggregates derived from both cuprates.[15]

The ^{6}Li NMR spectra contain vital new information.[12b] In [D_8]THF at $-80\,^{\circ}$C, the 1:1 and 2:1 reagents give rise to peaks at $\delta = -1.40$ ($\Delta\nu_{1/2} = 1$ Hz) and -1.18 ($\Delta\nu_{1/2} = 5$ Hz), respectively.[16] In the sample with 1.3:1 stoichiometry in [D_8]THF, there is a single peak at an intermediate chemical shift ($\delta = -1.25$, $\Delta\nu_{1/2} = 1$ Hz) instead of two peaks, as in the corresponding ^{15}N spectrum (Figure 1b). Apparently, an exchange process renders the Li ions equivalent, but not the N atoms. The ^{6}Li spectrum of BuCu(C^{15}N)^{6}Li in [D_{10}]diethyl ether is a single peak at $\delta = -0.87$ ($\Delta\nu_{1/2} = 2$ Hz). The major ^{6}Li peak in the spectrum of the 2:1 reagent in [D_{10}]diethyl ether is $\delta = -0.66$ ($\Delta\nu_{1/2} = 20$ Hz). The usual samples of the 2:1 reagent in this solvent had minor peaks at $\delta = 1.03$ and 1.90 (10.8% and 10.6% of the total area). These peaks have not been definitively assigned;[17] nevertheless, it is clear from the ^{15}N and ^{6}Li spectra that the situation in diethyl ether is much more complex than had previously been appreciated.

No ^{6}Li-^{15}N couplings could be observed for either the 1:1 or 2:1 reagent in [D_{10}]diethyl ether at temperatures down to $-110\,^{\circ}$C.[18] This is not unexpected: ^{6}Li-^{13}C couplings have not been observed for organocuprates $R_2CuLi \cdot LiI$, $R_2CuLi \cdot LiCN$ or RCu(CN)Li (R = Me, Et, Bu, Ph),[3, 6] in spite of the fact that the corresponding organolithium compounds RLi do exhibit such couplings.[14] In light of the ^{6}Li NMR results presented above, rapid exchange of Li is responsible for the lack of coupling with this nucleus.

The only discernible ^{13}C-^{15}N coupling is the cyano-doublet ($J = 11.7$ Hz) at $\delta = 149.35$ ($\Delta\nu_{1/2} = 7$ and 9 Hz) in the ^{13}C spectrum of BuCu(C^{15}N)^{6}Li in [D_8]THF. Broadening precluded measurement of coupling in the CN peak ($\delta = 158.82$,

 © WILEY-VCH Verlag GmbH, D-69451 Weinheim, 1998 1433-7851/98/3703-0315 $ 17.50+.50/0

$\Delta\nu_{1/2} = 35$ Hz) for $Bu_2Cu^6Li \cdot {}^6LiC^{15}N$ in this solvent. In [D_{10}]diethyl ether $BuCu(C^{15}N)^6Li$ has a broad peak at $\delta =$ 150.96 ($\Delta\nu_{1/2} = 80$ Hz), and the best spectrum of $Bu_2Cu^6Li \cdot {}^6LiC^{15}N$ has one at $\delta = 159.55$ ($\Delta\nu_{1/2} = 80$ Hz). Previously, ^{13}C NMR peaks at $\delta = 152$ and 163 were assigned without theoretical justification to "higher order" species.[5b]

The ^{15}N NMR chemical shifts measured for the 2:1 organocuprate in this study can be interpreted with the aid of calculations. Relative ^{15}N shifts were calculated by using Chesnut's locally dense basis set concept.[19] The calculations (Becke3LYP/6-311G*/GIAO)[20] were performed on the methyl analogues of **1**–**6** (R = Me) which also have one coordinated H_2O per Li to approximate ethereal solvation. We denote these hydrated methyl derivatives, which are the usual model compounds,[9, 11] as **1a**–**6a**. They were also performed on CN^- and TMSCN. We have scaled all the calculated ^{15}N NMR shifts so that TMSCN is set at the literature value $\delta = -77.7$.[13, 21] The ^{15}N NMR shift for "naked" CN^- is then $\delta = -125.8$, which is in reasonable agreement with the observed values for aqueous KCN ($\delta = -104$ to -106),[21] especially when the effect of solvation is considered. The calculated shifts for **1a**–**3a** are $\delta = -113.9$, -161.9, and -81.1, respectively, and for **5a** the calculated value is $\delta = -185.5$. Higher order structure **6a** has a calculated shift of $\delta = -81.2$. Only structure **1a** gives good agreement with the measured values (ca. $\delta = -118$) for the 2:1 species in this study.

There is no evidence that any of the minor species observed in solutions of the 2:1 reagent are higher order cuprates, which in any event would be unfavorable energetically.[11] Moreover, our results do not indicate how tightly the R_2Cu^- core in **1** is bonded to the $LiCNLi^+$ moiety, nor do they rule out minor equilibrium amounts of other species such as **2** or **3** (see below).

The IR stretching frequencies calculated for cyanide in methyl analogues **1a** and **3a** (2101 and 2099 cm^{-1}, respectively) are consistent with the observed value for $Me_2CuLi \cdot LiCN$ in THF (2115 cm^{-1}).[10] A recent ^{13}C NMR study by Berger et al. concluded that the "dimethylcuprate core" in $Me_2CuLi \cdot LiCN$ is the same as in "halide-free" Me_2CuLi,[22a] which is consistent with **1**–**3**, but not **5**. Cryoscopy indicates that $Me_2CuLi \cdot LiCN$ is essentially monomeric in THF,[22b] which is consistent with **1**–**3** or **5**, although some dissociation was postulated. ^{15}N NMR spectroscopy is the first technique that allows all the structures that have been proposed for the major component of the 2:1 reagent to be ruled out except **1**, which is in good agreement with both ^{15}N NMR and IR measurements.

We believe that the location of the CN is now "triangulated" by two independent experimental techniques and by calculations. These results establish that the very useful[23, 24] organocopper compounds prepared from two equivalents of RLi and one equivalent of CuCN are cyanide-modified Gilman reagents and not "higher order cyanocuprates." Consequently, they should be called *cyano-Gilman reagents* and written $R_2CuLi \cdot LiCN$ in analogy with other Gilman reagents based on linearly bonded copper(I) structural units ($R_2CuLi \cdot LiI$, $R_2CuLi \cdot LiBr \cdot DMS$ (DMS = dimethyl sulfide), $R_2CuLi \cdot LiOTf$, etc.[23]). NMR spectroscopic measurements were responsible for the first doubt about the higher order formulation of the cyanocuprates,[3, 6, 25] and they have now come full circle to definitively settle the ensuing controversy.[24]

Experimental Section

All NMR spectra were obtained on a Varian Unity 500 spectrometer at the canonical frequencies (^{15}N: 50.65; ^{13}C: 125.7; ^6Li: 73.6 MHz). All NMR shifts were calculated by using the "low frequency positive" convention.[13b] ^6Li NMR spectra were referenced with external 0.3 M ^6LiCl in [D_4]methanol set at $\delta = 0$. ^{13}C NMR spectra were referenced to the solvent signals: $\delta =$ 14.60 (ether) or $\delta = 25.37$ (THF). ^{15}N NMR spectra were referenced with 4 M TMSCN in [D_8]THF set at $\delta = -81.7$.[13c]

$CuC^{15}N$ (12.7 mg, 0.14 mmol, MSD Isotopes) was sealed under Ar in an NMR tube (∅ 5 mm) with a rubber septum and Teflon tape. A 0.5 mL aliquot of freshly-distilled [D_{10}]diethyl ether was added by syringe and the contents were sonicated before being cooled to $-78\,^\circ C$ (dry ice/acetone). A 30 μL aliquot of 2 M Bu^6Li (0.06 mmol, precise titer determined by Gilman double-titration)[12a] in pentane was added, and the mixture was sonicated at $0\,^\circ C$ for 1.0 min. It was then cooled to $-78\,^\circ C$ for 3 min, and the cycle was repeated two more times. The tube was inserted in a ceramic spinner, wiped with an ethanol-soaked tissue, and lowered into the NMR probe, precooled to $-80\,^\circ C$. The ^{13}C NMR spectrum was obtained to confirm the identity of the product,[3, 6] and then the ^{15}N and ^6Li spectra were measured.

Another 30 μL of 2 M Bu^6Li was added to the tube, and the above procedure was repeated to get high-quality spectra of 0.2 M $BuCu(C^{15}N)^6Li$. A small amount of $CuC^{15}N$ remained at the bottom of the tube to make sure none of the 2:1 reagent was present. (None was detected by ^{13}C, ^{15}N, or ^6Li NMR.) When the Bu^6Li was added all at once to $CuC^{15}N$ in [D_{10}]diethyl ether, the spectrum resembled the one in Figure 2b.

Addition of a third 30 μL aliquot gave a mixture of 1:1 and 2:1 reagents, which was analyzed by ^{13}C NMR spectroscopy to determine the ratio of cyano-carbon atoms and from this the effective titer of the Bu^6Li. The ratio of these reagents was also determined by integration of the ^{15}N NMR spectra. For the final sample of 2:1 reagent, a total of 1.90 equiv of Bu^6Li was used, as calculated from the effective titer.

Received: August 22, 1997 [Z10844IE]
German version: *Angew. Chem.* **1998**, *110*, 327–331

Keywords: aggregations · copper · density functional calculations · lithium · NMR spectroscopy

[1] For earlier uses of CuCN in organocopper chemistry, see a) N. V. Kondyreva, D. A. Fomina, *Zh. Russ. Fiz.-Khim. O-va, Chast Khim.* **1915**, *47*, 190–198; b) H. Gilman, J. M. Straley, *Rec. Trav. Chim. Pays-Bas.* **1936**, *55*, 821–834.
[2] J.-P. Gorlier, L. Hamon, J. Levisalles, J. Wagnon, *J. Chem. Soc. Chem. Commun*. **1973**, 88.
[3] S. H. Bertz, *J. Am. Chem. Soc.* **1991**, *113*, 5470–5471.
[4] B. H. Lipshutz, R. S. Wilhelm, D. M. Floyd, *J. Am. Chem. Soc*. **1981**, *103*, 7672–7674.
[5] a) B. H. Lipshutz, J. A. Kozlowski, R. S. Wilhelm, *J. Org. Chem*. **1984**, *49*, 3943–3949; b) See also B. H. Lipshutz, S. Sharma, E. L. Ellsworth, *J. Am. Chem. Soc*. **1990**, *112*, 4032–4034.
[6] S. H. Bertz, *J. Am. Chem. Soc.* **1990**, *112*, 4031–4032.
[7] a) B. H. Lipshutz, R. S. Wilhelm, J. A. Kozlowski, *Tetrahedron* **1984**, *40*, 5005–5038: "These species are differentiated from 'lower order' or Gilman-like cuprates, R_2CuLi, in that the Cu-cluster contains an additional ligand (originally negatively charged). Hence, they are formally Cu^I dianionic salts." b) See also B. H. Lipshutz, B. James, *J. Org. Chem*. **1994**, *59*, 7585–7587.
[8] a) T. Stemmler, J. E. Penner-Hahn, P. Knochel, *J. Am. Chem. Soc.* **1993**, *115*, 348–350; b) T. M. Barnhart, H. Huang, J. E. Penner-Hahn, *J. Org. Chem*. **1995**, *60*, 4310–4311; c) T. M. Barnhart, J. E. Penner-Hahn, *Physica B* **1995**, *208&209*, 709–710.
[9] T. L. Stemmler, T. M. Barnhart, J. E. Penner-Hahn, C. E. Tucker, P. Knochel, M. Böhme, G. Frenking, *J. Am. Chem. Soc*. **1995**, *117*, 12489–12497.

 © WILEY-VCH Verlag GmbH, D-69451 Weinheim, 1998 1433-7851/98/3703-0316 $ 17.50+.50/0

[10] H. Huang, K. Alvarez, Q. Lui, T. M. Barnhart, J. P. Snyder, J. E. Penner-Hahn, *J. Am. Chem. Soc.* **1996**, *118*, 8808 – 8816.
[11] a) J. P. Snyder, S. H. Bertz, *J. Org. Chem.* **1995**, *60*, 4312 – 4313; b) J. P. Snyder, D. P. Spangler, J. R. Behling, B. E. Rossiter, *ibid.* **1994**, *59*, 2665 – 2667; c) J. P. Snyder, G. E. Tipsword, D. P. Spangler, *J. Am. Chem. Soc.* **1992**, *114*, 1507 – 1510.
[12] a) Bu^{6}Li was prepared in pentane by the method of G. Hilmersson, Ö. Davidsson, *Organometallics* **1995**, *14*, 912 – 918; b) NMR samples were prepared as described in S. H. Bertz, A. S. Vellekoop, R. A. J. Smith, J. P. Snyder, *ibid.* **1995**, *14*, 1213 – 1220, except that 5 mm tubes were used instead of 10 mm. See also Experimental Section.
[13] a) B. Wrackmeyer, *Z. Naturforsch. B* **1988**, *43*, 923 – 926; b) D. E. J. Arnold, S. Cradock, E. A. V. Ebsworth, J. D. Murdoch, D. W. H. Rankin, D. C. J. Skea, R. K. Harris, B. J. Kimber *J. Chem. Soc. Dalton Trans.* **1981**, 1349 – 1351; c) reference [13a] reports $\delta = -77.7$ vs. nitromethane for TMSCN and reference [13b] observes $\delta = 254.7$ vs. tetramethylammonium iodide (both with ca. 10% [D_6]benzene for lock). The latter is $\delta = -82.6$ vs. nitromethane. We measure $\delta = -79.7$ vs. nitromethane, which is close to the average ($\delta = -80.1$) of the previous measurements. Since nitromethane freezes at $-29\,^\circ$C, we believe more work needs to be done on a primary standard, and we provisionally take the TMSCN shift to be $\delta = -77.7$, as listed in a critical review.[21] For 4 M TMSCN in [D_8]THF, we measure $\delta = -81.7$ on this scale. Since the calculated shifts are referenced to the same value as the experimental ones, our conclusions are independent of the standard.
[14] a) G. Fraenkel, A. M. Fraenkel, M. J. Geckle, F. Schloss, *J. Am. Chem. Soc.* **1979**, *101*, 4745 – 4747; b) D. Seebach, R. Hässig, J. Gabriel, *Helv. Chim. Acta* **1983**, *66*, 308 – 337; c) for a recent review see *Lithium Chemistry-A Theoretical and Experimental Overview* (Eds.: A.-M. Saspe, P. von R. Schleyer), Wiley, Chichester, **1995**.
[15] Similar observations have been reported for PhCu and Ph_2CuLi: S. H. Bertz, G. Dabbagh, X. He, P. P. Power, *J. Am. Chem. Soc.* **1993**, *115*, 11 640 – 11 641.
[16] a) There are also small peaks at $\delta = 0.56$ and 1.26 (each about 5% of the total area) in the ^{6}Li spectrum of the 2:1 reagent which may be attributable to CN-free cuprates, presumably similar to "halide-free" cuprates: E. C. Ashby, J. J. Watkins, *J. Am. Chem. Soc.* **1977**, *99*, 5312 – 5317; b) see also reference [25a].
[17] These minor peaks may be assigned to ^{6}LiC^{15}N and Bu^{6}Li, respectively, possibly in the form of a 1:1 complex. The "LiCN" was not detectable in the ^{15}N spectra of these samples, due to its low concentration and the broadness of its peak. One preparation contained about 20% of the presumed ^{6}LiC^{15}N · Bu^{6}Li (^{6}Li peaks at $\delta = 0.95$ and 1.83) and had a ^{15}N peak at $\delta = -67.5$ ($\Delta\nu_{1/2} = 95$ Hz). The peak at $\delta = 1.83$ was assigned to Bu^{6}Li by a standard addition experiment.
[18] The samples froze out at $-120\,^\circ$C. This was also true with the mixed solvent system THF/[D_{10}]diethyl ether/pentane.
[19] a) D. B. Chesnut, *Rev. Comput. Chem.* **1996**, *8*, 245 – 297; b) D. B. Chesnut, *Ann. Rep. NMR Spectr.* **1994**, *29*, 71 – 122; c) D. B. Chesnut, B. E. Rusiloski, K. D. Moore, D. A. Egolf, *J. Comput. Chem.* **1993**, *14*, 1364 – 1375; d) D. B. Chesnut, K. D. Moore, *ibid.* **1989**, *10*, 648 – 659.
[20] a) A. D. Becke, *J. Chem. Phys.* **1993**, *98*, 5648 – 5652; b) P. J. Stevens, F. F. Devlin, C. F. Chablowski, M. J. Frisch, *J. Phys. Chem.* **1994**, *98*, 11 623 – 11 627.
[21] M. Witanowski, L. Stefaniak, G. A. Webb, *Ann. Rep. NMR Spectr.* **1993**, *25*, 214 – 219. These authors use the opposite convention for ^{15}N NMR shifts as in reference [13], for example, TMSCN at $\delta = 77.7$.
[22] a) T. A. Mobley, F. Müller, S. Berger, *J. Am. Chem. Soc.* **1998**, *120*, in press; b) A. Gerold, J. T. B. H. Jastrzebski, C. M. P. Kronenburg, N. Krause, G. van Koten, *Angew. Chem.* **1997**, *109*, 778 – 780; *Angew. Chem. Int. Ed. Engl.* **1997**, *36*, 755 – 757.
[23] a) S. H. Bertz, E. H. Fairchild in *Encyclopedia of Reagents for Organic Synthesis*, (Ed.: L. Paquette), Wiley, New York, **1995**, pp. 1312 – 1315 (CuBr), 1341 – 1343 (CuCN), 1346 – 1349 (CuI); b) S. H. Bertz, G. Dabbagh, L. M. Williams, *J. Org. Chem.* **1985**, *50*, 4414 – 4415 (CuOTf).
[24] B. H. Lipshutz in *Advances in Metal-Organic Chemistry*, *Vol. 4* (Ed.: L. S. Liebeskind), JAI Press, Greenwich CT, **1995**, pp. 1 – 64. The dispute was succinctly stated in the title of reference [5b]: "'Higher Order' Cyanocuprates $R_2Cu(CN)Li_2$: Discrete Reagents or 'Lower Order' LiCN-Modified Gilman Cuprates?"
[25] Two classes of bona fide higher order cuprates that do not contain CN are known: a) S. H. Bertz, G. Dabbagh, *J. Am. Chem. Soc.* **1988**, *110*, 3668 – 3670 (aryl); b) F. Olbrich, J. Kopf, E. Weiss, *Angew. Chem.* **1993**, *105*, 1136 – 1138; *Angew. Chem. Int. Ed. Engl.* **1993**, *32*, 1077 – 1079 (alkynyl).

Analysis of the Symmetry of Crystal Packing Forces by Methyl Proton Tunneling: A Strategy for the Unambiguous Assignment of the Magnetic Jahn – Teller Effect in Molecules**

Upali A. Jayasooriya,* Roderick D. Cannon, Christopher E. Anson, Elisha Karu, Ahmed K. Saad, John P. Bourke, Gordon J. Kearley, and Ross P. White

Recent work on polynuclear complexes of magnetic metal ions is tending to confirm a hypothesis that was put forward some time ago in which it was stated that in such complexes there is an inherent tendency towards structural distortion with lowering of symmetry, due to spin-frustration or the magnetic Jahn – Teller effect.[1] For example, according to X-ray diffraction studies the complex $[Cu_4OCl_6(OPPh_3)_4]$ crystallizes in a cubic lattice in which the molecules are located on sites of tetrahedral symmetry; however, recent FTIR measurements have revealed a lower symmetry, as shown by splittings of the vibrational frequency of the central oxygen atom.[2] Other systems have triangular clusters, and inelastic neutron scattering (INS) measurements have shown that these deviate from equilateral symmetry at low temperatures.[3] But before attempting to assign structural anomalies to intrinsic forces within the metal atom cluster as such, it is important to consider to what extent they may be driven by extrinsic forces, such as crystal packing or steric hindrance between peripheral groups in the ligands, unrelated to electronic forces at the center.

One classic approach to such problems is to compare structures of two materials that are chemically as similar as possible, apart from the asymmetry of the electron configuration. This has worked well in studies of Jahn – Teller effects in mononuclear systems, for example by comparing structures of copper(II) and zinc(II) complexes with identical ligands and counterions.[4] A similar approach to the phenomenon of spin-frustration or magnetic Jahn – Teller effect would need isostructural pairs of magnetic and nonmagnetic polynuclear

[*] Dr. U. A. Jayasooriya, Dr. R. D. Cannon, Dr. C. E. Anson, Dr. E. Karu, Dr. A. K. Saad, J. P. Bourke, Dr. G. J. Kearley, Dr. R. P. White
School of Chemical Sciences, University of East Anglia
Norwich, NR4 7TJ (UK)
Fax: Int. code + (44) 1603 259396
E-mail: u.jayasooriya@uea.ac.uk

[**] We thank the Science and Engineering Research Council for support. U.A.J. acknowledges the hospitality of the Institut Laue-Langevin, Grenoble, France. We are grateful to Dr. Paul Wood for crystallographic calculations.

 © WILEY-VCH Verlag GmbH, D-69451 Weinheim, 1998 1433-7851/98/3703-0317 $ 17.50+.50/0

complexes, but no suitable materials are known at present. Another approach to this problem is to embed the magnetic cluster at the center of a large "soft" ligand environment, and place this in turn at a crystal lattice point that is close to the idealized high symmetry. In such a strategy, what is needed is a technique that can sense structural anomalies at the periphery of the complex. If such anomalies are *not* found, but the central cluster is still found to be distorted, the case for saying that the distortion is intrinsic will be strong.

Herein we present the phenomenon of rotational tunneling of protons in units such as methyl groups as a sensitive tool for detecting extrinsic structural distortions. Using a test substance whose structure and spectra have been well studied, we show that six peripheral methyl groups can be distinguished into at least three structural types reflecting small differences in local environment.

A preliminary investigation of the proton tunneling in salts of the chromium complex ion $[Cr_3O(OOCCH_3)_6(OH_2)_3]^+$ by using INS showed at least two features for the chloride salt, a single broad overlapping peak for the perchlorate, and none for the nitrate.[5] We have now measured new tunneling spectra of the chloride salt at higher resolution, and we have compared the normal salt with a sample containing a statistical mixture of CH_3 and CD_3 groups. The purpose of the latter experiment is to detect any coupling between adjacent methyl rotors. Relatively large differences in the tunneling frequencies between the CH_3 and CD_3 groups will result in a decoupling of these rotors. The results show that at least three methyl group environments can be distinguished. A detailed introduction to the application of INS including rotational tunneling is given in a special issue of the journal *Spectrochimica Acta*.[6]

$[Cr_3O(OOCCH_3)_6(H_2O)_3]Cl \cdot 6H_2O$ was synthesized as previously,[7] and a sample containing a statistical mixture of CH_3 and CD_3 groups was prepared by starting with an equimolar mixture of acetic acid and perdeuterioacetic acid. INS spectra were recorded on finely powdered samples sealed in aluminum cans; the thickness was calculated to provide about 10% total scattering. The detectors were calibrated based on a spectrum of vanadium metal. Data reduction was carried out with the standard programs PRIME and CROSSX available at the Institut Laue-Langevin.

The INS spectra of the labeled and unlabeled samples are shown in Figure 1. X-ray powder diffraction patterns of the two samples were identical confirming that they have the same crystal and molecular structure. The differences between the two INS spectra are striking: two peaks, A and D, in the all-^1H sample, reappear almost unchanged in frequency as A and D in the $^1H/^2H$ sample, but at least two other peaks, B and C, in the all-^1H sample, collapse into one broad peak E in the $^1H/^2H$ sample. An empirical Gaussian fitting to the $^1H/^2H$ sample spectrum is consistent with the intensity ratios A:E:D = 1:4:1.

At room temperature $[Cr_3O(OOCCH_3)_6(H_2O)_3]Cl \cdot 6H_2O$ crystallizes in the space group $P2_12_12$; four molecules per unit cell occupy crystallographically general sites.[8] Below a phase transition at about 211 K it changes to $P2_12_12_1$, with the unit cell doubled in size to contain two inequivalent sets of four trinuclear complex cations;[9] that is, there are twelve structurally distinct methyl groups. The C–C distances between the methyl groups are such that intramolecular coupling can be discounted; the shortest intermolecular C–C distances in X-ray crystal structure at room temperature[10] are consistent with intermolecular coupling. Four of the methyl-C atoms per molecule have nearest neighbor methyl-C atoms within a distance of 3.37–3.66 Å and the other two have their nearest neighbors at distances of 3.7 and 3.8 Å. These values may be compared with distances of about 3.5 Å in other acetate materials in which coupling between rotors has been observed.[11]

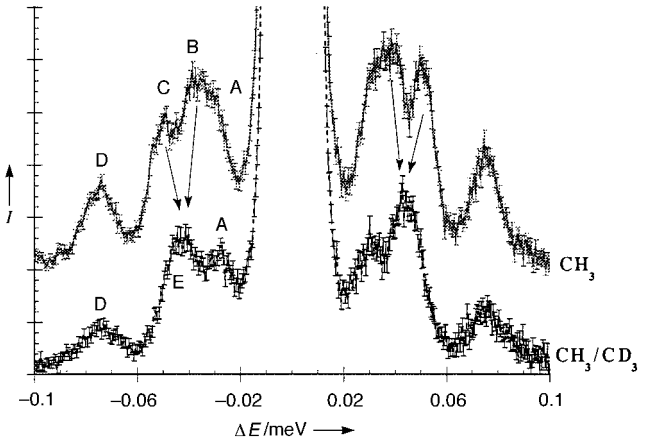


Figure 1. Methyl tunneling spectra of $[Cr_3O(OOCMe)_6(H_2O)_3]Cl \cdot 6H_2O$ recorded at $T = 2$ K (in the neutron down scattering mode) on the instrument IN5 at the Institut Laue-Langevin, Grenoble, France. Upper curve: Me = CH_3; lower curve: Me = 1:1 statistical distribution of CH_3 and CD_3 groups.

In the earlier work on the chloride salt, two possible reasons for the observed spectral profile were proposed, that is inequivalent environments of methyl groups, and coupling between pairs of very similar methyl groups, the two not being mutually exclusive. The observed intensity ratios suggest that both possibilities do in fact occur. That is, all twelve methyl groups are involved in tunneling, four of them rotating independently but grouped into two pairs with similar potentials to give the unshifted bands A and D, while the other eight are coupled intermolecularly in pairs, with similar interaction potentials, giving a set of overlapping peaks observed as bands B and C. On going over to the "scrambled" sample, which is a mixed crystal containing all possible molecules $[Cr_3O(OOCCH_3)_n(OOCCD_3)_{6-n}(H_2O)_3]^+$, the independent methyl groups remain unaffected, apart from a 50% reduction in numbers, but the coupled pairs become decoupled, and collapse to band E.[*]

From the widths and shapes of the observed spectral peaks in Figure 1, it is clear that these consist of many nearly coincident overlapping peaks. It may be possible to resolve them further by working at still lower temperatures, but with the present data we can still attempt an estimate of the methyl

[*] Another factor that should be taken into consideration in isotopic substitution experiments is lattice compression, which can produce blue shifts, but the lack of significant shifts of bands A and D, and also the observation of a red shift of band C, both suggest that lattice compression is not a significant complication here.

 © WILEY-VCH Verlag GmbH, D-69451 Weinheim, 1998 1433-7851/98/3703-0318 $ 17.50+.50/0

group rotation potentials and the inter-rotor coupling potentials. Such two-rotor systems have been described in detail,[11] though these were usually for simpler crystal structures in which the rotating pairs are coaxial. According to Clough et. al.,[12] the Hamiltonian operator for a pair of coaxially coupled methyl rotors is given by Equation (1), where B is a

$$\mathscr{H} = B\left(\frac{\partial^2}{\partial\theta^2}+\frac{\partial^2}{\partial\phi^2}\right)+V(\theta)+V'(\phi)+W(\theta,\phi) \quad (1)$$

constant, θ and ϕ are rotational coordinates of the two rotors, $V(\theta)$ and $V'(\phi)$ are the potentials for rotation of the methyl groups in their respective sites, and $W(\theta,\phi)$ is the coupling term which, considering only a threefold contribution, can be written according to Equation (2). For $V(\theta)$ and $V'(\phi)$ a Fourier series is used [Eq. (3)], where W and V_{3n} are constants and $N \leq 2$. $V'(\phi)$ is assumed to be equal to $V(\theta)$ in the simplified model used.

$$W(\theta,\phi) = \frac{W}{2}\{1-\cos 3(\theta-\phi)\} \quad (2)$$

$$V(\theta) = \sum_{n=0}^{N} V_{3n}\cos 3n\theta \quad (3)$$

The resulting energy level diagram is shown in Figure 2, which also shows the allowed transitions and their theoretical

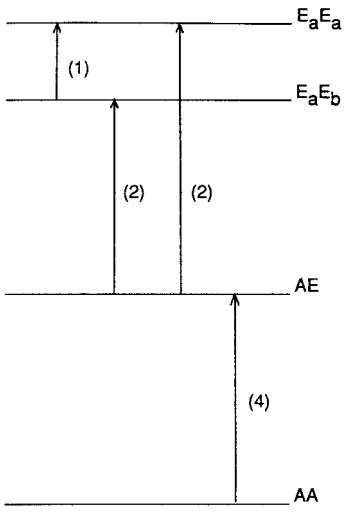


Figure 2. Energy level diagram showing the allowed transitions for two methyl groups coupled under a threefold potential. Energy levels are labeled with the symmetry species, according to reference [11]. Figures in parentheses are the relative intensities predicted for the INS spectrum.

relative intensities. A fit of this model to the spectrum of the all-H sample results in the band energies and assignments given in Table 1. The fit of calculated and observed spectra for the all H-sample is shown in Figure 3. The $(E_aE_a \leftarrow E_aE_b)$ transition is calculated to be at about 3 μeV, and is thus hidden within the elastic peak. Although the model used here is oversimplified, it provides a quantitative measure of the potentials felt by these peripheral methyl groups, which are due mainly to packing forces in the solid state.

Table 1. Summary of fitted tunneling energies ΔE [μeV] for $[Cr_3O(OOCMe)_6(H_2O)_3]Cl\cdot 6H_2O$ and its partially deuterated analogue.[a]

Me = CH_3 observed value[a]		calculated value[c]		Me = CH_3/CD_3 observed value[a]	
ΔE[b]	I_{rel}[b]	ΔE	I_{rel}	ΔE[b]	I_{rel}[b]
	1[d]	3	1		
27 (A)	2.25			26 (A)	1
	2[d]	39	2		
38 (B)	2[d]	40	2	43 (E)	4
50 (C)	4[d]	50	4		
75 (D)	2.25			77 (D)	1

[a] Letters in parentheses refer to bands labeled in Figure 1. For details of the fitting procedure see reference [14]. [b] Empirical fit to the curves shown in Figure 1. [c] Best fit to the upper curve shown in Figure 3. [d] Constrained value.

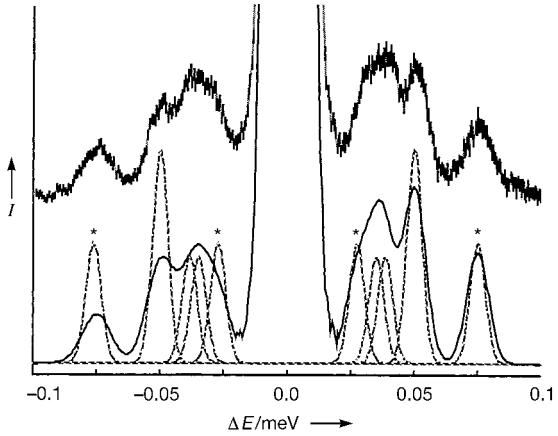


Figure 3. Methyl tunneling spectra of $[Cr_3O(OOCCH_3)_6(H_2O)_3]Cl\cdot 6H_2O$ recorded at $T = 2$ K (in neutron down scattering mode), showing the fit of the model described in the text. Upper curve: observed; lower curve: calculated. The bands labeled with an asterisk are tunneling transitions of the uncoupled methyl groups.

The vibrational spectrum of $[Cr_3O(OOCCH_3)_6(H_2O)_3]Cl\cdot 6H_2O$ in the region 100–150 cm^{-1} supports this interpretation. As measured by INS[5] it shows a strong peak at about 150 cm^{-1} and three others closely spaced at 100–130 cm^{-1}. A subsequent single-crystal Raman study has identified the 150 cm^{-1} band as the symmetric breathing mode of the oxo-centered metal triangle.[13] The other three peaks can therefore now be assigned to methyl torsions; the central peak is broader and stronger than the two side peaks, in agreement with the above conclusions on the methyl group environments.

The studies presented here clearly illustrate the sensitivity of the rotational tunneling of protons in methyl groups to the local environment. Polymetallic molecular systems with ligands such as carboxylic acids, provide useful systems for the investigation of the distortions that result from effects like the magnetic Jahn–Teller effect. As shown elsewhere,[3] the Cr_3 triangles in the present complex are "scalene" in the sense that all three Cr–Cr antiferromagnetic coupling constants are different. Inelastic magnetic neutron scattering and IR spectroscopy provide accurate information on the symmetry of the central metal core, while rotational tunneling of protons probes the symmetry of the external packing forces. Further

 © WILEY-VCH Verlag GmbH, D-69451 Weinheim, 1998 1433-7851/98/3703-0319 $ 17.50+.50/0

work including a low-temperature structure determination will be needed to establish whether or not there is a correlation between central and external geometries for this molecule. Other systems containing probable proton tunneling groups such as NH_3 will also be suitable candidates for this purpose.

Received: July 7, 1997 [Z10644IE]
German version: *Angew. Chem.* **1997**, *109*, 331 – 334

Keywords: carboxylato complexes · chromium · Jahn – Teller distortion · neutron scattering · packing effects

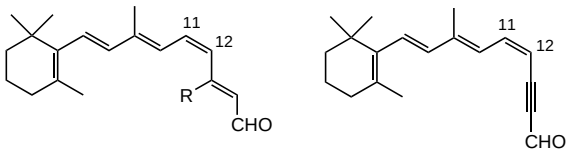
[1] T. Murao, *Phys. Lett. A* **1974**, *49*, 33.
[2] C. E. Anson, S. K. arapKoske, U. A. Jayasooriya, R. D. Cannon, *Spectrochim. Acta A* **1992**, *48*, 151.
[3] See for example: U. A. Jayasooriya, R. D. Cannon, R. P. White, G. J. Kearley, *Angew. Chem.* **1989**, *101*, 923; *Angew. Chem. Int. Ed. Engl.* **1989**, *28*, 930; U. A. Jayasooriya, R. D. Cannon, R. P. White, J. A. Stride, R. Grinter, G. J. Kearley, *J. Chem. Phys.* **1993**, *98*, 9303; R. D. Cannon, U. A. Jayasooriya, R. Wu, S. K. arapKoske, J. A. Stride, O. F. Nielsen, R. P. White, G. J. Kearley, D. Summerfield, *J. Am. Chem. Soc.* **1994**, *116*, 11869.
[4] C. J. Simmons, B. J. Hathaway, K. Amornjarusiri, B. D. Santarsiero, A. Clearfield, *J. Am. Chem. Soc.* **1987**, *109*, 1047.
[5] S. K. Bollen, N. Chaisa-ard, E. Karu, R. P. White, R. D. Cannon, U. A. Jayasooriya, C. J. Carlile, S. T. Robertson, U. Steigenberger, J. Tomkinson, *Spectrochim. Acta A* **1990**, *46*, 911.
[6] *Spectrochim Acta A* **1992**, *48*, 379ff.
[7] M. K. Johnson, D. B. Powell, R. D. Cannon, *Spectrochim. Acta A* **1981**, *37*, 995.
[8] S. C. Chang, G. A. Jeffrey, *Acta Crystallogr. Sect. B* **1970**, *26*, 673.
[9] M. Sorai, M. Tachiki, H. Suga, S. Seki, *J. Phys. Soc. Jpn.* **1971**, *30*, 750; K. J. Schenk, H. U. Gudel, *Inorg. Chem.* **1982**, *21*, 2253.
[10] C. E. Anson, J. P. Bourke, R. D. Cannon, U. A. Jayasooriya, M. Molinier, A. K. Powell, *Inorg. Chem.*, submitted.
[11] A. Heidemann, S. Clough, P. P. McDonald, A. J. Horsewill, K. Neumaier, *Z. Phys. B* **1985**, *58*, 141; F. Fillaux, C. J. Carlile, *Chem. Phys. Lett.* **1989**, *162*, 188; A. Prager, A. Heidemann, W. Hausler, *Z. Phys. B* **1986**, *64*, 447; G. J. Kearley, H. Blank, J. K. Cockcroft, *J. Chem. Phys.* **1987**, *86*, 5989; H. Blank, G. J. Kearley, *ibid.* **1987**, *87*, 6809.
[12] S. Clough, A. Heidemann, A. J. Horsewill, M. N. J. Paley, *Z. Phys. B* **1984**, *55*, 1.
[13] J. P. Bourke, R. D. Cannon, R. Grinter, U. A. Jayasooriya, *Spectrochim. Acta A* **1993**, *49*, 685.
[14] The detailed fitting procedure was as follows. On the basis of the observed spectra the coupling scheme referred to in the text was adopted. This gave the energy level scheme shown in Figure 2, and four bands with transition probabilities in the ratio 1:2:2:4. These were assigned as one low-energy transition (not observed), two overlapping transitions (band B), and a fourth transition (band C). Diagonalization of the Hamiltonian matrix within a refinement cycle allowed V and W to be adjusted to give a best fit to the observed transitions; the relative intensities are constrained to the calculated ratios. This gave $V = 62$ meV and $W = 21$ meV, and the energies listed in Table 1.

Stereocontrolled Synthesis of (11*Z*)-Retinal and Its Analogues**

Jun'ichi Uenishi,* Reiko Kawahama, Osamu Yonemitsu, Akimori Wada, and Masayoshi Ito

(11*Z*)-Retinal is a key chromophore in the visual system of the retina, which assembles with an apo-protein (opsin) to form rhodopsin.[1] When rhodopsin is exposed to photons, it is promoted to an excited state which induces a bleaching process by an enzymatic cascade. Thus, the signal is delivered to the brain through synaps, and vision is possible.[2] Although part of this mechanism was previously revealed, many unexplained interactions still remain for the visual pigments, and, in particular, the mode of action for sensing color has yet to be clarified. To study such a mechanism, pure (11*Z*)-retinal and its analogues are highly desired.[3] However, the stereoselective synthesis of pure (11*Z*)-retinals has been difficult, since they are unstable towards light, heat, acids, and bases; isomerization, condensation, or polymerization are promoted. Although a number of syntheses of (11*Z*)-retinal and its analogues have appeared, all required a separation of the stereoisomers at a certain stage.[3] The synthetic problem is largely due to the lack of a reliable method for controlling the (*Z*)-alkenyl unit at the C11 position in the conjugated pentaene system.

Since we succeeded in synthesizing conjugated polyenes bearing a (*Z*)-alkenyl component,[4] (11*Z*)-retinal was a natural target for our polyene syntheses. Furthermore, this synthetic method is able to supply a number of (11*Z*)-retinal derivatives in a stereochemically pure form. Here we describe the first strictly stereocontrolled synthesis of (11*Z*)-retinal (**1**) and its analogues **2** and **3**.



1 R = CH_3 **3**
2 R = H

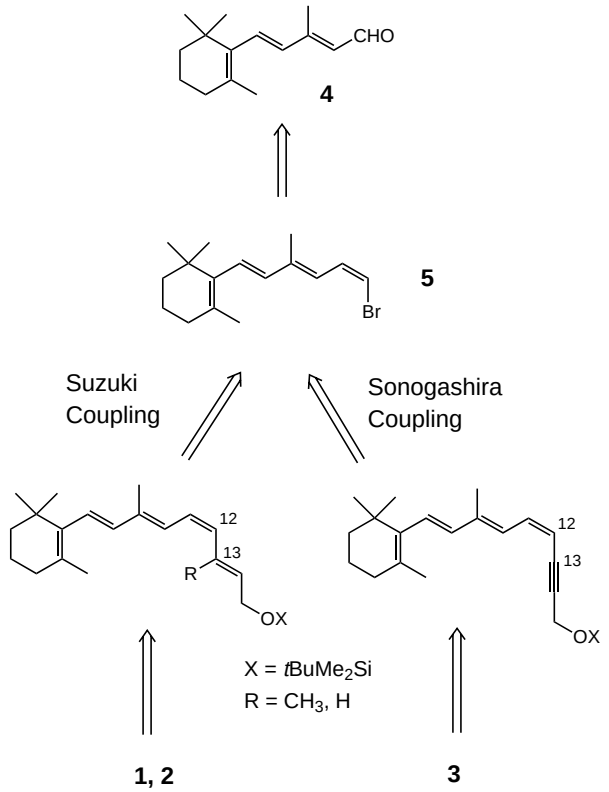
Scheme 1 summarizes the retrosynthesis of the (11*Z*)-retinals. Cleavage of the C12 – C13 bond gives rise to the important and flexible intermediate **5**, which couples with an appropriate alkenylboronic acid or alkyne by Pd-catalyzed cross-coupling reactions to afford **1**, **2**, and **3** with retention of

[*] Prof. Dr. J. Uenishi, Prof. Dr. O. Yonemitsu, Dr. R. Kawahama
Department of Chemistry, Faculty of Science
Okayama University of Science
Ridaicho, Okayama 700 (Japan)
Fax: Int. code + (81) 86 254-2891
E-mail: juenishi@chem.ous.ac.jp
Prof. Dr. A. Wada, Prof. Dr. M. Ito
Kobe Pharmaceutical University, Kobe (Japan)

[**] This work was supported by the Grant-in-Aid for Scientific research on Priority Area No. 08245101 from the Ministry of Education, Science, Sports and Culture of the Japanese Goverment, and a Special Grant for Cooperative Research administered by the Japan Private School Promotion Foundation.

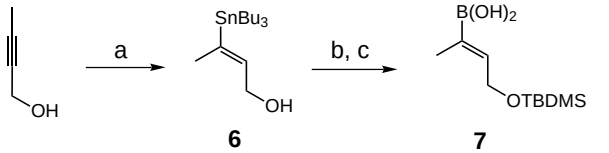
 © WILEY-VCH Verlag GmbH, D-69451 Weinheim, 1998 1433-7851/98/3703-0320 $ 17.50+.50/0

the geometries. It is important that this coupling is conducted very mildly without isomerization of the (11*Z*)-double bond in the conjugated pentaene. The key intermediate **5** can be obtained in geometrically pure form from the known aldehyde **4**[5] by the method we developed.[4]



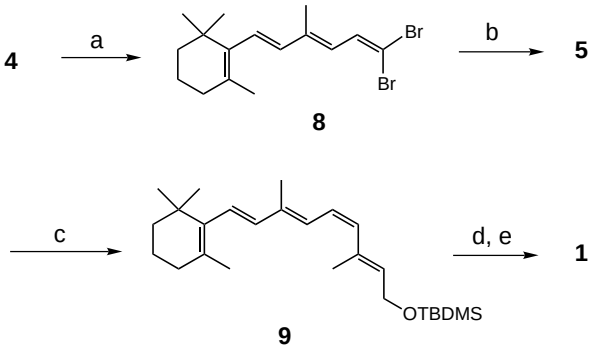
Scheme 1. Retrosynthesis of **1**–**3**; X = protecting group.

The synthesis of **1** requires the coupling partner **7**, which corresponds to the C13–C15 carbon chain; the synthesis of **7** is described in Scheme 2. A regio- and stereoselective addition of the tributylstannyl cuprate[6] to 2-butyn-1-ol gave (*E*)-3-tributylstannyl-2-buten-1-ol (**6**) in 83% yield.[7] Protection of the primary alcohol group of **6** with *t*BuMe$_2$SiCl (TBDMSCl) afforded the corresponding silyl ether in 93% yield. The tributylstannyl group was substituted with boronic acid in the three steps by the standard method:[8] 1) treatment of the alkenylstannane by alkenyllithium with BuLi, 2) quenching of the resulting alkenyllithium with triisopropyl boronate, and 3) hydrolysis of the boronate to boronic acid. The sequence gave **7** in 57% yield based on 2-butyn-1-ol.



Scheme 2. Synthesis of alkenylboronic acid **7**. a) $(Bu_3Sn)_2CuCNLi_2$, MeOH, THF, −10 °C; b) TBDMSCl, KH, THF, RT; c) 1. BuLi, THF, −78 °C; 2. B(O*i*Pr)$_3$; 3. aq HCl.

The construction of **1** from **4** is shown in Scheme 3. Aldehyde **4** was dibromomethylenylated at 0 °C with carbon tetrabromide and triphenylphosphane in dichloromethane[9] to afford **8** in 88% yield.[10] Stereoselective hydrogenolysis of **8** with tributyltin hydride in the presence of a catalytic amount

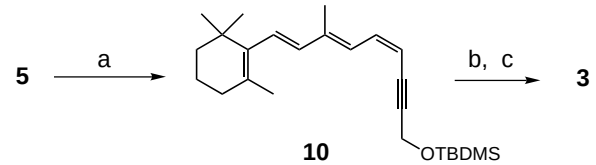


Scheme 3. Synthesis of **1**. a) CBr_4, PPh_3, CH_2Cl_2, 0 °C; b) cat. $[Pd(PPh_3)_4]$, Bu_3SnH, C_6H_6, RT; c) **7**, cat. $[Pd(PPh_3)_4]$, KOH, Ag_2CO_3, THF, RT; d) Bu_4NF, THF, RT; e) $BaMnO_4$, CH_2Cl_2, RT.

of $[Pd(PPh_3)_4]$ proceeded very cleanly to give **5** in 86% yield exclusively. This is an unstable molecule which decomposed easily upon exposure to light or acid. However, if kept in frozen benzene in the presence of a small amount of triphenylphosphane at −20 °C, **5** can be stored for one month. The Suzuki coupling of **5** with **7** was carried out in THF at room temperature in the presence of a catalytic amount of $[Pd(PPh_3)_4]$, Ag_2CO_3, and an aqueous solution of KOH to give **9** in 77% yield with retention of configuration. Removal of the silyl ether protecting group of **9** with tetrabutylammonium fluoride and successive oxidation with $BaMnO_4$ furnished isomerically pure **1** (85% yield over two steps). The spectroscopic data was in accordance with those reported for (11*Z*)-retinal.[11]

In the same manner as described for **1**, 13-demethyl-(11*Z*)-retinal (**2**) was obtained in 58% yield from **5**. Coupling of **5** with (*E*)-3-(*tert*-butyldimethylsilyl)oxy-1-propenyl-1-boronic acid[12] (90%, based on the recovery of **5**) followed by removal of the silyl ether protecting group (85%) and oxidation of the alcohol (76%) afforded **2** without the formation of any other stereoisomers.[13]

Palladium-catalyzed cross-coupling of **5** with O-protected propargyl alcohol introduced a C13 alkynyl component to form **3** instead of the *E*-ethenyl functionality in **1**. Scheme 4 depicts the synthesis of **3**. Intermediate **5** was coupled with



Scheme 4. Synthesis of **3**. a) *tert*-Butyldimethylsilyl propargyl ether, cat. $[Pd(PPh_3)_4]$, cat. CuI, *i*Pr$_2$NH, C_6H_6, RT; b) Bu_4NF, THF, RT; c) $BaMnO_4$, CH_2Cl_2, RT.

 © WILEY-VCH Verlag GmbH, D-69451 Weinheim, 1998 1433-7851/98/3703-0321 $ 17.50+.50/0

tert-butyldimethylsilyl propargyl ether in the presence of $[Pd(PPh_3)_4]$ (5 mol%), CuI, and diisopropylamine in benzene under the standard Sonogashira conditions[14] to give **10** in 88% yield. The reaction proceeded without isomerization of the (11*Z*)-double bond. After the TBDMS group was quantitatively removed with Bu_4NF, the primary alcohol obtained was oxidized with $BaMnO_4$ to give **3** (68% yield over two steps).[15]

We have demonstrated an efficient and concise synthesis of geometrically pure (11*Z*)-retinals, in which a construction of the conjugated pentaene system involving the (*Z*)-alkenyl unit is achieved. (11*Z*)-Retinals prepared by this method exhibit perfect purity in their geometry. An advantage of this method is that it can be used to prepare a wide range of (11*Z*)-retinals and thus offers a further development in the research of vision.

Experimental Section

8: PPh_3 (1.92 g, 7.32 mmol) was added all at once to an ice-cooled, stirred solution of **4** (400 mg, 1.83 mmol) and CBr_4 (912 mg, 2.75 mmol) in CH_2Cl_2 (30 mL). The mixture was stirred for 5 min at the same temperature and then purified by column chromatography (silica gel, hexane) to give a mixture of **8** and retroionylidene bromide (638 mg, 8.8:1 ratio) in a combined yield of 98%. Oil; $R_f = 0.62$ (hexane); ^{1}H NMR (300 MHz, $CDCl_3$): $\delta = 1.03$ (6H, s), 1.44–1.50 (2H, m), 1.57–1.66 (2H, m), 1.71 (3H, d, $J = 0.9$ Hz), 1.91 (3H, d, $J = 1.2$ Hz), 2.01 (2H, br t, $J = 6.2$ Hz), 6.01 (1H, d, $J = 10.9$ Hz), 6.13 (1H, d, $J = 16.1$ Hz), 6.33 (1H, dd, $J = 16.1$, 0.8 Hz), 7.27 (1H, d, $J = 10.9$ Hz); ^{13}C NMR (75 MHz, $CDCl_3$): $\delta = 13.5$, 19.2, 21.7, 28.9 (2C), 33.1, 34.2, 39.6, 90.7, 125.7, 129.6, 130.0, 133.6, 136.8, 137.6, 139.5; MS (70 eV): *m*/*z* (%): 376 (M^+, 52), 374 (M^+, 100), 372 (M^+, 50), 361 (19), 359 (34), 357 (20), 295 (11), 293 (11), 214 (29), 199 (38); HR-MS calcd for $C_{16}H_{22}Br_2$ (M^+): 376.0047, 374.0068, 372.0088; found: 376.0043, 374.0089, 372.0089.

5: A solution of Bu_3SnH (0.84 mmol, 2.27 mL, 0.37 M in benzene) was added to a mixture of **8** (298 mg, 0.8 mmol) and $[Pd(PPh_3)_4]$ (37 mg, 0.032 mmol) in benzene (5.7 mL) at room temperature. The mixture was stirred for 20 min, diluted with hexane (30 mL), washed with water (2 mL) and brine (2 mL), and dried over $MgSO_4$. The extract was concentrated under reduced pressure below 10 °C and purified by column chromatography (alumina, hexane) to give **5** (203 mg) in 86% yield. After addition of PPh_3 (30 mg), the mixture was frozen in benzene at −20 °C for storage. Oil; $R_f = 0.59$ (hexane); UV (hexane): $\lambda_{max} = 301$, 239 nm; ^{1}H NMR (300 MHz, $CDCl_3$): $\delta = 1.03$ (6H, s), 1.44–1.49 (2H, m), 1.57–1.67 (2H, m), 1.72 (3H, d, $J = 0.8$ Hz), 1.94 (3H, d, $J = 1.0$ Hz), 2.02 (2H, br t, $J = 6.2$ Hz), 6.18 (1H, d, $J = 16.2$ Hz), 6.20 (1H, d, $J = 7.1$ Hz), 6.30 (1H, d, $J = 16.2$ Hz), 6.33 (1H, d, $J = 11.0$ Hz), 6.98 (1H, dd, $J = 11.0$, 7.1 Hz); ^{13}C NMR (75 MHz, $CDCl_3$): $\delta = 13.3$, 19.2, 21.7, 28.9 (2C), 33.0, 34.2, 39.6, 108.2, 124.8, 128.9 (2C), 129.8, 137.2, 137.6, 139.7; MS (70 eV): *m*/*z* (%): 296 (M^+, 85), 294 (M^+, 99), 281 (21), 279 (18), 215 (100), 199 (35); HR-MS calcd for $C_{16}H_{23}Br$ (M^+): 296.0963, 294.0983; found: 296.0958, 294.0979.

9: $[Pd(PPh_3)_4]$ (42 mg, 0.036 mmol), an aqueous solution of KOH (7.2 mL, 2 N), and Ag_2CO_3 (398 mg, 1.44 mmol) were successively added at room temperature to a mixture of **5** (104 mg, 0.36 mmol) and **7** (268 mg, 0.88 mmol) in degassed THF (2.6 mL). The reaction mixture was stirred for 3 h at the same temperature, diluted with 10% ether in hexane (40 mL), washed with water (3 × 5 mL) and brine (5 mL), and dried over $MgSO_4$. The organic extract was condensed under reduced pressure below 10 °C, and the oily residue purified by column chromatography (silica gel, diethyl ether/hexane, 2/98) to give **9** (111 mg) in 77% yield. The material is very light-sensitive, and should be handled in the dark. Oil; $R_f = 0.18$ (hexane); UV (hexane): $\lambda_{max} = 322$, 236 nm; ^{1}H NMR (300 MHz, C_6D_6): $\delta = 0.08$ (6H, s), 0.99 (9H, s), 1.11 (6H, s), 1.44–1.51 (2H, m), 1.54–1.63 (2H, m), 1.73 (3H, s), 1.76 (3H, d, $J = 0.8$ Hz), 1.85 (3H, d, $J = 1.1$ Hz), 1.95 (2H, br t, $J = 6.2$ Hz), 4.26 (2H, d, $J = 6.6$ Hz), 5.88 (1H, t, $J = 6.6$ Hz), 5.90 (1H, d, $J = 11.8$ Hz), 6.28 (1H, d, $J = 16.0$ Hz), 6.38 (1H, d, $J = 16.0$ Hz), 6.38 (1H, dd, $J = 12.0$, 11.8 Hz), 6.88 (1H, d, $J = 12.0$ Hz); ^{13}C NMR (75 MHz, C_6D_6): $\delta = -5.0$, 12.3, 17.2, 18.4, 19.7, 21.9, 26.1 (2C), 29.1, 33.2, 34.5, 39.9, 60.4, 125.2, 127.0, 127.4, 129.1, 132.4, 133.4, 134.3, 136.8, 138.3, 138.9; MS (70 eV): *m*/*z* (%): 400 (M^+, 100), 385 (9), 343 (8), 269 (8), 254 (12), 199 (9); HR-MS calcd for $C_{26}H_{44}OSi$ (M^+): 400.3162; found: 400.3167.

10: A mixture of **5** (100 mg, 0.34 mmol), *tert*-butyldimethylsilyl propargyl ether (115 mg, 0.68 mmol), diisopropylamine (95 μL, 0.68 mmol), $[Pd(PPh_3)_4]$ (20 mg, 0.017 mmol), and CuI (6.5 mg, 0.034 mmol) in degassed benzene (3.4 mL) was stirred at room temperature for 30 min. The reaction mixture was diluted with hexane and washed with water (2 mL × 2) and brine (2 mL). The organic layer was dried over $MgSO_4$ and evaporated under reduced pressure below 10 °C. The crude mixture was purified by column chromatography (silica gel, diethyl ether/hexane, 2/98) to give **10** (115 mg) in 88% yield. The material is very light-sensitive, and should be handled in the dark. Oil; $R_f = 0.17$ (hexane); UV (hexane): $\lambda_{max} = 324$, 252 nm; ^{1}H NMR (300 MHz, $CDCl_3$): $\delta = 0.15$ (6H, s), 0.93 (9H, s), 1.03 (6H, s), 1.44–1.49 (2H, m), 1.57–1.66 (2H, m), 1.72 (3H, d, $J = 0.9$ Hz), 1.95 (3H, d, $J = 0.9$ Hz), 2.02 (2H, br t, $J = 6.0$ Hz), 4.53 (2H, d, $J = 2.5$ Hz), 5.46 (1H, d, $J = 10.6$ Hz), 6.17 (1H, d, $J = 16.0$ Hz), 6.27 (1H, d, $J = 16.0$ Hz), 6.56 (1H, d, $J = 12.1$ Hz), 6.76 (1H, dd, $J = 12.1$, 10.6 Hz); ^{13}C NMR (75 MHz, $CDCl_3$): $\delta = -5.0$, 12.7, 18.3, 19.2, 21.7, 25.9 (2C), 28.9, 33.1, 34.2, 39.6, 52.5, 82.6, 95.2, 107.6, 126.9, 128.7, 129.8, 136.2, 137.4, 137.7, 139.1; MS (70 eV): *m*/*z* (%): 384 (M^+, 31), 369 (3), 327 (2), 149 (100); HR-MS calcd for $C_{25}H_{40}OSi$ (M^+): 384.2849; found: 384.2838.

Received: August 5, 1997 [Z 10782 IE]
German version: *Angew. Chem.* **1998**, *110*, 334–336

Keywords: alkenes · bioorganic chemistry · cross-coupling · palladium · retinoids

[1] R. R. Birge, *Annu. Rev. Biophys. Bioeng.* **1981**, *10*, 315–354; J. E. Dowling, *The Retina*, Harvard University Press, Cambridge, **1987**.
[2] K. Nakanishi, R. Crouch, *Isr. J. Chem.* **1995**, *35*, 235–272; R. R. Rando, *Angew. Chem.* **1990**, *102*, 507–526; *Angew. Chem. Int. Ed. Engl.* **1990**, *29*, 461–480; J. C. Saari, *The Retinoids, Biology, Chemistry and Medicine*, 2nd ed. (Eds.: M. B. Sporn, A. B. Roberts, D. S. Goodmann), Raven, New York, **1994**, chap. 9, pp. 351–395.
[3] Reviews: R. S. H. Liu, A. E. Asato, *Tetrahedron* **1984**, *40*, 1931–1969; M. Dawson, P. D. Hobbs, *The Retinoids, Biology, Chemistry and Medicine*, 2nd ed. (Eds.: M. B. Sporn, A. B. Roberts, D. S. Goodmann), Raven, New York, **1994**, chap. 2, pp. 5–178; recent synthesis of (11*Z*)-retinals: B. Borhan, R. Kunz, A. Y. Wang, K. Nakanishi, N. Bojkova, K. Yoshihara, *J. Am. Chem. Soc.* **1997**, *119*, 5758–5759; A. Wada, Y. Tanaka, N. Fujioka, M. Ito, *Bioorg. Med. Chem. Lett.* **1996**, *6*, 2049–2052, and references therein.
[4] J. Uenishi, R. Kawahama, O. Yonemitsu, J. Tsuji, *J. Org. Chem.* **1996**, *61*, 5716–5717; J. Uenishi, R. Kawahama, Y. Shiga, O. Yonemitsu, J. Tsuji, *Tetrahedron Lett.* **1996**, *37*, 6759–6762.
[5] R. W. Dugger, C. H. Heathcock, *Syn. Commun.* **1980**, *10*, 509–515; J. A. Pardoen, P. P. Mulder, E. M. M. van Den Berg, J. Lugtenburg, *Can. J. Chem.* **1985**, *63*, 1431–1435; A. Wada, S. Hiraishi, M. Ito, *Chem. Pharm. Bull.* **1994**, *42*, 757–759.
[6] J.-F. Betzer, J. Ardisson, J. -Y. Lallemand, A. Pancrazi, *Tetrahedron Lett.* **1997**, *38*, 2279–2282.
[7] **6**: Oil; $R_f = 0.21$ (EtOAc/hexane, 1/9); IR (neat): $\tilde{\nu} = 3326$ cm^{-1}; ^{1}H NMR (300 MHz, $CDCl_3$): $\delta = 0.86$–0.93 (15H, m), 1.24–1.38 (6H, m), 1.41–1.55 (6H, m), 1.70 (1H, br s), 1.88 (3H, s), 4.26 (2H, d, $J = 6.0$ Hz), 5.75 (1H, tq, $J = 6.0$, 1.8 Hz); ^{13}C NMR (75 MHz, $CDCl_3$): $\delta = 9.0$, 13.6, 19.3, 27.3, 29.1, 58.8, 139.3, 142.3.
[8] H. C. Brown, T. E. Cole, *Organometallics* **1983**, *2*, 1316–1319.
[9] F. Ramirez, N. B. Desai, N. McKelvie, *J. Am. Chem. Soc.* **1962**, *84*, 1745–1747.
[10] This yield was determined by ^{1}H NMR spectroscopy for a mixture of **8** and the unseparable by-product 10-bromo-3,5,7,9-tetraene (retroionylidene bromide), which results from direct bromination of **4** under the reaction conditions. However, the by-product decomposed easily within several hours at room temperature.
[11] Y. Katsuta, M. Sakai, M. Ito, *J. Chem. Soc. Perkin Trans. 1* **1993**, 2185–2192.

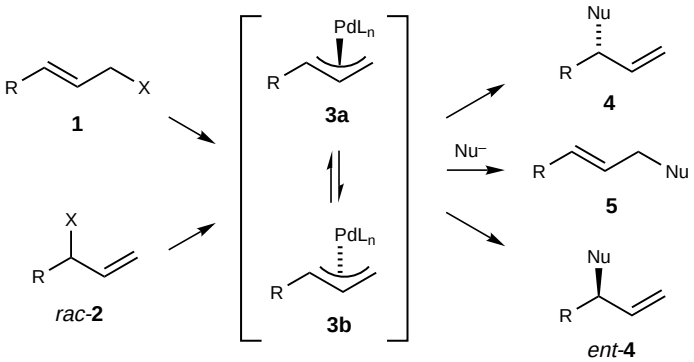
 © WILEY-VCH Verlag GmbH, D-69451 Weinheim, 1998 1433-7851/98/3703-0322 $ 17.50+.50/0

[12] (*E*)-1-[3-(*tert*-Butyldimethylsilyl)oxy-1-propenyl]-1,3,2-benzodioxaborole could be used instead of the boronic acid for this reaction.
[13] **2**: Oil; $R_f = 0.34$ (EtOAc/hexane, 5/95); IR (KBr): $\tilde{\nu} = 1677, 1580\ cm^{-1}$; UV (EtOH): $\lambda_{max} = 379, 243$ nm; ^1H NMR (300 MHz, C_6D_6): $\delta = 1.11$ (6H, s), 1.44 – 1.50 (2H, m), 1.53 – 1.63 (2H, m), 1.72 (3H, s), 1.76 (3H, d, $J = 1.0$ Hz), 1.95 (2H, br t, $J = 6.5$ Hz), 5.79 (1H, m), 6.01 (1H, dd, $J = 15.1$, 7.7 Hz), 6.27 (1H, d, $J = 16.1$ Hz), 6.35 – 6.47 (3H, m), 7.12 (1H, dd, $J = 15.1$, 12.0 Hz), 9.42 (1H, d, $J = 7.7$ Hz); ^{13}C NMR (75 MHz, C_6D_6): $\delta = 12.4$, 19.6, 21.9, 29.1 (2C), 33.3, 34.5, 39.8, 124.8, 126.2, 130.1, 130.4, 132.2, 133.8, 137.9, 138.0, 141.0, 144.8, 192.2; FAB-MS: *m/z*: 271 (M^++H); HR-MS calcd for $C_{19}H_{27}O$ (M^++H): 271.2062; found: 271.2068.
[14] K. Sonogashira, Y. Tohda, N. Hagihara, *Tetrahedron Lett.* **1975**, 4467 – 4470.
[15] **3**: Oil; $R_f = 0.23$ (EtOAc/hexane, 15/85); IR (KBr): $\tilde{\nu} = 2160, 1659, 1584\ cm^{-1}$; UV (EtOH): $\lambda_{max} = 370, 252$ nm; ^1H NMR (300 MHz, C_6D_6): $\delta = 1.04$ (6H, s), 1.35 – 1.45 (2H, m), 1.50 – 1.60 (2H, m), 1.61 (3H, s), 1.63 (3H, s), 1.89 (2H, br t, $J = 6.5$ Hz), 5.16 (1H, d, $J = 10.5$ Hz), 6.20 (1H, d, $J = 16.0$ Hz), 6.36 (1H, br d, $J = 16.0$ Hz), 6.62 (1H, dd, $J = 12.1$, 10.5 Hz), 6.78 (1H, d, $J = 12.1$ Hz), 8.91 (1H, d, $J = 1.2$ Hz); ^{13}C NMR (100 MHz, C_6D_6): $\delta = 15.6$, 19.6, 21.8, 29.1 (2C), 33.2, 34.5, 39.8, 91.9, 96.5, 104.6, 127.0, 130.8, 131.4, 137.6, 137.7, 142.9, 143.1, 175.4; MS (70 eV): *m/z* (%): 268 (M^+); HR-MS calcd for $C_{19}H_{24}O$ (M^+): 268.1826; found: 268.1814.

New Ligands for Regio- and Enantiocontrol in Pd-Catalyzed Allylic Alkylations

Roger Prétôt and Andreas Pfaltz*

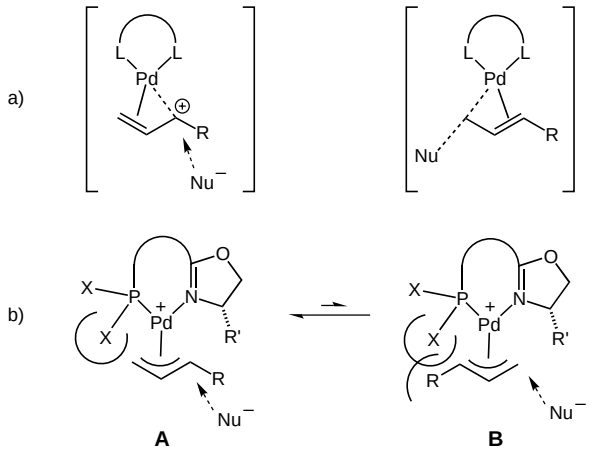
During the last few years dramatic progress has been made in the enantiocontrol of palladium-catalyzed allylic alkylations. New chiral ligands have been developed which can induce impressive levels of enantioselectivity in reactions with stabilized carbanions and various N-, O-, and S-nucleophiles.[1] However, the lack of regiocontrol is often a problem. For example, monosubstituted allylic substrates such as **1** and **2** (R = aryl) generally react predominantly at the unsubstituted allyl terminus (Scheme 1).[2] Consequently, the achiral, linear product **5** is formed rather than the chiral, branched isomer **4** or its enantiomer *ent*-**4**, which are the preferred products for applications in asymmetric synthesis. Although predominant formation of the branched isomers has been observed with achiral catalysts derived from other metals[3] (most notably W and Ir), the development of enantioselective catalysts for this class of substrate remains a challenge.



Scheme 1. Pd-catalyzed allylic alkylations generally produce the same products, regardless of whether substrate **1** or **2** is employed.

In 1995 we reported on the conversion of (*E*)-3-aryl-2-propenylphosphates **1** (R = aryl, X = OP(O)(OEt)$_2$) into chiral malonic acid derivatives **4** (Nu = CH(CO$_2$Me)$_2$).[4] High enantiomeric excesses and moderate to good regioselectivities were achieved with a tungsten catalyst prepared from the chiral (phosphanyloaryl)dihydrooxazole ligand **6a**[5] (see Scheme 3). The corresponding (*Z*) isomers and racemic substrates **2**, on the other hand, afford low enantioselectivities, in contrast with analogous Pd-catalyzed reactions, which generally proceed via rapidly equilibrating allyl intermediates and, therefore, in most cases give identical results with these three types of substrates.

Here we describe a new class of palladium catalysts that afford good enantio- and regioselectivities with both achiral and racemic aryl-substituted substrates **1** and **2**. The design of these catalysts was based on the following considerations: 1) Nucleophilic attack by an S_N2-type process should take place preferentially at the less substituted allyl terminus, whereas the opposite regioselectivity would be expected in an S_N1-like reaction via a cationic transition state (Scheme 2a).



Scheme 2. Nucleophilic attack in the Pd-catalyzed allylic alkylation. a) Transition states in S_N1- (left) and S_N2-like (right) processes. b) Steric encumbrance introduced by bulky substituents X on the P atom of the ligand favors attack of the substituted allyl terminus.

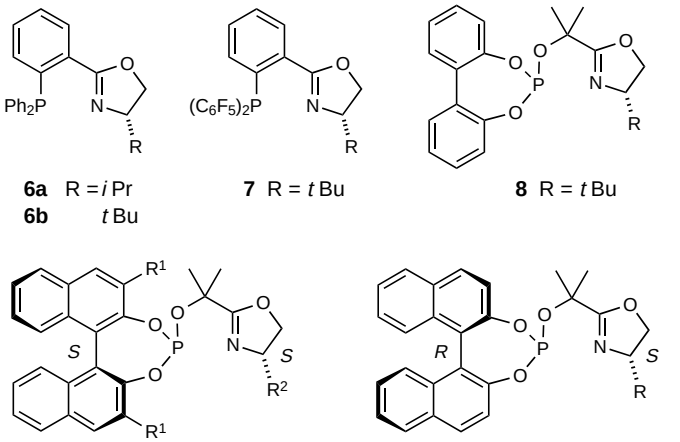
In order to enhance the S_N1 character, we decided to introduce electronegative substituents at the coordinating P atom that render the Pd center more electrophilic. 2) Steric factors affecting the equilibrium between allyl intermediates **A** and **B** also can play an important role (Scheme 2b). Bulky groups at the P atom are expected to destabilize isomer **B** as well as the transition states of the reaction pathways leading from **B** to the corresponding substitution products. Therefore, a pathway via **A** should be preferred and, assuming that nucleophilic attack at the allyl terminus *trans* to the Pd – P

[*] Prof. Dr. A. Pfaltz, Dipl.-Chem. R. Prétôt
Max-Planck-Institut für Kohlenforschung
Kaiser-Wilhelm-Platz 1, D-45470 Mülheim an der Ruhr (Germany)
Fax: Int. code + (49) 208-306 2992
E-mail: pfaltz@mpi-muelheim.mpg.de

 © WILEY-VCH Verlag GmbH, D-69451 Weinheim, 1998 1433-7851/98/3703-0323 $ 17.50+.50/0

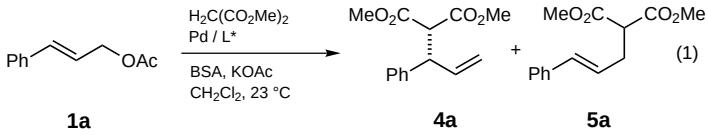
bond is electronically favored,[6] reaction at the substituted allyl end should be facilitated. Although there are certainly other factors affecting the regioselectivity, these straightforward concepts put us on the right track.

Replacement of the phenyl groups at the P atom of **6b** by electron-withdrawing pentafluorophenyl groups (→**7**, Scheme 3)[7] shifted the regioselectivity in the desired direction from 4:96 to 48:57 (Table 1). A similar effect was observed when ligand **8** was used, which has a biphenylphosphite group in place of the diphenylphosphane substituent.



6a R = *i* Pr
6b *t* Bu
7 R = *t* Bu
8 R = *t* Bu
9a R^1 = H R^2 = *t* Bu
9b H *i* Pr
9c H Ph
9d Me *t* Bu
10 R = *t* Bu

Scheme 3. Chiral ligands L* tested in the Pd-catalyzed allylic alkylation.



1a **4a** **5a**

Table 1. Results of enantioselective allylic alkylation [Eq. (1)] using different ligands L*.[a]

L*	Yield [%][b]	*ee* of **4a** [%][c]	**4a**:**5a**[d]
6b	90	78	4:96
7	87	84	47:53
8	75	81	63:37
9a	84	86	69:31
9a	86	90	76:24[e]
10	80	79	46:54
9b	92	77	68:32
9c	84	91	39:61
9d	88	92	55:45

[a] 1 mol% $[Pd(C_3H_5)Cl]_2$, 2.4 mol% L*, 50°C, CH_2Cl_2, 2 h; 2 equiv of $CH_2(CO_2Me)_2$ and *N*,*O*-bis(trimethylsilyl)acetamide (BSA), 4 mol% KOAc, 23°C, 18 h.[12] [b] Total yield of purified (*S*)-**4a** and (*E*)-**5a** after chromatography. [c] Determined by HPLC (Chiralcel OJ).[4] All reactions gave the (*S*)-(−) enantiomer. [d] Determined by GC analysis of the crude reaction mixture and ^{1}H NMR analysis after chromatography. [e] Reaction in benzene.

The regio- and enantioselectivities could be further improved by introduction of a second stereogenic unit derived from binaphthol. The best results were obtained with ligand (*S*,*S*)-**9a**; the (*R*,*S*) diastereomer **10**, derived from (*R*)-binaphthol, gave lower regio- and enantioselectivities. Apparently, the enantioselectivity is determined largely by the chiral dihydrooxazole ring. The chiral binaphthol unit has a minor, but still significant effect. The analogous isopropyldihydrooxazole ligand **9b** gave a somewhat lower *ee* value; the phenyldihydrooxazole ligand **9c**, on the other hand, was inferior in terms of regioselectivity. Introduction of two *ortho*-methyl groups in the binaphthol system (→**9d**) improved the enantioselectivity, but the regioselectivity decreased. The best results were achieved with ligand **9a** in benzene at 23°C (90% *ee*, **4a**:**5a** 76:24; Table 1) and in dichloromethane at −35°C (88% *ee*, 79:21).

Even better regio- and enantioselectivities were obtained with 1-naphthyl-substituted allylic acetates **1b** and **2b** (Table 2). The achiral substrates **1a**–**1c** afforded essentially the same regio- and enantioselectivities as the corresponding racemic isomers **2**. Apparently, the intermediate allyl complexes undergo rapid isomerization before they react with the nucleophile in the slower selectivity-determining step. The limitations of these catalysts become apparent with substrates **1d** and **2e**, which react with distinctly lower selectivities.

Table 2. Allylic alkylation of various substrates **1** and *rac*-**2** using ligand **9a** (Scheme 1; X = OAc, Nu = $CH(CO_2Me)_2$).[a]

	R	Yield [%][b]	*ee* of **4** [%][c]	**4**:**5**[d]
1b	1-naphthyl	87	94(*S*)	95:5
2b	1-naphthyl	91	96(*S*)	96:4
1c	2-naphthyl	72	88	77:23
2c	2-naphthyl	71	89	74:26
2a	phenyl	82	88(*S*)	66:34
1d	methyl	75	41[e]	30:70
2e	$(CH_3)_2C{=}CH$	72	51	75:25[f]

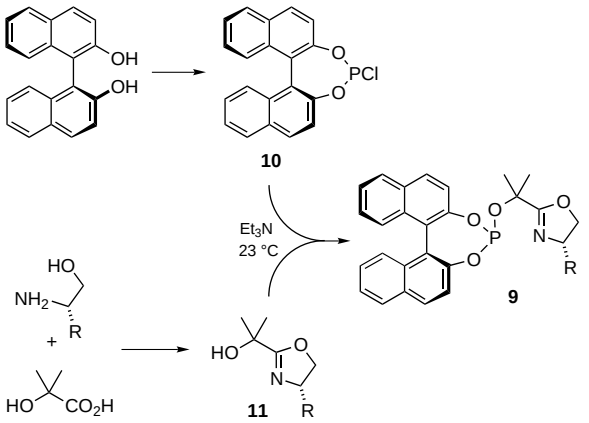
[a] For experimental conditions see Table 1. [b] Total yield of **4** and **5** after chromatography. [c] Determined by HPLC analysis (Chiralcel OJ and OD-H). Configurations of **4a** and **4b** were assigned by comparison to ref. [4]. [d] Determined by GC analysis of the crude reaction mixture and ^{1}H NMR analysis after chromatography. [e] Determined by GC analysis (Chiraldex G-TA). [f] Reaction in benzene.

A comparison of 3-phenyl-2-propenyl acetate **1a** with the corresponding *p*-methoxyphenyl- and *p*-cyanophenyl-2-propenyl acetates confirms that the regioselectivity is strongly affected by electronic factors. While the electron-donating *p*-methoxy substituent enhances the regioselectivity from 69:31 to 76:24 in favor of the chiral isomer (76% *ee*), the cyano group has the opposite effect, resulting in a reversed product ratio of 13:87 with the linear isomer **5** as the main product.

The synthesis of ligands **9** is straightforward (Scheme 4). Starting from various amino alcohols, hydroxy acids, and diols, a wide range of analogues can be readily prepared in this way. Libraries of ligands that are accessible by this route could be used to further optimize the selectivities obtained so far.

Our results demonstrate how the regioselectivity of allylic alkylations can be changed by systematic modification of the electronic and steric properties of the ligand attached to the

 © WILEY-VCH Verlag GmbH, D-69451 Weinheim, 1998 1433-7851/98/3703-0324 $ 17.50+.50/0 *Angew. Chem. Int. Ed.* **1998**, *37*, No. 3



Scheme 4. Synthesis of ligands **9**. The preparation of compounds **10**[10] and **11**[11] is described elsewhere.

palladium catalyst. By using a new type of chiral P,N ligand, practically useful enantio- and regioselectivities have been obtained in the reaction with 1- and 3-aryl-2-propenyl acetates.[8] Although at present the range of substrates that afford good selectivities is limited to aryl-substituted derivatives, the concepts used for the design of ligands **9** may serve as guidelines for the development of new catalysts for different classes of substrates. In addition, these ligands have other possible applications in asymmetric catalysis.[9]

Experimental Section

9a: All reactions were performed under argon in degassed solvents. A solution of **10**[10] (1.1 g, 3.2 mmol) in toluene (10 mL) was added dropwise to Et_3N (2.6 g, 25.7 mmol) in toluene (20 mL) at $-78^\circ C$. This solution was stirred for 5 min at $-78^\circ C$ before a solution of **11**[11] (0.6 g, 3.2 mmol) in toluene (5 mL) was added quickly. The solution was allowed to gradually warm up to room temperature and stirred for 12 h. The white precipitate was removed by filtration. Evaporation of the solvent afforded a yellow oil, which was purified by column chromatography (silica gel, 3.0×20 cm; *n*-hexane/EtOAc 4/1, $R_f = 0.4$) to afford (*S*,*S*)-**9a** (890 mg, 56%) as an amorphous solid. $[\alpha]_{589} = +269$ ($CHCl_3$, $c = 3.1$, 23°C); ^{1}H NMR (200 MHz, $CDCl_3$): $\delta = 0.96$ (s, 9H; *t*Bu), 1.65 (s, 3H; Me), 1.75 (s, 3H; Me), 3.95–4.00 (m, 1H; HCN), 4.20–4.35 (m, 2H; CH_2O), 7.22–7.52 (m, 8H; arom. CH), 7.89–7.96 (m, 4H; arom. CH); ^{13}C NMR (75 MHz, $CDCl_3$): $\delta = 25.8$ (*t*Bu), 28.1 (d, $J = 7.9$ Hz; Me), 28.2 (d, $J = 5.7$ Hz; Me), 33.9 (*t*Bu), 69.7 (CH_2O), 75.7 (CHN), 77.2 (C), 121.9/122.4 (arom. CH), 123.2 (arom. C), 124.5 (d, $J =$ 3.1 Hz; arom. C), 124.6/124.8/125.8/126.0/126.9/127.0/128.1/128.2/129.3/130.0 (arom. CH), 131.1/131.4/132.7/132.8 (arom. C), 147.9 (d, $J = 2.3$ Hz; arom. C), 148.0 (d, $J = 3.7$ Hz; arom. C), 168.3 (C=N); ^{31}P NMR (100 MHz, $CDCl_3$): $\delta = 151.5$.

Catalytic reactions (Tables 1 and 2) were carried out according to the literature procedure.[12] Purification and analytical data of the products are described elsewhere.[3b, 4].

Received: July 28, 1997 [Z 10745 IE]
German version: *Angew. Chem.* **1998**, *110*, 337–339

Keywords: allylic alkylations · asymmetric catalysis · dihydrooxazoles · N ligands · palladium · P ligands

[1] a) B. M. Trost, D. L. Van Vranken, *Chem. Rev.* **1996**, *96*, 395–422; b) T. Hayashi in *Catalytic Asymmetric Synthesis*, (Ed.: I. Ojima), VCH, New York, **1993**, pp. 325–365.

[2] a) For a discussion of the various regioselectivity-determining factors, see: B. M. Trost, M.-H. Hung, *J. Am. Chem. Soc.* **1984**, *106*, 6837–6839; b) systematic study of the influence of the ligand: B. Åkermark, K. Zetterberg, S. Hansson, B. Krankenberger, A. Vitagliano, *J. Organomet. Chem.* **1987**, *335*, 133–142; M. P. T. Sjögren, S. Hansson, B. Åkermark, A. Vitagliano, *Organometallics* **1994**, *13*, 1963–1971.

[3] a) W: B. M. Trost, M.-H. Hung, *J. Am. Chem. Soc.* **1983**, *105*, 7757–7759; b) see also: G. C. Lloyd-Jones, J. Lehmann, *Tetrahedron* **1995**, *51*, 8863–8874; c) Ir: R. Takeuchi, M. Kashio, *Angew. Chem.* **1997**, *109*, 268–270; *Angew. Chem. Int. Ed. Engl.* **1997**, *36*, 263–265; d) Mo: B. M. Trost, M. Lautens, *Tetrahedron* **1987**, *43*, 4817–4840; e) Ru: T. Kondo, H. Ono, N. Satake, T. Mitsudo, Y. Watanabe, *Organometallics* **1995**, *14*, 1945–1953; S.-W. Zhang, T. Mitsudo, T. Kondo, Y. Watanabe, *J. Organomet. Chem.* **1993**, *450*, 197–207.

[4] G. C. Lloyd-Jones, A. Pfaltz, *Angew. Chem.* **1995**, *107*, 534–536; *Angew. Chem. Int. Ed. Engl.* **1995**, *34*, 462–464.

[5] a) P. von Matt, A. Pfaltz, *Angew. Chem.* **1993**, *105*, 614–615; *Angew. Chem. Int. Ed. Engl.* **1993**, *32*, 566–568; A. Pfaltz, *Acta Chem. Scand. B* **1996**, *50*, 189–194; b) J. Sprinz, G. Helmchen, *Tetrahedron Lett.* **1993**, *34*, 1769–1772; G. Helmchen, S. Kudis, P. Sennhenn, H. Steinhagen, *Pure Appl. Chem.* **1997**, *69*, 513–518; c) G. J. Dawson, C. G. Frost, J. M. J. Williams, S. J. Coote, *Tetrahedron Lett.* **1993**, *34*, 3149–3150; J. M. J. Williams, *Synlett* **1996**, 705–710.

[6] J. Sprinz, M. Kiefer, G. Helmchen, M. Reggelin, G. Huttner, O. Walter, L. Zsolnai, *Tetrahedron Lett.* **1994**, *35*, 1523–1526; J. M. Brown, D. J. Hulmes, P. J. Guiry, *Tetrahedron* **1994**, *50*, 4493–4506; A. Togni, U. Burckhardt, V. Gramlich, P. S. Pregosin, R. Salzmann, *J. Am. Chem. Soc.* **1996**, *118*, 1031–1037; P. E. Blöchl, A. Togni, *Organometallics* **1996**, *15*, 4125–4132; T. R. Ward, *ibid.* **1996**, *15*, 2836–2838.

[7] Synthesis of **7**: O. Loiseleur, Dissertation, University of Basel, **1996**.

[8] After completion of this work analogous regioselective reactions of 3-aryl-2-propenyl acetates **1** with dimethyl methylmalonate catalyzed by a chiral monophosphane–Pd complex were reported (**4**:**5** = 4:1, 68–86% *ee*; R = Ph): T. Hayashi, M. Kawatsura, Y. Uozumi, *J. Chem. Soc. Chem. Commun.* **1997**, 561–562.

[9] Cu-catalyzed 1,4-addition of organozinc reagents to enones: A. K. H. Knöbel, I. H. Escher, A. Pfaltz, *Synlett* **1997**, 1429–1431.

[10] N. Green, T. P. Kee, *Synth. Comm.* **1993**, *23*, 1651–1657.

[11] J. V. Allen, J. M. J. Williams, *Tetrahedron: Asymmetry* **1994**, *5*, 277–282; L. N. Pridgen, G. Miller, *J. Heterocycl. Chem.* **1983**, *20*, 1223–1230.

[12] P. von Matt, G. C. Lloyd-Jones, A. B. E. Minidis, A. Pfaltz, L. Macko, M. Neuburger, M. Zehnder, H. Rüegger, P. S. Pregosin, *Helv. Chim. Acta* **1995**, *78*, 265–284.

Synthesis of a New Class of Solvent-Sensitive Fluorescent Labels

James J. La Clair*

Charge transfer (CT) labels such as 5-(dimethylamino)-naphthalene-1-sulfonyl (dansyl) chloride have been used extensively for the detection, characterization, and localization of carbohydrates, phospholipids, proteins, oligonucleotides, and numerous other synthetic and natural substances.[1] These materials typically experience shifts in their UV/Vis absorption and/or fluorescence bands depending on the nature of their solvent shells.[2] This effect together with modifications of fluorescence lifetimes, extent of intersystem crossing, and fluorescence quantum yield have encouraged

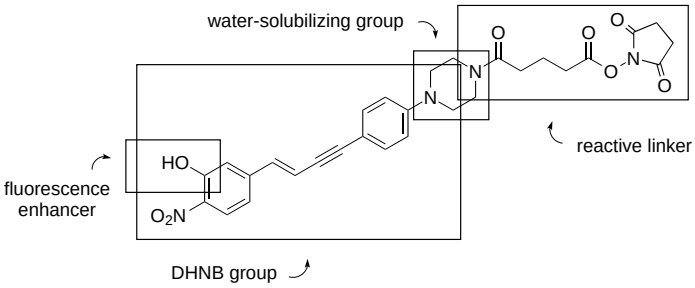
[*] Prof. J. J. La Clair
Department of Molecular Biology
The Scripps Research Institute
10550 North Torrey Pines Road, La Jolla, CA 92037 (USA)
Fax: Int. code + (1) 619 784-2584
E-mail: laclair@scripps.edu

 © WILEY-VCH Verlag GmbH, D-69451 Weinheim, 1998 1433-7851/98/3703-0325 $ 17.50+.50/0

the use of such compounds as practical sensors for monitoring interactions between biologically relevant macromolecules.[3] Because of the extent of its aromaticity, the dansyl group absorbs light between $\lambda = 190$ and 400 nm, limiting its excitation primarily to the ultraviolet region.[4] We describe here the synthesis of a new class of intramolecular charge-transfer labels that absorbs both visible and ultraviolet light, displays dramatic solvent sensitivity, and can be detected at the single-molecule level.

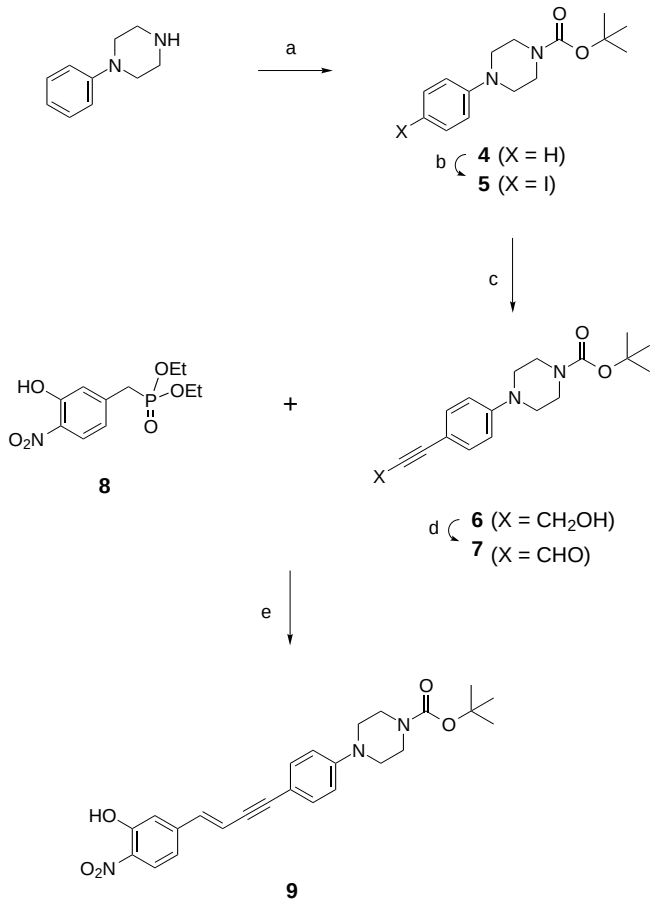
Recent studies have shown that fluorescence from 1-[4-(*N,N*-dimethylamino)phenyl]-4-(3-hydroxy-4-nitrophenyl)-3-(*E*)-buten-1-yne (DHNB) is dramatically affected by the nature of its solvent shell, whereas its UV/Vis absorption is altered only minimally.[5] For example, DHNB dissolved in methanol absorbs light with a maximum at 421 nm ($\varepsilon = 50\,800\ cm^{-1}M^{-1}$) and fluoresces at 528 nm with a quantum efficiency of 0.000017. However, in a nonpolar aprotic solvent such as *n*-hepane the absorption maximum undergoes a bathochromic shift to 435 nm ($\varepsilon = 47\,400\ cm^{-1}M^{-1}$), and the fluorescence quantum yield is enhanced by approximately 1000-fold to 0.0188 and 0.0205 at 593 and 570 nm, respectively. In an effort to devise new systems for monitoring the interactions of single molecules, we employed DHNB to selectively detect single aggregates of a complex consisting of a carbohydrate and a protein.[5] This communication describes the synthesis of a family of DHNB derivatives that can be used to label a wide variety of biologically significant molecules.

Scheme 1 depicts the current design, which mimics the functionality in the DHNB group. A hydroxy group adjacent



Scheme 1. Design of a new fluorescence label.

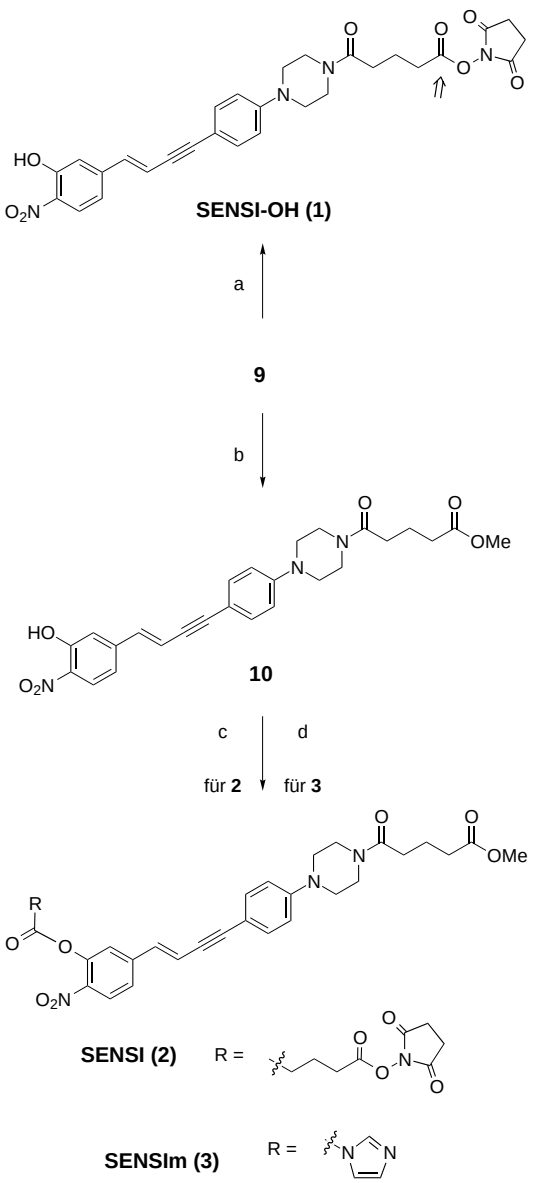
to the nitro group enhances the fluorescence quantum yield and serves as a site for the attachment of an additional functionality.[6] The dimethylamino group of DHNB was then replaced with a piperazine unit, which not only enhances the water solubility of the dye but also provides a handle for further linkage. *N*-Phenylpiperazine was chosen as the starting material for this synthesis because it is commercially available and inexpensive (ca. 1 DM per gram). Synthesis of the model compound begins with the halogenation of protected piperazine **4**[7] with iodine in a biphasic mixture of aqueous sodium bicarbonate and dichloromethane (Scheme 2). After one recrystallization, iodide **5** was coupled with the aid of transition metal catalysis to the C terminus of propargyl alcohol. The resulting alcohol **6** was then oxidized to aldehyde **7** with manganese dioxide, and subsequently



Scheme 2. a) Di-*tert*-butyl dicarbonate, Et_3N, DMAP, CH_2Cl_2, 0 °C → RT, 94 %; b) 1. iodine, $NaHCO_3$, CH_2Cl_2, H_2O, 12–15 °C, 10 min; 2. RT, 30 min, 90 %; c) propargyl alcohol, $[PdCl_2(PPh_3)_2]$, CuI, Et_3N, THF, RT, 18 h, 85 %; d) MnO_2, CH_2Cl_2, RT, 6 h, 98 %; e) 1. addition of NaHMDS in THF to **8** in DMF, 0 °C → RT, 1 h; 2. addition of **7** in THF, −20 °C → RT, 8 h, 62 %.

condensed with the dianion of phosphate **8**[6] to produce **9** (Table 1). The overall yield of this process ranged from 41 to 45 % on a one-gram scale. Deprotection of piperazine **9** with sulfuric acid in wet tetrahydrofuran provided a junction for attachment of a wide variety of reactive linkages. For example, the amine-reactive label SENSI-OH (**1**) was prepared by allowing the deprotected piperazine to react with glutaric anhydride and then converting the terminal carboxylic acid group into an *N*-hydroxysuccinimide ester functionality with 1-ethyl-3-(3-dimethylaminopropyl)carbodiimide (EDC; Scheme 3). The phenol function can also be used as a site for linkage, as shown in SENSI (**2**). Attachment to this site offers the advantage that the bond can be broken hydrolytically. Synthesis of **2** was achieved by converting the *t*boc-protected derivative **9** into **10**[8] (Table 1, *t*boc = *tert*-butoxycarbonyl), which in turn reacted with *N*-hydroxysuccinimidyl glutaryl chloride to provide **2**. Other systems, such as the one-carbon-linked SENSIm (**3**), were prepared by the same route. These three derivatives readily reacted with bovine serum albumin (BSA) under standard conditions. Addition of four equivalents of **1** per equivalent of BSA provided conjugates containing approximately 2.1 molecules of dye per molecule of BSA. The efficiency of the two phenol-

 © WILEY-VCH Verlag GmbH, D-69451 Weinheim, 1998 1433-7851/98/3703-0326 $ 17.50+.50/0 *Angew. Chem. Int. Ed.* **1998**, *37*, No. 3



Scheme 3. a) 1. H_2SO_4, H_2O, THF, RT; 2. glutaric anhydride, THF, RT, 2 h; 3. *N*-hydroxysuccinimide, EDC, THF, RT, 12 h, 81%; b) 1. H_2SO_4, H_2O, THF, RT; 2. glutaric anhydride, THF, RT, 2 h; 3. EDC, MeOH, THF, RT, 4 h, 77%; c) *N*-hydroxysuccinimidyl glutaryl chloride, DMAP, THF, RT, 12 h, 64%; d) *N,N*-carbonyldimidazole (2.5 equiv), DMAP (0.05 equiv), THF, RT, 14 h, 72%.

linked derivatives **2** and **3** was much lower (1.2 and 0.8 fluorescent units per molecule of BSA, respectively). This is probably a result of hydrolysis of the phenolic ester linkage during coupling. The conjugates of BSA with **2** and **3** were stable between pH 5.9 and 8.1, where only minimal dye release was visible during dialysis.[9] However, considerable hydrolysis occurred outside this region, often leaving only small amounts of label intact.

The spectroscopic properties of the new materials resemble those of DHNB. For instance, the UV/Vis absorption maximum of **10** was red-shifted by 33 nm upon changing the solvent from *n*-heptane to methanol (Table 2). The extinction coefficient was largest in aromatic solvents such as benzene and toluene, and decreased with increasing polarity. The intensity of the B band was between 14 and 63% greater than that of the K band in most solvents other than DMF.[10] The fluorescence band of **10** shifted by 111 nm and was 120 times more intense when methanol was replaced by *n*-heptane. Enhancement of fluorescence intensity was only one-eighth that observed with the parent DHNB. This may be due to the fact that the piperazine ring has a greater tendency to conjugate with the aryl π system than the dimethylamino group, which restricts its freedom to rotate and form additional fluorescence states.[11] As indicated in Table 3, single

Table 1. Selected physical data for **1**–**3**, **5**–**7**, **9**, and **10**.

1 ($C_{29}H_{28}N_4O_8$, 560.56): $R_f = 0.41$ (ethyl acetate/toluene/methanol 10/1/1); m.p. 223.1–225.6 °C; ^{1}H NMR (300 MHz, $CDCl_3$): $\delta = 10.6$ (s, 1H), 8.04 (d, $J = 8.8$ Hz, 1H), 7.38 (d, $J = 8.7$ Hz, 2H), 7.09 (d, $J = 1.6$ Hz, 1H), 7.01 (dd, $J = 1.6$, 8.8 Hz, 1H), 6.87 (d, $J = 16.1$ Hz, 1H), 6.83 (d, $J = 8.7$ Hz, 2H), 6.54 (d, $J = 16.1$ Hz, 1H), 3.73 (dd, $J = 4.8$, 4.9 Hz, 2H), 3.63 (dd, $J = 4.8$, 4.9 Hz, 2H), 3.24 (m, 4H), 2.83 (s, 4H), 2.74 (t, $J = 6.7$ Hz, 2H), 2.52 (t, $J = 7.2$ Hz, 2H), 2.10 (dddd, $J = 6.7$, 6.7, 7.2, 7.2 Hz, 2H); ^{13}C NMR (63 MHz, $CDCl_3$/[D_6]DMSO, 2/1): $\delta = 18.9$, 24.4, 29.0, 29.8, 43.5, 46.5, 46.8, 113.1, 113.9, 115.5, 116.3, 124.4, 131.6, 135.9, 149.2, 168.3

2 ($C_{35}H_{36}N_4O_{11}$, 688.69): $R_f = 0.62$ (ethyl acetate/toluene/methanol 10/1/1); m.p. 161.1–162.9 °C; ^{1}H NMR (300 MHz, $CDCl_3$): $\delta = 8.08$ (d, $J = 8.5$ Hz, 1H), 7.37 (d, $J = 8.7$ Hz, 2H), 7.35 (dd, $J = 1.1$, 8.5 Hz, 1H), 7.20 (d, $J = 1.1$ Hz, 1H), 6.90 (d, $J = 16.1$ Hz, 1H), 6.83 (d, $J = 8.7$ Hz, 2H), 6.51 (d, $J = 16.1$ Hz, 2H), 3.75 (t, $J = 4.9$ Hz, 2H), 3.65 (s, 3H), 3.63 (t, $J = 4.9$ Hz, 2H), 3.23 (m, 4H), 2.83 (s, 4H), 2.80 (t, $J = 7.1$ Hz, 2H), 2.42 (t, $J = 7.1$ Hz, 4H), 2.20 (quint, $J = 7.1$ Hz, 2H), 1.96 (quint, $J = 7.1$ Hz, 2H), 1.23 (t, $J = 7.1$ Hz, 2H); ^{13}C NMR (53 MHz, $CDCl_3$): $\delta = 19.4$, 20.3, 25.6, 29.8, 32.1, 32.4, 33.0, 41.1, 45.0, 48.0, 48.4, 51.6, 87.1, 113.1, 114.4, 115.3, 122.0, 123.8, 126.5, 133.0, 136.3, 140.1, 143.7, 144.5, 168.0, 169.0, 170.3, 173.7

3 ($C_{30}H_{29}N_5O_7$, 571.59): $R_f = 0.12$ (ethyl acetate/*n*-hexane 1/1); m.p. 192.5–193.1 °C; ^{1}H NMR (300 MHz, $CDCl_3$): $\delta = 8.04$ (d, $J = 8.8$ Hz, 1H), 7.67 (s, 1H), 7.38 (d, $J = 8.6$ Hz, 2H), 7.10 (s, 2H), 7.01 (d, $J = 8.8$ Hz, 1H), 6.88 (d, $J = 16.0$ Hz, 1H), 6.84 (d, $J = 8.7$ Hz, 2H), 6.54 (t, $J = 16.0$ Hz, 1H), 3.74 (m, 2H), 3.66 (s, 3H), 3.63 (m, 2H), 3.24 (m, 4H), 2.42 (t, $J = 7.1$ Hz, 2H), 1.97 (quint, $J = 7.1$ Hz, 2H), 0.85 (t, $J = 7.1$ Hz, 2H)

5 ($C_{15}H_{21}IN_2O_2$, 388.25): $R_f = 0.85$ (ethyl acetate/*n*-hexane 1/1); m.p. 153.1–153.8 °C; ^{1}H NMR (300 MHz, $CDCl_3$): $\delta = 7.50$ (d, $J = 8.7$ Hz, 2H), 6.65 (d, $J = 8.7$ Hz, 2H), 3.54 (dd, $J = 5.2$, 5.2 Hz, 2H), 3.07 (dd, $J = 5.2$, 5.2 Hz, 2H), 1.45 (s, 9H); ^{13}C NMR (63 MHz, $CDCl_3$): $\delta = 28.4$, 48.9, 118.5, 137.8, 150.8, 154.6

6 ($C_{18}H_{24}N_2O_3$, 316.40): $R_f = 0.52$ (ethyl acetate/hexane 1/1); m.p. 158.2–159.1 °C; ^{1}H NMR (300 MHz, $CDCl_3$): $\delta = 7.30$ (d, $J = 8.8$ Hz, 2H), 6.77 (d, $J = 8.9$ Hz, 2H), 4.44 (s, 2H), 3.53 (dd, $J = 5.2$, 5.2 Hz, 4H), 3.13 (dd, $J = 5.2$, 5.2 Hz, 4H), 1.45 (s, 9H); ^{13}C NMR (63 MHz, $CDCl_3$): $\delta = 28.4$, 48.4, 51.6, 80.0, 85.9, 113.1, 115.5, 132.8, 150.8

7 ($C_{18}H_{22}N_2O_3$, 314.38): $R_f = 0.74$ (ethyl acetate/*n*-hexane 1/1); m.p. 103.5–104.7 °C; ^{1}H NMR (300 MHz, $CDCl_3$): $\delta = 9.34$ (s, 1H), 7.48 (d, $J = 8.9$ Hz, 2H), 6.81 (d, $J = 8.9$ Hz, 2H), 3.55 (dd, $J = 5.5$, 5.5 Hz, 4H), 3.13 (dd, $J = 5.5$, 5.5 Hz, 4H), 1.46 (s, 9H); ^{13}C NMR (63 MHz, $CDCl_3$): $\delta = 28.4$, 47.2, 80.2, 89.4, 98.1, 108.2, 114.5, 135.3, 152.5, 154.6, 176.6

9 ($C_{25}H_{27}N_3O_5$, 449.20): $R_f = 0.83$ (ethyl acetate/*n*-hexane 1/1); m.p. 214.3–216.0 °C; ^{1}H NMR (300 MHz, $CDCl_3$): $\delta = 10.7$ (s, 1H), 8.03 (d, $J = 8.8$ Hz, 1H), 7.37 (d, $J = 8.8$ Hz, 2H), 7.07 (d, $J = 1.5$ Hz, 1H), 7.00 (dd, $J = 1.5$, 8.8 Hz, 1H), 6.87 (d, $J = 16.0$ Hz, 1H), 6.83 (d, $J = 8.9$ Hz, 2H), 6.53 (d, $J = 16.0$ Hz, 2H), 3.55 (dd, $J = 5.2$, 5.2 Hz, 4H), 3.20 (dd, $J = 5.2$, 5.2 Hz, 4H), 1.46 (s, 9H); ^{13}C NMR (63 MHz, [D_6]DMSO): $\delta = 28.4$, 48.1, 87.2, 114.8, 115.3, 116.6, 117.7, 125.6, 133.0, 136.9, 145.9, 151.1, 154.2

10 ($C_{30}H_{29}N_5O_7$, 571.59): $R_f = 0.13$ (ethyl acetate/*n*-hexane 1/1); m.p. 166.3–168.0 °C; ^{1}H NMR (300 MHz, $CDCl_3$): $\delta = 10.6$ (s, 1H), 8.02 (d, $J = 8.8$ Hz, 1H), 7.36 (d, $J = 8.8$ Hz, 2H), 7.07 (d, $J = 1.5$ Hz, 1H), 6.89 (dd, $J = 1.5$, 8.8 Hz, 1H), 6.86 (d, $J = 16.0$ Hz, 1H), 6.81 (d, $J = 8.9$ Hz, 2H), 6.51 (d, $J = 16.0$ Hz, 2H), 3.74 (t, $J = 1.4$ Hz, 2H), 3.65 (s, 3H), 3.62 (t, $J = 1.4$ Hz, 2H), 3.22 (m, 4H), 2.40 (dt, $J = 1.4$, 6.6 Hz, 2H), 1.95 (quint, $J = 7.2$ Hz, 2H), 1.22 (t, $J = 7.2$ Hz, 2H)

 © WILEY-VCH Verlag GmbH, D-69451 Weinheim, 1998 1433-7851/98/3703-0327 $ 17.50+.50/0

Table 2. UV/Vis absorption maxima ($\lambda_{A,max}$), range, extinction coefficients (ε), fluorescence maxima ($\lambda_{F,max}$), range, and quantum yields (Φ_F) for **10** in anhydrous solvents.[a]

Solvent	E_T[b]	$\lambda_{A,max}$[c] [nm]	ε [$cm^{-1}M^{-1}$]	λ_A range[d] [nm]	$\lambda_{F,max}$ [nm]	Φ_F[e]	λ_F range[d] [nm]
n-heptane	30.9	425	72500	190 – 505	595	0.082	575 – 740
		305	61800		579	0.079	
toluene	33.9	422	71700	190 – 495	601	0.041	510 – 730
		314	62800				
benzene	34.5	420	119300	190 – 495	606	0.057	520 – 730
		318	93700				
THF	37.4	412	65200	190 – 510	596	0.0067	450 – 760
		306	47500				
ethyl acetate	38.1	410	85100	190 – 495	624	0.0086	440 – 725
		310	60500				
$CHCl_3$	39.1	422	59200	190 – 505	666	0.0061	460 – 780
		316	46900				
CH_2Cl_2	41.4	422	69400	190 – 505	657	0.0051	450 – 670
		316	47200				
acetone	42.2	410	67400	190 – 495	468	0.0053	430 – 565
DMF	43.8	468	32900	190 – 515	473	0.0039	405 – 510
		364	73200				
DMSO	45.0	390	44900	190 – 510	480	0.0021	425 – 545
		310	34700				
acetonitrile	46.0	398	45300	190 – 495	473	0.0014	430 – 585
		316	34100				
n-butanol	50.2	406	45700	190 – 490	586	0.0019	432 – 705
		316	28200				
ethanol	51.9	394	63900	190 – 490	482	0.0016	425 – 690
		318	40800				
methanol	55.5	392	46700	190 – 485	490	0.00068	425 – 545
		318	28500				

[a] The reported data have been averaged over several iterations with deviations of less than 5%. Unavoidable traces of moisture undoubtedly decreased the intensity of these values. Precautions were taken to minimize contact with moisture, and all solvents were either purchased dry or distilled. [b] E_T is a measure of solvent polarity. See ref. [2a]. [c] The K band is defined as the lower and the B band as the higher wavelength band. [d] The range is defined as the region within which the signal intensity exceeded 5% of the maximum absorption or fluorescence. [e] Quantum yields were standardized against the value 0.70 for rhodamine B in ethanol.

Table 3. Single-molecule detection of **10**.[a]

Solvent	Detection limit [nM][b]	Extent of decomposition after 5 min [%]
n-heptane	0.015	1
THF	12	4
$CHCl_3$	0.95	3
acetone	14	4
DMF	17	3
acetonitrile	89	2
ethanol	128	2
methanol	205	5
water	625	4

[a] Excitation with an argon ion laser at 457 nm (0.5 mW). The fluorescence was observed through a filter with a cutoff at 545 nm. [b] The detection limit is the concentration at which transients from single molecules were no longer resolved from the baseline.

molecules derived from these dyes were detectable at submicromolar concentrations in polar solvents (e.g., THF, chloroform, acetone, acetonitrile, DMF, ethanol, methanol, and water) with the aid of a confocal fluorescence correlation spectrometer.[12] Single molecules were detected at far lower concentrations in nonpolar solvents such as *n*-heptane, providing a gain in response of approximately 40000 for selective detection of single molecules. Investigations into the use of these markers as a probe for interactions between molecules and lipophilic surfaces are currently in progress.

Experimental Section

5: Di-*tert*-butyl dicarbonate (4.5 g, 20.6 mmol) was added in small portions over 15 min to a mixture of *N*-phenylpiperazine (3.0 mL, 19.6 mmol), triethylamine (8.2 mL, 58.9 mmol), and 4-dimethylaminopyridine (DMAP; 86 mg) in anhydrous CH_2Cl_2 (100 mL) at 0 °C. Ten minutes after addition was complete the mixture was warmed to room temperature (RT). After 1.5 h it was diluted with CH_2Cl_2 (200 mL) and water (100 mL), and extracted. The aqueous phase was further extracted with CH_2Cl_2 (2 × 100 mL). The combined organic extracts were washed with saturated aqueous NaCl, dried over Na_2SO_4, and concentrated to yield 4.87 g (94%) of **4**. Iodine (5.0 g, 19.7 mmol) was added over 45 min to a mixture of **4** (5.46 g, 20.8 mmol) and $NaHCO_3$ (2.62 g, 31.2 mmol) in CH_2Cl_2 (80 mL) and water (60 mL), which was kept between 12 and 15 °C. After addition was complete the mixture was warmed to room temperature, and this temperature was maintained for 30 min. The mixture was then diluted with CH_2Cl_2 (500 mL) and water (100 mL), and the organic phase was collected and washed consecutively with water (50 mL), a solution ofL sodium thiosulfate (100 m), water (2 × 100 mL), and a saturated solution of aqueous NaCl (100 mL). The crude product was dried over Na_2SO_4, concentrated, and recrystallized from *n*-hexane/THF (10/1) to yield 6.95 g (90%) of **5**.

9: A mixture of **5** (1.17 g, 3.02 mmol), $[PdCl_2(PPh_3)_2]$ (21.2 mg, 0.032 mmol), and CuI (5.7 mg, 0.032 mmol) in THF (2 mL) and triethylamine (5 mL) was degassed by rapid bubbling of dry argon through it for 15 min. 2-Propyn-1-ol (0.193 mL, 3.32 mmol) was then added to the vigorously stirred mixture. Three hours later a second batch of $[PdCl_2(PPh_3)_2]$ and CuI was added. The reaction was complete within 18 h. Strict maintenance of an argon atmosphere was crucial to the yield of this step. The crude solution was filtered through silica gel (30 g) with methanol/ethyl acetate (5/95), and the eluate was concentrated. Flash chromatography (SiO_2, ethyl acetate/hexane 1/3) led to pure **6** (815.2 mg,

 © WILEY-VCH Verlag GmbH, D-69451 Weinheim, 1998 1433-7851/98/3703-0328 $ 17.50+.50/0 *Angew. Chem. Int. Ed.* **1998**, *37*, No. 3

85%). Activated MnO_2 (0.507 g, 5.83 mmol) was added to **6** (615.0 mg, 1.94 mol) in CH_2Cl_2 (18 mL) at RT. After 6 h the reaction mixture was purified directly by flash chromatography (SiO_2, ethyl acetate/hexane 1/3), yielding 602.1 mg (98%) of **7**. Sodium bis(trimethylsilyl)amide (4.79 mL, 1.0 M in THF, 4.79 mmol) was added to a solution of phosphonate **8** (621 mg, 2.15 mmol) in DMF (6.0 mL) at 0 °C. The solution was warmed to RT after 30 min at 0 °C and kept at RT for 20 min, after which it was again cooled to −20 °C. A solution of aldehyde **7** (376.5 mg, 1.19 mmol) in THF (10 mL) was added by syringe. After 8 h at room temperature water (5 mL) was added, the pH adjusted to 7 with 5% aqueous HCl, and the mixture further diluted with a saturated solution of aqueous NaCl (10 mL). The crude product was obtained by extraction with THF/CH_2Cl_2 (1/9, 3 × 40 mL), drying over Na_2SO_4, and concentration. Flash chromatography (SiO_2, $CHCl_3$/hexane 1/2) and recrystallization from *n*-heptane/THF (10/1) yielded 331.4 mg (62%) of **9**.

1: Concentrated sulfuric acid (130 μL) was added to **9** (82.1 mg, 0.178 mmol) in THF/H_2O (1/9, 9 mL) at 0 °C. After 20 min a saturated solution of aqueous sodium bicarbonate was added until a pH of 6.5 was reached, followed by a saturated solution of aqueous NaCl (15 mL). The crude product was obtained by extraction with THF/CH_2Cl_2 (1/9, 3 × 60 mL), drying over Na_2SO_4, and concentration. The residue was treated with glutaric anhydride (26.4 mg, 0.231 mmol) and DMAP (≈3 mg) in anhydrous THF (8 mL). After 2 h at room temperature *N*-hydroxysuccinimide (40.9 mg, 0.356 mmol) was added followed by EDC (119.4 g, 0.623 mmol). Twelve hours later water (10 mL) was added, and the pH adjusted to 6.5 with dilute Hcl. The mixture was extracted with THF/CH_2Cl_2 (1/9, 3 × 80 mL), dried over Na_2SO_4, and evaporated. Recrystallization from *n*-heptane/THF (2.5/1) provided 80.7 mg (81%) of pure **1**.

2: Concentrated sulfuric acid (80 μL) was added to **9** (49.5 g, 0.107 mmol) in THF/H_2O (1/9, 5 mL) at 0 °C. After 20 min a saturated solution of aqueous sodium bicarbonate was introduced until the pH reached 7.0, followed by a saturated solution of aqueous NaCl (10 mL). The crude product was obtained by extraction with THF/CH_2Cl_2 (1/9; 3 × 40 mL), drying over Na_2SO_4, and concentration. The residue was immediately dissolved in anhydrous THF (5 mL) and treated with glutaric anhydride (14.6 mg, 0.128 mmol) and DMAP (≈2 mg). After 2 h at room temperature anhydrous methanol (0.2 mL) was added followed by EDC (61.7 mg, 0.321 mmol). Esterification was complete after 4 h (TLC). Water (10 mL) was then added, and the product isolated by adjustment of the pH to 6.5 with dilute HCl followed by extraction with THF/CH_2Cl_2 (1/9, 3 × 40 mL), drying with Na_2SO_4, and rotary evaporation. Recrystallization from *n*-hexane/THF (3/1) provided 39.2 mg (77%) of pure **10**. *N*-Hydroxysuccinimidyl glutaryl chloride (81.1 mg, 0.327 mmol) was added to **10** (41.9 mg, 0.0953 mmol) and DMAP (ca. 1 mg) in anhydrous THF (5 mL). After 12 h at room temperature water was added (10 mL), and the product isolated by adjustment of the pH to 6.5 with dilute HCl followed by extraction with THF/CH_2Cl_2 (1/9, 3 × 30 mL). The extract was dried over Na_2SO_4 and concentrated by rotary evaporation. Recrystallization from a mixture of *n*-heptane/THF (3/1) led to 40.9 mg (64%) of **2**.

Coupling with BSA: Bovine serum albumin (BSA) used in these studies was purchased from Sigma, product A7030. A solution of **1** (1.2 mg, 2.14 μmol) in DMF (50 μL) was added in five portions to a solution of BSA (35.9 mg, 0.54 μmol) in a phosphate-buffered solution of NaCl (PBS, 5 mL; 0.15 mM NaCl, 8.1 mM Na_2HPO_4, 1.5 mM NaH_2PO_4). The mixture was allowed to react to completion for 8 h at room temperature, diluted with water (5 mL), dialyzed extensively against water (Spectra/por MWCO 12000–14000), and lyophilized to dryness. An absorption spectrum was recorded from 2–3 mg of this material, which was dissolved in 500 μL of PBS. The approximate number of fluorophores per protein molecule was then calculated based on the known absorption of **1** in PBS and the concentration of labeled BSA.

Received: July 14, 1997 [Z10681IE]
German version: *Angew. Chem.* **1998**, *110*, 339–343

[1] N. Seiler, *Meth. Biochem. Anal.* **1970**, *18*, 259.
[2] a) C. Reichardt, *Chem. Rev.* **1994**, *94*, 2319; b) E. M. Kosower, M. Mohammad, *J. Am. Chem. Soc.* **1971**, *93*, 2713; c) M. J. Kamlet, J.-L. M. Abboud, R. W. Taft, *ibid.* **1977**, *99*, 8325.
[3] a) G. Weber, D. H. R. Laurence, *J. Biochem.* **1954**, *56*, xxxi; b) J. Stryer, *J. Mol. Biol.* **1965**, *13*, 482; c) J. A. Gally, G. M. Edelman, *Biochim. Biophys. Acta* **1965**, *94*, 175; d) R. P. Cory, R. R. Becker, R. Rosenbluth, I. Isenberg, *J. Am. Chem. Soc.* **1968**, *90*, 1643; e) R. F. Chen, *Arch. Biochem.* **1967**, *120*, 609; f) C. R. Guest, R. A. Hochstrasser, C. G. Dupuy, D. J. Allen, S. J. Benkovic, D. P. Millar, *Biochemistry* **1991**, *30*, 8759.
[4] This can be circumvented through use of two- or multi-photon excitation, see C. Xu, W. W. Webb, *J. Opt. Soc. Am. B*, **1996**, *13*, 481.
[5] J. J. La Clair, *J. Am. Chem. Soc.* **1997**, *119*, 7676.
[6] J. J. La Clair, *Proc. Natl. Acad. Sci. USA*. **1997**, *94*, 1623. For studies on similar materials, see a) D. M. Shin, D. G. Whitten, *J. Phys. Chem.* **1988**, *92*, 2945; b) S. Akiyama, K. Tajima, S. Nakatsuji, K. Nakashima, K. Abiru, M. Watanabe, *Bull. Chem. Soc. Jpn.* **1995**, *68*, 2043.
[7] Piperazine **4** was prepared by allowing *N*-phenylpiperazine to react with di-*tert*-butyl dicarbonate, triethylamine, and DMAP in dichloromethane. For an alternative route, see M. Perez, P. Potier, S. Halazy, *Tetrahedon Lett.* **1996**, *37*, 8487.
[8] Compound **9** was converted into **10** to increase the yield in subsequent manipulations.
[9] The extent of hydrolysis was determined by monitoring the loss in absorption at 400 nm after 5 h of dialysis at the designated pH.
[10] For the assignment of K and B bands, see A. Burawoy, *Ber. Dtsch. Chem. Ges.* **1930**, *63*, 3155. Enhancement of the B band was significantly greater in protic (54–63%) than in aprotic media (14–47%).
[11] One possible explanation is that this is due to the lack of additional twisted intramolecular charge-transfer (TICT) states through minimization of rotation about the aryl–piperidine bond. For work describing TICT states see: a) Z. Grabowski, K. Rotkiewicz, A. Siemiarczuk, D. J. Cowley, W. Baumann, *Nouv. J. Chim.* **1979**, *3*, 443; b) W. Rettig, *Angew. Chem.* **1986**, 98, 969; *Angew. Chem. Int. Ed. Engl.* **1986**, *25*, 971; c) C. Rulliere, Z. R. Grabowski, J. Dobkowski, *Chem. Phys. Lett.* **1987**, *137*, 408; d) M. Vogel, W. Rettig, *Ber. Bunsenges. Phys. Chem.* **1985**, *137*, 408.
[12] Single-molecule studies were conducted with an Eigen–Rigler confocal fluorescence correlation spectrometer. All samples were excited at 457 nm (0.5 W) with an argon ion laser (Lexel, Waldbronn, Germany). The laser beam was passed through a water-immersible objective (Zeiss Plan Neofluar 40 × 0.9) and directed toward a droplet of the material attached through a drop of water and a hanging cover slip (Fisher 12-5454-101). The samples were contained in a 20-μL gold well and were filtered through a porous glass filter immediately prior to use. Fluorescence was collected through the same objective and filtered with a 545-nm cutoff filter. a) M. Eigen, R. Rigler, *Proc. Natl. Acad. Sci. USA* **1994**, *91*, 5740; b) R. Rigler, *J. Biotech.* **1995**, *41*, 177.

Keywords: dyes · fluorescence labeling · solvatochromism

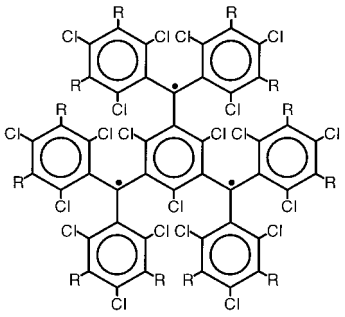
 © WILEY-VCH Verlag GmbH, D-69451 Weinheim, 1998 1433-7851/98/3703-0329 $ 17.50+.50/0

Crystal Structures of Chiral Diastereoisomers of a Carbon-Based High-Spin Molecule**

Josep Sedó, Nora Ventosa, Daniel Ruiz-Molina, Montserrat Mas, Elies Molins, Concepció Rovira, and Jaume Veciana*

The study of organic magnetic materials constitutes a whole field of basic research which has grown because of the capacity of covalent bonds to enhance magnetic interactions.[1] Owing to the versatility of organic synthesis, organic materials can be prepared that display two or more unusual physicochemical properties simultaneously, for instance, magnetism and electron transfer or electron transport.[2a–c] Nevertheless, there are still no examples of purely organic materials that have magnetic properties and are chiral;[3] novel properties are expected for such compounds.[4] Here we report for the first time the crystal structures of the stereoisomers and the resolution of optically active enantiomers of a purely organic high-spin molecule having carbon radical centers.

Open-shell compound **1** was synthesized by an established two-step procedure from its chlorinated hydrocarbon precursor.[5a–c] Both its electrochemical and spectroscopic properties



1 R = H
2 R = Cl

(Table 1) are similar to those of the previously described perchlorinated analogue **2**,[5c] but the absence of chlorine atoms in all *meta* positions leads to an improved solubility in apolar solvents and, apparently, a greater tendency to form high-quality single crystals. For triphenylmethyl-based molecules with three radical centers such as **1** theoretical studies[5,6] led us to assume that only two pairs of enantiomers were expected,[5c] one having C_2 symmetry and one showing D_3 symmetry. Crystallization efforts in *n*-alkanes yielded systematically the same kind of crystalline material. One of these samples afforded a single crystal of **1**/*n*-heptane 1:1 clathrate suitable for X-ray diffraction which, once solved, showed the

Table 1. Electrochemical and spectroscopic properties of **1** and **2**.

	1	**2**[a]
$E^{1/2}$[b]	− 0.07	− 0.41
	− 0.35	− 0.71
	− 0.62	− 1.00
$\lambda(\varepsilon)$[c]	377 (7.2×10^4)	388 (9.1×10^4)
	495 (3.1×10^3)	508 (4.6×10^3)
	539 (3.0×10^3)	558 (4.4×10^3)

[a] Data of **2** are from ref. [5c] and are given for comparison. [b] Standard reduction potentials ($E^{1/2}$) measured in V vs. $Ag^+/AgCl$ in 0.1 M (tBu$_4$N)PF$_6$ solution of CH_2Cl_2 using Pt wires as working and counter electrodes; [c] Wavelengths (λ) in nm and molar extinction coefficients (ε) in $M^{-1}cm^{-1}$.

structure of the C_2 diastereomer (Figure 1, top).[7a] Only once were we lucky enough to get a single crystal of **1**/*n*-pentane 2:1 clathrate[7b] containing the D_3 diastereomer (Figure 1, bottom). Both crystal structures are centrosymmetric and contain racemic mixtures of enantiomers. Molecules such as **1** and **2** may be thought of as constituted of three triphenylmethyl moieties sharing the innermost ring. From the conformational point of view, the overall molecular symmetry is determined by the combined helicities—plus (*P*) or minus (*M*)—of all the propellerlike moieties. In a D_3 conformation all three moieties have the same helicity (in other words, the combined helicity is either *PPP* or *MMM* depending on the enantiomer in question). In contrast, in a C_2 conformation the helicity of one of the moieties is opposite to that of the other two (in other words, the combined helicity of its enantiomers is either *MMP* or *PPM*). In terms of geometry, the helicity in each moiety may be expressed by the sign of the torsion angle defined by the following four atoms: the bridge-C(ar) atom of the innermost ring, the radical-C atom, the bridge-C(ar) atom of an external aromatic ring, and the *ortho*-C(ar) atom of the ring that is *syn* with respect to the first bridge-C(ar) atom. The noncoplanarity is thus accounted for by the absolute value of this torsion angle (Figure 1, insets). As a matter of fact, molecules of **1**/*n*-heptane clathrate show average torsion angles of $48 \pm 5°$, $48 \pm 2°$, and $-45 \pm 3°$, while those of **1**/*n*-pentane clathrate have average angles of $50 \pm 2°$, $49 \pm 2°$, and $49 \pm 1°$. Notwithstanding minor distortions due to crystal packing forces, these values indicate that the structures formally correspond to C_2 and D_3 conformations of **1**, respectively. The degree of noncoplanarity in each moiety is very similar to that found in simple triphenylmethyl monoradicals,[5a] indicating that the strongest steric interactions by far are those in the immediate surroundings of the radical center inside each moiety. Moreover, in both conformers all the distances between the geometrical centers of aromatic rings belonging to different moieties are greater than 5 Å, and no van der Waals contacts between atoms of different moieties are evident. Overall, triphenylmethyl moieties of **1** can be considered to be fairly independent of each other, regardless of the specific conformation. The three open-shell centers of both diastereomers show no or small deviations from planarity of at most 0.10 Å, which is in agreement with the values measured for analogous monoradicals.[5a] Bond lengths such as C(radical) – C(ar) average out at 1.46 ± 0.01 Å for the C_2 isomer and 1.49 ± 0.04 Å for the D_3, implying partial delocalization of the unpaired electron towards the aromatic

[*] Prof. J. Veciana, Dipl.-Eng. J. Sedó, Dr. N. Ventosa, Dr. D. Ruiz-Molina, Dr. M. Mas, Dr. E. Molins, Dr. C. Rovira
Institut de Ciència de Materials de Barcelona (CSIC)
Campus de la UAB, E-08193 Bellaterra (Spain)
Fax: Int. code + (34) 3-5805729
E-mail: vecianaj@icmab.es

[**] Financial support for this project was provided by the Dirección General de Investigación Científica y Técnica (grant no. PB96-0862-C02-01) and the Comissió Interdepàrtàmetàl de Recerca i Innovació Tecnològica (CIRIT) (grant no. GRQ95-00507). J. S. and D. R. thank the Generalitat de Catalunya for their doctoral fellowships.

 © WILEY-VCH Verlag GmbH, D-69451 Weinheim, 1998 1433-7851/98/3703-0330 $ 17.50+.50/0

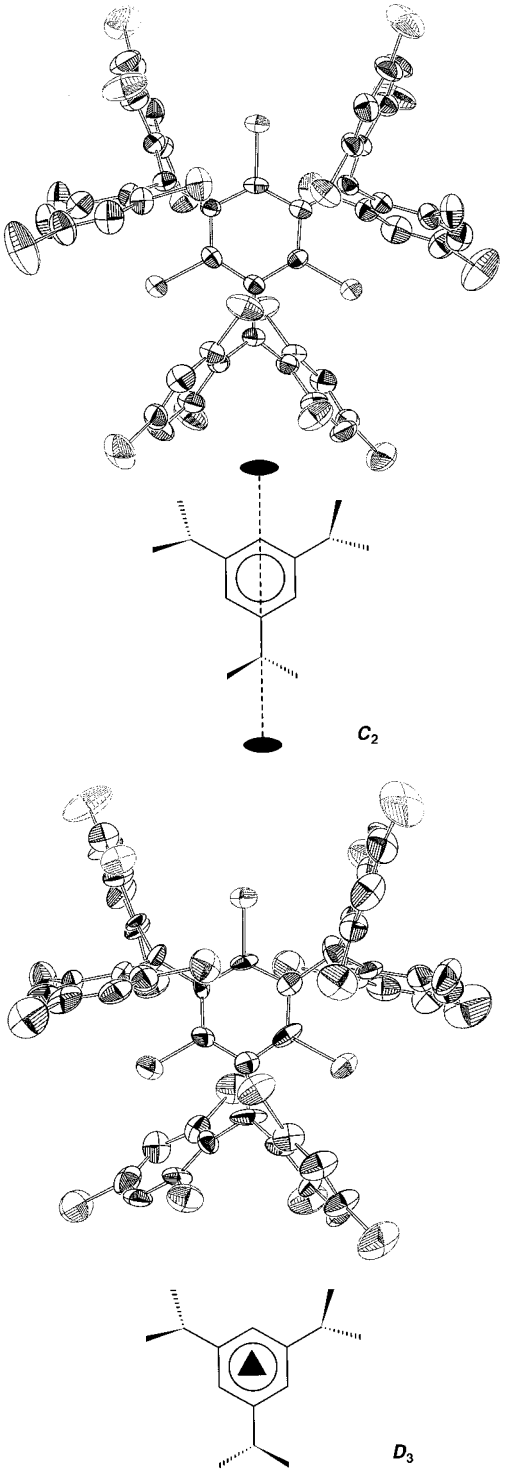


Figure 1. ORTEP views of the crystallized diastereomers of **1** having C_2 (top) and D_3 symmetry (bottom). Insets show schematically the orientation of the principal symmetry axis for each diastereomer.

rings. Other relevant bond lengths such as C(ar)–C(ar) (1.39 ± 0.03 Å for the C_2 isomer, 1.38 ± 0.03 Å for the D_3) and C(ar)–Cl (1.73 ± 0.01 Å and 1.74 ± 0.03 Å, for the C_2 and D_3 isomers, respectively) largely coincide with those observed in highly chlorinated triphenylmethyl radicals.[5a] Intermolecular distances in both crystals are very similar to those observed in analogous monoradical compounds[5a] so that regions with the largest spin densities of neighboring molecules are far away from each other.

Standard reversed-phase HPLC confirmed that **1** crystallizes in a single diastereomeric form (C_2) almost systematically, in the same way as its perchlorinated analogue **2**.[5c] This diastereomer is the most abundant one in solution, even though in such media it converts very slowly into the other diastereomer at room temperature, indicating a high energy barrier for this process. Such a dynamic process can be quenched by lowering the temperature and it can be therefore properly characterized. Thus, we determined an equilibrium constant at 298 K for the interconversion process in acetonitrile/THF (2:1) of $K_{eq} = C_2/D_3 = 0.34 \pm 0.01$. This value remains largely unchanged in other solvent mixtures such as toulene/CH_2Cl_2 (3:1). Kinetic studies of the C_2/D_3 equilibrium yielded an activation free energy of $\Delta G^{\neq}_{298} = 93 \pm 1$ kJ mol^{-1}. We carried out analytical chiral chromatography on the pure C_2 diastereomer of **1** in hexane/2-propanol (90:10) using an on-line dual detection technique (UV and polarimetry) in order to resolve the C_2 diastereomer into its optically active enantiomers. As expected, the UV signal recorded throughout shows two peaks (Figure 2) which, in spite of a slight overlap, can be mathematically deconvoluted. The area of

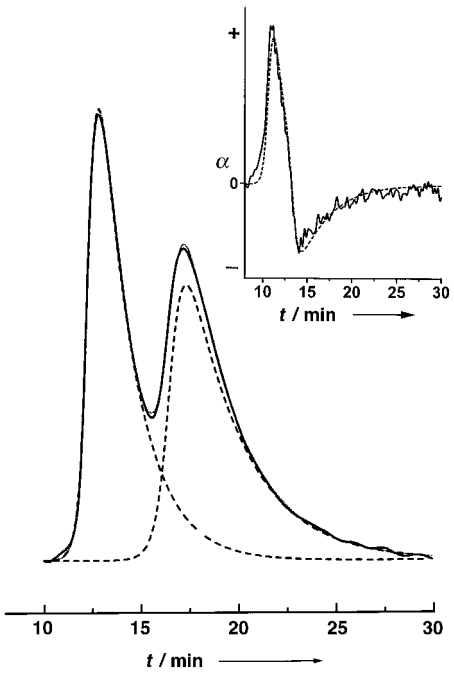


Figure 2. HPLC resolution of the C_2 racemic mixture of **1**. UV signal (240 nm); heavy line: experimental; thin line: simulated; dashed line: deconvoluted peaks. The ratio of peak areas is 1.04 ± 0.02. Inset: polarimetric signal (589 nm); solid line: experimental; dashed line: simulated. The separation was carried out using a Daicel CHIRALPAK OT(+) column (0.46 × 25 cm) with a flow rate of 1.0 mL min^{-1}, *n*-hexane/2-propanol (9:1) at 261 K.

both peaks is the same, as required for the resolution of any racemic mixture. This data was used further to simulate the polarimetric signal (Figure 2, inset). Despite a poor signal-to-noise ratio due to the concentration of the chiral species, an

 © WILEY-VCH Verlag GmbH, D-69451 Weinheim, 1998 1433-7851/98/3703-0331 $ 17.50+.50/0

excellent agreement between simulation and experiment was found, fully confirming the resolution of the two truly enantiomeric species.

The ESR spectrum of the C_2 diastereomer of **1** in frozen media shows a pattern characteristic of a single molecule in a quartet spin state. The derived zero-field splitting parameters (Table 2) are in accordance with the assignment of nonaxial

Table 2. Zero-field splitting parameters and principal g values of **1** and **2** obtained from their ESR spectra.[a]

	1		**2**[b]	
Symmetry	C_2	D_3	C_2	D_3
$\lvert D' \rvert$ [c]	36.5	46.0	38.5	53.5
$\lvert E' \rvert$ [c]	3.3	0	1.1	0
g_x	2.0013	2.0028	2.0029	2.002
g_y	2.0035	2.0028	2.0029	2.0024
g_z	2.0023	2.0033	2.0012	2.0024

[a] Spectra recorded in glassy toluene/CH_2Cl_2 (3:1) at 165 K. [b] From ref. [5c]. [c] Values of zero-field splitting parameters ($\lvert D' \rvert$, $\lvert E' \rvert$) are given in G.

C_2 symmetry to this species. The data were then used to simulate the ESR dipolar spectrum of an equilibrated mixture of the two diastereomers of **1** (Figure 3). The overall shape of

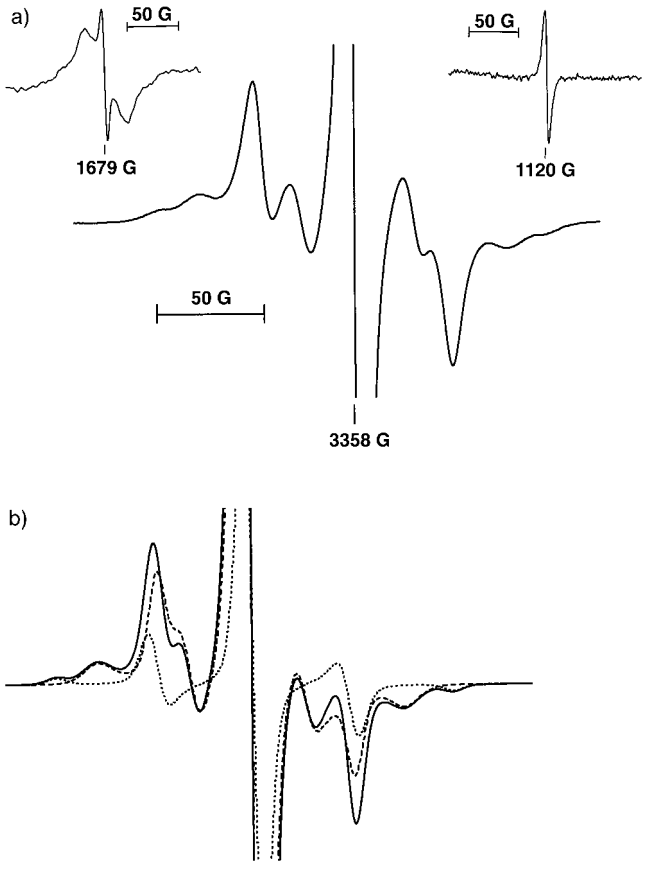


Figure 3. ESR spectrum of an equilibrated mixture of C_2 and D_3 diastereomers in a glassy toluene/CH_2Cl_2 (3:1) matrix at 165 K. a) Experimental; b) simulated; solid line: mixture; heavy dashed line: C_2 isomer; light dashed line: D_3 isomer. Insets show the half-field signal at 115 K (left), and the one-third-field signal at 5 K (right).

the spectrum requires the presence of about 25 % of another diastereomer with axial symmetry. This finding is in full agreement with the expected D_3 symmetry of **1** as well as with the C_2/D_3 equilibrium ratio estimated by HPLC analysis. At higher concentrations of the radical, and in accordance with the expected $S = 3/2$ spin state for the molecule, both the $\Delta M_s = \pm 2$ ($g \sim 4$) and $\Delta M_s = \pm 3$ ($g \sim 6$) signals at half and one-third of the original field, respectively, are clearly observed in the ESR spectra (Figure 3, insets). Since signals in the $g \approx 6$ spectral range only for states higher than or equal to a quartet, the evidence of the latter signal provides straightforward proof of the spin state of **1**. The dependence of the integrated intensity of this signal with temperature followed the Curie law in the temperature range 4–70 K, confirming that **1** has a $S = 3/2$ high-spin ground state in diluted, frozen solutions. Furthermore, both magnetic susceptibility and magnetization measurements on a polycrystalline sample of **1** showed Curie–Weiss behavior typical of a robust quartet state ($S = 3/2$) with thermally inaccessible (up to 300 K) low-spin excited states, ($C = 1.83$ emu K mol^{-1} and $\theta = -0.3$ K) although the structure is nonplanar.[8] The very low value of the Weiss constant indicates that the intermolecular interactions are very weak and, if anything, antiferromagnetic. Therefore, the overall magnetic behavior is close to that of an ideal paramagnet, in complete agreement with the long intermolecular distances observed in the reported crystal structures.

We have described the synthesis and most relevant properties of the first purely organic high-spin molecule which was resolved into its enantiomers by chiral HPLC. The isomerism was characterized by a combination of indirect techniques and, for the first time, by single-crystal X-ray diffraction. In this respect, the two solid-state structures, each corresponding to a different diastereomer of the molecule, constitute the first two examples of crystal structures of a carbon-based high-spin radical.

Received: July 28, 1997 [Z10747IE]
Revised version: September 23, 1997
German version: *Angew. Chem.* **1998**, *110*, 344–347

Keywords: chirality · helical structures · isomerizations · magnetic properties · radicals

[1] For reviews on organic magnetic materials, see: a) J. S. Miller, A. J. Epstein, *Angew. Chem.* **1994**, *106*, 399; *Angew. Chem. Int. Ed. Engl.* **1994**, *33*, 385; b) O. Kahn, *Molecular Magnetism*, VCH, New York, **1993**; *Proceedings of the International Symposium on Chemistry and Physics of Molecular Based Magnetic Materials* (Ed.: J. S. Miller), Salt Lake City, **1994**; c) H. Iwamura, N. Koga, *Acc. Chem. Res.* **1993**, *26*, 346.

[2] a) M. Kurmoo, A. W. Graham, P. Day, S. J. Coles, M. B. Hurtshouse, J. L. Caulfield, J. Singleton, F. L. Pratt, W. Hayes, L. Ducasse, P. Guionneau, *J. Am. Chem. Soc.* **1995**, *117*, 12209; b) M. M. Wienk, R. A. J. Janssen, *ibid.* **1997**, *119*, 4492. c) J. Sedó, D. Ruiz, J. Vidal-Gancedo, C. Rovira, J. Bonvoisin, J.-P. Launay, J. Veciana, *Adv. Mater.* **1996**, *8*, 748.

[3] The combination of magnetic and certain optical properties in a given material can give rise to two distinct, but related phenomena—photomagnetism and magnetooptical effects. Photomagnetism may be described as the change in the magnetic response of a material that results from its exposure to electromagnetic radiation, whereas a

 © WILEY-VCH Verlag GmbH, D-69451 Weinheim, 1998 1433-7851/98/3703-0332 $ 17.50+.50/0

magnetooptical effect is the effect that a magnetic material has on electromagnetic radiation. See: C. J. O'Connor in *Molecular Magnetism: From Molecular Assemblies to the Devices* (Eds.: E. Coronado, P. Delhaès, D. Gatteschi, J. S. Miller), Kluwer, Dordrecht, **1996**, p. 521.

[4] Magnetochiral dichroism and other magnetooptical effects have been predicted for molecules containing both magnetic and optically active centers. For theoretical background, see a) N. B. Baranova, Y. V. Bogdanov, B. Y. Zeldovich, *Opt. Commun.* **1977**, *22*, 243; b) L. D. Barron, J. Vrbancich, *Mol. Phys.* **1982**, *93*, 78. For recent experimental research, see c) R. Graziotti, D. K. Maude, G. Rikken, *Annual Report of the Grenoble High Magnetic Field Laboratory* **1996**, 85.

[5] a) O. Armet, J. Veciana, C. Rovira, J. Riera, J. Castañer, E. Molins, J. Rius, C. Miravitlles, S. Olivella, J. Brichfeus, *J. Phys. Chem.* **1987**, *91*, 5608; b) J. Veciana, C. Rovira, M. I. Crespo, O. Armet, V. M. Domingo, F. Palacio, *J. Am. Chem. Soc.* **1991**, *113*, 2552; c) J. Veciana, C. Rovira, L. Ventosa, M. I. Crespo, F. Palacio, *ibid.* **1993**, *115*, 57.

[6] K. Mislow, *Acc. Chem. Res.* **1976**, *9*, 26.

[7] For both structures, reflection intensities were measured at $T=$ 293(2) K with $Mo_{K\alpha}$ radiation (0.70926 Å) and a $\omega/2\theta$ scan mode; a Lorentz polarization correction and an empirical psi-scan absorption correction were applied (C. K. Fair, MolEN package). The structures were solved by direct methods (G. M. Sheldrick, SHELXS 86, **1990**) and refined by full matrix least squares on $|F^2|$ (G. M. Sheldrick, SHELXS 93, **1993**). H atoms were introduced in calculated positions and were refined isotropically with two global temperature factors, one for the H atoms of the molecule and the other for those of the included solvent. a) Crystal structure of **1**-D_3: $C_{45}H_{12}Cl_{21}\cdot 1/2\ C_5H_{12}$, orthorhombic, space group *Pbca*, $a=12.104(2)$, $b=21.903(6)$, $c=44.26(1)$ Å, $V=11733.9(5)$ Å^3, $\rho_{calc}=1.509$ g cm^{-3}, $Z=8$, $\mu=1.007$ mm^{-1} (max. transmission: 99.96%, min. transmission: 95.29%), crystal dimensions: $0.29\times0.17\times0.10$ mm^3. 8666 Independent reflections were collected ($2\theta_{max}=46.88^\circ$) and used for the refinement of 622 parameters. Final statistics were $R=0.0890$ for 2442 observed reflections ($I>2\sigma(I)$). Maximum and minimum residual electron densities 1.777 and -0.498 e Å^{-3}. b) Crystal structure of **1**-C_2: $C_{45}H_{12}Cl_{21}\cdot 1/2\ C_7H_{16}$, triclinic, space group $P\bar{1}$, $a=14.929(1)$, $b=15.226(2)$, $c=16.802(2)$ Å, $\alpha=63.69(1)$, $\beta=65.13(1)$, $\gamma=64.20(1)^\circ$, $V=2957.2(6)$ Å^3, $\rho_{calc}=1.511$ g cm^{-3}, $Z=2$, $\mu=1.002$ mm^{-1} (max. transmission: 99.89%, min. transmission: 94.09%), crystal dimensions: $0.35\times0.20\times0.12$ mm^3. 10776 Independent reflections were collected ($2\theta_{max}=49.94^\circ$) from which 10385 independent ($R_{inf}=0.0294$) reflections were used for the refinement of 625 parameters. Final statistics were $R=0.0626$ for 5731 reflections ($I>2\sigma(I)$). Maximum and minimum residual electron densities 1.079 and -0.603 e Å^{-3}. Crystallographic data (excluding structure factors) for the structures reported in this paper have been deposited with the Cambridge Crystallographic Data Centre as supplementary publication no. CCDC-100586. Copies of the data can be obtained free of charge on application to CCDC, 12 Union Road, Cambridge CB2 1EZ, UK. Fax: Int. code +(49)1223336-033; e-mail: deposit@ccdc.cam.ac.uk.

[8] This result is in contrast with other reports that show that large deviations from planarity change the spin preferences against the classical topology rule. See: a) S. Fang, M. S. Lee, D. A. Hrovat, W. T. Borden, *J. Am. Chem. Soc.* **1995**, *117*, 6727; b) Z. Jingping, M. Baumgarten, *Chem. Phys. Lett.* **1997**, *269*, 187.

A Chemically and Electrochemically Switchable [2]Catenane Incorporating a Tetrathiafulvalene Unit**

Masumi Asakawa, Peter R. Ashton, Vincenzo Balzani,* Alberto Credi, Christoph Hamers, Gunter Mattersteig, Marco Montalti, Andrew N. Shipway, Neil Spencer, J. Fraser Stoddart,* Malcolm S. Tolley, Margherita Venturi,* Andrew J. P. White, and David J. Williams*

Highly efficient constructions of mechanically interlocked molecules,[1] such as catenanes and rotaxanes, have followed rapidly in the wake of the development of self-assembly[2] in synthetic supramolecular chemistry.[3] The opportunity now exists to control the relative dispositions of one component with respect to the other(s) in such molecules by either chemical[4] or electrochemical[4a, 5] means. In this context, the tetrathiafulvalene[6] (TTF) unit represents a particularly attractive building block, since it can be oxidized sequentially and reversibly to the monocation ($E_{1/2}=+0.32$ V) and the dication ($E_{1/2}=+0.72$ V). Its redox properties, together with its ability to form[7, 8] a strong green 1:1 complex in both the solution and solid states with cyclobis(paraquat-*p*-phenylene) tetrakis(hexafluorophosphate),[9] have been largely responsible for its incorporation into the thread-like components of pseudorotaxanes,[10] as well as into catenanes[11] and rotaxanes.[8, 12] Here, we describe 1) the self-assembly of a [2]catenane comprising a macrocyclic polyether ring with two π-electron-rich "stations"—namely a 1,5-dioxynaphthalene moiety and a TTF unit—and the π-electron-deficient cyclobis(paraquat-*p*-phenylene),[9] 2) its solid-state structure and superstructure, 3) its spectroscopic characterization in solution, and 4) its ability to be switched both chemically and electrochemically, at the molecular level, between two different "states".

[*] Prof. J. F. Stoddart,[+] Dr. M. Asakawa, Dr. G. Mattersteig, Dr. A. N. Shipway, Dr. N. Spencer, P. R. Ashton, C. Hamers, M. S. Tolley
School of Chemistry, University of Birmingham
Edgbaston, Birmingham B15 2TT (UK)

Prof. V. Balzani, Prof. M. Venturi, Dr. A. Credi, Dr. M. Montalti
Dipartimento di Chimica "G. Ciamician"
Università di Bologna
Via Selmi 2, I-40126 Bologna (Italy)
Fax: Int. code +(39) 51 259-456
E-mail: vbalzani@ciam.unibo.it

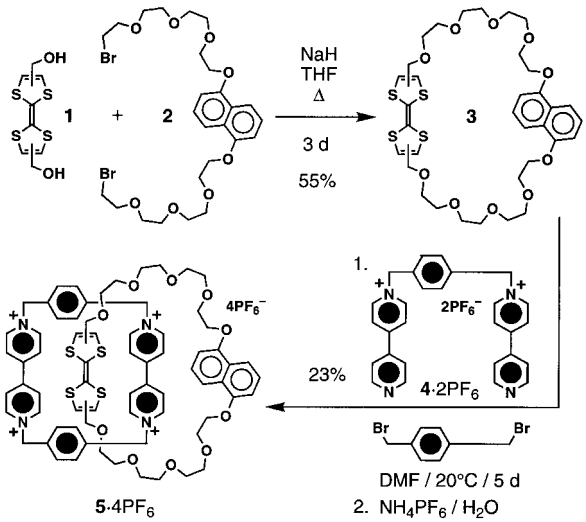
Prof. D. J. Williams, Dr. A. J. P. White
Chemical Crystallography Laboratory
Department of Chemistry, Imperial College
South Kensington, London SW7 2AY (UK)
Fax: Int. code +(44) 171 594-5804

[+] Current address:
Department of Chemistry and Biochemistry
University of California at Los Angeles
405 Hilgard Avenue, Los Angeles, CA-90095 (USA)
Fax: Int. code +(1) 310 206-1843
E-mail: stoddart@chem.ucla.edu

[**] This research was sponsored in the UK by the Deutsche Forschungsgemeinschaft, the Royal Society, and the Engineering and Physical Sciences and the Biotechnology and Biological Sciences Research Councils, and in Italy by the University of Bologna (Funds for Selected Research Topics) and CNR (Progetto Strategico Tecnologie Chimiche Innovative). This work has been carried out within the framework of the EU TMR project FMRX-CT96-0076.

 © WILEY-VCH Verlag GmbH, D-69451 Weinheim, 1998 1433-7851/98/3703-0333 $ 17.50+.50/0

The [2]catenane $\mathbf{5}\cdot 4PF_6$ was self-assembled in 23% yield, as a pure compound, by employing a "*cis*–*trans*" isomeric mixture of the crown ether incorporating TTF (**3**) as a template for the formation of catenated cyclobis(paraquat-*p*-phenylene) from $\mathbf{4}\cdot 2PF_6$ and paraxylylene dibromide (Scheme 1). A 55% yield of **3** was obtained by treatment of



Scheme 1. The self-assembly of the [2]catenane $\mathbf{5}\cdot 4PF_6$ in which the TTF crown ether **3** obtained from diol **1** and dibromide **2** in the presence of a base serves as template for the formation of the cyclobis(paraquat-*p*-phenylene) tetracation.

the TTF-diol **1**[13] with NaH in THF containing the dibromide **2**.[14] Slow diffusion of iPr_2O into a MeCN solution of $\mathbf{5}\cdot 4PF_6$ produced deep bluish-green crystals suitable for X-ray structural analysis.[15] In the solid state the TTF portion of the crown ether is positioned on the "inside" of the tetracationic cyclophane and the 1,5-dioxynaphthalene ring system "alongside" it[16] (Figure 1). The TTF is steeply inclined to the plane of the cyclophane, its central C–C bond subtending an angle of 74° to this plane—a value that is noticeably larger than the 66° observed in the 1:1 complex formed[7,8] between TTF and the cyclobis(paraquat-*p*-phenylene) tetracation.[9] It is important to note that, of the two

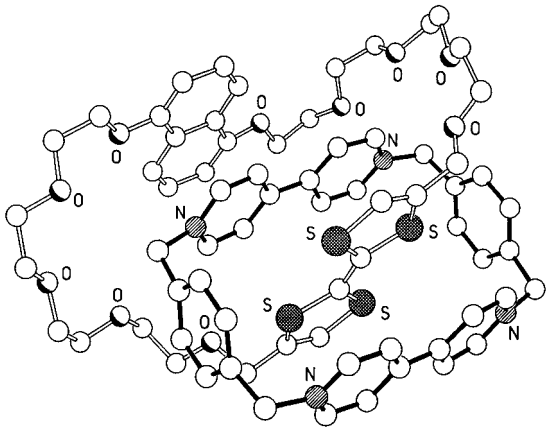


Figure 1. A ball-and-stick representation of the solid-state structure of the [2]catenane $\mathbf{5}^{4+}$.

possible constitutional isomers of the disubstituted TTF, *only* the "*trans*" isomer is observed in the solid state; the [2]catenane structure thus displays a chiral plane.[17] The complex is stabilized by the normal combination of $\pi-\pi$ stacking interactions[18] and [C–H···O] hydrogen bonds[19] from α-bipyridinium hydrogen atoms (the latter, in one instance, to the second oxygen atom from the TTF in one polyether chain and, in the other, to the first oxygen atom from the TTF in the other polyether chain).[20] The catenane molecules pack to form "conventional" polar stacks with a 3.29 Å separation between the 1,5-dioxynaphthalene and bipyridinium ring systems of *C*-face centrally translated molecules.

The UV/Vis spectrum of the [2]catenane $\mathbf{5}\cdot 4PF_6$ (Figure 2, curve a) reveals a charge transfer (CT) absorption band centered on 835 nm ($\varepsilon = 3500\,M^{-1}cm^{-1}$) characteristic of structures containing a TTF unit "inside" the tetracationic

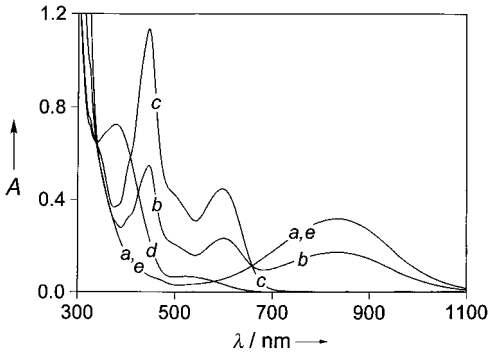


Figure 2. Absorption spectra (MeCN, 298 K) of a 9×10^{-5} M solution of [2]catenane $\mathbf{5}^{4+}$ (curve a) and of the same solution after addition of 0.4, 1.0, and 2.0 equiv of $Fe(ClO_4)_3$ (curves b–d). Addition of 2 equiv of ascorbic acid gives back the original spectrum (curve e).

cyclophane.[10] Furthermore, no absorption band is observed in the 500–560 nm region for the CT interaction that would result from the 1,5-dioxynaphthalene moiety's being located "inside" the cyclophane.[5e] Not only does the ^1H NMR spectrum (Figure 3a) recorded in CD_3CN support this conclusion, it also indicates[21] that only *one* of the two constitutional isomers possible for the arrangement with the TTF unit "inside" the tetracationic cyclophane—almost certainly the "*trans*" isomer, which is the only isomer observed in the solid state (Figure 1)—is present.

We hypothesized that it should be possible to trigger total and completely reversible redox switching between the two translational "isomers" of the [2]catenane $\mathbf{5}^{4+}$ by either chemical or electrochemical means (Scheme 2). We now demonstrate the truth of this hypothesis in a series of experiments where the redox switching of the [2]catenane between two different "isomeric" states [$\mathbf{5}^{4+}$ and $\mathbf{5}^{5+}$ and/or $\mathbf{5}^{6+}$] is monitored by ^1H NMR and UV/Vis spectroscopy (when the switching is driven chemically) and by cyclic voltammetry (when the switching is driven electrochemically).

The chemical switching of $\mathbf{5}^{4+}$ was performed by redox reactions. In the ^1H NMR experiments, oxidation of the TTF unit of $\mathbf{5}^{4+}$ (concentration: 3.6×10^{-3} M) was carried out in

 © WILEY-VCH Verlag GmbH, D-69451 Weinheim, 1998 1433-7851/98/3703-0334 $ 17.50+.50/0

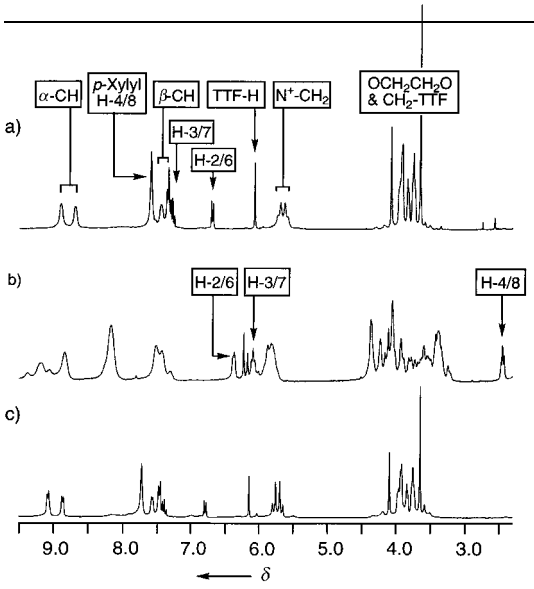
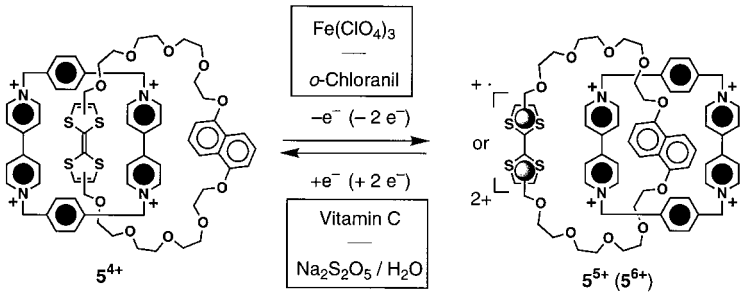


Figure 3. Partial ^{1}H NMR spectra (300 MHz) recorded in CD_3CN of a 3.6×10^{-3} M solution of the [2]catenane $\mathbf{5}^{4+}$ (a), after addition if 2 equiv of *o*-chloranil (b), and after reduction of $\mathbf{5}^{4+}$ with 2.2 equiv of $Na_2S_2O_5$ and isolation of the [2]catenane $\mathbf{5}^{4+}$ as its PF_6^- salt (c).



Scheme 2. The chemically and electrochemically triggered redox switching of [2]catenane.

CD_3CN with two equivalents of *o*-chloranil. After oxidation, the resonance (Figure 3b) for the protons attached to the 4- and 8-positions of the 1,5-dioxynaphthalene moiety is shifted significantly to higher fields and is centered on $\delta = 2.45$: the proton resonances for H-2/6 and H-3/7 appear at $\delta = 6.27$ and $\delta = 5.99$, respectively. The difference between the δ values for H-4/8, H-2/6, and H-3/7 upon oxidation of the TTF unit of the [2]catenane with *o*-chloranil and those of the free, unoxidized macrocycle are -5.33, -0.64, and -1.37, respectively. They are of a similar magnitude to those previously reported[5e, 14, 21] and so support the conclusion that the 1,5-dioxynaphthalene moiety of the macrocycle is encircled by the tetracationic cyclophane after oxidation of the TTF group. Moreover, the integrals for these particular resonances indicate that this mechanical state is the one that is populated exclusively. The ^{1}H NMR spectrum exhibits very little paramagnetic peak broadening, indicating[22] the preferential formation of the oxidized species $\mathbf{5}^{6+}$. Reduction of $\mathbf{5}^{6+}$ with 2.2 equivalents of $Na_2S_2O_5$ in CD_3CN in the presence of a few drops of H_2O and subsequent counterion exchange with NH_4PF_6, followed by evaporation of the solvent, washing of the dark green residue with H_2O, drying, and redissolving it in CD_3CN, yielded an ^{1}H NMR spectrum (Figure 3c) that was virtually identical with the original one (Figure 3a), confirming that the TTF unit is once again residing inside the cavity of the tetracationic cyclophane as shown in $\mathbf{5}^{4+}$ in Scheme 2.

In the UV/Vis experiments ($\mathbf{5}^{4+}$ concentration: 9×10^{-5} M), $Fe(ClO_4)_3$ was used as an oxidant in MeCN solution. As shown in Figure 2, addition of the oxidant (up to 1 equiv) caused a continuous decrease in the intensity of the CT band at 835 nm, characteristic of the encircling of the TTF unit by the tetracationic cyclophane. Accompanying this decrease, an increase in the intensity of the absorption bands with $\lambda_{max} =$ 450 and 600 nm, characteristic of the mono-oxidized form of the TTF unit,[23] was observed (Figure 2, curve c). As a consequence of these spectral variations, the color of the solution changes from dark green to maroon. The CT band ($\lambda_{max} = 515$ nm) due to the encirclement of the naphthalene moiety by the tetracationic cyclophane,[5b,e] expected on the basis of the ^{1}H NMR results, cannot be seen because it is hidden by the more intense bands of the oxidized TTF unit. Further addition of the oxidant (up to 2 equiv) caused the disappearance of the absorption bands of mono-oxidized TTF and formation of a new band ($\lambda_{max} = 375$ nm), which may be attributed to the bis-oxidized TTF unit.[24] An important observation is that the band due to the encirclement of the naphthalene moiety by the tetracationic cyclophane can now be seen (Figure 2, curve d). On addition of 1 equiv of ascorbic acid (as reductant), the bands of the TTF radical cation were completely restored. Further addition of 1 equiv of ascorbic acid yielded the original absorption spectrum with the characteristic CT band due to the encirclement of the TTF unit by the tetracationic cyclophane (Figure 2, curve e). Identical spectral changes have been obtained with Ag powder as reductant in place of ascorbic acid.

In conclusion, the ^{1}H NMR and UV/Vis experiments show clearly that the oxidation/reduction cycle of the TTF unit causes switching between the two translational "isomers" of $\mathbf{5}^{4+}$ (Scheme 2).

Switching can also be induced electrochemically. On electrochemical oxidation,[25] the two processes involving the TTF unit ($+0.28$ and $+0.70$ V vs SCE in crown ether **3**) and, at more positive potentials, the oxidation of the 1,5-dioxynaphthalene moiety ($+1.17$ V vs SCE in **3**) are expected.[26] Furthermore, since the ^{1}H NMR spectroscopic data show that the only observed "isomer" of $\mathbf{5}^{4+}$ has the TTF unit residing in the "inside" position, in the catenane the first oxidation of the TTF unit should be displaced toward more positive potentials relative to those of the free crown ether **3**. This prediction is confirmed by the experimental results. However, contrary to what happens in the crown ether, the first oxidation process of the TTF unit is characterized by a very large separation between the anodic and cathodic peaks. On increasing the scan rate, the former moves toward more positive potentials, the latter toward less positive potentials. At a scan rate of 50 mV s^{-1}, there is only one anodic peak at $+0.80$ V vs SCE, whose current intensity indicates the occurrence of a bielectronic process. Therefore, at this potential, the second oxidation of TTF also takes place; this process is reversible (halfwave potential $+0.76$ V vs SCE) as indicated by the cathodic part of the scan. The oxidation of the 1,5-dioxy-

 © WILEY-VCH Verlag GmbH, D-69451 Weinheim, 1998 1433-7851/98/3703-0335 $ 17.50+.50/0

naphthalene moiety is strongly displaced toward positive potentials (+1.60 V vs SCE) relative to those of the free crown ether.

The scan-rate dependence of the separation between the anodic and cathodic peaks of the first oxidation process of the TTF unit of $\mathbf{5}^{4+}$ indicates that oxidation is followed by a reaction taking place on the time scale of the electrochemical experiment.[27] The nature of such a reaction is elucidated by the following observations: 1) the second oxidation of the TTF unit is reversible, which shows that the system does not undergo any further reaction after one-electron oxidation; 2) the strongly positive potential value for oxidation of the 1,5-dioxynaphthalene moiety indicates that it is trapped within the tetracationic cyclophane.[28] These features strongly suggest that the action taking place as a consequence of the first oxidation of the TTF unit is the circumrotation of the macrocyclic polyether with respect to the tetracationic cyclophane to yield the translational "isomer" with the 1,5-dioxynaphthalene moiety positioned "inside" the cyclophane (Scheme 2). This observation is consistent with the dethreading observed[10b] upon one-electron oxidation of a pseudorotaxane in which a TTF-containing thread is located "inside" the tetracationic cyclophane. We have also found by fluorescence measurements that a 1,5-dioxynaphthalene-containing thread like **2** replaces the TTF unit "inside" the tetracationic cyclophane when the TTF moiety is mono-oxidized.

We have shown that total and completely reversible switching between the two translational "isomers" of catenane $\mathbf{5}^{4+}$ can be performed by either chemical or electrochemical oxidation/reduction cycles.[29] The process, which is accompanied by a clearly detectable color change, can be followed by ^{1}H NMR spectroscopy, UV/Vis spectroscopy, and cyclic voltammetry. This result represents a further step toward the design of chemical systems whose structures and properties can be controlled by use of external stimuli.

Experimental Section

3: NaH (288 mg, 12.0 mmol) was suspended in dry, degassed THF (280 mL) and a mixture of the diol **1**[13] (925 mg, 3.50 mmol), and the dibromide **2**[14] (2.24 g, 3.50 mmol) in dry, degassed THF (250 mL containing 50 mg of both LiBr and CsOTs) was added with stirring during 20 h while refluxing under Ar. After refluxing and stirring had been continued for a further 72 h, the reaction mixture was cooled down to 10°C, and wet THF (20 mL) was added with care. The solvents were removed under vacuum, and the residue extracted into CH_2Cl_2 (2 × 250 mL). The combined organic layers were washed with saturated aqueous NaCl solution (50 mL) and H_2O (4 × 30 mL), before being dried ($MgSO_4$) and concentrated under reduced pressure to afford a residue which was subjected to column chromatography (SiO_2:CH_2Cl_2/MeOH 30:1). The macrocycle **3** was isolated as a yellow wax (1.61 g, 55%). MS (LSI): $m/z = 740$ [M^+]; ^{1}H NMR (CD_3CN, 300 MHz, 25°C): $\delta = 3.40-3.72$ (m, 26H), 3.84–3.94 (m, 6H), 4.18–4.28 (m, 6H), 6.85–6.95 (m, 2H), 7.31–7.41 (m, 2H), 7.47–7.84 (m, 2H); ^{13}C NMR (CD_3CN, 75.1 MHz, 25°C): $\delta = 51.9$, 62.0, 69.1, 70.2, 70.4, 71.2, 71.6, 72.1, 73.4, 106.9, 115.1, 118.6, 126.5, 127.6, 155.3. Elemental analyses calcd for $C_{34}H_{44}O_{10}S_4$: C 55.11, H 5.99, S 17.31; found C 54.99, H 5.98, S 17.4.

$\mathbf{5}\cdot 4PF_6$: A solution of **3** (1.39 g, 1.88 mmol), $\mathbf{4}\cdot 2PF_6$ (1.33 g, 1.88 mmol) and *p*-xylylene dibromide (496 mg, 1.88 mmol) in dry, degassed DMF (125 mL) was stirred under Ar for 5 days, and then the solvent was removed under vacuum. After the residue had been extracted with CH_2Cl_2, MeCN was added. Undissolved polymeric material was filtered off, and the MeCN solution concentrated to a residue, which was subjected to column chromatography (SiO_2, MeOH:2N NH_4Cl:$MeNO_2$ 4:1.5:1.5). The darkish green fraction was collected, the solvent evaporated off, the residue dissolved in H_2O (100 mL), and a saturated aqueous solution of NH_4PF_6 was added until no further precipitation occurred. The precipitate was filtered off, washed with H_2O (2 × 10 mL), and dried under vacuum. The pure [2]catenane $\mathbf{5}\cdot 4PF_6$ was obtained as a bluish-green solid (808 mg, 23%). M.p. 300°C; MS (LSI): $m/z = 1840$ [M^+], 1695 [$M-PF_6$]$^+$, 1551 [$M+H-2PF_6$]$^+$, 1406 [$M+H-3PF_6$]$^+$; ^{1}H NMR (CD_3CN, 300 MHz, 25°C): $\delta = 3.50-4.00$ (m, 32H), 4.08 (br s, 4H), 5.55–5.78 (m, 8H), 6.08 (br s, 2H), 6.68–6.73 (m, 2H), 7.24-7.31 (m, 2H), 7.32–7.37 (m, 4H), 7.40–7.60 (m, 4H), 7.60–7.70 (m, 10H), 8.65–8.75 (m, 4H), 8.85–9.00 (m, 4H); ^{13}C NMR (CD_3CN, 75.1 MHz, 25°C): $\delta = 65.2$, 68.5, 68.6, 70.4, 70.5, 70.7, 71.1, 71.3, 71.6, 72.0, 106.6, 114.6, 119.8, 125.0, 125.3, 126.9, 133.5, 136.7, 143.9, 144.3, 145.5, 146.4, 154.6. Elemental analysis calcd for $C_{70}H_{76}F_{24}N_4O_{10}S_4P_4$: C 45.66, H 4.16, N 3.04, S 6.96; found C 45.55, H 4.28, N 3.18, S 7.1.

Received: June 2, 1997
Revised version: October 23, 1997 [Z10499IE]
German version: *Angew. Chem.* **1998**, *110*, 357–361

Keywords: catenanes · charge transfer complexes · molecular devices · redox switching · self-assembly · supramolecular chemistry

[1] D. B. Amabilino, J. F. Stoddart, *Chem. Rev.* **1995**, *95*, 2725–2828.
[2] a) J. S. Lindsey, *New J. Chem.* **1991**, *15*, 153–180; b) G. M. Whitesides, J. P. Mathias, C. T. Seto, *Science (Washington, DC)* **1991**, *254*, 1312–1319; c) D. Philp, J. F. Stoddart, *Synlett* **1991**, 445–458; d) D. S. Lawrence, T. Jiang, M. Levett, *Chem. Rev.* **1995**, *95*, 2229–2260; e) D. Philp, J. F. Stoddart, *Angew. Chem.* **1996**, *108*, 1242–1286; *Angew. Chem. Int. Ed. Engl.* **1996**, *35*, 1154–1196.
[3] M. C. T. Fyfe, J. F. Stoddart, *Acc. Chem. Res.*, **1997**, *30*, 393–401
[4] a) R. A. Bissell, E. Córdova, A. E. Kaifer, J. F. Stoddart, *Nature* **1994**, *369*, 133–137; b) M. J. Gunter, M. R. Johnston, *J. Chem. Soc. Chem. Commun.* **1994**, 829–830; c) P. R. Ashton, S. Iqbal, J. F. Stoddart, N. D. Tinker, *Chem. Commun.* **1996**, 479–481; d) R. Ballardini, V. Balzani, A. Credi, M. T. Gandolfi, S. J. Langford, S. Menzer, L. Prodi, J. F. Stoddart, M. Venturi, D. J. Williams, *Angew. Chem.* **1996**, *108*, 1056–1059; *Angew. Chem. Int. Ed. Engl.* **1996**, *35*, 978–981; e) M. Asakawa, S. Iqbal, J. F. Stoddart, N. D. Tinker, *ibid.* **1996**, *108*, 1054–1056 and **1996**, *35*, 976–978; f) D. B. Amabilino, C. O. Dietrich-Buchecker, A. Livoreil, L. Pérez-García, J.-P. Sauvage, J. F. Stoddart, *J. Am. Chem. Soc.* **1996**, *118*, 3905–3913; g) A. Credi, V. Balzani, S. J. Langford, J. F. Stoddart, *ibid.* **1997**, *119*, 2679–2681; h) M. V. Martínez-Diaz, N. Spencer, J. F. Stoddart, *Angew. Chem.* **1997**, *109*, 1991–1994; *Angew. Chem. Int. Ed. Engl.* **1997**, *36*, 1904–1907.
[5] a) A. Livoreil, C. O. Dietrich-Buchecker, J.-P. Sauvage, *J. Am. Chem. Soc.* **1994**, *116*, 9399–9400; b) P. R. Ashton, R. Ballardini, V. Balzani, A. Credi, M. T. Gandolfi, S. Menzer, L. Pérez-García, L. Prodi, J. F. Stoddart, M. Venturi, A. J. P. White, D. J. Williams, *ibid.* **1995**, *117*, 11171–11197; c) D. J. Cárdenas, A. Livoreil, J.-P. Sauvage, *ibid.* **1996**, *118*, 11980–11981; d) J.-P. Collin, P. Gaviña, J.-P. Sauvage, *Chem. Commun.* **1996**, 2005–2006; e) P. R. Ashton, R. Ballardini, V. Balzani, S. E. Boyd, A. Credi, M. T. Gandolfi, M. Gómez-López, S. Iqbal, D. Philp, J. A. Preece, L. Prodi, H. G. Ricketts, J. F. Stoddart, M. S. Tolley, M. Venturi, A. J. P. White, D. J. Williams, *Chem. Eur. J.* **1997**, *3*, 152–170.
[6] a) T. Jørgensen, T. K. Hansen, J. Becher, *Chem. Soc. Rev.* **1994**, *23*, 41–51; b) A. J. Moore, M. R. Bryce, *Synthesis* **1997**, 407–409.
[7] D. Philp, A. M. Z. Slawin, N. Spencer, J. F. Stoddart, D. J. Williams, *J. Chem. Soc. Chem. Commun.* **1991**, 1584–1586.
[8] P.-L. Anelli, M. Asakawa, P. R. Ashton, R. A. Bissell, G. Clavier, R. Górski, A. E. Kaifer, S. J. Langford, G. Mattersteig, S. Menzer, D. Philp, A. M. Z. Slawin, N. Spencer, J. F. Stoddart, M. S. Tolley, D. J. Williams, *Chem. Eur. J.* **1997**, *3*, 1113–1135.
[9] M. Asakawa, W. Dehaen, G. L'abbé, S. Menzer, J. Nouwen, F. M. Raymo, J. F. Stoddart, D. J. Williams, *J. Org. Chem.* **1996**, *61*, 9591–9595.
[10] a) W. Devonport, M. A. Blower, M. R. Bryce, L. M. Goldenberg, *J. Org. Chem.* **1997**, *62*, 885–887; b) M. Asakawa, P. R. Ashton, V.

 © WILEY-VCH Verlag GmbH, D-69451 Weinheim, 1998 1433-7851/98/3703-0336 $ 17.50+.50/0

Balzani, A. Credi, G. Mattersteig, O. A. Matthews, M. Montalti, N. Spencer, J. F. Stoddart, M. Venturi, *Chem. Eur. J.* **1997**, *3*, 1992 – 1996.

[11] a) T. Jørgensen, J. Becher, J.-C. Chambron, J.-P. Sauvage, *Tetrahedron Lett*. **1994**, *35*, 4339 – 4342; b) Z.-T. Li, P. C. Stein, J. Becher, D. Jensen, P. Mørk, N. Svenstrup, *Chem. Eur. J.* **1996**, *2*, 624 – 633; c) Z.-T. Li, J. Becher, *Chem. Commun*. **1996**, 639 – 640; d) J. Becher, Z.-T. Li, P. Blanchard, N. Svenstrup, J. Lau, M. Brøndsted Nielsen, P. Leriche, *Pure Appl. Chem*. **1997**, *69*, 465 – 470; e) Z.-T. Li, J. Becher, *Synlett* **1997**, 557 – 560; f) M. Brønsted Nielsen, Z.-T. Li, J. Becher, *J. Mater. Chem*. **1997**, *7*, 1175 – 1187.

[12] P. R. Ashton, R. A. Bissell, N. Spencer, J. F. Stoddart, M. S. Tolley *Synlett* **1992**, 923 – 926.

[13] R. Andreu, J. Garín, J. Orduna, M. Savirón, J. Cousseau, A. Gorgues, V. Morisson, T. Nozdryn, J. Becher, R. P. Clausen, M. R. Bryce, P. J. Skabara, W. Dehaen, *Tetrahedron Lett*. **1994**, *35*, 9243 – 9246.

[14] P. R. Ashton, J. Huff, S. Menzer, I. W. Parsons, J. A. Preece, J. F. Stoddart, M. S. Tolley, A. J. P. White, D. J. Williams, *Chem. Eur. J.* **1996**, *2*, 31 – 44.

[15] Crystal data for $\mathbf{5}\cdot 4\,PF_6\cdot 6\,MeCN$: monoclinic, space group *Cc* (no. 9), $a = 21.780(1)$, $b = 16.294(1)$, $c = 27.436(2)$ Å, $\beta = 93.94(1)^\circ$, $V = 9713.9(8)$ Å^3, $Z = 4$, $\rho_{calcd} = 1.428$ g cm^{-3}, $\mu(Cu_{K\alpha}) = 24.5$ cm^{-1}, $T = 203$ K, 6549 independent reflections measured, 5555 observed with $|F_o| > 4\sigma(|F_o|)$, $2\theta \leq 114^\circ$, refined on F^2 to $R_1 = 0.072$, $wR_2 = 0.183$ for 1023 parameters. The polarity of the structure was determined from the Flack parameter. The data were collected on a Siemens P4/RA diffractometer with ω scans and graphite monochromated $Cu_{K\alpha}$ radiation. The structure was solved by direct methods. The non-hydrogen atoms of the crown, the PF_6^- anions, and the included MeCN molecules were refined anisotropically; due to a shortage of observed data, the non-hydrogen atoms of the tetracation were refined isotropically. Crystallographic data (excluding structure factors) for the structure reported in this paper have been deposited with the Cambridge Crystallographic Data Center as supplementary publication no. CCDC-100460. Copies of the data can be obtained free of charge on application to CCDC, 12 Union Road, Cambridge CB2 1EZ (fax: int. code + (44) 1223 336-033; e-mail: deposit@ccdc.cam.ac.uk).

[16] The $OC_6H_{10}O$ vector of the "alongside" 1,5-dioxynaphthalene moiety is inclined by 18° to the mean plane of the tetracation.

[17] The [2]catenane molecules crystallize in a noncentrosymmetric space group, which contains a glide plane. Hence there are equal numbers of enantiomeric molecules present in the crystal.

[18] C. A. Hunter, J. K. M. Sanders, *J. Am. Chem. Soc*. **1990**, *112*, 5525 – 5534; C. A. Hunter, *Chem. Soc. Rev.* **1994**, *23*, 101 – 109.

[19] a) G. R. Desiraju, *Angew. Chem*. **1995**, *107*, 2541 – 2558; *Angew. Chem. Int. Ed. Engl*. **1995**, *34*, 2311 – 2327; b) T. Steiner, *Chem. Commun*. **1997**, 727 – 734.

[20] The mean interplanar separations between the "inside" disubstituted TTF ring system and the "inside" and "alongside" bipyridinium units are 3.43 and 3.37 Å, respectively; the separation between the "alongside" 1,5-dioxynaphthalene moiety and the "inside" bipyridinium unit is 3.31 Å. Hydrogen bonds between α-bipyridinium hydrogen atoms on the "inside" bipyridinium unit and the two polyether oxygen atoms have the following geometries: [C ··· O] 3.39 and 3.12 Å, [H ··· O] 2.43 and 2.40 Å; C–H ··· O angles 174° and 132°. The diametrically opposite sulfur atoms adjacent to the "*trans*"-substituted carbon atoms lie about 3.6 Å from the centroids of their proximal para-xylylene rings.

[21] When a 1,5-dioxynaphthalene moiety is located "inside" the tetracationic cyclophane, the H-4,8 protons resonate (M. Asakawa, P. R. Ashton, S. E. Boyd, C. L. Brown, R. E. Gillard, O. Kocian, F. M. Raymo, J. F. Stoddart, M. S. Tolley, A. J. P. White, D. J. Williams, *J. Org. Chem*. **1997**, *62*, 26 – 37) at very high field ($\delta = 2.1 – 2.6$). The fact that these naphthalene ring protons in the [2]catenane give rise to a masked signal (identified by a COSY experiment) in the region $\delta = 7.60 – 7.70$ confirms unequivocally that the 1,5-dioxynaphthalene moiety of the macrocycle is not located inside the tetracationic cyclophane. Intimate encirclement of the TTF unit by the tetracationic cyclophane was confirmed by 2D ROESY experiments (400 MHz, CD_3CN, 31°C, 200 ms mixing time), which display cross-peaks between the OCH_2 protons attached to the TTF core, and both the α-bipyridinium and the *p*-xylyl protons of the tetracationic cyclophane. No cross-peaks could be observed indicating that none of the 1,5-dioxynaphthalene moiety is located inside!

[22] The reduction potential of *o*-chloranil (+0.83 V: L. Horner, E. Geyer, *Chem. Ber.* **1965**, *98*, 2016 – 2045) substantiates the formation of the dicationic TTF species $\mathbf{5}^{6+}$. The UV/Vis spectrum (concentration: 9×10^{-5} M) recorded in MeCN shows no absorbance at $\lambda_{max} = 600$ nm, which is characteristic of $\mathbf{5}^{5+}$. The other typical band for the mono-oxidized TTF species at $\lambda_{max} = 450$ nm is hidden by the more intense band of *o*-chloranil ($\lambda_{max} = 435$ nm). Clear evidence for the presence of the bisoxidized TTF unit is provided by mass spectrometry. When examined with electrospray ionization (VG ProSpec mass spectrometer) in MeCN as solvent, the predominant ions observed for a 3:1 mixture of $\mathbf{5}^{4+}$ and *o*-chloranil are $m/z = 775$ and 468. They correspond to the loss of two and three PF_6^- counterions. On observation of the isotopic abundances for these species, the ion corresponding to loss of two counterions at $m/z = 775$ is doubly charged, as evidenced by the 0.5 u separation between the isotopes. The ion at $m/z = 468$ is shown to be triply charged with an isotopic separation of 0.3 u. A freshly prepared sample obtained after mixing *o*-chloranil and $\mathbf{5}^{4+}$ in a 2:1 ratio shows a peak at $m/z = 898$ as the most abundant in the spectrum. This peak corresponds to the incorporation of one counterion derived from *o*-chloranil into the [2]catenane. Once again, this species was found to be doubly charged by examination of isotopic abundances. Additionally, the spectrum shows peaks at $m/z = 775$ and 468. These peaks are the major ones for a sample recorded after standing for one week. The isotopic separations of these ions confirm that they are doubly ($m/z = 775$) and triply ($m/z = 468$) charged species. None of the spectra obtained show evidence for the presence of a monocationic species. As expected with reference to the second oxidation potential of the crown ether **3**, oxidation with *o*-chloranil yields preferentially $\mathbf{5}^{6+}$. We would like to thank one of the referees for asking us to comment on the nature of the oxidation state of the TTF unit.

[23] S. Hünig, G. Kiesslich, H. Quast, D. Scheutzow, *Liebigs Ann. Chem*. **1973**, 310 – 323.

[24] G. Schukat, E. Fanghänel, *J. Prakt. Chem*. **1985**, *327*, 767 – 774.

[25] The electrochemical experiments were carried out in argon-purged MeCN solutions with a Princeton Applied Research 273 multipurpose instrument interfaced to a personal computer, with cyclic voltammetry and differential pulse voltammetry techniques. The exact configuration and procedures for these measurements have been reported in Ref. [5e].

[26] A detailed study of the interesting electrochemical behavior of crown ether **3** will be reported elsewhere.

[27] The alternative explanation, based on lack of reversibility of the electrode process due to restricted access to the inside TTF unit, can be ruled out on consideration of the behavior observed for all the catenanes and rotaxanes previously investigated. See, for example: a) Ref. [5b]; b) P. R. Ashton, R. Ballardini, V. Balzani, M. Belohradsky, M. T. Gandolfi, D. Philp, L. Prodi, F. M. Raymo, M. V. Reddington, N. Spencer, J. F. Stoddart, M. Venturi, D. J. Williams, *J. Am. Chem. Soc*. **1996**, *118*, 4931 – 4951.

[28] We have found that oxidation of a 1,5-dioxynaphthalene moiety in "alongside" and "inside" positions occurs at +1.30 and +1.55 V vs SCE, respectively, in a catenane made of the cyclobis(paraquat-*p*-phenylene) tetracation and a crown ether (1/5DN38C10) containing two 1,5-dioxynaphthalene moieties.

[29] Since, strictly speaking, $\mathbf{5}^{4+}$ and $\mathbf{5}^{5+}$($\mathbf{5}^{6+}$), with their different oxidation states, are *not* isomers, we have introduced quotation marks round the term *isomer(s)* in our discussion of these two catenated species.

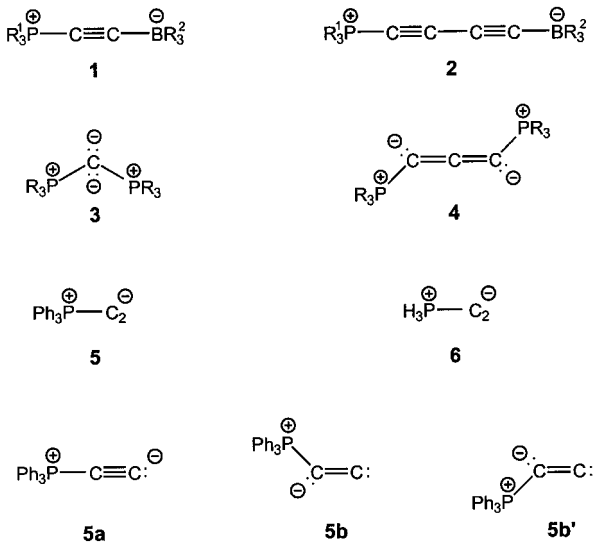
 © WILEY-VCH Verlag GmbH, D-69451 Weinheim, 1998 1433-7851/98/3703-0337 $ 17.50+.50/0

Triphenylphosphonioacetylide: A Species Isoelectronic with Isocyanides

Hans Jürgen Bestmann,* Wilhelm Frank, Claus Moll, Andreas Pohlschmidt, Timothy Clark, and Andreas Göller

In memory of Gerrit L'abbé

We have for some time been interested in "naked" carbon chains such as **1**–**4**, which are stabilized by donor and acceptor groups.[1, 2] Carbon chains stabilized by donors and acceptors have an even number of carbon atoms with betaine-like character (**1**, **2**), whereas the corresponding compounds



stabilized with two donors have an odd number of carbons and belong to the heterocumulene ylides (**3**, **4**).[3] In the course of this work, questions arose regarding the structure, stability, and reactivity of **5**, in which the C_2 unit is only stabilized by a single donor without an acceptor. This compound can be described by structures **5a** and **5b**/**5b′**. The former can be viewed as a triphenylphosphonioacetylide, whereas **5b**/**5b′** would be regarded as (methylenecarbenylidene)triphenylphosphoranes. Compound **5** is thus isoelectronic with isocyanides.

We utilized several computational techniques to determine the bond lengths, angles, and charge distribution in **5**: the semiempirical MO packages VAMP 6.1[4] and SPARTAN 4.1.1[5] with the PM3 Hamiltonian operator,[6] as well as ab initio [7, 8] and density functional theory (DFT)[9] techniques within Gaussian94.[10] Ab initio and DFT calculations relied on the following methods and basis sets:[8] HF/6-31G(d),[11] MP2/6-31G(d),[12, 13] MP2/6-311+G(d,p), and Becke3LYP/6-311+G(d).[9] Stationary points were characterized as minima or transition states at the appropriate level of calculation. NMR chemical shifts and coupling constants were calculated by the IGLO method[14] with DeMon 1.0.[15] In this case, PW91/IGLO-II//Becke3LYP/6-31G(d) was used for **5**, and PW91/IGLO-III//Becke3LYP/6-311+G(d) for the unsubstituted model compound **6**.

According to semiempirical calculations (Table 1), **5** is linear (P-C_α-C_β 179.98°). The most important bond lengths are

Table 1. Calculated geometries and energies for **5**.

Quantity	PM3	Becke3LYP/6-31G(d)
C–C [pm]	124.1	126.1
C–P [pm]	154.8	167.6
P–C(Ph) [pm]	180.4	183.8
C-P-C(Ph) [°]	112.3	110.2
E_{total}	180.471[a]	−1112.37540[b]
NIMAG[c]	0	1
ZPE[d]	175.424[a]	0.28353[b]

[a] In kcal mol^{-1}. [b] In Hartree. [c] NIMAG: Number of imaginary frequencies. [d] ZPE: Zero-point energy.

154.8 pm (P–C_α) and 124.1 pm (C_α–C_β); the latter is slightly longer than a C–C triple bond.[16] The PPh_3 group bears a net positive charge of +1.14 centered on the phosphorus atom (+2.14 on the P atom, −1.00 on all the phenyl rings combined). The most negative site is at C_α with a charge of −1.18, whereas C_β is practically neutral with a charge of +0.04 (Table 2).

Dipole moments for the individual atoms were derived with the help of the natural atomic orbital point charge (NAO-PC) method.[17] These experimentally nonobservable variables are a measure of the anisotropy of the atomic polarizability. The β-carbon atom in **5** has a dipole moment of 2.00 D, one of the largest yet ascertained with this technique. The molecule has essentially C_{3v} symmetry (the planes of the three phenyl rings intersect at angles of 120° at the P-C-C axis).

DFT Becke3LYP/6-31G(d) optimization (with the symmetry constrained to C_{3v}) gives slightly different values (Table 1). The C_α–C_β and P–C_α distances are 126.1 and 167.6 pm, respectively, and these bonds are expected to become somewhat longer upon inclusion of electron correlation. Atomic charges derived from an natural bond orbital (NBO) population analysis (C_α: −1.01, C_β: +0.02, P: +1.70, PPh_3: +0.99) agree well with those obtained by the NAO-PC method, which can be seen as a confirmation of the effectiveness of semiempirical techniques. Calculation of the normal vibrations for **5** at the Becke3LYP/6-31G(d) level results in one imaginary vibration with a frequency of −53 cm^{-1}. This vibration, which may be a result of numerical errors in the DFT integration, corresponds to a slight bending of the P-C-C unit.

To obtain more information about whether **5** is linear or not, we performed calculations at higher levels on the model compound **6**. H_3P–C_2 was therefore first optimized with C_{3v} symmetry (Table 3). At the RHF/6-31G(d), MP2/6-31G(d), and Becke3LYP/6-311+G(d) levels, this structure proved to be a minimum on the energy hypersurface. Only the structure optimized at the MP2/6-311+G(d,p) level proved to be a second-order saddle point with two imaginary vibrations. Structure **6** was therefore optimized without symmetry constraints (C_1, Table 3). The resulting geometry deviates

[*] Prof. Dr. H. J. Bestmann, Dr. W. Frank, Dipl.-Chem. C. Moll, Dr. A. Pohlschmidt, Priv.-Doz. Dr. T. Clark, Dr. A. Göller
Institut für Organische Chemie der Universität Erlangen-Nürnberg
Henkestrasse 42, D-91054 Erlangen (Germany)
Fax: Int. code + (49) 9131 85-6864
E-mail: bestmann@organik.uni-erlangen.de

 © WILEY-VCH Verlag GmbH, D-69451 Weinheim, 1998 1433-7851/98/3703-0338 $ 17.50+.50/0

Table 2. Atomic charges for **5** and **6** determined at different levels of theory.

Atom	**5**[a]	**5**[b]	**6**[c]	**6**[d]	**6**[e]	**6**[f]
C_β	+0.04	+0.02	−0.04 to +0.03	−0.11	−0.34	−0.42
C_α	−1.18	−1.01	−0.58 to −0.60	−0.38	−0.16	+0.06
P	+2.14	+1.70	+0.58 to +0.62	+0.40	+0.47	+0.08
H/Ph[g]	−1.00	−0.71	−0.06 to +0.06	+0.09	+0.03	+0.28

[a] PM3. [b] Becke3LYP/6-31G(d). [c] HF/6-31G(d), HF/6-31+G(d), HF/6-311+G(d,p). [d] MP2/6-31G(d). [e] MP2/6-311+G(d,p). [f] Becke3LYP/6-311+G(d). [g] Sum of all residuals on P.

Table 3. Calculated geometries and energies for **6** with various symmetries.

Symmetry	Quantity	RHF/6-31G(d)	MP2/6-31G(d)	MP2/6-311+G(d, p)	Becke3LYP/6-311+G(d)
C_{3v}	C−C [pm]	124.3	127.3	126.9	125.6
	C−P [pm]	164.4	165.3	165.6	165.2
	P−H [pm]	138.8	140.5	140.0	141.1
	C-C-P [°]	180.0	180.0	180.0	180.0
	C-P-H [°]	116.0	116.3	115.6	116.3
	E_{total} [Hartree]	−418.02689	−418.36887	−418.46541	−419.23912
	NIMAG[a]	0	0	2	0
	ZPE[b]	0.03856	0.03601	0.03541	0.03461
C_1	C−C [pm]	124.3	127.3	127.0	125.7
	C−P [pm]	164.4	165.3	165.7	165.3
	P−H [pm]	138.8	140.5	140.0	141.1
	C-C-P [°]	179.9	179.9	172.1	179.9
	C-P-H [°]	116.0	116.9/116.3	115.5/115.6	116.2
	E_{total} [Hartree]	−418.02885	−418.36887	−418.46543	−419.23912
	NIMAG[a]	0	0	0	0
	ZPE[b]	0.03856	0.03601	0.03569	0.03467

[a] NIMAG: Number of imaginary frequencies. [b] ZPE: Zero-point energy.

slightly from C_s symmetry, and **6** is nonlinear with a P-C-C angle of 172°. We assume that the corresponding angle is similar in **5**.

Calculations at all levels agree that the P-C-C unit can be bent very easily (frequencies 0–100 cm^{-1}). The difference in energy between **6** with C_{3v} symmetry and **6** with C_1 symmetry is only 0.00002 Hartree (0.01 kcal mol^{-1}) at the MP2/6-311+G(d,p) level; the nonlinearity should have no experimentally observable consequences. The calculated geometries show short C−C distances (124.3–127.3 pm) that suggest a C−C triple bond, as for the triphenyl compound. The P−C bond lengths (164.4–165.6 pm) are also short and lie in the range of formal P−C double bonds (cf. CH_2=PH 167.5 pm at the MP2/6-31G(d) level). The C-P-C(Ph) angle in the phenyl-substituted compound **5** is, as expected, somewhat smaller than the analogous C-P-H angle in **6**.

Coulson and Mulliken charges are very similar for semiempirical (PM3) and ab initio Hartree–Fock calculations. The phosphorus atom carries less charge in **6** because charge delocalization to the phenyl rings is not possible. Atom C_β is essentially neutral, C_α negatively charged, and P positive (+0.6 e). Methods that take electron correlation into account (MP2 and DFT) give results with the opposite trends, dependent on the basis set. The changes are most extreme for Becke3LYP/6-311+G(d) calculations: C_β now has a partial negative charge (−0.42e), whereas the other atoms are all slightly positive.

The three highest occupied molecular orbitals of **6** (Figure 1) are two almost degenerate orthogonal π orbitals (HOMO and HOMO − 1) with C−C bonding character and

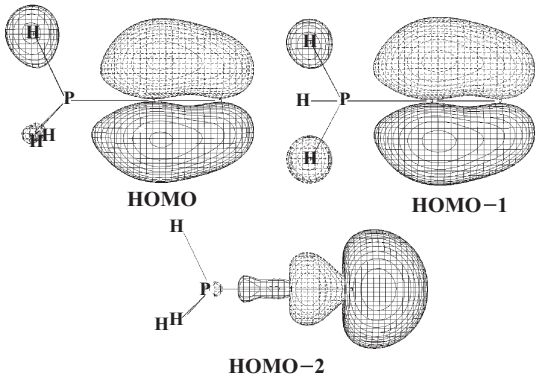


Figure 1. The orbitals HOMO, HOMO − 1, and HOMO − 2 for **6** (HF/6-31G(d)//Becke3LYP/6-311+G(d), PSI88[18]).

a σ orbital (HOMO − 2) with a large orbital lobe beyond C_β (lone pair) and significant C−C bonding character. Strong polarization of all three MOs leads to an accumulation of electron density at the lone pair and on C_α this is not fully reflected in the calculated net atomic charges. In **5**, only the ordering of these three MOs is changed (Figure 2). In this case, the lone pair is the HOMO (σ orbital). All these calculations point to the fact that it is not possible to formulate a single Lewis structure for **5** that correctly reproduces the geometry and charge distribution.

To synthesize **5** a solution of the known (silylethinyl)phosphonium salt **7**[19] in dichloromethane was added dropwise to benzyltrimethylammonium fluoride (**8**) in the same solvent at

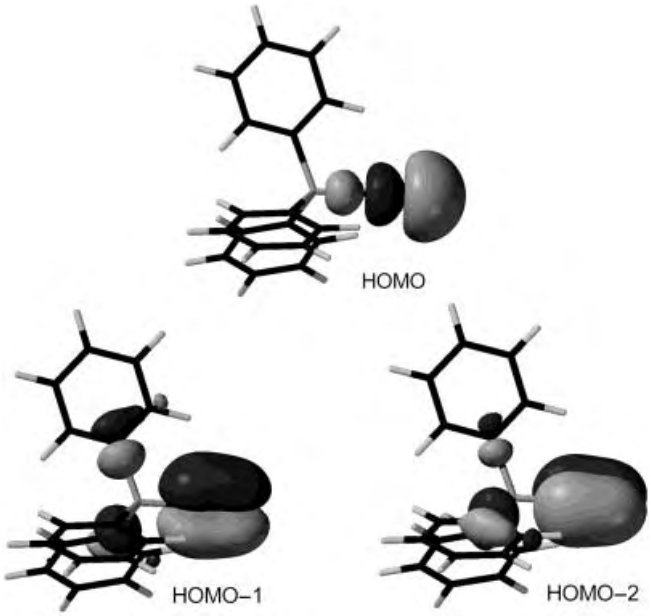
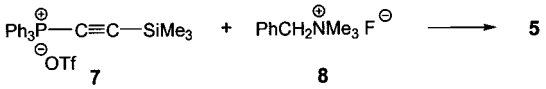


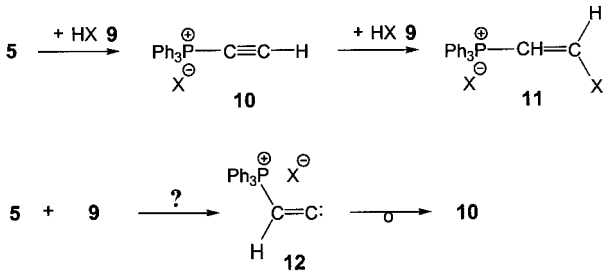
Figure 2. The orbitals HOMO, HOMO – 1, and HOMO – 2 for **5** (PM3/Spartan 4.1.1).

– 90 °C. The low-temperature (– 78 °C) ^{31}P NMR spectrum of the product showed (apart from small amounts of by-products) only one signal at $\delta = -13.85$. The signals of starting material **7** at ($\delta(^{31}P) = 5.22$, $\delta(^{29}Si) = -9.78$) had disappeared. Since **5** is stable only at low temperature and



decomposes upon warming to room temperature, all spectra were recorded at – 78 °C. Because the ^{13}C NMR data were not completely clear, we prepared ^{13}C-enriched **7**.[20] The corresponding ^{13}C NMR spectrum showed doublets for C_α and C_β (C_α: $\delta = 83.87$, $^1J(P,C) = 161.7$ Hz; C_β: $\delta = 133.03$, $^2J(P,C) = 18.4$ Hz). After desilylation of **7** to **5** the signals for C_α and C_β appeared at $\delta = 83.15$ (d, $^1J(P,C) = 132.4$ Hz) and 228.90 (d, $^2J(P,C) = 12.8$ Hz). These data support the results of the calculations extremely well (Table 4). The large downfield shift in the signal for C_β in **5** with respect to that for **7** (over 95 ppm) shows that this atom is electron deficient. The observed P–C_α coupling constant lies between the usual values for alkenyl- (ca. 90 Hz)[21] and alkinylphosphonium salts (ca. 180 Hz),[22] indicating some nonlinearity of the molecule in solution.[23] The ^{31}P NMR spectrum of ^{13}C-labeled **5** shows (apart from a singlet at – 13.687 ppm for the ^{12}C isotopomer) two doublets at $\delta = -13.693$ and – 13.710, which result from coupling of C_α or C_β of the two ^{13}C isotopomers with the phosphorus atom. The ^{31}P NMR signal of **5** is shifted upfield, as are those for **4** ($R^2 = C_6H_5$)[2] and other phosphaallene ylides.[24] The IR spectrum of **5** shows a sharp peak at 1957 cm^{-1} (**7**: 2135 cm^{-1}); cumulated ylides also absorb in this range.[23]

Compound **5** reacts with acids HX (**9**) initially to form ethinylphosphonium salts **10**, which could be characterized by ^{31}P NMR spectroscopy as intermediates between – 78 and – 30 °C (Scheme 1). A possible insertion into the H–X bond,



Scheme 1. Reaction of **5** with **9** (X = OMe, Cl, OCOMe) and possible reaction pathways that proceed directly via **10** or via carbene intermediate **12**.

which might be expected on the basis of the carbene structure **5b**/**5b**′, is not observed. At about 0 °C a further reaction with **9** takes place to give the vinylphosphonium salts **11**, which are formed as mixtures with widely differing *Z*:*E* isomeric ratios.[25] We assume that electrophilic attack at the β-carbon atom of **5** occurs to lead to a dynamic back-polarization of electron density from C_α to C_β. In principle, nucleophilic attack on the negatively charged α-carbon atom might be possible to form the vinylidenecarbenephosphonium salt **12**, which would be expected to undergo rapid rearrangement to the ethinylphosphonium salt **10** (Scheme 1).[26] However, in a series of experiments (e.g., reaction with electrophiles in the presence of alkenes) we found no evidence for the formation of carbene **12** or similar intermediates substituted at the α-carbon atom. Reaction of **5** with trifluoromethanesulfonic acid methyl ester (**13**) gives the propinylphosphonium salt **14**.



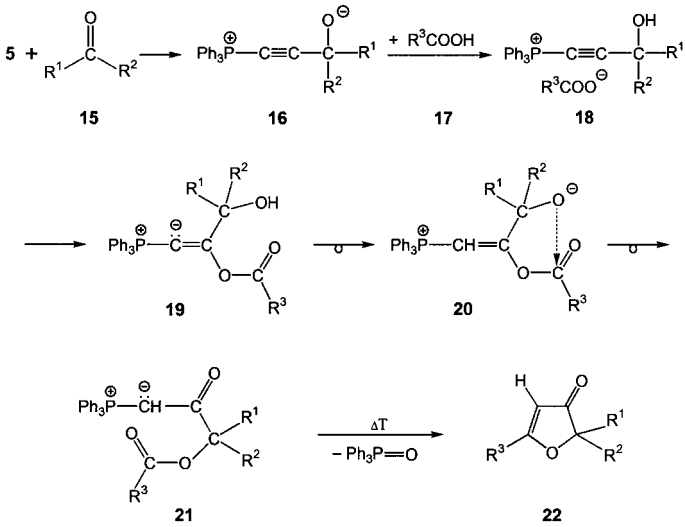
We further investigated whether **5**, which is isoelectronic with isocyanides, undergoes reactions analogous to the Passerini reaction.[27] We therefore treated solutions of **5** at – 78 °C with a ketone (**15**) and then at – 40 °C with carboxylic acid **17** (Scheme 2), and isolated the corresponding (3-acyloxy-2-oxo-alkylidene)triphenylphosphorane **21** about five hours later (Table 5). We assume that betaine **16** is initially formed and then is protonated by **17** to give alkynylphospho-

Table 4. Structurally relevant spectroscopic data for **5** and **7**.

	$\delta(^{31}P)/J(P,C)$ [Hz]	$\delta(^{29}Si)/J(Si,P)$ [Hz]	$\delta(^{13}C)/J(P,C)$ [Hz]	IR [cm^{-1}]
7[a]	5.22 (s)/ –	– 9.78 (d)/3.5 (^3J)	83.87 (d, C_α)/161.7 (^1J) 133.03 (d, C_β)/18.4 (^2J)	2135
5[b]	– 13.710 (d)/132.1 (^1J) – – 13.693 (d)/12.3 (^2J) – 13.687 (s)/ –		83.15 (d, C_α)/132.4 (^1J) 228.90 (d, C_β)/12.8 (^2J)	1957
5[c]	– 45.8	–	61.6 (C_α)/108.9 (^1J) 285.8 (C_β)/ – 57.0 (^2J)	–

[a] Determined in $CDCl_3$ at room temperature, IR as KBr pellet. [b] Determined in CH_2Cl_2 or CD_2Cl_2 at – 78 °C. [c] Calculated at the PW91/IGLO-II//Becke3LYP/6-31G(d) level.

 © WILEY-VCH Verlag GmbH, D-69451 Weinheim, 1998 1433-7851/98/3703-0340 $ 17.50+.50/0 *Angew. Chem. Int. Ed.* **1998**, *37*, No. 3



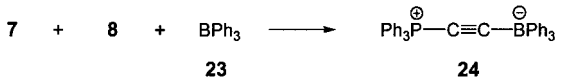
Scheme 2. Reaction of **5** that resembles the Passerini reaction.

Table 5. Acyl ylides **21** and furanones **22** prepared from **5**, ketones, and carboxylic acids.

	R^1	R^2	R^3	**21** [%]	M.p. [°C]	**22** [%]	M.p. [°C]
a	Me	*t*Bu	*p*-$MeOC_6H_4$	40	–	76	89
b	Et	Ph	*p*-$MeOC_6H_4$	42	170	82	97
c	Me	Me	*p*-$MeOC_6H_4$	45	172	83	93
d	Me	Me	Me	54	146	–	–

nium salt **18**. The carboxylate anion then adds at the position β to phosphorus in a slow reaction at room temperature. The resulting phosphaallene ylide **19** in turn undergoes a proton shift to provide **20**. The reaction sequence is terminated by an acyl shift to give **21**. The similarity between this sequence and the Passerini reaction is clear. Upon heating in benzene or toluene at reflux, acyl ylides **21** undergo an intramolecular Wittig reaction[28] to yield 2,2,5-trisubstituted 3(2*H*)-furanones **22** (cf. Table 5).

If **7** is desilylated in the presence of triphenylborane (**23**) at $-78\,^{\circ}C$, (triphenylphosphonioethinyl)triphenylborate (**24**),[29] which belongs to the phosphonioboratoacetylenes **1**, is formed in 84% yield. A comparison of the X-ray crystal structure of **24**[29] with that of **1**,[1] in which one phenyl is replaced by a



methyl group, shows no significant differences. The C_α–C_β distance in **24** (124.3 pm) is slightly greater than that in the analogue (121.6 pm), [1] and both molecules are slightly bent (**24**: P-C_α-C_β 177°, B-C_β-C_α 171.3°).

Experimental Section

All operations were carried out under a nitrogen atmosphere and in absolute solvents.

5 (in solution): **8** (169 mg, 1.0 mmol) was dissolved/suspended in CH_2Cl_2 (2 mL) and cooled to $-90\,^{\circ}C$. A solution of **7** (509 mg, 1.0 mmol) in CH_2Cl_2 (3.5 mL) was added dropwise over a period of 10 min. A deep red solution was obtained, which appeared yellow when viewed as a thin layer. To complete the reaction, the mixture was stirred for about 10 min and allowed to warm to $-78\,^{\circ}C$. Smaller batches (0.6 mmol) in absolute CD_2Cl_2 were prepared to obtain low-temperature spectra.

21: To a solution of **5** at $-78\,^{\circ}C$ was added an aromatic or aliphatic ketone (**16**, 5.0 mmol). The mixture was first allowed to react for 10 min at $-78\,^{\circ}C$, and then maintained for 30 min at $-40\,^{\circ}C$ before an aromatic or aliphatic carboxylic acid (**17**, 0.8 mmol) was added. The mixture was allowed to warm to room temperature and then stirred for 5 h. From this point on, a nitrogen atmosphere was no longer necessary. The solution was evaporated to 2 mL and washed with Et_2O (10 mL), and the residue was twice precipitated from CH_2Cl_2/Et_2O (little CH_2Cl_2). The oily red residue was discarded. The combined ether phases were evaporated, and the crude acyl ylides **21** chromatographed over silica gel with ethyl acetate as eluent.

Received: August 15, 1997 [Z10819IE]
German version: *Angew. Chem.* **1998**, *110*, 347–351

Keywords: ab initio calculations · betaines · isoelectronic analogues · ylides

[1] H. J. Bestmann, H. Behl, M. Bremer, *Angew. Chem.* **1989**, *101*, 1303; *Angew. Chem. Int. Ed. Engl.* **1989**, *28*, 1219.
[2] H. J. Bestmann, D. Hadawi, H. Behl, M. Bremer, F. Hampel, *Angew. Chem.* **1993**, *105*, 1198; *Angew. Chem. Int. Ed. Engl.* **1993**, *32*, 1205.
[3] H. J. Bestmann, *Angew. Chem.* **1977**, *89*, 361; *Angew. Chem. Int. Ed. Engl.* **1977**, *16*, 349.
[4] G. Rauhut, A. Alex, J. Chandrasekhar, T. Steinke, W. Sauer, B. Beck, M. Hutter, P. Gedeck, T. Clark, VAMP 6.1, Oxford Molecular Ltd., Magdalen Centre, Oxford Science Park, Sandford-on-Thames, Oxford, OX4GA, England, **1997**.
[5] SPARTAN Version 4.1.1, Wavefunction Inc., 18401 Von Karman, Suite 370, Irvine, CA 92715, USA.
[6] J. J. P. Stewart, *J. Comput. Chem.* **1989**, *10*, 209, 221; *ibid.* **1991**, *12*, 320.
[7] W. J. Hehre, R. Ditchfield, P. von R. Schleyer, J. A. Pople, *ab initio Molecular Orbital Theory,* Wiley, New York, **1986**.
[8] J. B. Foresman, A. Frisch, *Exploring Chemistry with Electronic Structure Methods*, Gaussian Inc., Pittsburgh, **1993**.
[9] R. G. Parr, W. Yang, *Density Functional Theory of Atoms and Molecules*, Oxford Science Publications, New York, **1989**.
[10] M. J. Frisch, G. W. Trucks, H. B. Schlegel, P. M. W. Gill, B. G. Johnson, J. R. Robb, T. Cheeseman, G. A. Keith, J. A. Peterson, K. Montgomery, M. A. Raghavachari, V. G. Al-Laham, J. V. Zakrzewski, J. B. Ortiz, J. Foresman, B. B. Cioslowski, A. Stefanov, M. Nanayakkara, C. Y. Challacombe, P. Y. Peng, W. Ayala, M. W. Chen, J. L. Wong, E. S. Andres, R. Replogle, R. L. Gomperts, D. J. Martin, J. S. Fox, D. J. Binkley, J. Defrees, A. Baker, J. P. Stewart, M. Head-Gordon, C. Gonzalez, J. A. Pople, Gaussian Inc., Pittsburgh, PA, **1995**.
[11] a) W. J. Hehre, R. Ditchfield, J. A. Pople, *J. Chem. Phys.* **1972**, *56*, 2257; b) P. C. Hariharan, J. A. Pople, *Theor. Chim. Acta* **1973**, *28,* 213; c) M. S. Gordon, *Chem. Phys. Lett.* **1980**, *76*, 163.
[12] C. Møller, M. S. Plesset, *Phys. Rev.* **1934**, *46,* 618.
[13] a) R. Krishnan, J. A. Pople, *Int. J. Quantum Chem*. **1978**, *14,* 91; b) R. Krishnan, M. Frisch, J. A. Pople, *J. Chem. Phys.* **1980**, *72,* 4244.
[14] a) W. Kutzelnigg, U. Fleischer, M. Schindler, *NMR Basic Princ. Prog.* **1990**, *23*, 165; b) W. Kutzelnigg, *J. Chem. Phys.* **1982**, *76*, 1919.
[15] a) V. G. Malkin, O. L. Malkina, L. A. Eriksson, D. R. Salahub in *Modern Density Functional Theory* (Ed.: J. M. Seminario, P. Politzer), Elsevier, Amsterdam, **1995**.
[16] Compare the C_α–C_β bond length in cumulated ylides: H. Burzlaff, R. Haag, E. Wilhelm, H. J. Bestmann, *Chem. Ber.* **1985**, *118*, 170.
[17] G. Rauhut, T. Clark, *J. Comput. Chem.* **1993**, *14*, 503; B. Beck, G. Rauhut, T. Clark, *ibid.* **1994**, *15*, 1064.
[18] PSI88: a) D. L. Severance, W. L. Jorgensen, Department of Chemistry, Yale University, New Haven, CT 06511, USA, **1988**; b) modified by H. Roth.
[19] P. J. Stang, C. M. Critell, *J. Org. Chem.* **1992**, *57*, 4305.
[20] ^{13}C enrichment to 25% at both C_α and C_β, although in different molecules. The synthesis of the ^{13}C-labeled compounds will be described elsewhere.
[21] T. A. Albright, W. Freeman, E. E. Schweizer, *J. Am. Chem. Soc.* **1975**, *97*, 2946.

 © WILEY-VCH Verlag GmbH, D-69451 Weinheim, 1998 1433-7851/98/3703-0341 $ 17.50+.50/0

[22] H. J. Bestmann, L. Kisielowski, *Chem. Ber.* **1983**, *116*, 132.
[23] Compare the P–C_α coupling in phosphacumulene ylides: H. J. Bestmann, G. Schmidt, *Chem. Ber.* **1980**, *113*, 3369.
[24] H. J. Bestmann, K. Roth, *Tetrahedron Lett.* **1981**, *22*, 1181.
[25] NMR data for the previously unknown (*Z*)-**11a** (X = Cl): ^{1}H NMR (400 MHz, $CDCl_3$, RT): $\delta = 7.62$ (dd, 1H, ^2J(P,H) = 16.17 Hz, ^3J(H,H) = 8.85 Hz, H on C_α), 7.86 (m, 15H, aromatic H), 8.03 (dd, 1H, ^3J(P,H) = 35.09 Hz, ^3J(H,H) = 8.85 Hz, H on C_β); ^{13}C NMR (100.4 MHz, $CDCl_3$, RT): $\delta = 111.90$ (d, ^1J(P,C) = 91.5 Hz, C_α), 117.21 (d, ^1J(P,C) = 91.6 Hz, *ipso*-C), 130.45 (d, ^3J(P,C) = 13.7 Hz, *meta*-C), 133.33 (d, ^2J(P,C) = 12.2 Hz, *ortho*-C), 135.32 (d, ^4J(P,C) = 3.1 Hz, *para*-C), 147.83 (d, ^2J(P,C) = 7.6 Hz, C_β).
[26] Review of alkylidene carbenes: P. J. Stang, *Chem. Rev.* **1978**, *78*, 283; *Acc. Chem. Res.* **1982**, *15*, 348.
[27] Review: I. Ugi, *Angew. Chem.* **1962**, *74*, 9; *Angew. Chem. Int. Ed. Engl.* **1962**, *1*, 8.
[28] Cf. H. J. Bestmann, G. Schade, H. Lütke, T. Mönius, *Chem. Ber.* **1985**, *118*, 2640.
[29] **24**: colorless crystals, m.p. 203–205 °C (decomp); IR: $\tilde{\nu} = 2090$ cm^{-1} (C≡C); ^{1}H NMR (60 MHz, [D$_5$]pyridine): $\delta = 7.1$–8.0 (m, 30H, aromatic H); ^{13}C NMR (100.4 MHz, [D$_5$]pyridine): $\delta = 71.3$ (d, ^1J(P,C) = 186.2 Hz, C_α), 122.3 (d, ^1J(P,C) = 99.2 Hz, *ipso*-C, P-phenyl), 124.4 (s, *para*-C, B-phenyl), 127.3 (s, *ortho*-C, B-phenyl), 130.3 (d, ^3J(P,C) = 13.7 Hz, *meta*-C, P-phenyl), 133.3 (d, ^2J(P,C) = 12.2 Hz, *ortho*-C, P-phenyl), 134.8 (d, ^4J(P,C) = 3.0 Hz, *para*-C, P-phenyl), 135.5 (s, *meta*-C, B-phenyl), 157.6 (s, *ipso*-C, B-Phenyl); ^{31}P NMR (161.7 MHz, [D$_5$]pyridine): $\delta = 0.04$; ^{11}B NMR (128 MHz, C_6D_6): $\delta = -11.2$.

A Three-Dimensional Framework with Accessible Nanopores: $RbCuSb_2Se_4 \cdot H_2O$**

Jason A. Hanko and Mercouri G. Kanatzidis*

The synthesis of nonoxidic chalcogen-based open frameworks is motivated by the prospect of obtaining interesting semiconducting analogues of zeolites.[1] Planned syntheses of open-framework structures based on germanium and tin sulfides were reported in 1989.[2] This discovery led to a rapid expansion in this area, and compounds such as $[Et_4N]_2Cu_2Ge_4S_{10}$,[3] $[Me_4N]_2MGe_4S_{10}$ (M = Mn,[4, 5] Fe,[5, 6] Co,[5] Zn[5]), and $[Me_4N]_6(Cu_{0.44}Ge_{0.56}S_{0.73})Ge_4S_{10}$[7] were prepared. Hydrothermal synthesis is a common route to these materials. Solid-state lattices can be generated by the self-assembly of the appropriate molecular building blocks in the presence of organic template ions. Using this approach, we have demonstrated that $[EQ_3]^{3-}$ (E = As, Sb; Q = S, Se) units are versatile building blocks from which interesting compounds such as KBi_3S_5,[8] $[Ph_4P]InSe_{12}$,[9] $[Me_4N]HgAs_3S_6$,[10] $[Me_4N]RbBiAs_6S_{12}$,[11] and $[Co(en)_3]CoSb_4S_8$[12] can be made. A transition metal is not necessary for the formation of extended structures. Several of these germanium,[13] tin,[14–22] and antimony sulfide[23, 24] frameworks are also accessible by condensation of molecular building blocks.

Here we report on the new three-dimensional material $RbCuSb_2Se_4 \cdot H_2O$ (**1**), which was prepared by heating CuCl with Rb_3SbSe_3[25] and Ph_4PBr in H_2O at 130 °C. The black needlelike crystals are insoluble in common organic solvents. Compound **1** has a three-dimensional framework in which tetrahedral Cu centers are connected to both pyramidal $SbSe_3$ and square-pyramidal $SbSe_5$ units.[26] The novel feature of this framework is the presence of large channels running along the [010] direction (Figure 1). The channels have an irregular

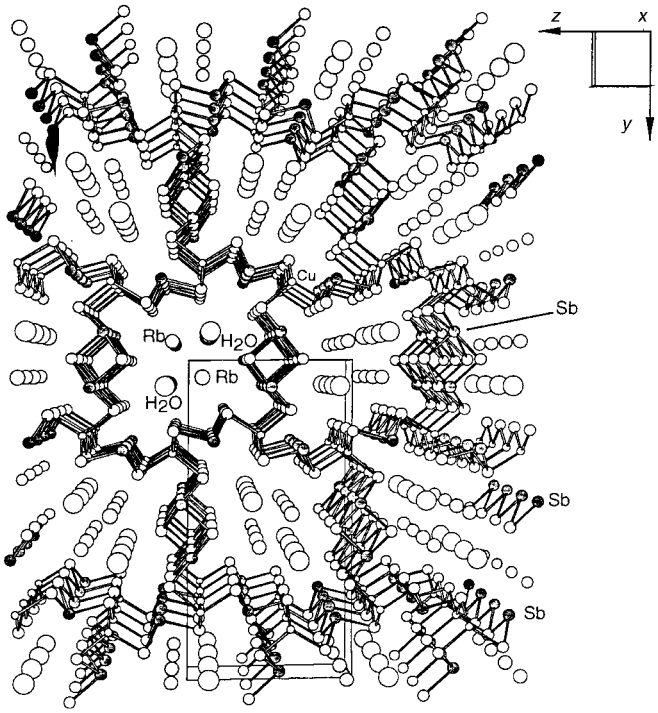


Figure 1. View of the structure of **1** along the *b* axis showing the channels occupied by the rubidium centers and water molecules.

cross section with dimensions of 11.29 × 10.52 × 8.16 Å (Figure 2). Another unique feature is the presence of two kinds of $[SbSe_2]_n^{n-}$ chains which run parallel to the channels. One is a single $[SbSe_2]_n^{n-}$ chain of corner-sharing pyramids in which all of the terminal Se centers on the same side; the Sb–Se bond lengths range from 2.556(4) to 2.726(3) Å (av 2.66(5) Å), and the Se-Sb-Se angles from 95.5(1) to 99.1(1)°. The other contains associated double $\{[SbSe_2]_2\}_n^{2n-}$ chains with Sb–Se bond lengths in the range 2.585(4)–2.972(3) Å (av 2.83(8) Å) and Se-Sb-Se angles between 84.8(1) and 173.9(1)°. Such double chains are also found in Sb_2Se_3.[27] Figure 2 highlights the two different $[SbSe_2]_n^{n-}$ chains. The $[SbSe_2]_n^{n-}$ single chains are connected to the Cu atoms to give corrugated $CuSbSe_2$ sheets composed of alternating rows of tetrahedrally coordinated Cu and pyramidally coordinated Sb units. These sheets are held together by the $\{[SbSe_2]_2\}_n^{2n-}$ double chains, which complete the tetrahedral coordination sphere of the Cu atoms

[*] Prof. M. G. Kanatzidis, J. A. Hanko
Department of Chemistry and
Center for Fundamental Materials Research
Michigan State University
East Lansing, MI 48824 (USA)
Fax: Int. code + (1) 517 353-1793
E-mail: kanatzid@argus.cem.msu.edu

[**] Financial support from the Petroleum Research Fund (administered by the American Chemical Society) and from the National Science Foundation is gratefully acknowledged. M.G.K. is a Camille and Henry Dreyfus Teacher Scholar (1993–1998). This work made use of the SEM facilities of the Center for Electron Optics at Michigan State University.

 © WILEY-VCH Verlag GmbH, D-69451 Weinheim, 1998 1433-7851/98/3703-0342 $ 17.50+.50/0

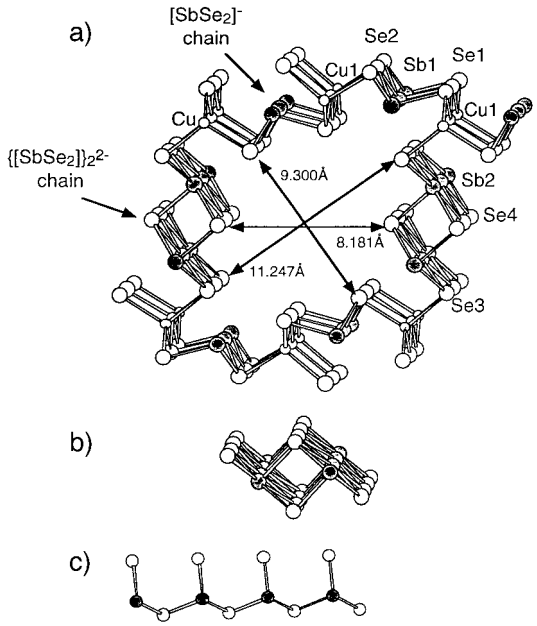


Figure 2. a) Section of the framework of **1** (Rb cation and water molecule omitted for clarity) with selected bond lengths [Å] and angles [°]: Cu(1)–Se(1) 2.489(3), Cu(1)–Se(1′) 2.489(3), Cu(1)–Se(2) 2.499(6), Cu(1)–Se(4) 2.480(5), Sb(1)–Se(1) 2.556(4), Sb(1)–Se(2) 2.726(3), Sb(1)–Se(2′) 2.726(3), Sb(2)–Se(3) 2.585(4), Sb(2)–Se(3′) 2.972(3), Sb(2)–Se(3″) 2.972(3), Sb(2)–Se(4) 2.823(3), Sb(2)–Se(4′) 2.823(3); Se(2)-Sb(1)-Se(1) 99.1(1), Se(2′)-Sb(1)-Se(1) 99.1(1), Se(2)-Sb(1)-Se(2′) 95.5(1), Se(3)-Sb(2)-Se(4) 89.7(1), Se(3)-Sb(2)-Se(3′) 84.8(1), Se(4)-Sb(2)-Se(4′) 91.2(1), Se(4)-Sb(2)-Se(4) 88.5(1), Se(3)-Sb(2)-Se(4) 91.3(1), Se(3)-Sb(2)-Se(4) 173.9(1), Se(4)-Cu(1)-Se(1) 110.6(1), Se(1)-Cu(1)-Se(1′) 108.4(1), Se(2)-Cu(1)-Se(4) 108.4(1), Se(2)-Cu(1)-Se(1) 109.4(1). b) View of the $[SbSe_2]_2^{2-}$ double chain. c) View of the $[SbSe_2]_n^{n-}$ single chain.

and form the three-dimensional framework. The Cu centers have a slightly distorted tetrahedral coordination environment. The Cu–Se bonds range from 2.480(5) to 2.499(6) Å, and the Se-Cu-Se angles from 108.4(1) to 110.6(1)°.

Thermogravimetric analysis (TGA, Figure 3) showed two significant weight loss steps. A one-step mass loss of 2.65 % at 200 °C corresponds to the loss of the water molecule (calcd 2.47 %). This was followed by a one-step mass loss, with a shoulder, of 22.48 % at 380 °C, corresponding to the loss of two Se atoms (calcd 22.33 %). The X-ray diffraction pattern of the remaining powder, which had been heated to 600 °C, indicated the presence of a crystalline solid; however, it did not match that of Sb_2Se_3 or any known Cu/Se or Cu/Sb/Se phase. The thermal stability of the material after loss of the water molecule was investigated by interrupting the TGA at 300 °C and cooling to room temperature. The powder X-ray diffraction pattern of the residue did not match that of **1**, showing that the loss of the water molecule results in the collapse of the framework. Compound **1** exhibits topotactic ion-exchange properties, a key criterion for assessing the performance of the framework as a host. The facile removal of Rb^+ ions indicates substantial mobility of the alkali metal ions and water molecules in the tunnels. By using a mild solid-state exchange method developed by us,[28] the Rb^+ cations can readily be exchanged with other, smaller cations such as Li^+, Na^+, and NH_4^+, which were used in the form of their iodides. The degree of exchange was determined by energy dispersive spectrosopy (EDS). The compositions of the exchanged materials were $Rb_{0.2}Li_{0.8}CuSb_2Se_4$, $Rb_{0.2}Na_{0.8}CuSb_2Se_4$, and $Rb_{0.4}(NH_4)_{0.6}CuSb_2Se_4$, for the Li^+, Na^+, and NH_4^+ ions, respectively.

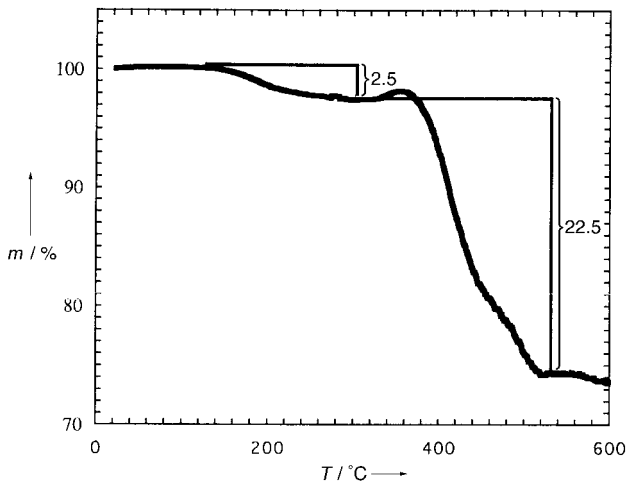


Figure 3. Therogravimetric analysis of **1** in the temperature range 25–600 °C.

The optical spectrum of **1** reveals the presence of a sharp optical gap of 1.32 eV, which suggests that the material is a semiconductor. The far-IR spectrum of **1** shows a broad absorption around 211 cm^{-1}, which can be tentatively assigned to Cu–Se stretching modes. The Raman spectrum of **1** displays a single strong band at about 233 cm^{-1}, which is assigned to Sb–Se stretching modes, and two shoulders at about 209 and 186 cm^{-1}, which are assigned to Cu–Se stretching vibrations.

Compound **1** has a unique structure and is the first example of a quaternary selenoantimonate with an open three-dimensional framework and proven ion-exchange properties.

Experimental Section

1 was synthesized by heating a mixture of CuCl (0.01 g, 0.10 mmol), Rb_3SbSe_3 (0.186 g, 0.30 mmol), Ph_4PBr (0.168 g; 0.40 mmol), and H_2O (0.2–0.5 mL) at 130 °C for 3 d in a sealed Pyrex tube. The product was isolated by washing with copious degassed methanol and dried with ether. The resulting product was a 50/50 mixture of black needles of $RbCuSb_2Se_4 \cdot H_2O$ and red platelets. The SEM/EDS analysis of the red platelets gave an average composition of $PCu_{2.0}Sb_{3.3}Se_{3.2}$, which suggests that they contains Ph_4P^+ ions.

Received: July 24, 1997 [Z10727IE]
German version: *Angew. Chem.* **1998**, *110*, 354–356

Keywords: antimony · chalcogens · ion exchange · selenium · semiconductors

[1] C. L. Bowes, G. A. Ozin, *Adv. Mater.* **1996**, *8*, 13–28.
[2] R. L. Bedard, S. T. Wilson, L. D. Vail, J. M. Bennett, E. M. Flanigen in *Zeolites: Facts, Figures, Future. Proceedings of the 8th International Zeolite Conference* (Eds.: P. A. Jacobs, R. A. van Santen), Elsevier, Amsterdam, **1989**, pp. 375–387.
[3] K. Tan, A. Darovsky, J. B. Parise, *J. Am. Chem. Soc.* **1995**, *117*, 7039–7040.
[4] O. M. Yaghi, Z. Sun, D. A. Richardson, T. L. Groy, *J. Am. Chem. Soc.* **1994**, *116*, 807–808.

 © WILEY-VCH Verlag GmbH, D-69451 Weinheim, 1998 1433-7851/98/3703-0343 $ 17.50+.50/0

[5] O. M. Yaghi, D. A. Richardson, G. Li, C. E. Davis, T. L. Groy, *Materials Research Society Symposium Proceedings,* **1994**, *371*, 15 – 19.
[6] C. L. Bowes, A. J. Lough, A. Malek, G. A. Ozin, S. Petrov, D. Young, *Chem. Ber.* **1996**, *129*, 283 – 287.
[7] K. Tan, Y. Ko, J. B. Parise, A. Darovsky, *Chem. Mater.* **1996**, *8*, 448 – 453.
[8] T. J. McCarthy, T. A. Tanzer, M. G. Kanatzidis, *J. Am. Chem. Soc.* **1995**, *117*, 1294 – 1301.
[9] S. P. Dhingra, M. G. Kanatzidis, *Science*, **1992**, *258*, 1769 – 1772.
[10] J.-H. Chou, M. G. Kanatzidis, *Chem. Mater.* **1995**, *7*, 5 – 8.
[11] J.-H. Chou, M. G. Kanatzidis, *Inorg. Chem.* **1994**, *33*, 1001 – 1002.
[12] H.-O. Stephan, M. G. Kanatzidis, *J. Am. Chem. Soc.* **1996**, *118*, 12226 – 12227.
[13] D. M. Nellis, Y. Ko, S. Koch, J. B. Parise, *J. Chem. Soc. Chem. Commun.* **1995**, 541 – 542.
[14] Y. Ko, K. Tan, D. M. Nellis, S. Koch, J. B. Parise, *J. Solid State Chem.* **1995**, *114*, 506 – 511.
[15] J. B. Parise, Y. Ko, K. Tan, D. M. Nellis, S. Koch, *J. Solid State Chem.* **1995**, *117*, 219 – 228.
[16] Y. Ko, C. L. Cahill, J. B. Parise, *J. Chem. Soc. Chem. Commun.* **1994**, 69 – 70.
[17] T. Jiang, G. A. Ozin, R. L. Bedard, *Adv. Mater.* **1994**, *6*, 860 – 865.
[18] H. Ahari, G. A. Ozin, R. L. Bedard, S. Petrov, D Young, *Adv. Mater.* **1995**, *7*, 370 – 374.
[19] H. Ahari, C. L. Bowes, T. Jiang, A. Lough, G. A. Ozin, R. L. Bedard, S. Petrov, D. Young, *Adv. Mater.* **1995**, *7*, 375 – 378.
[20] J. B. Parise, Y. Ko, *Chem. Mater.* **1994**, *6*, 718 – 720.
[21] T. Jiang, A. J. Lough, G. A. Ozin, D. Young, *Chem. Mater.* **1995**, *7*, 245 – 248.
[22] G. A. Marking, M. G. Kanatzidis, *J. Alloys Compd.*, **1997**, *259*, 122 – 128.
[23] J. B. Parise, *Science* **1991**, *251*, 293 – 294.
[24] X. Wang, F. Liebau, *J. Solid State Chem.* **1994**, *111*, 385 – 389.
[25] H. Sommer, R. Hoppe, *Z. Anorg. Allg. Chem.* **1977**, *430*, 199 – 210.
[26] a) Crystal structure analysis of **1**: $T = -148\,^{\circ}C$, orthorhombic, space group *Pnma* (no. 62), $a = 11.0765(1)$, $b = 4.0369(2)$, $c = 21.4629(8)$ Å, $V = 956.73(5)$ Å^3, $Z = 4$, $\rho_{calcd} = 5.027\ g\,cm^{-3}$, crystal dimensions $0.24 \times 0.01 \times 0.01$ mm, $\mu(Mo_{K\alpha}) = 27.92\ cm^{-1}$, $Mo_{K\alpha}$ radiation ($\lambda = 0.71073$ Å), Siemens SMART Platform CCD diffractometer, data collection at 10 s per frame; Lorentzian, polarization, and empirical absorption corrections[26b] were applied (min./max. transmission = 0.719); index ranges $-12 \le h \le 13$, $-22 \le l \le 26$, $-3 \le k \le 5$, $2\theta_{max} = 55.1^{\circ}$; of 5058 measured reflections, 1150 were independent ($R_{int} = 0.179$). The structure was solved by direct methods and refined with the SHELXTL-5[26c] package of programs, refinement on F^2, 59 variables, $R = 0.0767$, $wR2 = 0.1518$, GOF = 1.150, min./max. reidual electron density $+4.443/-2.691$ e Å^{-3} for data with $F_o^2 > 2\sigma(F_o^2)$. Further details of the crystal structure investigation may be obtained from the Fachinformationszentrum Karlsruhe, D-76344 Eggenstein-Leopoldshafen, Germany (fax: int. code + (49)7247-808-666 (Frau S. Höhler-Schlimm); E-mail: crysdata@fiz-karlsruhe.de), on quoting the depository number CSD-407337; b) H. R. Blessing, *Acta. Crystallogr. Sect. A* **1995**, *51*, 175 – 189. c) G. M. Sheldrick, SHELXTL: Version 5, Siemens Analytical X-ray Instruments Inc., Madison, WI 53719, **1994**.
[27] T. W. Tideswell, F. H. Kruse, J. D. McCullough, *Acta. Crystallogr. Sect. A* **1957**, *10*, 99 – 102.
[28] a) K. Chondroudis, M. G. Kanatzidis, *J. Am. Chem. Soc.*, **1997**, *119*, 2574 – 2575; b) K. Chondroudis, M. G. Kanatzidis, unpublished results.

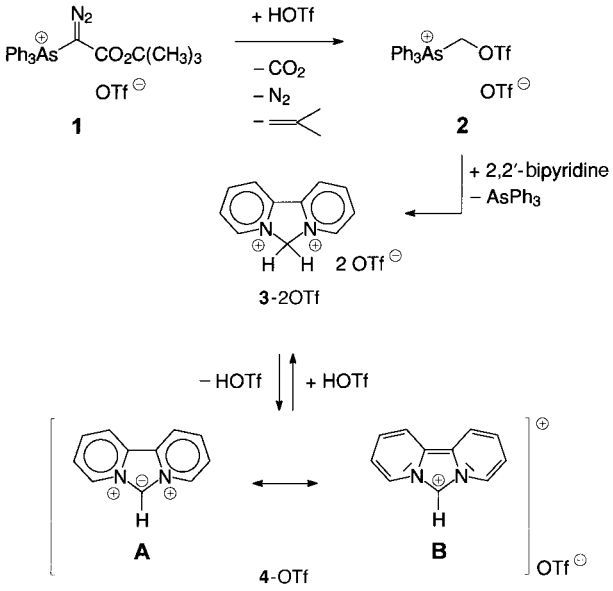
Generation and Trapping Reactions of a Formal 1:1 Complex between Singlet Carbon and 2,2′-Bipyridine**

Robert Weiss,* Silvia Reichel, Matthias Handke, and Frank Hampel

Dedicated to Professor George A. Olah on the occasion of his 70th birthday

2,2′-Bipyridine is a classical chelating ligand for metals as well as nonmetals in different oxidation states and bonding types.[1,2] However, to our knowledge analogous complexes are unknown for all oxidation states of carbon. Here we report a first compound of this kind. In 1994 we described the first S_N reactions at the α-carbon atom of aryliodonio diazo compounds.[3] Using $AsPh_3$ as nucleophile, we obtained the diazo compound **1**, which served as starting material for the new class of compounds.

The reaction of **1** with trifluoromethanesulfonic acid (HOTf, Scheme 1) afforded the arsonium salt **2** in high yield



Scheme 1. Synthesis of **3**-2 OTf and its deprotonation to **4**-OTf.

as the result of an acid-induced fragmentation of the *tert*-butyl ester functionality, followed by a proto-dediazonation.[4] Compound **2** is a potent 1,1-bis(electrophile) which reacted with a host of neutral nucleophiles to form symmetrical and unsymmetrical geminal bis(onio)-substituted salts.[5] Accordingly, the reaction of **2** with 2,2′-bipyridine provided the cyclic bis(onio)-substituted salt **3**-2 OTf, a bis(azonia) analogue of fluorene. Under the reaction conditions, this C–H-acidic

[*] Prof. Dr. R. Weiss, Dipl.-Chem. S. Reichel, Dipl.-Chem. M. Handke, Dr. F. Hampel
Institut für Organische Chemie der Universität Erlangen-Nürnberg
Henkestrasse 42, D-91054 Erlangen (Germany)
Fax: Int. code + (49) 9131-859132
E-mail: rweiss@organik.uni-erlangen.de

[**] This work was supported by the Deutsche Forschungsgemeinschaft and the Fonds der Chemischen Industrie.

 © WILEY-VCH Verlag GmbH, D-69451 Weinheim, 1998 1433-7851/98/3703-0344 $ 17.50+.50/0

compound was converted into **4**-OTf with excess 2,2′-bipyridine (Scheme 1) and isolated as **4**-Br after anion exchange (yield: 75% relative to **2**); this salt crystallizes more readily.[6] Figure 1 shows the result of the X-ray structure analysis of **4**-Br · H_2O.[7]

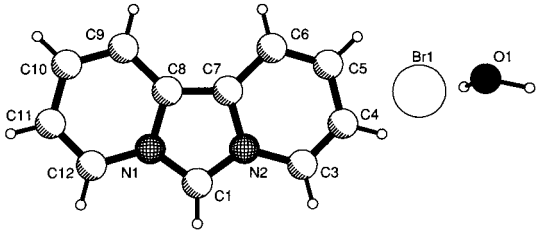
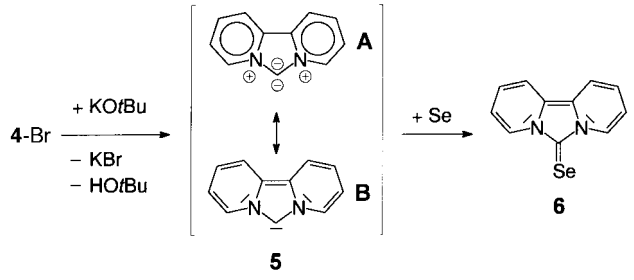


Figure 1. Structure of **4**-Br · H_2O in the crystal. Important bond lengths [Å] and angle [°]: C1–N1 1.338, N1–C8 1.394, C7–C8 1.387, C8–C9 1,41, C9–C10 1.34, C10–C11 1.41, C11–C12 1.33, C12–N1 1.39; N1-C1-N2 107.6.

A noticeable feature in the ^1H NMR spectra of **4**-Br and **4**-OTf is the large $^1H-^{13}C$ coupling constant (232.59 Hz) for the C–H bond in the five-membered ring. This coupling constant almost corresponds to sp hybridization of the C atom in this bond (the exact value is $sp^{1.15}$).[8] A PM3 calculation, combined with an NBO analysis,[9] provided a hybridization of $sp^{1.23}$. This unprecedented result can also be reached qualitatively by applying Bent's rules:[10] The carbon atom bridging the six-membered rings in **4** ("bridging C atom") has two strongly electronegative substituents (the N centers), which should induce a higher p character in the C hybrid orbitals associated with them. This automatically leads to a higher s proportion in the remaining σ orbital of the bridging C atom with a trigonal-planar environment.

With an excess of HOTf in THF, **4**-Br was quantitatively converted into the dicationic salt **3**-2 OTf, the first σ complex of an S_E reaction at an imidazolium system to be isolated. The $^1H-^{13}C$ coupling constant of 170.65 Hz for the geminal C–H bonds corresponds to $sp^{1.93}$ hybridization in these bonds, which is highly unusual for a saturated C atom.[8]

Salt **4**-Br was deprotonated to the neutral species **5** in a fast and quantitative reaction with KO*t*Bu in THF at $-30\,^\circ C$ (Scheme 2). Under these reaction conditions, **5** was stable for several hours. The ^{13}C NMR spectrum of the reaction mixture shows five signals in the range of $\delta = 114-129$ and a sixth signal at $\delta = 196.41$ for the bridging C atom. This value is shifted upfield only slightly with respect to the corresponding signals for Arduengo carbenes[11] and, according to research by Chen et al. on dimerized Arduengo carbenes,[12] cannot be ascribed to a dimer of **5**. Compound **5** can be trapped in high yields by a number of electrophiles.[13] For example, the reaction with selenium led to the chalcogenone **6**, which was characterized by X-ray structure analysis (Figure 2).[14]



Scheme 2. Subsequent reactions of **4**-Br.

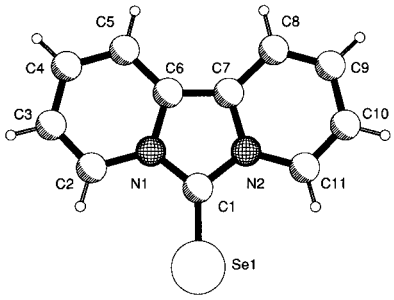
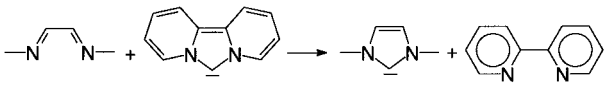


Figure 2. Structure of **6** in the crystal. Important bond lengths [Å] and angle [°]: Se1–C1 1.826, C1–N1 1.364, C1–N2 1.378, N1–C6 1.39, C6–C7 1.377, N1–C2 1.39, C2–C3 1.34, C3–C4 1.41, C4–C5 1.34, C5–C6 1.41; N1-C1-N2 103.8.

Compound **6** is characterized by a large degree of localization of the double bonds of the hydrocarbon moiety and partial delocalization in the selenourea structural element. The C(Se)–N bonds are longer and the C–Se bond is shorter in **6** than in an open-chain selenourea (each by about 0.04 Å).[16] This indicates that the hybridization of the bridging C atom corresponds to that in **4**-Br.

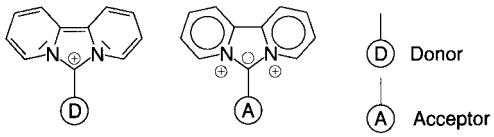
The two-step deprotonation of dication **3** leads to a far-reaching electronic reorganization. Whereas **3** contains two aromatic rings, **4** (in **4**-Br · H_2O, see Figure 1) is characterized by resonance structure **4B** (see Scheme 1) with a reduced bipyridine subsystem. Further deprotonation of **4** should then lead to an even more strongly localized π system, which according to ab initio calculations (3-21G*)[17] is better represented by the resonance structure **5B** (typical of arduengo carbenes) than by the bis(ylide) form **5A** (see Scheme 2). The latter is probably relevant for the description of excited states and gives an indication of the structural relationship of this class of compounds with "true" bis(ylides) such as carbodiphosphoranes. These were recognized early on as formal complexes of an excited singlet C atom with two molecules of triorganophosphane as stabilizing donor ligands.[18] By analogy, **5** can be seen as a chelate complex of such a C atom and 2,2′-bipyridine. Model calculations (3-21G*) for C1-transfer reactions with suitable reaction partners show that this view, beyond formal considerations, is supported by thermodynamics. Therefore, **5** should react according to the isodesmic Equation (1) with *N,N*′-dimethyl-



1,4-diazabutadienein a highly exothermic reaction ($\Delta H_f = -51.06$ kcal mol^{-1}) to the corresponding stable imidazol-2-ylidene and 2,2′-bipyridine. This should render **5** much more suitable for C1 transfer than Arduengo carbenes. Kinetic factors should be decisive for the experimental realization.

 © WILEY-VCH Verlag GmbH, D-69451 Weinheim, 1998 1433-7851/98/3703-0345 $ 17.50+.50/0

When an electrophile is coordinated to the nucleophile **5**, two electronic limiting cases can be distinguished for the resulting adducts: If the substituent at the bridging C atom shows donor character, resonance structure **7** dominates (e.g. selone **6**). If, on the other hand, the substituent is an acceptor, the adduct is characterized by resonance structure **8** with complementary polarization. We have already experimentally verified this structural classification.[19] Introducing carbene **5** into organic and inorganic substrates thus creates a type of



7 **8**

ligand which optimally adapts to the electronic needs of the substrate. The two-step bipyridinium redox system of **5**, which is immanent in the system, can flexibly fulfill the electronic demands on the bridging C atom with its reduced (situation in **7**) and oxidized forms (situation in **8**) as a built-in umpolung reagent. Corresponding adducts of Arduengo carbenes do not show a comparable electronic flexibility.

Experimental Section

All reactions were carried out under a nitrogen atmosphere with anhydrous, N_2-saturated solvents in Schlenk vessels. Correct elemental analyses (C,H,N) are available.

2: Diazo compound **1** (4.560 g, 7.65 mmol) was dissolved in CH_2Cl_2 (20 mL), and HOTf (0.71 mL, 8.0 mmol) added. After gas formation had ceased the mixture was stirred for 36 h at room temperature; the color became brown-red in the process. The solution was then concentrated under vacuum to about 5 mL. The white product was precipitated with Et_2O (150 mL), isolated by filtration, washed with Et_2O (25 mL), and dried under vacuum for 2 h; yield: 4.303 g (91 %). ^{1}H NMR (400 MHz, $CDCl_3$): $\delta = 6.52$ (s, 2H; CH_2), 7.73 (m, 12H; C_6H_5), 7.82 (m, 3H; C_6H_5); ^{13}C NMR (100 MHz, $CDCl_3$): $\delta = 68.51$ (CH_2), 118.13 (C1), 118.16 (q, ^1J(C,F) = 320 Hz; $F_3CSO_3CH_2$), 120.47 (q, ^1J(C,F) = 320 Hz; $F_3CSO_3^-$), 131.24 (C3/C5), 133.05 (C2/C6), 135.10 (C4); ^{19}F NMR (470 MHz, $CDCl_3$, C_6F_6): $\delta = -73.07$ ($F_3CSO_3CH_2$), -78.62 ($F_3CSO_3^-$).

4-Br: A solution of **2** (1.208 g, 1.95 mmol) in CH_3CN (60 mL) was treated with 2,2′-bipyridine (0.671 g, 4.30 mmol) and heated at reflux for 5 d. After removal of the solvent under vacuum the residue was stirred for 2 h in Et_2O (50 mL), filtered, washed with Et_2O (15 mL), and dried for 2 h under vacuum. The solid was dissolved in CH_2Cl_2 (50 mL), and a solution of Bu_4NBr (1.290 g, 4.00 mmol) in CH_2Cl_2 (10 mL) added. After 2 h the mixture was filtered to remove insoluble components. A yellow-brown solid was then precipitated with Et_2O (100 mL), isolated by filteration, washed with Et_2O (20 mL), and dried under vacuum for 2 h. Crystallization from EtOH afforded dark yellow **4**-Br; yield: 0.365 g (75 %). Crystals suitable for X-ray structure analysis formed in a supersaturated solution in EtOH at ambient temperature. ^{1}H NMR (400 MHz, [D$_6$]DMSO): $\delta = 7.56$ (m, 4H), 8.69 (m, 2H), 9.07 (m, 2H), 10.40 (s, 1H); ^{13}C NMR (100 MHz, [D$_6$]DMSO): $\delta = 116.01$ (bridging C atom), 118.76, 120.38, 121.71, 122.65, 123.34.

3-2 OTf: Salt **4**-Br (0.295 g, 1.18 mmol) was suspended in (THF) 20 mL, and HOTf (0.23 mL, 2.61 mmol) added at $-20\,^\circ$C. After 18 h the mixture was filtered. The white solid isolated was washed with THF (10 mL) and Et_2O (10 mL), and was dried under vacuum for 2 h; yield: 0.497 g (90 %). ^{1}H NMR (400 MHz, CD_3CN): $\delta = 7.41$ (s, 2H; CH_2), 8.41 (m, 2H), 8.97 (m, 4H), 9.35 (m, 2H); ^{13}C NMR (100 MHz, CD_3CN): $\delta = 77.65$ (CH_2), 120.72 (q, ^1J(C,F) = 320 Hz; CF_3), 125.28, 131.35, 142.95, 144.21, 150.34.

5: KO*t*Bu (0.065 g, 0.58 mmol) was added to a suspension of **4**-Br (0.097 g, 0.39 mmol) in THF (3 mL) at $-30\,^\circ$C. After 30 min the inorganic components (KBr, excess KO*t*Bu) were removed by filteration over Celite at $-60\,^\circ$C. The orange filtrate was examined with NMR spectroscopy. ^{13}C NMR (100 MHz, THF, $-30\,^\circ$C, [D$_6$]acetone): $\delta = 114.12$, 117.44, 117.64, 121.83, 128.72, 196.41.

Received: August 4,1997 [Z10771IE]
German version: *Angew. Chem.* **1998**, *110*, 352 – 354

Keywords: carbenes · diazo compounds · hybridization · imidazolylidenes

[1] a) W. A. E. McBryde, *A Critical Review of Equilibrium Data for Proton and Metal Complexes of 1,10-Phenanthroline, 2,2′-Bipyridin and Related Compounds*, IUPAC Chem. Data Ser., no. 17, Pergamon, Oxford, **1978;** b) E. D. McKenzie, *Coord. Chem. Rev.* **1971**, *6*, 187.
[2] D. Kummer, K.-E. Gaißer, T. Seshadri, *Chem. Ber.* **1977**, *110*, 1950.
[3] R. Weiss, J. Seubert, F. Hampel, *Angew. Chem.* **1994**, *106*, 2038; *Angew. Chem. Int. Ed. Engl.* **1994**, *33*, 1952.
[4] An analogous fragmentation of a triphenylphosphonio-substituted diazoacetic ester was already reported: M. Regitz, A. E. M. Tawfik, H. Heydt, *Liebigs Ann. Chem.* **1981**, 1865.
[5] a) R. Weiss, M. Handke, S. Reichel, F. Hampel, unpublished results; b) see also R. Weiss, R. Roth, *Synthesis* **1987**, 870.
[6] This salt had already been synthesized in low yield (25 %) by an alternative method: I. C. Calder, W. H. F. Sasse, *Aust. J. Chem.* **1965**, *18*, 1819.
[7] Crystal structure data for **4**-Br · H_2O: $C_{11}H_{11}BrN_2O$, $M_r = 267.13$, triclinic, space group $P1$, $a = 7.288(2)$, $b = 9.721(2)$, $c = 9.758(2)$ Å, $\alpha = 119.80(3)$, $\beta = 90.97(3)$, $\gamma = 110.52(3)^\circ$, $Z = 2$, $V = 546.1$ Å^3, $\rho_{calcd} = 1.625$ g cm^{-3}; red needles, crystal dimensions: $0.30 \times 0.30 \times 0.20$ mm^3. The data were collected on a Nonius Mach3 single-crystal diffractometer with monochromated (graphite) $Mo_{K\alpha}$ radiation ($\lambda = 0.71073$ Å) at T = 293(2) K and a scan range of $2.47^\circ < \theta < 26.28^\circ$. The absorption correction was carried out with ψ scans. Of 2390 reflections measured, 2205 were independent and 1605 with $I > 2\sigma(I)$. The structure was solved with direct methods (SHELXS 86). The 136 parameters were refined on F^2 with all data according to the least-squares method using SHELXL 93 (G. M. Sheldrick, Göttingen, **1993**). The hydrogen atoms were fixed in idealized positions with a riding model; R values of refinement: $R1 = 0.0363$ for $I > 2\sigma(I)$ and $wR2 = 0.1026$ for all data; min./max. residual electron density 0.377/ -0.536 e Å^{-3}.[15]
[8] N. Muller, D. E. Pritchard, *J. Chem. Phys.* **1959**, *31*, 768.
[9] J. P. Forster, F. Weinhold, *J. Am. Chem. Soc.* **1980**, *102*, 7211.
[10] H. A. Bent, *Chem. Rev.* **1961**, *61*, 275.
[11] A. J. Arduengo III, H. V. Rasika Dias, R. L. Harlow, M. Kline, *J. Am. Chem. Soc.* **1992**, *114*, 5530.
[12] Arduengo carbenes: $\delta(^{13}C) = 210 - 220$, corresponding dimers (tetraazafulvalenes): $\delta(^{13}C) = 127$: T. A. Taton, P. Chen; *Angew. Chem.* **1996**, *108*, 1098; *Angew. Chem. Int. Ed. Engl.* **1996**, *35*, 1011.
[13] S. Reichel, Dissertation, Universität Erlangen-Nürnberg, planned in **1998**.
[14] Crystal structure data for **6**: $C_{11}H_8N_2Se$, $M_r = 247.15$, triclinic, space group $P1$, a = 7.163(2), b = 9.054(2), c = 9.070(2) Å, $\alpha = 93.46(3)$, $\beta = 112.74(3)$, $\gamma = 112.69(3)^\circ$, $Z = 2$, $V = 485.1$ Å^3, $\rho_{calcd} = 1.692$ g cm^{-3}; yellow plates, crystal dimensions: $0.25 \times 0.10 \times 0.10$ mm^3. The data were collected on a Nonius Mach3 single-crystal diffractometer with monochromated (graphite) $Mo_{K\alpha}$ radiation ($\lambda = 0.71073$) at T = 293(2) K and a scan range of $3.09^\circ < \theta < 26.29^\circ$. The absorption correction was carried out with ψ scans. Of 2105 reflections measured, 1975 were independent and 1198 with $I > 2\sigma(I)$. The structure was solved with direct methods (SHELXS 86). The 127 parameters were refined on F^2 with all data according to the least-squares method using SHELXL 93 (G. M. Sheldrick, Göttingen, **1993**). The hydrogen atoms were fixed in idealized positions with a riding model; R values of refinement: $R1 = 0.0376$ for $I > 2\sigma(I)$ and $wR2 = 0.1110$ for all data; max./min. residual electron density: 0.318/ -0.392 e Å^{-3}.[15]
[15] Crystallographic data (excluding structure factors) for the structures reported in this paper have been deposited with the Cambridge Crystallographic Data Centre as supplementary publication no. CCDC-100542. Copies of the data can be obtained free of charge on application to CCDC, 12 Union Road, Cambridge CB2 1EZ, UK (fax: int. code + (44) 1223-336033; e-mail: deposit@ccdc.cam.ac.uk).

 © WILEY-VCH Verlag GmbH, D-69451 Weinheim, 1998 1433-7851/98/3703-0346 $ 17.50+.50/0

[16] *N,N′*-Dimethylselenourea: C–Se 1.866, C(Se)–N 1.32 Å: H. M. K. K. Pathirana, T. J. Weiss, J. H. Reibeneis, R. A. Zingaro, E. A. Meyers, *Z. Kristallogr.* **1994**, *209*, 697.
[17] With the length of the [0] bridge between the six-membered rings, calculated with ab initio methods, as an indicator: **3**: 1.461, **4**: 1.379, **5**: 1.353 Å.
[18] H. Schmidbaur, *Angew. Chem.* **1983**, *95*, 980; *Angew. Chem. Int. Ed. Engl.* **1983**, *22*, 907.
[19] We will report on compounds of this type separately.

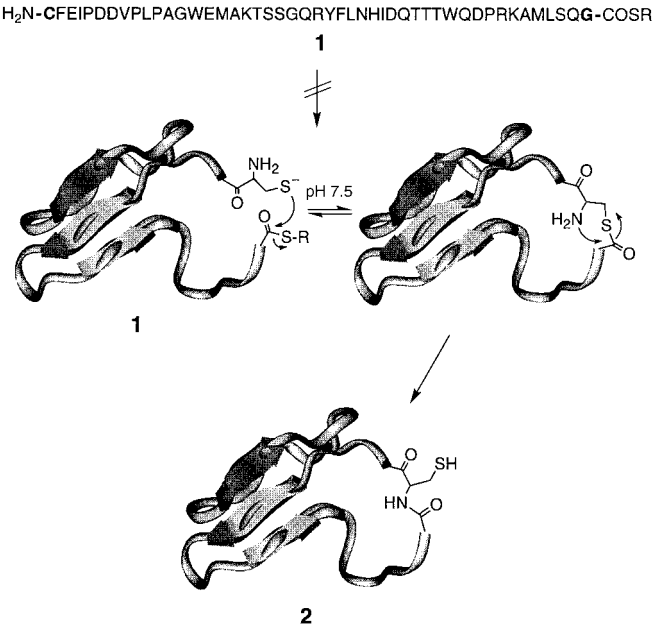
Chemical Synthesis of a Circular Protein Domain: Evidence for Folding-Assisted Cyclization**

Julio A. Camarero, Joanna Pavel, and Tom W. Muir*

The chemical-ligation approach to the condensation of peptide fragments offers a unique route for generating proteins possessing both natural[1] and unnatural topology.[2] Of the various architectures possible, one of the most fascinating from the perspective of both protein engineering and protein folding is the circular topology.[3] Although head-to-tail cyclization is commonly used to constrain the structure of small peptides,[4] relatively little is known about the affect of this modification on the structure and function of a protein. Indeed, the bulk of our current knowledge is based on the pioneering work of Creighton and co-workers on a cyclized version of bovine pancreatic trypsin inhibitor (BPTI) prepared by random chemical cross-linking.[3] Here we demonstrate that a backbone-cyclized protein domain, prepared by an intramolecular version[5] of Kent's native chemical ligation,[6] is able to spontaneously fold into a functional, native-like conformation. In addition, we provide evidence that the rate of cyclization is related to the folded state of the protein.

Our initial studies on protein cyclization focussed on the WW domain from the human Yes kinase-associated protein (YAP).[7] This protein domain possesses a globular structure composed of a three-stranded antiparallel β sheet which positions the flexible N and C termini in close proximity.[8] Given that native chemical ligation is tolerant to the presence of chemical denaturants,[6] it was anticipated that insights into the effect of this juxtaposition on the chemical reaction rate would be forthcoming.

The strategy used to synthesize the circular WW domain is shown in Scheme 1. Key to our approach was the generation



Scheme 1. Synthesis of the circular WW protein domain **2**.

of the linear polypeptide precursor **1**, which contains both groups necessary for native chemical ligation: an N-terminal cysteine residue and a C-terminal thioester group.[9] Cyclization of fully unprotected **1** to give the circular WW domain **2** was remarkably clean and extremely rapid (Figure 1). The ligation product was characterized as **2** by a combination of

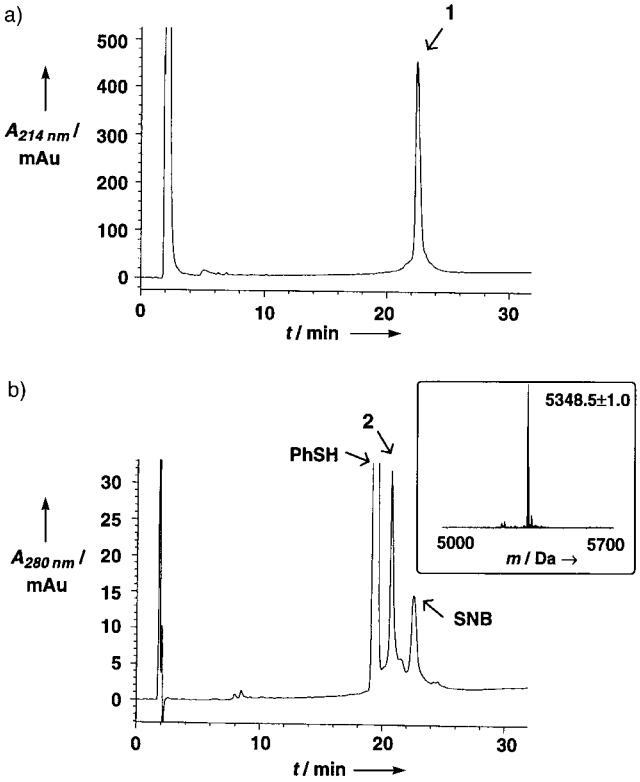


Figure 1. a) Analytical HPLC chromatogram of the purified linear precursor **1**. b) The crude ligation mixture after 2 min of reaction on the same scale as in a). mAu = 10^{-3} of full scale absorbance units. SNB = *S*-(5-sulfenyl-2-nitrobenzoic acid), the by-product. Inset: ES-MS of purified **2**.

[*] Dr. T. W. Muir, Dr. J. A. Camarero, J. Pavel
The Laboratory of Synthetic Protein Chemistry
The Rockefeller University
Box 223, 1230 York Avenue, New York, NY 10021 (USA)
Fax: Int. code + (1) 212 327-7358
E-mail: muirt@rockvax.rockefeller.edu

[**] This work was performed under the auspices of the Rockefeller University. J.A.C. was supported by a postdoctoral fellowship from the Ministerio de Educacion y Ciencia of Spain. T.W.M. gratefully acknowledges the support of the US National Institutes of Health (GM55843-01). We are grateful to Dr. Sean Cahill for help with NMR experiments, and Dr. Harmut Oschkinat for useful discussions and for providing NMR assignments of the recombinant YAP WW domain–ligand complex.

 © WILEY-VCH Verlag GmbH, D-69451 Weinheim, 1998 1433-7851/98/3703-0347 $ 17.50+.50/0

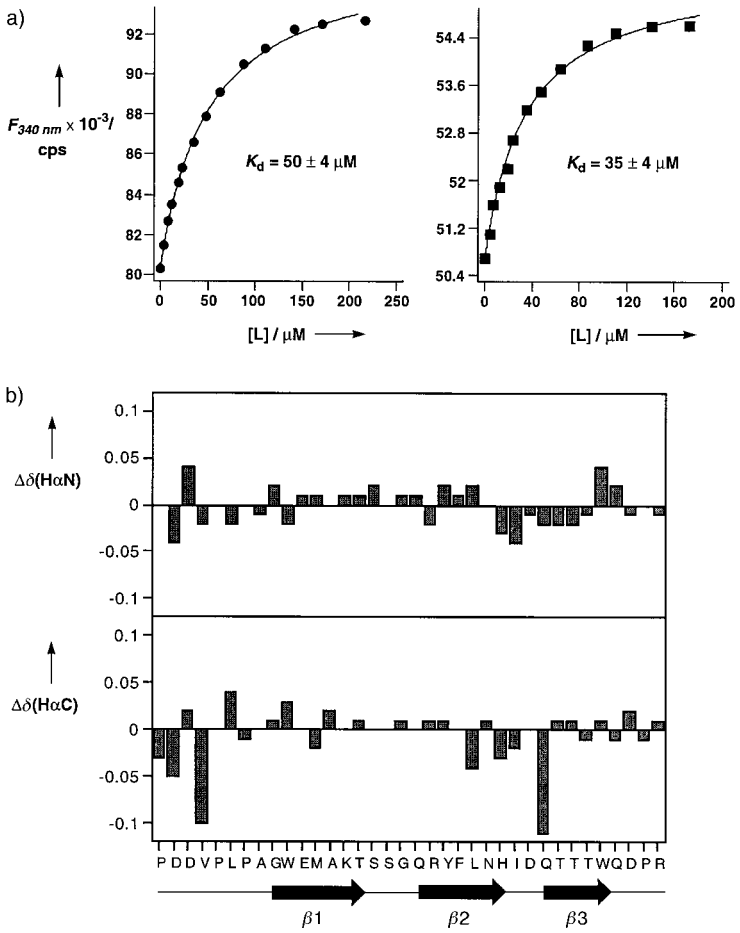


Figure 2. a) Binding of the linear (●) and circular (■) forms of the WW domain to the proline-rich ligand Ac–GTPPPPYTVG–NH_2 (L); cps = counts per scan. b) Summary of the ^{1}H NMR assignments for the main-chain protons: $\Delta\delta$(HαN) and $\Delta\delta$(HαC) are the deviations in the chemical shifts of the backbone protons in the circular WW domain from those in the the linear WW domain. The location of the secondary structure elements are shown at the bottom.[8]

electrospray mass spectrometry (ES-MS), tryptic digestion, and Edman sequencing.[10]

The YAP WW domain binds to proline-rich peptides containing the consensus sequence PPxY.[11] A fluoresence-based ligand-binding assay was used to study the functional consequences of backbone cyclization of the YAP WW domain (Figure 2a). As predicted based on the native structure of the protein, cyclization of the WW domain has no deleterious effect on ligand-binding activity. Indeed, the circular protein has a slightly higher affinity for ligands than its linear counterpart (dissociation constants $K_{d(cyclic)} = 35$ and $K_{d(linear)} = 50\,\mu$M).[12] Interestingly, the ligand affinity was the same regardless of whether the cyclic protein had been prepared in the presence or absence of 6 M guanidinium chloride (GdmCl), suggesting that the folding process is not inhibited by the cyclic topology.

The solution structures of the circular and linear YAP WW domains complexed to ligands were studied by two-dimensional homonuclear NMR spectroscopy. Deviations in the chemical shifts for the main-chain protons in the core β-sheet structure of the linear[13] and circular domains were uniformly less than 0.05 ppm, indicating that the same global fold is common to both versions of the molecule (Figure 2b). The NMR samples were prepared by simply dissolving the proteins, which had been purified by HPLC, in phosphate buffer containing the ligand. Given that HPLC purification is denaturing, this again indicates that the circular protein, like its linear counterpart, can spontaneously fold in the presence of the ligand.

The influence of the fold in the WW domain on the cyclization rate was investigated by performing the reaction in the presence and absence of chemical denaturant. Addition of 6 M GdmCl to the ligation buffer had a marked effect on the rate of cyclization: The reaction was approximately one order of magnitude faster under folding conditions than under unfolding conditions (Figure 3). Interestingly, linear polypeptide **1** was cleanly converted into cyclic **2**, regardless of whether 6 M GdmCl was present or absent in the ligation buffer. This rate enhancement on going from unfolding to folding conditions is significant and can be understood in terms of the proximity of the N and C termini within the native conformation of the protein. Under folding conditions the local concentration of the cysteinyl and thioester reactive functionalities would be expected to be higher than under unfolding conditions; this leads to a more rapid reaction for the former.[14] Therefore, the cyclization reaction is assisted by the native conformation of the protein.

We have generated a functional circular version of a WW protein domain by intramolecular chemical ligation. It is expected that several emerging areas in protein engineering will benefit from the ability to efficiently prepare backbone-cyclized polypeptides from unprotected linear precursors. For example, backbone cyclization provides a general way of constraining minimized protein sequences and complements the use of disulfide bonds.[15] Equally, new opportunities are created in sequence permutation by combining chemoselective cyclization with subsequent main-chain cleavages. Finally, our observation that the kinetics of protein cyclization are sensitive to changes in protein structure

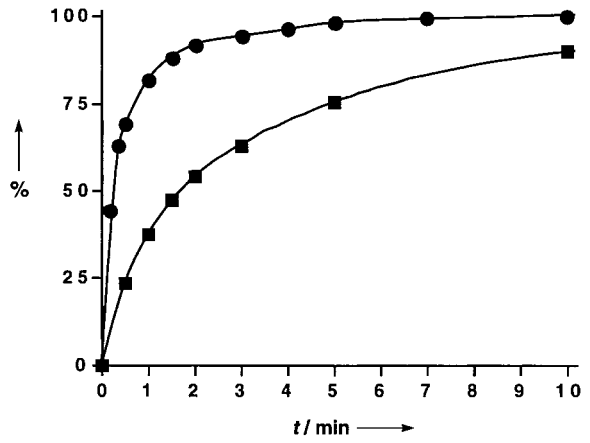


Figure 3. Progress of the cyclization under folding (0 M GdmCl, ●) and unfolding conditions (6 M GdmCl, ■).

 © WILEY-VCH Verlag GmbH, D-69451 Weinheim, 1998 1433-7851/98/3703-0348 $ 17.50+.50/0

suggests a potential application of this approach in the study of protein-structure dynamics.

Experimental Section

All peptide synthesis were carried out according to the in situ neutralization/HBTU activation protocol for Boc solid-phase peptide synthesis (HBTU = benzotriazol-1-yl-*N*-tetramethyluronium hexafluorophosphate).[16] Peptide thioester **1** was prepared by selective thioesterification of the corresponding peptide thioacid (prepared on a glycine–thioester support)[17] with 5,5′-dithiobis(2-nitrobenzoic acid) (DTNB, Ellman's reagent) as previously described[5a] and purified by preparative HPLC. ES-MS: observed mass: 5546.3(1.4) Da; calcd for $C_{244}H_{361}N_{65}O_{76}S_4$: 5545.5 (monoisotopic), 5549.0 (average isotope composition).

Cyclization: Purified **1** (0.4 μmol, 2.2 mg) was dissolved to a final concentration of about 50 μM in a freshly degassed buffer containing 0.1 M sodium phosphate and 1 mM ethylenediamine tetraacetate (EDTA) at pH 7.5 and 0.05 volume % each of PhSH and BnSH. In cyclization reactions carried out under unfolding conditions, 6 M GdmCl was included in the above buffer. To monitor the course of the reaction, small aliquots (50 μL) of the reaction mixture were periodically removed, quickly quenched by addition of 5% trifluoroacetic acid in water (20 μL), and investigated by analytical HPLC. The degree of conversion of **1** into **2** was calculated based on the absorption at 280 nm. The overall yield for the cyclization reaction following HPLC purification was 1.8 mg (0.32 μmol, 81%). Circular protein **2** was characterized by ES-MS and tryptic digestion. ES-MS: observed mass: 5348.5(1.0) Da; calcd for $C_{237}H_{356}N_{64}O_{72}S_3$: 5346.5 (monoisotopic), 5350.0 (average isotope composition).

Tryptic digestion of **2**: Cyclic **2** (100 μg) was dissolved in 0.1 M tris(hydroxymethyl)aminomethane (Tris)/HCl buffer (pH 8.4, 200 μL). Lyophilized trypsin (10 μg, sequencing grade, Sigma) was then added, and the reaction maintained at 37 °C for 3 h; a solution of 1,4-dithiothreitol (DTT, 50 mM, 20 μL) was subsequently added. The three expected fragments T1 (H–AMLSQGCFEIPDDVPLPAGWEMAK–OH), T2 (H–TSSGQR–OH), and T3 (H–YFLNHIDQTTTWQDPR–OH) were isolated by HPLC and characterized by ES-MS and Edman sequencing.

The isotherms for ligand binding were obtained by monitoring the intrinsic Trp fluoresence at 340 nm as a function of the concentration of the ligand at 22 °C. In all cases, the protein concentration was kept at 2 μM in a buffer containing 40 mM sodium phosphate, 50 mM NaCl, and 1 mM DTT at pH 7.2. Equilibrium dissociation constants were extracted from the curves by assuming a 1:1 receptor–ligand complex.[18]

Two-dimensional ^{1}H NMR spectra were measured on a Bruker DPX-400 spectrometer (400.132 MHz). The NMR samples were dissolved in a buffer containing 10 mM sodium phosphate, 100 mM NaCl, 1 mM [D_{10}]DTT, 0.02% NaN_3, and 10% D_2O at pH 6.2. A series of TOCSY and NOESY experiments[19] were recorded at 278 K on samples containing both linear and circular WW domains with WW ligand (protein concentrations 0.6–1.2 mM; ratio of peptide to protein 3:1). Typical mixing times were 30 ms for TOCSY experiments and 50–250 ms for NOESY experiments.

Received: June 30, 1997 [Z 10614 IE]
German version: *Angew. Chem.* **1998**, *110*, 361–364

Keywords: cyclizations · peptides · protein structures · solid-phase synthesis

[1] a) T. W. Muir, *Structure* **1995**, *3*, 649–652; b) C. J. A. Wallace, *Curr. Opin. Biotech.* **1995**, *6*, 403–410.
[2] a) P. E. Dawson, S. B. H. Kent, *J. Am. Chem. Soc.* **1993**, *115*, 7263–7266; b) A. Nefzi, X. Sun, M. Mutter, *Tetrahedron Lett.* **1995**, *36*, 229–230; c) L. E. Canne, A. R. Ferre-D'Amare, S. K. Burley, S. B. H. Kent, *J. Am. Chem. Soc.* **1995**, *117*, 2998–3007; d) J. Shao, J. Tam, *ibid.* **1995**, *117*, 3893–3899; e) K. J. Rose, *ibid.* **1994**, *116*, 30–33 ; f) T. W. Muir, M. J. Williams, M. H. Ginsberg, S. B. H. Kent, *Biochemistry* **1994**, *33*, 7701–7708.
[3] a) D. P. Goldenberg, T. E. Creighton, *J. Mol. Biol.* **1984**, *179*, 527–545; b) D. P. J. Goldenberg, *J. Cell. Biochem.* **1985**, *29*, 321–335; c) D. P. Goldenburg, T. E. Creighton, *J. Mol. Biol.* **1983**, *165*, 407–413.
[4] a) V. J. Hruby, *Life Science* **1982**, *31*, 189–199; b) H. Kessler, *Angew. Chem.* **1982**, *94*, 509–520 ; *Angew. Chem. Int. Ed. Engl.* **1982**, *21*, 512–523; c) J. Rizo, L. M. Gierasch, *Ann. Rev. Biochem.* **1992**, *61*, 387–418.
[5] a) J. A. Camarero, T. W. Muir, *Chem. Commun.*, **1997**, 1369–1370; b) L. Zhang, J. P. Tam, *J. Am. Chem. Soc.* **1997**, *119*, 2363–2370.
[6] P. E. Dawson, T. W. Muir, I. Clark-Lewis, S. B. H. Kent, *Science* **1994**, *266*, 776–779.
[7] WW domains are a novel class of protein modules which are found in a variety of signal-transducing and cytoskeletal proteins. Reviews: a) M. Sudol, *Prog. Biophys. Molec. Biol.* **1996**, *65*, 113–132; b) M. Sudol, H. I. Chen, C. Bougeret, A. Einbond, P. Bork, *FEBS Letters* **1995**, *369*, 67–71.
[8] M. J. Macias, M. Hyvonen, E. Baraldi, J. Schultz, M. Sudol, M. Saraste, H. Oschkinat, *Nature* **1996**, *382*, 646–649.
[9] To facilate native ligation, Cys and Gly were added at the N and C termini, respectively, of the core WW sequence (residues 165–209 of the human YAP protein).
[10] Cyclic protein **2** was digested with trypsin, and the peptide fragment encompassing the ligation site (AMLSQ**GC**FEIPDDVPLPAGWEMAK) characterized by Edman sequencing.
[11] H. I. Chen, M. Sudol, *Proc. Natl. Acad. Sci. USA* 1995, 92, 7819–7823.
[12] The linear WW domain was also chemically synthesized by Boc solid-phase protein synthesis and purified by standard procedures.
[13] Residues located at the immediate N and C termini could not be unambiguously assigned in either the linear or cyclic WW domains.
[14] Large effective molarities were described for many intramolecular organic reactions: F. M. Menger, *Acc. Chem. Res.* **1985**, *18*, 128–134.
[15] B. Li, J. Y. K. Tom, D. Oare, R. Yen, W. J. Fairbrother, J. A. Wells, B. C. Cunningham, *Science* **1995**, *270*, 1657–1660.
[16] M. Schnolzer, P. Alewood, A. Jones, D. Alewood, S. B. H. Kent, *Int. J. Pept. Protein Res.* **1992**, *40*, 180–193.
[17] D. Yamashiro, C. H. Li, *Int. J. Pept. Protein Res.* **1988**, *31*, 322–334.
[18] A. R. Viguera, J. L. Arrondo, A. Musacchio, M. Saraste, L. Serrano, *Biochemistry* **1994**, *33*, 10925–10933.
[19] a) A. Bax, D. G. Davis, *J. Magn. Reson.* **1985**, *65*, 355–360; b) A. Kumar, R. R. Ernst, K. Wuthrich, *Biochem. Biophys. Res. Commun.* **1980**, *95*, 1–6.

A Symmetrically Bridging Triarylsilyl Ligand in a Dinuclear Rhodium Complex: Synthesis and Structure of [LRh(H)(μ-Cl)(μ-SiAr$_2$)(μ-SiAr$_3$)Rh(H)L] (Ar = Ph, *p*-FC$_6$H$_4$; L = P*i*Pr$_3$)**

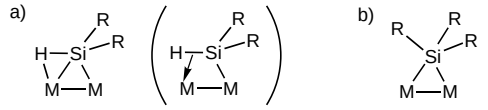
Kohtaro Osakada,* Take-aki Koizumi, and Takakazu Yamamoto*

Bridging coordination of a secondary silyl group ($SiHR_2$) in dinuclear complexes has become common for late transition metals.[1] The complexes reported so far contain both a σ bond between Si and one metal and a three-center, two-electron bond (3c–2e; π bond) between the Si–H group and the second metal center (Scheme 1a).

[*] Prof. Dr. K. Osakada, Prof. Dr. T. Yamamoto, T. Koizumi
Research Laboratory of Resources Utilization
Tokyo Institute of Technology
4259 Nagatsuta, Midori-ku, Yokohama 226 (Japan)
Fax: Int. code + (81) 45 924-5276
E-mail: kosakada@res.titech.ac.jp

[**] This work was supported by the Japanese Ministry of Education, Science, Culture, and Sports for Grants-in-Aid for Scientific Research (nos. 09239212 and 09440229). T.K. is grateful to the Japan Society for Promotion of Science for a Grant-in-Aid as a JSPS fellow.

 © WILEY-VCH Verlag GmbH, D-69451 Weinheim, 1998 1433-7851/98/3703-0349 $ 17.50+.50/0



Scheme 1. Common (a) and seldom (b) coordination modes of secondary and tertiary silyl groups in dinuclear metal complexes.

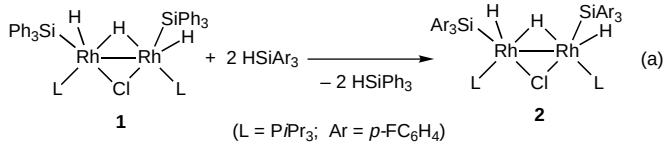
The μ-η^1,η^2-coordination of the ligand results in two M–Si bond lengths that are significantly different from each other. Complexes with a tertiary silyl ligand in a bridging coordination (Scheme 1b) seem to be less stable than with a primary or secondary silyl ligand, since it has no Si–H group to stabilize M-Si-M coordination by Si-H-M 3c–2e bonding. Multinuclear Cu complexes whose metal centers are bridged by extremely bulky $Si(SiMe_3)_3$ ligands were isolated.[2] Dinuclear complexes with a bridging tertiary silyl ligand are of interest as models for the transition state of the migration of the tertiary silyl ligand from one metal to the other in a dinuclear framework (Scheme 2).[3, 4] Bridging coordination of PR_3 ligands that are isolobal to SiR_3^- ligands has already been



Scheme 2. Migration of a tertiary silyl group to the second metal center in dinuclear metal complexes.

established.[5] Here we report the synthesis and structure of novel dinuclear Rh complexes with a bridging triarylsilyl ligand that coordinates symmetrically to the two Rh centers.

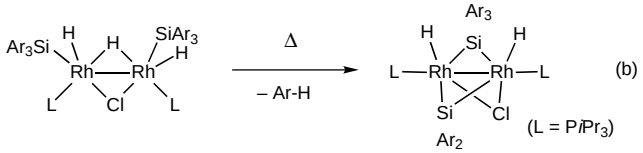
Complex **1**[6] is readily converted into its fluorine-substituted derivative **2**[7] [Eq. (a)]. Both **1** and **2** undergo thermal



(a)

(L = P*i*Pr$_3$; Ar = *p*-FC$_6$H$_4$)

reaction at 70 °C in toluene to afford complexes **3** and **4** under liberation of benzene and fluorobenzene, respectively, in quantitative yields [Eq. (b)].



(b)

1: Ar = C_6H_5, **2**: Ar = *p*-FC_6H_4 **3**: Ar = C_6H_5, **4**: Ar = *p*-FC_6H_4

Figure 1 shows the molecular structure of **4**, which has two Rh centers bridged by chloride, bis(4-fluorophenyl)silylene, and tri(4-fluorophenyl)silyl ligands.[8] The distances from the Rh centers to the Si atom of the triarylsilyl ligand are similar (2.444(4), 2.487(3) Å) and significantly longer than the bond lengths between the Si center of the silylene ligand and the Rh

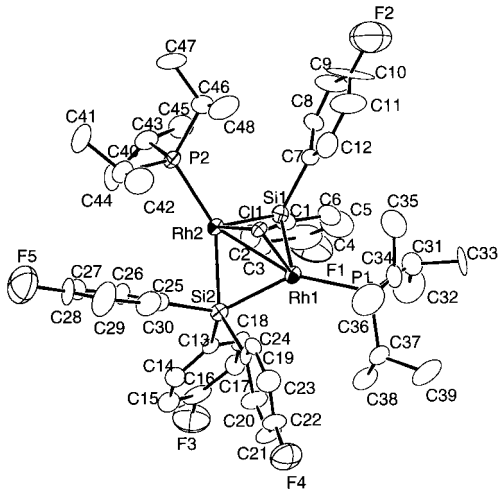


Figure 1. A perspective ORTEP drawing of the crystal structure of **4**. Selected bond lengths [Å] and angles [°]: Rh1–Rh2 2.684(2), Rh1–P1 2.320(4), Rh2–P2 2.337(3), Rh1–Cl1 2.551(3), Rh2–Cl1 2.534(3), Rh1–Si1 2.290(2), Rh2–Si1 2.250(3), Rh1–Si2 2.444(4), Rh2–Si2 2.487(3), Si1–C1 1.91(1), Si1–C7 1.90(2), Si2–C13 1.90(1), Si2–C19 1.931(8), Si2–C25 1.88(1); P1-Rh1-Rh2 160.10(10), P2-Rh2-Rh1 153.5(1), P1-Rh1-Cl1 111.2(1), P2-Rh2-Cl1 105.2(1), P1-Rh1-Si1 114.7(1), P2-Rh2-Si1 110.2(1), P1-Rh1-Si2 142.0(1), P2-Rh2-Si2 149.6(1), Rh1-Si1-Rh2 72.48(8), Rh1-Si1-C1 120.3(3), Rh1-Si1-C7 118.7(4), Rh2-Si1-C1 124.4(5), Rh2-Si1-C7 115.6(3), C1-Si1-C7 104.0(5), Rh1-Si2-Rh2 65.94(10), Rh1-Si2-C13 118.2(4), Rh1-Si2-C19 80.4(4), Rh1-Si2-C25 133.8(5), Rh2-Si2-C13 123.6(3), Rh2-Si2-C19 129.4(4), Rh2-Si2-C25 77.6(4), C13-Si2-C19 105.1(4), C13-Si2-C25 105.2(6), C19-Si2-C25 103.9(4).

centers (2.290(3), 2.250(3) Å). They are longer than the Rh–Si bond lengths already reported (2.203–2.379 Å)[9] and comparable even to that in a Rh-H-Si 3c–2e bond (2.487 Å).[1d] This is in contrast to the structure of Cu complexes containing $Si(SiMe_3)_3$ ligands, in which the Cu–Si bonds to the bridging and nonbridging ligands do not show significant differences in length.[3] The NMR spectra of **3** and **4** are consistent with the above structure. The ^{1}H NMR spectra show peaks due to two equivalent nonbridging hydrido ligands at $\delta = -17.40$ and -17.60, respectively;[10] the positions of the hydrogen atoms were not determined in the crystal structure analysis of **4**.

The ^{1}H and ^{31}P{^{1}H} NMR spectroscopic measurements of the thermal transformation of **1** to **3** in C_6D_6 revealed there are no Rh complexes other than **1** and **3** throughout the reaction. Conversion of **1** into **3** obeys first-order kinetics ($k = 4.41 \times 10^{-5}\ s^{-1}$ at 333 K). This indicates that the reaction proceeds in an intramolecular fashion, most probably by oxidative addition of a Si–C bond of an arylsilyl ligand onto the metal center followed by coupling of the phenyl group of this ligand with a hydride ligand and release of benzene. Activation of Si–C bonds under mild conditions has been found for reactions of various organotransition metal complexes.[1g, 11]

We succeeded in isolating rhodium complexes with a symmetrically bridging triarylsilyl ligand. The complexes show unexpectedly thermal stability, although the Rh–Si bond is significantly longer than common Rh–Si single bonds. Smooth conversion of a nonbridging triarylsilyl ligand into a bridging one corroborates the proposed mechanism for migration of the silyl ligand between the metal centers in dinuclear complexes (Scheme 2).

 © WILEY-VCH Verlag GmbH, D-69451 Weinheim, 1998 1433-7851/98/3703-0350 $ 17.50+.50/0 *Angew. Chem. Int. Ed.* **1998**, *37*, No. 3

Experimental Section

3: A solution of **1** (264 mg, 0.24 mmol) in toluene (5 mL) was stirred for 2 h at 70 °C. During the reaction the color of the solution changed from yellow to orange. Gas-chromatographic analysis of the solution showed quantitative formation of benzene. The $^{31}P\{^1H\}$ NMR spectrum of the mixture after the reaction showed only the signal for **3**. Addition of pentane caused separation of **3** as yellow-orange crystals, which were collected by filtration and recrystallized from toluene/pentane (71 mg, 29% yield). The similar reaction of **2** gave **4** in 51% yield.

The kinetic measurements of the conversion were carried out in a thermostatted (70 °C) NMR probe by following the changes in the intensities of the ^1H NMR signal for the hydrido ligands of **1**. Dioxane was used as an internal standard.

Received: August 19, 1997 [Z10834IE]
German version: *Angew. Chem.* **1998**, *110*, 364–366

Keywords: bridging ligands · rhodium · Si ligands

[1] a) W. A. G. Graham, *J. Organomet. Chem.* **1986**, *300*, 81, and references therein; b) U. Schubert, *Adv. Organomet. Chem.* **1990**, *30*, 151, and references therein; c) R. Carreño, V. Riera, M. A. Ruiz, Y. Jeannin, M. Philoche-Levisalles, *J. Chem. Soc. Chem. Commun.* **1990**, 15; d) M. D. Fryzuk, L. Rosenberg, S. J. Rettig, *Organometallics* **1991**, *10*, 2537; *ibid.* **1996**, *15*, 2871; e) H. Suzuki, T. Takao, M. Tanaka, Y. Moro-oka, *J. Chem. Soc. Chem. Commun.* **1992**, 476; f) T. Takao, S. Yoshida, H. Suzuki, M. Tanaka, *Organometallics* **1995**, *14*, 3855; g) B. K. Campion, R. H. Heyn, T. D. Tilley, *ibid*. **1992**, *11*, 3918; h) R. S. Simons, C. A. Tessier, *ibid*. **1996**, *15*, 2604.

[2] a) A. Heine, D. Stalke, *Angew. Chem.* **1993**, *105*, 90; *Angew. Chem. Int. Ed. Engl.* **1993**, *32*, 121; b) A. Heine, R. Herbest-Irmer, D. Stalke, *J. Chem. Soc. Chem. Commun.* **1993**, 1729.

[3] a) P. Braunstein, M. Knorr, B. Hirle, G. Reinhard, U. Schubert, *Angew. Chem.* **1992**, *104*, 1641; *Angew. Chem. Int. Ed. Engl.* **1992**, *31*, 1583; b) M. Knorr, P. Braunstein, A. Tiripicchio, F. Ugozzoli, *Organometallics* **1995**, *14*, 4910; c) M. Knorr, E. Hallauer, V. Huch, M. Veith, P. Braunstein, *ibid*. **1996**, *15*, 3868.

[4] W. Lin, S. R. Wilson, G. S. Girolami, *Organometallics* **1994**, *13*, 2309.

[5] R. Bender, P. Braunstein, A. Dedieu, Y. Dusausoy, *Angew. Chem.* **1989**, *101*, 931, *Angew. Chem. Int. Ed. Engl.* **1989**, *28*, 923.

[6] K. Osakada, T. Koizumi, T. Yamamoto, *Organometallics* **1997**, *16*, 2063.

[7] **2**: ^1H NMR (C_6D_6, TMS): $\delta = 7.59$ (dd, $^3J(H,H) = 9$, $^3J(H,F) = 2$ Hz, 12H; aromatic H), 6.90 (t, $^3J(H,H) = {}^3J(H,F) = 9$ Hz, 12H; aromatic H), 1.54 (m, $^3J(P,H) = 7$ Hz, 6H; P–CH), 0.82 (br, 36H; CH_3), −12.55 (tt, $^1J(Rh,H) = 58$, $^2J(P,H) = 25$ Hz, 1H; Rh-H-Rh), −16.07 (AA′ part of an AA′MM′XX′ pattern, 2H; Rh–H); $^{31}P\{^1H\}$ NMR (C_6D_6, 85% H_3PO_4): $\delta = 54.2$ (AA′ part of an AA′XX′ pattern).

[8] Crystallographic data for **4**: $C_{48}H_{64}ClF_5P_2Rh_2Si_2$, $M_r = 1095.41$, monoclinic, space group $P2_1/c$ (no. 14), $a = 18.146(10)$, $b = 12.806(8)$, $c = 21.512(9)$ Å, $\beta = 90.39(3)°$, $V = 4998$ Å^3, $Z = 4$, $\mu = 8.74$ cm^{-1}, $F(000) = 2248$, $\rho_{calcd} = 1.455$ g cm^{-3}. The final R factor was 0.075 ($Rw = 0.059$) for 7999 reflections with $I > 3\sigma(I)$. Data collection on a RIGAKU-AFC5R diffractometer at 298 K with graphite-monochromated $Mo_{K\alpha}$ radiation ($\lambda = 0.71073$ Å). The structure was solved with the program teXsan. Crystallographic data (excluding structure factors) for the structure reported in this paper have been deposited with the Cambridge Crystallographic Data Centre as supplementary publication no. CCDC-100766. Copies of the data can be obtained free of charge on application to CCDC, 12 Union Road, Cambridge CB2 1EZ, UK (fax: int. code + (49) 1223-336033; e-mail: deposit@ccdc.cam.ac.uk).

[9] a) K. W. Muir, J. A. Ibers, *Inorg. Chem.* **1970**, *9*, 440; b) M.-J. Fernandez, P. M. Bailey, P. O. Bentz, J. S. Ricci, T. F. Koetzle, P. M. Maitlis, *J. Am. Chem. Soc.* **1984**, *106*, 5458; c) F. L. Joslin, S. R. Stobart, *J. Chem. Soc. Chem. Commun.* **1989**, 504; d) D. L. Thorn, R. L. Harlow, *Inorg. Chem.* **1990**, *29*, 2017; e) K. Osakada, K. Hataya, Y. Nakamura, M. Tanaka, T. Yamamoto, *J. Chem. Soc. Chem. Commun.* **1993**, 576; *ibid.* **1995**, 2315.

[10] **3**: ^1H NMR (C_6D_6, TMS): $\delta = 6.9 - 8.2$ (m, 25H; aromatic H), 1.18 (m, $^3J(P,H) = 7$ Hz, 6H; P–CH), 0.95 (m, 36H; CH_3), −17.40 (AA′ part of an AA′MM′XX′ pattern, 2H; Rh–H); $^{31}P\{^1H\}$ NMR (C_6D_6, 85% H_3PO_4): $\delta = 57.4$ (AA′ part of an AA′XX′ pattern); $^{29}Si\{^1H\}$ NMR (C_6D_6, TMS): $\delta = 157.8$ (t, $^2J(P,Si) = 50$ Hz), 28.7 (tt, $^2J(P,Si) = 50$, $^1J(Rh,Si) = 8$ Hz). **4**: ^1H NMR (C_6D_6, TMS): $\delta = 6.76 - 7.88$ (m, 20H; aromatic H), 1.12 (m, 6H; P–CH), 0.86 (m, 36H; CH_3), −17.60 (AA′ part of an AA′MM′XX′ pattern, 2H; Rh–H); $^{31}P\{^1H\}$ NMR (C_6D_6, 85% H_3PO_4): $\delta = 58.2$ (AA′ part of an AA′XX′ pattern).

[11] a) M. Auburn, M. Ciriano, J. A. K. Howard, M. Murray, N. J. Pugh, J. L. Spencer, F. G. A. Stone, P. Woodward, *J. Chem. Soc. Dalton Trans.* **1980**, 659; b) D. E. Hendriksen, A. A. Oswald, G. B. Ansell, S. Leta, R. V. Kastrup, *Organometallics* **1989**, *8*, 1153; c) S. K. Thomson, G. B. Young, *ibid*. **1989**, *8*, 2068; d) P. Burger, R. G. Bergman, *J. Am. Chem. Soc.* **1993**, *115*, 10462; e) T. Rappert, O. Nürnberg, H. Werner, *Organometallics* **1993**, *12*, 1359; f) M. Baum, B. Windmüller, H. Werner, *Z. Naturforsch. B* **1994**, *49*, 859; g) D. Huang, R. H. Heyn, J. C. Bollinger, K. G. Caulton, *Organometallics* **1997**, *16*, 292.

A Glucose-Containing Ether Lipid (Glc-PAF) as an Antiproliferative Analogue of the Platelet-Activating Factor**

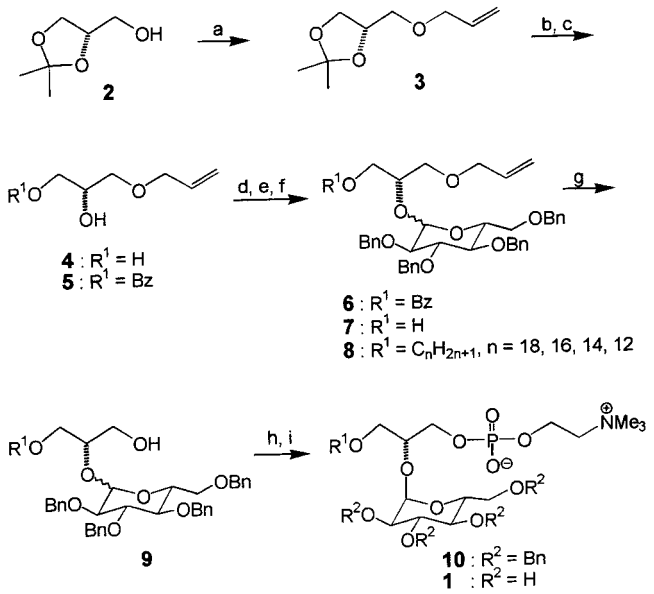
Michael Mickeleit, Thomas Wieder, Michael Arnold, Christoph C. Geilen, Johann Mulzer, and Werner Reutter*

It has long been known that the platelet-activating factor (PAF) is a biologically highly active phosphoglyceride,[1] and various PAF analogues have been reported as inhibitors of proliferation.[2] However, since synthetic phospholipids are strongly cytotoxic, their therapeutic use has hitherto been restricted to topical applications.[3] We reported earlier the synthesis of a new type of glyceroglucolecithin (Glc-PC)[4] which displayed antiproliferative activity without cytotoxicity at concentrations below 10 μmol L^{-1}. We now present the glycoside of the ether analogue [1-*O*-octadecyl-2-*O*-α-D-glucopyranosyl-*sn*-glycero(3)]phosphorylcholine (Glc-PAF, **1**), which is formally derived from the PAF by exchanging the 2-acyl group for a glucose molecule.

The glycerol skeleton is provided by the starting material (*S*)-isopropylidene glycerol (**2**),[5] whose hydroxyl group is protected as the allyl ether functionality in **3** for introduction of the end groups (Scheme 1). The primary hydroxyl group of the diol **4** released upon acid hydrolysis cannot react directly to form an ether, and it is therefore first converted into a terminal benzoate ester group.[6] Compound **5** undergoes

[*] Prof. Dr. W. Reutter, Dr. T. Wieder
Institut für Molekularbiologie und Biochemie der Freien Universität Arnimallee 22, D-14195 Berlin (Germany)
Fax: Int. code + (49) 30838-2141
Prof. Dr. J. Mulzer
Institut für Organische Chemie der Universität Wien (Austria)
Dr. M. Mickeleit
Institut für Organische Chemie der Freien Universität Berlin
Priv.-Doz. Dr. Dr. C. C. Geilen, M. Arnold
Haut- und Poliklinik des Universitätsklinikums Benjamin Franklin Freie Universität Berlin

[**] These investigations were supported by the Bundesministerium für Bildung, Wissenschaft, Forschung und Technologie (W.R.), zentrale Mittel (FNK) der Freien Universität Berlin, the Fonds der Chemischen Industrie, and the Deutsche Forschungsgemeinschaft (Ge 641/3-3).



Scheme 1. Synthesis of **1**. a) NaH, allyl bromide, THF, 0 °C (98 %); b) AcOH/H_2O (60/40) (73 %); c) BzCl, DMAP, py, 0 °C (76 %); d) 2,3,4,6-tetra-*O*-benzyl-β-D-glucopyranosyl fluoride, $AgClO_4$, $SnCl_2$, 4-Å molecular sieves, Et_2O, −15 °C (81 %); e) KOH/MeOH (30 %), MeOH, (91 %); f) NaH, RBr, THF, 80 °C (83–98 %); g) Pd/C (10 %), *p*-toluenesulfonic acid, MeOH/*i*PrOH/H_2O (4/4/1), 80 °C (70–94 %); h) 1. $POCl_3$, Et_3N, $CHCl_3$, 0 °C; 2. choline tosylate, py, 0 °C (47–74 %); i) H_2 (2 atm), Pd/C (5 %), MeOH (71–97 %); Bn = benzyl, Bz = benzoyl, DMAP = 4-(dimethylamino)pyridine, py = pyridine, R = C_nH_{2n+1}, n = 18, 16, 14, 12.

reaction with 2,3,4,6-tetra-*O*-benzyl-β-D-glucopyranosyl fluoride[8] at the secondary alcohol functionality to provide glycoside **6**[9] according to Mukaiyama et al.[7] After saponification of the benzoate, the resulting compound **7** is converted into the ether with the appropriate alkyl bromide. Since the activity of choline-containing phospholipid analogues strongly depends on the length of the alkyl chain,[10] the chain length of the ether introduced at this stage (C_{18}, C_{16}, C_{14}, and C_{12}) corresponds to that of a biologically relevant derivative. Formation of the ether is highly temperature-dependent, and complete conversion into **8** does not occur until 80 °C.

Before introducing the final glycerol substituent (i.e. the phosphate), the original allyl ether must be cleaved by hydrogenolysis.[11] Alcohol **9** is then esterified with phosphoryl chloride, and the resulting dichloroester is immediately converted into the desired phosphocholine derivative **10** with choline tosylate.[12,13] Cleavage of the benzyl protecting groups presented considerable problems in the synthesis of the ester analogue Glc-PC. The ethers are, however, much more reactive, and the products are obtained in good yields after only short periods of hydrogenation. Starting from **2**, gram quantities of **1** were synthesized in nine steps with a total yield of 25 %.[14]

The biological activity of **1** was determined in a serum-free cell-culture system of human keratinocytes (HaCaT cells) by measuring three typical cell parameters. First, it was shown that **1** (n = 18) is nontoxic at concentrations below 4 μmol L^{-1} (Figure 1 a). Higher concentrations cause marked cell damage; the median lethal dose (LD_{50}) was 9 μmol L^{-1}. The growth-inhibitory properties of **1** were then investigated. As

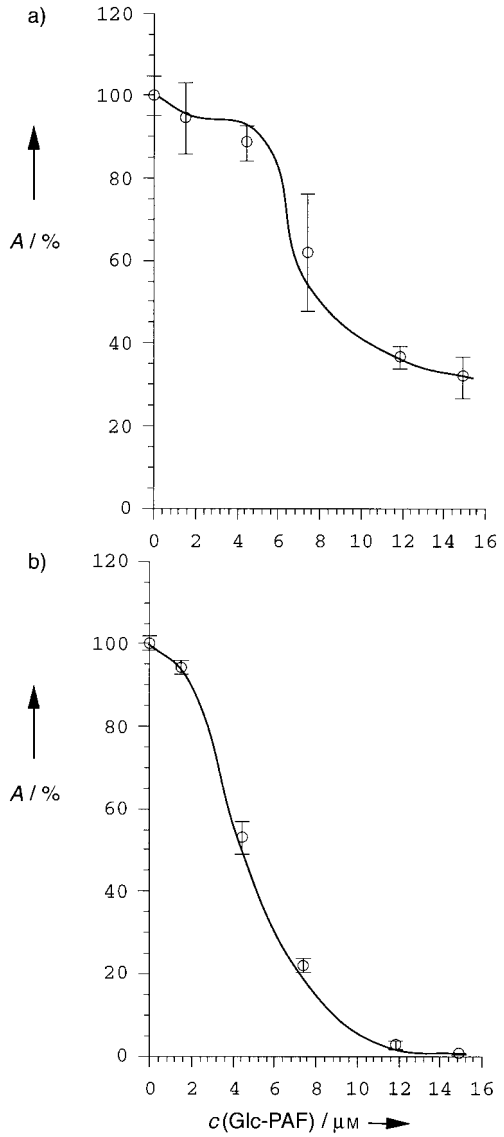


Figure 1. Influence of **1** (n = 18) on the viability (a) and proliferation (b) of HaCaT cells. Both are expressed as a percentage A of the value measured for the control experiment; c = concentration. Four experiments were carried out per data point. See the Experimental Section for details.

shown in Figure 1 b, nontoxic concentrations of **1** (n = 18) as low as 4 μmol L^{-1} inhibit proliferation. The inhibition curve shows a half-maximal inhibitor concentration (IC_{50}) of 4.8 μmol L^{-1}, which is well below the LD_{50} value. In view of the detergentlike structure of **1**, cytotoxicity may be attributed to cell lysis and/or the initiation of programmed cell death (apoptosis),[15] which is characterized biochemically by the appearance of ordered arrangements of internucleosomal DNA fragments.[16] To further characterize the cell death caused by **1**, we determined the proportion of apoptotic HaCaT cells by measuring the number of cytosolic nucleosomes after treatment of the cells for 20 h with the synthetic ether lipid. At low but antiproliferative concentrations of **1** (n = 18; 1.5, 4.5 and 7.4 μmol L^{-1}), the number of apoptotic cells showed a concentration-dependent increase; the greatest (tenfold) increase was observed for 7.4 μmol L^{-1} (Figure 2). At concentrations of 14.9 and 29.8 μmol L^{-1} there was a marked decrease in the number of apoptotic cells, as

 © WILEY-VCH Verlag GmbH, D-69451 Weinheim, 1998 1433-7851/98/3703-0352 $ 17.50+.50/0

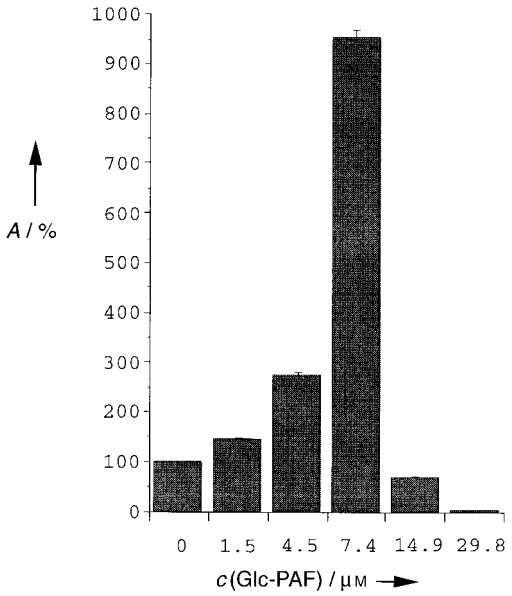


Figure 2. Influence of **1** ($n = 18$) on the apoptosis of HaCaT cells, which is expressed as the percentual enrichment A of apoptotic cells in comparison to the control experiment; c = concentration. Four experiments were carried out per data point. See the Experimental Section for details.

determined by the presence of cytosolic nucleosomes. This indicates that the cells were damaged by lysis at these higher concentrations. According to these data, **1** is a proliferation inhibitor which initiates programmed cell death in keratinocytes at concentrations below 7.5 μmol L^{-1}. Compared with the above-mentioned Glc-PC ($LD_{50} = 17$ μmol L^{-1} and $IC_{50} = 9$ μmol L^{-1} under the experimental conditions described above), **1** ($n = 18$) is not only biologically more active, but also more toxic. The synthesis of other derivatives with 2-glycosidic substituents and different alkyl side chains will be necessary to determine the structure – activity relationships of this new type of compound.

Experimental Section

Cell culture: The spontaneously immortalized human keratinocyte cell line HaCaT[17] was incubated in serum-free keratinocyte growth medium.[18] Compound **1** was dissolved directly in the keratinocyte growth medium.

Cytotoxicity test: Confluent HaCaT cells were incubated for 6 h with different concentrations of **1**. The cytotoxicity of **1** for HaCaT cells was determined in comparison with the control experiments (which did not contain **1**) by measuring the activity of alkaline phosphatase as described.[19]

Measurement of proliferation: HaCaT cells were sown at a cell density of about 20000 cells per cm^2. After adhesion the cells were incubated for 48 h with different concentrations of **1**. The cell count was determined as described[20] after staining with 0.1 % crystal violet in PBS, and compared with the control.

Measurement of apoptosis: Confluent HaCaT cells adapted to keratinocyte growth medium were treated for 20 h with different concentrations of **1**. The medium was removed, and the adherent cells released from the dish with a solution containing 0.1 % trypsin and 0.02 % ethylenediaminetetraacetic acid (EDTA). The cells were then washed off with serum-containing medium (10 % fetal-calf serum in Rosewell Park Memorial Institute (RPMI) medium) and combined with the previously removed medium. The cells were pelleted by centrifugation for 5 min at 300 g, washed once with serum-containing RPMI medium, and pelleted again. The cell pellet was incubated for 30 min in 1 mL of lysis buffer, and the resulting lysate centrifuged for 10 min at 13000 g to remove nonbound antibodies. Nucleosomes were then determined in the lysate and in the control with a commercially available enzyme-linked immunosorbent assay (ELISA) from Boehringer Mannheim according to the instructions provided by the manufacturer. An aliquot of each sample (20 μL) was pipetted into a well of a streptavidin-coated microtiter plate followed by immune reagent (80 μL; made up of 1 part peroxidase-conjugated anti-DNA antibody, 1 part biotinylated anti-histone antibody, and 18 parts incubation buffer) and incubated for 2 h at room temperature. After threefold washing incubation buffer, and the quantity of bound peroxidase-conjugated anti-DNA antibody was quantified by a peroxidase-catalyzed color reaction with measurement at 405 nm in the ELISA reader. The increase in the number of apoptotic cells was calculated by comparing the extinction of the treated sample with that of the corresponding control. The specificity of the method was tested by applying it to cells treated with suitable apoptosis-inducing substances (cell membrane-penetrating ceramides). In addition, electron microscopy of the treated cells revealed typical apoptotic changes, such as membrane evaginations and chromatin condensations, which were correlated with the results of the ELISA test.

Received: July 2, 1997 [Z10624IE]
German version: *Angew. Chem.* **1997**, *110*, 371 – 373

Keywords: apoptosis · glycosides · phospholipids · platelet-activating factor · proliferation inhibitors

[1] D. J. Hanahan, *Annu. Rev. Biochem.* **1986**, *55*, 483 – 509.
[2] M. Modollel, R. Andreesen, W. Pahlke, U. Brugger, P. G. Munder, *Cancer Res.* **1979**, *39*, 4681 – 4686; E. M. Scholar, *Cancer Lett.* **1986**, *33*, 199 – 204; T. Wieder, A. Haase, C. C. Geilen, C. E. Orfanos, *Lipids* **1995**, *30*, 389 – 393.
[3] C. Unger, W. Damenz, E. A. M. Fleer, D. J. Kim, A. Breiser, P. Hilgard, J. Engel, G. Nagel, H. Eibl, *Acta Oncol.* **1989**, *28*, 213 – 217; S. Clive, R. C. F. Leonard, *Lancet* **1997**, *349*, 621 – 622.
[4] M. Mickeleit, T. Wieder, K. Buchner, C. Geilen, J. Mulzer, W. Reutter, *Angew. Chem.* **1995**, *107*, 2879 – 2881; *Angew. Chem. Int. Ed. Engl.* **1995**, *34*, 2667 – 2669.
[5] R. M. Hanson, *Chem. Rev.* **1991**, *91*, 437 – 475.
[6] The dibenzoate forms in 9 % and the regioisomeric monobenzoate in 12 % yield. The regioisomers were separated by preparative HPLC.
[7] T. Mukaiyama, Y. Murai, S. Shoda, *Chem. Lett.* **1981**, 431 – 432.
[8] G. H. Posner, S. H. Haines, *Tetrahedron Lett.* **1985**, *26*, 5 – 8.
[9] The anomers are formed in the ratio $\alpha:\beta = 9:1$.
[10] C. C. Geilen, A. Haase, T. Wieder, D. Arndt, R. Zeisig, W. Reutter, *J. Lipid Res.* **1994**, *35*, 625 – 632.
[11] R. Boss, R. Scheffold, *Angew. Chem.* **1976**, *88*, 578 – 579; *Angew. Chem. Int. Ed. Engl.* **1976**, *15*, 558 – 559.
[12] G. Hirth, H. Saroka, W. Bannwarth, R. Barner, *Helv. Chim. Acta* **1983**, *66*, 1210 – 1240.
[13] At this stage the anomers were separated by HPLC ($MeOH/CH_2Cl_2$ 4/1). The final product **1** is the pure α-anomer
[14] Selected physical properties and spectroscopic data of **1** ($n = 18$): colorless, amorphous solid; m.p. 225 °C, $[\alpha]_D^{20} = +50.9$ ($c = 0.7$ in CH_3OH); ^1H NMR (500 MHz, CD_3OD): $\delta = 0.90$ (t, $J = 6.25$ Hz, 3 H), 1.18 – 1.38 (m, 30 H), 1.56 (m_c, 2 H), 3.20 (s, 9 H), 3.31 – 3.49 (m, 4 H), 3.58 – 3.80 (m, 8 H), 3.95 – 4.08 (m, 3 H), 4.30 (m_c, 2 H), 5.06 (d, $J =$ 3.75 Hz, 1 H); MS (FAB^+): m/z (%): 672 (4.0), 510 (5.6), 224 (9.4), 184 (39.4), 166 (26.4), 86 (100), 58 (65.7).
[15] J. Kerr, A. Wyllie, A. Currie, *Br. J. Cancer* **1972**, *26*, 239 – 257.
[16] A. Wyllie, *Nature* **1980**, *284*, 555 – 556.
[17] P. Boukamp, R. T. Petrussevska, D. Breitkreutz, J. Hornung, A. Markham, N. E. Fusenig, *J. Cell Biol.* **1988**, *106*, 761 – 771. The cells were provided by Dr. N. E. Fusenig (DKFZ, Heidelberg) und maintained in a liquid-culture medium.
[18] C. C. Geilen, M. Bektas, T. Wieder, C. E. Orfanos, *FEBS Lett.* **1996**, *378*, 88 – 92.
[19] J. G. Culvenor, A. W. Harris, T. E. Mandel, A. Whitelaw, E. Ferber, *J. Immunol.* **1981**, *126*, 1974 – 1977.
[20] R. J. Gillies, N. Didier, M. Denton, *Anal. Biochem.* **1986**, *159*, 109 – 113; C. C. Geilen, R. Haase, K. Buchner, T. Wieder, F. Hucho, W. Reutter, *Eur. J. Cancer* **1991**, *27*, 1650 – 1653.

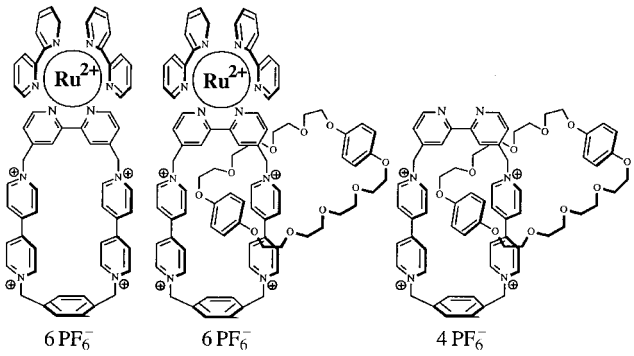
 © WILEY-VCH Verlag GmbH, D-69451 Weinheim, 1998 1433-7851/98/3703-0353 $ 17.50+.50/0

Artificial Photosynthesis: Mimicking Redox Asymmetry**

Andrew C. Benniston,* Philip R. Mackie, and Anthony Harriman*

One intriguing aspect of the bacterial photosynthetic reaction center (RC) is the redox asymmetry of the cofactors: Electron transfer proceeds only along the L branch of an almost symmetrically twinned set of reagents.[1, 2] The M branch is apparently excluded, since the effective dielectric constant of the surrounding medium differs.[3, 4] A slightly higher polarity around the L branch favors electron transfer along this direction,[5] although the reaction can be made to proceed along the M branch in mutagenically modified RC complexes.[6] We now describe a model system that is similar to the RC complex: The two chemically identical electron acceptors bound to the primary donor have different reduction potentials because of their environment. This effect is achieved by wrapping an electron-donating crown ether around one of the acceptor moieties, thereby excluding access to polar solvent molecules and further attenuating its electron affinity with charge-transfer interactions.

Cyclophane **1** [functionalized with ruthenium(II) bis(2,2′-bipyridine)], the corresponding metalated [2]catenane **2**, and the free catenated ligand **3** were synthsized by standard



1 **2** **3**

procedures[7] and characterized by ^{1}H NMR spectroscopy and mass spectrometry. For **2** and **3**, as with analogous nonmetalated [2]catenanes, an electron-poor tetracationic 4,4′-bipyridinium-based cyclophane is interlocked with a complementary electron-donating macrocycle.[8]

The structural feature that is most important to the present study is the asymmetry of the two 4,4′-bipyridinium dications bound to the metal complex in **2**. The absence of a suitable internal ^{1}H NMR probe prevented direct measurement of the rate at which the macrocycle migrates between these two cationic units. Such studies were possible for **3** in [D$_6$]acetone; in particular, signals for the degenerate 6,6′ protons of the 2,2′-bipyridine unit are readily observable from $+25$ to $-60\,^\circ$C. At the coalescence temperature ($T_c = -33\,^\circ$C) the rate constant for this process was estimated as 88 s^{-1}, and the Gibbs energy of activation as 12.5 kcal mol^{-1}. The rate of interchange at the coalescence temperature, which corresponds to a lifetime of about 11 ms, indicates that the two interlocked rings in **2** are frozen on the time scale of the electron transfer.

Electrochemical studies of **2** in deoxygenated acetonitrile showed that the metal center undergoes a quasi-reversible one-electron oxidation with a half-wave potential E^0 of 1.29 ± 0.02 V versus the standard calomel electrode (SCE). At higher potentials, oxidation peaks can be resolved for the external ($E^0 = 1.44 \pm 0.02$ V vs. SCE) and internal ($E^0 = 1.73 \pm 0.04$ V vs. SCE) hydroquinol units of the crown ether. Upon reversing the scan, reduction peaks for the external ($E^0 = -0.32 \pm 0.01$ V vs. SCE) and internal ($E^0 = -0.45 \pm 0.01$ V vs. SCE) viologens were observed before the appearance of a two-electron peak ($E^0 = -0.85 \pm 0.03$ V vs. SCE) corresponding to formation of the neutral viologens. Similar electrochemical behavior was found for the nonmetalated **3** and for related [2]catenanes.[8, 9] The redox potentials for internal and external viologens differ because of a) the relative accessibility to polar solvent molecules and b) the interaction with electron-donating hydroquinol units. These factors combine to introduce significant (130 meV) redox asymmetry into **2**. The metal center in cyclophane **1** is oxidized at $E^0 = 1.29 \pm 0.02$ V vs. SCE, whereas the 4,4′-bipyridinium-based cyclophane undergoes one-electron reduction at $E^0 = -0.28 \pm 0.01$ V vs. SCE.

Because of the inherent redox asymmetry in **2**, we might expect light-induced electron transfer to occur selectively from the metal center to the external viologen in view of the more favorable thermodynamic driving force. To ensure that the rate of the forward electron transfer does indeed depend on the driving force, we first studied the noncatenated system **1**. Although **1** is not luminescent at room temperature, weak luminescence characteristic of the metal complex was observed at 77 K upon excitation at 565 nm. Transient absorption spectral studies at 20 °C indicate that the triplet excited state of the Ru^{II} complex, which is formed within the laser pulse, has a lifetime of (12 ± 2) ps; the parent compound tris(2,2′-bipyridine)ruthenium(II) has a lifetime of about 1 μs. After decay of the triplet state the spectra show the presence of a mixture of the Ru^{III} complex and the singly reduced form of the 4,4′-bipyridinium-based cyclophane. Decay of these redox intermediates occurred by first-order kinetics with a lifetime of (35 ± 3) ps. The overall reaction is fast because of the close proximity of the reactants; a similar conclusion was reached by Mallouk et al. for a related system that, however, was not part of a cyclophane.[10]

[*] Dr. A. C. Benniston, P. R. Mackie
Chemistry Department
University of Glasgow
Glasgow G12 8QQ (UK)
Fax: Int. code + (44) 141 330-4888
E-mail: andrewb@chem.gla.ac.uk.
Prof. A. Harriman
Laboratoire de Photochimie, E.C.P.M.
Université Louis Pasteur
1 rue Blaise Pascal, F-67008 Strasbourg Cedex (France)
Fax: Int. code + (33) 388 416-825
E-mail: harriman@chimie.u-strasbg.fr.

[**] This work was supported by the University of Glasgow, the EPSRC, and Nuffield Foundation (A.C.B.), and The Royal Society of London (A.H.). A JWT Jones travel fellowship (A.C.B.) and the EPSRC funded mass spectrometry service at the University of Swansea are also gratefully acknowledged.

 © WILEY-VCH Verlag GmbH, D-69451 Weinheim, 1998 1433-7851/98/3703-0354 $ 17.50+.50/0

The triplet energy of the metal complex was determined to be about 1.90 eV from the low-temperature emission spectrum. The thermodynamic driving force[11] for light-induced reduction of the viologen subunits in acetonitrile was estimated as $\Delta G^0 \approx -0.36$ eV, which indicates that the reaction is likely to fall within the "normal Marcus region".[12]

Charge recombination is much more favorable ($\Delta G^0 \approx -1.60$ eV) and is likely to occur within the "inverted Marcus region". These expectations were confirmed by measuring the rates of forward and reverse electron transfer between -30 and $+65\,^{\circ}C$. The activation energies E_A of (0.070 ± 0.002) and (0.010 ± 0.001) eV, respectively, were derived from the linear Arrhenius plots for forward and reverse electron transfer. The total reorganization energy λ for forward electron transfer was calculated to be about 0.85 eV based on Marcus theory [Eq. (1)].[12]

$$E_A = \left(\frac{(\lambda + \Delta G^0)^2}{4\lambda}\right) \quad (1)$$

The rate constant for the forward electron transfer (k_{CS}), but not that of the charge recombination (k_{CR}), depends on the polarity of the surrounding solvent, as expressed in terms of the static dielectric constant ε_S. In highly polar solvents such as propylene carbonate ($\varepsilon_S = 62$), k_{CS} has an optimal value of about $10^{11}\,s^{-1}$ but decreases progressively as the polarity is reduced (Figure 1), subject to solubility restrictions.

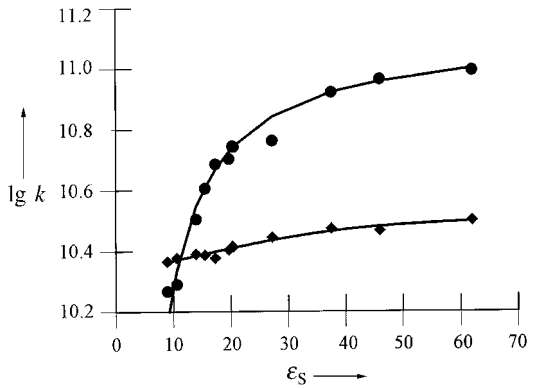


Figure 1. Effect of the dielectric constant on the rate constants for the forward electron transfer (●) and subsequent charge recombination (◆) measured for **1** after laser excitation at 565 nm. Solvents used (ε_S): propylene carbonate (62), dimethyl sulfoxide (46), acetonitrile (37.5), propionitrile (27.2), isobutyronitrile (20.4), butyronitrile (20.3), valeronitrile (19.7), hexanenitrile (17.3), 4-methylvaleronitrile (15.5), octanenitrile (13.9), 1,2-dichloroethane (10.6), dichloromethane (8.9).

Because the electron transfer is under activation control (i.e., $-\Delta G^0 \approx 0.4\lambda$), we attribute the decreased rate to a smaller thermodynamic driving force in less polar solvents due to weaker solvation of reactants and products. The important conclusion of these studies is that k_{CS} increases with increasing solvent polarity and with increasing temperature.

Similar transient spectroscopic studies were made with the catenane **2**, whose two electron-poor arms show disparate reduction potentials in acetonitrile. Laser excitation resulted in immediate formation of the triplet excited state of the ruthenium(II) complex, which decayed by first-order kinetics with a lifetime of (17 ± 2) ps. The triplet state decayed by way of electron transfer to the adjacent cyclophane ($k_{CS} \approx 5.9 \times 10^{10}\,s^{-1}$), as demonstrated by transient absorption spectroscopy (Figure 2), followed by subsequent charge recombination ($k_{CR} \approx 2.4 \times 10^{10}\,s^{-1}$) to restore the ground state. The redox intermediates survive for about (42 ± 4) ps. By measuring the rate of the forward electron transfer in acetonitrile as a function of temperature, the activation energy for this process was found to be (0.062 ± 0.002) eV. In contrast, charge recombination, which must occur in the inverted Marcus region ($\Delta G^0 \approx -1.6$ eV), is almost activationless. Upon application of Equation (1), λ is estimated to be about 0.75 eV; the forward electron transfer lies in the normal Marcus region ($-\Delta G^0 \approx 0.4\lambda$), in which the rate increases with increasing driving force.

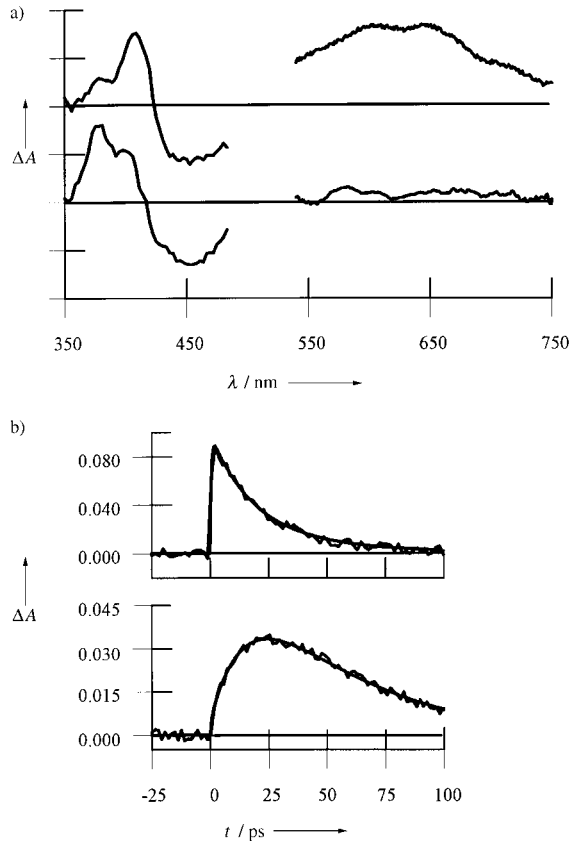


Figure 2. a) Transient differential absorption spectra recorded 1 ps (lower curve) and 25 ps (upper curve) after laser excitation of **2** in acetonitrile at 20 °C. b) Decay profiles showing formation and decay of the triplet state of the ruthenium(II) complex at 370 nm (top) and of the radical ion pair at 620 nm (bottom).

Consequently, the rate of electron transfer to the external viologen ($\Delta G^0 = -0.32$ eV) is expected to exceed that to the internal viologen ($\Delta G^0 = -0.19$ eV). Indeed, providing that λ and the electronic-coupling matrix element are identical for both viologens, a redox asymmetry of 130 meV would create a fivefold difference in rate. Therefore, electron transfer to the external viologen should account for about 85 % of the overall

 © WILEY-VCH Verlag GmbH, D-69451 Weinheim, 1998 1433-7851/98/3703-0355 $ 17.50+.50/0

deactivation of the excited state. This remains a theoretical hypothesis, however, since the two viologens cannot be distinguished by spectroscopic means. Even so, it seems reasonable to anticipate that highly directional electron transfer can be induced by environmental effects of the type proposed here.

Experimental Section

The syntheses of **1**, **2**, and **3** starting from readily prepared 4,4′-bis-(methylene-4,4′-bipyridinium)-2,2′-bipyridyl bis(hexafluorophosphate) have been reported.[7] Solvents were purified by standard methods, and dielectric constants were taken from the literature.[13] For all laser spectroscopic studies, excitation was carried out at 565 nm with a 0.3-ps laser pulse delivered from a Nd-YAG pumped pyromethene dye laser similar to that described in ref. [14].

1: Yield: 64 mg, 70 %; ^{1}H NMR (360 MHz, CD_3COCD_3, 298 K): $\delta = 6.15$ (s, 4H), 6.25 (s, 4H), 7.55 – 7.79 (m, 12H), 7.90 (s, 4H), 7.91 – 8.11 (m, 4H), 8.23 (m, 4H), 8.51 (d, 4H, $J = 6.2$ Hz), 8.70 – 8.85 (m, 6H), 9.33 – 9.55 (m, 8H); FAB-MS (nitrobenzyl alcohol(NBA)/CH_3CN matrix): *m*/*z*: 1737 $[M - PF_6]^+$, 1591 $[M - 2PF_6]^+$, 1446 $[M - 3PF_6]^+$.

2: Yield: 40 mg, 68 %; ^{1}H NMR (360 MHz, CD_3COCD_3, 298 K): $\delta = 3.45$ – 3.48 (m, 4H), 3.61 – 3.63 (m, 8H), 3.69 – 3.72 (m, 8H), 3.79 – 3.85 (m, 12H), 3.93 – 4.10 (m, 4H), 6.10 (s, 4H), 6.23 (s, 4H), 6.26 (s, 4H), 7.57 – 7.73 (q, 4H, $J = 7.5$ Hz), 7.92 – 7.94 (d, 2H, $J = 6$ Hz), 7.98 (s, 4H), 8.00 – 8.02 (d, 2H, $J =$ 5.3 Hz), 8.02 – 8.22 (m, 10H), 8.23 – 8.31 (q, 4H, $J = 7.8$ Hz), 8.34 – 8.36 (d, 2H, $J = 5.7$ Hz), 8.82 – 8.87 (m, 6H), 8.98 (m, 4H), 9.34 – 9.36 (d, 4H, $J =$ 5 Hz); ES-MS (CH_3CN/H_20/HCOOH): *m*/*z*: 661 $[M - 3PF_6]^{3+}$, 460 $[M - 4PF_6]^{4+}$, 339 $[M - 5PF_6]^{5+}$.

3: Yield: 100 mg, 20 %; ^{1}H NMR (360 MHz, CD_3COCD_3, 298 K): $\delta = 3.46$ (m, 8H), 3.61 (m, 8H), 3.89 – 3.93 (m, 16H), 6.08 (s, 4H), 6.15 (s, 4H), 7.94 (m, 2H), 8.00 (s, 4H), 8.10 – 8.14 (2 × d, 8H, $J = 8$ Hz), 8.18 (m, 2H), 8.90 – 8.92 (d, 2H, $J = 5$ Hz), 9.27 – 9.29 (d, 4H, $J = 5.2$ Hz), 9.32 – 9.34 (d, 4H, $J =$ 7 Hz); FAB-MS (NBA matrix): *m*/*z*: 1569 $[M - PF_6]^+$, 1425 $[M - 2PF_6]^+$, 1280 $[M - 3PF_6]^+$, 1135 $[M - 4PF_6]^+$.

Received: July 31, 1997 [Z 10759 IE]
German version: *Angew. Chem.* **1998**, *110*, 376 – 378

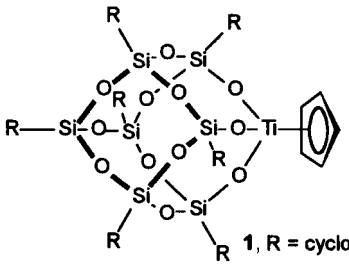
Keywords: catenanes · cyclophanes · electron transfer · photochemistry · photosynthesis

[1] J. Deisenhofer, H. Michel, *Angew. Chem.* **1989**, *101*, 872; *Angew. Chem. Int. Ed. Engl.* **1989**, *28*, 829.
[2] R. Huber, *Angew. Chem.* **1989**, *101*, 849; *Angew. Chem. Int. Ed. Engl.* **1989**, *28*, 848.
[3] O. El-Kabbani, C.-H. Chan, D. Tiede, J. R. Norris, M. Schiffer, *Biochemistry* **1991**, *30*, 5361.
[4] H. Treutlein, K. Schulten, A. T. Brünger, M. Karplus, J. Deisenhofer, H. Michel, *Proc. Natl. Acad. Sci. USA* **1992**, *89*, 75.
[5] M. A. Steffen, K. Lao, S. G. Boxer, *Science* **1994**, *264*, 810.
[6] B. A. Heller, D. Holten, C. Kirmaier, *Science* **1995**, *269*, 940.
[7] a) A. C. Benniston, P. R. Mackie, A. Harriman, *Tet. Lett.* **1997**, *38*, 3577: b) D. Philp, J. F. Stoddart, *SynLett.* **1991**, *7*, 445, and references therein.
[8] D. B. Amabilino, P.-L. Anelli, P. R. Ashton, G. R. Brown, E. Cordova, L. A. Godinez, W. Hayes, A. E. Kaifer, D. Philp, A. M. Z. Slawin, N. Spencer, J. F. Stoddart, M. S. Tolley, D. J. Williams, *J. Am. Chem. Soc.* **1995**, *117*, 11142.
[9] P.-L. Anelli, P. R. Ashton, R. Ballardini, V. Balzani, M. Delgado, M. T. Gandolfi, T. T. Goodnow, A. E. Kaifer, D. Philp, M. Pietraszkiewicz, L. Prodi, M. V. Reddington, A. M. Z. Slawin, N. Spencer, J. F. Stoddart, C. Vicent, D. J. Williams, *J. Am. Chem. Soc.* **1992**, *114*, 193.
[10] E. H. Yonemoto, R. L. Riley, Y. L. Kim, S. J. Atherton, R. H. Schmehl, T. E. Mallouk, *J. Am. Chem. Soc.* **1992**, *114*, 8081.
[11] Calculated from redox potentials and corrected for electrostatic effects according to J. Kroon, J. W. Verhoeven, M. N. Paddon-Row, A. N. Oliver, *Angew. Chem.* **1991**, *103*, 1398; *Angew. Chem. Int. Ed. Engl.* **1991**, *30*, 1358.
[12] R. A. Marcus, *Ann. Rev. Phys. Chem.* **1964**, *15*, 155.
[13] J. A. Riddick, W. B. Bunger in *Organic Solvents. Physical Properties and Methods of Purification. Techniques of Chemistry Vol II* (Ed.: A. Weissberger) Wiley-Interscience, New York, **1970**.
[14] J.-P. Collin, A. Harriman, V. Heitz, F. Odobel, J.-P. Sauvage, *J. Am. Chem. Soc.* **1994**, *116*, 5679.

Solid-Phase Immobilization of a New Epoxidation Catalyst**

Simon Krijnen, Hendrikus C. L. Abbenhuis,* Rob W. J. M. Hanssen, Jan H. C. van Hooff, and Rutger A. van Santen

The heterogenization of homogeneous catalysts is an important topic in liquid-phase oxidation catalysis.[1] Recently we reported on the use of the titanium(IV) silsesquioxane $[\{(c\text{-}C_6H_{11})_7Si_7O_{12}\}Ti(\eta^5\text{-}C_5H_5)]$ **1**[2] as an active and robust homogeneous catalyst for alkene epoxidation.[3] Under the catalytic conditions employed, **1** is stable and does not leach



titanium, which makes it an attractive candidate for heterogenization. Here we report on the immobilization of **1** in an MCM-41 molecular sieve,[4] for which we especially exploited its strong adsorption in the MCM-41 channel. The resulting self-assembled materials are active, truly heterogeneous, and recyclable catalysts for alkene epoxidation in the liquid phase.

The adsorption of the silsesquioxane **1** from hexane into an MCM-41 molecular sieve occurs quickly and can be followed easily by UV/Vis spectroscopy in solution by monitoring its intense 216 nm band. We investigated MCM-41 molecular sieves with Si/Al ratios of 42, 125, and ∞. The adsorption kinetics of **1** are typical for "single-file diffusion",[5] indicating that its actual adsorption takes place inside the MCM-41 channels. Because of this fast and complete adsorption, the loading of **1** can be adjusted easily by varying its total amount in solution. The maximum loading for the MCM-41 host with a Si/Al ratio of 42 was found to be 97 milligrams of **1** per gram

[*] Dr. H. C. L. Abbenhuis, S. Krijnen, R. W. J. M. Hanssen, Prof. Dr. J. H. C. van Hooff, Prof. Dr. R. A. van Santen
Schuit Institute of Catalysis
Eindhoven University of Technology
P. O. Box 513, 5600 MB Eindhoven (The Netherlands)
Fax: Int. code + (31) 402455054
E-mail: tgtaea@chem.tue.nl

[**] S. K. thanks the Netherlands Institute for Catalysis Research (NIOK) for financial support. H. C. L. A. received a fellowship from the Royal Netherlands Academy of Arts and Sciences (KNAW). We are grateful to Solvay Deutschland GmbH for financial support.

 © WILEY-VCH Verlag GmbH, D-69451 Weinheim, 1998 1433-7851/98/3703-0356 $ 17.50+.50/0

of MCM-41 (i.e. 4.3 mg Ti/g MCM-41). FT-IR analysis of MCM-41 materials (KBr pellet) with a maximum loading of **1** showed, superimposed on the vibration bands characteristic for MCM-41, bands typical for **1**: cyclohexyl and cyclopentadienyl C–H vibrations (2854, 2928 cm^{-1}) together with a very characteristic cyclopentadienyl C–C vibration (1449 cm^{-1}).

The titanium silsesquioxane containing materials efficiently catalyze the epoxidation of cyclooctene at 50°C with *tert*-butyl hydroperoxide (Table 1, Figure 1). The scope of the reaction

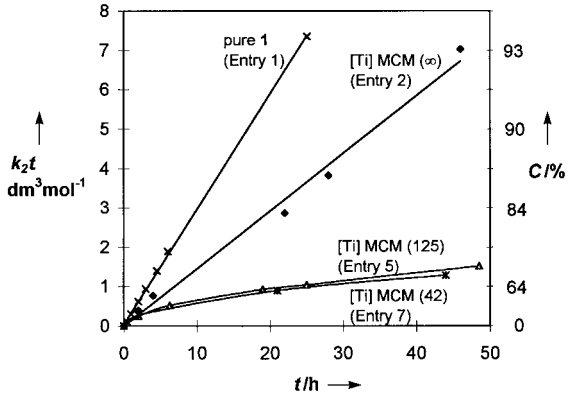


Figure 1. Second-order rate parameter k_2t for the catalytic epoxidation with [Ti] catalysts (Table 1, entries 1, 2, 5, 7). Left axis: $k_2t = 1/[A]_t - 1/[A]_0$ ($[A]_t$ = concentration of cyclooctene at time t and $[A]_0$ = concentration of cyclooctene at $t = 0$). Right axis: conversion C versus time t. All reactions were performed with equimolar amounts of alkene and dried *tert*-butyl hydroperoxide (7.2 mmol each) in hexane (4.0 mL).

includes also the epoxidation of norbornene and 1-octene.[3] With the aluminum-free MCM-41 molecular sieves, in particular, high catalytic activity and heterogeneity was obtained. The data show that the presence of aluminum in MCM-41 reduces the activity of the catalyst (Table 1, entries 2–7).[6] Moreover, under epoxidizing conditions these catalysts quantitatively leached **1** from its aluminum-containing mesoporous host, thus rendering the catalysis homogeneous.

Fortunately, the undesired leaching of the aluminum-containing catalysts can be completely stopped when the MCM-41 molecular sieves are treated with the silylating agent $SiCl_2Ph_2$ prior to catalysis (Table 1, entries 3, 5, 7).[7] The unresolved phenyl signals of the $(\text{-O-})_2SiPh_2$ functions are found in the ^{13}C MAS NMR spectrum (100 MHz) at $\delta = 127.3$ and $\delta = 134.3$. BET analysis on an impregnated MCM-41 sample clearly showed a decrease in both pore diameter and mesopore volume upon adsorption of the silsesquioxane **1** as well as an increase in surface area due to the additional surface of **1** (Table 2). The effect of the silylation is also expressed in both a reduced pore diameter and a reduced mesopore volume.

Table 1. Activity of **1** immobilized in mesoporous MCM-41 or silica for the epoxidation of cyclooctene.[a]

Entry	[Ti] Catalyst (Si/Al ratio)	Silylated samples[c]	Heterogeneous?[d]	Conv. [%][e] [mol mol^{-1} h^{-1}]	TOF[f]
1	**1**	–	–	95	287
2	[Ti]-MCM (∞)	–	yes	84	202
3	[Ti]-MCM (∞)	silylated	yes	77	184
4	[Ti]-MCM (125)	–	no	–[g]	–
5	[Ti]-MCM (125)	silylated	yes	65	160
6	[Ti]-MCM (42)	–	no	–[g]	–
7	[Ti]-MCM (42)	silylated	yes	55	178
8	[Ti]-silica	–	no	–[g]	–
9	[Ti]-silica	silylated	no	–[g]	–
10	MCM (∞)	–	–	10	–
11	MCM (125)	–	–	21	–
12	MCM (42)	–	–	14	–

[a] All reactions were performed with equimolar amounts of alkene and dried *tert*-butyl hydroperoxide (1.8 mmol each) in hexane (1.0 mL) and with 60 mg catalyst. [b] Catalysts with the prefix [Ti] contain complex **1** (1.2 mg Ti/g MCM-41); otherwise reference is being made to blank experiments without **1**. [c] $SiCl_2Ph_2$ was used as the silylating agent. [d] Catalysts are defined as heterogeneous when at 30% conversion and after direct filtration, no subsequent conversion takes place in the filtrate. [e] Conversion of cyclooctene determined by ^1H NMR spectroscopy after 22 h. Selectivities towards the epoxide >95%. [f] Initial turnover frequency (TOF) determined after 2 h. [g] Since the reaction was homogeneous the conversion is not relevant.

Table 2. BET results for the series of aluminum-free MCM-41 materials employed in catalysis.[a]

Entry[b]	Cat.	Surface area [$m^2 g^{-1}$]	Modus pore diameter [nm]	Micropore volume [$cm^3 g^{-1}$]	Mesopore volume [$cm^3 g^{-1}$]
10	MCM (∞)	552	2.9	0.20	0.15
2	[Ti]-MCM (∞)	610	2.7	0.20	0.10
3	[Ti]-MCM (∞) silylated	540	2.3	0.16	0.05

[a] All data have a maximum error of 5%; the error in the mesopore volume is roughly 20%. The [Ti]-MCM-41 samples were loaded with 25 milligrams of **1** per gram of MCM-41. [b] Entries as in Table 1.

The activity of the aluminum-containing heterogeneous catalysts obtained by the silylation procedure decreased in the course of alkene epoxidation (see Figure 1). Interestingly, the aluminum-free catalyst showed no deactivation at all, in either silylated or nonsilylated form. The kinetic data obtained for heterogeneous catalysis employing [Ti]-MCM-41 (∞) and for homogeneous catalysis by the complex **1** can be described by overall second-order rate equations (see Figure 1). All heterogeneous catalysts can be easily recovered by filtration; the aluminum-free catalyst can even be reused at least three times without an apparent loss of activity.

Even when a smaller silylation agent like $SiCl_2(CH_3)_2$ is used, an active, heterogeneous, nonleaching catalyst is obtained. This result indicates that the apolarity of the framework determines whether the catalyst will leach its active complex **1**, and not that **1** is physically trapped by the silylating agent.

The influence of the polarity of the framework on the adsorption of substrates was investigated by monitoring the competitive adsorption of 1,2-epoxyoctane and 1-octene. When an aluminum-containing MCM-41 molecular sieve was used, the 1,2-epoxyoctane/1-octene ratio decreased from 1 to 0 in several minutes, while in the case of an aluminum-free MCM-41 this ratio levels off at about 0.2. This demonstrates that the affinity of the hydrophilic aluminum-contain-

 © WILEY-VCH Verlag GmbH, D-69451 Weinheim, 1998 1433-7851/98/3703-0357 $ 17.50+.50/0

ing MCM-41 for the more polar epoxide is higher than that of the relatively hydrophobic aluminum-free MCM-41 framework. This observation is supported by thermogravimetric analysis, which indicated that both the water content and the dehydration temperature for the aluminum-free MCM-41 (1%, 49°C) are much lower than that of the the aluminum-containing MCM-41 (5%, 60°C). The higher polarity of the aluminum-containing MCM-41 materials is likely to induce leaching.[8] In contrast, the degree of apolarity of an aluminum-free MCM-41 molecular sieve is ideal for both strong adsorption of the catalyst, leading to a heterogeneous system, and diffusion of the organics through the MCM-41 channel. In contrast to physically enclosed systems, this will lead to a *self-assembled heterogeneous catalyst* that is prone to neither leaching nor deactivation.[9]

Conventional silica gel (Silica Grace SG360, total pore volume ca. $0.9-1.0\ cm^3\,g^{-1}$, surface area roughly $600\ m^2\,g^{-1}$) also adsorbs complex **1**. During catalyst testing, however, this material undergoes a significant degree of leaching (see Table 1). From this finding we conclude that a silica with channel-type pores such as an aluminum-free MCM-41 molecular sieve is essential for an irreversible adsorption of the silsesquioxane complex.

Experimental Section

The different MCM-41 samples were prepared following the procedure used by Beck et al.[10] and adapted by Busio et al.[4] In a typical adsorption experiment 50 mL of a 10^{-3} M solution of **1**[2b] in hexane (p.a., Acros) was added slowly to a suspension of 2 g of dried MCM-41 in hexane (50 mL), and the suspension was stirred for 24 h. The impregnated MCM-41 was subsequently filtered off, washed with hexane (3×20 mL), and dried in air at 80°C for 24 h.

In a typical silylation experiment 0.5 g of a dried and degassed impregnated MCM-41 sample was refluxed in a solution of 70 mL of hexane with 2.5 g of dichlorodiphenylsilane (96%, Acros) under an inert atmosphere for 72 h. The obtained material was filtered off, washed with hexane (3×20 mL) and acetone (p.a., Acros, 3×20 mL), and dried in air at 80°C for 24 h.

Received: August 11, 1997 [Z10799IE]
German version: *Angew. Chem.* **1998**, *110*, 374–376

Keywords: epoxidations · heterogeneous catalysis · immobilization · titanium · zeolites

[1] Different procedures with this goal have been reported: isomorphous substitution: a) M. Taramasso, G. Perego, B. Notari (Enichem), US Pat. **1983** 4 410 501; *Chem. Abstr.* **1981,** *95*, 206272k; for a recent review see: b) I. W. C. E. Arends, R. A. Sheldon, M. Wallau, U. Schuchardt, *Angew. Chem.* **1997**, *109*, 1190; *Angew. Chem. Int. Ed. Engl.* **1997**, *36*, 1144; grafting of complexes in molecular sieves: c) T. Maschmeyer, F. Rey, G. Sankar, J. M. Thomas, *Nature* **1995**, *378*, 159; ship-in-a-bottle catalysts, for a review see: d) D. E. De Vos, F. Thibault-Starzyk, P. P. Knops-Gerrits, R. F. Parton, P. A. Jacobs, *Macromol. Symp.* **1994**, *80*, 157; for a recent publication: e) K. J. Balkus, Jr., A. K. Khanmamedova, K. M. Dixon, F. Bedioui, *Appl. Catal. A* **1996**, *143*, 159. For a recent highlight see: R. Murugavel, H. W. Roesky, *Angew. Chem.* **1997**, *109*, 491; *Angew. Chem. Int. Ed. Engl.* **1997**, *36*, 477.

[2] a) F. J. Feher, T. A. Budzichowski, K. Rahimian, J. W. Ziller, *J. Am. Chem. Soc.* **1992**, *114*, 3859; b) I. E. Buys, T. W. Hambley, D. J. Houlton, T. Maschmeyer, A. F. Masters, A. K. Smith, *J. Mol. Catal.* **1994**, *86*, 309.

[3] H. C. L. Abbenhuis, S. Krijnen, R. A. Van Santen, *Chem. Commun.* **1997**, 331.

[4] M. Busio, J. Jänchen, J. H. C. Van Hooff, *Microporous Mater.* **1995**, *5*, 211.

[5] J. Kärger, M. Petzold, H. Pfeifer, S. Ernst, J. Weitkamp, *J. Catal.* **1992**, *136*, 283.

[6] A. Corma, P. Esteve, A. Martínez, *J. Catal.* **1996**, *161*, 11.

[7] For a related approach involving enzymes in MCM-41 materials: J. F. Díaz, K. J. Balkus, Jr., *J. Mol. Catal. B Enzymes* **1996**, *2*, 115.

[8] a) J. Jänchen, M. Busio, M. Hintze, H. Stach, J. H. C. Van Hooff, *Stud. Surf. Sci. Catal.* **1997**, 105, 1731; b) C. Y. Chen, H. X. Li, M. E. Davis, *Microporous Mater.* **1993**, *2*, 17.

[9] K. T. Wan, M. E. Davis, *Nature* **1994**, *370*, 449.

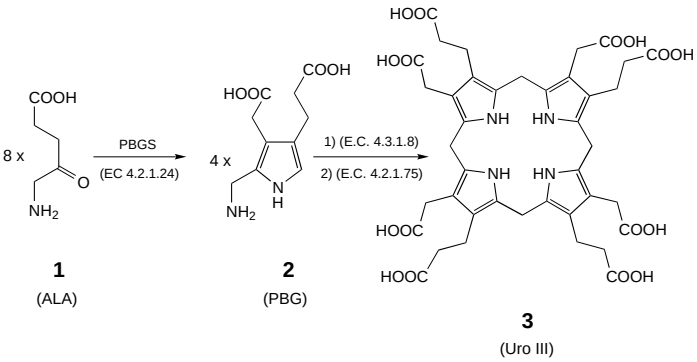
[10] J. S. Beck, J. C. Vartuli, W. J. Roth, M. E. Leonowicz, C. T. Kresge, K. D. Schmitt, C. T.-W. Chu, D. H. Olson, E. W. Sheppard, S. B. McCullen, J. B. Higgens, J. L. Schlenker, *J. Am. Chem. Soc.* **1992**, *114*, 10834.

A Biomimetic Synthesis of a Porphobilinogen Precursor Using a Mukaiyama Aldol Reaction**

André R. Chaperon, Thomas M. Engeloch, and Reinhard Neier*

Dedicated to Professor Dieter Seebach on the occasion of his 60th birthday

The tetrapyrrolic "pigments of life" fulfill many different functions and therefore have a special position among natural pigments.[1] The structures of the intermediates (δ-aminolevulinic acid (ALA, **1**) and porphobilinogen (PBG, **2**)) leading to uroporphyrinogen (Uro) III (**3**), the precursor of all tetrapyrroles, were determined in the early 1950s (Scheme 1).[2] Even early on, the second and third steps of this elegant and convergent biosynthesis could be mimicked chemically.[3]



Scheme 1. Biosynthesis of uroporphyrinogen III (**3**). PBGS = porphobilinogen synthetase.

[*] Prof. Dr. R. Neier, Dr. A. R. Chaperon, Dipl.-Chem. T. M. Engeloch
Institut de Chimie, Université de Neuchâtel
Av. Bellevaux 51, CH-2000 Neuchâtel (Switzerland)
Fax: Int. code + (41)32 718-2511
E-mail: reinhard.neier@ich.unine.ch

[**] This work was supported by the Swiss National Science Foundation and the Fonds der Basler Chemischen Industrie. This work contains parts of the Ph.D. theses of A. R. C. (Thèse de Doctorat, Université de Neuchâtel, 1996) and T. M. E. (Thèse de Doctorat, in preparation). We thank H. Bursian and Dr. S. Claude (Neuchâtel) for measuring the NMR spectra.

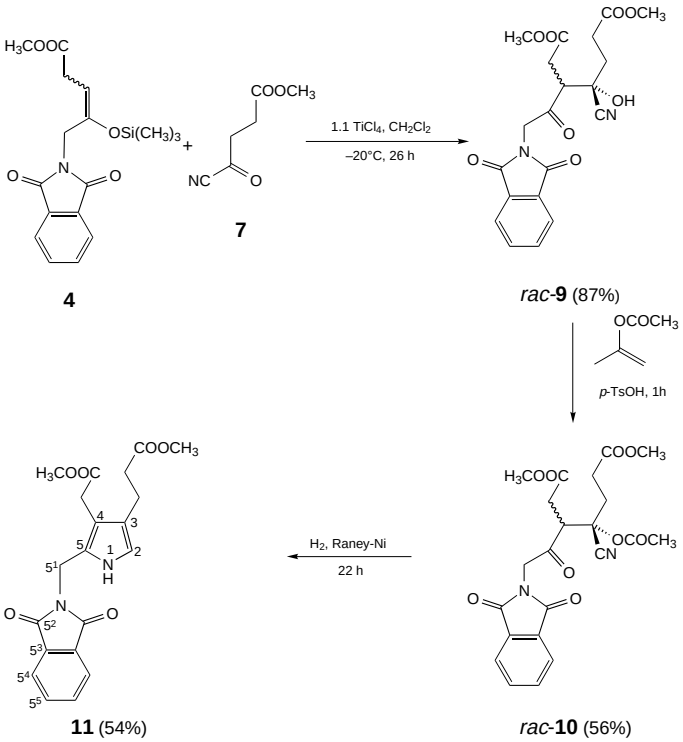
 © WILEY-VCH Verlag GmbH, D-69451 Weinheim, 1998 1433-7851/98/3703-0358 $ 17.50+.50/0

In this context the question arose whether the biosynthesis of porphobilinogen (**2**), which formally corresponds to a Knorr synthesis, could be imitated in the test tube.[4] Despite efforts in different laboratories the process could not be imitated satisfactorily so far. We are examining whether one can imitate the mechanism for the biosynthesis of **2** proposed by Shemin and Nandi[5] and use it for the synthesis of pyrroles.[6] We report here on the synthesis of an N-protected derivative of PBG, which relies on the Mukaiyama aldol reaction.[7] Since the structure determination of **2** 40 years ago, six different synthetic strategies have been developed.[2a, 8] Despite the simplicity of the structure, the synthesis of this natural product in large quantities has remained difficult. In recent years several groups have developed novel approaches to porphobilinogen (**2**).[9]

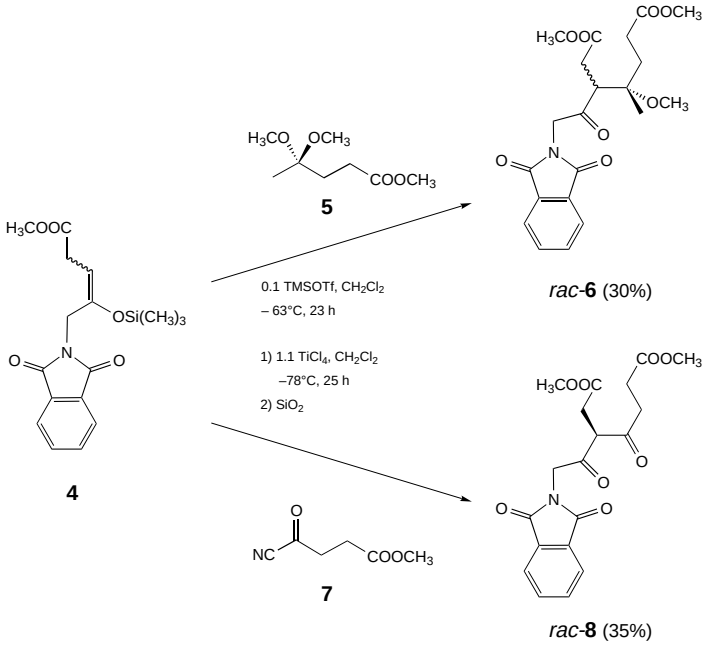
The starting point for our synthesis was the preparation of alkyl-substituted pyrroles using the two-step procedure consisting of a Mukaiyama aldol reaction followed by the reduction of the azido function to give the amino group.[6] The silyl enol ether **4**, obtained from 5-phthalimidomethyllevulinate in 93% yield, was required as starting material for our synthesis.[10] Because **4** is not very nucleophilic, we were unable to couple it under standard conditions with the acetal of 5-azidomethyllevulinate.[6] At temperatures below -40°C $TiCl_4$ was not active enough to catalyze the aldol reaction. At temperatures above -40°C we only could observe decomposition of the starting materials. When we used Lewis acids like TMSOTf[11] or the "super-Lewis acid" $(TMS)B(OTf)_4$ described by Davis[12] we could induce the aldol reaction with the dimethyl acetal of methyllevulinate (**5**). We applied the conditions described by Noyori et al.[11a] with 0.11 equiv TMSOTf as catalyst and were able to isolate 30% of the pure diastereoisomer *rac*-**6** (Scheme 2).

Even with these Lewis acids the crucial C–C bond formation could not be achieved when protected precursors of 5-aminolevulinate were employed. Increasing the reactivity of the carbonyl component seemed the most promising way to solve the problem. When **4** was allowed to react with acylcyanide **7**, the cyanohydrin could be detected in the crude reaction product. However, after aqueous extraction and purification by column chromatography the hydrolysis product *rac*-**8** was obtained in 35% yield (Scheme 2).

Under optimized conditions at -20°C and with $TiCl_4$, which had been freed from HCl by distillation over polyvinylpyridine, the aldol product *rac*-**9** was obtained in 60 to 87% yield (Scheme 3). One diastereoisomer of the aldol



Scheme 3. Synthesis of the protected porphobilinogen **11**.



Scheme 2. Aldol reaction with silyl enol ether **4**.

product *rac*-**9** could be obtained in 47% yield in analytically pure form after crystallization. Attempts to reduce the cyanohydrin *rac*-**9** directly met with limited success. For the synthesis we protected crude *rac*-**9** by reaction with 2-propenol acetate; the acetylated aldol product *rac*-**10** was obtained in 56% yield. Even the reduction of *rac*-**10** proved to be difficult, but finally we were able to reduce *rac*-**10** smoothly at 65°C under 120 atm H_2 in the presence of Raney nickel. After column chromatography we obtained the protected porphobilinogen **11**[13] in 54% yield and in analytically pure form. Removal of the protecting groups in two steps has been described previously.[14]

We were able to obtain the protected porphobilinogen **11** in a convergent way starting from two easily obtainable starting materials. The central step of the synthesis is the Mukaiyama aldol reaction between the regioselectively formed silyl enol ether **4** as the nucleophile and acylcyanide **7** as the electrophile. Reducing the acetylated cyanohydrin *rac*-**10** yields directly the protected porphobilinogen **11**. This synthesis

 © WILEY-VCH Verlag GmbH, D-69451 Weinheim, 1998 1433-7851/98/3703-0359 $ 17.50+.50/0

follows the proposal for the biosynthesis made by Nandi and Shemin almost 30 years ago. In contrast to the published syntheses of **11**, the correctly functionalized side chains are introduced with the two starting materials used for the synthesis of the pyrrole ring; subsequent functionalization is therefore not necessary. The bonds formed in this synthetic scheme are the same as those formed in the biosynthesis catalyzed by porphobilinogen synthase. The overall yield starting from 5-phthalimidomethyllevulinate is 25%. The synthesis can be used to obtain selectively labeled porphobilinogen.

Received: July 21, 1997 [Z10707IE]
German version: *Angew. Chem.* **1998**, *110*, 369–371

Keywords: aldol reactions · biomimetic synthesis · bioorganic chemistry · porphobilinogen · porphyrinoids

[1] B. Franck, A. Nonn, *Angew. Chem.* **1995**, *107*, 1941–1957; *Angew. Chem. Int. Ed. Engl.* **1995**, *34*, 1795–1811.
[2] a) R. Neier in *Advances in Nitrogen Heterocycles, Vol. 2* (Ed.: C. J. Moody), JAI Press, Greenwich, **1996**, pp. 35–146; b) P. M. Jordan in *Biosynthesis of Tetrapyrroles* (Ed.: P. M. Jordan), Elsevier, Amsterdam, **1991**, pp. 1–66; c) F. J. Leeper in *Chlorophylls* (Ed.: H. Scheer), CRC Press, Boca Raton, **1991**, pp. 407–464; d) A. R. Battersby, F. J. Leeper, *Chem. Rev.* **1990**, *90*, 1261–1274.
[3] a) D. Mauzerall, *J. Am. Chem. Soc.* **1960**, *82*, 2605–2609; b) *ibid.* **1960**, *82*, 2601–2605; c) L. F. Tietze, H. Geissler, *Angew. Chem.* **1993**, *105*, 1087–1090; *Angew. Chem. Int. Ed. Engl.* **1993**, *32*, 1038–1040.
[4] a) E. K. Jaffe, J. S. Rajagopalan, *Bioorg. Chem.* **1990**, *18*, 381–394; b) B. Franck, H. Stratman, *Heterocycles* **1981**, *15*, 919–923; c) A. I. Scott, C. A. Townsend, K. Okada, M. Kajiwara, *Trans. N. Y. Acad. Sci.* **1973**, *35*, 72–79.
[5] a) D. Shemin in *The Enzymes* (Ed.: P. D. Boyer), Academic Press, New York, **1972**, pp. 323–337; b) D. L. Nandi, D. Shemin, *J. Biol. Chem.* **1968**, *243*, 1236–1242.
[6] a) H. Bertschy, A. Meunier, R. Neier, *Angew. Chem.* **1990**, *102*, 828–830; *Angew. Chem. Int. Ed. Engl.* **1990**, *29*, 777–778; b) A. Meunier, R. Neier, *Synthesis* **1988**, 381–383; c) H. Bertschy, Dissertation, Universität Freiburg im Uechtland, **1991**; d) A. Meunier, Dissertation, Universität Freiburg im Uechtland, **1989**.
[7] a) T. Mukaiyama, *Org. React.* **1982**, *28*, 203–331; b) *Angew. Chem.* **1977**, *89*, 858–866; *Angew. Chem. Int. Ed. Engl.* **1977**, *16*, 817–825; c) K. Banno, T. Mukaiyama, *Chem. Lett.* **1975**, 741.
[8] R. B. Frydman, B. Frydman, A. Valasinas in *The Porphyrins, Vol. VI* (Ed.: D. Dolphin), Academic Press, New York, **1979**, pp. 1–123.
[9] a) C. Y. De Leon, B. Ganem, *Tetrahedron* **1997**, *53*, 7731–7752; b) *J. Org. Chem.* **1996**, *61*, 8730–8731; c) M. Adamczyk, R. E. Reddy, *Tetrahedron* **1996**, *52*, 14689–14700; d) *Tetrahedron Lett.* **1995**, *36*, 9121–9124.
[10] R. D. Miller, D. R. McKean, *Synthesis* **1979**, 730–732.
[11] a) S. Murata, R. Suzuki, R. Noyori, *J. Am. Chem. Soc.* **1980**, *102*, 3248; b) C. Mukai, S. Hashizume, K. Nagami, M. Hanaoka, *Chem. Pharm. Bull.* **1990**, *38*, 1509–1512.
[12] A. P. Davis, M. Jaspars, *Angew. Chem.* **1992**, *104*, 475–477; *Angew. Chem. Int. Ed. Engl.* **1992**, *31*, 470–471.
[13] NMR data of the protected porphobilinogen **11**: ^{1}H NMR (200 MHz, $CDCl_3$): $\delta = 8.56$ (br. s, 1H, NH), 7.83–7.76 (m, 2H, HC5^4, HC5$^{4'}$), 7.73–7.67 (m, 2H, HC5^5, HC5$^{5'}$), 6.49 (d, $J = 2.7$ Hz, 1H, HC2), 4.80 (s, 2H, H_2C5^1), 3.67 (s, 3H, H_3C3^4), 3.65 (s, 3H, H_3C4^3), 3.64 (s, 2H, H_2C4^1), 2.72 (pseudo t, $J \approx 7.6$ Hz, 2H, H_2C3^1), 2.53 (pseudo triplet, $J \approx 7.3$ Hz, 1H, H_2C3^2); ^{13}C NMR (100 MHz, $CDCl_3$): $\delta = 174.4$ (s, C3^3), 173.1 (s, C4^2), 169.0 (s, C5^2, C5$^{2'}$), 134.7 (d, C5^5, C5$^{5'}$), 132.7 (s, C5^3, C5$^{3'}$), 125.3 (s, C5), 124.0 (s, C5^4, 5$^{4'}$), 122.2 (s, C4), 116.0 (d, C2), 113.7 (s, C3), 52.6 (q, C3^4), 52.1 (q, C4^3), 35.3 (t, C3^2), 33.0 (t, C5^1), 30.3 (t, C4^1), 21.2 (t, C3^1).
[14] G. W. Kenner, J. Rimmer, K. M. Smith, J. F. Unsworth, *J. Chem. Soc. Perkin Trans. 1* **1977**, 332–340.

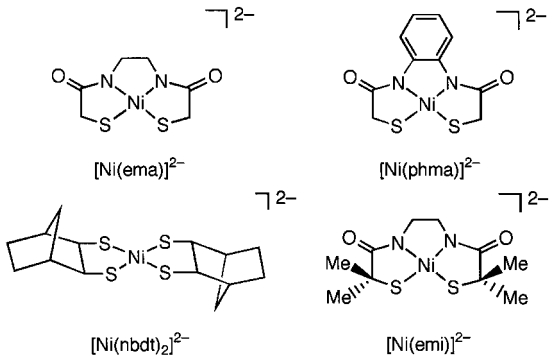
First Isolation and Structural Characterization of a Nickel(III) Complex Containing Aliphatic Thiolate Donors**

Jan Hanss and Hans-Jörg Krüger*

Dedicated to Professor Richard H. Holm on occasion of his 65th birthday

The discovery of a nickel site with a thiolate-rich ligand environment in hydrogenases some 15 years ago stimulated considerable interest in nickel(II) thiolate complexes and their redox behavior.[1] Because of the recent crystal structure determination of the enzyme from the sulfate-reducing bacterium *Desulfovibrio gigas*, the initial description of the nickel site as a mononuclear metal center was revoked, and the heterobimetallic nature firmly established.[2] Efforts towards modeling the structure and reactivity of the active site in nickel-containing hydrogenases are now shifting from the synthesis of mononuclear nickel thiolate complexes towards the synthesis of thiolato-bridged iron–nickel complexes. However, one of the original tasks for inorganic chemists has, to our knowledge, never been accomplished: namely, the preparation *and* isolation of a stable mononuclear nickel(III) complex with aliphatic thiolate donors[3] in the coordination environment. Here we report on the first successful isolation and structural characterization of such a complex.

Previous endeavors to synthesize mononuclear nickel(III) complexes with aliphatic thiolates utilized the nickel(II) complexes depicted in Scheme 1.[4] Although solutions of



Scheme 1. Nickel(II) complexes with aliphatic thiolate ligands which have been used to electrochemically generate nickel(III) complexes in solution.[4]

the relatively stable nickel(III) complexes $[Ni(nbdt)_2]^-$ and $[Ni(emi)]^-$[4] could be electrochemically generated, no solid compounds were isolated. Recently, we showed that stable copper(II) and even copper(III) complexes can be prepared with the quadruply deprotonated ligand *N*,*N*′-1,2-phenylenebis(2-sulfanyl-2-methylpropionamide) (H_4phmi).[5] With respect to its donor-atom set, H_4phmi is related to some of the

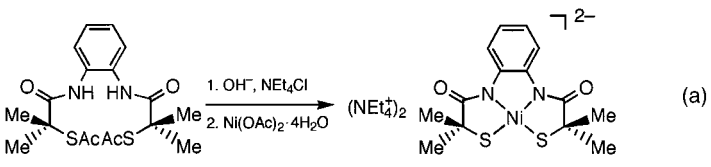
[*] Dr. H.-J. Krüger, J. Hanss
Institut für Anorganische und Angewandte Chemie der Universität
Martin-Luther-King-Platz 6, D-20146 Hamburg (Germany)
Fax: Int. code + (49) 40 4123-2893
E-mail: krueger@xray.chemie.uni-hamburg.de

[**] This work was supported by the Deutsche Forschungsgemeinschaft.

 © WILEY-VCH Verlag GmbH, D-69451 Weinheim, 1998 1433-7851/98/3703-0360 $ 17.50+.50/0

ligands depicted in Scheme 1. In general, nickel(III) complexes are more difficult to synthesize than copper(III) complexes, because Ni^{III}/Ni^{II} redox potentials are more positive than those of isostructural Cu^{III}/Cu^{II} redox pairs.[6] In addition, presumably due to the presence of an unpaired electron, nickel(III) complexes display a more pronounced tendency to decompose than the corresponding copper(III) complexes. One of the major obstacles to the synthesis of nickel(III) thiolate complexes is autoreduction of the metal ion by the coordinated thiolates with concomitant formation of disulfides.[7] This seems to be less of a problem when the thiolate-donor functionality is somewhat sterically protected, as in $[Ni(nbdt)_2]^-$ and $[Ni(emi)]^-$. For nickel(III) amidate complexes, a well-known decomposition pathway involves the presence of a hydrogen atom in an α position with respect to the amidato functionality.[8] Because no hydrogen atom is present in an α position to any donor functionalities in H_4phmi, in contrast to the amidethiol ligands used in previous studies, this ligand was deemed suitable for synthesizing nickel(III) complexes that are stable enough to be isolated.

The red nickel(II) complex $(NEt_4)_2[Ni(phmi)]$ (**1**) was prepared according to Equation (a). Based on the diamagnetism and electronic absorption spectrum of the complex, a



(a)

$(NEt_4)_2[Ni(phmi)]$ **1**

square-planar coordination geometry is attributed to the nickel ion. Owing to severe disorders in the crystal lattice of **1**, a structure determination was carried out on a single crystal of $K(PPh_4)[Ni(phmi)]$ (**2**).[9] As expected, the nickel ion is coordinated to two deprotonated amide and two thiolate groups. In agreement with the results for **1**, the NiN_2S_2 coordination environment in **2** is essentially square planar, and the nickel ion deviates from the least-squares N_2S_2 plane by only 0.022 Å. The potassium ion bridges the two thiolate sulfur atoms (3.173 – 3.208 Å) and is further bound in a tetrahedral geometry to two amide oxygen atoms of adjacent $[Ni(phmi)]^{2-}$ moieties (2.559 – 2.672 Å). Despite the coordinated potassium ion, the average Ni–N and Ni–S bond lengths of 1.879 ± 0.005 and 2.171 ± 0.005 Å, respectively, (see legend of Figure 1) are very similar to those found in $[Ni(ema)]^{2-}$.[4b] Electrochemical data suggest that in solution the potassium ion is no longer bound to the complex anion $[Ni(phmi)]^{2-}$.

The cyclic voltammograms of complexes **1** and **2** in acetonitrile reveal an electrochemically reversible oxidation at -0.71 V (versus the ferrocene/ferrocenium redox potential; all following potentials are given with respect to this redox pair). Quantitative electrolysis at -0.51 V provides a blue solution after the passage of 0.98 electrons per complex anion; upon re-reduction of the solutions at -0.91 V, more than 95% of the original nickel(II) complex is recovered. Spectrophotometric examination of the stability of the dissolved oxidized complex over time reveals that even after 50 days under an atmosphere of nitrogen 90% of the complex $[Ni(phmi)]^-$ is still present. This observation warrants the claim that isolation of the oxidized species is feasible. Indeed, quantitative bulk electrolysis of **2** in acetonitrile results in analytically pure crystals of blue $(PPh_4)[Ni(phmi)]$ (**3**) after recrystallization from acetone/diethyl ether.

The structure determination of **3** (Figure 1)[9] demonstrates that the coordination environment and the square-planar coordination geometry around the nickel ion are preserved upon oxidation (the nickel ion deviates from the least-squares

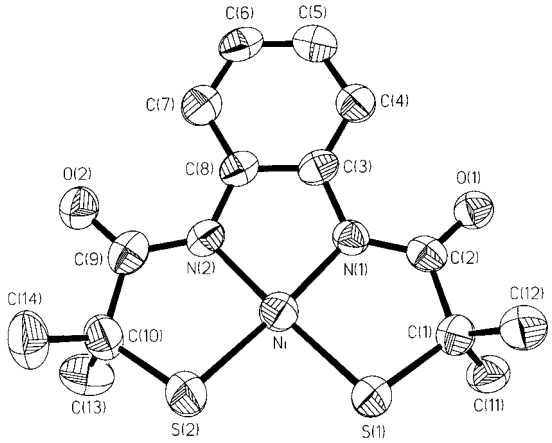


Figure 1. Perspective view of the structure of the $[Ni(phmi)]^-$ ion in **3** (thermal ellipsoids at the 50% probability level) and the atom-numbering scheme. Selected bond lengths [Å] and angles [°] in the $[Ni(phmi)]^-$ ion [in the two crystallographically independent $[Ni(phmi)]^{2-}$ ions in the crystal lattice of **2**]: Ni–S(1) 2.119(3) [2.168(1), 2.174(1)], Ni–S(2) 2.109(3) [2.166(1), 2.174(1)], Ni–N(1) 1.849(6) [1.878(2), 1.874(2)], Ni–N(2) 1.863(7) [1.882(2), 1.880(2)]; S(1)-Ni-S(2) 93.11(11) [96.09(3), 96.10(3)], S(1)-Ni-N(1) 90.40(22) [89.35(6), 89.20(6)], S(1)-Ni-N(2) 176.19(24) [175.18(6), 174.89(6)], S(2)-Ni-N(1) 175.59(23) [174.07(6), 174.66(6)], S(2)-Ni-N(2) 90.27(23) [88.73(6), 88.96(6)], N(1)-Ni-N(2) 86.31(30) [85.85(8), 85.74(8)].

N_2S_2 plane by 0.007 Å). Within a distance of 6 Å there are no axial donor atoms at the nickel ion. With respect to **2**, the average Ni–N and Ni–S bond lengths in **3** are reduced to 1.856 ± 0.007 Å and 2.114 ± 0.005 Å, respectively. A comparison of the C–C and C–N bond lengths of the phenylenediamide moieties of **2** and **3** indicates essentially no change within the 3σ criterion. In addition, these bond lengths are very different from those reported for an oxidized cobalt complex,[10] in which oxidation does take place at the phenylenediamide portion of the ligand (Table 1). Although the interatomic S–S distance substantially decreases from 3.224 Å in **2** to 3.069 Å in **3**, there is no bonding interaction between the two sulfur atoms. These structural results serve as the first piece of evidence that the oxidation is mainly metal-centered. A substantial shortening of the Ni–N and Ni–S bonds is not expected to occur, since the electron is not removed from a strongly σ-antibonding orbital during the oxidation of the nickel(II) complex. The rather modest decrease of 0.023 Å for the Ni–N bonds is related to the stronger electrostatic interactions between the more electro-

 © WILEY-VCH Verlag GmbH, D-69451 Weinheim, 1998 1433-7851/98/3703-0361 $ 17.50+.50/0

Table 1. Bond lengths [Å] in the phenylenediamide moieties of $[Ni(phmi)]^{2-}$, $[Ni(phmi)]^{-}$, $[Co^{III}(L)]^{-}$, and $[Co^{II}(L)]$.

	$[Ni(phmi)]^{2-}$[a]	$[Ni(phmi)]^{-}$	$[Co^{III}(L)]^{-}$[b]	$[Co^{II}(L)]$[b]
N(1)–C(3)	1.420(3)	1.419(9)	1.415(3)	1.353(6)
N(2)–C(8)	1.414(3)	1.412(10)	1.406(3)	1.353(6)
C(3)–C(4)	1.399(3)	1.389(11)	1.376(4)	1.398(7)
C(4)–C(5)	1.396(4)	1.390(11)	1.387(4)	1.350(8)
C(5)–C(6)	1.382(4)	1.361(12)	1.380(4)	1.428(10)
C(6)–C(7)	1.399(4)	1.387(11)	1.386(4)	1.350(8)
C(7)–C(8)	1.401(3)	1.401(11)	1.387(4)	1.398(7)
C(3)–C(8)	1.422(3)	1.414(11)	1.411(4)	1.432(9)

[a] Averaged bond lengths from the two crystallographically distinct complex anions. [b] From ref. [10], with the numbering schemes adapted to those of complexes **2** and **3**.

positive central ion and the negatively charged ligand donor atoms. The slightly greater decrease in the Ni–S bond length by 0.057 Å may be explained by the lack of a potassium ion bridging the two sulfur atoms in **3**.

The magnetic moment of **3** is 1.78 μ_B, which corresponds to a low-spin complex. As with $[Ni(emi)]^{-}$,[4b] no ESR spectrum is observed for **3** at room temperature or at 100 K. However, at 10 K a spectrum of solid **3** doped into the isomorphous crystal lattice of the diamagnetic complex $(PPh_4)[Cu(phmi)]$ reveals a very broad rhombic signal with apparent g values at 2.55, 2.14, and 2.00. This indicates a short electron spin relaxation time due to a relatively small energy separation between the electronic ground and excited states. This conclusion is also supported by the observation that the NIR region of the electronic absorption spectrum of **3** contains a d–d transition at rather low energy (5120 cm^{-1}). In the presence of excess pyridine (py) in the solution of **3**, the powder spectrum of the frozen solution at 100 K (Figure 2)

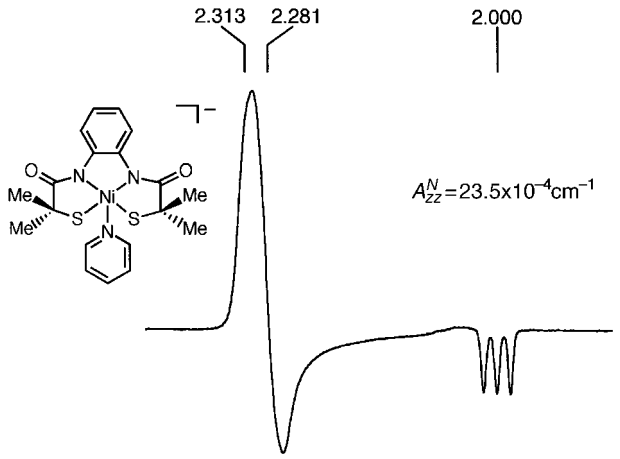


Figure 2. X-band ESR spectrum of a frozen solution of $[Ni(phmi)(py)]^{-}$ ions in dimethylformamide containing excess pyridine at 100 K (the g values are indicated).

shows a nearly axial signal with g values at 2.313, 2.281, and 2.000. The splitting of the g_z component into three lines of equal intensities due to superhyperfine coupling ($A_z^N = 25$ G) with the nuclear spin ($I_N = 1$) of a single nitrogen donor atom is consistent with the formation of the monoadduct $[Ni(phmi)(py)]^{-}$. The formation of a similar monoadduct upon addition of pyridine to a solution containing the complex $[Ni(emi)]^{-}$ was reported.[4b] The large anisotropy and the average g values of 2.23 and 2.20 for $[Ni(phmi)]^{-}$ and $[Ni(phmi)(py)]^{-}$, respectively, indicate that the unpaired electron mainly resides in a metal-based orbital. The fact that g_x and g_y are larger than g_z and that g_z is 2.00, together with the observation of a superhyperfine splitting of the g_z component, clearly establish a $\ldots(d_{z^2})^1$ electron configuration for the ground state of $[Ni(phmi)(py)]^{-}$. The observation of an ESR spectrum at 100 K only after addition of pyridine is interpreted to mean that axial coordination of a pyridine molecule raises the energy of the d_{z^2} orbital enough to cause less mixing between the ground and the excited states and, therefore, an increase of the electron spin relaxation time.

The results presented here reveal that the oxidized species contains an authentic nickel(III) ion coordinated to aliphatic thiolate groups. In dimethylformamide, the Ni^{III}/Ni^{II} redox potential of **1** (–0.78 V) is about 120 mV more positive than that of $[Ni(emi)]^{2-}$, although the stability of the oxidized complex $[Ni(emi)]^{-}$ is inferior to that of **3**. Therefore, our investigation demonstrates that the stability of nickel(III) thiolate complexes is determined only to a certain extent by the lowest possible redox potential; abolishing or at least retarding possible decomposition pathways (e.g. by introducing steric hindrance around the thiolate donors or by avoiding the presence of any hydrogen atoms in an α position to the donor functionalities in the ligand) plays a larger role, at least for the currently discussed amidato–thiolato nickel complexes.

The original challenge for inorganic chemists to prepare *and* isolate stable nickel(III) complexes with aliphatic thiolates in the coordination sphere has finally been met. However, as with the recently reported copper complexes, the stabilization of the high oxidation state of the nickel ion is only achieved because the highly polarizable, negatively charged nitrogen donor atoms of the deprotonated amide functionalities can supply the electropositive metal ion with sufficient electron density to avoid autoreduction of the nickel(III) ion by the coordinated aliphatic thiolates.

Experimental Section

1: Under strictly anaerobic conditions, a solution of *N*,*N*′-1,2-phenylene-bis(*S*-acetyl-2-sulfanyl-2-methylpropionamide) (200 mg, 0.5 mmol), KOH (140 mg, 2.5 mmol), and NEt_4Cl (166 mg, 1.0 mmol) in absolute EtOH (40 mL) was stirred for 0.5 h before a suspension of $Ni(OAc)_2\cdot 4H_2O$ (124 mg, 0.5 mmol) in absolute EtOH (30 mL) was added. After the reaction mixture was heated at reflux for a short time, the solvent was completely removed in vacuo. The residue was treated with CH_3CN (40 mL), and the resulting red solution filtered. Slow diffusion of Et_2O into the solution in CH_3CN afforded a red crystalline material, which was collected, washed with Et_2O, and dried in vacuo to yield analytically pure **1** (235 mg, 75 % yield). Elemental analysis calcd for $C_{30}H_{56}N_4NiO_2S_2$: C 57.41, H 8.99, N 8.93; found: C 57.18, H 8.85, N 8.90; absorption spectrum (CH_3CN): λ_{max} (ε_M) = 550 (85.6), 439 (280), 359 (7020), 248 (36 900), 232 nm (37 600); ^1H NMR (360 MHz, CD_3CN, anion): $\delta = 8.64$ (dd, 2H), 6.46 (dd, 2H), 1.23 (s, 12H).

Complex **2** was synthesized analogously with PPh_4Cl. However, based on the elemental analysis and the NMR spectrum, **2** is contaminated with $(PPh_4)_2[Ni(phmi)]$.

3: In a glove box, a mixture of $K(PPh_4)[Ni(phmi)]$ and $(PPh_4)_2[Ni(phmi)]$ (0.336 mmol based on the passed charge) in CH_3CN (10 mL) containing

 © WILEY-VCH Verlag GmbH, D-69451 Weinheim, 1998 1433-7851/98/3703-0362 $ 17.50+.50/0

0.05 M PPh_4Cl as supporting electrolyte was exhaustively oxidized at −0.51 V. The electrolysis was carried out at a platinum-net electrode with a PAR Model 273A Potentiostat/Galvanostat controlled by the PAR Model 270 Research Electrochemistry Software. After the oxidation was completed, the electrolyte PPh_4Cl was precipitated by diffusion of Et_2O into the resulting blue solution. Removal of the solvent from the filtered solution yielded a dark blue solid, which was redissolved in acetone (10 mL) under nitrogen. Diffusion of Et_2O into this solution afforded analytically pure **3** as dark blue, leafletlike crystals (128 mg, 54 % yield). Elemental analysis calcd for $C_{38}H_{36}N_2NiO_2PS_2$: C 64.60, H 5.14, N 3.97; found: C 64.63, H 5.12, N 4.12; absorption spectrum (CH_3CN): λ_{max} (ε_M) = 1953 (54.5), 940 (sh, 3410), 843 (3970), 573 (1330), 388 (3070), 337 (sh, 3710), 274 (sh, 21 400), 266 (sh, 25 700), 253 (sh, 28 700), 230 nm (60 600).

Received: May 28, 1997
Revised version: August 25, 1997 [Z 10488 IE]
German version: *Angew. Chem.* **1998**, *110*, 366 – 369

Keywords: high-valent metal ions · nickel · redox chemistry · S ligands

[1] A. F. Kolodziej, *Prog. Inorg. Chem.* **1994**, *41*, 493.

[2] a) A. Volbeda, M. H. Charon, C. Piras, E. C. Hatchikian, M. Frey, J. C. Fontecilla-Camps, *Nature* **1995**, *373*, 580; b) A. Volbeda, E. Garcin, C. Piras, A. L. de Lacey, V. M. Fernandez, E. C. Hatchikian, M. Frey, J. C. Fontecilla-Camps, *J. Am. Chem. Soc.* **1996**, *118*, 12 989.

[3] The synthesis of nickel(III) complexes with aliphatic thiolate ligands is considerably more difficult than that of complexes with thiolates in which the sulfur donor atom is bound to a sp^2-hybridized carbon atom owing to the lower redox potential of the thiolate functionality and, therefore, the greater propensity towards disulfide formation. In addition, the authenticity of the trivalent oxidation state of the nickel ion has to be verified for all complexes in which the thiolate sulfur atom is directly bound to a sp^2-hybridized carbon atom whose p orbital is part of an extended π molecular orbital system. Structural characterizations of mono- and dinuclear nickel(III) complexes with aryl thiolate ligands have been reported: a) C. Mahadevan, M. Seshasayee, P. Kuppusamy, P. T. Manoharan, *J. Cryst. Spectrosc.* **1985**, *15*, 305; b) J. Ochocki, P. Chaudhuri, W. L. Driessen, R. A. G. de Graaff, F. B. Hulsbergen, J. Reedijk, *Inorg. Chim. Acta* **1990**, *167*, 15; c) M. Köckerling, G. Henkel, *Chem. Ber.* **1993**, *126*, 951; d) J. D. Franolic, W. Y. Wang, M. Millar, *J. Am. Chem. Soc.* **1992**, *114*, 6587.

[4] a) S. Fox, Y. Wang, A. Silver, M. Millar, *J. Am. Chem. Soc.* **1990**, *112*, 3218; b) H.-J. Krüger, G. Peng, R. H. Holm, *Inorg. Chem.* **1991**, *30*, 734.

[5] J. Hanss, H.-J. Krüger, *Angew. Chem.* **1996**, *108*, 2989; *Angew. Chem. Int. Ed. Engl.* **1996**, *35*, 2827.

[6] a) F. P. Bossu, D. W. Margerum, *Inorg. Chem.* **1977**, *16*, 1210; b) J. M. Anast, D. W. Margerum, *ibid.* **1982**, *21*, 3494.

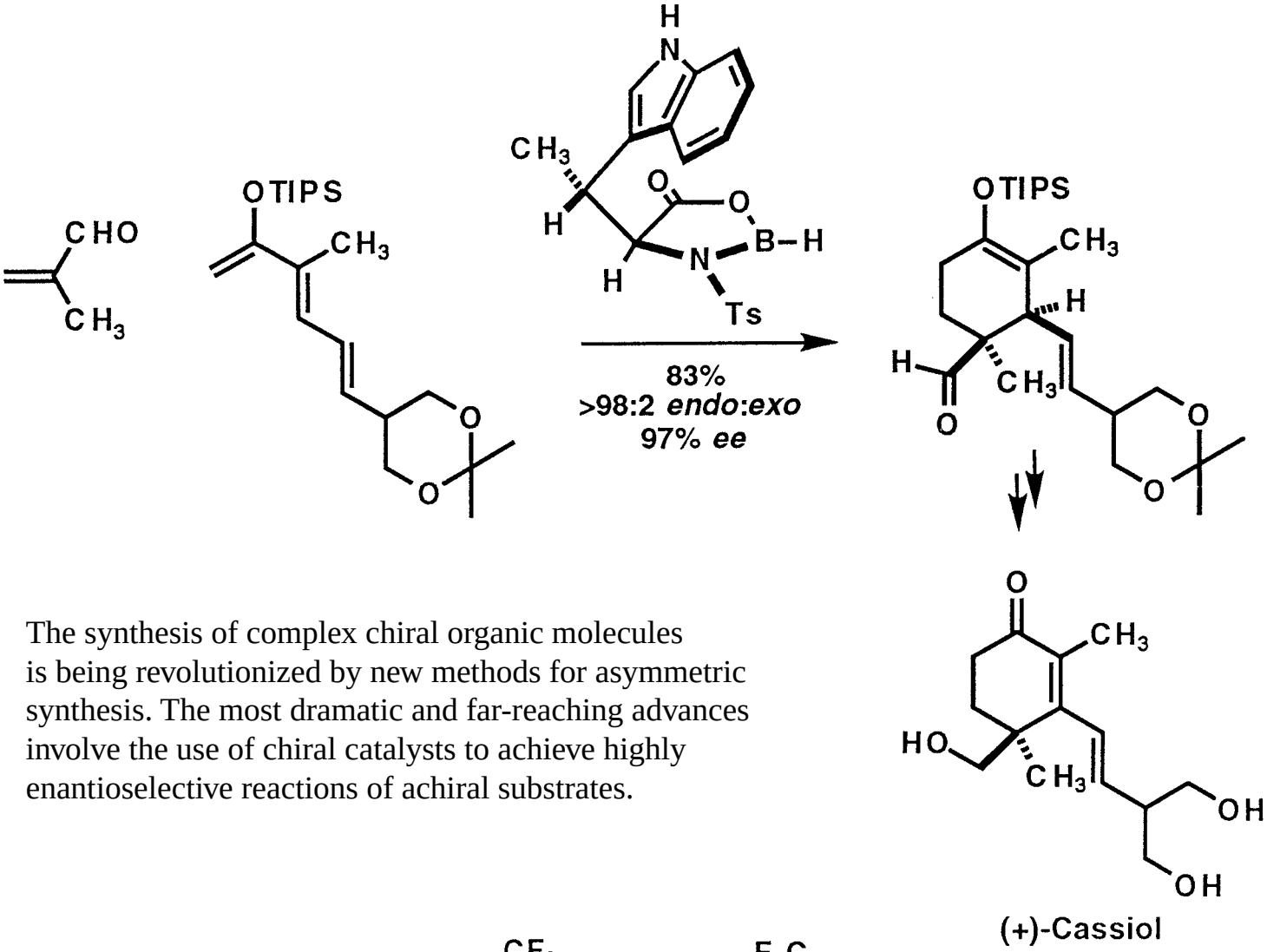
[7] H.-J. Krüger, R. H. Holm, *Inorg. Chem.* **1989**, *28*, 1148.

[8] S. T. Kirksey, Jr., T. A. Neubecker, D. W. Margerum, *J. Am. Chem. Soc.* **1979**, *101*, 1631.

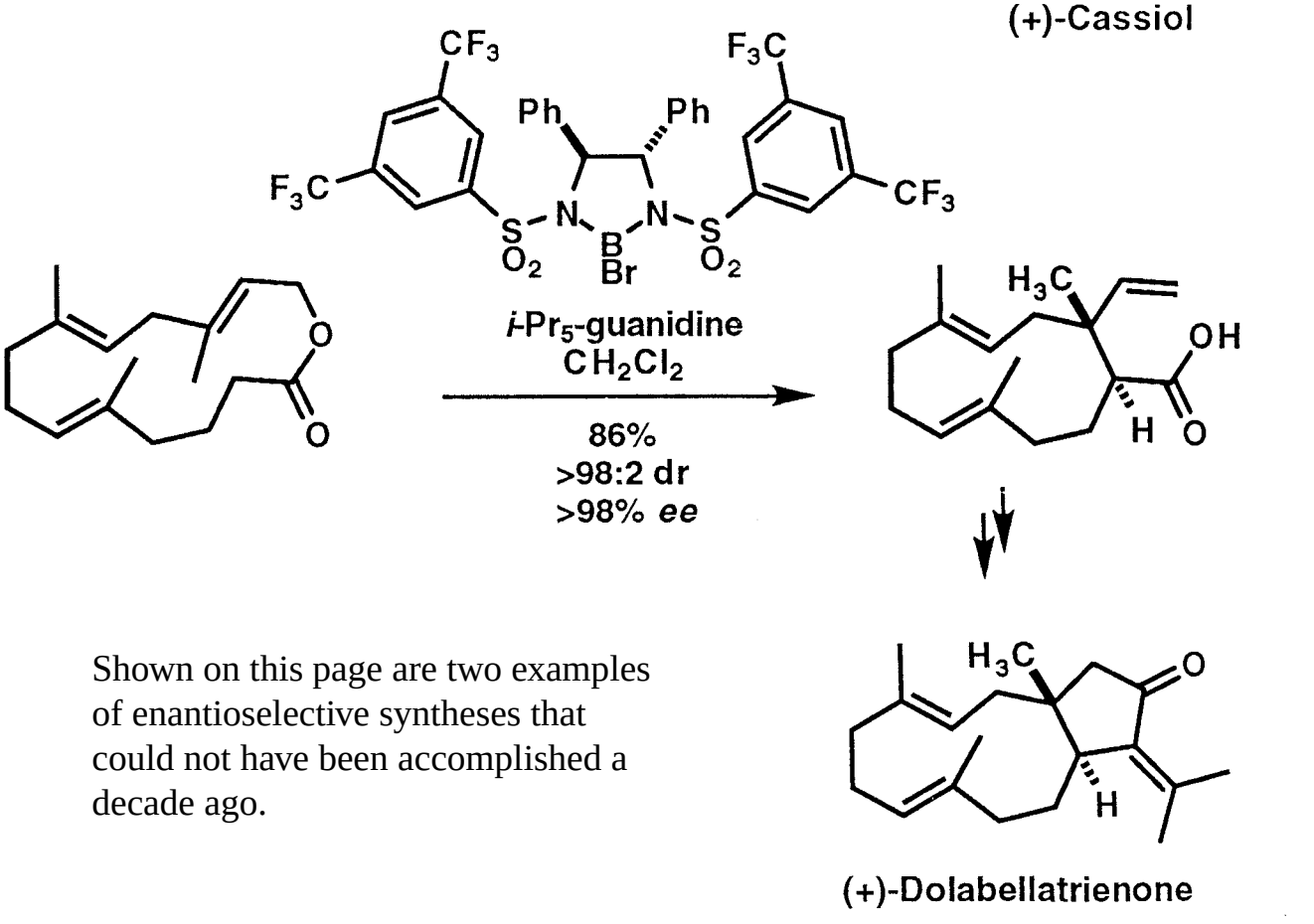
[9] Crystallographic data for **2**: triclinic, space group $P\bar{1}$, $a = 13.149(2)$, $b = 14.778(3)$, $c = 19.541(6)$ Å, $\alpha = 88.00(2)$, $\beta = 72.99(1)$, $\gamma = 77.96(1)^\circ$, $V = 3550(1)$ Å^3, $Z = 4$, $\rho_{calcd} = 1.395$ g cm^{-3}; $T = 153$ K; 2θ range $4.6^\circ < 2\theta < 50^\circ$; 12 577 unique reflections (9891 with $F_o > 4\sigma(F_o)$), $\mu(Mo_{K\alpha}) = 8.63$ cm^{-1}; 853 parameters; $R = 0.0333$ ($F_o > 4\sigma(F_o)$). Crystallographical data for **3**: monoclinic, space group $P2_1/n$, $a = 14.157(7)$, $b = 11.342(4)$, $c = 21.032(5)$ Å, $\beta = 98.92(2)^\circ$, $V = 3336(2)$ Å^3, $Z = 4$, $\rho_{calcd} = 1.407$ g cm^{-3}; $T = 153$ K; 2θ range $7^\circ < 2\theta < 120^\circ$; 4954 unique reflections (2546 with $F_o > 4\sigma(F_o)$), $\mu(Cu_{K\alpha}) = 27.54$ cm^{-1}; 418 parameters; $R = 0.0678$ ($F_o > 4\sigma(F_o)$). Crystallographic data (excluding structure factors) for the structures reported in this paper have been deposited with the Cambridge Crystallographic Data Centre as supplementary publication no. CCDC-100 465. Copies of the data can be obtained free of charge on application to CCDC, 12 Union Road, Cambridge CB2 1EZ, UK (fax: int. code + (49) 1223-336 033; e-mail: deposit@ccdc.cam.ac.uk).

[10] H_4L = 5,6-(4,5-dichlorobenzo)-3,8,11,13-tetraoxo-2,2,9,9-tetramethyl-12,12-diethyl-1,4,7,10-tetraazacyclotridecane; T. J. Collins, R. D. Powell, C. Slebodnick, E. S. Uffelman, *J. Am. Chem. Soc.* **1991**, *113*, 8419.

 © WILEY-VCH Verlag GmbH, D-69451 Weinheim, 1998 1433-7851/98/3703-0363 $ 17.50+.50/0



The synthesis of complex chiral organic molecules is being revolutionized by new methods for asymmetric synthesis. The most dramatic and far-reaching advances involve the use of chiral catalysts to achieve highly enantioselective reactions of achiral substrates.



Shown on this page are two examples of enantioselective syntheses that could not have been accomplished a decade ago.

ANGEWANDTE CHEMIE © WILEY-VCH

The Catalytic Enantioselective Construction of Molecules with Quaternary Carbon Stereocenters

Elias J. Corey* and Angel Guzman-Perez

The catalytic asymmetric synthesis of structurally complex naturally occurring organic molecules and other highly useful chiral substances represents a new frontier for synthetic chemistry and an ideal testing ground for the remarkable new synthetic chiral catalysts, whose impact on all of chemistry promises to be profound. Catalytic enantioselective methodology provides a powerful new option for synthesis planning and execution, which complements the use of chiral starting materials, chiral controller groups (auxiliaries), or enzymic catalysis. The synthesis of complex molecules with quaternary (fully substituted) stereocenters, one of the most demanding tasks in multistep synthesis, presents simultaneously a challenge to catalytic enantioselective processes and an opportunity to demonstrate their power and potential. In addition, the problems that inevitably arise in the execution of a synthesis of a complex molecule provide a stimulus and a sense of direction for new discovery. In this article several of the most promising new catalytic enantioselective methods are reviewed from the point of view of their application to the construction of complex chiral molecules with quaternary stereocenters. It is safe to predict that this field of chemistry will grow enormously in the coming decades and will have great intellectual and practical impact.

Keywords: asymmetric catalysis · chirality · enantioselective addition · quaternary stereocenters · total synthesis

1. Introduction

Organic chemistry has undergone a revolution in the last two decades. The development of new and highly enantioselective processes has become a major focus of chemical synthesis, and the use of chiral catalysts is displacing chiral auxiliaries and reagents as the method of choice for asymmetric synthesis. An efficient chiral catalyst allows for large quantities of optically active product to be obtained on use of relatively small amounts of enantiopure material, without the need for the removal and recovery of a chiral auxiliary. Furthermore, the most practical catalytic methods utilize an inexpensive and readily available chiral ligand, and provide high and predictable enantioselectivity across a wide range of substrates.[1] The application of such catalytic asymmetric reactions to the synthesis of challenging natural products has assumed increasing importance not only to demonstrate their value, but also to understand these methods better and improve them, thereby increasing their generality. The asymmetric construction of molecules with quaternary carbon stereocenters, that is, carbon centers with four different nonhydrogen substituents, represents a very challenging and dynamic area in organic synthesis. The preparation of compounds containing these centers with *catalytic* enantioselective reactions is particularly demanding. This review presents a concise survey of some modern and highly selective methods for the catalytic construction of these compounds, using representative recent examples. The many excellent noncatalytic, diastereoselective, or biochemical methods will not be discussed here.[2]

[*] Prof. E. J. Corey, Dr. A. Guzman-Perez
Department of Chemistry and Chemical Biology,
Harvard University
12 Oxford Street, Cambridge, MA, 02138 (USA)
Fax: (+1) 617-495-0376
E-mail: corey@chemistry.harvard.edu

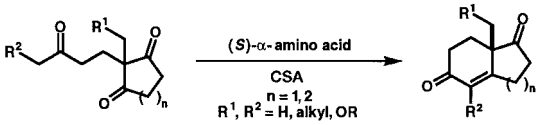
2. Catalytic Methods Applicable to the Direct Synthesis of All-Carbon-Substituted Quaternary Carbon Stereocenters

2.1. Robinson Annulation and Intramolecular Aldol Reaction Catalyzed by Amino Acids

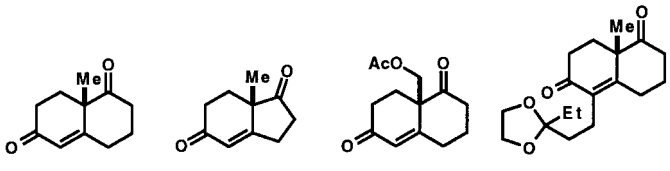
The enantioselective version of the classical Robinson annulation has been applied to the synthesis of optically active diketones, which are useful in the preparation of a variety of terpenes and other natural products. The transformation involves the discrimination between two enantiotopic carbonyl groups in an intramolecular aldol reaction, which involves

 © WILEY-VCH Verlag GmbH, D-69451 Weinheim, 1998 1433-7851/98/3704-0389 $ 17.50+.50/0

an enamine of the triketone and the chiral α-amino acid catalyst (Scheme 1). For example, the fused bicyclic compounds shown in Scheme 2, which include the Wieland–Miescher ketone, were prepared in this manner. The products could be recrystallized until optically pure.[3]



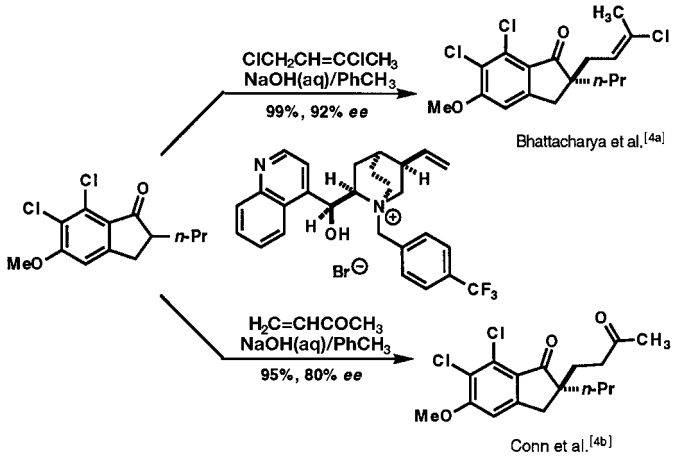
Scheme 1. Enantioselective aldol cyclization. CSA = (+)-camphorsulfonic acid.



Scheme 2. Chiral products from amino acid catalyzed cyclization of achiral precursors, including the Wieland–Miescher ketone (extreme left).

2.2. Alkylation and Michael Addition Reactions

Alkylations and Michael additions are useful and versatile reactions; however, few instances of highly enantioselective catalytic versions of these transformations for the synthesis of quaternary stereocenters have been demonstrated to date. A noteworthy example is the use of the phase-transfer catalyst *N*-(4-trifluoromethylbenzyl)cinchoninium bromide by Merck scientists for the synthesis of alkylated indanones as promising drug candidates (Scheme 3).[4]



Scheme 3. Enantioselective alkylation by phase-transfer catalysis.

2.3. Diels–Alder Reactions

The Diels–Alder cycloaddition is arguably one of the most useful and powerful transformations available to the synthetic chemist. Great effort has been devoted to the development of catalytic enantioselective versions of this reaction.[5] The enantioselective Diels–Alder reaction of 2-substituted acroleins is particularly interesting, because it provides products with a quaternary stereocenter. Scheme 4 presents a collection of Lewis acid catalysts (**1**–**10**) that have been applied successfully to the asymmetric Diels–Alder reaction of 2-substituted acroleins.[6]

The asymmetric Diels–Alder reactions of 2-haloacroleins have attracted considerable attention not only because of the high reactivity and selectivity obtained with these dienophiles, but also because of the exceptional synthetic versatility of the resulting adducts.[6d] The excellent enantioselectivities resulting from the reactions of 2-bromoacrolein and 2-chloroacrolein with a variety of dienes are summarized in Scheme 5. In

Elias J. Corey, born 1928 in Methuen about 50 km north of Boston, studied Chemisty from 1945 to 1950 at the Massachusetts Institute of Technology, where he gained his doctorate for work on synthetic penicillins under John C. Sheehan. In January 1951 he joined the University of Illinois at Urbana-Champaign as an Instructor in Chemistry and was promoted to full Professor in 1956 at the early age of 27. Since 1959 he has been at Harvard University. His many scientific successes were crowned with the Nobel Prize for Chemistry in 1990. For as long as he can remember he has enjoyed study, adventure, and discovery.

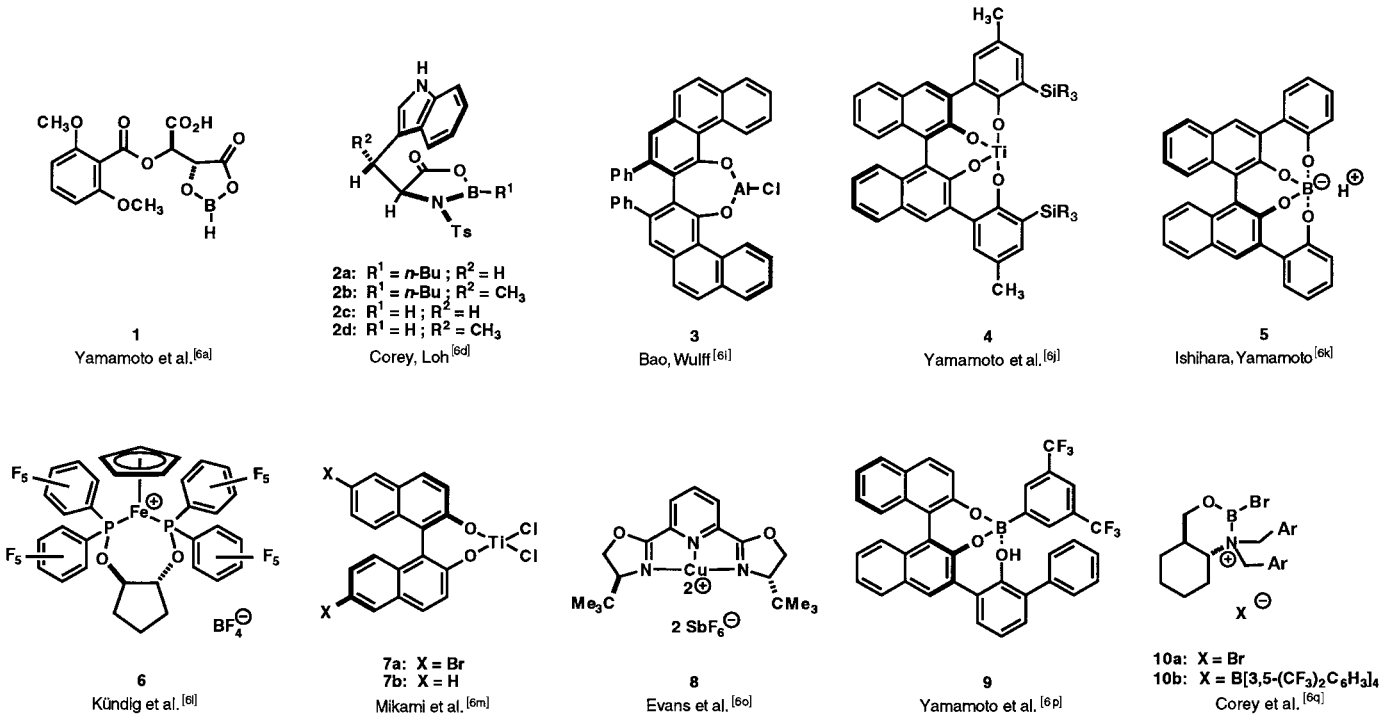


E. J. Corey



A. Guzman-Perez

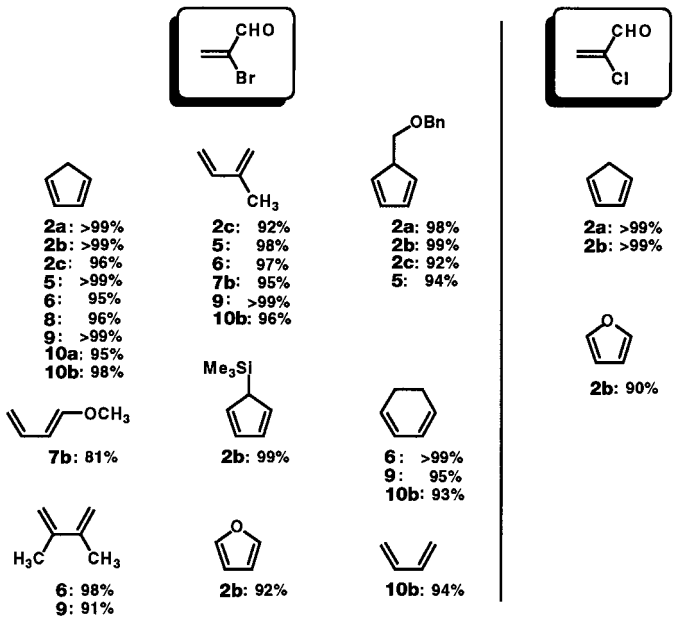
Angel Guzman-Perez was born in 1967 in Mexico City (Mexico) and obtained his Bachelor's degree in Chemistry at the National Autonomous University of Mexico. He worked for a year (1990–1991) at Syntex Research (Palo Alto, California, USA) in the medicinal chemistry department and then joined the Ph.D. program at Harvard University under the direction of Professor E. J. Corey to study new methods for the asymmetric synthesis of natural products. He received the Ph.D. degree in Chemistry in 1997 and now works in drug discovery at Pfizer Central Research (Groton, Connecticut, USA).



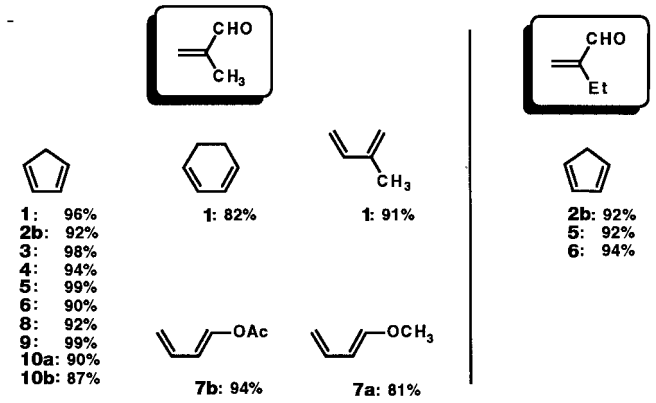
Scheme 4. Effective catalysts for the synthesis of Diels–Alder adducts with quaternary stereocenters. R = *o*-tolyl, Ar = 3,5-$Me_2C_6H_3$.

addition, 2-alkylacroleins such as 2-methylacrolein and 2-ethylacrolein produce favorable results with several dienes, but are less versatile than their 2-halo counterparts as shown in Scheme 6. Furthermore, certain 2,3-disubstituted acroleins afford promising selectivities in the reaction with cyclopentadiene (Scheme 7).

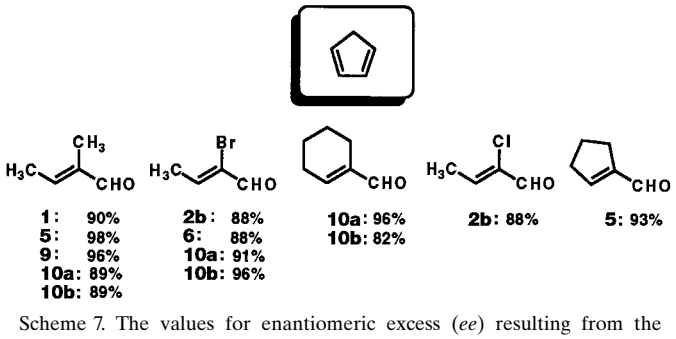
The application of these reactions to the total synthesis of natural products (especially with catalysts **2**) has recently commenced. For example, Marshall and Xie synthesized a



Scheme 5. The values for enantiomeric excess (*ee*) resulting from the asymmetric Diels–Alder reaction of 2-bromoacrolein and 2-chloroacrolein with several dienes on catalysis with the indicated compounds.

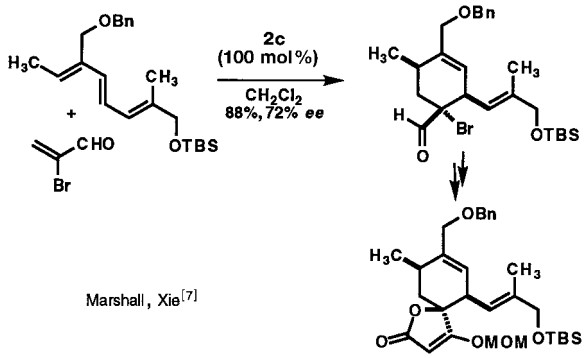


Scheme 6. The values for enantiomeric excess (*ee*) resulting from the asymmetric Diels–Alder reaction of 2-methylacrolein and 2-ethylacrolein with several dienes on catalysis with the indicated compounds.



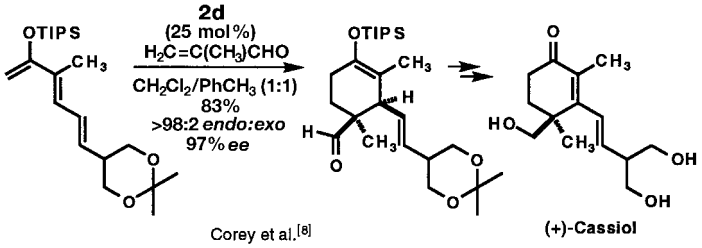
Scheme 7. The values for enantiomeric excess (*ee*) resulting from the asymmetric Diels–Alder reaction of several 2,3-disubstituted acroleins with cyclopentadiene on catalysis with the indicated compounds.

Diels–Alder cycloadduct bearing a quaternary stereocenter using stoichiometric amounts of catalyst **2c**, and converted it into the spirotetronate subunit of kijanolide (Scheme 8).[7]



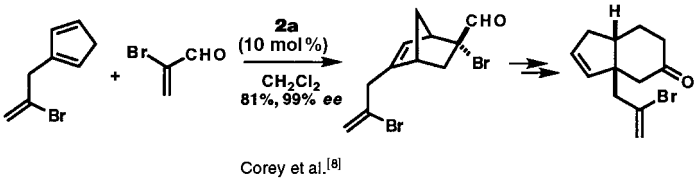
Scheme 8. Enantioselective Diels–Alder route to the spirotetronate unit of kijanolide. MOM = methoxymethyl, TBS = *tert*-butyldimethylsilyl.

Furthermore, the enantioselective Diels–Alder reaction between a trisubstituted electron-rich open-chain diene and 2-methylacrolein catalyzed by oxazaborolidine **2d** was used to accomplish an efficient synthesis of the potent antiulcer agent cassiol in 97% *ee* (Scheme 9). The high enantioselectivity of the key cycloaddition is the collective result of critical modifications to the substrate, catalyst, and reaction solvent.[8]



Scheme 9. Enantioselective total synthesis of (+)-cassiol. TIPS = triisopropylsilyl.

Finally, a Diels–Alder reaction involving catalyst **2a** was used as a key step in an especially simple enantioselective synthesis of gibberellic acid via the bicyclic ketone shown in Scheme 10.[8]



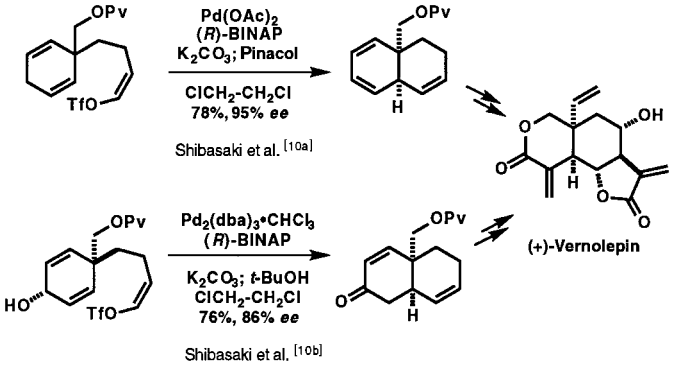
Scheme 10. Catalytic enantioselective Diels–Alder reaction for the synthesis of gibberellic acid.

2.4. Heck Reactions

The enantioselective version of the intramolecular Heck reaction is an extremely effective C–C bond construction. Its utility has already been demonstrated in the synthesis of several natural products containing quaternary stereocenters. Two general strategies have been applied in this field: the differentiation of enantiotopic olefinic bonds in molecules with prochiral quaternary centers and the differentiation of the enantiotopic faces of C–C double bonds.[9]

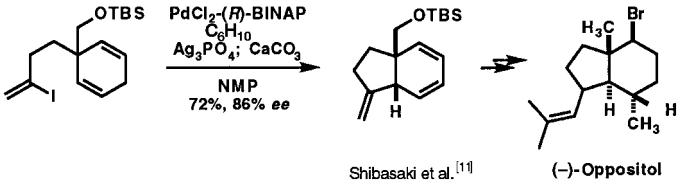
2.4.1. Heck Reactions That Differentiate between Enantiotopic Groups

The asymmetric synthesis of vernolepin has been accomplished in two ways by Shibasaki and co-workers (Scheme 11). The key step in both cases is the differentiation of enantiotopic C–C double bonds by an intramolecular Heck reaction.[10]



Scheme 11. Asymmetric intramolecular Heck reaction for the synthesis of vernolepin. BINAP = 2,2′-bis(diphenylphosphino)-1,1′-binaphthyl, dba = dibenzylidenacetone, PV = pivaloyl.

Furthermore, the synthesis of a *cis*-hydrindan was accomplished employing a similar strategy as outlined in Scheme 12. The product of this Heck reaction allowed for the formal asymmetric synthesis of oppositol and prepinnaterpene. Interestingly, the use of an *endo*-vinyl iodide instead of the *exo*-vinyl iodide shown afforded product in only 3% *ee*.[11]

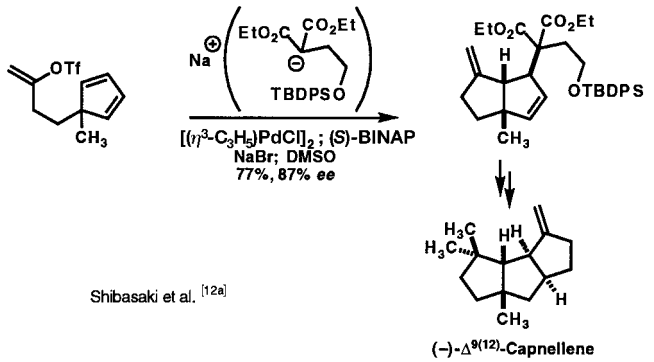


Scheme 12. Synthesis of (−)-oppositol. NMP = *N*-methyl-2-pyrrolidone.

The asymmetric Heck reaction has also been applied to the synthesis of compounds containing two fused five-membered rings by the use of prochiral cyclopentadienyl systems. The transformation initially generates a π-allylpalladium species, which is then trapped with a suitable nucleophile to complete the catalytic cycle. Nucleophiles that have been used for this purpose include acetate, an amine, and dicarbonyl-stabilized enolates. For example, in the synthesis of $\Delta^{9(12)}$-capnellene the π-allyl intermediate was captured with a malonate anion to provide the desired product of 87% *ee* with complete diastereo- and regioselectivity (Scheme 13).[12]

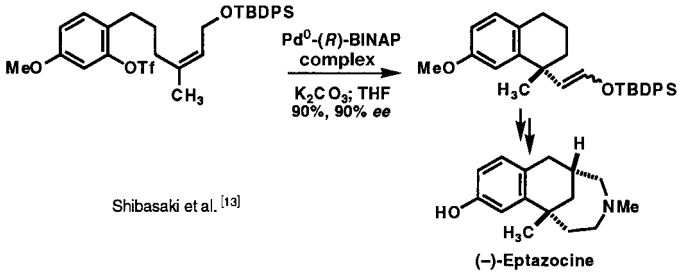
2.4.2. Heck Reactions That Differentiate between Enantiotopic Faces

The use of an intramolecular Heck reaction that differentiates between enantiotopic faces was demonstrated by Shibasaki and co-workers for the synthesis of eptazocine. The



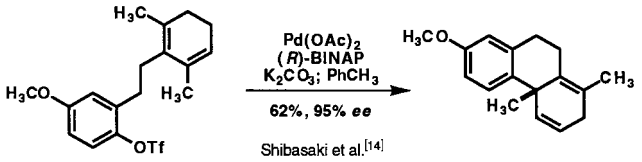
Scheme 13. Heck alkylation/cyclization route to (−)-capnellene. TBDPS = *tert*-butyldiphenylsilyl.

Z-olefinic substrate provided better results than the corresponding *E* isomer (Scheme 14).[13]



Scheme 14. Enantioselective synthesis of (−)-eptazocine.

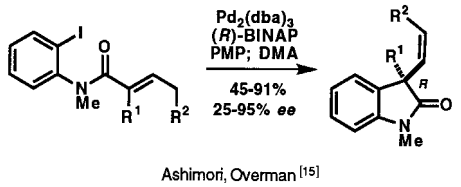
A synthetic intermediate in the synthesis of a number of diterpenes, including kaurene, abietic acid, and a bruceantin analogue, was prepared by a regio- and face-selective Heck reaction (Scheme 15).[14]



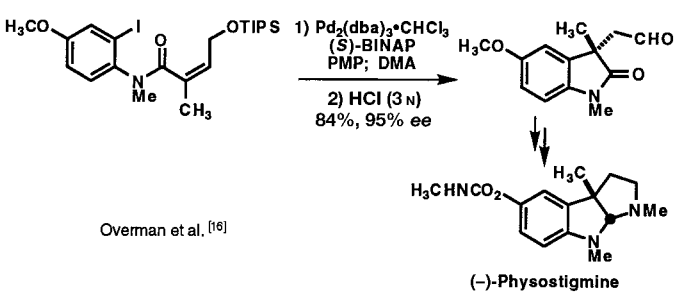
Scheme 15. Enantioselective route to hydrophenanthrenes.

Overman and Ashimori reported the construction of several 2-oxindoles from the corresponding aryl iodides through intramolecular Heck reactions. Either enantiomeric product, depending upon whether the HI scavenger used is Ag_3PO_4 or 1,2,2,6,6-pentamethylpiperidine (PMP), can often be obtained with good enantioselectivity by using a single enantiomer of BINAP (Scheme 16). The reason for this behavior is not known.[15]

The enantioselective synthesis of physostigmine was accomplished with the methodology outlined above. As observed by Shibasaki and co-workers in their eptazocine synthesis, the *Z* olefin provided better results than the corresponding *E* isomer (Scheme 17).[16, 17]



Scheme 16. Enantioselective route to 2-oxoindolines. DMA = *N*,*N*-dimethylacetamide, PMP = 1,2,2,6,6-pentamethylpiperidine. If PMP is used instead of $AgNO_3$, the *S* enantiomer is formed (74–99%, 63–81% *ee*).

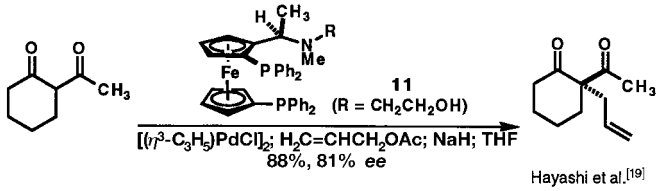


Scheme 17. Enantioselective route to (−)-physostigmine.

2.5. Palladium-Catalyzed Allylation Reactions[18]

2.5.1. Allylation Reactions That Differentiate between Enantiotopic Faces

The palladium-catalyzed allylation of active methine compounds employing a chiral ferrocene diphosphane ligand (**11**, R = CH_2CH_2OH) was reported by Hayashi and co-workers. For example, the sodium enolate of 2-acetylcyclohexanone undergoes a face-selective reaction with a chiral η^3-allylpalladium species generated in situ from allyl acetate and a catalytic Pd^0 complex with this ligand (Scheme 18). The high



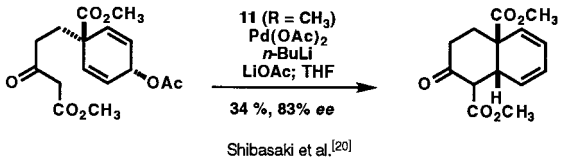
Scheme 18. Enantioselective alkylation of a 1,3-diketone.

enantioselectivity obtained with this ligand is ascribed to secondary attractive interactions between the terminal hydroxyl group of the ligand and the approaching prochiral enolate of the diketone.[20]

2.5.2. Allylation Reactions That Differentiate between Enantiotopic Groups

An intramolecular palladium-catalyzed allylation reaction was used by Shibasaki and co-workers to accomplish the differentiation of enantiotopic olefinic bonds in a molecule with a prochiral quaternary center. This strategy is reminiscent of the one discussed in the context of the Heck reaction (Section 2.4) and results in the enantioselective establishment of a quaternary stereocenter. The best results are obtained

with the indicated *trans* diastereomer of the substrate instead of the *cis* diastereomer, and with **11** (R = CH_3) as the ligand (Scheme 19).[20]



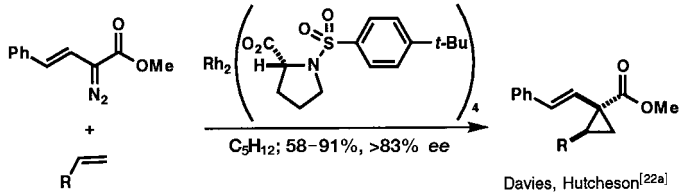
Scheme 19. Enantioselective intramolecular alkylation.

2.6. Rhodium-Catalyzed Cyclopropanation Reactions

The reaction of olefins with α-diazocarbonyl compounds in the presence of chiral rhodium or copper catalysts offers significant potential as a general method for the asymmetric synthesis of cyclopropanes. Rhodium(II) catalysts have been especially useful for the synthesis of optically active cyclopropanes containing quaternary stereocenters.[21]

2.6.1. Intermolecular Cyclopropanation Reactions

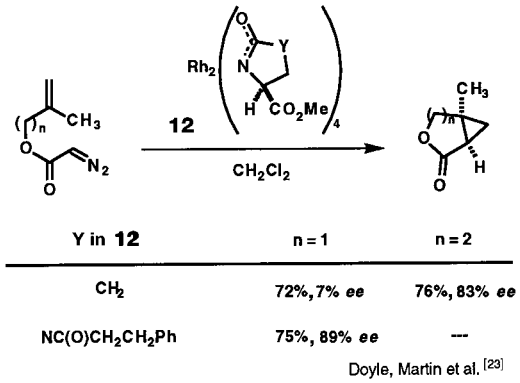
The intermolecular rhodium-catalyzed asymmetric cyclopropanations often result in products of good enantioselectivity but low *diastereoselectivity*. A noteworthy example of a rhodium-catalyzed intermolecular cyclopropanation that proceeds with both high diastereo- and enantiocontrol utilizes methyl (*E*)-2-diazo-4-phenylbut-3-enoate as shown in Scheme 20. The presence of a vinyl substituent on the diazo compound is essential for obtaining good selectivities in this reaction.[22]



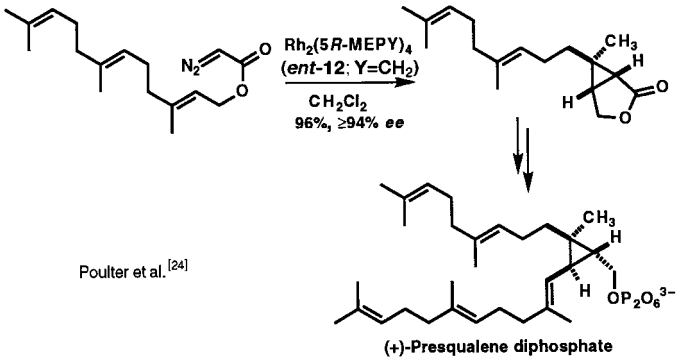
Scheme 20. Catalytic enantioselective intermolecular [2+1] cycloaddition.

2.6.2. Intramolecular Cyclopropanation Reactions

Unlike intermolecular cyclopropanations, the intramolecular reactions can only produce one diastereomer due to geometric constraints of the fused bicyclic product, and accordingly have seen substantially more use in synthesis. The enantioselective intramolecular reaction of a variety of alkenyl diazoacetates catalyzed by chiral rhodium carboxamides [Rh_2(5*S*-MEPY)$_4$] (**12**, Y = CH_2) and [Rh_2(4*S*-MPPIM)$_4$] (**12**, Y = NC(O)CH_2CH_2Ph) was studied by Doyle, Martin, and co-workers. Optically active bicyclic lactones containing quaternary stereocenters are obtained when 1,1-disubstituted and trisubstituted olefins are used in the reaction (Scheme 21).[23] This methodology was applied by Poulter and co-workers to the efficient asymmetric synthesis of presqualene diphosphate (Scheme 22).[24]



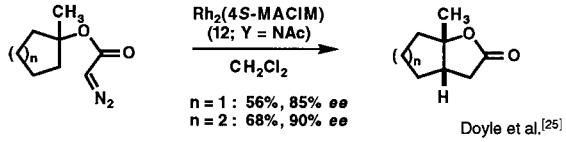
Scheme 21. Catalytic enantioselective intramolecular [2+1] cycloaddition.



Scheme 22. Enantioselective synthesis of (+)-presqualene diphosphate.

2.7. Rhodium-Catalyzed C–H Insertion Reactions

In addition to cyclopropanation reactions, rhodium(II) catalyzes the selective intramolecular insertion of diazoacetates into C–H bonds. The enantioselective version of this reaction[21a] allows for the differentiation of enantiotopic aliphatic C–H bonds of molecules with prochiral quaternary stereocenters. The resulting bicyclic lactones are obtained in high optical purity (Scheme 23).[25]



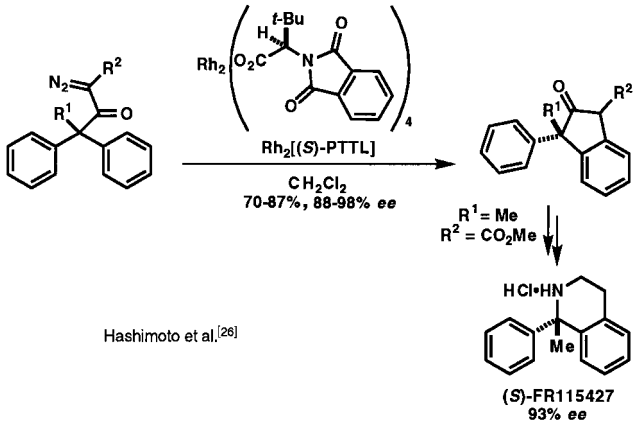
Scheme 23. Enantioselective cyclization by intramolecular C–H insertion.

In addition, an asymmetric rhodium-catalyzed aromatic C–H bond insertion has also been demonstrated and applied to the total synthesis of FR115427 (Scheme 24).[26]

3. Catalytic Methods Applicable to the Synthesis of Heteroatom-Substituted Quaternary Carbon Stereocenters

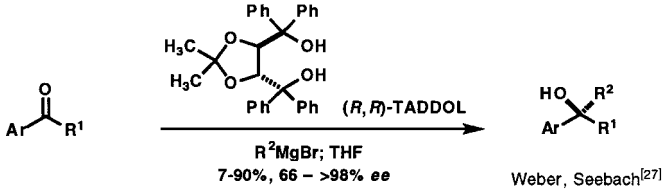
3.1. Addition of Carbon Nucleophiles to Ketones

A conceptually straightforward approach to the preparation of enantiopure tertiary alcohols is the addition of



Scheme 24. Enantioselective synthesis of (*S*)-FR115427.

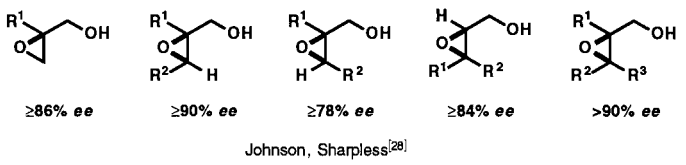
organometallic reagents to prochiral ketones in the presence of a chiral catalyst. This approach, which simultaneously forms a stereocenter and a C–C bond, has been realized for the synthesis of secondary alcohols from aldehydes. Recently, Seebach and Weber developed an effective asymmetric addition of alkyl Grignard reagents to ketones with stoichiometric amounts of (*R*,*R*)-TADDOL as shown in Scheme 25. The best results are obtained with alkyl aryl ketones. The chiral ligand was also used in substoichiometric amounts but this resulted in somewhat lower enantioselectivity.[27]



Scheme 25. Enantioselective carbonyl alklylation.

3.2. Katsuki–Sharpless Asymmetric Epoxidation Reactions (KSAE)

The KSAE of allylic alcohols is, to date, one of the most predictable and widely used catalytic asymmetric reactions. The reaction (employing diethyl or diisopropyl tartrate, *tert*-butylhydroperoxide, titanium(IV) isopropoxide, and molecular sieves in CH_2Cl_2 or toluene) provides 2,3-epoxy alcohols containing quaternary centers as shown in Scheme 26 in

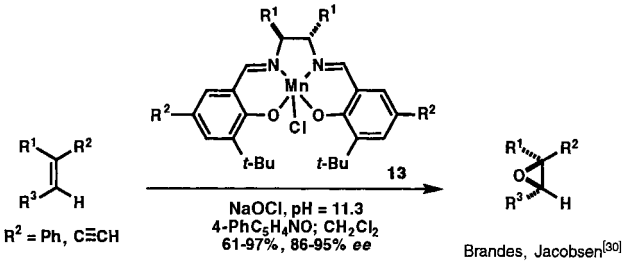


Scheme 26. Chiral 2,3-epoxy alcohols from Katsuki–Sharpless oxidation.

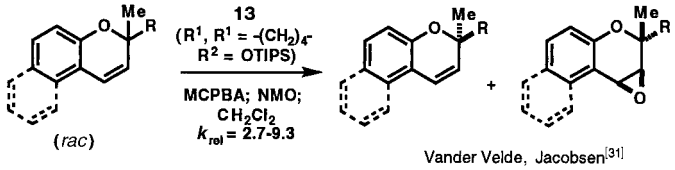
excellent enantioselectivity when 2-substituted, disubstituted, and trisubstituted allylic alcohols are used. The KSAE has been applied in numerous occasions to the synthesis of molecules containing quaternary stereocenters, and the topic has been extensively reviewed; consequently, it will not be discussed here.[28]

3.3. Jacobsen Epoxidation Reactions

The Jacobsen epoxidation of conjugated *cis*-disubstituted and trisubstituted olefins catalyzed by manganese–salen complexes (**13**) is highly enantioselective (Scheme 27).[29] Epoxides with quaternary stereocenters are obtained from the latter olefin class.[30] Furthermore, the kinetic resolution of racemic chromenes with the Jacobsen epoxidation exhibits promising relative rate (k_{rel}) values (Scheme 28).[31]



Scheme 27. Jacobsen enantioselective epoxidation.

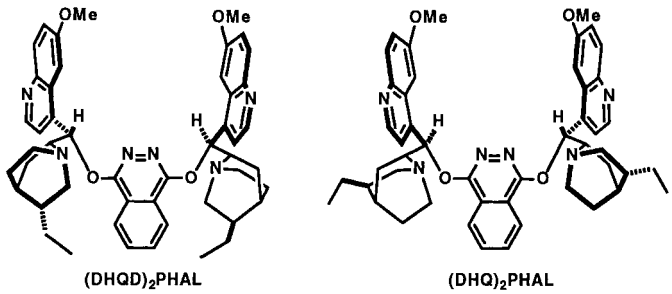


Scheme 28. Kinetic resolution by Jacobsen epoxidation. MCPBA = *m*-chloroperbenzoic acid, NMO = *N*-methylmorpholin-*N*-oxide.

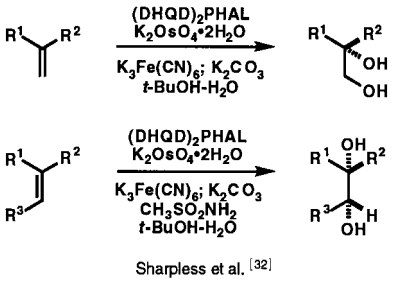
3.4. Sharpless Asymmetric Dihydroxylation Reactions

The cinchona alkaloid catalyzed asymmetric dihydroxylation (AD) has emerged as one of the most general methods for the enantioselective functionalization of olefins. The most common catalysts for the reaction are bis(cinchona) alkaloids such as the quinidine derivative $(DHQD)_2PHAL$ and its pseudo-enantiomer, the quinine derivative $(DHQ)_2PHAL$ (Scheme 29). Products containing quaternary stereocenters are typically obtained in high enantioselectivity by AD of 1,1-disubstituted and trisubstituted olefins (Scheme 30). A variety of groups can be tolerated on or near the olefinic carbons, such as ketone, ester, amide, halogen, sulfide, ether, carbamate, and silane functionalities. Furthermore, enynes and polyenes have been oxidized regio- and enantioselectively.[32] Although the AD of tetrasubstituted olefins is challenging, promising results have been reported (Scheme 31).[33]

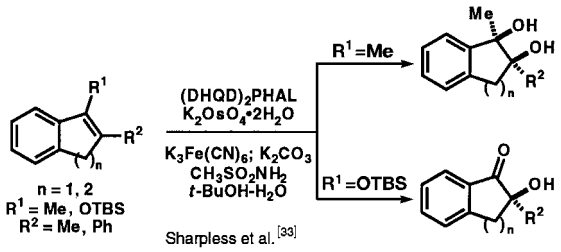
Applications to the synthesis of complex molecules have begun to emerge. A regioselective asymmetric dihydroxyla-



Scheme 29. Ligands for the Sharpless asymmetric dihydroxylation reaction.



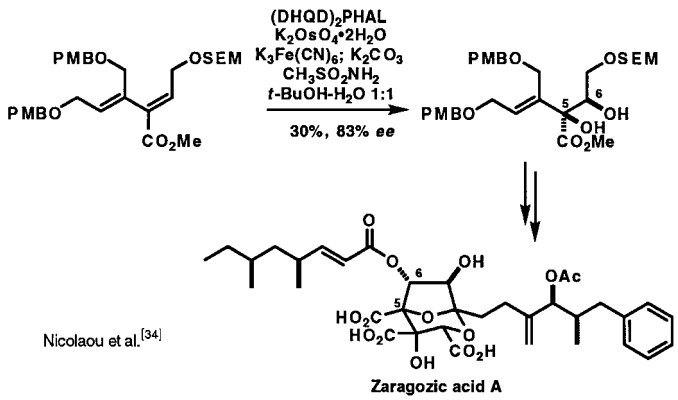
Scheme 30. Sharpless asymmetric dihydroxylation.



Scheme 31. Asymmetric dihydroxylation of tetrasubstituted olefins.

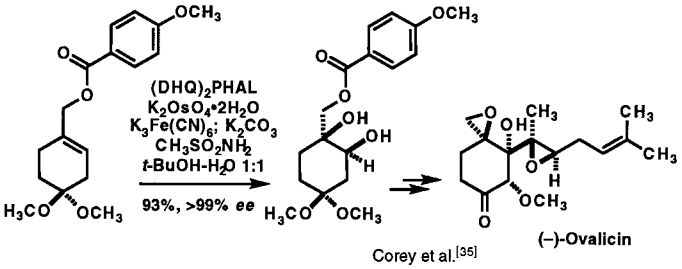
tion introduced the absolute stereochemistry in Nicolaou's synthesis of zaragozic acid A (Scheme 32).[34]

The key step in the synthesis of ovalicin is a novel application of the Sharpless asymmetric dihydroxylation in which a 4-methoxybenzoyl group is attached to the allylic alcohol substrate to produce a dramatic enhancement in enantioselectivity from 18% *ee* to greater than 99% *ee*



Scheme 32. Asymmetric dihydroxylation route to zaragozic acid A. In the asymmetric dihydroxylation, 44% of the starting material is recovered. PMB = *p*-methoxybenzyl, SEM = 2-(trimethylsilyl)ethoxymethyl.

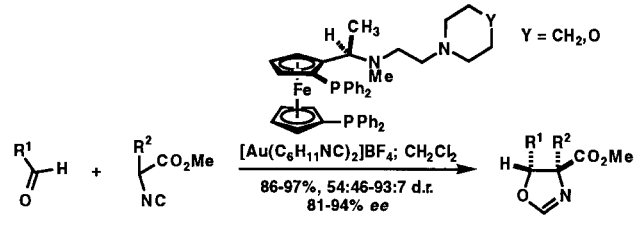
(Scheme 33).[35] The development of this novel application was guided by a mechanistic model recently proposed for AD, which predicted the specific binding of the 4-methoxybenzoyl unit of the substrate to the U-shaped binding pocket of the cinchona alkaloid/OsO_4 catalyst.[36] The reaction was extended to the highly selective dihydroxylation of a variety of allylic 4-methoxybenzoates, homoallylic 4-methoxyphenyl ethers, and other related compounds.[37, 38]



Scheme 33. Enantioselective synthesis of (−)-ovalicin.

3.5. Gold-Catalyzed Aldol Reactions

Aldol-type reactions form one of the most important classes of C–C bond forming transformations due to their ability to generate highly functionalized compounds. A noteworthy example of the catalytic enantioselective aldol processes that are currently becoming available to the synthetic chemist is the gold(I)-catalyzed reaction between α-isocyanocarboxylates and aldehydes.[39] In particular, methyl 2-alkylisocyanoacetates undergo this reaction in the presence of a gold(I) complex with chiral bis(phosphino)ferrocene ligands to afford the corresponding optically active 4-methoxycarbonyldihydrooxazoles (Scheme 34). These useful heterocycles can be hydrolyzed to enantiomerically enriched α-alkylserines and α-alkylthreonines.[40]



Scheme 34. Ito–Hayashi enantioselective route to dihydrooxazoles.

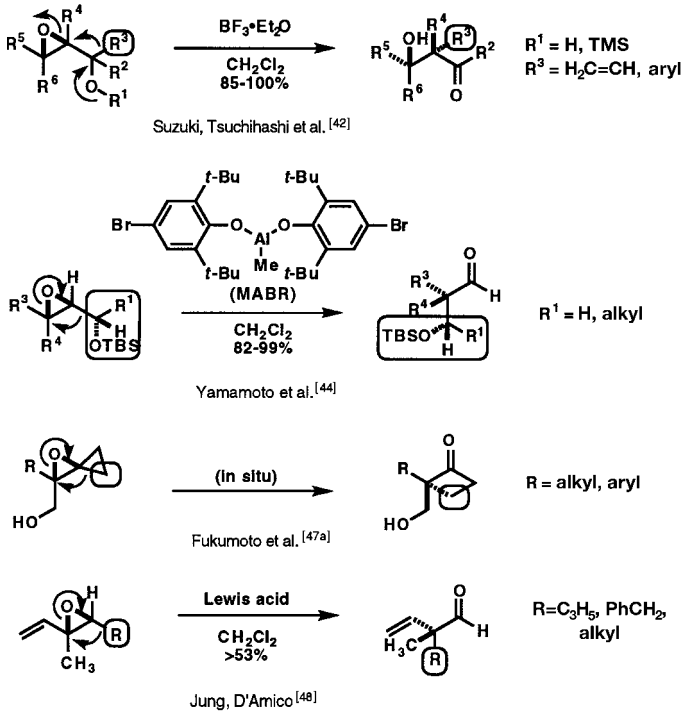
4. Methods Applicable to the Indirect Synthesis of Quaternary Carbon Stereocenters by a Catalytic Asymmetric Reaction Followed by Chirality Transfer

Intramolecular chirality-transfer reactions (also called self-immolative reactions), in which a chiral center is sacrificed as another is enantiospecifically created, are important for the construction of molecules containing quaternary stereocenters. Often in these approaches, a *catalytic enantioselective*

reaction is used to establish an initial chiral center. Subsequently, an *enantiospecific* intramolecular reaction, typically a rearrangement, destroys the original center and transfers the chirality to a newly created quaternary carbon atom. Commonly, a heteroatom-substituted stereocenter is destroyed at the expense of a less readily established all-carbon-substituted quaternary center.

4.1. Asymmetric Epoxidation—1,2-Rearrangement Strategies[41]

As discussed in Section 3.2, the KSAE of allylic alcohols is a general and predictable reaction that makes optically active 2,3-epoxy alcohols readily available. Consequently, the enantiospecific 1,2-rearrangement of these epoxides and their derivatives has been thoroughly studied and can be subdivided into four groups: the Suzuki–Tsuchihashi, Yamamoto, Fukumoto, and Jung variants (Scheme 35). The last three rearrangements are all mechanistically very similar but differ in the epoxide substituents, migrating group, and Lewis acid used.



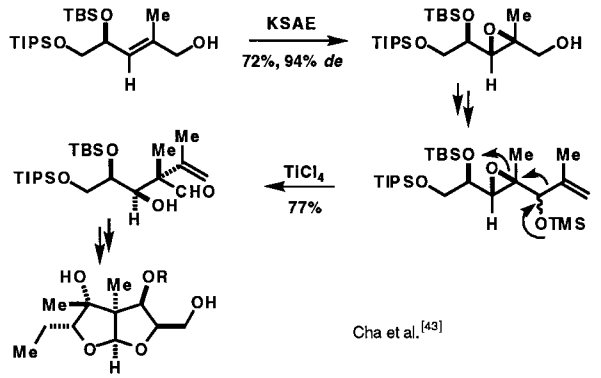
Scheme 35. Cationic rearrangements of chiral oxiranes.

4.1.1. Suzuki–Tsuchihashi Epoxide Rearrangements

The Suzuki–Tsuchihashi rearrangement is mechanistically similar to the pinacol rearrangement and results in the 1,2-migration of a vinyl or aryl group.[42] It was applied together with a KSAE to the synthesis of the bis(tetrahydrofuran) core of asteltoxin (Scheme 36).[43]

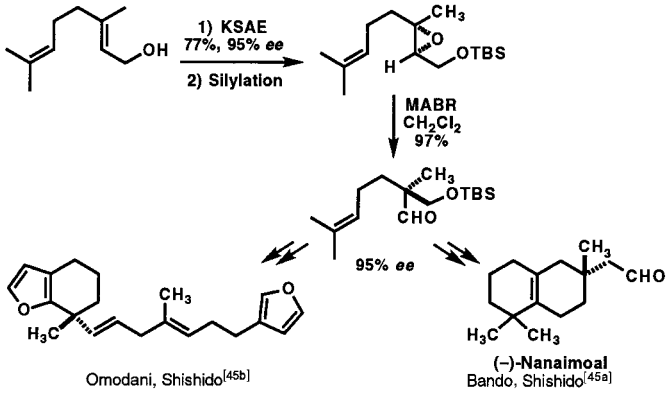
4.1.2. Yamamoto Epoxide Rearrangements

The Yamamoto rearrangement involves the 1,2-migration of a 1-(*tert*-butyldimethylsilyloxy)alkyl group, typically a 1-



Scheme 36. Enantioselective synthesis of a (+)-asteltoxin subunit.

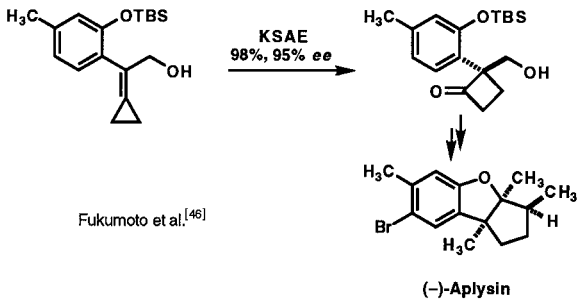
(*tert*-butyldimethylsilyloxy)methyl group.[44] A KSAE, followed by silylation and Yamamoto rearrangement, was utilized for the synthesis of nanaimoal and of the enantiomer of a naturally occurring marine furanoterpene (Scheme 37).[45]



Scheme 37. Synthesis of (−)-nanaimoal and the enantiomer of a natural marine furanterpene.

4.1.3. Fukumoto Epoxide Rearrangement

The Fukumoto variant is notable in that a stereospecific rearrangement occurs spontaneously during the KSAE of a 2-substituted 2-cyclopropylidenethanol. The natural product aplysin was synthesized in this manner (Scheme 38).[46, 47]

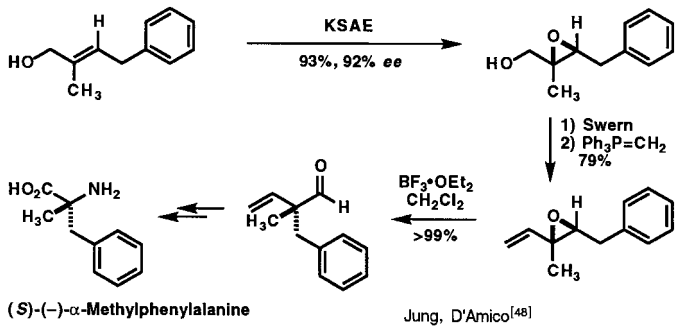


Scheme 38. Synthesis of (−)-aplysin.

4.1.4. Jung Epoxide Rearrangement

The Jung rearrangement of optically active vinyl epoxides is relatively flexible with respect to the migrating group. It was

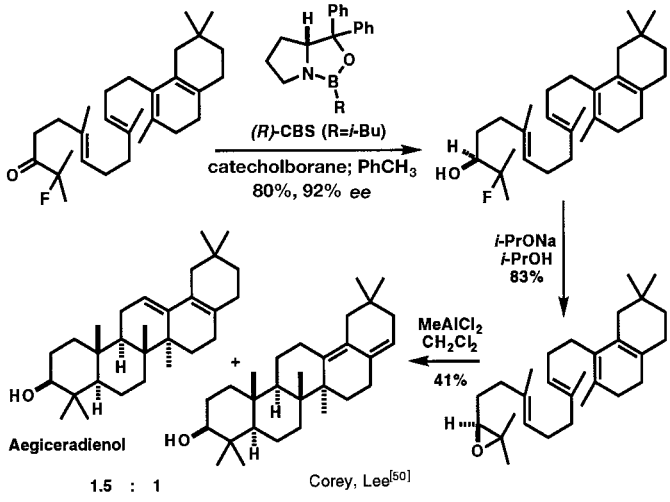
applied to the synthesis of (*S*)-(−)-α-methylphenylalanine as shown in Scheme 39.[48]



Scheme 39. Synthesis of (*S*)-(−)-α-methylphenylalanine by Jung rearrangement.

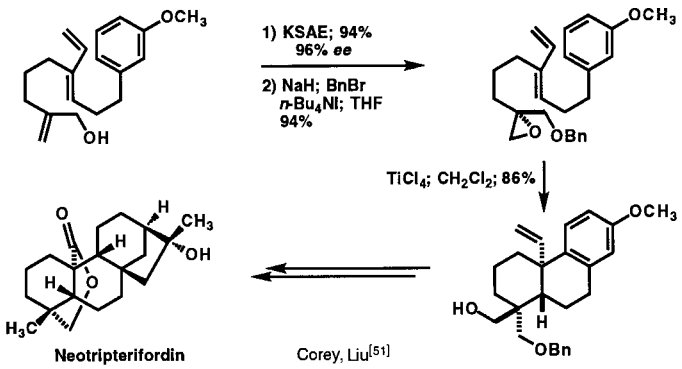
4.2. Chirality Transfer by Cationic Cyclization Reactions

The Lewis acid promoted olefin-cation cyclization[41] of optically active epoxides has been applied to the enantiospecific synthesis of molecules with quaternary stereocenters. For instance, the synthesis of β-amyrin, erythrodiol, and oleanolic acid was accomplished through the common intermediate aegiceradienol, itself a natural product, as shown in Scheme 40. Aegiceradienol was prepared stereospecifically by oxazaborolidine-catalyzed (CBS) reduction[49] of the indicated α-fluoroketone to provide the corresponding fluorohydrin in high enantiomeric purity, followed by ring-closure to the epoxide and enantiospecific olefin-cation cyclization. The latter reaction results in the formation of three new quaternary stereocenters, two new tertiary stereocenters, and three new rings in a single synthetic operation.[50]



Scheme 40. Enantioselective route to pentacyclic triterpenes.

Recently, the synthesis of neotripterifordin was accomplished by a Katsuki–Sharpless asymmetric epoxidation followed by a stereospecific olefin-cation double cyclization, which provided exclusively the indicated intermediate with three stereocenters in high yield (Scheme 41).[51, 52]

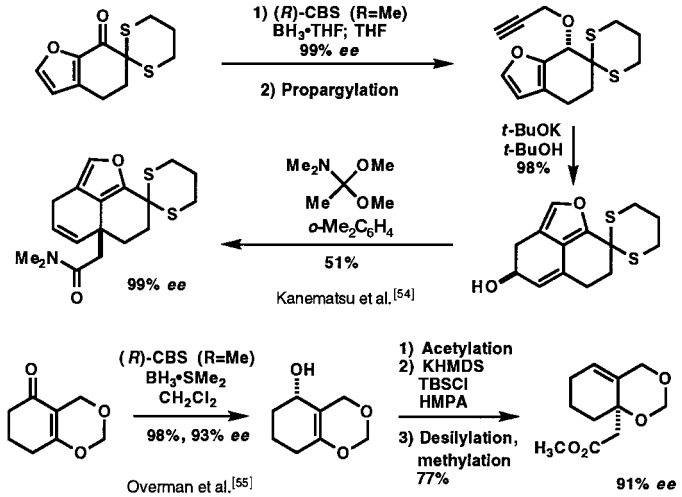


Scheme 41. Enantioselective synthesis of neotripterifordin.

4.3. Strategies Based on the Claisen Rearrangement[53]

4.3.1. Chirality Transfer by Claisen Rearrangements

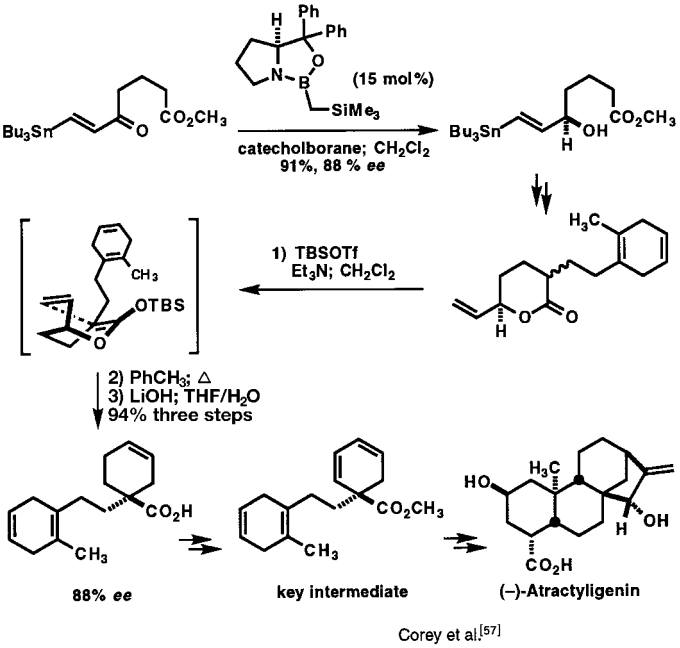
The Claisen rearrangement has been a mainstay of organic synthesis due to its wide applicability and high stereospecificity. Additionally, it is an excellent method for the transfer of chirality from an optically active secondary alcohol to a quaternary carbon center. This approach is especially useful, because several types of allylic alcohols are available by catalytic enantioselective reactions. For example, the preparation of a useful key intermediate for the synthesis of naturally occurring fused furans was accomplished by a sequence involving a highly enantioselective CBS reduction, a furan ring transfer reaction, and an enantiospecific Claisen rearrangement (Scheme 42).[54]



Scheme 42. Introduction of angular substituents by enantioselective CBS reduction followed by Claisen rearrangement. KHMDS = potassium bis(trimethylsilyl)amide.

Likewise, the basic skeleton of the cardenolides was stereospecifically synthesized by Overman and co-workers through the CBS reduction of a tetrasubstituted enone, followed by an Ireland–Claisen rearrangement of the resulting allylic alcohol (Scheme 42). The rearrangement proceeds with high stereochemical fidelity as evidenced by the high enantiomeric excess of the product.[55]

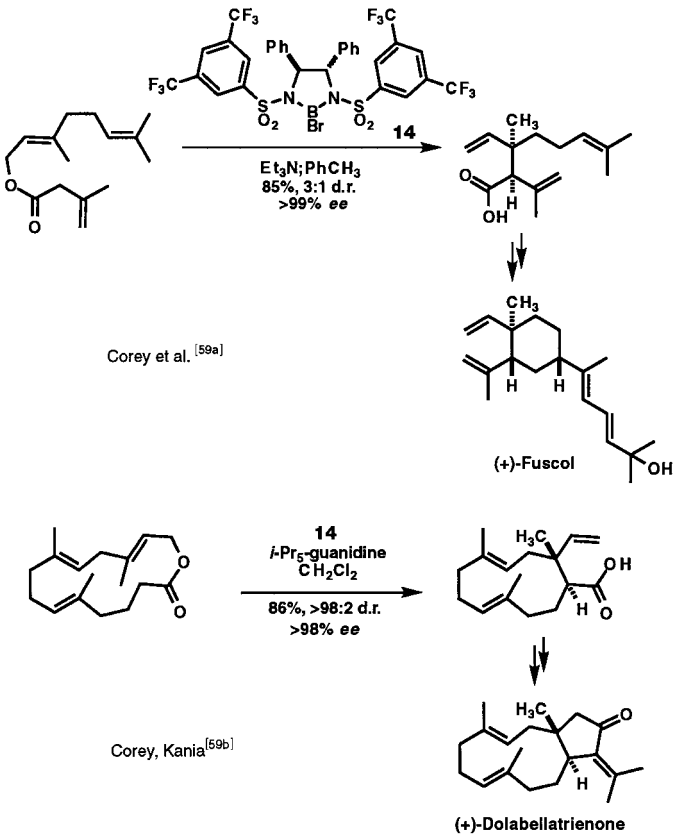
Furthermore, the challenging quaternary carbon center of a key intermediate for the synthesis of atractyligenin was established by the CBS reduction of a β-tri-*n*-butylstannyl enone followed by chirality transfer from the resulting secondary alcohol to the desired quaternary site by an Ireland–Claisen rearrangement (Scheme 43). The high enantioselectivity obtained in the CBS reduction is a result of remote steric interactions[56] between the β-tri-*n*-butylstannyl substituent of the enone and the trimethylsilylmethyl group on the boron atom of the catalyst, which strongly disfavor the minor diastereomeric reduction pathway.[57]



Scheme 43. Enantioselective synthetic route to (−)-atractyligenin.

4.3.2. *Claisen Rearrangements with Chiral Reagents*

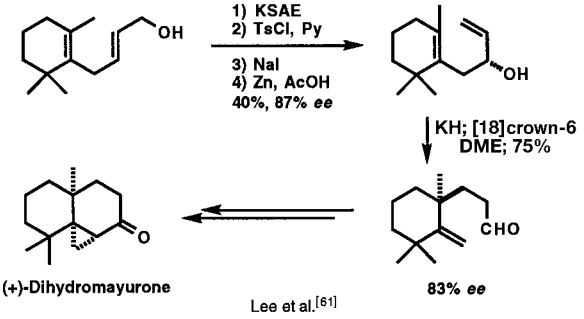
The Ireland–Claisen rearrangement of several allylic esters with chiral diazaborolidine reagent **14** results in substituted 4-alkenoic acids of high enantiomeric and diastereomeric purity.[58] This process has been utilized successfully to install the quaternary stereocenters in fuscol and dolabellatrienone (Scheme 44). Although these transformations require stoichiometric amounts of the chiral boron compound, the reagent is readily available and recyclable, and it provides outstanding results.[59]



Scheme 44. Asymmetric synthesis of cyclic diterpenoids by enantioselective Claisen rearrangement.

4.4. Strategies Based on Anionic Oxy-Cope Rearrangements

The anionic oxy-Cope rearrangement[60] is an alternative method for the transfer of chirality from a secondary alcohol to a quaternary stereocenter. For example, in a synthesis of dihydromayurone the stereochemistry of a secondary allylic alcohol is installed by KSAE. Subsequently, this alcohol undergoes anionic oxy-Cope rearrangement to generate a quaternary stereocenter through a putative chairlike transition state with approximately 95% stereochemical fidelity (Scheme 45).[61]



Scheme 45. Enantioselective synthesis of (+)-dihydromayurone by oxy-Cope rearrangement.

5. Summary and Outlook

The progress in the catalytic asymmetric synthesis of molecules containing quaternary carbon stereocenters, both by direct and indirect methods, has been astounding. Despite these impressive recent advances, many unsolved problems remain. These include limitations with regard to scope and frequent practical problems associated with catalyst preparation and use, especially on large scale. Nonetheless, continued exploratory research on catalytic enantioselective method-

ology and the underlying basis for enantioselectivity can be expected to provide new and powerful methods for the construction of a wide range of complex molecules.

We are grateful to the Schering-Plough Corporation, the National Institutes of Health, and the National Science Foundation for generous financial support.

Received: August 25, 1997 [Z250IE]
German version: *Angew. Chem.* **1998**, *110*, 402 – 415

[1] Recent review: R. Noyori, *Asymmetric Catalysis in Organic Synthesis*, Wiley, New York, **1994**.

[2] Reviews: a) K. Fuji, *Chem. Rev.* **1993**, *93*, 2037 – 2066; b) S. F. Martin, *Tetrahedron* **1980**, *36*, 419 – 460; c) R. Wang, X.-W. Yang, *Huaxue* **1996**, *54*, 169 – 192.

[3] a) U. Eder, G. Sauer, R. Wiechert, *Angew. Chem.* **1971**, *83*, 492 – 493; *Angew. Chem. Int. Ed. Engl.* **1971**, *10*, 496 – 497; b) Z. G. Hajos, D. R. Parrish, *J. Org. Chem.* **1974**, *39*, 1615 – 1621; c) Y. Tamai, Y. Mizutani, H. Hagiwara, H. Uda, N. Harada, *J. Chem. Res. (M)* **1985**, 1746 – 1787; d) E. J. Corey, S. C. Virgil, *J. Am. Chem. Soc.* **1990**, *112*, 6429 – 6431; e) H. Hagiwara, H. Uda, *J. Org. Chem.* **1988**, *53*, 2308 – 2311.

[4] a) A. Bhattacharya, U.-H. Dolling, E. J. J. Grabowski, S. Karady, K. M. Ryan, L. M. Weinstock, *Angew. Chem.* **1986**, *98*, 442 – 443; *Angew. Chem. Int. Ed. Engl.* **1986**, *25*, 476 – 477; b) R. S. E. Conn, A. V. Lovell, S. Karady, L. M. Weinstock, *J. Org. Chem.* **1986**, *51*, 4710 – 4711; c) U.-H. Dolling, P. Davis, E. J. J. Grabowski, *J. Am. Chem. Soc.* **1984**, *106*, 446 – 447; d) D. L. Hughes, U.-H. Dolling, K. M. Ryan, E. F. Schoenewaldt, E. J. J. Grabowski, *J. Org. Chem.* **1987**, *52*, 4745 – 4752.

[5] Recent reviews: a) H. B. Kagan, O. Riant, *Chem. Rev.* **1992**, *92*, 1007 – 1019; b) U. Pindur, G. Lutz, C. Otto, *Chem. Rev.* **1993**, *93*, 741 – 761; c) L. Deloux, M. Srebnik, *Chem. Rev.* **1993**, *93*, 763 – 784; d) K. Maruoka, H. Yamamoto in *Catalytic Asymmetric Synthesis* (Ed.: I. Ojima), VCH, New York, **1993**, Chapter 9; e) A. Togni, L. M. Venanzi, *Angew. Chem.* **1994**, *106*, 517 – 547; *Angew. Chem. Int. Ed. Engl.* **1994**, *33*, 497 – 526.

[6] Catalyst **1**: a) K. Furuta, S. Shimizu, Y. Miwa, H. Yamamoto, *J. Org. Chem.* **1989**, *54*, 1481 – 1483; b) K. Ishihara, Q. Gao, H. Yamamoto, *J. Am. Chem. Soc.* **1993**, *115*, 10412 – 10413; c) K. Ishihara, Q. Gao, H. Yamamoto, *J. Org. Chem.* **1993**, *58*, 6917 – 6919. Catalyst **2**: d) E. J. Corey, T.-P. Loh, *J. Am. Chem. Soc.* **1991**, *113*, 8966 – 8967; e) E. J. Corey, T.-P. Loh, T. D. Roper, M. D. Azimioara, M. C. Noe, *ibid.* **1992**, *114*, 8290 – 8292; f) E. J. Corey, T.-P. Loh, *Tetrahedron Lett.* **1993**, *34*, 3979 – 3982; g) T.-P. Loh, Ph. D. Thesis, Harvard University, January **1994**; h) Ref. [8]. Catalyst **3**: i) J. Bao, W. D. Wulff, A. L. Rheingold, *J. Am. Chem. Soc.* **1993**, *115*, 3814 – 3815. Catalyst **4**: j) K. Maruoka, N. Murase,H. Yamamoto, *J. Org. Chem.* **1993**, *58*, 2938 – 2939. Catalyst **5**: k) K. Ishihara, H. Yamamoto, *J. Am. Chem. Soc.* **1994**, *116*, 1561 – 1562. Catalyst **6**: l) E. P. Kündig, B. Bourdin, G. Bernardinelli, *Angew. Chem.* **1994**, *106*, 1931 – 1934; *Angew. Chem. Int. Ed. Engl.* **1994**, *33*, 1856 – 1858. Catalyst **7**: m) K. Mikami, Y. Motoyama, M. Terada, *J. Am. Chem. Soc.* **1994**, *116*, 2812 – 2820; n) Y. Motoyama, M. Terada, K. Mikami, *Synlett* **1995**, 967 – 968. Catalyst **8**: o) D. A. Evans, J. A. Murry, P. von Matt, R. D. Norcross, S. J. Miller, *Angew. Chem.* **1995**, *107*, 864 – 867; *Angew. Chem. Int. Ed. Engl.* **1995**, *34*, 798 – 800. Catalyst **9**: p) K. Ishihara, H. Kurihara, H. Yamamoto, *J. Am. Chem. Soc.* **1996**, *118*, 3049 – 3050. Catalyst **10**: q) Y. Hayashi, J. J. Rohde, E. J. Corey, *J. Am. Chem. Soc.* **1996**, *118*, 5502 – 5503.

[7] J. A. Marshall, S. Xie, *J. Org. Chem.* **1992**, *57*, 2987 – 2987.

[8] E. J. Corey, A. Guzman-Perez, T.-P. Loh, *J. Am. Chem. Soc.* **1994**, *116*, 3611 – 3612.

[9] Recent review: M. Shibasaki, C. D. J. Boden, A. Kojima, *Tetrahedron* **1997**, *53*, 7371 – 7395.

[10] a) K. Ohrai, K. Kondo, M. Sodeoka, M. Shibasaki, *J. Am. Chem. Soc.* **1994**, *116*, 11737 – 11748; b) K. Kondo, M. Sodeoka, M. Mori, M. Shibasaki, *Synthesis* **1993**, 920 – 930; c) *Tetrahedron Lett.* **1993**, *34*, 4219 – 4222; d) Y. Sato, S. Watanabe, M. Shibasaki, *Tetrahedron Lett.* **1992**, *33*, 2589 – 2592.

[11] a) Y. Sato, T. Honda, M. Shibasaki, *Tetrahedron Lett.* **1992**, *33*, 2593 – 2596; b) Y. Sato, M. Mori, M. Shibasaki, *Tetrahedron: Asymmetry* **1995**, *6*, 757 – 766.

[12] a) T. Ohshima, K. Kagechika, M. Adachi, M. Sodeoka, M. Shibasaki, *J. Am. Chem. Soc.* **1996**, *118*, 7108 – 7116; b) K. Kagechika, T. Ohshima, M. Shibasaki, *Tetrahedron* **1993**, *49*, 1773 – 1782; c) K. Kagechika, M. Shibasaki, *J. Org. Chem.* **1991**, *56*, 4093 – 4094.

[13] T. Takemoto, M. Sodeoka, H. Sasai, M. Shibasaki, *J. Am. Chem. Soc.* **1993**, *115*, 8477 – 8478, and structure correction: **1994**, *116*, 11207.

[14] K. Kondo, M. Sodeoka, M. Shibasaki, *Tetrahedron: Asymmetry* **1995**, *6*, 2453 – 2464.

[15] A. Ashimori, L. E. Overman, *J. Org. Chem.* **1992**, *57*, 4571 – 4572.

[16] A. Ashimori, T. Matsuura, L. E. Overman, D. J. Poon, *J. Org. Chem.* **1993**, *58*, 6949 – 6951.

[17] a) L. E. Overman, *Pure & Appl. Chem.* **1994**, *66*, 1423 – 1434. Other important work in this area: Spirotricyclic dienones: b) N. E. Carpenter, D. J. Kucera, L. E. Overman, *J. Org. Chem.* **1989**, *54*, 5846 – 5848; halenaquinone and halenaquinol: c) A. Kojima, T. Takemoto, M. Sodeoka, M. Shibasaki, *J. Org. Chem.* **1996**, *61*, 4876 – 4877; xestoquinone: d) S. P. Maddaford, N. G. Andersen, W. A. Cristofoli, B. A. Keay, *J. Am. Chem. Soc.* **1996**, *118*, 10766 – 10773.

[18] Review: B. M. Trost, D. L. Van Vraken, *Chem. Rev.* **1996**, *96*, 395 – 422.

[19] T. Hayashi, K. Kanehira, T. Hagihara, M. Kumada, *J. Org. Chem.* **1988**, *53*, 113 – 120.

[20] T. Takemoto, Y. Nishikimi, M. Sodeoka, M. Shibasaki, *Tetrahedron Lett.* **1992**, *33*, 3531 – 3532.

[21] Recent reviews: a) M. P. Doyle, *Aldrichimica Acta* **1996**, *29*, 3 – 11; b) M. P. Doyle in *Catalytic Asymmetric Synthesis* (Ed.: I. Ojima), VCH, New York, **1993**, Chapter 3; c) V. K. Singh, A. DattaGupta, G. Sekar, *Synthesis* **1997**, 137 – 149; d) Ref. [23b].

[22] a) H. M. L. Davies, D. K. Hutcheson, *Tetrahedron Lett.* **1993**, *34*, 7243 – 7246; b) E. J. Corey, T. G. Gant, *Tetrahedron Lett.* **1994**, *35*, 5373 – 5376.

[23] a) M. P. Doyle, Q.-L. Zhou, A. B. Dyatkin, D. A. Ruppar, *Tetrahedron Lett.* **1995**, *36*, 7579 – 7582; b) M. P. Doyle, R. E. Austin, A. S. Bailey, M. P. Dwyer, A. B. Dyatkin, A. V. Kalinin, M. M. Y. Kwan, S. Liras, C. J. Oalmann, R. J. Pieters, M. N. Protopopova, C. E. Raab, G. H. P. Roos, Q.-L. Zhou, S. F. Martin, *J. Am. Chem. Soc.* **1995**, *117*, 5763 – 5775.

[24] D. H. Rogers, E. C. Yi, C. D. Poulter, *J. Org. Chem.* **1995**, *60*, 941 – 945.

[25] M. P. Doyle, Q.-L. Zhou, C. E. Raab, G. H. P. Roos, *Tetrahedron Lett.* **1995**, *36*, 4745 – 4748.

[26] a) N. Watanabe, T. Ogawa, Y. Ohtake, S. Ikegami, S. Hashimoto, *Synlett* **1996**, 85 – 86; b) N. Watanabe, Y. Ohtake, S. Hashimoto, M. Shiro, S. Ikegami, *Tetrahedron Lett.* **1995**, *36*, 1491 – 1494.

[27] a) B. Weber, D. Seebach, *Angew. Chem. Int.* **1992**, *104*, 96; *Angew. Chem. Int. Ed. Engl.* **1992**, *31*, 84 – 86; b) B. Weber, D. Seebach, *Tetrahedron* **1994**, *50*, 6117 – 6128.

[28] R. A. Johnson, K. B. Sharpless in *Catalytic Asymmetric Synthesis* (Ed.: I. Ojima), VCH, New York, **1993**, Chapter 4.4, and references therein.

[29] Review: E. N. Jacobsen in *Catalytic Asymmetric Synthesis* (Ed.: I. Ojima), VCH, New York, **1993**, Chapter 4.2.

[30] B. D. Brandes, E. N. Jacobsen, *J. Org. Chem.* **1994**, *59*, 4378 – 4380.

[31] S. L. Vander Velde, E. N. Jacobsen, *J. Org. Chem.* **1995**, *60*, 5380 – 5381.

[32] Leading reference: a) H. Becker, K. B. Sharpless, *Angew. Chem.* **1996**, *108*, 447 – 449; *Angew. Chem. Int. Ed. Engl.* **1996**, *35*, 448 – 451; recent review: b) H. C. Kolb, M. S. VanNieuwenhze, K. B. Sharpless, *Chem. Rev.* **1994**, *94*, 2483 – 2547.

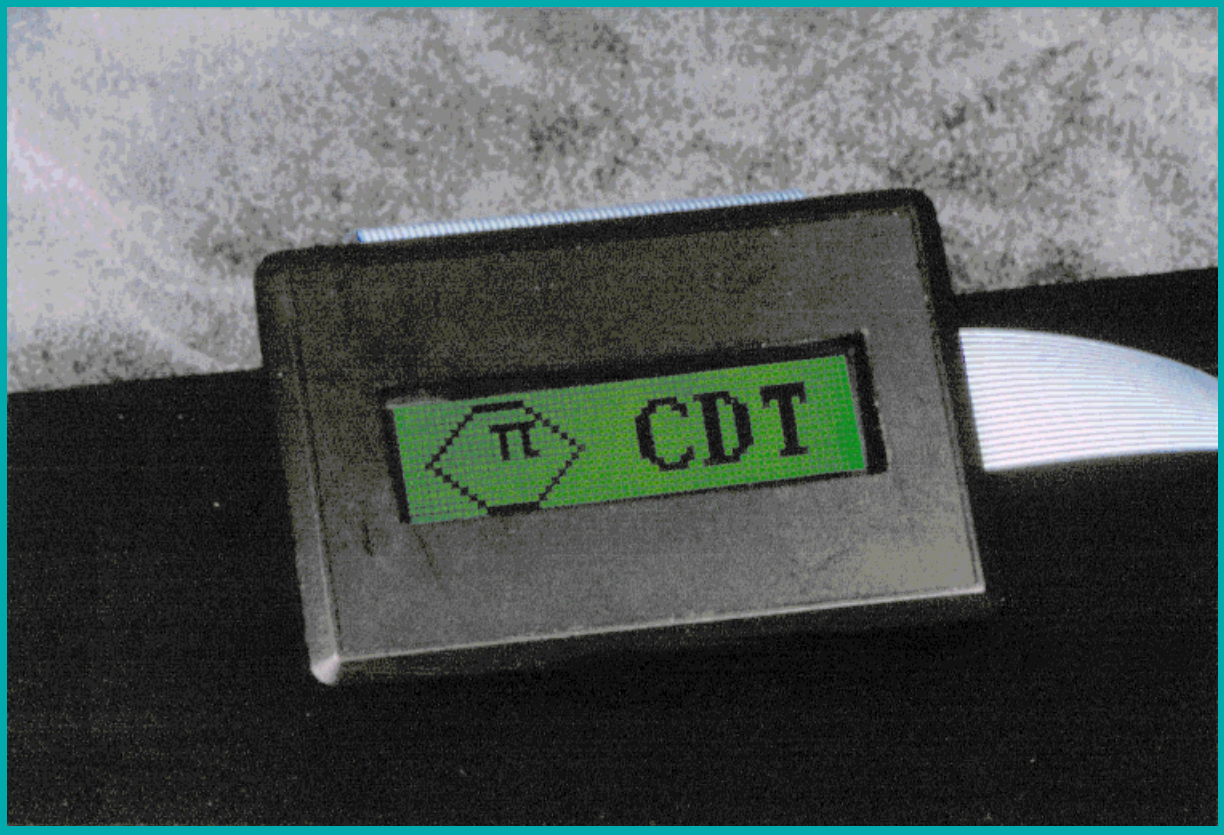
[33] K. Morikawa, J. Park, P. G. Andersson, T. Hashiyama, K. B. Sharpless, *J. Am. Chem. Soc.* **1993**, *115*, 8463 – 8464.

[34] K. C. Nicolaou, E. W. Yue, S. La Greca, A. Nadin, Z. Yang, J. E. Leresche, T. Tsuri, Y. Naniwa, F. De Riccardis, *Chem. Eur. J.* **1995**, *1*, 467 – 494.

[35] E. J. Corey, A. Guzman-Perez, M. C. Noe, *J. Am. Chem. Soc.* **1994**, *116*, 12109 – 12110.

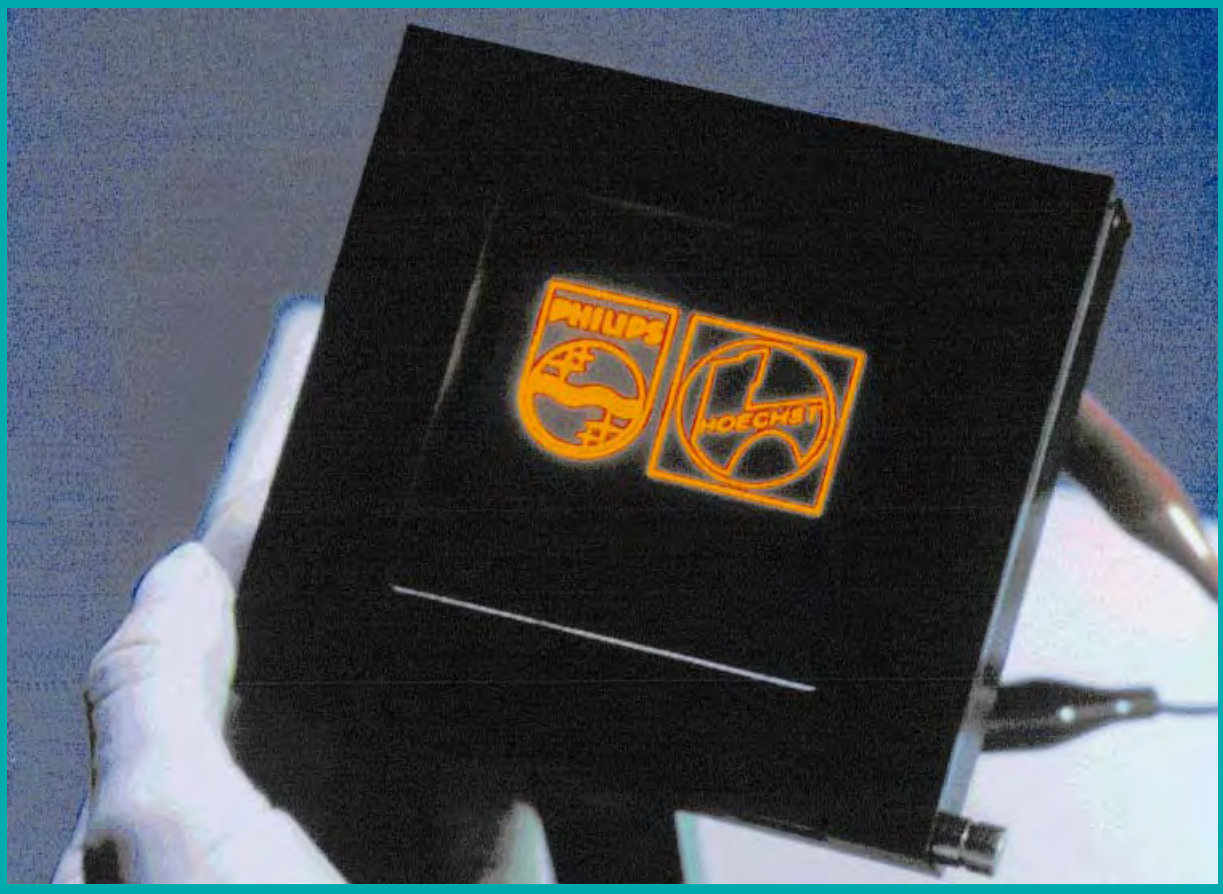
[36] a) E. J. Corey, M. C. Noe, *J. Am. Chem. Soc.* **1996**, *118*, 11038 – 11053; b) E. J. Corey, M. C. Noe, S. Sarshar, *J. Am. Chem. Soc.* **1993**, *115*, 3828 – 3929; c) E. J. Corey, M. C. Noe, S. Sarshar, *Tetrahedron Lett.* **1994**, *35*, 2861 – 2864; d) E. J. Corey, M. C. Noe, *J. Am. Chem. Soc.* **1996**, *118*, 319 – 329.

[37] a) E. J. Corey, A. Guzman-Perez, M. C. Noe, *J. Am. Chem. Soc.* **1995**, *117*, 10805 – 10816; b) E. J. Corey, A. Guzman-Perez, M. C. Noe, *Tetrahedron Lett.* **1995**, *36*, 3481 – 3484.
[38] Other recent applications of the AD to the synthesis of natural products with quaternary stereocenters: camphotecin: a) F. G. Fang, S. Xie, M. W. Lowery, *J. Org. Chem.* **1994**, *59*, 6142 – 6143; b) D. P. Curran, S.-B. Ko, *ibid.* **1994**, *59*, 6139 – 6141. Duocarmycin A: c) D. L. Boger, J. A. McKie, T. Nishi, T. Ogiku, *J. Am. Chem. Soc.* **1996**, *118*, 2301 – 2302.
[39] Recent review: M. Sawamura, Y. Ito in *Catalytic Asymmetric Synthesis* (Ed.: I. Ojima), VCH, New York, **1993**, Chapter 7.2.
[40] a) Y. Ito, M. Sawamura, E. Shirakawa, K. Hayashizaki, T. Hayashi, *Tetrahedron* **1988**, *44*, 5253 – 5262; b) *Tetrahedron Lett.* **1988**, *29*, 235 – 238.
[41] Recent reviews on epoxide rearrangements: a) B. Rickborn in *Comprehensive Organic Synthesis*, *Vol. 3* (Eds.: B. M. Trost, I. Fleming), Pergamon, Oxford, **1991**, Chapter 3.3; b) G. Magnusson, *Org. Prep. Proced. Int.* **1990**, *22*, 547 – 574.
[42] M. Shimazaki, H. Hara, K. Suzuki, G.-i. Tsuchihashi, *Tetrahedron Lett.* **1987**, *28*, 5891 – 5894.
[43] J. V. Raman, H. K. Lee, R. Vleggaar, J. K. Cha, *Tetrahedron Lett.* **1995**, *36*, 3095 – 3098.
[44] a) K. Maruoka, T. Ooi, H. Yamamoto, *J. Am. Chem. Soc.* **1989**, *111*, 6431 – 6432; b) K. Maruoka, T. Ooi, S. Nagahara, H. Yamamoto, *Tetrahedron* **1991**, *47*, 6983 – 6998.
[45] a) T. Omodani, K. Shishido, *J. Chem. Soc. Chem. Commun.* **1994**, 2781 – 2782; b) T. Bando, K. Shishido, *Chem. Commun.* **1996**, 1357 – 1358.
[46] H. Nemoto, M. Nagamochi, H. Ishibashi, K. Fukumoto, *J. Org. Chem.* **1994**, *59*, 74 – 79.
[47] Other applications: α-cuparenones: a) H. Nemoto, H. Ishibashi, M. Nagamochi, K. Fukumoto, *J. Org. Chem.* **1992**, *57*, 1707 – 1712; mesembrine: b) H. Nemoto, T. Tanabe, K. Fukumoto, *J. Org. Chem.* **1995**, *60*, 6785 – 6790.
[48] M. E. Jung, D. C. D′Amico, *J. Am. Chem. Soc.* **1995**, *117*, 7379 – 7388.
[49] a) E. J. Corey, R. K. Bakshi, S. Shibata, *J. Am. Chem. Soc.* **1987**, *109*, 5551 – 5553; b) E. J. Corey, R. K. Bakshi, S. Shibata, C. P. Chen, V. K. Singh, *ibid.* **1987**, *109*, 7925 – 7926; c) E. J. Corey, S. Shibata, R. K Bakshi, *J. Org. Chem.* **1988**, *53*, 2861 – 2863; d) E. J. Corey, R. K. Bakshi, *Tetrahedron Lett.* **1990**, *31*, 611 – 614; e) E. J. Corey, *Pure Appl. Chem.* **1990**, *62*, 1209 – 1216; reviews: f) V. K. Singh, *Synthesis* **1992**, 605 – 617; g) S. Wallbaum, J. Martens, *Tetrahedron: Asymmetry* **1992**, *3*, 1475 – 1504.
[50] E. J. Corey, J. Lee, *J. Am. Chem. Soc.* **1993**, *115*, 8873 – 8874.
[51] E. J. Corey, K. Liu, *J. Am. Chem. Soc.* **1997**, *119*, 9929 – 9930.
[52] Other examples of enantiospecific olefin-cation cyclizations: copalol: a) N. K. N. Yee, R. M. Coates, *J. Org. Chem.* **1992**, *57*, 4598 – 4608; aphidicolin: b) S. P. Tanis, Y.-H. Chuang, D. B. Head, *J. Org. Chem.* **1988**, *53*, 4929 – 4938; scalarenedial: c) E. J. Corey, G. Luo, L. S. Lin, *J. Am. Chem. Soc.* **1997**, *119*, 9927 – 9928; dammarenediol II: d) E. J. Corey, S. Lin, *J. Am. Chem. Soc.* **1996**, *118*, 8765 – 8766.
[53] Recent review on the Ireland – Claisen rearrangement: S. Pereira, M. Srebnik, *Aldrichimica Acta* **1993**, *26*, 17 – 29.
[54] K. Kanematsu, A. Nishizaki, Y. Sato, M. Shiro, *Tetrahedron Lett.* **1992**, *33*, 4967 – 4970.
[55] W. Deng, M. S. Jensen, L. E. Overman, P. V. Rucker, J.-P. Vionnet, *J. Org. Chem.* **1996**, *61*, 6760 – 6761.
[56] C. J. Helal, P. A. Magriotis, E. J. Corey, *J. Am. Chem. Soc.* **1996**, *118*, 10938 – 10939.
[57] E. J. Corey, A. Guzman-Perez, S. E. Lazerwith, *J. Am. Chem. Soc.* **1997**, *119*, 11769-11776.
[58] E. J. Corey, D.-H. Lee, *J. Am. Chem. Soc.* **1991**, *113*, 4026 – 4028.
[59] a) E. J. Corey, B. E. Roberts, B. R. Dixon, *J. Am. Chem. Soc.* **1995**, *117*, 193 – 196; b) E. J. Corey, R. S. Kania, *ibid.* **1996**, *118*, 1229 – 1230; For another chiral reagent that affords molecules with quaternary stereocenters, see: c) A. Krebs, U. Kazmaier, *Tetrahedron Lett.* **1996**, *37*, 7945 – 7946.
[60] a) D. A. Evans, A. M. Golob, *J. Am. Chem. Soc.* **1975**, *97*, 4765 – 4766. Review: b) R. K. Hill in *Comprehensive Organic Synthesis Vol. 5* (Eds.: B. M. Trost, I. Fleming), Pergamon, Oxford, **1991**, Chapter 7.1.
[61] E. Lee, I.-J. Shin, T.-S. Kim, *J. Am. Chem. Soc.* **1990**, *112*, 260 – 264.



Cambridge Display Technology, photograph taken in the Photo Department at the University Chemical Laboratory of the University of Cambridge.

Green and red-orange are only two of the many possible colors that can be produced with polymer-based light-emitting devices.



Collaboration between Hoechst and Philips.

ANGEWANDTE CHEMIE © WILEY-VCH

Electroluminescent Conjugated Polymers—Seeing Polymers in a New Light

Arno Kraft, Andrew C. Grimsdale, and Andrew B. Holmes*

A major recent development in the field of molecular electronics has been the discovery of electroluminescent conjugated polymers—that is, fluorescent polymers that emit light when excited by the flow of an electric current. These materials may now challenge the domination by inorganic materials of the commercial market in light-emitting diodes. Conjugated polymers are particularly versatile because their physical properties (color, emission efficiency) can be fine-tuned by manipulation of their chemical structures. The development of polymer-based light-emitting devices has been accompanied by an increased understanding of the processes involved in device function and breakdown, and the systematic modification of the properties of the emissive polymers by synthetic design has become a vital component in the optimization of light-emitting devices. In this account we present an overview of the synthesis and properties of electroluminescent polymers and demonstrate through examples the development of the field. There are many aspects of fundamental science to be studied in order to realize commercial applications of this serendipitous discovery. Opportunities for synthesis abound.

Keywords: conjugation · electrochemistry · luminescence · materials science · polymers

1. Introduction

The role of polymers in the electronics industry has been traditionally associated with insulating properties, whether these be for isolating metallic conductors or for use in photoresist technology. From that starting point it was the pioneering work of MacDiarmid, Heeger, and Shirakawa et al. that inspired chemists and physicists to consider the opportunity of using polymers as conductors. While the scientific community had started to accept the concept of conjugated polymers as semiconductors, no-one was prepared for the discovery of the plastic sandwich that would emit light when simply connected to a battery. The discovery in Cambridge of electroluminescence (EL), that is the emission of light when excited by flow of an electric current, in conjugated polymers[1] has provided a new impetus to the development of light-emitting devices (LEDs) for display and other purposes.[2] Organic electroluminescent displays represent an alternative to the well-established display technologies based on cathode-ray tubes and liquid-crystal displays (LCDs), particularly with respect to large-area displays for which the existing methods are not well suited.

Inorganic electroluminescent materials have been known for many years, and LEDs based on these materials have been commercially available since the early 1960s. They have been widely used in a variety of applications. EL from molecular organic materials was discovered about the same time, but it was only in the mid-1980s that devices using fluorescent organic dyes showing brightnesses and operating voltages suitable for commercial applications were developed by Tang and Van Slyke,[3] and by Saito and Tsutsui et al.[4] Monochromatic displays based on such devices are reportedly due to be released on the commercial market in 1997 or 1998.[5, 6] Inorganic semiconducting and organic dye materials have to be deposited as thin films by the relatively expensive techniques of sublimation or vapor deposition, which are not well suited to fabrication of large-area devices. For these reasons, the possibility of using fluorescent conjugated polymers, which can be readily deposited from solution as thin films over large areas by spin-coating or doctor blade techniques, is most attractive. Considerable research efforts have gone into the development of electroluminescent polymers for use in LEDs, and in this review we aim to give an overview of the progress made in this area. Polymer LEDs are expected to have commercial applications as backlights

[*] Dr. A. B. Holmes,[+] Dr. A. C. Grimsdale
University Chemical Laboratory
Lensfield Road, Cambridge CB21EW (UK)

[+] Other address:
Department of Chemistry
Melville Laboratory for Polymer Synthesis
Pembroke Street, Cambridge CB23RA (UK)
Fax: (+44) 1223-334866
E-mail: abh1@cus.cam.ac.uk

Dr. A. Kraft
Institut für Organische Chemie und
Makromolekulare Chemie II der Universität
Universitätsstrasse 1, D-40225 Düsseldorf (Germany)

[**] A list of abbreviations is given in the Appendix.

 © WILEY-VCH Verlag GmbH, D-69451 Weinheim, 1998 1433-7851/98/3704-0403 $ 17.50+.50/0

for liquid crystal displays and as the emissive material in alphanumeric displays within the near future.

Aspects of the properties of conjugated polymers and organic electroluminescence have previously been reviewed. These reviews are listed in Table 1.

Table 1. Recent reviews on conjugated polymers and electroluminescence.

First author	Topic
May	polymer electronics[2]
Patil	optical properties[7]
Friend	polymer LEDs[8]
Bradley	electroluminescent polymers[9]
Holmes	EL in conjugated polymers[10]
Fox	light-emitting plastics[11]
Baigent	conjugated polymer EL[12]
Yam	polymer electronics[13]
Greenham	physics of conjugated polymers[14]
Gymer	organic EL displays[15]
Rothberg	organic EL[16]
Salbeck	EL with organic compounds[17]
Salaneck	conjugated polymer interfaces[18]
Sheats	organic EL devices[19]
Lovinger	organic transistors[20]
Feast	synthesis of conjugated polymers[21]
Yang	polymer EL and LECs[22]
Friend	polymer device structures[23]
Díaz-García	plastic lasers[24]
Deussen	organic LEDs[323]
Hide	photonic applications[324]

2. Poly(phenylene vinylene)s—A Case History

Electroluminescence in conjugated polymers was first discovered during investigations into the electrical properties of poly(1,4-phenylene vinylene) (PPV; **6**),[1] the simplest and cheapest poly(arylene vinylene).

2.1. The Synthesis of Poly(*p*-phenylene vinylene)—Precursor Polymer Routes

PPV (**6**) is a bright yellow, fluorescent polymer. Its emission maxima at 551 nm (2.25 eV) and 520 nm (2.4 eV) are in the yellow-green region of the visible spectrum. The polymer is insoluble, intractable, and infusible. Any synthesis of PPV directly from a monomer produces an insoluble material, which cannot be easily processed; solution processing by spin-coating is, however, particularly desirable as it yields high-quality transparent thin films for the production of polymer



A. Holmes



A. Kraft



A. Grimsdale

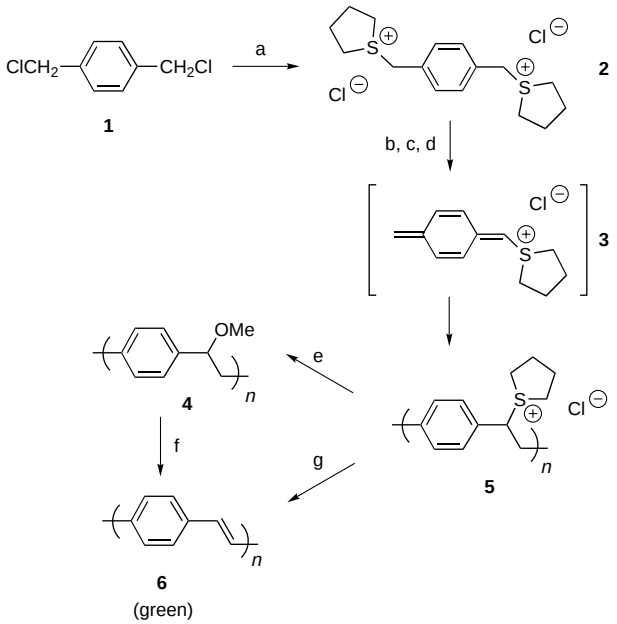
Andrew Holmes was born in Melbourne, Australia, in 1943 and received his early education at the University of Melbourne. He obtained his Ph.D. in 1971 in the field of annulene chemistry with Prof. Franz Sondheimer at University College London, and then carried out postdoctoral research at the Eidgenössische Technische Hochschule, Zürich with Prof. A. Eschenmoser on the total synthesis of vitamin B_{12}. In 1972 he was appointed University Demonstrator (Assistant Lecturer) and in 1977 Lecturer in the University Chemical Laboratory at the University of Cambridge. In 1989 he commenced a collaboration with Prof. R. H. Friend in molecular electronics, which led to the discovery of electroluminescence of poly(para-phenylene vinylene). *Dr. Holmes has been the Director of the Melville Laboratory for Polymer Synthesis since 1994. Current research interests embrace the synthesis of functional macromolecules and biologically active natural products.*

Arno Kraft, born 1961 in Darmstadt, Germany, studied chemistry at the Universität Würzburg. He then worked in the group of Prof. M. Christl on the synthesis of and NMR spectroscopic investigations of benzvalene derivatives, and obtained his Ph.D. in 1989. After a brief stay with Prof. G. Erker, he joined Andrew Holmes as a postdoctoral research fellow. During the following three years he worked on the development of electroluminescent polymers and charge-transporting materials. He left Cambridge in 1993 to start independent research for his habilitation at the Universität Düsseldorf. His current interests include highly soluble and, at the same time, highly self-associating and self-assembling dendrimers and branched macromolecules.

Andrew Grimsdale, born 1963 in Waiouru, New Zealand, is a graduate of the University of Auckland. He worked on the synthesis of analogues of biologically active drimane sesquiterpenes with Prof. R. C. Cambie and obtained his Ph. D. in 1990. He then joined Prof. A. Pelter at the University of Wales in Swansea, where he investigated photochromic and electroactive organic materials. In 1994 he moved to Cambridge where he began research with Andrew Holmes into novel electroluminescent polymers. In 1997 he returned to Auckland.

EL devices. This dilemma is conveniently resolved by the use of a solution-processible precursor polymer. The sulfonium precursor route to PPV was introduced by Wessling and Zimmerman,[25, 26] and was subsequently modified and optimized by other groups.[27–29] The principle has been applied, not only to PPV and its derivatives, but also to a whole range of PPV-related copolymers.

Scheme 1 outlines the standard preparation of PPV (**6**).[28] Treatment of 1,4-bis(dichloromethyl)benzene (**1**) with tetrahydrothiophene results in the formation of the bis-sulfonium



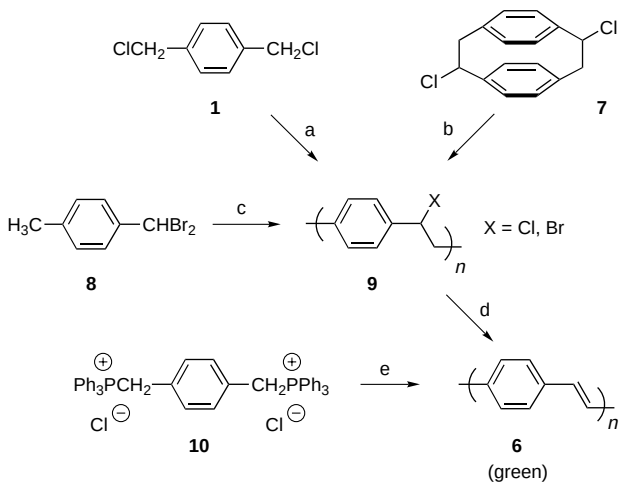
Scheme 1. Synthesis of PPV (**6**): a) tetrahydrothiophene, MeOH, 65 °C; b) NaOH, MeOH/H_2O or Bu_4NOH, MeOH, 0 °C; c) neutralization (HCl); d) dialysis (water); e) MeOH, 50 °C; f) 220 °C, HCl(g)/Ar, 22 h; g) 180–300 °C, vacuum, 12 h.

salt **2**. Other sulfides such as dimethyl sulfide can be employed, but unwanted side reactions occur at sulfonio groups during subsequent steps.[27] Polymerization of a methanolic solution of monomer **2** is induced by the addition of slightly less than 1 mol equivalent of aqueous sodium hydroxide at 0–5 °C. If more base is used, the resulting polymer solutions become brightly colored owing to partial base-induced elimination of the sulfonio groups. The mechanism of this polymerization deserves further investigation. Studies[26, 30] have shown that the presence of radical trapping agents such as oxygen can severely lower the molecular weight of the polymer, which would suggest that the *p*-quinodimethane intermediate **3** undergoes radical polymerization, although anionic propagation cannot be completely excluded. The reaction is in practice best performed under an inert atmosphere and is terminated by neutralization with dilute hydrochloric acid. The almost colorless solutions of precursor polymer **5** are then dialyzed against distilled water to remove impurities having low molecular weight. The molar mass of the precursor polymer **5** cannot be determined easily by gel-permeation chromatography owing to the polyelectrolyte nature of the polymer. Treatment with refluxing methanol gives a neutral polymer **4** which on gel-permeation chromatography characterization shows a number-average molar mass M_n of $\geq 100000\ g\,mol^{-1}$.[31]

The precursor polymer **5** is converted into PPV (**6**) by heating thin films (spin-coated with thickness of typically 100 nm) in the temperature range of 180–300 °C for 12 h under vacuum (10^{-6} mbar).[1, 28] Under these conditions the by-products of the elimination (tetrahydrothiophene and hydrogen chloride) escape easily. It has been reported that traces of oxygen during the conversion step reduce the luminescence quantum efficiency in the final PPV film. This has been attributed to the formation of carbonyl groups that are believed to quench luminescence.[32–34] The formation of such groups was reported to be suppressed by performing the conversion in a reducing atmosphere of nitrogen and hydrogen.[32, 33] PPV prepared under these conditions has higher fluorescence and EL quantum efficiencies.[35] Our own experience is that a nitrogen atmosphere suffices. When conducting the elimination step under argon, Schwoerer et al.[36, 37] found that conversion already occurred at 160 °C. Vanderzande et al.[38] and Müllen et al.[29] then showed that the conversion temperature could be further reduced by using the bromide instead of the chloride salt of precursor polymer **5**, which allows the conversion to occur at temperatures as low as 100 °C. This enables LEDs to be fabricated on flexible polymer foil substrates, for example on indium-tin oxide (ITO)-coated poly(ethylene terephthalate) (PET). Films of PPV can also be deposited by Langmuir–Blodgett techniques[39] and by simple dip-coating. The resulting PPV shows remarkably good luminance properties given that these techniques contaminate PPV with surfactant residues.[40–43] Highly aligned free-standing thin films and fibers of PPV can be formed by pre-ordering the precursor polymer **5** in a lyotropic liquid-crystalline phase before thermal conversion.[44] This type of nanocomposite might show promise for polarized emission.

Other methods have also been exploited to prepare PPV suitable for LEDs. The materials produced by these routes, however, may differ from PPV prepared by the Wessling route in molar mass, molar mass distribution, film quality, nature and amount of defects and impurities, output of waste materials etc., and of course the resulting device efficiency and lifetimes may also vary considerably. A modified Wessling (quinodimethane) synthesis, based on the elimination of sulfinyl or sulfonyl groups instead of sulfonio groups, has been reported by Vanderzande et al.[45–47] Galvin et al.[48] favored a xanthate precursor polymer soluble in organic solvents and claimed that it gave better quality PPV films and higher device efficiencies than the standard route.

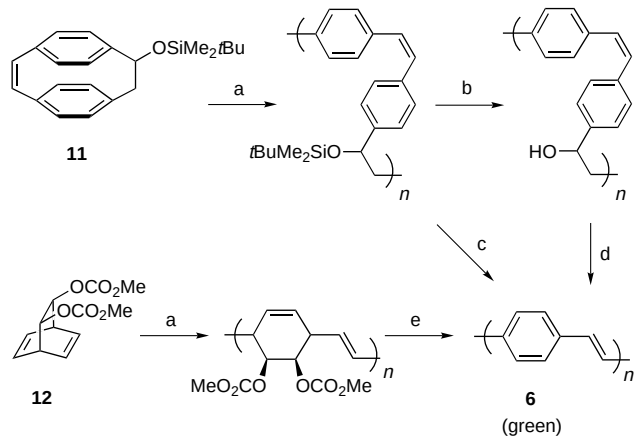
PPV films are also accessible by chemical vapor deposition (CVD) of compounds of type **1**[49] and **8** or of chlorinated cyclophane **7**.[50] In all cases the intermediate α-halo-precursor polymer **9** film is further converted to PPV **6** at 200 °C under vacuum (Scheme 2), but LEDs made with these films showed quite low (0.002 %) efficiencies (see Section 2.2).[49, 51] Electropolymerization of **10** gave PVV films, but absorption and emission spectra were blue-shifted with respect to material produced by other methods, indicating that the electropolymerized material had a shorter conjuga-



Scheme 2. Alternative synthetic routes to PPV (**6**): a) 500 – 700 °C, 0.01 mbar; b) 580 °C, 10 Pa; c) 800 – 900 °C, 0.01 mbar, then 60 °C, 0.1 mbar; d) 200 °C, vacuum; e) CH_3CN, 5.5 V.

tion length owing to incomplete elimination of the phosphonio groups.[52]

Ring-opening metathesis polymerization (ROMP) in principle offers the opportunity for precise control of polydispersity and microstructure. Applications to conjugated polymers such as polyacetylene are well-documented,[21] and promising routes to PPV are also emerging. The siloxy-substituted cyclophane **11**[53] or bicyclic monomer **12**[54] are typical substrates for ROMP and afford well-defined precursor polymers, which are converted to PPV **6** by thermal elimination (Scheme 3).



Scheme 3. ROMP routes to PPV (**6**): a) [Mo(=NAr)(=CHCMe$_2$Ph)-{OCMe(CF$_3$)$_2$}$_2$]; b) Bu$_4$NF; c) HCl(g), 190 °C; d) 105 °C; e) 280 °C.

2.2. Simple Electroluminescent Devices Based on PPV—A Basic Polymer LED

As a material, PPV has several advantages over classical inorganic light-emitting semiconductors. First the ease of processing permits PPV to be spread onto large areas and curved surfaces. Second PPV shows the tensile properties expected for a chain-extended polymer: its elastic moduli and tensile strength are almost as high as those of polyaramide fibers. This, of course, helps the polymer "to survive" under the harsh conditions prevailing during device operation.

In a light-emitting diode (LED) or electroluminescent device (Figure 1), the thin film of light-emitting material is sandwiched between two electrodes, one of which has to be

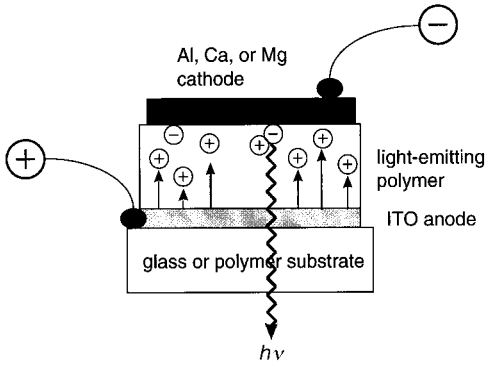


Figure 1. Schematic drawing of a single-layer electroluminescent device. An applied electric field leads to injection of holes (positive charges; the majority charge carriers in polymers such as PPV) and electrons (usually the minority charge carriers) into the light-emitting polymer film from the two electrode contacts. Formation of an electron-hole pair within the polymer may then result in the emission of a photon. Since holes migrate much more easily through PPV than electrons, electron-hole recombination takes place in the vicinity of the cathode.

semitransparent. Under an applied bias (voltage), oppositely charged carriers (electrons and holes) are injected into the emissive layer(s) from the opposing contacts, and are swept through the device by the high ($>10^5$ V cm^{-1}) electric field. Some of the electrons and holes combine within the emissive material to form triplet and singlet excited states. The singlets are indistinguishable from the excited states of photoluminescence (PL), the fluorescence process resulting from photoexcitation of the ground state (Figure 2).

A common measure of the efficiency of electroluminescent devices is the number of photons emitted per electron injected. This is the internal efficiency, which is based on the assumption that all the light generated is received by the viewer. External efficiencies are a factor of $2n^2$ smaller than internal efficiencies, where n is the refractive index of the polymer.[55] For a polymer having a typical refractive index of 1.4 this factor would be four, and external quantum efficiencies for the current family of polymers fall within the range 0.1 – 5 %.

It should also be noted that EL efficiencies are dependent on the distance of the emitting dipoles from the metal electrode.[56] Power conversion efficiences (W W^{-1}) are quoted by device engineers. These values are reached by multiplying the external quantum efficiency by the ratio of the photon energy and the drive voltage. The power efficiency should be as high as possible in order to maximize device longevity, and, at the same time, devices have to be bright at low current and low electric field. The luminous efficiency (lm W^{-1}) is the power conversion efficiency multiplied by the luminous efficacy (in lumens per watt).[19] The luminous efficacy is a conversion factor that takes account of the fact

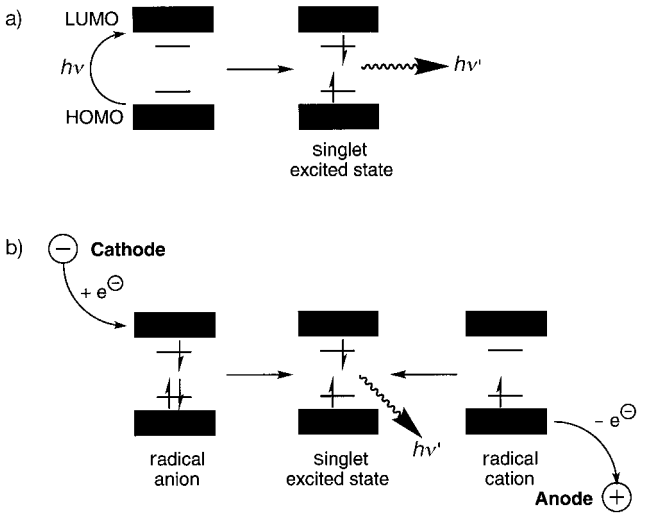


Figure 2. a) Irradiation of a fluorescent polymer excites an electron from HOMO to LUMO. In a typical conjugated polymer, two new energy states are generated upon relaxation within the original HOMO – LUMO energy gap and are each filled with one electron of opposite sign (singlet excited state). The excited polymer may then relax to the ground state with emission of light at a longer wavelength than that absorbed (photoluminescence). b) In a polymer LED, electrons are injected into the LUMO (to form radical anions) and holes into the HOMO (to form radical cations) of the electroluminescent polymer. The resulting charges migrate from polymer chain to polymer chain under the influence of the applied electric field. When a radical anion and a radical cation combine on a single conjugated segment, singlet and triplet exited states are formed, of which the singlets can emit light.

that the eye is more sensitive to green than to red and blue light. Current values reported for luminous efficiencies range between 1 – 2 lm W^{-1}, and values as high as 10 lm W^{-1} for the best devices have been reported. Luminance (cd m^{-2}) and luminance per unit of current density are also measures of device efficiency. Typical luminances for laptop displays are about 100 cd m^{-2}, but much higher luminances would be required for a matrix addressing scheme that avoids the need for thin film transistors behind each pixel.

The choice of the correct electrode combination is crucial to the operation of a polymer light-emitting diode (Figure 1). There has been considerable progress in understanding the dopant behavior of negatively charged metal contacts at the metal– polymer interface.[18] Single-layer devices are typically fabricated by solution-coating a thin film of polymer on indium-tin oxide (ITO)-glass and by vacuum evaporation of a cathode. These device structures will be denoted as ITO/polymer/metal in the remainder of this review. An early device configuration ITO/PPV/Ca had an average internal efficiency of 0.1 %.[57, 58] Glass or PET substrates with a thin (ca. 15 nm) transparent ITO layer are commercially available. The mixed-metal oxide has a high work-function, which matches the HOMO energy level of PPV and makes it convenient for hole injection (i.e. removal of an electron from the HOMO) into the polymer.

Other metals and oxides such as gold,[1] Al/Al_2O_3,[1] and SnO_2[59] have also been tested for electroluminescent polymers but in only a few cases gave better performance. Calcium as a result of its reactivity (especially its moisture sensitivity) may not be the preferred electrode for use in commercial devices unless excellent encapsulation can be realized, and a less reactive low-work-function metal would generally be favored. Aluminum has been a compromise, but the internal efficiency of a PPV light-emitting device using ITO and Al electrodes is only 0.01 % owing to poor electron injection.[58] Introduction of a thin layer of aluminum oxide between the PPV and Al layer (i.e., Al/Al_2O_3 as cathode) can result in a marked improvement in device efficiency as a result of carrier confinement.[60]

Heterostructure LEDs made from self-assembled multilayers of PPV and polyanions such as sulfonated polyaniline have also been constructed and found to emit bright yellow-green light with low turn-on voltages.[61–66] The self-assembled multilayer technique so far seems to enable exceptional control of the device thickness, and has recently been extended to include ruthenium-based complexes.[67] The improvement of power efficiency and stability of EL devices by addition of an extra charge-transporting layer between the PPV and the cathode[58, 68–77] is discussed in Section 3.2.

2.3. Solution-Processible Poly(phenylene vinylene)s—Direct Deposition of Electroluminescent Polymers

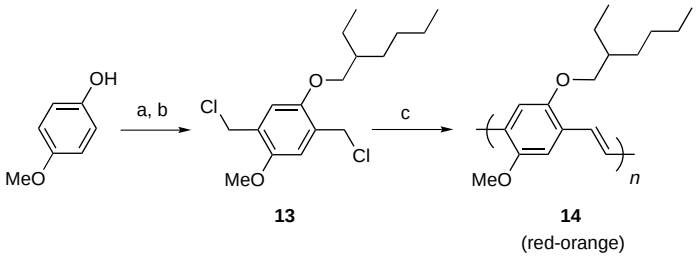
Following the discovery of electroluminescence in PPV, LEDs from PPV derivatives that are soluble in the conjugated form were reported independently by Ohnishi et al. at Sumitomo,[78] and by Braun and Heeger at Santa Barbara.[79, 80] Such soluble polymers no longer require thermal treatment during device fabrication, which is the drawback of the PPV precursor route, although they tend to have lower glass transition temperatures. It should be pointed out that, while the precursor polymer **5** is usually processed from methanolic solutions (and, like PPV, does not dissolve or swell in chloroform), almost all soluble PPV derivatives used in EL devices are processible from solvents that do not cause swelling of PPV or its precursor polymer **5**. This difference in solubility can be applied advantageously to the design of multilayer devices that consist of sandwich structures with layers of different polymers, for example, PPV and substituted PPVs (Section 3.3.).[81, 82]

Poly[(2,5-dialkoxy-1,4-phenylene)vinylene]s with at least one long, solubilizing alkoxy side chain (e.g., 2-ethylhexyloxy, 3,7-dimethyloctyloxy, 2-methylpentyloxy, or dodecyloxy)[78, 79, 83–87] dissolve in various organic solvents such as chloroform or tetrahydrofuran. In addition, their emission maximum is red-shifted [to ca. 590 nm (2.1 eV)] compared with that of PPV. The long side chains, which keep the conjugated polymer backbones apart from each other, apparently have a beneficial effect on the polymers' fluorescence and electroluminescence quantum yields.

Dialkoxy-substituted PPVs can be prepared by a sulfonium precursor route as described for the synthesis of PPV.[28, 86, 88–90] Although the Wessling route may be used to make soluble PPV derivatives, a dehydrohalogenation – condensation polymerization, first developed by Gilch et al.,[91] is generally preferred. It proceeds through base-promoted 1,6-elimination of 1,4-bis(halomethyl)benzene derivatives.[78, 84, 85, 92]

This shortens the preparation of the conjugated polymer by two steps, and can result in substantially increased yields. As with the Wessling procedure, the polymerization mechanism could involve a quinodimethane, an anionic intermediate, or a carbenoid species. Molar masses of soluble poly[(2,5-dialkoxyphenylene)vinylene]s, obtained by the polymerization of bis(chloromethyl) compounds with potassium *tert*-butoxide, are comparable with those obtained by the sulfonium precursor route.

Scheme 4 shows the synthesis of the most studied dialkoxy-PPV: MEH-PPV (**14**).[84, 86] The branched side chain in MEH-PPV has a favorable effect on the solubility of the polymer—



13 **14** (red-orange)

Scheme 4. Preparation of MEH-PPV (**14**): a) 3-(bromomethyl)heptane, KOH, EtOH, reflux, 16 h; b) HCHO, concd. HCl, dioxane, 20 °C, 18 h, reflux, 4 h; c) KO*t*Bu, THF, 20 °C, 24 h.

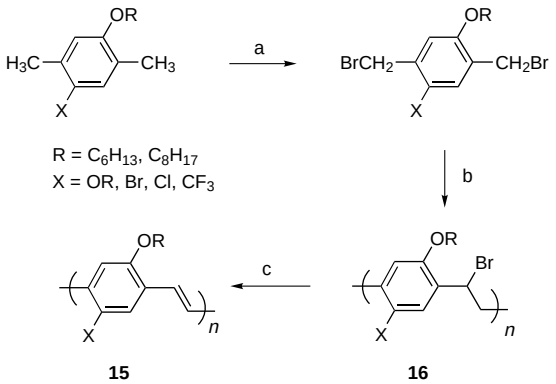
indeed, the polymer dissolves easily in solvents such as tetrahydrofuran, chloroform, or xylene. A related polymer **17** (OC_1C_{10}-PPV) with a 3,7-dimethyloctyloxy side chain has been been the subject of investigation by workers at Philips and Hoechst.[17]

The bis(chloromethyl) compound **13** is synthesized by alkylation of 4-methoxyphenol followed by chloromethylation.[79, 83, 84, 86] Polymerization of the monomer **13** is induced with a tenfold excess of potassium *tert*-butoxide in tetrahydrofuran and gives the bright red-orange MEH-PPV (**14**). Careful control of concentration is needed to avoid gelation. Purification involves several reprecipitations in methanol. A simple electroluminescent device (ITO/MEH-PPV/Ca) already achieves a quite respectable efficiency of 1.0 %.[79, 93] Insertion of a thin hole-blocking layer of poly(methyl methacrylate) film by Langmuir–Blodgett deposition is reported to give up to a fourfold increase in quantum efficiency with aluminum cathodes.[94] Devices have also been constructed with doped silicon as anode, thus opening the possibility of integrating polymer LEDs with silicon-chip technology.[95, 96]

Most of the reports of polymer LEDs described ITO on glass as the hole-injecting contact. Polyaniline (PANi), a long-known conducting polymer, presents an interesting alternative to ITO in devices using MEH-PPV, as, although it is deeply colored, it has an optical window coinciding with the maximum of emission for MEH-PPV. Using a layer of acid-doped PANi on ITO reduces the drive voltage of the device and causes an increase in device efficiency by a factor of 30 %. Such devices can produce peak luminances of over 10000 cd m^{-2} at drive voltages of 5 V, with external quantum efficiencies of 2–2.5 %, and luminous efficiencies of 3–4.5 lm W^{-1}.[97] Furthermore, replacement of the ITO-coated glass substrate by a polyaniline-coated PET sheet enables the manufacture of a flexible electroluminescent device.[83, 98] As the PET/PANi/MEH-PPV/Ca device consists of flexible polymers (with the exception of the calcium cathode), it can be safely deformed even during operation (inside a glove box). While this is an interesting application of PANi, it should be noted that ITO-coated PET is commercially available as an alternative flexible anode of reasonable mechanical stability.[36] A cylindrical polymer LED with layers of a transparent polyaniline electrode and MEH-PPV wrapped around a cylindrical metal cathode has been constructed; in this example the reactive electrode is protected by a sandwich of polymers.[99]

A significant recent development has been the introduction of a sulfonic acid-doped polyethylenedioxythiophene conducting polymer either in combination with ITO glass or alone as an anode. Quite spectacular improvements in device efficiency and reduction in drive voltage are observed in two-layer devices fabricated with this material.[100, 101] Gel-processing of a blend of MEH-PPV in polyethylene gives access to oriented films that show anisotropies of 60:1 in their fluorescence emission spectra; the preferred direction of emission is parallel to the draw axis.[102, 103] Rubbing alignment of a poly(dialkoxyphenylene vinylene) is the most effective way of orienting material to achieve polarized EL.[104, 326] Such oriented emission might find use for back-lighting in a liquid-crystal display. Orientation is also possible using Langmuir–Blodgett techniques for film deposition.[105]

Electroluminescent poly(2,5-dialkoxy-1,4-phenylene vinylene)s other than MEH-PPV have been similarly prepared.[85, 86, 106, 107] If less than one equivalent of base is used, a soluble α-halo precursor polymer **16** is obtained that can be converted into the conjugated polymer **15** (Scheme 5)[85, 108]—



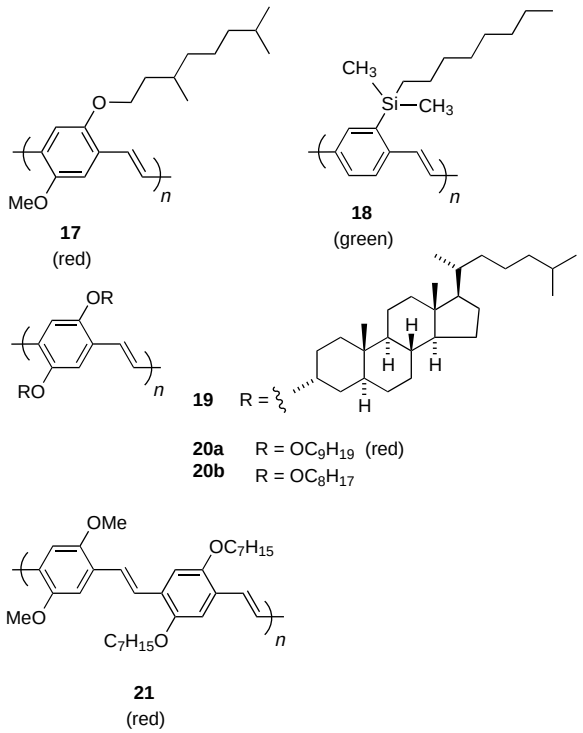
15 **16**

Scheme 5. The halo-precursor route to substituted PPVs: a) NBS, CCl_4, *hν*; b) KO*t*Bu, THF; c) 160–220 °C, vacuum, 4 h.

this is known as the halo-precursor route and has some advantages if the precursor polymer is more soluble, if vapor deposition methods are used, or if incomplete conversion to a partially conjugated polymer is envisaged (Section 3.1.).

Branched side chains, as in MEH-PPV, generally enhance solubility more than linear ones of identical length and number of carbon atoms or heteroatoms. With increasing size

of the alkoxy group, EL efficiency passes though a maximum and decreases again with even larger side chains;[78] very large substituents, for example cholestanoxy as in **19**,[106, 109] seem to overpower and "dilute" the semiconducting properties of the conjugated polymer (Scheme 6). The highest external EL



Scheme 6. Examples of soluble, dialkoxy-substituted PPV derivatives.

efficiency reported to date for a single layer device using dialkoxy-substituted PPV derivatives is 2.1% for a device made by Philips with **17**.[17] This polymer EL device has a luminance of 100 cd m^{-2} with a luminous efficiency of 3 lm W^{-1} at a drive voltage of 2.8 V. A group at Hoechst has achieved the same quantum efficiency and luminance with a flexible device using an ITO anode on PET, with a slightly lower luminous efficiency of 2 lm W^{-1} at a driving voltage of 3.4 V and a current density of 4.5 mA cm^{-2}.[17] The introduction of a silyl group as in DMOS-PPV (**18**) widens the band gap so as to give emission of green light.[110–114] Yoshino et al.[115] have employed poly(2,5-dinonyloxy-1,4-phenylene vinylene) (**20a**), which forms a nematic liquid-crystalline state upon melting. When cooled to room temperature, the polymer remains oriented and has a lower energy gap (2.08 eV) than in an unoriented film (2.21 eV) formed by casting from chloroform solution. Rubbing of a film of this material also induces molecular orientation, and gives rise to oriented electroluminescence.[116] This technique has also been applied to a smectic liquid-crystalline copolymer of distyrylbenzene linked by long chain polyester flexible spacer groups.[117]

Other polycondensations have been used to prepare soluble PPV derivatives. Wittig condensation of terephthaldicarboxaldehydes with arylene–bisphosphylidenes furnishes alternating PPV copolymers.[118] An alkoxy-substituted PPV copolymer (**21**) prepared in this manner was found to show orange (585 nm) emission.[118] Similar PPV copolymers have been prepared by Heck coupling of dihalobenzenes with divinylbenzenes.[119]

3. Improvement of Device Efficiency—Making EL Polymers Competitive

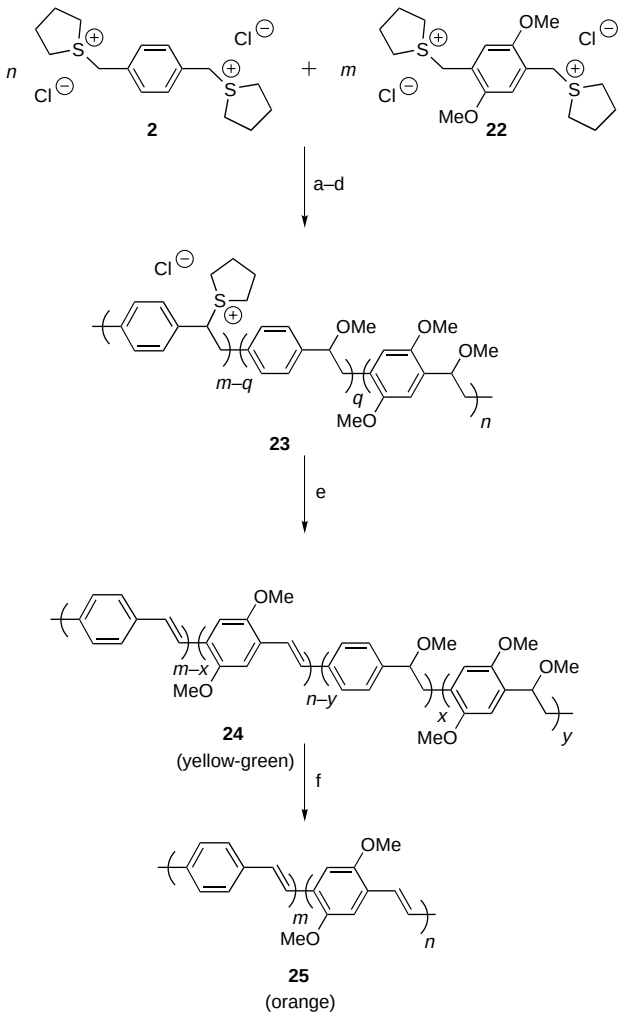
High efficiencies and reliability are the principle requirements of molecular and polymeric light-emitting materials for commercial applications.[19] The optimum goal is to obtain maximum power efficiency and brightness at minimum drive voltage and current density. This combination should afford devices having long lifetimes. The improvement of EL devices therefore requires optimization of the electroluminescent polymer and/or the device structure. Whereas it took about thirty years for an inorganic semiconductor to reach luminous efficiencies of several lm W^{-1}, organic light-emitting polymers have reached this level of performance in less than ten years. It is evident that the efficiencies of molecular and polymer organic LEDs have been dramatically improved in a short time, and are beginning to compete with those obtained for conventional inorganic LEDs.

3.1. The Use of Copolymers—Finessing the Properties

For the majority of conjugated polymers investigated so far, electron injection has proved to be more difficult than hole injection, that is, the polymers are more easily oxidized than reduced. This has been largely remedied by the use of metals with a low work-function (especially Ca) as the cathode material. However, calcium is highly susceptible to atmospheric degradation. Although this can be retarded by encapsulation, it would be beneficial to use less moisture- and oxygen-sensitive metals. If the barrier for electron injection from such metals is to be lowered, the polymer must be modified so that the energy of its LUMO matches the work function of the cathode. Copolymers of one kind or another present an attractive solution to this problem.

Copolymers containing a combination of different arylene units can be much more versatile than homopolymers and may even be chemically tuned to provide a range of materials with considerably improved EL properties. This was for the first time exemplified by statistical copolymers of PPV and poly[(2,5-dimethoxy-1,4-phenylene)vinylene], although other copolymers having interrupted conjugation have also been investigated.[57, 120–123]

By a modification of the sulfonium precursor route the two monomers **2** and **22** are copolymerized in the presence of sodium hydroxide in a water–methanol mixture (Scheme 7). The ratio of the units in the resulting (presumably statistical) copolymer **23** depends on the feed ratios of the two sulfonium salt monomers. The use of a solvent mixture leads to selective substitution of the sulfonio groups by methoxy groups. This occurs at a faster rate at those benzylic carbon atoms that are attached to the more activated dimethoxyphenylene rings. As a result, copolymer **23** has two leaving groups at the benzylic carbon atoms; the methoxy groups are adjacent to all the dimethoxyphenylene and a few phenylene units, and sulfonio

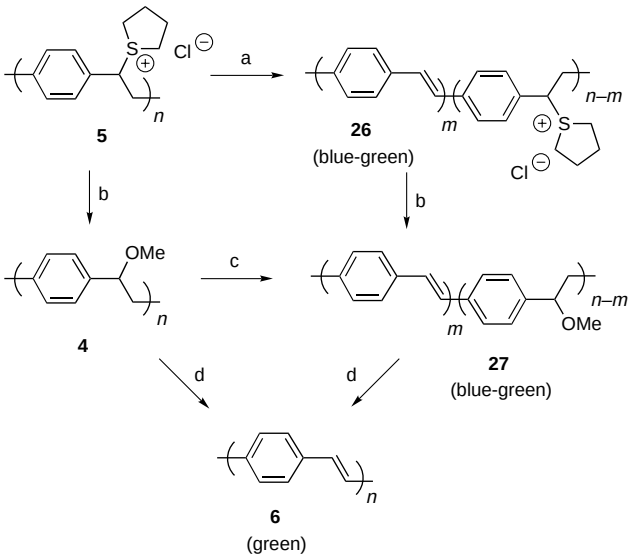


Scheme 7. Synthesis of PPV/dialkoxy-PPV copolymers: a) NaOH, MeOH/H_2O, 0 °C, 1 h; b) HCl; c) dialysis (water); d) MeOH; e) 220–300 °C, vacuum, 12 h; f) 220 °C, HCl(g)/Ar, 22 h.

groups are next to most of the phenylene units. Thermal conversion of thin (typical thickness 100 nm) films of **23** results in complete elimination of the sulfonio and only partial elimination of the methoxy leaving groups, which gives polymer **24** with interrupted conjugation. Complete elimination of all leaving groups to furnish the fully conjugated polymer **25** requires thermolysis under acidic conditions.

The electroluminescent device efficiency of polymer **24** varies with the composition of the copolymer and has its peak with a copolymer prepared from a 9:1 feed ratio of salts **2** and **22**. The maximum internal efficiency in this case is 0.3%, demonstrating a 30-fold improvement compared with that of PPV (0.01%) in the same device configuration (Al-Al_2O_3/polymer/Al).[120, 124] The shortening of the conjugated segments actually improves fluorescence yields and electroluminescence efficiency, probably originating from a reduction in nonradiative processes such as diffusion of the excited states to quenching sites. On the other hand, a large fraction of interruptions in the conjugated chain will lower the mobility of charged carriers. Somewhere in between lies an optimum for electroluminescence efficiency. The principle has been applied to other copolymers.[123] Alkoxy- and alkyl-substituted poly(phenylene vinylene)s prepared by the dehydrohalogenation route also yield interrupted copolymers having relatively high EL efficiencies.[123] In addition, statistical copolymer **23** has found use in forming lithographically patterned copolymers and waveguides.[120, 121]

A simple modification of the PPV synthesis gives access to PPV-derived blue-shifted light-emitting polymers with a high concentration of interruptions in the conjugated chain. Partial conversion of precursor homopolymers **4** or **5** produces statistical copolymers **26** and **27** with regions of saturated and unsaturated units (Scheme 8).[125, 126] The conversion of



Scheme 8. Synthesis of partially conjugated PPV copolymers: a) Bu_4NOH, MeOH; b) MeOH, 50 °C; c) 300 °C, vacuum, 12 h; d) 220 °C, HCl(g)/Ar, 22 h.

sulfonium precursor polymer **5** to **26** may be accomplished by either thermal or base treatment. Although **26** is prone to further elimination, Heeger et al. have found that conversion at 160 °C for 2 h gave a copolymer of the type **26** with fairly good long-term stability and emission efficiency.[127]

Another approach to raising the efficiency of PPV is the introduction of disorder into the chain, thus interfering with polymer chain packing. Son et al.[128] have synthesized amorphous PPV by using a modified Wessling procedure with a xanthate leaving group. The resulting PPV has a mixture of *cis*- and *trans*-alkene units, which affects conjugation and interferes with packing. Internal efficiencies of up to 0.22% for single-layer devices with aluminum cathodes and 2% for double-layer devices using an electron-transporting layer (see Section 3.2) are reported. It is not clear whether the improvements in efficiency arise from interruptions to conjugation or from reduced intermolecular order owing to the presence of *Z* double bonds. The authors favor the latter explanation.

Hörhold et al have reported poly(arylene vinylene)/poly(phenylene vinylene) alternating copolymers in which the arylene substituent carries in-chain phenylamino groups. These have the effect of dramatically reducing the oxidation potential compared with that of PPV-based polymers (and are therefore photoconductors), and offer interesting possibilities as electroluminescent materials as well.[129]

3.2. Multilayer Devices—Raising Device Efficiency with Additional Charge-Transporting Layers

The electroluminescent conjugated polymer devices discussed so far were mostly single layer devices, that is, they have the conjugated polymer sandwiched directly between anode (high work-function electrode) and cathode (low work-function electrode). Unless the barriers between these contacts and the HOMO (or LUMO) of the polymer are identical or zero, one type of charge carrier (either holes or electrons) will be preferentially injected. For a discussion of factors affecting charge injection the reader is referred to the article by Blom et al.[130] and the excellent reviews by Greenham and Friend,[14] and Sheats et al.[19].

For PPV, the injection of holes predominates. To increase the efficiency of devices, electron injection has to be significantly boosted. The use of certain additional layer(s) of materials can promote the passage of electrons through the layer and, at the same time, provides a barrier to the passage of holes. Such a layer is called an electron-conducting/hole-blocking (ECHB) layer. A suitable ECHB material should have an electron affinity equal to or greater than the electron affinity of PPV. As illustrated by Figure 3, holes are increasingly confined in the PPV layer, and the site of recombination of holes and electrons (where the emission takes place) is then moved away from the metal–polymer interface, which is known to act as a quenching site. In contrast, hole injection is not a problem with devices made from PPV. When a device with a hole-transporting layer (between the anode and the PPV layer) was tested, the efficiency of the device actually decreased, indicating that the main limiting factor in PPV-based LEDs is indeed electron injection and transport.[131]

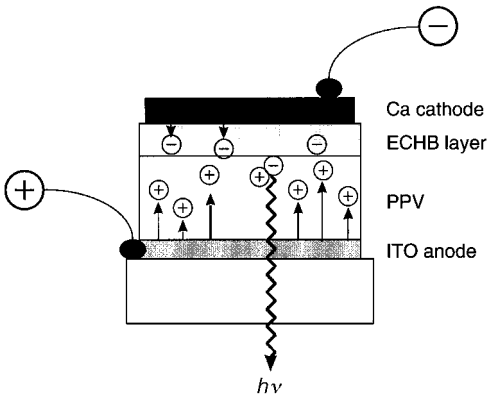
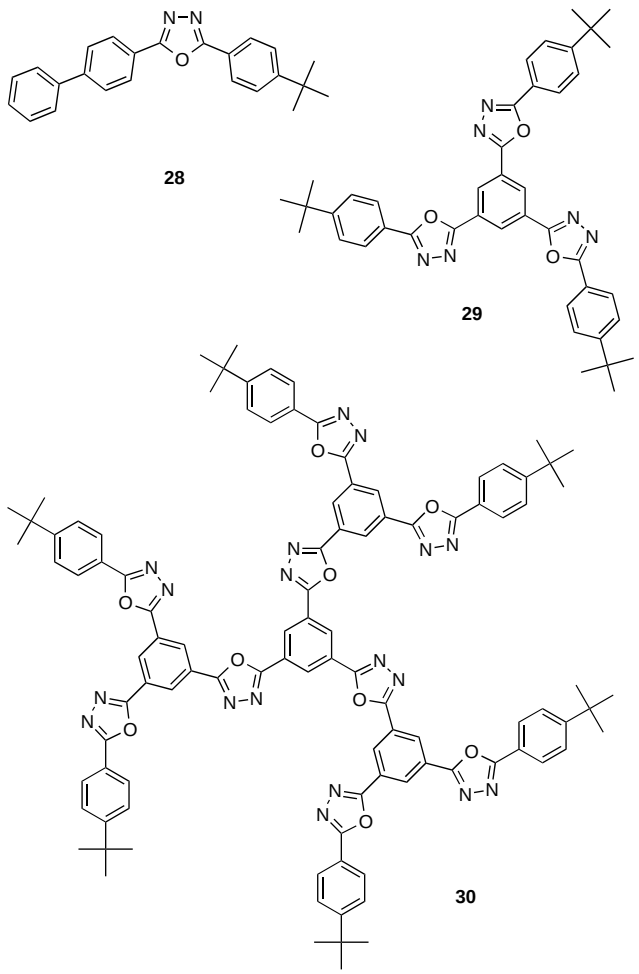


Figure 3. In this improved bilayer device structure for a polymer LED an extra ECHB layer has been inserted between the PPV and the cathode metal. The ECHB material enhances the flow of electrons but resists oxidation. Electrons and holes then accumulate near the PPV/ECHB layer interface. Charge recombination and photon generation occur in the PPV layer and away from the cathode.

The principle behind the design of ECHB materials is well exemplified by oxadiazoles, the first and most extensively investigated class of ECHB materials. Following the successful use of 2-(4-biphenylyl)-5-(4-*tert*-butylphenyl)-1,3,4-oxadiazole (PBD) (**28**) in sublimed film EL devices,[3, 4] PBD has long been a favored compound (Scheme 9). Oxadiazoles



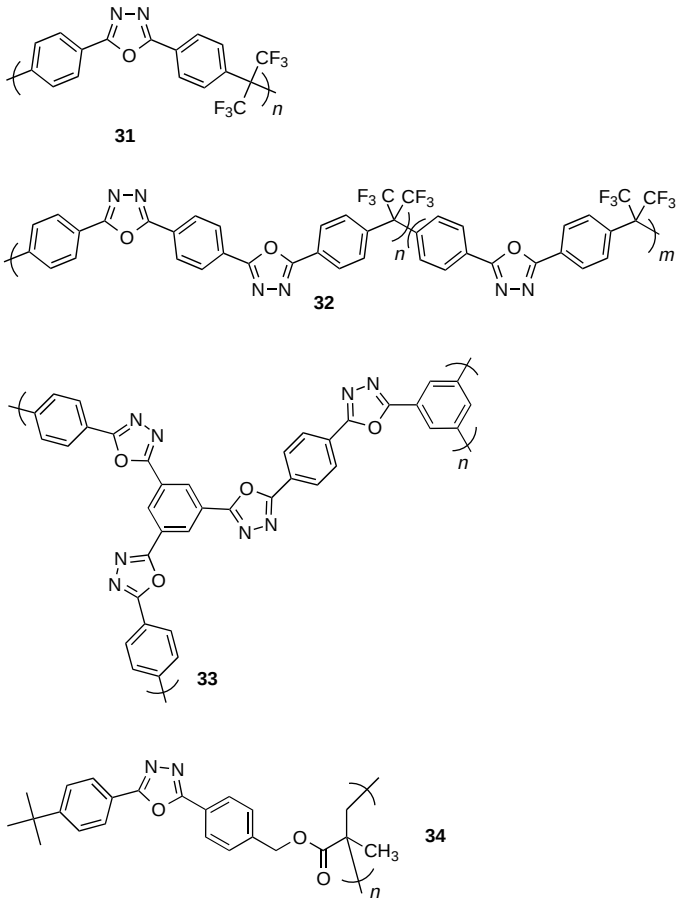
Scheme 9. Examples of oxadiazole-containing electron-transporting materials.

are electron-deficient, making PBD an extremely poor hole acceptor. It has a number of advantages: it is available in high purity, sublimes, can be spin-coated as a dispersion in a range of standard polymers such as poly(methyl methacrylate) (PMMA),[68] and can be blended with electroluminescent polymers.[112, 132–134] However, some incompatibilities with polymers exist that may lead to phase separation or crystallization especially at higher temperatures. Crystallization may be retarded by using a solid dispersion of PBD in an insulating polymer (PMMA).[68] As the ITO/PPV/PBD-PMMA/Ca device then becomes thicker owing to the extra layer, the voltage required to drive the device needs to be increased. This drawback is outweighed by a rise in internal EL efficiency from 0.1% (for an ITO/PPV/Ca device) to 0.8% (for ITO/PPV/PBD-PMMA/Ca). However, higher current densities cause a drop in device efficiency as a result of quenching by the high amount of accumulated holes at the PPV/PBD-PMMA interface.

The incorporation of identical redox sites within the same molecule has been used successfully in the design of charge-transporting compounds for electrophotography (photocopiers and laser printers). Since electron hopping is the main charge-transport mechanism in ECHB materials, increasing the number of (in this case) oxadiazole units would therefore

seem a promising way to improve the charge-transporting properties.[135] The idea was extended to the design of branched and highly symmetrical compounds such as the radialene **29**,[136] starburst structures,[137, 138] and small dendrimers like **30**.[138, 139] These materials have high glass-transition temperatures and form stable glasses, which minimize the problems of crystallization. Although the large numbers of branches in these materials should have made electron-transfer more efficient because of enhanced charge migration opportunities, they have not shown any improvement over PBD.

While low molar mass compounds are much easier to purify, incorporation of the active electron-transporting moieties into amorphous polymers should at least mitigate the problem of crystallization. Several polymeric analogs of PBD have been prepared with the oxadiazole unit either in the main or the side chain. A number of examples of poly(aromatic oxadiazole)s with satisfactory performance have been reported.[70, 72, 77, 136, 140] Solubility is mainly influenced by the frequency of solubilizing flexible spacer groups as in **31**, or the use of copolymer structures as in **32** (Scheme 10). A hyperbranched oxadiazole polymer **33**, which

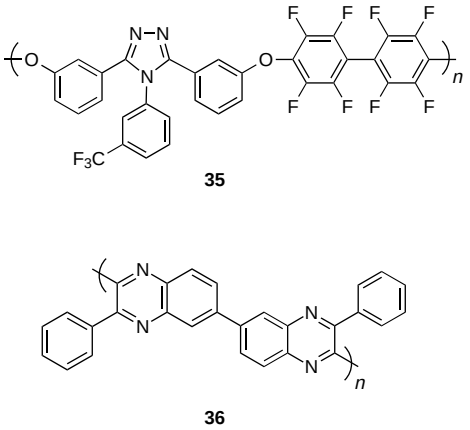


Scheme 10. Examples of oxadiazole-containing electron-transporting polymers.

is soluble in trifluoroacetic acid, was prepared by a one-step procedure, but its electron-transporting properties were mediocre, perhaps caused by defects within the polymer.[136]

Poly(methacrylate)s with ECHB-active oxadiazole side chains (e. g., **34**) have been prepared by radical polymerization and show good film-forming properties.[77, 141–143] However, their device performance has not fulfilled expectations, as higher drive voltages are required to achieve the improvement in efficiency.

Since oxadiazoles have not proved entirely successful as ECHB materials, attention has turned to other classes of materials. Nitrogen heterocycles such as 1,2,4-triazoles, 1,3,5-triazines,[325] or quinoxalines are of particular recent interest. The turn-on voltage in devices with an ECHB layer consisting of the polymer **35**, which contains a 1,2,4-triazole unit, is surprisingly unaltered from LEDs without an electron-transporting layer (Scheme 11).[69, 76] The electron-deficient nitro-



Scheme 11. Examples of a triazole- and a quinoxaline-containing electron-transporting polymer.

gen atoms in poly(phenyl quinoxaline) (**36**) also enhance the electron affinity of the polymer. This material has been shown to greatly enhance the efficiency of devices that use soluble PPV derivatives.[144] The materials discussed above have undoubtedly made a significant contribution towards improvement in device efficiency. A more successful approach may be to increase the electron affinity of the emissive polymer as will be discussed in Section 4.

3.3. Multilayer Devices with More Than One Electroluminescent Polymer—Towards White Light Emission

Other multilayer devices than those discussed in Section 3.2 can be constructed from at least two electroluminescent polymers. If carefully chosen, they show light emission from more than one layer provided that the polymers have small and controlled variations in energy gap from one layer to the next. This is necessary to avoid any build-up of space-charge at the interfaces between polymer layers. The first example of this type of LED consisted of an ITO/MEH-PPV/PPV/copolymer **24**/Ca device.[81] When one polymer is coated on top of another polymer layer, it is important that the process does not cause swelling or dissolution of the already deposited layer, and that good quality interfaces are obtained. Since

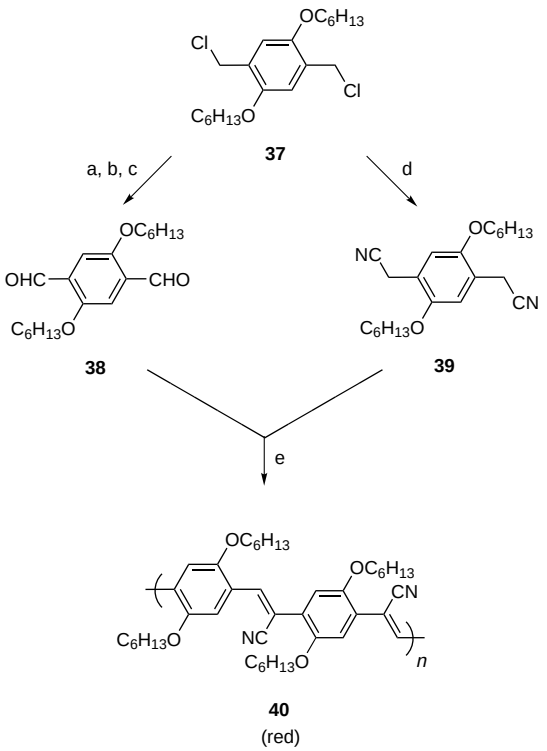
PPV and the sulfonium copolymer precursors are insoluble in chloroform, and MEH-PPV is insoluble in methanol, such a multilayer structure could be produced by spin-coating successive layers onto ITO without intermixing between MEH-PPV and the precursor layers. The precursor polymers **5** and **23** were then converted into the conjugated polymers and, after deposition of calcium, the device emitted orange light with the emission spectrum stretching from 800 nm (1.55 eV) through to 490 nm (2.5 eV). It was therefore concluded that electroluminescence occurred from both the red-light-emitting MEH-PPV, which was furthest away from the cathode, and from PPV, which showed yellow-green EL. The broadening of the emission spectrum further suggested how, in principle, to fabricate a white light source from a sandwich of several EL layers. A more recent multilayer device design developed by Yoshino et al.[145–147] uses layers of the blue-emitting polymer **75a** and of red-emitting materials such as the poly(3-alkylthiophene) **49a** separated by a charge-transport layer. Depending on the bias either red or blue light is emitted, while under alternating current bias emission from both materials is observed.

4. Polymers with Higher Electron Affinity—Luminescent Transport Layers

The ideal light-emitting polymer should be both fluorescent and avoid the need for an extra electron-transporting material. It should also function with cathode metals other than calcium. Calculations[148] have shown that a cyano substituent (and presumably other electron-withdrawing groups) on the ring or vinylene moiety of PPV lowers the HOMO and LUMO energies and increases the electron affinity of the polymer, thus improving the efficiency of electron injection and the potential efficiency of a polymer LED. Unfortunately, the Wessling (quinodimethane) route to poly(arylene vinylene)s is unsatisfactory when electron-withdrawing substituents are involved, and alternative polymerization or polycondensation methods need to be employed.

4.1. CN-PPV—Highly Luminescent Electron-Deficient Polymers

CN-PPV (**40**), a dialkoxy-substituted PPV derivative with cyano-groups on the vinylene units should be regarded as an alternating copolymer in this context. It is readily available by a Knoevenagel condensation[149] between equimolar amounts of the terephthaldehyde **38** and the benzene-1,4-diacetonitrile derivative **39**, both obtained from the same starting material **37**. The condensation reaction takes place upon addition of excess tetrabutylammonium hydroxide (or potassium *tert*-butoxide) in a tetrahydrofuran/*tert*-butanol mixture at 50 °C (Scheme 12).[150] Polymer **40** precipitates and can be easily isolated. Careful control of reaction conditions is required to avoid Michael additions (and consequently crosslinking), which may lead to polymers with inferior EL properties, and purification by reprecipitation is essential to obtain high quality polymer. CN-PPV is a brilliant



Scheme 12. Synthesis of CN-PPV (**40**): a) NaOAc; b) KOH, EtOH; c) pyridinium chlorochromate; d) NaCN; e) KO*t*Bu or Bu_4NOH, *t*BuOH, THF, 50 °C.

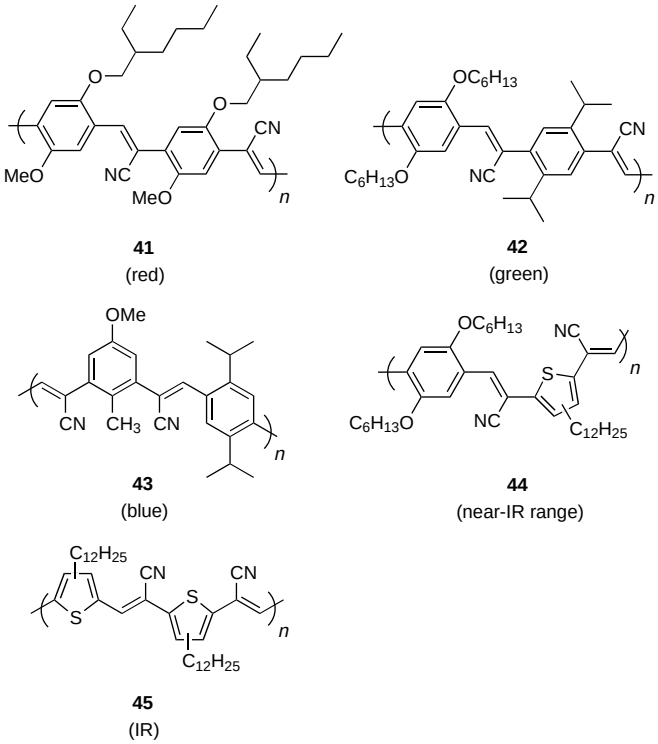
red, fluorescent material with a molar mass typical for polycondensates.

The HOMO–LUMO gap of CN-PPV (590 nm; 2.1 eV) is mainly determined by the effect of the alkoxy substituents, which also serve to promote solubility in chloroform, and thus ensure processibility of the conjugated polymer; the cyano substituents contribute only to an increase in the electron affinity of the polymer compared with PPV. Cyclic voltammetry studies show that the cyano groups shift the onset of reduction by about 0.6 V.[136] The low HOMO–LUMO gap of CN-PPV also indicates that the nitrile groups do not introduce any significant steric torsion in the conjugated poly(2,5-dialkoxyphenylene vinylene) chain.

Internal efficiencies of red-emitting ITO/CN-PPV/cathode devices can reach 0.2 % with calcium as well as aluminum cathodes. This is particularly noteworthy because other conjugated polymers such as PPV suffer from at least a tenfold reduction in efficiency when the electron-injecting contact is changed from Ca to Al. Since CN-PPV shows much higher electron affinity than PPV owing to the introduction of cyano groups, the device efficiency is now determined by hole injection at the ITO electrode. As a result of this, the introduction of a hole-transporting layer improves EL efficiencies considerably. PPV is a suitable hole-transporting polymer, and CN-PPV can be easily spin-coated on top of an insoluble PPV layer. Two-layer electroluminescent ITO/PPV/CN-PPV/cathode metal devices operate with very high internal (4 %) efficiencies.[151, 152] Significant lifetimes were only observed with high-quality polymer, demonstrating once more the importance of purification. The emission (λ_{max} =

710 nm) occurs exclusively from the lower energy CN-PPV, with no evidence of electroluminescence from the PPV layer. Although this appears to be in contrast to the multilayer devices discussed in Section 3.3, CN-PPV apparently acts more like a sink for charge carriers and excited states rather than to permit any emission from another EL polymer (namely PPV) to occur.

The synthetic route is extremely flexible and lends itself to considerable variation, enabling the synthesis of many other α-cyano PPV derivatives (Scheme 13).[123, 153] Some of these



Scheme 13. Color range available for CN-PPV derivatives.

show similarly high emission efficiencies in double-layer devices with PPV.[12, 154] In particular, MEH-CN-PPV (**41**) is processible in solvents such as toluene and exhibits very high EL device efficiencies. The improvement in processibility clearly contributes significantly to the improved device efficiency. A double layer device ITO/PPV/**41**/Al produces red-orange (600 nm) light with a power efficiency of 5 cd A^{-1} corresponding to a luminous intensity of over 1000 cd m^{-2} at a drive voltage of 6 V.[12, 154] This corresponds to a luminous efficiency of 2.5 lm W^{-1}.

Color variations over a wide range of wavelengths have been demonstrated. The bulky isopropyl substituents of **42** cause a blue-shift and green light emission (510 nm), while incorporation of *meta*-linkages, as exemplified by those in **43**, results in blue fluorescence. The thiophene group in **44** reduces the HOMO – LUMO energy gap to 1.75 eV (740 nm), and the polymer shows substantial emission in the near infrared region. An ITO/PPV/**44**/Al device was the first polymer-based IR-emitting LED.[155] Replacement of both arylene rings with thiophene groups in **45** reduces the energy gap even further to 1.56 eV (800 nm).[153, 156]

4.2. Other High-Electron-Affinity PPV Derivatives—Electron-Deficient Building Blocks

Apart from CN-PPV, other PPV derivatives with electron-withdrawing substituents, this time on the arylene ring, have been investigated for EL applications (Scheme 14). Poly-



46 (X=Cl) **47** (X=Br) (red) **48** (yellow-orange)

Scheme 14. High-electron-affinity PPV derivatives with electron-withdrawing groups on the aromatic ring.

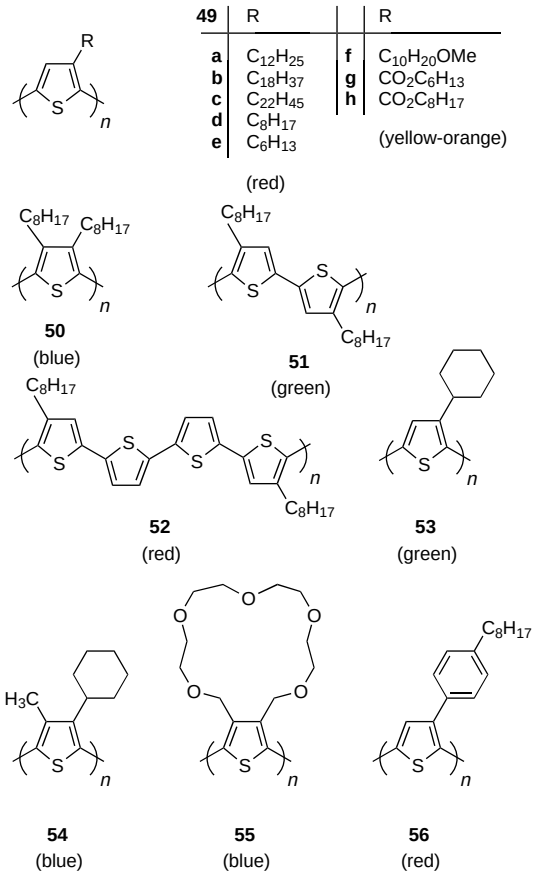
(phenylene vinylene)s **46** and **47** bearing halide and alkoxy groups on the ring are accessible through the Wessling method.[157] High molar masses required rigorous purification of the monomers and optimization of the polymerization conditions. We have found that PPV derivatives with bromo (**47**)[158] or trifluoromethyl (**48**) substituents[159, 160] can be readily obtained by a bromo-precursor route (see Scheme 5) or by Horner – Wittig polycondensation.[159] Polymer **48** in particular shows higher electron affinities than PPV. The halogen-substituted PPVs **46** and **47** were found to emit red ($\lambda_{max} = 620 - 630$ nm) light,[157] while the trifluoromethyl derivative **48** emits yellow to yellow-orange ($\lambda_{max} = 540 - 570$ nm) light. The PL quantum yields for **48** are much lower than for PPV and single-layer devices gave only weak emission, and EL internal efficiencies reached 0.01 % in double-layer devices with PPV as hole-injecting layer and Al as cathode.[160, 161] In view of their poor PL quantum yields these materials are more likely to prove useful as ECHB than as emissive materials.

5. Color Tuning—Varying the HOMO – LUMO Gap

A major advantage of polymers as EL materials is the ease with which their structures can be altered, thus enabling the chemist to tune the properties by modifying their structures. In this section we wish to illustrate both the wide range of polymer structures, which can be used for EL purposes, and also to show how the properties, especially the emission color, can be adjusted by varying the aromatic ring, the substituents, and the regioregularity of the conjugated polymer.

5.1. Poly(3-alkylthiophene)s—A Good Red

Poly(3-alkylthiophene)s provide a good example of how the color of emission can be varied in polymer LEDs by modifying both the polymer structure and the design of the devices (Scheme 15). Soluble poly(3-alkylthiophene)s **49** are readily prepared by the polymerization of the corresponding

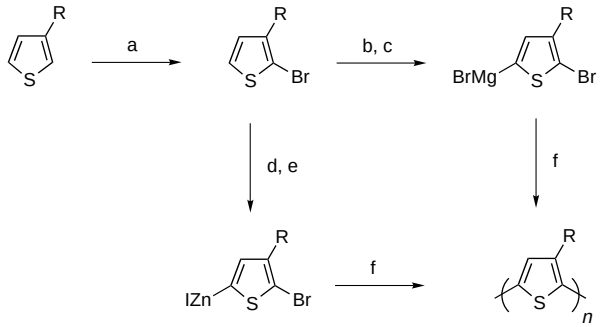


Scheme 15. Poly(alkylthiophene) derivatives and their emission color range.

3-alkylthiophene monomers in the presence of excess ferric chloride,[162] or by nickel-catalyzed coupling of dihalothiophenes with thiophene-bis(magnesium halide)s.[163, 164] Red electroluminescence (emission maxima at about 640 nm) from **49a–e**, which have alkyl chain lengths varying from 6 to 22 carbon atoms, has been reported by various groups.[165–169] The emission intensity became larger with increasing chain length, possibly owing to the improved confinement of excitons. Homopolymers based on 3-alkylthiophenes exhibit good red color purity, but they tend to have rather low fluorescence quantum yields. The use of charge carrier confinement layers[166] or doping with fluorescent dye materials[170] markedly increases device efficiency. Substitution of the hydrocarbon side chains as in **49f–h**[171, 172] produced a slight blue shift in the emission maximum and gave yellow-orange emission.

The emission frequency depends considerably on the nature and regularity of the side chains on the polymers. Hadziioannou et al.[173] studied alkylated polythiophenes **50**–**52** and reported that there was a correlation between their emission maximum and the inverse number of thiophenes between two consecutive head-to-head (2,2′-coupled) dyads. Thus the polymer **50** showed an emission maximum at 460 nm (2.7 eV), while **51** and **52** had emission maxima at 530 (2.35 eV) and 550 nm (2.25 eV), respectively. Similarly, the emission maximum for Holdcroft and Xu's[174, 175] poly(3-hexylthiophene) (**49e**) was blue-shifted with increasing amounts of head-to-head dyads. Similar blue shifts can be obtained by introducing bulky substituents; the cyclohexyl substituted polythiophene **53** has its emission maximum in the green (555 nm).[176–178] Blue emission can be obtained by substitution at both the 3- and 4-positions as in **54** (460 nm)[177–179] or **55** (470 nm).[180] Bilayer devices containing the 4-octylphenyl-substituted poly[α,α'-bithienyl] analogue of **56** and a thick layer of PBD **28** emit white light due to the simultaneous emission of three colors.[181] The red and green emission can be suppressed in favor of near ultraviolet emission (397 nm) for a device using a blend of the polythiophene **56** and **28** with a further layer of **28** as emissive material.[134] The blue shifts can be attributed to the twisting of the conjugated backbone out of coplanarity due to the bulky substituents.

Greater control of emission colors requires the ability to control polymer regioregularity. When thiophenes are polymerized with ferric chloride or by Grignard coupling reactions, the resulting polymers are regiorandom, with a preponderance of head-to-tail (2,5′-) coupling, varying from 52 to 80 % according to the method used.[164] Some control can be obtained in specific cases. For example, coupling of oligomeric alkylthiophenes results in regioregular copolymers,[173, 182] while polymerization of a 3-arylthiophene with ferric chloride under carefully controlled conditions can give high-molecular-weight, regioregular (94 % head-to-tail) polymers such as **56**[183] because the aryl group preferentially stabilizes the cationic charge in the intermediates at the 2-position. More general routes for the synthesis of regioregular (head-to-tail) poly(3-alkylthiophene)s have been developed by McCullough et al.[184–187] and Rieke et al.,[188, 189] who utilized nickel-catalyzed coupling of 2-halo-5-metallothiophenes (Scheme 16). These routes require extremely pure monomers for high molecular weights to be produced.



Scheme 16. Routes to regioregular poly(3-alkylthiophene)s: a) Br_2, HOAc, 15 °C; b) LiN*i*Pr$_2$, −40 °C; c) $MgBr_2$, diethyl ether, −40 °C; d) I_2, HNO_3, CH_2Cl_2; e) Rieke zinc; f) $[Ni(Ph_2PCH_2CH_2PPh_2)]Cl_2$ or $[Ni\{Ph_2PCH_2CH(CH_3)PPh_2\}]Cl_2$.

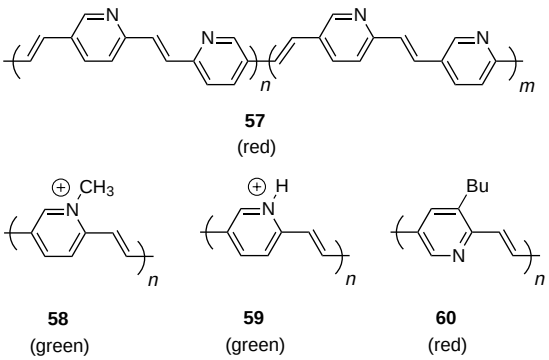
High regioregularity and a minimum amount of head-to-head dyads greatly influence the color of emission, and it is no surprise that the UV/Vis absorption spectrum of regioregular poly(3-hexylthiophene) (**49e**) indicates a longer conjugation length than observed for the corresponding regiorandom material.[190] McCullough et al. found that regioregular **49e** also showed a higher EL quantum efficiency than its regiorandom counterpart.[191] Comparison of regioregular

and regiorandom **49a** and **49e** prepared by us, however, showed no significant differences in their emission spectra or efficiencies.[192, 193]

The emissive properties of regioregular statistical copolymers can be tuned by varying the length of the alkyl side chain and the relative ratios of the organometallic monomers.[186, 194] We have also prepared poly(3-alkylthiophene) copolymers with side chains containing terminal azide groups which have enabled us to cross-link the deposited films so as to produce insoluble materials for use in multilayer devices.[195] Polarized emission from stretch-oriented polythiophenes has been observed.[196] An oriented film of poly[3-(10-methoxydecyl)thiophene] (**49f**) has been deposited by Langmuir–Blodgett techniques and shown to emit polarized electroluminescence.[197]

5.2. Electron-Deficient Aromatic Rings

Color control by alteration of substituents and regioregularity is also illustrated by the pyridine-based analogue **57** of PPV and its derivatives (Scheme 17). Stille coupling of 2,5-



Scheme 17. Pyridine-based analogues of PPV.

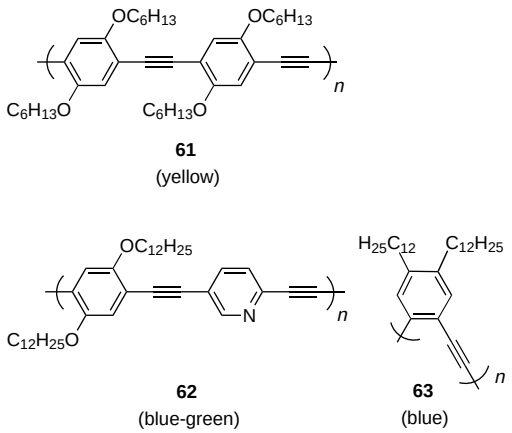
dibromopyridine and 1,2-bis(tributylstannyl)ethylene [198] gives **57** as an orange powder that is soluble in *m*-cresol. Alkylation and protonation furnish the N-alkylated **58** and N-protonated **59** derivatives, respectively. Both are soluble in chloroform although **58** tends to decompose in the presence of nucleophiles. Coupling of 3-butyl-2,5-dibromopyridine gives the substituted polymer **60**,[199, 200] which is soluble in conventional organic solvents.

The parent polymer **57** has a PL maximum in the red region (590 nm). The C-alkylated polymers **60** exhibit a red-shift to 630 nm, whereas a blue-shift to 540 nm is seen for the N-alkylated polymer **58**. Protonated polymer **59** has a more complex spectrum with emission maxima at 535 and 570 nm.

Owing to the lower symmetry of the pyridine ring, polymer **57** can exist in three regioisomeric forms: head-to-tail, head-to-head, and random. Swager et al.[201] have prepared the regioregular head-to-tail and head-to-head polymers and found that the three isomers show different UV/Vis absorption, PL, and EL emission spectra, with EL emission maxima of 575 nm (random), 584 nm (head-to-tail) and 605 nm (head-to-head).[202]

5.3. Poly(phenylene ethynylene)s—Stiffening the Polymer Chain

LEDs based on poly(phenylene ethynylene)s such as **61** (the dehydro-analogues of PPVs) are typically prepared by Sonogashira coupling of diethynylbenzenes and dihalobenzenes (Scheme 18).[203, 204] The synthesis and properties of poly-



Scheme 18. Examples of poly(phenylene ethynylene)s.

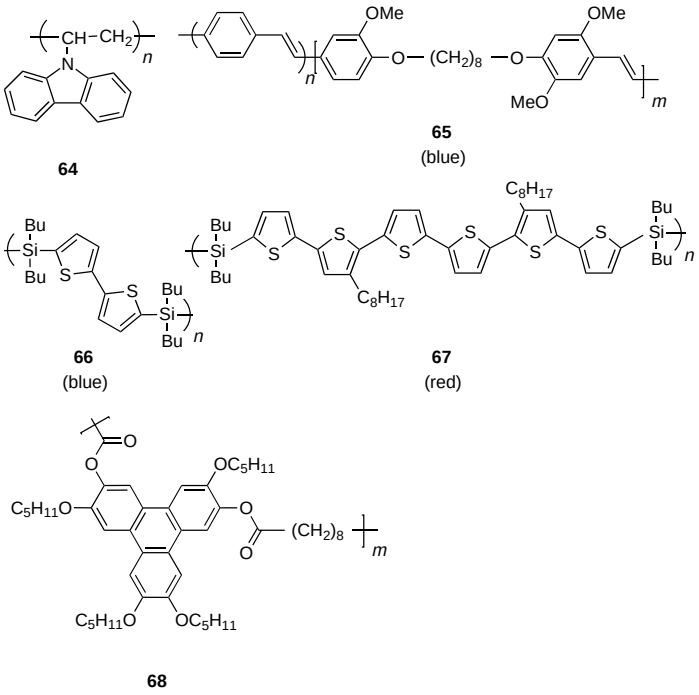
(arylene ethynylene)s have recently been reviewed by Giesa.[205] Poly(phenylene ethynylene) **61** shows yellow emission with maxima around 600 nm,[203, 206, 207] whereas the corresponding dialkoxy-PPVs give rise to red or red-orange emission. Incorporation of a 2,5-pyridinediyl unit (**62**) gives a blue-shift and blue-green emission ($\lambda_{max} = 480$ nm).[208] Blue (410 nm) emission is obtained from poly(3,4-dialkyl-1,6-phenylene ethynylene)s **63**,[209] prepared by palladium cross-coupling reaction of a 3,4-dialkyl-1,6-diiodobenzene and a 3,4-dialkyl-1,6-diethynylbenzene. Steric interactions may cause twisting of the polymer chain which reduces the effective conjugation length, but other factors also probably contribute to the overall emission characteristics. The poly(phenylene ethynylene)s have received some attention in the patent literature, but have been generally rather disappointing in EL applications.

5.4. Polymers with Isolated Chromophores—The Best of Both Worlds?

An alternative approach to designing a polymeric EL material is to blend a fluorescent dye in an inert polymer matrix such as polystyrene. Unfortunately, such blends often do not electroluminesce because the volume fraction of the electroactive species is too low. However, if an electroactive polymer such as poly(vinyl carbazole) (PVK) **64** is included, blends with tiny amounts of luminescent material can yield quite bright electroluminescent devices. An extension of this concept is to link the luminescent chromophore covalently to a polymer.

In polymers with isolated chromophores, the color is determined by altering the conjugation length of the chromophore. For example, Klavetter et al.[210] has prepared copolymers of type **65** by Wittig condensation using varying amounts of a flexible-chain dialdehyde and a bis-ylide

(Scheme 19). The emission peak of **65** ranges from 2.75 eV (460 nm) (blue) to 2.25 eV (550 nm) (yellow-green) depending on the amount of flexible linker content. Thus, the emission color can be easily altered by simply changing the comonomer feed ratio.



Scheme 19. Examples of polymers with isolated chromophores.

Hadziioannou et al. have prepared oligothiophene-dibutylsilane copolymers such as **66** or **67**[211–214] whose emission maxima range from blue (415 nm) for **66** to red (612 nm) for **67** according to the number of thiophene and silane units. The red-shift produced by increasing the number of silane units is slight and the emission color is mainly determined by the number of thiophene units. At present the advantages of the embedded chromophore polymers over the more traditional fully conjugated materials remain to be demonstrated.

Polymers that have special features of processibility in addition to high luminescent properties are particularly attractive. Much can be expected from improving supramolecular order. The recent work of Ringsdorf, Haarer et al. on discotic columnar phases involving triphenylene stacks shows much promise.[215] For example, the liquid-crystalline polymer **68** incorporating these structural features had a particular tendency to orient parallel to the film surface. Perhaps not surprisingly, this material showed steep current–voltage curves, low threshold fields, and high charge carrier mobilities.[216, 217]

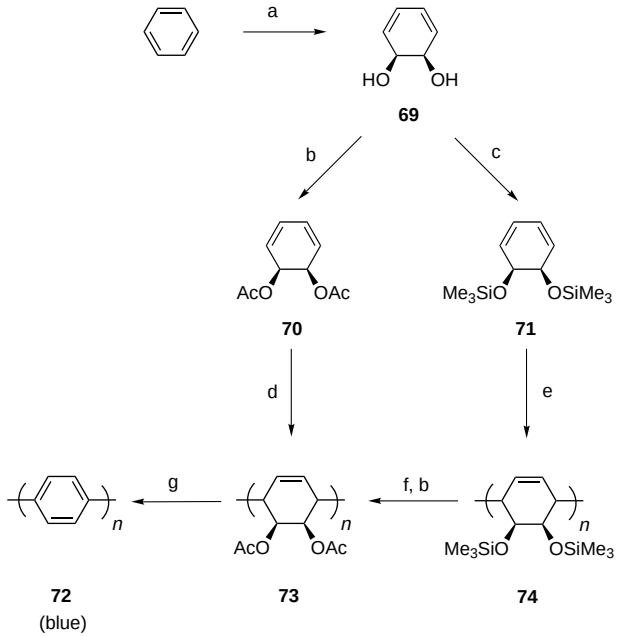
6. Blue Light-Emitting Polymers—The "Holy Grail"

The preceding sections outlined how a wide variety of conjugated electroluminescent polymers gives access to a whole range of emission colors. Multicolor display applications require at least three basic colors: red, green, and blue. Blue EL—already difficult to achieve with inorganic semiconductors—has been sought in conjugated polymers having a high HOMO–LUMO energy gap, and in copolymers containing high HOMO–LUMO, short conjugated segments. The search for a stable, highly efficient, bright blue light-emitting polymer continues. The following milestones have been passed.

6.1. Poly(*para*-phenylene)s—The Blue Paradigm

The design of blue-emitting electroluminescent polymers based on PPV-type materials with interrupted conjugation (Section 3.1) suffers from the drawback that emission occurs usually from the more conjugated segments, and the emission spectrum is therefore broadened and red-shifted. The alternative use of short, defined PPV oligomers will be discussed in succeeding sections (6.2 and 6.3). High HOMO–LUMO gap polymers are required for blue light emission. The first blue-emitting ($\lambda_{max} = 470$ nm) polymer LED was made by Yoshino et al.[218] using poly(9,9-dihexylfluorene) (**75a**) by oxidative coupling of the fluorene monomer with ferric chloride.[219, 220] This material has a poly(*para*-phenylene) (PPP) backbone, and derivatives of PPP **72** have been the focus of much research into the development of blue-emitting polymers. Higher polyarylenes have been little studied, possibly owing to the difficulties associated with their synthesis.

Leising et al.[221, 222] were the first to describe the use of PPP **72** as a blue light emitter [$\lambda_{max} = 459$ nm (2.7 eV)]. Like PPV, unsubstituted PPP is insoluble and not processible. Although films of oligomeric (9–10mer) poly(phenylene)s can be obtained by vacuum deposition,[223] the preparation of the polymer again requires suitable precursor routes (a topic recently reviewed by Gin and Conticello[224]). The original synthesis of unsubstituted PPP employs the ICI route based on *cis*-1,2-cyclohexadienediol (**69**) as starting material (Scheme 20).



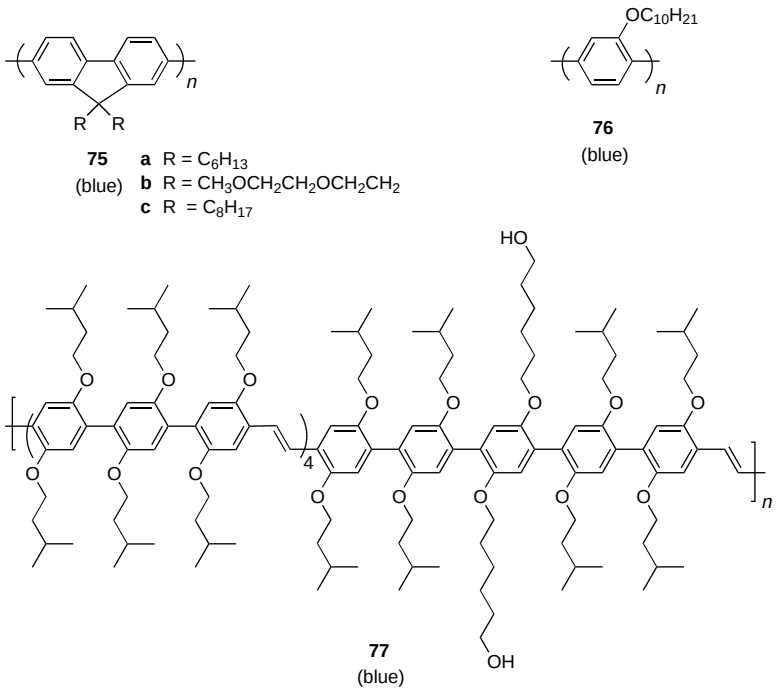
Scheme 20. Precursor routes to PPP (**72**): a) *Pseudomonas putida*; b) Ac_2O, pyridine; c) Me_3SiCl, DMAP, pyridine; d) azoisobutyronitrile AIBN, 70 °C; e) bis[(η^3-allyl)(trifluoroacetato)nickel(II)]; f) Bu_4NF, MeOH; g) 310–340 °C, Ar.

Radical-initiated polymerization of diacetate **70** furnishes the PPP precursor polymer **73**, which suffers from lack of stereoregularity and contains about 15% of 1,2-linkages.[225, 226] Thermal elimination of acetic acid finally gives the conjugated polymer **72** accompanied by some oligomer formation through chain scission. A number of other diesters have been polymerized by the same method (again with 10–15% of 1,2-linkages in the polymer) and thermally converted to PPP, of which the dimethyl carbonate and dipivaloyl esters yield the polymers with the highest molar masses.[227] Regioregular PPP is accessible through a nickel-catalyzed stereoregular polymerization of **71**. Despite the regioregularity and low polydispersity of the resulting polymer **74**, there are only limited reports on the electroluminescence of PPP derived from it.

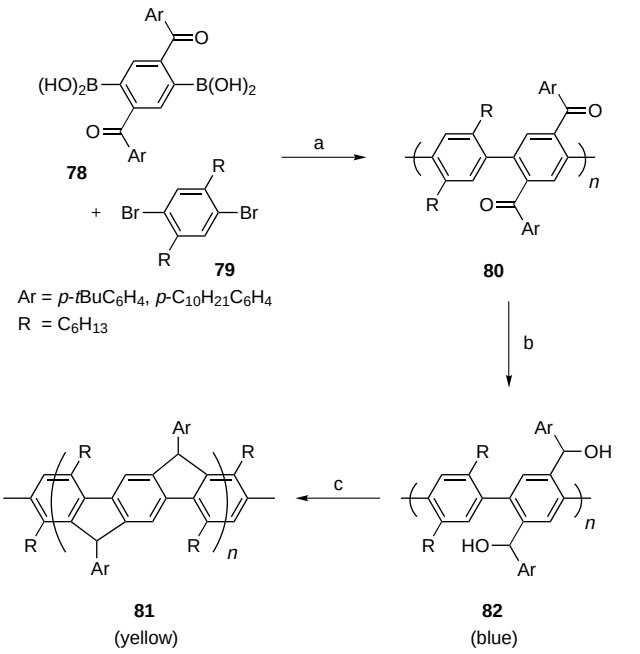
Much interest concentrates also on solution-processible poly(*para*-phenylene)s made soluble by suitable alkyl, aryl, alkoxy, or perfluoroalkyl[228] solubilizing groups. PPP derivatives with solubilizing alkyl side chains are the most important, and these are available through transition-metal-catalyzed polycondensations (reviewed by Schlüter and Wegner[229]), especially the Suzuki coupling of arylboronic acids and bromoarenes (optimized by Wegner et al.[230–232]), and the nickel-catalyzed coupling of substituted dihalobenzenes (reviewed by Yamamoto[233]), hydroquinone bistriflates,[234] or bis(mesylates).[235, 236] Although the degree of polymerization is usually rather limited, the molar masses of the polycondensates are sufficiently high (above 10000 g mol^{-1}) to form robust films for EL applications by spin-coating from solution. Various groups have used the resulting polymeric materials to make blue-emitting LEDs.[105, 237–242] The best devices so far reported have used the decyloxy derivative **76** (Scheme 21). External efficiencies of up to 3% have been achieved for double layer devices ITO/PVK/**76**/Ca, and of 0.8% with other, more air-stable, metal cathodes.[240] Polarized emission has been obtained from a device using an oriented Langmuir–Blodgett film of a dialkoxy PPP derivative.[105] Internal efficiencies of 4% have been measured for blue-emitting (460 nm) devices using the copolymer **77**, containing alternating terphenylene vinylene and quinquephenylene vinylene units, with calcium electrodes.[243]

The inclusion of solubilizing side groups on the PPP backbone has the drawback that the additional substituents twist the substituted phenylene rings considerably out of plane. This drastically decreases the interaction of the aromatic π-electron system, and an unwanted additional blue-shift in the emission spectrum compared with that for PPP is usually accompanied by a drop in fluorescence quantum yield. The twist cannot occur if the PPP backbone is planarized by incorporation into a ladder polymer. Scherf and Müllen were the first to show that structurally regular ladder-type polymers can be derived from a two-step route in which a soluble poly(*para*-phenylene) is prepared by a Suzuki aryl–aryl coupling of monomers **78** and **79**. After reduction of **80**, the resulting precursor polymer **82** is then subjected to another polymer-analogous intramolecular Friedel–Crafts ring-closing reaction to give **81**. The ladder formation occurs with surprisingly high regularity, and no indications of defects such as cross-linking or incomplete cyclization were found (Scheme 22).[244, 245] Molar masses of the structurally well-defined, soluble, ladder-type poly(para-phenylene)s (LPPPs) **81** are typically up to 20000 g mol^{-1}. The phenylene rings in the ladder polymers are almost planar and the homopolymer shows a broad emission between 650 and 450 nm in the solid state, in contrast to the polymer's sharp fluorescence emission around 450 nm in solution. The large Stokes shift (leading to yellow instead of blue light emission) is especially enhanced after annealing, and has been attributed to the formation of excimers owing to interchain interactions and π-stacking between the planarized conjugated segments.[246–249]

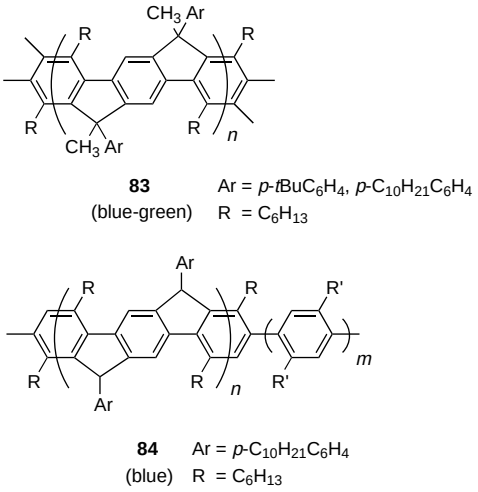
In some cases, blue emission has been observed from LPPP films but it remained unstable over time, again a result of the formation of yellow-emitting aggregates.[248] Slight structural variations have been suggested to inhibit the aggregation of planarized ladder-PPPs. After introduction of a methyl group at the methine bridge, the resulting ladder polymer **83**[250] shows stable blue-green emission with external efficiencies of up to 4% (Scheme 23).[251–253] Even more productive are random interruptions in the conjugated chain. In statistical copolymers **84**, called "step-ladder" copolymers, the conjugated chain is disrupted because the LPPP segments are connected by twisted oligophenylene spacers. These copolymers give stable films which remain blue-emitting even after annealing.[248] Pure blue emission with 0.1% internal efficiency can also be accomplished by diluting the ladder homopolymer (1–10 weight%) in a poly(vinylcarbazole) **64** hole-transporting poly-



Scheme 21. Examples of soluble PPP derivatives.



Scheme 22. Synthesis of ladder-PPP (**81**): a) $[Pd(PPh_3)_4]$; b) $LiAlH_4$; c) BF_3.

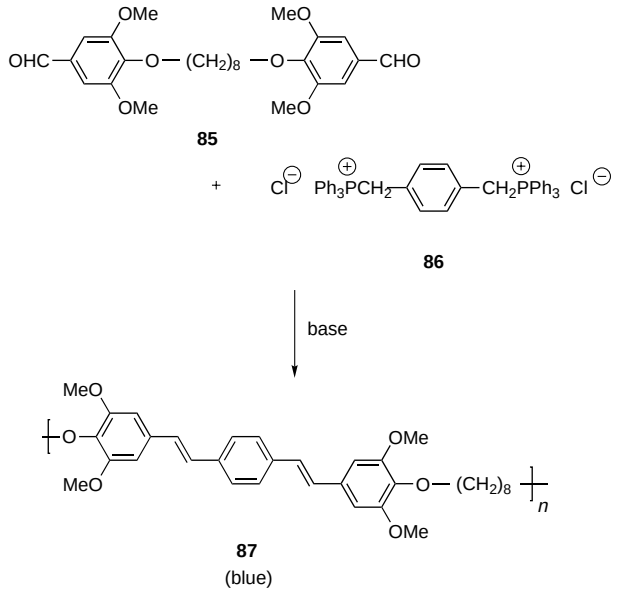


Scheme 23. Examples of blue-emitting, ladder-type PPP derivatives.

mer matrix.[254] This presumably inhibits aggregation. The above-mentioned poly(9,9-dihexylfluorene) (**75a**)[168, 218, 255] has a structure halfway between PPP and LPPP. A similar derivative BDOH-PF (**75b**) has been prepared by Pei and Yang.[256] Very little lifetime data is available for these materials as their development is in its infancy. However, the polyfluorene derivative **75c** has shown considerable promise in a number of applications.[257]

6.2. Polymers with Isolated Main-Chain Chromophores—Polycondensates by Wittig Reaction

Since the wavelength of the emitted light is dependent on the conjugation length of the chromophore, lowering this length will result in a blue-shift in the emission. One way to achieve a blue-emitting polymer, therefore, is to interrupt the conjugation of the polymer at short intervals with nonconjugated segments in between. As was discussed in Section 3.1 above, simple modification of the PPV synthesis gives access to PPV-derived blue light-emitting polymers with a high concentration of a fluorescent chromophore and, at the same time, with a statistical range of short conjugation lengths (see Scheme 8). This method, however, only allows limited control of the conjugation length. Another way to polymers with well-defined fluorescent π-electron systems makes use of a Wittig condensation of an arylene bisphosphonium salt **86** with a bisbenzaldehyde **85** already containing a spacer unit (Scheme 24). This has been used, for example, to make

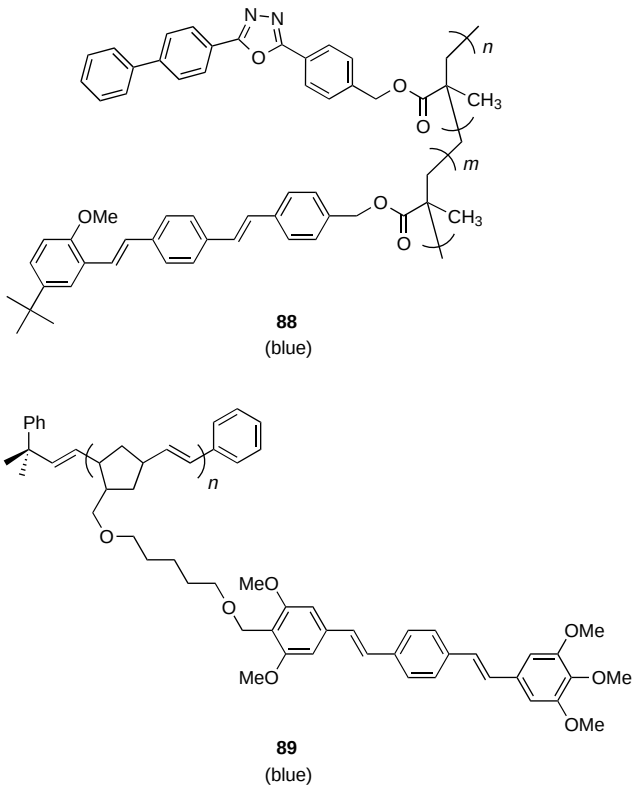


Scheme 24. Synthesis of a blue-emitting copolymers with isolated chromophore by Wittig reaction.

polycondensate **87** in which the oligomeric PPV segments are separated by flexible polymethylene spacers.[258–262] Such polyethers give blue or blue-green emission ($\lambda_{max} = 470-495$ nm).

6.3. Polymers with Conjugated Side-Chain Chromophores—"Comb" Lumophores

Another approach towards polymers with well-defined chromophores is based on polymers with luminescent conjugated side chains. As the backbone can now be any nonconjugated "standard" polymer, this enables, in principle, utilization of the considerable body of expertise developed in classical polymer synthesis to adjust the physical properties of the polymer. Our own efforts have concentrated on polymethacrylates such as the copolymers **88** bearing diaryloxadiazole charge-transporting and distyrylbenzene emissive units as side chains (Scheme 25).[74, 136, 141] Bilayer devices with **88** as emissive layer and PPV as hole-transport layer showed blue emission ($\lambda_{max} = 457$ nm) (with a tail in the yellow-green region, owing to emission from PPV, and an efficiency of 0.037 %). The polymers **88** unfortunately were not very stable,



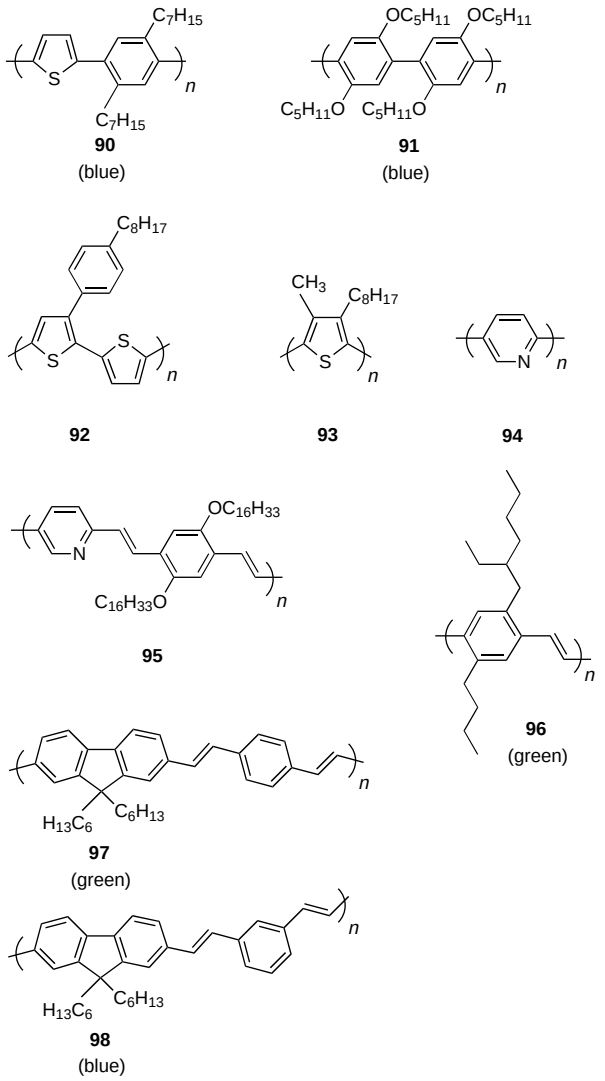
Scheme 25. Examples of electroluminescent polymers with side-chain chromophores.

degrading on storage, photoexcitation, and particularly during device operation. Significant improvements can be obtained by cross-linking.[143]

Schrock et al.[263] have used ROMP on a norbornene monomer with a side chain distyrylbenzene chromophore attached to produce polymer **89**, which shows blue ($\lambda_{max} =$ 475 nm) electroluminescence with 0.3% internal efficiency and a turn-on voltage of 12 V when calcium was the cathode. The efficiency increased to 0.55% for a blend of **89** and an oxadiazole electron-transporting material although the turn-on voltage was also raised considerably.

7. Blends and Combinations of Polymers with Other Materials—A Potpourri of Electroluminescent Materials

Improvements in electroluminescence efficiencies have been made by blending conjugated polymers. For example, Nishino et al.[264] found that blending the red-emitting polymers MEH-PPV (**14**) and poly(3-hexylthiophene) (**49e**) gave an initial increase in LED external efficiency up to a maximum of 1.7% (with a calcium cathode and 1 weight% of **49e**), which is twice the efficiency of a device made from pure MEH-PPV and three orders of magnitude higher than for pure **49e**. The emission spectra showed that the emitted light came from both polymers. Similarly, Salaneck et al.[265] have found that blue (2.6 eV, 490 nm) emission from the alternating copolymer **90**[266] was enhanced by blending it with the soluble PPP copolymer **91** (Scheme 26). A ratio of 1:9 for



Scheme 26. Examples of polymers used as blends, in SCALE and in other devices.

90:**91** produced the highest external quantum efficiency (1.9%) with a peak emission at 474 nm at a bias field of 6×10^7 V m^{-1}. Polymer **91** (460, 400 nm) as a single-layer ITO/**91**/Ca device emits two peaks at a bias field of 6×10^7 V m^{-1} and current density of 0.2 mA mm^{-2}.

Even greater enhancements in emission efficiency arise from blending conjugated polymers with partially conjugated polymers. Shim et al.[267, 268] found that blends of MEH-PPV (**14**) and a blue-emitting copolymer [similar to] **87** showed emission largely from **14**. The emission maximum was blue-shifted by 20–40 nm from that of MEH-PPV. The best efficiency (Al cathode, **87**:**14** = 15:1) was nearly 500 times greater than that for a device made from pure MEH-PPV. As blending of MEH-PPV with insulating polymers, for example polystyrene, enhances emission efficiency by a factor of less than 10, dilution effects clearly play only a minor part in the enhancement observed. The higher efficiency of the blend is therefore attributed to the charge-transporting properties of copolymer **87** leading to confinement of charge on MEH-PPV. Promising results with blends of the closely related polymers **97** and **98** offer opportunities for stable blue devices.[269]

Inganäs et al. have shown that blends of polymers with different emission colors are suitable for devices with variable-color, even white light emission. A blend of the polymers **53**, **54**, **56**, and **92** was used to construct a device in which emission can be tuned from red to green by controlling the applied voltage.[177, 178, 270] A similar blend of polymers **53**, **56**, and **93** in PMMA emits white light.[271] The PMMA acts as an insulating matrix and reduces the degree of exciton transfer between the polymers. Another approach employs a blend of a tristyrylamine in various host polymers such as the polyester Durel, polynorbornene, and poly(vinyl pyridine). The emission of the chromophore depends in this case strongly on the matrix.[216]

Devices can be constructed by using combinations of conjugated polymers and nonpolymeric materials. Yoshino et al.[272, 273] have shown that a device containing a mixture of red-orange-emitting **20b** and the green-emitting fluorescent dye tris(8-hydroxyquinolatino)aluminum produces a voltage-dependent variable emission of orange to green light. Blending of polythiophene **49e** with fluorescent dyes has been found to enhance the EL intensity at constant voltage by a factor of up to 70 with an increase in efficiency at constant luminance of up to 20-fold.[132, 274] With an oxadiazole dye as dopant, the emission color changed from red-orange to white when the voltage was increased.

8. Recent Advances

8.1. Degradation—Oxygen and Water

The one remaining obstacle to the widespread use of polymer LEDs is that, to date, their lifetimes remain lower than the best devices using inorganic or small-molecule organic compounds, although this gap is rapidly being closed. This is in part a result of the susceptibility of conjugated polymers towards oxidative degradation (a topic which has been recently reviewed by Cumpston, Jensen et al.).[275, 276] Studies on PPV have shown that photooxidation produces carbonyl defects that quench fluorescence.[33, 277, 278] Singlet oxygen has been implicated in the cleavage of vinylene groups in MEH-PPV (**14**) and bis (cholestanyloxy)-PPV (**19**), leading to ester or aldehyde groups.[279, 280] A study of PPV-based LEDs[281] revealed that exposure to air produced a drop in efficiency and an increase in threshold voltage, while degradation of the polymer is one of the primary processes involved in the breakdown of MEH-PPV-based LEDs.[282, 283] These results suggest that suitable protection from aerial oxidation may be a significant factor in improving the lifetime and efficiency of devices. Improvements in device design or encapsulation offer potential methods for achieving this. It should be noted that electrochemical dissolution of the metal electrodes at the electrode/polymer interface has been reported.[284] This is thought to lead to electrode failure due to corrosion.

8.2. Light-Emitting Electrochemical Cells—Lowering the Barrier to Charge Injection

A potentially significant new advance in the development of electroluminescent devices based on conjugated polymers has been the discovery[285–289] of light-emitting electrochemical cells (LECs) in which a conjugated polymer is blended with poly(ethylene oxide), a well-known ion-transporting polymer, and lithium trifluoromethanesulfonate as solid electrolyte. Application of a voltage above the bandgap energy (E_g/e), where e is the electron charge, results in p- and n-doping of regions adjacent to the anode and cathode respectively. A p-n junction is formed within the active layer, and positive and negative charge carriers combine with emission of a photon within the compensated p-n junction.[22]

With MEH-PPV (**14**) light emission is observed at a voltage < 2.5 V, with external efficiencies of up to 2%. Green emission with a luminance of 100 cd m^{-2} and an external quantum efficiency of 0.4% at a driving voltage of 4 V has been obtained from a device using PPV. Blue-green emission occurs when a soluble poly[9,9-bis(alkyl)fluorene] (BDOH-PF) (**75b**) serves as emitting polymer. Incorporation of the methoxyethoxyethyl substituents avoids the need for a two-phase blend with an extra ion-supporting polymer.[256] LECs have a high EL power efficiency, low operating voltages and allow the use of air-stable electrodes. A two-color LEC based on PPV and MEH-PPV has been made in which the emission color can be varied from red to green by altering the applied voltage.[290, 291] Some serious obstacles, still to be overcome in commercial realization of these devices, are the slow charging time (LECs are electrochemical batteries) and lifetimes under continuous operation, although promising results concerning these issues have been reported.[292, 293]

8.3. SCALE Devices—Using Alternating Current

Another new advance in device design has been the invention by Epstein and MacDiarmid et al.[294–300] of symmetrically configured, alternating current, light-emitting (SCALE) devices, which have the typical structure electrode/"insulating" polymer/emissive polymer/"insulating" polymer/electrode. The emissive layers used to date have been polypyridine **94** for blue and copolymer **95** for red light emission. Undoped (emeraldine base) polyaniline and polythiophene **49e** are typical "insulating" or electrode-modifying, nonemitting polymers for this type of device.

Use of **49e** with **95** as emissive layer gave a device in which the emission color varied depending on whether forward (590 nm) or reverse (635 nm) bias was applied. This is probably caused by charge recombination occurring at different interfaces in the two modes. With polyaniline, the EL spectra were essentially identical in both bias modes with a maximum at 635 nm. As with standard LEDs, one of the electrodes has to be transparent (ITO on glass), while air-stable metals such as Al, Cu, or Au have been used as the other electrode but, unlike standard LEDs, the two electrodes need not have dissimilar work-functions. Turn-on voltages are reported to be lower than those for the corresponding ITO/polymer/metal devices. Operation in alternating current mode also allows ion migration effects to be minimized. These devices remain to be developed to their full potential.

8.4. Lasers and Microcavities—Stimulated Emission and Superradiance

One method for the enhancement of emission in LEDs makes use of a microcavity structure in which the electroluminescent polymer is sandwiched between two planar, highly reflecting mirrors. When the polymer film thickness is of the order of the wavelength of the emitted light, the device acts as a resonator for a standing electromagnetic wave and produces a marked narrowing in the emission spectrum.[301–306] A microcavity device has been constructed by using ladder-type PPP **81** in which the emission color can be tuned from red to blue by altering the thickness of the polymer layer.[307]

Another microcavity device that uses PPV (**6**) as emissive layer has shown lasing activity with optical pumping, thus presenting the prospect of organic polymer-based lasers.[308] Similar optically pumped lasing and superradiance effects have been seen with other conjugated polymers.[309–317] Some investigators have questioned whether or not conjugated polymers will be capable of sustaining the high current densities necessary to realize electrically pumped lasing. The recent work by Bradley and Seidler and colleagues has shown that PPV films emitted light when a scanning tunneling microscope was used to inject charge at high current densities.[318]

9. Conclusion and Outlook

The prospects for the success of conjugated polymer-based LEDs as commercially viable display devices depend not only on the development of new materials, but also on progress in the design of devices. The three main factors (other than cost) that will determine the utility of polymer LEDs as light sources are their efficiencies (which control brightness for a given current), threshold or turn-on voltages (which affect power consumption), and lifetimes (over 10000 h are necessary for many commercial applications). With the appropriate choice of polymer and device design, external efficiencies of up to 4% can be obtained, which are comparable with the best EL devices based on inorganic or small molecule organic materials, and even much lower values suffice to give emission that is visible under ambient lighting. Turn-on voltages of 5 V or below have also been achieved by the use of charge-transporting layers, enabling devices to be run from low-power sources such as batteries.

The current best results for green materials (Table 2) are from Cambridge Display Technology with two-layer devices based on PPV (550 nm) prepared from a polyelectrolyte precursor copolymer as the emissive layer.[101] Photoluminescence efficiencies of about 50–80% have been reported for this material. Luminance efficiencies in excess of 2 lm W^{-1} and brightnesses in excess of 600 cd m^{-2} at 4 V and lifetimes of >1400 h at about 100 cd m^{-2} are now achievable. Another promising green polymer is the organic solvent-processible silylated DMOS-PPV (**18**) for which a respectable 0.1% external efficiency in a single-layer device with an Al cathode has been reported.[114, 319]

Table 2. Summary of promising light-emitting polymers across the range of the visible spectrum.

Polymer	Color(λ_{max} [nm])	Efficiency [%] [a]
MEH-PPV **14**[97]	red-orange (610)	2–4
OC_1C_{10}-PPV **17**[17]	red-orange (610)	2.1[b]
CN-PPV **40**[55, 150]	red (710)	0.87
MEH-CN-PPV **41**[12]	red-orange (600)	5.0
Polythiophene **49**[191]	red (662)	3.85×10^{-4}[b]
PPV **6**[101]	green (550)	0.3[c]
DMOS-PPV **18**[319]	green (500)	0.1[b]
BUEH-PPV **96**[322]	green (554)	3.2
BDOH-PF **75b**[256]	blue-green (450)	0.3[b]
PPP **72**[222]	blue (459)	0.01[b]
Blend **90**:**91** (1:10)[321]	blue (400–490)	2
DO-PPP **76**[240]	blue (440)	3
m-LPPP **83**[252]	blue-green (491)	0.1[b]
P3V/P5V **77**[243]	blue (460)	4[b]

[a] Unless otherwise indicated most devices are two-layer devices with a hole injecting layer between anode and emissive polymer. [b] Signifies single-layer device. [c] Estimated from the published data for a PPV device giving a luminous efficiency 1 lm W^{-1} at 4 V.

Exciting results for red emitters have emerged from three laboratories, all using closely related solvent-processible oxygenated PPV analogues. At UNIAX, MEH-PPV (**14**) ($\lambda_{max} = 610$ nm) in the configuration ITO/PANI-camphor sulfonate/MEH-PPV/Ca exhibited brightnesses of 100 cd m^{-2} at 2.4 V, 4000 cd m^{-2} at 4 V, and over 10000 cd m^{-2} at higher voltages. The external quantum efficiency was 2–2.5% and the luminous efficiency corresponded to 3–4.5 lm W^{-1}. Operating lifetimes in excess of 2000 h at 400–500 cd m^{-2} initial brightness were reported.[97] Two European companies, Philips and Hoechst, have achieved comparable results with OC_1C_{10}-PPV (**17**).[17] Philips reported an external quantum efficiency of 2.1% in the device configuration ITO/**17**/Ca.[87, 320] Luminous efficiencies up to 7 lm W^{-1} and lifetimes of several thousand hours at 100 cd m^{-2} were realized. Hoechst fabricated a flexible device based on a dialkoxy-PPV (probably OC_1C_{10}-PPV **17**) in the configuration PET-ITO/polymer/Ca, which demonstrated an external efficiency of 2.1%, a luminous efficiency of 2 lm W^{-1}, and a luminance of 100 cd m^{-2} at 3.4 V with a current density of 4.5 mA cm^{-2}.[17] Calculations based on the data reported by the Cambridge group show that MEH-CN-PPV (**41**) has a luminous efficiency of 5 lm W^{-1}.[12]

Some of the most interesting blue materials are based on polyphenylene and polyfluorene derivatives, but the major progress has been largely from academic laboratories, and serious industrial evaluation has still to be carried out. One of the best results has been obtained with the poly(2-decyloxy-1,4-phenylene) (**76**) ($\lambda_{max} = 440$ nm), which showed 1.8% external quantum efficiency in the single-layer device configuration ITO/**76**/Ca. Problems with polymer film quality were circumvented by using a second PVK buffer and hole injection layer. The two-layer device was more efficient (3%) and turned on at 15 V to reach a brightness of 490 cd m^{-2} at about 30 V.[240] The blends of copolymers **90** and **91** have already been mentioned as emitting blue light with external efficiency of about 2%.[321] The results highlight the general problem for blue emitters that the threshold

voltage is not far removed from that which induces dielectric breakdown. This makes the problem of obtaining good lifetime data considerable. These reservations should be qualified in the light of the recently reported stable devices made from the polyfluorenes **75b** and **75c**.[256, 257]

During the past seven years, a wide range of electroluminescent conjugated polymers and copolymers have been made that are suitable for use in LEDs. Alteration of their chemical structures by synthetic design has stimulated the preparation of polymer-based devices emitting in any part of the visible spectrum, and also in the near infrared. By the use of precursor methods thin films of insoluble and intractable materials can be produced. In view of the recent advances in polymer LEDs, efficiencies are now comparable with inorganic or dye-based devices, and ongoing work into improvement of device lifetimes makes the future for these devices promising.

A number of tasks still remain to be performed before the apparent bright prospects of conjugated EL polymers can be realized. Of the wide variety of polymers that have become available in the last seven years, only a few have been extensively studied, and the best materials have yet to be identified. The study of polymer EL devices is an interdisciplinary research area, combining semiconductor physics, polymer chemistry, and materials chemistry, and challenging tasks remain in all of these fields. Although much is known about simple device structures and common electrode materials, devices have yet to be optimized. We also need improved methods (which includes making the polymers more eco-friendly) for the preparation and purification of EL polymers. High purity polymers are required, and the challenge in polymer synthesis is to meet these requirements. High molar masses are advantageous for ensuring good film-forming properties. The long-term stability of polymers and polymer blends during storage and especially in the high electric fields found in operating devices also need to be improved. It will furthermore be necessary to develop suitable encapsulations for the protection of polymers and electrodes from environmental degradative influences. These challenges imply continuing scope for exciting and innovative research into the preparation and application of conjugated electroluminescent polymers. We are confident that markets will emerge for commercial polymer LED devices having a low information content – such as for mobile telephone displays, alphanumeric and backlit LCDs. While the horizon for high information content applications (such as flat-screen color TV) is still several years away, we expect that polymer LEDs will ultimately have a significant input in this area as well.

Appendix: List of Abbreviations

BDOH-PF	poly[9,9-bis(methoxyethoxyethyl)fluorene] **75b**
BUEH-PPV	poly[2-(2′-ethylhexyl)-5-butyl-1,4-phenylene vinylene] **96**
CN-PPV	poly[2,5-bis(hexyloxy)-1,4-phenylene-(1-cyanovinylene)] **40**
DMOS-PPV	poly[2-(dimethyloctylsilyl)-1,4-phenylene vinylene] **18**
DO-PPP	poly(2-decyloxy-1,4-phenylene) **76**
ECHB	electron-conducting/hole-blocking
EL	electroluminescence
HOMO	highest occupied molecular orbital
ITO	indium-tin oxide
LCD	liquid crystal display
LEC	light-emitting electrochemical cell
LED	light-emitting diode
LPPP	ladder-type poly(*para*-phenylene)
LUMO	lowest unoccupied molecular orbital
MEH-CN-PPV	poly[2-(2′-ethylhexyloxy)-5-methoxy-1,4-phenylene-(1-cyanovinylene)] **41**
MEH-PPV	poly[2-(2′-ethylhexyloxy)-5-methoxy-1,4-phenylene vinylene] **14**
OC_1C_{10}-PPV	poly[2-(3,7-dimethyloctyloxy)-5-methoxy-1,4-phenylene vinylene] **17**
P3V/P5V	copolymer **77**
PANi	polyaniline
PBD	2-(4-biphenylyl)-5-(4-*tert*-butylphenyl)-1,3,4-oxadiazole **28**
PDAF	poly(dialkylfluorene)
PET	poly(ethylene terephthalate)
PL	photoluminescence (fluorescence)
PMMA	poly(methyl methacrylate)
PPP	poly(*para*-phenylene) **72**
PPV	poly(*para*-phenylene vinylene) **6**
ROMP	ring-opening metathesis polymerization
SCALE	symmetrically configured, alternating current, light-emitting (diode)

This work has received financial support from the Engineering and Physical Sciences Research Council (EPSRC), the Commission of the European Community (ESPRIT Project No. 8013 "LEDFOS"), the Deutsche Forschungsgemeinschaft and ARC (British Council-Deutscher Akademischer Auslandsdienst). The work is a result of a longstanding collaboration between chemistry (A.B.H. and Dr. S. C. Moratti) and physics (Prof. R. H. Friend, Prof. D. D. C. Bradley, and Dr. N. C. Greenham). We acknowledge the contributions and helpful discussions from these colleagues and those at Cambridge Display Technology (Dr. P. May, Dr. C. Towns, Dr. K. Pichler, and Dr. K. Heeks).

Received: April 3, 1997 [A219IE]
German version: *Angew. Chem.* **1998**, *110*, 416 – 443

[1] J. H. Burroughes, D. D. C. Bradley, A. R. Brown, R. N. Marks, K. MacKay, R. H. Friend, P. L. Burn, A. B. Holmes, *Nature* **1990**, *347*, 539 – 541.
[2] P. May, *Phys. World* **1995**, *8(3)*, 52 – 57.
[3] C. W. Tang, S. A. Van Slyke, *Appl. Phys. Lett.* **1987**, *51*, 913 – 915.
[4] C. Adachi, S. Tokito, T. Tsutsui, S. Saito, *Jpn. J. Appl. Phys.* **1988**, *28*, L269 – L271.
[5] R. F. Service, *Science* **1996**, *273*, 878 – 880.
[6] H. Nakada, T. Tohma, *Inorganic and Organic Electroluminescence*, Wissenschaft-und-Technik-Verlag, Berlin, **1996**, pp. 385 – 390
[7] A. O. Patil, A. J. Heeger, F. Wudl, *Chem. Rev.* **1988**, *88*, 183 – 200.
[8] R. H. Friend, D. D. C. Bradley, A. B. Holmes, *Phys. World* **1992**, *5* (*11*), 42 – 46.
[9] D. Bradley, *Curr. Opin. Solid State Mater. Sci.* **1996**, *1*, 789 – 797.
[10] A. B. Holmes, D. D. C. Bradley, A. R. Brown, P. L. Burn, J. H. Burroughes, R. H. Friend, N. C. Greenham, R. W. Gymer, D. A.

Halliday, R. W. Jackson, A. Kraft, J. H. F. Martens, K. Pichler, I. D. W. Samuel, *Synth. Met.* **1993**, *141*, (March 5th *57*, 4031 – 4040.
[11] K. C. Fox, *New Sci.* **1994**, *141*, (March 5th), 33 – 37.
[12] D. R. Baigent, N. C. Greenham, J. Grüner, R. N. Marks, R. H. Friend, S. C. Moratti, A. B. Holmes, *Synth. Met.* **1994**, *67*, 3 – 10.
[13] P. Yam, *Sci. Am.* **1995**, *273*, (1), 74 – 79.
[14] N. C. Greenham, R. H. Friend, *Solid State Phys.* **1995**, *49*, 1 – 149.
[15] R. W. Gymer, *Endeavour* **1996**, *20*, 115 – 120.
[16] L. J. Rothberg, A. J. Lovinger, *J. Mater. Res.* **1996**, *11*, 3174 – 3187.
[17] J. Salbeck, *Ber. Bunsenges. Phys. Chem.* **1996**, *100*, 1666 – 1677.
[18] W. R. Salaneck, S. Stafström, J.-L. Brédas, *Conjugated Polymer Surfaces and Interfaces*, Cambridge University Press, Cambridge, **1996**.
[19] J. R. Sheats, H. Antoniadis, M. Hueschen, W. Leonard, J. Miller, R. Moon, D. Roitman, A. Stocking, *Science* **1996**, *273*, 884 – 888.
[20] A. J. Lovinger, L. J. Rothberg, *J. Mater. Res.* **1996**, *11*, 1581 – 1592.
[21] W. J. Feast, J. Tsibouklis, K. L. Pouwer, L. Groenendaal, E. W. Meijer, *Polymer* **1996**, *37*, 5017 – 5047.
[22] Y. Yang, *MRS Bull.* **1997**, *22(6)*, 31 – 38.
[23] R. H. Friend, G. J. Denton, J. J. M. Halls, N. T. Harrison, A. B. Holmes, A. Köhler, A. Lux, S. C. Moratti, K. Pichler, N. Tessler, C. Towns, *Synth. Met.* **1997**, *84*, 463 – 470.
[24] M. A. Díaz-García, F. Hide, B. J. Schwartz, M. R. Andersson, Q. Pei, A. J. Heeger, *Synth. Met.* **1997**, *84*, 455 – 462.
[25] R. A. Wessling, R. G. Zimmerman (Dow Chemical), US-B 3 401 152, **1968** [*Chem. Abstr.* **1968**, *69*, 87735q].
[26] R. A. Wessling, *J. Polym. Sci. Polym. Symp.* **1985**, *72*, 55 – 66.
[27] R. W. Lenz, C.-C. Han, J. Stenger-Smith, F. E. Karasz, *J. Polym. Sci. Polym. Chem.* **1988**, *26*, 3241 – 3249.
[28] P. L. Burn, D. D. C. Bradley, R. H. Friend, D. A. Halliday, A. B. Holmes, R. W. Jackson, A. Kraft, *J. Chem. Soc. Perkin Trans. 1* **1992**, 3225 – 3231.
[29] R. O. Garay, U. Baier, C. Bubeck, K. Müllen, *Adv. Mater.* **1993**, *5*, 561 – 564.
[30] F. R. Denton, P. M. Lahti, F. E. Karasz, *J. Polym. Sci. Polym. Chem.* **1992**, *30*, 2223 – 2231.
[31] D. A. Halliday, P. L. Burn, R. H. Friend, D. D. C. Bradley, A. B. Holmes, *Synth. Met.* **1993**, *55*, 902 – 907.
[32] F. Papadimitrakopoulos, K. Konstadinidis, T. M. Miller, R. Opila, E. A. Chandross, M. E. Galvin, *Chem. Mater.* **1994**, *6*, 1563 – 1568.
[33] F. Papadimitrakopoulos, M. Yan, L. J. Rothberg, H. E. Katz, E. A. Chandross, M. E. Galvin, *Mol. Cryst. Liq. Cryst.* **1994**, *256*, 663 – 669.
[34] V. H. Tran, V. Massardier, T. P. Nguyen, J. Davenas, *Polymer* **1996**, *37*, 2061 – 2065.
[35] H. H. Kim, R. G. Swartz, Y. Ota, T. K. Woodward, M. D. Feuer, W. L. Wilson, *J. Lightwave Technol.* **1994**, *12*, 2114 – 2120.
[36] M. Herold, J. Gmeiner, M. Schwoerer, *Acta Polym.* **1994**, *45*, 392 – 395.
[37] M. Herold, J. Gmeiner, W. Riess, M. Schwoerer, *Synth. Met.* **1996**, *76*, 109 – 112.
[38] A. Beerden, D. Vanderzande, J. Gelan, *Synth. Met.* **1992**, *52*, 387 – 394.
[39] Y. Nishikata, M. Kakimoto, Y. Imai, *Thin Solid Films* **1989**, *179*, 191 – 197.
[40] A. Wu, M. Jikei, M. Kakimoto, Y. Imai, S. Ukishima, Y. Takahashi, *Chem. Lett.* **1994**, 2319 – 2322.
[41] J. H. Kim, Y. K. Kim, B. C. Sohn, D.-Y. Kang, J.-I. Jin, C.-H. Kim, C.-H. Pyun, *Synth. Met.* **1995**, *71*, 2023 – 2024.
[42] A. Wu, M. Kakimoto, *Adv. Mater.* **1995**, *7*, 812 – 814.
[43] A. Wu, M. Jikei, M. Kakimoto, Y. Imai, S. Ukishima, Y. Takahashi, *Mol. Cryst. Liq. Cryst.* **1995**, *267*, 441 – 446.
[44] R. C. Smith, W. M. Fischer, D. L. Gin, *J. Am. Chem. Soc.* **1997**, *119*, 4092 – 4093.
[45] F. Louwet, D. Vanderzande, J. Gelan, *Synth. Met.* **1992**, *52*, 125 – 130.
[46] F. Louwet, D. Vanderzande, J. Gelan, *Synth. Met.* **1995**, *69*, 509 – 510.
[47] F. Louwet, D. Vanderzande, J. Gelan, J. Mullens, *Macromolecules* **1995**, *28*, 1330 – 1331.
[48] S. Son, A. J. Lovinger, M. E. Galvin, *Polym. Mater. Sci. Eng.* **1995**, *72*, 567 – 568.
[49] E. G. J. Staring, D. Braun, G. L. J. A. Rikken, R. J. C. E. Demandt, Y. A. R. R. Kessener, M. Bouwmans, D. Broer, *Synth. Met.* **1994**, *67*, 71 – 75.
[50] S. Iwatsuki, M. Kubo, T. Kumeuchi, *Chem. Lett.* **1991**, 1971 – 1974.
[51] O. Schäfer, A. Greiner, J. Pommerehne, W. Guss, H. Vestweber, H. Y. Tak, H. Bässler, C. Schmidt, G. Lüssem, B. Schartel, V. Stümpflen, J. H. Wendorff, S. Spiegel, C. Möller, H. W. Spiess, *Synth. Met.* **1996**, *82*, 1 – 9.
[52] W.-P. Chang, W.-T. Whang, P.-W. Lin, *Polymer* **1996**, *37*, 1513 – 1518.
[53] Y.-J. Miao, G. C. Bazan, *J. Am. Chem. Soc.* **1994**, *116*, 9379 – 9380.
[54] V. P. Conticello, D. L. Gin, R. H. Grubbs, *J. Am. Chem. Soc.* **1992**, *114*, 9708 – 9710.
[55] N. C. Greenham, R. H. Friend, D. D. C. Bradley, *Adv. Mater.* **1994**, *6*, 491 – 494.
[56] H. Becker, S. E. Burns, R. H. Friend, *Phys. Rev. B* **1997**, *56*, 1893 – 1905.
[57] P. L. Burn, A. B. Holmes, A. Kraft, A. R. Brown, D. D. C. Bradley, R. H. Friend, *Mater. Res. Soc. Symp. Proc.* **1992**, *247*, 647 – 654.
[58] N. C. Greenham, R. H. Friend, A. R. Brown, D. D. C. Bradley, K. Pichler, P. L. Burn, A. Kraft, A. B. Holmes, *Proc. SPIE Int. Soc. Opt. Eng.* **1993**, *1910*, 84 – 91.
[59] I. A. Hümmelgen, Y. D. Yadava, L. S. Roman, A. C. Arias, M. R. Fernandes, F. C. Nart, *Bull. Mater. Sci.* **1996**, *19*, 423 – 427.
[60] M. Meier, M. Cölle, S. Karg, E. Buchwald, J. Gmeiner, W. Riess, M. Schwoerer, *Mol. Cryst. Liq. Cryst.* **1996**, *283*, 197 – 202.
[61] A. C. Fou, O. Onitsuka, M. Ferreira, D. Howie, M. F. Rubner, *Polym. Mater. Sci. Eng.* **1995**, *72*, 160 – 161.
[62] A. C. Fou, O. Onitsuka, M. Ferreira, M. F. Rubner, B. R. Hsieh, *Mater. Res. Soc. Symp. Proc.* **1995**, *369*, 575 – 580.
[63] M. Onoda, K. Yoshino, *Jpn. J. Appl. Phys.* **1995**, *34*, L260 – L263.
[64] M. Onoda, K. Yoshino, *J. Appl. Phys.* **1995**, *78*, 4456 – 4462.
[65] A. C. Fou, O. Onitsuka, M. Ferreira, M. F. Rubner, B. R. Hsieh, *J. Appl. Phys.* **1996**, *79*, 7501 – 7509.
[66] M. Ferreira, O. Onitsuka, A. C. Fou, B. Hsieh, M. F. Rubner, *Mat. Res. Soc. Symp. Proc.* **1996**, *413*, 49 – 54.
[67] D. Yoo, A. Wu, J. Lee, M. F. Rubner, *Synth. Met.* **1997**, *85*, 1425 – 1426.
[68] A. R. Brown, D. D. C. Bradley, J. H. Burroughes, R. H. Friend, N. C. Greenham, P. L. Burn, A. B. Holmes, A. Kraft, *Appl. Phys. Lett.* **1992**, *61*, 2793 – 2795.
[69] M. Strukelj, F. Papadimitrakopoulos, T. M. Miller, L. J. Rothberg, *Science* **1995**, *267*, 1969 – 1972.
[70] Y. Yang, Q. Pei, *J. Appl. Phys.* **1995**, *77*, 4807 – 4809.
[71] X.-C. Li, M. Giles, J. Grüner, R. H. Friend, A. B. Holmes, S. C. Moratti, *Polym. Mater. Sci. Eng.* **1995**, *72*, 463 – 464.
[72] E. Buchwald, M. Meier, S. Karg, P. Pösch, H.-W. Schmidt, P. Strohriegl, W. Riess, M. Schwoerer, *Adv. Mater.* **1995**, *7*, 839 – 842.
[73] X.-C. Li, A. B. Holmes, A. Kraft, S. C. Moratti, G. C. W. Spencer, F. Cacialli, J. Grüner, R. H. Friend, *J. Chem. Soc. Chem. Commun.* **1995**, 2211 – 2212.
[74] X.-C. Li, F. Cacialli, M. Giles, J. Grüner, R. H. Friend, A. B. Holmes, S. C. Moratti, T. M. Yong, *Adv. Mater.* **1995**, *7*, 898 – 900.
[75] X.-C. Li, G. C. W. Spencer, A. B. Holmes, S. C. Moratti, F. Cacialli, R. H. Friend, *Synth. Met.* **1996**, *76*, 153 – 156.
[76] M. Strukelj, T. M. Miller, F. Papadimitrakopoulos, S. Son, *J. Am. Chem. Soc.* **1995**, *117*, 11 976 – 11 983.
[77] M. Meier, E. Buchwald, S. Karg, P. Pösch, M. Greczmiel, P. Strohriegl, W. Riess, *Synth. Met.* **1996**, *76*, 95 – 99.
[78] S. Doi, M. Kuwabara, T. Noguchi, T. Ohnishi, *Synth. Met.* **1993**, *57*, 4174 – 4179.
[79] D. Braun, A. J. Heeger, *Appl. Phys. Lett.* **1991**, *58*, 1982 – 1984.
[80] D. Braun, A. J. Heeger, H. Kroemer, *J. Electron. Mater.* **1991**, *20*, 945 – 948.
[81] A. R. Brown, N. C. Greenham, J. H. Burroughes, D. D. C. Bradley, R. H. Friend, P. L. Burn, A. Kraft, A. B. Holmes, *Chem. Phys. Lett.* **1992**, *200*, 46 – 54.
[82] N. C. Greenham, A. R. Brown, J. H. Burroughes, D. D. C. Bradley, R. H. Friend, P. L. Burn, A. Kraft, A. B. Holmes, *Proc. SPIE Int. Soc. Opt. Eng.* **1993**, *1910*, 111 – 119.
[83] G. Gustafsson, Y. Cao, G. M. Treacy, F. Klavetter, N. Colaneri, A. J. Heeger, *Nature* **1992**, *357*, 477 – 479.
[84] A. J. Heeger, D. Braun (UNIAX), WO-B 92/16023, **1992** [*Chem. Abstr.* **1993**, *118*, 157401j].
[85] G. J. Sarnecki, P. L. Burn, A. Kraft, R. H. Friend, A. B. Holmes, *Synth. Met.* **1993**, *55*, 914 – 917.

[86] F. Wudl, P. M. Allemand, G. Srdanov, Z. Ni, D. McBranch, *ACS Symp. Ser.* **1991**, *455*; F. Wudl (University of California), US-B 5189136, **1990** [*Chem. Abstr.* **1993**, *118*, 255575p].

[87] D. Braun, E. G. J. Staring, R. C. J. E. Demandt, G. L. J. Rikken, Y. A. R. R. Kessener, A. H. J. Venhuizen, *Synth. Met.* **1994**, *66*, 75 – 79.

[88] I. Murase, T. Ohnishi, T. Noguchi, M. Hirooka, *Synth. Met.* **1987**, *17*, 639 – 644.

[89] S. A. Askari, S. D. Rughooputh, F. Wudl, *Synth. Met.* **1989**, *29*, E129 – E134.

[90] D. A. Halliday, D. D. C. Bradley, P. L. Burn, R. H. Friend, A. B. Holmes, *Synth. Met.* **1991**, *41*, 931 – 934.

[91] H. G. Gilch, W. L. Wheelwright, *J. Polym. Sci. A1* **1966**, *4*, 1337 – 1349.

[92] W. J. Swatos, B. Gordon, *Polym. Prepr.* **1990**, *31*, 505 – 506.

[93] I. D. Parker, *J. Appl. Phys.* **1994**, *75*, 1656 – 1666.

[94] Y.-E. Kim, H. Park, J.-J. Kim, *Appl. Phys. Lett.* **1996**, *69*, 599 – 601.

[95] I. D. Parker, H. H. Kim, *Appl. Phys. Lett.* **1994**, *64*, 1774 – 1776.

[96] H. H. Kim, T. M. Miller, E. H. Westerwick, Y. O. Kim, E. W. Kwock, M. D. Morris, M. Cerullo, *J. Lightwave Technol.* **1994**, *12*, 2107 – 2113.

[97] G. Yu, *Synth. Met.* **1996**, *80*, 143 – 150.

[98] G. Gustafsson, G. M. Treacy, Y. Cao, F. Klavetter, N. Colaneri, A. J. Heeger, *Synth. Met.* **1993**, *57*, 4123 – 4127

[99] E. Westerweele, P. Smith, A. J. Heeger, *Adv. Mater.* **1995**, *7*, 788 – 790.

[100] S. A. Carter, M. Angelopoulos, S. Karg, P. J. Brock, J. C. Scott, *Appl. Phys. Lett.* **1997**, *70*, 2067 – 2069.

[101] J. C. Carter, I. Grizzi, S. K. Heeks, D. J. Lacey, S. G. Latham, P. G. May, O. R. de los Paños, K. Pichler, C. R. Towns, H. F. Wittmann, *Appl. Phys. Lett.* **1997**, *71*, 34 – 36.

[102] T. W. Hagler, K. Pakbaz, J. Moulton, F. Wudl, P. Smith, A. J. Heeger, *Polymer* **1991**, *32*, 339 – 342.

[103] T. W. Hagler, K. Pakbaz, K. F. Voss, A. J. Heeger, *Phys. Rev. B* **1991**, *44*, 8652 – 8666.

[104] M. Hamaguchi, K. Yoshino, *Appl. Phys. Lett.* **1995**, *67*, 3381 – 3383.

[105] V. Cimrová, M. Remmers, D. Neher, G. Wegner, *Adv. Mater.* **1996**, *8*, 146 – 149.

[106] F. Wudl, S. Höger, C. Zhang, K. Pakbaz, A. J. Heeger, *Polym. Prepr.* **1993**, *34*, 197 – 198.

[107] N. N. Barashkov, D. J. Guerrero, H. J. Olivos, J. P. Ferraris, *Synth. Met.* **1995**, *75*, 153 – 160.

[108] B. R. Hsieh, H. Antoniadis, D. C. Bland, W. A. Feld, *Adv. Mater.* **1995**, *7*, 36 – 38.

[109] C. Zhang, H. von Seggern, K. Pakbaz, F. Wudl, A. J. Heeger, *J. Electron. Mater.* **1993**, *22*, 413 – 417.

[110] S. Höger, J. J. McNamara, S. Schricker, F. Wudl, *Chem. Mater.* **1994**, *6*, 171 – 173.

[111] D.-H. Hwang, H.-K. Shim, J.-I. Lee, K.-S. Lee, *J. Chem. Soc. Chem. Commun.* **1994**, 2461 – 2462.

[112] C. Zhang, S. Höger, K. Pakbaz, F. Wudl, A. J. Heeger, *J. Electron. Mater.* **1994**, *23*, 453 – 458.

[113] D.-H. Hwang, I.-N. Kang, M.-S. Jang, H.-K. Shim, T. Zyung, *Polym. Bull.* **1996**, *36*, 383 – 390.

[114] S. T. Kim, D.-H. Hwang, X.-C. Li, J. Grüner, R. H. Friend, A. B. Holmes, H.-K. Shim, *Adv. Mater.* **1996**, *8*, 979 – 982.

[115] M. Hamaguchi, K. Yoshino, *Jpn. J. Appl. Phys.* **1994**, *33*, L1478 – L1481.

[116] M. Hamaguchi, K. Yoshino, *Jpn. J. Appl. Phys.* **1995**, *34*, L712 – L715.

[117] G. Lüssem, F. Geffarth, A. Greiner, W. Heitz, M. Hopmeier, M. Oberski, C. Unterlechner, J. H. Wendorff, *Liq. Cryst.* **1996**, *21*, 903 – 907.

[118] Z. Yang, B. Hu, F. E. Karasz, *Macromolecules* **1995**, *28*, 6151 – 6154.

[119] Z. Bao, Y. Chen, R. Cai, L. Yu, *Macromolecules* **1993**, *26*, 5281 – 5286.

[120] P. L. Burn, A. B. Holmes, A. Kraft, D. D. C. Bradley, A. R. Brown, R. H. Friend, R. W. Gymer, *Nature* **1992**, *356*, 47 – 49.

[121] P. L. Burn, A. Kraft, D. R. Baigent, D. D. C. Bradley, A. R. Brown, R. H. Friend, R. W. Gymer, A. B. Holmes, R. W. Jackson, *J. Am. Chem. Soc.* **1993**, *115*, 10117 – 10124.

[122] E. Z. Faraggi, H. Chayet, G. Cohen, R. Neumann, Y. Avny, D. Davidov, *Adv. Mater.* **1995**, *7*, 742 – 745.

[123] E. G. J. Staring, R. C. J. E. Demandt, D. Braun, G. L. J. Rikken, Y. A. R. R. Kessener, A. H. J. Venhuizen, M. M. F. van Knippenberg, M. Bouwmans, *Synth. Met.* **1995**, *71*, 2179 – 2180.

[124] A. Kraft, P. L. Burn, A. B. Holmes, D. D. C. Bradley, A. R. Brown, R. H. Friend, R. W. Gymer, *Synth. Met.* **1993**, *55*, 936 – 941.

[125] P. L. Burn, A. B. Holmes, A. Kraft, D. D. C. Bradley, A. R. Brown, R. H. Friend, *J. Chem. Soc. Chem. Commun.* **1992**, 32 – 34.

[126] A. R. Brown, P. L. Burn, D. D. C. Bradley, R. H. Friend, A. Kraft, A. B. Holmes, *Mol. Cryst. Liq. Cryst.* **1992**, *216*, 111 – 116.

[127] C. Zhang, D. Braun, A. J. Heeger, *J. Appl. Phys.* **1993**, *73*, 5177 – 5180.

[128] S. Son, A. Dodabalapur, A. J. Lovinger, M. E. Galvin, *Science* **1995**, *269*, 376 – 378.

[129] H. Rost, A. Teuschel, S. Pfeiffer, H. H. Hörhold, *Synth. Met.* **1997**, *84*, 269 – 270.

[130] P. W. M. Blom, M. J. M. Dejong, J. J. M. Vleggaar, *Appl. Phys. Lett.* **1996**, *68*, 3308 – 3310.

[131] A. Kraft, P. L. Burn, A. B. Holmes, D. D. C. Bradley, R. H. Friend, J. H. F. Martens, *Synth. Met.* **1993**, *57*, 4163 – 4167.

[132] M. Yoshida, H. Kawahara, A. Fujii, Y. Ohmori, K. Yoshino, *Jpn. J. Appl. Phys.* **1995**, *34*, L1237 – L1240.

[133] C. Zhang, H. von Seggern, B. Kraabel, H.-W. Schmidt, A. J. Heeger, *Synth. Met.* **1995**, *72*, 185 – 188.

[134] M. Berggren, M. Granström, O. Inganäs, M. Andersson, *Adv. Mater.* **1995**, *7*, 900 – 903.

[135] T. Tsutsui, E.-I. Aminaka, Y. Fujita, Y. Hamada, S. Saito, *Synth. Met.* **1993**, *57*, 4157 – 4162.

[136] X.-C. Li, A. Kraft, R. Cervini, G. C. W. Spencer, F. Cacialli, R. H. Friend, J. Grüner, A. B. Holmes, J. C. DeMello, S. C. Moratti, *Mat. Res. Soc. Symp. Proc.* **1996**, *413*, 13 – 22.

[137] J. Bettenhausen, P. Strohriegl, *Adv. Mater.* **1996**, *8*, 507 – 510.

[138] J. Bettenhausen, P. Strohriegl, *Macromol. Rapid Commun.* **1996**, *17*, 623 – 631.

[139] A. Kraft, *Chem. Commun.* **1996**, 77 – 79.

[140] Q. Pei, Y. Yang, *Chem. Mater.* **1995**, *7*, 1568 – 1575.

[141] F. Cacialli, X.-C. Li, R. H. Friend, S. C. Moratti, A. B. Holmes, *Synth. Met.* **1995**, *75*, 161 – 168.

[142] M. Greczmiel, P. Pösch, H.-W. Schmidt, P. Strohriegl, E. Buchwald, M. Meier, W. Riess, M. Schwoerer, *Macromol. Symp.* **1996**, *102*, 371 – 380.

[143] X.-C. Li, T.-M. Yong, J. Grüner, A. B. Holmes, S. C. Moratti, F. Cacialli, R. H. Friend, *Synth. Met.* **1997**, *84*, 437 – 438.

[144] D. O'Brien, M. S. Weaver, D. G. Lidzey, D. D. C. Bradley, *Appl. Phys. Lett.* **1996**, *69*, 881 – 883.

[145] M. Yoshida, A. Fujii, Y. Ohmori, K. Yoshino, *Jpn. J. Appl. Phys.* **1996**, *35*, L397 – L400.

[146] M. Hamaguchi, K. Yoshino, *Appl. Phys. Lett.* **1996**, *69*, 143 – 145.

[147] M. Yoshida, A. Fujii, Y. Ohmori, K. Yoshino, *Appl. Phys. Lett.* **1996**, *69*, 734 – 736.

[148] J.-L. Brédas, A. J. Heeger, *Chem. Phys. Lett.* **1994**, *217*, 507 – 512.

[149] H.-H. Hörhold, M. Helbig, *Makromol. Chem. Macromol. Symp.* **1987**, *12*, 229 – 258.

[150] N. C. Greenham, S. C. Moratti, D. D. C. Bradley, R. H. Friend, A. B. Holmes, *Nature* **1993**, *365*, 628 – 630.

[151] N. C. Greenham, F. Cacialli, D. D. C. Bradley, R. H. Friend, S. C. Moratti, A. B. Holmes, *Mat. Res. Soc. Symp. Proc.* **1994**, *328*, 351 – 360.

[152] S. C. Moratti, D. D. C. Bradley, R. H. Friend, N. C. Greenham, A. B. Holmes, *Mat. Res. Soc. Symp. Proc.* **1994**, *328*, 371 – 376.

[153] S. C. Moratti, R. Cervini, A. B. Holmes, D. R. Baigent, R. H. Friend, N. C. Greenham, J. Grüner, P. J. Hamer, *Synth. Met.* **1995**, *71*, 2117 – 2120.

[154] J. J. M. Halls, D. R. Baigent, F. Cacialli, N. C. Greenham, R. H. Friend, S. C. Moratti, A. B. Holmes, *Thin Solid Films* **1996**, *276*, 13 – 20.

[155] D. R. Baigent, P. J. Hamer, R. H. Friend, S. C. Moratti, A. B. Holmes, *Synth. Met.* **1995**, *71*, 2175 – 2176.

[156] S. C. Moratti, D. D. C. Bradley, R. Cervini, R. H. Friend, N. C. Greenham, A. B. Holmes, *Proc. SPIE Int. Soc. Opt. Eng.* **1994**, *2144*, 108 – 114.

[157] R. M. Gurge, A. Sarker, P. M. Lahti, B. Hu, F. E. Karasz, *Macromolecules* **1996**, *29*, 4287 – 4292.

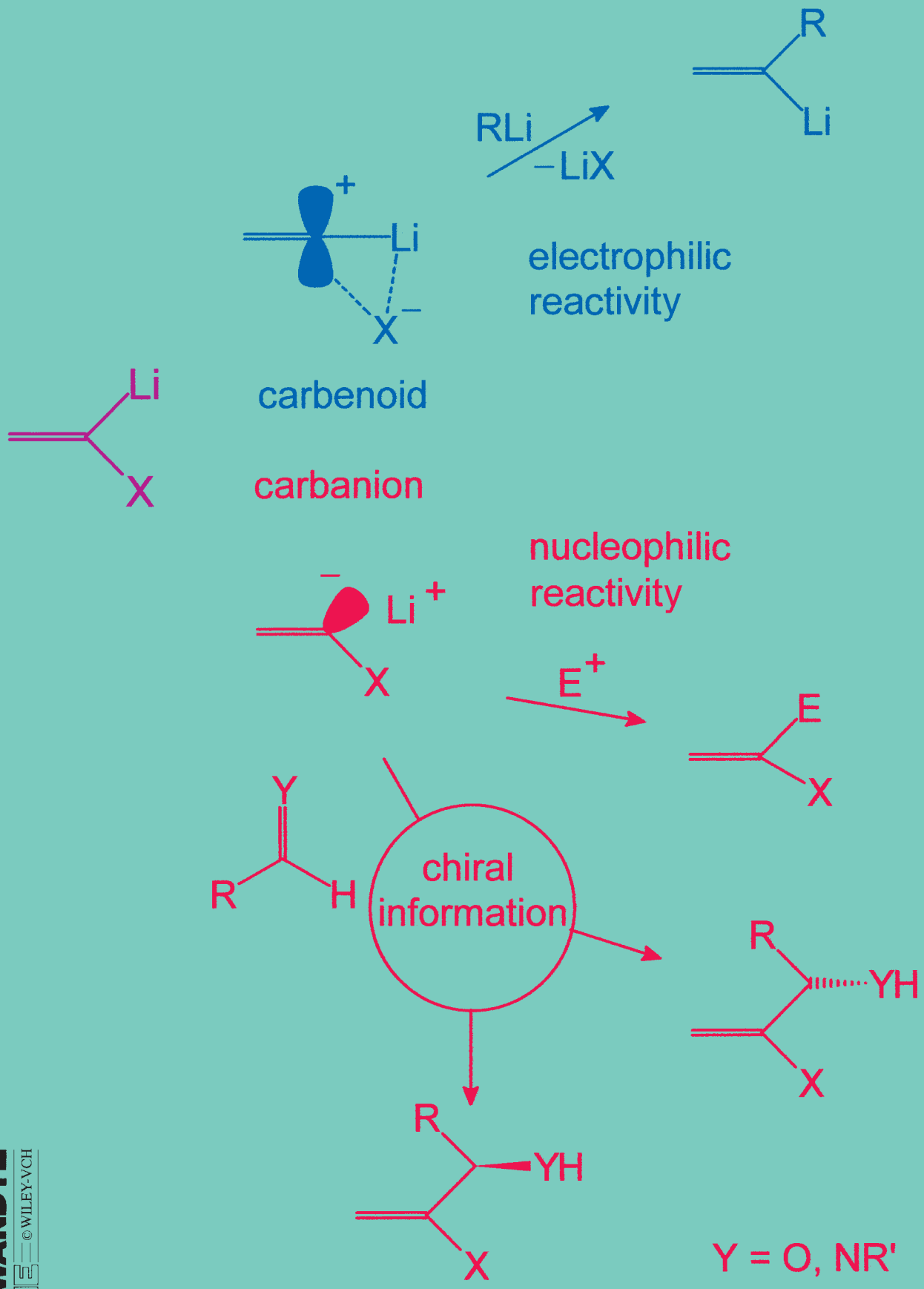
[158] G. J. Sarnecki, R. H. Friend, A. B. Holmes, S. C. Moratti, *Synth. Met.* **1995**, *69*, 545 – 546.

[159] A. Lux, A. B. Holmes, R. Cervini, J. E. Davies, S. C. Moratti, J. Grüner, F. Cacialli, R. H. Friend, *Synth. Met.* **1997**, *84*, 293 – 294.

[160] A. C. Grimsdale, X.-C. Li, F. Cacialli, J. Grüner, A. B. Holmes, S. C. Moratti, R. H. Friend, *Synth. Met.* **1996**, *76*, 165 – 167.
[161] A. Lux, S. C. Moratti, X.-C. Li, A. C. Grimsdale, J. F. Davies, P. R. Raithby, J. Grüner, F. Cacialli, R. H. Friend, A. B. Holmes, *Polym. Prepr.* **1996**, *37*, 202 – 203.
[162] M. Leclerc, F. M. Diaz, G. Wegner, *Makromol. Chem.* **1989**, *190*, 3105 – 3116.
[163] H. Mao, S. Holdcroft, *Macromolecules* **1992**, *25*, 554 – 558.
[164] H. Mao, B. Xu, S. Holdcroft, *Macromolecules* **1993**, *26*, 1163 – 1169.
[165] Y. Ohmori, M. Uchida, K. Muro, K. Yoshino, *Jpn. J. Appl. Phys.* **1991**, *30*, L1938 – L1940.
[166] Y. Ohmori, M. Uchida, K. Muro, K. Yoshino, *Solid State Commun.* **1991**, *80*, 605 – 608.
[167] D. Braun, G. Gustafsson, D. McBranch, A. J. Heeger, *J. Appl. Phys.* **1992**, *72*, 564 – 568.
[168] M. Uchida, Y. Ohmori, C. Morishima, K. Yoshino, *Synth. Met.* **1993**, *57*, 4168 – 4173.
[169] N. C. Greenham, A. R. Brown, D. D. C. Bradley, R. H. Friend, *Synth. Met.* **1993**, *57*, 4134 – 4138.
[170] A. Fujii, H. Kawahara, M. Yoshida, Y. Ohmori, K. Yoshino, *J. Phys. (D), Appl. Phys.* **1995**, *28*, 2135 – 2138.
[171] A. Bolognesi, C. Botta, Z. Geng, C. Flores, L. Denti, *Synth. Met.* **1995**, *71*, 2191 – 2192.
[172] M. Pomerantz, H. Yang, Y. Cheng, *Macromolecules* **1995**, *28*, 5706 – 5708.
[173] R. E. Gill, G. G. Malliaras, J. Wildeman, G. Hadziioannou, *Adv. Mater.* **1994**, *6*, 132 – 135.
[174] B. Xu, S. Holdcroft, *Macromolecules* **1993**, *26*, 4457 – 4460.
[175] B. Xu, S. Holdcroft, *Proc. SPIE Int. Soc. Opt. Eng.* **1993**, *1910*, 65 – 68.
[176] M. Berggren, G. Gustafsson, O. Inganäs, M. R. Andersson, O. Wennerström, T. Hjertberg, *Adv. Mater.* **1994**, *6*, 488 – 490.
[177] M. Berggren, O. Inganäs, G. Gustafsson, J. Rasmusson, M. R. Andersson, T. Hjertberg, O. Wennerström, *Nature* **1994**, *372*, 444 – 446.
[178] O. Inganäs, M. R. Andersson, G. Gustafsson, T. Hjertberg, O. Wennerström, P. Dyreklev, M. Granström, *Synth. Met.* **1995**, *71*, 2121 – 2124.
[179] M. R. Andersson, M. Berggren, O. Inganäs, G. Gustafsson, J. C. Gustafsson-Carlberg, D. Selse, T. Hjertberg, O. Wennerström, *Macromolecules* **1995**, *28*, 7525 – 7529.
[180] Y. Miyazaki, T. Yamamoto, *Chem. Lett.* **1994**, 41 – 44.
[181] M. Berggren, G. Gustafsson, O. Inganäs, M. R. Andersson, T. Hjertberg, O. Wennerström, *J. Appl. Phys.* **1994**, *76*, 7530 – 7534.
[182] M. C. Gallazzi, L. Castellani, G. Zerbi, P. Sozzani, *Synth. Met.* **1991**, *41*, 495 – 498.
[183] M. R. Andersson, D. Selse, M. Berggren, H. Järvinen, T. Hjertberg, O. Inganäs, O. Wennerström, J. E. Österholm, *Macromolecules* **1994**, *27*, 6503 – 6506.
[184] R. D. McCullough, R. D. Lowe, *J. Chem. Soc. Chem. Commun.* **1992**, 70 – 72.
[185] R. D. McCullough, R. D. Lowe, M. Jayaraman, D. L. Anderson, *J. Org. Chem.* **1993**, *58*, 904 – 912.
[186] R. D. McCullough, S. P. Williams, M. Jayaraman, J. Reddinger, L. Miller, S. Tristram-Nagle, *Mat. Res. Soc. Symp. Proc.* **1994**, *328*, 215 – 220.
[187] R. D. McCullough, S. P. Williams, S. Tristram-Nagle, M. Jayaraman, P. C. Ewbank, L. Miller, *Synth. Met.* **1995**, *69*, 279 – 282.
[188] T.-A. Chen, R. D. Rieke, *J. Am. Chem. Soc.* **1992**, *114*, 10087 – 10088.
[189] T.-A. Chen, X. Wu, R. D. Rieke, *J. Am. Chem. Soc.* **1995**, *117*, 233 – 244.
[190] C. A. Sandstedt, R. D. Rieke, C. J. Eckhardt, *Chem. Mater.* **1995**, *7*, 1057 – 1059.
[191] F. Chen, P. G. Mehta, L. Takiff, R. D. McCullough, *J. Mater. Chem.* **1996**, *6*, 1763 – 1767.
[192] K. A. Murray, S. C. Moratti, D. R. Baigent, N. C. Greenham, K. Pichler, A. B. Holmes, R. H. Friend, *Synth. Met.* **1995**, *69*, 395 – 396.
[193] N. C. Greenham, I. D. W. Samuel, G. R. Hayes, R. T. Phillips, Y. A. R. R. Kessener, S. C. Moratti, A. B. Holmes, R. H. Friend, *Chem. Phys. Lett.* **1995**, *241*, 89 – 96.
[194] R. D. McCullough, M. Jayaraman, *J. Chem. Soc. Chem. Commun.* **1995**, 135 – 136.
[195] K. A. Murray, A. B. Holmes, S. C. Moratti, R. H. Friend, *Synth. Met.* **1996**, *76*, 161 – 163.
[196] P. Dyreklev, M. Berggren, O. Inganäs, M. R. Andersson, O. Wennerstrom, T. Hjertberg, *Adv. Mater.* **1995**, *7*, 43 – 45.
[197] A. Bolognesi, G. Bajo, J. Paloheimo, T. Östergård, H. Stubb, *Adv. Mater.* **1997**, *9*, 121 – 124.
[198] M. J. Marsella, T. M. Swager, *Polym. Prepr.* **1992**, *33*, 1196 – 1197.
[199] J. Tian, C.-C. Wu, M. E. Thompson, J. C. Sturm, R. A. Register, M. J. Marsella, T. M. Swager, *Adv. Mater.* **1995**, *7*, 395 – 398.
[200] J. Tian, C.-C. Wu, M. E. Thompson, J. C. Sturm, R. A. Register, *Chem. Mater.* **1995**, *7*, 2190 – 2198.
[201] M. J. Marsella, D.-K. Fu, T. M. Swager, *Adv. Mater.* **1995**, *7*, 145 – 147.
[202] H. L. Wang, M. J. Marsella, D.-K. Fu, T. M. Swager, A. G. MacDiarmid, A. J. Epstein, *Polym. Mater. Sci. Eng.* **1995**, *73*, 473 – 474.
[203] L. S. Swanson, F. Lu, J. Shinar, Y. W. Ding, T. J. Barton, *Proc. SPIE Int. Soc. Opt. Eng.* **1993**, *1910*, 101 – 110.
[204] C. Weder, M. S. Wrighton, *Macromolecules* **1996**, *29*, 5157 – 5165.
[205] R. Giesa, *J. Macromol. Sci. Rev. Macromol. Chem. Phys.* **1996**, *36*, 631 – 670.
[206] L. S. Swanson, J. Shinar, Y. W. Ding, T. J. Barton, *Synth. Met.* **1993**, *55*, 1 – 6.
[207] C. Weder, M. J. Wagner, M. S. Wrighton, *Mat. Res. Soc. Symp. Proc.* **1996**, *413*, 77 – 84.
[208] K. Tada, M. Onoda, M. Hirohata, T. Kawai, K. Yoshino, *Jpn. J. Appl. Phys.* **1996**, *35*, L251 – L253.
[209] K. Yoshino, K. Tada, M. Onoda, *Jpn. J. Appl. Phys.* **1994**, *33*, L1785 – L1788.
[210] M. Hay, F. L. Klavetter, *J. Am. Chem. Soc.* **1995**, *117*, 7112 – 7118.
[211] G. G. Malliaras, J. K. Herrema, J. Wildeman, R. E. Gill, R. H. Wieringa, S. S. Lampoura, G. Hadziioannou, *Proc. SPIE Int. Soc. Opt. Eng.* **1993**, *2025*, 441 – 445.
[212] G. G. Malliaras, J. K. Herrema, J. Wildeman, R. H. Weiringa, R. E. Gill, S. S. Lampoura, G. Hadziioannou, *Adv. Mater.* **1993**, *5*, 721 – 723.
[213] J. K. Herrema, P. F. van Hutten, R. E. Gill, J. Wildeman, R. H. Wieringa, G. Hadziioannou, *Macromolecules* **1995**, *28*, 8102 – 8116.
[214] F. Garten, A. Hilberer, F. Cacialli, E. Esselink, Y. van Dam, B. Schlatmann, R. H. Friend, T. M. Klapwijk, G. Hadziioannou, *Adv. Mater.* **1997**, *9*, 127 – 131.
[215] D. Adam, F. Closs, T. Frey, D. Funhoff, D. Haarer, H. Ringsdorf, P. Schuhmacher, K. Siemensmeyer, *Phys. Rev. Lett.* **1993**, *70*, 457 – 460.
[216] T. Christ, V. Stümpflen, J. H. Wendorff, *Macromol. Rapid Commun.* **1997**, *18*, 93 – 98.
[217] T. Christ, B. Glüsen, A. Greiner, A. Kettner, R. Sander, V. Stümpflen, V. Tsukruk, J. H. Wendorff, *Adv. Mater.* **1997**, *9*, 48 – 52.
[218] Y. Ohmori, K. Uchida, K. Muro, K. Yoshino, *Jpn. J. Appl. Phys.* **1991**, *30*, L1941 – L1943.
[219] M. Fukuda, K. Sawada, K. Yoshino, *Jpn. J. Appl. Phys.* **1989**, *28*, L1433 – L1435.
[220] M. Fukuda, K. Sawada, K. Yoshino, *J. Polym. Sci. Polym. Chem.* **1993**, *31*, 2465 – 2471.
[221] G. Grem, G. Leditzky, B. Ullrich, G. Leising, *Adv. Mater.* **1992**, *4*, 36 – 37.
[222] G. Grem, G. Leditzky, B. Ullrich, G. Leising, *Synth. Met.* **1992**, *51*, 383 – 389.
[223] K. Miyashita, M. Kaneko, *Synth. Met.* **1995**, *68*, 161 – 165.
[224] D. L. Gin, V. P. Conticello, *Trends Polym. Sci.* **1996**, *4*, 217 – 223.
[225] D. G. H. Ballard, A. Courtis, I. M. Shirley, S. C. Taylor, *J. Chem. Soc. Chem. Commun.* **1983**, 954 – 955.
[226] D. G. H. Ballard, A. Courtis, I. M. Shirley, S. C. Taylor, *Macromolecules* **1988**, *21*, 294 – 304.
[227] D. R. McKean, J. K. Stille, *Macromolecules* **1987**, *20*, 1787 – 1792.
[228] M. Hamaguchi, H. Sawada, J. Kyokane, K. Yoshino, *Chem. Lett.* **1996**, 527 – 528.
[229] A.-D. Schlüter, G. Wegner, *Acta Polym.* **1993**, *44*, 59 – 69.
[230] T. Vahlenkamp, G. Wegner, *Macromol. Chem. Phys.* **1994**, *195*, 1933 – 1952.
[231] T. F. McCarthy, H. Witteler, T. Pakula, G. Wegner, *Macromolecules* **1995**, *28*, 8350 – 8362.
[232] M. Remmers, M. Schulze, G. Wegner, *Macromol. Rapid Commun.* **1996**, *17*, 239 – 252.
[233] T. Yamamoto, *Progr. Polym. Sci.* **1992**, *17*, 1153 – 1205.
[234] V. Percec, S. Okita, R. Weiss, *Macromolecules* **1992**, *25*, 1816 – 1823.
[235] V. Percec, J.-Y. Bae, M. Zhao, D. H. Hill, *Macromolecules* **1995**, *28*, 6726 – 6734.

[236] V. Percec, M. Zhao, J.-Y. Bae, D. H. Hill, *Macromolecules* **1996**, *29*, 3727 – 3735.
[237] F. L. Klavetter, G. Gustafsson, A. J. Heeger, *Polym. Mater. Sci. Eng.* **1993**, *69*, 153 – 154.
[238] W.-X. Jing, A. Kraft, S. C. Moratti, J. Grüner, F. Cacialli, P. J. Hamer, A. B. Holmes, R. H. Friend, *Synth. Met.* **1994**, *67*, 161 – 163.
[239] M. Hamaguchi, K. Yoshino, *Jpn. J. Appl. Phys.* **1995**, *34*, L587 – L589.
[240] Y. Yang, Q. Pei, A. J. Heeger, *J. Appl. Phys.* **1996**, *79*, 934 – 939.
[241] Y. Yang, Q. Pei, A. J. Heeger, *Synth. Met.* **1996**, *78*, 263 – 267.
[242] V. Cimrová, W. Schmidt, R. Rulkens, M. Schulze, W. Meyer, D. Neher, *Adv. Mater.* **1996**, *8*, 585 – 588.
[243] M. Remmers, D. Neher, J. Grüner, R. H. Friend, G. H. Gelinck, J. M. Warman, C. Quattrocchi, D. A. dos Santos, J.-L. Brédas, *Macromolecules* **1996**, *29*, 7432 – 7445.
[244] U. Scherf, K. Müllen, *Makromol. Chem. Rapid Commun.* **1991**, *12*, 489 – 497.
[245] U. Scherf, K. Müllen, *Macromolecules* **1992**, *25*, 3546 – 3548.
[246] G. Leising, G. Grem, G. Leditzky, U. Scherf, *Proc. SPIE Int. Soc. Opt. Eng.* **1993**, *1910*, 70 – 77.
[247] G. Grem, G. Leising, *Synth. Met.* **1993**, *55 – 57*, 4105 – 4110.
[248] J. Hüber, K. Müllen, J. Salbeck, H. Schenk, U. Scherf, T. Stehlin, R. Stern, *Acta Polym.* **1994**, *45*, 244 – 247.
[249] G. Grem, V. Martin, F. Meghdadi, C. Paar, J. Stampfl, J. Sturm, S. Tasch, G. Leising, *Synth. Met.* **1995**, *71*, 2193 – 2194.
[250] U. Scherf, A. Bohnen, K. Müllen, *Makromol. Chem.* **1992**, *193*, 1127 – 1133.
[251] G. Leising, G. Köpping-Grem, F. Meghdadi, A. Niko, S. Tasch, W. Fischer, L. Pu, M. W. Wagaman, R. H. Grubbs, L. Althouel, G. Froyer, U. Scherf, J. Huber, *Proc. SPIE Int. Soc. Opt. Eng.* **1995**, *2528*, 307 – 314.
[252] S. Tasch, A. Niko, G. Leising, U. Scherf, *Appl. Phys. Lett.* **1996**, *68*, 1090 – 1092.
[253] S. Tasch, A. Niko, G. Leising, U. Scherf, *Mat. Res. Soc. Symp. Proc.* **1996**, *413*, 71 – 76.
[254] J. Grüner, H. F. Wittmann, P. J. Hamer, R. H. Friend, J. Huber, U. Scherf, K. Müllen, S. C. Moratti, A. B. Holmes, *Synth. Met.* **1994**, *67*, 181 – 185.
[255] Y. Ohmori, M. Uchida, C. Morishima, A. Fujii, K. Yoshino, *Jpn. J. Appl. Phys.* **1993**, *32*, L1663 – L1666.
[256] Q. Pei, Y. Yang, *J. Am. Chem. Soc.* **1996**, *118*, 7416 – 7417.
[257] M. Grell, D. D. C. Bradley, M. Inbasekaran, E. P. Woo, *Adv. Mater.* **1997**, *9*, 798 – 802.
[258] I. Sokolik, Z. Yang, F. E. Karasz, D. C. Morton, *J. Appl. Phys.* **1993**, *74*, 3584 – 3586.
[259] Z. Yang, I. Sokolik, F. E. Karasz, *Macromolecules* **1993**, *26*, 1188 – 1190.
[260] Z. Yang, F. E. Karasz, H. J. Geise, *Macromolecules* **1993**, *26*, 6570 – 6575.
[261] D.-H. Hwang, I.-N. Kang, M.-S. Jang, H.-K. Shim, *Bull. Korean Chem. Soc.* **1995**, *16*, 135 – 138.
[262] T. Zyung, D.-H. Hwang, I.-N. Kang, H.-K. Shim, W.-Y. Hwang, J.-J. Kim, *Chem. Mater.* **1995**, *7*, 1499 – 1503.
[263] J.-K. Lee, R. R. Schrock, D. R. Baigent, R. H. Friend, *Macromolecules* **1995**, *28*, 1966 – 1971.
[264] G. Yu, H. Nishino, A. J. Heeger, T.-A. Chen, R. D. Rieke, *Synth. Met.* **1995**, *72*, 249 – 252.
[265] J. Birgerson, M. Fahlman, P. Bröms, W. R. Salaneck, *Synth. Met.* **1996**, *80*, 125 – 130.
[266] N. Tanigaki, H. Masuda, K. Kaeriyama, *Polymer* **1997**, *38*, 1221 – 1226.
[267] T. Zyung, J.-J. Kim, I.-N. Kang, D.-H. Hwang, H.-K. Shim, *Mat. Res. Soc. Symp. Proc.* **1996**, *413*, 103 – 107.
[268] I.-N. Kang, D.-H. Hwang, H.-K. Shim, T. Zyung, J.-J. Kim, *Macromolecules* **1996**, *29*, 165 – 169.
[269] H. N. Cho, D. Y. Kim, Y. C. Kim, J. Y. Lee, C. Y. Kim, *Adv. Mater.* **1997**, *9*, 326 – 328; *Proc. SPIE Int. Soc. Opt. Eng.* **1997**, *3418*, 151 – 159.
[270] M. Berggren, O. Inganäs, G. Gustafsson, M. R. Andersson, T. Hjertberg, O. Wennerström, *Synth. Met.* **1995**, *71*, 2185 – 2186.
[271] M. Granström, O. Inganäs, *Appl. Phys. Lett.* **1996**, *68*, 147 – 149.
[272] M. Uchida, Y. Ohmori, T. Noguchi, T. Ohnishi, K. Yoshino, *Jpn. J. Appl. Phys.* **1993**, *32*, L921 – L924.
[273] M. Yoshida, K. Yoshimoto, T. Akashi, M. Uchida, T. Kawai, Y. Ohmori, T. Noguchi, T. Ohnishi, K. Yoshino, *Synth. Met.* **1995**, *71*, 2111 – 2112.
[274] M. Yoshida, A. Fujii, Y. Ohmori, K. Yoshino, *Jpn. J. Appl. Phys.* **1995**, *34*, L1546 – L1549.
[275] B. K. Cumpston, K. F. Jensen, *Trends Polym. Sci.* **1996**, *4*, 151 – 157.
[276] B. H. Cumpston, I. D. Parker, K. F. Jensen, *J. Appl. Phys.* **1997**, *81*, 3716 – 3720.
[277] M. Yan, L. J. Rothberg, F. Papadimitrakopoulos, M. E. Galvin, T. M. Miller, *Phys. Rev. Lett.* **1994**, *73*, 744 – 747.
[278] T. Zyung, J.-J. Kim, *Appl. Phys. Lett.* **1995**, *67*, 3420 – 3422.
[279] B. H. Cumpston, K. F. Jensen, *Synth. Met.* **1995**, *73*, 195 – 199.
[280] R. D. Scurlock, B. Wang, P. R. Ogilby, J. R. Sheats, R. L. Clough, *J. Am. Chem. Soc.* **1995**, *117*, 10194 – 10202.
[281] S. Karg, W. Riess, M. Meier, M. Schwoerer, *Mol. Cryst. Liq. Cryst.* **1993**, *236*, 79 – 86.
[282] J. C. Scott, J. H. Kaufman, J. Salem, J. A. Goitia, P. J. Brock, R. DiPietro, *Mol. Cryst. Liq. Cryst.* **1996**, *283*, 57 – 62.
[283] J. C. Scott, J. H. Kaufman, P. J. Brock, R. DiPietro, J. Salem, J. A. Goitia, *J. Appl. Phys.* **1996**, *79*, 2745 – 2751.
[284] H. Aziz, G. Xu, *J. Phys. Chem. B* **1997**, *101*, 4009 – 4012.
[285] Q. Pei, G. Yu, C. Zhang, Y. Yang, A. J. Heeger, *Science* **1995**, *269*, 1086 – 1088.
[286] Y. Cao, G. Yu, A. J. Heeger, C. Y. Yang, *Appl. Phys. Lett.* **1996**, *68*, 3218 – 3220.
[287] Q. Pei, Y. Yang, G. Yu, C. Zhang, A. J. Heeger, *J. Am. Chem. Soc.* **1996**, *118*, 3922 – 3929.
[288] Q. Pei, Y. Yang, *Synth. Met.* **1996**, *80*, 131 – 136.
[289] G. Yu, Q. Pei, A. J. Heeger, *Appl. Phys. Lett.* **1997**, *70*, 934 – 936.
[290] Y. Yang, Q. Pei, *Appl. Phys. Lett.* **1996**, *68*, 2708 – 2710.
[291] Y. Yang, Q. Pei, *J. Appl. Phys.* **1997**, *81*, 3294 – 3298.
[292] Q. Pei, Y. Yang, G. Yu, Y. Cao, A. J. Heeger, *Synth. Met.* **1997**, *85*, 1229 – 1232.
[293] Y. Yang, Q. Pei, *Appl. Phys. Lett.* **1997**, *70*, 1926 – 1928.
[294] A. G. MacDiarmid, H.-L. Wang, J.-W. Park, D.-K. Fu, M. J. Marsella, T. M. Swager, Y. Wang, D. D. Gebler, A. J. Epstein, *Proc. SPIE Int. Soc. Opt. Eng.* **1995**, *2528*, 2 – 12.
[295] Y. Z. Wang, D. D. Gebler, J. W. Blatchford, S. W. Jessen, L. B. Lin, T. L. Gustafsson, H.-L. Wang, Y. W. Park, T. M. Swager, A. G. MacDiarmid, A. J. Epstein, *Proc. SPIE Int. Soc. Opt. Eng.* **1995**, *2528*, 54 – 61.
[296] Y. Z. Wang, D. D. Gebler, L. B. Lin, J. W. Blatchford, S. W. Jessen, H. L. Wang, A. J. Epstein, *Appl. Phys. Lett.* **1996**, *68*, 894 – 896.
[297] H. L. Wang, A. G. MacDiarmid, Y. Z. Wang, D. D. Gebler, A. J. Epstein, *Synth. Met.* **1996**, *78*, 33 – 37.
[298] A. J. Epstein, J. W. Blatchford, Y. Z. Wang, S. W. Jessen, D. D. Gebler, L. B. Lin, T. L. Gustafsson, H.-L. Wang, Y. W. Park, T. M. Swager, A. G. MacDiarmid, *Synth. Met.* **1996**, *78*, 253 – 261.
[299] H. Wang, F. Huang, A. G. MacDiarmid, Y. Z. Wang, D. D. Gebler, A. J. Epstein, *Synth. Met.* **1996**, *80*, 97 – 104.
[300] Y. Z. Wang, D. D. Gebler, D. K. Fu, T. M. Swager, A. J. Epstein, *Appl. Phys. Lett.* **1997**, *70*, 3215 – 3217.
[301] H. F. Wittmann, J. Grüner, R. H. Friend, G. W. C. Spencer, S. C. Moratti, A. B. Holmes, *Adv. Mater.* **1995**, *7*, 541 – 544.
[302] T. A. Fischer, D. G. Lidzey, M. A. Pate, M. S. Weaver, D. M. Whittaker, M. S. Skolnick, D. D. C. Bradley, *Appl. Phys. Lett.* **1995**, *67*, 1355 – 1357.
[303] M. Berggren, O. Inganäs, T. Granlund, S. Guo, G. Gustafsson, M. R. Andersson, *Synth. Met.* **1996**, *76*, 121 – 123.
[304] D. G. Lidzey, M. S. Weaver, T. A. Fisher, M. A. Pate, D. M. Whittaker, M. S. Skolnick, D. D. C. Bradley, *Synth. Met.* **1996**, *76*, 129 – 132.
[305] V. Cimrová, D. Neher, *J. Appl. Phys.* **1996**, *79*, 3299 – 3307.
[306] J. Grüner, F. Cacialli, R. H. Friend, *J. Appl. Phys.* **1996**, *80*, 207 – 215.
[307] V. Cimrová, U. Scherf, D. Neher, *Appl. Phys. Lett.* **1996**, *69*, 608 – 610.
[308] N. Tessler, G. J. Denton, R. H. Friend, *Nature* **1996**, *382*, 695 – 697.
[309] F. Hide, M. A. Díaz-García, B. J. Schwartz, M. R. Andersson, Q. Pei, A. J. Heeger, *Science* **1996**, *273*, 1833 – 1836.
[310] B. J. Schwartz, F. Hide, M. A. Díaz-García, A. J. Heeger, *Polym. Mater. Sci. Eng.* **1996**, *75*, 451 – 452.
[311] S. V. Frolov, M. Ozaki, W. Gellermann, Z. V. Vardeny, K. Yoshino, *Jpn. J. Appl. Phys.* **1996**, *35*, L1371 – L1373.

[312] H. J. Brouwer, V. V. Krasnikov, A. Hilberer, G. Hadziioannou, *Adv. Mater.* **1996**, *8*, 935 – 937.
[313] W. Holzer, A. Penzkofer, S.-H. Gong, A. Bleyer, D. D. C. Bradley, *Adv. Mater.* **1996**, *8*, 975 – 978.
[314] S. V. Frolov, W. Gellermann, M. Ozaki, K. Yoshino, Z. V. Vardeny, *Phys. Rev. Lett.* **1997**, *78*, 729 – 732.
[315] S. V. Frolov, W. Gellermann, Z. V. Vardeny, M. Ozaki, K. Yoshino, *Synth. Met.* **1997**, *84*, 471 – 472.
[316] S. V. Frolov, M. Ozaki, W. Gellermann, M. Shkunov, Z. V. Vardeny, K. Yoshino, *Synth. Met.* **1997**, *84*, 473 – 474.
[317] N. Tessler, G. J. Denton, R. H. Friend, *Synth. Met.* **1997**, *84*, 475 – 476.
[318] D. G. Lidzey, D. D. C. Bradley, S. F. Alvarado, P. F. Seidler, *Nature* **1997**, *386*, 135.
[319] D.-H. Hwang, S. T. Kim, H.-K. Shim, A. B. Holmes, S. C. Moratti, R. H. Friend, *Chem. Commun.* **1996**, 2241 – 2242.
[320] E. G. J. Staring, *Philos. Trans. R. Soc. Math. Phys. Eng. Sci.* **1996**, *80*, 111 – 117.
[321] J. Birgerson, K. Kaeriyama, P. Barta, P. Broms, M. Fahlman, T. Granlund, W. R. Salaneck, *Adv. Mater.* **1996**, *8*, 982 – 985.
[322] M. R. Andersson, G. Yu, A. J. Heeger, *Synth. Met.* **1997**, *85*, 1275 – 1276.
[323] M. Deußen, H. Bässler, *Chem. Unserer Zeit* **1997**, *31*, 76 – 86.
[324] F. Hide, M. A. Díaz-García, B. J. Schwartz, A. J. Heeger, *Acc. Chem. Res.* **1997**, *30*, 430 – 436.
[325] M. Thelekkat, R. Fink, P. Pösch, J. Ring, H.-W. Schmidt, *Polym. Prepr.* **1997**, *38*, 323 – 324.
[326] For a report by Meijer et al. in collaboration with Philips on circularly polarized electroluminescence from a polyldialkoxyphenylene vinylene), see E. Peeters, M. P. T. Christiaans, R. A. J. Janssen, H. F. M. Schoo, H. P. J. M. Dekkers, E. W. Meijer, *J. Am. Chem. Soc.* **1997**, *119*, 9909 – 9910.



ANGEWANDTE CHEMIE ©WILEY-VCH

α-Heteroatom-Substituted 1-Alkenyllithium Reagents: Carbanions and Carbenoids for C–C Bond Formation

Manfred Braun*

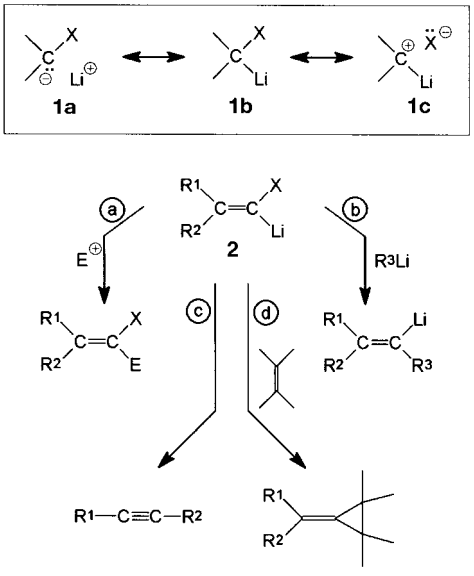
Dedicated to Professor Dieter Seebach on the occasion of his 60th birthday

Only the development of low-temperature methods has made it possible to synthesize in solution thermally unstable compounds substituted with a leaving group and a lithium atom at the same carbon center and to exploit their synthetic potential. 1-Alkenyllithium compounds with a heteroatom in the α position (α-heteroatom-substituted 1-alkenyllithium compounds) with geminal substitution of the vinyl carbon atom with an electronegative element and a lithium atom react as electrophilic carbenoids or nucleophilic carbanions depending on the type of heteroatom substituent and the temperature. Newer spectroscopic examinations and X-ray structure analyses, which are summarized here, have contributed substantially towards the understanding of this ambiphilia. After an overview of the most important methods for generating α-heteroatom-substituted 1-alkenyllithium compounds, the carbenoid reactivity of α-lithiated vinyl halides and vinyl ethers is illustrated. In contrast, the many possibilities for C–C bond formation are based on the carbanionic character of the α-heteroatom-substituted 1-lithioalkenes, which are also particularly well suited for carbonyl umpolung. The synthetic potential of such reagents is enlarged substantially with chiral representatives: Lithiated vinyl bromides find application in asymmetric syntheses of α-hydroxy and α-amino carbonyl compounds.

Keywords: asymmetric synthesis · lithium · nucleophilic additions · synthetic methods · umpolung

1. Introduction

Thermal lability and ambiphilic behavior are shown by compounds containing a lithium atom and an electronegative element as a leaving group on the same carbon center. Köbrich, whom we thank for seminal work in this field, used the term "carbenoid" for species **1**, which is usually highly reactive.[1] Whereas the resonance formula **1a** expresses the carbanionic character, the mesomeric structure **1c** highlights the electrophilic reactivity.[2] The ambiphilia is also detectable for alkene derivatives **2**. However, since stabilization of the carbon center increases with growing s content of the corresponding hybrid orbital,[3] the carbanionic reactivity is expressed more strongly in the sp^2-hybridized carbon atom and dominates completely when sulfur, the higher chalcogens, nitrogen, or phosphorus are used as heteroelements X. Numerous reactions with electrophiles prove the carbanionic reactivity (Scheme 1, reaction ⓐ). Since a C–C double bond substituted with a more electronegative element can in principle be converted into a carbonyl group by hydrolysis or ozonolysis, alkenyllithium compounds **2** are suitable equivalents of acyl anions and can be used as reagents for the umpolung of carbonyl reactivity.[4] Marked ambiphilia is



Scheme 1. Reactivities of vinylidene carbenoids **2** as carbanions (a), as electrophiles (b), with rearangement (c), and in cycloadditions (d).

[*] Prof. Dr. M. Braun
Institut für Organische Chemie und Makromolekulare Chemie der Universität
Universitätsstrasse 1, D-40225 Düsseldorf (Germany)
Fax: (+49) 211-81-13085
E-mail: braunm@uni-duesseldorf.de

 © WILEY-VCH Verlag GmbH, D-69451 Weinheim, 1998 1433-7851/98/3704-0431 $ 17.50+.50/0

observed for lithiated vinyl halides and vinyl ethers **2** (X = F, Cl, Br; OR). The surprising reaction of metalated vinyl bromides with alkyllithium compounds makes clear the electrophilic character of these carbenoids: In a nucleophilic, probably metal-supported, substitution the halide is replaced by the alkyl group with inversion of configuration (Scheme 1, reaction ⓑ).[5, 6] As a further feature of carbene-type reactivity, the intramolecular shift of a β-aryl, cyclopropyl, or hydrogen substituent (known as the Fritsch–Buttenberg–Wiechell rearrangement) occurs with the thermolabile α-lithiated vinyl halides **2** (X = Br, Cl; Scheme 1, reaction ⓒ). In the case of β-alkyl-substituted derivatives of **2** (X = Br, Cl), the cyclopropanation typical of carbenoids is also found (reaction ⓓ).[7]

Clearly, this chameleonlike chemical behavior of carbenoids **2** invited structural investigations to reach a better understanding of the different reactivities. Such studies were hampered for a long time by the thermal lability of alkenyllithium compounds, especially those with an α-halogen substituent. It was only in the last few years—in which the interest in carbenes and carbenoids increased[8]—that improved calculations, NMR studies, and finally X-ray structure analyses offered new insight into vinylidene carbenoids **2**. Köbrich had already predicted a larger s content of the C–Li bond and, therefore, a higher p content of the C–X bond in chloro- and bromo-substituted lithioalkenes.[1] Ab initio calculations show that carbenoids **1** and **2** have a comparatively high positive charge at the α-carbon atom and a LUMO that is low in energy.[9] These ideas are confirmed with systematic NMR spectroscopic studies on ^{6}Li-,^{13}C-labeled vinylidene carbenoids **2**:[10] The polarization of the carbon–halogen bond effects a significant deshielding of the α-carbon atom. Therefore, the resonance of the vinyl carbon atom *C in the cyclohexylidene derivative **3** is shifted downfield by $\Delta\delta$ = 101.6 when converted into the alkenyllithium compound **4**. Downfield shifts of $\Delta\delta = 40-280$ are also exhibited by other lithium carbenoids, which shows that the carbocationic structure **1c** has to be taken into account. If a hydrogen-atom substituent in an alkane is replaced by lithium, small upfield shifts of up to $\Delta\delta = 15$ are observed. Downfield shifts also occur to a lesser extent for α-hydrogen- and α-alkyl-substituted alkenyllithium compounds.[11]

The predictions concerning the rehybridization at the carbenoid carbon atom were thoroughly confirmed by an exciting[2] X-ray structure analysis of 1-chloro-2,2-bis(4-chlorophenyl)-1-lithioethene · tmeda · 2 thf (**5**, Figure 1; the second THF molecule is not shown since it is located on a free lattice position and is not bound to the Li atom), the first of a lithium carbenoid.[12] The C1–Cl1 bond is distinctly elongated (by

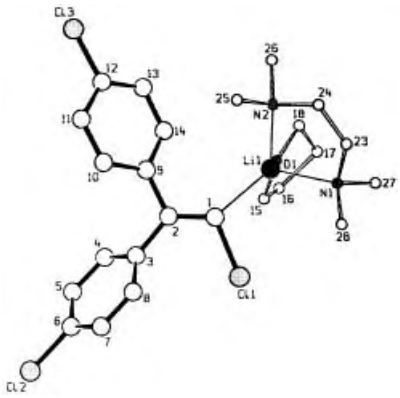
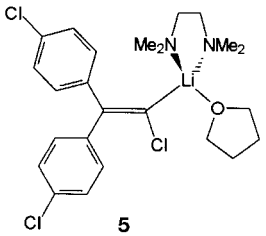
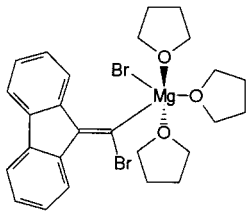


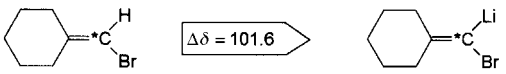
Figure 1. Crystal structure of **5**.



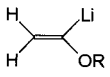
5



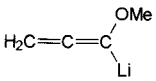
6



3 δ*C = 99.2 **4** δ*C = 200.8



7a: R = Et
7b: R = Me



8



Manfred Braun was born in Schwalbach near Saarlouis (Germany) in 1948. From 1966 until 1971 he studied chemistry at the Universität (Technischen Hochschule) Karlsruhe, and in 1975 he completed his doctorate under D. Seebach in Giessen. After a postdoc with G. Büchi at the Massachusetts Institute of Technology in 1975 and 1976 he joined H. Musso's research group at the Universität Karlsruhe and completed the habilitation there in 1981. Since 1985 he has been a professor of organic chemistry at the Heinrich-Heine-Universität Düsseldorf. He received the Liebig scholarship from the Fonds der Chemischen Industrie, the habilitation scholarship as well as the Heisenberg scholarship from the Deutsche Forschungsgemeinschaft, and the Karl Winnacker scholarship. Guest professorships led him to the Université de Rennes (France) and the University of Wisconsin in Madison (USA). His current research interests include the development of new synthetic methods (especially for asymmetric synthesis), organometallic chemistry, and syntheses of natural products.

12 pm) with respect to that in the non-lithiated compound. The Cl1-C1-C2 angle of 112.6(5)° is smaller than the 120° angle at sp^2-hybridized carbon atoms, whereas the Li1-C1-C2 angle is significantly larger (137.1(6)°). These results are easily explained with the high s character of the C–Li bond and the p content of the C–Cl bond. For a nonsolvated carbenoid **2** (X = Cl, OR), calculations predict a structure[13] in which the C–X bond is bridged by the lithium.[14] This contradiction to the crystal structure of **5** is probably due to the fact that the lithium atom is sufficiently solvated by TMEDA and tetrahydrofuran. The bond angles at the carbenoid carbon atom in **5** offer a simple explanation for the inversion that takes place during nucleophilic substitution at lithioalkenes **2** (Scheme 1, reaction ⓑ): apparently the "open" side (large C2-C1-Li angle) opposite the leaving group X offers the ideal trajectory for the nucleophilic alkyllithium compound. A distinct similarity to the alkenyllithium compound **5** is seen for the Grignard compound **6**, which is not surprising owing to the diagonal relationship in the periodic table. The C–Br bond in **6** is 10 pm longer than that in the corresponding vinyl bromide.[15]

1-Ethoxy-1-lithioethene (**7a**), which in contrast to the monomers **5** and **6** exists as polymeric chains in the crystalline state, also displays carbenoid character: With an average length of 142.8(7) pm, the C1–O bond is significantly elongated with respect to that normally seen in vinyl ethers (136 pm). The asymmetric unit presented in Figure 2 contains six $H_2C{=}C(Li)OEt$ molecules. Four of them form a distorted cubic Li_4C_4 tetramer, and the remaining two a second tetrameric aggregate.[16] According to ^{13}C NMR, ^{6}Li,^{13}C

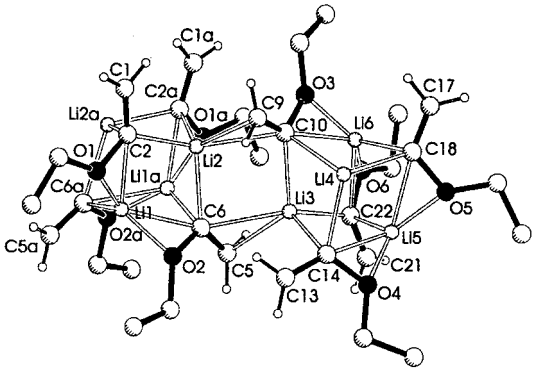
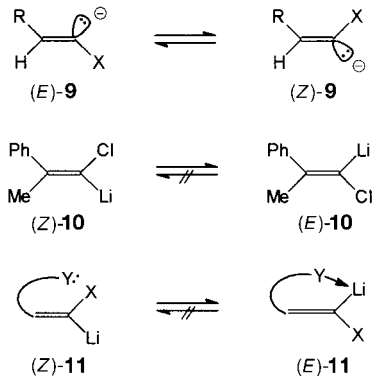


Figure 2. Detail of the crystal structure of polymeric **7a**.

HOSEY NMR, and IR spectroscopic studies, 1-lithio-1-methoxyallen (**8**) in tetrahydrofuran exists in the form of a dimeric nonclassical 1,3-bridged structure; this is also confirmed by ab initio model calculations on α-lithiohydroxyallene.[17]

Unlike alkyl anions, vinyl anions are regarded as configurationally stable; the calculated inversion barrier is about 35 kcal mol^{-1} in the case of the ethenyl anion (*E*)/(*Z*)-**9** (X = H).[18] This value was also experimentally confirmed for a series of 1-lithioalkenes with hydrogen, alkyl, and aryl groups as α substituents.[19] For preparative use, it is of great importance that if generated under mild conditions (low temperatures) the α-substituted 1-alkenyllithium reagents[20]



keep their configuration and react with electrophiles under retention. The lithioalkene (*Z*)-**10**, which is obtained at −110 °C, partially isomerizes to the more stable (*E*)-**10** upon warming to −85 °C, whereas the reverse reaction is not observed.[5] Therefore, two stereoselective transformations are possible: The respective vinylidene carbenoid with the higher energy configuration can be produced at temperatures below −105 °C without inversion and allowed to react under retention. In addition, the diastereomer becomes accessible if the alkenyllithium reagent is allowed to invert by raising the temperature to yield the thermodynamically more stable alkylidene carbenoid. This method can be applied with particular success when there are substituents in the *Z* position with respect to the lithium atom that contain donor centers at the right distance, so that the formation of chelates (*E*)-**11** (X = Cl, Br; Y = OR, NR_2) is possible. Admittedly the temperature can only be increased to about −85 °C because of the thermal lability of α-halogen α-lithioalkenes. On the other hand, metalated vinyl ethers are configurationally stable up to −20 °C for reactions with electrophiles in tetrahydrofuran.[21] Until the onset of decomposition, solutions of 1-ethoxy-1-lithioethene (**7a** · tmeda) show no coalescence of the signals for the vinyl protons in the ^1H NMR spectrum, as would be expected if inversion took place.[22] Also in the case of α-lithiated vinylthioethers, no *E*/*Z* isomerization occurs in tetrahydrofuran up to 0 °C; deprotonated vinyl sulfoxides and vinyl sulfones, on the other hand, are configurationally less stable.[23]

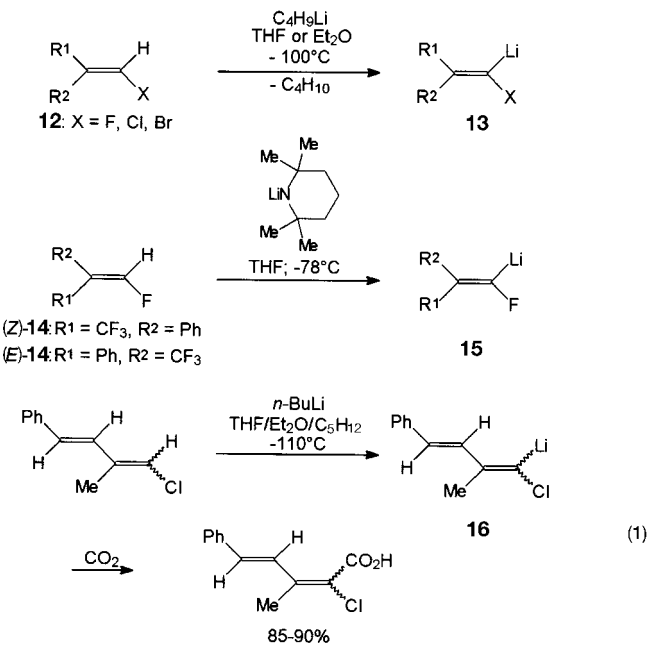
The selective generation of *E* and *Z* vinylidene carbenoids is growing in importance for synthetic applications of α-heteroatom-substituted 1-alkenyllithium compounds. This is particularly true when enantiomerically pure substances are to be produced by stereoselective transformations of such alkenyllithium compounds. This aspect of the chemistry of lithium carbenoids,[1, 2, 20, 24] which has so far received little notice, is the object of particular attention in this review.

2. Generation of α-Substituted 1-Alkenyllithium Compounds

2.1. Hydrogen–Lithium Exchange

α-Heteroatom-substituted 1-alkenyllithium compounds are usually generated quantitatively in solution under inert

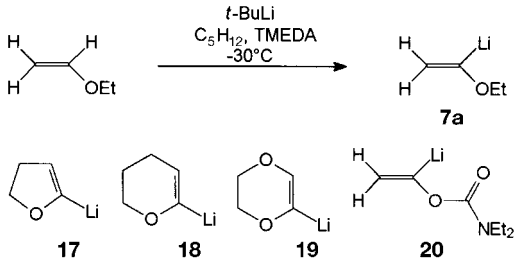
conditions at low temperatures and allowed to react further without isolation.[25] The acidity of vinyl-bound hydrogen atoms is sufficiently high due to the greater s proportion of the C–H bond compared with alkanes,[3] and deprotonation is possible with alkyllithium reagents such as *n*-, *sec*-, or *tert*-butyllithium. If the system to be metalated has one or several protons in the allyl position, the formation of the allyl instead of the vinyl anion can become the dominating rival reaction.[26] In alkenes with heteroatom substituents from Groups 15, 16, and 17, however, the α-hydrogen atom shows a higher acidity. Therefore, 1-halo-1-alkenes **12** can react with *n*- or *tert*-butyllithium in tetrahydrofuran or diethyl ether at $-100\,^{\circ}C$ to yield fluoro-, chloro-, and bromo-substituted 1-lithioalkenes **13**, whose existence can be confirmed in most cases by reaction with electrophiles.[24, 27] With vinyl fluorides and vinyl chlorides, deprotonation is very much faster than



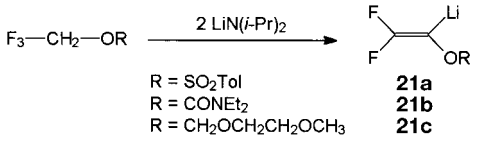
(1)

halogen–lithium exchange, which, however, can occur with bromoalkenes. Lithium-2,2,6,6-tetramethylpiperidide is also suitable for the metalation of vinyl fluorides **14** to form lithioalkenes **15**, which are stable up to $-78\,^{\circ}C$ and also retain their configuration.[28, 29] Particularly labile carbenoids such as the butadiene derivative **16** are advantageously generated[30] in the "Trapp mixture"[1]—a solvent mixture of tetrahydrofuran, diethyl ether, and pentane that has a low freezing point—and allowed to react further [Eq. (1)].

The metalation of an alkyl vinyl ether was first achieved by reaction with *tert*-butyllithium in pentane with TMEDA as a co-solvent [Eq. (2)].[31] 1-Ethoxy-1-lithioethene (**7a**) produced in this way can be characterized by NMR spectroscopy; the typical downfield shift for the carbenoid carbon atom can also be observed in this case ($\delta = 212$).[32] *tert*-Butyllithium in tetrahydrofuran[33] or tetrahydropyran[34] as well as a mixture of potassium *tert*-butoxide and butyllithium are also suitable for deprotonating alkyl alkenyl ethers. A series of α-lithiated vinyl ethers—such as 2-lithio-4,5-dihydrofuran (**17**),[32, 36, 37]



(2)

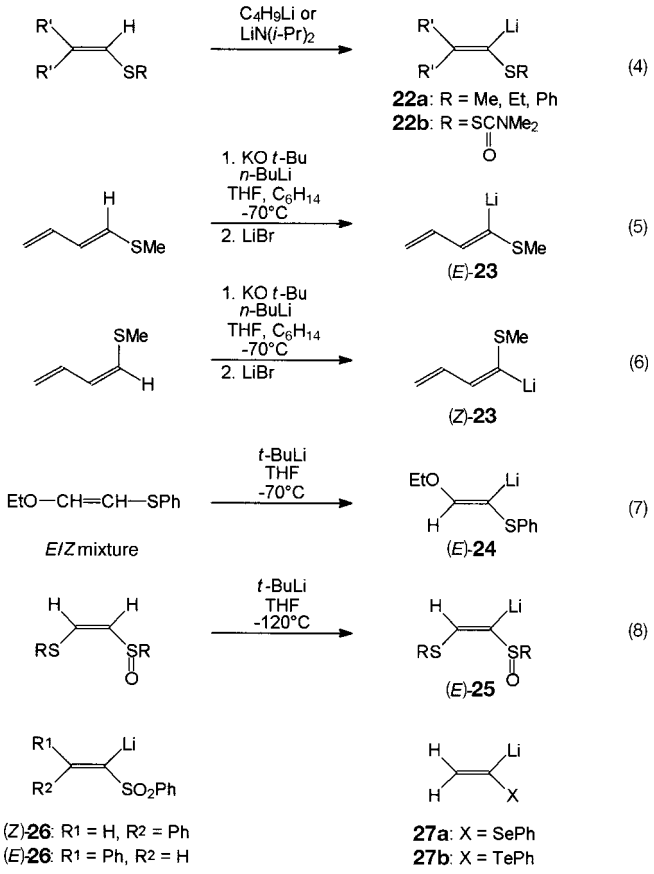


(3)

2-lithio-5,6-dihydropyran (**18**),[32, 38] and 2-litho-5,6-dihydro-1,4-dioxin (**19**)[39, 40]—as well as the metalated carbamide **20**[41] are available with this or a similar procedure. The metalated vinyl ethers are much more stable than the 1-halo-1-lithioalkenes; the lithiated dioxin **19** can supposedly be kept in solution at $20\,^{\circ}C$ for several days.[39]

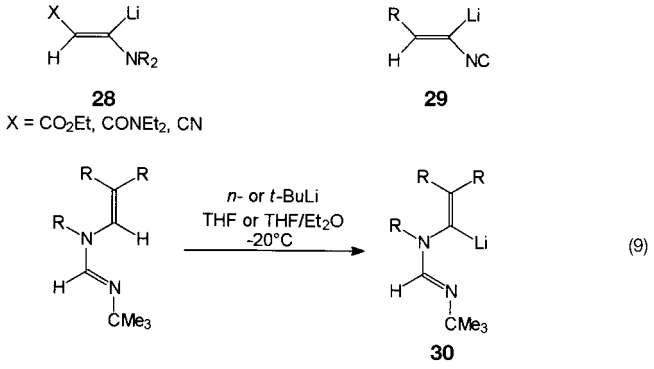
Lithiated enol esters **21a**[42] and **21b**,[43] which are substituted with two fluorides in the β position, are directly available from the corresponding esters of 2,2,2-trifluoroethanol [Eq. (3)]. In the reaction with two equivalents of lithium diisopropylamide the first step is probably elimination to yield the enol ester, which is immediately metalated in situ. Thus, the lithiated enol ether **21c** is also accessible.[44]

Considering the carbanion-stabilizing effect of the thio substituent, it comes as no surprise that alkyl and aryl vinyl sulfides[45–47] as well as thioesters[48] are easily converted into the alkenyllithium reagents **22a** and **22b**, respectively, by metalation [Eq. (4)]. Alkylthio-substituted derivatives of acrylic acid,[49] 1,2-bis(alkylthio)alkenes,[35a, 50] 1,4-dithiins,[51] and tetrathiafulvalene[52] can also be deprotonated in the same way. The lithiation of 1-methylthio-1,3-butadiene, however, can not be effected directly with butyllithium; instead, the potassium compound is produced and then transmetalated with lithium bromide [Eqs. (5), (6)].[53, 54] The diastereomers (*E*)- and (*Z*)-**23** thus available are configurationally stable below $-20\,^{\circ}C$.[54] The acidity of the α-positioned vinylic hydrogen atom is higher in alkylsulfinylalkenes[55, 56] than in the corresponding thioethers, and higher in these than in vinyl ethers. This is clearly shown in the regioselective metalations leading to the heteroatom-substituted lithioalkenes **24**[57] and **25** [Eqs. (7), (8)].[23] As expected, vinyl sulfones[58] and vinyl sulfoximines[59] are metalated even more easily, for example with methyllithium. The 1-arylsulfonyl-1-lithioalkenes thus available show low configurational stability unless they are already present as the thermodynamically favored isomer. Therefore, (*Z*)-**26** almost completely converts into the *E* isomer at $-60\,^{\circ}C$ in tetrahydrofuran.[60] The metalation of vinyl selenides and vinyl tellurides to give **27** is effected with comparatively weak bases such as lithium diisopropylamide or lithium hexamethylpiperidide[61] as well as with a mixture of potassium diisopropylamide and lithium *tert*-butoxide;[62]



apart from the formation of the α-seleno-substituted 1-lithioalkene **27a**,[63] elimination leading to the alkyne can also occur depending on the reaction conditions.[61]

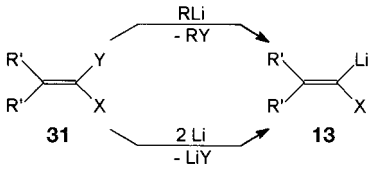
Enamines can only be deprotonated if additional carbanion-stabilizing groups are present either in the alkene skeleton or on nitrogen; in all cases *n*- or *tert*-butyllithium is necessary. Examples for the former substitution pattern are amides, esters and nitriles of β-aminoacrylic acid, whose lithium derivatives **28** ($R_2 = (CH_2)_4$, $(CH_2)_3$) are, however, extremely unstable and must be generated and allowed to react at



$-120\,^{\circ}C$.[64] Lithiated isonitriles **29** are similarly unstable,[65] whereas metalated amidines **30** [Eq. (9)] can be kept in solution at $-78\,^{\circ}C$, some even at $-20\,^{\circ}C$.[66] In contrast, vinyl phosphonates can already be deprotonated with lithium diisopropylamide.[67]

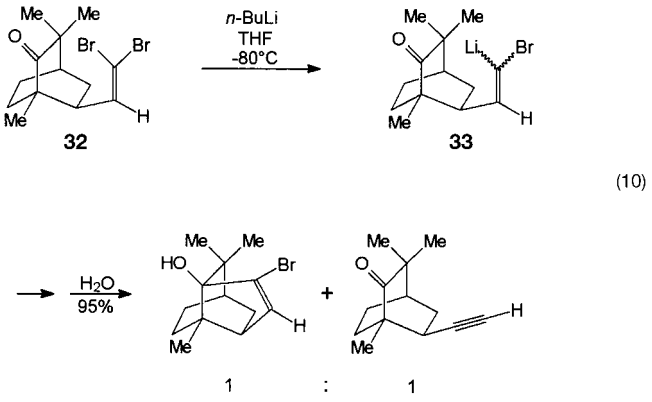
2.2. Halogen–Lithium Exchange

The most common method for generating alkylidene carbenoids **13** is halogen–lithium exchange in dihaloalkenes **31**. Particularly suitable reagents are *n*- or *tert*-butyllithium;



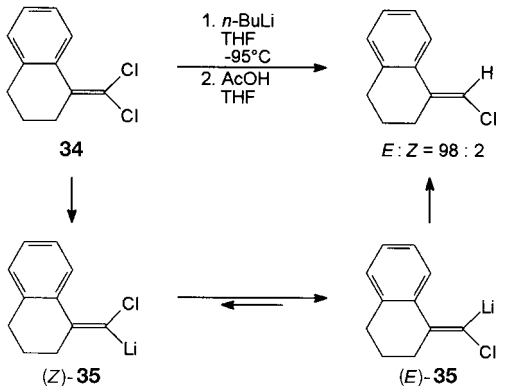
occasionally, metallic lithium is used. The efficiency of this method is documented in numerous examples.[24, 27]

The rate of halogen–lithium exchange increases when going from chlorine to iodine. Thus, only the bromine atom in 1-bromo-1-chloro- and 1-bromo-1-fluoroalkenes is replaced by the metal upon treatment with butyllithium.[6, 68] The reaction with *n*- or *tert*-butyllithium is so fast with the heavier halogens that it can compete with the addition of the alkyllithium compound: In the reaction of the dibromoalkene **32** with *n*-butyllithium, bromine–lithium exchange apparently takes place followed by the intramolecular nucleophilic addition of the lithioalkene **33** at the keto group or elimination to yield the alkyne [Eq. (10)].[69] Owing to the



high reaction rate, the halogen–lithium exchange is particularly suitable for generating the unstable halocarbenoids **13** since the reaction already takes place below $-100\,^{\circ}C$ in a fast and, for the most part, quantitative manner.

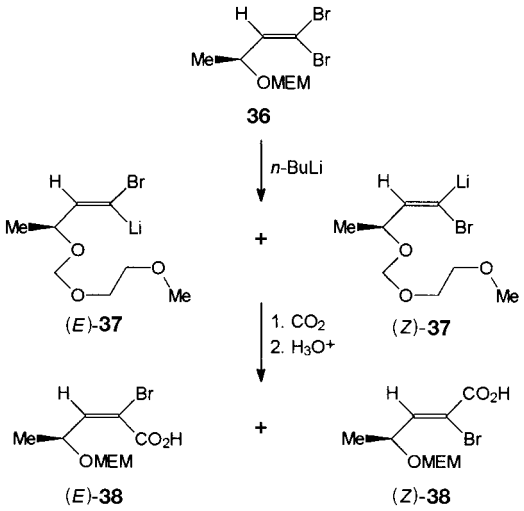
The stereochemistry of the reaction of butyllithium with 1,1-dibromo- and 1,1-dichloroalkenes, by which a halogen atom in a *Z* or *E* position with respect to a β substituent can in principle be replaced, is not uniform. As the example of the tetralin derivative **34** shows, bulky groups seem to favor lithiation in the *Z* position. The vinyl chloride obtained after protonation of **35** shows an *E*:*Z* ratio of over 98:2 [Eq. (11)].[70] As the formation of the diastereomer (*E*)-**35** by kinetically controlled attack on the sterically more hindered chlorine atom of alkene **34** is improbable, an equilibrium between (*Z*)-**35** and (*E*)-**35** is assumed in which



(11)

the *E* diastereomer is strongly favored. Apparently, the lithium atom requires less space than the halogen despite being solvated by the solvent.[71]

The effect a possible chelation has on the stereochemistry of the bromine–lithium exchange was investigated with the dibromoalkene **36**. Of the two diastereomeric lithiation

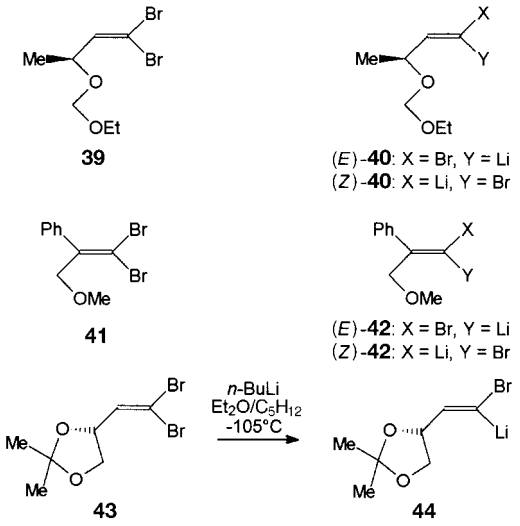


	(*E*)-**38** : (*Z*)-**38**
1.2 *n*-BuLi, THF	32 : 68
0.95 *n*-BuLi, Et_2O	>99 : 1

products **37**, the *E* diastereomer is without doubt thermodynamically more stable because of the lower space requirement of the lithium atom and particularly because of the possibility of intramolecular complexation by the methoxyethoxymethyl (MEM) ether protecting group. Surprisingly, treatment of the dibromoalkene **36** with 1.2 equivalents of *n*-butyllithium in tetrahydrofuran afforded the acids (*E*)- and (*Z*)-**38** in a ratio of 32:68 after carboxylation—apparently as a result of the kinetically favored substitution of the more easily accessible *trans* bromine atom by lithium. On the other hand, exclusive formation of the *E*-configured alkenyllithium compound **37** occurs when slightly less than one equivalent (0.95–0.98 equiv) of butyllithium is slowly added dropwise to a solution of **36** in diethyl ether at $-105\,^{\circ}C$. The diastereomeric carboxylic acids isolated after the reaction with dry ice are formed in a ratio of over 99:1.[72, 73]

The highly stereoselective bromine–lithium exchange in **36** can be explained as an equilibrium in which the two isomeric carbenoids (*E*)- and (*Z*)-**37** as well as the dibromoalkene **36** are involved. Since the latter is present in a slight excess, (*Z*)-**37** can enter into another bromine–lithium exchange with its partner **36**, so that finally the thermodynamically favored isomer (*E*)-**37** results as de facto the only lithioalkene [(*Z*)-**37** + **36** ⇌ (*E*)-**37** + **36**].[73] In an analogue fashion, the selective replacement of the *endo* bromine atom in 7,7-dibromonorcarane was effected.[74]

The outer oxygen atom of the MEM ether apparently plays an important role in the chelation of the lithium atom in the more stable isomer (*E*)-**37**: If the MEM unit is replaced by an ethoxymethoxy group (**39**), the bromine–lithium exchange in the dibromoalkene **39** only leads to an 87:13 mixture of (*E*)-**40** and (*Z*)-**40** under the conditions described for **36**.[73] This



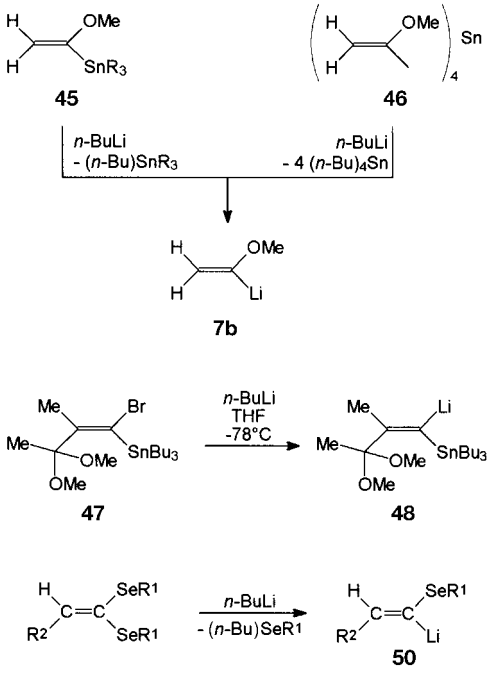
result is in accordance with lithiation of the methyl ether **41**, which affords the diastereomeric carbenoids (*E*)-**42** and (*Z*)-**42** in a ratio of 90:10 in a similar application of thermodynamic reaction control.[71a] On the other hand, the selective bromine–lithium exchange in the dibromoalkene **43** derived from isopropylidene glyceraldehyde is remarkable and leads predominantly (95:5) to the *E*-configured carbenoid **44**, as proven after protonation and carboxylation.[75]

Halogen–lithium exchange is also a method for producing 1-lithioalkenes with oxygen, sulfur, or nitrogen[57, 76] as the α heteroelements. However, it is in general only of preparative importance in special cases, such as with 1,2-dimethoxy-1-lithioethene.[77]

2.3. Metal–Lithium Exchange and Special Methods

Whereas the replacement of mercury, tin, or tellurium by lithium plays an important part in the synthesis of highly unstable di- and polylithiated alkenes,[78] the metal–lithium exchange leading to vinylidene carbenoids is limited to

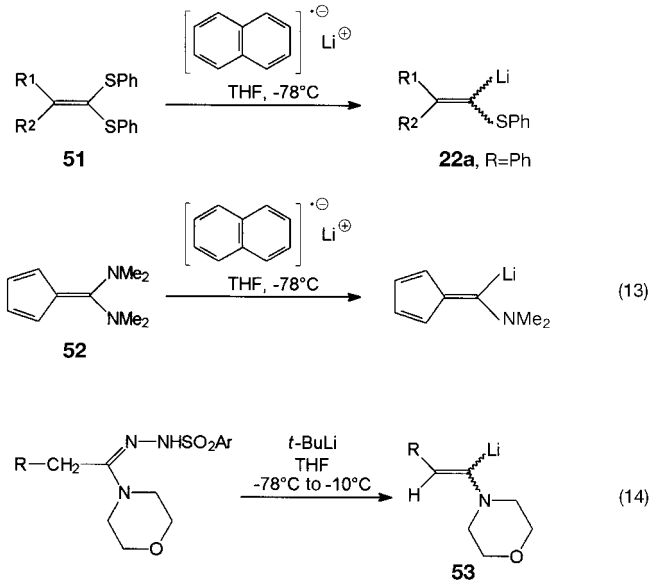
vinylstannanes and vinyl selenides. An alternative to metalation that is seldom used is the reaction of the vinylstannanes **45** and **46** with *n*-butyllithium to form 1-methoxy-1-lithioethene (**7b**) with concomitant formation of the appropriate tetraalkyltin compound.[79] Various α-lithiated vinyl sulfides



(12)

22a are also available by this method.[80] It is, however, unsuitable for generating 1-bromo-1-lithioalkenes **13** (X = Br): The corresponding alkenes, such as **47**, react with butyllithium by way of a bromine–lithium exchange to give metalated vinylstannanes **48**.[81] Clearly, the relatively slow and in principle reversible tin–lithium exchange cannot compete with the halogen–lithium exchange. The substitution of lithium by selenium is used merely for producing lithiated vinyl selenides **50** [Eq. (12)].[80, 82]

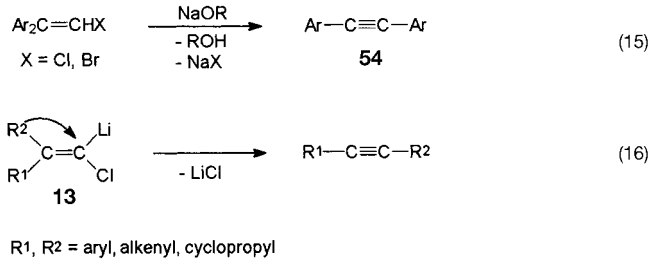
An efficient approach to lithiated vinyl sulfides **22a** is presented by reductive metalation of 1,1-bis(arylthio)ethenes **51** with lithium naphthalenide.[83, 84] The same reagent can also be used to metalate bis(dimethylamino)fulvene **52** [Eq. (13)].[85] The Shapiro reaction, which has found numerous applications in the generation of vinyl anions containing hydrogen or alkyl groups as α substituents,[86] seems to be the only efficient method for access to α-lithiated enamines **53**, which have no anion-stabilizing substituents [Eq. (14)].[87]



3. Reactions of 1-Alkenyllithium Reagents

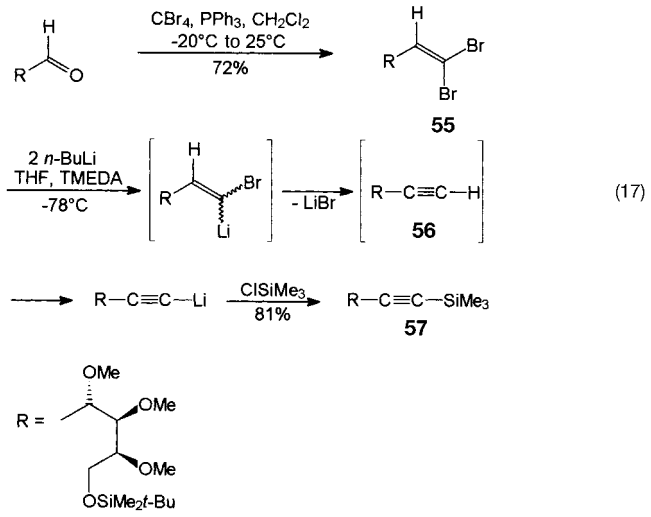
3.1. Reactions Typical of Carbenoids

Only the α-halo- and, to a lesser extent, the α-oxygen-substituted alkenyllithium compounds permit reactions that are typical of carbenoids; alkenyllithium compounds with α-sulfur and nitrogen atoms show carbanionoid reactivity exclusively. Whether 1-halo-1-lithioalkenes react as carbenoids or carbanions depends on the respective partner and, above all, on the reaction temperature. Long before α-halo vinyl anions were established as intermediates, products typical for carbenoid reactions were obtained and characterized: Fritsch, Buttenberg, and Wiechell independently observed at the end of the last century that tolanes **54** are formed upon treatment of 2,2-diaryl-1-haloethenes with sodium alkoxide [Eq. (15)].[88] This intramolecular rearrangement



also occurs in 1-halo-1-lithioalkenes **13** when at least one of the two β substituents is an aryl, alkenyl, or cyclopropyl group [Eq. (16)].[1] If two substituents are capable of undergoing this rearrangement, that in the *trans* position with respect to the halogen atom migrates almost exclusively.[89] The crystal structure of the carbenoid **5** (see Figure 1)[12] gives a plausible explanation for the stereochemistry of the Fritsch–Buttenberg–Wiechell rearrangement. The aryl moiety *cis* to Cl1 makes space for the chlorine atom (C1-C2-C3 129.5°), while that in the *trans* position is bent towards C1 (C1-C2-C9 116.5°). Therefore, migration of the *trans* aryl substituent becomes inevitable, and the free vinylidenecarbene can be ruled out as the intermediate.

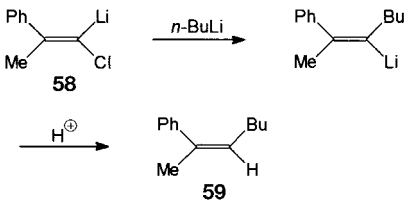
The hydride shift in 1-bromo- and 1-chloro-1-lithioalkenes that is analogous to this rearrangement also takes place at temperatures above $-70\,^{\circ}C$. The reaction is often used to transform aldehydes, which are initially converted into a dihalogenalkene (e.g. **55**) by carbonyl olefination,[90] into alkynes **56** with homologization [Eq. (17)]. If an excess of



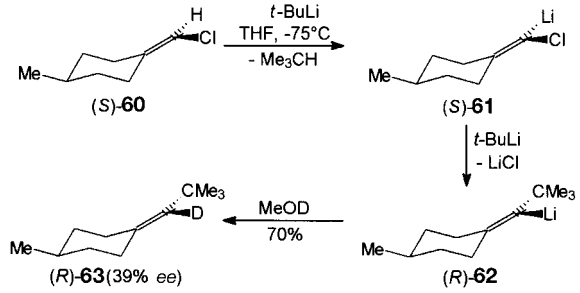
(17)

butyllithium is used the deprotonation of the alkyne is already effected in situ, and the reaction with an electrophile directly becomes possible.[90b, d, e, 91] This is illustrated by the formation of the silyl acetylene **57**.[90d]

The carbenoid, electrophilic character of 1-halo-1-lithioalkenes is seen clearly in their reaction with aryl or alkyllithium reagents. Köbrich and Ansari observed that alkene **59** is formed from the *E*-configured alkenyllithium compound **58** with excess butyllithium [Eq. (18)].[5] The

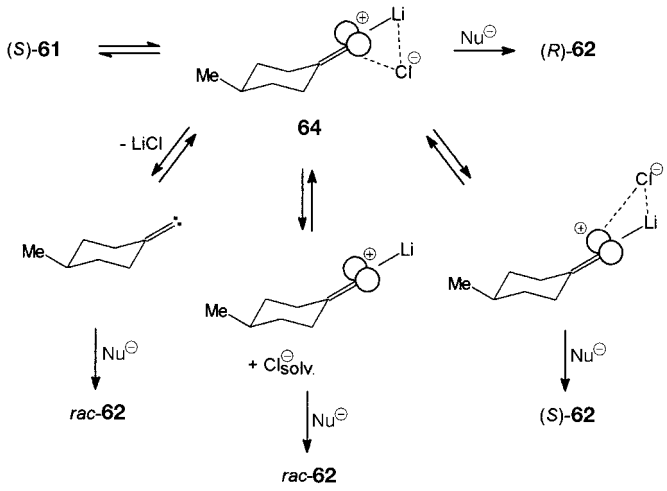


(18)



stereochemistry of the surprising reaction was investigated for the chiral chlorolithiocarbenoid **61** (and the corresponding bromine derivative).[6] Metalation of the (*S*)-vinyl chloride **60** with *tert*-butyllithium leads to the likewise *S*-configured carbenoid **61**. This reacts further with *tert*-butyllithium to the alkenyllithium compound **62**, which was detected by deuterolysis to alkene **63** with *R* configuration; this, however, exhibits an enantiomeric excess of only 39%.

Nucleophilic substitution at the vinylidene carbenoid **61**, which takes place with at least partial inversion, can be explained by the following mechanism: At a temperature

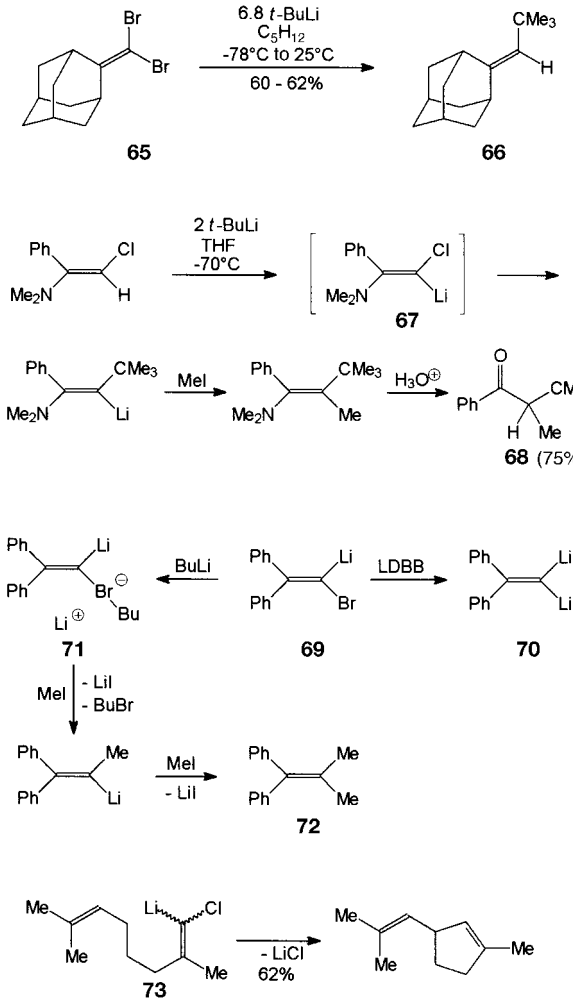


which is typical for every carbenoid, a loosening of the carbon–halogen bond takes place supported by the lithium atom, which remains bonded to the carbon atom ("metal-assisted ionization"). Thus, the nucleophilic vinyl anion **61** is transformed into an electrophilic species, the carbenoid **64**. Rehybridization occurs along with the ionization, and the positive charge is localized in the p orbital of the intimate ion pair. Whereas the lithium atom is colinear with the double bond, the chiral information is preserved by the chloride ion, which occupies one of the enantiotopic faces. The nucleophile Nu^- (in this case *tert*-butyllithium) enters on the side facing away from the chloride, resulting in inversion of configuration in **62** and, after deuterolysis, **63**. The observed partial racemization—that is, the formation of *rac*-**62**—could be caused by the separation of cation and anion by the solvent, the formation of an achiral carbene by completed α-elimination, or the migration of the chloride ion associated with the lithium atom to the enantiotopic face. The latter would lead to inversion of the configuration for **61**.

The ^{13}C NMR spectroscopic studies by Seebach et al.[10] are compatible with an assumed intimate ion pair **64**, which verifies the electrophilic character of the carbenoid carbon atom. The low-temperature crystal structure analysis of the vinylidene carbenoid **5** by Boche et al.[12] comes closer to the idea of the alkenyllithium compound **61** (nonlinearity of the C-C-Li bond); however, the beginning rehybridization is already indicated in this structure.

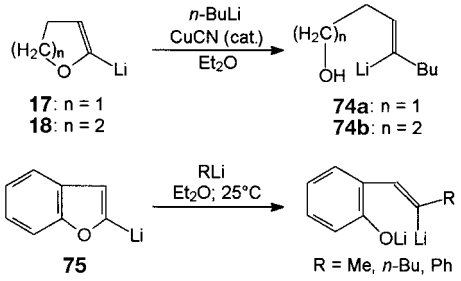
The nucleophilic attack of *tert*-butyllithium on the highly reactive vinylidene carbenoids allows the synthesis of sterically hindered alkenes: Thus, the reaction of the dibromoalkene **65**, which is available from adamantanone, affords neopentylideneadamantane **66**, with three bulky substituents at the double bond, in 62% yield.[92] A *tert*-butyl group can also be introduced into β-chloro enamines by making use of the carbenoid reactivity of the lithium compound formed in the primary deprotonation step. After hydrolysis of the enamine, the ketone **68** is finally obtained via **67** [Eq. (19)].[93]

There has been no lack of attempts to replace the remaining halogen atom by lithium in 1-bromo-1-lithioalkenes in order to acquire geminally dimetalated alkenes. This exchange is possible by, for example, the reaction of **69** with lithio-4,4'-di-*tert*-butyl biphenyl (LDBB) to form **70**. However, the



dilithium compound **70** is not formed in the reaction of **69** with butyllithium, as the alkylation to alkene **72** seems to show [Eq. (20)]. Rather in this case, the reaction with iodomethane proceeds successively with the participation of a quasi-dianion complex ("QUADAC") **71**.[2, 78]

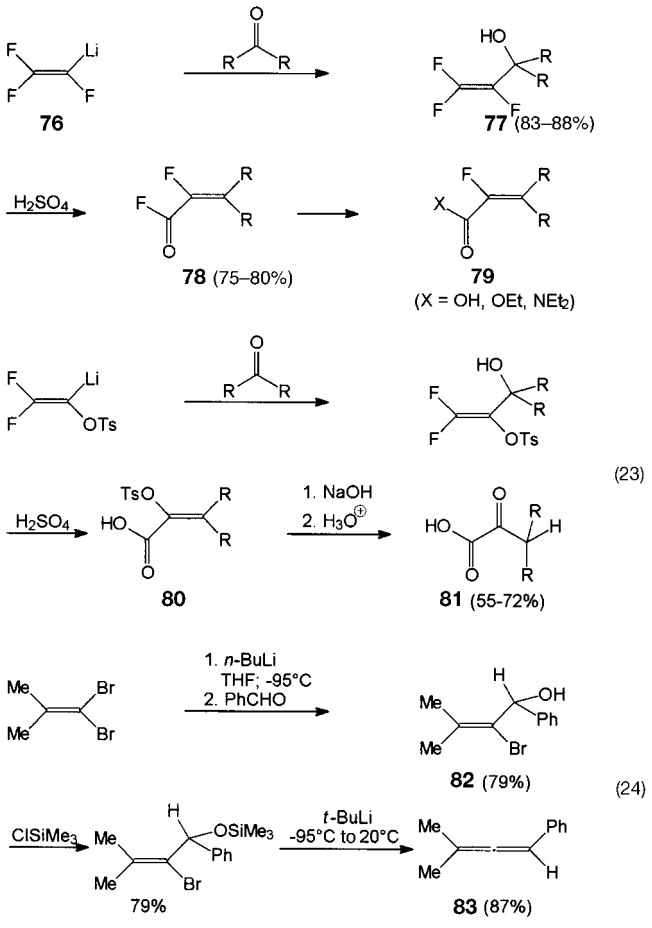
Finally, the carbenoid character of α-lithiated vinyl halides shows itself also in the formation of 1,2,3-butatrienes[94] as well as in the C–H insertion [for example with diene **73**,[95] Eq. (21)] and intramolecular cyclopropanations.[96] Reactivity typical of carbenoids is also displayed by α-lithiated vinyl ethers. For example, the metalated heterocycles **17** and **18** react with *n*-butyllithium to provide the substitution products **74a** and **74b**, respectively, with inversion of configuration at the carbenoid carbon atom.[97] For preparative purposes, the addition of catalytic amounts of CuCN is recommended.[98, 37c] α-Lithiated benzofuran (**75**) undergoes an analogous ring-opening reaction with alkyllithium compounds [Eq. (22)].[97]



3.2. Reactions Typical of Carbanions

α-Heteroatom-substituted 1-alkenyllithium compounds are usually employed as nucleophilic reagents with suitable electrophiles. In the case of the α-halo- and α-oxygen-substituted derivatives, the carbenoid reactivity can be suppressed by maintaining appropriately low temperatures (see **61** and **64**). No attempt will be made to list the reactions of the alkenyllithium reagents **2** with standard electrophiles; instead, synthetically important conversions of vinyl anions **2** and their follow-up reactions will be presented.

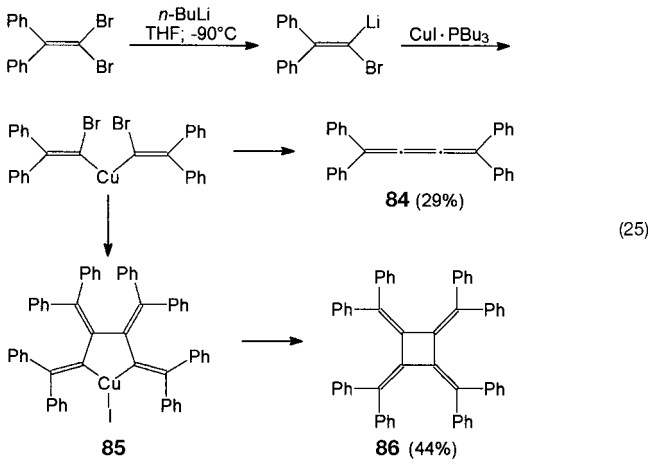
Trifluorovinyllithium **76**, which is available by deprotonation or chlorine–lithium exchange, reacts with ketones to carbinols **77**, as expected. Upon treatment with sulfuric acid,



the carbinols rearrange to acyl fluorides **78**, which can react further to yield α-fluoro-substituted acrylic acid derivatives **79**.[28] The α-sulfonyloxypropenoic acids **80** [Eq. (23)] available in a similar manner can be hydrolyzed to α-oxocarboxylic acids **81** in 55–72% overall yield [based on 2,2,2-trifluoroethyl *p*-toluenesulfonate, Eq. (23); see Section 2.1.].[42] The benzaldehyde adduct **82** of lithiated 1,1-dibromo-2-methyl

propene (**82**) serves as a precursor for an allene synthesis [Eq. (24)]: The hydroxy group is transformed into a leaving group by silylation; a second bromine–lithium exchange affords the allene **83** under spontaneous β-elimination.[20]

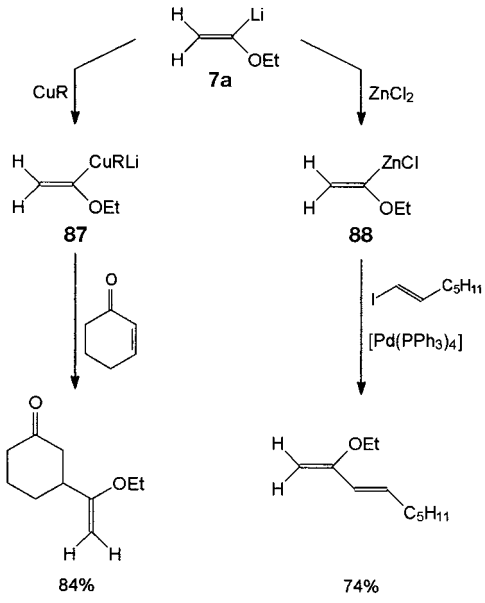
A simple synthesis of the [4]radialene skeleton starts from 1-bromo-2,2-diphenyl-1-lithioethene [Eq. (25)]. Transmetalation with $CuI \cdot PBu_3$ affords, in addition to cumulene **84**, tetramethylene cyclobutane **86** as the main product, whose formation is postulated to proceed via the cuprate **85** as an intermediate.[99]



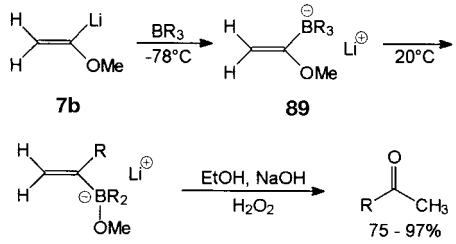
(25)

The metalation of vinyl ethers followed by reaction with electrophiles and hydrolysis is a simple and efficient method for carbonyl umpolung.[31] The range of applications is considerably increased by the possibility of transmetalating 1-lithioethenes **7a** and **7b**: Cuprates **87** allow 1,4-additions to α,β-unsaturated carbonyl compounds,[100] the zinc reagent **88** can be coupled with aryl or alkenyl iodides under palladium catalysis [Eq. (26)],[101] and the ate complex **89** produced in situ with trialkylborane reacts with transfer of an alkyl group upon warming [Eq. (27)].[102] Starting from an *E*/*Z* mixture of 1,2-dimethoxylithioethene, the tungsten and chromium carbene complexes **90** and **91** can be obtained [Eq. (28)], which, according to NMR spectroscopy, are present in the form of diethyl ether or tetrahydrofuran adducts as pure *Z* isomers.[77b] Further examples for the metalation of 1-alkenyl ethers with electrophiles and follow-up reactions are given in Table 1; it becomes clear that the versatility of the method is guaranteed especially by a particularly broad spectrum of substrates that ranges from simple vinyl ethers over methoxyallene[103, 104] to glucals.[105] In the case of the latter, tin–lithium exchange is used in addition to deprotonation.

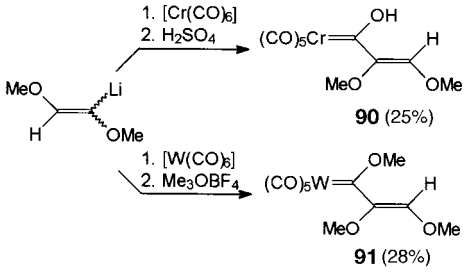
In principle, vinyl sulfides are also suitable as equivalents of acyl anions;[45–48] however, the liberation of the carbonyl group is in general more difficult than with vinyl ethers. An exception is given in the simple acid-catalyzed transformation of vinyl sulfide adducts with aldehydes to α-thiolated ketones **92** [Eq. (29)].[46a, 47a] Starting with the *ortho* lithiation of the benzamides **93**, deprotonation of the intermediate vinyl sulfide **94** offers a possibility for a quinone anellation in a one-pot reaction.[106]



(26)

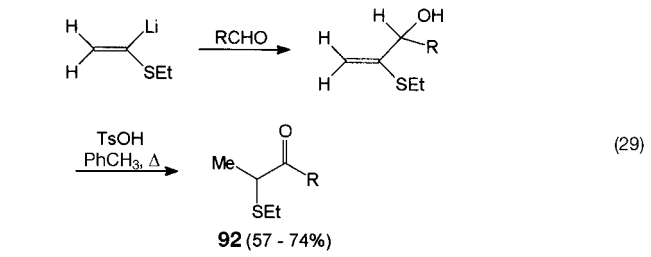


(27)

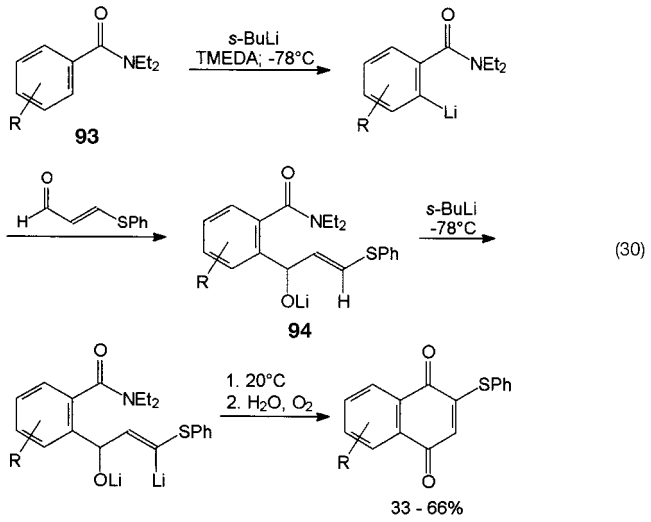


(28)

A new stereocenter is generated when α-heteroatom-substituted 1-alkenyllithium reagents are added to chiral aldehydes or ketones, and the formation of two diastereomeric products has to be anticipated. Reactions which proceed with high stereoselectivity and use enantiomerically pure carbonyl compounds as substrates are of particular interest ("substrate-induced stereoselectivity"[116]). It is hardly surprising that high diastereoselectivities in such reactions were only achieved with cyclic ketones; representative examples are shown in Table 1. The addition of the alkenyllithium compounds normally follows the same course as for other nucleophiles on the corresponding substrate.[117] Thus, estrone methyl ether is attacked by 1-methoxy-1-lithioethene (**7b**) exclusively from the α face[106]—a nucleophilic addition that is typical for 17-ketosteroids.[118] When polar organometallic compounds are allowed to react with α-alkoxy

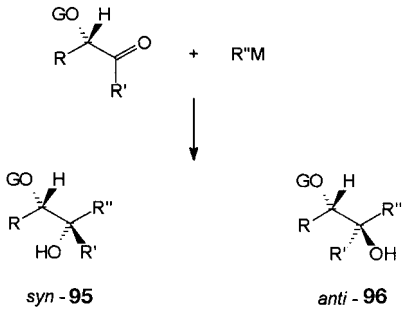


(29)



(30)

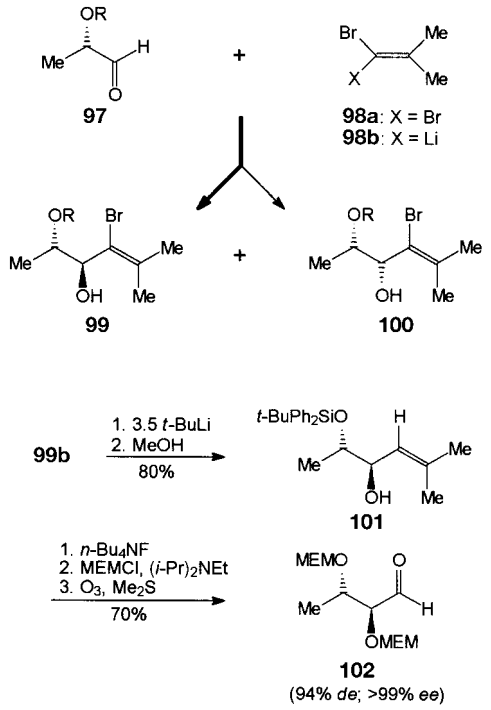
aldehydes or ketones whose carbonyl group is not integrated in a ring, the transformation to the alcohols **95**[117] is more or less stereoselective in the sense of "chelate control" (Scheme 2).[119] This result can plausibly be explained with



Scheme 2. Stereochemical process of the addition of polar organometallic compounds R″M to α-alkoxyaldehydes and -ketones (G = protecting group). Products of chelate control (left) and nonchelate control (right).

Cram's cyclic model.[120] "Nonchelate control"[119] leading to the diastereomeric carbinols **96**, sometimes referred to as Felkin – Anh selectivity,[121] can only be achieved with difficulty by adding lithiumorganic compounds to α-alkoxyaldehydes.[117] Therefore, the reactions of alkenyllithium compounds with chiral aldehydes are still characterized by unsatisfactory diastereoselectivity,[123] despite great progress in the area of acyclic stereoselection;[122] examples for this are also given in Table 1.

For some time now, we have used α-bromo-substituted 1-alkenyllithium reagents as nucleophilic acylating agents which allow stereoselective additions of formyl, formiate, and acyl d^1 synthons ($^-$CHO, $^-$COOH, $^-$COR) to aldehydes and imines.[72, 73, 124–130] The reaction of achiral 1-bromo-1-lithio-2-methyl-1-propene (**98b**), generated from the dibromoalkene **98a** by bromine – lithium exchange, with the MEM-protected enantiomerically pure (*S*)-lactaldehyde **97** is expected to result in the formation of the *syn* alcohol **100a** since the α-MEM ether moiety seems predestined to direct the reaction in the sense of chelate control (Scheme 3).[132] Surprisingly,



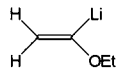
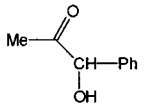
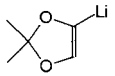
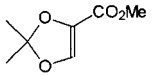
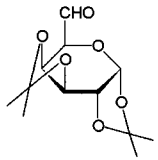
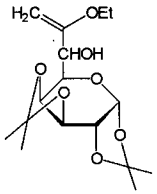
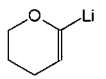
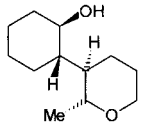
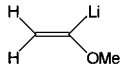
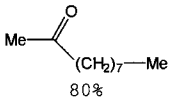
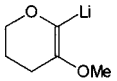
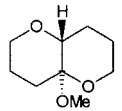
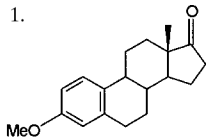
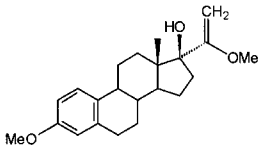
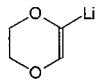
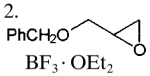
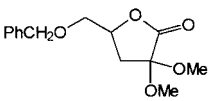
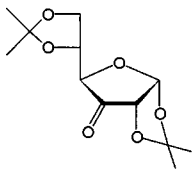
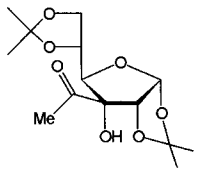
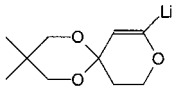
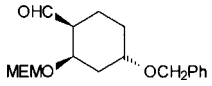
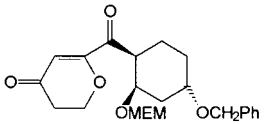
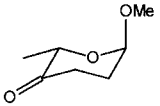
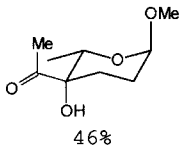
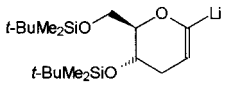
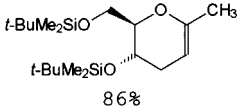
	R	99 : 100	99+100
97, 99, 100 a	MEM	92 : 8	92%
b	t-BuPh$_2$Si	>97 : 3	84%
c	ThexMe$_2$Si	95 : 5	93%

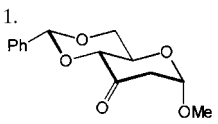
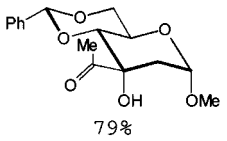
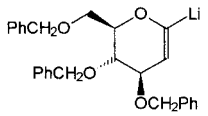
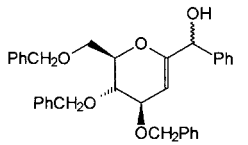
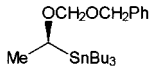
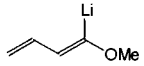
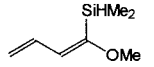
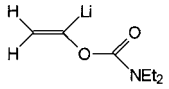
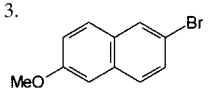
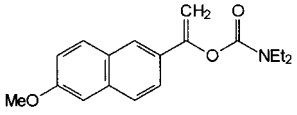
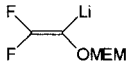
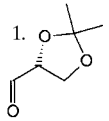
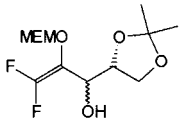
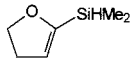
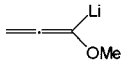
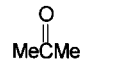
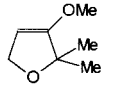
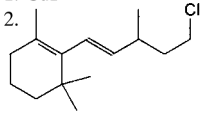
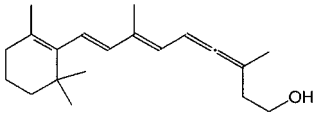
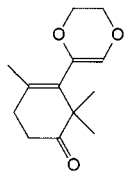
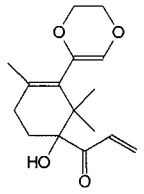
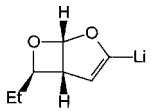
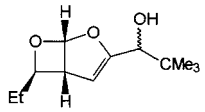
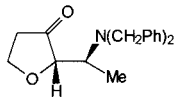
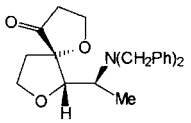
Scheme 3. Diastereoselective introduction of the formyl d^1 synthon $^-$CHO into lactaldehyde **97** by reaction with the lithioalkene **98b**. MEM = $MeOCH_2CH_2OCH_2$, Thex = $Me_2CH{-}CMe_2$.

however, the *anti*-carbinol **99a** is the favored product as a result of Felkin – Anh selectivity (*anti*:*syn* = 92:8). When the MEM group is replaced by silyl ethers (**97b**, **c**) the selectivity can be increased in favor of the nonchelate-controlled products (**99b**, **c**).[124, 126] To illustrate that the carbenoid **98b** can serve as an equivalent of a formyl d^1 synthon, the silyl ether **99b** (95% *de*) was transformed into the alkene **101** by another bromine – lithium exchange followed by protonation. Subsequent desilylation to the diol, protection of both hydroxy groups as MEM ethers, and ozonolysis led to the α,β-dialkoxyaldehyde **102** with a diastereomeric excess of 94%. Since the reaction starts with enantiomerically pure lactaldehyde and no racemization occurs during the course of the sequence, the enantiomeric excess is greater than 99%.[126]

The alkene **99c**, which is obtained with 90% *de* by the stereoselective reaction of the alkenyllithium compound **98b**,

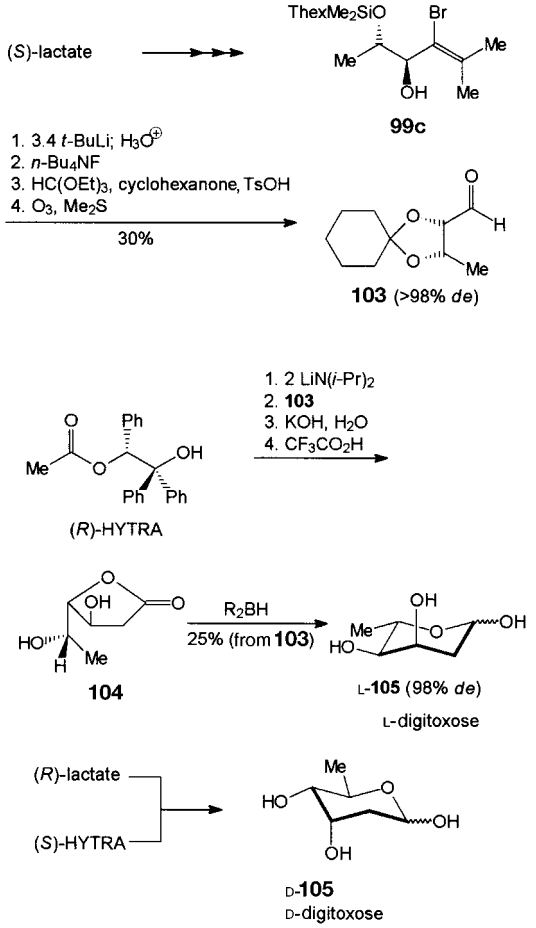
Table 1. Reactions of α-lithiated vinyl ethers.

α-Lithiated vinyl ether	Electrophile Follow-up reagents	Product Yield	Ref.	α-Lithiated vinyl ether	Electrophile Follow-up reagents	Product Yield	Ref.
	1. PhCHO 2. HCl, H_2O, MeOH	 57%	[31a]		1. $ClCO_2Me$	 72%	[67]
	1. 	 67% (1:1 diastereomeric mixture)	[31b]		1. Me_3Al 2.  3. $BF_3 \cdot OEt_2$	 78%	[38c]
	1. $Me(CH_2)_7I$ 2. HCl, H_2O, MeOH	 80%	[33]		1. $I(CH_2)_3OCH_2Ph$ 2. Me_3SiCl, NaI, MeCN 3. H_2, Pd/C 4. MeOH, H^+	 41%	[113]
	1. 	 83%	[107]		1. CuCN, LiCl 2.  $BF_3 \cdot OEt_2$ 3. 3-chloroperbenzoic acid 4. TsOH, MeOH 5. Ag_2CO_3, celite	 60%	[40e]
	1.  2. HCl, H_2O, dioxane	 37%	[108]		1.  2. H_3O^+ 3. Swern oxidation	 71%	[114]
	1.  2. HCl, H_2O, dioxane	 46%	[109]		1. CH_3I	 86%	[105a]

	1.  2. HCl, H_2O, dioxane	 79%	[109]		1. PhCHO	 89% (1:1 diastereomeric mixture)[b]	[105a]
	1. Bu_3SnCl 2. (*R*)-BINAL-H 3. $PhCH_2OCH_2Cl$, iPr_2NEt	 90% *ee*	[110]		1. Me_2SiHCl	 77%	[115]
	1. $ZnBr_2$ 2. $[PdCl_2(dppf)]$[a] (cat.) 3. 	 88%	[41d]		1. 	 26% (6:4 diastereomeric mixture)	[44b]
	1. Me_2SiHCl	 50%	[37a]		1.  2. KO*t*Bu, DMSO	 78%	[103a]
	1. CuI 2.  3. 2 MeLi	 55%	[111]		1.  2. TsOH, H_2O, acetone	 90%	[103e]
	1. Me_3C–CHO	 72% (1:1 diastereomeric mixture)	[112]		1.  2. KO*t*Bu, DMSO 3. H_2SO_4, THF	 84%[c]	[114]

[a] dppf = bis(diphenylphosphanyl)ferrocene. [b] Synthesized by tin–lithium exchange. [c] Diasteromeric ratio: 93:7.

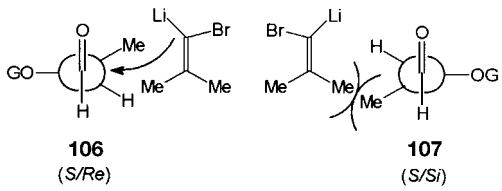
serves as the starting material for the synthesis of digitoxose (**105**) represented in Scheme 4.[127] As this carbohydrate is present in different organisms in both enantiomeric forms, a synthesis was conceived which leads to D- and L- digitoxose. The bromoalkene **99c** was first converted into the aldehyde



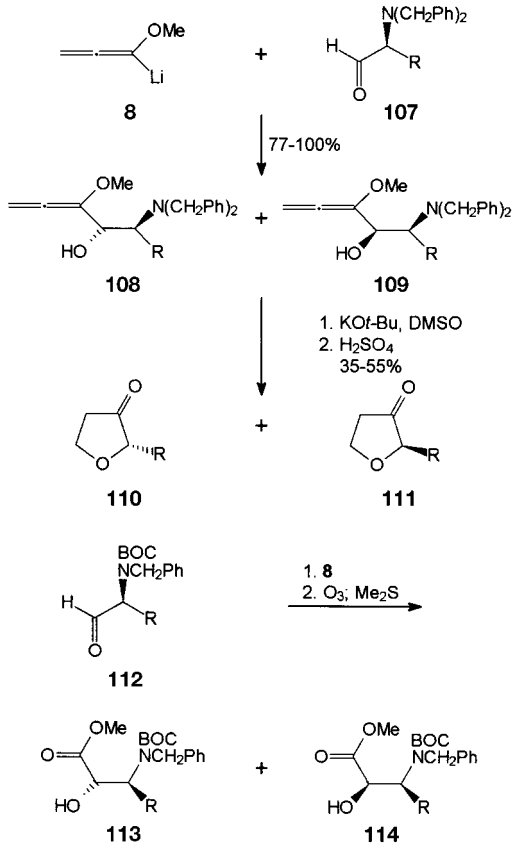
Scheme 4. Synthesis of L- and D-digitoxose.

103 (whose diastereomeric excess is increased to 98% *de* after distillation) by dehalogenation, transformation of the protecting group, and ozonolysis. Lengthening of the carbon backbone by introducing an acetate group proceeds successfully with (*R*)-HYTRA.[131] After removal of the minor diastereomer, the lactone **104** was transformed to L-digitoxose (L-**105**). Since both (*R*)-lactate (*ent*-**97c**) and (*S*)-HYTRA are easily available, D-digitoxose (D-**105**) was obtained in the analogous, enantiomeric sequence.

The extremely strong tendency of 1-bromo-1-lithio-1-alkenes to react in a nonchelate-controlled way, which stands in striking contrast to the low diastereoselectivity with α-unsubstituted 1-lithioalkenes, could be caused by the special structural properties of the carbenoid. Bearing in mind the high p character of the carbon–halogen bond as well as the small X–C=C angle involved, the Felkin–Anh model for the transition state (**106**) could offer an explanation for the preferred *ul* topicity[133] (i.e., attack at the *Re* face of the carbenoid **98b** on (*S*)-**97**): It seems plausible that the alternative reactive conformation **107** is less favored because of steric interaction between the methyl group of the chiral center in the aldehyde and the alkene.[126]



Similar stereochemical behavior with regard to chiral aldehydes is shown by the lithiated methoxyallene **8**, which also reacts with N,N-dibenzylated α-amino aldehydes **107** preferably with nonchelate control to yield *anti*-carbinols **108** (Scheme 5). Diastereomeric ratios **108**:**109** for these reactions

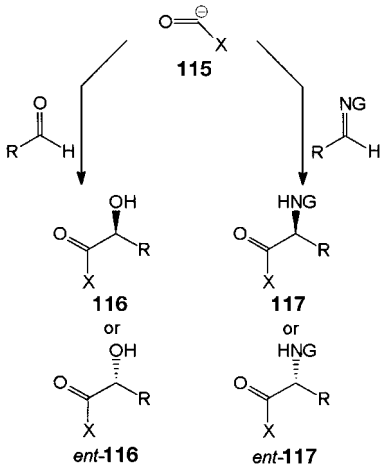


Scheme 5. Addition of lithiated methoxyallene **8** to N-protected α-amino aldehydes **107**. R = Me, $PhCH_2$, $Me_2CH–CH_2$.

can reach 80:20 to 95:5. Reaction with potassium *tert*-butoxide and subsequent acid hydrolysis enables the transformation of allenes **108**/**109** to furanones **110**/**111**.[103d, 134] On the other hand, ozonolysis of the adducts of **8** to the aldehydes **112** (diastereomeric ratios 74:26 to 85:15) offers an approach to N-protected α-hydroxy β-amino esters **113**/**114**.[135] The Felkin–Anh model also offers a plausible explanation for the nonchelate-controlled addition of the metalated allene **8**.

The enantioselective introduction of synthons **115** with umpoled carbonyl reactivity (d^1 reactivity[4]) into *achiral* aldehydes and imines was an unsolved problem of asymmetric

synthesis for a long time. This is surprising considering the large number of α-heteroatom-substituted carbanions[136] which serve as equivalents for the aforementioned synthons and have become extremely important reagents for carbon–carbon bond formation, however, leading to racemic products with aldehydes and imines. Enantiomerically pure acyloins and α-hydroxy carboxylic acids (**116** and *ent*-**116**, respectively) as well as α-amino acids and α-amino aldehydes (**117** and *ent*-**117**, respectively) can be obtained either by using chiral d^1 reagents or by combining achiral substrates with chiral additives (Scheme 6). With the second concept, the addition

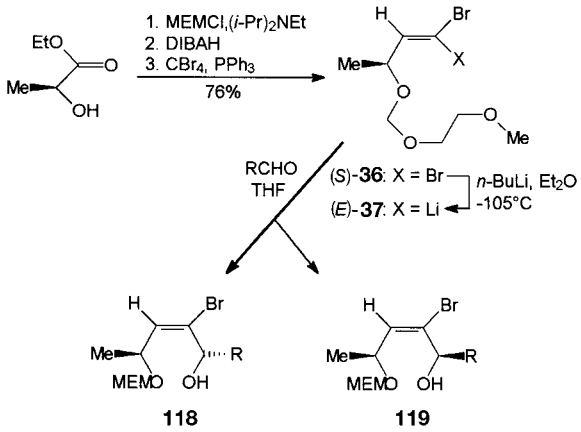


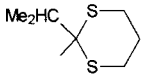
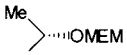
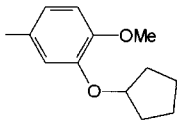
Scheme 6. Synthesis of enantiomerically pure α-hydroxy and α-amino-carbonyl compounds by the addition of chiral d^1 synthons **115** to aldehydes and imines. X = H, OH; G = protecting group.

of nucleophilic acylating agents in the presence of chiral ligands, only modest enantioselectivities are achieved for the most part.[137] On the other hand, α-heteroatom-substituted carbanions with covalently bound chiral auxiliaries are also rare;[138, 139] in some cases the chiral information is not easily introduced and is destroyed upon liberation of the target molecules, and in other cases the extent of stereoselectivity is modest.[140] More successful are different approaches which are not based on the direct addition of chiral synthons to aldehydes, but still lead to nonracemic α-hydroxy[141] and α-amino carbonyl compounds[142] in a roundabout way.

In the search for alkenyllithium reagents that serve as equivalents for d^1 synthons and can be enantioselectively introduced into aldehydes and imines, we followed the concept of a covalently bound auxiliary. Therefore, the chiral information should be localized in the allyl position of the vinyl anion and mediated by an ether group that chelates the lithium atom. These structural features are present in the 1-bromo-1-lithio-1-alkenes (*S*)- and (*R*)-**37**, which are available from the (*R*) and (*S*) lactates. Considerable stereoselectivity can only be expected for the addition to aldehydes or imines if the lithium atom is in the *Z* position with respect to the chelating ether group. This "conditio sine qua non" is met by the selective bromine–lithium exchange to (*E*)-**37** described in Section 2.2.

The dibromoalkene (*S*)-**36** is accessible in three steps from (*S*)-ethyl lactate on a 150-g scale by introduction of the MEM protecting group, reduction to the O-protected lactaldehyde,[143] and carbonyl olefination (Scheme 7).[90] (*R*)-Isobutyl



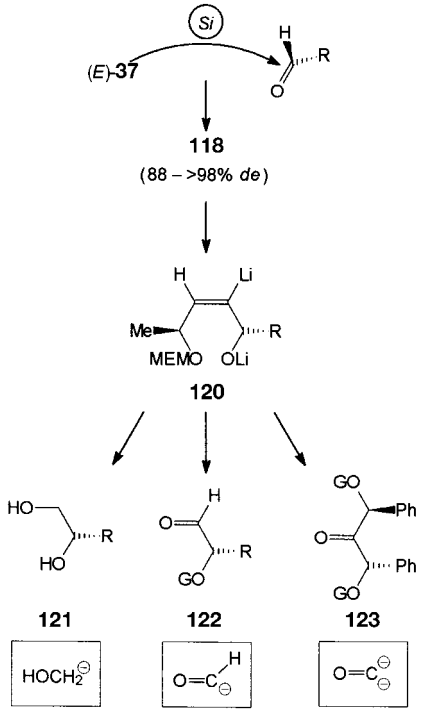
	R	118 : 119	118+119
118, 119 a	Me_2CH	94 : 6	87%
b	Me_2HC 	99 : 1	71%
c		95 : 5	92%
d		98 : 2	76%
e		96 : 4	95%
f	Ph	>99 : 1	93%
g		>99 : 1	92%

Scheme 7. Production and stereoselective addition of the lithioalkene (*E*)-**37** to aldehydes.

lactate is the analogous starting material for the enantiomeric sequence. The alkenyllithium reagent (*E*)-**37** generated from (*S*)-**36** at $-105\,^{\circ}C$ in diethyl ether adds to aliphatic and aromatic aldehydes with good diastereoselectivities after the addition of tetrahydrofuran. In all instances the *S*-configured lithioalkene **37** preferentially attacks the aldehyde from the *Re* face (*ul* topicity), and the predominant to almost exclusive formation of the diastereomers **118** results. In the case of the chiral *S*-configured aldehydes, combination with **37** leads to "matched pairs".[144] The tendency of the aldehydes to react with 1-bromo-1-lithioalkenes under nonchelate-control (substrate-induced) and the *ul* topicity displayed by the reagent (*S*)-**37** (reagent-induced) amplify each other, and allow the formation of carbinols **118c–e** with diastereomeric excesses of 90–96%. Whereas the reactions of (*E*)-**37** proceed with high stereoselectivity, those of analogous alkenyllithium compounds (H, Ph, SO_2Ph instead of Br in (*E*)-**37**) display only little differentiation between the enantiotopic faces of an aldehyde. Only the lithiated thioether (SMe instead of Br in (*E*)-**37**)[46c] shows a comparable diastereoselectivity.[145] If one

takes into account the importance of the outermost oxygen atom of the MEM ether group for the chelation of the lithium atom, it comes as no surprise that the bromolithioalkene (*E*)-**40** with a shorter ether protecting group only affords a 6:1 diastereomer mixture for the reaction with benzaldehyde.

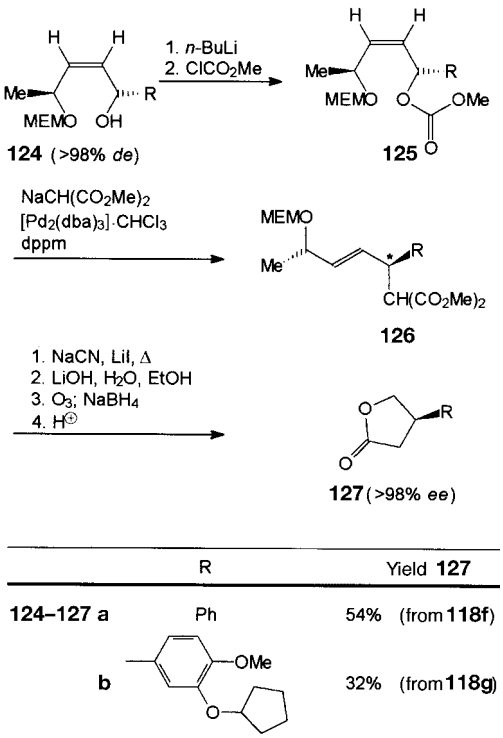
The dilithium compounds **120** can be obtained after one more halogen–lithium exchange in tetrahydrofuran from the bromoalkenes **118** (Scheme 8), which are available in 88 to



Scheme 8. Synthesis of 1,2-diols **121**, O-protected α-hydroxyaldehydes **122** and α,α'-dialkoxyketones **123** by stereoselective attack of the lithioalkene (*E*)-**37** on the *Si* face of aldehydes.

over 98% *de*. This step takes place under complete retention of configuration of the double bond, as proven by protonation to (*Z*)-alkenes.[146] Depending on the workup conditions of the subsequent ozonolysis, (*S*)-diols **121** or—after introduction of a protecting group at the alkene stage—O-protected α-hydroxyaldehydes (*S*)-**122** can be obtained. When the dilithium compound **120** (R = Ph) is allowed to react with benzaldehyde instead of a protic compound, the analogous sequence leads to C_2-symmetrical ketones **123**.[128] The enantiomeric excesses of products **121**, **122**, and **123** (the stereoselectively introduced synthon is given under each formula in Scheme 8) correspond to the respective diastereomeric excesses of the monobromoalkenes **118**.

The aryl-substituted allyl alcohols **124a**, **b**, which are obtained with over 98% *de* and an optical purity of 99% *ee* by protonation of **120**, serve as starting materials for an efficient palladium-catalyzed chirality transfer (Scheme 9).[130] For this the free hydroxy group of the alkenes **124**, which are present as pure *Z* isomers (this is essential, as shown below), is transformed into a leaving group by conversion into the carbonates **125**. The subsequent substitution with sodium dimethyl malonate in the presence of 4–5 mol% of the

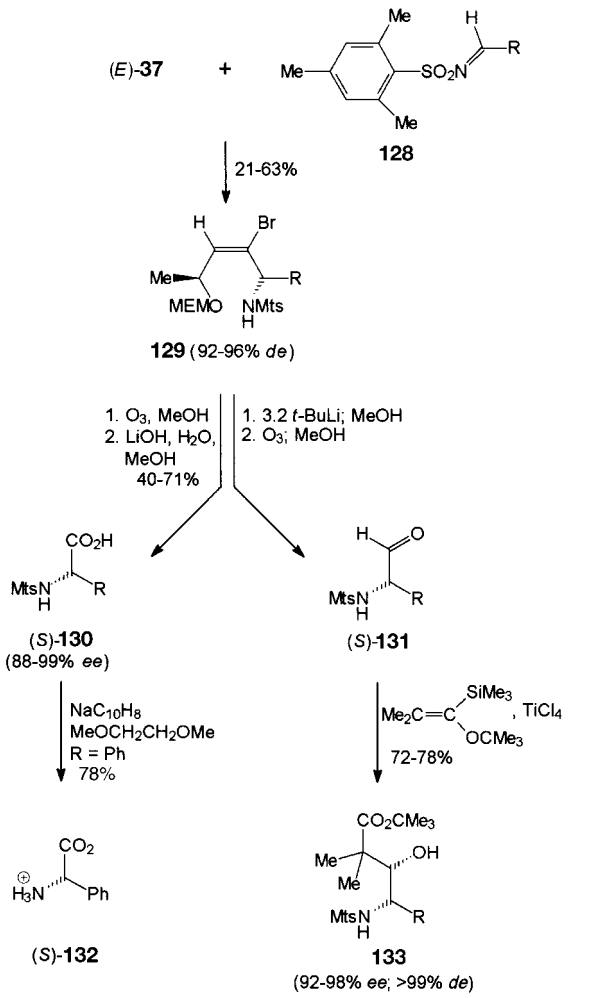


	R	Yield **127**
124–127 a	Ph	54% (from **118f**)
b	OMe	32% (from **118g**)

Scheme 9. Synthesis of chiral lactones **127** from allyl alcohols **124** by palladium-catalyzed chirality transfer.

dibenzylideneacetonepalladium complex $[Pd_2(dba)_3]\cdot CHCl_3$ and bis(diphenylphosphino)methane (dppm) affords the alkenes **126** as single isomers. This course of the reaction is unusual with respect to its stereo- and regiochemistry. Whereas palladium-catalyzed allylic substitutions usually proceed with overall retention due to the double inversion,[147] the stereochemical outcome of the conversion of **125** into **126** is in accordance with an inversion at the *C atom combined with rotation about the C–C double bond. These findings can plausibly be explained by assuming a displacement of the carbonate group (which fragments to sodium ethoxide and CO_2 in the process) by the metal with concomitant formation of a palladium π complex, rotation with a π-σ-π transformation,[148] and finally substitution of the palladium, once more with inversion, by the nucleophilic malonate. The completely regioselective exchange of carbonate for malonate without allyl shift, although the latter would lead to conjugation of the double bond with the aromatic system, is also unusual. Model studies[149] suggest that the MEM ether group is responsible for this, possibly by chelating the palladium atom. The lactones **127** can be obtained with over 98% enantiomeric purity from the alkenes **126** by decarboxylation and ozonolysis; derivative **127b** serves as an intermediate in the synthesis of the antidepressant (*R*)-rolipram.

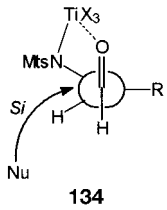
The *S*-configured lithioalkene (*E*)-**37** also adds to mesitylenesulfonylimines **128**, obtained from the corresponding aldehydes RCHO,[150] with preferred attack on the *Re* face with high diastereoselectivity to yield bromoalkenes **129** (Scheme 10). The cleavage of the double bond by ozonolysis in methanol leads directly to the methyl esters,[151] which are saponified without racemization to α-*N*-mesitylsulfonylcarboxylic acids (*S*)-**130**. The possibility of removing the



Scheme 10. Synthesis of N-protected α-amino acids (*S*)-**130** and α-amino alcohols (*S*)-**131** by stereoselective addition of lithioalkene (*E*)-**37** to sulfonylimines **128** and diastereoselective Mukaiyama aldol reaction of the α-amino aldehydes *(S)*-**131** to **133**.

mesitylsulfonyl (Mts) protecting group is shown with the example of the transformation into phenylglycine [(*S*)-**132**]; sodium in ammonia or sodium naphthalenide[152] proved to be the optimal reagents for deprotection without racemization.

As in the case of the allylic alcohols **118**, replacement of the bromine substituent by hydrogen by bromine–lithium exchange and protonation is also possible for the N-protected allylamines **129**. The subsequent ozonolysis then leads to α-sulfonylamino aldehydes (*S*)-**131**, which show the expected conformational lability but can nevertheless be isolated and used in further reactions. To illustrate their synthetic potential these compounds were used as substrates in Mukaiyama aldol reactions[153] with the silyl ketene acetal of *tert*-butyl isobutyrate in the presence of $TiCl_4$. This addition proceeds with very high diastereoselectivity in the sense of chelate control and affords diastereomerically pure alcohols **133** with enantiomeric purities of 92 to 98 % *ee*. The exclusive attack of the silyl ketene acetal on the *Si* face of the N-protected amino aldehyde can be plausibly explained with the transition state model **134**. The efficient chelate control of the Mts protecting group,[154] which was seldom used so far for amines, could also prove worthwhile in other substrates.



134

Whereas numerous enantioselective syntheses of α-amino acids are known[142] and a few possibilities for obtaining N-protected α-amino aldehydes[155] have become available, the direct approach by addition of chirally masked formyl or formiate d^1 synthons ($^-$CHO and $^-$COOH) to imines has not been attempted so far. Starting from dibromoalkene **36** or its enantiomer, which are both available from the enantiomerically pure lactates, it is clear that this concept leads to the target molecules with *R* or *S* configuration. For synthetic purposes the N-protected α-amino aldehydes **131** should be of even greater importance than the amino acids themselves.

4. Outlook

The exotic alkenyllithium compounds with electronegative heteroatom substituents in the α position, initially postulated to be short-lived intermediates in α-eliminations, have become useful reagents which can be readily generated in solution and whose chemical behavior is easily understood with the aid of new structural investigations. Owing to their ambiphilia they react with nucleophiles and, far more often, with electrophiles under formation of C–C bonds. Because of the structural unit of the heteroatom-substituted C–C double bond they are suitable for the umpolung of carbonyl reactivity. The possibilities for applying these reagents in asymmetric syntheses have already been demonstrated; further developments in this area can undoubtedly be expected. As far as the carbanionic reactions of the α-heteroatom-substituted alkenyllithium reagents are concerned, an essential future development should lie in the enantioselective control of nucleophilic additions by chiral complexing agents and ligands.

I wish to thank the Fonds der Chemischen Industrie and the Deutsche Forschungsgemeinschaft for supporting our research. The BASF AG helped us with generous gifts of chemicals. Our own research presented here is the result of the dedicated work of Dr. Hellmut Mahler, Dr. Kersten Opdenbusch, Dipl.-Chem. Claudia Unger, Dipl.-Chem. Jörg Moritz, and Dipl.-Chem. Jaykumar Rahematpura, to whom I wish to express my sincere gratitude.

Received: June 6, 1997 [A 233 IE]
German version: *Angew. Chem.* **1998**, *110*, 444–465
Translated by Linda Mundt, Düsseldorf (Germany)

[1] G. Köbrich, *Angew. Chem.* **1967**, *79*, 15–27; *Angew. Chem. Int. Ed. Engl.* **1967**, *6*, 41–52; *ibid.* **1972**, *84*, 557–570 and **1972**, *11*, 473–485.
[2] A. Maercker, *Angew. Chem.* **1993**, *105*, 1072–1074; *Angew. Chem. Int. Ed. Engl.* **1993**, *32*, 1023–1025.

[3] C. Lambert, P. von R. Schleyer, *Methoden Org. Chem. (Houben – Weyl) 4th ed. 1952 –*, Vol. E 19d, pp. 15 – 19.

[4] D. Seebach, *Angew. Chem.* **1979**, *91*, 259 – 278; *Angew. Chem. Int. Ed. Engl.* **1979**, *18*, 239 – 258; T. A. Hase, *Umpoled Synthons*, Wiley, New York **1987**.

[5] G. Köbrich, F. Ansari, *Chem. Ber.* **1967**, *100*, 2011 – 2020.

[6] M. Topolski, M. Duraisamy, J. Rachon, J. Gawronski, K. Gawronska, V. Goedken, H. M. Walborsky, *J. Org. Chem.* **1993**, *58*, 546 – 555.

[7] P. J. Stang, *Methoden Org. Chem. (Houben – Weyl)*, *4th ed. 1952 –*, Vol. E 19b, pp. 85 – 135.

[8] M. Regitz, *Angew. Chem.* **1991**, *103*, 691 – 693; *Angew. Chem. Int. Ed. Engl.* **1991**, *30*, 674 – 676; A. J. Arduengo III, R. L. Harlow, M. Kline, *J. Am. Chem. Soc.* **1991**, *113*, 361 – 363; A. J. Arduengo III, H. V. R. Dias, R. L. Harlow, M. Kline, *ibid.* **1992**, *114*, 5530 – 5534; D. Enders, K. Breuer, G. Raabe, J. Runsink, J. H. Teles, J.-P. Melder, K. Ebel, S. Brode, *Angew. Chem.* **1995**, *107*, 1119 – 1122; *Angew. Chem. Int. Ed. Engl.* **1995**, *34*, 1021 – 1023; M. Regitz, *ibid*. **1996**, *108*, 791 – 794 and **1996**, *35*, 725 – 728.

[9] P. von R. Schleyer, T. Clark, A. J. Kos, G. W. Spitznagel, C. Rohde, D. Arad, K. N. Houk, N. G. Rondan, *J. Am. Chem. Soc.* **1984**, *106*, 6467 – 6475.

[10] D. Seebach, H. Siegel, J. Gabriel, R. Hässig, *Helv. Chim. Acta* **1980**, *63*, 2046 – 2053; D. Seebach, R. Hässig, J. Gabriel, *ibid.* **1983**, *66*, 308 – 337.

[11] The apparent paradox that the α-carbon atom bears a positive partial charge in vinyl anions can, according to ab initio calculations, be explained by the fact that although the σ electron density is increased at the anionic carbon atom in the transition from ethene to the vinyl anion, a large reduction of the π electron density occurs at the same carbon atom: J. E. Williams, Jr., A. Streitwieser, Jr., *J. Am. Chem. Soc.* **1975**, *97*, 2634 – 2644; see also ref. [10]

[12] G. Boche, M. Marsch, A. Müller, K. Harms, *Angew. Chem*. **1993**, *105*, 1081 – 1082; *Angew. Chem. Int. Ed. Engl*. **1993**, *32*, 1032 – 1033.

[13] T. Clark, P. von R. Schleyer, *J. Chem. Soc. Chem. Commun.* **1979**, 883 – 884; *Tetrahedron Lett*. **1979**, 4963 – 4966; *J. Am. Chem. Soc*. **1979**, *101*, 7747 – 7748; see also ref. [9].

[14] In contrast, a crystal structure analysis of 2-lithiobenzofuran · tmeda clearly shows an interaction between the lithium and the oxygen atom: S. Harder, J. Boersma, L. Brandsma, J. A. Kanters, W. Bauer, R. Pi, P. von R. Schleyer, H. Schöllhorn, U. Thewalt, *Organometallics* **1989**, *8*, 1688 – 1696.

[15] G. Boche, K. Harms, M. Marsch, A. Müller, *J. Chem. Soc. Chem. Commun.* **1994**, 1393 – 1394.

[16] K. Sorger, W. Bauer, P. von R. Schleyer, D. Stalke, *Angew. Chem*. **1995**, *107*, 1766 – 1768; *Angew. Chem. Int. Ed. Engl*. **1995**, *34*, 1594 – 1596.

[17] C. Lambert, P. von R. Schleyer, E. U. Würthwein, *J. Org. Chem*. **1993**, *58*, 6377 – 6389.

[18] P. Caramella, K. N. Houk, *Tetrahedron Lett*. **1981**, *22*, 819 – 822; see also Y. Apeloig, P. von R. Schleyer, J. S. Binkley, J. A. Pople, *J. Am. Chem. Soc.* **1976**, *98*, 4332 – 4334; W. D. Laidig, H. F. Schaefer III, *ibid*. **1979**, *101*, 7184 – 7188; S. Nagase, K. Morokuma, *ibid*. **1978**, *100*, 1666 – 1672; S. I. Miller, W. G. Lee, *ibid*. **1959**, *81*, 6313 – 6319.

[19] D. Y. Curtin, J. W. Crump, *J. Am. Chem. Soc*. **1958**, *80*, 1922 – 1926; D. Y. Curtin, W. J. Koehl, Jr., *ibid*. **1962**, *84*, 1967 – 1973; D. Seyferth, L. G. Vaughan, *J. Organomet. Chem*. **1963**, *1*, 201 – 204; *J. Am. Chem. Soc.* **1964**, *86*, 883 – 890; R. W. M. ten Hoedt, G. van Koten, J. G. Noltes, *J. Organomet. Chem*. **1978**, *161*, C13 – 16; *ibid*. **1979**, *170*, 131 – 149; H. M. Walborsky, R. B. Banks, *Bull. Soc. Chim. Belg*. **1980**, *89*, 849 – 868, and references therein; R. Knorr, E. Lattke, *Tetrahedron Lett*. **1977**, 3969 – 3972; E. Lattke, R. Knorr, *Chem. Ber*. **1981**, *114*, 1600 – 1609; R. Knorr, E. Lattke, *ibid*. **1981**, *114*, 2116 – 2131; R. Knorr, E. Lattke, E. Räpple, *ibid*. **1981**, *114*, 1581 – 1591; R. Knorr, E. Lattke, F. Ruf, H.-U. Reissig, *ibid*. **1981**, *114*, 1592 – 1599.

[20] For a review of applications of halolithiocarbenoids in synthesis, see H. Siegel, *Top. Curr. Chem*. **1982**, *106*, 55 – 78.

[21] J. Hartmann, M. Stähle, M. Schlosser, *Synthesis* **1974**, 888 – 889; J. A. Soderquist, A. Hassner, *J. Am. Chem. Soc*. **1980**, *102*, 1577 – 1583.

[22] R. Knorr, T. von Roman, *Angew. Chem*. **1984**, 96, 349 – 350; *Angew. Chem. Int. Ed. Engl*. **1984**, *23*, 366.

[23] R. R. Schmidt, H. Speer, B. Schmid, *Tetrahedron Lett*. **1979**, 4277 – 4280.

[24] M. Braun, *Methoden Org. Chem. (Houben – Weyl) 4th ed. 1952 –*, Vol. E 19d, pp. 278 – 368.

[25] L. Brandsma, H. D. Verkruijsse, *Preparative Polar Organometallic Chemistry 1*, Springer, Berlin **1987**, pp. 3 – 23.

[26] The polarographically determined pK_a value of ethene is 36, whereas that of the allylic proton in propene is only 32; cf. K. P. Butin, I. P. Beletskaya, A. N. Kashin, O. A. Reutov, *J. Organomet. Chem*. **1967**, *10*, 197 – 210; see also H. F. Ebel, *Die Acidität der CH-Säuren*, Thieme, Stuttgart **1969**, p. 72.

[27] U. Schöllkopf, *Methoden Org. Chem. (Houben – Weyl) 4th ed. 1952 –*, Vol. 13/1, pp. 87 – 253.

[28] J.-F. Normant, J. P. Foulon, D. Masure, R. Sauvêtre, J. Villieras, *Synthesis* **1975**, 122 – 125; C. Chuit, R. Sauvêtre, D. Masure, M. Baudry, J.-F. Normant, J. Villieras, *J. Chem. Res. (S)* **1977**, 104; *J. Chem. Res. (M)* **1977**, 1147 – 1155; R. Sauvêtre, D. Masure, C. Chuit, J.-F. Normant, *Synthesis* **1978**, 128 – 130.

[29] a) J. L. Hahnfeld, D. J. Burton, *Tetrahedron Lett*. **1975**, 773 – 776; see also P. Tarrant, R. W. Whitfield, Jr., R. H. Summerville, *J. Fluorine Chem*. **1971/72**, *1*, 31 – 40; b) A. Pelter, J. Kvicala, D. E. Parry, *J. Chem. Soc. Perkin I* **1995**, 2681 – 2682; c) K. H. Dötz, J. Glänzer, *J. Chem. Soc. Chem. Commun* **1993**, 1036 – 1037; d) J. Burdon, P. L. Coe, I. B. Haslock, R. L. Powell, *Chem. Commun*. **1996**, 49 – 50.

[30] H. Fienemann, G. Köbrich, *Chem. Ber*. **1974**, *107*, 2797 – 2803; see also: G. Köbrich, B. Kolb, A. Mannschreck, R. A. Misra, *ibid*. **1973**, *106*, 1601 – 1611.

[31] a) U. Schöllkopf, P. Hänssle, *Liebigs Ann. Chem*. **1972**, *763*, 208 – 210; b) I. Hoppe, U. Schöllkopf, *ibid*. **1980**, 1474 – 1476; c) U. Schöllkopf, *Methoden Org. Chem. (Houben – Weyl) 4th ed. 1952 –*, Vol. 13/1, p. 116; d) For the metalation of alkyl allenyl ethers, see ref. [25, 103a].

[32] F. T. Oakes, J. F. Sebastian, *J. Org. Chem.* **1980**, *45*, 4959 – 4961.

[33] J. E. Baldwin, G. A. Höfle, O. W. Lever, Jr., *J. Am. Chem. Soc*. **1974**, *96*, 7125 – 7127.

[34] M. Shimano, A. I. Meyers, *Tetrahedron Lett*. **1994**, *35*, 7727 – 7730.

[35] a) L. Brandsma, H. Verkruijsse, *Preparative Polar Organometallic Chemistry 1*, Springer, Berlin 1987, chap. 3; b) J. Hartmann, M. Schlosser, *Helv. Chim. Acta* **1976**, *59*, 453 – 466; c) A. Deagostino, M. Mella, C. Prandi, P. Venturello, *J. Chem. Soc. Perkin I* **1995**, 2757 – 2760.

[36] R. K. Boeckman, Jr., K. J. Bruza, *Tetrahedron Lett*. **1977**, 4187 – 4190; *Tetrahedron* **1981**, *37*, 3997 – 4006.

[37] a) E. Lukevics, V. Gevorgyan, Y. Goldberg, J. Popelis, M. Gavars, A. Gaukhman, M. Shimanska, *Heterocycles* **1984**, *22*, 987 – 991; b) B. L. Groh, G. R. Magrum, T. J. Barton, *J. Am. Chem. Soc*. **1987**, *109*, 7568 – 7569; c) P. Kocienski, S. Wadman, K. Cooper, *ibid*. **1989**, *111*, 2363 – 2365; d) M. Schlosser, B. Schaub, B. Spahic, G. Sleiter, *Helv. Chim. Acta* **1973**, *56*, 2166 – 2170; e) B. Schaub, M. Schlosser, *ibid*. **1975**, *58*, 556 – 564; f) M. Stocks, P. Kocienski, D. K. Donald, *Tetrahedron Lett.* **1990**, *31*, 1637 – 1640.

[38] a) A. Lebouc, J. Delaunay, O. Riobé, *Synthesis* **1979**, 610 – 613; b) T. Cohen, M. Bhupathy, *Tetrahedron Lett.* **1983**, *24*, 4163 – 4164; c) A. Alexakis, J. Hanaizi, D. Jachiet, J.-F. Normant, L. Toupet, *ibid*. **1990**, *31*, 1271 – 1274; d) S. V. Ley, R. Leslie, P. D. Tiffin, M. Woods, *ibid* **1992**, *33*, 4767.–4770.

[39] R. W. Saylor, J. F. Sebastian, *Synth. Commun*. **1982**, *12*, 579 – 584.

[40] a) M. Fétizon, I. Hanna, J. Rens, *Tetrahedron Lett*. **1985**, *26*, 3453 – 3456; b) M. Fétizon, P. Goulaouic, I. Hanna, *ibid*. **1985**, *26*, 4925 – 4928; c) M. Fétizon, P. Goulaouic, I. Hanna, T. Prangé, *J. Org. Chem*. **1988**, *53*, 5672 – 5679; d) V. Blanchot, M. Fétizon, I. Hanna, *Synthesis* **1990**, 755 – 756; e) V. Blanchot-Courtois, I. Hanna, *Tetrahedron Lett*. **1992**, *33*, 8087 – 8090; f) N. Ruiz. M. D. Pujol, G. Guillaumet, G. Goudert, *ibid*. **1992**, *33*, 2965 – 2968.

[41] a) S. Sengupta, V. Snieckus, *J. Org. Chem*. **1990**, *55*, 5680 – 5683; b) P. Kocienski, N. J. Dixon, *Synlett* **1989**, 52 – 54; c) M. Tsukazaki, V. Snieckus, *Tetrahedron Lett*. **1993**, *34*, 411 – 414; d) S. Superchi, N. Sotomayor, G. Miao, B. Joseph, V. Snieckus, *ibid.* **1996**, *37*, 6057 – 6060.

[42] a) K. Tanaka, T. Nakai, N. Ishikawa, *Tetrahedron Lett*. **1978**, 4890 – 4810; b) J. Ichikawa, T. Sonoda, H. Kobayashi, *ibid*. **1989**, *30*, 1641 – 1644; c) *ibid*. **1989**, *30*, 5437 – 5438; d) J. Ichikawa, S. Hamada, T. Sonoda, H. Kobayashi, *ibid*. **1992**, *33*, 337 – 340; e) J. Ichikawa, T. Minami, T. Sonoda, H. Kobayashi, *ibid*. **1992**, *33*, 3779 – 3782; f) J. Ichikawa, C. Ikeura, T. Minami, *Synlett* **1992**, 739 – 740.

[43] A. J. Bennett, J. M. Percy, M. H. Rock, *Synlett* **1992**, 483 – 484; J. Lee, M. Tsukazaki, V. Snieckus, *Tetrahedron Lett*. **1993**, *34*, 415 – 418; P. J. Crowley. J. A. Howarth, W. M. Owton, J. M. Percy, K. Stansfield, *Tetrahedron Lett.* **1996**, *37*, 5975 – 5978; P. J. Crowley, J. M. Percy, K. Stansfield, *ibid.* **1996**, *37*, 8233 – 8236.

[44] a) J. M. Percy, *Tetrahedron Lett*. **1990**, *31*, 3931 – 3932; b) S. T. Patel, J. M. Percy, R. D. Wilkes, *Tetrahedron* **1995**, *51*, 9201 – 9216; S. T. Patel, J. M. Percy, R. D. Wilkes, *J. Org. Chem*. **1996**, *61*, 166 – 173.

[45] K. Oshima, S. Shimoji, H. Takahashi, H. Yamamoto, H. Nozaki, *J. Am. Chem. Soc*. **1973**, *95*, 2694 – 2695.

[46] a) M. Braun, *Tetrahedron Lett*. **1978**, 3695 – 3698; b) M. Braun, *Chem. Ber*. **1979**, *112*, 1495 – 1497; c) M. Braun, W. Hild, *Angew. Chem*. **1984**, *96*, 701 – 702; *Angew. Chem. Int. Ed. Engl*. **1984**, *23*, 723 – 724.

[47] a) R. C. Cookson, P. J. Parsons, *J. Chem. Soc. Chem. Commun*. **1976**, 990; *ibid*. **1978**, 821 – 822; b) B. Harirchian, P. Magnus, *ibid*. **1977**, 522 – 523; c) J. P. Marino, L. C. Katterman, *ibid*. **1979**, 946 – 947; d) P. G. McDougal, Y.-I. Oh, *Tetrahedron Lett* **1986**, *27*, 139 – 142; e) T. Takeda, H. Furukawa, T. Fujiwara, *Chem. Lett*. **1982**, 593 – 596; f) T. Takeda, H. Furukawa, M. Fujimori, K. Suzuki, T. Fujiwara, *Bull. Chem. Soc. Jpn.* **1984**, *57*, 1863 – 1869; g) M. Iwao, T. Kuraishi, *Tetrahedron Lett.* **1985**, *26*, 6213 – 6216.

[48] D. Hoppe, L. Beckmann, R. Follmann, *Angew. Chem*. **1980**, *92*, 305 – 306; *Angew. Chem. Int. Ed. Engl*. **1980**, *19*, 303.

[49] Y. Takahashi, H. Hagiwara, H. Uda, H. Kosugi, *Heterocycles* **1981**, *15*, 225 – 229; Y. Takahashi, H. Kosugi, H. Uda, *J. Chem. Soc. Chem. Commun*. **1982**, 496 – 497; R. R. Schmidt, R. Betz, *Angew. Chem*. **1984**, *96*, 420 – 421; *Angew. Chem. Int. Ed. Engl*. **1984**, *23*, 430 – 431; N. C. Barua, R. R. Schmidt, *Chem. Ber*. **1986**, *119*, 2066 – 2068; *Tetrahedron* **1986**, *42*, 4471 – 4474; A. Esswein, R. Betz, R. R. Schmidt, *Helv. Chim. Acta* **1989**, *72*, 213 – 223; A. J. Pallenberg, J. D. White, *Tetrahedron Lett*. **1986**, *27*, 5591 – 5594.

[50] R. R. Schmidt, B. Schmid, *Tetrahedron Lett* **1977**, 3583 – 3584.

[51] M. Schoufs, J. Meyer, P. Vermeer, L. Brandsma, *Recl. Trav. Chim. Pays-Bas.* **1977**, *96*, 259 – 263.

[52] D. C. Green, *J. Chem. Soc. Chem. Commun*. **1977**, 161 – 162; D. C. Green, R. W. Allen, *ibid*. **1978**, 832 – 833; D. C. Green, *J. Org. Chem*. **1979**, *44*, 1476 – 1479; E. Aharon-Shalom, J. Y. Becker, J. Bernstein, S. Bittner, S. Shaik, *Tetrahedron Lett* **1985**, *26*, 2783 – 2786; S. Rajeswari, Y. A. Jackson, M. P. Cava, *J. Chem. Soc. Chem Commun*. **1988**, 1089 – 1090; J. Y. Becker, J. Bernstein, M. Dayan, L. Shahal, *ibid*. **1992**, 1048 – 1049; J.-M. Fabre, J. Garin, S. Uriel, *Tetrahedron* **1992**, *48*, 3983 – 3990; G. Cooke, *Synth. Commun.* **1996,** *26*, 2917 – 2923.

[53] Cf. R. Muthukrishnan, M. Schlosser, *Helv. Chim. Acta* **1976**, *59*, 13 – 20, and ref. [35b].

[54] R. H. Everhardus, R. Gräfing, L. Brandsma, *Recl. Trav. Chim. Pays-Bas* **1978**, *97*, 69 – 72; R. H. Everhardus, H. G. Eeuwhorst, L. Brandsma, *J. Chem. Soc. Chem. Commun*. **1977**, 801 – 802.

[55] H. Okamura, Y. Mitsuhira, M. Miura, H. Takei, *Chem. Lett*. **1978**, 517 – 520; G. H. Posner, P.-W. Tang, J. P. Mallamo, *Tetrahedron Lett*. **1978**, 3995 – 3998; G. H. Posner, T. P. Kogan, S. R. Haines, L. L. Frye, *ibid*. **1984**, *25*, 2627 – 2630; R. A. Holton, H.-B. Kim, *ibid*. **1986**, *27*, 2191 – 2194.

[56] G. Solladié, G. Moine, *J. Am. Chem. Soc*. **1984**, *106*, 6097 – 6098; C. Alexandre, O. Belkadi, C. Maignan, *Synthesis* **1992**, 547 – 548.

[57] I. Vlattas, L. Della Vecchia, A. O. Lee, *J. Am. Chem. Soc*. **1976**, *98*, 2008 – 2010.

[58] J. J. Eisch, J. E. Galle, *J. Org. Chem.* **1979**, *44*, 3277 – 3279; 3279 – 3280; S. W. McCombie, B. B. Shankar, A. K. Ganguly, *Tetrahedron Lett*. **1985**, *26*, 6301 – 6304; S. W. McCombie, B. B. Shankar. A. K. Ganguly, A. Padwa, W. H. Bullock, A. D. Dyszlewski, *ibid*, **1987**, *28*, 4127 – 4130; N. S. Simpkins, *ibid*. **1987**, *28*, 989 – 992; T. Taguchi, G. Tomizawa, A. Kawara, M. Nakajima, Y. Kobayashi, *J. Fluorine Chem*. **1988**, *40* 171 – 182; C. Nájera, M. Yus, *Tetrahedron Lett*. *1987, 28*, 6709 – 6712; *J. Org. Chem*. **1988**, *53*, 4709 – 4715; *ibid*. **1989**, *54*, 1491 – 1499; M. Yamamoto, T. Takemori, S. Iwasa, S. Kohmoto, K. Yamada, *ibid*. **1989**, *54*, 1757 – 1760; P. L. Ibáñez, C. Nájera, *Tetrahedron Lett.* **1993**, *34*, 2003 – 2006.

[59] I. Erdelmeier, H.-J. Gais, *J. Am. Chem. Soc.* **1989**, *111*, 1125 – 1126; H.-J. Gais, H. Müller, J. Decker, R. Hainz, *Tetrahedron Lett*. **1995**, *41*, 7433 – 7436.

[60] H. Kleijn, P. Vermeer, *J. Organomet. Chem*. **1986**, *302*, 1 – 4.

[61] M. Sevrin, J. N. Denis, A. Krief, *Angew. Chem*. **1978**, *90*, 550 – 551; *Angew. Chem. Int. Ed. Engl*. **1978**, *17*, 526 – 527; H. J. Reich, W. W. Willis, Jr., P. D. Clark, *J. Org. Chem*. **1981**, *46*, 2775 – 2784; T. Kauffmann, H. Ahlers, *Chem. Ber*. **1983**, *116*, 1001 – 1008; S. L. Bender, M. R. Detty, M. W. Fichtner, N. S. Haley, *Tetrahedron Lett*. **1983**, *24*, 237 – 240.

[62] S. Raucher, G. A. Koolpe, *J. Org. Chem*. **1978**, *43*, 3794 – 3796.

[63] For the metalation of tetraselenofulvalenes, see S. Rajeswari, Y. A. Jackson, M. P. Cava, *J. Chem. Soc. Chem. Commun*. **1988**, 1089 – 1090.

[64] R. R. Schmidt, J. Talbiersky, P. Russegger, *Tetrahedron Lett*. **1979**, 4273 – 4276; R. R. Schmidt, J. Talbiersky, *Angew. Chem.* **1978**, *90*, 220 – 221*; Angew. Chem. Int. Ed. Engl*. **1978**, *17*, 204.

[65] U. Schöllkopf, D. Stafforst, R. Jentsch, *Liebigs Ann. Chem*. **1977**, 1167 – 1173.

[66] A. I. Meyers, P. D. Edwards, T. R. Bailey, G. E. Jagdmann, Jr., *J. Org. Chem*. **1985**, *50*, 1019 – 1026.

[67] F. M. Atta, R. Betz, B. Schmid, R. R. Schmidt, *Chem. Ber*. **1986**, *119*, 472 – 481.

[68] G. Zweifel, W. Lewis, H. P. On, *J. Am. Chem. Soc.* **1979**, *101*, 5101 – 5102; R. F. Cunico, Y.-K. Han, *J. Organomet. Chem*. **1978**, *162*, 1 – 16; A. Pelter, J. Kvicala, D. E. Parry, *J. Chem. Soc. Perkin I* **1995**, 2681 – 2683.

[69] H. Monti, P. Charles, *Synlett* **1995**, 193 – 194.

[70] A. Oku, T. Harada, K. Hattori, Y. Nozaki, Y. Yamaura, *J. Org. Chem.* **1988**, *53*, 3089 – 3098.

[71] a) T. Harada, T. Katsuhira, A. Oku, *J. Org. Chem*. **1992**, *57*, 5805 – 5807; b) D. Grandjean, P. Pale, *Tetrahedron Lett*. **1993**, *34*, 1155 – 1158; c) J. Barluenga, M. A. Rodríguez, P. J. Campos, G. Asensio, *J. Am. Chem. Soc.* **1988**, *110*, 5567 – 5568.

[72] H. Mahler, M. Braun, *Tetrahedron Lett.* **1987**, *28*, 5145 – 5148.

[73] H. Mahler, M. Braun, *Chem. Ber*. **1991**, *124*, 1379 – 1395.

[74] D. Seyferth, R. L. Lambert, Jr., *J. Organomet. Chem*. **1973**, *55*, C 53 – 57.

[75] M. Braun, J. Rahematpura, unpublished results.

[76] C. Wiaux-Zamar, J. P. Dejonghe, L. Ghosez, J.-F. Normant, J. Villieras, *Angew. Chem*. **1976**, *88*, 417 – 418; *Angew. Chem. Int. Ed. Engl*. **1976**, *15*, 371 – 372; G. Sauer, J. Heindl, H. Wachtel, *Tetrahedron Lett*. **1988**, *29*, 6425 – 6428.

[77] a) C. N. Skold, *Synth. Commun*. **1976**, *6*, 119 – 124; b) K. H. Dötz, W. Kuhn, U. Thewalt, *Chem. Ber*. **1985**, *118*, 1126 – 1132.

[78] A. Maercker, *Methoden Org. Chem. (Houben – Weyl) 4th ed. 1952* – , Vol. E 19d, pp. 448 – 566.

[79] J. A. Soderquist, G. J.-H. Hsu, *Organometallics* **1982**, *1*, 830 – 833; J. A. Soderquist, I. Rivera, *Tetrahedron Lett*. **1989**, *30*, 3919 – 3922; P. Kocienski, K. Jarowicki, S. Marczak, *Synthesis* **1991**, 1191 – 1200.

[80] B.-T. Gröbel, D. Seebach, *Chem. Ber.* **1977**, *110*, 867 – 877.

[81] R. K. Boeckman, Jr., J. E. Starrett, Jr., D. G. Nickell, P. E. Sum, *J. Am. Chem. Soc.* **1986**, *108*, 5549 – 5559.

[82] J. N. Denis, A. Krief, *Tetrahedron Lett*. **1982**, *23*, 3411 – 3414.

[83] T. Cohen, R. B. Weisenfeld, *J. Org. Chem*. **1979**, *44*, 3601 – 3603.

[84] The "thiophilic" addition of *n*-butyl- or methyllithium to specific thioketenes also leads to α-lithiated vinyl sulfides: E. Schaumann, W. Walter, *Chem. Ber*. **1974**, *107*, 3562 – 3573.

[85] T. Kawase, S.-I. Fujino, M. Oda, *Tetrahedron Lett*. **1990**, *31*, 545 – 548.

[86] M. Braun, *Methoden Org. Chem. (Houben – Weyl) 4th ed. 1952*-, Vol. E 19d, pp. 171 – 278.

[87] J. E. Baldwin, J. C. Bottaro, *J. Chem. Soc. Chem. Commun*. **1981**, 1121 – 1122.

[88] P. Fritsch, *Liebigs Ann. Chem*. **1894**, *279*, 319 – 323; W. P. Buttenberg, *ibid*. **1894**, *279*, 324 – 337; H. Wiechell, *ibid*. **1894**, *279*, 337 – 344.

[89] A. A. Bothner-By, *J. Am. Chem. Soc.* **1955**, *77*, 3293 – 3296; D. Y. Curtin, E. W. Flynn, R. F. Nystrom, *ibid*. **1958**, *80*, 4599 – 4601.

[90] a) F. Ramirez, N. B. Desai, N. McKelvie, *J. Am. Chem. Soc*. **1962**, *84*, 1745 – 1747; b) E. J. Corey, P. L. Fuchs, *Tetrahedron Lett*. **1972**, 3769 – 3772; c) H. J. Bestmann, H. Frey, *Liebigs Ann. Chem*. **1980**, 2061 – 2071; d) M. C. McIntosh, S. M. Weinreb, *J. Org. Chem*. **1993**, *58*, 4823 – 4832; e) D. Grandjean, P. Pale, J. Chuche, *Tetrahedron Lett*. **1994**, 35, 3529 – 3530; f) J. Villieras, P. Perriot, J.-F. Normant, *Synthesis* **1975**, 458 – 461; g) W. G. Salmond, M. C. Sobala, K. D. Maisto, *Tetrahedron Lett*. **1977**, 1237 – 1238; W. G. Salmond, *ibid*. **1977**, 1239 – 1240; h) A. Hosomi, M. Inaba, H. Sakurai, *ibid*. **1983**, 24, 4727 – 4728; i) L. F. Tietze, T. Neumann, M. Kajino, M. Pretor,

Synthesis **1995**, 1003 – 1006; j) M. T. Reetz, T. J. Strack, J. Kanand, R. Goddard, *J. Chem. Soc. Chem. Commun.* **1996**, 733 – 734.
[91] The generation of 1-propynyllithium from 1-chloro- and 1-bromo-1-propene by α-metalation is started in a similar way: D. J. Nelson, *J. Org. Chem*. **1984**, *49*, 2059 – 2061; J. Suffert, D. Toussaint, *ibid*. **1995**, *60*, 3550 – 3553.
[92] G. Olah, A. Wu, *Synthesis* **1990**, 885 – 886.
[93] L. Duhamel, J. M. Poirier, *J. Org. Chem.* **1979**, *44*, 3585 – 3586; see A. Kasatkin, R. J. Whitby, *Tetrahedron Lett.* **1997**, *38*, 4857 – 4860
[94] G. Köbrich, H. Heinemann, W. Zündorf, *Tetrahedron* **1967**, *23*, 565 – 584.
[95] R. H. Fischer, M. Baumann, G. Köbrich, *Tetrahedron Lett*. **1974**, 1207 – 1208.
[96] M. Baumann, G. Köbrich, *Tetrahedron Lett.* **1974**, 1217 – 1220.
[97] G. Boche, F. Bosold, J. C. W. Lohrenz, A. Opel, P. Zulauf, *Chem. Ber.* **1993**, *126*, 1873 – 1885.
[98] P. Kocienski, C. Barber, *Pure Appl. Chem*. **1990**, *62*, 1933 – 1940.
[99] M. Iyoda, H. Otani, M. Oda, Y. Kai, Y. Baba, N. Kasai, *J. Am. Chem. Soc.* **1986**, *108*, 5371 – 5372.
[100] C. G. Chavdarian, C. H. Heathcock, *J. Am. Chem. Soc*, **1975**, *97*, 3822 – 3823; R. K. Boeckman, Jr., K. J. Bruza, J. E. Baldwin, O. W. Lever, *J. Chem. Soc. Chem. Commun.* **1975**, 519 – 520; R. K. Boeckman, Jr., K. J. Bruza, *J. Org. Chem.* **1979**, *44*, 4781 – 4788.
[101] E. Negishi, F.-T. Luo, *J. Org. Chem*. **1983**, *48*, 1560 – 1562; C. E. Russell, L. S. Hegedus, *J. Am. Chem. Soc.* **1983**, *105*, 943 – 949.
[102] A. B. Levy, S. J. Schwartz, *Tetrahedron Lett.* **1976**, 2201 – 2204; A. B. Levy, S. J. Schwartz, N. Wilson, B. Christie, *J. Organomet. Chem*. **1978**, *156*, 123 – 132; see also S. Birkinshaw. P. Kocienski, *Tetrahedron Lett*. **1991**, *32*, 6961 – 6964, and ref. [42b, f].
[103] a) S. Hoff, L. Brandsma, J. F. Arens, *Recl. Trav. Chim. Pays-Bas* **1968**, *87*, 916 – 924; 1179 – 1184; *ibid*. **1969**, *88*, 609 – 619; b) J.-C. Clinet, G. Linstrumelle, *Tetrahedron Lett*. **1980**, *21*, 3987 – 3990; c) R. Zimmer, H.-U. Reissig, *Liebigs Ann. Chem.* **1991**, 553 – 562; d) S. Hormuth, H.-U. Reissig, *Synlett* **1991**, 179 – 180; e) I. Hanna, T. Prangé, R. Zeghdoudi, *Tetrahedron Lett.* **1996**, *37*, 7013 – 7016; f) S. Hormuth, W. Schade, H.-U. Reissig, *Liebigs Ann. Chem.* **1996**, 2001 – 2006; g) P. Kocienski, R. Whitby, Synthesis 1991, 1029 – 1038.
[104] Reviews of the metalation of methoxyallene and follow-up reactions: R. Zimmer, *Synthesis* **1993**, 165 – 178; R. Zimmer, F. A. Kahn, *J. Prakt. Chem.* **1996**, *338*, 92 – 94; for the generation and reactions of metalated diethylamino and alkylthio allene, see ref. [35a].
[105] a) P. Lesimple, J.-M. Beau, G. Jaurand, P. Sinaÿ, *Tetrahedron Lett*. **1986**, *27*, 6201 – 6204; b) K. A. Parker, C. A. Coburn, P. D. Johnson, P. Aristoff, *J. Org. Chem.* **1992**, *57*, 5547 – 5550; c) R. Preuss, R. R. Schmidt, *Liebigs Ann. Chem.* **1989**, 429 – 434; d) S. Maier, R. Preuss, R. R. Schmidt, *ibid*. 1990, 483 – 489; e) H. C. Zhang, M. Brakta, G. D. Daves, Jr., *Tetrahedron Lett*. **1993**, *34*, 1571 – 1574; f) P. Kocienski, K. Jarowicki, S. Marczak, *Synthesis* **1991**, 1191 – 1200.
[106] M. Iwao, T. Kuraishi, *Tetrahedron Lett*. **1985**, *26*, 6213 – 6216.
[107] J. E. Baldwin, O. W. Lever, Jr., N. R. Tzodikov, *J. Org. Chem*. **1976**, *41*, 2312 – 2314.
[108] J. S. Brimacombe, A. M. Mather, *J. Chem. Soc. Perkin I* **1980**, 269 – 272.
[109] J. S. Brimacombe, R. Hanna, A. M. Mather, T. J. R. Weakley, *J. Chem. Soc. Perkin I* **1980**, 273 – 276.
[110] R. S. Coleman, E. B. Grant, *J. Am. Chem. Soc*. **1995**, *117*, 10889 – 10904; cf. J. M. Chong, S. B. Park, *J. Org. Chem.* **1992**, *57*, 2220 – 2222; P. C.-M. Chan, J. M. Chong, *ibid.* **1988**, *53*, 5584 – 5586.
[111] R. Ruzziconi, M. Schlosser, *Angew. Chem*. **1982**, *94*, 865 – 866; *Angew. Chem. Int. Ed. Engl.* **1982**, *21*, 855.
[112] S. L. Schreiber, J. A. Porco, Jr., *J. Org. Chem* **1989**, *54*, 4721 – 4723.
[113] P. Cox, M. F. Mahon, K. C. Molloy, S. Lister, T. Gallagher, *Tetrahedron Lett.* **1988**, *29*, 1993 – 1996.
[114] A. B. Smith III, M. Fukui, *J. Am. Chem. Soc.* **1987**, *109*, 1269 – 1272.
[115] J. A. Soderquist, A. Hassner, *J. Org. Chem*. **1980**, *45*, 541 – 543; see also ref. [54] and P. G. McDougal, J. G. Rico, *J. Org. Chem*. **1987**, *52*, 4817 – 4819.
[116] G. Helmchen, *Methoden Org. Chem. (Houben – Weyl)* 4th ed. 1952 – , Vol. E 21a, pp. 1 – 74.
[117] Cf. R. M. Devant, H.-E. Radunz, *Methoden Org. Chem. (Houben – Weyl*) 4th ed. 1952 – , Vol. E 21b, pp. 1151 – 1334.
[118] Cf. G. Habermehl, P. E. Hammann, *Naturstoffchemie*, Springer, Berlin **1992**, chap. 2; L. F. Fieser, M. Fieser, *Steroids*, Reinhold, New York **1959**.
[119] M. T. Reetz, *Angew. Chem.* **1984**, *96*, 542 – 555; *Angew. Chem. Int. Ed. Engl.* **1984**, *23*, 556 – 569; *Acc. Chem. Res.* **1993**, *26*, 462 – 468.
[120] Reviews: D. J. Cram, F. A. Abd Elhafez, *J. Am. Chem. Soc*. **1952**, *74*, 5828 – 5835; D. J. Cram, D. R. Wilson, *ibid*. **1963**, *85*, 1245 – 1249; E. L. Eliel in *Asymmetric Synthesis*, Vol. 2, Part A (Ed.: J. D. Morrison), Academic Press, New York, **1983**, pp. 125 – 155; J. Mulzer, H.-J. Altenbach, M. Braun, K. Krohn, H.-U. Reissig, *Organic Synthesis Highlights*, VCH, Weinheim, **1991**, pp. 3 – 8.
[121] M. Chérest, H. Felkin, N. Prudent, *Tetrahedron Lett*. **1968**, 2199 – 2204, N. T. Anh, *Top. Curr. Chem*. **1980**, *88*, 145 – 162.
[122] Cf. E. L. Eliel, S. H. Wilen, L. N. Mander, *Stereochemistry of Organic Compounds*, Wiley, New York **1994**, pp. 835 – 990.
[123 See, for example, R. S. Coleman, A. J. Carpenter, *Tetrahedron Lett*. **1992**, *33*, 1697 – 1700; some stereoselective additions to chiral aldehydes with vinyl cuprates have been described: S. D. Burke, A. D. Piscopio, B. E. Marron, M. A. Matulenko, G. Pan, *Tetrahedron Lett*. **1991**, *32*, 857 – 858; P. Metz, A. Schoop, *Tetrahedron* **1993**, *49*, 10597 – 10608; *ibid*. **1995**, *51*, 9023 – 9030.
[124] M. Braun, H. Mahler, *Angew. Chem*. **1989**, *101*, 948 – 950; *Angew. Chem. Int. Ed. Engl*. **1989**, *28*, 896 – 898.
[125] M. Braun, H. Mahler, *Synlett* **1990**, 587 – 588.
[126] M. Braun, H. Mahler, *Liebigs Ann. Chem*. **1995**, 29 – 40.
[127] M. Braun, J. Moritz, *Synlett* **1991**, 750 – 752.
[128] M. Braun, J. Moritz, *Chem. Ber*. **1989**, *122*, 1215 – 1217.
[129] a) M. Braun, K. Opdenbusch, *Angew. Chem*. **1993**, *105*, 595 – 597; *Angew. Chem. Int. Ed. Engl*. **1993**, *32*, 578 – 580; b) M. Braun, K. Opdenbusch, *Liebigs Ann./Recueil* **1997**, 141 – 154.
[130] M. Braun, K. Opdenbusch, C. Unger, *Synlett* **1995**, 1174 – 1176.
[131] R. Devant, U. Mahler, M. Braun, *Chem. Ber.* **1988**, *121*, 397 – 406; M. Braun, S. Gräf, S. Herzog, *Org. Synth*. **1993**, *72*, 32 – 37; M. Braun, S. Gräf, *ibid*. **1993**, *72*, 38 – 47; M. Braun, H. Sacha, *J. Prakt. Chem.* **1993**, *335*, 653 – 668; M. Braun, H. Sacha, D. Galle, S. Baskaran, *Pure Appl. Chem*. **1996**, *68*, 561 – 564.
[132] W. C. Still, J. H. McDonald III, *Tetrahedron Lett*. **1980**, *21*, 1031 – 1034.
[133] For a definition of the descriptors *lk* (like) und *ul* (unlike), see D. Seebach, V. Prelog, *Angew. Chem*. **1982**, ***94***, 696 – 702; *Angew. Chem. Int Ed. Engl.* **1982**, *21*, 654 – 660.
[134] S. Hormuth, H.-U. Reissig, *J. Org. Chem*. **1994**, *59*, 67 – 73.
[135] S. Hormuth, H.-U. Reissig, D. Dorsch, *Liebigs Ann. Chem.* **1994**, 121 – 127.
[136] M. Braun, *Methoden Org. Chem. (Houben – Weyl) 4th ed. 1952 –* , Vol. E 19d, pp. 853 – 1138.
[137] D. Seebach, W. Langer, *Helv. Chim. Acta.* **1979**, *62*, 1701 – 1709; T. Mukaiyama, *Tetrahedron* **1981**, *37*, 4111 – 4119.
[138] D. Enders, P. Gerdes, H. Kipphardt, *Angew. Chem*. **1990**, *102*, 226 – 228; *Angew. Chem. Int. Ed. Engl*. **1990**, *29*, 179 – 181.
[139] An alternative is shown in the enantioselective enzymatic cyanohydrin formation; cf. F. Effenberger, T. Ziegler, S. Förster, *Angew. Chem*. **1987**, *99*, 491 – 492; *Angew. Chem. Int. Ed. Engl*. **1987**, *26*, 458; U. Niedermeyer, M.-R. Kula, *Angew. Chem.* **1990**, *102*, 423 – 425; *Angew. Chem. Int. Ed. Engl*. **1990**, *23*, 386 – 387.
[140] L. Colombo, C. Gennari, C. Scolastico, G. Guanti, E. Narisano, *J. Chem. Soc. Chem. Commun*. **1979**, 591 – 592; D. Enders, H. Lotter, *Angew. Chem.* **1981**, *93*, 831 – 832; *Angew. Chem. Int. Ed. Engl*. **1981**, *20*, 795 – 796.
[141] See ref. [73], and references therein.
[142] R. M. Williams, *Synthesis of Optically Active α-Amino Acids*, Pergamon, Oxford **1989**; J. Mulzer, H.-J. Altenbach, M. Braun, K. Krohn, H.-U. Reissig, *Organic Synthesis Highlights*, VCH, Weinheim, **1991**, pp. 300 – 305; D. Seebach, A. R. Sting, M. Hoffmann, *Angew. Chem.* **1996**, *108*, 2880 – 2921; *Angew. Chem. Int. Ed. Engl*. **1996**, *35*, 2708 – 2748, and references therein.
[143] T. R. Kelly, P. N. Kaul, *J. Org. Chem*. **1983**, *48*, 2775 – 2777.
[144] S. Masamune, W. Choy, J. S. Petersen, L. R. Sita, *Angew. Chem*. **1985**, *97*, 1 – 31; *Angew. Chem. Int. Ed. Engl*. **1985**, *24*, 1 – 30.
[145] Enantiomerically pure vinyl sulfoxides with sulfur as the stereogenic center only lead to high diastereoselectivities in special cases when they react with aldehydes; cf. ref. [56].

[146] Formal inversion of configuration due to change in the order of priority.
[147] S. A. Godleski in *Comprehensive Organic Synthesis, Vol. 4* (Eds.: B. M. Trost, I. Fleming, M. F. Semmelhack), Pergamon, Oxford **1991**, pp. 585–661; C. G. Frost, J. Howarth, J. M. J. Williams, *Tetrahedron: Asymmetry* **1992**, *3*, 1089–1122; B. M. Trost, D. L. Van Vranken, *Chem. Rev.* **1996**, *96*, 395–422, and references therein.
[148] T. Hayashi, A. Yamamoto, T. Hagihara, *J. Org. Chem.* **1986**, *51*, 723–727.
[149] M. Braun, C. Unger, unpublished results.
[150] G. Kresze, R. Albrecht, *Angew. Chem.* **1962**, *74*, 781–782; *Angew. Chem. Int. Ed. Engl.* **1962**, *1*, 595–596; R. Albrecht, G. Kresze, B. Mlakar, *Chem. Ber.* **1964**, *97*, 483–489; G. Kresze. W. Wucherpfennig, *Angew. Chem.* **1967**, *79*, 109–127; *Angew. Chem. Int. Ed. Engl.* **1967**, *6*, 149–167.
[151] Cf. K. Griesbaum, H. Keul, *Angew. Chem.* **1975**, *87*, 748–749; *Angew. Chem. Int. Ed. Engl.* **1975**, *14*, 716.
[152] J. Kovacs, U. R. Ghatak, *J. Org. Chem.* **1966**, *31*, 119–121; J. Rudinger, H. M. van den Brink-Zimmermannová, *Helv. Chim. Acta* **1973**, *56*, 2216–2226; S. Ji, L. B. Gortler, A. Waring, A. Battisti, S. Bank, W. D. Closson, *J. Am. Chem. Soc.* **1967**, *89*, 5311–5312; review: I. Schön, *Chem Rev.* **1984**, *84*, 287–297.
[153] T. Mukaiyama, *Org. React. N. Y.* **1982**, *28*, 203–331.
[154] N. Risch, M. Arend, *Methoden Org. Chem. (Houben–Weyl) 4th ed. 1952–*, Vol. E 21b, pp. 1848–1852, and references therein.
[155] T. Rein, R. Kreuder, P. von Zezschwitz, C. Wulff, O. Reiser, *Angew. Chem.* **1995**, *107*, 1099–1102; *Angew. Chem. Int. Ed. Engl.* **1995**, *34*, 1023–1025, and references therein.

EVENTS

PPG-SIPSY
is proud to announce the:

2nd Sipsy's Symposium

New frontiers in Asymmetric Synthesis

Nice
Museum of Modern Art

JUNE
22&23
1998

Please contact:
Jean-Claude CAILLE - PPG-SIPSY
ZI LA CROIX CADEAU - BP 79 - 49242 AVRILLÉ Cedex - France
Tel. : + 33 (0)2 41 43 32 11 - Fax : + 33 (0)2 41 42 76 55
E-mail. : sipsy@compuserve.com - Web site : www.sipsy.com

Scientific programme

The following topics will be covered:

- Recent progress in catalytic asymmetric reactions
- New catalytic asymmetric oxidation
- New chiral ligands
- Activation of racemic catalysts

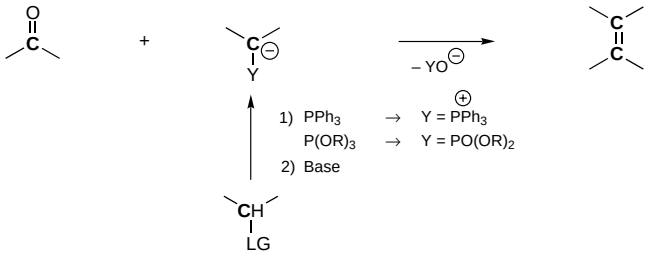
Lecturers

- V. Aggarwal - *Sheffield University*
- A. Alexakis - *UPMC Paris*
- C. Bolm - *Aachen University*
- E. Jacobsen - *Harvard University*
- H. Kagan - *University of Orsay (Paris-Sud)*
- P. Knochel - *Marburg University*
- M. Lipton - *Purdue University*
- K. Mikami - *Tokyo Institute of Technology*
- A. Pfaltz - *Max-Planck Institute*
- Y. Shi - *Colorado State University*
- A. Togni - *Zurich Institute of Technology*
- X. Zhang - *Penn State University*

Dithioacetals as an Entry to Titanium–Alkylidene Chemistry: A New and Efficient Carbonyl Olefination

Bernhard Breit*

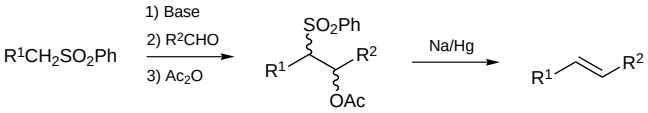
Reactions in which two halves of a complex molecule are linked by means of a convergent synthetic strategy belong to the most valuable framework-building reactions in organic synthesis. Especially successful are those reactions in which C–C double bonds are formed, such as the Wittig reaction and its variants according to Horner, Wadsworth, and Emmons (referred to here as Wittig-type reactions).[1] Decisive for the effectiveness of these methods is the simple preparative access to both individual components—a carbonyl compound as well as a Wittig-type reagent, which can be obtained, for instance, by the reaction of an alkyl halide with phosphanes or phosphites followed by deprotonation (Scheme 1). Only such



Scheme 1. Schematic representation of the Wittig and Horner–Wadsworth–Emmons reactions. LG = leaving group.

a simple and general approach enables the synthetic chemist to convert any two complex building blocks into carbonyl and Wittig-reagent components in a late step of the synthetic sequence. The components can be subsequently coupled by either an inter- or intramolecular olefination reaction.

However, Wittig-type reactions are also subject to certain limitations. One example is the *cis* selectivity upon use of nonstabilized ylides under salt-free reaction conditions. Fortunately, the Wittig-type reactions can be supplemented by the Julia–Lythgoe olefination (Scheme 2), which is a general method for preparing *trans*-disubstituted olefins.[2, 3] The components required for the Julia–Lythgoe olefination—the carbonyl and sulfone components—also meet the



Scheme 2. Stereoselective synthesis of disubstituted *trans*-olefins according to Julia and Lythgoe.

criterion of being readily available and allow the corresponding functionalization in a late synthetic step.

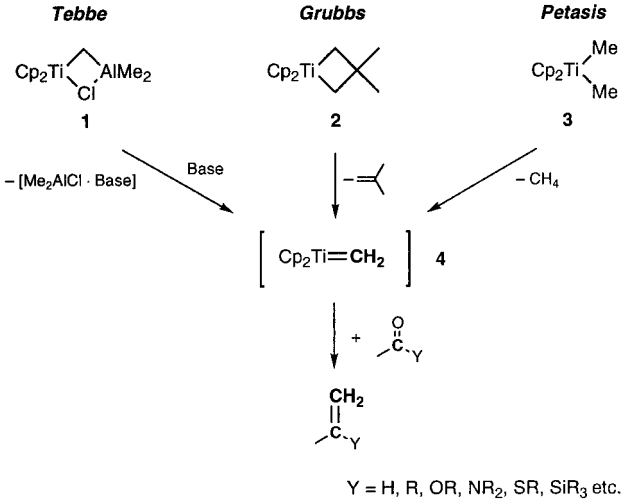
Another disadvantage of Wittig-type reactions is their limitation to aldehydes and ketones as the carbonyl component; carboxylic acid derivates are generally inert in this respect. Furthermore, Wittig-type reactions and Julia–Lythgoe olefinations both require a more or less basic reaction medium. Especially in the case of easily enolizable carbonyl compounds, this can lead to undesired side reactions such as elimination and racemization of adjacent stereocenters. The olefination of sterically demanding carbonyl substrates also clearly demonstrates the limitations of the Wittig reaction.

For this reason, considerable efforts have been devoted to finding improved olefination reagents that can overcome these shortcomings of both the Wittig-type reactions and Julia–Lythgoe olefinations. A milestone was already reached in 1978 by Tebbe, who recognized the usefulness of the titanium–aluminum complex **1** for carbonyl methylenations.[4] In addition to the Tebbe reagent **1**, the titanacyclobutane **2** reported by Grubbs[5] and the Petasis reagent **3**[6] are available for efficient methylenation of carbonyl compounds (Scheme 3). These reagents are reactive under neutral to slightly Lewis acidic conditions, which allows easily enolizable carbonyl compounds to be used in methylenation reactions without competing side reactions. Another advantage is the clean methylenation of carboxylic acid derivatives with formation of, for example, preparatively valuable enol ethers and enamines.[7]

A plausible intermediate of this olefination is the titanium–methylene species **4**, which is formed from **1** by removal of $AlMe_2Cl$ with a Lewis base, from **2** by fragmentation with elimination of isobutene, and from **3** by α-elimination and release of methane. However, none of these three routes to titanium–carbene complexes of type **4** proved to be generally applicable. Consequently, the use of these reagents in synthesis is essentially limited to the transfer of a methylene unit.[8] From a synthetic viewpoint, a general and easy route to

[*] Dr. B. Breit
Fachbereich Chemie der Universität
Hans-Meerwein-Strasse, D-35043 Marburg (Germany)
Fax: (+49) 6421-28-8917
E-mail: breit@ps1515.chemie.uni-marburg.de

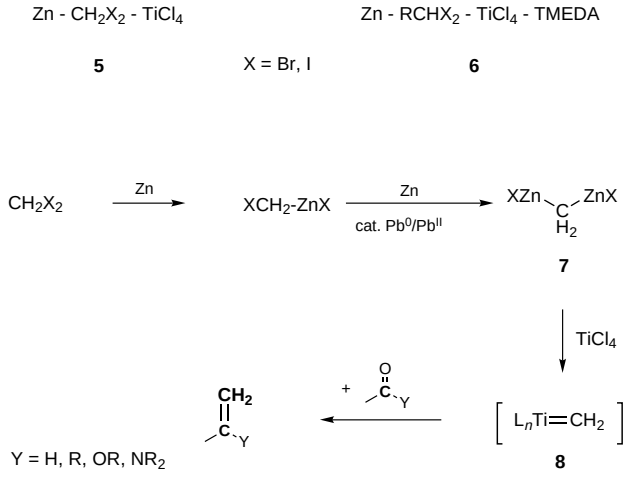
 © WILEY-VCH Verlag GmbH, D-69451 Weinheim, 1998 1433-7851/98/3704-0453 $ 17.50+.50/0



Scheme 3. Carbonyl methylenation with the titanium–methylene species **4** prepared from the Tebbe, Grubbs, or Petasis reagents (**1**–**3**).

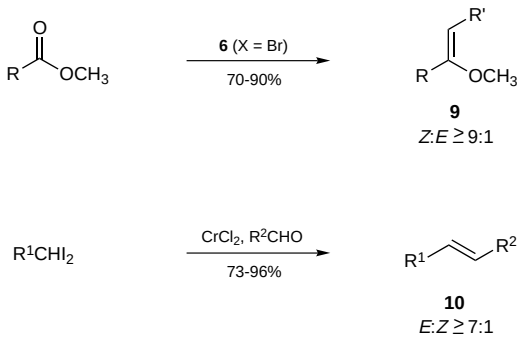
substituted titanium–alkylidene species and their use in carbonyl olefinations would be more desirable.

The first progress was made by Takai and Lombardo, who developed an in situ entry to titanium–alkylidene chemistry starting from the reagent combinations **5** and **6** (Scheme 4).[9] These reactions proceed via a *gem*-dizinc compound **7** (its formation is catalyzed by traces of lead or lead(II) salts), which is subsequently transmetalated with $TiCl_4$ to the titanium–alkylidene species **8**, the actual olefination reagent. To date, **8** has not been characterized in detail.[10] These in situ reagents exhibit chemoselectivities similar to those of the structurally defined methylenation reagents **1**–**3**.



Scheme 4. Takai–Lombardo reagents; TMEDA = *N*,*N*,*N*′,*N*′-tetramethylethylenediamine.

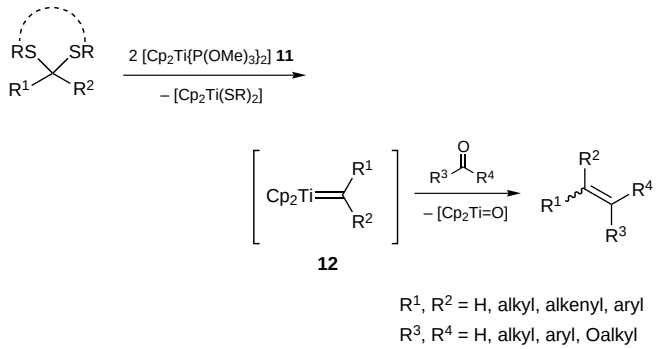
The advantage of the Takai–Lombardo reagents is the possibility of transferring substituted alkylidene units in addition to methylene units. The use of the olefination reagent **6** allows the general alkylidenation of carboxylic esters.[11] In this transformation, the (*Z*)-enol ethers **9** are obtained with high stereoselectivity (Scheme 5). A variation



Scheme 5. General alkylidenation of esters **9** and the synthesis of the disubstituted (*E*)-alkenes **10** starting from aldehydes and chromium(II) reagents according to Takai and Utimoto.

of this reaction was developed in 1986 by Takai and Utimoto, in which geminal dihaloalkanes were added to aldehydes in a reaction mediated by chromium dichloride. This led to the stereoselective formation of the corresponding *trans*-olefins **10**.[12] The major drawback of this method is the rather cumbersome access to the respective substituted dihalomethane compounds, which prevents a broad application of this reaction for synthesis.

The solution to the above problem was recently found by Takeda et al., who reported on the desulfurization of dithioacetals as a general and easy entry to titanium–alkylidene chemistry.[13] Dithioacetals, which are easily accessible from carbonyl compounds, are treated with the titanocene source $[Cp_2Ti\{P(OEt)_3\}_2]$(**11**), which was specifically developed for this purpose; the respective titanium–alkylidene species **12** is formed, presumably by desulfurization (Scheme 6). The most important subsequent reaction of this



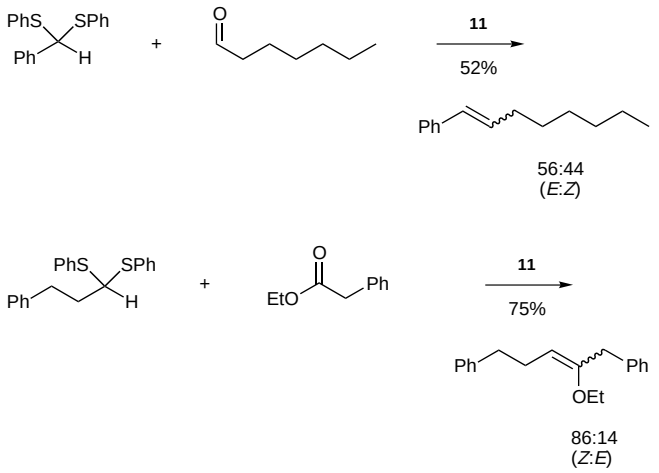
Scheme 6. Carbonyl olefination with titanium–alkylidene species **12** prepared from dithioacetals according to Takeda et al.

species is carbonyl olefination, which proceeds smoothly with aldehydes, ketones, and esters. The intermediates formed in these reactions exhibit a chemoselectivity spectrum similar to that of the titanium reagents **1**–**3**, **5**, and **6**. No limitations have yet been observed with respect to the structure of the dithioacetals; that is, even 1-substituted dithioacetals with β-hydrogen atoms can be converted. It is still unclear as to which functional groups can be tolerated in this reaction.

A clear disadvantage is the unsatisfactory stereoselectivity observed for the olefination of aldehydes so far. However, one

 © WILEY-VCH Verlag GmbH, D-69451 Weinheim, 1998 1433-7851/98/3704-0454 $ 17.50+.50/0

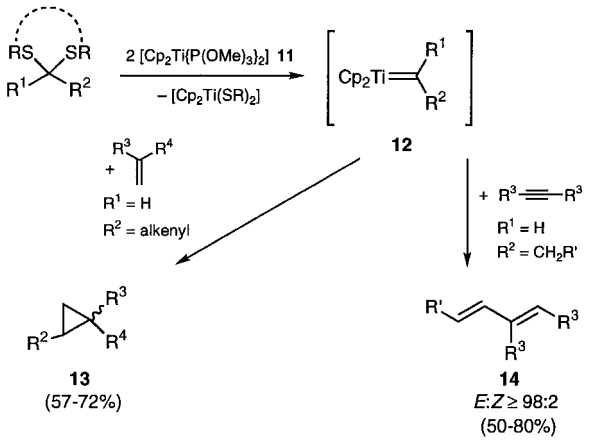
can easily envision that modifying the microenvironment of the reactive titanium center will bring about improvements. Better selectivities have been obtained in the olefination of carboxylic esters (Scheme 7).



Scheme 7. Stereoselectivity of the Takeda olefination.

The good accessibility of dithioacetals offers the possibility, as with Wittig-type reactions, to convert any two complex fragments into an olefin with the titanium reagent **11** in a late step of the synthetic sequence. This olefination is therefore as valuable as the Wittig-type reactions. Moreover, this reaction offers all the advantages of the titanium-mediated reactions that proceed in Lewis acidic media.

Interestingly, the subsequent reactions of the titanium–alkylidene species **12** obtained from dithioacetals are not limited to carbonyl olefinations. When the carbene complex is prepared in the presence of olefins, the latter are smoothly cyclopropanated (Scheme 8; →**13**).[14] Furthermore, the reaction of symmetrically disubstituted acetylenes with dithioacetals containing an α methylene unit provides the corresponding trisubstituted 1,3-diene **14** in a stereoselective fashion.[15]



Scheme 8. Reactions of the titanium–alkylidene species **12**, prepared from dithioacetals, with olefins and acetylenes.

Dithioacetals have already proven to be very useful in organic synthesis. For instance, they function as carbonyl protecting groups that can be used orthogonal to *O*,*O*-acetals.[16] The introduction of a dithioacetal leads to an umpolung of the carbonyl group (dithiane method according to Seebach).[17] As a result, any complex dithioacetal can be obtained by a deprotonation–alkylation sequence. This remarkable multifunctionality of the dithioacetal unit has now been expanded by the work of Takeda et al. with respect to the specific formation of titanium–alkylidene species. Although the subsequent chemistry of this species needs to be established in detail, the intermolecular carbonyl olefination has given a glimpse of the synthetic possibilities of this reaction strategy. In addition to the Wittig-type reaction and the Julia–Lythgoe olefination, this olefination variant has the potential of becoming another general olefination reaction which proceeds under Lewis acidic conditions.

German version: *Angew. Chem.* **1998**, *110*, 467–470

Keywords: alkylidene complexes · olefinations · synthetic methods · titanium

[1] a) A. Maercker, *Org. React.* **1965**, *14*, 270–490; b) M. Schlosser, *Top. Stereochem.* **1970**, *5*, 1–30; c) W. S. Wadsworth, Jr., *Org. React.* **1977**, *25*, 73–253; d) B. E. Maryanoff, A. B. Reitz, *Chem. Rev.* **1989**, *89*, 863–927; for the use of the Wittig reaction in the synthesis of complex natural products, see e) H. J. Bestmann, O. Vostrowsky, *Top. Curr.Chem.* **1983**, *109*, 85–163; f) K. C.Nicolaou, M. W. Härter, J. L. Gunzner, A. Nadin, *Liebigs Ann.* **1997**, 1283–1301.

[2] S. E. Kelly in *Comprehensive Organic Synthesis, Vol. 1* (Eds.: B. M. Trost, I.Fleming), Pergamon, Oxford, **1991**, p. 792 ff.

[3] Although the Schlosser modification of the Wittig reaction provides access to *trans*-olefins from nonstabilized ylides, the Julia–Lythgoe olefination has proven to be the method of choice for solving this synthetic problem today. a) M. Schlosser, K.-F. Christmann, *Justus Liebigs Ann. Chem.* **1967**, *708*, 1–35; b) M. Schlosser, K.-F. Christmann, A. Piskala, *Chem. Ber.* **1970**, *103*, 2814–2820.

[4] a) F. N. Tebbe, G. W.Parshall, G. S. Reddy, *J. Am. Chem. Soc.* **1978**, *100*, 3611–3613; b) S. H. Pine, R. Zahler, D. A. Evans, R. H. Grubbs, *J. Am. Chem. Soc.* **1980**, *102*, 3270–3272; c) S. H. Pine, R. J. Pettit, G. D. Geib, S. G. Cruz, C. H.Gallego, T. Tijerina, R. D. Pine, *J. Org. Chem.* **1985**, *50*, 1212–1216.

[5] a) T. R. Howard, J. B. Lee, R. H. Grubbs, *J. Am. Chem. Soc.* **1980**, *102*, 6876–6878; b) K. A. Brown-Wensley, S. L. Buchwald, L. Cannizzo, L.Clawson, S. Ho, D. Meinhardt, J. R. Stille, D. Straus, R. H. Grubbs, *Pure Appl. Chem.* **1983**, *55*, 1733–1744.

[6] N. A. Petasis, S.-P. Lu, E. I. Bzowej, D.-K. Fu, J. P. Staszewski, I. Akritopoulou-Zanze, M. A.Patane, Y.-H. Hu, *Pure Appl. Chem.* **1996**, *68*, 667–670.

[7] Review: S. H. Pine, *Org. React.* **1993**, *43*, 1–91.

[8] Reports have appeared on the olefination of carbonyl compounds with the use of dibenzyl-, bis[(trimethylsilyl)methyl]-, and dicyclopropyltitanocenes: a) N. A. Petasis, E. I. Bzowej, *J. Org. Chem.* **1992**, *57*, 1327–1330; b) N. A. Petasis, I. Akritopoulou, *Synlett* **1992**, 665–667; c) N. A. Petasis, E. I. Bzowej, *Tetrahedron Lett.* **1993**, *34*, 943–946; d) N. A. Petasis, J. P. Staszewski, D.-K.Fu, *ibid.* **1995**, *36*, 3619–3622.

[9] a) K. Takai, Y. Hotta, K. Oshima, H. Nozaki, *Tetrahedron Lett.* **1978**, 2417–2420; b) L. Lombardo, *ibid.* **1982**, *23*, 4293–4296; c) *Org. Synth.* **1987**, 65, 81–87; J. Hibino, T. Okazoe, K. Takai, H. Nozaki, *Tetrahedron Lett.* **1985**, *26*, 5579–5580; e) T. Okazoe, J. Hibino, K. Takai, H. Nozaki, *ibid.* **1985**, *26*, 5581–5584; f) K. Takai, O. Fujimura, Y. Kataoka, K. Utimoto, *ibid.* **1989**, *30*, 211–214.

[10] K. Takai, T. Kakiuchi, Y.Kataoka, K. Utimoto, *J. Org. Chem.* **1994**, *59*, 2668–2670.

[11] a) T. Okazoe, K. Takai, K.Oshima, K. Utimoto, *J. Org. Chem.* **1987**, *52*, 4410–4412; b) K. Takai, Y. Kataoka, T. Okazoe, K. Utimoto, *Tetrahedron Lett.* **1988**, *29*, 1065–1068.

[12] a) T. Okazoe, K. Takai, K. Utimoto, *J. Am. Chem. Soc.* **1987**, *109*, 951–953; b) K. Takai, K. Nitta, K. Utimoto, *ibid.* **1986**, *108*, 7408–7410;

 © WILEY-VCH Verlag GmbH, D-69451 Weinheim, 1998 1433-7851/98/3704-0455 $ 17.50+.50/0

c) K. Takai, Y. Kataoka, T. Okazoe, K. Utimoto, *Tetrahedron Lett.* **1987**, *28*, 1443 – 1446.
[13] Y. Horikawa, M. Watanabe, T. Fujiwara, T. Takeda, *J. Am. Chem. Soc.* **1997**, *119*, 1127 – 1128.
[14] Y. Horikawa, T. Nomura, M. Watanabe, T. Fujiwara, T. Takeda, *J. Org. Chem.* **1997**, *62*,3678 – 3682.
[15] T. Takeda, H. Shimokawa, Y. Miyachi, T. Fujiwara, *Chem. Commun.* **1997**, 1055 – 1056.
[16] P. J. Kocienski, *Protecting Groups*, Thieme, Stuttgart, **1994**, p. 171 – 178.
[17] a) D. Seebach, *Angew. Chem.* **1969**, *81*, 690 – 700; *Angew. Chem. Int. Ed. Engl.* **1969**, *8*, 639 – 649; b) B. T. Gröbel, D. Seebach, *Synthesis* **1977**, 357 – 402; c) D. Seebach, *Angew. Chem.* **1979**, *91*, 259 – 278; *Angew. Chem. Int. Ed. Engl.* **1979**, *18*, 239 – 258; d) P. C. Bulman Page, M. B. van Niel, J. C.Prodger, *Tetrahedron* **1989**, *45*, 7643 – 7677.

Direct Measurement of Dihedral Angles with High-Resolution NMR Spectroscopy

Marcel J. J. Blommers* and Wolfgang Jahnke

Since the discovery of the nuclear Overhauser effect (NOE)[1] and scalar coupling constants[2] decades ago, NMR-derived structure calculations of biomolecules largely depended on measurement of these two parameters.[3] Therefore, few scientists in this field expected that a new parameter for structure determination could be developed. The group of Griesinger at the University of Frankfurt recently changed this paradigm with the invention of an NMR method which directly measures angles between bond vectors.[4] The new parameter is widely applicable for isotopically labeled molecules and will certainly set a new direction in future design of experiments to determine the structure of biomolecules by NMR spectroscopy. The information extracted from these experiments will significantly improve the resolution of NMR structures and may provide new ways to obtain information on molecular dynamics.

The new parameter, cross-correlated dipolar relaxation (CCDR), can easily be explained in a simplified form. All coherences between nuclear spins that finally give rise to NMR signals relax (decay) with a certain rate and eventually disappear. In dipolar relaxation the relaxation of a spin is mediated by the fluctuating magnetic field caused by adjacent spins. Cross-correlated dipolar relaxation indicates that the dipolar coupled spin pair is not isolated, but experiences fluctuating magnetic fields from other spin pairs, which influence its relaxation rate. The dipolar interaction between these magnetic moments depends on the angle between them [Eq. (1) in which k is defined according to Eq. (2)].[5] θ is the

$$\mathrm{CCDR}_{ijkl} = k(3\cos^2\theta - 1) \quad (1)$$

$$k = \frac{2}{5}\frac{\gamma_i\gamma_j}{r_{ij}^3}\frac{\gamma_k\gamma_l}{r_{kl}^3}\left[\frac{\hbar\mu_0}{4\pi}\right]^2\tau_c \quad (2)$$

angle between the internuclear vectors that link nuclei i and j, and k and l (Figure 1). The internuclear distances r are well-known, and the rotational correlation time τ_c can be measured

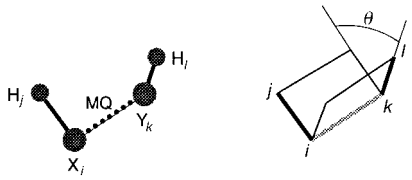


Figure 1. Schematic representation of a pair of bond vectors. The relaxation rate of the multiple quantum coherence (MQ) is dependent on the angle θ between the bond vectors.

independently. All other factors are constants. The angle θ between bond vectors is then the sole unknown in Equation (1) and can be readily and precisely determined by measurement of the cross-correlated dipolar relaxation rate. It should be emphasized that θ is measured *directly*, without the need of experimental calibration as, for example, the Karplus curve for J coupling constants.

Cross-correlated dipolar relaxation can conveniently be measured in novel triple-resonance experiments, that is, experiments that utilize the ^{1}H, ^{13}C, and ^{15}N nuclei in isotopically enriched biomolecules. In triple-resonance NMR experiments designed for that purpose, for example a nondecoupled heteronuclear multiple quantum experiment, each signal has a double doublet fine structure. The splitting of the signal is caused by the large one-bond couplings $^1J_{\mathrm{H,N}}$ and $^1J_{\mathrm{H,C}}$ (Figure 2). The individual lines of this double doublet relax with different rates due to the phenomenon of cross-correlated dipolar relaxation. Thus, the relaxation rate can be directly extracted from the intensity of individual lines [Eq. (3)]. CCDR is the relaxation rate, t is the time the

$$\mathrm{CCDR}_{ijkl} = \frac{1}{4t}\ln\left[\frac{I(\alpha\beta)I(\beta\alpha)}{I(\alpha\alpha)I(\beta\beta)}\right] \quad (3)$$

selected coherences experience relaxation, and I the signal intensities of the spin states $\alpha\alpha$, $\alpha\beta$, $\beta\alpha$, and $\beta\beta$. The relative

[*] Dr. M. J. J. Blommers, Dr. W. Jahnke
Core Technologies, Novartis Pharma AG
P.O. Box, CH-4002 Basel (Switzerland)
Fax: (+41) 61-697-3704
E-mail: marcel-jj.blommers@pharma.novartis.com

 © WILEY-VCH Verlag GmbH, D-69451 Weinheim, 1998 1433-7851/98/3704-0456 $ 17.50+.50/0

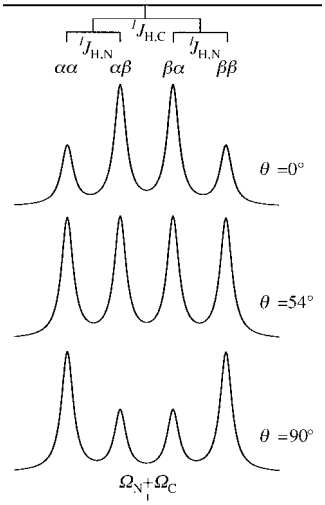


Figure 2. Cross-section through a double doublet signal obtained for each pair of correlated bond vectors. The signals represent double quantum coherence formed between N_i and C^{α}_{i-1} and are split by the $^1J_{H,N}$ and $^1J_{H,C^{\alpha}}$ couplings. The population of the spin states $\alpha\alpha$,$\alpha\beta$,$\beta\alpha$ and $\beta\beta$ is represented by the intensity of the individual peaks and is correlated with the angle θ between the H^N-N and $H-C^{\alpha}$ bond vector. The middle graph shows the magic angle condition where CCDR equals zero (Equation 2).

intensity of the individual lines thus reflects directly the relative orientation of the involved nuclei.

Cross-correlated dipolar relaxation can be measured between a variety of nuclei. The measurement requires two central nuclear spins, each of which is directly attached to a remote nuclear spin (Figure 1). The central spin and its attached remote spin must be connected by a large scalar coupling, and the remote spin must be the primary source of dipolar relaxation for the central spin. The two central spins do not need to be scalarly coupled, although the necessity to create multiple quantum coherence between them requires them to be close together in a scalar or dipolar coupled network. In practice, the central spins will be heteroatoms (for example, ^{13}C or ^{15}N in isotopically enriched biomolecules), and the remote spins will be their directly attached protons.

Reif et al.[4] chose the amide ^{15}N nucleus and the preceeding $^{13}C^{\alpha}$ nucleus as central nuclei, and their directly attached protons as remote nuclei. This choice of atoms allows the measurement of the angle θ between the H^N-N bond vector and the $H^{\alpha}-C^{\alpha}$ bond vector of the preceeding residue in the sequence (Figure 3). Assuming the planarity of the *trans* peptide bond between the two amino acid residues, the angle θ depends only on the protein backbone angle ψ. Measurement of θ is thus an indirect measurement of ψ, which is hard to determine with previous NMR technology.

The pulse sequence is similar to that in the conventional HN(CO)CA experiment,[6] which correlates the amide proton and the ^{15}N atom attached to it with the C^{α} atom of the preceeding amino acid residue. The main difference to the regular HN(CO)CA experiment is that the signal of C^{α} is recorded as double quantum coherence with amide nitrogen atom, and without decoupling of protons. A slice through the resulting 3D spectrum thus shows for every amino acid residue the double doublet of signals schematically shown in Figure 2. From the signal intensities of individual lines, the cross-correlated dipolar relaxation rate according to Equation (2), and the angles θ and ψ according to Equation (1) can be calculated. Reif et al. demonstrate the method with a small protein, rhodniin, for which they could determine a large number of ψ angles.

As with almost all NMR experiments, there is a limitation on the molecular size of biomolecules that can be investigated. The line widths of the individual lines of the double doublet (Figure 2) must be narrow relative to the one-bond scalar coupling of the central spin (^{13}C, ^{15}N) to the remote spin directly attached to it (the proton; 90 or 140 Hz, respectively). More importantly, the sensitivity of the experiment may become an issue for large biomolecules: large molecules tumble slowly in solution, and their coherences relax rapidly. During the (necessarily) long delays in the pulse sequence, a large portion of the magnetization will therefore relax before it is converted into detectable magnetization. This is particularly severe, since this type of (nondecoupled) multiple quantum coherence relaxes very rapidly. However, the cross-correlated relaxation rates grow with molecular weight analogous to the "normal" relaxation rates.

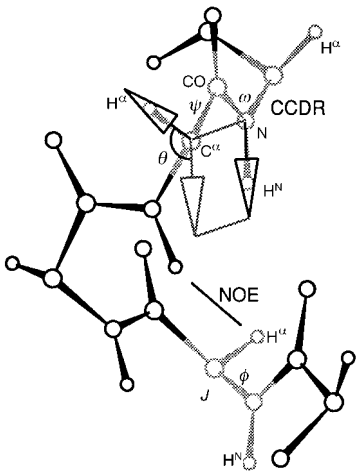


Figure 3. The measurement of cross-correlated dipolar relaxation (CCDR) yields the angles between bond vectors, such as the angle θ between the H^N-N vector and the $H-C^{\alpha}$ vector of the preceeding amino acid in the sequence. It complements information obtained from NOE and *J* coupling, that are schematically shown in the lower part of the figure.

Equation (2) is an approximation based on the assumption of isotropic tumbling of the rigid molecule. Thus, potential artefacts in the angle determination with Equation (1) can arise in the case of anisotropic tumbling, or in the presence of fast internal motions in the molecule.

Apart from its usefulness in biomolecular structure determination, measurement of cross-correlated dipolar relaxation may also help in the investigation of molecular dynamics. Cross-correlated dipolar relaxation involves a time scale that is different from the time scale for scalar coupling. In the case of internal motions, measurement of the three independent parameters, NOE, *J*, and CCDR will thus not necessarily yield identical results. Structures calculated on the basis of data that include experimental constraints from CCDR measurements may therefore be more accurate than structures calculated without CCDR information, but they are not necessarily more precise. The additional information from CCDR may be particularly important in the analysis of multiple-state equilibria, where the number of observables (NOEs and *J* coupling constants) has often not been sufficient, and the problem was consequently underdetermined. In such cases, new independent structural data may contribute to a more detailed picture of biomolecular structure, which includes structural and dynamical aspects.

 © WILEY-VCH Verlag GmbH, D-69451 Weinheim, 1998 1433-7851/98/3704-0457 $ 17.50+.50/0

Apart from the relaxation mechanism described here, other mechanisms like relaxation involving cross-correlation between dipole – dipole coupling and chemical shift anisotropy can also provide structural information[7]. The extraction of this information from the relaxation rates is, however, less straightforward than the CCDR method, mainly because many of the CSA tensors are not known. They may, however, be accessible from solid-state NMR. This relaxation mechanism is also expected to be explored with the aim of extracting structural information.

At high magnetic fields proteins with an intrinsic magnetic dipole moment experience a preferred orientation relative to the magnetic field. For these cases residual dipolar coupling can be measured, which provides information on the orientation of internuclear vectors relative to the molecular frame[8]. This method is interesting, since it gives structural information on the long-range relationships between parts of the molecules.

Measurement of cross-correlated relaxation has been described earlier for homonuclear cases[9] and is widely used in solid-state NMR.[10] It is the availablility of isotopically labeled biomolecules and their application in solution-state NMR that makes the new method so interesting. Presumably the method will be extended to determine additional structural parameters, such as the angles ϕ or χ_1, or even angles between bond vectors that are close in space but not close in sequence. It can be applied in a more general perspective, and beyond the scope of proteins, for example, in nucleic acids and small organic molecules. The new structural parameter is directly measured, without the use of experimental calibration, as, for example, in the case of coupling constants that need to be interpreted with Karplus-type curves. In addition, it is fortunate that this new parameter can be accessed rather easily without the need to produce new samples or to invest in new spectrometer hardware. The experiment is based on existing triple-resonance experiments, and uses an only slightly modified pulse sequence. It is likely that this method will rapidly gain acceptance in the field of biomolecular NMR and that it will soon be standard methodology for biomolecular structure determination by NMR.

German version: *Angew. Chem.* **1998**, *110*, 470 – 472

Keywords: conformation analysis · NMR spectroscopy · proteins · structure elucidation

[1] a) S. Macura, R. R. Ernst, *Mol. Phys.* **1980**, *41*, 95 – 117; b) D. Neuhaus, M. Williamson, *The Nuclear Overhauser Effect in Structural and Conformational Analysis*, VCH, New York, **1989**.

[2] a) M. Karplus, *J. Chem. Phys.* **1959**, *30*, 11 – 15; b) V. F. Bystrov, *Prog. NMR Spectrosc.* **1976**, *10*, 41 – 81.

[3] K. Wüthrich, *NMR of Proteins and Nucleic Acids*, Wiley, New York, **1986.**

[4] B. Reif, M. Hennig, C. Griesinger, *Science* **1997**, *276*, 1230 – 1233.

[5] J. Cavanagh, W. J. Fairbrother, A. G. Palmer III, N. J. Skelton, *Protein NMR Spectroscopy*, Academic Press, San Diego, **1996**, pp. 265 – 270.

[6] A. Bax, M. Ikura, *J. Biomol. NMR* **1991**, *1*, 99 – 104.

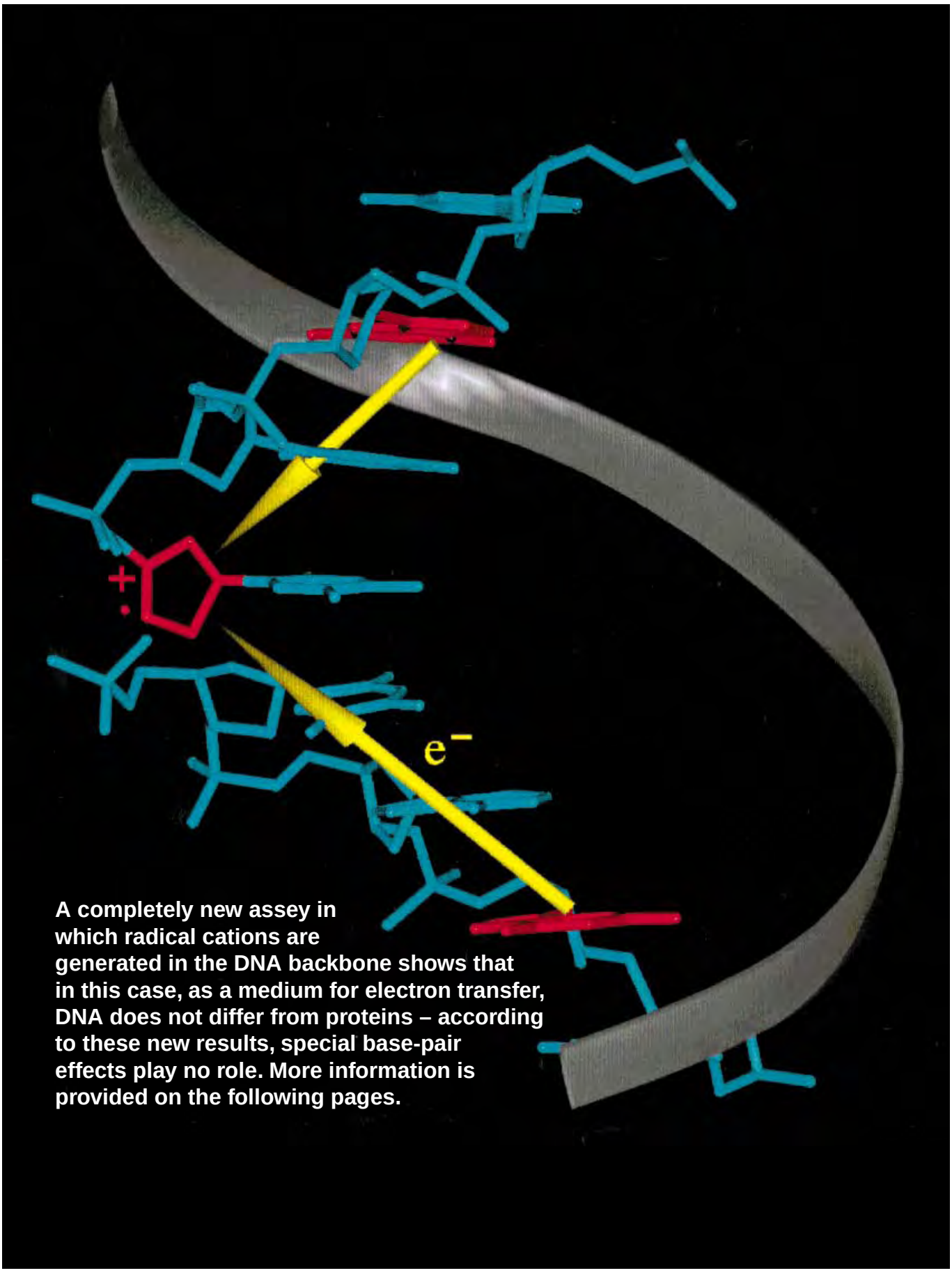
[7] M. Tessari, H. Vis, R. Boelens, R. Kaptein, G. Vuister, *J. Am. Chem. Soc.* **1997**, *119*, 8985 – 8990.

[8] J. R. Tolman, J. M. Flanagan, M. A. Kennedy, J. H. Prestegard, *Nat. Struct. Biol.* **1997**, *4*, 292 – 297; *PNAS* **1995**, *92*, 9279 – 9283; H. S. Kung, K. Y. Wang, I. Goljer, P. H. Bolton, *J. Magn. Reson. B* **1995**, *109*, 323 – 325; N. Tjandra, S. Grzesiek, A. Bax, *J. Am. Chem. Soc.* **1996**, *118*, 6264 – 6272; N. Tjandra, J. G. Omichinski, A. M. Gronenborn, G. M. Clore, A. Bax, *Nat. Struct. Biol.* **1997**, *4*, 732 – 738.

[9] a) C. Dalvit, G. Bodenhausen, *J. Am. Chem. Soc.* **1988**, *110*, 7924 – 2926; b) *Adv. Magn. Reson.* **1990**, *14*, 1 – 33.

[10] a) X. Feng, Y. K. Lee, D. Sandström, M. Eden, H. Maisel, A. Sebald, M. H. Levitt, *Chem. Phys. Lett.* **1996**, *257*, 314 – 320; b) X. Feng, P. J. E. Verdegem, Y. K. Lee, D. Sandström, M. Eden, P. Bovee-Geurts, W. J. de Grip, J. Lugtenburg, H. J. M. de Groot, M. H. Levitt, *J. Am. Chem. Soc.* **1997**, *119*, 6853 – 6857; c) K. Schmidt-Rohr, *ibid.* **1996**, *118*, 7601 – 7603.

 © WILEY-VCH Verlag GmbH, D-69451 Weinheim, 1998 1433-7851/98/3704-0458 $ 17.50+.50/0



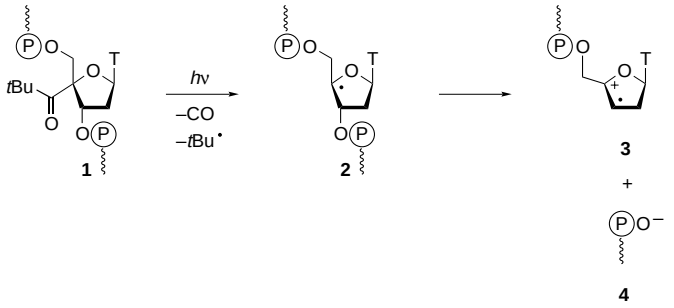
A completely new assey in which radical cations are generated in the DNA backbone shows that in this case, as a medium for electron transfer, DNA does not differ from proteins – according to these new results, special base-pair effects play no role. More information is provided on the following pages.

 © WILEY-VCH Verlag GmbH, D-69451 Weinheim, 1998 1433-7851/98/3704-0459 $ 17.50+.50/0

Electron Transfer through DNA in the Course of Radical-Induced Strand Cleavage**

Eric Meggers, Dirk Kusch, Martin Spichty, Uta Wille, and Bernd Giese*

In electron transfer (ET) reactions in proteins the transfer rates decrease by a factor of 10 for every 1.5 – 2.5 Å separation between reaction centers.[1] In sharp contrast to this generally accepted distance effect, studies on ET through the DNA have given contradictory results and raised a controversial discussion.[2] Depending upon the experimental probe either a minute[3] or a substantial[4] distance influence on the ET rate through DNA double strands was observed. In most of these studies the rates were determined by fluorescence quenching of photoactivated metal complexes or aromatic compounds attached to the DNA. In this communication we present a completely different assay that mimics the natural conditions of DNA reactions in a cell, and in which the ET through the DNA is measured by the chemical yield of a reduction step. The experimental method utilizes the spontaneous cleavage of a 4′-DNA radical **2**, which affords the radical cation **3** as a strong oxidant (Scheme 1).[5] We have observed that deoxy-



Scheme 1.

guanosine nucleotides within the DNA double strand can reduce this oxidized DNA fragment **3** and yield enol ether **5** by an ET step,[6] which mechanistically should be considered as a hole-transfer process.[4b–c, 7] The efficiency of this charge transfer depends upon the distance between the radical cation **3** and the guanine (G) base. It is important to note that in contrast to photoinduced ET studies, in our ground state experiments the ET is irreversible: there is no back transfer.

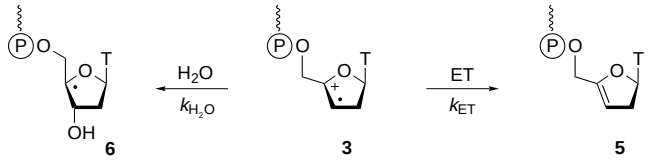
The experiments were carried out with DNA double strands in which one of the two DNA strands contained one 4′-acylated thymidine (T*) as in **1** that leads to radical cation **3** by Norrish type I cleavage (**1** → **2**) and subsequent heterolysis (**2** → **3** + **4**).[5b] The yield of phosphorylated oligonucleotide **4**, formed to the same extent as **3** in this reaction, is 71 – 89 %. The enol ether **5** was not detected when the double strands contained no G (Table 1, entries 1 and 2), but the yield reached 67 % if three guanosines were direct neighbors in the 5′- and 3′-direction (Table 1, entry 10).[8]

Table 1. Distance dependence of the electron transfer rates in single- and double-stranded DNA.

Entry	Sequence[a]	Δr [Å]	Yield of **5** [%][b,c]	$k_{ET,rel} \times 10^2$ [c]	Yield of **4** [%][b,c]
1	5′-dT$_5$T*T$_9$	-	-	-	81
2	5′-dT$_2$A$_3$T*T$_9$	-	-	-	78
3	5′-dG$_3$T$_2$T*T$_9$	14.1	< 0.2 (18)	< 0.25 (31)	80 (77)
4	5′-dT$_5$T*T$_2$G$_3$T$_4$	13.2	0.3	0.4	89
5	5′-dTG$_3$TT*T$_9$	11.1	1.2 (22)	1.6 (41)	76 (77)
6	5′-dT$_5$T*TG$_3$T$_5$	9.7	2.2	2.9	77
7	5′-dT$_2$C$_3$T*T$_9$	9.6	7.0	10	77
8	5′-dT$_2$G$_3$T*T$_9$	7.3	42 (30)	94 (45)	86 (96)
9	5′-dT$_5$T*G$_3$T$_6$	7.0	57 (36)	250 (92)	79 (75)
10	5′-dT$_2$G$_3$T*G$_3$T$_6$	-	67	310	89
11	5′-dT$_4$GT*T$_9$	7.3	24 (19)	52 (32)	71 (77)
12	5′-dT$_5$T*GT$_8$	7.0	41 (32)	100 (64)	83 (81)

[a] Sequence of the modified oligonucleotide; T* represents the 4′-acylated thymidine as in **1**; hybridization to the double strands was performed with the complementary, unmodified oligonucleotides. [b] Yields were obtained by HPLC. [c] Data for single strands in parentheses.

The yield of the enol ether **5** decreased from 57 to 0.3 % when the distance Δr[9,10] for the ET step increased from 7.0 to 13.2 Å (Table 1, entries 9 and 4). At a distance of 14.1 Å the reduction product **5** was not detectable: the ET reaction can no longer compete with other trapping reactions of the radical cation **3**. The main competition reaction is the addition of water (**3** → **6**, Scheme 2) that leads to further cleavage of the DNA.[11] Because of first-order or pseudo first-order conditions (excess of H_2O) the ratio between the rates of the ET reaction (k_{ET}) and all other trapping reactions (k_{trap})



Scheme 2.

like the water addition (k_{H_2O}) is given by the concentration ratio [**5**]/([**3**] – [**5**]).[12] Under the assumption that the competing reactions are not dependent upon the nucleotide sequence, we used the ratio k_{ET}/k_{trap} as the relative rate $k_{ET,rel}$ of the ET step (Table 1). In Figure 1 these relative rates are plotted against the distances Δr of the ET step according to Equation (1).[1]

$$k_{ET,rel} = A\, e^{-\beta \Delta r} \quad (1)$$

[*] Prof. Dr. B. Giese, Dipl.-Chem. E. Meggers, Dr. D. Kusch, Dipl.-Chem. M. Spichty, Dr. U. Wille
Institut für Organische Chemie
Universität Basel
St. Johanns-Ring 19, CH-4056 Basel
Fax: (+41) 61-267-1105
E-mail: giese@ubaclu.unibas.ch

[**] This work was supported by the Swiss National Science Foundation and the Volkswagen Foundation.

 © WILEY-VCH Verlag GmbH, D-69451 Weinheim, 1998 1433-7851/98/3704-0460 $ 17.50+.50/0

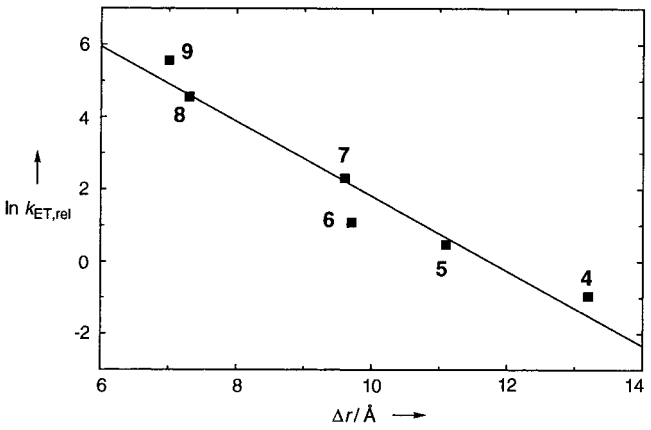


Figure 1. Distance dependence of electron transfer rates in double stranded DNA. The numbers at the data points correlate with the numbers at the arrows in Figure 2 and the entries in Table 1.

A linear dependence (correlation coefficient 0.97) of the rate ln $k_{ET,rel}$ upon the distance Δr of the ET reaction is observed. It is remarkable that the correlation holds even if the ET starts from the complementary strand (Table 1, entry 7) or from the cleaved strand (Table 1, entries 4, 6, and 9), and whether G is adjacent to the radical cation or separated by T bases. Figure 2 gives a graphical representation of this situation. The slope β of 1.0 ± 0.15 Å^{-1} in Figure 1 demonstrates that the ET rate decreases by a factor of 10 every 2.5 Å. Because this distance dependence is similar to ET reactions in proteins, it can be concluded that the hole transfer from the radical cation of the sugar phosphate backbone to the G base in DNA double strands does not benefit from base stacking effects (Figure 2).

From competition kinetic experiments with intermolecular electron donors (KI, methionine, selenomethionine, and $K_4[Fe(CN)_6]$) we deduced a rate of 10^6 M^{-1}s^{-1} for the addition of H_2O to the radical cation **3**.[13] With these data the rate coefficient of the electron transfer k_{ET} from G to a 7 Å distant deoxyribose radical cation (Table 1, entries 8 and 9) is 10^8 s^{-1}.[14]

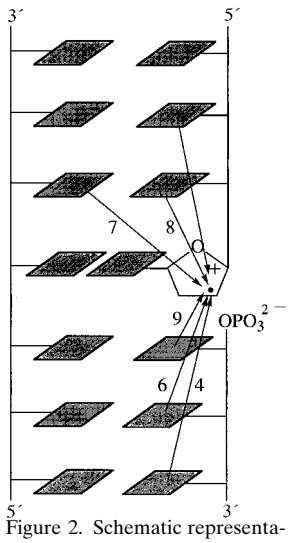


Figure 2. Schematic representation of the electron transfer (arrows) between guanine bases and the radical cation of the DNA sugar–phosphate backbone. The numbers at the arrows correlate with the numbers in Figure 1 and the entries in Table 1.

The β value of 1.0 Å^{-1} demonstrates that radical cation **3**, which is a reactive intermediate in the spontaneous strand cleavage of 4′-DNA radicals, can only be trapped efficiently by ET in DNA double strands if G bases are present in the immediate neighborhood. In sharp contrast the position of the deoxyguanosine has only little influence on the rate of the electron transfer in DNA single strands. As the data of Table 1 (entries 3 and 8) show, when two thymidine residues separate the G base from the deoxyribosyl radical cation **3**, the rate decreases by at least 400 in the double strand, but the same variation of the base sequence reduces the rate of electron transfer in single strands only by a factor of 1.5 (Table 1, data in parentheses). Obviously, single strands are flexible enough to adopt conformations in which the distance Δr between guanosine residues separated even by several nucleotides from the radical cation is short enough for a fast ET step. This assay opens new perspectives for the study of the conformation and flexibility of DNA molecules.

Experimental Section

The oligonucleotides were synthesized on a DNA synthesizer in 1 μmol scale. A standard procedure for 2-cyanoethyl phosphoramidites was used, except that the coupling of the 4′-pivaloyl-modified nucleoside was extended to 15 min. The resin of each synthesis was incubated in 1 mL concentrated ammonium hydroxide at 55°C overnight, and the mixture was subsequently lyophilized to dryness. The extracted crude oligonucleotide mixtures were purified by anion exchange chromatography and reversed phase HPLC. Finally, the oligonucleotides were passed through a sephadex column. The CD spectra of the modified double strands are very similar to those of the unmodified double strands and prove a B-DNA conformation. The UV melting temperatures T_m are decreased by the modification T* by only 0–2°C.

Irradiation experiments were carried out in poly(methyl methacrylate) cuvettes at 15°C by using a 500 W Hg high-pressure lamp with a 320 nm cut-off filter. A mixture of 2.0 nmol 4′-pivaloyl-modified oligonucleotide and 2.4 nmol complementary strand were dissolved in 300 μL buffer (20 mM sodium citrate pH 5.0 with 100 mM NaCl). Annealing of the complementary strand was achieved by heating to 70°C for 1 min and cooling down slowly to room temperature. The solutions were purged with argon for 30 min before photolysis. Single-stranded probes were irradiated for 4 min, double-stranded probes for 3 min. The irradiated solutions were analyzed by HPLC (Waters Symmetry C18, 3.5 μm, 100×4.6 mm) at 260 nm. Elution: Eluent A = 0.1M triethyl ammonium acetate (TEAA) pH 7.0; eluent B = acetonitrile. A typical gradient was 5% B for 2 min, then 5 to 13% B in 60 min; flow rate 1.5 mL min^{-1}, column temperature 30 or 50°C. Evaluation: The peak areas were divided by the calculated extinction coefficients of the corresponding oligonucleotides and quantified with external calibration. The identity of the products was determined by MALDI-TOF mass spectrometry, enzymatic digestion with analysis of the nucleotides, and by comparison of the reversed phase HPLC retention times with reference substances.

Received: September 25, 1997 [Z10971IE]
German version: *Angew. Chem.* **1998**, *110*, 474–476

Keywords: DNA cleavage · electron transfer · radical ions · radical reactions

[1] a) R. J. P. Williams, *J. Biol. Inorg. Chem.* **1997**, *2*, 373; b) S. S. Skourtis, D. N. Beratan, *ibid.* **1997**, *2*, 378; c) O. Farver, I. Pecht, *ibid.* **1997**, *2*, 387; d) C. C. Moser, C. C. Page, X. Chen, P. L. Dutton, *ibid.* **1997**, *2*, 393; e) J. R. Winkler, H. B. Gray, *ibid.* **1997**, *2*, 399, and references therein.

[2] a) D. N. Beratan, S. Priyadarshy, S. M. Risser, *Chem. Biol.* **1997**, *4*, 3; b) E. K. Wilson, *Chem. Eng. News* **1997**, *75* (8), 33; c) T. L. Netzel, *J. Chem. Educ.* **1997**, *74*, 646; d) G. Taubes, *Science* **1997**, *275*, 1420; e) U. Diederichsen, *Angew. Chem.* **1997**, *109*, 2411; *Angew. Chem. Int. Ed. Engl.* **1997**, *36*, 2317.

[3] a) C. J. Murphy, M. R. Arkin, Y. Jenkins, N. D. Ghatlia, S. H. Bossmann, N. J. Turro, J. K. Barton, *Science* **1993**, *262*, 1025; b) M. R. Arkin, E. D. A. Stemp, R. E. Holmlin, J. K. Barton, A. Hörmann, E. J. C. Olson, P. F. Barbara, *ibid.* **1996**, *273*, 475; c) D. B. Hall, R. E. Holmlin, J. K. Barton, *Nature* **1996**, *382*, 731; d) M. R. Arkin, E. D. A. Stemp, S. Coates-Pulver, J. K. Barton, *Chem. & Biol.* **1997**, *4*, 389;

 © WILEY-VCH Verlag GmbH, D-69451 Weinheim, 1998 1433-7851/98/3704-0461 $ 17.50+.50/0

e) P. J. Dandliker, R. E. Holmlin, J. K. Barton, *Science* **1997**, *275*, 1465; f) S. O. Kelley, R. E. Holmlin, E. D. A. Stemp, J. K. Barton, *J. Am. Chem. Soc.* **1997**, *119*, 9861; g) review: R. E. Holmlin, P. J. Dandliker, J. K. Barton, *Angew. Chem.* **1997**, *109*, 2830; *Angew. Chem. Int. Ed. Engl.* **1997**, *36*, 2715.

[4] a) F. D. Lewis, T. Wu, Y. Zhang, R. L. Letsinger, S. R. Greenfield, M. R. Wasielewski, *Science* **1997**, *277*, 673; b) A. M. Brun, A. Harriman, *J. Am. Chem. Soc.* **1992**, *114*, 3656; c) A. M. Brun, A. Harriman, *ibid.* **1994**, *116*, 10383; d) T. J. Meade, J. F. Kayyem, *Angew. Chem.* **1995**, *107*, 358; *Angew. Chem. Int. Ed. Engl.* **1995**, *34*, 352.

[5] a) C. von Sonntag, U. Hagen, A.-M. Schön-Bopp, D. Schulte-Frohlinde, *Adv. Radiat. Biol.* **1981**, *9*, 109; b) B. Giese, X. Beyrich-Graf, P. Erdmann, M. Petretta, U. Schwitter, *Chem. Biol.* **1995**, *2*, 367; c) A. Gugger, R. Batra, P. Rzadek, G. Rist, B. Giese, *J. Am. Chem. Soc.* **1997**, *119*, 8740.

[6] a) GC base pairs have lower oxidation potentials than AT base pairs: H. Sugiyama, I. Saito, *J. Am. Chem. Soc.* **1996**, *118*, 7063; b) M. Hutter, T. Clark, *ibid.* **1996**, *118*, 7574. In oxidative attack of DNA mainly G bases have been oxidized: c) D. T. Breslin, G. B. Schuster, *J. Am. Chem. Soc.* **1996**, *118*, 2311; d) D. Ly, Y. Kan, B. Armitage, G. B. Schuster, *ibid.* **1996**, *118*, 8747; e) I. Saito, M. Takayama, H. Sugiyama, K. Nakatani, *ibid.* **1995**, *117*, 6406; f) S. Steenken, S. V. Jovanovic, *ibid.* **1997**, *119*, 617.

[7] G. L. Closs, J. R. Miller, *Science* **1988**, *240*, 440.

[8] In the course of this ET step G must be oxidized to a radical cation that is known to undergo a fast deprotonation step yielding a very unreactive delocalized G radical. Since we cannot detect any damage at G sites, we assume that the G radical is repaired by hydrogen atom abstraction under anaerobic conditions. For structure, reactivity, and repair of deoxyguanosine radical cations, see: a) S. Steenken, *Chem. Rev.* **1989**, *89*, 503; b) L. P. Candeias, S. Steenken, *J. Am. Chem. Soc.* **1989**, *111*, 1094; c) S. V. Jovanovic, M. G. Simic, *Biochim. Biophys. Acta* **1989**, *1008*, 39.

[9] G triple units were chosen for the experiments on the distance dependence because they are the most potent electron donating sites in DNA (see ref. [6]). We suppose that the closest G is the initially oxidized base. This assumption is permitted since the change from a single G to a triple G unit in 3′- as well as in 5′-direction has nearly the same ET-acceleration effect of 2.5 and 1.8, respectively (Table 1, entries 8, 11, and 9, 12).

[10] For the determination of the distance Δr, the corresponding DNA duplex sequences were constructed in the B-form with the nucleic acid building tool in the program MacroModel V4.5. In order to mimic the planar enol ether radical cation **3**, the deoxyribose enol ether **5** was modeled into the DNA structure using the AMBER* force field implemented in MacroModel V4.5. Distances Δr were taken between the radical center C3′ of the radical cation and the G carbon atom 5 which has the highest electron density of the HOMO.

[11] Independent experiments with glutathione diethyl ester as a trap for radical **6** demonstrated that, in G-free DNA strands, the addition of water to radical cation **3** (**3** → **6**) occurs in about 70% yield.

[12] We determined the ratio k_{ET}/k_{trap} from the HPLC areas (corrected by the extinction coefficients) of 5′-phosphate **4** (A_4), whose concentration is equal to the overall yield of radical cation **3** (Scheme 1) and enol ether **5** (A_5). The ratio $A_5/(A_4 - A_5)$ is equal to k_{ET}/k_{trap}. Because these ratios turned out to be independent of the conversion, the reactions follow first- or pseudo first-order kinetics.

[13] We used one-electron donors like methionine, selenomethionine, KI, and $K_4[Fe(CN)_6]$ to reduce the radical cation **3** by intermolecular ET in competition to water addition. KI is the fastest ET quencher. Under the assumption that this ET proceeds in a nearly diffusion controlled way, we could determine a rate coefficient of $10^6\,M^{-1}s^{-1}$ by pseudo first-order kinetic experiments with different concentrations of KI.

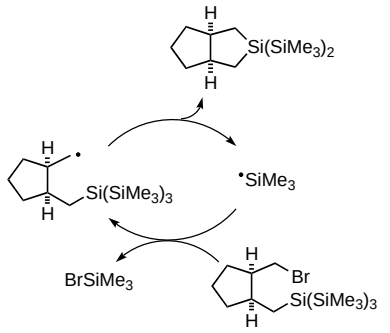
[14] Note added in proof (February 2, 1998): Similar ET rates at 7 Å were reported recently: K. Fukui, K. Tanaka, *Angew. Chem.* **1998**, *110*, 167; *Angew. Chem. Int. Ed.* **1998**, *37*, 158.

S_Hi Reactions at Silicon as Unimolecular Chain Transfer Steps in the Formation of Cyclic Alkoxysilanes**

Armido Studer*

Intermolecular transfer of bromine, iodine, phenylselenide, and aryltelluride groups between carbon-centered radicals is a well-established procedure for the synthesis of complex organic molecules.[1] In contrast (other than one example[2]), intramolecular transfer involving migration of selenium, tellurium or a halogen has not yet been observed. For the chalcogen group, only a single report describes the 1,4-transfer of a phenylsulfanyl group.[3] However, several reports on the intramolecular migration of stannyl or silyl groups have appeared.[4] The reasons for the facile intramolecular homolytic substitution (S_Hi) reaction at silicon or tin are not well understood.[5]

These S_Hi reactions can be used for the formation of silicon- or tin-containing heterocycles. Giese et al.[6] and Utimoto et al.[7] independently reported intramolecular homolytic substitutions at tris(trimethylsilyl)-substituted Si atoms by C-centered radicals. It was concluded that the trimethylsilyl radical generated during the intramolecular substitution acts as the chain carrier (Scheme 1). According to Curran's terminology,[8] this is an example of a unimolecular chain



Scheme 1. S_Hi reaction at tris(trimethylsilyl)-substituted silanes.

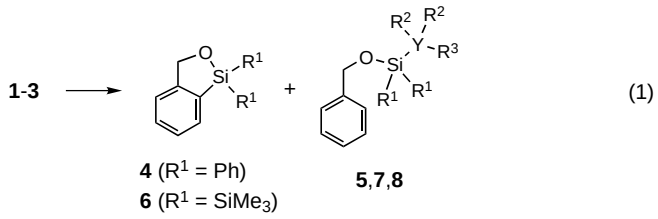
transfer (UMCT) reaction in which the key chain transfer step is a unimolecular process. After consideration of the results of Giese's and Utimoto's groups, we initiated further exploration of intramolecular homolytic substitutions at silicon. It was envisaged that this transformation would be a suitable UMCT step in bimolecular radical addition reactions, where either a silyl or a stannyl radical acts as the chain carrier. In addition, the cyclic silanes formed in these UMCT steps could be transformed into the corresponding alcohol derivatives by Tamao – Fleming oxidation.[9]

[*] Dr. A. Studer
Laboratorium für Organische Chemie
der Eidgenössischen Technischen Hochschule
ETH-Zentrum, Universitätstrasse 16, CH-8092 Zürich (Switzerland)
Fax: (+41) 1-632-1144,
E-mail: studer@org.chem.ethz.ch

[**] I am grateful to Prof. Dr. D. Seebach for generous financial support and to Prof. Dr. D. P. Curran for helpful discussions.

 © WILEY-VCH Verlag GmbH, D-69451 Weinheim, 1998 1433-7851/98/3704-0462 $ 17.50+.50/0

Initially, the S_Hi reaction of aryl radicals at differently substituted silanes was studied [Eq. (1)]. The required 2-halo-substituted benzyl silyl ethers **1**–**3** were synthesized from the



(1)

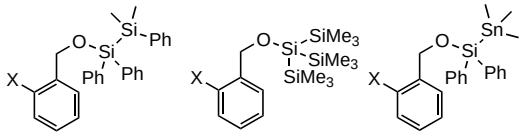
corresponding alcohols.[10] Reaction of disilane **1** with sub-stoichiometric amounts of Bu_3SnH (0.2 equiv) did not provide the desired alkoxysilane **4**. With 1.2 equivalents of $(TMS)_3SiH$ as initiator, 5% of **4** and 43% of the reduction product **5** were formed along with several unidentified side products. The reduction product was isolated in 38% yield (Table 1, entry 1).

Table 1. S_Hi reactions of aryl radicals at substituted silanes.[a]

Entry	Starting material	Conditions	Unchanged material [%]	Yield [%] (product)	Yield [%] (side product)
1	**1**	1.2 equiv $(TMS)_3SiH$ benzene, 0.04 M, AIBN reflux	–	5 (**4**)	43[b] (**5**)
2	**2**	0.2 equiv Bu_3SnH benzene, 0.04 M, AIBN (10%) reflux, syringe pump[c]	42	58 (**6**)	–
3	**2**	0.5 equiv Bu_3SnH benzene, 0.04 M, AIBN reflux	–	91 (**6**)	4 (**7**)
4	**2**	0.5 equiv $(TMS)_3SiH$ benzene, 0.04 M, AIBN (25%) reflux, syringe pump[d]	60	30 (**6**)	–
5	**2**	$Bu_3SnSnBu_3$ (10%) benzene, 0.1 M, acetone *hv*, 72 h	91	9 (**6**)	–
6	**2**	$Bu_3SnSnBu_3$ (10%) hexane, 0.1 M, acetone *hv*, 45 h	89	11 (**6**)	–
7	**3**	0.2 equiv Bu_3SnH benzene, 0.02 M, AIBN reflux	–	80[e] (**4**)	–

[a] Yields determined by ^1H NMR spectroscopy. AIBN = azoisobutyronitrile. [b] 38% yield of isolated product. [c] Bu_3SnH (0.08 M) and AIBN were dissolved in benzene and added over 7 h. [d] $(TMS)_3SiH$ (0.13 M) and AIBN were dissolved in benzene and added over 8 h. [e] 68% yield of isolated product.

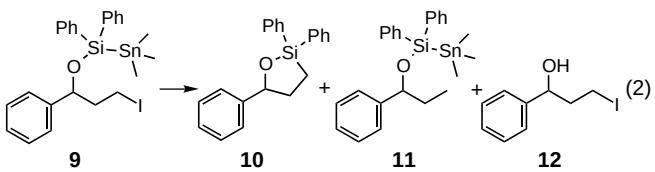
Slow addition of $(TMS)_3SiH$ did not provide better results. Presumably, the Si–Si bond in **1** is too strong to be efficiently cleaved by an aryl radical.[13] Addition of Bu_3SnH (0.2 equiv) by syringe pump to **2** in benzene (0.04 M) afforded alkoxysilane **6** and starting material **2** in a ratio of 58:42 (entry 2). No other side product derived from **2** could be observed. This clearly showed that the UMCT was occurring. However, even after careful optimization, it was still necessary to use up to 0.5 equivalents of initiator for complete reaction. For example, addition of Bu_3SnH (0.5 equiv) to a solution of **2** in benzene



1 (X = Br) **2** (X = Br) **3** (X = I)
5 (X = H) **7** (X = H) **8** (X = H)

(0.04 M) afforded **6** in 91% yield alongside the direct reduction product **7** (4% as determined by ^1H NMR analysis; entry 3). With $(TMS)_3SiH$ (0.5 equiv) as initiator, only 30% of cyclization product was formed (entry 4). Irradiation (300 W sun lamp, 72 hours) of a benzene solution of **2** containing hexabutylditin (0.1 equiv) and acetone as a sensitizer[14] afforded **6** (9%), along with 91% unchanged starting material (entry 5). A slightly faster reaction was observed in this case if benzene was replaced by hexane (entry 6). This is probably due to the fact that silyl radicals add to benzene and are thus prevented from propagating the chain.[15] With silyl ether **3** (0.02 M, benzene), quantitative consumption of the starting material was observed with only 0.2 equivalents of Bu_3SnH, added in two portions; alkoxysilane **4** formed in 80% yield as determined by ^1H NMR analysis (entry 7). No reduction product **8** was observed. Purification by reversed phase (RP) chromatography (RP-18 Nucleosil, Macherey-Nagel particle size 7, acetonitrile) afforded **4** in 68% yield. Apparently, due to the weaker bond energy,[16] the Si–Sn bond is superior to the Si–Si bond for applications to intramolecular homolytic substitutions at silicon.

To elaborate this UMCT process further, the cyclization of alkyl radicals was studied. To this end, iodide **9** was prepared (62%) from the corresponding iodoalcohol.[12] The UMCT reaction was studied under different conditions [Eq.(2)]. Under "atom transfer" conditions[17] on irradiation (300W sun lamp) of a benzene solution of **9** (0.1M) containing hexabutylditin (0.1 equiv) lead to complete consumption of **9** after 16 hours (Table 2, entry 1). Besides alkoxysilane **10** (87%, 66% after chromatography), the reduced silyl ether **11** (13%) was observed in the crude product.[18] Without addition of the ditin, under otherwise similar conditions, the reaction was much slower and iodoalcohol **12** (arising from desilylation of **9**) was formed as a side product (entry 2). Similar results were obtained if the reaction was conducted under atom transfer conditions with either hexaphenylditin (entry 3) or tetrakis (trimethylsilyl)silane[8b] (entry 4) as additives. The best result was obtained with Bu_3SnH as the initiator of the UMCT reaction. With 0.15 equivalents of



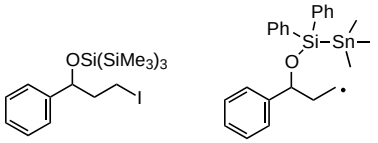
(2)

Table 2. Unimolecular chain transfer reaction of **9**.[a]

Entry	Conditions	**10** [%]	**11** [%]	**12** [%]
1	$Bu_3SnSnBu_3$ (10%), benzene 0.06 M, *hv*, 16 h	87	13	–
2	benzene, 0.1 M, *hv*, 36 h[b]	30	–	16
3	$Ph_3SnSnPh_3$ (10%), benzene 0.1 M, *hv*, 24 h	45	–	21
4	$(TMS)_4Si$ (10%), benzene 0.1 M, *hv*, 24 h	41	–	23
5	Bu_3SnH (15%), AIBN, benzene	89	4	–
6	Bu_3SnH (5%), AIBN, benzene	84	2	–

[a] Yields determined by ^1H NMR spectroscopy. [b] The reaction was stopped after 36 h; 16% of the starting material was detected.

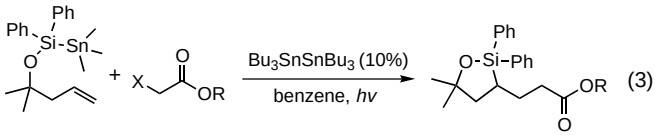
Bu_3SnH (added in three portions) the cyclic alkoxysilane **10** was formed in 89% yield with only 4% of the reduction product **11** (entry 5). As little as 0.05 equivalents of Bu_3SnH could be used for complete consumption of the starting material; however, a slight decrease of the yield (84%) was observed (entry 6). The desilylation product **12** was not seen in these tin hydride experiments. By competition experiments with $(TMS)_3SiH$,[6] a rate constant of $1.2 \times 10^6\,s^{-1}$ at 80° was estimated for the cyclization of radical **14** leading to **10**. In the case of iodide **13**, obtained by silylation ($(TMS)_3SiI$) of 3-



13 **14**

chloro-1-phenylpropan-1-ol followed by Finkelstein reaction (32% overall), no UMCT reaction could be observed under atom transfer conditions with $Bu_3SnSnBu_3$ (0.1 equiv) as the additive. Starting material **13** could be identified as the main component in the NMR spectrum of the crude product (65% recovered after chromatography). The reduction product (also independently synthesized) was formed in 5% yield.[19] As with some of the reactions described earlier, the Si–Si bond is not suitable for UMCT reactions based on S_Hi reactions at silicon.

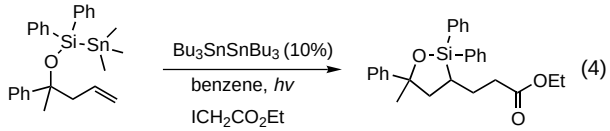
In order to demonstrate the preparative value of S_Hi reactions, bimolecular radical addition reactions with a subsequent S_Hi reaction were also studied. Radical acceptor **15** was prepared as previously described[12] from the corresponding tertiary alcohol (72%). Reaction of phenyl bromoacetate (1.2 equiv) with olefin **15** (0.3 M, benzene) under atom transfer conditions provided **16** [Eq. (3)]. Neither starting material nor side products derived from **15** could be identified in the NMR spectrum of the crude product.[20] Purification by



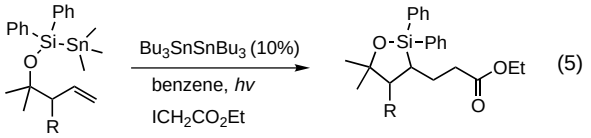
15 (X = Br, R = Ph) (X = I, R = Et) **16** (68%, R = Ph) **17** (56%, R = Et)

chromatography (SiO_2) afforded **16** in 68% yield. Under similar conditions, ethyl ester **17** was isolated in 56% yield starting from ethyl iodoacetate and **15**.[21] If the bimolecular reaction of **15** with phenyl bromoacetate was conducted with tin hydride (1 equiv Bu_3SnH, syringe pump, 0.2 M in benzene) only 26% of **16**, besides unchanged **15** (70%), was observed.

We also studied the cyclization reaction of chiral silyl ethers. The chiral olefins **18** and **19a**,**b** containing a stereogenic center either β or α to the double bond were synthesized as described above. UMCT reaction of **18** with ethyl iodoacetate under atom transfer conditions[17] provided alkoxysilane **20** as a 1.5:1 mixture of diastereoisomers in 67% yield [Eq. (4)].[22] Excellent selectivities were obtained for the



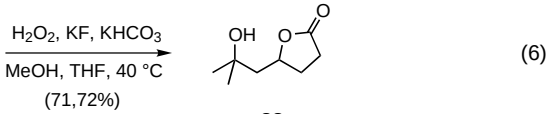
18 **20** (67%, *dr* = 1.5:1)



19a (R = Ph) **19b** (R = Me) **21** (R = Ph, 87%, only *trans*) **22** (R = Me, 76%, *trans*:*cis* = 22:1)

cyclization of the secondary radical formed after addition of the ethyl iodoacetate derived radical to **19a**,**b** [Eq. (5)]. With radical acceptor **19a** only the *trans* product **21** was observed (87% isolated yield).[23] With **19b** a somewhat lower (but still good) selectivity was obtained for the UMCT reaction with ethyl iodoacetate. The two isomers, *trans*-**22** and *cis*-**22** (22:1) were isolated as an inseparable mixture in 76% yield. To our knowledge, these are the first examples of such high stereocontrol in these types of homolytic substitution reactions.[4,24]

As the final step of the reaction sequence, Tamao–Fleming oxidation was performed on alkoxysilanes **16** and **17** according to known procedures [Eq. (6)].[11] Acidification after standard workup provided lactone **23**, which was isolated in good yields (71, 72%).



23

In summary, it has been shown that S_Hi reactions at silicon by C-centered radicals in γ-position of stannylated silyl ethers are efficient UMCT reactions providing cyclic alkoxysilanes, which can easily be converted into the corresponding diol derivatives. In addition, excellent 1,2 stereoinduction was obtained in the cyclization reaction of chiral silyl ethers.

Experimental Section

All irradiation experiments were carried out in sealed tubes with a 300W sun lamp (OSRAM 300W standard lamp, clear). Radical addition reaction:

 © WILEY-VCH Verlag GmbH, D-69451 Weinheim, 1998 1433-7851/98/3704-0464 $ 17.50+.50/0 *Angew. Chem. Int. Ed.* **1998**, *37*, No. 4

Silyl ether **19a** (150 mg, 0.28 mmol), ethyl iodoacetate (0.042 mL, 0.35 mmol), and $Bu_3SnSnBu_3$ (0.017 mL, 0.028 mmol) were dissolved under argon in benzene (1.1 mL). Irradiation for 16 hours and removal of the solvent afforded the crude product, which was purified by flash column chromatography (SiO_2, Et_2O/pentane 1/20) to give **21** (110 mg, 87 %) as a colorless oil. ^{1}H NMR (500 MHz, $CDCl_3$): $\delta = 0.86$ (t, $J = 7.1$, 3 H, CH_3), 1.06 (s, 3 H, CH_3), 1.47 (s, 3 H, CH_3), 1.59 – 1.67 (m, 1 H), 1.77 – 1.83 (m, 1 H), 2.19 (t, $J =$ 7.4, 2 H), 2.49 – 2.54 (m, 1 H, SiCH), 3.03 (d, $J = 13.3$, 1 H, PhCH), 3.78 – 3.89 (m, 2 H, CH_2O), 7.06 – 7.10 (m, 1 H, aromat.), 7.11 – 7.28 (m. 10 H, aromat.), 7.81 – 7.84 (m, 2 H, aromat.), 7.91 – 7.94 (m, 2 H, aromat.); ^{13}C NMR (125 MHz, $CDCl_3$): 14.19 (CH_3), 24.75 (CH_2), 25.53 (CH_3), 28.74 (CH), 30.08 (CH_3), 35.09 (CH_2), 59.99 (CH_2), 62.66 (CH), 82.14 (C), 127.10 (CH), 127.94 (CH), 128.29 (CH), 128,39 (CH), 128.42 (CH), 130.47 (CH), 130.53 (CH), 134.03 (C), 135.24 (CH), 135.66 (CH), 135.93 (C), 140.47 (C), 172.46 (C). EI-MS: m/z (%): 444.2 (3, M^+), 388.2 (9), 386.2 (100), 295.1 (12), 227.1 (81), 199.1 (63), 183.1 (53). C,H analysis calcd for $C_{28}H_{32}O_3Si$ (444.6): C 75.64, H 7.25, O 10.79, Si 6.32; found: C 75.41, H 7.34.

Received: September 11, 1997 [Z 10919 IE]
German version: *Angew. Chem.* **1998**, *110*, 507 – 510

Keywords: radical reactions · silicon · silyl ethers · tin

[1] D. P. Curran, *Synthesis* **1988**, 489; D. H. R. Barton, M. Ramesh, *J. Am. Chem. Soc.* **1990**, *112*, 891; D. P. Curran, E. Eichenberger, M. Collis, M. G. Roepel, G. Thoma, *ibid.* **1994**, *116*, 4279; D. Crich, C. Chen, J.-T. Hwang, H. Yuan, A. Papadatos, R. I. Walter, *ibid.* **1994**, *116*, 8937.
[2] J. T. Banks, H. Garcia, M. A. Miranda, J. Pérez-Prieto, J. C. Scaiano, *J. Am. Chem. Soc.* **1995**, *117*, 5049.
[3] M. C. Fong, C. H. Schiesser, *Aust. J. Chem.* **1992**, *45*, 475.
[4] C. H. Schiesser, L. M. Wild, *Tetrahedron* **1996**, *52*, 13265.
[5] C. H. Schiesser, M. L. Styles, L. M. Wild, *J. Chem. Soc. Perkin Trans. 2* **1996**, 2257.
[6] K. J. Kulicke, C. Chatgilialoglu, B. Kopping, B. Giese, *Helv. Chim. Acta* **1992**, *75*, 935.
[7] K. Miura, K. Oshima, K. Utimoto, *Bull. Chem. Soc. Jpn.* **1993**, *66*, 2348.
[8] a) D. P. Curran, J. Xu, E. Lazzarini, *J. Chem. Soc. Perkin Trans. 1* **1995**, 3049; b) D. P. Curran, J. Xu, *ibid.* **1995**, 3061; c) A. Martinez-Grau, D. P. Curran, *J. Org. Chem.* **1995**, *60*, 8332; d) D. P. Curran, J. Xu, E. Lazzarini, *J. Am. Chem. Soc.* **1995**, *117*, 6603; e) A. Martinez-Grau, D. P. Curran, *Tetrahedron* **1997**, *53*, 5679. For other UMCT reactions see: f) G. E. Keck, E. J. Enholm, J. B. Yates, M. R. Wiley, *Tetrahedron* **1985**, *41*, 4079; S. Kim, J. S. Koh, *J. Chem. Soc. Chem. Commun.* **1992**, 1377; J. Boivin, J. Camara, S. Z. Zard, *J. Am. Chem. Soc.* **1992**, *114*, 7909.
[9] G. R. Jones, Y. Landais, *Tetrahedron* **1996**, *52*, 7599.
[10] Silyl ether **1** was prepared according to known procedures[11] from 2-bromobenzyl alcohol and 1-chloro-2,2-dimethyl-1,1,2-triphenyldisilane (78 % yield). Compound **2** was obtained from the corresponding chlorosilane (imidazole, DMF, 87 %). Stannylated silyl ether **3** was synthesized from (diphenylsilyl)trimethyl tin chloride[12] and 2-iodobenzyl alcohol (85 %).
[11] M. Murakami, M. Suginome, K. Fujimoto, H. Nakamura, P. G. Andersson, Y. Ito, *J. Am. Chem. Soc.* **1993**, *115*, 6487.
[12] A. Kawachi, N. Doi, K. Tamao, *J. Am. Chem. Soc.* **1997**, *119*, 233.
[13] Compilation of Si – Si bond energies: R. Walsh, *Acc. Chem. Res.* **1981**, *14*, 246.
[14] M. Harendza, J. Junggebauer, K. Lessmann, W. P. Neumann, H. Tews, *Synlett* **1993**, 286.
[15] S. J. Cole, J. N. Kirwan, B. P. Roberts, C. R. Willis, *J. Chem. Soc. Perkin Trans 1* **1991**, 103. See also C. Chatgilialoglu, K. U. Ingold, J. C. Scaiano, *J. Am. Chem. Soc.* **1983**, *105*, 3292.
[16] M. F. Lappert, J. B. Pedley, J. Simpson, T. R. Spalding, *J. Organomet. Chem.* **1971**, *29*, 195.
[17] D. P. Curran, M.-H. Chen, D. Kim, *J. Am. Chem. Soc.* **1989**, *111*, 6265.
[18] So far the origin of the reduction product is not clear. When the UMCT reaction was conducted under higher dilution (0.01 M) no reduction product **11** was observed; however, unidentified side products were formed.
[19] Since no authentic sample of the desired cyclization product was available, it was not possible to determine by NMR analyis whether the UMCT product was formed in small quantities. Initiation of the UMCT reaction with Bu_3SnH did not provide better results.
[20] Interestingly, the presence of the reduction product in analogy to the formation of **11** could not be observed.
[21] The mediocre yield is due to partial decomposition of the products during chromatography.
[22] The diastereoisomers could not be separated. We could not determine which isomer was formed in excess.
[23] The relative configuration was assigned by NOE experiments.
[24] L. J. Benja min, C. H. Schiesser, K. Sutej, *Tetrahedron* **1993**, *49*, 2557; D. Colombani, B. Maillard, *ibid.* **1996**, *52*, 14855. Other stereoselective UMCT reactions: D. P. Curran, J. Xu, *Synlett* **1997**, 1102.

The Weak-Link Approach to the Synthesis of Inorganic Macrocycles**

Joshua R. Farrell, Chad A. Mirkin,* Ilia A. Guzei, Louise M. Liable-Sands, and Arnold L. Rheingold

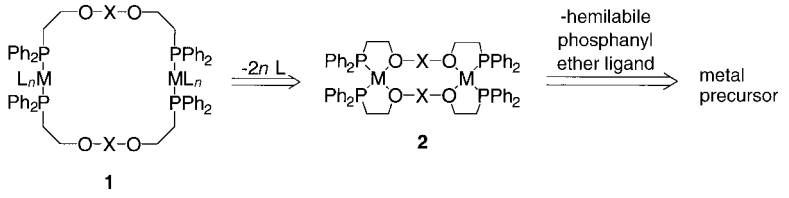
Inorganic and organometallic macrocycles have been topics of intense study with implications for host – guest chemistry, modeling of biological systems, catalysis, and even molecular electronics.[1] These structures can vary in size, shape (rings, squares, rectangles, and cylinders), and the number of metal centers that comprise the macrocycle.[2] One of the most popular synthetic strategies for macrocycles is the "molecular box, square, or rectangle strategy", which was pioneered by Fujita et al.[3] and has now been utilized by many;[4] this strategy uses conformationally rigid ligands bound to metal centers in a *cis* fashion to form tetranuclear complexes in exceptionally high yields. Although this strategy works well for rigid ligands, it will undoubtedly fail with flexible ones because of competing oligimerization and polymerization reactions.

Herein we report a new, general, high-yield (> 95 %) strategy for synthesizing homobimetallic macrocycles with chemically tailorable cavity properties from flexible ligands (Scheme 1). We refer to this strategy as the "weak-link approach" to the synthesis of inorganic macrocycles. In 1996 Steel and co-workers showed that the reaction between Ag^I and an aromatic ligand with multiple ligating sites resulted in the formation of dimetallocyclophanes.[5] These solid-state structures, which do not remain intact in solution, have ether

[*] Prof. C. A. Mirkin, J. R. Farrell
Department Of Chemistry
Northwestern University
2145 Sheridan Road, Evanston, IL 60208-3113 (USA)
Fax: (+1) 847-491-7713
E-mail: camirkin@chem.nwu.edu
I. A. Guzei, L. M. Liable-Sands, Prof. A. L. Rheingold
Department of Chemistry and Biochemistry, University of Delaware (USA)

[**] We acknowledge the National Science Foundation (CHE-9625391 and CHE-9357099) and the Petroleum Research Fund (no. 30759-AC3) for generously funding this research. C.A.M. also acknowledges an A. P. Sloan Foundation Fellowship and a Camille Dreyfus Teacher-Scholar Award.

 © WILEY-VCH Verlag GmbH, D-69451 Weinheim, 1998 1433-7851/98/3704-0465 $ 17.50+.50/0



Scheme 1. Retrosynthetic outline of the weak-link strategy for the synthesis of inorganic macrocycles. M = late transition metal, X = aromatic group.

oxygen atoms weakly coordinated to the Ag^I ions and exhibit arene–arene π-stacking interactions. Our strategy as presented in Scheme 1 takes advantage of 1) Steel's observation that 1,4-aryl diethers can bind weakly to late transition metals to form bimetallic compounds,[5] 2) hemilabile ligands,[6] and 3) π–π interactions between two aromatic groups that have been strategically incorporated into the ligands.

With this strategy, a target macrocyclic structure **1** is condensed in a retrosynthetic fashion to form the polycyclic compound **2**, which is made up of a series of fused thermodynamically stable rings with several strong (Rh–P) and weak (Rh–O, π–π interactions) chemical links (Scheme 1). This latter structure can be prepared with the appropriate hemilabile ligand and a metal compound, and once generated it can be opened into a series of structurally different macrocycles by adding a variety of ligands that can break its weak links. To demonstrate the viability of this strategy, we prepared the new hemilabile phosphanyl alkyl ether ligand **3** (1,4-bis[2-(diphenylphosphanyl)ethoxy]-2,3,5,6-tetramethylbenzene). It is synthesized by allowing dihydroxydurene[7] to react with two equivalents of 2-chloroethyl *p*-toluenesulfonate to form 1,4-bis[2-chloroethoxy]-2,3,5,6-tetramethylbenzene, followed by displacement of the chlorine atoms by -PPh_2 with $KPPh_2$ (overall yield 72%). Spectroscopic data for solutions of **3** are completely consistent with its proposed structure.[8] Significantly, ligand **3** reacts in a 1:1 stoichiometric ratio with a Rh^I precursor (formed by the reaction between $[\{RhCl(cot)_2\}_2]$ (cot = cyclooctene) and $AgBF_4$ in CH_2Cl_2) to provide the new, fused polycycle **4**[9] in almost quantitative yield (> 95%, Scheme 2). Consistent with this structural formulation, the ^{31}P NMR spectrum of **4** exhibits a resonance at $\delta = 61$ ($J_{Rh,P} = 213$ Hz), which is characteristic of a Rh^I complex with a square-planar, *cis*-phosphane, *cis*-ether coordination geometry.[10] Mass spectrometry and ^1H NMR spectroscopy also support this structural formulation.[9] In addition, the solid-state structure of **4**, as determined by a single-crystal X-ray diffraction study, is consistent with its assigned solution structure (Figure 1).[11] Complex **4** is made up of a series of fused, thermodynamically favorable five-membered rings.[12] The two durenylene moieties in **4** are coplanar and separated by only 3.32 Å, which is similar to the separation between carbon layers in graphite (3.35 Å)[12] and implies that π-stacking interactions play a role in stabilizing its structure. The Rh···Rh distance of 8.36 Å in **4** is clearly nonbonding.

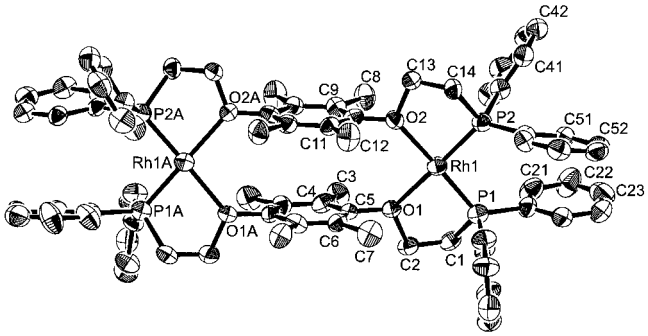
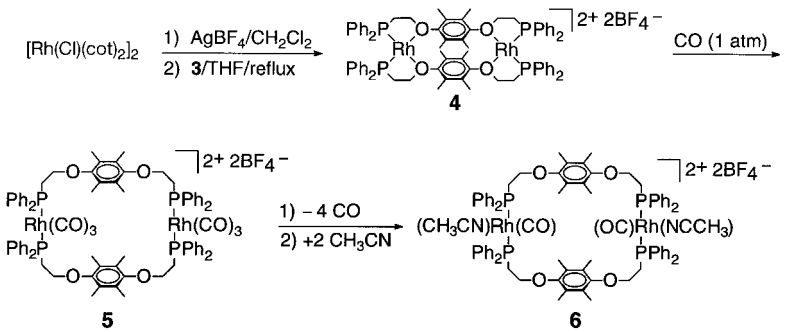


Figure 1. ORTEP drawing of complex **4** with thermal ellipsoids drawn at the 30% probability level. Hydrogen atoms are omitted for clarity. Selected bond distances [Å] and angles [°]: Rh(1)–Rh(1a) 8.362(10), Rh(1)–P(1) 2.169(3), Rh(1)–P(2) 2.172(3), Rh(1)–O(1) 2.247(7), Rh(1)–O(2) 2.217(7); P(1)-Rh(1)-P(2) 98.35(12), P(1)-Rh(1)-O(1) 81.3(2), P(1)-Rh(1)-O(2) 174.8(2), P(2)-Rh(1)-O(1) 173.9(2), P(2)-Rh(1)-O(2) 82.3(2), O(1)-Rh(1)-O(2) 98.7(2).

The weak Rh–O links in **4** can be broken with the more strongly coordinating ligand CO (1 atm) in CH_2Cl_2 to form the 26-membered macrocycle **5** (Scheme 2). Compound **5** was characterized in CD_2Cl_2 by ^1H and ^{31}P NMR spectroscopy.[13] The latter, which exhibits a doublet at $\delta = 21$ ($J_{Rh,P} = 88$ Hz), is highly diagnostic of a complex with trigonal-bipyramidal Rh^I.[14] Macrocycle **5** can be synthesized in one pot without isolating or purifying macrocycle **4** due to the high yields of all the synthetic steps involved.

Removal of solvent and CO from **5** under vacuum and dissolution of the product in acetonitrile results in the formation of the CH_3CN adduct **6**. This compound was spectroscopically characterized,[15] and all data are consistent with the formulated structure. For example, the IR spectrum of **6** in CH_2Cl_2 exhibits two ν_{CO} bands at 2008 (s) and 1971 cm^{-1} (w), and its ^1H NMR spectrum in CD_2Cl_2 shows a resonance at $\delta = 1.62$ for the coordinated CH_3CN ligands. The ^{31}P NMR spectrum of **6** in CD_2Cl_2 displays a single resonance at $\delta = 20.5$ (d) with a coupling constant ($J_{Rh,P} = 117$ Hz) that compares well with that reported for the analogous mononuclear compound $[Rh(PPh_3)_2(CO)(CH_3CN)][HC(SO_2CF_3)_2]$ ($J_{Rh,P} = 119$ Hz).[16]

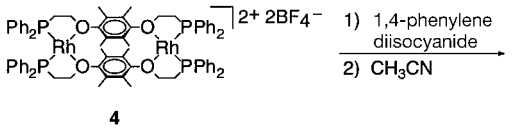
Interestingly, exposure of **4** to one equivalent of 1,4-phenylene diisocyanide in CD_2Cl_2 leads to the immediate formation of an uncharacterized or-



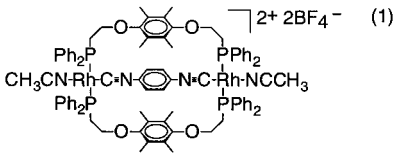
Scheme 2. Synthesis of compounds **4**–**6**.

 © WILEY-VCH Verlag GmbH, D-69451 Weinheim, 1998 1433-7851/98/3704-0466 $ 17.50+.50/0

ange precipitate, which is presumably an oligomer or polymer cross-linked by the bifunctional 1,4-phenylene diisocyanide. Introduction of ten equivalents of CH_3CN to a suspension of the precipitate results in the quantitative formation of **7** [Eq. (1)].[17] Compound **7** was characterized by ^1H, ^{31}P, and



4



7

NOE difference NMR spectroscopy. The proton resonances of the bound 1,4-phenylene diisocyanide have shifted 1.4 ppm upfield from those for the metal-free compound, which is indicative of $\pi-\pi$ interactions between the aromatic groups of the macrocycle and the complexed molecule.[18] The NOE difference spectrum shows an interaction between the protons of the complexed 1,4-phenylene diisocyanide and the methyl protons of the macrocycle. This NOE interaction clearly indicates that the 1,4-phenylene diisocyanide is bound inside the macromolecular cage. Furthermore, the solid-state structure of **7**, which was determined by a single-crystal X-ray diffraction study, is consistent with our structural formulation of **7** in solution (Figure 2).[19] In the solid state, the aromatic groups in **7** are uniformly separated by a distance of 4.24 Å, and the angles between the planes of the arenes are within 3.1° of being coplanar. The 1,4-phenylene diisocyanide is clearly situated inside the cage and bound to each Rh^I center.

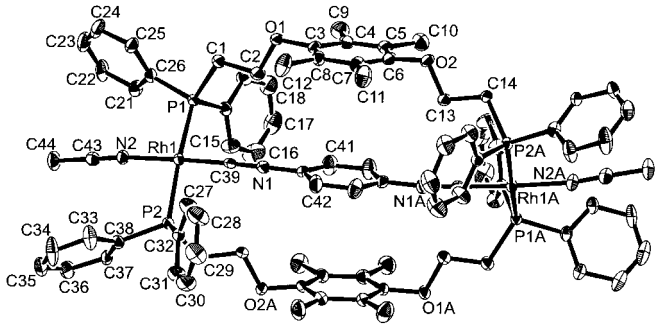


Figure 2. ORTEP drawing of complex **7** with thermal ellipsoids drawn at the 30% probability level. Hydrogen atoms are omitted for clarity. Selected bond distances [Å] and angles [°]: Rh(1)–Rh(1a) 11.598(13), Rh(1)–P(1) 2.343(6), Rh(1)–P(2) 2.326(6), Rh(1)–N(2) 2.06(2), Rh(1)–C(39) 1.85(2); P(1)-Rh(1)-P(2) 170.1(2), C(39)-Rh(1)-N(2) 177.4(10), N(2)-Rh(1)-P(2) 90.1(6), N(2)-Rh(1)-P(1) 89.8(6), C(39)-Rh(1)-P(2) 88.8(7), C(39)-Rh(1)-P(1) 91.0(7).

We have demonstrated the utility of this new synthetic strategy for the preparation of a novel class of homobimetallic macrocycles from flexible ligands in high yields and in one pot. These macrocycles contain Rh^I centers with steric and electronic environments that can be controlled through choice of ancillary ligands. Furthermore, we have taken advantage of the size of the macrocycle and the reactivity of the metal centers to demonstrate how such complexes can be used to direct the sequestration of bifunctional molecules.

Received: August 22, 1997 [Z10843IE]
German version: *Angew. Chem.* **1998**, *110*, 484–487

Keywords: macrocycles · P ligands · rhodium

[1] a) D. Philp, J. F. Stoddart, *Angew. Chem.* **1996**, *108*, 1242; *Angew. Chem. Int. Ed. Engl.* **1996**, *35*, 1154; b) D. S. Lawrence, T. Jiang, M. Levett, *Chem. Rev.* **1995**, *95*, 2229.
[2] a) C. A. Hunter, *Angew. Chem*, **1995**, *107*, 1181; *Angew. Chem. Int. Ed. Engl.* **1995**, *34*, 1079; b) A. W. Maverick, M. L. Ivie, J. H. Waggenspack, F. R. Fronczek, *Inorg. Chem.* **1990**, *29*, 2403.
[3] M. Fujita, J. Yazaki, K. Ogura, *J. Am. Chem. Soc.* **1990**, *112*, 5645.
[4] a) P. J. Stang, N. E. Persky, *Chem. Commun.* **1997**, 77; b) R. V. Slone, J. T. Hupp, C. L. Stern, T. E. Albrecht-Schmitt, *Inorg. Chem.* **1996**, *35*, 4096; c) P. M. Stricklen, E. J. Volcko, J. G. Verkade, *J. Am. Chem. Soc.* **1983**, *105*, 2494.
[5] C. M. Hartshorn, P. J. Steel, *Inorg. Chem.* **1996**, *35*, 6902.
[6] A. Bader, E. Lindner, *Coord. Chem. Rev.* **1991**, *108*, 27.
[7] A. D. Thomas, L. L. Miller, *J. Org. Chem.* **1986**, *51*, 4160.
[8] Compound **3**: ^1H NMR (CD_2Cl_2): $\delta = 7.46$ (m, 8H, PPh_2), 7.34 (m, 12H, PPh_2), 3.68 (q, 4H, OCH_2), 2.66 (t, 4H, PCH_2), 2.33 (s, 12H, CH_3); $^{31}P\{H\}$ NMR (CD_2Cl_2): $\delta = -22$ (s); MS (EI) *m/z*: 590.2 (M^+).
[9] Compound **4**: ^1H NMR (CD_2Cl_2): $\delta = 7.51$ (m, 16H, PPh_2), 7.39 (t, 8H, PPh_2), 7.30 (t, 16H, PPh_2), 3.62 (m, 8H, OCH_2) 2.66 (m, 8H, PCH_2), 2.34 (s, 24H, CH_3); MS (FAB^+): *m/z*: 1473 ($M^+ - BF_4^-$).
[10] E. T. Singewald, C. A. Mirkin, C. L. Stern, *Angew. Chem.* **1995**, *107*, 1725; *Angew. Chem. Int. Ed. Engl.* **1995**, *34*, 1624.
[11] a) Crystal structure data for **4** ($C_{76}H_{80}B_2F_8O_4P_4Rh_2$): trigonal, *P*31*c*, $a = 22.39145(5)$, $c = 26.4671(9)$ Å, $V = 12035.3(6)$ Å^3, $Z = 6$, $T = 218(2)$ K, $\rho_{calcd} = 1.292$ g cm^{-1}, $R(F) = 9.99$% for 8529 observed independent reflections ($3° \le 2\theta \le 56°$). b) Further details on the crystal structure investigation may be obtained from the Fachinformationszentrum Karlsruhe, D-76344 Eggenstein-Leopoldshafen, Germany (fax: (+49) 7247-808-666 (Frau S. Höhler-Schlimm); e-mail: crysdata@fiz-karlsruhe.de), on quoting the depository numbers CSD- 380141 (**4**) and -380142 (**7**).
[12] D. F. Shriver, P. Atkins, C. H. Langford, *Inorganic Chemistry*, 2nd ed., W. H. Freeman and Company, New York, **1997**.
[13] Compound **5**: ^1H NMR (CD_2Cl_2): $\delta = 7.60$ (m, 40H, PPh_2), 3.85 (m, 8H, OCH_2), 3.27 (m, 8H, PCH_2), 1.88 (s, 24H, CH_3).
[14] E. T. Singewald, X. Shi, C. A. Mirkin, S. J. Schofer, C. L. Stern, *Organometallics* **1996**, *15*, 3062.
[15] Compound **6**: ^1H NMR (CD_2Cl_2): $\delta = 7.72$ (m, 16H, PPh_2), 7.49 (m, 24H, PPh_2), 4.03 (m, 8H, PCH_2), 3.17 (m, 8H, OCH_2), 2.01 (s, 24H, CH_3), 1.62 (s, 6H, CH_3CN).
[16] A. R. Siedle, W. B. Gleason, R. A. Newmark, R. P. Skarjune, P. A. Lyon, C. G. Markell, K. O. Hodgson, A. L. Roe, *Inorg. Chem.* **1990**, *29*, 1667.
[17] Compound **7**: ^1H NMR (CD_2Cl_2): $\delta = 7.70$ (m, 16H, PPh_2), 7.53 (m, 24H, PPh_2), 5.96 (s, 4H, 1,4-$(CN)_2C_6H_4$), 3.54 (m, 8H, OCH_2), 3.27 (m, 8H, PCH_2), 1.80 (s, 24H, CH_3), 0.99 (s, 6H, CH_3CN); $^{31}P\{H\}$ NMR (CD_2Cl_2): $\delta = 18$ (d, $J_{Rh,P} = 125.0$ Hz).
[18] P. L.Anelli, P. R. Ashton, R. Ballardini, V. Balzani, M. Delgado, M. T. Gandolfi, T. T. Goodnow, A. E. Kaifer, D. Philp, M. Pietraszkiewicz, L. Prodi, M. V. Reddington, A. M. Z. Slawin, N. Spencer, J. F. Stoddart, C. Vicent, D. J. Williams, *J. Am. Chem. Soc.* **1992**, *114*, 193.
[19] Crystal structure data for **7** ($C_{101}H_{122}B_2C_{12}F_8N_4O_7P_4Rh_2$): tetragonal, $P4_12_12$, $a = 16.6807(1)$, $c = 39.1582(1)$ Å, $V = 10895.6(1)$ Å^3, $Z = 4$, $T = 223(2)$ K, $\rho_{calcd} = 1.266$ g cm^{-1}, $R(F) = 7.33$% for 9088 observed independent reflections ($3° \le 2\theta \le 56°$).

 © WILEY-VCH Verlag GmbH, D-69451 Weinheim, 1998 1433-7851/98/3704-0467 $ 17.50+.50/0

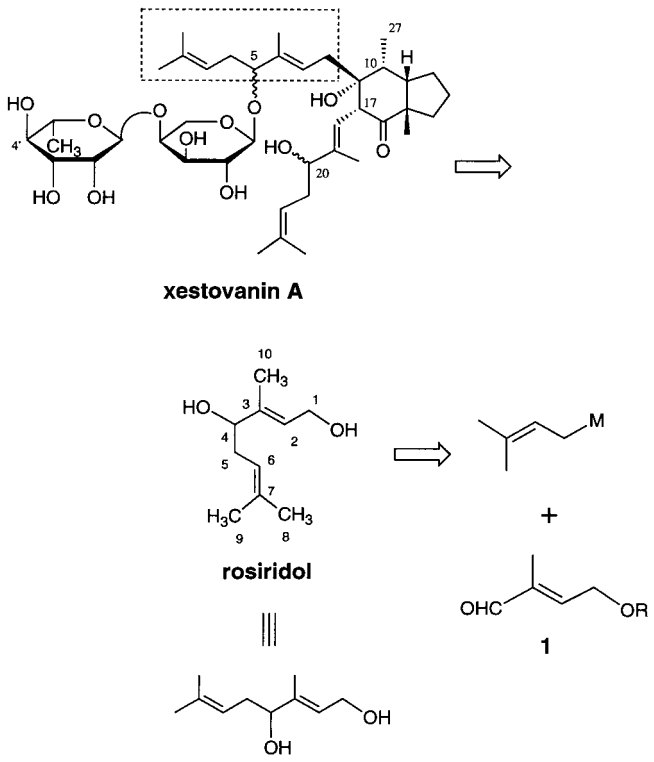
Regio- and Enantioselective Prenyl Anion Transfer: Application to the Total Synthesis of (−)-Rosiridol**

Bor-Cherng Hong,* Jang-Hsing Hong, and Yann-Chien Tsai

Dedicated to Professor E. J. Corey on the occasion of his 70th birthday

Monoterpenes have long been recognized as invaluable chiral precursors for the synthesis of various classes of natural products.[1] Many methodologies directed at the stereoselective synthesis of monoterpenes have been described. In recent years, stereoselective C–C bond forming reactions between allyl anions and carbonyl electrophiles have received a lot of attention.[2] We now describe a novel regio- and enantioselective prenyl anion addition to aldehyde **1** and its application to the first total synthesis of the monoterpene (−)-rosiridol.

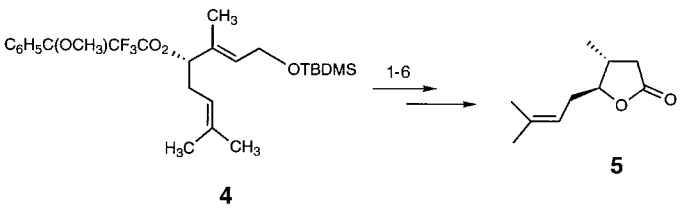
Our synthesis of xestovanin A[3] required the monoterpene rosiridol as a key intermediate (Scheme 1). Rosiridol has been isolated from several natural sources.[4] Although the structure of rosiridol had been reported, its absolute configuration remained unknown and to this date no total synthesis has been developed.[5, 6] In 1993 Manns isolated a new monoterpene from the leaves of *Cunila spicata* Benth (Lamiaceae) that bore close resemblance to the diacetate of rosiridol.[7] On the basis of this similarity the new monoterpene was named isorosiridol diacetate. However, there was a striking difference in the chemical shift of the C4 proton of rosiridol diacetate prepared from natural rosiridol ($\delta = 5.10$) and the C4 proton of this new monoterpene diacetate ($\delta = 5.70$). Based on de Haan's spectroscopic method and the ^{13}C NMR chemical shift of the C3 methyl group, Manns concluded that isorosiridol diacetate is (2*E*)-3,7-dimethylocta-2,6-diene-1,4-diol diacetate and that Kurkin's rosiridol could in fact be the *Z* isomer.



Scheme 1. Retrosynthesis of xestovanin A via rosiridol.

Retrosynthetic analysis indicates that rosiridol may be prepared by prenylation of aldehyde **1**.[8] Such carbonyl alkylations using prenyl metal anions are inherently problematic since both α and γ adducts are formed during the reaction, and in general, the γ adduct dominates.[9] Very few examples of α-selective carbonyl alkylations using prenyl anion are known.[10, 11] In fact, a practical and enantioselective α-alkylation of prenyl anion to aldehydes has never been reported.

We found that addition of the prenyl Grignard reagent, prenyllithium, or prenylzinc to aldehyde **1** provided the γ adduct **3** predominately (Table 1, entries 1–13). However, when prenylzinc was allowed to react with aldehyde **1** in the presence of HMPA for three days (THF, reflux), the α adduct **2** formed predominately (Table 1, entry 14).[12] Clearly, this is an equilibrium process in which the kinetic product **3** rearranges to the thermodynamic product **2** after prolonged heating (entries 13 and 14). Treatment of racemic alcohol **2** with (*R*)-α-methoxy-α-(trifluoromethyl)phenylacetyl chloride (Mosher chloride) afforded the corresponding Mosher esters, which were separated by HPLC and deprotected (KOH, MeOH; HF, THF, 90%) to give (−)- and (+)-rosiridol. The ^1H and ^{13}C NMR spectra of synthetic (−)-rosiridol are identical to those of natural (−)-rosiridol reported by Kurkin et al.[13] These results provide strong evidence that (−)-rosiridol is in fact (2*E*)-3,7-dimethylocta-2,6-diene-1,4-diol. To determine the absolute configuration at C4 of rosiridol, the Mosher ester **4** of (−)-rosiridol was converted into (−)-eldanolide (**5**) in six steps and 30% overall yield (Scheme 2).[14] Hence the structure of (−)-rosiridol can be assigned as (*S*)-(2*E*)-3,7-dimethylocta-2,6-diene-1,4-diol.



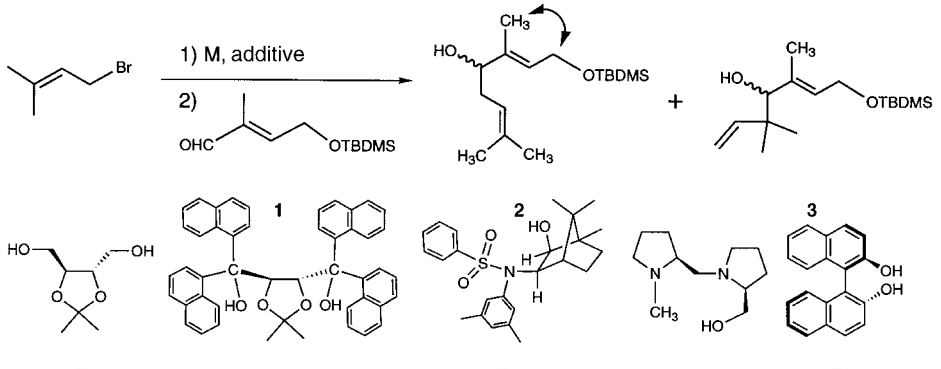
Scheme 2. 1. KOH, MeOH; 2. Ac_2O, Et_3N, 4-dimethylaminopyridine (DMAP), CH_2Cl_2; 3. HF, THF; 4. MnO_2, CH_2Cl_2; 5. MnO_2, KCN, MeOH; 6. $NaBH_4$, cat. $NiCl_2$, MeOH.

[*] Prof. B.-C. Hong, J.-H. Hong, Y.-C. Tsai
Department of Chemistry, National Chung-Cheng University
160, San-Hsing, Ming-Hsiung, Chia-Yi, 621
(Taiwan, Republic of China)
Fax: (+886) 5-272-1040
E-mail: che-bch@ccunix.ccu.edu.tw

[**] This work was supported by the National Science Council and National Chung-Cheng University. We thank Dr. S. Sarshar for valuable discussions and Prof. H. J. Borschberg for the spectrum of the tetrahydropyran derivative of rosiridol.

 © WILEY-VCH Verlag GmbH, D-69451 Weinheim, 1998 1433-7851/98/3704-0468 $ 17.50+.50/0

Table 1. Reaction of prenyl anion and aldehyde **1**.



A **B** **C** **D** **E**

Entry	M	Additive [equiv]	Solvent [h]	*T*	*t*	Products[b] **2**[a]:**3**	*R*/*S*(**2**)	Total yield [%][c]
1	Mg	0	THF	− 78°C	2	0:100		85
2	Mg	0	THF	reflux	2	0:100		85
3	Mg	0	THF	reflux	72	4:96		85
4	Mg	0	Et_2O	reflux	2	0:100		83
5	Mg	0	Et_2O	reflux	72	4:96		83
6	Li	0	THF	− 78°C	2	1:99		91
7	Li	0	THF	reflux	72	1:99		90
8	Zn	0	THF	− 78°C	2	1:99		93
9	Zn	0	THF	reflux	2	1:99		92
10	Zn	0	THF	reflux	72	7:93		90
11	Zn	0	Et_2O	reflux	2	0:100		89
12	Zn	0	Et_2O	reflux	72	6:94		87
13	Zn	HMPA (15)	THF	reflux	2	6:94		89
14	Zn	HMPA (15)	THF	reflux	72	**94:6**		89
15	Zn	**A** (1.5), HMPA (15)	THF	reflux	72	94:6	40/60	90
16	Zn	**A** (1.0), HMPA (15)	THF	reflux	72	94:6	43/57	90
17	Zn	**A** (0.2), HMPA (15)	THF	reflux	72	94:6	45/55	90
18	Zn	**B** (1.5), HMPA (15)	THF	reflux	72	94:6	19/81	89
19	Zn	**B** (1.0), HMPA (15)	THF	reflux	72	94:6	25/75	89
20	Zn	**B** (0.2), HMPA (15)	THF	reflux	72	94:6	31/69	89
21	Zn	**C** (1.5), HMPA (15)	THF	reflux	72	94:6	**3/97**	87
22	Zn	**C** (1.0), HMPA (15)	THF	reflux	72	94:6	12/88	87
23	Zn	**C** (0.2), HMPA (15)	THF	reflux	72	94:6	14/86	87
24	Zn	**D** (1.5), HMPA (15)	THF	reflux	72	94:6	57/43	86
25	Zn	**D** (1.0), HMPA (15)	THF	reflux	72	94:6	56/44	86
26	Zn	**D** (0.2), HMPA (15)	THF	reflux	72	94:6	54/46	86
27	Zn	**E** (1.5), HMPA (15)	THF	reflux	72	94:6	49/51	84
28	Zn	**E** (1.0), HMPA (15)	THF	reflux	72	94:6	49/51	84
29	Zn	**E** (0.2), HMPA (15)	THF	reflux	72	94:6	50/50	84

[a] The relative configuration of **2** was determined unambiguously by a 2D NOESY experiment. The spectrum, which shows key correlations between the protons on C1 and C10, supports the structure depicted in this table. [b] Optical purity assayed by preparation of the (*R*)-MTPA esters and analyzed by HPLC. [c] Yield of isolated product based on starting aldehyde.

Enantioselective alkylation of aldehydes using organozinc compounds in the presence of chiral Lewis acids is well known.[15] However, most Lewis acids decompose or lead to polymerization in refluxing THF. Since our prenylzinc reagent was stable under the reaction conditions, we postulated that addition of a chiral ligand to the reaction mixture may help induce some enantioselectivity in this already highly regioselective reaction. Various chiral ligands were employed and the corresponding enantiomeric excesses are summarized in Table 1 (entries 15 – 29). The best enantioselectivies were obtained with ligand **C**.[16] The use of catalytic amounts of chiral ligand did not affect the yield of the reaction; however, the enantioselectivity dropped slightly when substoichiometric amounts of ligand were used (entries 21 – 23).

Some preliminary experiments were conducted to shed light on the origin of the high enantioselectivity in this reaction. Racemate (±)-**3** was resolved by chiral HPLC (Daicel chiral OD column) and the individual enantiomers were subjected to the reaction conditions. Heating (+)-**3** in refluxing THF for 72 hours in the presence of RZnI and HMPA and in the absence of a chiral ligand produced (±)-**2**. However, when (±)-**3** was subjected to the same reaction conditions in the presence of chiral ligand **C**, adduct **2** was isolated with excellent enantiomeric excess (94% *ee*). The detailed mechanism of this reaction is unknown. However, the high enantioselectivity of **2** may be rationalized under the assumption that **3** is formed by a fast and reversible process whereas **2** is the product of a slow but irreversible reaction.

 © WILEY-VCH Verlag GmbH, D-69451 Weinheim, 1998 1433-7851/98/3704-0469 $ 17.50+.50/0

Experimental Section

To a suspension of zinc (200 mg, 3.06 mmol) in dry THF (10 mL) was added 4-bromo-2-methyl-2-butene (200 mg, 1.34 mmol), and the solution was stirred at room temperature for 1 h. The solution was filtered through a Schlenk filter and kept under argon for the following reaction. To a solution of (1*R*,2*S*,3*R*)-(+)-3-[*N*-benzenesulfonyl-*N*-(3,5-dimethylphenyl)amino]-2-bornanol (116 mg, 0.28 mmol) in dry THF (5 mL) was added the solution of prenylzinc bromide prepared above and the solution was stirred at room temperature for 15 min. The solution was treated with aldehyde **1** (40 mg, 0.19 mmol) and HMPA (0.5 mL, 2.87 mmol) and was heated to reflux for 72 h. A saturated aqueous solution of NH_4Cl (5 mL) was added into the reaction mixture. The solution was diluted with EtOAc (50 mL), washed with brine (30 mL), dried over $MgSO_4$, and concentrated in vacuo. The residue was purified by flash column chromatography with EtOAc/hexane (5/95) ($R_f = 0.38$ in EtOAc/hexane, 10/90) to give alcohol **2** as a colorless oil (47 mg, 87 % yield). IR (neat): $\tilde{\nu} = 3382$, 2930, 2921, 2847, 1466, 1378, 1254, 1107, 1061, 835, 775 cm^{-1}; ^1H NMR ($CDCl_3$, 400 MHz): $\delta = 5.53$ (t, $J =$ 5.5 Hz, 1H), 5.09 (t, $J = 7.2$ Hz, 1H), 4.21 (d, $J = 6.0$ Hz, 2H), 3.98 (t, $J =$ 5.5 Hz, 1H), 2.20 – 2.27 (m, 2H), 1.70 (d, $J = 1.0$ Hz, 3H), 1.62 (s, 6H), 1.59 – 1.63 (m, 1H), 0.88 (s, 9H), 0.05 (s, 6H); ^{13}C NMR ($CDCl_3$, 100 MHz): $\delta = 137.88$ (C), 134.81 (C), 125.97 (CH), 119.91 (CH), 76.59 (CH), 60.01 (CH_2), 34.02 (CH_2), 25.94 ($3 \times CH_3$), 25.82 (CH_3), 18.34 (C), 17.93 (CH_3), 12.03 (CH_3), – 5.13 ($2 \times CH_3$); MS: *m*/*z* (%): 284 (M^+, 1), 215 (48), 157 (23), 83 (100), 75 (92), 73 (62), 70 (25), 69 (28); HRMS calcd for $C_{16}H_{32}O_2Si$ (M^+): 284.2172; found: 284.2177.

Received: August 19, 1997 [Z 10829 IE]
German version: *Angew. Chem.* **1998**, *110*, 482 – 484

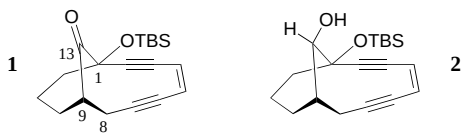
Keywords: alkylations · asymmetric synthesis · prenyl anions · rosiridol · total synthesis

[1] A. F. Thomas, Y. Bessière in *The Total Synthesis of Natural Products, Vol. 7* (Ed.: J. W. ApSimon), Wiley, New York, **1988**, pp. 275 – 454.
[2] W. R. Roush in *Comprehensive Organic Synthesis, Vol. 2* (Eds.: B. M. Trost, I. Fleming), Pergamon, Oxford, **1991**, pp. 1 – 53.
[3] For the isolation and structure determination of xestovanin, see: P. T. Northcote, J. Andersen, *J. Am. Chem. Soc.* **1989**, *111*, 6276; S. A. Morris, P. T. Northcote, R. J. Andersen, *Can. J. Chem.* **1991**, *69*, 1352.
[4] V. A. Kurkin, G. G. Zapesochnaya, A. N. Shchavlinskii, *Khim. Prir. Soedin.* **1985**, *5*, 632; V. A. Kurkin, G. G. Zapesochnaya, *ibid.* **1986**, *5*, 643; V. A. Kurkin, G. G. Zapesochnaya, I. A. Pautova, E. V. Avdeyeva, *Rastit. Resur.* **1995**, *31*, 27.
[5] 4-Hydroxy-3,7-dimethyl-2,6-octadienal was prepared by Iriye et. al. by a multiple-step sequence; the racemic compound showed growth inhibition activity against Sarcoma 180 and was more effective than citral: R. Iriye, T. Yorifuji, N. Takeda, A. Tatematsu, *Agric. Biol. Chem.* **1984**, *48*, 2923.
[6] The tetrahydropyran (THP) derivative of rosiridol was obtained as a side product (in ca. 2 % yield) from the oxidation of geraniol THP ether; see: H.-J. Borschberg, L. Jenny, *Helv. Chim. Acta.* **1995**, *78*, 715.
[7] D. Manns, *Planta Med*. **1993**, *59*, 171.
[8] Prepared by SeO_2 oxidation of the *tert*-butyldimethylsilyl (TBDMS) ether of prenyl alcohol: E. J. Corey, B. B. Snider, *J. Am. Chem. Soc.* **1972**, *94*, 2549.
[9] M. Clarembeau, A. Krief, *Tetrahedron Lett.* **1984**, *25*, 3629; B. Lipshutz, C. Hackmann, *J. Org. Chem.* **1994**, *59*, 7437; M. Uchida, K. Nakagawa, T. Negishi, S. Asano, K. Mori, *Biol. Chem.* **1981**, *45*, 369; V. Rautenstrauch, *Helv. Chim. Acta.* **1974**, *57*, 496.
[10] For a reversible α- and γ-alkylation process see: F. Barbot, P. Miginiac, *Tetrahedron Lett.* **1975**, 3829; G. Courtois, L. Miginiac, *J. Organomet. Chem.* **1974**, *69*, 1.
[11] Addition of crotylcerium to aldehydes gives the α adduct with moderate preference: B.-S. Guo, W. Doubleday, T. Cohen, *J. Am. Chem. Soc.* **1987**, *109*, 4710; D. W. McCullough, M. Bhupathy, E. Piccolino, T. Cohen, *Tetrahedron Lett.* **1991**, *47*, 9727.
[12] Alcohol **2** was converted into its THP derivative (HF, THF; dihydropyran (DHP), H^+; 82 %) and into rosiridal (1. Ac_2O, Et_3N, DMAP, CH_2Cl_2; 2. HF, THF; MnO_2, CH_2Cl_2; 76 %). Both compounds were identical in all aspects with those reported in the literature.[5, 6]
[13] The structure of rosiridol was further confirmed unambiguously by NOESY, COSY, HMQC, DEPT, and HMBC experiments. $[\alpha]_D^{25} = -7.1$ ($c = 0.4$ in acetone); lit.: $[\alpha]_D^{25} = -7.7$ ($c = 1.0$ in acetone).[4]
[14] This spectroscopic data of this product are identical with the data reported earlier. $[\alpha]_D^{25} = -52.3$, ($c = 1.4$ in EtOH); lit.: $[\alpha]_D^{25} = -52.4$ ($c = 1.5$ in EtOH); J.-P. Vigneron, R. Méric, M. Larchevêque, A. Debal, *Tetrahedron Lett.* **1982**, *23*, 5051.
[15] K. Soai, S. Niwa, *Chem Rev.* **1992**, *92*, 833; B. Schmidt, D. Seebach, *Angew. Chem.* **1991**, *103,* 100; *Angew. Chem. Int. Ed. Engl.* **1991**, *30*, 99; D. Seebach, L. Behrendt, F. Dorothee, *ibid.* **1991**, *103*, 991 and **1991**, *30*, 1008; R. Noyori, M. Kitamura, *ibid.* **1990**, *102*, 34 and **1991**, *30*, 49.
[16] Ligand **C** was purchased from Aldrich Chemical Co.

Actuating Cycloaromatization of a Bicyclo[7.3.1]enediyne by Annelation: An Example of Inverse Dependence on Bridge Atom Hybridization**

Michael H. Nantz,* David K. Moss, John D. Spence, and Marilyn M. Olmstead

The calicheamicin and esperamicin enediynes[1] have inspired numerous synthetic and mechanistic studies aimed toward understanding their DNA-cleaving activity.[2] In addition to natural calicheamicin γ_1^I,[3] many structural mimics have been synthesized and shown[4] to undergo the principal transformation responsible for the biological activity, Bergman cycloaromatization[5] of the 1,5-diyn-3-ene unit. We have been especially intrigued by the work of Magnus et al. who first determined the reactivity of bicyclo[7.3.1]enediyne analogues.[6] They showed that the bicyclo[7.3.1] ring of **1** is resistant to enediyne cycloaromatization at ambient temperature and reacts slowly[7] at 71 °C to form the corresponding C(2)–C(7) benzenoid product. In contrast, a change in the hybridization of the one-carbon bridge (C13) from sp^2 to sp^3 (**1** → **2**) was shown to effect a dramatic increase in the rate of cycloaromatization.[8] The tendency toward cycloaromatization was attributed to strain attenuation. These observations point toward the possibility of devising a bicyclo[7.3.1] model system wherein rehybridization of the one-carbon bridge may



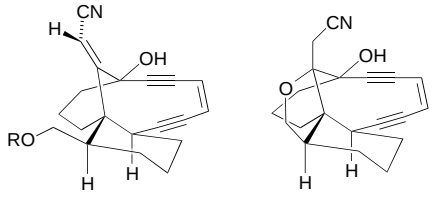
[*] Prof. M. H. Nantz, D. K. Moss, J. D. Spence, Dr. M. M. Olmstead
Department of Chemistry, University of California
Davis, CA 95616 USA
Fax: (+1) 916-752-8995
E-mail: mhnantz@ucdavis.edu

[**] Support of this work by the University of California Cancer Research Coordinating Committee is gratefully acknowledged.

 © WILEY-VCH Verlag GmbH, D-69451 Weinheim, 1998 1433-7851/98/3704-0470 $ 17.50+.50/0

occur through intramolecular reaction, analogous to the activation mode of the natural enediynes.[9]

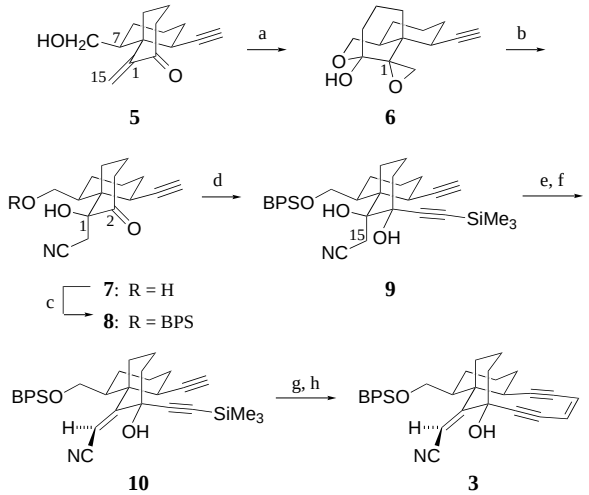
We report here on the synthesis of a system that incorporates these features. We have rigidly positioned a nucleophilic group near the bridging carbon by annelation of a cyclohexane ring to the C(8)–C(9) bond of the ten-membered carbocycle. To closely mimic the natural enediynes, a Michael acceptor group was chosen to replace the bridging carbonyl of **1**. These changes are illustrated in structure **3**. Enediyne **3** (R = Si*t*BuPh$_2$) has been prepared and unmasked to give **4**, the product of an intramolecular Michael addition to the one-carbon bridge of the bicyclo[7.3.1] system. A study of the



3 **4**

cycloaromatization kinetics for enediynes **3** and **4** has revealed that, in contrast to the Magnus system, rehybridization from sp^2 to sp^3 along the ten-membered ring serves to inhibit cycloaromatization.

Scheme 1 depicts a synthesis of **3** from spirocyclic enone **5**, which is available from monoethyl malonate in eight steps and 24% yield.[10] To convert C(1) of **5** into an electrophilic one-carbon bridge, C(1) was transformed into the β-center of a vinyl nitrile. Treatment of **5** with basic *tert*-butyl hydroperoxide in benzene[11] afforded a separable 7:1 mixture of epoxide diastereomers in 84% combined yield. The assigned stereochemistry at C(1) for the major isomer **6** is tentative.[12]

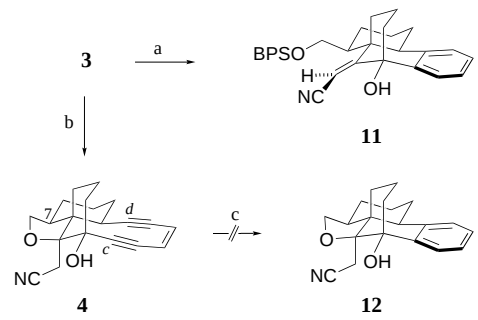


5 **6** **9** **10** **3**

Schema 1. a)*t*BuOOH, Triton-B, C_6H_6, room temperature (RT), 74%; b) Et_2AlCN (5 equiv), toluene, RT, 71%; c) BPSCl, *i*Pr$_2$NEt, DMAP, pyridine, reflux, 75%; d) LiCCTMS (10 equiv), $CeCl_3$ (15 equiv), THF, $-78\,^{\circ}C$, 88%; e) (imid)$_2$C=O, C_6H_6, reflux; f) DBU, C_6H_6, RT, 57% over two steps; g) NIS (2.2 equiv), $AgNO_3$ (0.5 equiv), acetone, $0\,^{\circ}C$, 94%; h) (*Z*)-Me$_3$SnCHCHSnMe$_3$ (2 equiv), [Pd(PPh$_3$)$_4$] (0.1 equiv), LiCl (2 equiv), DMF, $50\,^{\circ}C$, 57%. DMAP = 4-dimethylaminopyridine, imid = imidazol-1-yl, DBU = 1,8-diazabicyclo[5.4.0]undec-7-ene, NIS = *N*-iodosuccinimide.

Spectroscopic analysis indicates that **6** resides exclusively in its hemiacetal form. Hydrocyanation of **6** using Et_2AlCN according to the method of Nagata[13] gives adduct **7**, which was monosilylated under forcing conditions to afford the *tert*-butyldiphenylsilyl (BPS) derivative **8**. Examination of molecular models suggested that the 1,2-addition of an acetylide anion to C(2) of **8** might proceed stereoselectively to give the axial alkyne required for enediyne installation. Indeed, treatment of **8** with cerium trimethylsilylacetylide[14] generated in situ gave a single 1,2-addition product, assigned diyne **9**, in 88% yield. To differentiate the vicinal tertiary hydroxyl groups in **9** for selective elimination of the C(1) hydroxyl group, a cyclic carbonate was formed to exploit the acidity of the adjacent C(15) methylene position. Reaction of **9** with 1,1′-carbonyldiimidazole in benzene followed by treatment with DBU effected β-elimination of the carbonate to give a single vinyl nitrile stereoisomer in 57% yield. The least sterically encumbered transition state for carbonate elimination favors formation of the (*Z*) isomer, and, consequently, the elimination product has been assigned structure **10**. Completion of the enediyne carbocycle followed an approach developed by Danishefsky et al.[15] Treatment of diyne **10** with *N*-iodosuccinimide in the presence of catalytic silver nitrate converted each alkynyl group into an iodoalkynyl group.[16] Subsequent palladium-mediated cross coupling of the diiodide with (*Z*)-1,2-bis(trimethylstannyl)ethene[17] gave **3** in 57% yield. Enediyne **3** was readily purified and stored without notable change.[18]

Cycloaromatization studies were conducted in 1,4-cyclohexadiene. Enediyne **3** was heated to $37\,^{\circ}C$ to promote cycloaromatization (Scheme 2). At this temperature complete



4 **11** **12**

Schema 2. a) 1,4-Cyclohexadiene, $37\,^{\circ}C$, 2.5 d, 76%; b) *n*Bu$_4$NF (2.5 equiv), THF, RT, 46%; c) 1,4-cyclohexadiene, $60\,^{\circ}C$, 7 d.

consumption of starting enediyne requires roughly 2.5 days and gives benzenoid product **11** in 76% yield. The reactivity of **3** was assessed further by ^{1}H NMR analysis at temperatures ranging from 55 to $85\,^{\circ}C$. Analysis of the data provided the first-order rate constants shown in Table 1. Extrapolated to $37\,^{\circ}C$, the cycloaromatization rate of **3**, $k = 4.52 \times 10^{-5}\ s^{-1}$, is an order of magnitude faster than the extrapolated rate reported for **1**.[7] Molecular modeling of **3** predicts the transannular distance between the remote acetylenic carbons of the enediyne unit ($c-d$ distance[19]) to be identical to that measured in **1**.[20] Thus, the enhancement in reactivity is principally a function of cyclohexane annelation.[21] Presum-

 © WILEY-VCH Verlag GmbH, D-69451 Weinheim, 1998 1433-7851/98/3704-0471 $ 17.50+.50/0

Table 1. Kinetic parameters for the thermal cyclization of **3**.

T[°C]	k[s^{-1}]	$t_{1/2}$[min]
55	1.72×10^{-4}	67
62	4.13×10^{-4}	28
71	7.22×10^{-4}	16
78	1.20×10^{-3}	9.6
85	1.56×10^{-3}	7.4

ably the added cyclohexane ring serves to lower the transition state energy for 1,4-diyl formation.[22] Calculation of the differential strain energy (ΔSE) for the **3**→**11** transition according to the method of Maier et al.[23] suggests that the activation energy for the cyclization of **3** is 37% less than that for the cyclization of **1**. Although this approximation supports the postulated effect of the annulation, other factors may contribute and remain to be fully understood.

Compound **3** was treated with nBu$_4$NF to effect desilylation of the C(7) silyloxymethyl group. The liberated hydroxyl group spontaneously adds to the resident vinyl nitrile to give enediyne **4** (Scheme 2) as an isolable crystalline compound. X-ray crystallographic analysis of **4** (Figure 1) yielded a $c-d$ distance of 3.24 Å, a distance smaller than that calculated in **3**

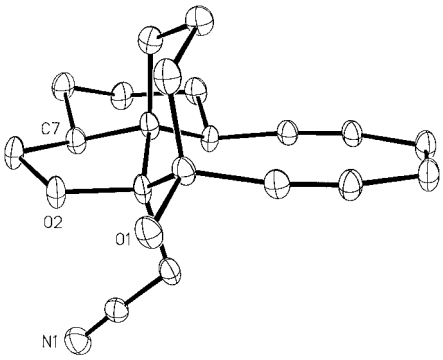


Abb. 1. X-ray crystal structure of enediyne **4**; for clarity 30% probability ellipsoids are depicted and H atoms are removed.

and well within the range for cycloaromatization.[24] However, and in stark contrast to the reactive enediyne **2**,[8] enediyne **4** is resistant to cycloaromatization at ambient temperature. Furthermore, when a solution of **4** in 1,4-cyclohexadiene was heated at 60°C for one week the enediyne was completely recovered. The stability of **4** constitutes an unusual reversal in the behavior of ten-membered enediynes that have undergone rehybridization. Prior to this example, a change in the hybridization of carbon along the enediyne core from sp^2 to sp^3 was known to facilitate cycloaromatization.[2]

Comparison of the calculated ΔSE[23] values for the **3**→**11** and **4**→**12** transformations suggests that enediyne **3** should undergo a more facile transition to its aromatized product; however, the unusual resistance of **4** to cyclization is not readily rationalized by this method.[25] The extraannular strain imparted by tetrahydrofuran annelation presumably is sufficient to deter cycloaromatization, a postulate that may be tested by expanding the heterocycle. Heating **4** at 90°C also failed to effect cycloaromatization; however, unlike the experiment at 60°C, **4** was gradually degraded to multiple products at this temperature. The cyclized product **12** was not detected in the product mixture.

Annelation of a bicyclo[7.3.1]enediyne core has been shown to alter the cycloaromatization reactivity typically controlled by the one-carbon bridge. Unlike prior systems, the enediyne containing an sp^3-hybridized bridging carbon atom is resistant to cycloaromatization whereas the immediate sp^2-hybridized precursor enediyne readily undergoes transformation to its benzenoid counterpart. Given the magnitude of the annulation effect on both actuating and deterring cycloaromatization, this controlling feature may prove to be useful for tuning enediyne systems for physiological applications.

Received: August 26, 1997 [Z10858IE]
German version: *Angew. Chem.* **1998**, *110*, 476–479

Keywords: annulation · cycloaromatizations · enediynes · kinetics · spiro compounds

[1] a) M. D. Lee, T. S. Dunne, M. M. Siegel, C. C. Chang, G. O. Morton, D. B. Borders, *J. Am. Chem. Soc.* **1987**, *109*, 3464, 3466; b) J. Golik, J. Clardy, G. Dubay, G. Groenwold, H. Kawaguchi, M. Konishi, B. Krishnan, H. Ohkum, K. Saitoh, T. W. Doyle, *ibid.* **1987**, *109*, 3461, 3462.

[2] For reviews of enediyne chemistry and biology, see a) J. W. Grissom, G. U. Gunawardena, D. Klingberg, D. Huang, *Tetrahedron* **1996**, *52*, 6453; b) M. E. Maier, *Synlett* **1995**, 13; c) K. C. Nicolaou, W.-M. Dai, *Angew. Chem.* **1991**, *103*, 1453; *Angew. Chem. Int. Ed. Engl.* **1991**, *30*, 1387; d) *Enediyne Antibiotics as Antitumor Agents* (Eds.: T. W. Doyle, D. B. Borders), Marcel Dekker, New York, **1994**.

[3] a) K. C. Nicolaou, C. W. Hummel, C. N. Pitsinos, M. Nakada, A. L. Smith, K. Shibayama, H. Saimoto, *J. Am. Chem. Soc.* **1992**, *114*, 10082; b) K. C. Nicolaou, C. W. Hummel, M. Nakada, K. Shibayama, C. N. Pitsinos, H. Saimoto, Y. Mizuno, K.-U. Baldenius, A. L. Smith, *ibid.* **1993**, *115*, 7625; c) S. A. Hitchcock, M. Y. Chu-Moyer, S. H. Boyer, S. H. Olson, S. J. Danishefsky, *ibid.* **1995**, *117*, 5750.

[4] For syntheses of calicheamicinone and calicheamicin analogues, see ref. [2] and D. L. J. Clive, Y. Bo, Y. Tao, S. Daigneault, Y.-J. Wu, G. Meignan, *J. Am. Chem. Soc.* **1996**, *118*, 4904.

[5] a) R. R. Jones, R. G. Bergman, *J. Am. Chem. Soc.* **1972**, *94*, 660; b) R. G. Bergman, *Acc. Chem. Res.* **1973**, *6*, 25; c) T. P. Lockhart, P. B. Comita, R. G. Bergman, *J. Am. Chem. Soc.* **1981**, *103*, 4082; d) see also: N. Darby, C. U. Kim, J. A. Salaun, K. W. Shelton, S. Takada, S. Masamune, *J. Chem. Soc. Chem. Commun.* **1971**, 1516.

[6] P. Magnus, R. T. Lewis, J. C. Huffman, *J. Am. Chem. Soc.* **1988**, *110*, 6921.

[7] The rate of cycloaromatization for enediyne **1** at 71°C was measured at $k = 1.07 \times 10^{-4}$ s^{-1}, $t_{1/2} = 2.10$ h; the extrapolated rate at 37°C is reported as $k = 1.85 \times 10^{-6}$ s^{-1}; see a) P. Magnus, S. Fortt, T. Pitterna, J. P. Snyder, *J. Am. Chem. Soc.* **1990**, *112*, 4986; b) P. Magnus, P. Carter, J. Elliott, R. Lewis, J. Harling, T. Pitterna, W. E. Bauta, S. Fortt, *ibid.* **1992**, *114*, 2544.

[8] Enediyne **2** undergoes complete cycloaromatization at 20°C within 30 min.[6]

[9] For examples of intramolecular triggering of bicyclo[7.3.1]enediynes, see a) J. N. Haseltine, S. J. Danishefsky, G. Schulte, *J. Am. Chem. Soc.* **1989**, *111*, 7638; b) J. N. Haseltine, S. J. Danishefsky, *J. Org. Chem.* **1990**, *55*, 2576; c) S. J. Danishefsky, M. D. Shair, *ibid.* **1996**, *61*, 16.

[10] a) J. D. Spence, L. E. Lowrie, M. H. Nantz, *Tetrahedron Lett.* **1995**, *36*, 5499; b) J. D. Spence, J. K. Wyatt, D. M. Bender, D. K. Moss, M. H. Nantz, *J. Org. Chem.* **1996**, *61*, 4014.

[11] N. C. Yang, R. A. Finnegan, *J. Am. Chem. Soc.* **1958**, *80*, 5845.

[12] The epoxidation selectivity decreased to 2:1 when the corresponding C(7) (*tert*-butyldiphenylsilyloxy)methyl derivative of **5** was treated under identical conditions, suggesting a shielding of the enone face *syn* to C(7).

 © WILEY-VCH Verlag GmbH, D-69451 Weinheim, 1998 1433-7851/98/3704-0472 $ 17.50+.50/0

[13] W. Nagata, M. Yoshioka, *Tetrahedron Lett.* **1966**, 1913.
[14] a) T. Imamoto, Y. Sugiura, N. Takiyama, *Tetrahedron Lett.* **1984**, *25*, 4233; b) For an experimental procedure to prepare anhydrous cerium chloride, see T. Imamoto in *Comprehensive Organic Synthesis Vol. 1* (Eds.: B. M. Trost, I. Fleming), Pergamon, Oxford, **1991**, p. 231.
[15] M. D. Shair, T. Yoon, S. J. Danishefsky, *J. Org. Chem.* **1994**, *59*, 3755.
[16] a) H. Hofmeister, K. Annen, H. Laurent, R. Wiechert, *Angew. Chem.* **1984**, *96*, 720; *Angew. Chem. Int. Ed. Engl.* **1984**, *23*, 727; b) T. Nishikawa, S. Shibuya, S. Hosokawa, M. Isobe, *Synlett* **1994**, 485.
[17] T. N. Mitchell, A. Amamria, H. Killing, D. Rutschow, *J. Organomet. Chem.* **1986**, *304*, 257.
[18] A sample of **3** was stored at $-20\,^{\circ}C$ for one week and analyzed. The ^1H NMR spectrum of this material was identical to the spectrum that was obtained from freshly purifed **3**.
[19] K. C. Nicolaou, G. Zuccarello, C. Riemer, V. A. Estevez, W.-M. Dai, *J. Am. Chem. Soc.* **1992**, *114*, 7360.
[20] The $c-d$ distance calculated for **3** is 3.39 Å, that measured for **1**[7] is 3.39 Å. The calculations were performed with the program PC Model 4.4 from Serena Software.
[21] The influence of benzannelation on the enediyne moiety has been documented, see K. C. Nicolaou, W.-M. Dai, Y. P. Hong, S.-C. Tsay, K. K. Baldridge, J. S. Siegel, *J. Am. Chem. Soc.* **1993**, *115*, 7944.
[22] J. P. Snyder, *J. Am. Chem. Soc.* **1990**, *112*, 5367.
[23] a) M. E. Maier, T. Brandstetter, *Tetrahedron* **1994**, *50*, 1435; b) M. E. Maier, D. Langenbacher, *Synlett* **1994**, 713.
[24] Crystal structure analysis: colorless, monoclinic, $P2_1/n$, $a=7.784(2)$, $b=20.371(6)$, $c=9.891(2)$ Å, $\beta=95.10(2)^{\circ}$, $V=1562.2(7)$ Å^3, $Z=4$, $\rho_{calcd}=1.307$ Mg m^{-3}, $T=130(2)$ K, full matrix refinement on F^2 (Siemens P4, SHELXTL 5, 2077 independent reflections, 1407 with $I>2\sigma(I)$), $R_1(F)=7.46$, $R_2(wF^2)=21.8\,\%$, GOF(F^2) = 1.066. Crystallographic data (excluding structure factors) for the structures reported in this paper have been deposited with the Cambridge Crystallogrphic Data Centre as supplementary publication no. CCDC-100780. Copies of the data can be obtained free of charge on application to CCDC, 12 Union Road, Cambridge CB21EZ, UK (fax: (+44) 1223-336-033; E-mail: deposit@chemcrys.cam.ac.uk).
[25] The difference in the ΔSE values for the cyclization of **4** and **3** was calculated to be 2.79 kcal mol^{-1}. Full theoretical calculations will be reported in a forthcoming account of this work.

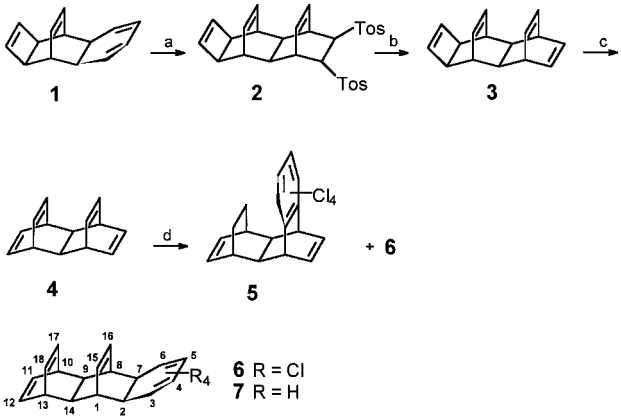
Tetrachloro-*p*-(*o*,*p*)-*o*-tribenzene: A Building Block for Diels–Alder Oligomers of Benzene and for a Laticyclic Conjugated Hexaene**

Wolfram Grimme,* Joachim Gossel, and Johann Lex

Dedicated to Professor Emanuel Vogel on the occasion of his 70th birthday

Some time ago we reported on *p*-(*o*,*p*)-*o*-tribenzene (**7**), the *endo*,*endo*-Diels–Alder trimer of benzene, and anticipated higher oligomers of this type.[1] However, experiments designed to dimerize the tribenzene by a Diels–Alder reaction failed up to 100 °C and 7.5 kbar, the limits of the compound's stability; dimerization apparently requires an activated tribenzene. We report here on tetrachloro-*p*-(*o*,*p*)-*o*-tribenzene (**6**), which undergoes a Diels–Alder reaction with itself under reverse electron demand.[2]

Cycloaddition of (*E*)-1,2-ditosylethene[3] to the tetracycle **1**[1] yields adduct **2**, which can be detosylated with sodium amalgam to pentacycle **3** (Scheme 1). In the next step the



Scheme 1. a) (*E*)-Ditosylethene, EtOAc, reflux, 24 h, 96 %; b) Na(Hg) 2 %, NaH_2PO_4, MeOH, 25 °C, 16 h, 85 %; c) 1. 2,5-dimethyl-3,4-diphenylcyclopentadienone dimer, benzene, 70 °C, 16 h, 95 %; 2. diethyl ether, low-pressure Hg burner, 2 h, 49 %; d) TCTD, benzene, 25 °C, 16 h, 95 %.

cyclobutene ring is degraded by the Dauben method,[4] which entails cycloaddition of 2,5-dimethyl-3,4-diphenylcyclopentadienone followed by photoextrusion of CO and 1,4-dimethyl-2,3-diphenylbenzene. The resulting sesquibicyclo[2.2.2]octadiene (**4**), synthesized previously by another route,[5] undergoes cycloaddition of tetrachlorothiophene dioxide (TCTD)[6] preferentially at one of the laticyclic conjugated double bonds. Through SO_2 extrusion and a dyotropic hydrogen transfer[7] at room temperature the arene **5** is formed. The desired tetrachlorotribenzene **6** is obtained from addition to one of the terminal double bonds (**6**:**5** = **1**:**3**).

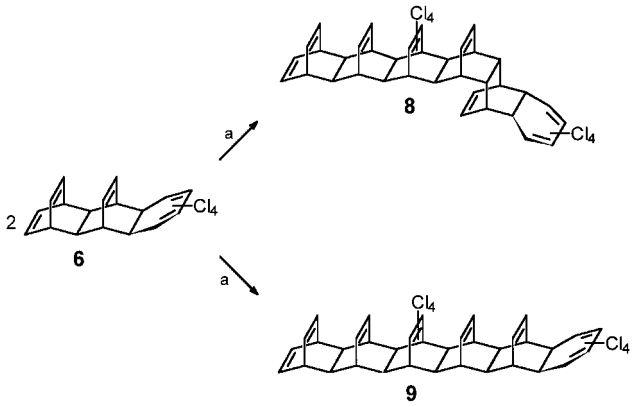
Compound **6** cycloreverts to benzene and tetrachlorobenzene at 110.8 °C with a half life of $t_{1/2}=52$ min, a reaction rate

[*] Prof. Dr. W. Grimme, Dr. J. Gossel, Dr. J. Lex
Institut für Organische Chemie der Universität
Greinstrasse 4, D-50939 Köln (Germany)
Fax: (+49) 221-470-5057
E-mail: grimme@uni-koeln.de

[**] This work was supported by the Deutsche Forschungsgemeinschaft.

which is similar to that of the parent tribenzene **7** ($t_{1/2}$ = 80 min) and supports our earlier conclusion[1] that the *para*-bonded benzene ring splits off first. Following cycloreversion of **6** in squalane in a differential scanning calorimeter (DSC7, Perkin–Elmer) at a heating rate of 40 K min^{-1}, one observes a heat of reaction of $\Delta H = -23.3$ kcal mol^{-1} in the range of 140–200 °C. Since at this temperature the heat of evaporation of two molar equivalents of benzene must be consumed, the heat of cycloreversion of **6** amounts to $\Delta H_r = -23.3 - 2 \times 7.7 = -38.7$ kcal mol^{-1}. A force-field calculation[8] gives $\Delta H_r = -41.7$ kcal mol^{-1} when one takes into account that the heat of dehydrogenation of 1,2,3,4-tetrachlorocyclohexa-1,3-diene is approximately 4.5 kcal mol^{-1}.[9]

For dimerization, **6** is heated in benzene for 24 h at 70 °C under a pressure of 7.5 kbar (Scheme 2). Subsequent liquid



Scheme 2. a) Benzene, 70 °C, 24 h, 7.4 kbar.

chromatography (silica gel, *n*-hexane) provides recovered **6** (40%) and, after changing the eluant to CCl_4, a mixture of lower oligomers (40%). Complete cycloreversion of this fraction to benzene/tetrachlorobenzene (2/1) after 72 h at 110 °C proves that only Diels–Alder oligomers are present. Medium-pressure liquid chromatography (LiChroprep Si 60, 15–25 μm, benzene/cyclohexane 1/10, 5 bar) permits isolation of the angular octachlorohexabenzene **8** (9%) and the linear all-*endo* isomer **9** (5%) from this mixture. The former shows two ^{1}H NMR signals above $\delta = 6.2$, which is characteristic of two nonlaticyclic conjugated double bonds, and a singlet at high field ($\delta = 1.59$) for two *endo* protons at the ring junction that interrupts the laticyclic conjugation (Table 1). The extended laticyclic conjugation of **9** gives rise to a broad band at 260–300 nm in the UV spectrum that is partly obscured by the hypsochromic portion of the tetrachlorocyclohexadiene absorption.

Cycloreversion of the two hexabenzenes begins at 110 °C with the successive extrusion of two *p*-bonded benzene units and results after 48 h in complete decomposition to benzene and tetrachlorobenzene. In the case of the linear hexabenzene **9**, short reaction times permit isolation of octachloropentabenzene **10** and octachlorotetrabenzene **11** (Scheme 3).

The favored dimerization of tribenzene **6** to the angular hexabenzene **8** demonstrates that, of the two double bonds at the bicyclic terminus of **6**, the one that is laticyclic conjugated

Table 1. Selected spectroscopic data for **5**, **6**, **8**–**15** (^{1}H NMR spectra at 300 MHz and ^{13}C NMR spectra at 75.5 MHz in $CDCl_3$ with TMS as internal standard).

5: M.p. 207 °C (hexane); ^{1}H NMR: $\delta = 6.55$, 6.21, 4.21, 2.35, 1.93, 0.74 (CH_2), 0.52 (CH_2); ^{13}C NMR: $\delta = 142.9$, 137.6, 128.7, 128.4, 42.2, 42.1, 33.7, 19.6; UV/Vis (*n*-hexane): λ_{max} (ε) = 244 (8000, sh), 225 nm (34500).

6: M.p. 145 °C (decomp); ^{1}H NMR: $\delta = 6.41$(m, 2H, 11,12-H), 5.86 (m, 2H, 17,18-H), 5.82 (m, 2H, 15,16-H), 3.41 (br s, 2H, 10,13-H), 3.10 (br s, 2H, 1,8-H), 3.05 (s, 2H, 2,7-H), 1.95 (s, 2H, 9,14-H); ^{13}C NMR: $\delta = 137.0$ (C-4,12), 132.3 (C-3,6), 131.5 (C-17,18), 123.3 (C-4,5), 50.3 (C-2,7), 41.7 (C-10,13), 41.5 (C-9,14), 39.8 (C-1,8); UV/Vis (*n*-hexane): λ_{max} (ε) = 320 (2500), 305 (4900), 298 (4600), 281 (3100), 268 nm (2500).

8: M.p. > 300 °C (decomp); ^{1}H NMR: $\delta = 6.38$, 6.30, 5.97, 5.76, 5.46, 3.35, 3.18, 3.09, 2.86, 2.85, 2.11, 1.98, 1.89, 1.59; ^{13}C NMR: $\delta = 137.3$, 133.3, 132.1, 131.8, 130.7, 125.9, 123.5, 74.4, 56.7, 50.9, 50.5, 43.5, 42.7, 41.6, 37.5, 35.4; UV/Vis (*n*-hexane): λ_{max} (ε) = 323 (2100), 307 (4000), 295 (3950), 278 (3100), 269 nm (2150); MS (FAB): *m/z* (%) = 742 (8) [$M^{\cdot+}$], 707 (4) [$M^{\cdot+}$ – Cl].

9: M.p. > 300 °C (decomp); ^{1}H NMR: $\delta = 6.37$, 5.78, 5.73, 5.52, 5.43, 3.34, 3.12, 3.04, 2.92, 2.84, 2.29, 2.23, 2.02, 1.88; ^{13}C NMR: $\delta = 137.2$, 133.3, 132.3, 131.7, 128.8, 128.2, 124.8, 123.4, 74.0, 56.3, 55.8, 50.1, 43.6, 42.2, 41.5, 38.9, 37.5, 37.2; UV/Vis (*n*-hexane): λ_{max} (ε) = 323 (2200), 307 (4000), 295 (3900), 278 (3700), 369 nm (3250); MS (FAB): *m/z* (%) = 742(6) [$M^{\cdot+}$], 707 (4) [$M^{\cdot+}$ – Cl].

10: M.p. > 300 °C (decomp); ^{1}H NMR: $\delta = 6.43$, 6.07, 5.78, 5.50, 3.85, 3.10, 2.95, 2.28, 2.26, 1.99; ^{13}C NMR: $\delta = 137.4$, 132.4, 131.8, 128.9, 124.8, 123.5, 74.6, 56.4, 55.8, 50.1, 42.3, 42.0, 38.9, 37.2; MS (FAB): *m/z* = 663 [M$^{\cdot+}$], 625 [$M^{\cdot+}$ – HCl].

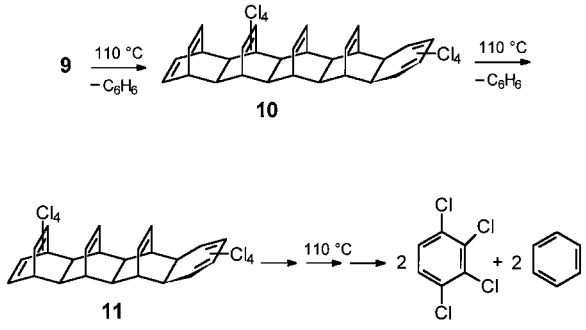
11: M.p. 280 °C (decomp); ^{1}H NMR: $\delta = 6.32$, 5.82, 5.56, 3.15, 3.09, 2.86, 1.98, 1.93; ^{13}C NMR: $\delta = 137.9$, 132.4, 128.6, 128.3, 124.9, 123.8, 74.6, 56.5, 50.1, 42.3, 38.7, 37.1.

12 (Two isomers with respect to the orientation of the ligand tfacac): m.p. 225 °C; ^{1}H NMR: $\delta = 6.30$, 5.61 (tfacac), 4.82, 4.32, 3.05, 2.99, 2.88, 2.12 (CH_3), 2.05 (CH_3), 1.38.

13: M.p. 285 °C; ^{1}H NMR: $\delta = 5.67$(tfacac), 4.45, 3.08, 2.88, 2.16 (CH_3), 1.52.

14: M.p. 191 °C (CH_2Cl_2); ^{1}H NMR: $\delta = 5.88$, 3.19, 3.15, 2.12; ^{13}C NMR: $\delta = 131.6$, 131.2, 123.6, 49.8, 40.3, 38.8.

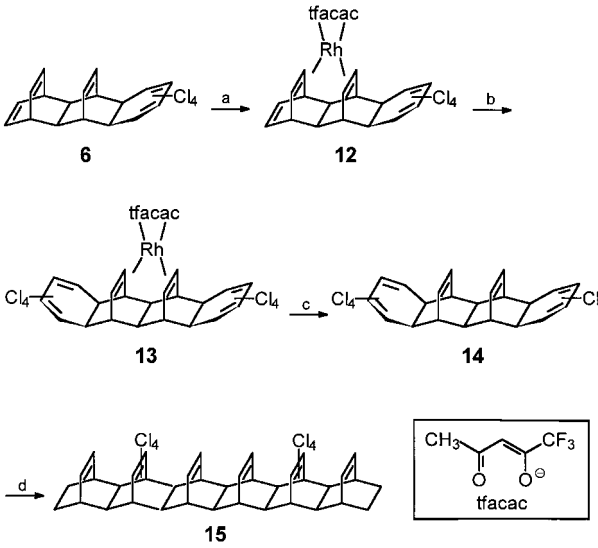
15: M.p. > 300 °C (decomp); ^{1}H NMR: $\delta = 5.92$, 5.44, 2.93, 2.88, 2.28, 2.25, 1.87, 1.43 (CH_2), 1.14 (CH_2); ^{13}C NMR: $\delta = 130.3$, 129.0, 124.6, 74.3, 55.9, 54.2, 44.2, 37.2, 31.4, 25.42; UV/Vis (*n*-hexane): λ_{max} (ε) = 260 nm (1500, sh); MS (FAB): *m/z* = 774 [$M^{\cdot+}$].



Scheme 3. Decomposition of **9** upon heating.

adds more rapidly to an electron-poor diene. This is the double bond that also adds nearly exclusively to TCTD, and protection is required to direct the reaction to the other double bond. Dicarbonyltrifluoroacetylacetonatorhodium[10] was chosen for this purpose because in $CHCl_3$ it binds to the two laticyclic conjugated double bonds of **6** to form diolefin complex **12** (Scheme 4). Masked tribenzene **12** adds TCTD at

 © WILEY-VCH Verlag GmbH, D-69451 Weinheim, 1998 1433-7851/98/3704-0474 $ 17.50+.50/0 *Angew. Chem. Int. Ed.* **1998**, *37*, No. 4



Scheme 4. a) $[Rh(tfacac)(CO)_2]$, $CHCl_3$, 50 °C, 16 h, 62 %; b) TCTD, hexane, 60 °C, 17 h, 59 %; c) CH_2Cl_2/aqueous NaCN 10 %, 3 min, 72 %; d) 10 equiv of dihydrobarrelene, THF, 75 °C, 96 h, 7.5 kbar, 57 %.

60 °C in hexane at the free double bond, which leads to complex **13** after subsequent loss of SO_2. The protecting group of **13** is conveniently cleaved with aqueous NaCN to yield the bifunctional diene **14**. Diels–Alder reaction of **14** with dihydrobarrelene utilizes the same structural elements that are responsible for oligomerization of tribenzene **6**. However, in this case reaction ceases on both sides after the first step. The resulting hexaene **15** consists of six *endo*-fused bicyclo[2.2.2]octene units, and its UV spectrum displays a broad shoulder at 240–290 nm ($\varepsilon = 1500$). An X-ray structural analysis[11] of **15**, recrystallized from CH_2Cl_2, shows that the basal C atoms are aligned on a circular arc of radius 9.57 Å encompassing an angle of 89° (Figure 1). One molecule of CH_2Cl_2 is located at the center of gravity of the segment.

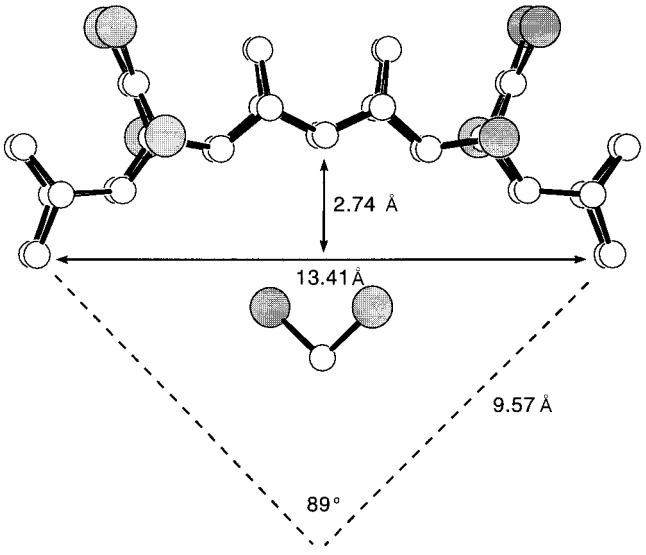


Figure 1. Molecular structure of **15** in the crystalline state. Hydrogen atoms have been omitted for clarity.

The structure of **15** indicates that the strategy used to obtain all-*endo* fusion of the bicyclo[2.2.2]octene units might make the synthesis of a ring of 24 *endo*-fused bicycles from four bifunctional dienes **14** and four Rh-protected dienophiles **4** possible. The closed laticyclic conjugation along its periphery would represent a new and interesting topology for a π-electron system. In principle, the proposed macrocycle could also be obtained by eightfold oligomerization of tribenzene **6**, but, as shown above, the formation of angular products is favored by this route.

Received: July 18, 1997 [Z10696IE]
German version: *Angew. Chem.* **1998**, *110*, 479–481

Keywords: arenes · cycloadditions · domino reactions · pi interactions · thermochemistry

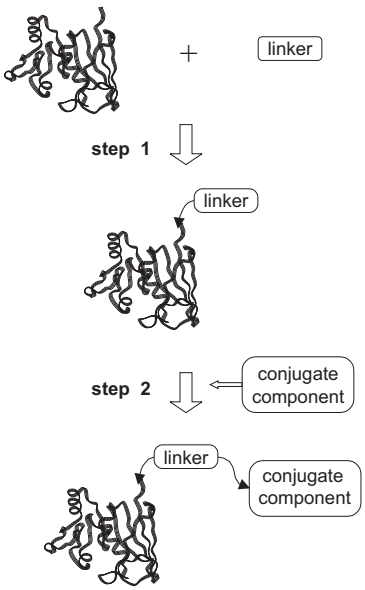
[1] W. Grimme, G. Reinhardt, *Angew. Chem.* **1983**, *95*, 636; *Angew. Chem. Int. Ed. Engl.* **1983**, *22*, 617–618.
[2] J. Sauer, H. Wiest, *Angew. Chem.* **1962**, *74*, 353; *Angew. Chem. Int. Ed. Engl.* **1962**, *1*, 269.
[3] O. De Lucchi, V. Lucchini, L. Pasquato, G. Modena, *J. Org. Chem.* **1984**, *49*, 596–604.
[4] W. G. Dauben, G. T. Rivers, R. J. Twieg, W. T. Zimmerman, *J. Org. Chem.* **1976**, *41*, 887–889.
[5] J. P. Melder, F. Wahl, H. Fritz, H. Prinzbach, *Chimia* **1987**, *41*, 426–428.
[6] M. S. Raasch, *J. Org. Chem.* **1980**, *45*, 856–867.
[7] K. Mackenzie, *J. Chem. Soc.* **1965**, 4646–4653.
[8] Force field MMX from PCMODEL4 (MM2 + π-VESCF routine, both by N. L. Allinger), Serena Software, Bloomington, IL, USA.
[9] W. Grimme, K. Pohl, J. Wortmann, D. Frowein, *Liebigs Ann.* **1996**, 1905–1916.
[10] F. Bonati, G. Wilkinson, *J. Chem. Soc.* **1964**, 3156–3160.
[11] Crystal structure data for **15**: $C_{38}H_{34}Cl_2 + CH_2Cl_2$, $M = 859.18$, crystal dimensions: $0.2 \times 0.1 \times 0.1$ mm, monoclinic, space group $C2/c$, $a = 17.994(4)$, $b = 16.901(4)$, $c = 4.006(3)$ Å, $\beta = 118.91(2)°$, $V = 3729(2)$ Å^3, $Z = 4$, $\rho_{calcd} = 1.531$ g cm^{-3}; $F(000) = 1760$; $\mu_{Mo} = 0.778$ cm^{-1}, $\theta_{max} = 27.04°$; 3159 measured, 3089 independent, and 1297 observed reflections ($F_o > 2\sigma > F_o^2$); $R_1 = 0.0617$, $wR_2 = 0.1722$. Nonius CAD4 diffractometer (room temperature, $Mo_{K\alpha}$ radiation, $\lambda = 0.71069$ Å). The structure was solved by direct methods and refined for all independent reflections against F^2(heavy atoms with anisotropic, H atoms with isotropic temperature factors). Programs used: MolEN (Nonius) for structure calculation and SHELXL-93 (G. M. Sheldrick, Universität Göttingen, Germany) for refinement. The calculations were performed in the Regionales Rechenzentrum der Universität zu Köln. Crystallographic data (excluding structure factors) for the structure(s) reported in this paper have been deposited with the Cambridge Crystallographic Data Centre as supplementary publication no. CCDC-100595. Copies of the data can be obtained free of charge on application to CCDC, 12 Union Road, Cambridge CB21EZ, UK (fax: (+44) 1223-336-033; e-mail: deposit@ccdc.cam.ac.uk).

 © WILEY-VCH Verlag GmbH, D-69451 Weinheim, 1998 1433-7851/98/3704-0475 $ 17.50+.50/0

Bioconjugation of Peptides by Palladium-Catalyzed C–C Cross-Coupling in Water**

Harald Dibowski and Franz P. Schmidtchen*

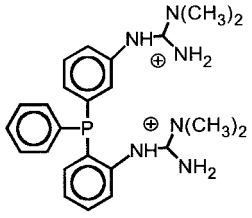
The biological activity of proteins in higher organisms frequently depends on their covalent modification with other substructures (e.g. prosthetic groups, saccharide chains, and membrane anchors). The attachment is performed in vivo at the enzymatic level and therefore cannot be directly controlled by methods of gene technology. An in vitro method for regioselectively attaching non-proteinogenic structural elements to a native folded protein would be a highly desirable tool supplementing the use of suitable cell lines. An obvious strategy would encompass a two-step process in which an amino acid containing some unique functionality is incorporated first into the primary sequence at the desired position (in Scheme 1 this is the N terminus of a folded protein) in a known manner.[1] In the second step this substructure would have to be linked with the second component to give the final bioconjugate (Scheme 1).



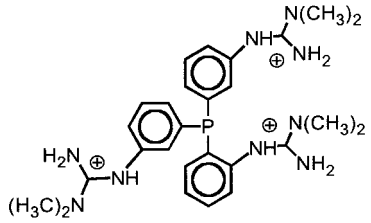
Scheme 1. Formation of a bioconjugate via an intermediate.

This second non-enzymatic step, apart from being chemoselective and establishing a permanent linkage of the two substructures, should allow coupling under mild reaction conditions in water to ensure that the fragile tertiary structure of the proteins is not damaged. Moreover, a high reactivity (rate constant) is mandatory in order to allow the bimolecular coupling to take place at the very small molar concentrations of the biopolymers within reasonable periods of time. Here we report that the palladium-catalyzed cross-coupling of aryl iodides with terminal alkynes, the Castro–Stephens–Sonogashira reaction[5] using a palladium–guanidinophosphane catalyst formed in situ, complies with these demands.

Water-soluble palladium catalysts for C–C cross-coupling usually employ sulfonated anionic triphenylphosphanes as ligands.[6] Under the basic reaction conditions required for Sonogashira reactions the proteins themselves carry a net negative charge as well, so that the catalytic process would have to overcome an electrostatic barrier. Experimental data indeed show that the catalytic activity of the cationic guanidinophosphanes **1** and **2**, which we recently synthesized, is well enhanced. In addition, these novel ligands are just as hydrophilic and substantially more stable against oxidation than their sulfonated analogues.[7]

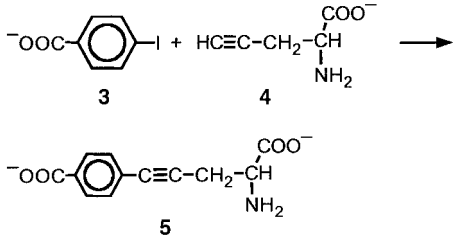


1



2

In preliminary experiments nonnatural free amino acids containing alkyne or iodoaryl groups were allowed to react with the corresponding reaction partners in aqueous acetonitrile (H_2O:CH_3CN = 7:3) at 50 °C. The reaction of *p*-iodobenzoate (**3**) with propargylglycine (**4**) gave the cross-coupled product **5** in 75 % yield after about three hours [Reaction (1)]



3 **4**

5

(1)

without formation of the product from alkyne homo-coupling. Under the same conditions (see Table 1) 3-iodotyrosine (**6**) reacted with propiolic acid [**7**; Reaction (2)] in 25 hours to give the C–C coupled product **8** (86 % yield), which could be isolated after acidic work-up and characterized by NMR spectroscopy. Longer reaction times or basic work-up caused the primary product **8** to rearrange cleanly in a known fashion to the benzofuran derivative **9**.

The same reaction course was observed under purely aqueous conditions (3-[tris(hydroxymethyl)methylamino]-1-propanesulfonic acid (TAPS) buffer, pH 8.3); therefore, the stage was set to test if the reaction conditions employed were influenced by the protein or were compatible with its catalytic function. We chose RNase A as our model protein, since this nuclease is readily available and its activity can be assayed

[*] Prof. Dr. F. P. Schmidtchen, Dr. H. Dibowski
Institut für Organische Chemie und Biochemie
der Technischen Universität München
Lichtenbergstrasse 4, D-85747 Garching (Germany)
Fax: (+49) 89-289-13345
E-mail: fpschmid@nucleus.org.chemie.tu-muenchen.de

[**] This work was supported by the Bundesminister für Bildung und Forschung (BMBF-project 03D 0002D6). We are also grateful to the Fonds der Chemischen Industrie for financial support.

 © WILEY-VCH Verlag GmbH, D-69451 Weinheim, 1998 1433-7851/98/3704-0476 $ 17.50+.50/0

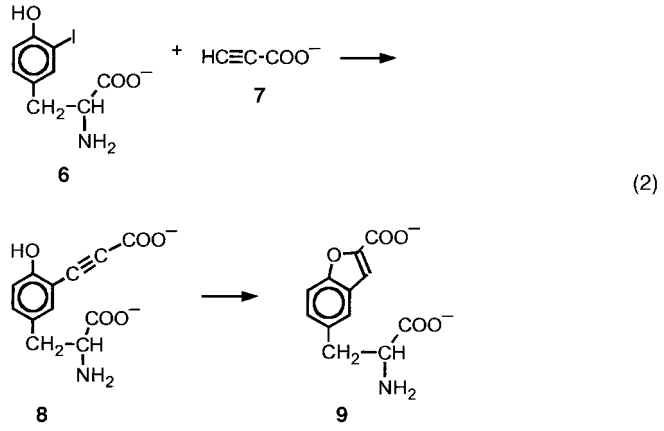
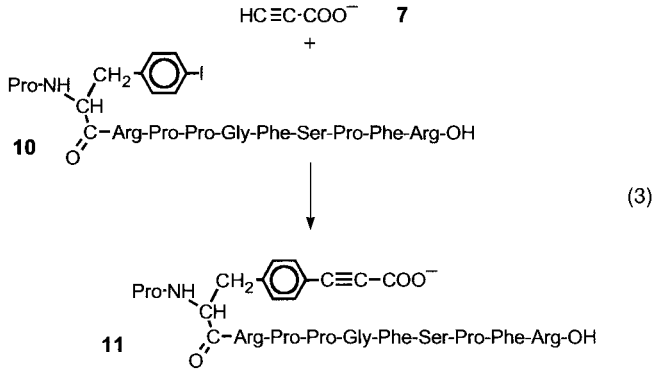


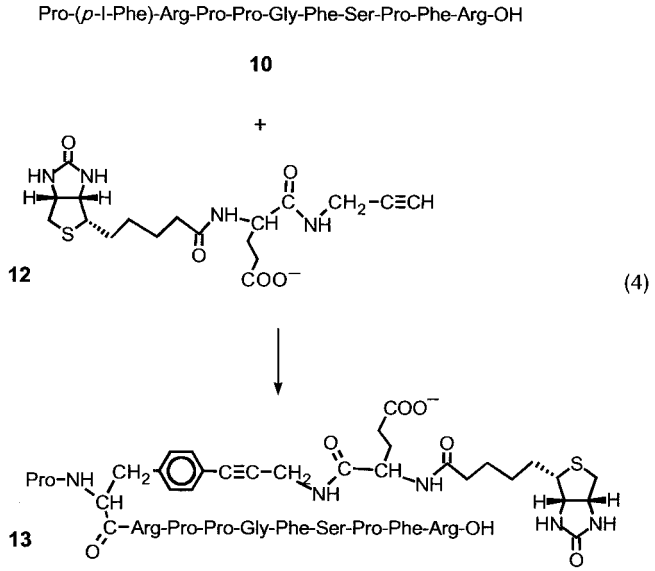
Table 1. Reaction conditions for the cross-couplings.[a]

Reaction	Solvent	Catalyst [mol%]	Yield [%]	*t* [min]
(1)	H_2O:CH_3CN = 7:3 $N(C_2H_5)_3$[b]	5	75	195
(2)	H_2O:CH_3CN = 7:3 $N(C_2H_5)_3$	5	86	120
(2)	0.2 M TAPS buffer pH 8.3 in H_2O	5[c]	89	140
(3)	0.2 M TAPS buffer pH 8.3 in H_2O	10[d]	75	240
(4)	0.2 M TAPS buffer pH 8.3 in H_2O	10	75	240

[a] T = 50 °C, unless noted otherwise. Substrate concentrations: iodoarene 10 mM, alkyne 20 mM. The catalyst solution was generated in situ by first mixing a solution containing 10 mM $Pd(OAc)_2$ and 50 mM **1**·Cl^- in water with 0.1 M CuI in acetonitrile in a volumetric ratio of 5:1 and then conditioning at 4° C under N_2 for five days. The activity of this stock solution was checked in regular intervals in standard catalysis reactions and remained constant for several weeks. [b] Iodoarene:alkyne = 1:1.4 with addition of four equivalents of hydroxylamine. [c] Ligand **2**. [d] Only four equivalents of ligand and one equivalent of CuI in the catalyst solution, T = 35 °C.



In close analogy peptides can be conjugated with biotin derivatives to provide a new access to the biotin–avidin technology[9] widely used in biological chemistry. In a demonstration biotinylglutamoylpropargylamide (**12**), a water-soluble biotin derivative, was allowed to react with **10** in aqueous TAPS buffer [pH 8.3; Reaction (4)]. After four



quickly by standard tests.[8] A comparison of the kinetics of Reaction (2) with and without the addition of RNase A (14 mg mL^{-1}) gave no qualitative difference in product formation, but the reaction in the presence of protein was markedly faster. The nuclease activity as well as its capillary electrophoretic behavior was determined before and after the reaction; it was not influenced at all by the palladium-catalyzed cross-coupling.

As an example of the regioselective C–C coupling of a multifunctional, free and unprotected peptide, Pro(*p*-I-Phe)-bradykinin (**10**) was allowed to react with propiolic acid [**7**; Reaction (3)]. The synthetic undecapeptide **10** itself can be synthesized in good yield from Pro(*p*-I-Phe)NH_2 and bradykinin[4a] by kinetically controlled reverse proteolysis with cathepsin C. Monitoring the reaction in aqueous TAPS buffer (pH 8.3) at 35 °C showed the clean formation of a single product in 91% yield after three hours. After it was isolated by HPLC, this compound was identified by FAB-MS (m/z = 1373; M^+) as the desired cross-coupling product.

hours a single product was formed in 75% yield, which was purified by gel chromatography and showed correct signals for the desired cross-coupling product in the electrospray mass spectrum [m/z = 1713 (M+H$^+$), 857 (M+2H$^+$), 572 (M+3H$^+$)]. The proof that this product possesses a competent biotin substructure was accomplished by affinity capillary electrophoresis (Figure 1). With incremental addition of the biotin-specific binding protein avidin to a sample of the reaction mixture that had not yet completely reacted, only the product peak was diminished to give a new protein complex.

The C–C cross-coupling catalyzed by palladium–guanidinoaryl–phosphane complexes thus allows the regioselective linking of iodoaryl and alkyne structures which are chemically rather stable and are orthogonal in their reactivity to almost all other functional groups in proteins. Their specific protection as well as general precautions for preserving the tertiary structure are therefore not necessary, since the native structure and function of the proteins remain unharmed under the extremely mild reaction conditions. A wide usage of

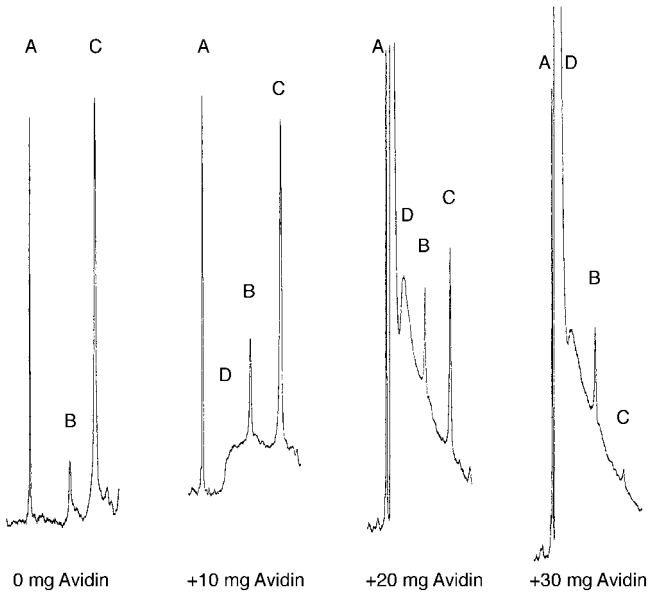


Figure 1. Affinity capillary electrophoresis of product **13** (C) from Reaction (4). A = catalyst complex, B = Pro(*p*-I-Phe)bradykinin (**10**), D = avidin – product complex. See text for further details.

this new method for the construction of structurally well-defined protein conjugates with nonnatural functions can be easily foreseen.

Received: September 24, 1998 [Z10964IE]
German version: *Angew. Chem.* **1998**, *110*, 487 – 489

Keywords: bioorganic chemistry · cross-coupling · palladium · P ligands · proteins

[1] In principal, known procedures include, among others, total synthesis, peptide-segment condensation,[2] in vitro protein biosynthesis,[3] and reverse proteolysis.[4]

[2] a) M. Brinkley, *Bioconjugate Chem*. **1992**, *3*, 2 – 13; b) H. D. Jakubke, *Angew. Chem*. **1995**, *107*, 189 – 191; *Angew. Chem. Int. Ed. Engl.* **1995**, *34*, 175 – 177; c) D. Hilvert, *Chem. Biol*. **1994**, *1*, 201 – 203; d) C. F. Liu, J. P. Tam, *J. Am. Chem. Soc*. **1994**, *116*, 4149 – 4153.

[3] a) D. V. Goeddel, *Methods Enzymol*. **1990**, *185*; b) J. Sambrook, E. F. Fritsch, T. Maniatis, *Molecular Cloning*, *a Laboratory Manual*, 2nd ed., Cold Spring Harbor Lab, Cold Spring Harbor, New York, **1989**.

[4] a) C. Gittel, F. P. Schmidtchen, *Bioconjugate Chem.* **1995**, *6*, 70 – 76; b) W. Kullmann, *Enzymatic Peptide Synthesis*, CRC, Boca Raton (FL), USA, **1987**; c) H. D. Jakubke, *Kontakte (Darmstadt)* **1991**, 60 – 72; d) *ibid.* **1992**, 46 – 60.

[5] a) R. D. Stephens, C. E. Castro, *J. Org. Chem.* **1963**, *28*, 3313 – 3315; b) C. E. Castro, E. J. Gaughan, D. C. Owsley, *ibid*. **1966**, *31*, 4071 – 4078; c) T. Sonogashira, Y. Tohda, N. Hagihara, *Tetrahedron Lett.* **1975**, 4467 – 4470.

[6] a) W. A. Herrmann, C. W. Kohlpaintner, *Angew. Chem*. **1993**, *105*, 1588 – 1609; *Angew. Chem. Int. Ed. Engl.* **1993**, *32*, 1524 – 1544; b) C. J. Li, *Chem. Rev*. **1993**, *93*, 2023 – 2035; c) A. Lubineau, J. Augé, Y. Quenceau, *Synthesis* **1994**, 741 – 760; d) R. Rossi, A. Carpita, F. Bellina, *Org. Prep. Proc. Int*. **1995**, *27*, 127 – 160.

[7] a) H. Dibowski, F. P. Schmidtchen, *Tetrahedron* **1995**, *51*, 2325 – 2330; b) A. Hessler, O. Stelzer, W. S. Sheldrick, H. Dibowski, K. Worm, F. P. Schmidtchen, *J. Org. Chem*. **1997**, *52*, 2362 – 2369.

[8] E. M. Crook, A. P. Mathias, B. R. Rabin, *Biochem. J.* **1960**, *74*, 234 – 238.

[9] a) E. A. Bayer, M. Milcheck, *Methods Biochem. Anal*. **1980**, *26*, 1 – 45; b) *Methods Enzymol*. **1990**, *184*, 138 – 160; c) Y. H. Chu, W. J. Lees, A. Stassinopulos, C. T. Walsh, *Biochemistry* **1994**, *33*, 10616 – 10621.

A Self-Replicating Peptide under Ionic Control**

Shao Yao, Indraneel Ghosh, Reena Zutshi, and Jean Chmielewski*

The self-replicating abilities of DNA, in addition to providing a genetic transfer mechanism for reproducing species, have played a significant role in the widespread development of biotechnology strategies.[1] DNA is unique in its self-replication, and species that rely on DNA for replication can adapt to environmental changes through natural selection. Recent examples of designed molecular systems capable of self-replication include nucleotide-based oligomers,[2] conjugates of adenine and Kemp's triacid,[3] peptides,[4] and micelles.[5] The production of a self-replicating molecule from a large molecular pool has been a more elusive target.[6] Recent work of Lee et al. demonstrated that peptides from the GCN4 leucine zipper domain self-replicate in an autocatalytic cycle.[4] We sought a peptidic self-replicating system that would be sensitive to environmental conditions and reproduce only under extreme conditions. We now describe a peptide that reproduces autocatalytically in an environmentally dependent manner.

The peptide K1K2 (Figure 1) was designed based on the sequence of the KK peptide of Zhou et al.[7] and on our peptide E1E2.[8] The K1K2 peptide contains Lys residues at

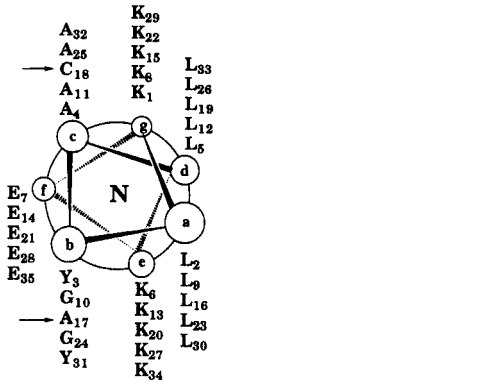


Figure 1. a) Helical wheel diagram of K1K2 showing the positions of the coiled-coil, heptad repeat (a – g). b) Peptide sequences employed in the study [R = $(CH_2)_2CONH_2$]. Ligation residues Ala and Cys are located at the solvent-exposed b and c positions, as indicated by the arrows.

[*] Prof. J. Chmielewski, S. Yao, I. Ghosh, R. Zutshi
Department of Chemistry, Purdue University
West Lafayette, IN 47907 (USA)
Fax: (+1) 765-494-0239
E-mail: chml@chem.purdue.edu

[**] This work was supported by the National Science Foundation (9457372-CHE). We are very grateful to Dr. G. von Kiedrowski for the generous gift of the program SimFit, and for his and Gary Knott's helpful advice.

 © WILEY-VCH Verlag GmbH, D-69451 Weinheim, 1998 1433-7851/98/3704-0478 $ 17.50+.50/0

the e and g positions of the leucine repeat, thus preventing formation of a stable coiled-coil conformation at acidic and neutral pH due to electrostatic repulsion. Under highly basic conditions or neutral conditions with high concentrations of shielding counterions, the repulsive forces would be minimized, thus allowing appropriate aggregation of the coiled-coil peptide. Ion-assisted nucleation of secondary structure has been demonstrated; however, a simultaneous nucleation in the presence of ions with concomitant autocatalysis has not yet been achieved.[7, 9, 10] In this work it was envisioned that the K1 K2 peptide would self-replicate from smaller fragments only under those conditions that promoted formation of a stable coiled-coil conformation and, therefore, template formation.

The two components of K1 K2, the thioester-containing K1 and the nucleophilic fragment K2, were designed to produce K1 K2 based on the chemical ligation method developed by Kent et al.[11] We anticipated that the coupling between K1 and K2 to form K1 K2 under acidic or neutral conditions would proceed by a nonautocatalytic pathway, in which K1 K2 exists mostly in a random coil, nontemplating conformation. The addition of certain salts such as $NaClO_4$ has been shown to enhance coiled-coil formation of peptides containing Lys residues in the e and g positions due to reduced electrostatic repulsion.[7, 9] These conditions, therefore, should promote the templating ability of K1 K2 for K1 and K2, leading to autocatalytic formation of K1 K2 at neutral pH.

Circular dichroism (CD) spectroscopy was used to assess the helical content of the designed peptides. The peptides were found to adopt a helical conformation with dependence on the salt concentration (Figure 2 a). The helical content of

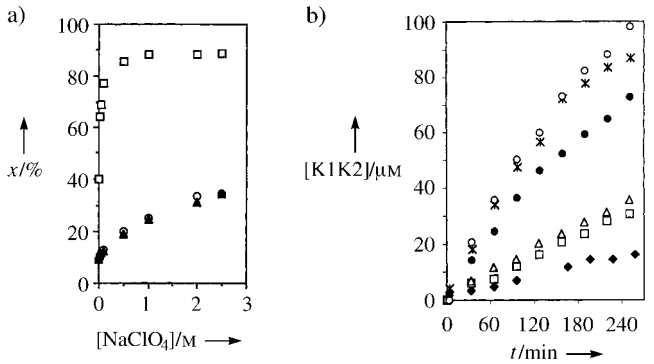


Figure 2. a) The helical content x of K1 K2 (□), K1 (○), and K2 (▲) as a function of $NaClO_4$ concentration. b) K1 K2 production as a function of time in MOPS buffer at pH 7.5 and with different concentrations of $NaClO_4$: 0 M $NaClO_4$ (◆), 0.25 M $NaClO_4$ (□), 0.5 M $NaClO_4$ (△), 0.75 M $NaClO_4$ (●), 1.0 M $NaClO_4$ (*), 2.0 M $NaClO_4$ (○).

K1 K2 reaches a maximum of 82% at 2.5 M $NaClO_4$,[12] presumably due to formation of a coiled-coil conformation when the protonated Lys residues are shielded, as was observed with K K.[7] The ratio of $\theta_{220\,nm}/\theta_{207\,nm}$ has been shown to correlate with the presence of a coiled-coil structure, and a value of 1.03 was obtained for K1 K2 at 1.0 M $NaClO_4$, which is in good agreement with the values for other coiled-coil peptides.[13] Addition of 50% trifluoroethanol, a solvent reported to disrupt interhelical interactions, to K1 K2 at 1.0 M $NaClO_4$ lowered the $\theta_{220\,nm}/\theta_{207\,nm}$ ratio to 0.89, a value indicative of a single-stranded α-helix.[13] The secondary structure of the shorter peptides, K1 and K2, was also dependent on the salt concentration with maximum helical contents of 34 and 35%, respectively, at 2.5 M $NaClO_4$. To ascertain whether K1 and K2 associate at 1.0 M NaClO4, CD spectra of equimolar mixtures of K1 and K2 were compared to the addition spectra of K1 and K2. No increase in helical content was observed with the mixture of peptides over that obtained with the individual peptides alone, suggesting a lack of association between K1 and K2.

Size exclusion chromatography was used to probe the aggregation state of K1 K2 in the presence of 0.5 M $NaClO_4$ at pH 7.5. An apparent molecular mass of approximately 18000 was obtained, which corresponds to a tetrameric structure under these conditions. Without added NaClO4, however, both monomeric and dimeric forms of K1 K2 were observed by size exclusion chromatography; this structural polymorphism has been described for other coiled-coil peptides.[14] The tetrameric form of K1 K2 was denatured with urea, and a two-state transition was observed by CD spectroscopy (Figure 3). A dissociation constant of $2.84 \pm 0.71 \times 10^{-32}\,M^3$ was obtained for K1 K2 at 0.75 M $NaClO_4$ by fitting the denaturation data with equations for a two-state model for the monomer-to-tetramer transition.[15]

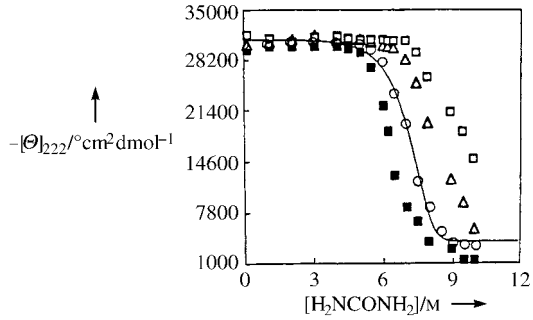


Figure 3. Urea denaturation of 50 μM K1 K2 at 0.5 M $NaClO_4$ (■), 0.75 M $NaClO_4$ (○), 1.25 M $NaClO_4$ (△), 1.5 M $NaClO_4$ (□), The data for 0.75 M $NaClO_4$ (○) are shown fit to a curve for a monomer–tetramer equilibrium.[15] [θ_{222}] is the mean residue ellipticity at 222 nm.

Since the conformation of K1 K2 can be controlled by the addition of salt, the production of K1 K2 from K1 and K2 was next investigated over the concentration range of 0 to 2.0 M $NaClO_4$. As the concentration of $NaClO_4$ in the reaction mixture was decreased from 2.0 M there was a concomitant decrease in the formation of K1 K2 (Figure 2 b). The significantly higher rate of K1 K2 formation at 1.0 and 2.0 M $NaClO_4$ as compared to that at other salt concentrations is presumably due to the coiled-coil and templating ability of the product K1 K2 under these conditions. As seen in Figure 3, the stability of the aggregate increases with increasing $NaClO_4$ concentration. At lower salt concentrations electrostatic repulsion from the protonated Lys residues likely results in uncoiling of K1 K2 and leads to a diminishing of its templating abilities for K1 and K2.

 © WILEY-VCH Verlag GmbH, D-69451 Weinheim, 1998 1433-7851/98/3704-0479 $ 17.50+.50/0

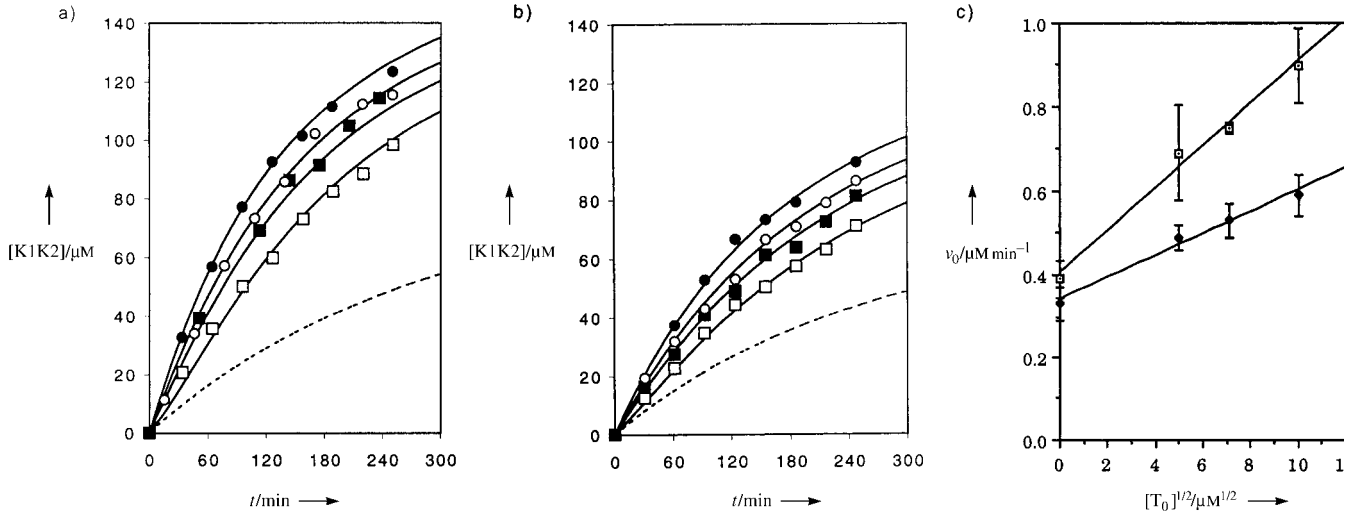


Figure 4. a) K1K2 production as a function of time for reaction mixtures of K1 and K2 containing different initial concentrations of K1K2 as the template at pH 7.5 in 250 mM MOPS (1% (v/v) 3-mercaptopropionic acid) containing 2.0 M $NaClO_4$; no K1K2 (□), 25 μM K1K2 (■), 50 μM K1K2 (○), 100 μM K1K2 (●). b) Same as a) except that the concentration of $NaClO_4$ in the solution was 0.75 M. Curves were generated with the program SimFit.[2d, e] The dashed lines represent the calculated production of K1K2 in the absence of autocatalysis. c) Initial rate v_0 of K1K2 formation as a function of the square root of the initial template concentration $[T_0]$ in 2.0 M $NaClO_4$ (□) and 0.75 M $NaClO_4$ (●). We assumed the following reaction equations for data analysis with SimFit: a) K1 + K2 → K1K2 with a rate constant of k_b; b) K1 + K2 + 0.5 K1K2 → 1.5 K1K2 with a rate constant of k_a; c) K1 → K1* with a hydrolysis rate of k_h.

The autocatalytic nature of the K1K2-forming reaction at pH 7.5 in the presence of $NaClO_4$ was unambiguously established by performing the coupling reaction between K1 and K2 at two different concentrations of $NaClO_4$ (0.75 and 2.0 M) in the presence of differing amounts of K1K2 as a template (Figure 4a and 4b). The production of K1K2 was accelerated by the presence of K1K2 as a template at both salt concentrations. In addition, the initial rate of product formation was found to be linearly proportional to the square root of the template concentration (Figure 4c), as is expected for an autocatalytic reaction.

The program SimFit[2d, e] was used to analyze the experimental results at concentrations of 2.0 and 0.75 M $NaClO_4$, and provided apparent rate constants, k_a, for the autocatalytic reaction of $24.6 \pm 1.5\ M^{-3/2}s^{-1}$ and $12.9 \pm 0.8\ M^{-3/2}s^{-1}$, rate constants, k_b, of the uncatalyzed reaction of $0.087 \pm 0.008\ M^{-1}s^{-1}$ and $0.082 \pm 0.009\ M^{-1}s^{-1}$, and rate constants, k_h, for the hydrolysis of the thioester-containing peptide fragment K1 of $2.78 \pm 0.25 \times 10^{-5}s^{-1}$ and $3.5+0.4 \times 10^{-5}s^{-1}$, respectively. These values provided an autocatalysis efficiency ($\varepsilon = k_a/k_b$) of approximately 280 and 160, respectively. While the rate constant for the uncatalyzed reaction was not appreciably affected by increasing concentrations of $NaClO_4$, the rate constant for autocatalytic K1K2 production increased from $12.9\ M^{-3/2}s^{-1}$ to $24.6\ M^{-3/2}s^{-1}$, presumably due to the enhanced coiled-coil and template formation.

Less than 5% of K1K2 was obtained in the ligation reaction upon addition of 50% trifluoroethanol, an agent known to inhibit coiled-coil formation.[13] Similarly the addition of 7 M urea to the ligation reaction in the presence of 1 M $NaClO_4$ reduced product formation to background reaction levels, also providing evidence for the role of K1K2 as a template for the reaction of K1 with K2. Additionally the rates of the reaction between K1 and K2 without added $NaClO_4$, in both the presence and absence of K1K2 at pH 7.5, were found to be identical, confirming that autocatalysis does not occur under conditions that do not promote the formation of a stable coiled-coil structure. Since K1K2 exists as a tetramer the templating species may be a coiled-coil trimer, although we cannot rule out the potential for a monomeric or dimeric template at the very low, initial concentrations of K1K2 during the early stages of the reaction.

We have successfully designed a self-replicating peptide that promotes its own production at high salt concentrations. At low salt concentrations autocatalysis is suppressed and the reaction with added template is indistinguishable from the background reaction. This self-replication reaction demonstrates that ionic control within the peptide autocatalysis regime is feasible, and we are applying this strategy to design self-replicating systems where cross-catalysis is possible under controlled conditions.

Experimental Section

Peptides K1K2 and K2 were synthesized by solid-phase peptide synthesis on the Rink resin[16] using Fmoc-based chemistry.[17] Peptide K1 was synthesized with a MBHA resin functionalized with Boc-Ala-$S(CH_2)_2CO_2H$[18] by using Boc-based chemistry with Kent's in situ neutralization method.[11] Cleavage of the peptide from the solid support with HF/anisole provided the thioester-containing peptide K1 (Figure 1). All peptide were purified to homogeneity by reversed-phase HPLC and characterized by mass spectrometry (plasma desorption) and amino acid analysis.

CD spectroscopy: The spectra for K1, K2, and K1K2 were recorded at 20°C in a 10 mM MOPS buffer at pH 7.5 (Buffer A). $NaClO_4$ and urea were added from stock solutions in Buffer A for salt dependence and denaturation studies. To ensure that no reaction took place during the measurements, Cys to Ala variants of K2 and K1K2 were used.

Size exclusion chromatography: A 1.8 cm × 98 cm column packed with Sephadex G-50 at 25°C and a flow rate of 0.34 mL min^{-1} was equilibrated with a buffer containing a) 100 mM phosphate, 0.5 M $NaClO_4$, pH 7.5; b) 100 mM phosphate, pH 7.5. A 75 μM solution of K1K2 (500 μL) was loaded onto the column, and the apparent molecular mass of the eluting

 © WILEY-VCH Verlag GmbH, D-69451 Weinheim, 1998 1433-7851/98/3704-0480 $ 17.50+.50/0

species was calculated by interpolation of a standard curve of carbonic anhydrase, cytochrome C, and aprotinin.

Reaction conditions: Mixtures of K1 (240 μM) and K2 (240 μM) were incubated at 23°C in 250 mM MOPS (1% (v/v) 3-mercaptopropionic acid), 0 to 2.0 M $NaClO_4$, at pH 7.5. At the indicated time interval 50 μL of the reaction mixture was evaluated by reversed-phase HPLC. The reaction products were identified by direct isolation and characterization by mass spectrometry, or by HPLC coinjection with authentic samples. Concentrations of product were determined by interpolation of peak areas from a standard curve.

Received: July 24, 1997 [Z 10729 IE]
German version: *Angew. Chem.* **1998**, *110*, 489 – 492

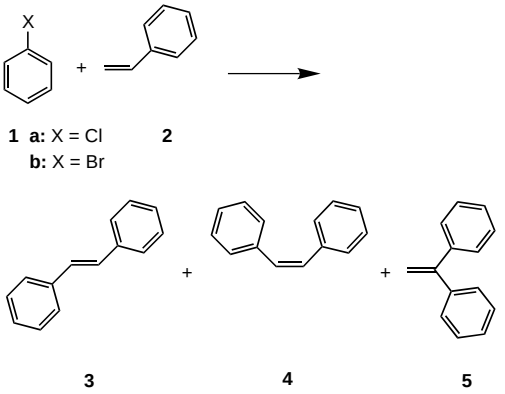
Keywords: bioorganic chemistry · peptides · self-replication · template synthesis

[1] A. Humphrey, *Ann. NY Acad. Sci.* **1995**, *758*, 356 – 365.
[2] a) G. von Kiedrowski, *Angew. Chem.* **1986**, *98*, 932; *Angew. Chem. Int. Ed. Eng.* **1986**, *25*, 932; b) G. von Kiedrowski, B. Wlotzka, J. Helbing, *ibid.* **1989**, *101*, 1259 and **1989**, *28*, 1235; c) G. von Kiedrowski, B. Wlotzka, J. Helbing, M. Matzen, S. Jordan, *ibid.* **1991**, *103*, 456 and **1991**, *30*, 423; d) D. Sievers, G. von Kiedrowski, *Nature* **1994**, *369*, 221; e) T. Achilles, G. von Kiedrowski, *Angew. Chem.* **1993**, *105*, 1225; *Angew. Chem. Int. Ed. Eng.* **1993**, *32*, 1198; f) G. von Kiedrowski, *Bioorg. Chem. Front.* **1993**, *3*, 113; g) W. S. Zielinski, L. E. Orgel, *Nature* **1987**, *327*, 346; h) L. E. Orgel, *ibid.* **1992**, *358*, 203; i) T. Li, K. C. Nicolaou, *ibid.* **1994**, *369*, 218.
[3] a) T. Tjivikua, P. Ballester, J. Rebek, *J. Am. Chem. Soc.* **1990**, *112*, 1249; b) J. S. Nowick, Q. Feng, T. Tjivikua, P. Ballester, J. Rebek, *ibid.* **1991**, *113*, 8831; c) E. A. Wintner, M. M. Conn, J. Rebek, *ibid.* **1994**, *116*, 8877; d) E. A. Wintner, B. Tsao, J. Rebek, *J. Org. Chem.* **1995**, *60*, 7997; e) E. A. Wintner, J. Rebek, *Acta Chem. Scand.* **1996**, *50*, 469.
[4] D. H. Lee, J. R. Granja, J. A. Martinez, K. Severin, M. R. Ghadiri, *Nature* **1996**, *382*, 525.
[5] P. A. Bachmann, P. L. Luisi, J. Lang, *Nature* **1992**, *357*, 57.
[6] For a review, see: L. E. Orgel, *Acc. Chem. Res.* **1995**, *28*, 109.
[7] a) N. E. Zhou, C. M. Kay, R. S. Hodges, *J. Mol. Biol.* **1994**, *237*, 500; b) W. D. Kohn, O. S. Monerra, C. M. Kay, R. S. Hodges, *ibid.* **1995**, *270*, 25495; c) H. Chao, M. E. Houston, S. Grothe, C. M. Kay, M. O'Connor-McCourt, R. T. Irvin, R. S. Hodges, *Biochemistry* **1996**, *35*, 12175.
[8] S. Yao, I. Ghosh, R. Zutshi, J. Chmielewski, *J. Am. Chem. Soc.* **1997**, *119*, 10559.
[9] Y. Goto, S. Aimoto, *J. Biol. Chem.* **1991**, *218*, 387 – 396.
[10] a) M. R. Ghadiri, C. Choi, *J. Am. Chem. Soc.* **1990**, *112*, 1630; b) R. Fuqiang, C. Yanqiu, P. B. Hopkins, *ibid.* **1990**, *112*, 9403.
[11] a) P. E. Dawson, T. W. Muir, I. Clark-Lewis, S. B. H. Kent, *Science* **1994**, *266*, 776; b) L. E. Canne, S. M. Walker, S. B. H. Kent, *Tetrahedron Lett.* **1995**, *36*, 1217; c) M. Schnolzer, P. Alewood, A. Jones, D. Alewood, S. B. H. Kent, *Int. J. Peptide Protein Res.* **1992**, *40*, 180; d) L. E. Canne, S. J. Bark, S. B. H. Kent, *J. Am. Chem. Soc.* **1996**, *118*, 5891.
[12] P. C. Lyu, J. C. Sherman, A. Chen, N. R. Kallenbach, *Proc. Natl. Acad. Sci. USA* **1991**, *88*, 5317.
[13] a) N. E. Zhou, C. M. Kay, R. S. Hodges, *J. Biol. Chem.* **1992**, *267*, 2664; b) S. Y. M. Lau, A. K. Taneja, R. S. Hodges, *ibid.* **1984**, *259*, 13253.
[14] L. Gonzalez, R. A. Brown, D. Richardson, T. Alber, *Nature Struct. Biol.* **1996**, *3*, 1002.
[15] R. Fairman, H. Chao, L. Mueller, T. B. Lavoie, L. Shen, J. Novotny, G. R. Matsueda, *Protein Sci.* **1995**, *4*, 1457.
[16] H. Rink, *Tetrahedron Lett.* **1987**, *28*, 3787.
[17] E. Atherton, R. C. Sheppard in *The Peptides, Vol. 9* (Eds.: E. Gross, J. Meienhofer), Academic Press, New York, **1987**.
[18] a) H. Hojo, S. Aimoto, *Bull. Chem. Soc. Jpn.* **1991**, *64*, 111; b) L. Zhang, J. P. Tam, *J. Am. Chem. Soc.* **1997**, *119*, 2363.

A New Catalyst System for the Heck Reaction of Unreactive Aryl Halides

Manfred T. Reetz,* Gunther Lohmer, and Renate Schwickardi

Although the palladium-catalyzed Heck reaction of aryl halides ArX (X = Cl, Br, I) with olefins is a standard C – C bond-forming reaction,[1] industrial applications are rare,[2] because the reactivity of aryl halides decreases drastically in the order ArI > ArBr > ArCl, which means that the cheap chlorides and even some bromides do not react with sufficiently high yields, turnover numbers (TON), and selectivities. In spite of recent progress, for example, use of certain palladacycles prepared from tris(*o*-tolyl)phosphane as catalysts in Heck reactions of bromo and activated chloro arenes,[3] the activation of unreactive aryl halides such as chlorobenzene remains a real challenge.[4] We report on a new and surprisingly simple catalyst system, which for the first time makes such coupling reactions possible in an unusually efficient manner.[5] We serendipitously discovered that the use of simple Pd salts such as $PdCl_2$ or $Pd(OAc)_2$ in the presence of tetraphenylphosphonium salts Ph_4PX (X = Cl, Br, I) leads to unexpectedly high catalytic activities.[6] Optimization of the reaction of chlorobenzene (**1a**) with styrene (**2**) to form the Heck products **3**, **4**, and **5** [Eq. (1)] showed that a ratio of Pd to Ph_4PX of 1:6 leads to the best results; sodium acetate is suitable as base and *N*,*N*-dimethylformamide (DMF) or *N*-methylpyrrolidinone (NMP) as solvent (Table 1).[7]



(1)

Another surprising discovery is that the use of small amounts of *N*,*N*-dimethylglycine (DMG) as additive leads to a pronounced improvement in regioselectivity.[7] Upon employing six equivalents of DMG relative to Pd and only 2 mol% of the Pd catalyst, the proportion of undesired regioisomer **5** is significantly reduced. Although no chemically engineered optimization was carried out, simple exploratory experiments showed that a further decrease in the amount of catalyst is certainly possible. Using 0.5 mol% catalyst a TON of 130 is reached. The same reaction with

[*] Prof. Dr. M. T. Reetz, Dipl.-Chem. G. Lohmer, R. Schwickardi
Max-Planck-Institut für Kohlenforschung
Kaiser-Wilhelm-Platz 1, D-45470 Mülheim an der Ruhr (Germany)
Fax: (+49) 208-306-2985
E-mail: reetz@mpi-muelheim.mpg.de

 © WILEY-VCH Verlag GmbH, D-69451 Weinheim, 1998 1433-7851/98/3704-0481 $ 17.50+.50/0

Table 1. Heck reaction of chlorobenzene (**1a**) with styrene (**2**) at 150°C.[a]

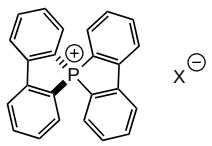
Catalyst	Solvent	*t* [h]	DMG [mol%]	Conversion [%]	Side products [%]	Selectivity [**3**:**4**:**5**]
$[Pd(CH_3CN)_2Cl_2]$	NMP	12	–	6	6	–
$[Pd(CH_3CN)_2Cl_2]\cdot 6Ph_4PCl$	DMF	8	–	89	11	86:1:13
$[Pd(CH_3CN)_2Cl_2]\cdot 6Ph_4PCl$	NMP	12	–	79	<1	84:1:15
$[Pd(CH_3CN)_2Cl_2]\cdot 6Ph_4PCl$	NMP	12	12	96	<1	96:1:3
$[Pd(CH_3CN)_2Cl_2]\cdot 6Ph_4PCl$	DMF	12	12	95	12	96:1:3
$[Pd(CH_3)_2(tmeda)]\cdot 6Ph_4PCl$[b]	NMP	12	9	85	<1	97:1:2
$[PdCl_2(Ph_3P)_2]\cdot 4Ph_4PCl$	DMF	6	–	77	7	85:1:14
$[\{Pd(\mu\text{-}Cl)(Ph_3P)(Ph)\}_2]$	NMP	12	–	14	8	83:2:15
$[\{Pd(\mu\text{-}Cl)(Ph_3P)(Ph)\}_2]\cdot 6Ph_4PCl$	NMP	12	–	86	<1	85:1:14
$[\{Pd(\mu\text{-}Cl)(Ph_3P)(Ph)\}_2]\cdot 6Ph_4PCl$	NMP	12	12	80	<1	97:1:2
$Pd(OAc)_2\cdot 6Ph_4PCl$	NMP	12	12	79	<2	97:1:2

[a] [a] Sodium acetate (2 equiv) as base; 2 mol% Pd catalyst. [b] tmeda = *N*,*N*,*N*′,*N*′-tetramethylethylenediamine.

bromobenzene (**1b**) and styrene (**2**) in NMP in the presence of as little as 0.05 mol% of the catalyst $[Pd(CH_3CN)_2Cl_2]\cdot 6Ph_4PCl$ also proceeded smoothly (24 h; 140°C; 77% Heck products **3**, **4**, and **5** in a ratio of 90:1:9; TON = 1300).

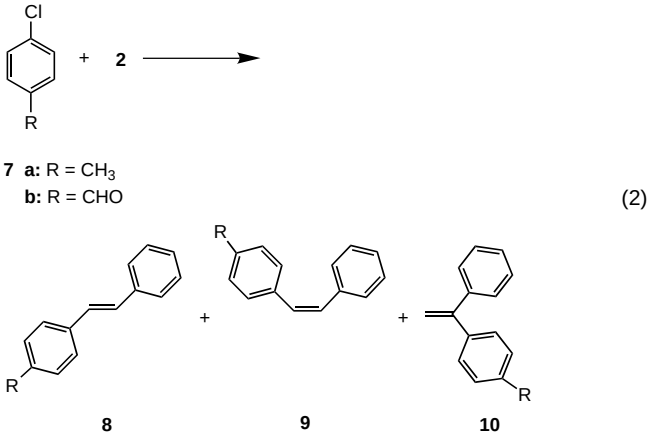
Interestingly, the influence of the phosphonium salt depends upon the nature of the halide counterion. Whereas the bromide is somewhat less effective than the chloride, the iodide turns out to be practically ineffective (<16% conversion after 8 h). Although detailed mechanistic studies remain to be carried out, we currently suspect that part or all of the reaction proceeds via the phosphonium salt. Ph_4PX are known to function as stoichiometric arylating agents in Pd-catalyzed Heck reactions, albeit in moderate yields.[8] Triphenylphosphane is thereby generated, which in our case becomes arylated back to the phosphonium salt in a known Pd-catalyzed process.[9]

It is currently unclear why the presence of Ph_4PX stabilizes the palladium so effectively, that is, why practically no undesired Pd precipitate is observed at such high temperatures. Anionic complexes[10] are probably formed on halide addition of Ph_4PX to such possible intermediates as $[(Ph_3P)Pd(Ph)X]$ or the dimeric form $[\{Pd(\mu\text{-}X)(Ph_3P)(Ph)\}_2]$. Indeed, the latter compound (X = Cl), which we were able to prepare easily as a relatively insoluble and difficult to characterize complex by reaction of $Pd(OAC)_2$ with Ph_4PCl in the presence of ethanol as the reducing agent,[11] is a highly active and thermally stable catalyst or precatalyst in the presence of excess Ph_4PCl. Accordingly, at 60–70°C the dimeric precursor is converted into a soluble and presumably anionic form. In addition, synthetically and mechanistically significant is the observation that the use of the spiro-type phosphonium salt **6a**,**b**[12] under the usual conditions of the test reaction leads to less than 4% conversion. This special phosphonium salt is particularly stable and does not undergo ring-opening arylation.



6 **a:** X = Cl
b: X = I

Should these hypotheses pertain, then the use of stoichiometric amounts of substituted aryl halides and catalytic amounts of $[Pd(CH_3CN)_2Cl_2]\cdot 6Ph_4PCl$ should afford scrambling products,[13] the amount of which is expected to depend upon the ratio of ArX to Ph_4PCl. Indeed, this was observed. For example, upon treating *p*-chlorotoluene (**7a**) with styrene (**2**) in the presence of $[Pd(CH_3CN)_2Cl_2]\cdot 6Ph_4PCl$ [2 mol%, NMP, 8 h, 150°C; Eq. (2)], not only the "normal" products **8a**,



7 **a:** R = CH_3
b: R = CHO

(2)

8 **9** **10**

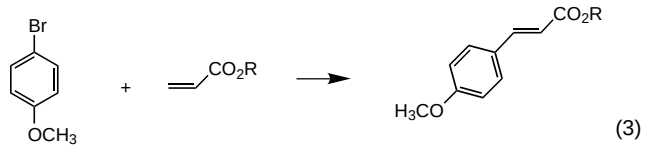
9a, and **10a** were formed in a ratio of 90:<1:10, but also the scrambling products **3**–**5** in a ratio of about 85:1:14 (conversion relative to **7a**: 66%; 30% normal products, 27% scrambling products). In the presence of DMG (12 mol%) the reaction proceeds similarly, but with increased regioselectivity (**8a**:**9a**:**10a** = 97:<1:3). The use of $[Pd(CH_3CN)_2Cl_2]\cdot 6(p\text{-tolyl})_4PCl$ as the catalyst (2 mol%, NaOAc, NMP, 19 h, 150°C) affords by nature solely the desired products **8a**, **9a**, and **10a** in a ratio of 90:<1:10 (58% conversion, 4% side products).

To suppress the amount of undesired scrambling products generally, it is not mandatory to prepare and use the corresponding phosphonium salt. Rather, it is simply necessary to reduce the amount of the catalyst $[Pd(CH_3CN)_2Cl_2]\cdot 6Ph_4PCl$. For example, the reaction of *p*-chlorobenzaldehyde (**7b**) with styrene (**2**) in presence of 0.1 mol% of $[Pd(CH_3CN)_2Cl_2]\cdot 6Ph_4PCl\cdot 6DMG$ (NaOAc, NMP, 48 h, 150°C) affords the desired products **8b**, **9b** and **10b** in a ratio of 98:<1:2 (98% conversion; TON = 950), and only 1% of undesired scrambling products **3**, **4**, and **5** [Eq. (2)].

The method can be applied to other substrates such as acrylates (**12**). Bromobenzene (**1b**) reacts smoothly with acrylate **12a** (0.01 mol% $[Pd(CH_3CN)_2Cl_2]\cdot 6Ph_4PCl$, NMP, 130°C; >97% yield, TON 9800). Reaction of the normally

 © WILEY-VCH Verlag GmbH, D-69451 Weinheim, 1998 1433-7851/98/3704-0482 $ 17.50+.50/0

sluggishly reacting *p*-bromoanisol **11** with the acrylate **12b** [Eq. (3)] leads to 71% of the desired product (TON 1300); only 1% scrambling product and no 1,1-regioisomers are formed.[14]

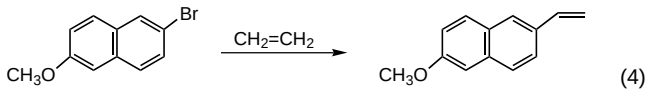


(3)

11 **12** **a:** R = *n*-C_4H_9 **13**

b: R = $CH_2CH(C_2H_5)C_4H_9$

In a further experiment the industrially relevant 2-bromo-6-methoxynaphthalene **14**[15] was treated with ethylene in the presence of 0.05 mol% $[Pd(CH_3CN)_2Cl_2]\cdot 6\,Ph_4PCl$ in a steel autoclave [NaOAc, *N*,*N*-dimethylacetamide as solvent, 24 h, 140°C, 20 bar; Eq. (4)]. The desired product **15** was obtained in 89% yield (conversion 97%, TON = 1800).



(4)

14 **15**

In summary, the combination of PdX_2 and Ph_4PX in the presence of DMG represents the currently most active and selective catalyst system for Heck reactions of normally unreactive aryl halides. Even the special palladacycles, recently described as being particularly active, fail in reactions of such substrates as chlorobenzene (**1a**).[3] Indeed, in our hands the coupling of **1a** and **2** with the usual palladacycle *trans*-di(μ-acetato)-bis[*o*-(di-*o*-tolylphosphino)benzyl]dipalladium[3] with or without DMG as an additive proceeded to less than 2% (TON = 1). The turnover number in the reaction of bromobenzene (**1b**) with acrylate (**12a**) is also significantly higher in our catalyst system (TON 9800 versus 48 for the palladacycle[3]). The same pertains to the reaction of *p*-bromoanisol (**11**; TON 1300 versus 87).[16] It remains to be seen whether our catalyst system is also effective in Suzuki coupling reactions, carbonylations, and aminations.

Received: September 3, 1997 [Z10884IE]
German version: *Angew. Chem.* **1998**, *110*, 492–495

Keywords: C–C coupling · Heck reaction · homogeneous catalysis · palladium · regioselectivity

[1] Reviews of Heck reactions: a) R. F. Heck, *Palladium Reagents in Organic Syntheses*, Academic Press, London, **1985**; b) J. Tsuji, *Palladium Reagents and Catalysts: Innovations in Organic Synthesis*, Wiley, Chichester, **1995**; c) A. de Meijere, F. E. Meyer, *Angew. Chem.* **1994**, *106*, 2473; *Angew. Chem. Int. Ed. Engl.* **1994**, *33*, 2379; d) W. Cabri, I. Candiani, *Acc. Chem. Res.* **1995**, *28*, 2; e) T. Jeffery, *Adv. Met.-Org. Chem*. **1996**, *5*, 153.

[2] B. Cornils, W. A. Herrmann, *Applied Homogeneous Catalysis with Organometallic Compounds*, VCH, Weinheim, **1996**.

[3] a) W. A. Herrmann, C. Brossmer, K. Öfele, C.-P. Reisinger, T. Priermeier, M. Beller, H. Fischer, *Angew. Chem.* **1995**, *107*, 1989; *Angew. Chem. Int. Ed. Engl.* **1995**, *34*, 1844; b) W. A. Herrmann, C. Brossmer, C.-P. Reisinger, T. H. Riermeier, K. Öfele, M. Beller, *Chem. Eur. J.* **1997**, *3*, 1357.

[4] a) V. V. Grushin, H. Alper, *Chem. Rev.* **1994**, *94*, 1047; b) Y. Ben-David, M. Portnoy, M. Gozin, D. Milstein, *Organometallics* **1992**, *11*, 1995; c) M. T. Reetz, G. Lohmer, *Chem. Commun.* **1996**, 1921; d) D. E. Kaufmann, M. Nouroozian, H. Henze, *Synlett* **1996**, 1091.

[5] M. T. Reetz, G. Lohmer, R. Schwickardi, DE-A 19712388.0, **1997**.

[6] The reaction of $PdCl_2$ with 2 equiv Ph_4PCl affords $(Ph_4P)_2[PdCl_4]$ as a crystalline compound, which we have characterized by X-ray crystallography. The compound is an active catalyst or pre-catalyst in Heck reactions, especially if an additional 4 equiv Ph_4PCl (relative to Pd) are employed.

[7] Typical procedure: A pyrex reaction flask was charged with $Pd(CH_3CN)_2Cl_2$ (5.2 mg, 0.02 mmol) and Ph_4PCl (45.0 mg, 0.12 mmol), degassed three times under vacuum, and then flushed with argon. Anhydrous sodium acetate (164.0 mg, 2.0 mmol), chlorobenzene (**1a**; 112.6 mg, 1.0 mmol) and styrene (**2**; 130.2 mg, 1.25 mmol) were added. Following the addition of 1 mL NMP (or DMF) the flask was closed, and the contents stirred for 30 min at 120°C and then 12 h at 150°C. After the usual workup, the mixture was analyzed by gas chromatography. The reaction was performed analogously with *N*,*N*-dimethylglycine (DMG) as additive.

[8] M. Sakamoto, I. Shimizu, A. Yamamoto, *Chem. Lett.* **1995**, 1101.

[9] a) Y. Hirusawa, M. Oku, K. Yamamoto, *Bull. Chem. Soc. Jpn*. **1957**, *30*, 667; b) L. Horner, G. Mummenthey, H. Moser, P. Beck, *Chem. Ber.* **1966**, *99*, 2782; c) C. B. Ziegler, R. F. Heck, *J. Org. Chem.* **1978**, *43*, 2941; d) T. Migita, T. Nagai, K. Kiuchi, M. Kosugi, *Bull. Chem. Soc. Jpn.* **1983**, *56*, 2869; e) L. Cassar, M. Foà, *J. Organomet. Chem*. **1974**, *74*, 75.

[10] Various anionic Pd-species have been postulated as possible intermediates in Heck reactions:[1] a) W. J. Scott, J. K. Stille, *J. Am. Chem. Soc.* **1986**, *108*, 3033; b) C. Amatore, A. Jutand, M. A. M'Barki, *Organometallics* **1992**, *11*, 3009; c) E. Negishi, T. Takahashi, K. Akiyoshi, *J. Chem. Soc. Chem. Commun*. **1986**, 1338.

[11] a) This compound as well as soluble derivatives were first prepared by Anderson by the reaction of $[\{PdCl(\mu\text{-}Cl)(PR_3)\}_2]$ with Ar_2Hg in yields of 20–40%: G. K. Anderson, *Organometallics* **1983**, *2*, 665; b) see also G. López, J. Ruiz, G. García, C. Vicente, J. M. Martí, M. D. Santana, *J. Organomet. Chem.* **1990**, *393*, C53; c) the reaction of $Pd(OAc)_2$ with 2 equiv Ph_4PCl at 25–60°C in DMF afforded only soluble adducts of the type $(Ph_4P)_2[Pd(OAc)_2Cl_2]$, whereas the same reaction in the presence of stoichiometric amounts of ethanol resulted in the formation of an insoluble light yellow solid material. The elemental analysis is in accord with $[\{PdCl(Ph_3P)(Ph)\}_n]$.

[12] a) D. Hellwinkel, *Top. Curr. Chem*. **1983**, *109*, 1. b) We thank Prof. Hellwinkel for a sample of **6b**. Compound **6a** was prepared by ion exchange.

[13] Scrambling products in conventional Heck reactions with phosphanes PAr^1_3 as ligands and Ar^2X as arylating agents are common:[1] a) K.-C. Kong, C.-H. Cheng, *J. Am. Chem. Soc.* **1991**, *113*, 6313; b) D. K. Morita, J. K. Stille, J. R. Norton, *ibid.* **1995**, *117*, 8576; c) W. A. Herrmann, C. Brossmer, K. Öfele, M. Beller, H. Fischer, *J. Mol. Catal. A: Chem.* **1995**, *103*, 133.

[14] Heitz has shown that in the $Pd(OAc)_2$-catalyzed reaction of bromobenzene (**1b**) with styrene (**2**) and other olefins, the nature of the base and the phosphane affects regioselectivity: S. Klingelhöfer, C. Schellenberg, J. Pommerehne, H. Bässler, A. Greiner, W. Heitz, *Macromol. Chem. Phys.* **1997**, *198*, 1511.

[15] M. Beller, A. Tafesh, W. A. Herrmann (Hoechst AG), EP 725049 A1, **1996** [*Chem. Abstr.* **1996**, *125*, 221376].

[16] Chloro arenes such as *p*-chlorobenzaldehyde (**7b**) are also practically inert in the presence of palladacycles as catalysts, unless an excess of Bu_4NBr was added (Jeffery conditions[1e]).[3]

 © WILEY-VCH Verlag GmbH, D-69451 Weinheim, 1998 1433-7851/98/3704-0483 $ 17.50+.50/0

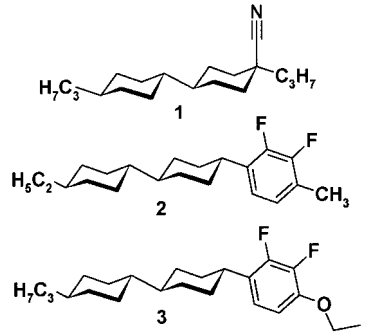
A Novel Type of Liquid Crystals Based on Axially Fluorinated Cyclohexane Units**

Peer Kirsch* and Kazuaki Tarumi

The recent boom in the development of multimedia liquid crystal displays (LCDs) has created a strong demand for new liquid crystalline materials with high clearing temperatures, high dielectric anisotropy ($\Delta\varepsilon$), and low rotational viscosity (γ_1).[1] Other desired properties with increasing importance for active matrix displays (AMDs) are high specific resistance (SR) and good voltage holding ratio (VHR) of LC mixtures.[2] Liquid crystals with highly fluorinated aromatic substructures meet most of these criteria and are now commonly used as major components of LC mixtures for AMDs with fast response times.[1]

Because of the strong dipole moment of the C–F bond, arenes with terminal or lateral fluorine substituents are well suited for achieving a strongly positive or negative dielectric anisotropy $\Delta\varepsilon$.[3] Unfortunately, the price to pay for such a high $\Delta\varepsilon$ is a decrease in the clearing temperature by about 25–30 K per fluorine substituent.[1] Especially fluorinated two-ring liquid crystals, whose major advantage is their low rotational viscosity, suffer from very low clearing points. Therefore, we are investigating structural modifications that improve the clearing points without losing the advantageous properties of fluorinated two- and three-ring systems.

Currently, most active matrix displays use liquid crystal mixtures with a positive dielectric anisotropy. In contrast, the recently introduced VA-TFT LCD (vertical alignment thin film transistor LCD)[4]—which offers a superior picture quality with a wide viewing angle (160°), high contrast, and video-compatible switching times (< 20 ms)—is based on a liquid crystal mixture with negative dielectric anisotropy and very low birefringence ($\Delta n \approx 0.08$). In the first generation of technically applicable materials (**1**, $\Delta\varepsilon = -8.2$; Scheme 1)[5] the negative $\Delta\varepsilon$ was achieved by means of the strong perpendicular dipole moment of a cyano group attached to an axial position of a dialkylbicyclohexane as mesogenic core structure. Unfortunately, nitriles in general cannot be used in AMDs because of their tendency to reduce the mixture's voltage holding ratio (VHR), which is a highly critical parameter for any kind of AMD technology.[1, 2] Nowadays, most AMD mixtures with negative $\Delta\varepsilon$ are based on second-generation materials such as the laterally difluorinated phenylbicyclohexanes **2** ($\Delta\varepsilon = -2.7$) or **3**[6] ($\Delta\varepsilon = -5.9$).

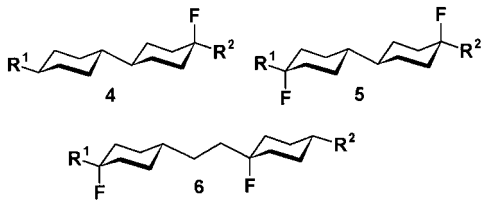


Scheme 1. Examples for first- (**1**) and second-generation (**2**, **3**) materials with negative dielectric anisotropy.

A general disadvantage of all compounds with the 2,3-difluorobenzene subunit is their relatively high rotational viscosity (**2**: $\gamma_1 = 184$; **3**: $\gamma_1 = 413$ mPa s), which leads to longer switching times. In addition, recent experience indicates that materials containing no heteroatoms other than fluorine display the best VHR values. Therefore, it would be desirable to replace compounds such as **3** (which contains an ether group) by a pure fluorohydrocarbon.

To reduce the driving voltage and therefore power consumption of VA-TFT displays, we looked for new liquid crystals with strongly negative dielectric anisotropy, low birefringence, high clearing points, and low rotational viscosity. These new materials should contain no aromatic substructures (which increase Δn) and no non-fluorine heteroatoms (which sometimes decrease the VHR).

A rational approach to this problem would be the attachment of one or more perpendicular dipoles to a nonaromatic mesogenic core structure. Especially suitable for this purpose are the tertiary axial positions of cyclohexane substructures of dialkyl bicyclohexanes, bis(cyclohexyl)ethanes, or their homologues (see **1**). If the axial hydrogen atom is replaced by fluorine, dipole moments perpendicular to the long molecular axis are created (**4**–**6**, Scheme 2). If more than one axial fluorine atom is introduced, the resulting C–F dipoles can be oriented parallel (**6**), which leads to mutual enhancement, or antiparallel (**5**), so that they cancel each other.



Scheme 2. Dielectrically negative target compounds with purely aliphatic mesogenic core structures containing axially fluorinated cyclohexyl subunits (R^1, R^2 are combinations of C_2H_5, C_3H_7, and C_5H_{11}).

In the search for new materials with improved mesogenic and viscoelastic properties in the 1980s, many attempts were made to synthesize liquid crystals containing axially fluorinated cyclohexane building blocks. The few examples known up to now were prepared by reaction of the respective tertiary cyclohexanol with diethylaminosulfur trifluoride (DAST),[5, 7] or by treating an alkylcyclohexane derivative with diluted

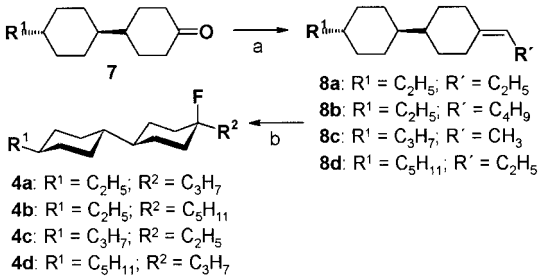
[*] Dr. P. Kirsch, Dr. K. Tarumi
Merck KGaA, Business Unit Liquid Crystals
D-64271 Darmstadt (Germany)
Fax: (+49) 6151-72-2593
E-mail: peer.kirsch@merck.de

[**] We thank A. Ruhl and R. Sander for experimental assistance, Dr. M. Bremer for helpful discussions about computational chemistry, and Dr. J. Krause, J. Haas, and H. Heldmann for the physical evaluation of the new substances. Part of this work was performed under the management of the Association of Super-Advanced Electronics Industries (ASET) in the R & D program of the Japanese Ministry of International Trade and Industry (MITI) supported by the New Energy and Industrial Development Organization (NEDO).

 © WILEY-VCH Verlag GmbH, D-69451 Weinheim, 1998 1433-7851/98/3704-0484 $ 17.50+.50/0

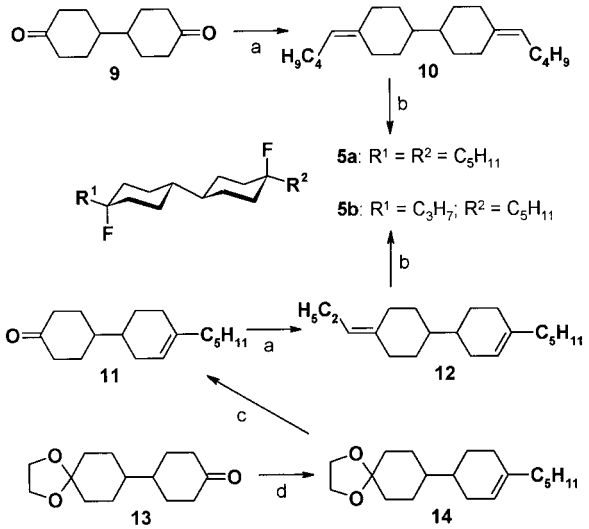
elemental fluorine.[8] Both procedures are potentially hazardous and unsuitable for large-scale syntheses. Furthermore, most of the axially fluorinated cyclohexane derivatives decomposed during purification or on extended storage. Here we report on an alternative approach, which also allows more complex compounds containing two or more axial fluorine atoms to be synthesized.

The syntheses of the axially monofluorinated bicyclohexanes **4** started from the corresponding cyclohexylcyclohexanones **7** (Scheme 3). A Wittig reaction furnished the

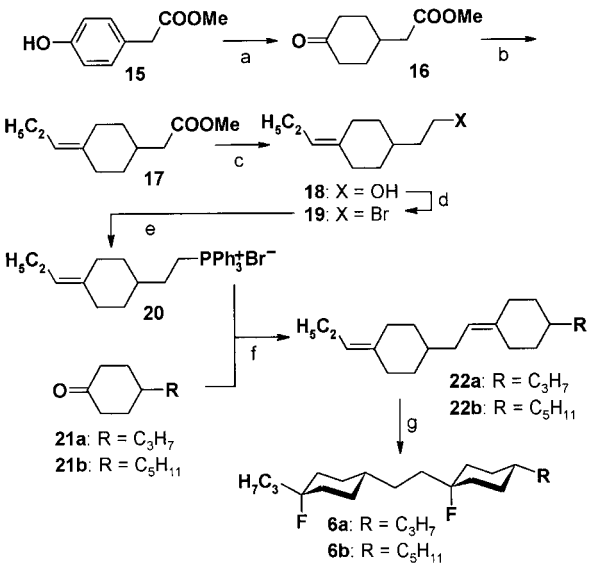


Scheme 3. Synthesis of the fluorobicyclohexanes **4a–d**: a) $R'CH_2PPh_3^+Br^-$, KO*t*Bu, THF; −10 °C→room temperature, 2 h (80–90%). b) 4 equiv of 70% HF/pyridine, CH_2Cl_2; room temperature, 18 h (15–50%; $R^2 = R'CH_2$).

alkylidenebicyclohexanes **8**, which were diluted with dichloromethane and treated with 70% HF/pyridine (Olah's reagent).[9] The crude products were extracted with *n*-heptane, and the extracts filtered through silica gel. Crystallization from *n*-heptane furnished the pure axially fluorinated compounds **4a–d** in 15–50% yield, mainly depending on the solubility of the product.[10] The more complex compounds **5a/b** and **6a/b** were synthesized analogously (Schemes 4 and 5).

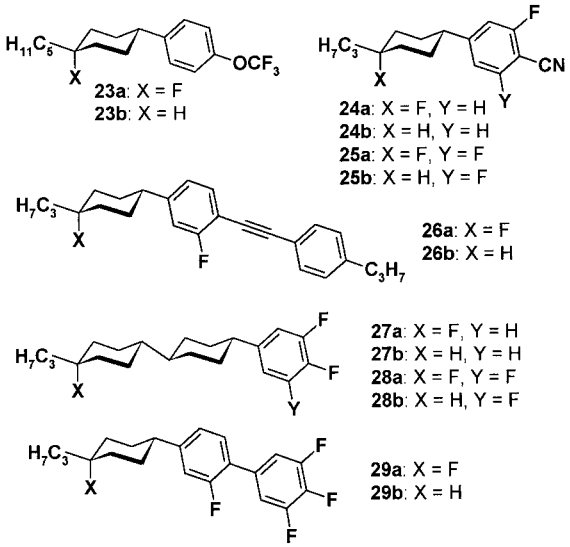


Scheme 4. Synthesis of the symmetric (**5a**) and unsymmetric (**5b**) difluorobicyclohexanes: a) $H_{11}C_5PPh_3^+Br^-$ or $H_7C_3PPh_3^+Br^-$, KO*t*Bu, THF; −10 °C→room temperature, 2 h (**10**: 85%, **12**: 74%). b) 122 equiv of 70% HF/pyridine, CH_2Cl_2; room temperature, 18 h (**5a**: 32%, **5b**: 26%). c) HCOOH, toluene; room temperature, 18 h (97%). d) 1. $C_5H_{11}MgBr$, THF; 2. cat. TsOH, ethylene glycol, toluene; azeotropic removal of water (32%).



Scheme 5. Synthesis of **6a** and **6b**: a) H_2, 5% Pd/C, toluene (89%). b) $H_7C_3PPh_3^+Br^-$, KO*t*Bu, THF; −10 °C→room temperature, 2 h (70%). c) $LiAlH_4$, THF; reflux, 3 h (88%). d) CBr_4, PPh_3, CH_3CN; −5 °C→room temperature, 18 h (69%). e) PPh_3, 1,3-dimethylhexahydro-2-pyrimidinone (DMPU); 75 °C, 18 h (63%). f) KO*t*Bu, THF; −10 °C→room temperature, 2 h (**22a**: 56%, **22b**: 29%). g) 19.5 equiv of 70% HF/pyridine, CH_2Cl_2; −15 °C→10 °C, 10 min (**6a**: 17%, **6b**: 18%).

In addition, we were interested in the general influence of axial fluorination on the physical properties of liquid crystals with different mesogenic core structures, including those with positive dielectric anisotropy. Therefore, we synthesized some representative compounds for comparison with their nonfluorinated analogues (**23–29**, Scheme 6).

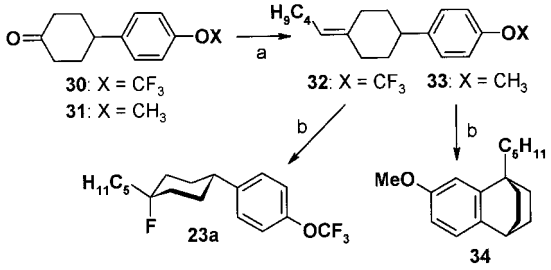


Scheme 6. Dielectrically positive target compounds and their nonfluorinated analogues.

Earlier publications on axially fluorinated cyclohexane derivatives[7, 8] mention the instability of these substances. Therefore, we first explored the limitations on the use of, for example, axially fluorinated phenylcyclohexane derivatives in the synthesis of more complex liquid crystalline materials.

 © WILEY-VCH Verlag GmbH, D-69451 Weinheim, 1998 1433-7851/98/3704-0485 $ 17.50+.50/0

The starting materials for all the newly synthesized compounds are the corresponding cyclohexanones, which were prepared by literature methods.[11] The hydrofluorination procedure functions very well for all alkylidenecyclohexylarenes with electron-withdrawing substituents and provides the axially fluorinated phenylcyclohexanes in good yields. An example is the smooth conversion of **32** into **23a** (Scheme 7).



Scheme 7. Synthesis of the axially fluorinated phenylcyclohexane derivative **23a** and the unexpected reaction product **34**: a) $H_{11}C_5PPh_3^+Br^-$, KO*t*Bu, THF; $-10\,^\circ C \rightarrow$room temperature, 2 h (**32**: 57%, **33**: 83%). b) CH_2Cl_2, ca. 100 equiv of 70% HF/pyridine; room temperature, 18 h (**23a**: 19%, **34**: quantitative according to GC, yield of isolated product 58%)

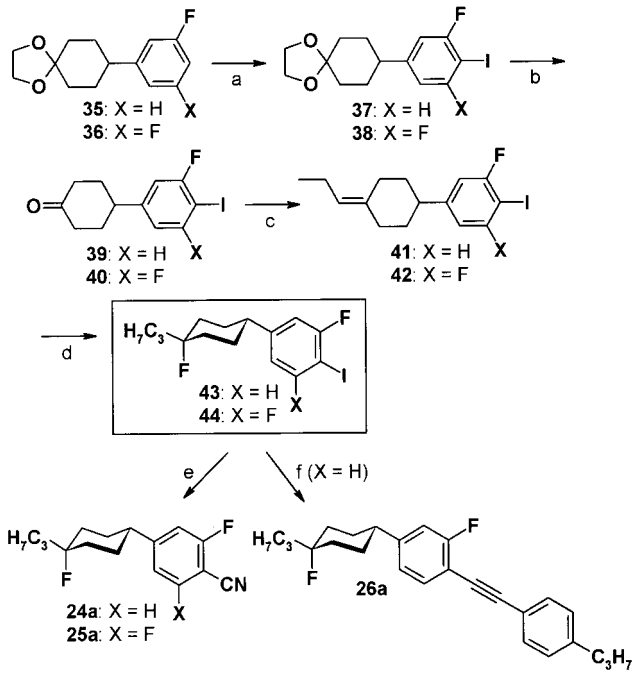
In contrast, for compound **33**, which contains an electron-donating methoxy group, the same hydrofluorination conditions result in quantitative formation of the benzobicyclooctane derivative **34**. The unexpected formation of this product can be explained by the intramolecular electrophilic attack of an intermediate carbocationic species on the activated methoxyphenyl group.[12]

As shown in Scheme 8, the building blocks **43** and **44** can be converted under drastic conditions into either the nitriles **24a** and **25a** (2 h at 120 °C) or, in the case of **44**, into the cyclohexyltolane **26a** (NEt_3 solvent, transition metal catalyst). To inhibit autocatalytic dehydrofluorination, the cyanation reaction was conducted in the presence of a small amount of 2,6-bis-*tert*-butylpyridine as a proton scavenger. The yields of both reactions were in the same range as for the analogous synthesis of the nonfluorinated liquid crystals **24b**, **25b**, and **26b**.

Under the same conditions as for the phenylcyclohexane derivatives, hydrofluorination with HF/pyridine in dichloromethane can also be used to prepare the more complex three-ring systems **27a**, **28a**, and **29a** (Scheme 6). The starting materials are the corresponding phenylcyclohexylcyclohexanones and the biphenylcyclohexanone.

All newly synthesized axially fluorinated cyclohexane derivatives are stable on extended storage at ambient temperature. In addition, their stability at elevated temperatures is clearly demonstrated by their successful conversion to cyano and alkinyl derivatives.

The evaluation of all the newly synthesized materials concentrated on mesogenic properties and electrooptic data, extrapolated from a standard LC mixture.[13] In LC displays pure liquid crystals are never used, but mixtures of typically 10 to 15 liquid crystalline components. Blending is the only method to achieve a broad nematic phase range and to adjust electrooptic and viscoelastic properties exactly to the specifications required for an optimal display performance. Many of the two-ring compounds display no mesophases as pure substances (see also Table 1) but are nevertheless indispensable components of the LC mixtures currently in use for displays. For this reason, the physical behavior of a new liquid



Scheme 8. Synthesis of the axially fluorinated phenylcyclohexane building blocks **43** and **44** and subsequent coupling reactions: a) 1. **35**: BuLi, KO*t*Bu, THF; $-100\,^\circ C$, 30 min; **36**: BuLi, THF; $-75\,^\circ C$, 30 min. 2. I_2, THF; metalation temperature $\rightarrow -25\,^\circ C$ (**37**: 61%, **38**: 65%). b) 98% HCOOH, toluene; room temperature, 18 h (**39**: 79%, **40**: 70%). c) $H_7C_3PPh_3^+Br^-$, KO*t*Bu, THF; $-10\,^\circ C \rightarrow$room temperature, 2 h (**41**: 84%, **42**: 70%). d) CH_2Cl_2, 4 equiv of 70% HF/pyridine; $-25\,^\circ C \rightarrow$room temperature, 1 h (**43**: 45%, **44**: 44%). e) *N*-Methylpyrrolidone, 0.1 equiv of 2,6-bis-*tert*-butylpyridine, 1.3 equiv of CuCN; 120 °C, 2 h (**24a**: 66%, **25a**: 25%). f) 4-Ethylphenylacetylene, 0.026 equiv CuI, 0.004 equiv $[PdCl_2(PPh_3)_2]$, NEt_3; room temperature, 3 h (29%).

Table 1. Physical properties of the axially fluorinated cyclohexane derivatives compared to their nonfluorinated analogues. To determine the extrapolated clearing points $T_{NI,extr}$, dielectric anisotropies $\Delta\varepsilon$, birefringences Δn, and rotational viscosities γ_1, see ref. [13]. The increase in the extrapolated clearing points ΔT_{NI} is calculated with respect to the corresponding nonfluorinated cyclohexane derivatives. The temperatures are given in °C, and the γ_1 values in mPa s. C = crystalline, N = nematic, I = isotropic. Numbers in parentheses denote monotropic phase transitions.

Entry	X	Mesophases	$T_{NI,extr}$	ΔT_{NI}	$\Delta\varepsilon$	Δn	γ_1
23a	F	C 32 I	−28.0	+16.2	5.9	0.079	–
23b	H	C 14 I	−44.2	–	5.6	0.089	38
24a	F	C 50 I	−15.6	+18.0	27.1	0.124	–
24b	H	C 39 N (−11) I	−33.6	–	26.0	0.123	98
25a	F	C 64 I	−50.0	+13.3	34.7	0.114	231
25b	H	C 57 I	−63.3	–	32.6	0.110	99
26a	F	C 107 N, decomp	218.3	+7.3	0.1	0.236	–
26b	H	C 81 N 197 I	211.0	–	1.3	0.234	–
27a	F	C 62 N, decomp	126.4	+0.4	4.9	0.080	293
27b	H	C 46 N 124 I	116.0	–	6.4	0.079	160
28a	F	C 73 N 115 I	89.4	+14.6	9.8	0.082	301
28b	H	C 66 N 94 I	74.8	–	9.7	0.075	171
29a	F	C 73 N (48.8) I	43.4	+18.4	16.0	0.126	292
29b	H	C 64 I	25.0	–	15.2	0.135	173

 © WILEY-VCH Verlag GmbH, D-69451 Weinheim, 1998 1433-7851/98/3704-0486 $ 17.50+.50/0

crystal in a complex mixture is of utmost importance for applied liquid crystal research.

For all dielectrically positive materials, axial fluorination has a significant effect on the mesogenic behavior: The melting points and the real and extrapolated[13] clearing points are increased by 10–20 K. Compounds **26a** and **27a** decompose with loss of HF above 120 °C. The nematic phase range of **28a** is broader by 14 K than than that of its nonfluorinated analogue **28b**. For **29a** there is a monotropic nematic phase, while **29b** exhibits no mesophase.

For **23**–**29** with a positive $\Delta\varepsilon$, axial fluorination has only a marginal effect on the electrooptic characteristics. For the weakly polar compounds **26a/b** and **27a/b** the dielectric anisotropy becomes smaller; for the other, more polar substances it increases slightly. Fluorination has no significant effect on the birefringence.

The rotational viscosity (γ_1) of a liquid crystal mixture is directly proportional to its switching time. To obtain the fast-switching LC mixtures required for multimedia displays, it is desirable to use single components with a γ_1 value as low as possible. For this reason, the extrapolated rotational viscosity[13] of a liquid crystalline compound is one of the most important parameters for evaluating new materials. Since there is also an empirical correlation of γ_1 with the clearing point and polarity of LC materials, it must always be seen in relation to these parameters. For all the newly synthesized compounds, axial fluorination approximately doubles the rotational viscosity. This increase probably outweighs the advantage of the higher clearing points for the three-ring compounds. However, for highly polar two-ring systems such as **25a**, the increased clearing point is a dramatic improvement and makes axially fluorinated phenylcyclohexanes a very promising class of substances for future application in AMDs.

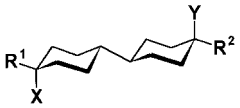
For the dielectrically negative materials, the results are somewhat different. Compared to the nonfluorinated dialkylbicyclohexanes **45** (Table 2),[14] the first axial fluorine substituent causes a dramatic increase in the extrapolated clearing point ($T_{NI,extr}$) by more than 50 K. Also the melting points and the S_B–I transition temperatures of the pure compounds **4** are increased by about 10–20 K. The general tendency to form smectic B (S_B) mesophases is not influenced by fluorination. As expected, the birefringence of **4** is even slightly lower than that of the nonfluorinated compounds **23**. The dielectric anisotropy $\Delta\varepsilon$ is between -2.1 and -2.4. Remarkably, the rotational viscosities of the axially monofluorinated bicyclohexanes are in the range of 50–75 mPa s, in contrast to 184 mPa s for the currently used material **2** (Table 3). With exception of the lower birefringence and the much lower γ_1 values, the axially fluorinated bicyclohexanes have quite similiar properties to aromatic compounds such as **2**.

Table 3. Physical properties of some conventional materials **1**, **2**, and **3** with negative dielectric anisotropy. Clearing points $T_{NI,extr}$, birefringences Δn, and rotational viscosities γ_1 are extrapolated from Merck liquid crystal mixture ZLI-4792, and dielectric anisotropies $\Delta\varepsilon$ from ZLI-2857.[13] The temperatures are given in °C, and the γ_1 values in mPa s. C = crystalline, S_B = smectic B, N = nematic, I = isotropic. Values in parentheses denote monotropic phase transitions.

Entry	Mesophases	$T_{NI,extr}$	$\Delta\varepsilon$	Δn	γ_1
1	C 34 N (19) I	14.1	−8.2	0.027	>400
2	C 58 N 106.2 I	107.8	−2.7	0.092	184
3	C 79 S_B (78) N 184.5 I	175.4	−5.9	0.096	413

The axially difluorinated bicyclohexanes **5** were synthesized in order to test the scope of our hydrofluorination method. We wanted to determine whether a second axial fluorine substituent leads to an increase in clearing point comparable to that resulting from the first one. This could result in extrapolated clearing points exceeding 150 °C. As shown in Table 1, the second fluorine substituent causes a slight decrease in the clearing point compared to the first substituent. The difluorinated compounds have low solubility in organic solvents. Since the C–F bonds were assumed to be aligned in opposite directions, we expected no significant

Table 2. Physical properties of the axially fluorinated bicyclohexanes **4** and **5** compared to their nonfluorinated analogues **45**. Clearing points $T_{NI,extr}$, dielectric anisotropies $\Delta\varepsilon$, birefringences Δn, and rotational viscosities γ_1 are extrapolated from ZLI-4792, and the $\Delta\varepsilon$ values for the dielecrically negative materials **4a–d**, **5a** and **5b** from ZLI-2857.[13] The increase in the extrapolated clearing points ΔT_{NI} is calculated with respect to the corresponding nonfluorinated dialkylbicyclohexanes **45**. The temperatures are given in °C, and the γ_1 values in mPa s. C = crystalline, S_B = smectic B, I = isotropic.

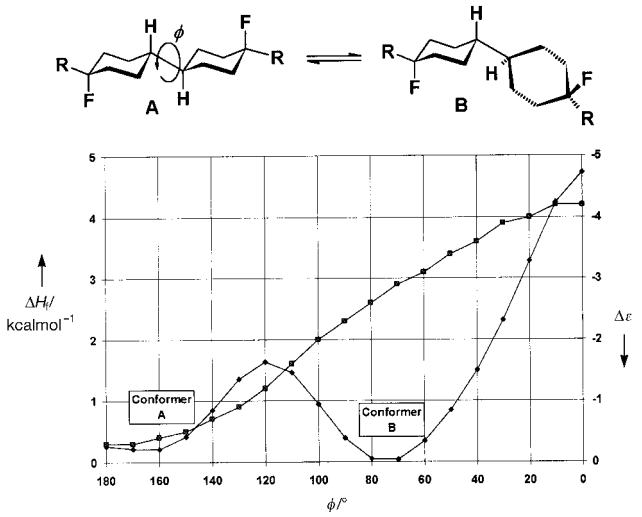


Entry	R^1	R^2	X	Y	Mesophases	$T_{NI,extr}$	ΔT_{NI}	$\Delta\varepsilon$	Δn	γ_1
4a	C_2H_5	C_3H_7	H	F	C 9 S_B 80 I	50.1	+33.4	−2.0	0.036	52
4b	C_2H_5	C_5H_{11}	H	F	? S_B 95 I	67.7	+56.9	−2.1	0.034	76
4c	C_3H_7	C_2H_5	H	F	C 31 S_B 80 I	28.5	+11.8	−2.4	0.048	51
4d	C_5H_{11}	C_3H_7	H	F	C 52 S_B 109 I	100.7	+44.5	−2.1	0.048	–
5b	C_5H_{11}	C_3H_7	F	F	C 142 I[a]	89.2	+33.0	−2.5	0.040	–
5a	C_5H_{11}	C_5H_{11}	F	F	C 100 S_B 153 I[a]	105.7	+28.7	−2.5	0.035	188
45a	C_2H_5	C_3H_7	H	H	C −3 S_B 68.2 I	16.7	–	−1.1	0.050	23
45b	C_2H_5	C_5H_{11}	H	H	C −16 S_B 77 I	10.8	–	−1.1	0.052	25
45c	C_5H_{11}	C_3H_7	H	H	C 22 S_B 98 I	56.2	–	−0.5	0.049	31
45d	C_5H_{11}	C_5H_{11}	H	H	C 41 S_B 114 I	77.0	–	–	–	–

[a] Decomposition.

 © WILEY-VCH Verlag GmbH, D-69451 Weinheim, 1998 1433-7851/98/3704-0487 $ 17.50+.50/0

dielectric anisotropy. To our surprise, **5a** and **5b** had $\Delta\varepsilon$ values that surpass those of their monofluorinated analogues. An explanation for this unexpected behavior is provided by AM1 calculations (Scheme 9):[15] apart from the approximately centrosymmetric conformation **A** with $\phi = 163.1^\circ$ ($\Delta\varepsilon_{calcd} = -0.4$) there is a *gauche* conformation **B** with $\phi = 74.8^\circ$ ($\Delta\varepsilon_{calcd} = -2.7$). If one assumes a Boltzmann distribution between conformer **A** with 42% and the energetically slightly preferred (190 cal mol^{-1}) conformer **B** with 58% occupation, this results in a calculated average $\Delta\varepsilon_{res}$ of -1.7 for **5a**. Comparative calculations on **45d** indicate that the axial fluorination of **5a** has no significant influence on this conformer equilibrium, and that the usual bicyclohexanes will show a similiar rotamer distribution. The γ_1 value of 188 mPa s for compound **5a** is quite high in comparison to the monofluorinated analogues, but it is still in the same range as for **2**, which has a similiar $\Delta\varepsilon$ and extrapolated clearing point T_{NI}.

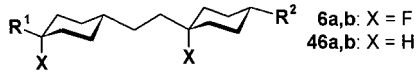


Scheme 9. Influence of the torsion angle ϕ (dihedral angle between the neighboring central axial hydrogen atoms) on the conformational energy ΔH_f and the dielectric anisotropy $\Delta\varepsilon$ of **5a**. –◆– = ΔH_f, –■– = $\Delta\varepsilon$.

The compounds containing two ethylene-bridged axially fluorinated cyclohexyl subunits in their mesogenic core structure, **6a** and **6b**, have significantly higher extrapolated clearing points than their nonfluorinated analogues (e.g., $\Delta T_{NI} = +21.5$ K for **6a**; Table 4). The general tendency to form S_B mesophases is not influenced by fluorination. The dielectric anisotropy of the bis(fluorocyclohexyl)ethanes **6** lies in the range of -4.2 to -4.6, in good agreement with the predictions of AM1 calculations. These values are about halfway between those of **2** and **3**, but in contrast to **3** these purely fluoroaliphatic materials have no adverse effect on the VHR. The rotational viscosity of **6b** is in the same range as that of the less polar **2**.

Making use of Olah's hydrofluorination method, we were able to synthesize multigram quantities of a variety of new liquid crystals with one or more axially fluorinated cyclohexane substructures. In spite of some reports on the inherent instability of this substance class, axially fluorinated synthetic building blocks were successfully subjected to drastic reaction conditions and provided yields in the same range as for the nonfluorinated analogues. Comparison of the physical properties of the axially fluorinated liquid crystals with their nonfluorinated analogues shows strongly increased clearing points T_{NI} accompanied by an (undesired) approximate doubling of the rotational viscosity γ_1. At least for low-viscosity, highly fluorinated two-ring liquid crystals, axial fluorination offers an interesting and useful method for improving their generally too low clearing points. We have obtained a new generation of superior liquid crystals with negative dielectric anisotropy. Due to their combination of low birefrincence, low rotational viscosity, and high clearing point, these materials are very well suited for application in recently emerging superior active matrix display technologies.

Table 4. Physical properties of liquid crystals based on ethylene-bridged axial fluorocyclohexane derivatives compared to their nonfluorinated analogues. Clearing points $T_{NI,extr}$, dielectric anisotropies $\Delta\varepsilon$, birefringences Δn, and rotational viscosities γ_1 are extrapolated from ZLI-4792, and the $\Delta\varepsilon$ values for the dielecrically negative materials **6a** and **6b** from ZLI-2857.[13] The temperatures are given in °C, and the rotational viscosities γ_1 in mPa s. C = crystalline, S_B = smectic B, I = isotropic.



Entry	R^1	R^2	X	Mesophases	$T_{NI,extr}$	ΔT_{NI}	$\Delta\varepsilon$	Δn	γ_1
6a	C_3H_7	C_3H_7	F	C 78 S_B 104 I	76.5	+21.5	−4.6	0.051	198
6b	C_3H_7	C_5H_{11}	F	C 68 S_B 120 I	81.5	–	−4.2	0.051	251
46a	C_3H_7	C_3H_7	H	C 36 S_B 73 I	55	–	–	–	–
46b	C_5H_{11}	C_5H_{11}	H	C 44 S_B 108 I	80	–	0.1	0.045	134

Experimental Section

4d: In a Teflon flask, a solution of **8d** (100 g, 0.36 mol) in CH_2Cl_2 (200 mL) was treated with 70% HF/pyridine (36.3 mL, 1.45 mol, 4 equiv) and stirred at room temperature for 18 h. The mixture was poured onto ice (300 g) and extracted three times with CH_2Cl_2 (100 mL). The combined organic extracts were washed to neutrality with a saturated solution of aqueous $NaHCO_3$ and dried over $MgSO_4$. After addition of pyridine (1%), the solution was evaporated to dryness to give 98 g of crude hydrofluorination product. The crude product was filtered over silica gel (*n*-heptane/pyridine 99/1) and crystallized from the same solvent at -20°C (38.4 g, 36%, purity according to HPLC: 99.5%; for mesophases see Table 2). ^{1}H NMR (500 MHz, $CDCl_3$, 303 K): $\delta = 0.85-1.56$ (m, 34H), 1.70–1.75 (m, 2H), 1.86–1.92 (mc, 1H); ^{19}F NMR (280 MHz, $CDCl_3$, 303 K): $\delta = -160.4$ (mc); MS (EI): $m/z = 276$ [M^+ – HF].

Received: August 28, 1997
Revised version: November 3, 1997 [Z10863/10864IE]
German version: *Angew. Chem.* **1998**, *110*, 501–506

Keywords: cyclohexane · fluorine · liquid crystals · mesophases

[1] a) D. Pauluth, T. Geelhaar, *Nachr. Chem. Tech. Lab.* **1997**, *45*, 9–15. b) W. H. de Jeu, *Physical Properties of Liquid Crystalline Materials*, Gordon & Breach, New York, **1980**.
[2] A. Sasaki, T. Uchida, S. Miyagami, *Japan Display '86* **1986**, 62.
[3] a) E. Bartmann, U. Finkenzeller, E. Poetsch, V. Reiffenrath, K. Tarumi, *22. Freiburger Arbeitstagung Flüssigkristalle*, March 31 – April 2, **1993**, contribution no. 8; b) E. Bartmann, J. Krause, K. Tarumi, *23. Freiburger Arbeitstagung Flüssigkristalle*, March 23–25, **1994**, contribution no. 27.

 © WILEY-VCH Verlag GmbH, D-69451 Weinheim, 1998 1433-7851/98/3704-0488 $ 17.50+.50/0

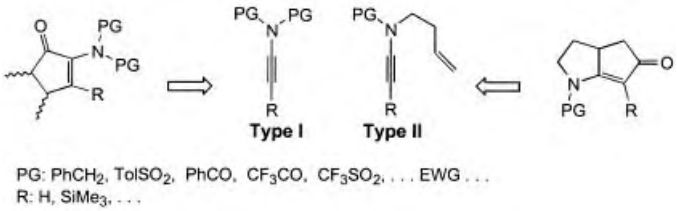
[4] K. Ohmuro, S. Kataoka, T. Sasaki, Y. Koike, *SID '97 Digest* **1997**, 845.
[5] R. Eidenschink, L. Pohl, M. Römer, B. Scheuble (Merck KGaA), DE-A 3231707 A1, **1982** [*Chem. Abstr.* **1984**, *101*, 63 770].
[6] a) A. E. F. Wächtler, V. Reiffenrath, J. Krause, G. Weber, U. Finkenzeller (Merck KGaA), EP-B 0364538, **1989** [*Chem. Abstr.* **1995**, *112*, 66 886]; b) V. Reiffenrath, J. Krause, H. J. Plach, G. Weber, *Liq. Crystals* **1989**, *5*, 159; c) K. Tarumi, M. Bremer, B. Schuler, *IEICE Trans. Electron.* **1996**, *E79-C*, 1035 – 1039.
[7] a) N. Mongelli, F. Animati, R. D'Alessio, L. Zuliani, C. Gandolfi, *Synthesis* **1988**, 310 – 313. b) R. Winters, Dissertation, Universität-GH-Paderborn, Germany, **1991**.
[8] S. Rozen, C. Gal, *J. Org. Chem.* **1987**, *52*, 2769 – 2779.
[9] G. A. Olah, J. T. Welch, Y. D. Vankar, M. Nojima, I. Kerekes, J. A. Olah, *J. Org. Chem.* **1979**, *44*, 3872 – 3881.
[10] Since all axially fluorinated cyclohexane derivatives tend to decompose under GLC conditions, the purity of the newly synthesized compounds was determined by HPLC. The regio- and stereoselectivity was verified by ^{1}H and ^{19}F NMR. The mass spectra usually indicated elimination of HF and display only the $[M^+ - 20]$ fragment instead of the molecular ion. Additional evidence for the desired *trans – trans* arrangement of the axial fluorine atoms are the high clearing points of all the newly synthesized compounds.
[11] a) D. Lednicer, D. E. Emmert, R. Lahti, A. D. Rudzik, *J. Med. Chem.* **1972**, *15*, 1239 – 1243; b) T. Taiho, K. San-nohe, S. Kajiya, T. Suzuki, K. Otsuka, T. Ito, J. Kamiya, M. Maruyama, *ibid.* **1989**, *32*, 351 – 357; c) M. Petrzilka, A. Germann, *Mol. Cryst. Liq. Cryst.* **1985**, *131*, 327 – 342; d) E. M. Sigman, G. L. Closs, *J. Phys. Chem.* **1991**, *95*, 5012 – 5017.
[12] A similiar type of reaction is described in L. Billet, G. Descotes, *Bull. Soc. Chim. Fr.* **1971**, 2626 – 2682.
[13] $T_{NI,extr}$, $\Delta\varepsilon$, Δn, and γ_1 were determined by linear extrapolation from a 10 % w/w solution in a standard host. For the dielectrically positive compounds, the commercially available Merck mixture ZLI-4792 ($T_{NI} = 92.8\,^\circ$C, $\Delta\varepsilon = 5.27$, $\Delta n = 0.0964$) was used. For the dielectrically negative materials, $\Delta\varepsilon$ was extrapolated from ZLI-2857 ($T_{NI} = 82.3\,^\circ$C, $\Delta\varepsilon = -1.42$, $\Delta n = 0.0776$). For the pure substances the mesophases were identified by optical microscopy, and the phase transition temperatures by differential scanning calorimetry (DSC).
[14] M. A. Osman, *Mol. Cryst. Liq. Cryst.* **1985**, *131*, 353 – 360.
[15] M. Bremer, K. Tarumi, *Adv. Mater.* **1993**, *5*, 842 – 848.

N-Functionalized 1-Alkynylamides: New Building Blocks for Transition Metal Mediated Inter- and Intramolecular [2+2+1] Cycloadditions**

Bernhard Witulski* and Thomas Stengel

Functionalized alkynes are versatile building blocks for transition metal mediated cycloadditions and cyclizations.[1] An exception in this respect are 1-alkynylamines (ynamines).[2] These electron-rich acetylene derivatives have certainly gained some significance with respect to transformations with electrophiles and to Diels – Alder reactions with inverse electron demand;[2, 3] nevertheless they were mostly ignored as building blocks in synthesis.[4] The latter can be attributed to a lack of functionality at the nitrogen atom, because previously known syntheses gave access to "simple" N,N-alkyl or aryl-substituted 1-alkynylamines only.[2a]

Herein we report on the synthesis of N-functionalized and electronically tunable 1-alkynylamines/1-alkynylamides of type **I** and **II** (Scheme 1), as well as their application in regio- and stereoselective inter- and intramolecular [2+2+1] cycloadditions. The protective groups (PGs) of these compounds perform two functions: On the one hand they might act as temporary masking groups of the primary or secondary amine moiety, on the other hand by varying their electron-withdrawing capacities—transformation of the amine into a carbamide, toluenesulfonamide, or trifluorsulfonamide—a tuning of electron density and reactivity of the neighboring triple bond should be possible.



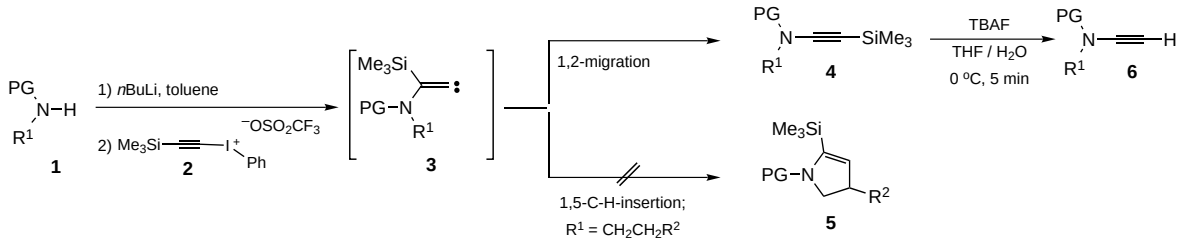
Scheme 1. 1-Alkynylamine and 1-alkynylamide building blocks of type **I** and **II**. EWG = electron-withdrawing group.

The key step for the synthesis of this new class of compounds is the ethynylation of the amides **1a – j** with the readily available trimethylsilylethynyliodonium triflate **2**.[5] Additions of nitrogen nucleophiles to alkynyliodonium salts, in which 2,3-dihydropyrroles are formed *via* alkylidene carbene intermediates and intramolecular 1,5-C – H insertions, were recently reported by Feldman et al.[6] With respect to the cases studied herein, and in accordance with a very high aptitude of silyl groups for 1,2-migrations towards carbenoid centers such as in **3**,[7] preferential formation of 1-alkynylamines and 1-alkynylamides (Scheme 2) is expected. Indeed the alkynes **4a – j** were obtained as single products after deprotonation of **1a – j** with *n*-butyllithium in toluene followed by addition of **2** at 20 °C (Table 1).[8] Dihydropyrroles **5** were not observed. This method is compatible with other functional groups (alkenyl-, alkynyl-, and alkoxycarbonyl residues). However, in some cases α-branched amides (**1h – j**) gave lower yields, reflecting an increase of steric hindrance in the nucleophilic addition of **1** to **2**. Desilylation with tetrabutylammonium fluoride (TBAF) in wet THF yielded the 1-alkynylamides **6a – j** in 78 – 98 % (Table 1). The acetylene derivatives **6** are often crystalline, air stable, and widely insensitive to hydrolysis. Unlike their *N,N*-dialkyl-substituted analogues, the 1-alkynylamides **4** and **6** withstand aqueous work-up procedures as well as chromatographic purification on silica gel. This stability and the ^{13}C NMR spectroscopic data,[9] which are atypical in comparison to those for regular ynamines, are results of electron-withdrawing features of the protective group (PG) affecting the alkyne moiety.

[*] Dr. B. Witulski, Dipl.-Chem. T. Stengel
Fachbereich Chemie der Universität
Erwin Schrödinger Strasse, D-67663 Kaiserslautern (Germany)
Fax: (+49) 631-205-3921
E-mail: Bernhard@chemie.uni-kl.de

[**] This work was supported by the Fonds der Chemischen Industrie. B. W. thanks the Fonds der Chemischen Industrie for a Liebig fellowship and Prof. Dr. Manfred Regitz for his generous support.

 © WILEY-VCH Verlag GmbH, D-69451 Weinheim, 1998 1433-7851/98/3704-0489 $ 17.50+.50/0



Scheme 2. Synthesis of functionalized 1-alkynylamides **6** (see Table 1).

Table 1. Ethynylation of **1** with **2** to give **4**, and its desilylation to give **6** (Figure 2).

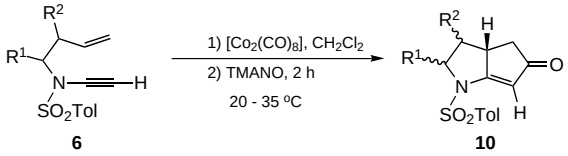
Entry	**1**	PG	R^1	**4**	Yield [%]	**6**	Yield [%]
1	**a**	$TolSO_2$	*n*Bu	**a**	86	**a**	95
2	**b**	$TolSO_2$	$PhCH_2$	**b**	75	**b**	95
3	**c**	CF_3SO_2	$PhCH_2$	**c**	65	**c**	55[a]
4	**d**	CF_3CO	$PhCH_2$	**d**	77	**d**	–[b]
5	**e**	PhCO	$PhCH_2$	**e**	81	**e**	98
6	**f**	$TolSO_2$	$CH_2{=}CH(CH_2)_2$	**f**	89	**f**	93
7	**g**	$TolSO_2$	$CH_2{=}CH(CHPh)CH_2$	**g**	70	**g**	78
8	**h**	$TolSO_2$	$CH_2{=}CHCH_2CH(Ph)$	**h**	28	**h**	89
9	**i**	$TolSO_2$	$CH_2{=}CHCH_2CH(n\text{Bu})$	**i**	50	**i**	91
10	**j**	$TolSO_2$	$(CH_2{=}CHCH_2)_2CH$	**j**	43	**j**	83

[a] Yields based on **1c**. [b] Not determined.

To explore the efficiency of these new building blocks in transition metal mediated transformations we tested their applicability in inter- and intramolecular Pauson–Khand reactions;[10] these [2+2+1] cycloadditions, which simultaneously form three bonds and up to two stereocenters in one step, are broadly recognized as reliable methods for generating five-membered rings.

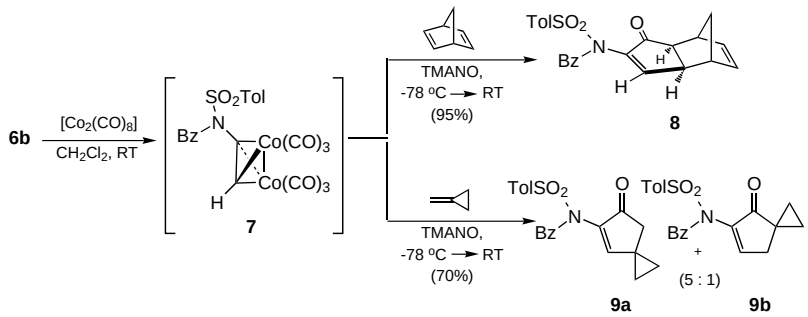
The $[Co_2(CO)_6]$-alkynylamide complex **7** forms almost quantitatively by addition of **6b** to a solution of $[Co_2(CO)_8]$ (1.1 equiv) in CH_2Cl_2. Complex **7** can be isolated; however, it was transformed immediately to [2+2+1] cycloaddition products by adding an olefin (norbornadiene, or methylenecyclopropane, −78 °C to RT, Scheme 3) and trimethylamine *N*-oxide (TMANO) as promoter.[11] Alternatively intermolecular cycloadditions could be initiated by heating to 80–90 °C, while omitting a promoter. Pauson–Khand reactions with **6b** gave yields of 95% for norbornadiene (only *exo* adduct **8** formed) and 70% for methylenecyclopropane (ratio of regioisomers **9a**:**9b** = 5:1). The cycloadditions were exceptionally regioselective with respect to 1-alkynylamide **6b,** and only α,β-unsaturated α-amidocyclopentenones were formed. Regio- and stereoselectivity with respect to the olefinic cycloaddition partner are comparable to those of other Pauson–Khand reactions.[9b, 12]

The steric and electronic effects that govern the regioselectivity of the *inter*molecular reaction are unfavorable for the use of a building block of type **II** in *intra*molecular [2+2+1] cycloadditions. Nevertheless in presence of the reaction promoter TMANO, *intra*molecular [2+2+1] cycloadditions yielded the products **10** in 40–60% after chromatographic purification[13] on aluminum oxide (Scheme 4, Table 2). Surprisingly, the intramolecular cycloadditions are exceedingly diastereoselective for β-branched (**6g**), as well as for α-branched 1-alkynylamides (**6h–j**)—in all cases only one diastereoisomer was observed. The elucidation of the structure of **10b** is based on NMR spectroscopic data and an X-ray structure analysis,[14] those of the bicyclic products **10c–e** on H,H- and C,H-COSY experiments[15] by analysis of distinct NOE relationships between the pseudoaxial protons of the pyrrole moiety (Table 2).



Scheme 4. $[Co_2(CO)_8]$-mediated intramolecular [2+2+1] cycloadditions of **6f–j** (see Table 2).

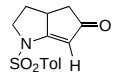
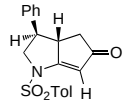
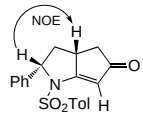
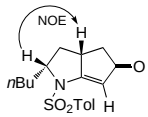
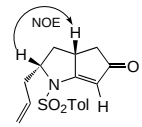
We consider the application of the type **I** and **II** building blocks in inter- and intramolecular Pauson–Khand reactions, cycloadditions frequently difficult to achieve with polarized acetylenes,[16] as evidence for a successful electronic modulation of the 1-alkynylamides introduced here. The preferred *exo*-orientation of the phenyl substituent of **10b** corresponds to that in carbocyclic analogues.[17] However, the observed diastereoselectivity is remarkable and should be attributed to governing effects of the toluenesulfonyl group. Similar arguments are advanced for the exclusive formation of **10c–e**. Pseudoaxial interactions between the α-substituent and the cobalt carbonyl fragment at the postulated reaction intermediate **B** seem to control the diastereoselectivity (Scheme 5).



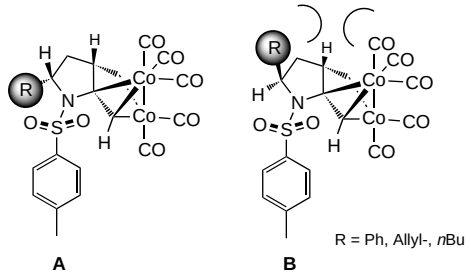
Scheme 3. $[Co_2(CO)_8]$-mediated intermolecular [2+2+1] cycloadditions of **6b** with norbornadiene and methylenecyclopropane.

 © WILEY-VCH Verlag GmbH, D-69451 Weinheim, 1998 1433-7851/98/3704-0490 $ 17.50+.50/0 *Angew. Chem. Int. Ed.* **1998**, *37*, No. 4

Table 2. Intramolecular [2+2+1] cycloadditions.

Entry	6	R^1	R^2		10	Yield [%][a]
1	**f**	H	H		**a**	40[b]
2	**g**	H	Ph		**b**	60
3	**h**	Ph	H		**c**	45
4	**i**	*n*Bu	H		**d**	54
5	**j**		H		**e**	50

[a] Yields obtained after column chromatography with Alox III/N. [b] Reaction at −78 to 25 °C.



A **B**

Scheme 5. Postulated reaction intermediates **A** and **B**.

The synthesis of functionalized and electronically modulated 1-alkynylamides and their application in intramolecular $[Co_2(CO)_8]$-mediated [2+2+1] cycloadditions outlines fundamental novel strategies for the stereoselective synthesis of nitrogen-containing heterocycles. The concept should be further applicable to other transition metal mediated cyclizations and cycloadditions.

Experimental Section

4g: *n*BuLi (5.19 mmol, 3.25 mL of a 1.6 M solution in hexane) was added to a solution of **1g** (1.3 g, 4.3 mmol) in absolute toluene (60 mL) under argon at 0 °C. After the mixture was allowed to warm to room temperature, iodonium salt **2** (1.13 g, 2.5 mmol) was added in small portions. The reaction mixture was stirred for 12 h and then filtered through a plug of silica gel. Purification by column chromatography (silica gel, petroleum ether:diethyl ether = 9:1 (v/v)) gave analytically pure **4g** (1.19 g, 3.0 mmol, 70 %). ^{1}H NMR (200 MHz, $CDCl_3$/TMS): $\delta = 0.15$ (s, 9H), 2.42 (s, 3H), 3.42–3.80 (m, 3H), 5.06–5.14 (m, 2H), 5.88–6.05 (m, 1H), 7.14–7.33 (m, $J = 8.1$ Hz, 7H), 7.67 (d, $J = 8.1$ Hz, 2H); ^{13}C NMR (100.6 MHz, $CDCl_3$): $\delta = 144.41$ (s), 140.1 (s), 134.46 (s), 137.53 (d), 129.44 (d), 128.60 (d), 127.94 (d), 127.74 (d), 126.98 (d); 117.11 (t), 94.86 (s), 73.93 (s), 55.22 (t), 48.06 (d), 21.58 (q), 0.14 (q); elemental analysis for $C_{22}H_{27}NO_2SiS$ (397.6): calcd.: C 66.46, H 6.84, N 3.52; found: C 66.85, H 6.60, N 3.44.

10b: **6g** (92 mg, 0.28 mmol) was added to a suspension of $[Co_2(CO)_8]$ (116 mg, 0.34 mmol) in CH_2Cl_2 at 20–36 °C. The formation of the cobalt carbonyl–**6g** complex was monitored by thin-layer chromatography (R_f: 0.48, SiO_2, petroleum ether:ethyl acetate = 8:2 (v/v)). After complete formation a solution of trimethylamine *N*-oxide (115 mg, 1.53 mmol) in CH_2Cl_2 (8 mL) was added by syringe pump over 2 h. The reaction mixture was then filtered through a plug of Alox III/N and eluted with CH_2Cl_2/ethyl acetate. Purification by column chromatography (Alox III/N, petroleum ether: diethyl ether = 1:1 (v/v)) gave analytically pure **10b** (60 mg, 0.17 mmol, 60 %).

10b: colorless plates, m. p.: 176–177 °C; ^{1}H NMR (400 MHz, $CDCl_3$/TMS): $\delta = 2.21$ (dd, $J = 16.7$ Hz, $J = 4.9$ Hz, 1H), 2.47 (s, 3H), 2.58 (dd, $J = 16.7$ Hz, $J = 6.7$ Hz, 1H), 3.00–3.08 (m, $J = 7.5$ Hz, 1H), 3.28–3.34 (m, $J = 2.1$ Hz, $J = 14.0$ Hz, $J = 4.9$ Hz, $J = 6.7$ Hz, 1H), 3.85 (dd, $J = 10.6$ Hz, $J = 10.6$ Hz, 1H), 4.30 (dd, $J = 10.6$ Hz, $J = 7.5$ Hz, 1H), 5.86 (d, $J = 2.07$ Hz, 1H), 7.15–7.39 (m, 7H), 7.81 (m, 2H); ^{13}C NMR (100.6 MHz, $CDCl_3$): $\delta = 205.58$ (s), 175.26 (s), 145.63 (s), 136.43 (s), 134.22 (s), 130.31 (d), 129.11 (d), 128.02 (d), 127.26 (d), 126.89 (d), 106.15 (d), 59.1 (t), 49.15 (d), 47.91 (d), 40.31 (t), 21.71 (q); elemental analysis for $C_{20}H_{19}NO_3S$ (353.4): calcd.: C 67.97, H 5.42, N 3.97; found: C 67.52, H 5.39, N 3.93.

Received: September 29, 1998 [Z 10986 IE]
German version: *Angew. Chem.* **1998**, *110*, 495–498

Keywords: alkynes · carbenes · cobalt · cycloadditions · heterocycles

[1] a) H.-W. Frühauf, *Chem. Rev.* **1997**, 97, 523–596; b) M. Lautens, W. Klute, W. Tam, *ibid.* **1996**, *96*, 49–92; c) D. F. Harvey, D. M. Sigano, *ibid.* **1996**, *96*, 271–288; d) E. Negishi, C. Copéret, S. Ma, S.-Y. Liou, F. Liu, *ibid.* **1996**, *96*, 365–393; e) I. Ojima, M. Tzamarioudaki, Z. Li, R. J. Donovan, *ibid.* **1996**, *96*, 635–662; f) *Modern Acetylene Chemistry* (Eds.: P. J. Stang, F. Diederich), VCH, Weinheim, **1995**; g) N. E. Schore. *Chem. Rev.* **1988**, *88*, 1081–1119.

[2] a) G. Himbert, *Methoden Org. Chem. (Houben-Weyl)*, **1993**, Vol. *E15,* p. 3267–3461; b) J. Collard-Motte, Z. Janousek, *Top. Curr. Chem.* **1986**, *130*, 89–132; c) G. Pitacco, E. Valentin in *The Chemistry of Amino, Nitroso and Nitro Compounds and their Derivatives, Supplement F, Part* 1 (Ed.: S. Patai), Wiley, Chichester, UK, **1982**, p. 624–714; d) J. Ficini, *Tetrahedron* **1976**, *32*, 1448–1486.

[3] a) A. Padwa, Y.Gareau, B. Harrison, A. Rodriguez, *J. Org. Chem.* **1992**, *57*, 3540–3545; b) D. L. Boger, M. Patel in *Prog. Heterocycl. Chem.* **1988**, *1*, 30–60.

[4] a) J. Ficini, *J. Organomet. Chem.* **1979**, *177*, 265–272; b) K. H. Dötz, I. Pruskil, *Chem. Ber.* **1978**, *111*, 2059–2063; c) J. Ficini, J. d'Angelo, S. Falou, *Tetrahedron Lett.* **1977**, 1645–1648; d) J. Ficini, *ibid.* **1979**, 1499–1502.

[5] a) P. J. Stang, V. V. Zhdankin, *Chem. Rev.* **1996**, *96*, 1123–1178; b) synthesis: P. J. Stang in ref. [1 f] p. 67–98.

[6] a) K. S. Feldman, M. M. Bruendl, K. Schildknegt, A. C. Bohnstedt, *J. Org. Chem.* **1996**, *61*, 5440–5452; b) K. Schildknegt, A. C. Bohnstedt, K. S. Feldman, A. Sambandam, *J. Am. Chem. Soc.* **1995**, *117*, 7544–7545.

[7] a) W. Kirmse, *Angew. Chem.* **1997**, *109*, 1212–1218; *Angew. Chem. Int. Ed. Engl.* **1997**, *36*, 1164–1170; b) R. Walsh, S. Untiedt, M. Stohlmeier, A. de Meijere, *Chem. Ber.* **1989**, *122*, 637–642; c) J. J. W. McDouall, H. B. Schlegel, J. S. Francisco, *J. Am. Chem. Soc.* **1989**, *111*, 4622–4627.

[8] All new compounds were characterized by ^{1}H, ^{13}C NMR, IR spectroscopy, mass spectrometry, C,H,N analysis and/or high-resolution mass spectrometry.

[9] Selected ^{13}C-NMR chemical shifts ($CDCl_3$) of the acetylene carbon atoms of the 1-alkynylamides: **4b**: $\delta = 95$ (s), 74 (s); **4c**: $\delta = 91$ (s), 76 (s); **4d**: $\delta = 92$ (s), 78 (s); **4e**: $\delta = 98$ (s), 76 (s); in comparison: trimethylsilyl-*N,N*-dialkyl-1-alkynylamines: $\delta = 111$ (s), 61 (s); **6b**: $\delta = 76$ (s), 60 (d); **6e**: $\delta = 79$ (s), 62 (d); in comparison *N*-methyl-*N*-phenyl-1-alkynylamine: $\delta = 84$ (s), 56 (d).

[10] Reviews: a) N. E. Schore in *Comprehensive Organic Synthesis*, *Vol. 5* (Eds.: B. M. Trost, I. Fleming), Pergamon, Oxford, **1991**, p. 1037–1064; b) N. E. Schore. *Org. React.* **1991**, *40*, 1–90; c) P. L. Pauson in

Organometallics in Organic Synthesis (Eds.: A. de Meijere, H. tom Dieck), Springer, Berlin, **1988**, p. 233; catalytic Pauson–Khand reactions: d) B. L. Pagenkopf, T. Livinghouse, *J. Am. Chem. Soc.* **1996**, *118*, 2285–2286, e) B. Y. Lee, Y. K. Chung, N. Jeong, Y. Lee, S. H. Hwang, *ibid.* **1994**, *116*, 8793–8794; f) N. Jeong, S. H. Hwang, Y. Lee, Y. K. Chung, *ibid.* **1994**, *116*, 3159–3160; natural product synthesis: g) J. Tormo, A. Moyano, M. A. Pericàs, A. Riera, *J. Org. Chem.* **1997**, *62*, 4851–4856; h) C. Johnstone, W. J. Kerr, U. Lange, *J. Chem. Soc. Chem. Commun.* **1995**, 457–458; i) T. F. Jamison, S. Shambayati, W. E. Crowe, S. L. Schreiber, *J. Am. Chem. Soc.* **1994**, *116*, 5505–5506; j) C. Exon, P. Magnus, *ibid.* **1983**, *105*, 2477–2478.

[11] a) A. R. Gordon, C. Johnstone, W. J. Kerr, *Synlett* **1995**, 1083–1084; b) N. Jeong, Y. K. Chung, B. Y. Lee, S. H. Lee, S.-E. Yoo, *ibid.* **1991**, 204–206; c) S. Shambayati, W. E. Crowe, S. L. Schreiber, *Tetrahedron Lett.* **1990**, *31*, 5289–5292.

[12] W. A. Smit, S. L. Kireev, O. M. Nefedov, V. A. Tarasov, *Tetrahedron Lett.* **1989**, *30*, 4021–4024.

[13] In all cases complete conversion of the starting material was observed. However the products were labile towards silica gel and tended to hydrolyze.

[14] Details of the X-ray analysis (U. Bergsträsser, B. Witulski, Universität Kaiserslautern, **1997)** will be published elsewhere.

[15] We would like to express our thanks to Prof. Dr. L. Ernst (Technische Universität Braunschweig) for NOE and 2D-NMR measurements.

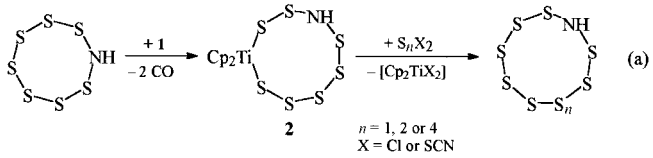
[16] a) M. Costa, A. Mor, *Tetrahedron Lett.* **1995**, *36*, 2867–2870; b) T. R. Hoye, J. A. Suriano, *J. Am. Chem. Soc.* **1993**, *115*, 1154–1156; c) M. E. Krafft, R. H. Romero, I. L. Scott, *J. Org. Chem.* **1992**, *57*, 5277–5278; d) F. Camps, J. M. Moretó, S. Ricart, J. M. Viñas, *Angew. Chem.* **1991**, *103*, 1540–1542; *Angew. Chem. Int. Ed. Engl.* **1991**, *30*, 1470–1472; e) M. E. Krafft, C. A. Juliano, I. L. Scott, C. Wright, M. D. McEachin, *J. Am. Chem. Soc.* **1991**, *113*, 1693-1703; f) I. U. Khand, P. L. Pauson, *J. Chem. Soc. Chem. Commun.* **1974**, 379.

[17] a) N. Jeong, B. Y. Lee, S. M. Lee, Y. K. Chung, S.-G. Lee, *Tetrahedron Lett.* **1993**, *34*, 4023–4026; b) P. Magnus, L. M. Prince, *ibid.* **1985**, *26*, 4851–4854.

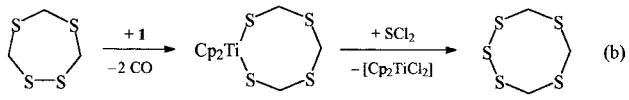
S_4NR (R = Methyl, *n*-Octyl) as Novel Chelating Ligands in Titanocene Complexes and First Synthesis of Small Sulfurimide Heterocycles S_nNR ($n = 5, 6$)**

Ralf Steudel,* Oliver Schumann, Jürgen Buschmann, and Peter Luger

Recently it has been shown that titanocene dicarbonyl $[Cp_2Ti(CO)_2]$ **1** reacts with the S–S bonds of certain homo- and heterocycles with insertion of the titanocene unit and liberation of the two CO ligands.[1] In this way a number of novel chelate complexes has been prepared that are useful reagents for the synthesis of new chain- and ringlike derivatives by ligand transfer reactions. Examples are the complexes **2** and **3**, which allowed the preparation of the cyclic sulfurimides S_8NH, S_9NH, $S_{11}NH$,[2] and of the natural product pentathiocane 1,3,5-$(CH_2)_3S_5$,[1b] respectively [Eq. (a), (b), $Cp = \eta^5$-C_5H_5].

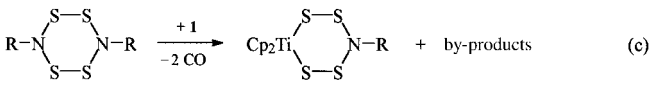


2 (a)



3 (b)

While cycloheptasulfurimide S_7NH and its organic derivatives S_7NR have been known for a long time,[3] the six- and seven-membered rings S_5NR and S_6NR have never been observed although the corresponding homocycles S_6 and S_7[4] as well as their carbon-substituted analogues CH_2S_5 and CH_2S_6[5] are well known as pure materials. Herein we show how cyclic penta- and hexasulfurimides may be prepared in very good yield by ligand transfer from the novel chelate complexes **4** and **5,** respectively. Complex **1** reacts in *n*-hexane at 20 °C with *N*-alkyl-substituted derivatives of the cyclic diimide $HN(\mu$-$S_2)_2NH$[6] to give titanocene derivatives which, however, do not contain the expected seven-membered but a six-membered metallacycle [Eq. (c), *n*Oct = *n*-octyl].



(c)

4 (R = Me)
5 (R = *n*Oct)
6 (R = *n*Oct; Cp = C_5H_4Me)

Contrary to the behavior of S_7NH and S_7NMe[2] there is no insertion into the S–S bond of the diimide, but one NR group is extruded (the fate of this group has not been investigated). Working with two different groups R (Me, *n*Oct) and two different cyclopentadienyl ligands (C_5H_5, C_5H_4Me) only *one* complex was obtained in each case (yields 25–34%). This contained the ligand SSN(R)SS, which has not been observed before.[7] Compound **4** forms black orthorhombic crystals with a melting point of 134 °C, while **5** and **6** are dark brown oils; all three compounds are stable in air for several days and soluble in *n*-hexane, dichloromethane, and carbondisulfide. Decomposition of the brown solutions occurs after several days at 20 °C.

Complex **4** was characterized by single-crystal X-ray structural analysis,[8] which revealed a metallacycle with a chair conformation (Figure 1) similar to the one in $[Cp_2TiS_5]$[9] and in the analogous complex $[Cp_2Ti(\mu$-$S_2)_2AsMe]$.[10] The molecules of **4** occupy general positions but approximately exhibit C_s symmetry. The geometrical parameters show the expected values, for example, d(S–S) = 206.0 pm, d(S–N) =

[*] Prof. Dr. R. Steudel, Dipl.-Chem. O. Schumann
Institut für Anorganische und Analytische Chemie der Technischen Universität, Sekr. C2
Strasse des 17. Juni 135, D-10623 Berlin (Germany)
Fax: (+49) 30-314-26519
E-mail: steudel@schwefel.chem.tu-berlin.de
Dr. J. Buschmann, Prof. Dr. P. Luger
Institut für Kristallographie der Freien Universität, Takustrasse 6, D-14195 Berlin (Germany)

[**] Sulfur Compounds, Part 204. This work was supported by the Deutsche Forschungsgemeinschaft (Sonderforschungsbereich 335). Part 203: K. Hassenberg, R. Steudel, *Phosphorus, Sulfur, Silicon*, in press.

 © WILEY-VCH Verlag GmbH, D-69451 Weinheim, 1998 1433-7851/98/3704-0492 $ 17.50+.50/0

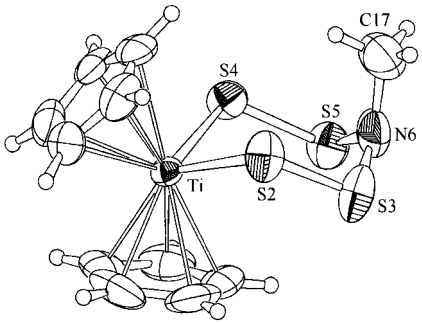


Figure 1. Structure of **4** in the crystal. Selected distances [pm], angles [°], and torsion angles [°]: Ti–S2 243.6(3), S2–S3 206.0(4), S3–N6 169.7(14), N6–S5 169.4(13), S5–S4 206.0(5), S4–Ti 244.4(4), N6–C17 146.0(2); S4-Ti-S2 93.99(13), S3-N6-S5 116.9(7), S3-N6-C17 116.0(11), S5-N6-C17 114.4(10); S4-Ti-S2-S3 53.8(2), Ti-S2-S3-N6 −64.4(5), S2-S3-N6-S5 80.5(7), S3-N6-S5-S4 −82.6(6), N6-S5-S4-Ti 67.2(5), S5-S4-Ti-S2 −54.7(2), S4-S5-N6-C17 57.7(11), S2-S3-N6-C17 −59.1(9).

169.4 and 169.7 pm. The methyl group of **4** is in an axial position. However, the coordination sphere of the nitrogen atom is only slightly pyramidal (sum of bond angles 347°). Similar observations have been made with several cyclic sulfurimides;[11] these findings have been explained by hyperconjugation of the nitrogen lone pair with the unoccupied σ^* orbitals at the neighboring S–S bonds.[12] The ^{1}H NMR spectra of **4** and **5** demonstrate that the six-membered rings are rigid at 23 °C (two signals for the Cp protons). That the connectivity of **5** is the same as in **4** follows from the ^{1}H NMR spectrum of the derivative **6**, which was prepared with C_5H_4Me ligands at the titanium atom. In the region of aromatic ring protons the spectrum consists of two triplets and one pseudo-quartet, indicating C_s symmetry; in the case of a lower symmetry (e.g., sequence of ring atoms TiSNSSS) up to eight signals are expected.

Complexes **4**–**6** react rapidly and quantitatively with either SCl_2 or S_2Cl_2 at 20 °C in CH_2Cl_2 to the novel cyclic sulfurimides **7** and **8** [Eq. (d)].

$$[Cp_2Ti(\mu\text{-}S_2)_2NR] + S_mCl_2 \rightarrow S_{4+m}NR + [Cp_2TiCl_2] \quad \text{(d)}$$

R = *n*Oct; **7** ($m = 1$), **8** ($m = 2$)

Compounds **7** and **8** are pale yellow oils rather than solids as a consequence of the long alkyl chain. They are soluble in *n*-hexane, CH_2Cl_2, and CS_2. In the EI mass spectra the molecular ions were observed with medium intensity; in addition, only signals of fragments of the types S_n^+ and S_nNR^+ were detected. Heterocycle **7** decomposes at 20 °C within a few hours, **8** within one day; however, both compounds may be kept at −25 °C for longer periods of time without decomposition. Decomposition products are S_8 and the homologous molecules S_nNnOct with $n \geq 6$. These species can easily be detected by reversed-phase HPLC analysis,[13] since the retention times systematically increase with increasing ring size. For comparison the eight-membered S_7NnOct has been prepared from S_7NH and *n*OctI.[14]

For the pure compounds S_nNnOct ($n = 5-7$) only *one* peak was observed in the HPLC analysis. The vibrational and ^{1}H NMR spectra of the three cyclic octyl-substituted sulfurimides differ markedly, allowing their identification even in mixtures. The chemical shifts of the α- and β-protons of the *n*-octyl groups depend on the ring size (Table 1).

Table 1. ^{1}H NMR chemical shifts (δ values) and signal multiplicities (200 MHz, $CDCl_3$, 23 °C) of S_nNnOct ($n = 5-7$).

S_5NnOct	S_6NnOct	S_7NnOct	
3.90 t (2H)	3.20 t (2H)	3.28 t (2H)	α-CH_2
1.60 q (2H)	1.70 q (2H)	1.69 q (2H)	β-CH_2
1.29 s br (10H)	1.30 s br (10H)	1.30 s br (10H)	-$(CH_2)_5$-
0.89 t (3H)	0.89 t (3H)	0.90 t (3H)	-CH_3

Our findings show that the reactivity of **1** towards sulfur compounds is more versatile than might have been anticipated. Thus, access is provided to novel and unexpected titanocene complexes, which, in turn, may serve as reagents in many new ligand transfer reactions as has been demonstrated by several groups for the now already classical case of $[Cp_2TiS_5]$.[15]

Experimental Section

4: Under an inert atmosphere **1** (304 mg, 1.3 mmol) in *n*-hexane (50 mL) was added dropwise over 2 h to 1,4-$S_4(NMe)_2$ (242 mg, 1.3 mmol) in *n*-hexane (30 mL) at 20 °C and stirred for an additional 15 h. The resulting precipitate was isolated, and the brown-black filtrate reduced in volume to give a dark brown oil, which was purified by column chromatography (SiO_2, *tert*-butyl methyl ether/*n*-hexane 1:2). Yield: 134 mg of needle-shaped black crystals (30%). ^{1}H NMR (200 MHz, $CDCl_3$, 23 °C): $\delta = 6.40$ (s, 5H), 6.21 (s, 5H), 2.29 (s, 3H); MS (144 °C, EI): 335 (M^+, 5%), 242 ($Cp_2TiS_2^+$, 98%), 209 (Cp_2TiS^+, 15%), 178 (Cp_2Ti^+, 100%); UV-Vis (methanol): $\lambda_{max} = 207$, 233, 313, 425, 481 nm (diode array detector).

5: As in the case of **4**, $[Cp_2Ti(CO)_2]$ (609 mg, 2.6 mmol) in *n*-hexane (80 mL) and 1,4-$S_4(Nn\text{Oct})_2$ (995 mg, 2.6 mmol) in *n*-hexane (70 mL). Yield: 627 mg of a dark brown oil (43%). Correct C,H,N,S analysis; ^{1}H NMR (200 MHz, $CDCl_3$, 23 °C): $\delta = 6.37$ (s, 5H), 6.22 (s, 5H), 2.25 (t, 2H), 1.47 (q, 2H), 1.25 (br s, 10H), 0.88 (t, 3H); UV-Vis (methanol): $\lambda_{max} = 210$, 233, 314, 428, 490 nm (diode array detector).

6: As in the case of **5**, $[(C_5H_4Me)_2Ti(CO)_2]$ (315 mg, 1.2 mmol) in *n*-hexane (50 mL) and 1,4-$S_4(Nn\text{Oct})_2$ (459 mg, 1.2 mmol) in *n*-hexane (50 mL). Yield: 138 mg of a dark brown oil (25%). ^{1}H NMR (200 MHz, $CDCl_3$, 23 °C): $\delta = 6.32$ (t, 2H), 6.25 (t, 2H), 6.07 (q, 4H), 2.39 (s, 3H), 2.39 (t, 2H), 1.97 (s, 3H), 1.49 (q, 2H), 1.25 (br s, 10H), 0.88 (t, 3H); UV-Vis (methanol): $\lambda_{max} = 212$, 240, 310, 432, 484 nm (diode array detector).

7: SCl_2 (0.32 mmol, 10 mL of a 0.032 M solution in CH_2Cl_2) was added dropwise to a solution of **5** (137 mg, 0.32 mmol) in dichloromethane (70 mL) at 20 °C. After the mixture had been stirred for 30 min, the orange-colored solution was filtered through a layer of SiO_2 (10 cm) to remove $[Cp_2TiCl_2]$. The yellow solution was reduced in volume to give **7** (80 mg, 87%). ^{1}H NMR (200 MHz, $CDCl_3$, 23 °C): $\delta = 3.90$ (t, 2H), 1.60 (q, 2H), 1.29 (br s, 10H), 0.89 (t, 3H); MS (60 °C, EI): 287 (M^+, 20%), 255 ($S_4Nn\text{Oct}^+$, 7%), 223 ($S_3Nn\text{Oct}^+$, 15%), 191 ($S_2Nn\text{Oct}^+$, 57%), 160 ($SNn\text{Oct}^+/S_5^+$, 11%), 126 ($Nn\text{Oct}^+$, 100%); UV-Vis (methanol): $\lambda_{max} =$ 220, 288 nm (diode array detector).

8: As in the case of **7**, S_2Cl_2 (0.056 mL, 0.7 mmol) and **5** (297 mg, 0.7 mmol) in dichloromethane (200 mL). Yield: 204 mg of a pale yellow oil (91%). ^{1}H NMR (200 MHz, $CDCl_3$, 23 °C): $\delta = 3.20$ (t, 2H), 1.70 (t, 2H), 1.30 (br s, 10H), 0.89 (t, 3H); MS (69 °C, EI): 319 (M^+, 16%), 255 ($S_4Nn\text{Oct}^+$, 32%), 191 ($S_2Nn\text{Oct}^+$, 13%), 160 ($SNn\text{Oct}^+/S_5^+$, 29%), 126 ($Nn\text{Oct}^+$, 100%); UV-Vis (methanol): $\lambda_{max} = 212$, 294 nm (diode array detector).

Received: September 15, 1997 [Z10923IE]
German version: *Angew. Chem.* **1998**, *110*, 515–517

Keywords: heterocycles · nitrogen · sulfur · titanium

[1] a) K. Bergemann, M. Kustos, P. Krüger, R. Steudel, *Angew. Chem.* **1995**, *107*, 1481; *Angew. Chem. Int. Ed. Engl.* **1995**, *34*, 1330. b) R. Steudel, M. Kustos, V. Münchow, U. Westphal, *Chem. Ber.* **1997**, *130*, 757.

[2] R. Steudel, K. Bergemann, J. Buschmann, P. Luger, *Angew. Chem.* **1996**, *108*, 2641; *Angew. Chem. Int. Ed. Engl.* **1996**, *35*, 2537.

[3] Reviews on cyclic S–N compounds: H. G. Heal, *The Inorganic Heterocyclic Chemistry of Sulfur, Nitrogen and Phosphorus*, Academic Press, London, **1980**; T. Chivers in *The Chemistry of Inorganic Homo- and Heterocycles*, *Vol. 2*, (Eds.: I. Haiduc, D. B. Sowerby), Academic Press, London **1987**, p. 793.

[4] Reviews on sulfur homocycles: R. Steudel, *Top. Curr. Chem.* **1982**, *102*, 149; R. Laitinen, P. Pekonen, R. J. Suontamo, *Coord. Chem. Rev.* **1994**, *130*, 1.

[5] Review on organic polysulfides: R. Steudel, M. Kustos, *Encyclopedia of Inorganic Chemistry*, *Vol. 7* (Ed.: B. King), Wiley, Chichester, **1994**, p. 4009.

[6] The diimides 1,4-$S_4(NR)_2$ with R = methyl and *n*-octyl were prepared under Ruggli–Ziegler dilution conditions from S_2Cl_2 and primary amines in *tert*-butyl methyl ether.

[7] a) Reaction of **1** with S_4N_4 yields inter alia $[Cp_2TiS_3N_2]$, containing a six-membered metallacycle with the sequence TiSSNSN: C. G. Marcellus, R. T. Oakley, W. T. Pennington, A. W. Cordes, *Organometallics* **1986**, *5*, 1395; b) review on transition metal complexes of inorganic sulfur–nitrogen ligands: T. Chivers, F. Edelmann, *Polyhedron* **1986**, *5*, 1661.

[8] Crystal structure analysis of **4**: $0.67 \times 0.08 \times 0.06$ mm, orthorhombic, *Fdd*2 (No. 43), $Z = 16$, $a = 2654.7(2)$, $b = 2812.6(2)$, $c = 746.1(2)$ pm, $V = 5570.8(16) \times 10^6$ pm^3, $\rho_{calcd} = 1.599$ g cm^{-3}, $2\theta_{max} = 52°$, $Mo_{K\alpha}$ radiation, $\lambda = 71.069$ pm, ω-2θ scan, $T = 291$ K, 1517 measured, 1467 independent, and 892 observed reflections, criterium: $I > 2\sigma(I)$, absorption correction (T_{min}/T_{max}) 1.135/1.064, structure solved by direct methods (program: SHELXS-86), refined versus F^2 (program: SHELXL-93) with anisotropic temperature factors for all non-hydrogen atoms, isotropic for hydrogen atoms, 155 refined parameters with $R = 0.057$, residual electron density (max/min): $0.67/-0.50$ e Å^{-3}. Further details of the crystal structure investigation may be obtained from the Fachinformationszentrum Karlsruhe, D-76344 Eggenstein-Leopoldshafen, Germany (fax: (+49) 7247-808-666 (Frau S. Höhler-Schlimm); e-mail: crysdata@fiz-karlsruhe.de) on quoting the depository number CSD-407339.

[9] E. F. Epstein, I. Bernal, *J. Organomet. Chem.* **1971**, *26*, 229.

[10] R. Steudel, B. Holz, J. Pickardt, *Angew. Chem.* **1989**, *101*, 1301; *Angew. Chem. Int. Ed. Engl.* **1989**, *28*, 1269.

[11] The sum of bond angles may be as large as 357° as in the structures of S_7NH and S_9NH. For S_7NH see: H.-J. Hecht, R. Reinhardt, R. Steudel, H. Bradaczek, *Z. Anorg. Allg. Chem.* **1976**, *426*, 43; S_9NH: ref. [1a].

[12] Y. Drozdova, R. Steudel, *Phosphorus, Sulfur, Silicon*, in press.

[13] On the HPLC analysis of sulfur–nitrogen heterocycles see: R. Steudel, D. Rosenbauer, *J. Chromatogr.* **1981**, *216*, 399.

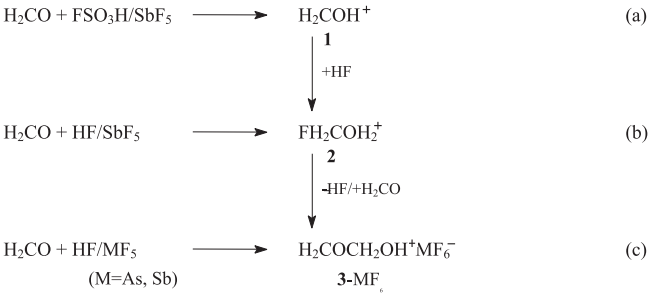
[14] Preparation in analogy to the synthesis of S_7NMe: B. A. Olsen, F. P. Olsen, *Inorg. Chem.* **1969**, *8*, 1739.

[15] M. Schmidt, B. Block, H. D. Block, H. Köpf, E. Wilhelm, *Angew. Chem.* **1968**, *80*, 660; *Angew. Chem. Int. Ed. Engl.* **1968**, *7*, 660; reviews on ligand transfer reactions: R. Steudel, M. Kustos, M. Pridöhl, U. Westphal, *Phosphorus, Sulfur, Silicon* **1994**, *93/94*, 61; R. Steudel in *The Chemistry of Inorganic Ring Systems*, (Ed.: R. Steudel), Elsevier, Amsterdam **1992**, p. 233

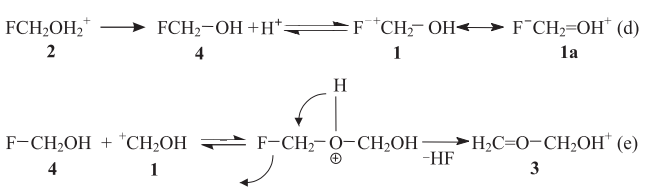
Formaldehyde in Super Acids: A Succession of Products from Carbenium through Oxonium Ion to Hydroxymethyl(methylidene)oxonium Salts

Rolf Minkwitz,* Stefan Schneider, and Hans Preut

The products of the reaction of formaldehyde with super acids were first examined by G. A. Olah et al.[1] The hydroxycarbonium ion **1** was identified in FSO_3H/SbF_5 [Eq. (a)] by NMR spectroscopy, and fluormethyloxonium ions **2** [Eq. (b)] were found after addition of HF or directly in HF/SbF_5.[2, 3] We attempted to isolate salts of monofluoromethanol, which is unknown in pure substance, from the HF solution according to Equation (b). Surprisingly, we obtained hydroxymethyl(methylidene)oxonium hexafluorometalate **3**-MF_6 at $-78°$C according to Equation (c) but no polymerization product of formaldehyde, as proposed by G. A. Olah et al.[3]



The formation of cation **3** might proceed in a simple way upon addition of formaldehyde to protonated formaldehyde **1**. However, no indications for **1** were found in the NMR spectra of the HF solution. Only signals for **2**, which exclusively exists in solution, were observed ($\delta(^{13}C) = 100.4$, $^1J_{C,F} = 222$ Hz); this confirms previous results by Olah et al. The stabilization in solution of protonated molecules for which the unprotonated form cannot be found is known and was recently described by Olah et al. for the example of protonated fluoroformic acid.[3, 4] The existence of cation **3** in solution cannot be proved. Considering the NMR spectroscopic results, it seems more likely that **3** is formed from **2** by a reversible electrophilic addition with subsequent elimination of HF [Eqs. (d) and (e)]. With the exception of **2**, no experimental proof was found for the intermediates which are formally required.



[*] Prof. Dr. R. Minkwitz, Dipl.-Chem. S. Schneider, Dr. H. Preut
Fachbereich Chemie der Universität
D-44221 Dortmund (Germany)
Fax: (+49) 0231-755-3797
E-mail: minkwitz@citrin.chemie.uni-dortmund.de

 © WILEY-VCH Verlag GmbH, D-69451 Weinheim, 1998 1433-7851/98/3704-0494 $ 17.50+.50/0

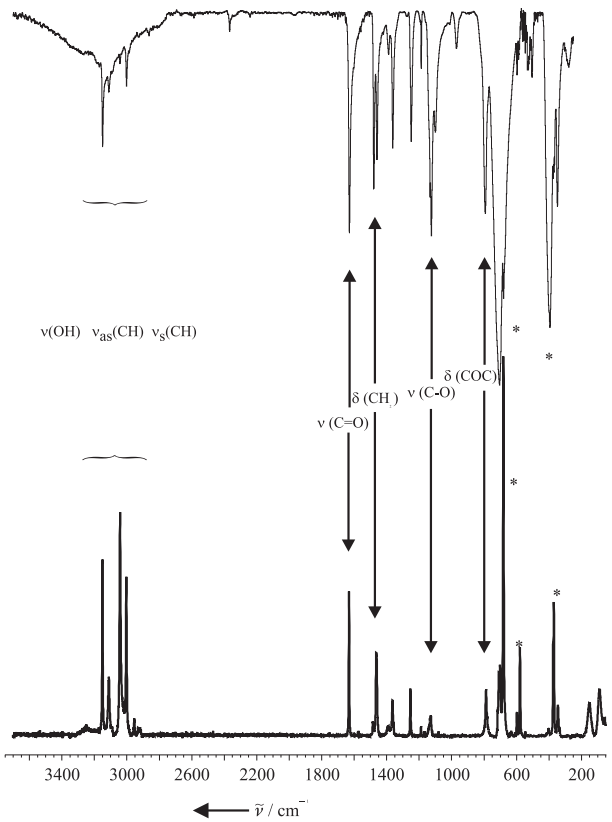


Figure 1. IR (top) and Raman spectra (bottom) of **3**-AsF_6 with labels for some vibrations of the cation. Vibrations of the anion are labeled with an asterisk. The IR spectrum was measured with a neat sample on a CsI plate at 233 K, and the Raman spectrum at 195 K.

Compounds **3**-MF_6 precipitate as colorless salts at either $-40\,^{\circ}C$ on concentrating the solution by removing HF or on cooling the solution to $-78\,^{\circ}C$. Vibrational spectroscopy provided the first indications for the presence of **3**, which was confirmed by a crystal structure analysis. The vibrational frequencies of **3** are in the expected range for molecules with comparable groups of atoms.[5] The symmetric and antisymmetric valence vibrations of the two CH_2 groups of the cation can be clearly distinguished in the Raman and IR spectra (Figure 1, Table 1).: ν_{as} for the methylidenic protons is observed at 3150 cm^{-1} (IR) and ν_s at 3041 cm^{-1} (Raman); ν_{as} for the methylic protons is at 3111 cm^{-1} (IR) and ν_s at 3002 cm^{-1} (Raman). Even if all work with DF/MF_5 systems is performed quickly, H/D exchange cannot be avoided.

In the crystalline state, cations and anions of **3**-MF_6 are connected by short H···F distances—the shortest interionic H···F contact is 217(8) pm (sum of the van der Waals radii 267 pm)—and a three-dimensional network is formed (Figure 2, Table 2).[6] In the C–O=C skeleton of **3** the lengths of the C(1)–O(1) single bonds and the C(2)–O(1) double bonds are increased compared to those in dimethyl ether (C–O 141.0 pm) or formaldehyde (C=O 120.8 pm).[7, 8]

The simplest molecule with a C–O=C skeleton is the methoxymethyl ion, $H_3COCH_2^+$, for which several ab initio calculations are known.[9–11] Values of 147.8 to 149.3 pm for the C–O bond and 121.5 to 124.0 for the C=O bond were calculated; corresponding bond angles values of 121.3 to 124.5° were predicted.[11] The C(2)-O(1)-C(1) bond angle and the C–O bond lengths in cation **3** are comparable with values predicted by ab initio methods.

Table 1. Vibrational frequencies [cm^{-1}] of ($X_2C^1OC^2X_2OX$)MF_6 [**3**-MF_6; M = As,Sb, X = H,D] and tentative assignments.[a]

M = As, X = H		M = Sb, X = H		M = As, X = H,D		M = Sb, X = H,D		Tentative
Raman	IR	Raman	IR	Raman	IR	Raman	IR	assignment
3250 vw	3250 b							ν(OH)
3149 m	3150 w	3150 vw	3120 sb	3151 m	3158 vw	n. d.[b]	n. d.[b]	$\nu_{as}(C^1H)$
3110 w	3111 vw	3112 vw		3113 m	3120 vw	n. d.[b]	n. d.[b]	$\nu_{as}(C^2H)$
3041 m	3033 vw	3041 w		3043 s	3051 vw	3030 m	3036 w	$\nu_s(C^1H)$
3002 m	3002 vw	3002 w		3003 m	3013 vw	2985 m	2990 w	$\nu_s(C^2H)$
				2404 w	2409 m	2404 w	2409 m	ν(OD)
				2345 w		2331 m	2333 m	ν_{as}(CD)
				2307 m	2317 vw	2288 m	2294 m	ν_s(CD)
1632 m	1629 m	1629 vw	1626 m	1629 m	1634 m	n. d.[b]	1637 m	ν(C=O)
			1480 m	1483 w	1484 w	1483 w	1484 m	δ(CH_2)
1464 w	1459 w	1461 vw	1455 m	1461 m	1468 w			δ(CH_2)
1393 vw								δ(CH_2)
1364 vw	1362 w	1364 vw	1364 w	1365 w	1369 m	1330 w		δ(COH)
1254 w	1249 w	1263 vw	1239 w	1258 w	1254 m	1271 w		δ(HCO)
		1185 vw	1193 vw	1194 vw	1201 m	1196 w	1201 m	τ(CH_2)
1130 vw	1132 w	1131 vw	1132 m	1135 w	1132 m			ν(C–O)
			1102 w	1097 w	1101 w	1092 w		ν_{as}(C–O)
		803 w	803 w	792 m	803 m			ρ(CH_2), δ(COC)
		564 w	563 w	567 m	558 m	561 m	558 m	ρ(CH_2)
				353 m	360 m	281 w		ω(CH_2)
				166 m				
682 vs		653 vs		685 vs		647 vs		ν(MF_6^-)
580 w		577 w		580 m		592 m		ν(MF_6^-)
	704 vs		666 vs		709 vs		666 vs	ν(MF_6^-)
	394 s		282 s		398 s		291 s	δ(MF_6^-)
371 m		289 m		380 m		384 m		δ(MF_6^-)

[a] Definitions of abbreviations: vw: very weak, w: weak, m: medium, s: strong, vs: very strong, b: broad. [b] Not determined.

 © WILEY-VCH Verlag GmbH, D-69451 Weinheim, 1998 1433-7851/98/3704-0495 $ 17.50+.50/0

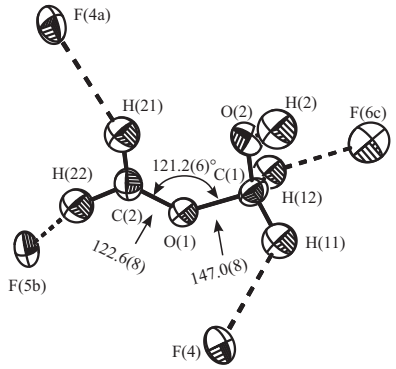


Figure 2. Structure of the cation **3** in the crystal with contacts, atom labels, and structural parameters for the central unit. Further distances [pm]: F4a $\cdots$ H21 236(8), F5b $\cdots$ H22 217(8), F6c $\cdots$ H12 244(8), F4 $\cdots$ H11 240(9). Symmetry operations: $x-1,+y,+z$ (a), $-x+1,-y,-z+1$ (b), $x,-y-0.5,+z+0.5$ (c).

Table 2. Selected bond lengths [pm] and angles [°] for **3**-AsF_6. Not all the atoms of the anion are shown in Figure 2.[a]

As(1)−F(2)	171.8(4)	C(2)-O(1)-C(1)	121.2(6)
As(1)−F(4)	171.0(4)	O(2)-C(1)-O(1)	108.8(5)
As(1)−F(6)	170.2(5)	F(1)-As(1)-F(4)	89.6(2)
O(1)−C(2)	122.6(8)	F(6)-As(1)-F(4)	90.4(3)
O(1)−C(1)	147.0(8)	F(1)-As(1)-F(2)	179.2(2)
O(2)−C(1)	132.5(8)		

[a] The standard deviations refer to the last digit.

Experimental Section

H_2CO was obtained and purified according to ref. [12]. AsF_5 was obtained by allowing the elements to reaction and purified by fractional condensation. SbF_5 was purified by fractional distillation, and HF was dried with fluorine.[13]

In a KEL-F reactor MF_5 (3 mmol; M = As, Sb) was dissolved in HF ($\approx$5 g). The solution was frozen at $-196\,^{\circ}C$, and then H_2CO (3 mmol) condensed onto the solution. The reaction mixture was allowed to warm slowly to $-40\,^{\circ}C$. The excess reactant was removed either at $-78\,^{\circ}C$ or at $-40\,^{\circ}C$ under a dynamic vacuum. Compound **3**-MF_6 remained as a colorless solid.

Instruments: Raman: Jobin–Yvon T64000, Ar^+ laser ($\lambda = 514.5$ nm) Spectra Physics; IR: Bruker IFS 133v; NMR: Bruker DPX300.

Received: July 11, 1997 [Z 10676 IE]
German version: *Angew. Chem.* **1998**, *110*, 510–512

Keywords: formaldehyde · IR spectroscopy · Raman spectroscopy · superacidic systems · oxonium ions

[1] G. A. Olah, D. H. O'Brien, M. Calin, *J. Am. Chem. Soc.* **1967**, *89*, 3582–3586.
[2] G. A. Olah, G. D. Mateescu, *J. Am. Chem. Soc.* **1971,** *93*, 781–782.
[3] G. A. Olah, S. Yu, G. Liang, G. D. Mateescu, M. R. Bruce, D. J. Donovan, M. Arvanaghi, *J. Org. Chem.* **1981**, *46*, 571–577.
[4] G. A. Olah, A. Burrichter, T. Mathew, Y. D. Vankar, G. Rasul, G. K. S. Prakash, *Angew. Chem.* **1997**, *109*, 1958–1961; *Angew. Chem. Int. Ed. Engl.* **1997,** 1875–1877.
[5] J. Weidlein, U. Müller, K. Dehnicke, *Schwingungsspektroskopie*, Thieme, Stuttgart, **1982.**
[6] Crystal structure analysis of **3**-AsF_6: crystals grown from HF, monoclinic, space group $P2_1/c$, $a = 632.0(4)$, $b = 1101.5(11)$, $c = 1031.5(6)$ pm, $\beta = 107.51(5)^{\circ}$, $V = 684.8(9) \times 10^6$ pm^3, $\rho_{calcd} = 2.425$ g cm^{-3}, crystal dimensions $0.20 \times 0.19 \times 0.12$ mm^3, $Mo_{K\alpha}$ radiation ($\lambda = 71.073$ pm), $2\theta/\omega$ scans, $2\theta_{max} = 50.0^{\circ}$, $T = 171$ K, 2910 measured reflections, 1199 independent reflections, 996 reflections used in the refinement, σ limit 2.0, Lp and absorption correction (ψ scans), $\mu(Mo_{K\alpha}) = 5.035$ mm^{-1}, min./max. transmission 0.78/0.91, structure solution: Patterson, difference-Fourier synthesis, SHELXS-86, SHELXL-93, PARST, PLATON, MISSYM, 114 free parameters; hydrogen atoms were experimentally determined and refined from ΔF, $R = 0.0485$, $wR = 0.1194$, $R = \Sigma\,||F_o| - |F_c||/\Sigma\,|F_o|$, refinement method: full-matrix least squares on F^2, min./max. residual electron density = 0.787/ − 0.980 eÅ^{-3}. Further details on the crystal structure investigation may be obtained from the Fachinformationszentrum Karlsruhe, D-76344 Eggenstein-Leopoldshafen, Germany (fax: (+49) 7247-808-666 (Frau S. Höhler-Schlimm); e-mail: crysdata@fiz-karlsruhe.de), on quoting the depository number CSD – 407344.
[7] U. Blukis, P. H. Kasai, R. J. Meyers, *J. Chem. Phys.* **1963**, *38*, 2753–2760.
[8] K. Takagi, T. Oka, *J. Phys. Soc. Jpn.* **1963**, *18*, 1174–1175.
[9] F. P. Lossing, *J. Am. Chem. Soc.* **1977**, *99*, 7526–7530.
[10] D. Farcasiu, J. A. Horsley, *J. Am. Chem. Soc.* **1980**, *102*, 4906–4911.
[11] R. J. Woods, C. W. Andrews, J. P. Bowen, *J. Am. Chem. Soc.* **1992**, *114*, 850–858.
[12] I. F. Walker, *J. Am. Chem. Soc.* **1933**, *55*, 2821–2826.
[13] R. Minkwitz, A. Kornath, W. Sawodny, *Angew. Chem.* **1992**, *104*, 648–649; *Angew. Chem. Int. Ed. Engl.* **1992,** *31*, 643–644.

Matrix Isolation and Characterization of a Reactive Intermediate in Olefin Oxidation with Chromyl Chloride**

Christian Limberg,* Ralf Köppe, and Hansgeorg Schnöckel

Although the oxidation of organic substrates by Cr^{VI} compounds has always been a useful tool in the hands of chemists, the course of such reactions and the nature of the intermediates have remained for the most part unknown. For example, the mechanism of C–H activation in the Etard reaction,[1] known since 1877, was only revealed in detail in 1995.[2] In the past, complex mechanisms were put forward for the oxidation of olefins with chromyl chloride CrO_2Cl_2[3, 4] that attempted to explain the great variety of products obtained on the basis of widely differing intermediates such as chromaoxetanes, chromium alkoxides, and epoxide complexes. None of these intermediates has ever been proven. The occurrence of carbonyl compounds among the products was explained by rearrangements of certain products during work-up,[3, 5] whereas more recent work highlights the relevance of intermediate chromium complexes of these carbonyl compounds. For example, ethylene reacts with the CrO_2^+ ion in the

[*] Dr. C. Limberg
Anorganisch-Chemisches Institut der Universität
Im Neuenheimer Feld 270, D-69120 Heidelberg (Germany)
Fax: (+49) 6221-54-5707
E-mail: limberg@sun0.urz.uni-heidelberg.de
Dr. R. Köppe, Prof. H. Schnöckel
Institut für Anorganische Chemie der Universität Karlsruhe (Germany)

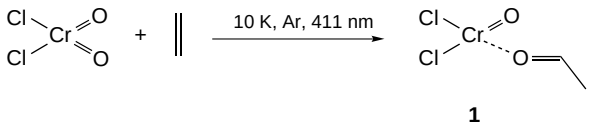
[**] C.L. is grateful to the Fonds der Chemischen Industrie and the Deutsche Forschungsgemeinschaft for scholarships and equipment, and to Professor G. Huttner for his generous support.

 © WILEY-VCH Verlag GmbH, D-69451 Weinheim, 1998 1433-7851/98/3704-0496 $ 17.50+.50/0

mass spectrometer to yield $O{=}Cr^{+}\cdots O{=}CHCH_3$.[6] The aim of the matrix studies presented here was to isolate intermediates in olefin oxidation with CrO_2Cl_2 in order to gain reliable information concerning the reaction mechanism. The investigations began with ethylene, the simplest olefin, and the first step was to identify the products formed on treatment with CrO_2Cl_2 under thermal conditions. The reaction of ethylene with CrO_2Cl_2 at $-80\,^{\circ}C$ in dichloromethane yields primarily 2-chloroethanol after isolation of the resulting Etard complex and work-up with wet acetonitrile. Therefore $CrOCH_2CH_2Cl$ fragments should be present in the Etard complex, and, consequently, **A** can be postulated as a possible intermediate.

$Cl(O{=})Cr{-}O{-}CH_2{-}CH_2{-}Cl$ **A**

In the next step, CrO_2Cl_2 was co-condensed with a mixture of ethylene and argon, the resulting matrix irradiated at 411 nm (activation of the $Cl\rightarrow Cr$ charge-transfer (CT) transition),[7] and the reaction followed by IR spectroscopy.[8] The spectra (Figure 1) show that a product has formed in good yield (approximately 40%) which produces an intense new band in the Cr=O region at 1009 cm^{-1}; this indicates the presence of only *one* Cr=O bond. In the Cr–Cl region, two new bands at 452 and 385 cm^{-1} appear suggesting that the $CrCl_2$ fragment is preserved during the reaction. This excludes **A** as the product. These findings tend to point to the fragment $O{=}CrCl_2$ as the inorganic part of the reaction product, and, consequently, CrO_2Cl_2 must have transferred one oxygen atom to the organic substrate ethylene. A new band at 1669 cm^{-1} helps to clarify the composition of the resulting organic product. This must belong to a carbonyl compound whose ν(C=O) band is shifted to lower wavenumber due to complexation with a Lewis acidic center (the formation of complexes, often only weakly bound, after photoreaction in noble gas matrices is commonly observed[9]). In addition, since investigations into the concentration dependence showed that only one equivalent of ethylene is involved in the reaction, the organic product must consist of a carbonyl compound with a C_2 unit ($O{=}CH_2$ can be excluded as the product[10]). Only acetaldehyde meets these requirements, and the connectivity **1** shown in reaction (1) can be assigned to



(1)

1

the product of the matrix experiment. Further proof was obtained by using $[D_4]$ethylene to synthesize the deuterated version of **1**, whose IR spectrum—when compared with that of the hydrogenated compound—showed all the changes expected in terms of the above interpretation: All bands assigned to the $O{=}CrCl_2$ fragment exactly maintained their previous positions, indicating that this fragment oscillates independently. The carbonyl band shows a slight shift ($\Delta\tilde{\nu} = 18\ cm^{-1}$) due to weak coupling to C–H modes (such as δ(CH)). All other bands show strong shifts due to the large contributions from C–H vibrations. When $^{18}O_2CrCl_2$[11] was used with the aim of synthesizing the ^{18}O isotopomer of **1**, significant shifts were only observed for three bands: the ν(C=O) band ($\Delta\tilde{\nu} = 29\ cm^{-1}$), the ν(Cr=O) band (43 cm^{-1}), and a further band at 852 cm^{-1} (26 cm^{-1}), which can be assigned as having principally δ(CCO) character. The remaining signals shift only marginally. Reaction of the mixed isotopomer $^{18}O^{16}OCrCl_2$ does not lead to new bands, which further proves the presence of only one Cr=O bond in **1**.

All these results already confirm **1** unequivocally as the product of the matrix experiments, but additional calcula-

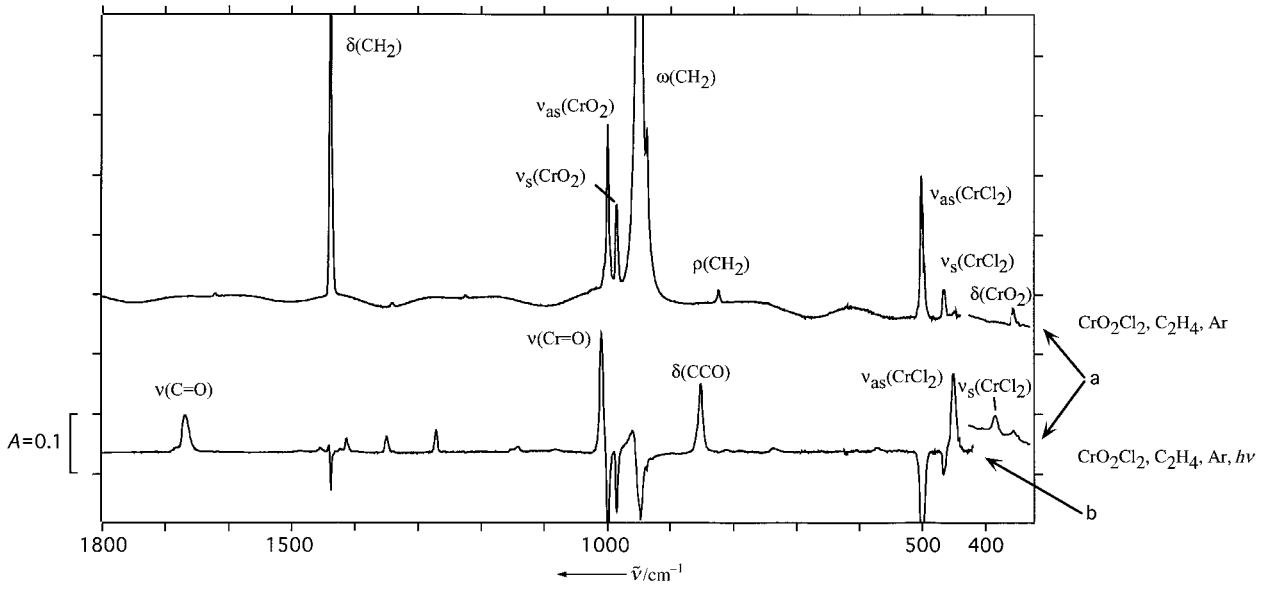
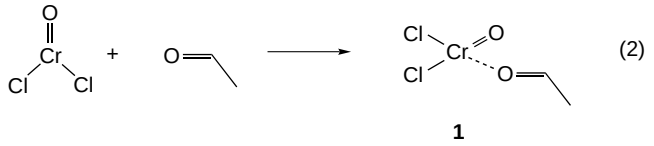


Figure 1. IR spectra of CrO_2Cl_2 in an ethylene/argon matrix (4/96) at 10 K in the region of 1800–330 cm^{-1}; upper trace: absolute spectrum (a) after deposition of the starting materials for 15 min; lower trace: difference spectrum (b) after irradiation at $\lambda = 411$ nm for 10 min. and the absolute spectrum (a) for the region below 400 cm^{-1} to give an impression of the conversion in the reaction. When the bands of the initial spectrum overlap with newly formed bands, the intensity ratios can be slightly perturbed upon spectrum subtraction.

 © WILEY-VCH Verlag GmbH, D-69451 Weinheim, 1998 1433-7851/98/3704-0497 $ 17.50+.50/0

tions—with respect to the structure of **1** on the one hand and in order to obtain information on the theoretically expected frequencies on the other—were of interest. Since DFT calculations (B3LYP, LanL2DZ, G94)[12] yielded good results for the structure of CrO_2Cl_2 (the maximum deviations in bond lengths and angles from those of the gas-phase structure[13] amounted to 0.03 Å and 2°, respectively), this method was employed for calculating the structure of **1**. The most stable *syn* conformation is energetically only 5.1 kJ mol^{-1} less stable than the most stable *anti* conformation. It is therefore the most likely structure of the product originating from a chromaoxetane[4] potentially generated in the primary step. However, because the latter intermediate step has never been proved and because conformers are photochemically interconvertable in matrices, a decision in favor of one structure or another cannot be made. Both show the features expected from the experimental IR spectra: the Cr=O bond is shorter than in CrO_2Cl_2, and the bond to the acetaldehyde oxygen atom is very strong (almost in the region of a Cr–O single bond[14]). This explains the significant shift of ν(C=O) to lower wavenumbers (observed: $\Delta\tilde{\nu} = 52$ cm^{-1} in comparison to free acetaldehyde[15]). The enthalpy of reaction (1) was calculated as -157.5 kJ mol^{-1}, whereas reaction (2) already proceeds exothermically with -144.4 kJ mol^{-1}. Therefore, product formation is also accounted for on energetic grounds.

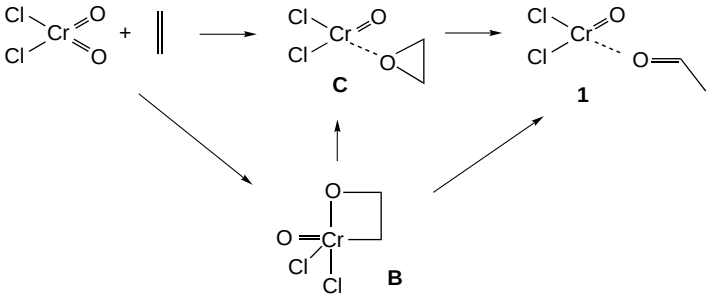


1

Calculations of the vibrational frequencies showed that the IR spectra of the two conformers differ only slightly[16] with respect to the error present in the calculations, thus preventing the assignment of one conformer to the experimental spectrum. However, as can be seen for the example of the most stable *syn* conformer in Table 1, the band pattern obtained experimentally could be reproduced qualitatively. The calculated shifts of the bands resulting from replacement of ^{16}O by ^{18}O agree very well with the experimental spectrum; any errors made previously cancel each other. In only one case (852 cm^{-1}) was the calculated shift too low.

The oxo chromium dichloride molecule in **1**, with chromium in the rare oxidation state of +IV, is particularly significant. This species was often mentioned as an important intermediate in oxidations with CrO_2Cl_2.[3, 4, 17] The experiments presented here describe for the first time the isolation and characterization of this fragment as complexed with acetaldehyde.

The fact that a primary product must exist between the substrate and **1**, which rearranges to **1** by a hydrogen shift, raises the question of the mechanism for the formation of **1**. In principle, the primary product could be a chromaoxetane **B**, which could then be the source of a photochemically generated diradical $^{\bullet}OCH_2CH_2^{\bullet}$ for which experimental data and MO calculations favor isomerization to acetaldehyde.[18] However, a more likely alternative is the intermediate formation of the oxirane adduct **C** in Scheme 1, either directly



Scheme 1. Possible mechanism for the formation of **1**.

from the starting materials or via **B**. The adduct **C** was mentioned previously as a possible intermediate[4] and could isomerize to form **1**. Such rearrangements of oxiranes to carbonyl compounds catalyzed by Lewis acids are widely known in synthetic chemistry,[19] and it is possible that in the present case the required activation energy is supplied photochemically and not thermally.[20] To compare the role of **1** in the reaction under inert conditions and irradiation with that under thermal conditions, a transfer of the results of the matrix experiments to preparative chemistry was attempted. As already mentioned, the reaction of ethylene with CrO_2Cl_2 at -50 °C in the dark followed by decomplexation of the Etard complex yields mainly chloroethanol. However, acetaldehyde (5%) was also present among the products, which

Table 1. Experimental frequencies $\tilde{\nu}$ in cm^{-1} measured after photolysis of an ethylene/argon (4/96) matrix doped with $Cr^{16}O_2Cl_2$ or $Cr^{18}O_2Cl_2$, and frequencies calculated with a combination of B3LYP/LanL2DZ for the most stable *syn* conformer of **1** (^{16}O and ^{18}O isotopomer, respectively) (the values in parentheses refer to relative intensities *I*; no scaling). The last column gives a qualitative assignment based on the calculations and the isotopic shifts.

$Cr^{16}O_2Cl_2$	$Cr^{18}O_2Cl_2$	$\Delta\tilde{\nu}(^{16}O - ^{18}O)$	calcd **1**(^{16}O) (*I*)	calcd $\Delta\tilde{\nu}(^{16}O - ^{18}O)$	Assignment
1669	1640	29	1651 (0.58)	26	ν(C=O)/ν(CC)/δ(CH)
1453	1453	0	1492 (0.15)	0	$\delta_{as}(CH_3)$
1413	1408	5	1483 (0.26)	4	$\delta_{as}(CH_3)$
1349	1349	0	1434 (0.37)	1	$\delta_s(CH_3)/\delta(CH)$
1271	1266	5	1418 (0.09)	7	$\delta_s(CH_3)/\delta(CH)$
1141	1141	0	1166 (0.18)	1	ν(CC)/δ(CCO)
1009	966	43	1104 (1.00)	47	ν(Cr=O)
852	826	26	932 (0.12)	6	δ(CCO)
			809 (0.08)	0	$\tau_r(CH_3)$,δ(CH)
			535 (0.12)	11	δ(CrOC)
452	451	1	425 (0.85)	0	$\nu_{as}(CrCl_2)$
385	379	6	362 (0.15)	7	$\nu_s(CrCl_2)$

 © WILEY-VCH Verlag GmbH, D-69451 Weinheim, 1998 1433-7851/98/3704-0498 $ 17.50+.50/0

could, in principle, originate in **1** incorporated in the Etard complex. When the matrix conditions are simulated by dissolving the two reactants in a Freon mixture at $-80\,^{\circ}C$ and quenching the resulting solution at 77 K to form a glass, the amount of acetaldehyde among the oxidation products increases to 35% after subsequent photolysis at 77 K and usual work-up; this is then comparable to the yield in the matrix experiment.[21] Therefore, **1** should also occur intermediately in the thermal reaction of ethylene with CrO_2Cl_2. Since other olefins are quantitatively oxidized to carbonyl compounds by CrO_2Cl_2 in thermal reactions,[3] intermediates analogous to **1** could play a more important role in these cases, although, of course, other mechanisms for the formation of carbonyl compounds are imaginable.[5]

The isolation of an intermediate in an olefin oxidation by CrO_2Cl_2 was achieved for the first time. The presence of this intermediate could explain the occurrence of carbonyl compounds in the product spectrum of such reactions.

Received: August 8, 1997 [Z10808IE]
German version: *Angew. Chem.* **1998**, *110*, 512 – 515

Keywords: chromium · ethylene · matrix isolation · intermediates · oxygenations

[1] A. L. Etard, *C. R. Hebd. Seances Acad. Sci.* **1877**, *84*, 127 – 129.
[2] G. K. Cook, J. M. Mayer, *J. Am. Chem. Soc.* **1994**, *116*, 1855 – 1868; *ibid*. **1995**, *117*, 7139 – 7156.
[3] M. A. Etard, H. M. Moissan, *C. R. Hebd. Seances Acad. Sci.* **1893**, *116*, 434 – 437; S. J. Cristol, K. R. Eilar, *J. Am. Chem. Soc.* **1950**, *72*, 4353 – 4356; R. A. Stairs, D. G. M. Diaper, A. L. Gatzke, *Can. J. Chem.* **1963**, *41*, 1059 – 1064; F. Freeman, P. J. Cameran, R. H. Dubois, *J. Org. Chem*. **1968**, *33*, 3970 – 3972; F. Freeman, R. H. Dubois, N. J. Yamachika, *Tetrahedron* **1969**, *25*, 3441 – 3446; F. Freeman in *Organic Syntheses by Oxidation with Metal Compounds* (Eds.: W. J. Mijs, C. R. H. I. de Jonge), Plenum, New York, **1986**, chapter 2, pp. 41 – 118.
[4] K. B. Sharpless, A. Y. Teranishi, J.-E. Bäckvall, *J. Am. Chem. Soc*. **1977**, *99*, 3120 – 3128.
[5] K. B. Sharpless, A. Y. Teranishi, *J. Org. Chem.* **1973**, *38*, 185 – 186.
[6] A. Fiedler, I. Kretzschmar, D. Schröder, H. Schwarz, *J. Am. Chem. Soc*. **1996**, *118*, 9941 – 9952.
[7] J. P. Jasinski, S. L. Holt, J. H. Wood, L. B. Asprey, *J. Chem. Phys.* **1975**, *63*, 757 – 771.
[8] The photolyses were performed with a 200-W Hg high-pressure arc lamp in combination with interference filters. The IR spectra were recorded on a Bruker-IFS-113 VFTIR spectrometer in the region of 4000 – 400 and 1000 – 200 cm^{-1} with a resolution of 1 cm^{-1}.
[9] R. N. Perutz, *Chem. Rev.* **1985**, *85*, 77 – 127.
[10] M. J. Almond, A. J. Downs, *J. Chem. Soc. Dalton Trans.* **1988**, 809 – 817; H. Khoshkhoo, E. R. Nixon, *Spectrochim. Acta A* **1973**, *29*, 603 – 612.
[11] $^{18}O_2CrCl_2$ was synthesized by the reaction of anhydrous $CrCl_3$ with $Na^{18}OH$, oxidation by Cl_2, and treatment of the resulting chromate with an excess of anhydrous HCl. The level of enrichment was approximately 70 – 80%. IR data for $Cr^{18}O_2Cl_2$ ($Cr^{18}O^{16}OCl_2$): $\tilde{\nu} = 960$ (992) [$\nu_{as}(CrO_2)$], 943 (951) [$\nu_s(CrO_2)$], 502 [$\nu_{as}(CrCl_2)$], 461 cm^{-1} [$\nu_s(CrCl_2)$].
[12] M. J. Frisch, G. W. Trucks, H. B. Schlegel, P. M. W. Gill, B. G. Johnson, M. A. Robb, J. R. Cheeseman, T. Keith, G. A. Petersson, J. A. Montgomery, K. Raghavachari, M. A. Al-Laham, V. G. Zakrzewski, J. V. Ortiz, J. B. Foresman, C. Y. Peng, P. Y. Ayala, W. Chen, M. W. Wong, J. L. Andres, E. S. Replogle, R. Gomperts, R. L. Martin, D. J. Fox, J. S. Binkley, D. J. Defrees, J. Baker, J. P. Stewart, M. Head-Gordon, C. Gonzalez, J. A. Pople, Gaussian, Inc., Pittsburgh, PA, **1995**.
[13] C. J. Marsden, L. Hedberg, K. Hedberg, *Inorg. Chem.* **1982**, *21*, 1115 – 1118.
[14] P. Stavropoulos, N. Bryson, M.-T. Youinou, J. A. Osborn, *Inorg. Chem.* **1990**, *29*, 1807 – 1811.
[15] C. O. Della Védova, O. Sala, *J. Raman Spectrosc.* **1991**, *22*, 505 – 507.
[16] The fact that some of the calculated bands deviate by approximately 100 cm^{-1} from the experimental values is not unusual for such calculations and presumably has its origin in slight deviations of the calculated structure from the real one. The structure of CrO_2Cl_2 calculated with the B-P functional and SV(P) basis sets (Turbomol [R. Ahlrichs, M. Baer, M. Haeser, H. Horn, C. Kölmel, *Chem. Phys. Lett.* **1989**, *162*, 165 – 169]) represents the real structure almost ideally ($\Delta r < 0.01$ Å, $\Delta(\text{angle}) < 1^{\circ}$), and therefore shows that this combination of functional and basis sets has to be considered more suitable for structure determination (the calculation of the frequencies is not possible) than the combination of B3LYP/LanL2DZ. The more reliable B-P/SV(P) structure of **1** differs slightly ($\Delta r < 0.05$ Å,$\Delta(\text{angle}) < 4^{\circ}$)from the B3LYP/LanL2DZ structure which forms the basis for the calculation of the spectrum. These differences can have drastic effects on the calculation. Accordingly, the deviations of the experimental IR spectrum calculated for chromyl chloride with the combination of B3LYP/LanL2DZ from the experimental spectrum were of the same magnitude. For DFT structure and frequency calculations for CrO_2Cl_2, see M. Torrent, P.Gili, M. Duran, M. Solà *J. Chem. Phys.* **1996**, *104*, 9499 – 9510. Differences in frequencies of the two most stable *syn* and *anti* conformations: $\nu_s(CrCl_2)$: 10, $\nu_{as}(CrCl_2)$: 6, $\delta(CCO)$: 18, $\nu(Cr{=}O)$: 20, $\nu(C{=}O)$: 1 cm^{-1}. The maximum deviation was obtained for a band that should be at 535 cm^{-1} for *syn*-**1** and at 576 cm^{-1} for *anti*-**1**, but which does not appear in the experimental spectrum due to low intensity; the calculated intensity ratios do not differ significantly.
[17] A. K. Rappé, W. A. Goddard III, *J. Am. Chem. Soc.* **1982**, *104*, 3287 – 3294.
[18] A. Lifshitz, H. Ben-Hamon, *J. Phys. Chem*. **1983**, *87*, 1782 – 1787; J. G. Serafin, C. M. Friend, *J. Am. Chem. Soc*. **1989**, *111*, 6019 – 6026; F. W. McLafferty, *Science (Washington DC)* **1990**, *247*, 925 – 929.
[19] R. O. C. Norman, J. M. Coxon, *Principles of Organic Synthesis*, 3rd ed., Chapman and Hall, London, **1993**, p. 590.
[20] C. Schmidt, Dissertation, Universität Giessen, Germany, **1995**.
[21] Whereas residual amounts of CrO_2Cl_2 do not react in the matrix experiment, free CrO_2Cl_2 reacts further thermally when the Freon mixture is warmed to temperatures that allow volatile components to be pumped off. The compounds produced by this route are also among the products.

Si_6, Si_{14}, and Si_{22} Rings in Iodide Silicides of Rare Earth Metals**

Hansjürgen Mattausch and Arndt Simon*

Numerous metal-rich halides MX_nA ($n \leq 2$) of rare earth metals M with interstitial atoms A = H,C,N,O have been prepared.[1–3] Recently we reported on boride and boride carbide halides.[4–6] Owing to the electropositive character of the rare earth metals, the interstitial atoms are present as anions, and in the case of carbon C_2^{6-} and C_2^{4-} units are found besides discrete C^{4-} ions.[1] In $M_4X_5B_4$ the boron atoms form rhomboids which are linked into chains.[6] Several factors influence the nature of the interstitial species: the number of

[*] Prof. Dr. A. Simon, Dr. H. Mattausch
Max-Planck-Institut für Festkörperforschung
Heisenbergstrasse 1, D-70569 Stuttgart (Germany)
Fax: (+49) 711-689-1642
E-mail: hansm@vaxff2.mpi-stuttgart.mpg.de

[**] We are grateful to C. Kamella for preparing the structural drawings, to R. Eger for help with the preparations, and to H. Gärttling for the diffractometer data.

 © WILEY-VCH Verlag GmbH, D-69451 Weinheim, 1998 1433-7851/98/3704-0499 $ 17.50+.50/0

electrons which can be donated by the MX_n framework[7] (thus determining the A – A bonding), the electronic balance between M – M, M – A, and A – A bonding, and the dimensions and distribution of voids in the metal atom arrangement.

So far, the only known compounds with silicon as interstitial atom are Gd_4I_5Si and Gd_3I_3Si.[8] Isolated Si atoms center Gd_6 octahedra, similar to carbon in the corresponding carbide halides. For binary rare earth silicides, however, structures involving Si – Si bonding exist, such as MSi,[9] which contains zig-zag chains, and MSi_2, which contains a three-dimensional network of Si atoms.[10] Compared to these binary and ternary[11] silicides, the variation of the halogen content in halide silicides offers an additional means for fine-tuning the valence-electron concentration and hence the nature of the Si Zintl anions. Since electron transfer to the interstitial Si species is decreased in the halide silicides, larger Si_n entities may be formed given appropriate geometrical conditions.

We prepared MISi (M = La, Ce, Pr), $La_4I_3Si_4$, and $La_5I_3Si_5$ by annealing stoichiometric mixtures of MI_3, M, and Si for several days.[12] The compounds were obtained as needles or laths with a metallic luster. Conductivity measurements[14] on pressed or sintered pellets revealed metallic behavior between 5 K and room temperature. The compounds are extremely sensitive towards moisture and ignite explosively upon contact with water.

Figure 1 depicts the characteristic M – Si building blocks in the structures of CeISi, $La_4I_3Si_4$, and $La_5I_3Si_5$.[15] All three

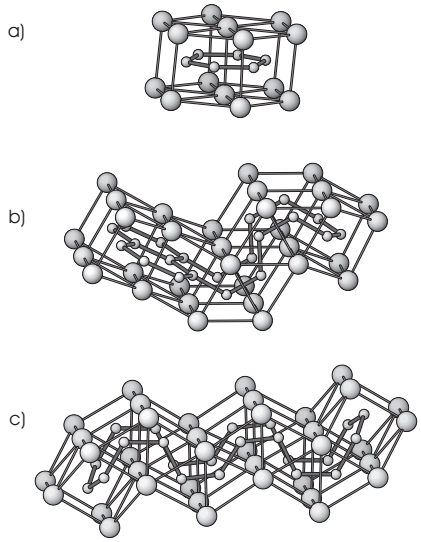


Figure 1. Building blocks in rare earth metal iodide silicides. Si and M atoms are represented by spheres of increasing size.[29] Silicon is coordinated by M in a trigonal-prismatic fashion. a) Si_6 rings with a Ce environment in CeISi, b) condensed Si_6 and Si_{14} rings with a La environment in $La_4I_3Si_4$, and c) Si_{22} rings with a La environment in $La_5I_3Si_5$.

structures contain Si_n rings (emphasized by bold lines): Si_6 rings which deviate from planarity by less than 7° are found in CeISi, planar Si_6 rings are condensed with strongly bent Si_{14} rings in $La_4I_3Si_4$, and Si_{22} rings are linked into corrugated layers in $La_5I_3Si_5$. All Si atoms are coordinated by M atoms in a trigonal-prismatic fashion, but the interconnection of the prisms differs in the three structures. There are two ways of fusing the prisms to attain optimal space filling[17] and these differ with respect to the relative directions of the quasi-threefold axes, which can be parallel (p) or orthogonal (o) to each other.[18] In the structure of CeISi prisms with (p) orientation form layers (see Figure 1a), and the occupation of the prism centers through Si results in Si_6 rings. The structural principle is closely related to that of β-$ThSi_2$.[19] Indeed, the structure of CeISi represents a two-dimensional section of the latter. As shown in the projection in Figure 2, the Ce-(SiSi)-Ce layers are surrounded on both sides by I atoms above the trigonal prism faces. The I-Ce-(SiSi)-Ce-I slabs with the sequence Cα(bc)αB are stacked parallel to (001) to provide close packing between layers of I atoms which are held together by van der Waals forces. The structure is in contrast with that of the composition-related compound $Gd_2Br_2C_2$, in which ethene-like C_2^{4-} anions occupy the octahedral voids of close-packed double layers of metal atoms.[20]

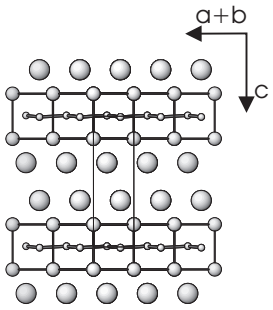


Figure 2. Projection of the structure of CeISi along [110]. The building blocks from Figure 1a are condensed to form layers parallel to the "threefold" axis of the trigonal prisms; between the layers are double layers of I atoms. Si, Ce, and I atoms are represented by spheres of increasing size.

Figure 3 shows the projection of the $La_4I_3Si_4$ structure along [010]. In contrast to CeISe the trigonal M prisms are fused in both (p) and (o) modes. Double strings of La_6 (o) prisms, shown as projections on the rectangular prism faces in Figure 3, are alternatingly condensed with (p) prisms to form corrugated layers parallel to (001). The (p)-linked prisms correspond to a section of the β-$ThSi_2$ structure (see insert of Figure 3) containing a ribbon of *trans*-condensed Si_6 rings formed from Si(1) and Si(2).

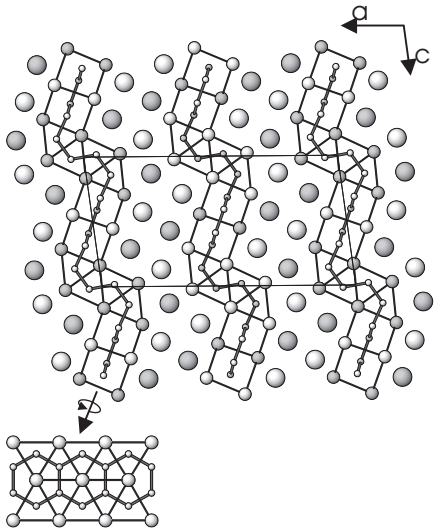


Figure 3. Projection of the structure of $La_4I_3Si_4$ along [010]. The building blocks from Figure 1a are condensed to form layers that are held together by the I atoms. The β-$ThSi_2$-analogous part of the structure is highlighted. Si, La, and I atoms are represented by spheres of increasing size.

 © WILEY-VCH Verlag GmbH, D-69451 Weinheim, 1998 1433-7851/98/3704-0500 $ 17.50+.50/0

The occupation of the (o) prisms by Si atoms and connection of these atoms with Si_6 rings (see Figures 1b and 3) leads to hitherto unknown Si_{14} rings composed of the atoms Si(1) – Si(4). In contrast to the nearly planar Si_6 rings (deviation from planarity less than 5°), the Si_{14} rings are strongly bent at Si(3) (∢ Si(4)-Si(3)-Si(3) = 115°).[21]

The Si_6 rings exhibit distances $d_{Si-Si} = 239$ and 244 pm and angles ∢ Si(1)-Si(1)-Si(2) = 119 and ∢ Si(1)-Si(2)-Si(2) = 121°. In spite of the different bonding modes of the atoms in the Si_{14} rings, the range of Si – Si distances is narrow (239 – 243 pm). Only the distance (2b)Si(3) – (2b)Si(3) in the bending position of the ring is significantly larger (247 pm). Using $d_n = 235 - 0.6 \lg n$[22] one calcultates Pauling bond orders of $n = 0.85$, 0.72, and 0.64 for the different Si – Si distances instead of the expected $n = 1.0$. Bond lengthening up to 10 pm was observed for singly charged (2b)X^- atoms (X = As, P) in phosphides and arsenides,[23] and in the case of $Li_{14}Si_6$ and related Li/Mg silicides single bond Si – Si distances of $d_0 =$ 251 – 258 pm were assumed.[24, 25] However, a value within this range is too large for the halide silicides. Apparently, the distances depend strongly on the cations, the other anions, and the nature of the Zintl anion.

The slightly puckered La-Si-Si-La layers in $La_4I_3Si_4$ are arranged parallel to (001) and linked through I atoms. Part of the I atoms belong to only one slab (I(1), I(2)), and others connect adjacent slabs (I(3)).

A similar arrangement of corrugated layers is found in $La_5I_3Si_5$, whose structure is shown as projection along [010] in Figure 4. Here the slabs are again connected by van der Waals contacts (I(3)) and La-I-La bridges (I(1), I(2)). In the shown projection, an (o) prism is followed by eight (p) prisms. Fusion of (o) prisms through common rectangular faces leads to chains, and condensation of the eight prisms in (p) orientation through common triangular faces leads to ribbons parallel to (010). Chains and ribbons together form layers. Alternatively the structure of $La_5I_3Si_5$ can be described in terms of a combination of sections of the α- and β-$ThSi_2$ structural types. In the central part of Figure 4, the α-$ThSi_2$ part is hatched and the β-$ThSi_2$ part is dotted. A block of the α-type in which an (o) prism surrounded by (p) prisms on both sides is followed by a section of the β-type with (p) prisms in *cis*, *trans* arrangement but with only (2b)Si atoms, as in silicides of the CrB type.[26] This formal decomposition of the structure indicates that besides $La_5I_3Si_5$ further compounds with a general composition $(M_2Si_2I)_a$ $(M_3Si_3I_2)_b$ may exist, where the coefficients a and b denote the number of condensed blocks of the α- and β-$ThSi_2$ structural type, respectively. The variation of a and b would allow different Si_n ring sizes to be synthesized. In the present case $a = b = 1$, the ring size corresponds to Si_{22}, and the rings are condensed parallel to (010) into layers. The Si – Si distances in the rings vary between 237 and 249 pm, independent of the functionality of the Si atoms, similar to $La_4I_3Si_4$ and CeISi. The bond angles deviate only slightly from 120° (114 – 120°); hence, the Si atoms are sp^2 hybridized. The lone pair on (3b)Si^- has p character, and those on (2b)Si^{2-} have sp^2 and p character.[11]

The description of $La_4I_3Si_4$, CeISi and La_5I_3Si within the Zintl – Klemm formalism corresponds to $(La^{3+})_4(I^-)_3Si_4^{6-} \cdot 3e^-$, $Ce^{3+}I^-Si^- \cdot e^-$, and $(La^{3+})_5(I^-)_3[(3b)Si^-]_1[(2b)Si^{2-}]_4 \cdot 3e^-$, respectively. One or three electrons per formula unit occupy bands with M – M bonding character. In agreement with the observed metallic conductivity and the results of band structure calculations,[27] these electrons are delocalized. Halide silicides of the rare earth metals are a new class of compounds with structures based on layers of the Zintl polyanions $Si^{1-}_{6/6}$ (Si_6), $Si^{2-}_{6/3}Si^{8-}_{8/2}$ (Si_{14}), and $Si^{2-}_{6/3}Si^{16-}_{16/2}$ (Si_{22}).

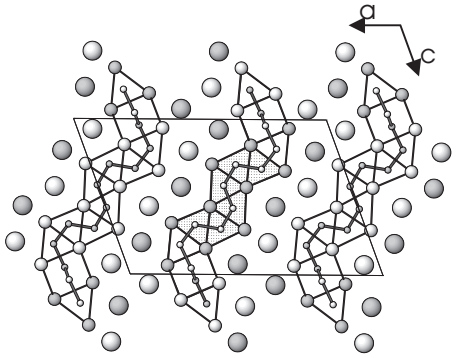


Figure 4. Projection of the structure of $La_5I_3Si_5$ along [010]. The lightly corrugated layers, made up of the units shown in Figure 1a, contain trigonal prisms around the Si atoms in the (p) and (o) orientation. The middle portion of the figure shows the partial structures that are analogous to α-$ThSi_2$ (hatched) and β-$ThSi_2$ (dotted). The I atoms connect the layers. Si, La, and I atoms are represented by spheres of increasing size.

Received: September 3, 1997 [Z10887IE]
German version: *Angew. Chem.* **1998**, *110*, 498 – 501
Keywords: iodine · lanthanides · silicon · solid-state structures

[1] A. Simon, H. Mattausch, G. J. Miller, W. Bauhofer, R. K. Kremer, *Handbook on the Physics and Chemistry of Rare Earth, Vol. 15* (Eds.: K. A. Gschneidner, Jr., L. Eyring), Elsevier, Amsterdam, 1991, p. 191.
[2] J. D. Corbett, *Modern Perspectives in Inorganic Crystal Chemistry* (Ed.: E. Parthé), Kluwer, Dordrecht, **1992**, p. 27.
[3] G. Meyer, *Chem. Rev.* **1988**, *88*, 93.
[4] H. Mattausch, A. Simon, *Angew. Chem.* **1995**, *107*, 1764; *Angew. Chem. Int. Ed. Engl.* **1995**, *34*, 1633.
[5] H. Mattausch, A. Simon, C. Felser, R. Dronskowski, *Angew. Chem.* **1996**, *108*, 1805; *Angew. Chem. Int. Ed. Engl.* **1996**, *35*, 1685.
[6] H. Mattausch, A. Simon, *J. Phys. Chem.* **1997**, *101*, 9951.
[7] A. Simon, E. Warkentin, *Z. Anorg. Allg. Chem.* **1983**, *497*, 79.
[8] D. Nagaki, A. Simon, H. Borrmann, *J. Less-Common Met.* **1989**, *156*, 193.
[9] D. A. Nagaki, A. Simon, *Acta Crystallogr. Sect. C* **1990**, *C46*, 1197.
[10] G. Bauer, H. Haag, *Z. Anorg. Allg. Chem.* **1952**, *267*, 198.
[11] A. Currao, J. Curda, R. Nesper, *Z. Anorg. Allg. Chem.* **1996**, *622*, 85.
[12] Tantalum capsules were filled with approximately 2 g of starting materials, sealed under 1 atm of Ar by arc welding, and heated in quartz glass ampoules for 18 d at 1270 K (LaISi; 90%), 6 d at 1270 K (CeISi; 80%), 3 d at 1220 K (PrISi; 60%), 30 d at 1270 K ($La_4I_3Si_4$; 50%), and 30 d at 1370 K ($La_5I_3Si_5$; 50%). The ampoules were then quenched to room temperature. The treatment of the rare earth metals and their triiodides are described in ref. [13]; Si (5N, Aldrich).
[13] H. Mattausch, H. Borrmann, R. Eger, R. K. Kremer, A. Simon, *Z. Anorg. Allg. Chem.* **1994**, *620*, 1889.
[14] L. J. van der Pauw, *Philips Res. Rep.* **1958**, *13*, 1.
[15] Full-matrix least-squares refinement on F^2.[16] Single-crystal data: a) four-circle diffractometer (CAD4, Enraf-Nonius); $Ag_{K\alpha}$ radiation; empirical absorption correction (ψ scan). CeISi: $P\bar{3}m1$; $a = 417.0(1)$, $c = 1167.6(5)$ pm. Ce: 0, 0, 0.1724(1); I: 1/3, 2/3, 0.3556(1); Si: 2/3, 1/3,

0.0057(3); (twin: $\bar{1}00$, $0\bar{1}0$, 001). $R_1 = 0.029$, $wR_2 = 0.071$ (all 325 independent reflections). Isotypic LaISi: $a = 421.9(2)$, $c = 1179.4(1)$ pm, PrISi: $a = 416.4(1)$, $c = 1161.9(1)$ pm. $La_5I_3Si_5$: $C2/m$; $a = 2401.9(1)$, $b = 425.34(2)$, $c = 1571.61(7)$ pm, $\beta = 119.38(1)^\circ$. La(1): 0.0856(1), 0, 0.5629(1); La(2): 0.3390(1), 0, 0.9422(1); La(3): 0.2622(1), 0, 0.6693(1); La(4): 0.1638(1), 0, 0.8339(1); La(5): 0.4826(1), 1/2, 0.7100(1); I(1): 0.3274(1), 1/2, 0.5627(1); I(2): 0.4091(1), 0, 0.7956(1); I(3): 0.0597(1), 1/2, 0.9334(1); Si(1): 0.0759(1), 1/2, 0.7076(1); Si(2): 0.2499(1), 1/2, 0.9599(1); Si(3): 0.9912(1), 1/2, 0.5731(1); Si(4): 0.2601(1), 1/2, 0.8098(1); Si(5): 0.1719(1), 1/2, 0.6806(1); $R_1 = 0.024$, $wR_2 = 0.051$ (all 3000 independent reflections). b) Image plate (IPDS, Stoe); $Mo_{K\alpha}$ radiation. $La_4I_3Si_4$: $C2/m$; $a = 2436.0(5)$, $b = 424.0(1)$, $c = 1257.0(3)$ pm, $\beta = 97.59(3)^\circ$. La(1): 0.5036(1), 0, 0.1653(1); La(2): 0.5747(1), 1/2, 0.4456(1); La(3): 0.3613(1), 0, 0.2918(1); La(4): 0.3548(1), 0, 0.9760(1); I(1): 0.6328(1), 0, 0.2889(1); I(2): 0.2014(1), 0, 0.5729(1); I(3): 0.2435(1), 0, 0.1311(1); Si(1): 0.5230(3), 0, 0.5902(2); Si(2): 0.5428(3), 1/2, 0.6828(2); Si(3): 0.5510(3), 1/2, 0.0168(2); S(4): 0.5967(3), 1/2, 0.8600(2); $R_1 = 0.044$, $wR_2 = 0.081$ (all 1952 independent reflections). Further details on the crystal structure investigation may be obtained from the Fachinformationszentrum Karlsruhe, D-76344 Eggenstein-Leopoldshafen, Germany (fax: (+49) 7247-808-666 (Frau S. Höhler-Schlimm); e-mail: crysdata@fiz-karlsruhe.de), on quoting the depository numbers CSD-407246 (CeISi), CSD-407247 ($La_4I_3Si_4$), and CSD-407248 ($La_5I_3Si_5$).

[16] G. M. Sheldrick, SHELXTL-PLUS, Göttingen, **1992** and SHELX-93, Göttingen, **1993**.

[17] Pure (p) stacking occurs in AlB_2 (also β-$ThSi_2$), and (p), (o) stacking in α-$ThSi_2$.

[18] R. Nesper, H. G. von Schnering, *Tschermaks Mineral. Petrogr. Mitt.* **1983**, *32*, 195.

[19] A. Brown, *Acta Crystallogr.* **1961**, *14*, 860.

[20] U. Schwanitz-Schüller, A. Simon, *Z. Naturforsch. B* **1985**, *40b*, 710.

[21] Taking into account different bonding functionalities of the Si atoms, the $^{2}_{\infty}Si_4^{6-}$ polyanion results from $(3b)Si(1)^{1-}_{6/3}(3b)Si(2)^{1-}_{6/3}$-$(2b)Si(3)^{2-}_{4/2}(2b)Si(4)\ ^{2-}_{4/2}$.

[22] L. Pauling, *Die Natur der chemischen Bindung*, Verlag Chemie, Weinheim, **1973**.

[23] H. G. von Schnering, *Homoatomic Rings, Chains and Macromolecules of Main-Group Elements,* Elsevier, New York, **1977**, p. 317.

[24] H. G. von Schnering, *Rheinisch Westfälische Akademie der Wissenschaften*, Westdeutscher Verlag, Opladen, **1984**, *N325*, 7.

[25] R. Nesper, *Habilitationsschrift,* Universität Stuttgart, **1988**.

[26] O. Schob, E. Parthé, *Acta Crystallogr.* **1965**, *19*, 214.

[27] QCPE program EHMACC by M.-H. Whangbo, M. Evains, T. Hughbanks, M. Kertesz, S. Wijeyesekera, C. Wilker, C. Zhenh, and R. Hoffmann; parameterization according to S. Alvarez.[28]

[28] Calculated with a PC version of an extended Hückel program (J. Köhler, unpublished results, **1993**).

[29] E. Dowty, ATOMS for Windows, Version 3.1, Shape Software, Kingsport, TN, USA, **1995**, 37663.

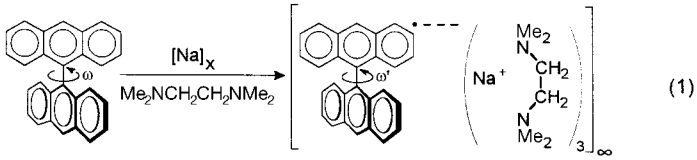
Tris(tetramethylethylenediamine-sodium)-9,9-bianthryl—The Salt of a π Hydrocarbon Radical Trianion with Three $Na^+ - C_\pi$ Contacts to One Molecular Half

Hans Bock,* Zdenek Havlas, Delia Hess, and Christian Näther

Dedicated to Professor Dieter Seebach on the occasion of his 60th birthday

Reductions of π hydrocarbons by sodium metal in aprotic solutions[1] of efficient cation-solvating ethers[2] facilitate the growth of single crystals (and thus the determination of the structures) of a wide variety of solvent-separated or solvent-shared contact-ion multiples containing radical ions, dianions, or even tetraanions.[1–3] Representative examples are the bare naphthalene radical anion that can be isolated from diglyme solution as a salt with an advantageously solvated sodium cation,[3a] the tetraphenylbutadiene dianion that crystallizes in stoichiometrically 1:1 solvent-separated and solvent-shared ion triples,[3b] or the rubrene tetraanion that has been structurally characterized as contact-ion quintuple with four THF-coordinated Na^+ countercations.[3c]

Still missing is a salt of a radical trianion. By reduction of 9,9′-bianthryl with sodium in a solution containing a mixture of tetramethylethylenediamine and benzene [Eq. (1)], the sodium salt of a π hydrocarbon radical trianion has been isolated as black blocks.[4a]



(1)

The structure determination of the radical trianion salt[4b] (Figure 1) reveals a surprise: In the solvent-shared contact ion quadruple, all three TMEDA-solvated sodium ions are η^6-coordinated to the same anthryl moiety of the 9,9′-bianthryl radical trianion (Figure 1B), whereas the perpendicular hydrocarbon residue forms only two η^1 and η^2 contacts to the centers Na1 and Na3 of an adjacent contact-ion aggregate in the *y* direction of the polymer string (Figure 1A, B). The shortest $Na^+ - C$ η^6 contacts are found for Na2 (average 269 pm); the ones for Na3 and Na1 of 285 and 289 pm are longer because of the additional relatively short contacts of

[*] Prof. Dr. H. Bock, Dipl.-Chem. D. Hess, Dr. C. Näther
Institut für Anorganische Chemie der Universität
Marie-Curie-Strasse 11, D-60439 Frankfurt am Main (Germany)
Fax: (+49) 69-7982-9188

Dr. Z. Havlas
Institute for Organic Chemistry and Biochemistry of the
Czech Academy of Sciences
Flemingova Nam 2, CS-11610 Prague 6 (Czech Republic)

[**] Interactions in Molecular Crystals, Part 140. The project was generously supported by the Hoechst AG, the Deutsche Forschungsgemeinschaft, the State of Hesse, and the Fonds der Chemischen Industrie. Part 139: H. Bock, M. Sievert, C. L. Bogdan, B. O. Kolbesen, A. Wittershagen, *Chem. Commun.* **1997**, submitted.

 © WILEY-VCH Verlag GmbH, D-69451 Weinheim, 1998 1433-7851/98/3704-0502 $ 17.50+.50/0

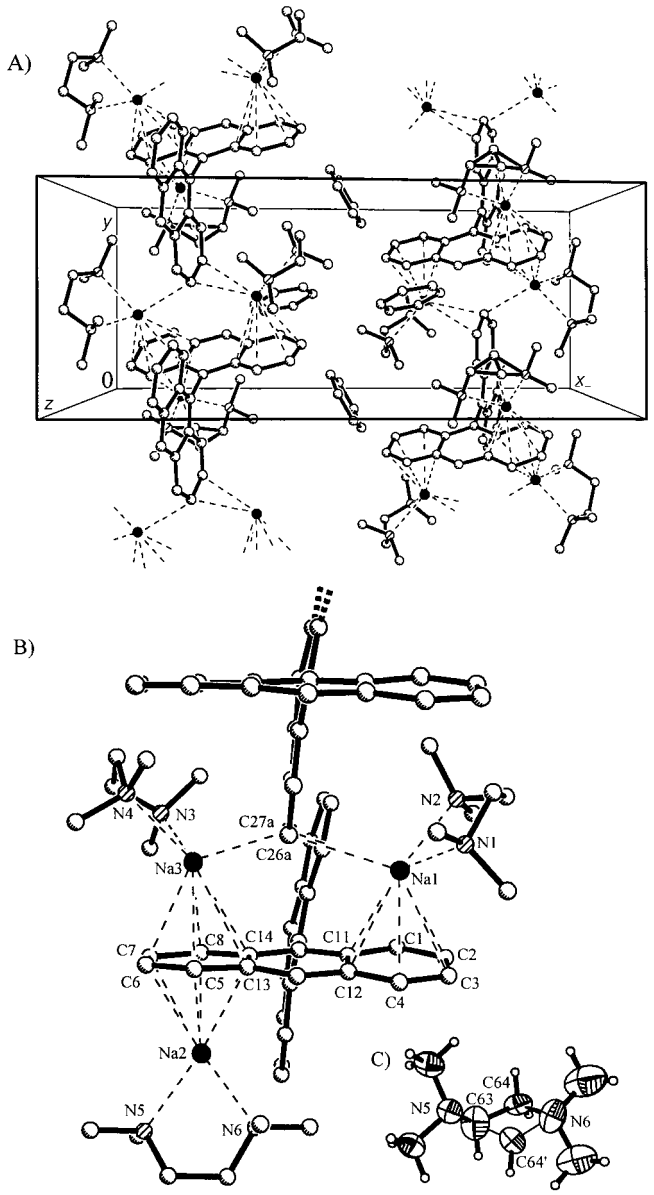


Figure 1. Single-crystal X-ray structure of tris(tetramethylethylenediamine-sodium)-9,9-bianthryl) · 1.5 benzene at 130 K. A) Unit cell (monoclinic, $P2_1/c$, $Z = 4$) along the crystallographic b axis, B) coordination sphere of the Na ions, and C) molecular structure of the disordered[4b] TMEDA ligand (thermal ellipsoids at 50% probability). Selected bond lengths [pm] and angles [°]: Na1 – C1/C12 272 – 302, Na3 – C5/C14 266 – 303, Na1 – C26a 283, Na1 – C27a 311, Na3 – C27a 274, Na2 – C5/C14 265 – 273, Na – N 240 – 251; ω(CC-CC) = 77.

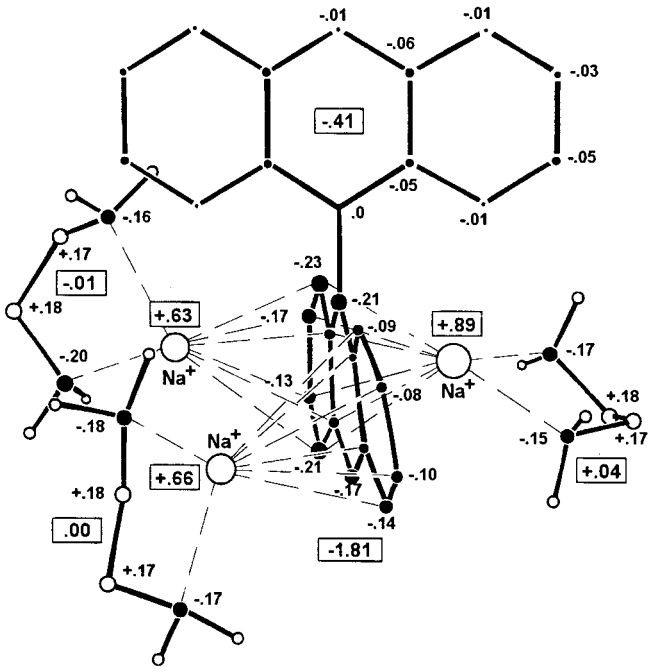


Figure 2. Charge distribution in the title compound determined by density functional calculations.[5] For reasons of space the zero before the comma has been omitted.

274 pm (Na3) and 283 pm (Na1) to the center C26a of the adjacent radical trianion in the polymer chain (Figure 1B).

The coordination of all three Na^+ ions to only one anthryl residue suggests a predominant delocalization of the negative charge within this half of the hydrocarbon, an assumption that is supported by density functional calculations with natural population analysis[5] based on the structural data (Figure 2).[4b] The largely contact-free bianthryl half holds only $\Sigma q^{\mu}_{DFT} = -0.41$ negative charge, in contrast to the threefold Na^+ complexed half with $\Sigma q^{\mu}_{DFT} = -1.91$. Values between $q^{\mu}_{DFT} = +0.63$ and $+0.66$ are predicted for the Na^+ centers at the six-membered ring substituted on both sides and $+0.89$ for that at the singly complexed one. Their reduced positive charges suggest small covalent bonding contributions to both the trianion and the TMEDA ligands. For the N centers of the amino groups coordinated within five-membered chelate rings to the Na^+ cations, charges q^{μ}_{DFT} between -0.15 and -0.20 result;[5] however, due to ($N^{\delta-} \leftarrow C^{\delta+}$) polarization the ethylenediamine ligands remain overall nearly neutral. The calculated polarity of $q^{\mu}_{DFT}(Na^+) \approx 0.7$ and $\Sigma q^{\mu}_{DFT}(2\,N) \approx -0.3$ illustrates the efficient TMEDA solvation of the Na^+ ions, essential for the formation of the radical trianion.[6]

Which consecutive steps within the network of equilibria[1] during the redox reaction (1) could lead to the formation of the contact ion quadruple with the unexpected threefold Na^+ coordination to only one bianthryl half (Figure 1)? On sodium metal reduction in dimethoxyethane (DME), an ether analogous to TMEDA, the solvent-separated salt of bianthryl radical monoanion, $[Na^+(dme)_3][9,9'\text{bianthryl}]$, crystallizes.[6] Cyclic voltammetry measurements[7] prove that bianthryl, twisted by about 80° due to H/H repulsion between the molecular halves,[6] represents an "electron storage" π system, which can be oxidized to its tetracation and reduced to its tetraanion.[7] According to ESR measurements, the twisted product of the two-electron reduction is a triplet diradical dianion.[7a] If the approach of a countercation is calculated on a MNDO/CI hypersurface,[8] configuration interaction predicts a biradical state with 10% admixture of a localized configuration corresponding to a dianion singlet state. The coordination of a second Na^+(TMEDA) lowers the negative charge in the contact-ion bianthryl residue into which the third electron must also be inserted.[8] Then the formation of a contact ion quadruple should result in a radical trianion doublet state. Even though other effects such as the stabiliza-

 © WILEY-VCH Verlag GmbH, D-69451 Weinheim, 1998 1433-7851/98/3704-0503 $ 17.50+.50/0

tion by the dimer contact Na2-C26a-Na3 (Figure 1B) are neglected, the extensive approximative calculations suggest the following course for as the reduction of bianthryl in a TMEDA/benzene solution at a sodium metal mirror: Via the radical anion an ESR-spectroscopically proven diradical dianion should be formed, which on further electron insertion adds all three $[Na(tmeda)]^+$ ligands to only one half of the bianthryl moiety (Figure 1B). According to the calculations, each coordination step should increase the total negative charge, which is essential for the contact ion formation.[1]

Attempts to prepare the sodium salt of a 9,9′-bianthryl tetraanion[9] under changed reduction conditions[3c] likewise yielded black crystals of the $[Na(pmdta)]^+$ salt of 10,10′-dihydro-9,9′-bianthryl dianion,[9] in which the two Na^+ counterions are coordinated between the mutually perpendicular molecular halves analogous to the tetraphenylethylene dianion.[1] This result is in accord with the cyclic voltammetrically irreversible third and fourth reduction potentials in solution,[7] but stimulates a search for Na^+ solvate ligands that stabilize the counterions better than the advantageous ether→amine exchange in the radical trianion salt reported here.

Received: July 15, 1997
Revised version: October 22, 1997 [Z10689IE]
German version: *Angew. Chem.* **1998**, *110*, 518 – 520

Keywords: arenes · density functional calculations · radical ions · reductions · tetraanions

[1] H. Bock, K. Ruppert, C. Näther, Z . Havlas, H.-F. Herrmann, C. Arad, I. Göbel, A. John, J. Meuret, S. Nick, A. Rauschenbach, W. Seitz, T. Vaupel, B. Solouki, *Angew. Chem.* **1992**, *104*, 595; *Angew. Chem. Int. Ed. Engl*. **1992**, *31*, 550.

[2] H. Bock, C. Näther, Z. Havlas, A. John, C. Arad, *Angew. Chem*. **1994**, *106*, 931; *Angew. Chem. Int. Ed. Engl*. **1994**, *33*, 875.

[3] a) H. Bock, C. Arad, C. Näther, Z. Havlas, *J. Chem. Soc. Chem. Commun*. **1995**, 2393. b) H. Bock, C. Näther, K. Ruppert, Z. Havlas, *J. Am. Chem. Soc*. **1992**, *114*, 6907. c) H. Bock, K. Gharagozloo-Hubmann, C. Näther, N. Nagel, Z. Havlas, *Angew. Chem*. **1996**, *108*, 720; *Angew. Chem. Int. Ed. Engl*. **1996**, *35*, 631.

[4] a) Preparation and single crystal growth: Sodium (100 mg, 4.35 mmol) was weighed into a Schlenck trap, dried by heating at 10^{-4} mbar, and a metal mirror was generated by distillation at 10^{-4} mbar. Under argon 9,9′-bianthryl (100 mg, 0.25 mmol) and dry TMEDA and benzene (4 mL each) were added. After 3 days the olive-green solution was covered by *n*-hexane (10 mL), and 4 days later black, air- and moisture-sensitive blocks crystallized. b) Crystal structure determination: Black blocks, $C_{28}H_{18}Na_3 \cdot 3\,C_6H_{16}N_2 \cdot 1.5\,C_6H_6$ ($M_r = 889.18$), $a = 2283.9(2)$, $b = 891.1(1)$pm, $c = 2542.7(2)$ pm, $\beta = 95.701\ (5)^\circ$, $V = 5149.3 \times 10^6$ pm^3 ($T = 150$ K), $\rho_{calcd} = 1.147$ g cm^{-3}, monoclinic, $P2_1/c$ (No. 14), $Z = 4$, Siemens P4 four-cycle diffractometer, $Mo_{K\alpha}$ radiation, $\mu = 0.09$ mm^{-1}, 8599 measured reflections within $3^\circ \le 2\Theta \le 48^\circ$, of which 7793 are independent and 7787 used for refinement ($R_{int} = 0.0294$). Structure solution by direct methods and difference Fourier technique (SHELXS-86), structure refinement against F^2 (SHELXL-93), 586 parameters, $w = 1/[\sigma^2(F_o^2) + (0.0450\,P)^2 + 3.20\,P]$, R for 5543 reflections $F_o > 4\sigma(F_o) = 0.0466$, R(all data) $= 0.1226$, GOOF $= 1.056$, residual electron density $0.28/-0.21$ e Å^{-3}. All C, N, O and Na are refined anisotropically, and the hydrogens (in geometrically ideal positions) with individual isotropic displacement parameters [$U(H)_{iso} = 1.2 \times U_{eq}(C_{arom.}/C_{methylene}) = 1.5 \times U_{eq}(C_{methyl})$] using the riding model. The asymmetric unit contains two independent benzene molecules at general positions as well as arranged around a crystallographic inversion center. The carbon center of one TMEDA ligand, disordered in two positions, has been refined with a split model (Figure 1C). Further details of the crystal structure determination may be obtained from the Fachinformationszentrum Karlsruhe, D-76344 Eggenstein-Leopoldshafen, Germany, (fax: (+49) 7247-808-666 (Frau S. Höhler-Schlimm); E-mail: crysdata§fiz-karlsruhe.de) on quoting the depository number CSD-380 145.

[5] The density functional calculations of DFT-B3LYP quality (C. Lee, W. Yang, R. G. Paar, *Phys. Rev. B* **1993**, *37*, 785) and with basis sets 6-31G** (H. Ditchfield, W. J. Hehre, J. A. Pople, *J. Chem. Phys.* **1971**, *42*, 724 and **1972**, *56*, 2257) have been performed with the program Gaussian 94 at the SNI SC900/4 computer of the Universität Giessen. Starting point are the structural data,[4b] but the 417 electrons of the contact-ion quadruple have been reduced by the exchange $CH_3 \rightarrow H$ in the TMEDA ligands to 321, yielding a total energy of -2136.3136907 a.u. The charge distribution of the polar complex has been approximated applying natural population analysis (A. E. Reed, R. B. Weinhold, F. Weinhold, *J. Chem. Phys.* **1985**, *107*, 6788). The spin populations calculated are: for the threefold coordinated bianthryl moiety only 0.043; however, for the largely uncomplexed bianthryl 0.354 and for the three $[Na(tmeda)]^+$ counterions 0.364 (Na1), 0.50 (Na2) and 0.274 (Na3).

[6] H. Bock, A. John, C. Näther, Z. Havlas, *Z. Naturforsch*. *B* **1994**, *49*, 1339.

[7] a) K. Müllen, M. Baumgarten, K. Müller, A. Böhnen, *Angew. Chem*. **1992**, *104*, 482; *Angew. Chem. Int. Ed. Engl*. **1992**, *31*, 448; b) J. Mortensen, J. Heinze, *J. Electroanal. Chem*. **1984**, *175*, 333 and M. Dietrich, J. Mortensen, J. Heinze, *Angew. Chem*. **1985**, *97*, 502; *Angew. Chem. Int. Ed. Engl*. **1985**, *24*, 508; c) cf. also M. Hoshino, K. Kimura, M. Imamura, *Chem. Phys. Lett*. **1973**, *20*, 294; d) W. Huber, K. Müllen, *J. Chem. Soc. Chem. Comm*. **1980**, 698.

[8] The presumed reduction pathway is approximated by MNDO/CI-calculations (cf. Z. Havlas, S. Nick, H. Bock, *Int. J. Quantum Chem.* **1992**, *44*, 449): In the dianion biradical ($\Delta H_f^{MNDO/CI} = 595$ kJ mol^{-1}) each anthracene moiety should be occupied by one electron, and MNDO runs with configuration interaction (6,6)- or (2,2)-CI yield negligibly small singlet/triplet energy splittings ($\Delta E_{S/T} < 0.000$). On approach of the first $[Na(tmeda)]^+$ under geometry optimization the enthalpy of formation is lowered to $\Delta H_f^{MNDO/CI} = 144$ kJ mol^{-1}, and the charge in the anthracene ring of the contact ion pairs of -0.80 is -0.16 smaller than that in the uncomplexed one. For the contact of the second $[Na(tmeda)]^+$, -196 kJ mol^{-1} at the same six-membered anthracene ring and -181 kJ mol^{-1} at the more distant one are calculated. The two biradical state contributions (27 % and 26 %) are comparable as are the singlet/triplet splittings (1.6 and 1.9 kJ mol^{-1}). The charges in the doubly complexed anthracene half are predicted to be -0.50 in contrast to -0.82 in the uncomplexed one. Dimers with additional contacts (Na3-C26a-Na1) have not been calculated.

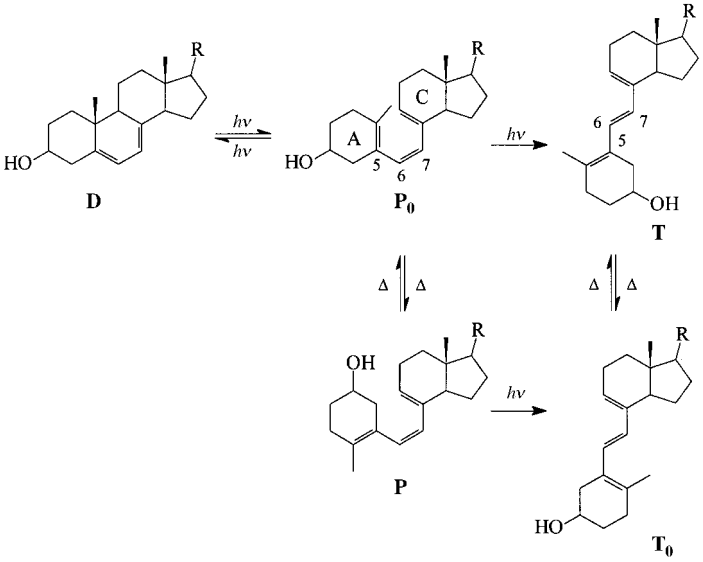
[9] H. Bock, Z. Havlas, D. Hess, C. Näther, unpublished; cf. D. Hess, Diplomarbeit, Universität Frankfurt, **1996**.

 © WILEY-VCH Verlag GmbH, D-69451 Weinheim, 1998 1433-7851/98/3704-0504 $ 17.50+.50/0

Low-Temperature Photochemistry of Previtamin D: A Hula-Twist Isomerization of a Triene**

Astrid M. Müller, Stefan Lochbrunner, Wolfram E. Schmid, and Werner Fuß*

For the investigation of the stereochemistry of chemical reactions it is advantageous if the conformers of the compounds employed can be distinguished based on their substitution patterns. Previtamin D, a triene in the steroid series, offers this possibility. Thermal interconversion of the conformers **P** and $\mathbf{P_0}$ can be suppressed in a cold matrix. Already in 1983 Havinga and co-workers irradiated previtamin D in a matrix at 92 K and found that in the *cis–trans* isomerization an unstable conformer ($\mathbf{T_0}$) of tachysterol forms initially and converts to the stable form **T** only when warmed up (Scheme 1).[1] The two conformers, whose UV spectra are clearly different, were assigned based on their circular dichroism. Havinga et al.[1] assumed that $\mathbf{P_0}$ is the thermodynamically more stable form of previtamin D, that it dominates at low temperature, and hence that $\mathbf{T_0}$ forms from $\mathbf{P_0}$.



Scheme 1. Photochemical and thermal reactions in the previtamin D system. **D**: 7-dehydrocholesterol; $\mathbf{P_0}$ and **P**: s-*cis,Z,*s-*cis* and s-*trans,Z,*s-*cis* conformers of previtamin D, respectively; **T** and $\mathbf{T_0}$: s-*trans,E,*s-*cis* and s-*cis,E,*s-*cis* conformers of tachysterol, respectively. (Actually it is a group of conformers for each, because the molecules are not planar and can have different helical sense, and because in particular the A ring is flexible.[4]) The subscript 0 in $\mathbf{P_0}$ and $\mathbf{T_0}$ denotes the thermally less stable conformer. R = $CH(CH_3)CH_2CH_2CH_2CH(CH_3)_2$.

We have established by direct photochemical ring opening of 7-dehydrocholesterol **D** in the cold matrix that the starting material has a ringlike geometry (Scheme 1). We irradiated a solution of **D** in the solvent mixture "EPA" (diethyl ether/2-methylbutane/ethanol 5/5/2) at 90 K with UV pulses (70 μJ, 10 ns at 291, 293, 295, and 297.5 nm) from a frequency-doubled rhodamine 6G laser. The reaction was carried out in a 1-cm cell, which was cooled by liquid nitrogen and surrounded by a vacuum jacket, and was monitored in a UV spectrometer. Only the conversion rates of **D** and $\mathbf{P_0}$ were different at the different wavelengths used, in accord with their respective absorption cross sections. A spectrum of $\mathbf{P_0}$ was reported previously.[2]

After generation of $\mathbf{P_0}$ further irradiation directly yields the stable conformer **T** of tachysterol, which was identified by its structured UV spectrum[1] (Figure 1). Kinetic measurements

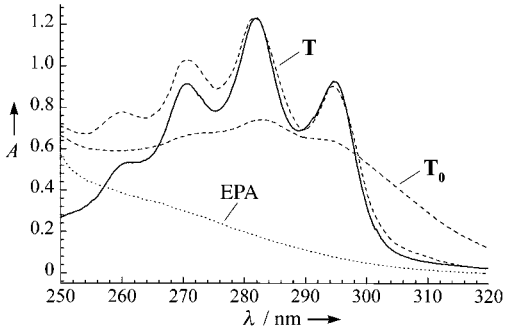


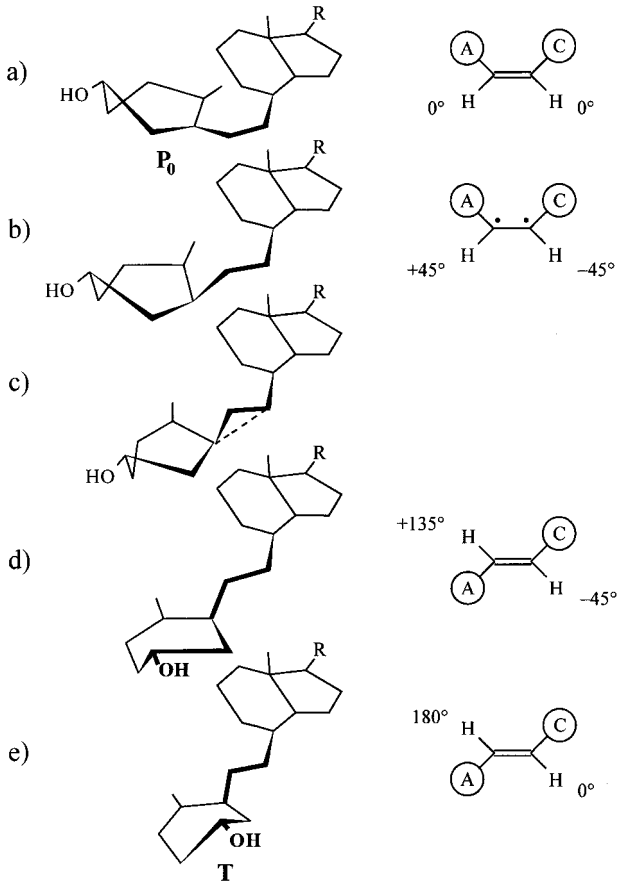
Figure 1. UV absorption of the two tachysterol conformers **T** and $\mathbf{T_0}$ according to ref.[1] (broken line; solvent absorption supposedly not subtracted, 92 K) and the spectrum of the final product of the irradiation at 90 K (solid line; absorption of EPA subtracted). *A*: absorbance; λ: wavelength.

on the previtamin D system indicate that thermal reactions are frozen out in the cold matrix.[3] Not the activation energy (16 kJ mol^{-1}) but rather the solvent viscosity η is mainly responsible for suppressing the conversion $\mathbf{P_0} \rightarrow \mathbf{P}$, whose rate is $\propto \eta^{-1}$.[3] The fact that we obtained a different product than Havinga et al.[1] implies that the starting compounds were different, too. Since the reaction we observed corresponds to $\mathbf{P_0} \rightarrow \mathbf{T}$, the process they observed[1] must be $\mathbf{P} \rightarrow \mathbf{T_0}$ (see Scheme 1). Furthermore it can be concluded that **P** is more stable than $\mathbf{P_0}$; this is consistent with the observed isomerization $\mathbf{P_0} \rightarrow \mathbf{P}$[3] and with some results[4, 5] of the force-field calculations.[4–6] Previous opinions about the relative stabilities of **P** and $\mathbf{P_0}$ were not uniform.[7] It should also be pointed out that tachysterol can form from both conformers of previtamin D, in contrast to the widespread opinion[4, 8] that $\mathbf{P_0}$ is only capable of ring closure.

It is evident from the positions of the methyl and hydroxyl groups that in the two *cis–trans* isomerizations the A ring reorients by 120° *without leaving the plane* (Scheme 1). This is reminiscent of the *cis–trans* isomerizations of Schiff bases by inversion at nitrogen. Inversion at carbon is, however, not possible. With the help of ball-and-stick models one can find another way (Scheme 2): Twisting C^6H and C^7H by about +45° and −45°, respectively, out of the plane only induces minor changes in the positions of the rings (Scheme 2b). When C^6H is turned a further 90° around the axis indicated by the broken line (Scheme 2c), the A ring reorients by 120° within the plane. Finally both CH groups can turn back into

[*] Dr. W. Fuß, A. M. Müller, S. Lochbrunner, Dr. W. E. Schmid
Max-Planck-Institut für Quantenoptik
D-85748 Garching (Germany)
Fax: (+49) 89-32905-200
E-mail: w.fuss@mpq.mpg.de

[**] We thank D. Proch for lending us his laser, M. Garavelli and M. Olivucci for stimulating discussions, R. S. H. Liu for valuable information, and V. E. Bondybey for kind support.



Scheme 2. Proposed geometrical pathway for the *cis–trans* isomerization. Only the C^6H group rotates substantially out of the plane, whereas the remaining parts of the molecule stay more or less in the plane while they reorient. The angles 0° and 180° only denote the planar reference geometry; the actual molecules in a) and e) are twisted for steric reasons.[4] The remaining angles are also only approximate.

the plane. A characteristic feature of this process is that only C^6H rotates substantially out of the plane. An equivalent description invokes the simultaneous rotation of the double bond and an adjacent single bond.

Our proposed mode of motion requires substantially less volume than the conventional concept, in which the terminal ligands move along a cone with an aperture of 120°. Hence this mode is possible even in a matrix. It was also postulated for rhodopsin[9, 10] and called a hula-twist isomerization, since only the central part of the molecule rotates. This mode of isomerization was proposed to rationalize how in the restricted opsin matrix the stiff polyene chain of the retinal chromophore can isomerize around a central double bond.[9, 10] The example presented here is the first experimental demonstration of the hula-twist isomerization.

Since the reaction $\mathbf{P_0} \rightarrow \mathbf{T}$ proceeds in a cold matrix, the hula-twist isomerization apparently has no appreciable activation energy. (The formation of tachysterol at low temperature is irreversible;[9] in other words, the back reaction seems to have an activation energy.) Hence the isomerization can also occur at higher temperatures and outside of a matrix. We assume that it probably corresponds to the normal path of *cis–trans* isomerization based on the following consideration.

Ultrafast photoreactions, including the *cis–trans* isomerization of hexatriene[11–13] and other polyenes, proceed along a continuous path from the upper (S_1) to the lower (S_0) potential energy surface. The transition from S_1 to S_0 occurs at a cone-shaped intersection of the two surfaces.[14–16] The molecular geometry at the conical intersection can be calculated by quantum chemistry. Remarkably, such calculations predict that this point on the potential energy surface (of 1,3,5-hexatriene) corresponds to a triangular substructure of the molecule similar to that in Scheme 2c, in which all the ligands are outside of the plane of the triangle and a bonding interaction exists between C^5 and C^7 (broken line in Scheme 2c).[17, 18] This prediction is shown in Figure 2 for (*Z*)-hexatriene. Thus quantum chemistry also

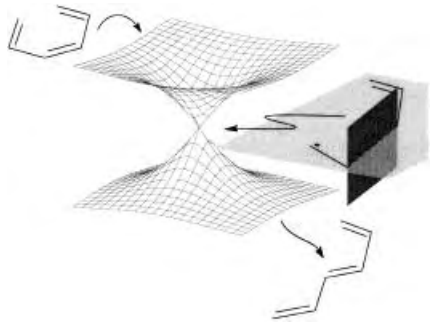


Figure 2. Transition from the excited to the ground state potential energy surface and associated geometries of (*Z*)-hexatriene.[17, 18]

supports the hula-twist mechanism and links it to the conical intersection and thus to electronic rather than steric effects. Since this three-center bond was found as an intermediate substructure for all polyenes calculated (butadiene to octatetraene),[18] it must be assumed that this pathway is standard for the *cis–trans* isomerization of nonpolar polyenes. Furthermore it is worth noting that the observed stereochemistry is the first experimental confirmation of the geometry predicted for a conical intersection.

A previous alternative proposal for a volume-saving isomerization ("bicycle-pedal mechanism") postulated the simultaneaous twist of two *double* bonds.[19] Our experiments do not allow a conclusion about this pathway since the terminal double bonds in previtamin D are sterically fixed. However, semiempirical calculations predict that the barrier for this path is higher in the excited state than in the ground state.[20] One argument against the hula-twist mechanism was that the expected conformer of bathorhodopsin, an intermediate of the rhodopsin isomerization, was not found by resonance Raman spectroscopy.[21] However, according to a previous proposal[22] the initial product is photorhodopsin which forms within about 100 fs,[23] whereas bathorhodopsin appears only within picoseconds.[24, 25] This period of time is long enough for single-bond isomerization in the ground state; therefore, a modified bicycle-pedal rotation of two single bonds can minimize the spatial demands according to ref. [10c]. Recent quantum chemical calculations indicate that the pentadieniminium cation has a conical S_1/S_0 intersection with a structure in which only the central double bond is

 © WILEY-VCH Verlag GmbH, D-69451 Weinheim, 1998 1433-7851/98/3704-0506 $ 17.50+.50/0

twisted by 90°.[27] This ion can serve as a model for the protonated Schiff base of retinal present in rhodopsin. In contrast to nonpolar polyenes, in highly polar double-bond systems no electronic reason exists for a hula-twist pathway, although steric reasons for it persist.

Received: August 14, 1997 [Z10814IE]
German version: *Angew. Chem.* **1998**. *110*, 520 – 522

Keywords: alkenes · conical intersections · isomerizations · photochemistry · reaction mechanisms

[1] a) P. A. Maessen, H. J. C. Jacobs, J. Cornelisse, E. Havinga, *Angew. Chem.* **1983**, *95*, 752; *Angew. Chem. Int. Ed. Engl.* **1983**, *22*, 718 – 719; *Angew. Chem. Suppl.* **1983**, 994 – 1004; b) H. J. C. Jacobs, *Pure Appl. Chem.* **1995**, *67*, 63 – 70.
[2] W. Fuss, S. Lochbrunner, *J. Photochem. Photobiol. A* **1997**, *105*, 159 – 164.
[3] W. Fuss, T. Höfer, P. Hering, K. L. Kompa, S. Lochbrunner, T. Schikarski, W. E. Schmid, *J. Phys. Chem.* **1996**, *100*, 921 – 927.
[4] W. G. Dauben, D. J. H. Funhoff, *J. Org. Chem.* **1988**, *53*, 5070 – 5075.
[5] O. G. Dmitrenko, personal communication, 1997.
[6] a) O. Dmitrenko, W. Reischl, *Monatsh. Chem.* **1996**, *127*, 445 – 453; b) O. G. Dmitrenko, I. P. Terenetskaya, W. Reischl, *J. Photochem. Photobiol. A* **1997**, *104*, 113 – 117.
[7] Review: P. A. Maessen, PhD thesis, University of Leiden, The Netherlands, **1983**.
[8] See, for example, O. G. Dmitrenko, A. A. Serikov, I. P. Terenetskaya, *J. Photochem. Photobiol. A* **1996**, *96*, 7 – 12.
[9] a) R. S. H. Liu, D. T. Browne, *Acc. Chem. Res.* **1986**, *19*, 42 – 48; b) R. S. H. Liu, A. E. Asato, *Proc. Natl. Acad. Sci. USA* **1985**, *82*, 259 – 263.
[10] For bacteriorhodopsin: a) K. Schulten, P. Tavan, *Nature* **1978**, *272*, 85 – 86; b) G. Orlandi, K. Schulten, *Chem. Phys. Lett.* **1979**, *64*, 370 – 374; c) R. S. H. Liu, D. Mead, A. E. Asato, *J. Am. Chem. Soc.* **1985**, *107*, 6609 – 6614.
[11] W. Fuss, T. Schikarski, W. E. Schmid, S. Trushin, K. L. Kompa, P. Hering, *J. Chem. Phys.* **1997**, *106*, 9386 – 9389.
[12] a) S. Lochbrunner, W. Fuss, K. L. Kompa, W. E. Schmid, *Chem. Phys. Lett.* **1997**, *274*, 491 – 498; b) S. H. Pullen, N. A. Anderson, L. A. Walker II, R. J. Sension, *J. Chem. Phys.* **1997**, *107*, 4985 – 4993.
[13] K. Ohta, Y. Naitoh, K. Saitow, K. Tominaga, N. Hirota, K. Yoshihara, *Chem. Phys. Lett.* **1996**, *256*, 629 – 634.
[14] M. Klessinger, J. Michl, *Excited States and Photochemistry of Organic Molecules*, VCH, New York, **1995**.
[15] M. Klessinger, *Angew. Chem.* **1995**, *107*, 597 – 599; *Angew. Chem. Int. Ed. Engl.* **1995**, *34*, 549 – 551.
[16] F. Bernardi, M. Olivucci, M. A. Robb, *Chem. Soc. Rev.* **1996**, *25*, 321 – 328.
[17] M. Olivucci, F. Bernardi, P. Celani, I. Ragazos, M. A. Robb, *J. Am. Chem. Soc.* **1994**, *116*, 1077 – 1085.
[18] P. Celani, M. Garavelli, S. Ottani, F. Bernardi, M. A. Robb, M. Olivucci, *J. Am. Chem. Soc.* **1995**, *117*, 11584 – 11585.
[19] A. Warshel, *Nature* **1976**, *260*, 679 – 683.
[20] a) S. Seltzer, *J. Am. Chem. Soc.* **1987**, *109*, 1627 – 1631; b) G. J. M. Dormans, G. C. Groenenboom, W. C. A. van Dorst, H. M. Buck, *ibid.* **1988**, *110*, 1406 – 1415.
[21] I. Palings, J. A. Pardoen, E. van den Berg, C. Winkel, J. Lugtenburg, R. A. Mathies, *Biochemistry* **1987**, *26*, 2544 – 2556.
[22] a) Y. Shichida, S. Matuoka, T. Yoshizawa, *Photobiochem. Photobiophys.* **1984**, *7*, 221 – 228; b) *Vision Res.* **1984**, *24*, 1455 – 1463.
[23] See, for example, a) G. G. Kochendoerfer, R. A. Mathies, *Isr. J. Chem.* **1995**, *35*, 211 – 226; b) Q. Wang, R. W. Schoenlein, L. A. Peteanu, R. A. Mathies, C. V. Shank, *Science* **1994**, *266*, 422 – 424.
[24] Reviews: a) R. R. Birge, *Biochem. Biophys. Acta* **1990**, *1016*, 293 – 327; b) R. M. Hochstrasser, C. K. Johnson, *Top. Appl. Phys.* **1988**, *65*, 357 – 417.
[25] In work other than ref. [23] (for example in ref. [26]) it is observed that in the 100-fs range a "hot" primary product initially forms which then assumes a more stable conformation and simultaneously cools down in the ps range. According to experience with hexatriene[12] the internal rotation in the hot primary product cannot be suppressed by cold solvent. We propose denoting only the (freezable) conformationally relaxed product as bathorhodopsin; only this product has been shown to have an all-*trans* configuration.[21]
[26] R. W. Schoenlein, L. A. Peteanu, Q. Wang, R. A. Mathies, C. V. Shank, *J. Phys. Chem.* **1993**, *97*, 12087 – 12092.
[27] M. Garavelli, P. Celani, F. Bernardi, M. A. Robb, M. Olivucci, *J. Am. Chem. Soc.* **1997**, *119*, 6891 – 6901.

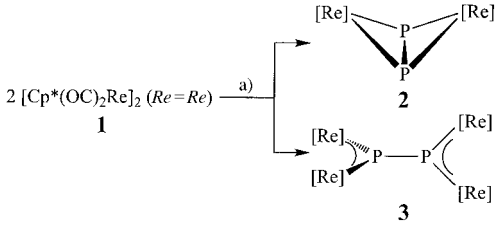
Activation of P_4 and P_2 by Transition Metal Complexes at Room Temperature**

Otto J. Scherer,* Markus Ehses, and Gotthelf Wolmershäuser

Dedicated to Professor Achim Müller on the occasion of his 60th birthday

The most important source of phosphorus for the preparation of complexes with P_n ligands[1] is white phosphorus P_4. The activation and cleavage of its P – P bonds[2] can be achieved in the presence of transition metal complex fragments both thermally at 60 – 190 °C as well as photochemically.[1]

The dropwise addition of a solution of white phosphorus in toluene to the dirhenium complex **1**[3] (Scheme 1) at room temperature gave, in addition to traces of complex **2**,[4] the tetranuclear complex **3** with a diphosphinidene ligand in approximately 40 % yield.



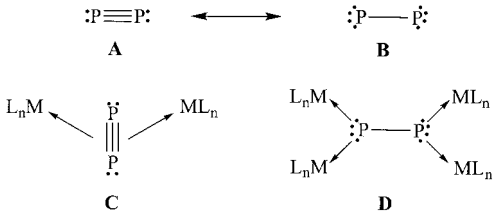
Scheme 1. P_4 activation at room temperature. a) P_4 (0.5 equiv), toluene, room temperature. [Re] = $Cp^*(CO)_2Re$.

The structures of **2** and **3** can be generally formulated as **C** (P_2 formally as a four-electron donor) and **D** (P_2 formally as an eight-electron donor), respectively. The structure type **C** with a P_2M_2 butterfly framework is relatively rare; it is observed for ML_n transition metal complex fragments with 14 and 16 valence electrons (VE).[1, 4] With 15-VE-ML_n complex fragments, polyhedra with P_2M_2 tetrahedrane frameworks are formed, which have been studied in detail.[1] In both cases the P_2 ligand is coordinated side-on as a π-electron donor

[*] Prof. Dr. O. J. Scherer, Dipl.-Chem. M. Ehses, Dr. G. Wolmershäuser[+]
Fachbereich Chemie der Universität
Erwin-Schrödinger-Strasse, D-67663 Kaiserslautern (Germany)
Fax: (+49) 631-205-2187
E-mail: oscherer@rhrk.uni.kl.de

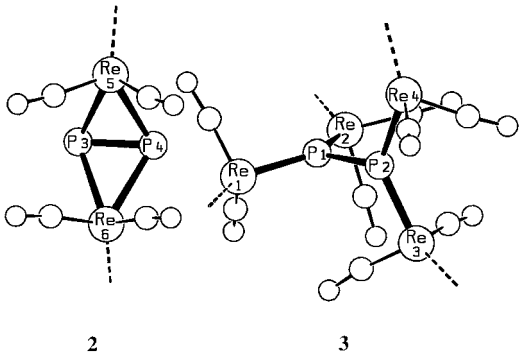
[+] X-ray crystal structure analyses.

[**] This work was supported by the Fonds der Chemischen Industrie and by the Graduiertenkolleg „Phosphorchemie als Bindeglied verschiedener chemischer Disziplinen".



(limiting structure **A**).[5] The diphosphinidene complex **3** contains a complex-stabilized form of the unusual mesomeric structure **B** of the P_2 molecule.

Complex **3** forms red crystals that can be manipulated for short periods in air. They are insoluble in hexane, soluble in toluene, and very soluble in dichloromethane. The compound is photolabile and decomposes slowly in solution above 40 °C. The ^{31}P NMR spectrum shows a singlet at $\delta = 690$.[6] Single crystals suitable for X-ray structure analyses have so far only been obtained in the form of cocrystals of complexes **2** and **3**. The results of the structure analysis[7] reveal that the bond lengths and angles of **2** (in the cocrystal) (Figure 1) differ only slightly from those of the "pure" complex **2**[4] (Table 1). Therefore we presume that the structure parameters of **3** in the cocrystal do not differ significantly from those of the "pure" complex.

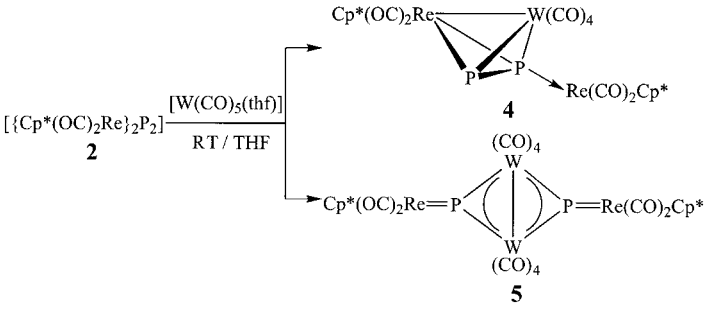


2 **3**

Figure 1. Structures of **2** and **3** in the cocrystal. Important bond lengths and angles are summarized in Table 1.

The P – P distance increases considerably on the transition from **2** (side-on-coordinated P_2; **C**) to the diphosphinidene complex **3** (P_2 formally as an 8σ-electron donor; **D**) whose P – P distance of 2.226(3) Å corresponds with that of a P – P single bond (in P_4: 2.21 Å) (Table 1). The Re1P1Re2/Re3P2Re4 planes are approximately orthogonal (91.1°); in the comparable diarsinidene complex $[\{Cp(OC)_2Mn\}_4As_2]$ (**6**)[8] the angle between the Mn_2As planes is 75.9°.[8b] The sum of angles at P1 and P2 of **3** equals 359.2° in each case. The Re – P bond in **3** (av 2.33 Å) is significantly shorter than the comparable bonds in **2** (2.56/2.54 Å (cocrystal/crystal)) and thus shows multiple-bond character.

Treatment of **2** with excess $[W(CO)_5(thf)]$ leads to two remarkable products (Scheme 2): compound **4** is to our knowledge the first structurally characterized example for the transformation of a M_2P_2 butterfly framework into a M_2P_2 tetrahedrane framework (42 → 40 VE, number of VE according to the Wade – Mingos rules;[9] see also reference [10]). At the same time the P_2 ligand of **2** (**C**) (which according to Table 1 shows multiple-bond character) is split into two P atoms at room temperature under formation of the tetranuclear complex **5**.



Scheme 2. P_2 activation at room temperature.

Complex **4** forms orange-red crystals, complex **5** dark red ones, which can be manipulated for short periods in air. They are insoluble in hexane, scarcely soluble in toluene, and well soluble in dichloromethane. Complex **5** decomposes gradually in solution. The ^{31}P NMR spectrum[6] of **4** with a chiral

Table 1. Selected bond lengths [Å] and angles [°] of complexes **2** (crystal[4] and cocrystal) and **3** (cocrystal only).[a]

3 in cocrystal		**2** in cocrystal		Crystals of **2**[4]	
P1 – P2	2.226(3)	P3 – P4	2.042(3)	P1 – P1′	2.032(8)
Re1 – P1	2.329(2)	Re5 – P3	2.566(2)	Re1 – P1	2.531(3)
Re2 – P1	2.335(2)	Re6 – P3	2.548(2)	Re1′ – P1′	2.531(3)
Re3 – P2	2.332(2)	Re5 – P4	2.561(2)	Re1 – P1′	2.555(3)
Re4 – P2	2.326(2)	Re6 – P4	2.565(2)	Re1′ – P1	2.555(3)
Re – Cp*[b]	1.99/1.99	Re5 – Cp*	1.95	Re – Cp*	1.95
	1.99/1.98	Re6 – Cp*	1.95		
Re1-P1-Re2	131.53(8)	P3-Re5-P4	46.94(8)	P1-Re1(1′)-P1′	47.1(2)
P2-P1-Re1	114.74(9)	P3-Re6-P4	47.06(8)		
P2-P1-Re2	112.97(9)	Re5-P3-Re6	105.71(8)	Re1-P1(1′)-Re1′	105.55(12)
Re3-P2-Re4	130.94(8)	Re5-P4-Re6	105.36(8)		
P1-P2-Re3	114.02(9)	P3-P4-Re5	66.65(9)	Re1-P1-P1′	67.1(2)
P1-P2-Re4	114.27(9)	P3-P4-Re6	66.03(9)	Re1′-P1′-P1	67.1(2)
		P4-P3-Re5	66.41(9)	Re1-P1′-P1	65.8(2)
		P4-P3-Re6	66.90(9)	Re1′-P1-P1′	65.8(2)

[a] Cp* denotes the center of the cyclopentadienyl ring. The torsion angle Cp*ReReCp* is 3.6° (in cocrystal) and 37.4° (in crystals of **2**). [b] In this case Re represents the center of Re1 – Re4.

 © WILEY-VCH Verlag GmbH, D-69451 Weinheim, 1998 1433-7851/98/3704-0508 $ 17.50+.50/0 *Angew. Chem. Int. Ed.* **1998**, *37*, No. 4

ReWPP′-tetrahedrane framework[11] contains two doublets ($\delta = -87.7/-188.7$, four-coordinate P atom; $^1J(P,P) = 545.3$ Hz) with tungsten satellites ($^1J(W,P) = 35/22$ Hz; cf. references [1, 4]). The crystal structure analysis[7] reveals a P–P distance of 2.067(2) Å for the $ReWP_2$ framework of **4** (Figure 2), a value that lies in the range observed for other

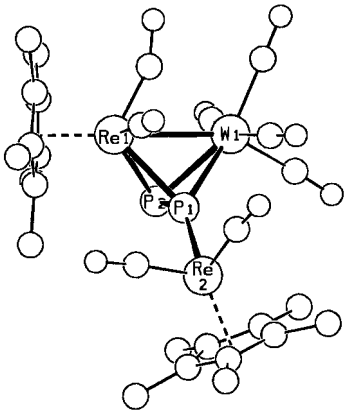


Figure 2. Crystal structure of **4**. P1–P2 2.067(2), Re1–P1 2.5151(11), Re1–P2 2.5205(12), Re2–P1 2.3255(11), Re1–W1 3.0667(3), W1–P1 2.5713(12), W1–P2 2.5388(13); P2-P1-Re2 137.83(6), Re2-P1-Re1 138.34(5), Re2-P1-W1 141.34(5), Re1-P1-W1 74.15(3).

complexes with M_2P_2 tetrahedrane frameworks.[1] The Re2–P1 bond length of 2.3255(11) Å corresponds to the average value of 2.33 Å in **3** (see Table 1). The mean value for Re–P bonds (2.52 Å) in the cluster differs only slightly from those in the Re_2P_2 butterfly framework of **2** (2.56/2.54 Å (cocrystal/crystal)).

The downfield shift of the ^{31}P NMR signal[6] of **5** ($\delta = 885$) is characteristic for planar-coordinated P atoms, which are surrounded by three metal complex fragments (in this case with metals of the 5d series; phosphinidene complexes). For instance, a value of $\delta = 977$ is found for $[\{Cp(OC)_2Mn\}_2(\mu_3\text{-}P)_2\{Fe_2(CO)_6\}]$(*Fe–Fe*) (**7**) with three complex fragments containing metals of the 3d series.[12]

The most interesting aspect of the structure of **5**[7] is the planar six-atom framework $Re_2P_2W_2$ (Figure 3). In contrast,

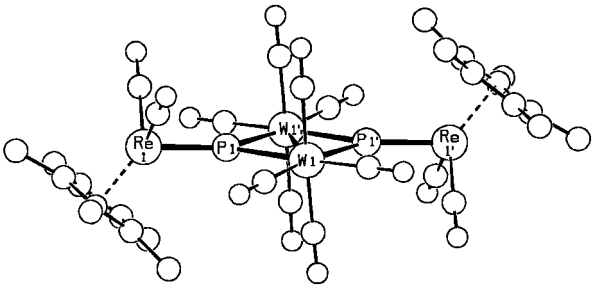


Figure. 3. Crystal structure of **5**. W1–W1′ 3.0523(7), W1(1′)–P1(1′) 2.439(2), W1(1′)–P1′(1) 2.440(2), Re1(1′)–P1(1′) 2.245(2), P1···P1′ 3.81; Re1(1′)-P1(1′)-W1(1′) 141.41(7), Re1(1′)-P1(1′)-W1′(1) 141.00(7), W1(1′)-P1(1′)-W1′(1) 77.45(5).

the comparable compounds **7**[12] and $[\{^{Me}Cp(OC)_2Mn\}_2(\mu_3\text{-}As)_2\{Mn_2(CO)_2(^{Me}Cp)_2\}]$ **(8),**[13] which were prepared from a P_1 complex or photochemically from the ^{Me}Cp derivative of **6**,[8b] respectively, and which were characterized by X-ray structure analyses, contain a M_2E_2 butterfly framework (M = Mn,Fe; E = As,P).[12, 13] The distance to the terminal Re group (P=Re) in **5** (2.245(2) Å) is particularly short. The sum of the angles at P1 and P1′ is 359.9°; the W–W bond length of 3.0523(7) Å lies in the range of a single bond, as observed for other ditungsten complexes.[14]

Experimental Section

2/3: **1** (435 mg, 0.58 mmol)[3, 4] was dissolved in toluene (40 mL) in a 50-mL-three-necked flask under exclusion of light. A solution of P_4 (ca. 20 mg, ca. 0.16 mmol) in toluene (ca. 5 mL) was added dropwise at room temperature, and the mixture was stirred at this temperature for a further 2 h. After removal of the solvent under vacuum, the residue was taken up in a small amount of toluene (ca. 5 ml) and transferred to a column (20 × 1.5 cm) packed with Al_2O_3 and petroleum ether. Several mg of a yellow-orange fraction containing **2/3** was initially eluted with petroleum ether/toluene (5/3), from which cocrystals of **2/3** were obtained by recrystallization from CH_2Cl_2/hexane (ca. 1/2) at −20 °C. Further chromatography gave an intense red fraction **3** (171 mg, 38 %); however, to date only very thin platelets have been obtained from crystallization.

4/5: **2** (98 mg, 0.12 mmol)[4] in THF (15 mL) was treated at room temperature with a solution of $[W(CO)_5(thf)]$ (ca. 0.70 mmol) in THF (45 mL), prepared by photolysis (10 min) of $[W(CO)_6]$ (261 mg). After 2.5 h (IR control) the reaction was complete and the solution was orange red. After removal of the solvent in vacuum, the residue was extracted with THF (4 × ca. 5 mL), silica gel was then added to the collected extracts, and the mixture was evaporated to dryness and transferred to a column (20 × 1.0 cm) packed with silica gel (activity grade II) and petroleum ether. An orange-red fraction was eluted with petroleum ether/toluene (1/1 to 1/2), from which **5** (10 mg) was isolated. Elution with the 1/2 solvent mixture subsequently gave **4** (39 mg, 29 %) as a red zone; red **5** (48 mg; overall yield 34 %) was obtained as the last fraction with toluene/diethyl ether (20/1 to 1/1).

Received: September 19, 1997 [Z 10949 IE]
German version: *Angew. Chem.* **1998**, *110*, 530–533

Keywords: P ligands · phosphinidenes · phosphorus · rhenium · tungsten

[1] Reviews: O. J. Scherer, *Angew. Chem.* **1990**, *102*, 1137–1155; *Angew. Chem. Int. Ed. Engl.* **1990**, *29*, 1104–1122; M. Scheer, E. Herrmann, *Z. Chem.* **1990**, *30*, 41–55.

[2] See also: D. E. C. Corbridge, *Phosphorus: An Outline of its Chemistry, Biochemistry and Technology*, 5th ed., Elsevier, **1995**, pp. 68–70.

[3] C. P. Casey, H. Sakaba, P. N. Hazin, D. R. Powell, *J. Am. Chem. Soc.* **1991**, *113*, 8165–8166; C. P. Casey, R. S. Carino, H. Sakaba, R. K. Hagashi, *Organometallics* **1996**, *15*, 2640–2649.

[4] O. J. Scherer, M. Ehses, G. Wolmershäuser, *J. Organomet. Chem.* **1997**, *531*, 217–221.

[5] K. I. Goldberg, D. M. Hoffmann, R. Hoffmann, *Inorg. Chem.* **1982**, *21*, 3863–3868.

[6] Spectroscopic data of compounds **3**–**5**: $\delta(^{31}P)$ (81.01 MHz, $CDCl_3$, 85 % H_3PO_4 external): **3**: 690 (s, 2P); **4**: −87.7 („d“, 1P, $^1J(P,P) = 545.3$ Hz, $^1J(W,P) = 35$ Hz), −188.7 („d“, 1P, $^1J(P,P) = 545.3$ Hz, $^1J(W,P) = 22$ Hz); **5**: 885 („s“, 2P, $^1J(W,P) = 85.4$ Hz); $\delta(^1H)$ (200.13 MHz, $CDCl_3$, $CHCl_3$ internal ($\delta = 7.25$); $T = 295$ K): **3**: 2.10 (s, 30H), 2.06 (s, 30H); **4**: 2.04 (s, 15H), 2.02 (s, 15H); **5**: 2.30 (s, 30H); IR (CH_2Cl_2): $\tilde{\nu}$(CO) [cm^{-1}]: **3**: 1968(s), 1935(s), 1922(sh), 1914(vs), 1890(s), 1871(m), 1862(m); **4**: 2040(vs), 1982(vs), 1950(s), 1913(m), 1894(m), 1857(m); **5**: 2017(s), 1974(vs, br.); 1943(m, sh), 1907(m).

[7] Crystal structure data of complexes **2/3** (in the cocrystal) and complexes **4** and **5** [in square brackets]: $C_{73}H_{92}Cl_2O_{12}P_4Re_6$ [$C_{28}H_{30}O_8P_2Re_2W$; $C_{32}H_{30}O_{12}P_2Re_2W_2$], $M_r = 2473.45$ [1112.71; 1408.60], monoclinic [monoclinic; triclinic], space group $P2_1/n$ [$P2_1/n$; $P\bar{1}$], $a = 14.485(2)$ [10.4887(6); 8.934(2)], $b = 15.8971(13)$ [17.9268(9);

 © WILEY-VCH Verlag GmbH, D-69451 Weinheim, 1998 1433-7851/98/3704-0509 $ 17.50+.50/0

9.801(2)], $c = 34.797(4)$ [17.1896(10); 12.071(3)] Å, $\alpha = 90$ [90; 82.20(2)], $\beta = 95.085(10)$ [94.768(6); 79.19(2)], $\gamma = 90$ [90; 67.21(2)]°, $V = 7981(2)$ [3221.0(3); 954.8(3)] Å^3, $Z = 4$ [4; 1], $\rho_{calcd} = 2.059$ [2.295; 2.450] g cm^{-3}, $T = 293(2)$ K, θ-range: 1.74–24.12 [2.20–25.93; 2.74–28.00]°, measured reflections: 46406 [45294; 16443], independent reflections: 12255 [5991; 4217] ($R_{int} = 0.0636$ [0.0694; 0.0620]), R values: final R values ($I > 2\sigma(I)$): $R1 = 0.0308$ [0.0247; 0.0353], $wR2 = 0.0685$ [0.0568; 0.0935], all data: $R1 = 0.0415$ [0.0303; 0.0420], $wR2 = 0.0738$ [0.0585; 0.0984]. Diffractometer: Stoe IPDS. Structure solution: direct methods [direct methods; Patterson]. Program used for solving the structure: SIR92 (Giacovazzo et al., 1993) [SHELXTL; SHELXS 86 (Sheldrick, 1990)]. Structure refinement: full-matrix least-squares methods against F^2. Program used for refining the structure: Siemens SHELXTL [SHELXTL; Siemens SHELXL 93 (Sheldrick, 1993)]. Data/parameters: 12248/904 [5991/381; 4217/232]. Crystallographic data (excluding structure factors) for the structures reported in this paper have been deposited with the Cambridge Crystallographic Data Centre as supplementary publication no. CCDC-100785. Copies of the data can be obtained free of charge on application to the CCDC, 12 Union Road, Cambridge CB2 1EZ (fax: (+44) 1223-336-033; e-mail: deposit@ccdc.cam.ac.uk).

[8] a) W. A. Herrmann, B. Koumbouris, T. Zahn, M. L. Ziegler, *Angew. Chem.* **1984**, *96*, 802–803; *Angew. Chem. Int. Ed. Engl.* **1984**, *23*, 812–813; W. A. Herrmann, B. Koumbouris, A. Schäfer, T. Zahn, M. L. Ziegler, *Chem. Ber.* **1985**, *118*, 2472–2488; b) G. Huttner, B. Sigwarth, O. Scheidsteger, L. Zsolnai, O. Orama, *Organometallics* **1985**, *4*, 326–332.

[9] D. M. P. Mingos, D. J. Wales, *Introduction to Cluster Chemistry*, Prentice-Hall, **1990**.

[10] J.-F. Halet, J.-Y. Saillard, *J. Organomet. Chem.* **1987**, *327*, 365–377.

[11] H. Vahrenkamp, *Adv. Organomet. Chem.* **1983**, *22*, 169–208, and references therein; *J. Organomet. Chem.* **1989**, *370*, 65–73, and references therein; F. G. A. Stone, *Pure Appl. Chem.* **1986**, *58*, 529–536, and references therein; O. J. Scherer, C. Vondung, G. Wolmershäuser, *Angew. Chem.* **1997**, *109*, 1360–1362; *Angew. Chem. Int. Ed. Engl.* **1997**, *36*, 1303–1305.

[12] H. Lang, L. Zsolnai, G. Huttner, *Angew. Chem.* **1983**, *95*, 1016–1017; *Angew. Chem. Int. Ed. Engl.* **1983**, *22*, 976–977.

[13] G. Huttner, U. Weber, B. Sigwarth, O. Scheidsteger, H. Lang, L. Zsolnai, *J. Organomet. Chem.* **1985**, *282*, 331–348.

[14] See for example: M. H. Linck, *Cryst. Struct. Commun.* **1973**, *3*, 379–382; G. Schmidt, R. Boese, *Chem. Ber.* **1976**, *109*, 2148–2153.

Functionalized Cross-Linked Copolymers: A "C_2-Symmetric" Solid-Phase Catalyst for Enantioselective Reactions**

Chris Halm and Mark J. Kurth*

Building on the pioneering work of Merrifield,[1] solid-phase synthesis,[2] polymer-supported reagents,[3] and polymer-bound catalysts[4] have revolutionized many aspects of synthetic chemistry. Most of these exploits were accomplished with styrene/divinylbenzene (PS/DVB) copolymers,[5] but there are notable exceptions.[6] Polymer-bound catalysts are typically prepared by covalent attachment of the catalytic moiety to the PS/DVB copolymer through the chloromethylated functionality (Merrifield's resin). While excellent enantioselectivities have been achieved with these heterogeneous catalysts,[7] this route to supported catalysts has been limited to placing the catalyst at a position pendant to the polymer backbone (**1**, Figure 1). What has been largely overlooked[8] is

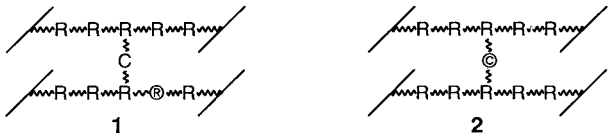


Figure 1. Functionalized resins. R: chain monomer; C: cross-linked monomer; ®: pendant functionalization; ©: cross-link functionalization.

a supported-catalyst strategy in which the catalytic moiety is located at the resin cross-link (**2**, Figure 1). We report here the rapid and convenient synthesis of this type of cross-link-functionalized resin by suspension copolymerization to yield a solid-phase "C_2-symmetric" catalyst (although the two polymer chains are not identical, the local environment is C_2-symmetric) for application in enantioselective transformations. We believe this unique cross-link functionalization provides the least disturbance to the symmetry of the catalytic center, because the two cross-linked polymer chains can be considered as symmetrically equivalent. Possible applications therefore benefit from a decrease in the number of competing diastereomeric transition states inherent in C_2-symmetric systems.[9] In most pendant catalysts, one arm of the auxiliary is attached to the polymer backbone while the other terminates with a small organic fragment, causing inherent dissymmetry between the auxiliaries. We believe cross-link-functionalized chiral resins may afford important processing advantages over pendant versions. For example, cross-link functionalization should minimize interactions between active sites which may positively influence reaction parameters such as catalytic turnover. In addition, resin-supported catalytic reagents can ease product purification as well as catalyst recovery and reuse.

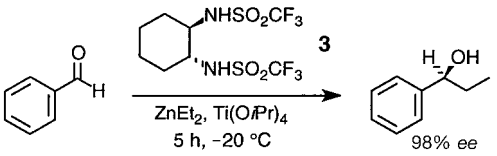
To obtain a cross-linked functionality, it was necessary to synthesize a monomeric chiral auxiliary (X) containing two polymerizeable units (i.e., $CH_2{=}CH{-}X{-}CH{=}CH_2$), which could then undergo suspension copolymerization with styrene. We reasoned that the resulting cross-link-functionalized polystyrene beads might provide an ideal opportunity for asymmetric catalysis, and selected enantioselective reductive alkylation of aldehydes as our target transformation.

Ohno and co-workers[10] reported that the chiral ligand **3** (1 mol%) together with titanium(IV) isopropoxide catalyzes the reductive alkylation of aldehydes (Scheme 1). We envisioned replacing the trifluoromethyl groups of **3** with styrenesulfonyl groups to give a cross-linking monomer (**4**) which, after copolymerization with styrene (**4** → **5**), could be evaluated for efficacy in the reaction of aromatic aldehydes and diethylzinc to form (*S*)-1-aryl-1-propanol. This auxiliary-mediated alkylation reaction was selected for our preliminary evaluation of cross-link efficacy in an enantioselective transformation because it competes with ligand-unassisted con-

[*] Prof. M. J. Kurth, C. Halm
Department of Chemistry
University of California
Davis, CA 95616 (USA)
Fax: (+1) 530-752-8995
E-mail: mjkurth@ucdavis.edu

[**] We are grateful to the National Science Foundation for financial support of this research.

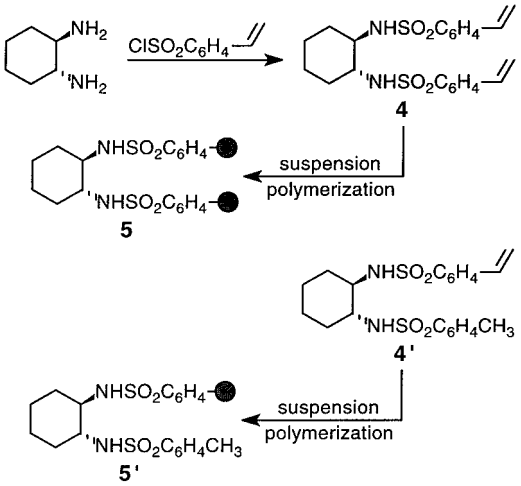
 © WILEY-VCH Verlag GmbH, D-69451 Weinheim, 1998 1433-7851/98/3704-0510 $ 17.50+.50/0



Scheme 1. Example for the enantioselective alkylation of aldehydes in toluene with disulfonamide **3** (1 mol%) as auxiliary.

version (i.e., formation of racemic product). Therefore, the objectives of this study were to place a chiral disulfonamide ligand at the cross-link of a polystyrene resin and to demonstrate that this ligand can successfully mediate enantioselective reductive alkylation of aldehydes in competition with ligand-unassisted conversion.

Disulfonamide **4** was readily prepared in 71% yield by the reaction of (*R*,*R*)-1,2-cyclohexanediamine[11] with styrenesulfonyl chloride[12] (CH_2Cl_2, 2 h, 0 °C). Subsequent copolymerization[13] of **4** with styrene afforded resin **5**, which is capable



of swelling, as beads, which were sorted with a series of macroporous filters of differing mesh size. Of course, the cross-link density of resin **5** can be manipulated by varying the ratio of monomers employed in the suspension copolymerization. For these studies we prepared **5** with cross-link densities from 0.25 to 2.5 mol% (this required a ratio of disulfonamide monomer to styrene of 1 to 10 wt%). Elemental analysis (C, H, N, S) was used to calculate the resin loading after copolymerization, which allowed us to submit the required amount of disulfonamide auxiliary (1–2 mol%) to the reaction.

In a control experiment, we first investigated the enantioselectivity of monomer **4** in the reaction of aromatic aldehydes and diethylzinc to form (*S*)-1-aryl-1-propanol. We were pleased to find that this auxiliary was as effective as triflate **3** (Table 1, compare entries 1–3 with 4–6). A significant difference between **3** and **4** is that the latter requires longer reaction times (5 h with **3** versus 24 h with **4**). This is probably due to the decreased Lewis acidity of the active Ti species derived from **4** compared to that derived from **3**.

With these results in hand, we turned to studying resin **5** as auxiliary for the same reaction. We were initially concerned that reagent transport to the polymeric active site, a requirement for resin-based disulfonamide, would fail to successfully compete with a ligand-unassisted reaction[11] of ArCHO with $ZnEt_2$/Ti(O*i*Pr)$_4$ and lead to products with low *ee* values. This problem was addressed by choosing a solvent which would swell the polymer sufficiently for reaction to take place. The measured swelling of **5** in toluene was more than four times the nonswollen volume. We later found that the use of nonswelling solvents such as hexane under identical reaction conditions gave products in low yields. It is precisely this swelling capacity in toluene that allowed for resin-bound reactions to occur at reasonable catalyzed rates. As presented in Table 1, resin **5** delivers (*S*)-1-aryl-1-propanol with *ee* values which nearly match those of solution reagents **3** or **4**. An advantage of resin-bound **5** is the ease of removal by simple filtration. This also allows for catalyst recycling; however, with 1–2 mol% catalyst, yields diminish from 82% with fresh catalyst down to about 60% with recycled catalyst.

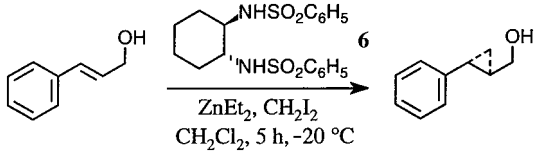
Table 1. Results of reactions with aldehydes RCHO according to Scheme 1.

Entry	R	Auxiliary[a]	Yield [%]	*ee* [%][b]
1	C_6H_5	**3**	98	98[c]
2	$C_6H_5CH{=}CH$	**3**	98	85–99[c, d]
3	*p*-ClC_6H_4	**3**	95	98
4	C_6H_5	**4**	96	98
5	$C_6H_5CH{=}CH$	**4**	98	70
6	*p*-ClC_6H_4	**4**	92	85
7	C_6H_5	**5**	82	98
8	$C_6H_5CH{=}CH$	**5**	80	63
9	*p*-ClC_6H_4	**5**	85	83
10	*p*-$MeOC_6H_4$	**5**	75	70
11	*o*-ClC_6H_4	**5**	85	56
12	*p*-MeC_6H_4	**5**	71	56
13	C_6H_5	**5′**	73	93

[a] 1–2 mol%. [b] Determined by ^{19}F NMR spectroscopy of Mosher's ester. [c] Ref. [10]. [d] With more than 1.2 equiv of diethylzinc, the *ee* values increased significantly.

In light of our results with **4** and **5**, we were not surprised that pendant ligand **5′** (prepared by suspension copolymerization of **4′**) also effectively mediates the reaction of aromatic aldehydes with diethylzinc to form (*S*)-1-phenyl-1-propanol. A comparison of cross-linked ligand **5** (Table 1, entry 7) and pendant ligand **5′** (entry 13) estabishes that the accessibility to cross-linked sites in this transformation is not compromised for **5**.

Solid-phase **5** also has applications in other enantioselective chemical transformations; for example, the cyclopropanation of allyl alcohols. Kobayashi et al.[14] reported that disulfonamide **6** catalyzes the cyclopropanation of cinnamyl alcohol with 65% *ee* (Scheme 2). The enantioselec-



Scheme 2. Example for enantioselective cyclopropanation with **6** (10 mol%) as catalyst.

 © WILEY-VCH Verlag GmbH, D-69451 Weinheim, 1998 1433-7851/98/3704-0511 $ 17.50+.50/0

tivity obtained with **5** parallels solution-phase results (Table 2, compare entry 3 with entries 1 and 2).[15] Again, the enantioselectivity of this transformation is compromised by effective

Table 2. Results of the cyclopropanation according to Scheme 2.

Entry	Disulfonamide[a]	Yield [%]	*ee* [%][b]
1	**4**	70	65
2	**5**	68	65
3	**6**	75	68[c]

[a] 10 mol%. [b] Determined by ^{19}F NMR spectroscopy of Mosher's ester. [c] Ref. [16].

competition of the ligand-unassisted reaction. As with other cyclopropanation studies,[16] lower temperatures do not increase the enantioselectivities (at $-78\,^{\circ}C$ the *ee* was still 65%). When a larger molar amount of resin catalyst was used (20 mol%), the yield improved to 90%, and enantioselectivities increased to 70% *ee*.

In conclusion, suspension copolymerization of the bis-styryl monomer **4** and styrene delivers cross-link-functionalized resin **5**, whose loadings are controlled by reagent stoichiometry. The solid-phase catalyst **5** effectively mediates the reductive alkylation of aryl aldehydes and the cyclopropanation of cinnamyl alcohol.

Experimental Section

Copolymerization: Water (100 mL) and gum arabic (6.0 g) were placed in a 200-mL Morton flask and stirred rapidly under N_2 at $75\,^{\circ}C$ for 30 min using a metal rotor to afford a homogenous mixture. Chlorobenzene (10 g), styrene (9 g), **4** (1 g), and benzoyl peroxide (0.15 g) were added, and the mixture was stirred such that very small suspended organic droplets formed ($600\ U\,min^{-1}$). After 30 min a stabilizer (Al_2O_3, 0.1 g) was added to avoid bead aggregation. After an additional 2 h the stirring rate was reduced dramatically ($130\ U\,min^{-1}$) to avoid bead sheering, and stirring was continued at $75\,^{\circ}C$ for another 16 h. The polymerization was halted by adding 1M HCl, the mixture washed with THF, and the polymer recovered by filtration. Approximately 75% of the material was collected by filtration; 25% was unrecoverable. However, 85% of the remaining beads had a diameter between 70 and 250 μm, which is suitable for solid supports (when compared with commercially available resins). With this method, the bead size could be reduced further by increasing the ratio of aqueous to organic phase and increasing the stirring rate with minimal effect on yield and bead shape. This is an attractive advantage considering reaction rates are often dependent on the diffusion of the reagents (the rate increased with smaller bead size).

Typical procedure for the reductive alkylation of aldehydes: To disulfonamide **5**, swollen in toluene, was added $Ti(O\mathit{i}Pr)_4$ (1.2 equiv). The mixture was heated at reflux for 30 min and cooled to $-70\,^{\circ}C$, and $ZnEt_2$ (1M in hexanes, 1.2 equiv) added slowly. At this point, an orange (not a yellow) color indicated catalyst activation. Without this color change, yields were often poor. Benzaldehyde was added, and the mixture stirred at -70 °C for an additional 5–24 h. The reaction was quenched with 1M HCl, the polymer removed by filtration, and the alcohol isolated by flash chromatography (silica gel, EtOAc/hexanes 1/3) after extraction with an organic solvent.

Cyclopropanation of cinnamyl alcohol: To disulfonamide **5**, swollen in CH_2Cl_2, was added $ZnEt_2$ (1M in hexanes, 2 equiv) and CH_2I_2 (3 equiv) at $-70\,^{\circ}C$, and the mixture was stirred for 1 h. Cinnamyl alcohol was added, and the reaction allowed to slowly warm to room temperature over 24 h. The reaction was quenched with 1M NaOH, the polymer collected by filtration, and the alcohol isolated by flash chromatography (silica gel, EtOAc/hexanes 1/4) after extraction with an organic solvent.

Received: August 25, 1997 [Z10847IE]
German version: *Angew. Chem.* **1998**, *110*, 523–525

Keywords: asymmetric catalysis · cross-linking · Lewis acids · polymers · sulfonamides

[1] R. B. Merrifield, *J. Am. Chem. Soc.* **1963**, *85*, 2149–2154.
[2] Reviews on solid-phase organic reactions: a) P. Hermkens, H. Ottenheijm, D. Rees, *Tetrahedron* **1997**, *53*, 5643–5678; b) *ibid.* **1996**, *52*, 4527–4554.
[3] a) J. Parlow, *Tetrahedron Lett.* **1995**, *36*, 1395–1396; b) P. Wipf, S. Venkatraman, *ibid.* **1996**, *37*, 4659–4662; c) A. Guyot, P. Hodge, D. Sherrington, H. Widdecke, *Reactive Polymers*, **1991**, *16*, 233–259.
[4] a) S. Itsuno, K. Kamahori, K. Watanabe, T. Koizumi, K. Ito, *Tetrahedron: Asymmetry* **1994**, *5*, 523–526; b) M. Zupan, D. Dolenc, *Tetrahedron* **1991**, *47*, 5025–5028; c) M. Zupan, N. Segatin, *Synth. Commun.* **1991**, *21*, 597–609; d) review: S. Schlick, E. Bortel, K. Dyrek, *Acta Polym.* **1996**, *47*, 1–15.
[5] J. S. Fruechtel, G. Jung, *Angew. Chem.* **1996**, *108*, 19–46; *Angew. Chem. Int. Ed. Engl.* **1996**, *35*, 17–42.
[6] a) H. Han, M. Wolfe, S. Brenner, K. Janda, *Proc. Natl. Acad. Sci. USA* **1995**, *92*, 6419–6423; b) R. Quarrell, T. Claridge, G. Weaver, G. Lowe, *Molecular Diversity* **1996**, *1*, 223–232; c) B. Zhao, G. Panigrahi, P. Sadowski, J. Krepinsky, *Tetrahedron Lett.* **1996**, *37*, 3093–3096; d) J. W. Labadie, T. L. Deegan, O. W. Gooding, K. Heisler, W. S. Newcomb, J. A. Porco, Jr., T. H. Tran, P. van Eikeren, *Polym. Mater. Sci. Eng.* **1996**, *75*, 389–390.
[7] a) S. Itsuno, Y. Sakurai, K. Ito, T. Maruyama, S. Nakahama, J. Frechet, *J. Org. Chem.* **1990**, *55*, 304–310; b) G. Liu, J. Ellman, *ibid.* **1995**, *60*, 7712–7713.
[8] a) B. De, B. Lohray, S. Sivaram, P. Dhal, *Tetrahedron: Asymmetry* **1995**, *9*, 2105–2108; b) F. Minutolo, D. Pini, P. Salvadori, *Tetrahedron Lett.* **1996**, *17*, 3375–3378.
[9] J. Whitesell, *Chem. Rev.* **1989**, *89*, 1581–1590.
[10] a) M. Yoshioka, T. Kawakita, M. Ohno, *Tetrahedron Lett.* **1989**, *13*, 1657–1660; b) H. Takahashi, *ibid.* **1989**, *50*, 7095–7098.
[11] For chiral resolution, see T. Whitney, *J. Org. Chem.* **1980**, *45*, 4214–4216.
[12] H. Kamogawa, A. Kanzawa, M. Kadoya, T. Naito, M. Nanasawa, *Bull. Chem. Soc. Jpn.* **1983**, *56*, 762–765.
[13] G. Odian, *Principles of Polymerization*, Wiley, New York, **1981**.
[14] a) H. Takahashi, M. Yoshioka, M. Ohno, S. Kobayashi, *Tetrahedron Lett.* **1992**, 18, 2575–2578; b) Lewis acid catalyzed cyclopropanations: A. Charette, C. Brochu, *J. Am. Chem. Soc.* **1995**, 117, 11367–11368.
[15] Enantioselectivities can be increased by replacing the phenyl with a nitrophenyl group in **6**, see S. Denmark, B. Christenson, S. O'Connor, *Tetrahedron Lett.* **1995**, *36*, 2219–2222.
[16] a) S. Denmark, B. Christenson, D. Coe, S. O'Connor, *Tetrahedron Lett.* **1995**, *36*, 2215–2218.

 © WILEY-VCH Verlag GmbH, D-69451 Weinheim, 1998 1433-7851/98/3704-0512 $ 17.50+.50/0

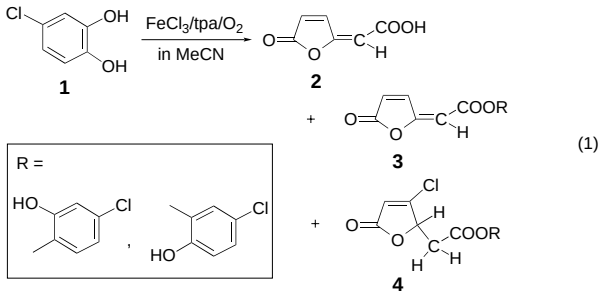
Oxygenative Cleavage of Chlorocatechols with Molecular Oxygen Catalyzed by Non-Heme Iron(III) Complexes and Its Relevance to Chlorocatechol Dioxygenases**

Takuzo Funabiki,* Tamio Yamazaki, Atsushi Fukui, Tsunehiro Tanaka, and Satohiro Yoshida

Numerous halogenated aromatic compounds are released that are difficult to degrade by chemical or biological oxidations into the environment. Recently, non-heme iron enzymes (chlorocatechol dioxygenases, CCD), which function in the degradation of mono- and polyhalocatechols, were purified.[1–5] This suggests the possibility of developing non-heme iron complexes which decompose halogenated arenes in a fashion similar to that of the chlorocatechol dioxygenases. We report here the first example of the oxidative cleavage of 3- and 4-chlorocatechols with molecular oxygen by a non-heme iron complex, which is accompanied with dehydrochlorination of the oxygenated products.

Recent remarkable progress in the enzymatic studies of oxygenases has clarified the native and substrate-bound species of some catechol dioxygenases;[6–9] however, very little is known about CCD, which contains a high-spin iron(III) ion in the active center.[1] Various types of functional models for catechol dioxygenases have been described[10–23] since the first model oxygenation by a bipyridine(pyridine)iron complex was reported.[10, 12] In these model studies 3,5-di-*tert*-butylcatechol (dtbc) was extensively used as a substrate, because the electron-donating substituents at the 3- and 5-positions facilitate the oxygenation of this catechol and prevent formation of polymer products.[24] Here we show that catechols with electron-withdrawing substituents can also be oxygenated catalytically by model iron complexes.

4-Chlorocatechol (4-Cl-catH_2, **1**) was oxygenated at 25 °C in acetonitrile under an O_2 atmosphere (1 atm). When an excess of **1** was oxygenated by the iron complex prepared in situ by mixing $FeCl_3$ and tris(2-pyridylmethyl)amine (tpa), the three oxidatively cleaved products **2**–**4** were obtained [Eq. (1)]. Compounds **3** and **4** are the 4-chlorocatechol esters



(1)

of **2** and chlorolactonic acid, respectively. No other product was detected. Both isomers of the 4-chlorocatechol esters, formed by modification of different hydroxyl groups, were observed for **3** and **4** by ^1H and ^{13}C NMR spectroscopy; however, they were not isolated separately.

Figure 1 A shows the time course of the oxygenation of **1**, which proceeded fairly slowly and catalytically to give the products in a ratio of (**2**+**3**):**4** ≈ 1:1.3. As shown in Figure 1 B, the presence of an excess of tpa was beneficial. The maximal yield was obtained for a tpa:Fe ratio of 10:1.

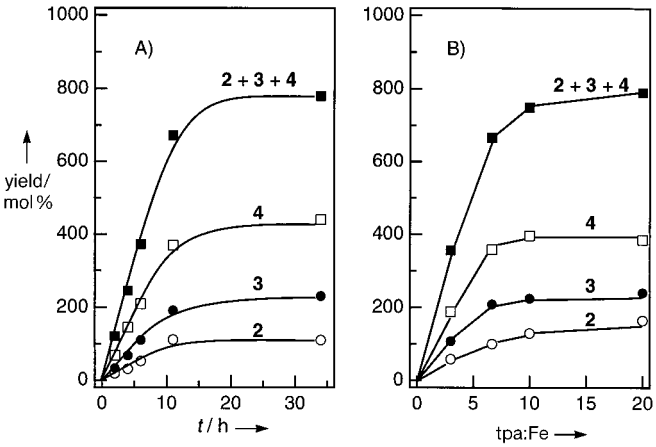


Figure 1. A) Time course of the oxygenation of **1** with O_2 catalyzed by the $FeCl_3$/tpa system. B) Effect of the tpa concentration. [$FeCl_3$] = 0.01 mmol, [tpa] = 0.1 mmol (A), [**1**] = 0.3 mmol in MeCN (5 mL). Yields [mol %] are based on the amount of Fe used.

The 4-chlorocatecholatoiron complex [Fe(tpa)(4-Cl-cat)]BPh_4 (**5**) was isolated; it exhibits ligand-to-metal charge-transfer (LMCT) absorption bands at 479 and 786 nm. Although the complex did not crystallize in a form suitable for crystallography, a preliminary X-ray absorption spectroscopic study[25] suggested a structure similar to that of [Fe(tpa)(dtbc)]BPh_4, in which the catecholate ligand chelates the iron center.[19] Complex **5** decomposes upon contact to O_2 in acetonitrile with exclusive formation of the oxygenated product **2**. Interestingly, no other product, such as the ester or the lactonic acid **4** (R = H), was formed. Figure 2 shows

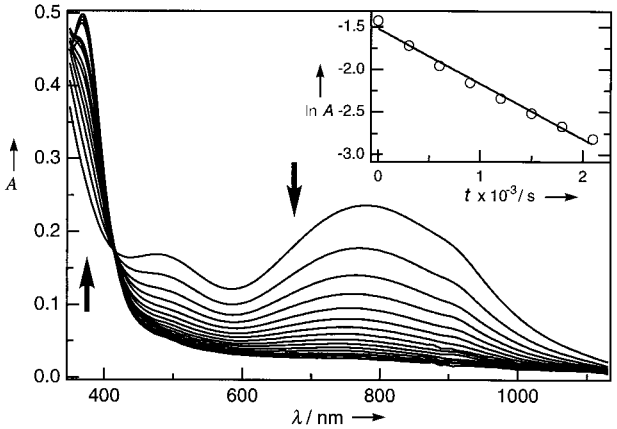


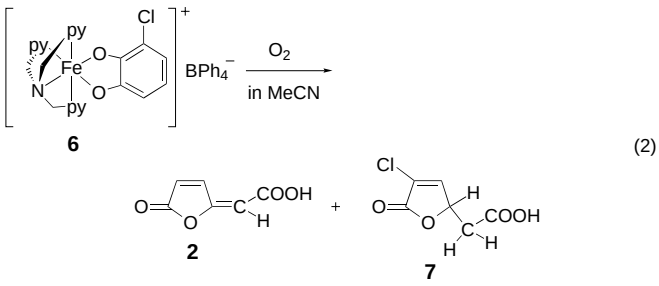
Figure 2. Oxygenation of **5** with O_2 monitored by electronic absorption spectroscopy in 5-min intervals at room temperature ([**5**] = 0.01 mmol in 5 mL MeCN under 1 atm of O_2). The arrows indicate the direction of the change in intensity of the absorption bands. Inset: plot of ln *A* vs. time *t*. *A* = absorption.

[*] Prof. T. Funabiki, T. Yamazaki, A. Fukui, T. Tanaka, S. Yoshida
Department of Molecular Engineering
Graduate School of Engineering,
Kyoto University
Kyoto 606-8501 (Japan)
Fax: (+81) 75-753-5925
E-mail: funabiki@scl.kyoto-u-ac.jp

[**] We thank the Japenese Ministry of Education, Science, and Culture for grants (nos. 07455322, 07305062, 0215239, and 0216238), and M. Kodera, Doshisha University, for measuring the FAB mass spectra.

 © WILEY-VCH Verlag GmbH, D-69451 Weinheim, 1998 1433-7851/98/3704-0513 $ 17.50+.50/0

the changes in the electronic absorption spectrum upon exposure of **5** to O_2, which indicates decomposition of the complex. The complex of 3-chlorocatechol [Fe(tpa)(3-Cl-cat)]BPh_4 (**6**) was also isolated; it exhibits LMCT bands at 532 and 766 nm. The reaction of **6** with O_2 gives mostly **2** with a small amount of **7** [Eq. (2), py = 2-pyridyl]. The pseudo-first-order rate constants evaluated from the disappearance of the



lowest energy CT bands in acetonitrile (Figure 2) were 8.4×10^{-2} for **5** and $6.4 \times 10^{-2}\,M^{-1}s^{-1}$ for **6** ($[O_2] = 8.1$ mM in acetonitrile,[26] pressure 1 atm; $1000 - 1500 \times 10^{-2}\,M^{-1}s^{-1}$ is reported for the dtbc analogue in different solvents[19]). The result that **5** is a slightly more reactive than **6** is different from the situation with the enzymatic system, in which the oxygenation of 3-chlorocatechol is a little faster than that of 4-chlorocatechol.[1, 24]

Figure 3 shows the effect of 2,6-lutidine on the catalytic conversion of **1** by **5** and by the complex prepared in situ from $FeCl_3$ and tpa. In contrast to the case of the in situ system, the oxygenation of **1** by **5** proceeds catalytically even without

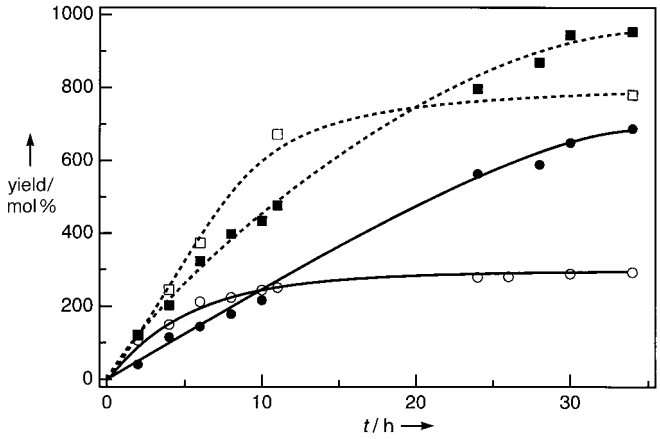
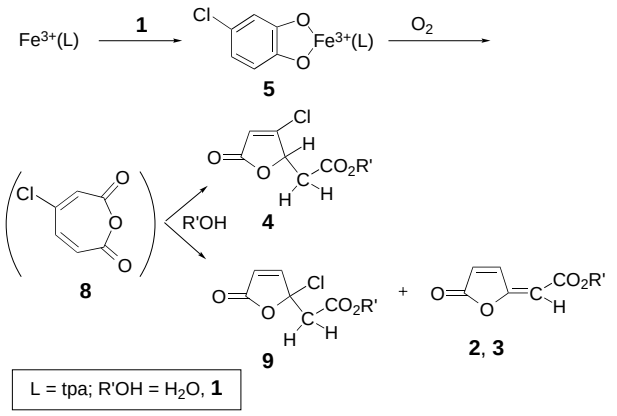


Figure 3. Effect of the addition of 2,6-lutidine on the yields of products in the oxygenation of **1** by **5** and by the complex prepared in situ from $FeCl_3$ and tpa. ○: **5**+**1** (1:29); ●: **5**+**1**+2,6-lutidine (1:29:333); □: $FeCl_3$+tpa+**1** (1:10:30); ■: $FeCl_3$+tpa+**1**+2,6-lutidine (1:10:30:333). $[FeCl_3] = [\mathbf{5}] =$ 0.2 mmol in MeCN (80 mL).

added tpa, and the reactivity is enhanced greatly by addition of 2,6-lutidine. A smaller effect was observed for the in situ system with an excess of tpa, except for the decrease in the initial rate. Since hydrogen chloride formed from $FeCl_3$ and by dehydrochlorination of the products binds to the tpa ligand, the addition of a base such as 2,6-lutidine or the presence of an excess of tpa are effective for maintaining the catalytic activity. However, the addition of these bases was not enough to prevent the termination of the reaction before complete conversion of **1**. This indicates that formation of HCl is not the sole cause of the deactivation. The stopping of the reaction even in the presence of **1** was accompanied by the disappearance of the LMCT band for the catecholate complexes. This suggests that the iron complexes are converted into inactive forms that are coordinated by product acids, as observed in the dtbc system.[19] Since the addition of base promoted the formation of esters rather than acid, it may be effective in retarding the formation of the inactive complexes coordinated by product acid.

It is reasonable to assume that the intradiol cleavage proceeds stepwise via the monooxygenated product **8**, similar to the case of dtbc.[12, 18, 19, 22, 23] The absence of **8** among the products must be due to the fact that it is more reactive with respect to water or chlorocatechols than the dtbc analogue. Esters are most probably formed directly from **8** by the reaction with chlorocatechols (Scheme 1) rather than by esterification of lactonic acids, since lactonic anhydrides react readily with water or alcohols.[27] This is reflected by the nearly constant ratio for **2**:**3**:**4** throughout the reaction (see Figure 1).



Scheme 1. Mechanism for the oxygenation of **1**.

Formation of oxygenated products from chlorocatecholatoiron complexes **5** and **6** suggests that these complexes are intermediates in the catalytic oxygenation. It is noticeable that the dehydrochlorinated product **2** is mainly formed from **5** and **6** in the absence of excess catechol. The selective formation of **2** is similar to the situation with the enzymatic system.[28] The dehydrochlorination occurs readily without extra catalysts in the model system, whereas manganese-containing chloromuconate cycloisomerases are known to catalyze the reaction in the enzymatic system.[29] In the model system other types of lactonic acids (e.g. **4**) are formed as catechol esters. The formation of esters is promoted by the presence of an excess of catechols and base such as 2,6-lutidine. It is likely that **8** is converted preferentially into **2** via **9** by reaction with water, but into both types of lactonic acid esters **4** and **9** by reaction with catechols.[27]

We have shown that the CCD model reaction is greatly dependent on the ligand. The ligand tpa is proved to be effective for the CCD model reaction, but it is not good

 © WILEY-VCH Verlag GmbH, D-69451 Weinheim, 1998 1433-7851/98/3704-0514 $ 17.50+.50/0

enough for oxygenation of polychlorocatechols. However, the present result suggests that oxygenation of polyhalocatechols will be possible by the development of ligands in the future.

Experimental Section

The oxygenations were performed in a 20-mL cylindrical flask at 25 °C and under 1 atm of O_2. MeCN (5 mL) was added to $FeCl_3$ (0.01 mmol), **1** (0.30 mmol), and tpa (0.1 mmol), and the solution stirred. Aliquots of the reaction solution (0.5 mL) were diluted with CH_2Cl_2, washed with 2 N HCl to remove iron complexes, and quantitatively analyzed by ^{1}H NMR spectroscopy by monitoring specific ^{1}H NMR peaks (naphthalene as internal reference) and using the gravimetric method.[14] The products were separated by preparative HPLC and identified by ^{1}H and ^{13}C NMR spectroscopy and high-resolution mass spectrometry. Two types of esters were detected for **3** and **4**, whose ratios were estimated to be about 2:1 for **3** and 1.4:1 for **4** based on the relative intensities of characteristic ^{13}C NMR signals for the products.

The 3- and 4-chlorocatecholatoiron complexes [Fe(tpa)(Cl-cat)]BPh_4 (**5** and **6**) were prepared by a modification of the reported methods.[19, 22] **5**: Elemental analysis calcd for $FeC_{48}H_{41}N_4O_2BCl$: C 71.34, H 5.11, N 6.93, Cl 4.39; found: C 71.05, H 5.25, N 6.88, Cl 4.40; FAB-MS: *m*/*z*: 488 ($M^+ - BPh_4$). **6**: Elemental analysis calcd for $FeC_{48}H_{41}N_4O_2BCl$: C 71.34, H 5.11, N 6.93, Cl 4.39; found: C 70.58, H 5.03, N 6.99, Cl 4.42.

The reaction of **5** or **6** with O_2 was started by adding MeCN (80 mL) to **5** or **6** (0.2 mmol) at 25 °C and under 1 atm of O_2. The oxygenations were also performed in the presence of **1** (5.8 mmol) and 2,6-lutidine (66.7 mmol).

2: HR-MS: *m*/*z* (E/I): 140.0113 (M^+); ^{1}H NMR ($CDCl_3$): $\delta = 5.96$ (d), 6.52 (dd), 8.37 (d); ^{13}C NMR ($CDCl_3$): 101.5, 125.1, 141.8, 161.9, 167.3, 169.6.

3 (mixture of two esters): HR-MS: *m*/*z* (E/I): 265.9980 (M^+); ^{1}H NMR ($CDCl_3$): $\delta = 6.17$ (d), 6.57 (dd), 8.40 (d), 6.92 – 7.19 (4-Cl-catH); ^{13}C NMR ($CDCl_3$): 100.3 (s), 100.4 (s), 125.5 (2s), 141.7 (2s), 162.5(2s), 163.1(s), 167.1 (2s), 118.2 – 147.7 (4-Cl-catH).

4 (mixture of two esters): HR-MS: *m*/*z* (E/I): 301.9750 (M^+); ^{1}H NMR ($CDCl_3$): $\delta = 2.91 - 3.45$ (m), 5.45 (dd), 6.27 (s), 6.77 – 7.13 (4-Cl-catH); ^{13}C NMR ($CDCl_3$): 36.6 (s), 36.7 (s), 79.5 (s), 79.6 (s), 118.4 (s), 159.1 (2s), 166.3 (s), 166.5 (s), 169.0 (2s), 117.8-148.4 (4-Cl-catH).

7: MS *m*/*z* (E/I): 176; ^{1}H NMR ($CDCl_3$): $\delta = 2.75$ (dd), 2.98 (dd), 5.38 (ddd), 7.48 (d); ^{13}C NMR ($CDCl_3$): 37.3, 76.2, 128.8, 146.4, 166.8, 172.1.

Received: August 22, 1997 [Z 10845 IE]
German version: *Angew. Chem.* **1998**, *110*, 527 – 530

Keywords: chlorocatechols · dioxygenases · enzyme mimetics · iron · non-heme iron complexes · oxygenations

[1] J. B. Broderick, T. V. O'Halloran, *Biochemistry* **1991**, *30*, 7349 – 7358.
[2] C. Hinteregger, M. Loidi, F. Streichsbier, *FEMS Microbiol. Lett.* **1992**, *97*, 261 – 266.
[3] C. B. Miguez, C. W. Greer, J. M. Ingram, *Can. J. Microbiol.* **1993**, *39*, 1 – 5.
[4] M. A. Bhat, T. Ishida, K. Horiike, C. S. Vaidyanathan, *Arch. Biochem. Biophys.* **1993**, *300*, 738 – 746.
[5] O. V. Maltseva, I. P. Solyanikova, L. A. Golovleva, *Eur. J. Biochem.* **1994**, *226*, 1053 – 1061.
[6] D. H. Ohlendorf, A. M. Orville, J. D. Lipscomb, *J. Mol. Biol.* **1994**, *244*, 586 – 608.
[7] A. M. Orville, N. Elango, D. H. Ohlendorf, J. D. Lipscomb, *J. Inorg. Biochem.* **1995**, *59*, 367.
[8] S. Han, L. D. Eltis, K. J. Timmis, S. W. Muchmore, J. T. Bolin, *Science* **1995**, *270*, 976 – 980.
[9] T. Senda, K. Sugiyama, H. Narita, T. Yamamoto, K. Kimbara, M. Fukuda, M. Sato, K. Yano, Y. Mitsui, *J. Mol. Biol.* **1996**, *255*, 735 – 752.
[10] T. Funabiki, H. Sakamoto, S. Yoshida, K. Tarama, *J. Chem. Soc. Chem. Commun.* **1979**, 754 – 755.
[11] T. Funabiki, A. Mizoguchi, T. Sugimoto, S. Yoshida, *Chem. Lett.* **1983**, 917 – 920.
[12] T. Funabiki, A. Mizoguchi, T. Sugimoto, S. Tada, M. Tsuji, H. Sakamoto, S. Yoshida, *J. Am. Chem. Soc.* **1986**, *108*, 2921 – 2932.
[13] T. Funabiki, T. Konishi, S. Kobayashi, A. Mizoguchi, M. Takano, S. Yoshida, *Chem. Lett.* **1987**, 719 – 722.
[14] T. Funabiki, I. Yoneda, M. Ishikawa, M. Ujiie, Y. Nagai, S. Yoshida, *J. Chem. Soc. Chem. Commun.* **1994**, 1453 – 1454.
[15] M. G. Weller, U. Weser, *J. Am. Chem. Soc.* **1982**, *104*, 3752 – 3754.
[16] M. G. Weller, U. Weser, *Inorg. Chim. Acta* **1985**, *107*, 243 – 245.
[17] D. D. Cox, S. J. Benkovic, L. M. Bloom, F. C. Bradley, P. J. Nelson, L. Que, Jr., D. E. Wallick, *J. Am. Chem. Soc.* **1988**, *110*, 2026 – 2032.
[18] D. D. Cox, L. Que, Jr., *J. Am. Chem. Soc.* **1988**, *110*, 8085 – 8092.
[19] H. G. Jang, D. D. Cox, L. Que, Jr., *J. Am. Chem. Soc.* **1991**, *113*, 9200 – 9204.
[20] A. Dei, D. Gatteschi, L. Pardi, *Inorg. Chem.* **1993**, *32*, 1389 – 1395.
[21] C. Sheu, A. Sobkowiak, S. Jeon, D. T. Sawyer, *J. Am. Chem. Soc.* **1990**, *112*, 879 – 881.
[22] W. O. Koch, H.-J. Krüger, *Angew. Chem.* **1995**, *107*, 2928 – 2981; *Angew. Chem. Int. Ed. Engl.* **1995**, *34*, 2671 – 2674.
[23] M. Duda, M. Pascaly, B. Krebs, *Chem. Commun.* **1997**, 835 – 836.
[24] "Oxygenases and Model Systems": T. Funabiki in *Catalysis by Metal Complexes*, *Vol. 19* (Eds.: R. Ugo, B. R. James), Kluwer, Dordrecht, **1997**, pp. 1 – 393 .
[25] T. Funabiki, T. Yamazaki, A. Fukui, T. Tanaka, S. Yoshida, unpublished results.
[26] D. T. Sawyer, *Oxygen Chemistry*, Oxford University Press, New York, **1991**, p. 21.
[27] T. R. Demmin, M. M. Rogic, *J. Org. Chem.* **1980**, *45*, 1153 – 1156.
[28] D. Ghosal, I.-S. You, D. K. Chatterjee, A. M. Chakrabarty, *Science* **1985**, *228*, 135 – 142.
[29] R. Blasco, R.-M. Wittich, M. Mallavarapu, K. N. Timmis, D. H. Pieper, *J. Biol. Chem.* **1995**, *270*, 29229 – 29235.

The Asymmetric Horner – Wadsworth – Emmons Reaction Mediated by An External Chiral Ligand**

Masashi Mizuno, Kunihiko Fujii, and Kiyoshi Tomioka*

The past decade has witnessed considerable activity in the area of asymmetric Horner – Wadsworth – Emmons (HWE) reactions of prochiral ketones for the synthesis of olefins with a chiral axis.[1] Asymmetric HWE reactions of anions derived from chiral phosphoranes,[2] phosphane oxides,[3] phosphonamides,[4] phosphonamidates,[5] and phosphonates[6] to produce chiral olefins have been well documented. Carboxylic acid derivatives with chiral alcohol[7] or amine[8] moieties also lead to chiral carbonyl olefination products. In spite of impressive progress with asymmetric reactions based on internal chiral auxiliaries, comparatively little effort has been

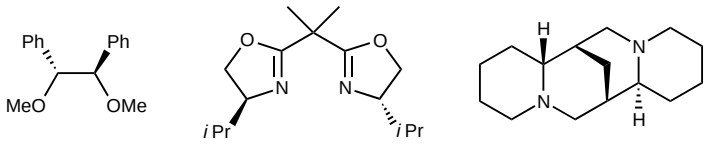
[*] Prof. Dr. K. Tomioka, M. Mizuno, K. Fujii
Graduate School of Pharmaceutical Sciences
Kyoto University
Yoshida, Sakyo-ku, Kyoto 606-01 (Japan)
Fax: (+81) 75-753-4604
E-mail: tomioka@pharm.kyoto-u.ac.jp

[**] We gratefully acknowledge financial support from the Japan Society for Promotion of Science (JSPS; RFTF-96P00302), the Japanese Ministry of Education, Science, Sports and Culture, and the Japanese Science and Technology Agency.

 © WILEY-VCH Verlag GmbH, D-69451 Weinheim, 1998 1433-7851/98/3704-0515 $ 17.50+.50/0

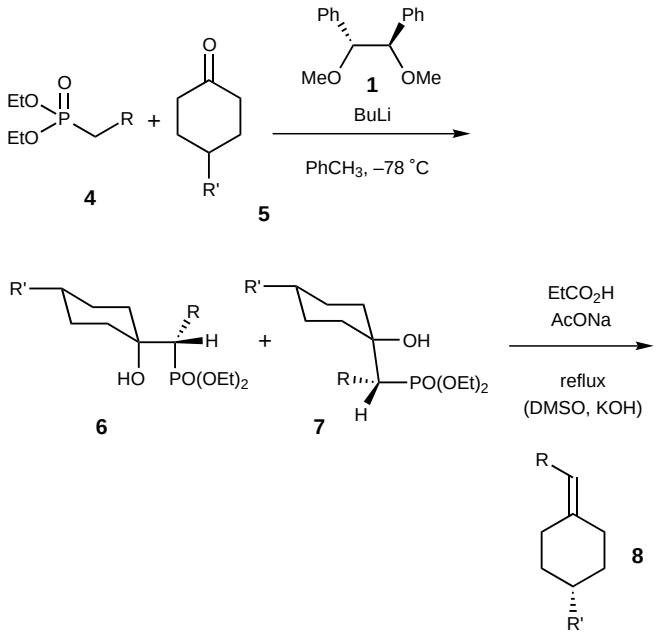
devoted to HWE or Wittig reactions controlled by external chiral ligands.[9, 10] We present here our approach to this problem, in which an achiral lithium phosphonate, controlled by an external chiral ligand, adds to a ketone, and the resulting chiral alcohol undergoes stereoselective olefination.[11]

Based on our previous studies on asymmetric reactions of lithiated carbonucleophiles,[12] chiral compounds **1**–**3** and



1 **2** **3**

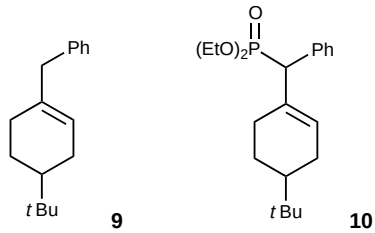
diethyl benzylphosphonate (**4**)[13] were chosen to be representative chiral ligands and the test nucleophile, respectively. Reaction of lithiated diethyl benzylphosphonate (**4**; R = Ph, 1.2 equiv) with 4-*tert*-butylcyclohexanone (**5**; R′ = *t*Bu) in the presence of **1** (1.4 equiv) in toluene at −78 °C for 0.5 h gave a separable diastereomeric mixture of (*S*)-*cis*-alcohol **6** and (*R*)-*trans*-alcohol **7** (R = Ph, R′ = *t*Bu)[14] in 82 and 12% *ee* and 89



4 **5** **6** **7** **8**

and 5% yield, respectively (Table 1, entry 1).[15] The chiral ligand **1** was recovered quantitatively.

Attempts to olefinate **6** (R = Ph, R′ = *t*Bu) by heating at 100 °C for 20 h in acetic acid[4, 16] gave an inseparable mixture of olefin **8** (R = Ph, R′ = *t*Bu) and isomerized olefin **9** in a ratio of 92:8 (73% yield) together with recovered **6** (9%). To minimize the production of **9** and to increase the conversion of **6**, compound **6** was heated in acetic acid at reflux in the presence of four equivalents of NaOAc for 2.5 h, which produced **8** in 79% yield and the dehydrated form of **10** in



9 **10**

14% yield. Compound **9** was not detected. Use of the less acidic propionic acid in place of acetic acid in the presence of NaOAc under reflux for 0.5 h gave **8** as the sole isolable product (85% yield). In the case of acid-sensitive compounds **6** or **8** (for example, allylidenecyclohexane), basic conditions were employed (KOH in DMSO, 50 °C, 0.5 h) to afford **8** in comparable yield.[3]

Heating **6** (82% *ee*, R = Ph, R′ = *t*Bu) with propionic acid/NaOAc it was readily provided (+)-(*S*)-benzylidene-4-*tert*-butylcyclohexane (**8**; R = Ph, R′ = *t*Bu) with 84% *ee* and no decrease in the enantiomeric purity of **6** (Table 1, entry 1). Heating **7** (12% *ee*, R = Ph, R′ = *t*Bu) also gave (+)-(*S*)-**8** with 12% *ee* in 76% yield, again without loss of enantiomeric purity in **7**. The absolute configuration of **8** (R = Ph, R′ = *t*Bu) was determined to be *S* by comparison of the specific rotation.[4b] Since the olefination is known to proceed in a *syn* fashion,[1] the absolute configurations of **6** and **7** (R = Ph, R′ = *t*Bu) are *S* and *R*, as indicated above. However, under the same addition reaction conditions, ligands **2**[17] and **3**[18] gave (*R*)- and (*S*)-**6** (R = Ph, R′ = *t*Bu) with only 15 and 17% *ee*, respectively.

Formation of a chelated complex with high enantioselectivity from the lithiated phosphonate and **1** requires warming the reaction mixture to 0 °C before adding **5**. In the absence of

Table 1. Asymmetric addition of phosphonates to 4-substituted cyclohexanones.

Entry	R	R′	**6**[a]		**7**[a]		**8**[b]		
			Yield [%]	*ee* [%]	Yield [%]	*ee* [%]	Yield [%]	*ee* [%]	Config.
1	Ph	*t*Bu	89	82	5	12	85	84	*S*
2	Ph	Me	92	71	7	0	84	70	*S*
3	Ph	Ph	94	64	4	51	80		
4	vinyl	*t*Bu	91	54	trace	–	83[c]	51	*S*
5	4-ClC_6H_4	*t*Bu	94	64	2	n.d.	84[c]		
6	1-naphthyl	*t*Bu	74	64	2	18	82[c]		
7	2-naphthyl	*t*Bu	99	90[d]	trace	–	84[c]		

[a] The *ee* values were determined by HPLC with a chiral stationary phase (Daicel Chiracel OD-H); n.d. = not determined. [b] The principal diastereomer **6** was transformed into **8**. The absolute configuration and *ee* value were established from the specific rotation of **8** (R = Ph, R′ = Me),[4b] (R = Ph, R′ = *t*Bu),[4b] and (R = vinyl, R′ = *t*Bu)[20]. The configuration was assigned by analogy to other olefins. [c] Olefination with DMSO/KOH at 50 °C. [d] The addition was carried out at −100 °C.

 © WILEY-VCH Verlag GmbH, D-69451 Weinheim, 1998 1433-7851/98/3704-0516 $ 17.50+.50/0

warming this reaction gave **6** (R = Ph, R′ = *t*Bu) with 79% *ee*.[19] Other 4-substituted cyclohexanones **5** were converted into the corresponding *cis*-alcohols **6** (R = Ph) and benzylidenecyclohexanes **8** (R = Ph) in 64-84% *ee* (Table 1, entries 1–3). Other diethyl phosphonates **4** (R = 4-ClPh, 1- and 2-naphthyl, vinyl) gave the corresponding alcohol **6** and olefins **8** in 51–90% *ee* (entries 4–7).

The reaction described, which is controlled by external chiral ligands, has the advantage that tedious steps in the synthesis of chiral phosphonate derivatives can be omitted. Furthermore, it may open the way to a catalytic asymmetric HWE reaction.

Experimental Section

A solution of BuLi in hexane (0.81 mL, 1.48 M, 1.2 mmol) was added to a solution of **1** (338 mg, 1.4 mmol) in toluene (6.5 mL) at −78 °C. After the mixtures was stirred for 0.5 h a solution of **4** (274 mg, 1.2 mmol) in toluene (2.0 mL) was added dropwise over 5 min. The solution was stirred for 0.5 h at −78 °C and then for 0.5 h at 0 °C. A solution of **5** (R′ = *t*Bu; 154 mg, 1.0 mmol) in toluene (2.0 mL) was added dropwise over 5 min at −78 °C, and the reaction mixture was stirred for 0.5 h at −78 °C before it was quenched with a saturated solution of aqueous NaCl (10 mL). The aqueous layer was extracted with ethyl acetate (3 × 10 mL) and the combined organic layers were washed with a saturated solution of aqueous NaCl (20 mL) and dried over sodium sulfate. Concentration followed by column chromatography (silica gel, hexane/ethyl acetate 5/1 then 1/1) gave (*S*)-**6** (R = Ph, R′ = *t*Bu; 340 mg, 89% yield, 82% *ee*) and (*R*)-**7** (R = Ph, R′ = *t*Bu; 18 mg, 5% yield, 12% *ee*) together with recovered **1** (337 mg, 90%).

A mixture of (*S*)-**6** (R = Ph, R′ = *t*Bu; 82% *ee*, 203 mg, 0.67 mmol) and sodium acetate (220 mg, 2.5 mmol) in propionic acid (1.0 mL) was stirred under reflux for 0.5 h. The mixture was allowed to cool to room temperature and then diluted with ethyl acetate (10 mL). The organic layer was washed successively with saturated solutions of sodium hydrogencarbonate (10 mL) and aqueous NaCl (10 mL), and then dried over sodium sulfate. Concentration and purification by column chromatography (silica gel, hexane) gave olefin (*S*)-**8** (R = Ph, R′ = *t*Bu; 156 mg, 85%) with 84% *ee*.

Received: September 23, 1997 [Z 10962 IE]
German version: *Angew. Chem.* **1998**, *110*, 525–527

Keywords: asymmetric synthesis · carbanions · lithium · olefinations

[1] a) L. Horner, *Pure Appl. Chem.* **1964**, *9*, 225–244; b) W. S. Wadsworth, Jr., W. D. Emmons, *J. Am. Chem. Soc.* **1961**, *83*, 1733–1738; c) W. S. Wadsworth, Jr., *Organic Reactions*, *Vol. 25*, Wiley, New York, **1977**, pp. 73–253; d) K. C. Nicolaou, M. W. Härter, J. L. Cunzner, A. Nadin, *Liebigs Ann.* **1997**, 1283–1301; e) E. L. Eliel, S. H. Wilen, *Stereochemistry of Organic Compounds*, Wiley, New York, **1994**, chap. 14.

[2] a) H. J. Bestmann, J. Lienert, *Angew. Chem.* **1969**, *81*, 751–752; *Angew. Chem. Int. Ed. Engl.* **1969**, *8*, 763–764; b) B. M. Trost, D. P. Curran, *J. Am. Chem. Soc.* **1980**, *102*, 5699–5700.

[3] N. J. S. Harmat, S. Warren, *Tetrahedron Lett.* **1990**, *31*, 2743–2746.

[4] S. Hanessian, S. Beaudoin, *Tetrahedron Lett.* **1992**, *33*, 7655–7658.

[5] S. E. Denmark, C.-T. Chen, *J. Am. Chem. Soc.* **1992**, *114*, 10674–10676.

[6] a) T. Takahashi, M. Matsui, N. Maeno, T. Koizumi, *Heterocycles*, **1990**, *30*, 353–357; b) K. Narasaka, E. Hidai, Y. Hayashi, J.-L. Gras, *J. Chem. Soc. Chem. Commun.* **1993**, 102–104; c) K. Tanaka, Y. Ohta, K. Fuji, T. Taga, *Tetrahedron Lett.* **1993**, *34*, 4071–4074.

[7] a) I. Tömösközi, G. Janzso, *Chem. Ind. (London)* **1962**, 2085–2086; b) H.-J. Gais, G. Schmiedl, W. A. Ball, J. Bund, G. Hellmann, I. Erdelmeier, *Tetrahedron Lett.* **1988**, *29*, 1773–1774; c) H. Rehwinkel, J. Skupsch, H. Vorbrüggen, *ibid.* **1988**, *29*, 1775–1776; d) N. Kann, T. Rein, *J. Org. Chem.* **1993**, *58*, 3802–3804; e) T. Furuta, M. Iwamura, *J. Chem. Soc. Chem. Commun.* **1994**, 2167–2168; f) T. Mandai, Y. Kaihara, J. Tsuji, *J Org. Chem.* **1994**, *59*, 5847–5849.

[8] A. Abiko, S. Masamune, *Tetrahedron Lett.* **1996**, *37*, 1077–1080.

[9] F. Toda, H. Akai, *J. Org. Chem.* **1990**, *55*, 3446–3447.

[10] T. Kumamoto, K. Koga, *Chem. Pharm. Bull.* **1997**, *45*, 753–755.

[11] K. Tomioka, *Synthesis* **1990**, 541–549.

[12] H. Fujieda, M. Kanai, T. Kambara, A. Iida, K. Tomioka, *J. Am. Chem. Soc.* **1997**, *119*, 2060–2061.

[13] Phosphonates used in this work were prepared by the Arbuzov reaction.

[14] There are many examples for the equatorial attack of phosphonate anions.[4, 5] The signals for benzylmethyl protons in **6** and **7** appeared at $\delta = 3.09$ and 3.50, consistent with literature values; see also J. E. Anderson, *J. Chem. Soc. Perkin 2* **1974**, 10–13.

[15] All new compounds were fully characterized.

[16] Treatment of **6** or **7** under Denmark's optimized neutral conditions[5a] led to recovery of the starting alcohol, not to **8**.

[17] A. Pfaltz, *Acc. Chem. Res.* **1993**, *26*, 339–345.

[18] P. Beak, A. Basu, D. J. Gallagher, Y. S. Park, S. Thayumanavan, *Acc. Chem. Res.* **1996**, *29*, 552–560.

[19] Repeated experiments without warming to 0 °C also led to slightly decreased *ee* values.

[20] M. Duraisamy, H. M. Walborsky, *J. Am. Chem. Soc.* **1983**, *105*, 3252–3264.

Methylalumoxane MCM-41 as Support in the Co-Oligomerization of Ethene and Propene with $[\{C_2H_4(1\text{-indenyl})_2\}Zr(CH_3)_2]$**

Lieven K. Van Looveren,* Daneel F. Geysen, Karen A. Vercruysse, Bart H. Wouters, Piet J. Grobet, and Pierre A. Jacobs

With the advent of single-site metallocene catalysts, the field of polymerization of α-olefins has been drastically changed.[1] Next to geometric manipulation of the metallocene structure to induce stereoregular polymerization, substitution or reduction of the excessive amounts of methylalumoxane (MAO) is an important challenge. MAO acts as a weakly coordinating anion and activates the metallocene structure. Heterogenization of the alumoxane structure on support materials like silica and alumina may be a solution to minimize the amounts of MAO. However, after impregnation of MAO or trimethylaluminum (TMA), addition of supple-

[*] Ir. L. K. M. Van Looveren, Ir. D. F. M. C. Geysen, Ir. B. H. J. Wouters, Ir. K. A. L. Vercruysse, Prof. Dr. P. J. Grobet, Prof. Dr. Ir. P. A. Jacobs
Centrum voor Oppervlaktechemie en Katalyse
Departement Interfasechemie, K. U. Leuven
Kardinaal Mercierlaan 92, B-3001 Heverlee (Belgium)
Fax: (+32) 16-321998
E-mail: lieven.vanlooveren@agr.kuleuven.ac.be

[**] This work was supported by an IUAP-PAI grant of the Belgian government. L.K.V.L. thanks IWT for a research grant. P.J.G. acknowledges the FWO for a research position. The constructive comments of D. De Vos are appreciated as well.

 © WILEY-VCH Verlag GmbH, D-69451 Weinheim, 1998 1433-7851/98/3704-0517 $ 17.50+.50/0

mentary MAO or TMA is still necessary to obtain catalytic activity. Moreover, the obtained polymers show a broadened molecular weight distribution.[2]

We describe a new heterogeneous alumoxane derivative generated by in situ hydrolysis of TMA in the mesopores of the siliceous molecular sieve MCM-41. The spectroscopic and physicochemical features of the solids obtained point to the formation of an MAO phase chemically linked to the pore walls of the support. This MAO phase is accessible for interaction with zirconocene and does not require supplementary MAO for co-oligomerization of ethene and propene. Especially at low concentrations the MAO-MCM-41 is catalytically more active than the corresponding silica-based MAO derivative or the homogeneous system. The molecular weight and physical properties of the co-oligomers are dependent on the pore size of MCM-41, which suggests shape-selective oligomerization. The main advantage of in situ alumoxane synthesis over physisorption is that cluster aggregation is prevented. The subtle balance between anchoring to the MCM-41 surface and delocalization of the negative charge determines the weakly coordinating properties of the alumoxane compound.

The siliceous mesoporous molecular sieves MCM-41 were synthesized according to published procedures with different quaternary ammonium compounds as surfactant.[3, 4] If $C_nH_{2n+1}(CH_3)_3N^+X^-$ with $n = 10$, 14, or 16 are used, d_{100} spacings of 2.89, 3.50 and 3.99 nm, respectively, result. Various silica sources (Ludox, Cab-O-Sil, and TEOS) were used for the synthesis. The alumoxane-MCM-41 materials were prepared by controlled in situ hydrolysis of TMA in a continuously stirred, cooled reactor at 273 K. During TMA treatment the OH overtone at 6900 cm^{-1} and the combination band at 5208 cm^{-1} of the water-containing MCM-41 disappear, while a CH overtone and a combination band appear at 5952 and 4386 cm^{-1}, respectively.[5] At the same time a charge transfer band (Al→O), characteristic for an alumoxane-type structure,[6] shows up as a broad band around 300 nm in the diffuse reflectance spectrum. ^{13}C *c*ross-*p*olarized (CP) *m*agic *a*ngle *s*pinning (MAS) NMR spectrum of alumoxane-MCM-41 reveals the presence of a broad band at $\delta = -7.4$, assigned to the methyl group of the alumoxane compound. No sharp signal of associated TMA ($\delta = -5.3$) is superimposed on this broad band, indicating complete conversion of TMA into alumoxane.[7] The fate of the silanol groups is followed by ^{29}Si CP-MAS NMR (Figure 1). The CP mode selectively highlights the Si atoms with bound hydroxyl groups, such as $[Si(OSi)_2(OH)_2]$ (Q_2, $\delta = -91.6$) and $[Si(OSi)_3(OH)]$ (Q_3, $\delta = -100.6$).[8] Si atoms with four neighboring Si atoms (Q_4) are silent in the CP mode. The disappearance of the Q_2 and Q_3 resonances after treatment with TMA clearly demonstrates the covalent bonding of the alumoxane to the silanol groups of the MCM-41. The ^{27}Al MAS NMR spectrum of the alumoxane-MCM-41 (Figure 2) displays a broad resonance between $\delta = 0$ and 80 due to the interaction of the Lewis acidic Al center of the alumoxane with the O bridging atoms of the mesoporous support. Different Al environments with tri-, tetra-, penta-, or hexacoordinated Al may contribute to this band. The ^{27}Al MAS NMR spectrum of the MAO-physisorbed system as well as of pure MAO does not reveal these particular coordinations, because of strong internal clustering of the alumoxane structure (Figure 2).

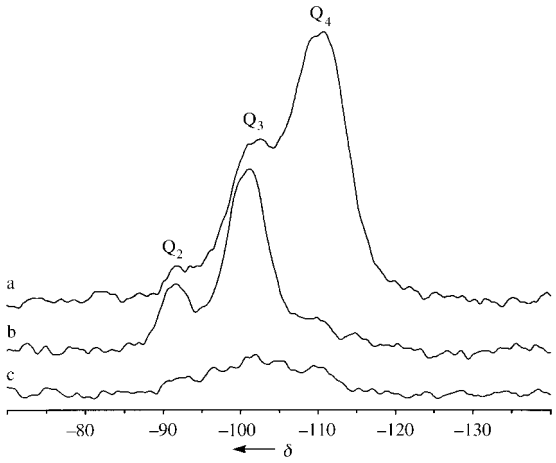


Figure 1. a) ^{29}Si MAS NMR spectrum of hydrated MCM-41 synthesized with Ludox. b) ^{29}Si CP-MAS NMR spectrum of hydrated MCM-41 and c) of alumoxane-MCM-41.

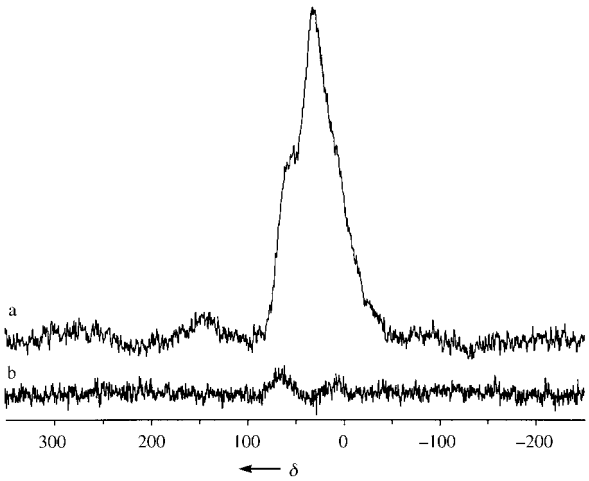


Figure 2. ^{27}Al MAS NMR spectrum of a) alumoxane-MCM-41 (3000 accumulations) and of b) MAO physisorbed onto MCM-41 (10000 accumulations).

Electron probe microanalysis (EPMA) reveals an average Si/Al ratio of 0.88, with a deviation as small as 0.11. Thus 72 mol% of the added TMA is incorporated as alumoxane, which is homogeneously distributed in the mesoporous host. The alumoxane formation reduces the average pore diameter of MCM-41 from 2.75 to 2.40 nm and its surface area from 880 to 470 $m^2 g^{-1}$. Capillary condensation within the pores of the alumoxane-MCM-41 disappears, which illustrates that the uniform pores are narrowed from mesoporous to microporous dimensions.

To obtain the final catalyst, *rac*,*meso*-ethylenebis(1-indenyl)dimethylzirconium ($[\{C_2H_4(ind)_2\}Zr(CH_3)_2]$) was added to a vigorously stirred suspension of in situ prepared alumoxane-MCM-41 in toluene. Table 1 shows representative activities for the co-oligomerization of ethene and propene with $[\{C_2H_4(ind)_2\}Zr(CH_3)_2]$/alumoxane-MCM-41 with various

 © WILEY-VCH Verlag GmbH, D-69451 Weinheim, 1998 1433-7851/98/3704-0518 $ 17.50+.50/0

Table 1. Co-oligomerization of ethene and propene with the *ansa*-metallocene $[\{C_2H_4(ind)_2\}Zr(CH_3)_2]$ on alumoxane-MCM-41 at 343 K in toluene.

Entry	Support components[a]	Al/Zr[b]	Activity[c]	M_n[d]	M_w/M_n[d]	P [mol %][e]
1	Ludox, C_{16}	180	4.12	1280	1.99	55.8
2	Ludox, C_{14}	180	3.85	1730	1.94	54.6
3	Ludox, C_{16}	360	4.37	830	1.97	58.0
4	Cab-O-Sil, C_{10}	360	4.32	880	2.00	57.9
5	Ludox, C_{16}	90	3.55	1890	1.99	53.5
6	TEOS, C_{16}	360	4.45	790	1.87	56.4
7	TEOS, C_{16}	180	4.34	830	2.08	55.9
8	TEOS, C_{16}	90	4.30	940	2.13	55.8
9	TEOS, C_{16}	40	3.88	1280	1.94	55.3
10	Ludox, C_{16}[f]	90	2.43	5590	–	56.7
11	Ludox, C_{16}[f]	90	2.43	960	2.46	45.1

[a] The MCM-41 samples were synthesized from Ludox, Cab-O-Sil, or TEOS as silica source with C_{16}TMACl, C_{14}TMABr, or C_{10}TMABr as surfactant. [b] The Al/Zr ratio was determined based on the Al content of the alumoxane-MCM-41. [c] Co-oligomerization activity (10^6 g(per mol Zr) h^{-1}) of the zirconocene after 75 min reaction time. [d] The number-average molecular weight (M_n) in g mol^{-1} and polydispersity (M_w/M_n) of the co-oligomer were correlated to polystyrene standards and determined on a GPC Chrompack Microgel 3 Mix column with a refractive index detector. [e] P = overall mol % propene incorporated in the co-oligomer chain, based on GC conversion after 75 min. [f] The oligomerization temperature of reactions 10 and 11 was 308 K and 373 K, respectively.

Al/Zr ratios. The polydispersity of the co-oligomer is always around 2, pointing to the occurrence of single-site catalysis.

There is, however, a clear pore size effect. Narrowing the pore size by altering the surfactant chain length during synthesis (entries 1–4) results in an increase of the molecular weight and alters the physical properties of the product from liquid (pour point 253 K) to wax (pour point 265 K). The effect of the pore size on the molecular weight is more pronounced at a lower Al/Zr ratio (entries 1 and 2). A smaller pore diameter of the alumoxane-MCM-41 is expected to lower the incorporation of metallocene molecules into the tubular pores of the host, which is reflected in a decreased oligomerization activity.

Generally, at a smaller Al/Zr ratio, the activity decreases and the molecular weight increases, because less propene is incorporated in the co-oligomer chain (entries 1, 3, and 5). Increasing the reaction temperature from 308 K (entry 10) to 343 K (entry 5) has a positive effect on the oligomerization activity and decreases the molecular weight. A further increase of the reaction temperature to 373 K (entry 11) has a negative influence on the activity and increases the molecular weight. At such high temperatures, the decreased solubility of propene in the reaction solvent becomes a limiting factor.

When tetraethyl orthosilicate (TEOS) is used as Si source instead of Ludox in the MCM-41 synthesis, the oligomerization activity increases and the molecular weight decreases for all Al/Zr ratios studied (compare entries 3, 1, and 5 with 6, 7, and 8, respectively). The surfactant chain length was identical in both series of samples. The ^{29}Si MAS NMR spectrum of the hydrated MCM-41 synthesized with TEOS shows a clear decrease in silanol content, as reflected by lower Q_2/Q_4 and Q_3/Q_4 ratios of 6.6×10^{-2} and 4.2×10^{-1} respectively, relative to the Ludox sample ($Q_2/Q_4 = 9.2 \times 10^{-2}$ and $Q_3/Q_4 = 4.4 \times 10^{-1}$). A decrease in the Q_2 and Q_3 concentrations is expected to provide less docking points for the alumoxane on the mesoporous support. This may increase the charge delocalization in the alumoxane structure, hereby producing a more weakly coordinating anion and a higher activity.

In Table 2 the alumoxane-MCM-41 is compared with homogeneous MAO and different alumoxane derivatives under identical reaction conditions. The oligomerization activity of the optimal alumoxane-MCM-41 sample (Table 1, entries 6, 7, and 8) exceeds that of the homogeneous system (Table 2, entries 1, 2, and 3) at all Al/Zr ratios tested. The alumoxane-MCM-41 (Table 1, entry 9) even retains a high activity at a reduced Al/Zr ratio of 40, where the homogeneous system is catalytically inert. A lower activity was also observed when alumoxane was formed on an amorphous, pyrogenic silica (Aerosil; Table 2, entry 4). The higher accessible surface area for the metallocene catalyst in the alumoxane-MCM-41 than in the alumoxane-Aerosil reduces the possibility of deactivation by binuclear complex formation, which is reported as the most probable way to form inactive sites after immobilization.[9] Physisorption of commercial MAO on MCM-41 results in a heterogeneous support with a much higher Si/Al ratio (3.27 ± 0.42 by EPMA measurement) than that for the in situ formed alumoxane. With such a physisorbed system lower activities than with the homogeneous system have been observed in the isotactic polymerization of propene with *rac*-$[\{C_2H_4(ind)_2\}ZrCl_2]$.[10] Moreover, in our oligomerization setup no significant activity is observed for the MAO-physisorbed system at an Al/Zr ratio of 90 (Table 2, entry 5). It seems therefore more appropriate to anchor and to finely distribute the alumoxane structure onto the silanol groups of the mesoporous material by in situ hydrolysis.

Table 2. Comparison of the co-oligomerization of ethene and propene with $[\{C_2H_4(ind)_2\}Zr(CH_3)_2]$ on different alumoxane derivatives at 343 K in toluene.

Entry	Support	Al/Zr	Activity	M_n	M_w/M_n	P [mol %]
1	MAO[a]	360	4.34	840	2.05	58.1
2	MAO[a]	180	4.14	1110	2.14	57.8
3	MAO[a]	90	4.15	1150	2.06	57.9
4	Aerosil[b]	360	2.81	2170	1.91	47.6
5	MAO on MCM-41[c]	90	–	–	–	–

[a] Reference experiment under homogeneous conditions. [b] Alumoxane-Aerosil is synthesized by in situ hydrolysis of TMA. [c] MAO is physisorbed on MCM-41 synthesized with Ludox as silica source and C_{16}TMACl as surfactant. (see footnote [e] of Table 1 for definition of P).

Experimental Section

Support syntheses: Typically, MCM-41 was synthesized from a gel with the molar composition of SiO_2:TEAOH:C_{16}TMACl:H_2O 1.00:0.21:0.30:44.81. The silica source was Ludox AS 40, and the templating agent tetraethylammonium hydroxide (TEAOH) and hexadecyltrimethylammonium chloride (C_{16}TMACl). After heating at 383 K for 24 hours in an autoclave, washing with water and ethanol, the sample was dried and calcined at 813 K for 10 hours. X-ray diffraction (Siemens D5000, $Cu_{K\alpha}$ source with $\lambda =$

0.1542 nm) showed the four peaks of MCM-41 between 1° and 12° (2θ) A d_{100} spacing of 3.99 nm was observed after calcination. In the synthesis of MCM-41 with C_{14}TMABr, a similar gel composition was made. A d_{100} spacing of 3.50 nm was observed after calcination. In the synthesis of MCM-41 with C_{10}TMABr as surfactant, the molar composition of the gel was SiO_2:TMAOH:C_{10}TMABr:Na_2O:H_2O 1.00:0.09:0.32:0.09:63.45. A d_{100} spacing of 3.03 nm was observed after calcination. In the same way MCM-41 was obtained with TEOS as Si source with the following composition: TEOS:C_{16}TMACl:NaOH:H_2O = 1.00:0.11:0.49:54.09.

In situ hydrolysis of TMA: The calcined MCM-41 samples and Aerosil 380 (Degussa) were equilibrated against a relative humidity of 79.3% at room temperature; thereafter they contained 16–27 wt% of sorbed water. The water-saturated sample was suspended in 270 mL toluene in the reactor, which was flushed with nitrogen and cooled to 273 K under continuous stirring for 1 h. TMA (2.0 M solution in toluene) was diluted in 20 mL toluene and added slowly to the suspension to give a water/Al ratio of 1. The alumoxane-MCM-41 was filtered, washed with toluene, and dried under inert atmosphere. Diffuse reflectance measurements were performed on a Varian Cary 05 UV/Vis/NIR spectrophotometer. Nitrogen sorption isotherms were recorded at 77 K with an Omnisorp 100 CX from Coulter. EPMA measurements were obtained on a JEOL JXA 733 scanning electron microscope using pure SiO_2 and Al_2O_3 as standards. ^{29}Si MAS NMR was performed on a BRUKER AMX 300 spectrometer operating at 59.62 MHz with excitation pulses of 3.5 μs and a spinning frequency of 4 kHz. ^{29}Si CP-MAS NMR was measured with a contact time of 1 ms. ^{27}Al MAS NMR measurements were carried out on a BRUKER MSL 400 with a resonance frequency of 104.26 MHz for Al, excitation pulses of 0.61 μs, and a spinning frequency of 12 kHz.

Catalyst preparation: [{C_2H_4(ind)$_2$}Zr(CH_3)$_2$] (0.036 mmol), obtained from the dichloride [{C_2H_4(ind)$_2$}ZrCl_2] by alkylation with TMA, was added under nitrogen atmosphere to the suspension of in situ prepared alumoxane-MCM-41 (Al/Zr ratios of samples were 360, 180, 90, and 40). Physisorption of MAO (85 g of a 10 wt% solution in toluene, Witco) on the calcined MCM-41 sample (0.77 g) was performed for 3 h at room temperature under inert atmosphere. The suspension was filtered and washed several times with toluene. Chemical analysis of the support shows that only 2.5 mol% of the added Al is anchored to the MCM-41 structure.

Co-oligomerization reactions: The reactions were performed for 75 min in a 600 mL water-cooled batch reactor (Parr) continuously fed with a flow of methane (491 mL min^{-1}), ethene (700 mL min^{-1}), propene (1400 mL min^{-1}), nitrogen (40 mL min^{-1}) and hydrogen (500 mL min^{-1}) at an overall pressure of 0.7 MPa. The solvent and the gases used were carefully dried over a molecular sieve (5 Å, Merck). The gas outlet was monitored by GC to calculate the conversion (methane as internal standard).

Received: August 28, 1997 [Z 10866 IE]
German version: *Angew. Chem.* **1998**, *110*, 540–543

Keywords: aluminum · heterogeneous catalysis · metallocenes · oligomerizations · zeolite analogues

[1] a) H. Sinn, W. Kaminsky, H. J. Vollmer, R. Woldt, *Angew. Chem.* **1980**, *92*, 396; *Angew. Chem. Int. Ed. Engl.* **1980**, *19*, 390; b) F. R. W. P. Wild, L. Zsolnai, G. Huttner, H. H. Brintzinger, *J. Organomet. Chem.* **1982**, *232*, 233; c) W. Kaminsky, K. Külper, H. H. Brintzinger, F. R. W. P. Wild, *Angew. Chem.* **1985**, *97*, 507; *Angew. Chem. Int. Ed. Engl.* **1985**, *24*, 507.

[2] a) J. C. W. Chien, D. He, *J. Polym. Sci.* **1991**, *12*, 367; b) M. Kaminaka, K. Soga, *Makromol. Chem. Rapid Commun.* **1992**, *13*, 221; c) M. Kaminaka, K. Soga, *Makromol. Chem.* **1992**, *194*, 1745; d) W. Kaminsky, F. Renner, *Makromol. Chem. Rapid Commun.* **1993**, *14*, 239; e) W. Kaminsky, *Macromol. Chem. Phys.* **1996**, *197*, 3907.

[3] a) C. T. Kresge, M. E. Leonowicz, W. J. Roth, J. C. Vartuli, J. S. Beck, *Nature* **1992**, *359*, 710; b) J. S. Beck, J. C. Vartuli, W. J. Roth, M. E. Leonowicz, C. T. Kresge, K. D. Schmitt, C. T.-W. Chu, D. H. Olson, E. W. Sheppard, S. B. McCullen, J. B. Higgins, J. L. Schlenker, *J. Am. Chem. Soc.* **1992**, *114*, 10834.

[4] a) J. S. Beck, C. T.-W. Chu, I. D. Johnson, C. T. Kresge, M. E. Leonowicz, W. J. Roth, J. C. Vartuli (Mobil Oil Corporation), WO-B 91/11390, **1991** [*Chem. Abstr.* **1991**, *115*, 139158 U]; b) J. S. Beck, J. C. Vartuli, C. T. Kresge, *Chem. Mater.* **1994**, *6*, 1816.

[5] X. S. Zhao, G. Q. Lu, A. K. Whittaker, G. J. Millar, H. Y. Zhu, *J. Phys. Chem. B* **1997**, *101*, 6525.

[6] E. Giannetti, G. M. Nicoletti, R. Mazzocchi, *J. Polym. Sci.* **1985**, *23*, 2117.

[7] D.-H. Lee, S.-Y. Shin, *Macromol. Symp.* **1995**, *97*, 195.

[8] G. Engelhardt, D. Michel, *High-resolution Solid-State NMR of Silicates and Zeolites*, Wiley, Chichester, **1987**.

[9] W. Kaminsky, R. Steiger, *Polyhedron* **1988**, *7*, 2375.

[10] a) J. Tudor, D. O'Hare, *J. Chem. Soc. Chem. Commun.* **1997**, 603; b) Y. S. Ko, T. K. Han, J. W. Park, S. I. Woo, *Macromol. Rapid Commun.* **1996**, *17*, 749.

Iterative Nucleophilic and Electrophilic Additions to Coordinated Cyclooctatetraene: An Efficient Route to *cis*-5,7-Disubstituted 1,3-Cyclooctadienes**

Jürgen Heck,* Gerhard Lange, and Oliver Reimelt

Dedicated to Professor Wolfgang Beck on the occasion of his 65th birthday

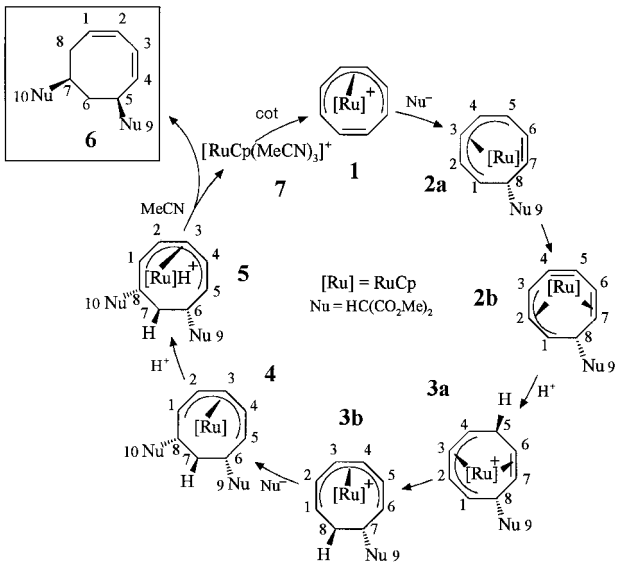
Hitherto, cyclooctatetraene (cot) played only a minor role as a starting material in the stereocontrolled synthesis of *cyclo*-C_8 compounds.[1, 2] From the point of view of synthetic chemistry, cot became more interesting as a complexing ligand.[3] It is usually functionalized by electrophilic substitution[4] and addition,[5] and more recently by photochemical reactions;[6] however, nucleophilic addition has seldom been used thus far despite its synthetic potential.[7, 8] With an iterative method involving nucleophilic and electrophilic additions, *cis*-5,7-difunctionalized 1,3-cyclooctadiene has now been prepared for the first time by a very simple route. These kinds of cyclooctadienes containing two stereogenic centers are representatives of a rare,[9] but remarkable class of compounds that show great synthetic potential with regard to terpenoid *cyclo*-C_8 compounds.

The starting material for our studies of the stereo- and regioselective functionalization of cot is [Ru(Cp)(η^6-cot)]$^+$ (**1**, Cp = cyclopentadienyl), which can be recovered after completion of the reaction cycle (Scheme 1). The first nucleophilic addition of the dimethyl malonate anion to **1** occurs *exo* to the metal center[10] and leads initially, as expected,[11] to the 1,2,3,4,5-η-cyclooctatrienyl complex **2a**, which gradually rearranges to the 1,2,3-η:6,7-η-haptomer **2b**.[12] The thermal stability of **2a** is sufficient, however, to allow, for the most part, its separation from **2b** by chromatographic methods. The stereochemistry of both haptomers can

[*] Prof. Dr. J. Heck, Dr. G. Lange, O. Reimelt
Institut für Anorganische und Angewandte Chemie der Universität
Martin-Luther-King-Platz 6, 20146 Hamburg (Germany)
Fax: (+49) 40-4123-6349
E-mail: heck@chemie.uni-hamburg.de

[**] This work was supported by the Deutsche Forschungsgemeinschaft (HE 1309/2-1). We thank BASF for the donation of cyclooctatetraene.

 © WILEY-VCH Verlag GmbH, D-69451 Weinheim, 1998 1433-7851/98/3704-0520 $ 17.50+.50/0



Scheme 1. Reaction cycle for the formation of *cis*-5,7-disubstituted 1,3-cyclooctadiene **6**.

unequivocally be determined by $^1H-{}^1H$ and $^1H-{}^{13}C$ correlation NMR spectra. Essential for the analysis of the ^1H NMR spectra is the coupling of the proton on the C atom that carries the nucleophile (C8): in **2a** this proton couples with neighboring protons of a coordinated and a noncoordinated C=C double bond, and in **2b** the proton on C8 exclusively couples with protons of metal-bound C atoms.

To further functionalize the *cyclo*-C_8 ligand, an electrophilic addition is performed by protonating **2b** with HBF_4, which takes place at position 5. The *cyclo*-C_8 ligand in the product cation **3a** shows 1,2,3,4-η:6,7-η coordination, but rearranges within several days at room temperature to a 1,2,3,4,5,6-η bonding mode (**3b**). The different hapticity of the two isomers is clearly evident from 2D correlation NMR spectra. An important difference between the ^1H NMR spectra of **3a** and **3b** results from the vicinal position of the *endo*-cyclic CH_2 group with respect to the C atom on which the nucleophilic addition in **3b** occurred; only $^1H-{}^1H$ coupling to metal-bound CH units is observed for the CH_2 group in **3a**. Protonation experiments with partially deuterated HBF_4 indicate a metal-assisted 1,5-H migration, as the deuterium atom remains *endo* relative to the Ru center in both **3a** and **3b**.[13]

The second nucleophilic addition is targeted at the terminal C atom of the metal-bound part of the ligand in **3b** farthest away from the first nucleophile. In this way, the 6,8-difunctionalized cyclooctadienyl complex **4** is formed, whose ^1H and ^{13}C NMR spectra have considerably fewer resonance signals than the corresponding spectra of **2a**, **b** and **3a**, **b** (Table 1) due to the local C_s symmetry of the *cyclo*-C_8 ligand. This result proves that the second nucleophile, like the first, is added *exo* to the metal center. It is noteworthy that **4** is formed exclusively even from mixtures of **3a** and **3b** in which the molar amount of **3b** is much less than the molar amount of **4** obtained.

Compound **4** can be protonated to the complex cation **5**, which shows a ^1H NMR spectrum very similar to that of **4**.

Table 1. Selected Spectroscopic data for **2**–**6**.[a]

2a: ^1H NMR (360 MHz, C_6D_6): $\delta = 4.43$ (s, Cp), 3.38 (s, CH_3), 3.27 (s, CH_3), 4.41 (m, 1-H), 4.30 (dd, 2-H), 5.51 (m, 3-H, 6-H), 4.10 (dd, 4-H), 3.66 (t, 5-H), 5.89 (m, 7-H), 3.74 (m, 8-H), 3.31 (d, 9-H); $^{13}C\{^1H\}$ NMR (50 MHz, C_6D_6): $\delta = 79.6$ (Cp), 169.3, 168.9 (C=O), 51.8, 51.6 (CH_3), 39.1 (C-1), 75.5 (C-2), 99.5 (C-3), 76.4 (C-4), 40.4 (C-5), 129.3 (C-6), 126.6 (C-7), 43.2 (C-8), 60.3 (C-9)

2b: IR (Nujol): $\tilde{\nu} = 1733$ (C=O), 1651 cm^{-1} (C=C); ^1H NMR (360 MHz, C_6D_6): $\delta = 4.34$ (s, Cp), 3.34 (s, CH_3), 3.90 (dd, 1-H), 3.38 (dd, 2-H), 4.57 (dd, 3-H), 5.44 (dd, 4-H), 5.73 (dd, 5-H), 3.86 (dd, 6-H), 2.95 (t, 7-H), 4.48 (m, 8-H), 4.00 (d, 9-H). $^{13}C\{^1H\}$ NMR (50 MHz, C_6D_6): $\delta = 80.5$ (Cp), 58.3 (CH_3) 169.3, 168.9 (C=O), 31.4 (C-1), 78.4 (C-2), 65.3 (C-3), 134.7 (C-4), 136.6 (C-5), 68.5 (C-6), 23.5 (C-7), 40.3 (C-8), 52.1 (C-9). MS (70 eV): *m*/*z* (%): 401 (91) [M^+]

3a: IR (Nujol): $\tilde{\nu} = 1733$ (C=O), 1252–1156 (C–O), 1048 cm^{-1} (BF_4); ^1H NMR (360 MHz, [D_6]acetone): $\delta = 5.59$ (s, Cp), 3.72 (s, CH_3), 3.67 (s, CH_3), 4.79 (t, 1-H), 5.60 (m, 2-H), 5.81 (t, 3-H) 4.56 (m, 4-H), 3.22 (m, 5_{endo}-H), 1.81 (m, 5_{exo}-H), 3.63 (m, 6-H), 3.92 (t, 7-H), 4.17 (m, 8-H), 3.09 (d, 9-H); $^{13}C\{^1H\}$ NMR (50 MHz, [D_6]acetone): $\delta = 83.8$ (Cp), 52.1 (CH_3), 167.7 (C=O), 41.4 (C-1), 90.6 (C-2), 90.9 (C-3), 32.3 (C-4), 17.9 (C-5), 52.3 (C-6), 35.6 (C-7), 33.2 (C-8), 55.2 (C-9), partially deuterized **3a** $\delta = 17.6$ (t, $^1J_{C,D} = 24.6$ Hz, C-5); MS (70 eV) *m*/*z* (%): 401 (18) [M^+][b]

3b: ^1H NMR (360 MHz, [D_6]acetone): $\delta = 5.67$ (s, Cp), 3.73 (s, CH_3), 3.65 (s, CH_3), 6.11 (dd, 1-H), 5.43 (m, 2-H), 6.96 (t, 3-H), 6.84 (dd, 4-H), 6.26 (t, 5-H), 5.42 (m, 6-H), 3.92 (m, 7-H), 1.63 (m, 8_{endo}-H), −0.95 (m, 8_{exo}-H), 3.40 (d, 9-H); $^{13}C\{^1H\}$ NMR (50 MHz, [D_6]acetone): $\delta = 87.2$ (Cp), 52.3 (CH_3), 86.7 (C-1), 85.7 (C-2), 105.6 (C-3), 95.5 (C-4), 83.3 (C-5), 78.0 (C-6), 27.4 (C-7), 32.3 (C-8), 58.0 (C-9); partially deuterized **3b**: $\delta = 27.1$ (t, $^1J_{C,D} = 20.3$ Hz, C-7)

4: IR (KBr): $\tilde{\nu} = 2988$, 2947, 2923, 1729 (C=O), 1228 cm^{-1} (C–O); ^1H NMR (360 MHz, C_6D_6): $\delta = 4.45$ (s, Cp), 3.37, (s,CH_3) 3.35 (s, CH_3), 3.84 (dm, 1-H, 5-H), 4.01 (dd, 2-H, 4-H), 5.63 (t, 3-H), 2.83 (dddd, 6-H, 8-H), 1.30 (dt, 7_{endo}-H), 0.19 (m, 7_{exo}-H), 3.41 (d, 9-H, 10-H); $^{13}C\{^1H\}$ NMR (50 MHz, C_6D_6): $\delta = 80.2$ (Cp), 61.6 (CH_3), 169.1, 168.8 (C=O), 44.1 (C-1, C-5), 72.3 (C-2, C-4), 103.1 (C-3), 42.9 (C-6, C-8), 27.8 (C-7), 51.6 (C-9, C-10); partially deuterized **4**: $\delta = 27.4$ (t, $^1J_{C,D} = 17.4$ Hz, C-7); MS (70 eV): *m*/*z* (%): 532 (11) [M^+]

5: IR (KBr): $\delta = 3117$ (CH), 2956 (CH), 1732 (C=O), 1244 (C–O), 1058 cm^{-1} (BF_4); ^1H NMR (360 MHz, CD_2Cl_2): $\delta = 5.52$ (s, Cp), 3.76 (s, CH_3), 3.72 (s, CH_3), 3.85 (t, 1-H, 5-H), 5.58 (m, 2-H, 4-H), 7.05 (t, 3-H), 2.66 (m, 6-H, 8-H), 1.24 (m, 7_{endo}-H), 0.27 (m, 7_{exo}-H), 3.36 (d, 9-H, 10-H), −10.6 (s, RuH)

6: IR (Nujol): $\tilde{\nu} = 1742$ (C=O), 1253, 1156, 1024 cm^{-1} (C–O); ^1H NMR (360 MHz, $CDCl_3$): $\delta = 3.761$, 3.754, 3.747, 3.736 (s, 4x3 H, CH_3), 5.84 (m, 1-H), 6.02 (dd, $^3J_{2,3} = 3.3$ Hz, $^3J_{1,2} = 10.7$ Hz, 2-H), 5.95 (dd, $^3J_{3,4} = 11.0$ Hz, $^3J_{2,3} = 3.3$ Hz, 3-H), 5.60 (dd, $^3J_{3,4} = 11.0$ Hz, $^3J_{4,5} = 8.0$ Hz, 4-H), 2.88 (m, 5-H), 1.49 (m, 6-H), 1.26 (m, 6′-H), 2.14 (m, 7-H), 2.30 (m, 8-H), 1.88 (m, 8′-H), 3.47 (d, $^3J_{5,9} = 8.2$ Hz, 9-H), 3.33 (d, $^3J_{7,10} = 7.7$ Hz, 10-H); ^{13}C NMR (50 MHz $CDCl_3$): $\delta = 169.0$, 168.2 (C=O), 57.9, 57.2 (C-9, C-10), 52.4 (CH_3) 132.0, 130.6, 127.8, 126.8 (C-1–C-4), 38.2, 35.5, 31.7, 31.4 (C-5–C-8); MS (70 eV): *m*/*z* (%): 368 (4) [M^+], 336 (5), 305 (8), 276 (13), 236 (17), 189 (20), 176 (49), 133 (21), 117 (89), 105 (100)

[a] Assignment of the NMR signals according to Scheme 1. [b] [M = **3b** – BF_4].

However, with the exception of the signals for 1-H and 5-H, the corresponding resonance signals of the metal-bound parts of the ligands are shifted more than 1 ppm downfield. Moreover a resonance signal is observed at $\delta = -10.6$, which is characteristic for a metal-bound H atom.

When **5** is dissolved in acetonitrile, the *cyclo*-C_8 ligand is cleaved spontaneously. $[Ru(Cp)(MeCN)_3]^+$ (**7**) is formed, which can react with cot to recover **1** again. The organic product was unequivocally identified with the aid of 1D and 2D NMR spectra as isomerically pure *cis*-5,7-disubstituted 1,3-cyclooctadiene (**6**). Compound **6**, which is also formed

when **4** is protonated directly in the presence of acetonitrile, is obtained in 46% yield with respect to the starting cot complex **1**!

Experimental Section

2a,b: A solution of sodium dimethyl malonate (286 mg, 1.8 mmol) in THF (20 mL) was added dropwise to a suspension of **1**-PF_6 (748 mg, 1.8 mmol) in THF (50 mL) at −78 °C. After warming to room temperature the solvent was removed under reduced pressure. The residue was extracted with diethyl ether, and the extract filtered through kieselguhr. After removal of the solvent the product was obtained as a pale yellow powder (yield: 561 mg, 78%). The haptomers **2a** and **2b** were, for the most part, separated by column chromatography (Al_2O_3/5% H_2O, toluene/diethyl ether 1/1). Elemental analysis calcd for $C_{18}H_{20}O_4Ru$ (401.41): C 53.86, H 5.02; found: C 54.12, H 5.18.

3a,b: A mixture of **2a** and **2b** (652 mg, 1.6 mmol) was dissolved in diethyl ether (50 mL) and allowed to react with $HBF_4 \cdot OEt_2$ (54%, 0.23 mL) at −78 °C. After warming to room temperature the mixture was filtered, and the residue washed several times with diethyl ether. The yellow filter residue was dissolved in CH_2Cl_2. The mixture of the products **3a** and **3b** was precipitated with diethyl ether and dried under vacuum (yield: 724 mg, 93%). The composition varied according to the duration of the reaction and the work-up. For the partial deuteration a corresponding amount of HBF_4/H_2O dissolved in D_2O was used instead of $HBF_4 \cdot OEt_2$. Elemental analysis calcd for $C_{18}H_{21}BF_4O_4Ru$ (489.23): C 44.19, H 4.33; found: C 43.49, H 4.38.

4: A solution of sodium dimethyl malonate (223 mg, 1.45 mmol) in THF (20 mL) was added to a suspension of **3a** and **3b** (645 mg, 1.3 mmol) in THF (50 mL) at room temperature. The work-up of the reaction mixture was analogous to that for the synthesis of **2**. Compound **4** was obtained as yellow crystals (yield: 558 mg, 80%). Elemental analysis calcd for $C_{23}H_{28}O_8Ru$ (533.52): C 51.78, H 5.29; found: C 51.63, H 5.60.

5: The protonation was carried out as for **2a,b** (see above). $HBF_4 \cdot OEt_2$ (54%, 0.22 mL) was added to a solution of **4** (613 mg, 1.15 mmol) in diethyl ether (40 mL) at −65 °C. Compound **5** (yield: 581 mg, 82%) was isolated as a yellow powder which slowly decomposed in solution. Elemental analysis calcd for $C_{23}H_{29}BF_4O_8Ru$ (621.34): C 44.46, H 4.70; found: C 44.13, H 4.69.

6: $HBF_4 \cdot OEt_2$ (54%, 0.16 mL, 1.16 mmol) was added to a solution of **4** (617 mg, 1.16 mmol) and acetonitrile (0.2 mL, 3.48 mmol) in diethyl ether (60 mL) at −78 °C. The suspension was warmed to room temperature and filtered. The yellow residue was washed with diethyl ether. After removal of the solvent **6** (yield: 287 mg, 67%) remained as an oil. The extraction residue was also dried under vacuum and identified by ^1H NMR spectroscopy as $[Ru(Cp)(CH_3CN)_3]BF_4$ (**7**). Elemental analysis calcd for $C_{18}H_{24}O_8$ (368.37): C 58.69, H 6.57; found: C 58.87, H 6.91.

Cleavage of **6** from **5**: Acetonitrile (2 mL) was added to a suspension of **5** (56 mg, 0.09 mmol) in diethyl ether (25 mL) at room temperature. The mixture was stirred for one hour, and worked up as in the preparation of **6** from **4**. **6**: 32 mg (97%), **7**: 33 mg (97%).

Received: September 1, 1997 [Z10873IE]
German version: *Angew. Chem.* **1998**, *110*, 533 – 535

Keywords: cyclooctadiene · cyclooctatetraene · nucleophilic additions · ruthenium · stereoselective synthesis

[1] G. Schröder, *Cyclooctatetraen*, Verlag Chemie, Weinheim, **1965**; G. I. Fray, R. G. Saxton, *The Chemistry of Cyclooctatetraene and its Derivates*, Cambridge University Press, Cambridge, **1978**.

[2] a) L. A. Paquette, *Tetrahedron* **1975**, *31*, 2855 – 2883; *Angew. Chem.* **1990**, *102*, 642 – 660, *Angew. Chem. Int. Ed. Engl.* **1990**, *29*, 609 – 627; *Acc. Chem. Res.* **1993**, *26*, 57 – 62; b) J. S. Moore, C. B. Gorman, R. H. Grubbs, *J. Am. Chem. Soc.* **1991**, *113*, 1704 – 1712; c) N. A. Petasis, M. A. Patane, *Tetrahedron* **1992**, *48*, 5757 – 5821.

[3] G. Deganello, *Transition Metal Complexes of Cyclic Polyolefins*, Academic Press, New York, **1979**, pp. 156 – 321.

[4] B. F. G. Johnson, J. Lewis, G. L. P. Randall, *J. Chem. Soc. A* **1971**, 422 – 429.

[5] S. M. Brookhart, S. K. Noh, F. J. Timmers, Y. H. Hong, *Organometallics* **1988**, *7*, 2458 – 2465; G. Alibrandi, B. E. Mann, *J. Chem. Soc. Dalton Trans.* **1992**, 1439 – 1442; N. G. Connelly, M. Gilbert, A. G. Orpen, J. B. Sheridan, *ibid.* **1990**, 1291 – 1300; N. G. Connelly, P. M. Hopkins, A. G. Orpen, J. Slater, *ibid.* **1992**, 3303 – 3310; L. A. Paquette, S. V. Ley, S. Maiorana, D. F. Schneider, M. J. Broadhurst, R. A. Boggs, *J. Am. Chem. Soc.* **1975**, *97*, 4658 – 4667.

[6] J. H. Rigby, S. Scribner, M. J. Heeg, *Tetrahedron Lett.* **1995**, *36*, 8569 – 8572; C. G. Kreiter, R. Eckert, *Chem. Ber.* **1997**, *130*, 9 – 12.

[7] a) A. J. Pearson, *Pure Appl. Chem.* **1983**, *55*, 1767 – 1779; H.-J. Knölker in *Organic Synthesis via Organometallics* (Eds.: K. H. Dötz, R. W. Hoffmann), Vieweg, Braunschweig, **1991**, pp. 119 – 147; b) A. J. Pearson, M. N. I. Khan, J. C. Clardy, He Cun-heng, *J. Am. Chem. Soc.* **1985**, *107*, 2748 – 2757; A. J. Pearson, S. Balasubramanian, K. Srinivasan, *Tetrahedron* **1993**, *49*, 5663 – 5672.

[8] J. Evans, B. F. G. Johnson, J. Lewis, D. J. Yarrow, *J. Chem. Soc. Dalton Trans.* **1974**, 2375 – 2380.

[9] According to our literature research only three(!) representatives of this type of compound have been reported, all of which show a *trans* configuration in the 5,7 position: a) H. Zhang, *Hebei Shifan Daxue Xuebao*, *Ziran Kexueban* **1987**, *1*, 13 – 15; b) M. Kroener, *Chem. Ber.* **1967**, *100*, 3162 – 3171.

[10] P. T. Beurskens, W. P. Bosman, H. C. Brussaard, J. Heck, M. Maters, J. M. Smits, R. J. M. Kleingebbink, *J. Organomet. Chem.* **1994**, *469*, 197 – 203.

[11] S. G. Davies, M. L. H. Green, D. M. P. Mingos, *Tetrahedron* **1978**, *34*, 3047 – 3077.

[12] a) For isomers which differ only in the order, but not in the number of connectivities of the ligand atoms to the central atom, we suggest the term hapticity isomers (haptomers). We were able to demonstrate the formation of 1,2,3-η:6,7-η-haptomers based on the crystal structure analysis of a vinyl-substituted cyclooctatrienyl Ru complex;[12b] the half-life of **2a** in solution at 60 °C is about 15 h; b) G. Lange, Dissertation, Universität Hamburg, **1996**.

[13] E. T. K. Haupt, J. Heck, M. Maters, B. Voss, M. Damen, *Organometallics* **1995**, *14*, 44 – 48.

$Ti_2Nb_6Cl_{14}O_4$: A Unique 2D – 1D Network Combination in Niobium Cluster Chemistry**

Ekaterina V. Anokhina, Michael W. Essig, and Abdessadek Lachgar*

The formation of clusters by metal – metal bonding is characteristic of many compounds with early transition metals in low oxidation states.[1] The most common structural motif in reduced niobium halides and oxides is the cluster unit $[(Nb_6L^i_{12})L^a_6]^{n-}$ (L = F, Cl, Br, O).[2, 3] It is based on an octahedron of Nb atoms surrounded by twelve inner (L^i) and six outer ligands (L^a). In compounds obtained through solid-state synthesis, these units can be present as discrete anions (as in $KLuNb_6Cl_{18}$,[4] $In_2Li_2Nb_6Cl_{18}$,[5] and $Rb_4Al_2Nb_{35}O_{70}$[6]) or link to each other by sharing outer and/or inner ligands to form various polymeric structures (as in

[*] Prof. Dr. A. Lachgar, E. V. Anokhina, M. W. Essig
Department of Chemistry,
Wake Forest University
Winston-Salem, NC 27109 (USA)
Fax: (+1) 336-758-4656
E-mail: lachgar@wfu.edu

[**] This work was supported in part by a grant from the Research and Publication Fund, Wake Forest University.

 © WILEY-VCH Verlag GmbH, D-69451 Weinheim, 1998 1433-7851/98/3704-0522 $ 17.50+.50/0

Nb_6Cl_{14},[7] $NaNb_6Cl_{15}$,[8] $InNb_6Cl_{15}$,[9] and $LaNb_7O_{12}$[10]). Experimental and theoretical investigations have shown that valence electrons that are available for metal–metal interactions in these compounds are distributed among a_{1g}, t_{1u}, t_{2g}, and a_{2u} energy states.[3, 11] The energy of the a_{2u} state is determined by the balance between its Nb–Nb bonding character and Nb–L antibonding character. In niobium oxides, the a_{2u} state is overall antibonding, leading to compounds with a valence-electron concentration (VEC) that ranges from 13 to 15 (with 14 being preferred). In niobium halides, however, the a_{2u} state is overall nonbonding and is partially or fully occupied, leading to compounds with a VEC of 15 or 16 (with 16 being preferred). Modification of these cluster units by introduction of both halogen and oxygen as ligands can lead to changes in electronic configuration, charge, and symmetry, and is, therefore, conducive to formation of new structural types. Indeed, the recently reported oxohalides $ScNb_6Cl_{13}O_3$ and $Cs_2LaTa_6Br_{15}O_3$ crystallize in structure types that have no analogues among halide or oxide clusters.[12]

To explore correlations that exist between stoichiometry, structure types, and VEC in the niobium oxohalide clusters, we are investigating the system $Nb/NbCl_5/Nb_2O_5/Ti$. We recently obtained and structurally characterized the oxochloride $Ti_2Nb_6Cl_{14}O_4$, which crystallizes in an original structure type. In this compound niobium clusters form layers linked to each other through zigzag chains of edge-sharing $[TiCl_4O_2]$ octahedra (Figure 1).[13]

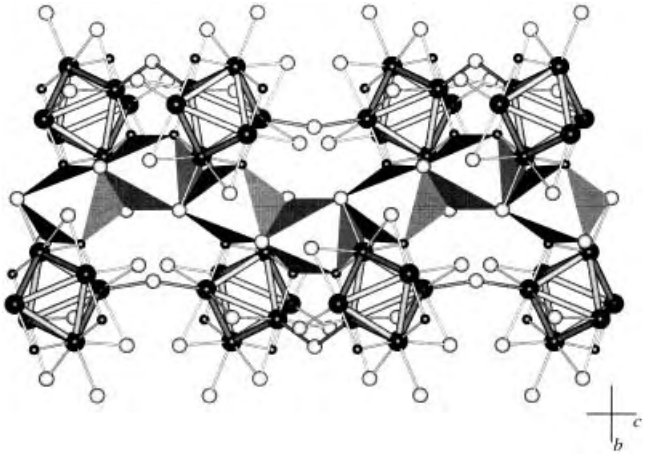


Figure 1. View of the structure of $Ti_2Nb_6Cl_{14}O_4$ in approximately the $\vec{a}$ direction. Large dark spheres, small dark spheres, and light spheres represent Nb, O, and Cl atoms, respectively. $[TiCl_4O_2]$ octahedra are highlighted.

The basic cluster unit $[(Nb_6Cl^i_8O^i_4)Cl^a_6]^{6-}$ has four oxygen and eight chlorine atoms as inner ligands and six chlorine atoms as outer ligands, and exhibits $\bar{1}$ symmetry (Figure 2). The Nb_6 octahedra are distorted owing to the difference in size and charge of the oxide and chloride ligands. The Nb–Nb bond distances range from 2.8174(7) to 2.8350(7) Å for oxygen-bridged niobium atoms, and from 2.9469(7) to 2.9916(7) Å for chlorine-bridged ones. These distances compare well with those in $ScNb_6Cl_{13}O_3$ (2.805(1) – 3.007(1) Å).[12a] The average niobium–ligand distances ($\bar{d}$(Nb–O^i) = 2.026 Å, $\bar{d}$(Nb–Cl^i) = 2.4536 Å, $\bar{d}$(Nb–Cl^a) = 2.6067 Å) are in good agreement with typical values in niobium oxide and chloride clusters.[3, 12c]

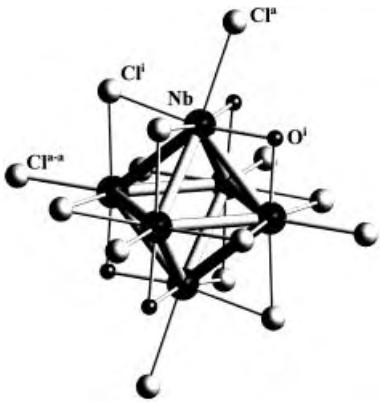


Figure 2. View of the $[(Nb_6Cl^i_8O^i_4)Cl^a_6]^{6-}$ cluster in $Ti_2Nb_6Cl_{14}O_4$.

Each cluster shares four outer chlorine atoms with four neighboring clusters, leading to the formation of pseudo-square layers $^2_\infty[(Nb_6Cl^i_8O^i_4)Cl^a_2Cl^{a-a}_{4/2}]^{4-}$ parallel to the *ac* plane (Figure 3). Adjacent layers are shifted with respect to each other by $1/2\,\vec{c}$. The layers have a buckled appearance resulting from about $\pm 28^\circ$ canting of the clusters from the normal to the layers and bent Nb-Cl^{a-a}-Nb bridges (Nb-$Cl(1)^{a-a}$-Nb 165, Nb-$Cl(2)^{a-a}$-Nb 131°). These layers are similar to those present in the binary compound Nb_6Cl_{14}, in which they are bridged through outer–inner chlorine atoms to form a three-dimensional framework. In contrast to Nb_6Cl_{14}, the layers in $Ti_2Nb_6Cl_{14}O_4$ are connected to each other through zigzag chains (parallel to the $\vec{c}$ direction) of edge-sharing $[TiCl_4O_2]$ octahedra.

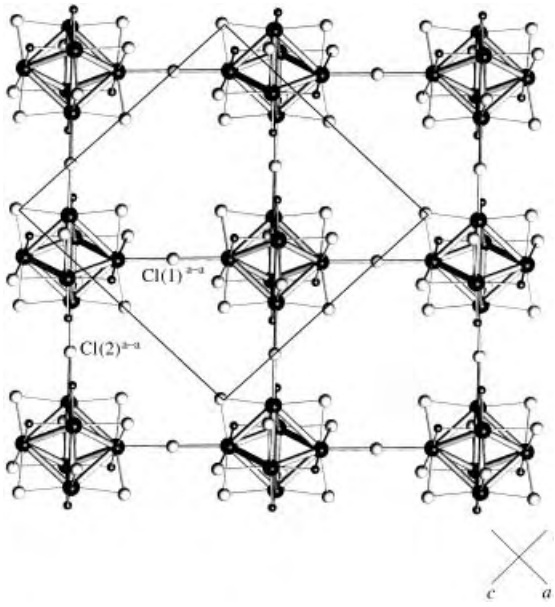


Figure 3. View of a $^2_\infty[(Nb_6Cl^i_8O^i_4)Cl^a_2Cl^{a-a}_{4/2}]^{4-}$ cluster layer in $Ti_2Nb_6Cl_{14}O_4$. Large dark spheres, small dark spheres, and light spheres represent Nb, O, and Cl atoms, respectively.

Titanium atoms occupy two inequivalent positions, Ti(1) and Ti(2), that alternate throughout the chain (Figure 4). In

 © WILEY-VCH Verlag GmbH, D-69451 Weinheim, 1998 1433-7851/98/3704-0523 $ 17.50+.50/0

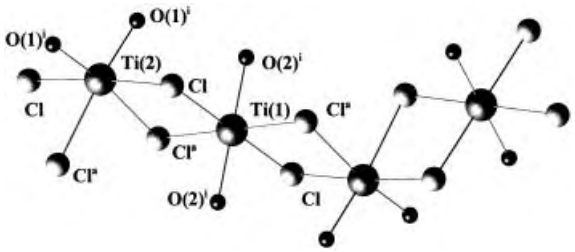


Figure 4. Section of an infinite chain of $[TiCl_4O_2]$ octahedra. Bond lengths [Å]: Ti(1)–O(2) 2.001(2), Ti(1)–Cl 2.4243(10), Ti(1)–Cl^a 2.4569(10), Ti(2)–O(1) 1.913(2), Ti(2)–Cl 2.4305(11), Ti(2)–Cl^a 2.5438(11).

the $[Ti(1)Cl_4O_2]$ octahedron, oxygen atoms are located in *trans* positions with respect to each other, whereas the oxygen atoms in $[Ti(2)Cl_4O_2]$ are in *cis* positions. Each *trans*-$[TiCl_4O_2]$ octahedron shares two opposite edges with two adjacent *cis*-$[TiCl_4O_2]$ octahedra, which in turn share their skew edges with adjacent *trans*-$[TiCl_4O_2]$ octahedra. This results in a zigzag *cis*–*trans* chain. To our knowledge, this is the first example of this type of linkage of octahedra into chains in titanium compounds. Titanium octahedra usually form rutile-like (*trans*) or brookite-like (*cis*) chains. Among other transition metal compounds, *cis*–*trans* chains were found in $AM_3(P_2O_7)_2$ (A = Sr, Ba; M = Co, Ni).[14] Two of the four chlorine atoms and both oxygen atoms coordinating to titanium also serve as outer and inner ligands for the clusters, respectively. Each *trans*-$[TiCl_4O_2]$ octahedron connects two clusters from adjacent layers, whereas each *cis*-$[TiCl_4O_2]$ octahedron bridges two clusters within the same layer. The remaining two chlorine atoms coordinate only to titanium atoms. The chains are separated from each other by empty channels running between the layers in the $\vec{c}$ direction (Figure 5). The minimum distance from the center of the channel to chlorine atoms is 2.350 Å.

The oxidation state of both Ti(1) and Ti(2) estimated from bond-valence sums is +3.[15] This implies that the number of valence electrons per niobium cluster in $Ti_2Nb_6Cl_{14}O_4$ is 14, as in $ScNb_6Cl_{13}O_3$ and $Cs_2LaTa_6Br_{15}O_3$. Although this conclusion needs to be experimentally verified, other oxidation states of titanium such as +2 or +4 seem to be less plausible. The former suggests an unstable electronic configuration for the cluster (VEC of 12), and the latter (implying a VEC of 16) does not agree with observed intracluster bond distances.[12c]

The combination of one- and two-dimensional sublattices in this new oxochloride is unprecedented for compounds with octahedral clusters. The novelty of the structural features in $Ti_2Nb_6Cl_{14}O_4$ indicates that further investigations into the chemistry of niobium oxohalides will undoubtedly lead to the discovery of many compounds with original structure types.

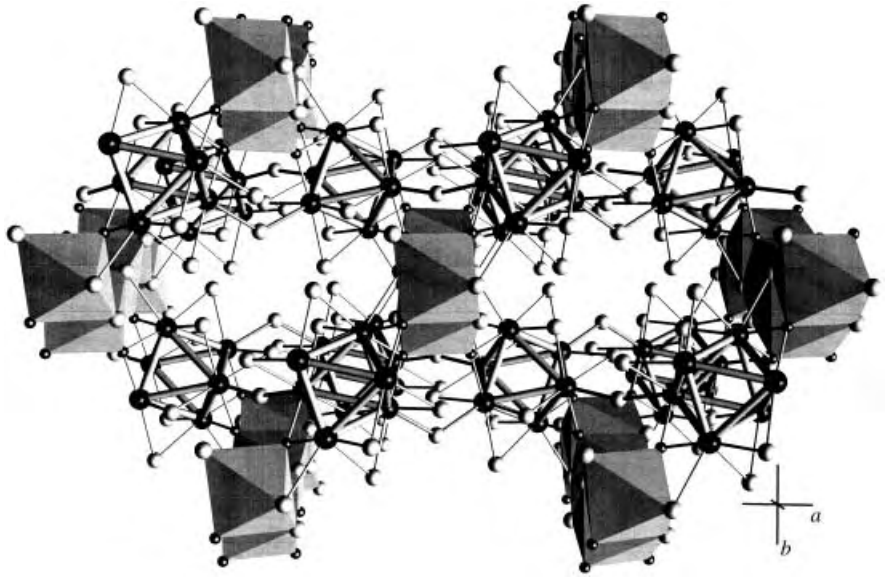


Figure 5. Perspective view of the structure of $Ti_2Nb_6Cl_{14}O_4$ in the $\vec{c}$ direction showing channels. Large dark spheres, small dark spheres, and light spheres represent Nb, O, and Cl atoms, respectively. $[TiCl_4O_2]$ octahedra are highlighted.

Experimental Section

A few crystals of the title compound were initially obtained by a reaction designed to yield $TiNb_6Cl_{18}$ in which contaminated $NbCl_5$ (probably containing $NbOCl_3$) was used. Subsequently, $Ti_2Nb_6Cl_{14}O_4$ was synthesized in high yield (> 90 %) from stoichiometric amounts of Nb powder, Ti foil, $NbCl_5$, and Nb_2O_5. The mixture (handled under a dry atmosphere) was placed in a quartz tube, sealed under vacuum, heated at 720 °C for 60 h, and cooled to room temperature within 3 h. The compound was obtained as black (dark brown when ground) columnlike crystals. The product was identified by comparing its X-ray powder diffraction pattern to that calculated based on crystal structure data for $Ti_2Nb_6Cl_{14}O_4$. The crystals did not undergo any noticeable decomposition in air.

Received: May 12, 1997
Revised version: October 30, 1997 [Z10430IE]
German version: *Angew. Chem.* **1998**, *110*, 538 – 540

Keywords: clusters · niobium · titanium

[1] A. Simon, *Angew. Chem.* **1988**, *100*, 163 – 188; *Angew. Chem. Int. Ed. Engl.* **1988**, *27*, 159 – 183.
[2] a) H. Schäfer, H. G. von Schnering, *Angew. Chem.* **1964**, *76*, 833 – 849; b) C. Perrin, M. Sergent, *Eur. J. Solid State Inorg. Chem.* **1991**, *28,* 933 – 948.
[3] J. Köhler, G. Svensson, A. Simon, *Angew. Chem.* **1992**, *104*, 1463 – 1483; *Angew. Chem. Int. Ed. Engl.* **1992**, *31*, 1437 – 1456.
[4] S. Ihmaïne, C. Perrin, O. Peña, M. Sergent, *J. Less Common Met.* **1988**, *137,* 323 – 332.
[5] A. Lachgar, H.-J. Meyer, *J. Solid State Chem.* **1994**, *110*, 15 – 19.
[6] M. J. Geselbracht, A. M. Stacy, *J. Solid State Chem.* **1994**, *110*, 1 – 5.
[7] A. Simon, H. G. von Schnering, H. Wöhrle, H. Schäfer, *Z. Anorg. Allg. Chem.* **1965**, *339*, 155 – 170.
[8] M. E. Sägebarth, A. Simon, H. Imoto, W. Weppner, G. Kliche, *Z. Anorg. Allg. Chem.* **1995**, *621*, 1589 – 1596.
[9] H. Womelsdorf, H.-J. Meyer, A. Lachgar, *Z. Anorg. Allg. Chem.* **1997**, *623*, 908 – 912.
[10] J. Xu, T. Emge, M. Greenblatt, *J. Solid State Chem.* **1996**, *123*, 21 – 29.
[11] T. Hughbanks, *Prog. Solid State Chem.* **1989,** *19,* 329 – 372.
[12] a) S. Cordier, C. Perrin, M. Sergent, *Eur. J. Solid State Inorg. Chem.* **1994**, *31*, 1049 – 1060; b) S. Cordier, C. Perrin, M. Sergent, *J. Solid State Chem.* **1995**, *120*, 43 – 48; c) C. Perrin, S. Cordier, S. Ihmaïne, M. Sergent, *J. Alloys Compd.* **1995**, *229*, 123 – 133.
[13] Crystal structure data for $Ti_2Nb_6Cl_{14}O_4$: monoclinic, space group *C*2/*c* (no. 15), *a* = 12.729(3), *b* = 14.570(3), *c* = 12.586(3) Å,

 © WILEY-VCH Verlag GmbH, D-69451 Weinheim, 1998 1433-7851/98/3704-0524 $ 17.50+.50/0

$\beta = 95.38(3)^\circ$, $V = 2323.9(8)$ Å^3, $Z = 4$, $\rho_{calcd} = 3.469$ Mg m^{-3}, $F(000) = 2240$, $\lambda(Mo_{K\alpha}) = 0.71073$ Å, $\mu(Mo_{K\alpha}) = 5.116$ mm^{-1}, $T = 298$ K. Of 11197 reflections collected in the range $2.1 \le 2\theta \le 53.1^\circ$ using the $\theta - 2\theta$ scan mode, 5132 were independent. Lorentzian polarization and empirical absorption corrections ($T_{min} = 0.252$, $T_{max} = 0.317$) were applied, and the structure solved and refined against F^2 using SHELX86 and SHELXL93 (G. M. Sheldrick, Universität Göttingen) with 5131 reflections (all unique reflections except for one with very negative F^2). All atoms were refined anisotropically. $R_1 = 0.058$, $wR_2 = 0.063$ for 121 parameters; max./min. residual electron density: 1.444/ − 0.924 e Å^{-3}. Further details on the crystal structure investigation may be obtained from the Fachinformationszentrum Karlsruhe, D-76344 Eggenstein-Leopoldshafen, Germany (fax: (+49) 7247-808-666 (Frau S. Höhler-Schlimm); e-mail: crysdata@fiz-karlsruhe.de), on quoting the depository number CSD-406839.

[14] K.-H.Lii, P. F.Shin, T.-M. Chen, *Inorg. Chem.* **1993**, *32*, 4373-4377.

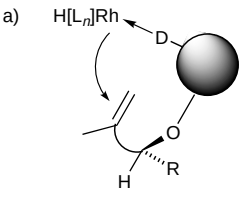
[15] I. D.Brown, D.Altermatt, *Acta Crystallogr. Sect. B* **1985**, *41*, 244 – 247.

ortho-Diphenylphosphanylbenzoyl-Directed Cuprate Addition to Acyclic Enoates**

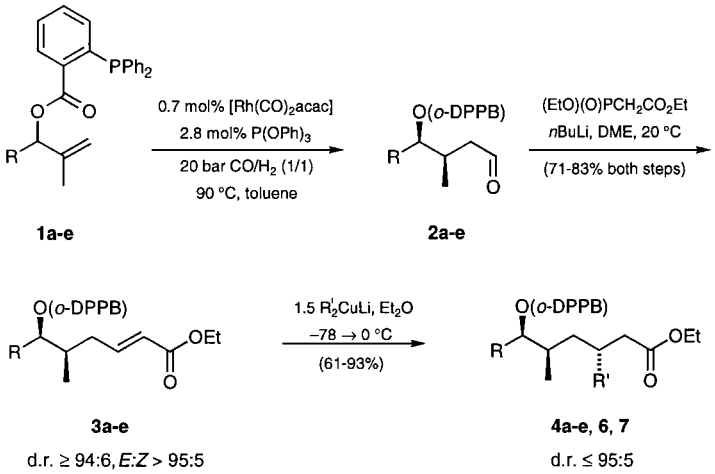
Bernhard Breit*

Reactions for constructing carbon skeletons, which lead to the formation of new stereogenic centers, are efficient transformations in organic synthesis. The control of stereoselectivity in such a process can be effected by either the reagent or the substrate. However, the latter is particularly difficult to achieve for acyclic substrates because of their structural flexibility. To overcome this problem, one has to make more efficient use of the chirality information inherent in the substrate. This can be achieved with the aid of a catalyst-directing group, which has been used successfully to control stereoselectivity in the rhodium-catalyzed hydroformylation of acyclic olefins (Scheme 1).[1] We report here that *ortho*-diphenylphosphanylbenzoyl (*o*-DPPB), the catalyst-directing group succesfully used in the hydroformylation reactions, can be employed in a subsequent step as a reagent-directing group for the diastereoselective addition of Gilman cuprates to α,β-unsaturated enoates (Scheme 1).

Enoates **3** were chosen as the test substrates, because a stereoselective 1,4-addition of an organometallic reagent that transfers a methyl group would provide the structural building blocks found in biologically important natural products of the polyketide class (e.g. the antitumor agent dictyostatin 1 and the ionophor calcimycin).[2, 3] Enoates **3** were obtained by *o*-DPPB-directed diastereoselective hydroformylation followed by Horner – Wadsworth – Emmons (HWE) olefination of the crude hydroformylation products (**2** → **3**) in good yields (71 – 83 %), diastereoselectivities (*syn*:*anti* ≥ 94:6), and *E*/*Z* selectivities (> 95:5).



Scheme 1. Working hypothesis for the *o*-DPPB group (shown schematically as a sphere; D = donor) a) as a catalyst-directing group and b) with the examples of hydroformylation and conjugated addition of cuprates.



Treatment of **3a** with 1.5 equivalents of lithium dimethyl cuprate provided the 1,4-addition product **4a** (93 %) in a diastereomer ratio of 95:5 (Table 1, entry 1).[4] To determine the relative configuration, **4a** was transformed into the δ-lactone **5** by standard reactions (Scheme 2). A 2D NOESY NMR experiment with **5** confirmed the axial position of the proton at C3 as well as the methyl group at C5, that is, an *anti* relationship between the two 1,3-positioned methyl groups of the acyclic 1,4-addition product **4a**.

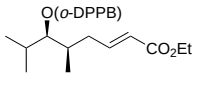
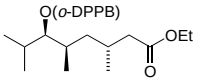
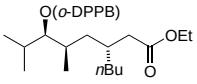
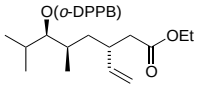
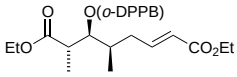
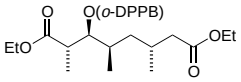
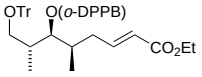
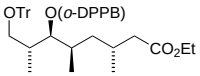
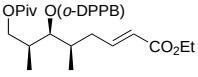
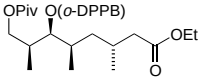
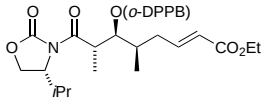
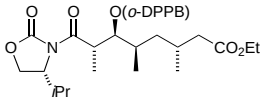
This reaction is not restricted to the transfer of a methyl group. Therefore, the addition of lithium di-*n*-butyl cuprate also proceeded with excellent diastereoselectivity (→*anti*-**6**, d.r. > 95:5, entry 2). In the case of lithium divinyl cuprate the diastereoselectivity was lower (→*anti*-**7**, d.r. = 80:20, entry 3).

With regard to the preparation of important building blocks of polyketide natural products, the addition of dimethyl cuprate is the most important reaction. Combining stereoselective *o*-DPPB-directed hydroformylation, HWE olefination, and stereoselective *o*-DPPB-directed cuprate addition provided access to acyclic building blocks with up to four stereogenic centers (→**4b** – **e**, entries 4 – 7). The 1,4-addition product **4b** is a potential C13 – C20 building block of the ionophor calcimycin, since it has the correct relative configuration at the four stereogenic centers. In addition, **4e** possesses the correct absolute configuration of this polyketide (entries 4 and 7).[3]

[*] Dr. B. Breit
Fachbereich Chemie der Universität
Hans-Meerwein-Strasse, D-35043 Marburg (Germany)
Fax: (+49) 6421-28-8917
E-mail: breit@ps1515.chemie.uni-marburg.de

[**] This work was supported by the Fonds der Chemischen Industrie and the Deutsche Forschungsgemeinschaft (SFB 260). The author thanks M. Dauber for skillful experimental assistance and Prof. R. W. Hoffmann for his generous support as well as the companies BASF and Degussa for their gifts of chemicals.

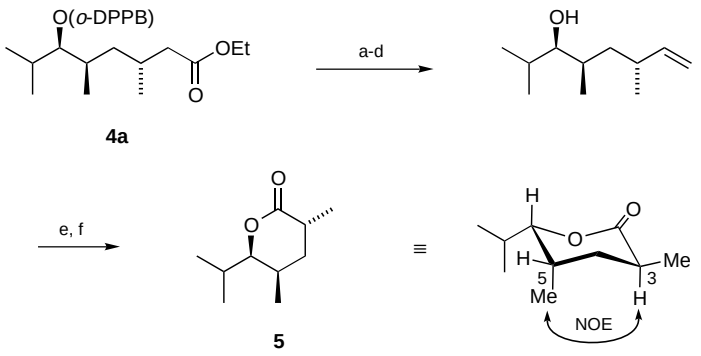
Table 1. Results of the diastereoselective conjugate addition of Gilman cuprates to enoates **3**.

Entry	Enoate	Major diastereomer[a]	Yield [%][b]	d.r. (*anti*:*syn*)[c]
1	 **3a**	 **4a**	93	95:5
2	**3a**	 **6**	68	95:5
3	**3a**	 **7**	61	80:20
4	 **3b**	 **4b**	68	95:5
5	 **3c**	 **4c**	71	86:14
6	 **3d**	 **4d**	60	85:15
7	 (−)-**3e**	 (−)-**4e**	75	95:5

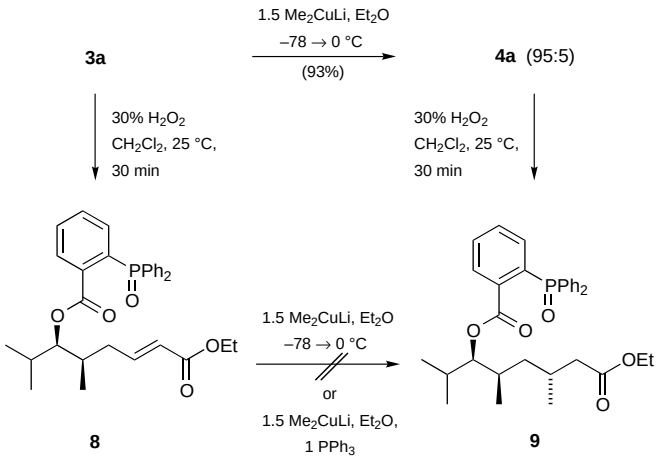
[a] The cuprate additions were performed according to the experimental procedure described for **3a**. Tr = Ph_3C, Piv = $(H_3C)_3CCO$.[b] After purification by flash chromatography. [c] Determined from ^1H NMR spectra of the crude product.

Even though the *o*-DPPB group represents an intrinsically coordinating functionality, it has not yet been proven that it is actually the origin of the observed diastereoselectivity.[5] An experiment which could give further mechanistic insight should be cuprate addition to enoate **8**, which differs from **3a** only by oxidation of the phosphane functionality to a phosphane oxide. This should suppress the ability of the *o*-DPPB group to coordinate to a cuprate. If the *o*-DPPB group does not play a significant role in controlling diastereoselectivity, one should also observe diastereoselectivity with derivative **8**. For that reason compounds **3a** and **8** were subjected to identical reaction conditions. Whereas the phosphane **3a** yielded the 1,4-addition product **4a** in 93% yield and with a diastereomer ratio of 95:5, the phosphane oxide **8** gave only unselective decomposition products besides recovered starting material.[6] Evidently, the phosphane functionality of the *o*-DPPB group is essential for a successful addition of dimethyl cuprate to the enoates **3**. However, the importance of the intramolecular attachment of the phosphane is still unclear.[7]

To address this issue, the phosphane oxide **8** was again treated with dimethyl cuprate under the identical conditions used above with one exception: the addition of one equivalent of triphenylphosphane as an external ligand.



Scheme 2. Determination of the relative configuration of **4a** by transformation into the δ-lactone **5**: a) $LiAlH_4$ (3 equiv), Et_2O, 0 → 25 °C, 2 h (94%); b) TsCl (1.1 equiv), pyridine (4 equiv), CH_2Cl_2 (0.2 M), 25 °C (72%); c) *o*-$NO_2C_6H_4SeCN$ (1.1 equiv), $NaBH_4$ (1.2 equiv), DMF, 25 °C, 6 h (100%); d) 30% H_2O_2 (10 equiv), THF, 3 h (96%); e) O_3, CH_2Cl_2, −78 °C, then PPh_3 (1.1 equiv), −78 → 25 °C (99%); f) PCC on Al_2O_3 (2 equiv), CH_2Cl_2, 36 h (70%).



 © WILEY-VCH Verlag GmbH, D-69451 Weinheim, 1998 1433-7851/98/3704-0526 $ 17.50+.50/0

Again, besides recovered starting material, only unspecified decomposition products were found. Not even a trace of the expected 1,4-addition product **9**, which was prepared independently by oxidation of **4a**, could be identified by NMR spectroscopy.

These results indicate that stereoselective cuprate addition to enoates **3** proceeds by an intramolecular transfer of the cuprate to one of the two diastereotopic enoate faces that is mediated by the *o*-DPPB group. Thus, the *o*-DPPB group controls reactivity as well as stereoselectivity. In addition to the already known ability of the *o*-DPPB group to act as catalyst-directing group, this system has also the potential to act as an organocuprate-directing functionality.

Experimental Section

3a→**4a** (entry 1 in Table 1): To a solution of lithium dimethylcuprate—prepared from CuI (143 mg, 0.75 mmol) and a 1.11M solution of methyl lithium (1.35 mL, 1.5 mmol) in Et_2O at $-5\,^{\circ}C$—in Et_2O (5 mL) was added dropwise a solution of **3a** (251 mg, 0.5 mmol) in Et_2O (2.5 mL). The mixture was stirred for 1 h at $-78\,^{\circ}C$, the cold bath removed, and the mixture allowed to warm to $0\,^{\circ}C$ within 15 min. The reaction mixture was stirred for another 75 min at $0\,^{\circ}C$ and then quenched by adding a saturated solution of aqueous NH_4Cl (2.5 mL). The mixture was diluted with *tert*-butyl methyl ether (25 mL) and 15% aqueous NH_3 (20 mL). The mixture was shaken vigorously until both phases were homogenous. The aqueous phase was separated and extracted with *tert*-butyl methyl ether ($2\times$ 10 mL). The combined organic phases were dried over Na_2SO_4, and the solvent removed in vacuo. NMR spectroscopic analysis of this crude product revealed a diastereomer ratio of 95:5. Flash chromatography with petroleum ether/*tert*-butyl methyl ether furnished 241 mg of **4a** (93%) as a colorless, highly viscous oil.[8]

Received: September 18, 1997 [Z 10943 IE]
German version: *Angew. Chem.* **1998**, *110*, 535 – 538

Keywords: asymmetric synthesis · copper · hydroformylations · synthetic methods

[1] a) B. Breit, *Angew. Chem.* **1996**, *108*, 3021 – 3023; *Angew. Chem. Int. Ed. Engl.* **1996**, *35*, 2835 – 2837; b) B. Breit, *Liebigs Ann.* **1997**, 1841 – 1851; c) B. Breit in *Organic Synthesis via Organometallics* (Eds.: G. Helmchen, J. Dibo, D. Flubacher, B. Wiese), Vieweg, Braunschweig, **1997**, pp. 139 – 146; d) B. Breit, *Chem. Commun.* **1997**, 591 – 592.

[2] G. R. Pettit, Z. A. Cichacz, F. Gao, M. R. Boyd, J. M. Schmidt, *J. Chem. Soc. Chem. Commun.* **1994**, 1111 – 1112.

[3] a) M. O. Chaney, P. V. Demarco, N. D. Jones, J. L. Occolowitz, *J. Am. Chem. Soc.* **1974**, *96*, 1932 – 1933; b) D. A. Evans, C. E. Sacks, W. A. Kleschick, T. R. Taber, *ibid.* **1979**, *101*, 6789 – 6791.

[4] The addition of higher order cuprates to structurally similar acyclic enoates having a methyl-substituted stereocenter in the δ-position proceeded in a stereorandom fashion: B. H. Lipshutz, *Tetrahedron Lett.* **1983**, *24*, 127 – 130.

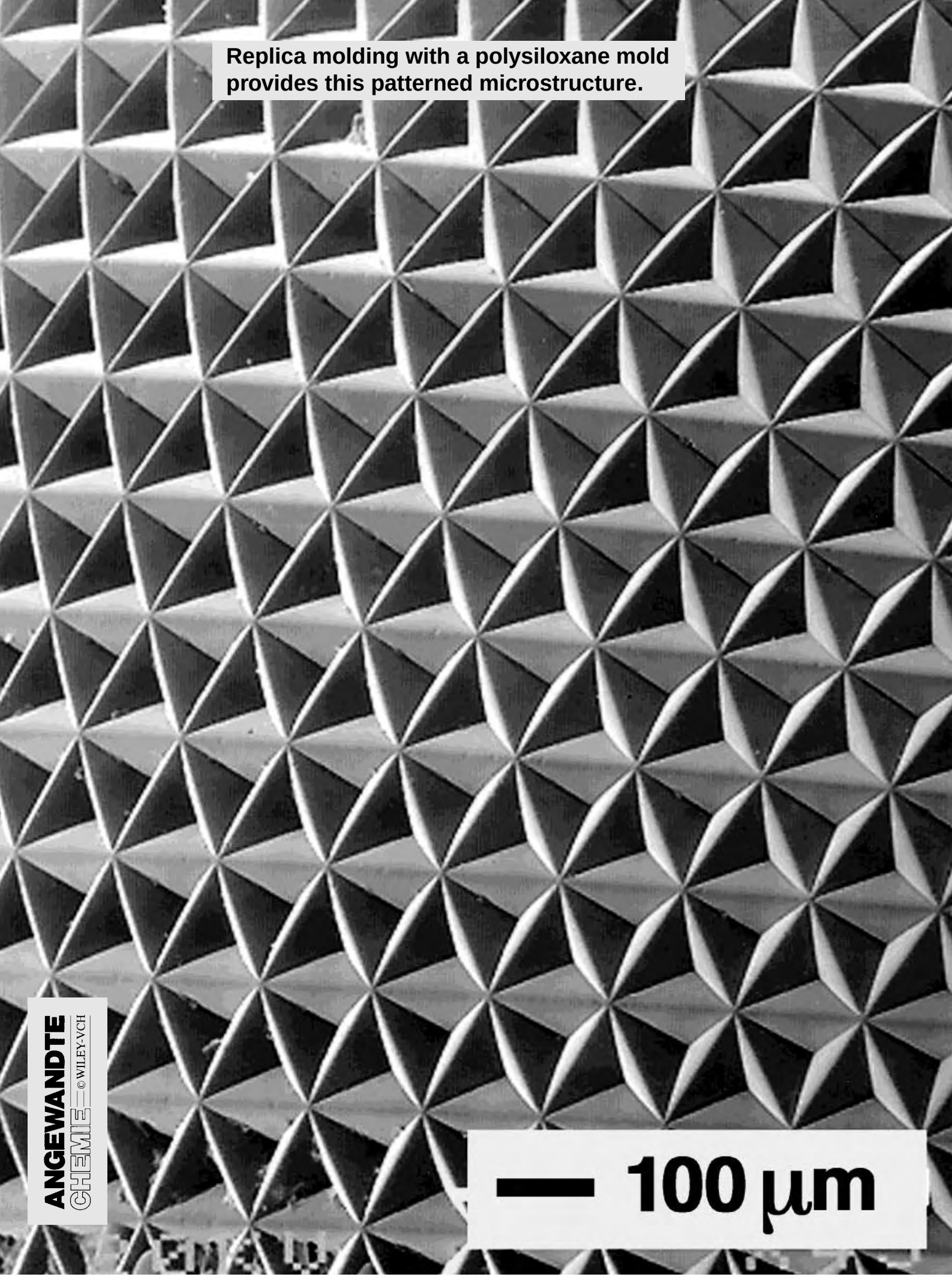
[5] The ability of phosphanes to coordinate to Gilman cuprates is known: a) X-ray crystal structure analysis of $[Cu(fluorenyl)_2(PPh_3)]^-[Li(thf)_4]^+$: A. J. Edwards, M. A. Paver, P. R. Raithby, M.-A. Rennie, C. A. Russell, D. S. Wright, *Organometallics* **1994**, *13*, 4967 – 4972; b) NMR investigations of $[LiI\cdot n Bu_2Cu(Pn Bu_3)Li]$: J. S. Filippo, Jr., *Inorg. Chem.* **1978**, *17*, 275 – 283.

[6] The addition of Gilman cuprates to enoates is generally not a synthetically useful reaction. Alternative reaction pathways such as 1,2-addition are often preferred. See ref. [4] and G. H. Posner, *Org. React.* **1972**, *19*, 1 – 113. For more recent reviews on organocuprate chemistry, see B. H. Lipshutz, S. Sengupta, *Org. React.* **1992**, *41*, 135 – 631; N. Krause, A. Gerold, *Angew. Chem.* **1997**, *109*, 194 – 213; *Angew. Chem. Int. Ed. Engl.* **1997**, *36*, 186 – 204.

[7] The addition of PPh_3 to the Gilman cuprate Ph_2CuLi was claimed to increase the reactivity and yield of a 1,4-addition: C. Jallabert, H. Riviere, P. W. Tang, *J. Organomet. Chem.* **1976**, *104*, 1 – 8.

[8] Selected physical data for **4a**: ^1H NMR (300 MHz, $CDCl_3$): $\delta = 0.7$ (m, 12H, $4CH_3$), 1.0 (m, 1H), 1.1 (m, 4H), 1.7 – 2.1 (m, 5H), 4.0 (q, $J =$ 7.2 Hz, 2H, OCH_2), 4.7 (dd, $J = 7.2$, 5.0 Hz, 1H, HCO), 6.8 (m, 1H, ArH), 7.2 – 7.3 (m, 12H, ArH), 8.0 (m, 1H, ArH); ^{13}C NMR (75.469 MHz, $CDCl_3$): $\delta = 13.51$, 14.23, 17.98, 19.05, 19.30, 27.62, 29.45, 31.80, 40.54, 42.62, 59.99, 82.80, 128.05, 128.35 (d, $J_{C,P} = 7.2$ Hz, 4C), 129.45 (2C), 130.45, 131.76, 133.90 (d, $J_{C,P} = 20.8$ Hz, 2C), 134.0 (d, $J_{C,P} = 21.1$ Hz, 2C), 134.21 (the signal for one *ipso* aryl C atom, expected at $\delta = 134$ as a doublet, is hidden by the signals at $\delta = 133.90$ and 134.21), 138.21 (d, $J_{C,P} = 12.2$ Hz, 2C), 141.15 (d, $J_{C,P} = 28.3$ Hz), 166.30 (d, $J_{C,P} = 2.6$ Hz), 172.78; ^{31}P NMR (81.015 MHz, $CDCl_3$): $\delta = -2.8$; elemental analysis calcd for $C_{32}H_{39}O_4P$ ($M_r = 518.6$): C 74.11, H 7.58; found: C 74.08, H 7.63.

 © WILEY-VCH Verlag GmbH, D-69451 Weinheim, 1998 1433-7851/98/3704-0527 $ 17.50+.50/0



ANGEWANDTE CHEMIE © WILEY-VCH

Soft Lithography

Younan Xia and George M. Whitesides*

Microfabrication, the generation of small structures, is essential to much of modern science and technology; it supports information technology and permeates society through its role in microelectronics and optoelectronics. The patterning required in microfabrication is usually carried out with photolithography. Although it is difficult to find another technology with more dominant influence, photolithography nonetheless has disadvantages. The sizes of the features it can produce are limited by optical diffraction, and the high-energy radiation needed for small features requires complex facilities and technologies. Photolithography is expensive; it cannot be easily applied to nonplanar surfaces; it tolerates little variation in the materials that can be used; and it provides almost no control over the chemistry of patterned surfaces, especially when complex organic functional groups of the sorts needed in chemistry, biochemistry, and biology are involved. We wished to develop alternative, non-photolithographic microfabrication methods that would complement photolithography. These techniques would ideally circumvent the diffraction limits of photolithography, provide access to three-dimensional structures, tolerate a wide range of materials and surface chemistries, and be inexpensive, experimentally convenient, and accessible to molecular scientists. We have developed a set of such methods that we call "soft lithography", since all members share the common feature that they use a patterned elastomer as the mask, stamp, or mold. We describe here soft lithography, and survey its ability to provide routes to high-quality patterns and structures with lateral dimensions of about 30 nm to 500 μm in systems presenting problems in topology, materials, or molecular-level definition that cannot (or at least not easily) be solved by photolithography.

Keywords: elastomers · materials science · patterning · supramolecular chemistry

1. Introduction

The ability to generate small structures is central to modern science and technology. There are many opportunities that might be realized by making new types of small structures, or by downsizing existing structures.[1] The most obvious examples are in microelectronics, where "smaller" has meant better—less expensive, more components per chip, faster operation, higher performance, and lower power consumption—since the invention of transistors in 1947.[2] It is also clear that many interesting new phenomena occur at nanometer dimensions: Examples include electronic processes such as quantum size effect (QSE),[3] Coulomb blockade,[4] and single-electron tunneling (SET).[4]

Microfabrication has its foundations in microelectronics, and it will continue to be the basis for microprocessors, memories, and other microelectronic devices for information technology in the foreseeable future. It is also increasingly being applied in areas outside of microelectronics (Figure 1).[5–9] Miniaturization and integration of a range of devices have resulted in portability; reductions in time, cost, reagents, sample size, and power consumption; improvements in detection limits; and new types of functions.

Photolithography is the most successful technology in microfabrication.[10] It has been the workhorse of semiconductor industry since its invention in 1959: Essentially all integrated circuits are made by this technology. The photolithographic techniques currently used for manufacturing microelectronic structures are based on a projection-printing system (usually called a stepper) in which the image of a reticle is reduced and projected onto a thin film of photoresist that is spin-coated on a wafer through a high numerical aperture lens system. The resolution R of the stepper is subject to the limitations set by optical diffraction according to the Rayleigh Equation (1),[10a] where λ is the wavelength of

$$R = k_1\lambda/\mathrm{NA} \quad (1)$$

the illuminating light, NA the numerical aperture of the lens system, and k_1 a constant that depends on the photoresist. Although the theoretical limit set by optical diffraction is usually about $\lambda/2$, the minimum feature size that can be ob-

[*] Prof. G. M. Whitesides, Dr. Y. Xia
Department of Chemistry and Chemical Biology
Harvard University
12 Oxford Street, Cambridge, MA 02138 (USA)
Fax: (+1) 617-495-9857
E-mail: gwhitesides@gmwgroup.harvard.edu

 © WILEY-VCH Verlag GmbH, D-69451 Weinheim, 1998 1433-7851/98/3705-0551 $ 17.50+.50/0

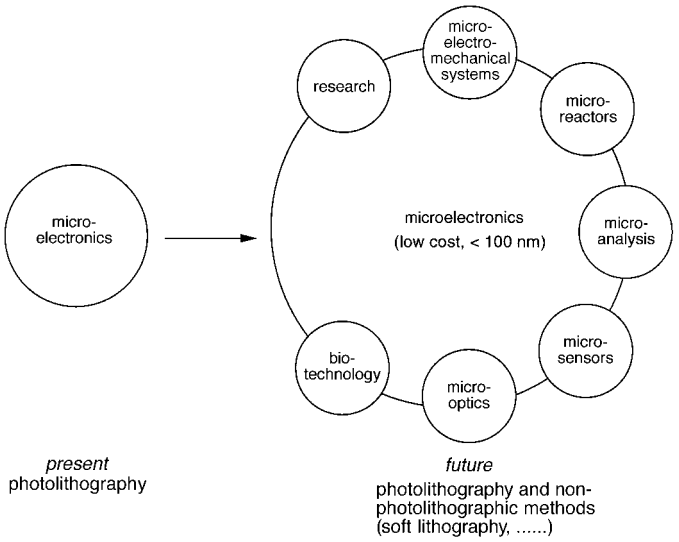


Figure 1. Microelectronics is based on photolithography and is very important, but the more expensive technology to surmount the "100-nm barrier"—a critical point in reducing feature sizes set by a combination of diffraction limitations to projected images and the lack of lenses that are transparent at wavelengths below 160 nm—make the future of photolithography on this small scale unclear. In addition, new opportunities in microfabrication are emerging as new types of microsystems (right) are developed; for these opportunities, photolithography is not always the best option. For most applications, cost is a dominant parameter.

tained is approximately the wavelength (λ) of the light used. As a result, illuminating sources with shorter wavelengths are progressively introduced into photolithography to generate structures with smaller feature sizes (Table 1).[10c] As structures become increasingly small, they also become increasingly difficult and expensive to produce.

In the late 1960s and early 1970s, Gorden Moore, founder of both Fairchild Semiconductor and Intel, projected that the number of transistors in an integrated circuit would double every 18 months or so. This prediction was later known as Moore's Law.[2] Over the past three decades many trends in the semiconductor industry have followed this law (Figure 2) thanks to continuous developments in photolithography that have allowed the size of features to decrease by a factor of approximately one-half every three years (Table 1). It is plausible that features as small as 100 nm can be manufactured optically in the future by employing advanced mask/resist technologies and deep UV (DUV) radiation.[10d] Below this size, however, it is generally accepted that current strategies for photolithography may be blocked by optical diffraction and by the opacity of the materials used for making lenses or supports of photomasks. New approaches must be developed if Moore's Law is to extend into the range below

Table 1. The recent past, present, and future of semiconductor technology.[10c, 12]

Year	Lithographic method	Resolution [nm][a]	Bits (DRAM)[b]
	Photolithography (λ[nm])		
1992	UV (436), *g* line of Hg lamp	500	16 M
1995	UV (365), *i* line of Hg lamp	350	64 M
1998	DUV (248), KrF excimer laser	250	256 M
2001	DUV (193), ArF excimer laser	180	1 G
2004	DUV (157), F_2 excimer laser	120	4 G
2007	DUV (126), dimer discharge from an argon laser	100	16 G
2010	*Advanced lithography* extreme UV (EUV, 13 nm) soft X-ray (6–40 nm) focused ion beam (FIB) electron-beam writing proximal-probe methods	<100[c]	>16 G

[a] The size of the smallest feature that can be manufactured. [b] The size of the dynamic random access memory (DRAM). [c] These techniques are still in early stages of development, and the smallest features that they can produce economically have not yet been defined.

Younan Xia was born in Jiangsu, China, in 1965. He received a B.S. degree from the University of Science and Technology of China in 1987, and then worked as a graduate student for four years at the Fujian Institute of Research on the Structure of Matter, Academia Sinica. He came to the United States in 1991, and received a M.S. degree from the University of Pennsylvania (with A. G. MacDiarmid) in 1993 and a Ph.D. degree from Harvard University (with G. M. Whitesides) in 1996. He is currently Assistant Professor of Chemistry at the University of Washington in Seattle. His research interests include micro- and nanofabrication, self-assembled monolayers, inorganic functional materials, nanomaterials, conducting polymers, microanalytical systems, microelectromechanical systems, and novel devices for optics, optoelectronics, and display.



Y. Xia



G. M. Whitesides

George M. Whitesides was born in 1939 in Louisville, Kentucky, USA. He received an A.B. degree from Harvard University in 1960 and a Ph.D. degree from the California Institute of Technology (with J. D. Roberts) in 1964. He was a member of the faculty of the Massachusetts Institute of Technology from 1963 to 1982. He joined the Department of Chemistry of Harvard University in 1982 and was department chairman from 1986 to 1989; he is now Mallinckrodt Professor of Chemistry. His present research interests include biochemistry, surface chemistry, materials science, molecular virology, optics, self-assembly, bioanalytical chemistry, microelectromechanical systems, and microfluidics.

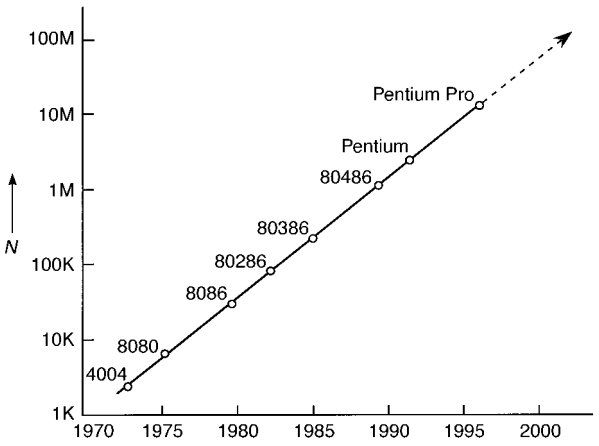


Figure 2. The integration trend given by Moore's law, and how microprocessors manufactured by Intel have followed this law since 1973;[2b, c] N = number of transistors per chip. This curve reflects the general trend of miniaturization achieved by microlithography; it also applies to other devices such as RAMs, DRAMs, and Motorola microprocessors.

100 nm. Advanced lithographic techniques currently being explored for this regime include extreme UV (EUV) lithography, soft X-ray lithography, electron-beam writing, focused ion beam writing, and proximal-probe lithography.[11, 12] These techniques are capable of generating very small features, but their development into practical commercial methods for low-cost, high-volume processing still requires great ingenuity: EUV and X-ray techniques, for example, will probably require the development of reflective optics.[10d]

The continued shrinking of feature sizes toward 100 nm poses new technical challenges for photolithography, but, even for microfabrication on the micrometer scale, it may not be the only and/or best microfabrication method for all tasks. For example, it is expensive (both in capital and operating cost), which makes it less than accessible to chemists, biologists, and material scientists; it cannot be easily adopted for patterning nonplanar surfaces;[13] it is largely ineffective in generating three-dimensional structures;[11a] it is poorly suited for introducing specific chemical functionalities; it is directly applicable to only a limited set of materials used as photoresists;[14] and it integrates well with semiconductor materials, but not necessarily with glass, plastics, ceramics, or carbon. These limitations suggest the need for alternative microfabrication techniques. The development of practical methods capable of generating structures smaller than 100 nm for a range of materials represents a major task, and is one of the greatest technical challenges now facing microfabrication.[11, 12]

A number of non-photolithographic techniques have been demonstrated for fabricating (and in some cases for manufacturing) high-quality microstructures and nanostructures (Table 2).[15–38] This review will focus on the soft lithographic techniques that we are currently exploring: microcontact printing (μCP),[34] replica molding (REM),[35] microtransfer molding (μTM),[36] micromolding in capillaries (MIMIC),[37] and solvent-assisted micromolding (SAMIM).[38] Collectively, we call these techniques "soft lithography",[33] because in each case an elastomeric stamp or mold is the key element that transfers the pattern to the substrate and, more broadly, because each uses flexible organic molecules and materials rather than the rigid inorganic materials now commonly used in the fabrication of microelectronic systems (Table 3).

Table 2. Non-photolithographic methods for micro- and nanofabrication.

Method	Resolution[a]	Ref.
injection molding	10 nm	[15, 16]
embossing (imprinting)	25 nm	[17, 18]
cast molding	50 nm	[19, 20]
laser ablation	70 nm	[21, 22]
micromachining with a sharp stylus	100 nm	[23]
laser-induced deposition	1 μm	[24]
electrochemical micromachining	1 μm	[25]
silver halide photography	5 μm	[26]
pad printing	20 μm	[27]
screen printing	20 μm	[28]
ink-jet printing	50 μm	[29, 30]
electrophotography (xerography)	50 μm	[31]
stereolithography	100 μm	[32]
soft lithography		[33]
microcontact printing (μCP)	35 nm	[34, 84f]
replica molding (REM)	30 nm	[35]
microtransfer molding (μTM)	1 μm	[36]
micromolding in capillaries (MIMIC)	1 μm	[37]
solvent-assisted micromolding (SAMIM)	60 nm	[38]

[a] The lateral dimension of the smallest feature that has been generated. These numbers do not represent ultimate limits.

Soft lithography generates micropatterns of self-assembled monolayers (SAMs)[39] by contact printing, and also forms microstructures in materials by embossing (imprinting)[17, 18] and replica molding.[19, 20] Figure 3 shows the general procedure for soft lithography in a technique we call "rapid prototyping" and whose components we describe in Section 2.5. The strength of soft lithography is in replicating rather than fabricating the master, but rapid prototyping and

Table 3. Comparison of photolithography to soft lithography.

	Photolithography	Soft lithography
definition of patterns	rigid photomask (patterned Cr supported on a quartz plate)	elastomeric stamp or mold (a PDMS block patterned with relief features)
materials that can be patterned directly	photoresists (polymers with photosensitive additives)	photoresists[e]
	SAMs	SAMs[a] unsensitized polymers[b–e] (epoxy, PU, PMMA, ABS, CA, PS, PE, PVC)[f] polymer precursors[c, d] (of carbon materials and ceramics) polymer beads[d] conducting polymers[d] colloidal materials[a, d] sol–gel materials[c, d] organic and inorganic salts[d] biological macromolecules[d]
current limits to resolution	ca. 250 nm	see Table 2
minimum feature size	ca. 100 nm (?)	10 (?) – 100 nm

[a] μCP. [b] REM. [c] μTM. [d] MIMIC. [e] SAMIM. [f] PU: polyurethane; PMMA: poly(methyl methacrylate); ABS: poly(acrylonitrile-butadiene-styrene); CA: cellulose acetate; PS: polystyrene; PE: polyethylene; PVC: poly(vinyl chloride).

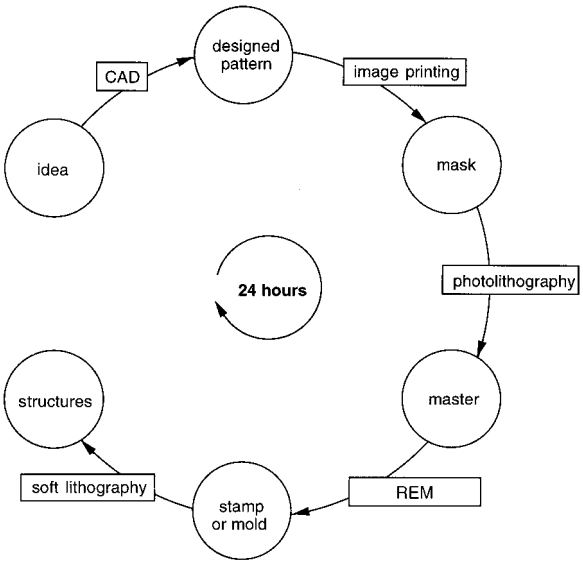


Figure 3. The rapid prototyping procedure for soft lithography. The pattern is composed and transferred to a CAD file, and printed on a transparent sheet of polymer with a commercial image setter. This patterned sheet is used in contact photolithography to prepare a master in a thin film of photoresist; a negative replica of this master in an elastomer becomes the stamp or mold for soft lithography. The overall procedure from design to stamp takes less than 24 hours to complete.

the ability to deform the elastomeric stamp or mold give it unique capabilities even in fabricating master patterns. Soft lithographic techniques require remarkably little capital investment and are procedurally simple: They can often be carried out in the ambient laboratory environment. They are not subject to the limitations set by optical diffraction and optical transparency (the edge definition is set, in principle, by van der Waals interactions and, in practice, by the properties of the materials involved), and they provide alternative routes to structures that are smaller than 100 nm without the need for advanced lithographic techniques. They also offer access to new types of surfaces, optical structures, sensors, prototype devices, and systems that could be difficult to fabricate by photolithographic procedures. Our aim in this review is to explain and examine the principles, processes, materials, and limitations of this new class of patterning techniques, and to describe their ability to form patterns and structures of a wide variety of materials with features that range from nanometers to micrometers in size.

2. Key Strategies of Soft Lithography

2.1. Self-Assembly

The obvious technical challenges to extending current photolithography to features that are smaller than 100 nm make it possible to at least consider radically new approaches to microfabrication. Both chemistry and biology can help in the development of new methodologies for microfabrication through contributions of a surprisingly broad range, both practical and conceptual. Among the conceptually new strategies offer possible routes to both smaller features and lower costs, self-assembly has been the most fully explored and is closest to practical realization.[40]

Self-assembly is the spontaneous organization of molecules or objects into stable, well-defined structures by noncovalent forces.[40] The key idea in self-assembly is that the final structure is close to or at thermodynamic equilibrium; it therefore tends to form spontaneously and to reject defects. Self-assembly often provides routes to structures having greater order than can be reached in non-self-assembling structures. The final structure is predetermined by the characteristics of the initial subunits: The information that determines the final structure is coded in the structures and properties of the subunits (e.g., shapes and surface functionalities). Self-assembly is ubiquitous in nature:[41] Processes such as folding of proteins and tRNAs as well as formation of the DNA double helix serve as biological illustrations of the potential of self-assembly in microfabrication. Various strategies of self-assembly have been developed and employed to fabricate two- and three-dimensional structures with dimensions ranging from molecular, through mesoscopic, to macroscopic sizes.[42–45]

2.2. Self-Assembled Monolayers

Self-assembled monolayers (SAMs) are the most widely studied and best developed examples of nonbiological, self-assembling systems.[39, 46] They form spontaneously by chemisorption and self-organization of functionalized, long-chain organic molecules onto the surfaces of appropriate substrates. SAMs are usually prepared by immersing a substrate in the solution containing a ligand that is reactive toward the surface, or by exposing the substrate to the vapor of the reactive species. Table 4 lists a number of systems known to give SAMs;[47–65] new systems are still being developed.

The best characterized systems of SAMs are alkanethiolates $CH_3(CH_2)_nS^-$ on gold (Figure 4).[47] Alkanethiols chemisorb spontaneously on a gold surface from solution and form adsorbed alkanethiolates. This process is assumed to occur with loss of dihydrogen; the fate of the hydrogen atom is still

Table 4. Substrates and ligands that form SAMs.

Substrate	Ligand or Precursor	Binding	Ref.
Au	RSH, ArSH (thiols)	RS–Au	[39, 46, 47]
Au	RSSR′ (disulfides)	RS–Au	[39, 46, 48]
Au	RSR′ (sulfides)	RS–Au	[39, 46, 49]
Au	RSO_2H	RSO_2–Au	[50]
Au	R_3P	R_3P–Au	[51]
Ag	RSH, ArSH	RS–Ag	[39, 52]
Cu	RSH, ArSH	RS–Cu	[39, 53]
Pd	RSH, ArSH	RS–Pd	[39, 54]
Pt	RNC	RNC–Pt	[39, 55]
GaAs	RSH	RS–GaAs	[56]
InP	RSH	RS–InP	[57]
SiO_2, glass	$RSiCl_3$, $RSi(OR')_3$	siloxane	[39, 46, 58]
Si/Si–H	$(RCOO)_2$ (neat)	R–Si	[59]
Si/Si–H	$RCH{=}CH_2$	RCH_2CH_2Si	[60]
Si/Si–Cl	RLi, RMgX	R–Si	[61]
metal oxides	RCOOH	$RCOO^- \cdots MO_n$	[62]
metal oxides	RCONHOH	$RCONHOH \cdots MO_n$	[63]
ZrO_2	RPO_3H_2	$RPO_3^{2-} \cdots Zr^{IV}$	[64]
In_2O_3/SnO_2 (ITO)	RPO_3H_2	$RPO_3^{2-} \cdots M^{n+}$	[65]

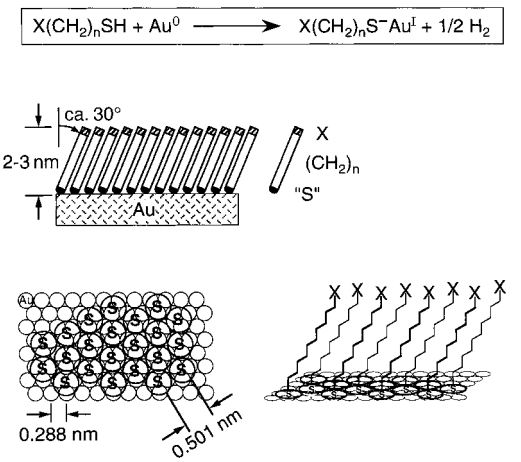


Figure 4. Representation of a highly ordered monolayer of alkanethiolate formed on a gold surface. The sulfur atoms form a commensurate overlayer on Au(111) with a $(\sqrt{3}\times\sqrt{3})R30^\circ$ structure, whose thickness is determined by the number of methylene groups (n) in the alkyl chain. The surface properties of the monolayer can be easily modified by changing the head group X. The alkyl chains $(CH_2)_n$ extend from the surface in a nearly all-*trans* configuration. On average they are tilted approximately 30° from the normal to the surface to maximize the van der Waals interactions between adjacent methylene groups.

not established. Sulfur atoms bonded to the gold surface bring the alkyl chains into close contact; these contacts freeze out configurational entropy and lead to an ordered structure. For carbon chains of up to approximately 20 atoms, the degree of interaction in a SAM increases with the density of molecules on the surface and the length of the alkyl backbones. Only alkanethiolates with $n>11$ form the closely packed and essentially two-dimensional organic quasi-crystals supported on gold that characterize the SAMs most useful in soft lithography.[46d] The formation of ordered SAMs on gold from alkanethiols is a relatively fast process: Highly ordered SAMs of hexadecanethiolate on gold can be prepared by immersing a gold substrate in a solution of hexadecanethiol in ethanol (ca. 2 mM) for several minutes, and formation of SAMs during microcontact printing may occur in seconds. This ability to form ordered structures rapidly is one of the factors that ultimately determine the success of microcontact printing.

The structures and properties of SAMs from alkanethiolates on gold have been examined using a number of techniques (Table 5).[66–82] It is generally accepted that sulfur atoms form a $(\sqrt{3}\times\sqrt{3})R30^\circ$ overlayer on the Au(111) surface (see Figure 4). Optical and diffraction techniques can only reveal the level of average order in SAMs (i.e., the dominant lattices and their dimensions) over the probed area (typically a few square millimeters). Recent STM studies show that these systems are heterogeneous and structurally complex: The alkyl chains may form a "superlattice" at the surface of the monolayer, that is, a lattice with a symmetry and dimension different from that of the underlying hexagonal lattice formed by sulfur atoms.[46d] These results indicate that the order in the top part of SAMs is not dictated solely by the sulfur atoms directly bonded to the gold surface, but also depends strongly on the intermolecular interactions between the alkyl backbones. When alkanethiolates are terminated in head groups other than methyl, it becomes even more complicated to predict and determine the structures of the SAMs.

Table 5. Techniques for characterizing SAMs of alkanethiolates on gold.

Property of SAMs	Technique	Ref.
structure and order	scanning probe microscopy	[66, 67]
	STM, AFM, LFM	[135]
	infrared spectroscopy	[39e, 68]
	low-energy helium diffraction	[69]
	X-ray diffraction	[70]
	transmission electron diffraction	[71]
	surface Raman scattering	[72]
	sum frequency spectroscopy (SFS)	[73]
composition	X-ray photoelectron spectroscopy (XPS)	[74]
	temperature programmed desorption (TPD)	[75]
	mass spectrometry (MS)	[76]
wettability	contact angle	[77]
thickness	ellipsometry	[78]
coverage and/or	quartz crystal microbalance (QCM)	[79]
degree of perfection	surface acoustic wave (SAW) device	[80]
	electrochemical methods	[81]
defects	STM and AFM	[66, 67]
	wet etching	[82]

SAMs of alkanethiolates on gold exhibit many of the features that are most attractive about self-assembling systems: ease of preparation, density of defects low enough to be useful in many applications, good stability under ambient laboratory conditions, practicality in technological applications, and amenability to controlling interfacial properties (physical, chemical, electrochemical, and biochemical) of the system. As a result, SAMs are excellent model systems for studies on wetting, adhesion, lubrication, corrosion, nucleation, protein adsorption, and cell attachment.[46, 83] SAMs are also well suited as ultrathin resists or passivating layers for fabrication of patterns and structures with lateral dimensions in the nanometer to micrometer range.

Patterning SAMs in the plane of the surface has been achieved by a wide variety of techniques (Table 6).[84–104] Each technique has advantages and disadvantages. Only micro-

Table 6. Techniques that have been used for patterning SAMs.

Technique	SAMs	Resolution[a]	Ref.
microcontact printing (μCP)			[84]
	RSH/Au	35 nm	[34, 84f, 85]
	RSH/Ag	100 nm	[86]
	RSH/Cu	500 nm	[87]
	RSH/Pd	500 nm	[88]
	RPO_3H_2/Al	500 nm	[89]
	siloxane/SiO_2	500 nm	[90, 145]
photooxidation	RSH/Au	10 μm	[91]
photo-cross-linking	RSH/Au	10 μm	[92]
photoactivation	RSH/Au	10 μm	[93]
	siloxane/glass	10 μm	[94]
photolithography/plating	siloxane/SiO_2	500 nm	[95]
electron-beam writing	RSH/Au	75 nm	[96]
	RSH/GaAs	25 nm	[97]
	siloxane/SiO_2	5 nm	[98]
focused ion beam writing	RSH/Ag	10 μm	[99]
neutral metastable atom writing	RSH/Au	70 nm	[100]
	siloxane/SiO_2	70 nm	[101]
SPM lithography	RSH/Au	10 nm	[84f, 102]
micromachining	RSH/Au	100 nm	[23, 103]
micropen writing	RSH/Au	10 μm	[104]

[a] The lateral dimension of the smallest feature that has been generated.

contact printing will be discussed in this review since it is the one that seems to offer the most interesting combination of convenience and new capability.

2.3. Contact Printing, Replica Molding, and Embossing

Contact printing is an efficient method for pattern transfer.[105] A conformal contact between the stamp and the surface of the substrate is the key to its success. Printing has the advantage of simplicity and convenience: Once the stamp is available, multiple copies of the pattern can be produced using straightforward experimental techniques. Printing is an additive process; the waste of material is minimized. Printing also has the potential to be used for patterning large areas. Although contact printing is most suitable for two-dimensional fabrication, it has also been used to generate quasi-three-dimensional structures through combination with other processes such as metal plating.[106]

Replica molding duplicates the information—for example, the shape, the morphology, and the structure—present in a master. It is a procedure that accommodates a wider range of materials than does photolithography. It also allows duplication of three-dimensional topologies in a single step, whereas photolithography is not able to replicate such structures. It has been used for the mass production of surface relief structures such as diffraction gratings,[107] holograms,[108] compact disks (CDs),[19, 20] and microtools.[109] Replica molding with an appropriate material (usually in the form of a precursor) enables highly complex structures in the master to be faithfully duplicated into multiple copies with nanometer resolution in a reliable, simple, and inexpensive way.[110–112] The fidelity of replica molding is determined by van der Waals interactions, wetting, and kinetic factors such as filling of the mold. These physical interactions should allow more accurate replication of features that are smaller than 100 nm than does photolithography, which is limited by optical diffraction.[10]

Embossing is another cost-effective, high-throughput manufacturing technique that imprints microstructures in thermoplastic materials.[17, 18] The manufacturing of CDs based on imprinting in polycarbonate with nickel masters[17a] and of holograms by imprinting in SURPHEX photopolymer (DuPont) with fused quartz masters[17f] are two typical examples of large-volume commercial applications of this technique. Until recently embossing had not been seriously developed as a method for fabricating and manufacturing structures of semiconductors, metals, and other materials used in microelectronic circuitry. The beautiful work by Chou et al. showed that embossing can be used to make features as small as 25 nm in silicon, and has attracted attention to the potential of this kind of patterning technique.[18]

We are extending the capability of these patterning techniques by bringing new approaches and new materials into these areas. In particular, a combination of self-assembly (especially of self-assembled monolayers) and pattern transfer using elastomeric stamps, molds, or masks constitutes the basis of soft lithographic methods.[33] It complements photolithography in a number of aspects and provides a wide range of new opportunities for micro- and nanofabrication.

2.4. Elastomeric Stamps and Molds

An elastomeric stamp, mold, or mask having relief structures on its surface is the key element of soft lithography.[33–38] It is usually prepared by replica molding (Figure 5) by casting

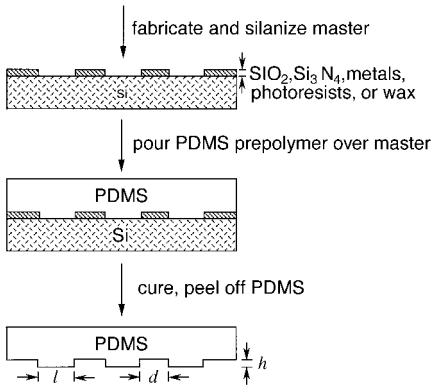


Figure 5. Schematic illustration of the procedure for casting PDMS replicas from a master having relief structures on its surface. The master is silanized by exposure to $CF_3(CF_2)_6(CH_2)_2SiCl_3$ vapor (ca. 0.5 h); each master can be used to fabricate more than 50 PDMS replicas. Representative ranges of values for h, d, and l are 0.2 – 20, 0.5 – 200, and 0.5 – 200 μm, respectively.

the liquid prepolymer of an elastomer against a master that has a patterned relief structure in its surface. The elastomer we used in most demonstrations is poly(dimethylsiloxane) (PDMS),[113] for example, Sylgard 184 from Dow Corning. We and other groups have also used other elastomers such as polyurethanes, polyimides, and cross-linked Novolac resin (a phenol formaldehyde polymer).[84, 85]

Several properties of PDMS are instrumental in the formation of high-quality patterns and structures in soft lithography. First, PDMS is an elastomer and conforms to the surface of the substrate over a relatively large area. PDMS is deformable enough such that conformal contact can even be achieved on surfaces that are nonplanar on the micrometer scale.[114] The elastic characteristic of PDMS also allows it to be released easily, even from complex and fragile structures. Second, PDMS provides a surface that is low in interfacial free energy (ca. 21.6×10^{-3} J m^{-2}) and chemically inert:[113] Polymers being molded do not adhere irreversibly to or react with the surface of PDMS. Third, PDMS is homogeneous, isotropic, and optically transparent down to about 300 nm:[115] UV cross-linking of prepolymers that are being molded is possible. It has been used to construct elastomeric optical devices for adaptive optics[116–119] and to fabricate photomasks for use in UV photolithography[120] and contact phase-shift photolithography.[121] Fourth, PDMS is a durable elastomer. We used the same stamp up to about 100 times over a period of several months without noticeable degradation in performance.[85] Fifth, the surface properties of PDMS can be readily modified by treatment with plasma followed by the formation of SAMs (Figure 6) to give appropriate interfacial interactions with materials that themselves have a wide range of interfacial free energies.[122]

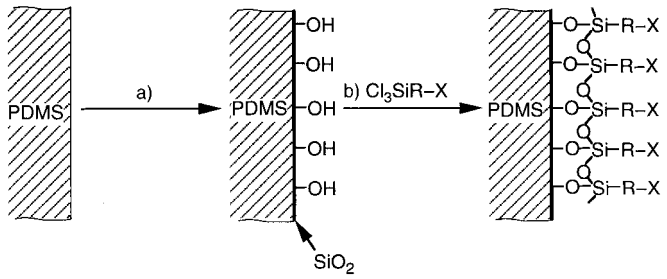


Figure 6. Schematic procedure for the modification of the PDMS surface. a) Treatment with an O_2 plasma; b) reaction with silyl chloride vapor. Different terminal groups X of the SAMs give different interfacial properties.[122]

The elastomeric character of PDMS is also the origin of some of the most serious technical problems that must be solved before soft lithography can be used in forming complex patterned structures (Figure 7). First, gravity, adhesion and

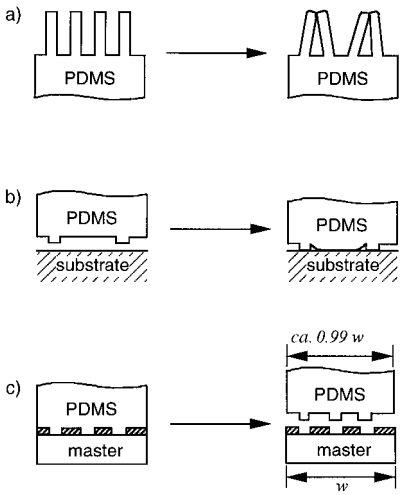


Figure 7. Schematic illustration of possible deformations and distortions of microstructures in the surfaces of elastomers such as PDMS. a) Pairing, b) sagging, c) shrinking.

capillary forces[123] exert stress on the elastomeric features and cause them to collapse and generate defects in the pattern that is formed.[124] If the aspect ratio of the relief features is too large, the PDMS microstructures fall under their own weight or collapse owing to the forces typical of inking or printing of the stamp. Delamarche et al. showed that the aspect ratios (l/h, Figure 5) of the relief structures on PDMS surfaces had to be between about 0.2 and 2 in order to obtain defect-free stamps.[124] They also found that collapsed parallel lines in PDMS could be restored by washing the stamp with sodium dodecylsulfate (SDS, ca. 1 % in water) followed by rinsing with heptane. Second, when the aspect ratios are too low, the relief structures are not able to withstand the compressive forces typical of printing and the adhesion between the stamp and the substrate; these interactions result in sagging. This deformation excludes soft lithography for use with patterns in which features are widely separated ($d \geq 20h$, Figure 5), unless nonfunctional "posts" can be introduced into the designs to support the noncontact regions. Third, achieving accurate registration without distorting the multilayer fabrication process is substantially more difficult with a flexible elastomer than with a rigid material. There are several other disadvantages that may limit the performance of PDMS for certain types of applications. For example, PDMS shrinks by a factor of about 1 % upon curing,[125] and PDMS can be readily swelled by nonpolar solvents such as toluene and hexane.[113, 126] We and other groups are beginning to address these problems associated with elastomeric materials: We recently found that we could use the Moiré technique to determine distortions of PDMS stamps or molds during soft lithography, and a method was identified for limiting the maximum distortions to less than 1 μm over areas of about 1 cm^2.[127] We believe that we will find solutions for most of these problems in the future by using new materials, new designs, and new configurations.

2.5. Masters and Rapid Prototyping

The utility of soft lithographic techniques is often limited by the availability of appropriate masters. In general, the master used to cast the PDMS stamp or mold is fabricated using microlithographic techniques such as photolithography[84] or micromachining,[128] or from available relief structures such as diffraction gratings or TEM grids.[129] Photolithography seems to be the most convenient method for generating complex patterns. Chrome masks are commercially available, but they are expensive (ca. $200 per square inch for features larger than 5 μm and ca. $500 per square inch for features between 1 and 5 μm). The time and expense involved in generating chrome masks are significant barriers to the use of photolithography by chemists and biologists. These barriers have also limited the development of soft lithography, and inhibited the use of microfabrication in a number of areas.

Recently we[130] and other groups[131] developed a system that allows fabrication of masters having feature sizes that are greater than or equal to 20 μm rapidly and at low cost (see Figure 3). In this technique we draw patterns using computer programs such as Freehand or AutoCAD and print them directly onto polymer sheets with a commercial laser-assisted image-setting system (e.g., Herkules PRO, resolution of 3387 dpi (dots per inch), Linotype-Hell Company, Hauppauge, NY). With this method photomasks, transparent polymeric sheets patterned with microstructures of black ink, can be made in a few hours at a cost of about $1 per square inch. Although these masks do not have the durability and dimensional stability required for use in the manufacturing of microelectronic devices, they are suitable for the rapid production of simple patterns that are well suited for prototyping microfluidic, microoptical, and microanalytical systems as well as for sensors.[5–9, 130] After the patterns on these polymer films are transferred into films of photoresists coated on silicon substrates using photolithography and developing, the resulting patterns can serve as masters to make the required PDMS stamps. Rapid prototyping allows the production of substantial numbers of simple microstructures rapidly and inexpensively. By combining this method with soft lithographic techniques, we can fabricate patterned

microstructures of polymers and metals within 24 hours after the design is completed. At present, the smallest feature size that can be achieved directly using this procedure is about 20 μm, a value that is limited by the resolution (ca. 3387 dpi) of the image-setting system. It should be possible to generate smaller features by using printers with higher resolutions. We believe that rapid prototyping paves the way for expanded use of microfabrication in chemistry and biology, especially when patterns may be complex but require only modest feature sizes.

3. Microcontact Printing

3.1. Principles of Microcontact Printing

Microcontact printing (μCP) is a flexible, non-photolithographic method that routinely forms patterned SAMs containing regions terminated by different chemical functionalities with submicron lateral dimensions.[84] The procedure is remarkably simple (Figure 8). An elastomeric PDMS stamp is used to transfer molecules of the "ink" to the surface of the substrate by contact. After printing, a different SAM can be formed on the underivatized regions by washing the patterned substrate with a dilute solution containing the second molecule. Microcontact printing was first demonstrated for SAMs of alkanethiolates on gold.[34] Its success relies on the rapid reaction of alkanethiols on gold and on the "autophobicity" of the resulting SAMs.[132] An exceptionally thoughtful STM study by Larsen et al. showed that for μCP with solutions of dodecanethiol in ethanol with concentrations greater than or equal to 10 mM, a contact time of longer than 0.3 s was enough to form highly ordered SAMs on Au(111) that are indistinguishable from those formed by adsorption from solution (Figure 9).[80f, 133] For μCP with hexadecanethiol (ca. 2 mM in ethanol), a contact time of about 10–20 s is usually used.[84]

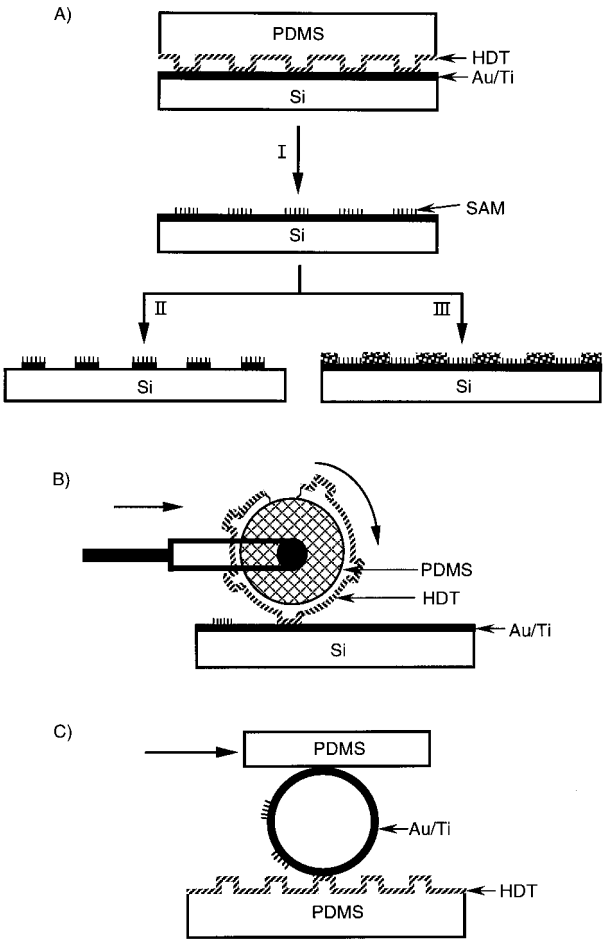


Figure 8. Schematic illustration of procedures for μCP of hexadecanethiol (HDT) on a gold surface: A) printing on a planar surface with a planar stamp (I: printing of the SAM, II: etching, III: deposition);[84] B) large-area printing on a planar surface with a rolling stamp;[147] C) printing on a nonplanar surface with a planar stamp.[149] After the "ink" (ca. 2 mM HDT in ethanol) was applied to the PDMS stamp with a cotton swab, the stamp was dried in a stream of N_2 (ca. 1 min) and then brought into contact with the gold surface (ca. 10–20 s).

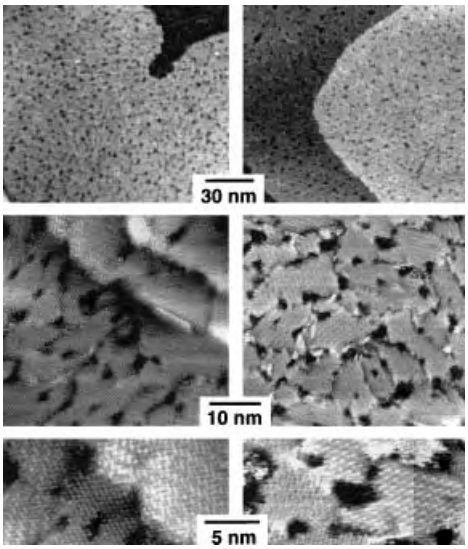


Figure 9. Comparison of STM images of SAMs of dodecanethiol (DDT) on Au(111) formed by μCP (left) and by adsorption from solution (right). The μCP was carried out with a solution of DDT in ethanol (ca. 100 mM) as the "ink" (the stamp was in contact with the gold surface for about 10 s); in the case of adsorption from solution the gold surface was equilibrated with a solution of DDT in ethanol (1 mM) for about 18 h (taken from Larsen et al.[133]).

Patterned SAMs formed by μCP can be visualized using a range of techniques such as scanning electron microscopy (SEM),[134] scanning probe microscopy (SPM),[135] secondary ion mass spectrometry (SIMS),[136] condensation figures (CFs),[136] and surface-enhanced Raman microscopy.[86b] Figure 10 compares the pattern in an original master with that of a SAM of hexadecanethiolate on gold formed by μCP with a PDMS stamp cast from this master. Figure 11 shows lateral force microscopy (LFM) images of a test pattern of SAMs of hexadecanethiolate on gold.[135b] The patterned SAMs of hexadecanethiolate formed by μCP seem to have an edge roughness less than about 50 nm.

We and other groups have extended μCP to a number of other systems of SAMs (see Table 6). The most useful systems are patterned SAMs of alkanethiolates on evaporated thin films of gold and silver, because both systems give highly ordered monolayers. Gold is interesting since it is widely used

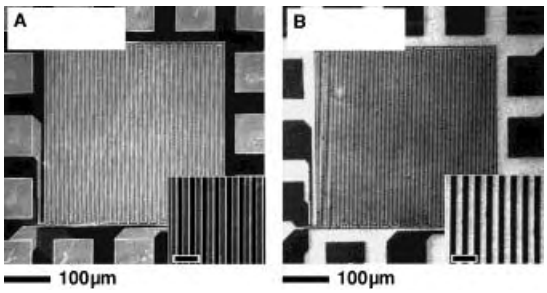


Figure 10. SEM images (at two different magnifications) of A) a master and B) the pattern of a SAM of HDT on gold formed by μCP (contact time ca. 10 s) with a PDMS stamp cast from this master. A planar PDMS stamp was used. The contrast in the image of the master (A) resulted from different heights and/or materials between regions. The dark regions on the SAM-patterned surface in image B represent the SAM of HDT, and the light regions underivatized gold. The scale bars in the insets correspond to 10 μm.

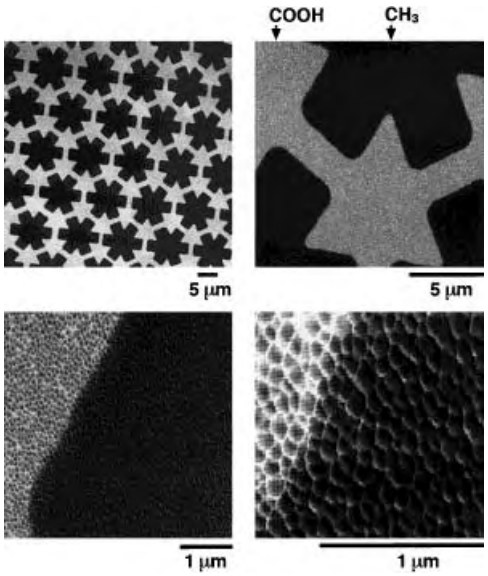


Figure 11. LFM images (at four different magnifications) of a gold surface patterned with SAMs terminated in different head groups. The surface was printed in HDT; the remaining regions were then derivatized with $HS(CH_2)_{15}COOH$ by immersing the patterned sample in a solution containing the second thiol. Relatively high frictional forces between the probe and the surface were detected in regions covered with a COOH-terminated SAM (light), and relatively low frictional forces were measured over regions covered with a CH_3-terminated SAM (dark).[135b]

as the material for electrodes in many applications,[137] and it is compatible with microelectronic devices based on GaAs (but not on silicon).[138] Silver is attractive because it is more convenient to etch than gold: Silver is chemically more reactive than gold and therefore dissolves more rapidly in most etchants;[86] the level of defects in SAMs of alkanethiolates on silver also seems to be lower than on gold.[86] Furthermore, silver is an excellent electrical and thermal conductor.[139] The system of siloxanes on HO-terminated surfaces is less tractable and usually gives disordered SAMs and in some cases submonolayers or multilayers.[140]

Patterned SAMs can be used as ultrathin resists in selective wet etching[84, 141] or as templates to control the wetting, dewetting, nucleation, growth, and deposition of other materials (Figure 8A, II and III).[142–145] They have also been used as supports to control both azimuthal and polar orientations of nematic liquid crystals (LCs).[146] The smallest features generated to date with a combination of μCP and selective etching are trenches etched in gold with lateral dimensions of approximately 35 nm.[84f] The minimum size of features that can be fabricated by μCP has still not been completely defined. Because the SAMs are only 1–3 nm thick, there is little loss in edge definition due to the thickness of the resist; the major determinants of edge resolution seem to be the fidelity of the contact printing and the anisotropy in the etching of the underlying metal. Absorbates on the surface of the substrate, the roughness of the surface, and materials properties (especially the deformation and distortion) of the elastomeric stamp also influence the resolution and feature size of patterns formed by μCP. Some tailoring of the properties of the PDMS stamp or development of new elastomeric materials optimized for the regime below 100 nm will be useful.

Microcontact printing is attractive because it is simple, inexpensive, and flexible. Routine access to clean rooms is not required (at least for fabricating structures that are larger than 20 μm by rapid prototyping and similar techniques), although occasional use of these facilities is convenient for making masters. The process is inherently parallel—that is, it forms the pattern over the entire area of the substrate in contact with the stamp at the same time—and thus suitable for forming patterns over large areas ($\geq 50\,cm^2$) in a single impression (Figure 8B).[147] The elastomeric PDMS stamp and the surface chemistry for the formation of SAMs can be manipulated in a number of ways to reduce the size of features generated by μCP.[148] It can, in principle, be used for many micro- and nanofabrication tasks and is a low-cost process. In particular, it can be applied to types of patterning where optically based lithography simply fails, for example, patterning nonplanar surfaces.[149]

3.2. Patterned SAMs as Ultrathin Resists in Selective Wet Etching

SAMs do not have the durability to serve as etch masks in conventional reactive-ion etching.[150] They are, however, efficient resists for certain types of wet etchants. Table 7 summarizes selective chemical etchants that have been studied for use with patterned SAMs.[84, 141] Many other selective etches are known for these and other materials, and they remain to be explored in conjunction with SAMs.[151]

Figure 12 shows SEM images of a series of test patterns of silver that were fabricated by μCP with hexadecanethiol followed by selective etching in aqueous solutions of ferricyanide.[86a] The SAM-derivatized regions were barely attacked by the etchant within the time required to remove the bare regions. These images represent the level of complexity, perfection, and scale that can be produced *routinely* with μCP. The ability to generate arrays of microstructures of coinage metals with controlled shapes and dimensions is directly useful in fabricating arrays of microelectrodes for sensors[8] and other electrochemical devices.[137] Another application of μCP is in the preparation of gold or silver patterns to be used

Table 7. Selective etchants that have been used with patterned SAMs generated by μCP (all wet etchants were used in aqueous solutions).

Surface	SAM	Etchant (approximate pH)	Ref.
Au	RS^-	$K_2S_2O_3/K_3[Fe(CN)_6]/K_4[Fe(CN)_6]$ (14)	[84, 85, 141]
		KCN/O_2 (14)	[34, 84, 85]
		$CS(NH_2)_2/H_2O_2$ (1)	[84e, 141]
Ag	RS^-	$Fe(NO_3)_3$ (6)	[84e, 86a]
		$K_2S_2O_3/K_3[Fe(CN)_6]/K_4[Fe(CN)_6]$ (7)	[84e, 86a, 141]
		$NH_4OH/K_3[Fe(CN)_6]/K_4[Fe(CN)_6]$ (12)	[84e, 86a]
		NH_4OH/H_2O_2 (12)	[84e, 86a]
		NH_4OH/O_2 (12)	[84e, 86a]
		KCN/O_2 (14)	[84e, 86a, 141]
Cu	RS^-	$FeCl_3$/HCl (1)	[84e, 87b]
		$FeCl_3/NH_4Cl$ (6)	[84e, 87b]
		H_2O_2/HCl (1)	[84e, 87a]
GaAs	RS^-	HCl/HNO_3 (1)	[84e, 97]
Pd	RS^-	HCl/HNO_3 (1)	[88]
Al	RPO_3^{2-}	HCl/HNO_3 (1)	[89]
Si/SiO_2	$RSiO_{3/2}$[a]	HF/NH_4F (2)	[90b]
glass	$RSiO_{3/2}$[a]	HF/NH_4F (partially selective)	[90b]

[a] These SAMs are formed by contact of $RSiCl_3$ or $RSi(OCH_3)_3$ with the substrates.

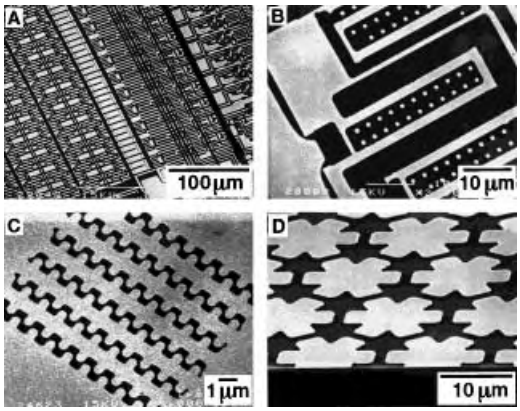


Figure 12. SEM images of test patterns on layers of silver (A, B, C: 50 nm thick; D: 200 nm thick) that were fabricated by μCP with HDT followed by chemical etching in an aqueous solution of ferricyanide. The patterns in A and B were printed with rolling stamps,[147] and those in C and D with planar stamps.[86a] The bright regions represent silver, and the dark regions Si/SiO_2 in which unprotected silver has dissolved.

as secondary masks in the etching of underlying substrates such as SiO_2, silicon, and GaAs.[152, 153] Figure 13 shows SEM images of microstructures in silicon that were fabricated by anisotropic etching of Si(100) in an aqueous solution containing KOH and 2-propanol with patterns of silver (50 nm thick) as masks.[86a, 154] The silver masks were in turn generated with a combination of μCP of hexadecanethiol and selective chemical etching.

SAMs and patterning by μCP illustrate a new approach to microfabrication. Although this combination is proving immediately useful in single-layer fabrication (e.g., sensors and microelectrode arrays), several issues remain to be solved before it can be considered for application in complex microelectronics. For example, the formation and distribution of defects in SAMs, especially under the conditions of chemical etching, must be understood. A recent study based on a method involving two-stage chemical amplification found that the density of defects in SAMs depended on the

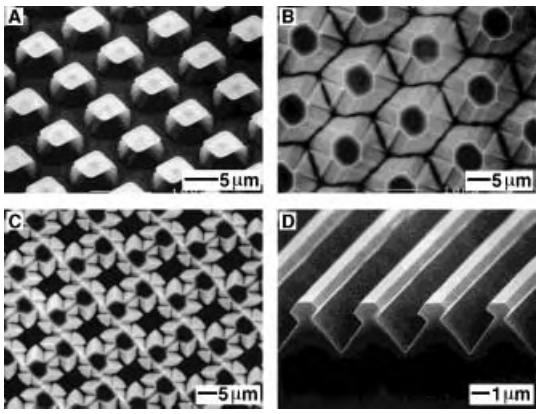


Figure 13. SEM images of silicon structures generated by anisotropic etching of Si(100) with patterned structures of silver or gold as masks.[86a, 120] The metal mask is still on the surface in A; it has been removed by immersion in aqua regia for B, C, and D. The structure in D was fabricated by a combination of shadow evaporation and anisotropic etching of Si(100).[153]

thickness of the gold layer, the length of the alkyl chain, and the conditions used for preparing the SAMs.[82] The density of defects in printed SAMs (in terms of pinholes in SAM-derivatized regions) measured using this technique was about 10^3 pits per mm^2 for 50 nm thick gold, and about 10 pits per mm^2 for 50 nm thick silver.[155] These densities are still too high to be useful for fabricating high-resolution microelectronic devices. The latter is, however, low enough that silver lines (200 nm thick and 50 μm wide) extending approximately 5 m in length are electrically continuous with no evidence of electrically significant defects.[130] The patterned microstructures fabricated using this procedure are acceptable for applications in many areas other than microelectronics, including the production of microelectromechanical systems (MEMS),[5] microanalytical systems,[6] sensors,[8] solar cells,[156] and optical components.[152b, 157]

3.3. Patterned SAMs as Passivating Layers in Selective Deposition

Through chemical control of the length of the polymethylene chain, the thickness of a SAM can be predetermined with a precision of about 0.1 nm. Organic synthesis also makes it possible to incorporate different functional groups (e.g., fluorocarbons, acids, esters, amines, amides, alcohols, nitriles, and ethers) into and/or at the termini of the alkyl chain.[39] With μCP, SAMs with different functional head groups can be organized into different patterns on a single surface and employed to control wetting, dewetting, nucleation, or deposition of other materials on this surface.[142–145]

Figures 14A and 14B shows how functionalities of SAMs influence the wetting and dewetting of liquids on SAM-patterned surfaces. These processes are determined by the minimization of free energies. They use self-assembly at two scales: the formation of SAMs at the molecular scale and the fabrication of structures of liquids at the mesoscopic scale. Figure 14A shows an optical micrograph of drops of water preferentially condensed on hydrophilic regions of a surface

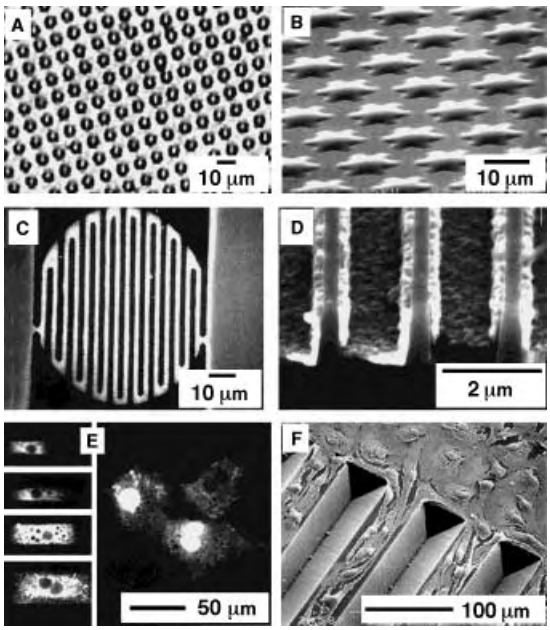


Figure 14. Demonstration of selective nucleation and deposition with patterned SAMs as templates. A) An optical micrograph of water condensed on a SAM-patterned gold surface.[142a] B) An SEM image of microstructures of polyurethane assembled by selective dewetting;[142b] only COOH-terminated regions were covered by water or polyurethane liquid. C) An SEM image of microstructures of $LiNbO_3$ on Si/SiO_2 produced with selective CVD.[145b] D) An SEM image of copper microstructures formed in silicon microtrenches with selective CVD.[145a] $LiNbO_3$ and copper only nucleated and grew on bare regions of SiO_2 underivatized by CH_3-terminated siloxane SAMs. E) Optical micrographs of hepatocytes placed on SAM-patterned (left) and bare surfaces (right).[143a] F) An SEM image of mammalian cells selectively attached to the plateaus of a contoured surface.[143b] In E and F the surfaces were derivatized by μCP in such a way that certain regions of the surface terminated in methyl groups whereas others terminated in oligo(ethylene glycol) groups. The matrix protein (fibronectin) only adsorbed to the methyl-terminated regions, and cells only attached to those regions where the matrix proteins were adsorbed.

patterned with SAMs terminated in carboxylic (COOH) and methyl groups (CH_3); no water condensed on the hydrophobic regions.[142a] Figure 14B shows an SEM image of patterned microstructures of polyurethane (PU) formed by selective dewetting.[142b] The liquid prepolymer of PU placed on the SAM-patterned surface selectively dewetted those regions derivatized with methyl groups (CH_3) and formed patterned structures on the hydrophilic regions terminated in hydroxyl groups (CH_2OH). The prepolymer was then solidified by curing under UV light. The organization of liquids into patterned arrays illustrates the use of controlled wettability in microfabrication. These patterned mcirostructures of polymers have been used as arrays of microlenses[142b] and optical waveguides.[142f]

Nuzzo et al. demonstrated selective chemical vapor deposition (CVD)[158] on Si/SiO_2 with printed SAMs of siloxanes as templates (Figures 14C, D).[145] The patterned SAMs directed the selective CVD by inhibiting nucleation: The material to be patterned only nucleated and grew on the bare regions underivatized with SAMs and formed continuous structures. This procedure could in principle be used to deposit a variety of materials selectively on many substrates without photolithography. The selective CVD of Cu may be useful in microelectronics processing, including the fabrication of thin-film interconnects (with feature sizes of ca. 0.5 – 100 μm) and selective filling of trenches and vias (representative microstructures having high aspect ratios) with feature sizes below about 1 μm.[159]

Patterned SAMs have also been used as templates to define and control the adsorption of extracellular matrix proteins and consequently the attachment of mammalian cells.[143] This technique makes it possible to place cells in predetermined locations in an array with defined shapes, sizes, and distances of separation. Figures 14E and 14F show SEM images of cells that have been selectively attached to a planar[143a] and a contoured surface,[143b] respectively. Using simple patterning procedures, it is possible to dictate the shape assumed by a cell that attaches to a surface and thus to control certain aspects of cell growth and protein secretion. This technique allows us to examine the influence of cell morphology on cell metabolism,[143d] and should be useful for applications in biotechnology that require analysis of individual cells cultured at high density and/or repeated access to cells placed in specified locations. The results of these studies may eventually shed light on complex phenomena such as contact inhibition of cell proliferation, or they may lead to new analytical systems based on arrays of cells.

3.4. Formation of Microstructures on Nonplanar Surfaces

Patterning on nonplanar surfaces has been a substantial challenge for photolithography and related techniques: even gently curved surfaces often cannot be patterned by photolithography because of limitations to depth of focus.[13] Because μCP involves conformal contact using an elastomeric stamp, it offers immediate advantages over photolithography in patterning nonplanar surfaces.[149]

Figure 8C illustrates one method for forming patterned microfeatures on surfaces of capillaries. A piece of flat PDMS stamp is used to control the movement of the capillary. Figures 15A and 15B show SEM images of test patterns of gold that were formed on gold-coated glass capillaries by μCP with hexadecanethiol followed by selective etching in an aqueous solution of cyanide.[149] They clearly show well-defined features of gold with dimensions of a few microns on capillaries with radii of curvature of about 500 μm (Figure 15A) and about 50 μm (Figure 15B). Microcontact printing can generate microstructures on planar and nonplanar surfaces with similar edge resolution. At present, there is no comparable technique for microfabrication on curved surfaces. Our recent demonstration of using electroless deposition rather than metal evaporation for preparing thin films of silver as the substrates for μCP of alkanethiols further simplifies the procedure for patterning nonplanar surfaces (even hidden surfaces such as the inside surfaces of hollow glass tubes).[114] The procedure based on μCP opens the door immediately to new types of electronic, optical, MEMS, and analytical structures including microtransformers (Figure 15C),[160] current carriers in microinductors,[160] microsprings

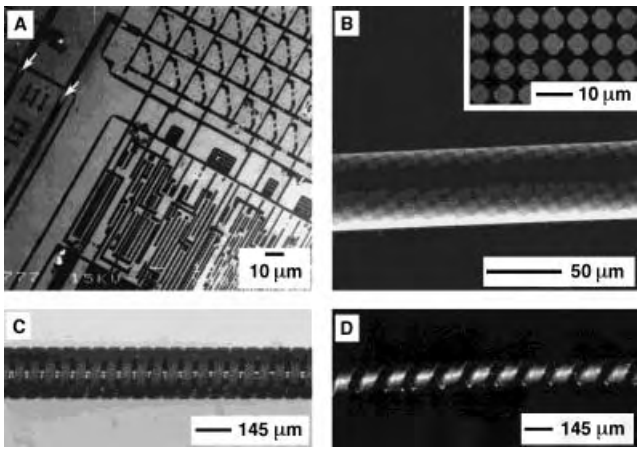


Figure 15. A, B) SEM images of test patterns of gold on curved surfaces (curvature 500 and 50 μm, respectively) that were fabricated by μCP with HDT followed by selective etching in an aqueous solution of KCN saturated with O_2.[149] C, D) Optical micrographs of a microtransformer[160] and a microspring[161] fabricated by μCP with HDT on silver (coated on the capillaries) followed by selective etching of silver and electroplating of nickel (C) and copper (D). The arrows in A indicate two defects caused by sagging.

(Figure 15 D),[161] in-fiber notch filters and Bragg gratings,[162] micro-coils for high-resolution NMR spectroscopy,[163] and intravascular stents.[164]

3.5. Microcontact Printing of Other Materials

Microcontact printing seems to be a general method for forming patterns of a variety of materials on surfaces of solid substrates through contact pattern transfer. We demonstrated μCP of protonic acids[165] and liquids containing suspended palladium colloids[106, 166] using similar procedures. Protonic acids were printed onto thin films of acid-sensitive photoresist.[167] They acted as the catalyst for the decomposition of the photoresist upon heating: Regions sensitized by acids became soluble in the basic developing solution. Colloids were also printed directly on a variety of substrates including glass, Si/SiO_2, and polymer films.[106, 166] The deposited colloids acted as catalysts for electroless deposition of metals (Figure 16). Microcontact printing of aqueous solutions containing biological molecules (e.g., proteins and enzymes) might also be possible, although formation of uniform monolayers of such materials using printing might be difficult.

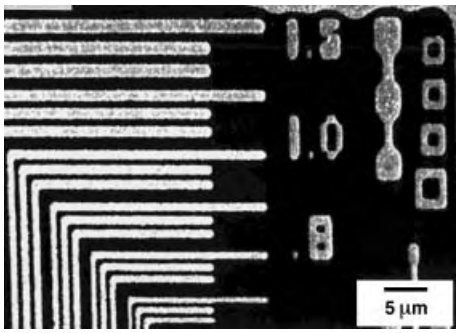


Figure 16. An SEM image of copper microstructures that were fabricated by electroless plating onto a pattern of electrocatalytic colloid particles of palladium. The palladium pattern was printed by μCP.[106]

4. Micromolding and Related Techniques

4.1. Replica Molding

Our procedure for replica molding (REM; Figure 17 A) differs from conventional procedures in the use of an elastomeric mold rather than a rigid mold.[35, 168] The elasticity

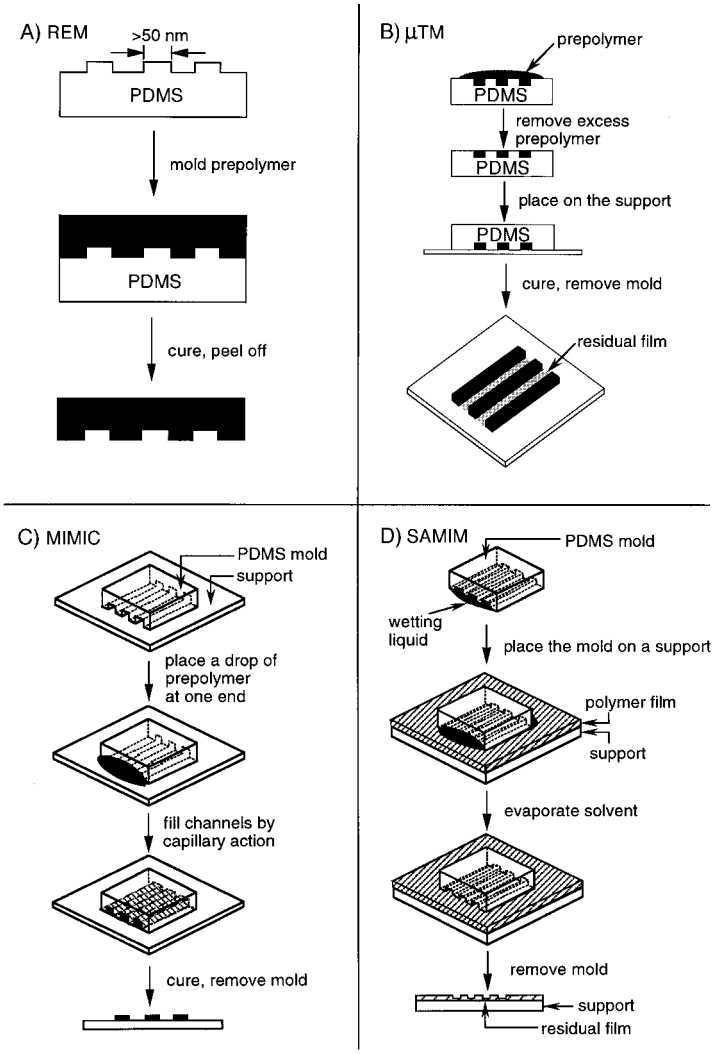


Figure 17. Schematic illustration of procedures for A) replica molding, B) microtransfer molding, C) micromolding in capillaries, and D) solvent-assisted micromolding.

and low surface energy of the elastomeric PDMS mold allows it to be released easily. An elastomeric mold also offers the opportunity to manipulate the size and shape of features present on the mold by mechanical deformation. The capability and versatility of this new procedure has been demonstrated for nanomanufacturing:[169] Conventional high-resolution nanolithographic techniques would be used to make masters, and these structures would then be duplicated into multiple copies by replica molding with organic polymers. This technique has also been adapted for the fabrication of topologically complex, optically functional surfaces that would be difficult to fabricate with other techniques.[35]

4.1.1. Nanomanufacturing

We demonstrated that replica molding against elastomeric molds is possible with a resolution on the nanometer scale.[169] Figure 18 shows AFM images of chromium structures on a master[170] and a PU replica prepared from a PDMS mold cast against this master. The most important feature of this replicated PU is the accuracy with which the vertical dimension is reproduced. The heights of the chromium lines on the original master were about 13 nm; the heights of the PU lines were about 8 nm. The prepolymer of PU used here shrinks less than 3% upon curing.[171] These images demonstrate that, within our ability to compare similar structures, this replica molding procedure duplicated structures within a few nanometers over substantial areas (ca. 1 mm^2).

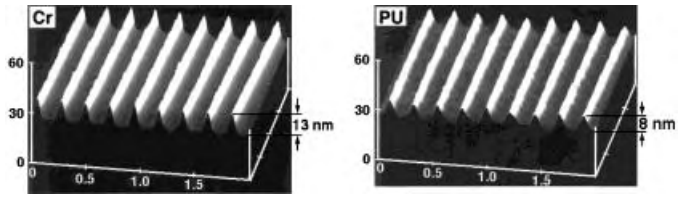


Figure 18. AFM images of chromium structures on a master and a PU replica prepared from a PDMS mold cast from this master.[169] The width is given in micrometers; the depth and height are given in nanometers.

We also monitored the quality of the replica structures generated from successive molds prepared from the same master.[169] Figure 19A shows the AFM image of gold structures on a master before it was used to cast PDMS molds; the gold master was prepared using a procedure including electron-beam writing in a resist, development of the lines, metal evaporation, and lift-off. Figure 19B shows an AFM image of this gold master after it had been used to cast seven PDMS molds. We observed no damage to the gold master after its repeated use (ten times) to form PDMS stamps. Figures 19C and 19D show AFM images of PU replicas generated from different PDMS molds. Again, we did not observe obvious change in the quality of these nanostructures on the PU replicas. These AFM images clearly demonstrate that this procedure is able to generate multiple copies of nanostructures starting from a single master. The simplicity and low cost of this procedure suggest its potential use in nanomanufacturing.

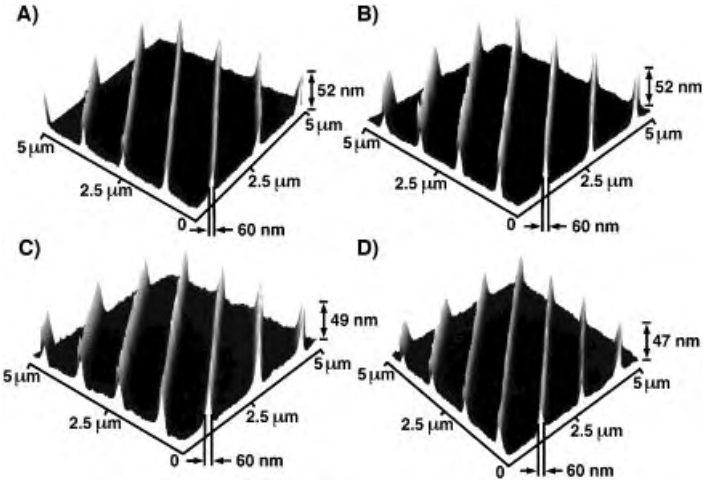


Figure 19. A, B) AFM images of gold structures on a master A) before it was used to cast PDMS molds and B) after it had been used to cast seven PDMS molds. C, D) AFM images of PU replicas produced from different PDMS molds cast from this master.[169]

A modification of the procedure, replica molding against an PDMS mold while it is bent mechanically, allows the fabrication of nanostructures with feature sizes smaller than those on the original master.[169] Figure 20A shows the AFM image of gold structures on another master with a feature size of about 50 nm, and Figure 20B the AFM image of a PU replica duplicated from a PDMS mold (cast from this gold master) while it was bent mechanically. The dimension of the features was reduced from 50 to 30 nm in this process.

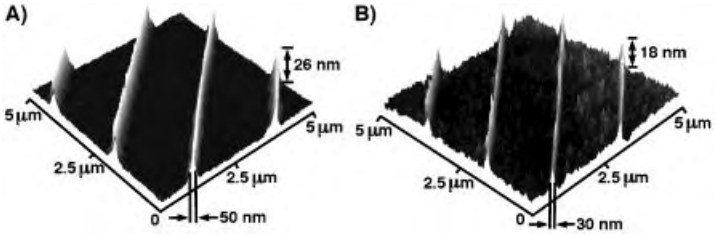


Figure 20. AFM images A) of Au structures on a master before it was used to cast PDMS molds and B) of a PU replica fabricated from a PDMS mold (cast from this master) while this mold was mechanically deformed by bending in a manner that generated narrower lines.[169]

The absence of techniques that are capable of generating and manufacturing nanostructures rapidly and economically represents one current limiting step in the area of nanoscience and nanotechnology.[12] This work based on replica molding demonstrates a practical protocol for fabricating structures as small as approximately 30 nm in organic polymers, and with an accuracy in vertical dimension as small as about 5 nm. Recently, Chou et al. demonstrated a related procedure that might also be included in soft lithography: embossing or imprinting in organic polymers with rigid masters. This method generates features in thermoplastic polymers with dimensions as small as about 25 nm.[18] Related work has also been demonstrated by groups at Phillips[19a] and IBM.[19b] These demonstrations make it clear that manufacturing (i.e., fabrication of multiple copies) of nanostructures of organic polymers is a practical reality. The ability to make both positive and negative polymeric replicas and to modify the dimensions and shapes of features present on elastomeric molds by mechanical deformation adds further flexibility to this methodology. Using nanostructures to generate electronically, optically, and magnetically functional components and systems will require the development of new technologies; the present work may provide one solution to the problem of mass production of nanostructures. Lessons learned from this process will be valuable in building more versatile systems.

4.1.2. Fabrication of Complex Optical Surfaces

Replica molding against a deformed PDMS mold provides a new strategy for making topologically complex structures and optically functional surfaces.[35, 168] It allows the sizes and shapes of features present on the surface of the mold to be changed in a controlled way (by mechanical compression, bending, stretching, or a combination of these deformations) and generates complex structures from simple, regular structures on planar surfaces. The highly isotropic deformation of the PDMS mold even permits patterned microstructures to be formed with gradients in size and shape. The relief features on the PDMS mold are reconfigured by mechanical deformation, and the deformed structures are replicated by casting an UV-curable liquid PU or a thermally curable epoxy against it. The capability and feasibility of this procedure has been demonstrated by the production of[35] 1) diffraction gratings with periods smaller than the original grating used as the master to cast the PDMS mold, 2) chirped, blazed diffraction gratings on planar and curved surfaces, 3) patterned microfeatures on the surfaces of approximately hemispherical objects, and 4) arrays of rhombic microlenses.

Figure 21 summarizes the typical procedures used in replica molding against elastomeric molds under mechanical deformation.[35] Figure 21 A shows the procedure for replica molding against a PDMS mold under mechanical compression. If desired, this procedure can be repeated, using the PU replica as the starting point, to make structures more complex than

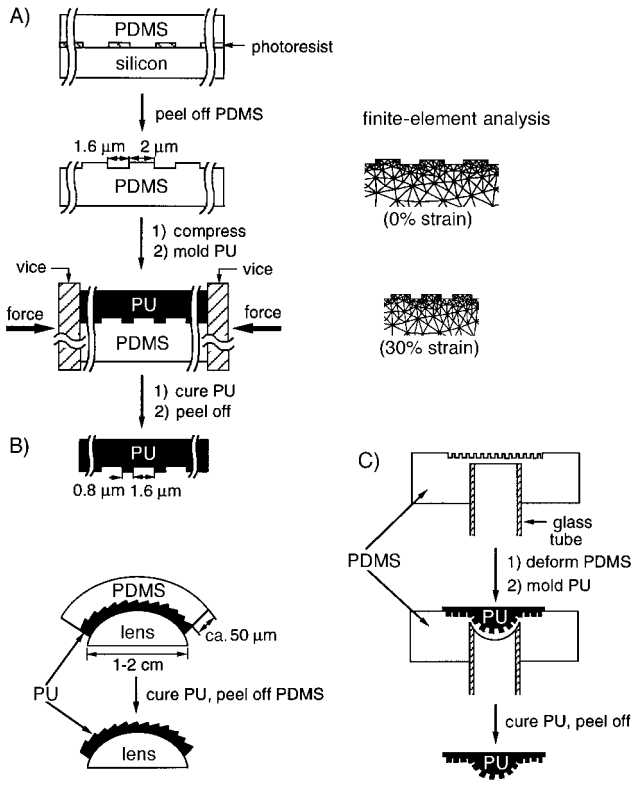


Figure 21. Schematic illustration of procedures for replica molding against elastomeric PDMS molds under A) mechanical compression, B) bending, and C) stretching.[35] The reconfigurated surfaces in PDMS are replicated with a UV-curable prepolymer of PU.

can be generated in one cycle (although with some degradation in the quality of the fabricated structures). Using a test structure of parallel lines, two cycles of compression and replication reduced the size of some features (that is, the recessed areas on the mold) from 1.6 μm to about 200 nm, and reduced the period of this test pattern from 3.6 to about 1.5 μm.[35] Figure 21 B illustrates the procedure that we used to fabricate diffraction gratings on cylindrical surfaces. A thin PDMS mold (ca. 50 μm thick) was bent to make conformal contact with a curved surface coated with a thin film of liquid PU. After curing the PU, the PDMS mold was removed to reveal the PU replica on the surface of the cylindrical substrate. Figure 21 C shows a similar procedure that was used to produce an approximately hemispherical object having micropatterned relief structures on its surface. A thin PDMS mold (ca. 1 mm thick) was mounted across the end of a hollow glass tube and deformed by applying positive or negative pressure through the tube. The resulting curved surface was then replicated in PU.

By compressing one end of the elastomeric mold more than the other, it was straightforward to fabricate a chirped diffraction grating, a grating whose period changes continuously with position.[172] More interestingly, the shape of the diffracting elements was largely preserved in this process: If we used a blazed grating as the starting master, the resulting chirped PU replica was also a blazed grating (Figure 22).[35] The period (Λ) of this chirped, blazed grating changed continuously from a value of about 1.55 to about 1.41 μm over a distance of approximetly 0.9 cm; the rate of chirping $d\Lambda/dz$ was approximately 1.6×10^{-5}. This grating was characterized in transmission at normal incidence. Figure 22 C shows the diffraction patterns (the zero-order and the two first-order peaks) of the PDMS mold, its PU replica, and the chirped PU grating. The first diffraction peak shifted continuously in position as the laser spot was scanned across the chirped grating along the z direction.

Figure 23 shows the SEM image of a hemispherical PU object with a pattern of corner cubes on its surface.[35, 168] The shape of this polymeric object can be easily tuned by changing the thickness of the PDMS mold or the applied pressure or both. We have made a range of different patterns and relief structures; the smallest feature had a size of about 1.5 μm.

4.2. Microtransfer Molding

In microtransfer molding (μTM, see Figure 17 B)[36] a drop of liquid prepolymer is applied to the patterned surface of a PDMS mold and the excess liquid is removed by scraping with a flat PDMS block or by blowing off with a stream of nitrogen. The filled mold is then placed in contact with a substrate and irradiated or heated. After the liquid precursor has cured to a solid, the mold is peeled away carefully to leave a patterned microstructure on the surface of the substrate.

Figure 24 shows SEM images of typical structures of polymers that were fabricated by μTM.[36] Microtransfer molding is capable of generating both isolated and interconnected microstructures (Figure 24 A). The most significant advantage of μTM over other microlithographic techniques is

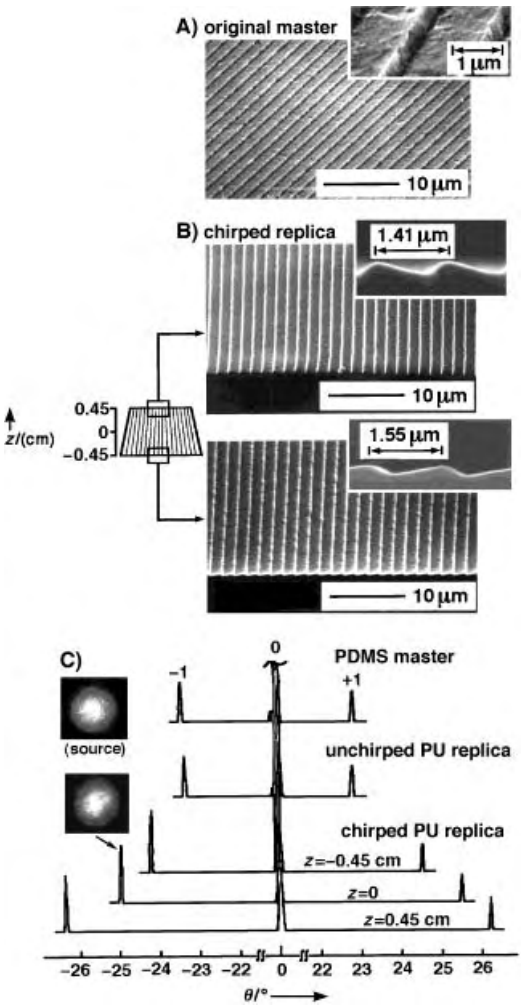


Figure 22. Cross-sectional SEM images of A) a commercial blazed diffraction grating and B) selective regions of a planar, chirped, blazed PU replica grating that was fabricated by molding against the PDMS mold while it was compressed asymmetrically. C) Diffraction patterns from the PDMS master, its PU replica, and the chirped PU grating. A He-Ne laser ($\lambda = 632.8$ nm) was used.[35]

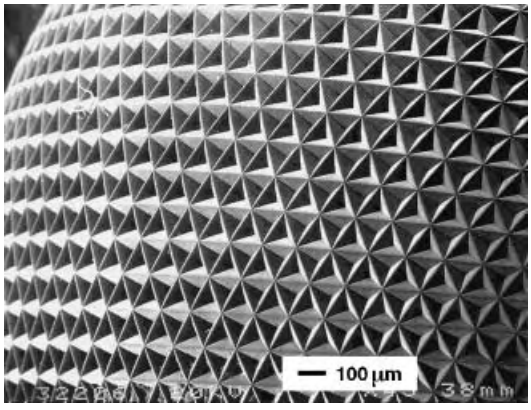


Figure 23. An SEM image of a dome-shaped object in polyurethane with patterned microstructures (corner cubes ca. 100 μm) on its surface that was formed by replica molding against a stretched PDMS mold.[35]

the ease with which it can fabricate microstructures on nonplanar surfaces, a characteristic that is essential for building three-dimensional microstructures layer by layer.

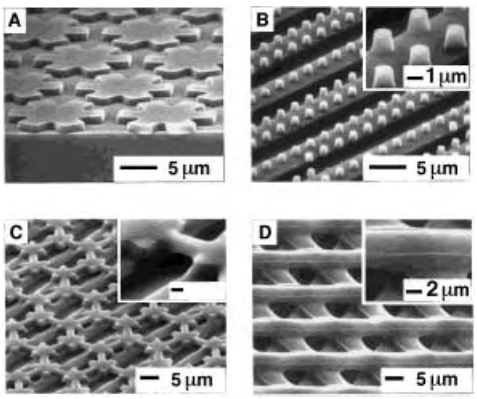


Figure 24. SEM images of polymeric microstructures fabricated by μTM:[36] A) patterned, isolated microstructures of PU on silver (one layer); B) isolated microcylinders of epoxy on 5-μm lines of epoxy supported on a glass slide (two layers); C) a continuous web of epoxy over a layer of 5-μm lines of epoxy supported on a glass slide (two layers); D) a three-layer structures on a glass slide made from a thermally curable epoxy.

Figure 24B shows microposts of thermally curable epoxy fabricated on an array of parallel lines made of the same material. Figure 24C shows a continuous polymeric web fabricated over separated polymer lines. Figure 24D shows a three-layer structure of epoxy fabricated by μTM. Analogues of these two- and three-dimensional microstructures may find potential application in integrated optics,[173] applied optics (as photonic crystals[174]), and tissue engineering.[175]

Microtransfer molding can generate microstructures over relatively large areas (ca. 3 cm^2) within a short period of time (ca. 10 min). It has been used to fabricate optical waveguides, couplers, and interferometers from organic polymers.[176] We fabricated arrays of polymeric waveguides (both single- and multimode) of 3 cm in length from thermally curable epoxies and UV-curable PU; both polymers could be pristine or doped with fluorescent dyes (e.g. rhodamine 6G).[36] An array of such waveguides could be turned into optical couplers and interferometers by tuning the separation between them; the coupling could also be controlled after fabrication by additional exposure to UV light.[176] Microtransfer molding also has the capability of forming patterned microstructures of a wide variety of other materials. Figures 25A and 25B show SEM images of microstructures of glassy carbon (an interdigitated capacitor and an optical deflector, respectively); the structures were fabricated by μTM with a polymeric precursor (a phenolic resin modified with furfuryl alcohol) followed by pyrolysis at elevated temperatures.[177] Figures 25C and 25D give SEM images of microstructures (an array of square pyramids and a free-standing membrane, respectively) of glasses fabricated from sol–gel precursors.[178] One important shortcoming of μTM in its current state of development is that microstructures fabricated on a flat surface usually have a thin film (ca. 100 nm) between the raised features. This film prevents the underlying substrate from being attacked by chemical etchants, and must be removed by reactive-ion etching with O_2 if we want to use these patterned structures of polymers as masks to control the etching of the underlying substrate. Although removing this film requires a separate

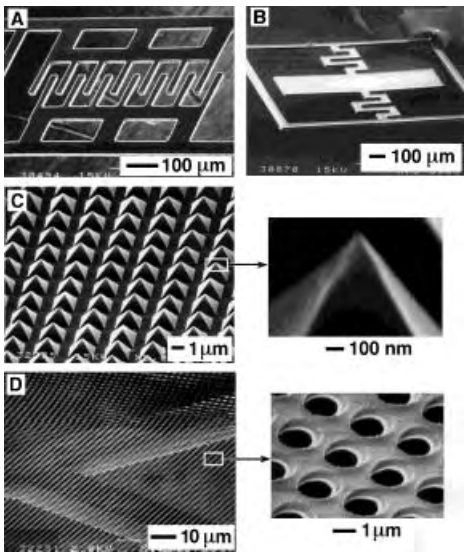


Figure 25. SEM images of A, B) microstructures of glassy carbon[177] and C, D) glasses fabricated by μTM and molding.[178] The retention of details in both procedures is very good.

step and is an inconvenience, we believe that μTM will find a broad application in microfabrication, especially for making three-dimensional microstructures.

4.3. Micromolding in Capillaries

Micromolding in capillaries (MIMIC) represents another non-photolithographic method that forms complex microstructures on both planar and curved surfaces.[37] In MIMIC (see Figure 17C) the PDMS mold is placed on the surface of a substrate and makes conformal contact with that surface; the relief structure in the mold forms a network of empty channels. When a low-viscosity liquid prepolymer is placed at the open ends of the network of channels, the liquid spontaneously fills the channels by capillary action. After filling the channels and curing the prepolymer into a solid, the PDMS mold is removed, and a network of polymeric material remains on the surface of the substrate. A variety of materials (see Table 3) have been used in this process[37] including prepolymers that are curable either with UV light or thermally,[179] precursors to carbons[177] or ceramics,[180] structural and functional polymers,[181, 182] polymer beads,[183] colloids,[184] inorganic salts,[184] sol–gel materials,[185] and biological macromolecules.[186]

Microfabrication based on MIMIC is remarkable for its simplicity and its fidelity in transferring the patterns from the mold to the polymeric structures that it forms. MIMIC is applicable to patterning a broader range of materials than is photolithography. MIMIC forms patterned structures in a single step, and patterning structures with multiple thicknesses (quasi-three-dimensional structures) is possible. The smallest features that we produced using this procedure were parallel lines with cross-sectional dimensions of about $0.1 \times 2\ \mu m^2$.[179] These dimensions were set by the PDMS molds that were available for use with this work; we have not tried molds with smaller features, and therefore the lower limit to the pattern definition that can be achieved by this technique has not been established.

MIMIC does have several limitations: 1) It requires a hydraulically connected network of capillaries; it cannot, therefore, form isolated structures or patterns on contoured surfaces. 2) Although capillary filling over a short distance (ca. 1 cm) can be achieved quickly and efficiently, the rate of filling over a large distance decreases significantly due to the viscous drag of the fluid in the capillary. 3) Since the rate of filling is proportional to the cross-sectional dimension of the capillary, the extremely slow filling of small capillaries may limit the usefulness of MIMIC in certain types of nanofabrication. Nevertheless, several groups have demonstrated that appropriate liquids could wet and fill nanometer-sized capillaries over short distances.[187, 188] 4) The forward ends of capillaries may fill incompletely if the hydraulic drag is sufficiently high.[189] Interestingly, capillaries with closed ends may fill completely if they are short; the gas in them appears to escape by diffusing into the PDMS.

4.3.1. The Principle of MIMIC

Capillary filling is a very simple and well-known phenomenon,[190] and the dynamics of wetting and spreading of liquids in capillaries has been studied systematically.[191] The flow of a liquid in a capillary occurs because of a pressure difference between two hydraulically connected regions of the liquid mass, and the direction of flow decreases this difference in pressure. In circular capillaries, the flow of a wetting liquid occurs initially in thin films that wet the capillary symmetrically; in noncircular capillaries the most rapid flow usually occurs in the corner regions.[191]

The rate of capillary filling is determined by the surface tension γ and viscosity η of the liquid, the radius of the capillary R, and the length of the filled section of the capillary z [Eq. (2); γ_{LV}, γ_{SV}, and γ_{SL} are liquid–vapor, solid–vapor, and solid–liquid interfacial free energies].[190] The rate of filling

$$\frac{dz}{dt} = \frac{R\gamma_{LV}\cos\theta}{4\eta z} = \frac{R(\gamma_{SV} - \gamma_{SL})}{4\eta z} \qquad (2)$$

is proportional to the cross-sectional dimension of the capillary as well as inversely proportional to the length of capillary that contains the liquid and to the viscosity of the liquid. The rate of filling decreases as the capillary fills or when a more viscous liquid is used.

The shape of the imbibition front strongly depends on the interfacial free energies. Kim et al. characterized the system and studied this relationship qualitatively using gold surfaces derivatized by SAMs of alkanethiolates terminated in different head groups (Figure 26).[189] In agreement with Equation (2), the product of the length of filling and the rate of filling $[z(dz/dt)]$ shows a linear dependence on the cosine of the advancing contact angles θ_a. The SEM images of the fronts (insets in Figure 26) indicate that different values of $\cos\theta_a$ result in different shapes of imbibing liquids: 1) For liquids with small advancing contact angles (Figure 26a, b) the imbibition fronts can be characterized as slipping films; 2) for liquids with intermediate advancing contact angles (Figure 26c, d) the shapes of the imbibition fronts consist of leading edges that suggest slipping films with shoulders; 3) for

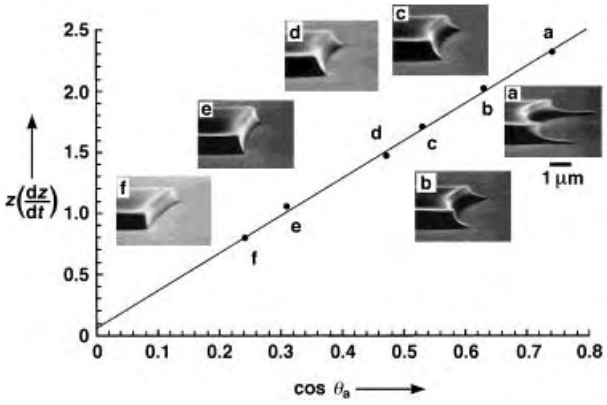


Figure 26. Dependence of the rate of capillary filling, represented by $z(dz/dt)$ in $10^4\ \mu m^2 s^{-1}$, and the imbibition shape (insets) on interfacial free energies of the surfaces[189] as described with the the dynamic contact angle θ_a between the liquid polymer and the SAM-derivatized surface.

liquids with high advancing contact angles (Figure 26e, f) the bulk liquids flow as a whole without having precursor structures. The imbibition shapes can be described as wedge or bulk-flow.

4.3.2. MIMIC of Solventless Systems

The capability and feasibility of MIMIC have been demonstrated by the fabrication of patterned structures from a variety of liquid prepolymers: PU, polyacrylates, and epoxies.[37, 179] These prepolymers have a shrinkage of less than 3% after curing.[171] The cured polymers, therefore, possess almost the exact dimensions and shapes of the channels in the surface of the PDMS mold; they can be directly used as masks in the etching of the underlying substrates. Figure 27 shows SEM images of polymeric microstructures that were fabricated by MIMIC. The polymer

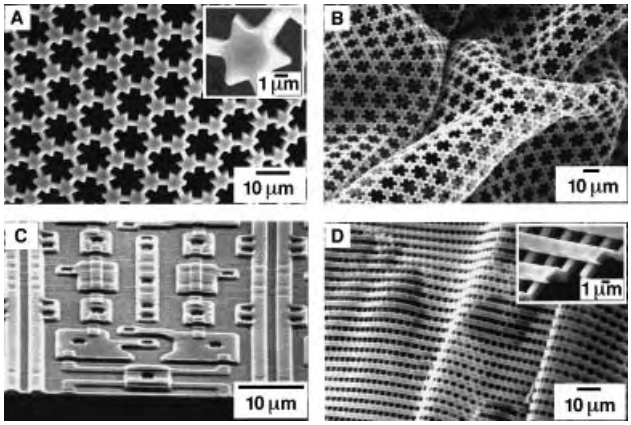


Figure 27. SEM images of polymeric microstructures fabricated by MIMIC from prepolymer of polyacrylate (A, C) and polyurethane (B, D) without solvents.[37, 179] The structures in B and D are freestanding; the buckling occurred during sample preparation and demonstrated their strength.

microstructure could be freed from the support by dissolving a sacrificial layer of glass or SiO_2 in an aqueous solution of HF/NH_4F (Figure 27B).[37] MIMIC also allows quasi-three-dimensional processing (i.e., patterning layers with different thicknesses) in a single step (Figure 27C).[179] Such complex arrays of micro and submicrometer scale channels filled completely; in some regions of these structures, features are connected to one another by channels with thicknesses of less than 100 nm. The support used in MIMIC could have relief patterns on its own surface. Figure 27D shows the SEM image of a free-standing microstructure of PU that was formed between two PDMS molds.[37, 179] Each PDMS mold has a relief pattern of parallel lines on its own surface. After the filling with liquid prepolymer and the curing of the prepolymer into a solid, the two PDMS molds were separated. The cross-linked polymeric microstructure remained on the surface of one of the two PDMS molds and could be easily released. These two layers of polymeric lines formed *one* interconnected polymeric microstructure. This type of free-standing microstructure, two layers with an independent relief structure in each, cannot be fabricated by photolithography.[10]

4.3.3. MIMIC of Systems with Solvents

Although MIMIC was developed based on prepolymers having no solvents, it has also been extended to those systems where solvents are involved.[182–186] The solvents were evaporated after the solutions had filled the channels. The only requirement seems to be that the solvent does not swell PDMS. It has been extremely difficult (or impossible) to fabricate patterned structures of those materials such as polymer beads (Figure 28A, B) and ceramics (Figure 28E, F)

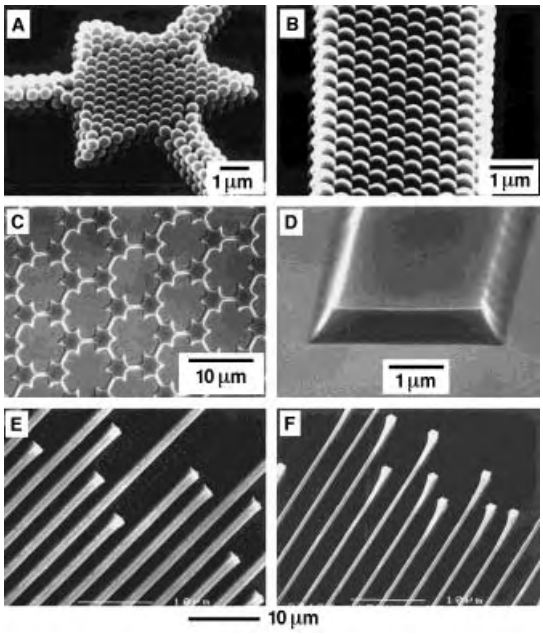


Figure 28. SEM images of patterned microstructures of A, B) polymer beads,[183] C, D) polyaniline emeraldine HCl salt,[182] and E, F) zirconium oxide[180] fabricated by MIMIC from their solutions in water, *N*-methyl-2-pyrrolidone, and ethanol, respectively. The crystallization of the polymer beads occured spontaneously. The structures of polyaniline were molded from a solution of polyaniline emeraldine base in *N*-methyl-2-pyrrolidone, and then converted into the conductive form of emeraldine salt by doping in aqueous HCl. The zirconium oxide was formed from a precursor polymer that has been molded into the structure shown in E. The precursor polymer was obtained from Chemat Technology (ZO9303), and was converted into ZrO_2 by heating at about 600 °C for 10 h. The ends of the lines deadhered from the substrate during thermal conversion.

with photolithography. Figure 28 shows SEM images of some patterned microstructures that were fabricated by MIMIC from systems involving solvents or suspending liquids. The ability to form patterned microstructures offers new opportunities for these materials. For example, the closely packed, multilayered structures of polymer beads are interesting for potential applications in chromatography and diffractive optics.[192] The ability to form patterned microstructures of conducting polymers provides a potential route to flexible, all-plastic electronic and optoelectronic devices.[193]

4.3.4. Fabrication of Functional Microelectronic Devices

Nuzzo et al. fabricated ferroelectric capacitors made up of thin films of Pt/Pb(Zr,Ti)O_3/Pt by μCP and selective CVD.[194] Recently Hu, Jeon et al. used MIMIC successfully to fabricate simple, electrically functional devices.[195–197] They demonstrated the fabrication of Schottky diodes,[195] GaAs/AlGaAs heterostructure field effect transistors (FETs),[196] and silicon metal oxide semiconductor FETs (MOSFETs).[197] The fabrication process for both types of transistors required at least three MIMIC steps and two registration steps. Figure 29 outlines the fabrication of the GaAs/AlGaAs heterostructure FET.[196] Figure 30 A shows the oblique view of the device. The source and drain are AuNiGe ohmic contacts, the channel is defined by a mesa etch, and the gate is a Cr/Au Schottky contact. In each step the pattern was defined by microstructures of PU formed by MIMIC (see Figure 29): Etching and evaporation were performed using these PU structures as the masks. Figure 30 B shows an optical micrograph of the FET, and Figure 30 C the performance of a representative GaAs/AlGaAs FET fabricated by this procedure. Its characteristics are similar to those of GaAs/AlGaAs FETs made using conventional photolithographic techniques as the patterning tools. The fabrication of the Si MOSFETs followed a similar procedure, but used PU microstructures to form the mask layers used during implantation of the silicon.[197] Although the feature sizes (16–26 μm) that characterize these devices are about 100 larger than those of state-of-the-art commercial devices (ca. 250 nm), these results established that soft lithography is compatible with the multilayer fabrication that has, up to now, been monopolized by photolithography and set a benchmark against which to measure further developments in this area.

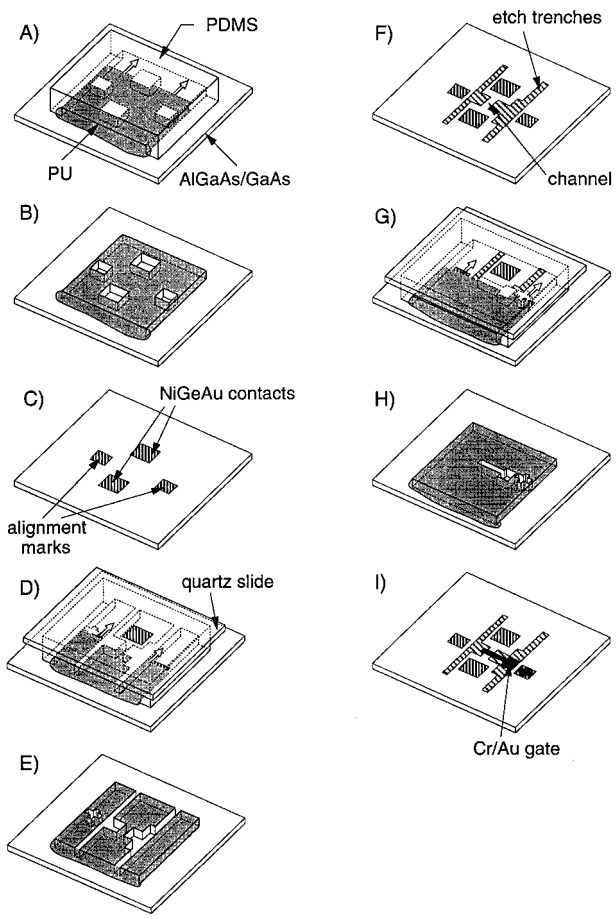


Figure 29. Schematic illustration of the procedure for the fabrication of GaAs/AlGaAs FETs.[196] A) Use MIMIC to define ohmic contacts and alignment marks. B) Cure PU, peel off the PDMS mold, and remove the thin film of PU adjoining the microstructures. C) Evaporate AuNiGe, lift off PU, anneal to form ohmic contacts for the source, and drain. D) Register and use MIMIC with another PDMS mold to define etch trenches. E) Cure PU, peel off the PDMS mold, and remove the connecting film of PU. F) Etch in an aqueous solution of citric acid and hydrogen peroxide to remove the 2DEG in the etched trenches. G) Register and use MIMIC with a third PDMS mold to define the gate. H) Cure PU, peel off the PDMS mold, and remove the thin film of PU. I) Evaporate Cr/Au and lift off PU to form the gate.

4.4. Solvent-Assisted Micromolding

Solvent-assisted micromolding (SAMIM) is a technique that allows fabrication of patterned, quasi-three-dimensional microstructures on the surfaces of polymeric substrates.[38] It can also be used to modify surface morphologies of polymers. The operational principle of this technique shares characteristics with both replica molding and embossing (see Figure 17 D). An elastomeric PDMS mold is wetted with a solvent that is a good solvent for the polymer, and is brought into contact with the surface of the polymer. The solvent dissolves (or swells) a thin layer of the polymer, and the resulting (probably gellike) fluid comprising polymer and solvent conforms to the surface topology of the mold. While the mold is maintained in conformal contact with the substrate, the polymer solidifies as the solvent dissipates and evaporates (probably by diffusion through the mold) to form relief structures with a pattern complementary to that on the surface of the mold.

SAMIM is an experimentally simple procedure. The key elements are wetting of the PDMS mold by a liquid that is a solvent for the polymer to be molded and conformal contact between the solvent-coated elastomeric mold and the substrate. The choice of solvent for a polymer determines the effectiveness and success of SAMIM. The solvent should rapidly dissolve or swell the surface of the polymer; it should not, however, swell the PDMS mold and thereby distort the mold and/or destroy the conformal contact between the polymer and the mold.[126] In general, the solvent should have a relatively high vapor pressure and a moderately high surface tension (e.g., methanol, ethanol, and acetone) to ensure rapid

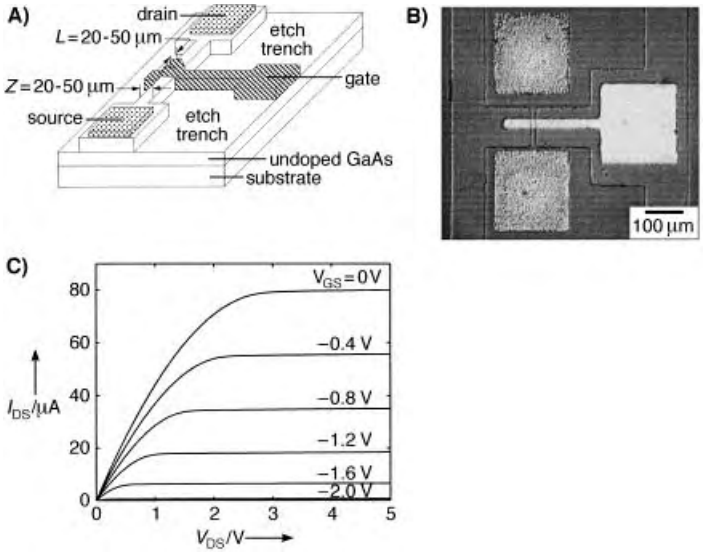


Figure 30. A) Schematic diagram of a GaAs/AlGaAs FET. B) Optical micrograph of a GaAs/AlGaAs FET fabricated by MIMIC (gate length $L = 26$ μm, gate width $Z = 16$ μm).[196] C) The performance of a representative GaAs/AlGaAs FET fabricated by this procedure.[196] I_{DS} = current between drain and source, V_{DS} = voltage between drain and source, V_{GS} = voltage between gate and source.

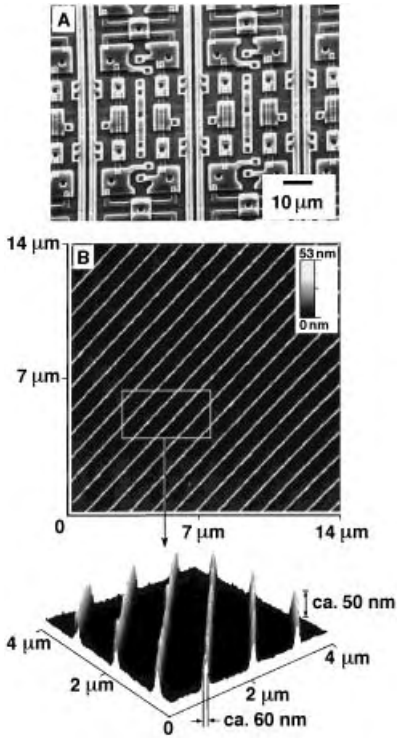


Figure 31. A) SEM and B) AFM images of polymeric microstructures fabricated by SAMIM.[38] The polymers used here were thin films (A: ca. 1.6 μm thick; B: ca. 0.4 μm thick) of a photoresist (Microposit 1805, Shipley) that was spin-coated on Si wafers. The solvent was ethanol.

evaporation of the excess solvent and minimal swelling of the PDMS mold. Dyes and inorganic salts can also be added to the solvent; they are subsequently incorporated into the resulting microstructures. Solvents with low vapor pressures (e.g., ethylene glycol and dimethyl sulfoxide) are not well suited for SAMIM. Surface modification[122] of the PDMS mold may be required when solvents with high surface tensions are used since they only partially wet the PDMS surface. Many nonpolar solvents (e.g., toluene and dichloromethane) cannot be used in SAMIM because they can swell the PDMS mold.

Replication of patterns with complex topology is practical in a single step by SAMIM. This procedure is also suitable for forming patterned relief microstructures over a large area and is applicable to a variety of polymers when appropriate solvents are selected, for example, ethanol or 2-propanol for Microposit photoresists (a phenol formadehyde resin) or acetone for polystyrene, poly(methyl methacrylate), cellulose acetate, and poly(acrylonitrile-butadiene-styrene). Figure 31 A shows the SEM image of patterned relief structures formed on a polystyrene film with acetone as the solvent.[38] These quasi-three-dimensional features are well defined and clearly resolved. A common characteristic of patterned microstructures generated by SAMIM is that the resulting structures are adjoined by a thin film of the polymer. These films can sometimes be removed by homogeneous thinning by reactive-ion etching with O_2. Figure 31 B shows AFM images of the smallest features that we have generated in a thin film of photoresist by SAMIM with ethanol as the solvent: parallel lines that are about 60 nm in width and about 50 nm in height.[38]

SAMIM can generate quasi-three-dimensional microstructures or morphologies on the surface of a polymer using a solvent that can soften the polymer without affecting the PDMS mold. SAMIM differs from other existing techniques (e.g., embossing with a rigid master[18] or MIMIC) in several ways. First, it uses an elastomeric rather than a rigid mold. Second, it uses a solvent instead of increased temperatures to "soften" the surface of the polymer. The process is simple, rapid, and does not require specialized equipment or a system for pressing the mold into the substrate. Third, it does not suffer from slow rates of capillary filling, which limits MIMIC to relatively small areas; it is also not restricted to fabrication of hydraulically connected structures. Fourth, it can be used with a wide range of polymers or prepolymers: the only requirement seems to be a solvent that dissolves the polymer of the substrate and wets the surface of the PDMS mold but does not significantly swell the mold.

5. Summary and Outlook

As fabrication of microstructures grows in importance in a wide range of areas—from microelectronics through optics, microanalysis, combinatorial synthesis, display, and MEMS to cell biology—the utility of new methods for patterning will certainly increase. The techniques of soft lithography—self-assembly, contact printing, micromolding, and contact phase-shift photolithography[115]—illustrate the potential for application of the largely unexplored, non-photolithographic procedures for micro- and nanofabrication to these new areas.

Soft lithography offers immediate advantages (Table 8) in applications in which photolithography clearly falters or fails: For example, manufacturing below the scale of 100 nm, patterning on nonplanar surfaces, fabrication of three-dimensional structures, patterning of functional materials other than

Table 8. Advantages and disadvantages of soft lithography.

Advantages
- convenient, inexpensive, accessible to chemists, biologists, and material scientists
- basis in self-assembly tends to minimize certain types of defects
- many soft lithographic processes are additive and minimize waste of materials
- readily adapted to rapid prototyping for feature sizes $>20\ \mu m$
- isotropic mechanical deformation of PDMS mold or stamp provides routes to complex patterns
- no diffraction limit; features as small as 30 nm have been fabricated
- nonplanar surfaces (lenses, optical fibers, and capillaries) can be used as substrates
- generation and replication of three-dimensional topologies or structures are possible
- optical transparency of the mask allows through-mask registration and processing
- good control over surface chemistry, very useful for interfacial engineering
- a broad range of materials can be used: functional polymers, sol–gel materials, colloidal materials, suspensions, solutions of salts, and precursors to carbon materials, glasses, and ceramics
- applicable to manufacturing: production of indistinguishable copies at low cost
- applicable in patterning large areas

Disadvantages and Problems
- patterns in the stamp or mold may distort due to the deformation (pairing, sagging, swelling, and shrinking) of the elastomer used
- difficulty in achieving accurate registration with elastomers ($<1\ \mu m$)
- compatibility with current itegrate-circuit processes and materials must be demonstrated
- defect levels higher than for photolithography
- μCP works well with only a limited range of surfaces; MIMIC is slow; REM, μTM, and SAMIM leave a thin film of polymer over the surface

photoresists, and modification of surfaces. Figure 32 summarizes the current state of development of soft lithography as well areas in which its potential is particularly clear. Most work in soft lithography has concentrated on single-step processing; our recent successes in multilayer fabrication requiring registration (albeit with features of about 20 μm) has established a modest potential in multilayer structures and functional microelectronic devices.[194–197] This demonstration paves the way for the evaluation of soft lithographic techniques in microelectronics, although serious technological use will require substantial further development.

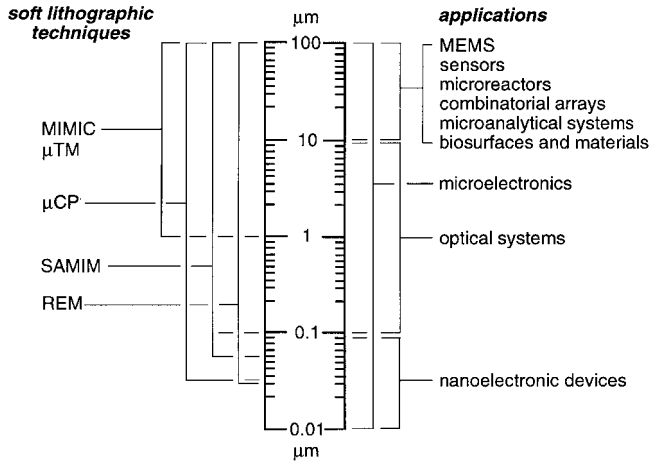


Figure 32. Summary of the current state of development of soft lithographic techniques and areas in which these techniques find applications.

Photolithography will of course continue as the dominant technology in microfabrication of technologically sophisticated semiconductor devices and systems for the foreseeable future. There are, however, many existing and emerging uses for soft lithography that take advantage of (or require) the characteristics of these techniques. Soft lithographic materials offer experimental simplicity and flexibility in forming certain types of patterns. Procedures involving relatively large features ($>1\ \mu m$) can be conducted in an unprotected laboratory environment, and thus are especially useful in laboratories that do not have routine access to the facilities normally used in microfabrication, or for which the capital cost of equipment is a serious concern. At the current state of development, they can replace photolithographic techniques in many problems of microfabrication where requirements for precise alignment, continuity, isolation, and uniformity in the final patterns are relaxed: for example, production of single-level structures for use in microelectrode arrays, sensors, biosensors, and microanalytical systems. Simple display devices, optical components, and elementary microelectronic devices also now seem practical. The initial success of soft lithography also suggests that it will be useful to reexamine other relatively undeveloped patterning techniques (see Table 2) for their potential for application in emerging technologies or in high-resolution patterning.

A number of issues remain to be solved before soft lithography invades the core applications of photolithography, that is, those in microelectronics. First, high-resolution (≤ 20 nm) registration with elastomeric materials must be demonstrated. The distortion and deformation associated with elastomeric materials must also be managed, and pattern transfer must be made exactly reproducible. Second, the quality of the patterns and structures produced must be improved. These patterns, especially for narrow lines, are not yet compatible with the levels of quality required for microfabrication of complex electronic devices. The formation and distribution of defects in SAMs, and especially their influence on the quality of patterns formed when they are used as resists for etching, must be understood and improved. Third, the compatibility of these patterning techniques with the range of processes used in the production of microelectronic circuitry must be explored. In particular, systems that form SAMs directly on semiconductors and are optimized for compatibility with current processes (especially etching with reactive ions) and materials are required.

Researchers and manufacturers of microstructures have specific requirements of any microlithographic technology: flexibility during the development process; reproducibility, reliability, and simplicity during manufacturing; and cost-effectiveness for commercial success. Judged against these standards, soft lithography has the potential to become an important addition to the field of micro- and nanofabrication, although it is still in an early stage of technical development.

This work was supported in part by the Office of Naval Research (ONR) and the Defense Advanced Research Projects Agency (DARPA). This work made use of Material Research Science and Engineering Center (MRSEC) Shared Facilities supported by the National Science Foundation (NSF) under

award number DMR-9400396. We thank our colleagues and collaborators for their essential contributions to this work: Colin Bain, Paul Laibinis, John Folkers, Hans Biebuyck, Ralph Nuzzo, Mark Wrighton, and Mara Prentiss (SAMs); Amit Kumar, Hans Biebuyck, Nicholas Abbott, James Wilbur, John Rogers, Rebecca Jackman, Gabriel López, and Ralph Nuzzo (μCP); Enoch Kim, Xiao-Mei Zhao (molding and related techniques); Dong Qin (rapid prototyping); John Rogers, Kateri Paul, and Joanna Aizenberg (contact phase shift photolithography); and Junmin Hu, Noo-Li Jeon, Ralph Nuzzo, and Robert Westervelt (fabrication of microelectronic devices). We also thank Dr. Hans Biebuyck for providing the STM images shown in Figure 9, and the IBM Zurich group for providing data before publication.

Received: July 4, 1997 [A239IE]
German version: *Angew. Chem.* **1998**, *110*, 568 – 594

[1] General reviews on nanoscience and nanotechnology: a) *Science* **1991**, *254*, 1300 – 1342; b) G. A. Ozin, *Adv. Mater.* **1991**, *4*, 612 – 649; c) G. Stix, *Sci. Am.* **1995**, *272*(2), 90 – 96.

[2] General accounts on the development of microelectronics: a) R. W. Keyes, *Phys. Today* **1992**, *45*(8), 42 – 48; b) C. R. Barrett, *MRS Bull.* **1993**, *28*(7), 3 – 10; c) R. F. Service, *Science* **1996**, *273*, 1834 – 1836; d) G. Moore, *Electrochem. Soc. Interf.* **1997**, 18 – 23.

[3] General reviews on QSE: a) M. Sundaram, S. A. Chalmers, P. F. Hopkins, A. C. Gossard, *Science* **1991**, *254*, 1326 – 1335; b) M. A. Kastner, *Phys. Today* **1993**, *46*(1), 24 – 31; c) M. A. Reed, *Sci. Am.* **1993**, *270*(1), 118 – 123; d) H. Weller, *Angew. Chem.* **1993**, *105*, 43 – 56; *Angew. Chem. Int. Ed. Engl.* **1993**, *32*, 41 – 53.

[4] General reviews on SET: a) K. K. Likharev, *IBM J. Res. Dev.* **1988**, *32*, 144 – 158; b) M. H. Devoret, D. Esteve, C. Urbina, *Nature* **1992**, *360*, 547 – 553; c) K. K. Likharev, T. Claeson, *Sci. Am.* **1992**, *269*(6), 80 – 85.

[5] General reviews on microelectromechanical systems (MEMS): a) K. D. Wise, K. Najafi, *Science* **1991**, *254*, 1335 – 1342; b) J. Bryzek, K. Peterson, W. McCulley, *IEEE Spectrum* **1994**, *31*(5), 20 – 31; c) N. C. MacDonald, *Microelectron. Eng.* **1996**, *32*, 49 – 73; d) G. T. A. Kovacs, K. Petersen, M. Albin, *Anal. Chem.* **1996**, *68*, 407A – 412A.

[6] General reviews and highlights on microanalytical systems: a) R. E. Service, *Science* **1995**, *268*, 26 – 27; b) A. Manz, *Chimia* **1996**, *59*, 140 – 145; c) D. Craston, S. Cowen, *Chem. Br.* **1996**(10), 31 – 33; d) P. Day, *ibid.* **1996**(7), 29 – 31; e) A. Goffeau, *Nature* **1997**, *385*, 202 – 203.

[7] Recent reports on microoptics: a) Y. A. Carts, *Laser Focus World* **1994**, *30*, 67 – 71; b) S. S. Lee, L. Y. Lin, M. C. Wu, *Appl. Phys. Lett.* **1995**, *67*, 2135 – 2137; c) M. C. Wu, L. Y. Lin, S. S. Lee, C. R. King, *Laser Focus World* **1996**, *32*, 64 – 68.

[8] General reviews on microsensors: a) H.-J. Galla, *Angew. Chem.* **1992**, *104*, 47 – 50; *Angew. Chem. Int. Ed. Engl.* **1992**, *31*, 45 – 47; b) P. Kleinschmidt, W. Hanrieder, *Sens. Actuators A* **1992**, *33*, 5 – 17; c) M. J. Vellekoop, G. W. Lubking, P. M. Sarro, A. Venema, *ibid.* **1994**, *44*, 249 – 263; d) G. Fuhr, T. Müller, T. Schnelle, R. Hagedorn, A. Voigt, S. Fiedler, W. A. Arnold, U. Zimmermann, B. Wagner, A. Heuberger, *Naturwissenschaften* **1994**, *81*, 528 – 535; e) J. Bryzek, *Sensors* **1996,** 7, 4 – 38.

[9] Recent reviews on combinatorial synthesis: *Chem. Rev.* **1997**, *97*, 347 – 509.

[10] General reviews on photolithography: a) S. Okazaki, *J. Vac. Sci. Technol. B* **1991**, *9*, 2829 – 2833; b) H. J. Jeong, D. A. Markle, G. Owen, F. Pease, A. Grenville, R. von Bünau, *Solid State Technol.* **1994**, *37*, 39 – 47; c) M. D. Levenson, *ibid.* **1995**, *38*, 57 – 66; d) L. Geppert, *IEEE Spectrum* **1996**, *33*(4), 33 – 38.

[11] General reviews on microlithographic techniques: a) W. M. Moreau, *Semiconductor Lithography: Principles and Materials*, Plenum, New York, **1988**; b) D. Brambley, B. Martin, P. D. Prewett, *Adv. Mater. Opt. Electron.* **1994**, *4*, 55 – 74; c) *Handbook of Microlithography, Micromachining, and Microfabrication, Vol. 1* (Ed.: P. Rai-Choudhury), SPIE Optical Engineering Press, Bellingham, WA, **1997**.

[12] General reviews on nanolithography: a) R. F. W. Pease, *J. Vac. Sci. Technol. B* **1992**, *10*, 278 – 285; b) F. Cerrina, C. Marrian, *MRS Bull.* **1996**, *31*(12), 56 – 62; c) *Microelectron. Eng.* **1996**, *32*, 1 – 418.

[13] See, for example, a) W. D. Deninger, C. E. Garner, *J. Vac. Sci. Technol. B* **1988**, *6*, 337 – 340; b) R. G. Vadimsky, *ibid.* **1988**, *6*, 2221 – 2223.

[14] General reviews on photoresists: a) E. Reichmanis, L. F. Thompson, *Chem. Rev.* **1989**, *89*, 1273 – 1289; b) R. D. Miller, G. M. Wallraff, *Adv. Mater. Opt. E1ectron.* **1994**, *4*, 95 – 127; c) A. Reiser, H.-Y. Shih, T.-F. Yeh, J.-P. Huang, *Angew. Chem.* **1996**, *108*, 2609 – 2620; *Angew. Chem. Int. Ed. Engl.* **1996**, *35*, 2428 – 2440.

[15] Injection molding on the micrometer scale: a) P. E. J. Legierse, J. H. T. Pasman in *Polymers in Information Storage Technology*, Plenum, New York, **1989**, p. 155; b) W. Michaeli, R. Bielzer, *Adv. Mater.* **1991**, *3*, 260 – 262; c) T. E. Huber, L. Luo, *Appl. Phys. Lett.* **1997**, *70*, 2502 – 2504.

[16] Injection molding on the nanometer scale: a) P. Hoyer, N. Baba, H. Masuda, *Appl. Phys. Lett.* **1995**, *66*, 2700 – 2702; b) H. Masuda, K. Fukuda, *Science* **1995**, *268*, 1466 – 1468; c) P. Hoyer, *Adv. Mater.* **1996**, *8*, 857 – 859.

[17] Embossing on the micrometer scale: a) J. S. Winslow, *IEEE Trans. Consumer Electron.* **1976** (Nov.), 318 – 326; b) H. W. Lehmann, R. Widmer, M. Ebnoether, A. Wokaun, M. Meier, S. K. Miller, *J. Vac. Sci. Technol. B* **1983**, *1*, 1207 – 1210; c) C. M. Rodia, *Proc. SPIE Int. Soc. Opt. Eng.* **1985**, *529*, 69 – 75; d) K.-H. Schlereth, H. Bötther, *J. Vac. Sci. Technol. B* **1992**, *10*, 114 – 117; e) M. Emmelius, G. Pawlowski, H. W. Vollmann, *Angew. Chem.* **1989**, *101*, 1475 – 1501; *Angew. Chem. Int. Ed. Engl.* **1989**, *28*, 1445 – 1471; f) F. P. Shvartsman in *Diffractive and Miniaturized Optics* (Ed.: S.-H. Lee), SPIE Optical Engineering Press, Bellingham, WA, **1993**, pp. 165 – 186.

[18] Embossing on the nanometer scale: a) S. Y. Chou, P. R. Krauss, P. J. Renstrom, *Appl. Phys. Lett.* **1995**, *67*, 3114 – 3116; b) *Science* **1996**, *272*, 85 – 87; c) M. T. Gale in *Micro-Optics: Elements, Systems and Applications* (Ed.: H. P. Herzig), Taylor & Francis, London, **1997**, pp. 153 – 179.

[19] Cast molding on the micrometer scale: a) H. C. Haverkorn van Rijsewijk, P. E. J. Legierse, G. E. Thomas, *Philips Tech. Rev.* **1982**, *40*, 287 – 297; b) J. G. Kloosterboer, G. J. M. Lippits, H. C. Meinders, *ibid.* **1982**, *40*, 198 – 309.

[20] Cast molding on the nanometer scale: B. D. Terris, H. J. Mamin, M. E. Best, J. A. Logan, D. Rugar, *Appl. Phys. Lett.* **1996**, *69*, 4262 – 4264.

[21] Laser ablation on the micrometer scale: a) U. Reblan, H. Endert, G. Zaal, *Laser Focus World* **1994**, *30*, 91 – 96; b) S. A. Weiss, *Photonics Spectra* **1995**, *29*(10), 108 – 114; c) M. A. Roberts, J. S. Rossier, P. Bercier, H. Giault, *Anal. Chem.* **1997**, *69*, 2035 – 2042.

[22] Laser ablation on the nanometer scale: a) D. Y. Kim, S. K. Tripathy, L. Li, J. Kumar, *Appl. Phys. Lett.* **1995**, *66*, 1166 – 1168; b) M. Müllenborn, H. Dirac, J. W. Peterson, *ibid.* **1995**, *66*, 3001 – 3003; c) N. Kramer, M. Niesten, C. Schönenberger, *ibid.* **1995**, *67*, 2989 – 2991.

[23] N. L. Abbott, A. Kumar, G. M. Whitesides, *Chem. Mater.* **1994**, *6*, 596 – 602.

[24] a) T. J. Hirsch, R. F. Miracky, C. Lin, *Appl. Phys. Lett.* **1990**, *57*, 1357 – 1359; b) V. Malba, A. F. Bernhardt, *ibid.* **1992**, *60*, 909 – 911; c) A. Miehr, R. A. Fisher, O. Lehmann, M. Stuke, *Adv. Mater. Opt. Electron.* **1996**, *6*, 27 – 32.

[25] M. Datta, *J. Electrochem. Soc.* **1995**, *142*, 3801 – 3806.

[26] a) H. Tabei, S. Nara, K. Matsuyama, *J. Electrochem. Soc.* **1974**, *121*, 67 – 69; b) A. Rose, P. K. Weimer, *Phys. Today* **1989**, *42*(9), 24 – 32; c) M. R. V. Sahyun, *CHEMTECH* **1992**, *22*(7), 418 – 424.

[27] S. Leppävuori, J. Väänänen, M. Lothi, J. Remes, A. Uusimäki, *Sens. Actuators A* **1994**, *41/42*, 593 – 596.

[28] H. Moilanen, J. Lappalainen, S. Leppävuori, *Sens. Actuators A* **1994**, *43*, 357 – 365.

[29] General reviews and highlights on ink-jet printing: a) M. Döring, *Philips Tech. Rev.* **1982**, *40*, 192 – 198; b) E. Anczurowski, J. Oliver, R. H. Marchessault, *CHEMTECH* **1986**, *16*(5), 304 – 310; c) C. Wu, *Sci. News* **1997**, *151*, 205.

[30] Application of ink-jet printing in combinatorial systhesis: a) A. P. Blanchard, R. J. Kaiser, L. E. Hood, *Biosens. Bioelectron.* **1996**, *11*,

687 – 690; b) A. V. Lemmo, J. T. Fisher, H. M. Geysen, D. J. Rose, *Anal. Chem.* **1997**, *69*, 543 – 551.
[31] a) M. Stolka, *CHEMTECH* **1989**, *19*(8), 487 – 495; b) Q. M. Pai, B. E. Springett, *Rev. Mod. Phys.* **1993**, *65*, 163 – 211.
[32] a) D. C. Neckers, *CHEMTECH* **1990**, *20*(10), 616 – 619; b) T. M. Bloomstein, D. J. Ehrlich, *Appl. Phys. Lett.* **1992**, *61*, 708 – 781; c) F. T. Wallenberger, *Science* **1995**, *267*, 1274 – 1275; d) O. Lehmann, M. Stuke, *ibid.* **1995**, *270*, 1644 – 1646.
[33] Short reviews on soft lithography: a) Y. Xia, Dissertation, Harvard University, USA, **1996**; b) X.-M. Zhao, Y. Xia, G. M. Whitesides, *J. Mater. Chem.* **1997**, *7*, 1069 – 1074; c) D. Qin, Y. Xia, J. A. Rogers, R. J. Jackman, X.-M. Zhao, G. M. Whitesides, *Top. Curr. Chem.* **1998**, *194*, 1 – 20; d) G. M. Whitesides, Y. Xia, *Annu. Rev. Mater. Sci.* **1998**, *28*, 153 – 184.
[34] A. Kumar, G. M. Whitesides, *Appl. Phys. Lett.* **1993**, *63*, 2002 – 2004.
[35] Y. Xia, E. Kim, X.-M. Zhao, J. A. Rogers, M. Prentiss, G. M. Whitesides, *Science* **1996**, *273*, 347 – 349.
[36] X.-M. Zhao, Y. Xia, G. M. Whitesides, *Adv. Mater.* **1996**, *8*, 837 – 840.
[37] E. Kim, Y. Xia, G. M. Whitesides, *Nature* **1995**, *376*, 581 – 584.
[38] E. Kim, Y. Xia, X.-M. Zhao, G. M. Whitesides, *Adv. Mater.* **1997**, *9*, 651 – 654.
[39] General reviews on SAMs: a) C. D. Bain, G. M. Whitesides, *Angew. Chem.* **1989**, *101*, 522 – 528; *Angew. Chem. Int. Ed. Engl.* **1989**, *28*, 506 – 512; b) G. M. Whitesides, P. E. Laibinis, *Langmuir* **1990**, *6*, 87 – 96; c) A. Ulman, *Introduction to Thin Organic Films: From Langmuir – Blodgett to Self-Assembly*, Academic Press, Boston, **1991**; d) J. D. Swalen, *Annu. Rev. Mater. Sci.* **1991**, *21*, 373 – 408; e) L. H. Dubois, R. G. Nuzzo, *Annu. Rev. Phys. Chem.* **1992**, *43*, 437 – 463.
[40] General reviews on self-assembly: a) J.-M. Lehn, *Angew. Chem.* **1990**, *102*, 1347 – 1362; *Angew. Chem. Int. Ed. Engl.* **1990**, *29*, 1304 – 1319; b) G. M. Whitesides, J. P. Mathias, C. T. Seto, *Science* **1991**, *254*, 1312 – 1319; c) G. M. Whitesides, *Sci. Am.* **1995**, *273*(9), 146 – 149.
[41] a) T. E. Creigton, *Proteins: Structures and Molecular Properties*, Freeman, New York, **1983**; b) W. Sanger, *Principles of Nucleic Acid Structures*, Springer, New York, **1986**; c) H. Ringsdorf, B. Schlarb, J. Venzmer, *Angew. Chem.* **1988**, *100*, 117 – 162; *Angew. Chem. Int. Ed. Engl.* **1988**, *27*, 113 – 158.
[42] Self-assembly on the molecular scale: a) J.-M. Lehn, *Angew. Chem.* **1988**, *100*, 91 – 114; *Angew. Chem. Int. Ed. Engl.* **1988**, *27*, 89 – 112; b) J. S. Lindsey, *New J. Chem.* **1991**, *15*, 153 – 180; c) E. E. Simanek, J. P. Mathias, C. T. Seto, D. Chin, M. Mammen, D. M. Gordon, G. M. Whitesides, *Acc. Chem. Res.* **1995**, *28*, 37 – 44; d) V. Percec, J. Heck, G. Johansson, D. Tornazos, M. Kawosumi, *Pure Appl. Chem.* **1994**, *A31*, 1031 – 1070.
[43] Self-assembly on the nanometer scale: a) C. A. Mirkin, R. L. Letsinger, R. C. Mucic, J. J. Storhuff, *Nature* **1996**, *382*, 607 – 609; b) A. P. Alivisator, K. P. Johnsson, X. Peng, T. E. Wilson, C. J. Loweth, M. P. Bruchez, Jr., P. G. Schurtz, *Nature* **1996**, *382*, 609 – 611.
[44] Self-assembly on the micrometer scale: a) A. S. Dimitov, K. Nagayama, *Langmuir* **1996**, *12*, 1303 – 1311; b) M. Trau, S. Sankaran, D. A. Saville, I. A. Aksay, *Nature* **1995**, *374*, 437 – 439; c) S.-R. Yeh, M. Seul, B. I. Shraiman, *ibid.* **1997**, *386*, 57 – 59; d) A. van Blaaderen, R. Ruel, P. Wiltzius, *ibid.* **1997**, *385*, 321 – 324.
[45] Self-assembly on the millimeter scale: a) A. Terfort, N. Bowden, G. M. Whitesides, *Nature* **1997**, *386*, 162 – 164; b) N. Bowden, A. Terfort, J. Carbeck, G. M. Whitesides, *Science* **1997**, *276*, 233 – 235.
[46] Recent reviews on SAMs: a) J. Xu, H.-L. Li, *J. Coll. Interf. Sci.* **1995**, *176*, 138 – 149; b) A. Ulman, *MRS Bull.* **1995**, *30*(6), 46 – 51; c) A. R. Bishop, R. G. Nuzzo, *Curr. Opin. Coll. Interf. Sci.* **1996**, *1*, 127 – 136; d) E. Delamarche, B. Michel, H. A. Biebuyck, C. Gerber, *Adv. Mater.* **1996**, *8*, 719 – 729.
[47] See, for example, a) P. Fenter, A. Eberhardt, P. Eisenberger, *Science* **1994**, *266*, 1216 – 1218; b) E. Delamarche, B. Michel, H. Kang, C. Gerber, *Langmuir* **1994**, *10*, 4103 – 4108; c) S. V. Atre, B. Liedberg, D. L. Allara, *ibid.* **1995**, *11*, 3882 – 3893; d) P. Wagner, M. Hegner, H.-J. Güntherodt, G. Sernenza, *ibid.* **1995**, *11*, 3867 – 3875.
[48] See, for example, a) H. A. Biebuyck, G. M. Whitesides, *Langmuir* **1994**, *10*, 1825 – 1831; b) H. Schönherr, H. Ringsdorf, *ibid.* **1996**, *12*, 3891 – 3897.
[49] E. B. Throughton, C. D. Bain, G. M. Whitesides, R. G. Nuzzo, D. L. Allara, M. D. Porter, *Langmuir* **1988**, *4*, 365 – 385.
[50] J. E. Chadwick, D. C. Myles, R. L. Garrell, *J. Am. Chem. Soc.* **1993**, *115*, 10364 – 10365.
[51] K. Uvdal, I. Persson, B. Liedberg, *Langmuir* **1995**, *11*, 1252 – 1256.
[52] See, for example, a) P. Fenter, P. Eisenberger, J. Li, N. Camillone III, S. Bernasek, G. Scoles, T. A. Ramnanarayanan, K. S. Liang, *Langmuir* **1991**, *7*, 2013 – 2016; b) A. Dhirani, M. A. Hines, A. J. Fisher, O. Ismail, P. Guyot-Sionnest, *ibid.* **1995**, *11*, 2609 – 2614.
[53] See, for example, a) H. Keller, P. Sirnak, W. Schrepp, J. Dembowski, *Thin Solid Films* **1994**, *244*, 799 – 805; b) M. Itoh, K. Nishihara, K. Aramaki, *J. Electrochem. Soc.* **1995**, *142*, 3696 – 3704; c) J. B. Schlenoff, M. Li, H. Ly, *J. Am. Chem. Soc.* **1995**, *117*, 12528 – 12536.
[54] T. R. Lee, P. E. Laibinis, J. P. Folkers, G. M. Whitesides, *Pure Appl. Chem.* **1991**, *63*, 821 – 828.
[55] J. J. Hickman, P. E. Laibinis, D. I. Auerbach, C. Zou, T. J. Gardner, G. M. Whitesides, M. S. Wrighton, *Langmuir* **1992**, *8*, 357 – 359.
[56] See, for example, a) C. W. Sheen, J.-X. Shi, J. Martensson, A. N. Parikh, D. L. Allara, *J. Am. Chem. Soc.* **1992**, *114*, 1514 – 1515; b) C. D. Bain, *Adv. Mater.* **1992**, *4*, 591 – 594; c) J. F. Dorsten, J. E. Maslar, P. W. Bohn, *Appl. Phys. Lett.* **1995**, *66*, 1755 – 1757.
[57] Y. Gu, Z. Lin, R. A. Butera, V. S. Smentkowski, D. H. Waldeck, *Langmuir* **1995**, *11*, 1849 – 1851.
[58] See, for example, a) M. J. Wirth, R. W. P. Fairbank, H. O. Fatunmbi, *Science* **1997**, *275*, 44 – 47; b) J. B. Brzoska, I. B. Azouz, F. Rondelez, *Langmuir* **1994**, *10*, 4367 – 4373; c) D. L. Allara, A. N. Parikh, F. Rondelez, *ibid.* **1995**, *11*, 2357 – 2360.
[59] M. R. Linford, C. E. D. Chidsey, *J. Am. Chem. Soc.* **1993**, *115*, 12631 – 12632.
[60] M. R. Linford, P. Fenter, P. M. Eisenberger, C. E. D. Chidsey, *J. Am. Chem. Soc.* **1995**, *117*, 3145 – 3155.
[61] A. Bansal, X. Li, I. Lauermann, N. S. Lewis, S. I. Yi, W. H. Weinberg, *J. Am. Chem. Soc.* **1996**, *118*, 7225 – 7226.
[62] See, for example, a) D. L. Allara, R. G. Nuzzo, *Langmuir* **1985**, *1*, 54 – 71; b) P. E. Laibinis, J. J. Hickinan, M. S. Wrighton, G. M. Whitesides, *Science* **1989**, *245*, 845 – 847; c) Y.-T. Tao, M.-T. Lee, S.-C. Chang, *J. Am. Chem. Soc.* **1993**, *115*, 9547 – 9555.
[63] J. P. Folkers, C. B. Gorman, P. E. Laibinis, S. Buchholz, G. M. Whitesides, R. G. Nuzzo, *Langmuir* **1995**, *11*, 813 – 824.
[64] Reviews: a) G. Cao, H.-G. Hong, T. E. Mallouk, *Acc. Chem. Res.* **1992**, *25*, 420 – 427; b) M. E. Thompson, *Chem. Mater.* **1994**, *6*, 1168 – 1175; c) H. E. Katz, *ibid.* **1994**, *6*, 2227 – 2232.
[65] T. J. Gardner, C. D. Frisbie, M. S. Wrighton, *J. Am. Chem. Soc.* **1995**, *117*, 6927 – 6933.
[66] A recent review on STM studies: G. E. Polner, *Chem. Rev.* **1997**, *97*, 1117 – 1127.
[67] Recent AFM studies: a) C. A. Alves, E. L. Smith, M. D. Porter, *J. Am. Chem. Soc.* **1992**, *114*, 1222 – 1227; b) G.-Y. Liu, M. B. Salmeron, *Langmuir* **1994**, *10*, 367 – 370.
[68] See, for example, M. R. Anderson, M. N. Evaniak, M. Zhang, *Langmuir* **1996**, *12*, 294 – 300.
[69] See, for example, N. Camillone III, T. Y. B. Leung, P. Schwartz, P. Eisenberger, G. Scoles, *Langmuir* **1996**, *12*, 2737 – 2746.
[70] See, for example, W. B. Caldwell, D. J. Campbell, K. Chen, B. R. Herr, C. A. Mirkin, A. Malik, M. K. Durbin, P. Dutta, K. G. Huang, *J. Am. Chem. Soc.* **1995**, *117*, 6071 – 6082.
[71] See, for example, L. Strong, G. M. Whitesides, *Langmuir* **1988**, *4*, 546 – 558.
[72] M. A. Bryant, J. E. Pemberton, *J. Am. Chem. Soc.* **1991**, *113*, 3629 – 3637.
[73] See, for example, a) Q. Du, E. Freysz, Y. R. Shen, *Science* **1994**, *264*, 826 – 828; b) C. D. Bain, *J. Chem. Soc. Faraday Trans.* **1995**, *91*, 1281 – 1296.
[74] See, for example, J. P. Folkers, P. E. Laibinis, G. M. Whitesides, *Langmuir* **1992**, *8*, 1330 – 1341.
[75] L. H. Dubois, B. R. Zegarski, R. G. Nuzzo, *J. Am. Chem. Soc.* **1990**, *112*, 570 – 579.
[76] See, for example, a) Y. Li, J. Huang, R. T. McIver, Jr., J. C. Hemminger, *J. Am. Chem. Soc.* **1992**, *114*, 2428 – 2432; b) M. J. Tarlov, J. G. Newman, *Langmuir* **1992**, *8*, 1398 – 1405; c) T. D. McCarley, R. L. McCarley, *Anal. Chem.* **1997**, *69*, 130 – 136.
[77] See, for example, a) C. D. Bain, G. M. Whitesides, *J. Am. Chem. Soc.* **1988**, *110*, 3665 – 3666; b) D. J. Olbris, A. Ulman, Y. Shnidman, *J. Chem. Phys.* **1995**, *102*, 6885 – 6873.

[78] See, for example, C. D. Bain, E. B. Throughton, Y.-T. Tao, J. Evall, G. M. Whitesides, R. G. Nuzzo, *J. Am. Chem. Soc.* **1989**, *111*, 321 – 335.

[79] See, for example, a) D. A. Buttry, M. D. Ward, *Chem. Rev.* **1992**, *92*, 1355 – 1379; b) T. W. Schneider, D. A. Buttry, *J. Am. Chem. Soc.* **1993**, *115*, 12391 – 12397; c) D. S. Karpovich, G. J. Blanchard, *Langmuir* **1994**, *10*, 3315 – 3322; d) C. Fruböss, K. Doblhofer, *J. Chem. Soc. Faraday Trans.* **1995**, *91*, 1949 – 1953.

[80] M. D. Ward, D. A. Buttry, *Science* **1990**, *249*, 1000 – 1007.

[81] See, for example, a) S. Li, R. M. Crooks, *Langmuir* **1993**, *9*, 1951 – 1954; b) A. Badia, R. Back, R. B. Lennox, *Angew. Chem.* **1994**, *106*, 2429 – 2432; *Angew. Chem. Int. Ed. Engl.* **1994**, *33*, 2332 – 2335; c) F. P. Zamborini, R. M. Crooks, *Langmuir* **1997**, *13*, 122 – 126.

[82] X.-M. Zhao, J. L. Wilbur, G. M. Whitesides, *Langmuir* **1996**, *12*, 3257 – 3264.

[83] General reviews on interactions between SAMs and proteins/cells: a) M. Mrksich, G. M. Whitesides, *TIBTECH* **1995**, *13*, 228 – 235; b) *Annu. Rev. Biophys. Biomol. Struc.* **1996**, *25*, 55 – 78.

[84] Previous reviews on microcontact printers: a) J. L. Wilbur, A. Kumar, E. Kim, G. M. Whitesides, *Adv. Mater.* **1994**, *6*, 600 – 604; b) A. Kurnar, N. L. Abbott, E. Kim, H. A. Biebuyck, G. M. Whitesides, *Acc. Chem. Res.* **1995**, *28*, 219 – 226; c) G. M. Whitesides, C. B. Gorman in *Handbook of Surface Imaging and Visualization* (Ed.: A. T. Hubbard), CRC Press, Boca Raton, FL, **1995**, pp. 713 – 733; d) J. L. Wilbur, A. Kumar, H. A. Biebuyck, E. Kim, G. M. Whitesides, *Nanotechnology* **1996**, *7*, 452 – 457; e) Y. Xia, X.-M. Zhao, G. M. Whitesides, *Microelectron. Eng.* **1996**, *32*, 255 – 268; f) H. A. Biebuyck, N. B. Larsen, E. Delamarche, B. Michel, *IBM J. Res. Dev.* **1997**, *41*, 159 – 170.

[85] Microprinting of alkanethiols on gold: A. Kumar, H. Biebuyck, G. M. Whitesides, *Langmuir* **1994**, *10*, 1498 – 1511.

[86] Microprinting of alkanethiols on silver: a) Y. Xia, E. Kim, G. M. Whitesides, *J. Electrochem. Soc.* **1996**, *143*, 1070 – 1079; b) X. M. Yang, A. A. Tryk, K. Hasimoto, A. Fujishima, *Appl. Phys. Lett.* **1996**, *69*, 4020 – 4022.

[87] Microprinting of alkanethiols on copper: a) T. P. Moffat, H. Yang, *J. Electrochem. Soc.* **1995**, *142*, L220 – L222; b) Y. Xia, E. Kim, M. Mrksich, G. M. Whitesides, *Chem. Mater.* **1996**, *8*, 601 – 603.

[88] Microprinting of alkanethiols on palladium: L. Goetting, N.-L. Jeon, G. M. Whitesides, unpublished results.

[89] Microprinting of RPO_3H_2 on Al/Al_2O_3: L. Goetting, G. M. Whitesides, unpublished results.

[90] Microprinting of siloxanes on Si/SiO_2: a) Y. Xia, M. Mrksich, E. Kim, G. M. Whitesides, *J. Am. Chem. Soc.* **1995**, *117*, 9576 – 9577; b) P. M. St. John, H. G. Craighead, *Appl. Phys. Lett.* **1996**, *68*, 1022 – 1024; c) D. Wang, S. G. Thomas, K. L. Wang, Y. Xia, G. M. Whitesides, *ibid*. **1997**, *70*, 1593 – 1595.

[91] Photooxidation of alkanethiolate SAMs on gold: a) J. Huang, J. C. Hemminger, *J. Am. Chem. Soc.* **1993**, *115*, 3342 – 3343; b) M. J. Tarlov, D. R. F. Burgess, Jr., G. Gillen, *ibid*. **1993**, *115*, 5305 – 5306; c) J. Huang, D. A. Dahlgren, J. C. Hemminger, *Langmuir* **1994**, *10*, 626 – 628; d) S.-W. Tam-Chang, H. A. Biebuyck, G. M. Whitesides, N. Jeon, R. G. Nuzzo, *ibid*. **1995**, *11*, 4371 – 4382; e) D. A. Hutt, E. Cooper, L. Parker, G. J. Leggett, T. L. Parker, *ibid*. **1996**, *12*, 5494 – 5497.

[92] Photo-cross-linking of alkanethiolate SAMs on gold: a) K. C. Chan, T. Kim, J. K. Schoer, R. M. Crooks, *J. Am. Chem. Soc.* **1995**, *117*, 5875 – 5876; b) T. Kim, K. C. Chan, R. M. Crooks, *ibid*. **1997**, *119*, 189 – 193.

[93] Photoactivation of alkanethiolate SAMs on gold: a) E. W. Wollman, C. D. Frisbie, M. S. Wrighton, *Langmuir* **1993**, *9*, 1517 – 1520; b) D. J. Pritchard, H. Morgan, J. M. Cooper, *Angew. Chem.* **1995**, *107*, 84 – 86; *Angew. Chem. Int. Ed. Engl.* **1995**, *34*, 91 – 93.

[94] See, for example, A. C. Pease, D. Solas, E. J. Sullivan, M. T. Cronin, C. P. Holmes, S. P. A. Fodor, *Proc. Natl. Acad. Sci. USA* **1994**, *91*, 5022 – 5026.

[95] Recent reviews: a) W. J. Dressick, J. M. Calvert, *Jpn. J. Appl. Phys.* **1993**, *32*, 5829 – 5839; b) J. M. Calvert, *Thin Films* **1995**, *20*, 109 – 141.

[96] J. A. M. Sondag-Huethorst, H. R. J. van Helleputte, L. G. Fokkink, *Appl. Phys. Lett.* **1994**, *64*, 285 – 287.

[97] M. Lercel, R. C. Tiberio, P. F. Chapman, H. G. Craighead, C. W. Sheen, A. N. Parikh, D. L. Allara, *J. Vac. Sci. Technol. B* **1993**, *11*, 2823 – 2828.

[98] M. J. Lercel, H. G. Craighead, A. N. Parikh, K. Seshadri, A. L. Allara, *Appl. Phys. Lett.* **1996**, *68*, 1504 – 1506.

[99] G. Gillen, S. Wight, J. Bennett, M. J. Tarlov, *Appl. Phys. Lett.* **1994**, *65*, 534 – 536.

[100] a) K. K. Berggren, A. Bard, J. L. Wilbur, J. D. Gillaspy, A. G. Heig, J. J. McClelland, S. L. Rolston, W. D. Phillips, M. Prentiss, G. M. Whitesides, *Science* **1995**, *269*, 1255 – 1257; b) K. K. Berggren, R. Younkin, E. Cheung, M. Prentiss, A. J. Black, G. M. Whitesides, D. C. Ralph, O. T. Black, M. Tinkham, *Adv. Mater.* **1997**, *9*, 52 – 55.

[101] K. S. Johnson, K. K. Berggren, A. J. Black, A. P. Chu, N. H. Dekker, D. C. Ralph, J. H. Thywissen, R. Youkin, M. Prentiss, M. Tinkham, G. M. Whitesides, *Appl. Phys. Lett.* **1996**, *69*, 2773 – 2775.

[102] See, for example, a) C. B. Ross, L. Sun, R. M. Crooks, *Langmuir* **1993**, *9*, 632 – 636; b) E. Delamarche, A. C. F. Hoole, B. Michel, S. Wilkes, M. Despont, M. E. Weiland, H. Biebuyck, *J. Phys. Chem. B* **1997**, *101*, 9263 – 9269.

[103] a) N. L. Abbott, J. P. Folkers, G. M. Whitesides, *Science* **1992**, *257*, 1380 – 1382; b) N. L. Abbott, D. R. Rolison, G. M. Whitesides, *Langmuir* **1994**, *8*, 267.

[104] A. Kumar, H. Biebuyck, N. L. Abbott, G. M. Whitesides, *J. Am. Chem. Soc.* **1992**, *114*, 9188 – 9189.

[105] A. Voet, *Ink and Paper in the Printing Process*, Interscience, New York, **1952**.

[106] P. O. Hidber, W. Helbig, E. Kim, G. M. Whitesides, *Langmuir* **1996**, *12*, 1375 – 1380.

[107] See, for example, a) M. C. Hutley, *Diffraction Gratings*, Academic Press, New York, **1982**; b) B. L. Ramos, S. J. Choquette, *Anal. Chem.* **1996**, *68*, 1245 – 1249.

[108] M. Nakano, N. Nishida, *Appl. Opt.* **1979**, *18*, 3073 – 3074.

[109] D. A. Kiewit, *Rev. Sci. Instrum.* **1973**, *44*, 1741 – 1742.

[110] Replication of features with dimensions below the micron scale has also been used in microscopy to aid in visualizing fragile structures: *Electron Microscopy Preparation Technology Accessories and Consumable*, Bal-TEC Products, Middlebury, CT, **1992**, catalogue no. 5B.

[111] S. L. Goodman, P. A. Sims, R. M. Albrecht, *Biomaterials* **1996**, *17*, 2087 – 2095.

[112] a) F. L. Dickert, S. Thierer, *Adv. Mater.* **1996**, *8*, 987 – 990; b) L. Schweitz, L. I. Anderson, S. Nilsson, *Anal. Chem.* **1997**, *69*, 1179 – 1183; c) D. Kriz, O. Ramström, K. Mosbach, *ibid*. **1997**, *69*, 345A – 349A; d) C. Pinel, P. Loisil, P. Gallezot, *Adv. Mater.* **1997**, *9*, 582 – 585.

[113] a) *Siloxane Polymers* (Eds.: S. J. Clarson, J. A. Semlyen), Prentice-Hall, Engleword, NJ, **1993**; b) J. F. Künzler, *Trends Polym. Sci.* **1996**, *4*, 52 – 59.

[114] Y. Xia, N. Venkateswaran, D. Qin, J. Tien, G. M. Whitesides, *Langmuir* **1998**, *14*, 363 – 371.

[115] A PDMS block that is about 1 mm thick has a transmittance of about 90 % at 325 nm.

[116] Elastomeric mirrors and diffraction gratings: J. L. Wilbur, R. J. Jackman, G. M. Whitesides, E. L. Cheung, L. K. Lee, M. G. Prentiss, *Chem. Mater.* **1996**, *8*, 1380 – 1385.

[117] Elastomeric optical modulators: a) J. A. Rogers, D. Qin, O. J. A. Schueller, G. M. Whitesides, *Rev. Sci. Instrum.* **1996**, *67*, 3310 – 3319; b) J. A. Rogers, O. J. A. Schueller, C. Marzolin, G. M. Whitesides, *Appl. Opt.* **1997**, *36*, 5792 – 5795.

[118] Elastomeric light valves: D. Qin, Y. Xia, G. M. Whitesides, *Adv. Mater.* **1997**, *9*, 407 – 409.

[119] Elastomeric photothermal detectors: J. A. Rogers, R. J. Jackman, O. J. A. Schueller, G. M. Whitesides, *Appl. Opt.* **1996**, *35*, 6641 – 6647.

[120] D. Qin, Y. Xia, A. J. Black, G. M. Whitesides, *J. Vac. Sci. Technol. B* **1998**, in press.

[121] J. A. Rogers, K. E. Paul, R. J. Jackman, G. M. Whitesides, *Appl. Phys. Lett.* **1997**, *70*, 2658 – 2660; *J. Vac. Sci. Technol. B* **1998**, in press.

[122] See, for example, a) G. S. Ferguson, M. K. Chaudhury, G. B. Sigal, G. M. Whitesides, *Science* **1991**, *253*, 776 – 778; b) M. K. Chaudhury, G. M. Whitesides, *ibid*. **1992**, *255*, 1230 – 1232; c) G. S. Ferguson, M. K. Chaudhury, H. A. Biebuyck, G. M. Whitesides, *Macromolecules* **1993**, *26*, 5870 – 5875; d) M. K. Chaudhury, *Biosens. Bioelectron.* **1995**, *10*, 785 – 788.

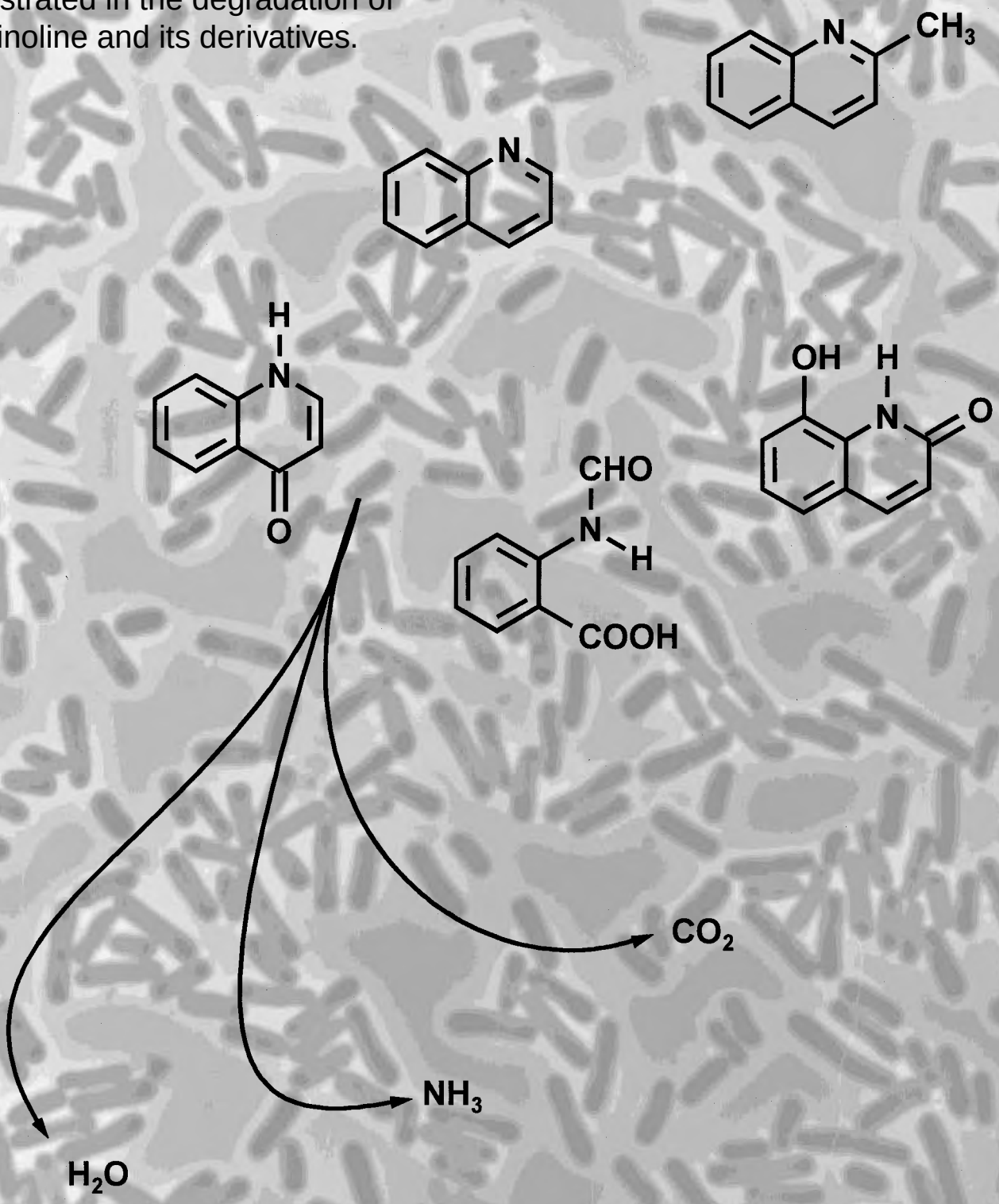
[123] See, for example, T. Tanaka, M. Morigami, N. Atoda, *Jpn. J. Appl. Phys.* **1993**, *32*, 6059 – 6061.

[124] E. Delamarche, H. Schmid, H. A. Biebuyck, B. Michel, *Adv. Mater.* **1977**, *9*, 741 – 746.

[125] For technical reports on thermally curable PDMS resins, see, for example, Dow Corning, Midland, MI, **1986**.
[126] L. C. DeBolt, J. E. Mark, *Macromolecules* **1987**, *20*, 2369 – 2374.
[127] J. A. Rogers, K. Paul, G. M. Whitesides, *J. Vac. Sci. Technol. B* **1998**, in press.
[128] Y. Xia, A. Zhuk, G. M. Whitesides, unpublished results.
[129] Y. Xia, J. Tien, D. Qin, G. M. Whitesides, *Langmuir* **1996**, *12*, 4033 – 4038.
[130] D. Qin, Y. Xia, G. M. Whitesides, *Adv. Mater.* **1996**, *8*, 917 – 919.
[131] For the economical production of masks using a desk-top publishing system, see M. Parameswaren, http://www.fas.sfu.ca/ensc/research/groups/micromachining/file2.html.
[132] H. A. Biebuyck, G. M. Whitesides, *Langmuir* **1994**, *10*, 4581 – 4587.
[133] N. B. Larsen, H. Biebuyck, E. Delamarche, B. Michel, *J. Am. Chem. Soc.* **1997**, *119*, 3017 – 3026.
[134] See, for example, a) G. P. López, H. A. Biebuyck, G. M. Whitesides, *Langmuir* **1993**, *9*, 1513 – 1516; b) G. B. López, H. A. Biebuyck, R. Härter, G. M. Whitesides, *J. Am. Chem. Soc.* **1993**, *115*, 10774 – 10781.
[135] See, for example, a) C. D. Frisbie, L. F. Rozsnyai, A. Noy, M. S. Wrighton, O. M. Lieber, *Science* **1994**, *263*, 2071 – 2073; b) J. L. Wilbur, H. A. Biebuyck, J. C. MacDonald, G. M. Whitesides, *Langmuir* **1995**, *11*, 825 – 831; c) G. Bar, S. Rubin, A. N. Parikh, B. I. Swanson, T. A. Zawodzinski, Jr., M.-H. Whangbo, *ibid.* **1997**, *13*, 373 – 377.
[136] G. P. López, H. A. Biebuyck, C. D. Frisbie, G. M. Whitesides, *Science* **1993**, *260*, 647 – 649.
[137] J. Heinze, *Angew. Chem.* **1993**, *105*, 1327 – 1349; *Angew. Chem. Int. Ed. Engl.* **1993**, *32*, 1268 – 1288.
[138] J. C. C. Tsai in *VLSI Technology* (Ed.: S. M. Sze), McGraw-Hill, New York, **1988**, pp. 272 – 326.
[139] C. Kittel, *Introduction to Solid State Physics*, 6th ed., Wiley, New York, **1986**, p. 110.
[140] a) N. L. Jeon, K. Finnie, K. Branshaw, R. G. Nuzzo, *Langmuir* **1997**, *13*, 3382 – 3391; b) A. N. Parikh, M. A. Schivley, E. Koo, K. Seshadri, D. Aurentz, K. Mueller, D. L. Allara, *J. Am. Chem. Soc.* **1997**, *119*, 3135 – 3143.
[141] Y. Xia, X.-M. Zhao, E. Kim, G. M. Whitesides, *Chem. Mater.* **1995**, *7*, 2332 – 2337.
[142] Selective wetting and dewetting: a) A. Kumar, G. M. Whitesides, *Science* **1994**, *263*, 60 – 62; b) H. A. Biebuyck, G. M. Whitesides, *Langmuir* **1994**, 10, 2790 – 2793; c) S. Palacin, P. C. Hidber, J.-P. Bourgoin, C. Miramond, C. Fermon, G. M. Whitesides, *Chem. Mater.* **1996**, *8*, 1316 – 1325; d) C. B. Gorman, H. A. Biebuyck, G. M. Whitesides, *ibid*. **1995**, *7*, 252 – 254; e) E. Kim, G. M. Whitesides, *ibid*. **1995**, *7*, 1257 – 1264; f) E. Kim, G. M. Whitesides, L. K. Lee, S. P. Smith, M. Prentiss, *Adv. Mater.* **1996**, *8*, 139 – 142.
[143] Selective attachment of cells: a) R. Singhvi, A. Kumar, G. P. Lopez, G. P. Stephanopoulos, D. I. C. Wang, G. M. Whitesides, D. E. Ingber, *Science* **1994**, *264*, 696 – 698; b) M. Mrksich, C. S. Chen, Y. Xia, L. E. Dike, D. E. Ingber, G. M. Whitesides, *Proc. Natl. Acad. Sci. USA* **1996**, *93*, 10775 – 10778; c) C. S. Chen, M. Mrksich, S. Huang, G. M. Whitesides, D. E. Ingber, *Science* **1997**, *276*, 1245 – 1248; d) M. Mrksich, L. E. Dike, J. Tien, D. E. Ingber, G. M. Whitesides, *Exp. Cell Res.* **1997**, *235*, 305 – 313.
[144] Selective deposition of polymers: a) C. B. Gorman, H. A. Biebuyck, G. M. Whitesides, *Chem. Mater.* **1995**, *7*, 526 – 529; b) P. Hammond, G. M. Whitesides, *Macromolecules* **1995**, *28*, 7569 – 7571; c) C. N. Sayre, D. M. Collard, *Langmuir* **1997**, *13*, 714 – 722; d) *J. Mater. Chem.* **1997**, *7*, 909 – 912; e) Z. Huang, P.-C. Wang, A. G. MacDiarmid, Y. Xia, G. M. Whitesides, *Langmuir* **1997**, *13*, 6480 – 6484.
[145] Selective CVD of copper and dielectric oxides: a) N. L. Jeon, R. G. Nuzzo, Y. Xia, M. Mrksich, G. M. Whitesides, *Langmuir* **1995**, *11*, 3024 – 3026; b) N. L. Jeon, P. G. Clem, R. G. Nuzzo, D. A. Payne, *J. Mater. Res.* **1995**, *10*, 2996 – 2999; c) N. L. Jeon, P. G. Clem, D. A. Payne, R. G. Nuzzo, *Langmuir* **1996**, *12*, 5350 – 5355; d) H. Yang, N. Coombs, G. A. Ozin, *Adv. Mater.* **1997**, *9*, 811 – 814.
[146] V. K. Gupta, N. L. Abbott, *Science* **1997**, *276*, 1533 – 1536.
[147] Y. Xia, D. Qin, G. M. Whitesides, *Adv. Mater.* **1996**, *8*, 1015 – 1017.
[148] a) Y. Xia, G. M. Whitesides, *J. Am. Chem. Soc.* **1995**, *117*, 3274 – 3275; b) Y. Xia, G. M. Whitesides, *Adv. Mater.* **1995**, *7*, 471 – 473; C) J. L. Wilbur, E. Kim, Y. Xia, G. M. Whitesides, *ibid*. **1995**, *7*, 649 – 652; d) Y. Xia, G. M. Whitesides, *Langmuir* **1997**, *13*, 2059 – 2067.
[149] R. J. Jackman, J. L.Wilbur, G. M. Whitesides, *Science* **1995**, *269*, 664 – 666.
[150] S. J. Moss in *The Chemistry of the Semiconductor Industry* (Eds.: S. J. Moss, A. Ledwidth), Chapman and Hall, New York, **1987**, pp. 390 – 413.
[151] W. Kern, C. A. Deckert in *Thin Film Processes* (Eds.: J. L. Vossen, E. Kern), Academic Press, New York, **1978**.
[152] a) E. Kim, A. Kumar, G. M. Whitesides, *J. Electrochem. Soc.* **1995**, *142*, 628 – 633; b) E. Kim, G. M. Whitesides, M. B. Freiler, M. Levy, J. L. Lin, R. M. Osgood, Jr., *Nanotechnology* **1996**, *7*, 266 – 269; c) T. K. Whidden, D. K. Ferry, M. N. Kozicki, E. Kim, A. Kumar, J. L. Wilbur, G. M. Whitesides, *ibid*. **1996**, *7*, 447 – 451.
[153] Y. Xia, G. M. Whitesides, *Adv. Mater.* **1996**, *8*, 765 – 768.
[154] K. E. Petersen, *Proc. IEEE* **1982**, *70*, 420 – 457.
[155] Y. Xia, X.-M. Zhao, G. M. Whitesides, unpublished results.
[156] A. Wang, J. Zhao, M. A. Green, *Appl. Phys. Lett.* **1990**, *57*, 602 – 604.
[157] N. Rajkumar, J. N. McMullin, *Appl. Opt.* **1995**, *34*, 2556 – 2559.
[158] A. E. Kaloyeros, M. A. Fury, *MRS Bull.* **1993**, *28*(6), 22 – 28.
[159] J. Li, T. E. Seidel, J. W. Mayer, *MRS Bull.* **1994**, *29*(8), 15 – 18.
[160] R. J. Jackman, J. A. Rogers, G. M. Whitesides, *IEEE Trans. Magn.* **1997**, *33*, 2501 – 2503.
[161] J. A. Rogers, R. J. Jackman, G. M. Whitesides, *J. Microelec. Sys.* **1997**, *6*, 184 – 192.
[162] J. A. Rogers, R. J. Jackman, G. M. Whitesides, J. L. Wagener, A. M. Vengsarkar, *Appl. Phys. Lett.* **1997**, *70*, 7 – 9.
[163] J. A. Rogers, R. J. Jackman, G. M. Whitesides, D. L. Olson, J. V. Sweedler, *Appl. Phys. Lett.* **1997**, *70*, 2464 – 2466.
[164] J. A. Rogers, R. J. Jackman, G. M. Whitesides, *Adv. Mater.* **1997**, *9*, 475 – 477.
[165] a) Y. Xia, G. M. Whitesides, unpublished results; b) C. Marzolin, A. Terfort, J. Tien, G. M. Whitesides, *Thin Solid Films* **1998**, in press.
[166] P. C. Hidber, P. F. Nealey, W. Helbig, G. M. Whitesides, *Langmuir* **1996**, *12*, 5209 – 5215.
[167] Reviews on acid-sensitive photoresists: a) E. Reichmanis, F. M. Houlihan, O. Nalamasu, T. X. Neenan, *Adv. Mater. Opt. Electron.* **1994**, *4*, 83 – 93; b) S. A. MacDonald, C. Willson, J. M. J. Frechet, *Acc. Chem. Res.* **1994**, *27*, 151 – 158.
[168] G. M. Whitesides, Y. Xia, *Photonics Spectra* **1997**, *31*(1), 90 – 91.
[169] Y. Xia, J. J. McClelland, R. Gupta, D. Qin, X.-M. Zho, L. L. Sohn, R. J. Celotta, G. M. Whitesides, *Adv. Mater.* **1997**, *9*, 147 – 149.
[170] J. J. McClelland, R. E. Scholten, E. C. Palm, R. J. Celotta, *Science* **1993**, *262*, 877 – 879.
[171] "Technical reports on UV-curable adhesives": Norland Products Inc., New Brunswick, NJ, USA.
[172] A. Suzuki, K. Tada, *Thin Solid Films* **1980**, *72*, 419 – 426.
[173] L. R. Dalton, A. W. Harper, B. Wu, R. Ghosn, J. Laquindanum, Z. Liang, A. Hubbel, C. Xu, *Adv. Mater.* **1995**, *7*, 519 – 540.
[174] See, for example, a) E. Ozbay, E. Michel, G. Tuttle, R. Biswas, M. Sigalas, K. M. Ho, *Appl. Phys. Lett.* **1994**, *64*, 2059 – 2061; b) J. D. Joannopoulos, P. R. Villeneuve, S. Fan, *Nature* **1997**, *386*, 143 – 149.
[175] N. A. Peppas, R. Langer, *Science* **1994**, *263*, 1715 – 1720.
[176] X.-M. Zhao, S. P. Smith, S. J. Waldman, G. M. Whitesides, M. Prentiss, *Appl. Phys. Lett.* **1997**, *71*, 1017 – 1019.
[177] a) O. J. A. Schueller, S. T. Brittain, G. M. Whitesides, *Adv. Mater.* **1997**, *9*, 477 – 480; b) O. J. A. Schueller, S. T. Brittain, C. Marzolin, G. M. Whitesides, *Chem. Mater.* **1997**, *9*, 1399 – 1406.
[178] C. Marzolin, S. P. Smith, M. Prentiss, G. M. Whitesides, *Adv. Mater.* **1997**, submitted.
[179] Y. Xia, E. Kim, G. M. Whitesides, *Chem. Mater.* **1996**, *8*, 1558 – 1567.
[180] Y. Xia, G. M. Whitesides, unpublished results.
[181] X.-M. Zhao, A. Stoddart, S. P. Smith, E. Kim, Y. Xia, M. Prentiss, G. M. Whitesides, *Adv. Mater.* **1996**, *8*, 420 – 424.
[182] Y. Xia, G. M. Whitesides, unpublished results.
[183] E. Kim, Y. Xia, G. M. Whitesides, *Adv. Mater.* **1996**, *8*, 245 – 247.
[184] E. Kim, Y. Xia, G. M. Whitesides, *J. Am. Chem. Soc.* **1996**, *118*, 5722 – 5731.
[185] a) M. Trau, N. Yao, E. Kim, Y. Xia, G. M. Whitesides, I. A. Aksay, *Nature* **1997**, *390*, 674 – 676; b) M. J. Lochhead, P. Yager, *Mater. Res. Soc. Symp. Proc.* **1997**, *444*, 105 – 110.
[186] E. Delamarche, A. Bernard, H. Schmid, B. Michel, H. Biebuyck, *Science* **1997**, *276*, 779 – 781.
[187] Filling of carbon nanotubes: a) P. M. Ajayan, S. Iijima, *Nature* **1993**, *361*, 333 – 334; b) E. Dujardin, T. W. Ebbesen, H. Hiura, K. Tanigaki, *Science* **1994**, *265*, 1850 – 1852.

[188] Filling of nanometer-sized pores in membranes: C. R. Martin, *Science* **1994**, *266*, 1961 – 1966.
[189] E. Kim, G. M. Whitesides, *J. Phys. Chem. B* **1997**, *101*, 855 – 863.
[190] D. Myers, *Surfaces, Interfaces, and Colloids*, VCH, New York, **1991**, pp. 87 – 109.
[l91] a) P. G. de Gennes, *Rev. Mod. Phys.* **1985**, *57*, 827 – 863; b) M. Dong, F. A. Dullien, I. Chatzis, *J. Coll. Interf. Sci.* **1995**, *172*, 21 – 31; c) M. Dong, I. Chatzis, *ibid*. **1995**, *172*, 278 – 288.
[192] See, for example, a) I. Peterson, *Sci. News* **1995**, *148*, 296 – 197; b) J. M. Weissman, H. B. Sunkara, A. S. Tse, S. A. Asher, *Science* **1996**, *274*, 959 – 960.
[193] See, for example, a) F. Gamier, R. Hajlaoui, A. Yassar, F. Srivastava, *Science* **1994**, *265*, 1684 – 1686; b) Z. Bao, Y. Feng, A. Dodabalapur, V. R. Raju, A. J. Lovinger, *Chem. Mater.* **1997**, *9*, 1299 – 1301.
[194] N. L. Jeon, P. G. Clem, D. Y. Jung, W. B. Lin, G. S. Girolami, D. A. Payne, R. G. Nuzzo, *Adv. Mater.* **1997**, *9*, 891 – 895.
[195] J. Hu, T. Deng, G. M. Whitesides, unpublished results.
[196] J. Hu, R. G. Beck, T. Deng, R. M. Westervelt, K. D. Maranowski, A. C. Gossard, G. M. Whitesides, *Appl. Phys. Lett.* **1997**, *71*, 2020 – 2022.
[197] N.-L. Jeon, J. Hu, M. K. Erhardt, R. G. Nuzzo, G. M. Whitesides, unpublished results.

The versatility and diversity of bacterial metabolism is well illustrated in the degradation of quinoline and its derivatives.



Various aerobic bacteria utilize these compounds as sole source of carbon and energy, leading to mineralization.

ANGEWANDTE CHEMIE ©WILEY-VCH

Bacterial Degradation of Quinoline and Derivatives—Pathways and Their Biocatalysts

Susanne Fetzner,* Barbara Tshisuaka, Franz Lingens, Reinhard Kappl, and Jürgen Hüttermann

In memory of Adolf Butenandt and Heinrich Hellmann

As a consequence of the continuous selection pressure exerted by the abiotic and biotic world, bacteria have evolved an immensely diverse potential to transform and even mineralize numerous organic compounds of both natural and xenobiotic origin. Quinoline (2,3-benzopyridine) derivatives were chosen as model compounds for studying the bacterial catabolism of heteroaromatic substances. The investigation of even this fairly limited spectrum of organic growth substrates yielded several catabolic pathways, which demonstrated the diversity of bacterial metabolism. However, common features of these aerobic pathways are enzyme-catalyzed hydroxylation reactions that prepare the substrate for the attack by ring-cleavage enzymes, and dioxygenolytic cleavage of the aromatic or heterocyclic ring. To develop a comprehensive understanding of enzyme-catalyzed reactions, various disciplines such as microbiology, biochemistry, biophysics, and molecular genetics need to contribute. The ultimate goals are to understand the mechanism of action of such biocatalysts, to get a view of the three-dimensional structure of the enzyme proteins, and to elucidate the molecular basis of reactivity. Such knowledge will allow us to understand metabolic processes on the molecular level, and it may also enable us to evaluate the potential of biocatalysts for use in industrial applications.

Keywords: enzymes · enzyme catalysis · heterocycles · metabolism · quinoline

1. Introduction

Quinolines and related N-heterocyclic compounds are ubiquitous environmental contaminants, typically released in association with coal gasification, fossil fuel processing activities, coal tar wastes, and creosote wood preservation. Compared with other azarenes occurring in coal tar and crude oil, quinolines have a relatively good solubility in water. The environmental persistence of these N-heterocyclic aromatic compounds is apparent from their detection in the tissues of fish,[1, 2] in sediments,[1, 3, 4] in urban air,[1, 4] in soils, and in groundwater, especially near landfills containing azarene-contaminated solid wastes, and near coal tar distillation and creosote wood preservation facilities.[1, 5]

N-heterocyclic aromatic compounds are of particular concern, because many are biologically more active than their homocyclic analogues. Quinoline is a hepatocarcinogen in mice and rats,[6] and quinoline and several derivatives have been shown to be indirect mutagens with the Ames assay.[4, 7] N-Heterocyclic amines, isolated from cooked food, pyrolysates of amino acids and protein, and heated mixtures of creatine, amino acids, and sugars exhibit mutagenic and carcinogenic activity towards bacteria and mammals.[8] Furthermore, potentially neurotoxic effects of halogen-substituted oxyquinolines were reported. Subacute myelo-optico neuropathy (SMON), which in the 1960s in Japan reached epidemic proportions, was suspected to be elicited by oxyquinoline derivatives under the names Entero-Vioform or Mexaform frequently used to treat enteric disorders.[9]

Nevertheless, quinoline derivatives are indispensable for various medicinal purposes. Cinchona bark, which contains quinine alkaloids, has been known for its therapeutic properties for more than three centuries.[10] Till today, quinine, primaquine, and resoquine are used as antimalarial agents. 8-Hydroxyquinolines are prescribed to treat infections of skin and intestine. Fluoro-substituted 4-quinolones are widely used due to their bactericidal effect against a number of gram-negative and some gram-positive pathogens.[11, 12] Continuous efforts to develop new fluoroquinolone compounds now allow a multiplicity of applications (for instance, in

[*] Priv.-Doz. Dr. S. Fetzner
Fachbereich Biologie der Universität
Postfach 2503, D-26111 Oldenburg (Germany)
Fax.: (+49) 441-798-3250

Dr. B. Tshisuaka, Prof. Dr. F. Lingens
Institut für Mikrobiologie der Universität Hohenheim
D-70593 Stuttgart (Germany)

Dr. R. Kappl, Prof. Dr. J. Hüttermann
Fachrichtung Biophysik der Universität des Saarlandes
D-66421 Homburg (Saar), (Germany)

 © WILEY-VCH Verlag GmbH, D-69451 Weinheim, 1998 1433-7851/98/3705-0577 $ 17.50+.50/0

treatment of leprosy and other mycobacterioses,[13] typhoid fever, and enteric infections such as drug-resistant shigellosis).[14]

Apart from these applications as pharmaceuticals, quinoline derivatives are also used as raw material and solvent in the manufacture of agrochemicals, dyes, and paints.[15] Quinoline yellow, produced by condensation of 2-methylquinoline and phthalic acid anhydride, is a coloring agent for food licensed in Germany as E104.

However, the widespread use of these N-heterocyclic aromatic compounds in our everyday life has led to an increase in the number of persons afflicted with allergies towards quinoline derivatives.[16]

Numerous quinoline derivatives are produced naturally, mainly by higher plants. By 1987 the structures of several hundred quinoline alkaloids had been established.[10] The quinine alkaloids mentioned above are mainly produced by subtropical trees belonging to the genera *Cinchona* and *Remija*. Papaverine from *Papaver somniferum* is a well-known isoquinoline alkaloid. However, formation of quinoline derivatives also occurs in mammals and insects: Kynurenic acid (1*H*-4-oxoquinoline-2-carboxylic acid) was first



S. Fetzner B. Tshisuaka F. Lingens R. Kappl J. Hüttermann

Susanne Fetzner, born in 1963 in Calw, Germany, studied biology at the Universität Hohenheim (1982–1988). Her graduate work under the direction of Prof. Dr. F. Lingens involved studies of the bacterial degradation of haloaromatic compounds and of a bacterial enzyme system that catalyzes a dehalogenation reaction. She received her doctoral degree in 1990 from the Universität Hohenheim. Following six years of postdoctoral work on microbial enzymes that catalyze hydroxylation reactions and ring cleavage of aromatic and heterocyclic compounds, she received her venia legendi for microbiology in 1996 from the Universität Hohenheim. Since 1996, she has been deputizing for the Professor of Microbiology at the Carl-von-Ossietzky-Universität Oldenburg. Her research interests include enzymology and genetic organization of catabolic pathways.

Barbara I. Tshisuaka, born in 1951 in Rudolstadt, Thuringia (Germany), spent ten years as Medical-technical assistant before studying Biology at the Universität Hohenheim (1984–1990). She obtained her doctorate in 1992 on the enzymatic hydroxylation of quinoline under the supervision of Professor F. Lingens. Still part of this research group she concentrates on bacterial molybdenum-containing hydroxylases and pterin-molybdenum cofactors, as well as on enzymatic and genetic topics concerning the microbial degradation of quinoline and its derivatives. Since her research in Brazil in 1996 she is also studying bacterial endoinulinases.

Franz Lingens, born in 1925, received his doctoral degree and venia legendi in Tübingen, and has worked at the Universität Hohenheim in Stuttgart since 1967. His research interests are the synthesis of amino acids with Mannich bases, the asymmetric three-carbon condensation, the Amadori rearrangement, anabolic and catabolic pathways in microorganisms, the biosynthesis of amino acids, riboflavin and pyrrolnitrin, the mechanisms of mutagenesis, biological halogenation and dehalogenation, microbial degradation of aromatic and heterocyclic compounds, and multicomponent enzyme systems, their properties and genetics.

Reinhard Kappl, born in 1956, studied Physics at the Universität Regensburg and the University of Colorado from 1975 and obtained his Diplom in 1982. He completed a doctorate at the Institut für Biophysik in Regensburg in 1988. Since 1986 he has been a scientific officer at the Institut für Biophysik und Physikalische Grundlagen der Medizin at the Universität des Saarlandes and the university clinic, Homburg/Saar.

Jürgen Hüttermann, born in 1942, began his Physics degree at the Universität Karlsruhe in 1961 and obtained his doctorate in 1969. After his habilitation at the Universität Regensburg in 1972, he was employed there as Wissenschaftlicher Rat and Professor. In 1984 he accepted the chair of Biophysics at the Universität des Saarlandes.

isolated from the urine of a dog by Liebig in 1853, and kynurin (1*H*-4-oxoquinoline) was isolated from pupae of the silk-moth *Bombyx mori* by Butenandt, Karlson, and Zillig.[17] Both kynurenic acid and kynurin are formed as degradation products of the aromatic amino acid tryptophan. Some bacteria belonging to the *Pseudomonas* group produce pseudans (2-*n*-alkyl-4-hydroxyquinoline derivatives) as secondary metabolites.[10, 18]

Presumably as a consequence of the natural occurrence of a variety of quinoline derivatives, bacteria have evolved strategies for metabolizing these heteroaromatic compounds.[19] In several laboratories bacterial strains that utilize quinoline or quinoline derivatives as their sole source of carbon and energy have been isolated from soil and water samples. The facile isolation of quinoline-degrading bacteria indicates that such organisms are widespread in nature. The metabolism of aerobic bacteria that grow on quinoline (derivatives) has been studied by the authors' group. Putative intermediates of the catabolic pathways were isolated and characterized, and enzymes catalyzing important steps of the degradative pathways have been purified and investigated. Unexpectedly, a novel type of ring-fission enzymes was discovered, namely, dioxygenases that catalyze the cleavage of two C–C bonds with concomitant formation of carbon monoxide—a quite exceptional way to break open a heterocyclic compound. Another important family of enzymes involved in the catabolic pathways are the molybdenum-containing hydroxylases, which in their active centers contain distinct forms of a pterin molybdenum cofactor.

The sophisticated enzyme proteins synthesized by all living organisms are fascinating objects to the scientist who tries to understand how these biocatalysts work. From a more practical point of view, however, such biocatalysts may well be suitable tools of applied chemistry. Particularly, hydroxylation reactions are important steps of various chemical syntheses for the manufacture of agrochemicals and pharmaceuticals. Biocatalysts such as molybdenum-containing hydroxylases offer substrate- and regiospecific hydroxylations free of side products, which may be difficult and/or expensive to achieve with conventional chemistry. Thus, it may be a prospect in the near future to produce hydroxylated intermediates with bacterial strains or isolated bacterial enzyme systems for use in subsequent syntheses.

2. Pathways of Aerobic Bacterial Degradation of Quinoline and Derivatives

2.1. General Features of Bacterial Utilization of Quinoline and Derivatives

Our studies on bacterial quinoline degradation started with the isolation of 16 bacterial strains capable of utilizing quinoline as sole source of carbon, nitrogen, and energy from soil and water samples, and from activated sludge of a sewage treatment plant.[20] Two strains belonging to the Gram-negative pseudomonads and the Gram-positive *Rhodococcus* strain B1 were chosen for more detailed investigation. From metabolic intermediates found in the growth medium, two different pathways for the degradation of quinoline were proposed[21] (Sections 2.3 and 2.5). In the initial step of both pathways, quinoline is converted into 1*H*-2-oxoquinoline. Actually, the bacterial degradation of quinoline derivatives as a rule starts with a hydroxylation reaction either in 2- or 4-position to the N atom. Labeling studies with $H_2{}^{18}O$ performed later with purified hydroxylating enzymes revealed that the oxygen atom incorporated into the product in almost all cases is derived from a water molecule, not from molecular oxygen.

When growing on quinoline (or its derivatives), many bacterial strains initially converted the substrate nearly quantitatively into such an 1*H*-2-oxo- or 1*H*-4-oxo- compound, which transiently accumulated in the culture medium before degradation proceeded. As an example, Figure 1 shows the accumulation of kynurenic acid (1*H*-4-oxoquinoline-2-carboxylic acid) during growth of a *Serratia* strain on quinaldic acid (quinoline-2-carboxylic acid). In general, such a massive

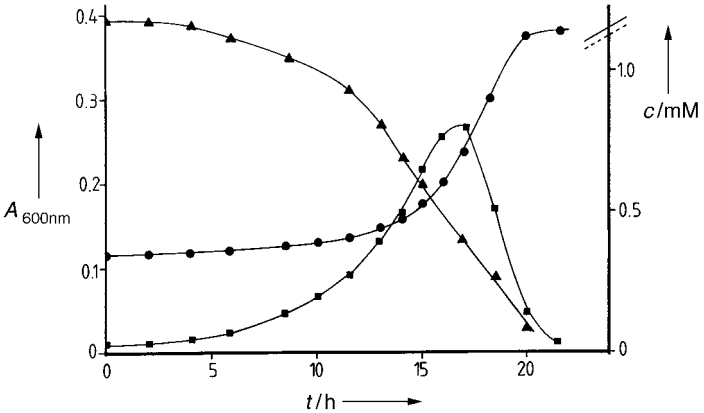


Figure 1. Growth of *Serratia marcescens* 2CC-1 on quinaldic acid. ●: Absorption (turbidity) at 600 nm (A_{600nm}) indicates the growth; ▲: *c*(quinaldic acid); ■: *c*(kynurenic acid).

accumulation of a metabolic intermediate is unusual. It may occur if the next enzyme of the catabolic pathway is a "bottleneck" due to its low catalytic activity. Another possibility is a differential regulatory mechanism such as sequential induction of distinct sets of catabolic genes, each set regulated by a specific effector (substrate), which activates gene expression when reaching a certain threshold concentration. Up to now, we do not know the reason for the observed accumulation of the 1*H*-2-oxo- or 1*H*-4-oxo-compounds. However, rapid initial hydroxylation may well be a vital function for instantaneous detoxification of quinoline (or derivatives), since the oxo compounds were found to be considerably less toxic for the bacteria than the unhydroxylated substrate.

Transient excretion into the culture broth of a catabolic intermediate is, of course, very helpful in establishing the reactions of a degradation pathway. Putative intermediates also can be obtained by the production and selection of mutants blocked in distinct catalytic steps of the pathway or by the use of antimetabolites, which are structural mimics of natural metabolites. Both methods may lead to accumulation of the metabolite prior to the block, or, less favorably, to the

accumulation of a transformation or decomposition product of the true intermediate. In contrast to such secondary products, true catabolic intermediates should disappear and support growth when fed to the bacteria. However, even a true intermediate may not be consumed if the bacterial cells fail to take up the exogenously supplied metabolite.

Nevertheless, purification of putative metabolic intermediates and structural determination with methods such as UV/Vis spectroscopy, mass spectrometry, ^{1}H and ^{13}C NMR spectroscopy and infrared spectroscopy finally may allow the formulation of a hypothetical reaction sequence. Currently four quinoline catabolic pathways of aerobic bacteria are known, which are presented in the following: the anthranilate pathway (Section 2.2), the 5,6-dihydroxy-1*H*-2-oxoquinoline pathway (Section 2.3), the 7,8-dihydroxy-1*H*-2-oxoquinoline pathway (Section 2.4), and the 8-hydroxycoumarin pathway (Section 2.5).

2.2. Anthranilate Pathway

The degradation of quinaldine (2-methylquinoline **1**) by *Arthrobacter* sp. Rü61a (Scheme 1a) is initiated by a hydroxylation at C4 of the substrate. The second step, a monooxygenation of the product **2** at C3, is followed by 2,4-dioxygenolytic cleavage of 1*H*-3-hydroxy-4-oxoquinaldine (**3**). This rather unique ring cleavage reaction (cf. Section 3) yields carbon monoxide and *N*-acetylanthranilate (**4**). The hydrolysis product anthranilate **5** is further degraded via catechol **6** and the well-known 2-oxoadipate pathway into Krebs cycle intermediates.[22] An analogous pathway of 1*H*-4-oxoquinoline (**7**) degradation via the hydroxylated intermediates **8** and **9** to anthranilate **5** has been found in *Pseudomonas putida* 33/1 (Scheme 1a).[23] Thus, in the anthranilate pathway, cleavage of the N-heterocyclic ring occurs prior to benzene ring cleavage.

2.3. 5,6-Dihydroxy-1*H*-2-oxoquinoline Pathway

Comamonas testosteroni 63 degrades 3-methylquinoline (**11**) via 5,6-dihydroxy-1*H*-3-methyl-2-oxoquinoline (**19**), which is proposed to undergo cleavage of the benzene ring, since 3-methyl-2,5,6-trihydroxypyridine (**21**) was isolated as N-heterocyclic intermediate (Scheme 1b).[24] 5,6-Dihydroxy-1*H*-2-oxoquinoline (**18**) presumably also is an intermediate in the degradation of quinoline (**10**) by *Comamonas testosteroni* 63,[25] *Pseudomonas putida* K1,[26] *Rhodococcus* sp. B1,[21] a *Moraxella* sp.,[27] and perhaps a *Nocardia* sp.[28] An aromatic *ortho*-dihydroxy derivative such as **18** or **19** might either derive from a dioxygenase-catalyzed formation of a dihydrodiol followed by a dehydrogenase reaction, or it might be formed in two monooxygenase-catalyzed steps. In the case of the 1*H*-(3-methyl-)2-oxoquinolines (**12** or **13**), which are converted by *Comamonas testosteroni* 63, a 5,6-dioxygenase was shown to catalyze the formation of the corresponding 5,6-dihydrodiol **14** or **15** (Scheme 1b).[25]

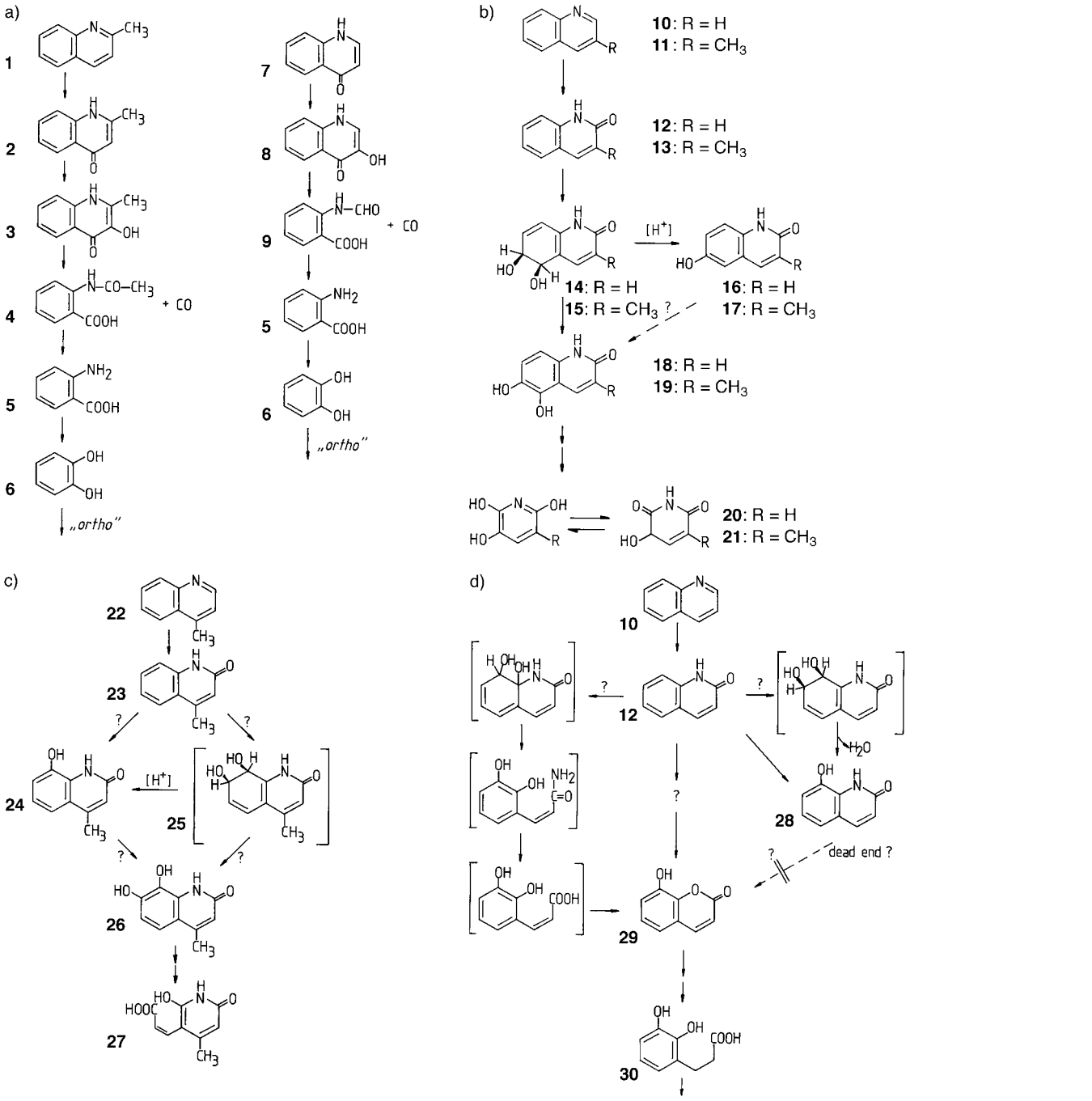
2.4. 7,8-Dihydroxy-1*H*-2-oxoquinoline Pathway

Similar to the pathway described in Section 2.3, the 7,8-dihydroxy-1*H*-2-oxoquinoline pathway also proceeds via an *ortho*-dihydroxy benzenoid compound, which probably undergoes benzene ring cleavage. 7,8-Dihydroxy-1*H*-2-oxoquinoline derivatives are key intermediates in the degradation of 4-methylquinoline (**22**) by *Pseudomonas putida* K1[26] (Scheme 1c), of 4-hydroxyquinoline by a soil pseudomonad,[29] and of kynurenic acid.[30, 31] The 8-monohydroxy derivative **24** of 1*H*-4-methyl-2-oxoquinoline (**23**) has been found as metabolite in the acidic extracts of the culture broth of the 4-methylquinoline degrader *Pseudomonas putida* K1 (Scheme 1c),[26] but this compound might be a dead-end product derived from dehydration of a hypothetical 7,8-dihydrodiol (**25**) rather than a true intermediate. The putative 7,8-dioxygenases of these pathways have not been investigated yet. However, in the degradation pathway of kynurenic acid by *Pseudomonas fluorescens*, the *cis*-7,8-dihydrodiol was detected as metabolite.[30]

2.5. 8-Hydroxycoumarin Pathway

Whereas in both pathways outlined in Scheme 1b and 1c the benzene nucleus is cleaved prior to the pyridine ring, there is a unique pathway of quinoline (**10**) degradation involving preferential cleavage of the N-heterocyclic ring and formation of 8-hydroxycoumarin (**29**, Scheme 1d). This pathway of quinoline degradation was first described by Shukla,[32] and it was also found in two *Pseudomonas* strains by our group.[21] However, the reaction sequence of quinoline degradation remains to be elucidated: Only a few metabolites have been identified as true intermediates, and the mechanism of N-heterocyclic ring cleavage per se is unknown. In *Pseudomonas putida* 86,[21] *Pseudomonas fluorescens* 3,[21] *Pseudomonas pseudoalcaligenes*, and *Pseudomonas stutzeri*,[32] 1*H*-2-oxoquinoline (**12**), 1*H*-8-hydroxy-2-oxoquinoline (**28**), 8-hydroxycoumarin (**29**), and 2,3-dihydroxyphenylpropionate (**30**) were found as metabolites. Compounds **29** and **30** appear to be true intermediates, but the mode of formation for **30** from **29** or from another hypothetical intermediate is not known yet. However, the enzymes catalyzing the first and second step of this pathway were investigated. Quinoline 2-oxidoreductase from *Pseudomonas putida* 86, which catalyzes the formation of 1*H*-2-oxoquinoline (**12**), was characterized thoroughly (Section 4.2).

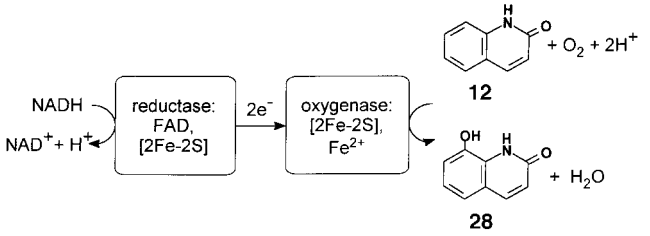
1*H*-2-Oxoquinoline 8-monooxygenase, which in the next step catalyzes the formation of 1*H*-8-hydroxy-2-oxoquinoline (**28**), consists of two inducible protein components, a "reductase" and "oxygenase" component. These protein components comprise a short electron transfer chain from the exogenous electron donor NADH via the redox centers of the reductase component (FAD and [2Fe-2S] ferredoxin) to the redox centers of the oxygenase (Rieske-type [2Fe2S] clusters), and finally to a proposed mononuclear Fe^{2+} center of the oxygenase component (Scheme 2). The latter is believed to activate molecular oxygen, and is thus the site of substrate oxygenation.[33] The subsequent steps of the degradation



Scheme 1. Pathways of the aerobic bacterial degradation of quinoline and its derivatives. a) Anthranilate pathway: degradation of quinaldine (**1**) by *Arthrobacter* sp. Rü61a[22] and degradation of 1*H*-4-oxoquinoline (**7**) by *Pseudomonas putida* 33/1.[23] b) 5,6-Dihydroxy-1*H*-2-oxoquinoline pathway: degradation of quinoline (**10**) and 3-methylquinoline (**11**) by *Comamonas testosteroni* 63.[24] c) 7,8-Dihydroxy-1*H*-2-oxoquinoline pathway: degradation of 4-methylquinoline by *Pseudomonas putida* K1.[26] d) 8-Hydroxycoumarin pathway: degradation of quinoline (**10**) by *Pseudomonas putida* 86,[21] *Pseudomonas fluorescens* 3,[21] *Pseudomonas stutzeri*, and *Pseudomonas pseudoalcaligenes*.[32]

pathway are speculative (Scheme 1d), since the failure to detect further proposed enzymes so far has precluded the detailed elucidation of the 8-hydroxycoumarin pathway.

Despite our current knowledge of a number of catabolic pathways, the metabolic route for the degradation of a quinoline derivative by a bacterial strain cannot be predicted. In *Comamonas testosteroni* 63, quinoline (**10**) and 3-methylquinoline (**11**) both are metabolized along the same pathway (Section 2.3), presumably by the same set of catabolic enzymes.[25] In contrast, *Pseudomonas* sp. K1 utilizes 4-methylquinoline (**22**) in the 7,8-dihydroxy-1*H*-2-oxoquinoline pathway (Section 2.4), but presumably degrades quinoline (**10**) along the 5,6-dihydroxy-1*H*-2-oxoquinoline pathway (Section 2.3); thus with this strain, each substrate induces the expression of a separate set of catabolic enzymes.[26] Fundamentally, the unsubstituted quinoline was degradable along three different pathways (those of Sections 2.3, 2.4, and 2.5), depending on the bacterial strain.



Scheme 2. Reaction catalyzed by 1*H*-2-oxoquinoline 8-monooxygenase, a two-component enzyme system from *Pseudomonas putida* 86.[33]

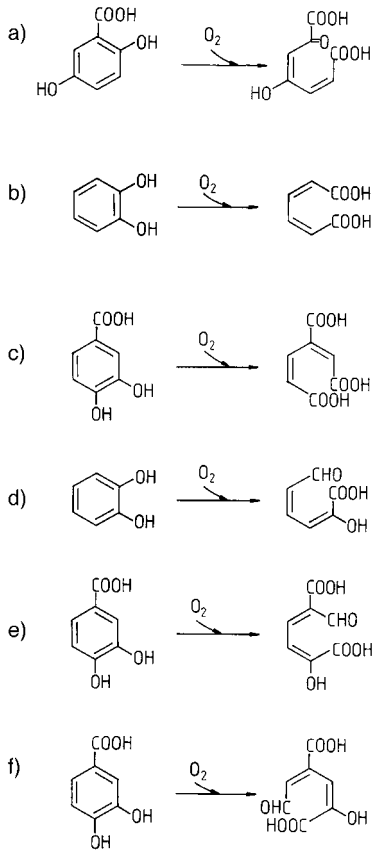
The catabolic pathways, deduced in early studies mainly from the isolation and characterization of metabolites, should be considered as tentative hypotheses, which are to be substantiated by the detection and characterization of the enzymes catalyzing each individual step of the proposed pathway. To confirm the conversions proposed, and, furthermore, to get an insight into the molecular mechanism of enzyme-catalyzed reactions, our further studies concentrated on the characterization of some catabolic enzymes. The structural and catalytic properties of the enzyme proteins were investigated, and in some cases the nucleotide sequences of the genes encoding degradative enzymes were determined and subjected to comparative analyses.

3. Dioxygenases Catalyzing the Ring-Opening Step in the Bacterial Degradation of Heterocyclic Compounds

Ring cleavage is the crucial step in the microbial degradation of aromatic and heterocyclic compounds. The aerobic biodegradation of benzenoid compounds generally proceeds with the introduction of two hydroxy groups *ortho* or *para* to each other, followed by cleavage by a dioxygenase to generate aliphatic compounds as intermediates (Scheme 3). Gentisate 1,2-dioxygenase, and the "intradiol" and "extradiol" enzymes that catalyze *ortho* and *meta* cleavage, respectively, of catecholic substrates, are well-characterized nonheme iron dioxygenases.[34, 35] In contrast, most enzymes that catalyze the cleavage of heterocyclic compounds are less understood.

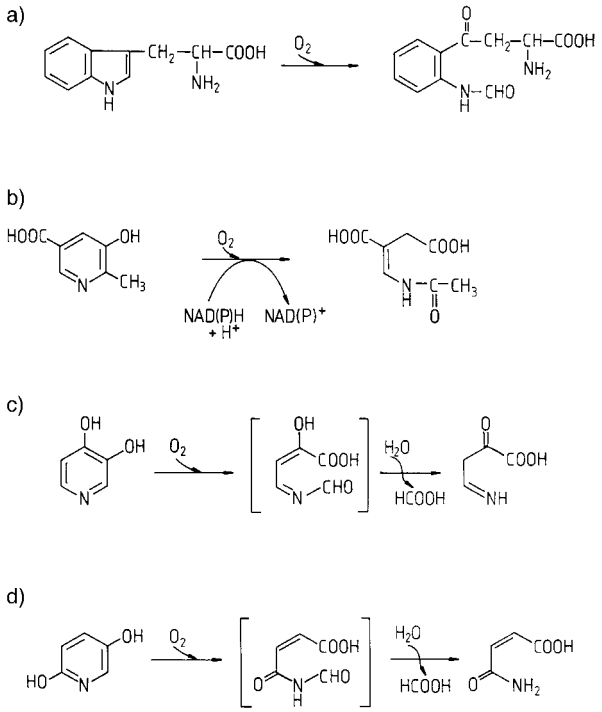
Different types of enzymes are involved in various heterocyclic ring cleavage reactions: L-Tryptophan 2,3-dioxygenases (Scheme 4a) from several bacterial strains are heme-containing enzymes.[34] 2-Methyl-3-hydroxypyridine-5-carboxylate oxygenase (Scheme 4b) is an NAD(P)H-dependent FAD-containing dioxygenase.[36] 3,4-Dihydroxypyridine dioxygenase from *Agrobacterium* sp. probably catalyzes an extradiol cleavage reaction, forming 3-(N-formyl)-formiminopyruvate, which upon hydrolysis would yield the observed products formate and 3-formiminopyruvate (Scheme 4c).[37] In an analogous reaction catalyzed by 2,5-dihydroxypyridine 5,6-dioxygenases from various strains (Scheme 4d), the hydrolysis products maleamate and formate were identified.[38] The latter enzymes require Fe^{2+} and a thiol donor such as dithiothreitol, cysteine, or glutathion for activity. However, the lability of these enzymes precluded extensive characterization.

In the anthranilate pathway of quinaldine (**1**) and 1*H*-4-oxoquinoline (**7**) degradation, we found an unusual way to break open the N-heterocyclic ring, involving cleavage of two C–C bonds with concomitant release of carbon monoxide (Section 2.2, Scheme 1a). Carbon monoxide forming enzymes are very rare. Known for some time is the mammalian microsomal heme monooxygenase system, which in the presence of molecular oxygen and NADPH forms CO and biliverdin IXα from iron protoporphyrin IX.[39] However, two enzymes are known which, in a manner analogous to that of the prokaryotic 2,4-dioxygenases active in the anthranilate pathway, catalyze an oxidative cleavage of two C–C bonds with concomitant CO release, namely, the eukaryotic flavonol 2,4-dioxygenase produced by *Aspergillus flavus*,[40, 41] and the prokaryotic aci-reductone oxidase (CO-forming) from *Klebsiella pneumoniae*.[42, 43] The latter is operative in the methionine salvage pathway, catalyzing 1,3-dioxygenolytic cleavage of the 1,2-dihydroxy-3-keto-*S*-methylthiopentene anion **32** to *S*-methylthiopropionic acid, CO, and formate. The substrates of all these dioxygenases show common structural features, since they all possess a double bond between C2 and C3 (C1 and C2), a hydroxyl group at C3 (C2), and a carbonyl group at C4 (C3) (Scheme 5).

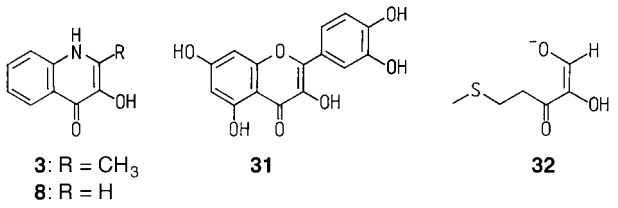


Scheme 3. Reactions catalyzed by aromatic ring cleavage dioxygenases: b, c) "*ortho*" cleavage; d)–f): "*meta*" cleavage. a) Gentisate 1,2-dioxygenase, b) catechol 1,2-dioxygenase, c) protocatechuate 3,4-dioxygenase, d) catechol 2,3-dioxygenase, e) protocatechuate 2,3-dioxygenase, f) protocatechuate 4,5-dioxygenase.

The bacterial CO-forming dioxygenases that catalyze N-heterocyclic ring cleavage reactions in the degradation of quinaldine and 1*H*-4-oxoquinoline are small monomeric proteins, which cleave their respective substrate in the presence of dioxygen, without any need of additional



Scheme 4. Reactions catalyzed by N-heterocyclic ring cleavage dioxygenases. Catalysis by a) tryptophan 2,3-dioxygenase, b) 2-methyl-3-hydroxypyridine-5-carboxylate oxygenase, c) 3,4-dihydroxypyridine dioxygenase, d) 2,5-dihydroxypyridine dioxygenase.



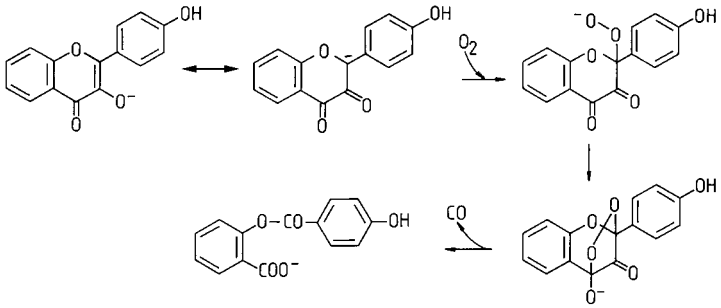
3: R = CH_3 **31** **32**
8: R = H

Scheme 5. Organic substrates of dioxygenases that catalyze cleavage of two C–C bonds with concomitant CO formation. **3** and **8**: substrates of 1*H*-3-hydroxy-4-oxoquinaldine 2,4-dioxygenase and 1*H*-3-hydroxy-4-oxoquinoline 2,4-dioxygenase, respectively.[44, 45] **31**: substrate of flavonol 2,4-dioxygenase.[40, 41] **32**: substrate of aci-reductone oxidase.[42, 43]

cosubstrates or metal ions. In oxygen isotope incorporation studies with an atmosphere of 50% $^{18}O_2$ and 50% $^{16}O_2$, two oxygen atoms of either $^{18}O_2$ or $^{16}O_2$ were incorporated at C2 and C4 of the respective substrates, indicating that these unusual enzymes indeed are 2,4-dioxygenases.[44, 45]

Flavonol 2,4-dioxygenase ("quercetinase"), which catalyzes an analogous 2,4-dioxygenolytic CO release from the O-heterocyclic flavonol quercetin **31**, was reported to contain two atoms of Cu^{II} per molecule.[40] Chemically, flavonols are known to form stable Cu^{II} chelates, presumably by coordination at the 3-hydroxy and 4-carbonyl group. Based on the model reaction of Cu^{II}-flavonolate-catalyzed oxygenation of flavonols, which exclusively gives quercetinase-like products in good yields, the mononuclear Cu^{II} cofactor was proposed to activate the flavonol substrate for dioxygen attack by formation of a Cu^{II} complex.[46]

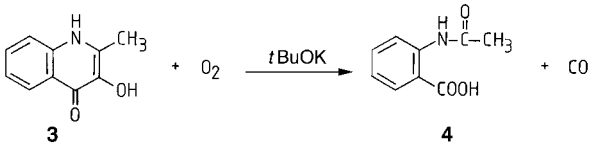
However, base-catalyzed autoxidation of flavonols was found to provide a nonenzymatic model for the reaction of flavonol 2,4-dioxygenase: when the 3-hydroxy group is deprotonated and the carbonyl character at C4 is retained, 3-hydroxyflavones undergo base-catalyzed oxygenolysis to give the corresponding depsides (phenolic carboxylic acid esters) and CO in excellent yields.[47] O_2 appears to be incorporated into the deprotonated form of the flavonol, yielding a peroxy intermediate, which upon intramolecular nucleophilic attack forms a five-membered cyclic peroxide (Scheme 6). Corresponding depside formations occur on use



Scheme 6. Proposed mechanism of base-catalyzed dioxygenolytic cleavage of the anion of **31** with concomitant CO formation.[47]

of bis(salicylidene)ethylenediaminatocobalt(II) ([Co^{II}(salen)]) as catalyst (salen = *N*,*N*′-bis(salicylidene)ethylene).[48] Catalytically active cobalt–oxygen complexes are considered to act as a base rather than as an oxidizing agent. Based on base-catalyzed model reactions, a direct ionic process was postulated for the flavonol 2,4-dioxygenase reaction.[47, 48]

Base-catalyzed chemical dioxygenation provides an analogous nonenzymatic model for the reaction of the 2,4-dioxygenases that catalyze N-heterocyclic ring cleavage: 1*H*-3-Hydroxy-4-oxoquinaldine (**3**) and 1*H*-3-hydroxy-4-oxoquinoline (**8**) were reactive towards molecular oxygen in the presence of the base catalyst potassium *tert*-butoxide in the aprotic solvent *N*,*N*-dimethylformamide. CO, *N*-acetylanthranilate (**4**), and anthranilate (**5**, resulting from amide hydrolysis) were formed from 1*H*-3-hydroxy-4-oxoquinaldine (**3**; Scheme 7). Analogously, **5** was identified as the hydrolysis



3 **4**

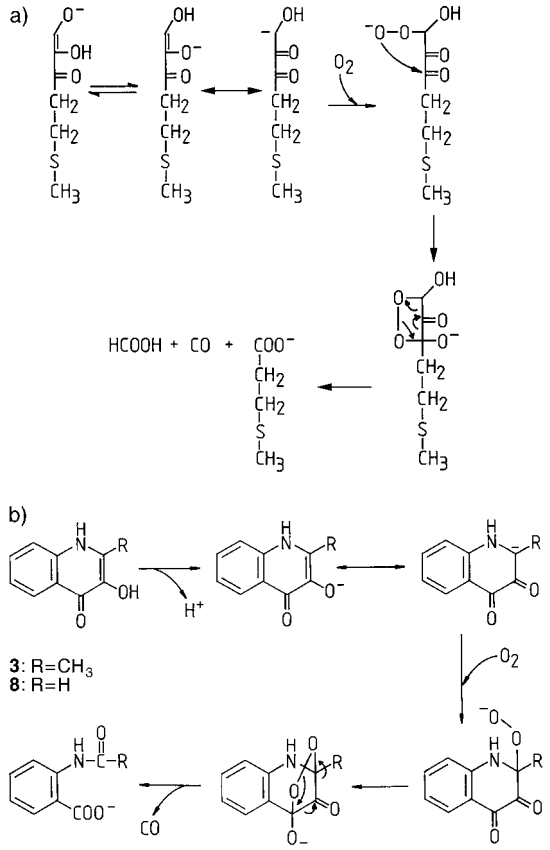
Scheme 7. Base-catalyzed dioxygenolytic cleavage of 1*H*-3-hydroxy-4-oxoquinaldine (**3**).[45]

product after base-catalyzed dioxygenolytic decarbonylation of **8**. When the assay was performed under anaerobic conditions, both **3** and **8** were completely recovered after neutralization of the samples. Thus, base catalysis mimics the enzyme-catalyzed 2,4-dioxygenolytic decarbonylation of the N-heterocyclic compounds **3** and **8**.[45]

In contrast to quercetinase, where Cu^{II} may act as a base, both 1*H*-3-hydroxy-4-oxoquinoline- and 1*H*-3-hydroxy-4-oxoquinaldine 2,4-dioxygenase do not contain any metal or other cofactor. Thus, a functional group of an amino acid residue may act as a base catalyst. However, the active site residue(s)

proposed to activate the N-heterocyclic substrates for dioxygen attack remain to be identified.[45]

Recently, the properties of the 1,3-dioxygenolytic aci-reductone oxidase from *Klebsiella pneumoniae* were reported.[43] Analogous to the 2,4-dioxygenases involved in the anthranilate pathway of quinaldine (**1**) and 1*H*-4-oxoquinoline (**7**) degradation, this 1,3-dioxygenolytic enzyme also appears to contain neither a chromophoric nor a metallic cofactor. The authors also propose a quercetinase-like reaction mechanism, involving formation of a substrate carbanion and addition of dioxygen at C1 of the carbanion tautomer to form a hydroperoxy anion, which in a nucleophilic attack may react with the C3 carbonyl, yielding a five-membered cyclic peroxide intermediate, which then decomposes (Scheme 8a). It is not yet known whether dioxygenase-catalyzed oxygen incorporation into the substrate carbanion involves formation of radical anions as intermediates, as described for the oxygenation of various carbanions.[49] Wray and Abeles[43] suggested a stepwise single-electron transfer from the carbanion to molecular oxygen for the formation of the peroxy anion. However, as discussed by Nishinaga et al. for base-catalyzed oxygenations,[47, 50] a direct one-step ionic mechanism, not involving a free-radical-chain process, may also be possible for the reaction of the carbanion with molecular oxygen. Scheme 8b summarizes the tentative hypothesis on the mechanism of 2,4-dioxygenolytic CO formation from **3** and **8**. Further studies are necessary to elucidate the molecular mechanism of dioxygenase-catalyzed oxidative cleavage of two C–C bonds with concomitant release of CO.



Scheme 8. Proposed mechanisms of dioxygenase-catalyzed formation of CO for the a) aci-reductone oxidase from *Klebsiella pneumoniae*,[43] b) 1*H*-3-hydroxy-4-oxoquinoline 2,4-dioxygenase from *Pseudomonas putida* (R = H) and 1*H*-3-hydroxy-4-oxoquinaldine 2,4-dioxygenase from *Arthrobacter* sp. Rü 61 a (R = CH_3).[45]

4. Molybdenum-Containing Enzymes

4.1. The Pterin Molybdenum Cofactors

Bacterial utilization of quinoline and its derivatives as a rule depends on the availability of traces of molybdate in the culture medium. In contrast, growth of the bacterial strains on the first intermediate of each catabolic pathway, namely, the 1*H*-2-oxo or 1*H*-4-oxo derivatives of the quinoline compound (Scheme 1a–d), was not affected by the availability of molybdate. This observation indicated a possible role of the trace element molybdenum in the initial hydroxylation at C2 or C4 of the quinoline derivatives.

Molybdenum plays an essential role in the biogeochemical cycles of nitrogen, sulfur, and carbon. In enzymes molybdenum occurs as part of redox-active cofactors. The molybdenum-dependent nitrogenases, synthesized exclusively by prokaryotes, are well known. The nitrogenase "MoFe-protein" contains an iron–molybdenum cofactor (FeMoCo), in which molybdenum is part of an unusual iron–molybdenum–sulfur cluster.[51] At the iron–molybdenum cofactor, nature performs its own "Haber-Bosch process", reducing the atmospheric nitrogen to ammonium. Apart from nitrogenase, all other molybdoenzymes described contain a pterin molybdenum cofactor.

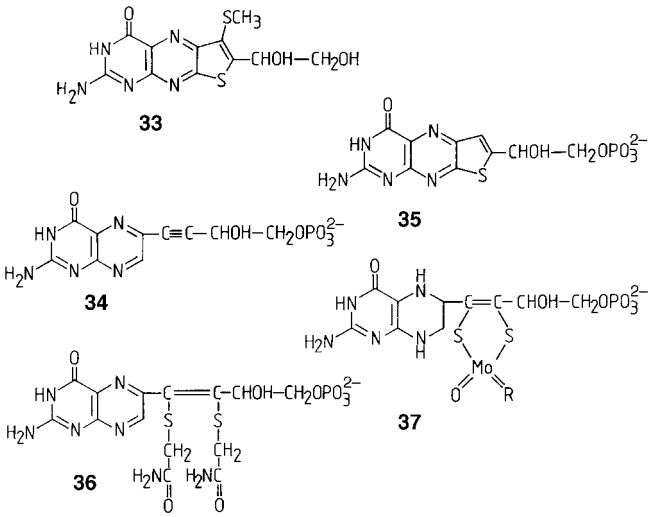
The reactions catalyzed by the enzymes dependent upon the pterin molybdenum cofactor all involve the transfer of an oxygen atom to or from a substrate molecule in a two-electron redox reaction. This large family of enzymes comprises, for example, nitrate reductase, sulfite oxidase, formate dehydrogenase, carbon monoxide dehydrogenase, arsenite oxidase, and various molybdenum-containing hydroxylases from pro- and eukaryotic sources such as aldehyde oxidase (EC 1.2.3.1) and various aldehyde dehydrogenases, purine hydroxylase, and xanthine dehydrogenase (EC 1.1.1.204)/xanthine oxidase (EC 1.1.3.22).[52–55] A number of bacterial enzymes that catalyze hydroxylations of pyridine carboxylic acids, quinoline derivatives and other N-heterocyclic compounds (see Section 4.2) also are molybdenum-containing hydroxylases.

Hydroxylation reactions are ubiquitous in the metabolic pathways of all living organisms. The majority of known hydroxylating enzymes, namely, the mono- and dioxygenases, utilize dioxygen as the source of the oxygen atom incorporated into the substrate. In this reaction reducing equivalents are consumed. In contrast, the molybdenum-containing hydroxylases utilize water as the ultimate source of the oxygen atom, and they generate rather than consume reducing equivalents according to the overall stoichiometry in Equation (1).

$$RH + H_2O \rightarrow ROH + 2\,e^- + 2\,H^+ \quad (1)$$

In the pterin molybdenum cofactor of molybdenum-containing hydroxylases, molybdenum is coordinated to molybdopterin or to a molybdopterin dinucleotide. Unlike many other organic cofactors known, these pterin cofactors in their native form are not amenable to isolation. Thus, the classical cofactor assays of reassociation with concomitant reconstitution of enzymatic activity are not feasible. The structural determination of the pterin molybdenum cofactors was severely hampered by the fact that these cofactors, once separated from the enzyme protein, immediately decayed into a multitude of fluorescent oxidation products.

In 1940, Koschara isolated tiny amounts of a sulfur-containing compound out of 1000 L of human urine.[56] He called it urothione, but at that time he naturally did not perceive that he had discovered the metabolic excretion product of the pterin molybdenum cofactor. The laborious isolation was repeated nearly 30 years later by Goto et al.,[57] who determined the structure of urothione (**33**). Its origin, however, still remained an enigma until 1982, when Johnson and Rajagopalan realized the metabolic relationship between the pterin molybdenum cofactor (**37**) and urothione.[58] From the known structures of urothione and of two fluorescent degradation products of the cofactor, called "form A" (**34**) and "form B" (**35**), a structural model of the pterin molybdenum cofactor was deduced. The model was confirmed by the characterization of an alkylated derivative of the pterin molybdenum cofactor, bis(carboxamidomethyl)-molybdopterin (camMPT **36**; Scheme 9).[58, 59]

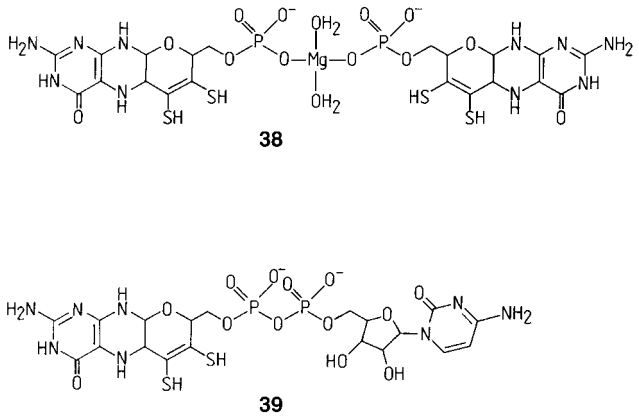


Scheme 9. Structures of pterin molybdenum cofactors and related compounds.[59] R = O, S, Se.

The generation of alkylated derivatives of the pterin molybdenum cofactor was an important accomplishment, since it allowed the discovery of the molybdopterin dinucleotides. The latter previously had escaped detection because of the common practice of demonstrating the presence of a pterin molybdenum cofactor in an enzyme by its conversion into **34** or **35**. The conditions required for these transformations are so harsh that pyrophosphate linkages are cleaved. Thus, **34** or **35** were found, irrespective of whether molybdopterin or a molybdopterin dinucleotide was primarily present. Direct evidence for the existence of a dinucleotide form of the pterin molybdenum cofactor was obtained in 1990, when an alkylated cofactor derivative was isolated from dimethylsulfoxide reductase from *Rhodobacter sphaeroides*, which upon treatment with nucleotide pyrophosphatase yielded camMPT (**36**) and GMP, thus establishing molybdopterin guanine dinucleotide (MGD) as organic part of the pterin molybdenum cofactor.[60] Shortly thereafter, molybdopterin cytosine dinucleotide (MCD) was found in carbon monoxide dehydrogenase from *Pseudomonas carboxydoflava*.[61] Since then, MGD and MCD have been found in a number of molybdenum-containing enzymes. Whereas enzymes depending on the pterin molybdenum cofactor as a rule specifically harbor either molybdopterin, MCD, or MGD, formylmethanofuran dehydrogenase from *Methanobacterium thermoautotrophicum* utilizes MGD, molybdopterin adenine dinucleotide, and molybdopterin hypoxanthine dinucleotide, that is, several purine dinucleotides of the pterin molybdenum cofactor.[62]

Major steps towards the elucidation of the structural features of the pterin molybdenum cofactor(s) were the analyses by X-ray diffraction methods of the crystal structures of aldehyde ferredoxin oxidoreductase from *Pyrococcus furiosus* (a hyperthermophilic archaeon),[63] of aldehyde oxidoreductase from the sulfate reducer *Desulfovibrio gigas*,[64] and of dimethylsulfoxide reductase from the phototrophic bacteria *Rhodobacter sphaeroides* and *Rhodobacter capsulatus*.[65]

Aldehyde ferredoxin oxidoreductase from *Pyrococcus furiosus* consists of two identical subunits, each containing a [4Fe-4S] cluster and a tungsten cofactor that is analogous to the pterin molybdenum cofactor. Each subunit of aldehyde ferredoxin oxidoreductase contains two pterin molecules, linked through their phosphate groups that coordinate axial sites of one magnesium ion. The two pterin molecules coordinate one tungsten atom through four sulfur donor atoms. No protein ligands were coordinated to the tungsten atom. The pterin system was modified to contain a third ring formed by closure of the side-chain hydroxyl with the pterin ring at C7 (Scheme 10). This revised bis(molybdopterin) structure (**38**) led to the proposal that in the dinucleotide forms of the pterin molybdenum cofactor, a single molecule of



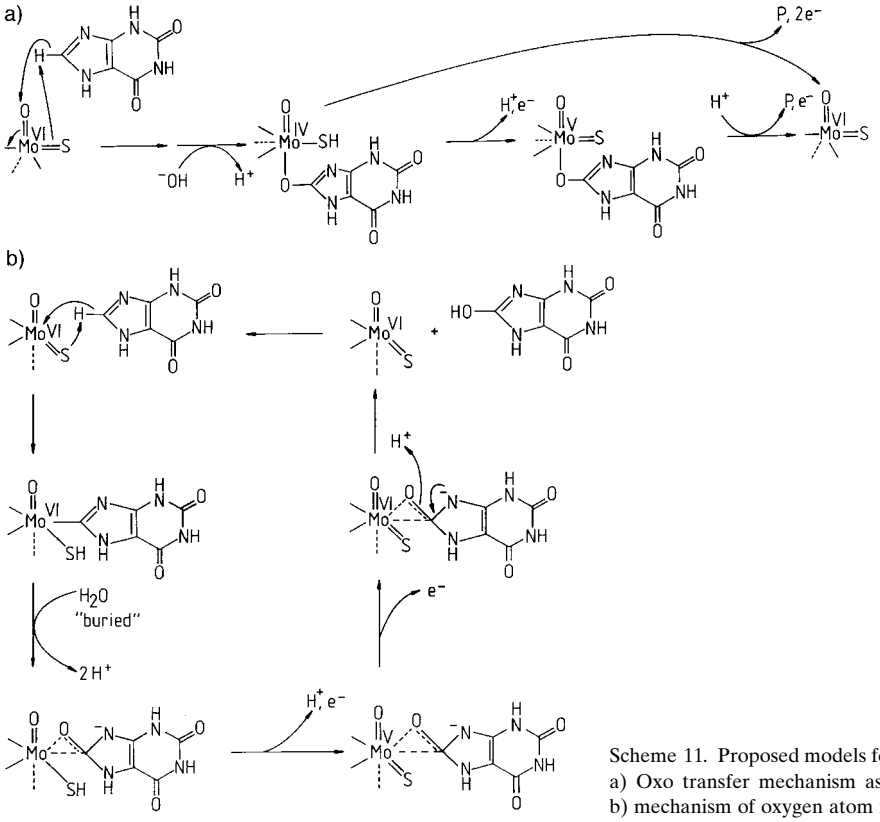
Scheme 10. Structural models for variants of the pterin molybdenum cofactor according to Chan et al.[63]

the pterin dinucleotide could possibly coordinate the molybdenum center, and that the second pterin of the bis(molybdopterin) may be replaced by the nucleotide, if the sugar hydroxyl oxygen atoms are utilized for metal ligation instead of the second dithiolene group.[63]

Aldehyde oxidoreductase from *Desulfovibrio gigas* is a homodimeric enzyme, in which each subunit contains two different [2Fe2S] clusters and one MCD as dinucleotide form of the pterin molybdenum cofactor. The amino acid sequence of this aldehyde oxidoreductase shares no homology to the tungstoprotein aldehyde ferredoxin oxidoreductase from *Pyrococcus furiosus* described above. However, analogous to the bis(molybdopterin) cofactor of aldehyde ferredoxin oxidoreductase, the molybdopterin forms a tricyclic system in which the pterin ring is annealed to a pyran ring (**39**, Scheme 10). The Mo^{VI} center present in the oxidized form of the enzyme is pentacoordinated by two dithiolene sulfur and three oxygen ligands, which were identified as two oxo (Mo=O) and one water ligand ($Mo-OH_2$).[64]. The structure, however, is at variance with the suggestion by Chan et al.[63] of an involvement of the sugar hydroxyl groups in molybdenum binding.

Characterization of the crystal structure of aldehyde oxidoreductase from *Desulfovibrio gigas* also provided insight into some mechanistic features of aldehyde oxidation and internal electron transfer. The oxygen transferred to the substrate may either derive from the water molecule nearest to the molybdenum, or it is one of the molybdenum's ligands. The transfer of the oxo ligand of the molybdenum was suggested earlier for the xanthine oxidase reaction by Hille and co-workers.[55] According to this model, the catalytically labile oxygen of the Mo=O group is transferred to substrate with each catalytic cycle. Since water is the ultimate source of the oxygen incorporated into product, the oxo group of the molybdenum center must be regenerated from solvent. Thus, a reaction initiated by proton abstraction followed by carbanion attack on Mo=O was proposed, as outlined in Scheme 11a.[55] However, recent ^{17}O and ^{13}C electron nuclear double resonance (ENDOR) spectroscopy and kinetic studies, which indicated a molybdenum–carbon bond formation in the catalytic action of xanthine oxidase, and structural analyses of the *Desulfovibrio gigas* aldehyde oxidoreductase led to the proposal of an alternative mechanism, not involving direct participation of the oxo ligand group but transfer of the molybdenum-bound water molecule to the substrate.[66] The catalytic model for the xanthine oxidase reaction is referred to as "oxygen atom insertion" rather than "oxo transfer" and involves formal addition of the substrate across the Mo=S bond of the catalytic center of xanthine oxidase, followed by attack of a "buried" water molecule (in the vicinity of molybdenum and perhaps a ligand of it) on the bound substrate carbon. Thus, the oxygen incorporated into the uric acid product is proposed to originate from a "buried" water rather than the oxo group. The oxo molybdenum ligand in this mechanistic model plays no active part in the reaction (Scheme 11b).[66]

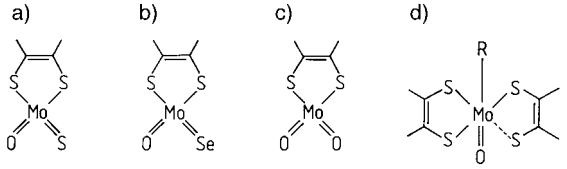
Structural data on dimethylsulfoxide reductase from *Rhodobacter sphaeroides* indicated that this protein represents a distinct group of pterin molybdenum cofactor-containing enzymes, unrelated to both the aldehyde ferredoxin oxidoreductase from *Pyrococcus furiosus* and the aldehyde oxidoreductase from *Desulfovibrio gigas* described above. The monomeric *Rhodobacter* dimethylsulfoxide reductase harbors



Scheme 11. Proposed models for the catalytic cycle of the xanthine oxidase reaction. a) Oxo transfer mechanism as proposed by Hille and co-workers,[55] P = product; b) mechanism of oxygen atom insertion as proposed by Howes et al.[66]

two MGDs that asymmetrically coordinate the molybdenum through their dithiolene groups. A protein ligand, namely, a side chain oxygen of a serine residue, additionally coordinates the metal.[65]

Based on the type of molybdenum center, the idea emerged that three fundamentally distinct classes of enzymes depending on the pterin molybdenum cofactor may be distinguished (Scheme 12):[65] Firstly, there are the enzymes possessing a



Scheme 12. Types of molybdenum(VI) centers in enzymes depending on the pterin molybdenum cofactor.[65] a) Monooxo-monosulfido-type, b) monooxo-monoselenido-type, c) dioxo-type, d) monooxo-type; R = serine, cysteine, selenocysteine.

monooxo-monosulfido-type molybdenum center (with xanthine oxidase as prototype). The *Desulfovibrio gigas* aldehyde oxidoreductase also belongs to this group of enzymes frequently referred to as the "xanthine oxidase family". Xanthine dehydrogenase and nicotinic acid dehydrogenase of certain anaerobic bacteria form a subgroup, since they apparently possess a monooxo-monoselenido-type molybdenum center, as demonstrated for nicotinic acid dehydrogenase (hydroxylase) from *Clostridium barkeri*.[67] The second group of enzymes, represented by sulfite oxidase, harbors a dioxo-type molybdenum center. The third group of enzymes can at best be described as possessing a monooxo-type molybdenum center. This group, with dimethylsulfoxide reductase as representative, is further characterized by a protein ligand at the molybdenum center. This ligand may be either a serine, as in dimethylsulfoxide reductase from *Rhodobacter sphaeroides* described above, a cysteine, or a selenocysteine residue. The latter was identified as molybdenum ligand in *Escherichia coli* formate dehydrogenase H.[68]

The molybdenum-containing hydroxylases that catalyze a hydroxylation either adjacent to the heteroatom or at C4 of the quinoline ring belong to the first group of enzymes, the xanthine oxidase family. All the enzymes characterized in greater detail by our group contained molybdopterin cytosine dinucleotide (MCD) with a monooxo-monosulfido-type molybdenum center.[69–75]

4.2. Molybdenum-Containing Hydroxylases Involved in the Bacterial Degradation of Quinoline and Derivatives

4.2.1. Biochemistry

4.2.1.1. Structural Features

Early studies on quinoline degradation by *Pseudomonas putida* 86 indicated that molybdenum was required for the biotransformation of quinoline (**10**) to 1*H*-2-oxoquinoline (**12**; cf. Section 4.1).[76] Since the molybdenum-dependent eukaryotic xanthine oxidases were known to exhibit a rather broad substrate specificity, catalyzing the hydroxylation of a number of N-heterocyclic compounds,[77] our observation of molybdenum-dependent quinoline hydroxylation at first led us tentatively to assume that a bacterial xanthine dehydrogenase might be involved in quinoline hydroxylation. This hypothesis, however, was disproved by the finding in *Pseudomonas putida* 86 of two distinct molybdenum-containing hydroxylases: the xanthine dehydrogenase purified from this strain was composed of two nonidentical subunits arranged in an $\alpha_4\beta_4$ structure, whereas the quinoline 2-oxidoreductase from the same strain was found to be a heterotrimeric protein ($\alpha_2\beta_2\gamma_2$). Both molybdenum-containing hydroxylases contain FAD and [2Fe2S] centers, but differ in their pterin molybdenum cofactor: the bacterial xanthine dehydrogenase possesses molybdopterin (MPT), wheras quinoline 2-oxidoreductase harbors molybdopterin cytosine dinucleotide (MCD) as organic part of the pterin molybdenum cofactor.[69, 78, 79] The enzymes show distinct substrate specificities. Neither is quinoline converted by xanthine dehydrogenase, nor are xanthine and hypoxanthine transformed by quinoline 2-oxidoreductase. Quinazoline (1,3-benzodiazine, **46**; see Scheme 14) was the only substrate found to be hydroxylated by both quinoline 2-oxidoreductase and xanthine dehydrogenase.

Quinoline 2-oxidoreductases, which catalyze the conversion of quinoline (**10**) into 1*H*-2-oxoquinoline (**12**), were purified not only from *Pseudomonas putida* 86, but also from *Rhodococcus* sp. B1 and *Comamonas testosteroni* 63.[25, 70, 76, 79] All three enzymes were found to be structurally complex molybdo iron–sulfur flavoproteins. The in vitro reaction requires the presence of an artificial electron acceptor. The physiological electron acceptor of the quinoline 2-oxidoreductases has not been identified yet.

Unlike the situation for quinoline, there are comparatively few reports on the bacterial catabolism of isoquinoline. Several bacterial strains capable of degrading isoquinoline as the sole source of carbon and energy were described.[80] All these strains appear to initially transform isoquinoline to 2*H*-1-oxoisoquinoline. The complete catabolic pathway(s), which in *Brevundimonas diminuta* 7 may involve degradation via phthalate and protocatechuate,[81] remain(s) to be elucidated.

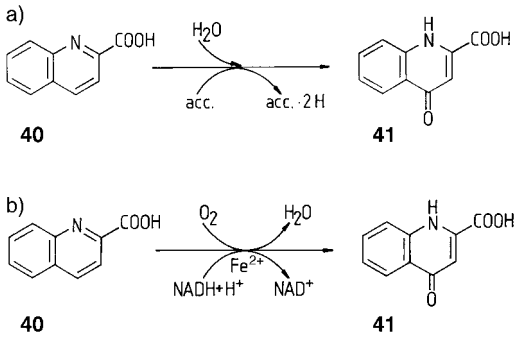
Isoquinoline 1-oxidoreductase, which catalyzes the hydroxylation at C1 of isoquinoline with concomitant reduction of a suitable electron acceptor, was purified from *Brevundimonas diminuta* 7.[75] The native enzyme is a heterodimeric molybdo iron–sulfur protein, lacking the flavin cofactor.

Quinaldine 4-oxidase from the Gram-positive bacterium *Arthrobacter* sp. Rü 61 a catalyzes the initial step in quinaldine (**1**) degradation[22] (Section 2.2, Scheme 1a): quinaldine is converted into 1*H*-4-oxoquinaldine (**2**) with concomitant reduction of an electron acceptor. The enzyme is able to function as oxidase or dehydrogenase, and molecular oxygen is proposed as physiological electron acceptor.[72] Hydroxylations in *para* position to the N-heteroatom were also described for two quinaldic acid 4-oxidoreductases.[74, 82]

Many bacterial molybdenum-containing hydroxylases that catalyze the nucleophilic attack of an N-heterocyclic compound either adjacent or *para* to the N-heteroatom are molybdo iron–sulfur flavoproteins, namely, xanthine dehydrogenases,[78, 83] nicotinate and 6-hydroxynicotinate dehydro-

genase from *Bacillus niacini*,[84] isonicotinate dehydrogenase from *Mycobacterium* sp. INA1,[85] nicotine dehydrogenase from *Arthrobacter oxidans*,[86] several quinoline 2-oxidoreductases,[25, 70, 76, 79] quinaldine 4-oxidase from *Arthrobacter* sp. Rü 61 a,[71, 72] quinoline 4-carboxylate 2-oxidoreductase from *Agrobacterium* sp. 1B,[73] and quinaldic acid 4-oxidoreductase from *Pseudomonas* sp. AK-2.[74] These prokaryotic enzymes, which contain a pterin molybdenum cofactor, iron–sulfur centers, and FAD, appear to be related to the eukaryotic molybdenum-containing hydroxylases aldehyde oxidase and xanthine oxidase. However, there are also prokaryotic molybdenum-containing hydroxylases without a flavin cofactor, such as the heterodimeric enzymes quinaldic acid 4-oxidoreductase from *Serratia marcescens* 2CC-1 and isoquinoline 1-oxidoreductase from *Brevundimonas diminuta* 7 mentioned already.[82, 75] The homodimeric aldehyde oxidoreductase from *Desulfovibrio gigas* discussed in Section 4.1 also belongs to this subgroup of molybdo iron–sulfur proteins.

As shown in Table 1, two quinaldic acid 4-oxidoreductases have been described, which differ in structure and in their set of redox-active centers. Both enzymes, however, catalyze a nucleophilic attack at C4 of quinaldic acid (**40**), incorporating the oxygen atom of a water molecule into the substrate. It is interesting to note that the very same conversion, that is, the formation of kynurenic acid (**41**) from **40**, in an *Alcaligenes* strain was catalyzed by a monooxygenase, which in an electrophilic attack incorporates an oxygen atom derived from molecular oxygen into the substrate (Scheme 13).[87]



Scheme 13. Enzyme-catalyzed conversion of quinaldic acid (**40**) to kynurenic acid (**41**).[87] a) Quinaldic acid 4-oxidoreductases from *Serratia marcescens* 2CC-1 and *Pseudomonas* sp. AK-2, b) quinaldic acid 4-monooxygenase from *Alcaligenes* sp. F2. acc. = electron acceptor.

Thus, the same reaction in different bacteria is accomplished by enzymes belonging to separate classes, differing fundamentally in their catalytic mechanism.

4.2.1.2. Substrate Specificity and Aldehyde Oxidation

Investigation of the substrate specificity of quinaldine 4-oxidase revealed that in addition to quinaldine, it converted 8-chloroquinaldine, quinoline, 2- and 8-monochloroquinoline, isoquinoline, and the benzodiazines cinnoline (1,2-benzodiazine), quinazoline (1,3-benzodiazine, **46**), and phthalazine (2,3-benzodiazine, **44**). Surprisingly, all these substrates (except **44**) elicited higher catalytic activities than quinaldine itself. Thus, the enzyme nomenclature is rather difficult: Despite its name, originally deduced from its role in quinaldine utilization by *Arthrobacter* sp. Rü 61 a (Scheme 1a),[22] the enzyme converts a number of N-heterocyclic substrates with a significantly higher conversion rate than quinaldine.[72]

To test whether other molybdenum-containing hydroxylases involved in the bacterial degradation of N-heteroaromatic compounds also convert such a broad range of substrates, the substrate specificities of quinaldine 4-oxidase, quinoline 2-oxidoreductase, and isoquinoline 1-oxidoreductase were compared (Table 2). Quinoline (**10**) was accepted as substrate by both quinaldine 4-oxidase and quinoline 2-oxidoreductase, yielding 1*H*-4-oxoquinoline and 1*H*-2-oxoquinoline, respectively. So, quinaldine 4-oxidase catalyzes the regiospecific attack in position 4, even if the carbon atom adjacent to the N-heteroatom is not blocked by a substituent. Isoquinoline and

Table 2. Enzyme-catalyzed hydroxylation of quinolines and benzodiazines.

Enzyme	Substrate	Product
quinaldine 4-oxidase	quinoline (**10**)	1*H*-4-oxoquinoline (**7**)
	quinaldine (**1**)	1*H*-4-oxoquinaldine (**2**)
	isoquinoline	2*H*-1-oxoisoquinoline
	phthalazine (**44**)	2*H*-1-oxophthalazine (**45**)
	quinazoline (**46**)	3*H*-4-oxoquinazoline (**48**)
	cinnoline	1*H*-4-oxocinnoline
quinoline 2-oxidoreductase	quinoline (**10**)	1*H*-2-oxoquinoline (**12**)
	quinazoline (**46**)	1*H*-2-oxoquinazoline
	quinoxaline (**42**)	1*H*-2-oxoquinoxaline (**43**)
isoquinoline 1-oxidoreductase	isoquinoline	2*H*-1-oxoisoquinoline
	phthalazine (**44**)	2*H*-1-oxophthalazine (**45**)
	quinazoline (**46**)	3*H*-4-oxoquinazoline (**48**)

Table 1. Molybdenum-containing hydroxylases involved in the bacterial degradation of quinoline derivatives.

Enzyme (organism)	*M* [kDa]	*M* [kDa] (subunits)	Structure	Moco[a, b]	FeS[b]	Flavin[b]
quinoline 2-oxidoreductase (*Pseudomonas putida* 86)	300	85, 30, 18	$\alpha_2\beta_2\gamma_2$	(2)MCD[c]	(2)[2Fe-2S]I (2)[2Fe-2S]II[e]	(2)FAD
quinaldine 4-oxidase (*Arthrobacter* sp. Rü 61 a)	340	82, 35, 22	$\alpha_2\beta_2\gamma_2$	(2)MCD[c]	(2)[2Fe-2S]I (2)[2Fe-2S]II[e]	(2)FAD
quinaldic acid 4-oxidoreductase (*Pseudomonas* sp. AK-2)	300	90, 34, 20	$\alpha_2\beta_2\gamma_2$	(2)MCD[c]	(8)Fe, (8)S	(2)FAD
quinaldic acid 4-oxidoreductase (*Serratia marcescens* 2CC-1)	100	80, 18	$\alpha\beta$	– [d]	(3–4)Fe	–
isoquinoline 1-oxidoreductase (*Brevundimonas diminuta* 7)	95	80, 16	$\alpha\beta$	(1)MCD[c]	(1)[2Fe-2S]I (1)[2Fe-2S]II[e]	–

[a] Pterin molybdenum cofactor. [b] In parentheses: number of cofactors per enzyme molecule. [c] Molybdopterin cytosine dinucleotide. [d] Not determined. [e] Deduced from EPR spectroscopic data.

phthalazine (**44**) are substrates not only for isoquinoline 1-oxidoreductase but for quinaldine 4-oxidase as well. Identical products were formed by the two enzymes, namely 2*H*-1-oxoisoquinoline and 2*H*-1-oxophthalazine (**45**), respectively. Quinazoline (**46**) is the only substrate accepted by all three enzymes (see Scheme 14). With quinaldine 4-oxidase and isoquinoline 1-oxidoreductase, 3*H*-4-oxoquinazoline (**48**) was produced, whereas quinoline 2-oxidoreductase hydroxylated at C2, that is, adjacent to both N1 and N3. Apparently, quinoline 2-oxidoreductase and isoquinoline 1-oxidoreductase hydroxylate their various substrates exclusively adjacent to an N-heteroatom. Quinaldine 4-oxidase is more versatile: whether the regiospecific nucleophilic attack is in *ortho* or in *para* position to an N-heteroatom depends on the substrate (Table 2).[72]

Apart from these prokaryotic enzymes, which are all involved in the bacterial degradation of quinoline and its derivatives, the eukaryotic molybdenum-containing hydroxylases xanthine oxidase from cow's milk and aldehyde oxidase from rabbit liver catalyze the oxidation of N-heterocycles, too.[77, 88] The latter two enzymes also convert aldehydes into the corresponding carboxylic acids.[89]

Since comparison of the amino acid sequence of isoquinoline 1-oxidoreductase with other molybdenum-containing hydroxylases revealed significant similarities with two aldehyde oxidoreductases, one from the industrial vinegar producer *Acetobacter polyoxogenes* and the other from the sulfate reducer *Desulfovibrio gigas* (Section 4.2.3),[90] substrate specificities of isoquinoline 1-oxidoreductase, quinoline 2-oxidoreductase, and quinaldine 4-oxidase towards various aldehydes were investigated. Surprisingly, quinaldine 4-oxidase and isoquinoline 1-oxidoreductase both catalyzed the oxidation of aromatic aldehydes. Benzaldehyde and salicylaldehyde (2-hydroxybenzaldehyde) turned out to be accepted best by quinaldine 4-oxidase. Cinnamaldehyde (3-phenyl-2-propenal) and vanillin (4-hydroxy-3-methoxybenzaldehyde) were also converted into the corresponding carboxylic acids, although at significantly lower rates, whereas short-chain aliphatic aldehydes were not oxidized. Isoquinoline 1-oxidoreductase markedly resembled quinaldine 4-oxidase in its substrate spectrum; salicylaldehyde and benzaldehyde were favorites. The aldehydes, however, were suicide substrates for isoquinoline 1-oxidoreductase. Quinaldine 4-oxidase and isoquinoline 1-oxidoreductase were more active towards aromatic than towards aliphatic aldehydes. This feature apparently does not apply for the prokaryotic aldehyde oxidoreductases described, which all convert short-chain aliphatic aldehydes far better than quinaldine 4-oxidase and isoquinoline 1-oxidoreductase do.[72] However, eukaryotic aldehyde oxidase, a molybdenum-containing enzyme well-characterized with respect to N-heterocyclic and aldehyde substrate specificity, appears to be similar to quinaldine 4-oxidase and isoquinoline 1-oxidoreductase in so far as it catalyzes the hydroxylation of N-heterocycles (such as quinoline, quinaldine, isoquinoline, cinnoline, quinazoline) and the oxidation of aromatic aldehydes with roughly comparable rates.[89]

In conclusion, molybdenum-containing hydroxylases show rather variable specificities, and even the distinction between aldehyde oxidoreductases and N-heterocycles hydroxylating enzymes remains a matter of discussion.[72] However, aldehydes are cytotoxic compounds due to their reactivity, and the molybdenum-containing hydroxylases active towards aldehydes may function as important detoxification enzymes for both the prokaryotic and the eukaryotic cell.

4.2.2. Biophysics

The internal electron transport chain of quinoline 2-oxidoreductase from *Pseudomonas putida* 86 is composed of four redox active centers (see also Table 1, Section 4.2.1.1)—FAD, two distinct [2Fe-2S] centers, and molybdenum-MCD. Each of these centers adopts a paramagnetic state during the redox cycle of the enzyme and can then be investigated by electron paramagnetic resonance (EPR) spectroscopy.[79]

Reduction of quinoline 2-oxidoreductase with dithionite or with quinoline led to the formation of an organic radical with 1.9 mT line width typical for a neutral (blue) flavin radical species and similar to eukaryotic xanthine oxidase (from cow's milk).[91] Two iron–sulfur centers were discernible by their EPR spectra: In the temperature range below 60 K distinct rhombic EPR signals were resolved. By comparison with xanthine oxidase, and according to the convention in literature, the rhombic iron–sulfur signals with the lower *g* anisotropy were designated FeS I and those with the larger *g* anisotropy FeS II, respectively (Figure 2a–c).[92, 93] The *g*

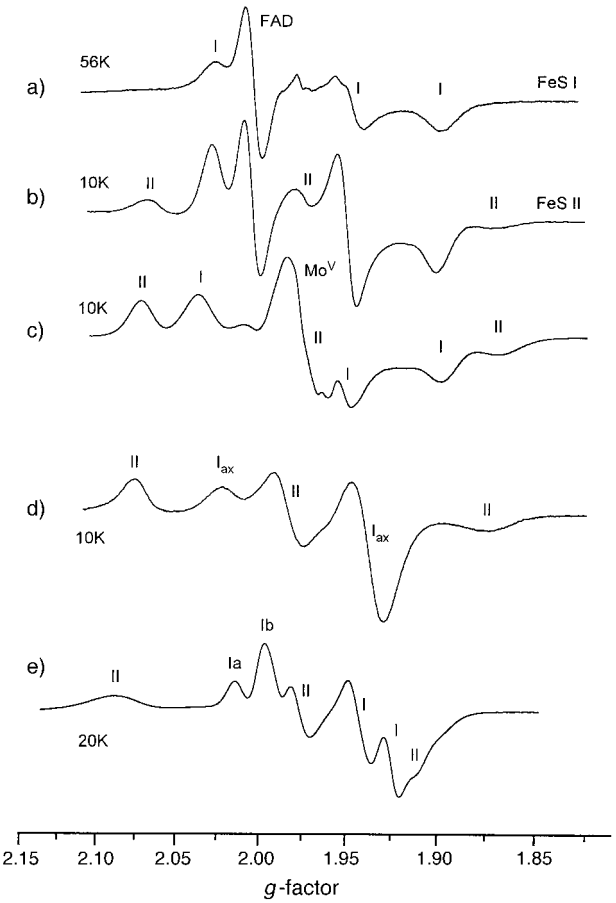


Figure 2. Comparison of the EPR signals of the iron–sulfur clusters. a)–c) Quinoline 2-oxidoreductase, a) reduced with dithionite, recorded at 56 K and b) at 10 K; c) reduced with quinoline, recorded at 10 K. The positions of the FAD radical signal as well as of a broadened Mo^V signal are indicated. d) Quinaldine 4-oxidase, reduced with dithionite, recorded at 10 K. e) Isoquinoline 1-oxidoreductase, reduced with dithionite, recorded at 20 K.

values of FeS I showed only little variation from those of the F–S centers in other proteins, implying similar stereochemical and electronic structures of the signal-generating FeS I species in the various pro- and eukaryotic enzymes. In the *g* factors for the FeS II signals, however, there were significant differences among the molybdenum-containing hydroxylases, indicative of a more pronounced variability of this signal-generating species.

The oxidation–reduction potentials, determined by titration with sodium dithionite solutions in the presence of various mediators, yielded values of -155 mV for FeS I and -195 mV for FeS II. These represent the highest redox potentials measured so far for [2Fe-2S] clusters of molybdenum-containing hydroxylases.

The molybdenum center is of fundamental interest as the putative site of substrate binding and catalysis. The EPR spectrum in Figure 3a of the oxidized quinoline 2-oxidoreductase (as isolated) recorded at 77 K resembles the Mo^V "resting" spectrum known from xanthine oxidase, aldehyde oxidase, and carbon monoxide oxidase.[79] It represents an inactive Mo^V species always present in low concentrations

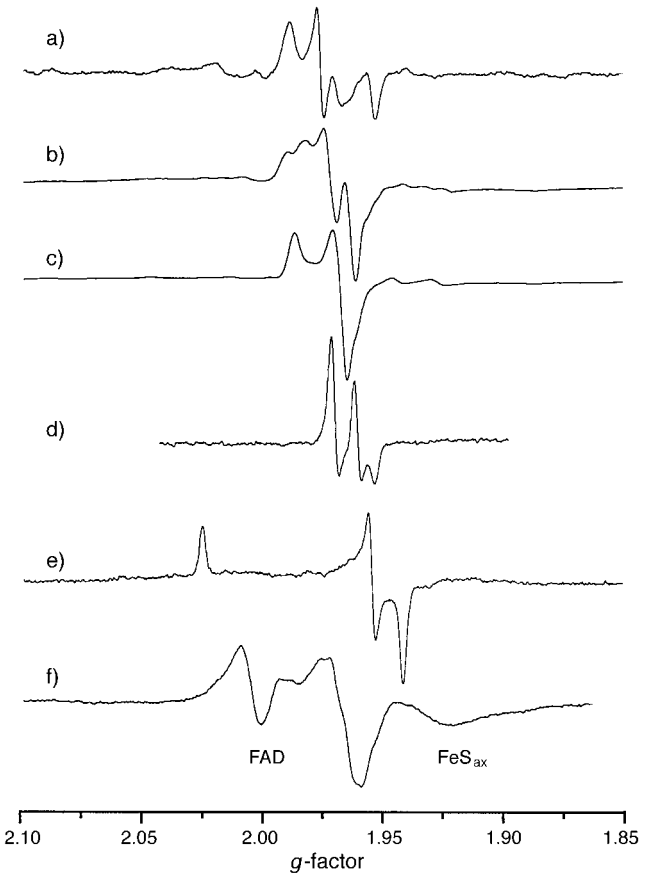


Figure 3. EPR signals of Mo^V species. a)–c): Quinoline 2-oxidoreductase. a) "Resting Q"; b) "rapid Q" in H_2O buffer; c) "rapid Q" in D_2O buffer; the hyperfine lines due to the thiol proton are no longer observed. d) "Slow Q" of the cyanide treated desulfo form. e) Isoquinoline 1-oxidoreductase: "very rapid I"; the signal was obtained by subtraction of spectra at different incubation times. f) Quinaldine 4-oxidase, reduced under anaerobic conditions with the substrate quinaldine (**1**). All spectra were recorded at 77 K.

(<5% of total Mo concentration) in the preparations. Reduction of the enzyme with its substrate or dithionite elicited an intense EPR spectrum of another Mo^V species (Figure 3b), designated "rapid Q" to characterize its origin and its similarity with the "rapid" signal of bovine xanthine oxidase.[92] Its prominent feature is a proton coupling of the sulfhydryl group, which is easily exchangeable in D_2O buffer in analogy to xanthine oxidase (Figure 3c). Small differences in the hyperfine coupling values obtained for the substrate-reduced and dithionite-reduced species reflect the influence of the substrate (or the product) in the vicinity of the Mo^V center, but direct spectral evidence for complex formation is not found by EPR. In ^{95}Mo-enriched quinoline 2-oxidoreductase hyperfine interaction of the metal nucleus with $I = 5/2$ leads to sixfold splitting of lines. Simulation of these hyperfine patterns points to a coincidence of one principal axis of the *g* and hyperfine tensor, which is typical for the presence of a complex with C_2 symmetry. The catalytically relevant "very rapid" Mo^V species, which is observed in xanthine oxidase in rapid freeze experiments on the millisecond time scale, could be isolated only in small amounts in quinoline 2-oxidoreductase by competitive binding of quinoline and the nonsubstrate quinaldine.

Quinoline 2-oxidoreductase from *Pseudomonas putida* 86 possesses a monooxo-monosulfido-type molybdenum center (see also Scheme 12) as shown by inactivation of the enzyme with cyanide with concomitant formation of thiocyanate, and reactivation of inactive enzyme by treatment with sulfide. Cyanide thus abstracts the so-called cyanolysable sulfur from the molybdenum center. In this inactive desulfo form of the enzyme the molybdenum center is thought to be of the dioxo type. In cyanide inactivation/sulfide reactivation experiments quinoline 2-oxidoreductase exhibits the same behavior as many other molybdo iron–sulfur flavoproteins. By analogy to the desulfo form of xanthine oxidase the Mo^V signal "slow Q" arising from the inactive desulfo quinoline 2-oxidoreductase was detected, which is characterized by a slightly rhombic *g* tensor and a proton interaction exchangeable in D_2O (Figure 3d).

In accordance with biochemical and genetic data, no free radical signal of a flavin-centered radical species was observed in EPR-spectroscopic analyses of isoquinoline 1-oxidoreductase from *Brevundimonas diminuta* 7. Two distinct rhombic EPR signals of iron–sulfur centers were discernible after reduction of the enzyme with dithionite or the substrate isoquinoline. At temperatures below 30 K a magnetic interaction between the iron–sulfur centers resulted in a pronounced splitting of the g_1 component of the FeS I signal (Ia, Ib in Figure 2e), indicating a spatial proximity of both clusters. While the FeS II signal occurred only in the temperature range below 40 K, FeS I signals were detectable already at 77 K, which is an unusual feature for a [2Fe-2S] center.

Upon reduction with its substrate isoquinoline the Mo^V species "rapid I" was readily observed, which again exhibited a strongly coupled proton exchangeable in D_2O, similar to the "rapid Q" signal of quinoline 2-oxidoreductase. A further Mo^V signal with nearly identical magnetic parameters to the "very rapid" species in quinoline 2-oxidoreductase and xanthine oxidase was detected in isoquinoline 1-oxidoreduc-

tase and called "very rapid I" (Figure 3e). Despite its name this signal persisted for at least 45 minutes, in contrast to its behavior as a short-lived intermediate such as in xanthine oxidase. It seems possible that a rather stable (partially inhibitory) complex between isoquinoline and the Mo^V center is formed in isoquinoline 1-oxidoreductase in the presence of an excess of substrate.

Quinaldine 4-oxidase and quinoline 2-oxidoreductase have a similar molecular mass and the same subunit and cofactor composition, whereas isoquinoline 1-oxidoreductase differs in these respects as indicated in Table 1 (Section 4.2.1.1). In order to compare these molybdenum-containing hydroxylases involved in bacterial catabolism of quinoline derivatives, the redox active centers of quinaldine 4-oxidase were additionally investigated by EPR spectroscopy.

Quinaldine 4-oxidase in the oxidized state (as isolated, aerobic conditions) did not elicit any EPR signal. Under anaerobic conditions, without substrate or reducing agent, an EPR signal of an organic radical species was observed. Upon addition of quinaldine to the enzyme this signal at $g = 2.0040$ was enhanced in intensity (Figure 3f). Its line width of 1.3 mT is characteristic for the anionic (red) flavin radical.[91] In contrast, for quinoline 2-oxidoreductase and eukaryotic xanthine oxidase the presence of a neutral (blue) radical species was deduced.

In dithionite reduced quinaldine 4-oxidase a distinct axial EPR signal of an iron–sulfur center (FeS I_{ax}) appeared at 77 K, which gained intensity at lower temperatures (Figure 2d and Figure 3f). In addition a second iron–sulfur center with rhombic symmetry was detectable below 60 K. This is at variance with the findings for quinoline 2-oxidoreductase and isoquinoline 1-oxidoreductase for which all centers provided rhombic symmetry. The pronounced axiality of the FeS I_{ax} center in quinaldine 4-oxidase should be associated with a more symmetrical ligand arrangement of the iron–sulfur cluster in this enzyme than in the other enzymes.

The generation of the "rapid" Mo^V species by addition of quinaldine to anaerobically prepared samples proved to be very sensitive to residual traces of oxygen. The corresponding axial "rapid" signal in Figure 3f exhibited a much lower spectral resolution than observed for the other enzymes, but still showed a decrease in the overall line width upon exchange of the buffer with D_2O. This is indicative for the presence of exchangeable protons at the molybdenum center, one of which probably is the sulfhydryl proton. In contrast to quinoline 2-oxidoreductase and isoquinoline 1-oxidoreductase neither the "resting" nor the "very rapid" type species could so far be detected spectroscopically.

The significant differences in EPR spectra of the three studied enzymes refer to the flavin radical, the iron–sulfur clusters, and the Mo^V signal-generating species. In particular, for Mo^V centers some spectral characteristics could be related to structural features. A more detailed understanding of the functional significance of the spectral observations for the various enzymes will be obtained from X-ray crystallographic data, which may allow for a correlation of electronic and electrochemical properties to the stereochemical arrangement of the redox active centers. In this context an important contribution is expected from the EPR-based high-resolution techniques electron nuclear double resonance (ENDOR) and electron spin echo envelope modulation (ESEEM) spectroscopy.

4.2.3. Genetics

In order to understand the binding of the redox-active centers by distinct peptide domains of the molybdenum-containing hydroxylases and to investigate the phylogenetic relationship of enzymes belonging to the xanthine oxidase family, the genes encoding isoquinoline 1-oxidoreductase and quinoline 2-oxidoreductase were cloned, sequenced, and subjected to comparative sequence analyses.[90, 94] The amino acid sequences of the small (IorA) and large (IorB) subunit, deduced from the nucleotide sequence of the *iorA* and *iorB* structural genes of the heterodimeric isoquinoline 1-oxidoreductase (cf. Table 1), indeed showed homologies 1) to the small (γ) and large (α) subunits of complex molybdenum-containing hydroxylases ($\alpha\beta\gamma/\alpha_2\beta_2\gamma_2$) possessing a pterin molybdenum cofactor with a monooxo–monosulfido-type molybdenum center, 2) to the N- and C-terminal regions of aldehyde oxidoreductase from *Desulfovibrio gigas*, and 3) to the N- and C-terminal domains of eukaryotic xanthine dehydrogenases. None of the regions of IorAB corresponded to the FAD-bearing middle domain of eukaryotic xanthine dehydrogenases, and there was no open reading frame putatively encoding an FAD-bearing peptide near the *iorAB* structural genes.[90]

The *qor* genes encoding quinoline 2-oxidoreductase from *Pseudomonas putida* 86 were found to be clustered in the transcriptional order 5'-*qorM-S-L*-3', corresponding to all other described structural genes of molybdenum-containing hydroxylases with $\alpha\beta\gamma$ or $\alpha_2\beta_2\gamma_2$ structure. We presume that both [2Fe-2S] centers are localized on the small, the FAD on the medium, and the pterin molybdenum cofactor as well as the substrate binding site on the large subunit, as discussed for the subunits or corresponding domains of other molybdenum-containing hydroxylases.[53, 90, 94–98]

An amino acid sequence alignment of the corresponding small subunits or domains of several pro- and eukaryotic enzymes belonging to the xanthine oxidase family with the small subunits of quinoline 2-oxidoreductase (QorS) and isoquinoline 1-oxidoreductase (IorA) revealed eight conserved cysteines, which are assumed to coordinate the two different [2Fe-2S] centers detected by EPR studies (cf. Section 4.2.2).[79, 92, 93, 99] The binding motif of the N-terminal [2Fe-2S] center (Figure 4a) is homologous to the signature sequence of bacterial and chloroplast-type [2Fe-2S]-ferredoxins, $[CX_4CX_2CX_nC]$ where X is any amino acid and n equals 11 for prokaryotic molybdenum-containing hydroxylases,[53, 98] 21 for eukaryotic molybdenum hydroxylases, and 29 or, in exception cases, 27 to 32 for bacterial and chloroplast-type ferredoxins. In contrast, the binding motif for the internal [2Fe-2S] cluster of the aligned small subunits has not been described in any other iron–sulfur protein and apparently is a distinct feature of the molybdenum-containing hydroxylases of pro- and eukaryotic organisms, where it is an absolutely conserved motif $[CX_2CX_{31}CXC]$ (Figure 4b).

a)

	★	↓					↓	★		↓					↓	
MenS	G	C	G	E	G	G	C	G	A	C	T	V	X_{18}	A	C	[42 - 73]
MauS	G	C	G	E	G	G	C	G	A	C	T	V	X_{18}	A	C	[45 - 76]
RatS	G	C	G	E	G	G	C	G	A	C	T	V	X_{18}	A	C	[41 - 72]
MelS	G	C	A	E	G	G	C	G	A	C	T	V	X_{18}	A	C	[46 - 77]
ObsS	G	C	A	E	G	G	C	G	A	C	T	V	X_{18}	A	C	[42 - 73]
BomS	G	D	G	E	G	G	C	G	A	C	T	V	X_{18}	A	C	[52 - 83]
HuhS	G	C	G	E	G	G	C	G	A	C	T	V	X_{18}	A	C	[46 - 77]
CalS	G	C	G	E	G	G	C	G	A	C	T	V	X_{18}	A	C	[55 - 86]
AspS	G	C	A	E	G	G	C	G	A	C	T	V	X_{18}	A	C	[72 - 102]
MopS	G	C	E	Q	G	Q	C	G	A	C	S	V	X_8	A	C	[39 - 60]
IorS	G	C	G	L	G	L	C	G	A	C	T	V	X_8	S	C	[38 - 59]
CsoS	G	C	E	T	G	I	C	G	A	C	S	V	X_8	S	C	[41 - 62]
CopS	G	C	D	T	S	H	C	G	A	C	T	V	X_8	S	C	[41 - 62]
NdhS	G	C	E	H	G	V	C	G	A	C	T	I	X_8	S	C	[47 - 68]
CooS	G	C	D	T	S	H	C	G	A	C	T	V	X_8	S	C	[41 - 62]
QorS	G	C	E	Q	G	V	C	G	S	C	T	I	X_8	S	C	[47 - 62]

b)

	★	↓	★		↓			★		★					★	+	↓	★	↓	+	+	★	
MenS	Q	C	G	F	C	T	P	G	X_8	L	X_{17}	-	-		N	L	C	R	C	T	G	Y	[112 - 153]
MauS	Q	C	G	F	C	T	P	G	X_8	L	X_{17}	-	-		N	L	C	R	C	T	G	Y	[114 - 155]
RatS	Q	C	G	F	C	T	P	G	X_8	L	X_{17}	-	-		N	L	C	R	C	T	G	Y	[110 - 151]
MelS	Q	C	G	F	C	T	P	G	X_8	L	X_{17}	-	-		N	L	C	R	C	T	G	Y	[116 - 157]
ObsS	Q	C	G	F	C	T	P	G	X_8	L	X_{17}	-	-		N	L	C	R	C	T	G	Y	[112 - 153]
BomS	Q	C	G	F	C	T	P	G	X_8	L	X_{17}	-	-		N	L	C	R	C	T	G	Y	[122 - 163]
HuhS	Q	C	G	F	C	T	P	G	X_8	L	X_{17}	-	-		N	L	C	R	C	T	G	Y	[116 - 157]
CalS	Q	C	G	F	C	T	P	G	X_8	L	X_{17}	-	-		N	L	C	R	C	T	G	Y	[125 - 166]
AspS	Q	C	G	F	C	T	P	G	X_8	L	X_{17}	-	-		N	L	C	R	C	T	G	Y	[141 - 182]
MopS	Q	C	G	F	C	S	P	G	X_8	L	X_{17}	H	R		N	A	C	R	C	T	G	Y	[99 - 142]
IorS	Q	C	G	Y	C	Q	S	G	X_8	L	X_{17}	-	-		N	L	C	R	C	G	T	Y	[96 - 137]
CsoS	Q	C	G	Y	C	T	P	G	X_8	L	X_{17}	-	-		N	L	C	R	C	T	G	Y	[100 - 141]
CopS	Q	C	G	F	C	T	P	G	X_8	L	X_{17}	-	-		N	L	C	R	C	T	G	Y	[100 - 141]
NdhS	Q	C	G	F	C	T	A	G	X_8	L	X_{17}	-	-		N	L	C	R	C	T	G	Y	[105 - 146]
CooS	Q	C	G	Y	C	T	P	G	X_8	L	X_{17}	-	-		N	L	C	R	C	T	G	Y	[101 - 142]
QorS	Q	C	G	F	C	T	A	G	X_8	L	X_{17}	-	-		N	L	C	R	C	T	G	Y	[106 - 147]

Figure 4. Alignment of amino acid sequences involved in binding of a) the N-terminal, ferredoxin-type [2Fe-2S] center and b) the internal [2Fe-2S] center of molybdenum-containing hydroxylases.[94] Numbers at the end of each line correspond to the amino acid number of the respective protein subunit or domain. Men = xanthine dehydrogenase of *Homo sapiens*; Mau = xanthine dehydrogenase of *Mus musculus*; Rat = xanthine dehydrogenase of *Rattus norvegicus*; Mel = xanthine dehydrogenase of *Drosophila melanogaster*; Obs = xanthine dehydrogenase of *Drosophila pseudoobscura*; Bom = xanthine dehydrogenase of *Bombyx mori*; Huh = xanthine dehydrogenase of *Gallus gallus*; Cal = xanthine dehydrogenase of *Calliphora vicina*; Asp = xanthine dehydrogenase of *Aspergillus nidulans*; Mop = aldehyde oxidoreductase of *Desulfovibrio gigas*; Ior = isoquinoline 1-oxidoreductase of *Brevundimonas diminuta* 7; Cso = quinaldic acid 4-oxidoreductase of *Pseudomonas* sp. AK-2; Cop = carbon monoxide dehydrogenase of *Pseudomonas thermocarboxydovorans* C2; Ndh = nicotine dehydrogenase of *Arthrobacter nicotinovorans*; Coo = carbon monoxide dehydrogenase of *Oligotropha carboxidovorans*; Qor = quinoline 2-oxidoreductase of *Pseudomonas putida* 86. S is small subunit or corresponding domain; ↓: conserved cysteine residues; ★: consistently conserved amino acid residues; + amino acid residues conserved in most sequences.

Since structural data on FAD binding by prokaryotic molybdo iron–sulfur flavoproteins are lacking, the mode of FAD binding in this subclass of enzymes belonging to the xanthine oxidase family is still unknown.

The large subunits of quinoline 2-oxidoreductase (QorL) and isoquinoline 1-oxidoreductase (IorB) probably contain the molybdopterin cytosine dinucleotide cofactor. QorL, IorB, and other large subunits or corresponding domains of a number of molybdenum-containing enzymes show significant homology to the C-terminal domain of aldehyde oxidoreductase from *Desulfovibrio gigas* (cf. Section 4.1). In this domain of the *Desulfovibrio gigas* enzyme, Romão et al. detected three molybdopterin binding amino acid segments and two dinucleotide binding segments.[64] Closely related signature sequences indeed are detectable in other molybdenum-containing enzymes belonging to the xanthine oxidase family: Figure 5 shows the sequence alignment of the molybdopterin binding and dinucleotide binding segments found in aldehyde oxidoreductase with putatively corresponding sequences of other molybdenum-containing hydroxylases. The first molybdopterin-contacting segment is the most conserved sequence of the five motifs. In aldehyde oxidoreductase from *Desulfovibrio gigas*, it contacts molybdopterin through F421 and G422, which are absolutely conserved in all aligned sequences (Figure 5).

However, the elucidation of structure and function of distinct conserved peptide domains of the molybdenum-containing hydroxylases must await further studies, such as investigation of the role of individual amino acid residues by site-directed mutagenesis, and, most significantly, X-ray structural analyses of crystallized enzyme proteins.

In analogy of the medium domain or subunit of other molybdenum-containing hydroxylases described, the medium subunit of quinoline 2-oxidoreductase (QorM) should contain the binding site for FAD.[53, 95, 96, 98, 100, 101] Several different dinucleotide (FAD, NAD/NADP, or ADP) binding motifs have been described.[102] All the FAD binding motifs comprise G-rich sequences, such as $[GXGX_2GX_3A]$ or $[GXGX_2GX_3G]$. A similar motif, $[GXGX_2AX_3A]$, is a site for NADP binding. None of these or other known motifs were detected in QorM or in the aligned sequences of nine eukaryotic xanthine dehydrogenases and five prokaryotic molybdenum-containing hydroxylases,[94] and the peptide domain proposed to bind the flavin cofactor of eukaryotic aldehyde oxidases also lacks such a consensus sequence.[103]

5. Future Prospects: Biotransformations Utilizing Molybdenum-Containing Hydroxylases?

For the manufacture of valuable intermediates for the synthesis of agrochemicals and pharmaceuticals, biotransformations with microbial strains or biocatalysts could provide versatile and economic alternatives to conventional chemical techniques. Chemical syntheses like hydroxylations of aromatic and heteroaromatic compounds usually require a high energy input. Furthermore, side-products that may be ex-

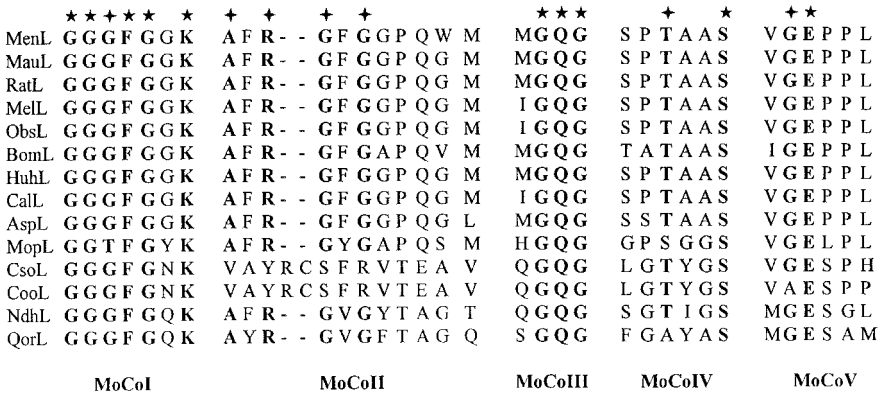


Figure 5. Alignment of amino acid sequences presumed to be involved in binding the pterin molybdenum cofactor of molybdenum-containing hydroxylases.[64, 94] MoCo I, MoCo II, MoCo III: putative molybdopterin binding segments; MoCo IV, MoCo V: putative dinucleotide binding segments.[64] The other abbreviations and the symbols are given in Figure 4. L is large subunit or corresponding domain.

pensive to separate and to dispose of may be formed, and the yields may be unsatisfactory. As a rule, however, biocatalysts possess substrate- and regiospecificities that are difficult to achieve by conventional chemistry, enabling the formation of defined products.

A number of hydroxylated quinolines, isoquinolines, and benzodiazines are important for the production of pharmaceuticals and agrochemicals:

1) Isocarbostyrils and carbostyrils: 2*H*-1-Oxoisoquinoline (isocarbostyril) is prepared chemically by treating isoquinoline in a KOH/NaOH or KOH/Na_2O melt.[104] Another possibility for the preparation of 2*H*-1-oxoisoquinolines is the Pd-catalyzed substitution of 2-bromobenzamides with ethylene and subsequent cyclization of the 2-ethenylbenzamide[105] or its preparation from *N*-propenyl-2-methylbenzamide.[106] Derivatives of 2*H*-1-oxoisoquinoline are widely used as drugs, fragrances, pharmaceuticals, and agrochemicals. In analogy to 2*H*-1-oxoisoquinoline, 1*H*-2-oxoquinoline (carbostyril, **12**) is prepared, for example, from quinoline (**10**) in a KOH/Na_2O or KOH/NaOH melt.[104] Other methods of chemical syntheses have been described. Carbostyril derivatives are useful as blood platelet aggregation inhibitors,[107] cardiotonic agents,[108] and neuroleptic agents.[109] Several 6-substituted carbostyrils were shown to inhibit vascular smooth muscle phosphodiesterases that hydrolyze cAMP and cGMP and thus may find application as therapeutic agents, for example, in cardiovascular disease.[110] Procaterol-HCl (5-[1-hydroxy-2-isopropylaminobutyl]-8-hydroxycarbostyril hydrochloride hemihydrate) is a sympathomimetic amine used as bronchodilator.[111]
2) Quinolones: "Quinolones" are generally defined as 1-substituted 1,4-dihydro-4-oxo-3-pyridinecarboxylic acids that have an additional ring fused at the 5,6-position. Quinolones, especially the 6-fluoroquinolones, have received considerable attention, and thousands of fluoroquinolone analogues have been disclosed. Fluoroquinolones are bactericidal agents against gram-negative and some gram-positive pathogens, and against mycobacteria and other intracellular bacteria, but they also exhibit promising activity against some categories of protozoa, such as *Leishmania*, *Trypanosoma*, and *Plasmodium* species, and thus may be useful in antimalaria therapy.[11–13, 112]
3) Hydroxylated benzodiazines: Quinoxalones, phthalazones, quinazolones: There are numerous patents for various methods to chemically synthesize 1*H*-2-oxoquinoxaline (**43**), which is manufactured as an intermediate for the production of agrochemicals, drugs, and dyes. The organophosphorus pesticide quinalphos (*O*,*O*-diethyl-*O*-quinoxaline-2-yl phosphorothioate) is used extensively for treatment of important crops in the tropical, subtropical, and temperate zones. For instance, lemon trees are sprayed with quinalphos for the control of the spherical mealybug *Nipaecoccus vastor*.[113] As pharmaceuticals, several 1*H*-2-oxoquinoxaline derivatives are useful in treating inflammatory and allergic diseases. 1,3-Dimethyl-1*H*-2-oxoquinoxaline, for instance, is a bronchodilator for asthma treatment.[114] For 2*H*-1-oxophthalazine **45**, too, there are numerous patents on different chemical syntheses. Substituted (2-biphenylyl)-2*H*-1-oxophthalazines are antipsychotics and antidepressants, and they are also used for the treatment of various inflammatory diseases.[115] Some 2*H*-1-oxophthalazine derivatives are vasoactive compounds and inhibit platelet aggregation.[116] Another important application of phthalazinones is for the preparation of photothermographic films.[117] Derivatives of quinazoline, especially the 3*H*-4-oxoquinazoline (**48**), also are used for the manufacture of pharmaceuticals such as antihypertensives, bronchodilators, anti-inflammatory agents, and central nervous system depressants.[118] A survey on biologically active quinazolones is given by Sinha and Srivastava, discussing their anthelmintic, central nervous system depressant, anti-inflammatory, cardiovascular, antimicrobial, and antitumor activities.[119]

In conclusion, carbostyril-, phthalazone-, quinazolone- and quinoxalone-based drugs are widely used as anti-inflammatory and cardiovascular agents, for the treatment of allergies, and as central nervous system depressants. Fluoroquinolones comprise a large class of antibacterial drugs, which are promising also for further therapeutic uses.

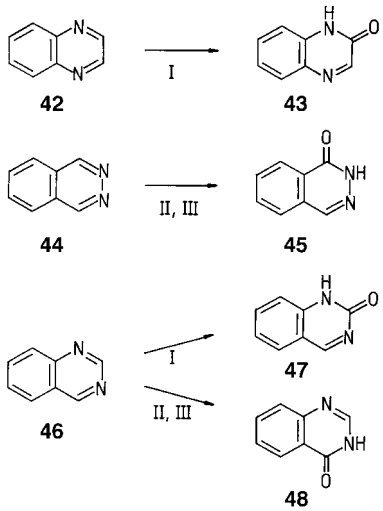
Up to now, these hydroxylated N-heterocyclic compounds almost exclusively are manufactured by chemical syntheses. The use of a bioconversion process, as exemplified in a Japanese patent, utilizing a *Pseudomonas* strain for the production of carbostyril (**12**) and/or 6-hydroxycarbostyril is rather exceptional.[120] However, hydroxylated quinolines, isoquinolines, and benzodiazines, useful as intermediates for further syntheses, alternatively might be produced by biotransformations, since biocatalysts enable substrate- and regiospecific hydroxylation free of side-products.

The molybdenum-containing hydroxylases may be utilized for the transformation of organic compounds such as quinolines and benzodiazines. Due to the observed accumulation of

the oxo compounds in the fermentation broth during growth of most bacterial strains on a quinoline derivative (cf. Section 1), such biotransformations even may be performed in a whole-cell system with the appropriate strain that degrades the N-heterocyclic compound in question. Cells of *Pseudomonas putida* 86, for instance, produce 1*H*-2-oxoquinoline (**12**) when growing on quinoline. High concentrations of quinoline prevent further degradation of **12**. Thus, it is even possible to harvest the product **12** from the culture broth in a crystalline state by regulating the concentration of the substrate quinoline during fermentation, first keeping it low in order to allow complete substrate utilization to obtain biomass, then increasing the quinoline concentration and maintaining it at a high level in order to accumulate **12**, which finally precipitates.

An efficient method to generate hydroxylated quinolines and benzodiazines, however, is biotransformation with a cometabolic process: The quinaldine-degrading strain *Arthrobacter* sp. Rü61a, for instance, does not grow on quinoline, but due to the broad substrate specificity of quinaldine 4-oxidase, cells of strain Rü61a—pregrown on quinaldine as carbon source in order to generate biomass and to induce the 4-hydroxylase—produce 1*H*-4-oxoquinoline from quinoline in excellent yields and free of side-products.

On the other hand, the isolated enzymes may be used as catalysts. The molybdenum-containing hydroxylases involved in the bacterial degradation of various N-heteroaromatic compounds offer several potential applications: Apart from the quinolines, some benzodiazines are accepted as substrates by isoquinoline 1-oxidoreductase, quinoline 2-oxidoreductase, and quinaldine 4-oxidase, yielding different hydroxylation products (Scheme 14):[72] Quinoxaline (**42**) is converted



Scheme 14. Hydroxylation of benzodiazines, catalyzed by various molybdenum-containing hydroxylases.[72] I: quinoline 2-oxidoreductase from *Pseudomonas putida* 86. II: isoquinoline 1-oxidoreductase from *Brevundimonas diminuta* 7. III: quinaldine 4-oxidase from *Arthrobacter* sp. Rü61a.

into 1*H*-2-oxoquinoxaline (**43**) by quinoline 2-oxidoreductase from *Pseudomonas putida* 86, and phthalazine (**44**) is converted into 2*H*-1-oxophthalazine (**45**) by both isoquinoline 1-oxidoreductase from *Brevundimonas diminuta* 7 and quinaldine 4-oxidase from *Arthrobacter* sp. Rü61a. The third benzodiazine, quinazoline (**46**), is hydroxylated at C4 by isoquinoline 1-oxidoreductase and quinaldine 4-oxidase, whereas quinoline 2-oxidoreductase catalyzes hydroxylation at C2 (Scheme 14).[72]

However, because biological systems have to be handled, the organic chemist would probably hesitate to consider a biochemical solution for a synthetic problem. At best, however, chemistry will supply economic precursors and enable efficient product isolation, whilst the critical step is catalyzed by an enzyme (or mixture of enzymes), or by whole cells. When using whole cells, growth and maintenance of a microbial strain in a fermentation system has to be set up, the conditions for biotransformation have to be optimized, and the biotransformation product must be purified from the culture broth. On the other hand, isolated enzymes, which may be obtained either in a crude or purified form, in a soluble or immobilized state, can be handled like a chemical catalyst. A number of applications, however, successfully use whole cells for bioconversion, such as LONZA's process to produce 6-hydroxynicotinic acid by regiospecific hydroxylation of nicotinic acid with a wild-type nicotinic acid degrading bacterial strain.[121] The bacterial enzyme involved in nicotinic acid hydroxylation also is a molybdenum-containing hydroxylase.

The more traditional biotransformation methods using whole cell systems or isolated biocatalysts and, additionally, modern techniques of molecular biology, such as cloning and (heterologous) expression of the hydroxylase genes and overproduction of the corresponding enzyme, will likely enable biotechnology to cooperate with chemistry.

6. Summary and Outlook

Microorganisms display enormous metabolic diversity and are primarily responsible for the cycling of organic compounds in the biosphere.

The pathways bacteria use to metabolize different classes of organic compounds are being studied extensively by many research groups. Biological attack on organic substances may lead to degradation, resulting ultimately in mineralization, or to transformation in which the main structure of the compound remains essentially unaltered. Mineralization of an organic compound generates carbon and energy for microbial growth. On the other hand, cometabolism, a process by which microorganisms in the obligatory presence of a growth substrate transform a non-growth substrate, is thought to play a significant role in the biotransformation and degradation of organic matter in the environment. Cometabolic conversions of N-heteroaromatic compounds may well take place in nature. However, the bacterial strains mentioned in this review article all were enriched and isolated from soil and water samples by offering quinoline (or a derivative) as sole source of carbon and energy, thus selecting for strains capable to grow on these compounds.

On investigating these bacterial isolates, four different catabolic pathways of aerobic utilization of quinoline derivatives were found. In some cases, minor amounts of side-

products (possible dead-end products) were formed in the culture broth, but degradation generally resulted in complete mineralization. Thus, bacteria have developed diverse and efficient strategies for metabolizing these N-heteroaromatic compounds. However, a detailed understanding of many degradative pathways is still lacking.

All the biochemical reactions taking place in an organism are governed by enzymes. The majority of these enzymes is highly selective, fundamentally exhibiting (depending on the reaction catalyzed) chemoselectivity, regioselectivity, and diastereoselectivity, and enantioselectivity. Detailed studies on the reactions involved in the bacterial degradation of quinoline and its derivatives have indeed revealed a number of interesting enzymes, such as the molybdenum-containing hydroxylases that catalyze regiospecific hydroxylations of their respective N-heteroaromatic substrate(s). Furthermore, unusual 2,4-dioxygenases that catalyze the cleavage of two C – C bonds with concomitant formation of carbon monoxide were discovered. However, although much is already known about the catalysts of aerobic degradation of N-heterocyclic compounds, there is still a great deal to be learned about the molecular mechanisms of enzyme-catalyzed reactions. Thus, study of bacterial enzymes progresses from physiological and biochemical investigations to a biophysical approach in order to understand how redox-active centers and cofactors work, to efforts to crystallize enzyme proteins in order to obtain structural data by X-ray diffraction methods, and to analysis of the genes encoding catabolic enzymes. Future research should also engage in the investigation of the regulatory mechanisms governing these catabolic pathways. These approaches may enable us to understand catalytic processes on the molecular level, and it may allow insight into the evolution of "enzyme families". From a practical point of view, the detailed investigation of the catalytic cycle and the study of the regulatory mechanisms of synthesis and the activity of an enzyme may help us to evaluate the potential of biocatalysts—either as whole cell systems or as isolated enzymes—for use in biotechnological processes.

We thank the Deutsche Forschungsgemeinschaft and the Fonds der Chemischen Industrie for financial support. We also would like to thank Dr. G. Collin and Dr. H. Höke, formerly Rütgerswerke AG, for their excellent cooperation.

Received: September 30, 1996
Revised version: April 14, 1997 [A 191 IE]
German version: *Angew. Chem.* **1998**, *110*, 596 – 617

[1] D. Warshawsky, *Environ. Carcinog. Ecotoxicol. Rev.* **1992**, *C10*, 1 – 71.
[2] D. L. Vassilaros, P. W. Stoker, G. M. Booth, M. L. Lee, *Anal. Chem.* **1982**, *54*, 106 – 112.
[3] R. C. Barrick, E. T. Furlong, R. Carpenter, *Environ. Sci. Technol.* **1984**, *18*, 846 – 854.
[4] J. Santodonato, P. H. Howard in *Hazard Assessment of Chemicals*, *Vol. 1* (Eds.: J. Saxena, F. Fisher), Academic Press, New York, **1981**, pp. 421 – 439.
[5] W. E. Pereira, C. E. Rostad, J. R. Garbarino, M. F. Hult, *Environ. Toxicol. Chem.* **1983**, *2*, 283 – 294; W. E. Pereira, C. E. Rostad, D. M. Updegraff, J. L. Bennett, *ibid*. **1987**, *6*, 163 – 176; D. H. Stuermer, D. J. Ng, C. J. Morris, *Environ. Sci. Technol.* **1982**, *16*, 582 – 587; J. G. Mueller, P. J. Chapman, P. H. Pritchard, *ibid*. **1989**, *23*, 1197 – 1201; M. G. Ondrus, T. R. Steinheimer, *J. Chromatogr. Sci.* **1990**, *28*, 324 – 330.
[6] K. Hirao, Y. Shinohara, H. Tsuda, S. Fukushima, M. Takahashi, N. Ito, *Cancer Res.* **1976**, *36*, 329 – 335.; E. J. LaVoie, S. Dolan, P. Little, C.-X. Wang, S. Sugie, A. Rivenson, *Food Chem. Toxicol.* **1988**, *26*, 625 – 629.
[7] M. Nagao, T. Yahagi, Y. Seino, T. Sugimura, N. Ito, *Mutat. Res.* **1977**, *42*, 335 – 342.
[8] T. Sugimura, *Mutat. Res.* **1988**, *205*, 33 – 39.
[9] Article in *Naturwiss. Rundsch.* **1971**, *24*, 492; H. E. Kaeser, R. Wüthrich, *Dtsch. Med. Wochenschr.* **1970**, *95*, 1685 – 1688; H.-H. Vogt, *Chem. Labor Betr.* **1979**, *30*, 296 – 297.
[10] M. Sainsbury in *Rodd's Chemistry of Carbon Compounds*, *Vol. IV*, *Part G*, (Ed.: S. Coffey), Elsevier, Amsterdam, **1978**, pp. 171 – 255; M. Sainsbury in *Rodd's Chemistry of Carbon Compounds*, *Suppl. Vol. IV*, *Part G*, (Ed.: M. F. Ansell), Elsevier, Amsterdam, **1987**, pp. 209 – 244.
[11] M. Neuman, A. Esanu, *Drugs Exp. Clin. Res.* **1988**, *14*, 385 – 391.
[12] A. Bryskier, *Int. J. Antimicrob. Agents* **1993**, *2*, 151 – 184.
[13] Y. X. Furet, J. C. Pechère, *Eur. J. Clin. Microbiol. Infect. Dis.* **1991**, *10*, 249 – 254.
[14] G. T. Keusch, *Rev. Infect. Dis.* **1988**, *10*, S199 – S205.
[15] G. Collin, H. Höke in *Ullmann's Encyclopedia of Industrial Chemistry*, *Vol. A22*, VCH, Weinheim, **1993**, pp. 465 – 469.
[16] D. Hutzler, I. Pevny, *Dermatosen* **1988**, *36*, 86 – 90; I. Pevny, D. Hutzler, *ibid*. **1988**, *36*, 91 – 98.
[17] a) J. Liebig, *Justus Liebigs Ann. Chem*. **1853**, *86*, 125; b) A. Butenandt, P. Karlson, W. Zillig, *Hoppe-Seyler's Z. Physiol. Chem.* **1951**, *288*, 125 – 129.
[18] M. Luckner in *Biosynthese der Alkaloide* (Eds.: K. Mothes, H. R. Schütte), VEB Deutscher Verlag der Wissenschaften, Berlin, **1969**, pp. 510 – 550; C. Ritter, M. Luckner, *Eur. J. Biochem.* **1971**, *18*, 391 – 400.
[19] G. Schwarz, F. Lingens in *Biochemistry of Microbial Degradation* (Ed.: C. Ratledge), Kluwer, Dordrecht, **1994**, pp. 459 – 486.
[20] G. Schwarz, E. Senghas, A. Erben, B. Schäfer, F. Lingens, H. Höke, *Syst. Appl. Microbiol.* **1988**, *10*, 185 – 190.
[21] G. Schwarz, R. Bauder, M. Speer, T. O. Rommel, F. Lingens, *Biol. Chem. Hoppe-Seyler* **1989**, *370*, 1183 – 1189.
[22] H.-K. Hund, A. de Beyer, F. Lingens, *Biol. Chem. Hoppe-Seyler* **1990**, *371*, 1005 – 1008.
[23] G. Bott, M. Schmidt, T. O. Rommel, F. Lingens, *Biol. Chem. Hoppe-Seyler* **1990**, *371*, 999 – 1003.
[24] S. Schach, G. Schwarz, S. Fetzner, F. Lingens, *Biol. Chem. Hoppe-Seyler* **1993**, *374*, 175 – 181.
[25] S. Schach, B. Tshisuaka, S. Fetzner, F. Lingens, *Eur. J. Biochem.* **1995**, *232*, 536 – 544.
[26] A. Rüger, G. Schwarz, F. Lingens, *Biol. Chem. Hoppe-Seyler* **1993**, *374*, 479 – 488.
[27] D. J. W. Grant, T. R. Al-Najjar, *Microbios* **1976**, *15*, 177 – 189.
[28] O. P. Shukla, *Biol. Mem.* **1987**, *13*, 115 – 131.
[29] T. R. Al-Najjar, R. J. Grout, D. J. W. Grant, *Microbios Lett.* **1976**, *1*, 157 – 163.
[30] H. Taniuchi, O. Hayaishi, *J. Biol. Chem.* **1963**, *238*, 283 – 293.
[31] S. Dagley, P. A. Johnson, *Biochim. Biophys. Acta* **1963**, *78*, 577 – 587.
[32] O. P. Shukla, *Appl. Environ. Microbiol.* **1986**, *51*, 1332 – 1342; O. P. Shukla, *Microbios* **1989**, *59*, 47 – 63.
[33] B. Rosche, B. Tshisuaka, S. Fetzner, F. Lingens, *J. Biol. Chem.* **1995**, *270*, 17836 – 17842; B. Rosche, S. Fetzner, F. Lingens, W. Nitschke, A. Riedel, *Biochim. Biophys. Acta* **1995**, *1252*, 177 – 179; B. Rosche, B. Tshisuaka, B. Hauer, F. Lingens, S. Fetzner, *J. Bacteriol* **1997**, *179*, 3549 – 3554.
[34] F. S. Sariaslani, *Crit. Rev. Biotechnol.* **1989**, *9*, 171 – 257, and references therein.
[35] A. E. True, A. M. Orville, L. L. Pearce, J. D. Lipscomb, L. Que, Jr., *Biochemistry* **1990**, *29*, 10847 – 10854, and references therein I. Bertini, F. Briganti, S. Mangani, H. F. Nolting, A. Scozzafava, *ibid.* **1994**, *33*, 10777 – 10784, and references therein D. M. Arciero, J. D. Lipscomb, *J. Biol. Chem.* **1986**, *261*, 2170 – 2178, and references therein M. R. Harpel, J. D. Lipscomb, *ibid.* **1990**, *265*, 6301 – 6311, 22187 – 22196; C. Nakai, K. Horiike, S. Kuramitsu, H. Kagamiyama, M. Nozaki, *ibid.* **1990**, *265*, 660 – 665, and references therein S. A.

Wolgel, J. E. Dege, P. E. Perkins-Olson, C. H. Juarez-Garcia, R. L. Crawford, E. Münck, J. D. Lipscomb, *J. Bacteriol.* **1993**, *175*, 4414 – 4426, and references therein.
[36] L. G. Sparrow, P. P. K. Ho, T. K. Sundaram, D. Zach, E. J. Nyns, E. E. Snell, *J. Biol. Chem.* **1969**, *244*, 2590 – 2600.
[37] G. K. Watson, C. Houghton, R. B. Cain, *Biochem. J.* **1974**, *140*, 277 – 292.
[38] E. J. Behrman, R. Y. Stanier, *J. Biol. Chem.* **1957**, *228*, 923 – 945; J. J. Gauthier, S. C. Rittenberg, *ibid.* **1971**, *246*, 3737-3742, 3743 – 3748; C. G. Orpin, M. Knight, W. C. Evans, *Biochem. J.* **1972**, *127*, 819 – 831; R. B. Cain, C. Houghton, K. A. Wright, *ibid.* **1974**, *140*, 293 – 300.
[39] R. Tenhunen, H. S. Marver, R. Schmid, *J. Biol. Chem.* **1969**, *244*, 6388 – 6394; M. D. Maines, *FASEB J.* **1988**, *2*, 2557 – 2568.
[40] T. Oka, F. J. Simpson, *Biochem. Biophys. Res. Commun.* **1971**, *43*, 1 – 5.
[41] H. G. Krishnamurty, F. J. Simpson, *J. Biol. Chem.* **1970**, *245*, 1467 – 1471; T. Oka, F. J. Simpson, J. J. Child, Sister C. Mills, *Can. J. Microbiol.* **1971**, *17*, 111 – 118; T. Oka, F. J. Simpson, H. G. Krishnamurty, *ibid.* **1972**, *18*, 493 – 508.
[42] J. W. Wray, R. H. Abeles, *J. Biol. Chem.* **1993**, *268*, 21466 – 21469.
[43] J. W. Wray, R. H. Abeles, *J. Biol. Chem.* **1995**, *270*, 3147 – 3153.
[44] I. Bauer, A. de Beyer, B. Tshisuaka, S. Fetzner, F. Lingens, *FEMS Microbiol. Lett.* **1994**, *117*, 299 – 304.
[45] I. Bauer, N. Max, S. Fetzner, F. Lingens, *Eur. J. Biochem.* **1996**, *240*, 576 – 583.
[46] G. Speier in *Dioxygen Activation and Homogeneous Catalytic Oxidation* (Ed.: L. I. Simándi), Elsevier, Amsterdam, **1991**, pp. 269 – 278.
[47] A. Nishinaga, T. Tojo, H. Tomita, T. Matsuura, *J. Chem. Soc. Perkin Trans. I* **1979**, 2511 – 2516.
[48] A. Nishinaga, T. Tojo, T. Matsuura, *J. Chem. Soc. Chem. Commun.* **1974**, 896 – 897.
[49] G. A. Russell, *Pure Appl. Chem.* **1967**, *15*, 185 – 206.
[50] A. Nishinaga, T. Shimizu, T. Matsuura, *Chem. Lett.* **1977**, 547 – 550.
[51] a) *Molybdenum Enzymes*, *Cofactors*, *and Model Systems* (Eds.: E. I Stiefel, D. Coucouvanis, W. E. Newton), American Chemical Society, Washington, DC, **1993**; b) B. K. Burgess in ref. [51 a], pp. 144 – 169; c) D. C. Rees, J. Kim, M. M. Georgiadis, H. Komiya, A. J. Chirino, D. Woo, J. Schlessman, M. K. Chan, L. Joshua-Tor, G. Santillan, P. Chakrabarti, B. T. Hsu in ref. [51 a], pp. 170 – 185; d) J. W. Peters, K. Fisher, D. R. Dean, *Annu. Rev. Microbiol.* **1995**, *49*, 335 – 366; e) A. Müller, E. Krahn, *Angew. Chem.* **1995**, *107*, 1172 – 1179; *Angew. Chem. Int. Ed. Engl.* **1995**, *34*, 1071 – 1078.
[52] R. C. Bray, *Q. Rev. Biophys.* **1988**, *21*, 299 – 329.
[53] J. C. Wootton, R. E. Nicolson, J. M. Cock, D. E. Walters, J. F. Burke, W. A. Doyle, R. C. Bray, *Biochim. Biophys. Acta* **1991**, *1057*, 157 – 185.
[54] R. S. Pilato, E. I. Stiefel in *Bioinorganic Catalysis* (Ed.: J. Reedijk), Dekker, New York, **1993**, pp. 131 – 188.
[55] R. Hille in ref. [51 a], pp. 22 – 37; *Biochim. Biophys. Acta* **1994**, *1184*, 143 – 169; R. Hille, T. Nishino, *FASEB J.* **1995**, *9*, 995 – 1003; R. Hille, *Chem. Rev.* **1996**, *96*, 2757 – 2816.
[56] W. Koschara, *Hoppe-Seyler's Z. Physiol. Chem.* **1940**, *263*, 78 – 79.
[57] M. Goto, A. Sakurai, K. Ohta, H. Yamakami, *J. Biochem.* **1969**, *65*, 611 – 620.
[58] J. L. Johnson, K. V. Rajagopalan, *Proc. Natl. Acad. Sci. USA* **1982**, *79*, 6856 – 6860.
[59] K. V. Rajagopalan, J. L. Johnson, *J. Biol. Chem.* **1992**, *267*, 10199 – 10202; K. V. Rajagopalan in ref. [51 a], pp. 38 – 49.
[60] J. L. Johnson, N. R. Bastian, K. V. Rajagopalan, *Proc. Natl. Acad. Sci. USA* **1990**, *87*, 3190 – 3194.
[61] J. L. Johnson, K. V. Rajagopalan, O. Meyer, *Arch. Biochem. Biophys.* **1990**, *283*, 542 – 545.
[62] G. Börner, M. Karrasch, R. K. Thauer, *FEBS Lett.* **1991**, *290*, 31 – 34.
[63] M. K. Chan, S. Mukund, A. Kletzin, M. W. W. Adams, D. C. Rees, *Science* **1995**, *267*, 1463 – 1469.
[64] M. J. Romão, M. Archer, I. Moura, J. J. G. Moura, J. LeGall, R. Engh, M. Schneider, P. Hof, R. Huber, *Science* **1995**, *270*, 1170 – 1176; M. J. Romão, R. Huber *Structure and Bonding* **1998**, *90*, 69 – 95.
[65] H. Schindelin, C. Kisker, J. Hilton, K. V. Rajagopalan, D. C. Rees, *Science* **1996**, *272*, 1615 – 1621; F. Schneider, J. Löwe, R. Huber, H. Schindelin, C. Kisker, J. Knäblein, *J. Mol. Biol.* **1996**, *263*, 53 – 69.
[66] B. D. Howes, R. C. Bray, R. L. Richards, N. A. Turner, B. Bennett, D. J. Lowe, *Biochemistry* **1996**, *35*, 1432 – 1443; R. Huber, P. Hof, R. O. Duarte, J. J. G. Moura, I. Moura, M.-Y. Liu, J. LeGall, R. Hille, M. Archer, M. J. Romão, *Proc. Natl. Acad. Sci. USA* **1996**, *93*, 8846 – 8851.
[67] V. N. Gladyshev, S. V. Khangulov, T. C. Stadtman, *Proc. Natl. Acad. Sci. USA* **1994**, *91*, 232 – 236; V. N. Gladyshev, S. V. Khangulov, T. C. Stadtman, *Biochemistry* **1996**, *35*, 212 – 223.
[68] V. N. Gladyshev, S. V. Khangulov, M. J. Axley, T. C. Stadtman, *Proc. Natl. Acad. Sci. USA* **1994**, *91*, 7708 – 7711.
[69] D. Hettrich, B. Peschke, B. Tshisuaka, F. Lingens, *Biol. Chem. Hoppe-Seyler* **1991**, *372*, 513 – 517.
[70] B. Peschke, F. Lingens, *Biol. Chem. Hoppe-Seyler* **1991**, *372*, 1081 – 1088.
[71] A. de Beyer, F. Lingens, *Biol. Chem. Hoppe-Seyler* **1993**, *374*, 101 – 110.
[72] I. Stephan, B. Tshisuaka, S. Fetzner, F. Lingens, *Eur. J. Biochem.* **1996**, *236*, 155 – 162.
[73] G. Bauer, F. Lingens, *Biol. Chem. Hoppe-Seyler* **1992**, *373*, 699 – 705.
[74] M. Sauter, B. Tshisuaka, S. Fetzner, F. Lingens, *Biol. Chem. Hoppe-Seyler* **1993**, *374*, 1037 – 1046.
[75] M. Lehmann, B. Tshisuaka, S. Fetzner, P. Röger, F. Lingens, *J. Biol. Chem.* **1994**, *269*, 11254 – 11260.
[76] R. Bauder, B. Tshisuaka, F. Lingens, *Biol. Chem. Hoppe-Seyler* **1990**, *371*, 1137 – 1144.
[77] T. A. Krenitzky, S. M. Neil, G. B. Elion, G. H. Hitchings, *Arch. Biochem. Biophys.* **1972**, *150*, 585 – 599.
[78] D. Hettrich, F. Lingens, *Biol. Chem. Hoppe-Seyler* **1991**, *372*, 203 – 211.
[79] B. Tshisuaka, R. Kappl, J. Hüttermann, F. Lingens, *Biochemistry* **1993**, *32*, 12928 – 12934.
[80] P. Röger, A. Erben, F. Lingens, *Biol. Chem. Hoppe-Seyler* **1990**, *371*, 511 – 513; J. Aislabie, S. Rothenburger, R. M. Atlas, *Appl. Environ. Microbiol.* **1989**, *55*, 3247 – 3249; J. Aislabie, N. K. Richards, T. C. Lyttle, *Can. J. Microbiol.* **1994**, *40*, 555 – 560; O. P. Shukla, *Microbios Lett.* **1990**, *45*, 89 – 96.
[81] P. Röger, G. Bär, F. Lingens, *FEMS Microbiol. Lett.* **1995**, *129*, 281 – 286.
[82] S. Fetzner, F. Lingens, *Biol. Chem. Hoppe-Seyler* **1993**, *374*, 363 – 376.
[83] Q. Xiang, D. E. Edmondson, *Biochemistry* **1996**, *35*, 5441 – 5450.
[84] M. Nagel, J. R. Andreesen, *Arch. Microbiol.* **1990**, *154*, 605 – 613.
[85] A. Kretzer, K. Frunzke, J. R. Andreesen, *J. Gen. Microbiol.* **1993**, *139*, 2763 – 2772.
[86] W. Freudenberg, K. König, J. R. Andreesen, *FEMS Microbiol. Lett.* **1988**, *52*, 13 – 18.
[87] B. Bubeck, B. Tshisuaka, S. Fetzner, F. Lingens, *Biochim. Biophys. Acta* **1996**, *1293*, 39 – 44.
[88] M. P. Coughlan in *Molybdenum and Molybdenum-Containing Enzymes* (Ed.: M. P. Coughlan), Pergamon, Oxford, **1980**, pp. 119 – 185.
[89] C. Beedham, *Drug Metab. Rev.* **1985**, *16*, 119 – 156, and references therein.
[90] M. Lehmann, B. Tshisuaka, S. Fetzner, F. Lingens, *J. Biol. Chem.* **1995**, *270*, 14420 – 14429.
[91] G. Palmer, F. Müller, V. Massey in *Flavins and Flavoproteins* (Ed.: H. Kamin), University Park Press, Baltimore, **1971**, pp. 123 – 140.
[92] R. C. Bray in *The Enzymes* (Ed.: P. D. Boyer), Academic Press, New York, **1975**, pp. 300 – 419.
[93] R. C. Bray, N. A. Turner, J. LeGall, B. A. S. Barata, J. J. G. Moura, *Biochem. J.* **1991**, *280*, 817 – 820.
[94] M. Bläse, C. Bruntner, B. Tshisuaka, S. Fetzner, F. Lingens, *J. Biol. Chem.* **1996**, *271*, 23068 – 23079.
[95] S. Grether-Beck, G. L. Igloi, S. Pust, E. Schilz, K. Decker, R. Brandsch, *Mol. Microbiol.* **1994**, *13*, 929 – 936.
[96] D. M. Pearson, C. O'Reilly, J. Colby, G. W. Black, *Biochim. Biophys. Acta* **1994**, *1188*, 432 – 438.
[97] U. Thoenes, O. L. Flores, A. Neves, B. Devreese, J. J. van Beeumen, R. Huber, M. J. Romão, J. LeGall, J. J. G. Moura, C. Rodrigues-Pousada, *Eur. J. Biochem.* **1994**, *220*, 901 – 910.
[98] A. Glatigny, C. Scazzocchio, *J. Biol. Chem.* **1995**, *270*, 3534 – 3550.
[99] R. K. Hughes, B. Bennett, R. C. Bray, *Biochemistry* **1992**, *31*, 3073 – 3083.

[100] R. K. Hughes, W. A. Doyle, A. Chovnick, J. R. S. Whittle, J. F. Burke, R. C. Bray, *Biochem. J.* **1992**, *285*, 507 – 513.
[101] Y. Amaya, K. Yamazaki, M. Sato, K. Noda, T. Nishino, T. Nishino, *J. Biol. Chem.* **1990**, *265*, 14170 – 14175.
[102] D. W. Rice, G. E. Schulz, J. R. Guest, *J. Mol. Biol.* **1984**, *174*, 483 – 496; R. K. Wierenga, P. Terpstra, W. G. J. Hol, *ibid.* **1986**, *187*, 101 – 107; G. Eggink, H. Engel, G. Vriend, P. Terpstra, B. Witholt, *ibid.* **1990**, *212*, 135 – 142; I. Hanukoglu, T. Gutfinger, *Eur. J. Biochem.* **1989**, *180*, 479 – 484; C. C. Correll, M. L. Ludwig, C. M. Bruns, P. A. Karplus, *Protein Sci.* **1993**, *2*, 2112 – 2133.
[103] M. Li Calzi, C. Raviolo, E. Ghibaudi, L. De Gioia, M. Salmona, G. Cazzaniga, M. Kurosaki, M. Terao, E. Garattini, *J. Biol. Chem.* **1995**, *270*, 31037 – 31045; R. M. Wright, G. M. Vaitaitis, C. M. Wilson, T. B. Repine, L. S. Terada, J. E. Repine, *Proc. Natl. Acad. Sci. USA* **1993**, *90*, 10690 – 10694.
[104] J. J. M. Vandewalle, E. De Ruiter, H. Reimlinger, R. A. Lenaers, *Chem. Ber.* **1975**, *108*, 3898 – 3899.
[105] T. Izumi, Y. Nishimoto, K. Kohei, A. Kasahara, *J. Heterocycl. Chem.* **1990**, *27*, 1419 – 1424.
[106] L. E. Fisher, J. M. Muchowski, R. D. Clark, *J. Org. Chem.* **1992**, *57*, 2700 – 2705.
[107] T. Nishi, F. Tabusa, T. Tanaka, T. Shimizu, T. Kanbe, Y. Kimura, K. Nakagawa, *Chem. Pharm. Bull.* **1983**, *31*, 1151 – 1157.
[108] G. Leclerc, G. Marciniak, N. Decker, J. Schwartz, *J. Med. Chem.* **1986**, *29*, 2427 – 2432, 2433 – 2438; N. Decker, M. Grima, J. Velly, G. Marciniak, G. Leclerc, J. Schwartz, *Arzneim. Forsch./Drug Res.* **1987**, *37*, 1108 – 1112.
[109] K. Banno, T. Fujioka, T. Kikuchi, Y. Oshiro, T. Hiyama, K. Nakagawa, *Chem. Pharm. Bull.* **1988**, *36*, 4377 – 4388.
[110] C. Lugnier, M. Bruch, J.-C. Stoclet, M.-P. Strub, M. Marivet, C. G. Wermuth, *Eur. J. Med. Chem.-Chim. Ther.* **1985**, *20*, 121 – 125.
[111] T. Shimizu, H. Mori, E. Tabusa, S. Morita, G. Miyamoto, Y. Yasuda, K. Nakagawa, *Xenobiotica* **1978**, *8*, 349 – 358.
[112] D. Bouzard in *Recent Progress in the Chemical Synthesis of Antibiotics* (Eds.: G. Lukacs, M. Ohno), Springer, Berlin, **1990**, pp. 249 – 283; M. P. Wentland, J. B. Cornett, *Annu. Rep. Med. Chem.* **1985**, *20*, 145 – 154.
[113] I. K. Nazer, *J. Agric. Entomol.* **1986**, *3*, 304 – 309;
[114] C. M. Hall, H. G. Johnson, (Upjohn Co., USA), US 4181724, **1980** [*Chem. Abstr.* **1980**, *92*, 135453 v].
[115] P. K. Chakravarty, E. M. Naylor, A. Chen (Merck and Co., Inc., USA) PCT Int. Appl. WO 9410151, **1994** [*Chem. Abstr.* **1994**, *121*, 83355k].
[116] S. Ito, H. Azuma, N. Funayama, T. Kubota, S. Sekizaki-Ohyama, M. Ishikawa, *Rep. Inst. Med. Dent. Eng. Tokyo Med. Dent. Univ.* **1990**, *24*, 41 – 48.
[117] Asahi Chemical Industry Co., Ltd., Japan, JP 8216445, **1982** [*Chem. Abstr.* **1982**, *97*, 47183e]; H. Sato, S. Horie, N. Sekikawa, H. Ono (Fuji Photo Film Co., Ltd., Japan), JP-A 75-89009, DE 2632656, **1977** [*Chem. Abstr.* **1977**, *86*, 171487u].
[118] T. H. Cronin (Pfizer Inc.), US-A 700309, DE 2206946, **1971** [*Chem. Abstr.* **1972**, *76*, 3889b]; A. M. Farghaly, I. Chaaban, M. A. Khalil, A. A. Bekhit, *Alexandria J. Pharm. Sci.* **1990**, *4*, 52 – 56; A. S. A. Gallardo, ES-B 360677, **1970** [*Chem. Abstr.* **1971**, *74*, 100094e]; D. D. Mukerji, S. R. Nautiyal, C. R. Prasad, *Indian J. Pharm. Sci.* **1978**, *40*, 44 – 47; V. K. Pandey, *Biol. Mem.* **1985**, *11*, 213 – 215.
[119] S. Sinha, M. Srivastava, *Prog. Drug Res.* **1994**, *43*, 143 – 238.
[120] H. Kawashima, H. Sueyoshi (Nippon Steel Corp., Japan)] JP 05304973 [93304973], **1993** [*Chem. Abstr.* **1994**, *120*, 132464 K].
[121] H. G. Kulla, *Chimia* **1991**, *45*, 81 – 85; P. Lehky, H. Kulla, S. Mischler (LONZA), EP-B 0152948, **1985** [*Chem. Abstr.* **1985**, *103*, 159132 m].

Deposition of Data from X-Ray Structure Analyses

In order to make life easier for authors and referees the Cambridge Crystallographic Data Centre (CCDC) and the Fachinformationszentrum Karlsruhe (FIZ) have unified their procedures for the depostion of data from single-crystal X-ray structure analyses.

Prior to submitting a manuscript please deposit the data for your compound(s) **electronically** at the appropriate date base, that is, at the CCDC for organic and organometallic compounds and at the FIZ for inorganic compounds. Both data bases will be pleased to provide help (see our *Notice to Authors* in the first issue of this year). In general, you will receive a depository number from the data base within two working days after electronic deposition; please include this number with the appropriate standard text (see our Notice to Authors) in your manuscript. This will enable the referees to retrieve the structure data quickly and efficiently if they need this information to reach their decision.

This is now the uniform procedure for manuscripts submitted to the journals *Advanced Materials, Angewandte Chemie, Chemistry—A European Journal,* the *European Journal of Inorganic Chemistry,* and the *European Journal of Organic Chemistry.*

"Self-Assembly" in Organolanthanide Chemistry: Formation of Rings and Clusters

Reiner Anwander*

The cyclopentadienyl ligand is ubiquitous in organolanthanide chemistry, and due to its steric bulk, rigidity, and thermal and chemical stability it is often referred to as a stabilizing backbone.[1] Variation of the substitution pattern of the cyclopentadienyl anion directs the solubility, reactivity, and molecular structure of the resulting complexes, and promising precursor compounds for the catalysis[2] and material sciences evolve.[3] The bonding in organometallic compounds of the large and hard rare earth cations is commonly described as predominantly ionic.[4] Consequently, in the absence of bulky ligands the metal centers extend their coordination number by intermolecular ligand bridges. However, such oligomerization reactions are as a rule undesired and afford products which are hard to characterize. Therefore, a steady challenge in preparative organolanthanide chemistry is the synthesis of mononuclear, soluble complexes, as in the case of well-defined precatalyst systems. In this hunt for discrete molecules the "less soluble products" were often not given the necessary attention. Recently, an increasing number of more highly associated rare earth cyclopentadienyl compounds with intriguing structural features have been reported. Their structural motifs range from infinite chains and band structures to isolated rings and clusters.[5] A decisive criterion for the formation of ring and cluster structures is the relative number of cyclopentadienyl ligands per metal center, the "Cp/Ln" ratio (Table 1).

Cp/Ln ≥ 2

The ionic character of cyclopentadienyl derivatives becomes obvious in the structural chemistry of homoleptic complexes $Ln^{II}Cp_2$ and $Ln^{III}Cp_3$. Depending on cation size and substitution pattern of the cyclopentadienyl ligand discrete molecules and oligomeric rings or polymeric chains can be observed.[1] However, biscyclopentadienyl or "lanthanidocene" complexes of type Cp_2LnCl have always attracted increased attention, and derivatives of the latter are meanwhile established in homogeneous catalysis.[2] Heteroligands X (e.g., H^-, Cl^-, NR_2^-, OR^-) and the presence of neutral donor ligands (e.g., THF, OEt_2) markedly influence the structure of the usually formed mononuclear or X-bridged dinuclear complexes "Cp_2LnXL". Cleavage of the donor ligands from thermally stable rare earth cyclopentadienyl derivatives is best achieved by the "toluene method"[6] and often leads to the formation of more highly associated complexes. In the presence of sterically demanding Cp ligands like, for example, pentamethylcyclopentadienyl (Cp*), dinuclear X-bridged complexes are routinely formed.[7] On the other hand, unsubstituted Cp ligands also favor polymeric X-bridged chain and band structures and sometimes even finite ladder motifs.[1]

Thermal cleavage of L or "steric degradation" of the heteroligand X can also result in self-assembly, producing ring systems. In 1985 Bottomley et al. first described the formation

Table 1. Organolanthanide rings and clusters involving cyclopentadienyl ligands.

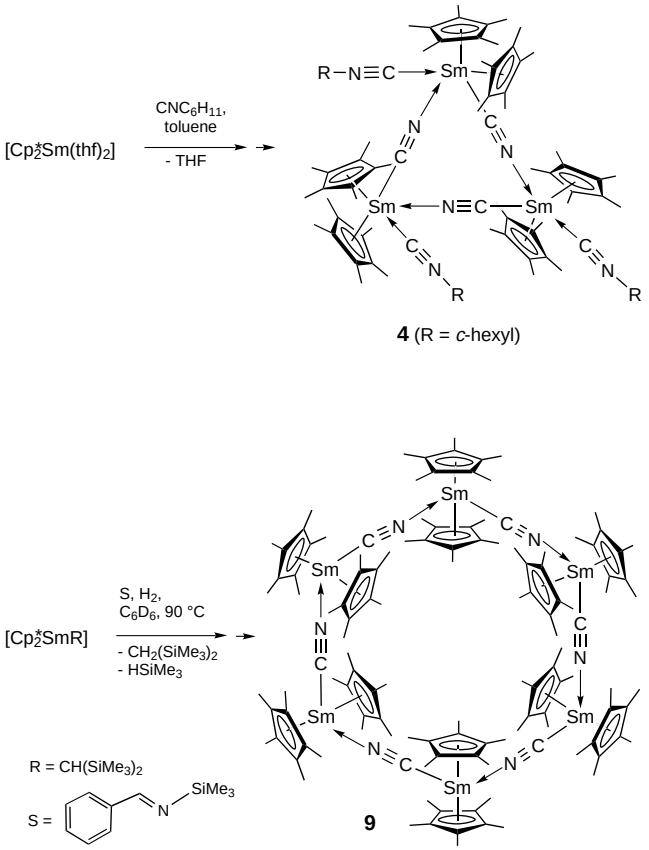
Formula[a]	Cp/Ln (ring atoms)	Ref.
rings		
$[\{(C_5H_5)_2Sc(\mu\text{-}F)\}_3]$ **1**	2 (6)	[8]
$[\{(C_5H_4tBu)_2Sm(\mu\text{-}F)\}_3]$ **2**	2 (6)	[9]
$[\{(C_5Me_5)_2Sm(\mu\text{-}Cl)\}_3]$ **3**	2 (6)	[10]
$[\{(C_5Me_5)_2Sm(CNC_6H_{11})(\mu\text{-}CN)\}_3]$ **4**	2 (9)	[11]
$[\{(C_5H_4Me_2\text{-}1,3)_2Y(\mu\text{-}H)\}_3]$ **5**	2 (6)	[12a]
$[(C_5Me_5)_6Sm_3(\mu\text{-}SiH_3)(\mu_3\text{-}\eta^1,\eta^1,\eta^2\text{-}SiH_2\text{-}SiH_2)]$ **6**	2 (6)	[13]
$[\{(C_5Me_5)_2Sm(\mu\text{-}SiH_3)\}_3]$ **7**	2 (6)	[13]
$[(C_5Me_5)_6Yb(\mu\text{-}F)_4]$ **8**	1.5 (8)	[14]
$[\{(C_5Me_5)_2Sm(\mu\text{-}CN)\}_6]$ **9**	2 (18)	[16]
rings with a central atom		
$[\{(C_5H_5)_2Er\}_3(\mu_3\text{-}H)(\mu\text{-}H)_2(\mu\text{-}Cl)][Li(thf)_4]$ **10**	2 (6)	[12b]
$[\{(C_5H_5)_2Y(\mu\text{-}OCH_3)\}_3(\mu_3\text{-}H)]_2[Li(thf)_3]_2$ **11**	2 (6)	[12c]
$[\{(C_5H_4)_2Lu\}_3(\mu\text{-}H)_2(\mu_3\text{-}H)]$ **12**	2	[15a]
clusters		
$[(C_5H_3tBu_2\text{-}1,3)LuH]_4[AlH_4(OEt_2)]_2[AlH_4]_2$ **13**	1	[15b]
$[(C_5Me_5)_6Yb_5(\mu_4\text{-}F)(\mu_3\text{-}F)_2(\mu\text{-}F)_6]$ **14**	1.2	[17]
$[Nd_6(2,4\text{-}C_7H_{11})_6Cl_{12}(thf)_2]$ **15**[b]	1	[18]
$[(C_5Me_4SiMe_2tBu)_6Yb_6(\mu_3\text{-}I)_8][Li(thf)_4]_2$ **16**	1	[19]
clusters with a central atom		
$[(C_5H_5)_5Yb_5(\mu_5\text{-}O)(\mu_3\text{-}OCH_3)_4(\mu\text{-}OCH_3)_4]$ **17** (Ln = Yb, **17a**; Gd, **17b**)	1	[20]
$[(C_5Me_5)_6Sm_6Se_{11}]$ **18**	1	[21]
$[(C_5H_5)_3Yb_3(\mu_3\text{-}Cl)_2(\mu\text{-}Cl)_3(thf)_3][(C_5H_5)_6Yb_6(\mu_6\text{-}Cl)(\mu\text{-}Cl)_{12}]$ **19**	1	[22]
$[(C_5H_5)_{12}Sm_{12}(\mu_3\text{-}Cl)_{24}]$ **20**	1	[22]

[a] Except for **8** [Yb^{II}/Yb^{III}] and **16** [Yb^{II}] all derivatives contain Ln^{III}.
[b] $(2,4\text{-}C_7H_{11})$ = 2,4-dimethylpentadienyl.

[*] Dr. R. Anwander
Anorganisch-chemisches Institut
Technische Universität München
Lichtenbergstrasse 4, D-85747 Garching (Germany)
Fax: (+49) 89-2891-3473
E-mail: anwander@arthur.anorg.chemie.tu-muenchen.de

 © WILEY-VCH Verlag GmbH, D-69451 Weinheim, 1998 1433-7851/98/03705-0599 $ 17.50+.50/0

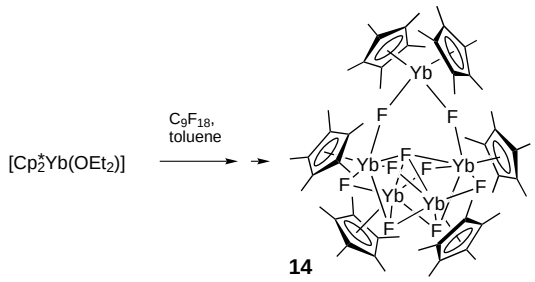
of a ring structure with more than two rare earth atoms and without a central atom for $[Cp_2Sc(\mu\text{-}F)]_3$ (**1**).[8] Later on similar ring arrangements were found for Cp/Ln = 2 (e.g., **2**–**7**, Table 1).[9–13] The 8-ring structure of **8** is a rare exception, displaying a Cp/Ln ratio of 1.5.[14] The presence of small and hard ligands like H^- and F^- seems to encourage ring formation. Additionally, a ring-stabilizing effect is observed by centrally positioned atoms like the (μ_3-H) atoms in complexes **10** and **11**, even accomplishing the exchange of bridging ligands.[12,15] The largest ring system so far was recently isolated in the group of Marks. The 18-membered $[Sm(CN)]_6$ ring in **9** exhibits a S_6-symmetric chair conformation and is formed by a thermal heteroligand degradation according to Scheme 1.[16] In the presence of coordinating isonitrile ligands Evans et al. could isolate a nine-membered $[Sm(CN)]_3$ ring even earlier (**4**, Scheme 1).[11]



Scheme 1. Formation of $[Sm(CN)]_n$ ring structures through ligand degradation.

Cp/Ln < 2

A lower Cp/Ln ratio inevitably creates further coordination sites at the metal center. This favors the formation of oligonuclear metal–ligand cluster compounds, mostly with total absence or at least a clearly substoichiometric amount of denucleating donor ligands (**13**–**20**, Table 1).[15,17–22] A by-product (**14**) isolated by Watson et al. in 1989 according to Scheme 2 turned out to be a "ring–cluster hybrid" with Cp/Ln = 1.2, which nicely underlines this trend.[17] While the

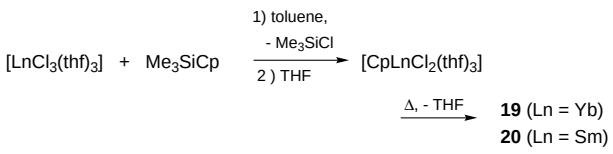


Scheme 2. Formation of Yb^{III} ring-cluster hybrids through fluorination of a Yb^{II} complex (C_9F_8 = perfluoro-2,4-dimethyl-3-ethylpent-2-ene).

"Cp'_2Yb" unit participates in a six-membered ring, the "Cp*Yb" units form a "butterfly cluster".[23]

The class of monocyclopentadienyl systems (Cp/Ln = 1) was neglected for a long time due to its apparent "steric unsaturation".[24] In the meantime however, even for these rare earth derivatives some catalytic activity was detected.[25]

The formation of cluster compounds with Cp/Ln = 1 was first established for oxo-centered, heteroleptic alkoxide clusters (**17**, Ln = Yb, Gd).[20] The recently isolated "Sm_6Se_{11}" cluster **18** confirms the stabilizing effect of centrally positioned heteroatoms in Ln^{III} clusters.[20] These so-called interstitial atoms can often be observed in metal-rich rare earth halides.[26] On the other hand, the outer ligand sphere of the dianionic, highly symmetrical "Yb_6I_8" cluster **16** seems to compensate the lower charge density at the softer Yb^{II} fairly well.[19] A recent publication of Kretschmer, Teuben, and Troyanov finally pushed organolanthanide cluster compounds into the center of interest,[22] abandoning former terms such as "random product" or "result of insufficient handling techniques". Starting with an improved synthesis of complexes $[CpLnCl_2(thf)_x]$[27] where ate complex formation is prevented under mild reaction conditions (Scheme 3), desolvation/



Scheme 3. Improved synthesis of monocyclopentadienyl rare earth complexes.

recrystallization procedures lead to less soluble products, which could be identified by X-ray analysis as highly symmetrical cyclopentadienyl clusters (Figure 1).

The "self-organization" of 12 "$CpSmCl_2$" fragments in **20**, producing a highly symmetrical icosahedral cluster unit with a molecular formula of $Cp_{12}Sm_{12}Cl_{24}$, is so far unique in transition metal chemistry. The electrostatic stabilization of the Sm_{12} icosahedron through a centered Cl_4 tetrahedron inspires a discussion whether even larger anion clusters could be enclosed in even larger metal cation clusters. Surprisingly, under similar crystallization conditions the smaller and more Lewis acidic Yb^{III} forms a cation–anion pair with a reduced degree of aggregation. This behavior is certainly directed by the cation size. However, because of increased affinity of the

 © WILEY-VCH Verlag GmbH, D-69451 Weinheim, 1998 1433-7851/98/03705-0600 $ 17.50+.50/0

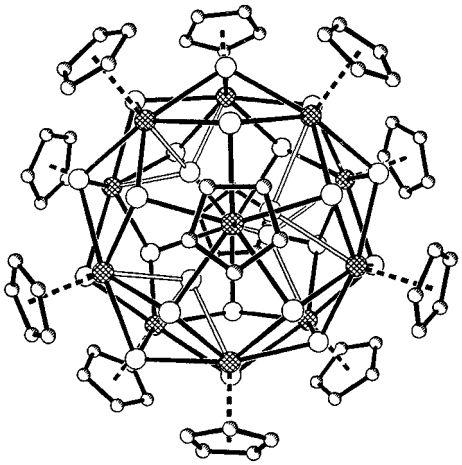


Figure 1. Molecular structure of $[Cp_{12}Sm_{12}Cl_{24}]$ (**20**).

Yb^{III} cation for THF, the desolvation is uncomplete. Therefore, comparison based on size effects remains rather vague. Again, a central μ_6-Cl atom stabilizes the anionic $[Cp_6Yb_6Cl_{13}]^-$ cluster.

"Self-assembly" along with other metalorganic rare earth compounds

While relatively few ring and cluster structures with Cp ligands could be isolated so far, cluster formation has long been an integral part of rare earth alkoxide chemistry.[28] In contrast to the purely academic interest for cyclopentadienyl cluster compounds, studies of alkoxide clusters are of considerable importance for the sol–gel technology (as model for precursor and intermediate compounds).[29] Due to their electronic and steric equivalence to the cyclopentadienyl ligand, alkoxide ligands are often discussed as alternative auxiliary ligands.[30] In homoleptic as well as in heteroleptic alkoxide complexes the presence of "central spherical charge density" like chloride, oxo and hydroxo functionalities often account for the driving force of cluster formation. But also desolvation may play a decisive role.[30] The self-organization to certain cluster sizes like in **21**–**26** seems to be partly influenced by the intra- and intermolecular coordination of additional neutral ligands.[29–33] From a thermodynamic and structural viewpoint a most interesting feature of alkoxide chemistry is the formation of rings. This is demonstrated with the intriguing 20-membered ring structure of decameric **27**[33] and the 8-ring structure of **28**[34] which is stabilized through agostic interactions (Scheme 4).

$[Nd_6(\mu_6\text{-Cl})(\mu_3\text{-O}i\text{Pr})_2(\mu\text{-O}i\text{Pr})_9(O i\text{Pr})_6]$ **21**

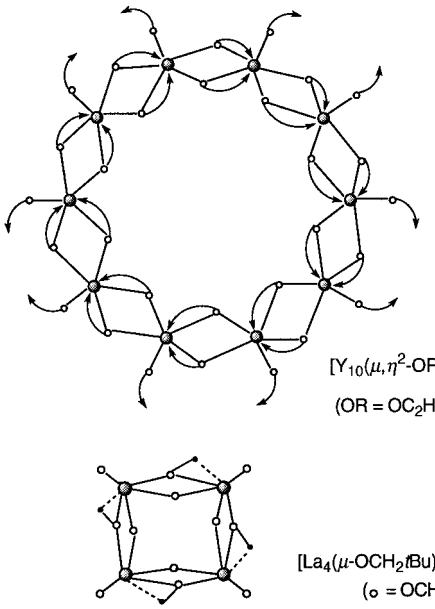
$[Y_5(\mu_5\text{-O})(\mu_3\text{-O}i\text{Pr})_4(\mu\text{-O}i\text{Pr})_4(O i\text{Pr})_5]$ **22**

$[Y_{14}(\mu_4\text{-O})_2(\mu_3\text{-Cl})_2(\mu_3\text{-O}t\text{Bu})_4(\mu\text{-O}t\text{Bu})_{14}(\mu\text{-Cl})_8(O t\text{Bu})_{10}(\text{thf})_4]$ **23**

$[Lu_4(\mu_4\text{-O})(\mu_3\text{-OH})(\mu_3,\eta^2\text{-OR})(\mu,\eta^2\text{-OR})_3(\mu,\eta^1\text{-OR})(\eta^1\text{-OR})_4]$ **24**
$R = CMe_2CH_2OMe$

$[Gd_6(\mu_4\text{-O})(\mu_3,\eta^2\text{-OR})_4(\mu,\eta^2\text{-OR})_6(\mu,\eta^1\text{-OR})_2(\eta^1\text{-OR})_4]$ **25**
$R = C_2H_4OMe$

$[Pr_8(\mu_4\text{-O})_4(\mu_3,\eta^2\text{-OR})_4(\mu,\eta^2\text{-OR})_8(\mu,\eta^1\text{-OR})_2(\eta^1\text{-OR})_2(OPMe_3)_2]$ **26**
$R = C_2H_4OMe$



Scheme 4. Ring formation in rare earth alkoxide chemistry.

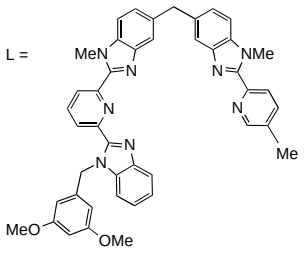
The most recent developments in classic rare earth coordination chemistry concerning "self-organization" also require mention. Large, oligonuclear heterobimetallic clusters of type **29**[35a] and **30** (with a central μ_{12}-ClO_4 anion)[35b] may be useful not only for the synthesis of magnetic nanomaterials. The study of intermetallic, magnetic interactions could also help to unravel the nature of high-temperature superconductivity in the related metal oxides. The self-assembly of heterobimetallic complexes **31** is based on polyfunctionalized podate ligands, whose single ligand segments code for different metal cations.[36] This concept creates fascinating possibilities for the development of programmable, molecular luminescent probes, as well as biological and analytical sensors.

Finally it can be concluded that organolanthanide cluster syntheses (still) cannot yet be planned and are inevitably characterized by random self-organization. Recently, Schnöckel

$[La_8Cu_{12}(\mu\text{-OH})_{24}(NO_3)_{21.2}(Hmhp)_{13}(H_2O)_{5.5}][NO_3]_{2.8}\cdot 2\,Hmhp$ **29**
Hmhp = 6-methyl-2-hydroxypyridine

$[Gd_6Cu_{12}(\mu_{12}\text{-}ClO_4)(\mu_3\text{-OH})_{24}(\mu\text{-pyb})_{12}(H_2O)_{18}][ClO_4]_{17}\cdot n\,H_2O$ **30**
pyb = pyridineacetate

$[LaZnL_3][ClO_4]_5$ **31**



et al. reported an alternative route to metalorganic cluster synthesis: Reaction of Al^I iodide and $Li[N(SiMe_3)_2]$ resulted in the extraordinary cluster **32**.[37] The chemical relationship of

$[Al_{77}\{N(SiMe_3)_2\}_{20}]^{2-}\,2\,[Li(OEt_2)_3(\mu\text{-}I)Li(OEt)_2]^{+}\cdot 2\,C_7H_8$ **32**

rare earth elements and aluminum certainly has to be discussed, and reduced halides are well investigated, especially in rare earth chemistry.[26] Apart from chain, layer, and network structures isolated clusters are also formed, often containing interstitial main group atoms or electron-rich transition metals. Could these cluster associations possibly be transformed to soluble, molecular compounds by allowing them to react with, for example, $Li[N(SiMe_3)_2]$?

German version: *Angew. Chem.* **1998**, *110*, 619 – 622

Keywords: clusters · cyclopentadienyl complexes · lanthanides · multinuclear complexes · ring structures

[1] a) H. Schumann, J. A. Meese-Marktscheffel, L. Esser, *Chem. Rev.* **1995**, *95*, 865 – 986; b) F. T. Edelmann in *Comprehensive Organometallic Chemistry II, Vol. 4* (Eds.: E. W. Abel, F. G. A. Stone, G. Wilkinson), Pergamon, Oxford, **1995**, Chap. 2.

[2] F. T. Edelmann, *Top. Curr. Chem.* **1996**, *179*, 247 – 276.

[3] Y. K. Gun'ko, F. T. Edelmann, *Comm. Inorg. Chem.* **1997**, *19*, 153 – 184.

[4] K. N. Raymond, C. W. Eigenbrot, Jr., *Acc. Chem. Res.* **1980**, *13*, 276 – 283.

[5] Organolanthanide clusters have already been isolated as catalytically active species in diene oligomerization reactions, like $[\{Al_3Nd_6(\mu_3\text{-}Cl)_6(\mu\text{-}Cl)_6(\mu\text{-}Et)_9Et_5(O\mathit{i}Pr)\}_2]$: C. Shan, Y. Lin, J. Ouyang, Y. Fan, G. Yang, *Makromol. Chem.* **1987**, *188*, 629 – 635.

[6] C. J. Burns, R. A. Andersen, *J. Organomet. Chem.* **1987**, *325*, 31 – 37.

[7] W. J. Evans, S. E. Foster, *J. Organomet. Chem.* **1992**, *433*, 79 – 94.

[8] F. Bottomley, D. E. Paez, P. S. White, *J. Organomet. Chem.* **1985**, *291*, 35 – 41.

[9] H. Schumann, M. R. Keitsch, J. Winterfeld, J. Demtschuk, *J. Organomet. Chem.* **1996**, *525*, 279 – 281.

[10] W. J. Evans, D. K. Drummond, J. W. Grate, H. Zhang, J. L. Atwood, *J. Am. Chem. Soc.* **1987**, *109*, 3928 – 3936.

[11] W. J. Evans, D. K. Drummond, *Organometallics* **1988**, *7*, 797 – 802.

[12] a) W. J. Evans, D. K. Drummond, T. P. Hanusa, R. J. Doedens, *Organometallics* **1987**, *6*, 2279 – 2285; b) W. J. Evans, J. H. Meadows, A. L. Wayda, W. E. Hunter, J. L. Atwood, *J. Am. Chem. Soc.* **1982**, *104*, 2015 – 2017; c) W. J. Evans, M. S. Sollberger, S. I. Khan, R. Bau, *J. Am. Chem. Soc.* **1988**, *110*, 439 – 446.

[13] a) S. Ya. Knjazhanskij, B. M. Bulychev, O. K. Kireeva, V. K. Belsky, G. L. Soloveichik, *J. Organomet. Chem.* **1991**, *414*, 11 – 22; b) S. Ya. Knjazhanskij, E. B. Lobkovsky, B. M. Bulychev, V. K. Belsky, G. L. Soloveichik, *ibid.* **1991**, *419*, 311 – 324.

[14] N. S. Radu, F. J. Hollander, T. D. Tilley, A. L. Rheingold, *Chem. Commun.* **1996**, 2459 – 2460.

[15] C. J. Burns, D. J. Berg, R. A. Andersen, *J. Chem. Soc. Chem. Commun.* **1987**, 272 – 273.

[16] Y. Obora, T. Ohta, C. L. Stern, T. J. Marks, *J. Am. Chem. Soc.* **1997**, *119*, 3745 – 3755.

[17] P. L. Watson, T. H. Tulip, I. Williams, *Organometallics* **1990**, *9*, 1999 – 2009.

[18] J. Sieler, A. Simon, K. Peters, R. Taube, M. Geitner, *J. Organomet. Chem.* **1989**, *362*, 297 – 303.

[19] S. P. Constantine, G. M. De Lima, P. B. Hitchcock, J. M. Keates, G. A. Lawless, *Chem. Commun.* **1996**, 2421 – 2422.

[20] a) W. J. Evans, M. S. Sollberger, *J. Am. Chem. Soc.* **1986**, *108*, 6095 – 6096; b) H. Schumann, G. Kociok-Köhn, J. Loebel, *Z. Anorg. Allg. Chem.* **1990**, *581*, 69 – 81.

[21] W. J. Evans, G. W. Rabe, M. A. Ansari, J. W. Ziller, *Angew. Chem.* **1994**, *106*, 2200 – 2201; *Angew. Chem. Int. Ed. Engl.* **1994**, *33*, 2110 – 2111.

[22] W. P. Kretschmer, J. H. Teuben, S. I. Troyanov, *Angew. Chem.* **1998**, *110*, 92 – 94; *Angew. Chem. Int. Ed. Engl.* **1998**, *37*, 88 – 90.

[23] The structural chemistry of oxo-centered cyclopentadienyl clusters additionally emphasizes this trend: a) A. Zalkin, D. J. Berg, *Acta Crystallogr. Sect. C* **1989**, *45*, 1630 – 1631; b) X. Zhou, H. Ma, Z. Wu, X. You, Z. Xu, X. Huang, *J. Organomet. Chem.* **1995**, *503*, 11 – 13.

[24] R. Poli, *Chem. Rev.* **1991**, *91*, 509 – 551.

[25] R. Taube, H. Windisch, *J. Organomet. Chem.* **1994**, *472*, 71 – 77.

[26] Reviews: a) J. D. Corbett, *Pure Appl. Chem.* **1984**, *56*, 1527 – 1543; b) G. Meyer, *Chem. Rev.* **1988**, *88*, 93 – 107; c) A. Simon, H.-J. Mattausch, G. J. Miller, W. Bauhofer, R. K. Kremer in *Handbook on the Physics and Chemistry of Rare Earths, Vol. 15* (Eds.: K. A. Gschneidner, Jr., L. Eyring), Elsevier, **1991**, pp. 191 – 285.

[27] a) S. Manastyrskyj, R. E. Maginn, M. Dubeck, *Inorg. Chem.* **1963**, *2*, 904 – 905; b) C. S. Day, V. W. Day, R. D. Ernst, S. H. Vollmer, *Organometallics* **1982**, *1*, 998 – 1003; c) M. Adam, X.-F. Li, W. Oroschin, R. D. Fischer, *J. Organomet. Chem.* **1985**, *296*, C19 – C22; d) P. N. Hazin, J. C. Huffman, J. W. Bruno, *Organometallics* **1987**, *6*, 23 – 27.

[28] R. C. Mehrotra, A. Singh, *Chem. Soc. Rev.* **1996**, 1 – 13.

[29] L. G. Hubert-Pfalzgraf, *New J. Chem.* **1995**, *19*, 727 – 750.

[30] W. J. Evans, M. S. Sollberger, *Inorg. Chem.* **1988**, *27*, 4417 – 4423.

[31] R. A. Andersen, D. H. Templeton, *Inorg. Chem.* **1978**, *17*, 1962 – 1965.

[32] R. Anwander, F. C. Munck, T. Priermeier, W. Scherer, O. Runte, W. A. Herrmann, *Inorg. Chem.* **1997**, *36*, 3545 – 3552.

[33] O. Poncelet, L. G. Hubert-Pfalzgraf, J.-C. Daran, R. Astier, *J. Chem. Soc. Chem. Commun.* **1989**, 1846 – 1848.

[34] D. M. Barnhart, D. L. Clark, J. C. Gordon, J. C. Huffman, J. G. Watkin, B. D. Zwick, *J. Am. Chem. Soc.* **1993**, *115*, 8461 – 8462.

[35] a) A. J. Blake, R. O. Gould, C. M. Grant, P. E. Y. Milne, S. Parsons, R. E. P. Winpenny, *J. Chem. Soc. Dalton Trans.* **1997**, 485 – 495; b) X.-M. Chen, S. M. J. Aubin, Y.-L. Wu, Y.-S. Yang, T. C. W. Mak, D. N. Hendrickson, *J. Am. Chem. Soc.* **1995**, *117*, 9600 – 9601.

[36] C. Piguet, *Chimia* **1996**, *50*, 144 – 153.

[37] A. Ecker, E. Weckert, H. Schnöckel, *Nature* **1997**, *387*, 379 – 381.

 © WILEY-VCH Verlag GmbH, D-69451 Weinheim, 1998 1433-7851/98/03705-0602 $ 17.50+.50/0

New Developments in Superacid Chemistry: Characterization of $HC{\equiv}O^+$ and $FC{\equiv}O^+$ Cations

Ted S. Sorensen*

Mainly through the efforts of Nobel laureate George Olah and his co-workers over a period of 35 years, a sizeable inventory of small, weakly basic molecules have been protonated by superacids. Some exceedingly simple systems have nevertheless remained problematic, including the single-carbon bases CO and CO_2. However, the year 1997 saw some significant developments in this area, highlighted by a publication describing the NMR and IR spectra of the long-sought $HC{\equiv}O^+$ cation and a paper by the Olah group on $FC{\equiv}O^+$, a missing member in the series of haloformyl cations (and directly related to O-protonated carbon dioxide, $HOC{\equiv}O^+$).

The detailed characterization of acylium ions, RCO^+, by Olah and co-workers in 1963[1] together with a copious literature[2] on Friedel–Crafts acylations long ago settled questions concerning the structure of these electrophiles. However, the direct observation of the simplest member of this family, HCO^+, has been elusive. A major difference between RCO^+ and HCO^+ concerns the acid–base equilibria in which they are involved; HCO^+ is in equilibrium with carbon monoxide [Eq. (a)], whereas a much more basic ketene is the neutral equilibrium partner of RCO^+ salts with an α-H atom in the R group.

$$CO + [H^+] \rightleftharpoons HC{\equiv}O^+ \qquad \text{(a)}$$

There is of course considerable indirect evidence for an HCO^+-like intermediate or transition state, since carbon monoxide in a solution of acid will formylate activated arenes (the well-known Gattermann–Koch reaction).[3] Furthermore, the reactivity of CO with arenes and adamantane in superacids such as SbF_5/HSO_3F (1/1) has been reported[4] along with the suggestion that the acylating species is an activated $HC{\equiv}O^+$ molecule, either diprotonated or protosolvated.[5] With this background in mind, the recent report of the direct in situ observation of $HCO^+_{(s)}$ by de Rege et al.[6] is a most noteworthy event.

The key to success was the use of the strongest known member of the superacid family, HF/SbF_5 (1:1), together with the use of pressurized NMR and IR cells in which a gaseous pressure of carbon monoxide could be maintained in contact with the neat solution-phase acid during the measurements. These experimental conditions are not overly novel (Olah previously reported NMR experiments with pressurized CO), but some courage is involved given the corrosive nature of the superacid and the gaseous pressures. The NMR spectra of ^{13}C-enriched carbon monoxide show signals for three species in addition to those for the excess HF/SbF_5 (which serves as a "solvent"). These were identified as H_3O^+ (a common trace contaminant of HF/SbF_5 mixtures), complexed formyl fluoride ($H(F)C{=}O\cdots SbF_5$), and the elusive $HC{\equiv}O^+$ cation. Formyl fluoride is the F^- adduct of $HC{\equiv}O^+$, and there is an analogy here with protonated formaldehyde, which forms protonated fluoromethanol and other cations in HF/SbF_5.[7, 8]

The ^{13}C NMR signal assigned to $HC{\equiv}O^+$ is a singlet at $\delta = 139.5$ (85 atm), which is in very good agreement with a value of $\delta = 136$ calculated for $HC{\equiv}O^+_{(g)}$ with ab initio methods. The worrysome absence of $^{13}C-{}^1H$ coupling was attributed to a rapid exchange of $HC{\equiv}O^+$ with excess HF/SbF_5; indeed, only one ^1H signal is seen for these hydrogen atoms. However, the authors report an NOE for the ^{13}C signal when this ^1H signal is irradiated, an indication that appreciable amounts of $HC{\equiv}O^+$ are present.

de Rege et al. also reported IR measurements of superacids under external ^{12}CO (and ^{13}CO) pressure. In addition to a relatively sharp signal for the $^{12}C{-}O$ and $^{13}C{-}O$ stretching mode in the complexed formyl fluoride, they observed a very broad absorption at 2110 (^{12}C) and 2060 cm^{-1} (^{13}C). Since no other carbonyl peak was observed, any signal from "free" $CO_{(s)}$ would have to be below the limits of detection. The extreme broadness of the $HC{\equiv}O^+$ carbonyl stretch was attributed to a strong interaction of this cation with either SbF_5 or the counterion (or both).

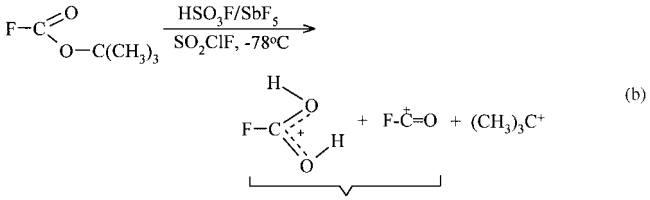
There are two possibilities for the rapid exchange of hydrogen atoms observed in the NMR spectra: either an acid–base exchange involving a small equilibrium concentration of "free" CO or, as previously suggested by Olah,[5, 9] an equilibrium involving a diprotonated $HC{\equiv}O^+H$ cation. However, the results of de Rege et al. show that the basicity of carbon monoxide is near the limit of what the strongest superacid will protonate, since parallel experiments with pressurized CO in HSO_3F/SbF_5 (1/1) or HF/SbF_5 (1/1) in SO_2ClF (both slightly weaker superacid systems) did not produce the ^{13}C NMR signal at $\delta = 139.5$ attributed to $HC{\equiv}O^+$. If the CO protonation by HF/SbF_5 (1/1) were truly "complete", there would have been no need for the NMR experiments under pressure. Given this, the rapid exchange of hydrogen atoms seems more likely to involve an equilibrium with "free" CO.

The combined evidence for the observation of $HC{\equiv}O^+$ is strong but not totally conclusive. The ultimate proof for its existence may be provided by an X-ray structure, which is not an entirely unreasonable expectation given the recent work of Laube[10] and Minkwitz.[11]

[*] Prof. Dr. T. S. Sorensen
Department of Chemistry
University of Calgary
Calgary, Alberta T2N 1N4 (Canada)
Fax: (+1) 403-289-9488
E-mail: sorensen@acs.ucalgary.ca

 © WILEY-VCH Verlag GmbH, D-69451 Weinheim, 1998 1433-7851/98/03705-0603 $ 17.50+.50/0

In another notable publication in the area of superacids, Olah et al.[12] reported the direct observation of the fluoroformyl acylium ion, $F\overset{+}{C}{=}O$, together with direct NMR characterization of protonated fluoroformic acid $FC(OH)_2^+$. The Olah group had previously reported[13] the analogous $Cl\overset{+}{C}{=}O$, $Br\overset{+}{C}{=}O$, and $I\overset{+}{C}{=}O$ cations, but have only now managed to obtain $F\overset{+}{C}{=}O$. The route to $F\overset{+}{C}{=}O$ involved the protolytic cleavage of *tert*-butyl fluoroformate in a SO_2ClF solution of HSO_3F/SbF_5 (1/1) at $-78^\circ C$ [Eq. (b)]. The $F\overset{+}{C}{=}O$



(b)

species was observed as a doublet at $\delta = 117.5$ ($J_{CF} = 322.4$ Hz) in the ^{13}C NMR spectrum, which is in reasonably good agreement with calculated values of $\delta = 131.1$ (IGLO) and 124.5 (GIAO-MP2).

Although $F\overset{+}{C}{=}O$ is superficially related to $H\overset{+}{C}{=}O$, the better analogy is to O-protonated carbon dioxide, $HO\overset{+}{C}{=}O$. Like $H\overset{+}{C}{=}O$, the $HO\overset{+}{C}{=}O$ cation has been detected in outer space, and a number of gas-phase studies of this species have been reported. Olah and Shen[14] reported indirect evidence for superacid protonation of CO_2 (and even diprotonated CO_2 has been suggested as a reactive intermediate[5]), but in the gas phase the proton affinity of CO_2 is 11.0 kcal mol^{-1} *less* than for CO.[15] It is somewhat superficial to compare gas-phase heats of protonation with possible solution-phase behavior, but since CO now appears to be among the weakest bases which can be protonated by the strongest superacid system, the evidence for $HO\overset{+}{C}{=}O_{(s)}$ needs to be more direct (and the recent work with $H\overset{+}{C}{=}O$ offers a good template). Unlike the case of CO, there is little evidence for the electrophilic carboxylation of arenes by CO_2/acid in solution. In this regard the $(Hal)\overset{+}{C}{=}O$ cations can serve as surrogates for aromatic carboxylation, although side reactions are usually a problem. The related $H_3CO\overset{+}{C}{=}O$ cation has also been reported,[16] but methyl chloroformate in superacid appears to be an alkylating rather than acylating agent; nevertheless, the gas-phase acylation of arenes by $H_3CO\overset{+}{C}{=}O$ has been shown.[17]

The protonated fluoroformic acid cogenerated along with $F\overset{+}{C}{=}O$ is a very interesting species in its own right. As in the case of $F\overset{+}{C}{=}O$, fluoroformic acid can be compared most closely with carbonic acid. Both free acids are extremely labile ($HFCO_2$ has not yet been characterized) but form stable mono anions FCO_2^- and $HOCO_2^-$. In earlier elegant work, Olah and White reported the preparation of monoprotonated carbonic acid,[18] and the present paper now extends this observation to protonated fluoroformic acid.

For the future, the development of techniques for generating higher gas pressures for the NMR and IR detection of labile carbocations would be rewarding. Furthermore, the continuing use of direct methods for analyzing structures—for example, single-crystal X-ray or powder methods—is to be encouraged.

German version: *Angew. Chem.* **1998**, *110*, 623 – 624

Keywords: carbocations · carbon monoxide · formyl fluoride · monofluoromethanol · superacidic systems

[1] G. A. Olah, W. S. Tolgyesi, S. J. Kuhn, M. E. Moffatt, I. J. Bastien, E. B. Baker, *J. Am. Chem. Soc.* **1963**, *85*, 1328.
[2] G. A. Olah, *Friedel – Crafts Chemistry*, Wiley, New York, **1973**.
[3] L. Gattermann, J. A. Koch, *Chem. Ber.* **1897**, *30*, 1622.
[4] a) O. Farooq, M. Marcelli, G. K. Surya Prakash, G. A. Olah, *J. Am. Chem. Soc.* **1988**, *110*, 864; b) G. A. Olah, K. Laali, O. Farooq, *J. Org. Chem.* **1985**, *50*, 1483; c) G. A. Olah, F. Pelizza, S. Kobayashi, J. A. Olah, *J. Am. Chem. Soc.* **1976**, *98*, 296; d) M. Tanaka, J. Iyoda, Y. Souma, *J. Org. Chem.* **1992**, *57*, 2677; e) M. Tanaka, M. Fujiwara, H. Ando, *ibid.* **1995**, *60*, 3846.
[5] G. A. Olah, *Angew. Chem.* **1993**, *105*, 805; *Angew. Chem. Int. Ed. Engl.* **1993**, *32*, 767.
[6] P. J. F. de Rege, J. A. Gladysz, I. T. Horváth, *Science* **1997**, *276*, 776.
[7] a) G. A. Olah, D. H. O'Brien, M. Calin, *J. Am. Chem. Soc.* **1967**, *89*, 3582; b) G. A. Olah, G. D. Mateescu, *ibid.* **1971**, *93*, 781; c) G. A. Olah, S. Yu, G. Liang, G. D. Mateescu, M. R. Bruce, D. J. Donovan, M. Arvanaghi, *J. Org. Chem.* **1981**, *46*, 571.
[8] R. Minkwitz, S. Schneider, H. Preut, *Angew. Chem.* **1998**, *110*, 510, *Angew. Chem. Int. Ed.* **1998**, *37*, 494.
[9] a) G. A. Olah, K. Dunne, Y. K. Mo, P. Szilagyi, *J. Am. Chem. Soc.* **1972**, *94*, 4200; b) G. A. Olah, A. Germain, H. C. Lin, D. A. Forsyth, *ibid.* **1975**, *97*, 2928.
[10] T. Laube, *Acc. Chem. Res.* **1995**, *28*, 399.
[11] R. Minkwitz, S. Schneider, M. Seifert, H. Hartl, *Z. Anorg. Allg. Chem.* **1996**, *622*, 1404, and references therein.
[12] G. A. Olah, A. Burrichter, T. Mathew, Y. D. Vankar, G. Rasul, G. K. Surya Prakash, *Angew. Chem.* **1997**, *109*, 1958; *Angew. Chem. Int. Ed. Engl.* **1997**, *36*, 1875.
[13] J. W. Bausch, G. K. Surya Prakash, G. A. Olah, *J. Am. Chem. Soc.* **1991**, *113*, 3205.
[14] G. A. Olah, J. Shen, *J. Am. Chem. Soc.* **1973**, *95*, 3582.
[15] a) S. G. Lias, J. F. Liebman, R. D. Levin, *J. Phys. Chem. Ref. Data* **1984**, *13*, 695; b) J. E. Del Bene, M. J. Frisch, *Int. J. Quantum Chem. Quantum Chem. Symp.* **1989**, *23*, 371.
[16] G. A. Olah, P. Schilling, J. M. Bolinger, J. Nishimura, *J. Am. Chem. Soc.* **1974**, *96*, 2221.
[17] P. Giacomello, F. Pepi, *J. Phys. Chem.* **1993**, *97*, 4421.
[18] G. A. Olah, A. M. White, *J. Am. Chem. Soc.* **1968**, *90*, 1884.

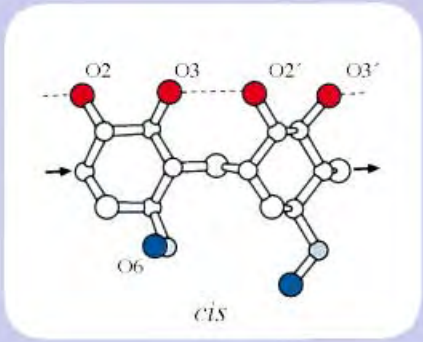
 © WILEY-VCH Verlag GmbH, D-69451 Weinheim, 1998 1433-7851/98/03705-0604 $ 17.50+.50/0

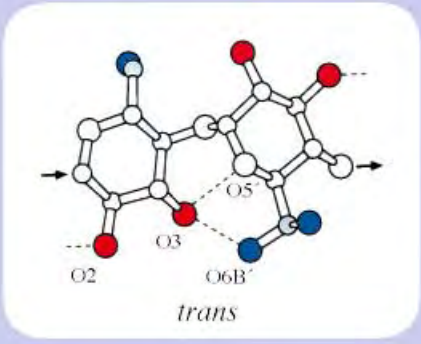
Band Flip as New Structural Motif in Amylose





In the well–known cyclodextrins, all glucose units are *cis*-oriented and connected by O3···O2′ hydrogen bonds forming cyclically closed bands. In larger cyclodextrins (cycloamyloses) with 10 and more glucoses, strain induced in the macrocycle is relieved by two 180° flips to *trans* orientation between diametrically opposed glucose units. These two "band flips" are stabilized by hydrogen bonds (O3···O5′ and O3···O6′), and lead to butterflylike structures. In the figures, cyclodextrins with 7 and 14 glucoses are shown; atoms O2, O3 are red, O6 blue, C6 grey, arrows mark chain direction, and dashed lines indicate hydrogen bonds.









 © WILEY-VCH Verlag GmbH, D-69451 Weinheim, 1998 1433-7851/98/3705-0605 $ 17.50+.50/0

Strain-Induced "Band Flips" in Cyclodecaamylose and Higher Homologues**

Joël Jacob, Katrin Geßler,* Daniel Hoffmann, Haruyo Sanbe, Kyoko Koizumi, Steven M. Smith, Takeshi Takaha, and Wolfram Saenger*

Cycloamyloses (CAs) are cyclic molecules composed of $\alpha(1-4)$-linked glucoses in $^4C_1$ chair conformation. The smallest members, α-, β-, and γ-cyclodextrin (cyclohexa-, cyclohepta-, and cyclooctaamylose; CA6, CA7, and CA8, respectively), are cone-shaped and form inclusion complexes.[1] Because all glucose units are *cis*-oriented, O2 and O3 hydroxyl groups are on the wide side of the cone, and the O6 hydroxyl groups are on the narrow side. This gives rise to a bandlike cyclic structure. The central, hydrophobic cavity is coated with C3–H and C5–H atoms, and glycosidic O4 oxygen atoms. The cone structures are stabilized by intramolecular hydrogen bonds ($O2(n)\cdots O3(n-1)$) between the adjacent *cis* glucose residues. The exocyclic torsion angles (χ^5 O5-C5-C6-O6) are preferentially $-$*gauche*, but if O6 is hydrogen bonded to a guest molecule, this torsion angle may adopt the $+$*gauche* form.

From CA6 to CA8 the size of the annulus increases, with a concomittant decrease of curvature, and the coplanar O4 atoms form regular hexagons, heptagons, or octagons. For CA9 (δ-cyclodextrin), however, the O4 atoms describe an ellipse distorted into the shape of a boat.[2] The hydrogen-bonded O2 and O3 hydroxyl groups are at the wider "hull" side and arranged in a circle as observed for CA6 to CA8, but with small indentations. As indicated by molecular modeling, the distorted boat-shaped structure of CA9 is enforced by steric strain resulting from the size of the larger macrocycle.[3]

Is there a limit where steric strain induces conformational instability if the cyclodextrin macrocycle is further enlarged? Larger CAs became available by preparative scale treatment of amylose with cyclodextringlucanotransferases.[4] ^{13}C NMR spectroscopy on the series from CA6 to CA26[5] showed only one sharp signal for each of the six glucose carbon atoms indicating that glucose residues of the individual molecules are identical on the NMR time scale. Increasing the macrocycle size mainly affects signals of the C1 and C4 atoms, while resonances of the other carbons are only marginally influenced. For CA6 to CA8, C1 and C4 signals occur at $\delta \approx 102.4$ and $\delta \approx 81.8$, respectively; for CA10 and the higher homologues, they shift to $\delta \approx 100.2$ and $\delta \approx 78.3$, suggesting some as yet undefined structural differences. The signals for CA9 are intermediate, C1 at $\delta = 100.9$ and C4 at $\delta = 79.2$. The change in C1 and C4 signals between CA8 to CA10 indicates a clear distinction between two structural types. According to its ^{13}C NMR signals, CA9 could occur in both forms, the observed singlets being indicative of rapid structural changes well below the millisecond time range.

CA10 and CA14 (ε- and ι-cyclodextrin or cyclodeca- and cyclotetradecaamylose) crystallized from aqueous solution as 20.3 and 27.3 hydrates, respectively. X-ray analyses[6] show that both crystals belong to the monoclinic space group *C*2 with half a molecule in the asymmetric unit; the second half is related by crystallographic symmetry. The molecular shapes of CA10 and CA14 are very different than those of the smaller CA6 to CA9 (Figures 1 and 2). This is due to the flipping of

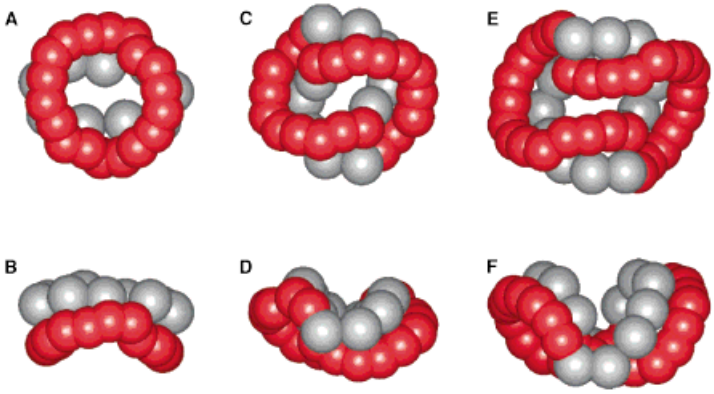


Figure 1. Schematic representation each in top and side views of the molecular structures of CA9 (A and B, respectively), CA10 (C and D, respectively), and CA14 (E and F, respectively). In Figures 1C and 1E the band flips occur where the course of the O2, O3, and C6 atoms is broken. For clarity, only O2, O3 (red), and C6 (grey) atoms are drawn. For numbering of O2, O3 hydroxyl groups, see Figure 4.

about 180° in *trans* orientation of two diametrically opposed glucoses, so that the ring of intramolecular $O2(n)\cdots O3(n-1)$ hydrogen bonds (for atom numbering see ref. [7,8]), which is still present in CA9, is disrupted (Figures 1C,E and 3A,B). As a consequence, the molecules are clearly divided into two halves connected at the flip sites called "band flips", as the typical band structure of amylose is interrupted; the central cavities are no longer open and round as in the smaller homologues but resemble narrow grooves. In a pictorial description, the molecules adopt the shape of a butterfly in which the wings are formed by cyclodextrin-like structures and the conformational band flips are located at the body.

There are significant conformational differences between CA10 and CA14. In CA10 the flipped glucose unit 1 is stabilized in orientation by a three-center hydrogen bond with O3(5′) as donor, namely $O3(5')\cdots O5(1)$ 3.21 Å and $O3(5')\cdots O6(1)B$ 2.74 Å; O6(1)B adopts the less preferred $+$*gauche*

[*] Dr. K. Geßler, Prof. Dr. W. Saenger, Dipl.-Chem. J. Jacob
Institut für Kristallographie der Freien Universität
Takustrasse 6, D-14195 Berlin (Germany)
Fax: (+49) 30-838-6702
E-mail: gessler@chemie.fu-berlin.de
Dr. D. Hoffmann
GMD-SCAI, Schloss Birlinghoven, Sankt Augustin (Germany)
H. Sanbe, Prof. K. Koizumi
School of Pharmaceutical Sciences, Mukogawa Women's University, Hyogo (Japan)
Prof. S. M. Smith
Institute of Cell and Molecular Biology, University of Edinburgh (UK)
Dr. T. Takaha
Biochemical Research Laboratory, Ezaki Glico Co., Ltd., Osaka (Japan)

[**] This work was supported by the Deutsche Forschungsgemeinschaft (SA 196/26-1), the Fonds der Chemischen Industrie, the Bundesministerium für Bildung und Forschung, the EU (ERB-CHRX-CT94-0469), and the High Performance Computing Center (HLRZ) at GMD-SCAI. We thank Prof. Takaji Fujiwara for coordinates of cyclononaamylose, Irene Brüdgam and Dr. Matthias Schneider for help with data collection, and Prof. K. Yamaki and her staff at Mukogawa Women's University for measuring the ^{13}C NMR spectra.

 © WILEY-VCH Verlag GmbH, D-69451 Weinheim, 1998 1433-7851/98/3705-0606 $ 17.50+.50/0

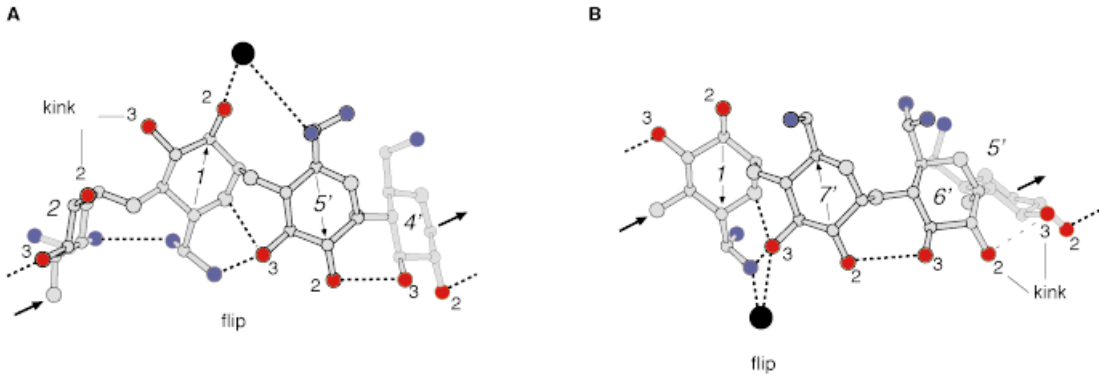


Figure 4. Structural details of kink and bond-flip sites in CA10 (A) and CA14 (B) viewed from the center of the molecules. Water oxygen atoms are represented in pink; O2, O3 are numbered and red, O6 are blue. The kink in CA10 (A) is stabilized by an unusual hydrogen bond between O6 hydroxyl groups (O6(1)A $\cdots$ O6(2)B 3.06 Å). The O2(2) $\cdots$ O3(1) distance at this kink site is too long (3.94 Å) to be a hydrogen bond, whereas in CA14, the O2(6′) $\cdots$ O3(5′) distance of 3.40 Å is indicative of a long, weak hydrogen bond. The orientations of the glucose units at the flip sites are marked by arrows, and thick arrows at O4 and C1 atoms at both ends of the flip sites delineate the course of the CA chain. Drawn with the program MOLSCRIPT.[19]

causes a herringbone-type arrangement. Consequently, the crystal structures of CA10 and CA14 combine the two packing motifs already identified in inclusion complexes of the smaller cyclodextrins.[12]

The CHARMM force field was used to minimize the energy of the X-ray structures (with calculated H positions)[13] of CA6 to CA10 and CA14. The solvation energy was calculated using the Poisson-Boltzmann program SOLVATE.[14] The sum of force field and solvation energies per glucose unit is similar for all molecules and ranges from -7.42 kcal mol^{-1} (CA6) to -7.94 kcal mol^{-1} (CA10). The individual energy terms in that sum vary significantly, especially for CA10 and CA14; the Coulombic energy per glucose unit is 2 kcal mol^{-1} higher in CA10 than in CA9, this difference being balanced by the more relaxed torsion angle energies and the better solvation of CA10 and CA14.

All very large CAs may exhibit comparable structures, because in CA14 the band-flip site forms short O2(n) $\cdots$ O3($n-1$) hydrogen bonds to preceding and following *cis* glucose residues. Additional glucose residues in larger CAs may be added at the flip sites to form strings of O2(n) $\cdots$ O3($n-1$) hydrogen-bonded glucose residues in *cis* orientation as in cyclodextrins, and the kink may vary (and even disappear), depending on residual strain energy. The two antiparallel strings may approach each other and associate across the center of the molecule through hydrogen bonds between O2 and O3 hydroxyl groups (see caption of Figure 3B). Since the strings will be twisted as a result of their O2(n) $\cdots$ O3($n-1$) hydrogen bonding, we anticipate that they will form a left-handed antiparallel double helix (Figure 2E) as observed in the crystal structure of (p-nitrophenyl-α-maltohexaoside)$_2 \cdot$ Ba(I$_3$)$_2 \cdot$ 27 H$_2$O.[15]

A recent preliminary note[16] reports the structure of CA10 crystallized from a 1:1 mixture of water and acetonitrile. The crystals are identical to ours and did not form a complex with the organic solvent. This suggests that the inclusion properties of CA10 are different to the cyclodextrins CA6 to CA8, which accommodate acetonitrile.[17] In CA10 and the higher homologues the cavities are so distorted into narrow grooves that probably only guest molecules with geometries that exactly fit these grooves can form inclusion complexes. This could open avenues for very specific host–guest interactions with the larger CA molecules.

The situation could be different with CAs large enough to form an antiparallel double helix (Figure 2E) containing a central, channel-like cavity that may accommodate guest molecules.[15a] This view is supported by the observation[18] that CA50 and larger amyloses show properties similar to linear amylose. They form precipitates from aqueous solutions if higher alcohols or long fatty acids are added and produce blue or brown complexes with iodine (the color depends on size).

Received: August 28, 1997 [Z10867IE]
German version: *Angew. Chem.* **1998**, *110*, 625–629

Keywords: conformation analysis · cyclodextrins · structure elucidation

[1] J. Szejtli, *Cyclodextrin Technology*, Kluwer, Dordrecht, **1988**; W. Saenger, *Angew. Chem.* **1980**, *92*, 343–361; *Angew. Chem. Int. Ed. Engl.* **1980**, *19*, 344–362; in *Inclusion Compounds*, *Vol. 2* (Eds.: J. L. Atwood, J. E. D. Davies, D. D. MacNicol), Academic Press, London, **1984**, pp. 231–260; K. Harata in *Inclusion Compounds*, *Vol. 5* (Eds.: J. L. Atwood, J. E. D. Davies, D. D. MacNicol), Academic Press, London, **1991**, pp. 311–344.

[2] T. Fujiwara, N. Tanaka, S. Kobayashi, *Chem. Lett.* **1990,** 739–742.

[3] D. Hoffmann, unpublished results.

[4] a) T. Takaha, M. Yanase, H. Takata, S. Okada, S. M. Smith, *J. Biol. Chem.* **1996**, *271*, 2902–2908; b) Y. Terada, M. Yanase, H. Takata, T. Takaha, S. Okada, *ibid.* **1997**, *272*, 15729–15733.

[5] CA mixtures, produced by cyclodextringlycosyltransferase acting on synthetic amylose,[4b] were purified by HPLC and characterized by time-of-flight (TOF) MS. ^{13}C NMR spectra (125.65 MHz) of the CAs were recorded at 2–3 % (w/v) in D$_2$O at 50°C on a JOEL GSX-500 spectrometer.

[6] X-ray data of CA10[7] measured at 20°C with a CAD4 diffractometer on an FR571 rotating anode X-ray generator (Enraf-Nonius) with Ni-filtered Cu$_{K\alpha}$ radiation. Monoclinic, space group $C2$, $a = 29.242(5)$, $b = 9.981(1)$, $c = 19.319(2)$ Å, $\beta = 120.97(2)°$, $V = 4834.7$ Å^3 with half a molecule in the asymmetric unit, composition $(C_6H_{11}O_5)_{10} \cdot 20.7\,H_2O$, $\rho_{calcd} = 1.380$ g cm^{-3}, 3158 unique reflections. Structure determined by direct methods (SIR92) and full-matrix least-squares refinement (SHELXL76). Crystallographic R factor 9.31 % for 2760 data with $F \geq 3\sigma_F$. O6 hydroxyl groups of glucose residues 1–3 and 5 doubly disordered; 17 water positions, some partially (0.3–1.0) occupied.

 © WILEY-VCH Verlag GmbH, D-69451 Weinheim, 1998 1433-7851/98/3705-0608 $ 17.50+.50/0

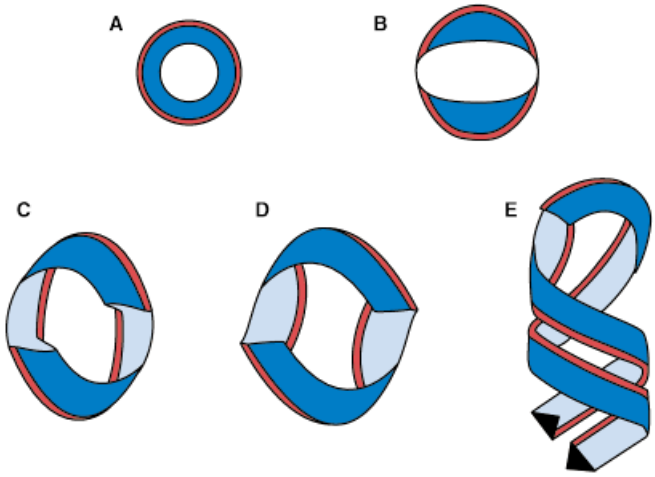


Figure 2. Illustration of folding schemes, thick red and thin black lines connect O2 to O3 and O6 atoms, respectively. Shown are annular, unstrained CA7 (A) and strained CA9 (B), and elliptically distorted CA10 (C), CA14 (D) and the proposed antiparallel left-handed, double helical form (only half a molecule) for larger cycloamyloses (E). The band flips in CA10, CA14 and larger CA occur where the red lines are broken.

form (Figure 4A). Between glucose residues 1 and 2, a kink increases the O2(2)···O3(1) distance to 3.94 Å, so this hydrogen bond is broken, but an unusual hydrogen bond between the O6 hydroxyl groups of these glucose units (O6(1)A···O6(2)B 3.08 Å) is formed and contributes to the stabilization of the kink (Figure 4A). The remaining glucose residues (2 to 5) are in cyclodextrin-like arrangement with interglucose O2(n)···O3($n-1$) hydrogen bonding distances in the range 2.89 to 3.03 Å.

In CA14, the flipped glucose 1 is held in orientation by the three-center hydrogen bonds O3(7′)···O6(1)B (3.05 Å) and O3(7′)···O5(1) (3.32 Å) reminiscent of the geometry around the flip site in CA10 (Figure 4B), with O6(1)B in the less preferred +*gauche* orientation. There is also a kink which, in contrast to CA10, does not directly follow the band-flip site but occurs between glucose residues 5′ and 6′, and is stabilized by a long (weak) O2(6′)···O3(5′) hydrogen bond of 3.40 Å. All other O2(n)···O3($n-1$) hydrogen bonds are in the common range (2.75–2.89 Å).

The band flip is best described by torsion angles ϕ and ψ commonly used to define oligosaccharide conformation.[9] They are in the normal range for the O2(n)···O3($n-1$) hydrogen-bonded glucose residues in the two halves ($\phi = 94$–110°, $\psi = 97^\circ$–135°). However, for the flipped glucose residues these torsion angles are $\phi = 84^\circ$ and $\psi = -65^\circ$ between residues 5′ and 1 in CA10 and $\phi = 82^\circ$, $\psi = -69^\circ$ between residues 7′ and 1 in CA14. In spite of these structural peculiarities, all glucose residues in CA10 and CA14 are in $^4C_1$ conformation and unstrained as indicated by Cremer and Pople[10] puckering parameters (not shown), and by the angles O4(n)···O4($n-1$)···O4($n-2$) subtended by O4 atoms (127–146° for CA10 and 132–145° for CA14).

The crystal packing of the butterflylike molecules CA10 and CA14 is very similar and of the channel type frequently observed for the smaller ring-shaped cyclodextrins and the related, chemically modified (cyclo(1–4)-α-D-rhamnopyranosyl-(1–4)-α-L-rhamnopyranoso)decasaccharide.[11] The CA10 and CA14 molecules are stacked head-to-tail along the crystallographic twofold rotation axes (parallel to the *b* axis), which have comparable lengths (9.981 Å for CA10 and 10.138 Å for CA14), implying that the differences in molecular size are accounted for by differences in the dimensions of the *a* and *c* axes. In contrast to the common channel structures, however, the cavities of CA10 and CA14 are so narrow that no continuous channel filled by guest molecules can form. The intermolecular contacts between the stacks are reminiscent of those observed in cage-type cyclodextrin packing motifs, and the butterflylike shape of the CA10 and CA14 molecules

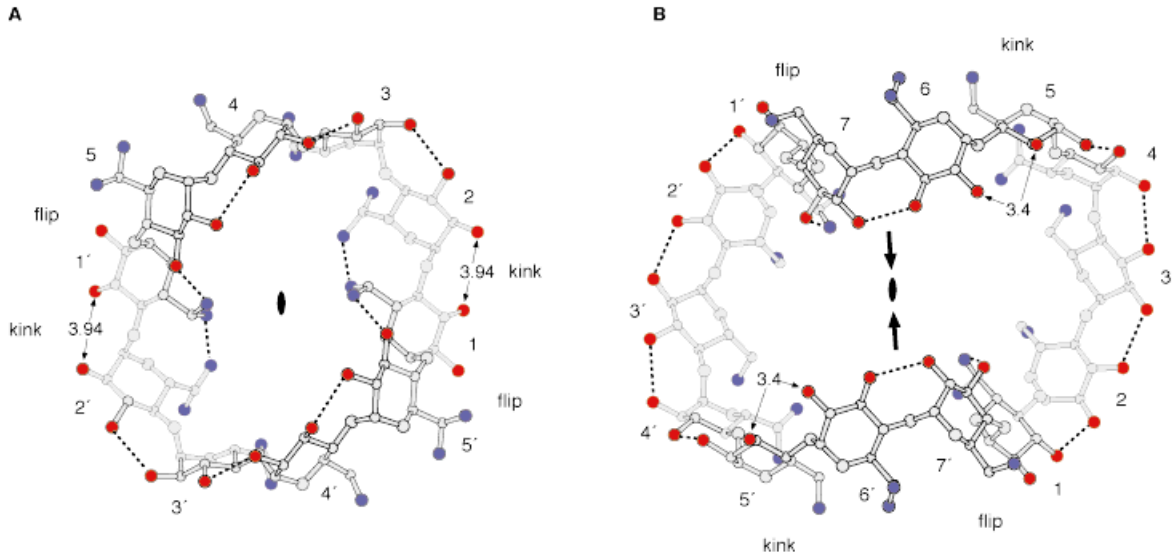


Figure 3. Molecular structures of CA10 (A) and CA14 (B). For clarity water molecules are omitted. Crystallographic twofold rotation axes are marked (⧫), glucose residues in the two asymmetric units are denoted with primed and unprimed numbers. O2 and O3 are red, O6 blue. O6 oxygen atoms of glucoses 1–3 and 5 in CA10 and 1, 4, 6 in CA14 are doubly disordered. Dotted lines suggest possible hydrogen bonds with smaller O···O distances than 3.5 Å. In CA14 the arrows in bold in the center indicate how glucose residues might approach each other in larger cycloamyloses to form antiparallel double helical structures with hydrogen bonds between O2 and O3 hydroxyl groups (see also Figure 2E). Drawn with the program MOLSCRIPT.[19]

 © WILEY-VCH Verlag GmbH, D-69451 Weinheim, 1998 1433-7851/98/3705-0607 $ 17.50+.50/0

Crystal structure analysis of CA14[7] as reported for CA10. Monoclinic, space group $C2$, $a = 36.750(9)$, $b = 10.138(2)$, $c = 21.236(4)$ Å, $\beta = 116.18(2)^\circ$, $V = 7093.5$ Å^3 with half a molecule in the asymmetric unit, composition $(C_6H_{11}O_5)_{14} \cdot 27.3\,H_2O$, $\rho_{calcd} = 1.301$ g cm^{-3}, 4633 unique X-ray reflections. Crystallographic R factor 9.71 % for 3478 data with $F \geq 3\sigma_F$. O6 hydroxyl groups of glucose residues 1, 4, and 6 doubly disordered; 24 water positions, some partially (0.3 – 1.0) occupied. A. Altomare, G. Cascarano, C. Giacovazzo, A. Guagliardi, M. C. Burla, G. Polidori, M. Camalli, *J. Appl. Cryst.* **1994**, *27*, 435; G. M. Sheldrick, SHELXL76 *Program for Crystal Structure Determination*, University of Cambridge, UK, **1976**.

[7] Crystallographic data (excluding structure factors) for the structures reported in this paper have been deposited with the Cambridge Crystallographic Data Centre as supplementary publication no. CCDC-100 656. Copies of the data can be obtained free of charge on application to CCDC, 12 Union Road, Cambridge CB2 1EZ, UK (fax: (+44) 1223-336-033; e-mail: deposit@ccdc.cam.ac.uk).

[8] Atom numbering: O2(4) means oxygen atom O2 in glucose residue 4; units with primed labels belong to the second half of the molecule. Disordered O6(n)A is in the preferred $-$*gauche* and O6(n)B in the less common $+$*gauche* orientation.

[9] Definition of ϕ and ψ torsion angles: O5(n)-C1(n)-O4($n-1$)-C4($n-1$) and C1(n)-O4($n-1$)-C4($n-1$)-C3($n-1$); see IUPAC rules: *Eur. J. Biochem.* **1983**, *131*, 5 – 7.

[10] C. Cremer, J. A. Pople, *J. Am. Chem. Soc.* **1975**, *97*, 1354 – 1358.

[11] G. Gattuso, S. Menzer, S. A. Nepogodiev, J. F. Stoddart, D. J. Williams, *Angew. Chem.* **1997**, *109*, 1615 – 1617; *Angew. Chem. Int. Ed. Engl.* **1997**, *36*, 1451 – 1454.

[12] W. Saenger, *Isr. J. Chem.* **1985**, *25*, 43 – 50.

[13] Convergence after 5000 energy minimization steps (Newton – Raphson, no cutoff, dielectric constant of 1.0); B. R. Brooks, R. E. Bruccoleri, B. D. Olafson, D. J. States, S. Swaminathan, M. Karplus, *J. Comp. Chem.* **1983**, *4*, 187 – 217.

[14] SOLVATE program with two cubic grids (focusing) of side length 81×1.0 Å and 101×0.3 Å. Atomic charges and radii as provided by the CHARMM22 force field. Dielectric constants inside and outside the atoms of the CA molecules were set to 1.0 and 78.3, respectively: D. Bashford, Program SOLVATE, The Scripps Research Institute, La Jolla, CA 92037 (USA), private communication.

[15] a) W. Hinrichs, G. Büttner, M. Steifa, C. Betzel, V. Zabel, B. Pfannemüller, W. Saenger, *Science* **1987**, *238*, 205 – 208; b) W. Hinrichs, W. Saenger, *J. Am. Chem. Soc.* **1990**, *112*, 2789 – 2796; c) W. Schulz, H. Sklenar, W. Hinrichs, W. Saenger, *Biopolymers* **1993**, *33*, 363 – 375.

[16] H. Ueda, T. Endo, H. Nagase, S. Kobayashi, T. Nagai, *J. Inclusion Phenom. Mol. Recognit. Chem.* **1996**, *25*, 17 – 20.

[17] T. Aree, J. Jacob, W. Saenger, H. Hoier, *Carbohyd. Res.*, in press.

[18] T. Takaha, unpublished results.

[19] P. J. Kraulis, *J. Appl. Crystallogr.* **1991**, *24*, 946 – 950.

Combinatorial Approach to the Hydrothermal Synthesis of Zeolites

Duncan E. Akporiaye,* Ivar M. Dahl, Arne Karlsson,* and Rune Wendelbo*

Recent automated combinatorial chemical methods have been developed for systematic production and evaluation of materials in the fields of organic[1] and inorganic[2] chemistry. Until now, however, there have not been any reports of methods capable of dealing with the special conditions used in the synthesis of zeolites, such as temperatures above the normal boiling point of the reaction mixture and under elevated pressures. To address this problem we have developed an autoclave[3] capable of carrying out at least 100 crystallizations under hydrothermal conditions at temperatures up to 200 °C (Figure 1). The simplest most inexpensive design consists of a Teflon block in which 100 reaction chambers are formed by cylindrical holes, having properly designed profiles to accommodate Teflon-coated septa, which seal the chambers when they are "sandwiched" in between two steel plates.

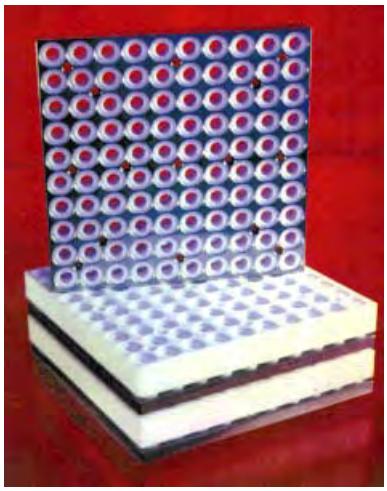


Figure 1. View of the multiautoclave showing the mode of stacking of the Teflon blocks and one of the alternative designs using Teflon inserts.

An important advantage of the system design, which highlights its versatility, is the capability of stacking identical synthesis blocks, allowing an expansion in the third dimension and the parallel synthesis of the order of 1000 combinations in one experiment. The autoclave fits into the compartment of commercial pipette robots for convenient formulation of the synthesis gels. After crystallization, the contents of the autoclave can be washed in situ before further processing. Procedures for a fully automated powder X-ray diffraction analysis of the arrays of materials that are obtained are in progress. To

[*] Dr. D. E. Akporiaye, Dr. A. Karlsson, Dr. R. Wendelbo, I. M. Dahl
Sintef Applied Chemistry
P. O. BOX 124, Blindern, N-0314 Oslo (Norway)
Fax: (+47) 2206-7350
E-mail: Duncan.Akporiaye@chem.sintef.no
Arne.Karlsson@chem.sintef.no
Rune.Wendelbo@chem.sintef.no

 © WILEY-VCH Verlag GmbH, D-69451 Weinheim, 1998 1433-7851/98/3705-0609 $ 17.50+.50/0

illustrate the functioning and potential of the autoclave, two different types of experiments were carried out.

The first experiment involved the detailed evaluation of the ternary phase system Na_2O-Al_2O_3-SiO_2-H_2O, perhaps the most intensively studied of all zeolite syntheses and known to produce several different zeolite structures when the compositional and environmental factors (temperature, time, water content, oxide sources, etc.) are varied. The phase diagram displayed in Figure 2a is reproduced from the very early work

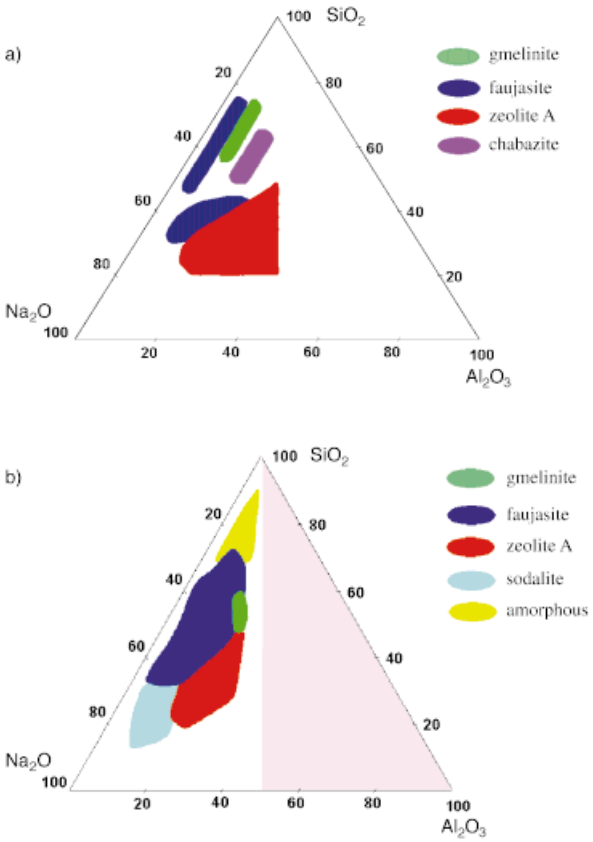


Figure 2. Ternary phase diagram of the Na_2O-Al_2O_3-SiO_2-H_2O system. a) As compiled by Breck from a range of individual syntheses and b) by using the multiautoclave. The light red region is inaccessible due to solubility constraints.

of Breck[4] conducted at temperatures around 100 °C by using colloidal silica and water contents in the range of 90–98 mol %. We have reinvestigated the whole phase diagram in a single experiment under truly identical conditions using the multiautoclave to cover all relevant compositional space. The array of synthesis mixtures were obtained by combining appropriate amounts of three solutions containing the sources of alumina, silica, and soda, respectively. Coordinates in the ternary phase diagram were regularly distributed, giving a total volume of each sample gel of no more than 0.5 mL.

The new results are presented in Figure 2b. As expected the crystalline phases zeolite A, faujasite, and gmelinite were obtained in discrete regions, with some batches containing more than one phase in the boundary regions. The results obtained are only partly in agreement with those of Breck, probably because only the bulk chemical composition of the reaction mixtures were reproduced. Nevertheless, the region for crystallization of zeolite A coincides almost perfectly, and we obtained faujasites in the regions where Breck reported zeolites X and Y. Interestingly, we also obtained faujasite in the regions where Breck reported chabazite and gmelinite, and finally, sodalite was obtained in a rather extended region in the sodium-rich end, which is partly blank in Breck's diagram. While the water content varied to some extent among the syntheses reported by Breck, in the present experiment the water content has been fixed rigorously with respect to the total system. Subsequently, the phase diagram can be extended in the third dimension by varying the water content to produce stability fields that would appear as solid volumes within a quaternary phase diagram.

As a next step in increasing the complexity, the Na_2O-Al_2O_3-SiO_2 system was modified by introducing additional cations. Thus, the goal of the second experiment was to make use of the multiautoclave to screen the effect of binary, ternary, and quaternary cation combinations by using tetramethylammonium hydroxide (TMAOH),[5] Li ions, and Cs ions,[6] in addition to Na ions.

We chose a strategy in which three-quarters of the synthesis capacity was dedicated to the screening of the two ternary combinations Li_2O-TMA_2O-Na_2O-Al_2O_3-SiO_2 and Cs_2O-TMA_2O-Na_2O-Al_2O_3-SiO_2, the remaining quarter covering an experimental mixture-design involving all four cations. In effect, these experiments span a quaternary phase diagram in the range of molar ratios between 0 and 1.0 for Na_2O and 0 and 0.9 for Li_2O, Cs_2O, and TMA_2O.

Under these conditions, the major phase is analcime (ANA) whenever Cs is present in the gels (Figure 3). In the

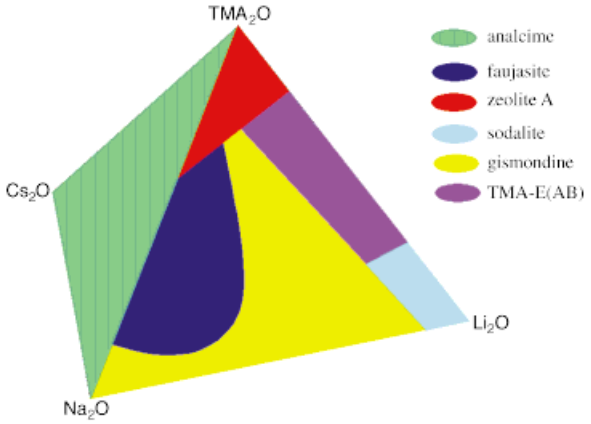


Figure 3. Quaternary phase diagram of the four oxides TMA_2O, Cs_2O, Li_2O (molar ratios 0–0.9), and Na_2O (molar ratios 0–1.0) in the system R_2O-Na_2O-Al_2O_3-SiO_2-H_2O, in which R_2O is the sum of the oxides of the four univalent cations.

absence of Cs, five different zeolites were formed, all of which have been obtained previously by using various combinations of the cations. The screening of the TMA_2O-Li_2O-Cs_2O-Na_2O-Al_2O_3-SiO_2 system maps the zeolite phases and approximate stability regions that may be expected under the synthesis conditions specified below and would serve as a starting point for more detailed studies in a manner similar to that of the first example. These results demonstrate a potential improvement in efficiency of two orders of magnitude achievable by applying combinatorial strategies. In our

 © WILEY-VCH Verlag GmbH, D-69451 Weinheim, 1998 1433-7851/98/3705-0610 $ 17.50+.50/0

opinion, these strategies will play a significant role in the development of catalysts and absorbents through the use of highly specialized and dedicated multifunctional units for sample preparation and identification/characterization, and through operation with a minimum of manual intervention.

Experimental Section

Routine X-ray diffraction analysis was carried out on small sample quantities (1–10 mg) with steps of 0.05° (2θ) and counting times of 0.5 s. For selected diffractograms, the quality was enhanced greatly by using maximum likelihood noise filtration strategies.

Mixing procedures: For the Na_2O-Al_2O_3-SiO_2 system, the composition of the reaction mixtures was defined according to relation (1) (molar ratios) in which $a/(a+x+y+z)=0.95$.

$$x\,Na_2O{:}y\,Al_2O_3{:}z\,SiO_2{:}a\,[H_2O] \quad (1)$$

For the TMA_2O-Cs_2O-Li_2O-Na_2O-Al_2O_3-SiO_2-H_2O system, the composition of the reaction mixtures were defined according to relation (2) in which $0 \le r, s, t \le 12.15$; $1.45 \le x \le 13.6$; $r+s+t+x=13.6$; $a/(a+r+s+t+x+y+z)=0.93$; $z/y=17.3$; $0 \le r/x \le 8.8$.

$$r\,TMA_2O{:}s\,Cs_2O{:}t\,Li_2O{:}x\,Na_2O{:}y\,Al_2O_3{:}z\,SiO_2{:}a\,[H_2O] \quad (2)$$

The mixtures were prepared by using the following sequence of aqueous solutions 1) NaOH; 2) LiOH; 3) CsOH; 4) TMAOH; 5) Ludox LS 30 % silica sol; 6) $NaAlO_2$ + NaOH. The water contents were corrected for by adding distilled water, giving a total volume of 0.5 mL. The sequence of mixing was elaborated in separate experiments before it was applied to all 100 syntheses. Homogenization of the mixtures was performed in a number of ways; for the prototype presented here, we chose to stir the autoclave contents consecutively, after the addition of all reagents, by using a simple stirring device. The gel mixtures were aged for 24 h at room temperature and the autoclave subsequently placed in an oven for one and six days at 100 °C, for the above-mentioned mixtures, respectively. Washing and isolation of the products was done in situ in the autoclave block by removing both top and bottom seals (Figure 1), and the products were flushed onto a single plate/sheet of adsorbent material with water. Once the products were thoroughly washed, they were transferred to sample holders ready for X-ray analysis and dried at room temperature.

Received: June 20, 1997 [Z 10580 IE]
German version: *Angew. Chem.* **1998**, *110*, 629–631

Keywords: combinatorial chemistry · heterogeneous catalysis · hydrothermal synthesis · solid-state chemistry · zeolites

[1] *Acc. Chem. Res.* **1996**, 29, 112–170 (Special issue, Eds.: A. W. Czarnik, J. A. Ellmann).
[2] X. D. Xiang, X. Sun, G. Briceño, Y. Lou, K. A. Wang, H. Chang, W. G. Wallace-Freedman, S. W. Chen, P. G. Schultz, *Science* **1995**, 268, 1738–1740.
[3] D. E. Akporiaye, I. M. Dahl, A. Karlsson, R. Wendelbo, Norwegian patent application number 97.0788.
[4] D. W. Breck, *Structure, Chemistry and Use of Zeolite Molecular Sieves*, Wiley, New York, **1974**.
[5] P. D. Hopkins, *ACS Symp. Ser.* **1989,** 398, 153–160.
[6] C. Colella, M. de Gennaro, *ACS Symp. Ser.* **1989**, 398, 196–208.

$[Mo_{12}S_{12}O_{12}(OH)_{12}(H_2O)_6]$: A Cyclic Molecular Cluster Based on the $[Mo_2S_2O_2]^{2+}$ Building Block

Emmanuel Cadot, Bernadette Salignac, Sabine Halut, and Francis Sécheresse*

Dedicated to Professor Achim Müller on the occasion of his 60th birthday

Polyoxoanions of tungsten, molybdenum, and vanadium have been the subject of interest since their wide variety of compositions, structures, and properties gave rise to numerous important applications.[1] Polyoxometalates are regarded as models for MO_3 oxide surfaces, and they are very strong acids and active oxidation catalysts. For example, the superacid $H_3[PW_{12}O_{40}]$ promotes esterification reactions and activates C_6 alkanes,[2] while salts of $[PMo_{12}O_{40}]^{3-}$ catalyze the mild oxidation of isobutyric acid to methacrylic acid.[3]

Conversely, alumina-supported molybdenum and tungsten sulfides are hydrogenation catalysts with applications in the hydrodesulfuration of crude oil and the activation of dihydrogen.[4] If these compounds are regarded as functional analogues of the active surface of MoS_2, then binary compounds with discrete M–S units could serve as models for studying the reactivity of the corresponding solids.[5] However, thiometalates are far less common than oxometalates.[6] In addition to their remarkable structural diversity, polyoxometalates can contain a large number of metal centers. In contrast, only low-nuclearity thiometalates have been obtained so far by sulfurization of oxo precursors.[7] Therefore, the synthesis of high-nuclearity sulfur-containing species by combining polyoxometalate and thiometalate chemistry represents a stimulating challenge.

The first method for introducing sulfur into a Keggin-type polyoxoanion was illustrated by the synthesis of α-$[PW_{11}NbSO_{39}]^{4-}$, by selective substitution of the terminal oxygen atom of an Nb=O group by a sulfur atom, and its subsequent characterization.[8] The second technique was the stereospecific addition of an $[Mo_2S_2O_2]^{2+}$ fragment to the cavity-containing polyanion γ-$[SiW_{10}O_{36}]^{8-}$.[9] These strategies are convenient for preparing thio complexes that are derived from well-defined structural types, but are unsuitable for the synthesis of new structures or frameworks with higher sulfur contents.

Here we present a new method for increasing the sulfur content; it is based on the one-step self-condensation of sulfur-containing building blocks. The $[Mo_2S_2O_2]^{2+}$ unit was first prepared by selective oxidation of the terminal S_2 ligands of $[(S_2)MoO(\mu_2\text{-}S)_2MoO(S_2)]^{2-}$ with iodine.[10, 11] The self-condensation reaction was performed by controlled addition of potassium hydroxide to an aqueous solution of the building

[*] Prof. F. Sécheresse, Dr. E. Cadot, B. Salignac
Institut Lavoisier, UMR C 173 du CNRS
Université de Versailles Saint-Quentin
45 avenue des Etats-Unis, 78035 Versailles (France)
Fax: (+33) 1-39254381
E-mail: secheres@chimie.uvsq.fr
[**] Dr. S. Halut
Université Pierre et Marie Curie, Paris (France)

 © WILEY-VCH Verlag GmbH, D-69451 Weinheim, 1998 1433-7851/98/3705-0611 $ 17.50+.50/0

block. The title compound was isolated as pale orange crystals and fully characterized by X-ray structure analysis.[12] The IR spectrum exhibited intense bands at 969 and 535 cm^{-1}, attributed to ν(Mo=O) and ν(Mo-OH-Mo) vibrations, respectively, and less intense absorptions at 493 (ν(Mo-S-Mo)), 413, and 346 cm^{-1}.

The formula of the cluster is $[Mo_{12}S_{12}O_{12}(OH)_{12}(H_2O)_6]$. A noteworthy feature of the structure is the cyclic arrangement of the neutral Mo_{12} cluster, which creates a central cavity (Figure 1, top). Six $\{Mo_2O_2S_2\}$ units are connected to each other by hydroxo double bridges; the coordination spheres of the Mo centers are completed by a terminal oxygen atom and a water molecule that is coordinated to two neighboring molybdenum atoms. Two types of Mo – Mo bonds are present in the cluster: short Mo – Mo distances within the building blocks (2.798(1) – 2.814(1) Å), and long Mo – Mo distances between the building blocks (3.289(1) – 3.317(1) Å). The short Mo – Mo distances in the $\{Mo_2O_2S_2\}$ units are similar to those in related polychalcogenide compounds and in the precursor, suggesting that the original single $Mo^V - Mo^V$ single bond is retained during the self-condensation process. The title compound can be described as a ring of alternately edge- and face-sharing octahedra (Figure 1, bottom). An S – S edge links the two octahedra of the same building block, and the building blocks are linked through common faces consisting of two OH ligands and one water molecule. The overall cyclic architecture constructed from the $\{Mo_2O_2S_2\}$ building blocks has a cavity of about 11 Å in diameter filled with six water molecules, each of which is bound to two adjacent metal centers.

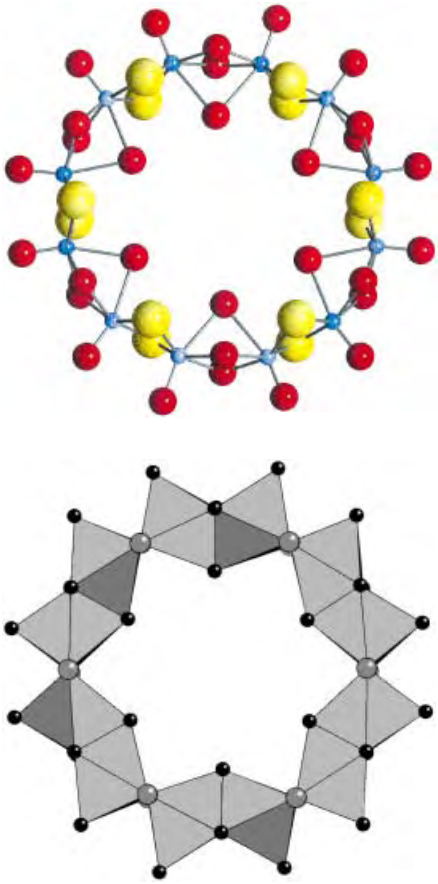


Figure 1. Views of the Mo_{12} cluster. Top: ball-and-stick model showing the Mo_{12} ring with the inner cavity (blue: Mo, red: O, yellow: S). Bottom: polyhedral representation showing the connectivity of the building blocks. Oxygen (black) and sulfur atoms (grey) are emphasized.

A noteworthy chemical property of this cluster is the reversibility of the self-condensation reaction. Acidification of the title compound results in the starting material $[Mo_2O_2S_2]^{2+}$, which can be recondensed by addition of hydroxide.

Experimental Section

Iodine (9 g, 35.4 mmol) and KI (16 g, 96.3 mmol) were dissolved in hydrochloric acid (70 mL, 1 M). $(NMe_4)_2[Mo_2O_2S_6]$[13] (10 g, 17.7 mmol) was suspended in an aqueous solution of KI (60 mL, 0.7 M), and the iodine solution was slowly added to the suspension with vigorous stirring. The resulting solution was heated to 50 °C for 10 min. The insoluble material formed (mainly solid sulfur and tetramethylammonium iodide) was removed by filtration. The red filtrate was cooled to 0 °C to complete the precipitation of the remaining tetramethylammonium iodide, and after filtration an aqueous solution of potassium hydroxide (4 M) was slowly added until the pH stabilized at about 1.5. A yellow microcrystalline solid precipitated. After cooling to 0 °C, the solid was collected by filtration, washed with cold ethanol, and dried with ether (yield 6 g). Pale orange crystals were obtained by dissolving 0.2 g of the yellow microcrystalline powder in 20 mL of distilled water and allowing the solution to stand for several hours at room temperature.

Crystal data for $H_{64}O_{50}S_{12}Mo_{12}$: $M_r = 2400.46$, monoclinic, $P2_1/c$, $a = 17.972(5)$, $b = 19.835(4)$, $c = 19.461(6)$ Å, $\beta = 99.9(2)^\circ$, $V = 6842(3)$ Å^3, $Z = 4$, $T = 20$ °C, $\rho_{calcd} = 2.33$ g cm^{-3}, $Mo_{K\alpha}$ radiation ($\lambda = 0.71069$ Å), $\mu = 25.1$ cm^{-1}. Data were collected on a Nonius CAD4 diffractometer. The structure was solved by direct methods and refined on F_o^2 by full-matrix least-squares methods with the program Crystals. All non-hydrogen atoms were refined anisotropically. $R_1 = 0.064$ and $wR_2 = 0.074$ for 8745 unique reflections with $I > 3\sigma(I)$ and 669 parameters. The figures were prepared with the program CrystalMaker (Interactive Crystallography for the Apple Macintosh, CrystalMaker Software, Lynxvale Ltd, 20 Trumpington Street, Cambridge, CB2 1QA, England). Further details of the crystal structure investigation may be obtained from the Fachinformationszentrum Karlsruhe, D-76344 Eggenstein-Leopoldshafen, Germany (fax: (+49) 7247-808-666 (Frau S. Höhler-Schlimm); e-mail: crysdata@fiz-karlsruhe.de), on quoting the depository number CSD-407925.

Received: August 4, 1997 [Z 10776 IE]
German version: *Angew. Chem.* **1998**, *110*, 631 – 633

Keywords: clusters · polyoxometalates · molybdenum · thiometalates

[1] *Polyoxometalates: From Platonic Solids to Anti-Retroviral Activity* (Eds: M. T. Pope, A. Müller), Kluwer, Dordrecht, **1994**.
[2] Y. Yzumi, K. Urabe, *Chem. Lett.* **1981**, 663.
[3] M. Misono, *Catal. Rev.-Sci. Eng.* **1987**, *29*, 269.
[4] O. Weisser, S. Landa, *Sulfide Catalysts, Their Properties and Applications*, Pergamon, New York, **1973**; M. Rakowski DuBois, *Chem. Rev.* **1989**, *89*, 1.
[5] W. Eltzner, M. Breysse, M. Lacroix, M. Vrinat, *Polyhedron* **1986**, *5*, 203.
[6] M. T. Pope, A. Müller, *Angew. Chem.* **1991**, *103*, 56; *Angew. Chem. Int. Ed. Engl.* **1991**, *30*, 422.
[7] A. Müller, E. Diemann, *Adv. Inorg. Chem. Radiochem.* **1987**, *31*, 89.
[8] a) E. Cadot, V. Béreau, F. Sécheresse, *Inorg. Chim. Acta* **1995**, *29*, 39; b) E. Radkov, Y. J. Lu, R. H. Beer, *Inorg. Chem.* **1996**, *35*, 552.
[9] E. Cadot, V. Béreau, B. Marg, S. Halut, F. Sécheresse, *Inorg. Chem.* **1996**, *25*, 3099.
[10] K. F. Miller, A. E. Bruce, J. L. Corbin, E. I. Stiefel, *J. Amer. Chem. Soc.* **1980**, *102*, 5102.
[11] D. Coucouvanis, A. Toupadakis, A. Hadjikriacou, *Inorg. Chem.* **1988**, *27*, 3273.
[12] T. Shibahara, *Coord. Chem. Rev.* **1992**, *123*, 73.
[13] A. Müller, E. Krickemeyer, U. Reinsch, *Z. Anorg. Allg. Chem.* **1980**, *470*, 35.

 © WILEY-VCH Verlag GmbH, D-69451 Weinheim, 1998 1433-7851/98/3705-0612 $ 17.50+.50/0

Mesoporous Silica from Lyotropic Liquid Crystal Polymer Templates

Christine G. Göltner,* Susanne Henke, Markus C. Weissenberger, and Markus Antonietti

Mesoporous nanostructures are regularly structured solids with pore sizes between 20 and 500 Å and a narrow pore size distribution. They are a welcome supplement to classical zeolites, the application of which was previously restricted because of their limited highest pore diameter of 13 Å.[1,2] Mesoporous ceramic oxides have large specific surface areas and are potential candidates for chemical and physical processes, such as chromatography and catalysis.[3–5] Since the discovery of M41S in 1992,[6] many research groups have focused their interests on mesoporous materials.[7] M41S is formed by a surfactant-assisted reaction pathway as a result of the attractive electrostatic interaction between a ceramic precursor and an ionic amphiphile (sometimes counterion-mediated), upon which a surfactant-rich gel phase precipitates from solution.[8-11] The structure of M41S-type materials depends sensitively on the preparation conditions, as a delicate balance between charge density and volume has to be maintained. Since M41S is obtained as a fine, porous precipitate from a heterogeneous reaction mixture, these nanostructured ceramic oxides have extraordinarily large specific surface areas.[12]

An alternative approach to mesoporous molecular sieves is the exploitation of nonionic surfactants (primary amines) at low concentration,[13] which affords similar materials to M41S. Mesoporous ceramic oxides obtained in the presence of oligoethylene oxide surfactants[14] are less regular than M41S (as determined by X-ray diffraction, which usually reveals just one diffraction peak), but still exhibit high specific surface areas and narrow pore size distributions. Pinnavaia et al. attributed the templating effect to the presence of wormlike surfactant micelles.[14,15] Their results clearly show that there is a displacement mechanism caused by nonionic micellar aggregates.

An alternative route towards ordered mesoporous ceramic nanostructures is the utilization of lyotropic liquid crystal phases as structure-directing media.[16,17] Here, the sol–gel synthesis of the inorganic nanostructure takes place in the ordered environment of a bulk surfactant mesophase: the polycondensation of a water-soluble monomer (e.g., silicic acid) is confined within the aqueous domains of a microphase-separated medium, which acts as a template for the nanostructure. The bulk liquid crystal approach has many advantages over previous routes towards inorganic nanostructures. The resulting ceramic oxide is a direct cast of the liquid crystalline phase, which indicates a high degree of control over the structure. Further, mesoporous ceramic oxides prepared in liquid crystalline phases can be obtained as monoliths (large, crack-free objects, which usually are not macroscopically aligned), because the product is generated by solidifying a homogeneous bulk liquid crystal as opposed to being precipitated from a heterogeneous mixture in the case of M41S. (A certain particle size, if required, can always be achieved after synthesis by grinding and subsequent sifting, and a large particle size of heterogeneous catalysts also facilitates catalyst recovery.)

Using the lyotropic phases of classical nonionic surfactants (low molecular weight amphiphiles) as templates typically affords particles sizes from 300 mm to several millimeters. This big particle size of silica has the effect that the surface area is to a large extent determined by the internal nanostructure and not by the particle surface, an important aspect with respect to size-exclusion processes.[12]

In this paper we describe the preparation of mesoporous silica from lyotropic liquid crystalline polymer templates. Amphiphilic block copolymers (ABCs), like low molecular weight surfactants, can form micelles when mixed with water or other suitable solvents.[18] Accordingly, more complex aggregate structures, namely, lyotropic liquid crystalline phases, are formed at higher polymer concentrations.

ABC templates are expected to show a number of advantages. Firstly, the compatibility of a polymeric amphiphile can be chemically adjusted to the desired product by established procedures of polymer chemistry. Thus, a significant extension of the chemical toolbox for the preparation of mesoporous materials is provided. Secondly, the higher molecular weight slows down exchange and structural relaxation kinetics of the aggregation structures, which makes these lyotropic liquid crystals kinetically less sensitive to phase changes. At the same time, a larger size of the templating lyotropic aggregate is achieved, which directly determines the pore diameter as well as the wall thickness of the mesoporous materials. In addition, such templates should facilitate the preparation and handling of large monoliths, because the resulting hybrid materials are expected to show an improved elasticity and ductility.

In our experiments we employed amphiphilic block copolymers consisting of an apolar polystyrene block (S) and a polar polyethylene oxide block (E) of equal molecular weight (the SE tensides) as polymer templates.[19] The average molecular weight was 1000 g mol^{-1} per block for SE 10/10 and 3000 g mol^{-1} per block for SE 30/30. The polyethylenoxide block's distribution was narrow, whereas the polystyrene block exhibited the Schulz–Flory distribution as a result of a radical polymerization mechanism.

The lyotropic phases of the polymeric SE surfactants investigated are extraordinarily stable. SE 10/10 is characterized by birefringent fluid phases between 45 and 80 % (w/w) above 45°C, although the diffuse textures do not allow any

[*] Dr. C. G. Göltner, Dipl.-Chem. S. Henke, Dipl.-Chem. M. C. Weissenberger, Prof. Dr. M. Antonietti
Max-Planck-Institut für Kolloid- und Grenzflächenchemie
Kantstrasse 55, D-14513 Teltow-Seehof (Germany)
Fax: (+49) 3328-46204
E-mail: goeltner@mpikg-teltow.mpg.de

[**] The authors would like to thank C. Burger and M. A. Micha for the X-ray diffractograms as well as many helpful discussions, S. Funari and G. Rapp for access to the EMBL beam line, P. Klobes and A. Zimathies (Bundesanstalt für Materialforschung und -prüfung, Berlin) for the adsorption isotherms, S. Gross for the density determinations, and B. Klein for invaluable assistance with the preparations. The company Th. Goldschmidt AG is gratefully acknowledged for supplying the amphiphilic block copolymers and the Max-Planck-Gesellschaft for financial support.

 © WILEY-VCH Verlag GmbH, D-69451 Weinheim, 1998 1433-7851/98/3705-0613 $ 17.50+.50/0

phase assignment into the classical scheme of liquid crystal phase structures. SE 30/30, as expected, is less soluble in water than its smaller analogue, and it has a higher melting point and Krafft temperature. However, like SE 10/10, it forms a broad mesophase between 45 and 65 % (w/w). The liquid crystalline phases of both block copolymers are thermally very stable, as no clearing point was observed up to 100 °C. Mesoporous silica was prepared in the same way as reported previously.[16,20] In the following the polymer-templated silica will be referred to as SE 10/10-silica and SE 30/30-silica, depending on the template in which it was generated.

As expected, the use of lyotropic polymer templates for the synthesis of nanostructured ceramic oxides has the advantage that macroscopic, transparent monoliths are obtainable, which, once the template is removed, could be suitable for separation processes. The crack-free monoliths can be obtained in considerable size (Figure 1) from the lyoptropic phase of SE 10/10 and are stable in a closed vessel. Exposure to dry air causes cracks to appear in the monolith; future studies will reveal which method of drying can avoid this problem.

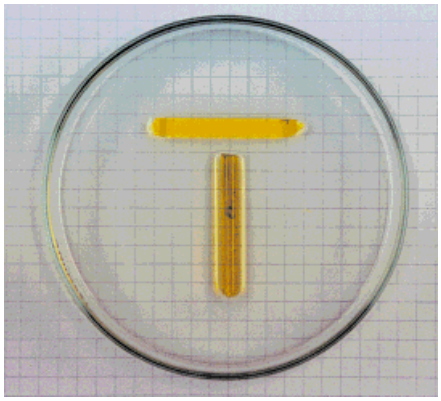


Figure 1. Silica monoliths (dyed with methyl orange for better visibility) templated with SE 10/10. The background lines are 5 mm apart.

After calcination the mesoporous silicas obtained from liquid crystalline polymer templates exhibit specific surface areas of about 500 $m^2 g^{-1}$, as found by nitrogen BET measurements.[22] From the type II adsorption–desorption isotherm (Figure 2), a narrow pore size distribution around 3 nm can be calculated (see the Horvath–Kawazoe plot in Figure 2). Thermogravimetric analysis (TGA) revealed an average content of organic matter of 53 % (w/w), which can be completely removed by either calcination or solvent extraction. Transmission electron microscopy (TEM) pictures of the ultramicrotomed, calcined materials shows the regular, porous structure of the polymer-templated silicas (Figure 3).

Quantitative evaluation of the TEM data reveals a larger pore diameter for SE 10/10-silica than that calculated from the desorption branch of the adsorption iotherm, but it confirms the narrow pore size distribution. This deviation can be explained by the "ink bottle" shape of the pores, which gives rise to the type II isotherm with its pronounced hysteresis.[21] The evaluation of the sorption data according to Barret, Joyner, and Halenda (BJH) gave an average pore radius of

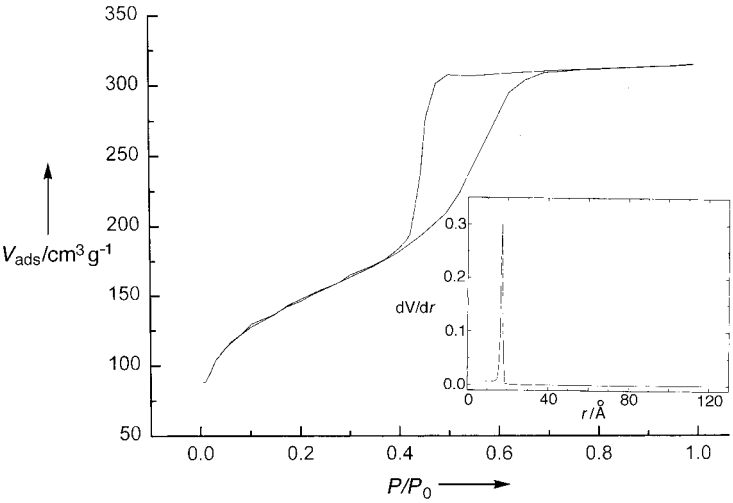


Figure 2. Nitrogen BET adsorption isotherm of SE 10/10-silica. Inset: Horwath–Kawazoe plot, depicting the pore size distribution. P is the equilibrium pressure of the adsorbate, P_0 the saturation pressure of the adsorbate at the temperature of the adsorbent; dV/dr is the derivative of the nitrogen volume adsorbed with respect to the pore diameter r of the adsorbent.

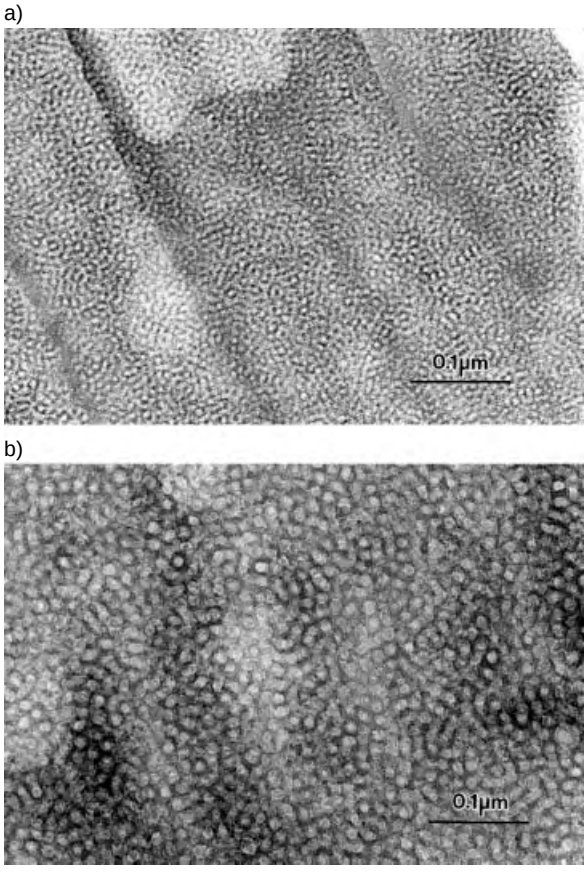


Figure 3. TEM micrographs of calcined silicas: a) SE 10/10 silica, b) SE 30/30 silica. Both samples were embedded in epoxy resin and ultramicrotomed.

4 nm as calculated from the adsorption branch of the isotherm, and 3 nm calculated from the desorption branch. The interpretation of the sorption data with respect to pore diameter should therefore be regarded with caution.

 © WILEY-VCH Verlag GmbH, D-69451 Weinheim, 1998 1433-7851/98/3705-0614 $ 17.50+.50/0

The TEM pictures clearly demonstrate that both polymeric templates produce equally structured, highly porous materials. With knowledge about the stoichiometry and the absence of macroscopic volume shrinkage during gelation (as proven by the monolith production), we can calculate a porosity of about 80 vol% which is very high for a material with three-dimensional form stability.

The structure of these silicas has nothing in common with any simple lyotropic phase structure. The TEM pictures can be compared with those reported by Pinnavaia et al., who used ethylene oxide monoethers and Pluronics as templates.[14] This research group applied the surfactants in concentrations much lower than the ones necessary to provide a lyotropic liquid crystalline phase. The structure of those materials was described as distorted hexagonal; however, no cylindrical structure of the silicas, which would be expected for a classical hexagonal lyotropic mesophase (H_I-phase), could be detected. Furthermore, similar structures have been observed for block copolymers and assigned to a hexagonal phase.[22] It is interesting to note that a very similar silica mesostructure was found in marine diatoms[23] and named "continuous silica". Such structures seem to be an optimal compromise between porosity and mechanical stability in nature for the purpose of lightweight design.

Small-angle synchrotron X-ray scattering[24] provides a deeper insight into this novel structure of mesoporous silicates. The small-angle X-ray diffractograms of SE 10/10-silica and SE 30/30-silica (Figure 4) show the same qualitative and quantitative features, indicating that both materials belong to the same type of phase structure. As expected, the

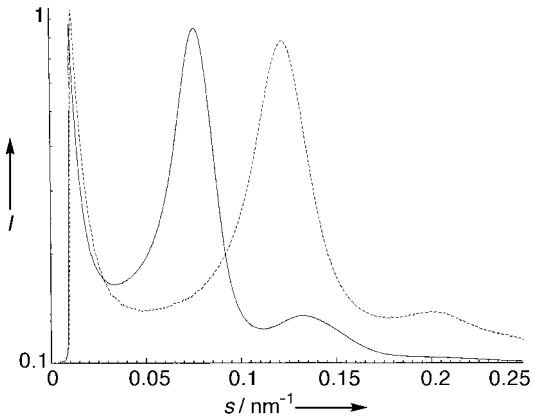


Figure 4. Synchrotron X-ray diffractograms of SE 10/10-silica (broken line) and SE 30/30-silica (solid line). I = rel. intensity.

X-ray reflections are shifted according to the different molecular weight and size of the template employed. The diffractograms typically show three reflections, of which the higher order ones are not resolved as simple peaks. The degree of order exceeds the one of the corresponding systems described by Pinnavaia et al., who reported only one broad first-order scattering peak. Since the diffractograms of SE 10/10 and SE 30/30 contain several scattering reflections, an L_3-phase as a template can be excluded.[25]

From the first-order scattering peak, we calculate a Bragg distance of 8.2 nm (SE 10/10 silica, 8.7 nm before calcination) and 13.3 nm (SE 30/30 silica, 14.1 nm before calcination). This is in good agreement with the pore-to-pore distances observed in the transmission electron micrographs. The the next higher-order peak can be described by the superposition of two Lorentz peaks, and fitting these reveals that they can be indexed according to a two-dimensional hexagonal packing. The high intensity and broadening of the peaks can be attributed to high order on a local scale, but also to a low correlation length ξ. From the width of the scattering peaks, the ξ value, a measure of the size of coherent hexagonal domains, is calculated to be of the order of about four times the pore-to-pore distance. The size of these hexagonal domains is limited by frequent branching points at a typical 120° angle ("tripods", as observed in the TEM pictures), which interconnect the silica rods and give rise to a three-dimensional continuity of the silica phase. This phase structure might be located between a cylindrical hexagonal, the bicontinuous cubic (gyroid), and a hexagonally perforated lamellar phase (the latter two consisting of tripods connected with a defined rotation angle), as it exhibits a statistical arrangement of structural elements of all three "pure" symmetry groups.

This phase structure turned out to be independent of temperature, amphiphile concentration, and silica content over wide ranges, as shown in a set of experiments in which the composition of the reaction mixture is varied. The structure of the materials does not change upon solvent extraction and calcination, as shown by small-angle X-ray diffraction studies at all stages. The volume shrinkage of 6–7% on calcination is much less than that observed when using low molecular weight surfactant phases as templates (up to 21%).

It was shown that the lyotropic liquid crystalline phases of amphiphilic block copolymers are very promising templates for the generation of mesoporous materials. It is not only possible to extend the long Bragg distance of classical mesoporous materials to 8–13 nm; macroscopic monolithic objects can also be obtained. The resulting phase morphology of a hexagonal continuous silica turned out to be stable over a wide range of accessible experimental parameters. Further experiments with more homodisperse model templates will show whether this is due to the polydispersity of the polymeric template or whether it is a general feature of such strongly segregating block copolymers.

In addition, the full potential of polymeric templates, which is gained by the careful chemical adjustment (using chemical functionality) of the interface between template and casting should allow the extension of this technique to other materials, such as mesoporous polymers or semiconductors. Finally, the regular porous structure of such structures is expected to be useful for enclosing nanometer-sized objects, such as enzymes and chemically active colloids.

Received: November 28, 1997
Revised version: October 27, 1997 [Z 9829 IE]
German version: *Angew. Chem.* **1998**, *110*, 633–636

Keywords: amphiphiles · block copolymers · mesoporosity · silicates · sol–gel processes

 © WILEY-VCH Verlag GmbH, D-69451 Weinheim, 1998 1433-7851/98/3705-0615 $ 17.50+.50/0

[1] M. E. Davies, C. Saldarriaga, C. Montes, J. Garces, C. Crowder, *Nature* **1988**, *331*, 698.
[2] L. B. McCusker, C. Baerlocher, E. Jahn, M. Bülow, *Zeolites* **1991**, *11*, 308.
[3] P. Behrens, *Adv. Mater.* **1993**, *5*, 127.
[4] D. Antonelli, J. Ying, *Curr. Opin. Coll. Interf. Sci.* **1996**, *1*, 523.
[5] K. R. Kloekstra, H. van Bekkum, *J. Chem. Soc. Chem. Commun.* **1995**, 1005, and references therein.
[6] C. T. Kresge, M. E. Leonowicz, W. J. Roth, J. C. Vartuli, J. S. Beck, *Nature* **1992**, *359*, 710.
[7] C. G. Göltner, M. Antonietti, *Adv. Mater.* **1997**, *9*, 431.
[8] J. S. Beck, J. C. Vartuli, W. J. Roth, M. E. Leonowicz, C. T. Kresge, K. D. Schmitt, C. T.-W. Chu, D. H . Olson, E. W. Sheppard, S. B. McCullen, J. B. Higgins, J. L. Schlenker, *J. Am. Chem. Soc.* **1992**, *114*, 10834.
[9] A. Monnier, F. Schüth, Q. Huo, D. Kumar, D. Margolese, R. S. Maxwell, G. D. Stucky, M. Krishnamurty, P. Petroff, A. Firouzi, M. Janicke, B. F. Chmelka, *Science* **1993**, *261*, 1299.
[10] Q. Huo, D. I. Margolese, U. Ciesla, D. G. Demuth, P. Feng, T. E. Gier, P. Sieger, A. Firouzi, B. F. Chmelka, F. Schüth, G. D. Stucky, *Chem. Mater.* **1994**, *6*, 1176.
[11] Q. Huo, D. I. Margolese, U. Ciesla, P. Feng, T. E. Gier, P. Sieger, R. Leon, P. M. Petroff, F. Schüth, G. D. Stucky, *Nature* **1994**, *368*, 317.
[12] G. S. Attard, M. Edgar, J. W. Emsley, C. G. Göltner, *MRS Symp. Proc.* **1996**, *425*, 185.
[13] P. T. Tanev, M. Chibwe, T. J. Pinnavaia, *Nature* **1994**, *368*, 321.
[14] S. A. Bagshaw, E. Prouzet, T. J. Pinnavaia, *Science* **1995**, *269*, 242.
[15] S. A. Bagshaw, T. J. Pinnavaia, *Angew. Chem.* **1996**, *108*, 1180; *Angew. Chem. Int. Ed. Engl.* **1996**, *108*, 1102.
[16] G. S. Attard, J. C. Glyde, C. G. Göltner, *Nature* **1995**, *378*, 366.
[17] G. S. Attard, M. Edgar, C. G. Göltner, *Acta Mater.* **1998**, in press.
[18] M. Antonietti, S. Förster, J. Hartmann, S. Oestreich, *Macromolecules* **1996**, *29*, 3800.
[19] The polymers were supplied by the company Th. Goldschmidt AG.
[20] The amphiphilic block copolymer (2 g) is dissolved in tetramethylorthosilicate (TMOS, 4 g), which is then hydrolyzed by adding dilute hydrochloric acid (pH 2, 2 g). Initially, an isotropic mixture is obtained. Methanol is removed by evaporation in vacuo (25 Torr, 30°C), upon which the reaction mixture turns viscous and birefringent. The subsequent sol–gel process is carried out at room temperature (50°C for SE 30/30) in an open flask. After 12 h the liquid crystalline mixtures are solid and, after extraction of a major portion of the template with acetone for 24 h, are calcined at 550°C (12 h under nitrogen, 12 h under oxygen).
[21] a) K. S. W. Sing, D. H. Everett, R. A. W. Haul, L. Moscov, R. A. Pierotti, J. Rouguerol, T. Siemieniewska, *Pure Appl.Chem.* **1985**, *57*, 603; b) S. J. Gregg, K. S. W. Sing, *Adsorption, Surface Area, and Porosity*, Academic Press, London, **1982**.
[22] *Interpenetrating Polymer Networks* (Eds.: D. Klempner, L. H. Sperling, L. A. Utracki), Advances in Chemistry Series, ACS, Washington, DC, **1994**, p. 239.
[23] *Biomineralization: Chemical and Biochemical Perspectives* (Eds.: S. Mann, J. Webb, R. J. P. William), VCH, Weinheim, **1992**.
[24] The X-ray data were recorded on the EMBL beam line in Hamburg.
[25] The X-ray data were fitted with Lorentzian functions. The normalized peak positions for the first three peaks are 1.00, 1.73, and 2.00, which indicates a hexagonal symmetry of the packing.

Why Does the Active Form of Galactose Oxidase Possess a Diamagnetic Ground State?**

Jochen Müller, Thomas Weyhermüller, Eckhard Bill, Peter Hildebrandt, Linda Ould-Moussa, Thorsten Glaser, and Karl Wieghardt*

Dedicated to Professor Gottfried Huttner on the occasion of his 60th birthday

The fungal enzyme galactose oxidase (GO) contains in its active site a square-pyramidally coordinated Cu^{II} ion (d^9) with an O-bound tyrosyl radical (Tyr 272) in the equatorial plane (see Figure 1). This catalytically active copper(II)–tyrosyl radical form is EPR-silent and has been proposed to possess a diamagnetic ground state ($S = 0$).[1a] The unpaired electron in the $d_{x^2-y^2}$ magnetic orbital of the Cu^{II} ion is then intramolecularly *antiferromagnetically* coupled to the electron of in the half-occupied π orbital of the tyrosyl radical. This is somewhat surprising, because in all known Cu^{II}–semiquinonate complexes this intramolecular exchange coupling is *ferromagnetic*, yielding an $S = 1$ ground state.[2] What is the mechanism of the exchange coupling in GO?

A catalytically inactive form of GO (pH = 4.5) containing a reduced Cu^{II}-tyrosinate moiety has been characterized by X-ray crystallography (Figure 1).[3] It has been shown that the conformation of the coordinated Tyr 272 ligand is fixed by π stacking with the tryptophane residue Trp 290. It is assumed that one-electron oxidation of Tyr 272 yielding the coordinated tyrosyl ligand does not change the conformation of the phenyl ring or the Cu-O-C bond angle significantly.

Recently Tolman et al.[4] and we[5] have reported some low molecular weight, structurally characterized Cu^{II}–phenolate complexes that can be chemically or electrochemically oxidized to generate relatively stable Cu^{II}-phenoxyl species.[6] These complexes are EPR-silent; they possess a diamagnetic ($S = 0$) ground state.[7] In these compounds the coordinated phenolate ligands are connected to the coordinated macrocycle 1,4,7-triazacyclononane (Figure 2); a six-membered chelate ring $\overline{Cu^{II}NCCCO}$ is formed. It is then natural to assume that the conformation of the chelate ring does not change upon one-electron oxidation of the phenolate to a coordinated phenoxyl.

A qualitative analysis of the relative orientations of the magnetic orbitals of the Cu^{II} ion ($d_{x^2-y^2}$) and of the phenoxyl radical (the half-occupied π orbital) reveals that they are strictly orthogonal at an Cu^{II}-O-C bond angle α of 180°, irrespective of the dihedral angle β between the x,y plane at the Cu^{II} ion and the phenyl ring of the radical ligand (Figure 3). According to the Goodenough–Kanamori rules

[*] Prof. Dr. K. Wieghardt, Dipl.-Chem. J. Müller, Dr. T. Weyhermüller, Dr. E. Bill, Dr. P. Hildebrandt, Dr. L. Ould-Moussa, Dipl.-Chem. T. Glaser
Max-Planck-Institut für Strahlenchemie
Stiftstrasse 34–36, D-45470 Mülheim an der Ruhr (Germany)
Fax: +(49) 208-306-3952
E-mail: wieghardt@mpi-muelheim.mpg.de

[**] We gratefully acknowledge financial support of this work from the Fonds der Chemischen Industrie. P. H. thanks the DFG for a Heisenberg-stipend.

 © WILEY-VCH Verlag GmbH, D-69451 Weinheim, 1998 1433-7851/98/3705-0616 $ 17.50+.50/0

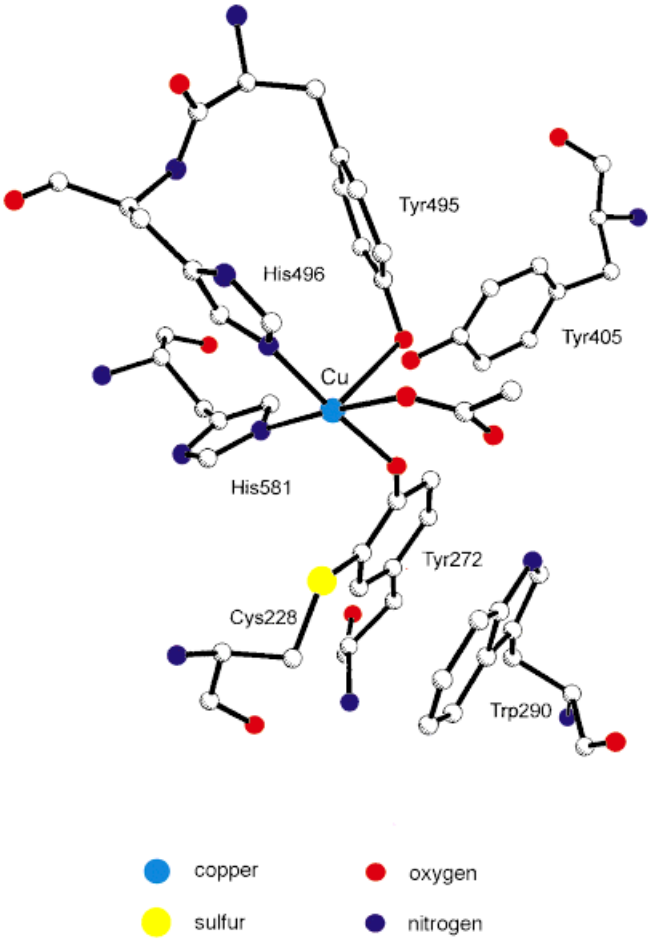
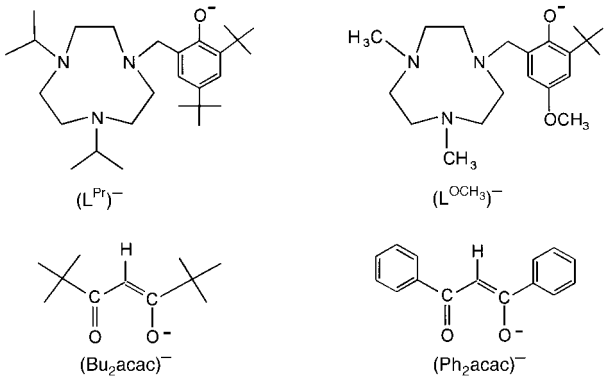


Figure 1. Schematic representation of the active site of galactose oxidase (pH = 4.5).[3]



$[L^{Pr}Cu^{II}Cl]$	**1**[4]
$[L^{OCH_3}CuCl]$	**2**
$[L^{OCH_3}Cu^{II}(Ph_2acac)]$	**3**
$[L^{OCH_3}Cu^{II}(Bu_2acac)]$	**4**

Figure 2. Ligands and complexes.

for exchange coupling a ferromagnetic coupling will then stabilize the triplet ground state ($S = 1$). If the observed bond angle α is in the range 125–135°, the magnitude of the dihedral angle β determines the multiplicity of the electronic ground state: at $\beta = 0°$ the magnetic orbitals are again strictly

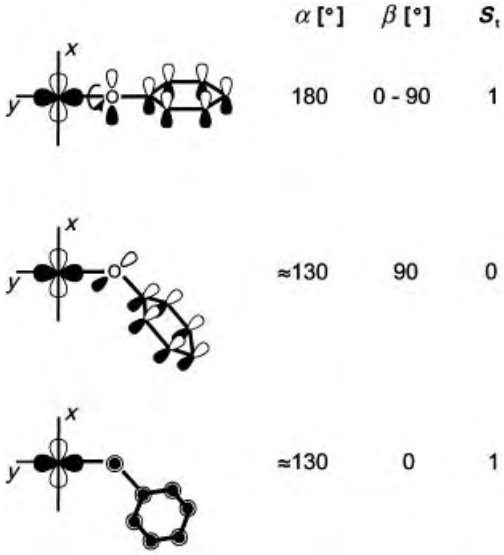


Figure 3. Relative orientations of the magnetic orbitals of the Cu^{II} ion ($d_{x^2-y^2}$) in the x,y plane relative to that of the half-occupied π orbital of the phenoxyl radical. α: Cu-O-C bond angle. β: dihedral angle between the x,y plane and the plane of the phenyl ring of the coordinated phenoxyl. S_t: expected electronic ground state.

orthogonal and $S = 1$ is the ground state, but at $\beta \approx 90°$ the significant overlap between the magnetic orbitals stabilizes a singlet ground state ($S = 0$). In GO the bond angle α is about 129° and $\beta \approx 75°$, which according to the above analysis results in an $S = 0$ ground state—as is observed.

We were able experimentally to corroborate the above analysis as follows: We synthesized the mononuclear complexes **2**, **3**, and **4** (Figure 2) all of which contain the tetradentate macrocyclic anion $(L^{OCH_3})^-$. Complex **2** is five-coordinate; its structure is proposed to be very similar to that of **1**, which has been analyzed by X-ray crystallography.[4]

In **3** and **4** the chloro ligand is replaced by the didentate β-diketonates Ph_2acac^- and Bu_2acac^-, which enforces the coordination number 6 at the Cu^{II} ions. Figure 4 displays the structure of **3**.[8] The *cis*-$Cu^{II}N_3O_3$ polyhedron exhibits a marked tetragonal Jahn–Teller distortion: The Cu–N and Cu–O bond lengths of the N(2)-Cu(1)-O(2) axis (z axis) are both longer than the corresponding lengths in x and y direction. The unpaired electron occupies a $d_{x^2-y^2}$ metal orbital as in the square-pyramidal Cu^{II} ion in **2**. This has been corroborated by the EPR spectra of these Cu^{II} complexes.

Cyclic voltammograms of **2**, **3**, and **4** recorded in CH_2Cl_2 (20°C, 0.10 M $[(n\text{Bu})_4\text{N}]PF_6$) exhibit in the potential range from 0.2 to −1.2 V vs. ferrocenium/ferrocene (Fc^+/Fc) one reversible one-electron oxidation ($E_{1/2}$ vs Fc^+/Fc for **2**: −0.015 V; **3**: −0.33 V; **4**: −0.42 V). Figure 5 shows the UV/Vis spectra of **4** and **2**, as well as their electrochemically one-electron oxidized forms $[\mathbf{4}]^{\bullet+}$ and $[\mathbf{2}]^{\bullet+}$. The intense absorption maxima of $[\mathbf{4}]^{\bullet+}$ at 391, 411, and 477 nm are characteristic of the phenoxyl radical. The resonance Raman (RR) spectrum of $[\mathbf{4}]^{\bullet+}$ in CH_2Cl_2 ($\lambda_{exc} = 413$ nm) displays the typical strong C–O phenoxyl stretching mode at 1509 cm^{-1} and a weaker C=C vibration at 1602 cm^{-1}.[5] The energy difference Δ of 107 cm^{-1} between these two modes conclusively demonstrates that the phenoxyl radical is O-bound to the Cu^{II} ion.[9]

 © WILEY-VCH Verlag GmbH, D-69451 Weinheim, 1998 1433-7851/98/3705-0617 $ 17.50+.50/0

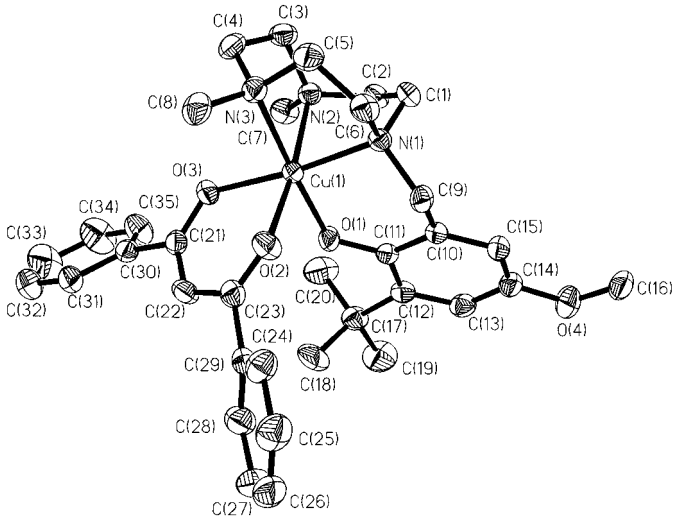


Figure 4. Structure of **3** in the crystal. Selected bond lengths [Å] and angles [°]: Cu(1)–O(1) 1.914(2), Cu(1)–O(2) 2.330(2), Cu(1)–O(3) 1.994(2), Cu(1)–N(1) 2.04782), Cu(1)–N(2) 2.333(2), Cu(1)–N(3) 2.125(2), O(1)–C(11) 1.325(3), O(3)–C(21) 1.268(3), O(2)–C(23) 1.243(3), C(21)–C(22), 1.392(4), C(22)–C(23) 1.421(4); Cu(1)-O81)-C(11) 129.2(2), N(3)-Cu(1)-O(1) 176.9(1), O(3)-Cu(1)-N(1) 173.7(1), O(2)-Cu(1)-N(2) 172.0(1).

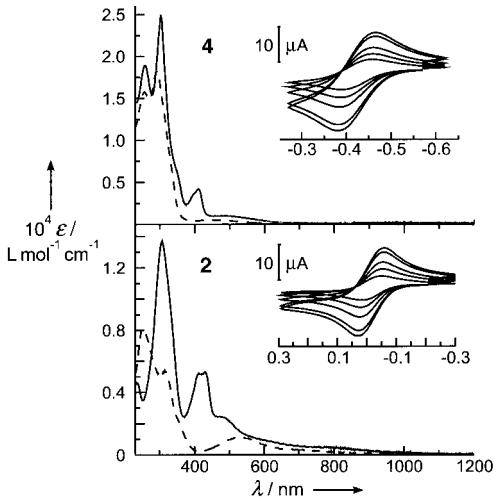


Figure 5. UV/Vis spectra (CH_2Cl_2) of **4** and **2** (broken lines) and of the electrochemically generated oxidized forms $[\mathbf{4}]^{\bullet+}$ and $[\mathbf{2}]^{\bullet+}$ (solid lines). The insets show the cyclic voltammograms of **4** and **2** in CH_2Cl_2 (0.10 M $[(n\mathrm{Bu})_4\mathrm{N}]PF_6$) at different scan rates (50–500 mV s^{-1}).

This difference Δ is only 79 cm^{-1} for the uncoordinated free 2,6-di-*tert*-butyl-4-methoxyphenoxyl radical.[10] Very similar UV/Vis and RR spectra have been obtained for the radical complexes $[\mathbf{2}]^{\bullet+}$ and $[\mathbf{3}]^{\bullet+}$. Compounds $[\mathbf{2}]^{\bullet+}$, $[\mathbf{3}]^{\bullet+}$, and $[\mathbf{4}]^{\bullet+}$ contain the same coordinated radical ligand $(L^{OCH_3})^{\bullet}$.

We then recorded the X-band EPR spectra of the electrochemically generated radical species $[\mathbf{2}]^{\bullet+}$, $[\mathbf{3}]^{\bullet+}$, and $[\mathbf{4}]^{\bullet+}$ in frozen CH_2Cl_2 solution in the temperature range 4–60 K. Solutions of $[\mathbf{2}]^{\bullet+}$ displayed no signal with the exception of a weak signal of **2** (<4%). This has also been reported by Tolman et al.[4] for $[\mathbf{1}]^{\bullet+}$. We conclude that both $[\mathbf{1}]^{\bullet+}$ and $[\mathbf{2}]^{\bullet+}$ containing a five-coordinate Cu^{II} ion possess a diamagnetic ground state ($S=0$). In contrast, frozen solutions of $[\mathbf{3}]^{\bullet+}$ and $[\mathbf{4}]^{\bullet+}$ are EPR-active. Figure 6 shows the spectrum of $[\mathbf{3}]^{\bullet+}$. A

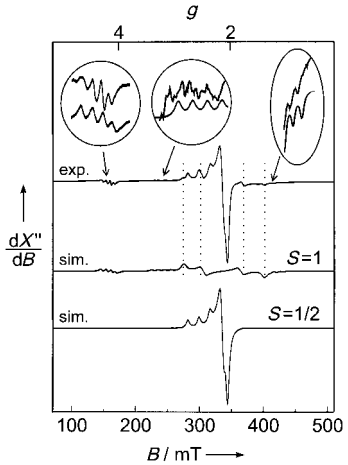


Figure 6. X-band EPR spectrum of electrochemically generated $[\mathbf{3}]^{\bullet+}$ in CH_2Cl_2 (0.10 M $[(n\mathrm{Bu})_4\mathrm{N}](PF_6)$) at 16 K. Conditions: frequency 9.6463 GHz, 100.6 mW; modulation amplitude 19.7 G, modulation frequency 100 kHz. For details of the simulations see ref. [11]. In the enlarged parts of the spectra the upper line represents the experimental data and the lower line a simulation.

typical triplet spectrum with hyperfine structure is observed in addition to a weak signal at $g \approx 2.0$ due to a mononuclear Cu^{II} successor species (decomposition?). From the temperature dependence of the triplet spectrum a ferromagnetic coupling constant of $J = 16 \pm 3$ cm^{-1} ($\mathscr{H} = -2JS_1S_2$; $S_1 = S_2 = {}^1/_2$) was established. The spectrum of $[\mathbf{4}]^{\bullet+}$ is similar, but the hyperfine structure was not resolved.

These spectroscopic results reveal that $[\mathbf{2}]^{\bullet+}$ possesses an (S=0) ground state, whereas $[\mathbf{3}]^{\bullet+}$ and $[\mathbf{4}]^{\bullet+}$ have an (S=1) ground state, although in all three species the same radical ligand $(L^{OCH_3})^{\bullet}$ is coordinated to a Cu^{II} ion.

A comparison of the bond angle α and the dihedral angle β in five-coordinate **1**[4] with the corresponding angles in six-coordinate **3** shows that increasing the coordination number from 5 to 6 does not change α significantly (125.2° in **1** vs. 129.2° in **3**), whereas β decreases by nearly 10° from 27.4° in **1** to 17.6° in **3**. This structural change induces the change of the sign of the exchange coupling from antiferromagnetic in $[\mathbf{1}]^{\bullet+}$ and $[\mathbf{2}]^{\bullet+}$ to ferromagnetic in $[\mathbf{3}]^{\bullet+}$ and $[\mathbf{4}]^{\bullet+}$. This is in excellent qualitative agreement with the above analysis of the orientation of the magnetic orbitals (Figure 3).

Experimental Section

All new compounds yielded correct C, H, N analyses and mass spectra. The ligand $L^{OCH_3}H$ as well as $Na(L^{OCH_3})$ was synthesized according to published procedures.[9]

2: To a solution of $Na(L^{OCH_3})$ (0.37 g, 1.0 mmol) in tetrahydrofuran/*n*-pentane mixture (30/10 mL) was added dehydrated $CuCl_2$ (0.134 g; 1.0 mmol). After stirring for 1 h at 20°C the volume of the reaction mixture was reduced by rotary evaporation to yield microcrystalline, violet **2**; yield 0.21 g (47%).

3: A solution of $Na(L^{OCH_3})$ (0.37 g, 1.0 mmol) and $[Cu^{I}(NCCH_3)_4](BF_4)$ (0.32 g, 1.0 mmol) in dry CH_3OH (30 mL) was stirred at 20°C for 20 min in the presence of air. To the deep violet solution was added K[Ph_2acac] (0.26 g, 1.0 mmol). Within a few minutes a brown-green precipitate of **3** formed. Recrystallization from CH_2Cl_2/CH_3CN (1/1) afforded single crystals suitable for X-ray crystallography; yield 0.28 g (44%).

4: A solution of $Na(L^{OCH_3})$ (0.37 g, 1.0 mmol) and $Cu^{I}Cl$ (0.099 g, 1.0 mmol) in dry CH_3OH (30 mL) was stirred in the presence of air for 20 min. To the

 © WILEY-VCH Verlag GmbH, D-69451 Weinheim, 1998 1433-7851/98/3705-0618 $ 17.50+.50/0 *Angew. Chem. Int. Ed.* **1998**, *37*, No. 5

clear brown solution was added K[Bu_2acac] (0.22 g, 1.0 mmol), and stirring was continued for 10 min. Dropwise addition of H_2O (5 mL) and filtration initiated the precipitation of brown-green crystals of **4** within 5 h; yield 0.31 g (52 %).

Physical data of complexes: UV/Vis (CH_2Cl_2): λ_{max} nm (ε[L mol^{-1} cm^{-1}]): **2**: 252 (8.1×10^3), 315 (5.3×10^3), 532 (1.2×10^3); **3**: 254 (2.71×10^4), 334 (1.67×10^4), 358 (1.60×10^4); **4**: 256 (1.6×10^4), 293 (1.8×10^4), 451(500). [**2**]$^{\cdot+}$: 236 (4.5×10^3), 308 (1.4×10^4), 413 (5.1×10^3), 431 (5.2×10^3), 485 (2.4×10^3); [**3**]$^{\cdot+}$: 270 (2.6×10^4), 304 (2.4×10^4), 352 (2.2×10^4), 412 (6.1×10^3); [**4**]$^{\cdot+}$: 259 (1.9×10^4), 303 (2.5×10^4), 347sh (6.4×10^3), 391 (3.2×10^3), 411 (4.0×10^3), 477(990).

The radical complexes [**2**]$^{\cdot+}$, [**3**]$^{\cdot+}$, and [**4**]$^{\cdot+}$ were generated in CH_2Cl_2 solution (0.10 M [$(n$Bu$)_4$N]PF_6) by coulometry. X-Band EPR spectra (CH_2Cl_2, 10 K, 9.45 GHz): g_x, g_y, g_z ($A_x = A_y$, A_z [10^{-4} cm^{-1}]): **2**: 2.05, 2.05, 2.24 (20, 180); **3**: 2.05, 2.06, 2.26 (21.7, 176); **4**: 2.06, 2.07, 2.25 (0, 175).

Received: September 12, 1997 [Z10917IE]
German version: *Angew. Chem.* **1998**, *110*, 637 – 640

Keywords: bioinorganic chemistry · copper · oxidases · phenoxyl complexes · radical ions

[1] a) J. W. Whittaker in *Metalloenzymes Involving Amino Acid Residue and Related Radicals*, *Vol. 30* (Eds.: H. Sigel, A. Sigel), Marcel Dekker, New York, **1994**, pp. 315 – 360; b) P. F. Knowles, N. Ito in *Perspectives in Bio-inorganic Chemistry, Vol. 2* (Eds.: R. W. Hay, J. R. Dilworth, K. B. Nolan), Jai Press, London, **1993**, pp. 207 – 244.

[2] a) C. G. Pierpont, C. W. Lange, *Progr. Inorg. Chem.* **1994**, *41*, 331; b) C. Benelli, A. Dei, D. Gatteschi, L. Pardi, *Inorg. Chem.* **1990**, *29*, 3409. c) O. Kahn, R. Prins, J. Reedijk, J. S. Thompson, *ibid.* **1987**, *26*, 3557.

[3] N. Ito, S. E. V. Phillips, C. Stevens, Z. B. Ogel, M. J. McPherson, J. N. Keen, K. D. S. Yadav, P. F. Knowles, *Nature* **1991**, *350*, 87; b) N. Ito, S. E. V. Phillips, C. Stevens, Z. B. Ogel, M. J. McPherson, J. N. Keen, K. D. S. Yadav, P. F. Knowles, *Faraday Discuss. Chem. Soc.* **1992**, *93*, 75; c) N. Ito, S. E. V. Phillips, K. D. S. Yadav, P. F. Knowles, *J. Mol. Biol.* **1994**, *238*, 794.

[4] a) J. A. Halfen, Y. G. Young, Jr., W. B. Tolman, *Angew. Chem.* **1996**, *108*, 1832; *Angew. Chem. Int. Ed. Engl.* **1996**, *35*, 1687; b) J. A. Halfen, B. Jazdzewski, S. Mahapatra, L. M. Berrean, E. C. Wilkinson, L. Que, Jr., W. B. Tolman, *J. Am. Chem. Soc.* **1977**, *119*, 8217.

[5] A. Sokolowski, H. Leutbecher, T. Weyhermüller, R. Schnepf, E. Bothe, E. Bill, P. Hildebrandt, K. Wieghardt, *J. Biol. Inorg. Chem.* **1997**, *2*, 444.

[6] Other Cu^{II} phenoxyl complexes have been generated in solution: a) D. Zurita, I. Gautier-Luneau, S. Menage, J.-L. Pierre, E. Saint-Aman, *J. Biol. Inorg. Chem.* **1997**, *2*, 46; b) S. Itoh, S. Takayama, R. Arakawa, A. Furuta, M. Komatsu, A. Ishida, S. Takamuku, S. Fukuzumi, *Inorg. Chem.* **1997**, *36*, 1407.

[7] The complex described in ref. [6a] is an exception. It has the phenoxyl radical in apical position of the Cu^{II} square pyramid. An (S=1) ground state has been proposed.

[8] X-ray structure analysis of **3**: Brown-green crystal ($0.42\times0.60\times0.49$ nm); $C_{35}H_{45}CuN_3O_4$, $M_r = 635.3$, monoclinic, space group $P2_1/c$, $a = 15.407(3)$, $b = 11.490(2)$, $c = 18.438(4)$ Å, $\beta = 101.69(3)^\circ$, $V = 3196(1)$ Å^3, $Z = 4$ at 293(2) K; $\rho_{calcd} = 1.32$ g cm^{-3}; $\mu_{Mo} = 0.726$ mm^{-1}, semiempirical absorption correction. Full-matrix least-squares refinement based on F with 6083 reflections with [$I > 2\sigma(I)$] and 388 variables, final R values: $R(F) = 0.037$ and $wR(F) = 0.091$. Intensities were measured on an Enraf-Nonius CAD-4 diffractometer. The crystallographic data were deposited as supplementary publication no. CCDC-100759 at the Cambridge Crystallographic Data Centre. Copies of the data are available from CCDC, 12 Union Road, GB-Cambridge CB2 1EZ (fax: (+44) 1223-336-033; e-mail: deposit@ccdc.cam.ac.uk).

[9] A. Sokolowski, J. Müller, T. Weyhermüller, R. Schnepf, P. Hildebrandt, K. Hildenbrand, E. Bothe, K. Wieghardt, *J. Am. Chem. Soc.* **1997**, *119*, 8889.

[10] R. Schnepf, A. Sokolowski, J. Müller, V. Bachler, K. Wieghardt, P. Hildebrandt, *J. Am. Chem. Soc.*, in press.

[11] In the first-derivative representation (dX″/dB) of the EPR spectrum (Figure 6) an apparently dominant signal of a Cu^{II} compound ($S = 1/2$) is detected; its intensity, however, represents only 10 % of the doubly integrated total signal. In a broad field range the oxidation product [**3**]$^{\cdot+}$ displays typical resonances of a triplet spectrum with small zero-field splitting ($D < h\nu$) as is observed for spin pairs ($S_1 = S_2 = 1/2$). $\Delta m = 1$ signals at $g < 2$ (350 – 430 mT) are clearly detected, as well as the typical half-field transitions with $\Delta m = 2$ at $g = 4$, which display a clearly resolved Cu hyperfine splitting ($I = 3/2$). The spectrum was simulated with a spin Hamiltonian for an effective spin $S = 1$ (strong coupling case) and parameters $D = 0.086$ cm^{-1}, $E/D = 0.13$, $g = (2.034, 2.021, 2.10)$ and $\boldsymbol{A} = (20, 20, 100)\times10^{-4}$ cm^{-1}. For the local spin of the Cu^{II} ion ($S = 1/2$) we obtained $\boldsymbol{a}_{Cu} = (40, 40, 200)\times10^{-4}$ cm^{-1}, $\boldsymbol{g}_{Cu} = (2.07, 2.04, 2.20)$ by using the usual spin projection technique. These values are similar to those obtained for the Cu^{II} ion in **3**. Since the signals are observed down to 4 K, the spin triplet is the ground state of [**3**]$^{\cdot+}$, owing to an intramolecular ferromagnetic coupling. The splitting energy $2J$ between the triplet and (EPR-silent) singlet has been determined from the temperature dependence of the intensities(IT vs. T) by a fitting procedure to the Boltzmann function IT = const. $(1 + \exp(2J/kT)^{-1})$ in the temperature range 4 – 60 K. For I the peak-to-peak amplitudes of the measured derivative spectra at $g = 4$ were used, because the resonances are not perturbed by signals of the Cu^{II} impurity.

Synthesis and Characterization of the First Double-Bridged Tetraselenafulvalenophanes**

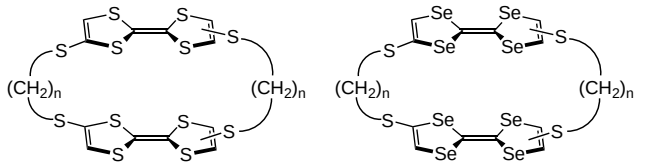
Kazuo Takimiya, Akinobu Oharuda, Atsushi Morikami, Yoshio Aso, and Tetsuo Otsubo*

Since the discovery of the tetrathiafulvalene/tetracyano-*p*-quinodimethane complex (TTF – TCNQ) as the first low-dimensional organic metal,[1] TTF derivatives with modified frameworks have been examined in order to develop yet more superior organic conductors.[2] One of the basic modifications is dimerization of TTF, which makes it possible to prepare charge-transfer complexes of given stoichiometry.[3] To date, a variety of dimeric TTFs have been thus synthesized and characterized.[4] Among them, tetrathiafulvalenophanes (TTF phanes) are of current interest, because in such sophisticated systems the two TTF units can adopt a unique sandwich structure and interact strongly with each other.[5, 6] We have recently found that the double-layered TTF phanes **1** are especially good electron donors, forming highly conductive radical cation salts. The high conductivities are induced by strong intra- and intermolecular nonbonding interactions between the sulfur atoms incorporated in the TTF moieties.[6] Since nonbonding interactions between selenium atoms are generally more effective than those of sulfur, tetraselenaful-

[*] Prof. Dr. T. Otsubo, Dr. K. Takimiya, A. Oharuda, A. Morikami, Prof. Dr. Y. Aso
Department of Applied Chemistry
Faculty of Engineering, Hiroshima University
Kagamiyama, Higashi-Hiroshima 739 (Japan)
Fax: (+81) 824-22-7191
E-mail: otsubo@ipc.hiroshima-u.ac.jp

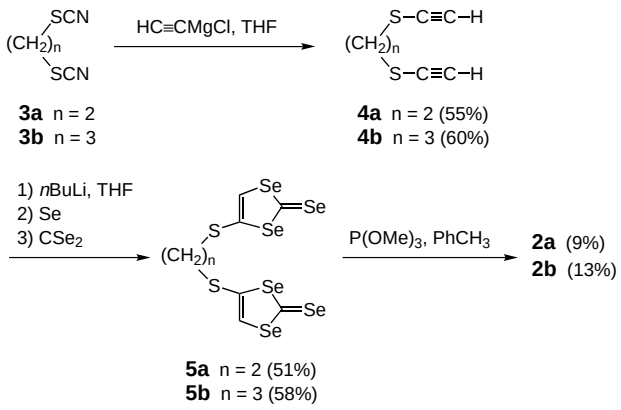
[**] This work was supported by Grants-in-Aid for Scientific Research from the Ministry of Education, Science, Sports and Culture of Japan.

valenophanes (TSF phanes) should be even better electron donors. To our knowledge, however, TSF phanes have not yet been described. We report here on the synthesis and properties of the first examples, double-bridged TSF phanes **2**.



1a n = 2 **2a** n = 2
1b n = 3 **2b** n = 3

TSF phanes **2** were synthesized according to the three-stage route shown in Scheme 1. The key step is the ready



3a n = 2 **4a** n = 2 (55%)
3b n = 3 **4b** n = 3 (60%)

1) *n*BuLi, THF
2) Se
3) CSe_2

$P(OMe)_3$, $PhCH_3$

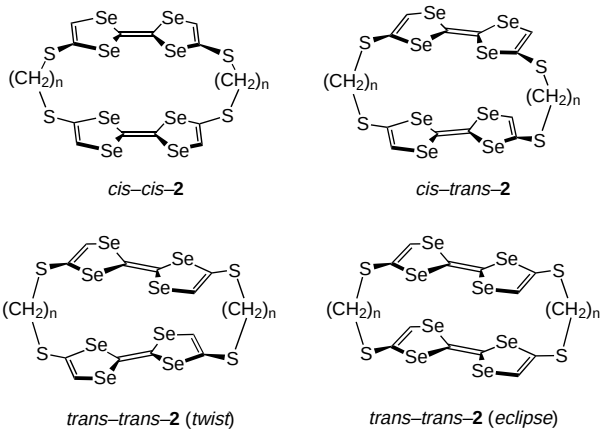
2a (9%)
2b (13%)

5a n = 2 (51%)
5b n = 3 (58%)

Scheme 1. Synthesis of TSF phanes **2a** and **2b**.

preparation of the bridged precursors, bis(1,3-diselenole-2-selones) **5**. Our recent improved synthetic method for 1,3-diselenole-2-selone derivatives[7] was successfully applied to the preparation of **5**: bis(ethynylthio)alkanes **4**, obtained from dithiocyanatoalkanes **3** and ethynylmagnesium chloride, were metalated with butyllithium in tetrahydrofuran, and then treated consecutively with selenium powder and carbon diselenide to give **5a** and **5b** in moderate yields (51 and 58%, respectively). The subsequent double-coupling reaction of **5** induced by trimethyl phosphite in refluxing toluene gave the desired TSF phanes **2a** and **2b** in 9 and 13% yield, respectively.

In analogy to the TTF phanes **1**, the TSF phanes **2** are expected to exist as a mixture of four diasteromers: *cis-cis*-**2**, *cis-trans*-**2**, and *twist* and *eclipse trans-trans*-**2**. Indeed, the ^1H NMR spectra of the crude products display five singlets for the fulvalenic protons, of which a pair of singlets corresponds to the *cis-trans* isomer and the remaining singlets to the other isomers. Recrystallization of a mixture of **2a** isomers from hot carbon disulfide/benzene gave a red columnar material, which was assigned on the basis of its NMR analysis to be the *cis-trans* isomer. In addition, during the NMR measurement in solution the compound slowly isomerized into the other isomers, an observation previously made for the TTF phanes **1**. The precise molecular structure of the *cis-trans* isomer was



cis–cis–**2** *cis–trans*–**2**

trans–trans–**2** (*twist*) *trans–trans*–**2** (*eclipse*)

determined by an X-ray crystallographic analysis (Figure 1).[8] The two TSF units are almost planar and stacked with partial overlap. The shortest distance between Se atoms in the stacked TSF units is 3.92 Å, which is slightly longer than the normal van der Waals contact (3.8 Å). In the crystal structure the TSF phane **2a** is stacked with other molecules to make a stacking column, but there are no intermolecular Se···Se contacts between the stacked molecules.

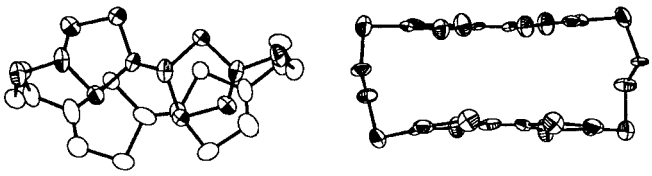


Figure 1. X-ray crystal structure of *cis-trans*-**2a** (ORTEP plots): top view (left) and side view (right).

Recrystallization of **2b** from carbon disulfide gave orange prisms, which were shown by X-ray crystallographic analysis to be the *cis-cis* isomer (Figure 2). In contrast to the almost

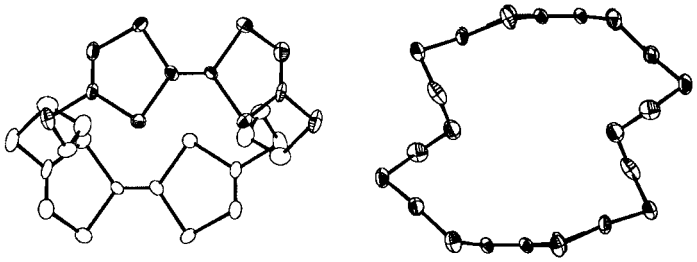
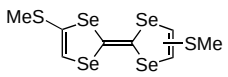


Figure 2. X-ray crystal structure of *cis-cis*-**2b** (ORTEP plots): top view (left) and side view (right).

planar TSF in *cis-trans*-**2a**, the TSF frameworks of *cis-cis*-**2b** are strongly bent, with dihedral angles of 24.3 and 42.9° between the central and the outer ethylene units. The molecule as a whole assumes an *anti* conformation. The two TSF units do not overlap and there is no close, nonbonding Se···Se contact. The crystal structure of **2b** unlike **2a** contains no intermolecular stacking, and instead some face-to-edge interactions through very short Se···Se contacts existing between the neighboring TSF phanes.

 © WILEY-VCH Verlag GmbH, D-69451 Weinheim, 1998 1433-7851/98/3705-0620 $ 17.50+.50/0

The cyclic voltammogram of the TSF phane **2a** shows two reversible one-electron redox waves ($E_{1/2} = 0.47$ and 0.62 V) and one quasi-reversible two-electron redox wave ($E_{1/2} =$ 0.96 V), and the pattern is very similar to that of the TTF phane **1a**. The splitting of the first and second redox processes is ascribed to a marked through-space interaction between the two TSF units. When compared with the first half-wave oxidation potential of 4,4′(5′)-bis(methylthio)tetraselenafulvalene (BMT-TSF) ($E_{1/2} =$ 0.57 V), the low potential shift of the first oxidation of **2a** indicates that the resulting monocationic state is stabilized by transannular charge delocalization. The high potential shift of the second oxidation reflects destabilization of the dicationic state due to transannular coulombic repulsion. The finding that the combined third and fourth oxidation wave is higher than the second oxidation potential of BMT-TSF ($E_{1/2} =$ 0.86 V) also supports large coulombic repulsion in the tri- and tetracationic states. The cyclic voltammogram of **2b**, which has longer methylene bridges, shows only two broad two-electron redox waves at $E_{1/2} = 0.51$ and 0.93 V. The two TSF units do not interact strongly enough to split the first and second redox processes.



BMT-TSF

Preliminary attempts to electrocrystallize **2a** from a chlorobenzene solution containing a small amount of 2-propanol and with tetrabutylammonium perchlorate as supporting electrolyte gave thin black needles of the radical cation salt **2a** · ClO_4. Its conductivity at room temperature is 3.5 S cm^{-1}, which is one order of magnitude higher than that of its sulfur counterpart, **1a** · ClO_4 (0.16 S cm^{-1}).[6] This suggests interaction of the selenium atoms incorporated in the TSF phane.

Experimental Section

All reactions were performed in a nitrogen atmosphere. Cyclic voltammetry was conducted in benzonitrile containing 0.1 M [nBu$_4$N]ClO_4 with an Ag/AgCl standard electrode and Pt working and counter electrodes. Electrical conductivity was measured on a single crystal with a four-probe technique.

4a: To a stirred solution of ethynylmagnesium chloride[9] (0.61 mol) in anhydrous THF (450 mL) was added **3a**[10] (21.5 g, 149 mmol) at 0°C, and the mixture was stirred for 12 h at room temperature. The reaction mixture was then poured into ice water (1 L) and extracted with CH_2Cl_2 (3 × 300 mL). The extract was washed with water and dried ($MgSO_4$). After evaporation of the solvent, the residue was purified by column chromatography (silica gel, hexane) and recrystallized from hexane to give colorless plates of **4a** (11.6 g, 55 %). M.p. 40 – 40.5°C; ^{1}H NMR (400 MHz, $CDCl_3$): $\delta = 2.84$ (s, 2H; CH), 3.08 (s, 4H; CH_2); IR (KBr): $\tilde{\nu} = 2035$ cm^{-1} (C≡C); Elemental analysis calcd for $C_6H_6S_2$ (142.23): C 50.67, H 4.25; found: C 50.62, H 4.21.

4b: Yield 60 %; colorless oil; b.p. 74°C/1.5 mmHg; ^{1}H NMR (400 MHz, $CDCl_3$): $\delta = 2.24$ (quintet, $J = 6.8$ Hz, 2H; CH_2), 2.78 (s, 2H; CH), 2.89 (t, $J = 6.8$ Hz, 4H; SCH_2); IR (neat): $\tilde{\nu} = 2041$ cm^{-1} (C≡C); Elemental analysis calcd for $C_7H_8S_2$ (156.26): C 53.81, H 5.16; found: C 53.76, H 5.16.

5a: According to the recently reported procedure,[7] a solution of **4a** (142 mg, 1 mmol) and TMEDA (0.61 mL, 4 mmol) in anhydrous THF (10 mL) was treated successively with 1.6 N nBuLi in hexane (1.25 mL, 2 mmol), selenium powder (158 mg, 2 mmol), carbon diselenide (0.14 mL, 2.2 mmol), and water/THF (1/1 v/v, 20 mL). Water (30 mL) was added to the reaction mixture, and the insoluble materials were removed by filtration and washed with MeOH (30 mL). The filtrate and washings were combined and concentrated, and the residue was recrystallized from chlorobenzene to give purple plates of **5a** (324 mg, 51 %). M.p. 142 – 143°C; ^{1}H NMR (400 MHz, CS_2/$CDCl_3$): $\delta = 3.11$ (s, 4H; CH_2), 7.98 (s, 2H; CH); IR (KBr): $\tilde{\nu} = 899$ cm^{-1} (C=Se); Elemental analysis calcd for $C_8H_6S_2Se_6$ (640.02): C 15.01, H 0.94; found: C 15.23, H 0.95.

5b: Yield 58 %; purple plates from chloroform; m.p. 100 – 101°C; ^{1}H NMR (400 MHz, CS_2/$CDCl_3$): $\delta = 2.07$ (quintet, $J = 7.1$ Hz, 2H; CH_2), 2.97 (t, $J =$ 7.1 Hz, 4H; SCH_2), 7.91 (s, 2H; CH); IR (KBr): $\tilde{\nu} = 920$ cm^{-1} (C=Se); Elemental analysis calcd for $C_9H_8S_2Se_6$ (654.02): C 16.53, H 1.23; found: C 16.53, H 1.14.

2a: A mixture of **5a** (319 mg, 0.5 mmol) and trimethyl phosphite (2.4 mL, 20 mmol) in toluene (40 mL) was refluxed for 10 min. After evaporation of the solvent, the residual solid was extracted with CS_2 (50 mL) and purified by column chromatography (silica gel, CS_2, $R_f = 0.2$) to give a reddish purple solid as an isomeric mixture of **2a** (21 mg, 9 %). M.p. 194°C (decomp); ^{1}H NMR (400 MHz, CS_2/[D_6]acetone): $\delta = 2.94 – 3.09$ (m; CH_2), 7.288, 7.304, 7.345, 7.371, 7.375 (each s; fulvalenyl H); MS (positive-ion FAB): $m/z = 965$ [M^+] with an isotopic pattern for eight selenium atoms; Elemental analysis calcd for $C_{16}H_{12}S_4Se_8$ (964.19): C 19.93, H 1.25; found: C 19.96, H 1.19. Recrystallization from benzene/CS_2 afforded red columnar crystals of *cis-trans*-**2a**: m.p. 184°C (decomp); ^{1}H NMR (400 MHz, CS_2/[D_6]acetone): $\delta = 2.94 – 2.98$ (m, AA′BB′, 4H; CH_2), 3.05 – 3.09 (m, AA′BB′, 4H; CH_2), 7.304 (s, 2H; fulvalenyl H), 7.375 (s, 2H; fulvalenyl H).

2b (isomeric mixture): Yield 13 %; m.p. 159°C (decomp); ^{1}H NMR (400 MHz, CS_2/[D_6]acetone): $\delta = 2.03 – 2.15$ (m; CH_2), 2.76 – 2.88 (m; CH_2), 7.285. 7.287, 7.310, 7.321, 7.368 (each s; fulvalenyl H); MS (positive-ion FAB): $m/z = 993$ [M^+] with an isotopic pattern for eight selenium atoms; Elemental analysis calcd for $C_{18}H_{16}S_4Se_8$ (992.24): C 21.79, H 1.63; found: C 21.81, H 1.53. Recrystallization from CS_2 gave orange prisms of *cis-cis*-**2b**: m.p. 198°C (decomp); ^{1}H NMR (400 MHz, CS_2/[D_6]acetone): $\delta = 2.046$ (quintet, $J = 7.6$ Hz, 4H; CH_2), 2.830 (t, $J = 7.6$ Hz, 8H; CH_2), 7.310 (s, 4H; fulvalenyl H).

Received: September 17, 1998 [Z10938IE]
German version: *Angew. Chem.* **1998**, *110*, 640 – 642

Keywords: conducting materials · cyclophanes · heterocycles · radical ions · selenium · through-space interactions

[1] J. Ferraris, D. O. Cowan, V. Walatka, Jr., J. H. Perlstein, *J. Am. Chem. Soc.* **1973**, *95*, 948 – 949.
[2] G. Schukat, A. M. Richter, E. Fanghänel, *Sulfur Rep.* **1987**, *7*, 155 – 240; G. Schukat, E. Fanghänel, *ibid.* **1993**, *14*, 245 – 390; G. Schukat, E. Fanghänel, *ibid.* **1996**, *18*, 1 – 294.
[3] T. Otsubo, Y. Kochi, A. Bitoh, F. Ogura, *Chem. Lett.* **1994**, 2047-2050.
[4] The extensive chemistry of dimeric TTFs was recently reviewed: T. Otsubo, Y. Aso, K. Takimiya, *Adv. Mater.* **1996**, *8*, 203 – 211; see also: M. Adam, K. Müllen, *ibid.* **1994**, *6*, 439 – 459.
[5] J. Ippen, C. Tao-pen, B. Starker, D. Schweitzer, H. A. Staab, *Angew. Chem.* **1980**, *92*, 51 – 52; *Angew. Chem. Int. Ed. Engl.* **1980**, *19*, 67 – 69; F. Bertho-Thoraval, A. Robert, A. Souizi, K. Boubekeur, P. Batail, *J. Chem. Soc. Chem. Commun.* **1991**, 843 – 845; M. Adam, V. Enkelmann, H.-J. Räder, J. Röhrich, K. Müllen, *Angew. Chem.* **1992**, *104*, 331 – 333; *Angew. Chem. Int. Ed. Engl.* **1992**, *31*, 309 – 310; K. Matsuo, K. Takimiya, Y. Aso, T. Otsubo, F. Ogura, *Chem. Lett.* **1995**, 523 – 524; K. Takimiya, Y. Shibata, K. Imamura, A. Kashihara, Y. Aso, T. Otsubo, F. Ogura, *Tetrahedron Lett.* **1995**, *36*, 5045 – 5048; J. Tanabe, T. Kudo, M. Okamoto, Y. Kawada, G. Ono, A. Izuoka, T. Sugawara, *Chem. Lett.* **1995**, 579 – 580; K. Takimiya, K. Imamura, Y. Shibata, Y. Aso, F. Ogura, T. Otsubo, *J. Org. Chem.* **1997**, *62*, 5567 – 5574; S. Yunoki, K. Takimiya, Y. Aso, T. Otsubo, *Tetrahedron Lett.* **1997**, *38*, 3017 – 3020.
[6] K. Takimiya, Y, Aso, F. Ogura, T. Otsubo, *Chem. Lett.* **1995**, 735 – 736; K. Takimiya, Y, Aso, T. Otsubo, *Synth. Met.* **1997**, *86*, 1891 – 1892.
[7] K. Takimiya, A. Morikami, T. Otsubo, *Synlett* **1997**, 319 – 321.
[8] X-ray crystal structure analyses were conducted with a Rigaku AFC6C four-circle diffractometer ($Cu_{K\alpha}$ radiation, $\lambda = 1.54178$ Å, graphite monochromator, $T = 296$ K, ω-2θ scan, $2\theta_{max} = 126°$). The structures were solved by direct methods and refined by full-matrix least-squares on $|F|$. All calculations were performed using the crystallographic software package teXsan (Molecular Structure Cor-

 © WILEY-VCH Verlag GmbH, D-69451 Weinheim, 1998 1433-7851/98/3705-0621 $ 17.50+.50/0

poration, **1985** and **1992**). Crystal data for *cis-trans*-**2a**: $C_{16}H_{12}S_4Se_8$, $M = 964.19$, red columnar crystal ($0.25 \times 0.13 \times 0.06$ mm^3), monoclinic, space group $P2_1/n$, $a = 8.304(3)$, $b = 22.611(3)$, $c = 13.678(2)$ Å, $\beta = 103.71(2)^\circ$, $V = 2494.9(8)$ Å^3, $Z = 4$, $\rho_{calcd} = 2.567$ g cm^{-3}, $\mu = 168.70$ cm^{-1}, $R = 0.060$, $R_w = 0.051$, 4214 measured reflections, 3903 independent reflections, 2459 observed reflections [$I > 3.0\sigma(I)$], 253 refined parameters. Crystal data for *cis-cis*-**2b**: $C_{18}H_{16}S_4Se_8$, $M = 992.24$, red prismatic crystal ($0.42 \times 0.42 \times 0.30$ mm^3), monoclinic, space group $P2_1/a$, $a = 10.378(2)$, $b = 13.198(2)$, $c = 10.683(2)$ Å, $\beta = 113.78(1)^\circ$, $V = 1339.1(4)$ Å^3, $Z = 2$, $\rho_{calcd} = 2.461$ g cm^{-3}, $\mu = 157.43$ cm^{-1}, $R = 0.059$, $R_w = 0.070$, 4197 measured reflections, 2671 independent reflections, 2300 observed reflections [$I > 3.0\sigma(I)$], 136 refined parameters. Crystallographic data (excluding structure factors) for the structures reported in this paper have been deposited with the Cambridge Crystallographic Data Center as supplementary publication no. CCDC-100683. Copies of the data can be obtained free of charge on application to CCDC, 12 Union Road, Cambridge CB2 1EZ (fax: int. code + (44) 1223-336033; e-mail: deposit@ccdc.cam.ac.uk).

[9] A. B. Holmes, C. N. Sporikou, *Org. Synth. Coll. Vol. VIII* **1993**, 606–609.

[10] P. Allen, Jr., *J. Am. Chem. Soc.* **1935**, *57*, 198–199; S. Yoneda, H. Kitano, K. Fukui, *Kogyo Kagaku Zasshi* **1962**, *65*, 1816–1819 [*Chem. Abstr.* **1963**, *59*, 2679e].

A Bifunctional Lewis Acidic Spacer in Self-Assembled Molecular Stairs and Ladders**

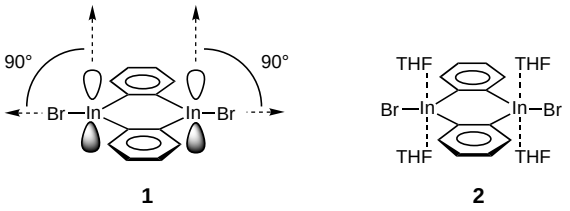
François P. Gabbaï,* Annette Schier, and Jürgen Riede

Neutral polyfunctional Lewis acids are becoming a well-established class of compounds which serve as anion receptors[1] and catalysts.[2] An emerging field of application concerns their use as electrophilic spacers in molecular self-assembly. Whereas a great number of self-assembled coordination macromolecules have been obtained by linking metallic centers with polyfunctional Lewis bases,[3] the use of organometallic polyfunctional Lewis acids as linker unit between nucleophiles has been only scarcely examined. For example, bis(stannyl)methanes[4a] and mercury crown compounds[4b, c] can form polymers or oligomers. More recently, palladium- and platinum-based cationic linkers were used as building blocks for the synthesis of coordination dendrimers[5a] and molecular hexagons.[5b] Considering the growing interest in coordination macromolecules[6] as microporous solids[7] and catalysts,[8] Lewis acidic spacers constitute an appealing novelty which greatly broadens the scope of the possible assembly sets. Here we report our findings on the use of a neutral bifunctional Lewis acidic spacer in the synthesis of self-assembled molecular stairs and ladders.

[*] Dr. F. P. Gabbaï, Dr. A. Schier, J. Riede
Anorganisch-chemisches Institut
der Technischen Universität München
Lichtenbergstrasse 4, D-85747 Garching (Germany)
Fax: (+49) 89-2891-3125
E-mail: f.gabbai@lrz.tu-muenchen.de

[**] This work was supported by the European Union (Training and Mobility of Researchers Program) and the Deutsche Forschungsgemeinschaft. We thank Prof. H. Schmidbaur for the necessary technical equipment.

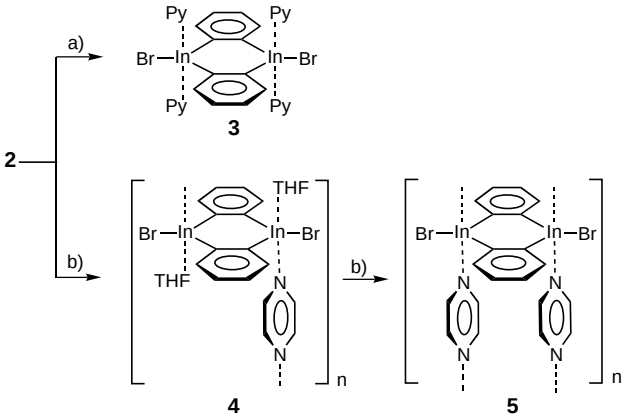
The synthesis and structure of the first *ortho*-phenyleneindium complexes were reported in 1996 and 1997.[9] *ortho*-Phenyleneindium bromide is dimeric (**1**) and was isolated as the tetrakis(THF) adduct **2**.[9a] This simple molecule contains



1 **2**

two electrophilic indium centers positioned at the opposite apexes of a flat six-membered ring. Since the vacant indium p orbitals are oriented orthogonal to the plane containing the diindacycle, **1** appears to be well suited for the formation of coordination macromolecules with building blocks assembled at 90° angles.[10]

To assess the lability of the coordinated THF molecules, a solution of **2** in THF was treated with an excess of pyridine. Crystals of **3** formed instantaneously at 25 °C (Scheme 1). The



Scheme 1. Reaction of 2 with pyridine (py) and pyrazine in THF at 25 °C. a) Excess pyridine; b) 2 equiv of pyrazine.

solid-state structure of **3**[11] is very similar to that of **2**, however, the axial positions of the indium coordination sphere in **3** are occupied with pyridine instead of THF ligands.

The isolation of **3** gave us a clue as to which type of nucleophile to combine with **1** for synthesizing a coordination polymer. Addition of one or two equivalents of pyrazine to a solution of **2** in [D_8]THF did not result in the formation of a precipitate. Moreover, as suggested by the fact that the chemical shifts of the aromatic proton of **2** and pyrazine are the same,[12] there is no strong association in solution. Pyrazine remains essentially unligated, and **1** still exists as its tetrakis(THF) adduct **2**. However, upon slow cooling of a solution of **2** in THF with one or two equivalents of pyrazine, crystals of a new compound (**4**·2THF) formed (Scheme 1). The ^{1}H NMR spectrum indicated the presence of one molecule of pyrazine and four molecules of THF per molecule of **1**.[12] Upon exposure to a dry, inert atmosphere, crystals of **4** become brittle through partial loss of THF, as indicated by elemental analysis. Compound **4** crystallizes with two inter-

stitial THF molecules and consists of polymeric [**1**-(THF)$_2$-pyrazine]$_n$.[11] Figure 1 shows a portion of a polymeric chain. The diindacycle is planar within experimental error, and the bromine atoms are displaced by 0.274 Å out of the plane containing the phenylene rings and the indium atoms. Each indium atom is in a trigonal-bipyramidal coordination geometry which does not exhibit any noteworthy angular distortion. The two phenylene rings and the bromine atom are at the equatorial sites. The axial positions are unsymmetrically occupied by one THF and one pyrazine molecule. The In–C, In–Br, and In–O(1) bond lengths fall within the expected range and are similar to those in **2**.[9a] The In–N distance of 2.478(5) Å is almost equal to the mean In–N distance in **3** (2.477 Å).

Examination of the cell-packing diagram reveals the polymeric nature of **4**. The "infinite chains" run parallel to one another and do not form any short interchain contacts. The monomeric units **1**-(THF)$_2$-pyrazine are linked through a single In–N linkage. All diindacycles are parallel to one another, and the In″-In-In′ angle of 94.8° approaches normality (Figure 1). Thus, chains of **4** are reminiscent of stairs in which the diindacycles constitute the steps. The solvate THF molecules occupy the void space between the chains and are not involved in intermolecular contacts.

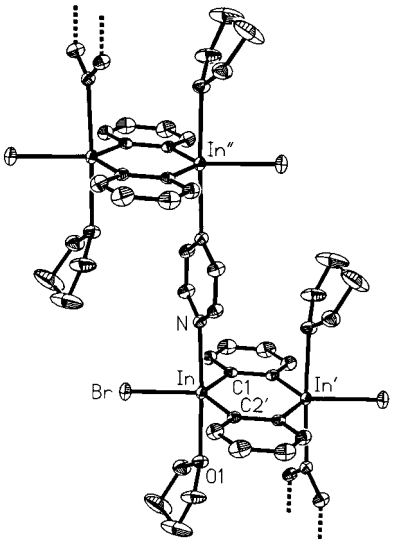


Figure 1. View of two monomeric units of polymer **4**; ORTEP drawing at the 30% probability level. Selected bond lengths [Å] and angles [°]: In–C(1) 2.156(3), In–C(2)′ 2.151(3), In–Br 2.542(1), In–O(1) 2.463(4), In–N 2.478(3); C(1)-In-C(2)′ 124.0(1), C(1)-In-Br 113.1(1), C(2)′-In-Br 122.7(1), N-In-O(1) 177.6(1).

Stoichiometric control of the assembly of **1** with pyrazine was our next aim. When the ratio of pyrazine to **1** in THF was increased to four, crystals of a novel compound (**5**·2THF) precipitated spontaneously (Scheme 1). The pale yellow needles obtained have strongly anisotropic mechanical properties and are easily cleaved along the direction of growth axis. The ^{1}H NMR spectrum revealed the presence of two molecules of pyrazine and two molecule of THF per molecule of **1**.[12] However, as observed for **4**·2THF, loss of THF occurs rapidly at 25 °C when the crystals are exposed to a dry, inert atmosphere. Definitive structural insights were gained from an X-ray study.[11] Compound **5** crystallizes with two interstitial THF molecules and consists of polymeric [**1**-(pyrazine)$_2$]$_n$. The structure of the monomeric unit can be derived from that of **3** by replacing the four axial pyridine ligands by two bridging pyrazine ligands (Figure 2).

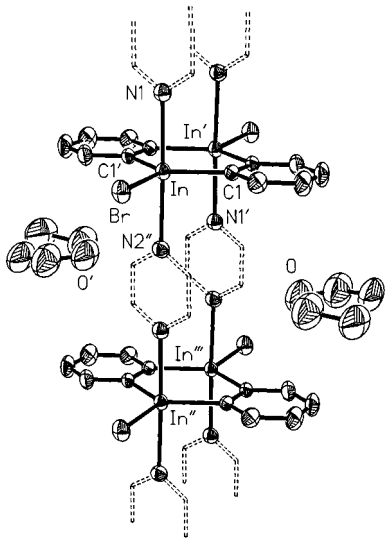


Figure 2. View of two monomeric units of polymer **5** with the interstitial THF molecules; ORTEP drawing at the 30% probability level. The disordered pyrazine molecules are represented by dotted lines in their average positions. Selected bond lengths [Å] and angles [°]: In–C(1) 2.159(3), In–Br 2.523(1), In–N(1) 2.528(4), In–N(2)″ 2.540(4); C(1)-In-C(1)′ 122.4(2), C(1)-In-Br 118.8(1), N(1)-In-N(2)″ 176.5(1).

All distances and angles in **5** are similar to those in **3** and **4** with the exception of the appreciably longer In–N distances (2.528(4) – 2.540(4) Å). As in **4**, the infinite chains run parallel to one another and do not form any short interchain contacts. In contrast to **4**, the monomeric units of **5** are assembled through two In–N linkages. Thus, chains of **5** ressemble a ladder in which the diindacycles constitute the rungs, and the [In-pyrazine]$_n$ sequences the legs. With In′-In-In″ and In-In′ – In‴ angles of 88.6 and 91.4°, respectively, the cavity generated between the indiviual rungs of the ladder approximately resembles a rectangular space of 7.8 × 3.6 Å (In–In′ × N1′–N2″). The THF molecules are position halfway between the rungs and do not penetrate the cavity deeply enough to be involved in short intermolecular contacts.

Polymers **4** and **5** are insoluble in nonpolar sovents. However, upon being heated in their THF mother liquors for a short time at reflux, the polymers dissolve completely. This process is reversible, and both polymers spontaneously reform upon cooling. When heated in the solid state, **4** and **5** first become brittle (0 – 50 °C) and then decompose at 380 and 300 °C, respectively.

The present results demonstrate that bifunctional Lewis acids are useful building blocks for coordination macromolecules, and that they can be regarded as electrophilic spacers. The system **1**/pyrazine/THF is versatile, and the stoichiometry and composition of the assembly can be controlled.

 © WILEY-VCH Verlag GmbH, D-69451 Weinheim, 1998 1433-7851/98/3705-0623 $ 17.50+.50/0

Experimental Section

3: Compound **3** spontaneously crystallized from a solution of **1**-$(THF)_2$ (40 mg, 58 μmol) in THF (0.5 mL) upon addition of pyridine (25 μL, 310 μmol). Yield: 79 % (40 mg); m.p. 235 °C (decomp); elemental analysis calcd for $C_{32}H_{28}Br_2In_2N_4$: C 44.7, H 3.3, N 6.5; found: C 44.3, H 3.3, N 6.2.

4·2THF and **5**·2THF: **1**-$(THF)_2$ (69 mg, 100 μmol) and pyrazine (16 mg, 200 μmol for **4**·2THF and 32 mg, 400 μmol for **5**·2THF) were mixed in Schlenck tubes, and THF (2 mL) was added. The resulting solutions were slowly concentrated until crystalline material started to appear on the sides of the tubes. All solids were then redissolved by heating the solutions at reflux for a short time. Upon slow cooling of the solutions from 60 to −15 °C, **4**·2THF and **5**·2THF were obtained as crystals in 67 % (80 mg) and 60 % yields (50 mg), respectively. Compounds **4**·2THF and **5**·2THF spontaneously loose THF at 25 °C. Elemental analysis carried out on "withered" samples indicated a THF depletion of 78 % for **4**·2THF and 34 % for **5**·2THF after one week at 25 °C under atmospheric pressure.

Received: October 15, 1998 [Z11038IE]
German version: *Angew. Chem.* **1998**, *110*, 646 – 648

Keywords: indium · ladder polymers · Lewis acids · metallacycles · supramolecular chemistry

[1] Reviews: a) B. Dietrich, *Pure Appl. Chem.* **1993**, *65*, 1457; b) D. E. Kaufmann, A. Otten, *Angew. Chem.* **1994**, *106*, 1917 – 1920; *Angew. Chem. Int. Ed. Engl.* **1994**, *33*, 1832 – 1834; c) M. F. Hawthorne, Z. Zheng, *Acc. Chem. Res.* **1997**, *30*, 267 – 276; d) F. P. Schmidtchen, M. Berger, *Chem. Rev.* **1997**, *97*, 1609 – 1646.

[2] a) T. Ooi, M. Takahashi, K. Maruoka, *J. Am. Chem. Soc.* **1996**, *118*, 11307 – 11308; b) J. D. Wuest, B. Zacharie, *ibid.* **1985**, *107*, 6121 – 6123.

[3] a) J. L. Atwood, J. E. D. Davies, D. D. MacNicol, F. Vögtle, K. S. Suslick, *Comprehensive Supramolecular Chemistry*, *Vol.* 9, Pergamon, Oxford, **1996**; recent reviews: b) E. C. Constable, *J. Chem. Commun. Chem. Soc.* **1997**, 1073 – 1080; c) A. Williams, *Chem. Eur. J.* **1997**, *3*, 15 – 19; d) H. Plenio, *Angew. Chem.* **1997**, *109*, 358 – 360; *Angew. Chem. Int. Ed. Engl.* **1997**, *36*, 348 – 350.

[4] a) M. Austin, K. Gebreyes, H. G. Kuivila, K. Swami, J. A. Zubieta, *Organometallics* **1987**, *6*, 834 – 842; b) Z. Zheng, C. B. Knobler, M. D. Mortimer, M. F. Hawthorne, *Inorg. Chem.* **1996**, *35*, 1235 – 1243; c) I. A. Tikhonova, F. M. Dolgushin, A. I. Yanovsky, Y. T. Struchkov, A. N. Gavrilova, L. N. Saitkulova, E. S. Shubina, L. M. Epstein, G. G. Furin, V. B. Shur, *J. Organomet. Chem.* **1996**, *508*, 271 – 273.

[5] a) W. T. S. Huck, R. Hulst, P. Timmerman, F. C. J. M. van Veggel, D. N. Reinhoudt, *Angew. Chem.* **1997**, *109*, 1046 – 1049; *Angew. Chem. Int. Ed. Engl.* **1997**, *36*, 1006 – 1008; b) P. J. Stang, N. E. Persky, J. Manna, *J. Am. Chem. Soc.* **1997**, *119*, 4777 – 4778.

[6] a) C. Janiak, *Angew. Chem.* **1997**, *109*, 1499 – 1502; *Angew. Chem. Int. Ed. Engl.* **1997**, *36*, 1431 – 1434; b) P. Ball, *Designing the Molecular World*; Princeton University Press, New Jersey, **1994**.

[7] a) M. Kondo, T. Yoshitomi, K. Seki, H. Matsuzaka, S. Kitagawa, *Angew. Chem.* **1997**, *109*, 1844 – 1846; *Angew. Chem. Int. Ed. Engl.* **1997**, *36*, 1725 – 1727; b) O. M. Yaghi, H. Li, *ibid.* **1995**, *107*, 232 – 234 and **1995**, *34*, 207 – 209; c) S. Subramanian, M. J. Zaworotko, *ibid.* **1995**, *107*, 2295 – 2297 and **1995**, *34*, 2127 – 2129; d) O. M. Yaghi, H. Li, *J. Am. Chem. Soc.* **1996**, *118*, 295 – 296. e) G. B. Gardner, D. Venkataraman, J. S. Moore, J. S. Lee, *Nature* **1995**, *374*, 792 – 795.

[8] M. Fujita, Y. J. Kwon, S. Washizu, K. Ogura, *J. Am. Chem. Soc* **1994**, *116*, 1151 – 1152.

[9] a) F. P. Gabbaï, A. Schier, J. Riede, D. Schichl, *Organometallics* **1996**, *15*, 4119 – 4121; b) M. A. Dam, T. Nijbacker, B. C. de Pater, F. J. J. de Kanter, O. S. Akkerman, F. Bickelhaupt, W. J. J. Smeets, A. L. Speck, *ibid.* **1997**, *16*, 511 – 512.

[10] a) P. Losier, M. J. Zawortko *Angew. Chem.* **1996**, *108*, 2957 – 2960; *Angew. Chem. Int. Ed. Engl.* **1996**, *35*, 2779 – 2782; b) M. Fujita, Y. J. Kwon, O. Sasaki, K. Yamaguchi, K. Ogura, *J. Am. Chem. Soc.* **1995**, *117*, 7287 – 7288; c) J. Whiteford, C. V. Lu, P. J. Stang, *ibid.* **1997**, *119*, 2524 – 2533; d) M. Fujita, *J. Synth. Org. Chem. Jpn.*, **1996**, *54*, 953; e) H. Rauter, I. Mutikainen, M. Blomberg, C. J. L. Lock, P. Amo-Ochoa, E. Freisinger, L. Randaccio, E. Zangrando, E. Charparin, B. Lippert, *Angew. Chem.* **1997**, *109*, 1353 – 1357; *Angew. Chem. Int. Ed. Engl.* **1997**, *36*, 1296 – 1231.

[11] Crystal structure analyses: Enraf Nonius CAD4 diffractometer, $Mo_{K\alpha}$ radiation ($\lambda = 0.71073$ Å). The data were corrected for Lorentzian and polarization effects and for absorption [psi scans]. The structure were solved with direct methods (SHELXS-86), and refined against F^2 (SHELXL-93).[13] Hydrogen atoms were calculated in idealized geometry and allowed to ride on their corresponding C atom with isotropic contributions ($U_{iso(fix)} = 1.5\,U_{eq}$ of the attached C); non-hydrogen atoms were refined with anisotropic displacement parameters with the exception of those of one pyridine ring in **3** [N22 – C225], which was treated isotropically as a rigid group. The pyrazine rings in **5**·2THF are disordered and were refined in split positions. The function minimized was $wR2 = \{[\Sigma w(F_o^2 - F_c^2)^2]/\Sigma[w(F_o^2)^2]\}^{1/2}$, $w = [\sigma^2(F_o^2) + (ap)^2 + bp]^{-1}$, $p = (F_o^2 + 2F_c^2)/3$. Structure data: **3**: $C_{32}H_{28}Br_2In_2N_4$, $M_r = 858.04$, triclinic, $a = 9.489(1)$, $b = 9.915(1)$, $c = 16.846(2)$ Å, $\alpha = 88.21(1)$, $\beta = 87.47(1)$, $\gamma = 86.72(1)^\circ$, space group $P\bar{1}$, $Z = 2$, $V = 1580.1(3)$ Å^3, $\rho_{calcd} = 1.803$ g cm^{-3}, $F(000) = 832$, $T = -80$ °C, $\mu(Mo_{K\alpha}) = 40.15$ cm^{-1}, $T_{min}/T_{max} = 0.731/0.999$; of 9904 measured reflections [$(\sin\theta/\lambda)_{max} = 0.64$ Å^{-1}], 6780 were used for the refinement of 319 refined, R_1 (wR_2) = 0.0404 (0.1000), $a = 0.0437$, $b = 5.39$, residual electron densities: $+1.91/-0.94$ e Å^{-3}. **4**·2THF: $C_{32}H_{44}Br_2In_2N_2O_4$, $M_r = 904.15$, monoclinic, $a = 8.716(1)$, $b = 10.609(1)$, $c = 19.359(2)$ Å, $\beta = 91.46(1)^\circ$, space group $P2_1/c$, $Z = 2$, $V = 1789.5(3)$ Å^3, $\rho_{calcd} = 1.689$ g cm^{-3}, $F(000) = 900$, $T = -74$ °C, $\mu(Mo_{K\alpha}) = 35.57$ cm^{-1}, $T_{min}/T_{max} = 0.757/0.999$; of 3688 measured reflections [$(\sin\theta/\lambda)_{max} = 0.64$ Å^{-1}], 3583 were used for the refinement of 190 parameters, R_1 (wR_2) = 0.0277 (0.0641), $a = 0.0318$, $b = 1.10$, residual electron densities: $+1.02/-0.93$ e Å^{-3}. **5**·2THF: $C_{28}H_{32}Br_2In_2N_4O_2$, $M_r = 864.04$, monoclinic, $a = 12.365(1)$, $b = 16.231(1)$, $c = 7.830(1)$ Å, $\beta = 93.88(1)^\circ$, space group $C2/m$, $Z = 2$, $V = 1567.9(3)$ Å^3, $\rho_{calcd} = 1.792$ g cm^{-3}, $F(000) = 824$, $T = +20$ °C, $\mu(Mo_{K\alpha}) = 40.50$ cm^{-1}, $T_{min}/T_{max} = 0.834/0.999$; of 2896 measured reflections [$(\sin\theta/\lambda)_{max} = 0.64$ Å^{-1}], 1432 were used for the refinement of 111 parameters, R_1 (wR_2) = 0.0292 (0.0626), $a = 0.0769$, $b = 0.20$, residual electron densities: $+0.62/-0.67$ e Å^{-3}. Further details on the crystal structure investigation may be obtained from the Fachinformationszentrum Karlsruhe, D-76344 Eggenstein-Leopoldshafen, Germany (fax: (+49) 7247-808-666 (Frau S. Höhler-Schlimm); e-mail: crysdata@fiz-karlsruhe.de), on quoting the depository number CSD 407782, CSD 407781, and CSD 407780.

[12] Incremental addition of pyrazine (2×4 mg, 2×50 μmol) to **2** (34 mg of **1**-$(THF)_2$,[9a] 50 μmol) in [D_8]THF (0.5 mL) did not result in any change in the chemical shift of the aromatic protons of **2** and pyrazine. For **3** – **5**, heating the samples for a short time to 65 °C was necessary to obtain solutions. For **4** and **5**, the ^{1}H and ^{13}C chemical shifts of the diindacycle phenylene atoms are the same as those measured for **2**.[9a] The ^{1}H and ^{13}C chemical shifts of the pyrazine atoms in **4** and **5** correspond exactly to those measured for the free bases in [D_8]THF. **3:** ^{1}H NMR (400 MHz, [D_8]THF): $\delta = 7.13$ (m, 4H; H(2, 3,6, 7)), 7.33 (m, 8H; H(3, 5), py), 7.57 (m, 4H; H(1, 4, 5, 8)), 7.75 (m, 4H; H(4), py), 8.54 (m, 8H; H(2, 6), py); ^{13}C NMR (400 MHz, [D_8]THF): $\delta = 125.0$ (s, C(3, 5), py), 127.7 (s, C(2, 3, 6, 7)), 137.7 (s, C(1, 4, 5, 8), 137.8 (s, C(4), py), 150.4 (s, C(2, 6)) 170.2 (s, *C*In).

[13] SHELXL 93, G. M. Sheldrick, Program for the Refinement of Structures, Universität Göttingen, **1993**. SHELXTL PLUS, Program Package for Structure Solution and Refinement, Version 4.2, Siemens Analytical Instruments Inc., Madison, WI, **1990**.

 © WILEY-VCH Verlag GmbH, D-69451 Weinheim, 1998 1433-7851/98/3705-0624 $ 17.50+.50/0

Dioldehydratase Binds Coenzyme B_{12} in the "Base-On" Mode: ESR Investigations on Cob(II)alamin**

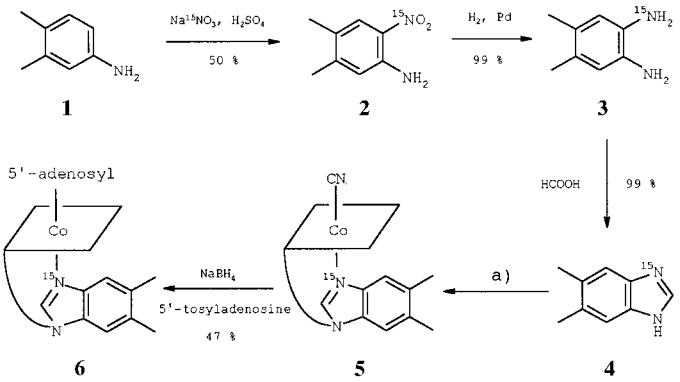
Andreas Abend, Rainer Nitsche, Vahe Bandarian, Erhard Stupperich, and János Rétey*

For several coenzyme B_{12}-dependent enzymes it has been shown that in the enzyme–coenzyme complex the axial dimethylbenzimidazole ligand of cobalt is replaced by the imidazole of a histidine residue in the polypeptide chain.[1] Two X-ray structure analyses[2, 3] as well as ESR spectra of the complexes with ^{15}N-labeled apoenzymes and unlabeled coenzyme led to this unexpected finding.[4, 5]

The ESR spectra of Cob(II)alamin is distinguished by an octet of triplets. The hyperfine splitting responsible for the octet arises from the interaction of the unpaired electron with the ^{59}Co nucleus [$I(^{59}Co) = 7/2$)].[6, 7] Interaction of the axial (but not the equatorial) nitrogen ligands with the unpaired electron, which resides mainly in the d_{z^2} orbital, leads to superhyperfine splitting. This results in a triplet (having lines with an intensity ratio of 1:1:1) in the case of ^{14}N, and in a doublet in the case of the heavy isotope ^{15}N [$I(^{15}N) = 1/2$).

More recent studies have indicated that the binding mode is not the same for all coenzyme B_{12}-dependent enzymes, but that there are "base-off" and "base-on" classes.[8, 9] In the latter, the dimethylbenzimidazole ligand is proposed to remain coordinated to the cobalt ion in the enzyme–coenzyme complex. To provide direct proof for the "base-on" binding mode for the dioldehydratase from *Salmonella typhimurium* we synthesized a sample of coenzyme B_{12} in which one of the nitrogen atoms of the dimethylbenzimidazole ligand is labeled with ^{15}N (Scheme 1).

3,4-Dimethylaniline (**1**) was nitrated with $Na^{15}NO_3$ in concentrated sulfuric acid, and the resulting 4,5-dimethyl-[2-^{15}N]nitroaniline (**2**) was catalytically reduced to [1-^{15}N]1,2-diamino-4,5-dimethylbenzene (**3**). Reaction of **3** with concentrated formic acid afforded [^{15}N]5,6-dimethylbenzimidazole (**4**), which was isolated in crystalline (m.p. 200°C) form. Compound **4** was biosynthetically incorporated into vitamin B_{12} (**5**) by using propionibacteria. The ^1H NMR spectrum of **5** unambiguously showed a geminal $^1H-^{15}N$ coupling. Reduction of **5** with $NaBH_4$ and subsequent reaction with 5′-tosyladenosine[11, 12]



Scheme 1. Synthesis of coenzyme B_{12} in which one the the nitrogen atoms of the dimethylbenzimidazole ligand is ^{15}N labeled. a) Propionibacteria.

afforded coenzyme B_{12} **6** labeled with one ^{15}N isotope in its dimethylbenzimidazole ligand.

The gene coding for dioldehydratase in *Salmonella typhimurium*[13] was subcloned in the expression vector pT7.7[14] and overexpressed in *E. coli*. When the cells were broken down by sonification, the enzyme remained in the insoluble cell debris, which was separated from the soluble proteins by centrifugation. Extraction of the membrane-bound enzyme with sodium cholate (46 mM) provided soluble dioldehydratase, which was subsequently purified by gel filtration (Pharmacia, HiLoad 26/60, Superdex 200 prep grade) in the presence of 125 mM 1,2-propanediol and 23 mM sodium cholate. The enzyme was electrophoretically homogeneous and had a specific activity of 95 U mg^{-1}.

For measuring the ESR spectra[16] the enzyme solution was concentrated to 60 mg mL^{-1} (250 μM), and 250 μL thereof was incubated with 60 nmol coenzyme B_{12} for 30 min at 37°C in the dark. Subsequent gel filtration on a Sephadex-G-25 column removed the possible excess free coenzyme. The high resolution of the axial spectrum at low field (2700–3000 G) provides additional evidence for the binding of the coenzyme to the enzyme. After addition of 60 nmol glycolaldehyde the samples were transfered into ESR vials, incubated for 24 h at room temperature without protection from light. The exposure to daylight led to homolysis of the cobalt–carbon bond and formation of cob(II)alamin and an organic radical. As a control, the free coenzyme was also submitted to homolysis in a potassium phosphate buffer (50 mM, pH 6.8) containing 10% glycerol and 5% 1,2-propanediol.

Figure 1 shows the ESR spectrum of free, unlabeled cob(II)alamin and the expanded region around 3400 G. In contrast, the spectrum of cob(II)alamin with (1-^{15}N)dimethylbenzimidazole as ligand has a doublet instead of the triplet in the same region (Figure 2). Although based on the labeling pattern half of the coordinating ligands should bear a ^{14}N atom in the first ligand sphere of the cobalt, the resulting triplet is apparently buried. Simulation of the ESR spectrum in the same region (3400 G, Figure 3) shows that at a linewidth of 8 G no superhyperfine splitting due to ^{14}N is discernible. The experimental spectrum shows the sum of the superhyperfine splittings arising from the coordination of both nitrogen atoms to the cobalt.

[*] Prof. Dr. J. Rétey, Dipl.-Chem. Rainer Nitsche
Institut für Organische Chemie der Universität
Richard-Willstätter-Allee, D-76128 Karlsruhe (Germany)
Fax: (+49) 721-6084823
E-mail: biochem@ochhades.chemie.uni-karlsruhe.de

Dr. A. Abend, V. Bandarian
Institute for Enzyme Research, University of Wisconsin-Madison
1710 University Avenue, Madison, WI 53705-4098 (USA)

Dr. E. Stupperich
Angewandte Mikrobiologie der Universität
Albert-Einstein Allee 11, D-89069 Ulm (Germany)

[**] This work was supported financially by the European Union, the Deutsche Forschungsgemeinschaft, and the Fonds der Chemischen Industrie. We thank Dr. T. A. Bobik, Gainesville, FL, for providing us with the gene coding for diodehydratase from *Salmonella typhimurium*, and Prof. P. A. Frey, Madison, WI, for discussions and support for A. A.

 © WILEY-VCH Verlag GmbH, D-69451 Weinheim, 1998 1433-7851/98/3705-0625 $ 17.50+.50/0

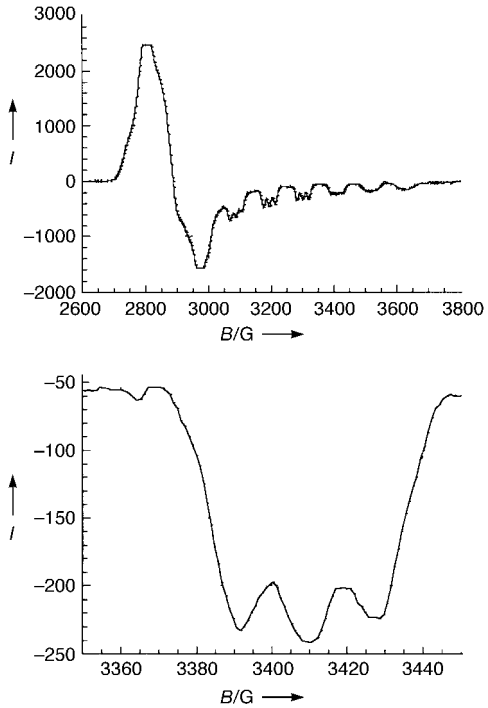


Figure 1. ESR spectrum of the free, unlabeled cob(II)alamin (top) and expansion of the triplet at 3400 G (bottom). Intensity I in arbitrary units.

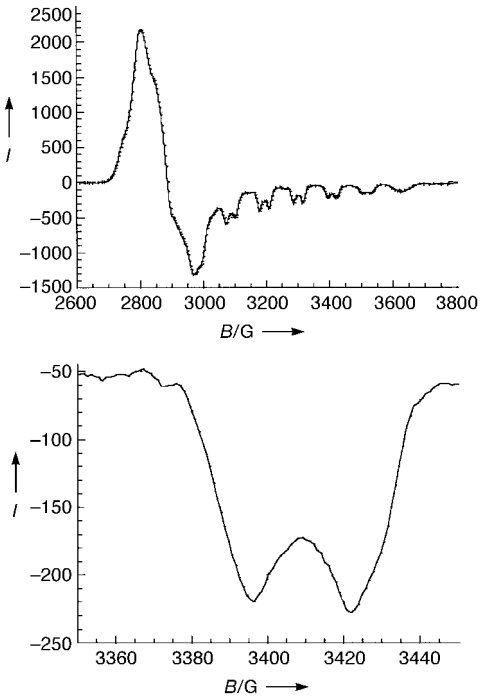


Figure 2. ESR spectrum of the free cob(II)alamin labeled with ^{15}N in the dimethylbenzimidazole ligand (top) and expansion of the doublet at 3400 G (bottom). Intensity I in arbitrary units.

The ESR spectra of the dioldehydratase B_{12} inhibitor complexes are similar but not identical (Figure 4). The dominant signal of the inhibitor radical at 3300 G ($g = 2$) obscures the superhyperfine splitting at lower fields. However, the multiplet structure of the superhyperfine splittings can be readily seen at higher fields. The region at 3400 G

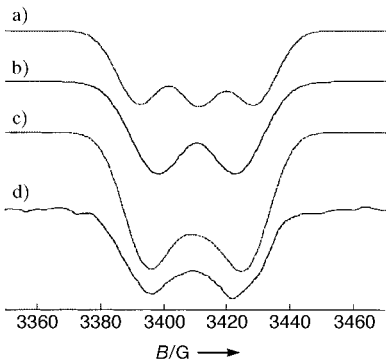


Figure 3. Section of the simulated ESR spectra (3350 – 3470 G) for the free (not enzyme-bound) cob(II)alamin in solution. a) The spectrum expected for coordination of the cobalt with ^{14}N and b) that with ^{15}N coordination. c) Sum of spectra a) and b). d) The experimental spectrum. Intensity I in arbitrary units.

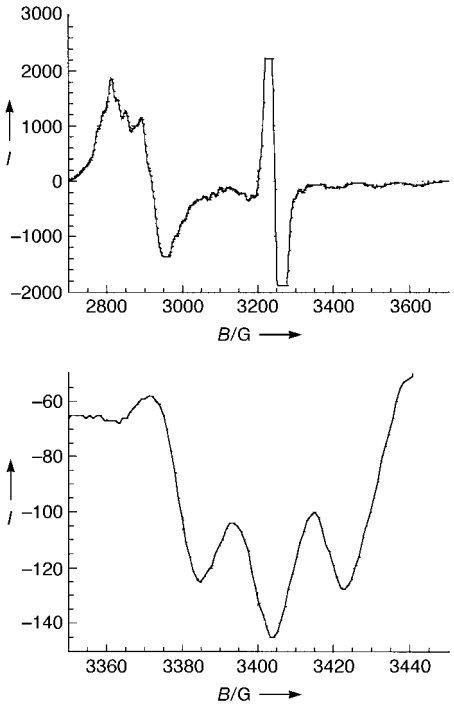


Figure 4. ESR spectrum of the unlabeled cob(II)alamin bound to dioldehydratase (top) and expansion of the triplet at 3400 G (bottom). Intensity I in arbitrary units.

contains a triplet for the enzyme complex with unlabeled cob(II)alamin (Figure 4), whereas a doublet is seen in the spectrum of the complex with [^{15}N]cob(II)alamin (Figure 5). It is noteworthy that the coupling constant A_N in free cob(II)-alamin is smaller than that in the enzyme-bound coenzyme. In the spectra of free cob(II)alamin we found $A_N = 18$ G for the unlabeled (^{14}N) and 26 G for the ^{15}N-labeled coenzyme. The ratio of the coupling constants $A_{^{15}N}/A_{^{14}N}$ compares favorably with the quotient of the theoretically expected gyromagnetic nuclear ratio of 1.44. The coupling constant for the cobalt is 105 G.

In the spectrum of the enzyme-bound cob(II)alamin A_N is 20 G for the unlabeled and 31 G for the ^{15}N-labeled coenzyme. Hence the ratio of the coupling constants is calculated to 1.5. Since the experimentally determined coupling constant

 © WILEY-VCH Verlag GmbH, D-69451 Weinheim, 1998 1433-7851/98/3705-0626 $ 17.50+.50/0

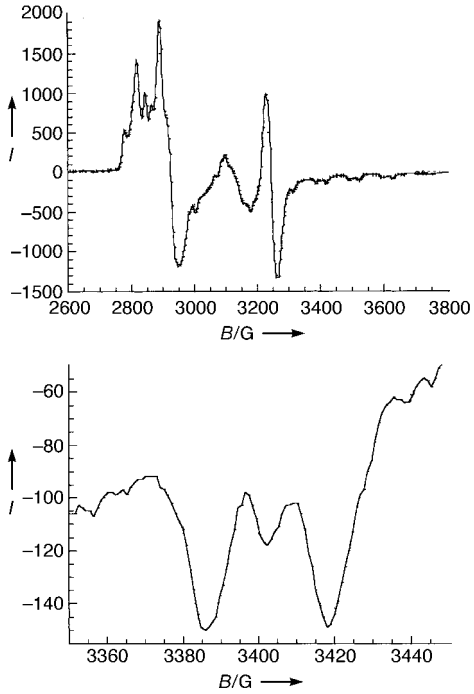


Figure 5. ESR spectrum of the ^{15}N-labeled cob(II)alamin bound to dioldehydratase (top) and expansion of the doublets with the partially obscured triplet at 3400 G (bottom). Intensity *I* in arbitrary units.

arises from the sum of the overlapping spectra, it is larger than that expected for the unlabeled (^{14}N) coenzyme. This conclusion is confirmed by the simulated spectra (Figure 6a, b).

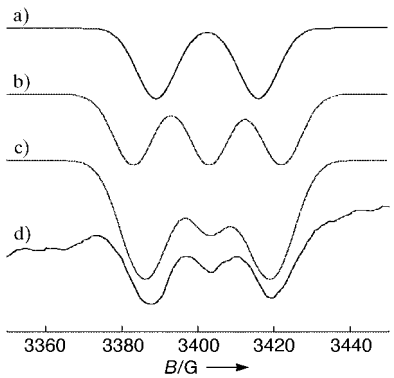


Figure 6. Section of the simulated ESR spectra (3350 – 3450 G) for the enzyme-bound cob(II)alamin in solution. a) The spectrum expected for coordination of cobalt with ^{15}N and b) that with ^{14}N coordination. c) Sum of spectra a) and b). d) The experimental spectrum. Intensity *I* in arbitrary units.

For these we assumed coupling constants of 20 G for ^{14}N and 28 G for ^{15}N (the gyromagnetic nuclear ratio is thus 1.4, the assumed linewidth 6 G). The simulated spectrum (Figure 6c) in the region around 3400 G is consistent with the experimental spectrum. The sum of the simulated individual spectra results in a spectrum similar to the experimental one.

We chose glycolaldehyde as a suicide inhibitor because it had been reported to cause immediate homolysis of the cobalt – carbon bond in the dioldehydratase-bound coenzyme B_{12}.[17] The initially formed 5′-deoxyadenosyl radical most likely abstracts a hydrogen atom from glycolaldehyde, leading to a stable enzyme-bound inhibitor radical. Characterization of this radical is in progress. The results presented here provide unambiguous evidence that dioldehydratase binds coenzyme B_{12} in the "base-on" mode.

Received: August 28, 1997 [Z10862IE]
German version: *Angew. Chem.* **1998**, *110*, 643 – 645

Keywords: bioorganic chemistry · coenzymes · EPR spectroscopy · isotopic labeling · vitamin B_{12}

[1] E. Stupperich, H. J. Eisinger, S. P. J. Albracht, *Eur. J. Biochem.* **1990**, *193*, 105.
[2] F. Mancia, N. H. Keep, A. Nakagawa, P. F. Leadlay, S. McSweeney, B. Rasmussen, P. Bösecke, O. Diat, P. R. Evans, *Structure* **1996**, *4*, 339.
[3] C. L. Drennan, S. Huang, J. T. Drummond, R. G. Matthews, M. L. Ludwig, *Science* **1994**, *266*, 1669.
[4] R. Padmakumar, S. Taoka, R. Padmakumar, R. Banerjee, *J. Am. Chem. Soc.* **1995**, *117*, 7033.
[5] O. Zelder, B. Beatrix, F. Kroll, W. Buckel, *FEBS Letters* **1995**, *369*, 252.
[6] J. R. Pilbrow in *B_{12}, Vol. 1* (Ed.: D. Dolphin), Wiley, New York, **1982**, p. 431.
[7] J. R. Pilbrow, W. E. Winfield, *Mol. Phys.* **1973**, *25*, 1073.
[8] T. Toraya, lecture at the 4th European Symposium on Vitamin B_{12} and B_{12}-Proteins, Innsbruck, Austria, **1996**; in *Vitamin B_{12} and B_{12} Proteins* (Eds.: B. Kräutler, D. Arigoni, B. T. Golding), WILEY-VCH, Weinheim, **1998**, p. 303.
[9] L. Poppe, E. Stupperich, W. E. Hull, T. Buckel, J. Rétey, *Eur. J. Biochem.* **1997**, *250*, 303.
[10] J. A. Hörig, P. Renz, *J. Biol. Chem.* **1978**, *253*, 7410.
[11] D. Dolphin, *Methods Enzymol.* **1971**, *18C*, 34.
[12] H. P. C. Hogenkamp, W. H. Pailes, C. Brownson, *Methods Enzymol.* **1971**, *18C*, 57.
[13] A generous gift of Dr. T. A. Bobik, Gainesville, FL, USA.
[14] S. Tabor, C. C. Richardson, *Proc. Natl. Acad. Sci. USA* **1985**, *82*, 1074.
[15] D. E. McGee, J. H. Richards, *Biochemistry* **1981**, *20*, 4293.
[16] ESR measurements were carried out as follows: The ESR vials containing the samples were immerged in liquid nitrogen, and spectra were recorded with a Varian E-3 ESR spectrometer under the following conditions: 9.09 GHz; 10 G modulation amplitude; 100 kHz modulation frequency; 10 mW power of the microwave beam; 2000 G sweepwidth; 2048 data points; $T = 77$ K.
[17] O. W. Wagner, H. A. Lee Jr., P. A. Frey, R. H. Abeles, *J. Biol. Chem.* **1966**, *241*, 1741.

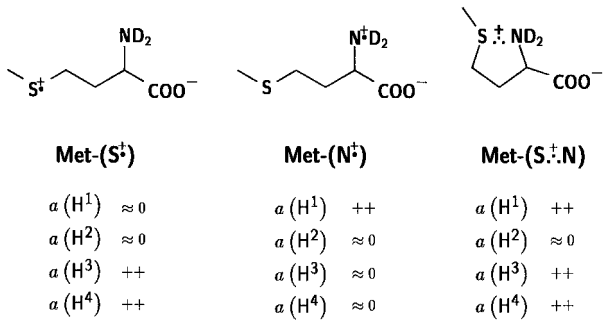
 © WILEY-VCH Verlag GmbH, D-69451 Weinheim, 1998 1433-7851/98/3705-0627 $ 17.50+.50/0

CIDNP Spectroscopic Observation of ($S.^{+}.N$) Radical Cations with a Two-Center Three-Electron Bond During the Photooxidation of Methionine**

Martin Goez,* Jaroslaw Rozwadowski, and Bronislaw Marciniak

Considerable effort has been devoted to investigating photoinduced[1] and radiation-induced oxidations[2] of sulfur-containing amino acids.[3] A major motivation of these studies has been that the reactions of these residues in proteins are thought to play an important role for long-range electron transfer across cell membranes[4a] and for oxidative damage of cell components.[4b]

The primary step of the sensitized photoreactions is photoinduced electron transfer from the amino acid to the sensitizer;[1] the same radical cations that are formed in this process are also early intermediates in the radiolysis experiments.[2] On the basis of UV/Vis spectroscopic evidence it was concluded[1d,g,2c–e] that in the case of methionine (Met) and related compounds the initial open-chain radical cations stabilize by the formation of cyclic structures Met-($S.^{+}.N$) with an intramolecular two-center three-electron bond between sulfur and nitrogen (Scheme 1[5,6]). Although the



Scheme 1.

($S.^{+}.N$) species are generally accepted intermediates in these reactions, to date there exists virtually no direct structural proof by methods that are sensitive to the distribution of unpaired spin density (i.e., magnetic resonance techniques). The only exception is a solid-state study in which poorly resolved EPR spectra exhibiting only a ^{14}N splitting were obtained during pulse radiolysis of Met in concentrated aqueous solutions of lithium halides below 160 K.[7] Here we report the first magnetic resonance observation in the liquid phase of the ($S.^{+}.N$) species derived from methionine.

[*] Prof. Dr. M. Goez
Fachbereich Chemie der Universität Halle-Wittenberg
Kurt-Mothes-Strasse 2, D-06120 Halle/Saale (Germany)
Fax: (+49) 345-5527229
E-mail: goez@chemie.uni-halle.de
Dr. J. Rozwadowski, Prof. Dr. B. Marciniak
Faculty of Chemistry, Adam Mickiewicz University Poznan (Polen)

[**] This work was supported by the DAAD, the Volkswagenstiftung, and the Committee of Scientific Research, Poland (grant no. 2P303049 06)

EPR spectroscopy of these radical cations is hampered by the fact that they are very short-lived in liquid solution. Measurements of chemically induced dynamic nuclear polarizations (CIDNP)[8] provide another method to probe the structures and spin-density distributions of radical intermediates that is exactly tailored for this situation. The polarizations are generated by nuclear spin sorting in radical pairs, which in turn is caused by the concomitant action of nuclear spin dependent intersystem crossing (by the interplay of Zeeman and hyperfine interactions) and electron spin selective reactions of the pairs (cage recombination is usually possible in the singlet state only.) Detection is accomplished by recording the NMR spectrum of the diamagnetic reaction products, in which the polarizations manifest themselves as anomalous line intensities.

The efficiency of spin sorting increases with increasing hyperfine coupling constant a_i of the proton or nucleus in question. Hence, the relative polarization intensities of the different protons in the products, the polarization pattern,[9] reflect the relative hyperfine coupling constants in the radicals. As the buildup of the polarizations is complete after the lifetime of the paramagnetic intermediates (nanoseconds or even shorter) but the polarizations persist in the diamagnetic products for the spin-lattice relaxation time T_1 (seconds for protons), the polarization pattern may be regarded as the frozen signature of the intermediate radicals. CIDNP spectroscopy is therefore sensitive to faster processes than is EPR spectroscopy. It is also in some respect more helpful for characterizing radical intermediates, because the CIDNP spectrum immediately establishes a correspondence between a particular value a_i and a particular nucleus i in the products.

CIDNP spectra observed in the photoreactions of methionine with 4-carboxybenzophenone (CB) in D_2O at pH 5.8 and 12.2 are shown in Figure 1. By a special pulse sequence,[11] the NMR signals of all unreactive molecules in the sample were eliminated, and the spectra display pure CIDNP signals only. Protons H_3 and H_4 of Met (i.e., those adjacent to sulfur) bear strong polarizations in both experiments, whereas H^1 (in the α position with respect to nitrogen) is unpolarized at pH 5.8 but strongly polarized at pH 12.2. Referring to equal numbers of protons (two equivalent protons H^3 *vs.* one proton H^1), integration of the signals shows that the ratio of CIDNP intensities $P(H^1)$: $P(H^3)$ is about 1.3 in the limit of high pH. At intermediate pH the polarization pattern lies between the two extremes. All these CIDNP signals appear in absorption. Proton H^2 ($\delta = 1.8...2.0$ ppm, depending on pH) is unpolarized. Owing to deprotonation of the amino function at higher pH (pK_{a2} of Met in D_2O was determined to be 9.65 ± 0.09 by NMR titration), the resonance frequencies of the methionine protons, especially of H^1, shift considerably with pH. However, comparison with the NMR signals in the dark renders the assignment given beyond doubt.

The mechanism relevant for the polarizations of the substrate Met is shown in Scheme 2. The triplet state ^{3}CB of the sensitizer is quenched by electron transfer[1] from Met to give a triplet radical pair $\overline{^{3}CB^{-}\cdot\ Met^{+}\cdot}$. The exact localization of the unpaired spin density in the methionine radical cation $Met^{+}\cdot$ (the three possibilities—the sulfur-centered radical

 © WILEY-VCH Verlag GmbH, D-69451 Weinheim, 1998 1433-7851/98/3705-0628 $ 17.50+.50/0

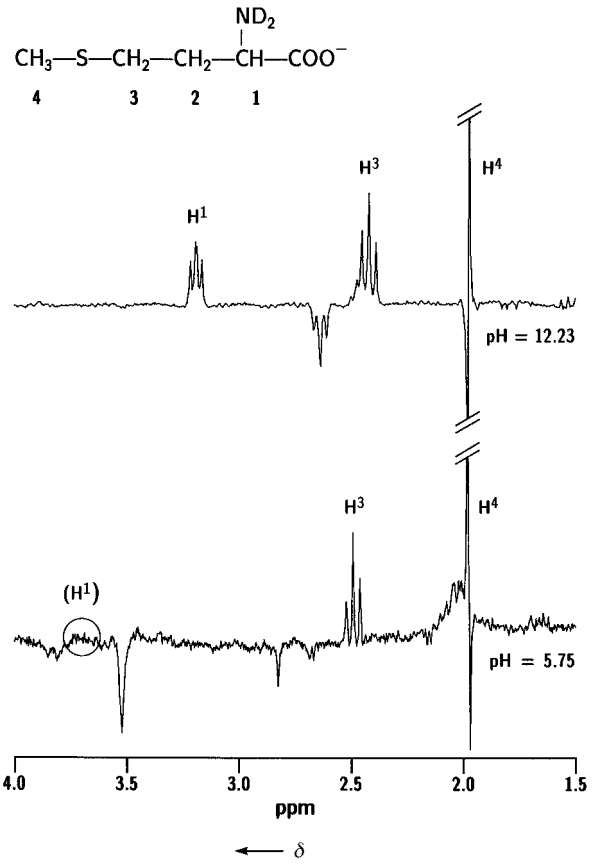
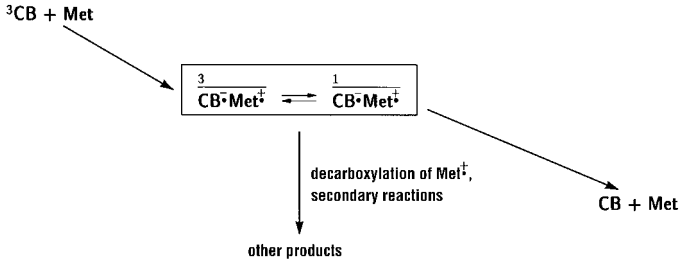


Figure 1. Background-free ^{1}H-CIDNP spectra (250 MHz) obtained in the photoreactions of 4-carboxybenzophenone with methionine in D_2O at pH 5.75 (bottom) and 12.23 (top).[10] Only the spectral region of interest is shown, and only the resonance of the methionine protons (compare the formula at the top)[6] are assigned. The spectra were normalized with respect to the triplet of H^3.



Scheme 2.

cation Met-(S^+), the nitrogen-centered radical cation Met-(N^+), and the species Met-($S^{+}.N$) with the two-center three-electron bond—are displayed in Scheme 1[5,6]) is of no consequence for the basic mechanism of Scheme 2: In any case, back electron transfer is feasible for singlet pairs $^1\overline{CB^-\cdot Met^+}$ only, because the radical pairs are 18 kJ mol^{-1} lower in energy than ^{3}CB[1e] and the triplet energy of the amino acid is even higher than that of the sensitizer.[1f]

Decarboxylation of Met^+ ultimately produces other products, some of them spin-polarized (compare the CIDNP spectra). However, this pathway cannot lead back to Met. Hence, all complications due to the rich secondary chemistry[1d] of the system are avoided by analyzing only the polarizations of the regenerated starting amino acid Met.

Comparison with model compounds[1f]—*S*-methylcysteine, which forms sulfur-centered radical cations only, for Met-(S^+), and alanine, in which the radical cation is necessarily nitrogen-centered, for Met-(N^+)—shows the *g* values of both Met-(S^+) and Met-(N^+) to be larger than that of CB^-. The *g* value of Met-($S^{+}.N$) (see also ref. [7]) must fall between that of Met-(S^+) and Met-(N^+) owing to the increased spin-orbit coupling in the sulfur-containing species Met-($S^{+}.N$) with the two-center three-electron bond compared to Met-(N^+), and is therefore also larger than that of CB^-. For any of the three methionine-derived radical cations, the nonnegligible proton hyperfine coupling constants must be positive because their source is hyperconjugation;[12] for Met-(S^+) and Met-(N^+) this is confirmed by CIDNP experiments[1f] on the above-mentioned model compounds. According to Kaptein's rule,[13] the observed absorption signals for the protons of Met are thus consistent with the reaction mechanism in Scheme 2 (triplet precursor, $\mu = +1$; singlet product, $\varepsilon = +1$; $\Delta g > 0$; positive a_i values).

The distribution of proton hyperfine coupling constants in Met-(S^+), Met-(N^+), and Met-($S^{+}.N$) is expected to be totally different; large values of a_i should only occur for protons on carbon atoms adjacent to the heteroatom(s) bearing the unpaired spin density, that is, for H^3 and H^4 in Met-(S^+), H^1 in Met-(N^+), and H^1 *as well as* H^3 and H^4 in Met-($S^{+}.N$) (compare Scheme 1). As far as Met-(S^+) and Met-(N^+) are concerned, this is again borne out by the CIDNP results[1f] for *S*-methylcysteine and alanine.

The polarization pattern of Met observed at pH 5.8 (Figure 1, bottom trace) therefore clearly points to the sole intermediacy of the sulfur-centered radical cation Met-(S^+). This is not surprising because the amino function is almost completely protonated under these conditions (pK_{a2} − pH ≈ 3.9) and it therefore cannot function as an electron donor, neither in the quenching process nor in formation of a two-center three-electron bond. In contrast, the polarization pattern at pH 12.2 (about 2.7 units above pK_{a2}, top trace of Figure 1) might be compatible either with the parallel occurrence of Met-(S^+) and Met-(N^+)—that is, with quenching of ^{3}CB by electron transfer from both sulfur and nitrogen—or generation of these polarizations in the radical cation Met-($S^{+}.N$) with the two-center three-electron bond. However, a clear decision between these alternatives is possible by comparison with *S*-methylcysteine, in which the distance between the sulfur and nitrogen termini is shorter by one CH_2 unit. While this shortening cannot have a noticeable influence on the redox potentials of the sulfur center and of the amino function because these groups are still isolated by a saturated C_2 chain, it renders impossible formation of a ($S^{+}.N$) species because this would involve a four-membered ring. The polarization pattern in the photoreaction of CB with *S*-methylcysteine at a pH value well above pK_{a2} of the amino acid unambiguously demonstrates that quenching of ^{3}CB takes place by electron transfer from sulfur only; electron transfer from nitrogen does not participate to any measurable degree.[1f] This finding therefore rules out electron transfer from nitrogen also in the methionine system. The fact that the rate constants for quenching of ^{3}CB by Met at pH 6.8 and 11.5 are practically identical (2.6×10^9 *vs.* 2.7×10^9 M^{-1}s^{-1})[1d]

 © WILEY-VCH Verlag GmbH, D-69451 Weinheim, 1998 1433-7851/98/3705-0629 $ 17.50+.50/0

provides additional corroboration. The polarization pattern of the top trace in Figure 1 must therefore be due to the radical Met-(S.$^{+}$.N) of methionine with the two-center three-electron bond.

In our high magnetic field (5.9 T) and with the substantial difference Δg of the radical pair involved, there is approximate proportionality between polarization intensity and the hyperfine coupling constant.[8] Furthermore, it is reasonable to assume that the formation of Met-(S.$^{+}$.N) from the sulfur-centered radical cation Met(S$^{+\cdot}$)—which must be the primary methionine-derived radical because in the ground state the interaction between the lone pairs of sulfur and nitrogen is repulsive—is fast on the CIDNP timescale because this reaction is exergonic and the rate-limiting step should be diffusion of the linked sulfur and nitrogen moieties towards one another. Under these conditions the distribution of the unpaired spin density ϱ in the radical cation Met-(S.$^{+}$.N) can be estimated from the limiting ratio of CIDNP intensities P (H^{1}): P (H^{3}) at high pH by using McConnell-type relationships.[12] Taking the dimeric radical cation of tetrahydrothiophene (a (H$^{\alpha}$) = 0.93 mT;[14] this value must be doubled to describe a radical cation in which ϱ is located on a single sulfur atom) and the radical cation of *N*-methylpyrrolidine (average of the splittings the methylene α protons 4.25 mT)[15] as model compounds, one obtains that in the species Met-(S.$^{+}$.N) with the two-center three-electron bond about one third of the unpaired spin density is shifted from sulfur to nitrogen ($\varrho_S : \varrho_N = 0.64 : 0.36$). The calculated ratio ($\varrho_S : \varrho_N = 0.74 : 0.26$)[7] is somewhat higher but, as the authors of reference [7] pointed out, the STO-3G* method used underestimates the spin density at nitrogen.

Received: September 18, 1997 [Z 10942IE]
German version: *Angew. Chem.* **1998**, *110*, 649 – 651

Keywords: amino acids · CIDNP spectroscopy · NMR spectroscopy · photochemistry · radical ions

[1] a) S. G. Cohen, S. Ojanpera, *J. Am. Chem. Soc.* **1975**, *97*, 5633 – 5634; b) K. Bobrowski, B. Marciniak, G. L. Hug, *ibid.* **1992**, *114*, 10279 – 10288; c) B. Marciniak, K. Bobrowski, G. L. Hug, *J. Phys. Chem.* **1993**, *97*, 11937 – 11943; d) K. Bobrowski, G. L. Hug, B. Marciniak, H. Kozubek, *ibid.* **1994**, *98*, 537 – 544; e) B. Marciniak, G. L. Hug, J. Rozwadowski, K. Bobrowski, *J. Am. Chem. Soc.* **1995**, *117*, 127 – 134; f) M. Goez, J. Rozwadowski, B. Marciniak, *ibid.* **1996**, *118*, 2882 – 2891; g) G. L. Hug, B. Marciniak, K. Bobrowski, *J. Photochem. Photobiol. A* **1996**, *95*, 81 – 88.

[2] a) K.-O. Hiller, B. Masloch, M. Göbl, K.-D. Asmus, *J. Am. Chem. Soc.* **1981**, *103*, 2734 – 2743; b) K.-O. Hiller, K.-D. Asmus, *J. Phys. Chem.* **1983**, *87*, 3682 – 3688; c) K.-D. Asmus, M. Göbl, K.-O. Hiller, S. Mahling, J. Mönig, *J. Chem. Soc. Perkin Trans. 2* **1985**, 641 – 646; d) K.-D. Asmus, in ref. [3], pp. 155 – 172, and references therein; e) D. Pogocki, G. Burlinska, T. Wasowicz, J. Sadlo, K. Bobrowski, *Mol. Phys. Rep.* **1994**, *6*, 224 – 229.

[3] *Sulfur-Centered Reactive Intermediates in Chemistry and Biology* (Eds.: C. Chatgilialoglu, K.-D. Asmus), Plenum Press, New York, **1991**.

[4] a) W. A. Prütz, in ref. [3], pp. 389 – 399; b) C. Schöneich, K. Bobrowski, J. Holcman, K.-D. Asmus in *Oxidative Damage and Repair. Chemical, Biological, and Medical Aspects* (Ed.: K. E. J. Davies), Pergamon Press, New York, **1991**, pp. 380 – 385.

[5] Scheme 1 shows the three types of radical cations derived from methionine (sulfur-centered radical cation Met-(S$^{+\cdot}$), nitrogen-centered radical cation Met-(N$^{+\cdot}$), and radical cation Met-(S.$^{+}$.N) with a two-center three-electron bond. The distribution of proton hyperfine coupling constants a in each radical is given schematically below the respective structural formula. Proton H^{1} is attached to the carbon atom bearing the amino group (compare the formula in Figure 1).

[6] For simplicity, protonation equilibria are omitted in Scheme 1 and Figure 1; that is, methionine and its radical cations are displayed in their deprotonated forms, which is present above the respective pK_{a2} value. Because of H/D exchange with the solvent, the nitrogen atom bears no protons but only deuterons in our experiments.

[7] M. H. Champagne, M. W. Mullins, A.-O. Colson, M. D. Sevilla, *J. Phys. Chem.* **1991**, *95*, 6487 – 6493.

[8] a) *Chemically Induced Magnetic Polarization* (Eds.: L. T. Muus, P. W. Atkins, K. A. McLauchlan, J. B. Pedersen), Reidel, Dordrecht, **1977**; b) K. M. Salikhov, Yu. N. Molin, R. Z. Sagdeev, A. L. Buchachenko, *Spin Polarization and Magnetic Effects in Radical Reactions*, Elsevier, Amsterdam, **1984**.

[9] a) H. D. Roth, M. L. Manion, *J. Am. Chem. Soc.* **1975**, *97*, 6886 – 6888; b) H. D. Roth in ref. [8a], pp. 53 – 61.

[10] Other experimental parameters: [CB] = 2×10^{-3} M, [Met] = 2×10^{-2} M, pH value adjusted by addition of KOH and measured with a glass electrode; room temperature, excitation wavelength 308 nm, 10 laser flashes per acquisition, 16 transients per spectrum. For details concerning the CIDNP setup, see ref. [1f]. The method for background suppression is described in ref. [11].

[11] M. Goez, *Chem. Phys. Lett.* **1992**, *188*, 451 – 456.

[12] A. Carrington, A. D. McLachlan, *Introduction to Magnetic Resonance*, Harper & Row, New York, **1969**.

[13] R. Kaptein, *J. Chem. Soc. Chem. Commun.* **1971**, 732 – 733.

[14] B. C. Gilbert, D. K. C. Hodgeman, R. O. C. Norman, *J. Chem. Soc. Perkin Trans. 2* **1973**, 1748 – 1752.

[15] R. W. Eastland, D. N. R. Rao, M. C. R. Symons, *J. Chem. Soc. Perkin Trans. 2* **1984**, 1551 – 1557.

A Fully Encapsulated Acetylenediide in $Ag_2C_2 \cdot 8\,AgF$**

Guo-Cong Guo, Gong-Du Zhou, Qi-Guang Wang, and Thomas C. W. Mak*

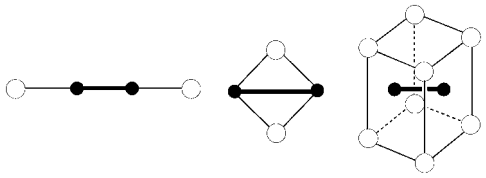
Silver acetylide (silver carbide), Ag_2C_2, is highly explosive when dry, and violent decomposition occurs upon mechanical shock and on heating to 120 – 140 °C.[1] Several double salts of silver acetylide with other silver compounds are known,[2–4] but only silver acetylide/silver nitrate (1/6) has been structurally characterized.[5–6]

Up to now the linear structure **I** of silver acetylide (Figure 1) was inferred from its chemical properties, which are consistent with those of a molecular compound but differ greatly from those of the ionic carbides of Group 1 and 2

[*] Prof. T. C. W. Mak, G.-C. Guo, Prof. Q.-G. Wang,[+]
Prof. G.-D. Zhou[++]
Department of Chemistry
The Chinese University of Hong Kong
Shatin, New Territories, Hong Kong (China)
Fax: (+852) 26035057
E-mail: tcwmak@cuhk.edu.hk
[+] On sabbatical from Lanzhou University, Lanzhou (China)
[++] On sabbatical from the Department of Chemistry, Peking University, Beijing (China)

[**] This work was supported by Hong Kong Research Grants Council Earmarked Grant CUHK 456/95P and Direct Grant A/C 2060090 of The Chinese University of Hong Kong.

 © WILEY-VCH Verlag GmbH, D-69451 Weinheim, 1998 1433-7851/98/3705-0630 $ 17.50+.50/0



I II III

Figure 1. Modes for the coordination of the acetylenediide C_2^{2-} to metal atoms: end-on M_2C_2 (**I**), side-on M_2C_2 (**II**), and encapsulated in a metal cage $C_2@M_8$ (**III**).

elements, such as Na_2C_2 and CaC_2. Owing to the low solubility of silver acetylide, its crystal structure is unknown. However, the existence of a cationic $[C_2@Ag_8]$ cage moiety in $Ag_2C_2 \cdot 6\,AgNO_3$[6] implies that the C_2^{2-} group (acetylenediide, often referred to as the acetylide dianion) in silver acetylide prefers a double π-bridged (**II**) or fully encapsulated coordination mode (**III**), or is present as a mixture of linear and π-bridged structures to give a linear structure.

The double π-bridged structure **II** was postulated for the dilithioacetylene monomer Li_2C_2 on the basis of calculations,[7] and since then similar π interactions in polar alkali metal acetylides[8] and alkaline earth metal acetylides[9] have been studied and extensively discussed. Here we report the synthesis and characterization of $Ag_2C_2 \cdot 8\,AgF$, in which an acetylenediide is completely enclosed within the Ag_9 cage of a chandelierlike arrangement of ten silver atoms.

A single-crystal X-ray structure analysis of $Ag_2C_2 \cdot 8\,AgF$ showed the presence of an exohedral Ag atom attached to the apex of a cationic Ag_9 cage, whose cavity is filled by an undisordered acetylenediide, C_2^{2-} (Figure 2, top). The resulting $[C_2@Ag_9]Ag$ assembly has a twofold symmetry axis that passes through Ag1 and Ag2 and bisects the C≡C bond. The cationic Ag_9 cage can be described as a capped square antiprism of approximate C_{4v} symmetry from which all four edges of the expanded capped face have been removed. Hitherto the only known example of an analogous cluster is $[C_2@Ag_8]$ in $Ag_2C_2 \cdot 6\,AgNO_3$, in which eight Ag atoms form the vertices of a rhombohedron that completely encages the threefold disordered C_2^{2-} dianion.[6]

The Ag···Ag distances in the $[Ag_9]Ag$ framework range from 2.8441(4) to 3.0863(5) Å. They are comparable to the Ag···Ag distance of 2.89 Å in silver metal[10] and hence suggest the existence of weak Ag···Ag interactions of the same order of magnitude. There are three arrangements of fluoride ions around the six different silver centers. The atoms Ag1 and Ag2 are each bonded to four F atoms to form a tetragonal pyramid with Ag–F distances of 2.392(2)–2.471(2) Å; Ag3 and Ag4 each have two F neighbors at a distance of 2.196(2)–2.485(2) Å, and Ag5 and Ag6 each have three F neighbors at a distance of 2.299(2)–2.571(2) Å (Figure 2, bottom). Thus the crystal structure of $Ag_2C_2 \cdot 8\,AgF$ consists of a three-dimensional framework in which F atoms act as bridges between adjacent $[C_2@Ag_9]Ag$ moieties.

As shown in the bottom of Figure 2, the atom C1 forms three shorter bonds (represented by broken lines) with Ag3, Ag4, and Ag6. The bond lengths are 2.311(4), 2.247(4), and 2.110(4) Å, respectively. Notably, they are shorter and longer, respectively, than those of silver atoms π-bonded (average

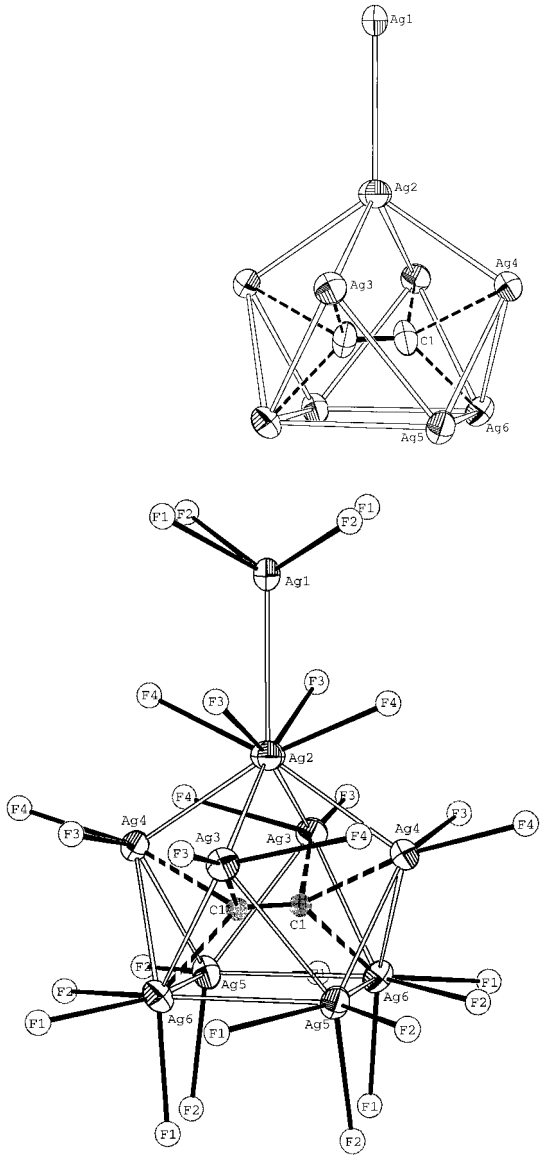


Figure 2. Crystal structure of $Ag_2C_2 \cdot 8\,AgF$. Top: chandelierlike $[Ag_9]Ag$ assembly accommodating a C_2^{2-} species in its cavity. The thermal ellipsoids are drawn at the 35% probability level. Bottom: coordination environment of the individual silver atoms in the $[C_2@Ag_9]Ag$ moiety. Selected bond lengths [Å] and angles [°]: Ag3–C1 2.3114, Ag4–C1 2.2474, Ag5–C1 2.1104, C1–C1A 1.1757; C1-Ag2-C1A 25.92, Ag3-C1-C1A 116.24, Ag4-C1-C1A 122.84, Ag6-C1-C1A 138.41.

2.452 Å) and σ-bonded (average 2.057 Å) to the C≡CR groups in the alkynyl complexes $[Ph_3PAgC{\equiv}CPh]_4 \cdot 3.5\,THF$ and $[Me_3PAgC{\equiv}CSiMe_3]_\infty$.[11] The bond angles between the enclosed acetylenediide and individual silver atoms (Ag-C1-C1A) are in the range of 116.2(4)–138.4(1)°, and are comparable to those between the C_2^{2-} species and "equatorial" Ag atoms in $Ag_2C_2 \cdot 6\,AgNO_3$.[6] The distance of 2.620(4) Å between the C_2^{2-} entity and "axial" atom Ag2 in the present compound is longer than the corresponding distances (2.45 and 2.56 Å) in $Ag_2C_2 \cdot 6\,AgNO_3$.[6] In contrast to the tetranuclear complex $[Cu_4(\mu\text{-dppm})_4(C{\equiv}C)][BF_4]_2$ (dppm = 1,2-bis(diphenylphosphanyl)methane),[12] in which the nearly coplanar bonding between the central C_2^{2-} ligand (C–C 1.26(2) Å) and peripheral Cu atoms allows a clear

distinction to be made between σ and π coordination modes, the bonding interaction between the C_2^{2-} group and the cage Ag atoms in $Ag_2C_2 \cdot 8\,AgF$ is ambiguous, as in the case of $Ag_2C_2 \cdot 6\,AgNO_3$. In the complex $[(TiN_4Et_8)(C_2)(Li)_2(TiN_4Et_8)]^{2+}$ ($H_2N_4Et_8$ = *meso*-octaethylporphyrin), the sandwiched C_2 species is bonded to pairs of Ti and Li atoms in the end-on (**I**) and side-on (**II**) modes (see Figure 1), respectively, and has a C–C bond length of 1.30(1) Å.[13] The fully encapsulated coordination mode of the dicarbido group C_2^{n-} occurs in a number of transition metal clusters.[14] However, in many instances the C_2 unit can be considered to be formally derived from complete deprotonation of ethane ($n = 6$), ethylene ($n = 4$), or the vinylidene ligand ($n = 4$), as the C–C bond length generally lies between 1.32 and 1.60 Å.[15] The very short C1–C1A bond length of 1.175(7) Å in $Ag_2C_2 \cdot 8\,AgF$ is comparable to that of acetylene (1.205 Å) and indicates that the encapsulated acetylenediide retains the triple-bond character of the starting material silver acetylide, as was confirmed by laser Raman spectroscopy (see Experimental Section). Molecular orbital calculations on ethanido clusters indicated that the C_2 entity enters into a synergic bonding interaction with the skeletal molecular orbitals of the metal cage, and the C–C bond length correlates with the degree of metal-to-ligand backbonding.[16] A similar molecular orbital picture may account for stabilization of the highly explosive silver acetylide by trapping the acetylide dianion inside a variety of polyhedral metal cages through formation of silver(I) double salts.

Experimental Section

Ag_2C_2: A slow stream of acetylene gas was bubbled into a stirred aqueous solution of silver nitrate at room temperature until saturation was reached. The white precipitate of Ag_2C_2 was isolated by filtration, washed several times with deionized water, and temporarily stored in wet form in the dark. **Caution**: Ag_2C_2 should never be dried or kept for a prolonged period, and only a small quantity should be used in any chemical reaction.

Moist Ag_2C_2 was added to 2 mL of a concentrated aqueous solution of AgF (about 40%) in a plastic vessel with stirring until saturated. The excess of Ag_2C_2 was filtered off, and the solution was placed in a desiccator charged with P_2O_5. In the course of two days colorless crystals of $Ag_2C_2 \cdot 8\,AgF$ were obtained. The laser Raman spectrum of this crystalline product, as measured on a Renishaw Raman Image Microscope System 2000, exhibits a doublet of about equal intensity at 2104.5 and 2168.6 cm^{-1} in the $\Delta\nu(C{\equiv}C)$ region, which arises from Fermi resonance between the stretching vibration of C_2^{2-} and the first overtone of the laser excitation line at 1125.3 cm^{-1}.

Crystal structure analysis: A colorless crystal of dimensions $0.03 \times 0.03 \times 0.04$ mm was mounted in a 0.3 mm Lindemann glass capillary and used for data collection on a Rigaku RAXIS IIC imaging plate diffractometer with graphite-monochromatized $Mo_{K\alpha}$ radiation ($\lambda = 0.71073$ Å) from a rotating-anode generator powered at 50 kV and 90 mA. Thirty-one oscillation frames were recorded in the range of $\phi = 0 - 180^\circ$ with $\Delta\phi = 5.0^\circ$ and 8 min exposure per frame. Crystal data for $Ag_2C_2 \cdot 8\,AgF$: $M_r = 1254.7$, tetragonal, space group $P\bar{4}$ (no. 81), $a = 7.464(1)$, $c = 10.337(1)$ Å, $V = 575.9(1)$ Å^3, $T = 293$ K, $Z = 2$, $\rho_{calcd} = 7.236$ g cm^{-3}, $F(000) = 1108$, $\mu(Mo_{K\alpha}) = 166.82$ cm^{-1}, absorption corrections applied by using ABSCOR, relative transmission factors in the range 0.788–1.0. A total of 1888 reflections were collected in the 2θ range 4.0–52.0° ($-9 \le h \le 9$, $0 \le k \le 9$, $-12 \le l \le 12$) and led to 1040 unique reflections ($R_{int} = 5.05\%$), 988 of which with $I > 2\sigma(I)$ were considered as observed. The structure was solved by direct methods and refined by full-matrix least squares on F^2 by using the Siemens SHELXTL/PC package of crystallographic software.[17] All non-hydrogen atoms were refined anisotropically. Further details of the crystal structure investigations may be obtained from the Fachinformationszentrum Karlsruhe, D-76344 Eggenstein-Leopoldshafen, Germany (fax: (+49) 7247-808-666 (Frau S. Höhler-Schlimm); e-mail: crysdata@fiz-karlsruhe.de), on quoting the depository number CSD-407646.

Received: September 26, 1997
Revised version: November 7, 1997 [Z 10976 IE]
German version: *Angew. Chem.* **1998**, *110*, 652–654

Keywords: acetylene · carbides · clusters · fluorine · silver

[1] N. R. Thompson in *Comprehensive Inorganic Chemistry*, *Vol. 3* (Eds.: J. C. Bailar, Jr., H. J. Emeléus, R. Nyholm, A. F. Trotman-Dickenson), Pergamon, Oxford, **1973**, p. 102.
[2] J. A. Shaw, E. Fisher, *J. Am. Chem. Soc.* **1946**, *68*, 2745.
[3] R. Vestin, E. Ralf, *Acta Chem. Scand.* **1949**, *3*, 101–124.
[4] A. D. Redhouse, P. Woodward, *Acta Crystallogr.* **1964**, *17*, 616–617.
[5] J. Osterlof, *Acta Crystallogr.* **1954**, *7*, 637.
[6] a) X.-L. Jin, G.-D. Zhou, N.-Z. Wu, Y.-Q. Tang, H.-C. Huang, *Acta Chem. Sin. Chin. Ed.* **1990**, *48*, 232–236; b) T. C. W. Mak, G.-D. Zhou, *Crystallography in Modern Chemistry: a Resource Book of Crystal Structures*, Wiley-Interscience, New York, **1992**, pp. 288–289.
[7] Y. Apeloig, P. von R. Schleyer, J. S. Binkley, J. A. Pople, W. L. Jorgensen, *Tetrahedron Lett.* **1976**, 3923–3926.
[8] B. Goldfuss, P. von R. Schleyer, F. Hampel, *J. Am. Chem. Soc.* **1997**, *119*, 1072–1080.
[9] a) C.-C. Chang, B. Srinivas, M.-L. Wu, W.-H. Chiang, C.-S. Hsiung, *Organometallics* **1995**, *14*, 5150–5159; b) E. Ruiz, P. Alemany, *J. Phys. Chem.* **1995**, *99*, 3114–3119.
[10] J. Emsley, *The Elements*, Clarendon, Oxford, **1989**, p. 174.
[11] C. Brasse, P. R. Raithby, M.-A. Rennie, C. A. Russell, A. Steiner, D. S. Wright, *Organometallics* **1996**, *15*, 639–644.
[12] V. W.-W. Yam, W. K.-M. Fung, K.-K. Cheung, *Angew. Chem.* **1996**, *108*, 1213–1215; *Angew. Chem. Int. Ed. Engl.* **1996**, *35*, 1100–1103.
[13] S. De Angelis, E. Solari, C. Floriani, A. Chiesi-Villa, C. Rizzoli, *Angew. Chem.* **1995**, *107*, 1200–1202; *Angew. Chem. Int. Ed. Engl.* **1995**, *34*, 1092–1094.
[14] a) V. G. Albano, P. Chini, S. Martinengo, M. Sansoni, D. Strumulo, *J. Chem. Soc. Dalton Trans.* **1978**, 459–463; b) A. Arrigoni, A. Ceriotti, R. Della Pergola, G. Longoni, M. Manassero, N. Masciocchi, M. Sansoni, *Angew. Chem.* **1984**, *96*, 290–291; *Angew. Chem. Int. Ed. Engl.* **1984**, *23*, 322–323; c) A. Ceriotti, G. Longoni, G. Piro, L. Resconi, M. Manassero, N. Masciocchi, M. Sansoni, *J. Chem. Soc. Chem. Commun.* **1985**, 1402–1403; d) M. I. Bruce, M. R. Snow, E. R. Tiekink, M. L. Williams, *ibid.* **1986**, 701–702; e) M. Akita, Y. Moro-oka, *Bull. Chem. Soc. Jpn.* **1995**, *68*, 420–432.
[15] R. B. King, *J. Organomet. Chem.* **1997**, *536/537*, 7–15.
[16] J.-F. Halet, D. M. P. Mingos, *Organometallics* **1988**, *7*, 51–58.
[17] a) G. M. Sheldrick in *Crystallographic Computing 6: A Window on Modern Crystallography* (Eds.: H. D. Flack, L. Párkányi, K. Simon), Oxford University Press, Oxford, **1993**, pp. 111–122; b) SHELXTL/PC Version 5 Reference Manual, Siemens Energy & Automation, Inc., Madison, WI, **1996**.

 © WILEY-VCH Verlag GmbH, D-69451 Weinheim, 1998 1433-7851/98/3705-0632 $ 17.50+.50/0

Synthesis of Unsaturated Nine-Membered Ring Ethers (Δ^3-Oxonenes) Containing a *Z*- or *E*-Configurated Double Bond: Thermodynamic versus Kinetic Control in Palladium-Catalyzed Allylic Cyclizations**

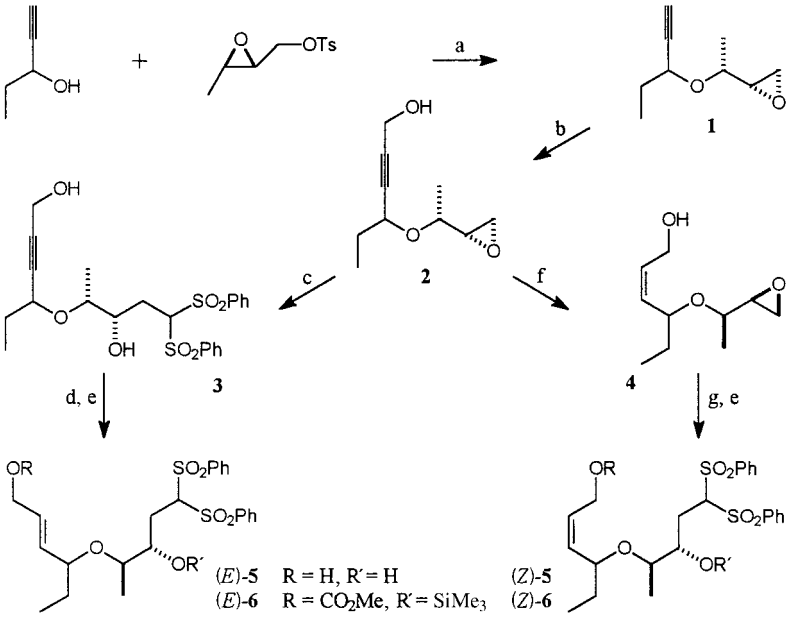
Jens Pohlmann, Christopher Sabater, and H. M. R. Hoffmann*

Dedicated to Professor Heribert Offermanns on the occasion of his 60th birthday

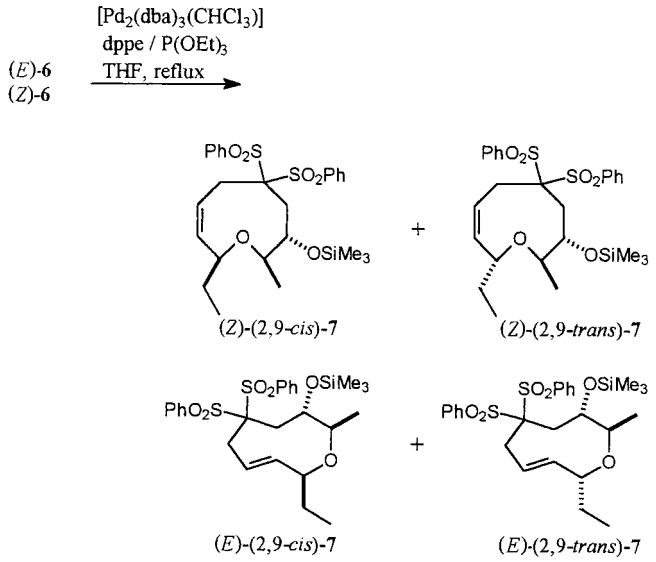
Medium-ring ethers ($n = 8-10$) occur in a variety of marine natural products, and efforts continue towards their total synthesis.[1] Of the currently known, unsaturated nine-membered ring ethers most contain *Z*-configurated double bonds. *E*-configurated, monocyclic Δ^3-oxonenes, either natural or unnatural, appear to be unknown.[2] We here report a simple and efficient stereoselective synthesis of both *Z*- and *E* -configurated Δ^3-oxonenes starting from a single advanced intermediate.

The cyclization precursors were prepared as outlined in Scheme 1. A key reaction was the BF_3-mediated regioselective opening of the crotyl alcohol derived epoxytosylate with 1-pentyn-3-ol. Although this secondary alcohol is a weak nucleophile and has to attack a secondary epoxide carbon in an S_N2-type displacement, the preparation of **1** proceeded with complete inversion and regioselectivity in 70% yield.[3] Thus the highly functionalized α,α'-di-*sec*-alkyl ether **1** is accessible in two steps with full control over two stereocenters by a simple procedure.[4] Hydroxymethylation of the triple bond provided propargylic alcohol **2**, which served as advanced intermediate en route to cyclization precursors (*E*)-**6** and (*Z*)-**6**.

Cyclization of (*E*)-**6** as well as (*Z*)-**6** with catalytic amounts of palladium(0) and in the presence of a ligand (1,2-bis(diphenylphosphanylethane (dppe), $P(OEt)_3$)[5] provided strained **7** in reproducible, good yield (Scheme 2, Table 1).[6] Seven-membered ring ethers are not formed, in agreement with early work on the preparation of related carbocycles.[5b, e] Separation and identification of the cyclization products was not trivial. Only the cyclic ether (*Z*)-(2,9-*cis*)-**7** could be purified by standard chromatography. The TLC plate showed an additional spot which could not be resolved further. NMR spectra were inconclusive but suggested that more than one isomer might be formed in dynamic distribution. Eventually, the experimental conditions in entry 8 provided a clue because the product mixture was rich in two *E*-configurated diastereomers. Recrystallization from ether gave single crystals of (*E*)-(2,9-*trans*)-**7** suitable for X-ray diffraction analysis.[7] Given the NMR spectrum of this diastereomer, the spectra of the *E*- and *Z*-configurated cyclic ethers **7** could be assigned.



Scheme 1. Synthesis of cyclization precursors (*E*)- und (*Z*)-**6**: a) 1. $BF_3 \cdot Et_2O$, CH_2Cl_2; 2. K_2CO_3, MeOH, 70%; b) *n*BuLi, $(CH_2O)_n$, THF, 98%; c) 1. ethyl vinyl ether, cat. *p*-TsOH, CH_2Cl_2; 2. $(PhO_2S)_2CH_2$, *n*BuLi, $BF_3 \cdot Et_2O$, THF; 3. aq. HCl, THF, 45%; d) Red-Al, THF, 62%; e) 1. MeO_2CCl, Py, CH_2Cl_2; 2. bis(trimethylsilyl)acetamide, THF, 77% (*E* isomer), 59% (*Z* isomer); f) Lindlar catalyst, H_2, MeOH, 97%; g) 1. ethyl vinyl ether, cat. *p*-TsOH, CH_2Cl_2; 2. $(PhO_2S)_2CH_2$, *n*BuLi, $BF_3 \cdot Et_2O$, THF; 3. aq. HCl, THF, 89%.



Scheme 2. Cyclization of (*E*)- and (*Z*)-**6**.

[*] Prof. Dr. H. M. R. Hoffmann
Institut für Organische Chemie der Universität
D-30167 Hannover (Germany)
Fax: (+49) 511-762-3011
E-mail: hoffmann@mbox.oci.uni-hannover.de
Dr. J. Pohlmann
California Institute of Technology, Pasadena, CA 91125 (USA)
Dr. C. Sabater
Dragoco Gerberding & Co. AG, D-37601 Holzminden (Germany)

[**] This work was supported by the Fonds der Chemischen Industrie (PhD fellowships for J. P. and C. S.) and the Deutsche Forschungsgemeinschaft. We thank Dr. R. Wartchow, Institut für Anorganische Chemie der Universität Hannover, for the X-ray crystal structure analysis and Dr. J. M. Goodman, University of Cambridge, for calculations, and Degussa for a gift of palladium salts.

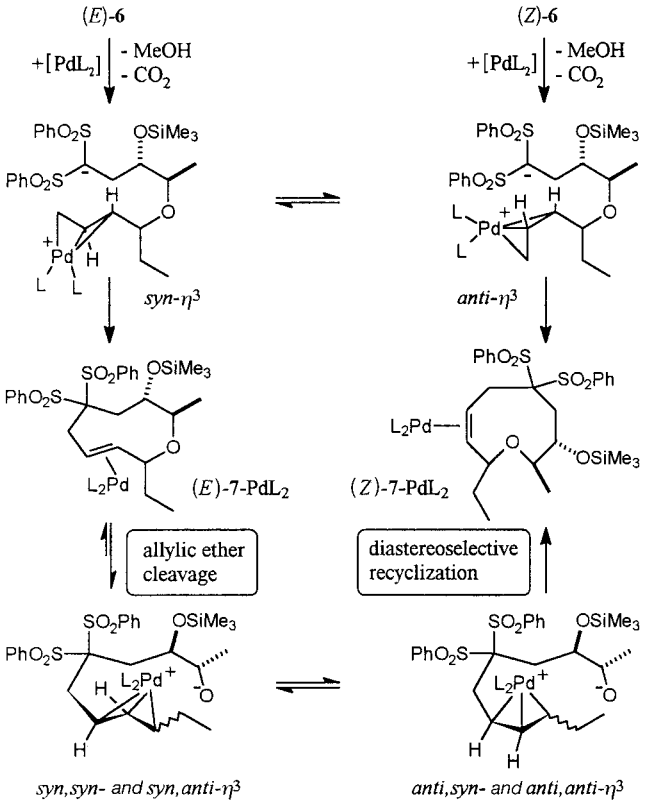
Table 1. Cyclization results.

Entry	Precursor	Ligand [mol%]	Cat. [mol%]	Add. time [h]	Reaction time [h]	(*Z*)-**7**:(*E*)-**7**	(*Z*)-(2,9-cis)-**7**: (*Z*)-(2,9-*trans*)-**7**	Yield [%]
1	(*E*)-**6**	dppe, 25	5	5.5	7	1.7:1	1:12	82
2	(*E*)-**6**	dppe, 45	10	6	17	2.5:1	1:12	83
3	(*E*)-**6**	dppe, 45	10	15	18	4.5:1	1:7	70
4	(*E*)-**6**	dppe, 45	10	13	17	7.5:1	1:4	67
5	(*E*)-**6**	$P(OEt)_3$, 50	5	5	8	0.25:1	1:10	68
6	(*E*)-**6**	$P(OEt)_3$, 50	5	5	20	0.75:1	1:5	53
7	(*Z*)-**6**	dppe, 22	5	7	8	7:1	1:3	80
8	(*Z*)-**6**	$P(OEt)_3$, 50	5	7	8.5	0.07:1	–	81

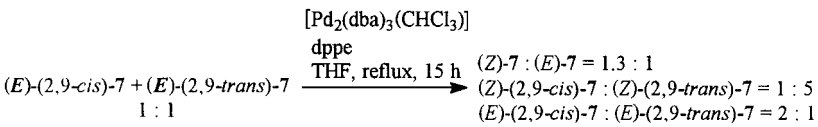
The product distribution depended on the type of ligand and reaction time. Surprisingly, the configuration of the double bond in the cyclization precursors (*E*)-**6** and (*Z*)-**6** also played an important role.[8] Proper choice of the reaction conditions allowed preparation of either predominantly *E*- or *Z*-configurated nine-membered ring ether. Furthermore, formation of (*Z*)-(2,9-*cis*)-**7** and (*Z*)-(2,9-*trans*)-**7** was diastereoselective with respect to the configuration at allylic carbon C-2. Epimer (*Z*)-(2,9-*trans*)-**7** was the major product (Table 1). The isolated *E*- and *Z*-configurated nine-membered ring ethers were resubjected to the conditions of allylic alkylation. Whereas the (*Z*) ethers were stable, the energy-rich (*E*) ethers isomerized to the less strained (*Z*) isomers. Furthermore, these experiments showed that (*E*)-(2,9-*trans*)-**7** (higher energy content) isomerized faster than (*E*)-(2,9-*cis*)-**7** (Scheme 3).

A unique feature of the cyclization is the palladium-mediated cleavage of the strained, nine-membered ring ethers (*E*)-(2,9-*cis*)-**7** and (*E*)-(2,9-*trans*)-**7** (Scheme 4).[9] This allylic ether cleavage and subsequent recyclization account not only for the observed *E*/*Z* isomerization of the olefinic double bond, but also for the diastereoselective formation of (*Z*) ethers. The C–O bond heterolysis generates at least four η^3-allylpalladium complexes (*syn,syn*, *syn,anti*, *anti,syn*, and *anti,anti*) in addition to the two initially formed η^3-complexes (*syn* and *anti*). Scheme 4 is simplified, since the allyl π-faces are diastereotopic. Hence, the number of η^3 complexes and therefore discrete allyl cation equivalents must be doubled from six to twelve. The presence of two and three further chiral centers along the carbon chain increases the manifold of possible organopalladium intermediates even further.

For the preparation of the more stable *Z*-configurated nine-membered ring ethers, the dppe ligand is advantageous, irrespective of the configuration of the double bond in the cyclization precursor (Table 1, entries 4 and 7). The precursor (*E*)-**6** requires extended reaction times for formation of the (*Z*) ether (cf. entry 4, $Z{:}E = 7.5{:}1$ and entry 1, $Z{:}E = 1.7{:}1$), presumably as a consequence of thermodynamic control. Comparison of entries 2 and 4 shows that the time required for the addition of the cyclization precursor to the catalyst solution also plays a role. Given a total reaction time of 17 h, fast addition (6 h vs. 13 h) increases the amount of (*E*) ether (cf. entry 2, $Z{:}E = 2.5{:}1$ and entry 4, $Z{:}E = 7.5{:}1$).[10] For the selective formation of the less stable (*E*) ether a maximum of kinetic control is required. Triethyl phosphite, a monodentate ligand with considerable backbonding capability, renders the η^3-allyl palladium complex more ionic and speeds cyclization. The effect of shortening the reaction time is shown in entries 5 and 6. The amount of (*E*) ether increases with shorter reaction times. The system of choice for high kinetic control and almost exclusive formation of *E*-configurated cyclic ether is the energy-rich precursor (*Z*)-**6** in combination with $P(OEt)_3$ as a ligand (entry 8).



Scheme 4. Simplified cyclization mechanism.

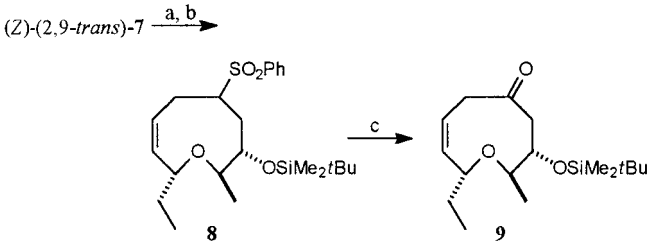


Scheme 3. Isomerization of *E*-configurated unsaturated ethers.

With a view to the synthesis of natural products and the *Laurencia* ethers, we examined the refunctionalization of the 1,1-bissulfone moiety of the cyclization products. Standard conditions for the reduction to a methylene group (NaHg in buffered methanol)[11] were unsatisfactory and led to partial cleavage

 © WILEY-VCH Verlag GmbH, D-69451 Weinheim, 1998 1433-7851/98/3705-0634 $ 17.50+.50/0 *Angew. Chem. Int. Ed.* **1998**, *37*, No. 5

of the allylic ether. In contrast, reductive monodesulfonylation with SmI_2 provided sulfone **8**.[12] Subsequent oxidative desulfonylation[13] afforded the ketone **9** as a functionalized intermediate, well endowed for further synthetic manoeuvres (Scheme 5).



Scheme 5. Refunctionalization of 1,1-bissulfone. a) 1. SmI_2, MeOH, THF; 2. aq. HCl, THF, 87%; b) tBuMe$_2$SiCl, imidazole, DMF, 75%; c) lithium diisopropylamide (LDA), MoO_5/pyridine/hexamethylphosphoric triamide (MoOPH), THF, 70%.

The epoxyether alkynol **2** is readily accessible from inexpensive starting materials and serves as a key intermediate for preparing *E*- and *Z*-configurated cyclization precursors. Thanks to the installation of three stereochemical labels we have been able to unravel some of the beautiful mechanistic complexity of organopalladium catalysis. Intramolecular allylic alkylation has been tuned to both (*E*)- and (*Z*)-Δ^3-oxonenes with high stereocontrol. The chemical yield of the nine-membered ring products remains respectable throughout, especially in view of the cleavage of the allylic ether and subsequent recyclization. The weakened bond between the allylic carbon and oxygen in *E*-configurated ring ethers generates a cascade of stereo- and structurally isomeric organopalladium intermediates. Finally, the 1,1-bissulfone refunctionalization is valuable in the synthesis of naturally occurring *Z*-configurated cyclic ethers. Strained *E*-configurated monocyclic Δ^3-oxonenes, which have apparently been unknown, are higher in energy than the corresponding (*Z*) isomers[7] and of intrinsic general interest. They are also analogues of natural products for evaluation of biological activity.

Experimental Section

General procedure for the Pd^0-catalyzed cyclization: A flame-dried, two-necked flask was charged with [$Pd_2(dba)_3CHCl_3$] (dba = dibenzylideneacetone) and ligand. The apparatus was evacuated and refilled with N_2 three times. Solvent (THF) was added such that the solution was 0.02 M with respect to starting material. The reaction mixture was heated to reflux and the cyclization precursor (0.02 M in THF) was added by syringe. After complete addition, the reaction mixture was heated to reflux for a further 1–15 h. The solvent was removed and the crude product was purified by chromatography. For further experimental details and spectroscopic data see reference [14].

Received: September 19, 1998 [Z10948IE]
German version: *Angew. Chem.* **1998**, *110*, 656–659

Keywords: allyl complexes · cyclizations · medium-sized rings · palladium

[1] a) M. C. Elliot, *Contemp. Org. Synth.* **1997**, *4*, 238–259; b) *ibid.* **1994**, *1*, 457–474; c) C. J. Moody, M. J. Davies in *Studies in Natural Product Chemistry, Vol. 10* (Ed.: Atta-ur-Rahman), Elsevier, Amsterdam, **1992**, pp. 201–239; d) medium-ring lactones: G. Rousseau, *Tetrahedron* **1995**, *51*, 2777–2849.
[2] CAS-online search up until August 1997.
[3] A. Brandes, U. Eggert, H. M. R. Hoffmann, *Synlett* **1994**, 745–747.
[4] No attempt was made to control the third stereocenter by using enantiopure 1-pentyn-3-ol in the first step, since the configuration of this chiral center is partially lost on cyclization (Scheme 4).
[5] For accounts of the extensive primary literature and Pd-mediated allylic alkylations see: a) J. Tsuji, *Palladium Reagents and Catalysts. Innovations in Organic Synthesis*, Wiley, Chichester, **1997**; b) B. M. Trost, D. L. Van Vranken, *Chem. Rev.* **1996**, *96*, 395–422; c) C. G. Frost, J. Howarth, J. M. J. Williams, *Tetrahedron: Asymmetry* **1992**, *3*, 1089–1122; d) S. A. Godleski in *Comprehensive Organic Synthesis, Vol. 4* (Eds.: B. M. Trost, I. Fleming, M. F. Semmelhack), Pergamon, Oxford, **1991**, pp. 585–661; e) B. M. Trost, *Angew. Chem.* **1989**, *101*, 1199–1219; *Angew. Chem. Int. Ed. Engl.* **1989**, *28*, 1173–1192.
[6] Other names: 2,3,4,5,6,9-hexahydrooxonine, 3,4-didehydrooxonane.
[7] R. Wartchow, J. Pohlmann, H. M. R. Hoffmann, unpublished. The X-ray data and torsion angles agree well with independent calculations (full Monte Carlo search of the ring system with MacroModel/MM2* MacroModel – An Integrated Software System for Modeling Organic and Bioorganic Molecules Using Molecular Mechanics: F. Mohamadi, N. G. J. Richards, W. C. Guida, R. Liskamp, M. Lipton, C. Caufield, G. Chang, T. Hendrickson, W. C. Still, *J. Comp. Chem.* **1990**, *11*, 440–467). A conformation search of the *cis* analogue gave a structure very much lower in energy (35 kJ mol^{-1} lower than the *trans* isomer). For comparison, carbocyclic *cis*-cyclononene is only 16 kJ mol^{-1} lower in energy than *trans*-cyclononene: J. M. Goodman, personal communication.
[8] η^3-Allylpalladium complexes have long been assumed to undergo a rapid *syn*–*anti* equilibration via η^1 intermediates, prior to nucleophilic addition. This is not the case here, which shows *contra* Curtin–Hammett behavior. For recent references to pertinent literature see J. D. Oslob, B. Åkermark, P. Helquist, P.-O. Norrby, *Organometallics* **1997**, *16*, 3015–3021; reference [5].
[9] H. M. R. Hoffmann, A. Brandes, *Tetrahedron* **1995**, *51*, 155–164; see also A. Brandes, H. M. R. Hoffmann, *ibid.* **1995**, *51*, 145–154.
[10] Fast addition is assumed to cause fast decomplexation of palladium bonded to the strained cyclic ether in [{(*E*)-**7**}PdL_2]. Consequently, palladium-induced allylic ether cleavage is suppressed and there is less isomerization from *E*- to *Z*-configurated cyclic ether.
[11] H. Muth, M. Sauerbier, *Methoden Org. Chem. (Houben-Weyl)*, Vol. 4/1c, **1980**, pp. 664–665.
[12] S. Chandrasekhar, J. Yu, J. R. Falck, C. Mioskowski, *Tetrahedron Lett.* **1994**, *35*, 5441.
[13] R. D. Little, S. O. Myong, *Tetrahedron Lett.* **1980**, *21*, 3339.
[14] J. Pohlmann, Dissertation, Universität Hannover, **1997**.

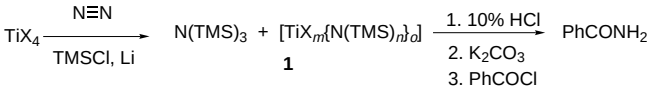
 © WILEY-VCH Verlag GmbH, D-69451 Weinheim, 1998 1433-7851/98/3705-0635 $ 17.50+.50/0

Fixation of Atmospheric Nitrogen: Synthesis of Heterocycles with Atmospheric Nitrogen as the Nitrogen Source**

Miwako Mori,* Katsutoshi Hori, Masaya Akashi, Masanori Hori, Yoshihiro Sato, and Mayumi Nishida

Since nitrogen fixation was first described by Vol'pin, Shur, et al.[1b, c] and van Tamelen et al.[1d, e] in the early 1960s there have been reports of molecular nitrogen fixation by various transition metals.[1] It is well known that nitrogenase catalyzes the reduction of atmospheric nitrogen to NH_3, fixation of atmospheric nitrogen in the laboratory remains quite challenging.[1d, e] Here we report the first example of the fixation of atmospheric nitrogen by TiX_4-Li-TMSCl[2] and the synthesis of heterocycles with atmospheric nitrogen as the nitrogen source (TMS = trimethylsilyl).

To examine whether atmospheric nitrogen can be fixed in titanium–nitrogen complexes of the type **1**,[2] we first



attempted to prepare $PhCONH_2$ as a product of nitrogen fixation with benzoyl chloride. A solution of $TiCl_4$ (1.0 equiv) and TMSCl (10.0 equiv) in THF was stirred in the presence of Li (10.0 equiv, porous) under dry air at room temperature for 24 h. The solution turned black with a green tinge. After hydrolysis the solution was made basic with K_2CO_3. To this was added a solution of PhCOCl in benzene, and the mixture was stirred overnight. After the usual workup, we were pleased to identify $PhCONH_2$ in 88% yield. Various titanium complexes such as $[Cp_2TiCl_2]$ and $Ti(OiPr)_4$ were applicable to this reaction, and $TiCl_4$ also gave good results (Table 1).

This means that atmospheric nitrogen can be fixed in the form of titanium–nitrogen complexes **1**. We next tried to synthesize N-heterocycles with dry air or molecular nitrogen as the nitrogen source using a TiX_4-Li-TMSCl system.[2] To a solution of cyclohexadione derivative **2a** and CsF in THF was added a solution of **1** in THF prepared under dry air from $TiCl_4$, Li, and TMSCl. The resulting mixture was heated at reflux overnight. After the usual workup indole derivative **3a** was obtained in 56% yield (Table 2, entry 1). When molecular nitrogen was used instead of air, **3a** was obtained in 86% yield.[2b] Similar treatment of diketone **2b** led to pyrrole derivative **3b** in moderate yield (entry 2). Michael addition of **1** to **2c** followed by condensation with the associated keto group proceeded smoothly at room temperature to give the tetrahydroindole derivative **3c** in good yield (entry 3). Lactams **3d**[3] and **3e** were obtained in a similar manner from the activated esters **2d** and **2e** (entries 4 and 5), respectively, which also contain keto groups and were prepared from the corresponding carboxylic acids by treatment with $ClPO(OEt)_2$. Interestingly, use of dry air as the nitrogen source gave nearly the same results as with molecular nitrogen.

We next investigated whether $TiCl_4$ could act as a catalyst.[2] To a solution of **1**—prepared under dry air from $TiCl_4$ (1 equiv), TMSCl (50 equiv), and Li (50 equiv)—in THF was added a solution of **2a** (10 equiv) and CsF (25 equiv) in THF. The mixture was heated at reflux for 24 h. After hydrolysis of the crude product indole derivative **3a** was isolated in 220% yield based on $TiCl_4$.[4] This means that nitrogen can be fixed catalytically from dry air in the form of $N(TMS)_3$, which acts as a ligand for titanium.

Table 1. Yields [%] of benzamide.[a]

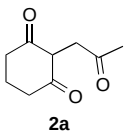
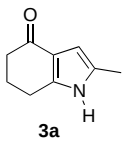
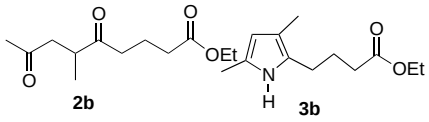
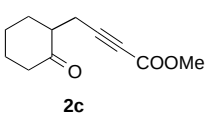
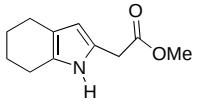
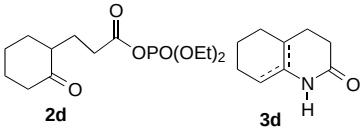
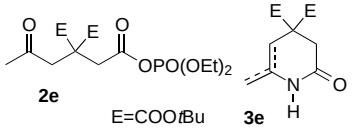
TiX_4	N_2 (pure)	Air
$TiCl_4$	90	88
$Ti(OiPr)_4$	91	80

[a] Yields are based on the titanium compound.

[*] Prof. Dr. M. Mori, K. Hori, M. Akashi, M. Hori, Y. Sato, M. Nishida
Faculty of Pharmaceutical Sciences
Hokkaido University
Sapporo 060 (Japan)
Fax: (+81) 11-721-6045
E-mail: mori@pharm.hokudai.ac.jp

[**] We thank the Hokkaido Foundation for the Promotion of Scientific and Industrial Technology for their support of this work. Supporting information for this contribution is available on the www under www/wiley-vch.de/home/angewandte.

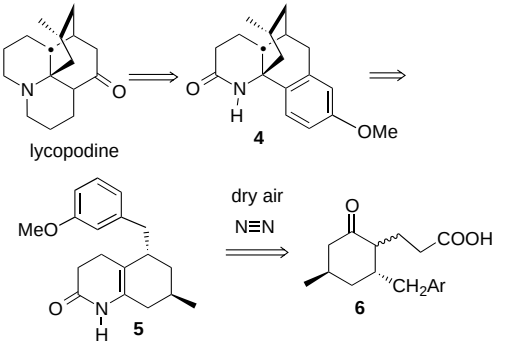
Table 2. Synthesis of heterocycles with fixed nitrogen.[a]

Entry	Substrate	Product	TiX_4	Yield [%][b] (N_2 Source)
1			$TiCl_4$ $TiCl_4$	86 (N_2) 56 (air)
2			$TiCl_4$ $TiCl_4$	51 (N_2) 37 (air)
3			$TiCl_4$ $Ti(OiPr)_4$ $Ti(OiPr)_4$	90 (N_2) 82 (N_2[c]) 72 (air[c])
4			$Ti(OiPr)_4$ $Ti(OiPr)_4$	58 (N_2) 60 (air)
5			$Ti(OiPr)_4$ $Ti(OiPr)_4$	51 (N_2) 50 (air)

[a] Complex **1** was prepared from TiX_4 (1.25 equiv), Li (12.5 equiv), and TMSCl (12.5 equiv) in THF under pure nitrogen or dry air at room temperature over 24 h. The reaction with **1** was conducted in the presence of CsF (5 equiv) in THF under reflux (24 h). [b] The yields are based on the substrate. [c] The reaction was carried out at room temperature (24 h).

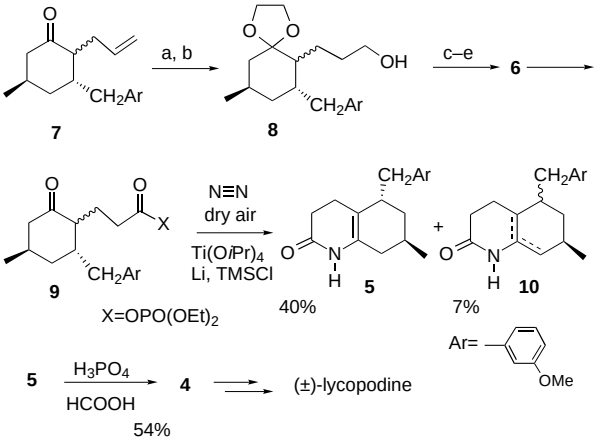
 © WILEY-VCH Verlag GmbH, D-69451 Weinheim, 1998 1433-7851/98/3705-0636 $ 17.50+.50/0

We then attempted to prepare the key intermediate in the synthesis of (±)-lycopodine[5] with dry air as the nitrogen source (Scheme 1). The total synthesis of (±)-lycopodine was achieved by Stork and co-workers[6] starting with the tetracycle **4**, which was obtained from lactam **5**. It was our intent to generate **5** from carboxylic acid **6** with dry air as the nitrogen source.



Scheme 1. Retrosynthesis of lycopodine.

Ketalization of **7**, which was easily prepared from 5-methyl-2-cyclohexenone,[7] followed by hydroboration and subsequent treatment with H_2O_2 in aqueous NaOH led to compound **8**, which was transformed into carboxylic acid **6** by oxidation and removal of the protecting group (Scheme 2).



Scheme 2. Synthesis of the lycopodine precursors **4** and **5**. a) $TMSOCH_2CH_2OTMS$, TMSOTf, 88%; b) $(Sia)_2BH$, then H_2O_2, NaOH, 98%; c) PCC; d) TsOH, acetone/H_2O; e) $NaClO_2$, KH_2PO_4, 2-methyl-2-butene, 67% based on **8**. Tf = Trifluoromethanesulfonate, Sia = 1,2-dimethylpropyl, PCC = pyridinium chlorochromate, Ts = 4-toluenesulfonyl.

A solution of **9**, derived from **6** and $ClPO(OEt)_2$, in THF together with **1**—prepared from $Ti(OiPr)_4$, Li, and TMSCl under dry air—was heated at reflux for 36 h; lactam **5** was then isolated in 40% yield along with a mixture of the stereoisomeric compounds **10**[8] in 7% yield. The melting point of **5** was in complete agreement with that reported in the literature.[6a, b] Conversion of **5** into **4** proceeded smoothly according to the procedure of Stork et al.

Thus, a formal total synthesis of (±)-lycopodine has been achieved with the aid of complexes of type **1** prepared from dry air; fixation of atmospheric nitrogen for the synthesis of heterocyclic compounds is clearly feasible. Notable characteristics of this procedure are the following: 1) the reaction is simple (a THF solution of $TiCl_4$ or $Ti(OiPr)_4$ and TMSCl in the presence of Li need only be stirred under dry air at room temperature), 2) $TiCl_4$ acts as a catalyst, and 3) nitrogen fixed from dry air can be introduced directly into organic compounds to produce useful heterocyclic compounds.

Received: October 8, 1997 [Z11020IE]
German version: *Angew. Chem.* **1998**, *110*, 659–661

Keywords: heterocycles · lycopodine · nitrogen fixation · titanium

[1] a) M. Hidai, Y. Mizobe, *Chem. Rev.* **1995**, *95*, 1115; b) M. E. Vol'pin, V. B. Shur, *Dokl. Akad. Nauk SSSR*, **1964**, *156*, 1102; c) M. E. Vol'pin, M. A. Ilatovskaya, L. V. Kosyakova, V. B. Shur, *J. Chem. Soc. Chem. Commun.* **1968**, 1074; d) E. E. van Tamelen, D. Seeley, S. Schneller, H. Rudler, W. Cretney, *J. Am. Chem. Soc.* **1970**, *92*, 5251; e) E. E. van Tamelen, *Acc. Chem. Res.* **1970**, *3*, 361; f) A. Yamamoto, M. Ookawa, S. Ikeda, *J. Chem. Soc. Chem. Commun.* **1969**, 841; g) K. Shiina, *J. Am. Chem. Soc.* **1972**, *94*, 9266; h) M. Mori, Y. Uozumi, M. Shibasaki, *Tetrahedron Lett.* **1987**, *28*, 6187; i) Y. Uozumi, N. Kawasaki, E. Mori, M. Mori, M. Shibasaki, *J. Am. Chem. Soc.* **1989**, *111*, 3725; j) Y. Uozumi, M. Mori, M. Shibasaki, *J. Chem. Soc. Chem. Commun.* **1991**, 81.

[2] a) M. Kawaguchi, S. Hamaoka, M. Mori, *Tetrahedron Lett.* **1993**, *34*, 6907; b) M. Mori, M. Kawaguchi, M. Hori, S. Hamaoka, *Heterocycles* **1994**, *39*, 729; c) M. Hori, M. Mori, *J. Org. Chem.* **1995**, *60*, 1480.

[3] D. Elad, D. Ginsburg, *J. Chem. Soc.* **1953**, 4137.

[4] When the same reaction was carried out under nitrogen gas, the indole derivative **3a** was isolated in 273% yield.

[5] a) K. Wiesner, *Fortschr. Chem. Org. Naturst.* **1962**, *20*, 271; b) D. B. MacLean, *Alkaloids (NY)* **1968**, *10*, 305.

[6] Total synthesis of (±)-lycopodine: a) G. Stork, R. A. Kretchmer, R. H. Schlessinger, *J. Am. Chem. Soc.* **1968**, *90*, 1647; b) G. Stork, *Pure Appl. Chem.* **1968**, *36*, 383; c) C. H. Heathcock, E. F. Kleinman, E. S. Binkley, *J. Am. Chem. Soc.* **1982**, *104*, 1054; d) C. H. Heathcock, E. F. Kleinman, *Tetrahedron Lett.* **1979**, 4125; e) C. H. Heathcock, E. F. Kleinman, E. S. Binkley, *J. Am. Chem. Soc.* **1978**, *100*, 8036; f) E. Wenkert, C. A. Broka, *J. Chem. Soc. Chem. Commun.* **1984**, 714; g) W. A. Ayer, W. R. Bowman, T. C. Joseph, P. Smith, *J. Am. Chem. Soc.* **1968**, *90*, 1648; h) D. Schuman, H. J. Muller, A. Nauman, *Liebigs Ann. Chem.* **1982**, 1700; i) S. W. Kim, Y. Bando, Z. I. Horii, *Tetrahedron Lett.* **1978**, 2293; j) T. Momose, S. Uchida, T. Imanishi, S. Kim, N. Takahashi, Z. I. Horii, *Heterocycles* **1977**, *6*, 1105; k) G. A. Kraus, Y. S. Hon, *ibid.* **1987**, *25*, 377; l) G. A. Karus, Y. S. Hon, *J. Am. Chem. Soc.* **1985**, *105*, 4341.

[7] W. Oppolzer, X. Petrzilka, *Helv. Chim. Acta* **1978**, *61*, 2755.

[8] The mixture consists of a pure constitutional isomer of **5** together with *cis*-**5** and the corresponding constitutional isomer. When *trans*-3-(3-methoxybenzyl)-5-methylcyclohexanone was synthesized by the reaction of 5-methyl-2-cyclohexenone with 3-methoxybenzylmagnesium chloride in the presence of CuI, a small amount of the *cis* isomer was obtained: A. Padwa, M. A. Brodney, J. P. Marino, Jr., S. M. Sheehan, *J. Org. Chem.* **1997**, *62*, 78.

 © WILEY-VCH Verlag GmbH, D-69451 Weinheim, 1998 1433-7851/98/3705-0637 $ 17.50+.50/0

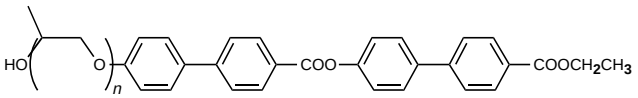
Cubic and Columnar Supramolecular Architectures of Rod–Coil Molecules in the Melt State**

Myongsoo Lee,* Byoung-Ki Cho, Heesub Kim, and Wang-Cheol Zin

Diblock molecules consisting of a rigid rod block and a flexible coil block provide the opportunity to study novel aspects of liquid-crystalline supramolecular structures. In general, classical rodlike molecules are arranged with their long axes parallel to each other to give rise to nematic and/or layered smectic types of supermolecular structures in the melt state. In contrast, diblock molecules consisting of different immiscible coil segments induce columnar or cubic types of supramolecular assemblies in addition to lamellar structures in a selective solvent.[1] Unlike rodlike molecules, coil–coil diblock copolymers also self-assemble into various supramolecular architectures with curved interfaces in the melt state due to conformational freedom associated with a long flexible chain.[2] A combination of these structural principles can provide a novel class of self-assembling materials since this rod–coil diblock system shares certain general characteristics of both lyotropic diblock molecules and thermotropic calamitic molecules.

Rod–coil molecules show lamellar or micellar microphase-separated domains depending on the volume fraction of coil segments in the molecules, although molecular order within the rod blocks in the melt state was not described.[3] In 1996 we published[4, 5] that rod–coil molecules consisting of a molecular rod and a poly(ethylene oxide) coil exhibit a microphase-separated lamellar structure of nanoscale dimensions in the crystalline phase as well as in the melt state; this leads to a smectic supramolecular structure. The binary mixture of these rod–coil molecules and lithium triflate induces micellar mesophases that are dependent on the salt concentrations.[5] This experimental system enabled us to study further their thermotropic phase behavior.

The design of the rod–coil diblock molecules was based on an extended rodlike molecule consisting of two biphenyl units.[4–6] The extended rods of this type can exhibit calamitic mesomorphism; however, unlike amphiphilic diblock macromolecules, rod molecules cannot form cubic or columnar phases with curved interfaces owing to steric reason. To introduce block segregation character, we synthesized rod–coil diblock molecules **1**–**3** consisting of a molecular rod and a poly(propylene oxide) coil (Figure 1). The coil portion is bulkier than poly(ethylene oxide) at the same degree of polymerization and is not able to crystallize because of the side methyl group in the propylene oxide unit. Therefore, these rod–coil diblock molecules can be considered as either small block copolymers or large smectogens.



1 n=7 k 62.1 s_C 108.6 s_A 122.8 i

2 n=12 k 38.7 bcc 69.6 i

3 n=15 k 23.0 bcc 41.1 col 46.1 i

Figure 1. Structure and phase behavior of **1**–**3**. The transition temperatures are given in °C; k: crystalline; s_A: smectic A; s_C: smectic C; bcc: bicontinuous cubic; col: hexagonal columnar; i: isotropic phase. The phase-transition temperatures are obtained from the second heating curves of the DSC measurements with a scan rate of 3 °C min^{-1}.

Rod–coil molecules **1**–**3** (see Table 1 for spectroscopic data) containing poly(propylene oxide) groups with various degrees of polymerization n were synthesized by a procedure similar to that previously described.[4, 6] The resulting rod–

Table 1. Spectroscopic data of **1**–**3**.

1: ^{1}H NMR (250 MHz, $CDCl_3$, TMS): $\delta = 8.26$ (d, $J = 8.2$ Hz, 2H; *o* to COOphenyl), 8.13 (d, $J = 8.2$ Hz, 2H; *o* to $COOCH_2$), 7.65–7.72 (m, 6H; *m* to COOphenyl, *m* to biphenylcarboxylate, and *m* to $COOCH_2$), 7.60 (d, $J =$ 8.6 Hz, 2H; *m* to $CH(CH_3)O$), 7.34 (d, $J = 8.4$ Hz, 2H; *o* to biphenylcarboxylate), 7.04 (d, $J = 8.3$ Hz, 2H; *o* to $CH(CH_3)O$), 4.58 (m, 1H; $OCH_2CH(CH_3)$), 4.41 (q, $J = 7.1$ Hz, 2H; CH_2CH_3), 3.18–3.92 (m, 20H; OCH_2CH), 1.35–1.45 (m, 6H; CH_2CH_3 and $CH(CH_3)$Ophenyl), 0.90–1.30 (m, 18H; $OCH_2CH(CH_3)$); ^{13}C NMR (62.5 MHz, $CDCl_3$, TMS): $\delta = 166.4$, 165.0, 158.6, 158.5, 151.1, 146.0, 144.6, 137.7, 132.1, 130.7, 130.1, 129.3, 128.3, 127.3, 126.9, 126.6, 122.2, 116.4, 72.3–76.0, 67.2, 65.5, 61.0, 18.4–16.9, 14.3; elemental analysis calcd for $C_{49}H_{64}O_{12}$: C 69.65, H 7.63; found: C 69.69, H 7.30.

2: ^{1}H NMR (250 MHz, $CDCl_3$, TMS): $\delta = 8.24$ (d, $J = 7.8$ Hz, 2H; *o* to COOphenyl), 8.12 (d, $J = 7.7$ Hz, 2H; *o* to $COOCH_2$), 7.65–7.71 (m, 6H; *m* to COOphenyl, *m* to biphenylcarboxylate, and *m* to $COOCH_2$), 7.59 (d, $J =$ 8.5 Hz, 2H; *m* to $CH(CH_3)O$), 7.34 (d, $J = 8.5$ Hz, 2H; *o* to biphenylcarboxylate), 7.04 (d, $J = 8.6$ Hz, 2H; *o* to $CH(CH_3)O$), 4.58 (m, 1H; $OCH_2CH(CH_3)$), 4.41 (q, $J = 7.1$ Hz, 2H; CH_2CH_3), 3.15–3.91 (m, 35H; OCH_2CH), 1.34–1.45 (m, 6H; CH_2CH_3 and $CH(CH_3)$Ophenyl), 0.90–1.30 (m, 33H; $OCH_2CH(CH_3)$); ^{13}C NMR (62.5 MHz, $CDCl_3$, TMS): $\delta = 166.4$, 165.0, 158.6, 158.5, 151.1, 146.1, 144.7, 137.8, 132.1, 130.7, 130.1, 129.3, 128.4, 127.3, 127.0, 126.6, 122.2, 116.4, 72.9–75.5, 67.2, 65.6, 61.0, 16.9–18.4, 14.3; elemental analysis calcd for $C_{64}H_{94}O_{17}$: C 67.70, H 8.34; found: C 67.72, H 8.48.

3: ^{1}H NMR (250 MHz, $CDCl_3$, TMS): $\delta = 8.25$ (d, $J = 7.8$ Hz, 2H; *o* to COOphenyl), 8.12 (d, $J = 7.7$ Hz, 2H; *o* to $COOCH_2$), 7.65–7.71 (m, 6H; *m* to COOphenyl, *m* to biphenylcarboxylate, and *m* to $COOCH_2$), 7.59 (d, $J =$ 8.5 Hz, 2H; *m* to $CH(CH_3)O$), 7.31 (d, $J = 8.5$ Hz, 2H; *o* to biphenylcarboxylate), 7.04 (d, $J =$ 8.6 Hz, 2H; *o* to $CH(CH_3)O$), 4.58 (m, 1H; $OCH_2CH(CH_3)$), 4.41 (q, $J = 7.1$ Hz, 2H; CH_2CH_3), 3.15–3.92 (m, 44H; OCH_2CH), 1.34–1.45 (m, 6H; CH_2CH_3 and $CH(CH_3)$Ophenyl), 0.85–1.35 (m, 42H; $OCH_2CH(CH_3)$); ^{13}C NMR (62.5 MHz, $CDCl_3$, TMS): $\delta = 166.4$, 165.0, 158.6, 158.5, 151.0, 146.0, 144.6, 137.7, 132.0, 130.7, 130.1, 129.3, 128.3, 127.3, 126.9, 126.6, 122.2, 116.3, 72.6–76.0, 67.1, 65.5, 60.9, 16.9–18.4, 14.3; elemental analysis calcd for $C_{73}H_{112}O_{20}$: C 66.95, H 8.62; found: C 67.24, H 8.71.

[*] Prof. M. Lee, B.-K. Cho
Department of Chemistry
Yonsei University
Shinchon 134, Seoul 120-749 (Korea)
Fax: (+82) 2-364-7050
E-mail: mslee@alchemy.yonsei.ac.kr
H. Kim, Prof. W.-C. Zin
Department of Materials Science and Engineering
Pohang University of Science and Technology (Korea)

[**] This work was supported by the Ministry of Education Republic of Korea (BSRI 96-3422) and the Korea Science and Engineering Foundation (1996)

 © WILEY-VCH Verlag GmbH, D-69451 Weinheim, 1998 1433-7851/98/3705-0638 $ 17.50+.50/0

coil molecules were characterized by differential scanning calorimetry (DSC) and thermal optical polarized microscopy (Figure 1). Upon heating of **1** ($n=7$) the crystalline phase goes into a smectic C phase at 62.1 °C, which in turn undergoes transformation into a smectic A phase.

In contrast, no birefringence between crossed polarizers could be observed upon melting of **2** ($n=12$) at 38.7 °C. The DSC results indicate an additional phase transition at 69.6 °C, which is accompanied by a significant decrease in viscosity; this strongly suggests the existence of a cubic mesophase in the range of 38.7 – 69.6 °C.[7] This is also confirmed by X-ray scattering experiments, which exhibit the same diffraction pattern (except that the lattice constant is smaller) as for the low-temperature mesophase of **3**.

Rod – coil molecule **3** ($n=15$) exhibits a crystalline melting transition into an optical isotropic cubic mesophase followed at higher temperatures by a hexagonal columnar mesophase, which in turn undergoes isotropization at 46.1 °C. Upon cooling the isotropic liquid, a spherulitic growing of texture can first be observed with a final development of pseudo-focal conic domains that are characteristic of a hexagonal columnar mesophase of conventional discotic mesogens.[8] On further cooling the hexagonal columnar phase, isotropic rectangular and rhombic areas with straight edges appear on the pseudo-focal conic domains. These regions then grow until the entire field of view is dark; this behavior is characteristic of the cubic mesophase (Figure 2).[7]

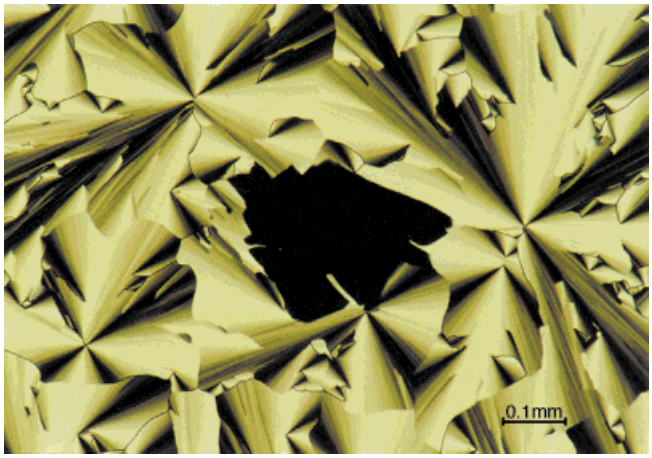


Figure 2. Representative optical polarized micrograph (100 × magnification) of the texture of **3** observed at the transition from the hexagonal columnar phase (pseudo-focal conic domains) to the cubic phase (dark area with straight edges) at 41 °C upon cooling.

To confirm the assignments of the mesophases, both small-angle (SAXS) and wide-angle X-ray scattering (WAXS) experiments were performed with **3** at various temperatures (Figure 3). The X-ray diffraction pattern of **3** in the crystalline state displays three reflections with q spacings of 0.84, 1.64, and 2.44 nm^{-1} in the small-angle region (Figure 3a), whereas two sharp reflections are observed in the wide-angle region. From the analysis of all available data, we can conclude that the crystalline phase of **3** is a lamellar structure with a periodicity of 7.5 nm. Comparison with the calculated length

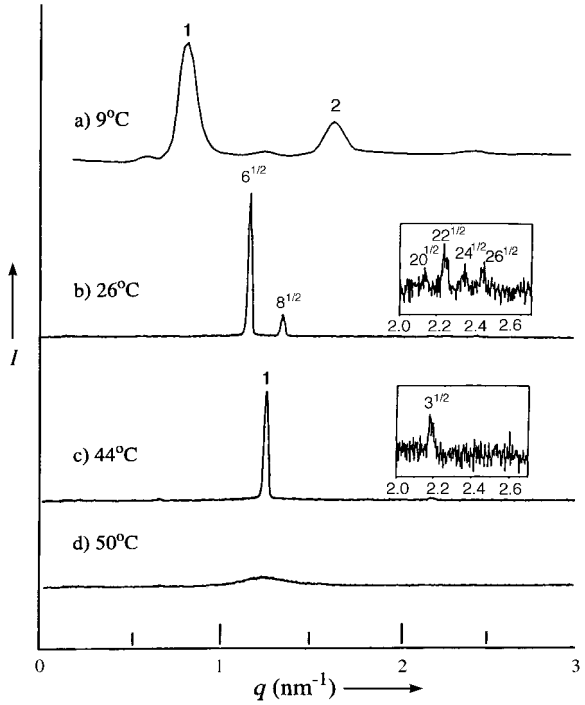


Figure 3. SAXS spectra of **3** obtained at different temperatures plotted against q ($=4\pi\sin\theta/\lambda$). Spectrum (a) was measured with Ni-filtered $Cu_{K\alpha}$ radiation and corrected for slit-length smearing. Spectra (b) through (d) were measured with synchrotron radiation at the 3C2 X-ray beam line ($\lambda=$ 0.1608 nm) at the Pohang Accelerator Laboratory.

of a fully extended molecular unit of 8.6 nm suggests that this periodicity arises from monolayers with packing similar to that in a related rod – coil molecule.[5]

In the liquid-crystalline phase at 26 °C, two strong and four weak reflections are observed at the relative positions $\sqrt{6}$, $\sqrt{8}$, $\sqrt{20}$, $\sqrt{22}$, $\sqrt{24}$, and $\sqrt{26}$ (Figure 3b). The positions of these reflections can be indexed as the (211), (220), (420), (332), (442), and (431) reflections of *Ia*3*d* symmetry.[9] From the observed d spacing of the (211) reflection, the value giving the best fit for the cubic lattice parameter a is 13.2 nm. At a wide angle only a diffuse halo remains as evidence for the melting of the aromatic rods. On the basis of the X-ray diffraction data described above and the thermal behavior, which exhibits an intermediate phase between the lamellar and columnar structures, the cubic phase can be best described as a bicontinuous cubic phase with *Ia*3*d* symmetry.[2, 9]

Upon further heating to 45 °C, **3** displays two sharp reflections with q spacings of 1.25 and 2.14 nm^{-1} whose SAXS pattern obeys the ratio of $1:\sqrt{3}$ (Figure 3c), which is characteristic of the two-dimensional hexagonal structure (hexagonally packed array of cylindrical micelles).[2] In contrast, only a diffuse halo can be observed in the WAXS pattern. These results together with observations from optical microscopy support that the high-temperature mesophase of **3** displays a disordered hexagonal columnar mesophase with a lattice constant of 5.8 nm. In the isotropic phase, **3** shows only broad, diffuse scattering in the small-angle region, which is most probably due to the existence of dynamic density inhomogeniety in the diblock melt.

Such molecular organizations in molecular rods are in striking contrast to what is generally accepted for the

 © WILEY-VCH Verlag GmbH, D-69451 Weinheim, 1998 1433-7851/98/3705-0639 $ 17.50+.50/0

relationship between molecular structure and the mesomorphic phase of thermotropic liquid crystals. The phase behavior in our rod–coil system can be explained by the fact that the main factor governing the geometry of the supramolecular architecture in the liquid-crystalline phase is the anisotropic aggregation of rod segments and the consequent space-filling requirements as well as entropic limitations due to the flexibility of the coil.[10–13] The lamellar structure observed in the crystalline phase for **3** or in the liquid -crystalline phase for **1** is still the most efficient packing of melt chains, which is similar to that of smectogens with low molar mass. With increasing temperature (in the case of **3**) or increasing volume fraction of coil segments, however, space crowding of the coil segments would be larger. Lamellar ordering of rods would confine junctions between rods and coils to a flat interface with a relatively high density of grafting sites, which forces a strong stretching of the coils away from the interface, and the system becomes energetically unfavorable. Consequently, the lamellar structure of the rod–coil molecule will break apart into interwoven networks of branched cylinders to lead to a bicontinuous cubic phase and then discrete cylinders; this gives rise to a hexagonal columnar phase in which coil stretching is reduced.

Although this explanation is qualitatively consistent with theoretical predictions for the phase behavior of rod–coil diblock molecules, that of our system is in contrast to the predicted specific supramolecular structures such as the various "hockey-puck" phases.[11] In this respect, our system provides access to a large variety of experimental and theoretical investigations to understand fully the complete range of supramolecular structures formed by rod–coil diblock molecules. This is essentially an unexplored area of research.

In summary, the rod–coil molecules which can be considered as either small diblock copolymers or large smectogens were observed to organize into bicontinuous cubic and hexagonal columnar mesophases as a function of volume fraction of the coil segments or temperature. This behavior differs significantly from that predicted for this type of molecule.[10–13]

Received: September 2, 1997 [Z 10881 IE]
German version: *Angew. Chem.* **1998**, *110*, 661–663

Keywords: columnar phases · cubic phases · liquid crystals · mesophases · supramolecular chemistry

[1] "Liquid Crystals": H. Stegemeyer, *Top. Phys. Chem.* **1994**, *3*.
[2] M. A. Hillmyer, F. S. Bates, K. Almdal, K. Mortensen, A. J. Ryan, J. P. Fairclough, *Science* **1996**, *271*, 976–978; F. S. Bates, *ibid.* **1991**, *251*, 898–901; S. Foster, A. K. Khandpur, J. Zhao, F. S. Bates, I. W. Hamley, A. J. Ryan, W. Bras, *Macromolecules* **1994**, *27*, 6922–6935.
[3] J. T. Chen, E. L. Thomas, C. K. Ober, G. Mao, *Science* **1996**, *273*, 343–346; J. T. Chen, E. L. Thomas, C. K. Ober, S. S. Hwang, *Macromolecules* **1995**, *28*, 1688–1697; L. H. Ladzilowski, B. O. Carraher, S. I. Stupp, *ibid.* **1997**, *30*, 2110–2119; L. H. Ladzilowski, S. I. Stupp, *ibid.* **1994**, *27*, 7747–7753; S. I. Stupp, V. LeBonheur, K. Walker, L. S. Li, K. E. Huggins, M. Keser, A. Amstutz, *Science* **1997**, *276*, 384–389. We thank a referee for bringing our attention to this work.
[4] M. Lee, N.-K. Oh, *J. Mater. Chem.* **1996**, *6*, 1079–1086.
[5] M. Lee, N.-K. Oh, H.-K. Lee, W.-C. Zin, *Macromolecules* **1996**, *29*, 5567–5573; M. Lee, N.-K. Oh, *Mol. Cryst. Liq. Cryst.* **1996**, *280*, 283–288.
[6] M. Lee, N.-K. Oh, W.-C. Zin, *Chem. Commun.* **1996**, 1787–1788.
[7] D. Demus, L. Richter, *Texture of Liquid Crystals*, Verlag Chemie, Weinheim, **1978**; G. W. Gray, J. W. Goodby, *Smectic Liquid Crystals, Texture and Structures*, Leonard Hill, Glasgow, **1984**.
[8] C. Destrade, P. Foucher, H. Gasparoux, N. H. Tinh, A. M. Levelut, J. Malthete, *Mol. Cryst. Liq. Cryst.* **1984**, *106*, 121–146; C. Destrade, N. H. Tinh, H. Gasparoux, J. Malthete, A. M. Levelut, *ibid.* **1981**, *71*, 111–117.
[9] J. M. Seddon, *Biochemistry* **1990**, *29*, 7997–8002; V. Luzzati, P. A. Spegt, *Nature* **1967**, *215*, 701–704.
[10] A. N. Semenov, *Mol. Cryst. Liq. Cryst.* **1991**, *209*, 191–199; A. N. Semenov, S. V. Vasilenco, *Sov. Phys. JETP Engl. Transl.* **1986**, *63*, 70–79.
[11] D. R. M. Williams, G. H. Fredrickson, *Macromolecules* **1992**, *25*, 3561–3568.
[12] A. Halperin, *Macromolecules* **1990**, *23*, 2724–2731.
[13] E. Raphael, P. G. de Gennes, *Makromol. Chem. Macromol. Symp.* **1992**, *62*, 1–17.

Superconductivity and Chemical Bonding in Mercury

Shuiquan Deng, Arndt Simon,* and Jürgen Köhler

Dedicated to Professor Hartmut Bärnighausen on the occasion of his 65th birthday

Recently a hypothesis on the chemical origin of superconductivity was proposed which is based on a tendency for pairwise localization of conduction electrons.[1] In crystalline phases, in which chemical bonding is adequately described by the electronic band structure, a prerequisite for superconductivity seems to be the simultaneous occurrence of bands with large dispersion, "steep bands", and those with "flat bands" at the Fermi level E_F. The flat bands provide a vanishing Fermi velocity for some conduction electrons in the normal conducting state. This view is formally similar to a physical model based on the interplay of itinerant electrons in a wide band with local pairs of electrons in a narrow band.[2] However, in extracting the flat band/wide band features from calculated band structures we address the specific chemical bonding in actual superconductors.

Following arguments introduced by Krebs,[3] who suggested that the necessary condition for superconductivity is a crystal orbital that is nodeless in certain directions, Johnson and Messmer used SCF-Xα-SW cluster calculations to obtain remarkably accurate results for the superconducting characteristics of a number of elements and compounds.[4] However, this real space approach is based on clusters rather than infinite solids; in terms of a band structure, Γ point configurations are considered.

[*] Prof. Dr. A. Simon, Dr. S. Deng, Dr. J. Köhler
Max-Planck-Institut für Festkörperforschung
Heisenbergstrasse 1, D-70569 Stuttgart (Germany)
Fax: (+49) 711-689-1091
E-mail: remon@simpow.mpi-stuttgart.mpg.de

 © WILEY-VCH Verlag GmbH, D-69451 Weinheim, 1998 1433-7851/98/3705-0640 $ 17.50+.50/0

Superconductivity has been discovered with mercury (T_c = 4.2 K).[5] Here we report on our studies of the electronic properties of the metal at the normal conducting state based on calculations of the Fermi surface, the total density of states (DOS), and the orbital analysis of the projected band structure. We are particularly interested in the occurrence of flat bands at the Fermi level E_F, and the character of chemical bonding for the states that belong to these bands. The term flat band refers to a section of a band, which falls into a narrow energy window centered by E_F, where the group velocities of the electrons approach zero. The width of the energy window should correspond to the Debye frequency; however, to account for inaccuracies of the band structure calculation, the window was fixed at a forty times larger value. We used the LMTO method[6] to calculate the energy dispersion $E(\boldsymbol{k})$ in the irreducible Brillouin zone (BZ).[7] After $E(\boldsymbol{k})$ was obtained, the scalar velocity field[12] in the whole BZ was calculated, and the maximum velocity as well as the positions and shapes of the flat bands were determined, the latter by using our own program.[13] The regions of the flat band are quite small. In order to analyze their bonding properties it is sufficient to choose one $\boldsymbol{k}$ point. Crystal orbital overlap population (COOP) curves[14] at some individual $\boldsymbol{k}$ point—not averaged over the entire BZ—were used as a bonding indicator for the flat band. To achieve this, we used the semiempirical extended Hückel (EH) method[15, 16] to carry out the bonding analyses.[17] The obtained bands below E_F were in good agreement with the LMTO bands.

The band structure of Hg serves as a particularly easy-to-analyze example to illustrate the flat band/steep band scenario. As Figure 1 shows, the total DOS at E_F has no local maximum and is very low ($N(E_F) = 0.29$ states/(eV · cell)). The bands have 6p and 6s character. The narrow 5d bands lie 5.6 to 8.7 eV below E_F. Hence, the electrons in the d bands do not contribute to the metallic and superconducting properties of Hg. Figure 1 also shows the energy dispersion $E(\boldsymbol{k})$ for seven bands up to E_F along three symmetry lines in the BZ.

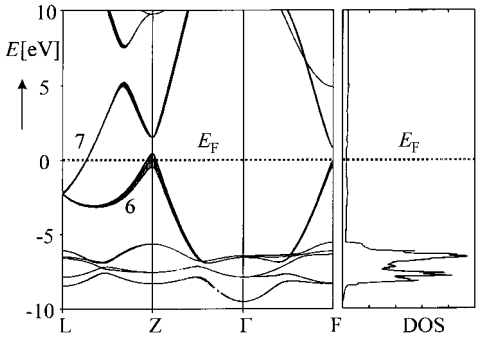


Figure 1. Band structure calculated for special symmetry directions and the total DOS of Hg. The fatness of the bands illustrates the contribution of the p_z orbital.

The highest occupied band (band 7) crosses the Fermi level, while the maxima of the next lowest band (band 6) approaches E_F at the Z and F points. It is worth mentioning that band 6 crosses E_F in other parts of the BZ. The flat bands at F and Z exhibit pure p character as p (ungerade) does not mix with s (gerade) at the special points. The "fat band" representation indicates the exclusive p_z orbital character of the flat band in Z (see below). In agreement with earlier results obtained both by relativistic APW calculations[18] and by de Haas–van-Alphen measurements,[19] our calculated Fermi surface (Figure 2) is composed of six electronic lenses (band 7) centered at the large hexagonal faces and a multiply connected surface of holes (band 6). The Fermi velocity on each lens decreases from the face center to the edge of the lens, while that on the multiply connected Fermi surface is low when it rides on the edge of the large hexagonal face of the BZ, and high when it rides on the edge of the rectangular face.

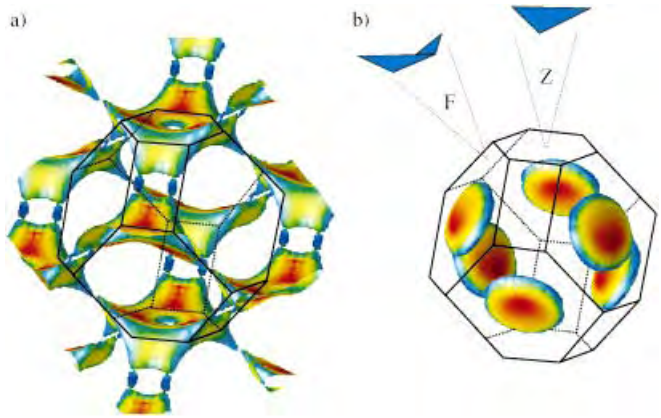


Figure 2. Fermi surface of Hg for band 6 (a) and band 7 (b) (Brillouin zone outlined). The increasing velocity of the electrons is represented by the change from blue to red. The isovelocity surface for band 6 around the F and Z points at a value of 0.03 (atomic units) is additionally shown in b). The two features are magnified by a factor of 100; they lie within the range of $E_F \pm 0.28$ eV.

Band 7, the steep band, crosses the Fermi level with various velocities throughout the BZ; the largest value is 1.29 (in atomic units). The highest value for the velocity of electrons within the energy window of $E_F \pm 0.28$ eV is 1.88 for band 7 and 1.83 for band 6. The maxima of band 6 at Z and F, which fall into the same energy window, meet the flat band, where the electron velocities become zero. In the energy window $E_F \pm 0.28$ eV this special condition only holds for these two $\boldsymbol{k}$ points in the whole BZ. Hence, the great majority of the conduction electrons exhibits high velocities. In this energy window the isovelocity surface at a value of 0.03 is plotted for band 6 in Figure 2, illustrating the shapes and locations of the flat band characteristics and giving evidence for their very limited extensions.

The self-consistently calculated and the fitted semiempirical band structure are in good agreement for all bands up to E_F, which provides added support for the accuracy of the analysis of the bonding properties of the flat bands on the basis of the semiempirical results. The interaction between nearest neighbors (2.986 Å) averaged over the whole BZ is of weakly bonding character for the band states around E_F. This particularly holds for the flat band states in band 6, as can be shown more explicitly with COOP curves calculated specifically for the Z and F points.

 © WILEY-VCH Verlag GmbH, D-69451 Weinheim, 1998 1433-7851/98/3705-0641 $ 17.50+.50/0

The crystal orbital of Hg at the Z point is purely p_z character (see Figure 1), as revealed by LMTO and EH calculations, while at the F point the orbital is a hybrid of Hg p_z, p_y, and p_x orbitals (with dominating p_z contribution). The crystal orbitals in band 6 are plotted for the Z and F point, respectively, in Figure 3. In both cases the imaginary part of the crystal orbital is very small and thus neglected. The crystal orbital at Z has the D_{3d} symmetry of the Z point in the BZ, while that at F has C_{2h} symmetry.

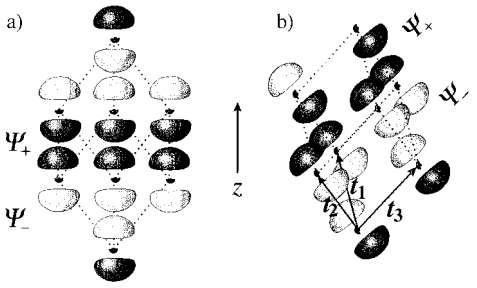


Figure 3. The crystal orbitals at Z (a) and F (b) in band 6. In a) the state is composed of pure p_z, while in b) the orbital at the origin of the primitive lattice is a hybrid of $-0.2642p_x$, $-0.4577p_y$, and $-0.5633p_z$. In both cases, the Ψ_+ and Ψ_- indicate two nodeless bonding systems, which are composed of the positive and the negative lobes of the orbitals, respectively.

At Z the orbital interactions along all three primitive lattice vectors (2.986 Å) are of $\sigma(p_z-p_z)$ type, while that along the short face diagonal direction (3.457 Å) is of $\pi(p_z-p_z)$ type. However, as the lobes of the p_z orbital do not point directly in the directions of the lattice vectors, the σ bonding is quite weak. At the F point, the orbital interactions along $\boldsymbol{t}_1$ and $\boldsymbol{t}_2$ are of σ(p – p) type, while those along the $\boldsymbol{t}_3$ direction are of π(p – p) type. In the $\boldsymbol{t}_1\boldsymbol{t}_2$ plane the orbital interactions along the $\boldsymbol{t}_1-\boldsymbol{t}_2$ direction are also of π(p – p) type, while those in the $\boldsymbol{t}_1\boldsymbol{t}_3$ and $\boldsymbol{t}_2\boldsymbol{t}_3$ planes are of σ(p – p) type. As shown in Figure 3a, for the Z point, $\pi(p_z\text{-}p_z)$ bonding occurs in planes perpendicular to the threefold axis and results in layers without nodes. Nodes occur between adjacent layers. According to Figure 3b, at the F point the nodeless bonding systems occur in layers that are oblique to the threefold axis, and these layers are again separated by nodal planes. The topologies of the crystal orbitals of the flat bands perfectly agree with those thought to be essential for superconductivity.[3, 4]

Our results suggest a rather visual scenario for the occurrence of superconductivity in mercury (and other conventional superconductors). According to the band structure the conduction electrons in mercury have large Fermi velocities except for a few that are at rest. The latter need to become singlet electron pairs in order to undergo condensation into the superconducting state.[20] Pairing can be achieved by coupling of the flat band states to dynamical lattice distortions, phonons, which modulate the bonding character of the band states in the maxima. A sufficient lowering of these states provides the spin pairing energy. Phonons periodically change the position of the flat band relative to E_F, and when the top of the flat band lies above E_F the electron pairs are scattered into states of steep bands near E_F. Vice versa, the electrons scatter into the so-created empty flat band states to become paired. At T_c the paired state becomes stable through condensation, and as the flat band states are periodically depleted they are continuously filled from the large reservoir of electrons in steep bands, thus creating more and more bosons.

Provided our hypothesis is correct, then two aspects are worth mentioning. First, in the band structure of Hg flat bands only lie at E_F when relativistic effects are considered in the calculations, otherwise the flat bands are located approximately 1 eV below E_F. Hence, mercury is a relativistic superconductor. Second, the flat bands have such tiny extensions that the identification of this feature, if responsible for superconductivity, rather resembles the search for a needle in a haystack.[21]

Received: September 3, 1997 [Z10888IE]
German version: *Angew. Chem.* **1998**, *110*, 664 – 666

Keywords: ab initio calculations · bond theory · extended Hückel calculations · mercury · superconductors

[1] A. Simon, *Angew. Chem.* **1997**, *109*, 1873; *Angew. Chem. Int. Ed. Engl.* **1997**, *36*, 1788.
[2] V. B. Geshkenbein, L. B. Ioffe, A. I. Larkin, *Phys. Rev. B* **1997**, *55*, 3173; J. Ranninger, J. M. Robin, *Physica C* **1995**, *253*, 279; R. Micnas, J. Ranninger, S. Robaszkiewicz, *Rev. Modern Phys.* 1990, 62, 113; A. S. Alexandrov, J. Ranninger, *Phys. Rev.* B **1981**, *23*, 1796; *ibid.* **1981**, *24*, 1164; J. Ranninger in *Polarons and Bipolarons in High-T_C Superconductors and Related Materials*, (Eds.: E. K. H. Salje, A. S. Alexandrov, W. Y. Liang), Cambridge University Press, Cambridge, **1995**, p. 67.
[3] H. Krebs, *Prog. Solid State Chem.* **1975**, *9*, 269.
[4] K. H. Johnson, R. P. Messmer, *Synthetic Metals* **1983**, *5*, 151.
[5] H. Kamerlingh-Onnes, *Akad. van Wetenschapen (Amsterdam)* **1911**, *14*, 113.
[6] Self-consistent first-principles linear muffin-tin orbital method: O. K. Andersen, O. Jepson, M. Sob in *Electronic Band Structure and its Applications* (Ed.: M. Yussouff), Springer, Berlin, **1986,** p. 1 – 57.
[7] The "combined correction"[8] to the atomic sphere approximation was used to get more accurate one-electron Hamiltonian and overlap matrices. The exchange-correlation potential of the density functional theory was obtained in the local density approximation (LDA) applied by Barth and Hedin.[9] The scalar-relativistic effect was considered through this calculation by solving the Dirac rather than the Schrödinger equation. All $\boldsymbol{k}$ space integrations were performed with the tetrahedron method[10] by using 4237 irreducible $\boldsymbol{k}$ points, and basis sets of 6s, 6p, 5d, and 5f orbitals; the 5f orbitals were down-folded.[11] These orbitals can carry charges, but make no contributions to the dimensions of Hamiltonian and overlap matrices, which saves calculation time and avoids possible distortions for the phase shifts of the high partial waves, or even the ghost band. To avoid too large atomic sphere overlap (1.6842 Å), we inserted an interstitial sphere with a radius of 0.8924 Å into the structure at (0,0,0.8832). Thus the actual basis set for the Hg calculations also includes 1s and 2p LMTOs of the interstitial, with 2p down-folded at the same level as that of the above-mentioned f orbitals.
[8] O. K. Andersen, *Phys. Rev.* B **1975**, *12*, 3060.
[9] U. von Barth, L. Hedin, *J. Phys.* C **1971**, *4*, 2064.
[10] P. Blöchl, O. Jepsen, O. K. Andersen, *Phys. Rev.* B **1994**, *49*, 16223.
[11] W. R. L. Lambrecht, O. K. Andersen, *Phys. Rev.* B **1986**, *34*, 2439.
[12] The group velocity of an electron is defined as $\boldsymbol{v}(\boldsymbol{k})=(1/\hbar)\nabla_k E(\boldsymbol{k})$, however, we use the term "velocity" for the scalar $v(\boldsymbol{k})=\sqrt{v(k)\cdot v(k)}$.
[13] S. Deng, Max-Planck-Institut für Festkörperforschung, Stuttgart **1997**.
[14] T. Hughbanks, R. Hoffmann, *J. Am. Chem. Soc.* **1983**, *105*, 3528.
[15] G. A. Landrum, YAeHMOP: Another EHMO package, Cornell University, Ithaca, NY (USA), **1997**.

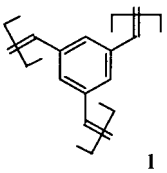
 © WILEY-VCH Verlag GmbH, D-69451 Weinheim, 1998 1433-7851/98/3705-0642 $ 17.50+.50/0

[16] The structural data used in this calculation are $a = 2.986$ Å, $\alpha = 70.743$, space group $R\bar{3}m$. All calculations are based on the primitive unit cell rather than the conventional one.The symbols of special $\boldsymbol{k}$ points in the BZ and the Cartesian system have been taken from Bradely and Cracknell.[17] EH parameters: H_{ii} [eV] (coefficients ζ_1) for Hg: 6s −13.68 (2.649), 6p −8.47 (2.631); 5d −17.50 (6.436); double ς functions were used: 5d C_1 0.6438, ς_2 3.032, and C_2 0.5215.
[17] C. J. Bradely, A. P. Cracknell, *The Mathematical Theory of Symmetry in Solids*, Clarendon, Oxford, **1972**.
[18] S. C. Keeton, T. L. Loucks, *Phys. Rev.* **1966**, *146*, 429; *ibid.* **1966**, *152*, 548; *ibid.* **1968**, *168*, 672.
[19] G. B. Brandt, J. A. Rayne, *Phys. Rev.* **1966**, *148*, 644.
[20] F. London, *Phys. Rev.* **1938**, *54*, 947.
[21] Calculations on the other polymorphs of mercury would serve as test cases for our criteria on the occurrence of superconductivity, however, the lack of knowledge concerning the structures prevents such calculations.

Stilbenoid Dendrimers**

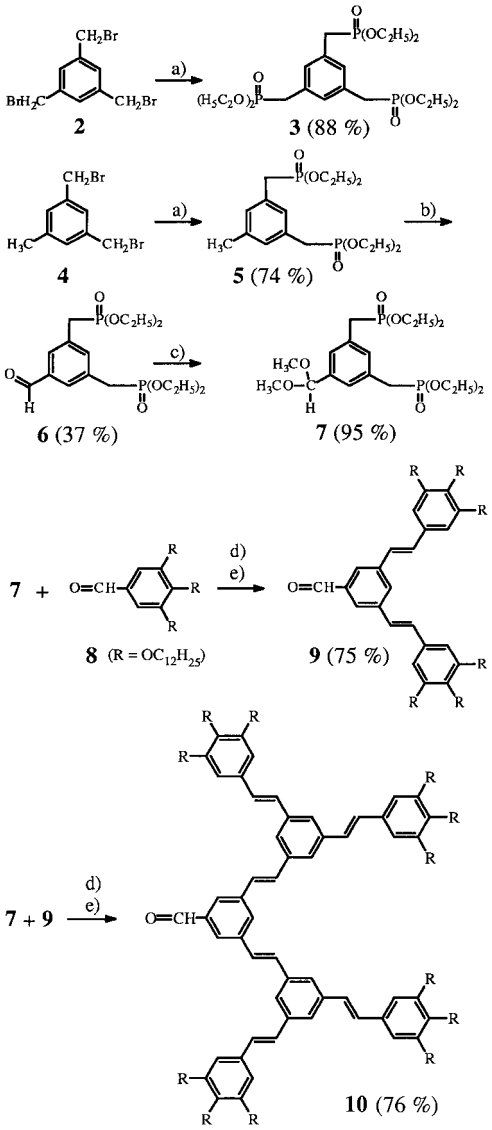
Herbert Meier* and Matthias Lehmann

Stilbenoid compounds show interesting photophysical and photochemical properties and are therefore appropriate for various applications in materials science.[1] Besides use in well-established areas such as optical brighteners, new applications are increasingly becoming apparent, including light-emitting diodes (LED), nonlinear optics (NLO), and optical imaging, storage, and switching techniques.



1

Through the incorporation of stilbenoid chromophores into dendrimers,[2] the design of which is also of considerable interest, we envisioned the new structural concept **1**. The convergent syntheses, coupled for individual generations, are depicted in Schemes 1 and 2. The required *E*-configured double bonds were formed by the Wittig–Horner reaction. The readily available tris(phosphonate) **3**[3] was used as a basic unit to form the core. Aldehyde **8**[4] and the bis(phosphonic acid) derivative **7**[5] with a protected aldehyde functionality served as building blocks for generating the dendrons; aldehydes **9**[6] and **10**[7] were obtained via **7** (Scheme 1). This procedure permitted the preparation of three generations of dendrimers (**1a**–**c**) from **3** and **8**, **9**, and **10** (Scheme 2). Tris(dodecyloxy)phenyl groups were attached to the periphery in order to enhance solubility and, as discussed below, to induce liquid crystalline (LC) behavior. The *trans* selectivity of the Wittig–Horner reaction is sufficiently high in this series of stilbenoid compounds to generate all-*trans* isomers **1a**–**c** within the limits of NMR detection. ^{1}H and ^{13}C NMR spectroscopy confirms the threefold symmetry of dendrimers **1a**–**c**. The observed chemical shifts are all very similar within this series of compounds (Table 1).



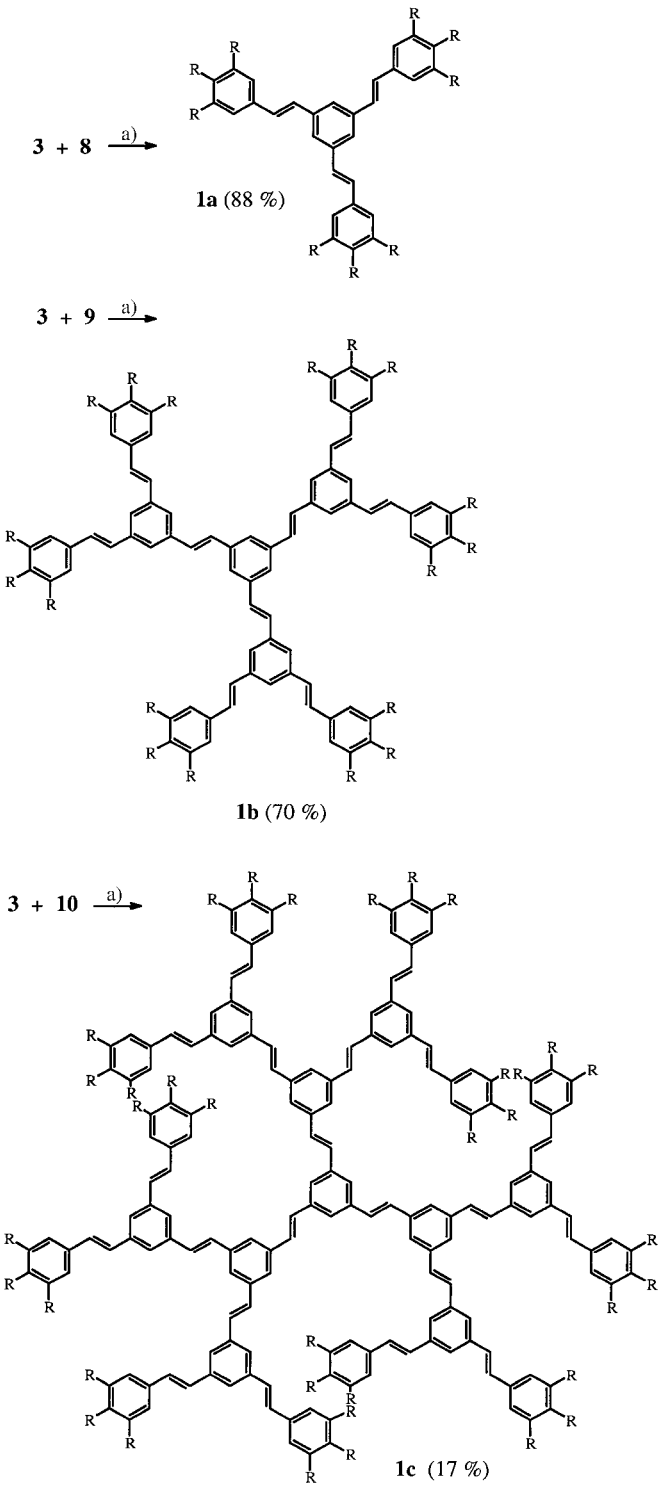
Scheme 1. Synthesis of the dendrimer precursors. a) $P(OC_2H_5)_3$, 160 °C; b) NBS (CCl_4), Fe (H_2O), 100 °C; c) CH_3OH, $HC(OCH_3)_3$, Dowex 50W-X8; d) $KOC(CH_3)_3$ (THF); e) HCl ($CHCl_3$).

The MALDI-TOF technique proved to be excellent for determining the molecular masses of **1a**–**c**. The discrepancy between the measured and calculated *m/z* values amounts to no more than one mass unit. For example, for **1c** with the molecular formula $C_{606}H_{996}O_{36}$ we obtained the value 8859.6, whereas the calculated mean for the peak of this molecular ion M^+ is 8858.6. The yields presented in Scheme 2 refer to dendritically pure compounds whose formation is assured by the convergent synthesis. A small amount of the "two-branched" compound, formed when only two molecules of **10** reacted with **3**, could only be detected in the crude product of **1c** with the MALDI-TOF method.

The aggregation of the stilbenoid dendrimers is especially interesting. Neat **1a** and **1b** generate two liquid crystalline phases each (D_{hd}: discotic hexagonal disordered phase; D_{rd}: discotic rectangular disordered phase; D_{ob}: discotic oblique

[*] Prof. Dr. H. Meier, Dipl.-Chem. M. Lehmann
Institut für Organische Chemie der Universität
J.-J. Becherweg 18-22, D-55099 Mainz (Germany)
Fax: (+49) 6131 395-396
E-mail: hmeier@mzdmza.zdv.uni-mainz.de

[**] This work was supported by the Deutsche Forschungsgemeinschaft and the Fonds der Chemischen Industrie.



Scheme 2. Synthesis of the three dendrimer generations **1a–c**. a) $KOC(CH_3)_3$ (THF).

phase). We obtained the following phase transitions for the two dendrimers from differential scanning calorimetric (DSC) measurements:

1a: k – 11 °C/59 kJ mol^{-1} – D_{hd} – 31 °C/4 kJ mol^{-1} – D_{rd} – 61 °C/8 kJ mol^{-1} – i

1b: k – 0 °C/52 kJ mol^{-1} – D_{hd} – 32 °C/4 kJ mol^{-1} – D_{ob} – 99 °C/17 kJ mol^{-1} – i

The data represent onset temperatures for phase transitions and the corresponding changes in enthalpy ΔH_o in the second heating curve. The DSC diagram for **1c** shows only melting of the alkoxy chains at −36 °C. Steric hinderance in the periphery of **1c** is probably too great for formation of an LC phase.

The mesophases of **1a** and **b** were characterized by polarization microscopy and X-ray scattering. Figure 1 shows the texture of the D_{ob} phase of **1b**; the corresponding parameters from X-ray analysis are provided in Table 2.

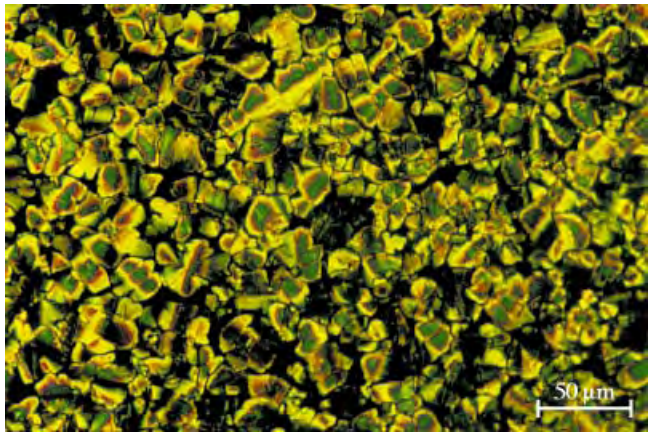


Figure 1. Texture of the D_{ob} phase of the second-generation dendrimer **1b**. The photograph was made with a polarization microscope after cooling to 45.9 °C.

Table 2. Parameters for X-ray scattering of the D_{ob} phase of **1b** (determined at 86 °C with CuK_α irradiation: $a = 42.0$ Å, $b = 38.0$ Å, $\gamma = 115°$).

Bragg reflections			d [Å]	
h	k	l	measured	calculated
1	0	0	38.0	38.0
0	1	0	32.4	32.6
0	−1	0	32.4	32.4
1	1	0	21.0	20.8
2	−1	0	21.0	20.7
2	0	0	19.2	19.0
−1	2	0	18.1	18.0
0	2	0	16.6	16.3
2	2	0	16.1	16.2

Table 1. Chemical shifts in the ^{1}H NMR spectra of **1a–c** (δ values in $CDCl_3$, TMS as internal standard).

1	CH_3	CH_2	*p*-OCH_2	*m*-OCH_2	Peripheral arom. H	Other arom. H	Peripheral olef. H[a]	Other olef. H[b]
a	0.85	1.1–1.9	3.96	4.02	6.72 (6H)	7.49 (3H)	7.00, 7.10	–
b	0.85	1.2–1.9	3.96	4.02	6.74 (12H)	7.55 (9H), 7.62 (3H)	7.02, 7.11	7.23 (6H)
c	0.83	1.1–1.8	3.7–4.0		6.69 (24H)	7.53 (6H), 7.55 (12H) 7.62 (3H), 7.69 (6H) 7.71 (3H)	6.97, 7.07	7.27 (12H), 7.34 (6H)

[a] AB, $^3J = 16.1 \pm 0.1$ Hz. [b] Singlets.

 © WILEY-VCH Verlag GmbH, D-69451 Weinheim, 1998 1433-7851/98/3705-0644 $ 17.50+.50/0

Electron-scattering investigations and model calculations that are currently in progress should provide more detailed characterization of the molecular self-assembly. Liquid crystalline properties are presumably destroyed by the segment mobility of an increasing number of stilbene units; in principle, the number of conformers is doubled per double bond, but for symmetry reasons the maximum number of 2^n (e.g., 2^{21} for the third generation) cannot be reached.

The tendency to aggregate increases from **1a** through **1b** to **1c**. Figure 2 shows the temperature dependence of ^{1}H NMR

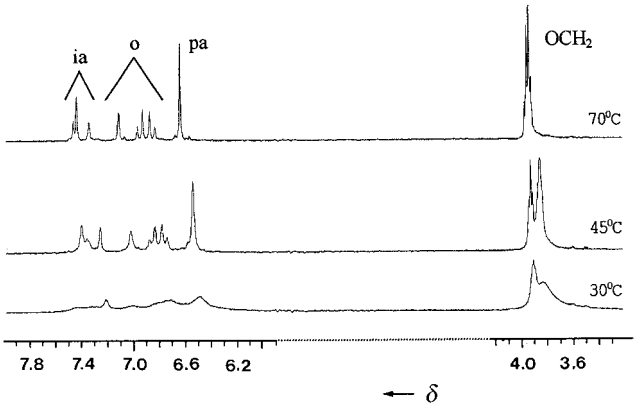


Figure 2. Temperature-dependent ^{1}H NMR spectra (400 MHz) of **1b** in C_6D_{12} (4.6×10^{-3} M). ia: inner aromatic protons; o: olefinic protons; pa: aromatic protons on the peripheral benzene rings.

spectra of **1b** in [D_{12}]cyclohexane. Whereas the spectrum in $CDCl_3$ at 20 °C exhibits quite normally resolved signals, aggregation in cyclohexane causes considerable line broadening, which has its origin in reduced segment mobility. The effect is so pronounced for **1c** that no highly resolved ^{1}H NMR spectrum can be obtained even by heating the sample.

Temperature- and concentration-dependent aggregation in nonpolar solvents can also be followed with fluorescence spectroscopy. For example, a 10^{-8} M solution of **1b** in cyclohexane shows two fluorescence maxima at $\lambda = 399$ and $\lambda = 419$ nm; however, only a broad band with a single bathochromically shifted maximum at 424 nm is obtained for a 10^{-4} M solution. In chloroform or dichloromethane the fluorescence band is independent of concentration. The interaction especially between the electron-rich peripheral benzene rings and the solvent molecules (which exhibit acceptor properties) is apparently so strong that dendrimer molecules no longer form aggregates. In dichloromethane, all three dendrimers **1a**–**c** show a UV absorption with $\lambda_{max} =$ 329 nm, which decreases upon irradiation. Decomposition progresses are especially fast in the aggregated state in cyclohexane.[8]

With respect to structure, **1a**–**c** are most closely related to the stiff dendrimers consisting of tolan building blocks.[9, 10] However, the aggregation, phase behavior, and photochemistry of the stilbenoid dendrimers have not been found with the tolan system so far,[11] nor was this expected in the case of photochemistry. Further investigations of conformational mobility and charge and energy transfers are currently in progress.

Received: August 4, 1997
Revised version: October 16, 1997 [Z10772IE]
German version: *Angew. Chem.* **1998**, *110*, 666–669

Keywords: aggregations · dendrimers · liquid crystals · stilbenes · supramolecular chemistry

[1] H. Meier, *Angew. Chem.* **1992**, *104*, 1425; *Angew. Chem. Int. Ed. Engl.* **1992**, *31*, 1399.
[2] a) G. R. Newkome, C. N. Moorefield, F. Vögtle, *Dendritic Molecules.* VCH, Weinheim **1996**; b) J. M. Fréchet, C. J. Hawker, I. Gitsov, J. W. Leon, *J. Macromol. Sci. Pure Appl. Chem.* **1996**, *A33*, 1399.
[3] L. Y. Malkes, N. P. Kovalenko, *Zh. Organ. Khim.* **1966**, *2*, 297 [*Chem. Abstr.* **1966**, *65*, 2188a].
[4] H. Meier, E. Prass, G. Zerban, F. Kosteyn, *Z. Naturforsch.* **1988**, *43b*, 889.
[5] **7**: Oil, ^{1}H NMR ($CDCl_3$): $\delta = 1.19$ (t, 12H, CH_3), 3.09 (d, ^2J(H,P) = 22.0 Hz, 4H, CH_2P), 3.25 (s, 6H, OCH_3), 3.95 (m, 8H, OCH_2), 5.31 (s, 1H, CH), 7.16 (m, 1H, 2-H), 7.23 (d, 2H, 4-H, 6-H).
[6] **9**: M.p. 66 °C, ^{1}H NMR ($CDCl_3$): $\delta = 0.86$ (m, 18H, CH_3), 1.40–1.85 (m, 120H, CH_2), 3.98 (t, 4H, OCH_2), 4.01, (t, 8H, OCH_2), 6.72 (s, 4H, arom. H), 7.00/7.13 (AB, $^3J = 16.2$ Hz, 4H, olef. H), 7.80 (t, 1H, 4-H), 7.85 (d, 2 H, 2-H, 6-H), 10.04 (s, 1H, CHO).
[7] **10**: M.p. 106 °C, ^{1}H NMR ($CDCl_3$): $\delta = 0.87$ (m, 36H, CH_3), 1.24–1.86 (m, 240H, CH_2), 3.97 (t, 8H, OCH_2), 4.03 (t, 16H, OCH_2), 6.74 (s, 8H, arom. H), 7.24/7.29 (AB, $^3J = 16.1$ Hz, 4H, olef. H), 7.55 (m, 6 H, arom. H), 7.88 (t, 1H, 4-H), 7.94 (d, 2H, 2-H, 6-H), 10.09 (s, 1H, CHO).
[8] Decomposition of the stilbenoid chromophores is almost complete; that is, the C–C double bonds disappear through formation of intermolecular C–C single bonds. For the 21 double bonds of **1c** and the 9 double bonds of **1b** these are processes that lead to very complex structures. In the case of **1a** we were able to isolate two diastereomeric dimers with three four-membered rings each; see J. Juriew, T. Skorochodova, J. Merkushew, W. Winter, H. Meier, *Angew. Chem.* **1981**, *93*, 285; *Angew. Chem. Int. Ed. Engl.* **1981**, *20*, 269.
[9] Z. Xu, B. Kyan, J. S. Moore, *Advances in Dendritic Macromolecules* **1994**, *1*, 69.
[10] P.-W. Wang, Y.-J. Liu, C. Devadoss, P. Bharathi, J. S. Moore, *Adv. Mater.* **1996**, *8*, 237.
[11] Shortly after submission of this work a paper was published by Pesak and Moore[12] on dendritic columnar liquid crystals from tolan building blocks; liquid crystalline dendrimers on a different molecular basis have been described, for example, by Percec et al.,[13] Mülhaupt, Frey, et al.,[14] Wendorff et al.,[15] and Lattermann et al.[15, 16] Note added in proof (February 19, 1998): After submission of this manuscript a somewhat related dendrimer system with stilbene building blocks was described: S. K. Deb, T. D. Maddux, L. Yu, *J. Am. Chem. Soc.* **1997**, *119*, 9079.
[12] D. J. Pesak, J. S. Moore, *Angew. Chem.* **1997**, *109*, 1709; *Angew. Chem. Int. Ed. Engl.* **1997**, *36*, 1636.
[13] a) V. Percec, P. Chu, G. Ungar, J. Zhou, *J. Am. Chem. Soc.* **1995**, *117*, 11441; b) V. Percec, G. Johansson, G. Ungar, J. Zhou, *ibid.* **1996**, *118*, 9855; c) V. S. K. Balagurusamy, G. Ungar, V. Percec, G. Johansson, *ibid.* **1997**, *119*, 1539.
[14] K. Lorenz, D. Holter, B. Stuhn, R. Mülhaupt, H. Frey, *Adv. Mater.* **1996**, *8*, 414.
[15] U. Stebani, G. Lattermann, M. Wittenberg, J. H. Wendorff, *Angew. Chem.* **1996**, *108*, 1941; *Angew. Chem. Int. Ed. Engl.* **1996**, *35*, 1858.
[16] J. H. Cameron, A. Facher, G. Lattermann, S. Diele, *Adv. Mater.* **1997**, *9*, 398.

 © WILEY-VCH Verlag GmbH, D-69451 Weinheim, 1998 1433-7851/98/3705-0645 $ 17.50+.50/0

Polariton-Induced Color Tuning of Thin Dye Layers**

Lars Dähne,* Erwin Biller, and Helmut Baumgärtel

The control of light absorption of supramolecular dye systems[1] is important for their technical application in photography,[2] xerography,[3] and electrooptical devices.[1, 3] The absorption energy of organic dyes depends on molecular parameters such as extension and delocalization of the conjugated π-electron system[4] as well as on intermolecular interactions between the dye and the surrounding medium.[1, 5] Since dyes are mostly applied in the solid state, the investigation and exploitation of such interactions are necessary. Up to now, three intermolecular interactions are widely known:

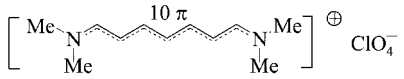
1. Polar dyes exhibit solvatochromism due to the influence of the solvent on the delocalization of the π-electron system.[5]
2. Charge-transfer transitions occur between dye molecules having unequal electron density. These are characterized by weak and broad absorption bands.[5]
3. Transition dipole interactions between dye molecules in aggregates and crystals yield intensive and often narrow absorption bands, shifted either to the red (J-aggregates) or to the blue (H-aggregates) relative to the monomer.[6, 7]

Furthermore, the absorption wavelength of anisotropic dye crystals can vary depending on the directional dispersion of polaritons;[8, 9] this phenomenon was rather unfamiliar until now. In contrast to the well-known excitons (electronic excitations in solids), polaritons include the interaction of excitons with the polarization of the crystal induced by optical excitation.[8] For weakly absorbing materials the difference is small, but for densely packed dye molecules unusual optical properties appear, which cannot be described by excitons alone. The interaction between excitons and polarization leads to different energies of the transverse (E_T) and longitudinal excitons (E_L). The energy difference $\Delta E = E_L - E_T$ depends on the strength of the transition dipole moment M and on the dye density N following the Lyddane–Teller–Sachs Equation (a).[8]

$$(E_L^2 - E_T^2)/E_T^2 \sim |M|^2 N \qquad \text{(a)}$$

Within the energy region ΔE light waves cannot propagate in the dye crystal, but are strongly reflected; broad reflection bands and a metallic luster result. Due to the small penetration depth of light, transmission spectra cannot be measured directly. Hence, the absorption can only be calculated from the reflection spectra, with the Kramers–Kronig relation.[9] In this way a further peculiarity of polaritons was shown, which arises from the anisotropic distribution of dipole moments in the crystal. The absorption maximum does not exhibit the excitation energy of the excitons (E_T), but depends on the angle β between the wave vector of the light and the transition dipole moment (see Figure 4). The absorption maximum lies at E_T only if $\beta = 90°$, that is, for normal incidence of light the dipole moment must be parallel to the crystal face. Otherwise, for decreasing β the absorption maximum shifts to higher energy till the energy of the longitudinal exciton is reached. Simultaneously, the absorption intensity decreases, as the transition dipole moment is projected onto the crystal face under consideration. This extraordinary behavior can be explained by excitation of an electromagnetic wave, the polariton, having mixed longitudinal–transverse polarization.

The direct observation of polariton absorption requires a layer thickness of about 80 nm (which depends on the penetration depth of the light), a single crystallike arrangement of the molecules over a large area, and the option to change the molecule inclination relative to the layer plane. Such layers could not be prepared by common techniques such as spin-coating, evaporation, Langmuir–Blodgett (LB) techniques, or epitaxy,[14] but were achieved by a new method (thin layer aggregation, TLA)[11] for salts of the dye 1,7-bis(dimethylamino)heptamethine cation BDH^+ (Scheme 1).



Scheme 1. The streptopolymethine dye 1,7-bis(dimethylamino)heptamethine perchlorate ($BDH^+ClO_4^-$).

In different crystals of this dye the values of both M and N are especially high, resulting in extraordinarily strong splittings with ΔE up to 14000 cm^{-1}.[10] The TLA method is based on the aggregation/crystallization of dye molecules in thin amorphous layers of an undercooled melt of $BDH^+ClO_4^-$. The originally prepared BDH^+ layers showed a high microscopical disorder, which prevented the observation of color variation by polaritons.[11] By using higher temperatures for the aggregation process, homogeneous molecule orientation and a variation of molecule inclination was achieved.

Amorphous layers of $BDH^+ClO_4^-$ were obtained by fast spin-coating of $BDH^+ClO_4^-$ solutions in acetone on quartz substrates.[11] We chose a layer thickness of approximately 80 nm, which yielded a maximal optical density of 2.5 in the absorption bands. After an incubation time of some minutes a few nuclei were formed in the layer. These grew radially to large spherulites with diameters up to 20 mm. The assembled structures exhibit strong dichroism. All microphotographs and spectroscopic investigations were therefore performed with linearly polarized light (Figure 1), which avoids the superposition of the two transition moments, excludes pleochroism effects,[12] and gives the genuine dichroic colors due to light absorption. In contrast, similar pictures of liquid crystals, taken between crossed polarizers, only shows apparent colors due to birefringence. Interference effects could be excluded as origin of the observed colors. Variation of layer thickness changed only the intensity and not the position of the absorption band. Furthermore, interference at layers of 80 nm can appear only in case of very high refractive indices

[*] Dr. L. Dähne, E. Biller, Prof. H. Baumgärtel
Institut für Physikalische und
Theoretische Chemie der Freien Universität
Takustrasse 3, D-14195 Berlin (Germany)
Fax: (+49) 30-838-6612
E-mail: daehne@chemie.fu-berlin.de

[**] This work was supported by the Deutsche Forschungsgemeinschaft.

 © WILEY-VCH Verlag GmbH, D-69451 Weinheim, 1998 1433-7851/98/3705-0646 $ 17.50+.50/0

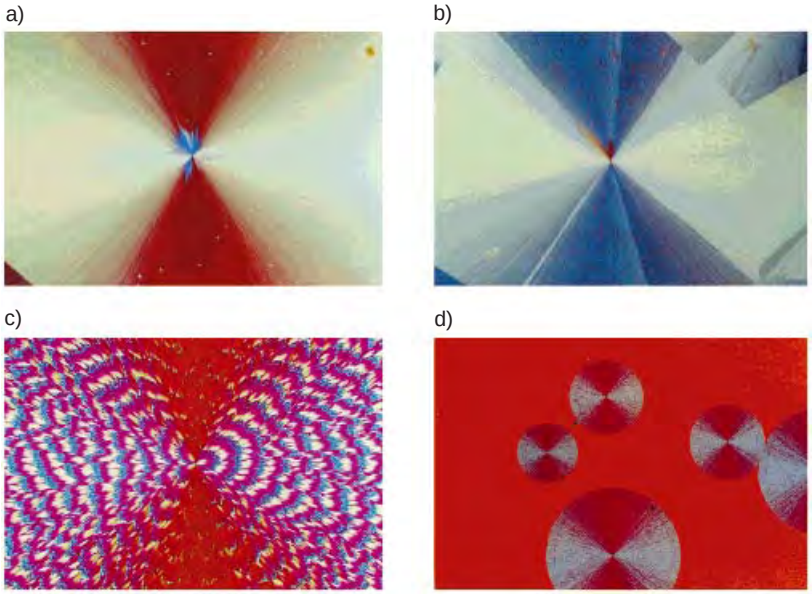


Figure 1. Microphotographs of $BDH^+ClO_4^-$ layers, aggregated at different temperatures (picture size $600 \times 900\ \mu m^2$, horizontally polarized light in transmission). a) Aggregation at 110°C, red/colorless region; b) aggregation at 110°C, blue/colorless region; c) aggregation at 88°C; d) aggregation at 20°C; the red layer is the amorphous phase.

n, which could be reached at most in the absorption maximum.

The growth process was performed at different temperatures between 20 and 155°C and at constant absolute air moisture of $12\ g\,m^{-3}$, because moisture also influenced the aggregation process. For that purpose, freshly prepared amorphous layers were transferred to a heating plate having electronically controlled temperature. The growth velocity depends on the temperature and increases from $0.35\ \mu m\,s^{-1}$ at 25°C to about $400\ \mu m\,s^{-1}$ at 140°C. The melting point (155–157°C) of the formed layers is independent of the aggregation temperature, which points to an identical aggregate structure. Four different layer types were obtained within following temperature regions:

1. Thin-layer aggregation at 90–155°C: Aggregation in this temperature interval yields spherulites that exhibit two differently colored layer regions. In light polarized in tangential (T) direction with respect to the aggregate circle (T polarization), one region is red (Figure 1a) and the other one blue (Figure 1b), whereas both are colorless in light polarized in radial (R) direction (R polarization). The polarized UV/Vis spectra were taken with a microspectralphotometer on $4 \times 4\ \mu m^2$ points of the spherulites (Figure 2a). Only for T polarization do they show an absorption band at 574 nm for the red/colorless and at 628 nm for the blue/colorless region. The layer spectra agree well with the dichroic absorption spectra of the $BDH^+ClO_4^-$ single crystal (Figure 2a), calculated from reflection spectra of crystal faces, where $\beta = 90°$.[13] The two absorption bands arise from two molecular directions in the unit cell of the $BDH^+ClO_4^-$ crystal[15]. Interactions between the molecular transition dipole moments lead to two perpendicularly oriented excitonic components m_+ (639 nm, blue) and m_- (591 nm, red; Figure 3).[7, 13] The total transition moment M of the crystal is distributed in the m_+ and m_- component in the ratio 1:2. Thus, the components show a fairly large splitting of $\Delta E_+ = 5400\ cm^{-1}$ and $\Delta E_- = 11\,400\ cm^{-1}$. Because the sensitivity of the solid-state spectra to the molecule arrangement is high,[10] two conclusions could be drawn from the good

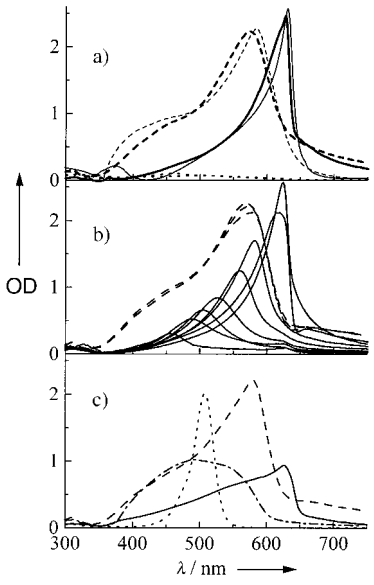


Figure 2. Spectra of optical density OD of $BDH^+ClO_4^-$: a) samples aggregated at 110°C: blue/colorless region (T polarization; bold —); m_+ component of the single crystal[13] (—); red/colorless region (T polarization; bold – – –); m_- component of the single crystal (– – –); both layer regions (R polarization; ···); b) sample aggregated at 88°C: spectra from eight successive points within one color period: R polarization (—), T polarization (– – –; due to the similarity of the spectra only three are shown); c) BDH^+ monomer in methanol (···); amorphous layer (–·–·–); sample aggregated at 20°C: R polarization (—), T polarization (– – –).

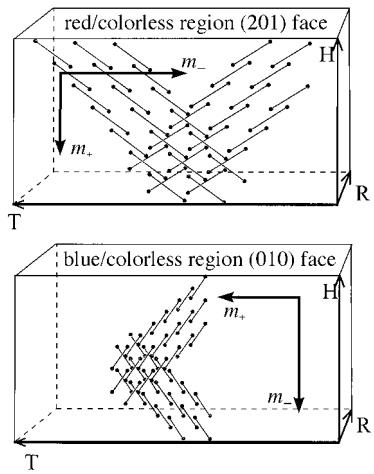


Figure 3. Orientation of BDH^+ cations (sketched as dumbbells) and the transition moments of the m_+ and m_- component in the red/colorless and blue/colorless region of the layer aggregated at 110°C; H: layer height, T: tangential direction, R: radial and growth direction (derived by spectroscopic data and X-ray structure analysis).[15]

 © WILEY-VCH Verlag GmbH, D-69451 Weinheim, 1998 1433-7851/98/3705-0647 $ 17.50+.50/0

Table 1. Spectroscopic data of the transition dipole components m_+ and m_- of $BDH^+ClO_4^-$ in single crystals[10] and in the ordered layer.

	$\lambda(m_+)$ transverse [nm]	$\lambda(m_+)$ longitudinal [nm]	$\lambda(m_-)$ transverse [nm]	$\lambda(m_-)$ longitudinal [nm]	Ratio of oscillator strengths f_+/f_-	M.p. [°C]
layer	628	430	574	345[a]	0.456	155–157
crystal	639	475	591	353	0.464	176–178

[a] Not exactly determinable.

agreement of layer and crystal spectra (Table 1). Firstly, layer and crystal structure are similar, although deviations in melting point (of 21 °) and absorption wavelength (of 11 and 17 nm) indicate small differences, which however, might be caused by the small layer thickness, too. Secondly, the layers virtually have the long- and short-range order of a single crystal within large regions. This is remarkable, because such high degree of order is hardly achievable by common layer preparation methods.[1, 14, 18] The apparently higher layer absorption in the long-wavelength region is caused by the layer reflection (Figure 2a). For both layer regions, the arrangement of BDH^+ was derived from the spectroscopic data and the known single-crystal structure.[15] As only one absorption band exists in each region, one excitonic component has to be perpendicular to the layer plane ($\beta = 0°$, Figure 3). Due to the orthogonality of m_+ and m_-, the other component is parallel to the surface ($\beta = 90°$). This is fulfilled for the blue/colorless region in the case of the (010) crystal face where only m_+ is observable and for the red/colorless region in the case of an approximate (201) face, where only m_- absorbs light. None of these crystal faces were formed by crystal growth of $BDH^+ClO_4^-$ in solution. It is not quite clear yet which factors in the TLA process influence the ratio between both regions.

2. TLA at temperatures between 40 and 90°C: Layers formed at these temperatures exhibit in growth direction for R polarization a periodical variation of color in the order colorless, yellow, orange, red, violet and blue (Figure 1c). For T polarization, the color always remains red. The period length increases from 2 μm at a growth temperature of 40°C to approximately 100 μm at 88°C and becomes infinite for the red/colorless region (Figure 1a) above 90°C. The polarized absorption spectra were taken step by step in growth direction within one period. While T polarization yielded almost the same absorption spectrum for every point with a maximum at 574 nm, for R polarization the absorption bands shifted from 435 nm to 628 nm (Figure 2b). Neither the aggregate structure nor the layer thickness changed remarkably within the period as indicated by the same melting point, the almost constant absorption spectrum for T polarization, and a nearly flat surface profile measured by atomic force microscopy.[16] Therefore, the observed color variation can only be caused by directional dispersion of polaritons. A successive widening of the angle β_+ between m_+ and the layer normal increases the absorption intensity and shifts the absorption maximum from $E_L = 430$ nm at $\beta_+ \approx 0°$ to $E_T = 628$ nm at $\beta_+ = 90°$ according to the polariton model (Figure 4).[8, 9] The m_- component always lies in T direction ($\beta_- = 90°$) yielding the unchanged absorption spectra at 574 nm (Figure 2b). The reason for the periodical change of orientation might be mechanical stress

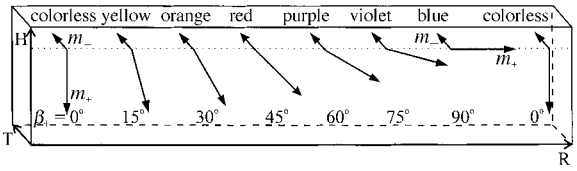


Figure 4. Orientation of the transition moments m_+ and m_- within one color period of a layer aggregated at 88°C; H: layer height, T: tangential direction, R: radial and growth direction; β_+: angle between m_+ component and face normal.

in the layer, possibly caused by different growth rates on the interfaces or by the deviation between growth and aggregate direction. Similar phenomena are known from self-organization processes, such as the crystal growth in undercooled melts of salol.[17]

3. TLA below 40°C: Aggregation at strong undercooling leads to period lengths below the spatial resolution of the microscope. Consequently, an unusually broad spectrum was measured for R polarization,[11] which arises from the superposition of all spectra within one period (Figure 2c). In contrast to spherulites prepared at higher temperatures the positions of both dichroic absorption bands depend sensitively on the humidity and other parameters and can vary by up to 15 nm.[11] Spectra of dyes are generally broader in thin layers than in solution. As possible molecular explanations for this phenomenon $\pi-\pi$ interactions, charge transfer transitions and light scattering are discussed.[1, 18] Our results show that polariton effects, especially at strong absorbing dyes, also have to be taken into account. Not only do different orientations of crystallites lead to the superposition of different spectra, but even in case of a single-crystal arrangement the absorption bands of dye J aggregates are broadened (Figure 2a) as a result of dramatic changes of the refractive index n within the energy region ΔE.[13] If the refractive index function is taken into account by calculation, the aggregate absorption in layers is as narrow as the J band in solution.[9, 10]

The results prove for the first time the strong directional dependence of absorption energy of excitonic polaritons in transparent dye layers. The observation of this phenomenon was possible because of the nearly single crystallike deposition of dye aggregates in thin layers and to the variation of the molecule's inclination relative to the substrate in the TLA process. The findings offer an important engineering opportunity for tuning the absorption behavior of thin dye layers without changing the thickness, the molecular structure, the crystal structure, or the substrate.

Received: July 9, 1998 [Z10659IE]
German version: *Angew. Chem.* **1998**, *110*, 669–672

 © WILEY-VCH Verlag GmbH, D-69451 Weinheim, 1998 1433-7851/98/3705-0648 $ 17.50+.50/0

Keywords: aggregation · crystal growth · polymethines · solid-state spectroscopy · thin films

[1] a) J. Fabian, H. Nakazumi, M. Matsuoka, *Chem. Rev.* **1992**, *92*, 1197 – 1226; b) J.-M. Lehn, *Angew. Chem.* **1990**, *102*, 1347 – 1362; *Angew. Chem. Int. Ed. Engl.* **1990**, *29*, 1304 – 1319.
[2] T. Tani, *J. Imag. Sci.* **1990**, *34*, 143 – 151.
[3] a) K. Y. Law, *Chem. Rev.* **1993**, *93*, 449 – 486; b) P. Ball, *Nature* **1993**, *362*, 123 – 125; c) C. Liu, H. Pan, M. A. Fox, A. J. Bard, *Science* **1993**, *261*, 897 – 899.
[4] S. Dähne, *Science* **1978**, *199*, 1163 – 1167.
[5] M. Klessinger, J. Michl, *Lichtabsorption und Photochemie organischer Moleküle*, VCH, Weinheim, **1989**, pp. 117 – 126.
[6] V. Czikkely, H. D. Försterling, H. Kuhn, *Chem. Phys. Lett.* **1970**, *6*, 11 – 14.
[7] A. S. Davydov, *Theory of Molecular Excitons*, McGraw-Hill, New York, **1962**, pp. 23 – 47.
[8] a) D. L. Mills, E. Burstein, *Rep. Prog. Phys.* **1974**, *37*, 817 – 925; b) G. J. Small, M. A. Connolly, S. H. Stevenson, *Chem. Phys.* **1988**, *128*, 157 – 168.
[9] a) H. J. Hesse, F. Fuhs, G. Weiser, L. v. Szentpaly, *Phys. Stat. Sol. b* **1976,** *76*, 817 – 826; b) R. K. Ahrenkiel, *J. Opt. Soc. Am.* **1971**, *61*, 1651 – 1655.
[10] L. Dähne, G. Reck, A. Horvath, G. Weiser, *Adv. Mater.* **1996**, *8*, 486 – 490; L. Dähne, Habilitation thesis, Berlin, **1997**.
[11] L. Dähne, *J. Am. Chem. Soc.* **1995**, *117*, 12855 – 12860.
[12] E. E. Wahlstrom, *Optical Crystallography*, 5th ed., Wiley, New York, **1979**, pp. 232 – 234.
[13] L. Dähne, A. Horvath, G. Weiser, *Chem. Phys.* **1995,** *196*, 307 – 316.
[14] Z. Bao, A. J. Lovinger, A. Dodalapur, *Adv. Mater.* **1997**, *9*, 42 – 44.
[15] L. Dähne, G. Reck, *Z. Kristallogr.* **1995**, *210*, 40 – 43.
[16] L. Dähne, J. Tao, G. Mao, *Langmuir* **1998**, *14*, 565 – 569
[17] W. C. McCrone in *Physics and Chemistry of the Organic Solid State*, *Vol. 2* (Eds.: D. Fox, M. M. Labes, A. Weissberger), Wiley, New York, **1965**, pp. 726 – 766.
[18] a) H. Böttcher, *J. Prakt. Chem.* **1992**, *334*, 14 – 24; b) S. Jäger, H. Böttcher, *Adv. Mater.* **1996**, *8*, 93 – 97.

A Chemosensor for Citrate in Beverages**

Axel Metzger and Eric V. Anslyn*

The high specificity of antibodies and enzymes makes them the current tools of choice for sensing and quantitating structurally complex molecules in a mixture of analytes. However, the sophistication of rationally designed and synthetic receptors is now high enough that their use as sensors is realistic.[1] Neutral and cationic analytes such as sugars,[2] metal ions,[3] creatinine,[4] and arenes,[5] as well as a few anions,[6] have been targeted.[7] Until now, the vast majority of synthetic sensors have not demonstrated the sensitivity and selectivity necessary to analyze solutions in which contaminates are competitive. For example, almost all past studies focused upon the analysis of solutions of analyte alone. Herein, we demonstrate that a chemosensor, a synthetic receptor coupled with a signaling element,[8] can be used to analyze for a specific compound in a multicomponent aqueous solution in a manner similar to that of antibody-based biosensors in immunoassays.

Immunoassays are facile because a simple competition approach is most often employed.[9] When the solution to be analyzed, which contains an unlabeled antigen, is added to the receptor, a labeled antigen is released and hence a signal change results. Such competition assays have not been widely exploited with synthetic receptors. As long as the chemosensor has useful selectivity for its analyte within an application, results comparable to those obtained with antibodies would be expected. Further, immunoassays typically rely on fluorescence spectroscopy.[10] Fluorescence emission appears at longer wavelengths than excitation, and hence the background signal is typically low, resulting in very high sensitivity.[11]

Considering antibody analysis methods and the current state of the art using synthetic receptors, we had two goals in mind. The first was to demonstrate that synthetic receptors can be selective enough for their analytes to sense and quantitate them in competitive media. We defined competitive media as water that is relatively high in ionic strength and other contaminants. Our second goal was to show that a competition assay could be quite readily applied to any synthetic receptor. For accomplishing these goals, citrate seemed to be an ideal analyte.[12]

Since at neutral pH citrate has a charge of minus three, it is quite distinctive from other possible interfering species. Hence, a receptor complementary to citrate in both charge and hydrogen bonding ability would likely not suffer interference from many other competing analytes, such as salts, mono- and dicarboxylic acids, and sugars.

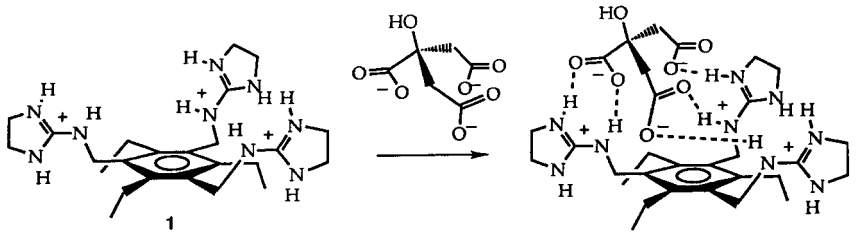
We recently reported that receptor **1** is selective for the recognition of citrate in water over di- and monocarboxylates, phosphates, sugars, and simple salts.[13a] The receptor binds citrate better than simple dicarboxylic acids and monocarboxylic acids by factors of approximately 35 and 700, respectively.[13b] The receptor consists of three guanidinium groups for hydrogen bonding and charge pairing[14] with citrate.[13c] The steric gearing imparted by ethyl groups on the 2-, 4-, and 6-positions[15] ensures that the guanidinium moieties are preorganized on the same face of the benzene ring. This conformation yields several hydrogen bonds and three sets of ionic interactions in the host – guest complex (as shown in Scheme 1), leading to good binding in water ($K_a = 6.8 \times 10^3\,\text{M}^{-1}$).

Our assay for citrate employed an ensemble of 5-carboxyfluorescein (**2**, a fluorescent probe) and **1**. Carboxyfluorescein **2** was chosen since it is commercially available, it has two carboxylates for binding with host **1**, and only very small quantities proved to be necessary (typically 5 to 18 μM). The absorbance/fluorescence of probe **2** is very sensitive to pH changes, and therefore a buffer to maintain constant pH was necessary in the sensing experiments.[16] It is well known that any charged buffer will act as a competitor for the binding

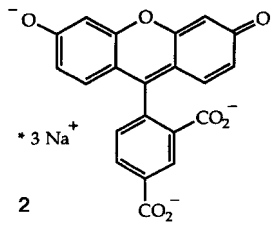
[*] Prof. Dr. E. V. Anslyn, Dr. A. Metzger
Department of Chemistry and Biochemistry
The University of Texas at Austin
Austin, TX 78712 (USA)
Fax: (+1) 512-471-8696
E-mail: anslyn@ccwf.cc.utexas.edu

[**] This work was supported by the National Science Foundation and The Welch Foundation, as well as by a Sloan Award and a Dreyfus Teacher Scholar Award to E. V. A.

 © WILEY-VCH Verlag GmbH, D-69451 Weinheim, 1998 1433-7851/98/3705-0649 $ 17.50+.50/0



Scheme 1.



sites in charged receptors. To compensate for this effect and to enhance the affinity towards citrate, methanol was added to the buffered solutions. The most advantageous solvent system was 25% water in methanol by volume (5 mM HEPES buffer at pH 7.4). UV/Vis spectroscopy was employed to determine the binding constant of complex **1**·**2** ($K_a = 4.7 \times 10^3\,\text{M}^{-1}$) under the conditions of our sensing assay, using the Benesi–Hildebrand method.[17] In the same solvent system a binding constant of $2.9 \times 10^5\,\text{M}^{-1}$ was determined for citrate·**1**, by using a competition assay in which citrate was added to a solution of host **1** and probe **2**, and the change in absorbance of **2** was monitored.[18] This binding constant is certainly of a magnitude appropriate for sensing citrate at milli- and micromolar concentrations.

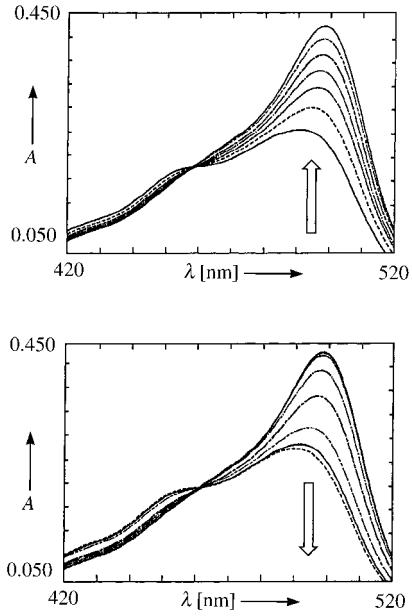


Figure 1. UV spectra of **2**. Top: Addition of **1** to a solution of **2** at constant concentration (14 μM) causes an increase of the absorption A. The curve with the lowest absorptivity was obtained with **2** alone. Bottom: Addition of citrate to a solution containing both **1** (74 μM) and **2** (14 μM) at constant concentrations causes a decrease of the absorption. The curve with the highest absorptivity was measured without citrate present.

We reasoned that binding between **1** and **2** would lower the pK_a of the phenol moiety of **2** due to the positively charged microenvironment presented by **1**. This shift in pK_a would cause the phenol moiety to be in a higher state of protonation when **2** is free in solution. The absorbance or fluorescence of **2** is known to decrease with higher protonation of the phenol.[16] Hence, we predicted that upon introduction of citrate to a mixture of **1** and **2** the absorbance and fluorescence of **2** would decrease. As shown in Figure 1, the intensity of the absorbance of **2** ($\lambda_{max} = 498$ nm) increases with addition of host **1** to a constant concentration of probe **2**, and as predicted the intensity decreases upon addition of citrate to the ensemble of **1** and **2**. The same effect was seen in the fluorescence spectrum ($\lambda_{max} = 525$). This cycling of absorbance and fluorescence could typically be repeated five times before any significant signal degradation occurred.

Calibration curves for the concentration of citrate were generated by incrementally adding citrate to a solution having constant concentrations of **1** and **2**. Addition of succinate to the sensing ensemble (**1**·**2**) resulted in small absorbance (fluorescence) changes, but the addition of acetate, salt, or sugars resulted in essentially no changes (Figure 2). Therefore common contaminants present in beverages (e.g. malate, ascorbate, lactate, benzoate, phosphate) should not effect our sensing assay. This was verified by the success of the method with soft drinks.

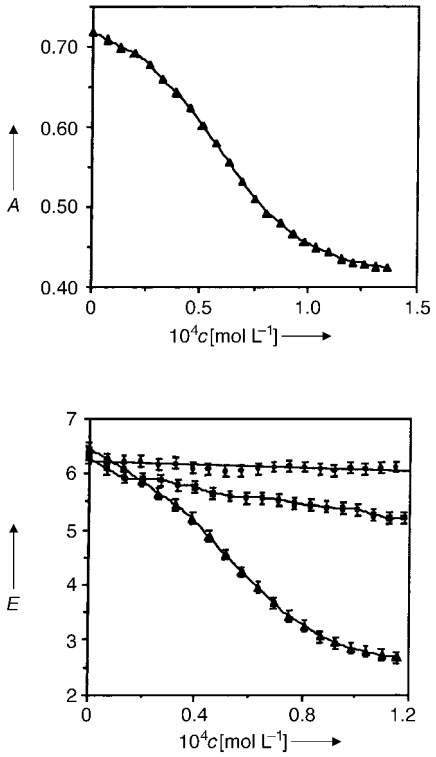


Figure 2. Calibration curves used for the sensor assay (75% methanol, 25% water, 5 mM HEPES buffer, pH 7.4).[19] Top: UV calibration curve (75 mM **1**, 14 mM **2**, $\lambda = 498$ nm). A = absorption, c = concentration of citrate. Bottom: Fluorescence calibration curves (75 mM **1**; 14 mM **2**; excitation at $\lambda = 490$ nm; emission E at $\lambda = 525$ nm). Addition of citrate (▲), succinate (■), and acetate (●) to the sensing assay.

 © WILEY-VCH Verlag GmbH, D-69451 Weinheim, 1998 1433-7851/98/3705-0650 $ 17.50+.50/0

Finding the concentration of citrate in a large number of beverages was simply a matter of adding between 2 and 50 μL of the beverage to the sensing ensemble, determining the absorbance or fluorescence, and reading the amount of citrate off the calibration curves. The results for several drinks are given in Table 1. To verify the accuracy of the method, known concentrations of citrate dissolved in water were tested, and an NMR technique for measuring citrate was also used as a control. All three methods agree within 10% (except for the beverage "Mountain Dew"), and the agreement between the absorption and emission is typically within 3%. Repetitive measurements indicated a standard deviation not larger than 3%. To demonstrate that competitive media can be analyzed, sport drinks which are very high in electrolyte content (i.e. ionic strength) were tested. "All Sport", for example, contains polyphosphates, benzoate, KH_2PO_4/H_3PO_4, and chloride salts. To show that the method works in the presence of large amounts of sugar, we analyzed "Mountain Dew", a soft drink very high in fructose and sucrose. In fact, the high saccharide concentrations makes the NMR method inaccurate due to a lack of sensitivity in integration of the citrate signal. Finally, to show that the method does not respond to other analytes in the absence of citrate, we analyzed "Coca Cola" and "Diet Coke", soft drinks containing either no citrate or very low concentrations of citrate, respectively. In all cases the sensor ensemble was effective.[20]

Table 1. Concentration of citrate [mM] in beverages determined by different methods.

	Gravimetric	NMR	**1**+**2**, absorption	**1**+**2**, emission
citrate model solution	30.1	–	30.3	29.9
calibration solution	1.33	–	1.205	1.39
orange juice	–	43.1	44.1	44.7
Gatorade	–	15.95	15.05	15.1
Powerade	–	12.4	11.1	11.3
All Sport	–	7.4	7.1	8.1
Mountain Dew	–	7.95	5.5	5.4
tonic water	–	21.0	21.15	20.8
Coca Cola	–	0	0	<0.5
Diet Coke	–	<0.2	<0.4	<0.7

In summary, when the receptor is selective for its guest within a given application, such a receptor can be used in situations typically reserved for antibodies. Further, competition assays can be applied to synthetic receptors, creating very facile assays. Both these concepts can be extended to any synthetic receptor. In fact, we are currently working on using a similar strategy for the sensing of even more complex molecules such as neurotransmitters.

Experimental Section

The detection limit for citrate under the experimental conditions described is approximately 5 mM. By either increasing the amount of methanol and/or manipulating the ratio of **1** and **2**, one can quantitate citrate down to approximately 100 μM as long as the concentrations of competitive components remain below the cross-reactivity concentrations given in ref.[13b].

Conditions for the UV/Vis determination of citrate: 5 mM HEPES buffer, 94 μM **1**, 18 μM 5-carboxyfluorescein in 25 vol% water/75 vol% methanol. The conditions used for fluorescence were the same as for the UV/Vis experiments except that **1** (84 μM) and 5-carboxyfluorescein (5 μM) were more dilute. The average of three scans was used to determine one value. The beverages were adjusted to pH 7.4 using NH_4OH prior to addition to the ensemble.

For the NMR assay the beverage was first filtered through Celite. Aliquots were then adjusted to pH 7.4 with NH_4OH and lyophilized. NMR titration method was used with standard solutions of THF and acetonitrile in D_2O. After integration of the citrate signal, the citrate concentration in the beverage tested was calculated.

Received: July 8, 1997 [Z10654IE]
German version: *Angew. Chem.* **1998**, *110*, 682–684

Keywords: analytical methods · chemosensors · citrate · guanidinium salts · host–guest chemistry

[1] M. A. Morttellaro, D. G. Nocera, *CHEMTECH* **1996**, *26*, 17; D. Diamond, M. A. McKervey, *Chem. Soc. Rev.* **1996**, 16; *Fluorescent Chemosensors for Ion and Molecule Recognition* (Ed.: A. W. Czarnik), Am. Chem. Soc., Washington, D. C., **1992**; *Chemosensors of Ion and Molecule Recognition* (Eds.: J.-P. Desvergne, A. W. Czarnik), Kluwer, New York, **1997**; A. P. de Silva, C. P. McCoy, *Chem. Ind.* **1994**, 992; A. P. de Silva, H. Q. N. Gunaratne, P. L. M. Lynch, *J. Chem. Soc. Perkin Trans. 2* **1995**, 685; R. A. Bissell, A. P. de Silva, H. Q. N. Gunaratne, P. L. M. Lynch, G. E. M. Maguire, K. R. A. S. Sandanayake, *Chem. Soc. Rev.* **1992**, *21*, 187; R. A. Bissell, A. P. de Silva, H. Q. N. Gunaratne, P. L. M. Lynch, G. E. M. Maguire, C. P. McCoy, K. R. A. S. Sandanayake, *Top. Curr. Chem.* **1993**, *168*, 223; D. N. Reinhoudt, *Sensors Actuators B* **1995**, *24–25*, 33; R. J. W. Lugtenberg, Z. Brzozka, A. Casnati, R. Ungarro, J. F. J. Engbersen, D. N. Reinhoudt, *Anal. Chim. Acta* **1995**, *310*, 263.

[2] J. Yoon, A. W. Czarnik, *J. Am. Chem. Soc.* **1992**, *114*, 5874; T. D. James, K. R. A. S. Sandanayake, S. Shinkai, *Angew. Chem.* **1994**, *106*, 2287; *Angew. Chem. Int. Ed. Engl.* **1994**, *33*, 2207; T. D. James, K. R. A. S. Sandanayake, S. Shinkai, *Nature* **1995**, *374*, 345.

[3] S.-Y. Hong, A. W. Czarnik, *J. Am. Chem. Soc.* **1993**, *115*, 3330; A. P. de Silva, H. Q. N. Gunaratne, M. Gunnlaugsson, M. Nieuwenhuizen, *J. Chem. Soc. Chem. Commun.* **1996**, 1967; R. Y. Tsien, *Biochemistry* **1980**, *19*, 2396; A. P. de Silva, H. Q. N. Gunaratne, G. E. M. Maguire, *J. Chem. Soc. Chem. Commun.* **1994**, 1213; H. A. Godwin, J. M. Berg, *J. Am. Chem. Soc.* **1996**, *118*, 6514.

[4] T. W. Bell, Z. Hou, Y. Luo, M. G. B. Drew, E. Chapoteau, B. P. Czech, A. Kumar, *Science* **1995**, *269*, 671.

[5] Z. Pikramenou, K. M. Johnson, D. G. Nocera, *Tetrahedron Lett.* **1993**, *34*, 3531.

[6] D. H. Vance, A. W. Czarnik, *J. Am. Chem. Soc.* **1994**, *116*, 9397.

[7] S. R. Adams, A. T. Harootunian, Y. J. Buechler, S. S. Taylor, R. Y. Tsien, *Nature* **1991**, *349*, 694.

[8] A chemosensor is a device that requires molecular recognition not relying on a biotic recognition element. A. W. Czarnik, *Acc. Chem. Res.* **1994**, *27*, 302.

[9] *Monoclonal Antibodies: Principles and Applications* (Eds.: J. R. Birch, E. S. Lennox), Wiley, New York, **1995**.

[10] A. W. Czarnik, *Chem. Biol.* **1995**, *2*, 423.

[11] L. Fabbrizzi, A. Poggi, *Chem. Soc. Rev.* **1995**, *24*, 197.

[12] P. N. Kale, P. G. Adsule, *Handbook of Fruit Science and Technology*, Chapter 3 ("Citrus"), **1995**, pp. 39–65.

[13] a) A. Metzger, V. M. Lynch, E. V. Anslyn, *Angew. Chem.* **1997**, *109*, 911–914; *Angew. Chem. Int. Ed. Eng.* **1997**, *36*, 862–865. b) Dissociation constants for citrate, succinate, and acetate are 147 μM, 4.5 mM, and >0.1 M, respectively. This yields cross-reactivities of simple dicarboxylic acids and monocarboxylic acids of approx-

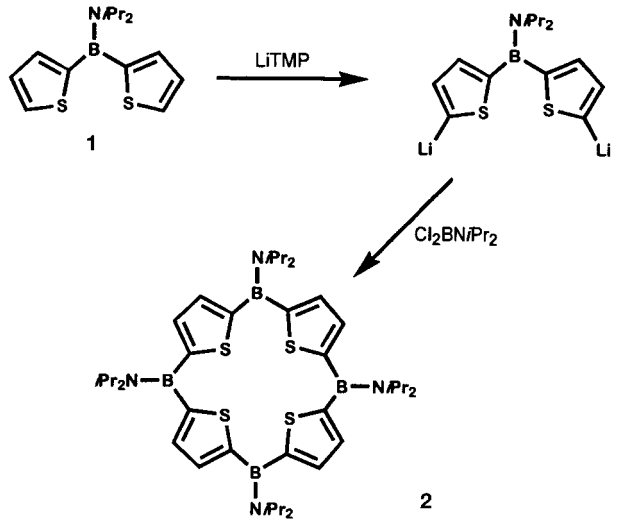
imately 28% and 0.14%, respectively. c) The unsymmetrical binding shown was revealed by X-ray crystal structure analysis.
[14] C. L. Hannon, E. V. Anslyn, *Bioorg. Frontiers* **1993**, *3*, 143.
[15] K. V. Kilway, J. S. Siegel, *J. Am. Chem. Soc.* **1995**, *114*, 255.
[16] J. Bramhall, J. Hofmann, R. DeGuzman, S. Montestruque, S. Schell, *Biochemistry* **1987**, *26*, 6330; M. L. Graber, D. DiLillo, B. L. Friedman, E. Pastoriza-Munoz, *Anal. Biochem.* **1986**, *156*, 202.
[17] H. A. Benesi, J. H. Hildebrandt, *J. Am. Chem. Soc.* **1949**, *71*, 2703;
F. Diederich, K. Dick, D. Griebel, *J. Am. Chem. Soc.* **1986**, *108*, 2273.
[18] K. A. Connors, *Binding Constants, The Measurement of Molecular Complex Stability*, Wiley, New York, **1987**.
[19] Typical immunoassay calibration curves show hyperbolic behavior while sigmoidal behavior is common with semilogarithmic plots (J. Wyman, S. J. Gill, *Binding and Linkage*, University Science Books, Mill Valley, CA, USA, **1990**, pp. 55–57). We have sigmoidal behavior in linear plots because **1** is in large excess over **2**. As we add citrate it first binds to the free **1** before it competes significantly with **2**.
[20] We have further validated the method by HPLC analyses. A series of citric acid samples obtained from an industrial source were analyzed by our fluorescence method. The results were compared to those determined independently by the industrial donor using their in-house HPLC protocol. In all cases the results differed by at most 5%.

A Boron-Bridged Tetrathiaporphyrinogen**

Francis H. Carré, Robert J.-P. Corriu,* Thomas Deforth, William E. Douglas,* Walter S. Siebert,* and Wolfgang Weinmann

Few porphyrinoid macrocycles based on thiophene are known,[1] and to our knowledge none containing boron have been previously described, although various mono- and diborylthiophenes were isolated many years ago.[2] The first thiophene-containing porphyrinoids to be reported were a colorless carbon-bridged tetrathiaporphyrinogen and the violet tetrathiaporphyrin dication generated from it on oxidation.[3] Their more soluble ethyl-substituted analogues have also been described,[4] as has a carbon-bridged neutral aromatic porphyrinoid based on thiophene.[5] Recently silicon-bridged silatetrathiaporphyrinogens and a phosphorus-bridged phosphatetrathiaporphyrinogen have been reported.[6] Several such silicon-bridged macrocycles based on thiophene have also been prepared.[7]

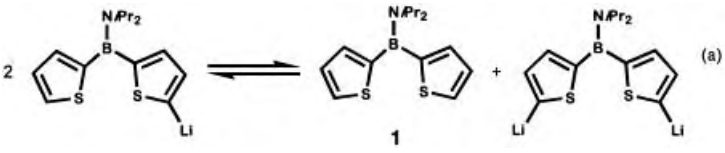
The novel boron-bridged tetrathiaporphyrinogen **2** reported here (see Scheme 1), which contains both Lewis base (sulfur) and Lewis acid (boron) sites, was isolated during an investigation into the synthesis of polymers containing boron and thiophene (or other aromatic) units in the backbone. Initial evidence for the formation of **2** was found in the mass spectrum of the product obtained from the reaction of Cl_2BNiPr_2 with 2,5-dilithiothiophene. The yield can be improved by starting from the *N*,*N*-diisopropyl derivative **1** of the previously reported *N*,*N*-dimethyl-1,1-di-2-thienylboranamine[2b] in which part of the porphyrinoid ring structure has been preformed. Thus, dimetalation of **1** followed by treatment with the stoichiometric quantity of Cl_2BNiPr_2 gave **2** in 62% yield (Scheme 1); no polymer formation was observed. To avoid any attack at boron, the sterically hindered



Scheme 1.

strong base lithium 2,2,6,6-tetramethylpiperidide (LiTMP) was used.

Remarkably, even monolithiation of **1** and treatment with the aminodichloroborane gives rise to **2**. As with the corresponding silicon system,[8] this can be explained in terms of the equilibrium between **1** and the mono- and dilithiated species [Eq. (a)].



Crystals of **2** suitable for an X-ray structure determination[9] were obtained from a solution of the crude reaction product in

[*] Prof. R. J.-P. Corriu, Dr. W. E. Douglas, Dr. F. H. Carré, Dr. T. Deforth, Dr. W. Weinmann
CNRS UMR 5637
Université Montpellier II
Place E. Bataillon, F-34095 Montpellier cedex 5 (France)
Fax: (+33) 467143888
E-mail: corriu@univ-montp2.fr
Prof. Dr. W. S. Siebert
Anorganisch-Chemisches Institut der Universität
Im Neuenheimer Feld 270, D-69120 Heidelberg, (Germany)
Fax: (+49) 6221-54-5609
E-mail: ci5@ix.urz.uni-heidelberg.de

[**] T.D. and W.W. thank the European Commission for fellowships under contract no. ERBCHBGCT940539 of the Human Capital and Mobility (Institutional Fellowships) Programme. Financial support to W.W. by the Deutsche Forschungsgemeinschaft (SFB 247) is gratefully acknowledged. Professor J. Lapasset (GDPC, Université Montpellier II) is thanked for helpful discussions concerning the crystal structure determination.

 © WILEY-VCH Verlag GmbH, D-69451 Weinheim, 1998 1433-7851/98/3705-0652 $ 17.50+.50/0

CH_2Cl_2/*n*-hexane (2/1). The four boron atoms of the macrocycle are not in the same plane (Figure 1), unlike the planar arrangement of the bridging groups in the corresponding carbo-[3a] and silatetrathiaporphyrinogens.[6a] Macrocycle **2** has a $\bar{4}$ symmetry axis, whereas the latter two compounds are centrosymmetric. The distance between neighboring sulfur

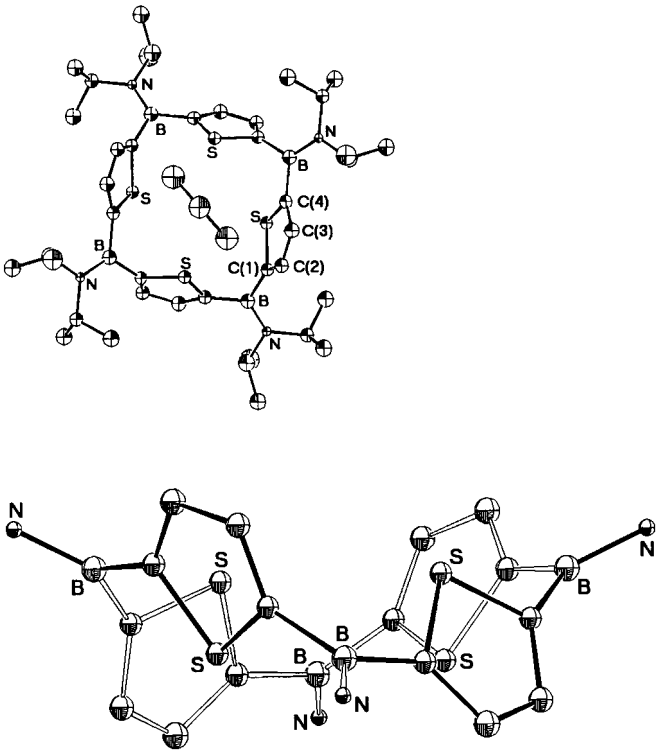


Figure. 1. Structure of **2** (ORTEP drawing). Top: Viewed along the $\bar{4}$ axis (only the CH_2Cl_2 molecule situated below the ring is shown; the position of the other CH_2Cl_2 molecule can be found by performing the $\bar{4}$ symmetry operation); bottom: perspective view of the central ring of **2** (*i*Pr groups omitted for clarity). The ellipsoids are drawn at the 30% probability level. Selected distances [Å] with standard deviations in parentheses: C(4)–B 1.569(6), B–N 1.408(6), C(1)–C(2) 1.343(6), C(2)–C(3) 1.408(6), S–C(1) 1.726(4), S–C(4) 1.728(4), C(3)–C(4) 1.368(6), B–C(1) 1.579(6).

atoms (3.74 Å) is greater than twice the van der Waals radius of sulfur (3.60 Å).[10] The distance between opposite sulfur atoms is 5.01 Å. The two molecules of CH_2Cl_2 contained in the unit cell (situated above and below the ring) are too remote to interact with the porphyrinogen.

Since **2** is colorless and nonplanar, the electrons are probably not delocalized in the macrocycle. Moreover, the B–C distance (1.57 Å) is that expected for a single bond (1.56 Å),[11] and the chemical shift of the signal for the boron atoms in **2** ($\delta = 40$) lies close to that for **1** ($\delta = 37$) in the region expected for such thienylboranamine derivatives.[2b, 12] The thiophene units show the bond-length relation C(1)–C(2) < C(2)–C(3) (Figure 1), whereas for electron-delocalized systems such as porphyrins the reverse is generally so.[3a] Any appreciable ring current or communication between the thiophene aromatic systems through the boron atoms can therefore be ruled out.

Further studies on **2** are in progress in the Heidelberg laboratory, concerning in particular its oxidation and complexation chemistry. It is expected that these properties should be interesting in view of the electron-donor/electron-acceptor nature of **2**.

Experimental Section

1: Thiophene (10.5 g, 125 mmol) was added drop by drop from a syringe to a solution of *n*BuLi (125 mmol) and *N*,*N*,*N*′,*N*′-tetramethylethylenediamine (TMEDA; 20 mL, 133 mmol) in *n*-hexane (100 mL) at 0°C. After the reaction mixture had been allowed to warm to room temperature, it was stirred for 1 h, then cooled to −60°C, and treated drop by drop with Cl_2BNiPr_2[13] (11.5 g, 63 mmol) in *n*-hexane (50 mL). The stirred mixture was allowed to warm to room temperature overnight, and the LiCl precipitate was removed by filtration through a glass frit (porosity 3). The solvent and TMEDA were removed under vacuum. Distillation (92°C, 10^{-2} mbar) of the residue yielded 13.93 g (80.5%) of **1**. M.p. 37°C; ^{1}H NMR ($CDCl_3$): $\delta = 7.52$-7.49 (m, 2H; H_{Ar}), 7.14-7.08 (m, 4H; H_{Ar}), 4.11 (sept, $J =$ 6.8 Hz, 2H; $CH(CH_3)_2$), 1.30 (d, $J = 6.8$ Hz, 12H; $CH(CH_3)_2$); ^{13}C NMR ($CDCl_3$): $\delta = 145$ (br, C_{Ar}), 133.2/129.2/127.4 (C_{Ar}), 49.8 ($CH(CH_3)_2$), 24.7 ($CH(CH_3)_2$); ^{11}B NMR ($CDCl_3$): $\delta = 37$; MS (70 eV, EI): *m*/*z* (%) 277 (6) [M^+], 262 (84) [$M^+ - CH_3$], 177 (20) [$M^+ - NiPr_2$], 111 (100) [$BNiPr_2^+$].

2: A solution of **1** (2.50 g, 9 mmol) in *n*-hexane (10 mL) was added drop by drop to a solution of LiTMP, freshly prepared by treating TMP (2.54 g, 18 mmol) with *n*BuLi (18 mmol) in *n*-hexane. After some seconds a suspension of the dilithiated product was formed. The reaction mixture was stirred for 1 h at room temperature, and then a solution of Cl_2BNiPr_2[13] (0.82 g, 4.5 mmol) in *n*-hexane (10 mL) was added drop by drop at room temperature. The reaction mixture was stirred at 50°C for 3 h. Volatile material was pumped off, and the crude product was taken up in toluene (10 mL). The resulting solution was filtered through a glass frit (porosity 3), and the toluene was removed under vacuum. Crystallization from CH_2Cl_2/*n*-hexane (2/1) afforded **2** in 62% yield. M.p. 182°C (decomp); ^{1}H NMR ($CDCl_3$): $\delta = 7.19$ (s, 8H; H_{Ar}), 4.08 (sept, $J = 6.8$ Hz, 8H; $CH(CH_3)_2$), 1.24 (d, $J = 6.8$ Hz, 48H; $CH(CH_3)_2$); ^{13}C NMR ($CDCl_3$): $\delta = 151$ (br, C_{Ar}), 131.1 (C_{Ar}), 49.4 ($CH(CH_3)_2$), 24.7 ($CH(CH_3)_2$); ^{11}B NMR ($CDCl_3$): $\delta = 40$; MS (FAB^+): *m*/*z* (%): 773 (61) [$M^+ + H$], 758 (17) [$M^+ + H - CH_3$], 673 (9) [$M^+ + H - NiPr_2$] , 102 (100) [$HNiPr_2$+H].

Received: September 4, 1997 [Z10890IE]
German version: *Angew. Chem.* **1998**, *110*, 654–656

Keywords: boron · heterocycles · macrocycles · porphyrinogens · thiophene

[1] E. Vogel, *J. Heterocycl. Chem.* **1996**, *33*, 1461.
[2] a) W. Siebert, *Chem. Ber.* **1970**, *103*, 2308; b) B. Wrackmeyer, H. Nöth, *ibid.* **1976**, *109*, 1075.
[3] a) E. Vogel, P. Röhrig, M. Sicken, B. Knipp, A. Herrmann, M. Pohl, H. Schmickler, J. Lex, *Angew. Chem.* **1989**, *101*, 1683; *Angew. Chem. Int. Ed. Engl.* **1989**, *28*, 1651; b) E. Vogel, *Pure Appl. Chem.* **1990**, *62*, 557.
[4] E. Vogel, M. Pohl, A. Herrmann, T. Wiss, C. König, J. Lex, M. Gross, J. P. Gisselbrecht, *Angew. Chem.* **1996**, *108*, 1677; *Angew. Chem. Int. Ed. Engl.* **1996**, *35*, 1520.
[5] Z. Hu, M. P. Cava, *Tetrahedron Lett.* **1994**, *35*, 3493.
[6] a) B. König, M. Rödel, P. Bubenitschek, P. G. Jones, *Angew. Chem.* **1995**, *107*, 752; *Angew. Chem. Int. Ed. Engl.* **1995**, *34*, 661; b) B. König, M. Rödel, P. Bubenitschek, P. G. Jones, I. Thondorf, *J. Org. Chem.* **1995**, *60*, 7406.
[7] P. Chicart, Dissertation, Université de Montpellier II, **1989**.
[8] T. Kauffmann, H.-H. Kniese, *Tetrahedron Lett.* **1973**, 4043.
[9] Crystal structure analysis of **2**: Enraf-Nonius automatic diffractometer, $Mo_{K\alpha}$, $\lambda = 0.71069$ Å, graphite monochromator, 163 K. Data collection, solution, and refinement: $\omega - \theta$ scan, direct methods with subsequent Fourier recycling. SHELXL-93 [G. M. Sheldrick, *SHELXL-93, A Program for Crystal Structure Determination*, Institüt für Anorganische Chemie der Universität Göttingen (Germany), **1993**]. $C_{42}H_{68}B_4N_4S_4Cl_4$, tetragonal, space group $P\bar{4}2_1c$, $a = 13.668(4)$, $c = 14.204(2)$ Å, $V = 2653.4(13)$ Å^{-3}, $Z = 2$, $\rho_{calcd} = 1.179$ gcm^{-3}. $4 < 2\theta < 50$. crystal dimensions $0.19 \times 0.18 \times 0.11$ mm^3. Of 1329 unique

 © WILEY-VCH Verlag GmbH, D-69451 Weinheim, 1998 1433-7851/98/3705-0653 $ 17.50+.50/0

reflections 982 assumed as observed with $I > 2\sigma(I)$. Refinement of 134 parameters with anisotropic thermal parameters for non-hydrogen atoms gave $R = 0.037$, $wR = 0.103$ (on F^2), and $S = 0.913$. Crystallographic data (excluding structure factors) for the structure reported in this paper have been deposited with the Cambridge Crystallographic Centre as supplementary publication no. 100475. Copies of the data can be obtained free of charge on application to CCDC, 12 Union Road, Cambridge CB2 1EZ, UK (fax: (+44) 1223-336-033; e-mail: deposit@chemcrys.cam.ac.uk).

[10] A. Bondi, J. Phys. Chem. **1964**, *68*, 441.

[11] *International Tables for X-ray Crystallography, Vol. III*, Kynoch Press, Birmingham, **1968**, p. 275.

[12] H. Nöth, B. Wrackmeyer in *NMR Basic Principles and Progress; Vol. 14, Nuclear Magnetic Resonance Spectroscopy of Boron Compounds* (Eds.: P. Diehl, E. Fluck, R. Kosfeld), Springer, Berlin, **1978**, pp. 169-170.

[13] W. Gerrard, H. R. Hudson, E. F. Mooney, *J. Chem. Soc.* **1960**, 5168.

Carbohydrate – Arene Interactions Direct Conformational Equilibrium of a Flexible Glycophane in Water**

Juan Carlos Morales and Soledad Penadés*

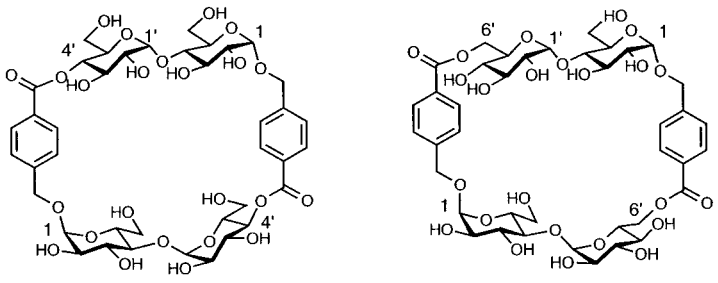
The confluence of many weak intermolecular forces is crucial for carbohydrate recognition processes. Knowledge about these forces derives mainly from the crystal structure analyses and NMR spectroscopy of complexes between oligosaccharides and lectins, antibodies, or periplasmic binding proteins.[1] These studies show that beyond the expected intermolecular forces always found in biological associations (hydrogen bonding, van der Waals forces, hydrophobic effects), stacking interactions between aromatic side chains and saccharides play an important role in stabilizing the complexes.[1,2] Besides the interactions at atomic level, change in oligosaccharide conformation on binding[3] and desolvation effects[4] are essential in determining the structural and energetic properties associated with carbohydrate recognition. Oligosaccharides observed in solution exist as an ensemble average of all possible conformations, and proteins may select oligosaccharide conformations that pre-exist in solution, or induce changes in the oligosaccharide upon binding. This selection has consequences in the thermodynamics of binding;[5] therefore it is important to assess which factors determine the conformation to be bound. However, the inherent oligosaccharide flexibility and the lack of strong intermolecular interactions places extreme demands on these studies.[3]

[*] Dr. S. Penadés, J. C. Morales
Instituto de Investigaciones Químicas, CSIC
Isla de la Cartuja, Américo Vespucio s/n
E-41092 Seville (Spain)
Fax: (+34) 95-446-0565
E-mail: penades@cica.es

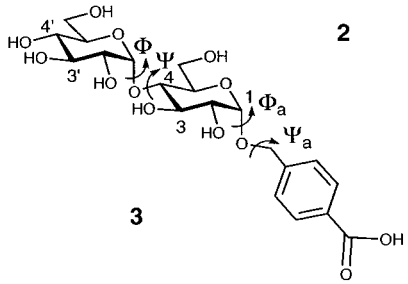
[**] We thank Dr. M. Bruix, Dr. Jiménez-Barbero and Dr. P. Nieto for NMR help. Financial support by the DGICYT is gratefully acknowledged. J.C.M. thanks the Ministerio de Educacion y Ciencia for a fellowship.

Model systems can also help to understand all these molecular aspects of carbohydrate recognition. In previous work we have designed and synthesized a new type of model receptor (glycophanes) to study carbohydrate binding in water.[6] Glycophanes consist of disaccharides and aromatic segments, and may be considered as cyclodextrin – cyclophane hybrids. With these receptors we have shown, for the first time, the existence of lipophilic interactions in water between carbohydrate surfaces.[7] We have now prepared two new glycophanes **1** and **2**, made up from maltose (4-*O*-(α-D-glucopyranosyl)-D-glucopyranose), the constituent disaccharide of cyclodextrins, and (4-hydroxymethyl)benzoic acid as aromatic segment. The linkage of the aromatic ring to either position 4′ or 6′ of the maltose molecule confers different flexibility on the receptors and different topologies than those present in cyclodextrins. This will allow us to compare the influence of the maltose presentation on the interactions of these receptors with a series of common ligands. In this paper we present evidence that carbohydrate – arene stacking is more important that hydrogen-bonding interactions for the dynamic behavior of the more flexible glycophane **2**. This glycophane adopts a folded conformation in water as a result of intramolecular interactions between a glucose moiety and a phenyl ring. This interaction induces a change in the maltose conformer distribution that is not observed in the more rigid glycophane **1**. Water is necessary for this hydrophobic collapse, which is not observed in methanol or dimethylsulfoxide. The conformational properties of **1** and **2** were assessed by NMR spectroscopy, as well as molecular mechanics and dynamics simulations. Model systems for binding carbohydrate in water based on sugar – arene interactions have been previously reported.[8]

Glycophane **1** was synthesized from maltose, and glycophane **2** was obtained in almost quantitative yield by spontaneous transacylation of glycophane **1** in water.[9] Significant upfield shifts (up to $\Delta\delta = 0.4$) were observed for the H1, H2, and H4 protons of **2** relative to the corresponding protons of the reference compounds **1** and **3**, indicating close proximity of the aromatic rings to the β face of the glucose



1 **2**



3

Table 1. Significant ^{1}H chemical shifts (δ) for **1**, **2**, and **3** at 30°C in different solvents.

	1			**2**			**3**		
Proton	D_2O	MeOH	DMSO	D_2O	MeOH	DMSO	D_2O	MeOH	DMSO
H1	5.08	5.24	4.87	4.67	5.14	4.85	5.04	5.09	4.77
H2	3.63	>3.7	>3.2	3.21	>3.6	>3.2	3.61	3.67	>3.2
H4	3.62	>3.7	>3.2	3.45	>3.6	>3.2	3.67	3.75	>3.2

units. Based on space-filling models, this proximity should force glycophane **2** to adopt a folded conformation that places the maltose molecule in a conformation rather different from that found in the solid state for maltose and cyclodextrins.[10] To test whether the driving force for this conformational change is interaction between sugar and arene units, additional experiments were carried out. Comparison of the ^{1}H NMR spectra of **1**, **2**, and **3** in [D_4]methanol, a protic solvent, shows similar chemical shifts for the H1, H2, and H4 protons of the reducing glucose unit in the three compounds. The same result is obtained in [D_6]dimethylsulfoxide ([D_6]DMSO), where hydrophobic interactions are not favored either (Table 1). In contrast, upon addition of [D_4]methanol to a solution of **2** in D_2O, the H1, H2, and H4 protons of the reducing glucose show large deshielding (up to $\Delta\delta = 0.70$), whereas for the rest of the protons regular downfield shifts of about $\Delta\delta = 0.20 - 0.33$ are observed, indicating an equilibrium between different conformations. Temperature also affects this equilibrium (Figure 1). Decreasing the temperature shifts the equilibrium toward the conformation with sugar–arene interactions, as indicated by the upfield shift of H1, H2, and H4 protons. As the temperature increases, the other conformers are favored. In the case of glycophane **1** or compound **3**, no significant changes in chemical shifts are observed on changing the temperature. Also, neither for **1** nor for **2** or **3** are significant changes in chemical shifts in [D_4]methanol solution observed over a broad range of temperatures (−50 to 55°C).

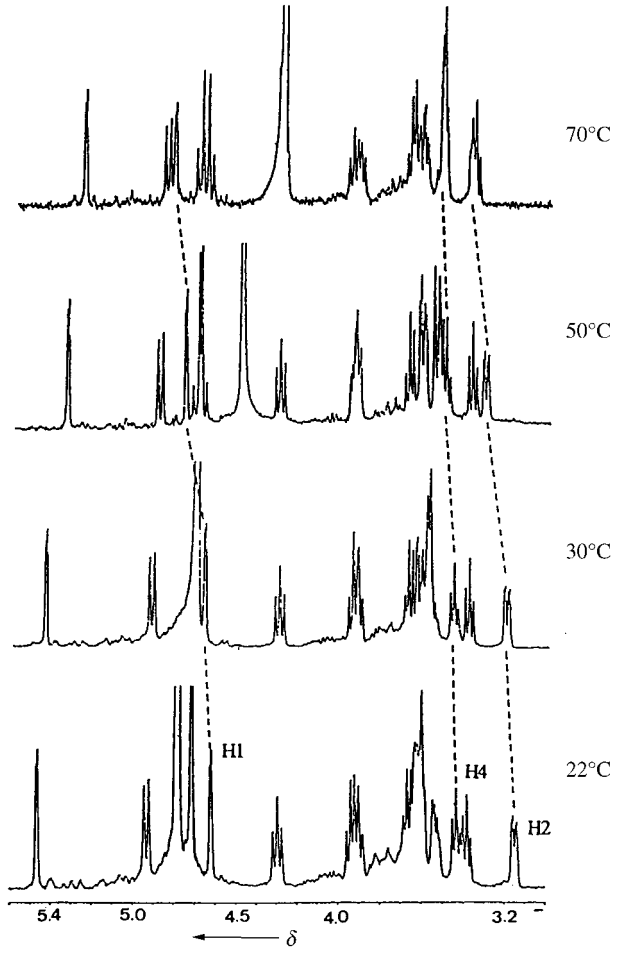


Figure 1. ^{1}H NMR spectra (500 MHz) of glycophane **2** in D_2O at different temperatures.

Molecular mechanics simulations by a Monte Carlo (MC) approach[11] show for glycophane **1** only one family of conformers (Figure 2A), in which the glucose moieties adopt

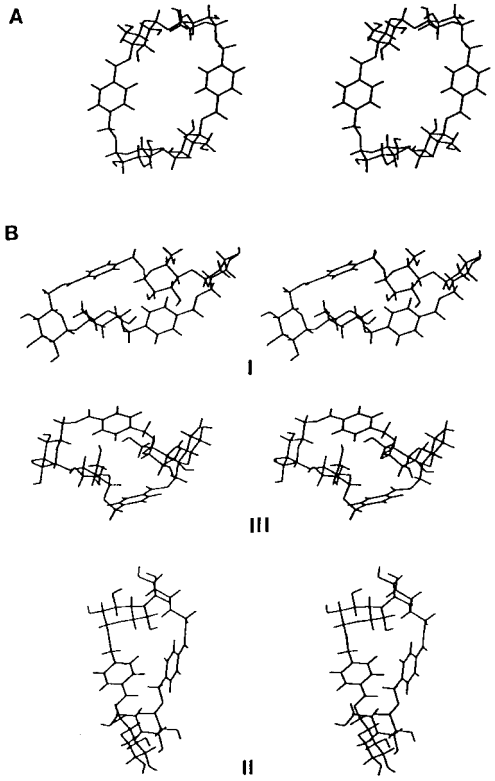


Figure 2. Stereoviews of the global minimun of glycophane **1** (A) and three conformations of glycophane **2** (B) obtained by the Monte Carlo search.

the expected $^4C_1$ chair conformation and the interglycosidic angles Φ (H1′-C1′-O1′-C4) and ψ (C1′-O1′-C4-H4) are −4 and −30°, respectively. This minimum is similar to the minimum B (−3 and −30°, respectively) found for maltose in solution.[12b] The glycosidic angle Φ_a(H1-C1-O1-CH_2) is 68°, in agreement with the *exo*-anomeric effect, and the torsion angle ψ_a(C1-O1-CH_2-C_{Ph}) is −170°, which allows the receptor to form the cavity. All conformers possess a hydrogen bond between 2′-OH and 3-OH. The structure of this minimum resembles that of cyclodextrins. For glycophane **2**, three

 © WILEY-VCH Verlag GmbH, D-69451 Weinheim, 1998 1433-7851/98/3705-0655 $ 17.50+.50/0

Table 2. Experimental and calculated ROESY data (%) for **1** and **2** in D_2O at 500 MHz at different temperatures.

	1			**2**				
	30 °C T-ROESY [a]	30 °C ROESY	Calcd ROESY	30 °C T-ROESY	25 °C T-ROESY	8 °C T-ROESY	Calcd ROESY [b]	Calcd ROESY [c]
H1′/H2′	4.6 (1.0)[d]	8.5 (1.0)	8.0 (1.0)	4.4 (1.0)	7.0 (1.0)	7.8 (1.0)	9.6 (1.0)	9.21 (1.0)
H1′/H3	< 1.0 (0.1)	< 1.0 (< 0.1)	1.1 (0.12)	1.4 (0.32)	1.2 (0.17)	1.2 (0.15)	3.3 (0.34)	2.92 (0.31)
H1′/H4	7.5 (1.63)	10.7 (1.25)	14.3 (1.8)	7.4 (1.68)	7.0 (1.0)	5.3 (0.68)	2.2 (0.23)	6.94 (0.75)

[a] T-ROESY experiments (350 ms mixing time) were carried out to minimize Hartmann–Hahn effects. T. L. Hwang, A. J. Shaka, *J. Am. Chem. Soc.* **1992**, *114*, 3157–3158. [b] All conformers were taken into account. [c] ROEs calculated for conformers **II** and **III**. [d] The number in brackets is the ratio between ROEs and H1′/H2′ ROE.

different families of conformers were found in the MC search. The global minimum (**I**, Figure 2B) shows a folded structure with a double sugar–arene stacking interaction. The interglycosidic angles Φ/Ψ are approximately $-55°/-60°$, the angle ψ deviating slightly from the minimum A (Φ/Ψ $-60°/-40°$) found for maltose and maltose derivatives in solution.[12] The Φ_a angle is 69°; however, the angle Ψ_a adopts a value of 70° to allow stacking between the aromatic ring and the β face of the reducing glucose (glycophane **1**: $-170°$). In this conformation a hydrogen bond between 2′-OH and 3-OH is not possible. The second family of conformers (**II**, Figure 2B) does not show sugar–arene stacking interactions. The receptor is closed by π–π face-to-edge interactions between the aromatic moieties. The interglycosidic angles Φ/Ψ are 11°/15°, similar to those found for maltose in the solid state.[10] This conformer is 22 kJ mol^{-1} more energetic than the folded family of conformers. A third family (**III**, Figure 2B) of conformers, with a similar energy to the nonfolded conformer was also obtained. All conformers are asymmetric and show sugar–arene stacking in only one of the reducing glucoses. These conformers are intermediates in the equilibrium between conformers **I** and **II** (Figure 2B). Molecular dynamics simulations[11] confirm the stability of the global minima found for **1** and **2** in the MC search. The starting conformations do not change during the 500 ps MD simulations at 300 K. The conformers **II** and **III** of **2** were also stable at this temperature. However, at higher temperatures in the simulation ($T = 500$ K) a transition of the glycosidic linkage conformation, after 300 ps in a maltose unit and after 400 ps in the other one, transforms these conformers into the global minimum **I**, which was stable for the rest of the MD run.

The existence of the folded conformation in **2** was also proven by comparison of the calculated and experimental rotating frame Overhauser enhancements (ROEs) between H1′/H3 and H1′/H4 protons of the maltose moiety. The distance between these interresidue protons reflects the glycosidic linkage conformation. The ROEs have been obtained at different temperature and are referred to the H1′/H2′ intraresidue ROE. The calculated ROEs for **1** and **2** were obtained from the MC calculation employing a quantitative approach with a full relaxation matrix.[13] For glycophane **1** a good agreement between experimental and calculated ROEs was found (Table 2). The calculated ROESY spectrum for **2** corresponds to a high population of the folded conformation; therefore a weak experimental H1′/H4 ROE should be expected. In contrast, the experimental ROEs observed for **2** at 30°C are similar to those for **1**. However, as the temperature decreases, the ratio between H2′ and H4 ROEs decreases, and at 8°C this ratio is smaller than 1 (Table 2), indicating an increase in the H1′–H4 distance, as is to be expected for a greater population of the folded conformation in glycophane **2**. Additionally, the observation of exclusive NOEs between the aromatic protons and the H2, H4, and H6 protons of the reducing glucose moiety at 5°C (Figure 3) definitively confirms the existence of the folded conformation in water as a result of sugar–arene intramolecular interactions.

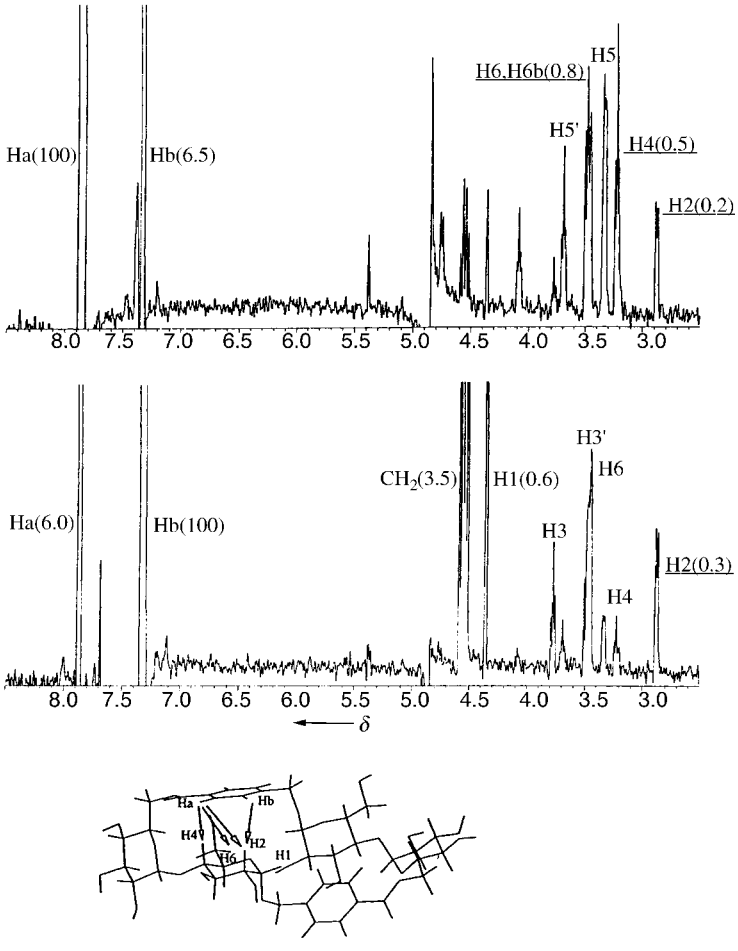


Figure 3. Cross-sections through the signals of the aromatic protons H_a (top spectrum) and H_b (bottom spectrum) from the 2D NOESY spectra (Brucker 600 MHz, 300 ms, 5°C, D_2O) of **2** showing the exclusive NOEs Ha/H2, Ha/H4 and the Hb/H6 of the folded conformation. Below the spectra is the folded conformation of **2** in which the arrows depict the expected NOEs.

 © WILEY-VCH Verlag GmbH, D-69451 Weinheim, 1998 1433-7851/98/3705-0656 $ 17.50+.50/0

The results presented here show that the maltose unit in glycophane **2** is rather flexible and that temperature and solvent, in conjunction with the presence of defined sugar–arene interactions influence its conformational equilibrium. Cyclodextrins together with glycophanes **1** and **2** are good examples of the existence of different conformers of the same disaccharide. It follows that the maltose units in these three compounds should also show different conformational entropies. This may have consequences in the thermodynamics of binding[5] of these maltose-containing compounds to a receptor, for example, the maltose-binding protein.

Received: June 27, 1997
Revised version: September 23, 1997 [Z 10609 IE]
German version: *Angew. Chem.* **1998**, *110*, 673–676

Keywords: carbohydrates · glycophanes · molecular dynamics · molecular recognition · NMR spectroscopy

[1] W. I. Weis, K. Drickamer, *Annu. Rev. Biochem.* **1996**, *65*, 360–473, and references therein.
[2] a) J. C. Spurlino, L. E. Rodseth, F. A. Quiocho, *J. Mol. Biol.* **1992**, *226*, 15–22; b) J. L. Asensio, F. J. Cañada, M. Bruix, A. Rodriguez-Romero, J. Jiménez-Barbero, *Eur. J. Biochem.* **1995**, *230*, 621–633.
[3] a) R. J. Woods, *Curr. Opin. Struct. Biol.* **1995**, *5*, 591–598, and references therein; b) T. Peters, B. M. Pinto, *ibid*. **1996**, *6*, 710–720, and references therein.
[4] R. U. Lemieux, *Acc. Chem. Res.* **1995**, *29* , 373–380.
[5] J. P. Carver, *Pure Appl. Chem.* **1993**, *65,* 763–770.
[6] J. M. Coterón, C. Vicent, C. Bosso, S. Penadés, *J. Am. Chem. Soc.* **1993**, *115*, 10066–10076.
[7] J. Jimenéz-Barbero, E. Junquera, M. Martin-Pastor, S. Sharma, C. Vicent, S. Penadés, *J. Am. Chem. Soc.* **1995**, *117*, 11198–11204.
[8] a) K. Kobayashi, Y. Asakawa, Y. Kato, Y. Aoyama, *J. Am. Chem. Soc.* **1992**, *114*, 10307–10313; b) B.-L. Poh, Ch. M. Tan, *Tetrahedron* **1993**, *49*, 9581–9592.
[9] J. C. Morales, S. Penadés, *Tetrahedron Lett.* **1996**, *37*, 5011–5014.
[10] a) M. E. Gress, G. A. Jeffrey, *Acta Crystallogr. Sect. B* **1977**, *33*, 2490–2495; b) K. Lindner, W. Saenger, *Acta Crystallogr. Sect. B* **1982**, *38*, 203–210.
[11] MM3* force field and GB/SA solvation model as integrated in MACROMODEL version 4.5 were used. One of the ester bonds was chosen as the ring closure bond. For the starting geometry the glycosidic torsion angles ϕ/Ψ were set at the minimum $-3°/-30°$ and Φ_a/Ψ_a at $-60°/-180°$. The hydroxymethyl at position 5′ in **2** was set *gt* as indicated by $J_{5'6'R} = 10.2$ Hz and $J_{5'6'S} < 1$ Hz. For more computational details see ref. [7].
[12] a) A. S. Shashkov, G. M. Lipkind, N. K. Kochetkov, *Carbohydr. Res.* **1986**, *147*, 175–182; b) S. N. Ha, L. J. Madsen, J: W. Brady, *Biopolymers* **1988**, *27*, 1927–1952; c) V. Tran, A. Buleon, A. Imberty, S. Perez, *ibid*. **1989**, *28*, 679–690; d) T. Peters, B. Meyer, R. Stuike-Prill, R. Somorjai, J.-R. Brisson, *Carbohydr. Res.* **1993**, *238*, 49–73; e) K.-H. Ott, B. Meyer, *ibid.* **1996**, *281*, 11–34.
[13] J. L. Asensio, J. Jiménez-Barbero, *Biopolymers* **1995**, *35*, 55–73. ROESY spectra were calculated assuming isotropic motion and external relaxation of 0.1 s^{-1}. A τ_c value of 0.27 ns was used in order to get the best match between experimental (Varian Unity 500) and calculated ROEs.

$[M^{II}(tcne)_2] \cdot x CH_2Cl_2$ (M = Mn, Fe, Co, Ni) Molecule-Based Magnets with T_c Values Above 100 K and Coercive Fields up to 6500 Oe**

Jie Zhang, Jürgen Ensling, Vadim Ksenofontov, Philipp Gütlich, Arthur J. Epstein, and Joel S. Miller*

Molecule-based magnets possessing spins on organic radicals is a growing area of increasing contemporary interdisciplinary research.[1, 2] Two classes of organic radicals have been particularly effective in stabilizing molecule-based magnets. These are the strong electron acceptors, such as tetracyanoethylene (TCNE), and dinitroxides. Several classes[2] of magnets are based on these radicals, namely, metallocene and manganoporphyrin electron transfer salts of TCNE (e.g., $[FeCp_2^*]^{\cdot+}[TCNE]^{\cdot-}$ (Cp* = pentamethylcyclopentadienyl) and $[Mn(tpp)]^{+}[TCNE]^{\cdot-}$ (H_2TPP = *meso*-tetraphenylporphyrin)), and $[Mn^{II}(hfac)_2]$ (hfac = hexafluoroacetylacetonate) adducts of dinitroxides (e.g., $(Me_2C_2)_2(NO)_2CR$, R = Me, Et, *i*Pr, etc.), $[V(tcne)_x] \cdot y$ solvent,[3, 4] as well as a few dinitroxides. Unlike the other classes of molecule-based magnets, there is only one example of a room temperature magnet $[V(tcne)_x] \cdot y$ solvent, and due to its high ordering temperatures ($T_c \sim 400$ K) and unknown structure, more examples of this class of materials are necessary to understand the chemistry and physics. Herein, we report the preparation and preliminary magnetic properties of $[M(tcne)_2] \cdot x CH_2Cl_2$ (M = Fe (**1**), Mn (**2**), Co (**3**), Ni (**4**)) magnets.[5]

$[Fe(tcne)_2] \cdot x CH_2Cl_2$ (**1**) is prepared from the reaction of iron(II) iodide,[3] which was used in the form of the MeCN solvate, and TCNE. Both reactants were dissolved in CH_2Cl_2, and upon mixing the product rapidly precipitated. After washing with CH_2Cl_2 the material was dried in vacuo at 30 °C overnight.[6] The IR spectrum of compound **1** exhibits three sharp ν_{CN} bands at 2221 (m), 2277 (s), and 2174 (s) cm^{-1} (Table 1); the width of these absorptions may depend on the precursors and other conditions.[6] These absorptions are consistent with those for the coordinated radical anion $[TCNE]^{\cdot-}$. They are similar to the ν_{CN} bands for $[V(tcne)_x] \cdot y CH_2Cl_2$, but are sharper and occur at higher energies. In contrast, however, to the amorphous $[V(tcne)_x] \cdot y CH_2Cl_2$, **1** is partly crystalline according to the X-ray powder pattern (Figure 1). Indexing of this pattern has been thwarted as the

[*] Prof. J. S. Miller, J. Zhang
Department of Chemistry, University of Utah
315 S. 1400 E. RM Dock, Salt Lake City, UT 84112-0850 (USA)
Fax: (+1) 801 581-8433
E-mail: jsmiller@chemistry.utah.edu
J. Ensling, V. Ksenofontov, Prof. P. Gütlich
Institut für Anorganische Chemie und Analytische Chemie der Universität
Staudingerweg 9, D-55099 Mainz (Germany)
Prof. A. J. Epstein
Department of Physics, The Ohio State University
Columbus, OH 43210-1106 (USA)

[**] The authors appreciate the constructive comments and insight provided by Prof. E. Coronado (Universidad de Valencia), Dr. C. M. Wynn, and Mr. M. Girtu (The Ohio State University), and gratefully acknowledge the support from the US Department of Energy (Grant No. DE-FG03-93ER45504) and the ACS-PRF (Grant No 30722-AC5).

 © WILEY-VCH Verlag GmbH, D-69451 Weinheim, 1998 1433-7851/98/3705-0657 $ 17.50+.50/0

Table 1. IR ν_{CN} absorption bands, saturation magnetization M_s, ordering temperature T_c, and exchange energy J for $[M(tcne)_2]\cdot x\,CH_2Cl_2$ (M = V, Mn, Fe, Co, Ni).

Synthesis[a]	ν_{CN} [cm^{-1}]				M_s[b]	T_c	J[c]
	vw	m	s	s	[emu Oe mol^{-1}]	[K]	[K]
$[V(CO)_6]$[6]			2189	2153	10300	ca. 400	53
$MnI_2\cdot 0.75\,CH_3CN$	2280	2224	2181	2171	19000	107	6.1
$FeI_2\cdot 0.75\,CH_3CN$	2279	2221	2177	2174	16900	121	10
$CoI_2\cdot 1.67\,CH_3CN$	2284	2230	2187	2167	8000	44	5.9
$NiI_2\cdot 1.05\,CH_3CN$	2290	2237	2194	(shoulder)	15800	44	11

[a] The given reactant was allowed to react with TCNE in CH_2Cl_2. [b] At 2 K and 5 T. [c] See text.

unit cell and space group for the low-symmetry pattern has yet to be identified. Elemental and thermal gravimetric analyses are consistent with the formulation in which x lies between 0.4 and 1.1.

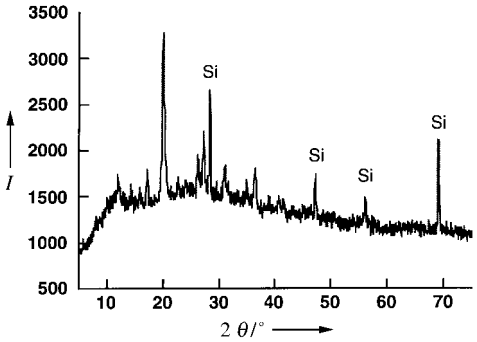


Figure 1. X-ray powder diffraction pattern[10] for $[Fe(tcne)_2]\cdot 0.75\,CH_2Cl_2$. The reflections marked with Si are attributed to an internal Si standard. I = relative intensity.

The oxidation and spin state of **1** was determined by ^{57}Fe Mössbauer spectroscopy. Within the detection limits only one iron site is observed. Above 95 K the sample shows absorptions with large chemical shift ($\delta = 1.23(1)$ mms^{-1}) and quadrupole coupling ($\Delta E_q = 3.26(1)$ mms^{-1}) indicative of penta- or hexacoordinate, high-spin Fe^{II} compounds[7] (Figure 2). As the sample is cooled below 95 K, the spectra become more complex due to magnetic splitting ($\delta = 1.24(1)$ mms^{-1}; $\Delta E_q = 3.31(1)$ mms^{-1}, $H_{int} = 229(1)$ KOe, Figure 2). The onset of the magnetic splitting is in agreement with the critical temperature determined by magnetic studies (vide infra).

Preliminary magnetization studies show that $[Fe(tcne)_2]\cdot 0.75\,CH_2Cl_2$ has a complex magnetic behavior that is essentially independent of the method of preparation and the amount of solvent.[6] The susceptibility cannot be fit to the Curie–Weiss law, $\chi \propto (T-\theta)^{-1}$, as expected for high-spin d^6 Fe^{II} centers in an octahedral environment with spin-orbit coupling.[8] A spontaneous magnetization occurs at temperatures below a T_c of 121 K as determined from the intercept of the slope of the magnetization as a function of temperature (Figure 3). At 2 K the magnetization shows complex, poorly understood responses to the field, reminiscent of metamagnetic behavior (Figure 4). At 5 T and 2 K the observed magnetization is about 16900 emu Oe mol^{-1}; however, higher fields are necessary to achieve saturation. This value of saturation magnetization corresponds to three $S = 1/2$ spins

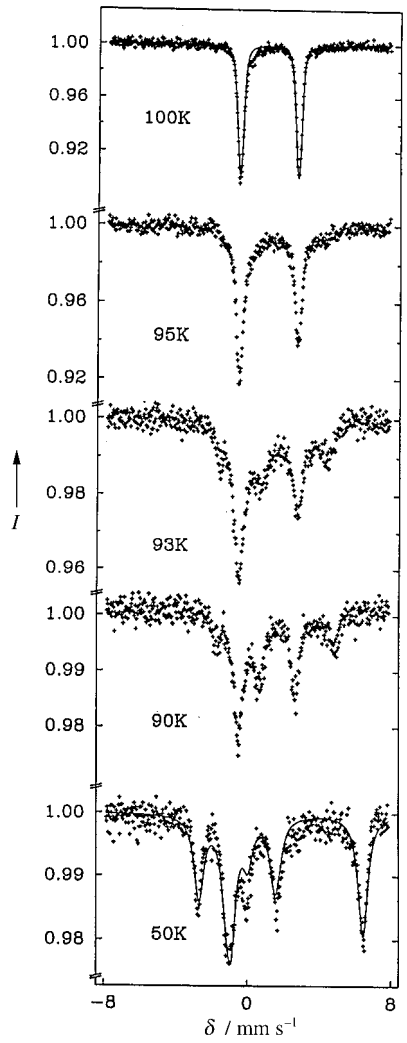


Figure 2. ^{57}Fe Mössbauer spectra of **1** at 50, 90, 93, 95, and 100 K. I = intensity.

and is 63% larger than the value for $[V(tcne)_x]\cdot y\,CH_2Cl_2$ (10300 emu Oe mol^{-1}) prepared from $[V(CO)_6]$.[4] It also exceeds the value (11200 emu Oe mol^{-1}) expected from antiferromagnetic coupling between an $S = 2$ Fe^{II} site and two $S = 1/2$ $[TCNE]^{\bullet -}$ ions. In addition it is substantially less than the value expected from ferromagnetic coupling (33500 emu Oe mol^{-1}). Although the T_c value shows little or no dependence on the synthetic route, the hysteresis loops taken at 2 K, which again are indicative of metamagnetic behavior, show a strong variation in the coercive field H_c, ranging from 300 to 3000 G (Figure 4). The detailed behavior

 © WILEY-VCH Verlag GmbH, D-69451 Weinheim, 1998 1433-7851/98/3705-0658 $ 17.50+.50/0

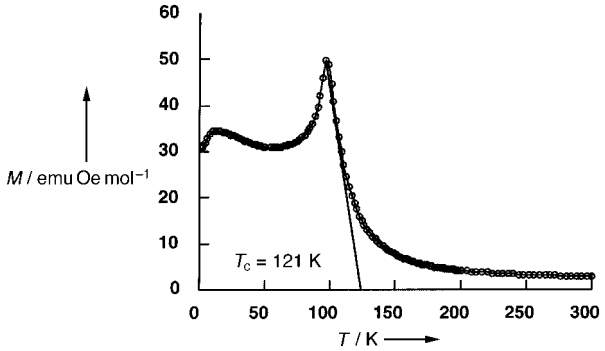


Figure 3. Zero-field cooled magnetization as function of temperature for $[Fe(tcne)_2]\cdot 0.75\,CH_2Cl_2$.

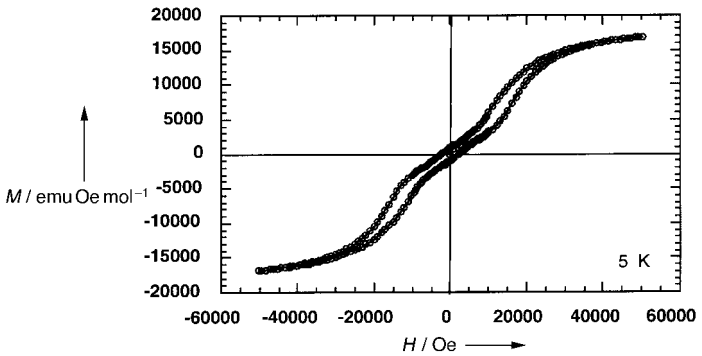


Figure 4. Representation of a hysteresis $M(H)$ for $[Fe(tcne)_2]\cdot 0.75\,CH_2Cl_2$ at 2 K. The observed coercive field for this sample is 2300 Oe, and the sample saturates to 16900 emu Oe mol^{-1}.

of the field and zero-field cooled curves also exhibits a strong dependency on reaction conditions and aging. In addition, a metastable impurity, which contributes to a broad transition around 150 K, exists for materials made from $[FeI_2]\cdot x\,CH_3CN$ and TCNE when the reaction time is less than four days.

Compound **1** shows remarkable thermal stability. The IR spectrum, the X-ray powder pattern, and the magnetic measurements on a sample treated at 130 °C for 38 h, suggest that the chemical and structural features of the materials are preserved after the heat treatment, except for the loss of solvent molecules. Some thermal degradation is apparent from magnetic measurements on a sample treated at 180 °C, and the IR spectrum indicates massive decomposition when the material is heated to 200 °C. The thermal gravimetric analytical data show that although desolvation starts at temperatures as low as 40 °C, it does not approach completion until the sample decomposes. As CH_2Cl_2 is a noncoordinating solvent, such high desolvation temperature may be attributed to the fact that **1** is likely a three-dimensional network, and the trapped CH_2Cl_2 can only be completely released when the structure collapses. Although **1** is not pyrophoric like $[V(tcne)_x]\cdot y$ solvent, it does decompose in air. A Fluorolube mull of **1** shows signs of H_2O absorption after being exposed to air for 40 min. Prolonged exposure to air causes the broadening and shift of the ν_{CN} to 2230 cm^{-1} and the sample also becomes amorphous.

Similar reactions of TCNE and acetonitrile solvates of MI_2 led to $[M(tcne)_2]\cdot x\,CH_2Cl_2$ (M = Mn (**2**), Co (**3**), Ni (**4**)). Preliminary studies indicate magnetic order with T_c values of 44 K for **3** and **4** and 107 K for **2** (see Table 1). These values are significantly lower than that reported for analogous vanadium compounds.[9] By using the mean-field expression $T_c = JzS(S+1)/3k_B$ (J = exchange energy, k_B = Boltzmann's constant, and z = number of nearest neighbors) for $H = -2J\mathbf{S_a}\cdot\mathbf{S_b}$ and by assuming z = 6, the following order for the J values is determined: $[V(tcne)_x]\cdot y$ solvent $\gg$ **4** $\approx$ **1** $>$ **2** $\approx$ **3** (see Table 1). The powder diffraction data indicate that **2** is isostructural to **1**;[10] however, for **3** and **4** the solids diffract poorly and do not appear to be isomorphous to **1**. Based upon the composition and the similarity of the ν_{CN} absorptions for **2**–**4**, we assign all the metals to the divalent oxidation state. Likewise, the previously elusive oxidation state of vanadium in the room temperature magnet $[V(tcne)_x]\cdot y\,CH_2Cl_2$ is also assigned the divalent oxidation state.

Hysteresis is observed for **1**, **3**, and **4** (but not **2**) below T_c; however, as observed for $[V(tcne)_x]\cdot y\,CH_2Cl_2$[3, 4] the coercive field varies from sample to sample. Nonetheless, we observe coercive fields ranging from 300 Oe (**4**) to a large 6500 Oe (**3**). The shape of the hysteresis curves is characteristic of metamagnetic behavior and along with more detailed magnetic studies, including ac measurements, will be the focus of future research.

Hence, a new synthetic route enabling the preparation of several new molecule-based magnets of the composition $[M^{II}(tcne)_2]\cdot x\,CH_2Cl_2$ has been identified. These new magnets have T_c values that exceed 100 K and coercive fields as great as 6500 Oe.

Received: August 21, 1997 [Z10851IE]
German version: *Angew. Chem.* **1998**, *110*, 676–679

Keywords: iron · magnetic properties · radicals · tetracyanoethylene

[1] *Mol. Cryst. Liq. Cryst.* **1989,** *176* (*Proceedings on the Conference on Ferromagnetic and High Spin Molecular Based Materials* (Eds.: J. S. Miller, D. A. Dougherty)); *NATO ARW Molecular Magnetic Materials*, **1991**, *E198* (*Proceedings on the Conference on Molecular Magnetic Materials* (Eds.: O. Kahn, D. Gatteschi, J. S. Miller, F. Palacio)); *Mol. Cryst. Liq. Cryst.* **1993**, *232/233* (*Proceedings on the Conference on the Chemistry and Physics of Molecular Based Magnetic Materials* (Eds.: H. Iwamura, J. S. Miller)); *ibid.* **1995**, *271–274* (*Proceedings on the Conference on Molecule-based Magnets* (Eds.: J. S. Miller, A. J. Epstein)); *ibid.* **1997**, *305/306* (*Proceedings on the Conference on Molecular-Based Magnets* (Eds.: K. Itoh, T. Takui, J. S. Miller)); M. M. Turnbull, T. Sugimoto, L. K. Thompson, *ACS Symp. Ser.* **1996**, *644*.

[2] Reviews: a) A. L. Buchachenko, *Russ. Chem. Rev.* **1990**, *59*, 307; O. Kahn, *Struct. Bonding (Berlin)* **1987**, *68*, 89; *Molecular Magnetism*, VCH, New York, **1993**; b) A. Caneschi, D. Gatteschi, R. Sessoli, P. Rey, *Acc. Chem. Res.* **1989**, *22*, 392; D. Gatteschi, *Adv. Mater.* **1994**, *6*, 635; c) J. S. Miller, A. J. Epstein, W. M. Reiff, *Acc. Chem. Res.* **1988**, *21*, 114; J. S. Miller, A. J. Epstein, W. M. Reiff, *Science* **1988**, *240*, 40; *Chem. Rev.* **1988**, *88*, 201; J. S. Miller, A. J. Epstein in *New Aspects of Organic Chemistry* (Eds.: Z. Yoshida, T. Shiba, Y. Ohsiro), VCH, New York, **1989**, p. 237; *Angew. Chem.* **1994**, *106*, 399; *Angew. Chem. Int. Ed. Engl.* **1994**, *33*, 385; *Adv. Chem. Ser.* **1995**, *245*, 161.

[3] a) J. M. Manriquez, G. T. Yee, R. S. McLean, A. J. Epstein, J. S. Miller, *Science* **1991**, *252*, 1415; b) J. S. Miller, G. T. Yee, J. M. Manriquez, A. J. Epstein in ref. [3d], p. 461 (*La Chim. La Ind.* **1992**, *74*, 845); c) A. J. Epstein, J. S. Miller in ref. [3d], p. 475 (*La Chim. La Ind.* **1993**, *75*, 185); d) *Proceedings of Nobel Symposium NS-81 Conjugated Polymers and Related Materials: The Interconnection of Chemical and Electronic Structure*, Oxford University Press, Oxford, **1993**.

 © WILEY-VCH Verlag GmbH, D-69451 Weinheim, 1998 1433-7851/98/3705-0659 $ 17.50+.50/0

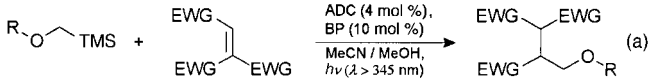
[4] J. Zhang, P. Zhou, W. B. Brinckerhoff, A. J. Epstein, C. Vazquez, R. S. McLean, J. S. Miller, *ACS Sym. Ser.* **1996**, *644*, 311.
[5] G. S. Girolami, G. Wilkinson, A. M. R. Galas, M. Thornton-Pett, M. B. Hursthouse, *J. Chem. Soc. Dalton Trans.* **1985**, 1339.
[6] Compound **1** can also be synthesized by reacting $[FeI_2]\cdot x\,CH_3CN$ or $[Fe^{II}(NCMe)_4]\{B[3,5\text{-}(CF_3)_2C_6H_3]_4\}_2$ with $[nBu_4N]TCNE$ in CH_2Cl_2.
[7] P. Gütlich, R. Link, A. Trautwein in *Inorganic Concepts 3: Mössbauer Spectroscopy and Transition Metal Chemistry*, Springer, Berlin, **1988**, p 19, 56–77.
[8] a) J. S. Griffith, *The Theory of Transition Metal Ions*, Cambridge University Press, Cambridge, **1961**, p. 271. b) If the Fe^{II} was in a tetrahedral geometry, the deviations from Curie–Weiss behavior are consistent with strong antiferromagnetic interactions between high-spin $S=2$ Fe^{II} and $S=1/2$ $[TCNE]^{\bullet-}$ above 240 K ($\theta=-120$ K) and strong ferromagnetic coupling between 115 and 185 K ($\theta\sim+100$ K).
[9] As observed for the preparation of $[V(tcne)_x]\cdot y$ solvent,[3, 4] reactions of $[M^{II}I_2]\cdot x$MeCN (M = Mn, Fe, Co, Ni) in MeCN led to magnetic materials with reduced T_c values.
[10] Powder diffraction data: corrected d spacing [Å] (normalized intensity): M = Fe: 7.393 (38), 5.123 (25), 4.425 (100), 3.266 (25), 2.862 (21), 2.462 (21); M = Mn: 7.455 (15), 5.210 (17), 4.470 (100), 3.314 (33), 2.912 (25), 2.494 (23).

α-Silyl Ethers as Hydroxymethyl Anion Equivalents in Photoinduced Radical Electron Transfer Additions**

Guido Gutenberger, Eberhard Steckhan,* and Siegfried Blechert

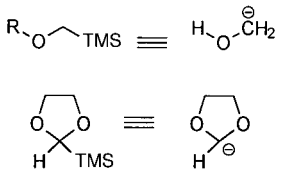
Hydroxymethyl anion equivalents (d^1-synthons) are desirable umpoled synthetic building blocks in organic chemistry.[1] In one of the very rare descriptions of its successful generation Hoppe et al. lithiated carbamates in the presence of (−)-sparteine.[2] Addition of nucleophilic hydroxy- or alkoxymethyl radicals to electron-poor alkenes can be considered as a general alternative. The oxidation of ethers, for example electrochemically,[3] provides the desired radical after one-electron oxidation and deprotonation; however, due to their high oxidation potentials ethers are difficult to oxidize. Besides, the generated alkoxy radical would be further oxidized immediately to the corresponding carbenium ion. The oxidation potential can be decreased significantly by introducing a silyl group to the position α to oxygen.[4] Nevertheless, also in this case further oxidation of the radical to the corresponding cation after desilylation cannot be avoided. Following our recent investigations of aminomethyl radicals[5] we are now presenting a new method for the generation of hydroxymethyl anion equivalents by photoinduced electron transfer catalysis (PET catalysis) starting from α-silyl ethers. This approach provides protected α-hydroxymethyl radicals under mild,[6] nonoxidizing conditions. A multiple-step alternative for the generation of α-silyloxyalkyl radicals is the radical Brook rearrangement of β-silylalkoxy radicals, which are accessible by radical cyclization of ω-bromoacylsilanes.[7]

In our method one-electron oxidation generates an intermediate α-silyl ether radical cation, which fragments with cleavage of the silyl group as an electrofuge. In the presence of catalytic amounts of 9,10-anthracenedicarbonitrile (ADC; 4 mol%) and biphenyl (BP; 10 mol%), irradiation with UV/Vis light leads to the addition of α-silyl ethers to acceptor-substituted alkenes. In this way, γ-acceptor-substituted ethers and alcohols can be prepared (Scheme 1).



Scheme 1. PET-catalyzed addition of α-silyl ethers to acceptor-substituted alkenes. EWG = electron-withdrawing group, TMS = trimethylsilyl, R = benzyl, TBDMS, methyl.

The α-silyl ethers **1**–**4** employed react as hydroxymethyl anion equivalents or, in the case of 2-trimethylsilyl-1,3-dioxolane (**5**), as formyl anion equivalents (Scheme 2). Consequently, this reaction can be considered to be a new route, analogous to the Michael addition, for the direct addition of hydroxymethyl groups to electron-poor alkenes.



Scheme 2. α-Silyl ethers and acetals as d^1-synthons.

We studied this transformation with the starting materials listed in Table 1. Methoxymethyltrimethylsilane (**1**) was successfully tested in addition reactions with methyl 2-cyanocrotonate (**6**) to give **11**. Because of the difficult cleavage of the methyl ether to generate the free OH function, trimethylsilylmethanol and other α-silyl ethers carrying readily cleavable protecting groups were examined. Reaction of the unprotected trimethysilylmethanol leads, according to GCMS analysis, to a product formed by addition of a trimethylsilyloxymethyl radical to the electron-poor double bond. Isolation of the product was impossible due to its instability. An explanation for the formation of this product would be deprotonation at the carbon or oxygen atom of the intermediate radical cation generated under electron transfer conditions. Subsequent Brook rearrangement[7, 8] would give the trimethylsilyloxymethyl radical.

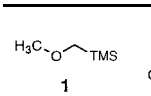
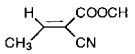
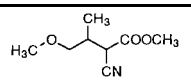
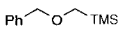
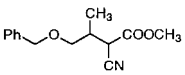
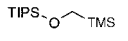
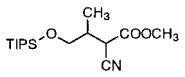
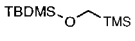
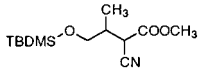
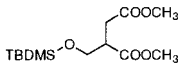
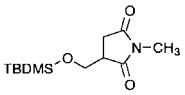
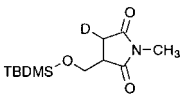
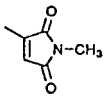
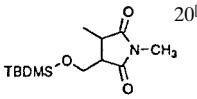
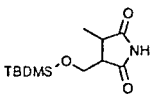
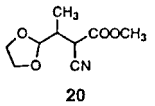
Next we investigated the behavior of α-silyl ethers carrying protecting groups on oxygen that can be cleaved easily like trimethylsilyl, *tert*-butyldimethylsilyl (TBDMS; **4**), benzyl (**2**), and triisopropylsilyl (TIPS; **3**). The addition product obtained from a trimethylsilyl-protected α-silyl ether is identical, according to GCMS analysis, to that formed from trimethyl-

[*] Prof. Dr. E. Steckhan, Dipl.-Chem. G. Gutenberger
Kekulé Institut für Organische Chemie und
Biochemie der Universität
Gerhard-Domagk-Strasse 1, D-53121 Bonn (Germany)
Fax: (+49) 228-735683
E-mail: steckhan@uni-bonn.de
Prof. Dr. S. Blechert
Institut für Organische Chemie der Technischen Universität Berlin

[**] This work was supported by the Volkswagen-Stiftung (I/71748), the Fonds der Chemischen Industrie, and BASF AG.

 © WILEY-VCH Verlag GmbH, D-69451 Weinheim, 1998 1433-7851/98/3705-0660 $ 17.50+.50/0

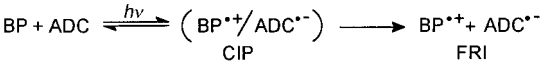
Table 1. Photoinduced radical additions of α-silyl ethers to electron-poor alkenes.

α-Silyl ether	Alkene	Product [a]	Yield [%]	d.r.
 1	 6	 11	46 [b]	
 2	6	 12	64 [c]	2:1
 3	6	 13	25 [b]	
 4	6	 14	42 [c]	1.8:1
4	 7	 15	38 [b]	2.5:1
4	 8	 16	42 [b]	
4	8	 17	55 [c] 20 [b] 21 [b, d]	2.5:1 – –
4	 9	 18	20 [b, e, f]	–
4	 10	 19	18 [b, d]	86:14
 5	6	 20	15 [b, d] 50 [b]	86:14 1.9:1

[a] All addition products were characterized by ^{13}C and ^{1}H NMR spectroscopy, and MS, HRMS, and CHN elemental analysis. [b] Yields of isolated products. [c] Yield determined by gas chromatography using a calibration curve. [d] Lower yields were obtained due to the easy polymerization of cyclic alkenes. [e] In presence of CH_3OD. [f] Overlapping NMR signals prevented determination of d.r.

silylmethanol. Also in this case, the product could not be isolated due to its instability. However, all other α-silyl ethers form the expected products. Of the α-silyl ethers, the TBDMS-protected derivative **4** proved to react most effectively with the acceptor-substituted alkenes **6**–**10**.

Compound **5** served as a model of an acyl anion equivalent. Cyclic α-silyl ethers and acetals are known to adopt a conformation in which the free π-electrons of the oxygen and the Si–C σ bond[4] are "in plane". This leads to faster, nucleophile-assisted desilylation. The higher yield is presumably due to the increased reactivity of the radical (Table 1). The reactivity is influenced not only by the different O-protecting groups but also by the radical acceptors. When aliphatic, electron-poor alkenes such as methyl 2-cyanocrotonate (**6**) are used, only poor diastereoselectivity (d.r. = 1.8:1 to 2.5:1) is observed (Table 1). A possible explanation might be the free rotation around the C–C single bond. Application of cyclic, electron-poor alkenes like 1,3-dimethyl-1*H*-pyrrole-2,5-dione (**9**) and 3-methyl-1*H*-pyrrole-2,5-dione (**10**), however, results in considerably higher diastereoselectivity with a *cis:trans* ratio of 86:14 (Table 1). The *cis* product is formed preferentially under kinetic control. This behavior can be explained on the basis of the mechanism. ET quenching between the primary electron donor BP ($E_{ox} = 1.98$ V vs. SCE) and photochemically excited ADC* ($E_{red}(S1) = 2.0$ V vs. SCE)[9] generates the biphenyl radical cation (Scheme 3), which subsequently oxidizes the α-silyl ether ($E_{ox} = 1.41 - 1.66$ V vs. $Ag/AgNO_3$)[10] to give its

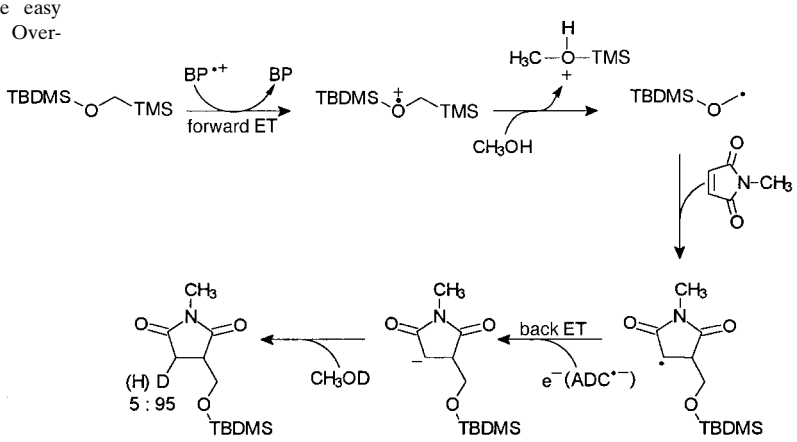


Scheme 3. Redox photosenzitation with ADC und BP. CIP = contact radical ion pair, FRI = free radical ions.

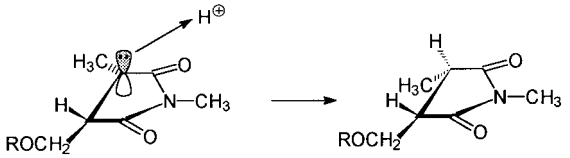
radical cation through a one-electron transfer reaction (redox photosensitization)[11] (Scheme 4). After cleavage of the silyl group,[12] the resulting nucleophilic radical is trapped by an electron-poor alkene. Back electron transfer from the ADC radical anion to the radical addition product and protonation complete the electron transfer catalytic cycle.

We wondered whether the α-carbonyl radical abstracts hydrogen from the solvent, or whether the carbanion intermediate is protonated. By using CH_3OD instead of CH_3OH as the solvent, we proved that the carbanion intermediate is protonated preferentially. GCMS analysis indicated the ratio of deuterated to nondeuterated product to be 95:5. The product itself shows no H/D exchange under the same reaction conditions.

The diastereoselectivity results from preferred protonation of the carbanion intermediate from the sterically less hindered side under kinetic control (Scheme 5). By treatment of the *cis* product with methoxide in methanol, the thermodynamically more stable *trans* product can be formed.



Scheme 4. Proof of protonation of the anionic intermediate.



Scheme 5. Model for stereochemical control of the protonation step.

In addition to the intermolecular additions to electron-poor alkenes described here, intramolecular cyclization of α-silyl ethers having electron-poor double bonds also seems promising.

Experimental Section

General conditions for PET reactions: A jacketed Schlenk tube was charged with a solution of the α-silyl ethers **1**–**5** in acetonitrile/methanol (2/1) containing ADC (4 mol%) and BP (10 mol%). The electron-poor alkenes **6** and **7**, each dissolved in 3 mL of CH_3CN, were added before irradiation, solutions of **8**–**10** were added dropwise during irradiation. A 450 W xenon-arc lamp with a wavelength filter ($\lambda > 345$ nm) was used as a light source. The solutions were degassed with argon prior to and during irradiation and thermostated by water-cooling.

11: (analogous for **12**–**15** and **20**): A mixture of **1** (350 mg, 2.9 mmol), **6** (543 mg, 4.3 mmol), BP (45 mg), and ADC (7 mg) was dissolved in 20 mL of acetonitrile and 10 mL of methanol. During subsequent irradiation for 11 h two 10-mg portions of ADC were added every 3–4 h (27 mg total). Evaporation of the solvent followed by flash chromatography on silica gel (first separation: ethyl acetate/*n*-heptane 1/5; $R_f = 0.31$), (second separation: petroleum ether/dichloromethane 2/1; $R_f = 0.1$)) provided 228.5 mg (46%) of a light yellow oil. The signal doubling observed in the ^1H and ^{13}C NMR spectra indicates the formation of diastereomers. The data for the diastereomers are separated by slashes. ^1H NMR (400 MHz, $CDCl_3$): $\delta =$ 0.98/1.05 (d, $J = 6.8$ Hz, 3H), 2.45–2.6 (m, 1H), 3.18–3.22 (1H), 3.25/3.3 (s, 3H), 3.31–3.4 (m, 1H), 3.51/3.9 (d, $J = 4.2$ Hz, 1H), 3.73/3.75 (s, 3H); ^{13}C NMR (100.6 MHz, $CDCl_3$): $\delta = 12.9/14.9$, 34.6/35.1, 40.2/41.3, 53.1/53.3, 58.9/59.0, 74.0, 114.8/115.4, 166.2/166.6; MS (EI, 70 eV): *m/z* (%): 171 (1) [M^+], 140 (7), 109 (7), 72 (58), 45 (100); HRMS (EI, 70 eV): calcd for $C_8H_{13}NO_3$: 171.0895; found 171.0890; CHN analysis calcd for $C_8H_{13}NO_3$: C 56.13, H 7.65, N 8.18; found C 56.40, H 7.83, N 7.64.

18: (analogous for **16**, **17**, and **19**): A mixture of **4** (348 mg, 1.6 mmol), ADC (21.8 mg, 0.09 mmol), and BP (24.6 mg, 0.16 mmol) were dissolved in 20 mL of acetonitrile and 10 mL of methanol. A solution of **9** (300 mg, 2.4 mmol) in 3 mL of CH_3CN was added dropwise to the reaction mixture, which was irradiated for 18 h. Evaporation of the solvent and subsequent flash chromatography on silica gel (cyclohexane/ethyl acetate 10/1; $R_f =$ 0.05) provided 115 mg (18%) of a light yellow oil. The data refer to the *cis* product. The relative configuration was determined by NOE experiments. ^1H NMR (500 MHz, C_6D_6): $\delta = -0.11$ (s, 3H), -0.09 (s, 3H), 0.70 (s, 9H), 1.26 (d, $J = 6.9$ Hz, 3H), 2.76–2.85 (m, 2H), 2.88 (s, 3H), 3.42–3.45 (dd, $J = 10.0$ Hz, $J = 2.0$ Hz, 1H), 3.86–3.89 (dd, $J = 10.0$ Hz, $J = 3.2$ Hz, 1H); ^{13}C NMR (100.6 MHz, $CDCl_3$): $\delta = 181.1$, 179.0, 60.4, 47.1, 37.6, 26.0, 25.1, 18.3, 9.7, -5.2, -5.3; MS (EI, 70 eV): *m/z* (%): 270 (1) [$M^+ - H$], 256 (41), 214 (100), 156 (4), 129 (4), 75 (14); HRMS (EI, 70 eV): calcd. for $C_{13}H_{25}NO_3Si$: 271.1603; found: 256.1371 [$M^+ - 15$]; CHN analysis calcd for $C_{13}H_{25}NO_3Si \cdot 1/6\,H_2O$: C 57.53, H 9.28, N 5.16; found: C 56.99, H 9.26, N 5.27.

Received: September 12, 1997 [Z10916IE]
German version: *Angew. Chem.* **1998**, *110*, 679–681

Keywords: electron transfer · photochemistry · radical ions · silicon

[1] J. E. Saavedra in *Umpoled Synthons* (Ed.: T. A. Hase), Wiley, New York, **1987**.

[2] P. Sommerfeld, D. Hoppe, *Synlett* **1992**, 764; W. Guarnieri, M. Grehl, D. Hoppe, *Angew. Chem.* **1994**, *106*, 1815; *Angew. Chem. Int. Ed. Engl.* **1994**, *33*, 1734.

[3] K. D. Ginzel, E. Steckhan, D. Degner, *Tetrahedron* **1987**, *43*, 5797; T. Shono, Y. Matsumura, O. Onomura, Y. Yamada, *Synthesis* **1987**, 1099.

[4] J. Yoshida, T. Maekawa, T. Murata, S. Matsunaga, S. Isoe, *J. Am. Chem. Soc.* **1990**, *112*, 1962; J. Yoshida, *Top. Curr. Chem.* **1994**, *170*, 39.

[5] E. Meggers, E. Steckhan, S. Blechert, *Angew. Chem.* **1995**, *107*, 2317; *Angew. Chem. Int. Ed. Engl.* **1995**, *34*, 2137.

[6] M. A. Brumfield, S. L. Quillen, U. C. Yoon, P. S. Mariano, *J. Am. Chem. Soc.* **1984**, *106*, 6855.

[7] Y. M. Tsai, K.-H. Tang, W.-T. Jiaang, *Tetrahedron Lett.* **1996**, *37*, 7767; D. P. Curran, W.-T. Jiaang, M. Palovich, Y.-M. Tsai, *Synlett* **1993**, 403.

[8] J. M. Harris, I. MacInnes, J. C. Walton, B. Maillard, *J. Organomet. Chem.* **1991**, *403*, C25.

[9] Reduction potentials of the most important sensitizers: H. D. Roth, *Top. Curr. Chem.* **1992**, *163*, 131; S. L. Murov, J. Carmichael, G. L. Hug, *Handbook of Photochemistry*, 2nd ed., Marcel Dekker, New York, **1993**.

[10] G. Gutenberger, *Diploma Thesis*, Universität Bonn **1996**; see also ref. [4].

[11] S. Tazuke, N. Kitamura, *J. Chem. Soc. Chem. Commun.* **1977**, 515; T. Majima, C. Pac, A. Nakasone, H. Sakurai, *J. Am.Chem. Soc.* **1981**, *103*, 4499.

[12] J. P. Dinnocenzo, S. Farid, J. L. Goodman, I. R. Gould, W. P.Todd, S. L. Mattes, *J. Am. Chem. Soc.* **1989**, *111*, 8973.

Heck Reactions without Salt Formation: Aromatic Carboxylic Anhydrides as Arylating Agents**

Massoud S. Stephan,* Antonius J. J. M. Teunissen, Gerard K. M. Verzijl, and Johannes G. de Vries*

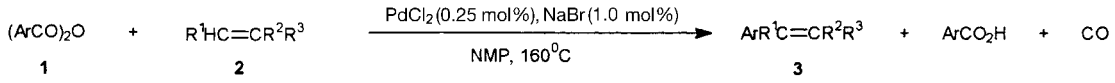
The Friedel-Crafts reaction is still the most commonly used method for the attachment of a carbon fragment to an aromatic ring. From an industrial point of view the reaction is less desirable because of the highly corrosive conditions and the concomitant formation of a large amount of waste. Recently the Heck reaction has come into the spotlight as a means of arylating double bonds.[1] Though the reaction has a wide scope, the arylating agent is limited to aryl bromides, iodides, or triflates, aroyl halides, arylsulfonyl halides, and aryldiazonium salts. In all cases a stoichiometric amount of base is required to neutralize the acid that is formed during the reaction. In addition, an equivalent amount of halide salt is formed as waste.

The development of a stable palladium catalyst, based upon a palladacycle, has allowed the conversion of activated aryl chlorides with high turnover numbers and has brought the Heck reaction into the industrial realm.[2] But also in this reaction a stoichiometric amount of chloride salt is formed as waste product. There clearly is a need for a cheap aryl source that does not lead to the formation of halide salts in the Heck reaction.

[*] Dr. M. Stephan, Dr. J. G. de Vries, A. J. J. M. Teunissen, G. K. M. Verzijl
DSM Research, Dept. Fine Chemicals
PO Box 18, NL-6160 MD Geleen (The Netherlands)
Fax: (+31) 46-476-7604
E-mail: j.g.vries-de@research.dsm.nl

[**] We thank Dr. Paul L. Alsters for stimulating discussions.

 © WILEY-VCH Verlag GmbH, D-69451 Weinheim, 1998 1433-7851/98/3705-0662 $ 17.50+.50/0



Scheme 1. Heck reaction of olefins **2** with aromatic carboxylic anhydrides **1**. For Ar, R^1, R^2, and R^3, see Table 1.

The solution to this problem lies in the use of aromatic carboxylic anhydrides as the arylating source.[3] Thus, heating benzoic anhydride (**1**, Ar = Ph) and *n*-butyl acrylate (**2**; R^1, R^2 = H, $R^3 = CO_2Bu$) in an *N*-methylpyrrolidinone (NMP) solution containing $PdCl_2$ (0.25 mol %) and NaBr (1.0 mol %) at 160°C for 90 min led to complete conversion of benzoic anhydride and formation of (*E*)-*n*-butyl cinnamate with 90 % selectivity (Scheme 1). The product was isolated in 77 % yield by evaporation of solvent, followed by extraction of the benzoic acid in hot water and purification of the residue by distillation (Table 1, entry 1). Side products in the reaction are benzoic acid and carbon monoxide. The latter can be easily burnt to carbon dioxide. Benzoic acid can be recycled into its anhydride.

A number of different palladium catalyst precursors can be used, such as $PdCl_2$, Na_2PdCl_4 and Na_2PdCl_6; however, they all require a catalytic amount of chloride or bromide for optimal activity (iodide was much less active).[4] Figure 1 shows the dependence of the yield *y* of **3** in the reaction between benzoic anhydride and *n*-butyl acrylate at 155°C after 1 h on the amount of sodium halide used. Alkali metal halides can be used as well as tetraalkylammonium halides or tetraalkylphosphonium halides. Initially we were not sure about the role of the tetraalkylammonium halide, as it has been shown that tetraalkylammonium salts can induce the formation of giant palladium clusters, known catalysts in the Heck reaction.[5, 6] However, use of non-halide tetraalkylammonium salts led to much slower reactions. These results seem to support a mechanism based upon halide-ligated palladium(0) catalyst[7, 8] as suggested by Jeffery.[4] This seems quite reasonable as Yamamoto et al. have shown that benzoic anhydride oxidatively adds to zerovalent $[(PMe_3)_2(C_6H_5CH{=}CH_2)Pd]$ and can be homogeneously hydrogenated to benzaldehyde and benzoic acid with this catalyst.[9] However, using electrospray mass spectrometry we have so far been unable to detect any halide-ligated Pd^0 complexes, leaving open the possibility that the reaction proceeds by a Pd^{II}/Pd^{IV} mechanism.[10]

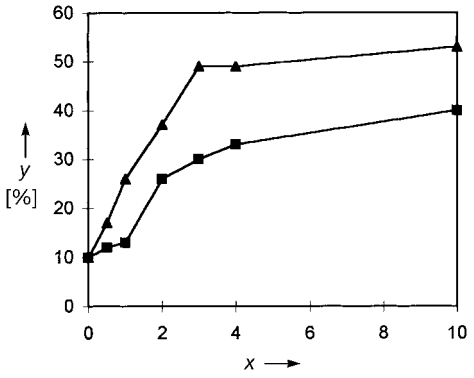


Figure 1. Dependence of yield *y* of **3** at 155°C after 1 h on halide: palladium ratio *x* for the reaction of benzoic acid with *n*-butyl acrylate at 155°C after 1 h. ■ NaCl, ▲ NaBr.

Phosphane ligands are not required in this reaction, which is thus more attractive as an industrially viable method. In fact, use of $[PdCl_2(PPh_3)_2]$ or $[Pd(PPh_3)_4]$, even in the presence of added halide, resulted in inferior conversions and selectivities. $[(PhCN)_2PdCl_2]$ also gave good results in conjunction with halides.

A wide variety of olefins can be arylated under similar conditions at temperatures ranging between 140–190°C. Olefins with electron withdrawing groups generally give high yields of the β-arylated products.[11] Even butyl methacrylate was arylated in good yield, though double-bond isomerization of the product resulted in a mixture of isomers.[12] Terminal olefins are good substrates, but in this case double-bond isomerization is very rapid, causing formation of a mixture of isomeric olefins. Unfortunately, at the relatively high reaction temperature arylation also took place at the internal positions. This was proven by hydrogenating the product mixture of the

Table 1. Palladium-catalyzed arylation of olefins **2** with aromatic carboxylic anhydrides **1**.[a]

Entry	Ar	R^1	R^2	R^3	Time (min)	Conversion of **1** (%)	Yield of **3** (%) (GC yield %)
1.	Ph	H	H	CO_2Bu	90	100	77 (90)
2.	Ph	H	H	nC_8H_{17}	90	85	60 (95)
3.	Ph	H	H	Ph	120	90	76 (85)[g]
4.	Ph	$-(CH_2)_6-$		H	120	100	54 (85)
5.	Ph	O*c*-C_6H_{11}	H	H	120	80	α (25)
6.[b]	Ph	H	H	CN	180	90	60 (E/Z = 75/20)
7.	Ph	H	Me	CO_2Bu	90	100	62[h]
8.[c, d]	Ph	CO_2Bu	CO_2Bu	H	180	100	73 (E/Z = 7/2) (90)
9.	Ph	$N(CH_2)_3CO$	H	H	90	100	25 (α/β-E = 20/5)[j]
10.[c]	[e]	H	H	CO_2Bu	60	100	75 (80)
11.	[f]	H	H	CO_2Bu	90	100	77 (85)

[a] Conditions: see Experimental Section; T = 160°C, unless otherwise noted. [b] Reaction at 140°C. [c] Reaction at 190°C. [d] Maleate. [e] *p*-$MeOC_6H_4$. [f] 2-Furyl. [g] 1,1′-Diphenylethene (11 %) also formed. [h] *n*-Butyl α-benzylacrylate (10 %) also formed. [j] *N*-Benzoyl-2-pyrrolidinone was also isolated in 58 % yield.

 © WILEY-VCH Verlag GmbH, D-69451 Weinheim, 1998 1433-7851/98/3705-0663 $ 17.50+.50/0

phenylation of 1-decene (H_2, Pd/C), which gave a mixture of all five possible phenyldecane isomers. Cyclooctene gave a mixture of phenylcyclooctenes in addition to some diphenylcyclooctene.

Arylations with olefins carrying electron-donating substituents were less successful. Vinyl esters invariably reacted by cleavage of the carbon–oxygen bond leading to the formation of styrene and stilbene. Reaction of cyclohexyl vinyl ether gave some Heck product (25% yield) in which phenylation had exclusively taken place in the α position.[11] *N*-vinyl-2-pyrrolidinone was arylated to give a mixture of isomeric *N*-styrylpyrrolidinones ($\alpha:\beta = 4:1$) in 25% yield of the isolated product. A major side product was *N*-benzoyl-2-pyrrolidinone (58%).

Other aromatic carboxylic anhydrides reacted similarly. *p*-Methoxybenzoic anhydride required a slightly higher temperature (190°C) for the reaction with *n*-butyl acrylate to go to completion. Furanoic anhydride was successfully used to furylate *n*-butyl acrylate.

In conclusion, we have discovered an environmentally benign method to arylate olefins. The products of these reactions can be hydrogenated to arylalkanes or oxidized as in the Wacker reaction to aryl alkyl ketones, thus providing a clean alternative to the Friedel–Crafts reaction.

Experimental Section[13]

A 300 mL Schlenk-tube, fitted with a rubber septum inlet and equipped with magnetic stirring, is charged with $(PhCO)_2O$ (23 g, 100 mmol), $PdCl_2$ (45 mg, 0.25 mmol), and NaBr (103 mg, 1 mmol). After repeated degassing under vacuum and purging with argon, nHex$_2$O (10 mmol) as internal standard, dibutyl maleate (28.0 mL, 120 mmol) and NMP (100 mL) are successively injected. The Schlenk tube is heated at 190°C for 3 h. The course of the reaction is monitored by gas chromatography (CP-Sil 8 CB column). A mixture of dibutyl phenylfumarate and dibutyl phenylmaleate (7:2) is obtained by fractional distillation (170°C/3 Torr) of the crude reaction mixture in 73% yield.

Received: July 24, 1997
Revised version: November 11, 1997 [Z10728IE]
German version: *Angew. Chem.* **1998**, *110*, 688–690

Keywords: alkenes · anhydrides · arenes · C–C coupling · homogeneous catalysis

[1] a) R. F. Heck, *Org. React.* **1982**, *27–390*, 345; b) R. F. Heck in *Comprehensive Organic Synthesis*, *Vol.4*, (Eds.: B. M. Trost, I. Fleming), Pergamon, Oxford, **1991**, 833–863; c) A. de Meijere, F. E. Meyer, *Angew. Chem.* **1994**, *106*, 2473–2506; *Angew. Chem. Int. Ed. Engl.* **1994**, *33*, 2379–2411; d) W. Cabri, I. Candiani, *Acc. Chem. Res.* **1995**, *28*, 2–7; e) J. Tsuji, *Palladium Reagents and Catalysts-Innovations in Organic Synthesis*, Wiley, Chichester, UK, **1995**.

[2] a) W. A. Herrmann, C. Brossmer, K. Öfele, C.-P. Reisinger, T. Priermeier, M. Beller, H. Fischer, *Angew. Chem.* **1995**, *107*, 1989-1992; *Angew. Chem. Int. Ed. Engl.* **1995**, *34*, 1844–1847; b) W. A. Herrmann, C. Brossmer, C.-P. Reisinger, T. H. Riermeier, K. Öfele, M. Beller, *Chem. Eur. J.* **1997**, *3*, 1357–1364.

[3] The rhodium-catalyzed benzoylation of styrene with benzoic anhydride has been reported: K. Kokubo, M. Miura, M. Nomura, *Organometallics* **1995**, *14*, 4521–4524.

[4] T. Jeffery, *Tetrahedron* **1996**, *52*, 10113–10130, and references herein.

[5] Halides are not a prerequisite for the formation of clusters aided by tetraalkylammonium salts: M. T. Reetz, S. A. Quaiser, *Angew. Chem.* **1995**, *107*, 2461–2463; *Angew. Chem. Int. Ed. Engl.* **1995**, *34*, 2240–2241.

[6] a) M. Beller, H. Fischer, K. Kühlein, C.-P. Reisinger, W. A. Herrmann, *J. Organomet. Chem.* **1996,** *520*, 257–259; b) M. T. Reetz, R. Breinbauer, K. Wanninger, *Tetrahedron Lett.* **1996**, *37*, 4499–4502.

[7] The role of chloride-ligated palladium phosphane complexes in oxidative addition reactions has been discussed: a) C. Amatore, M. Azzabi, A. Jutand, *J. Am. Chem. Soc.* **1991**, *113*, 8375–8384; b) C. Amatore, A. Jutand, A. Suarez, *J. Am. Chem. Soc.* **1993**, *115*, 9531–9541.

[8] We have observed the reduction of $PdCl_2$ to Pd black in NMP solutions at room temperature. This might be due to amine impurities in the solvent.

[9] K. Nagayama, F. Kawataka, M. Sakamoto, I. Shimizu , A. Yamamoto, *Chem. Lett.* **1995**, 367–368.

[10] On taking samples from the reaction mixture at 160°C and directly injecting these in the mass spectrometer (Finnigan Navigator) we found evidence for the following anionic complexes: $[PdCl_3]^-$ (or more likely the bridged dimer $[Pd_2Cl_6]^{2-}$), an adduct of $[PdCl_3]^-$ and benzoic acid, and $[Cl_3Pd(CO)]^-$).

[11] For a discussion on the factors influencing the stereochemical and regiochemical outcome of Heck reactions, see refs. [1b, 1c] and a) A. Spencer, *J. Organomet. Chem.* **1982**, *240*, 209–216; b) C.-M. Andersson, A. Hallberg, *J. Org. Chem.* **1988**, *53*, 235–239.

[12] M. Beller, T. H. Riermeier, *Tetrahedron Lett.* **1996**, *37*, 6535–6538.

[13] Use of only 0.1 mol% of $PdCl_2$ and 0.4 mol% halide is also possible without reducing the yield; reaction times increase to 3–5 h.

Synthesis of Microporous Transition Metal Oxide Molecular Sieves with Bifunctional Templating Molecules**

Tao Sun and Jackie Y. Ying*

Porous inorganic materials have been widely studied, and the mechanism by which their structures form remains an area of great interest. When synthesized with high surface area and narrow pore size distribution, these structures are highly useful as active and/or selective catalytic materials.[1] Inorganic and organic cations have been frequently used to construct microporous zeolitic frameworks, but our understanding of their function in the process remains rather limited and disparate.[2] In contrast, a more generalized approach for formation of mesoporous structures has been developed in the last five years with the discovery of M41S silicates by Mobil scientists.[3] Through charge matching between the hydrophilic head groups of surfactant molecules and inorganic precursors, silicates and surfactants can be self-assembled into supramolecular aggregates with long-range order of packing.[4] Upon removal of surfactants through

[*] Prof. J. Y. Ying, T. Sun
Department of Chemical Engineering
Massachusetts Institute of Technology
Cambridge, MA 02139 (USA)
Fax: (+1) 617-258-5766

[**] This work was supported by the Packard Foundation, the Dreyfus Foundation, and the National Science Foundation (CTS-9257223, DMR-9400334). The authors thank D. M. Antonelli for helpful discussions, and Z. Zhang and M. Frongillo (M. I. T. CMSE) for assistance with TEM.

 © WILEY-VCH Verlag GmbH, D-69451 Weinheim, 1998 1433-7851/98/3705-0664 $ 17.50+.50/0

calcination or organic washes, mesoporous silicates with ordered porous arrays can be achieved.

More recently, a ligand-assisted templating approach was developed to ensure proper precursor–template interaction and micellar self-assembly prior to precursor hydrolysis.[5] In this way a family of hexagonally packed mesoporous transition metal oxides termed TMS1 was derived by Antonelli and Ying.[5, 6] For example, Nb-TMS1, a niobium oxide analogue of the hexagonally packed mesoporous silicate-based MCM-41, was produced by first establishing a covalent bond between the niobium ethoxide precursor and an amine templating agent.[5] Narrow pore size distributions and high surface areas were obtained upon template removal from such systems by organic washes or calcination. By adjusting the molar ratio of metal precursor to templating molecule, new mesostructured transition metal oxides with a hexagonal *P*63/*mmc* phase (TMS2) and a lamellar phase (TMS4) could also be derived.[5b] Increasing the amine chain length also led to a new cubic *Pm*3*n* phase (TMS3).[5b] These approaches allowed mixed metal oxide molecular sieves to be easily achieved, and provided the fundamental chemical flexibility associated with compositional control and homogeneity. This, coupled with the possibility of tailoring pore sizes in the range of 20 to 100 Å, offers exciting new opportunities in catalytic and gas adsorption applications.

The hexagonally packed mesoporous structures of both MCM-41 and TMS1 were constructed around surfactant assemblies by a supramolecular templating mechanism.[3–7] The surfactant molecules have a hydrophilic head group and a hydrophobic hydrocarbon tail, and these species are organized into micellar rods under the proper conditions. The micellar cross section determines the pore diameter and can be varied by changing the length of the hydrocarbon chain of the surfactant; the chains usually range between 12 and 20 C atoms. Thus far, such a supramolecular templating approach has been utilized only in the derivation of mesoporous materials with pore openings larger than 20 Å. To generate microporous metal oxides, Maier et al. have developed a sol–gel technique to produce amorphous silicate-based mixed oxides with a narrow pore size distribution and a surface area as high as $523\,m^2g^{-1}$.[8] In our study, the goal is to generate microporous structures systematically by controlling the micellar dimensions by a self-assembly approach. We report herein a novel approach that enables us to achieve microporous transition metal oxides by the introduction of a second hydrophilic functional group to the tails of amine-templating molecules.

In a typical synthesis, niobium ethoxide was added to an ethanolic solution of 1,12-diaminododecane to prepare a solution of the niobium diamine complex. This complex was then hydrolyzed in an aqueous solution at ambient conditions and then hydrothermally treated at temperatures ranging between 96 to 180 °C for four or five days. The light brown solids produced were collected, washed, and dried at 180 °C for 24 h to further condense the niobium oxide framework. The diamine molecules were effectively removed by an acidic alcohol wash at temperatures varying from 25 to 80 °C, depending on the pH of the solution and the duration of washing. The porous sample obtained was designated as Nb-TMS6. The microporosity of Nb-TMS6 was illustrated by the type I nitrogen adsorption–desorption isotherm in Figure 1. The Nb-TMS6 sample possesses a Brunauer-Emmet-Teller

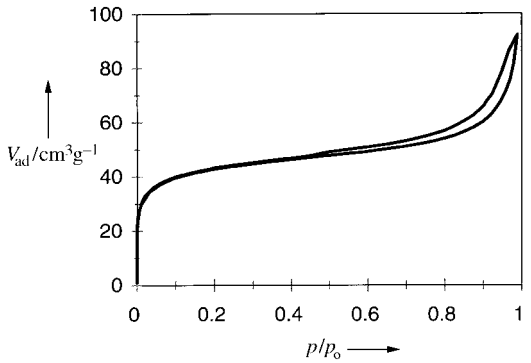


Figure 1. N_2 adsorption and desorption isotherms (V_{ad} = volume adsorbed, p/p_0 = relative pressure) of microporous Nb-TMS6 synthesized with a Nb:1,12-diaminododecane molar ratio of 1:0.5 at 180 °C. The isotherms were collected on a Micromeritics 2010 Gas Adsorption Analyzer.

(BET) surface area of $150\,m^2g^{-1}$ or higher, depending on the exact diamine removal conditions. The transmission electron micrograph (TEM) shown in Figure 2 further confirms the

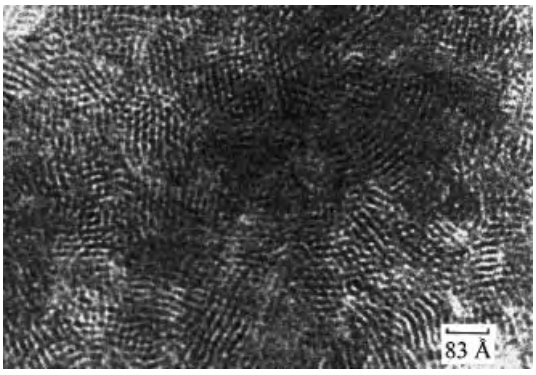


Figure 2. TEM image of as-prepared Nb-TMS6, synthesized with a Nb:1,12-diaminododecane molar ratio of 1:0.5 at 180 °C. This image was obtained with a 200 kV JEOL 002B transmission electron microscope.

microporous nature of Nb-TMS6 synthesized with diaminododecane. Unlike Nb-TMS1 and Nb-TMS3, which displayed long-range packing of mesopores in a hexagonal and a cubic arrangement, respectively, the packing of micropores in Nb-TMS6 appeared to be rather disordered with no clearly defined crystal phases.

The X-ray diffraction (XRD) pattern of Nb-TMS6 synthesized with diaminododecane (Figure 3) showed an intense (100) peak at 18.4 Å, and weaker peaks at 9.95 Å and 6.04 Å. The d_{100} spacing of 18.4 Å in Nb-TMS6 is much smaller than the d_{100} spacing of 28.0 Å in mesoporous Nb-TMS1 synthesized with dodecylamine.[5b] This confirms that the diamine molecules self-assemble by a mechanism very different from that of the monoamine molecules, leading to much finer porous structures upon their removal from the inorganic framework. Close examination of the high diffraction angles revealed the presence of a few weak peaks, which may be

 © WILEY-VCH Verlag GmbH, D-69451 Weinheim, 1998 1433-7851/98/3705-0665 $ 17.50+.50/0

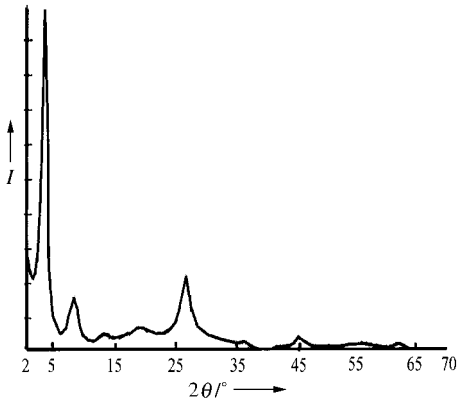


Figure 3. XRD patterns of as-prepared Nb-TMS6 synthesized with a Nb:1,12-diaminododecane ratio of 1:0.5, and aged at 180 °C for four days. The XRD patterns were obtained with a Siemens D5000 θ-θ diffractometer with $Cu_{K\alpha}$ radiation ($\lambda = 1.5418$ Å). I = intensity in arbitrary units.

attributed to minor impurities from a dense phase containing niobium oxide.

In addition to diaminododecane, we have investigated shorter chain diamine molecules as templating agents in an effort to derive even finer microporous structures. As shown in Figure 4, the (100) peak position shifted from 18.4 Å to 14.4 Å as the length of the diamine hydrocarbon chain was

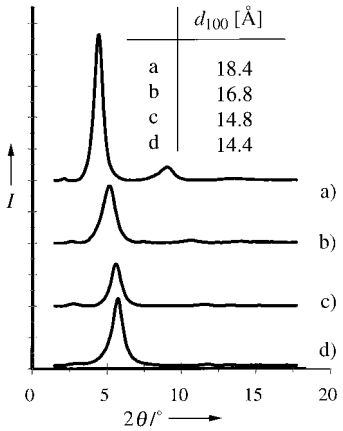


Figure 4. XRD patterns of as-prepared Nb-TMS6 synthesized with a) 1,12-diaminododecane, b) 1,10-diaminodecane, c) 1,8-diaminooctane, and d) 1,7-diaminoheptane as templating agents. The samples were prepared with a Nb:diamine ratio of 1:0.5 at 180 °C. I = intensity in arbitrary units.

decreased from twelve C atoms to seven C atoms. The intensity of the (100) peak and the resolution of the higher order peaks were greater for the samples synthesized with longer diamine molecules. The lower order in pore packing of the samples associated with shorter diamine molecules may be due to the relatively lower hydrophobicity of the shorter hydrocarbon chains. Despite the lack of well-defined pore packing, this synthetic approach allows us to systematically tailor novel microporous structures with high surface areas for transition metal oxide molecular sieves.

The diamine template molecules could not be properly removed from the oxide framework without structure collapse by treating the materials at elevated temperatures or under high vacuum. The departure of diamines may be accounted for by a weight loss of 21 % in the as-prepared Nb-TMS6 at 325 °C in thermogravimetric analysis. This temperature for template removal is much higher than that in MCM-41 materials,[3] indicating a very strong interaction between niobium oxide and the diamine molecules. However, if the templates are removed by washing with acidic alcohol, the materials can retain their microporous structure and XRD pore packing order up to 400 °C. The covalent nature of the bonding between diamine and niobium is also unique at relatively high pH; synthesis at pH below 5 yields only amorphous materials since the head groups of the templating molecule will be protonated as ammonium cations and cannot donate electrons to empty d orbitals of niobium to form strong chemical interactions.

The present study illustrates for the first time that long-chain diamine molecules can be used to construct microporous oxides. This approach is in contrast to the conventional surfactant templating of mesoporous phases and is distinct from the typical molecular templating of zeolitic structures. Our synthesis was made possible because the hydrophilic affinity of the templating molecules was tailored by introducing more than one functional group to the hydrocarbon chain. As in the synthesis of Nb-TMS1,[5] we have chosen amine as the functional group for deriving Nb-TMS6 since the bonding between nitrogen and niobium is expected to be very strong. This should allow aging at high temperatures and leave the templating molecule in place for full condensation of the niobium oxide framework. In the case of Nb-TMS6, that the N – Nb bond formation was expected to be highly favorable was further exploited to facilitate self-assembly between the two functional groups of diamines with the niobium alkoxide precursors. A smaller micellar dimension is achieved with a diamine than with a monoamine of the same hydrocarbon chain length. The resulting smaller supramolecular template has led to the successful derivation of a novel microporous transition metal oxide molecular sieve, in contrast to the mesoporous structures obtained by using monoamine templates. Our approach enables the fine-tuning of the pore size below 20 Å by varying the chain length of a bifunctional molecule for not only niobium oxide, but also tantalum oxide, and titanium oxide. The resulting family of microporous transition metal oxides and mixed metal oxides offers exciting new flexibility in designing molecular sieves targeted for size selectivity and chemical functionality.

Received: January 13, 1997
Revised version: November 5, 1997 [Z9987IE]
German version: *Angew. Chem.* **1998**, *110*, 690 – 693

Keywords: micelles · microporosity · molecular sieves · niobium · template synthesis

[1] a) I. E. Maxwell, *Adv. Catal.* **1982**, *31*, 1 – 76; b) J. M. Thomas, *Angew. Chem. Int. Ed. Engl.* **1988**, *27*, 1673 – 1691; c) W. F. Holderich, H. van Bekkum, *Stud. Surf. Sci. Catal.* **1991**, *58*, 631 – 726.
[2] M. E. Davis, R. F. Lobo, *Chem. Mater.* **1992**, *4*, 756 – 768.
[3] a) C. T. Kresge, M. E. Leonowicz, W. J. Roth, J. C. Vartuli, J. S. Beck, *Nature* **1992**, *359*, 710 – 712; b) J. S. Beck, J. C. Vartuli, W. J. Roth, M. E. Leonowicz, C. T. Kresge, K. D. Schmitt, C. T.-W. Chu, D. H. Olson, E. W. Sheppard, S. B. McCullen, J. B. Higgins, J. L. Schlenker, *J. Am.*

 © WILEY-VCH Verlag GmbH, D-69451 Weinheim, 1998 1433-7851/98/3705-0666 $ 17.50+.50/0

Chem. Soc. **1992**, *114*, 10834–10843; c) J. S. Beck, J. C. Vartuli, G. J. Kennedy, C. T. Kresge, W. J. Roth, S. E. Schramm, *Chem. Mater.* **1994**, *6*, 1816–1821.

[4] a) A. Monnier, F. Schüth, Q. Huo, D. Kumar, D. I. Margolese, R. S. Maxwell, G. D. Stucky, M. Krishnamurty, P. Petroff, A. Firouzi, M. Janicke, B. F. Chmelka, *Science* **1993**, *261*, 1299–1303; b) Q. Huo, D. I. Margolese, U. Ciesla, P. Feng, T. E. Gier, P. Sieger, R. Leon, P. M. Petroff, F. Schüth, G. D. Stucky, *Nature* **1994**, *368*, 317–321; c) Q. Huo, D. I. Margolese, G. D. Stucky, *Chem. Mater.* **1996**, *8*, 1147–1160.

[5] a) D. M. Antonelli, J. Y. Ying, *Angew. Chem.* **1996**, *108*, 461–464; *Angew. Chem. Int. Ed. Engl.* **1996**, *35*, 426–430; b) D. M. Antonelli, A. Nakahira, J. Y. Ying, *Inorg. Chem.* **1996**, *35*, 3126–3136.

[6] a) D. M. Antonelli, J. Y. Ying, *Chem. Mater.* **1996**, *8*, 874–881; b) *Angew. Chem.* **1995**, *107*, 2202–2206; *Angew. Chem. Int. Ed. Engl.* **1995**, *34*, 2014–2017; c) M. S. Wong, D. M. Antonelli, J. Y. Ying, *Nanostr. Mater.* **1997**, *9*, 165–168; d) D. M. Antonelli, J. Y. Ying, *Curr. Opin. Coll. Interf. Sci.* **1996**, *1*, 523–529.

[7] a) C.-Y. Chen, H. X. Li, M. E. Davis, *Microporous Mater.* **1993**, *2*, 17–26; b) C.-Y. Chen, S. L. Burkette, H. X. Li, M. E. Davis, *ibid.* **1993**, *2*, 27–34.

[8] W. F. Maier, J. A. Martens, S. Klein, J. Heilmann, R. Parton, K. Vercruysse, P. A. Jacobs, *Angew. Chem.* **1996**, *108*, 222–224; *Angew. Chem. Int. Ed. Engl.* **1996**, *35*, 180–182.

Polymers for 193-nm Microlithography: Regioregular 2-Alkoxycarbonylnortricyclene Polymers by Controlled Cyclopolymerization of Bulky Ester Derivatives of Norbornadiene**

Q. Jason Niu and Jean M. J. Fréchet*

The rapid advances in miniaturization of microelectronic devices require that new imageable and etch-resistant polymeric materials be developed for use in 193-nm microlithography. Current research has focused on alicyclic polymers featuring adamantane or norbornane repeating units since such rigid units have been shown to be effective in terms of dry etch resistance.[1, 2] The absence of conjugated double bonds in these alicyclic building blocks is also a favorable feature since the polymers must be transparent at 193 nm. We now report the first synthesis of regioregular, uncross-linked poly(2-alkoxycarbonylnortricyclenes) that may be used for 193-nm microlithography.

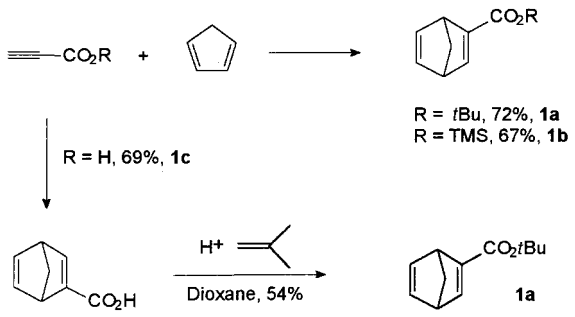
In the early 1980s we described a novel family of chemically amplified resists for deep-UV (248 and 254 nm) microlithography.[3] These resists, which have been used commercially for more than a decade, operate on the basis of acid-catalyzed deprotection of a polymer in a process that renders the final product soluble in aqueous base. The chemistry of these resists is now well understood and has been reviewed recently.[4]

[*] Prof. J. M. J. Fréchet, Dr. Q. J. Niu
Department of Chemistry, University of California at Berkeley
Berkeley, CA 94720-1460 (USA)
Fax: (+1) 510-643-3079
E-mail: frechet@cchem.berkeley.edu

[**] This work was supported by the Office of Naval Research. The authors thank Dr. R. Meagley (UC-Berkeley) and Dr. R. Allen (IBM) for assistance in the imaging experiments performed at IBM Almaden Research Laboratory (San Jose, CA).

Early work by Graham et al. described the free radical polymerization of 2-ethoxycarbonylbicyclo[2.2.1]-2,5-heptadiene to afford an irregular product possessing a structure with more than one repeating nortricyclene-type unit as well as some unsaturated norbornene-type units.[5] As a result of a competing 5,6-directed polymerization, high conversion could not be achieved without gelation of the polymer. Our approach to overcome this problem, while both preserving the high reactivity of the C2–C3 double bond towards free-radical polymerization and introducing an imageable functional group in the side chain of the resulting polymer, is to increase the size of the ester group at the 2-position. This increased steric bulk of the monomer inhibits intermolecular addition at the crowded 2-position while favoring internal cyclopropanation through reaction with the neighboring C5–C6 double bond. As a result, monomers such as 2-*tert*-butoxycarbonylbicyclo[2.2.1]-2,5-heptadiene (**1a**) and 2-trimethylsiloxycarbonyl bicyclo[2.2.1]-2,5-heptadiene (**1b**), which have bulky ester groups, undergo ring-closing cyclopolymerization[6] instead of normal vinyl addition.

The bulky monomers **1a** and **1b** used in the preparation of the regioregular polynortricyclenes were obtained in good yield by Diels–Alder addition of propiolic acid esters to cyclopentadiene (Scheme 1).



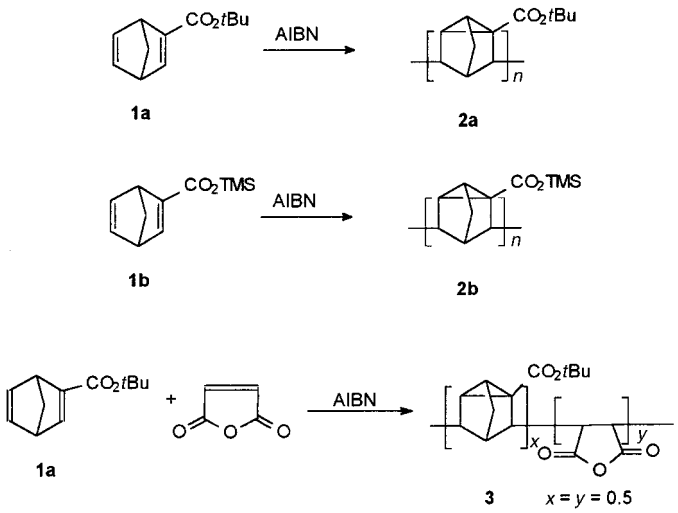
Scheme 1. Synthesis of **1a** and **1b**.

Conversion of the adduct of propiolic acid and cyclopentadiene to the desired *tert*-butyl diene ester is also possible through acid-catalyzed esterification with 2-methylpropene. Monomer **1a** was easily purified by flash chromatography, while monomer **1b** was purified by vacuum distillation. These 2-substituted bicyclo[2.2.1]-2,5-heptadiene derivatives are colorless oils, which slowly polymerize upon extended storage at room temperature but can be stored for months as 10–25% solutions in dichloromethane at $-20^{\circ}C$ under nitrogen. In the presence of oxygen the monomers have a strong tendency to polymerize even at low temperature.

As shown in Scheme 2, the cyclopolymerizations of **1a** and **1b** were carried out using 0.5–2% of azoisobutyronitrile (AIBN) as the free-radical initiator in benzene at $65^{\circ}C$ for 20 hours. A relatively large amount of AIBN (e.g. 2 mol%) is preferred for this polymerization since imaging applications generally require materials having a modest number average molecular weight.[4]

The resulting polymer **2a** was precipitated from methanol, while acetonitrile was used for the precipitation of **2b** to avoid complete loss of the trimethylsilyl protecting groups. All the

 © WILEY-VCH Verlag GmbH, D-69451 Weinheim, 1998 1433-7851/98/3705-0667 $ 17.50+.50/0



Scheme 2. Copolymerization of **1a** and **1b**.

polynortricyclenes that were obtained in 56–75% yield after precipitation and drying (Table 1) could readily be redissolved in most organic solvents including THF, benzene, acetone, chloroform, dichloromethane, and cyclohexane,

Table 1. Cyclopolymerization of **1a** and **1b** with AIBN as free-radical initiator (I).

T [°C]	[M] [wt%]	[I] [mol%]	M_n	M_w	Yield [%]
65	33 (**1a**)	2	15400	29100	56
65	50 (**1a**)	2	26900	59100	71
65	50 (**1a**)	0.5	44100	153500	66
75	50 (**1a**)	2	35000	107800	75
5	100 (**1a**)[a]	0	37200	83800	37
65	50 (**1a**)[b]	2	43500	172200	74
65	50 (**1b**)	2	20700	40800	67
65	50 (**1b**)	2	19500	33700	65

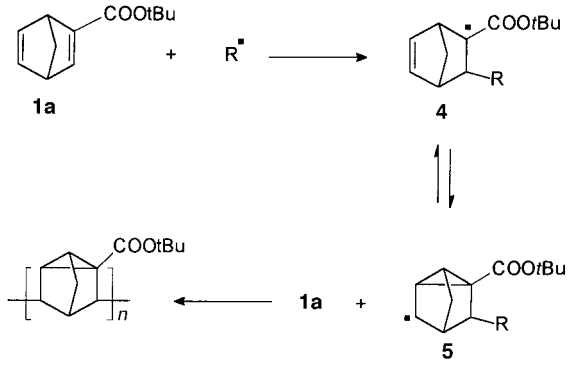
[a] Spontaneous bulk polymerization. [b] Polymerization performed in 2-methylpropanol.

which confirmed the absence of cross-linking. Table 1 also reports the results of a spontaneous polymerization that occurred in the bulk with a sample of monomer kept in a refrigerator for an extended time in the presence of oxygen. Obviously this spontaneous polymerization affords only a low yield of polymer (37%), but the product obtained is also free of cross-linking. The results of GPC analyses in THF are given in Table 1. All of the materials have a polydispersity in the range expected for a free-radical polymerization.

The FTIR spectrum of polymer **2a** displays a peak characteristic of carboxylic esters at 1750 cm^{-1} and no peaks arising from the C=C bond of the monomer (1605 and 1560 cm^{-1}). The ^1H NMR and ^{13}C NMR spectra after polymerization show both the complete disappearance of the vinyl resonances and the appearance of new ^1H NMR resonances centered at $\delta = 1-2$, corresponding to the saturated polymer backbone. The ^{13}C NMR spectrum of polymer **2a** also shows a chemical shift typical for a cyclopropyl carbon at $\delta = 21.4$ (in $CDCl_3$), providing further evidence for the nortricyclene structure. In the case of **2b**, the cyclopropyl carbon signal is seen at $\delta = 22.9$ (in [D_5]pyridine).

Differential scanning calorimetry (DSC) analysis of nortricyclene polymer **2a** shows no glass transition below the temperature of polymer decomposition. Thermogravimetric analysis (TGA) of this polymer shows a large loss in weight below 240°C, corresponding to the loss of the thermally labile *tert*-butyl ester groups. This thermal elimination is key to the ultimate application of polymer **2a** in a chemically amplified resist system.[3, 4, 7] It occurs at a temperature similar to those observed for several tertiary, allylic, and benzylic esters of poly(4-vinyl benzoic acid) used previously as positive/negative tone high-temperature resists for 248- or 254-nm microlithography.[8] In addition, a sudden weight loss of ~7% is observed at about 380°C in the TGA trace of polymer **2a**, which corresponds to the retro-Diels–Alder reaction of the polymer to form carbene and to break the bridge in the polymer backbone. Risse had also observed this phenomenon in the study of the TGA of poly(norbornene).[9] The TGA trace of polymer **2b** shows that this polymer is stable up to 300°C, then slowly decomposes above that temperature.

Bicyclo[2.2.1]-2,5-heptadiene, a model compound of monomers **1a** and **1b**, reacts with a variety of compounds to give the nortricyclene-type products, and formation of the cyclopropyl ring is believed to be the driving force for these reactions.[10] Although Graham et al.[5] had proposed two reaction pathways for the polymerization of 2-ethoxycarbonylbicyclo-[2.2.1]-2,5-heptadiene, our data shows that only one mechanism can account for the polymerization of bulky 2-alkoxycarbonylbicyclo[2.2.1]-2,5-heptadiene monomers (Scheme 3).



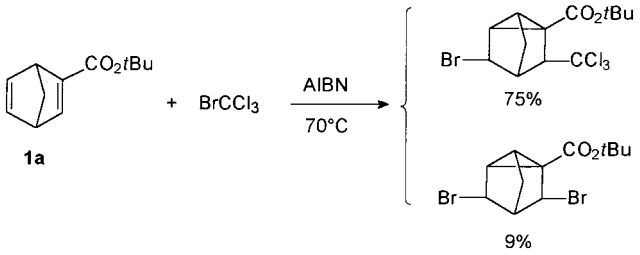
Scheme 3. Mechanism of the free-radical cyclopolymerization of **1a**.

It is apparent that the polymerization of such bicyclo[2.2.1]-2,5-heptadiene monomers requires a suitable substituent (e.g. ester group) to both activate one of the double bonds and provide resonance stabilization for the initially formed radical **4**. Instead of acting as a propagation point for the addition of more monomer, this stabilized free radical can also readily react with the unactivated double bond, which is held in close proximity, in a ring-closing process that affords radical intermediate **5**, which, in turn, serves as the point of propagation. Therefore, in order to facilitate cyclization and simultaneously block 2,3-vinyl addition, which would leave residual double bonds in the growing polymer chain, sufficient steric bulk is required at the 2-position of these bicycloheptadiene systems. Theoretical calculations on intramolecular

 © WILEY-VCH Verlag GmbH, D-69451 Weinheim, 1998 1433-7851/98/3705-0668 $ 17.50+.50/0

ring-closing processes by Gravel et al.[11] have shown that cyclopropanation is a favorable process in activated norbornene structures. In addition, Mathias and co-workers[6] have reported a similar effect in the cyclopolymerization of linear bifunctional acrylate monomers: the bis-*tert*-butyl ester yielded a soluble product, while the corresponding unhindered bis-ethyl esters cross-linked upon polymerization.

Further support for the free-radical addition mechanism involving both double bonds is provided by model studies, in which bromotrichloromethane is added to **1a** under conditions analogous to those employed in the polymerizations. After workup, two nortricyclene derivatives were isolated in 84% total yield (Scheme 4). In contrast, a similar reaction



Scheme 4. Model reaction: addition of $BrCCl_3$ to **1a**.

with 2-ethoxycarbonylbicyclo[2.2.1]-2,5-heptadiene affords a complex mixture of products too numerous to warrant further characterization. These results also indicate that the steric interactions between the *tert*-butoxycarbonyl substituents in this model system favor intramolecular cyclopropanation and thus control the regioselectivity of the final products.

For a preliminary assessment of the value of the nortricyclene moieties for 193-nm imaging, a 1:1 copolymer of **1a** and maleic anhydride was prepared. A solution of copolymer **3** containing a photoacid generator was then imaged with a 193-nm excimer laser to afford the high-resolution images with feature sizes well below 0.20 nm (Figure 1).

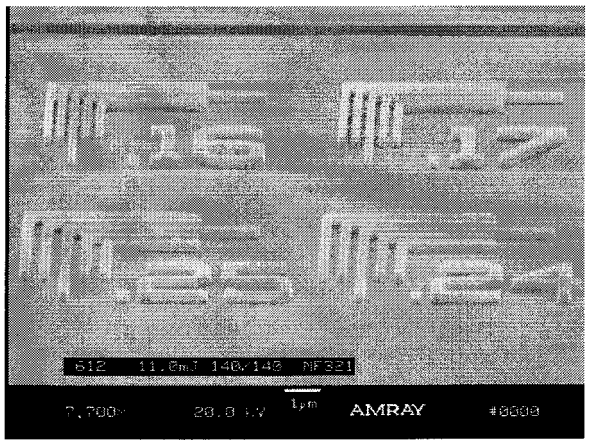


Figure 1. Image obtained with copolymer **3** by exposure to a 193-nm excimer laser and development with aqueous base.

The polymerization of bulky monomers such as 2-alkoxycarbonylbicyclo[2.2.1]-2,5-heptadiene can be accomplished without gelation to afford stable polymers with regioregular nortricyclene repeating backbone units. Polymers containing nortricyclene units derived from **1a** and **1b** or derivatives thereof are being applied successfully in combination with suitable photoacid generators as chemically amplified photoresist materials[7] in state-of-the art 193-nm microlithography.

Experimental Section

1a: Freshly distilled cyclopentadiene (4.0 g, 0.061 mol) was added to *tert*-butyl propiolate[12] (5.0 g , 0.04 mol) in benzene (5.0 g). The reaction mixture was heated to 60°C for 24 h in a sealed tube and cooled to room temperature. After removal of the solvent, the resulting mixture was separated by column chromatography to afford **1a** as a colorless oil (5.56 g , 72%). FTIR (neat): $\tilde{\nu}$ = 3000, 1715, 1605, 1560, 1490, 1465, 1300, 1155 cm^{-1}; ^1H NMR ($CDCl_3$): δ = 7.50 (d, 1H), 6.90 (m, 1H), 6.70 (m, 1H), 3.83 (s, 1H), 3.66 (s, 1H), 2.10 (m, 2H), 1.47 (s, 9H); ^{13}C NMR ($CDCl_3$): δ = 164.3, 154.1, 151.1, 143.7, 141.7, 79.9, 74.2, 51.3, 49.9, 28.1; C,H analysis calcd for $C_{12}H_{16}O_2$: C 74.97, H 8.39; found: C 74.79, H 8.16.

1b: To a solution of trimethylsilyl propiolate[13] (7.5 g, 0.052 mol) in 7.5 g of benzene was added freshly distilled cyclopentadiene (4.2 g, 0.064 mol). The solution was heated at 60°C for 24 h in a sealed tube. After cooling, the reaction mixture was distilled under vacuum to afford 7.2 g (67%) of product, which is moisture sensitive. FTIR (neat): $\tilde{\nu}$ = 2970, 1680, 1595, 1555, 1330, 1295, 1250, 1155, 1055, 855 cm^{-1}; ^1H NMR ($CDCl_3$): δ = 7.59 (d, 1H), 6.91 (m, 1H), 6.71 (m,1H), 3.84 (s, 1H), 3.68 (s, 1H), 2.13 (m, 2H), 0.28 (s, 9H); ^{13}C NMR: δ = 164.9, 156.6, 151.0, 143.8, 141.5, 74.4, 51.5, 49.9, −0.2. C,H analysis calcd for $C_{11}H_{16}SiO_2$, or $(C_{11}H_{16}SiO_2)_n$: C 63.42, H 7.74; found: C 63.49, H 7.90; FAB-MS: *m/z*: 208.093 [M^+] (calcd: 208.092).

Polymerization of **1a**: Freshly purified **1a** (2.0 g, 0.010 mol) was mixed with 2.0 g benzene. After the solution had been purged with nitrogen for 10 min, AIBN (33 mg, 0.00020 mol) was added, and the resulting mixture was heated at 65°C under nitrogen for 20 h. After cooling, the solution was diluted with 5 mL THF and added to methanol (ca. 500 mL). The precipitated polymer was collected by filtration, washed thoroughly with methanol, and then dried under vacuum for 24 h to afford a finely divided, white polymer (1.42 g, 71%). FTIR (KBr): $\tilde{\nu}$ = 3000, 1715, 1485, 1450, 1360, 1165, 1120 cm^{-1}; ^1H NMR ($CDCl_3$): δ = 1.0–2.4 (m, 16H); ^{13}C NMR ($CDCl_3$): δ = 172.5, 79.7, 44.4, 38.9, 32.5, 28.1, 21.4; C,H analysis calcd for $(C_{12}H_{16}O_2)_n$: C 74.97, H 8.39; found: C 75.16, H 8.35.

Polymerization of **1b**: Freshly purified **1b** (2.08 g, 0.010 mol) was mixed with 2.08 g benzene. After the solution had been purged with nitrogen for 10 min, AIBN (33 mg, 0.00020 mol) was added, and the resulting mixture was heated at 65°C under nitrogen for 20 h. After cooling, the solution was diluted with 5 mL THF and added to acetonitrile (ca. 500 mL). The precipitate was filtered and washed through with acetonitrile. It was then dried under vacuum for 24 h to afford a white powder polymer (1.39 g, 67%). FTIR (KBr): $\tilde{\nu}$ = 2960, 1700, 1420, 1255, 1125, 1045, 845 cm^{-1}; ^1H NMR ($CDCl_3$): δ = 1.0–2.4 (m, 7H), 0.3 (s, 9H); ^{13}C NMR ([D_5]pyridine): δ = 176.2, 45.4, 39.1, 33.0, 30.2, 28.5, 22.9, 2.2; C,H analysis calcd for $(C_{11}H_{16}SiO_2)_n$: C 63.42, H 7.74; found: C 63.49, H 7.90. The TMS protecting groups in **2b** can be removed to give the nortricyclene carboxylic acid polymer by simply using methanol as the precipitation solvent.

Copolymer **3**: A mixture of freshly purified monomer **1a** (3.84 g, 0.020 mol) and maleic anhydride (1.96 g, 0.020 mol) in benzene (5.80 g) was purged with nitrogen for 10 min, AIBN (0.131 g, 0.00080 mol) was added, and the mixture was heated at 65°C under nitrogen for 20 h. After cooling, the solution was diluted with 10 mL THF and poured into methanol (ca. 500 mL). The precipitated polymer was collected by filtration, washed with methanol, and dried under vacuum for 24 h to afford 4.88 g (84%) copolymer **3**. GPC (THF, calibrated with polystyrene standards): M_n = 11400; M_w = 21600; IR (KBr): $\tilde{\nu}$ = 2950, 1860, 1785, 1610 cm^{-1}; ^1H NMR ($CDCl_3$): δ = 0.8–3.4 (m, 14H); ^{13}C NMR ($CDCl_3$): δ = 171.4, 81.7, 46.0, 38.9, 31.1, 28.0, 25.9; C,H analysis calcd for 1:1 copolymer: C 66.19, H 6.25; found: C 64.75, H 6.26.

Imaging of copolymer **3**: A solution of 99 wt% **3** and 1 wt% triphenylsulfonium hexafluoroantimonate in propylene glycol methyl ether acetate (12% of solid content) was filtered through a 0.45 μm filter, then spin-coated at 2500 rpm on an antireflection-treated silicon wafer. After heating at 140°C for 1 min, the 0.35-μm thick film was exposed (11 mJ cm^{-2})

 © WILEY-VCH Verlag GmbH, D-69451 Weinheim, 1998 1433-7851/98/3705-0669 $ 17.50+.50/0

through a mask to a 193-nm excimer laser. The wafer was then heated to 140°C for 1 min and developed with 0.52 N aqueous tetramethylammonium hydroxide (0.5 min) to afford the image shown in Figure 1.

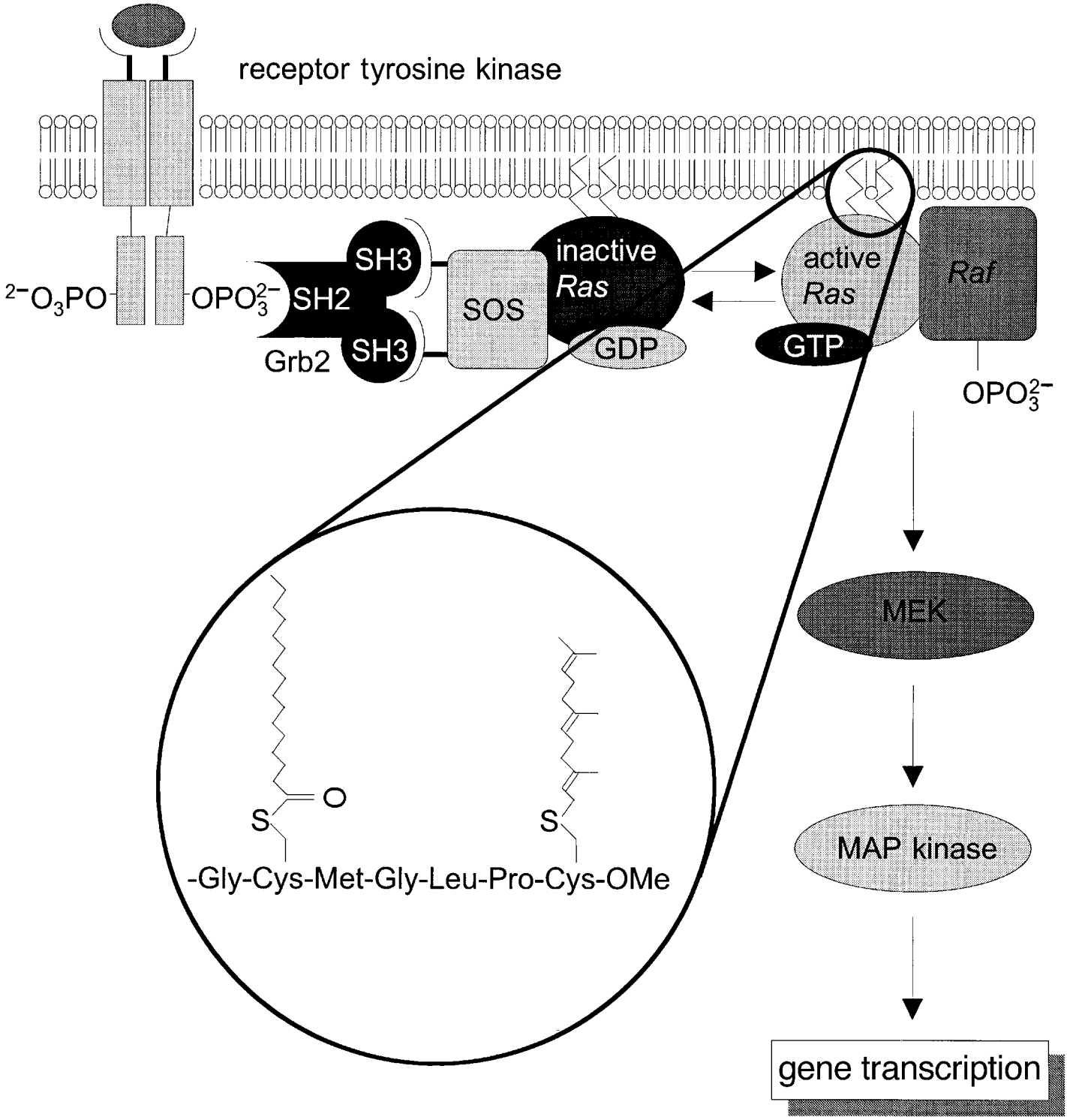
Model reaction: A mixture of **1a** (1.30 g, 0.0068 mole), $BrCCl_3$ (5.38 g, 0.0272 mol), and AIBN (0.022 g, 0.000132 mol) was heated at 70°C for 5 h. After the unreacted $BrCCl_3$ had been removed under vacuum, the residue was separated by flash chromatography to afford two solid products. Major product (1.99 g, 75%): m.p. 105–106°C; FTIR (neat): $\tilde{\nu}$ = 2975, 1705, 1475, 1365, 1315, 1165 cm^{-1}; ^1H NMR ($CDCl_3$): δ = 4.03 (s, 1H), 3.32 (d, 1H), 2.73 (s, 1H), 2.40 (d, 1H), 2.20 (dd, 2H), 2.26 (d,1H), 1.45 (s, 9H); ^{13}C NMR ($CDCl_3$): δ = 166.2, 98.8, 81.7, 63.3, 51.6, 46.3, 36.5, 33.9, 28.2, 28.0, 22.7; C,H analysis calcd for $C_{13}H_{16}BrCl_3O_2$: C 39.98, H 4.13; found: C 40.04, H 4.29. Minor product (0.22 g, 9%): m.p. 77–79°C; IR (neat): $\tilde{\nu}$ = 3005, 1715, 1485, 1375, 1295, 1165 cm^{-1}; ^1H NMR ($CDCl_3$): δ = 4.01 (s, 1H), 3.96 (s, 1H), 2.67 (s, 1H), 2.26 (m. 4H), 1.46 (s, 9H); ^{13}C NMR ($CDCl_3$): δ = 168.9, 81.7, 63.9, 53.0, 46.3, 34.6, 34.3, 29.5, 28.0, 25.0; C,H analysis calcd for $C_{12}H_{16}Br_2O_2$: C 40.94, H 4.58; found: C 40.75, H 4.66.

Received: June 16, 1997 [Z 10553 IE]
German version: *Angew. Chem.* **1998**, *110*, 685–688

Keywords: microlithography · photoresists · polymerizations

[1] K. Nakano, K. Maeda, S. Iwasa, J. Yano, Y. Ogura, E. Hasegawa, *Proc. SPIE Int. Soc. Opt. Eng.* **1994**, *2155*, 194.
[2] R. D. Allen, R. Sooriyakumaran, J. Opitz, G. W. Wallraff, R. A. Dipietro, G. Breyta, D. C. Hofer, R. Kunz, U. Okoroanyanwu, C. G. Willson, *Proc. SPIE Int. Soc. Opt. Eng.* **1996**, *2724*, 334, and references therein.
[3] J. M. J. Fréchet, E. Eichler, H. Ito, C. G. Willson, *Polymer* **1983**, 24, 995; USA 4,491,628, **1985**; J. M. J. Fréchet, H. Ito, C. G. Willson, *Proc. Microcircuit Eng.* **1982**, 260; C. G. Willson, H. Ito, J. M. J. Fréchet, T. G. Tessier, F. M. Houlihan, *J. Electrochem. Soc.* **1986**, 133, 181.
[4] S. A. MacDonald, C. G. Willson, J. M. J. Fréchet, *Acc. Chem. Res.* **1994**, *27*, 151.
[5] P. J. Graham, E. I. Buhle, N. J. Pappas, *J. Org. Chem.* **1961**, *26*, 4658.
[6] L. J. Mathias, R. M. Warren, S. Huang, *Macromolecules* **1991**, *24*, 2036; L. J. Mathias, T. Tsuda, *ibid.* **1993**, *26*, 4734.
[7] J. M. J. Fréchet, Q. J. Niu, patents pending, assigned to Cornell Research Foundation, Ithaca, NY 14853.
[8] H. Ito, C. G. Willson, J. M. J. Fréchet, *Proc. SPIE Int. Soc. Opt. Eng.* **1987**, *771*, 24.
[9] W. Risse, C. Mehler, *Macromol. Symp.* **1995**, *89*, 433.
[10] *Chem. Eng. News* **1957**, *35*(7), 23.
[11] R. W. Denis, J. R. Rancourt, E. Ghiro, F. Boutonnet, D. Gravel, *Tetrahedron Lett.* **1993**, *34*, 209.
[12] F. Sondheimer, N. Stjernstriom, D. Rosenthal, *J. Org. Chem.* **1959**, *24*, 1280.
[13] H. H. Hergott, G. Simchen, *Synthesis*, **1980**, 626.

 © WILEY-VCH Verlag GmbH, D-69451 Weinheim, 1998 1433-7851/98/3705-0670 $ 17.50+.50/0



Biological signal transduction regulates important cellular functions such as growth, differentiation, and metabolism. In recent years much progress has been made in the investigation of individual signal pathways. Synthesis of partial structures of proteins involved in signal transduction and other biologically active compounds has helped to elucidate important interactions in molecular detail and to achieve a better understanding of these processes.

ANGEWANDTE CHEMIE © WILEY-VCH

Organic Synthesis and Biological Signal Transduction

Klaus Hinterding, Daniel Alonso-Díaz, and Herbert Waldmann*

Dedicated to Professor Dieter Seebach on the occasion of his 60th birthday

Today, many biological phenomena are being investigated and understood in molecular detail, and organic chemistry is increasingly directed towards biological phenomena. Thus, the field of "bioorganic chemistry", which encompasses both biological and chemical research, has developed at the border between these two disciplines. The interplay of organic chemistry and biology will be illustrated in this review with biological signal transduction as an example. For signal transmission through tyrosine kinase receptors and the Ras protein and through G protein coupled receptors, it will be shown how, starting from a biological phenomenon, structural information can be obtained that leads to the development of new chemical methods and syntheses, and subsequently to new reagents for biological studies. In particular, bioorganic research on protein tyrosine kinases, interactions with SH2 and SH3 domains, protein farnesyltransferase, applications of peptide conjugates and inositol phosphate derivatives, protein kinases A and C, protein phosphatases, and ligand-induced dimerization of proteins will be presented.

Keywords: bioorganic chemistry · enzyme inhibitors · peptide conjugates · signal transduction · synthetic methods

What interests us all is finding that deep current—in my case, the most rational understanding of life: its reduction to the molecular details of chemistry.
A. Kornberg[1]

My idea is that chemistry is the central science. Everything that goes on in biology or medicine has a chemical basis.
R. Lerner[2]

1. Introduction

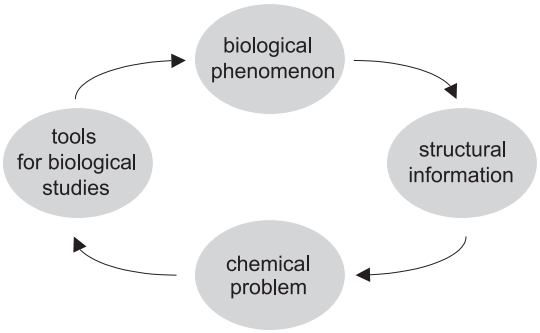
Biological processes are based on chemical reactions and depend on the structure and interactions of the molecules involved. In principle, all biological processes can be reduced to chemical ones: biology is molecular.[3] This insight has influenced current biological research, especially in recent years. Today, many biological phenomena are being investigated and understood in molecular detail, and the increasingly important field of structural biology[4] is becoming more prominent on the horizon of organic chemistry. Just as the dimensions of objects studied in biology have become smaller, organic chemistry has turned increasingly to larger molecules and systems. Owing to the high performance of organic synthesis today, even the most complicated of these natural and active compounds that are recognized as biologically relevant can be synthesized, and noncovalent interactions between large natural molecules that determine processes such as protein–protein and protein–DNA interactions and recognition phenomena at cell surfaces are the focus of "supramolecular chemistry". As the kinds and dimensions of the subjects of biological and organic chemical research have become more similar, these sciences have begun to permeate one another and a growing interdisciplinary field has been established at their interface: "bioorganic chemistry".

Although this term has been used for some time,[5] it still does not have a clear, firm definition (and there is not necessarily a need for this). In our opinion, a "bioorganic chemist" performs active research in chemistry *and* (!) biology[6]: he or she unites the "two cultures of chemistry and biology".[7] However, the emphasis of the research may lie on the chemical or biological side and can, for example, focus on the application of methods and tools of organic chemistry to study biological problems or the use of biological techniques to address chemical problems. These nuances can be more precisely expressed by the terms "chemical biology" and "biological chemistry".

One possible scenario for successful combination of biological and organic chemical research is illustrated in Scheme 1. Here, a well-known biological phenomenon is analyzed for the structures of the molecules involved; these

[*] Prof. Dr. H. Waldmann, Dr. K. Hinterding, Dr. D. Alonso-Díaz
Institut für Organische Chemie der Universität
Richard-Willstätter-Allee 2, D-76128 Karlsruhe (Germany)
Fax: (+49) 721-608-4825
E-mail: waldmann@ochhades.chemie.uni-karlsruhe.de

 © WILEY-VCH Verlag GmbH, D-69451 Weinheim, 1998 1433-7851/98/3706-0689 $ 17.50+.50/0



Scheme 1. Possible cooperation between organic synthesis and biology in "bioorganic chemistry".

may be active compounds or biomacromolecules of low molecular weight. Based on this structural information, unsolved synthesis problems are identified and tackled. This is true innovation in the field of organic synthesis. Once these problems have been conquered, the methods and syntheses developed are used to build up new reagents for studying the biological phenomenon under consideration; these are subsequently used in biological experiments. In the ideal case, these reagents are used to glean new knowledge which could not have been obtained (or only with great difficulty) with classical biological techniques. New structural information is derived from this new knowledge foundation, and the cycle of bioorganic research as outlined above starts over again.

In this review the successful interlocking of biological and organic chemical research according to the scenario above will be presented with "biological signal transduction" as an example of current relevance.

2. Biological Signal Transduction[8, 9]

For multicellular organisms to maintain functional and survival capacity, growth, differentiation, and metabolism of a large number of cells must be coordinated by synthesis, secretion, and recognition of signal molecules, sometimes over relatively large distances. Once the signal has been conveyed through the plasma membrane of the target cell, the message is relayed to the cell interior by intracellular signal cascades, and a reaction is triggered. According to their physical characteristics, extracellular signal substances (hormones) are recognized by receptors in the cell interior (lipophilic hormones which can diffuse through the plasma membrane, e.g. steroids and thyroid hormone) or they are bound to receptors on the cell surface (hydrophilic hormones which cannot pass through the cell membrane by diffusion, e.g. peptide hormones and small charged molecules such as adrenaline and histamine).[10] Finally, the signal is switched off and the reaction of the cell to the signal substance ends. The activity of the latter class of hormones and associated signal mediation has been the subject of particularly intensive


H. Waldmann


D. Alonso-Díaz


K. Hinterding

Herbert Waldmann, born in 1957, studied chemistry at the Universität Mainz (Germany) and finished his Ph.D. there in 1985 with Horst Kunz. After a postdoc at Harvard University with George Whitesides, he returned to the Universität Mainz in 1986 and finished his habilitation in 1991. From 1991 to 1993 he was Professor of organic chemistry at the Universität Bonn, and then became Full Professor (Chair) of organic chemistry at the Universität Karlruhe. He has been awarded, among others, the Friedrich-Weygand-Preis, a stipend from the Fonds der Chemischen Industrie, and the Carl-Duisberg-Preis from the Gesellschaft Deutscher Chemiker. His research covers many areas such as diastereo- and enantioselective synthesis, the chemistry of peptides, carbohydrates, and alkaloids, and the use of enzymes in organic chemistry. A main theme of this current work is the combination of methods from organic chemistry with biological techniques, in particular for the synthesis and application of new reagents and tools to study biological questions such as the control of signal transduction pathways.

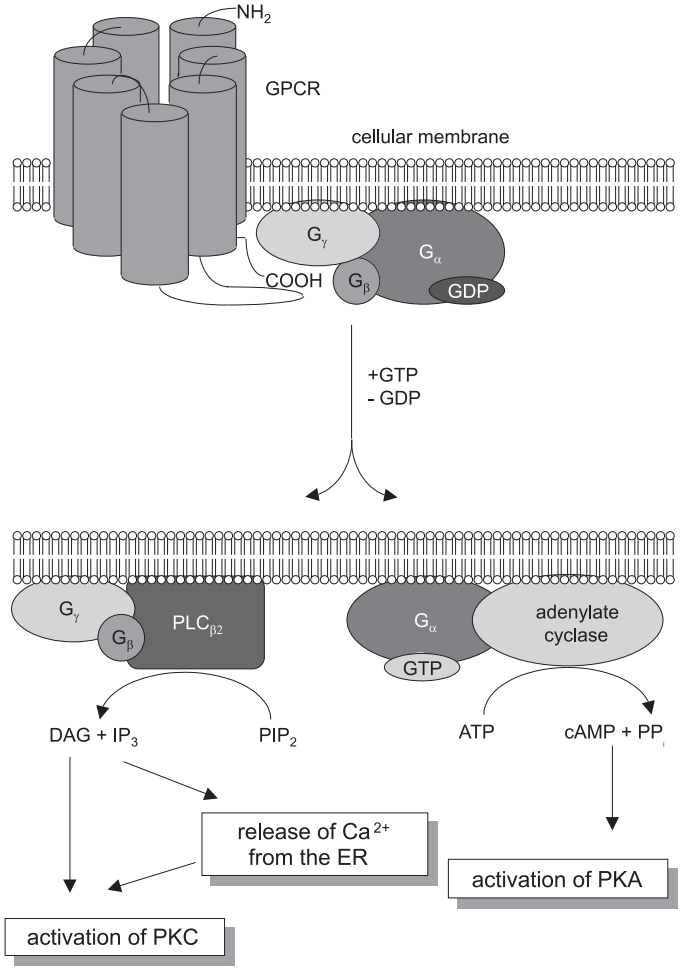
Daniel Alonso-Díaz, born in 1960 in Sabadell (Barcelona, Spain), studied chemistry at the Universidad Autónoma de Barcelona, where he finished his Ph.D. in 1991 on the synthesis of natural products. Afterwards, he conducted research in the pharmaceutical industry and coordinated a Eureka project of the European Union. In 1995 he joined the group of H. Waldmann as a postdoc with a Marie Curie fellowship, where he worked on the total synthesis of biologically active molecules.

Klaus Hinterding, born in 1969 in Neuenkirchen (Germany), studied chemistry between 1989 and 1991 in Freiburg. After a one-year stay at the University of Edinburgh (UK), where he worked on the synthesis of ruthenium and osmium clusters in the group of B. F. G. Johnson, he finished his Diplom in chemistry in 1994 with H. Waldmann in Karlsruhe. He completed his Ph.D. in 1997 on the synthesis of inhibitors for cellular signal transduction processes.

bioorganic research. The knowledge obtained from this work is the central theme of this review.[11] In the following sections the most important intracellular signal cascades relevant to this class of hormones, for which the mode of action has been adequately explained at the cellular and molecular level, are outlined.

2.1. Signal Transduction through G Protein Coupled Receptors and Heterotrimeric G Proteins [8, 9, 12–24]

Many hormonal messengers—for example, adrenaline, noradrenaline, glucagon, corticotropin, luteinizing hormone, and follicle-stimulating hormone—and also signals associated with senses such as taste,[23] smell, and vision[24] are recognized at the cell surface by G protein coupled receptors[12] (GCPRs) made up of seven transmembrane helices (Scheme 2). An

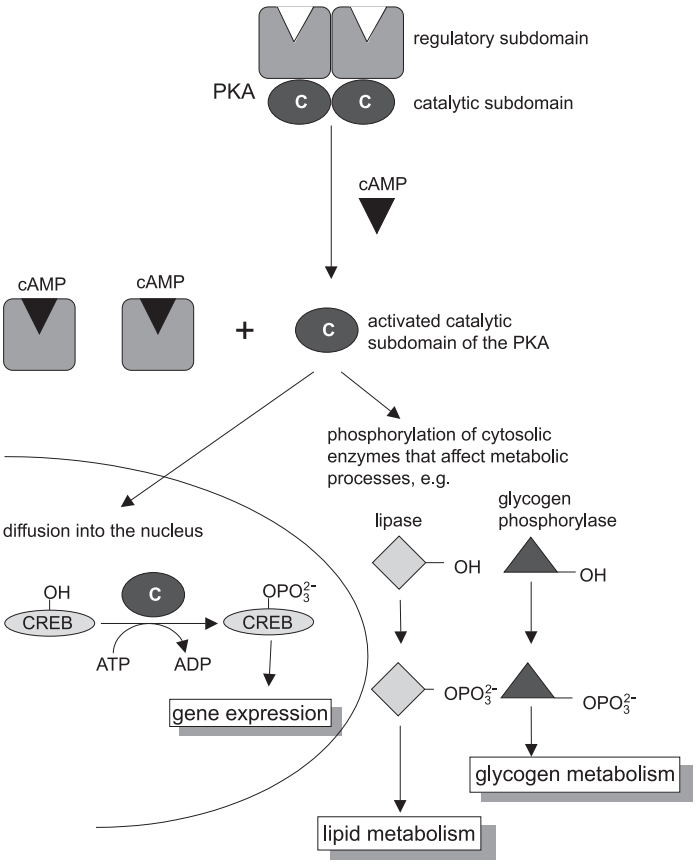


Scheme 2. Formation of "second messengers" in signal transduction through G protein coupled receptors and heterotrimeric G proteins.

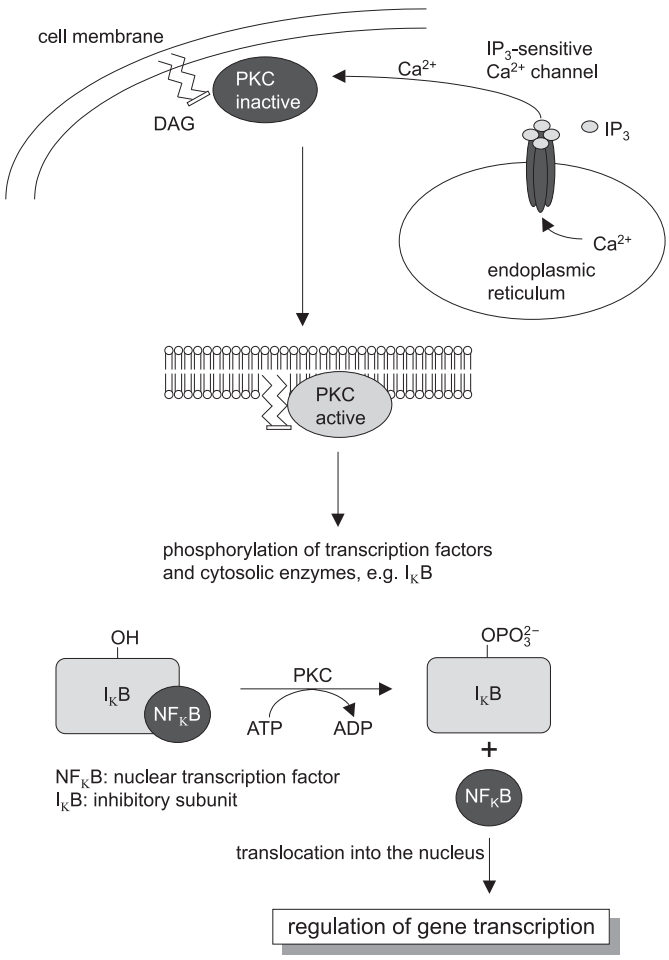
intracellular loop between helices 5 and 6 and the C terminus of the receptor, which is also cytosolic, interact with a heterotrimeric guanine nucleotide binding protein (G protein) located in the membrane. G proteins are made up of three different subunits (G_α, G_β, G_γ),[13–15] of which the α unit has a bound GDP molecule in the inactive form. As a consequence of the interaction with the receptor, GDP is exchanged for GTP on the α unit and the heterotrimeric complex dissociates into G_α/GTP and G_β/G_γ. This activation of the G protein by nucleotide exchange and dissociation is followed by hydrolysis of GTP to GDP and renewed formation of the inactive (but available for reactivation) GDP-binding heterotrimeric complex; thus, the signal is switched off. Before the signal is cancelled, however, G_α/GTP and G_β/G_γ trigger various intracellular signal cascades. If this complicated mechanism is disturbed by external agents, it results in serious complications, both for the cells involved and for the whole organism. For example, cholera toxin brings about a permanent binding of GTP to the α unit of a particular G protein (G_s) and thus continous stimulation of adenylate cyclase, which leads to massive diarrhea. On the other hand, pertussis toxin, which causes whooping cough, inactivates the α unit of the G_0 protein and inhibits stimulation of phospholipase C.

Depending on the heterotrimeric complex from which it is released, G_α/GTP can have a stimulatory ($G_{s\alpha}$) or inhibitory ($G_{i\alpha}$) effect on adenylate cyclase, an enzyme also located in the plasma membrane that catalyzes cyclization of ATP to cyclo-AMP (cAMP) when stimulated (see Scheme 2). This "second messenger" then activates cAMP-dependent protein kinases of Group A (PKA)[16] by releasing their catalytic subunits from an inactive tetrameric complex. According to cell type, PKA then activates various enzymes by phosphorylating them at serine or threonine residues. In liver and muscle cells, for example, activation of PKA takes place when adrenaline binds to the relevant G protein coupled receptors, and leads to degradation of glycogen to glucose 1-phosphate, that is, to mobilization of glucose from the depot form (Scheme 3). In fat-storing adipocytes, an enzyme cascade triggered by adrenaline results in release of fatty acids (Scheme 3). Binding of corticotropin to a G_s-coupled receptor stimulates biosynthesis of steroid hormones, such as cortisol, in the cells of the adrenal cortex. In ovarian cells, the follicle-stimulating hormone triggers increased biosynthesis of estradiol and progesterone, which are needed for expression of female sexual characteristics. In addition, protein kinase A can diffuse into the cell nucleus and stimulate transcription factors, which subsequently activate expression of many genes.

The G_β/G_γ complex (and also G_α) activates the membrane-bound phospholipase $C_{\beta 2}$ ($PLC_{\beta 2}$), which cleaves the plasma membrane lipid phosphatidylinositol 4,5-bisphosphate (PIP_2) to diacylglycerol (DAG) and inositol 1,4,5-trisphosphate (IP_3). These substances act as second messengers.[17–19] IP_3 diffuses through the cytosol once it has been released, and is bound by a specific receptor on the endoplasmic reticulum (ER) that opens a channel allowing Ca^{2+} ions to flow from the ER into the cytosol (Scheme 4). Ca^{2+} now functions as a further second messenger that is needed, for example, for activation of protein kinases. DAG remains in the plasma membrane where it binds, together with Ca^{2+} ions and phosphatidylserine, to a class of serine/threonine protein kinases of Group C (PKC; Scheme 4).[20–22] These molecules, which are inactive in



Scheme 3. Activation of protein kinase A and subsequent signal transmission to cytosolic enzymes and transcription factors. CREB = cAMP response element binding protein.



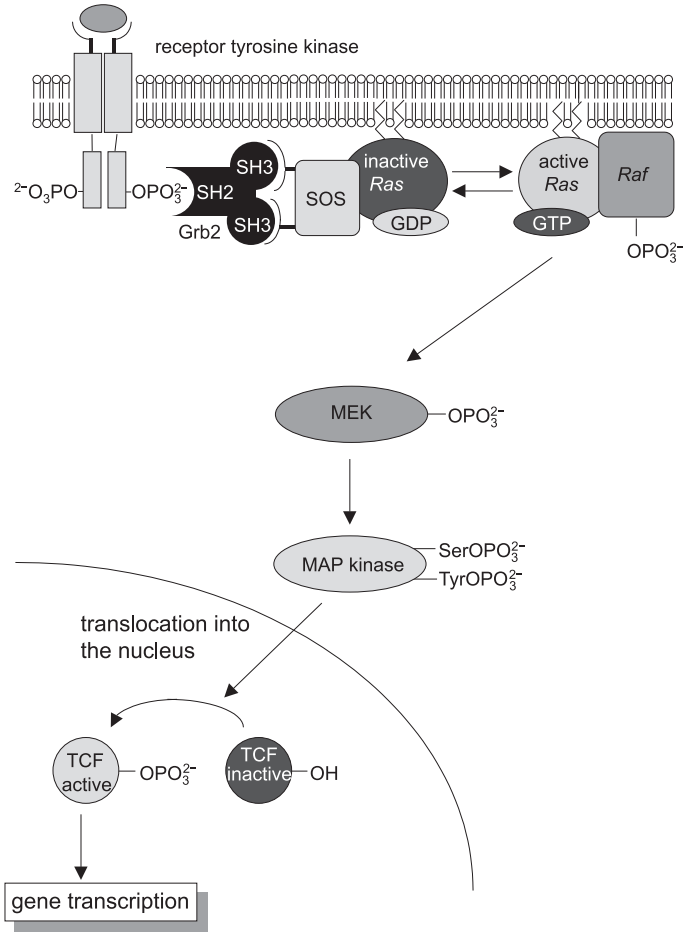
Scheme 4. Activation of protein kinase C by the IP_3/DAG signal pathway and subsequent activation of the transcription factor $NF_\kappa B$.

their cytosolic form, phosphorylate other enzymes after membrane localization, and thus influence a multitude of cell reactions. It is especially relevant that PKC also phosphorylates transcription factors and can thus, according to cell type, induce or suppress the synthesis of particular mRNA molecules. Threrefore, protein kinase C plays an important role in the regulation of cell growth, and it follows that a defective PKC function can lead to misregulated growth and ultimately transformation of the cell (see Section 2.5).

2.2. Signal Transduction through Receptor Tyrosine Kinases and Nonreceptor Tyrosine Kinases—The Ras/MAP Kinase Signal Transduction Cascade[9, 25–33]

Many of the polypeptide hormones that influence cell proliferation and differentiation bind to cell-surface receptors which have tyrosine kinase activity (receptor tyrosine kinases, RTKs). These include the receptors for the epidermal growth factor (EGF), the insulin-like growth factor 1 (IGF-1), the nerve growth factor (NGF) and the platelet-derived growth factor (PDGF), which influence growth, differentiation, and division of epidermal, endothelial, and epithelial cells (EGF), sensory and sympathetic neurons (NGF), and cells of the connective tissue, granulocytes, and the nervous system (PDGF).

The receptor tyrosine kinases, which are monomeric in the active form, are made up of an extracellular binding domain, a single membrane-spanning α helix, and a cytosolic domain with tyrosine kinase activity. On binding an extracellular ligand, the receptors dimerize and the kinase domain of one receptor molecule recognizes and phosphorylates tyrosine residues of the other monomeric unit (Scheme 5). The phosphorylated receptors are subsequently recognized by adaptor molecules, which are not signal molecules themselves but serve to bind the receptor to signal molecules. Of particular importance is the growth factor receptor binding protein 2 (Grb2); this binds, with the help of a SH2 domain (SH2 = sarcoma homology 2), to the peptide sequence of the receptor in which the phosphotyrosine is located. Grb2 also contains two SH3 domains that recognize proline-rich sequences in another adaptor protein, Sos (son of sevenless, named after a Drosophila mutant; Scheme 5). Thus, the cytosolic proteins Grb2 and Sos are localized on the inner side of the cell membrane and correctly aligned. Sos then interacts with the inactive, GDP-binding form of the protein Ras (from rat sarcoma) located in the membrane. Ras exchanges GDP for GTP following interaction with the Grb2/Sos complex, which acts as a kind of "molecular glue"; Grb2/Sos functions as a guanine nucleotide exchange factor (GEF). This activates Ras, which then acts as a molecular switch and diverts the signal arriving from the tyrosine kinase receptor by non-



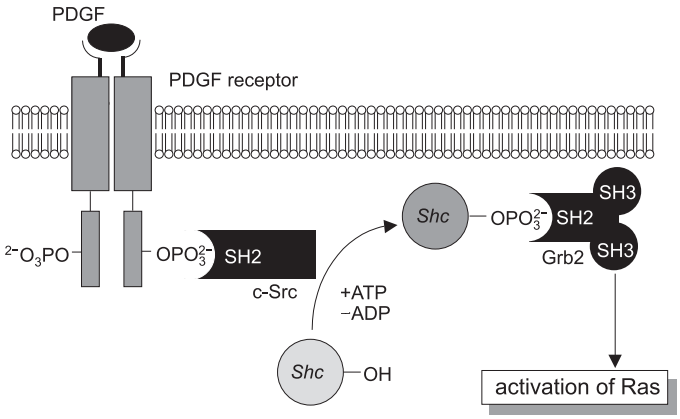
Scheme 5. Signal transduction by the Ras/MAP kinase cascade.

covalent protein – protein interactions to a cascade of protein phosphorylations and into the cell interior (Scheme 5). Ras has weak GTPase activity that hydrolyzes the bound GTP to GDP and thereby terminates the signal. This process is also accelerated by the GAP protein (GTPase-activating protein).

The activated, GTP-binding form of Ras binds to the N terminus of the serine/threonine kinase Raf and localizes Raf (analogous to immobilization of Sos to Grb2) on the plasma membrane. With its C terminus, Raf now binds the protein kinase MAP kinase kinase (MAP = mitogen activated protein)—also known as MEK (from MAP and ERK, extracellular signal regulated kinase)—and phosphorylates it. This activated MEK has tyrosine and serine/threonine kinase activity (dual specificity kinase) and phosphorylates the protein MAP kinase, which is also a serine/threonine-specific kinase. The activated MAP kinase now phosphorylates and activates other kinases, such as the ribosomal S6 kinase; it also diffuses into the cell nucleus and phosphorylates transcription factors there, for example the ternary complex factor (TCF, also known as Elk-1) and the Jun protein, which are thereby activated and stimulate expression of the corresponding genes.

In some cases, the Ras/MAP kinase cascade and the GPCR signal pathway influence the expression of the same gene. In this manner, many genes can be expressed very rapidly by a concerted interlocking of various signal chains. Another way for signal chains to mutually influence each other is the activation of elements of one cascade by members of another (cross talk). PKC and other serine/threonine kinases can phosphorylate MEK and other members of the Ras cascade,[30] and thus establish a cross-link between the GPCR signal pathway and the Ras cascade. Diverse further examples of cross talk are known between various signal cascades (see Section 3.2 and Scheme 12).[30]

Nonreceptor tyrosine kinases (NRTKs)[34]—that is, tyrosine kinases located on the cytosolic side of the plasma membrane without an extracellular domain—can also switch on the Ras cascade.[17, 31] This is how, through a SH2 domain, the NRTK c-Src recognizes the autophosphorylated, and thereby activated, PDGF receptor,[35] which itself has no Grb2 binding site (Scheme 6). c-Src phosphorylates the adaptor protein Shc



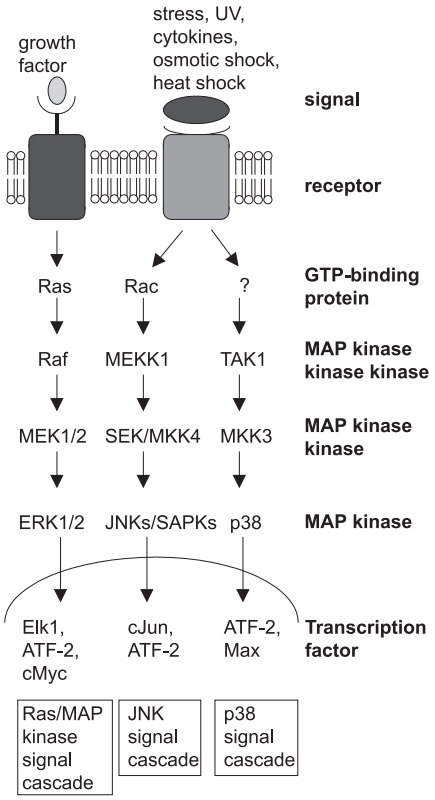
Scheme 6. Activation of the Ras signal cascade by nonreceptor tyrosine kinases (e.g., c-Src).

on a tyrosine residue and thus creates a binding site for the Grb2/Sos complex, which subsequently activates Ras (see above) and passes on the signal.

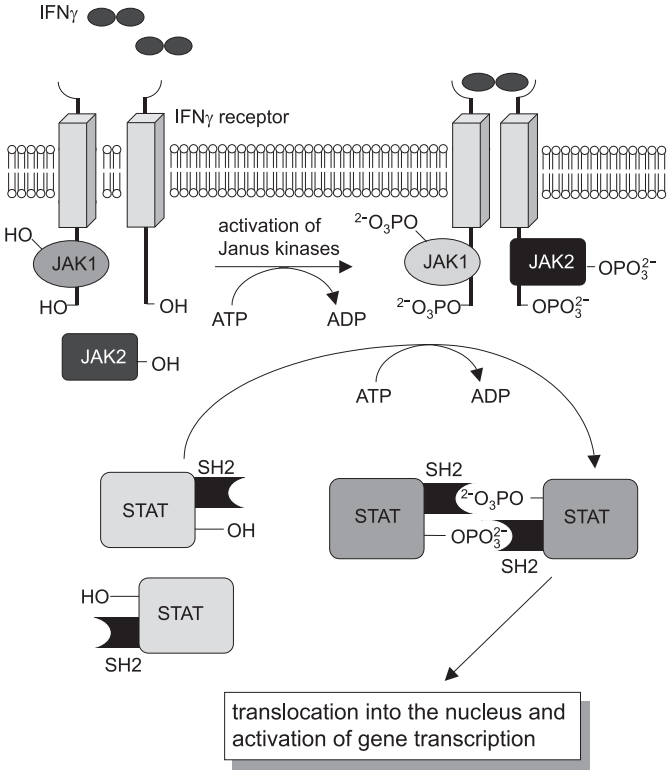
The Ras signal transduction cascade is of extreme physiological importance. It is central to the regulation of cell growth and differentiation, and a mistake in regulating this signal pathway can be one of the critical steps for cell transformation (see Section 2.5). The Ras path is highly conserved in different species,[9, 25–27] and its elements are used in the same way for transmission of growth signals in, for example, yeast, worms, flies, and mammals. Furthermore, it was recently shown that in mammalian cells there are at least three more signal transduction pathways, based on the same scheme as the Ras pathway, which conduct different extracellular signals to the cell nucleus (Scheme 7).[30] This includes, for example, information on stress due to UV light and ionizing radiation, alkylating reagents, osmotic and heat shock, and signals from inflammatory cytokines (see Section 2.3) such as the tumor necrosis factor α (TNF-α) and interleukin 1 (IL – 1).

2.3. Signal Transduction through Janus Kinases and STAT Molecules[9, 36, 37]

A very important pathway for signal transduction in which protein phosphorylation and protein – protein interactions



Scheme 7. Common elements of signal transduction cascades that are activated by growth factors, inflammatory cytokines, genotoxic reagents, and stress factors.



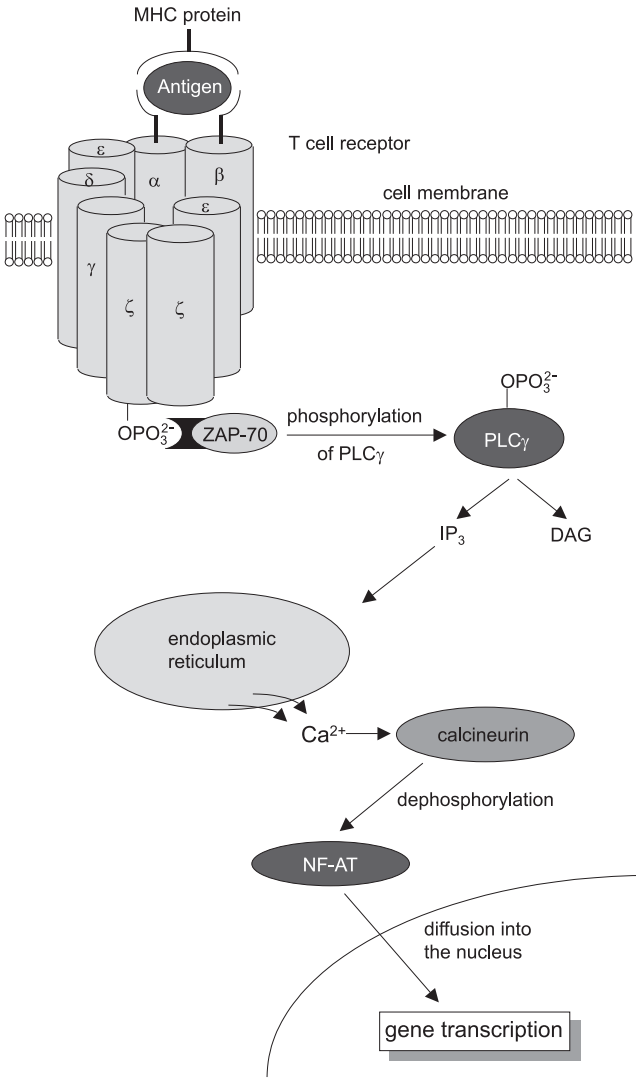
Scheme 8. The JAK/STAT signal transduction cascade. INFγ = interferon γ.

through SH2 domains (see Section 2.2) play a decisive role is for passing on signals triggered by cytokines. Cytokines are soluble proteins that influence growth, differentiation, and function of a variety of cells; they include, for example, interferons α, β, and γ as well as interleukins 2 to 7, 9 to 12, and 15. For example, the interferons are formed in, and secreted by, animal cells following a virus infection. When an interferon binds to plasma-membrane receptors on the target cell, cell growth is inhibited and synthesis is induced of proteins which give the target cell viral resistance.

When a cytokine binds to its receptor, the receptor dimerizes and leads to activation of Janus kinases (JAK or "just another kinase"), a class of tyrosine kinases that are noncovalently associated with the cytosolic domain of the receptor (Scheme 8). The JAK kinases then phosphorylate the receptor itself as well as the STATs (signal transducers and activators of transcription) that subsequently bind to it. On activation, these latent cytosolic transcription factors form homodimeric and heterodimeric complexes that migrate into the cell nucleus and induce transcription of cytokine-dependent genes there.

2.4. Signal Transduction through the T Cell Receptor[38–40]

The signal pathway starting from the T cell receptor (TCR) is essential for maintenance of the T cell dependent cellular immune response; this pathway uses the same transmission mechanism as the signal cascades previously described. On activation of the receptor by an antigen, the T cell first undergoes the transition from the G_0 phase to the G_1 phase; that is, it leaves the resting phase and prepares for cell division.[38] The complex T cell receptors are composed of eight noncovalently bound membrane-spanning subunits (α, β, γ, δ, ε_2, ζ_2). As soon as a macrophage presents an antigen fragment to the receptor through the proteins of the major histocompatibility complex (MHC proteins), the fragment is recognized and bound by the α and β subunits, and the eight individual strands aggregate (Scheme 9). The cytoplasmic domains are brought into spatial proximity and phosphorylated on tyrosine residues by an associated kinase (Lck or Fyn, kinases of the Src family). In particular, phosphorylation of the ζ subunit creates a binding site for the SH2 domain of the protein kinase ZAP-70. This kinase phosphorylates and activates phospholipase C_γ (PLC_γ), which releases inositol trisphosphate (see Section 2.1). This second messenger brings about the release of calcium ion from the endoplasmic reticulum into the cytosol, leading to activation of calcineurin, a Ca^{2+}-dependent Ser/Thr-specific protein phosphatase. Calcineurin now dephosphorylates the cytoplasmic part of the transcription factor NF-AT (nuclear factor of activated T cells), which migrates to the cell nucleus and directs transcription of certain genes responsible for the further correct course of the immune response.[39] As a result, the T cell expresses both the growth factor interleukin 2 (IL-2), which is released into the intracellular space, and also its receptor (IL-2-R), which is anchored in the plasma membrane as a transmembrane protein. This self-stimulation of the T cell



Scheme 9. Signal transduction by the T cell receptor.

(autocrine stimulation) brings about the transition from the G_1 phase to the S phase of the cell cycle and thus leads to division and multiplication of precisely the T cell that recognized the originally presented antigen (clonal selection).

This simple picture of T cell activation can be extended to include the overlap with other signal pathways (cross talk). IP_3 is also released by the GPCR signal pathway (see Section 2.1), and the tyrosine phosphorylated TCR can bind to the SH2 domain of certain adaptor proteins and is thereby linked to the Ras signal path.

2.5. Signal Transduction and Transformation of Cells[41, 42]

The influence of signal transduction cascades on the regulation of cell growth, division, and differentiation is of great importance. In normal cell growth, the interactions of the individual components of the signal cascades are precisely coordinated with one another. However, if a fault occurs in the regulation of an important signal cascade, the cell may be transformed; that is, its growth characteristics are changed and it can develop into a tumor cell. Transformation of a cell can be triggered by various mechanisms (e.g. by DNA-damaging chemical carcinogens), however, one of the most common causes is formation of an oncoprotein (i.e. the product of an oncogene, or cancer gene). Oncogenes are generally derived from normal cell genes responsible for controlling cell growth (protooncogenes), for example, by mutation, or incorrect or misregulated expression. Growth is mostly controlled by growth factors, their receptors, intracellular signal transducers, nuclear transcription factors and cell cycle control proteins. Most oncogenes code for proteins belonging to one of these five classes, whereby representatives of classes 1 – 4 are important elements of the signal transduction cascades described above.

Relatively few oncogenes are derived from genes for growth factors. Genes for growth factor receptors with tyrosine kinase activity can become oncogenes if, on mutation, they code for receptors with kinase activity that stay switched on in the absence of the respective ligand. However, in most cases, oncogenes of this class code for truncated receptors in which the extracellular ligand-binding domain is missing. The oncogene gives a permanent growth signal in both cases.

Most oncogenes derive from genes for proteins involved in intracellular signal transduction cascades. For example, mutations in the $G_{s\alpha}$ subunit of heterotrimeric G proteins (see Scheme 2) bring about loss of GTPase activity of these proteins, which results in continuous stimulation of cAMP synthesis. Therefore, pituitary cells with a mutated $G_{s\alpha}$ protein grow in an uncontrolled fashion owing to the resulting high levels of cAMP, and pituitary gland tumors develop. Similarly, mutations in *ras* genes mean that the Ras protein can no longer be converted from the active, GTP-binding state into the inactive GDP-binding form (see Scheme 5). Consequently, these highly conserved switches emit a permanent growth signal that can lead to tumor formation. Mutations in *ras* genes are found in many human tumors.

Mutations in genes for nonreceptor tyrosine kinases can also lead to oncogene formation. The kinase activity and therefore the signal transducing effect of Src (see Scheme 6) can be significantly reduced by phosphorylation of a tyrosine residue at the C terminus. If this phosphorylation site is altered (for example, in Rous sarcoma virus, the last 18 amino acids of the C terminus of Src are missing due to a deletion on the *src* gene), this possibility for regulation is absent and a permanent signal results. Activation of the transforming potential of the Raf serine/threonine kinase (see Scheme 5) also occurs by deletion of regulatory subunits of the normal cellular protein. The C terminus of Raf contains the kinase subunit, whereas the N terminus has two domains that are modulated by the kinase activity. These regulatory domains

are deleted in *raf* oncogenes, and the catalytically active C terminus of the enzyme functions in an uncontrolled manner. Oncogenes coding for nuclear transcription factors often manifest themselves by creating oncoproteins which change the transcription frequency of genes, for example, those coding for growth-stimulating proteins.

A class of oncogenes of great importance for the cell cycle code for tumor suppressors.[43, 44] These proteins monitor the operation of the cell cycle and prevent formation of tumors by arresting cells in the resting phase or even by inducing programmed cell death.[45, 46] If mutations occur in tumor suppressor genes, the cell cycle is no longer properly regulated and mutations accumulate.

The transforming effect of chemical compounds recognized as tumor promoters also arises because of their influence on signal transduction cascades. Whereas normal chemical carcinogens, such as alkylating reagents and polycyclic hydrocarbons, damage the DNA directly (tumor initiators), tumor promoters increase the probability of tumor formation by a tumor initiator. Phorbol esters and teleocidins belong to the tumor promoters. These substances activate protein kinase C by imitating the effect of diacyl glycerol (see Scheme 4).

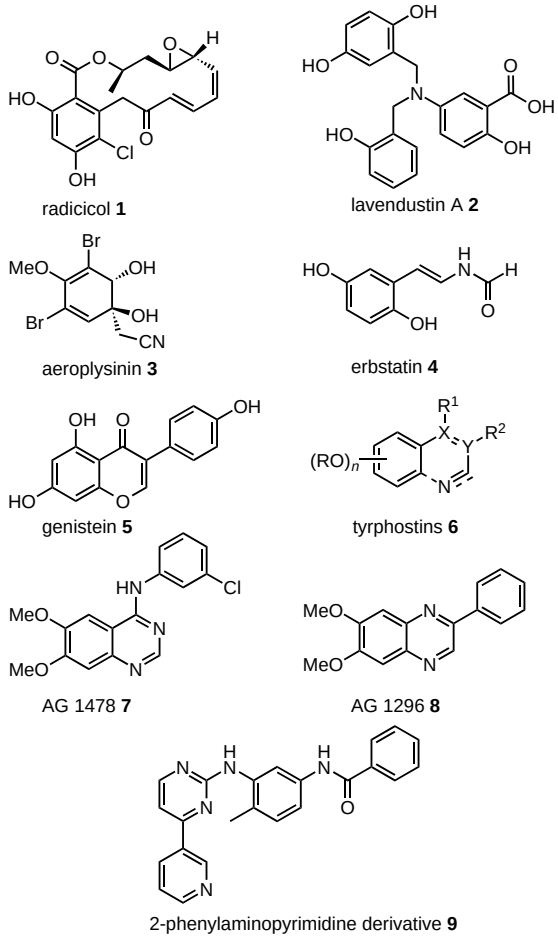
According to our current knowledge, carcinogenesis is generally triggered by several factors in a multistep process; cancer arises due to many effects acting together over a longer period of time. A single oncogene is usually not able to induce malignant growth by itself; different oncogenes must complement each other's activity. Human tumor cells embody several oncogenes, and probably several genetic changes (about four or five) would have to accumulate in a single cell for it to be transformed. Some mutations are particularly prominent because they attack at important points in the regulation of cell growth, division, and differentiation. In about 50% of all human tumors, mutations are found in the gene that codes for the tumor suppressor p53, which is therefore the most commonly occurring oncogene. Of almost equal importance is the *ras* oncogene which is mutated in about 40% of all human tumors. In some of the main types of cancer—such as cancer of the bowel, breast, or pancreas—the mutation rate of the *ras* oncogene is as high as about 80%.

Our understanding of intracellular signal transduction at the molecular level, and selective manipulation of these processes based on such knowledge, opens up fundamental new opportunities for study, and possibly also therapy, of malignant transformations. The rather apt expression "signal transduction therapy" was coined by A. Levitski for this new direction in "molecular medicine".[47]

3. Inhibition of Protein Tyrosine Kinases (PTKs)

PTKs play an important role in cellular signal transduction and the correct course of many genetic programs—for example, in the Ras signal cascade, the Jak/Stat signal pathway, and the TCR signal pathway (see Section 2.2, 2.3, and 2.4, respectively)—and half of all proto-oncogenes discovered so far code for proteins with PTK activity.[48] There is therefore an intensive search underway for selective inhibitors of PTKs.[49]

Such substances would enable selective interruption of the signal transduction cascades and branching of various signal paths to gain a better understanding of the molecular sequence of signal transmission. Furthermore, they could provide ways to treat diseases associated with abnormal PTK activity, such as cancer, psoriasis, restenosis, or septic shock.[49a] Examples of natural products with PTK-inhibiting activity are radicicol (**1**),[50] lavendustin A (**2**),[51] aeroplysinin (**3**),[52] erbstatin (**4**),[53] and genistein (**5**)[54] (Scheme 10).



Scheme 10. Structure of some natural products and synthetic compounds with PTK-inhibitory activity.

Owing to their interesting pharmacological profiles, these substances have already found various uses in biological research. However, the most potent of the currently available inhibitors originate from the synthetic laboratory.

With increasing knowledge of the structure of various PTKs (the primary structures are known for many different PTKs and show high homology in the catalytic domain;[55] furthermore, X-ray structures have been solved for the insulin receptor,[56] c-Src,[57] and some Ser/Thr kinases[58]) and derivation of important structural characteristics of enzyme inhibitors, it has been possible to make significant progress in the development of active and selective inhibitors in recent years. The assumption that it is practically impossible to produce selective ATP-competitive inhibitors (since the ATP binding sites of all PTKs, and even all kinases, share a high structural similarity) has been completely disproved. The

most active and selective inhibitors of the EGF receptor known to date and the PDGF receptor bind reversibly at the ATP binding site.

In the following sections, some examples of natural products with PTK-inhibitory activity and of synthetic inhibitors will be presented.

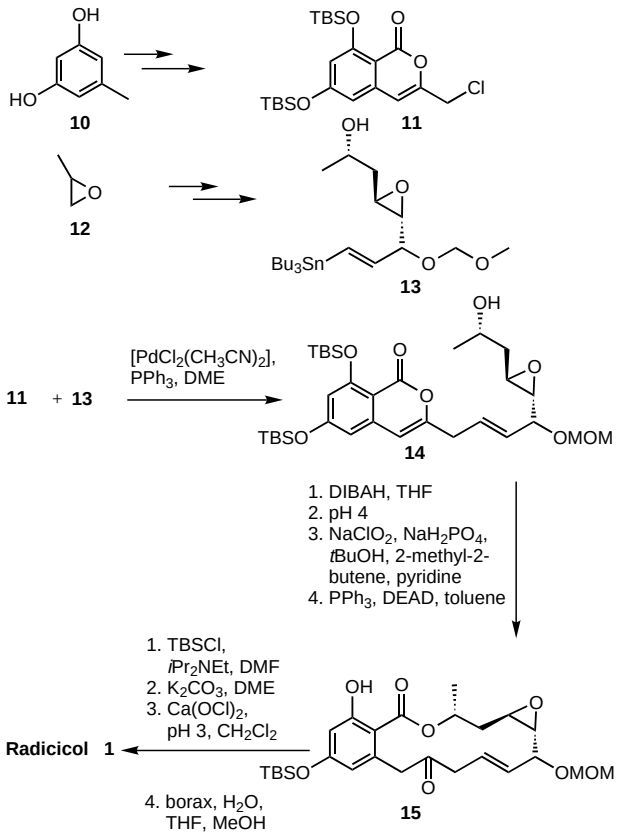
3.1. Radicicol

Radicicol (**1**, Scheme 10), a metabolite of the microparasite *Monocillium nordinii*,[59] shows a variety of biological activities (fungistatic, antitumor activity, PTK inhibitor). Since the natural product is difficult to isolate, the development of an efficient total synthesis provides the opportunity to produce enough material for biological and medical studies and to obtain analogues with altered biological properties.

Particular challenges for the synthesis are construction of the 14-membered macrolactone and a conjugated dienone epoxide unit with an *E* and a *Z* double bond. Based on molecular modeling experiments and the prediction that an established (*E*,*Z*)-dienone epoxide unit would hardly survive the conditions needed for a macrolactonization, the *Z* double bond was created by elimination following successful cyclization of the precursor **15** (Scheme 11) in the only total synthesis[60] published so far. Macrocycle **15** was retrosynthetically converted back into the isocoumarin derivate **14**, which was synthesized by palladium-catalyzed coupling of arene **11** and the vinyl stannane **13**, which contains all the stereogenic centers.

The isocoumarin derivate **11** was synthesized in eleven steps (total yield 31 %) starting from orcinol (**10**). After the free hydroxyl functionality was protected, a further substituent was introduced by a Friedel–Crafts acylation and, following elaboration of the *ortho* methyl group, it was cyclized to **11**.

In the case of the vinyl stannane **13**, particular attention must be paid to the absolute configuration of the three sterocenters: Whereas the two C atoms of the epoxide unit must be *R*-configured, the configuration of the hydroxy-substituted stereocenter must be variable according to whether the acyl functionality (with retention of stereochemistry) or the hydroxyl functionality (with inversion of configuration under S_N2 conditions) should be activated for the macrolactonization. The absolute configuration of the secondary alcohols can be adjusted as needed by nucleophilic opening of enantiomerically pure propylene oxide with lithiated propargyl alcohol that is protected at the hydroxyl functionality. The key steps of the subsequent synthesis were a stereospecific reduction of the acetylene to an (*E*)-allyl alcohol, a Sharpless epoxidation, and the extension of the carbon skeleton with a vinyl stannane. In a palladium-catalyzed Stille reaction, fragments **11** and **13** were coupled to isocoumarin **14**; following release of the ketocarboxylic acid by reduction with DIBAH and reoxidation (the silyl ether group ortho to the carboxyl functionality was selectively cleaved) the macrocycle was closed under Mitsunobu conditions (→**15**). The synthesis was finished with elimination of the MOM acetal, chlorination of the arene under mild conditions, and removal of the silyl protecting group.



Scheme 11. Synthesis of radicicol (**1**). DEAD = diethylazo dicarboxylate, DIBAH = diisobutylammonium hydride, MOM = methoxymethyl, TBS = *tert*-butyldimethylsilyl.

In addition to its activity as an antifungal antibiotic[59] and a tranquilizer,[61] radicicol was examined with particular intensity for its selective and potent PTK-inhibitory activity.[50] In an in vitro assay, the natural product inhibited autophosphorylation of the v-Src tyrosine kinase and phosphorylation of an exogenous substrate with an IC_{50} value of 0.1 $\mu g\,ml^{-1}$. In contrast, the serine/threonine kinases PKA and PKC were only inhibited by much higher concentrations of radicicol. Since the natural product also reduced the degree of phosphorylation of the v-Src kinase in vivo, it was possible to perform experiments on rat fibroblasts transformed by v-Src (SR-3Y1-2 cells); in these cells, radicicol converted the transformed phenotype back into the normal form and arrested the cells in the G_1 and G_2 phase of the cell cycle. When treatment with the macrolide was stopped, the fibroblasts adopted the form of the transformed species again. Since the specificity of activity in vivo was not lost, the morphology of cells transformed by c-*erb-B2* could also be normalized (c-*erb-B2* codes for a mutated, and thus permanently activated, receptor tyrosine kinase), whereas this did not occur with cells transformed by *v-raf-1* (*v-raf-1* codes for a serine/threonine kinase, see Section 2.2). By cultivating Friend leukemia cells in the presence of a low dose of radicicol, it was also demonstrated that phosphorylation and dephosphorylation at tyrosine residues play an important role in the differentation of cells: The fraction of differentiated cells that accumulated hemoglobin increased with increasing concentration of radicicol.

Investigations of structure–activity relationships (SAR), previously only performed for the antifungal activity of the natural product, showed that the biological activity decreased on modification of the macrocyclic ring, particularly of the epoxide function, whereas substitution of the aromatic ring had no influence on activity. Inhibition of the proliferation of HeLa cells, and thus antitumor activity of radicicol, was drastically increased by acylation of the phenolic OH group with stearic and palmitic acid as well as by conversion into an ether.[62] Even though initial investigations show that the PTK-inhibitory activity of radicicol disappears in the presence of reagents that can reduce the epoxide unit, such as dithiothreitol, further research in this area is overdue.

3.2. Tyrphostins

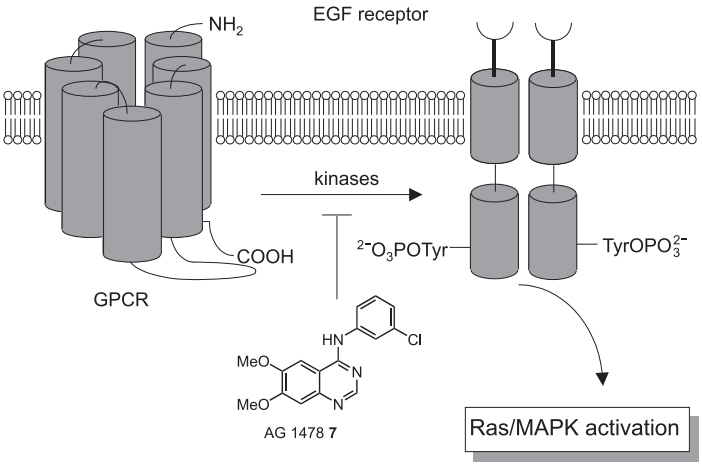
Tyrphostins **6** are particularly well-investigated synthetic PTK inhibitors whose structures are derived from those of erbstatin and tyrosine; they include compounds AG 1478 (**7**) and AG 1296 (**8**, Scheme 10).[49a, b, e] Several hundred representatives of this class of compounds, which are based on a donor-substituted styrene skeleton, have been synthesized and tested for their activity on a large number of kinases.

The majority of the PTK inhibitors found in this way had IC_{50} values in the low micromolar range; however, inhibitors of the newer generation (e.g., **7** and **8**) are often more active by three to four orders of magnitude and are also exceptionally specific for individual receptor subtypes.[49b, e] Tyrphostins are used, for example, to inhibit tumor growth,[63] to reverse transformation of cells,[64] to initiate cell differentiation,[65] to inhibit thrombin-induced platelet aggregation,[66] to inhibit activation of B cells,[67] T cells,[68] and other cell types, to stop growth of psoriatic keratinocytes,[69] and to protect experimental animals from lipopolysaccharide-induced septic shock.[70] In most cases, the molecular target of the inhibitor was precisely determined and, thus, its involvement in the cellular functions described could be demonstrated. These examples show the great potential of synthetic PTK inhibitors as potential medication for diseases such as cancer, restenosis, psoriasis, and sepsis. An interesting finding in these experiments was that, in certain cases, the active compound had to regulate not just a single kinase but rather a broad spectrum of enzymes to achieve the desired pharmaceutical effect.

Beyond the pharmaceutical interest, active and selective PTK inhibitors are also important for research into signal transduction mechanisms. For example, tyrphostin AG 1478 (**7**),[71] which is a highly selective inhibitor of autophosphorylation of the EGF receptor, was used to show that activation of the EGF receptor induced by UV light or strong oxidizing agents, such as H_2O_2, is caused by inhibition of phosphatases that serve to deactivate the receptor again.[72] Similar results were obtained ′with the equally specific tyrphostin AG 1296 (**8**) and the PDGF receptor.[73]

Kinases of the Src family play an important role in the development and progression of tumors, as demonstrated in particular for breast and colon cancer.[74] A 431 cells, which undergo constitutive autophosphorylation of the EGF receptor by autocrine secretion of TGFα (transforming growth factor α), display a tenfold increased activity of the Src kinase in comparison to other cells. It was possible to show that these phenomena are connected, since complete blocking of autophosphorylation of the EGF receptor upon addition of tyrphostin **7** also led to disappearance of the Src activity.[75] Thus, it was demonstrated that increased autophosphorylation of the EGF receptor can be responsible for overactivity of the Src kinase.

Whereas the individual steps of activation of the Ras/MAPK signal path by receptor tyrosine kinases are well understood (see Section 2.2), the activation of this kinase by GPCRs has not yet been explained. It was demonstrated in Rat-1 cells that receptor tyrosine kinases such as the EGF receptor can act as mediators of the mitogenic signals of the G protein coupled receptors; an intracellular crossover of the signal pathways takes place independent of the ligand (in this case, EGF; Scheme 12).[76] If rat fibroblasts are stimulated



Scheme 12. "Cross talk" between G protein coupled receptors and the EGF receptor. MAPK = MAP kinase.

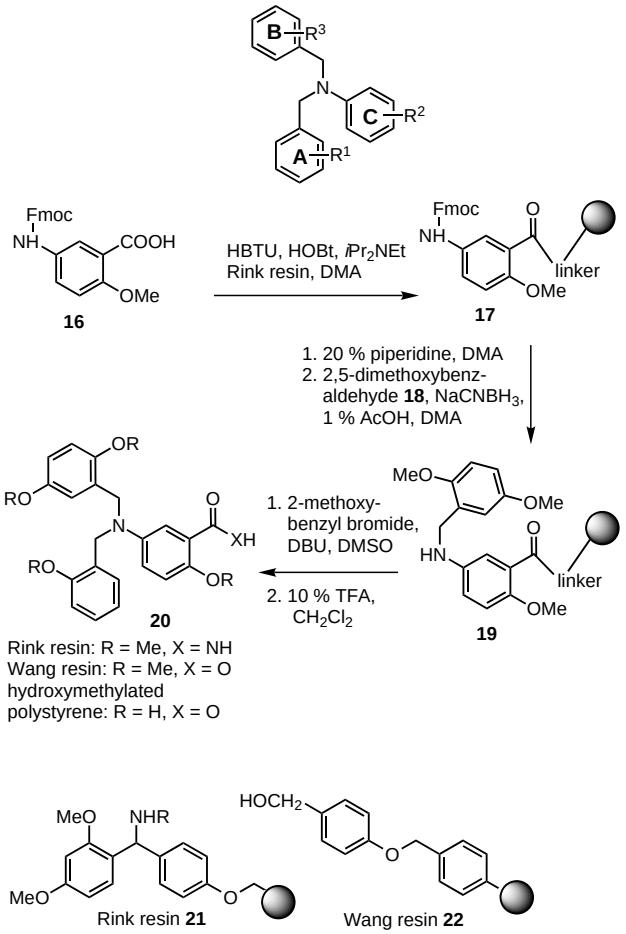
with GPCR agonists such as endothelin 1, lysophosphatidic acid, or thrombin, the receptor for epidermal growth factor is rapidly phosphorylated. If this covalent modification is blocked by addition of the tyrphostin **7** or by transfecting a dominant negative EGF-R mutant into the rat cells, synthesis of the DNA is interrupted and growth is thus stopped. These results give a clear example for crossover of different signal pathways and for the manner in which a membrane receptor, the GPCR, can intracellularly use the activity of another receptor, the EGF-R, without the action of its ligand, EGF. Furthermore, this investigation demonstrates the potential of the use of rapid, effective, and selective in vivo protein tyrosine kinase inhibitors to obtain biological knowledge.

3.3. Lavendustin A and Analogues

An elegant and promising alternative for creation of many potential inhibitors in the shortest time possible is the use of combinatorial chemistry.[77] The natural product lavendustin A (**2**) selectively inhibits the protein tyrosine kinase activity of the EGF receptor, whereas it only has a weak

effect on the activity of the cAMP-dependent kinases PKA or PKC.[78] Detailed kinetic studies show that the substance competes with ATP and peptide substrate, and it reduces the binding affinity of the kinase for both substrates significantly. From these observations, it was concluded that lavendustin A binds to the kinase domain, but outside the binding site for ATP and the peptide. As a target structure for the creation of analogues with modified biological activity by combinatorial synthesis, the substance has ideal properties: The basic skeleton can be assembled from three aromatic units by simple and effective reactions, and it can be bound to a solid phase through the phenolic functionalities or the carboxylic acid.[79]

For the combinatorial synthesis of 60 lavendustin A analogues, four benzyl bromides (**A**), five benzaldehydes (**B**), and three aromatic amino acids (**C**) were used; Rink resin (**21**), Wang resin (**22**), and hydroxymethylated polystyrene were used as polymers (Scheme 13). The Fmoc-protected amino



Scheme 13. Combinatorial synthesis of lavendustin A analogues. DBU = diazabicyclo[5.4.0]undec-7-ene, DMA = *N*,*N*-dimethylacetamide, DMSO = dimethyl sulfoxide, Fmoc = 9-fluorenylmethoxycarbonyl, HBTU = *O*-(benzotriazol-1-yl)-*N*,*N*,*N*′,*N*′-tetramethyluronium hexafluorophosphate, HOBt = 1-hydroxy-1*H*-benzotriazol. The solid support polystyrene is represented by a sphere; for the linker, see **21** and **22**.

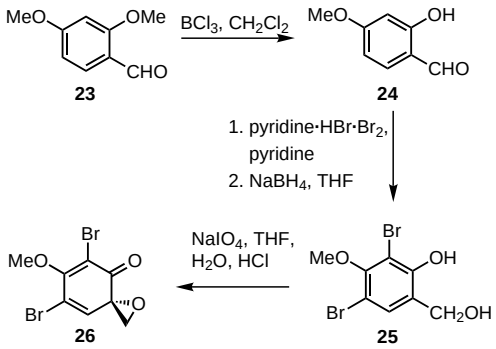
acids **16** (Fmoc = fluorenylmethoxycarbonyl) were first bound to the solid phase through the carboxy functionality (→**17**) and then N-deblocked by treatment with piperidine. Reductive amination with benzaldehydes (e.g. **18**) in the presence of sodium cyanoborohydride led to secondary amines **19**, which were then benzylated in a further step. On cleaving the target molecule from the polymeric phase under acidic (10 % TFA for the Rink resin, 50 % TFA for the Wang resin) or Lewis acid conditions (BBr_3 for hydroxymethylated polystyrene), the individual compounds were obtained protected at the hydroxyl functionality and in the free form. The yields were between 10 and 76 %; the purity was between 30 and 97 %.

3.4. 2-Phenylaminopyrimidine Inhibitors

Recently, 2-phenylaminopyrimidine derivatives were reported to be potent tyrosine kinase inhibitors.[80] By selective variation of the structure and the resulting preferred conformation, it was possible to obtain the highly potent and selective PGDF receptor inhibitor **9** (Scheme 10). Since the substance efficiently penetrates living cells, both autophosphorylation of the receptor and phosphorylation of other substrates were inhibited in vivo. Whereas the inhibitor has no effect on signal transduction stimulated by EGF, insulin, IGF-1, fibroblast growth factor, and phorbol ester, it did block PDGF-induced expression of the c-Fos mRNA in BALB/c 3T3 cells. Based on these findings, it was possible to block proliferation of cells that overexpress the oncogene *v-sis* (v-Sis is a PDGF receptor with a mutation in the transmembrane domain) and that grow due to autocrine PDGF production; the growth of cells transformed by EGF, IL3, and H-Ras was only inhibited by significantly higher concentrations of inhibitor. By feeding **9** to mice in which tumor cells transformed by *v-sis* and *c-sis* had been implanted, it was possible to demonstrate antitumor activity: The degree of tumor reduction was dependent on the dose administered.[81]

3.5. Aeroplysinin

Aeroplysinin (**3**) is a marine natural product which has been isolated in both enantiomeric forms from the sponges *Aplysina aerophoba*[82] and *Ianthella ardis*;[83] it has a highly substituted cyclohexadiene skeleton with two stereocenters. Of its many biological characteristics in addition to its antibiotic activity, its ability to inhibit phosphorylation of exogenous substrates of the EGF receptor in vitro and its antitumor effect on EGF receptor dependent cell lines have attracted attention.[52] However, attempts to investigate the activity of the natural product on autophosphorylation of the EGF receptor in vivo showed that application of the substance did not bring about any change in the phosphotyrosine content of cells.[84] This finding was explained by the high polarity of the *trans* diol unit, which makes it difficult for the substance to penetrate the lipophilic cell membrane. For this reason the more hydrophobic analogue **26** was synthesized (Scheme 14): It has much structural similarity with aeroplysinin, but instead of the diol function it embodies a less hydrophilic epoxyketone unit. This unit also has the advantage that it can be attacked by nucleophiles in the catalytic

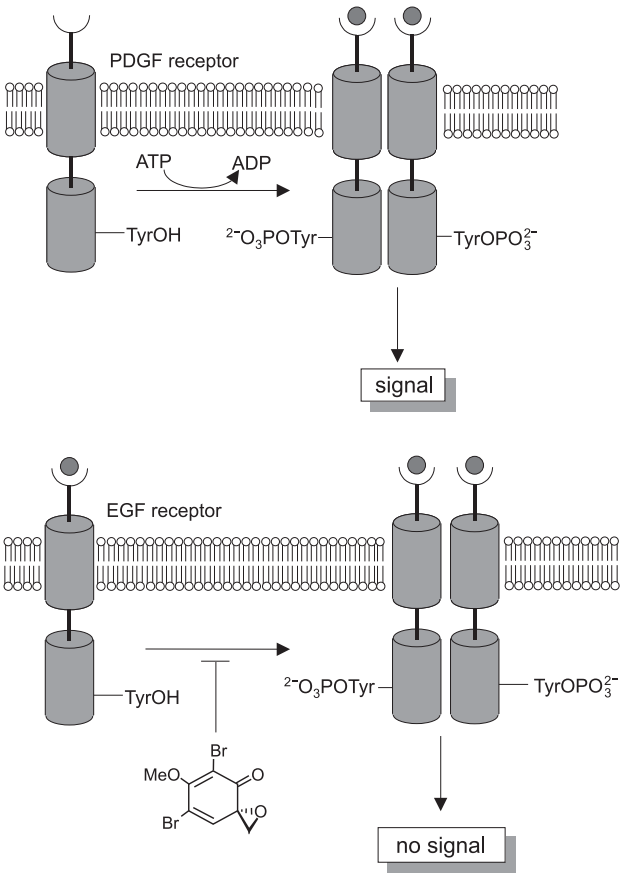


Scheme 14. Synthesis of the biologically active aeroplysinin analogue **26**.

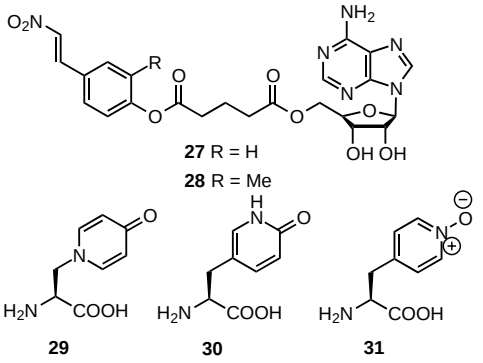
domain of the enzyme, enabling covalent modification, and thus irreversible inhibition, of the tyrosine kinase receptor. Analogue **26** was synthesized in four steps, starting from 2,5-dimethoxybenzaldehyde (**23**), by regioselective cleavage of a methyl ether, bromination, reduction to *ortho*-hydroxybenzyl alcohol, and subsequent Becker-Adler oxidation (total yield 50 %, Scheme 14).

The effect of **26** on autophosphorylation of the EGF receptor was investigated in immortalized rat cells which overexpress the human EGF receptor. The enzyme was inhibited with an IC_{50} value of 10 μM after only five minutes of incubation, whereas autophosphorylation of the PDGF receptor was not blocked, even at a tenfold higher concentration (100 μM, Scheme 15). By synthesis of further structurally related compounds, it was possible to show that the lipophilic bromine atoms and an electrophilic functional group are essential for this rapid in vivo activity. In addition, the epoxide function is opened and an unexpected rearomatization of the system takes place on reaction of **26** with nucleophiles, which supports the above-mentioned hypothesis of a possible covalent modification of the enzyme. The potent and selective activity of this synthetic inhibitor, which occurs almost directly after application of the substance, can now be used to selectively disrupt signals stimulated by EGF.

This is a particularly clear example of how organic synthesis and biological findings can be mutually fruitful: The (biological) observation of the lack of in vivo activity of a natural product leads to rational design and synthesis of an active inhibitor that can now be used in further biological and pharmaceutical experiments.



Scheme 15. Selective blocking of signal transduction by the EGF receptor with the synthetic aeroplysinin analogue **26**, which has no effect on the PDGF receptor (see text for details).



Scheme 16. Bisubstrate analogues and tyrosine mimetics.

3.6. Other Inhibitors

In another interesting experiment, putative bisubstrate analogues were synthesized based on the probable transition state for phosphate transfer from ATP to tyrosine residues.[85] Compounds **27** and **28** contain a nitrostyrene residue as a tyrosine mimetic, which is separated by an alkyl spacer from a glutaryl-adenosine unit that mimicks an ATP molecule (Scheme 16). Compounds **27** and **28** inhibited the EGF receptor with an IC_{50} value of less than 1 mM and also showed significant subtype selectivity for the PTKs v-*Abl* and c-*Src* and also for the Ser/Thr kinase PKC. In an in vivo system with strongly EGF-dependent epidermal murine keratinocytes, these compounds also demonstrated potent antiproliferative activity.

In addition, some publications describe attempts to obtain potent and specific inhibitors of certain tyrosine kinases by incorporating a modified tyrosine derivative in a substrate peptide of the particular kinase. Examples of tyrosine mimetics that should react irreversibly with nucleophilic side chains at the active center of the enzyme are L-3-deoxymimosine (**29**),[86] the pyridone **30**,[87] and the pyridine-*N*-oxide **31**[87], which should react with nucleophiles after O-phosphorylation by the enzyme. However, the observed biological activity was below expectations.

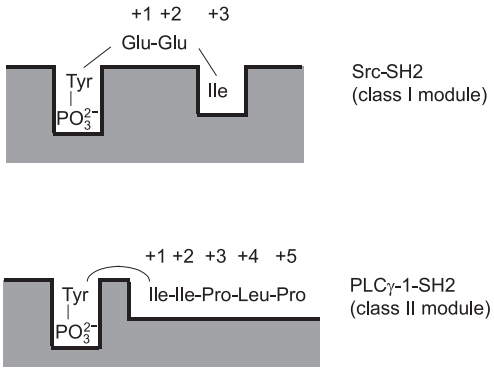
4. Investigation and Inhibition of Interactions with SH2 and SH3 Domains

Noncovalent interactions between proteins play a decisive role in biological phenomena. They are often mediated by modules that are used universally throughout nature and can be found in many proteins such as PTKs, lipid kinases, protein phosphatases, phospholipases, Ras-controlling proteins (see Section 2.2), transcription factors, and adaptor proteins in all eucaryotic cells.[88, 89] These units, which generally have conserved structures independent of the surrounding amino acids and the ligands involved, include the well-investigated SH2 and SH3 domains (see Section 2.2). Combinatorial synthesis of larger peptide libraries was successfully used for investigation of the interactions of SH2 and SH3 domains with their ligands and for discovery of the first modulators of these interactions. Natural products with similar activity are not known at present.

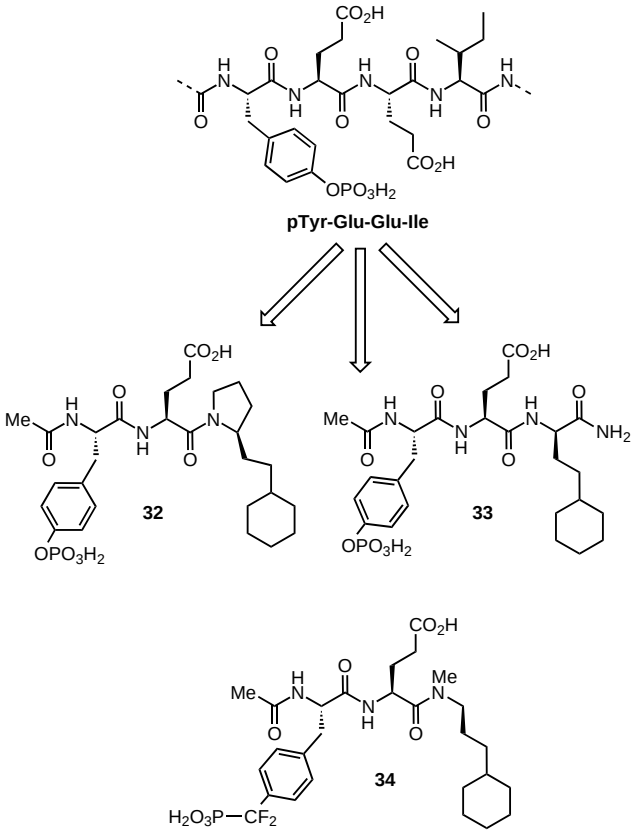
4.1. SH2 Domains

SH2 domains are clusters of about 100 amino acids that recognize and bind peptides phosphorylated on tyrosine residues; the affinity of the ligands is in the region of $K_D = 10-100$ nM.[90] With combinatorial chemistry, it was possible to find a structural basis for the interaction between SH2 domains of certain proteins and their specific binding partners.[91] A library was synthesized of $18^3 = 5832$ phosphopeptides with the general sequence Gly-Asp-Gly-pTyr-Xxx-Xxx-Xxx-Ser-Pro-Leu-Leu-Leu, in which the three Xxx residues were a variety of all natural amino acids except Cys and Trp; the affinity for 14 different SH2 domains was tested. It became apparent that two categories of SH2 domains can be differentiated: class I modules (which include the domains of the proteins Src, Fyn, Lck, Fgr, Abl, Crk, and Nck) bind motifs of the type pTyr-Xxx-Xxx-Ile/Pro (where Xxx is a hydrophilic amino acid), whereas class II modules (which appear in proteins such as p85, PLC$_\gamma$, and SHPTP2) prefer the motif pTyr-Yxx-Zzz-Yyy (where Yyy is a hydrophobic amino acid, and Zzz is any amino acid). With computerized sequence comparisons of the experimentally determined preferred motifs with the sequence of natural proteins, it was possible to identify potential new ligands and target molecules for the different SH2 domains in a straightforward manner. These predictions were confirmed for the binding partners of p85 and PLC$_\gamma$. With the help of NMR and X-ray data, the structures of the domains were determined both in the presence and absence of ligand.[92] Thus, the observed selectivity was explained at the molecular level, and it was shown that the pTyr residue is bound in a deep pocket by ionic (with the phosphate) and hydrophobic interactions (with the aromatic groups), whereas the C-terminal amino acids are either bound by a second pocket (class I domains; a quasi socket is formed here) or by a hydrophobic cleft (Scheme 17).

The high specificity with which the SH2 module of a certain protein recognizes the phosphotyrosine-containing sequences of a different protein makes inhibition or modification of this interaction a rewarding target for bioorganic and medical chemistry research, since it provides the opportunity to disrupt individual signal paths at precisely defined points with suitable substances. In particular, there has been no lack of attempts to find antagonists for the socketlike SH2 domain of the Src kinases which prefer the sequence pTyr-Glu-Glu-Ile (class II). The tetrapeptide analogues **32**, **33**, and **34** (Scheme 18), which all have a hydrophilic (pTyr) and a hydrophobic "plug" (Ile) for the SH2 "socket", have high binding affinities similar to those of longer peptide sequences with the naturally preferred motif (see above).[93, 94] Further



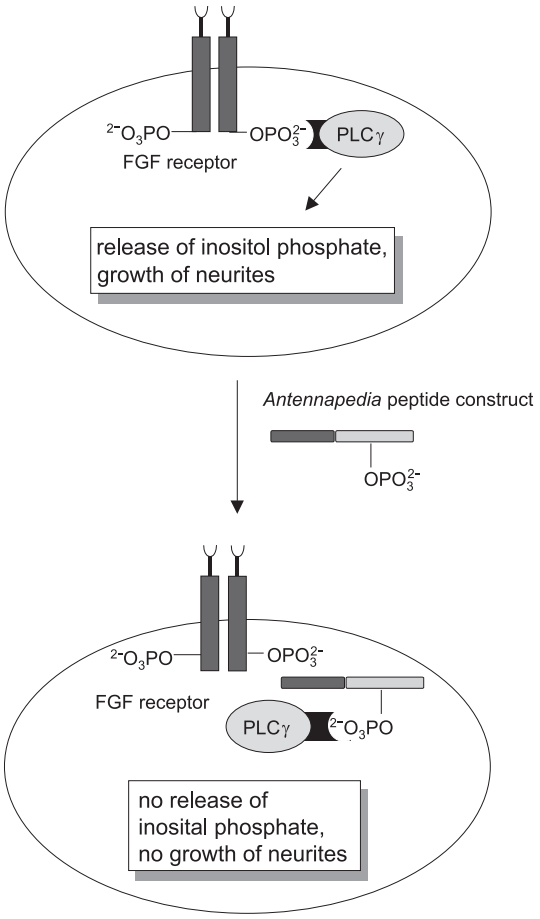
Scheme 17. Schematic representation of the structure of the two classes of SH2 domains.



Scheme 18. Inhibitors, derived from pTyr-Glu-Glu-Ile, of the interaction between the SH2 domain of c-Src and natural ligands.

work on this theme includes combinatorial synthesis of tyrosine-containing peptides[95] as well as the rational design and synthesis of phosphotyrosine peptide mimetics as ligands of c-Src.[96] In addition, conformationally rigid cyclic peptides that have phosphonomethylphenylalanine or phosphotyrosine residues were synthesized as inhibitors of the interaction between PTKs and the SH2 domains of different ligands.[97] The great potential of synthetic inhibitors is demonstrated, for example, by the finding that the pentapeptide acetyl-pTyr-Glu-Glu-Ile-Glu is able to block the interaction between Src and its cellular phosphoprotein partners in cell lysates (i.e. in vitro) even though the peptide has no antiproliferative effect on cells in vivo:[98] It cannot penetrate the cell membrane owing to its high polarity and is degraded by cellular phosphatases and peptidases.

Recently, however, a new and promising possibility for transport of peptide compounds through the membrane was reported. The SH2 domain of phospholipase C (see Section 2.1) recognizes the phosphotyrosine-containing sequences of receptors which are activated on binding their ligands, for example, the receptors for fibroblast growth factor (FGF), EGF, PDGF, or neurotrophin 3 (NT-3). This binding is necessary for hydrolysis of phospholipids and release of inositol phosphates. Phosphorylated peptides corresponding to the phosphotyrosine-containing sequences inhibit this binding in vitro.[99] A sequence of 16 amino acids from the *Antennapedia* protein, which can penetrate biological membranes and thereby transport other peptides and nucleotides,[100] was successfully used to transport these peptides into the cell interior. In an interesting experiment, this sequence was coupled to a nonapeptide corresponding to the sequence recognized by PLC_γ at the FGF receptor. The conjugate was investigated for its activity in cerebral neurons (Scheme 19).[101] Complete inhibition of release of inositol phosphates was achieved with a concentration of 1 $\mu g\,ml^{-1}$ of the phosphorylated peptide, whereas the unphosphorylated peptide showed no activity at all. To demonstrate that the active substance had actually penetrated into the cytoplasm, its uptake of a biotinylated derivative was followed by confocal microscopy. The peptide specifically inhibits FGF-stimulated hydrolysis of phospholipids: Treatment of the cells with PDGF or neurotrophin 3 led to release of inositol phosphates despite the presence of the active substance. Furthermore, it could be shown that activation of PLC_γ is necessary and sufficient for stimulation of FGF-induced growth of neurites, since this growth reaction was blocked in the presence of the peptide inhibitor. These findings document that, with this method, even polar peptides can be used for selective interruption of signal cascades. In the JAK/STAT pathway, the STAT proteins are activated by phosphorylation at tyrosine residues and subsequent dimerization of these transcription factors by interactions between phosphotyrosine and SH2 domains (see Section 2.3). As a result, they migrate into the cell nucleus and bind DNA there. This mechanism was elucidated with phosphotyrosyl peptides which, according to their sequence, were able to induce dissociation of the homodimer and thereby prevent formation of the protein–DNA complex.[102] Non-phosphorylated analogues of the peptide did not trigger this effect.



Scheme 19. In vivo inhibition of the binding of PLC_γ at the FGF receptor by an *Antennapedia* peptide construct.

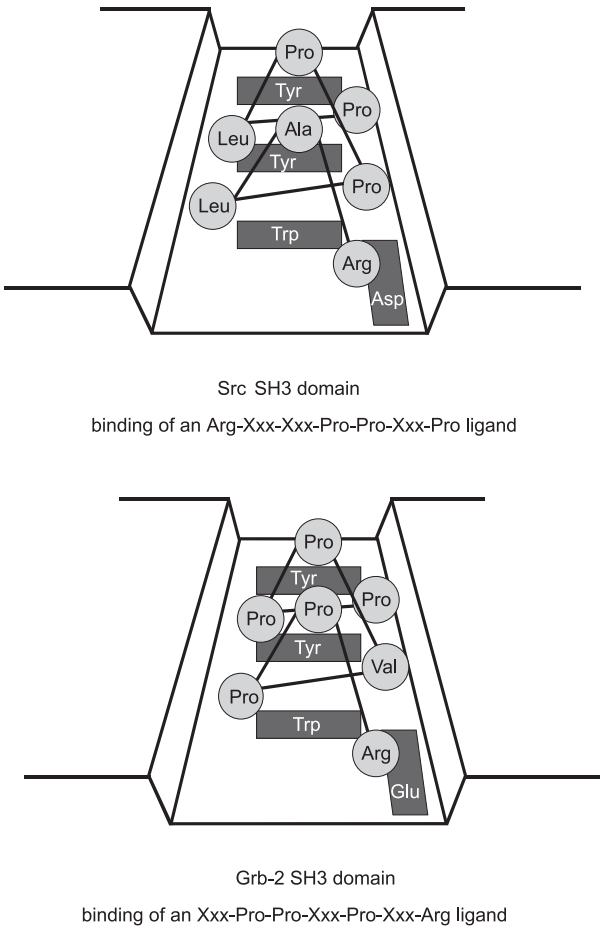
The human estrogen receptor (HER) is a transcription factor that is regulated by binding of a lipophilic hormone; it must also undergo homodimerization to bind to DNA and activate gene transcription. The role of phosphorylation of Tyr 537 of HER in dimerization and activation of the transcription factor was studied with a phosphotyrosine peptide that represents the immediate environment of this phosphorylation site.[103] This dodecapeptide completely inhibits binding of HER to the estrogen response element (ERE) of the DNA and was able, by specific binding of the receptor monomer, to prevent dimerization of the transcription factor. Unphosphorylated peptides and phosphopeptides with other amino acid sequences could not trigger this effect. Based on these findings, a mechanism similar to that for activation of the STAT proteins was postulated, that is, homodimerization by SH2-mediated interactions. A further interesting aspect of this work is that the peptide—in contrast to known antagonists such as clomiphen, tamoxifen and RU 486—inhibits the activity of the estrogen receptor without attacking the hormone binding site.

The protein-tyrosine phosphatase SH-PTP2 has two SH2 domains and, on stimulation by growth factors, it binds to the PDGF receptor, the EGF receptor, and also to the multiple tyrosine phosphorylated insulin receptor substrate 1 (IRS 1). Synthetic phosphotyrosyl peptides with sequence homology to IRS 1 were able to significantly increase dephosphorylation by the enzyme by allosteric activation.[104]

A tyrosyl phosphopeptide derived from EGF receptor, containing the Tyr 1068 of this protein, was used to inhibit interaction of the receptor with the adaptor protein Grb2. Infiltration of this peptide into cells leads to a weaker stimulation of the Ras protein and MAP kinase.[105]

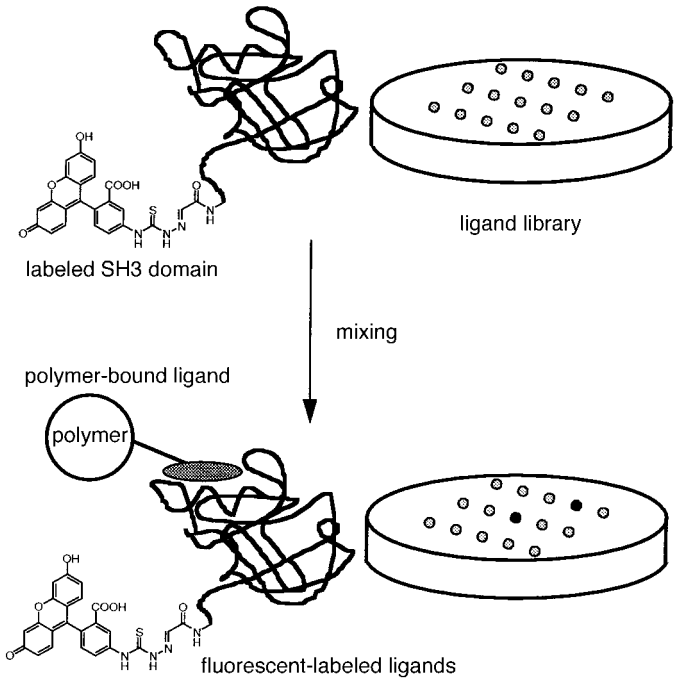
4.2. SH3 Domains

SH3 domains are made up of about 60 amino acids and bind proline-rich sequences that form a left-handed polyproline helix of type II (Scheme 20); the affinity of the peptide is in



Scheme 20. Possible orientation of the Pro-Pro-Xxx-Pro motif in SH3 domains of Src and Grb 2.

the region of $K_D = 5 - 100$ μM.[88] In addition to the determination of the structure of the domains and their ligands,[106] the investigation of the binding specificity and characteristics of this module was also accelerated with combinatorial chemistry.[107] Based on the observation that peptides with the sequence Pro-Pro-Xxx-Pro of the SH3 domain of phosphatidylinositol kinase were bound particularly well, a "biased" library of the general form Xxx-Xxx-Xxx-Pro-Pro-Xxx-Pro-Xxx-Xxx (where Xxx is any amino acid except cysteine) was synthesized which, with the Pro-Pro-X-Pro motif, should have a certain basic affinity to the SH3 domain used.[108] By combinatorial synthesis with the "split and combine" process, about two million different peptides were assembled on poly(dimethylacrylamide) beads, so that exactly one defined compound was attached to each bead. To detect binding of the potential ligands to the SH3 domain, the recombinant SH3 domain of the phosphatidylinositol 3-kinase was coupled to fluorescein-5-thiosemicarbazide following oxidization of the N-terminal serine to glyoxylamide, and the library was treated with this labeled protein (Scheme 21). Of 70 beads that bound

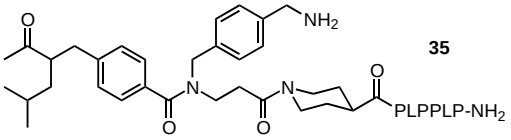


Scheme 21. Combinatorial synthesis of peptide ligands for the SH3 domain of the PI-3 kinase.

to the fluorescent protein, the 17 with the highest fluorescence were selected, and the attached peptides were sequenced by Edman degradation. The binding affinities measured for the ligands thus identified were amongst the highest known ($K_D = 8 - 30$ μM).

Interestingly, two classes of peptides were identified which differ in the location of a basic arginine residue at the C terminus of the common Pro-Pro-Xxx-Pro motif (Xxx-Pro-Pro-Leu-Pro-Xxx-Arg, class I ligands) in one case and at the N terminus (Arg-Xxx-Leu-Pro-Pro-Leu-Pro-Xxx-Xxx, class II ligands) in the other. Determination of the structure from the library of peptides that bind Src SH3 domains with multidimensional NMR techniques gave the surprising result that the helices of the ligand can be bound in two different orientations (Scheme 20). The arginine residue forms a salt bridge with either an aspartate or a glutamate residue in the binding pocket and thus determines the position of the peptide, whereas the side chains of the proline and leucine residues undergo hydrophobic interactions with aromatic amino acids in the protein.[109] Since these noncovalent bonds are common to all domain–ligand systems, the specificity of the SH3 module of a particular protein for its partner is mediated by interactions of the peptide with two of the central loops flanking the binding pocket (Scheme 20).

Identification of peptide-analogous ligands was achieved similarly with a combinatorial method. Four building units from a pool of 64 compounds were linked by amide and urethane bonds to a Pro-Leu-Pro-Pro-Leu-Pro sequence, which should guarantee orientation of the selected analogues in the manner of a class I ligand.[110] The affinity for SH3 domains of the ligands bound to the solid phase was determined with a biotinylated Src SH3 domain that binds to a complex of streptavidin and alkaline phosphatase and thus produces a detectable signal. From a library of 1.1 million compounds, 15 active ligands (e.g. **35**, Scheme 22) with small



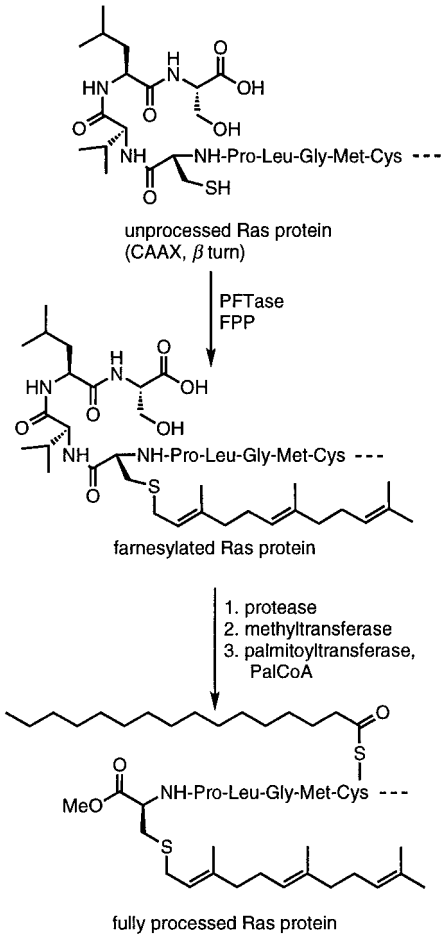
Scheme 22. Non-peptide ligand of the Src SH3 domain. P = Pro, L = Leu.

dissociation constants ($K_D = 3.4 - 30$ μM) were found. With the use of NMR spectroscopy, it was also shown that the binding specificity of peptide-analogous ligands arises from contacts other than those of the peptide binding partner. By designing substances that bind to both contact points, it should be possible to obtain very effective inhibitors for interactions with SH3 domains.[111]

5. Inhibition of the Ras Farnesyltransferase (PFTase)

Ras proteins function as central switches for signals given by growth factors that direct cell growth, cell differentiation, and other genetic programs.[112] The Ras proteins must be associated with the membrane to perform this function. They are anchored in the membrane by co- and post-translational modification of the C terminus of the polypeptide with lipid residues which bind the protein to membranes.[113] To this end, the cysteine of the C-terminal CAAX sequence (C is cysteine, A is generally an aliphatic amino acid, and X is methionine, serine, alanine, or glutamine) of a precursor protein is first enzymatically farnesylated during biosynthesis, the AAX part is then cleaved off by a specific protease, and the free terminal cysteine is finally converted into the methyl ester (Scheme 23). In addition, in H- and N-Ras a further lipid modification of cysteine occurs by formation of palmitoyl thioesters in the immediate vicinity of the CAAX motif. It was shown that farnesylation is essential for the transforming activity of mutated Ras proteins.[114] Inhibition of this lipid modification opens up various possibilities for studying signal transduction processes and for developing alternative medicinal – chemical strategies, for example in tumor therapy.[115]

Since the three-dimensional structure of the heterodimeric Ras farnesyltransferase was only recently obtained,[116] it was necessary to draw on information about substrate specificity as well as the conformation of the substrate in solution and bound to the enzyme (obtained from NMR spectroscopic investigations; the bound ligand Cys-Val-Trp-Met forms a β



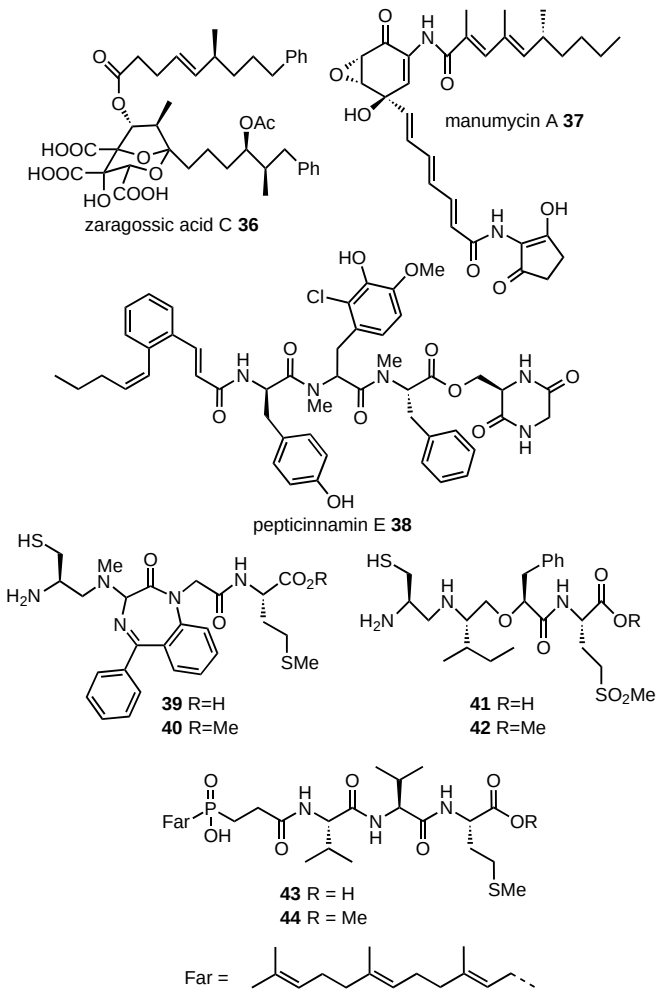
Scheme 23. Post-translational modification of the Ras protein. FPP = farnesyl pyrophosphate, Pal = palmitoyl.

loop of type III (Scheme 23))[117] to develop inhibitors of this enzyme. In addition, natural products with potent PFT-inhibiting activity were found in screening tests including, for example, zaragozic acids (e.g. **36**),[118] manumycin (**37**),[119] and pepticinnamin E (**38**)[120] (Scheme 24).

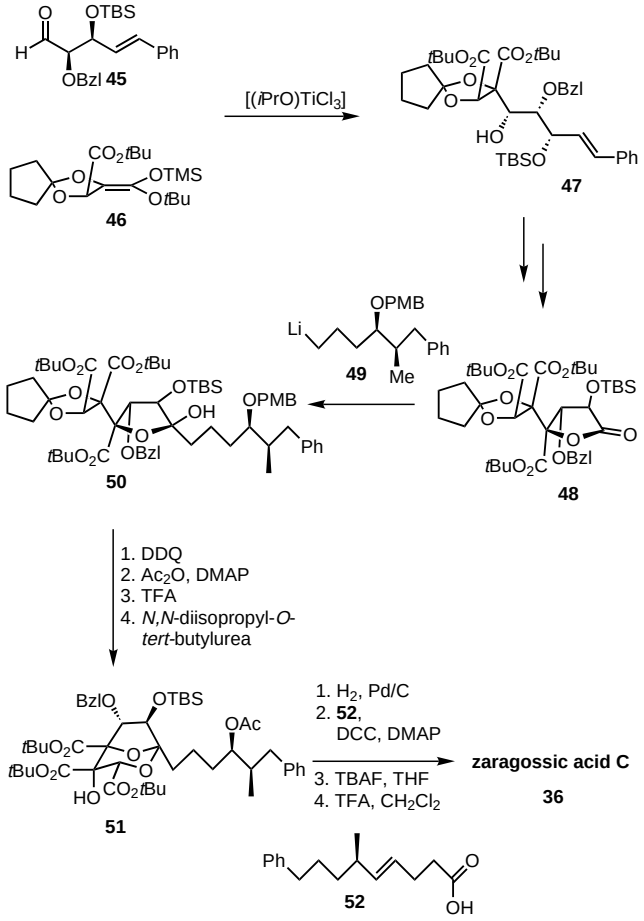
5.1. Naturally Occurring Ras Farnesyltransferase Inhibitors

5.1.1. Zaragozic Acids

The zaragozic acids (e.g. **36**, Scheme 24), first found in fungal cultures in the vicinity of the Spanish town Zaragoza, inhibit squalene synthase in addition to farnesyltransferase.[118] The high therapeutic potential of these complex compounds—which interfere with cholesterol biosynthesis and are therefore of interest for medical indications such as arteriosclerosis, hypertension, and cardiac infarct—was the reason for intensive research leading to the successful total synthesis of this new type of natural product.[121, 122] The biggest challenge was the stereospecific construction of the highly polar 2,8-dioxabicyclo[3.2.1]octane skeleton which carries three carboxy and three hydroxyl groups at five stereocenters. One of these hydroxyl groups must be selectively acylated with a fatty acid side chain. An alkyl side chain must also be attached.



Scheme 24. Inhibitors of the Ras farnesyltransferase.



Scheme 25. Synthesis of the zaragozic acid C. Bzl = benzyl, DCC = *N,N'*-dicyclohexylcarbodiimide, DDQ = 2,3-dichloro-5,6-dicyano-1,4-benzoquinone, DMAP = 4-dimethylaminopyridine, PMB = *para*-methoxybenzyl, TBAF = tetrabutylammonium fluoride.

After removal of the acyl side chain **52**, the resulting alcohol **51** can be retrosynthetically converted back into the lactol **50** (Scheme 25).[122] The latter is obtained by nucleophilic attack of the lithiated alkyl chain in **49** on the lactone **48**, which was obtained from dihydroxysuccinic acid. Assembly of the C_5–C_7 skeleton in **45** was achieved by a highly *syn*-diastereoselective Evans aldol reaction of a boron enolate with phenylacrolein and subsequent removal of the chiral auxiliary. The silyl ketene acetal **46**, which was obtained from the di-*tert*-butyl ester of dihydroxysuccininc acid, underwent a highly diasteroselective aldol reaction with aldehyde **45** to form alcohol **47**. With the help of standard transformations, **47** was converted into lactone **48**, which possesses all eight carbon atoms of the bicyclic skeleton as well as the equivalents of the alcohol and carboxyl groups. The C_1 side chain was introduced by addition of the organolithium compound **49** to **48**. After manipulation of the protecting groups on the side chain, lactol **50** was converted under acid conditions and by transacetalization into the desired bicyclic **51**, in which the carboxyl functionality was protected again as the *tert*-butyl ester. Selective cleavage of the benzyl ether, introduction of the acyl side chain **52**, and deprotection of the hydroxyl and carboxyl functionalities gave zaragozic acid C (**36**). This synthesis should be applicable to the preparation of zaragozic acid A, which only differs from **36** in the alkyl side chain. Noteworthy features of this total synthesis include the high degree of stereocontrol, the low number of steps (21 for the longest linear sequence), the associated high total yield of 15%, and the clever choice of protecting groups.

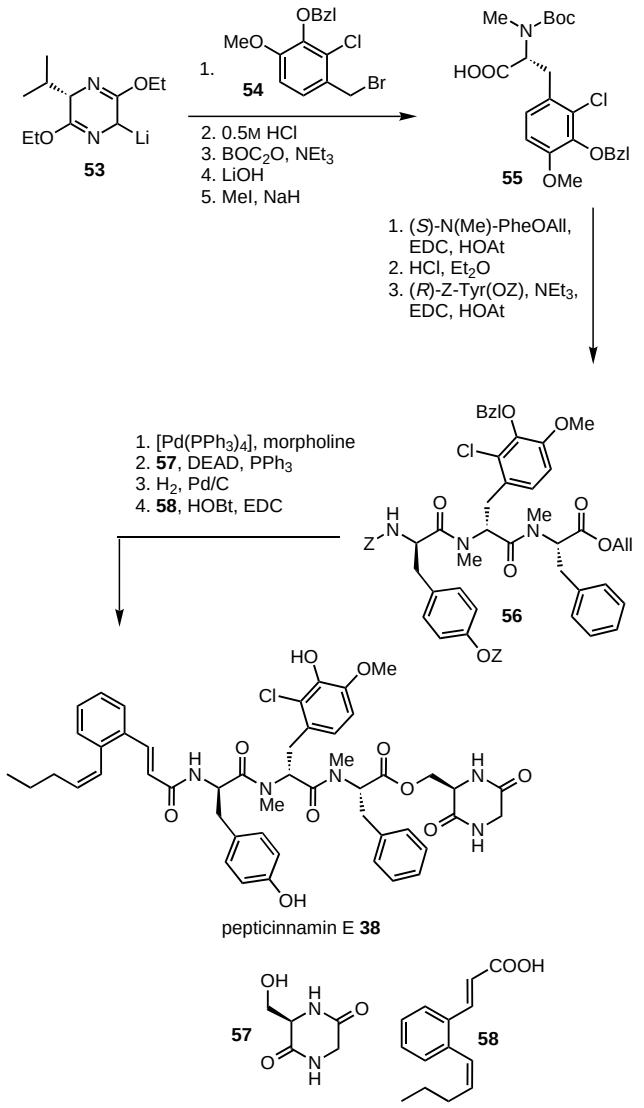
The zaragozic acids show very interesting biological activity: They interfere with the biosynthesis paths of cholesterol by inhibiting the squalene synthase that uses farnesyl pyrophosphate (FPP) as substrate. Zaragozic acid A was also identified as the inhibitor for another enzyme that uses FPP, the Ras farnesyltransferase. It was thereby shown that the natural product acts in competition with FPP rather than with the peptide substrate. Probably, the carboxy and hydroxyl functionalities mimick the bisphosphate, and the hydrophobic side chains imitate the isoprene part of the farnesyl pyrophosphate.[123] If inhibitors of the PFTase or squalene synthase are to be used in pharmaceutical or biological experiments, their selectivity for other prenyl-transferring enzymes—for example, the geranylgeranyl transferases (GGTases)—will be of great importance, since a large number of proteins are modified with the C_{20} diterpenes. By a slight modification of the alkyl side chain of zaragozic acid A, this selectivity was significantly improved; activity against PFTase was raised by a factor of 18, whereas activity against geranylgeranyl trans-

ferase was reduced by a factor of 2.7. These results suggest that other structural modifications may enable further improvement of these characteristics. It is interesting that, in intact cells, both compounds do not influence the function of the Ras protein, even at high concentrations and incubation times of 24 h. Here it can also be assumed that the compounds are too polar, owing to the carboxy and hydroxyl functionalities of the bicyclic core, to be able to penetrate the cell membrane; they would have to be masked to achieve any in vivo effects.

5.1.2. Pepticinnamin E

Pepticinnamin E (**38**, Scheme 24) was isolated from *Streptomyces* species and is a structurally interesting PFTase inhibitor.[120] One can speculate that the natural product is a transition state analogue for farnesyltransferase, in which the hydrophobic alkenyl acrylic acid imitates the prenyl residue and the conformationally rigid N-methylated peptide skeleton imitates the peptide substrate. A total synthesis of the natural product is of considerable interest since the absolute configuration of the unusual central amino acid is unknown. Furthermore, owing to its modular construction, the substance also permits various derivatizations and the combinatorial synthesis of analogues with modified biological activity.

For synthesis of pepticinnamin E[124] (**38**, Scheme 26), acrylic acid **58** was synthesized diastereomerically pure by esterification, *Z*-selective Wittig reaction, reduction to aldehyde, and *E*-selective Perkin reaction, starting from 2-carboxybenzaldehyde (total yield 31 %). The central unusual amino acid in the natural product was obtained in the form of both required enantiomers by a Schöllkopf reaction. For this, lithiated bis(lactim ether) **53** was alkylated with benzyl bromide **54**. Cleavage of the auxiliary, protection of the amino function, ester saponification, and methylation of the urethane gave amino acid **55** and its enantiomer, each in the enantiomerically pure form. The central tripeptide unit **56** was obtained by classical peptide coupling. The allyl ester was cleaved from **56** by Pd^0-mediated allyl transfer with morpholine as accepting nucleophile. Esterification of the carboxylic acid obtained with alcohol **57** by activation of the carboxy function with the help of carbodiimide or trichlorobenzoyl chloride only gave poor yields. Only nucleophilic attack of the carboxylic acid on alcohol **57**, activated according to Mitsunobu, gave the desired ester in satisfactory amounts. Following removal of all benzyl protecting groups, coupling with acrylic acid **58** delivered the natural product **38**.



Scheme 26. Synthesis of pepticinnamin E. All = allyl, Boc = *tert*-butyloxycarbonyl, EDC = *N*′-(3-dimethylaminopropyl)-*N*-ethylcarbodiimide, HOAt = 7-aza-1-hydroxy-1*H*-benzotriazole, *Z* = benzyloxycarbonyl.

5.1.3. Manumycin A

Manumycin A (**37**, Scheme 24), a natural product isolated from a *Streptomyces* species,[119] is an example of a class of structurally novel PFTase inhibitors. In addition to the complex parent compound, structurally simpler degradation products and derivatives also block the activity of the PFTase from yeast and rat brain. With the help of manumycin A, a simple test system for in vivo activity of the enzyme inhibitor was established for the development of the thread worm *Caenorabditis elegans*.[125] Both manumycin A and the basic aminoepoxycyclohexenone structure possess antitumor activity. The chemical synthesis[126] of analogues of the natural product should have great potential for providing highly active, selective, and metabolically stable enzyme inhibitors.

5.2. Peptidomimetics

Substances that compete with the peptide, in particular with the CAAX motif, should have particularly advantageous selectivity of inhibition toward other enzymes, since GGTases prefer different sequence motifs (CAAL, where L is leucine) to the PFTases.[115] Benzodiazepines such as **39** and **40** (Scheme 24) are CAAX peptidomimetics, whose central unit imitates a β turn. In addition, they bring the NH_2 terminus of the cysteine analogue and the COOH terminus of the methionine in spatial proximity; these can then complex a Zn^{2+} ion, which is essential for activity of the PFTase and

binding of the peptide substrate.[127] The free acid **39** inhibits the enzyme with an IC_{50} value of less than 1 nM, whereas in intact cells methyl ester **40**, despite its weaker in vitro activity, is significantly more potent; it can penetrate the plasma membrane better owing to its lower polarity. This property can be used to convert the morphology of cells that are transformed by *H-ras* back into the normal form and to inhibit growth of these cells. In contrast, the substance shows no effect on *src*-transformed and untransformed rat fibroblasts. The inhibitor therefore acts selectively on transformed cells and does not influence growth of normal cells. This result is noteworthy because farnesylation of the wild-type H-Ras protein is inhibited by the benzodiazepine, and H-Ras is involved in the growth of normal fibroblasts. Detailed examination of this unexpect result shows that inhibitor **40** reduces the amount of farnesylated H-Ras protein in cells that are both untransformed and transformed by *H-ras*. However, *only* in the transformed cells does this lead to the expected reduction of enzyme activity in the Ras cascade: Both the amount of phosphorylated Raf and the activities of MEK-1, MEK-2, and MAP kinase were reduced in the tumor cells.[128] In addition, stimulation of the Ras signal pathway was not influenced by EGF in normal or *src*-transformed cells. The normal cells apparently have the ability to activate the signal pathway with or without the reduced involvement of Ras. In fact, further experiments have shown that farnesylation of the K-Ras protein by the inhibitors is considerably less influenced than that of H-Ras. K-Ras is also a substrate of the GGTase I and can therefore be geranylgeranylated if activity of the PFTase is reduced.[129] Normal cells and *src*-transformed cells, in contrast to those transformed by *H-ras*, are able to compensate for loss of a Ras protein or an enzyme important for normal cell growth, by activation of alternative pathways.

5.3. Peptide Analogues

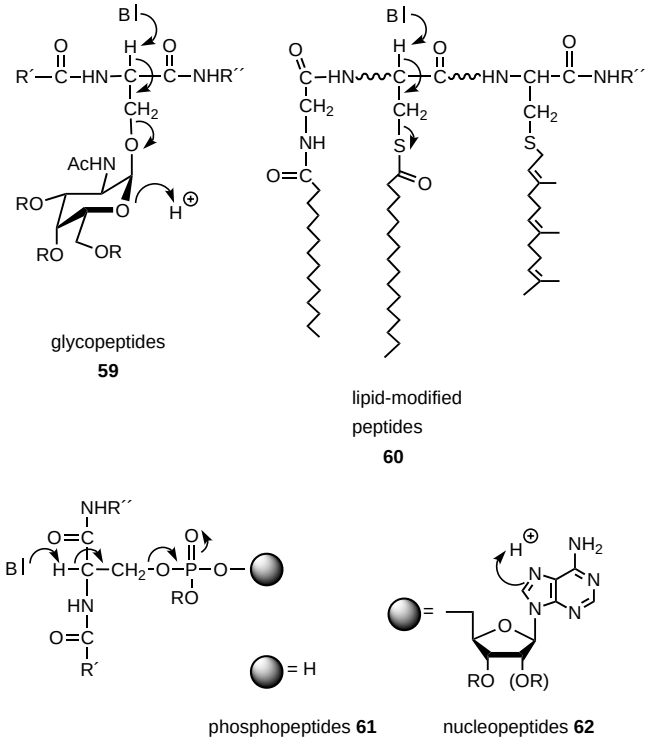
Another inhibitor obtained by rational design is the CAAX β turn mimetic **41** (Scheme 24).[130] It is an analogue of CAAX peptides in which peptide amide bonds are replaced by ether and amine groups. The compound inhibits the PFTase in vitro with an IC_{50} value of 1.8 nM and shows highly specific activity in comparison to inhibition of GGTase I. The less polar methyl ester **42** as prodrug showed better results in vivo and inhibits both farnesylation of the Ras protein and growth of *ras*-transformed cells, whereas proliferation of *raf*- or *mos*-transformed cells was not influenced. Growth of human pancreatic adenocarcinoma cells with mutated *K-ras*, *c-myc*, and p53 genes was inhibited by application of **42**. If the compound is administered over a period of five days to mice with implanted Ras-dependent tumors, tumor growth can be reduced by up to 66% compared to untreated mice, whereas the application of the antitumor antibiotic doxorubicin only resulted in 33% reduction under the same conditions. It is particularly noteworthy that treatment with the β-turn mimetic, in contrast to treatment with doxorubicin, was without any visible side effects such as weight loss.

5.4. Bisubstrate Inhibitors

The phosphinic acids **43** (R = H) and **44** (R = Me; Scheme 24) are examples of bisubstrate analogues for which, a priori, higher activity and selectivity compared to mimetics of the individual substrates alone might be expected.[115] Indeed, **43** is an effective in vitro inhibitor, and the prodrug **44** has activity in cells transformed by *H-ras* and—to a lesser extent—*K-ras*.[131] Prodrug **44** also inhibits growth of malignant cells of the neurofibromatosis type I, which are dependent on overactivation of the wild-type Ras protein.[132] These highly promising results are tempered, however, by the lower bioavailability and in vivo activity in comparison to the peptidomimetics.

6. Peptide Conjugates as Tools for Studying Biological Signal Transduction

The proteins involved in transduction of signals from the plasma membrane into the cell nucleus often have additional covalently linked structural units which are absolutely necessary for fulfillment of their biological function (Scheme 27).



Scheme 27. Structure and lability of peptide conjugates. B = base.

For example, the cell-surface receptors for growth factors (see Scheme 5) and the ligands recognized by them are often glycoproteins in which serine, threonine, and asparagine units are linked to oligosaccharides (**59**). The signal-transmitting proteins located in the membrane, such as the Ras protein, are lipid-modified at cysteine and glycine residues (**60**). In many cases, the signals are passed on by phosphorylating proteins to be switched on at serine, threonine (**61**), and tyrosine

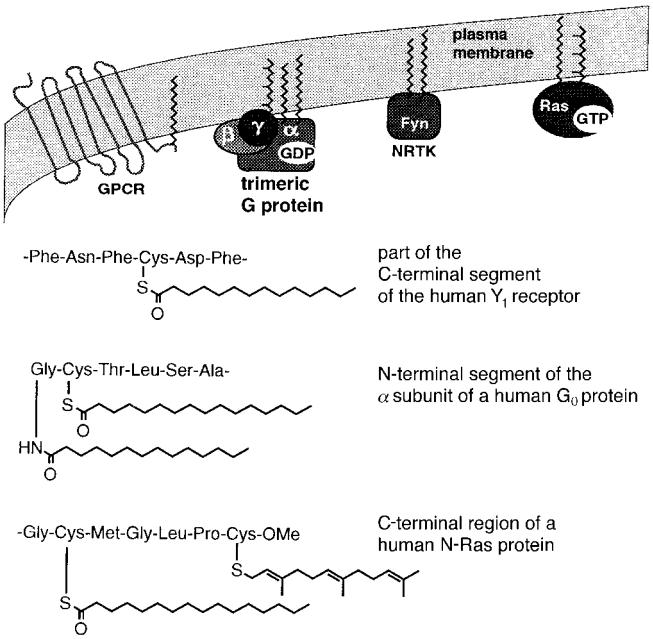
residues; DNA, which is often the target of the signal cascade, exists as a nucleoprotein in which serine, threonine, or tyrosine are linked as phosphoric acid esters to the nucleic acid chain (**62**).

Peptides containing the essential covalently modified structural units of these protein conjugates may be useful tools for studying their biological functions as well as for selectively manipulating the signal cascades in which they are involved (see below). However, synthesis of such peptide conjugates is hindered, by their multifunctionality, which requires the use of many orthogonally stable amino, hydroxyl, mercapto, carboxy, and phosphate protecting groups.[133–136] On the other hand, the peptide conjugates are also particularly acid and base labile. Thus at pH greater than 9, the side chain functionalities are cleaved from the serine glycosides **59**, the lipid-modified peptides **60**, and the phospho- and nucleopeptides **61** and **62** in a β elimination; the thioester in **60** hydrolyzes spontaneously in aqueous solution at pH greater than 7. In acid, there is a danger of anomerization or even cleavage of the *N*- and *O*-glycosidic bonds in **59** and **62**, and the olefins of the farnesyl residue in **60** are easily attacked by acids. In the synthesis of the peptide conjugates of type **59**–**62**, all reactions, particularly the removal of all the diverse protecting groups, must take place under mild (preferentially neutral) conditions, yet with complete preservation of orthogonal stability.

On one hand, peptide conjugates are of great interest as reagents and chemical tools for biological studies. On the other hand, their synthesis is a considerable challenge for organic chemistry. New, alternative synthetic methods must be developed in order to obtain complex peptide conjugates efficiently and with high selectively under very mild conditions. This area of organic synthesis offers an excellent opportunity for initiating bioorganic research as defined in Section 1. The chemistry of the peptide conjugates has received much attention in the last two decades, and has led to the development of high-performance synthetic methods and use of modified peptides in biological studies. In particular, efficient methods are now established for synthesizing glycopeptides[137] and phosphopeptides[138]. The use of enzyme-labile protecting groups[133–136] has been established as a valuable alternative to the classical chemical protecting group techniques, since enzymes often work under mild, neutral conditions, and combine high selectivity for the structural units that they recognize and the reactions they catalyze with broad substrate tolerance. The new synthetic methods resulting from this approach are the focus of the following discussion.

6.1. Lipid-Modified Peptides

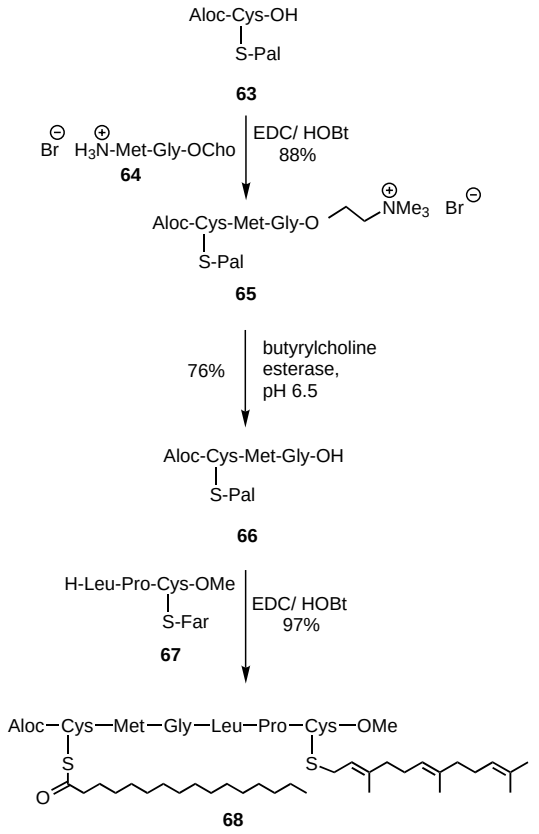
Signal-transducing proteins that are located in the plasma membrane often carry covalently attached lipid residues.[139, 140] Therefore, the C termini of many G protein coupled receptors are *S*-palmitoylated on cysteines; the α subunits of heterotrimeric G proteins and nonreceptor tyrosine kinases are myristoylated at N-terminal glycines and often S-palmitoylated in the immediate vicinity as well. The γ subunits of the G proteins contain an S-farnesylated or S-geranylgeranylated cysteine, and the Ras proteins are S-farnesylated and S-palmitoylated (Scheme 28).



Scheme 28. Structure of lipid-modified proteins bound to a plasma membrane. GPCR = G protein coupled receptor, NRTK = nonreceptor tyrosine kinase.

The lipid residues are necessary to localize the proteins to the site at which they perform their biological function, that is, in the plasma membrane. Therefore, the Ras proteins only fulfill their signal-tranducing function in both normal and transformed cells if they are membrane-bound. This is achieved by lipid modification; non-farnesylated Ras is cytosolic and inactive. Whether the correct lipid modification of proteins fulfills other biological functions and, for example, actively takes part in the process of signal transduction is unclear.[139, 140] There are indications that the interaction of Ras with its substrate Raf occurs through the C terminus of the Ras protein, and the lipid modification seems to play a role[142] (for a similar theory for the interaction of yeast Ras with its target protein, the adenylate cyclase, see ref. [177]). For the G protein coupled β_2 adrenoceptor, it was shown that desensitization following binding of an agonist (i.e. switching the signal off) is accompanied by depalmitoylation of the receptor.[143] Furthermore, addition of the agonist brings about an increase in the degree of palmitoylation of the $G_{s\alpha}$ protein of the β_2 adrenoceptor; its lipid-modified N terminus interacts better with the corresponding β,γ subunit and forms the original heterotrimeric, inactive complex (see Scheme 2, Section 2.1). This process also causes the signal to be switched off.[144] Whether the specific type of lipid modification of individual proteins is a form of subcellular addressing to certain intracellular membranes (e.g. by interaction with a receptor that recognizes lipid residues) is unclear.[141] Lipid-modified peptides have played an important role in the investigation of this last question.

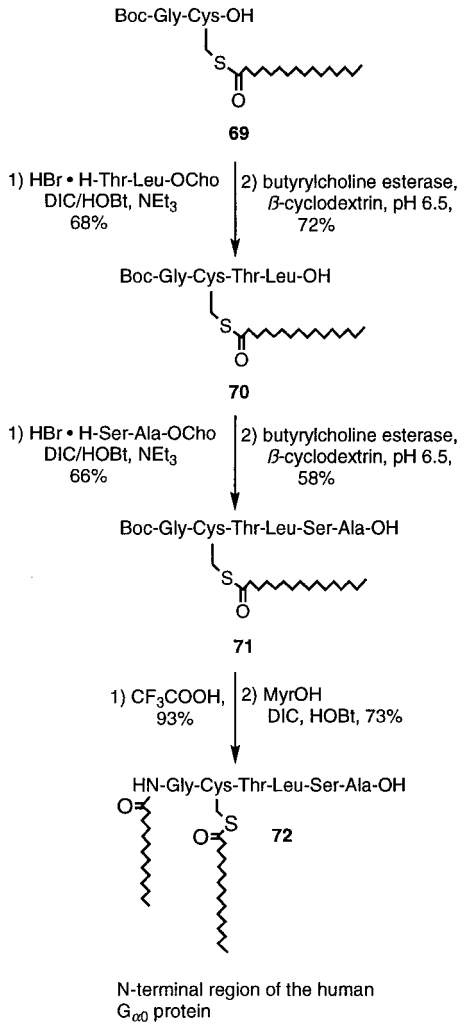
Enzymatic protecting group techniques[133–136] are particularly effective for synthesizing acid- and base-labile lipid-modified peptides. Thus, the choline ester was developed as an enzyme-labile carboxy protecting group that can be released under very mild conditions with butyrylcholine esterase from horse serum; at the same, it ensures better solubility in the aqueous media, which is necessary for biotransformation.[145] An example of its use is in the synthesis of the S-palmitoylated and S-farnesylated lipopeptide **68** of the human N-Ras protein (Scheme 29). The S-palmitoylated tripeptide choline ester **65**



Scheme 29. Chemoenzymatic synthesis of the farnesylated and palmitoylated C terminus of the human N-Ras protein with the enzyme-labile choline ester. Aloc = allyloxycarbonyl, Far = farnesyl, HOCho = choline.

was obtained from the cysteine derivative **63**. In the key step of the synthesis, **65** was completely released without attack at the thioester, which was more reactive under classical conditions, and without detectable β elimination. Extension of the peptide chain of the selectively demasked tripeptide **66** with the S-farnesylated tripeptide methyl ester **67** gave the target compound **68** in high yield.

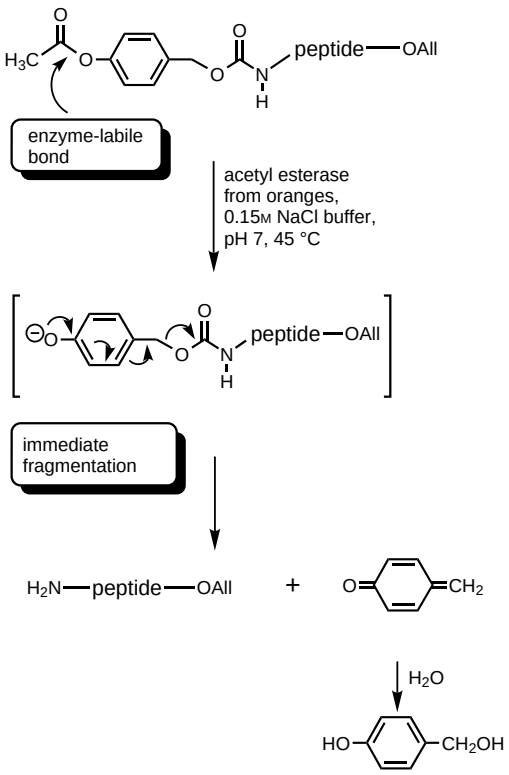
With a second application of this technique, the characteristic N-myristoylated and S-palmitoylated N-terminal hexapeptide of the α_0 subunit of a heterotrimeric $G_{\alpha 0}$ protein was synthesized[146] (Scheme 30). Starting from the S-palmitoylated dipeptide **69**, a tetrapeptide choline ester was synthesized and then enzymatically deblocked at the C terminus under very mild conditions to **70**. Again, there were no undesired side reactions. Successive chain extension and renewed



Scheme 30. Chemoenzymatic synthesis of the myristoylated and palmitoylated N terminus of the α subunit of a heterotrimeric α_0 protein with the enzyme-labile choline ester. DIC = diisopropylcarbodiimide, MyrOH = myristic acid.

choline esterase mediated deprotection delivered the Boc-masked peptide **71**, which was converted into the target compound **72** by cleavage of the urethane group and N-myristoylation.

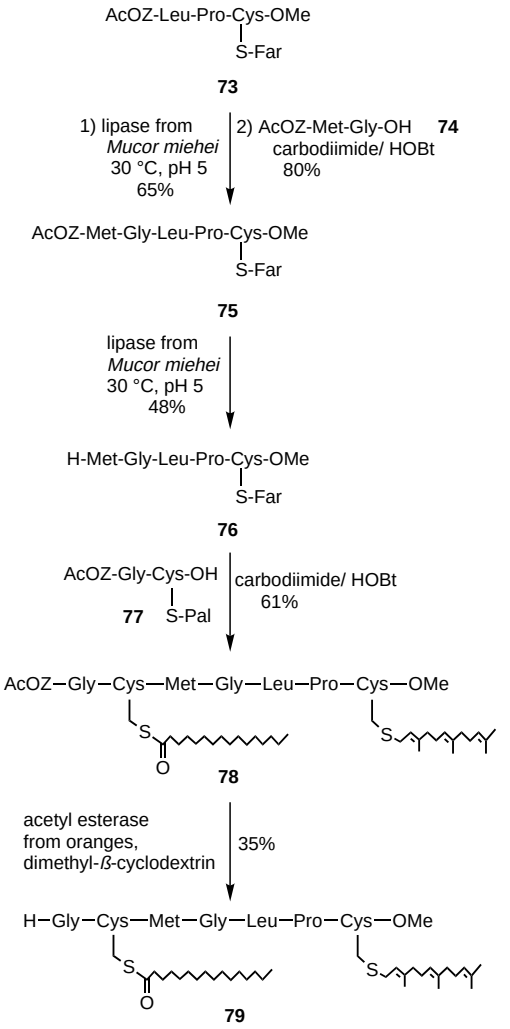
To synthesize acid- and base-labile lipid-modified peptides by N-terminal extension of the peptide chain, it was necessary to develop the first enzyme-labile urethane protecting group for the amino functionality of peptides (Scheme 31).[147] Since no biocatalyst is known for cleaving urethanes from peptides, a strategy was developed in which the enzyme removes a urethane without direct attack on the urethane structure. The p-acetoxybenzyloxycarbonyl (AcOZ) group used for this purpose contains a functional group (acetate) that the biocatalyst (an esterase or lipase) can recognize and that is bound through an enzyme-labile bond (an ester) to a second functional group (a *p*-hydroxybenzyl urethane); following cleavage of the enzyme-labile bond, the urethane undergoes spontaneous fragmentation with release of the desired peptide conjugate (Scheme 31). This is a general principle: Depending on the acyl residue selected (e.g., acetate or phenylacetate), enzymes with different selectivity (e.g., acetyl



Scheme 31. Enzyme-initiated cleavage of the AcOZ urethane protecting group.

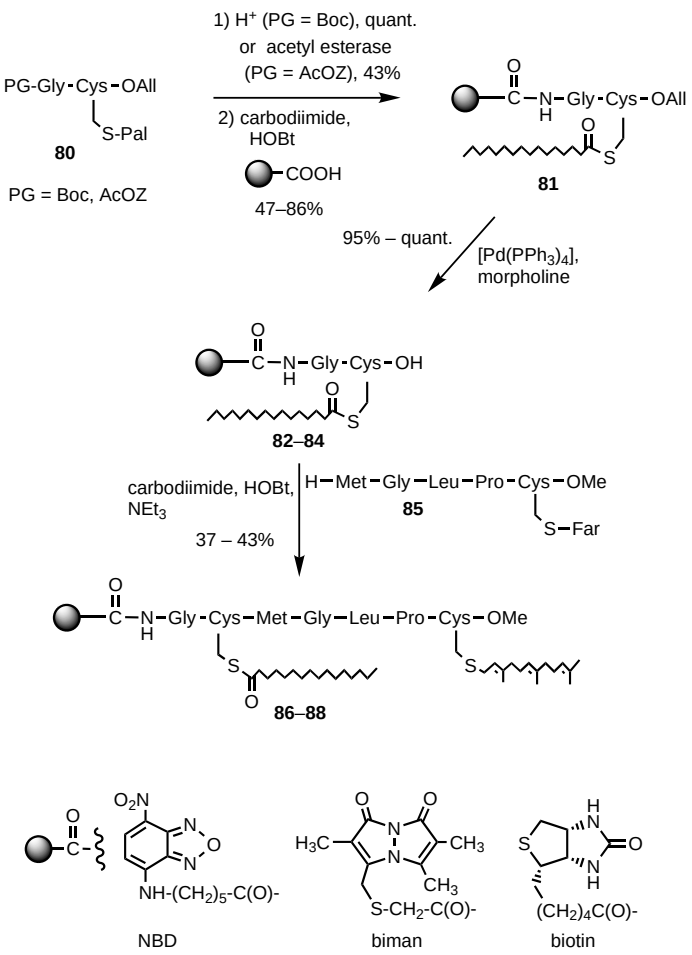
esterase or penicillin G acylase) can be used (see Schemes 32, 51, and 54), and the analogous C-terminal *p*-acyloxybenzyl esters can also be cleaved off by the same mechanism.[148] With the AcOZ urethane, the essential C-terminal lipid-modified heptapeptide ester of the N-Ras protein was constructed (Scheme 32).[147] Deblocking of the urethane-protected farnesylated tripeptide methyl ester **73** by enzyme-initiated fragmentation of the AcOZ group delivered the selectively deprotected peptide. Successive extension of the peptide chain with the AcOZ dipeptide **74** and renewed lipase-mediated release of the urethane protecting group gave the N-Ras pentapeptide **76**; this was condensed with the AcOZ-masked S-palmitoylated dipeptide **77** to give the fully protected lipid-modified heptapeptide **78**. It was subsequently possible to enzymatically release the N-terminal urethane from **78** to give the amino-deblocked Ras heptapeptide **79**, which is available for further chain extensions or linking to additional functional groups.

The enzymatic techniques described here have been proven to be flexible and efficient methods for synthesizing lipid-modified peptides that are both base- and acid-labile. Nevertheless, such conjugates could also be assembled by classical methods, although the different cysteine units to be modified had to be protected with a much more complicated procedure; in general, these were selectively unmasked and functionalized after completion of the peptide chain.[149, 150] If only base-labile palmitic acid thioesters are present in the compound to be demasked, the acid-labile Boc group may be used (see below); acid-labile peptides containing *S*-farnesylcysteine can be deblocked at the N terminus by cleavage of



Scheme 32. Chemoenzymatic synthesis of the C terminus of the human N-Ras protein with use of the enzyme-labile AcOZ urethane protecting group.

the Fmoc urethane.[151] In addition to enzymatic techniques, Pd^0-mediated release of allyl esters has also been demonstrated to be an efficient method for synthesizing sensitive lipid-modified peptides.[152] This protecting group technique demonstrated its potential in the development of a flexible building block system for synthesizing different lipid-modified N-Ras peptides carrying additional fluorophoric groups; owing to the fluorophore properties, these conjugates can be followed in biological and biophysical experiments. The AcOZ- or Boc-protected S-palmitoylated cysteine allyl ester **80** was selectively demasked at the N terminus either enzymatically or under acid conditions, and a fluorescent group was linked to the free amino function (Scheme 33). Without any attack at the palmitic acid thioester, release of the allyl ester was achieved in very high yield by Pd^0-mediated allyl transfer to morpholine as accepting nucleophile. The fluorescently labeled and S-palmitoylated dipeptides **82**–**84** thus obtained were then linked to the farnesylated N-Ras pentapeptide **85** to form Ras heptapeptides **86**–**88** with two lipid modifications; these were used in further biological and biophysical experiments (see below).



Scheme 33. Synthesis of labeled lipopetide derivatives for biological studies. NBD = 4-nitrobenzo-2-oxa-1,3-diazol, PG = protecting group.

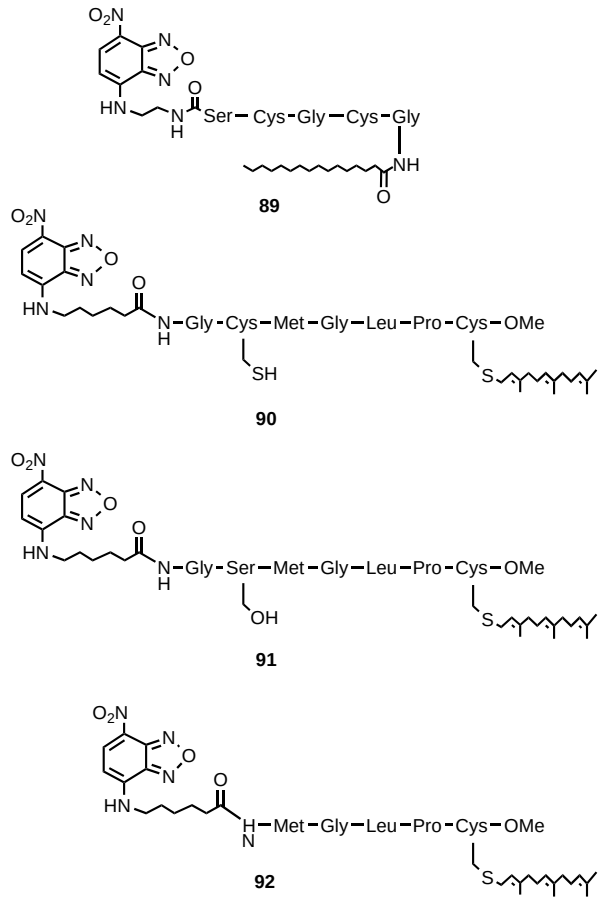
Lipid-modified peptides have been used in many ways as tools, for example, to study enzymes involved in introducing lipid residues into proteins and in processing lipidated proteins. In particular, they have been used to obtain knowledge about the importance of lipid residues in the function of lipid-modified proteins. Issues such as the contribution of different lipid residues to anchoring of proteins in membranes, and whether the type of lipid modification determines the localization of proteins in particular subcellular membranes under certain circumstances, have been addressed by combining biophysical and cell biology techniques for the lipopeptides obtained as described above.[153, 154]

In a series of biophysical investigations on the thermodynamics of the insertion of lipid-modified model peptides in vesicles functioning as model membranes, the contribution of the lipids to lipopeptide membrane affinity was determined.[149, 155–157] This showed that a N-myristoyl or a S-farnesyl group alone cannot contribute enough hydrophobic character to maintain stable membrane insertion of peptides, and therefore also of proteins. Peptides and proteins that carry only a single lipid modification are rapidly inserted into the membrane (within seconds), yet they are also rapidly exchanged between two different membranes (half-time on the order of seconds). A palmitoyl group provides the peptides with about 15-fold higher membrane affinity than a myristoyl residue, and a geranylgeranyl thioether has about the same effect. For a C terminal farnesylated and geranylgeranylated peptide modified as a methyl ester, the membrane affinity is ten times higher than for the analogous S-prenylated carboxylic acid. The C-terminal methylation of a farnesylated protein therefore has a greater effect on its distribution between cytosol and membrane, whereas a geranylgeranylated protein without esterification will be mostly membrane bound. Binding of simple modified peptides to model membranes is therefore strong in the thermodynamic sense but rapidly reversible. A single lipid modification cannot maintain stable insertion of a lipid-modified protein in a membrane.

However, a second lipid modification does achieve stable insertion. Biophysical model experiments on the kinetics of transfer of lipid-modified peptides from one model membrane to another[149, 158] showed that the half-time for transfer of a singly farnesylated or palmitoylated peptide is in the region of seconds. For peptides that are N-myristoylated and S-palmitoylated, or S-palmitoylated and S-farnesylated, the half-times are in the range of hours to days. These values are significantly larger than the half-time for turnover of S-acyl groups of membrane-associated proteins in vivo (≤ 2 h) or recycling of membrane-bound proteins that is mediated by escort proteins. These double lipid modifications give stable membrane binding in a biological context and on a biologically relevant time scale, and can be used as specific structural motifs to localize and anchor proteins in special subcellular membranes. In fact, the N-myristoyl/S-palmitoyl motif is found in nonreceptor tyrosine kinases and the α subunit of heterotrimeric G proteins, and H-Ras and N-Ras are S-palmitoylated and S-farnesylated.

This hypothesis was elegantly tested by in vivo studies with fluorescently labeled N-myristoylased[159] and S-farnesylated peptides.[152, 158, 159] Peptides **89** and **90** (Scheme 34), which represent forms of the N terminus of the human nonreceptor tyrosine kinase Lck and the human N-Ras protein with a single lipid modification, were S-palmitoylated in fibroblast cells; for analogous peptides in which the palmitoylatable cysteine residues were replaced by serine, such as **91**, no incorporation of palmitic acid could be detected. Palmitoylation was also observed for peptides in which the myristoyl residue had been exchanged for other fatty acids (C_{10} to C_{16}) or the farnesyl residue for other alkyl groups (*n*-undecyl, *n*-octyl, *trans*-geranyl).

The site of palmitoylation and the intracellular distribution of peptides with double lipid modification were determined with fluorescent microscopy techniques. This showed that the doubly lipid modified peptides formed from **89** and **90** were concentrated in the plasma membrane of fibroblast cells (Figure 1); this took place under conditions (15 °C) which exclude intracellular transport, for example, by vesicles. For analogous serinyl peptides such as **91** that do not become acylated (see below), such a selective distribution was not observed; the S-*n*-alkylated and geranylated analogues of **90** showed similar behavior. Peptides **89**–**91** were introduced into cells by fusion of the fibroblast membrane with vesicles containing the fluorescently labeled peptide. The results were also confirmed by microinjection of **92** and **86** (Scheme 33;



Scheme 34. Lipid-modified peptides with the NBD marker for biological studies.

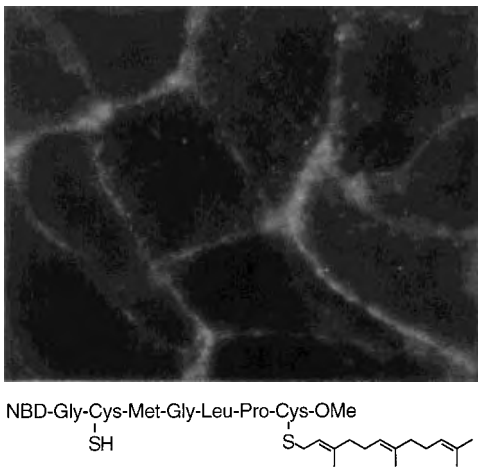


Figure 1. Fluorescence image of CV-1 fibroblasts after treatment with the NBD-labeled and farnesylated lipoheptapeptide **90**. The image shows that the fluorescence is concentrated in the plasma membrane.

NBD-labeled) and subsequent examination by confocal laser fluorescence microscopy.[152] This showed that the farnesylated, but no longer palmitoylatable, pentapeptide **92** was not selectively incorporated into a certain membrane; however, the doubly lipid modified **86** was selectively accumulated in the plasma membrane (Figure 2).

These findings, and those obtained from biophysical experiments, that doubly lipid modified (in contrast to singly

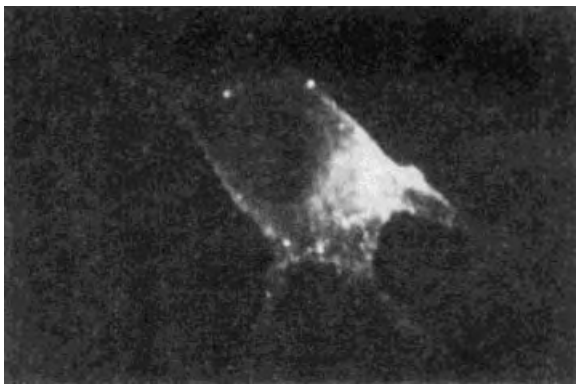
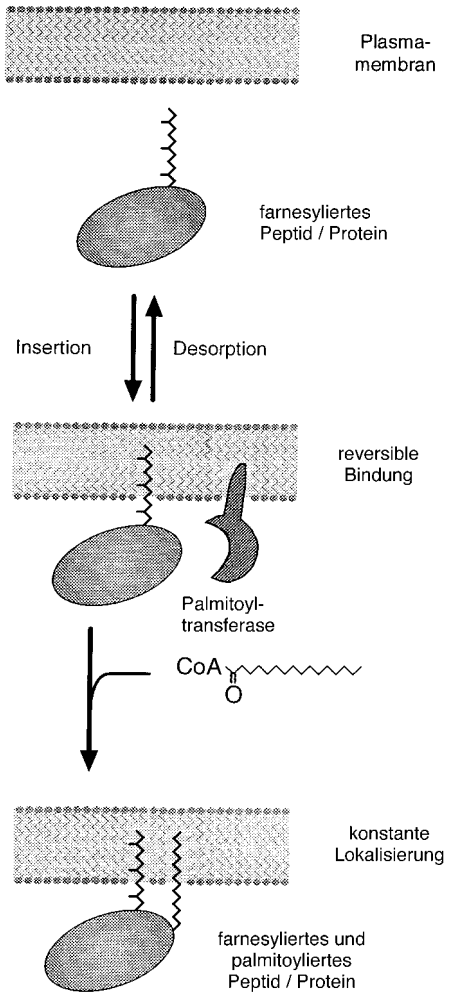


Figure 2. Fluorescence image of NIH-3T3 fibroblasts after microinjection of the NBD-labeled, farnesylated, and palmitoylated Ras heptapeptide **86**. The image shows that the peptide is localized in the plasma membrane.

modified) peptides only exchange very slowly between different membranes when a second lipid residue is introduced (see above) and should therefore concentrate in the cell compartment in which the second lipid modification takes place, led to the conclusion that S-palmitoylation of singly lipidated peptides (and therefore also singly modified proteins) takes place at the plasma membrane.

The results of the biophysical and cell biology investigations support a model[159] for specific localization of proteins by myristoylation/palmitoylation or farnesylation/palmitoylation. According to this model, the specific localization is not only determined by the lipid groups introduced in the course of the biosynthesis (in the case of Ras proteins, the farnesyl residue). Rather, the singly modified proteins can freely diffuse and insert in or desorb from different membranes (Scheme 35). It is only upon S-acylation in a certain membrane compartment that they remain localized in that membrane. In the case of the N-Ras peptide **90** and the $p56^{lck}$ peptide **89**, it is the plasma membrane in which the lipid-modified proteins are actually found. A membrane-bound protein S-acyltransferase that may be responsible for this modification was recently identified; it palmitoylates a farnesylated N-Ras peptide and also the H-Ras protein.[160] If the lipid-modified protein is no longer needed, or the signals transmitted by such proteins must be terminated (regulation of signal chains), the thioester can be cleaved again by a suitable hydrolase, initiating desorption of the protein from the membrane (Scheme 35).

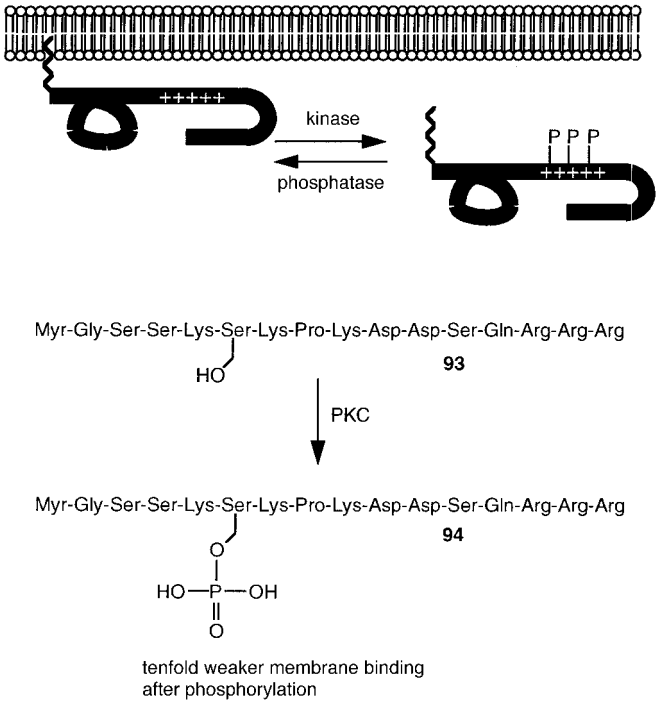
In addition to introduction of a second lipid residue, stable insertion of a protein in a membrane can also be achieved by combining a first lipid residue with a cluster of amino acids that are positively charged under physiological conditions and thus interact with the negatively charged cell membrane (Scheme 36).[153, 154] This cooperative interaction is reduced by phosphorylation of the proteins in the positively charged domains (i.e., by reducing the number of positive charges with negatively charged phosphate), and the protein desorbs from the membrane. The membrane insertion/desorption of proteins can be regulated in this way. A combination of a lipid residue with protonated basic amino acids is found in, for example, the N-myristoylated nonreceptor tyrosine kinase



Scheme 35. Model for insertion of lipid-modified proteins in the plasma membrane by additional S-palmitoylation.

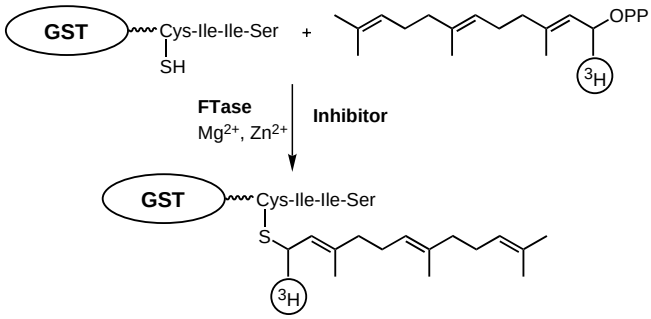
Src, the N-myristoylated alanine-rich C kinase substrate (MARCKS), and the S-farnesylated but not palmitoylated K-Ras protein. For MARCKS, regulation according to the model shown in Scheme 36 was proven by extensive mutation analysis; for the c-Src peptide **93** and the analogous phospholipopeptide **94**, which represent the N terminus of the protein, similar behavior was shown in experiments on a model membrane. The membrane binding of **93** was reduced tenfold on phosphorylation at Ser 12 by protein kinase C.[154] By investigating this and other similar issues with suitable lipid-modified peptides, it might be possible to obtain valuable information leading to development of heterologuous recombinant proteins and their direction to particular locations in the cell where they then influence signal transduction. Furthermore, the development of new active compounds that influence pathological signal mediation processes (e.g. through Ras) might gain a new impetus.

S-Farnesylated cysteinyl peptides have served as tools for studying and inhibiting all enzymes involved in the biosynthesis of S-farnesylated and C-terminal methylated proteins such as the Ras protein (Scheme 5, Scheme 23; see Sections 2.2 and 5). Farnesyltransferase, which transfers the farnesyl residue to the precursor protein, is inhibited with



Scheme 36. Regulation of membrane binding by combination of N-myristoylation with a polybasic amino acid sequence and phosphorylation.

an IC_{50} value in the millimolar range by farnesylated peptides which also have the subsequently cleaved C-terminal AAX sequence (Scheme 37).[161] However, an analogue masked



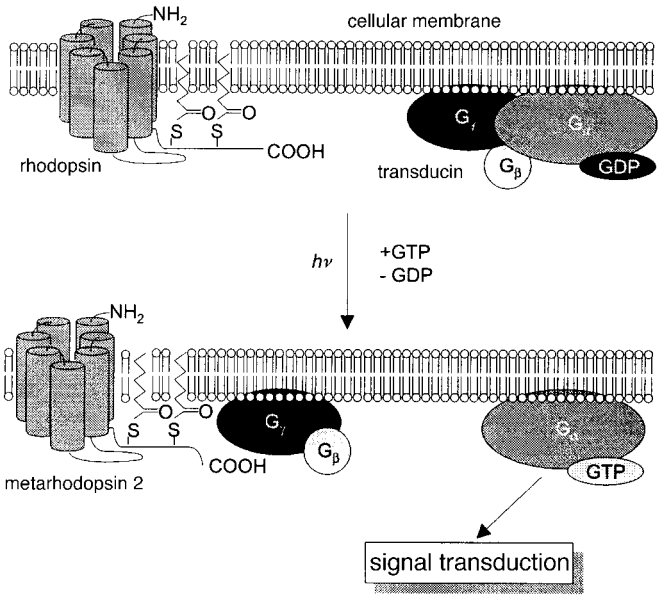
Inhibitor	IC_{50}
CAAX peptide	0.1 – 6 μM
S -farnesyl-CAAX-peptide	1.4 – 8.2 μM
S -farnesyl-Cys-OMe-peptide	no inhibition
Aloc-Cys(Pal)-Met-Gly-Leu-Pro-Cys(Far)-OMe **76**	5.5 mM

Scheme 37. Inhibition of the Ras farnesyltransferase by lipid-modified peptides. GST = glutathion S-transferase.

with a methyl ester which lacks the AAX peptide, corresponding to the processed form of the Ras protein, does not show any inhibitory activity.[151] Nevertheless, weak inhibition is observed if an esterified and also farnesylated and palmitoylated peptide is used as an inhibitor (Scheme 37). This finding indicates a possible feedback inhibition in the biosynthesis of the Ras protein.[151]

Similarly, tetrapeptides with isoprenylated N-terminal cysteine have been used to study proteinases that cleave the C-terminal AAX segment from the precursor protein.[141, 162, 163] It was shown that substrates of the enzyme must have an isoprenylated cysteine residue and that the biocatalyst recognizes the absolute configuration of the amino acids. Based on this knowledge, simple farnesyl peptide analogues were developed as inhibitors of the protease.[164] In addition, S-isoprenylated and simple alkylated peptides were used to track down a methyltransferase that creates the C-terminal methyl ester of the farnesylated protein.[141, 165, 166] This also showed that a farnesylated peptide was able to inhibit the methylation of a natural protein.

With lipid-modified peptides, the unsolved problem was tackled of whether lipid residues, in addition to their importance for membrane anchoring and localization of proteins, also have active roles in the biological function of lipid-modified proteins. The foremost questions here are whether there are specific receptors in the membrane that recognize farnesyl residues and whether the lipid residues are involved in controlling signal transduction processes, for example, through lipid–protein interactions. Signal transduction in photoreceptors through the G protein coupled receptor rhodopsin and the heterotrimeric G protein transducin was chosen as the biological system (see Section 2.1). Upon absorption of light, rhodopsin is activated to metarhodopsin 2, which then interacts with transducin and catalyzes exchange of GDP for GTP at the α subunit; the β,γ subunit is important in this exchange. The α unit with GTP then activates a cGMP-specific phosphodiesterase which transmits the signal to Na channels and thereby passes on the reaction to the light signal (Scheme 38).[141, 167] To test



R-Asp-Lys-Asn-Pro-Phe-Lys-Glu-Leu-Lys-Gly-Gly-Cys-OH
Far

95, R = H
96, R = Y

Scheme 38. Manipulation of signal transmission in the rhodopsin/transducin system by lipid-modified peptides.

whether coupling of the receptor to the G protein is mediated by its γ subunit, the farnesylated peptide **95**, which corresponds to the C terminus of the γ subunit, and *N*-acetyl-*S*-farnesylcysteine were examined as inhibitors of the interaction between rhodopsin and transducin.[168, 169] The peptide **95** stabilizes the active form of the receptor (metarhodopsin 2) and decouples it from transducin. Both the farnesyl residue and the amino acid sequence are important for the effect. It was concluded that the farnesyl residue is of direct importance for the protein–protein interaction and does not just function as a membrane anchor,[168] and that, with the help of S-prenylated cysteine analogues, the interaction of activated receptors with the β,γ subunits of G proteins can be specifically inhibited.[169] Subsequently, analogous peptides such as **96** were used to study the interaction between the α subunit of transducin and the β,γ complex, which can also be inhibited by **96**.[170]

Regardless of any doubt about the conclusions on rhodopsin/transducin drawn from the investigations described above,[141] different farnesyl cysteine analogues and farnesylated peptides show manifold physiological effects suggesting that these compounds interact with signal transduction processes. For example, they interfere with release of superoxide in neutrophiles[171, 172] in which isoprenylated Rac protein plays a role, they block thromboxane- or thrombin-induced platelet aggregation,[173, 174] and they influence the release of insulin from pancreatic cells.[175] These effects do not seem to be due to inhibition of processing of lipid-modified proteins. It seems likely that the isoprenylated peptides influence the function of isoprenylated G proteins, for example, by interaction with proteins in the sense of a receptor-ligand interaction in which they act as their target proteins.

Furthermore, a protein that binds prenylated CAAX peptides with high affinity was identified in microsomal membrane fractions of bovine brain; this protein could be a receptor for prenylated peptides.[176] For yeast Ras, the farnesyl residue of the protein probably serves not only to localize the protein on the plasma membrane but is also involved in the interaction of Ras with its target protein, the adenylate cyclase.[177]

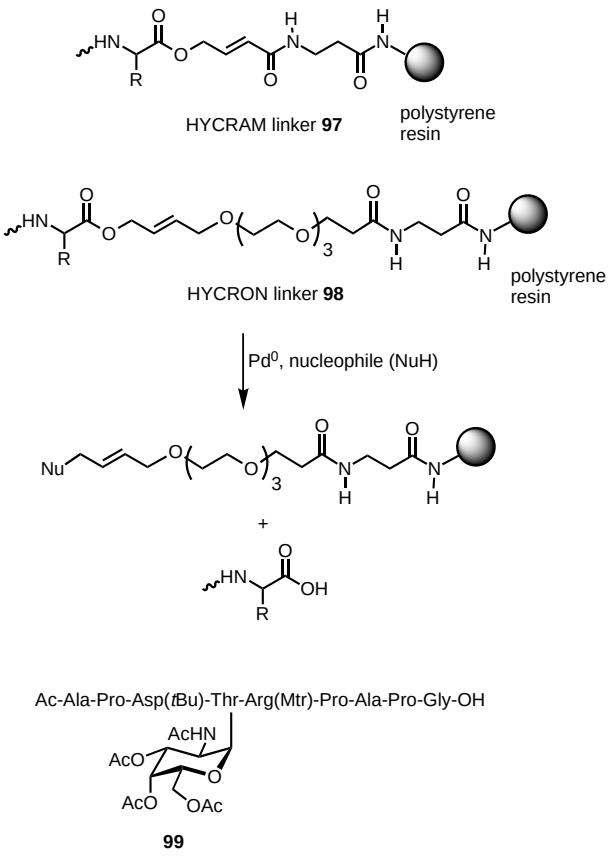
6.2. Glycopeptides

Many of the proteins localized on the extracellular face of the plasma membrane carry complex oligosaccharides. These glycoproteins are intensively involved in regulating communication between cells; they control cell–cell interactions and form cell-surface antigens.[178] Taking this into consideration, it is particularly noteworthy that glycoproteins have also been identified as tumor-associated antigens, that is, as antigens which appear on the surface of tumors but not on normal cells. In addition, many of the cell-surface receptors that take up extracellular signals and pass them through the plasma membrane into the cell interior are glycosylated. The carbohydrate and peptide structures are of importance for biological function of these protein conjugates, as shown, for example, for the proteins of the major histocompatibility

complex (MHC).[179] Whereas proteins with attached complex oligosaccharides almost exclusively fulfill extracellular biological functions on the cell surface, it was recently shown that glycosylation of proteins can play an important intracellular role (see Section 6.3).

Characteristic glycopeptides could be useful tools for investigation of the biological functions of glycoproteins. To synthesize these peptide conjugates, both in solution and on solid phase, powerful techniques for reversible blocking of the amino, carboxy, and alcohol groups have been developed in the last two decades[137] along with methods for gentle release from polymeric carriers.[180–183] Classical chemical synthesis of oligosaccharide units of glycoproteins has also reached a high level of efficiency.[137, 184] The first effective solid-phase techniques were developed to this end.[185]

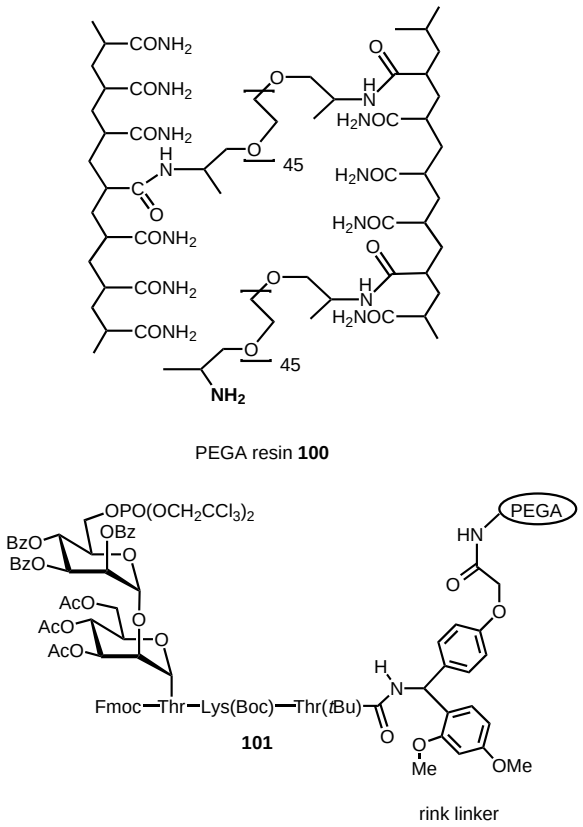
Owing to the performance of established classical chemical techniques, it is possible today to assemble glycosylated peptides on polymeric carriers with a high degree of efficiency. The allylic HYCRAM[180] (**97**) and HYCRON[181] linker groups (**98**, Scheme 39) are particularly advantageous



Scheme 39. Solid-phase glycopeptide synthesis with the HYCRAM and HYCRON linker groups. Mtr = 4-methoxy-2,3,6-trimethylbenzenesulfonyl.

since they permit gentle release of the sensitive glycopeptide from the solid phase in a Pd^0-catalyzed allyl transfer to N- and C-nucleophiles. With HYCRAM linkers, it was possible to synthesize many glycopeptides, with both the acid-labile Boc and base-labile Fmoc groups as protecting functionalities. However, the basic cleavage of the Fmoc group presented problems, for example, nucleophilic attack on the α,β-unsaturated amide group in **97**. Also, the glycopeptides could not be quantitatively released from the solid carrier in some cases. These disadvantages were overcome with the development of **98**. In **98**, a flexible oligoethylene glycol spacer ensures that the Pd^0 complex can progress well to the allylic group during cleavage; this group is no longer present as the α,β-unsaturated carbonyl functionality but rather as the ether and is therefore no longer competitively attacked by nucleophiles. With the HYCRON linker, the glycopeptide **99** was synthesized on a polymeric carrier and subsequently released in a high yield. The method has proven to be equally successful for synthesizing an eicosapeptide.

The PEGA resin **100** was recently developed as an advantageous alternative to the carriers based on polystyrene that are generally used (Scheme 40). In principle, it is made up

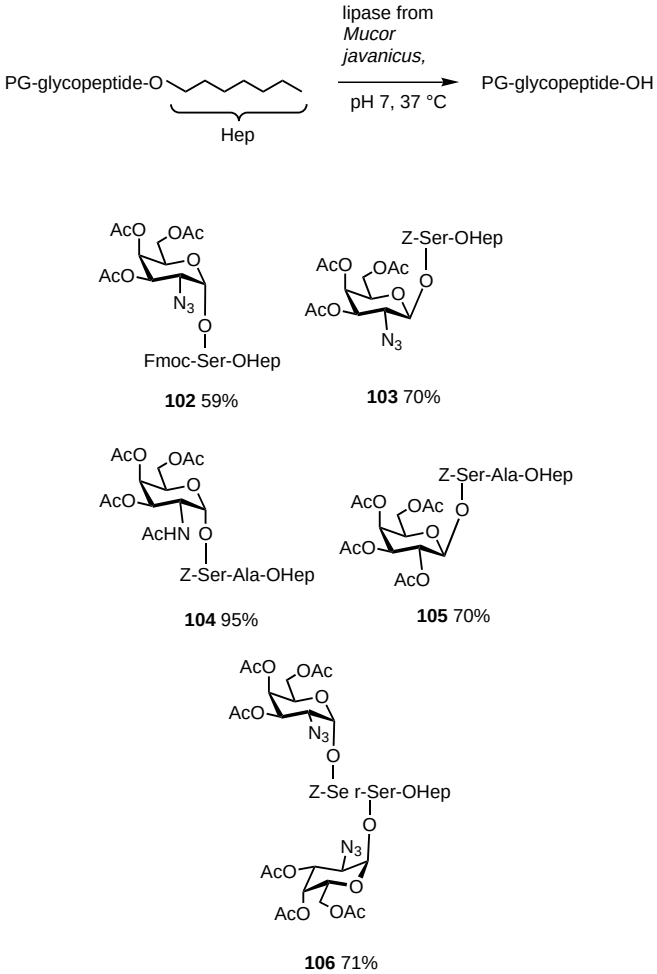


Scheme 40. Solid-phase glycopeptide synthesis on PEGA resin.

of poly(acrylamide) chains which are cross-linked by poly(ethylene glycol) units and carry additional free amino functionalities at which peptides and glycopeptides can be synthesized.[183] The hydrophilic PEGA resin swells very well in different solvents, and its interior is accessible to larger molecules and even enzymes owing to the flexible structure of the matrix. With PEGA resin, numerous glycosylated peptides were synthesized in automated solid-phase syntheses (Scheme 40).[182, 183, 186] Fmoc-urethane was used as N-terminal protecting group, and the glycopeptide to be synthesized was linked to the polymeric carrier through the acid-labile rink linker (see **101**, Scheme 40). Glycopeptides bound on the solid phase were thus synthesized by successive extension of the

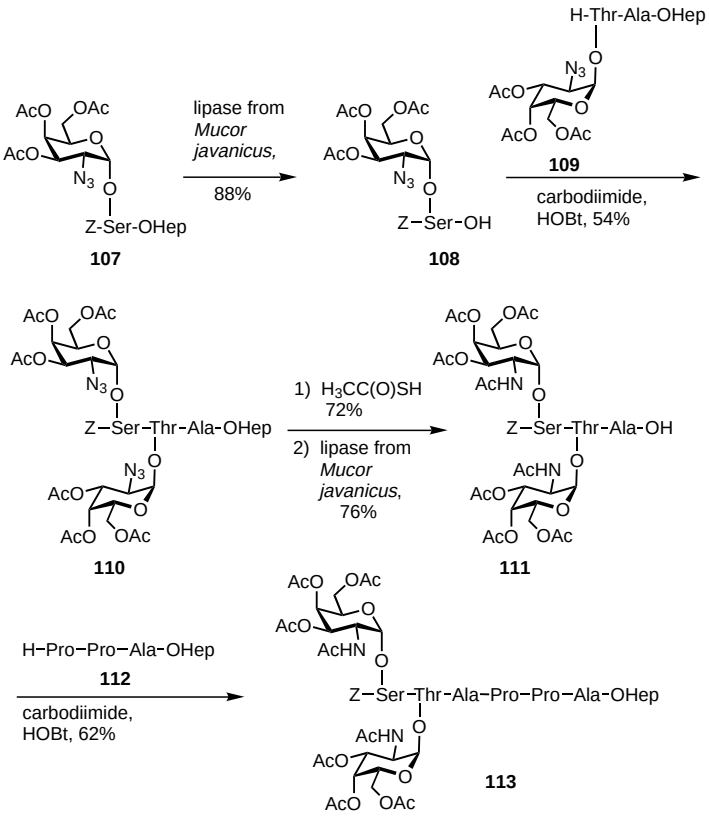
peptide chain. These glycoconjugates were cleaved from the solid phase under slightly acidic conditions and without unwanted side reactions. Glycopeptides can be reliably and efficiently synthesized today by this and other solid-phase techniques with automated methods.

Enzymatic methods have opened up valuable alternatives for selective deblocking of glycopeptides and for synthesis of their oligosaccharide units. For example, selective and gentle enzymatic deblocking of O-glycopeptides was achieved by lipase-mediated hydrolysis of the heptyl ester protecting group. The lipase from *Mucor javanicus* deblocks the C-terminus of the glycosylated amino acids and peptides **102**–**106** without unwanted attack on the N-terminal urethane and the carbohydrate protecting group (Scheme 41).[187] There was



Scheme 41. Chemoenzymatic glycopeptide synthesis with use of the enzyme-labile heptyl (Hep) protecting group (PG).

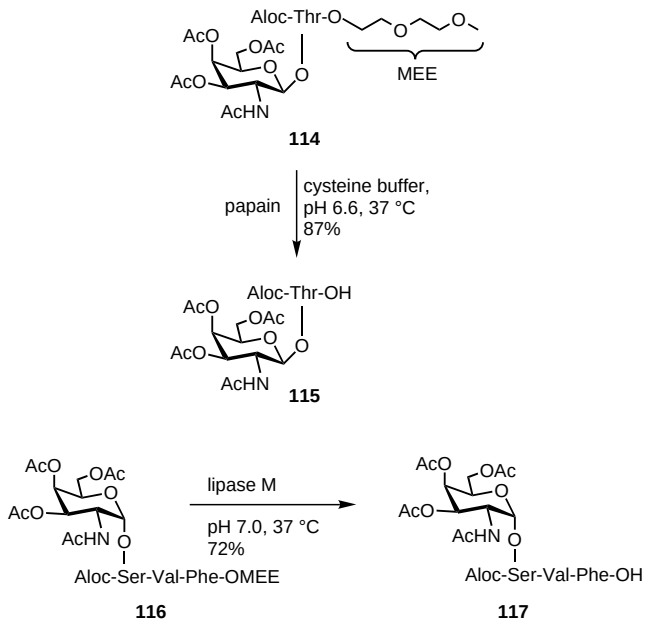
no anomerization or β-elimination under these mild conditions. With this enzymatic protecting group technique, the complex diglycohexapeptide **113** was synthesized; it contains the characteristic linkage region of a tumor-associated antigen found on the surface of human breast carcinomas (Scheme 42). Following selective C-terminal deblocking of the serine glycoside heptyl ester **107**, the carboxylic acid **108** that was released was condensed with the N-terminal deblocked glycopeptide ester **109** to form the diglycotripeptide **110**. The azido group of the latter was converted into the acetamide group, and subsequently the C terminus was selectively released again by enzyme-mediated hydrolysis without any unwanted side reactions (→**111**). The C-terminal extension of the peptide chain gave the desired peptide **113**.



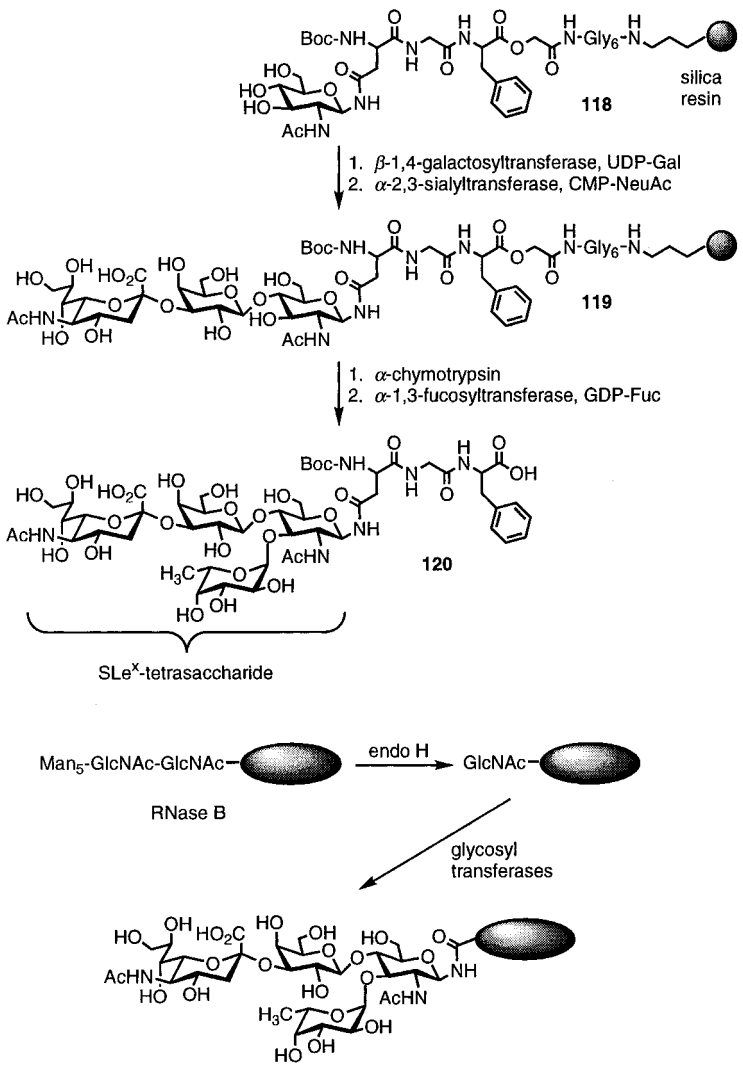
Scheme 42. Synthesis of glycopeptide **113**, which represents a characteristic section of a tumor-associated antigen.

If the very hydrophobic heptyl ester was used, there were problems due to the low solubility of the substrates and, thus, low rate of turnover, especially in the presence of similarly hydrophobic amino acids. These problems were solved by introducing the more hydrophilic 2-(*N*-morpholino)ethyl (MoEt)[188] and, in particular, the methoxyethoxyethyl (MEE) group.[189] The MEE ester was, for example, cleaved from the glycopeptide **116** by lipase-catalyzed hydrolysis (Scheme 43), and the threonine glycoside **114** could be deblocked at the C terminus by papain. The proteases papain, subtilisin, and thermitase were also used for demasking glycopeptide methyl[190] and even *tert*-butyl ester protecting groups.[191]

In the synthesis of glycopeptides, enzymatic transformations were also used to assemble the oligosaccharide. Thus, for example, the glycosylated asparaginyl peptide **118** was synthesized on a polymeric carrier (Scheme 44), and then regio- and stereospecific linking of a galactose and a neuraminic acid unit (→**119**) was achieved in two consecutive enzymatic glycosylations.[192] Following cleavage of the glycopeptide from the solid phase by chymotrypsin-mediated ester hydrolysis at the C terminus of a phenylalanine residue, the characteristic sialyl Lewis^X (SLe^X) tetrasaccharide was completed by fucosylation of the *N*-acetylglucosamine (→**120**).



Scheme 43. Enzymatic glycopeptide synthesis with use of the enzyme-labile methoxyethoxyethyl (MEE) ester.



Scheme 44. Enzymatic synthesis of peptides modified with sialyl Lewis^X and of proteins with glycosyl transferases.

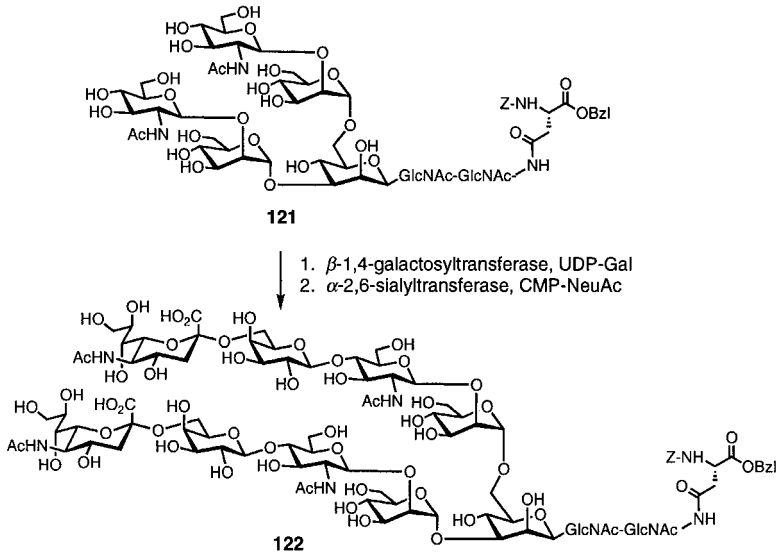
This technique also enabled in vitro synthesis of a glycosylated protein in an impressive manner.[193] For this, an oligosaccharide was cleaved off RNAase B with a glycosidase, and the remaining GlcNAc residue underwent successive enzymatic glycosylations until the protein was attached with the SLe^X tetrasaccharide attached (Scheme 44). With this enzymatic technique, which is based on a principle previously suggested for modifying unwanted glycans of recombinant glycoproteins,[194] it is possible to obtain glycosylated proteins with high homegeneity; this opens up new possibilities for studying the influence of carbohydrates on structure and function of glycoproteins.

A big advantage for the synthesis of complex glycopeptides is offered by combining classical chemical steps with enzymatic glycosylation steps. For example, glycopeptide **121** was synthesized with the help of established carbohydrate chemistry methods, and the oligosaccharide was subsequently extended to the undecasaccharide by enzymatic glycosylations (→**122**, Scheme 45).[195]

Synthetic glycopeptides produced both chemoenzymatically or by classical chemical methods, in solution or on solid phase, have often been used as inhibitors in experiments aimed at blocking the attachment of leucocytes to endothelial cells and the subsequent migration of leucocytes out of blood vessels as a reaction to acute and chronic inflammatory processes. During this process, proteins on the surface of the endothelial cells called selectins recognize complex glycoproteins on the leucocytes carrying the SLe^X carbohydrate epitope;[178, 196] this initiates the migration process.

This interaction was inhibited with glycopeptides with the aim of possibly developing a new therapeutic treatment. Based on data on the conformation of SLe^X in solution, the three-dimensional structure of the human E-selectin, and the structural elements needed for recognizing SLe^X by E-selectin, and supported by molecular modeling, the fucosylated peptides **123**–**125** and further analogues were synthesized and tested as inhibitors (Scheme 46).[197] The peptides each contain the necessary fucose, a structural element carrying a hydroxyl group that imitates the galactose of the SLe^X tetrasaccharide, and a glutaric acid, which functions as the equivalent of the negatively charged group of the sialic acid unit. Compound **123** proved to be as active as the natural SLe^X, whereas **124** and **125** were considerably better inhibitors.

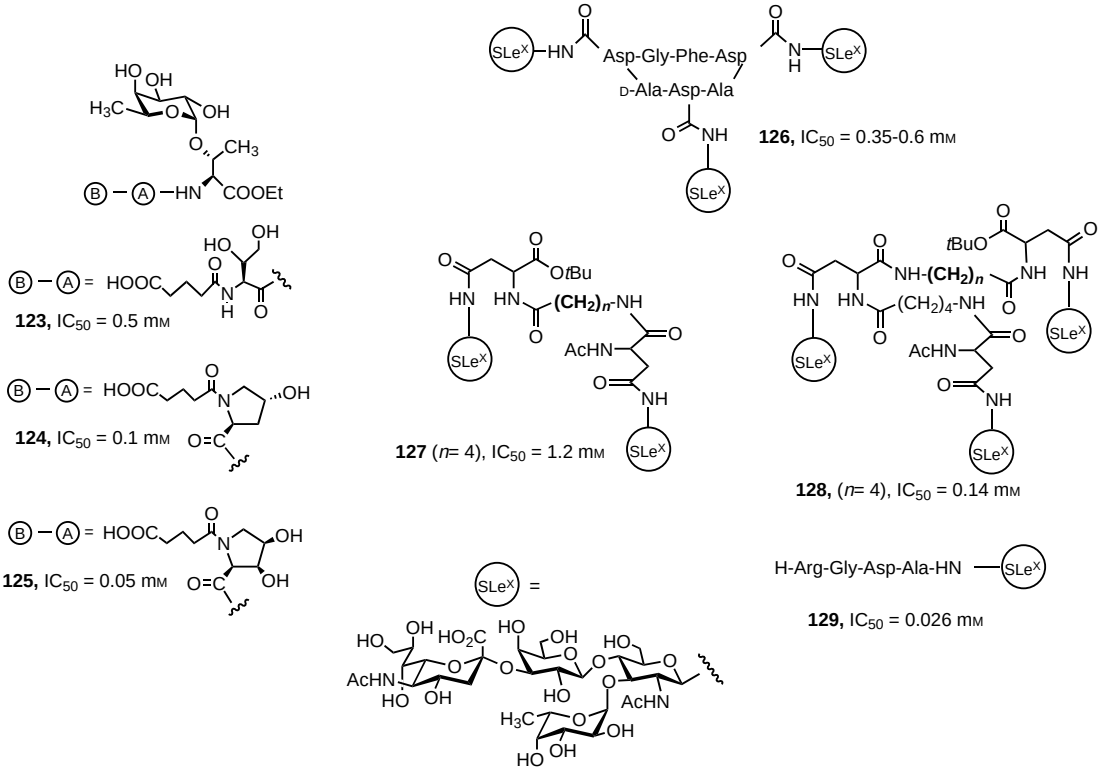
The assumption that the weak interaction of monomeric SLe^X in vivo is increased by "clustering" of ligands



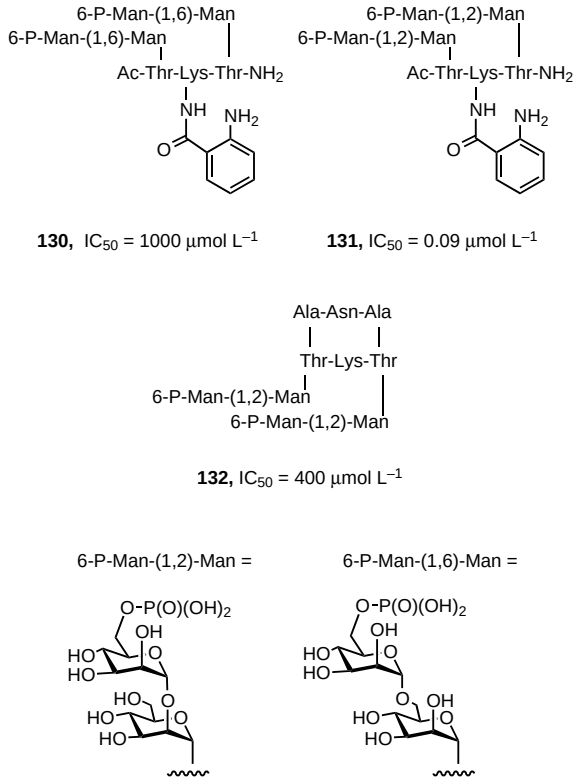
Scheme 45. Synthesis of a complex glycopeptide precursor by successive enzymatic glycosylations.

(multivalence) was examined with the multiple SLe^X glycopeptides **126**–**128** (Scheme 46). In a cell-adhesion test in which binding of **126** to recombinant E-selectin/immunoglobulin fusion proteins was compared to its binding to tumor cells carrying the SLe^X ligand, the trivalent glycopeptide was two to three times more active as an inhibitor than monomeric SLe^X building blocks.[198] In **127** and **128**, the distance of the SLe^X oligosaccharides from one another was varied to obtain information on the size and the spatial orientation of the SLe^X cluster.[199] The divalent ligands **127** were less active than the trivalent analogues **128**, and the inhibition actually depends on the number of methylene groups introduced as spacers. A considerable increase in the cell adhesion inhibitory activity was achieved by linking the SLe^X tetrasaccharide to the tripeptide Arg-Gly-Asp (RGD), which corresponds to the minimum sequence of many adhesion molecules and is, for example, recognized by integrin receptors. The adhesion hybrid **129** thus obtained showed an IC_{50} value of 26 μM in the cell assay and proved to be a very effective inhibitor of adhesion.[200]

Glycopeptides carrying the 6-O-phosphorylated mannose residue were used as reagents for studying the recognition of phosphorylated glycoproteins by the mannose 6-phosphate (Man-6-P) receptor.[186] Lysosomal enzymes carry oligosaccharides with Man-6-P residues. Through these carbohydrates, they are recognized by Man-6-P receptors, then correctly processed, and finally transported to the golgi apparatus. Misregulation of these steps is involved in inflammatory processes in the central nervous system. Based on the suggestion that a second oligosaccharide with two Man-6-P residues is the natural ligand for the receptor, diverse open-chain and cyclic glycopeptides such as **130**–**132** (Scheme 47) were synthesized. A phosphorylated mannose or a phosphorylated disaccharide with α(1,6)- or α(1,2)-linked mannoses was introduced into these compounds, and the length and sequence of the amino acid chains between the saccharides was varied.[186] The glycopeptides were then examined in a



Scheme 46. Synthetic sialyl Lewis^X mimetics.



Scheme 47. Synthetic phosphomannosyl glycopeptides and their inhibitory effect on the phosphomannose receptor.

specially developed ELISA test as inhibitors of binding of the Man-6-P receptor to an immobilized phosphomannan. A high binding affinity was obtained if the ligands are bidental and carry 6′-O-phosphorylated α(1,2)-linked disaccharides; monosaccharides and α(1,6)-linked disaccharides are considerably less active. Three to five amino acids as spacer between the two saccharides were favorable. Cyclic peptides seemed to be conformationally too stiff for good binding.

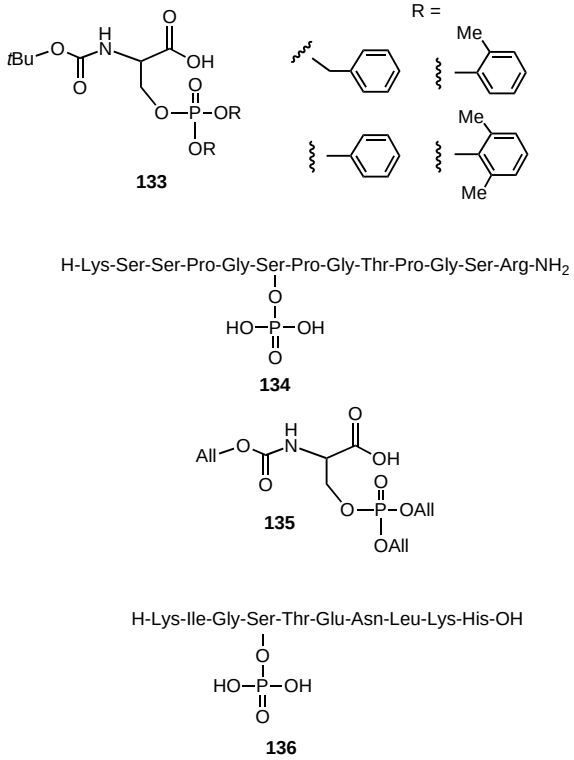
Since glycoproteins could represent the characteristic structures of tumor-associated antigens, corresponding synthetic glycopeptides have also been intensively used as reagents for developing antitumor vaccines.[201]

6.3. Phosphopeptides and Glycophosphopeptides

Protein kinase and phosphatase-mediated phosphorylation of proteins at serine, threonine, and tyrosine residues is used in all organisms to regulte many different intracellular processes, for example, signal transduction from the plasma membrane to the cell nucleus as well as direction of cell growth and division.[202] Characteristic phosphopetides were therefore repeatedly used as reagents for study and selective manipulation of such processes. The synthesis of phosphorylated serine and threonine peptides is impeded to a considerable extent by the extreme base lability of these peptide conjugates (see Scheme 27); protecting groups which can be released under mild conditions are required. However, peptides phosphorylated at tyrosine residues cannot lose the phosphate group by β-elimination, and are therefore much easier to synthesize.[138] The development of methods for their synthesis will not be discussed further here.

Serine/threonine phosphopeptides can in principle be made by post-synthesis phosphorylation of a separately synthesized peptide ("global phosphorylation strategy") or by stepwise synthesis of the target compound in solution or on solid phase with phosphorylated amino acid building units ("building block strategy"). The latter method is generally more flexible.

For the stepwise synthesis of phosphopeptides, Boc-protected building blocks such as **133** initially were used (Scheme 48); the phosphate protecting group had to be

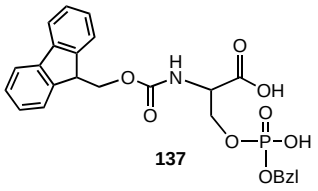


Scheme 48. Phosphopeptides synthesized with fully protected phosphoamino acid building blocks.

carefully chosen to avoid dephosphorylation under the conditions of Boc-group cleavage.[138, 203] Although this technique could be used to synthesize phosphopeptides, such as the partial sequence **134** of the Tau protein, on a polymeric carrier,[204] recently more advantageous synthetic building blocks were developed which were protected in other ways. Use of the N-terminal allyloxycarbonyl (Aloc) protecting group proved to be effective, for example. In a solid-phase synthesis of the Tau protein fragment **136**, the amino acid unit **135** was linked to a hexapeptide assembled on Wang resin with the base-labile N-terminal Fmoc group and acid-labile side-chain protecting groups.[205] By Pd^0-mediated release of the allyl protecting groups in the presence of Me_3SiN_3/Bu_4NF, the N terminus and the phosphate group were simultaneously deblocked without β-elimination. Extension of the peptide chain and subsequent release of the phosphopeptide from the resin, with simultaneous cleavage of the side-chain protecting groups, gave the desired peptide **136**. The disadvantage of this

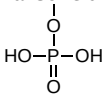
approach, however, is the simultaneous release of the phosphate group and amino functionality, since the latter can itself become activated during the subsequent peptide coupling.

The base-labile Fmoc protecting group, established as a standard method in solid-phase synthesis of nonmodified peptides and glycopeptides, cannot be used without further modification for synthesizing phosphopeptides, since serine and threonine phosphopeptides masked as phosphoric acid esters, unlike the more stable glycopeptides, lose the phosphate group by β-elimination and formation of α,β-dehydroalanyl peptides under the conditions for Fmoc cleavage.[206] This disadvantage was overcome, however, by introduction of the Fmoc-masked unit **137**, which only carries a phosphoric acid diester group (Scheme 49).[207, 208] The phosphate group is deprotonated under basic conditions and, as a poor leaving group, is no longer eliminated. It is stable with respect to treatment with piperidine, which is added to release the Fmoc group, and is apparently not activated upon subsequent extension of the peptide chain. With this building block, the phosphopeptides **138** and **139**, which represent phosphorylated partial sequences of the heat-shock protein 27, were synthesized on solid phase without any occurrence of the unwanted side reactions mentioned above.[208] This is therefore an efficient method for the flexible synthesis of phosphopeptides on polymeric carriers with the established N-terminal Fmoc group.



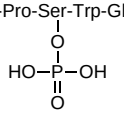
137

H-Ser-Gly-Val-Ser-Glu-Ile-OH



heat-shock protein 27 (87-92) **138**

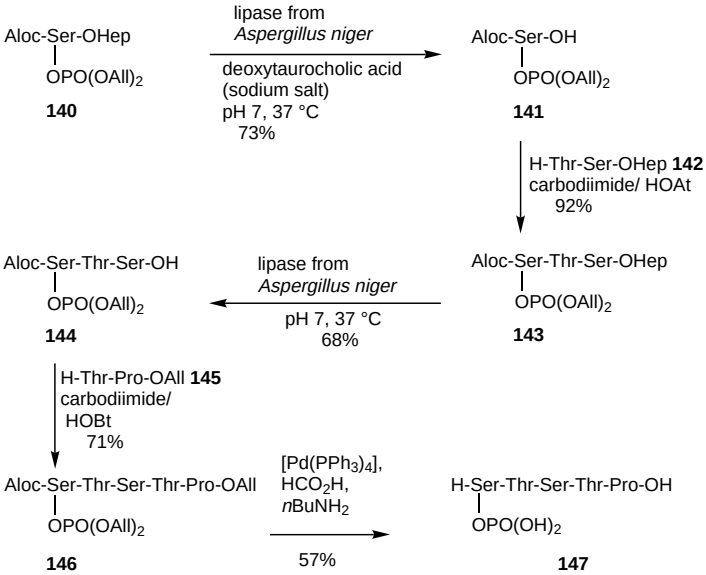
H-Leu-Leu-Arg-Ser-Pro-Ser-Trp-Glu-Pro-Phe-Arg-Cys-NH_2



heat-shock protein 27 (10-20)-Cys-NH_2 **139**

Scheme 49. Phosphopeptides synthesized with phosphoric acid diester **137**. The numbers in parentheses correspond to the sequence numbers in the protein.

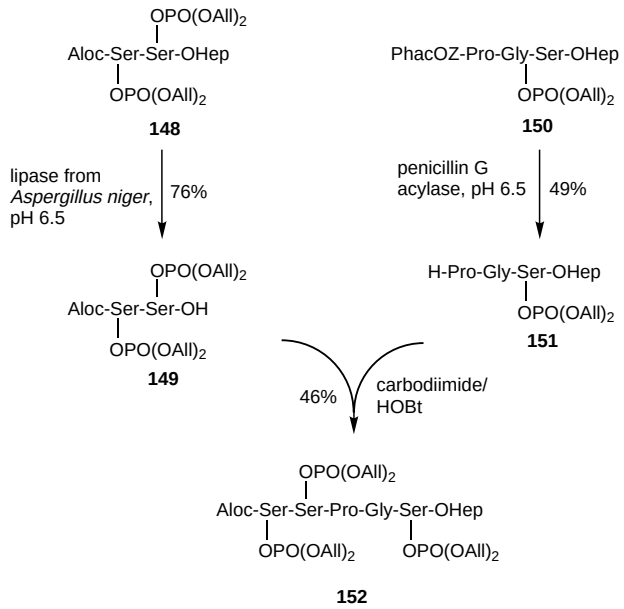
Enzymatic protecting group techniques have also provided interesting and advantageous alternatives to classical chemical methods in phosphopeptide synthesis. Thus, the phosphopentapetide **147** (Scheme 50), which is a characteristic section of the human Raf-1 kinase (see Section 2.2) was synthesized with lipase-mediated hydrolysis of the heptyl ester protecting group (see Section 6.2).[209] The fully protected phosphorylated serine heptyl ester **140** was selectively deblocked at the C terminus with the lipase from *Aspergillus niger*, and, following extension of the peptide chain, the enzyme released only the ester protecting group from the phosphotripeptide ester **143**. Renewed chain extension by a dipeptide and subsequent release of all allyl protecting groups gave the target compound **147**. The conditions for the enzymatic deblocking are so mild that there was no β-elimination of the phosphate residue from the phosphoric acid triester masked peptides.



Scheme 50. Chemoenzymatic phosphopeptide synthesis with the enzyme-labile heptyl ester.

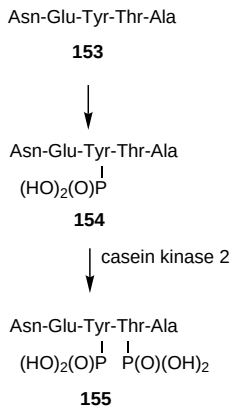
The N-terminal deblocking of phosphorylated peptides was achieved with the phenylacetoxybenzyloxycarbonyl (PhAcOZ) urethane protecting group.[210] This enzyme-labile urethane is an analogue of the AcOZ group described in Section 6.1 and was developed in the course of a phosphoglycopeptide synthesis (see below). On treating the PhAcOZ-masked phosphorylated tripeptide **150** with the enzyme penicillin G acylase, the terminal phenylacetic acid ester group was selectively cleaved off, and the spontaneous fragmentation shown in Scheme 31 was initiated. The phosphopeptide **151**, which is deblocked at the N terminus, that was released was then coupled with the doubly phosphorylated dipeptide **149** to give the pentapeptide **152** (Scheme 51), which is available for further C-terminal enzymatic deblocking. By selective lipase-mediated cleavage of the heptyl ester group, **149** was also obtained from the corresponding fully protected precursor **148**. An alternative possibility for selective N-terminal deblocking of phosphorylated peptides is by direct protection of the amino group with phenylacetic acid and biocatalyzed cleavage of the phenylacetamide with penicillin G acylase.[211]

Phosphorylated peptides have proven to be valuable tools in the study of signal cascades and the phosphoproteins involved therein. Phosphotyrosyl peptides have been repeatedly used in the elucidation of the binding specificity of signal transducing proteins which, for example, recognize phospho-



Scheme 51. Chemoenzymatic phosphopeptide synthesis with use of the enzyme-labile heptyl ester and the PhacOZ protecting group.

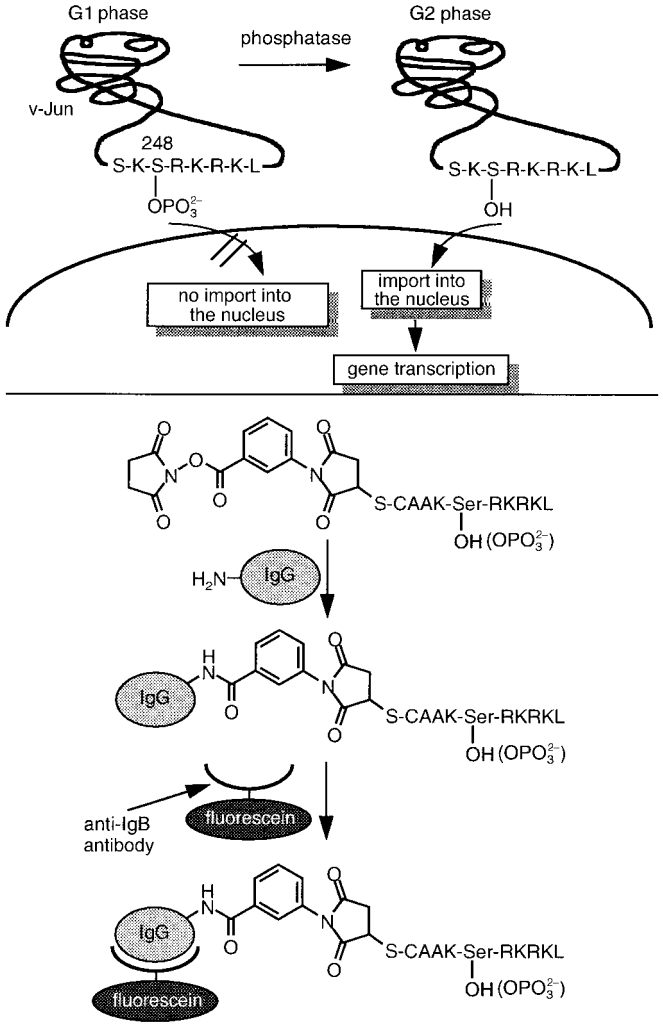
tyrosine residues in Ras and GPCR signal cascades with the help of SH2 domains (see Section 5). Targeted modulation of signal transmission by the JAK/STAT pathway was also achieved with such peptide conjugates (see Section 2.3). Furthermore, peptides modified with tyrosine phosphate which represent autophosphorylation sequences of tyrosine kinase receptors were used for determination of substrate tolerance of protein tyrosine phosphatases.[212] The substrate specificity of the Ser/Thr-specific casein kinase 2 was more closely defined with different phosphorylated peptides of the sequence Ala-Ser/Thr-Tyr-Ser-Ala,[213] which are derived from the phosphorylated form of the autophosphorylation site (Asn-Glu-Tyr-Thr-Ala) of the Src kinase family. Seven phosphopeptides were synthesized with the global phosphorylation strategy (see above) and tested as substrates for casein kinase 2. The enzymatic investigations showed that phosphorylation of the tyrosine residue favors the additional modification of the C-terminal serine; in the natural protein, the tyrosine phosphate group could function as the determinant for a subsequent second phosphorylation by casein kinase 2 at the adjacent C-terminal hydroxyamino acid (Scheme 52). This controlling activity explains why, in the case of the Src kinases, casein kinase 2 deviates from the typical substrate specificity, according to which the amino acid that is C-terminal to the target amino acid should be acidic.



Scheme 52. Enzymatic phosphorylation of a peptide with casein kinase 2.

A peptide in which a serine residue was phosphorylated was very elegantly used to elucidate the structural basis for the cell cycle dependent import of the tumorigenic transcription factor v-Jun in molecular detail.[214] In the G1 phase of the cell cycle, v-Jun is cytosolic. In this form, it is phosphorylated at Ser 248, that is, in the immediate vicinity of its nuclear localization sequence (NLS) which initiates active transport of the protein into the cell nucleus. In the G2 phase, the phosphoric acid ester is removed, however, and the protein concentrates in the cell nucleus. Apparently, the import of the v-Jun protein into the cell nucleus, which is essential for it to function as a transcription factor, is controlled by phosphorylation of the serine in the immediate vicinity of the NLS. That the phosphorylation has this crucial role in regulation of nuclear import was shown with the help of protein kinase and phosphatase inhibitors. In the presence of the serine kinase inhibitor staurosporin (see Section 7), the phosphorylation of v-Jun is suppressed, and the non-phosphorylated protein is transported into the nucleus in the G0, G1, and S phases of the cell cycle. The phosphatase inhibitor ocadaic acid (see Section 9.1) hinders dephosphorylation of the protein, however, and ensures that it also does not get into the nucleus in G2.

To test this hypothesis a phosphorylated peptide and the corresponding nonmodified peptide, both containing the serine residue in question and the NLS, were synthesized and linked to an immunoglobulin through an active ester (Scheme 53). Following microinjection of the protein conju-

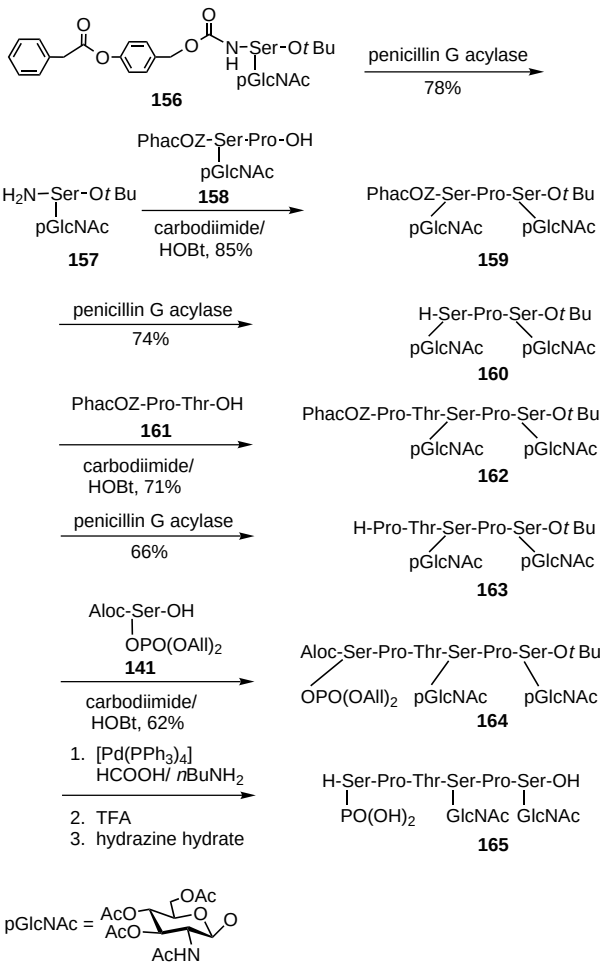


Scheme 53. Regulation of the nuclear import of v-Jun by phosphorylation.

gates into the cytosol of fibroblasts, their intracellular fate could be followed by fluorescence microscopy with a fluorescein-labeled anti-IgG antibody. This showed that the conjugate with the phosphorylated serine residue stayed in the cytosol, whereas the non-phosphorylated analogue was imported into the cell nucleus. Phosphorylated peptides have also often been used as antigenic structural units for creating monoclonal antibodies that recognize particular phosphoproteins.[205, 215] These antibodies serve, for example, as tools for immunodiagnosis of the Tau protein in Alzheimer's disease.

Recently, the glycosidic linkage of *N*-acetylglucosamine (GlcNAc) to the serine and threonine residues of intracellular proteins was reported as a new type of covalent intracellular protein modification.[216] The O-GlcNAc modification is similar to phosphorylation in many ways, especially with respect to its dynamic character and its ubiquitous occurrence, for example, in transcription factors such as Myc, the serum response factor (SRF), Jun, and Fos as well as oncogene products such as the tumor suppressors Rb and p53. Apparently, cells use reversible glycosylation with GlcNAc as a regulatory mechanism. In particular, it appears that phosphorylation and GlcNAc modification have a "yin–yang" relationship to one another, that is, they are not only similar but also often reciprocal to one another. The C-terminal domain of the human RNA polymerase II is multiply glycosylated in the cytosolic enzyme; however, the intranuclear enzyme is highly phosphorylated in the transcription complex and no longer glycosylated, whereby the phosphorylation and glycosylation sites are identical.[216, 217] Peptides containing both modifications could be valuable tools in answering the questions of whether the carbohydrate masks or even marks potential phosphorylation sites, and whether phosphorylation and glycosylation are involved in regulating nuclear import, or even influence transcription of the genetic code. The problems of both phosphopeptide and glycopeptide chemistry must be considered for their synthesis. However, with enzymatic protecting group techniques, the first synthesis of a complex phosphoglycopeptide which represents a characteristic section of the large C-terminal domain of the human RNA polymerase II was achieved.[218] Here, both lipase-mediated cleavage of heptyl ester groups (see Section 6.2) and enzyme-initiated fragmentation of a urethane protecting group (see above and Section 6.1) were employed.

On treating the fully protected glycosylated serine **156**, which includes the enzyme-labile PhAcOZ group at the N terminus (see Scheme 51), with penicillin G acylase, only the phenylacetic acid ester group was cleaved, and the fragmentation of the resulting phenolate shown in Scheme 31 led to release of the desired selectively deblocked amino acid **157** (Scheme 54). After being linked to a glycodipeptide, also PhAcOZ-protected, to form the diglycotripeptide **159**, penicillin G acylase rereleased the N terminus under very gentle conditions. A further cycle of chain extension and enzyme-initiated N-terminal deblocking gave the selectively deprotected diglycopentapeptide **163**. Subsequently, the allyl-masked serine derivative **141**, which was obtained by lipase-mediated cleavage of the heptyl protecting group from the corresponding ester (Scheme 50), was linked to the molecule.



Scheme 54. Chemoenzymatic synthesis of phosphoglycopeptide **165** with use of the enzyme-labile PhAcOZ protecting group.

Finally, successive release of all amino acid and carbohydrate protecting groups gave **165**.

Phosphoglycopeptides such as **146** have not yet been used in biological investigations. However, it was recently shown that a synthetic peptide modified with O-GlcNAc, corresponding to a repeat sequence of the C-terminal domain of the RNA polymerase II, inhibits in vivo gene transcription considerably.[219] The same effect was observed in the presence of an inhibitor of the enzymatic O-GlcNAc cleavage. These findings suggest that the O-GlcNAc modification is important for the transcription process. With synthetic phosphoglycopeptides, it should be possible to obtain valuable information about these and other biological processes.

6.4. Nucleopeptides

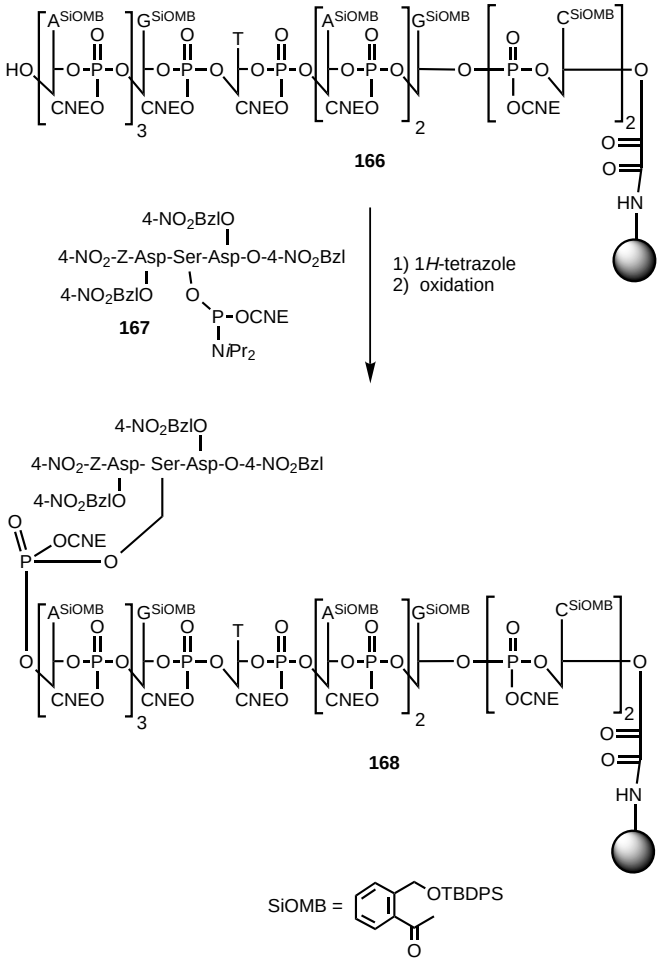
Nucleopeptides are involved in transcription of the genetic code in many different organisms. For example, formation of nucleopeptides plays a crucial role in priming replication of viruses,[220] DNA topoisomerases create nucleopeptides as part of their function,[221] and DNA exists as a nucleoprotein covalently linked to the matrix of the cell nucleus. Thus, characteristic nucleopeptides could open up many new

possibilities for studying gene transcription and particularly for developing new and alternative antiviral agents.

The synthesis of nucleopeptides presents in principle the same problems as that of phosphopeptides (see Section 6.3). However, the number of orthogonally stable protecting groups to be used increases considerably owing to the additional functional groups of the carbohydrates and nucleobases; also the acid lability of the purine N-glycoside forbids use of acid-labile protecting groups.

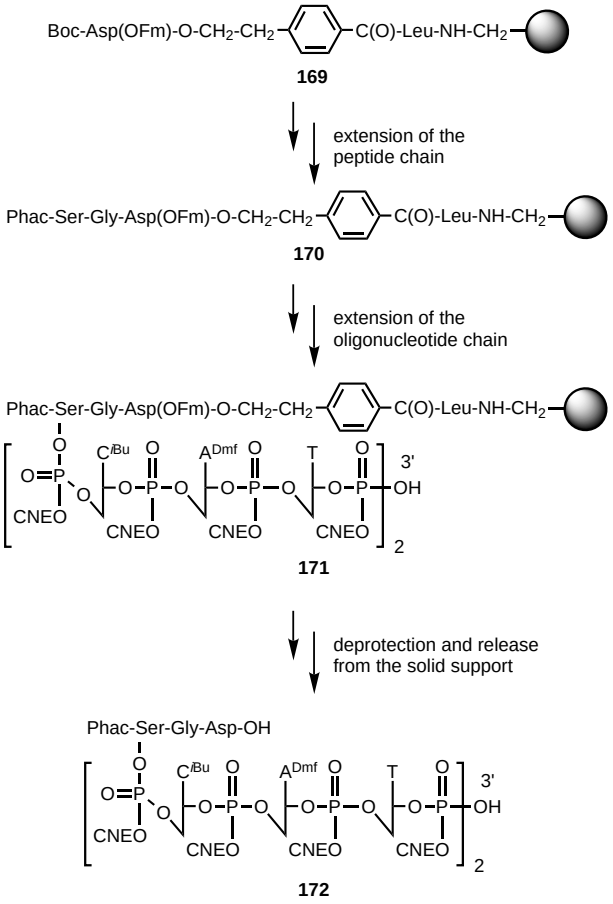
Initial work[222] showed that protecting groups established in peptide chemistry, such as allyl esters, often do not provide a suitable solution for this problem;[223] however, the first protecting group combinations were recently developed for synthesizing tyrosine nucleopeptides[223, 224] and serine/threonine nucleopeptides[223, 225–228] in solution and on polymeric carriers. Since the tyrosine derivatives—as in the case of phosphopeptides—are not destroyed by base-induced β-elimination, only synthesis of serine/threonine peptide conjugates are considered in this review.

Two general strategies were developed for the solid-phase synthesis of serine nucleopeptides. In a convergent method[225] the immobilized oligonucleotide **166** was first created and coupled to the separately synthesized peptide phosphoramidite **167** (Scheme 55). The protecting groups in the peptide



Scheme 55. Solid-phase synthesis of nucleopeptides by linking of a preformed peptide to an oligonucleotide. CNE = cyanethyl, TBDPS = *tert*-butyldiphenylsilyl.

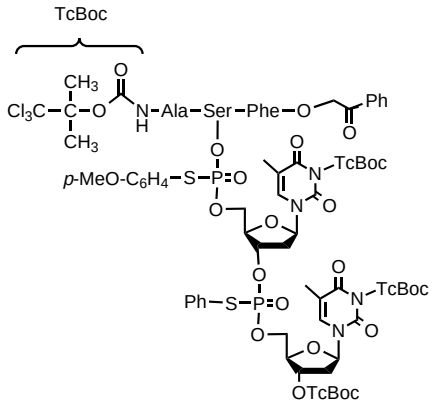
and oligonucleotide portions as well as the linker to the solid carrier were chosen so that the desired nucleopeptide was obtained in two concluding steps. Deblocking remained incomplete, however. An alternative procedure was the stepwise synthesis first of peptide **170** on a polymeric carrier by the Boc method followed by successive synthesis of the oligonucleotide chain[226] (Scheme 56). Subsequently, the linker to the polymeric carrier was cleaved by fluoride, and the base protecting groups were removed by treatment with concentrated ammonia. The desired nucleopeptide **172** was isolated in a total yield of 33 %. In neither case was it reported whether β-elimination occurred under the conditions used for cleavage.



Scheme 56. Solid-phase synthesis of nucleopeptides by successive extension of the peptide and nucleotide chains. Dmf = dimethylformamidinyl, Fm = fluorenylmethyl, Phac = phenylacetyl.

For the synthesis of nucleopeptides in solution, a strategy was successfully used in which the amino functionalities of the nucleobases and the N-terminal amino acids were protected with the trichloro-Boc group (TcBoc) and the C-terminus was protected as the phenacyl ester (Pac, Scheme 57).[227] In a convergent synthesis, a tripeptide was linked with a dinucleotide to give the nucleopeptide **173**; the protective functionalities mentioned were removed in one step without β-elimination.

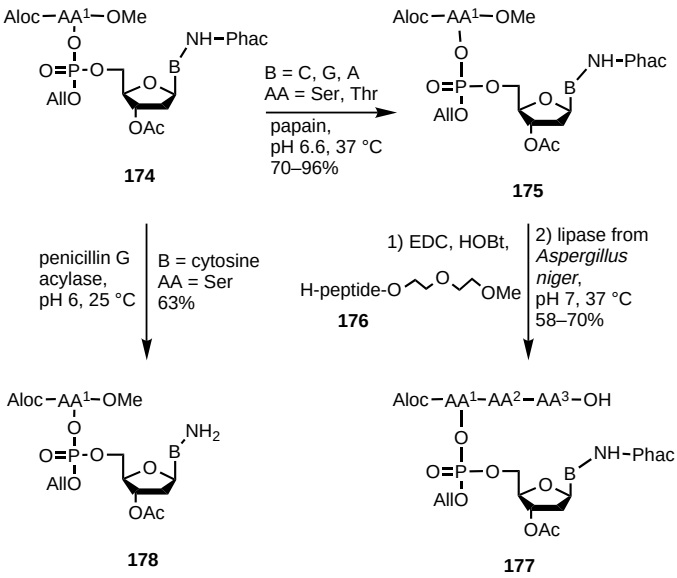
A stepwise flexible synthesis of nucleopeptides in solution, which, according to the previously described procedure, is not



173

Scheme 57. Combinations of protecting groups for the synthesis of nucleopeptides in solution.

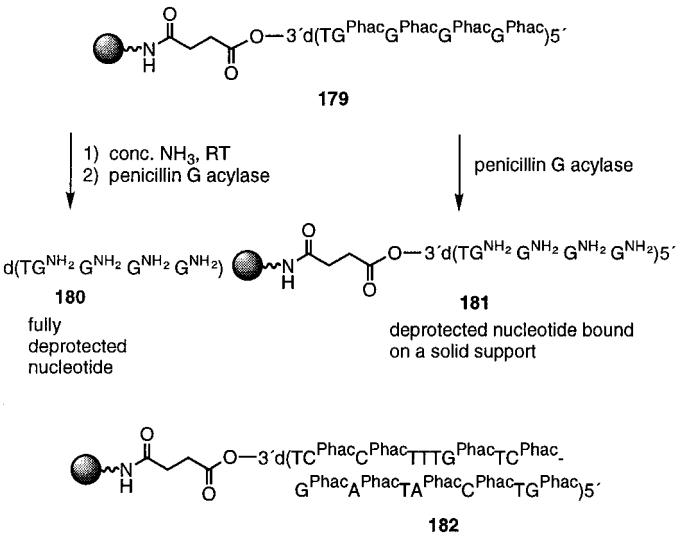
possible due to lack of orthogonality of the protecting groups, was achieved by combining classical chemical methods with enzymatic protecting group techniques,[228] however (Scheme 58). The nucleoamino acid **174** was synthesized for



Scheme 58. Nucleopeptide synthesis with use of enzyme-labile protecting groups.

this purpose, and the C-terminal methyl ester was cleaved off in high yield. Following extension of the amino acid chain with dipeptide diethylene glycol monomethyl ether (Dem) esters,[189] the selective C-terminal deblocking was performed again; the lipase from *Aspergillus niger* was the biocatalyst of choice. There was no β-elimination or attack on the other diverse protecting groups during the course of the enzymatic deblocking. On the other hand, the allyl protecting groups used could be selectively removed from **174** (B = cytosine) in a Pd^0-mediated transfer of the allyl groups, and the targeted deblocking of the amino functionality of the nuceobases of **174** was achieved by release of the phenylacetamide with penicillin G acylase.

This possibility for enzymatic deblocking of nucleobases is not limited to mononucleotides. For example, the PhAc-protected oligonucleotides **179** and **182** were synthesized on a solid carrier and cleaved off without deblocking the nucleobases[229] (Scheme 59). Release of all PhAc groups from the



Scheme 59. Enzymatic deblocking of the amino groups of oligoneucleotides in solution and on solid phase (controlled pore glass (CPG) beads, which are represented by spheres).

penta- and hexadecanucleotides was achieved by treatment with penicillin G acylase at pH 7 and room temperature. Furthermore, the enzyme even deblocked oligonucleotides such as **179** that were solid-phase anchored on the carrier (Scheme 59) without attacking the linker groups. This finding is of particular interest considering the possible application of biocatalysts in combinatorial synthesis on polymeric carriers.[230] Synthetic nucleopeptides have not yet been used for biological studies.

7. Modulation of the Activity of Protein Kinases C and A

Protein kinase C (PKC)[231] is a serine/threonine kinase that performs an important function in signal cascades in various cell types:[232] Cellular processes such as proliferation and differentiation are regulated by this function (see Section 2.1).[233–235] At present, at least 12 classes of the isoenzymes of PKC have been identified in mammalian cells,[236–238] which, according to the conditions required for activation, can be divided into three or four subfamilies.[239] The conventional PKC (cPKC) includes the isoenzymes α, β_1, β_2, β_3, and γ and requires calcium and diacyl glycerol (DAG) or phorbol ester for activation. The subfamily of the novel PKC (nPKC) includes the ε, δ, η, and o enzymes; their activity is independent of calcium but requires DAG or phorbol ester. The atypical PKC (aPKC) is represented by the subtypes ζ, δ, and τ, which function independent of calcium, diacyl glycerol, and phorbol esters, whereas the isoenzyme PKCμ has not been further classified. To perform its function, the latter

subtype requires membrane-bound phospholipids such as phosphatidylserine[233, 240] to localize the PKC at the plasma membrane. This illustrates that glycerolipids, sphingolipids and their metabolic products as well as phospholipases and phosphatidylinositol kinases can influence signal transduction processes (see Section 2.1).

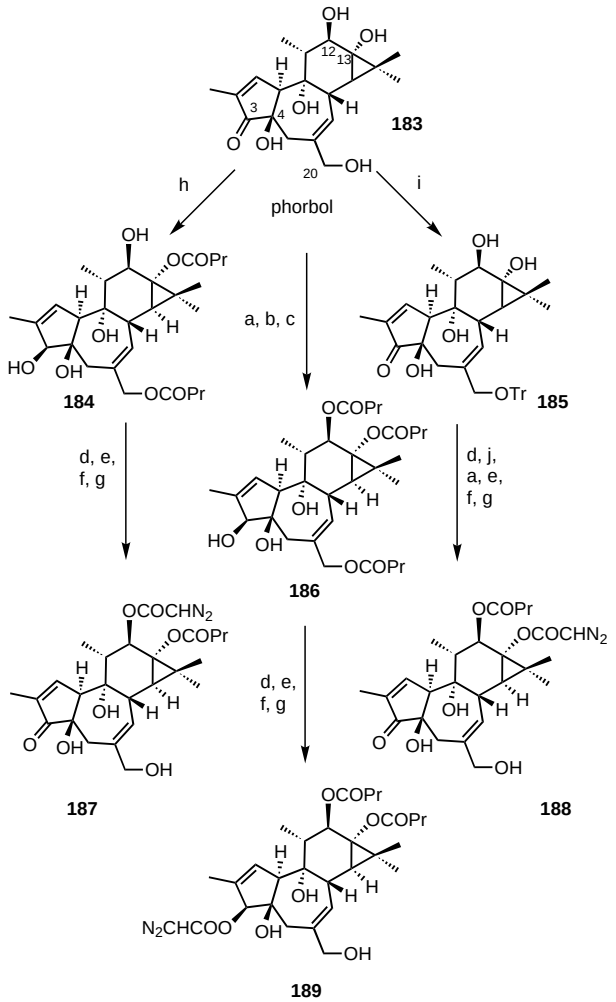
7.1. Modulation of the Activity of PKC by Binding to the Regulatory Domain

The activation of PKC by diacyl glycerol (see Section 2.1, Scheme 2) can also be achieved by various natural products such as the phorbol esters, teleocidins, bryostatins, and aplysia toxins.[241–245] With molecular modeling, an attempt was made to find a common pharmacophore for these structurally very different compounds.[246–251] This showed that a double cysteine rich motif in the C1 region of the PKC is necessary and sufficient for binding of diacyl glycerol;[244, 252–255] this finding was supported by an X-ray structural analysis of the complex of PKCδ and phorbol-13 acetate. Binding of the natural product to the protein through five hydrogen bridges creates a common hydrophobic surface and enables binding of the whole complex to the plasma membrane.[256] The structural requirements for formation of the PKC/activator/phospholipid aggregate are, however, for the most part unknown.

7.1.1. Phorbol Esters

Phorbol esters promote tumor growth by binding to the PKC and activating the enzyme over a long period, since, in contrast to DAG, they are metabolically stable. Two total syntheses of the structurally complex and synthetically very demanding phorbol ester have been published,[257a b] and diverse derivatives have been assembled starting from the natural product itself. For example, photoactivable substances carrying carbene precursors in the form of diazoacetyls on various hydroxyl groups of the molecule have been synthesized.[257c] Of six hydroxyl groups (on C3, C4, C9, C12, C13, and C20) those at C4 and C20 are probably needed for binding to the PKC, whereas that at C9 is sterically too well protected for a chemical derivatization. Starting from 12,13-phorbol dibutyrate, analogues with photolabile markers at C3, C12, and C13 were synthesized and tested for biological activity (Scheme 60). First, the relevant hydroxyl functionalities were esterified with Boc-glycine, and following cleavage of the Boc protecting group the free amine was diazotized. Selective hydrolysis of the butyl ester with $Ba(OH)_2$ in methanol gave the desired product.

To synthesize **189**, the three hydroxyl groups were acylated at C12, C13, and C20 with butyric acid anhydride in the presence of triethylamine and DMAP. Subsequently, reduction of the keto group with sodium borohydride/cerium trichloride and treatment with tetrabutylammonium fluoride (TBAF) selectively produced the biologically relevant β-alcohol **186**, which could be converted to the diazoacetic acid ester **189** with the procedure described above. If phorbol was acylated without addition of DMAP, a selective derivatization took place at C13 and C20 to provide the phorbol analogue



Scheme 60. Synthesis of photoactivable phorbol esters starting from phorbol. a) $[CH_3(CH_2)_2CO]_2O$, DMAP, NEt_3, CH_2Cl_2; b) $NaBH_4$, $CeCl_3$, MeOH; c) TBAF, THF; d) Boc-Gly, DMAP, NEt_3, DCC, THF; e) 1N HCl, AcOH; f) $NaNO_2$, H_2O/CH_2Cl_2, H_2SO_4; g) $Ba(OH)_2$, MeOH; h) $[CH_3(CH_2)_2CO]_2O$, NEt_3, THF/CH_2Cl_2; i) $(C_6H_5)_3CCl$, pyridine; j) $HClO_4$, MeOH.

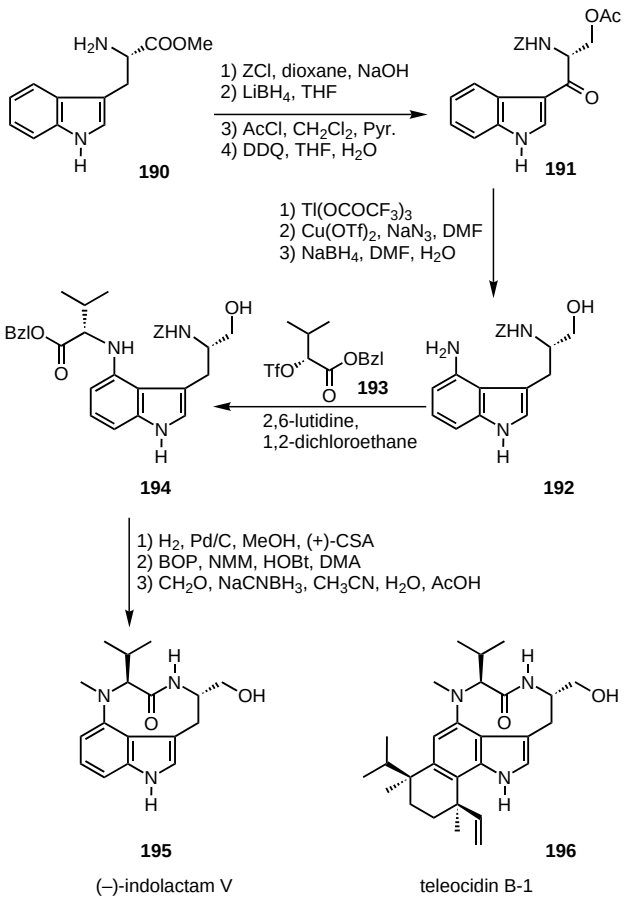
187, which is selectively labeled at C12. The various reactivities of the hydroxyl functionalities could also be used for labeling the C13 position (**188**). First, the most reactive primary alcohol was tritylated at C20, then the C13 position was selectively esterified with Boc-glycine. Following deprotonation of the primary hydroxyl groups, the C12,C20-dibutyl ester was obtained and selectively hydrolyzed to **188**.

The compounds synthesized were used in an investigation of the binding affinity and photoaffinity labeling of peptide C;[258] this represents a cysteine-rich subunit of the regulatory domain of PKCγ, and binds 12,13-[^{3}H]phorbol dibutyrate with high affinity in the presence of phosphatidylserine. Furthermore, like the PKC itself, it recognizes activators such as dioctanoyl glycerol and teleocidin B-4. Peptide C was not photolabeled by **187** and **188**, yet it was labeled by **189**. This indicates that the C3-hydroxyl group of the phorbol is close to the polar region of the phosphatidylserine in the bound complex.

Phorbol esters have been used in many different biological studies. For example, phorbol-12-myristate-13 acetate (PMA) triggers differentiation of the leukemia cell line HL60 into macrophage-like cells, which prove to be cytostatic and cytotoxic for malignant human cells in vitro.[259] Use of PMA also delivered information about the role of ceramide in inducing apoptosis through the Fas/Apo-1 cell-surface receptor. The effect triggered by ceramide was reduced by activation of PKC through PMA, which indicates that PKC modulates initiation of the ceramide-induced apoptosis.[260] The observation that different membrane transport processes are stimulated by PMA led to the conclusion that activation of PKC is involved in these processes and plays an important role in regulation of exocytosis, transport of receptors, and constitutive transport of proteins through the golgi complex.[261, 262] PMA was also successfully employed in studies of glucose uptake by translocation of the glucose transporter Glut 4 (see also Section 9.1). This showed that Glut 4 can be stimulated by insulin through PI3 kinase, through GTP (possibly through GTP-binding proteins), and through PKC (on activation by PMA).[263] Indications that PKC is also involved in signal mediation through nitric oxide formed in endothelial cells[264] were obtained with the phorbol derivative phorbol-12,13-dibutyrate (PDBu).[265] Thus incubation of rat hepatocytes led to release of the messenger NO. Finally, it has been shown with the help of PMA that a PMA-resistent isoform of PKC is directly involved in secretion of exocrine glands induced by the muscarinic agonist carbachol.[266]

7.1.2. Teleocidin and Indolactam V

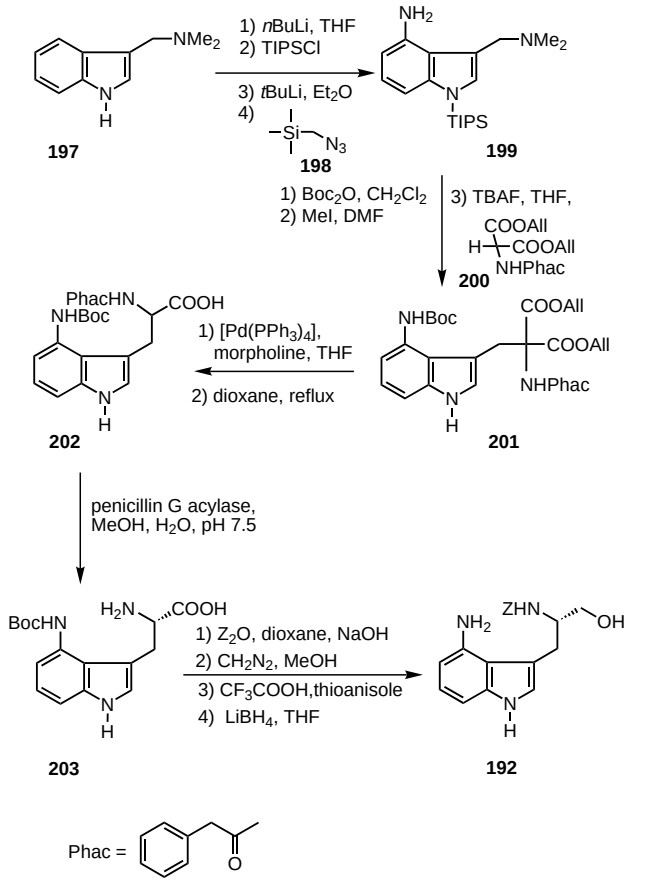
Teleocidin and indolactams are a family of indole alkaloids that promote tumor growth and, like phorbol ester, activate PKC. They were therefore used in studies of the biological relevance of this enzyme. The main problems in the total synthesis of these natural products,[267–273] all of which have the (−)-indolactam backbone (Scheme 61), were the regioselective substitution of the indole at C4 and C7, the ring closure to the nine-membered lactam ring, and control of the stereochemistry at C9 and C12 (see, for example, **195** and **196**, Scheme 61). Starting from L-tryptophan methyl ester, the ketone **191** was first obtained by protection of the amine, reduction of the ester with lithium borohydride, and subsequent acylation of the alcohol as well as a DDQ oxidation (Scheme 61).[270a] This ketone was metalated at the 4-position of the indole backbone with thallium(III) trifluoroacetate and converted to the 4-amino derivative **192** by treatment with sodium azide/copper triflate and subsequent reduction of the azido and keto functionalities. By a stereospecific reaction of the aminoindole **192** with the triflate **193** derived from D-valine, the missing stereocenter of the indolactam was assembled at C12. Hydrogenolysis released both the carboxyl and the amino functionalities so that lactam formation could be achieved with the help of 1-benzotriazolyloxytris(dimethylamino)phosphonium (BOP) hexafluorophosphate. The missing N-methyl group was introduced by reductive amination with formaldehyde in the presence of sodium cyanoborohydride.



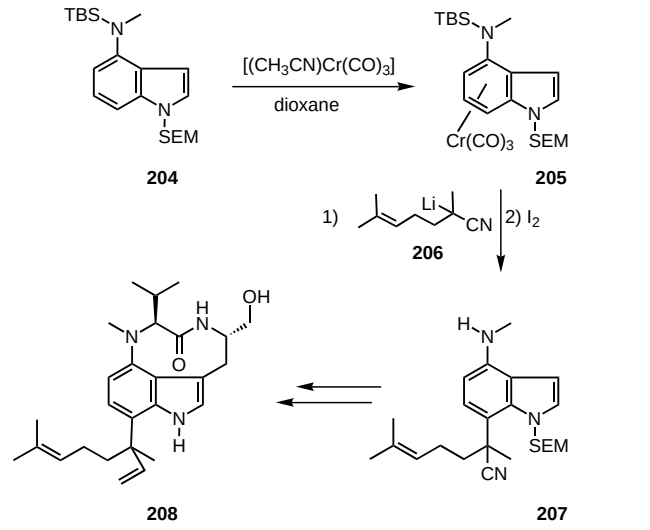
Scheme 61. Synthesis of (−)-indolactam V and teleocidin B-1. (+)-CSA = (+)camphorsulfonic acid, NMM = *N*-methylmorpholine, Tf = trifluoromethanesulfonyl.

In an alternative synthesis,[270b] the thallium reagent was avoided by selective lithiation at the 4-position of the TIPS-protected gramine **197** (TIPS = triisopropylsilyl) and introduction of the amino functionaliaty with trimethylsilylmethyl azide (Scheme 62). Following protection of the primary amine group, the side chain was assembled on an intermediary α,β-unsaturated imine by quaternization of the amine group and conjugated addition of phenylacetylaminodiallyl malonate. Cleavage of the allyl ester and decarboxylation of the dicarboxylic acid gave the racemic phenylacetamidotryptophan derivative, which was resolved into the enantiomers with penicillin G acylase. Amino acid **203**, which was selectively derivatized at the C4 position of the indole ring, could be converted into alcohol **192**, a precursor for indolactam V (see above).

The teleocidins have a greater PKC-activating effect than indolactam V owing to their higher lipophilicity, and, therefore, their synthesis[274, 275] and particularly the regioselective substitution at the 7-position has been given a great deal of attention. This derivatization was achieved by nucleophilic addition at an indole ring activated by a tricarbonylchromium fragment (Scheme 63). Furthermore, the C7 position of the indolactam V can be functionalized by a Vilsmeier formylation[276] to obtain a photolabile indolactam V derivative. For this, the indolactam V was protected as the acetate and then formylated at C7 of the indole backbone (→**209**). Condensation of the aldehyde with nitrohexane (hydrophobic residues

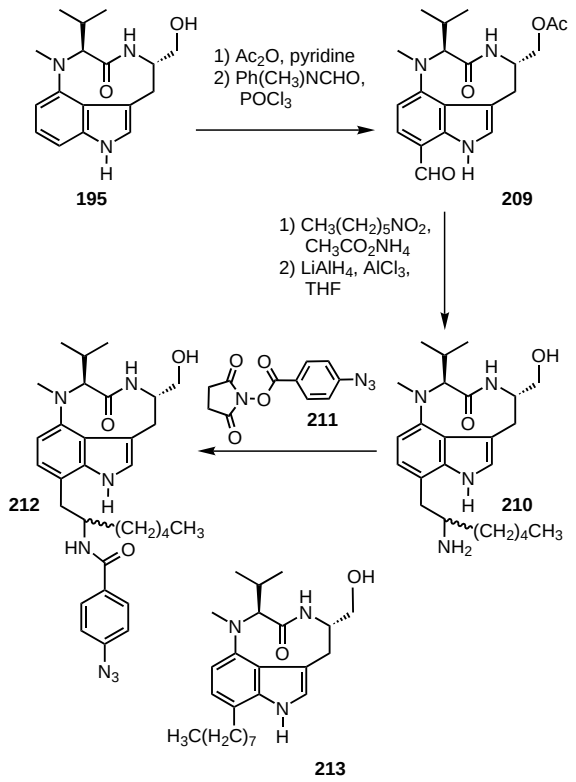


Scheme 62. Synthesis of the indolactam V precursor **192** with enzymatic racemate resolution.



Scheme 63. Synthesis of teleocidin **208**. SEM = trimethylsilylethoxymethyl.

at the C7 position of teleocidine seem to increase the tumor-promoting activity of this substance)[277] and subsequent reduction delivered amine **210**, to which ^{3}H-labeled succinimido 4-azidobenzoate (**211**) was added (Scheme 64). With these compounds in many different in vitro assay systems, attempts were made to identify the binding partners and



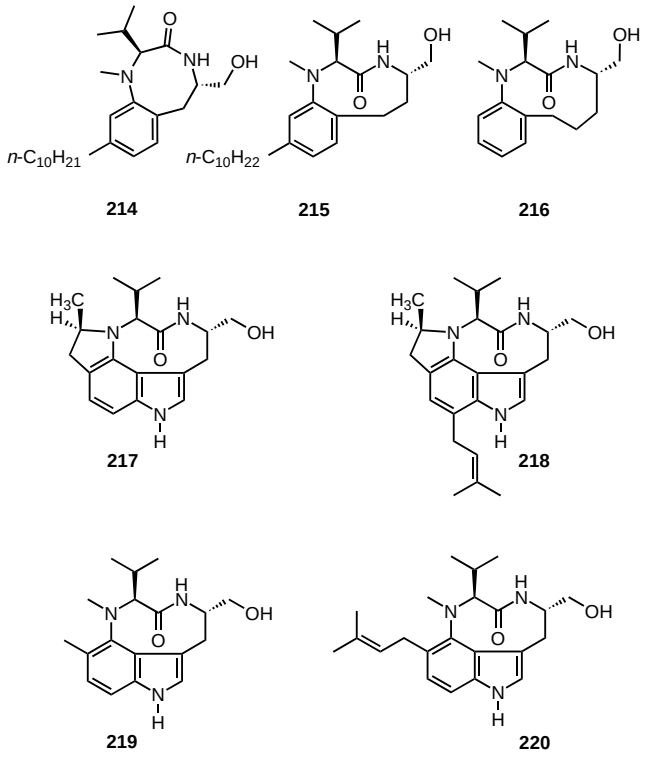
Scheme 64. Synthesis of the photolabile teleocidin derivative **212** and the biologically active (−)-7-octylindolactam (**213**).

binding sites of these natural-product analogues by photoaffinity labeling. These experiments were unsuccessful, however.

Indolactam V was used in mechanistic studies of the regulation of muscle contraction triggered by calcium/calmodulin-mediated activation of myosin kinase.[278, 279] Direct activation of PKC leads to contraction of arterioles, and indolactam V also proved to be a potent constrictor of small arteries. It was suggested that the alkaloid modulates the influence of Ca^{2+} on the contractile processes and brings about an increase in phosphorylation of myosin kinase.[280] Indolactam V was also used to develop a rapid and generally applicable phenotype assay of PKC activity for identification of PKC-activating or -inhibiting substances.[281] The (−)-7-octylindolactam **213** was successfully used in studies of the receptor for the inhibitory neurotransmitter γ-aminobutyric acid (GABA). GABA is recognized by two receptors ($GABA_A$ and $GABA_B$), which become desensitized on binding the ligand. Activation of PKC also leads to desensitization of $GABA_A$; use of **213** showed that the receptor is phosphorylated in this process. It is assumed that the purpose of the PKC signal system is to switch off receptors that were not completely desensitized by GABA. Finally, **213** was used in a study of phosphoinositide conversion in glioma cells. Conversion of this messenger substance is initiated by binding of an agonist to the ATP receptor, and it is assumed that PKC is involved in control of this process, by negative feedback. (−)-7-Octylindolactam and also PMA thus bring about desensitization by activation of PKC.[283]

7.1.3. Indolactam Analogues

Teleocidins and indolactams can adopt two stable conformations in solution, a twist conformation with a *cis* amide that is preferred by five- to eight-membered rings, and a sofa conformation with *trans* amide stucture that dominates for compounds with rings with ten or more members. To find out which of these two conformations is relevant for biological activity, different conformationally restricted analogues were designed, synthesized, and tested for biological activity.[273, 284–288] For example, the indole ring was exchanged for a benzene ring, and lactams were synthesized with different ring sizes that should adopt the twist (e.g. **214**) or the boat (**215** or **216**) conformation.[284] To ensure that the compounds were also sufficiently hydrophobic, a *n*-decyl chain was added to the arene. The activity of the compounds synthesized was examined in assays for growth inhibition, cell adhesion, and differentiation of human promyelocytic leukemia cells (HL-60) to monocytes. The twist conformation is the biologically active conformation of teleocidins. It was also possible to determine the optimal length of the alkyl side chains as 10 – 14 carbon atoms (Scheme 65).[285]



Scheme 65. Conformationally restricted indolactam analogues.

By replacing the indole backbone with a benzofuran ring, it was shown that the indole nitrogen atom influences the isoenzyme selectivity, but only plays a supporting role in the interaction with the PKC.[287] With an aza-Claisen *trans*-formation as the key step, analogues **217** and **218** with a twist conformation were synthesized. Examination of the biological activity of these and other derivatives as well as of the analogues **219** and **220**, which imitate the sofa conformation, also showed that it is the twist form that is biologically relevant.[288]

7.1.4 Other PKC Activators

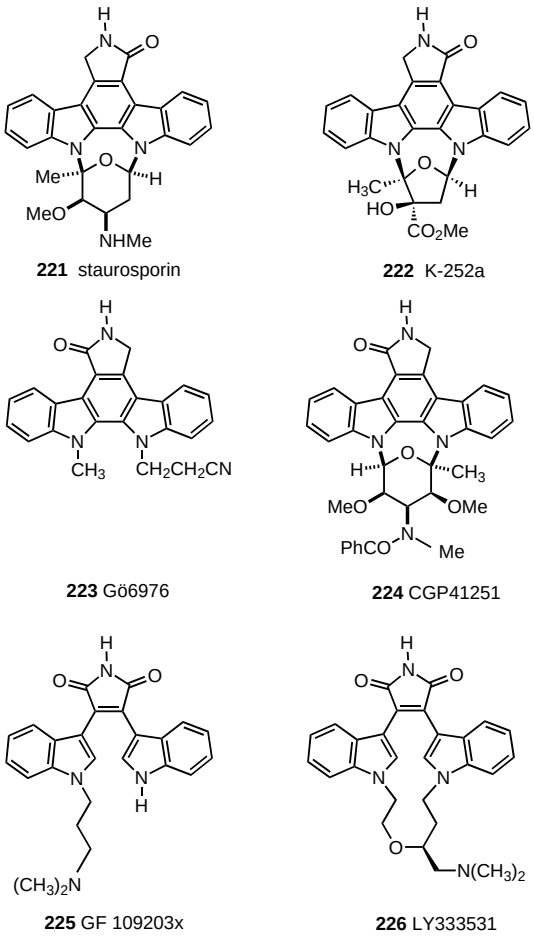
Diacyl glycerol (DAG) analogues were examined in detail as activators of PKC. This showed that the stereochemistry of the glycerol derivative is important for binding to the enzyme. *sn*-1,2-DAG analogues are recognized, *sn*-2,3- and 1,3-DAG derivatives are inactive. Two ester carbonyl groups and an alcohol were needed for activation.[289] The length of the acyl group may vary; *sn*-1,2-dibutyroyl glycerol is inactive, however, since it is taken up by membranes and forms micelles. Cyclic analogues were also synthesized but proved to be inactive. Of the diverse analogues examined, 1-oleoyl-2-acetyl-*sn*-glycerol (OAG) and 1,2-dioctanoyl-*sn* glycerol (DOG) turned out to be particularly valuable reagents for biological studies.[290] The high selectivity with which the DAG analogues recognize PKC indicates that at least three interactions with the enzyme are important; these are probably hydrogen bonds with the two ester carbonyl groups and the OH functionality.[291] Other PKC activators which will not be discussed here are mezerine,[292] 6-(*N*-decylamino)-4-hydroxymethylindole (DHI),[293] and ingenol.[294, 295]

7.2. Inhibition of PKC

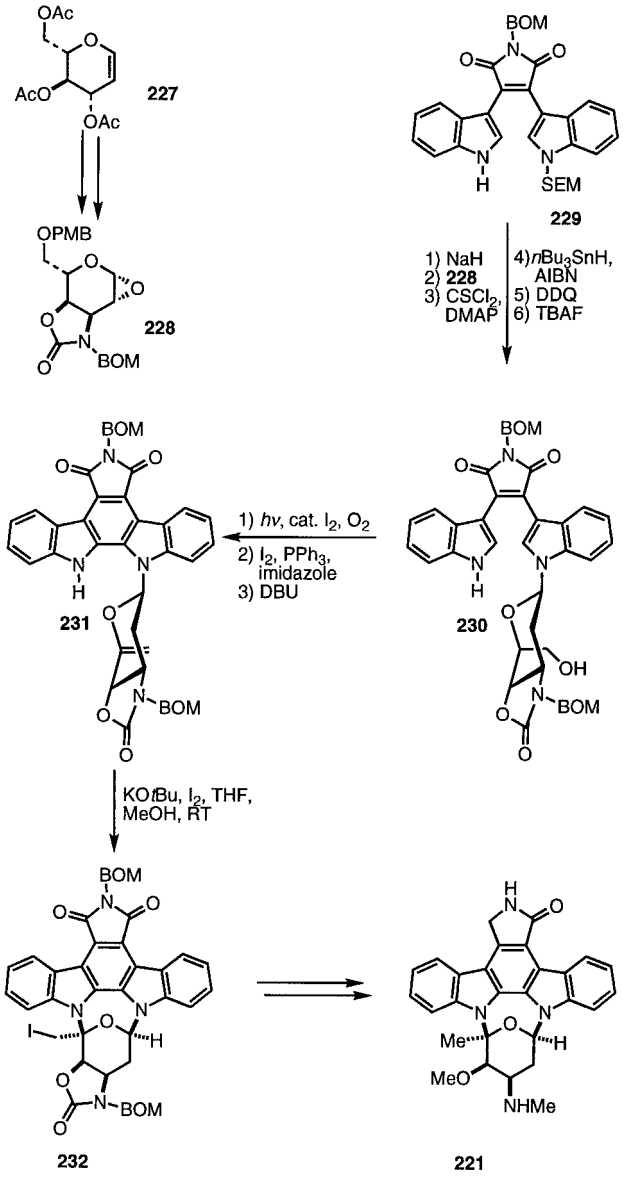
Since PKC has a decisive role in many different processes, discovery of selective inhibitors of this kinase is of great importance. Of particular interest is the development of inhibitors that show selectivity for the different isoenzymes (see Section 7). Staurosporin[296] and K-252a[297] are microbial products from the indole carbazole alkaloid family (Scheme 66) with potential antitumor activity. Staurosporin is one of the most potent PKC inhibitors known with activity in the nanomolar region,[298] and it interacts with the ATP binding site in the catalytic domain.[299, 300] The total synthesis of this natural product was recently reported;[301–304] one of the biggest synthetic challenges was to link two glycosidic bonds to the only weakly nuceolophilic indole nitrogen atoms.

The monosaccharide epoxide **228** used for this synthesis was obtained from tri-*O*-acetyl-L-glucal (**227**, Scheme 67).[301, 302] It proved to be a suitable glycosyl donor for linkage with the aglycon precursor **229**, which was obtained from N-BOM-masked dibromomaleinimide in a three-step sequence. The heterocycle was N-deprotonated and subsequently coupled with the epoxide **228** formed in situ. Following deoxygenation at the C2 position of the glycoside under Barton conditions and deprotection of the primary hydroxl group in the carbohydrate as well as of the second indole nitrogen atom, **230** was obtained. A photocyclization followed by conversion of the primary alcohol into the corresponding iodide and elimination of hydrogen iodide gave *exo*-glycal **231**. The key step in the synthesis was activation of the double bond with iodine accompanied by cyclization to **232**. Following dehalogenation, opening of the oxazolidinone, methylation, cleavage of the BOM group, and reduction of the imide to the amide, staurosporin and its enantiomer were produced.

(+)-Staurosporin and the closely related natural products (+)-K-252a, (+)-RK-286c, and (+)-MLR-52 were also ob-



Scheme 66. Structures of staurosporin, K-252-a, and analogues of these natural products.



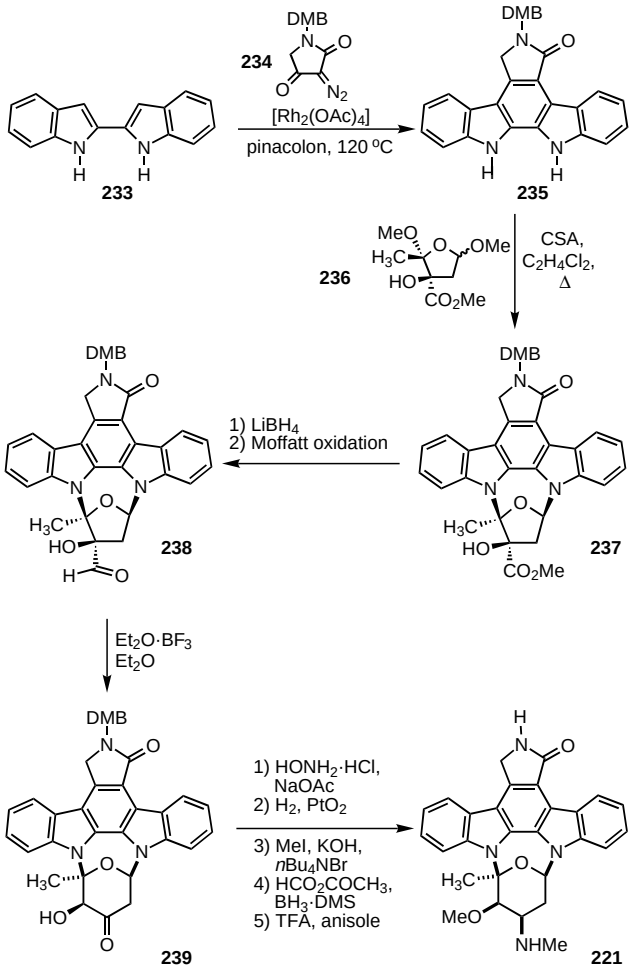
Scheme 67. Synthesis of staurosporin by successive glycosylations. AIBN = azobisisobutyronitrile, BOM = benzyloxymethyl.

tained starting from the common intermediate **239** (Scheme 68).[303, 304] For their synthesis, the carbene precursor **234** was allowed to react with the 2,2′-bis(indole) **233** in the presence of dirhodium tetraacetate to the 3,4-dimethoxybenzyl-protected aglycon **235**. In a cycloglycosylation reaction with the furanose derivative (−)-**236** in the presence of camphorsulfonic acid, the bis(indole) gave **237**, which underwent a ring extension to the pyran derivative **239** following reduction of the ester to the aldehyde upon treatment with boron trifluoride etherate. Reductive amination of the ketone via the oxime and alkylation delivered staurosporin in a total of 19 steps.

Investigation of staurosporin and isomeric compounds in two cell lines, on three human PKC isoenzymes, and on topoisomerase I showed that the spatial conformation of the lactam C5 carbonyl group and the pyranosyl C4′ methylamino functionality are more important for biological activity than the conformation of the pyranosyl C3′ methoxy functionality and the pyranosyl C2′ methyl group.[302]

Owing to the highly conserved structure of the catalytic domain of different protein kinases, staurosporin (**221**) and K-252a (**222**) are only unselective inhibitors, however,[305] so further analogues were synthesized to try to find more selective enzyme inhibitors. Examples are the analogues **223**–**225** (Scheme 66). Compound **223** belongs to a class of analogues in which the amino sugar was replaced by different alkyl substituents,[306] and it represents one of the most active and selective compounds of this type. The second class of inhibitors, of which **224** is an example, are semisynthetic derivatives of the natural product, whereby **224** inhibits PKC much more effectively than, for example, PKA and tyrosine kinases.[307] The third class are bis(indolyl) maleimides.[308–311]

An increased level of diacyl glycerol and the resulting long-lasting activation of PKC in macrovascular tissue is responsible for development of chronic vascular complications in diabetes.[312] The observation that the PKC isoenzyme β_2 is strongly expressed in the retina, heart, and aorta is particularly relevant to this problem. To determine whether this isoenzyme is responsible for the complications, inhibitors that specifically block this PKC subtype were needed.[313] The staurosporin analogue **226** proved to be a potent compound which was nontoxic and could be orally administered in a rat model. With **226**, the vascular misfunction could be



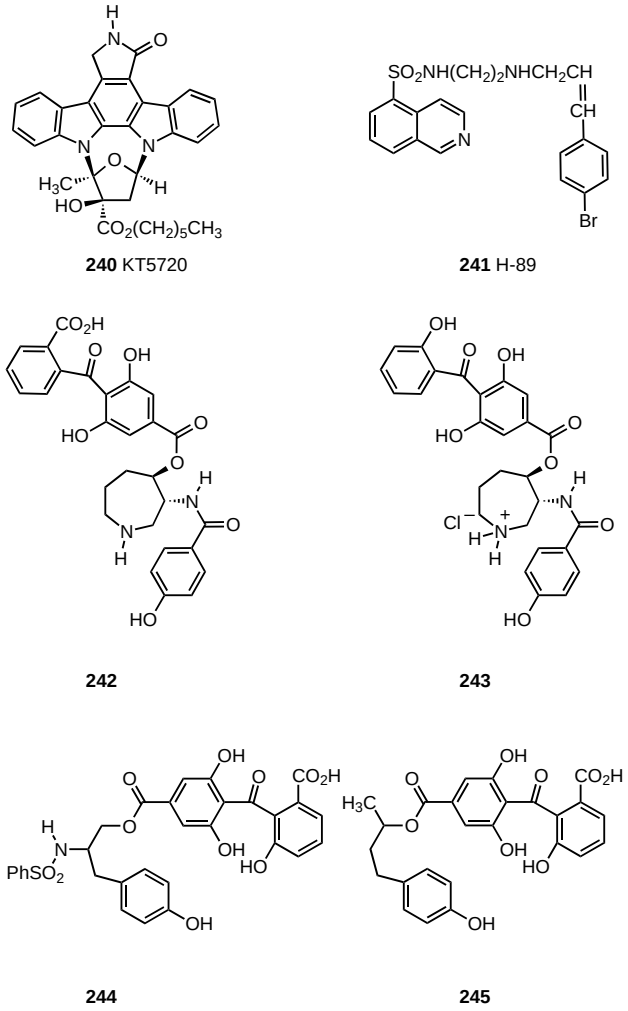
Scheme 68. Synthesis of staurosporin by cycloglycosylation and rearrangement.

corrected, and it was shown that the β_2 PKC isoenzyme is responsible for the corresponding complications in diabetes.

7.3. Inhibition of Protein Kinase A

Protein kinase A (PKA) is a serine/threonine kinase that is activated by cAMP upon stimulation of G protein coupled receptors; it transmits the incoming signal into the cell interior by phosphorylation of other target proteins (see Section 2.1). Since PKA is involved in many important processes, there is a lot of interest in developing selective inhibitors for this enzyme. PKA is made up of a heterotetrameric complex of two catalytic and two regulatory subunits. When cAMP binds to the regulatory subunit, the conformation of the enzyme changes and leads to release of the catalytic subunit, which then phosphorylates the target proteins.

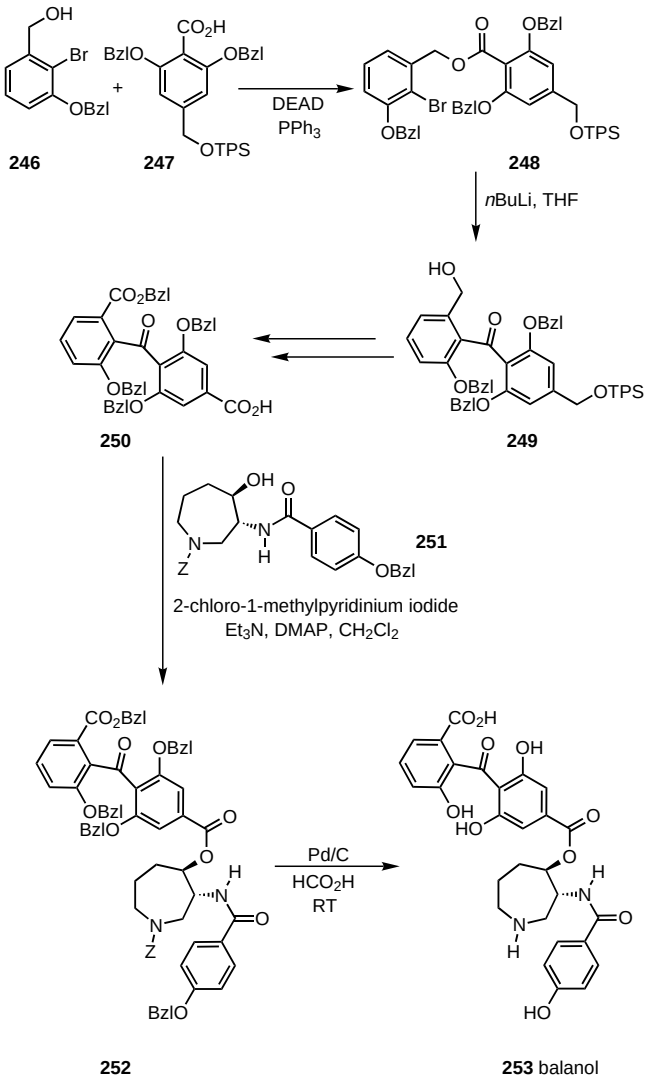
Some oligopeptides such as Ala-kemptide (kemptide = H-Leu-Arg-Arg-Ala-Ser-Leu-Gly-OH) and Asn-Ala-kemptide recognize and bind the PKA catalytic subunit, and inhibit enzyme activity by imitating the influence of the regulatory domain. Interest has been focused on non-peptide natural products and their derivatives, however, which has led to the discovery of two of the most selective nonpeptide inhibitors: KT 5720 (**240**), which is structurally related to staurosporin, and the isoquinolone sulfonamide derivative H-89 (**241**, Scheme 69).



Scheme 69. Inhibitors of protein kinase A.

The fungal metabolite balanol (**253**)[314–316] is also a PKA inhibitor ($IC_{50} = 4$ nM) which, however, inhibits PKC with equal efficiency. Several total syntheses of the natural product have been performed in order to develop analogues with higher selectivity.[317–321] In a convergent strategy to this end, two similarly complex partial structures of the molecule (**250** and **251**) were linked together, and the natural product was obtained by simple removal of the benzyl protecting groups (Scheme 70). Starting from D-serine, hexahydroazepine **251** was obtained in 15 steps (total yield 36%). To synthesize benzophenone **250**, the brominated benzyl alcohol **246** was linked to the aromatic carboxylic acid **247** in a Mitsunobu reaction to give ester **248**. Metalation with *n*-butyl lithium converted **248** into benzophenone **249**, from which the intermediate **250** was obtained by standard transformations. Esterification of **250** and **251** and subsequent deblocking produced balanol (**253**).

To elucidate which structural characteristics of the natural product are responsible for kinase inhibition, further balanol



Scheme 70. Convergent total synthesis of balanol. TPS = triphenylsilyl.

analogues were synthesized by the procedure described above.[318] Two of the compounds obtained, 10″-deoxybalanol (**242**) and 14″-decarboxybalanol hydrochloride (**243**), inhibited PKA more effectively than PKC and were more potent enzyme inhibitors than KT 5720 (**240**) and H-89 (**241**).[322] Balanol analogues in which the perhydroazepine ring and the *p*-hydroxybenzamide group are replaced by an acyclic unit, such as **244** and **245** (Scheme 69), show inhibitory activity. They inhibit PKC much more effectively than PKA and other serine/threonine kinases.[323]

8. Inositol Phosphate Analogues

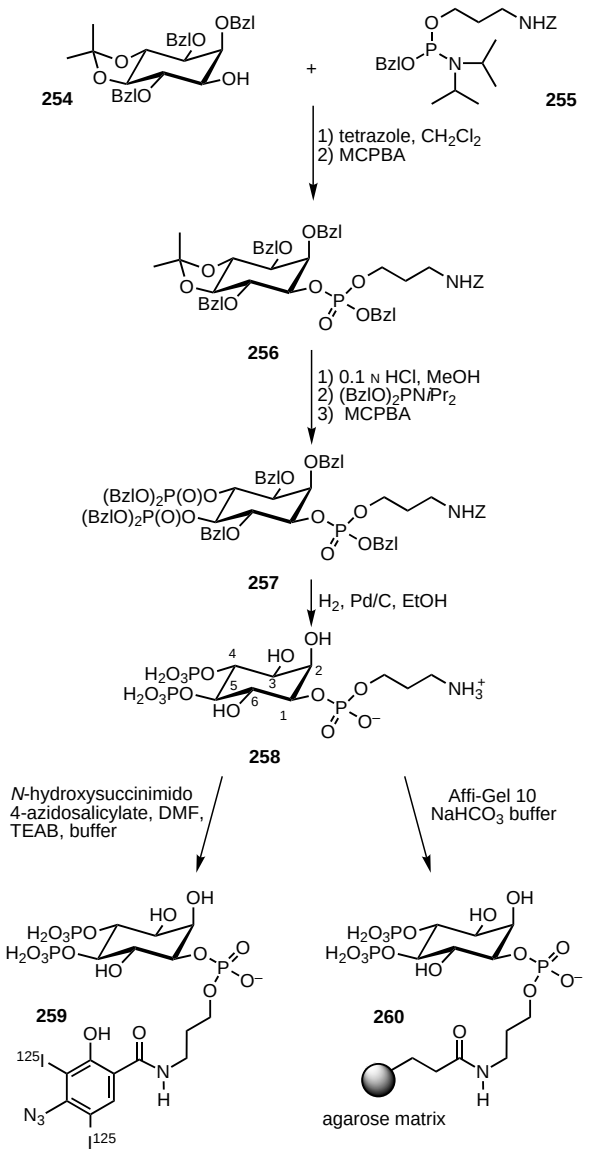
Inositol derivatives play a crucial role in signal transduction through heterotrimeric G proteins (see Section 2.1). Furthermore, they are also involved in other signal cascades. Activation of receptor tyrosine kinases can therefore lead to stimulation of the phosphoinositol-3 kinase (PI-3K),[324] which produces phosphatidylinositol 3,4,5-trisphosphate.[325] This is then converted into the corresponding 3,4-bisphosphate, which serves as a membrane anchor recognized by protein kinase B (PKB, *Akt*) through pleckstrin homology domains and thus brings about membrane localization of this protein. The PKB is subsequently activated by phosphorylation and switches on a further cascade.[326] Owing to the high biological relevance of inositol phosphate derivatives and the possibilities opened up for selective manipulation of physiological processes such as insulin secretion,[327, 328] a multitude of analogues have been synthesized and used as tools in biological studies and as lead substances for the development of new pharmaceuticals. As a result, the chemistry of inositol phosphates is highly developed and has been extensively reported in several reviews.[18, 19] Only a few newer developments and applications in biological studies will be presented here.

8.1. Inositol Phosphate Derivatives

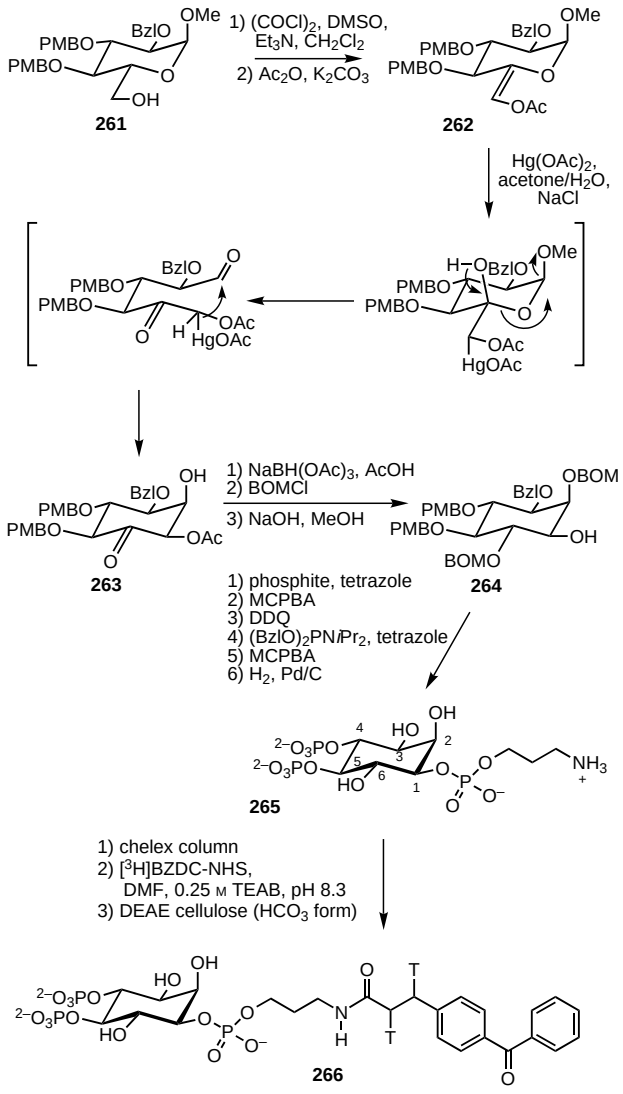
The focus of interest in inositol phosphate chemistry was particularly on the 1,4,5-trisphosphate and the investigation of the structural basis for the recognition of this mediator by the 1,4,5-IP_3 kinase, by the 1,4,5-IP_3 5-phosphatase, and by its receptor leading to calcium mobilization from intracellular reserves. By synthesizing a range of derivatives, it was possible to elucidate the molecular causes of these interactions in detail. According to these findings, the presence of the 4,5-bisphosphate motif seems to be essential for recognition by the receptor; furthermore, an additional phosphate group at the C1 position leads to increased release of Ca^{2+}. The presence of sterically demanding substituents at the C1 phosphate and the 2-OH group is tolerated. The phosphate group at C4 seems to be of particular importance for phosphorylation of the 1,4,5-IP_3 by the 1,4,5-IP_3 kinase. Modifications of the C5 phosphate are tolerated by the kinase; likewise, the C1 phosphate is important but not essential. For dephosphorylation of 1,4,5-IP_3 by the 5-phosphatase, the C1 phosphate group is probably of particular importance.

Based on this knowledge, derivatives suitable for photoaffinity labeling (**259**) were synthesized and an affinity matrix (**260**) was produced for further study of the 1,4,5-IP_3 receptor (Scheme 71).[329] For this purpose, the partially protected inositol **254** was converted into phosphate **256**, which could be selectively deblocked and phosphorylated to the 1,4,5-trisphosphate **257**. Subsequent removal of all benzyl protecting groups gave the inositol derivative **258**, from which the photoactivable and radioactively labeled 4-azidosalicylamide (**259**) and the affinity matrix **260** based on agarose could be synthesized. In an in vitro test system, trisphosphates **258** and **259** displaced [^{3}H]-myo-1,4,5-IP_3 from purified rat-brain receptors and released calcium from receptor preparations reconstituted in liposomes loaded with Ca^{2+}.[331] Both compounds were neither substrates nor inhibitors for the 1,4,5-IP_3 5-phosphatase and the 1,4,5-IP_3 kinase. With the immobilized derivative **260**, it was possible to isolate and purify receptors with good activity.

Recently, an improved general method was developed for the assembly of different enantiomerically pure IP_n derivatives and their functionalization to affinity matrices and



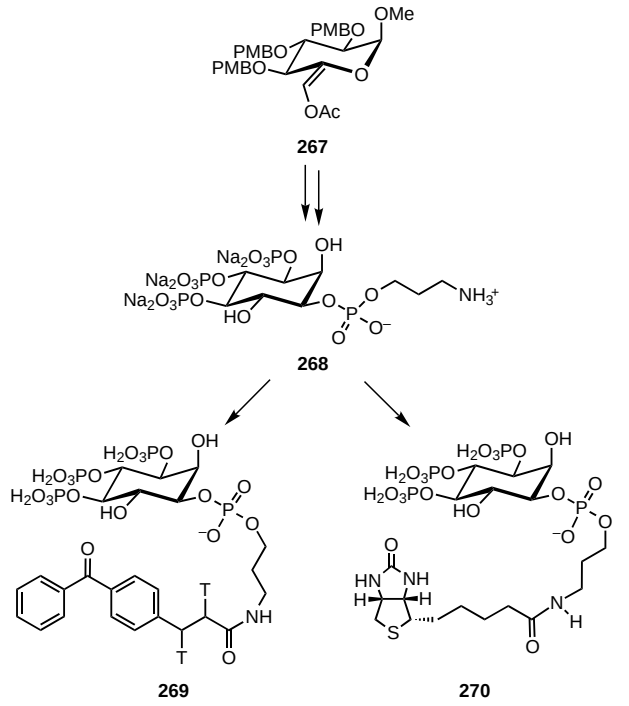
Scheme 71. Synthesis of inositol trisphosphates for photoaffinity labeling and production of an affinity matrix. MCPBA = *meta*-chloroperbenzoic acid, TEAB = tetraethylammonium bromide.



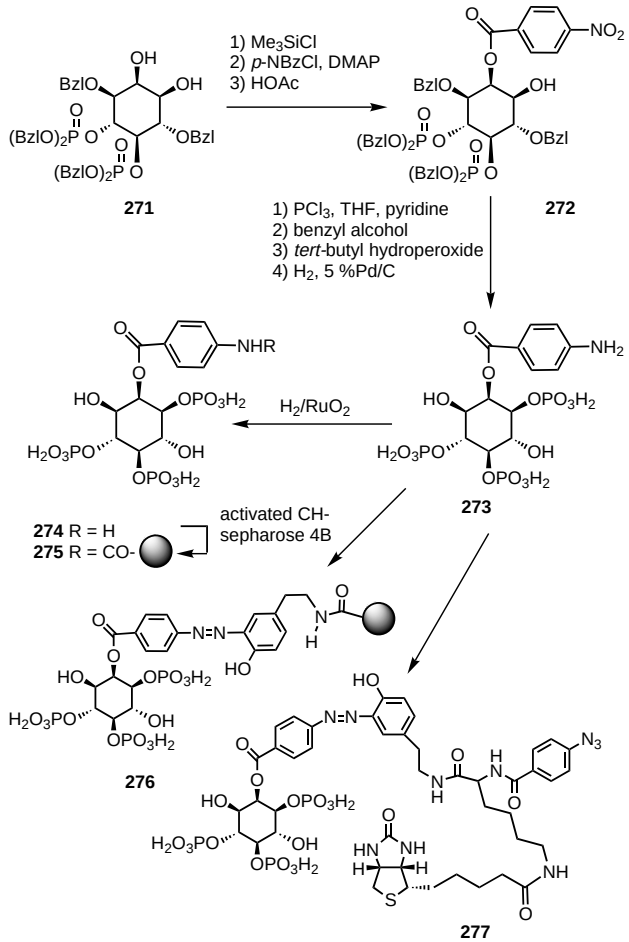
Scheme 72. Synthesis of an inositol phosphate analogue for biological studies. See Scheme 79 for the structure of BZDC-NHS (**308**), DEAE = diethylaminoethyl, T = ^{3}H.

photolabile analogues.[332] Starting from D-glucose, the differently protected glycoside **261**, which is selectively deblocked at the primary OH group, was synthesized, oxidized to the aldehyde, and converted into enol acetate **262** (Scheme 72). On treatment with mercury(II) acetate in aqueous solution, **262** reacted by ring opening and alternative ring closure to ionose **263**, which was stereoselectively reduced and then masked at 2-OH and 6-OH as the benzyloxymethyl (BOM) ether. Selective cleavage of the acetyl group enabled introduction of an aminoalkyl-modified phosphate group and following selective removal of the PMB groups, phosphorylation, and release of the remaining hydroxyl functionalities, derivative **265** was obtained. A radioactively labeled and photoactivable side chain was subsequently linked to the aminopropyl group (→**266**). Amide **266** was used, for example, to mark the PIP_2-binding pleckstrin homology (PH) domain of phospholipase C δ_1.[333, 334] By varying the pattern of protecting groups, 1,3,4,5-IP_4-tetrakisphosphates such as **269** and **270** were assembled with the same procedure (Scheme 73). Also IP_4 derivatives were used for producing affinity matrices and photoaffinity markers. With IP_4 affinity chromatography, different tetrakisphosphate receptors were purified. In addition, an IP_6 receptor was isolated and labeled.[335–337]

2-Acyl derivatives were also used as photoaffinity markers and for affinity chromatography (Scheme 74).[338] The synthesis started from the 4,5-bisphosphate **271**, which was obtained in five steps from D-*myo*-inositol. Manipulation of the protecting groups delivered the monohydroxyl derivative **272**, which—following phosphorylation, oxidation, and hydrogenolysis—gave trisphosphate **273**. Reduction of the aromatic ring gave the carboxylic acid derivative **274**. Compounds **273** and **274** were examined for interaction with the 1,4,5-IP_3 5-phosphatase and the 1,4,5-IP_3 3-kinase, exchange with D-[^{3}H]-1,4,5-IP_3, and ability to mobilize calcium ions. This showed that both analogues are substrates of the phosphatase and could release calcium from saponin-permeabilized[339–340]



Scheme 73. Synthesis of the inositol tetrakisphosphates **269** and **270**.

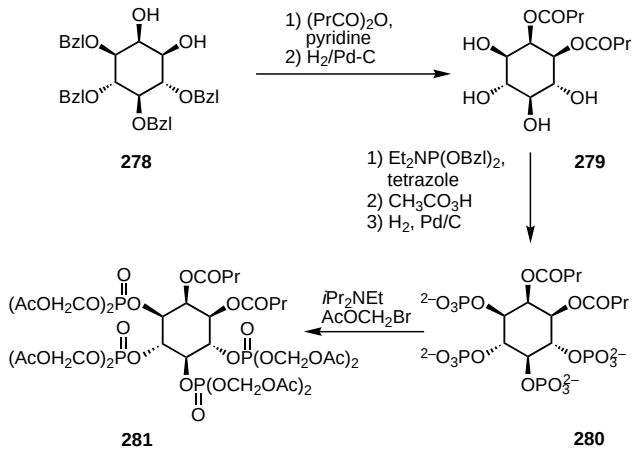


Scheme 74. Synthesis of the affinity matrices **275** and **276** as well as the biotinylated derivative **277**. *p*-NBzCl = *para*-nitrobenzyl chloride.

macrophages; only the D isomer of **274** was a substrate of the kinase, however. Likewise, displacement of D-[^{3}H]-1,4,5-IP_3 from its binding site in microsomal fractions of rat brain was observed. This led to the conclusion that the 2-OH functionality of the D-1,4,5-IP_3 is probably not involved in recognition by the receptor. Starting from derivatives **273** and **274**, affinity matrices such as **275** and **276** (Scheme 74) were produced for isolating corresponding cellular binding partners of 1,4,5-IP_3. To that end, **274** was coupled to an activated CH-sepharose 4B (→**275**). Amine **273**, following formation of the diazonium salt, opened up a route to matrix **276**. Similarly, the biotinylated analogue **277** was constructed, which could be detected without radioactive labeling with the biotin/avidin system. Labeling of a 1,4,5-IP_3 5-phosphatase from erythrocyte ghosts was achieved through the again activated amino functionality.[341]

The labeled analogues **266** and **269** were used as tools for isolating the cellular binding partner of the corresponding natural compounds and for labeling the exact sequences of the binding domains of these proteins. For example, the binding domain of the IP_3 receptor and of the PIP_2-binding protein were examined with [^{3}H]-BZDC-1,4,5-IP_3 (**266**).[333] In addition to the well-known role of the 4,5-bisphosphate in receptor recognition, it was also shown that the hydrophobic interaction is important for PLC isoenzymes for binding through the PH domain. Furthermore, four IP_4-binding proteins were isolated from rat brain, one of which was efficiently labeled by [^{3}H]-BZDC-1,4,5-IP_4 (**269**). This protein, called centaurin, has a PKC zinc finger and other domains in addition to the IP_4 binding domain; it also seems to be the first protein that binds PIP_3 more effectively than IP_4.[342]

Deblocked inositol phosphates cannot penetrate membranes at all, or only with great difficulty, owing to their high polarity; therefore, their use in biological studies is often limited. This problem was elegantly solved with the help of protected precursors such as **281** (Scheme 75).[343] In **281**, four



Scheme 75. Synthesis of a membrane-accessible inositol tetrakisphosphate analogue.

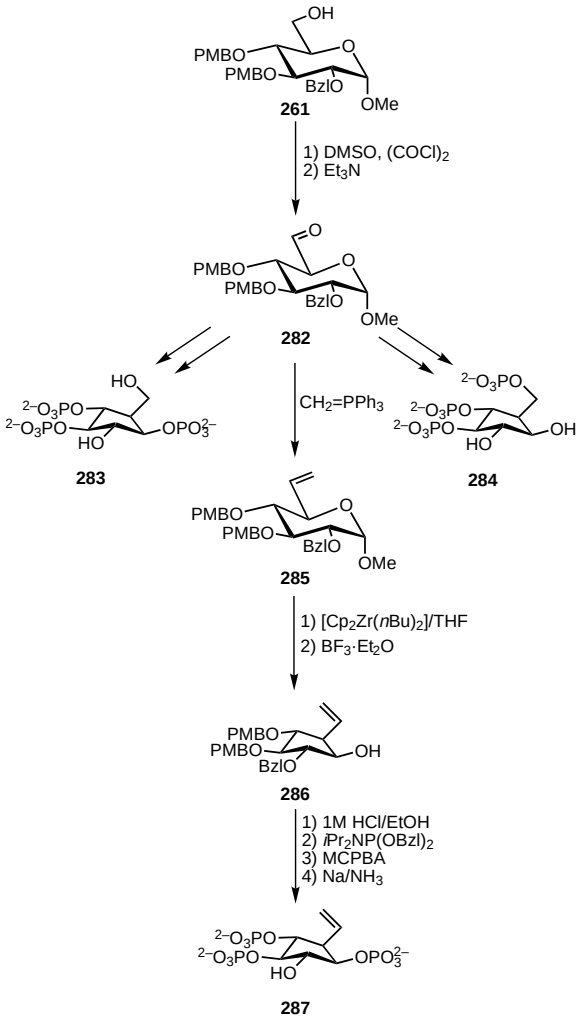
phosphate groups are protected as acetoxymethyl esters, and the OH groups of the inositol units are masked as butyrates. This lipophilic prodrug form of the inositol 3,4,5,6-tetrakisphosphate can penetrate membranes well and is intracellu-

larly deblocked by esterases and lipases to 3,4,5,6-IP_4 rapidly. With this reagent, it was possible to study the role of 3,4,5,6-IP_4 in the regulation of chloride secretion.[343] Chloride channels, which are regulated by cyclic nucleotides and the intracellular Ca^{2+} concentration, control the secretion of salt and liquid in intestinal epithelial cells; osmoregulation, pH balance, and neurotransmission also depend on the regulation of the chloride concentration. With **281**, it was shown that an increased flow of chloride ions brought about by raised Ca^{2+} concentration (e.g., triggered by histamine) is inhibited by 3,4,5,6-IP_4. The study also showed that, in the presence of a high 3,4,5,6-IP_4 concentration, chloride secretion is independent of Ca^{2+} concentration.

8.2. New Inositol Phosphate Analogues

The 1,4,5-IP_3 derivatives **287**, **283**, and **284** were developed as new inositol phosphate analogues with a modified ring; they have a five-membered ring instead of the cyclohexane structure (Scheme 76).[344] In **287** the positions 1, 4, 5, and 6 are still in the correct spatial orientation, but a C atom in the contracted ring is deleted. Several studies have shown that this C2 position is not needed for recognition by the 1,4,5-IP_3 receptor. To synthesize analogue **287**, the selectively deblocked glucose derivative **261** was synthesized and converted into the vinyl carbohydrate **285** by Swern oxidation and subsequent Wittig methylenation. Upon treatment with $[Cp_2Zr(n\mathrm{Bu})_2]$ and then with boron trifluoride etherate, **285** underwent a ring contraction to the vinyl cyclopentane **286**. Standard manipulations delivered the 1,4,5-IP_3 analogue **287**. With **287**, it was possible to mobilize calcium ions from 1,4,5-IP_3 receptors of platelets, although the concentration needed was higher than for 1,4,5-IP_3 itself.

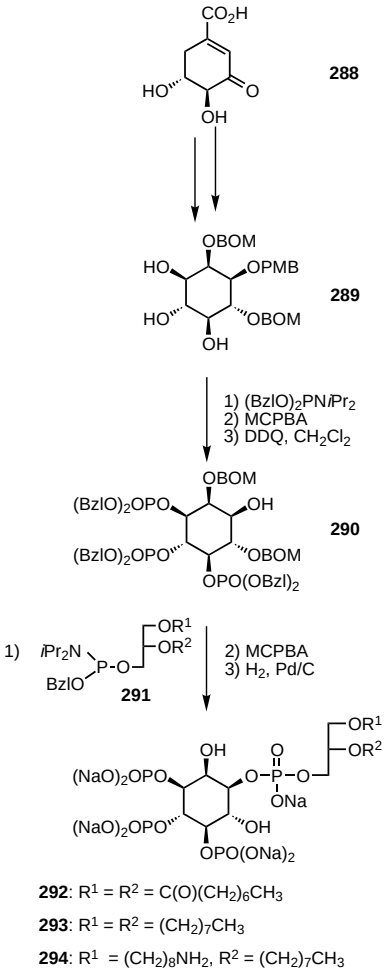
Starting from the intermediate **282**, analogues **283** and **284** were synthesized with the help of a ring contraction mediated by samarium(II) iodide. Compound **283** proved to be superior to the vinyl derivative **287** in mobilizing Ca^{2+}, whereas **284** hardly mobilized Ca^{2+} at all. These observations illustrate that a six-membered ring is not necessary for the development of 1,4,5-IP_3 agonists, and thus open up new perspectives for the investigation and disruption of the inositol signal pathways.



Scheme 76. Synthesis of ring-modified inositol phosphate analogues.

8.3. Analogues of Phosphatidylinositol Phosphates

Enantiomerically pure diester and diether analogues of PIP_2 and PIP_3 were constructed from compounds from the chiral pool, for example, dehydroshikimic acid (**288**, Scheme 77).

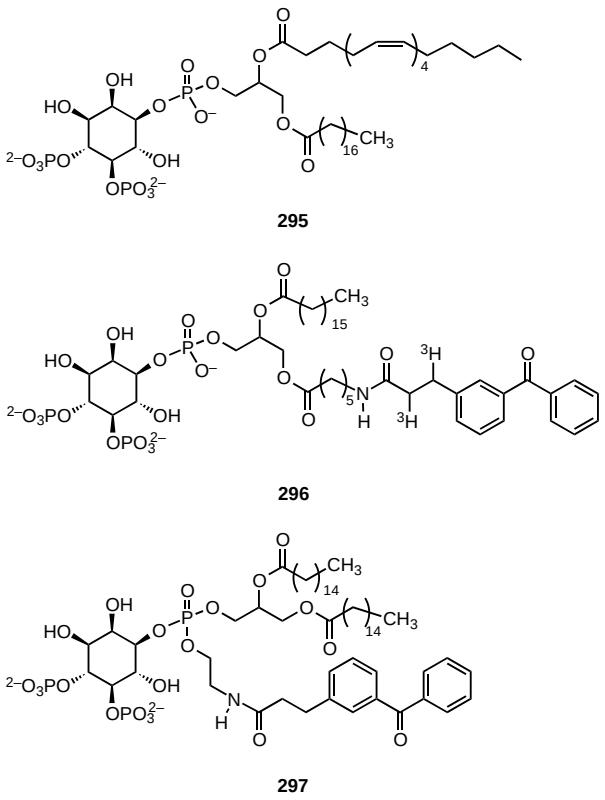


Scheme 77. Synthesis of phosphatidylinositol phosphates starting from dehydroshikimic acid.

To synthesize the ester or ether derivatives **292**–**294**, the natural product was first converted into triol **289**, which gave trisphosphate **290** on phosphorylation and removal of the PMB group. Condensation with the phosphoramidates **291**, oxidation with perchloric acid and deprotection gave the PIP_3 analogues **292**–**294**.[345] The water-soluble derivatives **292** and **293** stimulated the calcium-independent PKCδ, PKCε, and PKCη isoenzymes in vitro,[345, 346] whereas **294** can be used for coupling to antigens and for producing affinity matrices.

Based on the structure of PIP_3 **295** and the IP_3 analogues described, derivatives of PIP_3 with reporter groups, glycerol **296** and phosphotriester **297** were synthesized (Scheme 78).[322, 347, 348] Their synthesis started from the inositol derivatives **298** and **299** and used phosphoramidates **306** or **307** (Scheme 79). In the end product, the hydroxyl functionalities previously protected as PMB ethers are now phosphorylated; the alcohols previously protected as benzyl or benzyloxymethyl esters are now free. To incorporate reporter groups in the glycerol side chain, fragments **298** or **299** and **307** were coupled to one another and further elaborated; thus, PIP_2 and PIP_3 analogues were obtained. The PIP_2 and PIP_3 analogues modified at the phosphotriester (**304** and **305**) were similarly obtained following reaction of phosphoramidate **306** with inositol derivatives **298** and **299** and further elaboration.

These PIP_2 analogues and related compounds were used in photolabeling and fluorescence spectrometry tests. It was shown that the myristoylated alanine-rich C kinase substrate (MARCKS) brings about an encapsulation of PIP_2 and phosphatidylserine in lateral domains of the cell membrane through electrostatic interactions, and thus initiates a reversible inhibition of hydrolysis of PIP_2.[349]



295

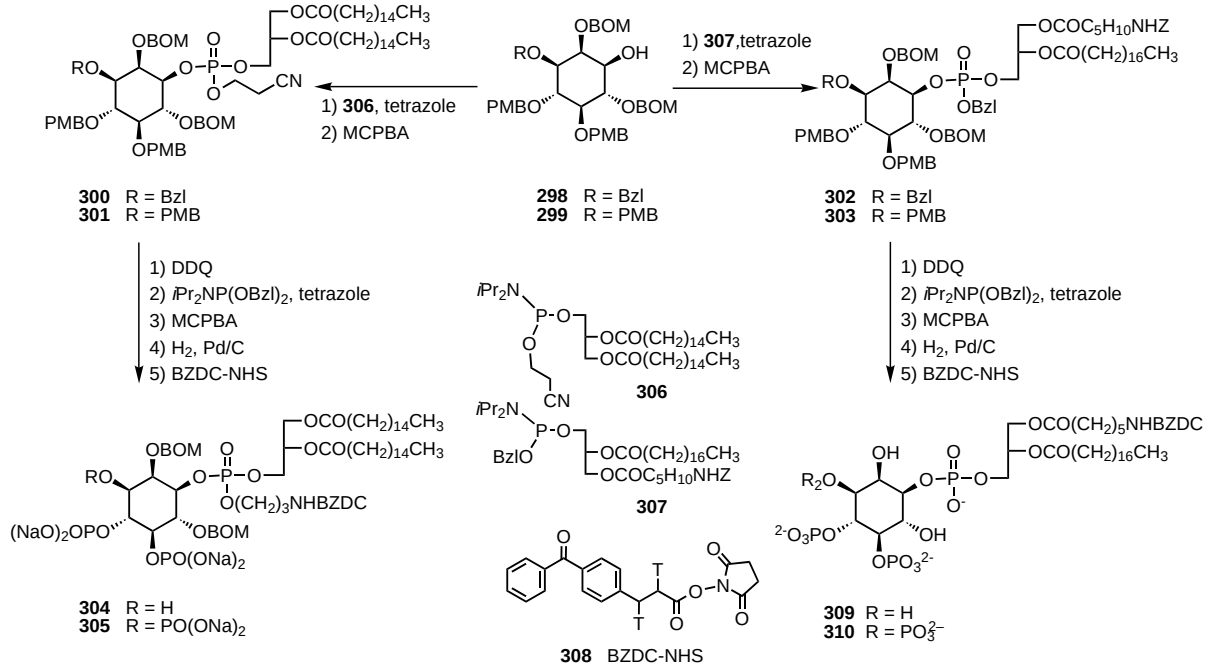
296

297

Scheme 78. Structures of phosphatidylinositol phosphate **295** and labeled analogues.

9. Inhibition of Phosphatases

Phosphorylation and dephosphorylation of proteins are critical components of signal transduction mechanisms that regulate cell differentiation and growth (see Sections 3, 6, and



300 R = Bzl
301 R = PMB

298 R = Bzl
299 R = PMB

302 R = Bzl
303 R = PMB

306

307

308 BZDC-NHS

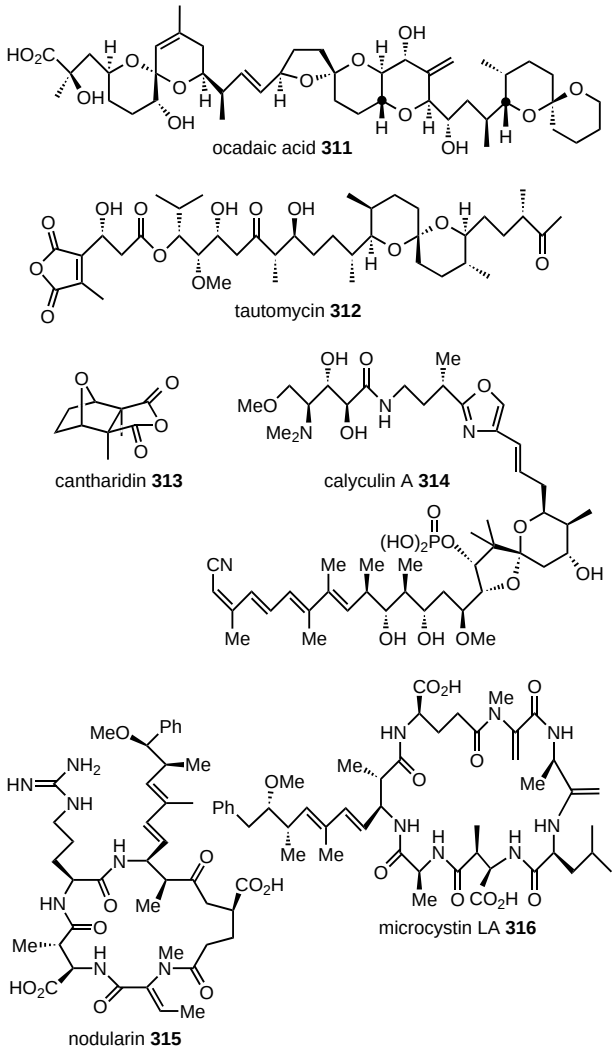
304 R = H
305 R = $PO(ONa)_2$

309 R = H
310 R = PO_3^{2-}

Scheme 79. Synthesis of labeled phosphatidylinositol phosphate analogues.

7). The position of this modulatable equilibrium is determined by the activity and concentration of protein kinases and phosphatases,[350] which reinforce or weaken one another according to the cellular context.[351] A disturbance of this balance can lead to disease and to transformation of the cell. In Sections 3 and 7, tyrosine- and serine/threonine-specific kinases were presented; in the following, their cellular opponents will be described.

Eucaryotic phosphatases[350] are structurally and functionally varied enzymes that are divided into several families. The Ser/Thr-specific phosphatases differ considerably in their catalytic domains from the "dual-specificity" phosphatases and from the tyrosine-specific phosphatases, which both have a high sequence homology. The structure of several serine/threonine and tyrosine phosphatases was obtained by crystal structure analysis. The catalytic mechanisms are also known.[352] The importance of these enzymes for cell physiology is underlined by the fact that they are often the target of microbial or viral attack. For example, λ-bacteriophage codes for a Ser/Thr phosphatase, the virulence plasmid from *Yersinia* for a Tyr phosphatase, and the *Vaccinia* virus for a phosphatase that dephosphorylates both Ser/Thr and Tyr residues.[350b] Inhibitors of these biocatalysts are important tools for in vivo investigations and have led to the discovery of a range of physiological functions of protein dephosphorylation. In particular, natural products such as ocadaic acid (**311**),[353] tautomycin (**312**),[354] calyculin A (**314**),[355] cantharidin (**313**),[356] nodularins such as (**315**),[357] and microcystins such as **316**[358] (Scheme 80) have been used. The special role of the phosphatase inhibitor FK 506 and cyclosporin A will be described in Section 10.



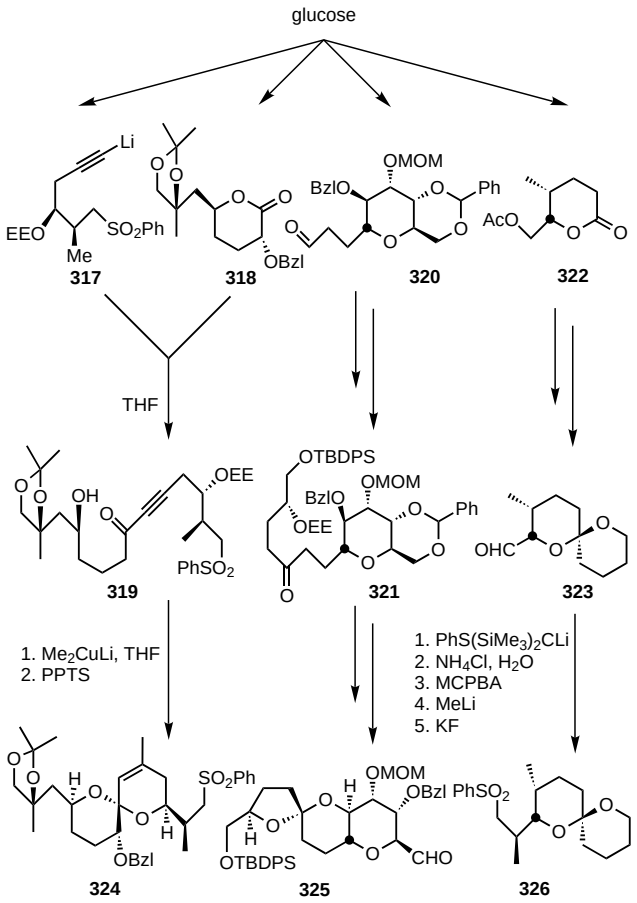
Scheme 80. Natural products that inhibit phosphatases.

9.1. Ocadaic Acid

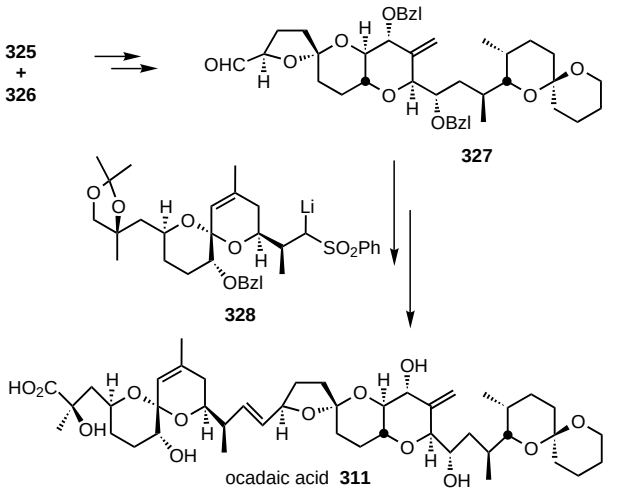
Ocadaic acid is a polyether derivative of a C_{38} fatty acid isolated from two different marine sponges.[353] In addition to its activity as a diarrheogenic shell-fish toxin, it has also been reported as a tumor promoter[359] and a specific Ser/Thr-phosphatase inhibitor.[360] Unlike the PKC-activating phorbol esters (see Section 7), it promotes tumor growth by inhibiting the dephosphorylation of the PKC's target proteins. Owing to its manifold biological activities and the interesting polyether structure with 17 steroecenters, the natural product is an exciting goal for a total synthesis. The correct assembly of the stereocenters is the biggest challenge. The complex molecule was retrosynthetically converted into fragments **324**–**326** (Scheme 81),[361] which were each assembled starting from glucose derivatives.

The key step in the synthesis of fragment **324**[362] (Scheme 81) was nucleophilic attack of acetylide **317** on lactone **318**, which are both obtained from glucose. The only carbon atom still missing was introduced by a stereoselective conjugate addition of a methyl cuprate to the acetylenic ketone **319**, and the ring was then closed to the spiroketal by acid catalysis. Fragment **325** (Scheme 81) was also synthesized from glucose.[363] Standard reactions gave aldehyde **320**, in which the benzylidene group fixed the conformation of the pyranosyl ring. The carbon backbone was extended by adding a lithiated sulfone with formation of ketone **321**. Selective manipulation of the protecting group enabled formation of the ketal and subsequently completion of fragment **325**. In the synthesis of the third fragment (Scheme 81), an enantiomerically pure glucose derivative also functioned as a starting material.[364] Following functionalization of the pyranose backbone, lactone **322** was opened with a lithiated sulfone and then converted into aldehyde **323**, which was converted into the alkene in a Petersen olefination. Stereoselective introduction of the missing methyl group was achieved by chelate-controlled heteroconjugate addition at the vinyl sulfone produced. This key step in the synthesis sequence was also used in the production of fragment **324**.

To complete the synthesis of the natural product **311** (Scheme 82),[365] phenylsulfone **326** was deprotonated, coupled with fragment **325**, and the phenylsulfone group subsequently removed. The correct stereochemistry of the newly created alcohol was set by oxidation and stereoselective reduction; further transformations then led to fragment **327**. This was coupled to the lithiated sulfone **328** with formation of the necessary olefin. Manipulation of the protecting groups and oxidation to the acid gave the natural product. The



Scheme 81. Synthesis of the individual fragments of ocadaic acid. EE = ethoxyethyl, PPTS = pyridinium-*p*-toluene sulfonate.



Scheme 82. Synthesis of ocadaic acid.

multitude of latent hydroxyl groups in the molecule called for a careful protecting group strategy. In the course of the synthesis, silyl (TBDPS), acetal (MOM, THP, benzylidene, ethoxyethyl) and acetyl protecting groups were used and were subsequently replaced by benzyl ethers, so that in the last step, complete deprotection of the molecule was achieved with lithium in ammonia.

The importance of ocadaic acid for investigating biological and medical phenomena is illustrated by the fact that in 1995 and 1996 this natural product was used in biological experiments described in about 450 and 400 publications, respectively. In particular, the ability of the natural product to selectively inhibit the Ser/Thr phosphatase PP2A (IC_{50} = 1 nM) without influencing the Ser/Thr phosphatase PP1 (IC_{50} = 330 nM) was put to use.[366] Fundamental knowledge was obtained in the investigation of programmed cell death, or apoptosis. By treating different cancer cell lines with ocadaic acid, it was shown that the cells already have the whole protein repertoire necessary for apoptosis, regardless of their position in the cell cycle.[367, 368] A de novo synthesis of additional proteins is not necessary. Phosphatases are thus involved in the signal cascade leading to apoptosis. However, further investigations are needed for better understanding of the whole process, since ocadaic acid is also able to protect lymphocytes from apoptosis induced by other reagents.[369]

In further experiments, the influence of ocadaic acid on K 562 leukemia cells was investigated.[370] Treatment with the natural product reduced expression of the genes *c-myc* and *max*. These code for proteins that play a key role in controlling cell growth and cell differentiation and which must heterodimerize in the cell nucleus for this function.[371] Reduction of expression of these genes induces apoptosis in the treated cells. It was shown with several reporter genes that the natural product does not cause general reduction of gene expression. In addition, PP2A is the only phosphatase that is inhibited. Treatment of the cells with the phosphatase inhibitor calyculin A (**314**, Scheme 80) gave similar results, whereas the ocadaic acid tetraacetate, which is inactive towards the enzymes, did not bring about any change in gene expression. One hypothesis that explains these observations is that the phosphatase PP2A dephosphorylates and activates transcription factors that are needed for transcription of *c-myc* and *max* (see Section 6.3).

The role of the phosphatase PP2A in resistance to insulin mediated by the tumor necrosis factor (TNF-α) was shown by treatment of skeletal muscle cells from rat with ocadaic acid.[372] The insulin resistance is caused because TNF-α blocks the insulin-stimulated phosphorylation of MEK triggered by Ras and Raf, and thus the subsequent activation of the MAP kinase (see Section 2.2). Cancellation of this effect by addition of ocadaic acid, and observation of increased PP2A activity on stimulation by TNF-α, indicate a role for this enzyme, which apparently dephosphorylates MEK and thereby inactivates it. In contrast, other phosphatase inhibitors such as orthovanadate or FK 506 (see Section 10) do not lead to removal of the TNF-α-mediated insulin resistance.

In further work on insulin-stimulated transport of glucose and translocation of a glucose transporter (Glut 4) from intracellular vesicles to the cell membrane, it was shown that ocadaic acid imitates the effect of insulin on human adipocytes: The rate of glucose transport is increased, and migration of Glut 4 to the cell membrane is stimulated.[373] In contrast to the insulin-stimulated signal path, the effect of ocadaic acid is independent of the activity of the PI-3 kinase, a lipid kinase. These findings suggest that several signal paths regulate glucose transport; this opens up new avenues for

treatment of diabetes. The exact cause of the effect of ocadaic acid has not been investigated further.

With ocadaic acid as a selective inhibitor of the PP2A phosphatase, at low concentrations of about 10 nM, this enzyme is involved in EGF-induced regulation of MAP kinase in A431 cells[374] and in hyperphosphorylation of the Tau protein, which is important in Alzheimer's disease.[375]

9.2. Calyculin A

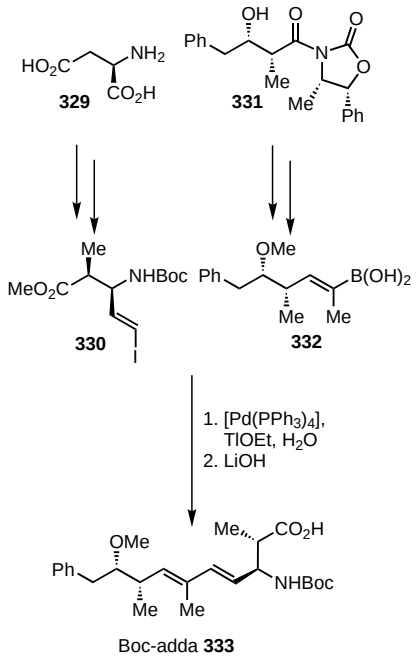
The secondary metabolite calyculin A (**314**, Scheme 80) was isolated in 1986 from a marine sponge[355] and was reported a bit later as a phosphatase inhibitor.[376] In contrast to ocadaic acid, which inhibits PP2A by a factor of 10–100 better than PP1, calyculin A blocks both enzymes with similar IC_{50} values. The relative stereochemistry of the natural product was obtained by a crystal structure analysis;[355] the absolute configuration was elucidated by a first total synthesis in which particular attention had to be paid to the hydrolysis-labile phosphate unit and the conjugated tetraene unit.[377] Calcyculin A has a broader enzyme specificity than ocadaic acid but otherwise has very similar biological activity.

If human tumor cells are exposed to γ-radiation or heat, intensive DNA fragmentation and morphological changes take place which are characteristic of apoptosis. In the presence of 20 nM calyculin A or 500 nM ocadaic acid, the programmed cell death is hindered, however.[378] Calyculin A has the same effect at low concentrations in photodynamic therapy (PDT). In this procedure for tumor treatment, apoptosis is triggered by laser radiation in cells which have been treated with photosensitive reagents. Alignment of the light source enables targeted destruction of malignant tissue. In leukemia cells from mice, the characteristic DNA fragmentation takes place very rapidly (within 30 min) after radiation.[379] Treatment of the cells with calyculin A prevents programmed cell death, whereas the PKC inhibitor staurosporin accelerates the process. From the very rapid occurrence of apoptosis, the authors concluded that photodynamic therapy initiates a late step in the whole process (this is probably the reason for the broad applicability of PDT; in contrast, chemotherapeutical agents influence earlier steps in programmed cell death which are no longer present or suppressed in tumor cells) and that a Ser/Thr phosphorylation/dephosphorylation is involved in a late stage of the signal transduction processes leading to cell death.

Calyculin A and ocadaic acid function as strong tumor promoters (see above and Section 9.1) in that they prevent dephosphorylation of target proteins of PKC; they have the same effect as activation of the Ser/Thr kinase by phorbol esters (see Section 7).[350b] Both natural products bring about translocation of PKC from the cytosol to the cell membrane in different cell types; calyculin A does this at lower concentrations (10 nM) than ocadaic acid (1 μM).[380] This membrane association is also initiated by phorbol esters and leads to activation of the kinase.[381] Despite differences in the structure and the cellular target proteins, the different natural products promote tumor growth in a similar way, by membrane localization of the PKC. Further applications of calyculin A include examination of the TNF-α-mediated insulin resistance,[382] modulation of the activity of the Ras farnesyltransferase by phosphorylation/dephosphorylation,[383] and the role of the phosphatases PP1 and PP2A in glucose-induced regulation of glycogen synthase.[384]

9.3. Nodularins and Microcystins

Nodularins such as **315**[357] and microcystins such as **316**[358] (Scheme 80) are cyclic penta- and heptapeptides, respectively, produced by cyanobacteria. These compounds are hepatotoxic and responsible for the poisonousness of water in which blue-green algae bloom. In addition, they function as potent inhibitors of the Ser/Thr phosphatases PP1 and PP2A and as tumor promoters. Both natural products are structurally related and have a common unusual β-amino acid, adda (**333**, Scheme 83), as well as D-*erythro*-β-methylaspartic acid.



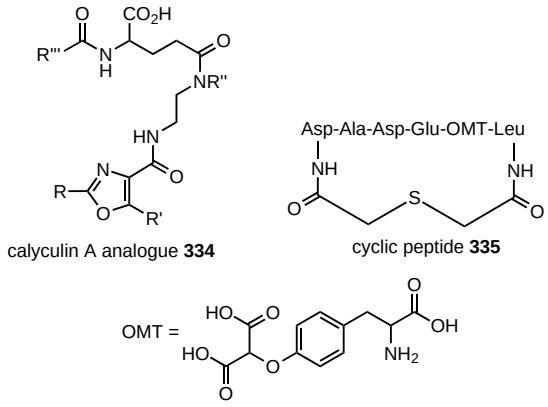
Scheme 83. Synthesis of Boc-adda.

Owing to their many biological properties, there is much interest in the synthesis of these natural products and of structurally related nonnatural analogues.[385] For this purpose, an efficient and stereospecific synthesis of **333** is required.[386] In a recently published initial total synthesis of microcystin LA,[385] **333** was obtained by a Suzuki coupling of the vinyl iodide **330**, which is obtained from a stereoselectively β-methylated aspartic acid, and boronic acid **332**, which was synthesized from the *syn*-aldol **331** (Scheme 83).

9.4. Other Inhibitors

An example for the development of new synthetic phosphatase inhibitors was recently reported.[387] Based on the few

available SAR[388] and molecular modeling investigations[389] concerning the activity of the naturally occurring inhibitors, the highly simplified calyculin A analogue **334** (Scheme 84)



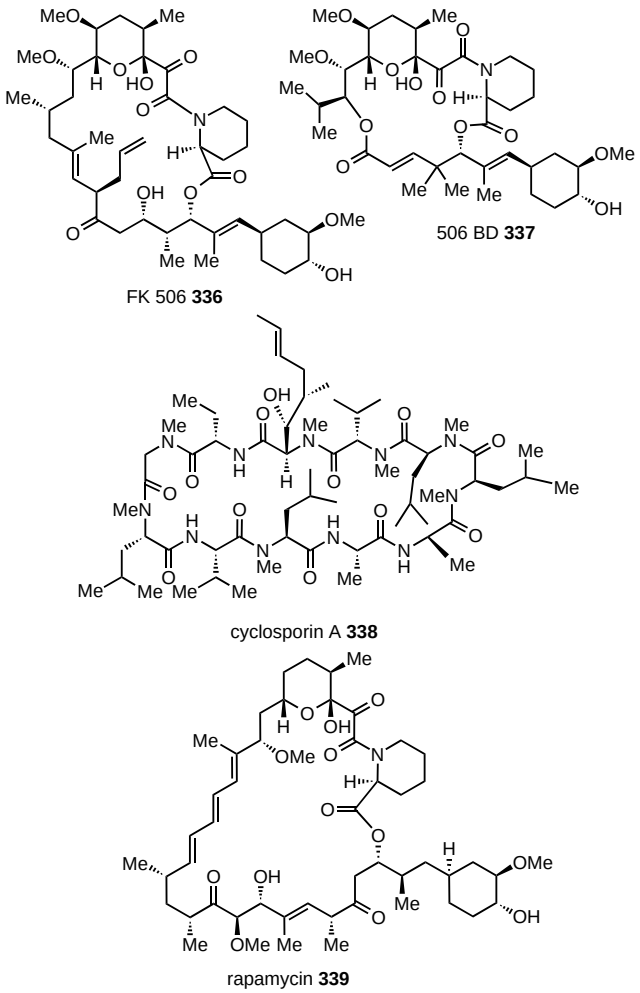
Scheme 84. Synthetic phosphatase inhibitors.

was designed, which contains an essential carboxylate functionality, a hydrophobic residue, and hydrogen donors and acceptors. With a combinatorial strategy, 18 derivatives of **334** were synthesized and tested for activity against the phosphatases PP1 and PP2A as well as in human breast cancer cells. Some compounds in the library blocked the enzyme activity (although at considerably higher concentrations than calyculin A), and in whole cell systems an antiproliferative activity developed, so that the planned further experiments promise interesting results.

Starting from the amino acids sequences of preferred substrates of individual phosphatases, it was also possible to synthesize selective peptide enzyme inhibitors. It is advantageous to replace phosphotyrosine with hydrolysis-labile derivatives such as phosphonomethylphenylalanine, difluorophosphonomethylphenylalanine, or *O*-malonyltyrosine (OMT). In this way, cyclic peptides derived from an autophosphorylation sequence of the EGF receptor were synthesized which were stable with respect to proteolysis. Those compounds that contained the OMT mimetic (e.g. **335**, Fig. 24) were potent in vitro inhibitors of the phosphatase PTP1.[390] It would be interesting to investigate whether there are structural similarities between this class of enzyme inhibitors and the microcystins and nodularins mentioned above.

10. Induced Dimerization of Proteins by Synthetic Ligands[391]

One of the most illustrative examples for the cross-fertilization of organic synthesis and biology is the elucidation of the mechanism of the immunosuppressants FK 506 (**336**) and cyclosporin (CsA, **338**; Scheme 85) as well as T cell activation (see Sections 2 and 4 and Scheme 9). Since this fascinating area of research has already been extensively described elsewhere,[392] it will only be mentioned briefly here. FK 506 and cyclosporin are natural products that block Ca^{2+}-dependent signal paths, and, due to their inhibitory effect on



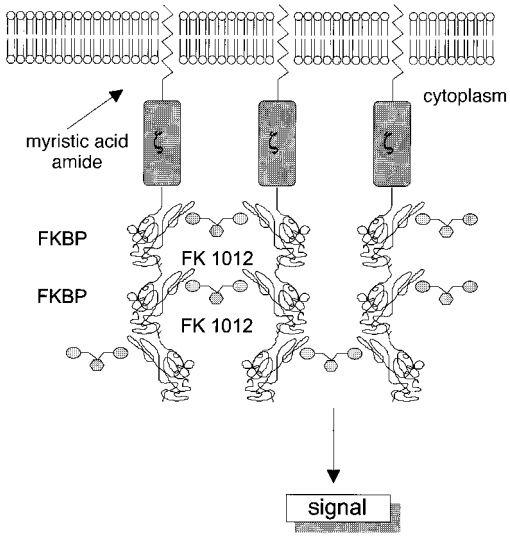
Scheme 85. Immunosuppressants and the synthetic ligand 506 BD.

the transcription of a range of genes in T cells, they have been used as immunosuppressants in organ transplantation. With immobilized derivatives of these ligands, their physiological receptor proteins, the immunophilins cyclophilin (Cyp) and FK 506 binding protein (FKBP) were identified. At first it was assumed that the activity of the natural products immuno suppressiol was due to inhibition of the rotamase activity of these proteins, which is essential for the activation of T cells. However, this hypothesis had to be abandoned when it was discovered that both rapamycin (**339**) and the fully synthetic FK 506 binding domain (506 BD, **337**; Scheme 85) bind to FKBP and inhibit its rotamase activity but that rapamycin inhibits a signal path other than that of FK 506 and CsA, and 506 BD does not inhibit any signal transmission. Building on the hypothesis that the ligand–receptor complex influences another molecule of the transduction cascade, the cellular binding partner of the "activated complex" of FK 506 and FKBP was found, again with the help of affinity chromatography. This turned out to be the calmodulin-dependent phosphatase calcineurin; its enzymatic activity is inhibited by binding to FK 506/FKBP but is not influenced by FK 506, FKBP, Cyp, rapamycin, 506 BD, or rapamycin/FKBP. This enzyme inhibition hinders phosphorylation of the transcription factor NF-AT (see Scheme 9) leading to arrest of the cell

cycle in the G_0 phase and thus to the observed immunosuppression. It is interesting that the phosphatase calcineurin is also inhibited by the complex of CsA and cyclophilin. The natural products have two protein-binding domains; they bind to the immunophilins with one and to calcineurin with the other, and can therefore be described as "chemical inducers of dimerization".[391] Stimulated by this work, quite new possibilities and concepts have grown from the investigation of signal transduction processes.

Ligand-mediated signal transduction processes are often initiated by di- or oligomerization of receptors.[393] However, the extracellular and transmembrane domains are only needed to a limited extent: Their function is primarily to bring the enyzmatically active intracellular domains into the immediate vicinity of one another so that, for example, a transphosphorylation can take place. Based on this assumption, a dimer was synthesized starting from FK 506 in which two FK 506 monomers are linked to one another through a functional group within the calcineurin binding domain.[394] This dimeric ligand, FK 1012 (**340**, Scheme 86), should still be able to bind FKBP, but inhibition of the TCR signal path by essential binding to the phosphatase calcineurin is no longer possible.

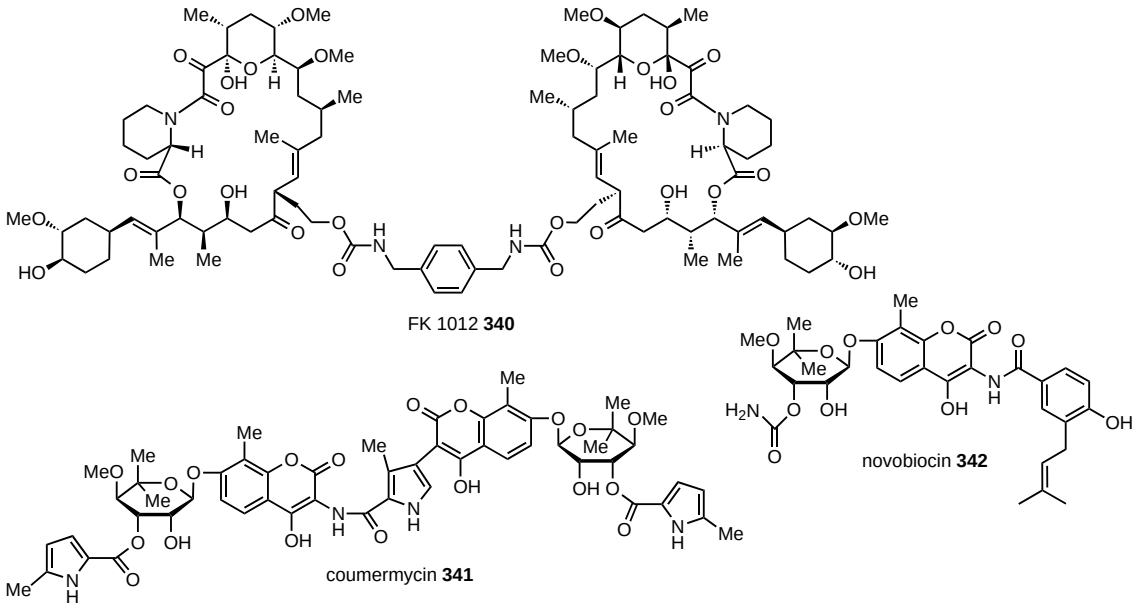
To show the applicability of this property in biological studies, Tag–Jurkat T cells were transfected with chimeric Src/ζ-FKBP receptors constructed from the N terminus of Src (this protein is myristoylated and thus brings about a membrane localization), the ζ-chain of the TCR (to induce a kinase cascade upon dimerization of the receptors, see Scheme 9), and several copies of the FKBP. On treating these cells with the synthetic dimer **340**, the receptors oligomerized in that the ligand bound them to one another through its FKBP binding site (Scheme 87). As a consequence of this artificial aggregation and the kinase cascade thereby initiated, activation of reporter genes was observed similar to that elicited by antibody cross-linking. If the myristoylation, and thus the membrane association of the receptor, was prevented by exchanging the N-terminal glycine of the Src protein for



Scheme 87. Activation of chimeric receptors by FK 1012.

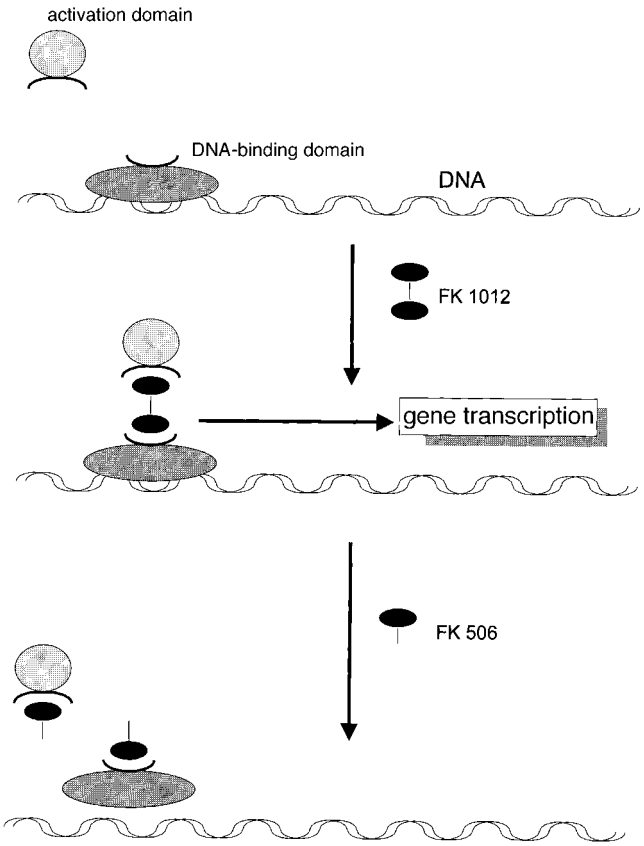
alanine, no activation of the signal path was detected. The same finding was observed if the receptor only contained one copy of FKBP, whereas three copies gave maximal activity. It was thus concluded that it is not the extracellular and the transmembrane domains of the TCR that are necessary for activating the TCR signal path; however, the receptor must be localized on the cytosolic side of the plasma membrane. Ligand-induced conformational changes in the T cell receptor apparently do not play an essential role. In addition, an oligomerization of the receptor seems to be necessary, but a simple dimerization by the synthesized ligands does not switch the signal cascade on. The artificial signal can be switched off by addition of the monomeric FK 506 or CsA; therefore, the transduction cascade can be activated or terminated on command.

This method was also used to selectively switch on transcription of genes. Transcription factors are made up of



Scheme 86. Ligands that induce protein dimerization and the monomeric novobiocin.

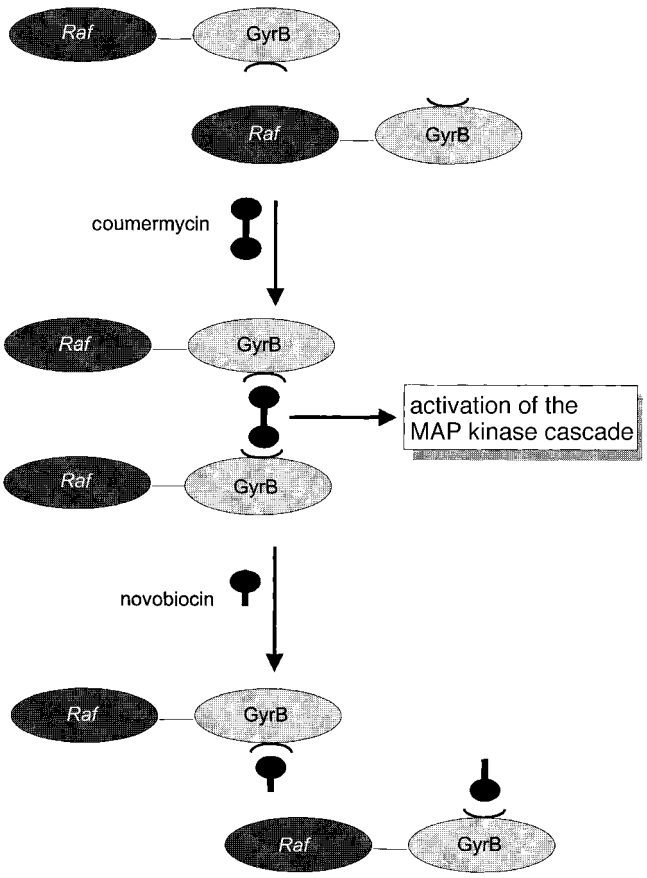
functionally different domains which mediate binding to DNA and activation of transcription independent of one another.[395] Since no covalent bonds are needed here, it is possible to bring such domains close to each other with the help of dimeric ligands and thus induce transcription. For this purpose, chimeric proteins were used, each containing FKBP and, in one case, a DNA-binding domain (GF3 or HF3), and in another, an activation domain (NF3V1); these were expressed in cells (Scheme 88).[396] Treatment of these cells



Scheme 88. Induction of gene transcription by a synthetic ligand.

with the ligand FK 1012 (**340**) led to the activation of transcription, which could be stopped by addition of the monomer FK 506. In addition, the observations suggest that the activation domain must be permanently bound to the DNA for maintenance of transcription and that a solitary occurrence of complex formation is not sufficient.

In a further investigation, signal transduction through the Raf kinase was examined with the help of induced dimerization.[397] Coumermycin (**341**, Scheme 86) is an antibiotic that binds to two molecules of the B subunit of a bacterial DNA gyrase (GyrB) and induces a dimerization. To investigate the mechanism that leads to activation of the Raf-1 kinase (see Section 2.2), chimeric Raf fusion proteins were created in which the GyrB subunit was linked to the C terminus of Raf. If these proteins were expressed in Cos cells, their catalytic activity (i.e., phosphorylation of MEK) could be induced by addition of the antibiotic **341** (Scheme 89). High doses of coumermycin or novobiocin (**342**, a monomeric analogue of coumermycin, Scheme 86) blocked the MEK activation; this



Scheme 89. Activation of the MAP kinase cascade by coumermycin-induced dimerization of the Raf kinase.

is consistent with the hypothesis of activation by dimerization. If a mutant of Raf (R89L), which does not interact with Ras and therefore should not be localized in the plasma membrane, was used for these experiments, the same coumermycin-dependent reaction was observed as for the wild-type protein. Dimerization of Raf kinase seems to be sufficient for activation, and a membrane localization is not necessary. The role of the Ras protein in the activation of Raf, according to these results, may be to induce aggregation of the kinase. Investigations in which dimerization of chimeric FKBP-Raf fusion proteins were induced with the help of FK 1012 led to similar results.[398]

With a dimer of the cyclosporin A, a Fas-mediated apoptosis was induced in cells in which the intracellular domain of the Fas receptor was expressed linked to cyclophilin.[391] A synthetic construct of FK 506 and cyclosporin A, FKCsA, was also successfully used for the aggregation of two different proteins.[399]

The potential of this conceptionally new class of active compounds is increased by the fact that they are generally orally applicable and are easily taken up by cells. For example, a therapeutic protein, human growth hormone (hGH), was produced with the help of the natural product rapamycin by controlling transcription in mice implanted with a cell construct.[400] The cell construct contained the hGH gene and two regulatory proteins which were equipped with recognition sequences for rapamycin.

11. Conclusions and Outlook

The examples described in this review for the successful interlocking of organic chemical and biological search to investigate and influence biological signal transduction are an impressive demonstration of the capabilities of interdisciplinary research in the field of bioorganic chemistry, according to the definition given in the introduction. Today, more and more biological phenomena are being investigated, elucidated, and understood in molecular detail at a rapidly increasing speed. For organic chemistry, this opens up a multitude of new spheres of activity, in which its capabilities can be used to the full extent and in which new, great, and important challenges are presented which must be taken up: In mastering them, organic chemistry can rise to a key role. For biology, bioorganic research presents new alternative possibilities to obtain results faster, more directly, and often with a greater degree of precision and clarity; in most cases, these results could hardly be achieved with methods established today, or only with much greater effort. Establishing bioorganic chemistry at the border between organic chemistry and biology as a capable and widely applicable field, such as physical chemistry between physics and chemistry, requires the readiness and will of organic chemists and biologists to step over the boundary to the neighboring discipline. The language and methods of the other must be learnt, and there must be mutual respect (and one must not just regard the neighboring science as a source of themes or substances) and dedication to the issues to be addressed with real cooperation. The future will show whether we can rise to this challenge.

Motivation to write this review came from our own work in linking organic chemical and biological research in the field of signal transduction at the Universität Mainz, Universität Bonn, and Universität Karlsruhe. Our work is mainly mentioned in Sections 3 and 5–7. The following persons (in alphabetical order) have been involved in the past and at present: D. Alonso-Díaz, D. Brom, A. Cotté, F. Eisele, S. Gabold, S. Glomsda, P. Hagenbuch, A. Heuser, K. Hinterding, V. Jungmann, D. Kadereit, T. Kappes, B. Klaholz, V. Klein, N. Kuder, K. Kuhn, Y. Li, T. Lipps, R. Machauer, B. Meseguer-Vidagany, E. Nägele, D. Owen, T. Pathak, T. Pohl, A. Reidel, J. Sander, M. Schelhaas, U. Schlede, D. Sebastian, T. Schmid, T. Schmittberger, S. Schulze, P. Stahl, F. Stieber, P. Stöber, T. Zelinski. For generous support of our work, we would like to thank the Deutsche Forschungsgemeinschaft, the Bundesministerium für Bildung und Forschung, the Fonds der Chemischen Industrie, the European Union, the Alexander-von-Humboldt-Stiftung, the Krupp Stiftung, Boehringer Mannheim GmbH, Bayer AG, BASF AG, Degussa AG, and Boehringer Ingelheim KG.

Received: June 17, 1997 [A 235 IE]
German version: *Angew. Chem.* **1998**, *110*, 716–780
Translated by Dr. J. Cooper, Frankfurt (Germany)

[1] A. Kornberg, *The Golden Helix—Inside Biotech Ventures*, University Science Books, Sausalito, CA (USA), **1995**, p. 4.
[2] *Chem. Eng. News* **1996**, *74*(20), 39.
[3] See also G. M. Whitesides, *Angew. Chem.* **1990**, *102*, 1247–1257; *Angew. Chem. Int. Ed. Engl.* **1990**, *29*, 1209–1219.
[4] This situation is also demonstrated by the founding of diverse new journals on the subject, which have been met with great interest and respect, for example, *Nature Structural Biology*, *Structure*, *Current Opinion in Structural Biology*.
[5] See, for example, H. Dugas, *Bioorganic Chemistry*, 3rd ed., Springer, New York, **1995**.
[6] Recently, the emphasis on biological aspects seems to have gained importance. Therefore, the Chemistry Department of Harvard University was recently renamed Department of Chemistry and Chemical Biology (and not Biological Chemistry!); Harvard University is also going to open an Institute for Chemistry and Cell Biology (*Chem. Eng. News* **1997**, *75*(24), 31) and at the Scripps Research Institute, the Skaggs Department of Chemical Biology has been opened.[2]
[7] See a) ref. [1], p. 13, b) A. Kornberg, *Chem. Biol.* **1996**, *3*, 3–5. In this essay, the author identifies one of the main differences between chemical and biological research as the different way that chemists and biologists tackle problems: "Chemists seek precise answers to well-defined problems, whereas biologists are content with approximate answers to complex problems" (ref. [7a], p. 14); "Chemists seem more conservative, analytical and clanish, […] They obtain precise data with relatively few and elegant techniques. […] Biologists on the other hand seem more artistic, eclectic and right-brain dominated. They focus on complex phenomena in cells and organisms using a wider range of techniques with less presicion." (ref [7b], p. 3–4). We are furthermore of the opinion that communication problems arise between biologists and chemists due to their education and the ways of thinking thereby impressed upon them. Therefore, for an organic chemist, the expression "glucose 6-phosphate" evokes a structural association and the biological function remains in the background, whereas a biologist will first think of the role of this carbohydrate derivative for instance in glycolysis, and the structure is secondary for him. Chemists and biologists look at different, yet inseparable, sides of the same coin.
[8] a) M. Rodbell, *Angew. Chem.* **1995**, *107*, 1549–1558; *Angew. Chem. Int. Ed. Engl.* **1995**, *34*, 1420–1428, b) A. G. Gilman, *ibid*. **1995**, *107*, 1533–1546 and **1995**, *34*, 1406–1419.
[9] For a comprehensive presentation, see a) H. Lodish, D. Baltimore, A. Berk, S. L. Zipursky, P. Matsudeira, J. Darnell, *Molekulare Zellbiologie*, 2nd ed, de Gruyter, Berlin, **1996**, chap. 20; b) G. Krauss, *Biochemie der Regulation und Signaltransduktion*, WILEY-VCH, Weinheim, **1997**.
[10] A third class is formed by lipophilic hormones with membrane receptors, such as the arachidonic acid derivatives, which are continuously produced and secreted by many cell types and are often degraded again in the immediate vicinity of the site at which they were biosynthesized.
[11] The influence on behaviour of other organisms of the same type by pheromones will not be discussed here.
[12] a) S. Watson, S. Arkinstall, *The G-Protein Linked Receptor Facts Book*, Academic Press, San Diego, **1994**, and references therein; b) G. H. Gold, E. N. Pugh, Jr., *Nature* **1997**, *385*, 677–679.
[13] L. Birnbaumer, *Annu. Rev. Pharmacol. Toxicol.* **1990**, *30*, 675–705.
[14] D. E. Coleman, S. R. Sprang, *Trends Biochem. Sci.* **1996**, *21*, 41–44.
[15] D. E. Clapham, *Nature* **1996**, *379*, 297–299, and references therein.
[16] S. S. Taylor, J. A. Buechler, W. Yonemoto, *Annu. Rev. Biochem*. **1990**, *59*, 971–1005.
[17] M. J. Berridge, *Nature* **1993**, *361*, 315–325.
[18] a) D. C. Billington, *The Inositol Phosphates*, VCH, Weinheim, **1993**; b) D. C. Billington, *Chem. Soc. Rev.* **1989**, *18*, 83–122.
[19] B. V. L. Potter, D. Lampe, *Angew. Chem.* **1995**, *107*, 2085–2125; *Angew. Chem. Int. Ed. Engl.* **1995**, *34*, 1933–1972.
[20] Y Asaoka, S. Nakamura, K. Yoshida, Y. Nishizuka, *Trends Biochem. Sci.* **1992**, *17*, 414–417.
[21] Y. Nishizuka, *Science* **1992**, *258*, 607–614.
[22] K. Buchner, *Eur. J. Biochem.* **1995**, *228*, 211–211.
[23] T. A. Gilbertson, S. C. Kumamon, *Chem. Biol.* **1996**, *3*, 233–237.
[24] P. A. Hargrave, J. H. McDowell, *FASEB J.* **1992**, *6* , 2323–2331.
[25] F. McCormick, *Nature* **1993**, *363*, 15–16.
[26] S. E. Egan, R. A. Weinberg, *Nature* **1993**, *365*, 781–783.
[27] M. S. Bogushi, F. McCormick, *Nature* **1993**, *366*, 643–654.

[28] M. Spaargaren, J. R. Bischoff, F. McCormick, *Gene Expression* **1995**, *4*, 345 – 356.
[29] *Intracellular Signal Transduction*, *Advances in Pharmacology 36* (Eds.: H. Hidaka, A. C. Nairin), Academic Press, San Diego, **1996**.
[30] a) B. Stein, D. Anderson, *Annu. Rep. Med. Chem.* **1996**, *31*, 289 – 298; b) C. E. Canman, M. B. Kastan, *Nature* **1996**, *384*, 213 – 214.
[31] M. L. Gishizky, *Annu. Rep. Med. Chem.* **1995**, *30*, 247 – 253.
[32] A. J. Bridges, *Chemtracts: Org. Chem.* **1995**, *8*, 73 – 107.
[33] D. L. Cadena, G. N. Gill, *FASEB J.* **1992**, *6*, 2334 – 2337.
[34] J. B. Bolen, *Oncogene* **1993**, *8*, 2025 – 2031.
[35] G. Alonso, M. Koegl, N. Mazurenko, S. A. Courtneige, *J. Biol. Chem.* **1995**, *270*, 9840 – 9848.
[36] P. Lamb, H. M. Seidel, R. B. Stein, J. Rosen, *Annu. Rep. Med. Chem.* **1996**, *31*, 269 – 278.
[37] J. E. Darnell Jr., I. M. Kerr, G. R. Stark, *Science* **1994**, *264*, 1415 – 1421.
[38] J. Kunz, M. N. Hall, *Trends Biochem. Sci.* **1993**, *18*, 334 – 338.
[39] G. R. Crabtree, N. A. Clipstone, *Annu. Rev. Biochem.* **1994**, *63*, 1045 – 1083.
[40] M. N. Pruschy, D. M. Spencer, T. M. Kapoor, H. Miyake, G. R. Crabtree, S. L. Schreiber, *Chem. Biol.* **1994**, *1*, 163 – 172.
[41] G. M. Cooper, *Oncogenes*, 2. Aufl., Jones and Bartlett, London, **1995.**
[42] Ref. [9], chap. 26.
[43] F. McCormick, P. Myers, *Chem. Biol.* **1994**, *1*, 7 – 9.
[44] T. Jacks, R. A. Weinberg, *Nature* **1996**, *381*, 643 – 644.
[45] C. B. Thompson, *Science* **1995**, *267*, 1456 – 1462.
[46] A. J. Hale, C. A. Smith, L. C. Sutherland, V. E. A. Stoneman, V. L. Longthorne, A. C. Culhane, G. T. Williams, *Eur. J. Biochem.* **1996**, *236*, 1 – 26.
[47] A. Levitzki, *Eur. J. Biochem.* **1994**, *226*, 1 – 13.
[48] T. Hunter, *Cell* **1991**, *64*, 249 – 270.
[49] Reviews: a) A. Levitzki, *FASEB J.* **1992**, *6*, 3275 – 3282; b) A. Levitzki, A. Gazit, *Science* **1995**, *267*, 1782 – 1788; c) T. R. Burke, Jr., *Stem Cells* **1994**, *12*, 1 – 6; d) T. R. Burke, Jr., *Drugs Future* **1992**, *17*, 119 – 131; e) D. W. Fry, *Annu. Rep. Med. Chem.* **1996**, *31*, 151 – 160.
[50] H. J. Kwon, M. Yoshida, Y. Fukui, S. Hoeinouchi, T. Beppu, *Cancer Res.* **1992**, *52*, 6926 – 6930.
[51] T. Onoda, H. Iinuma, Y. Sasaki, M. Hamada, K. Isschiki, H. Naganawa, T. Takeuchi, K. Tatsuta, K. Umezawa, *J. Nat. Prod.* **1989**, *52*, 1252 – 1257.
[52] M. H. Kreuter, R. E. Leake, F. Rinaldi, W. Müller-Klieser, A. Maidhof, E. G. Müller, H. C. Schröder, *Comp. Biochem. Physiol.* **1990**, *97B*, 151 – 158.
[53] H. Umezawa, M. Imoto, T. Sawar, K. Isshiki, N. Matsuda, T. Uchida, H. Finuma, M. Hamada, T. Takeuchi, *J. Antibiot.* **1986**, *39*, 170 – 173.
[54] T. Akiyama, J. Ishida, S. Nakagama, H. Ogawara, S. Watanabe, N. Itoh, M. Shibuya, Y. Fukami, *J. Biol. Chem.* **1987**, *262*, 5592 – 5595.
[55] K. J. Murray, W. J. Coates, *Annu. Rep. Med. Chem.* **1994**, *29*, 255 – 264.
[56] S. R. Hubbard, L. Wie, L. Elis, W. A. Hendrickson, *Nature* **1994**, *372*, 746 – 754.
[57] W. Xu, S. C. Harrison, M. J. Eck, *Nature* **1997**, *385*, 595 – 601; for the crystal structure of the Src kinase Hck, see F. Sicheri, I. Moarefi, J. Kuriyan, *ibid.* **1997**, *385*, 602 – 608.
[58] Erk2: F. M. Zhang, A. Strand, D. Robbins, M. H. Cobb, E. J. Goldsmith, *Nature* **1994**, *367*, 704 – 711; Cdk2: H. L. De Bondt, J. Rosenblatt, J. Jancarik, H. D. Jones, D. O. Morgan, S.-H. Kim, *Nature* **1993**, *363*, 595 – 602; PKA: D. R. Knighton, J. Zheng, L. F. Ten Eyck, V. A. Ashford, N.-H. Xuong, S. S. Taylor, J. M. Sowadski, *Science* **1991**, *253*, 407 – 414.
[59] P. Delmotte, J. Delmotte-Plaquee, *Nature* **1953**, *171*, 344 – 347.
[60] M. Lampilas, R. Lett, *Tetrahedron Lett.* **1992**, *33*, 773 – 776, 777 – 780.
[61] F. McCapra, A. I. Scott, P. Delmotte, J. Delmotte-Plaquee, *Tetrahedron Lett.* **1964**, *15*, 869 – 875.
[62] a) Y. Sugimura, K. Iino, Y. Tsujita, Y. Shimada, T. Kobayashi, T. Kagasaki (Sankyo Co. Ltd), EP-B EP 460950 A1, **1991** [*Chem. Abstr.* **1992**, *116*, 105970h]; b) G. J. Calton (Grace, W.R. & Co.), US-B 874,348, **1978** [*Chem. Abstr.* **1981**, *94*, 121499u].
[63] See, for example, T. Yoneda, R. M. Lyall, M. M. Alsina, P. E. Persons, A. P. Spada, A. Levitzki, A. Zilberstein, G. R. Mundy, *Cancer Res.* **1991**, *51*, 4430 – 4435.
[64] See, for example, M. Kovalenko, A. Gazit, A. Bohmer, C. Rorsman, L. Romstrand, C. H. Heldin, J. Waltenberger, F. D. Bohmer, A. Levitzki, *Cancer Res.* **1994**, *54*, 6106 – 6114.
[65] M. Anafi, A. Gazit, C. Gilon, Y. Benneriah, A. Levitzki, *FEBS Lett.* **1993**, *330*, 260 – 264.
[66] F. Rendu, A. Eldor, F. Grelac, C. Bachelot, A. Gazit, C. Gilon, S. Levytoledano, A. Levitzki, *Biochem. Pharmacol.* **1992**, *44*, 881 – 888.
[67] C. Roifman, K. Chin, A. Gazit, G. B. Mills, C. Gilon, A. Levitzki, *J. Immunol.* **1991**, *146*, 2965 – 2971.
[68] J. B. Stanley, R. Gorczynski, C. K. Huang, J. Love, G. B. Mills, *J. Immunol.* **1990**, *145*, 2189 – 2198.
[69] A. Dvir, Y. Milner, O. Chamsky, C. Gilon, A. Gazit, A. Levitzki, *J. Cell Biol.* **1991**, *113*, 857 – 865.
[70] A. Novogrodsky, A. Vanichkin, M. Patya, A. Gazit, N. Osherov, A. Levitzki, *Science* **1994**, *264*, 1319 – 1322.
[71] D. W. Fry, A. K. Kraker, A. McMichael, L. A. Ambroso, J. M. Nelson, W. R. Leopold, R. W. Connors, A. J. Bridges, *Science* **1994**, *265*, 1093 – 1095.
[72] A. Knebel, H. J. Rahmsdorf, A. Ullrich, P. Herrlich, *EMBO J.* **1996**, *15*, 5314 – 5325.
[73] F. D. Böhmer, A. Böhmer, A. Obermeier, A. Ullrich, *Analyt. Biochem.* **1995**, *228*, 267 – 273.
[74] a) M. S. Talamonti, M. S. Roh, G. E. Gallick, *J. Clinic. Invest.* **1993**, *91*, 53 – 60; b) A. E. Ottenhof, G. Rijksen, A. A. Michels, G. E. Staal, *Cancer Res.* **1993**, *52*, 4773 – 4778.
[75] N. Osherov, A. Levitzki, *Eur. J. Biochem.* **1994**, *225*, 1047 – 1053.
[76] H. Daub, F. U. Weiss, C. Wallasch, A. Ullrich, *Nature* **1996**, *9*, 557 – 560.
[77] Reviews: a) F. Balkenhohl, C. von dem Bussche-Hünnefeld, A. Lansky, C. Zechel, *Angew. Chem.* **1996**, *108*, 2437 – 2488; *Angew. Chem. Int. Ed. Engl.* **1996**, *35*, 2288 – 2337; b) L. A. Thompson, J. A. Ellman, *Chem. Rev.* **1996**, *96*, 555 – 600.
[78] C.-Y. J. Hsu, P. E. Persons, A. P. Spada, R. A. Bednar, A. Levitzki, A. Zilberstein, *J. Biol. Chem.* **1991**, *266*, 31, 21105 – 21112.
[79] J. Green, *J. Org. Chem.* **1995**, *60*, 4287 – 4290; see also R. Devraj, M. Cushman, *ibid.* **1996**, *61*, 9368 – 9373.
[80] J. Zimmermann, E. Buchdunger, H. Mett, T. Meyer, N. B. Lydon, P. Traxler, *Bioorg. Med. Chem. Lett.* **1996**, *6*, 1221 – 1226.
[81] E. Buchdunger, J. Zimmermann, H. Mett, T. Meyer, M. Müller, U. Regenass, N. B. Lydon, *Proc. Natl. Acad. Sci. USA* **1995**, *92*, 2558 – 2562.
[82] E. Fattorusso, L. Minale, G. Sodano, *J. Chem. Soc. Chem. Commun.* **1970**, 751 – 752.
[83] W. Fulmor, G. E. Van Lear, G. O. Morton, R. D. Mills, *Tetrahedron Lett.* **1970**, *52*, 4551 – 4552.
[84] H. Waldmann, K. Hinterding, A. Knebel. H. J. Rahmsdorf, P. Herrlich, *Angew. Chem.* **1997**, *109*, 1553 – 1555; *Angew. Chem. Int. Ed. Engl.* **1997**, *36*, 1541 – 1542.
[85] a) S. Peterli, R. Stumpf, M. Schweizer, U. Sequin, H. Mett, P. Traxler, *Helv. Chim. Acta* **1992**, *75*, 696 – 706; b) S. Peterli, D. Hubmann, U. Sequin, H. Mett, P. Traxler, *ibid.* **1994**, *77*, 59 – 69.
[86] E.-S. Lee, J. Jurayj, M. Cushman, *Tetrahedron* **1994**, *50*, 9873 – 9882.
[87] D. M. Andrews, M. Gregorou, T. C. M. Page, J. M. Peach, A. J. Pratt, *J. Chem. Soc. Perkin Trans. 1* **1995**, 1335 – 1340.
[88] T. Pawson, *Nature* **1995**, *373*, 573 – 580.
[89] G. B. Cohen, R. Ren, D. Baltimore, *Cell* **1995**, *80*, 237 – 248.
[90] B. Schaffhausen, *Biochim. Biophys. Acta* **1995**, *1242*, 61 – 75.
[91] Z. Songyang, S. E. Shoelson, M. Chandhuri, G, Gish, T. Pawson, W. G. Haser, F. King, T. Roberts, S. Ratnofsky, R. J. Lechleider, B. G. Neel, R. B. Birge, J. E. Fajardo, M. M. Chou, H. Hanafusa, B. Schaffhausen, L. C. Cantley, *Cell* **1993**, *72*, 767 – 778.
[92] a) G. Waksman, D. Kominos, S. C. Robertson, N. Pant, D. Baltimore, R. B. Birge, D. Cowburn, H. Hanafusa, B. J. Mayer, M. Overduin, M. D. Resh, C. B. Rios, L. Silverman, J. Kuriyan, *Nature* **1992**, *358*, 646 – 653; b) G. Waksman, S. E. Shoelson, N. Pant, D. Cowburn, J. Kuriyan, *Cell* **1993**, *72*, 779 – 790; c) M. J. Eck, S. K. Atwell, S. E. Shoelson, S. C. Harrison, *Nature* **1994**, *368*, 764 – 769; d) M. M. Zhou, R. P. Meadows, T. M. Logan, H. S. Yoon, W. S. Wade, K. S. Ravichandran, S. J. Burakoff, S. W. Fesik, *Proc. Natl. Acad. Sci. USA* **1995**, *92*, 7784 – 7788; e) S. M. Pascal, A. U. Singer, G. Gish, T. Yamazaki, S. E. Shoelson, T. Pawson, L. E. Kay, J. D. Forman-Kay, *Cell* **1994**, *77*, 461 – 472.

[93] M. S. Plummer, T. K. Sawyer, *Drug Des. Discovery* **1996**, *13*, 75 – 81.
[94] M. Rodriguez, R. Crosby, K. Alligood, T. Gilmer, J. Berman, *Lett. Peptide Sci*. **1995**, *2*, 1 – 6.
[95] Q. Lou, M. E. Leftwich, K. S. Lam, *Bioorg. Med. Chem*. **1996**, *4*, 677 – 682.
[96] M. S. Plummer, E. A. Lunney, K. S. Para, A. Shahripour, C. J. Stankovic, C. Humblet, J. H. Fergus, J. S. Marks, P. Herrera, S. Hubbell, A. Saltiel, T. K. Sawyer, *Bioorg. Med. Chem*. **1997**, *5*, 41 – 47.
[97] M. Nomizu, A. Otaka, T. R. Burke, Jr., P. P. Roller, *Tetrahedron* **1994**, *50*, 2691 – 2702.
[98] T. Gimer, M. Rodriguez, S. Jordan, R. Crosby, K. Alligood, M. Green, M. Kimery, C. Wagner, D. Kinder, P. Charifson, A. M. Hassel, D. Willard, M. Luther, D. Rusnak, D. D. Sternbach, M. Mehrota, M. Peel, L. Shampine, R. Davis, J. Robbins, I. R. Patel, D. Kassel, W. Burtzhart, M. Moyer, T. Bradshaw, J. Berman, *J. Biol. Chem*. **1994**, *269*, 31711 – 31719.
[99] D. J. McNamara, E. M. Dobrusin, G. Zhu, S. J. Decker, A. Saltiel, *Int. J. Pept. Protein Res*. **1994**, *43*, 240 – 248.
[100] L. Theodore, D. Derossi, G. Chassaing, B. Llirbat, M. Kubes, P. Jordan, H. Chneiweiss, P. Godement, A. Prochiantz, *J. Neurosci*. **1995**, *15*, 7158 – 7167.
[101] a) H. Hall, E. J. Williams, S. E. Moore, F. S. Walsh, A. Prochiantz, P. Doherty, *Curr. Biol*. **1996**, *6*, 580 – 587; b) review: A. Prochiantz, *Curr. Opin. Neurobiol*. **1996**, *6*, 629 – 634.
[102] K. Shuai, C. M. Horvath, L. H. Tsai Huang, S. A. Qureshi, D. Cowburn, J. E. Darnell, Jr., *Cell* **1994**, *76*, 821 – 828.
[103] S. F. Arnold, A. C. Notides, *Proc. Natl. Acad. Sci. USA* **1995**, *92*, 7475 – 7479.
[104] S. Sugimoto, T. J. Wandless, S. E. Shoelson, B. G. Neel, C. T. Walsh, *J. Biol. Chem*. **1994**, *269*, 13614 – 13622.
[105] M. Rojas, S. Y. Yao, Y.-Z. Lin, *J. Biol. Chem*. **1996**, *271*, 27456 – 27461.
[106] a) W. A. Lim, F. M. Richards, R. O. Fox, *Nature* **1994**, *372*, 375 – 379; b) A. Musacchio, M. Saraste, M. Wilmanns, *Nat. Struct. Biol*. **1994**, *1*, 546 – 551; A. Musacchio, M. Noble, R. Pauptit, R. Wierenga, M. Saraste, *Nature* **1992**, *359*, 851 – 855.
[107] J. K. Chen, S. L. Schreiber, *Angew. Chem*. **1995**, *107*, 1041 – 1058; *Angew. Chem. Int. Ed. Engl*. **1995**, *34*, 953 – 969.
[108] J. K. Chen, W. S. Lane, A. W. Brauer, A. Tanaka, S. L. Schreiber, *J. Am. Chem. Soc*. **1993**, *115*, 12591 – 12592.
[109] S. Feng, J. K. Chen, H. Yu, J. A. Simon, S. L. Schreiber, *Science* **1994**, *266*, 1241 – 1247.
[110] A. P. Combs, T. M. Kapoor, S. Feng, J. K. Chen, L. F. Daude-Snorr, S. L. Schreiber, *J. Am. Chem. Soc*. **1996**, *118*, 287 – 288.
[111] S. Feng, T. M. Kapoor, F. Shiron, A. P. Combs, S. L. Schreiber, *Chem. Biol*. **1996**, *3*, 661 – 670.
[112] M. Barbacid, *Annu. Rev. Biochem*. **1987**, *56*, 779 – 827.
[113] J. F. Hancock, A. I. Magee, J. E. Childs, C. J. Marshall, *Cell* **1989**, *57*, 1167 – 1177.
[114] J. F. Hancock, H. Paterson, C. J. Marshall, *Cell* **1990**, *63*, 133 – 139.
[115] Reviews: a) S. Ayral-Kaloustian, J. S. Skotnicki, *Annu. Rep. Med. Chem*. **1996**, *31*, 171 – 180; b) G. L. Bolton, J. S. Sebolt-Leopold, J. C. Hodges, *ibid*. **1994**, *29*, 165 – 174; c) J. E. Buss, J. C. Marsters, Jr., *Chem. Biol.* **1995**, *2*, 787 – 791; d) F. Tamanoi, *Trends Biochem. Sci*. **1993**, *18*, 350 – 353; e) R. M. J. Liskamp, *Angew. Chem*. **1994**, *106*, 313 – 315; *Angew. Chem. Int. Ed. Engl*. **1994**, *33*, 633 – 636.
[116] H. W. Park, S. R. Boduluri, J. F. Moomaw, P. J. Casey, L. S. Beese, *Science* **1997**, *275*, 1800 – 1807.
[117] K. S. Koblan, J. C. Culberson, S. J. Desolms, E. A. Giuliani, S. D. Mosser, C. A. Omer, S. M. Pitzenberger, M. J. Bogusky, *Protein Sci.* **1995**, *4*, 681 – 688.
[118] a) K. E. Wilson, R. M. Burk, T. Biftu, R. G. Ball, K. Hoogsteen, *J. Org. Chem*. **1992**, *57*, 7151 – 7158; b) J. D. Bergstrom, M. M. Kurtz, D. J. Rew, A. M. Amend, J. D. Karkas, R. G. Bosteor, V. S. Bansal, C. Dufresne, F. L. Van Middlesworth, O. D. Hensens, J. M. Liesch, D. L. Zink, K. E. Wilson, J. Onishi, J. A. Milligan, G. Bills, L. Kaplan, M. Nallin Omstead, R. G. Jenkins, L. Huang, M. S. Meinz, L. Quinn, R. W. Burg, T. Biftu, R. G. Ball, K. Hoogsteen, *Proc. Natl. Acad. Sci. USA* **1993**, *90*, 80 – 84; c) C. Dufresne, K. E. Wilson, S. B. Singh, D. L. Zink, J. D. Bergstrom, D. Rew, J. D. Polishook, M. Meinz, L. Huang, K. C. Silverman, R. B. Lingham, M. Mojena, C. Cascales, F. Pelaez, J. B. Gibbs, *J. Nat. Prod*. **1993**, *56*, 1923 – 1929; d) J. M. Dawson, J. E. Farthing, P. S. Marshall, R. F. Middleton, M. J. O'Neill, A. Shuttleworth, C. Stylli, R. M. Tait, P. M. Taylor, H. G. Wildman, A. D. Buss, D. Langley, M. V. Hayes, *J. Antibiot*. **1992**, *45*, 639 – 647; e) P. J. Sidebottom, R. M. Highcock, S. J. Lane, P. A. Procopiou, N. S. Watson, *ibid*. **1992**, *45*, 648 – 658; f) W. J. Blows, G. Foster, S. J. Lane, D. Noble, J. E. Piercey, P. J. Sidebottom, G. J. Webb, *ibid*. **1994**, *47*, 740 – 754.
[119] D. Van der Pyl, J. Inokoshi, K. Shiomi, H. Yang, H. Takeshima, S. Omura, *J. Antibiot*. **1992**, *45*, 1802 – 1805.
[120] K. Shiomi, H. Yang, J. Inokoshi, D. Van der Pyl, A. Nakagawa, H. Takeshima, S. Omura, *J. Antibiot*. **1993**, *46*, 229 – 234.
[121] a) E. M. Carreira, J. Du Bois, *J. Am. Chem. Soc*. **1994**, *116*, 10825 – 10826; b) K. C. Nicolaou, E. W. Yue, Y. Naniwa, F. De Ricondis, A. Nadin, J. E. Leresche, S. La Greca, Z. Yang, *Angew. Chem*. **1994**, *106*, 2306 – 2309; *Angew. Chem. Int. Ed. Eng*. **1994**, *33*, 2184 – 2187.
[122] D. A. Evans, J. C. Barrow, J. L. Leighton, A. J. Robichand, M. Sefkow, *J. Am. Chem. Soc*. **1994**, *116*, 12111 – 12112.
[123] J. B. Gibbs, D. L. Pampliano, S. D. Mosser, E. Rands, R. B. Lingham, S. B. Singh, E. M. Scolnick, N. E. Kohl, A. Oliff, *J. Biol. Chem*. **1993**, *268*, 7617 – 7620.
[124] K. Hinterding, P. Hagenbuch, J. Rétey, H. Waldmann, *Angew. Chem.* **1998**, in press; *Angew. Chem. Int. Ed.* **1998**, in press.
[125] a) M. Hara, M. Han, *Proc. Natl. Acad. Sci. USA* **1995**, *92*, 3333 – 3337; b) M. Hara, K. Akasaka, S. Akinaga, M. Okabe, H. Nakano, R. Gomez, D. Wood, M. Uh, F. Tamanoi, *ibid*. **1993**, *90*, 2281 – 2285.
[126] a) P. Wipf, Y. Kim. H. Jahn, *Synthesis* **1995**, 1549 – 1561; b) I. Kapfer, N. J. Lewis, G. MacDonald, R. J. K. Taylor, *Tetrahedron Lett*. **1996**, *37*, 2101 – 2104; c) L. Alcaraz, G. MacDonald, I. Kapfer, N. J. Lewis, R. J. K. Taylor, *ibid*. **1996**, *37*, 6619 – 6622.
[127] G. L. James, J. L. Goldstein, M. S. Brown, T. E. Rawson, T. C. Somers, R. S. McDowell, C. W. Crowley, B. K. Lucas, A. D. Levinson, J. C. Marsters, Jr., *Science* **1993**, *260*, 1937 – 1942.
[128] G. L. James, M. S. Brown, M. H. Cobb, J. L. Goldstein, *J. Biol. Chem*. **1994**, *269*, 27705 – 27714.
[129] G. L. James, J. L. Goldstein, M. S. Brown, *J. Biol. Chem*. **1995**, *270*, 6221 – 6226.
[130] N. E. Kohl, F. R. Wilson, S. D. Mosser, E. Guiliani, S. J. Desolms, M. W. Conner, N. J. Anthony, W. J. Holtz, R. P. Gomez, T.-J. Lee, R. L. Smith, S. L. Graham, G. D. Hartman, J. B. Gibbs, A. Oliff, *Proc. Natl. Acad. Sci. USA* **1994**, *91*, 9141 – 9145.
[131] a) D. V. Patel, E. M. Gordon, R. J. Schmidt, H. N. Weller, M. G. Young, R. Zahler, M. Barbacid, J. M. Carboni, J. L. Gullo-Brown, L. Hunikan, C. Ricca, S. Robinson, B. R. Seizinger, A. V. Tuomari, V. Manne, *J. Med. Chem*. **1995**, *38*, 435 – 442; b) V. Manne, N. Yan, J. M. Carboni, A. V. Tuomari, C. Ricca, J. Gullo-Brown, M. L. Andahazy, R. J. Schmidt, D. Patel, R. Zahler, R. Weinmann, C. J. Der, A. D. Cox, J. T. Hunt, E. M. Gordon, M. Barbacid, B. R. Seizinger, *Oncogene* **1995**, *10*, 1763 – 1779.
[132] N. Yan, C. Ricca, J. Fletcher, T. Glover, B. R. Seizinger, V. Manne, *Cancer Res.* **1995**, *55*, 3569 – 3575.
[133] M. Schelhaas, H. Waldmann, *Angew. Chem.* **1996**, *108*, 2192 – 2219; *Angew. Chem. Int. Ed. Engl.* **1996**, *35*, 2056 – 2083.
[134] H. Waldmann, D. Sebastian, *Chem. Rev.* **1994**, *94*, 911 – 937.
[135] T. Kappes, H. Waldmann, *Liebigs Ann.* **1997**, 803 – 813.
[136] B. Sauerbrei, T. Kappes, H. Waldmann, *Top. Curr. Chem.* **1997**, *186*, 65 – 86.
[137] a) H. Kunz, *Angew. Chem*. **1987**, *99*, 297 – 311; *Angew. Chem. Int. Ed. Engl.* **1987**, *26*, 294 – 308; b) M. Meldal, *Curr. Opin. Struct. Biol.* **1994**, *4*, 710 – 718.
[138] J. W. Perich in *Peptides and Protein Phosphorylation* (Ed.: B. E. Kemp), CRC Press, Boca Raton, FL (USA), **1990**, p. 289.
[139] P. J. Casey, *Science* **1995**, *268*, 221 – 225.
[140] G. Milligan, M. Parenti, A. I. Magee, *Trends Biochem. Sci* **1995**, *20*, 181 – 186.
[141] R. R. Rando, *Biochim. Biophys. Acta* **1996**, *1300*, 5 – 16.
[142] a) C.-D. Hu, K. Kariya, M. Tamada, K. Akasaka, M. Shirouzu, S. Yokoyama, T. Kataoka, *J. Biol. Chem.* **1995**, *270*, 30274 – 30277; b) T. Okada, T. Masuda, M. Shinkai, K. Kariya, T. Kataoka, *J. Biol. Chem*. **1996**, *271*, 4671 – 4678; c) D. Stokoe, F. McCormick, *EMBO J.* **1997**, *16*, 2384 – 2396.
[143] S. Moffet, B. Mouillac, H. Bonin, M. Bouvier, *EMBO J.* **1993**, *12*, 349 – 356.

[144] P. B. Wedegaertner, H. R. Bourne, *Cell* **1994**, *77*, 1063 – 1070.
[145] M. Schelhaas, S. Glomsda, M. Hänsler, H.-D. Jakubke, H. Waldmann, *Angew. Chem.* **1996**, *108*, 82 – 85; *Angew. Chem. Int. Ed. Engl.* **1996**, *35*, 106 – 109.
[146] T. Schmittberger, A. Cotté, H. Waldmann, *Chem. Commun.* **1998**, in press.
[147] H. Waldmann, E. Nägele, *Angew. Chem.* **1995**, *107*, 2425 – 2428; *Angew. Chem. Int. Ed. Engl.* **1995**, *34*, 2259 – 2262.
[148] H. Waldmann, F. Eisele, unpublished results.
[149] S. Shahinian, J. Silvius, *Biochemistry* **1995**, *34*, 3813 – 3822.
[150] L. Liu, G.-F. Jang, C. F. Farnsworth, K. Yokohama, J. A. Glomset, M. H. Gelb, *Methods Enzymol.* **1995**, *250*, 189 – 206.
[151] P. Stöber, M. Schelhaas, E. Nägele, P. Hagenbuch, J. Rétey, H. Waldmann, *Bioorg. Med. Chem.* **1997**, *5*, 75 – 83.
[152] H. Waldmann, M. Schelhaas, E. Nägele, J. Kuhlmann, A. Wittinghofer, H. Schroeder, J. R. Silvius, *Angew. Chem.* **1997**, *109*, 2334 – 2337; *Angew. Chem. Int. Ed. Engl.* **1997**, *36*, 2238 – 2241.
[153] R. S. Bhatnagar, J. I. Gordon, *Trends Cell Biol.* **1997**, *7*, 14 – 20.
[154] S. McLaughlin, A. Achren, *Trends Biochem. Sci* **1995**, *20*, 272 – 276.
[155] J. R. Silvius, F. l'Heureux, *Biochemistry* **1994**, *33*, 3014 – 3022.
[156] R. M. Peitzsch, S. McLaughlin, *Biochemistry* **1993**, *32*, 10436 – 10443.
[157] C. A. Buser, C. T. Sigal, M. D. Resh, S. McLaughlin, *Biochemistry* **1994**, *33*, 13093 – 13101.
[158] H. Schröder, R. Leventis, S. Rex, M. Schelhaas, E. Nägele, H. Waldmann, J. R. Silvius, *Biochemistry* **1997**, *36*, 13102 – 13109.
[159] H. Schroeder, R. Leventis, S. Shahinian, P. A. Walton, J. R. Silvius, *J. Cell Biol.* **1996**, *134*, 647 – 660.
[160] L. Liu, T. Dudler, M. H. Gelb, *J. Biol. Chem.* **1996**, *271*, 23269 – 23276.
[161] a) M. D. Schaber, M. B. O'Hara, V. M. Garsky, S. D. Mosser, J. D. Bergstrom, S. L. Moores, M. S. Marshall, P. A. Friedman, R. A. F. Dixon, J. B. Gibbs, *J. Biol. Chem.* **1990**, *265*, 14701 – 14704; b) S. L. Moores, M. D. Schaber, S. D. Mosser, E. Rands, M. B. O'Hara, V. M. Garsky, M. S. Marshall, D. L. Pompliano, J. B. Gibbs, *J. Biol. Chem.* **1991**, *266*, 14603 – 14610; c) D. L. Pompliano, E. Rands, M. D. Schaber, S. D. Mosser, N. J. Anthony, J. B. Gibbs, *Biochemistry* **1992**, *31*, 3800 – 3807.
[162] Y.-T. Ma, R. R. Rando, *Proc. Natl. Acad. Sci. USA* **1992**, *89*, 6275 – 6279.
[163] Y.-T. Ma, A. Chaudhuri, R. R. Rando, *Biochemistry* **1992**, *31*, 11722 – 11777.
[164] Y.-T. Ma, B. A. Gilbert, R. R. Rando, *Biochemistry* **1993**, *32*, 2386 – 2393.
[165] E. W. Tan, D. Pérez-Sala, F. J. Canana, R. R. Rando, *J. Biol. Chem.* **1994**, *266*, 10719 – 10722.
[166] R. C. Stephenson, S. Clarke, *J. Biol. Chem.* **1990**, *265*, 16248 – 16254.
[167] P. A. Hargrave, J. H. McDowelll, *FASEB J.* **1992**, *6*, 2323 – 2331.
[168] O. G. Kisselev, M. V. Ermolaeva, N. Gautam, *J. Biol. Chem.* **1994**, *269*, 21399 – 21402.
[169] A. Scheer, P. Gierschik, *Biochemistry* **1995**, *34*, 4952 – 4961.
[170] T. Matsuda, T. Takao, Y Shimonishi, A. Murata, T. Asano, T. Yoshizawa, Y. Fukada, *J. Biol. Chem.* **1995**, *269*, 30358 – 30363.
[171] J. Ding, D. J. Lu, D. Pérez-Sala, Y.-T. Ma, J. F. Maddox, B. A. Gilbert, J. A. Badwey, R. R. Rando, *J. Biol. Chem.* **1994**, *269*, 16837 – 16844.
[172] M. R. Philips, M. R. Phillinger, R. Staud, C. Volker, M. G. Rosenfeld, G. Weissmann, J. F. Starck, *Science* **1993**, *259*, 977 – 980.
[173] Y.-T. Ma, Q.-M. Shi, Y. H. Lim, S. H. McGrail, J. A. Ware, R. R. Rando, *Biochemistry* **1994**, *33*, 5414 – 5420.
[174] H. Akbar, W. Wang, R. Kornhauser, C. Volker, J. B. Stock, *Proc. Natl. Acad. Sci. USA* **1993**, *90*, 868 – 872.
[175] G. M. Bokoch, *Curr. Opin. Cell Biol.* **1994**, *6*, 212 – 218.
[176] J. A. Thissen, P. J. Casey, *J. Biol. Chem.* **1993,** *268*, 13780 – 13783.
[177] S. Bhattacharya, L. Chen, J. R. Broch, S. Powers, *Proc. Natl. Acad. Sci. USA* **1995**, *92*, 2984 – 2988.
[178] a) A. Varki, *Glycobiology* **1993**, *3*, 97 – 130; b) L. A. Lasky, *Science* **1992**, *258*, 964 – 969; c) S. Hakomori, *Adv. Cancer Res.* **1989**, *52*, 257 – 331; d) T. Feizi, *Nature* **1985**, *314*, 53 – 57; e) J. C. Paulson in *The Receptors*, *Vol. 2* (Ed.: M. Conn), Academic Press, New York, **1985**, pp. 131 – 219.
[179] S. J. Gendler, C. A. Lancaster, J. Taylor-Papadimitriou, T. Duhig, N. Peat, J. Burchell, L. Pemberton, E.-N. Lalani, D. Wilson, *J. Biol. Chem.* **1990**, *265*, 5286 – 5293.
[180] W. Kosch, J. März, H. Kunz, *React. Polym.* **1994**, *22*, 181 – 194.
[181] O. Seitz, H. Kunz, *J. Org. Chem.* **1997**,*62*, 813 – 826.
[182] a) M. Christiansen, M. Meldal, H. Bock, *J. Chem. Soc. Perkin Trans. 1* **1993**, 1453 – 1460; b) A. M. Jansson, K. J. Jensen, M. Meldal, J. Lomako, W. M. Lomako, C. E. Olsen, K. Bock, *ibid.* **1996**, 1001 – 1006.
[183] a) M. Meldal, *Tetrahedron Lett.* **1992**, *33*, 3077 – 3080; b) M. Meldal, F.-I. Auzanneau, O. Hindsgaul, M. C. Palcic, *J. Chem. Soc. Chem. Commun.* **1994**, 1849 – 1850.
[184] a) H. Paulsen, *Angew. Chem.* **1982**, *94*, 184 – 201; *Angew. Chem. Int. Ed. Engl.* **1982**, *21*, 155 – 172; b) R. R. Schmidt, *ibid.* **1986**, *98*, 213 – 236 and **1986**, *25*, 212 – 235; c) K. Toshima. K. Tasuda, *Chem. Rev.* **1993**, *93*, 1503 – 1531.
[185] a) J. Y. Roberge, X. Beebe, S. J. Danishefsky, *Science* **1995**, *269*, 202 – 204; b) R. Liang, L. Yan, J. Loebach, M. Ge, Y. Uozumi, K. Sekanina, N. Horan, J. Gildersleeve, C. Thompson, A. Smith, K. Biswas, W. C. Still, D. Kahne, *Science* **1996**, *274*, 1520 – 1522; c) K. C. Nicolaou, N. Winssinger, J. Pastor, F. DeRoose, *J. Am. Chem. Soc.* **1997**, *119*, 449 – 450.
[186] a) M. K. Christensen, M. Meldal, K. Bock, H. Cordes, S. Mouritsen, H. Elsner, *J. Chem. Soc. Perkin Trans 1* **1994**, 1299 – 1310; b) H. Franzyk, M. K. Christensen, R. M. Jorgensen, M. Meldal, H. Cordes, S. Mouritsen, K. Bock, *Bioorg. Med. Chem.* **1997**, *5*, 21 – 40.
[187] a) P. Braun, H. Waldmann, H. Kunz, *Bioorg. Med. Chem.* **1993**, *1*, 197 – 207; b) *Synlett* **1992**, 39 – 40.
[188] G. Braun, P. Braun, D. Kowalczyk, H. Kunz, *Tetrahedron Lett.* **1993**, *34*, 3111 – 3114.
[189] a) H. Kunz, D. Kowalczyk, P. Braun, G. Braun, *Angew. Chem.* **1994**, *106*, 353 – 355; *Angew. Chem. Int. Ed. Engl.* **1994**, *33*, 336 – 338; b) J. Eberling, P. Braun, D. Kowalcyk, M. Schultz, H. Kunz, *J. Org. Chem.* **1996**, *61*, 2638 – 2646.
[190] a) D. Cantacuzene, S. Attal, S. Bay, *Bioorg. Med. Chem. Lett.* **1991**, 197 – 200; b) D. Cantacuzene, S. Attal, S. Bay, *Biomed. Biochim. Acta* **1991**, *50*, 231 – 236; c) H. Ishii, K. Unabashi, Y. Mimura, Y Inoue, *Bull. Chem. Soc. Jpn.* **1990**, *63*, 3042 – 3043.
[191] M. Schulz, P. Hermann, H. Kunz, *Synlett* **1992**, 37 – 38.
[192] M. Schuster, P. Wang, J. C. Paulson, C.-H. Wong, *J. Am. Chem. Soc.* **1994**, *116*, 1135 – 1136.
[193] K. Witte, P. Sears, R. Martin, C.-H. Wong, *J. Am. Chem. Soc.* **1997**, *119*, 2114 – 2118.
[194] R. Schneider, M. Hammel, E. C. Berger, O. Ghisalba, J. Nuesch, D. Gygax, *Glycoconjugate J.* **1990**, *7*, 589 – 600.
[195] C. Unverzagt, *Angew. Chem.* **1996**, *108*, 2507 – 2510; *Angew. Chem. Int. Ed. Engl.* **1996**, *35*, 2350 – 2353.
[196] Short review: A. Giannis, *Angew. Chem.* **1994**, *106*, 188 – 191; *Angew. Chem. Int. Ed. Engl.* **1994**, *33*, 178 – 181.
[197] a) S.-H. Wu, M. Shimazaki, C.-C. Lin, W. J. Moore, G. Weitz-Schmidt, C.-H. Wong, *Angew. Chem.* **1996**, *108*, 106 – 108; *Angew. Chem. Int. Ed. Engl.* **1996**, *35*, 88 – 90; b) C. C. Lin, M. Shimazaki, M.-P. Heck, S. Aoki, R. Wang, T. Kimura, H. Ritzèn, S. Takayama, S.-H. Wu, G. Weitz-Schmidt, C.-H. Wong, *J. Am. Chem. Soc.* **1996**, *118*, 6826 – 6840.
[198] U. Sprengard, M. Schudok, W. Schmidt, G. Kretzschmar, H. Kunz, *Angew. Chem.* **1996**,*108*, 359 – 362; *Angew. Chem. Int. Ed. Engl.* **1996**, *35*, 321 – 324.
[199] G. Baisch, R. Öhrlein, *Angew. Chem.* **1996**, *108*, 1949 – 1952; *Angew. Chem. Int. Ed. Engl.* **1996**, *35*, 1812 – 1815.
[200] U. Sprengard, G. Kretzschmar, E. Bartnik, C. Hüls, H. Kunz, *Angew. Chem.* **1995**, *107*, 1104 – 1106; *Angew. Chem. Int. Ed. Engl.* **1995**, *34*, 990 – 993.
[201] a) T. Toyokuni, A. K. Singhal, *Chem. Soc. Rev.* **1995**, 231 – 242; b) B. M. Longenecker, M. Reddish, R. Koganty, G. D. MacLean, *Ann. N.Y. Acad. Sci*. **1993**, *690*, 276 – 291.
[202] a) *Protein Phosphorylation* (Ed.: F. Marks), VCH, Weinheim, **1996**; b) T. Hunter, M. Karin, *Cell* **1992**, *70*, 375 – 387; c) E. G. Krebs, *Angew. Chem.* **1993**, *105*, 1173 – 1180; *Angew. Chem. Int. Ed. Engl.* **1993**, *32*, 1122 – 1129; d) E. H. Fischer, *ibid.* **1993**, *105*, 1181 – 1188 and **1993**, *32*, 1130 – 1137.
[203] a) P. F. Alewood, J. W. Perich, R. B. Johns, *Tetrahedron Lett.* **1984**, *25*, 987 – 990; *ibid.* **1986**, *27*, 1373 – 1376; 1377 – 1380; b) M. Tsukamoto, R. Kita, K. Ishiguro, T. Uchida, K. Sato, *ibid.* **1991**, *32*, 7083 – 7086.

[204] K. Ishiguro, A. Omori, K. Sato, K. Tomizawa, T. Uchida, *Neurosci. Lett.* **1991**, *128*, 195 – 198.
[205] G. Shapiro, D. Büchler, C. Dalvit, P. Frey, M. del Carmen Fernandez, B. Gomez-Lor, E. Pombo-Villar, U. Stauss, R. Swoboda, C. Warichel, *Bioorg. Med. Chem.* **1997**, *5*, 147 – 156.
[206] a) A. Paquet, M. Johns, *Int. J. Pept. Protein Res.* **1990**, *36*, 97 – 103; b) S. Ferrari, W. Bannworth, S. J. Morley, N. F. Totty, G. Thomas, *Proc. Natl. Acad. Sci. USA* **1992**, *89*, 7282 – 7286.
[207] T. Vorherr, W. Bannwarth, *Bioorg. Med. Chem. Lett.* **1995**, *5*, 2661 – 2664.
[208] a) T. Wakamiya, K. Saruta, J. Yasuoka, S. Kusumoto, *Chem. Lett.* **1994**, 1099 – 1102; b) T. Wakamiya, T. Nishida, R. Togashi, K. Saruta, J. Yasuoka, S. Kusumoto, *Bull. Chem. Soc. Jpn.* **1996**, *69*, 465 – 468; c) T. Wakamiya, R. Togashi, T. Nishida, K. Saruta, J. Yasuoka, S. Kusumoto, S. Aimoto, K. Y. Kumagaye, K. Nakajima, K. Nagata, *Bioorg. Med. Chem.* **1997**, *5*, 135 – 145.
[209] a) D. Sebastian, H. Waldmann, *Tetrahedron Lett.* **1997**, 38, 2927 – 2930; b) D. Sebastian, A. Heuser, S. Schulze, H. Waldmann, *Synthesis* **1997**, 1098 – 1108.
[210] T. Zelinski, T. Pathak, H. Waldmann, unpublished results.
[211] a) H. Waldmann, A. Heuser, S. Schulze, *Tetrahedron Lett.* **1996**, *37*, 8725 – 8728; b) ref. [209b].
[212] R. L. Stone, J. E. Dixon, *J. Biol. Chem.* **1994**, *269*, 31323 – 31326, and references therein.
[213] J. W. Perich, F. Meggio, L. A. Pinna, *Bioorg. Med. Chem.* **1996**, *4*, 143 – 150.
[214] T. Tagawa, T. Kuroki, P. K. Vogt, K. Chida, *J. Cell Biol.* **1995**, *130*, 255 – 263.
[215] a) W.-K. Liu, W. T. Moore, R. T. Williams, F. L. Hall, S.-H. Yen, *J. Neurosci. Res.* **1993**, 371 – 376; b) W.-K. Liu, S.-H. Yen, *J. Neurochem.* **1996**, *66*, 1131 – 1139; c) P. Seubert, M. Mawal-Dewan, R. Barbour, R. Jakes, M. Goedert, G. V. W. Johnson, J. M. Litersky, D. Schenk, I. Lieberburg, J. Q. Trojanowski, V. M.-Y. Lee, *J. Biol. Chem.* **1995**, *270*, 18917 – 18922; d) K. Ishiguro, K. Sato, M. Takamatsu, J. Park, T. Uchida, K. Imakori, *Neurosci. Lett.* **1995**, *202*, 81 – 84.
[216] a) G. W. Hart, L. K. Kreppel, F. I. Comer, C. S. Arnold, D. M. Snow, Z. Ye, X. Cheng, D. DellaMauna, D. S. Caine, B. J. Earles, Y. Akimoto, R. N. Cole, B. K. Hayes, *Glycobiology* **1996**, *6*, 711 – 716; b) G. W. Hart, K. D. Greis, L.-Y. Dennis Dong, M. A. Blomberg, R.-Y. Chou, M.-S. Jiang, E. P. Roquemore, D. M. Snow, L. K. Kreppel, R. C. Cole, B. K. Hayes, *Pure Appl. Chem.* **1995**, *67*, 1637 – 1645.
[217] W. G. Kelly, M. E. Dahmus, G. W. Hart, *J. Biol. Chem.* **1993**, *268*, 10416 – 10424.
[218] a) T. Pohl, H. Waldmann, *Angew. Chem.* **1996**, *108*, 1829 – 1832; *Angew. Chem. Int. Ed. Engl.* **1996**, *35*, 1720 – 1723; b) *J. Am. Chem. Soc.* **1997**, *119*, 6702 – 6710.
[219] L. Medina-Vera, R. S. Haltiwanger, *Mol. Biol. Cell* **1994**, *5*, 340.
[220] a) M. Salas, *Annu. Rev. Biochem.* **1991**, *160*, 39 – 71; b) L. Blanco, J. M. Lázaro, M. de Vega, A. Bonnin, M. Salas, *Proc. Natl. Acad. Sci. USA* **1994**, *91*, 12198 – 12202.
[221] K. A. Henningfeld, T. Arslan, S. M. Hecht, *J. Am. Chem. Soc.* **1996**, *118*, 11701 – 11714.
[222] B. A. Juodka, *Nucleosides Nucleotides* **1984**, *3*, 445 – 483.
[223] E. Kuyl-Yeheskiely, C. M. Tromp, A. W. M. Lefebre, G. A. van der-Marel, J. H. van Boom, *Tetrahedron* **1988**, *44*, 6515 – 6523.
[224] a) H. Hotoda, Y. Ueno, M. Sekine, T. Hata, *Tetrahedron Lett.* **1989**, *30*, 2117 – 2120; b) C. M. Dreef-Tromp, H. van der Elst, J. E. van den Boogaart, G. A. van der Marel, J. H. van Boom, *Nucleic Acids Res.* **1992**, *20*, 2435 – 2439.
[225] C. M. Dreef-Tromp, J. C. M. van der Maarel, H. van der Elst, G. A. van der Marel, J. H. van Boom, *Nucleic Acids Res.* **1992**, *20*, 4015 – 4020.
[226] a) J. Robles, E. Pedroso, A. Grandas, *Tetrahedron Lett.* **1994**, *35*, 4449 – 4452; b) J. Robles, E. Pedroso, A. Grandas, *J. Org. Chem.* **1994**, *59*, 2482 – 2486.
[227] Y. Ueno, R. Saito, T. Hata, *Nucleic Acids Res.* **1993**, *21*, 4451 – 4457.
[228] H. Waldmann, S. Gabold, *Chem. Commun.* **1997**, 1861 – 1862.
[229] H. Waldmann, A. Reidel, *Angew. Chem.* **1997**, *109*, 642 – 644; *Angew. Chem. Int. Ed. Engl.* **1997**, *36*, 647 – 649.
[230] J. S. Früchtel, G. Jung, *Angew. Chem.* **1996**, *108*, 19 – 46; *Angew. Chem. Int. Ed. Engl.* **1996**, *35*, 17 – 42.
[231] M. Inoue, A. Kishimoto, Y. Takai, Y. Nishizuka, *J. Biol. Chem.* **1977**, *252*, 7610 – 7616.
[232] Y. Nishizuka, *Nature* **1984**, *308*, 693 – 698.
[233] Y. Nishizuka, *Science* **1992**, *258*, 607 – 614.
[234] M. J. Clemens, I. Trayner, J. Menaya, *J. Cell Sci.* **1992**, *103*, 881 – 887.
[235] M. J. Hubbard, P. Cohen, *Trends Biochem. Sci.* **1993**, *18*, 172 – 177.
[236] C. L. Ashendel, *Biochim. Biophys. Acta* **1985**, *822*, 219 – 242.
[237] L. V. Dekker, P. J. Parker, *Trends Biochem. Sci.* **1994**, *19*, 73 – 77.
[238] H. Hug, T. F. Sarre, *Biochem. J.* **1993**, *291*, 329 – 343.
[239] M. Gschwendt, S. Dieterich, J. Rennecke, W. Kittstein, H.-J. Mueller, F.-J. Johannes, *FEBS Lett.* **1996**, *392*, 77 – 80.
[240] Y. Asaoka, S. Nakamura, K. Yoshida, Y. Nishizuka, *Trends Biochem. Sci.* **1992**, *17*, 73 – 77.
[241] M. Castagna, Y. Takai, K. Kaibuchi, K. Sano, U. Kikkawa, Y. Nishizuka, *J. Biol. Chem.* **1982**, *257*, 7847 – 7851.
[242] M. Castagna, *Biol. Cell* **1987**, *59*, 3 – 14.
[243] U. Kikkawa, A. Kishimoto, Y. Nishizuka, *Annu. Rev. Biochem.* **1989**, *58*, 31 – 44.
[244] D. J. Burns, R. M. Bell, *J. Biol. Chem.* **1991**, *266*, 18330 – 18338.
[245] A. C. Newton, *Annu. Rev. Biophys. Biomol. Struct.* **1993**, *22*, 1 – 25.
[246] A. M. Jeffrey, R. M. J. Liskamp, *Proc. Natl. Acad. Sci. USA* **1986**, *83*, 241 – 245.
[247] P. A. Wender, K. F. Koehler, Nancy A. Sharkey, M. L. Dell'Aquila, P. M. Blumberg, *Proc. Natl. Acad. Sci. USA* **1986**, *83*, 4214 – 4218.
[248] A. Itai, Y. Kato, N. Tomioka, Y. Itaka, Y. Endo, M. Hasegawa, K. Shudo, H. Fujiki, S.-I. Sakai, *Proc. Natl. Acad. Sci. USA* **1988**, *85*, 3688 – 3692.
[249] P. A. Wender, C. M. Cribbs, K. F. Koehler, N. A. Sharkey, C. L. Herald, Y. Kamano, G. R. Pettit, P. M. Blumberg, *Proc. Natl. Acad. Sci. USA* **1988**, *85*, 7197 – 7201.
[250] H. Nakamura, Y. Kishi, M. A. Pajares, R. R. Rando, *Proc. Natl. Acad. Sci. USA* **1989**, *86*, 9672 – 9676.
[251] R. R. Rando, Y. Kishi, *Biochemistry* **1992**, *31*, 2211 – 2218.
[252] Y. Ono, T. Fujii, K. Ogita, K. Igarashi, T. Kuno, C. Tanaka, U. Kikkawa, Y. Nishizuka, *Proc. Natl. Acad. Sci. USA* **1989**, *86*, 4868 – 4871.
[253] A. F. G. Quest, E. S. G. Bardes, R. M. Bell, *J. Biol. Chem.* **1994**, *269*, 2961 – 2970.
[254] P. A. Wender, K. Irie, B. L. Miller, *Proc. Natl. Acad. Sci. USA* **1995**, *92*, 239 – 243.
[255] K. Irie, F. Koizumi, Y. Iwata, T. Ishii, Y. Yanai, Y. Nakamura, H. Ohigashi, P. A. Wender, *Bioorg. Med. Chem. Lett.* **1995**, *5*, 453 – 458.
[256] G. Zhang, M. G. Kazanietz, P. M. Blumberg, J. H. Hurley, *Cell* **1995**, *81*, 917 – 924.
[257] a) P. A. Wender, H. Kogen, H. Y. Lee, J. D. Munger, R. S. Wilhelm, P. D. Williams, *J. Am. Chem. Soc.* **1989**, *111*, 8957 – 8958; b) P. A. Wender, K. D. Rice, M. E. Schnute, *ibid.* **1997**, *119*, 7897 – 7898; c) K. Irie, T. Ishii, H. Ohigashi, P. A. Wender, B. L. Miller, N. Takeda, *J. Org. Chem.* **1996**, *61*, 2164 – 2173.
[258] P. A. Wender, K. Irie, B. L. Miller, *Proc. Natl. Acad. Sci. USA* **1995**, *92*, 239 – 243.
[259] J. B. Weinberg, *Science* **1981**, *213*, 655 – 657.
[260] C. G. Tepper, S. Jayadev, B. Liu, A. Bielawska, R. Wolff, S. Yonehara, Y. A. Hannun, M. F. Seldin, *Proc. Natl. Acad. Sci. USA* **1995**, *92*, 8443 – 8447.
[261] J. M. Backer, G. L. King, *Biochem. Pharmacol.* **1991**, *41*, 1267 – 1277.
[262] M. Fabbri, S. Bannykh, W. E. Balch, *J. Biol. Chem.* **1994**, *269*, 26848 – 26857.
[263] M. Todaka, H. Hayashi, T. Imanaka, Y. Mitani, S. Kamohara, K. Kishi, K. Tamaoka, F. Kanai, M. Shichiri, N. Morii, S. Narumiya, Y. Ebina, *Biochem. J.* **1996**, *315*, 875 – 882.
[264] C. J. Lowenstein, S. H. Snyder, *Cell* **1992**, *70*, 705 – 707.
[265] S. Hortelano, A. M. Genaro, L. Boscá, *J. Biol. Chem.* **1992**, *267*, 24937 – 24940.
[266] K. Möller, D. Benz, D. Perrin, H.-D. Söling, *Biochem. J.* **1996**, *314*, 181 – 187.
[267] J. Quick, B. Saha, P. E. Driedger, *Tetrahedron Lett.* **1994**, *35*, 8549 – 8552.
[268] M. F. Semmelhack, H. Rhee, *Tetrahedron Lett.* **1993**, *34*, 1395 – 1398.
[269] M. Mascal, C. J. Moody, A. M. Z. Slawin, D. J. Williams, *J. Chem. Soc. Perkin Trans. 1* **1992**, 823 – 830.

[270] a) T. P. Kogan, T. C. Somers, M. C. Venuti, *Tetrahedron* **1990**, *46*, 6623 – 6632; b) D. Alonso-Díaz, H. Waldmann, unpublished results.
[271] T. Masuda, S. Nakatsuka, T. Goto, *Agric. Biol. Chem.* **1989**, *53*, 2257 – 2260.
[272] A. P. Kozikowski, K. Sato, A. Basu, J. S. Lazo, *J. Am. Chem. Soc.* **1989**, *111*, 6228 – 6234.
[273] Y. Endo, K. Shudo, A. Itai, M. Hasegawa, S. Sakai, *Tetrahedron* **1986**, *42*, 5905 – 5924.
[274] M. F. Semmelhack, H. Rhee, *Tetrahedron Lett.* **1993**, *34*, 1399 – 1402.
[275] H. Muratake, M. Natsume, *Tetrahedron Lett.* **1987**, *28*, 2265 – 2268.
[276] K. Irie, S. Okuno, F. Koizumi, K. Koshimizu, H. Nishino, A. Iwashima, *Tetrahedron* **1993**, *49*, 10817 – 10830.
[277] K. Irie, N. Hagiwara, H. Tokuda, K. Koshimizu, *Carcinogenesis* **1987**, *8*, 547 – 552.
[278] R. A. Murphy, *FASEB J.* **1994**, *8*, 311 – 314.
[279] M. Nishikawa, S. Shirakawa, R. S. Adelestein, *J. Biol. Chem.* **1985**, *260*, 8978 – 8983.
[280] M. A. Hill, M. J. Davis, J. Song, H. Zou, *J. Pharmacol. Exp. Ther.* **1996**, *276*, 867 – 874.
[281] H.-L. Shieh, H. Hansen, J. Zhu, H. Riedel, *Mol. Carcinogen.* **1995**, *12*, 166 – 176.
[282] N. J. Leidenheimer, S. J. McQuilkin, L. D. Hahner, P. Whiting, R. A. Harris, *Mol. Pharmacol.* **1992**, *41*, 1116 – 1123.
[283] W.-W. Lin, D.-M. Chuang, *Neurochem. Int.* **1993**, *23*, 53 – 60.
[284] Y. Endo, M. Ohno, M. Hirano, A. Itai, K. Shudo, *J. Am. Chem. Soc.* **1996**, *118,* 1841 – 1855.
[285] Y. Endo, M. Yamaguchi, M. Hirano, K. Shudo, *Chem. Pharm. Bull.* **1996**, *44,* 1138 – 1140.
[286] A. P. Kozikowski, D. Ma, Y. Pang, P. Shum, V. Likic, P. K. Mishra, S. Macura, A. Basu, J. S. Lazo, R. G. Ball, *J. Am. Chem. Soc.* **1993**, *115,* 3957 – 3965.
[287] A. P. Kozikowski, D. Ma, L. Du, N. E. Lewin, P. M. Blumberg, *J. Am. Chem. Soc.* **1995**, *117*, 6666 – 6672.
[288] K. Irie, T. Isaka, Y. Iwata, Y. Yanai, Y. Nakamura, F. Koizumi, H. Ohigashi, P. A. Wender, Y. Satomi, H. Nishino, *J. Am. Chem. Soc.* **1996**, *118,* 10733 – 10743.
[289] B. Ganong, C. Loomis, Y. Hannun, R. M. Bell, *Proc. Natl. Acad. Sci. USA* **1986**, *83*, 1184 – 1188.
[290] J. Florin-Christensen, M. Florin-Christensen, J. M. Delfino, H. Rasmussen, *Biochem. J.* **1993**, *289*, 783 – 788.
[291] R. M. Bell, D. J. Burns, *J. Biol. Chem.* **1991**, *266*, 4661 – 4664.
[292] N. Rudra, N. Singh, M. Gupta, *J. Biosci.* **1996**, *21*, 477 – 485.
[293] R. Z. Kozlowski, M. L. J. Ashford, *Br. J. Pharmacol.* **1992**, *107*, 34 – 43.
[294] G. Krauter, C.-W. von der Lieth, R. Schmidt, E. Hecker, *Eur. J. Biochem.* **1996**, *242*, 417 – 427.
[295] S. Armstrong, C. E. Ganote, *Cardiovasc. Res.* **1994**, *28*, 1700 – 1706.
[296] S. Omura, Y. Iwai, A. Hirano, A. Nakagawa, J. Awaya, H. Tsuchiya, Y. Takahashi, R. Masuma, *J. Antibiot.* **1977**, *30*, 275 – 282.
[297] H. Kase, K. Iwahashi, Y. Matsuda, *J. Antibiot.* **1986**, *39*, 1059 – 1065.
[298] T. Tamaoki, H. Nomoto, I. Takahashi, Y. Kato, M. Morimoto, F. Tomita, *Biochem. Biophys. Res. Commun*. **1986**, *135*, 397 – 402.
[299] H. Kase, K. Iwahashi, M. Kaneko, Y. Matsuda, C. Murakata, S. Nakanishi, A. Sato, K. Yamada, M. Takahashi, *Biochem. Biophys. Res. Commun*. **1987**, *142*, 436 – 440.
[300] J. M. Herbert, E. Seban, J. P. Maffrand, *Biochem. Biophys. Res. Commun*. **1990**, *171*, 189 – 195.
[301] J. T. Link, S. Raghavan, S. J. Danishefsky, *J. Am. Chem. Soc.* **1995**, *117*, 552 – 553.
[302] J. T. Link, S. Raghavan, M. Gallant, S. J. Danishefsky, T. C. Chou, L. M. Ballas, *J. Am. Chem. Soc.* **1996**, *118*, 2825 – 2842.
[303] J. L. Wood, B. M. Stolz, H.-J. Dietrich, *J. Am. Chem. Soc.* **1995**, *117*, 10413 – 10414.
[304] J. L. Wood, B. M. Stoltz, S. N. Goodman, *J. Am. Chem. Soc.* **1996**, *118*, 10656 – 10657
[305] T. Tamaoki, H. Nakano, *Biotechnology* **1990**, *8*, 732 – 735.
[306] J. H. Hartenstein, J. Aranda, H. Barth, H. J. Betche, J. Kleinschroth, R. Reck, C. Rudolph, U. Trostmann, C. Schächtele, *Perspect. Med. Chem.* **1993**, 99 – 118.
[307] T. Meyer, U. Regenass, D. Fabbro, E. Alteri, J. Rösel, M. Müller, G. Caravatti, A. Matter, *Int. J. Cancer* **1989**, *43*, 851 – 856.
[308] P. D. Davis, C. H. Hill, E. Keech, G. Lawton, J. S. Nixon, A. D. Sedgwick, J. Wadsworth, D. Westmacott, S. E. Wilkinson, *FEBS Lett.* **1989**, *259*, 61 – 63.
[309] D. Toullec, P. Pianetti, H. Coste, P. Bellevergue, T. Grand-Perret, A. Ajakane, V. Baudet, P. Boissin, E. Boursier, F. Loriolle, L. Duhamel, D. Charon, J. Kirilovsky, *J. Biol. Chem.* **1991**, *266*, 5771 – 5781.
[310] P. D. Davis, C. H. Hill, G. Lawton, J. S. Nixon, S. E. Wilkinson, S. A. Hurst, E. Keech, S. E. Turner, *J. Med. Chem.* **1992**, *35*, 177 – 184.
[311] P. D. Davis, L. H. Elliott, W. Harris, C. H. Hill, S. A. Hurst, E. Keech, M. K. H. Kumar, G. Lawton, J. S. Nixon, S. E. Wilkinson, *J. Med. Chem.* **1992**, *35*, 994 – 1001.
[312] T. Inoguchi, R. Battan, E. Handler, J. R. Sportsman, W. Heath, G. L. King, *Proc. Natl. Acad. Sci. USA* **1992**, *89*, 11059 – 11063.
[313] H. Ishii, M. R. Jirousek, D. Koya, C. Takagi, P. Xia, A. Clermont, S.-E. Bursell, T. S. Kern, L. M. Ballas, W. F. Heath, L. E. Stramm, E. P. Feener, G. L. King, *Science* **1996**, *272*, 728 – 731.
[314] P. Kulanthaivel, Y. F. Hallock, C. Boros, S. M. Hamilton, W. P. Janzen, L. M. Ballas, C. R. Loomis, J. B. Jiang, *J. Am. Chem. Soc.* **1993**, *115*, 6452 – 6453.
[315] P. Kulanthaivel, Y. F. Hallock, C. Boros, S. M. Hamilton, W. P. Janzen, L. M. Ballas, C. R. Loomis, J. B. Jiang, *J. Am. Chem. Soc.* **1993**, *115*, 10468 – 10468.
[316] S. Ohsima, M. Yanagisawa, A. Katoh, T. Fujii, T. Sano, S. Matsukuma, T. Fuyumai, M. Fujui, K. Watanabe, K. Yokose, M. Arisawa, T. Okuda, *J. Antibiotics* **1994**, *47*, 639 – 647.
[317] K. C. Nicolau, M. E. Bunnage, K. Koide, *J. Am. Chem. Soc.* **1994**, *116*, 8402 – 8403.
[318] K. C. Nicolaou, K. Koide, M. E. Bunnage, *Chem. Eur. J.* **1995**, *1*, 454 – 466.
[319] J. W. Lampe, P. F. Hughes, C. K. Biggers, S. H. Smith, H. Hu, *J. Org. Chem.* **1994**, *59*, 5147 – 5148.
[320] J. W. Lampe, P. F. Hughes, C. K. Biggers, S. H. Smith, H. Hu, *J. Org. Chem.* **1996**, *61,* 4572 – 4581.
[321] C. P. Adams, S. M. Fairway, C. J. Hardy, D. E. Hibbs, M. B. Hursthouse, A. D. Morley, B. W. Sharp, N. Vicker, I. Warner, *J. Chem. Soc. Perkin Trans. 1* **1995**, 2355 – 2362.
[322] K. Koide, M. E. Bunnage, L. G. Paloma, J. R. Kanter, S. S. Taylor, L. L. Brunton, K. C. Nicolaou, *Chem. Biol.* **1995**, *2*, 601 – 608.
[323] J. M. Defauw, M. M. Murphy, G. E. Jagdmann, Jr., H. Hu, J. W. Lampe, S. P. Hollinshead, T. J. Mitchell, H. M. Crane, J. M. Heerding, J. S. Mendoza, J. E. Davis, J. W. Darges, F. R. Hubbard, S. E. Hall, *J. Med. Chem.* **1996**, *39*, 5215 – 5227.
[324] T. F. Franke, D. R. Kaplan, L. C. Cantley, *Cell* **1997**, *88*, 435 – 437.
[325] S. Spiegel, D. Foster, R. Kolesnick, *Curr. Opin. Cell. Biol*. **1996**, *8*, 159 – 167.
[326] B. A. Hemmings, *Science* **1997**, *275*, 628 – 630.
[327] C. A. Alter, B. A. Wolf, *Biochem. Biophys. Res. Commun.* **1995**, *208*, 190 – 197.
[328] B. A. Wolf, R. J. Konrad, C. A. Alter in *Frontiers of Insulin Secretion and Pancreatic B-Cell Research* (Eds.: P. R. Flatt, S. Lenzen), **1993**.
[329] G. D. Prestwich, J. F. Marececk, R. J. Mourey, A. B. Theibert, C. D. Ferris, S. K. Danoff, S. H. Snyder, *J. Am. Chem. Soc.* **1991**, *113*, 1822 – 1825.
[330] P. F. Worley, J. M. Baraban, S. Supattapone, V. S. Wilson, S. H. Snyder, *J. Biol. Chem.* **1987**, *262*, 12132 – 12136.
[331] C. D. Ferris, R. L. Huganir, S. Supattapone, S. H. Snyder, *Nature* **1989**, *342*, 87 – 89.
[332] G. D. Prestwich, *Acc. Chem. Res.* **1996**, *29*, 503 – 513.
[333] B. Mehrotra, J. T. Elliot, J. Chen, J. D. Olszewski, A. A. Profit, A. Chaudhary, M. Fukuda, K. Mikoshiba, G. D. Prestwich, *J. Biol. Chem.* **1997**, *272*, 4237 – 4244.
[334] K. M. Ferguson, M. A. Lemmon, J. Schlessinger, P. B. Sigler, *Cell* **1996**, *83*, 1037 – 1046.
[335] V. A. Estevez, G. D. Prestwich, *Tetrahedron Lett.* **1991**, *32*, 1623 – 1626.
[336] A. B. Theibert, V. A. Estevez, R. J. Mourey, J. F. Marececk, R. K. Barrow, G. D. Prestwich, S. H. Snyder, *J. Biol. Chem.* **1992**, *267*, 9071 – 9079.
[337] V. A. Estevez, G. D. Prestwich, *J. Am. Chem. Soc.* **1991**, *113*, 9885 – 9887.
[338] S. Ozaki, Y. Watanabe, T. Ogasawara, M. Hirata, T. Kanematsu, *Carbohydr. Res.* **1992**, *234*, 189 – 206.

[339] M. Hirata, Y. Watanabe, T. Ishimatsu, T. Ikebe, Y. Kimura, K. Yamaguchi, S. Ozaki, T. Koga, *J. Biol. Chem.* **1989**, *264*, 20303 – 20308.
[340] M. Hirata, F. Yanaga, T. Koga, T. Ogasawara, Y. Watanabe, S. Ozaki, *J. Biol. Chem.* **1990**, *265,* 8404 – 8407.
[341] Y. Watanabe, M. Hirata, T. Ogasawara, T. Koga, S. Ozaki, *Bioorg. Med. Chem. Lett.* **1991**, *1*, 399 – 402.
[342] L. P. Hammonds-Odie, T. R. Jackson, A. A. Profit, I. J. Blader, C. Turck, G. D. Prestwich, A. B. Theibert, *J. Biol. Chem.* **1996**, *271,* 18859 – 18868.
[343] M. Vajanaphanich, C. Schultz, M. T. Rudolf, M. Wasserman, P. Enyedi, A. Craxton, S. B. Shears, R. Y, Tsien, K. E. Barrett, A. Traynor-Kaplan, *Nature* **1994**, *371*, 711 – 714.
[344] D. J. Jenkins, A. M. Riley, B. V. L. Potter, *J. Org. Chem.* **1996**, *61*, 7719 – 7726.
[345] K. K. Reddy, M. Saady, J. R. Falck, *J. Org. Chem.* **1995**, *60*, 3385 – 3390.
[346] A. Toker, M. Meyer, K. K. Reddy, J. R. Falck, R. Aneja, D. J. Burns, L. M. Ballas, L. C. Cantley, *J. Biol. Chem.* **1994**, *269,* 32358 – 32367.
[347] J. Chen, A. A. Profit, G. D. Prestwich, *J. Org. Chem.* **1996**, *61*, 6305 – 6312.
[348] Q.-M. Gu, G. D. Prestwich, *J. Org. Chem.* **1996**, *61*, 8642 – 8647.
[349] M. Glaser, S. Wanaski, C. A. Buser, V. Bogulavsky, W. Rashidzada, A. Morris, M. Rebecchi, S. F. Scarlata, L. W. Runnels, G. D. Prestwich, J. Chen, A. Aderem, J. Ahn, S. McLaughlin, *J. Biol. Chem.* **1996**, *271,* 26187 – 26193.
[350] Reviews: a) K. J. Murray, W. J. Coates, *Annu. Rep. Med. Chem*. **1994**, *29*, 255 – 264; b) T. Hunter, *Cell* **1995**, *80*, 225 – 236; c) D. Barford, *Trends Biochem. Sci*. **1996**, *21*, 407 – 412; d) E. B. Fanman, M. A. Saper, *ibid*. **1996**, *21*, 413 – 417.
[351] W. Vogel, R. Lammers, J. Huang, A. Ullrich, *Science* **1993**, *259*, 1611 – 1614.
[352] Ser/Thr phosphatases: a) M. P. Egloff, P. T. W. Cohen, P. Reinemer, D. Barford, *J. Mol. Biol*. **1995**, *254*, 942 – 959; b) J. Goldberg, H. B. Huang, Y. G. Kwon, P. Greengard, A. C. Nairn, J. Kuriyan, *Nature* **1995**, *376*, 745 – 753; c) C. R. Kissinger, H. E. Parge, D. R. Knighton, C. T. Lewis, L. A. Pelletier, A. Tempcyk, V. J. Kalish, K. D. Tucker, R. E. Showalter, E. W. Moonaw, L. N. Gastinel, N. Habuka, X. H. Chen, F. Maldonado, J. E. Barker, R. Bacquet, J. E. Villafranca, *Nature* **1995**, *378*, 641 – 644; d) J. P. Griffith, J. L. Kim, E. E. Kim, M. D. Sintchak, J. A. Thomsen, M. J. Fitzgibbon, M. A. Fleming, P. R. Caron, K. Hsiao, M. A. Navia, *Cell* **1995**, *82*, 507 – 522; Tyr phosphatases: e) M. Zhang, R. L. Van Etten, C. V. Stauffacher, *Biochemistry* **1994**, *33*, 11097 – 11105; f) D. Barford, A. J. Flint, N. K. Tonks, *Science* **1994**, *236*, 1379 – 1404; g) J. A. Stuckey, H. L. Schubert, E. B. Fauman, Z. Y. Zhang, J. E. Dixon, M. A. Saper, *Nature* **1994**, *370*, 571 – 575; h) Z. C. Jia, D. Barford, A. J. Flint, N. K. Tonks, *Science* **1995**, *268*, 1754 – 1758; i) A. M. Bilwes, J. den Hertog, T. Hunter, J. P. Noel, *Nature* **1996**, *382*, 555 – 559; j) J. Yuvaniyama, J. M. Denu, J. E. Dixon, M. A. Saper, *Science* **1996**, *272*, 1328 – 1331; k) E. B. Fanman, C. Yuvaniyama, H. L. Schubert, J. A. Stuckey, M. A. Saper, *J. Biol. Chem*. **1996**, *271*, 18780 – 18788.
[353] K. Tachibana, P. J. Scheuer, Y. Tsukitani, H. Kikuchi, D. Van Engen, J. Clardy, Y. Gopichand, F. J. Schmitz, *J. Am. Chem. Soc*. **1981**, *103*, 2469 – 2471.
[354] X.-C. Cheng, T. Kihara, H. Kusakabe, J. Magae, Y. Kobayashi, R.-P. Fang, Z.-F. Ni, Y.-C. Shen, K. Ko, I. Yamaguchi, K. Isono, *J. Antibiot*. **1987**, *40*, 907 – 909.
[355] Y.-M. Li, C. Mackintosh, J. E. Cassida, *Biochem. Pharmacol*. **1993**, *46*, 1435 – 1443.
[356] Y. Kato, N. Fusetani, S. Matsunaga, K. Hashimoto, S. Fujita, T. Furuya, *J. Am. Chem. Soc*. **1986**, *108*, 2780 – 2781.
[357] a) K. L. Rinehart, K.-I. Harada, M. Namikoshi, C. Chen, C. A. Harvis, M. H. G. Munro, J. W. Blunt, P. E. Mulligan, V. R. Beasley, A. M. Dahlem, W. W. Carmichael, *J. Am. Chem. Soc*. **1988**, 110, 8557 – 8558; b) M. Namikoshi, B. W. Choi, R. Sakai, F. Sun, K. L. Rinehart, W. W. Carmichael, W. R. Evans, P. Cruz, M. H. G. Munro, J. W. Blunt, *J. Org. Chem*. **1994**, *59*, 2349 – 2357.
[358] M. Namikoshi, F. Sun, B. W. Choi, K. L. Rinehart, W. W. Carmichael, W. R. Evans, V. R. Beasley, *J. Org. Chem*. **1995**, *60*, 3671 – 3679.
[359] R. Nishiwaki-Matsushima, T. Ohta, S. Nishiwaki, M. Suganuma, K. Kohyama, T. Ishikawa, W. W. Carmichael, H. Fujiki, *J. Cancer Res. Clin. Oncol*. **1992**, *118*, 420 – 424.
[360] C. Bialojau, A. Takai, *Biochem. J*. **1988**, *256*, 283 – 290.
[361] M. Isobe, Y. Ichikawa, T. Goto, *Tetrahedron. Lett*. **1986**, *27*, 963 – 966.
[362] Y. Ichikawa, M. Isobe, D.-L. Bai, T. Goto, *Tetrahedron* **1987**, *43*, 4737 – 4748.
[363] Y. Ichikawa, M. Isobe, T. Goto, *Tetrahedron* **1987**, *43*,4749 – 4758.
[364] Y. Ichikawa, M. Isobe, H. Masaki, T. Kawai, T. Goto, *Tetrahedron* **1987**, *43*, 4759 – 4766.
[365] M. Isobe, Y. Ichikawa, D.-L. Bai, H. Masaki, T. Goto, *Tetrahedron* **1987**, *43*, 4767 – 4776.
[366] A. Takai, G. Mieskes, *Biochem. J*. **1991**, *275*, 233 – 239.
[367] M. C. Raff, *Nature* **1992**, *356*, 379 – 399.
[368] R. Boe, B. T. Gjertsen, O. K. Vintermyr, G. Houge, M. Lanotte, S. O. Doskeland, *Exp. Cell. Res*. **1991**, *195*, 237 – 246.
[369] Y. Ohoka, Y. Nakai, M. Mukai, M. Iwata, *Biochem. Biophys. Res. Commun*. **1993**, *197*, 916 – 921.
[370] A. Lerga, B. Belandia, M. D. Delgado, M. A. Cuadrado, C. Richard, J. M. Ortiz, J. Martin-Perez, J. Leon, *Biochem. Biophys. Res. Commun*. **1995**, *215*, 889 – 885.
[371] K. B. Marcu, S. A. Bossone, A. J. Patel, *Annu. Rev. Biochem*. **1992**, *61*, 809 – 860.
[372] N. Begum, L. Ragolia, M. Srinivasan, *Eur. J. Biochem*. **1996**, *238*, 214 – 220.
[373] C. M. Rondinone, U. Smith, *J. Biol. Chem*. **1996**, *271*, 18148 – 18153.
[374] N. Chajry, P.-M. Martin, C. Cocher, Y. Berthois, *Eur. J. Biochem*. **1996**, *235*, 97 – 102.
[375] L. Dupont-Wallois, P. E. Sautiere, C. Cocquerelle, B. Bailleul, A. Delacourte, M. L. Caillet-Boudin, *FEBS Lett.* **1995**, *357*, 197 – 201.
[376] H. Ishihara, B. L. Martin, D. L. Brautigan, H. Karahi, H. Ozaki, Y. Kato, N. Fusetani, S. Watabe, K. Hashimoto, D. Uemura, D. J. Hartshorne, *Biochem. Biophys. Res. Commun*. **1989**, *159*, 871 – 877.
[377] D. A. Evans, J. R. Gage, J. L. Leighton, *J. Am. Chem. Soc*. **1992**, *114*, 9434 – 9453; weitere Synthese**:** N. Tanimoto, S. W. Gerritz, A. Sawabe, T. Noda, S. A. Filla, S. Masamune*, Angew. Chem*. **1994**, *106*, 674 – 677; *Angew. Chem. Int. Ed. Engl*. **1994**, *33*, 673 – 675.
[378] Q. Song, M. F. Lavin, *Biochem. Biophys. Res. Commun*. **1993**, *190*, 47 – 55.
[379] Y. Luo, D. Kessel, *Biochem. Biophys. Res. Commun*. **1996**, *221*, 72 – 76.
[380] R. Gopalakrishna, Z. H. Chen, U. Gundimeda, *Biochem. Biophys. Res. Commun*. **1992**, *189*, 950 – 957.
[381] T. P. Thomas, R. Gopalakrishna, W. B. Anderson*, Methods Enzymol*. **1986**, *141*, 399 – 411.
[382] H. Kanety, R. Feinstein, M. Z. Papa, R. Hemi, A. Karasik, *J. Biol. Chem*. **1995**, *270*, 23780 – 23784.
[383] A. Kumar, M. H. Beresini, P. Dhawan, K. D. Mehta, *Biochem. Biophys. Res. Commun.* **1996**, *222*, 445 – 452.
[384] S. Pugazhenthi, B. Yu, R. R. Gali, R. L. Khandelwal, *Biochim. Biophys. Acta* **1993**, *1179*, 271 – 276.
[385] Synthesis of microcystin LA: J. M. Humphrey, J. B. Aggen, A. R. Chamberlin, *J. Am. Chem. Soc*. **1996**, 118, 11759 – 11770; see also H. Y. Kim, K. Stein, P. L. Toogood, *Chem. Commun*. **1996**, 1683 – 1684; Synthese von Nodularinanaloga: A. P. Mehrotra, D. Gani, *Tetrahedron Lett*. **1996**, *37*, 6915 – 6918; synthesis of Mmcrocystin/nodularin analogues: C. Taylor, R. J. Quinn, P. Alewood, *Bioorg. Med. Chem. Lett*. **1996**, *6*, 2107 – 2112.
[386] See, for example, a) F. D'Aniello, A. Mann, M. Taddei, *J. Org. Chem*. **1996**, *61*, 4870 – 4871; b) N. Sin, J. Kallmerten, *Tetrahedron Lett*. **1996**, *37*, 5645 – 5648; c) *ibid*. **1996**, *37*, 2349 – 2352.
[387] P. Wipf, A. Cunningham, R. L. Rice, J. S. Lazo, *Bioorg. Med. Chem*. **1997**, *5*, 165 – 177.
[388] a) S. Nishiwaki, H. Fujiki, M. Suganuma, H. Furuya-Suguri, *Carcinogenesis* **1990**, *11*, 1837 – 1841; b) A. Takai, M. Murata, K. Torigoe, M. Isobe, G. Mieskes, T. Yasumoto, *Biochem. J*. **1992**, *284*, 539 – 544; c) K. Sasaki, M. Murata, T. Yasumoto, G. Mieskes, A. Takai, *Biochem. J*. **1994**, *288*, 259 – 262.
[389] a) R. J. Quinn, C. Taylor, M. Sugamuna, H. Fujiki, *Bioorg. Med. Chem. Lett*. **1993**, *3*, 1029 – 1034; b) C. Taylor, R. J. Quinn, R.

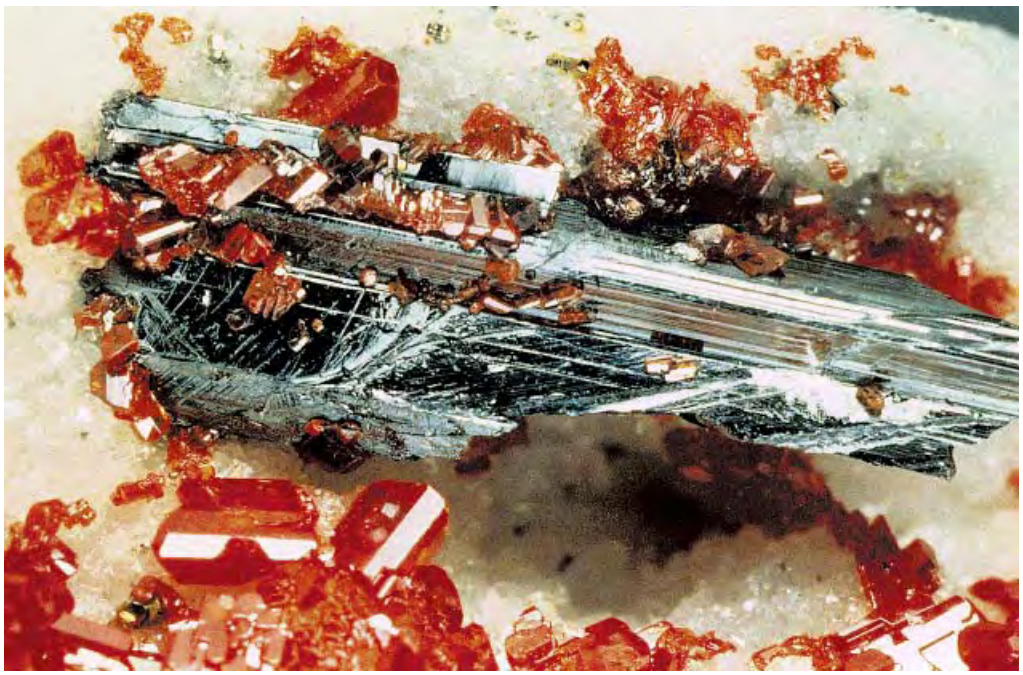
McCulloch, R. Nishiwaki-Matsushima, H. Fujiki, *ibid*. **1992**, 2, 299 – 302.
[390] M. Akamatsu, P. P. Roller, L. Chen, Z.-Y. Zhang, B. Ye, T. R. Burke, Jr., *Bioorg. Med. Chem*. **1997**, *5*, 157 – 163.
[391] G. R. Crabtree, S. L. Schreiber, *Trends Biochem. Sci*. **1996**, *21*, 418 – 422.
[392] a) M. K. Rosen, S. L. Schreiber, *Angew. Chem.* **1992**, *104*, 413 – 430; *Angew. Chem. Int. Ed. Engl*. **1992**, *31*, 384 – 400; b) S. L. Schreiber, *Science* **1991**, *251*, 283 – 287; c) J. Kunz, M. N. Hall, *Trends Biochem. Sci*. **1993**, *18*, 334 – 338.
[393] a) C.-H. Heldin, *Cell* **1995**, *80*, 213 – 223; b) D. J. Austin, G. R. Crabtree, S. L. Schreiber, *Chem. Biol*. **1994**, *1*, 131 – 136.
[394] a) D. M. Spencer, T. J. Wandless, S. L. Schreiber, G. R. Crabtree, *Science* **1993**, *262*, 1019 – 1024; b) M. N. Pruschy, D. M. Spencer, T. M. Kapoor, H. Miyake, G. R. Crabtree, S. L. Schreiber, *Chem. Biol*. **1994**, *1*, 163 – 172.
[395] a) R. Brent, M. Ptashne, *Cell* **1985**, *43*, 729 – 736; b) L. Keegan, G. Gill, M. Ptashne, *Science* **1986**, *231*, 699 – 704.
[396] S. N. Ho, S. R. Biggar, D. M. Spencer, S. L. Schreiber, G. R. Crabtree, *Nature* **1996**, *382*, 822 – 826.
[397] M. A. Farrar, J. Alberola-Ila, R. M. Perlmutter, *Nature* **1996**, *383*, 178 – 181.
[398] Z. Luo, G. Tzivion, P. J. Belshaw, D. Vavvas, M. Marshall, J. Avruch, *Nature* **1996**, *383*, 181 – 185.
[399] P. J. Belshaw, S. N. Ho, G. R. Crabtree, S. L. Schreiber, *Proc. Natl. Acad. Sci. USA* **1996**, *93*, 4604 – 4607.
[400] V. M. Rivera, T. Clackson, S. Natesan, R. Pollock, J. F. Amara, T. Keenan, S. R. Magari, T. Phillips, N. L. Courage, F. Cerasoli, D. A. Holt, M. Gilman, *Nature Medicine* **1996**, 2, 1028 – 1032.

Deposition of Data from X-Ray Structure Analyses

In order to make life easier for authors and referees the Cambridge Crystallographic Data Centre (CCDC) and the Fachinformationszentrum Karlsruhe (FIZ) have unified their procedures for the depostion of data from single-crystal X-ray structure analyses.

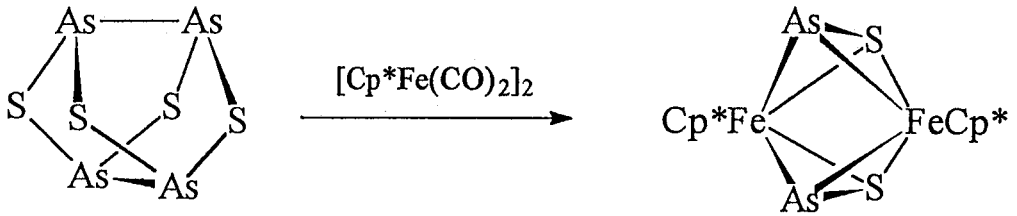
Prior to submitting a manuscript please deposit the data for your compound(s) **electronically** at the appropriate date base, that is, at the CCDC for organic and organometallic compounds and at the FIZ for inorganic compounds. Both data bases will be pleased to provide help (see our *Notice to Authors* in the first issue of this year). In general, you will receive a depository number from the data base within two working days after electronic deposition; please include this number with the appropriate standard text (see our Notice to Authors) in your manuscript. This will enable the referees to retrieve the structure data quickly and efficiently if they need this information to reach their decision.

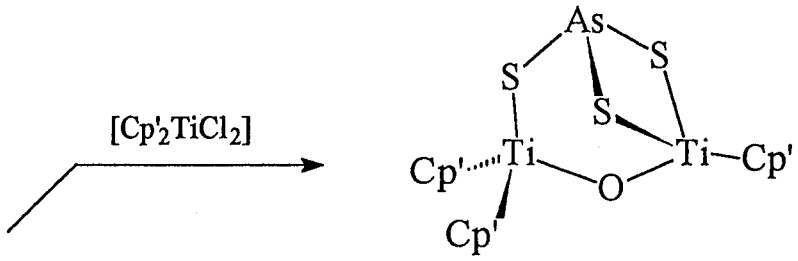
This is now the uniform procedure for manuscripts submitted to the journals *Advanced Materials, Angewandte Chemie, Chemistry—A European Journal,* the *European Journal of Inorganic Chemistry,* and the *European Journal of Organic Chemistry.*

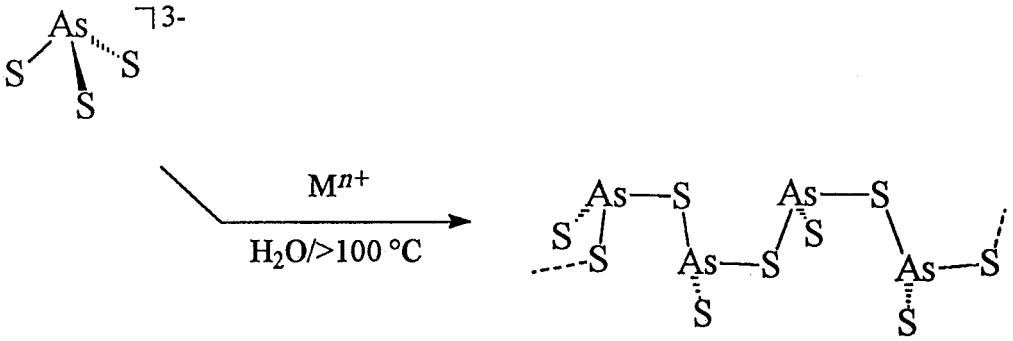


"AsS" (from As_4S_4) and AsS_2^- (from AsS_3^{3-}) are the smallest building blocks, which form the molecular cage of realgar (red) and the infinite $PbAs_2S_4$ chains in the sulfosalt mineral sartorite (black shining).

Examples of the compounds that are accessible in the laboratory from the above starting materials are illustrated below.







ANGEWANDTE CHEMIE © WILEY-VCH

Mixed Ligands from Group 15/16 Elements: Interface of Solid-State and Molecular Chemistry

Joachim Wachter*

Heteroatomic ligands E/X containing the elements P, As, Sb (E) and S, Se, Te (X) span the wide range from simple salts through to neutral and anionic cage molecules and on to solids. Their coordination chemistry with numerous metals, ranging from the formation of diatomic ligands in organometallic complexes to extended solid-state structures is currently the focus of a great deal of attention. Besides neutral clusters such as $E_4X_{3(4)}$, Zintl phases and covalent solids play an increasing role in the development of new E/X ligands. Typical synthetic strategies are the reduction of binary phases by nucleophilic complexes and the introduction of organometallic complex fragments ML_n (L = CO, cyclopentadienyl) into neutral and anionic cage molecules. The ligands can be classified into three groups: a) small, covalently bonded E/X ligands with different π-bond participation and a pronounced tendency for "self-condensation", b) heteroatomic Zintl anions, which are incorporated into electron precise complexes under partial fragmentation, and c) neutral cage molecules, which are useful for studying fragmentation mechanisms and for the construction of new hybride clusters with inorganic cores and peripheral organometallic groups. In this context labile "primary complexes" that still contain the intact inorganic cage are of particular interest. Structural and other aspects of the degradation and rearrangement of these clusters are discussed in terms of the main group and transition elements employed and the reaction conditions.

Keywords: main group elements · ligands · solid–state chemistry · transition metals

1. Introduction

Thiosalts of arsenic and antimony should be familiar to chemists from their earlier experiences in classical analytical chemistry; however, very few students realize at this stage the manifold varieties of these compounds in Nature. The building blocks are flat trigonal pyramids that condense under the influence of metal ions to give chain, band, and ring structures; thus, there is a certain resemblance to silicate chemistry. In this way the family of sulfosalts,[1] which are a structurally and optically fascinating class of compounds, has been established. Another natural product is the red realgar As_4S_4,[2] which is built up in a very different manner as a molecular cage, and which is frequently employed as ligand supplier for transition metal complexes. Synthetic solid-state compounds containing Group 15 thioanions are realized in the laboratory by means of hydro- and solventothermal procedures. This aspect is summarised in a topical review.[3]

[*] Dr. J. Wachter
Institut für Anorganische Chemie der Universität
Universitätsstrasse 31, D-93040 Regensburg (Germany)
Fax: (+49) 941-943-4439
E-mail: Joachim.Wachter@chemie.uni-regensburg.de

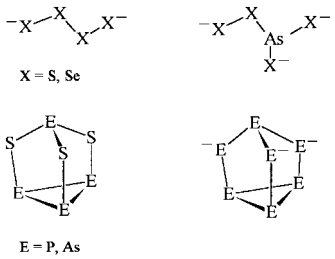
Molecular sections of solid-state structures produced in this way occur in mixed polyatomic anions, the nature of which ranges from centered anions (e. g. phosphate type) to main group element clusters, and in transition metal complexes. Syntheses and structural chemistry of mixed anions with respect to the Zintl ion concept have alreay been thoroughly summarized.[4] In addition to the stabilization of discrete anions by suitable cations, the synthesis of "transition metal carbonyl main group hybrid clusters"[5] is becoming increasingly important. Hereby covalent bonds between main group and transition elements are formed, which are similar to those typically found for complexes with unsubstituted ("naked") homoatomic ligands of Groups 15 and 16.

The quest for novel structures with pnicogen ligands "E" has been influenced in a decisive manner by the isolobal relationship P(As) $\longrightarrow$ CH.[6] In contrast, for the heavier homologues antimony and bismuth far fewer results are available.[7] The complex chemistry of chalcogen ligands "X" has been reviewed under different aspects: They tend, particularly in the case of the heavier elements, to oligomerize,[8] which gives rise to different chain lengths and manifold coordination properties and results in a wide structure chemistry.[9] The number of known complexes with homo-

 © WILEY-VCH Verlag GmbH, D-69451 Weinheim, 1998 1433-7851/98/3706-0751 $ 17.50+.50/0

atomic ligands is considerably greater than that of transition metal complexes with mixed ligands.

According to a proposal by Kanatzidis et al.,[10] the advantage of introducing trivalent E^- building blocks into polychalcogenide skeletons lies primarily in the additional branching possibilities offered (Scheme 1 top). On the other



Scheme 1. Substitution of an atom X by E^- in polychalcogenides provides a branching site (top), similar substitution in neutral sulfur-containing cage molecules gives Zintl ions (bottom).

hand the substitution of sulfur by E^- in neutral, mixed cage molecules, such as E_4S_3, provides a relationship to Zintl ions and their complexes (Scheme 1 bottom).[11] Extension of these formalisms gives rise to the question of how combinations from mE and nX ligands to mixed ligands E_mX_n may express the different coordinative and electronic properties of both element groups under the influence of reactive metal fragments.

The primary goals of this article are to summarize the rapidly growing body of knowledge on transition metal complexes with mixed ligands of the heavier elements—excluding NO and NS ligands[12,13]—and to find trends within a group of the periodic table. In addition to carbonyl complex fragments,[4,5] the role of cyclopentadienyl[*] and of other complexes in the stabilization of molecular aggregates will be examined. Examples from thioarsenate(III) chemistry will show that there is a steady transition from low molecular weight main group clusters to covalent solid-state structures, with and without incorporation of transition metals. Building blocks that are common or similar to polymeric solids and molecular compounds should stimulate the interest of the complex chemist in this ligand pool, which is at the interface of solid-state and molecular chemistry.

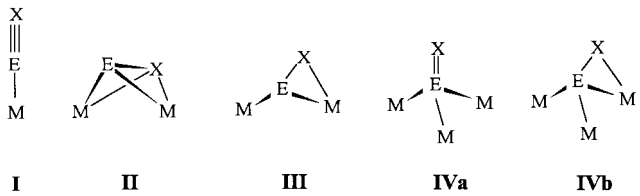
[*] Abbreviations used throughout the text: Cp = η^5-cyclopentadienyl, $Cp^{(*)}$ = any substituted Cp ligand, Cp* = C_5Me_5 and/or EtC_5Me_4, en = ethylendiamine, triphos = 1,1,1-tris(diphenylphosphinomethyl)ethane, np_3 = tris(2-diphenylphosphinoethyl)amine, PPN = bis(triphenylphosphane)iminium.

2. Synthetic and Structure Chemistry of Di- to Tetratomic Ligands

The simplest mixed ligands may be expressed by the combinations EX, E_2X, EX_2, E_2X_2, and EX_3. The coordination behavior of these ligands is correspondingly rich, and, apart from PS[14] and some EX_3 species (see Section 2.4), they do not exist in the free state nor in solution. The transition from discrete ions to extended structures is such a fluid one especially in the thioarsenite system that it seems appropriate to also treat its condensation reactions. Preferred methods for the syntheses of transition metal complexes are the fragmentation of E_4X_n cages (n = 3,4) and the chalcogenation of pnicogen ligands. In contrast extraction of binary or ternary chalcogenide/pnictide phases in polar solvents, for example ethylenediamine and in the presence of large organic cations, and reactions in superheated or supercritical aqueous and nonaqueous solvents[3] give, depending on the conditions, discrete ions or more or less extended structures.

2.1. EX Ligands

Diatomic ligands exist in the coordination forms **I**–**IV** (Scheme 2); it is noticable that with the exception of one complex of type **II** (in which X = Se) sulfur has been



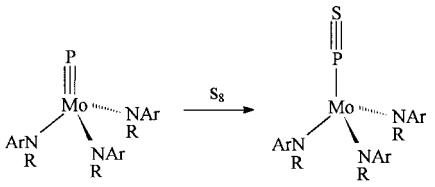
Scheme 2. Different coordination types for diatomic EX ligands.

employed as chalcogen X. In contrast to ligands containing one of the lighter elements N and O (one should note the rich complex chemistry of NO and NS,[12] but also the exotic PO[15]), there is a preferred tendency of the heavier elements for bridge formation. Semiempirical calculations[16] for the free molecules PO, PS, AsS, and AsSe indicate the following order for donor ability of the unpaired π electron located in the π* HOMO: PO > PS > AsS > AsSe. The energies of the two filled π bonding orbitals decrease in the reverse order AsSe > AsS > PS > PO; thus, better π-ligand-to-metal interactions are expected for AsSe, AsS, and PS than for PO.



Joachim Wachter was born in 1945. After studying chemistry at the Universität München he received his Ph.D. in 1976 under the supervision of Prof. Dr. H. Brunner at the Universität Regensburg. In 1978/79 he spent a year as a postdoctoral researcher with Prof. J. G. Riess in Nice, in 1987 and 1992 he was invited to the University of Dijon as professeur associé. Since 1977 he has headed a research group at the Universität Regensburg. His main scientific interests are the organometallic chemistry of the chalcogens and the mixed ligands of Group 15/16 elements, and the cluster chemistry of highly reactive tellurium.

The only example of coordination type **I** known to date is complex **1**. The existence of the terminal PS ligand was deduced from spectroscopic data and from the synthetic method [Eq. (1)]. Structural parameters are not yet available.[17]



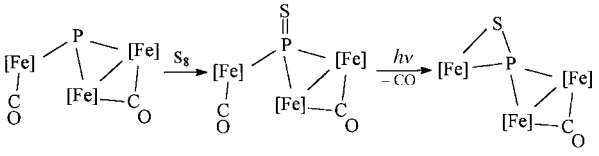
(1)

1

R = *t*Bu, Ar = 3,5-$Me_2C_6H_3$

The symmetrical bridge of the coordination type **II** belongs to the large family of diatomic η^2 ligands, which are formed from homonuclear E_2 (E = P, As)[6] and X_2 (X = S, Se)[9,18] ligands. Homonuclear examples for the η^1:η^2 coordination type **III** are thus far only found in chalcogenide complexes (X = S,[19] Se[20]), a heteronuclear example will be given in Section 2.1.1.

The coordination type **IVa** (X = S, E = P) is accessible by oxidative addition of sulfur to μ_3-P ligands (**2**, **4**).[21] This method should be more widely applicable because of the frequency of μ_3-E ligands (see also Eq. (6)). The μ_3-PS ligand (d_{P-S} = 2.008(5) Å) in **2** is capable of eliminating CO under formation of **3,** in which a five-electron donor of coordination type **IVb** is present [Eq. (2)]; however, structural data are not

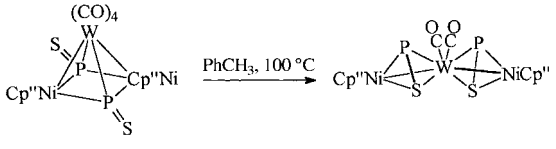


(2)

2 **3**

[Fe] = $C_5H_5Fe(CO)$

yet available.[21a] Whereas in the latter ligand all valence electrons of phosphorus are used for coordination, the bis(dimetallatetrahedrane) **5** contains two η^2-PS ligands. These are formed from the μ_3-PS bridges of cluster **4** by a rearrangement of the skeleton and a redistribution of the electrons in the ligand [Eq. (3)].[21c]



(3)

4 **5**

Cp'' = $C_5H_iPr_4$

A comparison of the P–S distances in **2, 4,** and **5** allows a cautious assignment of single- and double-bond regions (Table 1). The value found for the PS radical[14] is even shorter than these values, and in this regard it is of interest that the unpaired π* electron is preferentially located at phosphorus.[16]

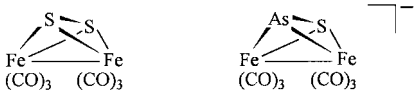
Table 1. Classification of diatomic EX ligands in transition metal complexes.

Ligand	Complex	d_{E-X} [Å]	n[a]	BO[b]	Ref.
PS[c]	–	1.8977	–	2.5	[14]
μ_3-PS	**2**	2.008(5)	3	2	[21a]
μ_3-PS	**4**	1.952(2)	3	2	[21c]
μ,η^2-PS	**5**	2.092(2)	5	1	[21c]
μ,η^2-AsS	**7**	2.227(2)	5	1	[23]
μ,η^2-AsS	**8**(S)	2.165(2)	5	1	[24]
μ,η^2-AsSe	**8**(Se)	2.281(3)	5	1	[25]
μ,η^1:η^2-AsS	**14**	2.170(4)	3	1	[31]

[a] Number of valence electrons. [b] Formal bond order. [c] Obtained from a $PSCl_3$/He discharge.

2.1.1. η^2-Bridging Ligands (Type II)

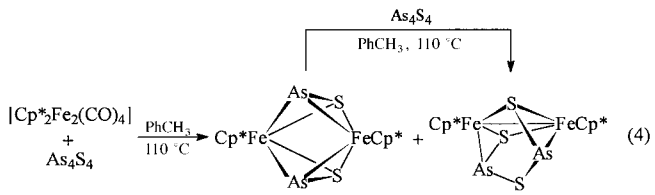
The η^2-EX ligands have one less valence electron than the X_2 ligands; thus, in isostructural complexes with the same central metal an additional negative charge is required. This formalism can be illustrated with the pair of complexes $[Fe_2(S_2)(CO)_6]$ (**6**)[22] and $[Fe_2(AsS)(CO)_6]^-$ (**7**).[23] Complex **7**



6 **7**

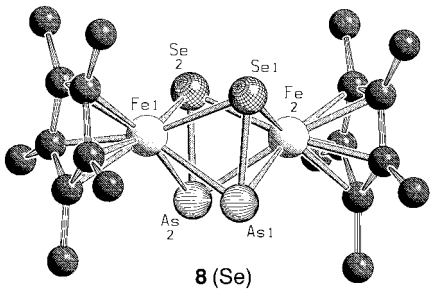
is formed by reductive coupling of $S_2O_4^{2-}$ and AsO_2^{2-} by $[Fe_3(CO)_{12}]$ under hydrothermal conditions, and serves as one of the first examples for the application of hydrothermal methods in organometallic chemistry.

Two η^2-EX ligands form the core of the sandwichlike Cp*Fe complex **8**(S), which is obtained together with the topologically completely different complex **9** in the reaction of $[Cp^*_2Fe_2(CO)_4]$ with As_4S_4 in boiling toluene [Eq. (4)].[24] In contrast, the analogous reaction with As_4Se_4 gives exclusively $[Cp^*_2Fe_2As_2Se_2]$ (**8**(Se)) (Figure 1).[25]



(4)

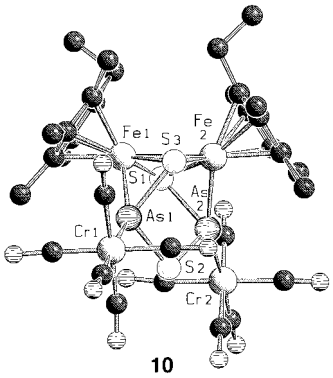
8(S) **9**



8 (Se)

Figure 1. Molecular structure of **8**(Se) in the crystal.

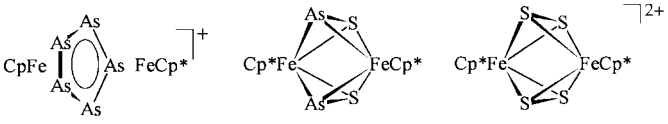
The structures of complexes **8** are characterized by two coplanar η^2-AsX bridges, whereas that of **9** contains a "basket" with an alternating AsS chain. Complex **8**(S) can be converted into **9** by reaction with mild sulfur donors [Eq. (4)]; the cage structure of **9** has been confirmed through the determination of the structure of the $Cr(CO)_5$ bisadduct **10** (Figure 2).[24] Although the incoming sulfur atom is incorporated between the two As atoms, a planar As_2S_3 ring is not formed (similar to the As_5 ring in **11**, see Scheme 3), but instead a five-membered twisted As–S chain. The $Cr(CO)_5$ groups in **10** are coordinated to both As atoms under considerable distortion of the tetrahedral geometry (angle Fe-As-Cr 145.8°). Further consequences of their steric interactions with the C_5Me_4Et ligands are the hindrance of free rotation of the cyclopentadienyl rings and the reformation of **9** by dissociation of the $Cr(CO)_5$ groups upon warming in solution.[24]



10

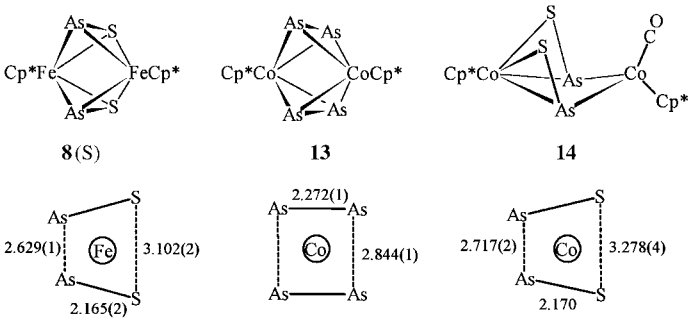
Figure 2. Molecular structure of $[(C_5Me_4Et)_2Fe_2As_2S_3\{Cr(CO)_5\}_2]$ (**10**) in the crystal.

Similar to the dication $[Cp^*_2Fe_2S_4]^{2+}$ (**12**),[26] complexes **8** possess 36 valence electrons (VE). From a structural point of view one may consider the "mixed" complex **8**(S) as a link between the "pure" sandwich complexes $[CpCp^*Fe_2As_5]^+$ (**11**)[27] (30 VE) and **12** (Scheme 3). The exclusive *cis* arrangement of the trapezoid-arranged AsS ligands gives rise to As–As distances in the range for single bonds (Scheme 4). The values of 2.629(1) Å (**8**(S)) and 2.587(3) Å (**8**(Se)), respectively, are at the upper limit of values determined to date for As–As bonds (e.g. 2.593(6) Å in β-As_4S_4[28] and 2.602(3) Å in diarsadisilabicyclo[1.1.0]butane[29]). In comparison the As_4 ligand plane in $[Cp^*_2Co_2As_4]$ (**13**) forms a rectangular middle deck in which the As_2 bridges are significantly separated from each other.[30]



11 **8**(S) **12**

Scheme 3. Examples for cyclopentadienyliron sandwich complexes containing homo- and heteroatomic ligands.



8(S) **13** **14**

Scheme 4. Comparison of the structures of complexes **8**(S), **13**, and **14** made by slicing through the ligand plane.

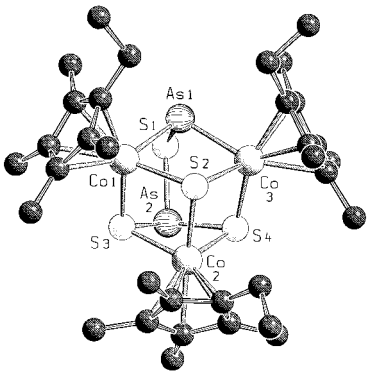
2.1.2. The η^1:η^2 Coordination Type III

Only one example is known for this coordination type thus far: In $[Cp^*_2Co_2(CO)(AsS)_2]$ (**14**) two η^1:η^2-AsS ligands form a trapezoid plane that is tilted towards one metal center.[31] The As–As distance is slightly longer than those in complexes **8** (see Scheme 4); in contrast, the As–S distances remain practically unchanged although each ligand now acts as a three-electron donor. A significantly longer As–S distance has been found in **7** (Table 1), which may be indicative of the π-acceptor properties of the EX ligands by increased back-donation through negative charge. Generally, all As–S distances discussed thus far are shorter than those reported for the trigonal AsS_3 pyramid (see Section 2.4.1).

Complex **14** is formed from $[Cp^*_2Co_2(CO)_2]$ and As_4S_4 as the main product in a relatively narrow temperature range around 80 °C. At higher temperatures formation of complexes **15**–**17** is favored, in which the As/S ratios deviate considerably from that in the starting material [Eq. (5)].[31] The structure of **15**[32] is analogous to that of **9**, apart from the lack of the metal–metal bond. Complex **16** also possesses an As_2S_3 core , but here a trigonal-pyramidal AsS_3 center acts as a triply bridging ligand; one arm of this is lengthened by one As (Figure 3). The structure of the arsenic-rich cluster **17** has not yet been determined.

$$[Cp^*_2Co_2(CO)_2] + As_4S_4 \xrightarrow{PhCH_3} |Cp^*_2Co_2(CO)As_2S_2| + |Cp^*_2Co_2As_2S_3| + |Cp^*_3Co_3As_2S_4| + |Cp^*_3Co_3As_4S_2| \quad (5)$$

14 **15** **16** **17**

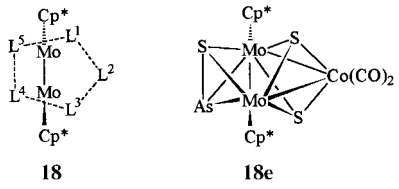


16

Figure 3. Molecular structure of $[(C_5Me_4Et)_3Co_3As_2S_4]$ (**16**) in the crystal.

2.1.3. Organometallic Sandwich Complexes

Sandwich complexes containing cyclopentadienyl Group 6 metal fragments and in particular their bonding have already been reviewed in detail, and thus they are mentioned only briefly here.[6]. In the combination with E/S ligands dimers of type **18** (M = Mo) are formed, in which parallel five-membered rings are the dominating structural element. Starting



18 **18e**

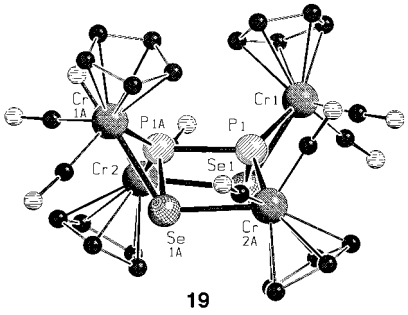
	L^1	L^2	L^3	L^4	L^5
a	P	P	P	P	S
b	As	As	As	As	S
c	P	S	P	S	S
d	As	S	As	S	S

from *cyclo*-E_5^-[27] the substitution of E by S leads to increasing distortion within the central five-membered ring. As a consequence first separation into a pair of ES/E_3 and then S_2/E_2S bridging ligands is observed, accompanied by a continuous decrease of π bonding[6] from **18a, b**[33,34] ("$(P/As)_4S$") to **18c, d**[34] ("$(P/As)_2S_3$" rings).

Formation of the 48-electron cluster **18e** from **18d** and $[Co_2(CO)_8]$ demonstrates that a main group ligand may be replaced by a complex fragment. All metal atoms achieve a closed valence shell in that the $Co(CO)_2$ fragment and the AsS ligand serve as 13-electron and 5-electron building blocks, respectively. The As–S distance in **18e,** the first example for an AsS ligand, is 2.237(3) Å.[35] As may also be replaced by P.

2.2. E_2X_2 Ligands

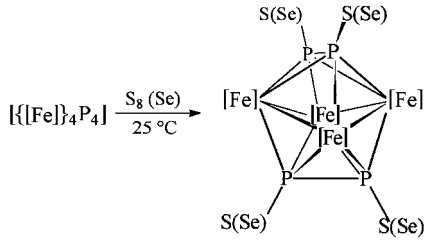
Whereas **8**(S) and **14** may be regarded at best as borderline cases for As_2S_2 ligands, a "real" P_2Se_2 ligand forms the backbone in $[\{CpCr(CO)_2\}_4P_2Se_2]$ (**19**), one of the many fragmentation products of the P_4Se_3 cage in its reactions with $[CpCr(CO)_3]_2$ (see Section 4.1.1). The approximate *Z*-like conformation in **19** seems to be forced by the four $CpCr(CO)_2$ fragments (Figure 4).[36] The P–P and P–Se distances



19

Figure 4. Molecular structure of $[\{CpCr(CO)_2\}_4P_2Se_2]$ (**19**) in the crystal.[36]

(2.237(5) and 2.250(3) Å, respectively) are both in the ranges for single bonds. Nearly planar P_2X_2 ligands (X = S, Se) form the characteristic units in the clusters **20**.[37] They have been synthesized by chalcogen addition to the E_2 ligands in $[Cp_4Fe_4P_4]$ [Eq. (6)]; the overall geometry of the clusters



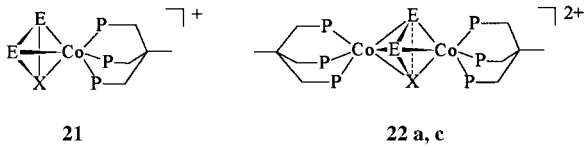
(6)

[Fe] = C_5H_5Fe **20**

does not alter. The P–P distances (av 2.38 Å) are not affected by the oxidation, whereas the P–S (av 1.965(8) Å) and P–Se distances (av 2.10 Å) are typical for double bonds (Table 1).

2.3. E_mX_{3-m} Ligands ($m = 1,2$; E = P, As; X = S, Se, Te)

The pseudo-tetrahedral clusters $[(triphos)Co(\eta^3\text{-}E_2X)]^+$ (**21**) contain the ligand combinations **a–e,** which are the preferred structural elements among triatomic E/X ligands.



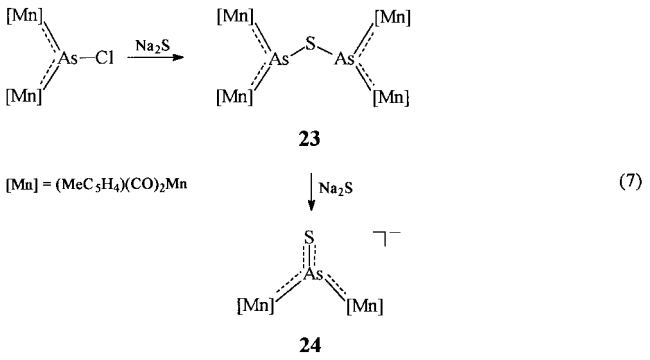
21 **22 a, c**

E	P	P	As	As	As
X	S	Se	S	Se	Te
	a	**b**	**c**	**d**	**e**

This class of compounds combines Co^{II} salts and triphos with the corresponding four-electron ligands, which arise from the fragmentation of E_4X_3 cage molecules (see Scheme 7) or As_2X_3 layers (X = Se, Te). Syntheses, structures, and reactions of these complexes have already been reviewed.[38] The electronic situation of the employed complex fragment determines whether heteroatomic (as in **21**) or homoatomic three-membered cycles (as in $[(triphos)Ni(P_3)]^+$[39] and $[Cp^*(CO)_2Mo(E_3)]$ (E = P, As)[34]) are extracted from the mixed E_4X_3 cage units.

Compounds **21a, c** react with $(triphos)Co^{II}$ to form the salts **22a, c**. These compounds belong to the class of 32-electron triple deckers. In contrast to their η^3-P_3 analogues[40] the ligand plane in these complexes is strongly distorted as shown by two rather different As–S distances (2.336(5) and 3.099(6) Å).[41]

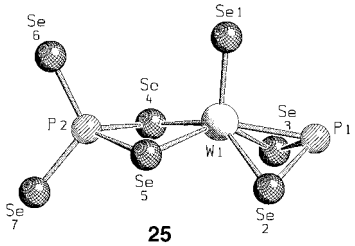
Complex **23** may be described as a bis(diarsinidene) compound in which sulfur functions as a bridge [Eq. (7)].[42] The trigonal-planar As atoms of the As_2S ligand are part of



(7)

the original 4π-electron system together with all the Mn centers. Complex **23** reacts with excess sulfide under cleavage of the S bridge to give **24**, the four-center 6π-electron system of which exhibits a relatively short (Table 1) As–S distance of 2.123(3) Å.[42]

The only known example for an EX_2 ligand is in $[W(=Se)PSe_4(PSe_2)]^{2-}$ (**25**) (Figure 5), which crystallizes as a PPh_4 salt.[43] The structural parameters are in agreement with a side-on coordinated heteroallyl ligand of the formal charge −1, making it isoelectronic with NO_2^-. The selenophosphate ligand will be commented on in more detail in Section 3.1.



25

Figure 5. Structure of the dianion of $(PPh_4)_2$ **25** in the crystal.[43]

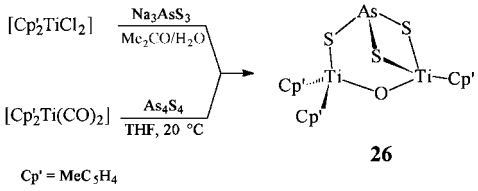
2.4. How Useful Are EX_3 Building Blocks as Ligands?

EX_3 building blocks are the only species among the di- to tetratomic element combinations that may be stabilized as ions in aqueous and nonaqueous solutions, though with some restrictions. In Nature they play an important role as the structure-determining component of the extensive mineral class of sulfosalts:[1] Trigonal ψ-EX_3 pyramids (E = As, Sb, Bi; X = S, Se, Te) with a stereochemically active lone pair of electrons (ψ) either form isolated EX_3 units or are "condensed" through common X bridges to give polymeric units of chains, bands, and rings.[44] As highly charged ligands they form mainly covalent solids with metals like Tl, Pb, Cu, Ag, Zn, Hg, Mn, Co, and Ni. For the complex and solid-state chemist, aspects of mineral genesis, that is the mobilization of thioarsenite, thioantimonite, and thiobismutite ions in the melt or in hydrothermal solutions as well as their conversion into the crystal lattice upon cooling[45] may be of interest in terms of the development of model systems based on soluble compounds as a means to understanding these processes. In the following it will be shown that through these efforts the number of potential ligands is growing rapidly.

2.4.1. Chemistry of Discrete Thioarsenate(III)

The simplest discrete thioanion of trivalent arsenic is obtained as Na_3AsS_3 by melting together Na_2S and As_2S_3.[46] Modern variants prefer the reaction of As_2S_3 with M_2S (M = K, Rb, Cs) in liquid NH_3.[47] Reaction of As_2S_3 with Na_2S in aqueous medium results in an unstable yellow solution, from which $(PPN)_3[AsS_3]$ may be isolated upon addition of (PPN)Cl.[48] Warming of such solutions leads under loss of sulfide and condensation to one-dimensional $NaAsS_2$ chains containing corner-linked AsS_3 pyramids (see Scheme 5).[49] In this context the question arises if and under what conditions the single steps of the condensations can be detected.

Initially, the first organometallic complex comprising an AsS_3 unit is presented: Complex **26** is formed in a metathesis reaction from $(PPN)_3[AsS_3]$ and $[(MeC_5H_4)_2TiCl_2]$ [Eq. (8)].[48] The only "flaw" is a μ-oxo ligand, which probably



26

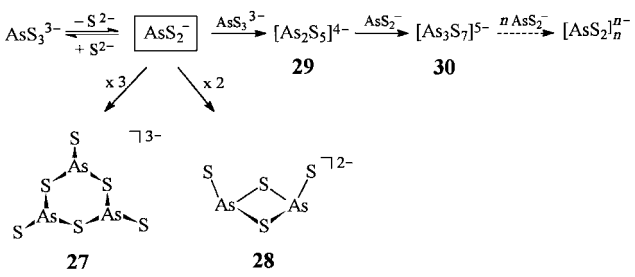
Cp' = MeC5H4

(8)

serves to stabilize the molecule. The same product is also obtained from the mild degradation of realgar As_4S_4 [Eq. (8)],[48] but it should be noted here that the starting material and the product possess different As–S connectivities (see Section 4.3). The electronically unequal Ti centers in **26** make the As–S distances in the AsS_3 bridge significantly different ($\Delta d = 0.07$ Å). In contrast to this the trigonal AsS_3 pyramid generally has equidistant As–S distances and equivalent S-As-S angles. An analysis of structural parameters of synthetic and natural sulfosalts reveals a range of 2.26–2.36 Å for d(As–S) and $98.0 \pm 2^\circ$ for the angles at As.[46, 50]

2.4.2. Polymetathioarsenite Compounds

AsS_3^{3-} solutions in liquid ammonia readily dissociate to give S^{2-} and metathioarsenite AsS_2^-.[51] Already in 1960 the investigation of the system AsO_2^-/HS^- under alkaline conditions led to the proposal of a trimerization of AsS_2^- to *cyclo*-$As_3S_6^{3-}$ (**27**) (Scheme 5).[52] Anion **27** is isolable in the form of $[As_3S_6]_2(enH_2)_3$,[53] by dissolving As_2S_3 in ethylendiamine;



Scheme 5. Partial steps of the metathioarsenite oligomerization realized under laboratory conditions.

the latter also provides the necessary protons for cation formation. In the chairlike **27** the exocyclic As–S bonds are about 0.15 Å shorter than the other As–S bonds.

The formally simplest oligomerization of AsS_2^- would lead to the dimer **28**. However, this ion has been synthesized only indirectly from As_4S_4 and potassium in the presence of 4,7,13,16,21,24-hexaoxa-1,10-diazabicyclo[8.8.8]hexacosane ([2.2.2]cryptand). Noteworthy in the structure of **28**[54] are the two edge-sharing AsS_3 pyramids; this building principle is not often observed in As/S sulfosalt chemistry.

The coordination potential of the anionic ligands is used in hydrothermal syntheses. In general a metal salt and a thioarsenate(III) substrate are heated under conditions given in Table 2.[3] The degree of condensation as well as the conformation of the chains are determined by the metal cations. Eventual excess of negative charge is compensated by large organic cations (e.g. Ph_4P^+, Me_4N^+), which can thus function as spacers between the anionic chains.

The simplest species in the metathioarsenite oligomerization (Scheme 5) is $[As_2S_5]^{4-}$ (**29**), which is realized in the reduction of MoO_3 by K_3AsS_3 (Table 2) as infinite sinusoidal chains in $[Mo_2O_2As_2S_7]_n^{2n-}$ (**31**) (Scheme 6).[55] In this compound **29** acts as a double chelate bridging two molecular $[Mo_2O_2S_2]^{2+}$ units. The thiophilic character of the latter is well documented in many coordination compounds with sulfides and polysulfides.[56] If, however, the original building blocks are connected in an all-*cis* configuration formation of soluble cyclic compounds should be possible, such as $[Mo_2O_2As_2S_7]_2^{4-}$ (**32**). The synthesis of this compound was postulated 13 years ago by Rauchfuss by an alternative route (see Section 3.4).[48]

The combination $BiCl_3/Rb_3AsS_3$ (Table 2) yields a two-dimensional network composed of the cyclic anion **27** and octahedrally coordinated Bi^{3+} ions. The layers are separated from each other by Me_4N^+ and Rb^+ ions.[47] The following member in the series is $[As_3S_7]^{5-}$ (**30**) (see Scheme 5), which may be realized by reaction of $InCl_3$ with K_3AsS_3 (Table 2). The insertion of an additional AsS_2 unit provides a further coordination site; thus, In^{3+} achieves the coordination number 5 (Figure 6).[47] In the dianion $[Hg_2As_4S_9]^{2-}$ (**33**) trigonal-planar Hg^{II} forms with the As_4S_9 chain eight-membered rings, which function as subunits of a one-dimensional structure.[57] At the end of the reaction sequence polymeric chains, such as

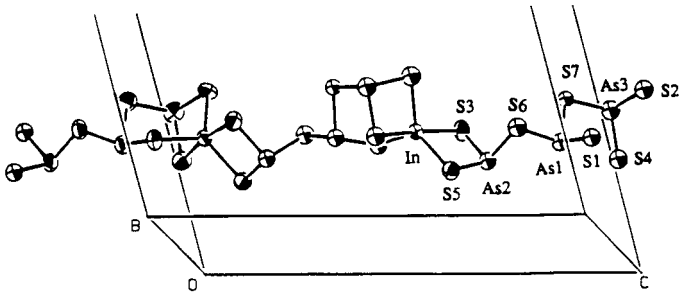
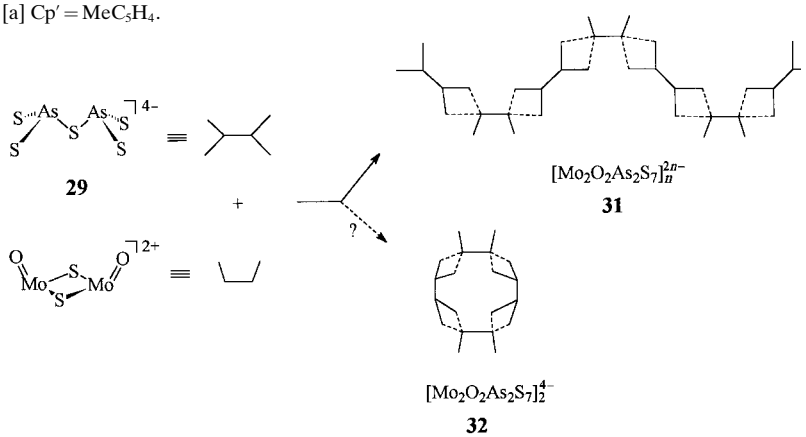


Figure 6. View of an $InAs_3S_7$ chain in the lattice of $(Ph_4P)_2[InAs_3S_7]$.[47]

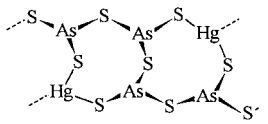
Table 2. Routes to thioarsenate(III) and selected polymetathioarsenite compounds.

Compound	As/S structural element	Starting materials	Reaction conditions	Ref.
M_3AsS_3	ψ-pyramid	As_2S_3, S_8, M (M = K, Rb, Cs)	NH_3 (liq)	[47]
Na_3AsS_3	ψ-pyramid	As_2S_3, Na_2S	melt	[46]
$(PPN)_3[AsS_3]$	ψ-pyramid	As_2S_3, Na_2S, (PPN)Cl	H_2O/EtOH	[48]
$[Cp'_3Ti_2(AsS_3)O]$ **26**[a]	ψ-pyramid	$[Cp'_2TiCl_2]$, Na_3AsS_3	acetone/H_2O	[48]
$[K(crypt)]_2[As_2S_4]$	**28**	As_4S_4, K, [2.2.2]cryptand	NH_3 (liq); CH_3CN	[54]
$(enH_2)_3[As_3S_6]_2$	**27**	As_2S_3, en	en, 20 °C	[53]
$(Me_4N)_2Rb[BiAs_6S_{12}]$	**27**	$BiCl_3$, Rb_3AsS_3, Me_4NCl	H_2O, 120 °C	[47]
$(Me_4N)_2[Mo_2O_2As_2S_7]$	**29**	MoO_3, K_3AsS_3, Me_4NCl	H_2O, 110 °C	[55]
$(Ph_4P)_2[InAs_3S_7]$	**30**	$InCl_3$, K_3AsS_3, Ph_4PBr	H_2O, 120 °C	[47]
$(Ph_4P)_2[Hg_2As_4S_9]$	**33**	$HgCl_2$, K_3AsS_3, Ph_4PBr	H_2O, 130 °C	[57]
$NaAsS_2$	$[AsS_2]_\infty$	As_2S_3, Na_2S	H_2O, 80 °C	[49]
$TlAsS_2$	$[AsS_2]_\infty$	As_2S_3, Tl_2S	H_2O, 225–340 °C	[58]

[a] Cp′ = MeC_5H_4.



Scheme 6. Schematic representation of the synthesis of one-dimensional **31**[55] and cyclic **32**[48] from $[As_2S_5]^{4-}$ (**29**) and $[Mo_2O_2S_2]^{2+}$.



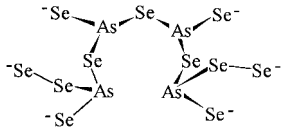
33

in $NaAsS_2$[49b, c] or $TlAsS_2$[58] are obtained. Common to all these compounds are edge-linked AsS_3 pyramids, the formation of which may be explained by "condensation" of AsS_3^{3-} under loss of sulfide.

Although the anions shown in Scheme 5 are preferentially incorporated into covalent lattices, **27** and **28** may also be obtained in discrete form. The single steps represented by the anionic ligands **27**–**30** may be considered as a model for the formation of sulfosalt minerals. Indeed *cyclo*-$[As_3S_6]^{3-}$ (**27**) exists as the essential unit in trechmannite, $AgAsS_2$,[59] and in axial conformation of the exocyclic sulfur atoms in smithite, $AgAsS_2$.[60] In contrast baumhauerite, $Pb_3As_4S_9$, is composed of As_3S_7 (**30**), As_4S_9, and As_5S_{11} chain fragments.[61] Examples for naturally occurring infinite chains are $TlAsS_2$ (lorandite),[62] which is also the first sulfosalt synthesized in the laboratory[58] (Table 2), and $PbAs_2S_4$[63] (sartorite).

2.4.3. Sulfosalt Compounds of the Heavier Homologues Sb, Bi and Se, Te

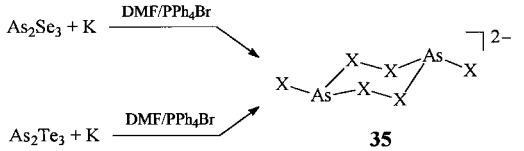
Compounds of the heavier homologues Sb, Bi, and Se, Te exhibit an increasing tendency for the formation of complex anions with a cage structure.[4, 64] Some of these anions have already been tested successfully as ligands in transition metal complexes (see Section 3). The following examples comprising structural elements analogous to the sulfosalts in Scheme 5 warrant mention in this context: the Se analogue of **27**[65] and the Sb/Se analogue of **28**[54] as discrete anions as well as the Se analogue of **29**[55] and the Sb analogue of **30**[66] in low dimensional structures ($[Mo_2O_2(\mu\text{-}Se_2)As_2Se_5]^{2-}$ and $[Ag_3Sb_3S_7]^{2-}$, respectively). However, analogies between the chemistry of thio- and selenoarsenates cannot always be drawn. For instance, the system $HgCl_2/K_2AsSe_3/Me_4NCl$ forms the novel structural unit **34** under conditions given in Table 2, and not the expected anion $[As_4Se_9]^{6-}$ (**33**):[67] Self-condensation of $AsSe_3^{3-}$[10] leads in this case to an $AsSe_4$ subspecies containing Se–Se bonds (see Section 3.2).



34

Like the As sulfosalts, ternary phases of the composition $MAsSe_2$ (M = Na, K, Rb, Cs) also consist of infinite chains,[68] as does $(NEt_4)[BiSe_2]$, which is very sensitive to hydrolysis.[69] The first selenobismutate is soluble in ethylendiamine and CH_3CN, probably under chain fragmentation. In contrast, the anionic $SbSe_2$ chains in $KSbSe_2$ consist of edge-sharing ψ-$SbSe_4$ tetrahedra.[70]

It is expected that anionic clusters, extracted from binary phases in strongly basic solvents and in the presence of suitable cations,[4] may be good candidates for ligands. How such compounds might appear is demonstrated by the cyclic dianions **35**, which have already gained some importance as ligand precursors (see Section 3.2). Formally, they may be formed by oxidative cyclization according to $2\,EX_3^{3-} \rightarrow E_2X_6^{2-} + 4\,e^-$, but actually the best synthesis is reduction of As_2Se_3[71] or As_2Te_3 [72,73] with potassium in DMF [Eq. (9)]. The system is very sensitive towards solvent effects, as has been reported elsewhere in detail.[74]



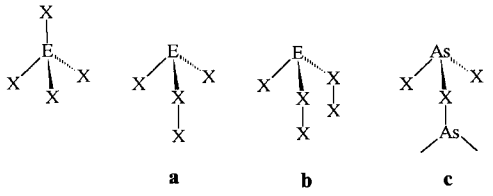
35
(X = Se, Te)

(9)

3. Mixed Zintl Anions as Ligands

In the synthesis of the molecular sulfosalt compounds **27** and **28** it has already been pointed out that basic solvents are able to convert binary E/X phases by electron transfer reactions under mild conditions into complex Zintl anions. This action is enhanced by working in polar solvents (e.g. DMF, en) and in the presence of alkali metals. The stabilization of the cluster anions is achieved by using large counterions, such as Me_4N^+ and Ph_4P^+, or by the addition of cryptands.[4,5]

For the application as ligands in transition metal complexes the mixed main group clusters prepared in this way must be selectively accessible and soluble in organic solvents. These conditions are best fulfilled by the cyclic anions $[As_2X_6]^{2-}$ (**35**) and $[P_2Se_8]^{2-}$ (**36**) (see Section 3.1), but it must be noted that these have never been incorporated completely into transition metal complexes; instead they are fragmented into penta- or hexaatomic E/X ligands. Pentaatomic E/X ligands may be divided into the subgroups **V** (central atom E with coordination number 4) and **VIa** (a trigonal-pyramidal structure type closely related to the sulfosalts, coordination number 3). Formally both structure types are related by the redox



a **b** **c**

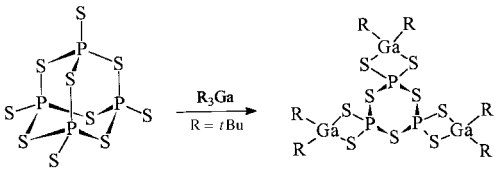
V **VI**

equation $\mathbf{V}^{3-} + 2\,e^- \rightleftharpoons \mathbf{VIa}^{3-}$. The examples realized thus far demonstrate that the equilibrium in the presence of transition metal complexes is on the right-hand side for arsenic chalcogenides, which favors the formation of X–X bonds. Heavier chalcogenides may form another dichalcogenido arm (**VIb**). If at the end of the side chain of **VIa** X is replaced by As, **VIc** is obtained; this structure type is realized for X = S in the μ_3-As_2S_3 ligand of **16**. Similar to tetrachalcogenido ligands[9c, 75] the dichalcothioarsenites **VIa**, **b** preferentally form five-membered chelate rings with metal ions of mostly covalent nature.

3.1. Thio- and Selenophosphate Complexes

In contrast to the abundance of ternary and quaternary solid-state compounds with anionic P/S and P/Se ligands,[76] molecular complexes with P/X ligands are still relatively rare. This is evidently related to the difficulties arising from the transfer of discrete PX_4^{3-} ions into compounds that are soluble in organic solvents, although they may be isolated from aqueous solutions as hydrates.[4]

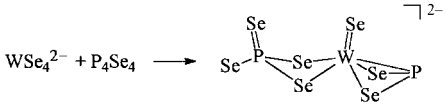
The first molecular example of a cyclic phosphorus(v) sulfide is **37,** which is obtained in the reaction of P_4S_{10} with t-Bu_3Ga [Eq. (10)] upon formally removing a P=S group from the top of the adamantane skeleton. The core of the molecule is a twisted P_3S_3 ring in which the integrated thiophosphate groups now function as chelate agents.[77]



(10)

37

The only known molecular example for a complex with the PSe_4 unit is $[W(=Se)PSe_4(PSe_2)]^{2-}$ (**25**).[43] This compound is obtained from vitreous P_4Se_4 and $(Ph_4P)_2[WSe_4]$ [Eq. (11)]. It

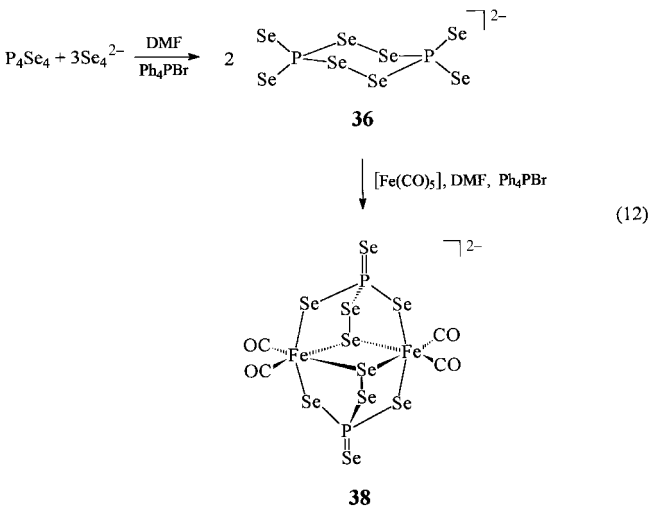


(11)

25

contains along with the side-on coordinated PSe_2 ligand a bidentate PSe_4 group, which most likely arises from oxidative Se addition at trivalent phosphorus (see Figure 5).

The usefulness of selenophosphates as ligands is documented by the cyclic phosphorus selenide **36,** which reacts with $[Fe(CO)_5]$ to give the dinuclear Fe^{II} complex **38** [Eq. (12)].[78]



(12)

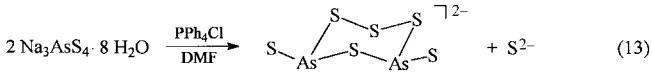
36

38

The original geometry around the P atom is maintained, but there is an increased amount of Se found in the two perselenophosphate ligands, which may indicate an intermediate existence of free selenium.

3.2. Dichalcoarsenate(III) Complexes

The lability of pentavalent thioarsenate is evident from the problems that arise when trying to convert Na_3AsS_4 hydrate into a salt soluble in organic solvents [Eq. (13)]: Upon loss of sulfide the six-membered ring **39** is formed, which is isomeric with **35** (X = S).[79] [Eq. (13)]. It contains two sulfur segments of different length and two As^{III} centers. In contrast to this

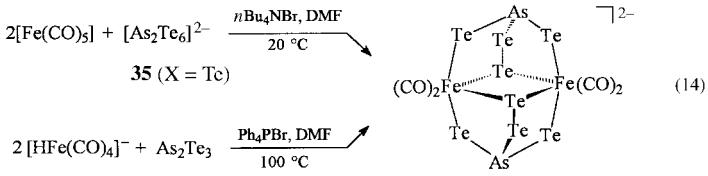


(13)

39

system, solutions of SbS_4^{3-} in ethylenediamine seem to be sufficiently stable.[69]

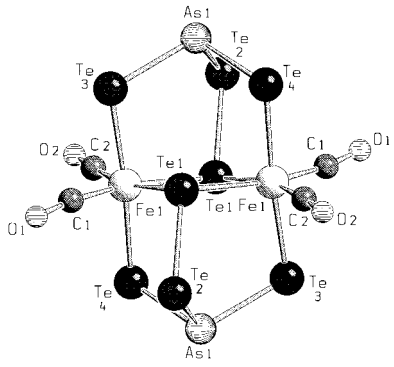
Whereas the ligand ability of **39** has not yet been tested, the cyclic dianion **35** (Te) reacts with $[Fe(CO)_5]$ to give **40** [Eq. (14)], which exibits a geometry comparable to that of **38**



(14)

40

(Figure 7).[73] This means that also in this reaction dichalcogen side arms are formed contrary to the original stoichiometry. Interestingly the same result is obtained upon reduc-

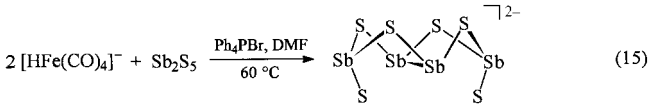


40

Figure 7. Structure of the dianion of $(nBu_4N)_2$–**40** in the crystal.[73]

tion of As_2Te_3 glass with $[HFe(CO)_4]^-$ [Eq. (14)], demonstrating that binary E/X phases may also be converted into mixed anionic cage ligands by means of nucleophilic transition metal complexes.

In contrast, base reduction of Sb_2S_5 with the same carbonyl reagent does not lead to a novel complex, but instead to the new main group cluster $[Sb_4S_6]^{2-}$ (**41**) with SbS wingtips in an unusual conformation [Eq. (15)].[80]

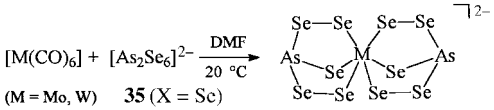


(15)

41

In principle the trigonal As^{III} pyramid is maintained during the reactions described by Equations (14) and (16) (see below). This means that liberated chalcogen, which is

obtained from partial decomposition of the ligand, is employed for the construction of new X–X bonds. Unusual large Se/metal ratios characterize the complexes **42** that are synthesized by complete decarbonylation of $[M(CO)_6]$ (M = Mo, W) under mild conditions [Eq. (16)].[81] The coaxial

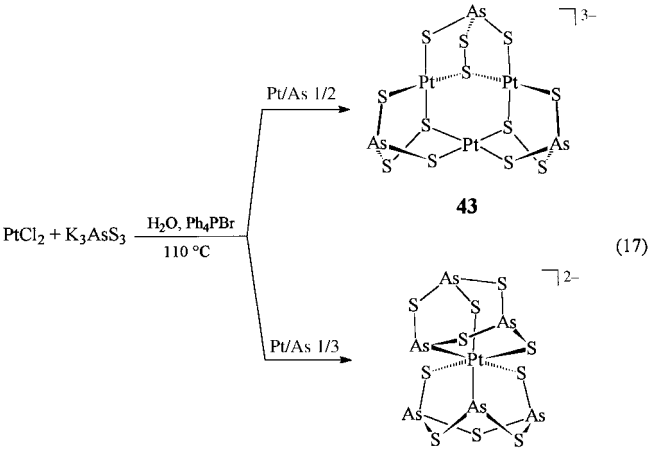


(16)

42

arrangement in the two $AsSe_5$ cages is striking, and may be explained by weak contacts (Se ··· Se 2.702–3.017 Å) between opposite Se atoms. The reaction type described in Equations (12), (14), and 16 resembles, in principle, the oxidative decarbonylation of metal carbonyls by polyselenides and polytellurides.[75] However, the creation of a new branching point by incorporation of the trivalent arsenic into the MX_4 ring causes a new electronic situation for the central metal.

Under hydrothermal conditions AsS_3^{3-} buildung blocks may undergo not only condensation reactions but also the formation of discrete clusters [Eq. (17)]. Depending on the



(17)

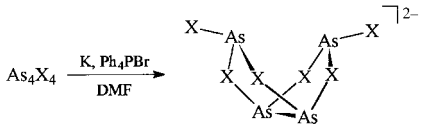
43

44

Pt/As ratio $[Pt_3(AsS_4)_3]^{3-}$ (**43**) and $[Pt(As_3S_5)_2]^{2-}$ (**44**) are formed from $PtCl_2$ and K_3AsS_3, both of which differ in terms of the oxidation states of Pt.[82] The dominating structural element in **43** (planar environment for Pt^{II}) are three AsS_4 groups of type **VIa**. The structure of **44** is characterized by two As_3S_3 rings, which with one of the As atoms and as well as two additional S atoms generate an octahedral environment at the Pt^{IV} center. This might indicate a possible participation of *cyclo*-$[As_3S_6]^{3-}$ (**27**), which would then be reduced by the originally present Pt^{II} to give $[As_3S_5]^{3-}$ and sulfide.[82]

3.3. Stabilization of Cage Anions in Metal Carbonyl Complexes

The $[As_4X_6]^{2-}$ compounds **45**[54, 71b, 83] are mixed cluster anions in which the basic realgar framework is still recognizable [Eq. (18)]. The nucleophilic AsX wingtips and the lone

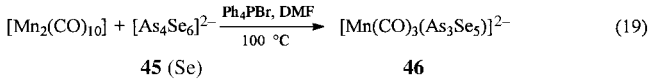


(18)

X = S, Se **45**

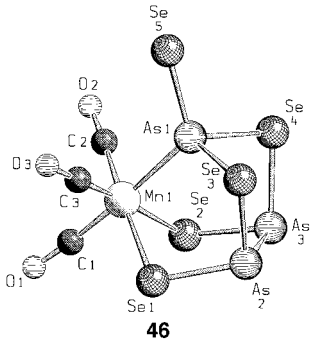
pairs of electrons of the cradle should increase the reactivity. Indeed reactions of **45**(Se) with transition metal carbonyl complexes exhibit reactivities between that of polychalcogenides[9c,75] and that of classical Zintl anions like E_7^{3-},[84] since depending on the metal carbonyl used not only M–X, but M–E bonds are formed.

To date, all investigations have been carried out with $[As_4Se_6]^{2-}$ (**45**(Se)), which reacts with $[Mn_2(CO)_{10}]$ to give the cluster **46** [Eq. (19)]. The core of the molecule may formally



(19)

be derived from the realgar cradle in that an As atom is replaced by a $Mn(CO)_3$ fragment (Figure 8).[73] Thus **45**(Se) already contains most of the preformed building blocks, since only the elimination of terminal "AsSe" seems to be necessary, whereas the final cyclization is achieved by coordination of As1 at Mn1. The As–Se distances in **46** may be divided into three categories: As1–Se5 (2.254(4) Å) is 0.07 Å shorter than As2–Se1 and 0.16 Å shorter than As1–Se3. The average As–Se distance of 2.354(4) Å is in a good agreement with the length expected for As–Se single bonds. Overall the ligand may be regarded as a six-electron donor of the formal charge −3, which results in a Mn^{I} center with 18 valence electrons.



46

Figure 8. Structure of the dianion of $(Ph_4P)_2$–**46** in the crystal.[73]

The complexes **47**[73] and **48**[81] are formed in the oxidative decarbonylation reaction of $[Fe(CO)_5]$ or $[M(CO)_6]$ (M = Mo, W) with **45**(Se) [Eq. (20)]. They may also be derived from known E/X cage structures, since they belong to the type of metal-substituted E_4X_3 cages in which one basal E atom is replaced by a ML_n fragment (see Section 4.2). In **47** and **48** two As_3Se_3 building blocks share a metal center as common corner. Although different conformations of the cages relative

$$[Fe(CO)_5] + [As_4Se_6]^{2-} \xrightarrow[100\ ^\circ C]{DMF} [Fe(CO)(As_3Se_3)_2]^{2-} \quad (20a)$$

45(Se) **47**

$$[M(CO)_6] + [As_4Se_6]^{2-} \xrightarrow[100\ ^\circ C]{DMF} [M(CO)_2(As_3Se_3)_2]^{2-} \quad (20b)$$

45(Se) **48**

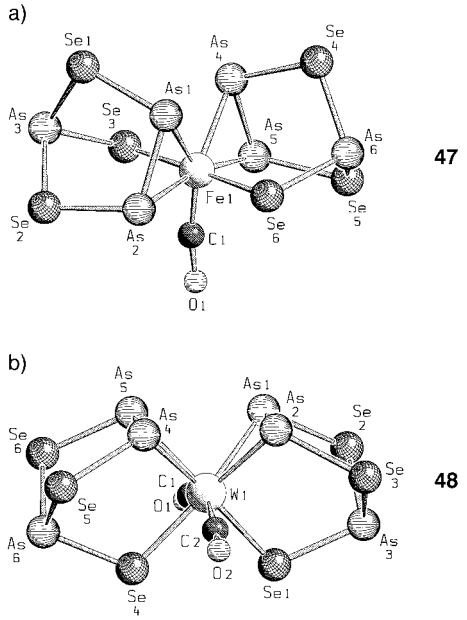
M = Mo, W

$\downarrow Se_8$

$[M(AsSe_5)_2]^{2-}$

42

to each other are possible only those with neighboring arsenic atoms are observed; slight differences in the arrangement of such As atoms are apparent in **47** and **48** (Figure 9). There is no explanation for the comparably short As–As distances (e.g. 2.381(4) Å in **47**) within the cage ligands (see Table 3).



47

48

Figure 9. The different conformations of the As_3Se_3 cages in a) **47**[73] and b) **48**[81] (Schakal plots). Counterion in the crystallographically investigated salts is $[Ph_4P]^+$.

Complex **47** may also be obtained by reduction of As_4Se_4 with $[HFe(CO)_4]^-$ in DMF at 100 °C. By contrast, under similar conditions As_2Te_3 gives the completely different structure **40** (see Eq. (14)). This difference might be a consequence of the different structures of the binary phases. The As_3Se_3 subunits in **48** can be transformed into polyselenidearsenate(III) ligands of type **VIb** in **42** by reaction of **48** with red selenium under elimination of CO [Eq. (20b)]. Notably, there is no oxidative addition of Se to arsenic under formation of structure type **V**, but a substitution of all As by Se atoms, which, in turn, reduces the degree of branching in the cradle.[81]

3.4. Cage Building Blocks Based on Tetrathio and Tetraseleno Metalates

Neutral cage molecules like As_4S_4 can be converted into mixed E/X cluster anions by alkali metal chalcogenides.[4] Similar nucleophilic effects are exerted by tetrathio and tetraselenometalates. The first reaction in this sense was that of MoS_4^{2-} with As_4S_4 [Eq. (21)] , in which the product **49** is a

$$MoS_4^{2-} + As_4S_4 \xrightarrow[20\ ^\circ C]{CH_3CN} \quad (21)$$

49

$\downarrow [MoO_2S_2]^{2-}$

$[Mo_2O_2As_2S_7]_2^{4-}$

32

combination of the complex fragment $[Mo_2O_2S_2]^{2+}$ and an $As_4S_{12}^{4-}$ chelate ligand.[48] The origin of the oxygen ligand is unclear. The close relationship to complexes containing sulfosalt units is demonstrated by the reaction of **49** with $[MoO_2S_2]^{2-}$ in which the excess sulfur is eliminated.[48] It is very likely that **32** possesses a cyclic structure in which $As_2S_5^{4-}$ units (**29**) may function as tetradentate chelate ligands (see Scheme 6).

In contrast, tetraselenometalates MSe_4^{2-} (M = Mo, W) form with As_4Se_4 clusters like **42** and **50** [Eq. (22)], which both contain $AsSe_5^{3-}$ ligands but have metals in different oxidation states. In the dinuclear tungsten(V) complex **50** a $W_2Se_3^{4+}$ core

$$MoSe_4^{2-} + As_4Se_4 \xrightarrow[25\ ^\circ C]{DMF} [Mo(AsSe_5)_2]^{2-} \quad (22a)$$

42

$$WSe_4^{2-} + As_4Se_4 \xrightarrow[25\ ^\circ C]{DMF} \quad (22b)$$

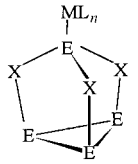
50

links the "terminal" cage ligands, which are slightly twisted towards each other.[85] Another method for the preparation of **42** (M = Mo) is the decarbonylation of $[Mo(CO)_6]$ with $[As_2Se_6]^{2-}$ (see Equation (16)). The reaction of WSe_4^{2-} with P_4Se_4 belongs to the same reaction type, and has already been outlined in Equation (11), but it gives a completely different result.

4. Activation of Neutral Cage Molecules

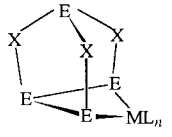
Among the mixed neutral main group clusters, the coordination chemistry of the cage molecules E_4X_n ($n = 3,4$; E = P, As; X = S, Se) has been investigated in detail.[38, 86] In contrast to mixed complex anions, "primary" complexes can be isolated under mild conditions with reactive transition metal complexes, that is intact inorganic cages stabilized by Lewis acidic complex fragments or peripheral sterically demanding

groups from organometallic components or multidentate phosphane chelates. Their stability is a function of the reaction partners and reaction conditions, which gives rise to very diverse fragmentation patterns and thus to the formation of ligand fragments of different size. As it is evident that all fragmentation reactions proceed via primary products, these will be discussed first.



51

E = P, As; X = S, Se



52

ML_n: see Table 3

4.1. Primary Complexation

4.1.1. E_4X_3 Cages (E = P, As; X = S, Se) as Ligands

E_4X_3 compounds exist as molecular cradles that are derived from the tetrahedron.[86] The compounds are easily synthesized by fusing together the elements, they are sufficiently soluble in organic solvents, and most importantly they possess reactive centers the nucleophilicity of which differ considerably.

Sterically demanding Lewis acidic complex fragments like $[M(CO)_5]$ (M = Mo, W) [87] and $[(np_3)M]$ (M = Ni, Pd)[88] coordinate to P_4X_3 (X = S, Se) to give complexes of the apical type **51**. The coordination pattern is in agreement with the electronic structure of P_4S_3, which predicts donor properties for the apical phosphorus comparable to those of tertiary phosphanes. The basal P_3 unit, however, should behave more like P_4.[89] Indeed edge-opening reactions are typical for P_4[90] and As_4.[30] Thus, oxidative addition of Ir^I or Pt^0 metal fragments to P_4S_3 leads to the complex type **52**.[91] The electronically unsaturated products dimerize or trimerize to yield stable aggregates (see Scheme 7, Section 4.2).

The complexation of intact As_4S_3 seems to be much more difficult, since to date there is only proof for one example each of η^1 (**51d**)[92] and η^2 coordination (**52c**) (Table 3).[31] Apical coordination as well as insertion into the base do not significantly influence the distances within the E_4X_3 cage, with the exception of the cleaved E–E bonds, which are clearly elongated.

Curiously, for a definite metal fragment there exists only one corresponding complex type. Therefore it is not yet known if there is any link between both forms **51** and **52**; for instance, in the form of a migration of a metal from the top to the base, and what role the X atoms might play in this. It would be important in this context to prove coordination to the sulfur bridge atoms, which in principle might be expected because of the excellent suitability of sulfur ligands as nucleophiles with respect to 16-electron complex fragments.[93] A first indication for the participation of bridging sulfur is the addition of up to four $M(CO)_5$ fragments (M = Mo, W) to P_4S_3. Nevertheless, there is only spectroscopic evidence and the structures have not been cofirmed.[86]

The role of organometallic radicals in the activation of the cages has still not been investigated in detail. A first example is the reaction of P_4X_3 (X = S, Se) with $(C_5H_5)Cr(CO)_3$ radicals arising from $[(C_5H_5)_2Cr_2(CO)_6]$ [Eq. (23)]. The for-

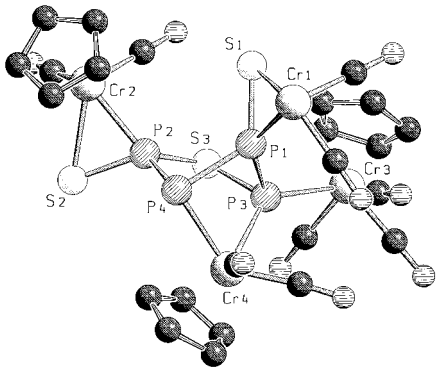
$$[(C_5H_5)_2Cr_2(CO)_6] \rightleftharpoons 2\ C_5H_5Cr(CO)_3\bullet$$
$$\downarrow P_4X_3/THF\ (X = S, Se)$$
$$[(C_5H_5)_4Cr_4(CO)_9(P_4X_3)]$$
53
$$\downarrow 60\ ^\circ C\ (X = Se)$$
$$[(C_5H_5)_4Cr_4(CO)_8(P_2Se_2)]$$
19 (23)

Table 3. E–E and E–X distances in complexes with $E_4X_{4(3)}$ and E_3X_3 building blocks and in the inorganic precursor cages.

Complex	n[a]	d(E–E) [Å]	d(E···E) [Å]	$d(E_{bas}–X)$ [Å]	$d(E_{ap}–X)$ [Å]	Ref.
$[(CO)_5Mo(P_4S_3)]$ **51a**	0	2.24(1)		2.12(4)	2.13(1)	[87]
$[(np_3)Ni(P_4S_3)]$ **51b**	0	2.23(1)		2.09(1)	2.12(1)	[88a]
$[(np_3)Ni(P_4Se_3)]$ **51c**	0	2.21(1)		2.238(5)	2.280(3)	[88b]
$[(CO)_5Cr(As_4S_3)]$ **51d**	0	2.484(5)		2.21(1)	2.21(1)	[92]
$\{IrCl(CO)(P_4S_3)(PPh_3)\}_2$ **52a**	1	2.265(5)[c]	3.055(5)			[91a]
$[Pt(P_4S_3)(PPh_3)]_3$ **52b**	1	2.22(1)	3.03(3)	2.11(2)[c]	2.10(2)[c]	[91b]
$[(C_5Me_4Et)Co(CO)(As_4S_3)]$ **52c**	1	2.470(1)	3.251(4)	2.209(4), 2.263(3)[b]	2.252(4)	[31]
$[(C_5H_5)_4Cr_4(CO)_9(P_4S_3)]$ **53a**	3	2.201(5)[c]		2.001(4)[d]		[94a, c]
$[(C_5H_5)_4Cr_4(CO)_9(P_4Se_3)]$ **53b**	3	2.237(5)[c]		2.250(3)[d]		[94b]
$[(C_5Me_4Et)Co(CO)(As_4S_4)]$ **54a**	1	2.519(6)	3.714(6)	2.252(7)[c]		[31]
$[(triphos)Rh(P_3S_3)]$ **57a**		2.165(6)				[100]
$[(triphos)Ir(P_3S_3)]$ **57b**		2.164(7)				[100]
$[(triphos)Rh(P_3Se_3)]$ **57c**		2.15(1)				[100]
$[Fe(CO)(As_3Se_3)_2]^{2-}$ **47**		2.381(4)		2.403(5)[c]	2.358(5)[c]	[73]
$[W(CO)_2(As_3Se_3)_2]^{2-}$ **48** (M = W)		2.356(7)[c]		2.440(7)[c]	2.354(8)[c]	[81]
P_4S_3		2.23(1)		2.09(1)	2.09(1)	[105]
P_4Se_3		2.22(1)		2.24(1)	2.24(1)	[106]
As_4S_3		2.45(1)		2.20(1)	2.22(1)	[107]
As_4S_4		2.569(1)[c]		2.237(2)[c]		[2, 28]
As_4Se_4[e]		2.57(1)		2.38(1)		[108]

[a] Number of edge openings. [b] Metal-coordinated As. [c] Average value. [d] $P–X_{terminal}$. [e] Structural parameters of As_4Se_3 are not known.[109]

mation of $[(C_5H_5)_4Cr_4(CO)_9(P_4X_3)]$ (**53a**) (X = S) and **53b** (X = Se) requires the cleavage of P–P *and* P–X cage bonds. As consequence of the formation of a new P–P bond in **53a** a central P_4S ring, in which all P atoms are linked to each other, is the characteristic feature (Figure 10).[94] The Cr centers are



53a

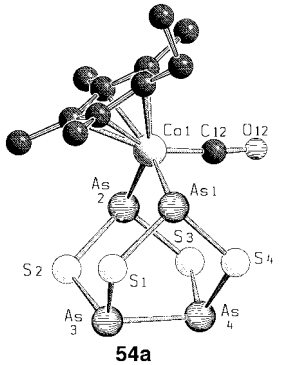
Figure 10. Molecular structure of $[Cp_4Cr_4(CO)_9(P_4S_3)]$ (**53a**)[94] in the crystal. The Cp ring at Cr1 is omitted for clarity.

either directly attached to the ring or coordinated to the peripheral P/X groups. Complexes **53a** and **53b** are thermally unstable, and lead to a series of fragmentation products (see below). The first isolable intermediate product in the case of **53b** is $[(C_5H_5)_4Cr_4(CO)_8(P_2Se_2)]$ (**19**) (see Equation (23) and Figure 4).

Only a few studies are known concerning the numerous other phosphorus sulfides that are derived from the P_4 tetrahedron. For example, the $P_4S_7/Mo(CO)_6$ system is handicapped by the low solubility of the inorganic cage and light sensitivity of the products.[86]

4.1.2. Complexes with As_4S_4 Ligands

Whereas the coordination behavior of E_4X_3 cage molecules has already been relatively well investigated, there are comparatively few results on E_4X_4 compounds.[95] A first hint for the possible activation of the complete realgar molecule by a complex is the insertion of "Cp*Co(CO)" (from $[Cp^*Co(CO)]_2$) into one of the two As–As bonds to give $[Cp^*Co(CO)As_4S_4]$ (**54a**) (Figure 11).[31] As in the E_4X_3 complexes of type **52** insertion of the Co fragment leads to considerable widening of the relevant As–As distance and angle; the other distances resemble those in the free ligand (Table 3). However, **54a** is only a by-product (the main products are **14**–**17**; see Eq. (5)); the same is also true for its homologue $[Cp^*Ir(CO)As_4S_4]$ (**54b**), which is formed from $[Cp^*_2Ir_2(CO)_3]$ and As_4S_4.[96] Thus, the systematic activation of realgar by coordinatively unsaturated transition metal fragments as well as their use in organometallic synthesis remains a desirable goal.



54a

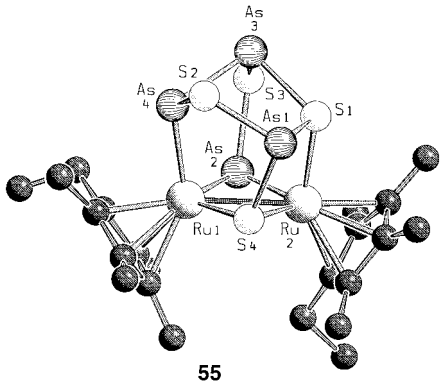
Figure 11. Molecular structure of $[(C_5Me_4Et)Co(CO)(\eta^2\text{-}As_4S_4)]$ (**54a**) in the crystal.

Reaction of $[Cp^*_2Ru_2(CO)_4]$ with β-As_4S_4[97] in boiling decane [Eq. (24)] gives $[Cp^*_2Ru_2As_4S_4]$ (**55**), which contains

$$[Cp^*_2Ru_2(CO)_4] \xrightarrow[C_{10}H_{22},\ 175\ ^\circ C,\ 24h]{\beta\text{-}As_4S_4} [Cp^*_2Ru_2As_4S_4] + Cp^*Ru(As_4S_4)RuCp^* \quad (24)$$

55 **56**

an As_4S_4 cage that is enlarged by two metal atoms (Figure 12). $[Cp^*_2Ru_2As_4S_2]$ (**56**) is formed as by-product in this reaction, and may be considered as a "classical" fragmentation



55

Figure 12. Molecular structure of $[(C_5Me_4Et)_2Ru_2As_4S_4]$ (**55**) in the crystal.

product.[98] A comparison of the As–S connectivities in **55** with those in known As_4S_4 forms reveals a structural relationship rather to the extremely rare As_4S_4(II),[99] since in this case it would only require insertion of both Cp*Ru fragments into the bonds As2–As4 and As2–S4 (Figure 13). However, a

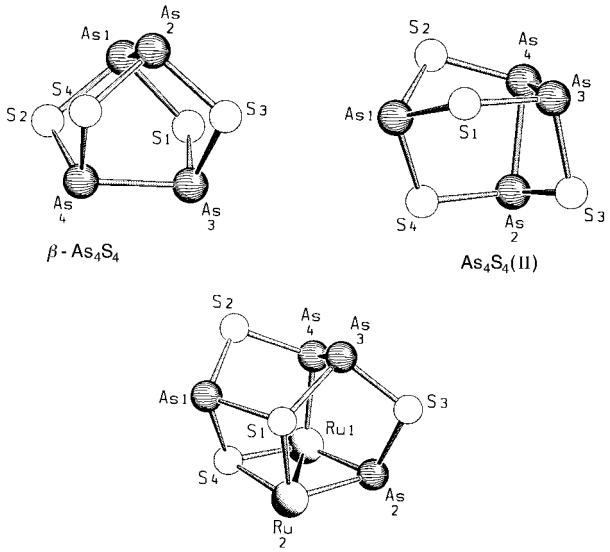
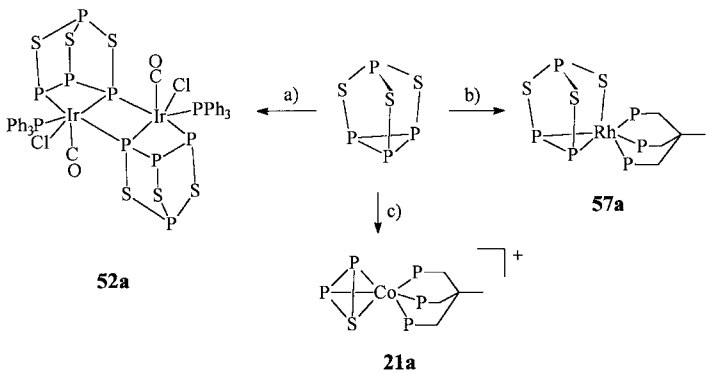


Figure 13. Comparison of the molecular structures of β-As_4S_4[2] and As_4S_4(II)[99] with the core of **55** (bottom) (Schakal plots).

phase transformation of β-As_4S_4 into As_4S_4(II) has been excluded;[28] thus **55** is more likely to be a recombination product of smaller intermediate building blocks. This hypothesis is also supported by the formation of **55** from phases that have lower sulfur contents such as As_4S_3 and As_2S_3.[98]

The sandwichlike structure of **56** is a result of the coplanar arrangement of the two As_2S ligands. The As atoms form an approximate square; the distances between 2.824(2) and 3.065(4) Å may indicate weak bonding interactions. Although S insertions into As–As bonds have not yet been described, the structural relationship to $[Cp^*_2Co_2(\mu\text{-}As_2)_2]$ (**13**) (see Scheme 4) is evident.[30]



Scheme 7. Representation of some of the different reaction modes of P_4S_3. a) Opening of a basal edge with $[IrCl(CO)(PPh_3)_2]$; b) substitution of one of the atoms in the base with $[\{RhCl(cod)\}_2]$/triphos; c) fragmentation of the cage with $Co(BF_4)_2$/triphos.

4.2. Metal-Substituted E_4X_3 Cages

Formal substitution of a P atom from the base of P_4X_3 (X = S, Se) by a ML_n fragment results in the complex type $ML_n(P_3X_3)$. In practice the neutral complexes [(triphos)$M(P_3X_3)$] (**57**) are formed by reaction of $[MCl(cod)]_2$ (M = Rh, Ir; cod = 1,5-cyclooctadiene) with P_4X_3[100] in the presence of triphos (Scheme 7). The interplay between the steric demand of the supporting ligands (triphos, np_3) and the electron configuration of the metal determines whether the cage is incorporated only by opening of a basal edge (**52a**) or if it is fragmented in a mild way to give the three-electron ligand present in **57**.[38] If, however, Co^{II} or Ni^{II} salts are used, P_2X or P_3 fragments are extruded from the base and transformed into η^3-ligands as in **21a** (Scheme 7).[38]

A comparison of the structure of complexes **57** with those of the initial cages reveals a slight but significant shortening of the basal P–P bonds. This is even more pronounced for the As–As bonds in the structurally related anionic As_3Se_3 clusters **47** and **48** (see Table 3).

The reaction of As_4S_4 with (triphos)M^I complexes (M = Rh, Ir) under comparable reaction conditions leads to [(triphos)-$M(As_3S_3)$] (**57b**), which is analogous to **57a**. Thus, in this case "AsS" elimination and a rearrangement of the cage skeleton are required.[101] Interaction of realgar with (triphos)M^{II} complexes (M = Co, Ni) leads to an even more drastic "decomposition" of the molecule, yielding [(triphos)$M(\eta^3\text{-}As_2S)$] (M = Co, **21c**).[38]

4.3. Fragmentation and Recombination Reactions in Organometallic Complexes

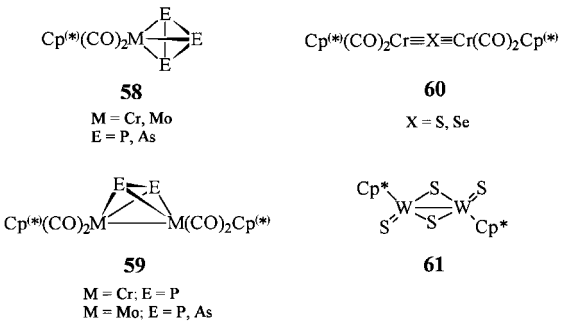
For many years the basic idea of the reactions of organometallic complexes with E/X cages was to obtain complexes as stable as possible under thermal conditions, despite the obvious risk of fragmentations. Dimeric, CO-containing cyclopentadienyl complexes with metal–metal multiple bonds or labile metal–metal single bonds have been employed as substrates. Modifying the reaction conditions has allowed more of the intermediate products to be isolated and their decomposition into the stable final products to be investigated systematically. Apart from the realization of new structures, this clearly shows the significance of small mixed ligands, which recombine under suitable conditions to give larger aggregates.

The dimers $[Cp^*_2M_2(CO)_4]$ ($M{\equiv}M$; M = Cr, Mo, W) preferentially react with $E_4X_{3(4)}$ to give products containing the E/X components of the original cage in separated form (Table 4, Scheme 8). The only exception are the mixed sandwich complexes $[Cp^*_2Mo_2P_4S]$ (**18a**) and $[Cp^*_2Mo_2E_2S_3]$ (**18c,d**). Little attention has been paid to the mechanism of formation of the metallatetrahedranes **58**, which reflect the simplest case of a recombination of atomic fragments. As possible intermediates one may consider complexes like **19** and **53**, which are formed in reactions with $CpCr(CO)_3$ radicals [Eq. (23)], but which fragment at higher temperatures to give **58**–**60**.[94] This system has allowed the activation and degradation of an inorganic cage to be investigated from the very beginning of the processes for the first time. Recent investigations in our group have shown that the fragmentation rate may be

Table 4. Product spectrum of the reactions of $[Cp^{(*)}_2M_2(CO)_{4(6)}]$ (M = Cr, Mo, W) with $E_4X_{3(4)}$ cage molecules.

Reactands	T [°C]	Intermediate products	E/X separated products[a]	Ref.
$[Cp_2Cr_2(CO)_6]/P_4S_3$	20–60	$[Cp_4Cr_4(CO)_9P_4S_3]$ **53a**	$[Cp(CO)_2CrP_3]$ **58a** $[\{Cp(CO)_2Cr\}_2P_2]$ **59a** $[\{Cp(CO)_2Cr\}_2S]$ **60a**	[94c]
$[Cp_2Cr_2(CO)_6]/P_4Se_3$	60	$[Cp_4Cr_4(CO)_9P_4Se_3]$ **53b** $[Cp_4Cr_4(CO)_8P_2Se_2]$ **19**	$[Cp(CO)_2CrP_3]$ **58a** $[\{Cp(CO)_2Cr\}_2P_2]$ **59a** $[\{Cp(CO)_2Cr\}_2Se]$ **60b**	[94b]
$[Cp^*_2Cr_2(CO)_6]/As_4S_4$	20		$[\{Cp^*(CO)_2Cr\}_2S]$ **60c**	[96]
$[Cp^*_2Cr_2(CO)_4]/As_4S_4$	110		$[Cp^*(CO)_2CrAs_3]$ **58b**	[96]
$[Cp^*_2Mo_2(CO)_4]/P_4S_3$	110		$[Cp^*(CO)_2MoP_3]$ **58c** $[\{Cp^*(CO)_2Mo\}_2P_2]$ **59b**	[34b]
$[Cp^*_2Mo_2(CO)_4]/As_4S_4$	100		$[Cp^*(CO)_2MoAs_3]$ **58d** $[\{Cp^*(CO)_2Mo\}_2As_2]$ **59c**	[34a]
$[Cp^*_2W_2(CO)_4]/As_4S_4$	110		$[Cp^*_2W_2S_4]$ **61**	[32]

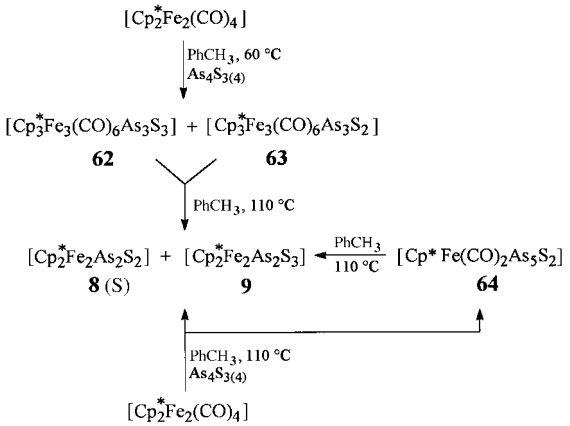
[a] Only in the reactions described in reference [34] were E/X mixed products obtained: $[Cp^*_2Mo_2P_4S]$ **18a**, $[Cp^*_2Mo_2P_2S_3]$ **18c** and $[Cp^*_2Mo_2As_2S_3]$ **18d**.



Scheme 8. Stable end products of the reactions of P_4X_3 (X = S, Se) and As_4S_4 with $[Cp^*_2M_2(CO)_{4(6)}]$ (M = Cr, Mo, W).

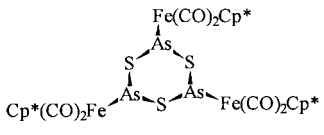
increased by the use of electron-rich ligands (Cp*) and slowed by employing relatively bulky $As_4S_4 \cdot Cr(CO)_5$ adducts.

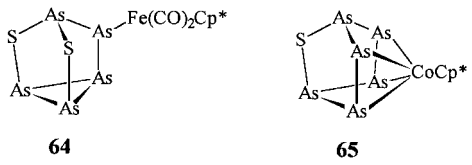
The AsS and As_2S_3 ligands in **8**(S) and **9** (see Eq. (4)) also do not stem directly from the inorganic cages, but from the intermediate products **62**–**64** that are characterized by very different As/S ratios. The complexes are stabilized by the 17-electron fragment $Cp^*Fe(CO)_2^{\bullet}$, and degradation to stable products containing comparatively slow ligands requires more drastic reaction conditions (Scheme 9).[102] The structures of



Scheme 9. The stepwise reaction of $[Cp^*_2Fe_2(CO)_4]$ with $As_4S_{3(4)}$.

the iron complexes **62** and **64** may be derived by analogies: complex **62** may be regarded as an As-metalated As_3S_3 ring resembling *cyclo*-$As_3S_6^{3-}$ (**27**),[53] whereas **64** may be formu-

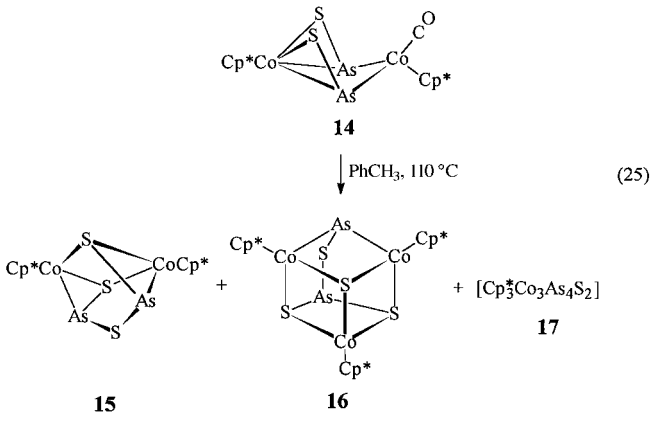




lated as a metalated derivative in the series E_4S_3, $E_5S_2^-$, E_6S^{2-}, and E_7^{3-} (see Scheme 1).

Complex **64** belongs to the structurally characterized class of Zintl ion complexes $[P_7\{Fe(CO)_2Cp\}_3]$,[11a] $[(P_7H)\{Mo(CO)_4\}]^{2-}$,[11b] and $[As_7\{Cr(CO)_3\}]^{3-}$.[103] A further member of this family is the Co complex **65**,[104] in which formally two As^- units replace two sulfur bridges in As_4S_3. As the base forms part of the bonding system (cleavage of one As–As bond), all As atoms are coordinated to the Cp*Co fragment, which achieves a closed valence shell.

Complex **65** arises from the system $[Cp^*_2Co_2(CO)_2]/As_4S_4$ (see Eq. (5)), which has been modified by addition of "$Cr(CO)_5$". The intermediary formed $As_4S_4 \cdot Cr(CO)_5$ adduct influences the nature of the products such that preferentially compounds rich in arsenic, such as **65** or $[Cp^*_2Co_2As_6]$,[30] are formed. In the original reaction sequence shown in Equation (5) complex **14** plays the key role, because controlled thermolysis of a solution of **14** in toluene results in products of different As/S stoichiometry and connectivity [Eq. (25)]. The



As-rich cluster **17** evidently serves to help maintain the As/S balance.[31] This reaction provided evidence for the first time for the synthesis of new organometallic main group clusters by the recombination of smaller ligand fragments.

In a certain way this behavior reflects the self-condensation of metathioarsenites. In agreement with this supposition, CO-containing intermediate products with smaller inorganic building blocks are precursors in the formation of the Ru cluster **55;** however, the structures of these are not yet clear.[98]

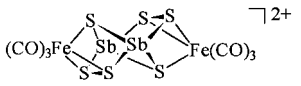
5. Summary and Outlook

The chemistry of mixed ligands from Group 15/16 elements represents a rapidly growing modern field, ranging from diatomic ligands, which are unstable in the free state or nonexistent, to polymers in natural and synthetic solids. In between are anionic and neutral main group clusters, which either serve as ligand precursors or (less frequently) are directly incorporated into metal complexes.

Discrete anions may form solids by condensation, a process that can be controlled by metal ions. The aggregates that are formed by recombination of ligand fragments require less space. Conversely, sections of solid-state structures are realized by introduction of negative charge and large counter-

ions or of organometallic complex fragments containing CO and Cp ligands. Whereas hydro- and solventothermal syntheses are already established as standard methods for the preparation of ternary and quaternary phases, their transfer to soluble complexes has, unlike the synthesis of polychalcogenido complexes[110] and in spite of preliminary successes, attracted little interest to date.

The focus of many studies are ligands based on As/S(Se). The use of the heavier pnicogens Sb and Bi should be stimulated by the fact that the classical Zintl ions Sb^{3-}[111] and Sb^{7-}[84b] can be incorporated into organometallic complexes. Promising candidates might be $Sb_6S_6^{2-}$,[80] $Sb_{12}Se_{20}^{4-}$,[112] $Sb_2S_{15}^{2-}$,[113] or fragments out of them. A first step in this direction might be the cationic cluster $[Fe_2(Sb_2S_6)(CO)_6]^{2+}$ (**66**), which represents a completely new type of compound. Furthermore it demonstrates impressively, that the development of new synthetic methods seems to have no limits: the cationic cluster **66** is formed as the SbF_6 salt from $[Fe(CO)_5]$ and $S_8(Sb_2F_{11})_2$ in liquid SO_2 by Sb transfer from the anion into a cationic sulfur complex.[114]



66

Although the presented area of research is mainly motivated by the fascination for the unusual and surprising structures, one should also always bear in mind the mechanisms and reaction pathways. Thus, metathesis reactions of mixed anions with transition metal halide complexes—the only example is shown in Equation (8)—represent an astonishingly neglected route, which might even be used for the incorporation of intact anionic clusters. In this way it should be possible to study the fragmentation mechanism as a function of the metal center, as has already been carried out for neutral cage molecules.

There are only a few indications of cage-opening reactions induced by radicals; these are mainly based on the one-electron fragments $CpCr(CO)_3^{\cdot}$ and $Cp^*M(CO)_2^{\cdot}$ (M = Fe, Ru). As this reaction type seems to be responsible for rearrangements, recombinations to new ligands, and even cage-expansion reactions, photochemical investigations should be intensified. In this context it is of great interest that realgar undergoes a light-induced rearrangement into para-realgar, which takes place even in the solid-state and which involves the cleavage of As – As bonds.[115]

I wish to thank my co-workers for their numerous contributions to this review. Dr. B. Nuber from the research groups of Prof. Dr. M. L. Ziegler and later Prof. Dr. G. Huttner (Heidelberg) is acknowledged for the numerous X-ray structure investigations. I am particularly indebted to Prof. Dr. H. Brunner for generous support, and to the Deutsche Forschungsgemeinschaft. I thank Prof. M. M. Kubicki (Dijon) for the semiempirical calculations of the free EX ligands, and W. Gabriel and B. Hofmann, Naturhistorisches Museum Bern for the photo used in the frontispiece.

Received: April 14, 1998
Revised version: September 3, 1997 [A 226 IE]
German version: *Angew. Chem.* **1998**, *110*, 782 – 800

[1] The name "sulfosalts" designates in mineralogic systematics complex sulfides that are derived from sulfur-containing arsenic acids: C. M. Gramaccioli, *Die Mineralien der Alpen*, Ott, Thun, **1978**, p. . 176; F. Klockmann, *Lehrbuch der Mineralogie*, Enke, Stuttgart, **1978**, p. 470.
[2] T. Ito, N. Morimoto, R. Sadanaga, *Acta Crystallogr.* **1952**, *5*, 775; D. J. E. Mullen, W. Nowacki, *Z. Kristallogr.* **1972**, *136*, 48.
[3] W. S. Sheldrick, M. Wachhold, *Angew. Chem.* **1997**, *109*, 214; *Angew. Chem. Int. Ed. Engl.* **1997**, *36*, 206.
[4] G. W. Drake, J. W. Kolis, *Coord. Chem. Rev.* **1994**, *137*, 131.
[5] J. W. Kolis, D. M. Young in *Chemistry, Structure, and Bonding of Zintl Phases and Ions* (Ed.: S. M. Kauzlarich), VCH, **1996**, p. 225.
[6] O. J. Scherer, *Angew. Chem.* **1990**, *102*, 1137; *Angew. Chem. Int. Ed. Engl.* **1990**, *29*, 1104; A.-J. DiMaio, A. L. Rheingold, *Chem. Rev.* **1990**, *90*, 169.
[7] K. H. Whitmire, *J. Coord. Chem.* **1988**, *17*, 95.
[8] M. Draganjac, T. B. Rauchfuss, *Angew. Chem.* **1985**, *97*, 745; *Angew. Chem. Int. Ed. Engl.* **1985**, *24*, 742; A. Müller, E. Diemann, *Adv. Inorg. Chem.* **1987**, *31*, 89.
[9] a) A. Müller, W. Jaegermann, J. H. Enemark, *Coord. Chem. Rev.* **1982**, *46*, 245; b) J. Wachter, *Angew. Chem.* **1989**, *101*, 1645; c) L. C. Roof, J. W. Kolis, *Chem. Rev.* **1993**, *93*, 1037.
[10] M. G. Kanatzidis, J.-H. Chou, *J. Solid State Chem.* **1996**, *127*, 186.
[11] a) G. Fritz, K. D. Hoppe, W. Hönle, D. Weber, D. Mujica, V. Manriquez, H. G. von Schnering, *J. Organomet. Chem.* **1983**, *249*, 63; R. Ahlrichs, D. Fenske, K. Fromm, H. Krautscheid, U. Krautscheid, O. Treutter, *Chem. Eur. J.* **1996**, *2*, 238; b) S. Charles, J. C. Fettinger, B. W. Eichhorn, *Inorg. Chem.* **1996**, *35*, 1540.
[12] W. A. Herrmann, *Angew. Chem.* **1991**, *103*, 835; *Angew. Chem. Int. Ed. Engl.* **1991**, *30*, 818.
[13] Ligands based on S/N are summarized in: P. F. Kelly, J. D. Woollins, *Polyhedron* **1986**, *5*, 607; T. Chivers, F. Edelmann, *ibid.* **1986**, *5*, 1661.
[14] K. Kawaguchi, E. Hirota, M. Ohishi, H. Suzuki, S. Takano, S. Yamamoto, S. Saito, *J. Mol. Spectrosc.* **1988**, *130*, 81.
[15] O. J. Scherer, J. Braun, P. Walther, G. Heckmann, G. Wolmershäuser, *Angew. Chem.* **1991**, *103*, 861; *Angew. Chem. Int. Ed. Engl.* **1991**, *30*, 852.
[16] Program PM3: J. J. P. Stewart, *J. Comput. Chem.* **1989**, *10*, 209, 221; M. M. Kubicki, personal communication.
[17] C. E. Laplaza, W. M. Davis, C. C. Cummins, *Angew. Chem.* **1995**, *107*, 2181; *Angew. Chem. Int. Ed. Engl.* **1995**, *34*, 2042.
[18] A. Müller, W. Jaegermann, J. H. Enemark, *Coord. Chem. Rev.* **1982**, *46*, 245.
[19] H. Chanaud, A. M. Ducourant, C. Gianotti, *J. Organomet. Chem.* **1980**, *190*, 201; H. Brunner, N. Janietz, W. Meier, G. Sergeson, J. Wachter, T. Zahn, M. L. Ziegler, *Angew. Chem.* **1985**, *97*, 1056; *Angew. Chem. Int. Ed. Engl.* **1985**, *24*, 1060.
[20] W. Chen, L. Y. Goh, *Organometallics* **1988**, *7*, 2020; C. Bianchini, D. Mani, C. Mealli, A. Meli, M. Sabat, F. Vizza, *Inorg. Chem.* **1988**, *27*, 3716; J. Amarasekera, E. J. Houser, T. B. Rauchfuss, C. L. Stern, *ibid.* **1992**, *31*, 1614.
[21] a) I.-P. Lorenz, W. Pohl, *Chem. Ber.* **1996**, *129*, 11; b) J. Foerstner, F. Olbrich, H. Butenschön, *Angew. Chem.* **1996**, *108*, 1323; *Angew. Chem. Int. Ed. Engl.* **1996**, *35*, 1323; c) O. J. Scherer, C. Vondung, G. Wolmershäuser, *ibid.* **1997**, *109*, 1360 and **1997**, *36*, 1303.
[22] W. Hieber, J. Gruber, *Z. Anorg. Allg. Chem.* **1958**, *296*, 91; C. H. Wei, L. F. Dahl, *Inorg. Chem.* **1965**, *4*, 1.
[23] B. K. Das, M. G. Kanatzidis, *Inorg. Chem.* **1995**, *34*, 6505.
[24] H. Brunner, L. Poll, J. Wachter, B. Nuber, *J. Organomet. Chem.* **1994**, *471*, 117.
[25] F. Leis, B. Nuber, J. Wachter, unpublished results.
[26] H. Brunner, A. Merz, J. Pfauntsch, O. Serhadli, J. Wachter, M. L. Ziegler, *Inorg. Chem.* **1988**, *27*, 2055.
[27] O. J. Scherer, C. Blath, G. Wolmershäuser, *J. Organomet. Chem.* **1990**, *387*, C21.
[28] E. J. Porter, G. M. Sheldrick, *J. Chem. Soc. Dalton Trans.* **1972**, 1347.
[29] M. Drieß, R. Janoschek, H. Pritzkow, *Angew. Chem.* **1992**, *104*, 449; *Angew. Chem. Int. Ed. Engl.* **1992**, *31*, 460.
[30] O. J. Scherer, K. Pfeiffer, G. Wolmershäuser, *Chem. Ber.* **1992**, *125*, 2367; O. J. Scherer, K. Pfeiffer, G. Heckmann, G. Wolmershäuser, *J. Organomet. Chem.* **1992**, *425*, 141.

[31] H. Brunner, B. Nuber, L. Poll, J. Wachter, *Angew. Chem.* **1993**, *105*, 1699; *Angew. Chem. Int. Ed. Engl.* **1993**, *32*, 1627; H. Brunner, H. Kauermann, L. Poll, B. Nuber, J. Wachter, *Chem. Ber.* **1996**, *129*, 657.

[32] H. Brunner, H. Kauermann, B. Nuber, J. Wachter, M. L. Ziegler, *Angew. Chem.* **1986**, *98*, 551; *Angew. Chem. Int. Ed. Engl.* **1986**, *25*, 557.

[33] A.-J. DiMaio, A. L. Rheingold, *Inorg. Chem.* **1990**, *29*, 798.

[34] a) I. Bernal, H. Brunner, W. Meier, H. Pfisterer, J. Wachter, M. L. Ziegler, *Angew. Chem.* **1984**, *96*, 428; *Angew. Chem. Int. Ed. Engl.* **1984**, *23*, 438; b) H. Brunner, U. Klement, W. Meier, J. Wachter, O. Serhadle, M. L. Ziegler, *J. Organomet. Chem.* **1987**, *335*, 339.

[35] H. Brunner, H. Kauermann, U. Klement, J. Wachter, T. Zahn, M. L. Ziegler, *Angew. Chem.* **1985**, *97*, 122; *Angew. Chem. Int. Ed. Engl.* **1985**, *24*, 132.

[36] L. Y. Goh, W. Chen, R. C. S. Wong, Z.-Y. Zhou, H. K. Fun, *Mendeleev Commun.* **1995**, 60.

[37] O. J. Scherer, G. Kemény, G. Wolmershäuser, *Chem. Ber.* **1995**, *128*, 1145.

[38] M. DiVaira, P. Stoppioni, *Coord. Chem. Rev.* **1992**, *120*, 259.

[39] M. DiVaira, L. Sacconi, P. Stoppioni, *J. Organomet. Chem.* **1983**, *250*, 183.

[40] M. DiVaira, F. Mani, S. Moneti, M. Peruzzini, L. Sacconi, P. Stoppioni, *Inorg. Chem.* **1985**, *24*, 2230.

[41] M. DiVaira, L. Sacconi, *Angew. Chem.* **1982**, *94*, 338; *Angew. Chem. Int. Ed. Engl.* **1982**, *21*, 330; M. DiVaira, P. Stoppioni, M. Peruzzini, *Polyhedron* **1987**, *6*, 351.

[42] C. Emmerich, G. Huttner, A. Asam, *J. Organomet. Chem.* **1993**, *447*, 71.

[43] S. C. O'Neal, W. T. Pennington, J. W. Kolis, *Angew. Chem.* **1990**, *102*, 1502; *Angew. Chem. Int. Ed. Engl.* **1990**, *29*, 1486.

[44] a) W. Nowacki, *Schweiz. Min. Petr. Mitt.* **1969**, *49*, 109; b) Y. Takeuchi, R. Sadanaga, *Z. Kristallogr.* **1969**, *130*, 346.

[45] a) B. A. Hofmann, *Mineral. Deposita* **1994**, *29*, 439; b) F. A. Schaufelberger in *Arsenic in the Environment, Part I* (Ed.: J. O. Nriagu), Wiley, New York, **1994**, p. 403.

[46] M. Palazzi, *Acta Crystallogr. Sect. B* **1976**, *32*, 3175.

[47] J.-H. Chou, M. G. Kanatzidis, *Inorg. Chem.* **1994**, *33*, 1001.

[48] G. A. Zank, T. B. Rauchfuss, S. R. Wilson, A. L. Rheingold, *J. Am. Chem. Soc.* **1984**, *106*, 7621.

[49] a) M. Palazzi, *Bull. Soc. Chim. Fr.* **1972**, 528; b) J. E. Iglesias, F. J. Zuniga, W. Nowacki, *Z. Kristallogr.* **1977**, *146*, 43; c) M. Palazzi, *Ann. Chim.* **1978**, *3*, 47.

[50] A. Edenharter, *Schweiz. Min. Petr. Mitt.* **1976**, *56*, 195.

[51] H. Behrens, L. Glasser, *Z. Anorg. Allg. Chem.* **1955**, *278*, 174.

[52] J. Angeli, P. Souchay, *C. R. Acad. Sci.* **1960**, *250*, 713.

[53] W. Sheldrick, J. Kaub, *Z. Naturforsch. B* **1985**, *40*, 19.

[54] D. M. Smith, C.-W. Park, J. A. Ibers, *Inorg. Chem.* **1996**, *35*, 6682.

[55] J.-H. Chou, J. A. Hanko, M. G. Kanatzidis, *Inorg. Chem.* **1997**, *36*, 4.

[56] D. Coucouvanis, A. I. Hadjikyriacou, *Inorg. Chem.* **1986**, *25*, 4317; A. I. Hadjikyriacou, D. Coucouvanis, *ibid.* **1987**, *26*, 2400.

[57] J.-H. Chou, M. G. Kanatzidis, *Chem. Mater.* **1995**, *7*, 5.

[58] A. Edenharter, T. Peters, *Z. Kristallogr.* **1979**, *150*, 169.

[59] T. Matsumoto, W. Nowacki, *Z. Kristallogr.* **1969**, *129*, 163.

[60] E. Hellner, H. Burzlaff, *Naturwissenschaften* **1964**, *51*, 35.

[61] P. Engel, W. Nowacki, *Z. Kristallogr.* **1969**, *129*, 178.

[62] A. Zemann, J. Zemann, *Acta Crystallogr.* **1959**, *12*, 1002; M. E. Fleet, *Z. Kristallogr.* **1973**, *138*, 147.

[63] Y. Iitaka, W. Nowacki, *Acta Crystallogr.* **1961**, *14*, 1291.

[64] C. J. Warren, D. M. Ho, R. C. Haushalter, A. B. Bocarsly, *Angew. Chem.* **1993**, *105*, 1684; *Angew. Chem. Int. Ed. Engl.* **1993**, *32*, 1646; B. Eisenmann, *ibid.* **1993**, *105*, 1764 and **1993**, *32*, 1693.

[65] W. S. Sheldrick, J. Kaub, *Z. Naturforsch. B* **1985**, *40*, 1020.

[66] P. T. Wood, G. L. Schimek, J. W. Kolis, *Chem. Mater.* **1996**, *8*, 721.

[67] J.-H. Chou, M. G. Kanatzidis, *J. Solid State Chem.* **1996**, *123*, 115.

[68] B. Eisenmann, H. Schäfer, *Z. Anorg. Allg. Chem.* **1979**, *456*, 87; W. S. Sheldrick, H.-J. Häusler, *ibid.* **1988**, *561*, 139.

[69] M. A. Pell, J. A. Ibers, *Inorg. Chem.* **1996**, *35*, 4559.

[70] G. Dittmar, H. Schäfer, *Z. Naturforsch. B* **1977**, *32*, 1346.

[71] a) C. H. E. Belin, M. M. Charbonnel, *Inorg. Chem.* **1982**, *21*, 2504; b) M. Ansari, J. A. Ibers, S. C. O'Neal, W. T. Pennington, J. W. Kolis, *Polyhedron* **1992**, *11*, 1877.

[72] C. H. E. Belin, *C. R. Acad. Sci. Ser. 2* **1984**, *298*, 691.

[73] T. M. Martin, P. T. Wood, G. L. Schimek, W. T. Pennington, J. W. Kolis, *Inorg. Chem.* **1995**, *34*, 4385.

[74] M. Wachhold, W. S. Sheldrick, *Z. Naturforsch. B* **1996**, *51*, 1235.

[75] J. W. Kolis, *Coord. Chem. Rev.* **1990**, *105*, 195.

[76] J. H. Chen, P. K. Dorhout, *Inorg. Chem.* **1995**, *34*, 5705; K. Chondroudis, T. J. McCarthy, M. G. Kanatzidis, *ibid.* **1996**, *35*, 840; J. H. Chen, P. K. Dorhout, J. E. Ostenson, *ibid.* **1996**, *35*, 5627; K. Chondroudis, M. G. Kanatzidis, *ibid.* **1995**, *34*, 5401; K. Chondroudis, T. J. McCarthy, M. G. Kanatzidis, *ibid.* **1996**, *35*, 3451.

[77] A. H. Cowley, D. Hellert, F. P. Gabbai, F. Olbrich, *Inorg. Chem.* **1995**, *34*, 3127.

[78] J. Zhao, W. T. Pennington, J. W. Kolis, *J. Chem. Soc. Chem. Commun.* **1992**, 265.

[79] K. Wendel, U. Müller, *Z. Anorg. Allg. Chem.* **1995**, *621*, 979.

[80] T. M. Martin, G. L. Schimek, W. T. Pennington, J. W. Kolis, *J. Chem. Soc. Dalton Trans.* **1995**, 501.

[81] S. C. O'Neal, W. T. Pennington, J. W. Kolis, *Inorg. Chem.* **1992**, *31*, 888.

[82] J.-H. K. Chou, M. G. Kanatzidis, *Inorg. Chem.* **1994**, *33*, 5372.

[83] E. J. Porter, G. M. Sheldrick, *J. Chem. Soc. A* **1971**, 3130.

[84] a) S. Charles, B. W. Eichhorn, A. L. Rheingold, S. G. Bott, *J. Am. Chem. Soc.* **1994**, *116*, 8077; b) U. Bolle, W. Tremel, *J. Chem. Soc. Chem. Commun.* **1994**, 217.

[85] S. C. O'Neal, W. T. Pennington, J. W. Kolis, *J. Am. Chem. Soc.* **1991**, *113*, 710.

[86] J. G. Riess, *ACS Symp. Ser.* **1983**, *232*, 17.

[87] R. Jefferson, H. F. Klein, J. F. Nixon, *Chem. Commun.* **1969**, 536; A. W. Cordes, R. D. Joyner, R. D. Shores, E. D. Dill, *Inorg. Chem.* **1974**, *13*, 132.

[88] a) M. DiVaira, M. Peruzzini, P. Stoppioni, *Inorg. Chem.* **1983**, *22*, 2196; b) *J. Organomet. Chem.* **1983**, *258*, 373.

[89] J. D. Head, K. A. R. Mitchell, L. Noodleman, N. L. Paddock, *Can. J. Chem.* **1977**, *55*, 669.

[90] O. J. Scherer, M. Swarowsky, G. Wolmershäuser, *Angew. Chem.* **1988**, *100*, 738; *Angew. Chem. Int. Ed. Engl.* **1988**, *27*, 694; *Organometallics* **1989**, *8*, 841; M. Scheer, C. Troitzsch, P. G. Jones, *Angew. Chem.* **1992**, *104*, 1395; *Angew. Chem. Int. Ed. Engl.* **1992**, *31*, 1377.

[91] a) C. A. Ghilardi, S. Midollini, A. Orlandini, *Angew. Chem.* **1983**, *95*, 800; *Angew. Chem. Int. Ed. Engl.* **1983**, *22*, 790; b) M. DiVaira, M. Peruzzini, P. Stoppioni, *J. Chem. Soc. Dalton Trans.* **1985**, 291.

[92] G. Roidl, B. Nuber, J. Wachter, unpublished results.

[93] H. Brunner, G. Gehart, J.-C. Leblanc, C. Moise, B. Nuber, B. Stubenhofer, F. Volpato, J. Wachter, *J. Organomet. Chem.* **1996**, *517*, 47, and references therein.

[94] a) L. Y. Goh, C. Wei, R. C. S. Wong, *Angew. Chem.* **1993**, *105*, 1838; *Angew. Chem. Int. Ed. Engl.* **1993**, *32*, 1728; b) *Phosphorus Sulfur Silicon Relat. Elem.* **1994**, *93 – 94*, 209; c) L. Y. Goh, W. Chen, R. C. S. Wong, *Organometallics* **1995**, *14*, 3886.

[95] R. Blachnik, P. Lönnecke, J. Nuß, *Z. Naturforsch. B* **1993**, *48*, 1175.

[96] L. Poll, Dissertation, Universität Regensburg, **1995**, 46.

[97] β-Realgar is the metastable high-temperature modification, which is obtained from fusing together the elements at 440 °C (G. B. Street, Z. A. Munir, *J. Inorg. Nucl. Chem.* **1970**, *32*, 3769 and ref. [28]). It is generally employed as substrate.

[98] H. Brunner, B. Nuber, L. Poll, G. Roidl, J. Wachter, *Chem. Eur. J.* **1997**, *3*, 57.

[99] A. Kutoglu, *Z. Anorg. Allg. Chem.* **1976**, *419*, 176.

[100] M. DiVaira, B. E. Mann, M. Peruzzini, P. Stoppioni, *Inorg. Chem.* **1988**, *27*, 3725.

[101] M. DiVaira, P. Stoppioni, M. Peruzzini, *Inorg. Chim. Acta* **1987**, *132*, 37.

[102] H. Brunner, L. Poll, J. Wachter, *Polyhedron* **1996**, *15*, 573.

[103] B. W. Eichhorn, R. C. Haushalter, J. C. Huffman, *Angew. Chem.* **1989**, *101*, 1081; *Angew. Chem. Int. Ed. Engl.* **1989**, *28*, 1032.

[104] H. Brunner, F. Leis, B. Nuber, J. Wachter, *Organometallics*, **1997**, *16*, 4954.

[105] Y. C. Leung, S. van Houten, A. Vos, G. A. Wiegers, E. H. Wiebenga, *Acta Crystallogr.* **1957**, *10*, 574.

[106] E. Keulen, A. Vos, *Acta Crystallogr.* **1959**, *12*, 323; G. R. Bruns, J. R. Rollo, R. J. H. Clark, *Inorg. Chem.* **1986**, *25*, 1145.

[107] H. J. Whitfield, *J. Chem. Soc. A* **1970**, 1800.

[108] T. J. Bastow, H. J. Whitfield, *J. Chem. Soc. Dalton Trans.* **1973**, 1739.

[109] T. J. Bastow, H. J. Whitfield, *J. Chem. Soc. Dalton Trans.* **1977**, 959.
[110] S.-P. Huang, M. G. Kanatzidis, *J. Am. Chem. Soc.* **1992**, *114*, 5477; *Inorg. Chem.* **1992**, *31*, 821; R. Seidel, R. Kliss, S. Weissgräber, G. Henkel, *J. Chem. Soc. Chem. Commun.* **1994**, 2791; B. K. Das, M. G. Kanatzidis, *Inorg. Chem.* **1995**, *34*, 1011, 5721; *J. Organomet. Chem.* **1996**, *513*, 1.
[111] W. J. Evans, S. J. Gonzales, J. W. Ziller, *J. Chem. Soc. Chem. Commun.* **1992**, 1138.
[112] T. M. Martin, P. T. Wood, J. W. Kolis, *Inorg. Chem.* **1994**, *33*, 1587.
[113] P. P. Paul, T. B. Rauchfuss, S. R. Wilson, *J. Am. Chem. Soc.* **1993**, *115*, 3316.
[114] G. W. Drake, G. L. Schimek, J. W. Kolis, *Inorg. Chem.* **1996**, *35*, 4534.
[115] D. L. Douglass, C. Shing, G. Wang, *Am. Mineralogist* **1992**, *77*, 1266.

Protein Mimicry: A New Dimension for Peptides as Lead Compounds?**

Ulrich Reineke and Jens Schneider-Mergener*

Four publications from 1996 and 1997 in *Science* and the *Proceedings of the National Academy of Science USA* concern the identification of peptides which emulate the biological functions of proteins.[1–4] Many biological processes are regulated by specific protein interactions with receptors located at the cell membrane. A large group of these receptors belong to the family of haemopoietic cytokine receptors. Their members have an N-terminal extracellular part comprising several domains responsible for ligand binding which is connected to the C-terminal signal-transduction domain through a transmembrane helix. Signal transduction takes place by homodimerization or heterooligomerization of the receptors with additional membrane-associated proteins after binding of the cytokine ligand.[5] As shown by X-ray crystal structure analyses of hormone–receptor complexes, such as that of the human growth hormone (hGH) with its receptor (hGHR; Figure 1, right),[6] ligand binding is mediated over a large contact surface area (500–1300 Å^2); around 30 amino acids from each partner are involved in the interaction. Owing to these observations it was long thought almost impossible to imitate such specific, high-affinity interactions with peptides or even smaller organic ligands. Pioneering work in this direction was first published in 1995 by J. Wells and co-workers at Genentec (San Francisco, California). They shortened the atrial natriuretic peptide (ANP) from 28 to 15 amino acids while retaining its activity.[7] The same group also suceeded in shortening the Z domain of protein A, which binds to the Fc region of immunoglobulins, from 59 to 33 amino acids while retaining its binding activity.[8] A breakthrough was achieved in 1996 by the group of W. Dower at Affymax Research Institute (Palo Alto, California) through the identification of a 20-mer peptide which emulates the function of the considerably larger protein erythropoietin (EPO, 165 aa). This protein mimic shows no sequence similarity to the protein, yet it can not only bind the erythropoietin receptor (EPOR), but also activate it. These properties can be explained by analyzing the X-ray crystal structure of a complex comprising two EPO receptors and a dimer of this peptide; the data were obtained by I. Wilson and co-workers at Scripps Research Institute (La Jolla, California).[2]

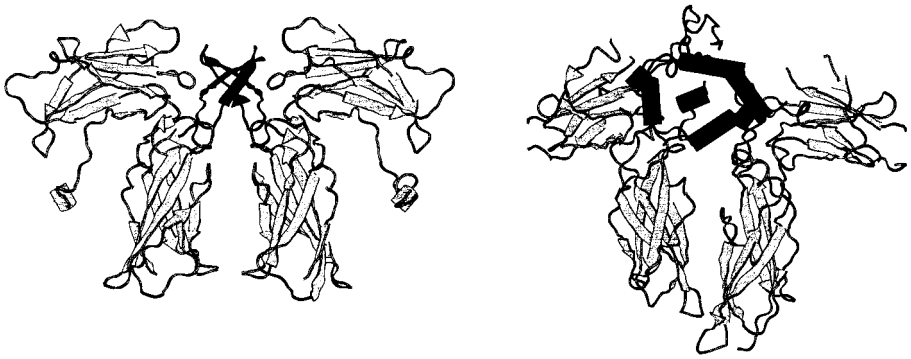


Figure 1. Schematic representation of the X-ray crystal structure of two erythropoietin receptors (gray) complexed with the erythropoietin mimic (black) identified by phage display.[2] The peptide binds the ligand as a homodimer. β-Folded sheets are shown as arrows, and α helixes as cylinders. Right: Schematic representation of the structure of the human growth hormone (hGH, black) complexed with two identical receptor molecules (hGHR, gray).[6] In the case of both receptors, only the soluble extracellular part was crystallized.

The identification of this peptide and the work on the atrial natriuretic peptide and Z domain of protein A were possible with the phage-display technique established in 1985 by G. Smith.[9] Since the beginning of the 1990s, this method has developed into a versatile means of biologically generating peptide libraries on the surface of phage.[10] The principal behind phage display is described in Figure 2. The basis for presenting different peptides on the filamentous phage surface is the cloning of random oligonucleotides in gene III or VIII of the phage genome (Figure 2). The serendipitous sequences in mutated genomes code for all the possible peptides corresponding to the number of randomized triplet

[*] Priv.-Doz. Dr. J. Schneider-Mergener,
Dipl.-Biochem. U. Reineke[+]
Institut für Medizinische Immunologie, Universitätsklinikum Charité
Humboldt-Universität
Schumannstrasse 20/21, D-10098 Berlin (Germany)
Fax: (+49) 30-2802-6460
E-mail: jens@immunologie.charite.hu-berlin.de

[+] Current address: Jerini BioTools GmbH, Berlin

[**] We wish to thank P. Fischer, A. Kramer, and U. Hoffmüller for a critical reading of the manuscript, and R. Stigler for help in creating the figures.

 © WILEY-VCH Verlag GmbH, D-69451 Weinheim, 1998 1433-7851/98/03706-0769 $ 17.50+.50/0

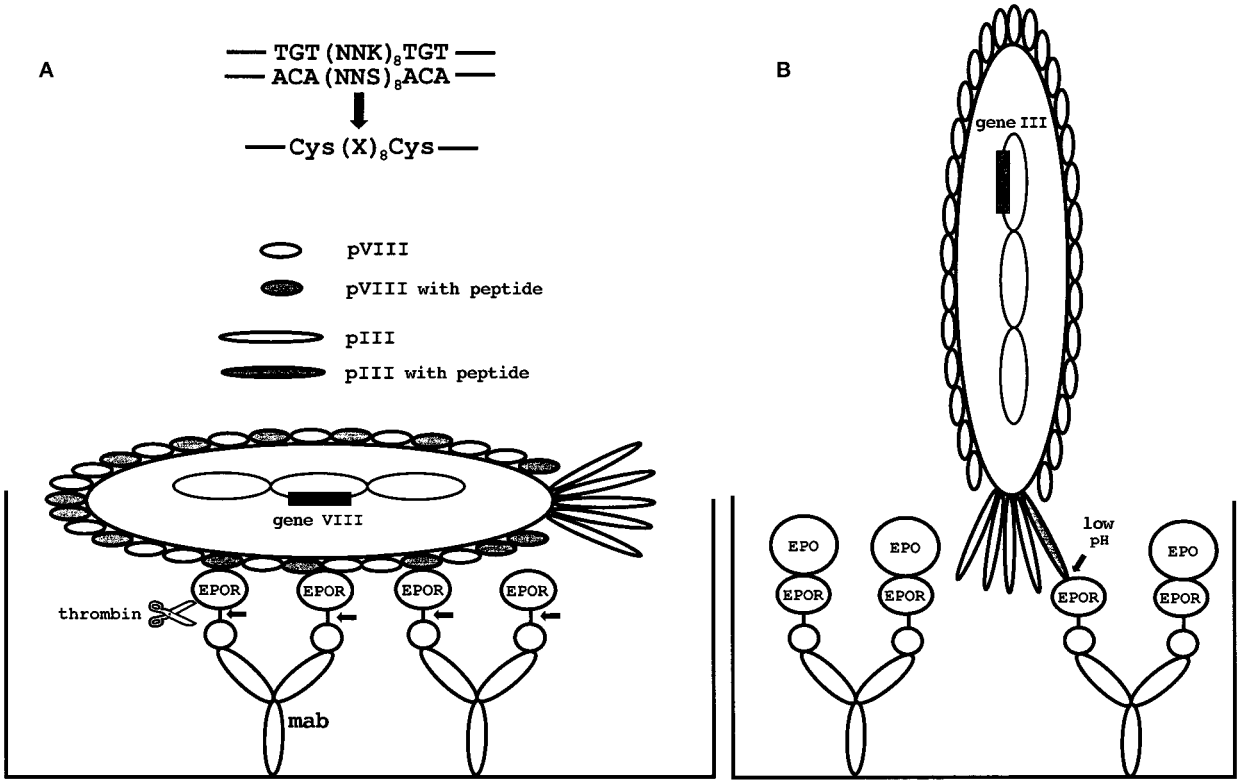


Figure. 2. A) Multivalent phage display on the phage coat protein pVIII. The randomized DNA sequence encoding the library of assorted peptides is cloned into gene VIII.[1, 10] Those triplets coding for all possible 20 amino acids (X) have any of the four nucleotides A, C, G, or T (N) in the first two positions, whereas the third position is occupied by only G or T (K) or, alternatively, A or C (S) in the complementary strand. This selection codes for all 20 amino acids; however, the number of possible stop codons is reduced from three to one. Both flanking triplets code for the cysteine residues that are important for the cyclic conformation. Only about 100 – 200 copies of the protein VIII (pVIII, small gray oval) contain the displayed peptide sequence. The information for the non-mutated coat protein (white oval), which is essential for phage replication, comes either from a second copy of the wild-type gene or through coinfection with a helper phage.[10] To screen the phage library, erythropoietin receptor fusion protein is fixed to microtiter plates by means of an antibody (mab). The bound phages can be eluted by cleavage at a thrombin cleavage site located between EPOR and the fusion region. B) Low-valency display on protein III (pIII) results in the presentation of 1 – 5 peptides. Screening in the presence of competing erythropoietin (EPO) selects for higher affinity binding phages compared to pVIII display. In these experiments, bound phage are eluted from EPOR under acid conditions.

codons. The phages destined to display a peptide sequence fused to the coat protein pIII or pVIII are propagated in bacteria. To do this, the mutated phage DNA must be introduced into the bacteria, a step known as transfection. Libraries of around 10^7 to 10^9 different phages are routine these days. By a step known as "panning", these repertoires are subjected to selection processes based on their affinity to an immobilized ligand. Phages which remain bound after particular selection pressures (e.g. elution conditions, competitive ligands) are subsequently eluted, propagated, and subjected to a further round of selection. After at least three rounds of enrichment, the peptide sequence of several ligand-binding phages can be determined by sequencing the relevant DNA region of gene III or VIII.

How was it possible with this technique to identify a peptide which can bind with high affinity to the erythropoietin receptor and also activate it?[1] The first step was conducted with a phage library in which the cyclic peptide sequence CXXXXXXXXC (C = cysteine, X = any of the 20 genetically encoded L-amino acids) was displayed on pVIII. With this multivalent display, around 100 to 200 copies of the peptide are present on the phage surface. Consequently, even phages displaying lower affinity peptides can bind to the ligand and be amplified (Figure 2 A). The extracellular domain of EPOR as a fusion protein was immobilized through an antibody against the fusion moiety. The EPOR-binding phages were eluted with the protease thrombin, which cleaves an internal amino acid sequence introduced between EPOR and the fusion region. This method identified the peptide CRIGPITWVC, which inhibits the EPO/EPOR interaction with a half-maximal constant (IC_{50}) of 10 μM. To find peptide sequences with higher affinity, a subsequent pIII (Figure 2 B) library of the type GGXXXCRIGPITWVCXXXGG was tested in the presence of EPO as competitor for phage/EPOR interactions. The library was constructed not only to increase the peptide length, but to permit substitutions within the loops. The best peptide obtained (GGT**YSC**HF**GPL**T**W**V**CKP**QGG) inhibited the EPO/EPOR interaction with an IC_{50} of 200 nM; the dissocoiation constant for the natural complex is 200 pM. Amino acids common to all the peptides in the last round of selection plus the cysteine residues essential for activity are highlighted. In addition, a variety of biological assays proved that the peptide (called EMP1 for "EPO-mimicking peptide") is able to activate EPOR, and, hence, is a promising lead compound for EPO mimics. Medical and commercial implications of such a

 © WILEY-VCH Verlag GmbH, D-69451 Weinheim, 1998 1433-7851/98/03706-0770 $ 17.50+.50/0

liason are immense. For example, recombinant human EPO is used in the therapy of renal anaemia following kidney insufficiency. The worldwide turnover volume of EPO in 1995 amounted to 2.6 billion dollars.

The same issue of *Science* in which the identification of EMP1 was published contained an article describing the crystallization and structural resolution of the $EPOR_2/EMP1_2$ complex and shedding light on how the astonishing protein mimicry by a peptide is possible (Figure 1, left).[2] All the amino acids in the EPO mimic EMP1 marked in bold in the previous paragraph are essential either for interactions with the receptor or the peptide conformation. EMP1 forms a double-stranded, antiparallel β sheet and dimerizes with a second EMP1 molecule at an angle of about 90° to form a four-stranded β sheet. This dimerization creates two identical EPOR binding sites. The receptor, as expected for a class-1 cytokine receptor, consists of two seven-stranded β-sheet domains. The interaction of EMP1 dimers with EPOR is achieved through four loops between the β-sheet strands of both receptor domains. Despite some differences in details, a fascinating similarity to the $hGH/hGHR_2$ complex is observed (Figure 1, right). The EPO/EPOR complex itself could not be crystallized to date. The interaction of EMP1 or hGH with their receptors is mediated through homologous amino acids in these receptors. In the hGH/hGHR complex, in addition to the four EPOR loops, two further loops make contact with the cytokine, which mirrors the size of hGH in comparison to EMP1 dimers.

How was it possible purely through selection for affinity to EPOR to obtain at the same time a functional dimeric peptide which dimerizes and activates the receptor? One explaination suggested by the authors is that EPOR is immobilized by a divalent antibody during the panning steps. This process could imitate the three-dimensional situation on the cell surface during receptor dimerization. It is also unclear whether the dimerization of EMP1 already takes place on the phage surface, or if it first occurs between free peptides. In any case, the relatively high affinity for EPOR is impressive (200 nM, as opposed to 200 pM for EPO), as is the specificity (related receptors are not bound) of this 20-mer protein mimic. For the comparable system hGH/hGHR, detailed studies into the contribution to the free binding energy made by particular amino acids were carried out. They revealed that only a few of the contact residues account for most of the free binding energy.[11] Since it probably applies to many systems, this "hot spot of binding" principal should make it possible to mimic larger protein-interaction surfaces by concentrating on the "energetic epitope". Indeed, at almost the same time the group at the Affymax Research Institute, again with the phage-display technique, identified an antagonistic 15-mer peptide which binds the type-1 interleukin-1 receptor with a dissociation constant of 2 nM.[4] This affinity resembles that of the IL-1 receptor antagonist (1.6 nM), a naturally occuring 20-kDa glycoprotein. However, with regard to its biological activity, the peptide is noticably poorer.

A third example of protein mimicry was published one year later, again by W. Dower and co-workers. With a phage display and later *E. coli* display, a 14-mer peptide was found which similarly binds the thrombopoietin receptor (TPOR) with very high affinity ($K_D \approx 2$ nM), although only weakly activating it.[3] However, synthetic dimerization of this peptide through a linker resulted in a half-maximal efficiency constant of 100 pM(!), which is identical to that of the natural ligand thrombopoietin (332 aa) and makes the peptide an attractive pharmacological lead compound. Thrombopoietin is the most important factor involved in the differentiation of bone-marrow stem cells to blood platelets and, in recombinant form, is currently being tested in clinical studies for thrombocytopenia therapy following chemotherapy or bone-marrow transplants. Analogous to the dimerization of the thrombopoietin mimic, W. Dower and co-workers recently reported a pseudosymetrical covalent dimerization of the erythropoietin mimic EMP1 through a lysine residue.[12] Each monomer is simultaeously synthesized either on its ε-amino group or on its α-amino functional end with a β-alanine linker. The two disulfide bridges are selectively joined by an orthogonal protection strategy. Compared to the noncovalently dimerized EMP1, this peptide, $EMP1_{K\text{-dimer}}$, has 100-fold higher affinity for EPOR and more than 10-fold better antagonistic activity in vivo.

The protein mimics described here form a new class of promising lead compounds for the synthesis of readily available active drugs that can be taken orally. Until now, there has existed no general strategy to block larger protein-contact surfaces based exclusively on chemical combinatorial methods; this is currently a bottleneck in drug discovery. The renaissance of peptides as lead compounds is dawning.

German version: *Angew. Chem.* **1998**, *110*, 801 – 804

Keywords: peptides · phage-display technology · protein mimetics · proteins · receptors

[1] N. C. Wrighton, F. X. Farrell, R. Chang, A. K. Kashyap, F. P. Barbone, L. S. Mulcahy, D. L. Johnson, R. W. Barrett, L. K. Jolliffe, W. J. Dower, *Science* **1996**, *273*, 458.
[2] O. Livnah, E. A. Stura, D. L. Johnson, S. A. Middleton, L. S. Mulcahy, N. C. Wrighton, W. J. Dower, L. K. Jolliffe, I. A. Wilson, *Science* **1996**, *273*, 464.
[3] S. E. Cwirla, P. Balasubramanian, D. J. Duffin, C. R. Wagstrom, C. M. Gates, S. C. Singer, A. M. Davis, R. L. Tansik, L. C. Mattheakis, C. M. Boytos, P. J. Schatz, D. P. Baccanari, N. C. Wrighton, R. W. Barrett, W. J. Dower, *Science* **1997**, *276*, 1696.
[4] S. D. Yanofsky, D. N. Baldwin, J. H. Butler, F. R. Holden, J. W. Jacobs, P. Balasubramanian, J. P. Chinn, S. E. Cwirla, E. Peters-Bhatt, E. A. Whitehorn, E. H. Tate, A. Akeson, T. L. Bowlin, W. J. Dower, R. W. Barrett, *Proc. Natl. Acad. Sci. USA* **1996**, *93*, 7381.
[5] J. A. Wells, *Curr. Opin. Cell. Biol.* **1994**, *6*, 163.
[6] A. M. de Vos, M. Ultsch, A. A. Kossiakoff, *Science* **1992**, *255*, 306.
[7] B. Li, J. Y. K. Tom, D. Oare, R. Yen, W. J. Fairbrother, J. A. Wells, B. C. Cunningham, *Science* **1995**, *270*, 1657.
[8] A. C. Braisted, J. A. Wells, *Proc. Natl. Acad. Sci. USA* **1996**, *93*, 5688.
[9] G. P. Smith, *Science* **1985**, *228*, 1315.
[10] G. P. Smith, J. K. Scott, *Methods Enzymol.* **1993**, *217*, 228.
[11] T. Clackson, J. A. Wells, *Science* **1995**, *267*, 383.
[12] N. C. Wrighton, P. Balasubramanian, F. P. Barbone, A. K. Kashyap, F. X. Farrell, L. K. Jolliffe, R. W. Barrett, W. J. Dower, *Nature Biotechnology.* **1997**, *15*, 1261.

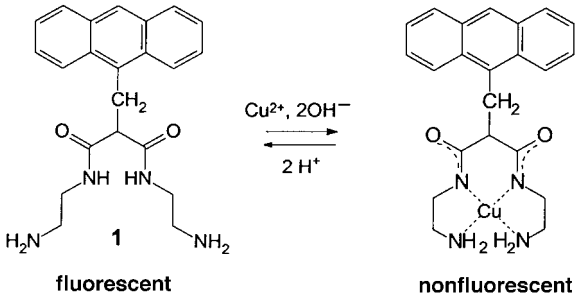
 © WILEY-VCH Verlag GmbH, D-69451 Weinheim, 1998 1433-7851/98/03706-0771 $ 17.50+.50/0

Fluorescent Chemosensors for Cu^{2+} Ions: Fast, Selective, and Highly Sensitive

Roland Krämer*

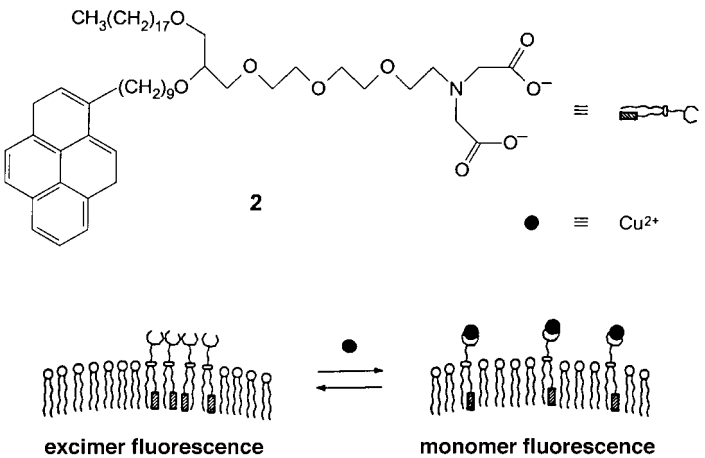
The design of chelating ligands for the selective complexation of metal ions has been an important goal of coordination and supramolecular chemistry for several decades. Chemical sensors for metal ions become accessible by combining a recognition event with an easily quantifiable signal event. The properties of an "ideal" sensor include high selectivity for one metal ion only, high sensitivity, fast and reversible (real-time) response, real-space response down to the micrometer level, and easy handling. Fluorescence signaling[1] offers the advantage of high sensitivity and can be directly used for sensors with fiber optic systems. A new generation of fluorescent reagents in which a chelating group and a fluorophore are discrete subunits of the same molecule[2] has the potential to fulfil the above-mentioned requirements. Recent attempts to apply these two-component systems to the detection of transition metal ions have been particularly successful in case of Cu^{2+} ions. This is not surprising, since among the more relevant transition metal ions, copper(II) has a particularly high thermodynamic affinity for typical N,O-chelate ligands and fast metal-to-ligand binding kinetics. Copper is a significant metal pollutant due to its widespread use, but it is also an essential trace element in biological systems. Whereas copper toxicity for humans is rather low compared with other heavy metals, certain microorganisms are affected by submicromolar concentrations. Compared with classical fluorescence reagents for Cu^{2+} detection in which the donor atoms are part of the fluorophore π-system,[3] the spatial separation of chelating group and fluorophore offers considerable flexibility in design. This is a prerequisite for the straightforward optimization of sensor properties with a view to specific applications.

The fluorosensor **1** of Fabrizzi et al. consists of a metal-binding dioxotetraaza unit linked to a light-emitting anthracene fragment (Scheme 1).[4] Compared with other copper(II) fluorosensors of this type described in recent years,[5] **1** combines a reversible response to nanomolar concentrations of Cu^{2+} in aqueous medium and low cross-sensitivity to certain transition metal ions and protons. When irradiated at 372 nm **1** displays an intense emission band at 415 nm. This fluorescence is quenched completely upon coordination of Cu^{2+} ions, presumably through a photoinduced metal-to-fluorophore electron-transfer mechanism. The copper concentration is determined by measurement of the fluorescence intensity with a fluorimeter. Binding and signaling are fast and fully reversible. The lower detection limit is 100 nM Cu^{2+}. At pH 7.1, equimolar concentrations of Mn^{2+}, Co^{2+}, Ni^{2+}, and Zn^{2+} do not affect the response for Cu^{2+}, since they do not bind to the receptor. Selectivity is due to the high affinity of Cu^{2+} for nitrogen donors and to the strong tendency to promote deprotonation of amide nitrogen atoms during complex formation. Metal-ion selectivity, binding kinetics, and proton cross-sensitivity are strongly dependent on the structure of the chelating group of the fluorescent sensor.[4]



Scheme 1. The binding of Cu^{2+} ions by **1**.

The membrane-based fluorosensor described by Arnold and coworkers is even more sensitive to Cu^{2+}.[6] Lipid **2** is functionalized with a fluorescent pyrene residue and a chelating iminodiacetate group. When added to distearoylphosphatidylcholine vesicles at pH 7.5, **2** forms aggregates within the parent membrane (Scheme 2). Upon excitation at



Scheme 2. Cu^{2+}-induced change in the fluorescence properties of a phospholipid membrane containing **2**.

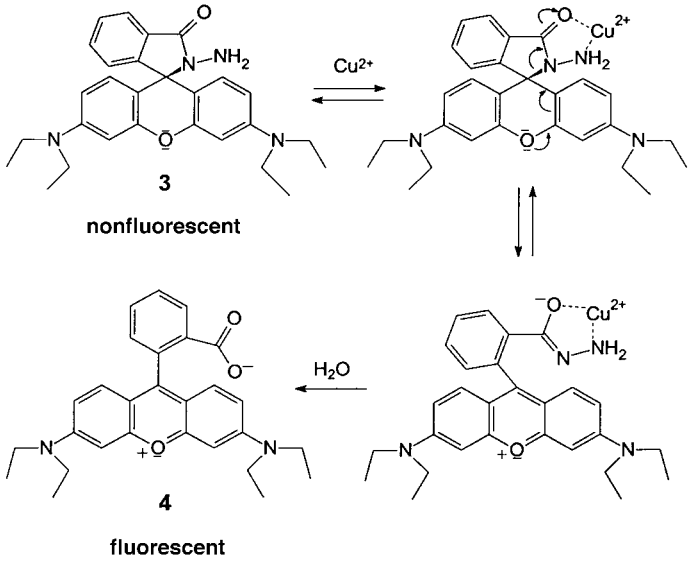
346 nm, the vesicles show two distinct bands in the fluorescence spectrum: a weak emission at 377 nm attributed to a small number of isolated monomers of **2**, and a broad and intense band at 470 nm attributed to aggregates of **2** (pyrene excimers). The addition of Cu^{2+} ions has a dramatic effect on the fluorescence spectrum. The monomer band increases, and the excimer band decreases. Unlike the previous example, copper ions are not directly involved in the fluorescence quenching mechanism. Complexation of copper by the iminodiacetate moiety induces a reorganization of the lipids (Scheme 2) by dispersion of **2** in the matrix, which results in an

[*] Dr. R. Krämer
Anorganisch-Chemisches Institut der Universität
Wilhelm-Klemm-Str. 8, D-48149 Münster (Germany)
Fax: (+49) 251-833-8366
E-mail: kramerr@nwz.uni-muenster.de

 © WILEY-VCH Verlag GmbH, D-69451 Weinheim, 1998 1433-7851/98/03706-0772 $ 17.50+.50/0

increase of the monomer-to-excimer ratio. The copper-induced changes in the fluorescence spectrum are fast and reversible, and can be used for quantification of Cu^{2+} down to a concentration of 5 nM. The sensor is at least 10 times more sensitive for Cu^{2+} than for Co^{2+}, Ni^{2+}, Mn^{2+}, and Ca^{2+}. Once again, selectivity is attributed to the high thermodynamic stability of the copper-iminodiacetate complex. Optimization of the system should soon lead to analytical applications such as monitoring Cu^{2+} concentrations by continuous-flow fluorimetry.

The rhodamine B hydrazide **3**[7] of Czarnik et al. is a "chemodosimeter" rather than a sensor in the strict sense, since the fluorimetric signaling is not reversible. Compound **3** is a nonfluorescent substance. Addition of Cu^{2+} ions results in N,O chelation by the hydrazide moiety and subsequently in a redox hydrolysis with release of fluorescent rhodamine B (**4**) (Scheme 3). Stoichiometric reagents for the fluorimetric



Scheme 3. Reaction of **3** with Cu^{2+} ions.

detection of copper are mainly redox-based and have been known for 30 years,[8] but Czarnik's dosimeter is the first based on a hydrolysis reaction.

The process is induced by the unique ability of Cu^{2+} ions to efficiently hydrolyze carboxylic acid derivatives with anchoring groups, such as α-amino esters, hydroxamic acids, and hydrazides. Analyte recognition and signaling are stoichiometric, irreversible processes. In a typical assay, excess **3** is added to the aqueous Cu^{2+} sample at pH 7.5 and the amount of released **4** is determined by fluorescence measurement (excitation 510 nm, emission 578 nm) after 2 minutes, when hydrolysis is complete. Copper concentrations down to 10 nM can be detected accurately with this method. Although the chemodosimeter method does not allow real-time monitoring, it is highly selective for copper due to a double selection process: response to the target metal ion requires both high affinity for the sensor molecule and hydrolytic reactivity of the metal ion. Many other metal ions (such as Mn^{2+}, Fe^{3+}, Cr^{3+}, Co^{2+}, Ni^{2+}, Zn^{2+}, Pb^{2+}, Hg^{2+}, Ag^{+}, Ca^{2+}, and Mg^{2+}) in equimolar amounts do not produce any increase in fluorescence intensity after 2 minutes.

A paper by B. Imperiali and co-workers[9] shows the potential of combinatorial methods for the optimization of sensor properties. Prompted by the Cu^{2+} binding site of serumalbumin a series of pentapeptides was synthesized. The metal ion was bound by the amino-terminal NH_2 group and the deprotonated amide-N atoms. The side chain of the N-terminal amino acid contains as fluorophore a 5-(dimethylamino)naphthalene-1-sulfonamide group, which does not participate in the metal coordination. Sensitivity and selectivity for Cu^{2+} are comparable with that for the fluorosensor **1**. The sensor properties can be modified in a simple way by variation of the amino acids. For example, the exchange of a glycin residue by β-alanine gives a distinctly better selectivity for Cu^{2+} in the presence of Ni^{2+}. The immobilization of the fluorescing peptide by covalent binding to a poly(ethylene glycol) matrix enables combinatorial peptide synthesis on a solid phase and a rapid screening of the metal-ion selectivity by observation of fluorescence quenching directly in the matrix.

The fluorescent Cu^{2+} sensors described here display outstanding sensitivity and selectivity. For many other metal ions, the development of highly selective reagents of this type is still a challenge. The combination of fluorophores with hydrolyzable groups may provide new systems for the specific determination of metal ions with high hydrolytic reactivity, for example lanthanide(III) and Pb^{2+} ions which efficiently cleave phosphate ester bonds.

German version: *Angew. Chem.* **1998**, *110*, 804 – 806

Keywords: analytical methods · copper · fluorescence spectroscopy · sensors

[1] A. P. de Silva, H. Q. N. Gunaratne, T. Gunnlaugsson, A. J. M. Huxley, C. P. McCoy, J. T. Rademacher, T. E. Rice, *Chem. Rev.* **1997**, *97*, 1515 – 1566.

[2] Systems in which fluorophore and donor atoms are separated by at least one CH_2 group have been denoted "conjugate fluoroionophores". Early representatives (see for example: L. R. Sousa, J. M. Larson, , *J. Am. Chem. Soc*. **1977**, *99*, 307) were active in organic media but could not be used for in-situ metal ion detection in aqueous solution.

[3] A. F. Gutierrez, A. M. De la Pena in *Molecular Luminescene Spectroscopy,* (Ed. S. G. Schulman), Wiley, New York, **1985**, pp. 371 – 546, and references therein.

[4] L. Fabrizzi, M. Licchelli, P. Pallavicini, A. Perotti, A. Taglietti, D. Sacchi, *Chem. Eur. J.* **1996**, *2*, 75 – 82; L. Fabrizzi, M. Licchelli, P. Pallavicini, A. Perotti, D. Sacchi, *Angew. Chem.* **1994**, *106*, 2051 – 2053; *Angew. Chem. Int. Ed. Engl.* **1994**, *33*, 1975 – 1977.

[5] J. Yoon, N. E. Ohler, D. H. Vance, W. D. Aumiller, A. W. Czarnik, *Tetrahedron Lett*. **1997**, *38*, 3845 – 3848; G. De Santis, L. Fabrizzi, M. Licchelli, C. Mangano, D. Sacchi, N. Sardone, *Inorg. Chim. Acta* **1997**, *257*, 69 – 76; E. U. Akkaya, M. E. Huston, A. W. Czarnik, *J. Am. Chem. Soc*. **1990**, *112*, 3590 – 3593.

[6] D. Y. Sasaki, D. R. Shnek, D. W. Pack, F. H. Arnold, *Angew. Chem*. **1995**, *107*, 994 – 996; *Angew. Chem. Int. Ed. Engl.* **1995**, *34*, 905 – 907.

[7] V. Dujols, F. Ford, A. W. Czarnik, *J. Am. Chem. Soc.* **1997**, *119*, 7386 – 7387.

[8] See for example: K. Ritchie, J. Harris, *Anal. Chem.* **1969**, *41*, 163 – 166.

[9] A. Torrado, G. K. Walkup, B. Imperali, *J. Am. Chem. Soc.* **1998**, *120*, 609 – 610.

 © WILEY-VCH Verlag GmbH, D-69451 Weinheim, 1998 1433-7851/98/03706-0773 $ 17.50+.50/0

From D-Arabinose to the Marine Natural Product Eleutherobin

Thomas Lindel*

In 1994 the soft coral *Eleutherobia* sp. was discovered as the source of a marine natural product with outstanding biological activity. In a bioassay-guided fractionation of its extract, Fenical et al. were able to attribute the cytotoxic activity to the glycosylated diterpenoid eleutherobin (**1**). The structure of **1** was elucidated by extensive 2D NMR spectroscopy and mass spectrometry (Figure 1).[1] The eunicellane carbon

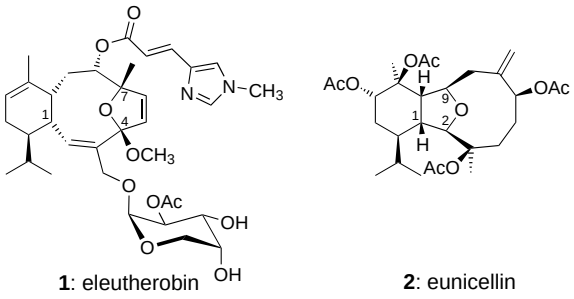


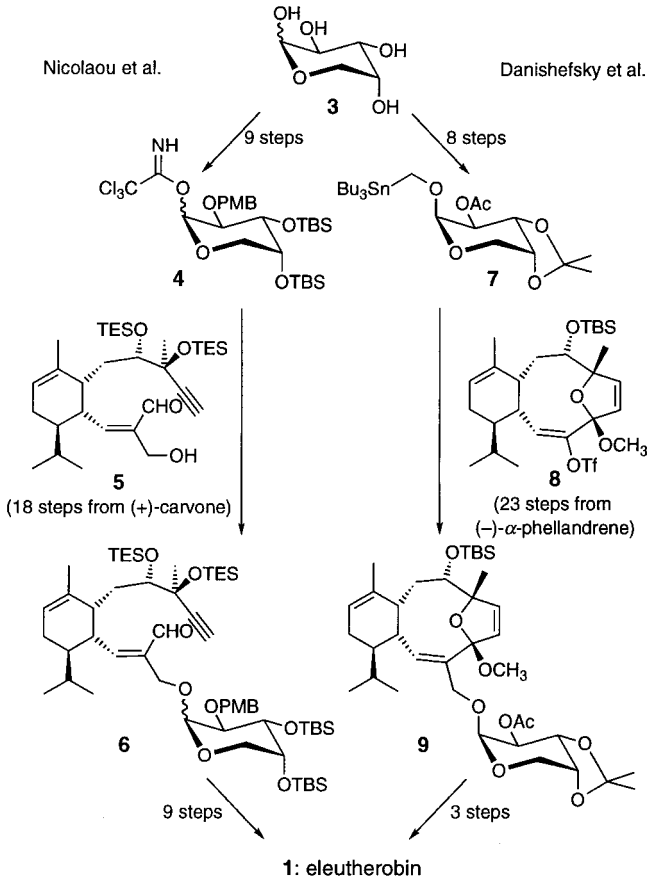
Figure 1. The marine natural products eleutherobin (**1**) and eunicellin (**2**).

skeleton of **1** is exclusive to natural products from gorgonians and alcyonaceans and it was observed for the first time in eunicellin (**2**) from *Eunicella stricta* in 1968.[2] Compounds **1** and **2** differ with respect to the position of their oxygen bridges, namely between C-2 and C-9 in **1** and between C-4 and C-7 in **2**. Other members of the small group of natural products with a 4,7-oxaeunicellane skeleton include the eleuthosides[3] and the nonglycosylated sarcodictyins[4] and valdivones[5] from related soft corals.

Eleutherobin (**1**) competes with paclitaxel (formerly known as taxol) for its binding at the microtubuli, inhibits their depolymerization, and thereby prevents the division of cancer cells.[6] Until 1994, paclitaxel had remained the only compound showing that mode of action, despite intense efforts.[7] Since then, additional natural products, the epothilones[8] and discodermolide[9], have shown the same effect. Eleutherobin (**1**) showed an in vitro cytotoxicity of about 10 – 15 nM (IC_{50}) against a diverse panel of tumor tissue cell lines with an approximate 100-fold increased potency toward selected breast, renal, ovarian, and lung cancer cell lines (National Cancer Institute (NCI)). It exhibited a similar tumor-type selectivity as paclitaxel (correlation coefficient 84%, COMPARE protocol[10], NCI).

From natural sources, eleutherobin (**1**) as well as the eleuthosides are available only in scarce amounts (0.01 – 0.02% of the dry weight of the rare alcyonacean *Eleutherobia* sp.). These are insufficient to explore their biochemical properties. This bottleneck was recently overcome by two total syntheses of eleutherobin (**1**) by Nicolaou et al.[11] and by Danishefsky et al.[12] Nicolaou et al. also synthesized the less cytotoxic sarcodictyin A.[11b]

Both research groups take advantage of the chiral pool and start from D-arabinose to synthesize their glycosylation building blocks **4** and **7**, respectively (Scheme 1). The two



Scheme 1. The synthetic strategies by Nicolaou et al. (left) and Danishefsky et al. (right). PMB = 4-methoxybenzyl; TBS = *tert*-butyldimethylsilyl; TES = triethylsilyl.

approaches differ strategically with regard to the order of the glycosylation step and the construction of the oxygen-bridged, ten-membered ring. While Nicolaou et al. make use of Schmidt's method and employ a trichloroacetimidate to glycosylate the monocyclic allylic alcohol **5**,[13] Danishefsky et al. first generate the norterpenoid tricycle **8**, which is then subjected to a modified Stille coupling to simultaneously introduce the missing carbon atom and the arabinose moiety.[14]

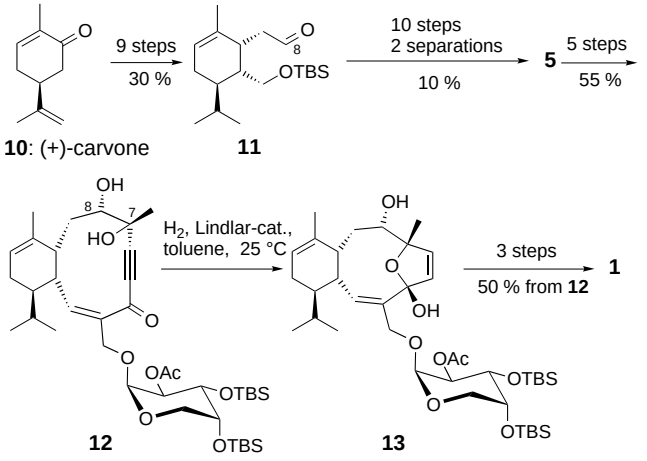
In both approaches, the required diastereomeric purity of the glycosylated intermediates **6** and **9**, respectively, is reached in a laborious way. Nicolaou et al. obtain **6** as a mixture of

[*] Dr. T. Lindel
Universität Heidelberg
Pharmazeutisch-chemisches Institut
Im Neuenheimer Feld 364, D-69120 Heidelberg (Germany)
Fax: (+49) 6221-546430
E-mail: lindel@convex.phazc.uni-heidelberg.de

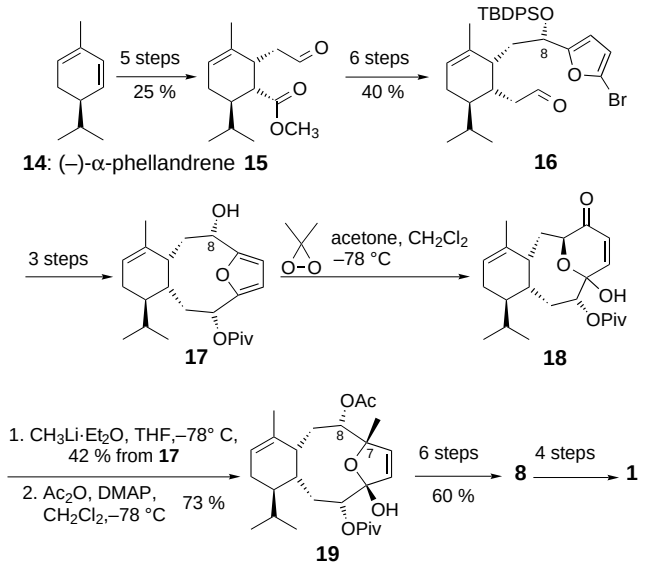
 © WILEY-VCH Verlag GmbH, D-69451 Weinheim, 1998 1433-7851/98/03706-0774 $ 17.50+.50/0

anomers from which the desired β-form is separated by column chromatography (α: 28%, β: 54%). Danishefsky et al. stereospecifically couple the anomerically pure arabinosyloxymethyl stannane **7** to the vinyl triflate **8**, but they obtain a yield of only 40–50%. In addition, **7** has to be separated from its α-anomer before use.

The monoterpenes (+)-carvone (**10**; Scheme 2) and (−)-α-phellandrene (**14**; Scheme 3) were chosen as the starting materials for the synthesis of the diterpenoid skeleton of eleutherobin (**1**) by Nicolaou et al. and Danishefsky et al., respectively. Again, both routes require the separation of



Scheme 2. Outline of the total synthesis of eleutherobin (**1**) by Nicolaou et al. TBS = *tert*-butyldimethylsilyl.



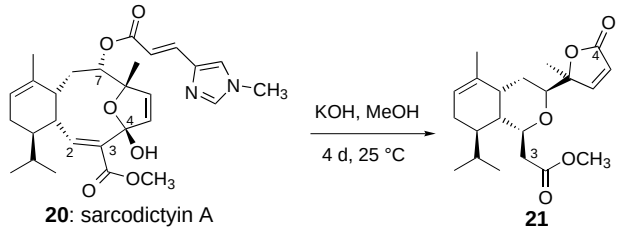
Scheme 3. Outline of the total synthesis of eleutherobin (**1**) by Danishefsky et al. DMAP = 4-dimethylaminopyridine; Piv = pivaloyl (CO*t*Bu); TBDPS = *tert*-butyldiphenylsilyl.

diastereomers by chromatography. The addition of 1-ethoxyvinyllithium to the TBS-protected aldehyde **11** (Scheme 2) leads to a mixture of diastereomeric alcohols (5:4 ratio in favor of the desired configuration at C-8), which is separated by Nicolaou et al. in a later step. Danishefsky et al. have to separate a mixture of diastereomeric alcohols after addition of 2-bromo-5-lithiofuran to their aldehyde **15** (Scheme 3), obtaining the desired diastereomer in a yield of 57%.

The key step of the synthesis by Nicolaou et al. is the stereoselective hydrogenation of the unsaturated cyclododecanone **12,** which was obtained through intramolecular acetylide–aldehyde condensation of **5**. The intermediate (*Z*)-olefin immediately rearranges to the tricyclic dihydrofuran **13** (Scheme 2). Solely the hydroxy group at the quaternary carbon atom C-7 takes part in the intramolecular formation of the hemiacetal. It can be concluded from the synthesis by Danishefsky et al. that the participation of the hydroxy group at C-8 could have been possible in that acetalization. Oxidation of the furan **17** (Scheme 3) by dimethyldioxirane at −78 °C gives the dihydropyranone **18**, because there appears to be no intermediate with a free hydroxy group at C-7. After nucleophilic methylation of **18**, the great preference of the cyclic system for the formation of a dihydrofuran ring becomes clearly visible. Treatment with acetic anhydride/DMAP leads to the selective acetylation of the ring oxygen atom of the dihydropyranone, and in the subsequent ring contraction to give **19**, it is substituted by the oxygen connected to C-7.

Both total syntheses of eleutherobin (**1**) are completed by the introduction of the (*E*)-*N*(6′)-methylurocanic acid moiety through acylation of the free hydroxy function at C-8, followed by the removal of the TBS- or isopropylidene protecting groups, respectively, in the arabinose side chain. The longest linear sequences are 28 steps in the case of the synthesis by Nicolaou et al. and 27 steps for that by Danishefsky et al.

The reactivity of the strained, tricyclic skeleton of the 4,7-oxaeunicellanes was previously studied by Pietra et al. in 1988, and their results could be of importance for an understanding of the chemical properties of these compounds.[4b] Treatment of sarcodictyin A (**20**) with methanolic potassium hydroxide led to the formation of the butenolide **21** (Scheme 4). The Michael acceptor property of the carbon



Scheme 4. The rearrangement of sarcodictyin A (**20**) observed by Pietra et al.

atom C-2 favors this rearrangement, leading to a relaxation of the strained ring system. After methanolysis of the *N*-methylurocanate, the newly formed hydroxy group attacks at C-2, and the fragmentation of the carbon–carbon bond between C-3 and C-4 by retro-Claisen condensation follows immediately thereafter.

The absolute stereochemistry of eleutherobin (**1**) had not been determined when the compound was first isolated, because priority was given to biological testing.[1] However,

results obtained by Pietra et al. strongly suggested the proposed absolute configuration of the diterpenoid 4,7-oxaeunicellane skeleton.[4] Of the enantiomeric arabinoses, the L-enantiomer appears to be favored in nature.[15] Therefore, it is remarkable that Nicolaou et al. and Danishefsky et al. could unambiguously identify the sugar unit of **1** as D-arabinose. In addition to a comparison of optical rotations, Danishefsky et al. even synthesized the L-arabinosyl diastereomer *neo*-eleutherobin.

In the tubulin depolymerization assay, synthetic eleutherobin (**1**) and two closely related analogues proved to be about as active as paclitaxel.[11a] It will be interesting to see whether the marine natural products containing a 4,7-oxaeunicellane skeleton will fulfill their promise.

German version: *Angew. Chem.* **1998**, *110*, 806 – 808

Keywords: antitumor agents · diterpenoids · eleutherobin · glycosides · natural products · total synthesis

[1] a) W. Fenical, P. R. Jensen, T. Lindel (University of California), US-A 5,473,057, **1995** [*Chem. Abstr.* **1996**, *124*, P194297z]; b) T. Lindel, P. R. Jensen, W. Fenical, B. H. Long, A. M. Casazza, J. Carboni, C. R. Fairchild, *J. Am. Chem. Soc.* **1997**, *119*, 8744 – 8745.

[2] O. Kennard, D. G. Watson, L. Riva di Sanseverino, B. Tursch, R. Bosmans, C. Djerassi, *Tetrahedron Lett.* **1968**, *9*, 2879 – 2884.

[3] S. Ketzinel, A. Rudi, M. Schleyer, Y. Benayahu, Y. Kashman, *J. Nat. Prod.* **1996**, *59*, 873 – 875.

[4] a) M. D′Ambrosio, A. Guerriero, F. Pietra, *Helv. Chim. Acta* **1987**, *70*, 2019 – 2027; b) *ibid.* **1988**, *71*, 964-976.

[5] Y. Lin, C. A. Bewley, D. J. Faulkner, *Tetrahedron* **1993**, *49*, 7977-7984.

[6] B. H. Long, A. M. Casazza, J. Carboni, C. R. Fairchild, T. Lindel, P. R. Jensen, W. Fenical, *Cancer Res.*, submitted.

[7] For the chemistry and biology of paclitaxel, see K. C. Nicolaou, W.-M. Dai, R. K. Guy, *Angew. Chem.* **1994**, *106*, 38 – 69; *Angew. Chem. Int. Ed. Engl.* **1994**, *33*, 15 – 44.

[8] a) G. Höfle, N. Bedorf, H. Steinmetz, D. Schomburg, K. Gerth, H. Reichenbach, *Angew. Chem.* **1996**, *108*, 1671 – 1673; *Angew. Chem. Int. Ed. Engl.* **1996**, *35*, 1567 – 1569; b) see also L. Wessjohann, *Angew. Chem.* **1997**, 109, 739 – 742; *Angew. Chem. Int. Ed. Engl.* **1997**, *36*, 715 – 718.

[9] E. ter Haar, R. J. Kowalski, E. Hamel, C. M. Lin, R. E. Longley, S. P. Gunasekera, H. S. Rosenkranz, B. W. Day, *Biochemistry* **1996**, *35*, 243 – 250.

[10] Information with regard to the COMPARE protocol established at the NCI are available in the internet: http://epnws1.ncifcrf.gov:2345/dis3d/itb/compare.html.

[11] a) K. C. Nicolaou, F. van Delft, T. Ohshima, D. Vourloumis, J. Xu, S. Hosokawa, J. Pfefferkorn, S. Kim, T. Li, *Angew. Chem.* **1997**, *109*, 2630 – 2634; *Angew. Chem. Int. Ed. Engl.* **1997**, *36*, 2520 – 2524; b) K. C. Nicolaou, J.-Y. Xu, S. Kim, T. Ohshima, S. Hosokawa, J. Pfefferkorn, *J. Am. Chem. Soc.* **1997**, *119*, 11353 – 11354.

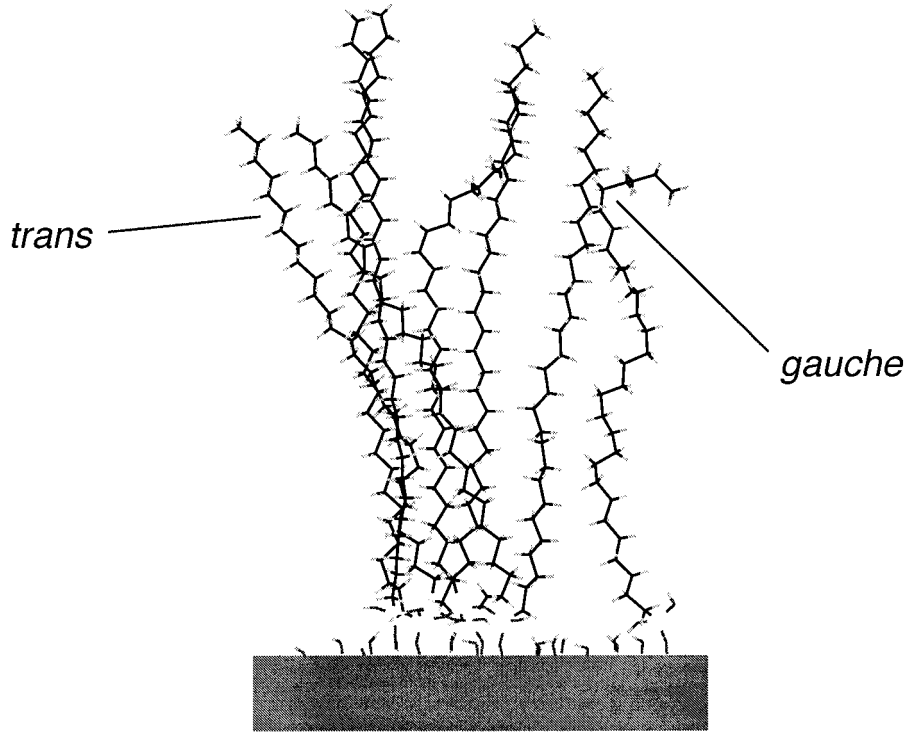
[12] a) X.-T. Chen, C. E. Gutteridge, S. K. Bhattacharya, B. Zhou, T. R. R. Pettus, T. Hascall, S. J. Danishefsky, *Angew. Chem.* **1998**, *110*, 195 – 197; *Angew. Chem. Int. Ed.* **1998**, *37*, 185 – 187; b) X.-T. Chen, B. Zhou, S. K. Bhattacharya, C. E. Gutteridge, T. R. R. Pettus, S. J. Danishefsky, *ibid.* **1998**, *110*, 835 – 838; *ibid.* **1998**, *37*, 789 – 792.

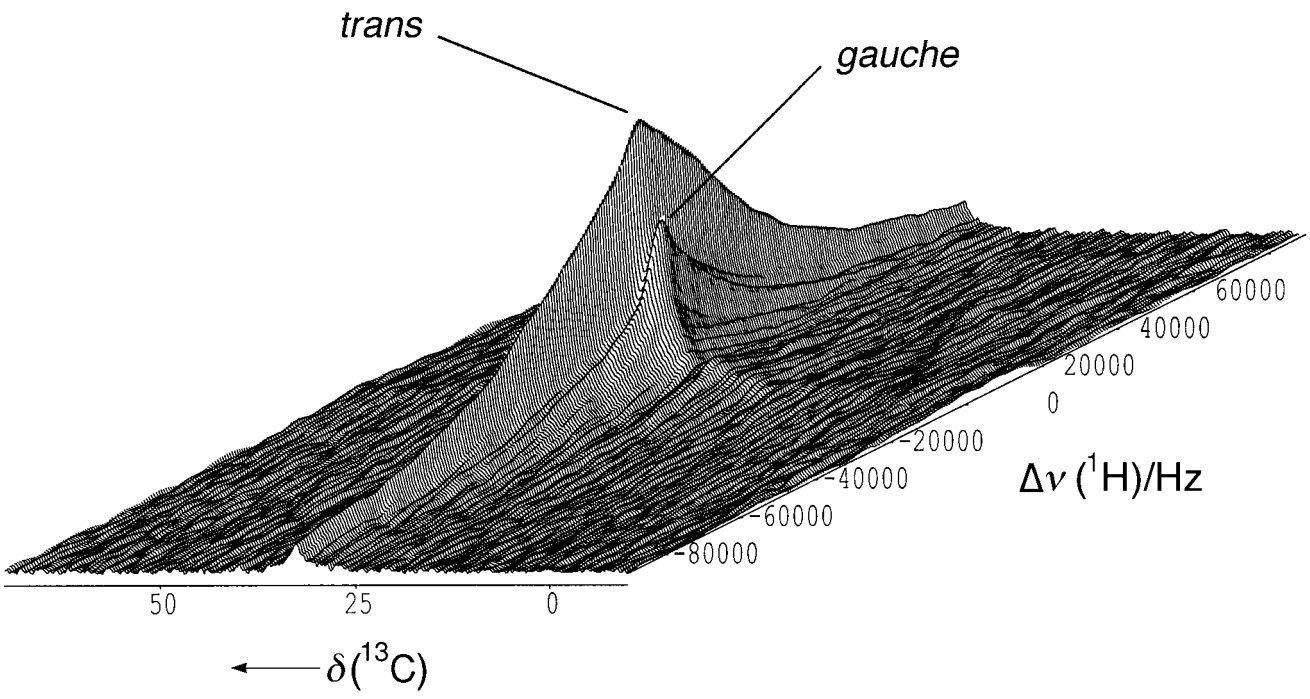
[13] R. R. Schmidt, K.-H. Jung in *Preparative Carbohydrate Chemistry* (Ed.: S. Hanessian), Marcel Dekker, New York, **1997**, p. 283 – 312.

[14] J. K. Stille, *Angew. Chem.* **1986**, *98*, 504 – 519; *Angew. Chem. Int. Ed. Engl.* **1986**, *25*, 508 – 524.

[15] *Römpp-Lexikon Naturstoffe* (Eds.: B. Fugmann, S. Lang-Fugmann, W. Steglich), Thieme, Stuttgart, **1997**, p. 52.

 © WILEY-VCH Verlag GmbH, D-69451 Weinheim, 1998 1433-7851/98/03706-0776 $ 17.50+.50/0





The dynamic behavior of the alkyl chains of a stationary C_{30} interphase for HPLC can be characterized with a 2D solid-state NMR spectrum. Find out more about the application of this method on the following pages.

 © WILEY-VCH Verlag GmbH, D-69451 Weinheim, 1998 1433-7851/98/3706-0777 $ 17.50+.50/0

Investigating the Selectivity of Triacontyl Interphases**

Klaus Albert,* Tanja Lacker, Martin Raitza, Matthias Pursch, Hans-Joachim Egelhaaf, and Dieter Oelkrug

In addition to the use of octyl- and octadecyl-modified silica gel (C_8 and C_{18} bonded phases) for the separation of isomeric mixtures by reverse-phase high-performance liquid chromatography (RP-HPLC), there is a progressive application of separation phases with triacontyl groups (C_{30} bonded phases). Owing to their specific selectivity, these materials are now widely employed especially for the analysis of carotenoids and tocopherol derivatives.[1–7] We present here an investigation of the structural parameters and interactions responsible for the specific separation behavior. The selectivity (selectivity factor α) of a chromatographic separation is dependent upon the interactive game of the stationary and mobile phases with the different analytes. Within this complicated interphase system, the mobile phase penetrates into the stationary component of the alkyl-modified silica gel in molecular dimension without forming a homogeneous solution. The different partition coefficients between mobile and stationary phases are responsible for the chromatographic separation within different components of a mixture.

Important parameters of the chromatographic interphase system are the structure and dynamics of the stationary phase, the composition of the mobile phase, and the steric and electronic structure of the analyte. To investigate the dynamic behavior of these complex systems, solid-state NMR, suspended-state MAS NMR (MAS = magic angle spinning), and fluorescence spectroscopies were combined with HPLC separations at various temperatures.

The investigated C_{30} interphase was prepared by the solution polymerization procedure, in which the partially hydrolyzed silane is tethered to the silica surface after partial polycondensation.[1, 4] The specific arrangement of the *n*-alkyl groups provided is reflected by the behavior of solid-state ^{13}C NMR spectra measured at various temperatures (Figure 1). Two clearly separated signals at $\delta = 30.0$ and 32.8 are observed for the carbon atoms of the methylene main chain at 305 and 315 K. At lower temperatures the low-field resonance is more intense, whereas the intensity of the high-field resonance increases with higher temperatures. According to solid-state ^{13}C NMR investigations of polyethylene, the signal at $\delta = 32.8$ is assigned to ordered alkyl-chain domains with *trans* conformations and that at $\delta = 30.0$ to more disordered domains

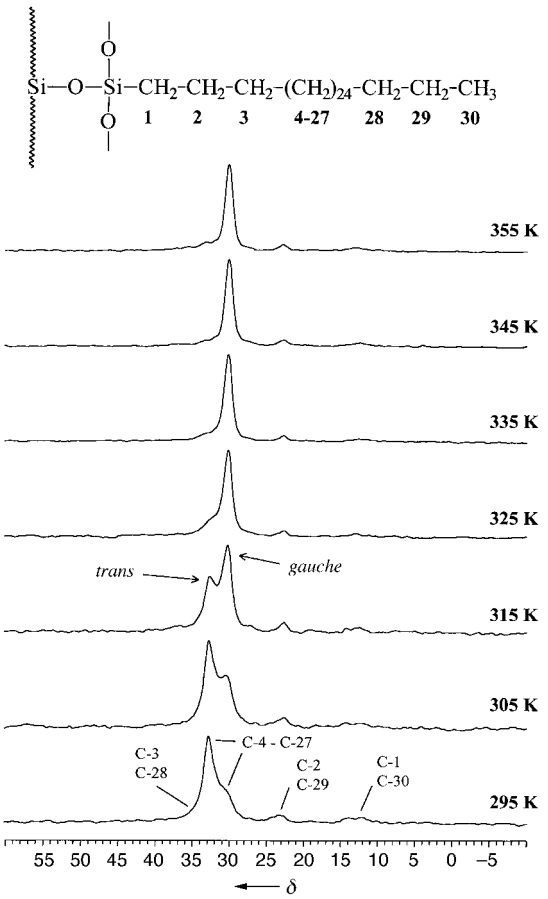


Figure 1. Temperature dependence of the ^{13}C CP/MAS NMR spectra (75.4 MHz) of the C_{30} phase.

with *gauche* conformations.[8] The described signal assignment can be checked with a two-dimensional wideline separation (WISE) experiment.[9] In Figure 2a the ^{13}C chemical shifts are plotted against the half-height widths $\Delta\nu$ of the proton signals. It is clearly evident from Figure 2b that the half-height widths for protons in *trans* conformations ($\delta(^{13}C) = 32.8$) is much larger (48 kHz) than that for protons in *gauche* conformations ($\delta(^{13}C) = 30.0$; 15 kHz). The half-height width for the signal of a methylene proton ensemble is reciprocal to the spin–spin relaxation time T_2 of the protons involved and thus to the averaged overall mobility. Therefore, more immobile *trans* conformations can unambigously be distinguished from flexible *gauche* conformations.

Both conformations of the *n*-alkyl chains can be interconverted by changing the temperature, as indicated in Figure 1. At 295 K mainly *trans* conformations exist beside minor amounts of *gauche* conformations, whereas above 335 K *gauche* conformations appear exclusively. Moreover, in the presence of a mobile phase—the medium in which the chromatographic separation takes place—*gauche* and *trans* conformations of the C_{30} alkyl chains can be detected by suspended-state MAS NMR spectroscopy.[7] The relative amounts of each conformation vary according to the composition of the mobile phase. *tert*-Butyl methyl ether (TBME), which is often used as a modifier in HPLC separations, leads to a preference for *gauche* conformations and thus increases the overall mobility of the alkyl chain.[7]

[*] Prof. Dr. K. Albert, Dipl.-Chem. T. Lacker, Dipl.-Phys. M. Raitza, Dr. M. Pursch
Institut für Organische Chemie der Universität
Auf der Morgenstelle 18, D-72076 Tübingen (Germany)
Fax: (+49) 7071-295875
E-mail: klaus.albert@uni-tuebingen.de
Dr. H.-J. Egelhaaf, Prof. Dr. D. Oelkrug
Institut für Physikalische und Theoretische Chemie der Universität Tübingen

[**] This work was funded by the Deutsche Forschungsgemeinschaft (LI 154/41-3 and LI 154/41-4) and the Fonds der Chemischen Industrie. We thank Bischoff Analysentechnik und -geräte GmbH, Leonberg, Germany for providing Prontosil silica gel.

 © WILEY-VCH Verlag GmbH, D-69451 Weinheim, 1998 1433-7851/98/3706-0778 $ 17.50+.50/0

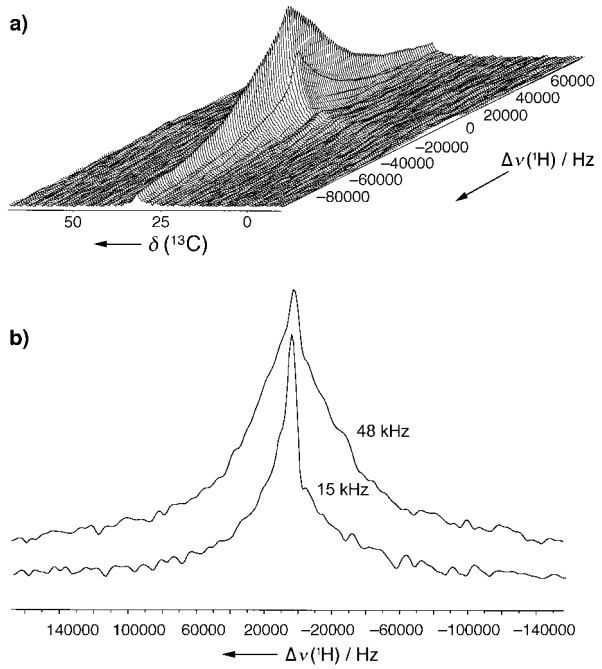


Figure 2. a) 2D WISE NMR spectrum of the C_{30} phase. b) ^{1}H wide-line spectra ($\Delta\nu$ in Hz) derived from the 2D WISE NMR spectrum of resonances for the *trans* and *gauche* conformations.

Suspended-state ^{13}C NMR spectra of a C_{30} phase were recorded at various temperatures (Figure 3) in methanol/TBME (75/25, v/v); this solvent mixture is preferably used for separating β-carotene isomers. At 295 K, the relative amounts of *trans* and *gauche* alkyl-chain conformations are basically the same as indicated by the solid-state NMR spectra. In analogy to the behavior observed in the solid-state NMR spectra, the population of *trans* and *gauche* conformations interchanges with increasing temperature (Figure 3).

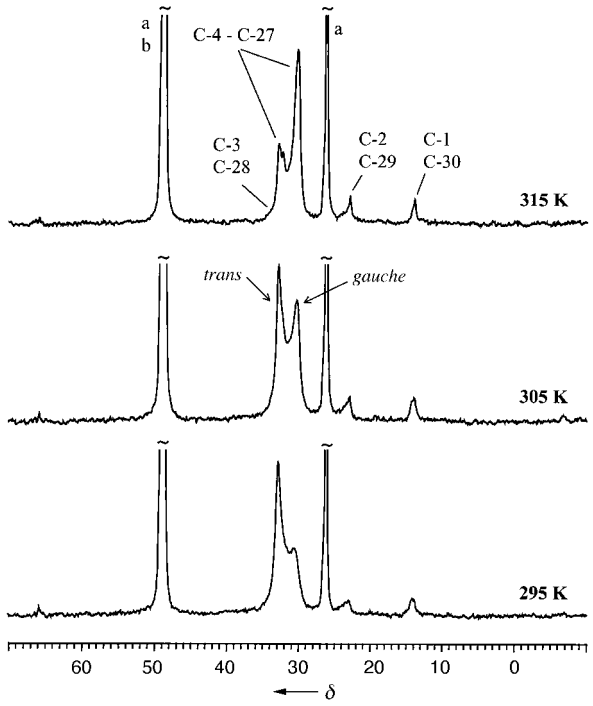


Figure 3. Temperature dependence of the suspended-state ^{13}C MAS NMR spectra (75.4 MHz) of the C_{30} phase in methanol/TBME (75/25, v/v). Solvent signals are indicated with a (TBME) and b (methanol).

A change in the arrangement of the alkyl chain, caused by an alteration in the composition of the mobile phase or temperature, should result in a different dynamic and chromatographic retention behavior of the analyte. In the case of analytes containing a fluorophoric group, the dynamic behavior in the interphase system can be determined from the rotation correlation time τ_R. This parameter is obtained from fluorescence anisotropy measurements.[10] The reciprocal value of the rotation correlation time τ_R is proportional to the rotation diffusion coefficient of the employed fluorescence probe and directly monitors the mobility in the interphase system.[10] Figure 4 clearly shows that the analyte employed, 1,6-diphenylhexatriene (DPH), increases its mobility with increasing temperature in the interphase system consisting of the C_{30} separation phase and acetonitrile/water as mobile phase. The average rotation correlation time $\bar{\tau}_R$ shown in Figure 4 were calculated from stationary fluorescence anisotropies and the corresponding fluorescence decline curves τ_F.

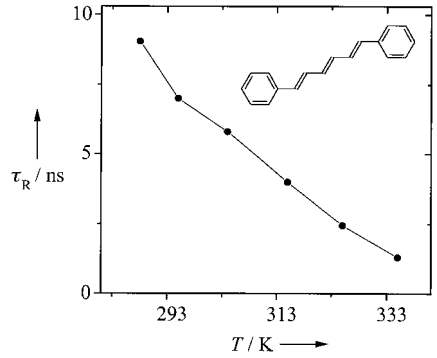


Figure 4. Temperature dependence of the average rotation correlation time $\bar{\tau}_R$ of DPH in the interphase system C_{30} phase – DPH – acetonitrile/water (50/50, v/v).

The overall picture of the temperature-dependent interphase system is illustrated by the separation of β-carotene isomers performed with the C_{30} phase at various temperatures. At 285 K the all-*trans* and the 9-*cis* isomers are well separated (Figure 5). An increase in temperature leads to decreased retention times and selectivity factors. Nonetheless, a good separation is achieved at 295 K with shorter retention times. No severe changes occur up to a temperature of 305 K, but between 305 and 315 K the separation capability of the C_{30} phase decreases, and there is coelution of both stuctural isomers at 315 K.

Parallel to the decrease in separation quality of the C_{30} phase, the increase in temperature between 295 and 315 K leads to a change in the ratio of *trans* to *gauche* conformations of the *n*-alkyl chain. The fraction of *trans* conformations continuously decreases with increasing temperature. Under the separation conditions used at 295 K the fraction of *trans* conformations is 70%, and decreases to 57% at 305 K and finally to 35% at 315 K. Therefore, the increased specific selectivity for the sterical recognition of structural isomers is

 © WILEY-VCH Verlag GmbH, D-69451 Weinheim, 1998 1433-7851/98/3706-0779 $ 17.50+.50/0

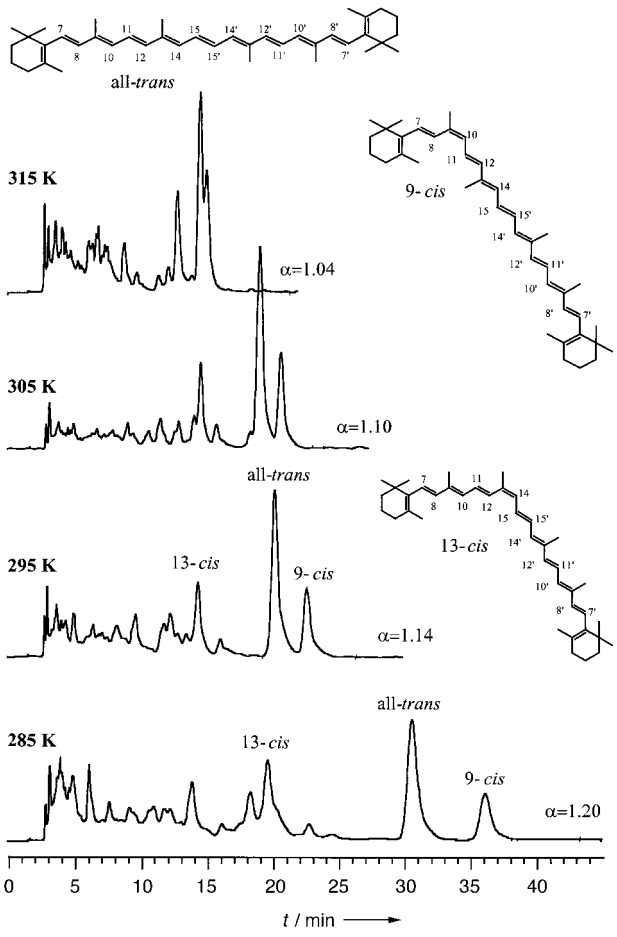


Figure 5. Separation of *cis* and *trans* isomers of β-carotene with a C_{30} phase at various temperatures. The indicated selectivities α refer to the relative retention behavior of the 9-*cis* and the all-*trans* isomers.

directed by the ratio of *trans* to *gauche* conformations of the C_{30} alkyl chains. A higher fraction of *trans* conformations improves the shape selectivity of the C_{30} phases. As far as practical applications are concerned, an important conclusion is that, in contrast to applications employing C_8 and C_{18} phases, temperature equilibration of the C_{30} column should be performed.

Experimental Section

The C_{30} interphase was synthesized by allowing silica gel (4 g, Prontosil, particle size 3 μm, pore size 200 Å, Bischoff, Leonberg, Germany) to react with trichloro-*n*-triacontylsilane (5 g, ABCR, Karlsruhe, Germany). The silane was dissolved in xylene (50 mL) at 343 K and decanted through a paper towel to silica gel suspended in xylene (50 mL). H_2O (1.0 mL) was added to start the reaction. After the mixture was heated at reflux for 10 h, the reaction product was isolated by filtration through a glass frit (P4) and washed with xylene, acetone, ethanol, H_2O, ethanol, acetone, and *n*-hexane.[1, 4]

NMR parameters: NMR spectra were recorded on a Bruker ASX300 spectrometer.^{13}C CP/MAS NMR measurements were performed with a 7-mm probe at a spinning rate (MAS) of 4000 Hz (pulse angle 90°, proton pulse length 6.5 μs, 2048 transients, contact time 6 ms, delay time 1 s, time domain 2K data points (TD) with a spectral width of (SW) 23 kHz, acquisition time 45 ms). Suspended-state NMR spectra were recorded with a 4-mm probe at a spinning rate of 3000 Hz (pulse angle 90°, pulse length 3.6 μs, 8000 transients, delay time 5 s, time domain 6K data points (TD) with a spectral width (SW) of 23 kHz, acquisition time 135 ms). All NMR measurements were performed after an equilibration time of 15 min.

2D WISE experiment: 650 transients per FID, time domain 2K data points (TD2) with a spectral width (SW2) of 23 kHz, acquisition time 45 ms, 64 increments (TD1) at 3 μs, spectral width (SW1) 333 kHz, contact time 500 μs, delay time 1 s, exponential multiplication with 20 Hz along F_2 and with 5000 Hz along F_1.

Fluorescence parameters: Stationary fluorescence anisotropies were determined in diluted suspensions (10^{-7} M solutions of DPH) on a Spex-222-Fluorolog spectrometer equipped with calcite polarizer prisms. The high dilution was necessary to prevent fluorescence depolarization by multiple scattering.

Chromatographic parameters: The separation material was added as a slurry in propan-2-ol to a stainless steel column (250 × 4.6 mm, Bischoff, Leonberg, Germany). The separation was carried out on a HP-1100 chromatographic system (Hewlett–Packard, Waldbronn, Germany) with methanol/TBME (75/25, v/v) as eluent (flow rate 1.0 mL min^{-1}, UV detection at 450 nm). An aliquot (10 μL) of a 0.05% solution of the β-carotene isomers was injected onto the column. The temperature of the HPLC separation was controlled by calibrating the column in a Haake K thermostat at the desired temperature.

Received: September 29, 1997
Revised version: November 17, 1997 [Z10985IE]
German version: *Angew. Chem.* **1998**, *110*, 809–812

Keywords: carotenoids · chromatography · fluorescence spectroscopy · NMR spectroscopy

[1] L. C. Sander, K. Epler Sharpless, N. E. Craft, S. A. Wise, *Anal. Chem.* **1994**, *66*, 1667–1674.
[2] C. Emenhiser, L. C. Sander, S. J. Schwartz, *J. Chromatogr. A* **1995**, *707*, 205–212.
[3] S. Strohschein, M. Pursch, H. Händel, K. Albert, *Fresenius J. Anal. Chem.* **1997**, *357*, 498–502.
[4] M. Pursch, S. Strohschein, H. Händel, K. Albert, *Anal. Chem.* **1996**, *68*, 386–393.
[5] K.-J. Yeum, S. L. Booth, J. A. Sadowski, C. Liu, G. Tang, N. I. Krinsky, R. M. Russel, *Am. J. Clin. Nutr.* **1996**, *64*, 594–602.
[6] F. Delgado-Vargas, O. Paredes-Lopez, *J. Agric. Food Chem.* **1997**, *45*, 1097–1102.
[7] S. Strohschein, M. Pursch, D. Lubda, K. Albert, *Anal. Chem.* **1998**, *70*, 13–18.
[8] W. L. Earl, D. L. Van der Hart, *Macromolecules* **1979**, *12*, 762–767.
[9] K. Schmidt-Rohr, J. Clauss, H.-W. Spiess, *Macromolecules* **1992**, *25*, 3273–3277.
[10] J. R. Lakowicz, *Principles of Fluorescence Spectroscopy*, Plenum Press, New York, **1982**.

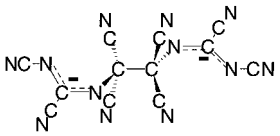
 © WILEY-VCH Verlag GmbH, D-69451 Weinheim, 1998 1433-7851/98/3706-0780 $ 17.50+.50/0

Structure and Properties of Tetracyanomanganate(II), $[Mn^{II}(CN)_4]^{2-}$, The First Paramagnetic Tetrahedral Cyanometalate Complex**

Wayne E. Buschmann, Atta M. Arif, and Joel S. Miller*

Cyanide is a well-known strong-field ligand that forms a large family of homoleptic cyanometalates.[1] Due to their small size and large stability constants these complexes have a propensity to be 18-electron complexes and coordinatively saturated. Examples include octahedral $[M(CN)_6]^{z-}$ (e.g., M = V, Cr, Mn, Fe, Co), and eight-coordinate $[M(CN)_8]^{z-}$ (e.g., M = Mo, W), as well as diamagnetic four-coordinate square-planar d^8 $[M(CN)_4]^{z-}$ (e.g., M = Ni^{II}, Pd^{II}, Pt^{II}), and tetrahedral d^{10} (e.g., M = Zn^{II}, Cd^{II}, Hg^{II}) complexes. $[Co^{II}(CN)_4]^{2-}$ also attests to the strong ligand field of CN, as such d^7 low-spin $S = 1/2$ square-planar complexes are rare.[1b] Interest in this class of compounds has recently been renewed because of the ferro- and ferrimagnetic ordering at both relatively high and ambient temperatures[2] as well as the reversible binding of oxygen.[3] Recently we prepared the $S = 3/2$ d^3 complex, $[PPN]_2[Mn^{IV}(CN)_6]$ (PPN = $[PH_3P{=}N{=}PPh_3]^+$),[4] and herein we report its photochemical degradation to 13-electron $[PPN]_2[Mn^{II}(CN)_4]$, the first member of a new class of magnetic tetrahedral coordinatively unsaturated cyanometalates.

Solutions of yellow $[Mn^{IV}(CN)_6]^{2-}$ decompose on exposure to light in a complex manner by a 10-electron process to several products including the {(1,1,2,2-tetracyano-1,2-ethanediyl)bis[imino(cyanomethylene)]}bis[cyanamide] dianion **1**[5] ($[C_{12}N_{12}]^{2-}$), and $[Mn^{II}(CN)_4]^{2-}$.[6] Crystals of $[PPN]_2[Mn^{II}(CN)_4]$ were studied by single-crystal X-ray diffraction (Figure 1).[7] The MnC and CN distances average 2.159 Å and 1.133 Å, and the C-Mn-C and Mn-C-N angles average 104.2° and 177.05°, respectively. The cation is typical with an average PN distance of 1.583 Å and P-N-P angle of 136.4°. Each anion is surrounded by eight cations in the solid state.



1

The 2.16 Å Mn^{II}–CN bonds are unusually long, and the CN bonds are marginally shorter than typical. The reported average Mn–CN (and CN) distances of $Na_4[Mn^{II}(CN)_6]\cdot 10H_2O$,[8a] $K_3[Mn^{III}(CN)_6]$,[8b] $Cs_2Li[Mn^{III}(CN)_6]$,[8c] and $[PPN]_2[Mn^{IV}(CN)_6]$[4] are 1.95 (1.16), 2.00 (1.14), 1.98 (1.15), and 1.97 (1.15) Å, respectively. The tetrahedral $K_2[Zn^{II}(CN)_4]$ complex has Zn–CN (and CN) bond lengths of 2.024 (1.157) Å.[9] This suggests that the CN^- ion is predominantly a σ-donor with essentially no π-backbonding, consistent with the IR and Raman data. The absence of Mn–CN multiple bond character makes $[Mn^{II}(CN)_4]^{2-}$ a good candidate to estimate the covalent radius of Mn^{II} in a similar manner used to estimate the covalent radii of $[M^0(dien)(CO)_3]$ (M = Mn, Cr).[10] Taking the average Mn–CN bond length of 2.16 Å and subtracting the radius of carbon (0.77 Å[11]) gives a value of 1.39 Å, the same as reported for $[Mn^0(dien)(CO)_3]$. This is reasonable, since the Mn^{II}–CN distance is 0.14 Å longer than the Zn^{II}–CN distance, which is consistent with the estimated difference (0.19 Å) in covalent radii of Mn^{II} and Zn^{II}.[11]

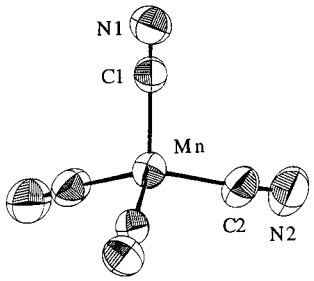


Figure 1. ORTEP drawing depicting $[Mn^{II}(CN)_4]^{2-}$ atom labeling and bond lengths; atoms shown as 30% probability ellipsoids. Selected bond lengths [Å] and angles [°]: Mn–C1 2.151 (6), Mn–C2 2.164 (5), C1–N1 1.139 (6), C2–N2 1.126 (5); C1-Mn-C2 104.1 (2), Mn-C1-N1 174.6 (5), Mn-C2-N2 179.5 (4).

The electronic structure can be determined from the magnetic properties. The strong-field character of the cyanide ligand, as observed for all other percyano-transition metal complexes, suggests the low-spin $^2T_2$ ground state ($S = 1/2$); however, the significantly smaller crystal-field splitting associated with T_d complexes than with O_h complexes suggests the high-spin $^6A_1$ ground state ($S = 5/2$). The high-spin $^6A_1$ ground state is confirmed by magnetic measurements with the observed moment of 5.99 μ_B in excellent agreement with the predicted spin-only value of 5.92 μ_B.

The $\tilde{\nu}_{CN}$ vibrational spectra of $[Mn^{II}(CN)_4]^{2-}$ has intense absorptions at 2202 cm^{-1} (MeCN, IR) and 2209 cm^{-1} (solid; Raman). These bands are assigned to the IR-allowed $\tilde{\nu}_5$ (F_{1u}) and Raman-allowed $\tilde{\nu}_1$ (A_{1g}) and $\tilde{\nu}_5$ (F_{2g}) modes,[12] respectively, by comparison with the assignments made for $K_2[Zn^{II}(CN)_4]$.[13] This assignment represents a pure metal-bound CN absorption without a contribution from d–π* back-bonding. Weak absorptions at approximately 298, 266, and 241 cm^{-1} are observed and assumed to be related to the $\tilde{\nu}_{MC}$ and $\tilde{\nu}_{MCN}$ (A_{1g}, E_g, and F_{2g}) modes, but assignments cannot be made without more information. These are about 50 cm^{-1} lower in energy than the three observed bands of $K_2[Zn^{II}(CN)_4]$ at 348 ($\tilde{\nu}_6$), 340 ($\tilde{\nu}_2$), 216 cm^{-1} ($\tilde{\nu}_3$).[12]

The room-temperature EPR spectrum of $[Mn^{II}(CN)_4]^{2-}$ in solution is typical of high-spin Mn^{II}.[14] At concentrations less than or equal to 1 mM the expected six-line hyperfine structure for ^{55}Mn ($I = 5/2$) is isotropic in solution and centered at $g = 2.003(1)$ with an average hyperfine coupling constant $|A| = 71 \pm 1$ G (Figure 2a).[15a] Because of the observation of isolated sites, the spectrum in frozen solution at 78 K changes to a rhombic lineshape, and there is a slight increase in the g value to 2.012(1).[15b] The temperature dependence of the lineshape has been reported previously for $Mn^{II}(ClO_4)_2$ in methanol upon cooling.[14e]

[*] Prof. J. S. Miller, W. E. Buschmann, A. M. Arif
Department of Chemistry,
University of Utah
315 S. 1400 E. RM Dock, Salt Lake City, UT 84112-0850 (USA)
Fax: (+1) 801-581-8433
E-mail: jsmiller@chemistry.utah.edu

[**] This work was supported by the U.S. Department of Energy (DE-FG03-93ER45504) and by the ACS-PRF (30722-AC5)

 © WILEY-VCH Verlag GmbH, D-69451 Weinheim, 1998 1433-7851/98/3706-0781 $ 17.50+.50/0

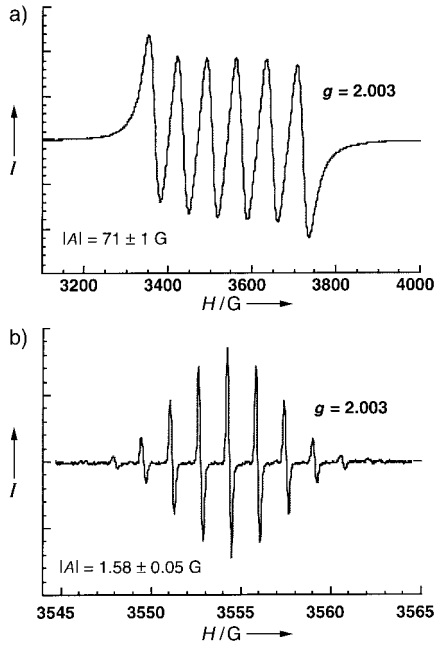


Figure 2. EPR spectrum of $[PPN]_2[Mn^{II}(CN)_4]$ at 300 K, 1.0 mM ($|A| = 71 \pm 1$ G) (a) and 1.5 mM ($|A|$ 1.58 ± 0.05 G) (b) in CH_2Cl_2 and 9.930 GHz; this is attributable to a cyanocarbon radical.

As the concentration is increased above about 1 mM, the six-line resonance pattern loses intensity, whereas a very narrow, sharp eleven-line resonance at $g = 2.003(1)$ with relative integrated peak areas of 0.026:0.063:0.23:0.51:0.83:1.00:0.83:0.51:0.23:0.063:0.026 grows (Figure 2b). The loss of signal intensity suggests some Mn^{II} nearest neighbor interactions leading to an EPR-silent integral spin system. Above 1.5 mM concentration this new resonance remains sharp and increases in intensity, while the original one is broadened into the baseline. The resonance is 16.0 G wide with an average hyperfine coupling constant $|A| = 1.58 \pm 0.05$ G, and the peak-to-peak linewidths are uniform within experimental resolution. An eleven-line pattern is characteristic of unpaired electrons delocalized between two Mn^{II} sites; however, the hyperfine splitting is unreasonably small, and the solution $\tilde{\nu}_{CN}$ shows no detectable changes even at about 10 mM. The hyperfine splitting is consistent with coupling of the unpaired electrons on $^{55}Mn^{II}$ to ^{14}N,[16] but since it lacks Mn^{II} hyperfine structure, the identity of this species is unknown, but most likely is a cyanocarbon radical.

There is a significant amount of intermolecular interactions in solution for $[Mn^{II}(CN)_4]^{2-}$ as shown by the concentration dependence of the EPR spectrum. Line broadening for aqueous Mn^{II} is not observed below 10 mM, presumably because a saturated coordination sphere inhibits intermolecular interactions, while a single broad resonance is still observed at 3.2 M.[14c] Due to the poor coordinating ability of the solvent and the ability of CN^- ions to bind to metal ions at both the C and N, the $[Mn^{II}(CN)_4]^{2-}$ ion likely distorts as it interacts with another $[Mn^{II}(CN)_4]^{2-}$ ion. This distortion could cause the CNs to twist away resulting in nonlinear MnCN bonds, which facilitate the observance of nitrogen hyperfine coupling.

The optical spectrum of $[Mn^{II}(CN)_4]^{2-}$ is atypical for a Mn^{II} ion[17] and does not obey Beer's law as its UV/Vis spectrum changes significantly with concentration, precluding assignment of the parity and spin forbidden d–d transitions. This behavior is consistent with the intermolecular interactions in solution noted from the EPR spectra.

Received: August 25, 1997 [Z10852IE]
German version: *Angew. Chem.* **1998**, *110*, 813–815

Keywords: EPR spectroscopy · magnetic properties · manganese

[1] a) A. G. Sharpe, *The Chemistry of Cyano Complexes of the Transition Metals*, Academic Press, New York, **1976**; b) S. J. Carter, B. M. Foxman, L. S. Stuhl, *Inorg. Chem.* **1986**, *25*, 2888; *J. Am. Chem. Soc.* **1984**, *10*, 4265; c) K. Dunbar, R. A. Heintz, *Prog. Inorg. Chem.* **1996**, *45*, 283.

[2] a) V. Gadet, T. Mallah, I. Castro, M. Verdaguer, *J. Am. Chem. Soc.* **1992**, *114*, 9213; b) T. Mallah, S. Ferlay, C. Auberger, C. Helary, F. L'Hermite, F. Ouahes, J. Vaissermann, M. Verdaguer, P. Veillet, *Mol. Cryst. Liq. Cryst.* **1995**, *273*, 141; c) S. Ferlay, T. Mallah, R. Ouahes, P. Veillet, M. Verdaguer, *Nature* **1995**, *378*, 701; d) W. R. Entley, G. S. Girolami, *Science* **1995**, *268*, 397; e) W. R. Entley, G. S. Girolami, *Inorg. Chem.* **1994**, *33*, 5165; f) W. R. Entley, C. R. Treadway, G. S. Girolami, *Mol. Cryst. Liq. Cryst.* **1995**, *273*, 153.

[3] D. Ramprasad, P. Pez, B. H. Toby, T. J. Markley, R. M. Pearlstein, *J. Am. Chem. Soc.* **1995**, *117*, 10 694.

[4] W. E. Buschmann, C. Vazquez, R. S. McLean, M. D. Ward, N. J. Jones, J. S. Miller, *Chem. Commun.* **1997**, 409.

[5] W. E. Buschmann, A. M. Arif, J. S. Miller, *J. Chem. Soc. Chem. Commun.* **1995**, 2343.

[6] A dry, deoxygenated solution of $[(Ph_3P)_2N]_2[Mn(CN)_6]$ (1.546 g, 0.847 mmol) in a 1:1 mixture of MeCN and CH_2Cl_2 (10 mL) was exposed to ambient sunlight until the color had changed from yellow to dark red. The solution was then layered with Et_2O to crystallize out burgundy-red prisms of $[(Ph_3P)_2N]_2[Mn(CN)_4]$ (314 mg; 30% yield). IR (Nujol): $\tilde{\nu}_{CN} = 2205 \pm 1\ cm^{-1}$; Raman: $\tilde{\nu}_{CN} = 2209 \pm 1\ cm^{-1}$; decomp. at 206°C. Elemental analysis calcd for $C_{76}H_{60}MnN_6P_4$: C 73.84, H 4.82, N 6.80; found: C 73.62, H 4.97, N 6.75. Thermolysis of $[(Ph_3P)_2N]_2[Mn(CN)_6]$ also led to $[(Ph_3P)_2N]_2[Mn(CN)_4]$. $(Et_4N)_2[Mn^{II}(CN)_4]$, which exhibits virtually identical spectroscopic properties, has also been prepared.

[7] Crystal data for $C_{76}H_{60}MnN_6P_4$, $M_r = 1236.20$, monoclinic, space group $C2/c$, $a = 23.001(6)$, $b = 12.810(3)$, $c = 23.820(8)$ Å, $\beta = 111.59(2)°$, $V = 6525.94$ Å^3, $Z = 4$, $\rho_{calcd} = 1.258\ g\,cm^{-3}$, $\lambda = 0.71073$ Å, crystal size $0.48 \times 0.47 \times 0.38$ mm, $T = 20°C$, $2\theta_{max} = 50°$, R_w (on F) [R (on F)] = 0.0500 [0.0425], for 3011 unique reflections with $I > 3\sigma(I)$. Data were collected on a CAD4 diffractometer, and the crystal structure solved with MOLEN software distributed by Enraf Nonius. Crystallographic data (excluding structure factors) for the structure reported in this paper have been deposited with the Cambridge Crystallographic Data Center as supplementary publication no. CCDC-179178. Copies of the data can be obtained free of charge on application to CCDC, 12 Union Road, Cambridge CB2 1EZ (fax: (+44) 1223-336-033; e-mail: deposit@ccdc.cam.ac.uk).

[8] a) N.-G. Vannerberg, *Acta Chem. Scand.* **1970**, *24*, 2335; b) A. Tullberg, N.-G. Vannerberg, *ibid.* **1974**, *28*, 551; c) B. I. Swanson, R. R. Ryan, *Inorg. Chem.* **1973**, *12*, 283.

[9] a) R. G. Dickinson, *J. Am. Chem. Soc.* **1922**, *44*, 774; b) A. Sequeira, R. Chidambaram, *Acta Crystallogr.* **1966**, *20*, 910.

[10] F. A. Cotton, D. C. Richardson, *Inorg. Chem.* **1966**, *5*, 1851.

[11] J. E. Huheey, E. A. Keiter , R. L. Keiter, *Inorganic Chemistry*, 4th ed., Harper Collins, New York, **1993**, p 292.

[12] A high-emission background of the $[PPN]_2[Mn^{II}(CN)_4]$ makes it difficult to obtain well-resolved Raman spectra of low-intensity absorptions even with a 764.925 nm (Ti sapphire) excitation line.

[13] L. H. Jones, B. I. Swanson, *J. Chem. Phys.* **1975**, *63*, 5401.

[14] a) I. S. Chan, B. M. Fung, H. Lütje, *J. Chem. Phys.* **1967**, *47*, 2121; b) B. B. Garrett, L. O. Morgan, *ibid.* **1966**, *44*, 890; c) C. C. Hinkley, L. O. Morgan, *ibid.* **1966**, *44*, 898; d) A. W. Nolle, L. O. Morgan, *ibid.*

 © WILEY-VCH Verlag GmbH, D-69451 Weinheim, 1998 1433-7851/98/3706-0782 $ 17.50+.50/0

1962, *36*, 378; e) L. Burlamacchi, E. Tiezzi, *Chem. Phys. Lett.* **1969**, *4*, 173.

[15] a) This resonance is about 384 G wide, and the peak-to-peak linewidths vary from 69 through 70, 71, and 72 to 73 ± 1 G from low to high field. b) This resonance is about 414 G wide with an average hyperfine coupling constant $|A| = 71 \pm 1$ G. The peak-to-peak linewidths are 56, 68, 73, 78, 80 ± 1 G from low to high field.

[16] a) J. R. Shock, M. T. Rogers, *J. Mag. Res.* **1975**, *18*, 157; b) H. A. Kuska, M. T. Rogers, *J. Chem. Phys.* **1965**, *42*, 3034; c) K. D. J. Root, M. C. R. Symons, *J. Chem. Soc. A* **1968**, 2366; d) M. B. D. Bloom, J. B. Raynor, M. C. R. Symons, *ibid.* **1972**, 3843.

[17] B. N. Figgis, *Introduction to Ligand Fields*, Wiley-Interscience, New York, **1966**, Chap. 9.

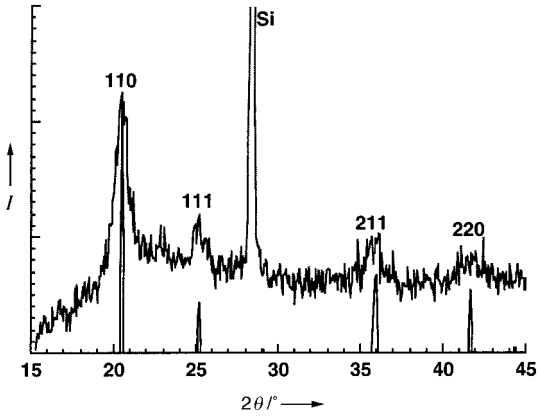


Figure 1. Observed (top) and calculated (lower) powder X-ray diffraction pattern for $Mn^{II}[Mn^{II}(CN)_4]$. The calculated pattern is for the $P\bar{4}3m$ space group with $a = 6.1229$ (5) Å. Silicon was used as an internal standard. I = intensity.

$Mn^{II}[Mn^{II}(CN)_4]$—A Magnetic Interpenetrating Three-Dimensional Diamondlike Solid**

Jamie L. Manson, Wayne E. Buschmann, and Joel S. Miller*

The preparation of the first paramagnetic tetrahedral tetracyanometalate[1] enables the construction new magnetic 3-D network solids, as $[Mn^{II}(CN)_4]^{2-}$ is a building block for the preparation of four-coordinate extended network structures akin to the interpenetrating diamondlike $Zn(CN)_2$.[2] Information on the magnetic properties of this new class of materials will enable a direct comparison to the six-coordinate Prussian Blue family of ordered magnets.[3]

The reaction of equimolar amounts of $[PPN]_2[Mn^{II}(CN)_4]$ (PPN = $[Ph_3P{=}N{=}PPh_3]^+$) and $[Mn^{II}(NCMe)_6]\{B[3,5\text{-}C_6H_3(CF_3)_2]_4\}$ leads to the immediate precipitation of a solid of composition $Mn(CN)_2$, formulated as Mn^{II}-$[Mn^{II}(CN)_4]$. This red solid exhibits an $\tilde{\nu}_{CN}$ absorption at 2170 cm^{-1}, shifted relative to the corresponding band of $[Mn^{II}(CN)_4]^{2-}$ by 32 cm^{-1} to lower energy, which suggests the lengthening of the CN bond upon coordination of its N atom to high-spin Mn^{II}. Based on the 2θ values and relative intensities, the powder pattern is assigned to the cubic $P\bar{4}3m$ space group with $a = 6.1229(5)$ Å (Figure 1).[4] This is consistent with an interpenetrating diamondlike (sphalerite) lattice (Figure 2), based on tetrahedral Mn^{II} sites with an $Mn^{II} \cdots Mn^{II}$ separation of 5.303 Å, which is 0.20 Å longer than the intermetallic distance found for $Zn(CN)_2$ and 0.23 Å longer than that in $K_2Mn^{II}[Mn^{II}(CN)_6]$.[7] Solvent is not evident from either IR or thermal gravimetric analyses. The interpenetrating structure would lead to a density twice the value of 0.775 g cm^{-3} (i.e., 1.550 g cm^{-3}) calculated for a noninterpenetrating structure; indeed, 1.68 g cm^{-3} is observed for a small sample.[8] Due to the inherent lability and coordinative unsaturation of the 13 e^- $[Mn(CN)_4]^{2-}$ building block in polar organic solvents, the CN ligand can dissociate or bind to other $[Mn(CN)_4]^{2-}$ ions permitting the competitive formation of by-products such as octahedral complexes. Consequently, some variability in the energy of the $\tilde{\nu}_{CN}$ band and in the magnetic properties is observed.

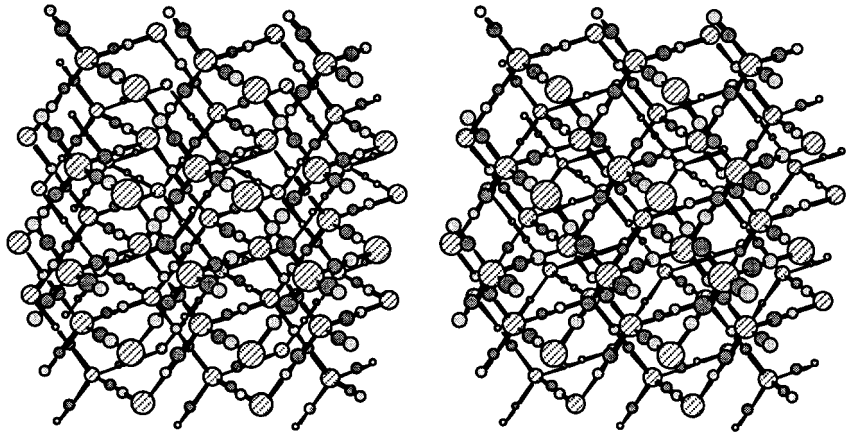


Figure 2. Stereoview of the proposed double-density interpenetrating diamondlike lattice for $Mn^{II}[Mn^{II}(CN)_4]$. The structure resembles that of sphalerite.

The room-temperature magnetic moment μ is 4.4μ_B, a value substantially lower than the predicted value (5.92μ_B) for uncoupled Mn^{II} ions with $S = 5/2$, but consistent with strong antiferromagnetic coupling. As depicted in Figure 3 the magnetic susceptibility χ gradually increases with decreasing temperature reaching a broad maximum, and then decreases rapidly upon further cooling to 2 K. The broad maximum is consistent with antiferromagnetic ordering, while the upturn at low temperature is assigned to impurities with $S = 5/2$. Mn^{II}

[*] Prof. J. S. Miller, J. L. Manson, W. E. Buschmann
Department of Chemistry,
University of Utah
315 S. 1400 E. RM Dock
Salt Lake City, UT 84112-0850 (USA)
Fax: (+)801-581-8433
E-mail: jsmiller@chemistry.utah.edu

[**] The authors appreciate the constructive comments and insight provided by Prof. E. Coronado (Universidad de Valencia), Prof. A. J. Epstein, Dr. C. M. Wynn, and Mr. M. Girtu (The Ohio State University), and gratefully acknowledge the support from the US Department of Energy (Grant No. DE-FG03-93ER45504) and the ACS-PRF (Grant No 30722-AC5).

 © WILEY-VCH Verlag GmbH, D-69451 Weinheim, 1998 1433-7851/98/3706-0783 $ 17.50+.50/0

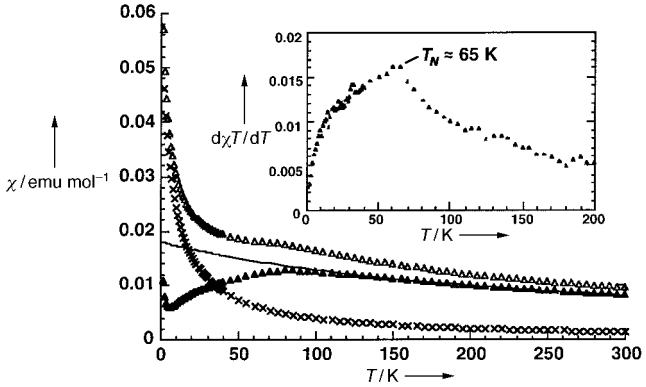


Figure 3. Uncorrected (△) and corrected (▲) molar magnetic susceptibility χ as a function of temperature T for $Mn^{II}[Mn^{II}(CN)_4]$, as well as that obtained after correction for a spin impurity (9.5%) containing Mn^{II} with $S = 5/2$ (×). The fit above 140 K to the Curie–Weiss expression is also presented (—). The inset shows the maximum at $T_N \sim 65$ K from the $d\chi T(T)/dT$ (▲) data.

spin impurities are believed to arise as a result of simultaneous formation of an insoluble oligomeric species as the solid precipitates from solution. Subtraction of a spin impurity[6] leads to the corrected susceptibility with a broad maximum at 80 K due to 3-D antiferromagnetic ordering (Figure 3). Above 140 K χ can be fitted by the Curie–Weiss expression, $\chi \propto (T-\theta)^{-1}$ with a strongly antiferromagnetic θ value of -240 K (Figure 4). The Neèl ordering temperature T_N is $\sim$65 K, as detemined from the maximum in the $d\chi T/dT$ data (Figure 3 inset). Alternating current susceptibility χ_{ac} below 75 K further substantiates antiferromagnetic ordering, as a peak in χ'' is not observed.

Although both $K_2Mn^{II}[Mn^{II}(CN)_6]$[3e] and $Mn^{II}[Mn^{II}(CN)_4]$ have $Mn^{II} \leftarrow C{\equiv}N \rightarrow Mn^{II}$ linkages (six for the former and four for the latter), the former has an uncompensated moment and is a ferrimagnet below 41 K, whereas the latter has a compensated moment and is an antiferromagnet with a higher ordering temperature. This is a consequence of the different electronic structures. Each substance has high-spin Mn^{II} ($S = 5/2$) centers bound to the N atoms. However, the six C-bound CN ligands provide a strong field and the Mn^{II} bound to them is low-spin ($S = 1/2$) and in contrast, as noted above, the tetrahedral Mn^{II} bound to C atoms of the CN ligands is high-spin ($S = 5/2$). Hence, $K_2Mn^{II}[Mn^{II}(CN)_6]$ has

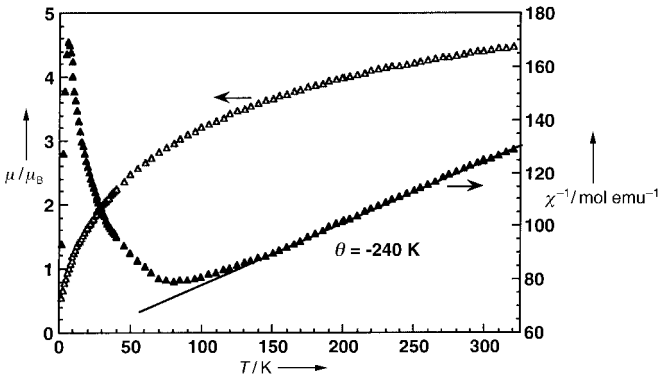


Figure 4. Corrected reciprocal molar magnetic susceptibility χ^{-1} (▲) and moment μ/μ_B (△) as a function of temperature T for $Mn^{II}[Mn^{II}(CN)_4]$. Above 140 K χ^{-1}(T) is linear and can be fitted by the Curie-Weiss expression with $\theta = -240$ K.

coupling between the high- and low-spin sites ($S = 5/2 - 1/2 = 2$) leading to an uncompensated moment, while both Mn^{II} centers have a spin $S = 5/2$ for $Mn^{II}[Mn^{II}(CN)_4]$ and lead to a compensated moment, that is, $S = 5/2 - 5/2 = 0$.

T_c can be estimated[3b, f] from Equation (a), where J is the nearest neighbor magnetic coupling constant, and C_{MC} and C_{MN} are the Curie constants for the C- and N-bound Mn^{II}

$$T_c \propto z J [C_{MC} C_{MN}]^{1/2} \qquad \text{(a)}$$

centers. For systems with a Landé factor g of 2, C is proportional to $S(S+1)$, and assuming identical J values the T_c for tetrahedral $Mn^{II}[Mn^{II}(CN)_4]$ should be 2.28 times greater than the 41 K (i.e., 93.5 K), which is observed for octahedral $K_2Mn^{II}[Mn^{II}(CN)_6]$. Since only 1.58 times the 41 K is observed, J for $Mn^{II}[Mn^{II}(CN)_4]$ must be smaller. This is consistent with the substantially longer $Mn^{II}-C$ bond (by about 0.20 Å), which reduces J. An independent estimation of J requires a model for a 3-D diamond-type Heisenberg system with $S = 5/2$, which at present does not exist.

In contrast to $Mn^{II}[Mn^{II}(CN)_4]$, $M'[Mn^{II}(CN)_4]$ ($M \neq Mn$) should have uncompensated moments and order ferrimagnetically. Studies on these materials are in progress.

Received: August 25, 1997 [Z10853IE]
German version: *Angew. Chem.* **1998**, *110*, 815–817

Keywords: magnetic properties · manganese · network structures

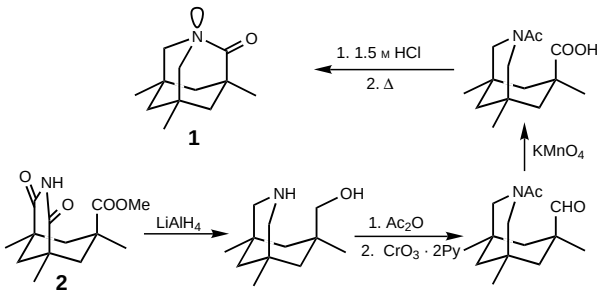
[1] W. E. Buschmann, A. M. Arif, J. S. Miller, *Angew. Chem.* **1998**, *110*, 813; *Angew. Chem. Int. Ed.* **1998**, *37*, 781.
[2] B. F. Hoskins, R. Robson, *J. Am. Chem. Soc.* **1990**, *112*, 1546.
[3] a) V. Gadet, T. Mallah, I. Castro, M. Verdaguer, *J. Am. Chem. Soc.* **1992**, *114*, 9213; b) T. Mallah, S. Ferlay, C. Auberger, C. Helary, F. L'Hermite, F. Ouahes, J. Vaissermann, M. Verdaguer, P. Veillet, *Mol. Cryst. Liq. Cryst.* **1995**, *273*, 141; c) S. Ferlay, T. Mallah, R. Ouahes, P. Veillet, M. Verdaguer, *Nature* **1995**, *378*, 701; d) W. R. Entley, G. S. Girolami, *Science* **1995**, *268*, 397; e) W. R. Entley, G. S. Girolami, *Inorg. Chem.* **1994**, *33*, 5165; f) W. R. Entley, C. R. Treadway, G. S. Girolami, *Mol. Cryst. Liq. Cryst.* **1995**, *273*, 153.
[4] Based upon the corrected (with respect to Si internal standard) *d*-spacings, a crude lattice parameter was calulated and peak indices using $Zn(CN)_2$ as a structural model.[2] Using LATPARM and assuming cubic symmetry the reflection indices along with *d*-spacings were refined. The refinement converged after only four cycles and generated a new lattice parameter with the standard deviation. The space group $P\bar{4}3m$ assumes an ordered arrangement of cyano ligands that is MnC_4 and $Mn\text{-}N_4$, which in reality may not be reasonable. Based on a random orientation of the cyano ligands, that is, $ZnCN_3$, ZnC_2N_2, ZnC_3N, ZnC_4, and ZnN_4, a lower symmetry space group, $Pn\bar{3}m$, has been proposed.[5] Altering the space group merely changes (slightly) the calculated peak intensities. A calculated X-ray diffraction pattern was generated with CRYSTALDIFFRACT[6] on using the refined lattice parameter and atomic positions of the isostructural $Zn(CN)_2$ compound. Therefore the calculated and experimental diffraction patterns are in excellent agreement.
[5] T. Kitazawa, S. Nishikiori, R. Kuroda, T. Iwamoto, *J. Chem. Soc. Dalton Trans.* **1994**, 1029
[6] D. C. Palmer, CRYSTALDIFFRACT. Cambridge University Technical Services Ltd. 20 Trumpington Street, Cambridge CB2 1QA, UK.
[7] The $Mn^{II} \cdots Mn^{II}$ separation is determined from the positions of the Mn centers (Mn Wyckoff positions: 1a Mn(1) 0,0,0; 3d Mn(2) 0,0,½ as follows: $3^{1/2}a/2$.
[8] The density of the material was determined by utilizing a CH_2I_2/CH_2Cl_2 mixture and weighing a 1.00 mL volume.
[9] The impurity (9.5%) is not a simple paramagnet, but possesses some antiferromagnetic coupling ($\theta = -9$ K). This coupling suggests nearest neighbor interactions among adjacent Mn^{II} sites.

 © WILEY-VCH Verlag GmbH, D-69451 Weinheim, 1998 1433-7851/98/3706-0784 $ 17.50+.50/0

The Most Twisted Amide: Structure and Reactions**

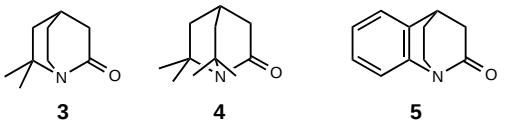
Anthony J. Kirby,* Igor V. Komarov, Peter D. Wothers, and Neil Feeder

We report the preparation, the crystal structure, and some remarkable chemistry of 1-aza-2-adamantanone (**1**). This is the extreme case of a twisted amide, in which overlap of the lone pair on the nitrogen atom with the π system of the carbonyl group is prevented by the rigid geometry of the tricyclic compound. It is prepared from the ester imide **2**[1] of the Kemp triacid by the simple route shown in Scheme 1.



Scheme 1. Synthesis of the twisted amide **1**. Py = pyridine.

The known examples of highly twisted amides (**3**–**5**)[2] are based on the tricyclo[2.2.2]octane skeleton. No detailed structural information is available for these compounds: Only



5 has even been crystallized, and there is evidence that all three polymerize on standing. In contrast, **1** is thermally very stable (m.p. 142–144 °C; it is conveniently purified by sublimation), and gives crystals suitable for structure determination.[3] This shows that the carbonyl group is accurately planar (the three bond angles at the C=O carbon atom add up to 359.9°), and the "amide" nitrogen atom pyramidal (the sum of three bond angles at N is 325.7°; Figure 1).[4] The N–C and C=O bond lengths are 1.475(11) and 1.196(5) Å: substantially longer and shorter, respectively, than expected (1.352, 1.233 Å)[5] for the amide group of an unconstrained tertiary δ-lactam. The twist angle[6] $\tau = 90.5°$ indicates that the nitrogen lone pair lies almost in the nodal plane (a molecular mirror plane) of the π system of the carbonyl group. The most

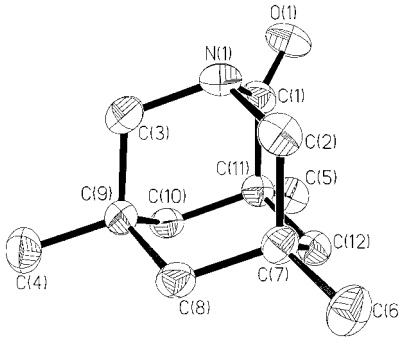
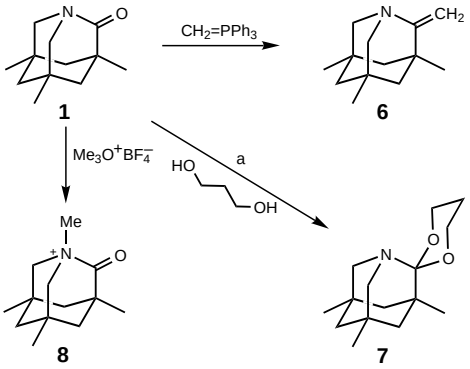


Figure 1. Molecular structure of **1** (ORTEP drawing; ellipsoids are drawn at the 30% probability level).[3] Hydrogen atoms are omitted for clarity.

twisted simple[7] amides for which crystal structures have been reported are two isomeric homologues of **5** that have twist angles of about 40°.[8]

In organic media **1** behaves spectroscopically and chemically as a ketone. The C=O group absorbs at 1732 cm^{-1} in the IR (both in solution in $CDCl_3$ and in a KBr disc), and its ^{13}C NMR chemical shift (in $CDCl_3$) is $\delta = 200$. It reacts with phosphorus ylids under the standard conditions of the Wittig reaction, for example, to form the twisted enamine **6** (Scheme 2), and even forms an "acetal" (**7**) when heated



Scheme 2. Characteristic reactions of the twisted amide **1**. a) p-Toluenesulfonic acid (cat.), benzene, reflux.

with a diol under acid catalysis. Compounds **1**, **6**, and **7** can be methylated at the nitrogen atom by methyl iodide;[7] however, the cation **8** obtained from **1** is an active alkylating and acylating agent, and Meerwein's reagent is needed to give a stable product in this case.

Perhaps most remarkable is the behavior of **1** in water. Pracejus measured an apparent pK_a of 5.3 for the twisted amide **3**.[2] His method (extrapolating the measured pH of a 50% neutralized solution to zero time) fails in the case of **1**, because it is rapidly hydrolyzed when dissolved in water containing a half equivalent of HCl (no signals for **1** were observed in a ^1H NMR spectrum taken in D_2O after 45 s). When the solution is titrated with base, two dissociations are observed with apparent pK_a values of 4.57 and 10.56 (at 25 °C). We take these to be the ionizations of the ring-opened amino acid: The solution shows ^{13}C NMR shifts (in D_2O containing 1% acetonitrile as standard) of $\delta = 188.1$ and 187.8 at pH 7.45 and 12.5, respectively, which are assigned to the

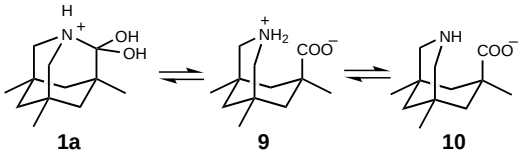
[*] Prof. A. J. Kirby, Dr. I. V. Komarov,[+]
Dr. P. D. Wothers, Dr. N. Feeder
University Chemical Laboratory
Cambridge CB2 1EW (UK)
Fax: (+44) 1223-336-362
E-mail: ajk1@cam.ac.uk

[+] Permanent address:
Institute of Organic Chemistry, Taras Shevchenko University, Kiev (Ukraine)

[**] I.V.K. acknowledges the award of a Royal Society–NATO Postdoctoral Fellowship for 1997.

 © WILEY-VCH Verlag GmbH, D-69451 Weinheim, 1998 1433-7851/98/3706-0785 $ 17.50+.50/0

carboxylate carbon atoms of zwitterion **9** and anion **10** [Eq. (1)]. However, at pH 3.30 there is no absorption in this



1a **9** **10** (1)

region, but a new peak at $\delta = 106.3$. This signal can be assigned with some confidence to the orthoamide carbon atom of the hydrate **1a**[11] of the conjugate acid of the twisted amide **1**: The very similarly substituted carbon atom of N-methylated **7** (which has been fully characterized) absorbs at $\delta = 111$ in $CDCl_3$.

Received: October 21, 1997 [Z11056IE]
German version: *Angew. Chem.* **1998**, *110*, 830 – 831

Keywords: amides · cage compounds · ketones · stereoelectronic effects

[1] K. S. Jeong, K. Paris, P. Ballester, J. Rebek, Jr., *Angew. Chem.* **1990**, *102*, 550 – 551; *Angew. Chem. Int. Ed. Engl.* **1990**, *29*, 555-556. We are grateful to Prof. Rebek, Jr. for detailed experimental instructions for the preparation of **2**.

[2] Compound **3**: H. Pracejus, *Chem. Ber.* **1959**, *92*, 988 – 993; Compound **4**: E. I. Levkoeva, E. S. Nikitskaya, L. N. Yakhontov, *Khim. Geterotsikl. Soedin*. **1971**, *3*, 378 – 384; Compound **5**: G. M. Blackburn, C. J.Skaife, I. T.Kay, *J. Chem. Res. Miniprint* **1980**, 3650 – 3669; V. Somayaji, R. S. Brown, *J. Org. Chem.* **1986**, *51*, 2676 – 2686.

[3] Crystal data for **1**: $C_{12}H_{19}NO$, $M_r = 193.28$, crystal dimensions $0.40 \times 0.20 \times 0.10$ mm, monoclinic, space group $P2_1/c$ (no. 14) $a = 8.962(8)$, $b = 6.298(16)$, $c = 19.399(7)$ Å $\beta = 97.38(5)^\circ$, $V = 1085.4(29)$ Å^3, $Z = 4$, $\rho_{calcd} = 1.183$ Mg m^{-3}, $\mu = 0.074$ mm^{-1}, $2\theta_{max} = 49.98^\circ$, $Mo_{K\alpha}$, $\lambda = 0.71069$ Å, data collected by the $\omega/2\theta$ method, $T = 150(2)$ K. Of 2040 measured reflections, 1909 were independent ($R_{int} = 0.0268$). Data reduction was performed within the TEXSAN program. The crystal structure was solved by direct methods with SIR92 and refined by full-matrix least squares on F^2 with SHELXL-93; final residuals (1909 included reflections, 137 parameters): $R1[I > 2\sigma(I)] = 0.0557$, $wR2 = 0.1232$, $S = 1.143$, ($w = 1/[\sigma^2(F_o^2) + (0.0526P)^2 + 0.3815P]$ where $P = (F_o^2 + 2F_c^2)/3$). Hydrogen atoms were fixed geometrically, riding on the relevant heavy atom, and refined with isotropic temperature factors; largest peak and hole in the final difference map: 0.165 and -0.201 e Å^{-3}, respectively. The C=O group is disordered over two sites: The bond lengths quoted for C=O and C–N represent the weighted mean values from the two disordered fragments. Crystallographic data (excluding structure factors) for the structure reported in this paper have been deposited with the Cambridge Crystallographic Data Center as supplementary publication no. CCDC-100711. Copies of the data can be obtained free of charge on application to CCDC, 12 Union Road, Cambridge CB2 1EZ (fax: (+44) 1223-336-033; e-mail: deposit@ccdc.cam.ac.uk).

[4] The figure of 325.7° is very similar to those observed for acyclic tertiary amines, and identical to that measured for the sum of the three bond angles at the N atoms of diazabicyclooctane: S. Sorriso in *The Chemistry of Functional Groups, Supplement F, Part 1* (Ed.: S. Patai), Wiley-Interscience, Chichester, **1982**, p. 1.

[5] F. H. Allen, O. Kennard, D. G. Watson, L. Brammer, A. G. Orpen, R. Taylor, *J. Chem. Soc. Perkin Trans. 2* **1987**, S1 – S19. The effect of the adjacent nitrogen appears to be to shorten the C=O bond in **1** with respect to that in a simple ketone: The mean value for cyclohexanones is 1.211(9) Å.

[6] The angle of twist (not a simple torsion angle) was defined by F. K.Winkler, J. D.Dunitz, *J. Mol. Biol.* **1971**, *59*, 169.

[7] We consider as simple amides compounds with only one N–C=O bond. The rotational barrier is significantly reduced if a second C=O (or C=S) group is attached to the same nitrogen atom.

[8] Relevant known structures: A. Greenberg, C. A. Venanzi, *J. Am. Chem. Soc.* **1993**, *115*, 6951-6957.

[9] The MeN^+ derivative of **7** is of special interest in the context of the reverse anomeric effect[10] and was the primary objective of this work. Our structural and conformational studies on this compound will be reported shortly.

[10] C. L. Perrin, *Tetrahedron*, **1995** *51*, 11901 – 11935.

[11] Protonated hydrates such as **1a**, high-energy intermediates in the acid-catalyzed hydrolysis of normal amides, are formed with particular ease from twisted amides[12] and derive further stabilization from the adamantane framework in our system.

[12] N. H. Werstiuk, R. S. Brown, Q. Wang, *Can. J. Chem.* **1996**, *74*, 524 – 532.

Amidoglycosylation of Polymer-Bound Glycals: A Complete Solid-Phase Synthesis of the Oligosaccharide Domain of the Lewis^b Blood Group Determinant**

Changsheng Zheng, Peter H. Seeberger, and Samuel J. Danishefsky*

Blood group determinants are a class of cell surface glycoconjugates that are involved in a variety of functions such as cell – cell adhesion, control of cell growth and differentiation, and immune response.[1] Docking of viral and bacterial pathogens is also often initiated through binding of cell surface carbohydrates.[2] In this regard the Lewis^b blood group antigen (Le^b) is of particular interest, as it has been identified as a mediator for the binding of *Helicobacter pylori* to human gastric epithelium.[3] Clinical studies have identified *H. pylori* as a causative agent in gastric and duadenal ulcers.[4] Antimicrobial treatments are currently the means of combatting infection.[5] Since bacterial attachment is a prerequisite to infection,[6] small-molecule lookalikes of the Le^b antennary structure may serve as therapeutic alternatives to broad-spectrum antibiotics.

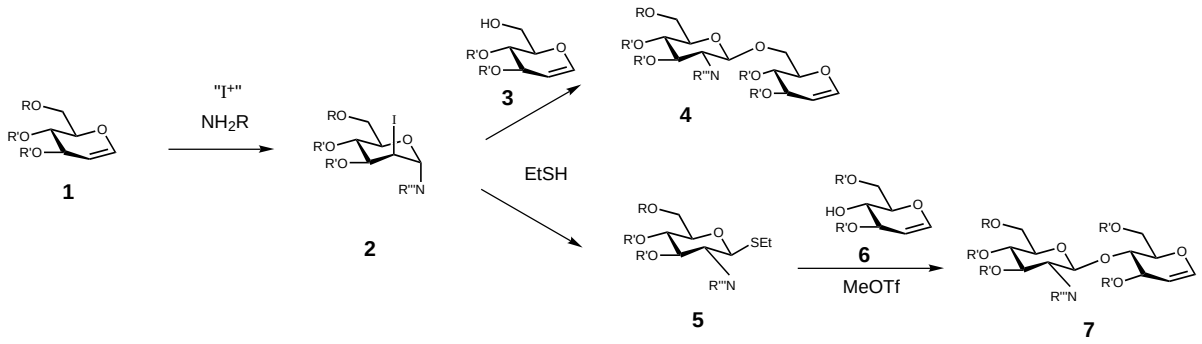
Although many carbohydrate antigens of the A, B, H, and Lewis families has been synthesized in solution phase, synthetic access has often been laborious and time-consuming.[6] A particularly desirable goal would be the development of generally applicable methods for the rapid assembly of oligosaccharides with a long-term view toward automation. Our laboratory has been investigating an approach in which glycals are key building blocks for the synthesis of oligosaccharides and glycoconjugates.[7] This approach has also proven to be amenable to the synthesis of complex structures on solid supports.[7]

Our solution-phase synthesis of glycosides of 2-deoxy-2-acetylamidoglucose (GlcNac) and -galactose (GalNAc) takes

[*] Prof. Dr. S. J. Danishefsky, Dr. C. Zheng, Dr. P. H. Seeberger
Laboratory for Bioorganic Chemistry
Sloan-Kettering Institute for Cancer Research
Box 106, 1275 York Avenue, New York, NY 10021 (USA)
Fax: (+1) 212-772-8691
E-mail: c-kandell@ski.mskcc.org

[**] This work was supported by the National Institutes of Health (CA-28824).

 © WILEY-VCH Verlag GmbH, D-69451 Weinheim, 1998 1433-7851/98/3706-0786 $ 17.50+.50/0



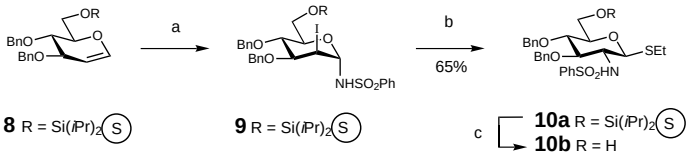
Scheme 1. Conversion of solid support bound glycals into thiodonors for amidoglycosylation. R = protecting group or solid support; R′, R″, R‴ = protecting groups; Tf = triflate.

advantage of sulfonamidoglycosylation. This sequence starts with the addition of a halonium arenesulfonamide to a glycal such as **1** to afford **2** (Scheme 1). The latter reacts with glycal acceptor **3** to afford **4**. The C2-α-sulfonamide group can be converted into a C2-α-acetamido function by any of several protocols.[8]

Our previous approaches towards the solid-phase synthesis of blood group determinants underscored a serious shortcoming in our polymer-based methodological arsenal. The glycal assembly method permitted rapid and concise access to β-glucosidic and β-galactosidic linkages where C2 carries a protected oxy group.[9] The solution-phase protocol of sulfonamidoglycosylation did not translate to the solid phase since silver ion catalysis is apparently needed in the direct coupling step. We had to take recourse to solution-phase azaglycosylation for the construction of *N*-acetylaminoglycosidic linkages prevalent in biologically important blood group determinants, as well as gangliosides.[10] Needless to say, protocols allowing for the efficient formation of these β-2-aminoglucosidic linkages in solid-phase syntheses would greatly facilitate the synthetic entry to a variety of biologically important targets.

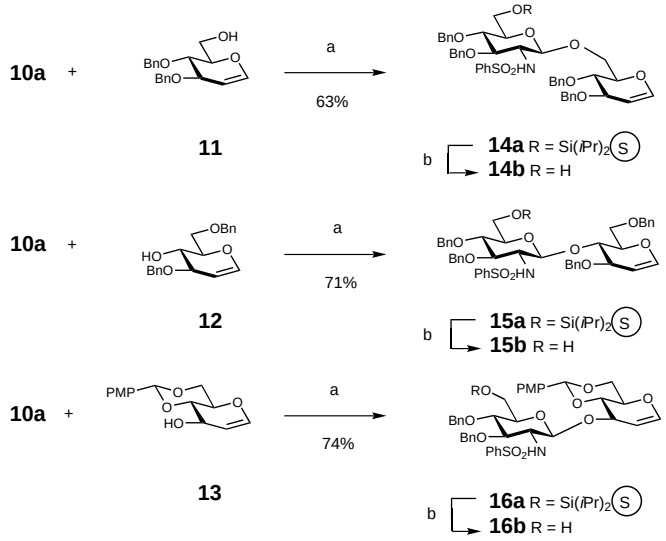
The strategy for success borrowed from a refinement in sulfonamidoglycosylation first demonstrated in solution phase. We found that such direct couplings with encumbered acceptors tended to fail or to occur in poor yield. The modification was developed for transformations with hindered or otherwise weakly reactive acceptors in a projected direct rearrangement – coupling sequence with a 2-β-iodo-1-α-arenesulfonamide donor. Our procedure required prior conversion of **2** to **5** through reaction with ethanethiolate. At this point system **5** serves as an effective donor with a hindered glycal acceptor of type **6** under promotion by methyl trifluoromethanesulfonate (triflate).

We therefore wondered about the transferability of this two-stage sulfonamidoglycosylation methodology to the solid phase. Herein we report the feasibility of converting support-bound glycals into ethylsulfanyl 2-amidoglucosyl donors. These donors were subsequently employed in the construction of β(1,3)-, β(1,4)-, and β(1,6)-2-aminoglucosidic linkages using glycal acceptors. This methodological advance paved the way to the solid-support synthesis of the Lewis^b pentasaccharide glycal. Polymer-supported glucal **8**[8] was treated with iodonium *sym*-collidine perchlorate to form iodosulfonamide **9** as an intermediate (Scheme 2). Rearrangement – displacement through the agency of ethanethiolate yielded the protected ethylsulfanyl glycosyl donor **10** (65%).



Scheme 2. Synthesis of polymer-bound ethylsulfanyl 2-amidoglucosyl donor **10**. a) $I(coll)_2ClO_4$, $PhSO_2NH_2$, CH_2Cl_2, 0°C; b) LHMDS/EtSH, DMF, $-40 \rightarrow 0$°C; c) TBAF/AcOH, THF, 40°C, 18 h. Bn = Benzyl, Ⓢ = polystyrene, coll = *sym*-collidine (2,4,6-trimethylpyridine), LHMDS = lithium bis(trimethylsilyl)amide, TBAF = tetrabutylammonium fluoride.

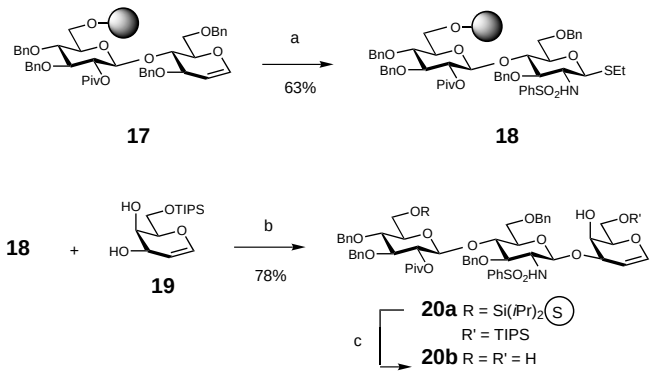
Recently, we have shown that support-bound thioglycosides bearing a protected hydroxyl functionality in the C2 position can be efficiently coupled to glycal acceptors by activation with methyl triflate as a thiophile.[11] One equivalent of the nonnucleophilic base di-*tert*-butylpyridine (DTBP) was added to stabilize the glycal linkage during the coupling experiments. These reaction conditions also proved successful in the case of the ethylsulfanyl 2-amidoglucosyl donors: the formation of β-2-aminoglucosyl (1,4)-linked disaccharide **15a** and β-2-aminoglucosyl (1,3)-linked disaccharide **16a** proceeded in over 70% yield (Scheme 3). The β-2-aminoglucosyl (1,6)-linked disaccharide **20a** was formed in lower yields; this result



Scheme 3. Synthesis of disaccharides with a polymer-bound ethylsulfanyl 2-aminoglucosyl donor. a) MeOTf, DTBP, molecular sieves (4 Å), CH_2Cl_2, $0° \rightarrow 20$°C, 8 h; b) TBAF/AcOH, THF, 40°C, 18 h. PMP = 4-methoxyphenyl.

was not unexpected based on the findings of the study in the C2-oxy series.

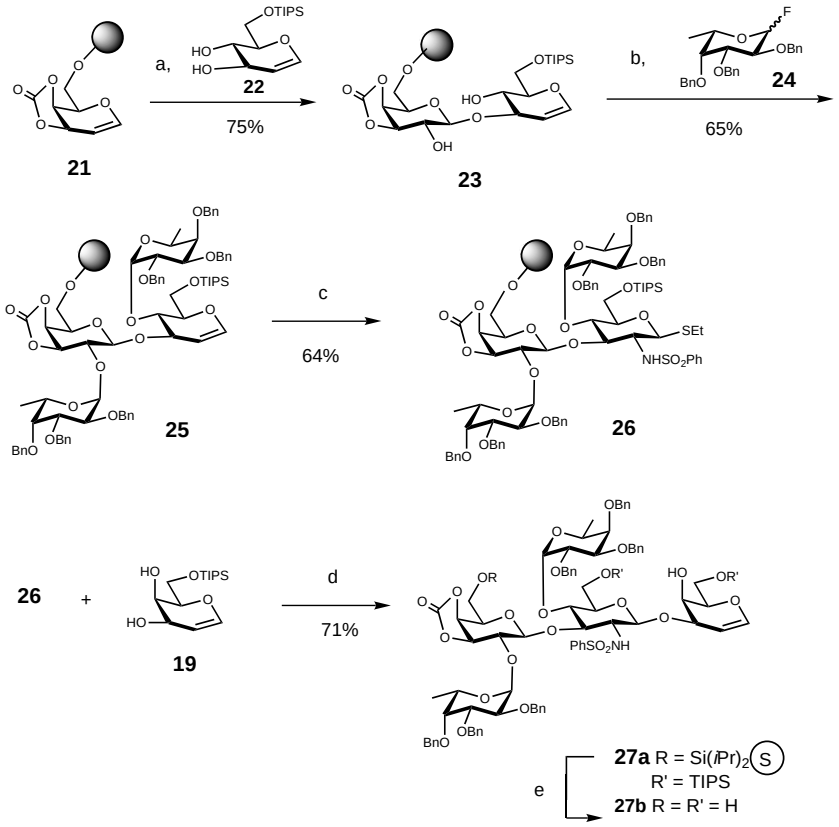
Good coupling yields and excellent selectivities were also obtained in the fashioning of a β-2-aminoglucosyl (1,3) linkage between the support-bound disaccharide donor **18a** and galactal acceptor **19** presenting two exposed hydroxyl functions. Trisaccharide **20a** was formed in 78% yield as the only isomer. (Scheme 4).



Scheme 4. Synthesis of a trisaccharide with polymer-bound ethylsulfanyl 2-aminoglycosyl donor. a) 1. $I(coll)_2ClO_4$, $PhSO_2NH_2$, CH_2Cl_2, 0°C; 2. LHMDS/EtSH, DMF, $-40 \rightarrow 0$°C; b) MeOTf, DTBP, molecular sieves (4 Å), CH_2Cl_2, $0 \rightarrow 20$°C, 8 h; c) TBAF/AcOH, THF, 40°C, 18 h. ● = polymer. TIPS = triisopropylsilyl.

After an efficient coupling protocol for the synthesis of β-2-amidoglucosidic linkages had been established, this methodology was applied to the synthesis of the Lewis[b] pentasaccharide glycal (Scheme 5). Our earlier synthesis failed at the stage of sulfonamidoglycosylation.[12] The tetrasaccharide glycal **25** had to be cleaved from the polymeric carrier and further elaborated by solution-based methods to form the Le[b] oligosaccharide domain in bioconjugatable form. Expanding now on these earlier advances, we converted branched tetrasaccharide **25**[12] into the ethylsulfanyl donor **26**. Coupling to galactal acceptor **19** yielded 71% of the desired pentasaccharide **27a** (Scheme 5). Retrieval of the pentasaccharide was accomplished with tetrabutylammonium fluoride to afford **27b** in 20% overall yield.

A major advance in solid-support oligosaccharide synthesis by the glycal assembly approach has now been achieved. A novel protocol for the conversion of support-bound glycals into ethylsulfanyl 2-amidoglycosyl donors has been developed. Coupling of these glycosyl donors was shown to proceed in good yields in the construction of a variety of different glycosidic linkages. This methodological advance together with other recent methodological progress has brought about a vast expansion of the arsenal of glycosidic linkages accessible by the glycal assembly approach where the donor moiety is linked to the solid support. The range of biologically important oligosaccharides and glycopeptides now accessible by solid-support synthesis is accordingly amplified. This fact was exemplified by preparation of the previously elusive Lewis[b] pentasaccharide glycal. The challenge of solid-support synthesis of blood group determinants, gangliosides, and carbohydrate tumor-associated antigens of increasing complexity is becoming eminently "doable".



Scheme 5. Solid-phase synthesis of the pentasaccharide glycal of the Lewis[b] blood group determinant. a) 1. DMDO, CH_2Cl_2; 2. **19**, $ZnCl_2$, THF; b) $Sn(OTf)_2$, DTBP, molecular sieves (4 Å), THF/toluene (1/4); c) 1. $I(coll)_2ClO_4$, $PhSO_2NH_2$, CH_2Cl_2, 0°C; 2. LHMDS/EtSH, DMF, $-40 \rightarrow 0$°C; d) MeOTf, DTBP, molecular sieves (4 Å), CH_2Cl_2, $0 \rightarrow 20$°C, 8 h; e) TBAF/AcOH, THF, 40°C, 18 h. DMDO = dimethyldioxirane.

Experimental Section

General procedure for the synthesis of polymer-bound ethylsulfanyl 2-amidoglucosyl donors: Polymer-bound glycal (loading: 0.6 mmol g^{-1}) was suspended in anhydrous CH_2Cl_2 under N_2 and cooled to 0°C. Benzenesulfonamide (8 equiv) and $I(coll)_2ClO_4$ (5.5 equiv) were added. The mixture was stirred at 0°C for 6 h and quenched with saturated $Na_2S_2O_3$ solution. The polymer was filtered and washed with water, acetone, DMSO, acetone, THF, and CH_2Cl_2. The iodosulfonamide intermediate was suspended in anhydrous DMF and cooled to -40°C. Ethanethiol (20 equiv) and LHMDS (8 equiv of a 1.0 M solution in THF) were added sequentially. The suspension was gradually warmed up to 0°C over 3 h and stirred for 5 h. The reaction mixture was quenched with saturated NH_4Cl, filtered, and washed with water, acetone, DMSO, acetone, and THF.

General procedure for the coupling of polymer-bound ethylsulfanyl 2-amidoglucosyl donors with glycal acceptors: Polymer-bound ethylsulfanyl 2-amidoglucoside and activated 4 Å molecular sieves (2 mg per 1 mg of polymer) were suspended in anhydrous CH_2Cl_2 under N_2 and cooled to 0°C. Di-*tert*-butylpyridine (20 equiv) was added and the

 © WILEY-VCH Verlag GmbH, D-69451 Weinheim, 1998 1433-7851/98/3706-0788 $ 17.50+.50/0

mixture was stirred for 30 min. Methyl triflate (20 equiv) was added dropwise, and the reaction mixture was warmed gradually to room temperature and stirred for 5 h. Triethylamine (60 equiv) was added and the reaction mixture stirred for 15 min. The polymer was filtered and suspended in acetone in order to remove the molecular sieves. The polymer was further washed with DMSO, acetone, CH_2Cl_2, and THF.

Analytical samples of the intermediates and the final product were cleaved from the solid support following published procedures[12] and were purified by flash column chromatography.

10b: ^{1}H NMR ($CDCl_3$): $\delta = 7.89$ (d, $J = 7.3$ Hz, 2 H, SO_2Ph), 7.46 (m, 1 H, SO_2Ph), 7.38 (m, 2 H, SO_2Ph), 7.34 – 7.18 (m, 10 H, Bn), 4.77 – 4.67 (m, 3 H), 4.64 (d, $J = 8.2$ Hz, 1 H), 4.59 (d, $J = 11$ Hz, 1 H), 3.84 – 3.78 (m, 1 H), 3.72 – 3.65 (m, 1 H), 3.63 – 3.57 (m, 2 H), 3.56 – 3.48 (m, 1 H), 3.45 – 3.39 (m, 1 H), 2.53 (q, $J = 7.6$ Hz, 2 H, SCH_2CH_3), 1.91 (m, 1 H), 1.14 (t, $J = 7.6$ Hz, 3 H, SCH_2CH_3); Positive-ion electrospray (ES) MS: *m/z*: 566.2 ($[M]^+ + Na^+$); Negative-ion ES MS: 578.2 ($[M]^- + Cl^-$).

27b: ^{1}H NMR ($CDCl_3$): $\delta = 7.86$ (m, 2 H), 7.68 – 7.56 (m, 3 H), 7.50 – 7.17 (m, 65 H), 6.24 (d, $J = 6.0$ Hz, 1 H), 5.29 – 5.25 (m, 1 H), 5.20 – 5.14 (m, 1 H), 5.11 – 4.99 (m, 7 H), 4.89 – 4.42 (m, 34 H), 4.37 – 4.28 (m, 3 H), 4.12 – 3.94 (m, 7 H), 4.00 – 3.82 (m, 8 H), 3.79 – 3.53 (m, 21 H), 1.11 – 1.04 (dd, $J = 6.3$, 6.2 Hz, 6 H); Positive-ion ES MS: 1490.5 ($[M]^+ + Na^+$); Negative-ion ES MS: 1466.7 ($[M]^- - H^+$).

Received: November 1, 1997 [Z 11109 IE]
German version: *Angew. Chem.* **1998**, *110*, 831 – 834

Keywords: glycals · glycosylations · oligosaccharides · solid-phase synthesis

[1] A. Varki, *Glycobiology* **1993**, *3*, 97; A. Giannis, *Angew. Chem.* **1994**, *106*, 188; *Angew. Chem. Int. Ed. Engl.* **1994**, *33*, 178; T. Feizi, *Curr. Opin. Struct. Biol.* **1993**, *3*, 701.
[2] P. Falk, T. Boren, S. Normark, *Methods Enzymol.* **1994**, *236*, 353, and references therein.
[3] T. Boren, P. Falk, K. A. Roth, G. Larson, S. Normark, *Science* **1993**, *262*, 1892.
[4] J. Alper, *Sciene* **1993**, *260*, 159.
[5] a) D. Y. Graham, G. M. Lew, P. D. Klein, D. G. Evans, D. J. Evans, Z. A. Saeed, H. M. Malaty, *Ann. Intern. Med.* **1992**, *116*, 705; b) E. Hentschel, G. Brandstatter, B. Dragosics, A. M. Hirschl, H. Nemeg, K. Schutze, M. Taufer, H. Wurzer, *N. Eng. J. Med.* **1993**, *328*, 308.
[6] For syntheses of the Le^b oligosaccharide see: S. S. Rana, J. J. Barlow, K. L. Matta *Carbohydr. Res.* **1981**, *96*, 231; U. Spohr, R. U. Lemieux *ibid.* **1988**, *174*, 211.
[7] S. J. Danishefsky, M. T. Bilodeau, *Angew. Chem.* **1996**, *108*, 1482; *Angew. Chem. Int. Ed. Engl.* **1996**, *35*, 1380; P. H. Seeberger, M. T. Bilodeau, S. J. Danishefsky, *Aldrichimica Acta* **1997**, *30*, 75.
[8] D. A. Griffith, S. J. Danishefsky, *J. Am. Chem. Soc.* **1990**, *112*, 5811; T. Hamada, A. Nishida, O. Yonemitsu, *ibid.* **1986**, *108*, 140.
[9] C. Zheng, P. H. Seeberger, S. J. Danishefsky, *J. Org. Chem.* **1998**, *63*, 1126.
[10] J. T. Randolph, S. J. Danishefsky, *Angew. Chem.* **1994**, *106*, 1538; *Angew. Chem. Int. Ed. Engl.* **1994**, *33*, 1470.
[11] For couplings of thiodonors with glycals see: P. H. Seeberger, M. Eckhardt, C. E. Gutteridge, S. J., Danishefsky *J. Am. Chem. Soc.* **1997**, *119*, 10064. For activation of thiodonors see: H. Lönn *Carbohydr. Res.* **1985**, *135,* 105; *ibid.* **1985**, *139,* 115; H. Lönn *J. Carbohydr. Chem.* **1987**, *6,* 301; P. Fügedi, P. J. Garegg *Carbohydr. Res.* **1986**, *149,* C9.
[12] J. T. Randolph, K. F. McClure, S. J. Danishefsky, *J. Am. Chem. Soc.* **1995**, *117*, 5712.

The Total Synthesis of Eleutherobin: A Surprise Ending**

Xiao-Tao Chen, Bishan Zhou, Samit K. Bhattacharya, Clare E. Gutteridge, Thomas R. R. Pettus, and Samuel J. Danishefsky*

In memory of John K. Stille

The "eleuthesides" comprise[1] a family of marine-derived natural products that exhibit cytotoxic activity.[1, 2] Most intriguing of these is eleutherobin (**1**),[3] which has a modality of action and a potency to warrant its inclusion with paclitaxel, the epothilones, and discodermolide as actual or potential anticancer agents of mechanistic commonality. The first total synthesis of eleutherobin (as well as that of sarcodictyin A) was recently disclosed by Nicolaou et al.[4]

Our own efforts pursuant to the synthesis of the eleuthesides were recently described.[5] The most advanced compound in our synthesis was the ketone **2**. We viewed this compound as a platform structure through which naturally occurring eleuthesides could be reached, and a large number of analogues could be fashioned. We turned to the synthesis of eleutherobin (**1**) from **2** (Scheme 1). The conventional approach to this kind of problem would be to develop a method to convert **2** into a suitable glycosyl acceptor (**3**) by overall addition of a C_1 fragment to carbon 3. We would also synthesize a glycosyl donor (cf. suitably activated arabinosyl donor **4**). Classical glycosylation could eventually lead to **1**. In this simple formulation, we do not yet address the question of the order of introduction of the sugar and the urocanic acid appendages.

It seemed possible that one-carbon homologation of enol triflate **5**[6] could serve as a possible route to reach acceptor **3**. In the event, ketone **2** was converted into **5** by deprotonation and enol triflation. We shall return to this compound shortly.

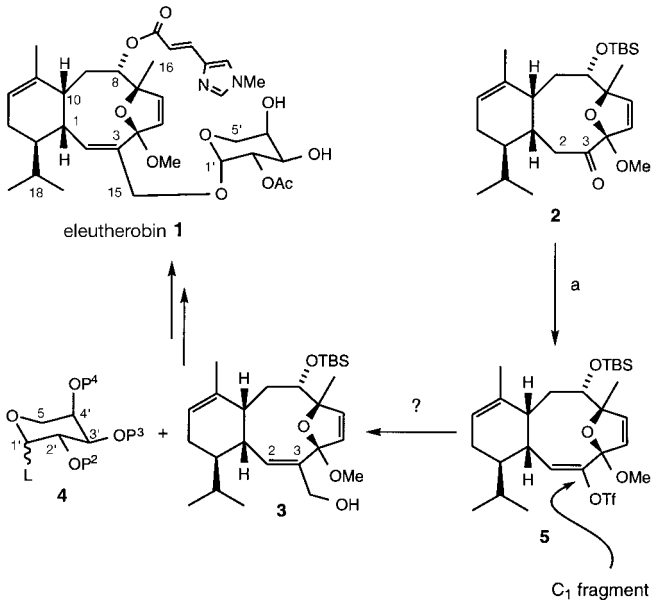
While the matter of the relative configurations of the aglycone and carbohydrate sectors of eleutherobin had not yet been proven to our satisfaction,[7] we began with the assumption that the compound is derived from D-arabinose.[4] Following peracetylation and introduction of an ethylthiol group at the anomeric carbon of D-arabinose, compound **6** became available (Scheme 2). Hydrolysis of the three acetate

[*] Prof. S. J. Danishefsky,[+] X.-T. Chen, B. Zhou, Dr. S. K. Bhattacharya, Dr. C. E. Gutteridge, Dr. T. R. R. Pettus
Department of Chemistry, Columbia University
Havemeyer Hall, New York, NY 10027 (USA)

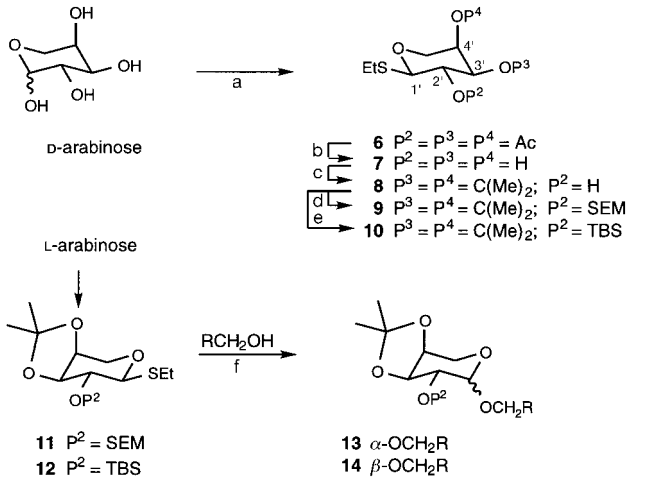
[+] Other address:
Laboratory for Bioorganic Chemistry,
The Sloan-Kettering Institute for Cancer Research
1275 York Avenue, New York, NY 10021 (USA)
Fax: (+1) 212-772-8691
E-mail: c-kandell@ski.mskcc.org

[**] Graduate Fellowships are gratefully acknowledged by X.-T.C. (Kanagawa Academy of Science and Technology) and B.Z. (Pharmacia - Upjohn). Postdoctoral Fellowships are gratefully acknowledged by C.E.G. (The Royal Commission for the Exhibition of 1851) and T.R.R.P. (The National Science Foundation). We are grateful to Vinka Parmakovich and Barbara Sporer of the Columbia University Mass Spectral Facility. We also thank Professor Fenical, University of California, San Diego, for kindly providing us spectral data and a copy of the NMR spectrum of natural eleutherobin.

 © WILEY-VCH Verlag GmbH, D-69451 Weinheim, 1998 1433-7851/98/3706-0789 $ 17.50+.50/0



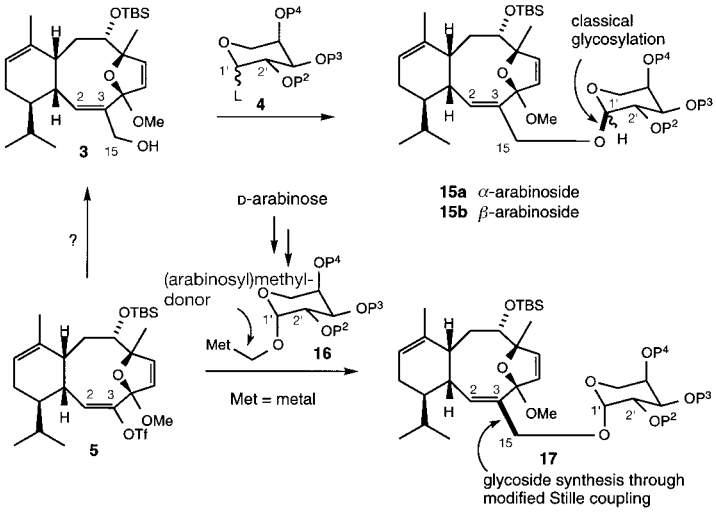
Scheme 1. Conventional glycosylation pproach toward the synthesis of **1**. a) KDA/THF, $-78\,^{\circ}C \rightarrow 0\,^{\circ}C \rightarrow -78\,^{\circ}C$, *N*-(5-cloro-2-pyridyl)triflimide $\approx$ 80%. KDA = potassium diisopropylamide; L = glycosyl donor function; P^2,P^3,P^4 = suitable protecting groups.



Scheme 2. Synthesis of the potential arabinosyl donors. a) Ac_2O, pyridine, DMAP, $0\,^{\circ}C \rightarrow 20\,^{\circ}C$, 100%; EtSH, $BF_3 \cdot Et_2O$, CH_2Cl_2, $20\,^{\circ}C$, 83% (α:β > 10:1); b) NaOMe, MeOH, $20\,^{\circ}C$, 100%; c) 2,2-dimethoxypropane, *p*-TsOH, $20\,^{\circ}C$, 96%; d) SEM-Cl, iPr_2NEt, CH_2Cl_2, $20\,^{\circ}C$, 82%; e) TBS-Cl, imidazole, DMAP, CH_2Cl_2, $20\,^{\circ}C$, 93%; f) MeOTf, DTBP, CH_2Cl_2/Et_2O (1:2), molecular sieves (4 Å), $0\,^{\circ}C$. DMAP = 4-dimethylaminopyridine; DTBP = 2,6-di-*tert*-butylpyridine; SEM = 2-(trimethylsilyl)ethoxymethyl; TBS = *tert*-butyldimethylsilyl.

groups gave rise to **7**. The *cis*-related vicinal hydroxy groups at carbons 3′ and 4′ were engaged in an isopropylidene linkage (see **8**). The lone hydroxy group at C2′ was protected either as a SEM ether (see **9**) or as a TBS ether (see **10**). Following an identical series of steps, starting with L-arabinose, the *ent*-compounds **11** and **12** were also in hand. We explored the use of these potential arabinosyl donors with a variety of model primary alcohol glycosyl acceptors such as benzyl or cinnamyl alcohol. Unfortunately, under a variety of activation conditions, we consistently encountered approximate 1:1 mixtures of α- and β-arabinosides (see **13** and **14** in L-series, Scheme 2).[8]

The thought of subjecting an acceptor of the type **3**, perhaps derivable from **5**, to a stereorandom glycosylation by a system of the type **4** (**3** + **4** → **15**) was dismaying (Scheme 3). This



Scheme 3. Glycosylation strategies. Met = metal.

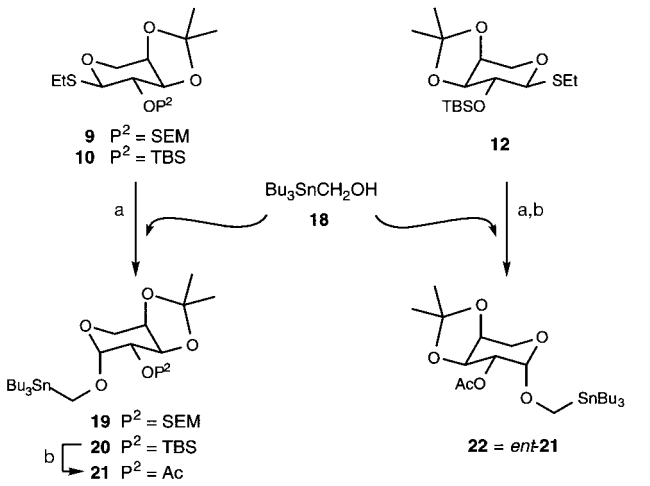
bleak prospect led us to wonder about the possibility of conducting the merger of the aglycone and carbohydrate domains in a nonconventional manner. The stereochemistry of the anomeric carbon of the carbohydrate domain would be defined in advance, (see (arabinosyl)methyl ("oxycarba") donor type **16**). Perhaps, a direct coupling of triflate **5** with **16** could be conducted to lead to the bidomainal compound **17**. Thus, formation of a carbon–carbon bond (C_3-C_{15}) rather than a conventional glycosylation ($C_{15}-O-C_{1'}$) would be used to join the domains.

For our first exploration into the possibility of such a coupling, we focused on a permutation wherein the metal in **16**[9] would be tin in the form of a tri-*n*-butylstannyl function. What we would be seeking would be an "sp^3 version" of the Stille reaction.[10] While there was precedent for transferring simple alkoxyalkyl ligands in a few select cases by an sp^3 Stille-like coupling,[11, 12] no one, to our knowledge, had reported on the possibility of delivering a fully developed carbohydrate by an "oxycarba" transfer through such a process.

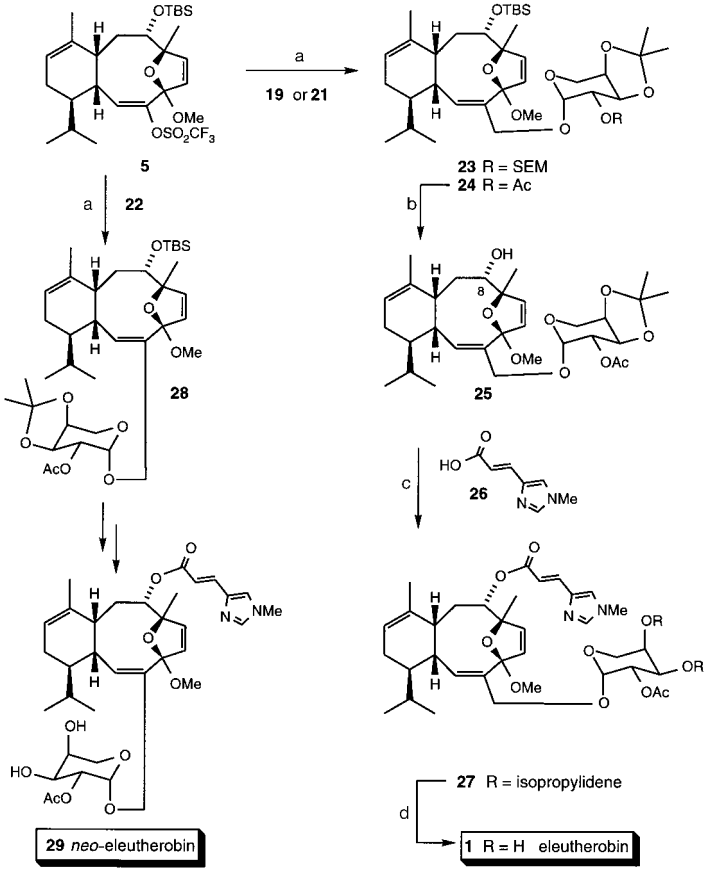
To explore this possibility, we synthesized the novel potential (arabinosyl)methyl donors **19** and **20** (Scheme 4). The previously described **9** was used as a classical donor in a Lönn–Garegg glycosylation[13] with tri-*n*-butylstannylmethanol (**18**).[14] We obtained a 93% yield of a 1:1 mixture of glycosides which was readily separated into its components. For the moment only the β-form[8] **19** was of interest. Similarly, the thioethyl donor, **10** served to glycosylate **18**, affording a 1:1 mixture of separable glycosides. Only the β form[8] **20** was employed. Cleavage of the TBS group and installation of an acetate led to **21**. In an identical way, the *ent*-(arabinosyl)-methyl donor **22** was prepared from **12**.

In the event, modified Stille coupling of vinyl triflate **5** with **19** or **21** gave rise, in 40–50% yields, to **23** and **24**, respectively (Scheme 5). From compound **24**, the pathway to eleutherobin (**1**) was straightforward. The hydroxy group at C8 was

 © WILEY-VCH Verlag GmbH, D-69451 Weinheim, 1998 1433-7851/98/3706-0790 $ 17.50+.50/0



Scheme 4. Synthesis of the (arabinosyl)methyl donors for Stille coupling. a) MeOTf, DTBP, CH_2Cl_2/Et_2O (1:2), molecular sieves (4 Å), 0 °C, 93 % (α:β = 1:1); b) TBAF, THF, 20 °C, ≈ 98 %; Ac_2O, DMAP, CH_2Cl_2, 20 °C, ≈ 99 %. DMAP = 4-dimethylaminopyridine; DTBP = 2,6-di-*tert*-butylpyridine; TBAF = tetrabutylammonium fluoride.



Scheme 5. Synthesis of eleutherobin and *neo*eleutherobin. a) $Pd(PPh_3)_4$, LiCl, 2-amino-5-chloropyridine, THF, △, ≈ 40 – 50 %; b) TBAF, THF, 20 °C, 67 %; c) DCC, DMAP, $PhCH_3$, 50 °C, ≈ 80 %; d)PPTS, MeOH, △, ≈ 70 %. DCC = dicyclohexylcarbodiimide, DMAP = 4-dimethylaminopyridine; PPTS = pyridinium *p*-toluenesulfonate; TBAF = tetrabutylammonium fluoride.

liberated (see compound **25**) and acylated with (*E*)-*N*(1)-methylurocanic acid **26**[15] to afford **27**, as shown. Removal of the acetonide protecting group, released eleutherobin itself. The 500 MHz NMR spectrum (and optical rotation) of fully synthetic eleutherobin corresponded very closely to the spectrum of natural eleutherobin, recorded and forwarded to us by Fenical et al.[16] A sample of naturally derived eleutherobin was not available for direct comparison in our laboratory.

At this stage, we could not be confident that the spectral consequences of having an enantiomeric L-arabinose-derived sugar domain attached to the same aglycone (i.e. *neo*eleutherobin, vide infra) would be significant. If the two domains were virtually noninteractive, the differences between the two permutations might be difficultly discernible. To check this point, we proceeded to synthesize the only viable alternative version of eleutherobin. For this purpose, **22** was coupled with vinyl triflate **5** to produce **28**. Following an identical series of steps used in the previous series, compound **29** was in hand.[17]

Examination of the 500 MHz NMR spectrum of **29**, which we call *neo*eleutherobin, revealed small, but clear-cut, differences with the spectrum of eleutherobin itself, provided by Fenical et al. Hence, we can rigorously assert that the relative chiralities of the aglycone and arabinose domains of eleutherobin are as shown in **1**, and that the total synthesis of eleutherobin has been accomplished.

We are hopeful that our synthesis, though not currently without weaknesses, will yield amounts of eleutherobin adequate for in vivo evaluation. The generation of families of analogues and their evaluation can certainly be accomplished. These efforts are under way. Moreover, the synthesis serves to highlight a new strategy for generation of certain kinds of glycosides. Studies directed toward establishing the scope and limitation of the modified Stille approach, as well as attempts to include other metals in the general paradigm, **5** + **16** → **17**, are in progress.

Received: December 22, 1997 [Z11287IE]
German version: *Angew. Chem.* **1998**, *110*, 835 – 838

Keywords: antitumor agents · eleutherobin · glycosylations · Stille coupling · total synthesis

[1] For sarcodictyins see: a) M. D'Ambrosio, A. Guerriero, F. Pietra, *Helv. Chim. Acta* **1987**, *70*, 2019; b) *ibid.* **1988**, *71*, 964.

[2] For eleuthosides see: S. Ketzinel, A. Rudi, M. Schleyer, Y. Benayahu, Y. Kashman, *J. Nat. Prod.* **1996**, *59*, 873. Pending development of an official name for this exciting family of natural products, we are referring to them as "eleuthesides" based on eleutherobin as the key member of the grouping.

[3] a) W. H. Fenical, P. R. Jensen, T. Lindel, (University of California) US-A 5,473,057, **1995** [*Chem. Abstr.*, **1996**, *124*, 194297z]; b) T. Lindel, W. H. Fenical, P. R. Jensen, B. H. Long, A. M. Casazza, J. Carboni, C. R. Fairchild, *J. Am. Chem. Soc.* **1997**, *119*, 8744; c) B. H. Long, C. R. Fairchild, A. J. Wasserman, J. Carboni, A. M. Casazza, W. H. Fenical, *Cancer Res.*, **1997**, in press. We thank Professor Fenical for providing us with these papers in advance of publication.

[4] a) K. C. Nicolaou, F. van Delft, T. Ohshima, D. Vourloumis, J. -Y. Xu, S. Hosokawa, J. Pfefferkorn, S. Kim, T. Li, *Angew. Chem.* **1997**, *109*, 2631; *Angew. Chem. Int. Ed. Engl.* **1997**, *36*, 2520. b) For the total synthesis of sarcodictyin A see: K. C. Nicolaou, J.-Y. Xu, S. Kim, T. Ohshima, S. Hosokawa, J. Pfefferkorn, *J. Am. Chem. Soc.* **1997**, *119*, 11353. c) For synthetic studies in the arabinose section of eleutherobin see: K. C. Nicolaou, J. I. Trujillo, K. Chibale, *Tetrahedron*, **1997**, *53*, 8751.

 © WILEY-VCH Verlag GmbH, D-69451 Weinheim, 1998 1433-7851/98/3706-0791 $ 17.50+.50/0

[5] X. -T. Chen, C. E. Gutteridge, S. K. Bhattacharya, B. Zhou, T. R. R. Pettus, T. Haskall, S. J. Danishefsky, *Angew. Chem.* **1998**, *110*, 196; *Angew. Chem. Int. Ed.* **1998**, *37*, 185.
[6] For use of *N*-(5-chloro-2-pyridyl)triflimide as a triflating reagent see: a) D. L. Comins, A. Dehghani, *Tetrahedron Lett.* **1992**, *33*, 6299; b) D. L. Comins, A. Dehghani, C. J. Foti, S. P. Joseph, *Org. Synth.* **1996**, *74*, 77.
[7] The data provided in references [2] and [3], pertaining to eleuthoside (A and B) and eleutherobin, respectively, do not rigorously establish the absolute stereochemical nature of the sugar domain. The total synthesis (ref. [4]) did not explicitly deal with the *neo*eleutherobin issue raised here.
[8] By conventions of carbohydrate nomenclature, α and β in the arabinose series correspond to the configurational relationship between C-1 and C-4 of the pyranoside. (For the nomenclature of carbohydrates see: A. D. McNaught *Carbohydr. Res.* **1997**, 197, 1). In terms of the structures presented here, α would correspond to the equatorial anomer and β to the axial one.
[9] For an interesting example of metalated [((tetrahydropyran-2-yl)-oxy)methyl] species see: D. K. Hutchinson, P. L. Fuchs, *J. Am. Chem. Soc.* **1987**, *109*, 4930.
[10] a) W. J. Scott, J. K. Stille, *J. Am. Chem. Soc.* **1986**, *108*, 3033. For reviews see: b) J. K. Stille, *Angew. Chem.* **1986**, *98*, 504; *Angew. Chem. Int. Ed. Engl.* **1986**, *25*, 508; c) T. N. Mitchell, *Synthesis* **1992**, 803; c) K. Ritter *ibid.* **1993**, 735.
[11] a) M. Kosugi, T. Sumiya, T. Ogata, H. Sano, T. Migita, *Chem. Lett.* **1984**, 1225; b) A. Majeed, Ø. Antonsen, T. Benneche, K. Undheim *Tetrahedron* **1989**, *45*, 993; c) G. K. Cook, W. J. Hornback, C. L. Jordan, J. H. McDonald III, J. E. Munroe *J. Org. Chem* **1989**, *54*, 582; d) J. P. Férézou, M. Julia, Y. Li, W. Liu, A. Pancrazi *Synlett* **1991**, 53.
[12] For selective alkyl transfer to a vinyl iodide using internal coordination at tin see: E. Vedejs, A. R. Haight, W. O. Moss *J. Am. Chem. Soc.* **1992**, *114*, 6556.
[13] a) R. J. Ferrier, R. W. Hay, N. Vethaviyasar, *Carbohydr. Res.* **1973**, *27*, 5; b) P. J. Garegg, C. Henrichson, T. Norberg, *ibid.* **1983**, *116*, 162; c) H. Lönn, *ibid.* **1985**, *139*, 105, 115.
[14] D. Seebach, N. Meyer *Angew. Chem.* **1976**, *88*, 484; *Angew. Chem. Int. Ed. Engl.* **1976**, *15*, 438. We also approached the synthesis of the stannyl methyloxy compounds (**19, 20** etc.) by a Schmidt-type (R. R. Schmidt, M. Reichrath, *Angew. Chem.* **1979**, *91*, 497; *Angew. Chem. Int. Ed. Engl.* **1979**, *18*, 466; R. R. Schmidt, *ibid.* **1986**, *98*, 213 and **1986**, *25*, 212) alkylation of the anomeric hydroxyl with tributylstannylmethyl iodide. For preparation of the alkylating agent see: a) S. L. Buchwald, R. B. Nielsen, J. C. Dewan, *Organometallics* **1989**, 8, 1593; b) D. E. Seitz, J. J. Carroll, C. P. Cartaya M. , S-H. Lee, A. Zapata *Synth. Commun.* **1983**, *13*, 129.
[15] a) See ref. [1a]; b) H. Mawlawi, M. C. Monje, A. Lattes, M. Riviére, *J. Heterocycl. Chem.* **1992**, *29*, 1621.
[16] **1**: $[\alpha]_D^{23} = -73.2$ ($c = 0.17$ in MeOH). Previous reports of $[\alpha]_D^{25}$ for eleutherobin were: -49.3 ($c = 3.0$ in MeOH)[3b] and -67.0 ($c = 0.2$ in MeOH).[4a]
[17] **29**: $[\alpha]_D^{23} = +44.5$ ($c = 0.09$ in MeOH).

Intermolecular Hydrogen Bonding between Water and Pyrazine**

Walther Caminati,* Laura B. Favero, Paolo G. Favero, Assimo Maris, and Sonia Melandri

Hydrogen bonds involving aromatic rings, especially those containing heterocyclic nitrogen atoms, are of fundamental importance in nature. For example, they are essential in base pairing of oligonucleotides, and they determine the tertiary structure and functions of biopolymers. Since all these processes occur in an aqueous environment, the corresponding interactions with water are also of particular interest.[1]

Although it had been speculated for many years that the π-electron cloud of aromatic rings could act as a hydrogen-bond acceptor, the position of hydrogen was first established unambiguously through rotational spectra from the 1:1 complex of benzene with water obtained in a supersonic expansion.[2, 3] Thus, it has been shown that the water molecule is located above the plane of the benzene ring, subject to nearly free internal rotation, with both hydrogen atoms pointing toward the π cloud.

Because aromatic nitrogen heterocycles are essential components of proteins and nucleotides, we thought it would be interesting to study the nature of the interactions of such compounds with water. Rotational transitions of pyridine/water have already been described, but that research project has since been abandoned.[4] Although pyrimidine is the most common six-membered aromatic ring in nature, we chose pyrazine (PRZ) as a prototype, because in this case only the spectrum of the complex is observable in the aromatic-ring/water mixture, since PRZ itself produces no rotational spectrum (the electric dipole moment μ is zero due to symmetry).

Evidence of hydrogen-bond formation between PRZ and water has been obtained from electronic spectra recorded in solution[5] and in an argon matrix,[6] but extensive efforts to observe the formation of such complexes in a supersonic expansion were unsuccessful.[7] The position of the hydrogen atom has not been precisely determined; nevertheless, the blue shift of the $n-\pi^*$ transition strongly suggests that the hydrogen atom is bound to the nitrogen atom. The effects of hydrogen bonding interactions on the electronic molecular spectra of PRZ/water complex and PRZ in solution have been investigated theoretically by Zeng et al.[8] In all cases the interpretations of experimental spectra rely on the assumption of a linear structure for the OH···N bond.

Molecular beam Fourier transform microwave (MBFTMW) spectrometers have frequently been used for the investigation of rotational spectra of molecular complexes of aromatic

[*] Prof. W. Caminati, Prof. P. G. Favero, Dr. A. Maris, Dr. S. Melandri
Dipartimento di Chimica "G. Ciamician" dell'Università
Via Selmi 2, I-40126 Bologna (Italy)
Fax: (+39) 51-259-456
E-mail: caminati@ciam.unibo.it
Dr. L. B. Favero
Istituto di Spettroscopia Molecolare del C.N.R.
Via Gobetti 101, I-40129 Bologna (Italy)

[**] We wish to thank Mr. A. Millemaggi for technical help, and the Ministero dell'Università e della Ricerca Scientifica e Tecnologica, as well as the C.N.R., for financial support.

 © WILEY-VCH Verlag GmbH, D-69451 Weinheim, 1998 1433-7851/98/3706-0792 $ 17.50+.50/0

molecules. Reported spectra include those of six-membered aromatic rings, either with rare gases[9–16] or with small polar molecules. [2, 3, 17] Since we were recently successful in investigating molecular complexes of six-membered aromatic molecules with a simpler technique[18–20]—supersonic jet millimeter-wave absorption spectroscopy—we decided to apply this technique to complexes of aromatic molecules with water as well.

PRZ has two types of proton-acceptor sites: the ring π cloud and the nitrogen lone pair; rotational constants of the complex have therefore been estimated according to two models: the water molecule is bound a) above the ring and subject to the same intermolecular distances as in the benzene/water complex, and b) in the plane of the ring, with a linear N···H–O arrangement and an N–H(O) bond length of 1.9 Å.[7] The geometry of PRZ was taken from the literature[21] under the assumption that it remains unaltered in the complex. From the derived rotational constants, and based on symmetry considerations, the following rotational spectra might have been expected: a μ_a-type spectrum in case a) and both μ_a- and μ_b-type spectra in case b) (μ_a and μ_b are dipole moments along the *a* and *b* axes).

In accordance with model b), the experimental spectrum showed several lines of type μ_b in the R branch, with high values for the quantum number *J* (overall angular momentum) and K_a (the component about the *a* axis for a prolate rotor). The latter is composed of two overlapping components as a result of quasi-degeneracy of the associated levels. All the observed transitions were split into two components, with a relative intensity of 5:3 or 3:5 depending on the parity of K_a. The intensity ratios alternate for consecutive k_a values. After assignment of the rotational spectrum of the complex with normal water, spectra of the isotopomers with D_2O, HDO, and $H_2{}^{18}O$ were investigated. The same types of spectra were observed for all four isotopomers with respect to the doubling of lines and the intensity ratios. It is interesting to note that in the case of the PRZ/HDO complex two isotopomers could in principle have been formed, in which either H or D is involved in the intermolecular bond (PRZ···H′OD and PRZ···D′OH, where H′ and D′ refer to the hydrogen atoms involved in the hydrogen bond), but only the spectrum of the PRZ···D′OH species was observed. This could be due to the lower zero-point energy of the PRZ···D′OH complex, since the energy of the PRZ–D stretching vibration would, in a harmonic approximation, be $1/\sqrt{2}$ as great as that in a PRZ···H vibration.

The two component lines of each transition are interstate transitions between the two sublevels of the ground state, which arise from a low-energy motion on a double-minimum potential energy surface. In order to analyze simultaneously the 0^+ and 0^- levels we used a coupled Hamiltonian operator based on Pickett's reduced axes system (RAS) [Eq. (1)], and $\boldsymbol{H}(0^+)$ and $\boldsymbol{H}(0^-)$ are given by Equations (2) and (3).[22, 23]

$$\boldsymbol{H} = \boldsymbol{H}(0^+) + \boldsymbol{H}(0^-) \quad (1)$$

$$\boldsymbol{H}(0^+) = \mathbf{H}_R(0^+) + \boldsymbol{H}_{CD}(0^+) \quad (2)$$

$$\boldsymbol{H}(0^-) = \boldsymbol{H}_R(0^-) + \boldsymbol{H}_{CD}(0^-) + \Delta E \quad (3)$$

$\boldsymbol{H}_R$ and $\boldsymbol{H}_{CD}$ are the rotational and centrifugal distortion Hamiltonian operators, and ΔE is the energy difference between the two states. Interaction terms of the type $F_{ab}(P_aP_b + P_bP_a)$, etc., provided by theory,[22, 23] were not taken into account here, as is usual for small ΔE values. The quartic centrifugal distortion parameters correspond to the irreducible representation $\mathbf{I}^r$ of Watson's "A" reduced Hamiltonian.[24]

Spectroscopic constants obtained with this approach are reported in Table 1. The centrifugal distortion parameters can be regarded as effective fitting parameters. For example, in a more detailed analysis the large values of the Δ_{JK} and Δ_K parameters could be interpreted in terms of low-energy bending motions of the water molecule relative to the ring, while the opposite signs of the δ_K parameters for the 0^+ and 0^- states are probably due to non-exact interpretation of the two potential minima involved in internal rotational motions of the water molecule.

As shown above, the water molecule is linked to the lone pair of the nitrogen atom through one of the two protons. The quasi-zero values of the inertial defects (-0.23, -0.14, -0.37, and -0.52 u Å^2, for normal H_2O, $H_2{}^{18}O$, HDO, and D_2O species, respectively) suggest full planarity of the complex. This is supported also by the r_s substitution coordinates, obtained by application of Kraitchmann's equations[25] to average values of the rotational constants of the two sublevels of the four isotopomeric complexes. They are reported in Table 2 and provide further indications regarding the structure of the complex. The small non-zero values of $|b|$ and $|c|$ for the oxygen atom and the hydrogen atom involved in the hydrogen bond are probably due to the large amplitude motions underlying this type of molecular complex (see, for example, ref. [19]), and are therefore compatible with zero

Table 1. Rotational constants, centrifugal constants, and energy differences between the two sublevels of the ground state for the pyrazine/water complexes.

	Prz···HOH		Prz···H^{18}OH		Prz···DOH		Prz···DOD	
	0^+	0^-	0^+	0^-	0^+	0^-	0^+	0^-
A [MHz]	6290.15(3)	6290.20(3)	6288.90(3)	6289.00(3)	6279.79(4)	6279.72(3)	6251.12(3)	6251.01(3)
B [MHz]	1466.15(5)	1466.07(6)	1374.12(6)	1374.10(6)	1439.7(1)	1439.3(1)	1377.85(4)	1377.53(5)
C [MHz]	1190.43(6)	1188.82(6)	1128.58(6)	1127.48(5)	1172.7(1)	1170.96(9)	1130.80(5)	1129.77(5)
Δ_J [kHz]	2.42(6)	−1.08(8)	1.76(6)	−0.68(7)	2.8(1)	−1.9(1)	1.77(5)	−1.16(7)
Δ_{JK} [kHz]	7.4(5)	19.8(6)	7.7(4)	17.0(4)	4.4(8)	22.9(9)	7.5(4)	19.0(5)
Δ_K [kHz]	−9.1(6)	−14.8(6)	−7.3(6)	−10.2(6)	−5(1)	−18.9(9)	−5.8(6)	−13.4(5)
δ_J [kHz]	−1.09(6)	1.13(6)	−0.7(1)	1.2(1)	−1.7(3)	0.9(2)	−0.45(4)	1.02(4)
δ_K [kHz]	52(6)	−47(7)	56(6)	−29(6)	80(10)	−79(11)	38(5)	−76(6)
ΔE [MHz]	68.8(7)		51.6(5)		96.0(8)		67.8(5)	

 © WILEY-VCH Verlag GmbH, D-69451 Weinheim, 1998 1433-7851/98/3706-0793 $ 17.50+.50/0

Table 2. Substitution coordinates [Å] for the pyrazine/water complexes. The geometries of the complexed molecules correspond to those of the uncomplexed species (see text). The atom involved in the hydrogen bond is in each case indicated by a prime.

r_s Coordinates		$\|a\|$		$\|b\|$		$\|c\|$	
Complex	Atom	exp.	calcd. [a]	exp.	calcd.[a]	exp.	calcd.[a]
Prz···H′OH	O	3.432(3)	3.441	0.18(5)	0.07	0.16(6)	0.0
	H′	2.526(6)	2.559	0.25(5)	0.30	0.27(6)	0.0
	H	3.977[b]	4.021	0.56	0.69	0.29	0.0
Prz···D′OH	D′	2.501(6)	2.533	0.25(6)	0.29	0.26(6)	0.0
	H	3.952(4)	3.997	0.56(3)	0.66	0.29(6)	0.0

[a] Calculated with hydrogen bond parameters from the r_0 structure (see Figure 1 and text). [b] Obtained from the *a* coordinate of H in the Prz···D′OH complex by addition of the difference between the *a* coordinates of H′ in the Prz···HOH and the Prz···D′OH complexes.

equilibrium values. The larger $|b|$ value for the hydrogen atom not involved in the hydrogen bond indicates that this atom does not lie along the *a* axis, but always lies in the *ab* plane.

Alternatively, a plausible structure with the distance parameters for the vibrational ground state r_0 has been calculated from the rotational constants. The geometries of the two subunits have been taken from literature data on the isolated molecules water and PRZ,[21] except that for PRZ, for which an r_0 structure is not available, the C-N-C angle was changed from 115.6 to 116.7°. The hydrogen bond parameters are provided in Figure 1, and r_s coordinates calculated with this r_0 structure are compared to the experimental values in Table 2. The equilibrium configuration of the complex is shown in Figure 1.

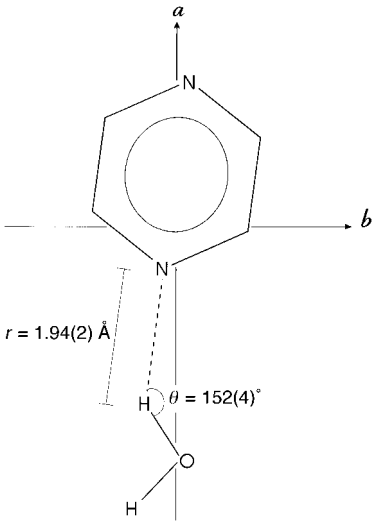


Figure 1. Geometry and principal axes system in the pyrazine/water complex.

The three translational and three rotational degrees of freedom of an isolated water molecule are replaced by six low-energy vibrational modes upon formation of the complex. One of these motions can be considered a stretching between the centers of mass of the two constituent molecules, while the remaining ones can be thought of as two bendings and three internal rotations of the complexed water moiety. Considering the equivalent configurations generated by these motions, and the fact that the water molecule can be bound to either of the two ring nitrogen atoms, the potential energy surface that describes the position of the water molecule with respect to the PRZ molecule is characterized by eight equivalent minima. Only one of the barriers connecting these minima can determine the vibrational spacings (ΔE) reported in Table 1 and is low enough to produce the doubling we have observed for all transitions. This motion can be interpreted as an internal rotation of the water molecule along the H–N bond relative to the ring. Going from one of the two equivalent minima to the other (see Figure 2) inverts the μ_b

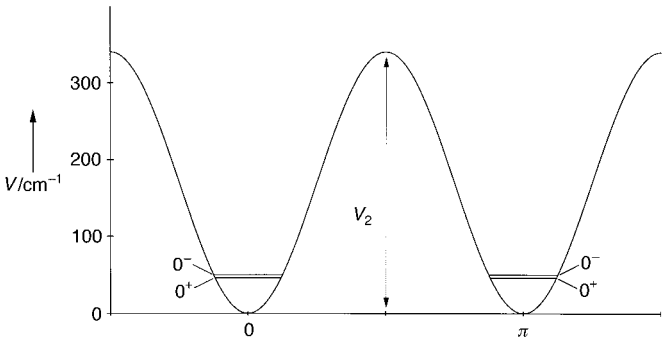


Figure 2. Potential energy function V for internal rotation of the water molecule with respect to the pyrazine ring.

component of the dipole moment, which implies that each μ_b-type transition takes place across the two vibrational sublevels. Furthermore, and in agreement with the permutation group theory of non-rigid molecules,[26, 27] the ratio of intensities of these transitions is established by the two pairs of equivalent hydrogen atoms on the ring; that is, 5:3 for rotational levels of the ground state (0^+) for even K_a, and 3:5 for odd K_a. The reverse is true for the 0^- state.

A quantitative description of this torsion has been obtained by application of Meyer's one-dimensional flexible model[28] to the ΔE splittings of the four isotopic species, with the V_2 parameter determined according to Equation (4), where τ is the internal rotational angle of the water molecule (coinciding with the O-H-N-C dihedral angle).

$$V(\tau) = 1/2\, V_2(1 - \cos 2\tau) \qquad (4)$$

The value of the N-H′-O angle also proved to be an important model parameter, related to the kinetic part of the motion, and it was determined to be about 140°, not very different from the value for the r_0 structure presented in Figure 1. The range 2π for τ has been resolved for the calculation into 21 mesh points.[28] The results of the calculations are shown in Table 3. Two different values of V_2 have

 © WILEY-VCH Verlag GmbH, D-69451 Weinheim, 1998 1433-7851/98/3706-0794 $ 17.50+.50/0

Table 3. Experimental values and energy differences obtained from the flexible model for internal rotation of the water molecule relative to the pyrazine ring in the four isotopomeric pyrazine/water complexes.

	Prz···HOH[a]	Prz···H^{18}OH[a]	Prz···DOH[b]	Prz···DOD[b]
$\Delta E_{exp.}$ [MHz]	68.8(7)	51.6(5)	96.0(8)	67.8(5)
$\Delta E_{calcd.}$ [MHz]	68.2	52.1	97.8	64.3

[a] Parameters utilized: $V_2 = 346\ cm^{-1}$, $\theta = 140°$. [b] Parameters utilized: $V_2 = 308\ cm^{-1}$, $\theta = 140°$.

been fitted, depending on the isotopic species of hydrogen (H′ or D′) involved in the hydrogen bond. A lowering in the V_2 value by about 10% occurs upon introduction of a deuterium atom into the hydrogen bond. This is probably related to the Ubbelohde effect:[29] that is, a shrinkage of the hydrogen bond upon deuteration, which also reduces the distances between the participating heavier atoms of the two subunits.

The two remaining torsional motions of the water subunit would imply rupture of the hydrogen bond, with a correspondingly higher barrier to internal rotation. As a consequence, we did not observe further splittings of the rotational lines due to these motions.

The effects of the two bending motions are reflected in the anomalously high values of the centrifugal distortion parameters Δ_{JK} and Δ_K, as described for several complexes of aromatic molecules with rare gases.[9–20]. Information regarding the force constants for these motions can be obtained in a rather straightforward way from the rotational spectrum when the complex is a symmetric top.[9] It can also be obtained through a more complicated procedure for molecular complexes with C_s symmetry,[30] but this task appears to be difficult in our particular case.

A comparison of our results on PRZ···H_2O with those obtained for the benzene/water complex[2, 3] shows that completely different hydrogen bonds characterize the two complexes. We believe that the type of interaction we have studied is one of the most common in nature, and that our results can therefore serve as a firm experimental starting model for the interpretation of similar linkages in more complicated natural systems.

Experimental Section

The Stark and pulse-modulated free jet absorption millimeter-wave spectrometer used in this study has already been described elsewhere.[18] Complexes were formed in a stream of argon saturated with water at room temperature and a pressure of about 2 bar that passed over samples of PRZ heated to about 40 °C. The mixture, at a stagnation pressure of 0.5 bar, was expanded to about 5×10^{-3} mbar through a pulsed nozzle (repetition rate 5 Hz) with a diameter of 0.35 mm, which produced an estimated "rotational" temperature of about 10 K. All samples involved commercial materials utilized without further purification. The accuracy of the frequency measurements is about 0.05 MHz.

Received: September 23, 1997 [Z10963IE]
German version: *Angew. Chem.* **1998**, *110*, 852 – 856

Keywords: hydrogen bonds · molecular dynamics · N ligands · rotational spectroscopy

[1] G. C. Pimentel, A. C. McClellan in *The Hydrogen Bond* (Ed.: L. Pauling), Freeman, San Francisco, **1960**.
[2] S. Suzuki, P. G. Green, R. E. Bumgarner, S. Dasgupta, W. A. Goddard III, G. A. Blake, *Science* **1992**, *257*, 942 – 945.
[3] H. S. Gutowsky, T. Emilsson, E. Arunan, *J. Chem. Phys.* **1993**, *99*, 4883 – 4892.
[4] a) R. L. Kuczkowski in *Microwave Information Letters* (Ed.: F. J. Lovas) **1995,** No. XXXVIII, p. 37; b) ibid. **1996**, No. XXXIX, p. 39.
[5] C. Marzzacco, *J. Am. Chem. Soc.* **1973**, *95*, 1774 – 1777.
[6] R. Rossetti, L. E. Brus, *J. Chem. Phys.* **1979**, *70*, 4730 – 4736.
[7] J. Wanna, J. A. Menapace, E. R. Bernstein, *J. Chem. Phys.* **1986**, *85*, 1795 – 1805.
[8] J. Zeng, C. Woywod, N. S. Hush, J. R. Reimers, *J. Am. Chem. Soc.* **1995**, *117*, 8618 – 8626.
[9] a) T. Brupbacher, A. Bauder, *Chem. Phys. Lett.* **1990**, *173*, 435 – 438; b) T. Brupbacher, J. Makarewicz, A. Bauder, *J. Chem. Phys.* **1994**, *101*, 9736 – 9746.
[10] T. D. Klots, T. Emilsson, H. S. Gutowsky, *J. Chem. Phys.* **1992**, *97*, 5335 – 5340.
[11] E. Arunan, T. Emilsson, H. S. Gutowsky, *J. Chem. Phys.* **1993**, *99*, 6208 – 6210.
[12] J.-U. Grabow, W. Stahl, *Z. Naturforsch. A* **1992**, *47*, 681 – 684.
[13] E. Jochims, W. Stahl, J.-U. Grabow, *J. Mol. Spectrosc.* **1993**, *158*, 278 – 286.
[14] E. Jochims, H. Mäder, W. Stahl, *J. Mol. Spectrosc.* **1996**, *180*, 116 – 120.
[15] T. D. Klots, T. Emilsson, R. S. Ruoff, H. S. Gutowsky, *J. Phys. Chem.* **1989**, *93*, 1255 – 1265.
[16] R. M. Spycher, D. Petiprez, F. L. Bettens, A. Bauder, *J. Phys. Chem.* **1994**, *98*, 11863 – 11869.
[17] M. Gerhards, M. Schmitt, K. Kleinermanns, W. Stahl, *J. Chem. Phys.* **1996**, *104*, 967 – 982.
[18] S. Melandri, G. Maccaferri, A. Maris, A. Millemaggi, W. Caminati, P. G. Favero, *Chem. Phys. Lett.* **1996**, *261*, 267 – 271.
[19] W. Caminati, S. Melandri, P. G. Favero, R. Meyer, *Chem. Phys. Lett.* **1997**, *268*, 393 – 400.
[20] W. Caminati, A. Millemaggi, P. G. Favero, J. Makarewicz, *J. Phys. Chem.* **1997**, *101*, 9272 – 9275.
[21] S. Cradock, P. B. Liescheski, D. W. H. Rankin, H. E. Robertson, *J. Am. Chem. Soc.* **1988**, *110*, 2758 – 2762.
[22] H. M. Pickett, *J. Chem. Phys.* **1972**, *56*, 1715 – 1723.
[23] H. M. Pickett, *J. Mol. Spectrosc.* **1991**, *148*, 371 – 377.
[24] J. K. G. Watson in *Vibrational Spectra and Structure, Vol. 6* (Ed.: J. R. Durig), Elsevier, New York, **1977**, pp. 1 – 89.
[25] J. Kraitchman, *Am. J. Phys.* **1953**, *21*, 17 – 25.
[26] H. C. Longuet-Higgins, *Mol. Phys.* **1963**, *6*, 445 – 460.
[27] P. R. Bunker, *Molecular Symmetry and Spectroscopy*, Academic Press, New York, **1979**, Chap. 12.
[28] R. Meyer, *J. Mol. Spectrosc.* **1979**, *76*, 266 – 300.
[29] A. R. Ubbelohde, K. J. Gallagher, *Acta Crystallogr.* **1955**, *8*, 71 – 83.
[30] R. P. A. Bettens, R. M. Spycher, A. Bauder, *Mol. Phys.* **1995**, *86*, 487 – 511.
[31] Measured transition frequencies for all complexes are available from the authors.

 © WILEY-VCH Verlag GmbH, D-69451 Weinheim, 1998 1433-7851/98/3706-0795 $ 17.50+.50/0

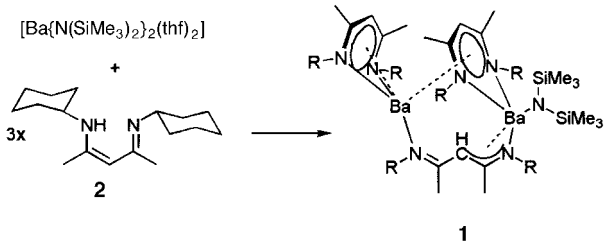
Alkaline Earth Diazapentadienyl Compounds: Structure of $[Ba_2\{(C_6H_{11})NC(Me)CHC(Me)N(C_6H_{11})\}_3\{(SiMe_3)_2N\}]$**

William Clegg, Simon J. Coles, Elaine K. Cope, and Francis S. Mair*

Dedicated to Dr. Ronald Snaith on the occasion of his 50th birthday

Interest in encapsulation of barium ions in covalent sheaths for chemical vapor deposition (CVD) of superconducting oxides has stimulated investigation of the coordination chemistry of barium. Of all ligand platforms, β-diketonates have been much the most studied,[1] followed by substituted cyclopentadienyl ligands.[2] Indeed, barium cyclopentadienyl complexes (and indenyl and fluorenyl complexes) comprise virtually the entire state of current structural knowledge of barium organometallic compounds.[2, 3] We chose to apply the diazapentadienyl (DAP) ligand system[4] to the problem of enforcing molecularity upon barium compounds for CVD. The DAP ligand has much in common with the β-diketonate family, but we reasoned on the basis of our earlier work on lithium complexes of this ligand class[4j] that it would be less likely to bridge two metals. Moreover, we considered that the DAP ligands may show some of the character of their pentadienyl parents,[5] thus adding to the recent extension of organometallic chemistry of barium beyond that of five-membered π-bonded rings (a solvate of the barium salt of 2-pyridylphenylmethane has been recently characterized).[6]

The reaction shown in Scheme 1 yielded small crystals of **1**. Solution and refinement of the structure of **1** from data collected by using synchrotron X-radiation[7] provided the first structural information on alkaline earth DAP complexes,[8] in which this versatile ligand type[4] is found in *three* different bonding modes, *two* of which are novel, all within the same dinuclear molecule.



Scheme 1. Synthesis of **1**. R = cyclohexyl.

The complex retains a single terminal bis(trimethylsilyl)-amido ligand from the starting material.[9] It is somewhat surprising that this amido unit, so often found in a bridging role, is terminal. Instead, the bridging function is undertaken by two DAP ligands in an unprecedented fashion (Figure 1):[10] One DAP ligand chelates Ba1 through N4 and N5 with bond lengths similar to those determined in β-ketoiminatobarium complexes.[11] The NCCCN core of this ligand is

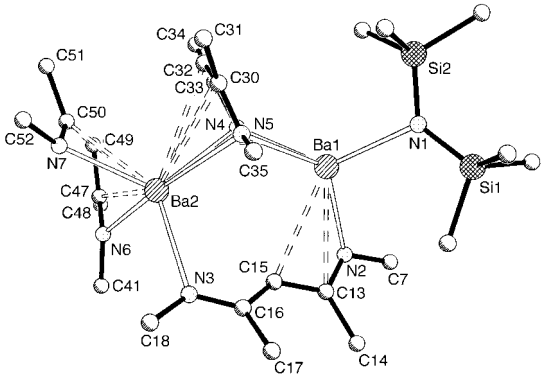


Figure 1. Crystal structure of **1**. Hydrogen atoms and methylene carbon atoms of the cyclohexyl groups are omitted for clarity. Selected bond lengths [Å]: Ba1 – N1 2.613(4), Ba1 – N2 2.703(4), Ba1 – N4 2.829(4), Ba1 – N5 2.841(4), Ba1 – C15 3.125(5), Ba1 – C13 3.192(5), Ba2 – N 7 2.635(4), Ba2 – N 6 2.689(4), Ba2 – N4 2.860(4), Ba2 – N3 2.873(4), Ba2 – N5 3.108(4), Ba2 – C50 3.161(5), Ba2 – C49 3.202(5), Ba2 – C30 3.210(5), Ba2 – C47 3.244(5), Ba2 – C32 3.345(5), Ba2 – C33 3.408(5), N2 – C13 1.327(7), N3 – C16 1.317(6), N4 – C30 1.335(7), N5 – C33 1.317(6), N6 – C47 1.313(7), N7 – C50 1.321(6), C13 – C15 1.425(7), C15 – C16 1.424(7), C30 – C32 1.429(7), C30 – C33 1.423(7), C47 – C49 1.426(8), C49 – C50 1.416(7).

nearly planar (root mean square (RMS) deviation: 0.017 Å), with a moderately obtuse envelope angle (defined as the angle between the NCCCN mean plane and the NBaN plane) of 139.9°. This unremarkable envelope angle[12] indicates that N4 and N5 are σ-bonded to Ba1. However, on the other side of this ring Ba2 lies at a much sharper envelope angle of 99.3°, which would seem to indicate that this ligand is π-bonding to Ba2. The Ba2 – C30, Ba2 – C32, and Ba2 – C33 lengths are somewhat longer than the π bonds in $[(i\mathrm{Pr}_4\mathrm{C}_5\mathrm{H})_2\mathrm{Ba}]$[2b] (mean Ba – C: 2.94(2) Å). Rather, the situation is more akin to that in $[Ba\{(Pz^*)_3Ge\}_2]$ ($Pz^* = 3,5$-dimethylpyrazol-1-yl),[13] where two Pz* rings bind to Ba side-on, principally through Ba – N contacts (mean Ba – N: 2.947 Å; cf. mean Ba2 – N4/N5: 2.984(5) Å). In the Pz* ring (a cyclic analogue of DAP), the Ba – C distances are also rather long (mean 3.409 Å).[13] However, the role of the bridging ligand in **1** as a π donor to Ba2 is not in doubt; its presence in that region forces the other bridging ligand into a most unusual conformation (vide infra). Another DAP ligand binds in a more conventional terminal mode, principally through N6 and N7, with rather shorter σ bonds to Ba2. The envelope angle of 107.9° and the shorter Ba – C bonds indicate considerable η^5 character.

The coordination of Ba2 is completed by a σ bond to N3 of the third DAP ligand, which in fact appears to bond more in

[*] Dr. F. S. Mair, E. K. Cope
Department of Chemistry, UMIST
PO Box 88, Manchester, M60 1QD (UK)
Fax: (+44) 161-236-7677
E-mail: frank.mair@umist.ac.uk
Prof. W. Clegg
Department of Chemistry, University of Newcastle
Newcastle upon Tyne, NE1 7RU (UK)
Dr. S. J. Coles
The Royal Institution of Great Britain
London, WA4 4AD (UK)

[**] The financial support of The Associated Octel Company (F.S.M.), UMIST (F.S.M., E.K.C.), EPSRC and CCLRC (W.C., S.J.C.), and the European Social Fund (E.K.C.) is gratefully acknowledged. We are indebted to Dr. S. Cooke of The Associated Octel Company for useful discussions.

 © WILEY-VCH Verlag GmbH, D-69451 Weinheim, 1998 1433-7851/98/3706-0796 $ 17.50+.50/0

the manner of a 1-aza-allyl fragment to Ba1. This novel opening of the ligand into a W-conjugated conformation is notable because methyl groups reside in the 2- and 4-positions (C14 and C17; Figure 1). A loose analogy may be drawn with pentadienylmagnesium, which adopts a W-conjugated, σ-C-bonded structure in its complex with tetramethylethyenediamine, but which is converted to a U-shaped structure in the 2,4-dimethyl-substituted congener, even while remaining as a η^1 ligand.[5] In **1** the disfavored Me – Me interaction is moderated by a slight out-of-plane twisting of the two methyl groups, but overall, the W-conjugated DAP fragment is close to planar (RMS deviation from N2-C13-C15-C16-N3 plane: 0.070 Å). The ligand adopts this unusual mode to relieve steric interaction between its own cyclohexyl groups and those of the other bridging ligand, these now being orthogonally disposed. Though the bond lengths within the W-conjugated DAP are indicative of full delocalization, Ba1 binds to the ligand in a η^3-1-aza-allyl mode, and lies 1.922 Å above the N2-C13-C15 plane. The most comparable structure is a recent 1-azapentadienyl complex in which potassium ions lie above and below the first three atoms of the delocalized anion to form a polymeric structure.[14] However, in that case the 1-azapentadienyl unit adopts a "sickle", and not a W conformation. Within Group 2 chemistry, there are no structurally characterized aza-allyl complexes, and within heavy alkaline earth organometallic chemistry as a whole there are only two noncyclic ligands in structurally determined complexes, $[Ca(2,4\text{-}tBu_2C_5H_5)_2(thf)]$, which also adopts a U-shaped η^5 conformation,[15] and the aforementioned $[Ba\{PhCH(C_5H_4N\text{-}2)\}_2(thf)\{MeO(CH_2)_2\}_2O]$.[6]

While we failed in our original intention to produce monomeric barium complexes for CVD due to the determination of the barium ions to raise their coordination number and hence the nuclearity of the molecule, the unexpected contortions undergone by the ligands in fulfilling this task have contributed to a new chapter in heavy alkaline earth organometallic chemistry,[3] a chapter which should rapidly expand if the prevalence for π bonding revealed here approaches that recently established for the similarly sized potassium ion.[16] Indeed, this prevalence may explain the differing regiochemistry and superior selectivity of electrophilic attack upon allylbarium reagents over their lithium or magnesium counterparts.[17] Other workers employing N-centered ligands of higher denticity have obtained monomeric barium complexes,[13, 18] though compounds with sufficiently low lattice energies to qualify as attractive CVD agents have yet to appear from this approach. We are continuing the search for the optimum encapsulation topology by replacing the cyclohexyl arms of our ligand with ether-containing lariats.[11]

Experimental Section

2: After the procedure of Hansson et al.,[19] addition of $TiCl_4$ (6 mL, 54.7 mmol) in *n*-hexane (10 mL) to an ice-cooled solution of cyclohexylamine (35 mL, 150 mmol) in *n*-hexane (75 mL) with stirring (10 min) caused formation of an orange solid. At room temperature, 2,4-pentanedione (2.5 mL, 25 mmol) was added dropwise. The mixture was agitated by magnetic stirring and ultrasound (1 h). Diethyl ether (100 mL) was added, and the mixture was filtered. Slow removal of solvent from the filtrate produced crystals (1.5 g, 23 %) of **2.** M.p. 58 – 60. ^{1}H NMR (200 MHz, $CDCl_3$): $\delta = 1.5 - 1.85$ (m, 20H, $CH(CH_2)_5$), 1.89 (s, 6H, *Me*CCHCMe), 3.4(quintet,2H, $CH(CH_2)_5$),4.39 (s, 1H, MeCC*H*CMe), 11.4 (br s, 1H, N*H*). FAB-MS: *m*/*z*: 263 [MH^+]. Satisfactory C, H, and N analyses were obtained.

1: Under a dry argon blanket, 40 – 60 petroleum ether (10 mL) was added to $[Ba\{N(SiMe_3)_2\}_2(thf)_2]$ (0.49 g, 0.825 mmol)[9] and **2** (0.256 g, 0.95 mmol). The solution was evaporated to dryness and redissolved in toluene (5 mL). Very small crystals of **1**·toluene (0.193 g, 0.147 mmol, 35.67 % based on barium) formed overnight at −25 °C. M.p. 126 – 130 °C. ^{1}H NMR (200 MHz, C_6D_6, 293 K): $\delta = 0.53$ (s, 18H, $Si(CH_3)_3$), 1.4 – 2.2 (m, 60H, $CH(CH_2)_5$), 2.22 (br s, 18H, $(CH_3C(NR)CHC(NRBa)CH_3)$, 3.58 (br septet, 6H, $N(CH(CH_3)_5)$, 4.3-5.3 (br s 3H, $CH_3C(NR)CHC(NRBa)$-CH_3). Satisfactory C, H and N analyses were obtained for **1**·toluene.

Received: September 8, 1997 [Z10900IE]
German version: *Angew. Chem.* **1998**, *110*, 841 – 843

Keywords: barium · bridging ligands · chemical vapor deposition · coordination modes · N ligands

[1] W. S. Rees in *Encyclopedia of Inorganic Chemistry*, *Vol. 1* (Ed.: R. B. King), Wiley, Chichester, **1994**, pp. 78-87, and references therein.

[2] a) T. P. Hanusa, *Polyhedron* **1990**, *9*, 1345; b) R. A. Williams, K. F. Tesh, T. P. Hanusa, *J. Am. Chem. Soc.* **1991**, *113*, 4843; c) R. A. Williams, T. P. Hanusa, J. C. Huffman, *J. Organomet. Chem.* **1992**, *429*, 143; d) G. Mosges, F. Hampel, P. von R. Schleyer, *Organometallics* **1992**, *11*, 1769; e) D. J. Burkey, R. A. Williams, T. P. Hanusa, *ibid.* **1993**, *12*, 1331; f) J. S. Overby, T. P. Hanusa, *ibid.* **1996**, *15*, 2205.

[3] D. Stalke, *Angew. Chem.* **1994**, *106*, 2256; *Angew. Chem. Int. Ed. Engl.* **1994**, *33*, 2168.

[4] Also termed β-diketeniminates and β-aminoiminates, DAP ligands have been known for some time but have recently attracted a surge of interest: a) J. E. Parks, R. H. Holm, *Inorg. Chem*. **1968**, *7*, 1408; b) P. C. Healy, M. R. Bendall, D. M. Dodderell, B. W. Skelton, A. H. White, *Aust. J. Chem*. **1979**, *32*, 727; c) A. C. Filipou, C. Völkl, R. D. Rogers, *J. Organomet. Chem*. **1993**, *463*, 135; d) D. Drees, J. Magull, *Z. Anorg. Allg. Chem*. **1994**, *620*, 814; e) *ibid*. **1995**, *621* 948; f) A. Mandel, J. Magull, *ibid.* **1995**, *621*, 941; g) M. F. Lappert, D.-S. Liu, *J. Organomet. Chem.* **1995**, *500*, 203; h) P. B. Hitchcock, J. Hu, M. F. Lappert, M. Layh, D.-S. Liu, J. R. Severn, T. Shu, *Anales de Química Int. Ed.* **1996**, *92*, 186, and references therein; i) P. B. Hitchcock, M. F. Lappert, S. Tian, *J. Chem. Soc., Dalton Trans.* **1997**, 1945; j) F. S. Mair, D. Scully, A. J. Edwards, P. R. Raithby, R. Snaith, *Polyhedron* **1995**, *14*, 2397.

[5] a)H Yasuda, A. Nakamura, *J. Organomet. Chem.* **1985**, *285*, 15; b) R. D. Ernst, *Chem. Rev.* **1988**, *88*, 1255.

[6] M. G. Gardiner, C. L. Raston, H. Viebrock, *Chem. Commun*. **1996**, 1795.

[7] R. J. Cernik, W. Clegg, C. R. A. Catlow, G. Bushell-Wye, J. V. Flaherty, G. N. Greaves, I. Burrows, D. J. Taylor, S. J. Teat, M. Hamichi, *J. Synchrotron Rad.* **1997**, *4*, 279.

[8] Crystal data: $C_{64}H_{113}Ba_2N_7Si_2$, $M_r = 1311.47$, triclinic, space group $P\bar{1}$, $a = 13.2834(2)$, $b = 14.2820(3)$, $c = 19.4521(4)$ Å, $\alpha = 80.399(1)$, $\beta = 88.190(1)$, $\gamma = 70.442(1)°$, $V = 3427.5(1)$ Å^3, $Z = 2$, $\rho_{calcd} = 1.271$ g cm^{-3}; synchrotron radiation (CCLRC Daresbury Laboratory Station 9.8,[6] silicon monochromator, 0.6879 Å), $\mu = 1.22$ mm^{-1}, $T = 160$ K. 17453 data (13177 unique, $R_{int} = 0.0363$, $\theta < 27°$), were collected on a Siemens SMART CCD diffractometer using narrow frames (0.3° in ω), and were corrected semiempirically for absorption and incident beam decay (transmission 0.54 – 1.00). The structure was solved by direct methods and refined by full-matrix least-squares on F^2 values of all data (G. M.Sheldrick, SHELXTL manual, Siemens Analytical X-ray Instruments, Madison WI, USA, 1994, version 5) to give $wR2 = \{\Sigma[w(F_o^2(F_c^2)_2]/\Sigma[w(F_o^2)^2]\}^{1/2} = 0.1088$, conventional $R = 0.0452$ for F values of 8223 reflections with $F_o^2 > 2\sigma(F_o^2)$, $S = 0.824$ for 690 parameters. Isotropic H atoms were constrained; other atoms were refined anisotropically. Residual electron density extremes were 1.33 and −1.50 e Å^{-3}. Crystallographic data (excluding structure factors) for the structures reported in this paper have been deposited with the Cambridge Crystallographic Data Center as supplementary publication

no. CCDC-100681. Copies of the data can be obtained free of charge on application to CCDC, 12 Union Road, Cambridge CB21EZ, UK (fax: (+44) 1223-336-033; e-mail: deposit@ccdc.cam.ac.uk).
[9] B. A. Vaartstra, J. C. Huffman, W. E. Streib, K. G. Caulton, *Inorg. Chem.* **1991**, *30*, 121.
[10] The only previously reported bridging DAP functions thus through a single, symmetrical N bridge, see ref. [4].
[11] D. L. Schulz, B. J. Hinds, D. A. Neumayer, C. L. Stern, T. J. Marks, *Chem. Mater.*, 1993, 1605.
[12] Values ranging from 180 to 110° have been previously observed; see ref. [4].
[13] A. Steiner, D. Stalke, *Inorg. Chem.* **1995**, *34*, 4846.
[14] P. B. Hitchcock, M. F. Lappert, Z. -X. Wang, *Chem. Commun.* **1996**, 1647.
[15] J. S. Overby, T. P. Hanusa, *Angew. Chem.* **1994**, *106*, 2300; *Angew. Chem. Int. Ed. Engl.* **1994**, *33*, 2191.
[16] D. A. Dougherty, *Science* **1996**, *271*, 163.
[17] A. Yanagisawa, S. Habaue, H. Yamamoto, *J. Am. Chem. Soc.* **1991**, *113*, 8955.
[18] a) S. K. Pandey, A. Steiner, H. W. Roesky, D. Stalke, *Angew. Chem.* **1993**, *105*, 625; *Angew. Chem. Int. Ed. Engl.* **1993**, *32*, 596; b) S. G. Dutremez, D. B. Leslie, W. E. Streib, M. H. Chisolm, K. G. Caulton, *J. Organomet. Chem.* **1993**, *462*, C1.
[19] R. Carlsson, U. Larsson, L. Hansson, *Acta Chim. Scand.* **1992**, *46*, 1211.

Structural and Spectroscopic Characterization of a Mononuclear Hydroperoxo–Copper(II) Complex with Tripodal Pyridylamine Ligands**

Akira Wada, Manabu Harata, Koji Hasegawa, Koichiro Jitsukawa,* Hideki Masuda,* Masahiro Mukai, Teizo Kitagawa, and Hisahiko Einaga

Hydroperoxo–copper species are key intermediates in biological oxidations catalyzed by copper enzymes, such as dopamine β-hydroxylase (DβH),[1] galactose oxidase (GO),[2] and superoxide dismutase (SOD).[3] Characterization of these hydroperoxo intermediates is very difficult due to their short lifetimes. Hydroperoxo– or alkylperoxo–copper(II) complexes could be used as model compounds of hypothetical reaction intermediates in these oxidations. Recently the spectroscopic characterization of binuclear hydroperoxo–copper(II) complexes and X-ray structural characterization of mononuclear acylperoxo–copper(II) complexes were reported by Karlin et al.[4] and Kitajima et al.[5] However, the thermal instability of these compounds prevented their complete characterization. To confirm the structural characterization of the $Cu^{II}-OOH^-$ species, we prepared a mononuclear copper complex with a newly designed tripodal pyridylamine ligand, bis(6-pivalamide-2-pyridylmethyl)-(2-pyridylmethyl)amine (bppa), and subjected it to reaction with hydrogen peroxide. Here we describe the structural and spectroscopic characterization of the resulting mononuclear hydroperoxo–copper complex cation $[Cu^{II}(bppa)(OOH^-)]^+$, the first example of an isolated copper–hydroperoxo species.

The addition of a large excess of hydrogen peroxide to a MeCN solution of $[Cu^{II}(bppa^-)]ClO_4$ (**1**)[6] or $[Cu^{II}(bppa)(CH_3COO)]ClO_4$ (**2**)[6] at room temperature resulted in a slight color change from greenish blue to green. The absorption spectra of the reaction product **3,** which is stable for a month at room temperature, exhibited well-separated bands in the d–d region at 830 nm ($\varepsilon = 250\,M^{-1}cm^{-1}$) and 660 nm ($\varepsilon = 150\,M^{-1}cm^{-1}$) and an intense band near 380 nm ($\varepsilon = 890\,M^{-1}cm^{-1}$). The ESR spectrum of a solution of **3** is typical of a trigonal-bipyramidal mononuclear copper complex ($g_\parallel = 2.004$, $g_\perp = 2.207$, $A_\perp = 75$, and $A_\parallel = 109$ G at 77 K in MeOH), suggesting that one of the axial positions has been coordinated by an anionic donor ligand such as a deprotonated hydrogen peroxo ion. The resonance Raman spectra of a solution of **3** in MeCN measured at room temperature (laser excitation wavelength 441.6 nm) revealed a strong resonance-enhanced Raman band at 856 cm^{-1}, which shifted to 810 cm^{-1} ($\Delta\tilde{\nu} = 46\ cm^{-1}$) when ^{18}O-labeled H_2O_2 was used. This range is characteristic for ν(O–O) vibrations of peroxide species and is in close proximity to those found in free $H_2{}^{16}O_2$ and $H_2{}^{18}O_2$ (873 and 826 cm^{-1}).[7] Interpretation of the vibrational data indicates that the hydroperoxo moiety is bound to the copper(II) ion and the intense absorption band near 380 nm can be assigned to the charge-transfer transition of the hydroperoxo group to copper(II) ion. The ESI mass spectrum of a solution of **3** in MeCN showed positive and negative ions with prominent peak clusters at *m/z* 584 and 784, the observed masses and isotope patterns of which corresponded to the $[Cu^{II}(bppa)(OOH^-)]^+$ and $\{[Cu^{II}(bppa)(OOH^-)](ClO_4)_2\}^-$ ions. The use of ^{18}O-labeled H_2O_2 caused these features to shift, as expected, to *m/z* 588 and 788. The intense green color of **3** is maintained throughout the mass spectroscopic experiment, suggesting that the complex is very stable. It is thus clear from these findings that **3** can be best formulated as $[Cu^{II}(bppa)(OOH^-)]^+$. The electronic absorption, ESR, resonance Raman, and ESI mass spectra, as described above, represent the first evidence for the successful synthesis of a mononuclear hydroperoxo–copper(II) complex in solution.

A solution of **3** in MeCN stored in a cold room produced a dark green crystal suitable for X-ray diffraction measurements. The crystal structure of the complex **3**[8] (Figure 1) revealed that the coordination geometry around the copper(II) ion is an axially compressed trigonal bipyramid. The three pyridine nitrogen atoms are in the equatorial plane (Cu–N(2A) 2.099(5), Cu–N(2B) 2.136(4), Cu–N(2C) 2.051(6) Å), and one of the axial positions is occupied by a nitrogen atom

[*] Dr. K. Jitsukawa, Dr. H. Masuda, A. Wada, M. Harata, K. Hasegawa, Dr. H. Einaga
Department of Applied Chemistry, Nagoya Institute of Technology
Showa-ku, Nagoya 466-8555 (Japan)
Fax: (+81) 52-735-5254
E-mail: masuda@ach.nitech.ac.jp
Dr. M. Mukai, Dr. T. Kitagawa
Institute for Molecular Science, Okazaki 444 (Japan)

[**] This work was supported by the Ministry of Education, Science, Sports, and Culture of Japan (K.J. and H.M.). We are grateful to T. Matsui, Kyoto University, for the ^{18}O-labeled H_2O_2 and Prof. Y. Watanabe, Institute for Molecular Science, Okazaki, for the use of the API-300 triple quadrupole mass spectrometer equipped with an ionspray interface (PE-Sciex, Thornhill, ON, Canada). Supporting information for this article is available on the WWW under http://www/wiley-vch.de/home/angewandte/ or from the author.

 © WILEY-VCH Verlag GmbH, D-69451 Weinheim, 1998 1433-7851/98/3706-0798 $ 17.50+.50/0

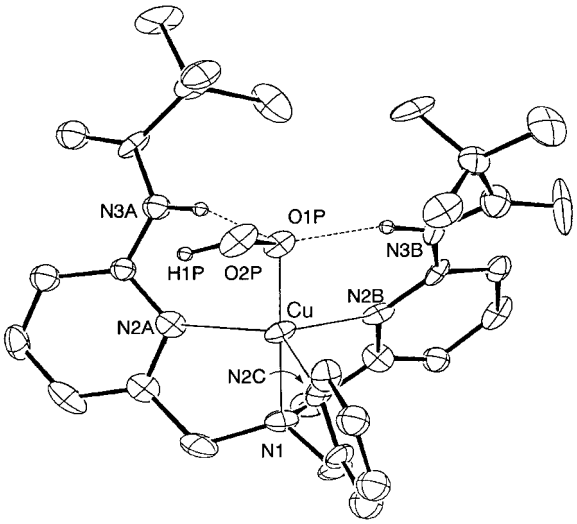


Figure 1. ORTEP representation of the $[Cu^{II}(bppa)(OOH^-)]^+$ cation in **3**. All hydrogen atoms, except for the hydroperoxo hydrogen and those of the amino group, have been omitted for clarity. Selected bond lengths [Å]: Cu–N(1) 1.999(5), Cu–N(2A) 2.099(5), Cu–N(2B) 2.136(4), Cu–N(2C) 2.051(6), Cu–O(1P) 1.888(4), O(1P)–O(2P) 1.460(6).

from the tertiary amine group (Cu–N(1) 1.999(5) Å). Interestingly, the other axial position is occupied by the hydroperoxide anion with a Cu–O(1P) bond length of 1.888(4) Å and a Cu-O(1P)-O(2P) angle of 114.5°. The O–O bond distance of 1.460(6) Å is in good agreement with that of H_2O_2 (1.490 Å),[7] and the O(1P)-O(2P)-H(1P) valence bond angle of 101.8° is similar to that in H_2O_2 (96–102°).[9] As previously demonstrated in Cu^{II}–tppa (tppa = tris(6-pivalamide-2-pyridylmethyl)amine) complexes with small molecules such as OH^- ($[Cu^{II}(tppa)(OH^-)]^+$)[10] and N_3^-, ($[Cu^{II}(tppa)(N_3^-)]^+$),[11] the two amine H atoms stabilize the hydroperoxide group (seen by the direction of two N–H bond vectors and distances between the peroxo oxygen atom and the hydrogen-bonded nitrogen atoms (O(1P)–N(3A) 2.78, O(1P)–N(3B) 2.79 Å).

These results clearly indicate that the novel copper complexes $[Cu^{II}(bppa^-)]ClO_4$ (**1**) or $[Cu^{II}(bppa)(CH_3COO)]ClO_4$ (**2**) react with hydrogen peroxide to generate $[Cu^{II}(bppa)(OOH^-)]^+$ (**3**).[12] It is also apparent that the N–H hydrogen bonding and hydrophobic *tert*-butyl groups contribute significantly to the stabilization of the extremely thermally unstable hydroperoxo species. We have confirmed that a particular arrangement of noncovalently interacting groups is essential for the coordination of small molecules such as HOO^- by metal complexes. These hydroperoxo complexes could serve as models for the active center in biological systems, and the elucidation of their chemistry, in particular the metal–oxygen interactions, will enable us to gain insight into the mechanism of the catalysis by copper oxygenase.

Received: July 7, 1997 [Z10642IE]
German version: *Angew. Chem.* **1998**, *110*, 874–875

Keywords: copper · enzyme models · peroxo complexes

[1] a) M. C. Brenner, J. P. Klinman, *Biochemistry*, **1989**, *209*, 249; b) L. C. Stewart, J. P. Klinman, *Annu. Rev. Biochem*. **1988**, *57*, 551.

[2] a) M. M. Whittaker, J. W. Whittaker, *J. Biol. Chem.* **1990**, *265*, 9610; b) N. Ito, S. E. V. Phillips, C. Stevens, Z. B. Ogel, M. J. Mcpherson, J. N. Keen, K. D. S. Yadau, P. F. Knowles, *Nature*, **1991**, *350*, 87; c) N. Ito, S. E. V. Phillips, K. D. S. Yadau, P. F. Knowles, *J. Mol. Biol*. **1994**, *131*, 794.

[3] a) J. A. Tainer, E. D. Getzoff, K. M. Beem, J. S. Richardson, D. C. Richardson, *J. Mol. Biol.* **1982**, *165*, 181; b) G. Condorelli, L. L. Costanzo, G. De Guidi, S. Giuffrida, E. Rizzarelli, G. Vecchio, *J. Inorg. Biochem*. **1994**, *54*, 257.

[4] a) K. D. Karlin, P. Ghosh, R. W. Cruse, A. Farooq, Y. Gultneh, R. R. Jacobson, N. J. Blackburn, R. W. Strange, J. Zubieta, *J. Am. Chem. Soc.* **1988**, *110*, 6769; b) R. R. Tahir, N. N. Murthy, K. D. Karlin, N. J. Blackburn, S. N. Shaikh, J. Zubieta, *Inorg. Chem.* **1992**, *31*, 3001; mono and binuclear copper(II) alkylperoxo complexes have also been synthesized: c) P. Ghosh, Z. Tyeklar, K. D. Karlin, R. R. Jacobson, J. Zubieta, *J. Am. Chem. Soc.* **1987**, *109*, 6889; d) I. Sanyal, P Ghosh, K. D. Karlin, *Inorg Chem.* **1995**, *34*, 3050.

[5] a) N. Kitajima, K. Fujisawa, Y. Moro-oka, *Inorg. Chem.* **1990**, *29*, 358; b) N. Kitajima, T. Katayama, K. Fujisawa, Y. Iwata, Y. Moro-oka, *ibid.* **1993**, *115*, 7872.

[6] a) Elemental analysis data for $[Cu^{II}(bppa^-)]ClO_4$ (**1**): calcd for $C_{28}H_{35}N_6O_6CuCl$: C 51.69, H 5.42, N 12.92; found: C 51.78, H 5.45, N 12.67; b) elemental analysis data for $[Cu^{II}(bppa)(CH_3COO^-)]ClO_4$ (**2**): calcd for $C_{30}H_{39}N_6O_8CuCl$: C 50.70, H 5.53, N 11.83; found: C 50.73, H 5.44, N 11.75.

[7] The vibrational spectra of $H_2{}^{16}O_2$ and $H_2{}^{18}O_2$ in MeCN yielded 873 and 826 cm^{-1} for the ν(O–O) vibration; a) O. Bain, P. A. Giguere, *Can. J. Chem.* **1955**, *33*, 527; b) R. C. Taylor, P. C. Cross, *J. Chem. Phys.* 1955, *24*, 41; c) S. Ahmad, J. D. McCallum, A. K. Shiemke, E. H. Appelman, T. M. Loehr, J. Sanders-Loehr, *Inorg. Chem.* **1988**, *27*, 2230.

[8] Single crystal X-ray diffraction data were collected at 295 K with an Enraf Nonius CAD4 four-circle diffractometer with $Mo_{K\alpha}$ radiation and a graphite monochromator ($\lambda = 0.71073$ Å), $2\theta_{max} = 52°$, Lorentz and polarization correction, an empirical absorption correction (based on Ψ scans). The structure was solved by direct methods and refined anisotropically for non-hydrogen atoms by full-matrix least-squares methods by using reflections with $I > 3\sigma(I)$. The weighting scheme $w^{-1} = \sigma^2(F_o)$ was applied to the data. All calculations were performed with the software package MoIEN. The hydrogen atoms were located from the difference Fourier maps, followed by parameter refinement. X ray structure data of **3**: $C_{28}H_{37}N_6O_8CuCl$, $M_r = 683$, monoclinic, space group $P2_1/a$, $a = 15.532(81)$, $b = 10.009(1)$, $c = 21.473(1)$ Å, $\beta = 107.489(4)°$, $V = 3184.0(3)$ Å^3, $Z = 4$, $\rho_{calcd} = 1.397$ g m^{-3}, $\mu = 8.21$ cm^{-1}, $F(000) = 1408.0$, $R = 0.062$, $R_w = 0.077$ for 3627 unique reflections. Crystallographic data (excluding structure factors) for the structure reported in this paper have been deposited with the Cambridge Crystallographic Data Centre as supplementary publication no. CCDC-100825. Copies of the data can be obtained free of charge on application to CCDC, 12 Union Road, Cambridge CB2 1EZ (fax: (+44) 1223-336-033; e-mail: deposit@ccdc.cam.ac.uk).

[9] a) W. C. Schumb, C. N. Satterfield, R. L. Wentworth, *Hydrogen peroxide*, Reinhold, New York, **1955**; b) R. L. Redington, W. B. Olsen, P. C. Cross, *J. Chem. Phys.* **1962**, *36*, 1311; c) R. H. Hund, R. A. Leacock, C. W. Petess, *J. Am. Chem. Soc.* **1952**, *74*, 4742.

[10] M. Harata, K. Jitsukawa, H. Masuda, H. Einaga, *Chem. Lett.* **1995**, *1*, 61.

[11] M. Harata, K. Jitsukawa, H. Masuda, H. Einaga, *J. Coord. Chem.* **1997**, in press.

[12] Elemental analysis data for $[Cu^{II}(bppa)(OOH^-)]ClO_4$ (**3**): calcd $C_{28}H_{37}N_6O_8CuCl$: C 49.12, H 5.45, N 12.28; found: C 49.10, H 5.31, N 12.10.

 © WILEY-VCH Verlag GmbH, D-69451 Weinheim, 1998 1433-7851/98/3706-0799 $ 17.50+.50/0

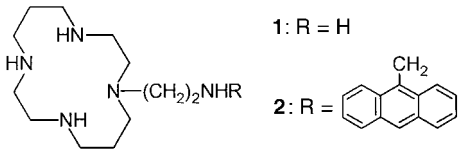
Controllable Intramolecular Motions That Generate Fluorescent Signals for a Metal Scorpionate Complex

Luigi Fabbrizzi,* Maurizio Licchelli, Piersandro Pallavicini, and Luisa Parodi

Molecular systems exist which contain a movable part, whose position can be varied through an external stimulus (addition of ions, change of the redox potential, illumination). Recent examples from supramolecular chemistry include rotaxanes of the π-donor-acceptor type, whose wheel can shuttle between two different stations following either a chemical or electrochemical command,[1] and copper-complexed catenates in which the Cu^{I}/Cu^{II} redox change triggers a half-turn of one of the rings.[2, 3] Systems of this type can be considered as elementary machines and are promising tools for information processing and storage at a molecular level.[4] The association of quick and reversible molecular movement with the generation of a distinct signal appears to be a useful step along this route.

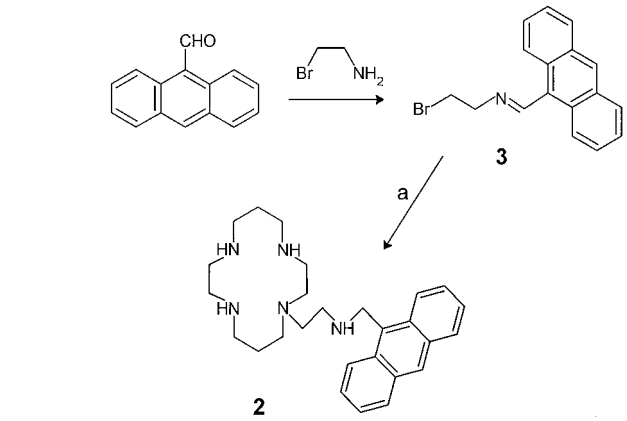
We report here a multicomponent, covalently linked molecular system whose movable part contains a light-emitting fragment and can be reversibly relocated to one of two topologically definite positions by changing the pH value. The appended lumophore is quenched in only one of the positions. Therefore, the pH-driven intramolecular motion is signalled (and visually perceived) through quenching or revival of the light emission.

The basic system is the nickel(II) complex of a 14-membered tetraaza macrocycle bearing an alkylamine side chain (**1**). Compounds of this type combine the rigidity and inertness of



the metal-bound macrocyclic ring with the flexibility and lability of the pendant arm.[5] In acidic solution, the protonated alkylamine side chain is forced away from the ring due to electrostatic repulsive effects; on increasing the pH value, the exocyclic nitrogen atom is deprotonated and coordinates to the metal center in an axial position. This reversible molecular motion can be followed both visually and spectrophotometrically: The protonated metal complex is yellow ($\lambda = 450$ nm; square planar, low spin), whereas the deprotonated form is blue-violet (d–d bands at $\lambda = 350$ and 525 nm in the visible region; octahedral, high spin). Functionalized macrocycles of type **1** are called scorpionands (or scorpiands), based on the analogy of an aggressive molecular "tail" that "stings" the chelated metal center from the top.[6] On varying the pH over a narrow interval ($pK_A \pm 1$), the side chain swings reversibly from one location to the other.

An anthracene fragment was appended through a methylene group to the scorpionand ethylamine side chain to give **2** (Scheme 1). Compound **2** will be indicated as B-L-An in the following discussion, where B denotes the macrocycle, L the alkylamine side chain, and An the fluorophore. Spectrofluorimetric titrations in $MeCN/H_2O$ (4/1) show a two-step behavior (Figure 1). First, the protonated form displays its maximum fluorescence. On addition of one equivalent of OH^- the fluorescence intensity I_F is quenched to 60%. Addition of a further equivalent of base completely quenches the fluorescence of the anthracene fragment. Fluorescence is revived to 60 and 100% on stepwise addition of two equivalents of acid.



Scheme 1. Synthesis of **2**: a) 1. cyclam (excess); 2. $NaBH_4$.

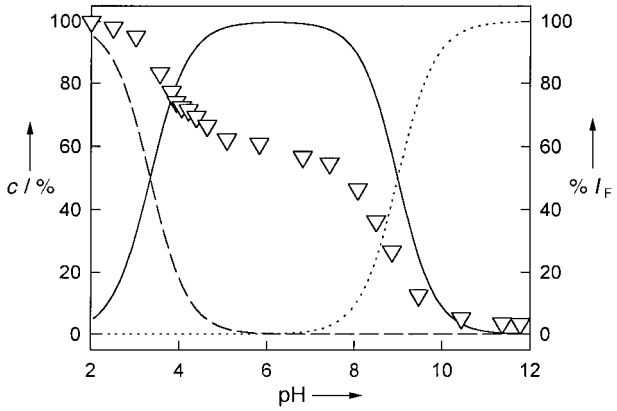


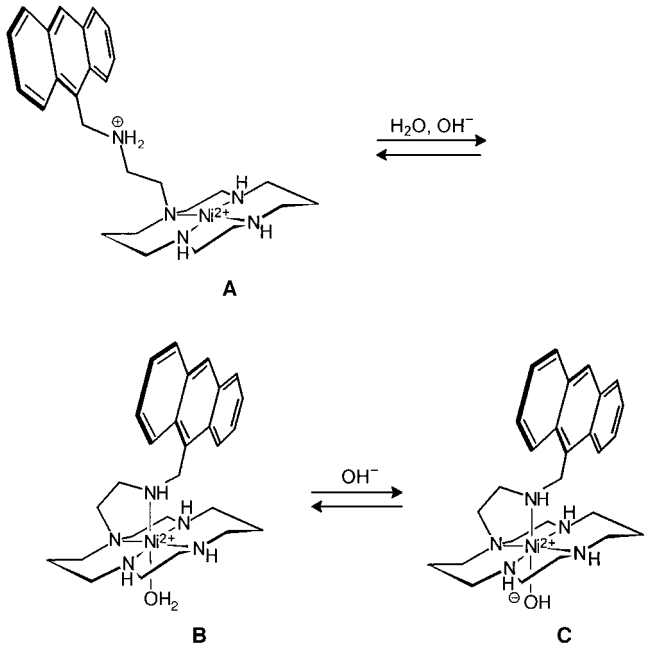
Figure 1. Distribution curves of the three Ni^{II} complexes of **2** (see Scheme 2; **A** dashed line, **B** solid line; **C** dotted line) in $MeCN/H_2O$ (4/1) and pH dependence of the fluorescence intensity I_F of the same solution (▽).

Nonlinear least-squares analysis of the potentiometric titration data indicated that three species were present in equilibrium in the pH range of 2–12. The species present in the strongly acidic region ($pH \leq 2$) displays an absorption band centerd at 460 nm, which is typical for a square-planar low-spin Ni^{II} species. This indicates that the amine side chain is protonated and does not coordinate to the metal center (this

[*] Prof. L. Fabbrizzi, Dr. M. Licchelli, Dr. P. Pallavicini, Dr. L. Parodi
Dipartimento di Chimica Generale
Università di Pavia
via Taramelli 12, I-27100 Pavia (Italy)
Fax: (+39) 382-528-544
E-mail: fabbrizz@ipv36.unipv.it

 © WILEY-VCH Verlag GmbH, D-69451 Weinheim, 1998 1433-7851/98/3706-0800 $ 17.50+.50/0

species is indicated as $[Ni^{II}(B\text{-}LH^{+}\text{-}An)]^{3+}$). Above pH 3 a proton is released, the band at 460 nm disappears, and a new band centered at 530 nm develops. This band is typically observed for an octahedral high-spin Ni^{II} complex (the band expected at 350 nm is hidden by the strong absorption by the An moiety). This indicates that above pH 3 the ethyl ammonium side chain is deprotonated and coordinates apically to the metal center; at the same time a water molecule coordinates to the opposite axial position to complete the octahedral arrangement. $[Ni^{II}(B\text{-}L\text{-}An)(H_2O)]^{2+}$ is present as the major species between pH 4 and 8. It is noteworthy that, due to the favorable contribution of the metal–ligand interaction, the pK_{A1} value for the deprotonation of the alkylammonium side chain in $[Ni^{II}(B\text{-}LH^{+}\text{-}An)]^{3+}$ (3.34 ± 0.02) is drastically lower than that observed for the reference system propyl(anthracen-9-ylmethyl)amine ($AnCH_2NHC_3H_7$, $pK_A = 8.91 \pm 0.02$) measured under the same conditions. A further deprotonation takes place at higher pH ($pK_{A2} = 8.99 \pm 0.02$). No variations are observed in the d–d absorption spectrum, and it is suggested that the proton is released from the axially bound water molecule to give $[Ni^{II}(B\text{-}L\text{-}An)(OH)]^{+}$. Above pH 10 this is the only species present. The stereochemical aspects of the three-component equilibrium are sketched in Scheme 2. The structures of the three species



Scheme 2. Protonation–deprotonation equilibrium of the scorpionate complex.

have been drawn based on semi-empirical calculations (PM3-transition metals within the Spartan package).

The results of the spectrofluorimetric titrations (I_F vs. pH) are given in the distribution diagram in Figure 1. At pH 2 or lower, $[Ni^{II}(B\text{-}LH^{+}\text{-}An)]^{3+}$ displays its maximum emission.[7] The measured I_F value is ten times lower than that observed for the reference system $AnCH_2NH_2^{+}C_3H_7$ in the same medium. The lower emission has probably to be ascribed to the presence of the linked Ni^{II} center: Occasional folding of the aliphatic linker may bring the fluorophore and the metal within the van der Waals contact distance, causing a substantial quenching of the excited fluorophore.[8] Above pH 4, the pendant arm is deprotonated and swings onto the metal center to give $[Ni^{II}(B\text{-}L\text{-}An)(H_2O)]^{2+}$. This process is accompanied by partial fluorescence quenching: The intensity I_F is reduced to 60% of that measured in acidic solution.

The nature of the quenching process operating in both $[Ni^{II}(B\text{-}LH^{+}\text{-}An)]^{3+}$ and $[Ni^{II}(B\text{-}L\text{-}An)(H_2O)]^{2+}$ can be explained by spectrofluorimetric studies at 77 K. In particular, vitrified ethanolic solutions of $[Ni^{II}(B\text{-}LH^{+}\text{-}An)]^{3+}$ and $[Ni^{II}(B\text{-}L\text{-}An)(H_2O)]^{2+}$ do not show any fluorescence enhancement, which suggests the occurrence of an energy transfer process. It should be noted that the Ni^{II} ion possesses low-energy half-filled d levels suitable for a double electron exchange energy transfer process. Furthermore, the occurrence of the occasional contact between Ni^{II} and the An* fragment is favored for $[Ni^{II}(B\text{-}L\text{-}An)(H_2O)]^{2+}$, in which the metal–fluorophore distance is distinctly smaller than in the protonated form $[Ni^{II}(B\text{-}LH^{+}\text{-}An)]^{3+}$. In particular, the distance between the Ni^{II} ion and the anthracene carbon atom connected to the linker, as calculated by molecular modeling, is 4.4 Å in $[Ni^{II}(B\text{-}L\text{-}An)(H_2O)]^{2+}$ and 7.7 Å in $[Ni^{II}(B\text{-}LH^{+}\text{-}An)]^{3+}$. This makes the occasional metal–fluorophore contact and occurrence of a double electron exchange more favorable in species B (Scheme 2) and accounts for a 60% decrease in the I_F value.

At pH 10 or higher, the axially bound water molecule is deprotonated: This simple act causes complete quenching of An fluorescence.[9] Again, the nature of the quenching can be inferred from spectrofluorimetric studies at 77 K. In particular, on freezing an ethanolic solution of $[Ni^{II}(B\text{-}L\text{-}An)(OH)]^{+}$ at this temperature, the fluorescence revives to the value observed for $[Ni^{II}(B\text{-}L\text{-}An)(H_2O)]^{2+}$ under the same conditions. This suggests that, at room temperature, an electron transfer (ET) process gives a significant additional contribution to the quenching of the photoexcited anthracene fragment.

The electron transfer may be due to either a $Ni^{II} \rightarrow {}^{*}An$ or an $An^{*} \rightarrow Ni^{II}$ process. Coordination by a tetraaza macrocycle and, in particular, by a scorpionand favors the oxidation of Ni^{II} to Ni^{III}, and additional quenching may be due to a $Ni^{II} \rightarrow An^{*}$ ET process. The decrease in the electrical charge due to axial coordination of hydroxide may favor the access to the Ni^{III} state and promote the $Ni^{II} \rightarrow An^{*}$ ET process. The occurrence of an $An^{*} \rightarrow Ni^{II}$ ET process seems less probable, as a reduction from Ni^{II} to Ni^{I} would not profit from the decrease in electrical charge associated with hydroxide coordination. The high quenching efficiency observed for the $[Ni^{II}(B\text{-}L\text{-}An)(OH)]^{+}$ form therefore results from the contribution of energy and electron transfer mechanisms involving the metal center.

The metal scorpionate reported here is a multicomponent molecular system whose movable part (the alkylamine side chain) can be made to oscillate between the metal center and a more distant point by the varying an external parameter, the pH value. The relocation of the side chain above the plane of the macrocyclic ring is induced by an increase in pH and is signalled by the partial quenching of the fluorescence of the

 © WILEY-VCH Verlag GmbH, D-69451 Weinheim, 1998 1433-7851/98/3706-0801 $ 17.50+.50/0

appended fluorophore. A further increase in pH does not influence the position of the side chain, but simply increases the quenching efficiency. Most of the previously reported fluorescence switches typically exhibit two states: on or off.[10, 11] Systems displaying multistage emission are more rare and include 2-naphthol[12] and a tin(IV) complex of a functionalized porphyrin.[13] Ligand **2** is a novel high/low/off fluorescence switch whose control has a mechanical nature.

Experimental Section

3: 2-Bromoethylamine was allowed to react with a stoichiometric amount of 9-anthracenecaraldehyde in CH_2Cl_2. The reaction mixture was dried over Na_2SO_4, filtered, and evaporated to dryness. The residue was recrystallized from *n*-hexane/diethyl ether (1/1); yield 45%. Correct C,H,N analysis.

2: Cyclam (0.48 g, 2.4 mmol) was disolved in hot toluene, and **3** (0.14 g, 0.45 mmol) added as a solid. The resulting solution was heated at reflux for 3 h and then cooled to room temperature. The ammonium salts of excess cyclam were removed by filtration, and the clear solution extracted with 0.1M NaOH to separate the remaining cyclam. The dried organic layer was filtered and evaporated to dryness. The resulting yellow oily substance was dissolved in EtOH (20 mL) and reduced with excess $NaBH_4$. Compound **2** was obtained as a pale yellow oil; yield (based on **3**) 70%. MS (ESI): 434 $[M+H^+]$. The NMR spectra were consistent with the proposed structure.

$[Ni^{II}(\mathbf{2})](ClO_4)_2 \cdot H_2O$: **2** (150 mg, 0.35 mmol) was dissolved in EtOH (30 mL), and a stoichiometric amount of an aqueous solution of 0.55M $Ni(ClO_4)_2$ added. The obtained mixture was heated at reflux for 2 h and then evaporated to dryness. The residue was recrystallized from water. $[Ni^{II}(\mathbf{2})](ClO_4)_2 \cdot H_2O$ was obtained as a pale brown solid; yield 63%. Correct C,H,N analysis; MS (ESI): 590 $[M - ClO_4]$.

Received: June 11, 1997
Revised version: November 7, 1997 [Z10535IE]
German version: *Angew. Chem.* **1998**, *110*, 838–841

Keywords: fluorescence · electron transfer · macrocycles · molecular devices · nickel

[1] R. A. Bissell, E. Córdova, A. E. Kaifer, J. F. Stoddart, *Nature* **1994**, *369*, 133.
[2] A. Livoreil, C. O. Dietrich-Buchecker, J. P. Sauvage *J. Am. Chem. Soc.* **1994**, *116*, 9399.
[3] D. J. Cárdenas, A. Livoreil, J. P. Sauvage, *J. Am. Chem. Soc.* **1996**, *118*, 11980.
[4] R. Ballardini, V. Balzani, M. T. Gandolfi, L. Prodi, M. Venturi, D. Philp, H. G. Ricketts, J. F. Stoddart, *Angew. Chem.* **1993**, *105*, 1363; *Angew. Chem. Int. Ed. Engl.* **1993**, *32*, 1301.
[5] T. A. Kaden, *Top. Curr. Chem.* **1984**, *121*, 157.
[6] P. Pallavicini, A. Perotti, B. Seghi, L. Fabbrizzi, *J. Am. Chem. Soc.* **1987**, *109*, 5139.
[7] The quantum yield for $[Ni^{II}(B\text{-}LH^+\text{-}An)]^{3+}$ is 0.083 in EtOH (0.27 for plain anthracene).
[8] The isolated component $[Ni^{II}(cyclam)]^{2+}$ quenches the emission of the reference compound $AnCH_2NH_2^+C_3H_7$ in aqueous MeCN by a bimolecular process. Reduction of I_F to 10% requires the addition of 4500 equivalents of $[Ni^{II}(cyclam)]^{2+}$. This emphasizes the "chelate effect" exerted by the aliphatic linker, which favors the intramolecular metal–fluorophore collisions in $[Ni^{II}(B\text{-}LH^+\text{-}An)]^{3+}$.
[9] One of the referees made the hypothesis that at pH 10 or above, a species of the composition $[Ni^{II}(B\text{-}L\text{-}An)(OH)Ni^{II}(B\text{-}L\text{-}An)]^{3+}$ could form: In this dinuclear species each cyclam subunit coordinates to its metal in a *cis* fashion, and the hydroxo group bridges the two Ni^{II} centers. Although hydroxo-bridged complexes are often observed in transition metal complexes in basic solution, this possibility can be ruled out in the present case: Complete quenching of fluorescence requires the addition of 2 equiv of OH^-, whereas 1.5 equiv are needed for the formation of the dinuclear species $[Ni^{II}(B\text{-}L\text{-}An)(OH)Ni^{II}(B\text{-}L\text{-}An)]^{3+}$. Furthermore, $[Ni^{II}(B\text{-}L\text{-}An)(OH)Ni^{II}(B\text{-}L\text{-}An)]^{3+}$, when replacing $[Ni^{II}(B\text{-}L\text{-}An)(OH)]^+$, did not fit well with the potentiometric titration data.
[10] A. P. de Silva, H. Q. N. Gunaratne, T. Gunnlaugsson, A. J. M. Huxley, C. P. McCoy, J. T. Rademacher, T. E. Rice, *Chem. Rev.* **1997**, 97, 1515.
[11] L. Fabbrizzi , A. Poggi, *Chem. Soc. Rev.* **1995**, 197.
[12] W. Klöpffer, *Adv. Photochem.* **1977**, *10*, 312.
[13] R. Grigg, W. D. J. A. Norbert, *J. Chem. Soc. Chem. Commun.* **1992**, 1298.

SIAM, a Novel NMR Experiment for the Determination of Homonuclear Coupling Constants**

Thomas Prasch, Peter Gröschke, and Steffen J. Glaser*

The most important NMR parameters for the determination of molecular conformations in solution are cross-relaxation rates and coupling constants.[1] With the help of empirical Karplus relations, vicinal coupling constants (^3J) yield information about dihedral angles. For example, in peptides and proteins the $^3J(H^N,H^\alpha)$ coupling is related to the backbone angle ϕ.[2] However, the quantitative determination of coupling constants is difficult if the line width is not significantly smaller than the coupling constants of interest (Figure 1). In the case of in-phase doublets (e.g. in NOESY[3]

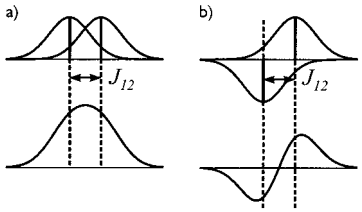


Figure 1. The apparent splittings of in-phase (a) and antiphase (b) doublets deviate markedly from the actual coupling constant J_{12} if the line width is not much smaller than J_{12}.[6] The individual doublet components are shown at the top and their superposition is shown at bottom. In this case the superimposed in-phase signal does not show any resolved splitting (a), whereas the apparent splitting of the superimposed antiphase signal is significantly larger than the coupling constant J_{12} (b).

[*] Priv.-Doz. Dr. S. J. Glaser, Dipl.-Chem. T. Prasch, Dipl.-Chem. P. Gröschke
Institut für Organische Chemie der Universität
Marie-Curie-Strasse 11, D-60439 Frankfurt (Germany)
Fax: (+49) 69-7982-9128
E-mail: sg@org.chemie.uni-frankfurt.de

[**] This work was supported by the Deutsche Forschungsgesellschaft (Gl 203/2-1 and Gl 203/1-5) and by the Fonds der Chemischen Industrie. T. P. thanks the Fonds der Chemischen Industrie for a doctoral fellowship and the Graduiertenkolleg (Gk oIII Eg-52/3-3) for support. All experiments were performed at the Large Scale Facility "Center for Biomolecular NMR at the University of Frankfurt"-(ERBFMGECT950034).

 © WILEY-VCH Verlag GmbH, D-69451 Weinheim, 1998 1433-7851/98/3706-0802 $ 17.50+.50/0

or TOCSY spectra[4]) the finite line width results in a reduced separation of the maxima of the two doublet lines (Figure 1a). This is in contrast to the case of antiphase doublets (e.g. in DQF-COSY spectra[5]), where the finite line width leads to an increased separation of the doublet maxima and hence to an apparent splitting that is larger than the actual coupling constant (Figure 1b).[6] However, the precise determination of coupling constants is possible irrespective of the experimental line form if both in-phase and antiphase multiplets are available.[7, 8]

Here we present a new experimental approach for the simultaneous acquisition of in-phase and antiphase multiplets that provides spectra with a minimum of overlap and markedly enhanced sensitivity compared to conventional methods. The experiment is based on the fact that several coherence transfer processes occur simultaneously during the mixing period τ of TOCSY experiments. For example, in a spin system consisting of two spins 1/2, polarization of the first spin (I_{1z}) is transformed not only into polarization of the second spin (I_{2z}), but also into zero-quantum coherence ($ZQ_y = I_{1y}I_{2x} - I_{1x}I_{2y}$) between the two spins [Eq. (1)].[4]

$$I_{1z} \rightarrow I_{1z}\cos^2(\pi J_{12}\tau) + I_{2z}\sin^2(\pi J_{12}\tau) - ZQ_y\sin(2\pi J_{12}\tau) \quad (1)$$

In conventional TOCSY experiments only the polarization transfer $I_{1z} \rightarrow I_{2z}$ is exploited, resulting in cross peaks with in-phase splitting in ω_1 and ω_2 (Figure 2a). The second transfer

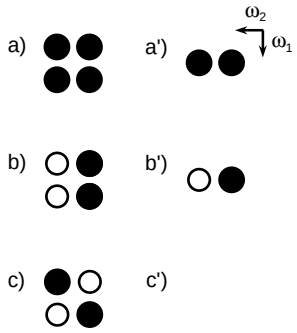


Figure 2. Schematic representation of characteristic multiplets in 2D NMR spectra: a) in-phase splitting in ω_1 and ω_2 (e.g. NOESY, ROESY, TOCSY, and ZQF-SIAM), b) in-phase splitting in ω_1 and antiphase splitting in ω_2 (DQF-SIAM), c) antiphase splitting in ω_1 and ω_2 (e.g. DQF-COSY). Positive signals are white, negative signals are black. a′)–c′) show the corresponding multiplets when ω_1 decoupling is used. In the first two cases this leads to a signal enhancement and to an improved resolution, whereas in the third case the signals completely cancel.

($I_{1z} \rightarrow ZQ_y$), which results in an in-phase splitting in ω_1 and an antiphase splitting in ω_2 (Figure 2b), was so far either ignored or suppressed.[4] The separation of polarization I_{2z} and zero-quantum coherence ZQ_y poses a problem because both terms have the same coherence order $p = 0$.[1] However, if the two mutually coupled spins have well-resolved chemical shifts, selective pulses can be used to convert the zero-quantum coherence ZQ_y selectively into double-quantum coherence ($DQ_y = I_{1y}I_{2x} + I_{1x}I_{2y}$) with coherence order $p = \pm 2$. The two terms I_{2z} and DQ_y can be conveniently selected with the help of a zero-quantum filter (ZQF) and a double-quantum filter (DQF), respectively (Figure 3a). It is even possible to realize

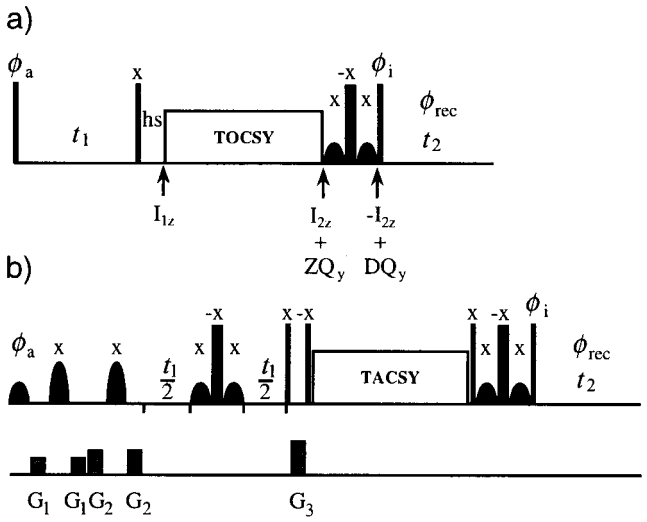


Figure 3. a) Schematic pulse sequence of a SIAM experiment (narrow vertical lines: 90° pulses; broad vertical lines: 180° pulses; bell-shaped symbols: selective 90° pulses acting only on spin I_1; hs: homospoil gradient; phase cycles of ϕ_a, ϕ_i, and ϕ_{rec}: see Experimental Section). For a two-spin system, the characteristic operators created during the sequence are indicated. b) Optimized SIAM experiment for the determination of $^3J(H^N,H^\alpha)$ couplings in peptides and proteins (see Experimental Section).

both filters by processing a single experimental data set in two different ways (see Experimental Section). Since this allows the *s*imultaneous acquisition of *i*n-phase and *a*ntiphase *m*ultiplets, we refer to the new method as the SIAM experiment. Because the cross peaks of both ZQF-SIAM and DQF-SIAM spectra have an in-phase splitting in ω_1, it is possible to further increase the resolution and the sensitivity by ω_1 decoupling[9](Figure 2a′, b′). This is not possible in a conventional DQF-COSY experiment with antiphase splittings in ω_1 and ω_2 (Figure 2c, c′). Figure 3b shows an optimized SIAM experiment with ω_1 decoupling and band-selective excitation for the quantitative determination of $^3J(H^N,H^\alpha)$ couplings in peptides and proteins. In addition, a band-selective TACSY mixing sequence (*ta*ilored *c*orrelation *s*pectroscopy)[10] is used which provides more efficient coherence transfer than a nonselective TOCSY sequence (*to*tal *c*orrelation *s*pectroscopy) (see Experimental Section).

Figures 4a and b show a section of the fingerprint region of the protein BPTI with H^N,H^α cross peaks; the ZQF-SIAM and DQF-SIAM spectra were obtained from the same experimental SIAM data set. For comparison, Figure 4c shows the corresponding region of a conventional DQF-COSY spectrum (same total measurement time). The resolution of the DQF-SIAM spectrum (Figure 4b) is markedly better than that of the DQF-COSY spectrum because of ω_1 decoupling. Furthermore, the intensity of the antiphase signals is significantly larger in the DQF-SIAM experiment. For example, the cross sections of the DQF-SIAM cross peaks of Ala 25, Ala 58, and Ile 18 are up to a factor of four more intense than those of the corresponding DQF-COSY cross peaks (see Figure 5). The fact that a ZQF-SIAM spectrum with in-phase splitting and a DQF-SIAM spectrum with antiphase splitting can be obtained from the same data set not only saves measurement time, but also guarantees that the in-phase and antiphase multiplets have identical center frequencies. This is not

 © WILEY-VCH Verlag GmbH, D-69451 Weinheim, 1998 1433-7851/98/3706-0803 $ 17.50+.50/0

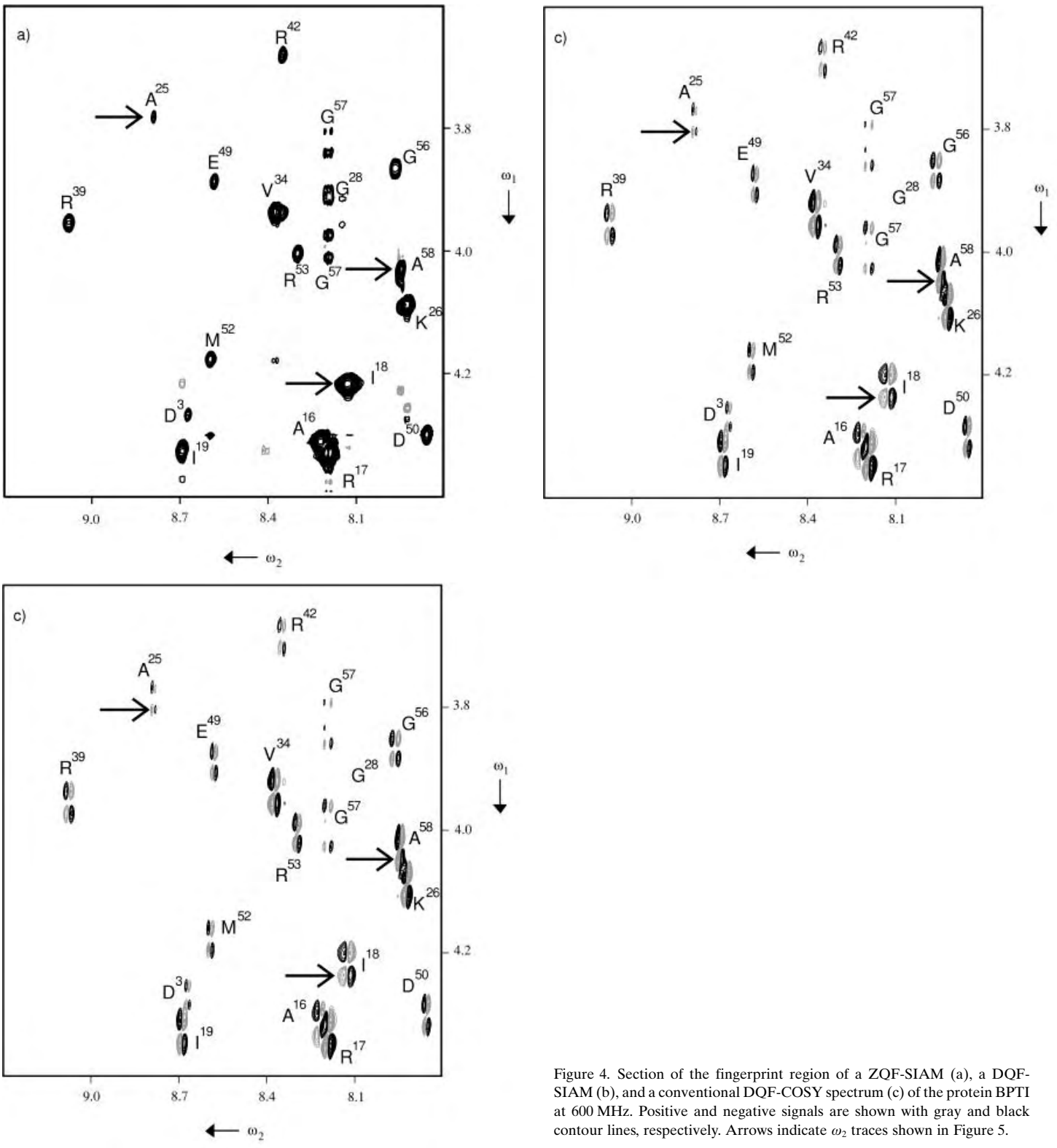


Figure 4. Section of the fingerprint region of a ZQF-SIAM (a), a DQF-SIAM (b), and a conventional DQF-COSY spectrum (c) of the protein BPTI at 600 MHz. Positive and negative signals are shown with gray and black contour lines, respectively. Arrows indicate ω_2 traces shown in Figure 5.

warranted if two different experiments (e.g. DQF-COSY and TOCSY) are acquired because of nonidentical sample heating. Hence, the novel SIAM experiment is almost ideally suited for the determination of $^3J(H^N,H^\alpha)$ coupling constants in peptides and proteins. Based on the traces of the ZQF-SIAM and DQF-SIAM cross peaks shown in Figure 5, $^3J(H^N,H^\alpha)$ coupling constants of (3.6 ± 0.25) Hz for Ala 25, (6.1 ± 0.25) Hz for Ala 58, and (9.7 ± 0.25) Hz for Ile 18 were determined by using the Keeler–Titman extraction procedure.[8] These coupling constants differ significantly from the apparent in-phase splittings of 0, 6.3, and 6.5 Hz, respectively.

 © WILEY-VCH Verlag GmbH, D-69451 Weinheim, 1998 1433-7851/98/3706-0804 $ 17.50+.50/0

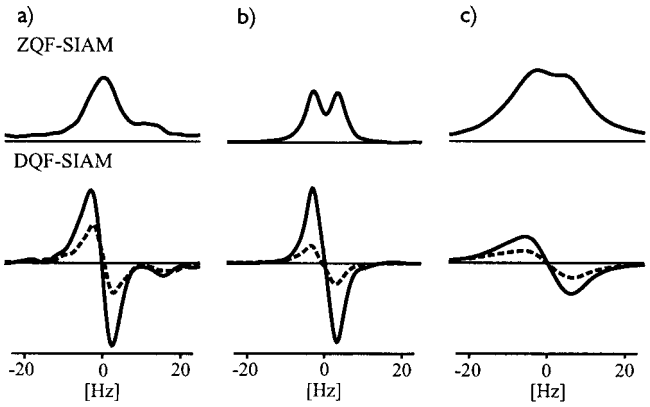


Figure 5. ω_2 traces of the (H^N,H^α) cross peaks of a) Ala 25, b) Ala 58, and c) Ile 18 (see arrows in Figure 4) with representative $^3J(H^N,H^\alpha)$ coupling constants and line widths. The top panels show the in-phase signals of the ZQF-SIAM spectrum and the bottom panels show the antiphase signals of the DQF-SIAM spectrum (solid lines). The dashed lines represent the antiphase signals of the conventional DQF-COSY spectrum for comparison.

The SIAM method is not restricted to the determination of $^3J(H^N,H^\alpha)$ couplings nor to applications to peptides and proteins. A necessary condition is that the two mutually coupled spins of interest (here H^N and H^α) have different chemical shifts. Furthermore it must be ensured that in large spin systems the pure in-phase and antiphase multiplets are not contaminated by other signals. A sufficient (but not necessary) condition for this is that the detected spin (here H^N) has no further coupling partners. Hence, the SIAM method complements the powerful E.COSY technique,[11] for which a third common coupling partner is mandatory.

Experimental Section

The SIAM technique is based on the conversion of zero-quantum coherence ZQ_y to double-quantum coherence DQ_y, which requires a band-selective inversion pulse with a simultaneous suppression of chemical shift evolution. This can be implemented by a composite pulse element consisting of a hard (nonselective) 180°_{-x} pulse sandwiched between two band-selective 90°_x pulses (see Figure 3). A ZQF- and a DQF-SIAM spectrum can be obtained from the same experimental data set if for each t_1 increment two free induction decays FID1(t_1,t_2) and FID2(t_1,t_2) with different phase cycles are acquired and stored separately. The phase cycle ϕ_i of the last 90° pulse (Figure 3) and the phase ϕ_{rec} of the receiver are ϕ_i = x, − x and ϕ_{rec} = x, − x for FID1(t_1,t_2), whereas for FID2(t_1,t_2) ϕ_i = y, − y and ϕ_{rec} = y, − y. Addition and subtraction of FID1(t_1,t_2) and FID2(t_1,t_2) yields, after a two-dimensional Fourier transformation, a ZQF- and a DQF-SIAM spectrum, respectively. Only an additional 90° phase correction in ω_2 is required for the DQF-SIAM spectrum.

The spectra shown in Figures 4 and 5 were acquired with the SIAM experiment shown in Figure 3b, which was optimized for the determination of $^3J(H^N,H^\alpha)$ couplings in peptides and proteins. The RF irradiation frequency was positioned at 6.2 ppm. The water signal was presaturated by CW irradiation for a duration of 2 s (not shown in Figure 3b). For band-selective excitation we used a H^α-selective 90° pulse (Q5)[12] with a duration of 3.731 ms and an offset of − 1.072 kHz in combination with two H^α-selective 180° pulses (Q3)[12] with a duration of 3 ms and an offset of − 1.072 kHz. (Offset frequency, amplitude, and duration of the band-selective pulses are matched for experiments at 600 MHz but can be scaled for applications at other spectrometer frequencies.) The two H^α-selective 180° pulses were bracketed by different B_0 gradients (G_1 = 15 G cm^{-1}, G_2 = 25 G cm^{-1}) with a duration of 1 ms each.[13] This made it possible to reduce the spectral width in ω_1 to 1 kHz and the number of t_1 increments to 200 (spectral width in ω_2: 4.194 kHz, 2048 complex data points in t_2). The phase ϕ_a was incremented by using the TPPI scheme.[14] A composite pulse consisting of two H^α-selective 90°_x pulses (Q5)and a nonselective 180°_{-x} pulse was used both for ω_1 decoupling in the center of t_1 and for the conversion of zero-quantum coherence ZQ_y to double-quantum coherence DQ_y at the end of the sequence. Prior to the mixing step, x magnetization was selected by two 90°_y pulses and a B_0 gradient (G_3 = 35 G cm^{-1}). The band-selective HNHA-TACSY sequence CABBY-1[10] was used in the mixing period. The radio frequency amplitude of CABBY-1 was 4.4 kHz, corresponding to a bandwidth of about 3.4 kHz, which allows efficient polarization and coherence transfer between H^α and H^N (in the range between 3.4 and 9.0 ppm). The mixing time used was 43 ms (according to relation (1) the optimal mixing time for the creation of zero-quantum coherence ZQ_y between H^N and H^α is given by $\tau = 1/(4J_{12})$ with $J_{12} = {}^3J(H^N,H^\alpha)$). For the clean conversion of ZQ_y to DQ_y it is important that the H^N spins can be inverted without affecting the H^α spins. This is usually possible because the H^N and H^α resonances are well separated. Overlap between H^α and H^β resonances (e.g. of Ser or Thr) does not pose a problem. Although this leads to a loss of sensitivity (due to incomplete ω_1 decoupling of the $^3J(H^\alpha,H^\beta)$ couplings and nonselective TOCSY transfer), the additional coherence terms (involving more than two spins) do not lead to any detectable signals if not all participating spins are coupled to the detected spin (H^N). As $^4J(H^N,H^\beta)$ couplings can be neglected, the H^α,H^N cross peaks in ZQF-SIAM and DQF-SIAM spectra show even in the presence of overlapping H^α and H^β resonances purely absorptive in-phase and antiphase splittings with respect to the desired $^3J(H^N,H^\alpha)$ coupling. (Only in the case of Gly, where H^N is coupled to H^α and $H^{\alpha'}$, can the H^α,H^N cross peaks of the ZQF-SIAM spectrum can contain in addition to the desired absorptive in-phase signals also dispersive signals in double antiphase with respect to H^α and $H^{\alpha'}$).

A SIAM experiment and a DQF-COSY experiment were acquired for the protein BPTI at a temperature of 310 K using the same band-selective excitation and the same total measurement time of 9.5 h with a total of 64 scans per t_1 increment (32 scans for FID1(t_1,t_2) and 32 scans for FID2(t_1,t_2) in the SIAM experiment). Except for the addition and subtraction of FID1(t_1,t_2) and FID2(t_1,t_2) for the ZQF-SIAM and DQF-SIAM spectrum, respectively, and an additional 90° phase correction (0th order) in ω_2 for the DQF-SIAM spectrum (as described above), the 2D spectra shown in Figure 4 were processed and scaled identically (no apodization in ω_2, skewed sinebell with a phase of 90° and a skew parameter of 0.8 in ω_1, polynomial baseline correction in ω_1 und ω_2). In order to increase the digital resolution of the traces shown in Figure 5, the traces were inversely Fourier transformed and the first 1024 points of the resulting interferograms were extended to 16384 points by using linear prediction with 110 poles. After a final Fourier transformation, the digital resolution of the traces was 0.25 Hz per point.

Received: July 30, 1997 [Z10752IE]
German version: *Angew. Chem.* **1998**, *110*, 817 – 821

Keywords: NMR spectroscopy · peptides · proteins · structure elucidation

[1] a) K. Wüthrich, *NMR of Proteins and Nucleic Acids*, Wiley, New York, **1986**; b) H. Kessler, M. Gehrke, C. Griesinger, *Angew. Chem.* **1988**, *100*, 507 – 554; *Angew. Chem. Int. Ed. Engl.* **1988**, *27*, 490 – 536; c) *Two-Dimensional NMR Spectroscopy* (Eds.: W. R. Croasmun, R. M. K. Carlson), VCH Publishers, New York, **1994**.

[2] A. Pardi, M. Billeter, K. Wüthrich, *J. Mol. Biol.* **1984**, *180*, 741 – 751.

[3] a) J. Jeener, B. H. Meier, P. Bachmann, R. R. Ernst, *J. Chem. Phys.* **1979**, *71*, 4546 – 4553; b) S. Macura, Y. Huang, D. Suter, R. R. Ernst, *J. Magn. Reson.* **1981**, *43*, 259 – 281.

[4] a) L. Braunschweiler, R. R. Ernst, *J. Magn. Reson.* **1983**, *53*, 521 – 528; b) A. Bax, D. G. Davis, *ibid.* **1985**, *65*, 355 – 360; c) S. J. Glaser, J. J. Quant in *Advances in Magnetic and Optical Resonance, Vol. 19* (Ed.: W. Warren), Academic Press, San Diego, **1996**, pp. 59 – 252.

[5] a) U. Piantini, O. W. Sørensen, R. R. Ernst, *J. Am. Chem. Soc.* **1982**, *104*, 6800 – 6801; b) M. Rance, O. W. Sørensen, G. Bodenhausen, G. Wagner, R. R. Ernst, K. Wüthrich, *Biochem. Biophys. Res. Commun.* **1983**, 117, 479 – 485.

 © WILEY-VCH Verlag GmbH, D-69451 Weinheim, 1998 1433-7851/98/3706-0805 $ 17.50+.50/0

[6] a) D. Neuhaus, G. Wagner, M. Vasak, J. H. R. Kägi, K. Wüthrich, *Eur. J. Biochem.* **1985**, *151*, 257–273; b) M. Eberstadt, G. Gemmecker, D. F. Mierke, H. Kessler, *Angew. Chem.* **1995**, *107*, 1813–1838; *Angew. Chem. Int. Ed. Engl.* **1995**, *34*, 1671–1695.
[7] a) H. Oschkinat, R. Freeman, *J. Magn. Reson.* **1984**, *60*, 164–169; b) H. Kessler, S. Seip in ref.[1c], pp. 619–654.
[8] a) J. Titman, J. Keeler, *J. Magn. Reson.* **1990**, *89*, 640–646; b) P. Huber, C. Zwahlen, S. J. F. Vincent, G. Bodenhausen, *J. Magn. Reson. A* **1993**, 103, 118–121.
[9] R. Brüschweiler, C. Griesinger, O. W. Sørensen, R. R. Ernst, *J. Magn. Reson.* **1988**, *78*, 178–185.
[10] J. Quant, T. Prasch, S. Ihringer, S. J. Glaser, *J. Magn. Reson. B* **1995**, *106*, 116–121.
[11] a) C. Griesinger, O. W. Sørensen, R. R. Ernst, *J. Am. Chem. Soc.* **1985**, *107*, 6394–6396; b) C. Griesinger, O. W. Sørensen, R. R. Ernst, *J. Chem. Phys.* **1986**, *85*, 6837–6852; c) C. Griesinger, O. W. Sørensen, R. R. Ernst, *J. Magn. Reson.* **1987**, *75*, 474–492.
[12] L. Emsley, G. Bodenhausen, *J. Magn. Reson.* **1992**, *97*, 135–148.
[13] T. L. Hwang, A. J. Shaka, *J. Magn. Reson. A* **1995**, *112*, 275–279.
[14] D. Marion, K. Wüthrich, *Biochem. Biophys. Res. Commun.* **1983**, *113*, 967–974.

Catalytic Hydrogenolysis at Low Temperature and Pressure of Polyethylene and Polypropylene to Diesels or Lower Alkanes by a Zirconium Hydride Supported on Silica-Alumina: A Step Toward Polyolefin Degradation by the Microscopic Reverse of Ziegler–Natta Polymerization

Véronique Dufaud* and Jean-Marie Basset*

Transition metal catalyzed polymerization of ethylene and propylene was discovered in the 1950s by Ziegler and Natta.[1] Since then, there have been many applications and a large production of these polymers. However, at the end of this century, the presence of such polyolefins in our daily life has reached such a level that its environmental consequences can no longer be underestimated. The solutions to overcome this environmental challenge with catalytic methods at low temperature and pressure are not known at the moment.[2] The scientific reasons for this deficit may be divided in two categories: the chemical inertness of polyolefins and the thermodynamic limitations to achieving the reverse of the Ziegler–Natta polymerization.

Although they are formed from olefins, polyolefins such as polyethylene or polypropylene are not "olefinic" materials since they become "paraffinic" upon polymerization. These long-chain paraffinic materials are extremely inert, and there is no simple way to transform them selectively, especially at moderate temperature, into valuable products.

[*] Dr. V. Dufaud, Dr. J.-M. Basset
Laboratoire de Chimie Organométallique de Surface
UMR 9986, CNRS-CPE Lyon
43 boulevard du 11 Novembre 1918, 69616 Villeurbanne Cédex (France)
Fax: (+33) 47243-1793
E-Mail: basset@coms1.cpe

It would be very fascinating to transform polyolefins into olefinic oligomers or monomers, which is theoretically possible from a mechanistic point of view according to the principle of microreversibility. The insertion of an olefin into a metal–alkyl bond, the key step in the Ziegler–Natta polymerization,[3] can be considered as the microscopic reverse of the β-alkyl transfer [Eq. (a); the polymer chain is



(a)

represented by Ⓟ].[4] However, since such transformations are thermodynamically impossible at moderate temperature, it is necessary to find solutions to overcome this limitation.

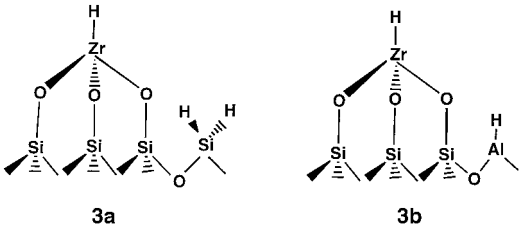
We report here that it is possible to polymerize ethylene or propylene to the corresponding polyolefins with a zirconium hydride supported on silica-alumina.[5] We also demonstrate that under hydrogen the same catalyst that can polymerize ethylene or propylene is able to cleave statistically all the C–C bonds of polyethylene or polypropylene to a range of short-chain saturated oligomers, diesels, or eventually methane, ethane, and lower alkanes.

We recently disclosed a new catalyst that is able to carry out the catalytic cleavage of the C–C bonds in several simple alkanes under hydrogen. The catalyst is a well-defined silica-supported zirconium monohydride ($\equiv SiO)_3ZrH$ (**1**)[6–8] that is obtained by surface organometallic chemical reactions.[9] For example, **1**, which is very electrophilic,[10] is able to cleave the C–C bonds of propane, butanes, and pentanes (but not ethane) under a moderate hydrogen pressure (<1 atm) and at mild temperatures (typically 25–150 °C).[11, 12] Considering that polyolefins are simply long-chain hydrocarbons, the catalytic cleavage of the C–C bonds in these higher alkanes might be possible with our electrophilic silica-supported zirconium hydride or some more strongly electrophilic supported zirconium hydride.

To render the supported zirconium hydride even more electrophilic than on silica, we treated tetraneopentylzirconium with the surface silanol groups of a silica-alumina that was partially dehydroxylated at 500 °C (silica-alumina$_{500}$). The reaction led to the formation of a surface species which can be formulated as $(\equiv SiO)ZrNp_3$ (**2**). Treatment of **2** with hydrogen at 150 °C provided the formation of a zirconium hydride supported on silica-alumina with the concommitant generation of silicon dihydride and aluminium hydride. Based on what is known for the structure of **1** on pure silica, we propose two structures for the zirconium hydride supported on silica-alumina (Scheme 1): One can be formulated as $(\equiv SiO)_3ZrH$ (**3a**), in which the zirconium hydride is a monohydride grafted to silica-alumina through three covalent bonds. This was already demonstrated for pure silica by several techniques including EXAFS.[8] The second structure **3b** is very similar. However, aluminium hydride groups could be in close proximity to the zirconium center, and the zirconium atom would be even more electrophilic than on pure silica.

When **3** was exposed to an ethylene pressure of 200 torr at room temperature, the IR spectrum of the solid showed the

 © WILEY-VCH Verlag GmbH, D-69451 Weinheim, 1998 1433-7851/98/3706-0806 $ 17.50+.50/0



Scheme 1. Proposed structures for **3**.

immediate disappearence of the band at 1635 cm^{-1} for the ν(Zr–H) vibration (Figure 1a and b). Simultaneously, very intense bands appeared in the region of 2970–2850 cm^{-1} and at 1380 cm^{-1}, which is characteristic of polyethylene.[13] The same catalyst is able to polymerize propylene at room

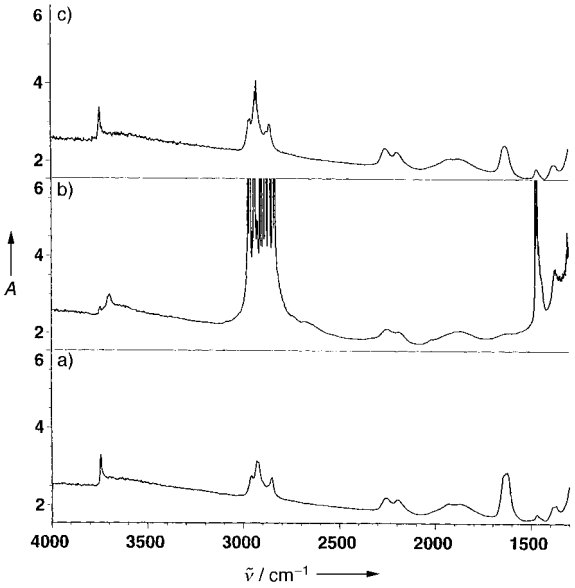


Figure 1. IR spectra of **3**. a) Pure **3**; b) after exposure to ethylene (200 torr) overnight at room temperature; c) after heating at 150 °C overnight under H_2 (300 torr).

temperature to polypropylene, as evidenced by IR spectroscopy (intensive, characteristic bands associated for ν(C–H) and δ(C–H) vibrations of polypropylene were observed).[13]

The polymers are formed by initial insertion of ethylene or propylene into the Zr–H bond followed by multiple insertions of the monomer into the resulting Zr–alkyl bond.[14] When the polyethylene bound to zirconium supported on silica-alumina was heated to 150 °C overnight under hydrogen (300 torr), hydrogenolysis of the polymer occured, as demonstrated by IR spectroscopy, gas chromatography/mass spectroscopy, and other experiments. The very intense bands in the IR spectrum at 2970–2850 cm^{-1} and 1380 cm^{-1} (attributed to the ν(C–H) and δ(C–H) vibrations of polyethylene, respectively) decreased dramatically in intensity with time, whereas the band for the ν(Zr–H) vibration at 1635 cm^{-1} reappeared (Figure 1c). Only methane, ethane, and higher alkanes were detected in the gas phase, which indicates that all the C–C bonds of the polymer were cleaved progressively under these conditions. After 15 hours of reaction only methane and ethane were detected. Similar results were obtained for polypropylene bound to zirconium supported on silica-alumina. Under appropriate conditions, catalyst **3** is apparently capable of catalyzing both olefin polymerization and hydrogenolytic degradation of the resulting polymer.

A logical application of this polymerization/hydrogenolysis reaction is therefore the degradation of commercial polyolefins under analogous conditions. In another series of experiments, samples of polyethylene of low molecular weight (C_{18} to C_{50}, Figure 2a) were brought into contact with catalyst **3** under hydrogen (1 atm) at 150 °C for varying periods of time. As represented on Figures 2 and 3, degradation of the polymer occurred; the product distribution depends on the reaction time.

After one hour of reaction 5% of the starting polyethylene had been converted into light alkanes. The distribution of the oligomers underwent significant changes (Figure 2b): The proportion of lower oligomers increased (especially below C_{18}), which demonstrates catalytic cleavage of the C–C skeleton of the initial polyethylene. Furthermore, in the fraction from C_{18} to C_{50}, for which the starting polymer contains only oligomers with an even number of carbon atoms, new peaks with an odd number of carbon atoms were detected. This shows that there is a statistical cleavage of all C–C bonds in the polymeric chain by the zirconium hydride. After two hours of reaction 25% of the starting polyethylene was converted into lower alkanes ($< C_9$, Figure 3). The amount of oligomers with an even number of carbon atoms was almost the same as that of oligomers with an odd number of carbon atoms; there was a broadening of the molecular-weight distribution and a shift toward the oligomers of low molecular weight (Figure 2c). After five hours of reaction only a fraction of oligomers between C_{10} and C_{17} persisted (corresponding to the hydrocarbons in diesel), and 84% of the initial polyethylene was converted into lower alkanes (C_1 to C_9; Figure 3). When the reaction was carried out for 62 hours, all the starting polyethylene was converted into light alkanes (Figures 2e and 3). Therefore, the reaction time has an effect on the distribution of product oligomers and light alkanes. For alkanes with less than nine carbon atoms, one obtains predominantly pentanes and hexanes at low conversion, whereas methane and ethane are the predominant products at higher conversions. This was expected from previous studies on alkane hydrogenolysis with similar catalysts.[11] In conclusion, catalyst **3** is able to cleave polyethylene under a low hydrogen pressure and at very moderate temperature. Further experiments carried out with low-density polyethylene of higher molecular weight ($M = 125\,000$) provided essentially similar results: 100% conversion of the initial polyethylene into saturated oligomers (after 5 h) or lower alkanes (last ten hours) at 150 °C. Catalyst **3** is also able to cleave commercial isotactic polypropylene ($M = 250\,000$) under hydrogen at about 190 °C and in the absence of any solvent. For example, 40% of the starting polypropylene was converted into lower alkanes after 15 hours of reaction at 190 °C (see Experimental Section). Furthermore, the reaction could be carried out in the presence of a solvent which is not hydrogenolyzed under reaction conditions (e.g. decaline, owing to steric constrains on β-alkyl elimination).[15]

 © WILEY-VCH Verlag GmbH, D-69451 Weinheim, 1998 1433-7851/98/3706-0807 $ 17.50+.50/0

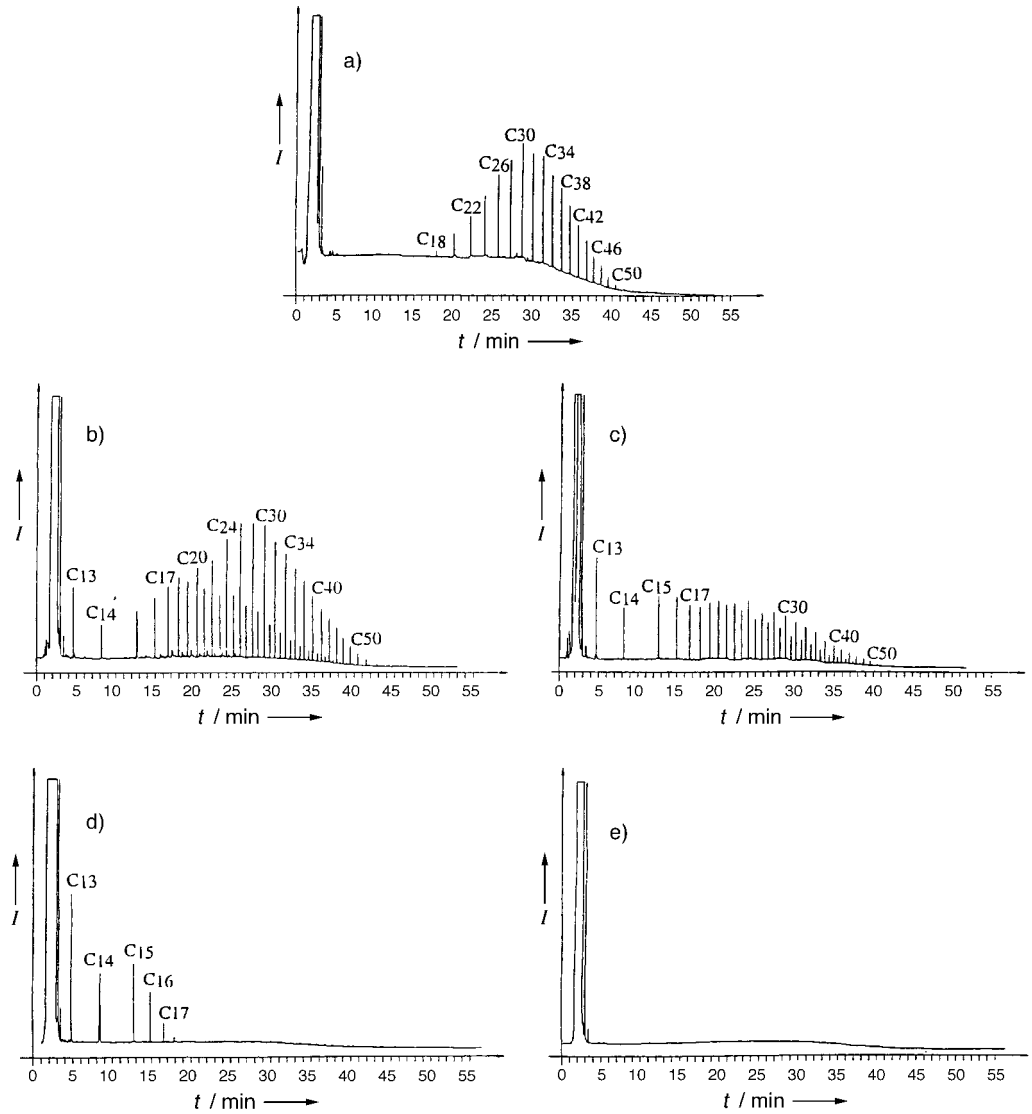


Figure 2. Gas chromatographic determination of the oligomer distribution. a) Initial polyethylene; b) after 1 h; c) after 2 h; d) after 5 h; e) after 62 h of reaction.

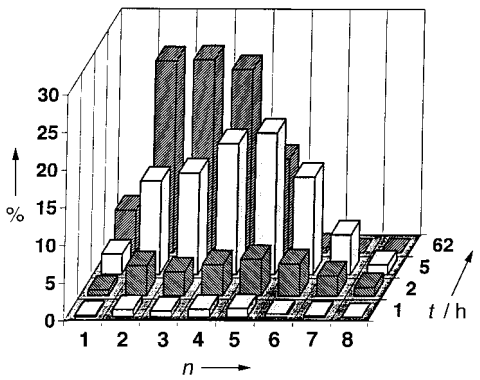
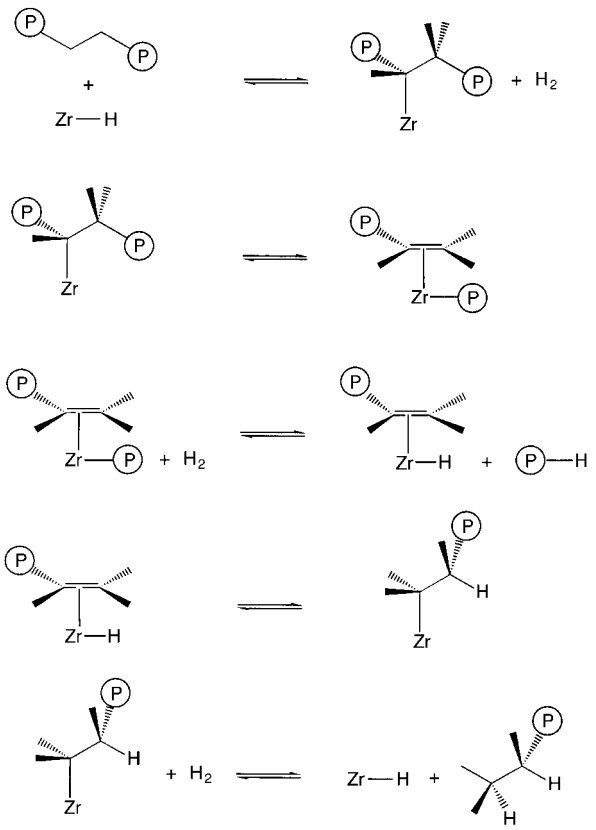


Figure 3. Product distribution of light alkanes C_nC_{2n+2} as a function of time t.

The mechanism of such polymerization/hydrogenolysis reactions is possibly based on elementary steps already known in organometallic chemistry, mainly the equilibrium insertion $\rightleftharpoons$ β-alkyl transfer. In and of itself, the β-alkyl transfer (the microscopic reverse of olefin insertion) would be thermodynamically unfavorable. However, based on our observations, we propose that a subsequent hydrogenation of olefinic double bonds renders the process of "hydrogenolytic polymer degradation" exothermic (Scheme 2).

The first step (Scheme 2) is a facile, unselective activation of a C–H bond in the paraffinic chain, which occurs by σ-bond metathesis with liberation of hydrogen. This kind of activation is now well described for early transition metals with a d^0 configuration[16] as well as for silica-supported zirconium hydride.[8, 11] The polymer is then unselectively grafted to the zirconium center through a σ bond. This can be proven by the fact that, at low conversion and in all the cases we described, statistical cleavage of C–C bonds along the polymer backbone produced small amounts of methane or ethane. This indicates that the C–H bonds at the ends of the oligomers are not particularly favored over those in the rest of the chain. Once the polymeric chain is linked to the zirconium center, a β-alkyl transfer is observed (Scheme 2, second reaction); a fraction of

 © WILEY-VCH Verlag GmbH, D-69451 Weinheim, 1998 1433-7851/98/3706-0808 $ 17.50+.50/0



Scheme 2. Proposed mechanism for the hydrogenolytic degradation of polyethylene.

the polymeric chain is grafted through a sigma bond to the metal, and another fraction is π-bonded through its terminal double bond to the metal. The final steps (Scheme 2, last three reactions) involve removal of the polymers by cleavage of the zirconium – carbon bond and hydrogenation of the terminal double bond.

Experimental Section

The IR spectra were recorded on a Nicolet 550 FT spectrometer, and the CP-MAS ^{13}C NMR spectra (75.47 MHz) on a Brucker MSL-300 spectrometer. The 90° ^{1}H pulse length was 5 μs, the contact time 15 ms, and the recycle delay 2 s. $ZrNp_4$ was prepared by a literature procedure.[17] All manipulations were performed in a glovebox or with high-vacuum techniques. Light alkanes were analyzed by gas chromatography (GC) with a capillary column of fused silica (CHROMPACK Al_2O_3/KCl; 50 m × 0.32 mm). Oligomers were extracted from the reaction medium with hot decaline and analyzed by gas chromatography (capillary column HT5 0.1 mm, 12 m, 0.22 mm internal diameter, covered with alumina). Typical chromatograms are given in Figure 2.

(≡SiO)$ZrNp_3$ (**2**): The reaction between $ZrNp_4$ and the surface silanol groups of a deuterated silica-alumina (Ketjen, 25% Al, 375 $m^2 g^{-1}$, dehydroxylated at 500 °C) led to the generation of a zirconium alkyl species on the surface and the liberation of about 1 mol of $[D_1]$2,2-dimethylpropane per mole of grafted zirconium [Eq. (b)]. The surface

$$\equiv Si{-}OH\,(D) + ZrNp_4 \rightarrow (\equiv SiO)ZrNp_3 + NpH\,(D) \qquad (b)$$

species was characterized with analytical and spectroscopic techniques, and the structure (≡SiO)$ZrNp_3$ (**2**) was proposed, in which the zirconium atom is σ-coordinated by three neopentyl ligands and grafted to the surface through one covalent bond to oxygen. **2**: Elemental analysis: C:Zr = 14:1 (expected value: 15:1); IR: $\tilde{\nu}$ = 2949 ($\nu_{as}(CH_3)$), 2900 ($\nu_{as}(CH_2)$), 2865 ($\nu_s(CH_3)$), 2822 ($\nu_s(CH_2)$), 1467 ($\delta_{as}(CH_3)\delta_s(CH_2)$), 1362 cm^{-1} ($\delta_s(CH_3)$); CP-MAS ^{13}C NMR: δ = 33.1 ($CH_2C(CH_3)_3$), 94.5 ($CH_2C(CH_3)_3$). Deuterolysis of **2** gave 2.7 mol of $[D_1]$2,2-dimethylpropane (expected value: 3 mol). Deuterolysis of **2** after polymerization gave 2.16 mol of $[D_1]$2,2-dimethylpropane (expected value if all the zirconium atoms are propagating centers: 2 mol).

(≡SiO)$_3$ZrH: Treatment of **2** with H_2 at 150 °C led to the formation of a zirconium monohydride supported of silica-alumina along with the concommitant generation of silicon dihydride and the partial formation of an aluminium hydride [Eq. (c)]. The reaction was monitored by IR

$$(\equiv SiO)ZrNp_3 + \equiv SiOSi\equiv + \equiv SiOAl= \xrightarrow{H_2} (\equiv SiO)_3ZrH + \equiv SiH_2 + =AlH + C_nH_{2n+2} \qquad (c)$$

spectroscopy. The broad band at 1635 cm^{-1} for the ν(Zr–H) vibration was displaced under D_2 and quantitavely restored under H_2. The band for the ν(Al–H) vibration was observed as a very weak signal at 1933 cm^{-1}. The bands for $\nu(Si(H)_2)$ vibrations appeared at 2260 and 2189 cm^{-1}.[8]

Polymerization of ethylene and propylene and hydrogenolytic depolymerization of the resulting polymers: These reactions were followed by IR spectroscopy. The monomer (ethylene or propylene, 200 torr) was introduced into the infrared cell and allowed to react with **3** at room temperature for 2 h. The excess of monomer was then removed for 4 h under vacuum. The polymer bound to zirconium supported on silica-alumina was then heated at 150 °C overnight under H_2 (300 torr).

Hydrogenolysis of polyethylene: A polyethylene of low molecular weight with a broad range of molecular weight (C_{20} to C_{50}; only oligomers with an even number of carbon atoms are included, see Figure 2a) was used for the kinetic experiments. In a typical experiment **3** (70 mg, 3 wt% Zr, 0.023 mmol Zr) was placed in a glass reactor with a volume of 482 mL, and polyethylene (115 mg; corresponding to 8 mmol of CH_2 units) was then introduced under an inert atmosphere. A hydrogen pressure of 10^5 Pa (corresponding to 19.7 mmol of H_2) was established in the reactor at room temperature. The reactor was heated at 150 °C for several hours. The hydrogenolyses were also conducted with a low-density polyethylene (M = 125 000) from Aldrich. The conversion into lower alkanes (C_1 to C_9) was calculated by dividing the number of moles of carbon in the product mixture by the number of moles of starting polymer (obtained by dividing the mass of the polymer by 14). The yields of the individual products (C_n) was determined by dividing the number of moles of carbon for a given product by the total number of moles of carbon in the starting polymer.

Hydrogenolysis of polypropylene: The polypropylene (M = 250 000) used in these experiments was purchased from Aldrich. According to the procedure described above, 40% of the starting polypropylene was converted into lower alkanes (methane: 11.6, ethane: 5.7, propane: 6.2, butanes: 7.2, pentanes: 6, hexanes: 2.8, heptanes: 0.5%) after 15 h at 190 °C.

Received: November 7, 1997 [Z11127IE]
German version: *Angew. Chem.* **1998**, *110*, 848 – 852

Keywords: depolymerizations · hydrogenolysis · polymerizations · zirconium

[1] a) K. Ziegler, *Angew. Chem.* **1955**, *67*, 543; b) K. Ziegler, H. Breil, E. Holzkamp, H. Martin, DE-B 973 626, **1960**; c) G. Natta, *J. Am. Chem. Soc.* **1955**, *77*, 1708; d) G. Natta (Montecatini Corp.), US-A 3 715 344, **1972**, [*Chem. Abstr.* **1973**, *78*, 1488661].

[2] a) P. L. Beltrame, P. Carniti, *Poly. Degrad. Stab.* **1989**, *26*, 209; b) Y. Ishihara, H. Nanbu, T. Ikemura, *Fuel* **1990**, *69*, 978; c) T. Hirota, F. N. Fagan, *Makromol. Chem. Macromol. Symp.* **1992**, *57*, 161; d) F. Dawans, *Inf. Chim.* **1994**, *356*, 85; e) F. Dawans, *Rev. Inst. Fr. Pet.* **1992**, *47*, 837; f) J. Shabtai, X. Xiao, W. Zmierczak, *Energ. Fuels* **1997**, *11*, 76.

[3] For olefin polymerization mechanism with conventional Ziegler – Natta catalysts, see a) P. Corradini in *Comprehensive Polymer Science*, *Vol. 4* (Ed.: Sir G. Allen), Pergamon, Oxford, **1988**, pp. 40; b) P. Cossee, *J. Catal.* **1964**, *3*, 80; c) E. J. Arlman, P. J. Cossee, *Catal.* **1964**, *3*, 99; d) H. Sinn, W. Kaminsky, *Adv. Organomet. Chem.* **1980**, *18*, 99. For olefin polymerization mechanism with metallocene catalysts, see

 © WILEY-VCH Verlag GmbH, D-69451 Weinheim, 1998 1433-7851/98/3706-0809 $ 17.50+.50/0

e) P. G. Gassman, M. R. Callstrom, *J. Am. Chem. Soc.* **1987**, *109*, 7875; f) H. Sinn, W. Kaminsky, H.-J. Vollmer, R. Woldt, *Angew. Chem.* **1980**, *92*, 396; *Angew. Chem. Int. Ed. Engl.* **1980**, *19*, 390; g) R. F. Jordan, *Adv. Organomet. Chem.* **1991**, *32*, 325; h) T. J. Marks, *Acc. Chem. Res.* **1992**, *25*, 57; i) J. J. Eisch, A. M. Piotrowski, S. K. Brownstein, E. J. Gabe, F. L. Lee, *J. Am. Chem. Soc.* **1985**, *107*, 7219; j) R. F. Jordan, C. S. Bajgur, R. Willett, B. Scott, *ibid.* **1986**, *108*, 7410.

[4] For β-methyl and β-alkyl elimination, see a) P. Watson, C. Roe, *J. Am. Chem. Soc.* **1982**, *104*, 6471; b) "Initiation of Polymerisation": P. L. Watson, T. Herskovitz, *ACS Symp. Ser.* **1983**, *212*, 459–479; c) W. Kaminsky, H. Luker, *Makromol. Chem. Rapid Commun.* **1984**, *5*, 225; d) P. L. Watson, G. W. Parshall, *Acc. Res.* **1985**, *18*, 51; e) E. Bunel, B. Burger, J. Bercaw, *J. Am. Chem. Soc.* **1988**, *110*, 976; f) L. Schock, T. J. Marks, *ibid.* **1988**, *110*, 7701; g) B. Burger, M. Thompson, D. Cotter, J. Bercaw, *ibid.* **1990**, *112*, 1566; h) J. Eshuis, Y. Tan, J. Teuben, J. Renkema, *J. Mol. Catal.* **1990**, *62*, 277; i) L. Resconi, F. Piemontesi, G. Franciscono, L. Abis, T. Fiorani, *J. Am. Chem. Soc.* **1992**, *114*, 1025; j) J. J. Eshuis, Y. Y. Tan, A. Meetsma, J. H. Teuben, J. Renkema, G. G. Evens, *Organometallics* **1992**, 11, 362; k) K. McNeill, R. A. Andersen, R. Bergman, *J. Am. Chem. Soc.* **1995**, *117*, 3625; l) A. D. Horton, *Organometallics* **1996**, *15*, 2675; m) L. D'ornelas, S. Reyes, F. Quignard, A. Choplin, J.-M. Basset, *Chem. Lett.* **1993**, 1931.

[5] V. Dufaud, J.-M. Basset (CPE Lyon), XF-B 9508552, **1995**, [*Chem. Abstr.* **1997**, *126*, 293772y].

[6] F. Quignard, C. Lecuyer, C. Bougault, F. Lefevbre, A. Choplin, D. Olivier, J.-M. Basset, *Inorg. Chem.* **1992**, *31*, 928.

[7] a) F. Quignard, A. Choplin, J.-M. Basset, *J. Chem. Soc. Chem. Commun.* **1991**, 1589; b) F. Quignard, C. Lecuyer, A. Choplin, D. Olivier, J.-M. Basset, *J. Mol. Catal.* **1992**, *74*, 353.

[8] J. Corker, F. Lefebvre, C. Lécuyer, V. Dufaud, F. Quignard, A. Choplin, J. Evans, J.-M. Basset, *Science* **1996**, *276*, 966.

[9] S. L. Scott, J.-M. Basset, *J. Mol. Catal.* **1994**, *86*, 5.

[10] Formally, **1** is a Zr^{IV} d^0 compound with eight electrons if one does not consider the $p_\pi - d_\pi$ interaction between the oxygen lone pair orbitals and the Zr orbitals.

[11] C. Lecuyer, F. Quignard, A. Choplin, D. Olivier, J.-M. Basset, *Angew. Chem.* **1991**, *103*, 1692; *Angew. Chem. Int. Ed. Engl.* **1991**, *30*, 1660.

[12] A proposed mechanism[7] includes the following elementary steps: 1) electrophilic activation of a C–H bond of the alkane by a highly electrophilic zirconium hydride on the surface by σ-bond metathesis, 2) β-alkyl migration with formation of an (alkyl)(olefin)zirconium complex, 3) hydrogenolysis of the alkylzirconium complex with liberation of an alkane and formation of a surface (hydride)(olefin)-zirconium complex, 4) insertion by the latter of the coordinated olefin into the Zr–H bond, and 5) hydrogenolysis of the new surface alkylzirconium species to give an alkane with regeneration of the electrophilic zirconium catalyst. No hydrogenolysis was observed with ethane owing to the lack of an alkyl group in the β-position.

[13] For polyethylene and polypropylene IR data, see C. Pouchert in *The Aldrich Library of Infrared Spectra*, **1981**, 3rd. ed.

[14] The polymerization of ethylene or propylene with alumina-supported zirconium hydrides is well known; see, for example, a) A. M. Pyle, K. J. Jens, *J. Mol. Catal.* **1986**, *38*, 337; b) V. A. Zakharov, Y. A. Ryndin, *ibid.* **1989**, *56*, 183; c) J. P. Candlin, H. Thomas, *Adv. Chem. Ser.* **1976**, *132*, 212; d) Y. I. Yermakov, V. A. Zakharov in *Coordination Polymerization* (Ed.: J. C. Chien), Academic Press, New York, **1975**, pp. 91; e) V. A. Zakharov, V. K. Dudchenko, A. I. Minkov, O. N. Efrimov, L. G. Khomyakova, V. P. Babenko, Y. I. Yermakov, *Kinet. Catal.* **1976**, *17*, 643; f) V. A. Zakharov, Y. I. Yermakov, *Catal. Rev. Sci. Eng.* **1979**, *19*, 67; g) L. E. Firment, *J. Catal.* **1983**, *82*, 196; h) P. J. Toscano, T. J. Marks, *J. Am. Chem. Soc.* **1985**, *107*, 653.

[15] S. Reyes, G. P. Niccolai, J.-M. Basset, unpublished results.

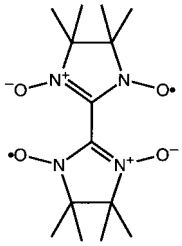
[16] a) D. R. McAlister, D. K. Erwin, J. E. Bercaw, *J. Am. Chem. Soc.* **1978**, *100*, 5966; b) J. E. Bercaw, *Adv. Chem. Ser.* **1978**, *167*, 136; c) M. E. Thompson, S. M. Baxter, A. R. Bulls, B. J. Burger, M. C. Nolan, B. D. Santarsiero, W. P. Schaefer, J. E. Bercaw, *J. Am. Chem. Soc.* **1987**, *109*, 203.

[17] S. A. King, J. Schwartz, *Inorg. Chem.* **1991**, *30*, 3771.

A Spin-Frustrated System Composed of Organic Radicals and Magnetic Metal Ions

Megumi Tanaka, Kenji Matsuda, Tetsuji Itoh, and Hiizu Iwamura*

Antiferromagnetically coupled spins in polynuclear complexes of paramagnetic metal ions[1] and π-cross-conjugated organic polyradicals[2] can be arranged in triangular, "butterfly"-shaped, tetrahedral, or cubane-like structures and combinations of these topologies. Consequently, these materials provide ample opportunities for delineating competing interactions in which two neighboring spins have to align in parallel in spite of the antiferromagnetic coupling. When a degenerate ground state ensues, the system is referred to as spin-frustrated. The versatility of molecule-based magnetic materials will be much enhanced in heterospin systems consisting of paramagnetic metal ions in conjunction with organic free radical bridging ligands.[3] The diradical 2,2′-bis(1-oxyl-3-oxide-4,4,5,5-tetramethylimidazolinyl) (bnn), which was first reported by Ullman et al.[4] and later characterized by Rey et al. with respect to its magnetic properties,[5] captured our attention as an interesting bis-bidentate paramagnetic ligand for magnetic metal ions. We report here a new spin-frustrated system consisting of manganese(II) bis(hexafluoroacetylacetonate) ([$Mn(hfac)_2$]) and bnn with a butterfly spin arrangement.



bnn

Complexation was effected by mixing anhydrous [$Mn(hfac)_2$] and bnn. Dark green crystals were obtained, and their composition was found to be 2:1, [$\{Mn(hfac)_2\}_2$-(bnn)], by elemental analysis.[6] The crystal and molecular structure (Figure 1) was determined by X-ray crystallographic analysis.[7] The molecular structure of bnn in the complex is very similar to that reported for free bnn.[5] The C1–C8 bond length of 1.44(2) Å is almost the same as that in the free ligand (1.439(3) Å), and the dihedral angle between the two "Ullman's nitronyl nitroxide radical" moieties is 55° in the complex as well as in bnn itself. These similarities suggest that the bnn ligand forms the [$Mn(hfac)_2$] complex with minimal structural perturbation and that the magnetic interaction between the two radical centers should only be marginally modified by complexation.

Magnetic measurements of [$\{Mn(hfac)_2\}_2$(bnn)] were performed on a SQUID susceptometer/magnetometer. The

[*] Prof. Dr. H. Iwamura, M. Tanaka, Dr. K. Matsuda, Dr. T. Itoh
Institute for Fundamental Research in Organic Chemistry
Kyushu University
6-10-1 Hakozaki, Higashi-ku, Fukuoka, 812-81 (Japan)
Fax: (+81) 92-642-2735
E-mail: iwamura@ms.ifoc.kyushu-u.ac.jp

[**] This work was supported by a Grant-in-Aid for COE Research "Design and Control of Advanced Molecular Assembly Systems" (no. 08CE2005) from the Ministry of Education, Science, Sports, and Culture, Japan. We acknowledge Prof. Katsuya Inoue of the Institute for Molecular Science for assisting with the X-ray crystal structure analysis. T.I. is thankful to the Japan Society for the Promotion of Science for a Postdoctoral Fellowship.

 © WILEY-VCH Verlag GmbH, D-69451 Weinheim, 1998 1433-7851/98/3706-0810 $ 17.50+.50/0

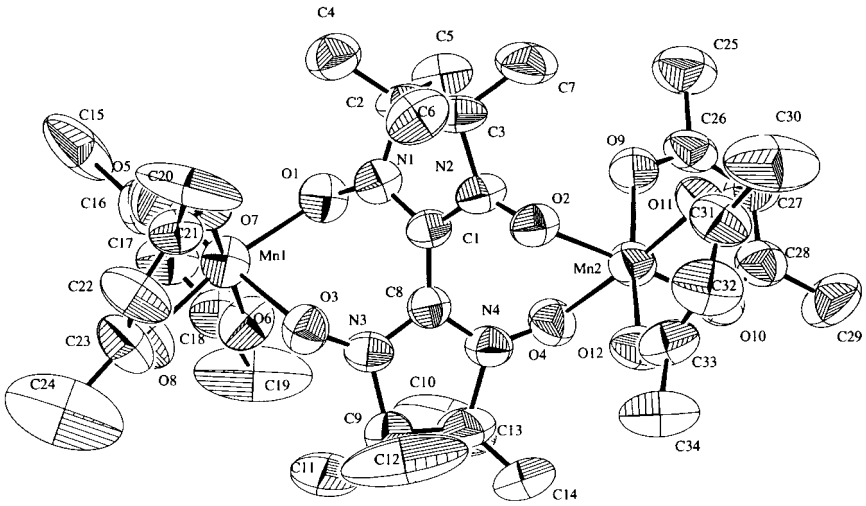


Figure 1. ORTEP drawing of [{Mn(hfac)$_2$}$_2$(bnn)] with thermal ellipsoids at the 50% probability level. The fluorine and hydrogen atoms are omitted for clarity. Selected bond lengths [Å] and angles [°]: C1–C8 1.44(2), Mn1–O1 2.150(8), Mn1–O3 2.201(9), O1–N1 1.28(1), O3–N3 1.28(1), N2–O2 1.28(1), N4–O4 1.25(1), O2–Mn2 2.168(7), O4–Mn2 2.18(1); O3-Mn1-O1 83.8(3), Mn1-O1-N1 126.8(6), N3-O3-Mn1 124.5(6), O2-Mn2-O4 84.8(3), Mn2-O4-N4 127.3(7), N2-O2-Mn2 121.6(6).

temperature dependence of the paramagnetic susceptibility χ at 500 G is presented as a χT vs. T plot in Figure 2. The χT values remained almost constant from 300 to 2 K.

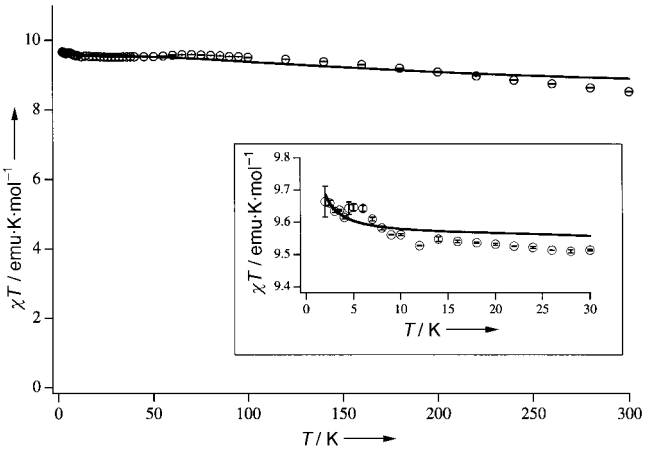


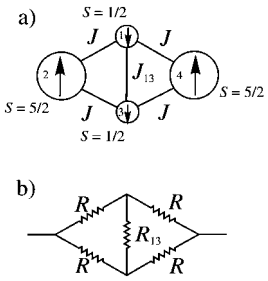
Figure 2. χT vs. T plot for [{Mn(hfac)$_2$}$_2$(bnn)] at 500 G. The solid line represents the theoretical curve (see text).

The spin Hamiltonian $\boldsymbol{H}$ for this butterfly system is given by Equation (1),[1b] where J is the exchange coupling parameter between the 3d spins of Mn^{II} and the 2p spins of the organic ligand (corresponding to the spins of the "wing" and the "body", respectively, of the butterfly), and J_{13} is the interaction between the two 2p spins of the organic ligand (Scheme 1a). The eigenvalues E are given by Equation (2); $\boldsymbol{S}_T = \boldsymbol{S}_1 + \boldsymbol{S}_2 + \boldsymbol{S}_3 + \boldsymbol{S}_4$, $\boldsymbol{S}_{13} = \boldsymbol{S}_1 + \boldsymbol{S}_3$ and $\boldsymbol{S}_{24} = \boldsymbol{S}_2 + \boldsymbol{S}_4$.

$$\boldsymbol{H} = -2J(\boldsymbol{S}_1\cdot\boldsymbol{S}_2 + \boldsymbol{S}_2\cdot\boldsymbol{S}_3 + \boldsymbol{S}_3\cdot\boldsymbol{S}_4 + \boldsymbol{S}_4\cdot\boldsymbol{S}_1) - 2J_{13}\boldsymbol{S}_1\cdot\boldsymbol{S}_3 \quad (1)$$

$$E = -J[S_T(S_T+1) - S_{13}(S_{13}+1) - S_{24}(S_{24}+1)] - J_{13}[S_{13}(S_{13}+1)] \quad (2)$$

A theoretical equation was derived for the temperature dependence of χ due to the Boltzmann distribution of the four spins among the energy levels and fitted to the observed data (Figure 2). The best fit provided $J/k_B = -68.1 \pm 4.6$ K and $J_{13}/k_B = -408 \pm 28$ K. The latter is close to that for the free ligand bnn (-447.4 K),[5] and its absolute value is about 10% smaller. Both J and J_{13} are negative, which confirms that any two neighboring spins are antiferromagnetically coupled. Therefore, the four-spin system must have a competing interaction, since two neighboring spins have to align in parallel in spite of the antiferromagnetic coupling.



Scheme 1. a) Spin alignment for the ground state of [{Mn(hfac)$_2$}$_2$(bnn)]; b) Wheatstone bridge.

The field dependence of the magnetization of [{Mn(hfac)$_2$}$_2$(bnn)] was measured at 2 K. The fitting of a theoretical Brillouin function to the observed data (Figure 3) suggests that the populated state is close to the $S = 4$ state (Scheme 1a). Although J_{13} is more negative than J, the latter wing–body antiferromagnetic interaction appears to dominate, and the two $S = 1/2$ spins of the bnn moiety are obliged to align in parallel. The butterfly configuration and two $S = 5/2$ spins of the manganese ions at the wing sites therefore play an important role in dictating this spin configuration.

Equation (2) reveals that the ground state is $S = 4$ when $6|J| > |J_{13}|$ or degenerate among $S = 0$, 1, 2, 3, 4, 4 and 5 when $6|J| = |J_{13}|$. The present case of $6|J| \approx |J_{13}|$ suggests the latter possibility, that is, a genuine spin-frustrated system.

The butterfly configuration of the four spins (Scheme 1a) and the ineffectiveness of a large J_{13} interaction in aligning the two body spins in antiparallel in [{Mn(hfac)$_2$}$_2$(bnn)] offer a

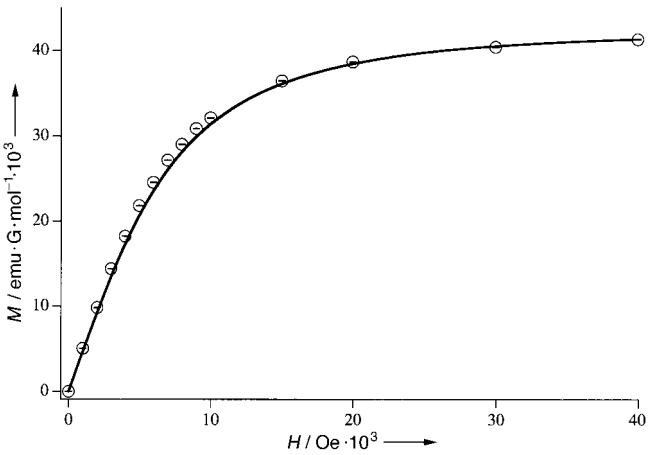


Figure 3. Dependence of the magnetization M of [{Mn(hfac)$_2$}$_2$(bnn)] on the field strength H at 2 K. The solid line indicates the theoretical curve for $S = 4$.

formal comparison of these systems with a Wheatstone bridge in an electric circuit (Scheme 1b). In a balanced Wheatstone bridge, no current flows through R_{13} even if R_{13} is very small. With respect to information processing at the molecular level, the mimicking of an electric circuit by molecular materials is instructive.[8]

We have succeeded in constructing a heterospin system which displays competing interactions between organic radicals and transition metal ions. In this system the large antiferromagnetic interaction was made ineffective by the butterfly spin configuration, and J and J_{13} are sufficiently large to realize the degeneracy of a ground-state spin-frustrated system.

Experimental Section

Preparation of the sample: A suspension of [Mn(hfac)$_2$]·2H$_2$O (165 mg, 0.32 mmol) in *n*-heptane (40 mL) was heated at reflux to remove H$_2$O by azeotropic distillation. The dark green solution obtained by adding bnn (50 mg, 0.16 mmol) in CH_2Cl_2 (20 mL) was concentrated on a rotary evaporator to remove CH_2Cl_2. The green precipitate was collected by filtration to afford dark green plates of [Mn$_2$(hfac)$_4$(bnn)] (153 mg, 76 %). The sample for X-ray crystallography was recrystallized from CH_2Cl_2/heptane: IR (KBr): $\tilde{\nu} = 1258, 1651, 3002\ cm^{-1}$.

Magnetic measurement: A fine-crystalline sample was mounted in a capsule and measured on a Quantum Design MPMS-5S SQUID susceptometer at 500 G. Corrections for the diamagnetic contribution were made with Pascal's constants.

Received: September 15, 1997 [Z 10924 IE]
German version: *Angew. Chem.* **1998**, *110*, 866 – 869

Keywords: magnetic properties · manganese · radicals

[1] a) J. Villaian, *J. Phys. C Solid State Phys.* **1977**, *10*, 1717 – 1734; b) J. B. Vincent, C. Christmas, H.-R. Chang, Q. Li, P. D. W. Boyd, J. C. Huffman, D. N. Hendrickson, G. Christou, *J. Am. Chem. Soc.* **1989**, *111*, 2086 – 2097; c) J. K. McCusker, J. B. Vincent, E. A. Schmitt, M. L. Mino, K. Shin, D. K. Coggin, P. M. Hagen, J. C. Huffman, G. Christou, D. N. Hendrickson, *ibid.* **1991**, *113*, 3012 – 3021; d) J. K. McCusker, C. A. Christmas, P. M. Hagen, R. K. Chadha, D. F. Harvey, D. N. Hendrickson, *ibid.* **1991**, *113*, 6114 – 6124; e) D. N. Hendrickson in *Research Frontiers in Magnetochemistry* (Ed.: C. J. O'Connor), World Scientific, Singapore, **1993**, pp. 87 – 108; f) O. Kahn, *Molecular Magnetism*, VCH, New York, **1993**, chap. 10.5; g) O. Kahn, *Chem. Phys. Lett.* **1997**, *265*, 109.

[2] a) K. Awaga, T. Okuno, A. Yamaguchi, M. Hasegawa, T. Inabe, Y. Maruyama, N. Wada, *Phys. Rev. B* **1994**, *49*, 3975 – 3981; b) J. Fujita, M. Tanaka, H. Suemune, N. Koga, K. Matsuda, H. Iwamura, *J. Am. Chem. Soc.* **1996**, *118*, 9347 – 9351.

[3] a) A. Caneschi, D. Gatteschi, P. Rey, *Prog. Inorg. Chem.* **1991**, *39*, 331 – 429; b) H. Iwamura, K. Inoue, T. Hayamizu, *Pure Appl. Chem.* **1996**, *68*, 243 – 252; c) N. Yoshioka, M. Irisawa, Y. Mochizuki, T. Kato, H. Inoue, S. Ohba, *Chem. Lett.* **1997**, 251 – 252; d) H. Oshio, T. Watanabe, A. Ohto, T. Ito, U. Nagashima, *Angew. Chem.* **1994**, *106*, 691 – 692; *Angew. Chem. Int. Ed. Engl.* **1994**, *33*, 670 – 671; e) D. Luneau, J. Laugier, P. Rey, G. Ulrich, R. Ziessel, P. Legoll, M. Drillon, *J. Chem. Soc. Chem. Commun.* **1994**, 741 – 742.

[4] E. F. Ullman, D. G. B. Boocock, *J. Chem. Soc. Chem. Commun.* **1969**, 1161 – 1162.

[5] F. Alies, D. Luneau, J. Laugier, P. Rey, *J. Phys. Chem.* **1993**, *97*, 2922 – 2925.

[6] Elemental analysis calcd for $C_{34}H_{28}N_4O_{12}F_{24}Mn_2$: C 32.66, H 2.26, N 4.48; found: C 32.72, H 2.26, N 4.52.

[7] Crystallographic data for [{Mn(hfac)$_2$}$_2$(bnn)]: $C_{34}H_{28}N_4O_{12}F_{24}Mn_2$, $M_r = 1250.45$, triclinic, space group $P\bar{1}$, $a = 13.305(1)$, $b = 18.617(1)$, $c = 11.0825(6)$ Å, $\alpha = 101.885(5)$, $\beta = 100.968(5)$, $\gamma = 103.359(6)^\circ$, $V = 2530.6(4)$ Å^3, $Z = 2$, $\rho_{calcd} = 1.641\ g\,cm^{-3}$, $\mu(Cu_{K\alpha}) = 54.26\ cm^{-1}$. Data were collected on a Rigaku AFC7R diffractometer at 296 K with $Cu_{K\alpha}$ radiation ($\lambda = 1.54178$ Å). The structure was solved by direct methods and refined to $R = 0.082$, $R_w = 0.079$, for 3677 unique reflections with $|F_o| > 1.5\sigma(|F_o|)$ and 685 parameters. Crystallographic data (excluding structure factors) for the structure reported in this paper have been deposited with the Cambridge Crystallographic Data Centre as supplementary publication no. CCDC-100688. Copies of the data can be obtained free of charge on application to CCDC, 12 Union Road, Cambridge CB2 1EZ, UK (fax: (+44) 1223-336-033; e-mail: deposit@ccdc.cam.ac.uk).

[8] a) A. Aviram, *J. Am. Chem. Soc.* **1988**, *110*, 5687 – 5692; b) A. P. deSilva, H. Q. N. Gunaratne, C. P. McCoy, *Nature* **1993**, *364*, 42 – 44; c) A. Credi, V. Balzani, S. J. Langford, J. F. Stoddart *J. Am. Chem. Soc.* **1997**, *119*, 2679 – 2681.

Silanediols: A New Class of Potent Protease Inhibitors**

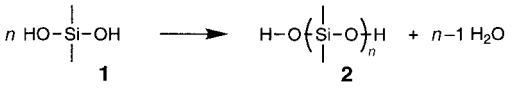
Scott McN. Sieburth,* Thomas Nittoli, Alfred M. Mutahi, and Luxuan Guo

Lower dialkylsilanediols, with their proclivity for self-condensation [Eq. (1)], are the cornerstone of the siloxane (silicone) industry, and siloxane polymers **2** have a reputation as stable and inert materials.[1] Dimethylsilanediol (**1**) is the best known siloxane monomer and the most prone to polymerization. In contrast, more sterically hindered silane-

[*] Prof. S. McN. Sieburth, Dr. T. Nittoli, Dr. A. M. Mutahi, L. Guo
Department of Chemistry
State University of New York at Stony Brook
Stony Brook, NY 11794-3400 (USA)
Fax: (+1) 516-632-8882
E-mail: ssieburth@ccmail.sunysb.edu

[**] This work was funded by The Center for Biotechnology, supported by the New York State Science and Technology Foundation and Wyeth-Ayerst Research. Funding for the NMR spectrometers used in this study was provided by the National Science Foundation (CHE9413510). T.N. was supported in part by a GAANN fellowship (P200A4014596). L.G. was supported by a Grant-in-Aid for undergraduate research from American Cyanamid.

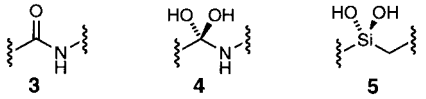
 © WILEY-VCH Verlag GmbH, D-69451 Weinheim, 1998 1433-7851/98/3706-0812 $ 17.50+.50/0



(1)

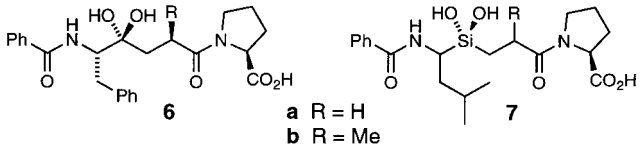
diols can be stable and in some cases will form oligomers only under forcing conditions.[2]

Organosilanes are inherently unnatural yet have no intrinsic toxicity.[3] As silicon is the element most similar to carbon, its derivatives have been the subject of many investigations in the search for bioactive materials.[4, 5] A dialkylsilanediol **5**[6, 7] should be an isosteric analogue of the tetrahedral hydrolysis intermediate **4** of a peptide amide **3**: The silicon atom of a



silanediol is most stable in a tetrahedral configuration, and the hydroxyl groups are excellent hydrogen bond donors and acceptors.[8, 9] Nevertheless, previous attempts to inhibit hydrolases with relatively simple silanediols[10] and silanetriols[11] found them to be inactive. Here we report the first synthesis of a silanediol-based dipeptide analogue and the discovery that these compounds can be potent inhibitors of the metalloproteases and, therefore, therapeutically important target molecules for medicinal chemistry.

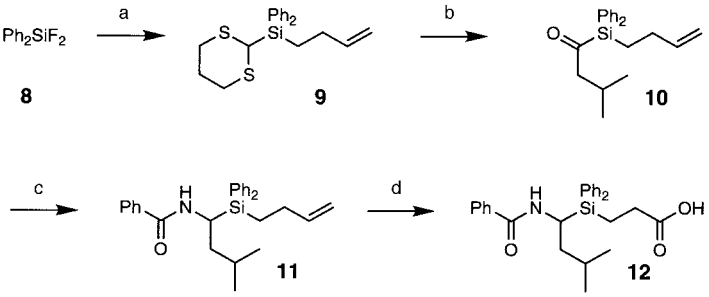
A ketone inhibitor (**6**, shown in the hydrated form) of angiotensin-converting enzyme (ACE) was used as a model for design of the silanediol inhibitor. This ketone is presumably hydrated at the active site of the enzyme.[12] The



silanediol analogue **7** differs from **6** in three significant ways: the central silicon atom, an isobutyl group in place of the benzyl group,[13] and the formation of **7** as a mixture of diastereomers.

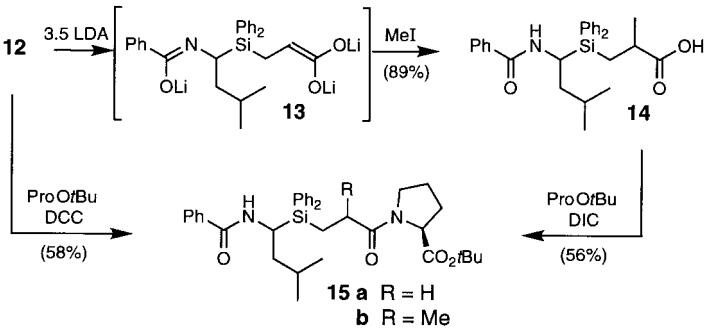
Synthesis of **7** required a silanol-protecting group. Phenyl groups were selected with the expectation that their hydrolysis with strong acid would be similar to standard peptide deprotection routines[14, 15] and would therefore be compatible with the amide groups in the molecule.

Preparation of **7** commenced with the sequential treatment of difluorodiphenylsilane[16] with 1-bromomagnesium-3-butene and 2-lithio-1,3-dithiane (Scheme 1).[17] The resulting 2-siladithiane **9** was deprotonated, alkylated with isobutyl bromide, and then hydrolyzed to yield the moderately stable silylketone **10**, which was reduced to the alcohol with lithium aluminum hydride. Mesylation of the alcohol and substitution with azide was followed by reduction with lithium aluminum hydride and benzoylation to give **11**. The alkene of **11** was then oxidatively cleaved under Weinreb conditions[18] to give



Scheme 1. Synthesis of diphenylsilane **12**. a) 1. C_4H_7MgBr (83%), 2. $C_4H_7S_2Li$ (96%); b) 1. *n*BuLi, *i*BuBr (92%), 2. $HgCl_2$, H_2O (88%); c) 1. $LiAlH_4$ (69%), 2. MsCl, NaN_3 (87%), 3. $LiAlH_4$, 4. PhCOCl (88%); d) OsO_4 (cat.), Jones reagent (96%). Ms = methanesulfonyl.

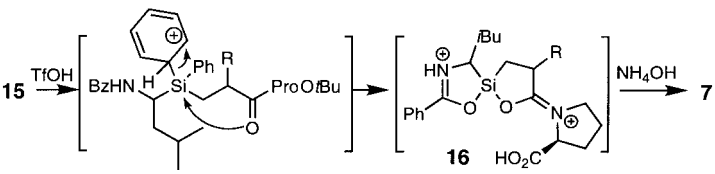
the carboxylic acid **12**. Introduction of the methyl group in the position α to the carboxyl group was achieved in good yield, albeit stereorandomly, by using the trianion **13** (Scheme 2).



Scheme 2. Synthesis of diphenylsilane **15**. LDA = lithium diisopropylamide, DCC = dicyclohexylcarbodiimide, DIC = diisopropylcarbodiimide.

Acids **12** and **14** were coupled with the *tert*-butyl ester of L-proline to give the silanediol precursors **15a** and **15b** as mixtures of two and four diastereomers, respectively.[17]

Reaction of phenyl groups on silicon with trifluoromethanesulfonic (triflic) acid is a routine method for the preparation of silyl triflates,[19, 20] and here it was combined with removal of the *tert*-butyl ester group. Consideration of the relative reactivities of the functional groups in **15** leads to the expectation that the protonated arylsilane will be intercepted by a nucleophilic neighboring amide carbonyl group rather than by triflate (Scheme 3). Therefore, a probable intermedi-



Scheme 3. Hydrolysis of **15** may be assisted by the amide carbonyl group. Tf = trifluoromethanesulfonyl, Bz = benzoyl.

ate in the acidic cleavage of the phenyl–silicon bond in nonnucleophilic solvents is the spirocyclic compound **16**. Hydrolysis of **16** was expected to be facile, as simple five-membered silyl ethers are strained.[21] In the event, treatment of **15a** and **15b** with triflic acid in dichloromethane at 0 °C for

30 min followed by addition of ammonium hydroxide led to **7a** and **7b** as diasteromeric mixtures that were very difficult to separate. Yields of isolated **7a** and **7b** after HPLC purification were 39% and 21%, respectively.

Silanediol mixtures **7a** and **7b** were tested as ACE inhibitors with use of the commercially available enzyme and substrate by the methods of Cushman[22] and Holmquist.[23] The measured IC_{50} values are listed in Table 1

Table 1. Inhibition of ACE by **6** and **7**.

	R	IC_{50} (**6**)[24]	IC_{50} (**7**)
a	H	3.2 nM	57 nM
b	Me	1.0 nM	14 nM

together with the reported values for **6a** and **6b**.[24] Notably for both **6** and **7**, introduction of the methyl group (R) in the position α to the amide carbonyl group increases the enzyme inhibition by a factor of 3–4. The more potent inhibitors **6b** and **7b** differ by a factor of 14. These differences in potency are likely to be due to the presence of low-activity diastereomers in the **7b** mixture and the replacement of an isobutyl group by a benzyl group in **6**.

Enantioselective synthesis of the isomers of **7** can be expected to improve the activity, and the chemistry reported here should be readily amenable to asymmetric control at all stereogenic centers. We have demonstrated the use of aryl groups as stable yet readily hydrolyzable protecting groups for silanols that are compatible with peptidomimetic silanediol synthesis. Silanediols **7a** and **7b** are the most complex silanediols reported to date and represent a new class of inhibitors for metalloproteases.

Experimental Section

Inhibition of ACE (EC 3.4.15.1, Sigma) was measured by monitoring the absorbance at 340 nm with a Perkin-Elmer Lambda 5 UV/Vis spectrophotometer. Samples were prepared in disposable polystyrene cuvettes and incubated at 37 °C. Each cuvette was charged with 1.0 mL of substrate (0.5 mM solution, pH 8.2, *N*-[3-(2-furyl)acryloyl]-L-phenylalanylglycylglycine, Sigma) and 0.1 mL of the porcine enzyme solution in a buffered human serum base (Sigma). Stock solutions of **7a** and **7b** were prepared in deionized water buffered with 0.3 M NaCl and 0.05 M Trizma (Sigma) to give a pH of 8.3 at 37 °C, and this solution was added to the cuvettes to achieve the desired concentration. Solutions with and without inhibitors were equilibrated at 37 °C for 5 min, and initial rates were measured. Captopril was used to calibrate the assay. Inhibition measurements were made three times at each concentration.

Received: September 3, 1997 [Z10883IE]
German version: *Angew. Chem.* **1998**, *110*, 845–847

Keywords: angiotensin-converting enzyme · enzyme inhibitors · peptidomimetics · silanols · structure–activity relationships

[1] F. O. Stark, J. R. Falender, A. P. Wright in *Comprehensive Organometallic Chemistry*, *Vol. 2* (Eds.: G. Wilkinson, F. G. A. Stone, E. W. Abel), Pergamon, New York, **1982**, pp. 305–363; S. S. Brown, T. C. Kendrick, J. McVie, D. R. Thomas in *Comprehensive Organometallic Chemistry II*, *Vol. 2* (Eds.: E. W. Abel, F. G. A. Stone, G. Wilkinson), Pergamon, New York, **1995**, pp. 111–135.

[2] P. D. Lickiss, *Adv. Inorg. Chem.* **1995**, *42*, 147–262.

[3] K. D. Friedberg, E. Schiller, W. B. Farnham in *Handbook on Toxicity of Inorganic Compounds* (Eds.: H. G. Seiler, H. Sigel), Marcel Dekker, New York, **1988**, pp. 595–617.

[4] R. Tacke, H. Linoh in *The Chemistry of Organic Silicon Compounds* (Eds.: S. Patai, Z. Rappoport), Wiley, New York, **1989**, pp. 1143–1206.

[5] S. McN. Sieburth in *Designing Safer Chemicals* (Eds.: S. C. DeVito, R. L. Garrett), American Chemical Society, Washington, DC, **1996**, pp. 74–83.

[6] Diphenylsilanediol is the only silanediol that has been found to be biologically active. For an excellent review, see ref. [4].

[7] Tacke has reported a series of silanols with outstanding activity as antagonists of the muscarinic receptors: R. Tacke, D. Reichel, M. Kropfgans, P. G. Jones, E. Mutschler, J. Gross, X. Huo, M. Waelbroeck, G. Lambrecht, *Organometallics* **1995**, *14*, 251–262, and references therein.

[8] R. West, L. S. Wilson, D. L. Powell, *J. Organomet. Chem.* **1979**, *178*, 5–9.

[9] R. Damrauer, S. R. Kass, C. H. DePuy, *Organometallics* **1988**, *7*, 637–640.

[10] R. E. Galardy, Z. P. Kortylewicz, *Biochem. J.* **1985**, *226*, 447–454.

[11] K. Curley, R. F. Pratt, *J. Am. Chem. Soc.* **1997**, *119*, 1529–1538.

[12] G. Shoham, D. W. Christianson, D. A. Oren, *Proc. Natl. Acad. Sci. USA* **1988**, *85*, 684–688.

[13] Initial attempts to prepare **7** with a benzyl group rather than an isobutyl group failed.

[14] J. P. Tam, R. B. Merrifield in *The Peptides*, *Vol. 9* (Eds.: S. Udenfriend, J. Meienhofer), Academic Press, New York, **1987**, pp. 185–248.

[15] F. Gharahdaghi, J. Mathers, S. M. Mische in *Techniques in Protein Chemistry III* (Ed.: R. H. Angeletti), Academic Press, New York, **1992**, pp. 199–208.

[16] H. J. Emeléus, C. J. Wilkins, *J. Chem. Soc.* **1944**, 454–456; C. Eaborn, *J. Chem. Soc.* **1952**, 2846–2849.

[17] Compounds **9**–**12** were fully characterized, and **14**, **15**, and **7** were characterized by mass spectrometry and ^{1}H NMR spectroscopy; **7a** and **15a** are 1:1 mixtures of diastereomers, and **7b**, **14**, and **15b** are approximately 1:1:1:1 mixtures. Full experimental details will be reported elsewhere.

[18] J. R. Henry, S. M. Weinreb, *J. Org. Chem.* **1993**, *58*, 4745.

[19] W. Uhlig, *Chem. Ber.* **1996**, *129*, 733–739.

[20] A. R. Bassindale, T. Stout, *J. Organomet. Chem.* **1984**, *271*, C1–C3.

[21] R. J. P. Corriu, C. Guérin, G. Guirand, *J. Chem. Soc. Chem. Commun.* **1979**, 8–9.

[22] D. W. Cushman, H. S. Cheung, *Biochem. Pharm.* **1971**, *20*, 1637–1648.

[23] B. Holmquist, P. Bünning, J. F. Riordan, *Anal. Biochem.* **1979**, *95*, 540–548.

[24] R. G. Almquist, J. Crase, C. Jennings-White, R. F. Meyer, M. L. Hoefle, R. D. Smith, A. D. Essenburg, H. R. Kaplan, *J. Med. Chem.* **1982**, *25*, 1292–1299.

 © WILEY-VCH Verlag GmbH, D-69451 Weinheim, 1998 1433-7851/98/3706-0814 $ 17.50+.50/0

Influence of the *trans* Substituent on N_2 Bonding in Iron(II)–Phosphane Complexes: Structure, Synthesis, and Properties of the Monomeric Adducts *trans*-$[FeXN_2(depe)_2]BPh_4$, X = Cl, Br**

Beatrix E. Wiesler, Nicolai Lehnert, Felix Tuczek,* Jörg Neuhausen, and Wolfgang Tremel

In our investigations on the bonding and activation of dinitrogen in transition metal complexes, we prepared the compound "*trans*-[{$FeCl(depe)_2$}$_2$(μ-N_2)]$(BPh_4)_2$" (depe = $Et_2PCH_2CH_2PEt_2$) according to a method described by Bellerby et al.[1] This compound is the only known example of an N_2-bridged iron(II) dimer with octahedral coordination of donor ligands, and thus is of interest as a potential phosphane-analogous N_2 precursor of diazene-bridged Fe^{II} dimers with an octahedral thiolate/thioether coordination environment.[2] We recently characterized the electronic and vibrational properties of these compounds.[3] The known dinuclear μ-N_2–Fe complexes include Fe^0 dimers with trigonal-bipyramidal coordination by P-donor and CO ligands besides N_2, as well as tetracoordinate Fe^{II} complexes with diphosphane and cyclopentadienyl co-ligands.[4] Otherwise, N_2-bridged octahedral complexes are only known for the higher homologues ruthenium(II) and osmium(II).

Doubts about the dimeric structure of the above-mentioned Fe–N_2–depe complex were raised in 1993 by Hughes et al. on the basis of a comparison with the analogous dmpe system (dmpe = $Me_2PCH_2CH_2PMe_2$), for which a monomeric structure was inferred from spectroscopic data.[5] Indeed, our X-ray crystallograpic characterization of the chloro and bromo depe complexes $[FeClN_2(depe)_2]BPh_4$ (**1**) and $[FeBrN_2(depe)_2]BPh_4$ (**2**) revealed a monomeric octahedral structure with end-on terminally bound dinitrogen *trans* to the halide ligand. This is the first X-ray structure of an $[FeXN_2P_4]^+$ complex with X = halide. Corresponding structures with X = H are known.[6]

The reaction of $[FeX_2(depe)_2]$ (X = Cl, Br)[7] with N_2 in methanol at room temperature yields an orange solution. After the addition of $NaBPh_4$, crystals of $[FeXN_2(depe)_2]BPh_4$ (X = Cl **1**[8], X = Br **2**[9]) precipitate. In the IR spectrum the N–N stretching mode is observed in a region typical for complexes in which N_2 is coordinated end-on (**1**: $\tilde{\nu}_{NN} = 2088$, **2**: $\tilde{\nu}_{NN} = 2091\ cm^{-1}$; cf. $\tilde{\nu}_{NN} = 2090\ cm^{-1}$ in $[FeHN_2(depe)_2]BPh_4$ (**3**)[7]) but at lower wavenumber than in the analogous, but not structurally characterized, compounds $[FeXN_2(dmpe)_2]BPh_4$ (X = Cl: $\tilde{\nu}_{NN} = 2105$, X = Br: $\tilde{\nu}_{NN} = 2107 cm^{-1}$).[10] A further band associated with the Fe(II)–N_2 unit is observed at 513 cm^{-1} (**1**) and 509 cm^{-1} (**2**). We succeeded in characterizing complexes **1** and **2** by Raman spectroscopy (30 K, 30 mW, excitation wavelength $\lambda = 514.5$ nm). The band for ν_{NN} was found at 2088 cm^{-1} for **1** and at 2090 cm^{-1} for **2**. Corresponding to the decrease in the intensity of the NN peak, rapid decay of the samples upon laser irradiation was observed.

Both **1** (Figure 1a, b) and **2** were studied by Mössbauer spectroscopy under nitrogen at various temperatures (Table 1). The spectrum of **1** at 300 K (Figure 1b) shows two doublets with quadrupole splittings ΔE_Q of 1.30 (I) and 2.66 $mm\,s^{-1}$ (II) and an isomer shift of $\delta = 0.21$ (I) and 0.41 $mm\,s^{-1}$ (II). Doublet (I) is assigned to complex **1**, which is in agreement with Mössbauer parameters given in the literature and a prediction by Silver.[11, 12] Correspondingly, ΔE_Q and δ were determined for complex **2** to be 1.34 and 0.23 $mm\,s^{-1}$, respectively (Table 1). Doublet (II) is attributed to the analogous N_2-free complex, because its intensity increases in a He atmosphere at room temperature (Figure 1c). Interestingly, this transformation is reversible: Repeating the measurement in an N_2 atmosphere again yields

Table 1. Mössbauer parameters of **1** and **2** under N_2 in $mm\,s^{-1}$ (δ vs. α-iron)

	T [K]	δ (I)	ΔE_Q (I)	δ (II)	ΔE_Q (II)
1	100	0.256(3)	1.398(5)	0.43(2)	2.64(3)
	150	0.244(4)	1.371(7)	0.38(3)	2.64(5)
	250	0.23(2)	1.31(3)	0.36(12)	2.65(24)
	300	0.21(1)	1.30(2)	0.41(3)	2.66(7)
2	150	0.268(8)	1.42(2)	0.39(1)	2.70(1)
	250	0.23(1)	1.39(3)	0.34(1)	2.61(3)
	300	0.23(2)	1.34(4)	0.33(1)	2.61(3)

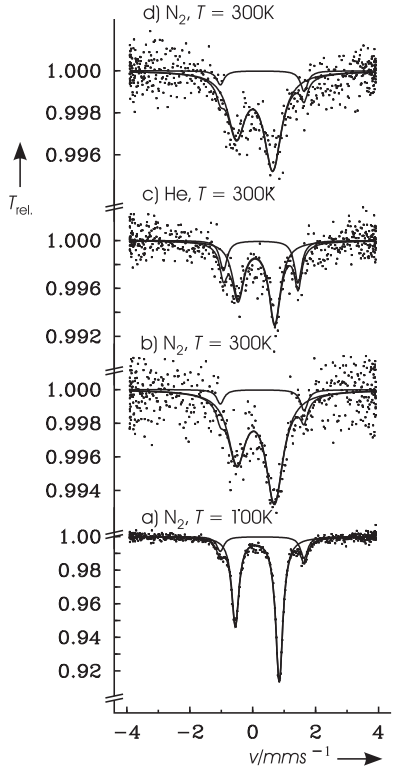


Figure 1. Mössbauer spectra of **1** under N_2 and He atmospheres. T_{rel} = relative transmission.

[*] Dr. F. Tuczek, Dipl.-Chem. B. E. Wiesler, Dipl.-Chem. N. Lehnert
Insitut für Anorganische und Analytische Chemie der Universität
Staudingerweg 9, D-55099 Mainz (Germany)
Fax: (+49) 6131-39-2990
E-mail: tuczek@iacgu7.chemie.uni-mainz.de
Dr. J. Neuhausen, Prof. Dr. W. Tremel
Insitut für Anorganische und Analytische Chemie der Universität
Becherweg 24, D-55099 Mainz (Germany)

[**] We thank S. Stauf for single-crystal X-ray measurements, Prof. Dr. P. Gütlich for providing the Mössbauer instruments, and the Deutsche Forschungsgemeinschaft (Tu 58-04/2) and Fonds der Chemischen Industrie for financial support.

 © WILEY-VCH Verlag GmbH, D-69451 Weinheim, 1998 1433-7851/98/3706-0815 $ 17.50+.50/0

the original spectrum (Figure 1d). Hence, the complex undergoes N_2 exchange at room temperature in the solid state, and the N_2-free product reversibly binds N_2 in the solid state. These observations demonstrate the lability of the Fe–N bond in these complexes.

The monomeric structure of **1** is shown in Figure 2. In the distorted octahedral environment of the iron atom, the end-on-bound N_2 is *trans* to the chloride ligand. One of the two

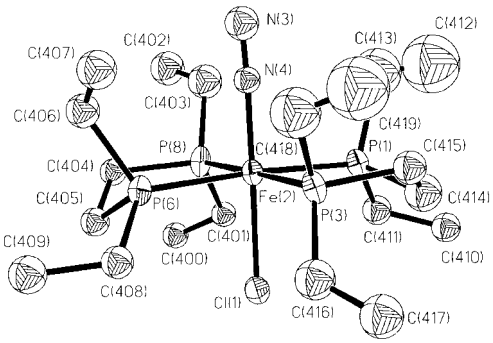


Figure 2. Structure of the cation of **1** (thermal ellipsoids are drawn at the 30% probability level; H atoms omitted for clarity). Selected bond lengths [Å] and angles [°]: Fe(2)–P(1) 2.293(3), Fe(2)–P(3) 2.294(4), Fe(2)–P(6) 2.280(3), Fe(2)–P(8) 2.298(4), Fe(2)–Cl(1) 2.311(3), Fe(2)–N(4) 1.784(9), N(3)–N(4) 1.073(11), P(3)-Fe(2)-P(6) 96.58(12), P(3)-Fe(2)-P(1) 84.63(12), P(6)-Fe(2)-P(8) 84.18(12), P(1)-Fe(2)-P(8) 94.54(12), P(3)-Fe(2)-N(4) 89.3(3), P(3)-Fe(2)-Cl(1) 89.71(12), P(1)-Fe(2)-N(4) 92.5(3), P(6)-Fe(2)-Cl(1) 86.64(12), Fe(2)-N(4)-N(3) 177.5(10).

independent cations in the unit cell exhibits a partial disorder between the chloride and dinitrogen ligands.[13] In the following discussion of bond lengths we exclusively consider the geometry of the undisordered cation (Figure 2). The N–N bond length is comparable to that in the related complex $[FeH(N_2)(depe)_2]BPh_4$ (**3**),[14] the Fe–N bond is slightly shorter, and the Fe–P bonds are considerably longer (**3**: N–N 1.070(12), Fe–N 1.825(7), Fe–P (av) 2.240 Å). Furthermore, the Fe–Cl bond is slightly shorter than those in $[FeHCl(depe)_2]$ (**4**)[15] and $[FeCl_2(depe)_2]$ (**5**)[16] (**4**: Fe–Cl 2.404(2), Fe–P (av) 2.208; **5**: Fe-Cl 2.344(2), Fe–P (av) 2.260 Å). We also obtained single crystals of $[FeBr(N_2)(depe)_2]BPh_4$ (**2**) that were suitable for an X-ray structure analysis. Initial results confirm that the cations in **2** are structurally analogous to those of **1**. However, due to the strong disorder of the ligands in the two symmetry independent cations, a precise determination of the geometry was not possible up to now.[17]

In general iron(II)–dinitrogen complexes are stable if they contain tertiary phosphane and hydride ions as co-ligands.[18] This is demonstrated by the ability of $[FeH_4(PEtPh_2)_3]$ and $[FeH(Ph_2PCH_2CH_2PPh_2)_2]BPh_4$ to fix dinitrogen from air.[19] In contrast, the dinitrogen ligands in **1** and **2** are only weakly bound. A possible explanation for this difference is that the bond between the transition metal and dinitrogen is dominated by π backbonding into the π* orbitals of N_2. This interaction can be enhanced by co-ligands that lower the effective nuclear charge Z_{eff} of the metal and thus raise the energy of the backbonding d orbitals. The hydride ion is the strongest σ donor and therefore has the greatest influence in this respect. This is in accordance with the observation that the bis-hydrido unit has as strong a bonding capability for N_2 as the hydride-free ruthenium and osmium complexes.[20] In comparison, halides are in general weaker donors and also have π-donor character. The latter is an additional disadvantage as the π-donor ligand mixes with the t_{2g} orbitals which are responsible for backbonding, and hence the Fe–N overlap is reduced. Molecular orbital calculations seem to confirm this assumption,[21] which is of general significance for the stability of transition metal–N_2 adducts.

In view of the weakness of the Fe–N bond, it is not surprising that **1** has a monomeric stucture, as the bridging coordination of N_2 requires a certain stability of the Fe–N bond. Therefore, the existence of bridged, octahedrally coordinated iron(II)–N_2 systems at room temperature appears very unlikely.

Received: October 7, 1997 [Z11010IE]
German version: *Angew. Chem.* **1998**, *110*, 856–858

Keywords: iron · Moessbauer spectroscopy · N_2 complexes · nitrogen fixation · P ligands

[1] J. M. Bellerby, M. J. Mays, P. L. Sears, *J. Chem. Soc. Dalton Trans.* **1976**, 1232–1236.
[2] D. Sellmann, A. Hennige, *Angew. Chem.* **1997**, *109*, 270–271; *Angew. Chem. Int. Ed. Engl.* **1997**, *36*, 276–278.
[3] a) N. Lehnert, B. Wiesler, F. Tuczek, A. Hennige, D. Sellmann, *J. Am. Chem. Soc.* **1997**, *119*, 8869–8878; b) N. Lehnert, B. Wiesler, F. Tuczek, A. Hennige, D. Sellmann, *ibid.* **1997**, *119*, 8879–8888
[4] a) H. Kandler, C. Gauss, W. Bidell, S. Rosenberger, T. Bürgi, I. L. Eremenko, D. Veghini, O. Orama, P. Burger, H. Berke, *Chem. Eur. J.* **1995**, *1*, 541–548; b) H. Berke, W. Bankhardt, G. Huttner, J. von Seyerl, L. Zsolnai, *Chem. Ber.* **1981**, *114*, 2754–2768; c) W. E. Silverthorn, *J. Chem. Soc. Chem. Commun.* **1971**, 1310–1311; d) D. Sellmann, E. Kleinschmidt, *J. Organomet. Chem.* **1977**, *140*, 211–219; e) D. Sellmann, E. Kleinschmidt, *Angew. Chem.* **1975**, *87*, 595–596; *Angew. Chem. Int. Ed. Engl.* **1975**, *14*, 571.
[5] D. L. Hughes, G. J. Leigh, M. Jimenez-Tenorio, A. T. Rowley, *J. Chem. Soc. Dalton Trans.* **1993**, 75–82.
[6] a) I. E. Buys, L. D. Field, T. W. Hambley, A. E. D McQueen, *Acta Cryst.* **1993**, *C49*, 1056–1059; b) A. Hills, D. L. Hughes, M. Jimenez-Tenorio, G. J. Leigh, *J. Organomet. Chem.* **1990**, *391*, C41–C44; c) see ref. [5].
[7] M. J. Mays, B. E. Prater, *Inorg. Synth.* **1974**, *15*, 21–28.
[8] All reactions were carried out under dry N_2 in a glovebox or by standard Schlenk techniques. All solvents were distilled under Ar from an appropriate drying agent prior to use. The spectra were measured with the following instruments: IR spectra (CsI pellets): Matson Instruments 2030 Galaxy FTIR spectrometer, UV/Vis spectra (methanol, N_2 atmosphere): Bruins Omega 10 spectrophotometer, NMR spectra: Bruker DRX 400.
A solution of $[FeCl_2(depe)_2]$ (0.4 g, 0.74 mmol) in MeOH (50 mL) was stirred at room temperature under N_2 over night. After the addition of $NaBPh_4$ (0.37 g, 1.1 mmol) in MeOH (10 mL), orange cubes of **1** precipitated slowly and were collected by filtration under N_2. Yield: 0.6 g (95%); ^{1}H NMR (400 MHz, $CDCl_3$, 233 K): $\delta = 1.19$ (m, CH_3), 1.88 (m, CH_2), 7.13 (m, Ph); ^{31}P NMR (200 MHz, solid state, 303 K): $\delta = 61.5$ (quin); ^{31}P NMR(400 MHz, $CDCl_3$, 233 K): $\delta = 65.7$ (s); IR (CsI): $\tilde{\nu}_{NN} = 2088\ cm^{-1}$; UV/Vis: $\lambda_{max}(\varepsilon) = 280$ (7575), 333 (sh; 2272), 382 (2020), 420 nm (sh; 1818 $L\,mol^{-1}\,cm^{-1}$); elemental analysis calcd for $C_{44}H_{68}BClN_2P_4Fe$ (850.99): C 62.1, H 8.1, N 3.3; found: C 62.0, H 8.2, N 2.0. Small amounts of oxygen caused an immediate color change of the orange solutions of **1** and **2** to red (**1**) or green (**2**). After the

 © WILEY-VCH Verlag GmbH, D-69451 Weinheim, 1998 1433-7851/98/3706-0816 $ 17.50+.50/0

addition of $NaBPh_4$, correpondingly colored needles precipitated, which regained an orange color under an N_2 atmosphere.

[9] A solution of $[FeBr_2(depe)_2]$ (0.35 g, 0.56 mmol) in MeOH (40 mL) was stirred at room temperature under N_2 overnight. After the addition of $NaBPh_4$ (0.28 g, 0.84 mmol) in MeOH (10 mL), orange prisms of **2** precipitated slowly and were collected by filtration under nitrogen. Yield: 0.45g (90%); ^{1}H NMR (200 MHz, CD_3OD, 303 K): $\delta = 1.19$ (m, CH_3), 1.98 (m, CH_2), 7.15 (m, Ph); ^{31}P NMR (400 MHz, CD_3OD, 233 K): $\delta = 63.8$ (s); IR (CsI): $\tilde{\nu}_{NN} = 2091\ cm^{-1}$; UV/Vis: $\lambda_{max}(\varepsilon) = 284$ (8666), 328 (sh; 4000), 394 nm ($1818\ L\,mol^{-1}\,cm^{-1}$); elemental analysis calcd for $C_{44}H_{68}BBrN_2P_4Fe$ (895.45): C 59.0, H 7.7, N 3.1; found: C 56.3, H 7.4, N 1.6.

[10] a) A. Hills, D. L. Hughes, M. Jimenez-Tenorio, G. J. Leigh, *J. Organomet. Chem*. **1990**, *391*, C41 – C44; b) see ref. [5].

[11] $\delta = 0.26\ mm\,s^{-1}$ and $\Delta E_Q = 1.42\ mm\,s^{-1}$ at 77 K; see ref. [5].

[12] J. Silver, *Inorg. Chim. Acta* **1991**, *184*, 235 – 242.

[13] X-ray structure analysis of **1**: An orange cube was mounted on a glass fiber by standard inert-gas techniques and cooled immediately. Crystal data for **1**: triclinic, $P\bar{1}$ ($\equiv$ no. 2), $a = 13.425(3)$, $b = 17.399(5)$, $c = 19.937(5)$ Å, $\alpha = 102.02(2)$, $\beta = 91.16(1)$, $\gamma = 95.7(3)^\circ$, $V = 4528(2)$ Å^3, $Z = 4$, $\rho_{calcd} = 1.248\ g\,cm^{-1}$, $\mu(Mo_{K\alpha}) = 0.566\ mm^{-1}$. The data were collected on a Siemens P4 diffractometer ($Mo_{K\alpha}$ radiation, $\lambda = 0.71073$ Å, graphite monochromator, $T = 203$ K) in the range $4 < 2\theta < 50^\circ$; 16528 (15785 symmetry independent) reflections were measured. The phase problem was solved by direct methods (SIR92), from which the heavy atoms were located. The other non-hydrogen atoms were found in subsequent cycles of refinements (SHELXL93) and difference Fourier maps. The hydrogen atoms were taken into account at idealized sites and with isotropic thermal parameters in the final cycle of refinement; 494 parameters, semiempirical absorption correction (ψ scan) $R1 = 0.077$ (3108 reflections with $F_o > 4\sigma(F_o)$), $wR2 = 0.202$ (all data). The unit cell contains two symmetrically independent cations. One of these cations shows some disorder of the chlorine and dinitrogen ligands. This disorder over the two *trans* positions (N_2, Cl) was modeled by partial occupation of these positions with Cl^- and N_2 with a fixed N – N bond length of 1.10 Å. The occupation ratio Cl^-:N_2 of the two positions was refined to 56:44 and 44:56, respectively. Anisotropic thermal parameters were refined for the heavy atoms (Fe, P, Cl); C and N atoms were refined isotropically. In the discussion of the molecular geomety, we exclusively describe the cation which is not disordered. Further details of the crystal structure investigations may be obtained from the Fachinformationszentrum Karlsruhe, D-76344 Eggenstein-Leopoldshafen, Germany (fax: (+49) 7247-808-666 (Frau S. Höhler-Schlimm); e-mail: crysdata@fiz-karlsruhe.de), on quoting the depository number CSD-407743.

[14] I. E. Buys, L. D. Field, T. W. Hambley, A. E. D. McQueen, *Acta Crystallogr. Sect. C* **1993**, *C49*, 1056 – 1059.

[15] B. E. Wiesler, F. Tuczek, C. Näther, W. Bensch, *Acta Crystallogr. Sect. C* **1998**, *54*, 44 – 46.

[16] M. V. Baker, L. D. Field, T. W. Hambley, *Inorg. Chem.* **1988**, *27*, 2872 – 2876.

[17] Preliminary crystal data of **2**: triclinic, P1 (no. 1), $a = 11.5727(3)$, $b = 13.3353(4)$, $c = 16.6220(3)$ Å, $\alpha = 108.23(1)$, $\beta = 101.235(2)$, $\gamma = 104.545(2)^\circ$, $V = 2251(1)$ Å^3, $Z = 2$, $\rho_{calcd} = 1.321\ g\,cm^{-1}$, $\mu(Mo_{K\alpha}) = 1.40\ mm^{-1}$.

[18] C. A. Ghilardi, S. Midollini, L. Sacconi, P. Stoppioni, *J. Organomet. Chem*. **1981**, *205*, 193 – 202.

[19] P. Giannoccaro, M. Rossi, A. Sacco, *Coord. Chem. Rev.* **1972**, *8*, 77 – 79; M. Aresta, P. Giannoccaro, M. Rossi, A. Sacco, *Inorg. Chim. Acta* **1971**, *5*, 203 – 206.

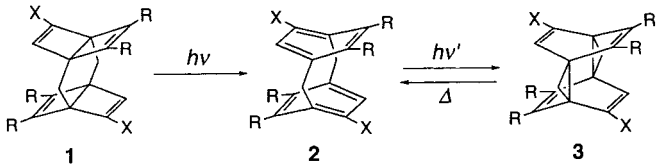
[20] M. Aresta, P. Giannoccaro, M. Rossi, A. Sacco, *Inorg. Chim. Acta* **1971**, *5*, 203 – 206.

[21] N. Lehnert, F. Tuczek, *J. Am. Chem. Soc.*, submitted.

A Kinetically Stabilized [1.1]Paracyclophane: Isolation and X-Ray Structural Analysis**

Hidetoshi Kawai, Takanori Suzuki, Masakazu Ohkita, and Takashi Tsuji*

In 1993 we reported preparation of the first [1.1]paracyclophane, the bis(methoxycarbonyl) derivative **2b**.[1] The low thermal stability of **2b** and of the subsequently synthesized **2a**[2]—both persistent only below $-20\,^\circ C$ in dilute solution—virtually precluded exploration of their physical and chemical properties. The lability of [1.1]paracyclophanes seems to arise from susceptibility of the bridgehead carbon atoms toward addition of numerous reagents, upon which the steric strain inherent in the system is largely relieved. In other words, it seems plausible that the [1.1]paracyclophane skeleton might be kinetically stabilized by the introduction of substituents that sterically shield all four bridgehead sites. Although fulfillment of such a requirement appears formidable at first, examination of molecular models suggests that kinetic stabilization of the [1.1]paracyclophane system might be achieved through **2c**, for which the appropriate precursor **1** should also be accessible. Here we report the isolation and X-ray structural analysis of **2c** as well as its interconversion with the corresponding transannular addition product **3c**.



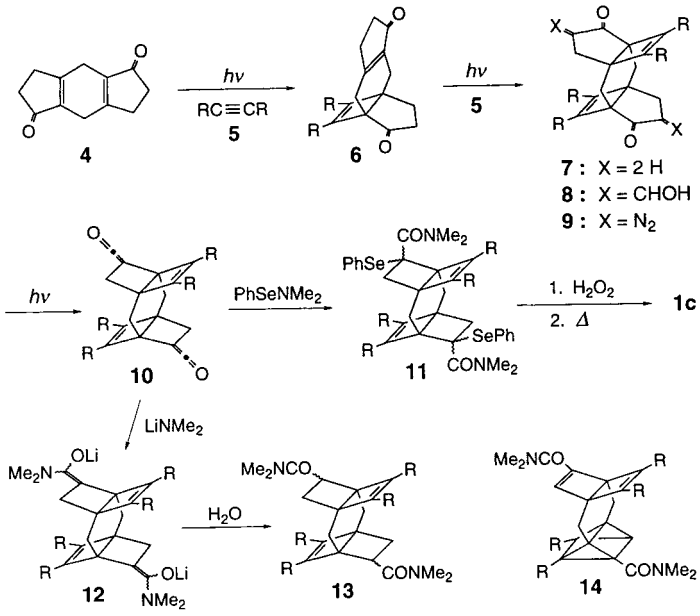
a: R = X = H **b**: R = H, X = CO_2Me **c**: R = CH_2SiMe_3, X = $CONMe_2$

The synthesis of precursor **1c** is outlined in Scheme 1. Although addition of **5**[3] to **6** was significantly slower than that of **5** to **4**,[2] *anti*-bis-adduct **7** was obtained after prolonged irradiation of **6** in a saturated solution of **5** in CH_2Cl_2. The conversion of **7** into **10** via **8**[4] and **9** proceeded uneventfully, and **10** was transformed into diamide **13** by addition of $LiNMe_2$ followed by hydrolysis. However, the carbon atoms adjacent to the amide groups in **13** are already so sterically hindered that initial attempts to prepare **11** (e.g. by reaction of **12**[5] with PhSeBr, and of **13** with KH/$PhSe_2$[6]) proved fruitless. Taking a hint from the reaction of (phenylselenyl)-amines with unsaturated carbonyl compounds,[7] we obtained **11** by the reaction of **10** with $PhSeNMe_2$.[8] Oxidation of **11** to the selenoxide and subsequent elimination of PhSeOH proceeded smoothly to afford **1c**.

Irradiation of **1c** in degassed *n*-decane with a low-pressure mercury lamp at $-20\,^\circ C$ led to formation of the corresponding

[*] Prof. Dr. T. Tsuji, H. Kawai, Prof. Dr. T. Suzuki, Dr. M. Ohkita
Division of Chemistry, Graduate School of Science
Hokkaido University, Sapporo 060 (Japan)
Fax: (+81) 11-746-2557
E-mail: tsuji@science.hokudai.ac.jp

[**] This research was supported by a Grant-in-Aid for Scientific Research (08454192) from the Japanese Ministry of Education, Science, Sport, and Culture.



Scheme 1. Preparation of **1c** ($R = CH_2Si(CH_3)_3$).

[1.1]paracyclophane **2c** (which exhibits absorption bands at $\lambda_{max} = 321$, 377, and 464 nm), isomer **3c** resulting from a secondary transannular [4+4] addition within **2c**, and a product to which structure **14** is tentatively assigned.[9] That **2c** has a much greater kinetic stability than **2a** or **2b** was clearly demonstrated when a dilute solution of **2c** was heated in the dark in the absence of air. The intensity of the UV/Vis absorptions due to **2c** remained unchanged for 2 h at 50 °C and decreased only by 8% after the solution was heated at 100 °C for 1.5 h. It should be recalled that **2a**,**b** are stable only below −20 °C in dilute solution. When **2c** was transformed into **3c** by irradiation in solution with light of wavelength greater than 420 nm and the resulting solution was allowed to stand in the dark at room temperature, the characteristic UV/Vis absorption due to **2c** slowly developed. This confirms the ability of **3c** to revert thermally into **2c** at ambient or higher temperatures (Figure 1).[10] Because **2c** is very susceptible to photochemical reaction to give **3c**,[11] and also because its high absorptivity extends to long wavelengths, photolysis of **1c** tends to afford mainly **3c** rather than the primary product **2c** except at very low conversion: Irradiation of **1c** with a high-pressure mercury lamp through Pyrex in benzene produced **2c**, **3c**, and **14** in yields of 5, 66, and 6%, respectively, after 80% conversion. Air-stable **3c** is readily isolated from the mixture as colorless crystals, and it can be converted quantitatively into **2c** upon mild heating as a solution in a deaerated solvent such as benzene or hexane. This facilitates the preparation of the fairly air-sensitive **2c** in pure form. Activation parameters for the cycloreversion are $\Delta H^{\ddagger} = (21.1 \pm 0.8)$ kcal mol^{-1} and $\Delta S^{\ddagger} = (-10.5 \pm 2.6)$ cal K^{-1} mol^{-1}, and the half-life of **3c** at 40.0 °C is (191 ± 2) min in *n*-hexane.[12] When a solution of **3c** in degassed benzene was heated at 45 °C for 15 h and then cooled to 5 °C, the resulting **2c** separated from solution in the form of orange-red crystals.

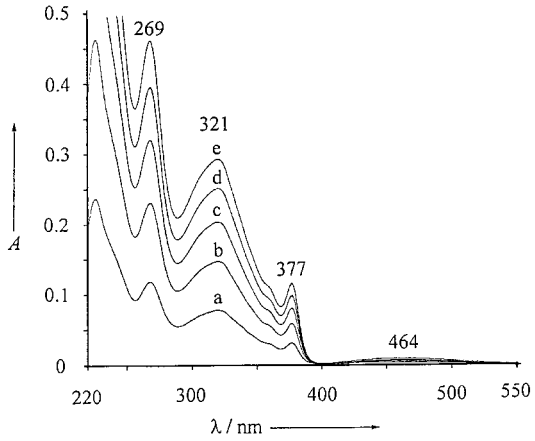


Figure 1. UV/Vis absorption observed upon heating a solution of **3c** in *n*-hexane at 48 °C for a) 30, b) 60, c) 90, d) 120, and e) 150 min. This is regarded as an indicator of the thermal regeneration of **2c**.

Table 1. Selected spectroscopic data for **1c**, **2c**, **3c**, and **14**.

1c: ^{1}H NMR (400 MHz, CD_2Cl_2, TMS): $\delta = -0.002$ (s, 18H), 0.002 (s, 18H), 1.28 (d, $J = 14.7$ Hz, 2H), 1.40 (dd, $J = 14.2$, 1.5 Hz, 2H), 1.47 (d, $J = 14.2$ Hz, 2H), 1.53 (dd, $J = 14.7$, 1.5 Hz, 2H), 2.22 (d, $J = 14.7$ Hz, 2H), 2.46 (d, $J = 14.7$ Hz, 2H), 2.91 (brs, 6H), 3.07 (brs, 6H), 6.69 (s, 2H); ^{13}C NMR (100 MHz, CD_2Cl_2, TMS): $\delta = -0.78$, −0.71, 16.74, 16.85, 35.19, 37.81, 51.91, 56.57, 143.97, 144.67, 149.20, 150.41, 164.51; IR (neat): $\tilde{\nu} = 1628$, 1578, 1248, 842 cm^{-1}; UV/Vis (*n*-hexane): $\lambda_{max}(\varepsilon) = 255$ nm (6900); EI-MS: *m/z* 666.3924 (calcd for $C_{36}H_{62}N_2O_2Si_4$: 666.3888).

2c: ^{1}H NMR (CD_2Cl_2): $\delta = -0.14$ (s, 18H), 0.00 (s, 18H), 2.08 (d, $J = 15.1$ Hz, 2H), 2.25 (d, $J = 15.1$ Hz, 2H), 2.41 (d, $J = 15.1$ Hz, 2H), 2.74 (d, $J = 15.1$ Hz, 2H), 3.07 (brs, 6H), 3.16 (brs, 6H), 3.61 (d, $J = 12.7$ Hz, 2H), 3.67 (d, $J = 12.7$ Hz, 2H), 7.67 (s 2H).

3c: ^{1}H NMR (CD_2Cl_2): $\delta = 0.00$ (s, 18H), 0.03 (s, 18H), 1.09 (dd, $J = 14.7$, 1.5 Hz, 2H), 1.43 (dd, $J = 14.7$, 1.5 Hz, 2H), 1.54 (d, $J = 6.8$ Hz, 2H), 1.55 (d, $J = 14.7$ Hz, 2H), 1.58 (d, $J = 14.7$ Hz, 2H), 2.12 (d, $J = 6.8$ Hz, 2H), 2.91 (s, 12H), 6.07 (s, 2H).

14: ^{1}H NMR ($CDCl_3$): $\delta = -0.01$ (s, 9H), 0.02 (s, 9H), 0.03 (s, 9H), 0.04 (s, 9H), 0.75 (d, $J = 15.1$ Hz, 1H), 0.90 (d, $J = 15.1$ Hz, 1H), 0.92 (d, $J = 15.1$ Hz, 1H), 1.07 (d, $J = 15.1$ Hz, 1H), 1.16 (d, $J = 12.7$ Hz, 1H), 1.20 (d, $J = 12.7$ Hz, 1H), 1.25–1.30 (m, 3H), 1.48 (d, $J = 14.1$ Hz, 1H), 2.09 (d, $J = 12.7$ Hz, 1H), 2.22 (d, $J = 12.7$ Hz, 1H), 2.87 (s, 3H), 2.97 (brs, 3H), 3.06 (s, 3H), 3.10 (s, 1H), 3.16 (brs, 3H), 6.38 (s, 1H).

The X-ray structural analysis reveals that **2c** has C_i symmetry in the crystalline state, and the [1.1]paracyclophane core is slightly distorted from ideal D_{2h} symmetry (Figure 2).[13] The transannular interatomic distance between the opposing bridgehead carbon atoms C2 and C12 is 2.376(5) Å (almost 1.0 Å less than the sum of the van der Waals radii), and the corresponding distances between nonbridgehead carbon atoms (C6–C10 and C7–C11) are 3.025(5) and 2.996(5) Å, respectively. The dihedral angle α between the mean plane of the four nonbridgehead aromatic carbon atoms and the plane of the adjoining flap is 25.6° on the side bearing the amide group and 24.3° on the other. The extent of out-of-plane bending of the bridging carbon atom, β, is 26.8° on the side nearer to the amide group and 22.9° on the far side.[14] Thus, the average total bending angle ($\alpha + \beta$) is 49.8°, the largest value ever reported for a paracyclophane and only slightly less than that calculated for [5]paracyclophane.[15, 16] As expected from an examination of molecular models, each of the nearly planar amide groups is slightly twisted from coplanarity with the adjoining aromatic ring, which places one

 © WILEY-VCH Verlag GmbH, D-69451 Weinheim, 1998 1433-7851/98/3706-0818 $ 17.50+.50/0

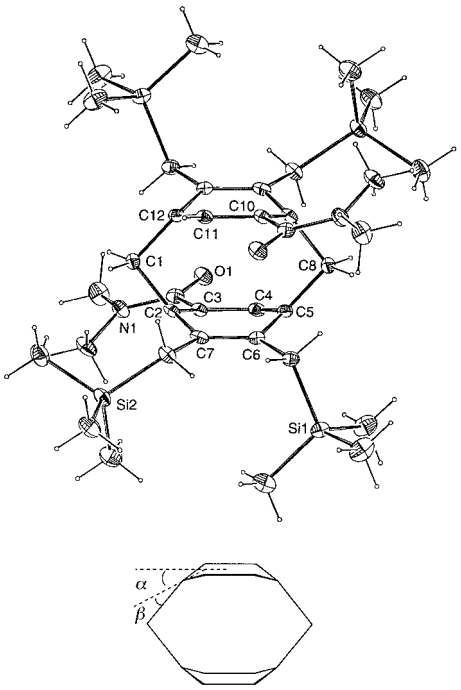


Figure 2. Crystal structure of **2c**. Selected bond lengths [Å] and angles [°]: C1–C2 1.560(6), C1–C12 1.551(6), C2–C3 1.421(6), C2–C7 1.422(6), C3–C4 1.400(6), C4–C5 1.386(6), C5–C6 1.443(6), C6–C7 1.396(6), C2–C12 2.376(5), C6–C10 3.025(5), C7–C11 2.996(5); C1-C2-C3 118.0(4), C1-C2-C7 117.9(4), C2-C1-C12 99.6(3), C3-C2-C7 116.5(4), C4-C5-C6 115.4(4), C4-C5-C8 118.2(4), C6-C5-C8 120.9(4).

of the N-methyl groups above the adjacent bridgehead carbon atom. Preferential adoption of a similar conformation in solution is supported by the observation of a positive NOE between protons of the methylene bridge and the N-methyl protons.[17] The trimethylsilyl groups preferentially occupy the space near the neighboring bridgehead carbon atoms, thereby minimizing repulsive steric interactions: mutual, transannular, and with the methylene bridges. Thus, the aromatic substituents of **2c** effectively shield the bridgehead carbon atoms from access by attacking reagents; this is certainly the reason for the remarkable stability of **2c**.

Received: September 15, 1997 [Z10928IE]
German version: *Angew. Chem.* **1998**, *110*, 827–829

Keywords: arenes · cyclophanes · photochemistry · strained molecules

[1] T. Tsuji, M. Ohkita, S. Nishida, *J. Am. Chem. Soc.* **1993**, *115*, 5284.
[2] T. Tsuji, M. Ohkita, T. Konno, S. Nishida, *J. Am. Chem. Soc.* **1997**, *119*, 8425.
[3] A. Guijarro, M. Yus, *Tetrahedron* **1995**, *51*, 231; H. J. Reich, I. L. Reich, K. E. Yelm, J. E. Holladay, D. Gschneidner, *J. Am. Chem. Soc.* **1993**, *115*, 6625.
[4] M. Regitz in *The Chemistry of Diazonium and Diazo Groups* (Ed.: S. Patai), Wiley, Chichester, **1975**, chap. 17.
[5] L. M. Baigrie, H. R. Seiklay, T. T. Tidwell, *J. Am. Chem. Soc.* **1985**, *107*, 5391; L. M. Baigrie, D. Lenoir, H. R. Seiklay, T. T. Tidwell, *J. Org. Chem.* **1985**, *50*, 2105; R. Häner, T. Laube, D. Seebach, *J. Am. Chem. Soc.* **1985**, *107*, 5396.
[6] H. J. Reich, *Org. React.* **1993**, *44*, 1; A. L. Cossey, L. Lombardo, L. N. Mander, *Tetrahedron*, **1980**, *21*, 4383; L. Lombardo, L. N. Mander, *J. Org. Chem.* **1983**, *48*, 2298.
[7] H. J. Reich, J. M. Renga, *J. Org. Chem.* **1975**, *40*, 3313.
[8] To our knowledge, the preparation of α-selenylated carboxamides through the reaction of ketene with selenylamines was previously unknown.
[9] As with **1a** and **1b**, a product resulting from the aromatization of only one of the Dewar-benzene moieties of **1c** was not detected in the photolysate.
[10] According to theoretical calculations, **2a** is more stable than **3a** by 26.2 kcal mol^{-1} at the B3LYP/6-31G* level and by 20.0 kcal mol^{-1} at the MP2/6-31G*//RHF/6-31G* level.[2]
[11] The photochemical transformation of **2** into **3** represents the first direct preparation of a *p,p′*-benzene dimer. To our knowledge, [2.2]paracyclophanes do not undergo such a transannular [4+4] addition under irradiation. Apparently, the photochemical reactivity of **2** is dictated by the geometrical constraint imposed upon it: the face-to-face arrangement of two bent benzene rings in close proximity. For photoadditions of aromatic compounds, see J. J. McCullough, *Chem. Rev.* **1987**, *87*, 811.
[12] The rate of this cycloreversion is comparable to those for known *p,p′*-benzene dimers: N. C. Yang, M. Chen, P. Chen, *J. Am. Chem. Soc.* **1984**, *106*, 7310; H. Gan, J. L. King, N. C. Yang, *Tetrahedron Lett.* **1989**, *30*, 1205.
[13] Crystal data for [1.1]paracyclophane **2c**·benzene: $C_{36}H_{62}N_2O_2Si_4 \cdot C_6H_6$, $M = 745.36$, $0.40 \times 0.40 \times 0.10$ mm^3, triclinic, $P\bar{1}$, $a = 9.564(3)$, $b = 10.156(5)$, $c = 12.299(5)$ Å, $\alpha = 98.86(4)$, $\beta = 108.85(3)$, $\gamma = 98.51(4)^\circ$, $V = 1092(1)$ Å^3, $(Z = 1)$, $\rho_{calcd} = 1.134$ g cm^{-1}. A total of 3640 independent reflections ($2\theta_{max} = 52^\circ$) were measured at $T = 203$ K (ω-2θ scan mode, $Mo_{K\alpha}$ radiation, $\lambda = 0.71073$ Å). No absorption correction was applied ($\mu = 1.097$ cm^{-1}). The structure was solved by direct methods (Crystan). Hydrogen atoms are located at the calculated positions. Refinement by the full-matrix least-squares method on F gave a final R value of 0.078 ($wR = 0.112$) for 3022 reflections with $I > 3\sigma(I)$ and 260 parameters. Residual electron density is 0.37 e Å^{-3}. Crystallographic data (excluding structure factors) for the structure reported in this paper have been deposited with the Cambridge Crystallographic Data Center as supplementary publication no. CCDC-100696. Copies of the data can be obtained free of charge on application to CCDC, 12 Union Road, Cambridge CB2 1EZ (fax: (+44) 1223-336-033; e-mail: deposit@ccdc.cam.ac.uk).
[14] There exists some ambiguity concerning the bending angles α and β since the nonbridgehead aromatic carbon atoms are displaced from the mean plane by 0.004–0.011 Å and the plane of the methylene bridge is not exactly orthogonal to that formed by the bridgehead and the adjacent aromatic carbon atoms.
[15] S. Grimme, *J. Am. Chem. Soc.* **1992**, *114*, 10542; M. von Arnim, S. D. Peyerimhoff, *Theor. Chim. Acta* **1993**, *85*, 43, and references therein.
[16] [5]Paracyclophanes so far prepared are not sufficiently stable to be isolated. D. S. van Es, F. J. J. de Kanter, W. H. de Wolf, F. Bickelhaupt, *Angew. Chem.* **1995**, *107*, 2728; *Angew. Chem. Int. Ed. Engl.* **1995**, *34*, 2553, and references therein.
[17] A weak NOE was also observed between the N-methyl and the aromatic protons. Therefore, the amide groups seem to flip-flop more or less freely in solution with respect to the aromatic rings.

 © WILEY-VCH Verlag GmbH, D-69451 Weinheim, 1998 1433-7851/98/3706-0819 $ 17.50+.50/0

Direct Preparation of Trifluoromethyl Ketones from Carboxylic Esters: Trifluoromethylation with (Trifluoromethyl)trimethylsilane**

Jürgen Wiedemann, Thomas Heiner, Gregorz Mloston, G. K. Surya Prakash,* and George A. Olah*

Trifluoromethyl ketones are potential inhibitors of hydrolytic enzymes because of their ability to form stable hydrates, thereby acting as transition-state analogues of substrates for such enzymes.[1] The trifluoroacetyl group is also a highly electron-withdrawing substituent. Methods for the synthesis of trifluoromethyl ketones are scarce.[2] While trifluoromethyl aryl ketones can be obtained by Friedel–Crafts acylations,[3] alicyclic and aliphatic trifluoromethyl ketones are usually available only by multistep synthetic operations.[4, 5] This restricts their use and makes it difficult to handle complicated intermediates for pharmacologically interesting targets.

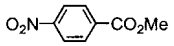
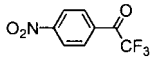
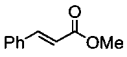
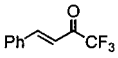
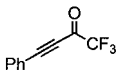
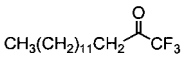
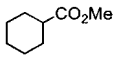
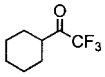
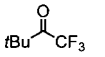
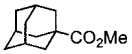
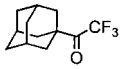
Trifluoromethyltrimethylsilane ($TMS\text{-}CF_3$, **2**) reacts with aldehydes and ketones under fluoride-induced trifluoromethyl transfer to yield trifluoromethyl alcohols.[6–8] The chemistry of $TMS\text{-}CF_3$ and related reagents was recently reviewed.[9] When α-keto esters are used as substrates in THF, $TMS\text{-}CF_3$ adds only to the keto group to give derivatives of Mosher's acid.[10] Simple unactivated esters are unreactive toward $TMS\text{-}CF_3$[11] in THF.

We now report on the first successful nucleophilic trifluoromethylation of esters with $TMS\text{-}CF_3$. This provides a straightforward and powerful synthetic tool to convert the ester functionality into the trifluoromethylcarbonyl group in one step without formation of double-addition products. A remarkable feature of this novel method is that it can be applied to non-enolizable as well as enolizable esters.

Reaction of methyl benzoate (**1a**) with $TMS\text{-}CF_3$ (1.25 equiv) in dry toluene smoothly gave 1,1,1-trifluoroacetophenone (**6a**) in 95% yield. The initiator, anhydrous tetrabutylammonium fluoride (TBAF; 2.5 mol% in THF) was added at $-78\,^{\circ}C$, and the reaction mixture was then allowed to warm slowly to room temperature, stirred for 18 h, and finally treated with 2 M hydrochloric acid. Addition of the initiator at $0\,^{\circ}C$ gave rise to mixtures of the corresponding trifluoromethyl ketone **6a** and bis-trifluoromethylated alcohol as a result of double addition.

Table 1 shows the optimized reaction conditions for each case. The yields are good to excellent. In anhydrous pentane as solvent, methyl myristate (**1e**) gave the corresponding trifluoromethyl ketone (**6e**) in 75% yield. α,β-Unsaturated methyl cinnamate (**1c**) gave exclusively the 1,2-addition product **6c** in 85% yield. Even sterically hindered esters, including methyl pivalate (**1g**) and methyladamantane 1-carboxylate (**1h**), reacted smoothly. However, in the case of methyl 3-phenylpropinate (**1d**), the desired product **6d** could not be isolated owing to extensive polymerization under the reaction conditions. In general, it is possible to use any nonpolar aprotic solvent, such as pentane, benzene, toluene, or dichloromethane. Although THF can also be used for some reactive esters such as **1a**, it is not the solvent of choice; THF undergoes slow ring opening by $TMS\text{-}CF_3$ under these conditions to yield detectable amounts of 5,5,5-trifluoro-1-trimethylsiloxypentane as a by-product. For the synthesis of low-boiling trifluoromethyl ketones, pentane is a good reaction medium, which nevertheless can be substituted by dichloromethane whenever solubility problems arise. The prerequisite for a successful reaction between esters and $TMS\text{-}CF_3$ is careful drying of all solvents and reagents. Therefore, a commercial solution of TBAF (1 M in THF) was dried for 4 h under a dry argon atmosphere over activated 4-Å molecular sieves (4 mL of solution per 1 g of molecular sieves) prior to use.

Table 1. Conditions and yields for reactions of $TMS\text{-}CF_3$ (1.25 equiv) with various esters induced by 2.5 mol% TBAF in THF.

	Reagent **1**	Solvent	t [h]	Product **6**	Yield [%]
a	$PhCO_2Me$	toluene	18		95
b		CH_2Cl_2	18		81
c		pentane	24		85
d		pentane	24		0[a]
e	$CH_3(CH_2)_{12}CO_2Me$	pentane	24		75
f		pentane	48		72
g	$tBu\text{-}CO_2Me$	pentane	72		68
h		pentane	72		70

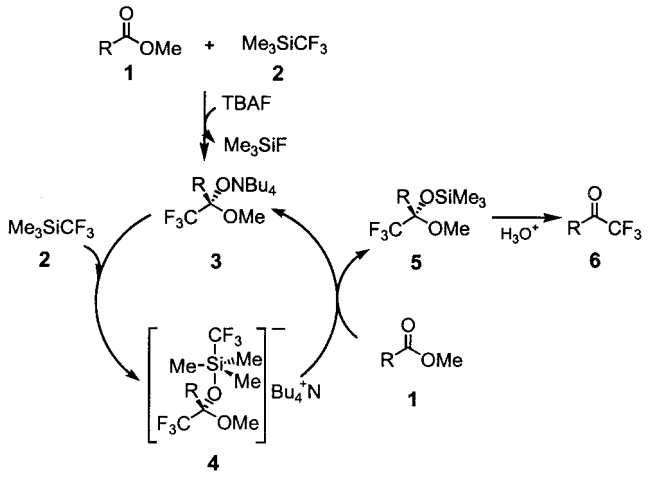
[a] Extensive polymerization.

[*] Prof. Dr. G. K. S. Prakash, Prof. Dr. G. A. Olah, Dr. J. Wiedemann, Dr. T. Heiner, Prof. Dr. G. Mloston
Donald P. and Katharine B. Loker Hydrocarbon Research Institute and
Department of Chemistry
University of Southern California
University Park, Los Angeles, CA 90089-1661 (USA)
Fax: (+1) 213-740-5087
E-mail: prakash@methyl.usc.edu
olah@methyl.usc.edu.

[**] Synthetic Methods and Reactions, Part 201. This work was generously supported by the Loker Hydrocarbon Research Institute and the US Air Force Office of Scientific Research (MURI program, Dr. C. Lee). J.W. and T.H. were supported by Feodor–Lynen Fellowships from the Alexander von Humboldt Foundation. Part 200: ref. [8].

 © WILEY-VCH Verlag GmbH, D-69451 Weinheim, 1998 1433-7851/98/3706-0820 $ 17.50+.50/0

The mechanism for TMS-CF_3 addition is shown in Scheme 1. In the initiation step of the nucleophilic trifluoromethylation, TBAF reacts with TMS-CF_3 to transfer a CF_3 group to the ester. This gives rise to the deprotonated hemiacetal **3**, the true catalytic species. The latter in turn



Scheme 1. Proposed mechanism for the fluoride-induced nucleophilic trifluoromethylation of carboxylic esters with TMS-CF_3.

activates a second molecule of TMS-CF_3 through formation of a negatively charged pentacoordinated silicon species **4**, which transfers a CF_3 group to another ester molecule, resulting in formation of **5** and simultaneous regeneration of the catalytic species **3**.

However, when the initiator is added at higher temperatures (at or above 0 °C), **3** may decompose to give a methoxide ion, and the intermediate trifluoromethyl ketone, because of its high reactivity, may be subject to a second addition reaction.

In summary, we have developed a versatile method for the simple and efficient preparation of trifluoromethyl ketones from methyl esters.

Received: September 17, 1997 [Z10939IE]
German version: *Angew. Chem.* **1998**, 110, 880 – 881

Keywords: fluorine · ketones · nucleophilic additions · synthetic methods

[1] M. H. Gelb, J. P. Svaren, R. H. Abales, *Biochemistry* **1985**, *24*, 1813 – 1817.
[2] J. P. Bague, D. Bonnet-Delphon, *Tetrahedron* **1991**, *47*, 3207 – 3258; Y. Yokoyama, K. Mochida, *Synlett* **1997**, 907 – 910.
[3] T. Keumi, M. Shimada, M. Takahashi, H. Kitajima, *Chem. Lett.* **1990**, 783 – 786.
[4] W. F. Cockburn, R. A. B. Bannard, *Can. J. Chem.* **1957**, *35*, 1285 – 1292.
[5] M. Nassal, *Liebigs Ann. Chem.* **1983**, 1510 – 1523.
[6] G. K. S. Prakash, R. Krishnamurti, G. A. Olah, *J. Am. Chem. Soc.* **1989**, *111*, 393 – 395; R. Krishnamurti, A. D. R. Bellew, G. K. S. Prakash, *J. Org. Chem.* **1991**, *56*, 984 – 989.
[7] S. P. Kotun, J. D. O. Anderson, D. D. DesMarteau, *J. Org. Chem.* **1992**, *57*, 1124 – 1131.
[8] J. S. Brunck, A. Koch, G. Mloston, S. Lehnhoff, P. Margaretha, G. K. S. Prakash, G. Rasul, A. R. Bau, G. Olah, *J. Org. Chem.*, submitted.
[9] G. K. S. Prakash, A. K. Yudin, *Chem. Rev.* **1997**, *97*, 757 – 786.
[10] P. Ramaiah, G. K. S. Prakash, *Synlett* **1991**, 643 – 644.

In Situ X-Ray Diffraction Study of the Initial Stages of Formation of MCM-41 in a Tubular Reactor**

Mika Lindén, Stephan A. Schunk, and Ferdi Schüth*

The successful preparation of MCM-41, a mesoporous silicate with hexagonally ordered cylindrical pores, has stimulated interest in this new class of composite materials since the pore sizes can be varied between 2 and 10 nm.[1, 2] Surfactants are used to induce the desired structure of the silicate polymer network. Usually, the synthesis of MCM-41 is carried out at surfactant concentrations at which the surfactant alone would not form a mesophase, which indicates a strong cooperative surfactant – silicate interaction. We describe here for the first time a continuous preparation of MCM-41 in a tubular reactor, which allows in situ X-ray diffraction (XRD) studies of the kinetics of mesophase formation on a mesoscopic length scale. The hexagonal mesophase is shown to form within the first three minutes of the reaction without passing through any intermediate phase. Different models have been developed to describe the formation of MCM-41. Beck et al.[2] proposed several possible pathways for the formation of such materials, and a more detailed, mechanistic model was presented by Monnier et al.[3] to account for the observation of an intermediate layered phase prior to reaching the hexagonal phase. This model introduced multidentate binding of silicate oligomers, preferred polymerization of silicate at the surfactant – silicate interface, and charge density matching as key factors in the formation of a surfactant – silicate mesophase. However, owing to the large number of different synthesis routes reported, each varying with respect to the silica source, surfactant concentration, pH, and the acid/base used etc., some of the reaction steps involved in the formation of the mesophase may differ depending on the applied experimental conditions. This is particularly important when organic precursors, such as tetraethoxysilane (TEOS), are used as the silica source, since their solubilities in aqueous solution are limited and therefore formation of an oil-in-water emulsion is expected as the initial reaction step. We describe here the results obtained by time-resolved in situ XRD measurements on the kinetics of formation of the hexagonal composite mesophase of such a system.

The reaction is too fast to allow data accumulation times long enough to obtain accurate kinetic data with a traditional setup for the investigation of liquids. To circumvent this problem, a tubular reactor was constructed and connected to a cell especially designed for XRD measurements of liquids; this allowed data accumulation times long enough to obtain a

[*] Prof. Dr. F. Schüth, Dr. M. Lindén,[+] Dipl.-Chem. S. A. Schunk
Institut für Anorganische Chemie der Universität
Marie Curie Strasse 11, D-60439 Frankfurt am Main (Germany)
Fax: (+49) 69-798-29260
E-mail: ferdi@schueth.chemie.uni-frankfurt.de
[+] Permanent address:
Department of Physical Chemistry, Åbo Akademi University,
Porthansgatan 3-5, SF-20500 Åbo (Finland)

[**] This work was supported by the EU project ERB-FMRX-CT96-0084.

good signal-to-noise ratio and allowed the reaction time to be varied. The experimental setup is shown schematically in Figure 1. Two peristaltic pumps are used to control the ratio of

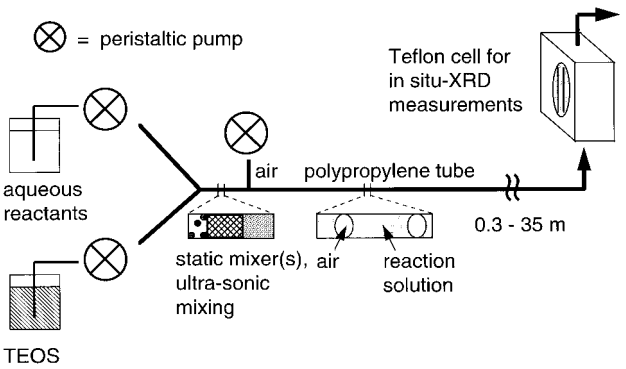


Figure 1. Schematic description of the tubular reactor setup. See Experimental Section for more details.

the aqueous to the hydrophobic reactants. TEOS is mixed with the aqueous solution, this solution is homogenized in an ultrasonic bath, passed through a series of static mixers, and subsequently passed through a tube ($\varnothing = 4$ mm) at a constant flow rate. The residence time of the reactants in the mixing step was 5–10 seconds. After mixing, air bubbles were introduced to prevent back-mixing in the tube; this resulted in approximately 20-cm-long trains of reaction solution separated by 3 cm of air. The residence time in the tube, that is the reaction time, is determined by the tube length. To ensure a good mixing of the reagents a small amount of *n*-butanol (BuOH) (BuOH:cetyltrimethylammonium bromide (CTAB) 1:4 w/w) was added to the aqueous solution. In order to exclude errors in the measured diffractograms, which arise from solid formation on the cell windows, data were accumulated for 4–10 minutes after which the reactor was flushed with distilled water and a background diffractogram was recorded. The background was then substracted from the original diffractogram. The experiment was repeated to give a total data accumulation time of 40 minutes. Fouling on the cell windows was detected mainly at short residence times (< 2 min), which was attributed to partial hydrolysis of TEOS; however, it never accounted for more than 15% of the measured signal. The reactor was cleaned prior to performing the next run by flushing with 0.2 M NaOH followed by large amounts of distilled water. The measured XRD patterns after different reaction times are shown in Figure 2. No peaks were observed for the pure surfactant solution, as expected for an isotropic micellar solution possessing no long-range order. However, a small-angle Bragg reflection appeared in the diffractogram upon addition of TEOS. The intensity of this reflection increased at longer reaction times due to the higher solid content of the solution. After a reaction time of only three minutes, two high-order peaks were resolved and indexed by assuming a hexagonal symmetry. No intermediate lamellar phase was detected. The solid product obtained after a reaction time of three minutes was immediately filtered and washed with water for further characterzation. The d_{100} spacing of 4.43 nm observed in the in situ measurements decreased to 4.0 nm upon drying at 90 °C (Figure 3). This

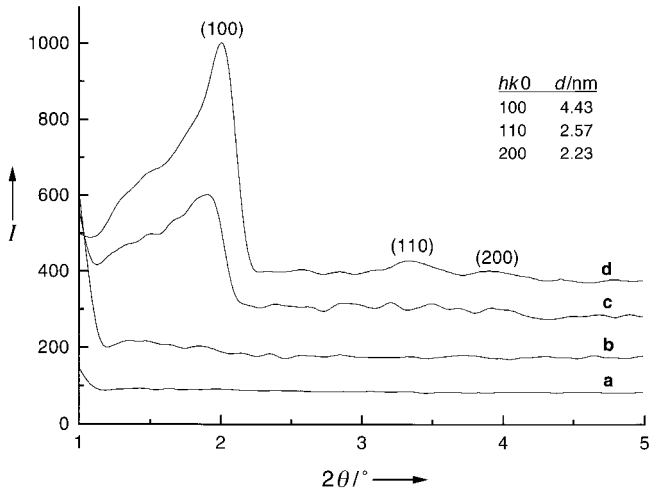


Figure 2. In situ XRD patterns of MCM-41 prepared in the tubular reactor in different reaction times. a) No added TEOS; after reaction times of b) 15 s, c) 90 s, and d) 180 s.

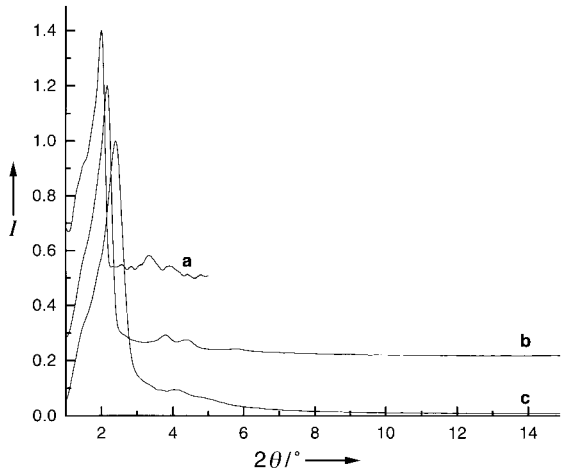


Figure 3. XRD patterns of MCM-41 prepared in the tubular reactor. a) In situ, reaction time 180 s, b) product isolated after 180 s and dried at 90 °C for 8 h, c) same sample as in b) but calcined at 550 °C for 6 h.

suggests that the wet sample was only partly condensed and that the removal of free and hydration water from the silicate–surfactant phase upon drying caused deswelling of the structure. These results are in good agreement with those presented in a recent study in which small-angle X-ray scattering (SAXS, ex situ) and EPR experiments were performed to study the formation of MCM-41.[4] The d_{100} spacing decreased further to 3.7 nm upon calcination at 550 °C. The XRD patterns of the dried and calcined product isolated after three minutes in the tubular reactor were identical to those obtained for the corresponding product prepared under stirring in an open beaker for one hour. This suggests that the mesostructure was more or less fully developed already at this stage although less condensed than the product prepared in an open beaker. Upon addition of TEOS the pH of the reaction solution decreased from 11.1 to 10.3, because of the presence of HCl traces in the TEOS solution and the formation of charged hydrolysis products. At this pH a variety of silicate species is known to form, ranging from monomers and dimers to oligomeric species with

 © WILEY-VCH Verlag GmbH, D-69451 Weinheim, 1998 1433-7851/98/3706-0822 $ 17.50+.50/0

different charges.[5] It is well known that oppositely charged polyions are preferentially adsorbed on to interfaces of charged surfactant assemblies.[6] Furthermore, since the TEOS droplets are presumably covered by the surfactant, the concentration of hydrolysis products close to the surfactant–water interface will be very high. However, polymerization of silicate species adsorbed on to the surfactant headgroups will also readily occur at this pH at a rate higher than in the bulk.[3] This makes it almost impossible to determine whether certain species are preferentially adsorbed at the micellar interface. However, it is most probable that the reason for the rapid formation of the hexagonal mesophase observed in this study is caused by strong cooperative adsorption of polyionic silicate oligomers, which induce the hexagonal ordering of the composite assemblies.

N_2-sorption measurements at 77 K were carried out to compare the pore system of the product isolated from the tubular reactor (denoted as MCM-41t) to that of the product of the batch reaction (denoted as MCM-41b). The XRD patterns were identical for both samples. In both cases a fully reversible type IV isotherm was observed, which is characteristic for MCM-41 materials (Figure 4). The adsorbed volume

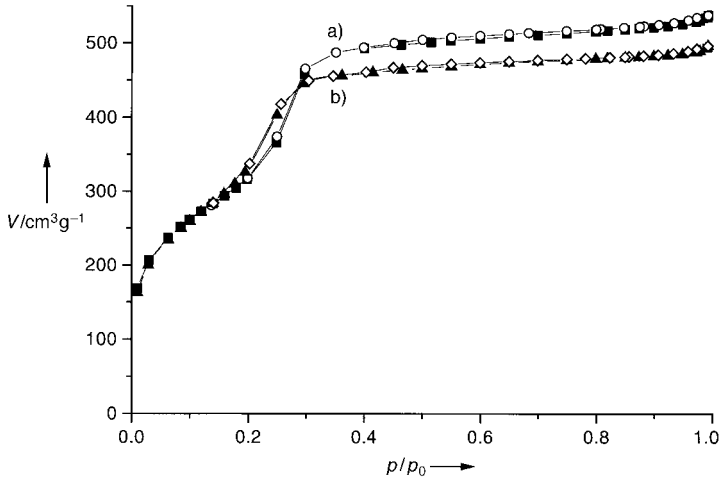


Figure 4. N_2-sorption isotherms of MCM-41 a) prepared as a batch synthesis in an open beaker, reaction time 60 min and b) prepared in the tubular reactor and isolated after 180 s.

increases linearly at low values of the relative pressure and then, because of secondary micropore filling inside the mesopores, it increases sharply between $p/p_o \approx 0.20-0.28$ for MCM-41t and 0.22–0.29 for the MCM-41b. The shift towards lower p/p_o values in the position of the sharp increase in the adsorption for MCM-41t compared to that for MCM-41b suggests that the pore diameter was slightly smaller for this sample. Pore sizes are difficult to calculate from the isotherms, since no good algorithms are available so far for this type of isotherm; however, the pore sizes are estimated to be around 2–3 nm.

In conclusion, we have for the first time carried out a continuous preparation of MCM-41 in a tubular reactor, which allows accurate in situ XRD measurements of the kinetics of formation of the hexagonal surfactant–silicate mesophase. The hexagonal phase was developed already after a reaction time of three minutes. In addition, the setup with a tubular reactor and an in situ XRD cell, which was developed to study fast processes with "slow" analytical techniques, may be used for other studies. Other analytical cells, like UV/Vis or Raman cells can be used, and there are few limitations with respect to the systems that can be studied. The concept introduced may thus be useful in a more general way.

Experimental Section

The composition of the reaction mixture by weight was: H_2O:NH_3 (25 wt %):CTAB:1-butanol:TEOS = 400:40:8:2:31. All experiments were carried out at 30 ± 2 °C.

Two Ismatec MCP peristaltic pumps were used to control the flow of the aqueous and the organic solutions in the tubular reactor. The tube was made of polypropylene with an inner diameter of 4 mm. The static mixing element was a stainless steel mixer (Sulzer, Switzerland) with five mixing elements of type SMXS DN 6. The XRD cell was built in house and consists of a Teflon body and PEEK (polyether ether ketone) windows (Goodfellow, 0.025 mm). The sample thickness between the polymer foils was 3 mm. Since the system was not optimized for the production of large amounts of product, the maximum running time before the reactor had to be cleaned was 15 min.

A STOE STADIP transmission X-ray diffractometer with a position sensitive detector (PSD) was used for all XRD experiments. For the in situ experiments data was accumulated between 0 and 6° (2θ). An ASAP 2010 (Micromeritics) sorptometer was used for the N_2-sorption measurements.

Received: July 8, 1997 [Z10650IE]
German version: *Angew. Chem.* **1998**, *110*, 871–873

Keywords: mesophases · mesoporosity · silicon · X-ray scattering · zeolite analogues

[1] a) C. T. Kresge, M.E: Leonowicz, W. J. Roth, J. C. Vartuli ,J. S. Beck, *Nature* **1992**, *359*, 710; b) J. S. Beck, J. C. Vartuli, W. J. Roth, M. E. Leonowicz, C. T. Kresge, K. D. Schmitt, C.T-W. Chu, D. H. Olson, E. W. Sheppard, S. B. McCullen, J. B. Higgins, J. L. Schlenker, *J. Am. Chem. Soc.* **1992**, *114*, 10843.
[2] Q. Huo, D. I. Margolese, U. Ciesla, P. Feng, T. E. Gier, P. Sieger, R. Leon, P. M. Petroff, F. Schüth, G. D. Stucky, *Nature* **1994**, *368*, 317.
[3] A. Monnier, F. Schüth, Q. Huo, D. Kumar, D. Margolese, R. S. Maxwell, G. D. Stucky, M. Krishnamurty, P. Petroff, A. Firouzi, M. Janicke, B. F. Chmelka, *Science* **1993**, *261*, 1299.
[4] J. Zhang, Z. Luz, D. Goldfarb,*J. Phys. Chem. B* **1997**, *101*, 7087.
[5] C. J. Brinker, G. W. Scherer, *Sol-Gel Science*, Academic Press, San Diego, CA, **1990.**
[6] J. N. Israelachvili, *Intermolecular & Surface Forces*, Academic Press, London, **1991.**

 © WILEY-VCH Verlag GmbH, D-69451 Weinheim, 1998 1433-7851/98/3706-0823 $ 17.50+.50/0

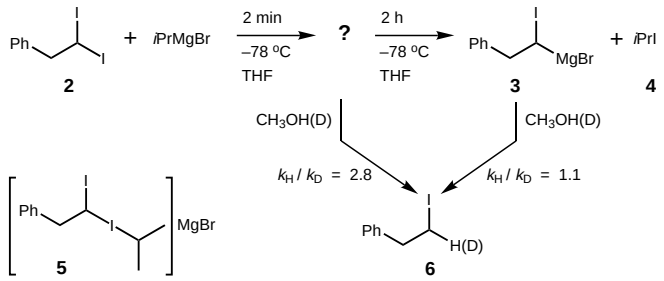
α-Iodoalkyl–Iodine–Ate Complexes as Observable Intermediates in the Iodine–Magnesium Exchange Reaction**

Volker Schulze, Mark Brönstrup, Volker P. W. Böhm, Peter Schwerdtfeger, Michael Schimeczek, and Reinhard W. Hoffmann*

Since its discovery by Wittig[1] and Gilman,[2] the halogen–metal exchange reaction has been the focus of mechanistic speculations:[3] Four-center transition states,[4] free radical chain reactions,[5] or reaction via a halogen–ate complex[6] have been discussed. Kinetic evidence for the formation of an intermediate—possibly the iodine–ate complex **1**—in the iodine–lithium exchange reaction [Eq. (a)] was reported by

$$R^1\text{–}I + Li\text{–}R^2 \underset{}{\overset{k_1}{\rightleftharpoons}} \underset{\mathbf{1}}{[R^1\text{–}I\text{–}R^2]^-\ Li^+} \xrightarrow{k_2} R^1\text{–}Li + I\text{–}R^2 \quad \text{(a)}$$

Reich.[7] He was subsequently able to observe spectroscopically the iodine–ate complex **1** ($R^1 = R^2 = Ph$).[8] In parallel, Calabrese successfully crystallized an ate complex (**1**, $R^1 = R^2 = C_6F_5$) in which the lithium cation is shielded by two TMEDA ligands.[9] We report here the direct observation of an iodine–ate complex (**5**) in the iodine–magnesium exchange reaction[10] of 1,1-diiodoalkanes **2** (Scheme 1).



Scheme 1. Formation of the iodine–ate complex in the iodine–magnesium exchange reaction of 1,1-diiodoalkane **2**.

Treatment of **2** with isopropylmagnesium bromide for two hours at $-78\,^\circ C$ in THF provided the carbenoid **3** quantitatively, as evidenced by the formation the iodoalkane **6** upon quenching with CH_3OH. When isopropylmagnesium bromide or diisopropylmagnesium was mixed with **2**, an intense yellow color formed immediately[11] and faded over about two hours. We surmised that the color could be caused by the ate complex **5**. Hints as to the nature of the species responsible for the color can be attained by comparing the kinetics of the decay in color with the time dependence of other observables of the system: Low-temperature UV/Vis spectroscopy of a 0.007 M solution of **2** showed an absorption at $\lambda_{max} = 409$ nm after addition of one equivalent of diisopropylmagnesium. The absorption disappeared at $-78\,^\circ C$ with a pseudo-first-order rate constant of $1.2 \times 10^{-4}\ s^{-1}$ (Figure 1); when two equivalents of diisopropylmagnesium were added the rate constant increased to $3.8 \times 10^{-4}\ s^{-1}$.

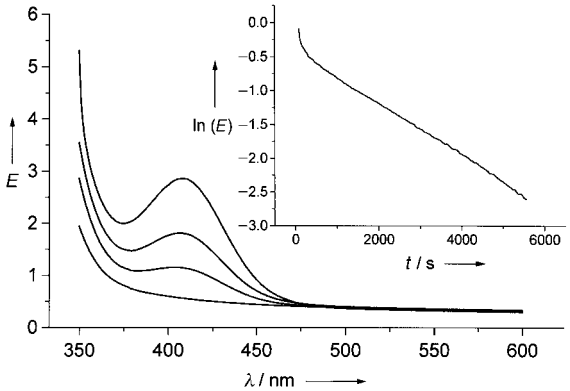


Figure 1. Time dependence of the UV/Vis spectra of the α-iodoalkyl–iodine–ate complex **5**.

Since the chromophore is the "fingerprint" of the species formed, we carried out calculations on the UV absorption expected for a model compound, the α-iodomethyl–iodine–ate anion **8**. CAS/MP2 calculations[12] reproduced the absorption characteristics of diiodomethane reasonably well. When applied to **8**, the same calculations resulted in a predicted absorption maximum at 431 nm, which is in qualitative agreement with our findings.

Still, the question remains whether the colored species is formed stoichiometrically as an intermediate en route from **2** to **3**, or whether it is formed in substoichiometric amounts in an unrelated side reaction. No clue was obtained by quenching the yellow solution after two minutes with methanol, which resulted again in the formation of the iodoalkane **6** (97%).

A short-lived intermediate may be characterized by a competition constant by which it selects between two reaction pathways.[13] We therefore quenched the reaction mixture with a 1:1 mixture of CH_3OH and CH_3OD. Quenching of the colorless solution after two hours showed that **3** is "protonated" with an apparent isotope effect of $k_H/k_D = 1.1$. However, quenching of the yellow solution two minutes after mixing of **2** with isopropylmagnesium bromide resulted in an apparent isotope effect of $k_H/k_D = 2.6$. This suggests that substantial amounts of a species different from **3** must be present in the yellow solution. Data for quenching at various time intervals (Figure 2) indicate that a species is initially formed which protonates with an isotope effect of about 2.8. The change in the isotope effect with time shows that that this species decays with a rate constant of $4.8 \times 10^{-4}\ s^{-1}$, which matches the rate of decrease in the intensity of the yellow color.

At this point we tried to characterize the intermediate by low-temperature rapid-injection ^1H NMR spectroscopy. To

[*] Prof. Dr. R. W. Hoffmann, Dr. V. Schulze, Dipl.-Chem. M. Brönstrup, Dipl.-Chem. V. P. W. Böhm, Dr. P. Schwerdtfeger, Dr. M. Schimeczek
Fachbereich Chemie der Universität
Hans-Meerwein-Strasse, D-35032 Marburg (Germany)
Fax: (+49) 6421-28-8917
E-mail: rwho@ps1515.chemie.uni-marburg.de

[**] This work was supported by the Deutsche Forschungsgemeinschaft (SFB 260) and the Fonds der Chemischen Industrie.

 © WILEY-VCH Verlag GmbH, D-69451 Weinheim, 1998 1433-7851/98/3706-0824 $ 17.50+.50/0

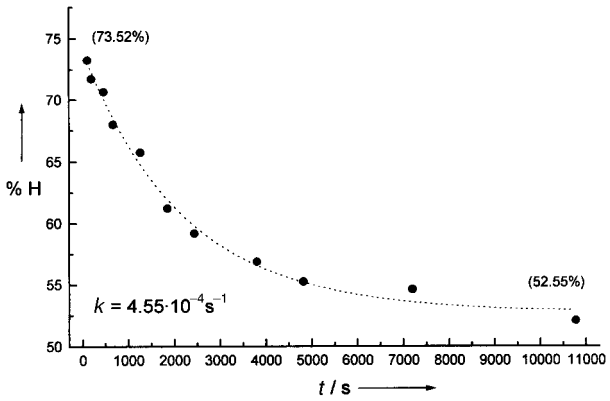


Figure 2. Proton content (%) in product **6** as a function of the time upon quenching with CH_3OH/CH_3OD. Conditions: 1.0 equiv of **2**, 0.8 equiv of *i*PrMgBr, THF, $-78\,^{\circ}C$, $c = 0.4$M.

this end, a solution of the diiodoalkane **2** in [D_8]THF was injected into a solution of diisopropylmagnesium in [D_8]THF at $-75\,^{\circ}C$. The ^1H NMR signals of the starting material **2** disappeared with a rate constant of $5 \times 10^{-2}\,L\,mol^{-1}\,s^{-1}$, whereas the signals of the (easier to observe) product **4** increased in intensity with a rate constant of $5 \times 10^{-4}\,s^{-1}$. This roughly 100-fold difference in rate requires the formation of an intermediate. The following ^1H NMR signals could be assigned to the intermediate: $\delta = 2.98$ (dd, $J = 12.7$, 7.9 Hz, 1H), 3.24 (t, $J = 11.9$ Hz, 1H), 3.45 (dd, $J = 10.4$ and 8.0 Hz, 1H).

The intensity of the signal at $\delta = 2.98$ decreased with a rate constant of $4 \times 10^{-4}\,s^{-1}$, which is again in line with the time dependence of the isotope effect upon quenching with methanol and with the time dependence of the decoloration. In view of the precedent set by Calabrese[9] and Reich[8] we feel confident that the intermediate observed is the iodine–ate complex **5**.

What is so special about the ate complex **5** that its lifetime becomes long enough to be observed under the ordinary conditions of the halogen–metal exchange reaction? The substantial stabilization has to be associated with the second iodine atom present, which helps to delocalize the negative charge. This is suggested by the results of ab initio calculations (Figure 3).[14, 15] They indicate that the negative charge in the ate complex **7** does not reside on the hypervalent iodine atom. Instead, it is evenly distributed to the carbon atoms in **7** and unevenly distributed to the two sides in the ate complex **8**. Preliminary information on the reactivity of such ate complexes shows that electrophiles (MgX^+, H^+) attack the ate complex **5** at the side carrying the larger part of the negative charge or, in other words, at the weaker and longer carbon–iodine bond.

The finding that iodine–ate complexes are readily protonated led us to the following experiment: When isopropylmagnesium chloride was added at $-78\,^{\circ}C$ to a solution containing **2** and 20 equivalents of CH_3OH/CH_3OD, the iodoalkane **6** was again obtained in 15% yield. Its isotope content revealed that protonation had occured at the stage of the ate complex **5** and not at that of the carbenoid **3**. This result challenges the notion[20] that halogen–metal exchange reactions can be carried out to completion in the presence of

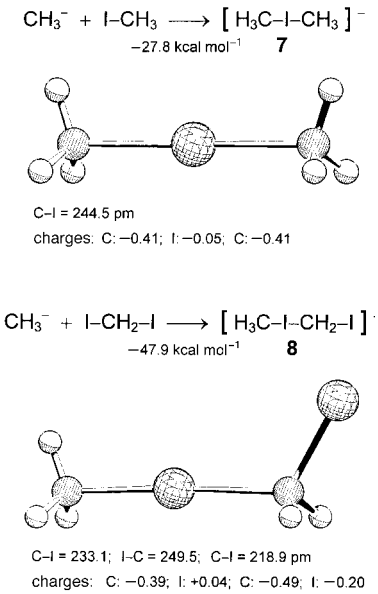


Figure 3. Calculated sructures of iodine–ate complexes.

proton donors. Our findings rather suggest that completion of the halogen–metal exchange reaction is foiled under these conditions, since protonation takes place at the stage of the intermediate ate complexes.[21] It may therefore be prudent to check which of the in situ trapping reactions or intramolecular reactions hitherto ascribed to organolithium compounds generated by halogen–metal exchange reactions are actually reactions of organolithium compounds and which are rather caused by halogen–ate complexes.[22]

Received: October 22, 1997 [Z11068IE]
German version: *Angew. Chem.* **1998**, *110*, 869–871

Keywords: ate complexes · carbenoids · hypervalent compounds · iodine · metalations

[1] G. Wittig, U. Pockels, H. Dröge, *Ber. Dtsch. Chem. Ges.* **1938**, *71*, 1903–1912.
[2] H. Gilman, W. Langham, A. L. Jacoby, *J. Am. Chem. Soc.* **1939**, *61*, 106–109.
[3] W. F. Bailey, J. J. Patricia, *J. Organomet. Chem.* **1988**, *352*, 1–46.
[4] J. Villiéras, *Bull. Soc. Chim. Fr.* **1967**, 1520–1532.
[5] a) H. R. Ward, R. G. Lawler, R. A. Cooper, *J. Am. Chem. Soc.* **1969**, *91*, 746–748; b) A. R. Lepley, R. L. Landau, *ibid.* **1969**, *91*, 748–749; c) E. C. Ashby, T. N. Pham, *J. Org. Chem.* **1987**, *52*, 1291–1300.
[6] G. Wittig, U. Schöllkopf, *Tetrahedron* **1958**, *3*, 91–93.
[7] H. J. Reich, N. H. Phillips, I. L. Reich, *J. Am. Chem. Soc.* **1985**, *107*, 4101–4103.
[8] a) H. J. Reich, D. P. Green, N. H. Phillips, *J. Am. Chem. Soc.* **1989**, *111*, 3444–3445; b) H. J. Reich, D. P. Green, N. H. Phillips, *ibid.* **1991**, *113*, 1414–1416.
[9] W. B. Farnham, J. C. Calabrese, *J. Am. Chem. Soc.* **1986**, *108*, 2449–2451.
[10] J. Villiéras, *Organomet. Chem. Rev. A.* **1971**, *7*, 81–94.
[11] This observation was made first by P. Meister in our Laboratory in 1992.
[12] The CAS/MP2 calculation[16] was performed with a relativistic effective core potential for iodine, which replaces the 46 core electrons.[17] The valence basis set for iodine is (8s,8p,1d)/[6s,6p,1d]. For carbon and hydrogen we used 6-311++G(d,p) basis sets.[18] The geometry of the model compound **8** was optimized at the MP2 level of theory with the same basis set. This was followed by a CAS/MP2

 © WILEY-VCH Verlag GmbH, D-69451 Weinheim, 1998 1433-7851/98/3706-0825 $ 17.50+.50/0

calculation with an active space of 45 configurations. All calculations were carried out with Gaussian 94.[19]
[13] R. Huisgen, *Angew. Chem.* **1970**, *82*, 783 – 820; *Angew. Chem. Int. Ed. Engl.* **1970**, *9*, 751 – 762.
[14] a) J. Cioslowski, P. Piskorz, M. Schimeczek, G. Boche, *J. Am. Chem. Soc.*, submitted; b) G. Boche, M. Schimeczek, J. Cioslowski, P. Piskorz, *J. Org. Chem.*, submitted.
[15] MP2(full) with 6-31++G(d)[18] for C and H; ECP and (4s,4p,1d)/[3s,3p,1d] for iodine. Charges quoted are AIM charges, cf. R. W. F. Bader, *Atoms in Molecules: A Quantum Theory*, Clarendon Press, Oxford **1994**.
[16] J. J. McDouall, K. Peasley, M. A. Robb, *Chem. Phys. Lett.* **1988**, *148*, 183 – 196.
[17] P. Schwerdtfeger, M. Dolg, W. H. E. Schwarz, G. A. Bowmaker, P. D. W. Boyd, *J. Chem. Phys.* **1989**, *91*, 1762 – 1774.
[18] a) R. Krishnan, J. S. Binkley, R. Seeger, J. A. Pople, *J. Chem. Phys.* **1980**, *72*, 650 – 654; b) T. Clark, J. Chandrasekhar, G. W. Spitznagel, P. von R. Schleyer, *J. Comp. Chem.* **1983**, *4*, 294 – 301.
[19] Gaussian 94 from Gaussian Inc., Pittsburgh, PA, **1995**.
[20] a) W. F. Bailey, J. J. Patricia, T. T. Nurmi, W. Wang, *Tetrahedron Lett.* **1986**, *27*, 1861 – 1864; b) A. Schmidt, G. Köbrich, R. W. Hoffmann, *Chem. Ber.* **1991**, *124*, 1253 – 1258; c) P. Beak, T. J. Musick, C. Liu, T. Cooper, D. J. Gallagher, *J. Org. Chem.* **1993**, *58*, 7330 – 7335, and references quoted.
[21] Such a possibility was explicitly discussed for the sulfoxide – lithium exchange reaction: G. Theobald, W. H. Okamura, *Tetrahedron Lett.* **1987**, *28*, 6565 – 6568.
[22] This may also apply to reactions ascribed to a 1,1-dilithioalkene,[23] as suggested by A. Maercker.[24]
[23] J. Barluenga, M. A. Rodriguez, P. J. Campos, *J. Am. Chem. Soc.* **1988**, *110*, 5567 – 5568.
[24] A. Maercker, B. Bös, *Main Group Metal Chem.* **1991**, *14*, 67 – 71.

Stabilities of Hydrogen-Bonded Supramolecular Complexes with Various Numbers of Single Bonds: Attempts To Quantify a Dogma in Host – Guest Chemistry**

Frank Eblinger and Hans-Jörg Schneider*

It is generally accepted that optimal preorganization for molecular recognition requires an optimal geometric fit between convergent binding sites A(H), A′(G), B(G), B′(G), etc. of host and guest molecules H and G.[1] If binding sites within host and/or guest are connected by single bonds, this can give rise to enthalpy or strain penalties if a transoid fragment must convert into a *gauche* conformation for an optimal orientation of binding sites. At the same time the presence of freely rotatable single bonds can lead to a loss of rotational freedom on complexation, which is generally regarded as a major drawback of, for instance, open-chain versus macrocyclic receptors. However, systematic analyses of complexes with crown and open-chain poly(ethylene glycol) ethers show that the formation of macrocyclic hosts is based to a large degree on enthalpy advantages (macrocyclic effect).[2]

Entropic contributions to the formation of noncovalent bonds are one of the most often invoked problems in molecular recognition, and until now they were among the least predictable factors. Systematic analyses of free energies of association ΔG_{cplx} of many supramolecular associations show little dependence of ΔG_{cplx} on the presence of single bonds in either host or guest molecule, and $\Delta\Delta G_{cplx}$ contributions from the different binding sites are generally additive.[3] However, most of the investigated complexes were constructed so as to avoid the presence of many freely rotatable bonds. This also holds for the few studies of noncovalent intramolecular interactions, which also show little strengthening upon rigidification of the underlying frameworks.[4] In the gas phase one expects rotational entropy contributions ΔS_{rot} of 13 – 21 $J\,mol^{-1}\,K^{-1}$ per single bond.[5, 6] If the rotations were completely frozen upon complex formation, which is expected only if rigid covalent bonds are formed,[6] the corresponding loss of free energy $\Delta\Delta G_{rot}$ would be 3.9 – 6.4 $kJ\,mol^{-1}$ at room temperature. For noncovalent interactions Williams et al. assume a value between 2 and 6 $kJ\,mol^{-1}$ per restricted bond.[7]

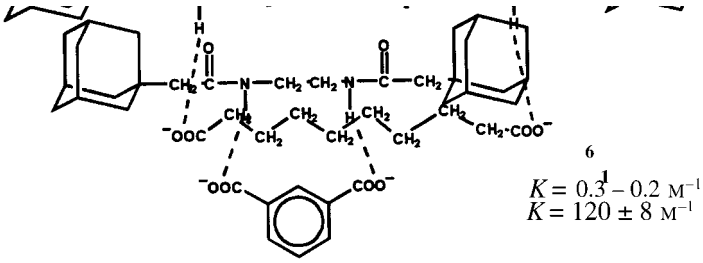
Unfortunately these numbers translate into a large uncertainty of prediction. The presence of only two nonrestricted bonds[8] in host and guest would correspond to differences in the association constant K of between 2 and 11 M^{-1}. Therefore, it seems to be essential to obtain experimental values for the change of free energy ΔG_{cplx} associated with the presence of single bonds in host – guest complexes. Surprisingly, there were no studies till now in which the number of single bonds in supramolecular complexes was systematically varied. We chose a series of α,ω-diamides as hydrogen-bond donors[9] and α,ω-dicarboxylates as acceptors.[10] The tetrabutylammonium salts of the latter are soluble in chloroform. The functional groups were connected by spacers of different length and flexibility (Scheme 1). The advantage of these chloroform-soluble compounds is that interactions other than hydrogen bonds are suppressed, and problems in the measurements, such as self-association and salt effects, are minimized.

The initially prepared amides of long-chain fatty acids were only sparingly soluble in chloroform, probably owing to strong dispersive interactions between the alkyl chains in the solid state. Therefore, derivatives with the bulky and more spherical adamantyl group were prepared from the corresponding adamantyl acid chloride and, as expected, were sufficiently soluble in chloroform. Dilution experiments with these amides in $CDCl_3$ in which the chemical shift of the NH protons was monitored gave dimerization constants $K < 30\,M^{-1}$, so that at least 85 % of the monomer was present in the observed concentration range ($\leq 5 \times 10^{-3}$ M). Equilibrium constants were determined according to ref. [11] and gave a satisfactory fit to a 1:1 model for the association between host and guest monomers (e.g., Figure 1). The spacers were chosen to allow contact between the corresponding binding sites without buildup of substantial strain; this was checked by computer-aided molecular modeling (Figure 2). All amide groups and the alkyl chains can retain their transoid

[*] Prof. Dr. H.-J. Schneider, Dipl.-Chem. F. Eblinger
FR 11.2 Organische Chemie der Universität des Saarlandes
D-66041 Saarbrücken (Germany)
Fax: (+49) 681-302-4105
E-mail: ch12hs@rz.uni-sb.de

[**] Supramolecular Chemistry, Part 76. This work was supported by the Deutsche Forschungsgemeinschaft and the Fonds der Chemischen Industrie. We thank Prof. A. Yatsimirski, UNAM Mexico, for literature references and valuable comments. Part 75: A. Roigk, R. Hettich, H.-J. Schneider, *Inorg. Chem.* **1998**, in press.

 © WILEY-VCH Verlag GmbH, D-69451 Weinheim, 1998 1433-7851/98/3706-0826 $ 17.50+.50/0

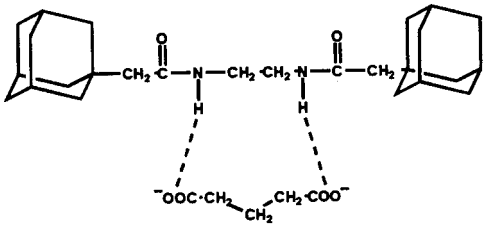


6

$K = 0.3 - 0.2\ \mathrm{M}^{-1}$

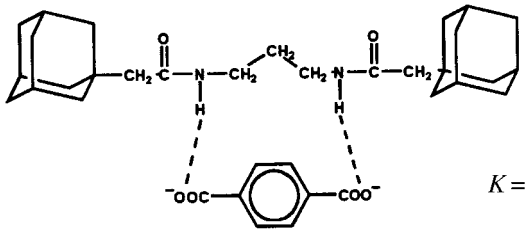
1

$K = 120 \pm 8\ \mathrm{M}^{-1}$



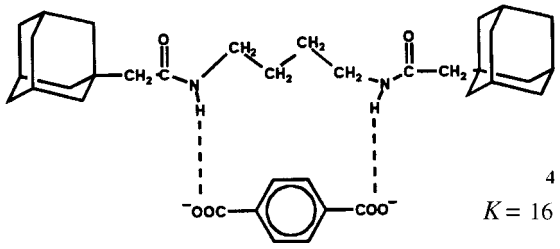
2

$K = 78 \pm 5\ \mathrm{M}^{-1}$



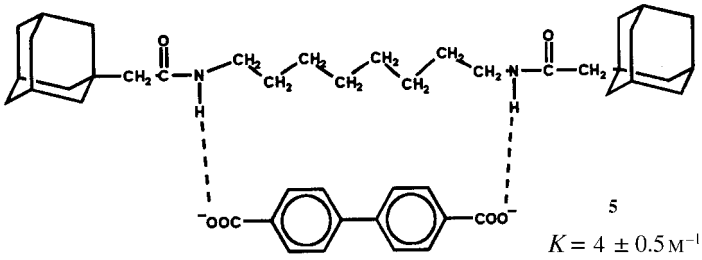
3

$K = 51 \pm 4\ \mathrm{M}^{-1}$



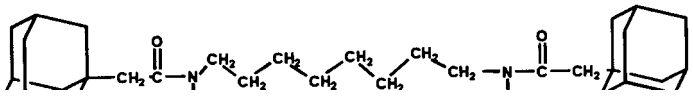
4

$K = 16 \pm 2\ \mathrm{M}^{-1}$



5

$K = 4 \pm 0.5\ \mathrm{M}^{-1}$



Scheme 1. Structures and association constants of complexes **1**–**6** in $CDCl_3$ at 298 K.

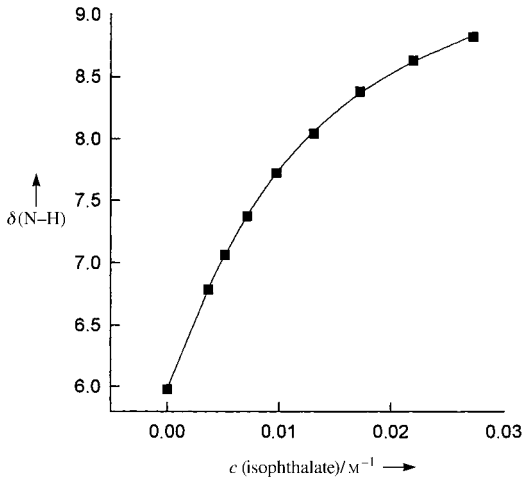
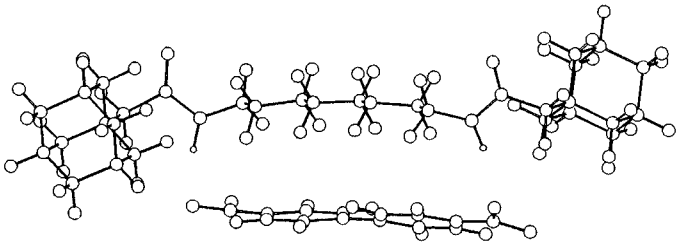


Figure 1. Experimental (dots) and calculated (line) chemical shifts of the NH protons in the titration of **1** in $CDCl_3$.



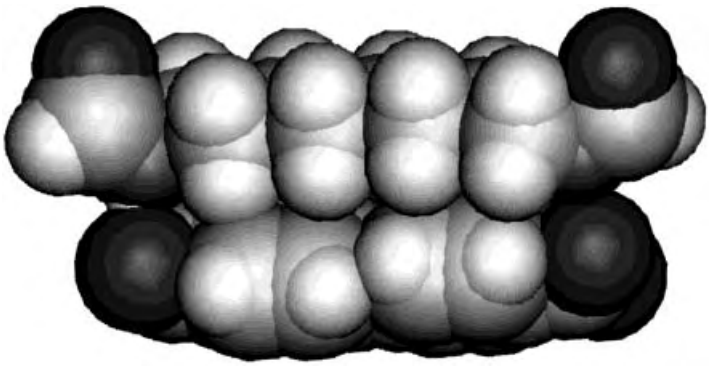


Figure 2. Quanta/CHARMm Structure of **5**. For the sake of clarity, the adamantyl groups are omitted from the space-filling model.

conformations on complexation. The chemical shifts of the NH protons at 100% complexation (complexation-induced shift, CIS), obtained by nonlinear least-squares fitting, were consistent and agreed with published CIS values for the deshielding of these protons in other amide associates.[10a, c, e, 12]

The measured ΔG_{cplx} values (Table 1) show a remarkably small decrease with increasing flexibility of the spacer between the binding sites. Thus, **1** and **2** (Scheme 1) differ only by 10% in complexation free energy, although **2** has two more rotatable bonds than **1**. Similarly small differences are found for the other complexes. Only if the number of single bonds n in both host and guest is increased to nine, that is, a total of 18 (**6**), does the association constant become too small to be obtained from a titration curve. It was therefore estimated by comparison of the observed NH chemical shifts with other CIS values.

 © WILEY-VCH Verlag GmbH, D-69451 Weinheim, 1998 1433-7851/98/3706-0827 $ 17.50+.50/0

Table 1. Experimental and calculated data for complexes **1**–**6**.

Complex	ΔG_{exp} [kJ mol^{-1}] (±5%)	n	ΔG_{calcd}[a] [kJ mol^{-1}]	pK_a[d]	ΔG_{calcd}[b] [kJ mol^{-1}]	CIS (±3%)
1	−11.9	3	−11.1	4.62	−11.9	3.9
2	−10.8	7	−7.1	5.41	−10.4	3.2
3	−9.7	4	−10.1	4.34	−9.3	3.1
4	−6.7	5	−9.1	4.34	−8.0	4.0
5	−3.4	9	−5.1	4.31	−2.6	3.9
6	+2.8–3.9[c]	18	+3.7	5.54	+3.4	3.1–4.0[c]

[a] $\Delta G_{calcd} = n \cdot 0.99 - 14.1$; $r = 0.941$. [b] $\Delta G_{calcd} = 6.14 + 1.31 \cdot n - 4.78 \cdot pK_a$. Plot: $\Delta G_{calcd} + 4.78 \cdot pK_a = 6.14 + 1.31 \cdot n$; $r = 0.995$. [c] Calculated from the NH shift at the highest possible concentration and from the highest or lowest CIS values of the other complexes. [d] From the Stability Constant Database, IUPAC and Academic Software, **1993**, Version 1.16.

The steadily decreasing ΔG_{cplx} values from **1** to **6** allow for the first time the derivation of at least an upper limit for the binding loss ΔG_{cplx} involved with the presence of single bonds. An almost linear correlation (correlation coefficient $r = 0.941$; slope $m = 0.99$) between ΔG_{cplx} and the number of freely rotatable bonds n indicates a constant additive contribution of a freely rotatable bond. If one also takes into account the CO–NH, Ph–Ph and Ph–CO bonds the correlation changes only slightly ($r = 0.973$, $m = 1.15$). Taking into account the differences in dicarboxylate basicity leads to an extended correlation of the form $\Delta G_{cplx} = s + m \cdot n + p \cdot pK_a$. Multilinear fitting then yields $s = 6.14$, $m = 1.31$, and $p = -4.78$. Although the correlation between ΔG_{cplx} and n is improved significantly ($r = 0.995$, Figure 3), the value of $m = 1.3$ kJ mol^{-1} per single

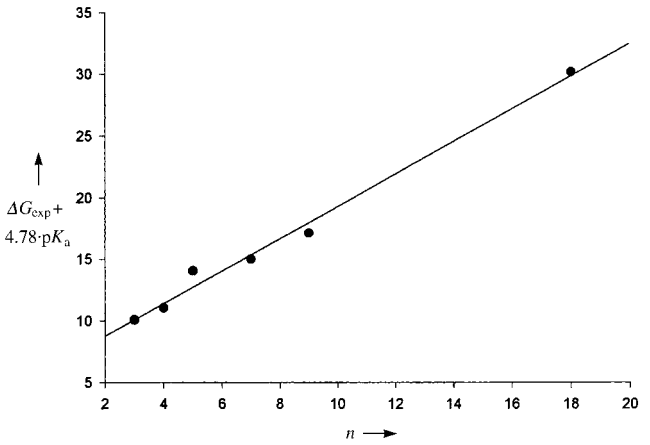
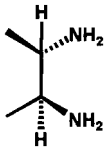


Figure 3. Plot of $(\Delta G_{exp} + 4.78 \cdot pK_a)$ versus the number of freely rotatable single bonds n. Regression: y axis intercept 6.14, slope $m = 1.31$, correlation coefficient $r = 0.995$, standard deviation 0.8.

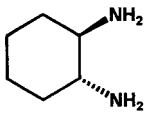
bond is close to that found without taking into account the different pK_a values and shows its relatively small influence. The intercept $s = 6.14$ leads through $\Delta\Delta G_{cplx} = 6.14 - 4.78 \cdot pK_a$ with corresponding pK_a values to association energies between −14.5 and −20.3 kJ mol^{-1}. These values are close to the typical values for interactions between two carboxylates and amides or amide-like groups in chloroform.[10a, c, d] These findings also confirm the reliability of the present analysis. The value of 1.3 kJ mol^{-1} for the loss of ΔG due to the presence of a single bond, which has been experimentally determined for the first time, is considerably lower than the previously proposed minimum values.[7]

One might expect that the entropic disadvantage will drastically increase with increasing binding strength.[6, 7] Indeed the dissociation rate constants in our relatively weak complexes approach $k = 10^6$ s^{-1} if diffusion-controlled association rates are assumed. Since rotational barriers[14] also lie in the range of $k = 10^6$ s^{-1}, dissociation of the complex would allow rotation to occur, especially as this would require only one of the two hydrogen bonds to be opened.[6, 7] However, even in much more stable complexes, such as those between transition metal ions and substituted ethylenediamines with association constants up to 10^8 times stronger than those with **1**–**6**, the presence of a rotatable bond does not substantially change ΔG_{cplx}, as exemplified by literature data[15] for complexes of **7** and **8** (Scheme 2). The relatively small sensitivity



7

	ΔG [kJ M^{-1}]
Ni^{2+}	43.6
Cu^{2+}	64.3



8

	ΔG [kJ M^{-1}]
Ni^{2+}	45.0
Cu^{2+}	63.5

Scheme 2. Free energies of association of complexes **7** and **8** with Ni^{2+} and Cu^{2+}.[15]

of ΔG to the presence of single bonds may partially be the result of enthalpy–entropy compensation, which seems to be typical for many noncovalent interactions.[16]

That the efficiency of molecular recognition processes obviously suffers less than generally assumed from the presence of rotatable bonds is of importance for the rational design of artificial receptors and effectors. The need to reduce the number of single bonds in a host compound has become an almost unquestioned dogma in synthetic host–guest chemistry. Since single bonds can better accommodate strain arising from the induced fit between ligand and receptor, better results will generally be achieved with more flexible host compounds. The acceptable number of rotatable bonds will depend on the strength of interaction between the complementary binding sites, which in many cases will compensate any disadvantages introduced by flexible bonds. It is noteworthy that that nature has developed nearly perfect systems for molecular recognition on the basis of linear peptides containing many single bonds.

Received: September 12, 1997 [Z10915IE]
German version: *Angew. Chem.* **1998**, *110*, 821–824

Keywords: adamantanes · diamides · host–guest chemistry · hydrogen bonds · molecular recognition

[1] D. J. Cram, *Angew. Chem.* **1986**, *98*, 1041; *Angew. Chem. Int. Ed. Engl.* **1986**, *25*, 1039.
[2] Y. Inoue, G. W. Gokel, *Cation Binding by Macrocycles*, Marcel Dekker, New York, **1990.**

 © WILEY-VCH Verlag GmbH, D-69451 Weinheim, 1998 1433-7851/98/3706-0828 $ 17.50+.50/0

[3] a) H.-J. Schneider, *Chem. Soc. Rev.* **1994**, *22*, 227; b) H.-J. Schneider, *Angew. Chem.* **1991**, *103*, 1419; *Angew. Chem. Int. Ed. Engl.* **1991**, *30*, 1417; group-contribution methods have long been used for estimating thermodynamic quantities of organic compounds: N. Cohen, S. W. Benson, *Chem. Rev.* **1993**, *93*, 2419; I. M. Klotz, R. M. Rosenberg, *Chemical Thermodynamics*, 5th ed., Wiley, New York, **1994**, chap. 22.
[4] G.-B. Liang, J. M. Desper, S. H. Gellman, *J. Am. Chem. Soc.* **1993**, *115*, 925.
[5] S. W. Benson, *Thermochemical Kinetics*, 2nd ed., Wiley, New York, **1967**.
[6] a) M. I. Page, W. P. Jencks, *Proc. Natl. Acad. Sci. USA* **1971**, *68*, 1678; b) M. I. Page, *Chem. Soc. Rev.* **1973**, *2*, 295; c) M. I. Page in *The Chemistry of Enzyme Action* (Ed.: M. I. Page), Elsevier, Amsterdam, **1984**, p. 1; d) W. P. Jencks, *Proc. Natl. Acad. Sci. USA* **1978**, *78*, 4046.
[7] a) D. H. Williams, M. S. Searle, M. S. Westwell, V. Mackay, P. Groves, D. A. Beauregard, *Chemtracts: Org. Chem.* **1994**, *7*, 133; b) M. S. Searle, D. H. Williams, U. Gerhard, *J. Am. Chem. Soc.* **1992**, *114*, 10697, and references therein.
[8] Even highly preorganized receptors such as Rebek's derivatives of Kemp acid contain at least two rotatable bonds: J. Rebek, Jr., *Angew. Chem.* **1990**, *102*, 261; *Angew. Chem. Int. Ed. Engl.* **1990**, *29*, 245.
[9] J. D. Joesten, L. J. Schaad, *Hydrogen Bonding*, Marcell Decker, New York, **1974**; G. A. Jeffrey, W. Saenger, *Hydrogen Bonding in Biological Structures*, Springer, Berlin, **1994**.
[10] Other studies with amide–carboxylate complexes: a) J. S. Albert, A. D. Hamilton, *Tetrahedron Lett.* **1993**, *34*, 7363; b) B. C. Hamann, N. R. Branda, J. Rebek, Jr., *ibid.* **1993**, *34*, 6837; c) E. Fan, S. A. van Arman, S. Kincaid, A. D. Hamilton, *J. Am. Chem. Soc.* **1993**, *115*, 369; d) C. Vincent, S. C. Hirst, F. Garcia-Tellado, A. D. Hamilton, *ibid.* **1991**, *113*, 5466; e) T. R. Kelly, M. H. Kim, *ibid.* **1994**, *116*, 7072.
[11] H.-J. Schneider, R. Kramer, S. Simova, U. Schneider, *J. Am. Chem. Soc.* **1988**, *110*, 6442.
[12] F. Garcia-Tellado, S. Goswami, S. K. Chang, S. J. Geib, A. D. Hamilton, *J. Am. Chem. Soc.* **1990**, *112*, 7393.
[13] C. Vincent, E. Fan, A. D. Hamilton, *Tetrahedron Lett.* **1992**, *33*, 4269.
[14] U. Berg, J. Sandström, *Adv. Phys. Org. Chem.* **1989**, *25*, 1.
[15] a) L. D. Pettit, J. M. L. Swash, *J. Chem. Soc. Dalton Trans.* **1977**, 697; b) P. Tilus, *Finn. Chem. Lett.* **1979**, 76.
[16] R. Lumry in *Bioenergetics and Thermodynamics* (Ed.: A. Braibanti), Reidel, Dordrecht, **1980**, p. 405, and references therein.

A Gas-Phase Model for the Pt^+-Catalyzed Coupling of Methane and Ammonia**

Massimiliano Aschi, Mark Brönstrup, Martin Diefenbach, Jeremy N. Harvey, Detlef Schröder,* and Helmut Schwarz*

Dedicated to Professor Heribert Offermanns on the occasion of his 60th birthday

The activation of methane has been referred to as one of the central challenges in contemporary chemical research.[1] In addition to various academic aspects, methane activation is of eminent industrial importance. One economically attractive process is the coupling of ammonia and methane according to reaction (1) to afford hydrogen cyanide, a valuable feedstock for chemical synthesis. Reaction (1) is, however, endothermic[2] by 61 kcal mol^{-1} and the thermochemical equilibrium must be shifted to the right by appropriate means. Two concepts have been pursued in the chemical industry,[3] both of which rely on platinum catalysts.[4] In the Degussa process, reaction (1) is performed at elevated temperatures (ca. 1500 K), while in the Andrussow synthesis of HCN, molecular oxygen is added to shift the energy balance by formation of water rather than molecular hydrogen.

$$CH_4 + NH_3 \rightarrow HCN + 3\,H_2 \quad (1)$$

Details of the reaction mechanism of the Pt-catalyzed coupling of methane and ammonia remain uncertain.[3] Gas-phase studies can complement catalyst research by providing information about the elementary steps of bond activation and formation as well as the characterization of possible reaction intermediates. Here, we describe the reactions of atomic platinum cations with methane and ammonia examined using Fourier transform ion cyclotron resonance (FTICR) mass spectrometry.[5–7]

As has been described previously,[8, 9] bare platinum cations dehydrogenate methane to afford the platinum carbene cation $[PtCH_2]^+$ with an apparent rate constant of $k = 8.2 \times 10^{-10}$ cm^3 molecule^{-1} s^{-1}.[9a] Subsequently, $[PtCH_2]^+$ reacts with an excess of methane to form $[PtC_2H_4]^+$ and higher $[PtC_nH_m]^+$ ions, but the associated rate constants are small as compared to that of reaction (2).[9a]

$$Pt^+ + CH_4 \rightarrow [PtCH_2]^+ + H_2 \quad (2)$$

$$Pt^+ + NH_3 \rightarrow [Pt(NH_3)]^+ \quad (3)$$

$$Pt^+ + NH_3 \not\rightarrow [PtNH]^+ + H_2 \quad (4)$$

When Pt^+ is allowed to interact with ammonia under FTICR conditions ($p \approx 10^{-8}$ mbar) only adducts such as $[Pt(NH_3)]^+$ and subsequently $[Pt(NH_3)_2]^+$ form. The association reaction (3) proceeds quite slowly ($k \approx 5 \times 10^{-13}$ cm^3 molecule^{-1} s^{-1}), even though B3LYP calculations predict an appreciable $Pt^+ - NH_3$ binding energy of 74 kcal mol^{-1}.[10, 11] Further, although dehydrogenation of ammonia to yield the NH fragment is less endothermic (101 kcal mol^{-1}) than that of methane to afford methylene (111 kcal mol^{-1}),[2] formation of $[PtNH]^+$ by means of reaction (4) is not observed. While this result may be attributed to kinetic barriers, the B3LYP calculations suggest that reaction (4) is endothermic by 17 kcal mol^{-1}, and thus its non-occurrence is a consequence of a thermodynamic restriction.

Mass-selected $[PtCH_2]^+$ reacts rapidly with ammonia ($k = 6.2 \times 10^{-10}$ cm^3 molecule^{-1} s^{-1}) to form three different product ions according to reactions (5a–c) in a ratio of 70:25:5.

$$[PtCH_2]^+ + NH_3 \rightarrow CH_2NH_2^+ + [PtH] \quad (5a)$$

$$[PtCH_2]^+ + NH_3 \rightarrow [Pt,C,N,H_3]^+ + H_2 \quad (5b)$$

$$[PtCH_2]^+ + NH_3 \rightarrow NH_4^+ + [PtCH] \quad (5c)$$

[*] Dr. D. Schröder, Prof. Dr. H. Schwarz, Dr. M. Aschi, Dipl.-Chem. M. Brönstrup, Dipl.-Chem. M. Diefenbach, Dr. J. N. Harvey, Institut für Organische Chemie der Technischen Universität Strasse des 17. Juni 135, D-10623 Berlin (Germany)
Fax: (+49) 30-314-21102
E-mail: schw0531@www.chem.tu-berlin.de

[**] This work was supported by the Deutsche Forschungsgemeinschaft and the Fonds der Chemischen Industrie. M. A. acknowledges support from the C.N.R. (Italy), and M. B. thanks the Fonds der Chemischen Industrie for a Kekulé scholarship. We thank P. E. M. Siegbahn for providing us with a basis set for platinum. We are indebted to Degussa AG for having brought this important topic to our attention.

Reaction (5c) represents a simple proton transfer from $[PtCH_2]^+$ to the ammonia base and will not be discussed further. Instead, we will focus on the formation of the iminium ion in reaction (5a), which clearly indicates the coupling of methane and ammonia concomitant with C–N bond formation. The assignment of the iminium structure to the ionic product of reaction (5a) is further supported by the finding that $[PtCD_2]^+$ reacts with ammonia to yield neutral [PtH] and $CD_2NH_2^+$; the latter undergoes proton but not deuteron transfer in its subsequent reaction with ammonia to yield NH_4^+. The combination of reactions (2) and (5a) together with deprotonation and dehydrogenation steps constitutes a route for the generation of HCN, which is summarized in Sequence 1. In this sequence platinum mediates the activation of methane and its coupling with ammonia, but does not intervene in the final steps to yield hydrogen cyanide. Notably, the dehydrogenation step (6d) in Sequence 1 is almost thermoneutral (0.3 kcal mol^{-1}),[2] thus it may readily occur at the elevated temperatures possibly needed to overcome kinetic barriers.[12]

Sequence 1

$$Pt^+ + CH_4 \rightarrow [PtCH_2]^+ + H_2 \quad (6a)$$

$$[PtCH_2]^+ + NH_3 \rightarrow CH_2NH_2^+ + [PtH] \quad (6b)$$

$$CH_2NH_2^+ + NH_3 \rightarrow NH_4^+ + CH_2NH \quad (6c)$$

$$CH_2NH \rightarrow HCN + H_2 \quad (6d)$$

$$[PtH] + NH_4^+ \rightarrow Pt^+ + NH_3 + H_2 \quad (6e)$$

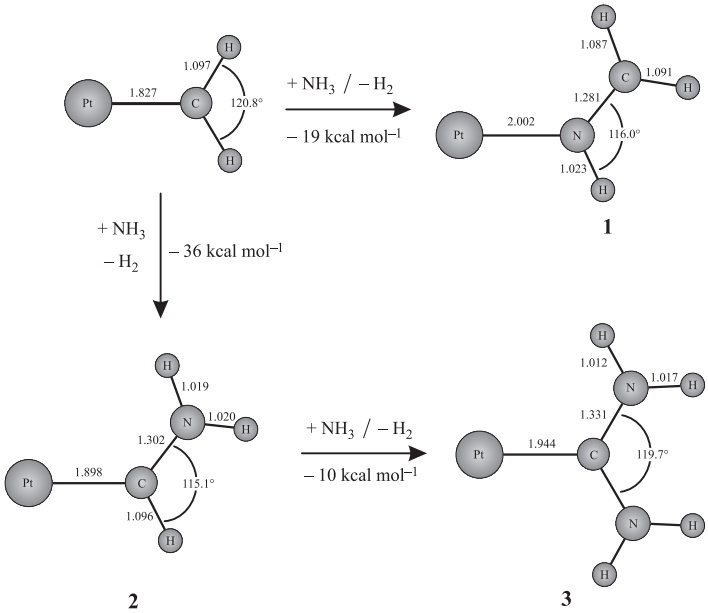
$$CH_4 + NH_3 \rightarrow HCN + 3\ H_2 \quad (1)$$

Let us now address the side reaction (5b) leading to the organometallic species $[Pt,C,N,H_3]^+$, for which two connectivities are considered. Formation of the formimine complex $[PtN(H)(CH_2)]^+$ (**1**) would imply that both hydrogen atoms of the molecular hydrogen in reaction (5b) are cleaved from the ammonia molecule in a 1,1-elimination. However, in the reaction of $[PtCD_2]^+$ with ammonia only HD is lost in this channel,[13] suggesting the occurrence of a 1,2-elimination formally leading to the aminocarbene complex $[PtC(D)(NH_2)]^+$ (**2**). With respect to the structural assignment of the $[Pt,C,N,H_3]^+$ ion, the subsequent ion/molecule reactions are quite revealing. $[Pt,C,N,H_3]^+$ reacts with ammonia in yet another dehydrogenation step to afford $[Pt,C,N_2,H_4]^+$, and when $[PtCD_2]^+$ is used as the initial reactant, all the deuterium label is lost in the dehydrogenation steps to afford $[Pt,C,N_2,H_4]^+$ exclusively. These results imply substitution of the hydrogen (deuterium) atoms of the carbene, and the proposed sequence of reactions (7a) and (7b) lends strong support to structure **2**.

$$[PtCD_2]^+ + NH_3 \rightarrow [PtC(D)(NH_2)]^+ + HD \quad (7a)$$

$$[PtC(D)(NH_2)]^+ + NH_3 \rightarrow [PtC(NH_2)_2] + HD \quad (7b)$$

The results of the B3LYP calculations are in accord with this assignment: the formation of **2** is approximately 17 kcal mol^{-1} more favorable than that of **1** and 33 kcal mol^{-1} more favorable than that of a η^2-bridged formimine complex, and also the second dehydrogenation to yield the diaminocarbene complex $[PtC(NH_2)_2]^+$ (**3**) is exothermic (Scheme 1).



Scheme 1. Geometries (bond lengths [Å] and angles [°]) of $[PtCH_2]^+$ and **1**–**3** (optimized at the B3LYP/6-31 + G* level) and relative energies for the reaction with ammonia (obtained at the B3LYP/6-311 + G**//B3LYP/6-31 + G* level of theory).

We stress, however, that the current theoretical results are only qualitative since the barriers en route to the products remain unknown. Nevertheless, complexes **2** and **3** formed in the reactions of $[PtCH_2]^+$ with ammonia are unprecedented gas-phase analogues to the metal complexes of Arduengo-type[14] aminocarbenes.[15, 16]

Can the aminocarbene complex **2** also contribute to the formation of hydrogen cyanide in the coupling of methane and ammonia? To address this question we subjected mass-selected $[Pt,C,N,H_3]^+$ to collisional activation. Dehydrogenation predominates to yield $[Pt,C,N,H]^+$ along with small amounts of Pt^+ and $[C,N,H_3]^+$ fragment ions. B3LYP calculations predict the formation of $[Pt(CNH)]^+$ (28 kcal mol^{-1}) and $[Pt(NCH)]^+$ (41 kcal mol^{-1}) to be the least endothermic processes, but at present we cannot assess the barriers associated with dehydrogenation of $[Pt,C,N,H_3]^+$. To further probe this aspect experimentally, we studied the reaction of bare platinum cations with methylamine.[17] Here, single (10%) and double (10%) dehydrogenation are observed, giving $[Pt,C,N,H_3]^+$ and $[Pt,C,N,H]^+$, respectively, along with predominating hydride transfer to yield $CH_2NH_2^+$ and neutral [PtH] (80%).

In perfect analogy to the $Pt^+/CH_4/NH_3$ system, only D_2, D_2 + HD, and [PtD] are lost as neutral fragments when CD_3NH_2 is used as a neutral reagent. Apparently the fact that the entrance energy of the reactants is somewhat higher for the Pt^+/CH_3NH_2 couple ($\Sigma\Delta H^\circ = 328$ kcal mol^{-1})[2] than for the $[PtCH_2]^+/NH_3$ system ($\Sigma\Delta H^\circ = 303$ kcal mol^{-1})[2, 9b, 18] is sufficient to surmount the barriers associated with double

 © WILEY-VCH Verlag GmbH, D-69451 Weinheim, 1998 1433-7851/98/3706-0830 $ 17.50+.50/0 *Angew. Chem. Int. Ed.* **1998**, *37*, No. 6

dehydrogenation to afford $[Pt,C,N,H]^+$. Further, the formation of $[Pt,C,N,H]^+$ rather than $[Pt,C,N,D]^+$ from Pt^+/CD_3NH_2 implies an intermediate complex with isonitrile coordination. Combination of reactions (2) and (6b) with a dehydrogenation and a desorption step suggests an additional route for the formation of hydrogen cyanide (Sequence 2).

Sequence 2

$$Pt^+ + CH_4 \rightarrow [PtCH_2]^+ + H_2 \quad (8a)$$

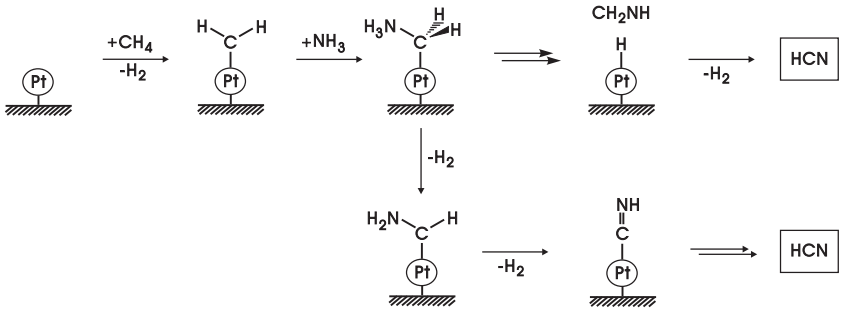
$$[PtCH_2]^+ + NH_3 \rightarrow [Pt,C,N,H_3]^+ + H_2 \quad (8b)$$

$$[Pt,C,N,H_3]^+ \rightarrow [Pt,C,N,H]^+ + H_2 \quad (8c)$$

$$[Pt,C,N,H]^+ \rightarrow Pt^+ + HCN \quad (8d)$$

$$CH_4 + NH_3 \rightarrow HCN + 3\ H_2 \quad (1)$$

Finally, let us extrapolate these results towards a working model for the heterogeneous catalysis of the methane/ammonia coupling according to reaction (1). In the first step an active platinum center brings about the dehydrogenation of methane to yield a surface-bound carbene intermediate (Scheme 2).[19] Next, ammonia approaches the carbon center



Scheme 2. Proposed mechanism for the platinum-catalyzed methane/ammonia coupling. Note that the isomerization HNC → HCN in the lower route may be facilitated by acid–base catalysis.

with subsequent C–N bond formation. This can either lead to gaseous formimine, which is then dehydrogenated to give HCN in the gas phase, or to a surface-bound aminocarbene, which may decompose to yield HCN at elevated temperatures. Thus, we suggest two independent routes for the formation of hydrogen cyanide, one of which occurs entirely on the surface and the other is terminated in the gas phase. Common to both pathways is the initial activation of methane at platinum. The possible existence of two parallel pathways for the formation of HCN may result in rather complex dependencies of the product yields on pressure and temperature. Currently, we are further exploring the reaction mechanism and the effect of oxygen as an additional reactant on the elementary steps, and we are attempting to design a catalytic routine for the gas-phase process under FTICR conditions.[9, 20]

Received: November 3, 1997 [Z11117IE]
German version: *Angew. Chem.* **1998**, *110*, 858–861

Keywords: ammonia · gas-phase chemistry · hydrogen cyanide · methane · platinum

[1] a) R. H. Crabtree, *Chem. Rev.* **1995**, *95*, 987; b) J. H. Lunsford, *Angew. Chem.* **1995**, *107*, 1059; *Angew. Chem. Int. Ed. Engl.* **1995**, *34*, 970.

[2] S. G. Lias, J. E. Bartmess, J. F. Liebman, J. L. Holmes, R. D. Levin, W. G. Mallard, *J. Phys. Chem. Ref. Data* **1988**, *17*, Suppl. 1. Part of the compilation is available on Internet under http://webbook.nist.gov/chemistry.

[3] a) D. Hasenberg, L. D. Schmidt, *J. Catal.* **1987**, *104*, 441, and references therein; b) N. Waletzko, L. D. Schmidt, *AIChE J.* **1988**, *34*, 1146; c) A. Bockholt, I. S. Harding, R. M. Nix, *J. Chem. Soc. Faraday Trans.* **1997**, *93*, 3869; d) D. Hasenberg, L. D. Schmidt, *J. Catal.* **1985**, *91*, 116.

[4] *Chemistry of the Platinum Group Metals* (Ed.: F. R. Hartley), Elsevier, Amsterdam, **1991**.

[5] The experiments were performed with a Spectrospin CMS 47X FTICR mass spectrometer, which has been described previously.[6] In brief, Pt^+ ions were generated by laser ionization of a platinum target in the external ion source and transferred to the analyzer cell, which was located within a superconducting magnet (7.05 T). Prior to the ion/molecule reactions the $^{195}Pt^+$ isotope was mass-selected by double-resonance techniques and thermalized with pulsed-in argon buffer gas. The reactions were studied at room temperature. Then, Pt^+ was reacted with ammonia, which was leaked in at pressures between 0.5 and 10×10^{-8} mbar. In the same manner, $[PtCH_2]^+$ was produced from Pt^+ and pulsed-in methane, mass-selected, and reacted with NH_3; similarly, the reactivity of subsequent product ions was examined. A complete analysis of the kinetic and thermochemical data including the secondary reactions as well as additional experiments will be published elsewhere.

[6] a) K. Eller, H. Schwarz, *Int. J. Mass Spectrom. Ion Processes* **1989**, *93*, 243; b) K. Eller, W. Zummack, H. Schwarz, *J. Am. Chem. Soc.* **1990**, *112*, 621.

[7] For a related study on the gas-phase coupling of CH_4 and CO_2 by Ta^+ cations, see: R. Wesendrup, H. Schwarz, *Angew. Chem.* **1995**, *107*, 2176; *Angew. Chem. Int. Ed. Engl.* **1995**, *34*, 2033.

[8] a) K. K. Irikura, J. L. Beauchamp, *J. Am. Chem. Soc.* **1991**, *113*, 2769; b) K. K. Irikura, J. L. Beauchamp, *J. Phys. Chem.* **1991**, *95*, 8344.

[9] a) R. Wesendrup, D. Schröder, H. Schwarz, *Angew. Chem.* **1994**, *106*, 1232; *Angew. Chem. Int. Ed. Engl.* **1994**, *33*, 1174; b) C. Heinemann, R. Wesendrup, H. Schwarz, *Chem. Phys. Lett.* **1995**, *239*, 75; c) M. Pavlov, M. R. A. Blomberg, P. E. M. Siegbahn, R. Wesendrup, C. Heinemann, H. Schwarz, *J. Phys. Chem. A* **1997**, *101*, 1567.

[10] The $Pt^+/CH_4/NH_3$ potential energy surface was characterized en gros at the B3LYP level. Nonmetallic atoms were calculated with a 6-31 + G* basis set, whereas a LANL2DZ basis set was used for platinum. The 60 platinum core electrons were treated with the corresponding LANL2DZ pseudopotential.[11] Full geometry optimization was performed at this level to yield geometries verified by frequency calculations and zero-point energy corrections. These geometries were then used to evaluate the energy based on B3LYP single-point calculations with the larger 6-311 + G** basis sets, and an extended valence basis set for platinum.[9c] Details of these and further computations, including transition structures, will be published elsewhere.

[11] M. J. Frisch, G. W. Trucks, H. B. Schlegel, P. M. W. Gill, B. G. Johnson, M. A. Robb, J. R. Cheeseman, T. Keith, G. A. Petersson, J. A. Montgomery, K. Raghavachari, M. A. Al-Laham, V. G. Zakrzewski, J. V. Ortiz, J. B. Foresman, C. Y. Peng, P. Y. Ayala, W. Chen, M. W. Wong, J. L. Andres, E. S. Replogle, R. Gomperts, R. L. Martin, D. J. Fox, J. S. Binkley, D. J. Defrees, J. Baker, J. P. Stewart, M. Head-Gordon, C. Gonzalez, J. A. Pople, Gaussian 94, Revision E.1, Gaussian, Inc., Pittsburgh, PA (USA), **1995**.

[12] At the B3LYP level of theory, the barrier associated with the unimolecular dehydrogenation of CH_2NH to yield HCN is substantial (93 kcal mol^{-1}), but is likely to be lowered significantly by bimolecular acid–base reactions which exhibit low barriers. Reaction (9) is such a base-catalyzed process.

 © WILEY-VCH Verlag GmbH, D-69451 Weinheim, 1998 1433-7851/98/3706-0831 $ 17.50+.50/0

$CH_2NH + NH_2^- \rightarrow CH_2N^- + NH_3$ (9a)
($\Delta H = 15$ kcal mol^{-1})
$CH_2N^- + NH_3 \rightarrow HCN + H_2 + NH_2$ (9b)
($\Delta H = -15$ kcal mol^{-1})
An acid-catalyzed sequence like that in reaction (10) is also conceivable.
$CH_2NH + NH_4^+ \rightarrow HCNH^+ + H_2 + NH_3$ (10a)
($\Delta H = 32$ kcal mol^{-1})
$HCNH^+ + NH_3 \rightarrow HCN + NH_4^+$ (10b)
($\Delta H = -32$ kcal mol^{-1})
($\Delta H = +32$ kcal mol^{-1})
$HCNH^+ + NH_3 \rightarrow HCN + NH_4^+$ (10b)
($\Delta H = -32$ cal mol^{-1})

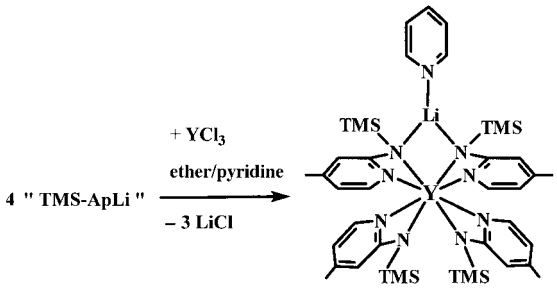
[13] Product distribution for $[PtCD_2]^+ + NH_3$: $[Pt,C,N,H_2,D]^+ + HD$ (20%), $CD_2NH_2^+ + PtH$ (70%), $NH_3D^+ + [PtCD]$ (10%).
[14] a) A. J. Arduengo III, R. L. Harlow, M. Kline, *J. Am. Chem. Soc.* **1991**, *113*, 361; b) A. J. Arduengo III, H. V. Rasika Dias, R. L. Harlow, M. Kline, *ibid.* **1992**, *114*, 5530; c) W. A. Herrmann, C. Köcher, *Angew. Chem.*, **1997**, 109, 2257, *Angew. Chem. Int. Ed. Engl.* **1997**, *36*, 2162.
[15] C. Heinemann, T. Müller, Y. Apeloig, H. Schwarz, *J. Am. Chem. Soc.* **1996**, *118*, 2023, and references therein.
[16] For a recent observation of C=NH$_2$ species on Pt(111) formed in the reaction of cyanogen and dihydrogen, see: P. Millis, D. Jentz, M. Trenary, *J. Am. Chem. Soc.* **1997**, *119*, 9002.
[17] For the heterogeneous catalysis of methylamine decomposition see: a) S. Y. Hwang, L. D. Schmidt, *J. Catal.* **1988**, *114*, 230; b) S. Y. Hwang, A. C. F. Kong, L. D. Schmidt, J. *Phys. Chem*. **1989**, *93*, 8327
[18] a) K. K. Irikura, W. A. Goddard, III, *J. Am. Chem. Soc.* **1994**, *116*, 8733; b) C. Heinemann, H. Schwarz, W. Koch, K. Dyall, *J. Chem. Phys.* **1996**, *104*, 4642.
[19] It should be noted that methane is also activated by neutral platinum atoms, by platinum clusters, and by bulk platinum: a) J. J. Carroll, J. C. Weisshaar, P. E. M. Siegbahn, C. A. M. Wittborn, M. R. A. Blomberg, *J. Phys. Chem.* **1995**, *99*, 14388; b) D. J. Trevor, D. M. Cox, A. Kaldor, *J. Am. Chem. Soc.* **1990**, *112*, 3742; c) M. Valden, N. Xiang, J. Pere, M. Pessa, *Appl. Surf. Sci.* **1996** , *99*, 83.
[20] For other examples of catalytic processes under FTICR conditions, see: a) M. M. Kappes, R. H. Staley, *J. Am. Chem. Soc.* **1981**, *103*, 1286; b) S. W. Buckner, B. S. Freiser, *ibid.* **1988**, *110*, 6606; c) K. K. Irikura, J. L. Beauchamp, *ibid.* **1989**, *111*, 75; d) D. Schröder, H. Schwarz, *Angew. Chem.* **1990**, *102*, 1468; *Angew. Chem. Int. Ed. Engl.* **1990**, *29*, 1433; e) P. Schnabel, M. P. Irion, K. G. Weil, *J. Phys. Chem.* **1991**, *95*, 9688; f) D. Schröder, A. Fiedler, M. F. Ryan, H. Schwarz, *ibid.* **1994**, *98*, 68; g) M. F. Ryan, D. Stöckigt, H. Schwarz, *J. Am. Chem. Soc.* **1994**, *116*, 9565; h) D. Stöckigt, H. Schwarz, *Lieb. Ann. Chem.* **1995**, 429.

Yttrate-Mediated Ligand Transfer and Direct Synthesis as a Route to Amidopalladium Complexes**

Anke Spannenberg, Perdita Arndt, and Rhett Kempe*

In the wide range of applications of palladium compounds,[1] amidometal complexes[2] have played only a secondary role to date.[3] Only a few examples of this reactive class of compounds have been reported.[3, 4] This could be due to difficulties in the synthesis or to the instability of these compounds which arise from the "unfortunate" combination of a soft metal with the hard amido ligand.[5] The development of new synthetic routes could help solve this problem. We report here on an yttrate-mediated ligand transfer as well as the direct synthesis as efficient routes to amido complexes of late transition metals.

The in situ reaction of lithiated 4-methyl-2-(trimethylsilylamino)pyridine (TMS-ApH) with dry YCl_3 in ether in the presence of pyridine gave the colorless yttrate complex **1** in good yields [Eq. (a)].



(a)

1

Aminopyridinato complexes of the early transition metals are rare,[6] and compounds with Group 3 metals, as well as the corresponding lanthanide complexes, have not yet been reported. The two sets of signals observed for the aminopyridinato ligands in the ^{1}H NMR spectrum of **1** (see Table 1) is explained by coordination to lithium. This was confirmed by X-ray structural analysis[7] (Figure 1). The lithium atom is sterically shielded and has trigonal planar coordination (sum of the angles 360°).[8] Because of the bridging function of the amido nitrogen atom, the $Y-N_{pyridine}$ bond in the Li-coordinated TMS-Ap ligands is significantly shorter than the $Y-N_{amido}$ bond. The yttrium–nitrogen bond lengths of the other two aminopyridinato ligands are equally long and indicate a delocalized bonding mode.[9] In the reaction of **1** with $ZrCl_4$ the complexed lithium is displaced by a $ZrCl_3$ unit to form the extremely unstable Y-Zr heterobimetallic complex **2**, which is also colorless [Eq. (b)]. Complex **2** acts as an intermediate in

[*] Dr. R. Kempe, Dr. A. Spannenberg, Dr. P. Arndt
Abt. Komplexkatalyse, IfOK an der Universität Rostock
Buchbinderstrasse 5–6, D-18055 Rostock (Germany)
Fax: (+49) 381-466-9374
E-mail: rkempe@chemie1.uni-rostock.de

[**] This work was supported by the Max-Planck-Gesellschaft and by the Fonds der Chemischen Industrie. We thank Prof. Rosenthal for his support.

 © WILEY-VCH Verlag GmbH, D-69451 Weinheim, 1998 1433-7851/98/3706-0832 $ 17.50+.50/0

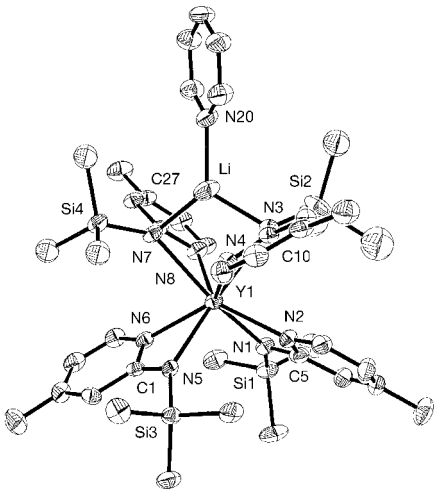
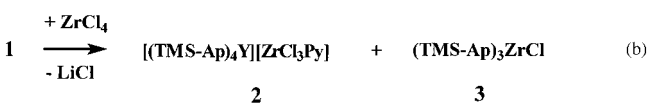
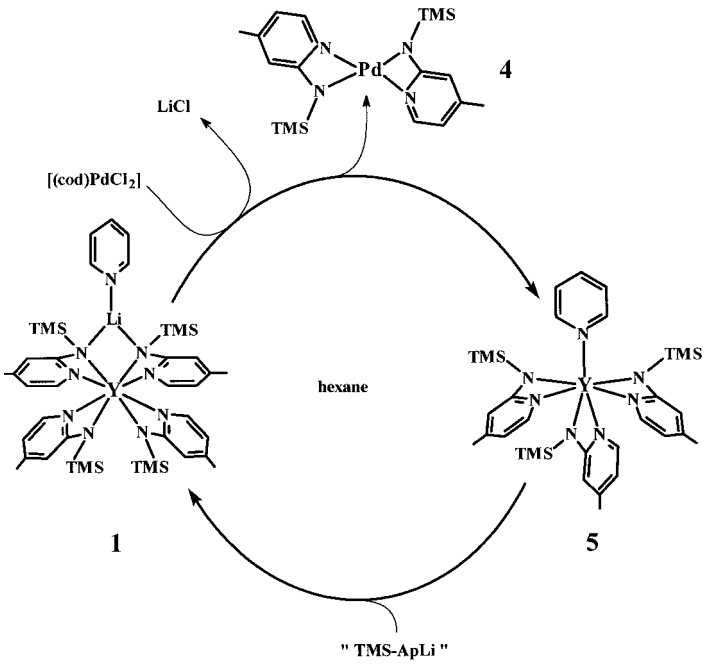


Figure 1. Crystal structure of **1** (thermal ellipsoids at the 30% probability level). Selected bond lengths [Å] and angles [°]: N1–Y 2.448(5), N2–Y 2.448(5), N3–Li 2.057(14), N3–Y 2.620(6), N4–Y 2.572(6), N5–Y 2.442(5), N6–Y 2.497(6), N7–Li 2.03(2), N7–Y 2.569(5), N8–Y 2.508(6), N20–Li 2.01(2); N1-Y-N2 56.3(2), N5-Y-N6 55.9(2), N8-Y-N7 54.5(2), N4-Y-N3 52.9(2), N20-Li-N7 129.0(7), N20-Li-N3 119.7(8), N7-Li-N3 111.1(7).

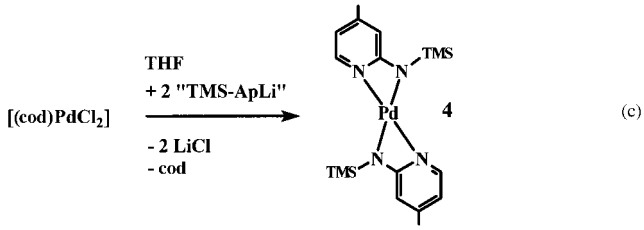


the transfer of ligands from yttrium to zirconium to produce $[(TMS\text{-}Ap)_3ZrCl]$ (**3**) as a side or decomposition product. An analogous ligand-transfer reaction also allows access to palladium complexes: the treatment of **1** with $[(cod)PdCl_2]$ in hexane (Scheme 1, top half) gave $[(TMS\text{-}Ap)_2Pd]$ (**4**) and $[(TMS\text{-}Ap)_3YPy]$ (**5**). This reaction seems laborious in comparison to a direct synthesis [Eq. (c)]; however, it can



Scheme 1. Yttrate-mediated synthesis of $[(TMS\text{-}Ap)_2Pd]$ (**4**).

be made more efficient, because compound **5**, in the presence of "TMS-ApLi", reacts to give **1** (Scheme 1, bottom half).[10] The latter can be explained by the coordinative unsaturation



of **5**.[11] Complex **1** can now participate in a further ligand-transfer reaction so that a cyclic reaction is possible. In order to test this premise, **1** was treated with an equimolar amount of $[(cod)PdCl_2]$ in hexane at temperatures below 0 °C, after 12 hours one equivalent of "TMS-ApLi" was added, and after a further 12 hours one equivalent of $[(cod)PdCl_2]$ was added. The last two steps were each repeated twice to give 1.25 equivalents of **4** after work-up. This corresponds to a turnover number (TON) of 2.5 with regard to the ligand transfer reaction. The sequential addition of the starting materials and excess $[(cod)PdCl_2]$ are essential in order to produce **4** catalytically. We explain this prerequisite by assuming that the reduction of $[(cod)PdCl_2]$ in the presence of "TMS-ApLi", which takes place even at low temperatures in hexane, can thus be suppressed. A control experiment, without **1** as the catalyst, produced no **4**; the treatment of "TMS-ApLi" and $[(cod)PdCl_2]$ in hexane at low temperatures (−78 to 0 °C) gave only the starting materials along with colloidal palladium after work-up, and mainly colloidal palladium was obtained at temperatures above 10 °C. In THF **4** can be obtained in 48% yield at a temperature of −30 °C by direct synthesis [Eq. (c)].[12]

Complex **4** is an orange, crystalline compound that exhibits a ^1H NMR spectrum with one simple set of signals, typical of TMS-Ap ligands (Table 1). The molecular structure, obtained by X-ray structural analysis[7] (Figure 2), shows two transoid-coordinated aminopyridinato ligands and a planar coordination geometry at the palladium center. The two, drastically different N-Pd-N angles [114.55(9)° and 65.45(9)°] confirm

Table 1. Selected analytical data of **1**, **2**, **4**, and **5**.

1: $C_{41}H_{65}LiN_9Si_4Y \cdot 0.5\,C_4H_{10}O$ (929.28): calcd C 55.58, H 7.59, N 13.57; found C 55.53, H 7.58, N 13.42; ^1H NMR ([D$_8$]toluene, 298 K): $\delta = 8.19$ (d, 2H, *o*-H, Py), 7.65 (br, 2H, Ap), 6.79 (t, 1H, *p*-H, Py), 6.46 (m, 2H, *m*-H, Py), 6.3–6.5 (br, 5H, Ap), 1.8 (br, 12H, Me), 0.06 (br, 36H, $SiMe_3$, Ap).

2: $C_{41}H_{65}Cl_3N_9Si_4YZr$ (1082.85): calcd C 45.48, H 6.05, N 11.64, Zr 8.42; found C 45.52, H 6.07, N 11.51, Zr 9.07. Since compound **2** does not dissolve without decomposition, an unambiguous characterization by NMR spectroscopy was not possible.

4: $C_{18}H_{30}N_4PdSi_2$ (465.05): calcd C 46.49, H 6.50, N 12.05; found C 46.78, H 6.56, N 12.09; ^1H NMR (C_6D_6, 303 K): (δ) = 7.50 (d, $J = 5.6$ Hz, 1H, H-6, Ap), 5.75 (s, 1H, H-3, Ap), 5.57 (d, $J = 5.6$ Hz, 1H, H-5, Ap), 1.72 (s, 3H, Me), 0.32 (s, 9H, $SiMe_3$).

5: $C_{32}H_{50}N_7Si_3Y$ (705.96): calcd C 54.44, H 7.14, N 13.89; found C 54.92, H 7.15, N 13.31; ^1H NMR (C_6D_6, 303 K): $\delta = 8.75$ (d, $J = 4.5$ Hz, 2H, *o*-H, Py), 7.74 (s, 3H, Ap), 6.82 (m, 1H, *p*-H, Py), 6.52 (m, 2H, *m*-H, Py), 6.35 (s, 3H, Ap), 5.98 (d, $J = 1.2$ Hz, 3H, Ap), 1.82 (s, 9H, Me), 0.28 (s, 27H, $SiMe_3$).

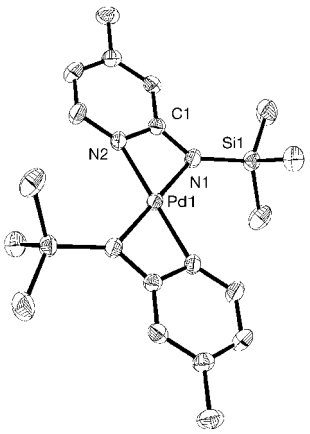


Figure 2. Crystal structure of **4** (thermal ellipsoids at the 30% probability level). Selected bond lengths [Å] and angles [°]: N1 – Pd 2.054(2), N2 – Pd 2.017(3); N2′-Pd-N1 114.55(9), N2-Pd-N1 65.45(9). Labeled and corresponding nonlabeled atoms are related by the following symmetry operators: $-x, -y, -z$.

the severe strain in the complex. The $Pd-N_{pyridine}$ bond length (2.017(3) Å) is shorter than that of $Pd-N_{amido}$ (2.054(2) Å), which verifies the delocalized bonding mode. Complex **5** is a colorless crystalline compound and its elemental analysis agrees with the composition of the structure depicted in Scheme 1. The ^{1}H NMR spectrum shows, along with the resonances of coordinated pyridine, a single simple set of signals typical of aminopyridinato ligands in trisaminopyridinato complexes[6b,f] (Table 1). Scheme 1 presents the probable mechanism of the yttrate-catalyzed ligand-transfer reaction. We also assume, in analogy to the reaction of compound **1** with $ZrCl_4$, that an intermediate Y-Pd complex is unstable and could not be isolated.

Currently we are investigating whether the yttrate-mediated transfer is the best method for the synthesis of amido complexes of the later transition metals in those cases in which the direct synthesis failed. Furthermore, we are trying to discover how the ligand-transfer reaction can be deliberately suppressed in order to obtain stable, heterodinuclear complexes.

Experimental Section

All work was performed under the exclusion of oxygen and moisture in an argon atmosphere.

1: A solution of 4-methyl-2-(trimethylsilylamino)pyridine[6a] (2.86 mL, 13.44 mmol) in ether (40 mL) at $-40\,^\circ$C was slowly treated with a solution of *n*BuLi in hexane (2.5 M, 5.4 mL, 13.44 mmol) and then stirred at room temperature for 2 h. The resulting "TMS-ApLi" solution was added to a suspension of YCl_3 (656 mg, 3.36 mmol) in ether (20 mL) containing pyridine (407 µL, 5.04 mmol). Since **1** is sensitive to light, the reaction must take place in the dark. After stirring for 48 h at room temperature, the reaction mixture was filtered, the solvent removed in vacuo, and the residue taken up in ether/hexane. Crystallization at $-30\,^\circ$C gave a colorless crystalline solid (1.92 g, 64%). M.p.: 109 °C.

2: A suspension of $ZrCl_4$ (141 mg, 0.6 mmol) in ether (5 mL) was treated with a solution of **1** (540 mg, 0.6 mmol) in ether (10 mL). The solution turned yellowish very quickly. It was filtered, the residue washed, and the volume of the filtrate greatly reduced in vacuo. The addition of hexane precipitated compound **2** (400 mg, 61%) as a white powder. M.p. (decomp.): 178 °C. [(TMS-Ap)$_3$ZrCl] **3** (30 mg, 22%) crystallized from the mother liquor (hexane/ether). M.p.: 268 °C.

Synthesis of **4** by yttrate-mediated ligand transfer: A solution of **1** (892 mg, 1 mmol) in hexane (10 mL) at 0 °C was added to a suspension of [(cod)$PdCl_2$] (285 mg, 1 mmol) in hexane (10 mL). The reaction mixture was kept in the dark between 0 and $-78\,^\circ$C until work-up. The reaction solution was stirred for 12 h and then treated with "TMS-ApLi" (1 mmol, prepared as described for **1**) and after a further 12 h further [(cod)$PdCl_2$] (285 mg, 1 mmol) was added. The last two steps were both repeated twice. After stirring for a further 12 h the LiCl formed was filtered off, the residue extracted three times with hexane, and the filtrate concentrated. Crystallization at $-30\,^\circ$C afforded orange needles of **4** (580 mg, 1.25 mmol).

Direct synthesis of **4**: A solution of "TMS-ApLi" (prepared as described for **1** from TMS-ApH (425 µL, 2 mmol), *n*BuLi (0.8 mL) in hexane (2.5 M, 2 mmol), and THF (20 mL)) was added at $-30\,^\circ$C to [(cod)$PdCl_2$] (286 mg, 1 mmol) in THF (20 mL). After 12 h at $-30\,^\circ$C, the solvent was removed in vacuo and the residue washed several times with hexane. LiCl was filtered off, and the combined filtrates concentrated in vacuo. Crystallization at $-30\,^\circ$C afforded **4** (226 mg, 48%).

Received: 8. September, 1997
Revised version: 20. November,1997 [Z10901IE]
German version: *Angew. Chem.* **1998**, *110*, 824 – 827

Keywords: amido complexes · N ligands · palladium · synthetic methods · yttrium

[1] J. Tsuji, *Palladium Reagents and Catalysts, Innovations in Organic Synthesis*, Wiley, Chichester, **1996**.

[2] Amidometal complexes correspond to the definition in M. F. Lappert, P. P. Power, A. R. Sanger, R. C. Srivastava, *Metal and Metalloid Amides*; Ellis Norwood Ltd., Chichester, **1980.**

[3] Amido complexes have been identified as important intermediates in palladium-catalyzed arylaminations: J. F. Hartwig, *Synlett* **1997**, 329 – 340.

[4] a) M. D. Fryzuk, C. D. Montgomery, *Coord. Chem. Rev.* **1989**, *95*, 1 – 40; b) J. V. Cuevas, G. Garcia-Herbosa, A. Muñoz, S. Garcia-Granda, D. Miguel, *Organometallics* **1997**, *16*, 2220 – 2222; c) M. S. Driver, J. F. Hartwig, *J. Am. Chem. Soc.* **1996**, *118*, 4206 – 4207; d) *ibid.* **1995**, *117*, 4708 – 4709; e) L. A. Villanueva, K. A. Abboud, J. M. Boncella, *Organometallics* **1994**, *13*, 3921 – 3931; f) J. M. Boncella, L. A. Villanueva, *J. Organomet. Chem.* **1994**, *465*, 297 – 304; g) J. Ruiz, M. T. Martinez, C. Vincente, G. Garcia, G. López, P. A. Chaloner, P. B. Hitchcock, *Organometallics* **1993**, *12*, 4321 – 4326; h) P. Espinet, M. Y. Alonso, G. Garcia-Herbosa, J. M. Ramos, Y. Jeannin, M. Philoche-Levisalles, *Inorg. Chem.* **1992**, *31*, 2501 – 2507; i) A. L. Seligson, R. L. Cowan, W. C. Trogler, *ibid.* **1991**, *30*, 3371 – 3381.

[5] a) R. G. Pearson, *J. Am. Chem. Soc.* **1963**, *85*, 3533 – 3539; b) *J. Chem. Educ.* **1968**, *45*, 581 – 586; c) *ibid.* **1968**, *45*, 643 – 654.

[6] Compounds of Group 4 elements: a) R. Kempe, P. Arndt, *Inorg. Chem.* **1996**, *35*, 2644 – 2649; b) R. Kempe, S. Brenner, P. Arndt, *Organometallics* **1996**, *15*, 1071 – 1074; c) M. Oberthür, P. Arndt, R. Kempe, *Chem. Ber.* **1996**, *129*, 1087 – 1091; d) H. Fuhrmann, S. Brenner, P. Arndt, R. Kempe, *Inorg. Chem.* **1996**, *35*, 6742 – 6745; e) A. Spannenberg, P. Arndt, M. Oberthür, R. Kempe, *Z. anorg. allg. Chem.* **1997**, *623*, 389 – 393; f) M. Oberthür, G. Hillebrand, P. Arndt, R. Kempe, *Chem. Ber./Recueil* **1997**, *130*, 789 – 794. Compounds of Group 5 elements: g) J. J. H. Edema, S. Gambarotta, A. Meetsma, A. L. Spek, N. Veldman, *Inorg. Chem.* **1991**, *30*, 2062 – 2066; h) M. Polamo, M. Leskelä, *Acta Chem. Scand.* **1997**, *51*, 449 – 454; i) *J. Chem. Soc. Dalton Trans.* **1996**, 4345 – 4349.

[7] X-ray structural analyses of **1** and **4**: STOE-IPDS diffractometer, graphite monochromatized $Mo_{K\alpha}$ radiation, $\lambda = 0.71069$ Å, structure solved by direct methods (SHELXS-86: G. M. Sheldrick, *Acta Crystallogr. Sect. A* **1990**, *46*, 467.), and refined with the full-matrix least-squares method against F^2 (SHELXL-93: G. M. Sheldrick, still unpublished), structural representation: XP (Siemens), compound **1**: $0.7 \times 0.4 \times 0.3$ mm, colorless prisms, space group $P2_1/n$, monoclinic, $a = 12.195(2)$, $b = 22.055(3)$, $c = 22.071(3)$ Å, $\beta = 97.60(2)^\circ$, $V = 5884(2)$ Å^3, $Z = 4$, $\rho_{calcd} = 1.104$ g cm^{-3}, 16848 measured, 8683 were independent of symmetry, of which 3876 were observed ($I \geq 2\sigma(I)$), $R = 0.066$, wR^2 (all data) = 0.176, 499 parameters. Compound **4**: $0.3 \times 0.15 \times 0.15$ mm, orange prisms, space group $P2_1/c$, monoclinic, $a = 7.773(11)$, $b = 11.644(2)$, $c = 12.372(2)$ Å, $\beta = 91.360(11)^\circ$, $V = 1119.5(3)$ Å^3, $Z = 2$, $\rho_{calcd} = 1.380$ g cm^{-3}, 3289 measured reflections, 1714 were independent of symmetry, of which 1366 were observed ($I \geq 2\sigma(I)$), $R = 0.026$, wR^2 (all data) = 0.066, 175 parameters. Crys-

 © WILEY-VCH Verlag GmbH, D-69451 Weinheim, 1998 1433-7851/98/3706-0834 $ 17.50+.50/0

tallographic data (excluding structure factors) for the structures reported in this paper have been deposited with the Cambridge Crystallographic Data Centre as supplementary publication no. CCDC-179-100685. Copies of the data can be obtained free of charge on application to CCDC, 12 Union Road, Cambridge CB2 1EZ, UK (fax: (+44) 1223-336-033; e-mail: deposit@ccdc.cam.ac.uk).

[8] Examples of trigonally coordinated Li: a) M. F. Lappert, M. J. Slade, A. Singh, J. L. Atwood, R. D. Rogers, R. Shakir, *J. Am. Chem. Soc.* **1983**, *105*, 302–304; b) L. M. Engelhardt, B. S. Jolly, P. C. Punk, C. L. Raston, B. W. Skeleton, A. H. White, *Aust. J. Chem.* **1986**, *39*, 133; c) P. G. Willard, M. A. Nichols, *J. Am. Chem. Soc.* **1991**, *113*, 9671–9673; d) H. Görls, B. Neumüller, A. Scholz, J. Scholz, *Angew. Chem.* **1995**, *107*, 732–735; *Angew. Chem. Int. Ed. Engl.* **1995**, *34*, 673–676.

[9] The negative charge of the aminopyridinato ligand is not localized on the amido nitrogen atom.

[10] Compound **5** is not accessible by transmetalation with YCl_3 and three equivalents "TMS-ApLi" (ether/pyridine); this procedure affords compound **1** instead.

[11] The "ate" complexes are very often observed for lanthanide ions: a) H. Schumann, *Angew. Chem.* **1984**, *96*, 475–493; *Angew. Chem. Int. Ed. Engl.* **1984**, *23*, 474–492; b) R. D. Köhn, G. Kociok-Köhn, H. Schumann in *Encyclopedia of Inorganic Chemistry* (Ed.: R. B. King), Wiley, New York, **1994**; c) C. J. Schaverien, *Adv. Organomet. Chem.* **1994**, *36*, 283–362; d) F. T. Edelmann in *Comprehensive Organometallic Chemistry II* (Eds.: E. W. Abel, F. G. A. Stone, G. Wilkinson), Pergamon, Oxford **1995**; e) H. Schumann, J. A. Meerse-Marktscheffel, L. Esser, *Chem. Rev.* **1995**, *95*, 865–986.

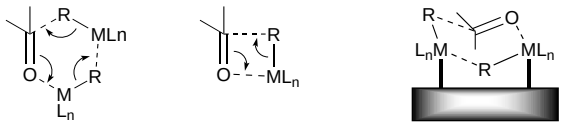
[12] Sincere thanks are due to the referee who provided this information.

Rate Acceleration in Nucleophilic Alkylation of Carbonyl Compounds with a New Template Containing Two Metallic Centers**

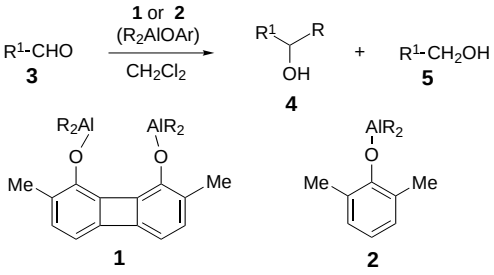
Takashi Ooi, Makoto Takahashi, and Keiji Maruoka*

The nucleophilic addition of reactive organometallic reagents to carbonyl compounds is undoubtedly one of the most thoroughly investigated of all organic transformations because of sustained interest in its mechanism and selectivity, as well as numerous applications to a variety of syntheses in the fields of natural products, pharmacology, and material science.[1]

The preferred transition state for addition of Grignard and organoaluminum reagents is often a cyclic six-membered array (**A**) that contains a carbonyl group and two molecules of organometallic reagent.[2] With the same reactants in a 1:1 ratio, a four-centered transition state (**B**) is also conceivable, although alkylation proceeds more slowly by this route. Hence, facilitation of the six-membered transition state **A** is



crucial in order to achieve high reactivity, particularly in the case of less reactive organometallic reagents. In this context, we became interested in designing new molecules of type **C** with two metallic centers that would permit simple alkylation of carbonyl compounds with otherwise less reactive alkylmetal species.[3] Here we report initial results with the modified bis(dialkylaluminum) reagent **1**, an efficient alkyl-transfer system for aldehydes (Scheme 1).[4]



Scheme 1. Alkylation of aldehydes with dialkylaluminum reagents.

Treatment of benzaldehyde (**3**; $R^1 = Ph$) with one equivalent of Me_3Al in CH_2Cl_2 at $-78\,^\circ C$ gave a long-lived monomeric 1:1 complex that gradually decomposed to 1-phenylethanol (**4**; $R^1 = Ph$, $R = Me$) on warming to $-20\,^\circ C$.[5] Use of (2,6-dimethoxyphenyloxy)dimethylaluminum (**2**, $R_2 = Me$) instead of Me_3Al significantly retarded the rate of alkylation under similar reaction conditions. Even use of excess **2** (2 equiv) failed to yield methylation product **4** at $-20\,^\circ C$. In marked contrast, however, methylation of benzaldehyde proceeded quite smoothly with one equivalent of 2,7-dimethyl-1,8-biphenylenedioxybis(dimethylaluminum) (**1**; $R = Me$) at $-20\,^\circ C$ to furnish after 4 h 1-phenylethanol (**4**; $R^1 = Ph$, $R = Me$) in 84% yield.[6] With higher alkyl derivatives of **1** ($R = Et$, Hex), alkylation was accompanied by concomitant formation of reduction product **5**, and different aldehydes gave equally good results (Table 1).

Table 1. Alkylation of aldehyde **3** with dialkylaluminum reagents.[a]

Entry	R^1	R	Reaction conditions [°C, h][a]	Yield of **4** and **5** [%][b] Use of **1**	Use of **2**
1	Ph	Me	−20,4	84	0
2	Ph	Et	−78,1; −40,2	71 (11)	10 (2)
3	Ph	Hex	−78,1; −40,1.5	60 (36)	6 (5)
4	*c*Hex	Me	−78,1; −40,3; −20,3	63	4[c]
5	*c*Hex	Et	−78,2; −40,3	52 (22)	10 (9)
6	*c*Hex	Et	−78,2; −40,3[d]	50 (20)	3 (2)
7	C_9H_{19}	Me	−20,4.5	86	< 1

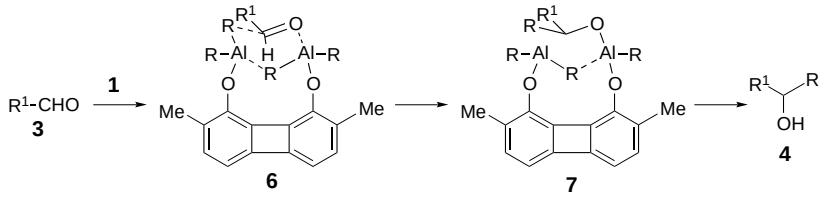
[a] Alkylation was carried out under the reaction conditions cited with **1** (1 equiv) or **2** (2 equiv) in CH_2Cl_2. [b] Yield of **5** in parentheses. [c] Aldol product through self-condensation. [d] Use of dilute CH_2Cl_2 solution.[7]

[*] Prof. K. Maruoka, M. Takahashi, Dr. T. Ooi
Department of Chemistry, Graduate School of Science
Hokkaido University
Sapporo, 060 (Japan)
Fax: (+81) 11-746-2557
E-mail: maruoka@sci.hokudai.ac.jp

[**] This work was partially supported by the Asahi Glass Foundation, the Akiyama Foundation, the Suhara Memorial Foundation, and a Grant-in-Aid for Scientific Research from the Japanese Ministry of Education, Science, Sports, and Culture.

 © WILEY-VCH Verlag GmbH, D-69451 Weinheim, 1998 1433-7851/98/3706-0835 $ 17.50+.50/0

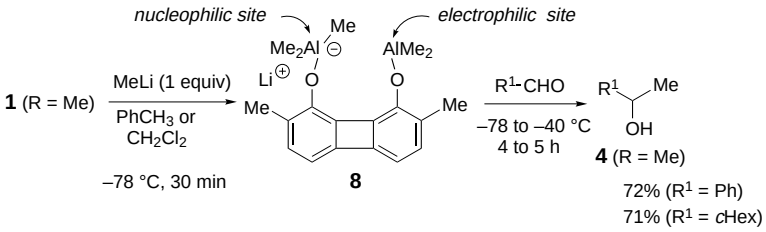
The observed rate acceleration is readily understandable in terms of the mechanism outlined in Scheme 2. Upon reaction of **1** with aldehyde **3**, the 1:1 coordination complex **6** is initially



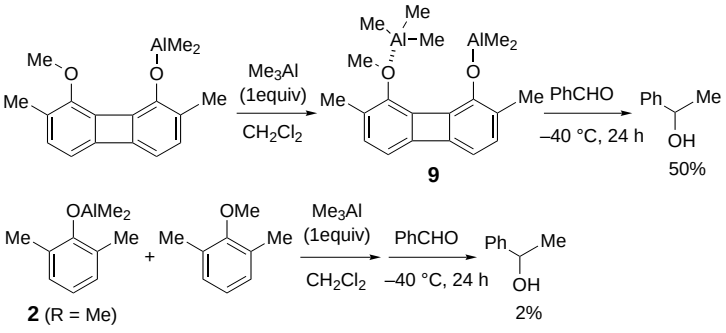
Scheme 2. Plausible mechanism for rapid alkylation of aldehydes with **1**.

formed, which is easily transformed by way of a cyclic six-membered transition state into alkylation product **7**.[6] Formation of the persistent alkoxyaluminum bond in **7** requires use of a stoichiometric amount of **1** for nucleophilic carbonyl alkylation. The formation of reduction product **5** as a by-product from bis(dialkylaluminum) reagent **1** when R = ethyl or hexyl is assumed to be a result of β-hydride transfer from the alkyl residue.

Our hypothesis is further supported by alkylation experiments with a modified system that also contains two metallic centers. Thus, initial treatment of bis(dimethylaluminum) derivative **1** (R = Me) with one equivalent of MeLi generates a new amphiphilic alkylation system **8** that possesses both an electrophilic and a nucleophilic center (Scheme 3). This compound proved to be much more effective than the



Scheme 3. Alkylation by way of the methyllithium adduct **9**.



Scheme 4. Methylation of benzaldehyde after coordination of Me_3Al with a methyl ether.

symmetric compound **1**, and carbonyl alkylation of aldehyde **3** with **8** proceeds even at temperatures between −78 and −40 °C (see entry 1 of Table 1). However, similar alkylations with monoaluminum derivative **2** (R = Me) and its complex with MeLi produced only traces of **4** (R = Ph; < 3% yield). This indicates that appropriate placement of the two metallic centers is essential for achieving the remarkable rate enhancement in the new amphiphilic alkylation.

To supply proof for the key element in the present suggestion we also prepared another system with two metallic centers (**9**, Scheme 4) on the assumption that proximity provided by coordination of the methyl ether to trimethylaluminum could still confer a certain degree of acceleration in carbonyl alkylation. Indeed, methylation of benzaldehyde with **9** proceeded smoothly at −40 °C to give 1-phenylethanol in 50% yield, whereas a simple combination of the monoaluminum species **2** (R = Me) and 2,6-dimethylanisole dramatically lowered the yield of methylation product under similar reaction conditions.

More appropriate choice of metals and a more sophisticated design for templates are the subjects of ongoing study.

Experimental Section

Alkylation of benzaldehyde (**3**; R^1 = Ph) with **1** (R = Me): A suspension of 2,7-dimethyl-1,8-biphenylenediol (106 mg, 0.5 mmol) in dry CH_2Cl_2 (5 mL) was carefully degassed, and a 2 M solution of Me_3Al in hexane (0.5 μL, 1 mmol) was added at room temperature under argon. The red solution was stirred for 30 min. After cooling to −78 °C, benzaldehyde (51 mL, 0.5 mmol) was added dropwise. The solution was allowed to warm to −20 °C, and stirring was continued for 4 h. The mixture was then poured into ice-cooled 1 N HCl and extracted with ether. The combined ethereal extracts were dried over Na_2SO_4. Evaporation of solvents and purification of the residual oil by column chromatography (silica gel, dichloromethane) gave 1-phenylethanol (**4**, R^1 = Ph, R = Me; 52 mg, 0.43 mmol) as a colorless oil (84% yield). ^{1}H NMR (300 MHz, $CDCl_3$, 20 °C, TMS): δ = 7.26–7.40 (5H, m, Ph), 4.91 (1H, dq, J = 3.6, 6.3 Hz, CH), 1.79 (1H, d, J = 3.6 Hz, OH), 1.51 (3H, d, J = 6.3 Hz, CH_3).

Received: September 2, 1997 [Z10880IE]
German version: *Angew. Chem.* **1998**, *110*, 875–877

Keywords: alkylations · aluminum · synthetic methods · template synthesis · transition states

[1] Review: E. C. Ashby, *Chem. Rev.* **1975**, *75*, 521.
[2] a) E. C. Ashby, R. B. Duke, H. M. Neuman, *J. Am. Chem. Soc.* **1967**, *89*, 1964; b) E. C. Ashby, *Pure Appl. Chem.* **1980**, *52*, 545.
[3] For asymmetric two-center catalysis, see H. Steinhagen, G. Helmchen, *Angew Chem.* **1996**, *108*, 2489; *Angew. Chem. Int. Ed. Engl.* **1996**, *35*, 2339.
[4] Reviews of organoaluminum chemistry: a) T. Mole, E. A. Jeffery, *Organoaluminum Compounds*, Elsevier, Amsterdam, **1972**; b) K. Maruoka, H. Yamamoto, *Angew. Chem.* **1985**, *97*, 670; *Angew. Chem. Int. Ed. Engl.* **1985**, *24*, 668; c) K. Maruoka in *Synthesis of Organometallic Compounds—A Practical Guide* (Ed.: S. Komiya), Wiley, New York, **1997**, Chap. 16, p. 364.
[5] a) E. C. Ashby, J. Laemmle, H. M. Neumann, *J. Am. Chem. Soc.* **1968**, *90*, 5179; b) T. Mole, J. R. Surtees, *Aust. J. Chem.* **1964**, *17*, 961.
[6] In the initial stages of the reaction, aldehyde **3** forms a chelation complex with **1** as a bidentate Lewis acid, which would be in equilibrium with another complex (**6**) in which the free electron pairs

 © WILEY-VCH Verlag GmbH, D-69451 Weinheim, 1998 1433-7851/98/3706-0836 $ 17.50+.50/0

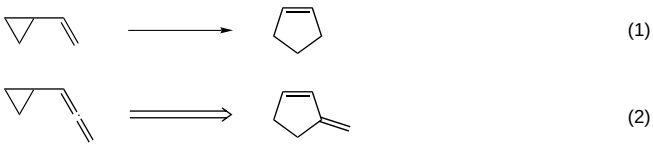
of the carbonyl groups and the alkylaluminum substituents are involved in the coordination. In a chelation complex, alkyl groups R are far removed from the carbonyl center due to the sp^3-like conformation of aluminum, so transfer of an R group from aluminum to the carbonyl center through an unfavorable four-membered transition state seems quite unlikely. See: T. Ooi, M. Takahashi, K. Maruoka, *J. Am. Chem. Soc.* **1996**, *118*, 11307; T. Ooi, E. Tayama, M. Takahashi, K. Maruoka, *Tetrahedron Lett.* **1997**, *38*, 7403. Other examples of bidentate Lewis acids: V. Sharma, M. Simard, J. D. Wuest, *J. Am. Chem. Soc.* **1992**, *114*, 7931; M. Reilly, T. Oh, *Tetrahedron Lett.* **1995**, *36*, 217; *ibid.* **1995**, *36*, 221.

[7] If the proposed mechanism is truly operative, it must be assumed that dilution would not affect the rate of alkylation with **1**, but would further retard reaction with **2**.

Rhodium(I)-Catalyzed Regioselective Ring-Expanding Rearrangement of Allenylcyclopropanes into Methylenecyclopentenes**

Minoru Hayashi, Tadashi Ohmatsu, Yun-Ping Meng, and Kazuhiko Saigo*

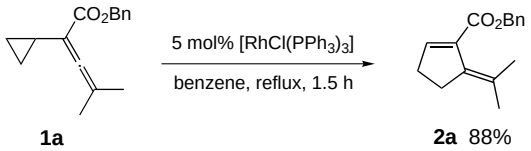
The vinylcyclopropane–cyclopentene rearrangement has attracted much attention owing to its potential synthetic utility.[1–3] The skeletal similarity between vinylcyclopropanes and allenylcyclopropanes led us to examine the rearrangement of allenylcyclopropanes into methylenecyclopentenes; the selective transformation has not yet been reported (Scheme 1).[3–5] Here we describe the first examples of the



Scheme 1. Similarity of the skeletal structures of vinylcyclopropanes and allenylcyclopropanes.

transition metal catalyzed selective transformation of allenylcyclopropanes into methylenecyclopentenes.

Our test of the hypothesis started with the allenylcyclopropane **1a**, which was easily prepared by palladium-catalyzed carbonylation of the benzyl carbonate of 2-methyl-4-cyclopropyl-3-butyn-2-ol. Heating allenylcyclopropane **1a** in refluxing benzene for 1.5 h in the presence of 5 mol% of $[RhCl(PPh_3)_3]$ gave the corresponding methylenecyclopentene **2a** in 88% yield (Scheme 2).



Scheme 2. Rhodium(I)-catalyzed rearrangement of cyclopropylallene **1a**.

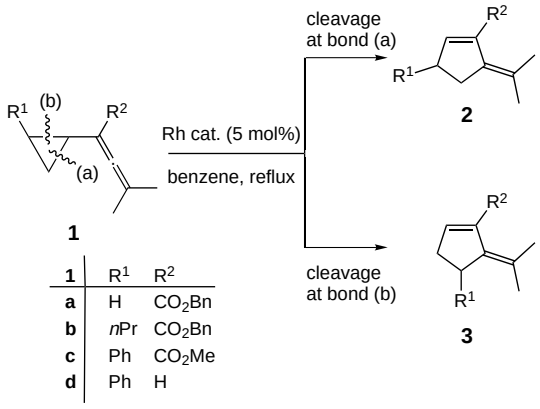
Wender and co-workers reported that a cationic rhodium(I) complex catalyzes the [5+2] cycloaddition of vinylcyclopropanes with alkynes faster than a neutral rhodium complex.[6] However, in our case, the cationic rhodium complex $[Rh(cod)_2]^+BF_4^-$ (cod = 1,5-cyclooctadiene) required a longer reaction time than $[RhCl(PPh_3)_3]$ to complete the rearrangement, although the initial reaction rate was faster (Table 1, entries 1 and 2). These reactions are the first examples of the selective rearrangement of an allenylcyclopropane into the corresponding methylenecyclopentene.

Table 1. Rhodium(I)-catalyzed rearrangement of allenylcyclopropanes

Entry	1	Cat.[a]	t [h]	Products[b]	Yield [%][c]	2:3[d]
1	**1a**	A	1.5	**2a**	88	–
2	**1a**	B	3	**2a**	88	–
3	**1b**	A	1	**2b/3b**	89	88:12
4	**1b**	C	3	**2b/3b**	98	>99:1
5	**1b**	B	10	**2b/3b**	89	>99:1
6	**1c**	A	3	**2c/3c**	99	69:31
7	**1c**	C	0.8	**2c/3c**	98	92:8
8	**1c**	B	14	**2c/3c**	95	5:95
9	**1d**	A	12	**2d/3d**	73	56:44
10	**1d**	D	12	**2d/3d**	79	15:85
11	**1d**	B	12	**2d/3d**	78	3:97

[a] Catalyst A: $[RhCl(PPh_3)_3]$, B: $[Rh(cod)_2]^+BF_4^-$, C: $[Rh(PPh_3)_3]^+BF_4^-$ (prepared in situ from an equimolar mixture of $[RhCl(PPh_3)_3]$ and $AgBF_4$), D: $[Rh(cod)(PPh_3)_2]^+BF_4^-$. [b] Satisfactory analytical and spectral data were obtained for all products listed here. [c] Yield of isolated product. [d] The isomer ratio was determined by ^1H NMR spectroscopy.

When the cyclopropane ring of the allenylcyclopropane bears a substituent, two isomers can be obtained on rearrangement, since there are two possibilities for carbon–carbon bond cleavage. Bond cleavage (a) gives methylenecyclopentene **2**, and cleavage (b) leads to the other regioisomer **3** (Scheme 3).



Scheme 3. Possible ring-opening reactions of the cyclopropane.

[*] Prof. K. Saigo, Dr. M. Hayashi, T. Ohmatsu, Y.-P. Meng
Department of Chemistry and Biotechnology, Graduate School of Engineering
The University of Tokyo
Hongo, Bunkyo-ku, Tokyo 113-8656 (Japan)
Fax: (+81) 3-5802-3348
E-mail: saigo@chiral.t.u-tokyo.ac.jp

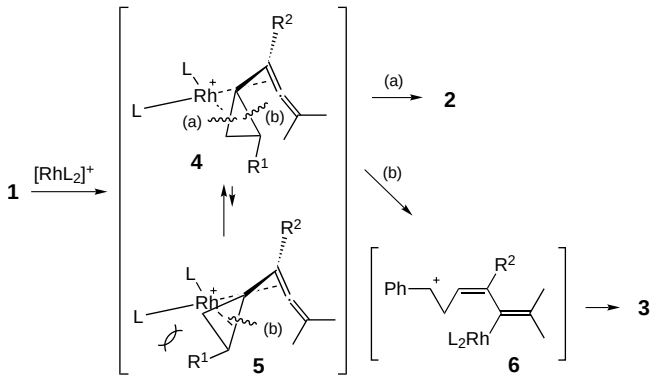
[**] This work was supported in part by the Ministry of Education, Science, Sports and Culture of Japan (Grant-in-Aid for General Science Research No. 09650932). M.H. is also grateful for financial support by Nissan Science Foundation.

 © WILEY-VCH Verlag GmbH, D-69451 Weinheim, 1998 1433-7851/98/3706-0837 $ 17.50+.50/0

In our first trial with Wilkinson's complex as catalyst, allenylcyclopropane **1b**, which has a propyl group on the cyclopropane ring, gave the corresponding rearranged products in 89% yield as a mixture of two regioisomers **2b** and **3b** (Table 1, entry 3). In contrast, high regioselectivity for **2b** was achieved by using a cationic rhodium catalyst prepared in situ from Wilkinson's complex and silver tetrafluoroborate (entry 4). Another cationic rhodium complex without phosphane ligands also gave **2b** in excellent yield and selectivity (entry 5). These results indicate that the rearrangement of alkyl-substituted allenylcyclopropanes proceeds preferably by cleavage of bond (a) of the cyclopropane ring when a cationic rhodium catalyst is used.

A contrasting result was obtained for phenyl-substituted allenylcyclopropanes **1c** and **1d**. The rearrangement of **1c** in the presence of $[Rh(PPh_3)_3]^+BF_4^-$ gave the rearranged product **2c** with the same regioselectivity as observed for **1b** (entry 7). However, in a complete reversal of regioselectivity, methylenecyclopentene **3c** was selectively obtained when $[Rh(cod)_2]^+BF_4^-$ was used as catalyst (entry 8).[7] Cationic rhodium catalysts with or without phosphane ligands preferentially gave **3d** when allenylcyclopropane **1d** was used as substrate (entries 10 and 11). Therefore, the regioselectivity of the rearrangement of phenyl-substituted allenylcyclopropanes depends not only on the cationic character of the catalyst but also on the electron density of the allenyl group of the substrate.

Although we have no direct evidence for the mechanism of this rearrangement, the regioselectivity could be explained as follows (Scheme 4): The product **2** can be formed by cleavage



Scheme 4. Possible mechanism for the rhodium(I)-catalyzed rearrangement of cyclopropylallenes.

of bond (a) in **4**, which is overwhelmingly preferred to **5** because of steric repulsion between the substituent on the cyclopropane ring and the ligands of the catalyst (entries 4 and 5). The selective formation of **3** from the phenyl-substituted allenylcyclopropanes **1c** and **1d** could be ascribed to ionic ring opening with cleavage of bond (b) followed by oxidative insertion of the metal center to form the phenyl-stabilized cation **6** (entries 8, 10, and 11). Owing to the relatively low electron density of the allenyl group in **1c**, the cationic catalyst with phosphane ligands may not be sufficiently cationic to cleave bond (b) in **1c**, so that **2c** is preferentially formed for steric reasons (entry 7). The low regioselectivity of the reactions catalyzed by $[RhCl(PPh_3)_3]$ (entries 3, 6, and 9) can be explained by assuming the formation of a trigonal-bipyramidal intermediate[8] in which the interaction of both bonds (a) and (b) with rhodium leads to a mixture of **2** and **3**.

The transition metal mediated vinylcyclopropane–cyclopentene rearrangement is a well-established process,[2, 9] and simple vinylcyclopropanes are known to give conjugated dienes.[10, 11] In contrast, the present rearrangement of allenylcyclopropanes gave exclusively the ring-expanded products, and no conjugated diene was detected.

Since allenylcyclopropanes having one or more substituents on the cyclopropane ring and/or in the allenyl moiety can be easily prepared, the present rearrangement could be applied to the synthesis of multifunctional molecules. Moreover, the resulting methylenecyclopentenes have an exomethylene moiety, as well as other functional groups, and can be converted into methylenecyclopentane or cyclopentanone derivatives.

Experimental Section

The rearrangement reactions were performed on a 0.2–0.3 mmol scale. To a solution of the catalyst (5 mol%) in benzene (20 mL per mmol of substrate) was added **1**, and the resulting mixture was heated under reflux until the reaction was complete (monitoring by TLC). The reaction mixture was diluted with an approximately equal volume of hexane and filtered through a short silica gel column (eluent: AcOEt/hexane 10/90–30/70) to remove the catalyst. Purification by column chromatography or preparative TLC afforded **2** and/or **3**. The catalyst $[Rh(PPh_3)_3]^+BF_4^-$ was prepared in situ by mixing Wilkinson's complex and silver tetrafluoroborate (1:1) prior to adding the substrate.

Received: September 5, 1997 [Z10891IE]
German version: *Angew. Chem.* **1998**, *110*, 877–879

Keywords: allenes · carbocycles · rearrangements · rhodium · small ring systems

[1] Reviews: T. Hudlicky, J. W. Reed in *Comprehensive Organic Synthesis, Vol. 5* (Eds.: B. M. Trost, I. Fleming, L. A. Paquette), Pergamon, Oxford, **1991**, pp. 899–970.

[2] Examples of transition metal mediated vinylcyclopropane–cyclopentene rearrangements: a) V. Aris, J. M. Brown, J. A. Conneely, B. T. Golding, D. H. Williamson, *J. Chem. Soc. Perkin Trans. 2* **1975**, 4–10; b) N. W. Alcock, J. M. Brown, J. A. Conneely, D. H. Williamson, *ibid.* **1975**, 962–971; c) M. Murakami, S. Nishida, *Chem. Lett.* **1979**, 927–930; d) T. Hudlicky, F. L. Koszyk, T. M. Kutchan, J. P. Sheth, *J. Org. Chem.* **1980**, *45*, 5020–5027; e) Y. Morizawa, K. Ohshima, H. Nozaki, *Tetrahedron Lett.* **1982**, *23*, 2871–2874.

[3] a) T. Hudlicky, T. M. Kutchan, S. M. Naqvi, *Org. React.* **1985**, *33*, 247–335; b) H. Hopf, *Methoden Org. Chem. (Houben-Weyl) 4th ed.* **1997**, Vol. E17c, pp. 2526–2537.

[4] The pyrolysis of an allenylcyclopropane resulted in the formation of a mixture of five- and six-membered rings; no regioselectivity was observed for the cyclopropane ring cleavage: D. E. Minter, G. J. Fonken, *Tetrahedron Lett.* **1977**, *18*, 1717–1720.

[5] There are a few reports dealing with the reactions of allenylcyclopropane derivatives: a) M. J. S. Dewar, G. J. Fonken, S. Kirschner, D. E. Minter, *J. Am. Chem. Soc.* **1975**, *97*, 6750–6753; b) W. R. Roth, T. Schmidt, H. Humbert, *Chem. Ber.* **1975**, *108*, 2171–2175; c) M. J. S. Dewar, G. J. Fonken, T. B. Jones, D. E. Minter, *J. Chem. Soc. Perkin Trans. 2* **1976**, 764–767; d) D. E. Minter, G. J. Fonken, *Tetrahedron Lett.* **1977**, *18*, 4149–4152; e) D. E. Minter, G. J. Fonken, F. T. Cook, *ibid.* **1979**, *20*, 711–714; f) Z. Komiya, S. Nishida, *J. Chem. Soc. Chem.*

 © WILEY-VCH Verlag GmbH, D-69451 Weinheim, 1998 1433-7851/98/3706-0838 $ 17.50+.50/0

Commun. **1982**, 429–430; g) L. P. Olson, J. J. Gajewski, *Tetrahedron Lett.* **1993**, *34*, 2895–2898; h) N. Iwasawa, Y. Owada, T. Matsuo, *Chem. Lett.* **1995**, 115–116.

[6] P. A. Wender, H. Takahashi, B. Witulski, *J. Am. Chem. Soc.* **1995**, *117*, 4720–4721.

[7] The structure of **3c** was confirmed by X-ray crystallography on 5-isopropylidene-4-phenyl-1-cyclopentenylmethyl 3,5-dinitrobenzoate, obtained by reduction of **3c** followed by esterification.

[8] A trigonal-bipyramidal structure was determined for a rhodacycle obtained from Wilkinson's complex and a vinylallene: M. Murakami, K. Itami, Y. Ito, *J. Am. Chem. Soc.* **1996**, *118*, 11672–11673.

[9] a) Z. Goldschmidt, B. Cramer, *Chem. Soc. Rev.* **1988**, *17*, 229–267; b) R. I. Khusnutdinov, U. M. Dzhemilev, *J. Organomet. Chem.* **1994**, *471*, 1.

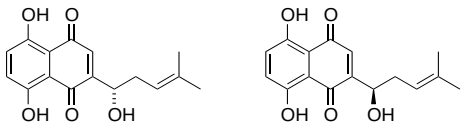
[10] The substrates of the rearrangement require another activating group other than a vinyl group, such as an electron-withdrawing group or a vinyl group on the ring and/or on the olefin.[2]

[11] a) P. A. Pinke, R. D. Stauffer, R. G. Miller, *J. Am. Chem. Soc.* **1974**, *96*, 4229–4234; b) R. G. Salomon, M. F. Salomon, J. L. C. Kachinski, *ibid.* **1977**, *99*, 1043–1054.

Concise and Efficient Total Syntheses of Alkannin and Shikonin**

K. C. Nicolaou* and David Hepworth

In ancient times extracts from the roots of *Alkanna tinctoria* in Europe and *Lithospermum erythrorhizon* in the Orient were used as natural purple dyes. More interestingly, Dioscorides recorded their use in ointments for the healing of wounds.[1] Early this century the enantiomeric naphthoquinones alkannin (**1**) and shikonin (**2**) (Scheme 1) were isolated[2] and identified[3] from these extracts. In fact, these natural products have been found in many species of Boraginaceae,[4] both as the free alcohols and ester derivatives—the ratio of enantiomers varies not only with species but also between the different derivatives.[5] More recently the wound-healing properties of these root extracts, which had drifted into folklore, were confirmed experimentally by Papageorgiou, and the active components identified as **1**, **2**, and closely related derivatives.[6] These natural products exhibit many other interesting biological effects including antibacterial,[7] antifungal,[8] anti-inflammatory,[9] antitumor,[10] analgesic,[9a,11] antipyretic,[12] and immunostimulatory[13] activities. In spite of the apparently simple molecular structures of **1** and **2**, short and efficient syntheses remained elusive. This, coupled with the extraordinary biological properties of these natural products, prompted us to investigate their total syntheses.

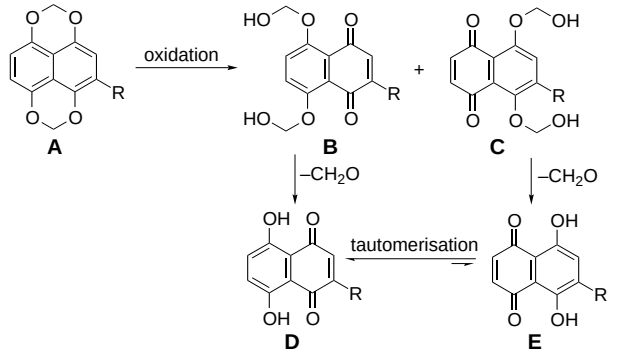


1 **2**

Scheme 1. Structures of alkannin (**1**) and shikonin (**2**).

Successful syntheses of **1** and **2** reported thus far have involved the use of 1,4,5,8-tetramethoxynaphthalene derivatives,[14] with only one exception.[15] While this protecting regime for the 5,8-dihydroxynaphthoquinone (naphthazarin) core has enabled the assembly of the side chain by several routes,[14] the final deprotection sequences to reveal the quinone system of the natural product are low-yielding and impractical. There are three major problems associated with the use of this protected system: a) initial oxidation using ceric ammonium nitrate (CAN) gives rise to two regioisomeric dimethoxynaphthoquinones with no or negligible selectivity.[14,16] Only one of these isomers can be converted into a naphthazarin in a single step;[14c,f,17] b) removal of the second pair of methyl protecting groups requires very harsh conditions ($Ag^{II}O$, HNO_3, dioxane) and gives only a poor yield of the naphthazarin derivative,[14a–f,18] and c) the drastic conditions for deprotection of the aromatic system make it prudent to protect the side-chain hydroxyl.[14e] The sensitivity of the natural products to acidic conditions[4a,14b] and to light and oxygen must also be addressed in designing efficient syntheses.[19]

We aimed to apply a novel protecting system for the naphthoquinone moiety, so that removal could be effected in one step (thus avoiding problems of regioselectivity of the oxidation) and under mild conditions compatible with an unprotected hydroxyl group. Furthermore, it was projected that this could be achieved through the use of the bismethyleneacetal derivatives of type **A** (Scheme 2). The isomers **D** and **E** should rapidly tautomerize in favor of the



A **B** **C** **D** **E**

Scheme 2. Strategy for the selective generation of **1** and **2** from bismethyleneacetal derivatives.

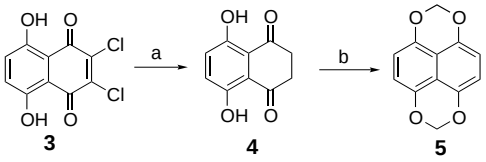
[*] Prof. Dr. K. C. Nicolaou, Dr. D. Hepworth
Department of Chemistry
and
The Skaggs Institute for Chemical Biology
The Scripps Research Institute
10550 North Torrey Pines Road, La Jolla, CA 92037 (USA)
Fax: (+1) 619-784-2469
and
Department of Chemistry and Biochemistry
University of California, San Diego
9500 Gilman Drive, La Jolla, CA 92093 (USA)

[**] We thank Prof. V. P. Papageorgiou for an authentic sample of alkannin and shikonin, Dr. M. R. Ghadiri and D. H. Lee for assistance with the CD spectra, and Drs. D. H. Huang and G. Suizdak for NMR and mass spectroscopic assistance, respectively. This work was financially supported by the National Institutes of Health (USA) and The Skaggs Institute for Chemical Biology.

 © WILEY-VCH Verlag GmbH, D-69451 Weinheim, 1998 1433-7851/98/3706-0839 $ 17.50+.50/0

desired form **D**, by virtue of the stabilizing effect of the electron-donating alkyl group (Scheme 2).[20]

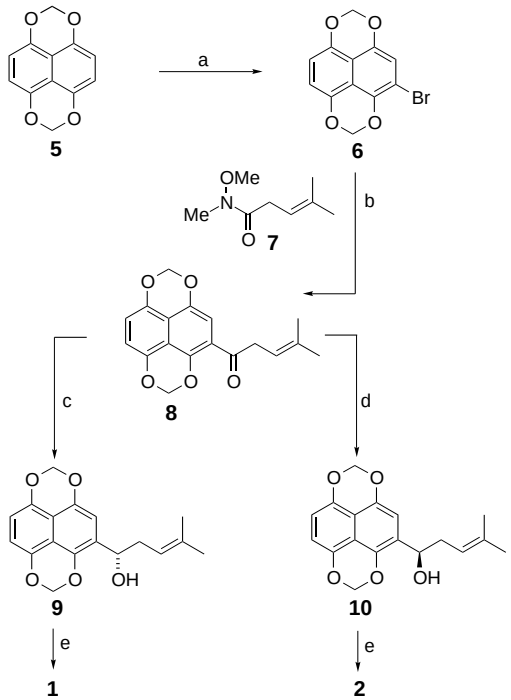
As 5,8-dihydroxy-1,4-naphthoquinone (naphthazarin) itself is prohibitively expensive, we expected that the more efficiently synthesized 2,3-dichloronaphthazarin (**3**) would provide us with a more viable source for the naphthoquinone core, since it can be readily produced in large quantities by Friedel–Crafts acylation.[21] Furthermore, we anticipated that an asymmetric ketone reduction would be an effective way of producing both enantiomers from a common late-stage intermediate. Thus, treatment of **3** with $SnCl_2$ in 4 M HCl at reflux causes reduction of the quinone with concomitant dechlorination to afford leuconaphthazarin (**4**) as its moderately air-sensitive diketo tautomer (Scheme 3).[22] Methyleneacetal formation according to the literature procedure provides intermediate **5** in good yield.[23]



Scheme 3. Synthesis of **5**: a) $SnCl_2$, 4 M HCl, reflux, 5 h, 90%; b) $BrClCH_2$, K_2CO_3, DMF, 100°C, 18 h, 70%. DMF = *N*,*N*-dimethylformamide.

Monobromination of **5** was achieved by treatment with *N*-bromosuccinimide (NBS) in $CHCl_3$ to afford **6** (70%) (Scheme 4). Halogen–metal exchange at low temperature using *t*BuLi followed by addition of the Weinreb amide **7**,[24] synthesized from the known carboxylic acid precursor by a standard procedure in 61% yield,[25] afforded ketone **8** as a yellow crystalline solid (63% plus 23% recovered **5**; Table 1). Asymmetric reduction of **8** was found to be most effective with diisopinocampheylchloroborane (DIP-Cl),[26] which provided enantiomeric alcohols **9** [with (+)-DIP-Cl] and **10** [with (−)-DIP-Cl] in excellent enantiomeric excesses ($\geq$98%)[27] and high yields (93%).

Attempts to reveal the naphthoquinone core from the methyleneacetal-protected system by using chemical oxidants (e.g. CAN, $Ag^{II}O$, MnO_2) gave disappointing results and required protection of the side-chain hydroxyl. However, mild anodic oxidation of the free hydroxy derivatives **9** and **10** avoided an undesirable protection–deprotection sequence. As envisioned, the one-step deprotection procedure allowed easy and relatively efficient access to each naturally occurring enantiomer, alkannin (**1**) and shikonin (**2**) (80% yield at ca. 50% conversion). Analytical data were consistent with those previously reported for the natural products (^{1}H NMR,[14,28] ^{13}C NMR,[14,28] IR,[14] UV,[3] HRMS,[14a,b] CD,[5a,14e] m.p.;[3] Table 1). Furthermore, the anodic oxidation was performed with a simple experimental set-up: an undivided cell with graphite electrodes, a constant external voltage across the cell (3 V),[29] 50% aqueous acetonitrile as solvent, and 1 M $LiClO_4$ as electrolyte. At less than 50% conversion, TLC analysis showed clean conversion to the desired product. Side products only began to appear as the reaction proceeded to higher



Scheme 4. Total synthesis of alkannin (**1**) and shikonin (**2**): a) NBS (1 equiv), $CHCl_3$, 25°C, 12 h, 70%; b) *t*BuLi (2 equiv), THF, −78°C, 1 h, then **7**, −78°C, 1.5 h, 63% (23% recovered **5**); c) (+)-DIP-Cl (1.5 equiv), THF, −40°C → −25°C, 3 h, then CH_3CHO (2 equiv), 0°C, 12 h, 93%, $\geq$98% *ee*; d) (−)-DIP-Cl (1.5 equiv), THF, −40°C → −25°C, 3 h, then CH_3CHO (2 equiv), 0°C, 12 h, 93%, $\geq$98% *ee*; e) anodic oxidation, CH_3CN/H_2O (1:1), $LiClO_4$ (1M), graphite electrodes, undivided cell, 3 V constant external voltage, 25°C, 80% at ca. 50% conversion.

Table 1. Selected physical properties of compounds **8**–**10**, **1**, and **2**.

8: R_f = 0.49; (silica gel, 10% Et_2O in hexanes); m.p. 110–117°C (decomp); IR (KBr): $\tilde{\nu}_{max}$ = 3072, 2966, 2911, 1666, 1622, 1598, 1480, 1425, 1378, 1251, 1218, 1169, 1049, 969 cm^{-1}; ^{1}H NMR (500 MHz, $CDCl_3$): δ = 7.34 (s, 1H; C^5-H), 6.98, 6.92 (AB, J = 8.3 Hz, 1H; C^6-H, C^7-H), 5.62 (s, 2H; CH_2O), 5.51 (s, 2H; CH_2O), 5.47 (tq, J = 6.9, 1.3 Hz, 1H; CH=C), 3.82 (d, J = 6.9 Hz, 2H; CH_2C=O), 1.77 (d, J = 1.0 Hz, 3H; *trans* CH_3), 1.68 (s, 3H; *cis* CH_3); ^{13}C NMR (125.7 MHz, $CDCl_3$): δ = 197.1, 145.8, 145.6, 144.6, 144.1, 135.4, 119.3, 117.1, 116.3, 115.0, 111.8, 110.1, 107.7, 91.7, 91.4, 43.5, 25.9, 18.3; HR-MS (fast atom bombardment; FAB) calcd for $C_{18}H_{17}O_5$ [M+H$^+$]: 313.1076; found: 313.1065.

9: R_f = 0.27 (silica gel, 33% Et_2O in hexanes); $[\alpha]_D^{22}$ = +80.2 (c = 1.48, $CHCl_3$); IR (thin film): $\tilde{\nu}_{max}$ = 3397, 2914, 1614, 1477, 1418, 1380, 1250, 1162, 1047, 1011, 973, 879, 823 cm^{-1}; ^{1}H NMR (500 MHz, $CDCl_3$): δ = 7.02 (s, 1H; C^3-H), 6.80, 6.77 (AB, J = 8.3, 1H; C^6-H, C^7-H), 5.51 (d, J = 5.0 Hz, 1H; CH_2O), 5.50 (d, J = 4.4 Hz, 1H; CH_2O), 5.46 (d, J = 5.2 Hz, 1H; CH_2O), 5.45 (d, J = 5.1 Hz, 1H; CH_2O), 5.19 (dt, J = 6.8, 1.2 Hz, 1H; CH=C), 5.13 (dd, J = 7.7, 5.5 Hz, 1H; C*H*OH), 2.53–2.42 (m, 3H; CH_2CHO*H*), 1.71 (s, 3H; CH_3), 1.61 (s, 3H; CH_3); ^{13}C NMR (125.7 MHz, $CDCl_3$): δ = 144.4, 144.3, 144.3, 140.3, 135.7, 125.2, 119.4, 114.8, 114.3, 108.8, 108.2, 106.8, 91.7, 91.5, 67.7, 67.7, 36.8, 25.8, 17.9; HR-MS (FAB) calcd for $C_{18}H_{19}O_5$: [M^+] 314.1154, found: 314.1144.

10: as for **9** except $[\alpha]_D^{22}$ = −80.2 (c = 1.26, $CHCl_3$).

1 and **2**: R_f = 0.55 [silica gel (prewashed with 10% AcOH in CH_2Cl_2), 33% Et_2O in hexanes]; ^{1}H NMR (400 MHz, $CDCl_3$): δ = 12.60 (s, 1H; $C^{5/8}$-H), 12.50 (s, 1H; $C^{5/8}$-H), 7.20, 7.18 (AB, J = 9.6, 1H; C^6-H, C^7-H), 7.17 (d, J = 1.2 Hz, 1H; C^3H), 5.20 (dt, J = 6.8, 1.3 Hz, 1H; CH=C), 4.92 (ddd, J = 7.9, 4.3, 1.0 Hz, 1H; C*H*OH), 2.68–2.62 (m, 1H; CH_2), 2.39–2.32 (m, 2H; CH_2CHO*H*), 1.76 (s, 3H; CH_3), 1.66 (s, 3H; CH_3); ^{13}C NMR (125.7 MHz, $CDCl_3$): δ = 180.6, 179.8, 165.5, 164.9, 151.4, 137.4, 132.4, 132.3, 131.8, 118.4, 112.0, 111.5, 68.4, 68.3, 35.7, 25.9, 18.1.

 © WILEY-VCH Verlag GmbH, D-69451 Weinheim, 1998 1433-7851/98/3706-0840 $ 17.50+.50/0 *Angew. Chem. Int. Ed.* **1998**, *37*, No. 6

conversion. We anticipate that the efficiency of this step may be further improved by employing more sophisticated electrochemical equipment, in particular, through precise voltage control.

In conclusion, we have developed a novel protecting system for 5,8-dihydroxynaphthoquinones, which may be removed easily under mild conditions. This development, together with a highly enantioselective ketone reduction, has allowed us to complete concise and practical syntheses of each of the enantiomers alkannin (**1**) and shikonin (**2**). Chemical synthesis and biological investigations of a series of structural analogues of the natural products, more diverse than simple ester derivatives, are now viable. Further studies into the chemical biology of these compounds are in progress.

Received: September 18, 1998 [Z 10945 IE]
German version: *Angew. Chem.* **1998**, *110*, 864 – 866

Keywords: asymmetric synthesis · naphthoquinones · natural products · oxidations · total synthesis

[1] a) P. Dioscorides in *De Materia Medica*, *Vol. IV.23* (Ed.: Max Wellman), Berloni Apud Weidmannos, Berlin, **1958**, pp. 187 – 188; b) R. Gunther in *The Greek Herbal of Dioscorides*, *Vol. IV*, Hafner, New York, **1968**, pp. 421.
[2] R. Majima, C. Kuroda, *Acta Phytochim. (Tokyo)* **1922**, *1*, 43 – 65.
[3] H. Brockmann, *Justus Liebigs Ann. Chem*. **1936**, *521*, 1 – 47.
[4] a) R. H. Thomson, *Naturally Occurring Quinones*, 2nd ed., Academic Press, New York, **1971**, pp. 248 – 251; b) *Naturally Occurring Quinones III, Recent Advances*, Chapman & Hall, New York, **1987**, pp. 219 – 223.
[5] a) H. Fukui, M. Tsukada, H. Mizukami, M. Tabata, *Phytochemistry* **1983**, *22*, 453 – 456; b) Y. Ikeda, N. Ishida, C. Fukaya, K. Yokoyama, M. Tabata, H. Fukui, G. Honda, *Chem. Pharm. Bull.* **1991**, *39*, 2351 – 2352.
[6] V. P. Papageorgiou, *Experientia* **1978**, *34*, 1499 – 1501.
[7] V. P. Papageorgiou, *Planta Med.* **1980**, *38*, 193 – 203, and references therein.
[8] G. Honda, F. Sakakibara, K. Yazaki, *J. Nat. Prod.* **1988**, *51*, 152 – 154.
[9] a) M. Hayashi, *Nippon Yakurigaku Zasshi* **1977**, *73*, 193 – 203; b) S. Tanaka, M. Tajima, M. Tsukada, M. Tabata, *J. Nat. Prod.* **1986**, *49*, 466.
[10] B.-Z. Ahn, K.-U. Baik, G.-R. Kweon, K. Lim, B.-D. Hwang, *J. Med. Chem.* **1995**, *38*, 1044 – 1047, and references therein.
[11] M. Hayashi, *Nippon Yakurigaku Zasshi* **1977**, *73*, 205 – 214.
[12] M. Hayashi, *Nippon Yakurigaku Zasshi* **1977**, *73*, 177 – 191.
[13] H. Wagner, B. Kreher, K. Jurcic, *Arzneim. Forsch.* **1988**, *38*, 273 – 275.
[14] a) A. Terada, Y. Tanoue, A. Hatada, H. Sakamoto, *J. Chem. Soc. Chem. Commun.* **1983**, 987 – 988; b) *Bull. Chem. Soc. Jpn.* **1987**, *60*, 205 – 213; c) A. M. Moiseenkov, N. N. Balaneva, V. L. Novikov, G. B. Elyakov, *Dokl. Akad. Nauk. SSSR* **1987**, *295*, 614 – 617; d) Y. Tanoue, A. Terada, Y. Sugyo, *J. Org. Chem.* **1987**, *52*, 1437 – 1439; e) M. Braun, C. Bauer, *Liebigs Ann. Chem.* **1991**, 1157 – 1164; f) V. L. Novikov, N. N. Balaneva, A. M. Moiseenkov, G. B. Elyakov, *Izv. Akad. Nauk, Ser. Khim.* **1992**, 1901 – 1910; g) S. Torii, K. Akiyama, H. Yamashita, T. Inokuchi, *Bull. Chem. Soc. Jpn.* **1995**, *68*, 2917 – 2922; h) E. A. Couladouros, Z. F. Plyta, A. T. Strongilos, V. P. Papageorgiou, *Tetrahedron Lett*. **1997**, *38*, 7263 – 7266.
[15] Y. Shimai, T. Koga, (Pias Co., Ltd.) JP-B 63156741, **1988** [*Chem. Abstr*. **1989**, *110*, 23567u].
[16] Y. Tanoue, A. Terada, *Bull. Chem. Soc. Jpn.* **1988**, *61*, 2039 – 2045.
[17] A low-yielding three-step sequence to deprotect the alternate regioisomer has been reported: see Ref. [14g].
[18] Other methods for demethylation of naphthazarin ethers (e.g. $AlCl_3$)[16] are incompatible with the acid-sensitive side chain of **1** and **2**.
[19] F. A. Chen, H. W. Cheng, A.-B. Wu, H.-C. Hsu, C.-Y. Chen, *Chem. Pharm. Bull.* **1996**, *44*, 249 – 251.
[20] R. E. Moore, P. J. Scheuer, *J. Org. Chem.* **1966**, *31*, 3272 – 3283.
[21] R. Huot, P. Brassard, *Can. J. Chem.* **1974**, *52*, 838 – 842.
[22] D. B. Bruce, R. H. Thomson, *J. Chem Soc.* **1955**, 1089 – 1096.
[23] F. Dallacker, J. Jacobs, W. Coerver, *Z. Naturforsch. B* **1983**, *38*, 1000 – 1007. Rigorous exclusion of oxygen is required to ensure the success of this reaction.
[24] S. Nahm, S. M. Weinreb, *Tetrahedron Lett.* **1981**, *22*, 3815 – 3818.
[25] J. Einhorn, C. Einhorn, J.-L. Luche, *Synth. Commun.* **1990**, *20*, 1105 – 1112.
[26] a) H. C. Brown, J. Chandrasekharan, P. V. Ramachandran, *J. Am. Chem. Soc.* **1988**, *110*, 1539 – 1546; b) P. V. Ramachandran, A. V. Teodorovic, M. V. Rangaishenvi, H. C. Brown, *J. Org. Chem.* **1992**, *57*, 2379 – 2386; c) R. K. Dar, *Aldrichimica Acta* **1994**, *27*, 43 – 51.
[27] The enantiomeric excesses were determined by 500 MHz ^{1}H NMR spectroscopic analysis of the Mosher's esters with each enantiomer of α-methoxytrifluoromethylphenylacetic acid chloride. In each case, only a single diastereoisomer could be observed: a) J. A. Dale, D. L. Dull, H. S. Mosher, *J. Org. Chem.* **1969**, *34*, 2543 – 2549; b) J. A. Dale, H. S. Mosher, *J. Am. Chem. Soc.* **1973**, *95*, 512 – 519; c) for a very convenient experimental method, see D. E. Ward, C. K. Rhee, *Tetrahedron Lett.* **1991**, *32*, 7165 – 7166.
[28] K. Inoue, M. Akaji, H. Inouye, *Chem. Pharm. Bull.* **1985**, *33*, 3993 – 3997.
[29] D. A. Frey, N. Wu, K. D. Moeller, *Tetrahedron Lett*. **1996**, *37*, 8317 – 8320.

A Naphthalene-Like Si_{10}^{10-} Unit in the Novel $^2_\infty[Si_{20}^{30-}]$ Planar Anion of $Sr_{13}Mg_2Si_{20}$**

Antonio Currao and Reinhard Nesper*

Dedicated to Professor Dieter Seebach on the occasion of his 60th birthday

In recent years, a large number of novel silicon Zintl anions[1] in the ternary and quaternary solids $M^1M^2Si_x$ and $M^1M^2M^3Si_x$ ($M^1 - M^3$ = alkali or alkaline earth metal) have been discovered and characterized.[2–5] Unequivocal evidence for a structure-directing influence of the metal atom on its respective Zintl anion Si_m^{n-} was observed relatively early; this effect may be exploited as a strategic aid in synthesis.[3] As was established for the oligomeric Si_m^{n-} polyanions, small, strongly polarizing cations (especially Mg^{2+}) coordinate formally highly charged terminal or isolated Si^{n-} anions, whereas larger, weakly charged cations are in the more highly networked regions of the polyanion.[2, 4] This phenomenon was used to tune the relative ratio of terminal to more highly networked atoms, the latter embedded deeper in the anion, while maintaining an identical valence electron count and mean bond order within the polyanion. In other words, the degree of disproportionation of the Si_x units is a function of the various cations and their respective stoichiometries. An unusual number of planar Si_m^{n-} polyanions have been reported

[*] Prof. Dr. R. Nesper, Dipl.-Chem. A. Currao
Laboratorium für Anorganische Chemie
der Eidgenössischen Technischen Hochschule
ETH-Zentrum
CH-8092 Zürich (Switzerland)
Fax: (+41)1-632-1149
E-mail: nesper@inorg.chem.ethz.ch

[**] This work was supported by the Swiss National Foundation (project no. 20-4322.958).

whose geometries are in strange contradication to the generally accepted notion that Si_m^{n-} units with multiple bonds should be more energetically stable than their isoelectronic singly bonded counterparts. For example, the doubly bound $[Si{=}Si]^{4-}$ monomer is energetically less stable than a $^1_\infty[(\text{-Si-Si})^{4-}]$ linear chain.

We present here a new polymeric $^2_\infty[Si_{20}^{30-}]$ anion with naphthalene-like planar ring systems that is consistent with the aforementioned unusual trends. $Sr_{13}Mg_2Si_{20}$ exists in the magnesium-poor region of the ternary phase system SrMgSi as a stable compound[6] that decomposes above 1253 K to SrSi, Sr_4Si_{6+x}, and $Sr_2Mg_{2-x}Si_3$. Long tempering below 1230 K readily provides pure-phase black products, mostly in powder form. Upon further tempering at 1240 K, beautiful, tiny, black single crystals of about 0.1 mm in diameter are obtained, which could be used for a structure determination.[4, 7]

$Sr_{13}Mg_2Si_{20}$ contains separated sheetlike silicon domains (Figures 1 a, lightly shaded area, and 1 b) that are formed from two interpenetrating $^2_\infty[Si_{20}^{30-}]$ polyanions with naphthalene-like Si_{10}^{10-} building blocks (Figure 2 a). The relatively open structure of this polyanion is dictated by the large Sr^{2+} ions, which form trigonal-prismatic assemblies in the region of the rings (Figure 1 a, darkly shaded area). Consistent with their aforementioned structure-directing influence, the Mg^{2+} ions coordinate exclusively the peripheral, highly charged Si atoms of the polymers.

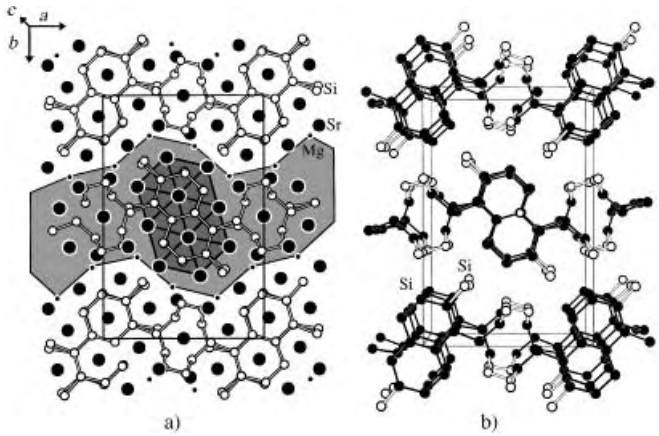


Figure 1. Structure of $Sr_{13}Mg_2Si_{20}$: a) Projection along the crystallographic *c* axis; the prismatic coordination of the Si_6 rings by the large Sr atoms is highlighted in gray (Si: large empty circles, Sr: large filled circles, Mg: small filled circles); b) perspective view of the Si_{20}^{30-} polymer anion sheets.

The polymeric $^2_\infty[Si_{20}^{30-}]$ anions contain two crystallographically independent planar Si_{10}^{10-} building blocks (Figures 1 and 2), each formed from a pair of condensed Si_6 rings. Each of these rings is bound by a terminal Si^{3-}center and a bridging, doubly branched Si_{10}^{20-} chain fragment (Figure 2 c). Each Si_{10}^{20-} unit bonds together four naphthalene-like fragments within a layer. In contrast to the other six Si atoms of the bridging piece, atoms Si9 and Si10 are not co-planar with one of the ring systems (Figure 2 a, c). Thus, a planar building block of sixteen Si atoms, $(Si_{10})^{ring}(Si)_2^{terminal}(Si_2)_2^{bridging}$, results.

On the basis of numerous new findings it has become apparent that in planar Zintl anions there is no general

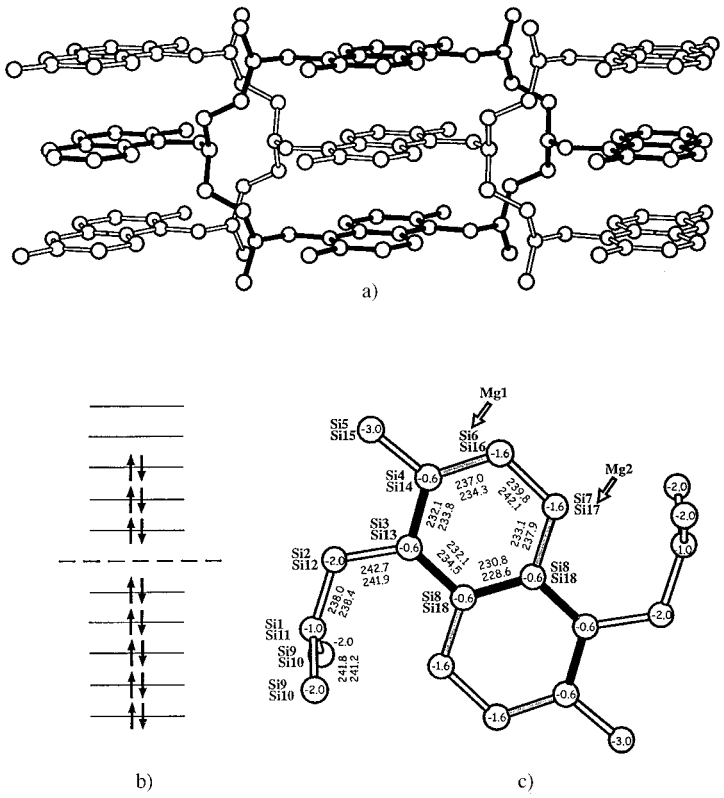


Figure 2. a) Interpenetration of the two polymeric Zintl anions in a layer of $Sr_{13}Mg_2Si_{20}$. b) Schematic MO diagram and electronic occupation of the π and π^* states in the double-ring system. (below and above, respectively, the dashed line). c) Labeling scheme, formal charges (inside the circles), and bond lengths (pm) in the planar Si_{16}^{22-} fragment. Atoms Si9 and Si10 do not belong to the ring system. The relatively short Si – Si bonds are darkened. Atoms Si6 and Si17 are also coordinated by Mg and are marked with arrows; they feature the longest bond lengths to neighboring Si atoms.

tendency towards the formation of aromatic systems (such as that observed for the CH arenes), even when the assembly into nearly or completely isometric rings is possible. This was corroborated by ring systems observed in Si and Ge Zintl anions.[2, 3, 8] In the title compound, there is indeed a difference between the bond lengths within the rings (230.8 to 239.8 pm); however, the distribution does not permit the assignment of localized double bonds (Figure 2 c). It is interesting that the somewhat longer bond lengths about Si6 and Si17 occur at two different Si sites in the two independent ring systems, and where the Si atoms are coordinated by Mg^{2+} ions. Even the exocyclic bonds do not show strikingly varied bond lengths, including those which one can confidently assign as Si – Si single bonds.[9] However, the mean Si – Si bond length (240.5 pm) is somewhat larger than that of the endocyclic bonds (234.6 and 235.2 pm). The double bonds are perhaps localized in the ring system.

Upon applying the (8 – N) rule and considering the planar groups, it is clear that the composition $Sr_{13}Mg_2Si_{20}$ does not contain sufficient valence electrons to achieve a completely singly bonded structure. Consequently, an incomplete occupation of the π^* states in the bicyclic system results. The π MO states are depicted schematically in Figure 2 b (owing to the low C_s symmetry, there are no degenerate π levels; this is also the case in naphthalene). The observed composition leads to a

 © WILEY-VCH Verlag GmbH, D-69451 Weinheim, 1998 1433-7851/98/3706-0842 $ 17.50+.50/0

degree of filling in which two of the five π* states remain unoccupied, which effectively results in two, relatively strongly delocalized double bonds in the bicyclic system. A completely singly bonded Si polymer of this type would require four additional valence electrons so that the π* levels would also be filled. The bond distances suggest that the (-Si4-Si3-Si8-Si7-)$_2$ and (-Si16-Si14-Si13-Si18-)$_2$ ring fragments carry the majority of the double-bond character (Figure 2c). We will report elsewhere on an explanation of why highly charged Zintl anions of Si are so frequently planar.[8]

The Si_{10}^{10-} units in the polyanion structure are ecliptically stacked (Figure 2a). Despite the relatively large distance of $c/2 = 4.91$ pm between neighboring rings, one-dimensional conductivity along the stacking direction could arise through π*–π* interactions. Such interactions were recently suggested for a related Group 14 compound in which bond lengths of 430 to 500 pm were observed between ecliptically stacked planar Zintl anions.[3, 4, 8] One-dimensional conductivity originates from interactions between ecliptically stacked ring systems, whereas semiconducting properties are observed in the perpendicular direction. Such semiconductors are at the border between intermetallic phases and common Zintl compounds, which strongly adhere to the valence rules. As their structural details can nevertheless be understood with electron-counting rules and a semiconducting character predominates, we call such compounds "extended Zintl phases". This description is supported by practically all of the band-structure calculations we have carried out to date on such silicides; all of the occupied electronic states are Si-centered (similar to the MO scheme in Figure 2b). In this respect, these species may be differentiated from intermetallic phases.

From a small number of examples, it can already be seen that topochemical reactions can be carried out on two-dimensional polyanions of silicon and germanium—such as those in $CaSi_2$,[10] Li_3NaSi_6,[11] and Li_7Ge_{12}[12, 13]—to afford new element modifications[11, 13] and siloxanes[14, 15]; this fosters a continued excitement in this area of research. In this respect, the Si polymer anions we recently discovered in $Ba_2Eu_3Si_7$,[15] Ca_3Si_4, $Ca_{14}Si_{19}$,[4, 2[and the title compound $Sr_{13}Mg_2Si_{20}$[4] could be of interest.

Received: March 3, 1997
Revised version: November 24, 1997 [Z 10185IE]
German version: *Angew. Chem.* **1998**, *110*, 843 – 845

Keywords: layered compounds · silicon · solid-state chemistry · structure elucidation · Zintl anions

[1] E. Zintl, *Angew. Chem.* **1939**, *52*, 1; W. Klemm, *Proc. Chem. Soc. London* **1959**, 329; H. G. von Schnering, *Angew. Chem.* **1981**, *93*, 44; *Angew. Chem. Int. Ed. Engl.* **1981**, *20*, 33; H. G. von Schnering, W. Hönle, *Chem. Rev.* **1988**, *88*, 243; H. Schäfer, B. Eisenmann, *Rev. Inorg. Chem.* **1981**, *3*, 29; R. Nesper, *Prog. Solid State Chem.* **1990**, *20*, 1.

[2] R. Nesper, A. Currao, S. Wengert in *Organosilicon Chemistry II, From Molecules to Materials* (Eds.: N. Auner, J. Weis), VCH, Weinheim, **1995**.

[3] A. Currao, J. Curda, R. Nesper, *Z. Anorg. Allg. Chem.* **1996**, *622*, 85.

[4] A. Currao, Dissertation, ETH Zürich, **1995**; Diplomarbeit, ETH Zürich, **1991**.

[5] C. Häussermann, R. Nesper, *Angew. Chem.* **1995**, *107*, 1593; *Angew. Chem. Int. Ed. Engl.* **1995**, *34*, 1462.

[6] Differential thermal analysis (DTA) investigations on probes of Sr/Mg/Si compositions 33.3/11.7/55 and 40/10/50 demonstrate that $Sr_{13}Mg_2Si_{20}$ decomposes peritectically above 1253 K. As established by a powder diagram, pure $Sr_{13}Mg_2Si_{20}$ may be obtained by tempering a sample of the former composition at 1223 K ($t_1 = 99$ h). The crystal investigated was isolated from a synthesis at 1243 K ($t_1 = 8$ d). At this temperature, $Sr_{13}Mg_2Si_{20}$ is the main product and Sr_4Si_7 and $SrSi_2$ are side products. In the products of syntheses at 1234 K ($t_1 = 10$ h) and 1243 K ($t_1 = 99$ h) for the latter composition, one finds predominantly $Si_{13}Mg_2Si_{20}$ with SrSi as a minor component. If either composition is subsequently tempered at about 1363 K ($t_1 = 30$ and 10 h, respectively) SrSi is obtained as the main component with minor Sr_4Si_7 and $Sr_2Mg_{2-x}Si_3$ impurities.

[7] Crystal structure: *Pbam* (no. 55), $a = 15.200(3)$, $b = 23.201(6)$, $c = 9.832(2)$ Å, $Z = 4$, $V = 3464.1$ Å^3, $\rho_{calcd} = 3.354$ g cm^{-3}, 2907 independent reflections ($R_{int\,F^2} = 0.176$), 2109 reflections with $F^2 > 2\sigma(F^2)$, $R(F^2) = 0.085$, $R_w(F^2) = 0.164$. Further details of the crystal structure determination may be obtained from the Fachinformationszentrum, Karlsruhe, D-76344 Eggenstein-Leopoldshafen, Germany (fax: (+49)7247-808-666 (Frau S. Höhler-Schlimm); e-mail: crysdata@fiz-karlsruhe.de), on quoting the depository number CSD-408183.

[8] R. Nesper, S. Wengert, unpublished results; see also S. Wengert, Dissertation, ETH Zürich, **1997**.

[9] H. Bock, *Angew. Chem.* **1993**, *105*, 413; *Angew. Chem. Int. Ed. Engl.* **1993**, *32*, 414.

[10] K. Janzon, H. Schäfer, H. Weiss, *Z. Naturforsch.* ***B*** **1968**, *23*, 1544; J. Evers, *J. Solid State Chem.* **1978**, *24*, 199.

[11] H. G. von Schnering, M. Schwarz, R. Nesper, *J. Less-Common Met.* **1988**, *137*, 297.

[12] A. Grüttner, R. Nesper, H. G. von Schnering, *Angew. Chem.* **1982**, *94*, 933; *Angew. Chem. Int. Ed. Engl.* **1982**, *21*, 912.

[13] A. Grüttner, Dissertation, Universität Stuttgart, **1982**.

[14] H. Kautsky, G. Herzberg, *Z. Anorg. Allg. Chem.* **1924**, *139*, 135.

[15] A. Weiss, G. Beil, H. Meyer, *Z. Naturforsch.* ***B*** **1979**, *34*, 25.

Formation of Adamantane-Like Structures by Reaction of Titanocene Fluorides with an Iminoalane**

Helge Wessel, Mavis L. Montero, Carsten Rennekamp, Herbert W. Roesky,* Peihua Yu, and Isabel Usón

Dedicated to Professor Sir John Meurig Thomas on the occasion of his 65th birthday

Imido transition metal complexes play an important role both in biological processes such as nitrogen fixation as well as in a series of industrial processes.[1] Cycloadditions, C–H activations, and ring-opening polymerizations can all be catalyzed by imido complexes.[1, 2] Numerous imidotitanium

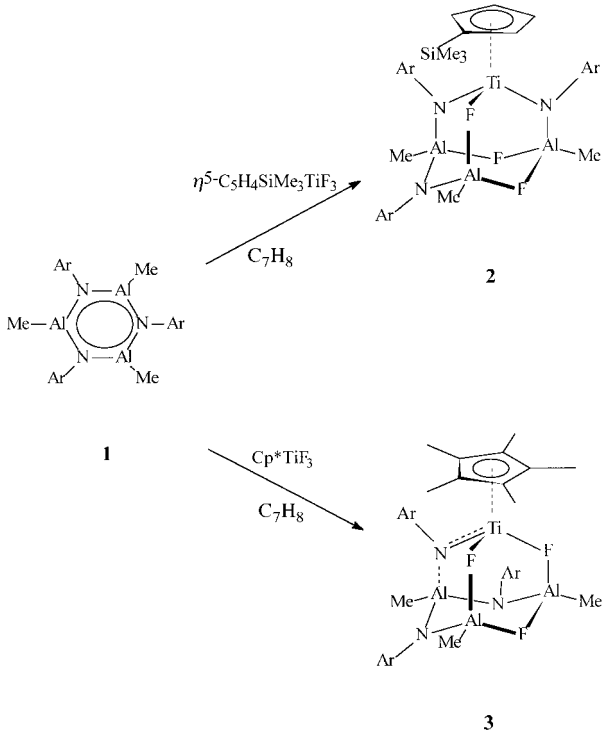
[*] Prof. Dr. H. W. Roesky, Dipl.-Chem. H. Wessel, Dr. M. L. Montero, Dipl.-Chem. C. Rennekamp, Dipl.-Chem. P. Yu, Dr. I. Usón
Institut für Anorganische Chemie der Universität
Tammannstrasse 4, D-37077 Göttingen (Germany)
Fax: (+49) 551-39-3373
E-mail: hroesky@gwdg.de

[**] This work was supported by the Deutsche Forschungsgemeinschaft, the Bundesministerium für Bildung, Forschung und Technologie and the Witco GmbH, Bergkamen. H. W. and C. R. thank the Fonds der Chemischen Industrie for Doctoral fellowships.

 © WILEY-VCH Verlag GmbH, D-69451 Weinheim, 1998 1433-7851/98/3706-0843 $ 17.50+.50/0

chlorides as well as the corresponding oxygen-containing complexes have recently been reported;[3] however, syntheses of fluorine-containing imido compounds have thus far remained elusive.

Herein, we report on the reaction of titanocene fluorides with the trimeric iminoalane **1**,[4] which exhibits quasiaromatic properties and contains Lewis acidic, three-coordinate aluminum centers. The reactions of **1** with η^5-$C_5H_4SiMe_3TiF_3$ and Cp*TiF_3 (Cp* = η^5-C_5Me_5) in toluene lead under fluorine–nitrogen metathesis to the adamantane-like cage compounds **2** and **3**, respectively (Scheme 1). These novel titanocene compounds were characterized by IR and NMR spectroscopy, mass spectrometry, and elemental analysis. Compound **2**[5] crystallizes in the triclinic space group $P\bar{1}$ and contains an $[(Al_3NF_2)(TiN_2F)]$ adamantane core (Figure 1). The structure of **2** consists of a six-membered Al_3NF_2 ring with μ_2-bridging fluorine and nitrogen atoms (av Al–F distance: 180.3 pm, av Al–N distance: 180.7 pm). The Al_3 plane resides in a chair conformation with an average Al-F-Al angle of 131.8° and an Al-N-Al angle of 116.4°. The Al_3 plane is capped by a μ_3-$F(NAr)_2TiC_5H_4SiMe_3$ ligand. The average Ti–N distance is 188.9 pm and the Ti–F distance 202.0 pm; the average Ti-N-Al angle is 116.5° and the Ti-F-Al angle 131.1°. The environment of the titanium atom is pseudotetrahedral. The $C_5H_4SiMe_3$ ligand completes this coordination sphere.



Scheme 1. Reactions of **1** with titanocene fluorides. Ar = 2,6-*i*$Pr_2C_6H_3$.

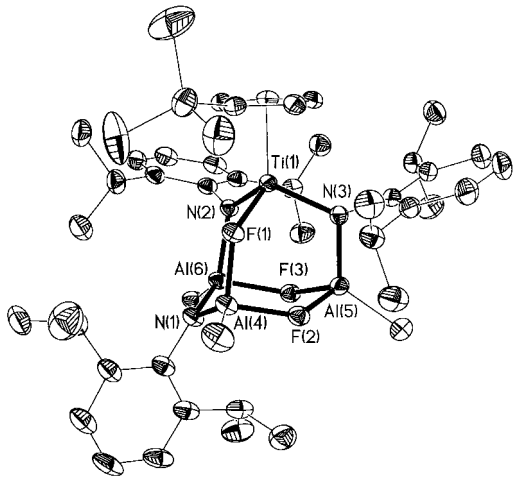
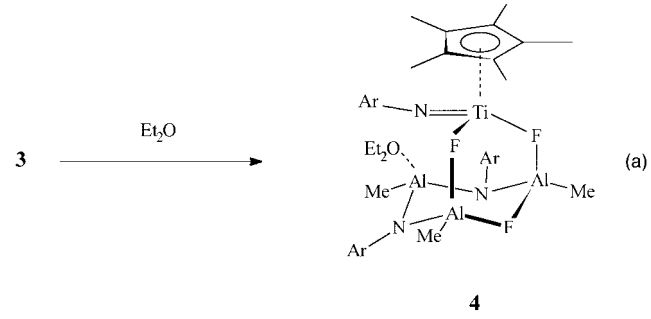


Figure 1. Molecular structure of **2** in the crystal. Selected distances [pm] and angles [°]: Al(4)–F(1) 176(1), Al(4)–N(1) 178(2), Al(4)–F(2) 181(1), Al(5)–F(3) 175(1), Al(5)–N(3) 183(2), Al(6)–F(3) 187(1), Al(6)–N(2) 193(2), Ti(1)–F(1) 202(1), Ti(1)–N(3) 191(2); Al(5)-F(2)-Al(4) 132.6(8), Al(4)-F(1)-Ti(1) 131.1(7), Al(4)-N(1)-Al(6) 116.4(9), Ti(1)-N(2)-Al(6) 117.8(9), N(1)-Al(6)-F(3) 102.6(8).

Treatment of **3** with the donor solvent diethyl ether leads to **4** through cleavage of an aluminum–nitrogen bond. This is the first compound, containing a titanium–nitrogen double bond obtained by a metathesis; hereby an intramolecular stabilization of such a double bond by fluorine was established for the first time.[8]



The ^{19}F NMR spectra of **2**–**4** contain signals for the Al–Ti-bridging fluorine atoms (**2**: $\delta = -151.9$; **3**: $\delta = -168.2$, -158.4; **4**: $\delta = -168.1$, -158.4), which are strongly shifted to higher field with respect to those of the starting materials ($\delta = 164.5$ and 124.0). This was also established for other compounds with Ti-F-Al substructures.[9] The signals at $\delta \approx -135$ are assigned to the Al-bridging fluorine atoms. These findings indicate that the structures of the compounds are similar in the solid state and in solution[9, 10] and confirm the structure formulated for **3**.

Compound **4** crystallizes in the monoclinic space group $P2_1/c$ (Figure 2). The structure of **4** consists of a six-membered Al_3N_2F ring with μ_2-bridging fluorine and nitrogen atoms (av Al–F distance: 181.4 pm, av Al–N distance: 182.4 pm). The Al_3 plane resides in a chair conformation with an Al-F-Al angle of 129.6° and an Al-N-Al angle of 125.6°. The atoms Al(1) and Al(2) are bridged by a μ_2-$F_2TiCp^*(NAr)$ ligand, the average Ti-F-Al angle is 142.4°. One diethyl ether molecule is coordinated at Al(3). The environment of the titanium atom is pseudotetrahedral, the coordination sphere is completed by the Cp* ligand. The average Ti–F distance is 204.4 pm. The Ti(1)–N(2) bond length of 173.0 pm[7] is considerably shorter than that in **2**, and is in accord with the lengths of Ti–N double bonds in other compounds.[8]

 © WILEY-VCH Verlag GmbH, D-69451 Weinheim, 1998 1433-7851/98/3706-0844 $ 17.50+.50/0 *Angew. Chem. Int. Ed.* **1998**, *37*, No. 6

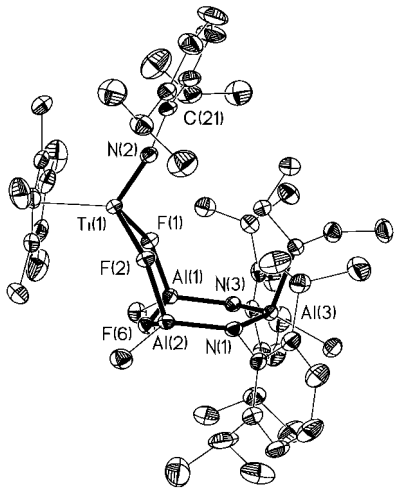


Figure 2. Molecular structure of **4** in the crystal. Selected distances [pm] and angles [°]: Ti(1) – N(2) 173(2), Ti(1) – F(2) 204(2), N(1) – Al(2) 180(2), F(1) – Al(1) 178(2), F(2) – Al(2) 178(2), F(6) – Al(1) 181(2); C(21)-N(2)-Ti(1) 167.9(2), N(1)-Al(3)-N(3) 113.2(11), Al(1)-F(6)-Al(2) 129.6(9), Al(1)-F(1)-Ti(1) 142.3(9).

Experimental Section

2: **1** (1.3 g, 2.0 mmol) in toluene (40 mL) was added dropwise to a solution of $C_5H_4SiMe_3TiF_3$ (0.48 g, 2.0 mmol) in toluene (40 mL) at 0 °C and stirred. The mixture was allowed to warm to room temperature and stirred for a further 12 h. After removal of the volatile components in vacuo the residue was washed with *n*-hexane (30 mL). Compound **2** (1.16 g, 65 %) was obtained as a red microcrystalline solid. Single crystals were obtained from toluene at – 22 °C over four weeks. M.p.: 190 °C; ^{1}H NMR (250 MHz, C_7D_8, TMS): $\delta = -1.12$ (d, 3H; $AlCH_3$), – 0.68 (t, 3H; $AlCH_3$), – 0.53 (dd, 3H; $AlCH_3$), 0.21 (s, 9H; $Si(CH_3)_3$), 1.09 – 1.65 (m, 36H; $CH(CH_3)_2$), 3.02 (sept., 1H; $CH(CH_3)_2$), 3.31 (sept., 1H; $CH(CH_3)_2$), 3.49 (sept., 1H; $CH(CH_3)_2$), 3.89 (m, 3H; $CH(CH_3)_2$), 5.53, 6.04, 6.11, 6.79 (4m, each 1H; $C_5H_4Si(CH_3)_3$), 6.90 – 7.15 (m, 9H; arom. H); ^{19}F NMR (235 MHz, C_7D_8, $CFCl_3$): $\delta = -151.9$ (d, 1F), – 133.4 (m, 1F), – 132.4 (m, 1F); IR (KBr, Nujol): $\tilde{\nu} = 1588, 1422, 1308, 1250, 1179, 1108, 1045, 891, 776, 637, 563, 432$ cm^{-1}; EI-MS: *m*/*z* (%): 891 (20, M^+), 162 (100, $C_{12}H_{18}$); elemental analysis: calcd for $C_{47}H_{73}Al_3F_3N_3SiTi$: C 63.1, H 8.2, F 6.4, N 4.7; found: C 62.7, H 8.2, F 6.3, N 4.7.

3: **1** (0.99 g, 1.5 mmol) in toluene (30 mL) was added dropwise to a solution of Cp^*TiF_3 (0.36 g, 1.5 mmol) in toluene (40 mL) at 0 °C and stirred. The mixture was allowed to warm to room temperature and stirred for a further 12 h. After removal of the volatile components in vacuo the residue was washed with *n*-hexane (30 mL). Compound **3** (0.81 g, 60 %) was obtained as a dark red solid. M.p.: 105 °C (decomp); ^{1}H NMR (200 MHz, C_6D_6, TMS): $\delta = -0.80$ (s, 3H; $AlCH_3$), – 0.60 (m, 3H; $AlCH_3$), – 0.15 (m, 3H; $AlCH_3$), 1.10 – 1.41 (m, 36H; $CH(CH_3)_2$), 1.98 (s, 15H; $C_5(CH_3)_5$), 2.60 (sept., 2H; $CH(CH_3)_2$), 3.05 (sept., 1H; $CH(CH_3)_2$), 3.25 (m, 2H; $CH(CH_3)_2$), 3.80 (sept., 1H; $CH(CH_3)_2$), 6.88 – 7.15 (m, 9H; arom. H); ^{19}F NMR (188 MHz, C_6D_6, $CFCl_3$): $\delta = -168.2$ (d, 1F), – 158.4 (t, 1F), – 135.9 (s, 1F); IR (KBr, Nujol): $\tilde{\nu} = 1455, 1422, 1383, 1268, 1178, 1040, 901, 793, 670, 571$ cm^{-1}; EI-MS: *m*/*z* (%): 593 (5, $M^+ - Cp^* - 4\ CH(CH_3)_2$), 162 (100, $C_{12}H_{18}$); elemental analysis: calcd for $C_{49}H_{79}Al_3F_3N_3Ti$: C 65.7, H 8.8, F 6.3, N 4.7; found: C 65.3, H 8.9, F 5.6, N 4.6.

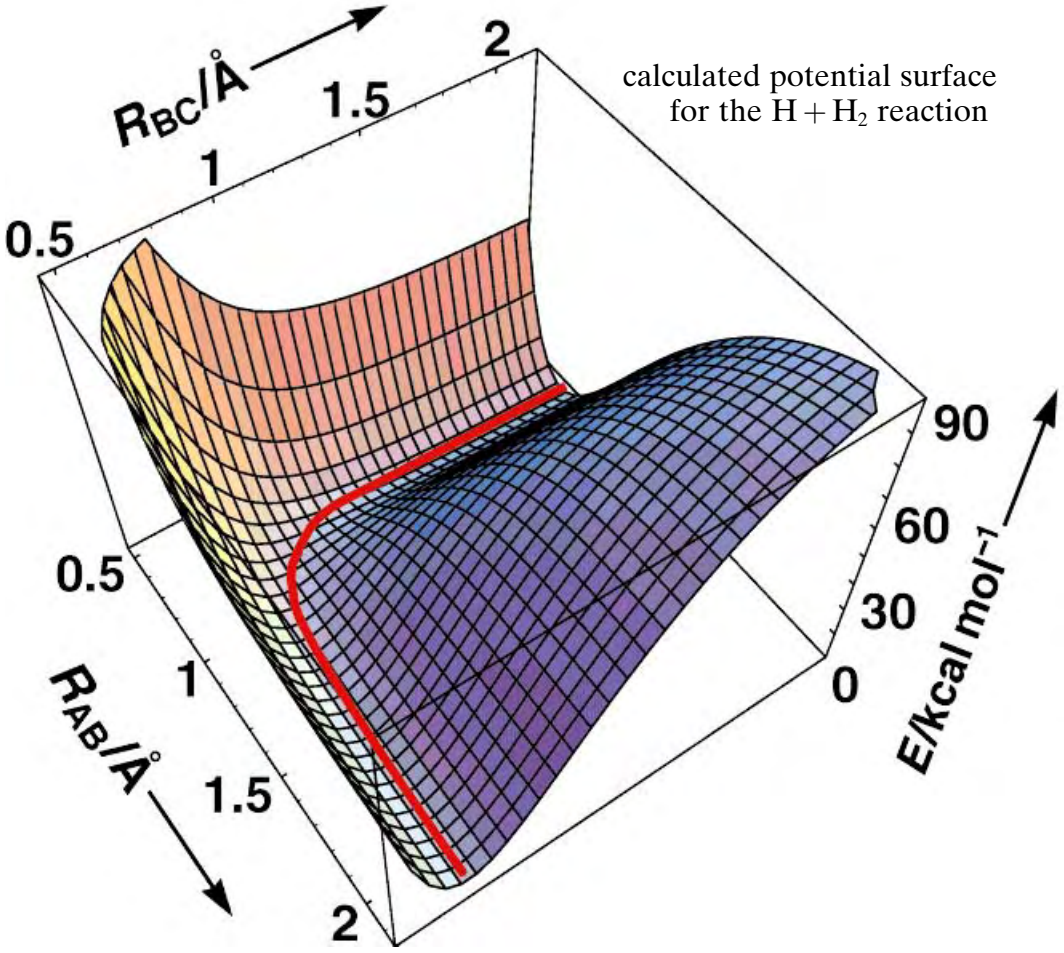
4: **3** (0.90 g, 1.0 mmol) was dissolved in diethyl ether (40 mL) at room temperature and then stirred for a further 2 h. Compound **4** crystallized at – 22 °C within 12 h. Compound **4** (0.75 g, 77 %) was obtained as a dark red crystalline solid. M.p.: 120 °C (decomp), ^{1}H NMR (200 MHz, C_6D_6, TMS): $\delta = -0.75$ (s, 3H; $AlCH_3$), – 0.60 (m, 3H; $AlCH_3$), – 0.15 (m, 3H; $AlCH_3$), 0.85 (t, 6H; CH_2CH_3), 1.10 – 1.41 (m, 36H; $CH(CH_3)_2$), 1.98 (s, 15H; $C_5(CH_3)_5$), 2.55 – 3.70 (several sept., 6H; $CH(CH_3)_2$), 3.25 (q, 4H; CH_2CH_3), 6.88 – 7.15 (m, 9H; arom. H); ^{19}F NMR (188 MHz, C_6D_6, $CFCl_3$): $\delta = -168.1$ (m, 1F), – 158.4 (m, 1F), – 139.4 (m, 1F); IR (KBr, Nujol): $\tilde{\nu} = 1590, 1430, 1380, 1260, 1187, 1101, 1040, 891, 796, 671, 566, 438$ cm^{-1}; EI-MS: *m*/*z* (%): 162 (100, $C_{12}H_{18}$); elemental analysis: calcd for $C_{53}H_{85}Al_3F_3N_3OTi$: C 65.6, H 8.7, Al 8.4, F 5.8, N 4.3; found C 65.0, H 8.6, Al 8.5, F 5.3, N 4.5.

Received: September 9, 1997 [Z 10906 IE]
German version: *Angew. Chem.* **1998**, *110*, 862 – 864

Keywords: aluminum · cage compounds · imido complexes · metathesis · titanium

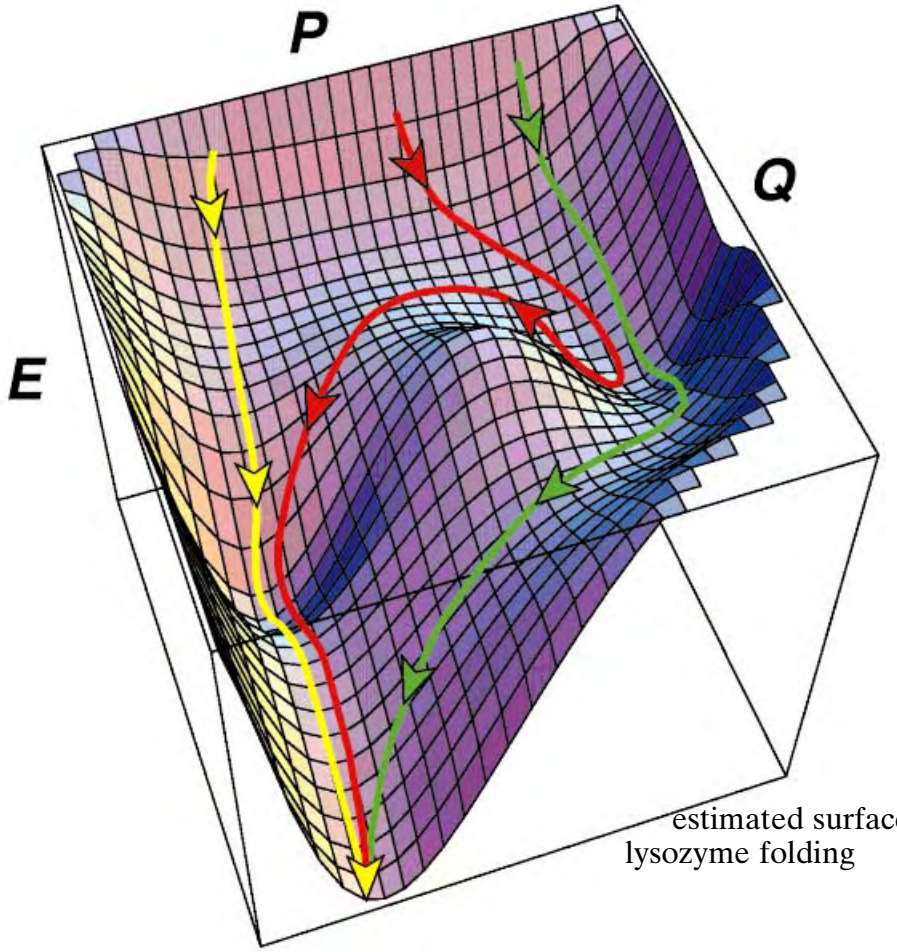
[1] D. E. Wigley, *Prog. Inorg. Chem.* **1994**, *42*, 239.
[2] V. C. Gibson, *Adv. Mater.* **1994**, *6*, 37.
[3] a) D. L. Thorn, R. L. Harlow, *Inorg. Chem.* **1992**, *31*, 3917; b) P. J. McKarns, G. P. A. Yap, A. L. Rheingold, C. H. Winter, *ibid.* **1996**, *35*, 5968.
[4] K. M. Waggoner, H. Hope, P. P. Power, *Angew. Chem.* **1988**, *100*, 1765; *Angew. Chem. Int. Ed. Engl.* **1988**, *27*, 1699.
[5] Crystal structure analyses:[11] **2**: $C_{47}H_{73}Al_3F_3N_3SiTi$, $M_r = 894.01$, triclinic, space group $P\bar{1}$, $a = 1312.9(3)$, $b = 1316.7(3)$, $c = 1662.6(3)$ pm, $\alpha = 74.62(3)$, $\beta = 81.93(3)$, $\gamma = 61.99(3)°$, $V = 2.446(1)$ nm^3, $Z = 2$, $\rho_{calcd} = 1.214$ mg m^{-3}, $F(000) = 956$, $\lambda = 71.073$ pm, $T = 133$ K, $\mu(Mo_{K\alpha}) = 0.299$ mm^{-1}. Crystal dimensions: $0.3 \times 0.3 \times 0.2$ mm^3, $4° \le 2\Theta \le 52°$; of the 51623 reflections collected, 9959 were independent and were used in the structure refinement of 541 parameters. The *R* values are $R1 = \Sigma \mid F_o - F_c \mid / \mid \Sigma F_o = 0.0424$ ($I > 2\sigma(I)$) and $wR2 = [\Sigma w(F_o^2 - F_c^2)^2/\Sigma wF_o^4]^{0.5} = 0.1152$ (all data); min./max. residual electron density = – 412/365 e nm^{-3}. **4** · 2 $C_4H_{10}O$: $C_{61}H_{105}Al_3F_3N_3O_3Ti$, $M_r = 1114.32$, monoclinic, space group $P2_1/c$, $a = 1622.2(6)$, $b = 2698(2)$, $c = 3047(2)$ pm, $\beta = 97.98(2)°$, $V = 13.20(1)$ nm^3, $Z = 8$, $\rho_{calcd} = 1.122$ mg m^3, $F(000) = 4832$, $\lambda = 71.073$ pm, $T = 133$ K, $\mu(Mo_{K\alpha}) = 0.155$ mm^{-1}. Crystal dimensions: $0.2 \times 0.3 \times 0.2$ mm^3, $4° \le 2\Theta < 52°$; of the 226699 reflections collected, 23381 were independent and were used in the structure refinement of 1479 parameters with 481 restraints. The *R* values are $R1 = 0.0559$ ($I > 2\sigma(I)$) and $wR2 = 0.1225$ (all data); min./max. residual electron density: – 547/792 e nm^{-3}.
[6] G. M. Sheldrick, *Acta Crystallogr.* **1990**, *A46*, 467.
[7] G. M. Sheldrick, SHELXL-93/96, program for crystal structure refinement, Göttingen, **1993**.
[8] a) Y. Bai, H. W. Roesky, H.-G. Schmidt, M. Noltemeyer, *Z. Naturforsch. B* **1991**, *47*, 603; b) H. W. Roesky, H. Voelker, M. Witt, M. Noltemeyer, *Angew. Chem.* **1990**, *102*, 712; *Angew. Chem. Int. Ed. Engl.* **1990**, *29*, 669; c) H. W. Roesky, T. Raubold, M. Witt, M. Noltemeyer, *Chem. Ber.* **1991**, *21*, 595; d) A. J. Blake, P. E. Collier, L. H. Gade, M. McPartlin, P. Mountford, M. Schubart, I. J. Scowen, *Chem. Commun.* **1997**, 1555.
[9] P. Yu, H. W. Roesky, A. Demsar, T. Albers, H.-G. Schmidt, M. Noltemeyer, *Angew. Chem.* **1997**, *109*, 1846; *Angew. Chem. Int. Ed. Engl.* **1997**, *36*, 1766.
[10] In the ^{19}F NMR spectra recorded at room temperature and at 70 °C the F atoms are inequivalent, which is attributed to the steric effects of the ligands.
[11] The data were collected on a Stoe-Siemens-Huber four-circle diffractometer with a Siemens-CCD area detector. The intensities were recorded with φ and ω scans. The data were integrated with the program SAINT. The structures were solved with direct methods (SHELXS-90/96)[6] and refined according to least-squares methods against F^2.[7] All non-hydrogen atoms were refined anisotropically. All hydrogen atoms were included in the refinement in geometrically ideal positions. All disorders were resolved with distance and ADP restraints and refined anisotropically. Crystallographic data (excluding structure factors) for the structures reported in this paper have been deposited with the Cambridge Crystallographic Data Centre as supplementary publication no. CCDC-100627. Copies of the data can be obtained free of charge on application to CCDC, 12 Union Road, Cambridge CB2 1EZ (fax: (+44) 1223-336-033; e-mail: deposit@ccdc.cam.ac.uk).

 © WILEY-VCH Verlag GmbH, D-69451 Weinheim, 1998 1433-7851/98/3706-0845 $ 17.50+.50/0



calculated potential surface for the $H + H_2$ reaction

A knowledge of the potential energy surface that determines the dynamics of a polypeptide chain is as important for understanding protein folding as is the potential surface for the $H + H_2$ reaction.



estimated surface for lysozyme folding

ANGEWANDTE CHEMIE ©WILEY-VCH

Protein Folding: A Perspective from Theory and Experiment

Christopher M. Dobson,* Andrej Šali, and Martin Karplus*

Proteins are involved in virtually every biological process, and their functions range from catalysis of chemical reactions to maintenance of the electrochemical potential across cell membranes. They are synthesized on ribosomes as linear chains of amino acids in a specific order from information encoded within the cellular DNA. To function, it is necessary for these chains to fold into the unique native three-dimensional structure that is characteristic for each protein. This involves a complex molecular recognition phenomenon that depends on the cooperative action of many relatively weak nonbonding interactions. As the number of possible conformations for a polypeptide chain is astronomically large, a systematic search for the native (lowest energy) structure would require an almost infinite length of time. Recently, significant progress has been made towards solving this paradox and understanding the mechanism of folding. This has come about through advances in experimental strategies for following the folding reactions of proteins in the laboratory with biophysical techniques, and through progress in theoretical approaches that simulate the folding process with simplified models. The most recent advances in this area are comparable in significance to those that took place in developing an understanding of reactions of small molecules some thirty years ago. In this article we review the present state of our knowledge of the protein folding reaction and compare the concepts that are emerging with those that are now established for simpler reactions. A major distinction between protein folding and reactions of small molecules is the heterogeneity of the folding process and the resulting complex interplay between entropic and enthalpic contributions to the free energy of the system during the reaction. A unified model for protein folding is outlined based on the effective energy surface of a polypeptide chain and its bias towards the native state. An understanding of folding is important for the analysis of many events involved in cellular regulation, the design of proteins with novel functions, the utilization of sequence information from the various genome projects, and the development of novel therapeutic strategies for treating or preventing debilitating human diseases that are associated with the failure of proteins to fold correctly.

Keywords: kinetics · molecular dynamics · protein folding · proteins · structure elucidation

[*] Prof. C. M. Dobson
Oxford Centre for Molecular Sciences, New Chemistry Laboratory
University of Oxford
South Parks Road, Oxford OX1 3QT (UK)
Fax: (+44) 1-865-275-921
E-mail: chris.dobson@chem.ox.ac.uk
Prof. M. Karplus
Department of Chemistry and Chemical Biology
Harvard University
12 Oxford Street, Cambridge, MA 02138 (USA)
Fax: (+1) 617-496-3204
email: marci@tammy.harvard.edu
and
Laboratoire de Chimie Biophysique, Institut Le Bel
Universite Louis Pasteur
F-67000 Strasbourg (France)
Fax: (+33) 388-60-83-63
E-mail: marci@brel.u-strasbg.fr
Prof. A. Šali
The Rockefeller University, New York, NY (USA)

1. Introduction

Reactions are central to chemistry. They range from simple exchange processes involving only a few atoms to protein folding, in which thousands of atoms take part. The understanding of a reaction is based on a knowledge of the role of the dominant interactions that determine the potential energy surface and a description of the dynamics leading from the reactants to the products. Substantial progress has been made in the past thirty years toward achieving this understanding for simple reactions through a combination of experimental developments and theoretical advances.[1] By contrast, protein folding is so complex that even the approaches to be used for its characterization are not fully defined.[2, 3] In this review, we begin by addressing some of the similarities and differences between simple chemical reactions and protein folding. Apart from the much greater complexity of protein folding, which requires the introduction of simplified theoretical models and

 © WILEY-VCH Verlag GmbH, D-69451 Weinheim, 1998 1433-7851/98/3707-0869 $ 17.50+.50/0

novel experimental approaches, a number of more general issues arise. Not the least of these is the presence of an ensemble of molecules differing substantially in their structure and dynamics at various stages of the folding reaction.

Globular proteins are synthesized as linear chains of amino acids. To carry out their functions, they must fold rapidly and reliably to a specific structure designed by evolution for the particular task (Figure 1). Although the folding process in a cell involves a range of catalytic and control systems,[4] the information for folding is contained in the amino acid sequence for many, if not all, proteins.[5] A protein sequence must satisfy two requirements: one thermodynamic and one kinetic.[2, 6] The thermodynamic requirement is that the molecules adopt a unique folded conformation (the native state) which is stable under physiological conditions. The kinetic requirement is that the denatured polypeptide chain can fold into the native conformation within a reasonable time. A polypeptide chain can adopt so many conformations that there must be a way to reach the native state in a time many orders of magnitude shorter than that required for a random search.[7] To obtain an estimate of this order of magnitude, one can assume that there are three configurations for each amino acid residue. If a protein is made up of a polypeptide chain consisting of 100 amino acids, there is a total of about 10^{49} conformations. If only 10^{-11} s were required to convert from one conformation into another, a random search of all conformations would still require 10^{36} s or about 10^{29} years. This led Levinthal to suggest "pathways" for protein folding.[8] Many theoretical attempts to "fold" pro-



C. M. Dobson



A. Šali



M. Karplus

Christopher Martin Dobson, born in Rinteln (Germany) in 1949, studied chemistry at the University of Oxford and completed his D. Phil. thesis on the NMR spectroscopy of proteins under the supervision of Professor R. J. P. Williams in 1975. After research fellowships in Oxford he moved to Harvard University in 1977 as an Assistant Professor of Chemistry. In 1980 he returned to the University of Oxford as a Lecturer and then Reader in Chemistry. He is presently Professor of Chemistry and Director-elect of the Oxford Centre for Molecular Sciences. In 1992 he was appointed a Howard Hughes International Research scholar, and in 1996 he was elected a Fellow of the Royal Society. His research interests have been focused on the development and application of NMR and other biophysical methods to biological and chemical problems. His recent activities have been directed particularly at unravelling the underlying mechanism of protein folding and determining its relevance to biological function and disease.

Andrej Šali, born in 1963 in Kranj (Slovenia), studied chemistry at the University of Ljubljana. He obtained his Ph.D. in 1991 at Birkbeck College, University of London with Professor T. L. Blundell in the area of comparative protein structure modelling. During a postdoctoral fellowship with Professor M. Karplus at Harvard University, he worked in the area of protein folding simulations. Since 1995 he has been an Assistant Professor at The Rockefeller University and is focusing on developing comparative modelling of protein structures and its applications in genomic research.

Martin Karplus, born in Vienna (Austria) in 1930, received his B.A. from Harvard College in 1950 and his Ph.D. from the California Institute of Technology in 1953. He worked at Oxford University as an National Science Foundation postdoctoral fellow from 1953 until 1955, when he joined the faculty of the University of Illinois. In 1960 Karplus became a professor at Columbia University, and in 1966 a professor at Harvard University. He was named Theodore William Richards Professor of Chemistry there in 1979. He is also Professeur Conventionné at the Université Louis Pasteur in Strasbourg. He is a member of the National Academy of Sciences (USA), the American Academy of Arts and Sciences, and the Netherlands Academy of Arts and Sciences. Early in his career Karplus studied magnetic resonance spectroscopy; of particular interest was his theoretical analysis of nuclear spin – spin coupling constants. He made fundamental contributions to the theory of reactive collisions between small molecules based upon trajectory calculations. He was one of the first researchers to apply many-body perturbation theory to atomic and molecular systems. He has studied reactions in biological molecules, such as the bonding of oxygen to hemoglobin and the photochemistry of visual pigments. His more recent work has been concerned with the development of molecular dynamics and other simulation methods for the elucidation of the properties of proteins and nucleic acids. He is now studying enzymatic reactions, protein folding, and the application of computational methods to combinatorial ligand design.

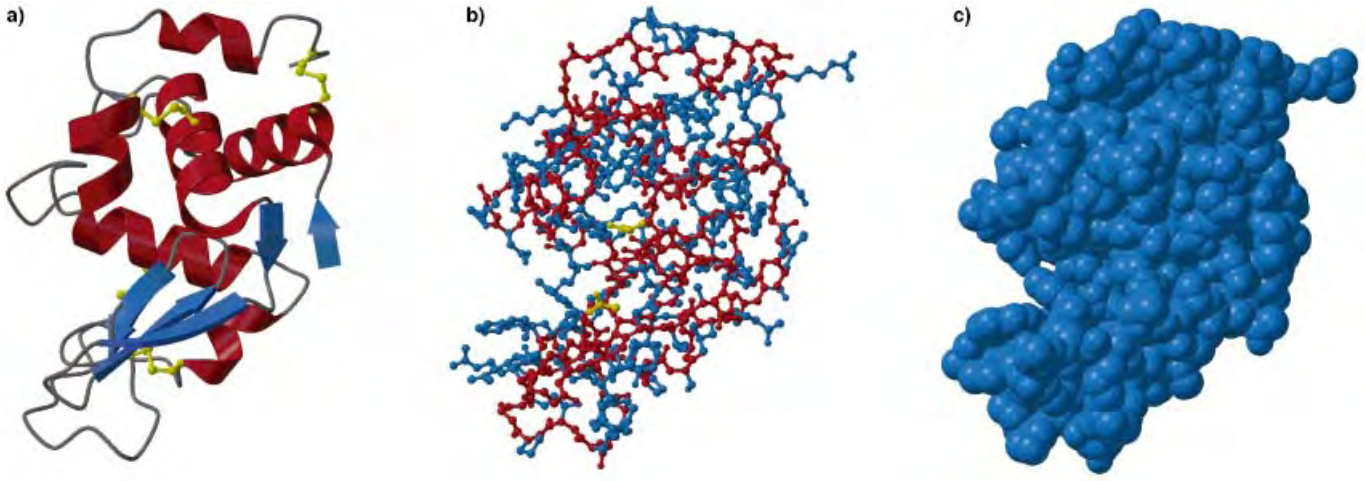


Figure 1. Different representations of the protein lysozyme (PDB code: 8LZT) drawn with the programs Molscript[163] and Render.[164] a) Ribbon diagram of the fold of the main chain of the protein with 129 residues. The α helices are shown as red spirals, and the β strands as blue arrows. The cross-links due to the disulfide bonds are shown in yellow. b) Ball-and-stick drawing in which the main chain is red, the side chains are blue, and the side chains involved in the catalytic mechanism are yellow. c) Space-filling view showing that the protein is a close-packed structure. Calculations with normal van der Waals radii indicate that more than 75 % of space is occupied.

teins based on the pathway concept have been made, but no one has succeeded in doing so,[9] in spite of some claims to the contrary. The difference between the limitations of what can be done on a computer in thousands of hours and what nature can do in less than a second clearly poses the question of the mechanism of protein folding, a question that has perplexed researchers for many decades.[10, 11]

Despite the long-standing interest in protein folding, it is only relatively recently that experiments to probe the details of the events that occur during the folding process have begun to be carried out.[3] As was the situation for reactions of small molecules thirty years ago,[12, 13] protein folding is now at the stage where theory and experiment can together make rapid progress toward an understanding of this complex process. Toward this end, a framework must be developed for interpreting the results of the new experimental techniques and for probing specific features of the folding reaction. In this review, we briefly outline some aspects of the reactions of small molecules to permit us to contrast them with the protein folding reaction. We then show how folding can be described in terms of existing theoretical and experimental results. Although the differences among proteins are often emphasized, the characteristics that emerge point to an underlying universality of the mechanism of folding when it is interpreted in terms of an averaged effective energy and the associated configurational entropy.

Because of recent theoretical and experimental advances in methods for studying the mechanism of protein folding, a review of this rapidly developing field addressed to chemists is particularly timely. Readers may wish to refer also to a number of other reviews directed more toward biologists and biophysicists that have appeared recently;[6, 14–17] they can serve to complement the present article. The viewpoint presented emphasizes our own work and experience, although we have profited greatly from the contributions of many others, cited in the list of references, to this exciting and rapidly developing field.

2. Energy Surfaces for Reactions of Small Molecules

The nature of any reaction, whether of a small molecule or a protein, is determined by the potential energy surface and the laws of dynamics.[1, 12, 13] The detailed experimental and theoretical analysis of simple chemical reactions is based on well-defined procedures. We briefly review them here to contrast the situation with that for proteins. Experimentally, the potential energy surface for a reaction is usually characterized first in a relatively crude way by measuring the reaction rate as a function of temperature to evaluate the activation energy E_A and the pre-exponential factor $A(T)$ in the Arrhenius formula; that is, the temperature-dependent rate constant is written as Equation (1). Most of the temper-

$$k(T) = A(T)\exp(-E_A/RT) \quad (1)$$

ature dependence arises from the exponential (Arrhenius) factor E_A/RT, whereas the factor $A(T)$ generally has only a weak temperature dependence. Measurements of $A(T)$ and E_A can be complemented by reactive scattering data obtained from studies with crossed molecular beams[12] and by measurements that permit direct observation of the transition state.[18] Such studies provide the details necessary to characterize the potential energy surface. Theoretical calculations can also be used to determine the potential energy surface, the reaction coordinate, and the transition state.[19] Finally, trajectory calculations, or their quantum-dynamical analogues, can be used to determine the overall rate constant and to simulate more detailed reactive scattering behavior.[13, 20] For a small number of simple reactions, the available theoretical descriptions are as accurate as the experimental results.[1, 20]

We consider briefly the simplest and best understood chemical reaction, the bimolecular exchange of a hydrogen atom with a hydrogen molecule. Only three internal coor-

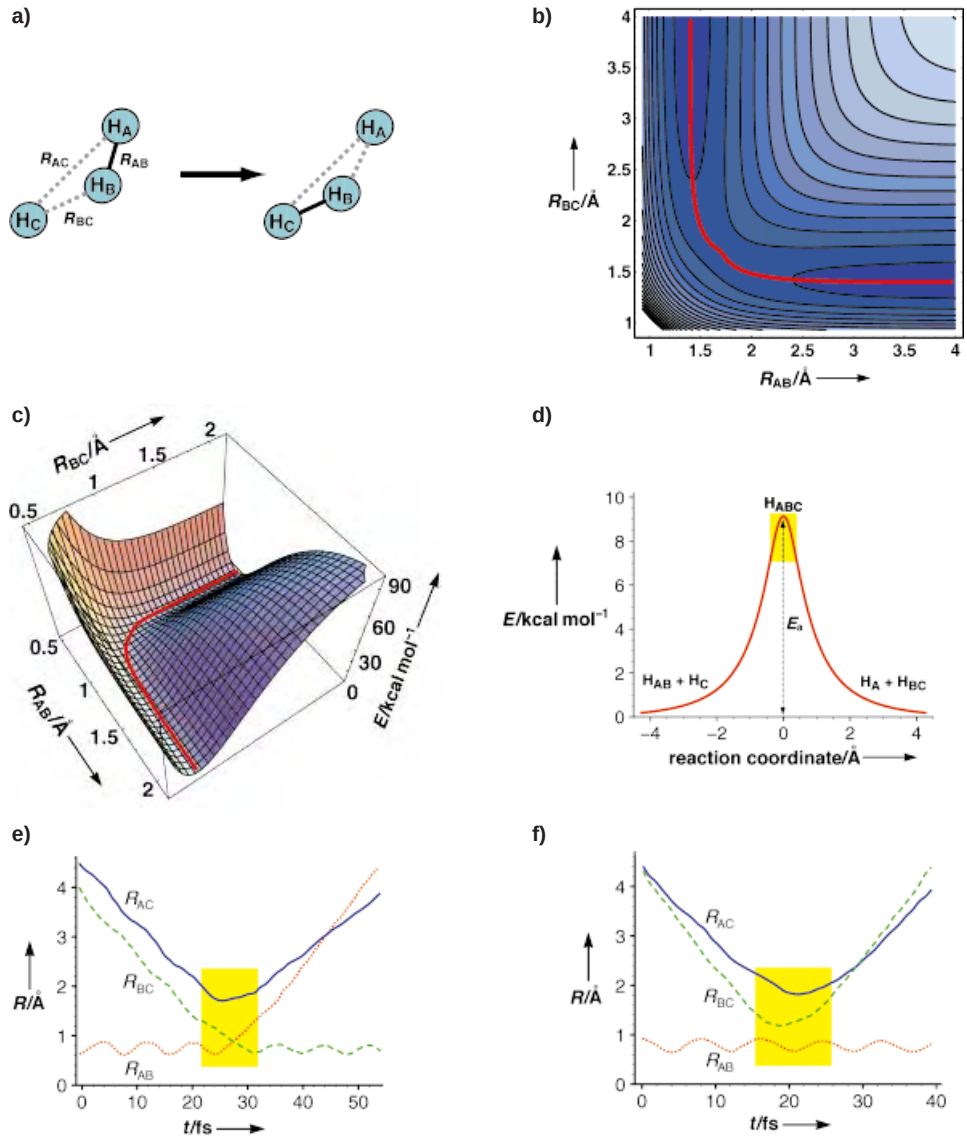


Figure 2. The exchange reaction between a hydrogen atom and a hydrogen molecule. a) Schematic representation of the reaction with definitions for the distances R_{AB}, R_{AC}, and R_{BC}. b) Contour plot of the potential energy surface for a linear collision as a function of the distances R_{AB} and R_{BC} with $R_{AC} = R_{AB} + R_{BC}$; the minimum-energy path is shown in red. c) Same as b), but in a three-dimensional representation. d) Energy along the reaction coordinate corresponding to the minimum-energy path in b) and c); the transition state is indicated in yellow. e) A typical trajectory for the reactive, three-dimensional collision; the three distances R_{AB}, R_{AC}, and R_{BC} are represented as a function of time. f) A typical trajectory for the nonreactive collision; shown as in e). In both e) and f) the interactions between the three atoms are limited to a very short time period (yellow background); this mirrors the narrow potential energy barrier in d). The results are adapted from references [13, 19].

dinates are needed to describe the reaction (Figure 2a). The atoms move on a potential energy surface, which gives the energy of the system as a function of the coordinates. This surface corresponds to the "energy landscape" for the H+H_2 reaction, Figures 2b and 2c show the surface for a collinear collision and the reaction coordinate, which is a combination of the degrees of freedom essential for characterizing the minimum-energy path from reactant to product. The energy along the reaction coordinate is shown in Figure 2d. At a nonzero temperature T the kinetic energies of the H atom and the H_2 molecule are such that the reaction does not follow the minimum-energy path. However, because the valley from reactants to products is narrow and well-defined and there is a highly localized transition state at the top of the barrier, the trajectories remain close to the minimum-energy path at room temperature. As we shall see later, the reaction path for proteins is much less well defined, and the folding polypeptide chain moves over a large region of the energy surface during the folding reaction. This means that, in contrast to H+H_2, the entropy as well as the energy play an important role in protein folding. The well-defined minimum-energy path for H+H_2 results in the simple trajectories shown in Figures 2e and 2f for a reactive and a nonreactive collision, respectively. In the reactive collision an atom approaches, collides with the molecule, and forms a new bond with one of the H atoms, while the other H atom leaves rapidly; the nonreactive collision looks very similar except that there is no exchange of atoms. All of the interesting behavior takes place in only 10 fs

over a very limited range of distances, which is shaded yellow in Figures 2d–f. The initial conditions (positions and velocities) and the interactions in this ultrashort event determine whether the collision is reactive or nonreactive.

3. Protein Folding Reactions

Protein folding reactions have very different characteristics from reactions of small molecules. For example, although the Arrhenius equation can be and often is applied to protein folding, the preexponential factor has a strong temperature dependence.[21] This indicates that protein folding has a complexity not present in most simple reactions. Furthermore, in contrast to the femtosecond time scale of the reactive event in the case of $H+H_2$ (Figure 2), the interactions between the different parts of the polypeptide chain are significant over the entire folding time of milliseconds or longer.

A better analogue for protein folding may be the condensation of atomic clusters (Figure 3), whose thermodynamics and kinetics have been studied in great detail.[22–24] Such clusters have a gas→liquid condensation, which corresponds to the transition from a denatured random coil to a compact but disorganized globule in a protein. If the temperature is low enough, the liquidlike clusters rearrange to an organized solid by a search that is analogous to that through a collapsed globule for the native state in a protein. Of course, a protein has a unique native state determined by its amino acid sequence, whereas clusters composed of identical atoms have many symmetry-related solid structures. In phase transitions of atomic clusters and proteins, multiple pathways are the rule and the transition from the liquid (compact globule) state to the solid (native) ground state is pseudo-first-order; that is, the two states are well-defined and separated by a free energy barrier.

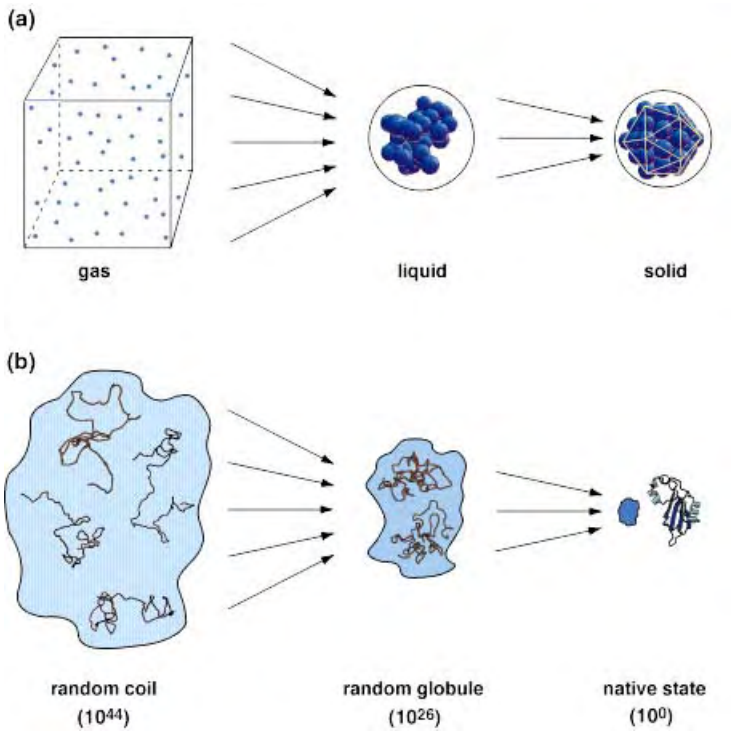


Figure 3. a) Schematic illustration of the phase transitions of a stable cluster consisting of 55 Lennard–Jones particles. The solid cluster has the structure of a Mackay icosahedron.[19] b) Schematic illustration of the corresponding transitions during protein folding. The protein barnase, composed of 110 amino acid residues, is used as an example. Carbon α traces are shown (prepared by the program Molscript).[163] The random coil and disorganized globule conformations were constructed to have radii of gyration of approximately 31 and 15 Å, respectively; the native structure has a radius of gyration of 13.4 Å. The numbers of possible main-chain conformations were calculated from the estimates of the main-chain entropy per residue; there are 2.57 and 1.7 conformations per residue in the random coil and random semicompact states, respectively.[55a] Therefore, the number of random coil states is $2.57^{109} \approx 10^{44}$, and the number of compact random globule states is $1.7^{109} \approx 10^{26}$.

Since proteins and atomic clusters have multidimensional potential energy surfaces involving a large number of degrees of freedom, instead of only three for $H+H_2$, there can be a multitude of local minima and transition regions. Furthermore, the structural changes in folding from the denatured (reactant) state to the native (product) state involve the entire protein, as does the rearrangement to the solid state of a liquid cluster.[22, 23] This suggests that approaches based on the statistical mechanics and dynamics of large systems[2, 25–28] can provide more insights concerning protein folding than the extrapolation from the behavior of small molecules.

An important difference between descriptions of reactions of small molecules and protein folding or cluster condensation is that it is useful to replace the potential energy surface of the former (Figure 2) by a temperature-dependent averaged effective energy surface for the latter. This surface corresponds to a Boltzmann-weighted average of the accessible energies for each value of an appropriately chosen progress variable. The value of the progress variable, which describes the approach to the native state, is obtained by averaging over many nonessential degrees of freedom. The resulting motion on the effective surface is expected to be diffusive.[14] Therefore, it can be described by a Kramers-type model,[29] similar to that appropriate for many solution reactions. An example is the very simple conformational changes from *gauche* to *trans* in liquid butane.[30] Of course, the protein folding reaction is much more complex since a multitude of conformational transitions in a long polypeptide chain are involved. In particular, both protein folding and the formation of solid clusters have a many-body character that plays an important role in the subsequent analysis.

As the comparison with atomic clusters suggests, it is not possible to define a *simple* reaction coordinate on the multidimensional effective energy surface for protein folding. Since there are many ways of reaching the native state, a single minimum-energy path or pathway, in the language of Levinthal,[8] is unlikely to dominate the folding reaction. A progress variable or variables must replace the reaction coordinate in analyses of protein folding. These variables describe the progress of the reaction from the initial to the final state, as does a reaction coordinate, but include the

possibility of many fundamentally different paths. This suggests that our knowledge of folding can never be as detailed as in the case of small molecules, and that we have to be careful in extending concepts from reactions of small molecules, even those catalyzed by enzymes, to protein folding.

If there is no simple reaction coordinate in protein folding, there is also no simple transition state. Indeed, even the rotation of a single side chain in a protein requires an extended region on the potential energy surface (a transition "seam") to describe the reaction.[31] It is likely that the most precise statement possible for the protein folding reaction will refer to a multidimensional transition region on the averaged effective energy surface that includes the structures from which the polypeptide chain folds rapidly and with high probability to the native state. There may be multiple transition regions with similar free energies but significantly different structures that do not interconvert rapidly, in which case parallel paths would contribute to the overall folding reaction. There is also the question of whether standard kinetic schemes, which use the concentrations of a small number of well-defined species, are appropriate for the protein folding reaction.

The temperature dependence of the stability of the various states in cluster formation (protein folding) is determined by the balance between the effective energy and the configurational entropy. The number of available states decreases by many orders of magnitude in the progression from the gas (random coil) through the liquid (compact globule) to the solid (native) state (Figure 3b). This could represent nothing more than the necessary reduction in the number of available states as the system becomes more organized (nativelike). Alternatively, the effective energy function may bias the motion in the direction of the native state and result in a more rapid reduction in the accessible configuration space. The latter is essential to obtain rapid folding of proteins and solidification of clusters. Therefore, the essential problem to be solved is how the system "finds" the ground state or, in other words, what in the nature of the effective energy surface and the resulting balance between energy and entropy determines whether the system can reach the ground state in a reasonable time or not.

4. Thermodynamics of Protein Folding

Prior to describing our current understanding of the folding reaction, it is useful to consider the thermodynamics of proteins. The free energy of the native state of a protein is only slightly lower than that of the denatured state under physiological conditions owing to a near cancellation of large energetic and entropic contributions. The major interactions are the nonbonded van der Waals and electrostatic terms in the potential energy function.[32] They act between the atoms of the protein and between the protein atoms and the solvent. For interpreting folding thermodynamics and dynamics, it is convenient to define an effective energy function that includes one essential part of the free energy of a polypeptide chain in solution. This corresponds to a "potential of mean force"[33] and is obtained from a Boltzmann average at the temperature of interest, of the polypeptide–solvent interactions over all positions of the solvent molecules for a given polypeptide configuration. A potential of mean force of the type considered here can be defined exactly for the system at equilibrium; that is, to describe the thermodynamics.[2] Extending such a potential of mean force to time-dependent phenomena, such as protein folding, requires that the relaxation of the solvent be fast compared to the protein motions involved in the folding reaction. This appears to be a good approximation, as illustrated in simulations of protein unfolding in water.[34, 35] Such an effective energy function, which strongly favors the native state, contains all contributions to the total free energy (e.g., the hydrophobic effect, solvation of polar groups and hydrogen bonding that involve both van der Waals and electrostatic interactions) except the configurational entropy, which strongly favors the denatured state. The latter arises from the fact that the conformation space available to the polypeptide main chain and side chains is much more restricted in the native state than in the denatured state.

Analysis of the contributions to the effective energy (i.e., the potential of mean force) indicates that the nonpolar groups strongly favor the folded state owing to the attractive van der Waals interactions in the tightly packed (solidlike) native structure and the hydrophobic effect, which favors the burial of nonpolar groups.[32, 36] By contrast, the polar groups (the peptide groups and the polar and charged side chains) make a much smaller contribution to the stability of the native state owing to a balance of the interactions in the interior of the protein and those with the solvent. For lysozyme, as an example, calculations show that the nonpolar groups contribute $450\,\mathrm{kcal\,mol^{-1}}$ and the polar groups contribute $87\,\mathrm{kcal\,mol^{-1}}$ at 25 °C to the free energy of denaturation.[36] The stabilization of the native state due to the effective energy term (about $537\,\mathrm{kcal\,mol^{-1}}$) is counterbalanced by a configurational entropy contribution of about $523\,\mathrm{kcal\,mol^{-1}}$ at 25 °C. This yields a net free energy of unfolding of $14\,\mathrm{kcal\,mol^{-1}}$ (on the order of $0.1\,\mathrm{kcal\,mol^{-1}}$ per residue), which is a typical value for globular proteins.[36] In contrast, the energy or enthalpy difference between the native and unfolded state can be significantly larger; for lysozyme at 25 °C, the unfolding enthalpy is $58\,\mathrm{kcal\,mol^{-1}}$.[36, 37]

An important feature of protein folding is that the overall structure, such as that represented in Figure 1, is determined by the sequence of the protein.[5] Native folds for three different proteins are illustrated in Figure 4. The difference in sequence gives rise to differences in the nature of the secondary structure (the regions of α-helix and β-sheet) and the tertiary structure (the overall folding pattern). Three-dimensional structures of approximately 6000 proteins have been determined by X-ray crystallography and NMR spectroscopy.[38] The domains in these proteins can be clustered into approximately 350 families of folds, which consist of sequences that have similar structures.[39] It has been estimated that only 1000 or so different folds exist.[39–41] This is a large number but much smaller (by a factor of about 100 or so) than the total number of different sequences in the human genome. Some folds are adopted by a large number of

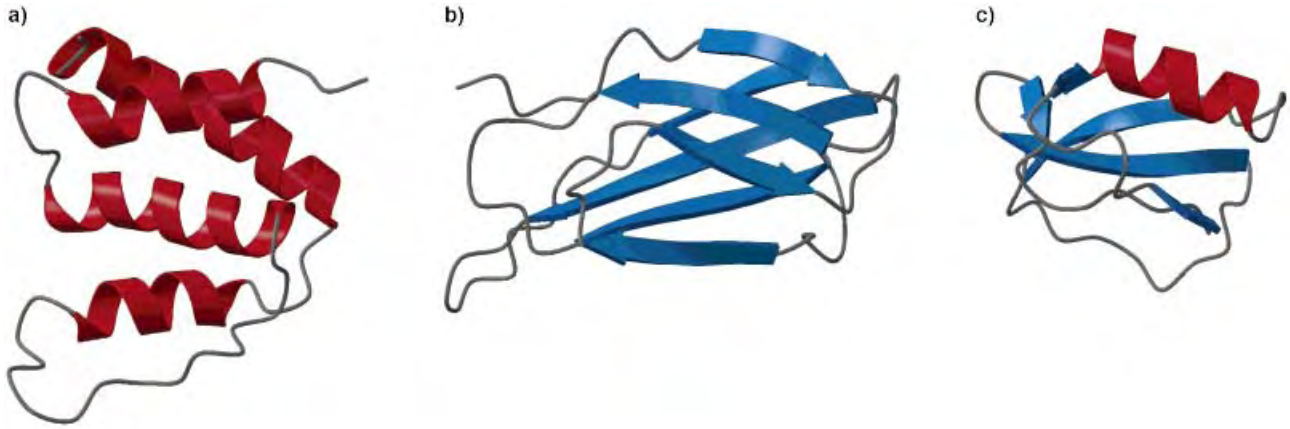


Figure 4. Structures of representative folds (teriary structure) of small proteins. a) Bovine acyl-coenzyme A binding protein (PDB code: 2ABD), an α-helical protein; b) Type-III module of the tenth domain of the human fibronectin (PDB code: 1TTG), a β-sheet protein; c) Barley chymotrypsin inhibitor 2 (PDB code: 2CI2), an α/β protein. Secondary-structure elements correspond to α helices (red) and β strands (blue). The figures were drawn with the programs Molscript[163] and Render.[164]

sequences, which is perhaps related to the stability of the fold[42] or to the robustness and speed of the folding process, but for any given sequence only one fold exists in almost all cases. The uniqueness of the native state arises from the fact that the interactions that stabilize the native structure significantly destabilize alternative folds of the same amino acid sequence; that is, sequences with a deep energy minimum for the native state have been generated through evolution to eliminate wrongly folded or partly unfolded structures at physiological temperatures. This "energy gap" between the native state and significantly misfolded structures[25, 55a] is a key element in the relation between sequence and structure and plays an important role in protein folding, as we describe in Section 5.

To relate the free energy of a protein to its conformations, it is necessary to describe the latter in terms of an order parameter. Qualitative curves of the free energy of the polypeptide chains in equilibrium as a function of the radius of gyration R_g, one possible order parameter for protein folding, are shown in Figure 5 for two different temperatures.[2, 43] At each value of R_g the free energy corresponds to a Boltzmann average over all values of the other internal coordinates, including those of the solvent. The form of the free energy curve is strongly dependent on the environmental conditions, particularly the temperature.

The curve in Figure 5a is valid for a temperature at which the native state is stable. It is significantly below the folding transition temperature, T_m, at which the native and denatured states have equal free energy. The native state is a deep, narrow minimum and thus satisfies the thermodynamic criterion for protein stability. In this minimum the atomic fluctuations have a magnitude of up to approximately 2 Å, and such motions take place on a picosecond to nanosecond time scale.[44] All structures visited by such fluctuations are very similar and correspond approximately to the differences between X-ray structures of proteins that are members of the same family (e.g., myoglobins and hemoglobins from the globin family[44]). Many simulations of molecular dynamics that use empirical potentials have explored this region of conformational space,[45] which is the one most relevant to

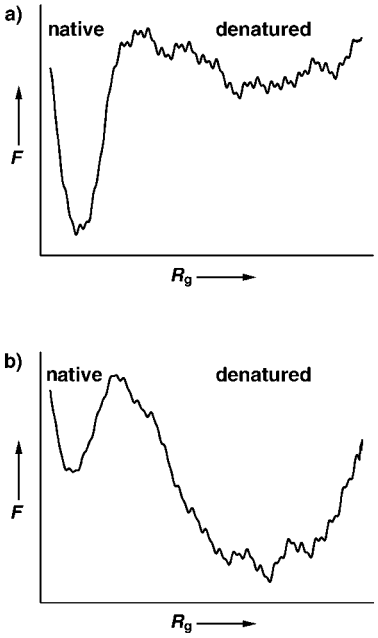


Figure 5. The free energy F of protein folding as a function of the radius of gyration at a) a temperature below T_m, at which the native state is stable, and b) a temperature above T_m, at which the denatured state is stable. The ranges corresponding to the native state and the denatured region are indicated. The curves are schematic but should be representative of real proteins.

protein function. The other region of the free energy curve corresponds to the vast number of configurations which make up the denatured state. In the folding process the polypeptide chain may go from a relatively extended random coil with large R_g to a disorganized compact globule that has liquidlike properties and from there to the native state. The length scale of the structural changes involved is on the order of 10 to 20 Å, and the time scale is in the microsecond to millisecond range. In other cases, the compact globule may lead to an intermediate with some order (e.g. nativelike secondary structure) that is often referred to as a "molten globule".[56] The regions corresponding to a random coil, a compact

globule, and the native state in protein folding have their analogues in the solid, liquid, and gaseous states of atomic clusters (see Figure 3). Phase diagrams for proteins and for simple protein models show the existence of these different phases.[2, 47, 48]

Figure 5b shows the free energy of a protein as a function of R_g at a temperature significantly above T_m. As the temperature is raised, the denatured state is stabilized by its increase in configurational entropy relative to the native state. The curve in Figure 5b also corresponds to the polypeptide chain under denaturing solvent conditions. Although the native minimum may be nearly unchanged, the random coil region has a lower free energy, primarily as a result of its energetic stabilization by better interactions of the unfolded polypeptide chain with the denaturant.[49] Evidence concerning the potential energy surface and the fluctuations characteristic of the different states can be derived from experimental studies; for example, from the rate with which amide group hydrogens in the protein exchange with solvent.[50]

5. Energy Surfaces for Protein Folding: A Theoretical Approach

To determine possible features of the protein folding reaction and the mechanism by which the Levinthal paradox is resolved, it is necessary to go beyond the simple one-dimensional representation used in Figure 5. In contrast to the $H+H_2$ reaction, where a reduction from three variables to one yields a reaction coordinate, a description that is useful for obtaining an understanding of the protein folding reaction requires a reduction from several thousand degrees of freedom to one or a few progress variables. Since the validity of such a reduction is not evident a priori, it must be attempted and justified a posteriori by comparison of theoretical predictions with experimental measurements.

Many phenomenological models for protein folding have been proposed over the years, but most of them were neither specific enough nor detailed enough to permit actual calculations; a recent review of these models is given in reference [51]. The introduction of lattice models with simplified potentials (see Appendix 1) has made possible simulations of folding for systems that include many of the essential complexities of the folding reaction (e.g., there is a Levinthal paradox) and yet are simple enough for a complete analysis (i.e., it is possible to obtain information at any level of detail for the folding process in such model systems). From the lattice simulations[6, 14–16] and statistical mechanical models,[25] insights into possible folding scenarios have been obtained. They provide a basis for exploring the general characteristics of the mechanism of folding for real proteins and for relating experiment to theory. In the following sections, we review the results obtained from lattice models and show what has been learned from them.

Although lattice models (see Appendix 1) are clearly oversimplified,[52] they play a role in the investigation of protein folding that is analogous to that of $H+H_2$ for chemical reactions. The general concepts developed from the detailed analysis of the $H+H_2$ reaction, which involves only three atoms, serve as a basis for the treatment of much more complex reactions with activation barriers. Moreover, the foundations of the theory of the transition state were developed by Wigner[53] for the $H+H_2$ reaction. Simple lattice models treat an amino acid as a single quasiparticle (without representing the side chains), use contact potentials rather than much more detailed potential functions, and restrict the motions to a lattice instead of three-dimensional space. Nevertheless, the detailed analysis of lattice models serves to provide concepts that are useful for understanding the folding reactions of real proteins.

To go beyond the thermodynamic description (Figure 5), it is necessary to find progress variables appropriate for the folding reaction. One possibility is the radius of gyration R_g (Figure 5). However, in some circumstances there is a relatively little change in R_g over the region of interest—for example, if the system goes from a disorganized globule to the native state while remaining compact. A more useful progress variable is the fraction of native contacts Q, which varies from a value near zero for the highly denatured (coil) state to unity for the native state. For the 27-mer, described in Appendix 1, there are 156 different possible contacts and 28 native contacts in a $3 \times 3 \times 3$ cube, whereas for a 125-mer,[54a] there are 3782 possible contacts and 176 native contacts in a $5 \times 5 \times 5$ cube. In a real protein, although there are many more "native contacts", a subset of 50 to 100 contacts can be chosen to define the native state.[54b] This supports the use of the native contacts as a progress variable for the folding reaction.

To visualize the reaction as a function of Q, we use a surface to represent the averaged effective energy and configurational entropy of the polypeptide chain as it folds from the denatured to the native state (Figures 6 and 7). Both quantities are calculated by averaging over a series of simulations for a given sequence. It is this type of average that is suggested by many-body statistical mechanics and by the comparison between protein folding and the formation of solids of rare gases (see Figure 3). The resulting values depend on the temperature of the system; that is, more conformations with higher energies are sampled along the folding trajectory at higher temperatures. Therefore, in drawing and interpreting a diagram, it is necessary to consider the temperature of the simulation.

Figures 6 and 7 show results obtained from folding simulations of a 27-mer lattice model;[30, 55a] this model system is expected to give results applicable to small proteins. Figure 6 corresponds to a low-temperature simulation, and Figure 7 to a high-temperature simulation. For both cases, the native state is stable (in accord with the diagram in Figure 5a), and folding occurs in a reasonable amount of time. At still lower temperatures, folding may be extremely slow because the chain cannot escape from local minima; at very high temperatures the native state is not stable, and the number of accessible conformations is so large that the Levinthal problem cannot be solved. The scenarios illustrated in Figures 6 and 7 could correspond to the behavior of different proteins under the same environmental conditions or to the same protein under different environmental conditions (see below). Since the resulting surfaces are based on statistical

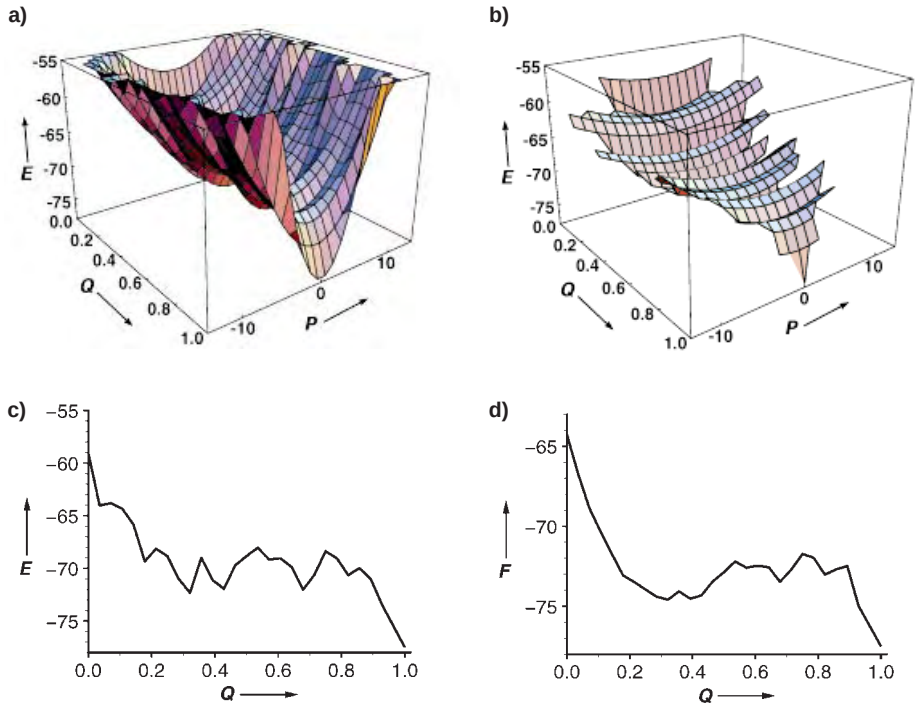


Figure 6. Lattice simulation of the folding of a 27-mer at low temperature. a) The averaged effective energy and the configurational entropy are shown as a function of the progress variable Q (see Appendix 1). At each value of Q, the cross-section of the surface is a parabola whose lowest point corresponds to the averaged effective energy $E(Q)$, and whose steepness is proportional to the configurational entropy $S(Q)$. The function $E(Q,P) = E(Q) + P^2[0.2/(S(Q)+1)]$ is used for illustrative purposes, where P is a measure of the available conformational space. b) The accessible energy surface, the part of the surface which is significantly populated in the reaction, is shown. The surface is obtained by cutting the edges of the surface in a) such that the length of the parabola at each value of Q is $4S(Q)+0.2$. c) The averaged effective energy E as a function of Q. d) The effective free energy F as a function of Q. The results are adapted from the data for sequence 43 in reference [28] for $T = 0.7$ (to relate T to a physical temperature $T = 1$ can be assumed equal to about 250 K.

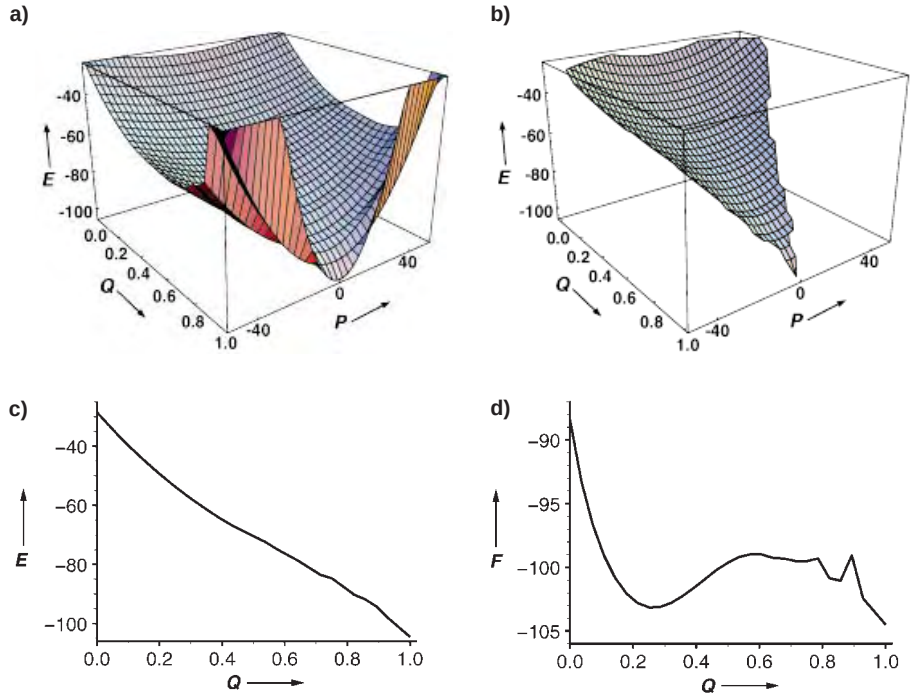


Figure 7. Lattice simulation of the folding of a 27-mer at high temperature. Figure a) – d) correspond to those in Figure 6. The same sequence as in Figure 6 was used except that the native state was stabilized by offsetting the energies of all 28 native contacts by a random number from a Gaussian distribution (mean value: $-0.8\,T$, standard deviation: $0.1\,T$); $T = 2.0$. The spike at $Q = 0.9$ may be a lattice artifact due to the very small number of states.

mechanical averages over the energies sampled in many trajectories, they appear smoother than the actual potential energy variation along individual trajectories, such as the one illustrated in Appendix 1. However, for drawing conclusions about the general behavior of the system, results of the type shown in Figures 6 and 7 are appropriate.

From the low-temperature averaged effective energy/entropy surface shown in Figures 6a and 6b, it is evident that the conformational space accessible to the protein molecules is limited, even at low Q. At the temperature corresponding to that in Figure 6, the polypeptide chain collapses to a disorganized ("misfolded") globule whose Q value is near that of the random coil (see Appendix 1). The configurational entropy at this temperature is sufficiently small that its destabilizing contribution to the free energy on collapse is compensated by the burial of hydrophobic groups, even in the absence of native contacts. As Q increases from 0.2 to 0.8, the average energy does not decrease significantly. In this region, the system makes a slow stochastic search within the collapsed state (see Appendix 1). As is evident from Figure 6c, the averaged effective energy surface is "rough"; that is, there are dips and crests along the valley floor due to the presence of energy barriers to reorganization within the collapsed state. The jagged edges of the accessible energy surface in Figure 6b reflect the "roughness" of the entropy as a function of Q. Intermediates would accumulate if the barriers were high enough or if the temperature was low enough. For the sequence of the 27-mer from which the results shown here were obtained,[28] there was no deviation from simple exponential kinetics in the lattice simulations, even at the lowest temperatures.[56] This indicates that traps do not play an important role; more complex behavior is found for other systems (see below). The transition region in the simulation is close to the native state ($Q \approx 0.7 - 0.9$), as indicated by the free energy profile (Figure 6d).

Furthermore, the simulations show that folding is highly cooperative in that only Q values near the random value of 0.2 and that of the native state ($Q = 1$) are significantly populated during the reaction.[55b]

Figure 7a shows the averaged effective energy/entropy surface at a high folding temperature; the accessible surface is shown in Figure 7b. Early in folding (e.g. for $Q = 0.2$), the surface is very broad, which indicates that the average system is sampling a very wide range of conformations; in fact, most of the random coil configurations that give rise to the Levinthal paradox are accessible. Each individual chain, of course, samples only a small part of the configuration space in moving on the surface. The surface becomes narrower fairly continuously, and the entropy decreases as Q increases to unity for the native structure. The averaged effective energy surface therefore acts as a funnel,[57] in that regardless of the initial position in conformational space, the molecules diffuse downward in energy towards the native state as a consequence of the increase in the number of stabilizing contacts. The steepness of the energy gradient is expected to be correlated with the energy of the native state relative to the average energy of the random coil conformations. This leads to the energy gap criterion mentioned above for the simultaneous optimization of thermodynamic stability and rapid folding.[25, 55a] It is valid for small proteins, as represented by the 27-mer, but more complex folding behavior is found for the 125-mer[54a] (see Section 7).

Despite the smoothness of the effective energy surface (Figure 7b), a transition state barrier in the free energy profile can exist. In simulations of the 27-mer, such a free energy barrier (Figure 7d) arises from a reduction of the chain entropy at large Q; that is, the number of accessible configurations decreases strongly as Q approaches the native state value (Figure 7b). This leads to a "constriction" in the folding funnel that results in an entropy "bottleneck". This can be compared with unimolecular dissociation reactions of small molecules, where a "bottleneck" also exists owing to the requirement that a sufficient fraction of the internal energy must be concentrated in the specific degree of freedom associated with the dissociation process.[1, 58]

For the high-temperature scenario in Figure 7, both the energy and entropy decrease essentially monotonically as the system approaches the native state. Thus, it is the balance between the rate of decrease of the energy and of the entropy that determines if there is a free energy barrier and where it occurs. A different balance between the averaged effective energy and the configurational entropy could move the transition barrier in the free energy to smaller values of Q than that shown in Figure 7d. A simple model based on a smooth funnel with a late barrier was used to obtain a kinetic description that provides additional insights into the folding reaction.[59]

A surface of the general form shown in Figure 7b is likely to result in fast folding, much faster than that expected on the surface shown in Figure 6b. The number of Monte Carlo steps required are on the order of 10^7 for Figure 7 (obtained from simulations) and 10^{10} for Figure 6; the latter is obtained from an extrapolation of Figure 8 (see below), because the Monte Carlo simulations required to obtain an accurate value would use too much computer time. When the order of magnitude arguments in Appendix 1 are applied, this corresponds to 10 ms for the fast folding (Figure 7) and 20 s for the slower folding (Figure 6). Both are in the range of actual folding times for real proteins. Figure 7 represents a simple, but nontrivial funnel; it is simple because the averaged effective energy decreases essentially monotonically in the direction of the native state, and it is nontrivial because the number of states that are accessible to the folding trajectories decreases more rapidly than the reduction calculated from the increase in Q. Folding scenarios based on Figure 7 are intuitive and appealing as a solution to the Levinthal paradox. They correspond to relatively rapid, biased diffusion of the progress variable to the native state; the rate-limiting step is the crossing of an entropic barrier. A description corresponding to a Kramers-type model[31, 60] would be appropriate for the reaction. Such a simple funnel is an idealized representation of one possible type of folding scenario. Lattice simulations have suggested alternative scenarios, like that shown in Figure 6, and more complex scenarios emerge when interpreting experiments or simulations of longer lattice chains (see Section 7). Also important is the fact that the various folding scenarios obtained from the lattice models give no information as to how the averaged effective energy surfaces arise from the sequence and its interactions (see Section 8).

For the scenarios in Figures 6 and 7, the probability of reaching the transition region is small, whether there is an entropic or an energetic barrier. However, it is far greater than in the unbiased random search considered by Levinthal, sufficiently so that these model systems are able to fold within a reasonable time. The essential element, as we have seen, is the bias of the averaged energy surface towards the native state, either by an energy gradient or by a restriction of the accessible conformation space, or both.

An important conclusion from Figures 6 and 7 is that the averaged effective energy and free energy surfaces for a protein have a strong temperature dependence, in contrast to the situation for simple chemical reactions such as $H+H_2$, for which the surfaces are almost independent of temperature. This arises from the minor role of the entropy in most reactions of small molecules and its essential importance in protein folding. There is a striking difference between the temperature dependence of the rate constants calculated for the two types of systems (Figure 8). The rate constant for the reaction $H+H_2$ (Figure 8a)[13] shows Arrhenius behavior, as expected from the reaction coordinate profile in Figure 2d. The reaction is dominated by the activation energy, and the activation entropy plays only a small role; this leads to an activation free energy that is nearly independent of temperature. For the protein folding reaction, the calculated behavior of $\ln k$ versus $1/T$ is shown in Figure 8b.[56] At low temperatures, there is an Arrhenius-like behavior. However, as the temperature increases, the behavior deviates significantly from that expected from the Arrhenius equation: The rate reaches a maximum and then decreases as the temperature increases further.

The calculated behavior shown in Figure 8b has been observed in experimental studies of the temperature dependence of rates of protein folding.[21, 61] Such a curved plot

indicates that the reaction is dominated by energy at low temperatures and by entropy at high temperatures. In both

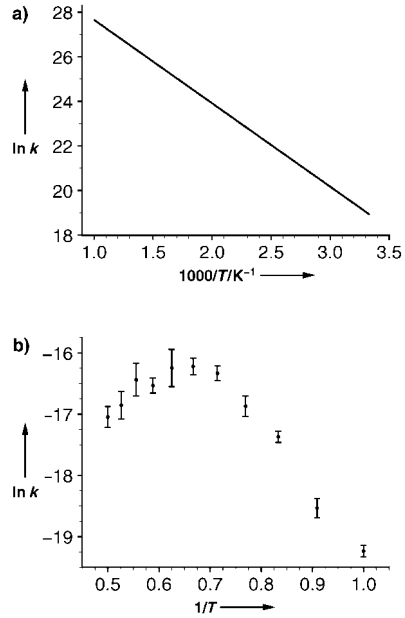


Figure 8. Arrhenius plots of $\ln k$ as a function of $1/T$ (in arbitrary units) for a) the $H+H_2$ reaction (adapted from reference [13]; k has the units $cm^3 mol^{-1} s^{-1}$ here), and b) the protein folding reaction for the same sequence as in Figure 6 (adapted from reference [56]; k is in Monte Carlo steps). To relate T to a physical temperature $T=1$ can be assumed equal to about 250 K.

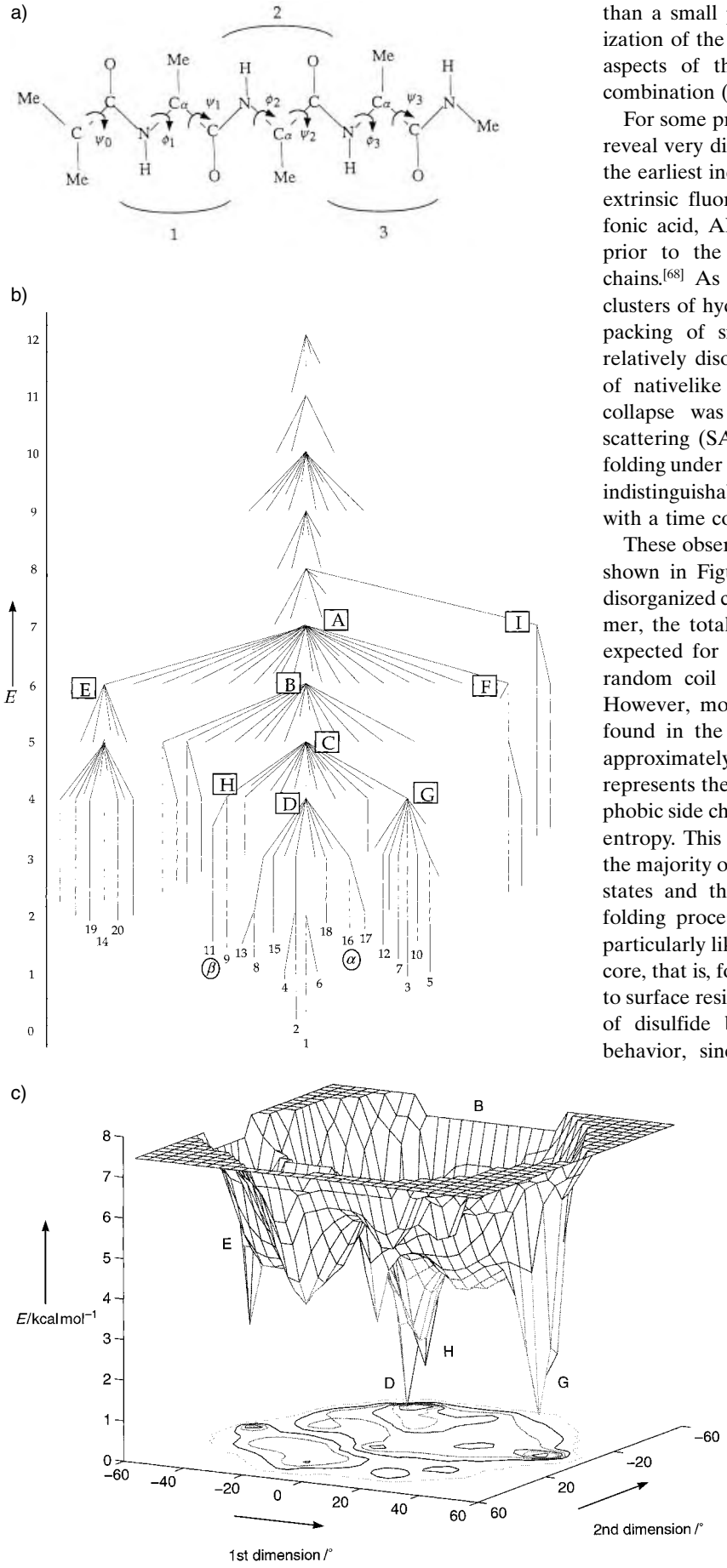
the simulations and experiment, there is a contribution from the activation heat capacity. However, the origin of this contribution may not be the same in the two cases, since the lattice attraction parameter is temperature-independent, whereas the hydrophobic interaction is not.[23] Unfolding, by contrast, is expected to show an Arrhenius-type temperature dependence owing to the large activation energy barrier for escaping from the native state, as shown schematically in Figure 5a. Experiments for lysozyme[61] and barnase[62] demonstrated such simple behavior; the rate constant varies with temperature as depicted in Figure 8a.

The two types of behavior illustrated in Figures 6 and 7 could occur for different systems at different temperatures, depending on the balance of energetic and entropic factors and their variation with temperature, as shown in Figure 8b. For a specific amino acid sequence at a physiological temperature, the observed behavior could be anywhere in the range of possibilities suggested by Figures 6 and 7. Folding scenarios that combine elements of both are likely; that is, funnellike behavior occurs for certain values of the progress variable, and a stochastic search is involved for others. The type of curve shown in Figure 8b for the folding rate constant as a function of temperature is expected to apply to most proteins, although the optimal folding temperature and the maximum folding rate will differ.

The results of lattice simulations point to the essential importance of the energy and free energy surfaces for real proteins. Although a detailed determination of the actual protein surface is beyond present computational possibilities, it is of interest to present here the results obtained for a very small model system: the alanine tetrapeptide described by a detailed atomic model.[63, 64] Figure 9a shows the peptide structure and the important dihedral angles that determine its conformation. In Figure 9b, the complex treelike structure of the multiminimum potential energy surface is indicated. A representation of the energy as a function of the two orthogonal coordinates (principal components) that give the best description is shown in Figure 9c. The basinlike, rather than funnellike, character of the overall surface is evident, as are many deep local minima. The surface is a relatively broad basin down to a certain energy (about 4 $kcal\,mol^{-1}$), at which point the various minima separate into individual basins. Because a protein has a hundred times as many soft dihedral angles as does this small peptide, and because the calculation was done in the absence of solvent (which might be expected to "soften" some of the local minima), it is difficult to extrapolate to the expected behavior for proteins. Nevertheless, the tetrapeptide makes clear that there can be many traps that must be avoided if the sequence is to fold rapidly to the energy minimum corresponding to the native state. How this happens is an essential question that has yet to be resolved, although with a much larger number of degrees of freedom, there will be an increased likelihood of avoiding barriers and traps.

6. Experimental Information on Energy Surfaces

A key objective of experimental studies of any reaction is to obtain information concerning the structures of the species involved as a function of time and to relate this information to the energy surface. Although this has been accomplished in detail only for $H+H_2$ and a few other reactions of small molecules (see Section 2), the insights obtained from studying them have provided a conceptual framework for a wide range of reactions, including most of those important in organic chemistry.[66] In the reactions of organic molecules, it is often true that only a small part of the molecule is actually involved, so that the analysis is not much more complex than for very simple reactions.[67] The problem is much more challenging for proteins because of the very wide range of structures that contribute in all but the final stages of the folding reaction, and because the entire polypeptide chain is involved. This means that it is necessary to determine the distribution function describing the contributing structures as a function of the progress variable. Only in some simple cases, such as those illustrated in Figures 6 and 7, is the time dependence of the *average* structure interpretable in terms of simple kinetic schemes, as in reactions of small molecules. Because of such complications, considerable ingenuity has been needed to devise methods appropriate for structural studies of protein folding (see Appendix 2). Moreover, many folding reactions take place in milliseconds to seconds, which is short compared with the conventional time scales of the techniques available for determining protein structures in solution. Most studies involve a rapid perturbation of the system from equilibrium so that the approach to the native state can be followed. Since no single experimental technique has been able to provide more



than a small part of the detail needed for a full characterization of the folding reaction, methods that probe different aspects of the developing structure have been used in combination (see Appendix 2).

For some proteins, probes for different aspects of structure reveal very different kinetic behavior during folding. One of the earliest indications of this was that for many proteins the extrinsic fluorescence of a dye (8-anilino-1-naphthalinesulfonic acid, ANS) added to the refolding solution develops prior to the intrinsic fluorescence of the aromatic side chains.[68] As the former is indicative of the formation of clusters of hydrophobic residues, and the latter of nativelike packing of side chains, this suggests that collapse to a relatively disorganized globule occurs before the formation of nativelike structure. More direct evidence for such a collapse was recently obtained from small-angle X-ray scattering (SAXS) studies of myoglobin.[69] After 100 ms of folding under acid conditions the radius of gyration is virtually indistinguishable from that of the native state, which is formed with a time constant of about 1 s under the same conditions.

These observations are consistent with the folding scenario shown in Figure 6, in which there is rapid formation of a disorganized collapsed globule. In the simulations with the 27-mer, the total number of contacts is large (≥ 20 of 28), as expected for a collapsed state; this is in contrast with the random coil state, which has seven contacts on average. However, most of these contacts are not those ultimately found in the native structure (the average value of Q is approximately 0.25). Such a disordered collapsed state represents the situation in which nonspecific burial of hydrophobic side chains compensates for the loss of configurational entropy. This can explain the experimental observation that the majority of tertiary interactions are not persistent in these states and that structural rearrangements are part of the folding process.[70, 71] Collapse to a disorganized globule is particularly likely for proteins with a substantial hydrophobic core, that is, for larger proteins for which the ratio of internal to surface residues is high. Other factors, such as the presence of disulfide bonds, may also contribute to this type of behavior, since the formation of cross-links reduces the

Figure 9. The conformation space for a blocked alanine tetrapeptide. a) The peptide and the important backbone dihedral angles ϕ and ψ are shown. b) Tree structure showing the 139 minima of the energy surface of the tetrapeptide; the energies of the minima (indicated by the lower ends of the lines) are given on the scale [kcal mol^{-1}] relative to the minimum energy. c) A simplified three-dimensional diagram of the energy surface of the main basin B, which includes the conformer of minimum energy (basin D), projected onto two principal components [a reduced representation relative to the seven soft dihedral angles specifying the conformation, see a)]. It is interesting to note that the accessible region is rather broad down to an energy of about 4 kcal mol^{-1}, where the different basins separate. Clearly there are many traps on this surface (adapted from references [63, 64]).

entropic penalty for collapse by limiting the disorder of the unfolded polypeptide chain.[72]

For several proteins (including the much-studied α-lactalbumin, which we use as an example) the nature of collapsed, but nonnative, states has been explored in some detail.[46, 73] In the case of α-lactalbumin, the far- and near-UV circular dichroism (CD) signals develop with very different kinetics in stopped-flow experiments (Figure 10b). This indicates that extensive secondary structure exists within a collapsed state prior to the formation of close-packed tertiary structure in the native state.[74] Studies of stable analogues of this kinetically formed collapsed state by a variety of techniques, including measurement of the degree of protection against hydrogen exchange, suggest that the secondary structure has at least some, and possibly extensive, nativelike character.[75, 76] Such secondary structure is not important in the folding of the 27-mer,[28, 55a] but simulations of a 125-mer lattice model (a $5 \times 5 \times 5$ cubic ground state) have shown that the existence of secondary structure speeds up the search in the collapsed state for the nativelike folding "core".[54a] More generally, an appropriate mix of short-range and long-range native contacts appears to be important for fast folding.

Experimental studies on α-lactalbumin have also provided indications of an overall nativelike fold, and of specific tertiary contacts for at least a core within these collapsed (molten) globules[77, 78] (Figure 11), whose important role in folding was originally proposed by Ptitsyn et al.[46, 79] Although

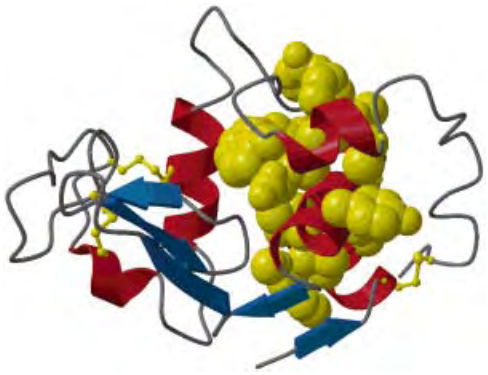


Figure 11. Results of NMR spectroscopic investigations into the protection against hydrogen exchange in the hydrophobic core of the molten globule state of equine lysozyme. The core is formed primarily from amino acid residues that in the native state form three of the four major α helices of the protein (helices A, B, and D); adapted from reference [78]. The α helices are shown in red, the β strands in blue, the disulfide bonds as ball-and-stick representations in yellow, and the side chains of the hydrophobic box core as a space-filling model in yellow; reduced values for the van der Waals radii are used in the latter.

recent experiments suggest that both native and nonnative contacts can exist within the α-lactulbumin molten globule,[80] the former appear to be crucial in defining the nature of the overall fold.[81] Folding of the polypeptide chain to the molten globule can have low cooperativity,[80, 82] while kinetic studies with NMR spectroscopy that monitor individual residues indicate that the close packing characteristic of the native state emerges in a highly cooperative manner.[83, 84] Folding of this type with a late transition state correlates with the simulation results in Figure 6.

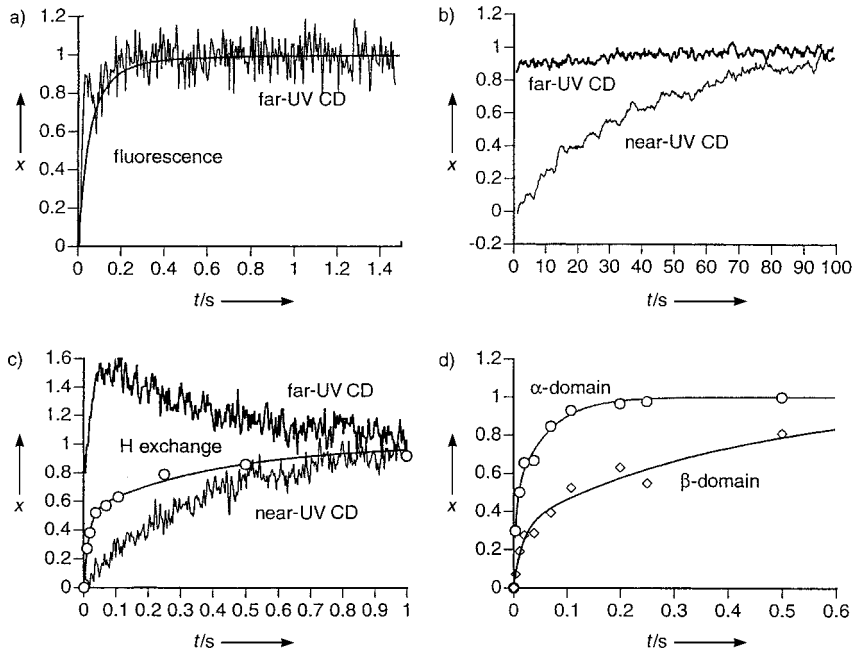


Figure 10. Experimental results from kinetic studies of protein folding. a) Far-UV CD and fluorescence data for the fibronectin domain, ^{10}FN III, shown in Figure 4b (x = fraction of the native signal). All experimental data follow a simple exponential curve.[165] b) Near- and far-UV CD for the apo form of bovine α-lactalbumin.[84] The former (a measure of tertiary structure) develops much more slowly than the latter (a measure of secondary structure). c) Near- and far-UV CD data as well as fraction of hydrogen exchange for hen lysozyme.[98] The overshoot in the far-UV CD indicates the development of nonnative interactions, and the protection against hydrogen exchange prior to the formation of the tertiary structure indicates the presence of intermediates with persistent structure. d) Details of the protection against hydrogen exchange shown in c). The two structural domains of lysozyme form protective structures at different rates, and the fast phase of protection in each indicates that some molecules fold on a "fast track" compared with the remainder of the population.

For some proteins, in contrast to those discussed above, the rate of development of the different aspects of structure, monitored by a variety of physical techniques, is very similar[3] (Figure 10a). This suggests that in these cases there is no significant concentration of partially folded species; that is, there are only small populations of molecules containing some, but not all, secondary-structure elements or displaying secondary structure in the absence of persistent tertiary interactions. A range of proteins with different folding topologies show this type of behavior.[3] The essential common feature appears to be that they are small (ca. 100 residues or less) and do not contain more than one domain in the native structure. The simplest interpretation is that the observed results arise from a kinetic "two-state" reaction; that is, at any given time there is a distribution of molecules consisting mainly of a mixture of "unfolded" polypeptide chains and essentially native ones.

This type of behavior could arise from a funnellike potential energy surface (see Figure 7), provided that there is a sufficient

entropy barrier to obtain single-exponential folding kinetics. The results of lattice simulations shown in Figure 7 yielded an entropic barrier that occurs late (at high Q). However, as already mentioned, an early barrier (at low Q) is also possible; in the latter case, only a small fraction of the native contacts would exist in the transition region. This would result in a "nucleation" mechanism, in which formation of a nucleus involving specific contacts of a small set of residues is the rate-determining step of the folding reaction.[85, 86] The free energy of the system begins to decrease only when the energetic stabilization from nativelike contacts is sufficient to overbalance the entropy loss due to the reduction in accessible conformations when the nucleus is formed; a detailed description of nucleation in sickle cell fiber formation by hemoglobin is of interest in this regard.[87] Simulations of lattice models obtained with sequences that maximize the energy gap between the ground state and the average energy of a random globule fold rapidly by a nucleation mechanism whose transition region corresponds to a Q value of about 0.2.[16, 86] Such a nucleus can still have a large entropy because many configurations are consistent with its existence. A nucleation mechanism has also been proposed for the folding of small proteins on the basis of experimental studies (see below).[88] There appears to be no case where the experimental data on the millisecond time scale are indicative of a gradual accumulation of structure in a small protein, as would be expected for a funnel without a free energy barrier.

For the nucleation-based folding mechanism, the specific structure of the nucleus, which is far from that of the native state, is of particular interest. A powerful approach for investigating this (transition state) region is based on protein engineering.[89] It involves mutating specific residues and measuring the change in the rates of folding and unfolding relative to the effect on the overall stability of the protein. As an example, if a residue has nativelike contacts in the transition region, a mutation would be expected to have approximately the same effect on the stability of the transition region as on that of the native state. Consequently, the mutation would perturb the folding rate but not the unfolding rate; if a residue has no transition-region contacts, the inverse would be true. By studying a large number of residue mutations in this way, a detailed characterization of the transition region is possible.[89] The method has been applied to several proteins, including the barley chymotrypsin inhibitor CI2,[90, 91] a fast-folding protein with two-state folding kinetics of the type discussed above. These experiments show that a small group of residues has nativelike contacts in the transition region. This set of residues is highly conserved in a sequence optimization simulation of CI2 and in a series of related sequences.[92] The results are suggestive of a broad transition region rather than a well-defined transition state, because an ensemble of species with very different structures can have the same or a similar nucleus.[93] A recent study of the folding kinetics of two forms of cytochrome c, which have very similar native structures but only 60 % sequence identity, also suggests an early transition region in which only the conserved regions have a well-defined structure.[54b, 94]

Although the two experimental scenarios for folding described in this section appear to be very different, they have a common feature: The folding process involves a search of conformational space for nativelike contacts that bring together residues in space. The difference in the averaged effective energy surface and the resulting kinetics reflects the importance of the contacts between specific residues. For certain sequences, a collapsed state is energetically favored over extended states, even if most of the contacts involve residues of only the appropriate type (e.g., those with hydrophobic side chains). In the case of folding on such a surface, the conformational search takes place within the collapsed state, and the reorganization of contacts to form the late transition region may involve overcoming significant barriers that would not be present in more expanded states. For other proteins, a collapsed structure is stable only with a set of highly specific and energetically favorable (nativelike) contacts. In this case, the search for a rather small nucleus can take place mainly in the unfolded state, and the transition region is early in the folding process. Mutations and/or changes in the environment can alter the averaged effective energy surface and change the details of the folding reaction by altering the balance between the effective energy and configurational entropy; this may result in a shift of the transition region. This effect has been observed experimentally in several proteins.[95, 96] Significant changes in the position of the transition region, which indicates its labile character and its critical dependence on the balance between the effective energy and entropy, have been found for a series of Ala $\rightarrow$Gly mutants (in which Ala was replaced by Gly) of a monomeric form of the fast folding λ-repressor protein.[97]

7. Complexities in Folding

Many reactions of small molecules have more complex kinetics than the $H+H_2$ reaction. There can be a series of intermediates and more than one product. The reaction-rate theory can readily be extended to include such features. Correspondingly for proteins, particularly larger ones, more complex behavior has been observed experimentally than for the cases discussed in the previous section. An approach to understanding their folding is to use the knowledge gained from simulations of the simpler systems to propose averaged effective energy surfaces that are consistent with the experimentally observed properties.

A schematic surface for a complex folding scenario is shown in Figure 12. It is based primarily on experiments with lysozyme and is generated so as to correspond to the results shown in Figures 10c and 10d. In particular, the surface incorporates features which account for two of the complexities observed in the folding process.[69, 98–101] The first of these is that distinct intermediate species accumulate during folding. This indicates that there are significant minima along the effective energy surface prior to the transition region for the formation of the native state. The second is that the native state appears more rapidly for some of the refolding molecules than for the remainder.[100, 101] This suggests that there are fast and slow folding trajectories and that a "ridge" in the energy surface inhibits exchange between them. Such results can be related to the mechanism of "kinetic partitioning" discussed by Guo

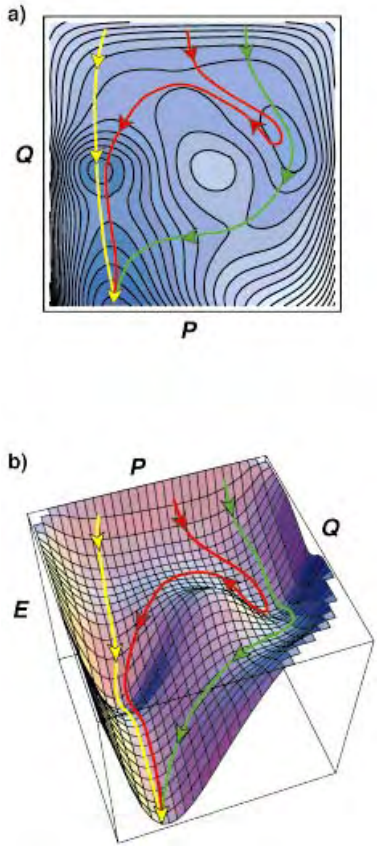


Figure 12. Averaged effective energy surface based on experimental data for the folding of lysozyme (see text, Appendix 2, and Figure 10) illustrated as a) a contour plot and b) a three-dimensional surface. Several possible folding trajectories are shown: a trajectory for fast folding (yellow); a trajectory for slow folding that crosses the high energy barrier (green); a trajectory for slow folding (red) that returns to a less folded state and then follows the valley corresponding to the trajectory for fast folding.

and Thirumalai.[102] Incorporating such behavior in an effective energy surface requires that the progress of the reaction be specified by more than the single native contact variable Q, which we have used for the simpler surfaces described above. At least one additional variable is required. It is indicative of our relative ignorance about the detailed mechanism of folding that there is not enough information to assign a specific physical meaning to the additional variable. It could, for example, involve the number of nonnative contacts in a partly folded state.[54c] This gives a measure of compactness, as would the exposed surface area.

Intermediates arise in the folding of lysozyme because persistent structure does not form cooperatively for the entire protein from the collapsed state that is generated early in the folding reaction; this collapse is represented by the steep drop at the top of Figure 12. Instead, nativelike structure develops independently in the two distinct domains that make up the native fold (see Figure 1); one domain is largely α-helical, and the other contains a substantial region of β sheet.[103] As one domain (the α-domain) folds faster than the other, a partially folded state with structure in the faster folding domain will result. In the surface of Figure 12 this corresponds to the deep minimum on the right-hand side. Within each domain the formation of persistent structure is largely cooperative, and can, but does not always (see below), take place on a time scale similar to that for the complete folding of a small, single-domain protein.[99, 101] The two domains coalesce in a slower step which is coupled to the formation of fully native character within the domains; this is indicated by the barrier on the left-hand side of Figure 12 along the yellow trajectory. In accord with these experiments, more than one folding domain was found in lattice simulations of longer chains.[54a, 104] The results suggest that domains[105] are likely to be an important feature of the folding of larger proteins, in contrast to small proteins (and short chains on lattices) in which the only cooperative unit may be the entire polypeptide chain.[3, 89]

There is abundant evidence that intermediates are common in the folding of all but the smallest of proteins. Important information concerning them can come from the results of protein-engineering experiments of the type discussed above for mapping the transition region. One of the larger proteins for which such studies exist is barnase, a 110-residue ribonuclease from *Bacillus amyloliquefaciens*.[89, 106] Like lysozyme, this protein forms a well-defined intermediate, in which substantial nativelike structure exists. The protein-engineering experiments show that additional nativelike structure is present in the transition region for folding, which occurs at significantly higher Q values than for small proteins such as CI2. As in lysozyme, the rate-determining step may involve the docking of partially preformed domains[89]

The observation of kinetic intermediates in the folding of larger proteins, including lysozyme and barnase, has prompted considerable discussion as to their significance.[76, 107–109] There are two extreme views. One is that these intermediates are productive and help to direct the folding process towards the native state by acting as templates for the formation of nativelike structure and restricting the conformations that need to be sampled. This can speed up the search and, once again, differentiates protein folding from reactions of small molecules, in which intermediates generally decrease the reaction rate. Alternatively, intermediates could represent kinetic traps that, for example, involve misfolded species which hinder the folding process and slow down formation of the native state; such intermediates appear in the lattice simulations of the 125-mer.[54a] This is the situation found for reactions of small molecules, in which an intermediate often decreases the rate, although it may play a crucial role in determining the product. It is likely that in protein folding both types of intermediates occur and that their role can depend on the amino acid sequence and the environmental conditions, as indicated by experiments on ubiquitin[96] and cytochrome c.[110]

The existence of both fast- and slow-folding molecules in lysozyme also sheds light on the role of intermediates in folding. In some systems distinct populations that fold with different rates are associated with isomerization of the protein backbone.[111] In particular, in an unfolded polypeptide chain *cis* and *trans* isomers of proline residues have comparable stability, and the barrier to their interconversion is large; the folding reaction for the molecules which exist in the nonnative isomeric state at the onset of folding therefore includes an additional slow step. In the case of lysozyme, however, the

origin of the kinetic heterogeneity does not appear to be associated with proline residues.[70, 100] The existence of parallel folding routes instead suggests that species with different conformations are generated relatively early in the folding reaction, and that significant barriers to the interconversion between the slow- and fast-folding populations exist; the slow-folding species have to go over a higher barrier to reach the native state or to unfold and return to the fast pathway (see Figure 12). The experimental studies indicate that the intermediate state populated on the slow -folding trajectories has elements of the nativelike structure within one of the two domains of the overall fold, whereas that populated on the fast-folding trajectory has such structures within both domains.[99, 101]

These findings imply that the rate-limiting step in the folding process for the slow-folding population of lysozyme molecules involves, at least to some extent, the reorganization of misfolded species.[70] As the collapsed states in lysozyme have substantial secondary structure and four disulfide bridges, it is not unreasonable that such rearrangement processes are subject to significant barriers and hence observable in experimental studies. The occurrence of this type of behavior is supported by the results of lattice simulations. In the collapsed globule seen in the 27-mer simulations, there are many nonnative contacts; that is, the number of contacts N is much larger than Q (see Appendix 1). Although the resulting species are not stable enough to be intermediates, they are manifest in a roughness of the effective energy surface for the low-temperature simulations (see Figure 6c). The energy surface is such that the polypeptide chain does not have to expand significantly to escape from the minima and progress toward the native state. Trajectories in which misfolded species are more important have been observed in lattice simulations of 125-mers.[54a,c] In these simulations, as already mentioned, a folding core or nucleus is formed early in the reaction. It consists of about 30 residues and has significant secondary structure. The folding trajectories show populations in which the remainder of the polypeptide chain condenses on this core and directly forms the native state, and others in which misfolded but relatively stable structures are formed that slow down the folding reaction. In the case of the latter, a slow step involving significant unfolding is required before reaching the native state; that is, Q is reduced substantially before it can again increase. This occurs, for example, for the trajectories in which two parts of the system have developed nativelike structure but have incorrect relative orientations. The results of the 125-mer simulations have much in common with the experimental data for lysozyme and also with recent results for cytochrome c.[96, 112]

8. A Unified View of Protein Folding

It is useful at this stage to present the general picture of protein folding that is beginning to emerge from heteropolymer theory, from lattice simulations of simplified models, and from experiments on real proteins; we do not repeat references in this section, which unifies the ideas and results presented earlier. When a polypeptide chain is placed under refolding conditions, the van der Waals and electrostatic interactions within the protein and between the protein and solvent stabilize the native state. However, the greater stability of the native state relative to the denatured state does not by itself explain how the polypeptide chain finds the former (a single state out of an astronomically large number of denatured configurations) starting from the latter. The essential element, as illustrated by the lattice simulations, is that the search is not random, but is significantly restricted by the fact that only a portion of the averaged effective energy surface is accessible (see Figures 6 and 7); that is, certain regions are too high in energy to be sampled with a significant probability by folding trajectories. Such restrictions on the space to be searched and an overall bias of the energy toward the native state mean that the polypeptide chain never faces the problem posed in the Levinthal paradox.

In one scenario of protein folding, the polypeptide chain collapses rapidly to a compact globule. Although the most significant factor leading to such an early collapse is the burial of hydrophobic groups, the nature of the collapse depends on the heterogeneity of the stabilizing interactions. The collapse can lead to a disorganized globule without specific contacts and with a relatively large configurational entropy, or to a compact structure with some highly probable contacts and a lower configurational entropy. In the former case, the collapse does not involve a search (i.e., contacts can be formed in any order), and it can be fast. Fluctuations within the collapsed state bring different groups into contact with each other, and the search for the critical contacts that are required to reach the transition region is the slow step. This type of folding has many elements that correspond to those associated with the effective energy and free energy surface shown in Figure 6.

Under other circumstances, chain collapse does not lead to a decrease in free energy unless specific contacts are formed. The search process that brings the required residues together can be aided by intrinsic structural preferences and the formation of hydrophobic clusters that exist even in the highly unfolded state. These rudimentary structural elements can be further stabilized by the formation of main-chain hydrogen bonds (e.g., as in neighboring β strands or in α helices), so that larger regions of structure are formed in a synergistic manner. Transient fluctuations of such nascent structures within a noncompact state lead to collapse only when the required stabilizing nativelike contacts are present. They constitute a "folding core" or "nucleus", about which the rest of the structure can coalesce. The slow step corresponds to the search for the core structure from which the system proceeds rapidly to the native state. There is a relatively early transition region, and proteins with such a free energy surface are likely to fold fast and in an apparently two-state manner. The less stable the native state is, the more nativelike contacts are needed for the compact molten globule state to be formed, and the slower is the folding process.

As proteins increase in size the scenarios become more complex, though the nature of the interactions remain the same and the folding mechanisms build on the elements described for smaller systems. The stochastic search or nucleation mechanism can involve finding a relatively local

folding core that is the size of a small protein, and additional restrictions on the search are required to permit folding in a reasonable time. These can be based, in part, on the chain preferences that already exist in the random coil state.[113, 114] Under native conditions, short-range interactions can give rise to structural features (e.g. β turns or nascent helices) which act as initiation sites to increase the probability of coalescing to structures involving longer range contacts. In many cases, incorrect structures will form that need to be undone. At the early stages of folding this is likely to be fast, but later in folding significant barriers to the rearrangement of misfolded elements may lead to slow steps in the folding process. High stability is important for formation of the core, so that it exists long enough for condensation of the rest of the polypeptide chain to be able to take place. Too much stability in noncore regions can lead to intermediates, some of which may be misfolded. Populations of folding chains may access different regions of conformational space. Therefore, they have to surmount different barriers, giving rise to heterogeneity in the folding kinetics. This type of folding, including complex kinetics, has been found in lattice simulations of larger proteins as well as in experiments. It is likely to occur when there exist relatively structured portions of the protein distant in the sequence that have to be brought together to form the native state.

From the above it follows that—although the events in the folding of different proteins, or of the same protein under different conditions, may appear to be very different—the underlying elements of the folding mechanism are the same. Folding is a progression in which nonnative and native contacts, some of which may be particularly important, stabilize nativelike features of the structure. The energy penalty for nonnative interactions, or misfolding, increases throughout the folding process. The polypeptide chain is directed by stabilizing interactions into productive regions of conformation space that permit an effective search for the native state. Although energy biases restricting the configuration space are essential for folding within a reasonable time, a continuous funnellike gradient in effective energy is not required and appears unlikely to exist in real proteins. A more "stepwise" behavior, involving the sampling of regions that are downhill in energy and other regions that are relatively constant (or even uphill) in energy on the effective energy surface, appears probable. Analogous behavior was observed in folding simulations of clusters of rare gases.[23] The trajectories followed by individual polypeptide chains are likely to be very different, at least initially, with an increasing number of common features as the system approaches the native state. It is only the ensemble of individual molecule trajectories which sample the full accessible configuration space.

To complete the above description of the folding process requires an understanding of how it is encoded in the sequence. It is the sequence which determines the energy surface of each particular protein. Such information cannot be obtained directly from the available lattice simulations. The simulations that have been used to explore the full conformation space are oversimplified and do not contain sufficient detail to relate the specific results to those for individual proteins. Nevertheless, the present analysis of the folding mechanism gives clues as to how folding might encode. An essential aspect of the process is that the specific nature of individual residues becomes more important as the polypeptide chain approaches the native state. The local interactions in the unfolded state lead to a significant probability for the formation of nascent nativelike helices and strands within the ensemble of rapidly interconverting conformers.[113, 114] As a folding polypeptide chain undergoes a collapse transition, the nonrandom distribution of residues of different character (e.g. those having hydrophobic or hydrophilic side chains) generates an architecture, or global fold, that has the general characteristics of the native state. However, at this stage of folding, which often results in a relatively disorganized globule, the specific nature of the residues is of little importance, and very different sequences with similar characteristics can generate the same overall fold.

In defining such an architecture, contacts between some residues are more important than others in bringing together regions of the polypeptide chain which are not close to each other in the sequence. Another essential aspect of finding the correct fold is the need to avoid highly destabilizing situations, such as an unbalanced charged residue in the protein interior. For the final assembly of the native state, the specific interactions in all parts of the sequence become important. The formation of the closely packed structure optimizes the van der Waals and other stabilizing interactions. Even one residue in a nonnative environment can significantly destabilize the structure (e.g., a side chain that introduces a large cavity in the core), though a plasticity towards the replacement of certain residues by others does exist.[115, 116] Because the native state is in a deep energy well, most of the polypeptide chains reach this state and remain there under folding conditions. These physical aspects of the thermodynamics and kinetics of protein folding have their analogue in the use of threading algorithms for identifying the structure associated with a given sequence.[9, 117–122]

The packing of side chains is unlikely to be involved in the resolution of the Levinthal paradox, and side chains are not included in the lattice models used in developing the concepts presented here. However, this packing may be essential for a first-order transition between the deep energy minimum associated with the native structure and the large population of loosely packed globules with backbone structures that are similar to the native state. Indeed, in attempts to design small proteins, it appears to be relatively easy to obtain a compact globule with the correct topology (e.g., a four-helix bundle).[123, 124] The difficult part is to modify such a globule so as to introduce the full nativelike properties that arise from the solidlike packing of side chains. The sequence of a real protein generates the deep native state minimum by a specificity that goes beyond that of the simple patterns of hydrophobic and hydrophilic side chains; the sequence permits specific residues to pack correctly to form the unique native structure. Such packing must be strong enough to overcome the additional entropy loss involved in going from the multiconformational molten globule to the unique native state. The final stage in folding thus involves the cooperative generation of highly compact structures in which specific side chain packing is likely to play a critical role.

9. Summary and Outlook

Detailed calculations for the $H+H_2$ reaction and the concept of reaction surfaces revolutionized the fundamental understanding of chemical reactions. The "new view",[107, 125, 126] which is based on averaged effective energy surfaces[28] or energy "landscapes",[14, 17, 127] plays a similar role in our understanding of protein folding. The new view has emerged from theoretical models and lattice simulations. The latter have played an essential role because they capture many of the complexities of protein folding, but are still sufficiently simple to permit detailed studies of the folding process.[6, 52] There is an essential difference in the new view from that of Levinthal presented in Section 1. The astronomically large number of states that exist for the denatured protein has to be searched in a random fashion to find the native state only if, with the exception of the native state, they all have essentially the same energies. This has been called the "golf-course model" of the energy surface.[25, 55a] As the simulations of lattice folding of the 27-mer demonstrate, even a set of random sequences contains a significant fraction that fold rapidly.[55a] The search through the denatured configurations is highly restricted because only a relatively small subset has energies low enough to be sampled at the given temperature. In addition, the search may be guided by the decrease in energy in the direction of the native state. This leads to a range of folding scenarios, in all of which there are many ways of going from the extended coil to the unique native state. The resulting multiplicity of folding populations requires that reduced progress variables on an averaged effective energy surface be used to describe protein folding as a replacement for the reaction coordinate on a potential energy surface for small molecules. The appropriate progress variable or variables must capture the essential features of the folding reaction and be accessible to experimental investigation. One type of progress variable (the fraction of nativelike contacts) has been shown to be sufficient for simple surfaces. However, as demonstrated in the analysis of lysozyme folding, additional variables are required for more complex systems. Furthermore, it has become clear that to reach an understanding of the underlying principles governing the folding reaction, the averaged effective energy and the configurational entropy need to be considered in addition to the total free energy. This is essential, for example, for an analysis of the non-Arrhenius behavior of protein folding as a function of temperature.

As a consequence of the large number of significant degrees of freedom, the transition "state" is much more complex than in reactions of small molecules. Lattice simulations suggest that there is likely to be a transition region or regions with many configurations that lead rapidly to the native state. If the transition region is late, it consists of an ensemble of structures that resemble the native state, and the interesting step involved in the resolution of the Levinthal paradox concerns the mechanism by which it is found. If the transition region is early in the folding process, it can involve a wide range of very different structures with only a small portion of the structure being well-defined. Knowledge of that portion of structure is then crucial for understanding the folding process.

An important result from the lattice studies is that the difference in behavior observed experimentally between proteins that fold rapidly (and without intermediates) from the extended coil state and those that pass through collapsed states and kinetic traps does not require a qualitative difference in the averaged effective energy surface. Instead, the differences in folding behavior can result from a change in the balance of the configurational entropy and the averaged effective energy as a function of the progress variable. It is possible experimentally to change from one type of behavior to another, for example by mutagenesis to incorporate more hydrophobic groups in the core of the protein (see Section 6).[96] In simulations, a change in behavior can be produced by reducing the temperature to decrease the entropic term (see Figures 6 and 7), and by increasing the attractive hydrophobic interaction between the amino acids.[128]

The multiplicity of ways of reaching the native state suggests that the use of simple kinetic schemes for the analysis of the protein folding reaction has to be reevaluated. As long as measurements on a certain time scale (usually milliseconds or longer) yield single-exponential behavior or the results can be described by a few exponential terms, a focus on "chemical" species is a useful way to summarize the reaction. However, the species may not represent the conformationally well-defined entities of reactions of small molecules, but may instead correspond to a broad distribution of structures. A simple scheme is appropriate if there is a separation of time scales; that is, the equilibration of the conformers corresponding to a given chemical species is fast relative to the interconversion of different species. For example, in the folding simulations corresponding to Figures 6 and 7, single-exponential kinetics are observed. This can be described by the standard scheme $U \rightarrow N$, in which the unfolded species U includes the random coil and collapsed globule region (10^{16} states in the 27-mer), and there is a single native state N. The collapse to a globule, which is an important part of the folding process, does not appear in the simplest kinetic scheme because it is fast and does not affect the overall reaction rate. Therefore, even if a simple kinetic model is able to describe the available data, this does not mean that the folding reaction is understood. The results of simulations and their analysis indicate that there are "hidden" complexities in the protein folding process; that is, proteins that fold with a "two-state" transition are likely to involve a multistage process if probed on a shorter time scale and exhibit more complex behavior on this time scale. This is analogous to the increase in the observed complexity with improvements in the experimental techniques found in other apparently simple reactions in proteins, such as ligand rebinding after photodissociation in myoglobin.[129]

Experiments that make it possible to study protein folding at shorter times and to higher structural resolution are clearly needed.[130] Such techniques are being implemented at the present time, and some preliminary results are already available. Of major importance is NMR spectroscopy, which is beginning to make it possible to study folding in real time.[84, 131, 132] Recent developments include the introduction of novel two-dimensional methods to study folding at the

level of individual residues[83] and the ability to observe at least some aspects of the folding process on a time scale of tens of milliseconds.[133] In addition, measurements of the nuclear Overhauser effect (nOe) to determine intramolecular distances can probe the development of native and nonnative contacts during folding, a crucial aspect of more detailed comparisons with simulations.[80] Other spectroscopic techniques that give specific structural information, such as IR[134] and vibrational Raman spectroscopy,[135] are also beginning to be applied to protein folding. Studies of the larger fluctuations in proteins at equilibrium, as probed by amide hydrogen exchange and other techniques, are being related to the effective energy surface for folding and unfolding.[136, 137]

Methods are currently being developed to probe the very early events in folding by using fast mixing devices or rapid initiation methods on the micro- to nanosecond time scale[138–142] Studies of unfolding[134] in the submicrosecond range are of interest as a complement to the examination of the folding process. Furthermore, such unfolding experiments can be compared directly with detailed all-atom simulations of unfolding initiated by high temperatures or low pH.[2, 34, 35, 143–145] Simultaneously with the experimental developments, theoretical approaches are being improved to permit more realistic studies of folding. These include, for example, all-atom calculations with an implicit model for the solvent,[54b] lattice models with explicit representation of the side chains,[146] simplified off-lattice models of polypeptide-like chains,[147] and the extension of methods for determining averaged effective energy and configurational entropy surfaces for the folding process to all-atom models of the protein and the solvent.[148] The continued increase in computer power is critical to progress in this area.

At their present level of detail, lattice simulations cannot determine the folding mechanism for any specific protein. The utility of the simulations is to suggest general concepts and possible mechanisms. Experiments are essential to show which, if any, of the proposed folding scenarios are correct and to suggest refinements of the models. Some tests of the conclusions from lattice simulations have been published already.[6, 88, 149] At the present stage our knowledge is not sufficient, however, to demonstrate that any protein has an effective energy surface that corresponds to a simple "funnel".[57] We indicated above that such a surface is unlikely to exist, if for no other reason than that there is no evolutionary pressure to create an idealized world for the theoretician. Nevertheless, the limitation of the available experimental data are such that qualitative interpretations in terms of funnels are adequate to describe a number of the folding studies[93] In this review, we have suggested how simulations and experiments can be used to go beyond such descriptions. It is necessary to first map out an approximate effective energy surface and its structural correlates, to describe the dynamics of folding on that surface, and to determine how the structure develops with time. Comparison of the results with more detailed structural information on shorter time scales from experiments can be used to improve the model and to serve as the basis for simulating more realistic models. This makes it likely that an understanding of the basic principles of the folding of real proteins will be achieved in the next few years.

The fundamental principles of protein folding have practical applications in the exploitation of advances in genomic research[150] and in the design of novel proteins with special functions.[151] In addition, it is important to underline that a process as critical for a living system as protein folding is aided by a sophisticated series of helper molecules. Enzymes speed up potentially slow events in folding such as proline isomerism and disulfide bond formation.[4, 111] Moreover, molecular chaperones serve to avoid intermolecular interactions in cells which would otherwise lead to aggregation in such an environment.[4, 152] Some molecular chaperones may also possess "unfoldase activity"[153] to permit misfolded proteins to escape from kinetic traps of the type discussed in Section 7. Their action can also be discussed in terms of energy surfaces such as those shown here for the folding of isolated systems.[154] However, at the present level of information, simple kinetic models yield satisfactory descriptions. Another intriguing problem is associated with the folding of proteins in membranes or at membrane surfaces. Experiments are just beginning to explore how this might occur.[155] Given the very large number of proteins associated with membranes, the nature of folding in a mainly hydrophobic, rather than hydrophilic, environment raises important questions.

In parallel with our developing knowledge of the principles of protein folding, it is being realized that folding and unfolding play an important role in the mechanism and control of a wide range of cellular processes. These include the translocation of proteins across membranes to their correct cellular compartments[155] and the regulation of the complex events occurring throughout the cell cycle.[156] In addition, the failure of proteins to fold correctly and efficiently is being associated with the malfunction of biological systems, and a substantial range of diseases is now known to be associated with the misfolding of proteins.[157] Some of these diseases, for example cystic fibrosis, result from mutations which interfere with the normal folding and secretion of specific proteins.[158] Others, such as Alzheimer's and Creutzfeldt – Jakob diseases, are associated with the later conversion of normal soluble proteins into insoluble amyloid plaques and fibrils.[159] Although such intermolecular interactions represent regions of conformational space outside those discussed in this review, the origin of the forces and the nature of the folding process is expected to be similar, except for the presence of the concentration dependence as an additional variable. There also exist normal proteins in which the monomer folds efficiently in dimeric or multimeric form.[160, 161] One of the proteins for which mutations are known to result in an amyloid-based disease is lysozyme,[162] whose folding behavior as a monomer was discussed extensively here. Recent studies have suggested that the aggregation-prone species giving rise to the formation of amyloid fibriles may be closely related to normal folding intermediates. A more detailed understanding of both normal and deviant folding behavior of proteins could therefore be important in efforts to develop novel therapeutic strategies to avoid or reverse the onset or consequences of such diseases.

We hope that we have been able to demonstrate that the mechanism of protein folding is one of the most fascinating problems in the field of chemical reactions. This review will be a success if it awakens the interest of chemists in this rapidly evolving subject and persuades some of them to contribute to its investigation.

Appendix 1. Lattice Models of Protein Folding

In a lattice model, the residues are positioned on a grid and have specific nearest neighbour interactions which depend on the residues involved. A cubic grid is used in the models discussed here,[28, 54a] although more complex lattices have been employed.[146] The folding process on the lattice takes place by local Monte Carlo moves of the residues until the native (lowest energy) configuration is reached. To illustrate the lattice models used in Figures 6 and 7, we consider a simple polypeptide chain with 27 amino acids (27-mer) and a folding trajectory of that chain. There are on the order of 10^{16} conformations of the chain on an infinite cubic lattice. Given a net hydrophobic attraction between the residues, the native state of the model protein corresponds to a $3 \times 3 \times 3$ cube (the structure on the far right in figure 13 d), which is fully occupied by the 27-mer polypeptide chain. There are 103 346 ways of threading a 27-mer through the cube. Which one of the possible threadings is the native state is determined by the sequence, that is, by the nature of the interactions between neighboring pairs of amino acids in any given conformation. Since there are 28 nearest neighbor contacts in the cube, the native state can be specified in terms of these contacts. In the model, simple contact potentials are used to represent the effective energy of a given configuration. This makes it possible to determine the thermodynamics and dynamics of the system with a reasonable amount of computer time.

Although the potentials used in the lattice simulations are simplified, the results provide general information on possible protein folding scenarios, which are the primary concern of this article. To determine the detailed behavior of specific proteins, more elaborate models and more accurate interaction potentials are required. The insights from folding simulations with lattice models and the complementary results of detailed all-atom model unfolding simulations can be combined with experimental data to achieve an understanding of protein folding. The contribution made by the simulations is that they enable the structures, energetics, and dynamics of reactions to be analyzed at a level of detail not accessible to experiment.

To illustrate the time course of a trajectory at a temperature near the folding transition temperature T_m, the energy E, the number of contacts N (a measure of the compactness that is similar to the radius of gyration), and the fraction Q of native contacts are shown in Figure 13 e. For a 27-mer, N goes from zero for the fully extended chain (no contacts) to 28 for the fully compact cube, whether or not it is in the native state. The number of contacts N increases before Q. This corresponds to a rapid collapse (in 10^4 Monte Carlo steps) and the formation of a disorganized relatively compact globule. The collapse is followed by a slow search (10^7 steps) through the 10^{10} semicompact states (the structure changes completely over about 10^3 steps, but the number of contacts remains high) until one of 10^3 states in the transition region is found. Since Q in the transition region is between 0.7 and 0.9 (which means 20 to 26 native contacts), the transition states resemble each other and the native state. From there, as expected for a transition state, there is rapid rearrangement (10^4 steps) to the native state.

An approximate relation between the number of Monte Carlo steps and the time can be obtained since the pseudodihedral angles in the lattice model (e.g., the dihedral angle formed by amino acids 2–5 in Figure 13 d) can be identified with the corresponding C_α-C_α-C_α-C_α pseudodihedral angles of a protein backbone. The rate for a change in the C_α pseudodihedral angle is on the order of $10^9\ s^{-1}$;[166, 167] therefore, 10^6 Monte Carlo steps correspond to about 10^{-3} s. In a typical folding simulation of the model protein, approximately 10^7 steps are required; this corresponds to 10 ms, a value comparable to that found experimentally for the folding of small proteins.

Appendix 2. Structural Studies of Protein Folding

Protein folding can be initiated in the laboratory in a variety of ways. One of the simplest is to unfold the protein in a high concentration of chemical denaturant, such as guanidinium chloride, and then to dilute the solution rapidly such that the denaturant concentration falls below that at which the native state is thermodynamically unstable. The question then is how to follow the structural changes that occur, given that folding is often complete in less than 1 s, and that (as the energy surfaces indicate) the structures of folding chains are extremely heterogeneous, at least until the final stages.

One strategy that has been developed is to use a battery of complementary stopped-flow and quenched-flow techniques, each of which is capable of monitoring a specific aspect of the formation of nativelike structure.[65, 98] This approach is illustrated schematically in Figure 14. For example, if the far-UV CD signal is followed as a function of time, the development of secondary structure (particularly helicity) can be monitored. If, in contrast, the near-UV CD signal is measured, the development of nativelike packing of aromatic side chains can be probed. The range of techniques being utilized in this way is increasing rapidly; one of the more remarkable developments is the ability to follow the overall dimensions of the protein (R_g) by means of time-resolved small-angle X-ray scattering.[69]

The dead time in even the best conventional mixing devices is typically a few milliseconds, but progress is being made to develop devices in which this is substantially reduced.[130] In addition, novel methods to initiate refolding reactions are being introduced.[138-142] These include the use of temperature jumps under conditions where cold denaturation takes place and an increase in temperature leads to refolding.[139, 141] In some cases, the rapid change of oxidation state of a metalloprotein can trigger the onset of the folding reaction.[140] With

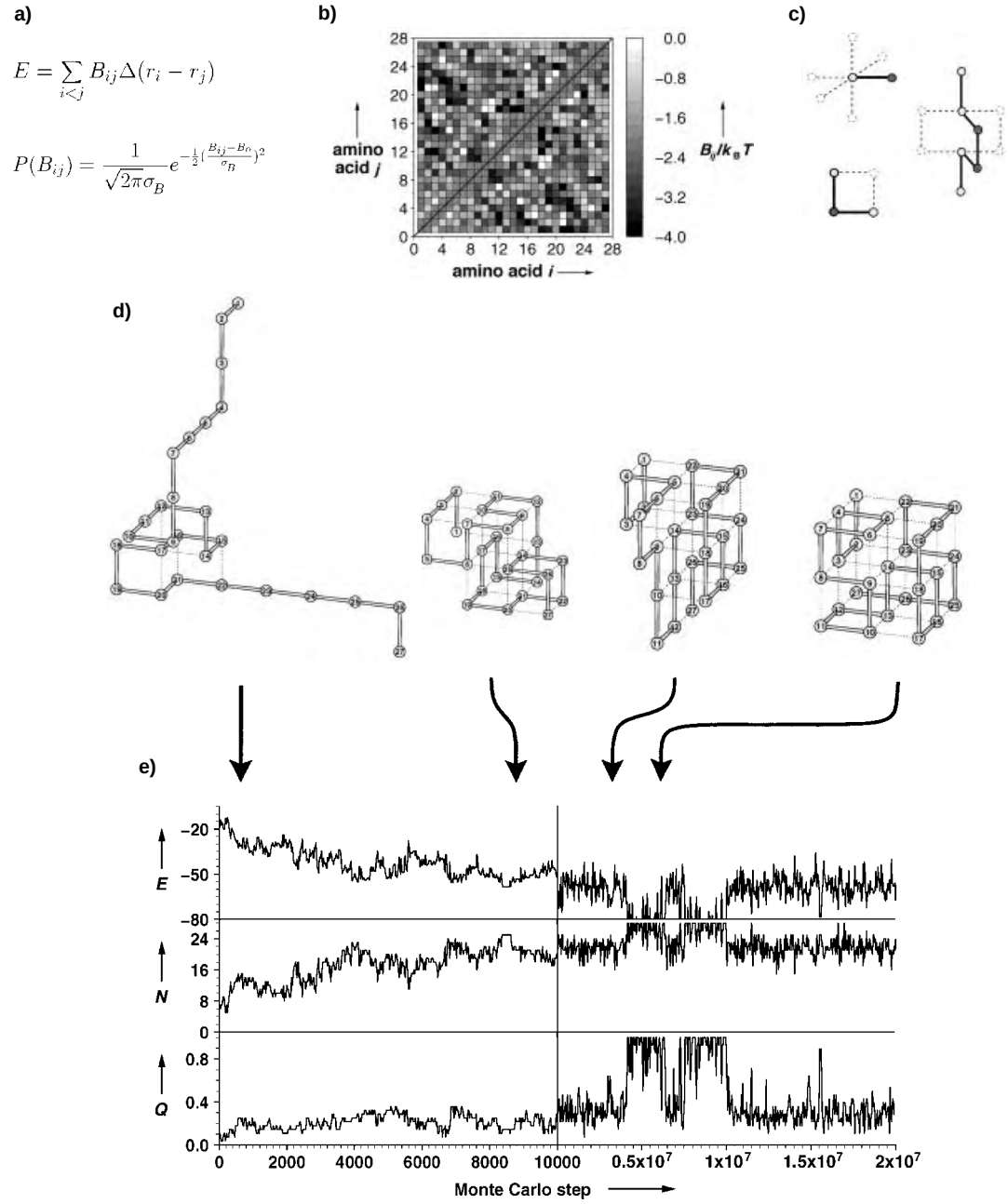


Figure 13. a) The total energy E of any chain configuration is a sum of residue contact energies B_{ij}, which themselves are derived from a Gaussian distribution with a mean value of B_0 and the standard deviation σ_B. The parameters r_i and r_j represent the position vectors of the residues with the sequence numbers i and j, respectively. The value of B_0 is $-2\,k_BT$ and corresponds to the average attraction between the monomers with which the hydrophobic effect is emulated. The standard deviation σ_B is k_BT and corresponds to the range in the contact energies of the amino acid residues. b) The contact energy matrix for the sequence used in e) and in Figure 3. c) The three allowed Monte Carlo moves: tail flip (top left), corner flip (bottom left), and the crankshaft move of two residues (right). d) Sample structures for the various parts of the folding trajectory shown in e), as indicated by the arrows (from left to right): a random coil, a disorganized semi-compact globule, a transition state, and the native state. f) Folding trajectory showing E, N, and Q as a function of the number of Monte Carlo steps; adapted from references [28, 55].

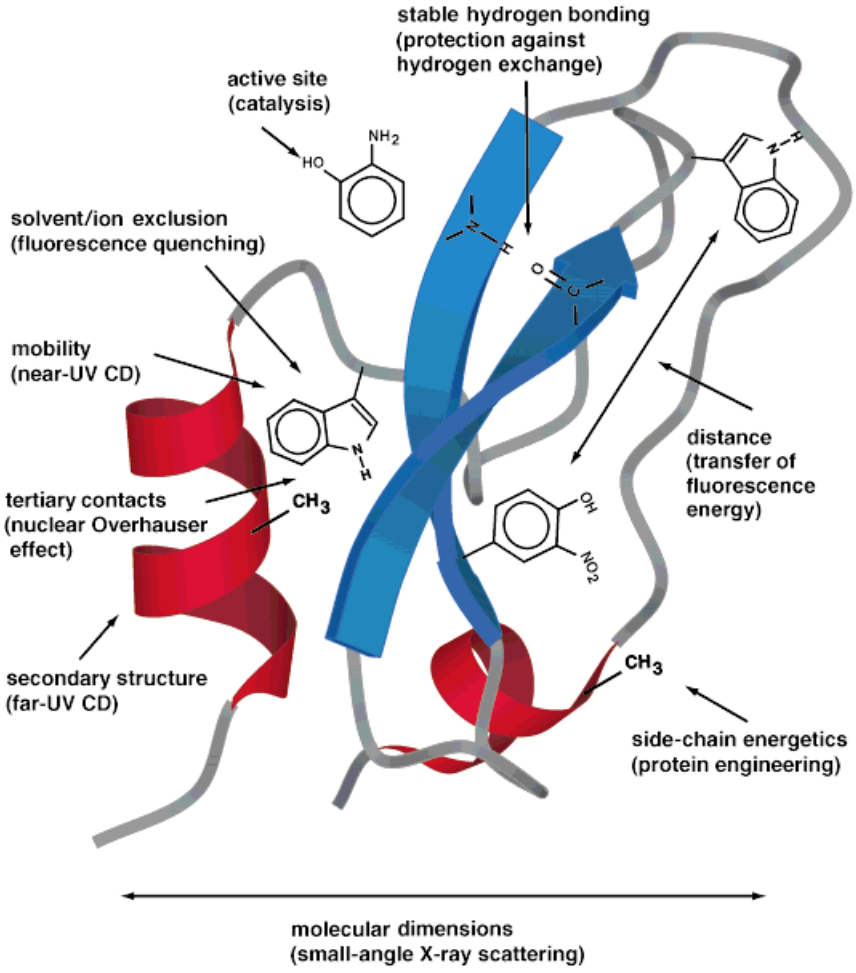


Figure 14. Schematic representation of some of the characteristics of a globular protein that can be followed during folding by physical techniques (stopped- or quenched-flow) with time resolution in the second to millisecond range; adapted from reference [130]. Examples of specific techniques able to probe the different features are indicated. Other properties that can be monitored but are not indicated include the existence of hydrophobic cavities and overall thermodynamic stability. Although no individual probe can monitor all of the structural changes during folding, the use of a set of complementary probes can provide a detailed picture of the distributions of conformations that are sampled at different stages of folding.

such approaches folding events on the micro- and submicrosecond time scale are becoming accessible.

A particular aim of structural studies is to probe interactions as they form at the level of individual residues. It is such data that can be compared directly with simulations. NMR spectroscopy has long been recognized as the approach by which this can be achieved, at least in principle. Considerable progress is now being made at realizing this goal in practice. If folding is relatively slow, on a time scale of seconds or longer, one-dimensional spectra can be recorded sequentially, and the spectral changes monitored.[131, 132] One example of such an experiment is depicted in Figure 15. Moreover, it has been shown that it is possible to monitor the folding reaction at the level of the individual residues of an isotopically labeled protein with a single two-dimensional experiment; this opens the way to high-resolution experiments.[83] Equally important has been the demonstration that laser-excitation methods of generating nuclear polarization (photo-CIDNP experiments; CIDNP = chemically induced dynamic nuclear polarization) allow the time scale on which events can be followed to be reduced to about 10 ms,[133] which brings time resolution of this NMR technique close to that of optical spectroscopic methods.

Another approach to using NMR spectroscopy to follow folding has been through hydrogen pulse labelling procedures.[50, 168, 169] This approach is based on the fact that labile hydrogens (e.g., those attached to the amide nitrogen atoms in peptide bonds) exchange rapidly with solvent hydrogen atoms in unfolded states, but are often protected from exchange when the protein folds as a result of the involvement of the amides in hydrogen bonds and through burial in the protein interior. At different times after initiation of the folding of a protein, the extent of protection of individual hydrogens can be monitored by applying at high pH a "labelling" pulse in which exposed amide hydrogens are replaced by deuterons. The exchange is then "quenched" at low pH (to slow hydrogen/deuterium exchange), and the protein is allowed to refold. The extent of labelling at different sites (monitored by NMR) then reflects the nature of the protein structure at the time of the labelling pulse during the folding process. The extent of labelling can also be monitored by mass spectrometry, an approach that provides key information on the distribution of structural heterogenicity during refolding.[170]

We thank Azat Badretdinov, Matthias Buck, Aaron Dinner, Alan Fersht, Andrew Miranker, Sheena Radford, Lorna Smith, and Eugene Shakhnovich for helpful discussions. We are grateful to Oren Becker for providing Figure 9, and Eric Feyfont for help in preparing Figures 1, 4, and 11. Partial support of this research came from the Biotechnology and

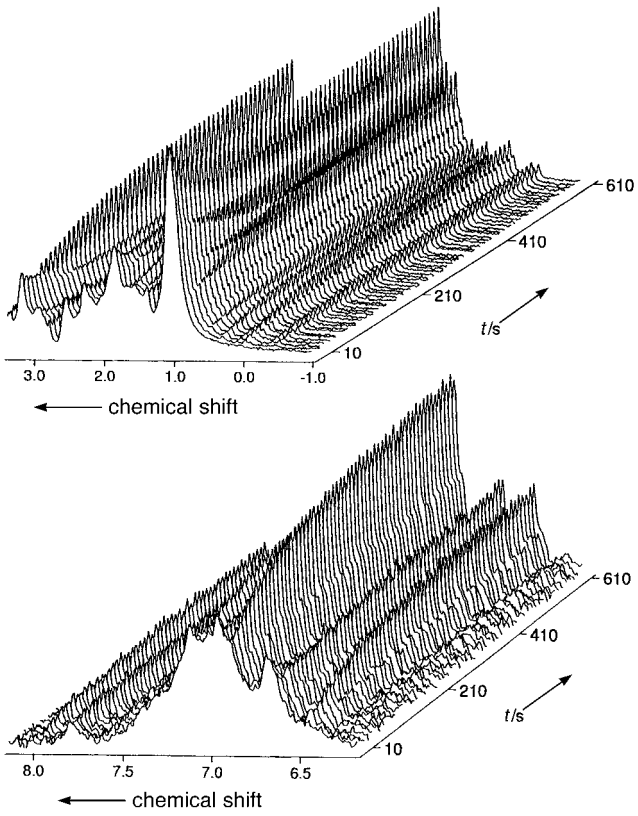


Figure 15. ^{1}H NMR spectroscopic investigation of protein folding in real time. Bovine α-lactalbumin dissolved in 6 M guanidinium chloride was injected into refolding buffer within an NMR instrument. Spectra were recorded at incremental time points between 1.2 s and 10.3 min after initiation of refolding; the stack plots show the changes in the spectral regions containing resonances for methyl and methylene groups (top) and aromatic side chains (bottom). The disappearance of the broad and overlapping signals of the initially formed disorganized globule state and the emergence of the well-resolved resonances characteristic of the native state are clearly evident; taken from reference [132].

Biological Research Council (C.M.D.), the Medical Research Council (C.M.D.), the Engineering and Physical Science Research Council (C.M.D.), the National Science Foundation (M.K.), the National Institutes of Health (M.K., A.S.), the Ministère de la Recherche et Centre National du Recherche Scientifique (M.K.), and the Alexander and Alexandrine Sinsheimer Fund (A.S.). The research of C.M.D. is supported in part by an International Research Scholar award from the Howard Hughes Medical Institute.

Received: July 14, 1997 [Z A242 IE]
German version: *Angew. Chem.* **1998**, *110*, 908 – 935

[1] R. E. Levine, R. B. Bernstein, *Molecular Reaction Dynamics and Chemical Reactivity*, Oxford University Press, Oxford, **1987**.
[2] "Protein Folding: Theoretical Studies of Thermodynamics and Dynamics": M. Karplus, E. Shakhnovich in *Protein Folding* (Ed.: T. E. Creighton), Freeman, San Francisco, **1992**, pp. 127 – 195.
[3] A. D. Miranker, C. M. Dobson, *Curr. Opin. Struct. Biol.* **1996**, *6*, 31 – 42.
[4] M.-J. Getting, J. Sambrook, *Nature* **1992**, *355*, 33 – 45.
[5] C. B. Anfinsen, *Science* **1973**, *181*, 223 – 230.
[6] M. Karplus, A. Šali, *Curr. Opin. Struct. Biol.* **1995**, *5*, 58 – 73.
[7] C. Levinthal in *Mossbauer Spectroscopy in Biological Systems*, *Proceedings of a Meeting held at Allerton House*, *Monticello*, *Illinois* (Eds.: P. Debrunner, J. C. M. Tsibris, E. Münck), University of Illinois Press, Urbana, **1969**, p. 22.
[8] C. Levinthal, *J. Chim. Phys.* **1968**, *65*, 44 – 45.
[9] J. Moult, T. Hubbard, S. H. Bryant, K. Fidelis, J. Pedersen, *Proteins: Struct. Funct. Genet. Suppl.* **1997**, *1*, 2 – 6.
[10] H. Wu, *Am. J. Physiol.* **1929**, *90*, 562.
[11] J. S. Fruton, *Molecules and Life*, Wiley, New York, **1972**.
[12] "Molecular Dynamics of Elementary Chemical Reaction (Nobel Lecture)": D. R. Herschbach, *Angew. Chem.* **1987**, *99*, 1251 – 1275; *Angew. Chem. Int. Ed. Engl.* **1987**, *26*, 1221 – 1243.
[13] M. Karplus, R. N. Porter, R. D. Sharma, *J. Chem. Phys.* **1965**, *43*, 3259 – 3287.
[14] J. D. Bryngelson, J. N. Onuchic, N. D. Socci, P. G. Wolynes, *Proteins: Struct. Funct. Genet.* **1995**, *21*, 167 – 195.
[15] K. A. Dill, S. Bromberg, K. Yue, K. M. Fiebig, D. P. Yee, P. D. Thomas, H. S. Chan, *Protein Sci.* **1995**, *4*, 561 – 602.
[16] E. I. Shakhnovich, *Curr. Opin. Struct. Biol.* **1997**, *7*, 29 – 40.
[17] K. A. Dill, H. S. Chan, *Nat. Struct. Biol.* **1997**, *4*, 10 – 19.
[18] A. H. Zewail, J. Polanyi, *Acc. Chem. Res.* **1995**, *28*, 119 – 124.
[19] R. N. Porter, M. Karplus, *J. Chem. Phys.* **1964**, *40*, 1105 – 1115.
[20] G. C. Schatz, *J. Phys. Chem.* **1996**, *100*, 12839 – 12847.
[21] M. Oliveberg, A. R. Fersht, *Proc. Natl. Acad. Sci. USA* **1995**, *92*, 8926 – 8929.
[22] D. J. Wales, *Science* **1996**, *271*, 925 – 929.
[23] K. D. Ball, R. S. Berry, R. E. Kunz, F.-Y. Li, A. Proykova, D. J. Wales, *Science* **1996**, *271*, 963 – 965.
[24] D. L. Freeman, J. D. Doll, *Annu. Rev. Phys. Chem.* **1996**, *47*, 43 – 80.
[25] J. D. Bryngelson, P. G. Wolynes, *J. Phys. Chem.* **1989**, *93*, 6902 – 6915.
[26] E. I. Shakhnovich, A. M. Gutin, *Biophys. Chem.* **1989**, *34*, 187 – 199.
[27] V. I. Abkevich, A. M. Gutin, E. I. Shakhnovich, *J. Chem. Phys.* **1994**, *101*, 6052 – 6062.
[28] A. Šali, E. Shakhnovich, M. Karplus, *Nature* **1994**, *369*, 248 – 251.
[29] H. A. Kramers, *Physica* **1940**, *7*, 284 – 293.
[30] R. W. Pastor, M. Karplus, *J. Chem. Phys.* **1989**, *91*, 211 – 218.
[31] S. H. Northrup, M. R. Pear, C.-Y. Lee, J. A. McCammon, M. Karplus, *Proc. Natl. Acad. Sci. USA* **1982**, *79*, 4035 – 4039.
[32] T. Lazaridis, G. Archontis, M. Karplus, *Adv. Protein Chem.* **1995**, *47*, 231 – 306.
[33] D. A. McQuarrie, *Statistical Mechanics*, Harper & Row, New York, **1976**, p. 641.
[34] A. Caflisch, M. Karplus, *Proc. Natl. Acad. Sci. USA* **1994**, *91*, 1746 – 1750.
[35] A. Caflisch, M. Karplus, *J. Mol. Biol.* **1995**, *252*, 672 – 708.
[36] G. I. Makhatadze, P. L. Privalov, *Adv. Protein Chem.* **1995**, *47*, 308 – 417.
[37] P. L. Privalov, *Adv. Protein Chem.* **1979**, *33*, 167 – 241.
[38] F. C. Bernstein, T. F. Koetzle, G. J. B. Williams, E. F. Meyer, Jr., M. D. Brice, J. R. Rodgers, O. Kennard, T. Shimanouchi, M. Tasumi, *J. Mol. Biol.* **1977**, *112*, 535 – 542.
[39] L. Holm, C. Sander, *Science* **1996**, *273*, 595 – 602.
[40] C. Chothia, *Nature* **1992**, *360*, 543 – 544.
[41] C. A. Orengo, D. T. Jones, J. M. Thornton, *Nature* **1994**, *372*, 631 – 634.
[42] A. V. Finkelstein, A. Y. Badretdinov, A. M. Gutin, *Proteins* **1995**, *23*, 142 – 150.
[43] A. R. Fersht, *Curr. Opin. Struct. Biol.* **1994**, *5*, 79 – 84.
[44] R. Elber, M. Karplus, *Science* **1987**, *235*, 318 – 321.
[45] C. L. Brooks III, M. Karplus, B. M. Pettitt, *Proteins: A Theoretical Perspective of Dynamics*, *Structure*, *and Thermodynamics (Advances in Chemical Physics, Vol. 71)*, Wiley, New York, **1988**.
[46] O. B. Ptitsyn, *Adv. Protein Chem.* **1995**, *47*, 83 – 229.
[47] A. Dinner, A. Šali, M. Karplus, E. Shakhnovich, *J. Chem. Phys.* **1994**, *101*, 1444 – 1451.
[48] D. Stigter, D. O. V. Alonso, K. A. Dill, *Proc. Natl. Acad. Sci. USA* **1991**, *88*, 4176 – 4180.
[49] C. Tanford, *Adv. Protein Chem.* **1970**, *24*, 1 – 95.
[50] W. Englander, P. Mayne, *Annu. Rev. Biophys. Biomol. Struct.* **1992**, *21*, 243 – 265.
[51] M. Karplus, D. L. Weaver, *Protein Sci.* **1994**, *3*, 650 – 668.

[52] E. Shakhnovich, *Folding Des.* **1996**, *1*, R50 – R54.
[53] E. P. Wigner, *Trans. Faraday Soc.* **1938**, *34*, 29.
[54] a) A. Dinner, A. Šali, M. Karplus, *Proc. Natl. Acad. Sci. USA* **1996**, *93*, 8356 – 8361; b) T. Lazaridis, M. Karplus, *Science* **1997**, *278*, 1928 – 1931; c) A. Dinner, M. Karplus, *Folding Des.* **1998**, in press.
[55] a) A. Šali, E. Shakhnovich, M. Karplus, *J. Mol. Biol.* **1994**, *235*, 1614 – 1636; b) A. Šali, E. Shakhnovich, M. Karplus, unpublished results.
[56] M. Karplus, A. Caflisch, A. Šali, E. Shakhnovich in *Modelling of Biomolecular Structures and Mechanisms* (Ed.: A. Pullman), Kluwer, Dordrecht, **1995**, pp. 69 – 84.
[57] J. N. Onuchic, P. G. Wolynes, Z. Luthey-Schulten, N. D. Socci, *Proc. Natl. Acad. Sci. USA* **1996**, *92*, 3626 – 3630.
[58] D. L. Bunker, *Theory of Elementary Gas Phase Reaction Rates*, Pergamon, Oxford, **1966**.
[59] R. Zwanzig, *Proc. Natl. Acad. Sci. USA* **1995**, *92*, 9801 – 9804.
[60] N. Socci, J. N. Onuchic, P. G. Wolynes, *J. Chem. Phys.* **1996**, *104*, 5860 – 5868.
[61] S. J. Segawa, M. Sugihara, *Biopolymers* **1984**, *23*, 2473 – 2488.
[62] M. Oliveberg, A. R. Fersht, *Biochemistry* **1996**, *35*, 2726 – 2737.
[63] O. M. Becker, M. Karplus, *J. Phys. Chem.* **1997**, *106*, 1495 – 1517.
[64] O. M. Becker, *J. Mol. Struct. (Theochem.)*, **1997**, *398*, 507 – 516.
[65] P. A. Evans, S. E. Radford, *Curr. Opin. Struct. Biol.* **1994**, *4*, 100 – 106.
[66] K. B. Wiberg, *Physical Organic Chemistry*, Wiley, New York, **1964**.
[67] D. R. Herschbach, M. S. Johnson, D. Rapp, *J. Chem. Phys.* **1959**, *31*, 1652 – 1661.
[68] O. B. Ptitsyn, R. H. Pain, G. V. Semisomov, E. Zerovnik, O. I. Razgulysev, *FEBS Lett.* **1990**, *262*, 20 – 24.
[69] D. Eliezer, P. A. Jennings, P. E. Wright, S. Doniach, K. O. Hodgson, H. Tsuruta, *Science* **1995**, *270*, 487 – 488.
[70] S. E. Radford, C. M. Dobson, P. A. Evans, *Nature* **1992**, *358*, 302 – 307.
[71] J. I. Guijarro, M. Jackson, A. F. Chaffotte, M. Delepierre, H. H. Mantsch, M. E. Goldberg, *Biochemistry* **1995**, *34*, 2998 – 3008.
[72] W. Kauzmann, *Adv. Protein Chem.* **1959**, *14*, 1 – 63.
[73] K. Kuwajima, *FASEB J.* **1996**, *10*, 102 – 109.
[74] M. Ikeguchi, M. Kuwajima, M. Mitani, S. Sugai, *Biochemistry* **1986**, *25*, 6965 – 6972.
[75] J. Baum, C. M. Dobson, P. A. Evans, C. Hanley, *Biochemistry* **1989**, *28*, 7 – 13.
[76] B. A. Schulman, C. Redfield, Z.-Y. Peng, C. M. Dobson, P. S. Kim, *J. Mol. Biol.* **1995**, *253*, 651 – 657.
[77] L. C. Wu, Z.-Y. Peng, P. S. Kim, *Nat. Struct. Biol.* **1995**, *2*, 281 – 286.
[78] L. A. Morozova, D. T. Haynie, C. Arico-Muendel, H. V. Van Dael, C. M. Dobson, *Nat. Struct. Biol.* **1995**, *2*, 871 – 875.
[79] D. A. Dolgikh, R. I. Gilmanshin, E. V. Brazhnikov, V. E. Bychkova, G. V. Semisotnov, S. Y. Venyaminov, O. B. Ptitsyn, *FEBS Lett.* **1981**, *136*, 311 – 315.
[80] J. Balbach, V. Forge, W. S. Lau, J. Jones, N. A. J. van Nuland, C. M. Dobson, *Proc. Natl. Acad. Sci. USA* **1997**, *94*, 7182 – 7185.
[81] B. Schulman, P. S. Kim, C. M. Dobson, C. Redfield, *Nat. Struct. Biol.*, in press.
[82] B. A. Schulman, P. S. Kim, *Nat. Struct. Biol.* **1996**, *3*, 682 – 687.
[83] J. Balbach, V. Forge, W. S. Lau, N. A. J. van Nuland, K. Brew, C. M. Dobson, *Science* **1996**, *274*, 1161 – 1163.
[84] J. Balbach, V. Forge, N. J. van Nuland, S. Winder, P. J. Hore, C. M. Dobson, *Nature Struct. Biol.* **1995**, *2*, 865 – 870.
[85] D. B. Weflaufer, *Proc. Natl. Acad. Sci. USA* **1973**, *70*, 697 – 701.
[86] V. E. Abkevich, A. M. Gutin, E. Shakhnovich, *Biochemistry* **1994**, *33*, 10026 – 10036.
[87] W. Eaton, *Adv. Protein Chem.* **1990**, *40*, 63 – 279.
[88] A. R. Fersht, *Proc. Natl. Acad. Sci. USA* **1995**, *92*, 10869 – 10873.
[89] A. R. Fersht, *FEBS Lett.* **1993**, *325*, 5 – 16.
[90] A. R. Fersht, L. S. Itzhaki, N. F. ElMasry, J. M. Matthews, D. E. Otzen, *Proc. Natl. Acad. Sci. USA* **1994**, *91*, 10426 – 10429.
[91] L. S. Itzhaki, D. E. Otzen, A. R. Fersht, *J. Mol. Biol.* **1995**, *254*, 260 – 288.
[92] E. Shakhnovich, V. Abkevich, O. B. Ptitsyn, *Nature* **1996**, *379*, 96 – 98.
[93] J. N. Onuchic, N. D. Socci, Z. Luthey-Schulten, P. G. Wolynes, *Folding Des.* **1996**, *1*, 441 – 450.
[94] G. A. Mines, T. Pascher, S. C. Lee, J. R. Winkler, H. B. Gray, *Chem. Biol.* **1996**, *3*, 491 – 496.
[95] M. S. Kay, R. L. Baldwin, *Nat. Struct. Biol.* **1996**, *3*, 439 – 445.
[96] S. Khorasanizadeh, I. D. Peters, H. Roder, *Nat. Struct. Biol.* **1996**, *3*, 193 – 205.
[97] R. E. Burton, C. S. Huang, M. A. Daugherty, T. L. Calderone, T. G. Oas, *Nat. Struct. Biol.* **1997**, *4*, 305 – 310.
[98] C. M. Dobson, P. A. Evans, S. E. Radford, *Trends Biochem. Sci.* **1994**, *19*, 71 – 72.
[99] S. E. Radford, C. M. Dobson, *Philos. Trans. R. Soc. London B* **1995**, *348*, 17 – 25.
[100] T. Kiefhaber, *Proc. Natl. Acad. Sci. USA* **1995**, *92*, 9029 – 9033.
[101] A. Matagne, S. E. Radford, C. M. Dobson, *J. Mol. Biol.* **1997**, *267*, 1068 – 1074.
[102] Z. Guo, D. Thirumalai, *Biopolymers* **1995**, *36*, 83 – 102.
[103] A. Miranker, S. E. Radford, M. Karplus, C. M. Dobson, *Nature* **1991**, *349*, 633 – 636.
[104] V. I. Abkevich, A. M. Gutin, E. I. Shakhnovich, *Protein Sci.* **1995**, *4*, 1167 – 1177.
[105] A. R. Panchenko, Z. Luthey-Schulten, P. G. Wolynes, *Proc. Natl. Acad. Sci. USA* **1996**, *93*, 2008 – 2113.
[106] A. R. Fersht, *Biochem. Soc. Trans.* **1994**, *22*, 267 – 273.
[107] R. L. Baldwin, *J. Biomol. NMR* **1995**, *5*, 103 – 109.
[108] T. E. Creighton, N. J. Darby, J. Kemmink, *FASEB J.* **1996**, *10*, 110 – 118.
[109] H. Roder, W. Colón, *Curr. Opin. Struct. Biol.* **1997**, *7*, 15 – 28.
[110] T. R. Sosnick, L. Mayne, S. W. Englander, *Proteins* **1996**, *24*, 413 – 426.
[111] F. X. Schmid in *Protein Folding* (Ed.: T. E. Creighton), Freeman, San Francisco, **1992**, pp. 197 – 241.
[112] T. R. Sosnick, L. Mayne, R. Hiller, S. W. Englander, *Nat. Struct. Biol.* **1994**, *1*, 149 – 156.
[113] V. Munoz, L. Serrano, *Proteins* **1994**, *20*, 301 – 311.
[114] L. J. Smith, K. Fiebig, H. Schwalbe, C. M. Dobson, *Folding Des.* **1996**, *1*, 95 – 106.
[115] M. Blaber, W. A. Baase, N. Gassuer, B. W. Matthews, *J. Mol. Biol.* **1993**, *246*, 317 – 330.
[116] M. H. J. Cordes, A. R. Davidson, R. T. Sauer, *Curr. Opin. Struct. Biol.* **1996**, *6*, 3 – 10.
[117] J. Novotny, R. E. Bruccoleri, M. Karplus, *J. Mol. Biol.* **1984**, *177*, 787 – 818.
[118] J. U. Bowie, R. Luthy, D. Eisenberg, *Science* **1991**, *253*, 164 – 170.
[119] A. V. Finkelstein, B. A. Reva, *Nature* **1991**, *351*, 497 – 499.
[120] M. J. Sippl, *J. Comput. Aided Mol. Des.* **1993**, *7*, 473 – 501.
[121] C. M. R. Lemer, M. J. Rooman, S. J. Wodak, *Proteins* **1995**, *23*, 337 – 355.
[122] D. T. Jones, J. M. Thornton, *Curr. Opin. Struct. Biol*. **1996**, *6*, 210 – 216.
[123] S. Kamtekar, J. M. Schiffer, H. Xiong, J. M. Babik, M. H. Hecht, *Science* **1993**, *262*, 1680 – 1685.
[124] M. H. Hecht, J. S. Richardson, D. C. Richardson, R. C. Ogden, *Science* **1990**, *249*, 884 – 891.
[125] S. C. Harrison, R. Durbin, *Proc. Natl. Acad. Sci. USA* **1985**, *82*, 4028 – 4030.
[126] R. L. Baldwin, *Nature* **1994**, *369*, 183 – 184.
[127] "Physics & Biology": H. Frauenfelder in *Physics in a Technological World* (Ed.: A. P. French), AIP, New York, **1988**, pp. 255 – 267.
[128] A. M. Gutin, V. I. Abkevich, E. I. Shakhnovich, *Biochemistry* **1995**, *34*, 3066 – 3076.
[129] P. J. Steinbach, A. Ansari, J. Berendzen, D. Braunstein, K. Chu, B. R. Cowen, D. Ehrenstein, H. Frauenfelder, J. B. Johnson, D. C. Lamb, *Biochemistry* **1991**, *30*, 3988 – 4001.
[130] K. W. Plaxco, C. M. Dobson, *Curr. Opin. Struct. Biol.* **1996**, *6*, 630 – 636.
[131] C. Freiden, S. D. Hoeltzli, I. J. Ropson, *Protein Sci.* **1993**, *2*, 2007 – 2014.
[132] N. A. J. van Nuland, J. Balbach, V. Forge, C. M. Dobson, *Nat. Struct. Biol.* **1995**, *2*, 865 – 870.
[133] P. J. Hore, S. Winder, C. H. Roberts, C. M. Dobson, *J. Am. Chem. Soc.* **1997**, *119*, 5049 – 5050.
[134] C. M. Phillips, Y. Mizutani, R. M. Hochstrasser, *Proc. Natl. Acad. Sci. USA* **1995**, *92*, 7292 – 7296.

[135] G. Wilson, L. Hecht, L. D. Barron, *J. Mol. Biol.* **1996**, *261*, 341 – 347.
[136] Y. Bai, S. W. Englander, *Proteins* **1996**, *24*, 145 – 151.
[137] D. Shortle, Y. Wang, J. R. Gillespie, J. O. Wrable, *Protein Sci.* **1996**, *5*, 991 – 1000.
[138] C. M. Jones, E. R. Henry, U. Hu, C.-K. Chan, S. D. Luck, A. Bhuyan, H. Roder, J. Hofrichter, W. A. Eaton, *Proc. Natl. Acad. Sci. USA* **1993**, *90*, 11860 – 11864.
[139] B. Nolting, R. Golbik, A. R. Fersht, *Proc. Natl. Acad. Sci. USA* **1995**, *92*, 10668 – 10672.
[140] T. Pascher, J. P. Chesick, J. R. Winkler, H. B. Gray, *Science* **1996**, *271*, 1558 – 1560.
[141] R. M. Ballew, J. Sabelko, M. Gruebele, *Proc. Natl. Acad. Sci. USA* **1996**, *93*, 5759 – 5764.
[142] W. A. Eaton, P. A. Thompson, C.-K. Chan, S. J. Hagen, J. Hofrichter, *Structure* **1996**, *4*, 113 – 1139.
[143] A. E. Mark, W. F. van Gunsteren, *Biochemistry* **1992**, *31*, 7745 – 7788.
[144] V. Daggett, M. Levitt, *Curr. Opin. Struct. Biol.* **1994**, *4*, 291 – 295.
[145] A. J. Li, V. Daggett, *Proc. Natl. Acad. Sci. USA* **1994**, *91*, 10430 – 10434.
[146] A. Kolinski, J. Skolnick, *Proteins* **1994**, *18*, 338 – 352.
[147] a) A. Guo, D. Thirumalai, J. D. Honeycutt, *J. Chem. Phys.* **1992**, *97*, 525 – 535.; b) Y. Zhou, M. Karplus, *Proc. Natl. Acad. Sci. USA* **1997**, *94*, 14429 – 14432.
[148] E. M. Boczko, C. L. Brooks III, *Science* **1995**, *269*, 393 – 396.
[149] A. R. Fersht, *Curr. Opin. Struct. Biol.* **1997**, *7*, 3 – 9.
[150] G. L. G. Miklos, G. M. Rubin, *Cell* **1996**, *86*, 521 – 529.
[151] J. S. Marvin, E. E. Corcoran, N. A. Hattangadi, J. V. Zhang, S. A. Gere, H. W. Hellinga, *Proc. Natl. Acad. Sci. USA* **1997**, *94*, 4366 – 4371.
[152] F. U. Hartl, *Nature* **1996**, *381*, 571 – 580.
[153] R. Zahn, S. Perrett, G. Stenberg, A. R. Fersht, *Science* **1996**, *271*, 642 – 645.
[154] M. Todd, G. Lorimer, D. Thirumalai, *Proc. Natl. Acad. Sci. USA* **1996**, *93*, 4030 – 4034.
[155] M. L. Riley, B. A. Wallace, S. L. Flitsch, P. J. Booth, *Biochemistry* **1997**, *36*, 192 – 196.
[156] R. W. King, R. J. Deshaies, J. M. Peters, M. W. Kirchner, *Science* **1996**, *274*, 1652 – 1659.
[157] P. J. Thomas, B.-H. Qu, P. L. Pederson, *Trends Biochem. Sci.* **1995**, *20*, 456 – 459.
[158] S. C. Hyde, P. Emsley, M. J. Hartshorn, M. M. Mimmack, U. Gileadi, S. R. Pearce, M. P. Galagher, D. R. Gill, R. E. Hubbard, C. F. Higgins, *Nature* **1990**, *346*, 362 – 365.
[159] S. B. Prusiner, *Biochemistry* **1992**, *31*, 12277 – 12288.
[160] C. D. Waldburger, T. Jonsson, R. T. Sauer, *Proc. Natl. Acad. Sci. USA* **1996**, *93*, 2629 – 2634.
[161] J. King, C. Haase-Pettingell, A. S. Robinson, M. Speed, A. Mitraki, *FASEB J.* **1996**, *10*, 57 – 66.
[162] D. R. Booth, M. Sunde, V. Bellotti, C. V. Robinson, W. L. Hutchinson, P. E. Fraser, P. N. Hawkins, C. M. Dobson, S. E. Radford, C. C. F. Blake, M. B. Pepys, *Nature* **1997**, *385*, 787 – 793.
[163] P. J. Kraulis, *J. Appl. Crystallogr.* **1991**, *24*, 946.
[164] E. A. Merritt, M. E. Murphy, *Acta Crystallogr. Sect. D* **1994**, *50*, 869 – 873.
[165] K. W. Plaxco, C. Spitzfaden, I. D. Campbell, C. M. Dobson, *Proc. Natl. Acad. Sci. USA* **1996**, *93*, 10703 – 10706.
[166] J. A. McCammon, S. H. Northrup, M. Karplus, R. M. Levy, *Biopolymers* **1980**, *19*, 2033 – 2045.
[167] K. Yapa, D. L. Weaver, M. Karplus, *Proteins: Struct. Funct. Genet.* **1992**, *12*, 237 – 265.
[168] J. B. Udgaonkar, R. L. Baldwin, *Nature* **1988**, *335*, 694 – 699.
[169] H. Roder, G. A. Elove, S. W. Englander, *Nature* **1988**, *335*, 700 – 704.
[170] A. Miranker, C. V. Robinson, S. E. Radford, R. T. Aplin, C. M. Dobson, *Science* **1993**, *262*, 896 – 900.

Deposition of Data from X-Ray Structure Analyses

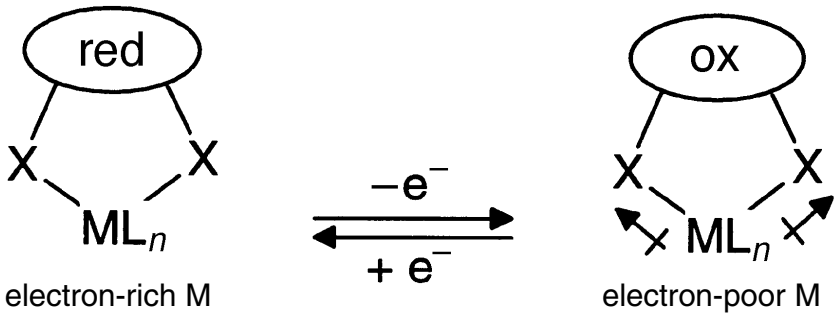
In order to make life easier for authors and referees the Cambridge Crystallographic Data Centre (CCDC) and the Fachinformationszentrum Karlsruhe (FIZ) have unified their procedures for the depostion of data from single-crystal X-ray structure analyses.

Prior to submitting a manuscript please deposit the data for your compound(s) **electronically** at the appropriate date base, that is, at the CCDC for organic and organometallic compounds and at the FIZ for inorganic compounds. Both data bases will be pleased to provide help (see our *Notice to Authors* in the first issue of this year). In general, you will receive a depository number from the data base within two working days after electronic deposition; please include this number with the appropriate standard text (see our Notice to Authors) in your manuscript. This will enable the referees to retrieve the structure data quickly and efficiently if they need this information to reach their decision.

This is now the uniform procedure for manuscripts submitted to the journals *Advanced Materials, Angewandte Chemie, Chemistry—A European Journal,* the *European Journal of Inorganic Chemistry,* and the *European Journal of Organic Chemistry.*

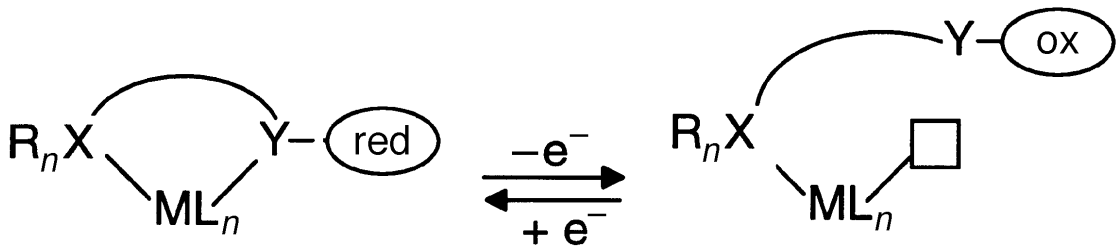
Use of redox-active ligands to control the reactivity of metal complexes

- substitutionally inert redox-switchable ligands

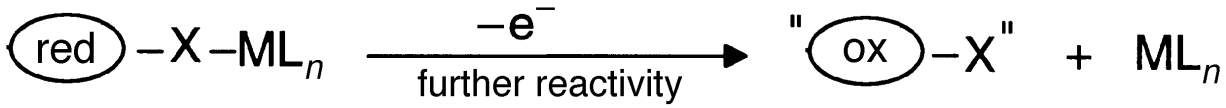


X = strongly binding ligand
Y = weakly binding ligand
R = substituent of tunable electronic nature
□ = ligand or solvent

- redox-switchable hemilabile ligands



- reactive fragment redox-switchable ligands



ANGEWANDTE CHEMIE © WILEY-VCH

Three ways to control the stoichiometric and catalytic activity of transition metal complexes by oxidation or reduction of a ligand. More about the design of such ligands is reviewed by A. M. Allgeier and C. A. Mirkin on the following pages.

Ligand Design for Electrochemically Controlling Stoichiometric and Catalytic Reactivity of Transition Metals

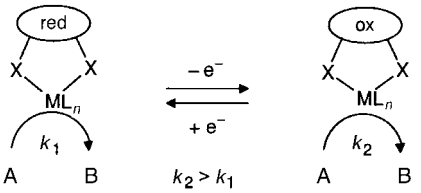
Alan M. Allgeier and Chad A. Mirkin*

Chemists have several tools at their disposal for studying and subsequently controlling reactivity. Recently, redox-active ligands were utilized in novel ways to control the reactivity of transition metal complexes. Several redox-active ligands undergo stable and reversible changes in oxidation state, which allows one to tune the electron richness of the ligand and the bound metal. In this contribution we present an overview of redox-active ligands, which have been categorized into three classes based on their mode of reactivity control. In addition, specific examples are presented which demonstrate the utility of redox-active ligands for controlling metal–ligand binding constants and both stoichiometric and catalytic reactions involving transition metals. In some cases, these oxidation state dependent changes in reactivity can be quite significant, and alter reaction rates by several orders of magnitude and ligand binding constants by many orders of magnitude. Further development of redox-active ligands will be anchored upon a firm understanding of the factors that influence the charge-dependent behavior of transition metal complexes of these ligands. Perspectives on the future direction of research in this area are presented, in particular with respect to the interest in new redox-active groups and potential applications in redox-switchable catalysis and materials for the separation of molecules.

Keywords: cyclic voltammetry · homogeneous catalysis · ligand effects · redox chemistry · substituent effects

1. Introduction

An electrode is one of the most powerful, yet most underutilized, reagents available to the synthetic chemist. It offers an almost unlimited source of or sink for electrons of mechanically tunable (through a potentiostat) free energy. These electrons can be used to effect oxidation or reduction of substrates directly at an electrode surface (e.g. reduction of H^+ to H_2)[1] or, alternatively, they can be used to reversibly interconvert a compound between two useful states of reactivity (Scheme 1). These compounds, which are often referred to as redox switches, have found extensive application in chemistry. The sensitivities of their formal potentials to their electronic and chemical environments have been exploited in the development of sensors for ions[2] and small molecules.[3] A key component of these complexes is a redox-active ligand that can be interconverted between two or more useful oxidation states through a series of applied potentials.



Scheme 1. Redox-active ligands can be used to reversibly alter the reactivity of transition metals. red = reduced form of the ligand, ox = oxidized form of the ligand, A = substrate, B = product.

[*] Prof. C. A. Mirkin, Dr. A. M. Allgeier
Department of Chemistry
Northwestern University
2145 Sheridan Road, Evanston, IL 60208-3113 (USA)
Fax: (+1) 847-491-7713
E-mail: camirkin@chem.nwu.edu

2. Perspective on Redox-Active Ligands

2.1. Overview of Redox-Active Ligands

Of significant interest to inorganic chemists has been the incorporation of redox-active groups into a variety of metal-binding ligands. Cryptand and crown sequestering agents which incorporate ferrocenyl,[2c, 4] cobaltocenyl,[2d, 5] anthraquinone,[6] and other redox-active groups have been synthesized.[7] These molecules have been used for the electrochemical recognition of alkali and alkaline earth metal cations,[2a,c,d, 4a–c, 7, 8] late transition metals, and some coinage metals.[2d, 4b, 9] They also offer electrochemical control over metal binding constants and have been used in a variety of electrochemically driven metal ion transport systems.[6, 10] In addition, redox switches have been designed for electrochemically detecting a variety of anionic and neutral guest

 © WILEY-VCH Verlag GmbH, D-69451 Weinheim, 1998 1433-7851/98/3707-0895 $ 17.50+.50/0

species.[2a,d, 11] These areas have been reviewed thoroughly and will not be treated further here.[2a,c,d, 4d]

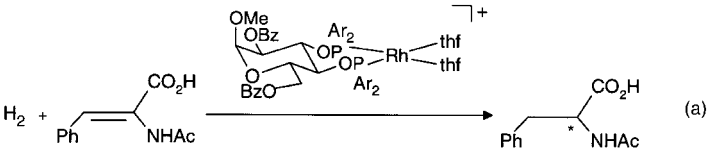
In addition to ligands that can be used to control the thermodynamic binding affinities of transition metals, several redox-active ligands that alter the reactivity of a bound transition metal as a function of ligand oxidation state have been designed and synthesized. This latter group of ligands, which provides electrochemical control over several stoichiometric and catalytic reactions of transition metals, constitutes the topic of this review (Scheme 1). By making use of the different stabilities of oxidation states associated with certain redox-active groups, researchers have designed ligands that when complexed to transition metals yield compounds with electrochemically switchable states of reactivity. Catalysts formed from these ligands may be inactive or sluggish in one oxidation state, but active following oxidation or reduction. Alternatively, they may show selectivities for specific transformations that depend upon the oxidation state of the complex.

Hembre and McQueen recently reported the use of a redox-active ligand as an electron shuttle in a catalytic process.[12] While the presence of the redox-active moiety is essential to the completion of the catalytic reaction, the moiety itself is not used to tune the reactivity of the bound transition metal. Such electrocatalysts are beyond the scope of the present review and will not be discussed further.

2.2. Alternative Methods for Controlling the Reactivity of Transition Metals

2.2.1. Ligand Substituent Effects

In general, the use of redox-active groups and electrochemistry offers some distinct advantages over complementary synthetic-based approaches to altering the reactivity of transition metals. With a redox-active group, one can control the electron richness of a ligand through mechanically driven electrochemical oxidation or reduction processes without the need for further conventional synthetic steps. Such adjustments in the electronic nature of the ligand can provide corresponding changes in the reactivity of the bound metal. Indeed, there are many examples that demonstrate how subtle changes in the electron-donating properties of a ligand can markedly affect the reactivity of transition metals.[13] For instance, in the enantioselective hydrogenation of acetamidoacrylates, chiral rhodium–diphosphonite catalysts bearing electron-donating substituents incorporated into the aryl (Ar) groups offer higher enantioselectivity than the corresponding catalysts with electron-withdrawing groups [Eq. (a)].[13h] One



(a)

drawback to the above experiment and others like it is the extensive synthetic work necessary to make ligands with varying degrees of electron richness. In contrast, one redox-active ligand can be shuttled between multiple states of charge and, therefore, multiple states of electron richness by electrochemically driven redox processes without extra conventional synthetic steps. Numerous studies have established a dependence of both stoichiometric[13a] and catalytic reactivity[13b–i] on substituent electronic effects; this bodes well for the use of redox-active ligands in the rational design of complexes with stoichiometric and catalytic chemistries that can be electrochemically controlled.


C. A. Mirkin

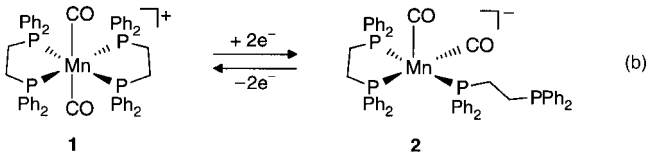

A. M. Allgeier

Chad A. Mirkin was born in Phoenix, AZ (USA) in 1963. After earning his B.S. in Chemistry at Dickinson College in Carlisle, PA in 1986 and a Ph.D. in Chemistry from the Pennsylvania State University in 1989, he worked as an NSF Postdoctoral Fellow at the Massachusetts Institute of Technology. In 1991 he became an Assistant Professor of Chemistry at Northwestern University; he is currently Charles E. and Emma H. Morrison Professor of Chemistry. He has an interdisciplinary research program aimed at the design, synthesis, and study of surface-confined electroactive materials. For his efforts in this area, he has won numerous awards including the 1998 E. Bright Wilson Award, the 1997 BFGoodrich Collegiate Inventors Award, a Camille Dreyfus Teacher-Scholar Award, an A. P. Sloan Foundation Fellowship, a Beckman Young Investigator Award, an ONR Young Investigator Award, a DuPont Young Professor Award, and an NSF Young Investigator Award.

Alan M. Allgeier was born in Erie, PA (USA) in 1971. He earned his B.S. in Chemistry at Case Western Reserve University in Cleveland, OH, where he performed research under Prof. Anthony J. Pearson. Subsequently, he studied inorganic chemistry at Northwestern University, and in 1997 received his Ph.D. with Prof. Chad A. Mirkin for his work on ferrocene-based redox-switchable ligands. He is currently a Research Chemist for DuPont and works in the field of catalysis.

2.2.2. Controlling the Reactivity of Transition Metals with Redox Processes at the Central Metal

In addition to ligand-based approaches for controlling the reactivity of transition metals, there are very effective metal-based approaches. By changing the d-electron count of a transition metal through a metal-based oxidation or reduction reaction, one can control the electronic and steric properties of the metal's coordination sphere. For example, when the six-coordinate manganese complex **1** is electrochemically reduced by a two-electron process, an electron count of 18 is maintained in that a phosphane ligand is dissociated to form **2** [Eq. (b)].[14] This can be an effective way of electrochemically

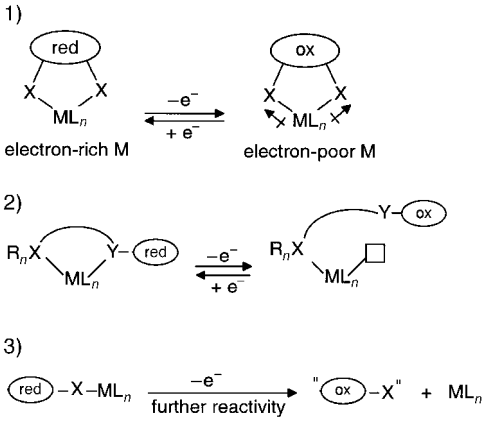


1 2 (b)

opening and closing a coordination site at a metal center. When this approach is applied to metal–arene complexes, interesting changes in arene hapticity are observed,[15] which often lead to reactivity inaccessible to the complexes before reduction.[16] In one example, electochemical reduction of a manganese–η^6-benzene complex leads to a cyclodimerization of the complexed arene.[16] Furthermore, complexes susceptible to this type of electrochemical reaction display a variety of behaviors associated with their redox reactions, including changes in the mode of ligand binding (e.g. linkage isomerism),[15, 17] redox-induced ligand exchange reactions,[18] geometrical isomerism,[19] and redox-induced binding or expulsion of a ligand.[14, 20] This approach has even been used in elaborate gas-separation schemes involving a Cu^{I}/Cu^{II} redox couple.[21] As opposed to ligand-based approaches to changing the reactivity of transition metals, these redox reactions based at the central metal *drastically* alter both the electronic (oxidation state) and steric environments of the bound metal and, therefore, the type of chemistry that the metal center might mediate. A ligand-based approach, however, allows for more subtle but substantial changes in the electronic properties of the transition metal without a formal change in the oxidation state of the metal. For studies which probe the impact of redox processes on catalytic performance, it is especially important that the complex remains in the catalytically relevant formal oxidation state.

2.3. Categorization of Redox-Active Ligands for Transition Metals

Although we have provided representative examples of the above chemistry, our goal is to survey the redox-active ligands designed for controlling the reactivity of transition metals. Such ligands may be categorized into three classes according to their method of altering the reactivity and coordinating properties of transition metals: 1) substitutionally inert, redox-active ligands, 2) redox-switchable hemilabile ligands (RHLs), and 3) redox-active ligands that are reactive (leaving) fragments in a transition metal complex (Scheme 2).



Scheme 2. Classification of redox-switchable ligands. 1) Substitutionally inert, redox-active ligands; X = strongly binding ligand. 2) Redox-switchable hemilabile ligands (RHLs); Y = weakly binding ligand, R = substituent of tunable electronic nature, □ = ligand or solvent. 3) Redox-active ligands that are released upon oxidation.

For ligands in class 1, the redox-active group is incorporated into a ligand which forms a strong, substitutionally inert interaction with a chosen transition metal. Changes in the oxidation state of the ligand affect the reactivity of the metal by altering its electronic nature without changing its formal oxidation state.[22] The RHLs (class 2), which were pioneered and have been extensively studied by our group,[23] are multidentate ligands with at least one substitutionally inert center (R_nX) and one substitutionally labile center (Y). A redox-switchable group is covalently attached to the substitutionally labile portion of the ligand, and, therefore, changes in the oxidation state of the redox-active group allow one to modulate the strength of the adjacent metal–ligand bond, in some cases leading to dissociation of the labile portion of the ligand.[23, 24] The substitutionally inert linkage serves to anchor the ligand to the metal center and provides tunability (through choice of the R group) with regard to the electronic properties of the metal center. This ligand type allows one to control a coordination site or set of coordination sites at a transition metal to which the ligand is bound, without changing the formal oxidation state of the metal center (Scheme 2). In contrast with ligands of class 1, which primarily offer electrochemical control of the electronic properties of the transition metals to which they are bound (without significant concomitant changes in steric properties), RHLs offer electrochemical control of both the steric and electronic environments of transition metals. If one is designing a catalytic system with electrochemically switchable selectivities for desired transformations, this could be quite useful. Finally, some metal complexes have redox-active ligands (class 3) which may be completely expelled as reactive fragments from the coordination sphere of the transition metal upon electrochemical oxidation or reduction, or change their mode or strength of binding (Scheme 2).[25] Although these ligands have thus far been primarily monodentate, they could in principle be easily extended to polydentate systems.

In addition to the aforementioned ligand types, several redox-active ligands and their metal complexes have been examined and characterized electrochemically; however, they

have not been studied with regard to their ability to change the reactivity of transition metals as a function of the oxidation state of the ligand.[19b–d, 26] Sometimes redox-active groups based on ferrocene or cobaltocene are incorporated into ligands for their structural properties, but not studied with regard to their electrochemical behavior.[4d, 9b, 26e–g, 27] Indeed, ferrocene-based ligands have been used in the design of several very effective and useful homogeneous catalysts.[4d] These systems will not be commented on further in this review.

3. Substitutionally Inert, Redox-Active Ligands

3.1. General Description

Changes in the oxidation state of a substitutionally inert, redox-active ligand affects the electronic nature of a bound metal by through-bond electron donation or withdrawal as well as through-space dipole interactions. This can be shown by examining the UV/Vis or IR spectroscopic properties of complexes bearing redox-active ligands and, especially, the changes in these properties upon oxidation or reduction of the ligand.[22a,b, 28]

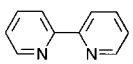
3.2. Dependence of the Carbonyl Stretching Frequency on the Oxidation State of the Ligand

3.2.1. Theoretical Basis

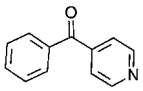
With respect to the dependence of the carbonyl stretching frequency on the oxidation state of the ligand, attention has been devoted primarily to metal–carbonyl complexes. The vibrational energies of carbonyl ligands are sensitive to the electronic nature of the metal to which they are bound, since electron density can be displaced from the metal into carbonyl π^* orbitals. This π backbonding results in a decrease in the C–O bond strength and, consequently, a decrease in the CO stretching frequency. Therefore, if a redox-active ligand undergoes a change in oxidation state that results in a change in the electronic character of the bound transition metal, this can be determined by an analysis of the ν_{CO} region of the IR spectrum. A large series of transition metal complexes (**3**–**17**) have been studied in this manner[22a,b, 28b–g,i,j] (Table 1); included are redox-active ligands which are more stable in their oxidized states (reducible ligands) and others which are more stable in their reduced state (oxidizable ligands). Reducible ligands lead to lower CO stretching frequencies, because

Table 1. Metal–carbonyl complexes with redox-active ligands.

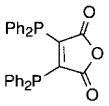
Complex[a]	Ref.	Ligand-based redox process	$\Delta\nu_{CO}$ [cm^{-1}]
3: *fac*-[ClRe(CO)$_3$(bpy)]	[28c]	1-e$^-$ reduction	−25 to −34
4: *fac*-[ClRe(CO)$_3$(4-bzpy)$_2$]	[28c]	1-e$^-$ reduction	−14 to −20
		2-e$^-$ reduction	−26 to −37
5: *fac*-[BrRe(CO)$_3$(bma)]	[28f]	1-e$^-$ reduction	−15 to −32
6: *fac*-[Re(CO)$_4$(dppc)]$^{2+}$	[22a]	1-e$^-$ reduction	−11 to −17
7: *fac*-[Re(CO)$_3$(dppc)(NCCH$_3$)]$^{2+}$	[22a]	1-e$^-$ reduction	−13 to −21
8: *fac*-[ClRe(CO)$_3$(dppf)]	[28d]	1-e$^-$ oxidation	12 to 20
9: *fac*-[ClRe(CO)$_3$(FcPPh$_2$)$_2$]	[28d]	1-e$^-$ oxidation	5 to 9
		2-e$^-$ oxidation	8 to 16
10: *fac*-[ClRe(CO)$_3$(FcPy)$_2$]	[28d]	2-e$^-$ oxidation	4 to 7
11: *fac*-[Re(CO)$_3${poly-(btbt)}(NCCH$_3$)]$^+$	[28e]	controlled-potential oxidation[b]	4 to 6
12: [Re(CO)$_5$Fc]	[28d]	1-e$^-$ oxidation	12 to 33
13: [LM(CO)$_5$]	[28g]	sequential	each $\approx$5
M = Cr, Mo, W; L = Fc$_x$PPh$_{3-x}$ (x = 1–3)		1-e$^-$ oxidations	
14: [M(CO)$_4$(dppbc)]	[28b]	1-e$^-$ oxidation	$\leq$30
M = Cr (**14a**), Mo (**14b**), W (**14c**)			
15: [(η^6-PhFc)Cr(CO)$_3$]	[22b]	1-e$^-$ oxidation	10 to 20
16: [(FcC)Co$_3$(CO)$_8$PPh$_3$]	[28i]	1-e$^-$ oxidation	13 to 19
17: [(FcCO)Os$_3$H(CO)$_{10}$]	[28j]	1-e$^-$ oxidation	6 to 8

[a] 

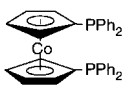
η^2-2,2-bipyridine (bpy)



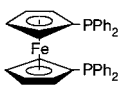
4-benzoylpyridine (4-bzpy)



η^2-2,3-bis(diphenylphosphanyl)maleic anhydride (bma)



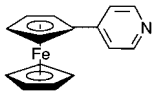
η^2-1,1′-bis(diphenylphosphanyl)cobalticene (dppc)



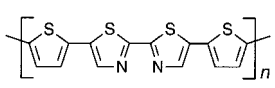
η^2-1,1′-bis(diphenylphosphanyl)ferrocene (dppf)



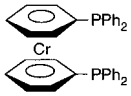
ferrocenyl (Fc)



4-ferrocenylpyridine (FcPy)

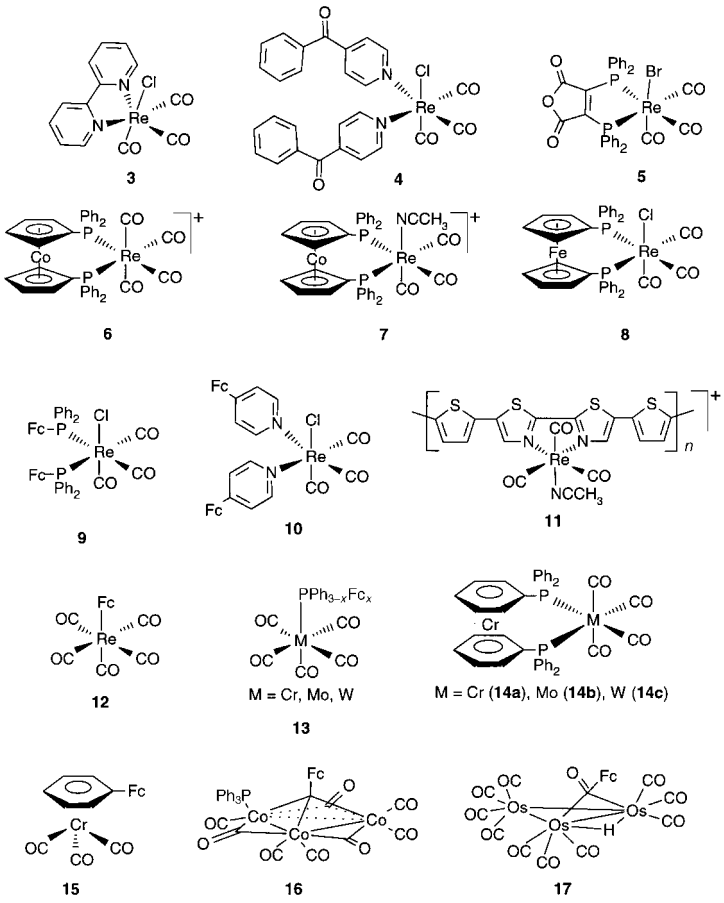


poly-[5,5′-bis(2-thienyl)-2,2′-bithiazole] (poly-(btbt))



η^2-1,1′-bis(diphenylphosphanyl(η^6-benzene))-chromium (dppbc)

[b] Oxidized at 1.5 V versus Ag wire



reduction increases the electron density at the metal, which results in increased π backbonding into the CO ligands. Conversely, oxidizable redox-active ligands deplete a metal center of electron density upon oxidation and thus lead to increased CO stretching frequencies. These ligands have been complexed to a variety of transition metal fragments including mononuclear rhenium–carbonyl complexes,[22a, 28c,d,f,i] Group 6 metal–carbonyl complexes,[28b,g] and several metal–carbonyl clusters.[28i,j]

3.2.2. *Factors Controlling the Magnitude of* $\Delta\nu_{CO}$

Examination of a series of structurally related complexes, such as the rhenium–carbonyl complexes[22a, 28c,d,f] **3**–**12** shown in Table 1, reveals some of the factors that control the magnitude of changes in ν_{CO} ($\Delta\nu_{CO}$) upon oxidation or reduction of a pendant redox-active ligand. Alterations in the relative orientation of the redox-active center and the central metal as well as in the distance separating them can lead to significant changes in $\Delta\nu_{CO}$. For example, **8** contains a chelating diphosphanylferrocene ligand, and **9** two monodentate Fc-functionalized phosphane ligands (Fc = ferrocenyl).[28d] Despite very similar coordination spheres for the two complexes, one-electron oxidation of **8** leads to approximately twice the increase in $\Delta\nu_{CO}$ over that of **9**. One clear difference between **8** and **9** is the proximity of the redox-active Fe center to the complexed Re atom. With a shorter Fe–Re distance (4.506(1) Å for **8** versus 5.157(2) and 5.519(2) Å for **9**)[28d] and two phosphane groups bound to the Re atom, the 1,1′-bis(diphenylphosphanyl)ferrocene (dppf) ligand of **8** withdraws more electron density from the Re center than the monodentate $FcPPh_2$ ligands of **9** when both complexes are transformed from their totally reduced state (see Table 1) to their singly oxidized states.[28d] Also affecting the charge-dependent carbonyl stretching frequencies are the electronic natures of the redox-active ligand and the bound metal as well as the degree of electronic communication between the two. Although complexes **9** and **10** both contain monodentate ferrocene-based ligands, the identity of the bridging group between the ferrocenyl group and the Re atom is different, and the distance separating the Fe and Re centers is greater in **10** than in **9**.[28d] Oxidation of **10** results in a product with a smaller $\Delta\nu_{CO}$ than the oxidation of **9**, which reflects that there is less electronic communication between the ferrocenyl group and the Re center in **10**.[28d] Like **9** and **10**, complexes **3**–**5** and **8** also contain redox-active ligand(s) and the $[XRe(CO)_3]$ fragment.[28c,d,f] The redox-active ligands have different electronic natures, however, and bring about a range of $\Delta\nu_{CO}$ values upon their oxidation or reduction. The above-mentioned factors are also observable in the comparison between **3** and **4**, which contain reducible pyridine-based ligands.[28c] Upon one-electron reduction, complex **3** with a bidentate bipyridine (bpy) ligand undergoes a larger average change in its CO stretching frequencies than **4**.[28c] Furthermore, the largest changes in CO stretching frequency occur for complexes with redox-active groups directly bound to a metal as in **3**[28c] and **12**.[28d] Examination of the complexes in Table 1 and the corresponding spectroscopic data shows how the charge-dependent behavior of such complexes can be tuned. Changes in the oxidation state in geometrically constrained (i.e., the redox center is fixed close in space to the metal center), bidentate, redox-active ligands perturb the electronic properties of the bound transition metals (i.e., $>\Delta\nu_{CO}$) more than changes in oxidation state for monodentate ligands that can move the redox-active group farther away from the metal center of interest. Additionally, by controlling the distance and the degree of electronic communication between a redox-active center and a metal, one can tune the magnitude of changes in physical properties (e.g. $\Delta\nu_{CO}$) and chemical reactivity (Section 3.3) that result from ligand-based redox processes.

3.2.3. *Qualitative Evaluation of Substituent Effects for Ferrocenyl and Ferrocenylium Ligands*

An interesting issue involving the use of ligands with redox-active substituents is the difference between substituent effects for the reduced and oxidized forms of the ligand. For example, what effect does switching from a ferrocenyl to a ferrocenylium group have upon the substituent effect? Although σ constants calculated from Taft equations have been determined for ferrocenyl and other metallocenyl substituents,[29] we are not aware of any such determination for ferrocenylium.

Although the impact of changing a substituent between its reduced and oxidized states will vary from system to system, examination of the literature provides some insight into the substituent effect of the ferrocenyl versus ferrocenylium

group. A series of structurally similar $[(\eta^6\text{-}C_6H_5X)Cr(CO)_3]$ complexes has been examined with regard to the effect of various aryl substituents (X) upon the CO stretching frequencies of the complexes.[30] This series can be compared to the oxidized and reduced forms of **15** (X = Fc or Fc^+) to determine the placement of ferrocenyl versus ferrocenylium within this series. Upon one-electron Fe-centered oxidation of **15**, the carbonyl stretching frequencies shift from $\nu_{CO} = 1964$ and 1887 cm^{-1} to 1974 and 1907 cm^{-1}.[22b] This suggests that in this class of compounds the ferrocenyl group is more electron-donating than Me or $SiMe_3$ (X = Me: $\nu_{CO} = 1969$ and 1889 cm^{-1}; X = $SiMe_3$: $\nu_{CO} = 1968$ and 1890 cm^{-1}), whereas a ferrocenylium group is more withdrawing than H but less so than COOMe (X = H: $\nu_{CO} = 1974$ and 1894 cm^{-1}; X = COOMe: $\nu_{CO} = 1985$ and 1911 cm^{-1}).[30] Knowledge of such electronic substituent effects should allow the experimentalist to predictably design transition metal complexes with switchable states of electron richness. However, this analysis will be highly dependent on the class of compound. For example, in the aforementioned series of compounds, the methoxy group is not a particularly strong π donor owing to the interaction of the arene with the Cr center (a similar effect has been observed for Rh^I–arene complexes),[31] and we have already seen that the positioning of a redox-active group in a complex can substantially affect its electronic perturbation on a complex.

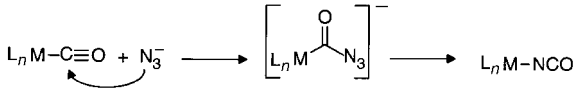
3.2.4. Application of Conducting Polymers

In connection with the influence of varying the electronic nature of a redox-active group, it is interesting to note that conducting polymers can be complexed to transition metals and serve as substitutionally inert, redox-active ligands. An example is polymer **11**, whose controlled-potential oxidation yields $\Delta\nu_{CO} = 4-6$ cm^{-1} (Table 1).[28e] Unlike other redox-active species which switch between integral amounts of charge, conducting polymers, in principle, allow access to a continuous range of intermediate states of charge because of their high electronic delocalization. Such effects may allow for tunable reactivity of a bound metal center, as opposed to switchable reactivity provided by other redox-active ligands. This depends upon the degree of electronic localization induced by the interaction between the metal centers and the conducting polymers. This issue has not yet been adequately addressed, in part because of the heterogeneous nature of conducting polymer–metal complexes and the difficulties associated with preparing and adequetely characterizing such complex materials.

3.3. Controlling Reactivity with Substitutionally Inert, Redox-Active Ligands

3.3.1. Nucleophilic Attack at Metal–Carbonyl Complexes

The above-mentioned studies indicate that the electron richness of metal–carbonyl complexes can be tuned by ligand-based redox processes. Since these effects are manifested in changes in ν_{CO}, they suggest that the rate of reactions involving these ligands also may be adjusted by ancillary ligand-based redox processes. Ideally suited for such a study are nucleophilic reactions at CO groups in transition metal–carbonyl complexes.[32] These reactions are selective, often proceeding to only one metal-containing product, and are generally irreversible.[32] Such reactions, for example azide or amine-*N*-oxide attack at a carbonyl group, have been thoroughly studied and are known to be first-order in both metal–carbonyl complex and nucleophile; the rate-determining step is nucleophilic attack on the CO group (Scheme 3).[32] Since carbonyl stretching frequencies are known to be

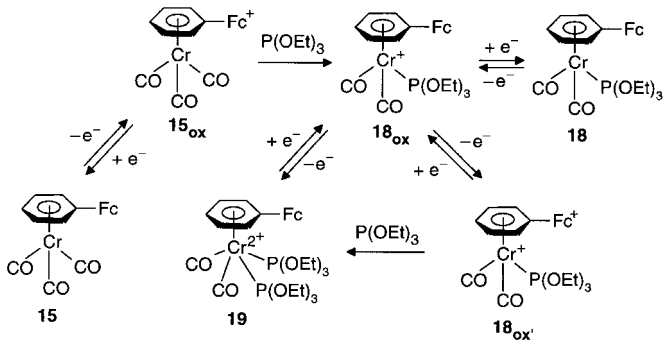


Scheme 3. Nucleophilic attack of an azide on a metal–carbonyl moiety; the first step is the rate-determining step.

dependent on the oxidation state of a pendant redox-active ligand, the electrophilicity of the carbonyl group should show a similar trend. Indeed, the rates of the reaction of **7** (Table 1) with three different amine-*N*-oxides also depend upon the state of charge of the (1,1′-bis(diphenylphosphanyl)cobalticene (dppc) ligand. For the reaction of trimethylamine-*N*-oxide, *N*-methylmorpholine-*N*-oxide, and dimethylaniline-*N*-oxide with **7**, the ratio k_{ox}/k_{red} is on average 200.[22a] Under a model of some simplified kinetic conditions, it was shown that the difference in reactivity between $\mathbf{7}_{ox}$ and $\mathbf{7}_{red}$ corresponds to $\Delta\Delta H^{\neq} = 3.1-3.2$ kcal mol^{-1}.[22a] Furthermore, the reaction of **6** (Table 1) with $[n\text{Bu}_4\text{N}][N_3]$ in acetonitrile is highly dependent on the state of charge of the cobaltocenyl moiety.[22a] In acetonitrile without added salt $\mathbf{6}_{ox}$ reacts 5400 times faster than $\mathbf{6}_{red}$;[22a] in 0.1 M $[n\text{Bu}_4\text{N}][PF_6]$ in acetontrile the rate is enhanced only by a factor of 2200.[22a] The differences in k_{ox}/k_{red} ratios for nucleophilic attack by neutral amine-*N*-oxides are larger than expected based on $\Delta\nu_{CO} = -11$ to -17 cm^{-1}, and suggest the possible involvement of electrostatic effects in further enhancing the rate of nucleophilic attack by N_3^-. Furthermore, the reaction rates are eight and three times slower for $\mathbf{6}_{ox}$ and $\mathbf{6}_{red}$, respectively, when the reactions are conducted in 0.1 M $[n\text{Bu}_4\text{N}][PF_6]$ in acetonitrile.[22a] The results indicate that $\mathbf{6}_{ox}$ is more sensitive to electrostatic effects and are consistent with $\mathbf{6}_{ox}$ having a greater attraction to the anionic nucleophile than $\mathbf{6}_{red}$. Further investigation verified the difference in the role of electrostatic effects between $\mathbf{6}_{ox}$ and $\mathbf{6}_{red}$. The nonelectrostatic contributions to the rate enhancements were studied, and the nonelectrostatic rate constant ratio between $\mathbf{6}_{ox}$ and $\mathbf{6}_{red}$ was determined to be $k_{ox}/k_{red}(\text{nonelectrostatic}) = 1100$.[22a]

3.3.2. Ligand Displacement and Addition

Substitutionally inert, redox-active ligands also can be used to control ligand displacement and ligand addition reactions (Scheme 4).[22b] Compound **15** displays rich yet complicated electrochemical behavior under a variety of conditions.[22b,e,f] In coordinating solvents, such as CH_3CN or DMF, one-electron oxidation of **15** occurs at the ferrocenyl group and is followed by intramolecular electron transfer from the Cr to

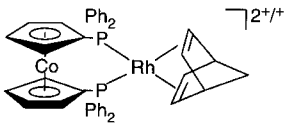


Scheme 4. A chromium complex with a redox-active ligand exhibits electrochemically modulated, reversible uptake and release of triethylphosphite.

the Fe center and rapid degradation of the complex.[22d] In dichloromethane, however, the oxidation process is reversible at reasonable scan rates ($0.5\,V\,sec^{-1}$) and activates the complex toward CO substitution by $P(OEt)_3$ to provide $\mathbf{18}_{ox}$ (Scheme 4).[22b] Interestingly, this substitution changes the formal potential of the Cr center such that an intramolecular electron transfer occurs between the Cr and the Fe center, effectively "closing" the redox switch (Scheme 4).[22b] The Cr center can subsequently be electrochemically reduced. The mechanism was supported by an examination of the behavior of the model compound $[(\eta^6\text{-}C_6H_6)Cr(CO)_3]$ and a comparison with authentic samples of the predicted product.[22b] The reactivity of **18** is also dependent on the oxidation state of the ligand (Scheme 4). Upon oxidation of $\mathbf{18}_{ox}$ an electron is removed from the ferrocenyl moiety to provide $\mathbf{18}_{ox'}$, which in the presence of $P(OEt)_3$ undergoes ligand addition (Scheme 4).[22b] Once again, phosphite addition to the Cr center increases the electron richness of the metal such that an intramolecular electron transfer occurs between the Cr center and the ferrocenylium group; this "closes" the redox switch and reestablishes an electron count of 18 for each metal center.[22b] One-electron reduction of **19** leads to phosphite expulsion and closes a cycle, which may be viewed as a reversible chemical uptake and release scheme.[22b] Significantly, even in the presence of $P(OEt)_3$, $[(\eta^6\text{-}C_6H_6)Cr(CO)_2P(OEt)_3]$ is degraded upon two-electron oxidation: This verifies the necessary involvement of the ferrocenyl group of **18** in the reversible uptake and release of phosphite.[22b]

Another interesting example of the use of a substitutionally inert, redox-active ligand to affect transition metal reactivity involves the ferrocenyl sulfide complex $[Rh\{\eta^2\text{-}(\eta^5\text{-}C_5H_5)Fe(\eta^5\text{-}C_5H_4SCH_2CH_2PPh_2)\}_2]^+$.[22c] In the reduced state, this complex does not react with acetonitrile; however, after ferrocenyl-based oxidation, it cleanly reacts with two equavalents of acetonitrile to form the diamagnetic octahedral Rh^{III} complex *cis-cis-trans*-$[Rh(CH_3CN)_2\{\eta^2\text{-}(\eta^5\text{-}C_5H_5)Fe(\eta^5\text{-}C_5H_4SCH_2CH_2PPh_2)\}_2]^+$. This appears to be the only example of a complex formed from a substitutionally inert, redox-active ligand which exhibits such oxidation state dependent ligand-uptake characteristics. Apparently oxidation of the ferrocenyl groups increases the Lewis acidity of the Rh center, which effects coordination of the acetonitrile ligand. This in turn results in a redistribution of electrons within the complex from Rh to the oxidized Fe centers. Therefore, conventional analogues of this ligand which have aryl substituents that vary in electron-withdrawing ability (e.g. NO_2, F) do not duplicate this effect. Indeed, in this system the ferrocenylium groups not only act as electron-withdrawing substituents but also provide an intramolecular means for effecting the Rh^I to Rh^{III} conversion with concomitant expansion of the complex's coordination sphere by acetonitrile ligand uptake.

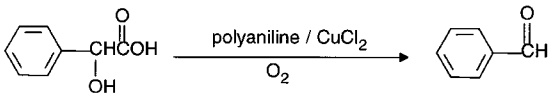
3.3.3. Catalytic Reactivity



20

In addition to stoichiometric reactions, catalytic reactions have been controlled with substitutionally inert, redox-active ligands. The traditional rhodium – diphosphane – norbornadiene catalyst **20** was synthesized with the chelating ligand dppc.[22d] The catalyst is active for the hydrogenation of cyclohexene to cyclohexane, and substantial rate enhancements (approximately 16-fold) are found for the reduced over the oxidized catalyst.[22d] This result was rationalized in terms of the reduced ligand having more basic phosphane groups. From isostructural complexes, hydrogenation rates are known to increase with increased phosphane basicity.[33] Catalyst **20** also has been employed in the hydrosilation of acetone. A trend in reactivity opposite to that for the hydrogenation reactions was observed; the catalyst derived from $\mathbf{20}_{ox}$ has a greater hydrosilation turnover frequency than the catalyst derived from $\mathbf{20}_{red}$.[22d] This phenomenological result was not further rationalized. These are important pioneering experiments because they demonstrate the concept and viability of redox-switchable catalysis through changes in the oxidation state of the ligand.

In complementary work, the reactivity of a heterogeneous catalyst comprised of polyaniline and $CuCl_2$ was tuned by adjusting the doping level of protonic acid, which is a chemical means of controlling the degree of oxidation of the polymer.[34] The complex catalytic system was used in the decarboxylative dehydrogenation of mandelic acid [Eq. (c)].



(c)

A comparison of two different protonic acid doping levels revealed that the less doped catalyst provided a faster rate of reaction.[34] Although the catalyst was inherently difficult to characterize, it was nonetheless clear that altering the doping level, and thus state of oxidation of the metal – polymer complex, provided a means of controlling the reactivity of the catalytic system.

4. Redox-Switchable Hemilabile Ligands (RHLs)

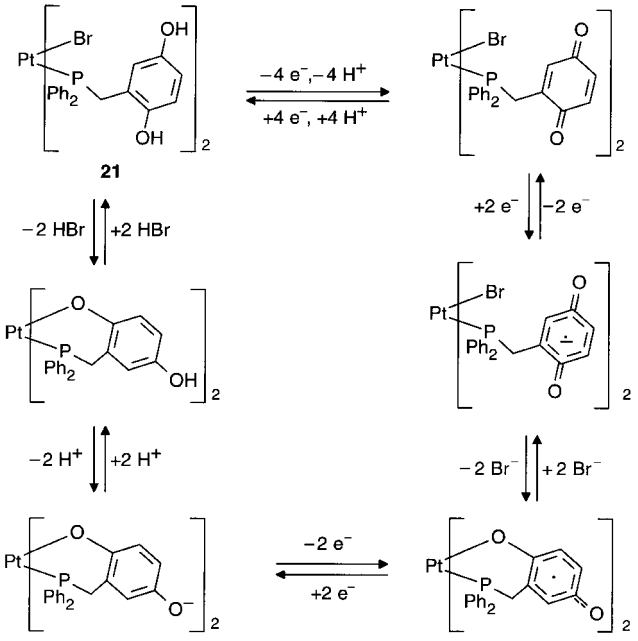
4.1. General Description

The RHLs (Scheme 2, class 2) have been designed and synthesized for complexation to a variety of metals.[23, 24]

Often phosphane ligands are used to form the substitutionally inert linkage to late transition metals; in these cases the alkyl- or arylphosphane substituents may be used to tailor the electronic nature of the metal center to which the RHL is bound. Weakly binding centers studied thus far include ethers,[23c] η^6-arenes,[23b] sulfides,[23c] η^1-thiophenes,[35] and η^1-quinones.[24] The redox groups employed have been the ferrocenyl moiety, quinones, and polythiophenyl derivatives. Changes in the state of charge of the redox group alter the strength of the bond between the metal and the labile group of the ligand; in some cases, this leads to dissociation of this group in favor of a stronger binding ligand or solvent molecule. Two initial entries into this area involved very different redox-active ligands.[23b, 24] Both studies took advantage of phosphanes as inert binding groups for late transition metals, but the redox-active group in one is a quinone, involving a proton-coupled redox process,[24] and the other utilizes ferrocene.[23b]

4.2. Controlling the Metal Coordination Sphere with RHLs

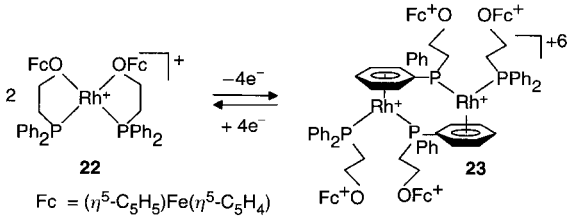
A Pt^{II} complex, and a similar Pd^{II} complex, bearing two phosphane ligands each with a pendant *p*-hydroquinonyl group exhibits both H^+- and electrochemically induced changes in its coordination sphere (Scheme 5).[24] When **21** is



Scheme 5. A quinone-based RHL exhibits proton-coupled, electrochemically modulated binding to Pt^{II}.

treated with sodium carbonate in methanol, the hydroquinone group is deprotonated, and the anionic oxygen atoms coordinate to the Pt center and displace Br^-.[24] The reaction is reversible, and **21** reforms upon treatment of the O,P-chelated complex with HBr. Similar changes in coordination sphere proceed under electrochemical conditions.[24] The cyclic voltammograms of **21** and its oxidized form (which contain quinonyl groups) exhibit irreversible waves at slow scan rates, which were attributed to reversible oxygen coordination accompanying displacement of Br^-, as outlined in Scheme 5.[24] These changes also can be effected with chemical oxidants and reductants in a medium with a controlled concentration of H^+.[24] A drawback to this approach, however, is the requirement of varying H^+ concentration to shuttle between the different chemical species of Scheme 5. This condition necessitates not only electrochemical changes but also chemical changes of the reaction medium (varying concentration of H^+).

A RHL system which avoids proton-coupled electrochemistry is based upon chelating ferrocenyl ether phosphane ligands bound to Rh^I [Eq. (d)].[23a] The Rh–O(ether) bond is

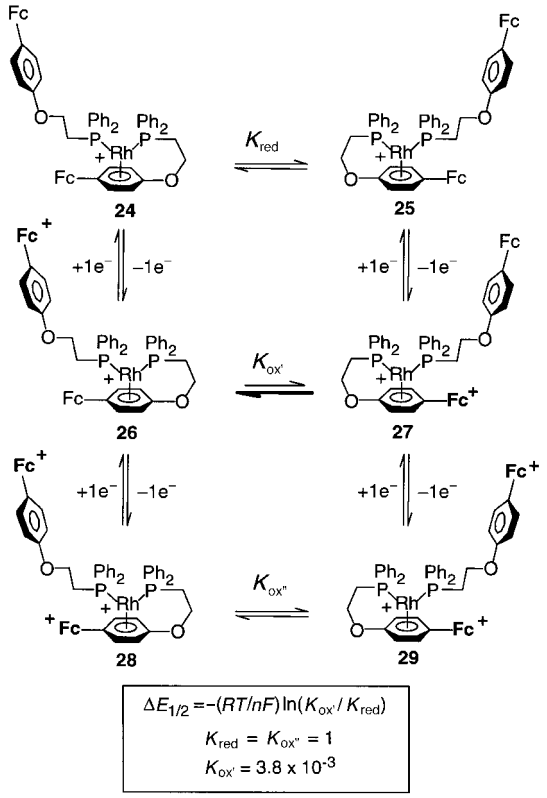


(d)

weak, and oxidation of the adjacent ferrocenyl group further weakens this bond to the extent of dissociation to form the η^6-arene-bridged dimer **23** [Eq. (d)].[23a] Cyclic voltammetry of **22** is consistent with the proposed transformation and exhibits scan rate dependent behavior, which allows for detection of intermediate species. Furthermore, this mode of arene-ligand binding was substantiated by a crystal structure determination of an intermediate in the proposed mechanism for the reaction depicted in Equation (d).[23a] The oxidation state dependent behavior of **22** is proof for the RHL concept; the electrochemical interconversion of the square-planar complex **22** and the arene-bridged dimer **23** (with "pianostool" geometry around each Rh center) shows how one can use RHLs to control the electronic and steric environment of transition metals. Furthermore, it provides a foundation for the synthesis and application of other complexes displaying similar and potentially useful behavior.

4.3. Determination of Thermodynamic and Kinetic Perturbations Induced by Oxidation of RHLs

In addition to ether moieties, η^6-arenes have been incorporated into redox-switchable hemilabile ligands,[31] and these ligands have been used to quantitatively determine the thermodynamic perturbation that results in a Rh^I–RHL complex upon ligand-based redox processes.[23b] The oxidation-induced thermodynamic perturbation in **24** was determined through analysis of cyclic voltammetry data and their relationship to a series of intramolecular arene–arene exchange reactions (Scheme 6). The cyclic voltammogram of **24** exhibits two reversible waves within a potential window common for ferrocenyl-based oxidation. These waves, whose half-wave potentials $E_{1/2}$ are separated by 143 mV, are assigned to the two ferrocenyl groups of **24**; the ferrocenyl group attached to the Rh-bound arene is oxidized at a more



Scheme 6. A degenerate exchange reaction can be used to evaluate the thermodynamic perturbation that results from RHL oxidation.

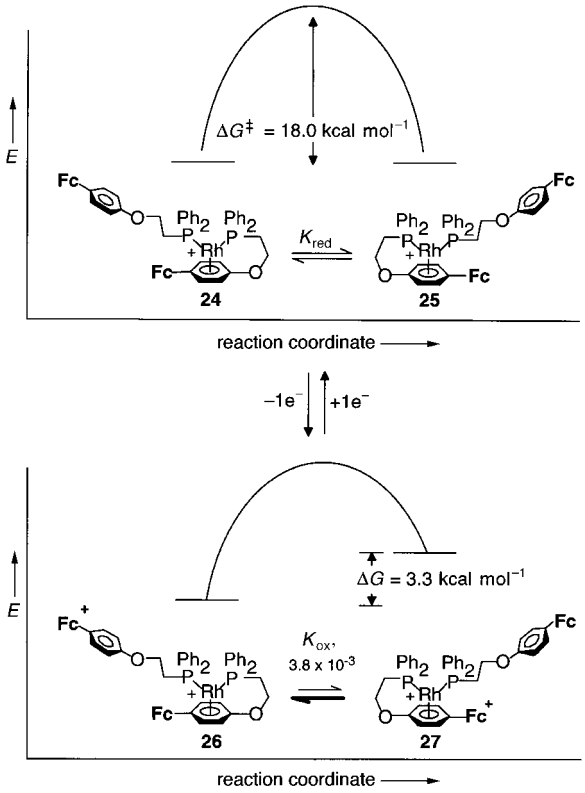


Figure 1. RHL oxidation in complex **24** results in a change in the equilibrium constant and in the Gibbs energy for an arene – arene exchange reaction.

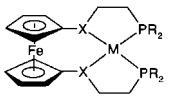
positive potential than the free ferrocenylarene.[23b] A ladder diagram was used to describe and evaluate the exchange processes (Scheme 6).[23b] Assuming that $E_{1/2}$ for the oxidation of **27** is equal to that for the oxidation of **24** to **26** allows for the determination of $K_{ox'}$. An equation derived from the Nernst equation—($\Delta E_{1/2} = -(RT/nF)\ln(K_{ox}/K_{red})$—can be used to calculate the ratio $K_{ox'}/K_{red}$. Since K_{red} (and $K_{ox''}$) describes a degenerate process, this analysis gives the absolute value of 3.8×10^{-3} for $K_{ox'}$. At 20 °C, $\Delta G = 3.3$ kcal mol^{-1}, which presumably represents the destabilization of the complex due to weakening of the η^6-arene – Rh interaction (Figure 1).[23b] Significantly, this type of analysis can in general be applied to any RHL complex that undergoes a degenerate exchange process. In the absence of a degenerate process, one cannot obtain the absolute thermodynamic perturbation that results from ligand oxidation. Instead, the cyclic voltammetry for such a process merely yields a ratio of equilibrium constants for the reaction involving the oxidized and reduced species.[23b]

In addition to the thermodynamic perturbation associated with RHL oxidation, the kinetic perturbation also has been evaluated for this unusual process. The degenerate arene – arene exchange reaction of **24** was detected and studied by exchange spectroscopy (EXSY), and kinetic parameters were determined (at $T = 20$ °C: $k = 0.36$ s^{-1}, $\Delta G^{\ddagger} = 18.0$ kcal mol^{-1}, $\Delta H^{\ddagger} = 22.5$ kcal mol^{-1}, $\Delta S^{\ddagger} = 15.3$ cal mol^{-1} K^{-1}).[23b] The arene exchange reactions between **26** and **27** as well as **28** and **29** were also studied by EXSY.[36] The rate of the exchange reaction for the singly oxidized compound **26** is nearly identical to that of **24**, which is consistent with a dissociative mechanism (at $T = 20$ °C: $k = 0.35$ s^{-1}, $\Delta G^{\ddagger} = 17.9$ kcal mol^{-1}, $\Delta H^{\ddagger} = 23.0$ kcal mol^{-1}, $\Delta S^{\ddagger} = 17.3$ cal mol^{-1} K^{-1}). The doubly oxidized **28**, however, has a higher rate of exchange than **24** or **26** (at $T = 20$ °C: $k = 0.54$ s^{-1}, $\Delta G^{\ddagger} = 17.2$ kcal mol^{-1}, $\Delta H^{\ddagger} = 12.8$ kcal mol^{-1}, $\Delta S^{\ddagger} = -15.3$ cal mol^{-1} K^{-1}). The results can be understood as the weaker Rh – arene bond in **28** leading to a greater rate of dissociation and exchange.[36] As will be discussed in Section 4.6, the oxidation of **24** significantly impacts its catalytic reactivity.

While the above work allowed for the determination of the impact of RHL oxidation upon complex stability, other work has provided insight into some of the fundamental factors (e.g. electrostatic and inductive effects, ligand geometry) which contribute to effects that depend on the oxidation state of the RHL. This work shows how such factors can be synthetically adjusted to tune the behavior of RHL complexes. The contributions of two factors toward weakening of the metal – ligand bonds were considered: 1) inductive withdrawal of electron density from the metal – ligand bond toward the electron-deficient redox-active group and 2) electrostatic repulsion between the cationic redox-active group and the bound cationic metal center. Several characteristics of RHL complexes influence the relative importance of the two above-mentioned factors: 1) the electronic nature of the ligand (the redox-active group and the phosphane moiety) and the bound transition metal, 2) the valency of the central metal, and 3) the distance separating the redox-active group and the metal atom. The electrochemical behavior of a series

of RHL complexes in which oxidizable RHLs are bound to cationic metal centers was investigated to address these fundamental factors (Table 2).[23c] Cyclic voltammetry was employed to record formal potentials, which are measures of the change in thermodynamic stability in the complex upon oxidation ($\Delta G = -nFE$). Additionally, ratios of ligand binding constants in the reduced and oxidized states were determined from cyclic voltammetry with minor assumptions.[23c] For example, oxidation of the ligand in **34** decreases its binding affinity for Rh ($K_{red}/K_{ox} = 4.43 \times 10^6$).[23c] These parameters were used to compare the compounds in Table 2.

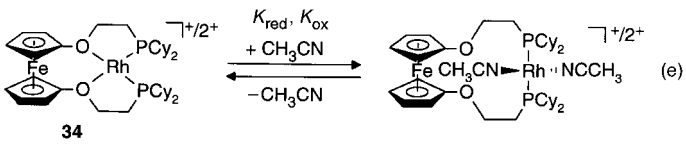
Table 2. Comparison of tetradentate RHLs and their metal complexes.



Complex	X	M	R	$E_{1/2}$ [mV][a]	K_{red}/K_{ox}
30	O	–	Ph	−203	–
31	O	–	Cy	−200	–
32	S	–	Ph	37	–
33	O	Rh^I	Ph	270[b]	$> 9.98 \times 10^7$
34	O	Rh^I	Cy	193	4.43×10^6
35	S	Rh^I	Ph	677[c]	1.27×10^{11}
36	O	Pd^{II}	Ph	420[b]	$> 1.58 \times 10^{10}$
37	O	Pd^{II}	Cy	388	9.88×10^9

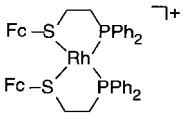
[a] Half-wave potential, except where noted. All values are quoted versus Fc/Fc^+. [b] Potential of anodic peak E_{pa}; appears to be irreversible at moderate scan rates ($< 1\ V\,s^{-1}$). [c] $E_{1/2}$ recorded at $100\ V\,s^{-1}$; at moderate scan rates the wave appears to be irreversible.

The influence of the electronic nature of the ligand is demonstrated by changing the weakly binding group from ether to sulfide, which significantly changes the electronic nature of the redox-active group. Ligand **30** undergoes reversible oxidation and reduction at a much lower potential than **32** (−203 vs. 37 mV), a reflection of the donation of π electron density from the ether into the ferrocenyl moiety.[23c] In addition, the electronic nature of the phosphane groups plays a significant role in determining the behavior of RHL complexes. In addition to Fe-based oxidations and reductions, electron transfer processes characterized as Rh^I/Rh^{II} redox couples can be observed by cyclic voltammetry. Although these couples have been characterized as one-electron oxidations/reductions by rotating disk electrode experiments, EPR data that unambiguously confirms the formation of paramagnetic Rh^{II} centers have not been obtained owing to the transient nature of the oxidized forms of these complexes. Nevertheless, all oxidized forms of complexes with phenyl-substituted ligands are unstable, as evidenced by irreversible oxidations at moderate scan rates. However, the electron-rich complex **34** with a cyclohexyl-substituted ligand has a relatively more stable "Rh^{II}" oxidation state, and exhibits reversible Fe- and Rh-based oxidations.[23c] Studies on other model complexes support this conclusion.[23c] Furthermore, relative to phenyl substituents, cyclohexyl groups "soften" the bound metal, reducing electrostatic repulsion and inductive electron withdrawal between the central metal and the redox-active group. This yields a modest decrease in oxidation potential, as shown by a comparison of **33** to **34** and **36** to **37**. The valency of the central metal also impacts the charge-dependent behavior of RHL–metal complexes. The Pd^{II} complexes **36** and **37** exhibit much higher half-wave potentials $E_{1/2}$ than their Rh^I counterparts **33** and **34**, respectively (Table 2). With X-ray crystallography it was shown that these square-planar complexes all have nearly identical Fe–M nonbonding separations of about 4.0 Å. Since this parameter is fixed, the differences between the Pd^{II} complexes and the Rh^I complexes reflect enhanced electrostatic repulsion between the central metal and the oxidized redox group. Since differences in electron-withdrawing effects are also present, it was clear that Pd^{II} complexes exhibit greater changes in their ligand binding constants than Rh^I complexes. Indeed, **37** exhibits a greater K_{red}/K_{ox} value (9.98×10^9)[23c] than any other reported redox-active metal–ligand complex that is stable in two oxidation states. Complex **35** exhibits a larger K_{red}/K_{ox} ratio, but its oxidized form has a short lifetime and must be detected by ultrafast voltammetry. Changes of this magnitude suggest that substantial changes in complex reactivity should occur upon ligand-based oxidation. Complex **34** shows just such a change in its reaction with acetonitrile [Eq. (e)]. The Rh–O bonds weaken upon oxidation of the ferrocenyl group, and the complex's binding constant for acetonitrile increases by 2.27×10^7.[23c]



34 (e)

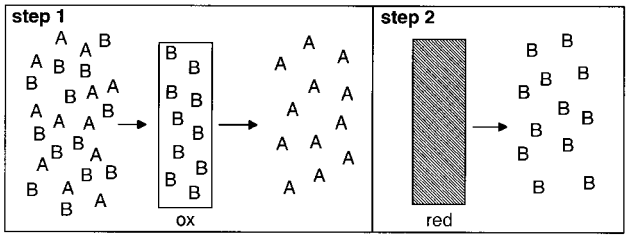
Although it is difficult to separate the contributions of electrostatic repulsion and inductive withdrawal in the oxidatively induced destabilization of RHL complexes, a comparison of electronically similar but structurally different complexes has addressed this issue for one class of RHLs. Complex **38** is a bis(phosphane)bis(sulfide)rhodium complex, just like **33** (Table 2); however, the former exhibits a much smaller K_{red}/K_{ox} value (3.87×10^3 vs. 1.27×10^{11}) for one-electron oxidation. The main difference between **35** and **38** is the geometric constraint imposed by the tetradentate ligand in **35**. As a result, the Rh–Fe separation in **35** is fixed and significantly shorter (4.055(7) Å) than that of **38** (≈ 5.2 Å).[23c] Owing to their shorter Rh–Fe separations, the contribution of electrostatic repulsion to the destabilization of tetradentate RHL complexes should be larger than in similar bidentate complexes. While the absolute contribution of electrostatic repulsion could not be directly extracted from the experiments in that study, results of cyclic voltammetry and the determined binding-constant ratios indicated that electrostatic repulsion significantly contributes to the destabilization of the RHL systems upon their oxidation.



38

4.5. Polymeric RHLs: A Glimpse at The Future

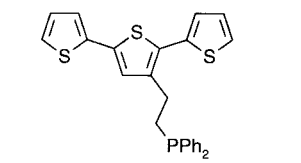
With regard to the application of RHL–transition metal chemistry to separation technology and heterogeneous catalysis, current work is aimed at extending these systems to polymeric supports. The envisioned transition metal complexes will be designed to exhibit selective binding of a desirable component of a multicomponent mixture (Scheme 7). Furthermore, this binding will be switchable, such that the desired component binds to the metal in a particular oxidation state of the ligand. Separation of the



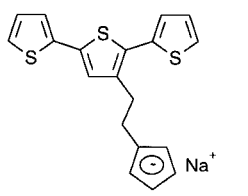
Scheme 7. RHL-modified membranes may be used in electrochemically controlled devices for the separation of small molecules.

resulting metal complex from the mixture followed by electrochemical switching of the ligand to the original oxidation state is expected to yield the purified component. Polymer-supported metal complexes will facilitate these separations of the metal–substrate complexes. Furthermore, they can be readily used to modify or construct functionalized membranes.[37] Two options exist for polymeric RHLs: conducting polymers and redox-active polymers. Conducting polymers are being incorporated into RHL–metal complexes in which the metal forms an intimate interaction with the polymer.[35] Oxidation of the polymer is expected to weaken this interaction by removing electron density from the polymer and thus the polymer–metal bond. As referred to in Section 3.2.4., conducting polymers (e.g. polythiophene, polypyrrole) offer potential advantages over other redox-active ligands because they can be oxidized to a range of intermediate oxidation states.[38a,b] In principle, this property, which results from the high electronic delocalization of the conducting polymer, can be taken advantage of in tuning, and not merely switching, the reactivity of RHL–transition metal complexes. Also of interest are redox-active polymers which bear electronically isolated redox-active groups (e.g. polyvinylferrocene). Although they do not allow for the "tunability" of highly conjugated conducting polymers, redox polymers do provide a heterogeneous support for RHL–metal complexes[39] and can be prepared with higher molecular weights than electrochemically deposited conducting polymers.

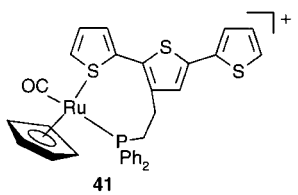
Toward the development of polymeric RHLs, several systems have been synthesized and preliminarily studied. Conducting polymer RHLs have been developed based on ligands **39**[35b] and **40**.[35a] Substituted terthiophenes were chosen as the monomer building blocks because of their favorable polymerization potentials as well as their ability to coordinate to transition metals in either an η^1 or η^5 binding mode. For example, Ru complexes **41** and **42** were prepared



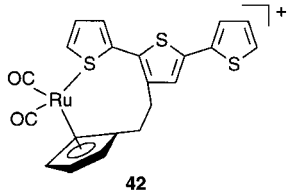
39



40



41

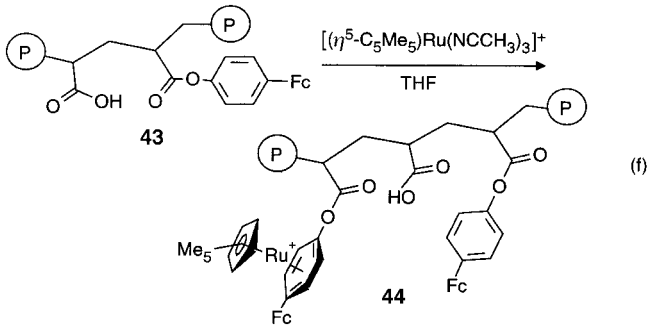


42

from ligands **39** and **40**, respectively. Both complexes were electrochemically polymerized in anodic fashion to form stable films confined to the electrode surface. A typical electrochemical response for poly-**41** is a reversible wave with $E_{pa} = 505$ mV and $E_{pc} = 435$ mV (vs. Fc/Fc^+); a color change from red to blue accompanies the polymer oxidation. The film is rapidly degraded at higher potentials. This demonstrates the importance of carefully designing a polymeric RHL that is electrochemically compatible with the metal center of interest. The stability of the polymer and the retention of the metal–thiophene complex upon oxidation was confirmed by IR spectroscopy with a comparison of the carbonyl stretching frequencies for **41** and poly-**41**: Both exhibit a ν_{CO} of about 1990 cm^{-1}. Importantly, the η^1-thiophenyl ligands in **41** and poly-**41** can be displaced by more strongly coordinating ligands such as CO and acetonitrile, demonstrating the hemilability of both the monomeric and polymeric ligands. Oxidation of polymers formed from **41** and **42** should deplete the metal–thiophenyl bonds of electron density and weaken this interaction. Polymer oxidation should not only accelerate the uptake reactions involving CO and acetonitrile, but also affect the equilibrium constants associated with these reactions. Significantly, this weakening, in principle, can be varied by controlling the degree of oxidation of the highly delocalized conducting polymeric ligands. However, with these preliminary test systems it has been difficult to separate the electronic effects associated with polymer oxidation from other effects, such as porosity changes and substrate partitioning coefficients. Nevertheless, incorporation of phosphinite, cyclopentadienyl, and phosphane moieties as substitutionally inert groups will lead to a variety of metal complexes with interesting and electrochemically controllable catalytic activity. Note that **41** is chiral and can easily be obtained enantiomerically pure; therefore, it may be a good initial candidate for developing chiral transition metal based materials that are suitable for electrochemically controllable separation of enantiomer pairs.

Under the class of redox polymers, a first-generation system was recently investigated. Inspired by complex **24** (Section 4.3), polymer **44** was prepared by modification of poly(acrylic acid), to incorporate ferrocenylarene sites (**43**), and subsequent complexation of the $[(\eta^5\text{-}C_5Me_5)Ru]^+$ frag-

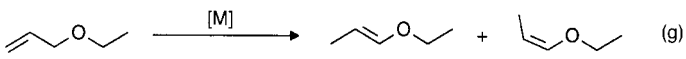
ment [Eq. (f)].[39] This new system is a model for the expansion of RHL–metal chemistry to redox polymers, and its exhibits an oxidation-induced change in binding constant



for Ru of over two orders of magnitude. The feasibility of using **43** for electrochemically controlling transition metal binding constants has provided motivation for the development of future polymeric RHLs incorporating *p*-ferrocenylphenyl acrylate.

4.6. Controlling Catalytic Reactivity with RHLs

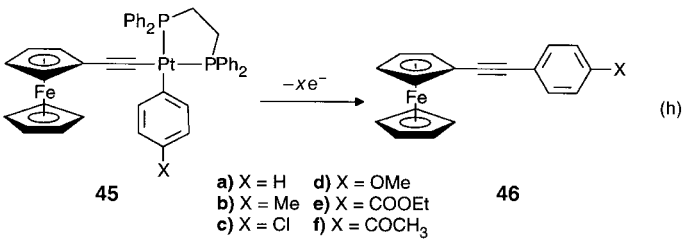
Although RHLs are still in the early stages of development, one ligand has been used to prepare a Rh^{I} catalyst with electrochemically switchable reactivity (**24**, see Figure 3). Recall that **24** exhibits an increase in the rate of intramolecular arene–arene exchange upon oxidation of both ferrocenyl groups (**28**; Section 4.3.) Complex **24** also behaves as an olefin-isomerization catalyst whose activity is dependent on the oxidation state of the RHL. For example, the isomerization of ethyl allyl ether to *cis*- and *trans*-1-propenyl ethyl ether proceeds smoothly with either **24** or **28**, but the rate of reaction is significantly higher with **28** (2–3 times higher) [Eq. (g)].[36] This difference in rate reflects the greater lability



of the ferrocenyliumarene ligand in **28** compared to the ferrocenylarene ligand in **24** (see Section 4.3). Significantly, the rate of reaction with the singly oxidized species **26** (Scheme 6) is nearly identical to that with the reduced catalyst **24**;[36] this shows the importance of oxidizing the multidentate RHL ligand.[36] This experiment to demonstrate the ability of RHLs to yield electrochemical control over a catalyst's reactivity sets the stage for further development of RHL–metal catalysts for more sophisticated and perhaps more useful reactions. The thermodynamic perturbation associated with the oxidation of **24** is fairly modest in comparison with some of the other complexes discussed in this review (e.g. **33**–**37**). Therefore, with the optimum design of RHL–transition metal catalysts, it is likely that substantially large oxidation state dependent changes in both catalytic activity and selectivity will be realized with this approach and other ligands.

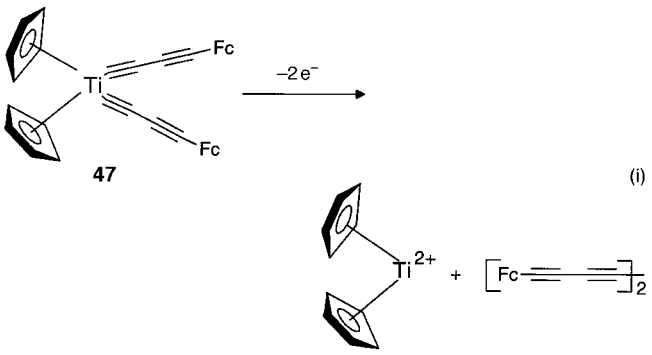
5. Redox-Active Ligands with Reactive (Leaving) Fragments

While the above-mentioned examples describe redox-active ligand–metal complexes whose chemistry may be altered in a reversible fashion, other workers have studied redox-active ligand–metal complexes that exhibit electrochemically induced irreversible changes in reactivity. In some cases ferrocene-containing alkynyl ligands take part in ligand-based oxidation-induced reductive eliminations [Eq. (h) and (i)].[25a,b] Prior to these studies it was shown that oxidation of a



metal center can induce reductive elimination as a means of returning electron density to the electron-deficient metal fragment.[40] According to recent work, this reaction can also be promoted in **45** by ligand-based chemical or electrochemical oxidation [Eq. (h)].[25b] The mechanism of the reaction was studied with electronic spectroscopy, and the first intermediate observed upon treatment of **45e** with a chemical oxidant was the ferrocenium version of **45e**.[25b] Unexpectedly, kinetic studies with **45a**–**f** showed that electron-withdrawing aryl substituents decrease the rate of reaction.[25b] One might expect that such substituents would reduce the electron density at the Pt^{II} center and increase the rate of reductive elimination. These data suggested that the initial rapid oxidation is followed by intramolecular electron transfer from the Pt^{II} center to the ferrocenylium group.[25b] Consistent with the results, one would expect electron-donating substituents to favor this process. In the final step reductive elimination occurs to yield the arylalkyne coupling product **46**.[25b] The fate of the Pt fragment was not discussed.

Similar oxidatively induced reductive elimination was observed for **47** [Eq. (i)].[25a] From a mechanistic point of



view, the reaction in Equation (i) must be different from that in Equation (h), because the electron-deficient d^0 Ti center is not likely to undergo the intramolecular oxidation observed for d^8 complexes (**45**). However, a comparison of the cyclic

voltammetry data of **47** to that of model compounds confirms that the oxidation of **47** results in removal of an electron from the ferrocenyl group.[25a] Rather than a metal →metal electron transfer as in **45**, initial oxidation of **47** is probably followed by electron transfer from the Ti–C bond to the ferrocenylium group to yield $[Cp_2Ti]^{2+}$ and two alkynyl radicals, which couple to yield the product.[25a]

6. Summary and Outlook

Redox-active ligands offer a novel tool for controlling the reactivity of transition metals with distinct advantages over other methods, such as variations in ligand substituents or redox reactions at the central metal. Redox groups with stable and reversible changes in oxidation state can be exploited for the development of transition metal complexes with switchable states of reactivity. The redox-active ligands which have appeared so far in the literature can be categorized into three classes: 1) substitutionally inert, redox-active ligands, 2) redox-switchable hemilabile ligands (RHLs), and 3) redox-active ligands which are reactive (leaving) fragments. Changes in the oxidation state of substitutionally inert ligands attenuate the electronic character of a bound metal, thereby yielding control over the carbonyl stretching frequency for a variety of metal–carbonyl complexes. Additionally, stoichiometric and catalytic reactivity may be controlled with substitutionally inert, redox-active ligands and RHLs. Indeed, oxidation of a redox-active ligand has led to rate enhancements by a factor as large as 5400 for nucleophilic attack at a metal–carbonyl complex.[22a]

A fundamental understanding of the factors that control the magnitude of changes in reactivity accompanying changes in the oxidation state of the ligand will allow for the rational design of future metal complexes with tunable states of reactivity. Toward this goal, degenerate exchange reactions were investigated to determine the thermodynamic and kinetic perturbations that result from oxidation of an RHL.[23b] Additionally, in a series of cationic phosphane ether RHL–metal complexes electrostatic repulsion was shown to be a significant factor in changing ligand binding constants. These binding constants can be tuned by choice of phosphane substituents, the bound central metal, and ligand geometry to provide very large oxidation-induced changes in binding constant (as high as 10^{11}).[23c]

The idea of electrochemically controlling the reactivity of transition metals with redox-active ligands is still in its infancy, and several challenges remain. A large percentage of the work reported here involves the use of metallocenes as redox groups; however, a wide array of other redox-active moieties are available to the synthetic chemist. Of special interest are reducible redox groups and those with three or more stable oxidation states, which would allow for a greater level of control over the reactivity of a transition metal complex. With such control, we envision the development of new and potentially useful catalysts with switchable reactivity or, alternatively, materials for new molecule-separation technologies. Redox-switchable catalysts may exhibit desirable changes in chemical selectivity as a function of oxidation state, or they may provide a means of interconverting a catalyst between a reactive active state and a more stable inactive state, thereby simplifying catalyst recovery. Regarding molecular separations, we believe the greatest potential exists in enantiomeric separations. Spurred by the high level of control which catalytic chemists have obtained in asymmetric catalysis, chiral transition metal complexes of redox-active ligands can be designed to exhibit electrochemically induced reversible uptake and release of molecular compounds. These systems could be used for the separation of enantiomer pairs that are critical to the pharmaceutical industry. Even if the metal centers used in Scheme 7 exhibit modest or even poor enantioselectivity, because the process can be repeated it can in principle provide high levels of purity of a desirable enantiomer. This could be a distinct advantage over asymmetric catalysis in which suitable product purities are often unattainable.

In short, this field has a great deal of promise. Significant strides have been made with regard to developing a fundamental understanding of how both the coordination environment and electronic character of a transition metal center can be controlled with the appropriate redox-active ligand and an applied potential. Although technologically useful systems have not yet been developed, in view of the current level of understanding it would not be surprising to see such systems emerge over the next decade.

C.A.M. acknowledges support by the National Science Foundation (NSF CHE-9625391 and CHE-9357099), the ACS Petroleum Research Fund (ACSPRF-30759-AC3), and the A. P. Sloan Foundation.

Received: January 29, 1997 [A 203 IE]
German version: *Angew. Chem.* **1998**, *110*, 936–952

[1] *Molecular Design of Electrode Surfaces* (Ed.: R. W. Murray), Wiley-Interscience, New York, **1992**.
[2] a) P. D. Beer, *Chem. Soc. Rev.* **1989**, *18*, 409; b) I. Rubinstein, *Anal. Chem.* **1984**, *56*, 1135; c) C. D. Hall in ref. [4d], p. 279; d) P. D. Beer, *Adv. Inorg. Chem.* **1992**, *39*, 79.
[3] a) C. A. Mirkin, M. S. Wrighton, *J. Am. Chem. Soc.* **1990**, *112*, 8596; b) C. A. Mirkin, J. R. Valentine, D. Ofer, J. J. Hickman, M. S. Wrighton in *Biosensors and Chemical Sensors: Optimizing Performance Through Polymeric Materials* (Eds.: P. G. Edelman, J. Wang), American Chemical Society, Washington D.C., **1992**, chap. 17.
[4] a) H. Plenio, R. Diodone, *J. Organomet. Chem.* **1995**, *492*, 73; b) J. C. Medina, T. T. Goodnow, M. T. Rojas, J. L. Atwood, B. C. Lynn, A. E. Kaifer, G. W. Gokel, *J. Am. Chem. Soc.* **1992**, *114*, 10583; c) C. D. Hall, S. Y. F. Chu, *J. Organomet. Chem.* **1995**, *498*, 221; d) *Ferrocenes. Homogeneous Catalysis, Organic Synthesis, Material Science* (Eds.: A. Togni, T. Hayashi), VCH, New York, **1995**.
[5] H. Plenio, D. Burth, *Organometallics* **1996**, *15*, 1151.
[6] L. E. Echegoyan, H. K. Yoo, V. J. Gatto, G. W. Gokel, L. Echegoyan, *J. Am. Chem. Soc.* **1989**, *111*, 2440.
[7] L. Echegoyan, G. W. Gokel, L. E. Echegoyen, Z.-H. Chen, H. Yoo, *J. Inclusion Phenom. Mol. Recognit. Chem.* **1989**, *7*, 257.
[8] T. Saji, *Chem. Lett.* **1986**, 275.
[9] a) G. DeSantis, L. Fabbrizzi, M. Licchelli, P. Pallavicini, A. Perotti, *J. Chem. Soc. Dalton Trans.* **1992**, 3283; b) M. Sato, M. Katada, S. Nakashima, H. Sano, S. Akabori, *ibid.* **1990**, 1979; c) P. Zanello, M. Casarin, L. Pardi, M. Herberhold, G.-X. Jin, *J. Organomet. Chem.* **1995**, *503*, 243; d) J. S. Kim, A. J. Bessire, R. A. Bartsch, R. A. Holwerda, B. P. Czech, *ibid.* **1994**, *484*, 47.

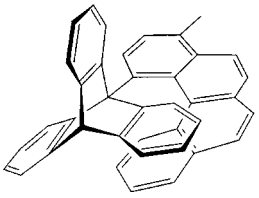
[10] a) Z. Chen, G. W. Gokel, L. Echegoyen, *J. Org. Chem.* **1991**, *56*, 3369; b) T. Saji, I. Kinoshita, *J. Chem. Soc. Chem. Commun.* **1986**, 716.
[11] B. Delavaux-Nicot, Y. Guari, B. Douziech, R. Mathieu, *J. Chem. Soc. Chem. Commun.* **1995**, 585.
[12] R. T. Hembre, J. S. McQueen, *Angew. Chem.* **1997**, *109*, 79; *Angew. Chem. Int. Ed. Engl.* **1997**, *36*, 65.
[13] a) B. J. Boone, D. P. Klein, J. W. Seyler, N. Q. Méndez, A. M. Arif, J. A. Gladysz, *J. Am. Chem. Soc.* **1996**, *118*, 2411; b) A. L. Casalnuovo, T. V. RajanBabu, T. A. Ayers, T. H. Warren, *ibid.* **1994**, *116*, 9869; c) A. Schnyder, L. Hintermann, A. Togni, *Angew. Chem.* **1995**, *107*, 996; *Angew. Chem. Int. Ed. Engl.* **1995**, *34*, 931; d) R. R. Schrock, R. T. DePue, J. Feldman, C. J. Schaverien, J. C. Dewan, A. H. Liu, *J. Am. Chem. Soc.* **1988**, *110*, 1423; e) H. Nishiyama, S. Yamaguchi, M. Kondo, K. Itoh, *J. Org. Chem.* **1992**, *57*, 4306; f) E. N. Jacobsen, W. Zhang, M. L. Güler, *J. Am. Chem. Soc.* **1991**, *113*, 6703; g) T. V. RajanBabu, T. A. Ayers, *Tetrahedron Lett.* **1994**, *35*, 4295; h) T. V. RajanBabu, T. A. Ayers, A. L. Casalnuovo, *J. Am. Chem. Soc.* **1994**, *116*, 4101; i) T. V. RajanBabu, A. L. Casalnuovo, *ibid.* **1992**, *114*, 6265.
[14] D. J. Kuchynka, J. K. Kochi, *Inorg. Chem.* **1988**, *27*, 2574.
[15] a) W. J. Bowyer, J. W. Merkert, W. E. Geiger, A. L. Rheingold, *Organometallics* **1989**, *8*, 191; b) W. J. Bowyer, W. E. Geiger, *J. Am. Chem. Soc.* **1985**, *107*, 5657.
[16] a) R. L. Thompson, S. J. Geib, N. J. Cooper, *J. Am. Chem. Soc.* **1991**, *113*, 8961; b) S. Lee, S. R. Lovelace, D. J. Arford, S. J. Geib, S. G. Weber, N. J. Cooper, *ibid.* **1996**, *118*, 4190.
[17] a) D. O. Silva, H. E. Toma, *Can. J. Chem.* **1994**, *72*, 1705; b) W. D. Harman, H. Taube, *J. Am. Chem. Soc.* **1988**, *110*, 5403; c) W. D. Harman, M. Sekine, H. Taube, *ibid.* **1988**, *110*, 2439; d) A. Yeh, N. Scott, H. Taube, *Inorg. Chem.* **1982**, *21*, 2542; e) D. Ooyama, N. Nagao, H. Nagao, Y. Miura, A. Hasegawa, K. Ando, F. S. Howell, M. Mukaida, K. Tanaka, *ibid.* **1995**, *34*, 6024.
[18] a) G. J. Bezems, P. H. Rieger, S. Visco, *J. Chem. Soc. Chem. Commun.* **1981**, 265; b) J. W. Hershberger, J. K. Kochi, *ibid.* **1982**, 212.
[19] a) D. J. Kuchynka, J. K. Kochi, *Organometallics* **1989**, *8*, 677; b) J. A. Wytko, C. Boudon, J. Weiss, M. Gross, *Inorg. Chem.* **1996**, *35*, 4469; c) A. Livoreil, C. O. Dietrich-Buchecker, J.-P. Sauvage, *J. Am. Chem. Soc.* **1994**, *116*, 9399; d) J. B. Fernandes, L. Q. Zhang, F. A. Schultz, *J. Electroanal. Chem.* **1991**, *297*, 145.
[20] a) M. Hecht, F. A. Schultz, B. Speiser, *Inorg. Chem.* **1996**, *35*, 5555; b) N. G. Connelly, D. J. H. Emslie, B. Metz, A. G. Orpen, M. J. Quayle, *Chem. Commun.* **1996**, 2289; c) X. H. Mu, F. A. Schultz, *Inorg. Chem.* **1992**, *31*, 3351; d) X. H. Mu, F. A. Schultz, *ibid.* **1995**, *34*, 3835.
[21] a) T. Suzuki, R. D. Noble, C. A. Koval, *Inorg. Chem.* **1997**, *36*, 136; b) P. A. Terry, R. D. Noble, D. Swanson, C. A. Koval, *Am. Inst. Chem. Eng.* **1997**, *43*, 1709; c) P. A. Terry, H. J. Walls, R. D. Noble, C. A. Koval, *ibid.* **1995**, *41*, 2556.
[22] a) I. M. Lorkovic, M. S. Wrighton, W. M. Davis, *J. Am. Chem. Soc.* **1994**, *116*, 6220; b) L. K. Yeung, J. E. Kim, Y. K. Chung, P. H. Rieger, D. A. Sweigart, *Organometallics* **1996**, *15*, 3891; c) I. Kourkine, C. Slone, C. A. Mirkin, *J. Am. Chem. Soc.*, submitted; d) I. M. Lorkovic, R. R. Duff Jr., M. S. Wrighton, *J. Am. Chem. Soc.* **1995**, *117*, 3617; e) C. Degrand, J. Besançon, A. Radecki-Sudre, *J. Electroanal. Chem.* **1984**, *160*, 199; f) C. Degrand, A. Radecki-Sudre, *J. Organomet. Chem.* **1984**, *268*, 63.
[23] a) E. T. Singewald, C. A. Mirkin, C. L. Stern, *Angew. Chem.* **1995**, *107*, 1725; *Angew. Chem. Int. Ed. Engl.* **1995**, *34*, 1624; b) C. A. Sassano, C. A. Mirkin, *J. Am. Chem. Soc.* **1995**, *117*, 11379; c) A. M. Allgeier, C. S. Slone, C. A. Mirkin, L. M. Liable-Sands, G. P. A. Yap, A. L. Rheingold, *ibid.* **1997**, *119*, 550.
[24] S. B. Sembring, S. B. Colbran, D. C. Craig, *Inorg. Chem.* **1995**, *34*, 761.
[25] a) Y. Hayashi, M. Osawa, K. Kobayashi, Y. Wakatsuki, *Chem. Commun.* **1996**, 1617; b) M. Sato, E. Mogi, S. Kumakura, *Organometallics* **1995**, *14*, 3157.
[26] a) J. C. Kotz, C. L. Nivert, *J. Organomet. Chem.* **1973**, *52*, 397; b) P. Le Floch, L. Ricard, F. Mathey, A. Jutand, C. Amatore, *Inorg. Chem.* **1995**, *34*, 11; c) M. Sato, K. Suzuki, H. Asano, M. Sekino, Y. Kawata, Y. Habata, S. Akabori, *J. Organomet. Chem.* **1994**, *470*, 263; d) P. Braunstein, L. Douce, F. Balegroune, D. Grandjean, D. Bayeul, Y. Dusausoy, P. Zanello, *New J. Chem.* **1992**, *16*, 925; e) M. Sato, S. Akabori, *Bull. Chem. Soc. Jpn.* **1989**, *62*, 3492; f) S. Akabori, S. Sato, M. Sato, Y. Takanohashi, *ibid.* **1989**, *62*, 1582; g) P. Zanello in ref. [4d], p. 317.
[27] a) P. D. Beer, J. E. Nation, M. E. Harman, M. B. Hursthouse, *J. Organomet. Chem.* **1992**, *441*, 465; b) A. W. Rudie, D. W. Lichtenberg, M. L. Katcher, A. Davison, *Inorg. Chem.* **1978**, *17*, 2859; c) T. Moriuchi, I. Ikeda, T. Hirao, *Organometallics* **1995**, *14*, 3578; d) *J. Organomet. Chem.* **1996**, *514*, 153; e) *Inorg. Chim. Acta* **1996**, *248*, 129.
[28] a) K. M. Kadish, A. Tabard, A. Zrineh, M. Ferhat, R. Guilard, *Inorg. Chem.* **1987**, *26*, 2459; b) C. Elschenbroich, F. Stohler, *Angew. Chem.* **1975**, *87*, 198; *Angew. Chem. Int. Ed. Engl.* **1975**, *14*, 174; c) C.-F. Shu, M. S. Wrighton, *Inorg. Chem.* **1988**, *27*, 4326; d) T. M. Miller, K. J. Ahmed, M. S. Wrighton, *Inorg. Chem.* **1989**, *28*, 2347; e) M. O. Wolf, M. S. Wrighton, *Chem. Mater.* **1994**, *6*, 1526; f) K. Yang, S. G. Bott, M. G. Richmond, *Organometallics* **1995**, *14*, 2387; g) J. C. Kotz, C. L. Nivert, J. M. Lieber, R. C. Reed, *J. Organomet. Chem.* **1975**, *91*, 87; h) H. Plenio, J. Yang, R. Diodone, J. Heinze, *Inorg. Chem.* **1994**, *33*, 4098; i) S. B. Colbran, B. H. Robinson, J. Simpson, *Organometallics* **1983**, *2*, 943; j) A. J. Arce, P. A. Bates, S. P. Best, R. J. H. Clark, A. J. Deeming, M. B. Hursthouse, R. C. S. McQueeen, N. I. Powell, *J. Chem. Soc. Chem. Commun.* **1988**, 478.
[29] S. P. Gubin, A. A. Koridze, N. A. Ogorodnikova, A. A. Bezrukova, B. A. Kvasov, *Izv. Akad. Nauk SSSR Ser. Khim.* **1981**, 929.
[30] A. D. Hunter, V. Mozol, S. D. Tsai, *Organometallics* **1992**, *11*, 2251.
[31] E. T. Singewald, X. Shi, C. A. Mirkin, S. J. Schofer, C. L. Stern, *Organometallics* **1996**, *15*, 3062.
[32] I. M. Lorkovic, R. R. Duff Jr., M. S. Wrighton, *J. Am. Chem. Soc.* **1995**, *117*, 3617, and references therein.
[33] a) W. R. Cullen, T.-J. Kim, F. W. B. Einstein, T. Jones, *Organometallics* **1985**, *4*, 346; b) *ibid.* **1983**, *2*, 714.
[34] M. Higuchi, I. Ikeda, T. Hirao, *J. Org. Chem.* **1997**, *62*, 1072.
[35] a) T. B. Higgins, C. A. Mirkin, unpublished results; b) D. A. Weinberger, T. B. Higgins, C. A. Mirkin, L. M. Liable-Sands, I. A. Guzei, A. L. Rheingold, *J. Am. Chem. Soc.*, submitted.
[36] C. S. Slone, C. A. Mirkin, G. P. A. Yap, I. A. Guzei, A. L. Rheingold, *J. Am. Chem. Soc.* **1997**, *119*, 10743.
[37] a) J. Qian, Y. Liu, H. Liu, T. Yu, J. Deng, *Fresenius J. Anal. Chem.* **1996**, *354*, 173; b) R. W. Baker, W. J. Koros, E. L. Cussler, R. L. Riley, W. Eykamp, H. Strathmann, *Membrane Separation Systems*, Noyes Data Corporation, Park Ridge, NJ, **1991**.
[38] a) P. Bäuerle, U. Segelbacher, K.-U. Gaudl, D. Huttenlocher, M. Mehring, *Angew. Chem.* **1993**, *105*, 125; *Angew. Chem. Int. Ed. Engl.* **1993**, *32*, 76; b) *Handbook of Conducting Polymers* (Ed.: T. A. Skotheim), Marcel Dekker, New York, **1986**.
[39] A. M. Allgeier, C. A. Mirkin, *Organometallics* **1997**, *16*, 3071.
[40] a) M. Almemark, B. Akermark, *J. Chem. Soc. Chem. Commun.* **1978**, 66; b) F. Mao, D. R. Tyler, D. Keszler, *J. Am. Chem. Soc.* **1989**, *111*, 130; c) T. T. Tsou, J. K. Kochi, *ibid.* **1978**, *100*, 1634; d) A. Pedersen, M. Tilset, *Organometallics* **1993**, *12*, 56.

Tilting at Windmills? The Second Law Survives

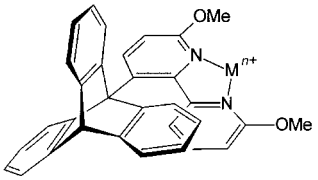
Anthony P. Davis*

The Second Law of Thermodynamics is surely among the most annoying of scientific principles. In puritan tones it dictates that we cannot do what we would so like to—extract useful work from the vast reservoirs of thermal energy surrounding us at ambient temperature. To counterbalance this stricture, it promises no reward or redemption. Ultimately we are condemned to perish in a sea of bleak uniformity, as entropy pursues its dismal end.[1] Sadly the Second Law seems also to be among the most secure of principles. The notion of a device which breaks it, exhibiting "perpetual motion of the second kind", has long been considered beyond the pale of respectable science, evidence of foolishness and perhaps even quackery.

In this context, it is remarkable and refreshing to see, within the pages of *Angewandte Chemie*, a piece of work that challenges the Second Law in a subtle and elegant fashion. Perhaps wisely, the authors make no explicit reference to the thermodynamic consequences of their experiments. However, their intentions are surely clear. Kelly and co-workers, of Boston College, Massachusetts, designed the molecule **1** as a



1



2

"molecular ratchet".[2] Its polycyclic structure is largely rigid, but has one degree of internal rotational freedom, about the single bond between the triptycene and benzophenanthrene units. As in the earlier "molecular brake" **2** from this group,[3] rotation about this bond is hindered by interference of the "pawl" with the "spokes" of the triptycene.

In the case of **2**, interest was centered on the controllability of the hindrance. In the presence of metal ions (as shown) the brake was "on", while in their absence rotation within the bipyridyl unit minimized its effect, so that the brake was "off".

[*] Prof. A. P. Davis
Department of Chemistry, Trinity College
Dublin 2 (Ireland)
Fax: (+353) 1-6712826
E-mail: adavis@mail.tcd.ie

In the case of **1** the focus is on the *asymmetric* nature of the helicene pawl. Because of its chiral, helical structure, its effect on the rotating triptycene depends strongly on the direction of rotation. As the triptycene rotates clockwise (as pictured in **1**), resistance builds up steadily, while for anticlockwise rotation a much steeper barrier intercedes (Figure 1). The situation

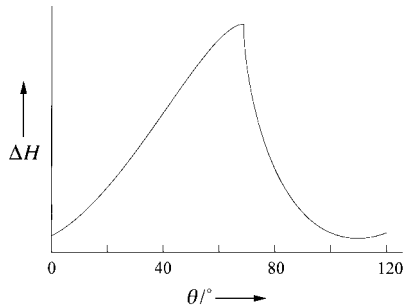


Figure 1. Calculated energy profile (AM1) for rotation about the helicene-triptycene bond in **1**. Increase in θ refers to clockwise rotation of the triptycene as viewed in the formula.

bears a close resemblance to that in a macroscopic ratchet (Figure 2). For the latter, motion in one direction is effectively prohibited, while motion in the other is relatively free. If the wheel were subjected to small, rapidly varying torques, rotation in the favored direction would presumably accumulate.

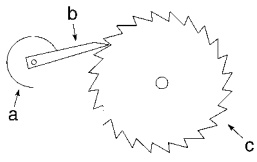


Figure 2. A macroscopic ratchet composed of a) spring, b) pawl, and c) wheel with asymmetric indentations.

So can this macroscopic picture be transferred to the microscopic scale? Will a "molecular ratchet" such as **1**, harboring thermal energy and therefore in constant motion, rotate preferentially in one direction? Before answering that question it is important to consider the consequences of a positive answer. Suppose that a molecular ratchet were linked to a microscopic pulley. If no load is applied to the system it would clearly rotate in one direction. If a very small load were applied this motion would slow, but not stop. The load would be raised, work would be done, and the only source of energy would be the thermal energy of the ratchet (which would cool).[4] The thermal energy could of course be replaced from the environment, so

 © WILEY-VCH Verlag GmbH, D-69451 Weinheim, 1998 1433-7851/98/03707-0909 $ 17.50+.50/0

that the motion would continue until the environs of the ratchet dropped below a critical temperature.

Less fancifully, the success of a molecular ratchet would imply the possibility of other devices, notably a "one-way membrane". Such a membrane would present asymmetric barriers to the passage of gas or liquid molecules, varying in energy profile depending on the direction of approach ("molecular trap-doors", to draw analogy with the macroscopic world).[5] Molecules would pass through more rapidly in the preferred direction, creating a pressure differential. The differential could be used to drive a turbine to generate electricity, with the thermal motion of the gas again the only source of energy. Although the gas would cool below ambient temperature, resupply of energy from the outside world would not be difficult. Our energy problems would be at an end.

Of course, the Second Law of Thermodynamics says that this cannot be achieved, just as the Principle of Microscopic Reversibility (which is connected to the Second Law through the above arguments) says that the rates of passage across a free energy surface between isoenergetic states must be equal in both directions. Can they be wrong? To determine the directional preference of **1**, Kelly et al. made elegant use of the NMR technique of spin polarization transfer.[6] Rotation of the triptycene is slow on the NMR timescale, so that separate signals are observed for the three aromatic "spokes". By polarizing a signal on one ring, then observing the spectrum after successive delays, the triptycene can be followed in its travels. Rotation with no directional preference results in polarization transfer at equal rates to both other environments. Transfer to just one of the other environments would imply unidirectional rotation, or racemization (a possibility that would then need to be discounted). The answer, sadly, is disappointing but predictable. Rotation occurs in both directions with equal ease, the principle of microscopic reversibility is upheld, and the Second Law survives.

Some would argue that this experiment was misconceived. To challenge the Second Law may be seen as scientific heresy (a nice irony, considering the Jesuit origins of Boston College), and the theoretical arguments against molecular ratchets and trapdoors are well-developed.[4, 5, 7] However, as scientists we should take the view that nothing is sacred, that experimental results outweigh all theoretical considerations, and that it is quite appropriate to revisit old questions as new techniques become available. The Boston College group should be congratulated on their courageous, if perhaps Quixotic, attempt at the "impossible". Wishful thinking will not make the Second Law disappear, but if there is any chance we can escape its deathly grip, surely we should take it.

German version: *Angew. Chem.* **1998**, *110*, 953 – 954

Keywords: molecular devices · molecular modeling · NMR spectroscopy · thermodynamics · triptycenes

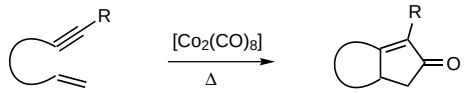
[1] For alternative (and more authoritative) perspectives on the Second Law, see: P. W. Atkins, *The Second Law: Energy, Chaos and Form*, W. H. Freeman, New York, **1994**, and references therein.
[2] T. R. Kelly, I. Tellitu, J. P. Sestelo, *Angew. Chem.* **1997**, *109*, 1969, *Angew. Chem. Int. Ed. Engl.* **1997**, *36*, 1866.
[3] T. R. Kelly, M. C. Bowyer, K. V. Bhaskar, D. Bebbington, A. Garcia, F. Lang, M. H. Kim, M. P. Jette, *J. Am. Chem. Soc.* **1994**, *116*, 3657.
[4] For a theoretical analysis of a related mechanism, see: R. P. Feynman, R. B. Leighton, M. Sands, *The Feynman Lectures on Physics, Vol. 1*, Addison-Wesley, Reading, MA, USA, **1963**, chap. 46.
[5] C. H. Bennett, *Sci. Am.* **1987**, *257*(5), 88.
[6] F. W. Dahlquist, K. J. Longmur, R. B. Du Vernet, *J. Magn. Reson.* **1975**, *17*, 406.
[7] For example, Feynman[4] points out that motions at the molecular level are perfectly elastic, and that, at thermal equilibrium, the pawl is in constant motion. When it lifts, rotations can occur in either direction with equal probability.

 © WILEY-VCH Verlag GmbH, D-69451 Weinheim, 1998 1433-7851/98/03707-0910 $ 17.50+.50/0

New Developments in the Pauson – Khand Reaction**

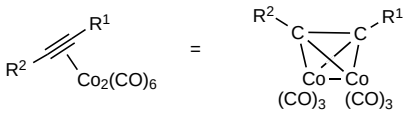
Oliver Geis and Hans-Günther Schmalz*

Metal mediated and catalyzed reactions have made significant contributions to organic synthesis over the past two decades.[1] One of the earliest and most useful of these is the Pauson – Khand carbon – carbon coupling reaction first reported in 1971.[2] In this reaction, a cyclopentenone is formed from an alkyne and an alkene in the presence of $[Co_2(CO)_8]$ with insertion of carbon monoxide in a formal [2+2+1] cycloaddition. The exceptional potential of this reaction has been demonstrated in many (mostly intramolecular) syntheses (Scheme 1).[3]



Scheme 1. The general pattern of the Pauson – Khand reaction.

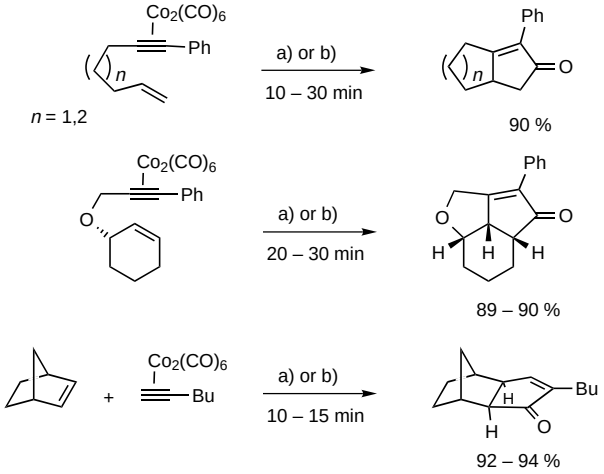
Although a catalytic approach was discussed in the initial publication,[2b] stoichiometric amounts of the metal were usually required to achieve acceptable yields. In most cases, the readily prepared and air-stable alkyne – $Co_2(CO)_6$ complexes (**1**) were heated (60 – 120 °C) with the alkene (occasionally under CO atmosphere), but long reaction times (often several days) were needed and the yields were frequently unsatisfactory.



1

Improved Reaction Conditions

Once the high synthetic value of the Pauson – Khand reaction was recognized, considerable efforts were made by several groups in the early 1990s to optimize the reaction conditions. An important improvement came with the use of tertiary amine N-oxides that generate free coordination sites at cobalt by oxidative removal of CO ligands. These reactions proceed rapidly at room temperature, often in high yields.[4] A very promising procedure for the stoichiometric Pauson – Khand reaction was described recently by Sugihara et al,[5] who discovered that the use of primary amines as solvent leads to a dramatic increase in reaction rates. Excellent yields are obtained within few minutes with only 3.5 equivalents of cyclohexylamine when the reactions are run in dichloromethane at 83 °C under argon. Alternatively, the reactions can be performed in a 1:3 mixture of 1,4-dioxane and 2 M aqueous ammonia at 100 °C (Scheme 2).

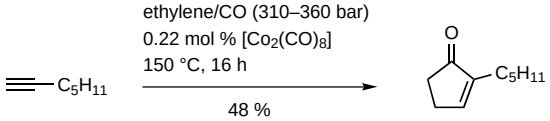


Scheme 2. Stoichiometric Pauson – Khand reactions according to Sugihara. a) 3.5 equiv of cyclohexylamine, 1,2-dichloroethane, 83 °C; b) 1,4-dioxane/2 N NH_3(aq) (1/3), 100 °C.

Catalytic Variants

Only catalytic Pauson – Khand reactions fulfil the criterion of atom economy,[6] and the use of stoichiometrical amounts of the transition metal is not acceptable commercially. It is not surprising, therefore, that several research groups have focused more recently on the development of catalytic variants.

Based on the work of Pauson and Billington,[2,7] Rautenstrauch et al. showed in their 1990 synthesis of the dihydrojasmonate precursor **2** (Scheme 3) that catalytic Pauson – Khand reactions are possible if high CO pressure and high temperature are used.[8] Korean laboratories have since found that more efficient transformations can be achieved with modified cobalt catalysts such as $[Co_2(CO)_8/P(OPh)_3]$, [(indenyl)Co(cod)] or $[Co(acac)_2/NaBH_4]$ under CO pressure or with $[Co_2(CO)_8]$ in supercritical fluids.[9] A very practical procedure was published recently by Pagenkopf and Livinghouse, who obtained high yields with photo-activation of $[Co_2(CO)_8]$ and low CO pressures (Scheme 4).[10]



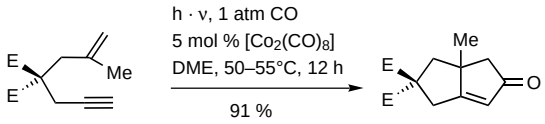
2

Scheme 3. Catalytic Pauson – Khand reactions according to Rautenstrauch.

[*] Prof. Dr. H.-G. Schmalz, Dipl.-Chem. O. Geis
Institut für Organische Chemie der Technischen Universität
Strasse des 17. Juni 135, D-10623 Berlin (Germany)
Fax: (+49) 30-3142-1105
E-mail: schmalz@wap0109.chem.tu-berlin.de

[**] O.G. thanks the Graduiertenkolleg "Synthetische mechanistische und reaktionstechnische Aspekte von Metallkatalysatoren" for a Ph.D. scholarship.

 © WILEY-VCH Verlag GmbH, D-69451 Weinheim, 1998 1433-7851/98/03707-0911 $ 17.50+.50/0

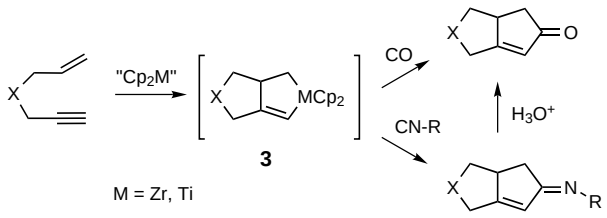


Scheme 4. Photochemically induced, catalytic Pauson–Khand reactions according to Livinghouse.

Although a whole series of carbonyl complexes of other transition metals (Fe, Mo, W, Ni) could only be used in stoichiometric Pauson–Khand reactions,[11] two Japanese laboratories have since independently reported efficient ruthenium-catalyzed (intramolecular) reactions. The desired cyclopentenones are formed in good to excellent yields in dimethylacetamide[12] or dioxane[13] in the presence of 2 mol% of $[Ru_3(CO)_{12}]$ at 140–160 °C and 10–15 atm CO pressure.

Pauson–Khand Type Reactions with Metallocenes

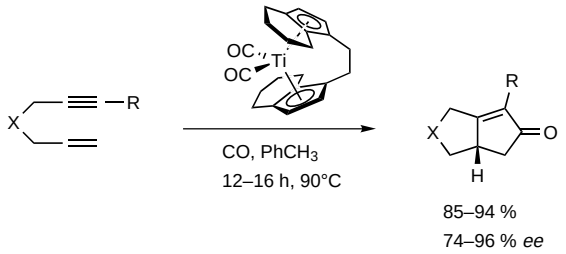
Negishi et al. have demonstrated that alkynes react with "zirconocene" generated in situ to give metallacyclopentene species of type **3**, which when treated with carbon monoxide afford typical Pauson–Khand products (Scheme 5).[14] Tamao



Scheme 5. Metallocene-mediated Pauson–Khand type reactions.

et al. have also shown that enynes react with isocyanides to form iminocyclopentenones in the presence of stoichiometric amounts of $[Ni(cod)_2/nBu_3P]$.[15] More recently, Buchwald and co-workers have developed a titanocene-based method in which the intermediate titanacyclopentenes are initially captured by isocyanides and the resulting imines are subsequently hydrolyzed to the cyclopentenones.[16] They have also succeeded in performing the reactions catalytically with trialkylsilylcyanides as isocyanide source and catalytic amounts of $[Cp_2Ti(PMe_3)_2]$ or, alternatively, a catalyst which is generated in situ from $[Cp_2TiCl_2]$ by addition of two equivalents of *n*BuLi or EtMgBr.[17] A Ni-based catalyst system ($[Ni(cod)_2]$/BDPEDA) has also proved to be efficient.[18]

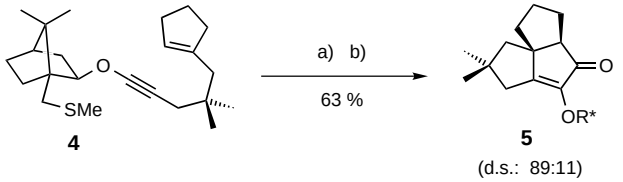
Recently Buchwald and co-workers devised an outstanding procedure for the direct, titanocene-catalyzed cyclocarbonylation of enynes.[19] This catalytic method has a number of advantages: it occurs at low CO pressure, tolerates a variety of functional groups including disubstituted alkenes, and gives the cyclopentenones in high yields (> 85%). This industrially attractive process was later modified to proceed enantioselectively. With 5–20% of $[(S,S)$-(EBTHI)$Ti(CO)_2]$ as chiral catalyst[20] the desired cyclopentenones are obtained in high enantiomeric purity (Scheme 6).[21]



Scheme 6. Catalytic enantioselective bicyclizations according to Buchwald.

Asymmetric Pauson–Khand Reactions

Considerable efforts have been made to develop asymmetrical variants of the classical Pauson–Khand reaction. Initial investigations have shown that compounds derived from cobalt complexes of type **1**, in which a carbonyl ligand is replaced by a chiral phosphane (glyphos), react with high enantioselectivity.[22] However, the procedure is too complex to be of preparative value. The concept of Kerr et al., who achieved significant enantioselectivities (max. 44% *ee*) in intermolecular Pauson–Khand reactions by employing chiral amine-oxides as promoters, appears more elegant.[23] A different approach was used by Pericàs, Moyano, Riera, and Greene, who observed high levels of asymmetric induction in Pauson–Khand reactions when chirally modified substrates were used.[24] The potential of this method was demonstrated in total syntheses of hirsutene,[25] brefeldin A,[26] and β-cuparenone.[27] The same concept was applied successfully in a recently published synthesis of (+)-15-norpentalenene in which the key step is the conversion of enyne **4** into the tricyclic product **5** (Scheme 7).[28] As the preparation of



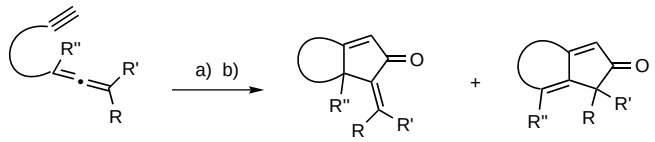
Scheme 7. A diastereoselective Pauson–Khand reaction with a chirally modified substrate according to Pericàs. a) 1.1 equiv of $[Co_2(CO)_8]$; b) 9 equiv of *N*-methylmorpholin-*N*-oxide, 20 °C.

chirally modified substrates always requires considerable effort, the attractiveness of the above-mentioned catalytic enantioselective method is obvious, and it would be interesting to test the Buchwald procedure with the achiral analogues of Pericàs' substrates.

Pauson–Khand Reactions with Allenes

Several authors have demonstrated that a Pauson–Khand type formation of methylenecyclopentenones from enynes, allenes, and carbon monoxide occurs with stoichiometric amounts of $[Fe_2(CO)_9]$ or $[Mo(CO)_6]$, and catalytically with $[Cp_2Ti(CO)_2]$.[29,19] Cazes et al. recently reported that cobalt-mediated inter- and intramolecular conversions of allenes with enynes are also possible (Scheme 8).[30] In these reac-

 © WILEY-VCH Verlag GmbH, D-69451 Weinheim, 1998 1433-7851/98/03707-0912 $ 17.50+.50/0

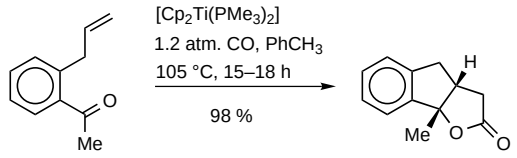


Scheme 8. Pauson–Khand reactions with allenes. a) $[Co_2(CO)_8]$; b) 6 equiv of *N*-methylmorpholin-*N*-oxide, THF/CH_2Cl_2, $-78 \rightarrow 20\,^{\circ}C$, 3 h.

tions, however, the formation of β-methylenecyclopentenone is favored and di- or trisubstituted allenes must be employed in intramolecular reactions, because less substituted allenes tend to polymerize in the presence of $[Co_2(CO)_8]$.

"Hetero-Pauson–Khand Reactions": Synthesis of γ-Butyrolactones

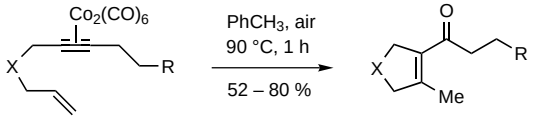
Buchwald and his group have also synthesized γ-butyrolactones successfully by a metallocene mediated cyclization of enones (and ynones) with carbon monoxide in a formal [2+2+1] addition, and have thus achieved the first hetero-Pauson–Khand reaction".[31] The reactions can be conducted in high yields with either stoichiometrical or catalytical amounts of $[Cp_2Ti(PMe_3)_2]$ as the example shown in Scheme 9.



Scheme 9. An example of a "hetero-Pauson–Khand reaction" according to Buchwald.

"Interrupted" Pauson–Khand Reactions

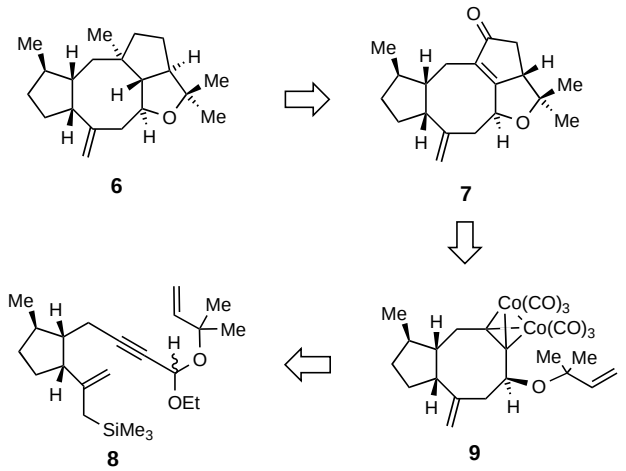
Krafft et al. have found that in the conversions of enyne-$Co_2(CO)_6$ complexes significant amounts of monocyclic by-products are obtained in addition to the desired cyclopentenones (via oxidation of the primary enyne cyclization product).[32] In fact, the conventional Pauson–Khand reaction can be almost totally suppressed if it is conducted in air. An example of an "interrupted Pauson–Khand reaction" is illustrated in Scheme 10.



Scheme 10. The "interrupted Pauson–Khand reaction" according to Krafft.

New Synthetic Applications of the Pauson–Khand Reaction

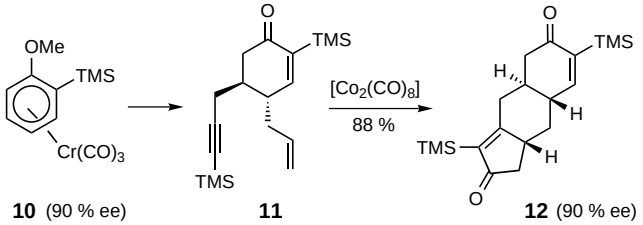
The high value of the Pauson–Khand reaction in the synthesis of natural products and other complex compounds was frequently demonstrated.[3] One of the most impressive examples is the recently published synthesis of the marine natural product (+)-epoxydictymene (**6**) by Schreiber and co-workers.[33] The synthetic strategy (Scheme 11) uses an



Scheme 11. Retrosynthetic strategy of the Schreiber synthesis of (+)-epoxydictymene.

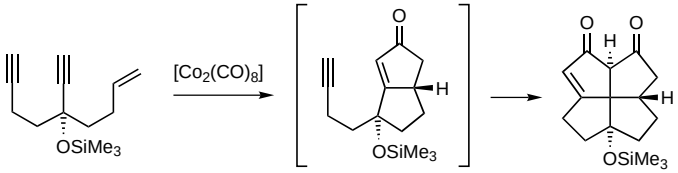
intramolecular Nicholas reaction[34] (the Lewis acid mediated conversion of **8**) for the preparation of the actual Pauson–Khand substrate **9**, which is then converted into the epoxydictymene precursor **7**.

A reaction sequence published recently by Kündig and co-workers also deserves notice:[35] In a one-pot reaction the planar chiral arene-$Cr(CO)_3$ complex **10** is first converted (with chirality transfer) into the enyne **11,** which then affords the tricyclic Pauson–Khand product **12** in high yield and completely diastereoselectively (Scheme 12).



Scheme 12. Combined arene-$Cr(CO)_3$ and Pauson–Khand chemistry according to Kündig.

Finally, sequential Pauson–Khand reactions (domino reactions) are possible.[36,37] A particularly fascinating application of this concept is the synthesis of a fenestrane by Keese and co-workers (Scheme 13).[36]



Scheme 13. Synthesis of a fenestrane by domino-Pauson–Khand reaction according to Keese.

Conclusions

The Pauson–Khand reaction (together with related metallocene-catalyzed transformations) has established a prominent place in the repertoire of synthetic organic chemists. Its

use enables the construction of complex molecules in a convergent and atom economic way starting from structurally simple precursors. High levels of enantioselectivity can be achieved. It is therefore not surprising that an increasing number of research groups is focusing on the further development of this reaction. In the era of combinatorial chemistry the conversion of solid-supported substrates is just one possiblity.[38]

German version: *Angew. Chem.* **1998**, *110*, 955 – 958

Keywords: cobalt · cycloadditions · homogeneous catalysis · metallocenes · Pauson – Khand reactions

[1] a) L. S. Hegedus, *Organische Synthese mit Übergangsmetallen*, VCH, Weinheim, **1995**; b) R. Noyori, *Asymmetric Catalysis in Organic Synthesis*, Wiley, New York, **1994**.

[2] a) I. U. Khand, G. R. Knox, P. L. Pauson, W. E. Watts, *J. Chem. Soc. Chem. Commun.* **1971**, 36; b) I. U. Khand, G. R. Knox, P. L. Pauson, W. E. Watts, M. I. Foreman, *J. Chem. Soc., Perkin Trans. 1* **1973**, 977; c) P. L. Pauson, I. U. Khand, *Ann. N. Y. Acad. Sci.* **1977**, *295*, 2.

[3] Reviews of the Pauson – Khand reaction: a) P. L. Pauson, *Tetrahedron* **1985**, *41*, 5855; b) P. L. Pauson in *Organometallics in Organic Synthesis* (Eds.: A. de Meijere, H. tom Dieck), Springer, Berlin, **1987**, p. 233; c) N. E. Schore, *Org. React.* **1991**, *40*, 1; d) in *Comprehensive Organic Synthesis, Vol 5* (Ed.: B. M. Trost), Pergamon, Oxford, **1991**, p. 1037; e) in *Comprehensive Organometallic Chemistry II, Vol. 12* (Eds.: E. W. Abel, F. G. A. Stone, G. Wilkinson), Pergamon, Oxford, **1995**, p. 703; review on metal-mediated cycloadditions: f) H.-W. Frühauf, *Chem. Rev.* **1997**, *97*, 523.

[4] a) S. Shambayati, W. E. Crowe, S. L. Schreiber, *Tetrahedron Lett.* **1990**, *31*, 5289; b) N. Jeong, Y. K. Chung, B. Y. Lee, S. H. Lee, S.-E. Yoo, *Synlett* **1991**, 204; c) A. R. Gordon, C. Johnstone, W. J. Kerr, *Synlett* **1996**, 1083.

[5] T. Sugihara, M. Yamada, H. Ban, M. Yamaguchi, C. Kaneko, *Angew. Chem.* **1997**, *109*, 2884; (for a related paper that also describes a method for the in situ complexation of alkynes with CoBr2, Zn and CO, see T. Rajesh, M. Periasamy, *Tetrahedron Lett.* **1998**, *39*, 117).

[6] a) B. M. Trost, *Science* **1991**, *254*, 1471; b) B. M. Trost, *Angew. Chem.* **1995**, *107*, 285; *Angew. Chem. Int. Ed. Engl.* **1995**, *34*, 259.

[7] D. C. Billington, W. J. Kerr, P. L. Pauson, C. F. Farnocchi, *J. Organomet. Chem.* **1988**, *356*, 213.

[8] V. Rautenstrauch, P. Mégard, J. Conesa, W. Küster, *Angew. Chem.* **1990**, *102*, 1441; *Angew. Chem. Int. Ed. Engl.* **1990**, *29*, 1413.

[9] a) N. Jeong, S. H. Hwang, Y. Lee, Y. K. Chung, *J. Am. Chem. Soc.* **1994**, *116*, 3159; b) B. Y. Lee, Y. K. Chung, N. Jeong, Y. Lee, S. H. Hwang, *J. Am. Chem. Soc.* **1994**, *116*, 8793; c) N. Y. Lee, Y. K. Chung, *Tetrahedron Lett.* **1996**, *37*, 3145; d) N. Jeong, S. H. Hwang, Y. W. Lee, Y. S. Lim, *J. Am. Chem. Soc.* **1997**, *119*, 10549.

[10] B. L. Pagenkopf, T. Livingstone, *J. Amer. Chem. Soc.* **1996** *118*, 2285.

[11] a) A. J. Pearson, R. A. Dubbert, *J. Chem. Soc., Chem. Commun.* **1991**, 202; b) A. J. Pearson, R. A. Dubbert, *Organometallics* **1994**, *13*, 1656; c) T. R. Hoye, J. A. Suriano, *Organometallics* **1992**, *11*, 2044; d) T. R. Hoye, J. A. Suriano, *J. Am. Chem. Soc.* **1993**, *115*, 1154; e) C. Mukai, M. Uchiyama, M. Hanaoka, *J. Chem. Soc. Chem. Commun.* **1992**, 1014; f) N. Jeong, S. J. Lee, *Tetrahedron Lett.* **1993**, *34*, 4027; g) L. Pagès, A. Llebaria, F. Camps, E. Molins, C. Miravitlles, J. M. Moretó , *J. Am. Chem. Soc.* **1992**, *114*, 10449.

[12] T. Kondo, N. Suzuki, T. Okada, T.-a. Mitsudo, *J. Am. Chem. Soc.* **1997**, *119*, 6187.

[13] T. Morimoto, N. Chatani, Y. Fukumoto, S. Murai, *J. Org. Chem.* **1997**, *62*, 3762.

[14] a) E.-i. Negishi, S. J. Holmes, J. M. Tour, J. A. Miller, *J. Am. Chem. Soc.* **1985**, *107*, 2568; b) E.-i. Negishi, F. E. Cederbaum, T. Takahashi, *Tetrahedron Lett.* **1986**, *27*, 2829; c) E.-i. Negishi, S. J. Holmes, J. M. Tour, J. A. Miller, F. E. Cederbaum, D. R. Swanson, T. Takahashi, *J. Am. Chem. Soc.* **1989**, *11*, 3336.

[15] a) K. Tamao, K. Kobayashi, Y. Ito, *J. Am. Chem. Soc.* **1988**, *110*, 1286; b) K. Tamao, K. Kobayashi, Y. Ito, *Synlett* **1992**, 539.

[16] R. B. Grossmann, S. L. Buchwald, *J. Org. Chem.* **1992**, *57*, 5803.

[17] a) S. C. Berk, R. B. Grossmann, S. L. Buchwald, *J. Am. Chem. Soc.* **1993**, *115*, 4912; b) *ibid*, **1994**, *116*, 8593; c) F. A. Hicks, S. C. Berk, S. L. Buchwald, *J. Org. Chem.* **1996**, *61*, 2713.

[18] M. Zhang, S. L. Buchwald, *J. Org. Chem.* **1996**, *61*, 4498.

[19] F. A. Hicks, N. M. Kablaoui, S. L. Buchwald, *J. Am. Chem. Soc.* **1996**, *118*, 9450.

[20] For the use of EBTHI complexes in enantioselective synthesis, see A. H. Hoveyda, J. P. Morken, *Angew. Chem.* **1996**, *108*, 1378; *Angew. Chem. Int. Ed. Engl.* **1996**, *35*, 1262.

[21] F. A. Hicks, S. L. Buchwald, *J. Am. Chem. Soc.* **1996**, *118*, 11688.

[22] a) P. Bladon, P. L. Pauson, H. Brunner, R. Eder, *J. Organomet. Chem.* **1988**, *355*, 449; b) H. Brunner, A. Niederhuber, *Tetrahedron Asym.* **1990**, *1*, 711; c) A. M. Hay, W. J. Kerr, G. G. Kirk, D. Middlemiss, *Organometallics* **1995**, *14*, 4986.

[23] a) W. J. Kerr, G. G. Kirk, D. Middlemiss, *Synlett* **1995**, 1085; b) W. J. Kerr, D. M. Lindsay, J. S. Scott, S. Watson, *OMCOS 9 Conference, Göttingen* **1997** (Poster No. 318).

[24] a) J. Castro, A. Moyano, M. A. Pericà s, A. Riera, A. E. Greene, *Tetrahedron Asym.* **1994**, *5*, 307; b) V. Bernardes, X. Verdaguer, N. Kardos, A. Riera, A. Moyano, M. A. Pericà s, A. E. Greene, *Tetrahedron Lett.* **1994**, *35*, 575; c) X. Verdaguer, A. Moyano, M. A. Pericà s, A. Riera, V. Bernardes, A. E. Greene, A. Alvarez-Larena, J. F. Piniella, *J. Am. Chem. Soc.* **1994**, *116*, 2153; d) S. Fonquerna, A. Moyano, M. A. Pericà s, A. Riera, *Tetrahedron* **1995**, *51*, 4239; e) S. Fonquerna, A. Moyano, M. A. Pericà s, A. Riera, *J. Am. Chem. Soc.* **1997**, *119*, 10225; f) E. Montenegro, M. Poch, A. Moyano, M. A. Pericà s, A. Riera, *Tetrahedron Lett.* **1998**, *39*, 335.

[25] J. Castro, H. Sörensen, A. Riera, C. Morin, A. Moyano, M. A. Pericà s, A. E. Greene, *J. Am. Chem. Soc.* **1990**, *112*, 9388.

[26] V. Bernardes, N. Kann, A. Riera, A. Moyano, M. A. Pericà s, A. E. Greene, *J. Org. Chem.* **1995**, *60*, 6670.

[27] J. Castro, A. Moyano, M. A. Pericàs, A. Riera, A. E. Greene, A. Alvarez-Larena, J. F. Piniella, *J. Org. Chem.* **1996**, *61*, 9016.

[28] J. Tormo, A. Moyano, M. A. Pericàs, A. Riera, *J. Org. Chem.* **1997**, *62*, 4851.

[29] a) R. Aumann, H.-J. Weidenhaupt, *Chem. Ber.* **1987**, *120*, 23; b) J. L. Kent, H. Wan, K. M. Brummond, *Tetrahedron Lett.* **1995**, *36*, 2407.

[30] a) M. Ahmar, F. Antras, B. Cazes, *Tetrahedron Lett.* **1995**, *36*, 4417; b) M. Ahmar, O. Chabanis, J. Gauthier, B. Cazes, *Tetrahedron Lett.* **1997**, *38*, 5277; c) M. Ahmar, C. Locatelli, D. Colombier, B. Cazes, *Tetrahedron Lett.* **1997**, *38*, 5281.

[31] a) N. M. Kablaoui, F. A. Hicks, S. L. Buchwald, *J. Am. Chem. Soc.* **1996**, *118*, 5818; b) N. M. Kablaoui, F. A. Hicks, S. L. Buchwald, *J. Am. Chem. Soc.* **1997**, *119*, 4424.

[32] M. E. Krafft, A. M. Wilson, O. A. Dasse, B. Shao, Y. Y. Chung, Z. Fu, L. V. R. Bonaga, M. K. Mollmann, *J. Am. Chem. Soc.* **1996**, *118*, 6080.

[33] a) T. F. Jamison, S. Shambayati, W. E. Crowe, S. L. Schreiber, *J. Am. Chem. Soc.* **1994**, *116*, 5505; b) T. F. Jamison, S. Shambayati, W. E. Crowe, S. L. Schreiber, *J. Am. Chem. Soc.* **1997**, *119*, 4353.

[34] K. M. Nicholas, *Acc. Chem. Res.* **1987**, *20*, 207.

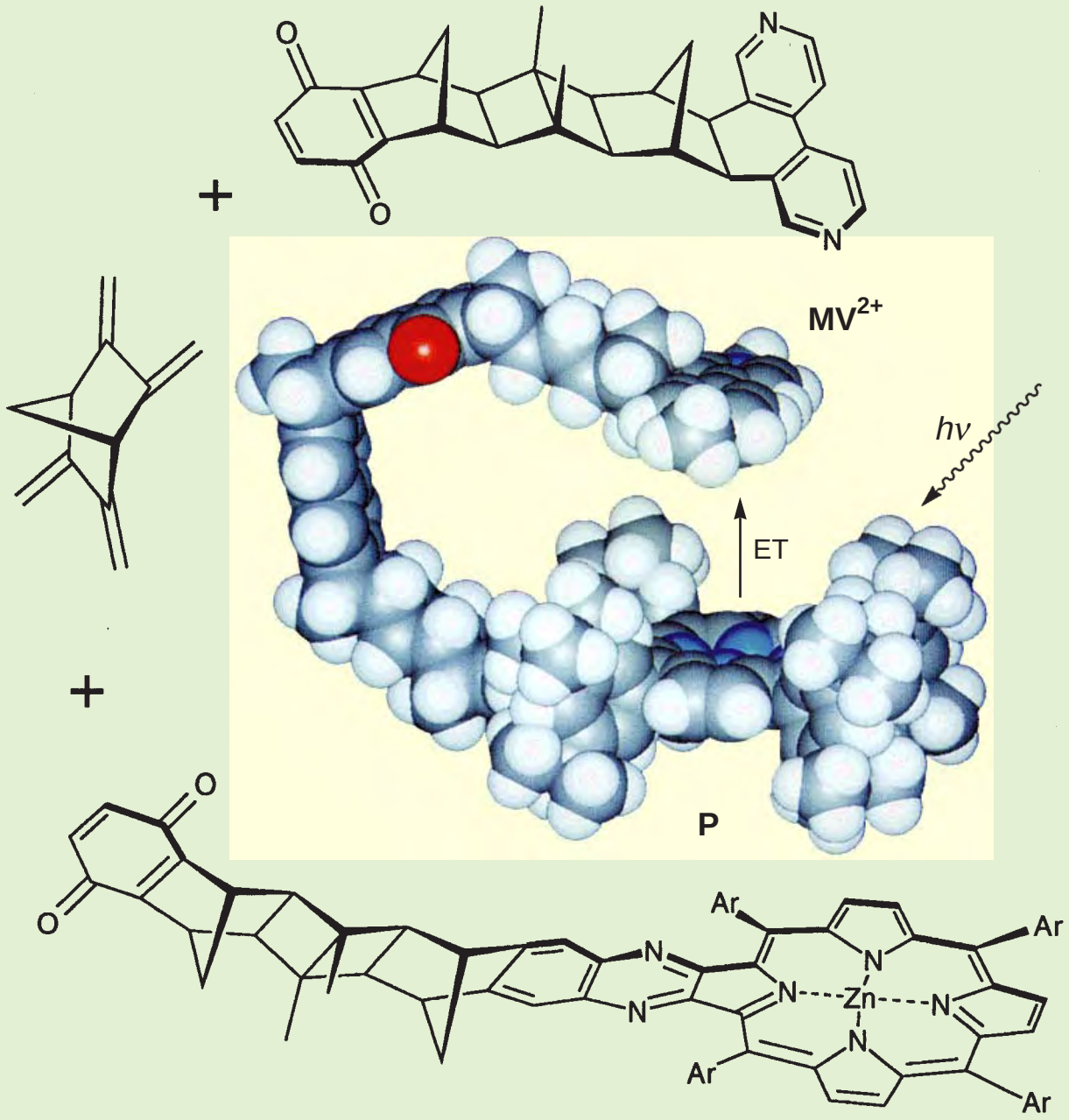
[35] A. Quattropani, G. Anderson, G. Bernardinelli, E. P. Kündig, *J. Am. Chem. Soc.* **1997**, *119*, 4773.

[36] M. Thommen, R. Keese, *Synlett* **1997**, 231.

[37] S. G. Van Ornum, J. M. Cook, *Tetrahedron Lett.* **1997**, *38*, 3657.

[38] a) G. L. Bolton, *Tetrahedron Lett.* **1996**, *37*, 3433; b) J. L. Spitzer, M J. Kurth, N. E. Shore, S. D. Najdi, *Tetrahedron* **1997**, *53*, 6791; c) G. L. Bolton, J. C. Hodges, J. R. Rubin, *Tetrahedron* **1997**, *53*, 6611.

 © WILEY-VCH Verlag GmbH, D-69451 Weinheim, 1998 1433-7851/98/03707-0914 $ 17.50+.50/0



The giant U-shaped tetrad shown above as a space-filling model (and surrounded by the reagents needed for its synthesis) contains porphyrin (P) and methyl viologen (MV^{2+}) chromophores. The terminal P and MV^{2+} units are only about 10 Å apart. Photophysical measurements demonstrate that rapid electron transfer occurs between these units, and that the resulting charge-separated state is remarkably stable towards charge recombination. More details are reported by Paddon-Row et al. on the following pages.

 © WILEY-VCH Verlag GmbH, D-69451 Weinheim, 1998 1433-7851/98/3707-0915 $ 17.50+.50/0

Efficient Photoinduced Electron Transfer in a Rigid U-Shaped Tetrad Bearing Terminal Porphyrin and Viologen Units**

Katrina A. Jolliffe, Toby D. M. Bell, Kenneth P. Ghiggino, Steven J. Langford, and Michael N. Paddon-Row*

Molecules constructed through the covalent attachment of donor and acceptor chromophores to rigid, saturated hydrocarbon bridges continue to provide important and fundamental insights into the characteristics of long-range intramolecular electron transfer (ET) processes.[1] By way of example, our experimental studies on diads involving the norbornyl bridge revealed that these bridges not only serve as a highly rigid scaffold that fixes the chromophores at well-defined separations and orientations with respect to each other, but they also play a crucial role in mediating the ET process by a superexchange or through-bond (TB) coupling mechanism.[1d, 2]

Recently, we extended these studies to the construction of novel trichromophoric compounds such as **1**, which exist in two rigid, noninterconverting diastereomeric *syn* and *anti* forms (Figure 1).[3] Interestingly, the charge recombination (CR) rate constants k_{CR} for the giant charge-separated (CS) states of **1** (i.e., $^{+\bullet}$DMA-bridge-DMN-bridge-DCV$^{\bullet-}$), generated following photoinduced ET, are at least an order of magnitude different for the *syn* and *anti* diastereomers ($k_{CR}^{syn} > k_{CR}^{anti}$).[4] This behavior is probably a consequence of the fact that the *syn* diastereomer possesses a U-shaped geometry with the terminal chromophores facing each other at a distance of about 15 Å. The orientation of chromophores in the *syn* diastereomer is conducive to a facile solvent-mediated CR process that is not available to the *anti* diastereomer.[4]

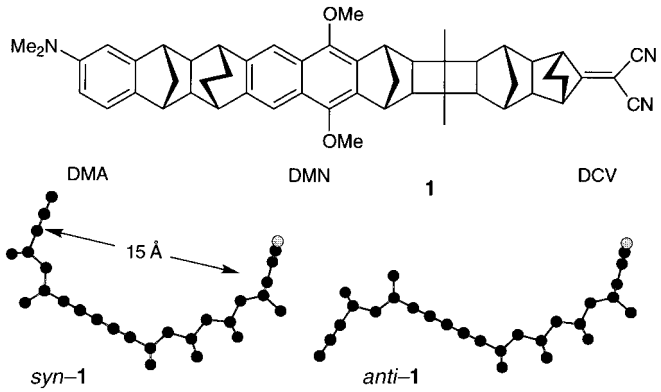


Figure 1. Calculated structures (AM1) of the *syn* and *anti* diastereomers of **1**. The *syn* and *anti* terms refer to the relative disposition of the methano or ethano groups in one bridge with respect to those on the other bridge. DMA = dimethylaminobenzene, DMN = 1,4-dimethoxynaphthaline, DCV = dicyanovinylidene.

To gain a better understanding of the importance of solvent-mediated ET processes, we and others[5] are presently designing and synthesizing rigid systems possessing U-shaped cavities of various dimensions. Here we describe the synthesis and photophysical properties of the *syn*,*syn*-tetrad $\mathbf{2}\cdot 2PF_6$ (Figure 2).[6] This compound is endowed with several features which make it well suited for studying photoinduced ET processes: 1) The porphyrin and methyl viologen chromophores serve as acceptable mimics of redox chromophores which participate in biological ET processes; 2) the synthetic strategy adopted to prepare $\mathbf{2}\cdot 2PF_6$ follows a "building-block" approach in which more than ten different types of chromophores[2, 7] can be incorporated into the methodology; 3) most importantly, the geometry-optimized structure (AM1) for *syn*,*syn*-$\mathbf{2}\cdot 2PF_6$ reveals that the porphyrin and viologen chromophores lie in roughly parallel planes approximately 10 Å apart. The near cofacial alignment of the two chromophores provides an excellent opportunity for exploring the role of solvent-mediated ET processes.

Tetrads of the type $\mathbf{2}\cdot 2PF_6$ may be synthesized[8] by a convergent pathway (Scheme 1 on page 918) involving the cycloaddition of tetraenes such as **3**[9] with dienophiles such as **4**[7b,c, 10] and **5**. Quinone **5** is formed by the reaction of **6**[11] with BBr_3 followed by oxidation[12] of the resulting hydroquinone (AgO/Ag_2O). When tetraene **3** is heated with **4** (0.3 equiv) in toluene at reflux under an inert atmosphere, the corresponding mono-adduct **7** is formed in nearly quantitative yield as a mixture of inseparable diastereomers. That no bis-adduct was produced clearly indicates the difference between the rates for the first and second cycloadditions,[13] thereby making it possible for **3** (or analogues thereof) to react sequentially with a range of dienophiles to yield the backbone of a range of tetrachromophoric systems.

Adduct **7** was converted in two steps into a mixture of *syn*- and *anti*-**8**. Separation of the two diastereomers by preparative thin-layer chromatography (TLC) gave pure *syn*- and *anti*-**8** in a ratio of 70:30. Although we cannot assign *syn* or *anti* stereochemistry to either stereoisomer with absolute certainty, precedence from similar Diels–Alder reactions[3, 14] strongly suggests that the major isomer has *syn* stereochemistry. Diene *syn*-**8** was heated with a large excess of quinone **5** (40 h/Δ/Ar/toluene) in the dark to give directly *syn*,*syn*- and *syn*,*anti*-**9**. Separation of the two newly formed diastereomers was achieved by column chromatography upon demetalation of the zinc compounds (2 M HCl/CH_2Cl_2) to give *syn*,*syn*-[15] and *syn*,*anti*-**10**. Matrix-assisted laser desorption and ionization (MALDI) mass spectrometry of both fractions yielded a parent ion peak at 2097 mass units, which is consistent with the calculated value for $[\mathbf{10}+2]^+$. Metalation of porphyrin *syn*,*syn*-**10** with $Zn(OAc)_2\cdot 2H_2O$, methylation of the bipyridyl unit (MeI/MeCN/Δ), and exchange of the counterion

[*] Prof. M. N. Paddon-Row, Dr. K. A. Jolliffe, Dr. S. J. Langford
School of Chemistry
University of New South Wales
Sydney, N.S.W. 2052 (Australia)
Fax: (+61) 2-9385-6141
E-mail: m.paddonrow@unsw.edu.au
T. D. M. Bell, Prof. K. P. Ghiggino
School of Chemistry, University of Melbourne (Australia)

[**] M.N.P.-R. and K.P.G. thank the Australian Research Council for continuing support of this research. The Australian Government is acknowledged for the award of an Australian Postgraduate Research Award to K.A.J. and T.D.M.B. as well as a APDF to S.J.L. We wish to thank Mr. M. J. Shephard for carrying out the AM1 structure optimization of $\mathbf{2}\cdot 2PF_6$, Dr. M. L. Scudder for the producing the photographs, and Dr. G. Wilson of the CSIRO Division of Molecular Sciences for assisting with the flash photolysis studies.

 © WILEY-VCH Verlag GmbH, D-69451 Weinheim, 1998 1433-7851/98/3707-0916 $ 17.50+.50/0

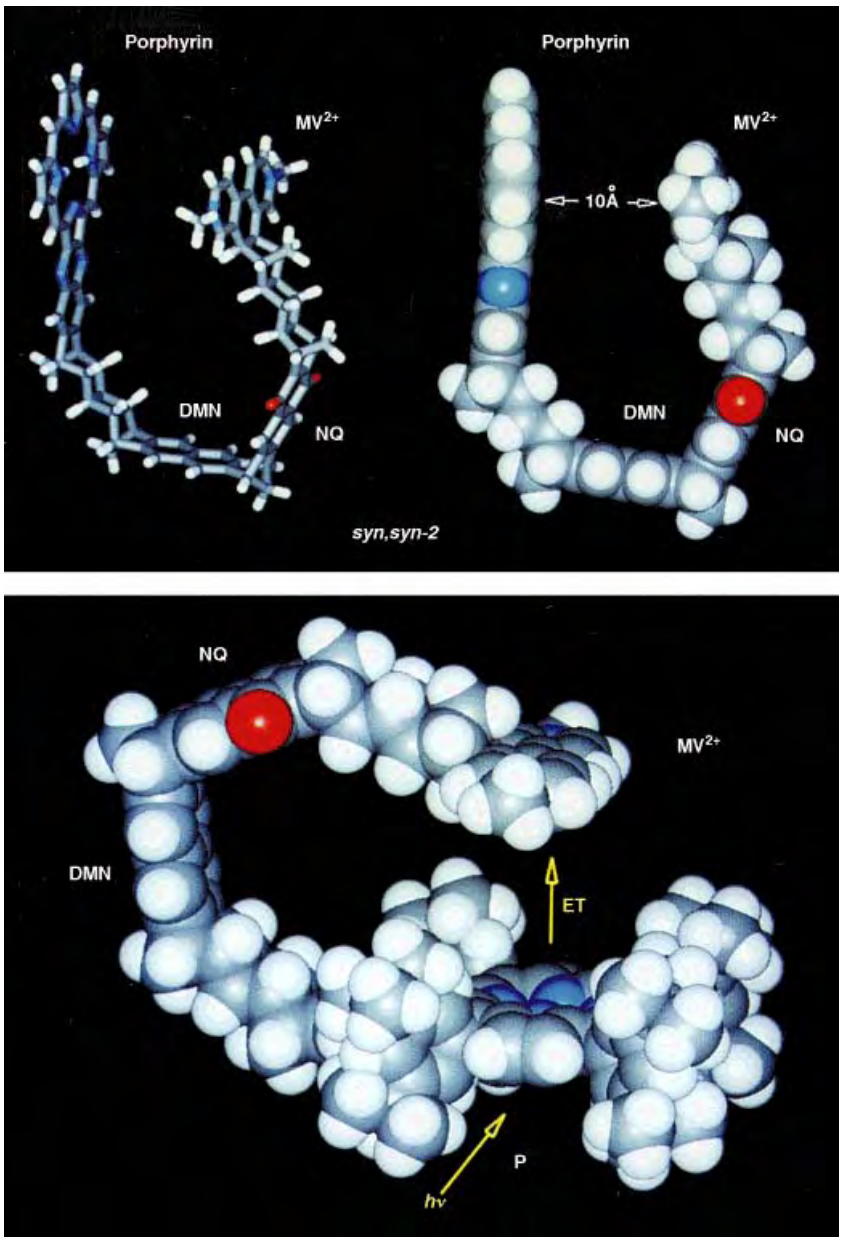
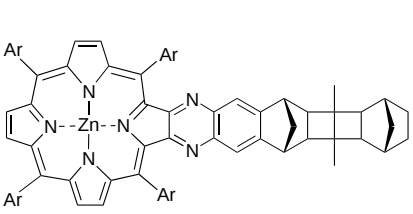


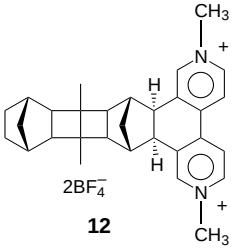
Figure 2. Top: Calculated structure (AM1) of metal-free base *syn*,*syn*-**2**·2PF$_6$ showing the near parallel orientation of the porphyrin and methyl viologen units. The 3,5-di-*tert*-butylphenyl and methoxy groups have been omitted for clarity. Bottom: A possible orientation of the *meso* aryl groups in the structure of basic *syn*,*syn*-**2**·2PF$_6$. MV = methyl viologen, NQ = naphthoquinone

(NH$_4$PF$_6$/aq Me$_2$CO) gave the desired tetrad *syn*,*syn*-**2**·2PF$_6$ in 72% yield. A MALDI mass spectrum of *syn*,*syn*-**2**·2PF$_6$ showed a parent ion at 2188 mass units, which corresponds to the molecular mass of $[\mathbf{2} - 2\,PF_6]^+$.

Evidence for photoinduced ET from the porphyrin to the viologen unit was obtained from time-resolved fluorescence and laser flash photolysis studies. The fluorescence lifetime of porphyrin emission from *syn*,*syn*-**2**·2PF$_6$ ($\tau = 330$ ps) was shorter than that of the porphyrin model compound **11** ($\tau =$ 1.16 ns; Ar = 3,5-di-*tert*-butylphenyl). This indicates the presence of an additional nonradiative process occurring in *syn*,*syn*-**2**·2PF$_6$ with a rate constant of $3 \times 10^9\ s^{-1}$ following photoexcitation. Laser flash photolysis of **11** resulted in a long-lived transient absorption ($\lambda_{max} \approx 500$ nm, $\tau = 400$ µs), which was attributed to the formation of a triplet state by intersystem crossing from the porphyrin singlet state. The transient spectrum of *syn*,*syn*-**2**·2PF$_6$ (Figure 3) was markedly different from that of **11** and exhibited additional



11

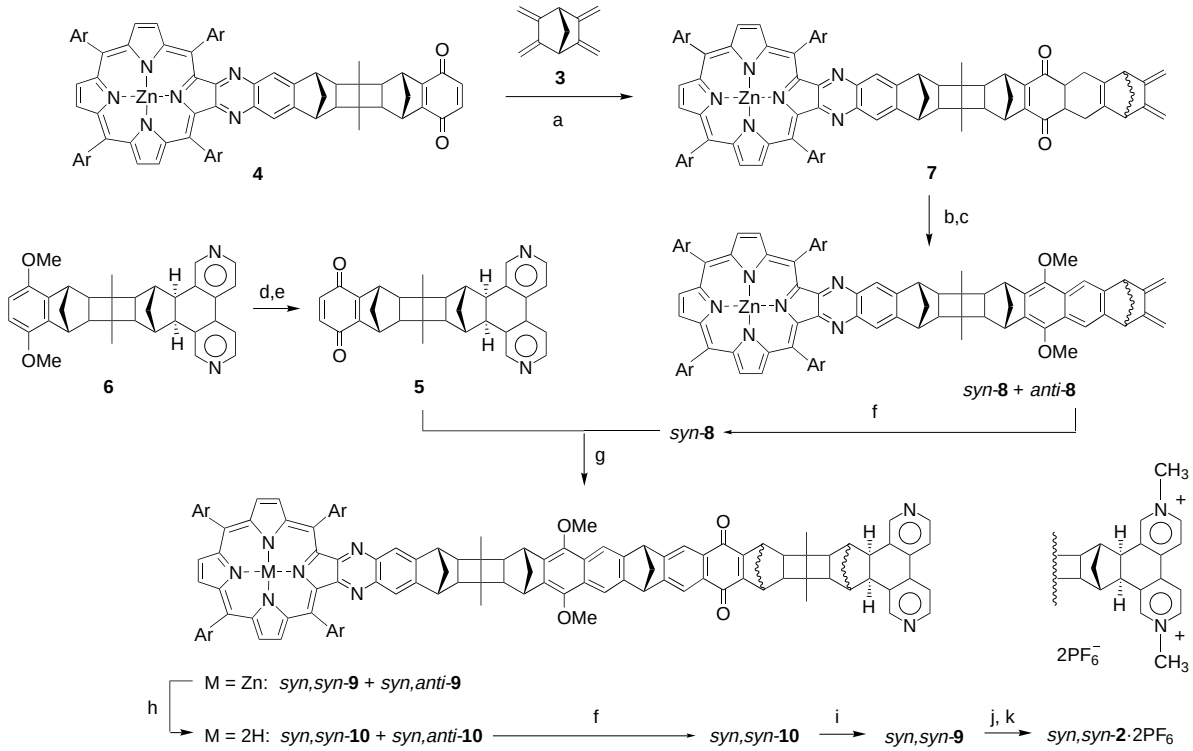


12

transient absorptions in the 580–690 nm and 700–800 nm spectral regions. Comparison with the spectrum of chemically reduced **12** enabled the assignment of the band at 580–690 nm to the methyl viologen radical ion, MV$^{\bullet+}$.

There remains an additional transient absorption above 690 nm. Previous work on other linked, porphyrin-based donor–acceptor molecules carried out by ourselves[16a] and others[16c] has assigned absorption in this spectral region to the

 © WILEY-VCH Verlag GmbH, D-69451 Weinheim, 1998 1433-7851/98/3707-0917 $ 17.50+.50/0



Scheme 1. Synthesis of tetrad *syn*,*syn*-**2**·2PF$_6$. a) Toluene, 80 °C, 99 %; b) K_2CO_3, Me_2CO, MeI, 86 %; c) DDQ, CH_2Cl_2, 83 %, separate isomers; d) BBr_3, CH_2Cl_2, 83 %; e) AgO, Ag_2O, CH_2Cl_2, 85 %; f) **5** (7 equiv), 40 h, reflux, $CH_3C_6H_5$; g) 2 M HCl, CH_2Cl_2, 60 % over two steps, separate isomers; h) $Zn(OAc)_2 \cdot 2H_2O$, MeOH, $CHCl_3$; i) MeI, MeCN, reflux; j) NH_4PF_6, H_2O, Me_2CO, 72 % over three steps. DDQ = 2,3-dichloro-5,6-dicyanobenzoquinone.

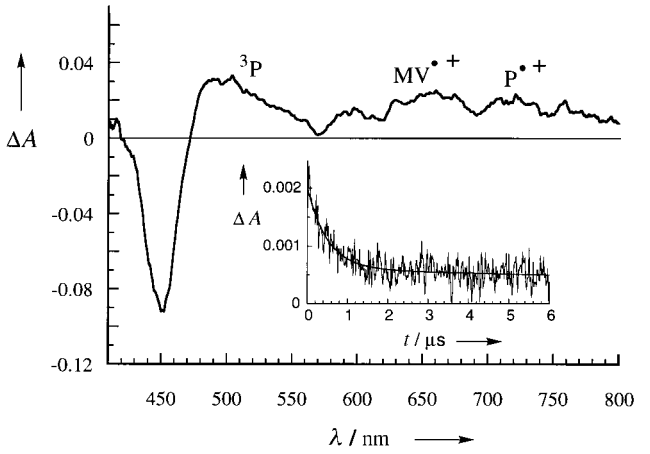


Figure 3. Transient absorption spectrum of *syn*,*syn*-**2**·2PF$_6$ in MeCN recorded 700 ns after photoexcitation along with assignments of the absorbing species. The inset shows the decay of the transient absorption at 650 nm. The data were obtained by fitting to Equation (1); $\tau_1 = 500$ ns, $\tau_2 = 32$ μs, $B/C = 2.33$.

$$\Delta A = B\,e^{(-t/\tau_1)} + C\,e^{(-t/\tau_2)} \quad (1)$$

porphyrin radical cation, P$^{\bullet+}$. Thus, the transient absorption spectra provide convincing evidence for photoinduced ET from locally excited porphyrin, P*, to MV^{2+} in *syn*,*syn*-**2**·2PF$_6$. The additional absorption near 500 nm (Figure 3) can be assigned to residual formation of a triplet state, whereas there is strong bleaching of the ground state in the region of the porphyrin Soret band at 450 nm.

The decay behavior of the transient spectrum is complex. Analysis of the decay kinetics in the region of the radical-ion absorbance yielded two components (inset of Figure 3). The contribution of the shorter component dominates (≈ 70 %) and decays with a lifetime of 500 ns (± 15 %) at 650 nm and 710 nm, whereas the longer component decays over tens of microseconds!

These results indicate that photoinduced ET occurs in *syn*,*syn*-**2**·2PF$_6$ with a quantum efficiency of 78 % and formation of the giant CS state P$^{\bullet+}$-DMN-NQ-MV$^{\bullet+}$. The ratio of the rates of charge separation to charge recombination is greater than 1400. The observation of efficient photoinduced ET from locally excited P* to MV^{2+} is surprising because, although the process is calculated[17] to be strongly exoergic (-0.77 eV), the P and MV^{2+} chromophores are remote in terms of spatial separation (10 Å) and connectivity (23 σ bonds). Three mechanisms could explain the observed ET dynamics: 1) direct, solvent-mediated ET from P* to MV^{2+}; 2) direct TB-mediated ET from P* to MV^{2+} through the orbitals of the bridge and the DMN and NQ units; 3) a two-step ET process in which TB-mediated ET from P* to NQ occurs first to generate the CS intermediate P$^{\bullet+}${bridge}NQ$^{\bullet-}$ followed by thermal ET from NQ$^{\bullet-}$ to MV^{2+}. Both steps are estimated to be exoergic, the first by about 0.25 eV,[7h, 17] and the second by about 0.52 eV[17]. The present experimental data are unable to discriminate between these mechanisms, although the solvent-mediated mechanism would appear to be more plausible than the other two mechanisms.[18] Further investigations are in progress to resolve both the matter of mechanisms and the origin of the complex decay kinetics of the CS species.

 © WILEY-VCH Verlag GmbH, D-69451 Weinheim, 1998 1433-7851/98/3707-0918 $ 17.50+.50/0

Experimental Section

Photophysical measurements were carried out at room temperature on solutions in MeCN which were thoroughly degassed by freeze-pump-thaw cycles. Transient decay experiments were performed with a laser flash photolysis apparatus that used the second harmonic of a Nd-YAG laser (Continuum) for photoexcitation at 530 nm. Transient species generated by the absorption of 5-mJ excitation pulses (pulse width 7 ns) were monitored at right angles to the excitation with a pulsed 150-watt high-pressure xenon lamp, a photomultiplier tube, and a digital oscilloscope. For transient spectra, the flash photolysis system (CSIRO Division of Molecular Sciences) incorporated an excimer laser excitation source (351 nm) and a gated diode array/optical multichannel analyser detector (Princeton Applied Research).

syn,*syn*-**10**: M.p. $> 300\,^{\circ}C$; ^1H NMR (600 MHz, $CDCl_3$): $\delta = -2.64$ (br s, 2H), 0.45 (m, 1H), 0.52 (s, 6H), 0.92 (m, 1H), 1.11 (s, 6H), 1.34 (m, 1H), 1.41 (s, 18H), 1.46 (s, 18H), 1.54 (s, 36H), 1.60 (s, 2H), 1.63 (m, 1H), 1.70 (s, 2H), 1.75 (m, 1H), 1.79 (m, 1H), 1.83 (s, 2H), 1.90 (s, 4H), 1.97 (m, 1H), 2.03 (m, 1H), 2.28 (s, 2H), 2.66 (AB q, 2H), 3.31 (d, $J = 5.1$ Hz, 2H), 3.34 (s, 2H), 3.46 (s, 2H), 3.67 (s, 2H), 3.94 (s, 6H), 4.56 (s, 2H), 6.01 (d, $J = 5.1$ Hz, 2H), 7.32 (s, 2H), 7.36 (t, $J = 1.5$ Hz, 2H), 7.67 (s, 2H), 7.82 (t, $J = 1.5$ Hz, 2H), 7.83 (t, $J = 1.8$ Hz, 2H), 7.86 (m, 2H), 7.89 (s, 2H), 7.91 (s, 2H), 8.12 (t, $J = 1.8$ Hz, 2H), 8.18 (t, $J = 1.8$ Hz, 2H), 8.86 (s, 2H), 9.03 (AB q, 4H); ^{13}C NMR (75.5 MHz, $CDCl_3$): $\delta = 8.8$, 9.5, 31.8, 31.9, 34.9, 35.1, 40.0, 40.7, 40.8, 41.0, 42.8, 43.0, 43.5, 43.8, 48.4, 48.6, 50.5, 50.6, 51.0, 52.6, 62.0, 63.2, 113.4, 115.0, 118.1, 119.2, 120.6, 121.2, 122.4, 126.4, 126.8, 128.0, 128.1, 128.6, 129.4, 129.5, 130.5, 131.7, 133.8, 134.1, 135.4, 137.6, 139.6, 140.3, 140.6, 141.2 144.7, 144.8, 145.7, 146.0, 148.4, 148.6, 148.8, 150.0, 150.7, 151.6, 152.6, 154.7, 155.8, 181.8; MS (MALDI): *m/z*: 2097 $[M+2]^+$.

syn,*syn*-**2**$\cdot 2PF_6$: M.p. $> 300\,^{\circ}C$; ^1H NMR (500 MHz, [D_6]acetone): $\delta = 0.68$ (s, 6H), 0.92 (m, 1H), 1.09 (m, 1H), 1.17 (s, 6H), 1.40 (s, 18H), 1.48 (s, 18H), 1.54 (s, 36H), 1.70 (m, 2H), 1.92 (m, 3H), 2.19 (m, 3H), 2.30 (s, 2H), 2.58 (AB q, 2H), 3.09 (s, 2H), 3.32 (s, 2H), 3.60 (s, 2H), 3.75 (s, 2H), 3.92 (s, 6H), 4.15 (s, 6H), 4.69 (s, 2H), 7.55 (m, 4H), 7.73 (m, 2H), 7.89 (s, 2H), 7.90 (m, 2H), 7.93 (m, 2H), 7.96 (s, 2H), 7.97 (m, 2H), 8.07 (m, 6H), 8.86 (AB q, 4H), 8.90 (br s, 2H); ^{13}C NMR (75.5 MHz, [D_6]acetone): $\delta = 8.4$, 8.8, 31.1, 31.3, 34.6, 34.7, 34.8, 40.7, 40.8, 40.9, 41.0, 42.8, 43.0, 43.6, 43.8, 47.9, 48.3, 49.6, 50.8, 50.9, 52.4, 61.1, 114.8, 118.0, 118.6, 120.3, 120.5, 121.1, 122.0, 123.7, 126.3, 127.7, 128.4, 128.9, 129.3, 131.1, 131.2, 131.5, 131.7, 135.0, 138.7, 139.6, 140.5, 141.5, 142.1, 142.3, 142.5, 144.6, 145.2, 147.9, 148.4, 148.6, 148.7, 148.8, 149.7, 149.8, 150.9, 152.1, 152.9, 156.3, 181.1; MS (MALDI): *m/z*: 2188 $[M - 2PF_6]^+$.

Received: November 14, 1997 [Z11160IE]
German version: *Angew. Chem.* **1998**, *110*, 959 – 964

Keywords: cycloadditions · electron transfer · isomerism · porphyrinoids · superexchange

[1] a) G. L. Closs, J. R. Miller, *Science* **1988**, *240*, 440; b) M. A. Newton, *Chem. Rev.* **1991**, *91*, 767; c) M. R. Wasielewski, *Chem. Rev.* **1992**, *92*, 435; d) M. N. Paddon-Row, *Acc. Chem. Res.* **1994**, *27*, 18.

[2] a) K. D. Jordan, M. N. Paddon-Row, *Chem. Rev.* **1992**, *92*, 395; b) M. N. Paddon-Row, K. D. Jordan in *Modern Models of Bonding and Delocalization* (Eds.: J. F. Liebman, A. Greenberg), VCH, New York, **1988**, chap. 3; c) M. J. Shephard, M. N. Paddon-Row, *J. Am. Chem. Soc.* **1997**, *119*, 5355.

[3] a) J. M. Lawson, M. N. Paddon-Row, *J. Chem. Soc. Chem. Commun.* **1993**, 1641; b) J. M. Lawson, D. C. Craig, A. M. Oliver, M. N. Paddon-Row, *Tetrahedron* **1995**, *51*, 3841.

[4] a) J. M. Lawson, M. N. Paddon-Row, W. Schuddeboom, J. M. Warman, A. H. A. Clayton, K. P. Ghiggino, *J. Phys. Chem.* **1993**, *97*, 13099; b) M. R. Roest, J. M. Lawson, M. N. Paddon-Row, J. W. Verhoeven, *Chem. Phys. Lett.* **1994**, *230*, 536; c) M. R. Roest, J. W. Verhoeven, W. Schuddeboom, J. M. Warman, J. M. Lawson, M. N. Paddon-Row, *J. Am. Chem. Soc.* **1996**, *118*, 1762.

[5] a) K. Kumar, Z. Lin, D. H. Waldeck, M. B. Zimmt, *J. Am. Chem. Soc.* **1996**, *118*, 243; b) J. N. H. Reek, A. E. Rowan, R. de Gelder, P. T. Beurskens, M. J. Crossley, S. de Feyter, F. de Schryver, R. J. M. Nolte, *Angew. Chem.* **1997**, *109*, 396; *Angew. Chem. Int. Ed. Engl.* **1997**, *36*, 361.

[6] The *syn*,*syn* and *syn*,*anti* diastereomers are defined by the relative orientation of the outer methano bridges to the central methano bridge which links DMN units to NQ units in **2**$\cdot 2PF_6$.

[7] a) H. K. Patney, M. N. Paddon-Row, *Synthesis* **1986**, 326; b) M. Antolovich, A. M. Oliver, M. N. Paddon-Row, *J. Chem. Soc. Perkin Trans. 2* **1989**, 783; c) M. Antolovich, P. J. Keyte, A. M. Oliver, M. N. Paddon-Row, J. Kroon, J. W. Verhoeven, S. A. Jonker, J. M. Warman, *J. Phys. Chem.* **1991**, *95*, 1933; d) A. Golka, P. J. Keyte, M. N. Paddon-Row, *Tetrahedron* **1992**, *48*, 7663; e) J. M. Lawson, A. M. Oliver, D. F. Rothenfluh, Y.-Z. An, G. A. Ellis, M. G. Ranasinghe, S. I. Khan, A. G. Franz, P. S. Ganapathi, M. J. Shephard, M. N. Paddon-Row, Y. Rubin, *J. Org. Chem.* **1996**, *61*, 5032; f) D. Rothenfluh, A. M. Oliver, M. N. Paddon-Row, *J. Chem. Soc. Perkin Trans. 2* **1996**, 639; g) P. T. Gulyas, S. J. Langford, N. R. Lokan, M. G. Ranasinghe, M. N. Paddon-Row, *J. Org. Chem.* **1997**, *62*, 3038.

[8] Detailed synthesis and NMR spectroscopic analysis justifying the stereochemistry will be shortly presented: K. A. Jolliffe, G. Ball, S. J. Langford, A. M. Oliver, A. Salek, M. N. Paddon-Row, unpublished results.

[9] O. Pilet, P. Vogel, *Helv. Chim. Acta* **1981**, *64*, 2563.

[10] Compound **4** differs from that reported in the literature[7b,c] in that the *meso* phenyl groups of the porphyrin unit have been replaced by the more lipophilic 3,5-di-*tert*-butylphenyl groups.

[11] D. C. Craig, K. P. Ghiggino, K. A. Jolliffe, S. J. Langford, M. N. Paddon-Row, *J. Org. Chem.* **1997**, *62*, 3038.

[12] G. Kaupp, H. Prinzbach, *Chem. Ber.* **1971**, *104*, 182.

[13] A. A. Pinkerton, D. Schwarzenbuch, J.-L. Birbaum, P.-A. Carrupt, L. Schwager, P. Vogel, *Helv. Chim. Acta.* **1984**, *67*, 1136.

[14] a) L. A. Paquette, A. G. Schaefer, J. F. Blount, *J. Am. Chem. Soc.* **1983**, *105*, 3642; b) G. Mehta, S. Padma, V. Pattabhi, A. Pramanik, J. Chandrasekhar, *ibid.* **1990**, *112*, 2942.

[15] Interestingly, the ^1H NMR spectrum of *syn*,*syn*-**10** exhibits a pair of doublets at $\delta = 3.31$ and 6.01 which was not seen for the other isomer. Based on COSY and TOCSY experiments, these resonances are attributed to the ring-fused bipyridyl protons. The upfield nature ($\Delta\delta > 2.5$) of these resonances is most likely a result of an intramolecular porphyrin ring current, which supports the presence of the U-shaped cavity in this molecule. This is reasonable since NOESY experiments indicated that NOEs exist between the signals at $\delta = 6.01$ and 3.31 and those of the inner peripheral protons, the β-pyrrolic protons, and several *tert*-butyl protons within the porphyrin unit. The only other option, that of an intermolecular interaction, can be ruled out on the basis of both ^1H NMR and UV dilution studies. Dilution experiments (10^{-2} to 10^{-5} M) resulted in no observable changes in the NMR spectrum or diversion from the Beer – Lambert law for *syn*,*syn*-**10**.

[16] a) T. D. M. Bell, T. A. Smith, K. P. Ghiggino, M. G. Ranasinghe, M. J. Shephard, M. N. Paddon-Row, *Chem. Phys. Lett.* **1997**, *268*, 223; b) K. P. Ghiggino, T. A. Smith, *Prog. Reac. Kin.* **1993**, *18*, 375; c) D. Kuciauskas, S. Lin, G. R. Seely, A. L. Moore, T. A. Moore, D. Gust, T. Drovetskaya, C. A. Reed, P. D. W. Boyd, *J. Phys. Chem.* **1996**, *100*, 15926.

[17] The Gibbs energy ΔG_{cs} for photoinduced ET can be estimated with the semi-empirical approach of Weller (A. Weller, *Z. Phys. Chem. Neue Folge* **1982**, *133*, 93). Calculation of ΔG_{cs} for photoinduced ET with the Weller equation requires the donor (P) and acceptor (MV^{2+}) redox potentials ($E^{ox}(D) = 1.11$[16] and $E^{red}(A) = -0.42$ eV[11]) measured in MeCN ($\varepsilon_s = 37.5$), the singlet energy of the lowest excited state of P ($E_{00} = 2.01$ eV[16]), the through-space separation between the P center and the MV^{2+} center ($R_c = 10$ Å), and the effective radii of the radical ion donor and acceptor ($r^+ \approx r^- = 4.5$ Å[11]).

[18] Mechanism 2 is unfavored because P and MV^{2+} are separated by 23 σ bonds; superexchange coupling through these bonds is expected to be weak. The first step of mechanism 3 involves a weakly exoergic process taking place over a comparatively large connectivity distance; it is expected to be inefficient. Mechanism 1 involves solvent-mediated ET between chromophores that are about 10 Å apart. There is experimental precedence that this mechanism is efficient for this interchromophore separation.[3, 5]

 © WILEY-VCH Verlag GmbH, D-69451 Weinheim, 1998 1433-7851/98/3707-0919 $ 17.50+.50/0

Synthesis and Structural Analysis of a Helical Coordination Polymer Formed by the Self-Assembly of a 2,2′-Bipyridine-Based *exo*-Ditopic Macrocyclic Ligand and Silver Cations**

Christian Kaes, Mir Wais Hosseini,* Clifton E. F. Rickard, Brian W. Skelton, and Allan H. White

Because transition metals exhibit numerous oxidation states and coordination geometries as well as a wide range of photochemical and magnetic properties, the design and preparation of coordination polymers, which may be regarded as metalloorganic networks, are topics of current interest.[1] Most of the known coordination polymers contain bis-monodentate ligands.[1, 2] Examples of coordination polymers based on bis-bidentate[3] and bis-tridentate ligands have also been reported.[4] Furthermore, there are numerous discrete polynuclear complexes with helical arrangements,[5] but only a few infinite helical coordination polymers.[6]

Using the molecular tectonics approach, which involves the self-assembly of complementary molecular building blocks ("tectons"),[7, 8] we have prepared compounds that exist as molecular networks in the solid state. These networks are based on weak van der Waals interactions between convex connectors and concave receptors[9] or on a combination of electrostatic and hydrogen bonding.[10] A further step in our strategy is the use of coordinative bonds for assembling metals and organic ligands into molecular networks. Here we report the design, synthesis, and structural analysis of a helical coordination polymer obtained by self-assembly of the ligand **7** with silver cations.

The overall topology of coordination polymers can be controlled by means of the coordination preferences of the metal center and the structure of the bridging ligand. Thus, for bis-bidentate exo ligands and metal cations that adopt a tetrahedral coordination geometry, one can envisage the formation of discrete cyclic or infinite linear polynuclear species. Depending on the structure of the ligand, one of these possibilities may be favored. With bis-bidentate exo ligands that adopt a planar conformation, only one-dimensional linear coordination polymers are conceivable (Figure 1a). With nonplanar bis-bidentate exo ligands that adopt a "roof-shaped" conformation, in addition to discrete cyclic polynuclearspecies such as the tetranuclear complex shown in Figure 1b, infinite one-dimensional networks of the "stair type" (Figure 1c), or single-stranded helical species (Figure 1d) may be formed. However, when constraints such as steric hindrance are imposed, one of the alternative structures may be favored.

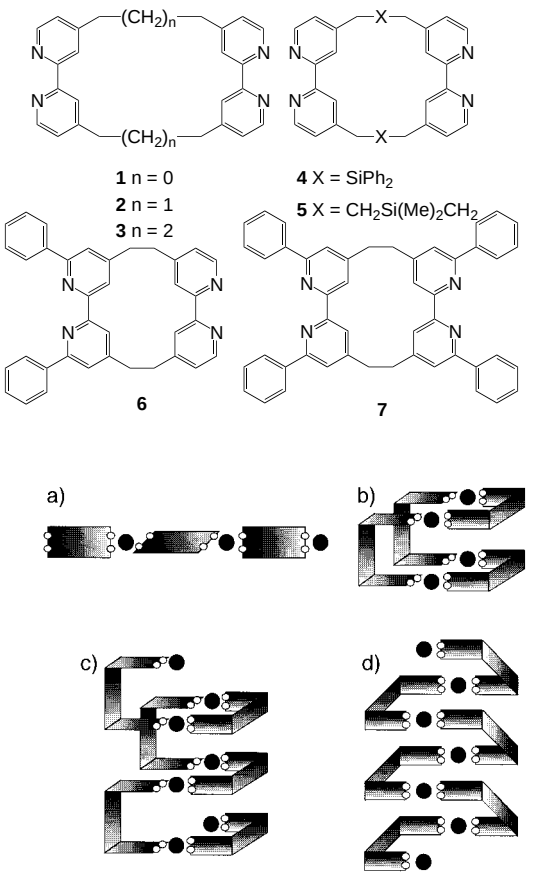


Figure 1. Schematic representation of different types of arrangements that can be obtained by self-assembly of exoditopic ligands and tetrahedrally coordinated metal cations: a) linear, c) "stair-type", d) helical coordination polymer and b) discrete tetranuclear species.

The conformational motion can be restricted, and the location of the metal centers and the distance between them controlled by using exo ligands based on macrocyclic frameworks.[11–14] We prepared exo ligands **1**–**7**, in which two 2,2′-bipyridine units are linked at the 4- and 4′-positions by different spacers.[14] Silver(I) was chosen as the metal because it forms kinetically labile complexes with 2,2′-bipyridine and can adopt a tetrahedral coordination geometry. We then attempted to synthesize a one-dimensional coordination polymer by the self-assembly of Ag^{I} and the *exo*-ditopic bis-chelate ligand **7** (Figure 2).

Treatment of **7** with 1.2 equivalents of $AgPF_6$ in CH_3CN at 25 °C for about 12 h gave a colorless, clear solution, which was evaporated to dryness. The solid thus obtained was redissolved in CH_3CN, and slow diffusion of toluene/hexane (1/1) into the solution gave morphologically uniform single crystals. The same type of crystals could also be grown without the evaporation step.

The solid-state structure of the coordination polymer was elucidated by an X-ray structure analysis,[15] which revealed

[*] Prof. Dr. M. W. Hosseini, C. Kaes
Laboratoire de Chimie de Coordination Organique (URA CNRS)
Université Louis Pasteur, Institut Le Bel
4, rue Blaise Pascal, F-67000 Strasbourg (France)
Fax: (+33) 388-416-266
E-mail: hosseini@chimie.u-strasbg.fr
Prof. Dr. C. E. F. Rickard
Department of Chemistry, University of Auckland
Private Bag 92019, Auckland (New Zealand)
Prof. Dr. A. H. White, Dr. B. W. Skelton
Department of Chemistry, University of Western Australia
Nedlands, WA 6907 (Australia)

[**] Molecular Tectonics, Part 7. We thank A. De Cian for helpful discussions, the CNRS and the Institut Universitaire de France (IUF) for financial support. C.K. thanks the Ministry of Education of Luxembourg for a scholarship. Part 6: ref. [9b]

 © WILEY-VCH Verlag GmbH, D-69451 Weinheim, 1998 1433-7851/98/3707-0920 $ 17.50+.50/0

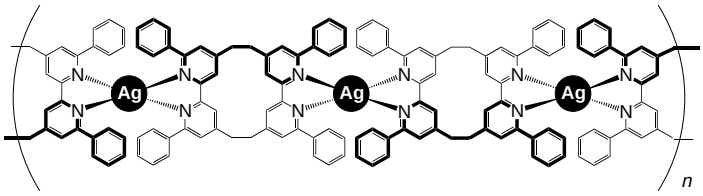


Figure 2. Infinite coordination polymer obtained by the self-assembly of the *exo*-ditopic ligand **7** and silver ions.

that the cationic component of the structure is a single-stranded helical network formed by alternate silver atoms and ligand **7**, which are mutually bridging (Figure 3). The helix

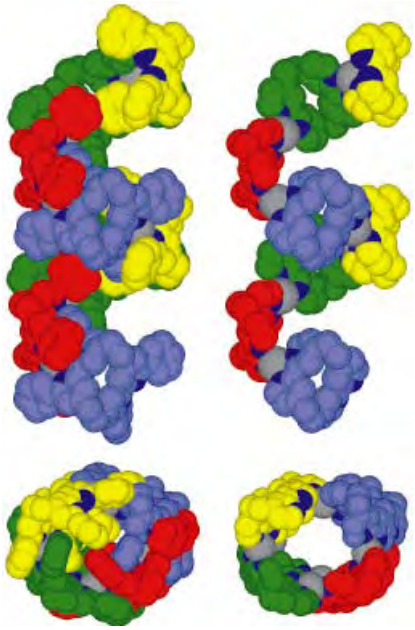


Figure 3. X-ray structure of the infinite single-stranded helical coordination polymer obtained by self-assembly of ligand **7** and silver cation. Projection of the cationic array along (top left) and normal (bottom left) to the polymer axis. For the sake of clarity, the same projections without the Ph groups at the 6 and 6′ positions are also shown on the right. Hydrogen atoms, anions, and CH_3CN molecules are omitted in both representations. The different colors of the ligands are merely intende to more clearly reveal the pitch of the helix.

extends along the crystallographic *a* axis, and two crystallographic twofold axes pass perpendicularly through the non-crystallographic axis. The fragment that determines the pitch of the single helix is composed of four Ag atoms and four ligand molecules. The interior of the helix is not empty, but occupied by phenyl groups (Figure 3). The interstices in the solid were occupied to different extents by CH_3CN molecules and PF_6^- anions.

The observed helical structure is derived from the primary structure of **7**, which adopts a roof-shaped conformation in the complex. However, since **7** is not chiral, a racemic mixture of both the right- and left-handed helical coordination polymers was obtained, as expected. The infinite network crystallized in the centrosymmetric space group *C*2/*c*. The roof-shaped conformation adopted by **7** was previously observed in the solid state for the *exo*-binuclear Ru^{II} complex of the analogous ligand **1**.[14b] This conformation was due to the shortness of the ethylene bridges connecting the two 2,2′-bipyridine units at the 4- and 4′-positions. Indeed, X-ray structural studies on Ru^{II} *exo*-binuclear complexes with ligands **3**[14d] and **5**[14e] showed that when the length of the spacer group is increased, both ligands adopt a planar conformation. In the trinuclear $Ru^{II}-Cu^{I}-Ru^{II}$ complex with two macrocycle **6**, both ligands also adopt a roof-shaped conformation.[14f]

In the one-dimensional network of Ag^+ and **7**, three crystallographically nonequivalent Ag atoms (Ag1, Ag2, Ag3) and two slightly different roof-shaped conformers of the ligands (L1 and L2) were identified (Figure 4), of which

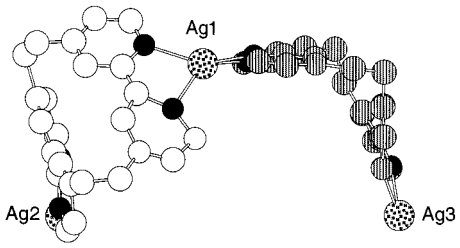


Figure 4. A section of the structure showing the crystallographically nonequivalent L1 (left) and L2 (right) conformers and three silver ions (see text for definition). For the sake of clarity, hydrogen atoms are omitted.

Ag2 and Ag3 are located on the crystallographic twofold axes. Ligands L1 and L2 differ in the conformation of the ethylene bridges (CCH_2CH_2C dihedral angles of 40.0 and 68.5° for L1; and −67.7 and −70.0° for L2). Consequently, two different Ag–Ag distances of 8.8 (Ag1–Ag2) and 9.8 Å (Ag1–Ag3) are present. For both L1 and L2, the two pyridine rings of each bipyridine unit were not coplanar. The average tilt angle of L1 is 20.5°, and that of L2 21.4°.

All silver atoms are coordinated to two sets of bipyridine units to give a AgN_4 coordination sphere in which the N-Ag-N angles range from 73.5 to 139.5° for Ag1, from 74.4 to 149.7° for Ag2, and from 73.6 to 153.9° for Ag3. For all three silver atoms, the Ag–N distances range from 2.30 (estimated standard deviation (esd): 0.8) to 2.47 (esd: 0.2) Å, and the bite angles of the ligands from 73.5(9) to 74.4(6)°. The interplanar (N_2Ag/AgN_2) dihedral angles are 70(1), 65.2(7), and 68(1)°.

Inspection of CPK models revealed that the formation of the helical structure with ligand **7** was probably due to the presence of phenyl groups at the 6- and 6′-positions. Indeed, for both discrete cyclic polynuclear species such as the tetranuclear complex (Figure 1b), and the infinite stair-type network (Figure 1c), the substitution of hydrogen atoms at the 6- and 6′-positions in ligand **1** by phenyl groups in ligand **7** could generate severe steric hindrance between phenyl groups of consecutive ligands. This assumption is supported by electrospray mass spectrometric studies on the Cu^{I} coordination polymer formed with ligand **7**, in which no peak corresponding to the cyclic tetranuclear complex was detected.

In conclusion, we have synthesized a single-stranded helical coordination polymer as a racemic mixture of left- and right-handed helices by self-assembly of an *exo*-ditopic ligand and silver. The structure of the infinite network was established by

 © WILEY-VCH Verlag GmbH, D-69451 Weinheim, 1998 1433-7851/98/3707-0921 $ 17.50+.50/0

single-crystal X-ray structure analysis. With the same combination of ligand and metal, the generation of optically pure left- or right-handed helices by using chiral anions is currently under investigation. Furthermore, the formation of linear coordination polymers (Figure 1a) with ligands such as **3** and **5** and silver or copper is also being studied.

Received: August 25, 1997
Revised version: November 24, 1997 [Z10855IE]
German version: *Angew. Chem.* **1998**, *110*, 970 – 973

Keywords: helical structures · coordination polymers · N ligands · self-assembly · silver

[1] R. Robson in *Comprehensive Supramolecular Chemistry*, *Vol. 6* (Eds.: D. D. Macnicol, F. Toda, R. Bishop), Pergamon, Oxford, **1996**, p. 733.
[2] T. L. Hennigar, D. C. MacQuarrie, P. Losier, R. D. Rogers, M. J. Zaworotko, *Angew. Chem.* **1997**, *109*, 1044; *Angew. Chem. Int. Ed. Engl.* **1997**, *36*, 972, and references therein.
[3] U. Velten, M. Rehahn, *Chem. Commun.* **1996**, 2639; S. Decurtins, R. Pellaux, A. Hauser, M. E. von Arx in *Magnetism: A Supramolecular Function*, *Vol. C484* (Ed.: O. Kahn), Kluwer, Dordrecht, Netherlands, **1996**, pp. 487.
[4] E. C. Constable, A. M. W. Cargill Thompson, *J. Chem. Soc. Dalton Trans.* **1992**, 3467; M. Ferigo, P. Bonhôte, W. Marty, H. Stoeckli-Evans, *ibid.* **1994**, 1549.
[5] J.-M. Lehn, *Supramolecular Chemistry*, *Concepts and Perspectives*, VCH, Weinheim, **1995**; E. C. Constable in *Comprehensive Supramolecular Chemistry*, *Vol. 9* (Eds.: J.-P. Sauvage, M. W. Hosseini), Pergamon, Oxford, **1996**; C. Piguet, G. Bernardinelli, B. Bocquet, O. Schaad, A. F. Williams, *Inorg. Chem.* **1994**, *33*, 4112.
[6] O. J. Gelling, F. van Bolhuis, B. L. Feringa, *J. Chem. Soc. Chem. Commun.* **1991**, 917; Y. Dai, T. J. Katz, D. A. Nichols, *Angew. Chem.* **1996**, *108*, 2230; *Angew. Chem. Int. Ed. Engl.* **1996**, *35*, 2109; B. Wu, W.-J. Zhang, S.-Y. Yu, X.-T. Wu, *Chem. Commun.* **1997**, 1795.
[7] M. Simard, D. Su, J. D. Wuest, *J. Am. Chem. Soc.* **1991**, *113*, 4696.
[8] X. Delaigue, E. Graf, F. Hajek, M. W. Hosseini, J.-M. Planeix in *Crystallography of Supramolecular Compounds*, *Vol. C480* (Eds.: G. Tsoucaris, J. L. Atwood, J. Lipkowski), Kluwer, Dordrecht, **1996**, p. 159; G. Brand, M. W. Hosseini, O. Félix, P. Schaeffer, R. Ruppert in *Magnetism: A Supramolecular Function*, *Vol. C484* (Ed.: O. Kahn), Kluwer, Dordrecht, **1996**, p. 129.
[9] a) F. Hajek, E. Graf, M. W. Hosseini, X. Delaigue, A. De Cian, J. Fischer, *Tetrahedron Lett.* **1996**, *37*, 1401; b) F. Hajek, E. Graf, M. W. Hosseini, A. De Cian, J. Fischer, *Angew. Chem.* **1997**, *109*, 1830; *Angew. Chem. Int. Ed. Engl.* **1997**, *36*, 1760, and references therein.
[10] O. Félix, M. W. Hosseini, A. De Cian, J. Fischer, *Angew. Chem.* **1997**, *109*, 83; *Angew. Chem. Int. Ed. Engl.* **1997**, *36*, 102; O. Félix, M. W. Hosseini, A. De Cian, J. Fischer, *Tetrahedron Lett.* **1997**, *38*, 1755; O. Félix, M. W. Hosseini, A. De Cian, J. Fischer, *ibid.* **1997**, *38*, 1933.
[11] O. Kocian, R. J. Mortimer, P. D. Beer, *Tetrahedron Lett.* **1990**, *31*, 5069; P. D. Beer, F. Szemmes, *J. Chem. Soc. Chem. Commun.* **1995**, 2245; M. Schmittel, A. Ganz, *ibid.* **1997**, 999.
[12] a) X. Delaigue, J. McB. Harrowfield, M. W. Hosseini, A. De Cian, J. Fischer, N. Kyritsakas, *J. Chem. Soc. Chem. Commun.* **1994**, 1579; b) X. Delaigue, M. W. Hosseini, A. De Cian, N. Kyritsakas, J. Fischer, *ibid.* **1995**, 609; c) X. Delaigue, M. W. Hosseini, *Tetrahedron Lett.* **1993**, *34*, 8112.
[13] G. Mislin, E. Graf, M. W. Hosseini, *Tetrahedron Lett.* **1996**, *37*, 4503; C. Drexler, M. W. Hosseini, A. De Cian, J. Fischer, *ibid.* **1997**, *38*, 2993.
[14] a) C. Kaes, M. W. Hosseini, R. Ruppert, A. De Cian, J. Fischer, *Tetrahedron Lett.* **1994**, *35*, 7233; b) *J. Chem. Soc. Chem. Commun.* **1995**, 1445; c) C. Kaes, M. W. Hosseini, A. De Cian, J. Fischer, *Tetrahedron Lett.* **1997**, *38*, 4389; d) *ibid.* **1997**, *38*, 3901; e) *Chem. Commun.* **1997**, 2229; f) C. Kaes, M. W. Hosseini, C. E. F. Rickard, A. H. White, B. W. Skelton, unpublished results.
[15] Suitable crystals were obtained from acetonitrile/toluene/hexane. Reflections were measured on an area detector. Crystal dimensions: $0.12 \times 0.10 \times 0.05$ mm (mounted in a capillary). $C_{48}H_{36}AgF_6N_4P \cdot 11/4\,CH_3CN$, $M_r = 1034.6$, monoclinic, space group $C2/c$, $a = 17.7806(8)$, $b = 34.529(2)$, $c = 38.715(2)$ Å, $\beta = 91.915(5)^\circ$, $V = 23756$ Å^3, $Z = 16$, $\rho_{calcd} = 1.15$ g cm^{-3}, $F(000) = 8456$, $T = 295$ K, monochromatized $Mo_{K\alpha}$ radiation, $\lambda = 0.71073$ cm; 27682 measured reflections ($R_{int} = 0.10$, $2\theta_{max} = 52.6^\circ$), of which 19624 were unique and were corrected for absorption. Final conventional $R = 0.11$ and $Rw = 0.11$ (statistically weighted) for 5092 observed reflections ($I > 3\sigma(I)$). $T_{min}/T_{max} = 0.35/0.86$ (SADABS), Xtal3.4 program system. Phenyl and pyridine rings were refined as rigid bodies, and the geometries of the anions and solvent molecules were constrained to "idealized" values, with isotropic thermal parameters. Ring 24n was modeled as disordered over two sets of sites of equal occupancy. Crystallographic data (excluding structure factors) for the structures reported in this paper have been deposited with the Cambridge Crystallographic Data Center as supplementary publication no. CCDC-100747. Copies of the data can be obtained free of charge on application to CCDC, 12 Union Road, Cambridge CB2 1EZ (fax: (+44) 1223-336-033; e-mail: deposit@ccdc.cam.ac.uk).

Alternating Ethene/Propene Copolymerization with a Metallocene Catalyst**

Margarete K. Leclerc and Robert M. Waymouth*

Metallocene catalysts have introduced an element of design into the construction of polyolefins of defined architecture.[1] Correlation of the catalyst structure with the structure of the resulting polymers has provided considerable insight into the mechanism of polymerization. For example, the syndiospecific polymerization of propene with [{(Cp)(Me_2C)(Flu)}$ZrCl_2$]-based catalysts strongly implicates a Cossee-type mechanism[2] in which the olefin inserts at alternating enantiotopic coordination sites with each insertion (Cp = cyclopentadienyl, Flu = fluorenyl).[3] Differentiation of the coordination sites by methyl substitution on the Cp ring in these systems yields hemiisotactic polypropene,[4–6] in which olefin insertion occurs alternately at an aspecific and isospecific coordination site; substitution of the Cp ring with the larger *tert*-butyl substituent yields isotactic polypropylene.[7,8] The latter result has been interpreted by invoking a "chain-skipping" mechanism in which the polymer chain "skips" out of the more sterically hindered site prior to olefin insertion, resulting in polyinsertions at only one isospecific coordination site.[9]

Metallocene catalysts have also proven useful for olefin copolymerization as copolymers produced with metallocene catalysts tend to have more random comonomer distributions and better compositional homogeneity than copolymers produced with heterogeneous catalysts.[1] However, metallocene catalysts also offer the possibility to design catalyst

[*] Prof. Dr. R. M. Waymouth, Dr. M. K. Leclerc
Department of Chemistry, Stanford University
Stanford, CA 94305 (USA)
Fax: (+1) 650-725-0259
E-mail: waymouth@leland.stanford.edu

[**] We acknowledge the National Science Foundation (NSF-CHE-9615699) and Amoco Chemical Company for support of this work. R.M.W. is a recipient of the NSF Alan T. Waterman Award, for which he is grateful. We thank Amoco for GPC analysis. We thank Prof. W Kaminsky for communicating his results prior to publication.

 © WILEY-VCH Verlag GmbH, D-69451 Weinheim, 1998 1433-7851/98/3707-0922 $ 17.50+.50/0

systems for *nonrandom* olefin copolymers. In particular, we sought to exploit the alternating-site insertion behavior proposed for bridged-fluorenyl complexes[3–8] to design catalysts for the alternating copolymerization of olefins. Herein we report the copolymerization of ethene and propene with catalysts derived from **2**/MAO and **3**/MAO (Figure 1; MAO = metylaluminoxane) to produce highly alternating ethene/propene copolymers (alt-EP), which, until recently,[10, 11]

[{(3-*t*BuCp)(Me_2C)(Flu)}$ZrMe_2$] **1**

[{(3-MeCp)(Me_2C)(Flu)}$ZrMe_2$] **2**

[{(3,4-Me_2Cp)(Me_2C)(Flu)}$ZrMe_2$] **3**

[{(Cp)(Me_2C)(Flu)}$ZrMe_2$] **4**

could be obtained only by hydrogenation of polyisoprene or 1,4-poly(pentadiene).[12,13] Soga et al. have recently reported that *meso*-[{(Me_2Si)(1-MeInd)}$ZrCl_2$]/MAO systems (Ind = indenyl) give alternating ethene/octene copolymers.[14]

Copolymerizations of ethene and propene with **1**/MAO, **2**/MAO, and **3**/MAO were carried out using a variety of monomer feed compositions. The sequence distributions of the polymers obtained were estimated by ^{13}C NMR spectroscopy. The experimental results are summarized in Table 1.

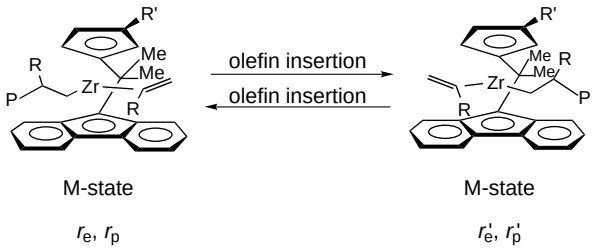


Figure 1. Olefin polymerization with **1**/MAO and **2**/MAO (R′ = *t*Bu and Me, respectively). R = H, Me.

Copolymers produced from **1**/MAO with ethene contents of 44–51 % exhibit random sequence distributions with no preferential formation of EPE and PEP triads even at equal E/P contents.[15] The copolymerization parameters r_1 and r_2 and their product $r_1 r_2 = 0.51 - 0.57$ are comparable to those obtained with other metallocenes.[16, 17] For these copolymers, satisfactory fits for the triad distributions were obtained only by the second-order Markovian model (Table 2); first-order Markovian statistics yielded poor fits. The second-order Markovian copolymerization parameters r_{11} and r_{21} show little variation for copolymers made under a variety of conditions. Moreover, the monomer distributions are very similar to those obtained with the unsubstituted system **4**/MAO.[18] These results, coupled with the observation that the

Table 1. E/P Copolymerization, reactivity ratios, and triad distribution.

Cat.[a] (T[°C])	% E in the Comonomer	% E in the Polymer	r_1[b]	r_2[b]	EEE	PEE + EEP	PEP	EPE	EPP + PPE	PPP
1/MAO (0)	14.7	51	3.94	0.144	8.6	24.8	18.0	19.6	19.9	9.1
1/MAO (20)	9.7	44	4.62	0.111	5.5	19.3	19.2	16.8	23.6	15.6
2/MAO (0)	9.7	49	1.56	0.022	1.9	11.3	37.4	35.9	11.6	1.9
2/MAO (20)	7.2	48	2.07	0.022	2.0	10.4	35.4	35.8	13.0	3.4
3/MAO (0)	7.1	48	1.59	0.017	0.9	10.0	37.7	39.3	9.8	2.3
3/MAO (20)	5.0	51	4.29	0.011	2.8	15.3	33.2	37.1	8.6	3.0

[a] [Zr] = $6.4 \times 10^{-6} - 1.76 \times 10^{-5}$ M; [Al] = $1.3 - 1.4 \times 10^{-2}$ M. [b] Based on the dyad distribution.[27]

Table 2. Calculated triad distribution and reactivity ratios.

Cat. (T[°C])	EEE	PEE + EEP	PEP	EPE	EPP + PPE	PPP	Fit [$\times 10^{-3}$][a]	Calcd parameters			
First-order Markovian model								r_1	r_2		
1/MAO (0)	8.6	25.0	18.2	19.6	22.3	6.3	16.1	3.99	0.097		
1/MAO (20)	5.6	20.9	19.6	16.8	26.6	10.5	36.5	4.98	0.085		
2/MAO (0)	0.8	10.8	37.4	35.9	13.8	1.3	8.6	1.34	0.021		
2/MAO (20)	1.3	13.6	35.4	35.8	12.8	1.1	9.4	2.46	0.014		
3/MAO (0)	1.0	12.3	37.7	39.3	9.1	0.6	7.0	2.13	0.009		
3/MAO (20)	2.3	17.3	33.2	37.1	9.5	0.6	9.4	4.89	0.007		
Second-order Markovian model								r_{11}	r_{22}	r_{12}	r_{21}
1/MAO (0)	8.6	24.8	17.6	20.0	19.9	9.1	3.0	4.04	0.157	0.085	4.10
1/MAO (20)	5.5	19.3	19.1	16.9	23.6	15.6	0.9	5.32	0.141	0.075	4.72
2/MAO (0)	3.0	8.8	37.4	35.9	11.8	3.2	6.6	6.29	0.058	0.018	1.09
2/MAO (20)	3.4	11.3	35.4	35.8	10.5	3.6	8.7	7.61	0.053	0.011	2.05
3/MAO (0)	2.7	10.4	37.7	39.3	7.2	2.7	6.1	6.79	0.057	0.007	1.80
3/MAO (20)	2.8	15.8	33.2	37.1	8.1	3.0	2.6	6.66	0.039	0.006	4.48
Alternating-site model								r_1	r_2	r_1'	r_2'
2/MAO (0)	0.9	10.6	37.4	35.9	13.6	1.6	7.0	1.14	0.048	1.88	0.012
2/MAO (20)	2.3	12.7	35.4	35.8	11.9	21.9	8.9	2.01	0.12	6.54	0.005

[a] χ^2 values.

 © WILEY-VCH Verlag GmbH, D-69451 Weinheim, 1998 1433-7851/98/3707-0923 $ 17.50+.50/0

PP sequences in copolymers made with catalyst **1**/MAO are isotactic,[19] provide strong experimental support for the "chain-skipping" hypothesis[9] according to which, following an olefin insertion, the polymer chain skips back to its initial coordination site—even in the presence of ethene.

In contrast to the results obtained with the *tert*-butyl-substituted catalyst **1**/MAO, the methyl-substituted catalyst **2**/MAO produced copolymers that show triad distributions with up to 70% EPE and PEP triads in approximately the same ratio (Figure 2). The copolymerization parameters and in

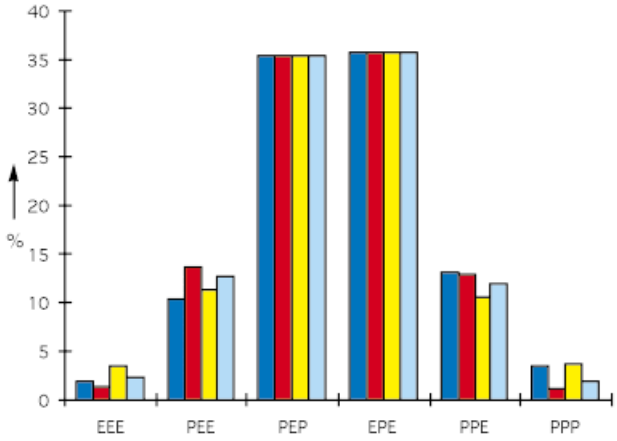
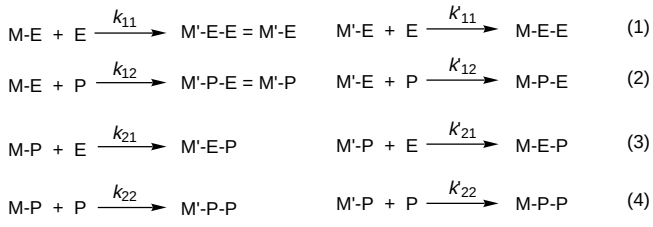


Figure 2. Triad distribution for E/P copolymer from **2** at 20 °C. Dark blue: experimental data, red: according to first-order Markovian model, yellow: according to second-order Markovian model, pale blue: according to the alternate site model.

particular the product of the reactivity ratios $r_1 r_2 = 0.028 - 0.034$ are unusually small for copolymers obtained from metallocenes.[11] As is typically observed for homogeneous catalysts the mass distribution is narrow ($M_n/M_w = 1.7 - 2.5$) for both catalyst systems. The triad distribution obtained by using catalyst **2**/MAO indicates a highly alternating monomer distribution. The percentage of alternating structures can be estimated to be 81% from the triad distribution.[20]

A mechanistic model was derived to interpret the comonomer distribution of the copolymers produced from catalysts (such as **1**/MAO and **2**/MAO) that have two different coordination sites. For this model, the standard copolymerization equations were written for each catalyst site, and it was assumed that the sites alternate with each insertion to give two states, M and M′ [Figure 1; Eqs. (1) – (4)].[21] This two-



state model yields two sets of reactivity ratios r_1, r_2 and r_1', r_2', which can be derived from the experimental triad distribution in terms of the probabilities of each insertion step.

The experimental triad distribution of copolymers from catalyst **2**/MAO gave satisfactory fits to all three statistical models (Table 2, Figure 2). Copolymerization parameters obtained from the first-order Markovian model $r_1 r_2 = 0.026 - 0.034$ and the second-order Markovian model are indicative of an alternating structure, as observed. Copolymerization parameters obtained from the alternating-site model show a large difference in the copolymerization parameters for the two sites (r_1,r_2 vs r_1',r_2'), which suggests that the reactivity ratios towards ethene and propene are different at the two reaction sites. While it is not necessary to invoke the switching model to fit the triad distribution (the first-order model is adequate), the derived reactivity ratios from the switching model are illuminating. In particular, for the polymer obtained at 20 °C, $r_1 = 2.01$ and $r_2 = 0.12$—values that are close to those observed for the unsubstituted catalyst **4**/MAO ($r_1 = 1.3$ and $r_2 = 0.20$).[17] In contrast, for the other site $r_1' = 6.54$ and $r_2' = 0.005$, which suggests a much larger preference for ethene insertion at this coordination site.

The E/P copolymerization with the symmetrical substituted complex **3**/MAO was investigated in order to determine if the reactivity ratios for this catalyst would match those derived from the switching-site model with **2**/MAO (r_1', r_2'). The copolymers obtained from **3**/MAO show also a triad distribution with predominant EPE and PEP triads. A degree of alternation of 83% (polymerization at 0 °C) can be estimated. The experimental triad distribution of copolymers from catalyst **3**/MAO gave satisfactory fits to both first- and second-order Markovian statistical models (Table 2), and the copolymerization parameters ($r_1 r_2$ values of 0.027 – 0.047) indicate an alternating structure. The reactivity ratios ($r_1 = 2.13 - 4.95$; $r_2 = 0.007 - 0.009$) are similar to those derived for r_1' and r_2' from the switching-site model for **2**/MAO, but the mechanism for alternating monomer incorporation by **3**/MAO *cannot be that as proposed for* **2**/MAO because **3**/MAO has two enantiotopic coordination sites which will have identical reactivity ratios. Preliminary analysis of the microstructure reveals that polymers derived from **2**/MAO are *isotactic*, while those from **3**/MAO are *atactic*,[12] strongly implicating different mechanisms for catalysts **2**/MAO and **3**/MAO.

Values for parameter r_1 for **3**/MAO (2.13 – 4.95) are close to reported values for other *ansa*-metallocene catalysts,[16, 17] but the r_2 values (0.007 – 0.009) are unusually small. This suggests that either k_{22} is small or k_{21} is large. Preliminary propene homopolymerization results for **3**/MAO indicate its activity towards propene polymerization is comparable to that of **1**/MAO and **2**/MAO, implying that k_{22} is not negligible. Therefore, the small ratio of k_{22} to k_{21} is likely due to a relatively large value for k_{21}. The parameters obtained by fitting to a second-order Markovian model point to similar interpretations: unusually small r_{22} and r_{12} values indicate a small ratio of propene versus ethene insertion into a propene-terminated chain. Presumably the encumbered ligand framework enforces a placement of a propene-terminated polymer chain such that the ratio of propene versus ethene insertion becomes uncommonly small. Further studies are underway to clarify the factors leading to alternating structures formed by these types of catalysts. While we had originally assumed that a dual

 © WILEY-VCH Verlag GmbH, D-69451 Weinheim, 1998 1433-7851/98/3707-0924 $ 17.50+.50/0

site catalyst (such as **2**/MAO) would be necessary for preparing alternating EP copolymers, the remarkable implication of the results with the catalyst **3**/MAO is that it appears possible to design catalysts with symmetric coordination sites that are capable of producing alternating structures of ethene and propene.[11]

In summary, we report the alternating copolymerization of ethene and propene with symmetric and nonsymmetric catalysts of type [{(RCp)(Me_2C)(Flu)}ZrMe_2]/MAO.[11] These studies show the potential of metallocenes for preparing copolymers of defined sequence distributions by controlling the reactivity ratios of olefins through appropriate ligand design.

Experimental Section

General: Copolymerizations were carried out in a mixture of propene (100 mL) and toluene (20 mL) with a constant supply of ethene at a pressure sufficient to give the desired E/P feed ratio.[22, 23] The reactions were started by injecting a solution of metallocenedimethyl and MAO in toluene (20 mL) under Ar pressure into an autoclave charged with propene (100 mL) and saturated with ethene at a total pressure of 5650 – 11 030 hPa. Low conversion and constant total pressure ensured a constant monomer feed. After 30 – 60 min the reaction was quenched by injection of methanol (20 mL). The copolymers were precipitated in methanol (200 mL) and dried at 40 °C under reduced pressure. Quantitative ^{13}C NMR spectra of polymer (300 mg) dissolved in a mixture of dichlorobenzene with 10% [D_6]benzene (4 mL) were used for compositional analyses. The monomer feed was calculated by using the fugacity equation and the experimentally estimated fugacity coefficient for ethene and propene.[23, 24]

(3,4-Me_2Cp)(Me_2C)(Flu): 3,4,6,6′ tetramethylfulvene was prepared from 1,2-dimethylcyclopentadienyl-Li[25] and acetone/pyrrolidine in methanol.[26] (3,4-Me_2Cp)(Me_2C)(Flu) was synthesized from 3,4,6,6′ tetramethylfulvene and fluorenyllithium according to reported procedures.[4] ^{1}H NMR (400 MHz, $CDCl_3$): $\delta = 7.71$ (d, 2H; arom.), 7.34 – 7.16 (m, 6H; arom.), 5.87 (s, 1H; CH), 4.09 (s, 1H; CH); 3.09 (s, 2H; CH_2), 2.01 (s, 3H; CH_3), 1.89 (s, 3H; CH_3), 1.01 (s, 6H; CH_3).

3: [{(3,4-Me_2Cp)(Me_2C)(Flu)}ZrCl_2] was synthesized from Li salt of the ligand and $ZrCl_4$ in CH_2Cl_2.[4] The resulting red crystals were treated with 2.2 equiv of MeLi in ether. Extraction with pentane gave **3,** which was recrystallized once from toluene/pentane. $\delta = 8.07$ (d, 2H; arom.), 7.50 (d, 2H; arom.), 7.32 (m, 2H; arom.), 7.07 (m, 2H; arom.), 5.15 (s, 2H; CH), 1.89 (s, 6H; CH_3), 1.87 (s, 6H; CH_3), – 1.17 (s, 6H; CH_3). C,H analysis: calcd for $C_{25}H_{28}Zr$ (419.75): C 71.53, H 6.74; found: C 71.27, H 7.01.

Received: September 8, 1997 [Z 10898 IE]
German version: *Angew. Chem.* **1998**, *110*, 964 – 967

Keywords: alkenes · copolymerizations · homogeneous catalysis · polymers · sandwich complexes

[1] H. H. Brintzinger, D. Fischer, R. Mülhaupt, B. Rieger, R. M. Waymouth, *Angew. Chem.* **1995**, *107*, 1255 – 1283; *Angew. Chem. Int. Ed. Engl.* **1995**, *34*, 1143 – 1170.
[2] J. Boor, *Ziegler-Natta Catalysts and Polymerizations*; Academic Press, New York, **1979**.
[3] J. A. Ewen, R. L. Jones, A. Razavi, J. D. Ferrara, *J. Am. Chem. Soc.* **1988**, *110*, 6255 – 6256.
[4] J. A. Ewen, M. J. Elder, R. L. Jones, L. Haspeslagh, J. L. Atwood, S. G. Bott, K. Robinson, *Makromol. Chem. Macromol. Symp.* **1991**, *48/49*, 253 – 295.
[5] A. Razavi, J. L. Atwood, *J. Organomet. Chem.* **1995**, *497*, 105 – 111.
[6] N. Herfert, G. Fink, *Makromol. Chem. Macromol. Symp.* **1993**, *66*, 157 – 178.
[7] J. A. Ewen, M. J. Elder in *Ziegler Catalysts* (Eds.: G. Fink, R. Mülhaupt, H. H. Brintzinger), Springer, Berlin, **1995**, pp. 99 – 109.
[8] A. Razavi, J. L. Atwood, *J. Organomet. Chem.* **1996**, *520*, 115 – 120.
[9] G. Guerra, L. Cavallo, G. Moskardi, M. Vacatello, P. Corradini, *Macromolecules* **1996**, *29*, 4834 – 4845.
[10] Following submission of this manuscript, Professor Kaminsky informed us of similar results from his laboratories: M. Arndt, W. Kaminsky, A-M. Schauwienold, U. Weingarten, *Macromol. Chem. Phys.* in press.
[11] Chien and Galimberti have recently reported that bisflourenyl metallocenes yield very small $r_1 r_2$ values in ethene/propene copolymerization implicating a tendency towards alternation: a) Z. Yu, M. Marques, M. Rausch, J. C. W. Chien, *J. Polym. Sci. part A* **1995**, *33*, 2795 – 2801; b) M. Galimberti, L. Resconi, E. Albizzati, *Eur. Pat. Appl.* 632066, **1995** [*Chem. Abstr.* **1995**, *123*, 11617r].
[12] L. Zetta, G. Gatti, G. Audisio, *Macromolecules* **1978**, *11*, 763 – 766.
[13] H. Chien, D. McIntyre, J. Cheng, M. Fone, *Polymer* **1995**, *36*, 2559 – 2565.
[14] T. Uozumi, K. Miyazawa, T. Sano, K. Soga, *Macromol. Rapid Commun.* **1997**, *18*, 883 – 889.
[15] Kaminsky et al. have recently reported the synthesis of alternating ethene/norbornene copolymers with this catalyst: W. Kaminsky, M. Arndt, I. Beulich, *Polym. Mater. Sci. Eng.* **1997**, *76*, 18 – 19.
[16] T. Uozumi, K. Soga, *Makromol. Chem.* **1992**, *193*, 823 – 831.
[17] A. Zambelli, A. Grassi, M. Galimberti, R. Mazzocchi, F. Piemontesi, *Makromol. Chem. Rapid Commun.* **1991**, *12*, 523 – 539.
[18] N. Herfert, P. Montag, G. Fink, *Makromol. Chem.* **1993**, *194*, 3167 – 3182.
[19] I. Tritto, Z.-Q. Fan, P. Locatelli, M. C. Sacchi, *Macromolecules* **1995**, *28*, 3342 – 3350.
[20] Two different types of errors are considered: a sequence of three consecutive monomer insertions (PPP or EEE) and a sequence of two consecutive monomer insertions (PP or EE). The amount of PPP and EEE errors can be calculated directly from the PPP and EEE triads. The percentage of PP and EE sequence errors can be estimated from the intensities of EEP + PEE (and EPP + PPE) triads minus twice the intensity of PPP and EEE triads (each EEE (or PPP) triad gives twice the amount of EEP + PEE (or PPE + EPP) triads). Therefore, the amount of nonalternating insertions *na* is given as *na* = [EEP + PEE] + [PPE + EPP] – [EEE] – [PPP].
[21] Full details of this model will be reported elsewhere.
[22] This method insures a reasonably constant monomer feed ratio throughout the polymerization.
[23] R. Kravchenko, R. M. Waymouth, *Macromolecules* **1998**, *31*, 1 – 6.
[24] J. B. Maxwell, *Databook on Hydrocarbons*; D. Van Nostrand Company, New York, **1950**.
[25] W. Mengele, J. Diebold, C. Troll, W. Röll, H.-H. Brintzinger, *Organometallics* **1993**, *12*, 1931 – 1935.
[26] K. J. Stone, R. D. Little, *J. Org. Chem.* **1984**, *49*, 1849.
[27] Y. Doi, R. Ohnishi, K. Soga, *Makromol. Chem. Rapid Commun.* **1983**, *4*, 169 – 174.

 © WILEY-VCH Verlag GmbH, D-69451 Weinheim, 1998 1433-7851/98/3707-0925 $ 17.50+.50/0

A Visual Tagging Process for Mix and Sort Combinatorial Chemistry

Joseph W. Guiles,* Carolina L. Lanter, and Ralph A. Rivero

Solid-phase synthesis (SPS) is an integral part of the combinatorial chemistry technology that is emanating from academic and industrial institutions worldwide.[1] The extension of solid-phase peptide synthesis[2] for the generation of small druglike molecules is an area of tremendous research interest.[3] Also this extension is performed rapidly, provides samples of good purity, and is amenable to robotics. These characteristics of SPS have been exploited for the rapid generation of large numbers of compounds as discrete samples or mixtures. Currently, major differences between utilizing discrete compounds versus mixtures exist, as was recently pointed out by Berk and Chapman.[4] The major differential aspect is the impact that synthesis and screening speed have on the rate at which one obtains information (e.g. development of structure – activity relationships). To date this is a distinguishing factor that determines at which step in the drug-discovery process either of these two approaches is applied.

A comparison of speed characteristics for combinatorial techniques as they apply to their roles in the drug-discovery process is depicted in Table 1. The ability to obtain modest quantities of compound (e.g. >10 mg) with a reliable purity makes parallel synthesis (entry 1) the method of choice for meeting the needs of lead optimization. Recent technological advances with robotics have transformed parallel synthesis into a "higher throughput" process. This improved ability is generally recognized as alleviating the tedium of multiple pipetting routines normally done by hand. However, the throughput capacity of this method is limited by the size of the parallel array platform, and therefore only marginal increases in throughput have been realized. In considering other techniques, chemically encoded mix and split (entry 4) provides a moderate information retrieval while maintaining a fast speed of library synthesis.[5] An additional chemical encoding technique makes use of covalently linked dyes for tagging and decoding by the absorption or fluorescence spectrum of the resin bead.[6] Lastly, the mix and sort technique (entry 5) that utilizes microreactors provides an avenue for moderate speed of library production and an expedient delivery of information.[7] These factors make this technique appealing from the standpoint of being useful for both lead identification and optimization. This led us to investigate alternative traceless encoding techniques. We describe here a noncovalent, color-coding strategy for performing mix and sort combinatorial chemistry.

Table 1. Combinatorial techniques and their characteristics.

Entry	Technique	Single substance/ mixture	Speed of library synthesis	SAR retrieval	Utility
1	parallel synthesis	single	slow	fast	lead optimization
2	parallel arrayed mixture[4]	mixture	moderate	moderate	lead identification
3	mix and split	mixture	fast	slow	lead identification
4	chemically encoded mix and split	mixture	fast	moderate	lead identification
5	mix and sort	single	moderate	fast	lead identification and optimization

Recent reports have exploited the use of noncovalent tagging strategies in conjunction with microreactors or porous containers (PCs).[7] The primary advantages of these techniques are the chemical inertness of the tags and the convenience of deciphering the encoded information (no additional tagging and untagging chemistry is required). However, this technology does necessitate computer tracking (a possible economic issue), and the current sizes of the tags consume a moderate amount of space inside the container (a possible yield issue). As a means to address these two problems, smaller and more economical tags were sought. Our objective was to utilize this variation of traceless encoded mix and sort for the generation of moderately sized three-dimensional libraries.

The process utilizes two sets of simple color codes: color-coded glass beads and color-coded container caps. The color codes are used after the mixing steps to sort into the matrix of a 96-well plate (Figure 1). The colored glass beads are chemically inert, whereas the colored polypropylene caps and the PCs are compatible with a wide variety of synthetic reagents.[8] In addition to the cost effectiveness of this method, very little internal container space is yielded to the tag, routinely allowing 10 – 15 mg of compound to be obtained. We consider this quantity to be the minimum amount necessary to meet the needs of lead identification and optimization.

This technique allows for two mix and split steps followed by sorting into a parallel array (Figure 1). The library is typically of an X-Y-Z format. The X and Y subunits are each assigned a set of eight bead colors and a set of twelve cap colors, and Z is added globally for each group of 96 wells. The size of the library is contingent upon the number of Z subunits available. With 20 Z subunits—that is, when 20 differently substituted reagents are attached in the third step of the process—20 separate 96-well plates, or 1920 compounds, are generated. Repeating the process for different sets of X and Y would of course lead to larger libraries. It is possible to

[*] Dr. J. W. Guiles,[+] C. L. Lanter
The R. W. Johnson Pharmaceutical Research Institute
1000 Route 202, P.O. Box 300
Raritan, NJ 08869 (USA)
Fax: (+1) 908-526-6469
Dr. R. A. Rivero
The R. W. Johnson Pharmaceutical Research Institute
Spring House, PA (USA)
[+] Current address:
Hoechst Marion Roussel, Inc.
Route 202 – 206, P.O. Box 6800
Bridgewater, NJ 08807-0800 (USA)
Fax: (+1) 908-231-4774
E-mail: joseph.guiles@hmrag.com

 © WILEY-VCH Verlag GmbH, D-69451 Weinheim, 1998 1433-7851/98/3707-0926 $ 17.50+.50/0

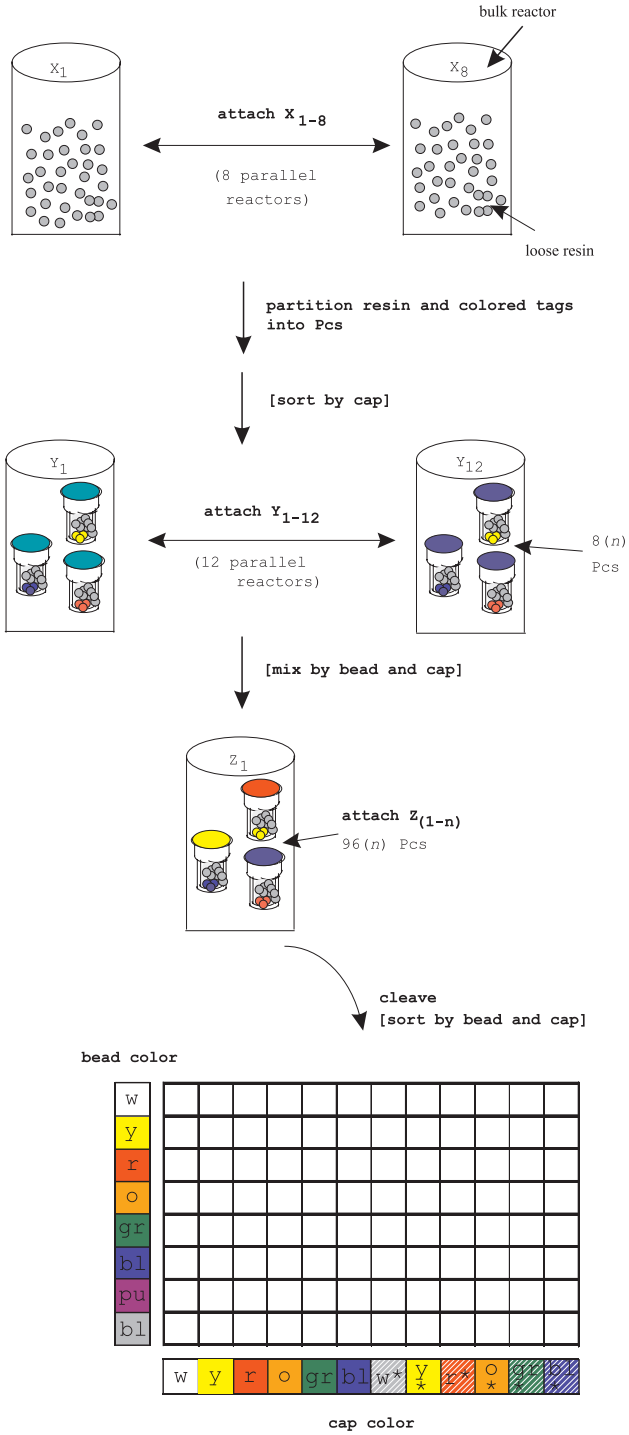
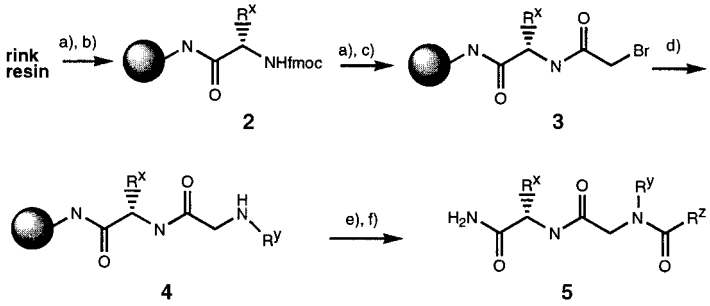


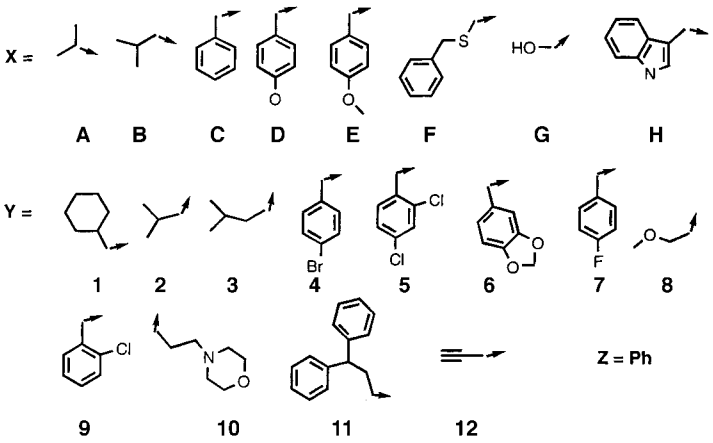
Figure 1. Mix and sort protocol for coding into porous containers.

construct W-X-Y-Z or larger libraries by attaching the additional subunits once the PCs have been sorted into the 96-well plate matrix. However, for these larger dimension libraries beyond the X-Y-Z format, the speed of handling 96 × Z plates for the additional synthetic steps becomes an issue. As depicted in Figure 1, the technique has facilitated the construction of moderately sized three-dimensional libraries.

To exemplify this technique, the synthesis of a library of N-substituted glycine-capped dipeptides is described (Scheme 1). The construction of pseudopeptides or peptoids[3e] was chosen owing to the reproducibility of the synthetic method and the availability of the subunits. The library was arrayed as eight X subunits, twelve Y subunits, and one Z subunit (corresponding to the groups R^x, R^y, and R^z (Schemes 1 and 2), and constituting the rows, columns, and



Scheme 1. Synthesis of pseudopeptides: a) piperidine/DMF (80/20); b) R^x–fmoc, DIC, 1M in CH_2Cl_2; c) bromoacetic acid, DIC, 1M in CH_2Cl_2; d) R^y–NH_2, 1M in CH_2Cl_2; e) PhCOCl, DIEA, 1M in CH_2Cl_2; f) CH_2Cl_2/TFA/TES (8.5/1.5/0.5). DIC = Diisopropylcarbodiimide, DIEA = *N*,*N*-diisopropylethylamine, DMF = dimethylformamide, fmoc = 9-fluorenylmethoxycarbonyl, TES = 2-[tris(hydroxymethyl)methylamino]ethanesulfonic acid, TFA = trifluoroacetic acid.



Scheme 2. Substituents R^x, R^y, and R^z in **2**–**5**.

number, respectively, of 96-well plates). Rink resin (6.8 g, meshed at 100–200 μm)[9] was used to attach the eight fmoc-protected amino acids. The resins derived from the same X subunit in the bulk reactors were then partitioned equally (ca. 35 mmol) into twelve different PCs. A small sample of individual colored beads was then added, coding for the X subunit, and the containers were sealed with the twelve possible different colored caps.[10] After this splitting operation was completed for all eight batches, the 96 PCs were segregated by cap color into twelve reaction vessels. At this point there were eight PCs in each vessel representing all eight X subunits. The fmoc group was then removed, and the twelve Y subunits were attached with standard peptoid chemistry.

After this process was complete, a mixing step combined the 96 unique samples into one vessel,[11] to which the Z subunit was then attached. The 96 samples from each

 © WILEY-VCH Verlag GmbH, D-69451 Weinheim, 1998 1433-7851/98/3707-0927 $ 17.50+.50/0

container are individually sorted into the wells of a polypropylene-fritted 96-well plate according to their bead and cap color, and subsequently treated with a cleavage reagent. The cleavage reagent was then collected by filtration under a slight vacuum into a second nonporous 96-well plate. The individual removable wells of this plate were preweighed before collection of the cleavage solution. Alternatively, we also utilized glass test tubes for this procedure. The tubes were preweighed, and a single porous container was added to each tube followed by the cleavage solution (1 mL). After approximately 20 minutes the porous container was removed above the liquid level and rinsed with a small aliquot of CH_2Cl_2. The volatile components were subsequently removed under vacuum, and the residue was treated with ether. The resulting solid products were isolated in a range of 9.1 – 15.6 mg with an overall average yield of 83.5 % for the six-step sequence. The purity of each sample is excellent, and the analytical data are consistent with the structures assigned for all samples.[12]

We have applied this inert two color encoding strategy for the rapid construction of moderately sized, discrete sample libraries. It presents a simple, cost-effective method for performing mix and sort combinatorial chemistry that does not rely upon robotics, computer monitoring controls, or spectroscopic techniques. The versatility of this technology may be applied not only for the identification of lead structures but also for their subsequent optimization.

Received: September 17, 1997 [Z 10940 IE]
German version: *Angew. Chem.* **1998**, *110*, 967 – 970

Keywords: combinatorial chemistry · microreactors · solid-phase synthesis

[1] a) L. A. Thompson, J. A. Ellman, *Chem. Rev.* **1996**, *96*, 555; b) J. A. Ellman, *Acc. Chem. Res.* **1996**, *29*, 132; c) S. H. DeWitt, A. W. Czarnik, *ibid.* **1996**, *29*, 114; d) M. A. Gallop, R. W. Barrett, W. J. Dower, S. P. A. Fodor, E. M. Gordon, *J. Med. Chem.* **1994**, 37, 1233; e) *ibid.* **1994**, 37, 1385.

[2] a) M. Bodanszky, *Principles of Peptide Synthesis*, Springer, Berlin, **1984**; b) M. Bodanszky, *The Practice of Peptide Synthesis*, Springer, Berlin, **1984**.

[3] Examples of oligo "nonpeptides": K. Burgess, J. Ibarzo, D. S. Linthicum, D. H. Russell, H. Shin, A. Shitangkoon, R. Totani, A. J. Zhang, *J. Am. Chem. Soc.* **1997**, *119*, 1556; b) J. A. W. Kruijtzer, R. M. J. Liskamp, *Tetrahedron Lett.* **1995**, *36*, 6969; c) J. M. Ostresh, G. M. Husar, S. E. Blondelle, B. Dorner, P. A. Weber, R. A. Houghten, *Proc. Natl. Acad. Sci. USA* **1994**, *91*, 11138; d) H. Kessler, *Angew. Chem.* **1993**, *105*, 572; *Angew. Chem. Int. Ed. Engl.* **1993**, *32*, 543; e) R. N. Zuckermann, J. M. Kerr, S. B. H. Kent, W. H. Moos, *J. Am. Chem. Soc.* **1992**, *114*, 10646.

[4] S. C. Berk, K. T. Chapman, *Bioorg. Med. Chem. Lett.* **1997**, *7*, 837.

[5] Chemical encoding: a) S. Brenner, R. Lerner, *Proc. Natl. Acad. Sci. USA* **1992**, *89*, 5381; b) J. Kerr, S. Banvill, R. Zuckermann, *J. Am. Chem. Soc.* **1993**, *115*, 2529; c) M. Ohlmeyer, R. Swanson, L. Dillard, J. Reader, G. Asouline, R. Kobayashi, M. Wigler, W. Still, *Proc. Natl. Acad. Sci. USA* **1993**, *90*, 10922; d) Z.-J. Ni, D. Maclean, C. P. Holmes, M. M. Murphy, B. Ruhland, J. W. Jacobs, E. M. Gordon, M. A. Gallop, *J. Med. Chem.* **1996**, *39*, 1601.

[6] B. J. Egner, S. Rana, H. Smith, N. Bouloc, J. G. Frey, W. S. Brocklesby, M. Bradley, *Chem. Commun*. **1997**, 735.

[7] a) R. W. Armstrong, P. A. Tempest, J. F. Cargill, *Chimia* **1996**, *50*, 258; b) E. J. Moran, S. Sarshar, J. F. Cargill, M. M. Shahbaz, A. Lio, A. M. M. Mjalli, R. W. Armstrong, *J. Am. Chem. Soc.* **1995**, *117*, 10787; c) K. C. Nicolaou, X.-Y. Xiao, Z. Parandoosh, A. Senyei, M. P. Nova, *Angew. Chem.* **1995**, *107*, 2476; *Angew. Chem. Int. Ed. Engl.* **1995**, *34*, 2289; d) X.-Y. Xiao, C. Zhao, H. Potash, M. P. Nova, *ibid.* **1997**, *109*, 799 and **1997**, *36*, 780.

[8] In our hands reactions performed above 50 °C with the containers mentioned in ref. [11] sporadically resulted in the loosening of the container tops and loss of resin from the container. More details are available from the manufacturer.

[9] H. Rink, *Tetrahedron Lett.* **1987**, *28*, 3787.

[10] The resin (ca. 70 mg) was placed in a PC obtained from IRORI Quantum Microchemistry, 11025 N. Torrey Pines Road, La Jolla, CA 92307 (USA). Alternative PCs have been described: R. A. Houghten, *Proc. Natl. Acad. Sci. USA* **1985**, *82*, 5131. The repetitive weighing was facilitated by employing 96-well plates to hold the empty PCs, and the resin was manually partitioned with an Accofil Powder Filler, available from M & O Perry Industries, Inc. 591 No. Smith Avenue Corona, CA 91720 (USA). The colored glass beads were obtained from a local fabric store and are colloquially termed "seed beads". The PCs are considerably more transparent for the lighter tinted colors, and the beads are easier to visualize when the container is moist with solvent. The caps are available in six separate colors from VWR as Eppendorf "Safe-Lock" microcentrifuge tubes (0.5 mL), are can be easily attached and detached by hand without the need for a hand tool. To obtain twelve different cap colors, a degenerate set of colors were prepared by etching the top surface of the cap.

[11] A glass-fritted vessel with a screw cap or an amber jar with a screw cap is routinely used.

[12] HPLC analysis was performed on a Hewlett-Packard ODS Hypersil column (5 μM, 4 × 125 mm) with monitoring at 220 nm. Elution was carried out with a solvent mixture A/B (A = 0.1 % TFA in water, B = 0.1 % TFA in acetonitrile); the amount of A was increased from 20 to 80 % over 20 min. A mass spectrum in the positive-ionization mode was recorded for all samples on a Hewlett-Packard electrospray mass spectrometer; selected ES-MS data: *m*/*z*: **A1** 374 [373], **B2** 348 [347], **C3** 396 [395], **D4** 510, 512 [510], **E7** 464 [463], **E9** 480 [479], **F7** 480 [479], **F10** 499 [498], **G5** 424 [424], **G11** 460 [459], **H10** 492 [491], **C12** 364 [363].

Ligand Self-Recognition in the Self-Assembly of a $[\{Cu(L)\}_2]^{2+}$ Complex: The Role of Chirality**

M. Athar Masood, Eric J. Enemark, and T. Daniel P. Stack*

A large interest in the assembly of discrete molecular architectures from smaller molecules has developed in recent years with the realization that these assemblies may show interesting chemical, physical, and mechanical properties.[1] Examples of metal-assisted self-assembly of independent ligands to form helices,[2–8] grids,[9] knots,[10, 11] cylinders,[12] platonic shapes,[13, 14] and circular helicates[15] quantitatively with labile metals represent impressive feats of molecular design and assembly.[3, 16–19] Many forms of supramolecular complexes are intrinsically chiral, even if the individual

[*] Prof. T. D. P. Stack, Dr. M. A. Masood, E. J. Enemark
Department of Chemistry, Stanford University
Stanford, CA 94305-5080 (USA)
Fax: (+1) 650-725-0259
E-mail: stack@leland.stanford.edu

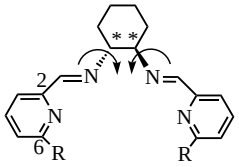
[**] Financial Support of this research is from the National Institutes of Health (GM-50730) and the Shell Foundation.

 © WILEY-VCH Verlag GmbH, D-69451 Weinheim, 1998 1433-7851/98/3707-0928 $ 17.50+.50/0

ligands are achiral. Achiral ligands can yield a racemic mixture of complexes such as a mixture of left- and right-handed helices under equilibrium conditions. Appropriately designed, enantiopure, polynucleating ligands can stereospecifically form a single, homochiral isomer[20] through "chiral-directed self-assembly", in which the chirality of all metal centers is identical and is dictated by ligand chirality.[1] Helices of this type have been synthesized quantitatively in solution with labile metals.[4, 6, 21] The homochirality of these complexes results from the enantiomeric purity of the starting components.

A more complex and perhaps more interesting situation arises when a mixture of ligands is used. In such systems, more types of complexes are possible. The biasing of ligand components to form a specific structural motif at equilibrium requires selective ligand recognition. Conceptually, the simplest form of selectivity is one of self-recognition whereby a single ligand type from a mixture of ligands is incorporated into each complex. An example of ligand self-recognition from a mixture of ligands with different numbers of chelating groups has been reported.[22] An example based on differences in distance between metal-chelating groups of ligands has also been reported.[23] A system is presented here that exhibits ligand self-recognition based solely on chirality in which the reaction of a racemic ligand mixture with metal ions generates only homochiral complexes.

The design of the ligand L^{6R} (Figure 1), meets three objectives needed for this study: conformational rigidity, preclusion of tetradentate ligation of a single metal, and chirality. These objectives are all accomplished by the



$^{RR}L^{6Br}$ R=Br(*R*,*R*)
$^{rac}L^{6Br}$ R=Br(*rac*)
$^{RR}L^{6H}$ R=H(*R*,*R*)
$^{rac}L^{6H}$ R=H(*rac*)

Figure 1. Nomenclature of the ligands used in this work.

incorporation of *trans*-1,2-diaminocyclohexane into the ligand backbone. Both the racemic ligands $^{rac}L^{6R}$ (R = Br, H) and the enantiomerically pure ligands[24] $^{RR}L^{6R}$ (R = Br, H) are readily prepared by Schiff base condensation of the appropriate diamine and 6-R-2-pyridinecarboxyaldehyde (R = Br,[25, 26] H). These ligands have geometric constraints that preclude tetradentate chelation of a single, first-row transition metal,[27, 28] and have only two effective degrees of rotational freedom, each about a N–C single bond (Figure 1). Models suggest that a binuclear metal complex, $[(ML)_2]$ complex could be generated from metals that prefer tetrahedral coordination such as Cu^{I}.

In $[D_6]$DMSO ^{1}H NMR titrations of $[Cu^{I}(MeCN)_4]^+$ with $^{rac}L^{6R}$ show the formation of a single metal complex with D_2 symmetry at a metal:ligand ratio of 2:2. As an addition of more ligand to this 2:2 complex does not result in the formation of any new metal complex, a cooperative assembly process is indicated. The existence of a single metal species suggests that the enantiomeric forms of $^{rac}L^{6Br}$ sort to form exclusively either a heterochiral, binuclear complex, $[Cu2(^{RR}L^{6Br})(^{SS}L^{6Br})]^{2+}$, or a racemic mixture of stereospecific, homochiral[6, 20] binuclear complexes, Λ,Λ-$[\{Cu(^{RR}L^{6Br})\}_2]^{2+}$ and Δ,Δ-$[\{Cu(^{SS}L^{6Br})\}_2]^{2+}$ (vide infra). The identical ^{1}H NMR spectrum of the metal complex compared with that of a titration with enantiopure ligand $^{RR}L^{6Br}$ indicates that a racemic mixture of homochiral metal complexes is formed [Eq. (1)]. The bromine atom of L^{6Br} does not appear

$$^{RR}L^{6Br} + {}^{SS}L^{6Br} + 2\ Cu^{+} \longrightarrow \begin{matrix} 1/2\ \Lambda,\Lambda\text{-}[\{Cu(^{RR}L^{6Br})\}_2]^{2+} \\ 1/2\ \Delta,\Delta\text{-}[\{Cu(^{SS}L^{6Br})\}_2]^{2+} \end{matrix} \quad (1)$$

$$2\ ^{RR}L^{6Br} + 2\ Cu^{+} \longrightarrow \Lambda,\Lambda\text{-}[\{Cu(^{RR}L^{6Br})\}_2]^{2+} \quad (2)$$

$$2\ ^{RR}L^{6H} + 2\ Cu^{+} \longrightarrow \Lambda,\Lambda\text{-}[\{Cu(^{RR}L^{6H})\}_2]^{2+} \quad (3)$$

important for the stereoselectivity[20] of the assembly, because $^{RR}L^{6H}$ also forms a single D_2-symmetric species in solution [Eqs. (2) and (3)]. In contrast, the bromine atom plays an important role in ligand self-recognition; $^{rac}L^{6H}$ assembles to two diastereomeric species in solution while $^{rac}L^{6Br}$ exclusively forms one enantiomeric pair.[29]

Crystal structures of the products of the equimolar reaction of Cu^{I} with either $^{RR}L^{6Br}$ or $^{rac}L^{6Br}$ support the interpretation of the behavior in solution. The enantiopure ligand generates a stereospecific binuclear species (Λ,Λ-$[\{Cu(^{RR}L^{6Br})\}_2]^{2+}$, Figure 2),[26] while $^{rac}L^{6Br}$ leads to a racemic mixture of homochiral binuclear species (Λ,Λ-$[\{Cu(^{RR}L^{6Br})\}_2]^{2+}$ and Δ,Δ-$[\{Cu(^{SS}L^{6Br})\}_2]^{2+}$) in the unit cell.[26] Comparison of the structures of the two $[\{Cu(^{RR}L^{6Br})\}_2]^{2+}$ entities indicates that they are nearly isostructural;[30] the greatest deviations occur in the positions of the pyridine rings. The complexes are effectively C_2-symmetric with a pseudo C_2 axis perpendicular to the Cu–Cu vector (Figure 2). The complex is significantly distorted from the idealized D_2 symmetry of a binuclear double helix; the pseudo twofold axes of the two metal

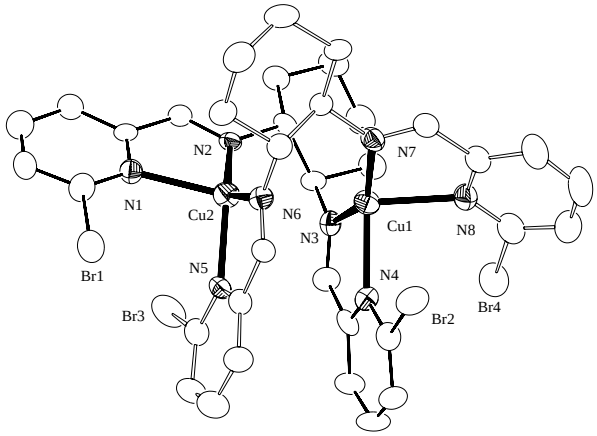


Figure 2. An ORTEP representation of the structure of Λ,Λ-$[\{Cu(^{RR}L^{6Br})\}_2]^{2+}$ nearly perpendicular to the Cu–Cu vector (50% probability thermal ellipsoids). Shaded ellipsoids and atom labels for the trigonal monopyramidal coordination environment of each copper center are given. One ligand is drawn with solid bonds while the other is drawn with open bonds. Selected distances [Å]: N3–Cu1, 1.968(5); N3–Cu1, 1.968(5); N4–Cu1, 2.145(5); N7–Cu1, 1.966(5); N1–Cu2, 2.186(6); N2–Cu2, 1.966(5); N5–Cu2, 2.096(5); N6–Cu2, 1.993(5).

 © WILEY-VCH Verlag GmbH, D-69451 Weinheim, 1998 1433-7851/98/3707-0929 $ 17.50+.50/0

coordination spheres (bisecting N4-Cu1-N8 and N1-Cu2-N5) are not collinear.[31] This distortion makes the complex qualitatively different from a traditional helical or side-by-side binuclear structure.[4] However, the presence of identical chirality at each metal center within a given complex supports a helix designation. A clear relationship between ligand and metal chirality is found in these homochiral structures: the (*R*) and (*S*) configurations of the ligand stereocenters solely associate with the *Λ* and *Δ* metal configurations, respectively, which demonstrates the stereospecificity of the reaction.[32, 33]

The coordination geometry of each metal is best described as distorted trigonal monopyramidal rather than tetrahedral (Figure 2). The coordinated atoms in the trigonal plane (equatorial ligand atoms) consist of one pyridine (N4; N5) and two imine nitrogen atoms (N3, N7; N2, N6), while a pyridine nitrogen atom (N1; N8) occupies the axial position. The two monopyramidal coordination spheres are arranged in a antiparallel sense; the trigonal basal planes are oriented at 18° to each other. The Cu – Cu distance is short at 3.1 Å. One pyridine nitrogen atom of each ligand occupies an axial position at one copper center and an equatorial position at the other. The two pyridine – imine chelate planes within a single ligand are close to perpendicular at 80°. The equatorial pyridine rings of the two ligands are π-stacked and almost in van der Waals contact.

The D_2 symmetry suggested by the ^{1}H NMR spectrum of both $[\{Cu(^{rac}L^{6Br})\}_2]^{2+}$ and $[\{Cu(^{RR}L^{6Br})\}_2]^{2+}$ is not consistent with the distinct equatorial and axial arrangement of the pyridine rings displayed in the solid-state structures. Rapid interconversion of the axial and equatorial pyridine groups must occur in solution. While a rapid dissociative mechanism cannot be excluded, a nondissociative rearrangement is presumed. Within a single complex, simultaneous inward disrotatory motion of all 4 N−C single bonds by 90° not only maintains bonding to the metal centers while interconverting the axial and equatorial pyridine moieties, but also maintains the chirality at each metal center. The lack of broadening of the ^{1}H resonances at 200 K in [D$_6$]acetone indicates that this process must have a low energy barrier. Molecular dynamic calculations with $[\{Cu(^{RR}L^{6Br})\}_2]^{2+}$ support this interconversion mechanism with a D_2-symmetric helix-like transition state.[34]

The most interesting aspect of this system is the ligand self-recognition in the assembly process. The reaction of $^{rac}L^{6Br}$ with Cu^{I} ions leads to two discrete homochiral, stereospecific metal complexes: *Λ*,*Λ*-$[\{Cu(^{RR}L^{6Br})\}_2]^{2+}$ and *Δ*,*Δ*-$[\{Cu(^{SS}L^{6Br})\}_2]^{2+}$. Identification of the key structural features that promote such behavior is important for future design of other selective assembling systems. While stereospecifity and self-recognition are not required to occur simultaneously, assembling components that are rigid and project chirality almost assures a direct correlation. This is readily visualized by the construction of a cube (Figure 3) or by analogy to the classic example of "la coupe du roi".[35] Two rigid homochiral units combine to generate a compact structure (the cube in Figure 3) while two heterochiral units assemble to a structure that is less compact. As complexes generally adopt configurations that minimize the surface-to-volume ratio (maximizing intramolecular van der Waals interactions), rigid building components should preferentially assemble to homochiral, stereospecific complexes. Such is the case of the complex $[\{Cu(^{rac}L^{6Br})\}_2]^{2+}$, which has building components that possess both limited flexibility and spacially projected chirality analogous to the building components of the cube (Figure 3).

This analysis would suggest that all conformationally restricted ligands that project their chirality would exhibit ligand self-recognition and assemble in a homochiral fashion. This is not the case with $^{rac}L^{6H}$, a ligand with similar structural attributes to $^{rac}L^{6Br}$. This ligand forms both homo- and heterochiral complexes in solution in a ratio of approximately 3:1 [Eq. (4)]. The enhanced ligand selectivity exhibited by

$$^{RR}L^{6H} + {}^{SS}L^{6H} + 2\ Cu^{+} \longrightarrow \begin{array}{l} 3/8\ \Lambda,\Lambda\text{-}[\{Cu(^{RR}L^{6H})\}_2]^{2+} \\ 3/8\ \Delta,\Delta\text{-}[\{Cu(^{SS}L^{6H})\}_2]^{2+} \\ 2/8\ \Lambda,\Lambda\text{-}[Cu_2(^{RR}L^{6H})(^{SS}L^{6H})]^{2+} \end{array} \quad (4)$$

$^{rac}L^{6Br}$ relative to $^{rac}L^{6H}$ probably does not arise from favorable nonbonded interactions of the bromine atoms within the complex formed, but rather through destabilization of unformed heterochiral complexes. With such energetics operative, such a system is not necessarily displaying "self-selective" behavior, but perhaps more accurately "opposite-deselective" behavior.

Experimental Section

The ligands $^{RR}L^{6H}$ and $^{rac}L^{6H}$ were prepared according to literature methods.[21] The ligands $^{RR}L^{6Br}$ and $^{rac}L^{6Br}$ were synthesized by reaction of

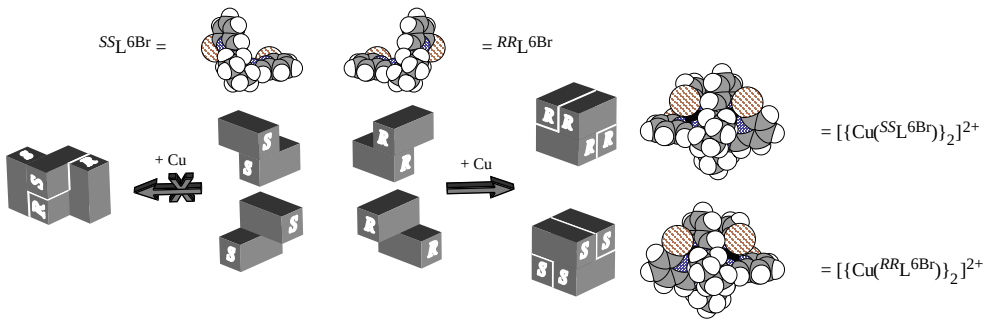


Figure 3. Self-assembly of a racemic mixture of rigid fragments to either a discrete heterochiral (Z-shaped) or homochiral (cube-shaped) species. The cube-shaped species is more compact. Space-filling drawings of the ligands ($^{RR}L^{6Br}$ and $^{SS}L^{6Br}$) and complexes (*Λ*,*Λ*-$[\{Cu(^{RR}L^{6Br})\}_2]^{2+}$ and *Δ*,*Δ*-$[\{Cu(^{SS}L^{6Br})\}_2]^{2+}$), are related to the appropriate rigid fragments and assembled products.

 © WILEY-VCH Verlag GmbH, D-69451 Weinheim, 1998 1433-7851/98/3707-0930 $ 17.50+.50/0

6-bromo-2-pyridine-carboxyaldehyde[25] with enantiomerically pure[24] or racemic *trans*-(1,2)-diaminocyclohexane (0.5 equiv), respectively. The metal complexes were prepared by equimolar reaction of ligand with $[Cu(MeCN)_4]CF_3SO_3$ in 1:1 CH_2Cl_2:CH_3CN, followed by evaporation of the solvent.

Crystal data for $[\{Cu(^{RR}L^{6Br})\}_2](CF_3SO_3)_2 \cdot CH_3CN \cdot (C_2H_5)_2O$:[36] Crystals were grown by slow diffusion of ether into a CH_2Cl_2:MeCN solution of the complex. Space group $P2_12_12_1$ (no. 19) with cell constants based on 9999 reflections ($4.5^\circ < 2\theta < 52.6^\circ$): $a = 12.3865(2)$, $b = 13.9288(1)$, $c = 32.2188(3)$ Å, $V = 5558.68(9)$ Å^3, $Z = 4$. Of 27076 reflections collected at 155 K, ($4.5^\circ < 2\theta < 52.6^\circ$), 10026 were unique. Full matrix refinement of 667 variables based on 6964 reflections with $F_o^2 > 3\sigma F_o^2$ and σ weights converged with final residuals of $R(R_w) = 0.036(0.039)$. The absolute configuration of the molecule was assigned by the chirality of the ligand (*R,R*).

Crystal data for $[\{Cu(^{rac}L^{6Br})\}_2](CF_3SO_3)_2 \cdot CH_3OH$:[36] Crystals were grown by slow diffusion of ether into a methanol solution of the complex. Space group $P2_1/c$ (no. 14) with cell constants based on 5586 reflections ($4.5^\circ < 2\theta < 47^\circ$): $a = 11.702(1)$, $b = 20.898(1)$, $c = 20.015(1)$ Å, $\beta = 92.725(1)^\circ$, $V = 4889.0(5)$ Å^3, $Z = 4$. Of 20478 reflections collected at 156 K ($4.5^\circ < 2\theta < 47.0^\circ$), 4795 were unique. Full matrix refinement of 613 variables based on 7227 reflections with $F_o^2 > 3\sigma F_o^2$ and σ weights converged with final residuals of $R(R_w) = 0.029(0.035)$. The $[\{Cu(^{RR}L^{6Br})\}_2]^{2+}$ and $[\{Cu(^{SS}L^{6Br})\}_2]^{2+}$ moieties are related by inversion.

Mass spectra were recorded at the University of California, San Francisco. ^{1}H NMR measurement conditions: 400 MHz, [D$_6$]DMSO, 25 °C, TMS (unless otherwise stated).

$^{rac}L^{6Br}$ and $^{RR}L^{6Br}$: ^{1}H NMR ($CDCl_3$): $\delta = 1.45$ (t, 2 H); 1.80 (s, 4 H); 1.90 (s, 2 H); 2.50 (s, 6 H); 2.75 (t, 4 H); 3.50 (t, 2 H); 7.45 (d, 2 H); 7.55 (t, 2 H); 7.90 (d, 2 H). UV/Vis (CH_2Cl_2): λ_{max} (ε, $M^{-1}cm^{-1}$) = 273 (10000), 232 nm (12500). Fast-atom-bombardment FABMS: $m/z = 451.0$ (found); 448.0 (calcd exact mass), 451.0 (calcd major isotope peak for $[C_{18}H_{19}Br_2N_4]^+$).

$^{rac}L^{6H}$ and $^{RR}L^{6H}$: ^{1}H NMR: $\delta = 1.48$ (m, 2 H); 1.80 (m, 6 H); 3.50 (m, 2 H); 7.38 (t, 2 H); 7.79 (t, 2 H); 7.85 (d, 2 H); 8.22 (s, 2 H; imine); 8.55 (d, 2 H). FABMS: $m/z = 293.1$ (found); 293.2 (calcd for $[C_{18}H_{21}N_4]^+$).

$[\{Cu(^{RR}L^{6Br})\}_2](CF_3SO_3)_2$ and $[\{Cu(^{rac}L^{6Br})\}_2](CF_3SO_3)_2$ ($M_r = 1325.6$): ^{1}H NMR: $\delta = 1.4$ (t, 1 H); 1.6 – 1.9 (pseudo dt, 2 H); 2.15 (d, 1 H); 4.05 (split s, 1 H); 7.75 (d, 1 H); 7.95 (t, 1 H); 8.9 (s, 1 H). LSIMS (LSI = liquid-secondary-ion): $m/z = 1176.7$ (found), 1177 (calcd for major isotope peak for $[(C_{18}H_{18}Br_2N_4)_2Cu_2(CF_3O_3S)]^+$); 512.9 (found), 513 (calcd major isotope peak for $[(C_{18}H_{18}Br_2N_4)Cu]^+$).

$[\{Cu(^{RR}L^{6H})\}_2](CF_3SO_3)_2$ and $[\{Cu(^{rac}L^{6H})\}_2](CF_3SO_3)_2$ ($M_r = 1010.0$): ^{1}H NMR: homochiral species: $\delta = 1.28$ (br. s, 2 H); 1.52 (br. s, 2 H); 1.75 (br. s, 2 H); 3.84 (br. s, 2 H); 7.54 (d, 2 H); 7.66 (d, 2 H); 7.97 (t, 2 H); 8.07 (d, 2 H); 8.75 (s, 2 H; imine). Heterochiral species for $^{rac}L^{6H}$ (only resonances distinguishable from the homochiral species are recorded): $\delta = 3.71$ (m, 1 H); 4.71 (m, 1 H); 7.88 (t, 2 H); 8.10 (m, 2 H); 8.30 (t, 2 H); 8.70 (s, 2 H); 9.12 (d, 2 H; imine). LSIMS: $m/z = 859.2$ (found), 859.3 (calcd major isotope peak for $[(C_{18}H_{20}N_4)_2Cu_2(CF_3O_3S)]^+$); 355.2 (found), 355.2 (calcd major isotope peak for $[(C_{18}H_{20}N_4)Cu]^+$).

Received: August 13, 1997
Revised version: December 12, 1997 [Z 10811 IE]
German version: *Angew. Chem.* **1998**, *110*, 973 – 977

Keywords: chirality · copper · N ligands · self-assembly · supramolecular chemistry

[1] J.-M. Lehn, *Supramolecular Chemistry: Concepts and Perspectives*, VCH, Weinheim, **1995**.
[2] R. C. Scarrow, D. L. White, K. N. Raymond, *J. Am. Chem. Soc.* **1985**, *107*, 6540 – 6546.
[3] J.-M. Lehn, A. Rigault, J. Siegel, J. Harrowfield, B. Chevrier, D. Moras, *Proc. Natl. Acad. Sci. USA* **1987**, *84*, 2565 – 2569.
[4] W. Zarges, J. Hall, J.-M. Lehn, C. Bolm, *Helv. Chim. Acta* **1991**, *74*, 1843 – 1852.
[5] R. Krämer, J.-M. Lehn, A. De Cian, J. Fischer, *Angew. Chem.* **1993**, *105*, 764 – 768; *Angew. Chem. Int. Ed. Engl.* **1993**, *32*, 703 – 706.
[6] E. J. Enemark, T. D. P. Stack, *Angew. Chem.* **1995**, *107*, 1082 – 1084; *Angew. Chem. Int. Ed. Engl.* **1995**, *34*, 996 – 998.
[7] M. Albrecht, S. Kotila, *Angew. Chem.* **1995**, *107*, 2285 – 2287; *Angew. Chem. Int. Ed. Engl.* **1995**, *34*, 2134 – 2136.
[8] E. J. Enemark, T. D. P. Stack, *Inorg. Chem.* **1996**, *35*, 2719 – 2720.
[9] G. S. Hanan, C. R. Arana, J.-M. Lehn, D. Fenske, *Angew. Chem.* **1995**, *107*, 1191 – 1193; *Angew. Chem. Int. Ed. Engl.* **1995**, *34*, 1122 – 1124.
[10] C. O. Dietrich-Buchecker, J.-P. Sauvage, *J. Am. Chem. Soc.* **1984**, *106*, 3043 – 3046.
[11] C. O. Dietrich-Buchecker, J.-P. Sauvage, N. Armaroli, P. Ceroni, V. Balzani, *Angew. Chem.* **1996**, *108*, 1190 – 1193; *Angew. Chem. Int. Ed. Engl.* **1996**, *35*, 1119 – 1121.
[12] P. Baxter, J.-M. Lehn, A. De Cian, J. Fischer, *Angew. Chem.* **1993**, *105*, 92 – 95; *Angew. Chem. Int. Ed. Engl.* **1993**, *32*, 69 – 72.
[13] R. W. Saalfrank, R. Burak, A. Breit, D. Stalke, R. Herbst-Irmer, J. Daub, M. Porsch, E. Bill, M. Müther, A. X. Trautwein, *Angew. Chem.* **1994**, *106*, 1697 – 1699; *Angew. Chem. Int. Ed. Engl.* **1994**, *33*, 1621 – 1623.
[14] T. Beissel, R. E. Powers, K. N. Raymond, *Angew. Chem.* **1996**, *108*, 1166 – 1168; *Angew. Chem. Int. Ed. Engl.* **1996**, *35*, 1084 – 1086.
[15] B. Hasenknopf, J.-M. Lehn, B. O. Kneisel, G. Baum, D. Fenske, *Angew. Chem.* **1996**, *108*, 1987 – 1990; *Angew. Chem. Int. Ed. Engl.* **1996**, *35*, 1838 – 1840.
[16] D. S. Lawrence, T. Jiang, M. Levett, *Chem. Rev.* **1995**, *95*, 2229 – 2260.
[17] J. P. Schneider, J. W. Kelly, *Chem. Rev.* **1995**, *95*, 2169 – 2187.
[18] R. Ziessel, M.-T. Youinou, *Angew. Chem.* **1993**, *105*, 929 – 932; *Angew. Chem. Int. Ed. Engl.* **1993**, *32*, 877 – 880.
[19] E. C. Constable, A. M. W. C. Thompson, P. Harveson, L. Macko, M. Zehnder, *Chem. Eur. J.* **1995**, *1*, 360 – 367.
[20] Homochirality refers to a metal complex in which all ligand stereocenters are of identical chirality. Stereospecificity refers to the generation of metal configurations that correlate with the chirality of the associated ligand.
[21] C. R. Woods, M. Benaglia, F. Cozzi, J. S. Siegel, *Angew. Chem.* **1996**, *108*, 1985 – 1987; *Angew. Chem. Int. Ed. Engl.* **1996**, *35*, 1830 – 1833.
[22] R. Krämer, J.-M. Lehn, A. Marquis-Rigault, *Proc. Natl. Acad. Sci. USA* **1993**, *90*, 5394 – 5398.
[23] D. L. Caulder, K. N. Raymond, *Angew. Chem.* **1997**, *109*, 1508 – 1510; *Angew. Chem. Int. Ed. Engl.* **1997**, *36*, 1439 – 1442.
[24] T. A. Whitney, *J. Org. Chem.* **1980**, *45*, 4214 – 4216.
[25] J. E. Parks, B. E. Wagner, R. H. Holm, *J. Organomet. Chem.* **1973**, *56*, 53 – 66.
[26] See experimental section for details.
[27] G. C. van Stein, G. van Koten, K. Vrieze, C. Brevard, A. L. Spek, *J. Am. Chem. Soc.* **1984**, *106*, 4486 – 4492.
[28] G. C. van Stein, G. van Koten, K. Vrieze, C. Brevard, *Inorg. Chem.* **1984**, *23*, 4269 – 4278.
[29] The ^{1}H NMR shows an approximately 3:1 mixture of two products, one the racemic mixture of homochiral complexes and the other a single heterochiral complex. Comparison of the chemical shifts with those from studies with the enantiopure ligand indicates that the major product is the homochiral species.
[30] The minimum root-mean-square difference for all non-hydrogen atoms is 0.24 Å.
[31] G. Bidan, B. Divisia-Blohorn, M. Lapkowski, J.-M. Kern, J.-P. Sauvage, *J. Am. Chem. Soc.* **1992**, *114*, 5986 – 5994.
[32] IUPAC, *IUPAC Nomenclature of Inorganic Chemistry*, Butterworths, London, **1970**.
[33] R. E. Ernst, M. J. O'Connor, R. H. Holm, *J. Am. Chem. Soc.* **1967**, *89*, 6104 – 6113.
[34] The molecular dynamics calculations (in vacuum at 297 K) were performed on a CACHE Scientific Workstation. While the parameters of the copper center for these calculations are certainly approximate, the calculations provide a way to visualize this facile interconversion.
[35] F. A. L. Anet, S. S. Miura, J. Siegel, K. Mislow, *J. Am. Chem. Soc.* **1983**, 1419 – 1426. As indicated by a reviewer, this particular example is not an authentic example of "la coupe du roi" in which an achiral object possessing at least S_4 symmetry is cut into two homochiral halves. In the case presented here, the assembly of two homochiral objects is still a chiral object.
[36] General crystallographic details: data collected on a Siemens SMART diffractometer with graphite-monochromated $Mo_{K\alpha}$ radiation ($\lambda =$

0.71069 Å). The structures were solved by direct methods (SHELX-86) and refined with teXsan (Crystal Structure Analysis Package, Molecular Structure Corporation). All non-hydrogen atoms were refined anisotropically. Hydrogen atoms were positioned at an idealized geometry 0.95 Å from their parent atoms before the last cycle of refinement. Further details on the crystal structure investigations may be obtained from the Fachinformationszentrum Karlsruhe, D-76344 Eggenstein-Leopoldshafen, Germany (fax: (+49) 7247-808-666; e-mail: crysdata@fiz-karlsruhe.de), on quoting the depository number CSD-406212 for $[\{Cu(^{RR}L^{6Br})\}_2](CF_3SO_3)_2 \cdot MeCN \cdot Et_2O$ and CSD-406213 for $[\{Cu(^{rac}L^{6Br})\}_2](CF_3SO_3)_2 \cdot MeOH$).

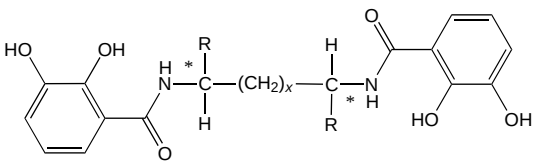


Figure 1. Structure of the bis-catecholamide ligands of this study (nomenclature given in Table 1).

Table 1. Nomenclature of the ligands and complexes.

x	R	*	Ligand	Product
0	H	–	$L_{et}^{H,H}$	Λ,Λ-$[Ga_2(L_{et}^{H,H})_3]^{6-}$/$\Delta,\Delta$-$[Ga_2(L_{et}^{H,H})_3]^{6-}$
0	Me	*S*	$^{SS}L_{et}^{Me,Me}$	$\Lambda,\Lambda,\Lambda,\Lambda$-$[Ga_4(^{SS}L_{et}^{Me,Me})_6]^{12-}$
0	Me	*rac*	$^{rac}L_{et}^{Me,Me}$	$\Lambda,\Lambda,\Lambda,\Lambda$-$[Ga_4(^{SS}L_{et}^{Me,Me})_6]^{12-}$/$\Delta,\Delta,\Delta,\Delta$-$[Ga_4(^{RR}L_{et}^{Me,Me})_6]^{12-}$
1	H	–	$L_{pr}^{H,H}$	Λ,Λ-$[Ga_2(L_{pr}^{H,H})_3]^{6-}$/$\Delta,\Delta$-$[Ga_2(L_{pr}^{H,H})_3]^{6-}$
1	Me	*R*	$^{RR}L_{pr}^{Me,Me}$	Λ,Λ-$[Ga_2(^{RR}L_{pr}^{Me,Me})_3]^{6-}$
1	Me	*rac*	$^{rac}L_{pr}^{Me,Me}$	$[Ga_2(^{RR}L_{pr}^{Me,Me})_3]^{6-} + [Ga_2(^{RR}L_{pr}^{Me,Me})_2(^{SS}L_{pr}^{Me,Me})]^{6-} + [Ga_2(^{RR}L_{pr}^{Me,Me})(^{SS}L_{pr}^{Me,Me})_2]^{6-} + [Ga_2(^{SS}L_{pr}^{Me,Me})_3]^{6-}$

Stereospecificity and Self-Selectivity in the Generation of a Chiral Molecular Tetrahedron by Metal-Assisted Self-Assembly**

Eric J. Enemark and T. Daniel P. Stack*

By design, a complex generated by metal-assisted self-assembly possesses a preconceived metal–ligand ratio (for example M_nL_n). However, several stoichiometries satisfy this ratio (M_2L_2, M_3L_3, M_4L_4,...), and recent results demonstrate that the actual stoichiometry of a supramolecular metal complex cannot be definitively predicted. A linear tris-bidentate ligand that forms a trinuclear triple helix with octahedrally coordinated metals (M_3L_3)[1] also generates a circular helix (M_5L_5) under different conditions.[2] More recently one bis-bidentate ligand generated a mixture of three rapidly equilibrating metal complexes $[(CuL)_n]^{n+}$ (n = 1–3).[3] Another ligand has been shown to generate both $[(FeL)_3]^{6+}$ and $[(FeL)_4]^{8+}$ complexes simultaneously.[4] In addition a binuclear $[(AgL_a)_2]^{2+}$ complex and a trinuclear $[(AgL_b)_3]^{3+}$ complex, where L_a and L_b are very similar bis-oxazoline ligands, have been crystallographically characterized.[5] The variety of stoichiometries observed with similar, or even identical ligands indicates that the factors discriminating such stoichiometries are rather subtle.

Supramolecular assemblies generated from octahedrally coordinated metals and bis-bidentate ligands include $[M_{2n}L_{3n}]$ complexes, where n can take the value 1,[6–17] 2,[18–22] and 4,[23] corresponding to 2:3, 4:6, and 8:12 complexes. Our previous investigations of the gallium complexes of a family of systematically varied bis(2,3-dihydroxybenzamide) ligands (Figure 1, Table 1, bis-catecholamide ligands) exclusively identified metal complexes of 2:3 stoichiometry: $[Ga_2L_3]^{6-}$ ($L = L_{et}^{H,H}$,[11, 24] $L_{pr}^{H,H}$,[9, 25] or $^{RR}L_{pr}^{Me,Me}$[9]). In contrast, our current work with $^{SS}L_{et}^{Me,Me}$ and $^{rac}L_{et}^{Me,Me}$ (rac = racemic) ligands demonstrates a 4:6 stoichiometry [Eq. (1)], in a structure that has been described as an "adamantanoid"[19] or as a tetrahedral cluster.[22]

$$4\ Ga^{3+} + 6\ ^{SS}L_{et}^{Me,Me} \rightarrow \Lambda,\Lambda,\Lambda,\Lambda\text{-}[Ga_4(^{SS}L_{et}^{Me,Me})_6]^{12-} \quad (1)$$

The $[Ga_4(^{SS}L_{et}^{Me,Me})_6]^{12-}$ complex has been characterized in the solid and in solution and is a stereoselectively formed tetrahedral cluster with T symmetry. More impressive is the exclusive assembly of an enantiomeric pair of homochiral tetrahedral clusters when the ligand is racemic rather than enantiopure [Eq. (2, 3)]. For a polynuclear species the term

$$4(m+n)\ Ga^{3+} + 6m\ ^{SS}L_{et}^{Me,Me} + 6n\ ^{RR}L_{et}^{Me,Me} \rightarrow m\ \Lambda,\Lambda,\Lambda,\Lambda\text{-}[Ga_4(^{SS}L_{et}^{Me,Me})_6]^{12-} + n\ \Delta,\Delta,\Delta,\Delta\text{-}[Ga_4(^{RR}L_{et}^{Me,Me})_6]^{12-} \quad (2)$$

$$4\ Ga^{3+} + 6\ ^{SS}L_{et}^{Me,Me} + 6\ ^{RR}L_{et}^{Me,Me} \not\rightarrow [Ga_4(^{SS}L_{et}^{Me,Me})_a(^{RR}L_{et}^{Me,Me})_{6-a}]^{12-} \quad (0 \le a \le 6) \quad (3)$$

homochiral refers to a metal complex that meets two criteria: 1) each ligand has the same chirality, and 2) all metal centers are in identical configurations. Any metal complex that does not simultaneously satisfy both criteria is considered to be heterochiral.

Reaction of Ga^{3+} and enantiopure $^{SS}L_{et}^{Me,Me}$ in the ratio 2:3 generates a single, highly symmetric, metal complex as demonstrated by an ^1H NMR spectrum that contains a single set of resonances. The complex has a tetrahedral structure of 4:6 stoichiometry with a Λ configuration at each metal center: $\Lambda,\Lambda,\Lambda,\Lambda$-$[Ga_4(^{SS}L_{et}^{Me,Me})_6]^{12-}$. The crystal structure of $(Me_4N)_{12}[Ga_4(^{SS}L_{et}^{Me,Me})_6] \cdot 42.5\,H_2O$ (Figure 2) shows the metal complex to be on a site with T point symmetry. A threefold axis passes through each metal center, and a twofold axis bisects each ligand. One-third of a metal center and half of a ligand comprise the unique portion of the metal complex. All four metal centers possess identical Λ configurations defined by the configuration of the enantiopure ligand.[26, 27] An

[*] Prof. T. D. P. Stack, E. J. Enemark
Department of Chemistry, Stanford University
Stanford, CA 94305-5080 (USA)
Fax: (+1) 650-725-0259
E-mail: stack@leland.stanford.edu

[**] This research was supported by the Shell Foundation and the Stanford Office of Technology and Licensing. We thank Dr. Fred Hollander and Dr. Ryan Powers at the University of California (CHEXRAY Berkeley) for collection of the X-ray diffraction data, and the University of California Mass Spectrometry Facility (Department of Pharmaceutical Chemistry, San Francisco). Supporting information for this article is available on the www under http://www/wiley-vch.de/home/angewandte/ or from the author.

 © WILEY-VCH Verlag GmbH, D-69451 Weinheim, 1998 1433-7851/98/3707-0932 $ 17.50+.50/0

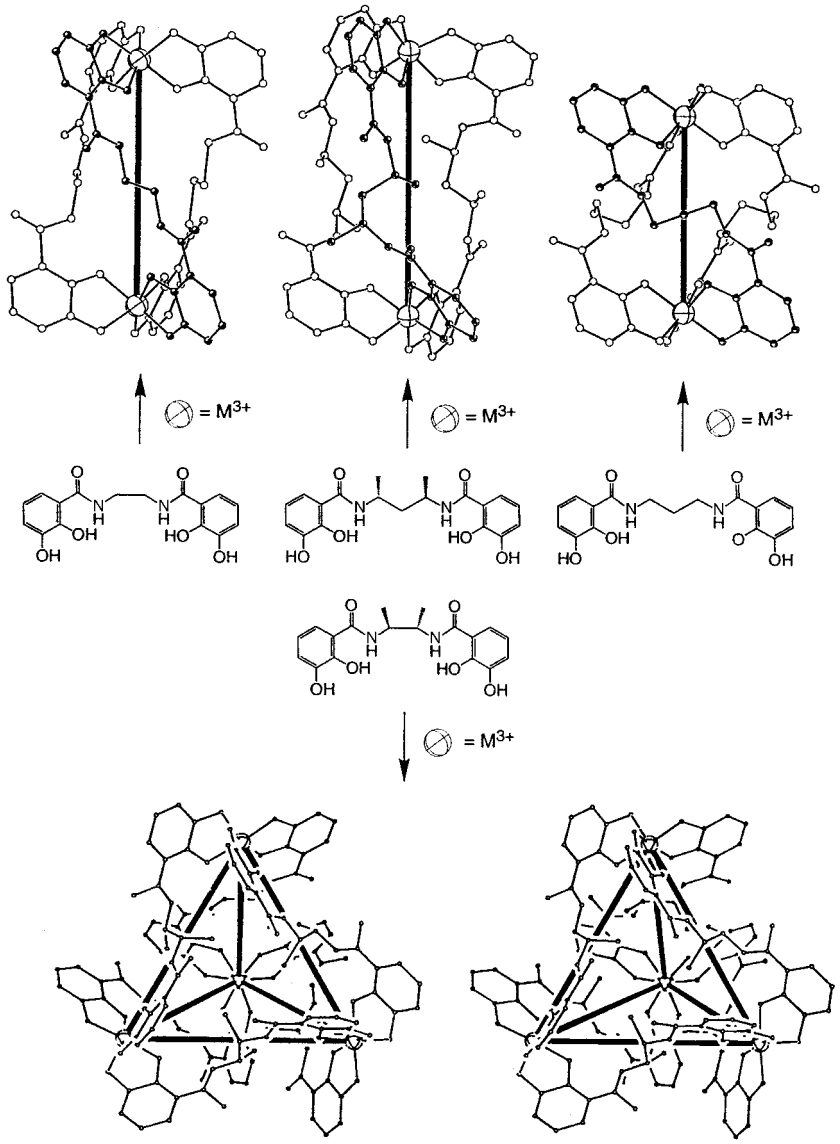


Figure 2. ORTEP representations of the structures of the complexes formed by each ligand. Atoms are represented as ideal spheres, and the metal–metal vectors are highlighted by thick lines. While $L_{et}^{H,H}$, $L_{pr}^{H,H}$, and $^{RR}L_{pr}^{Me,Me}$ each generate a helical 2:3 metal complex (top), $^{SS}L_{et}^{Me,Me}$ leads to a 4:6 tetrahedral cluster (bottom, shown as a stereoview).

identical configuration at each metal center produces a molecular topology with overall chirality. Such a tetrahedral topology has been observed previously in racemic mixtures with achiral ligands.[18, 19, 21] An achiral, S_4-symmetric, tetrahedral topology has also been demonstrated with two metals in a Λ configuration and two metals in a Δ configuration.[20, 22]

The highly symmetric, single set of ^{1}H NMR signals is consistent with the stereoselective formation in solution of the single *T*-symmetric tetrahedral cluster that is observed in the crystal structure analysis.[28] This stereoselectivity is analogous to that demonstrated in the formation of helical metal complexes.[5, 9, 13, 29–31] The enantiopure ligand $^{RR}L_{pr}^{Me,Me}$ selectively discriminates between three potential diastereomers (Λ,Λ; Λ,Δ; Δ,Δ) to generate a 2:3 left-handed helix: Λ,Λ-$[Ga_2(^{RR}L_{pr}^{Me,Me})_3]^{6-}$.[9] Stereoselective generation of $\Lambda,\Lambda,\Lambda,\Lambda$-$[Ga_4(^{SS}L_{et}^{Me,Me})_6]^{12-}$ from enantiopure $^{SS}L_{et}^{Me,Me}$ is statistically four times less probable. The observed isomer would comprise $^1/_{16}$ of a truly statistical mixture, while Λ,Λ-$[Ga_2(^{RR}L_{pr}^{Me,Me})_3]^{6-}$ would comprise $^1/_4$ of a purely statistical mixture of triply-bridged 2:3 complexes.

An impressive difference in specificity between the $L_{et}^{Me,Me}$ and $L_{pr}^{Me,Me}$ ligands is observed when the ligands are a racemic mixture rather than enantiopure. Racemic $^{rac}L_{pr}^{Me,Me}$ generates a mixture of diastereomeric metal complexes (Table 1)[9] while $^{rac}L_{et}^{Me,Me}$ produces only one enantiomeric pair of homochiral isomers in solution: $\Lambda,\Lambda,\Lambda,\Lambda$-$[Ga_4(^{SS}L_{et}^{Me,Me})_6]^{12-}$ and $\Delta,\Delta,\Delta,\Delta$-$[Ga_4(^{RR}L_{et}^{Me,Me})_6]^{12-}$ [Table 1 and Eqs. (2) and (3)]. This result is supported by a ^{1}H NMR spectrum of the $^{rac}L_{et}^{Me,Me}$ metal complex that is identical to the spectrum observed for enantiopure $[Ga_4(^{SS}L_{et}^{Me,Me})_6]^{12-}$. The ligands self-selectively sort based on their chirality in a stereospecific equilibrium. This process requires dramatic specificity since a total of 112 isomers are theoretically possible considering all combinations of four metal configurations with six ligand configurations and orientations.[32] The observed enantiomeric pair would comprise less than $^2/_{1024}$ of the hypothetical statistical mixture.[33]

Previous investigations of the Ga^{3+} complexes of simple alkyl-bridged bis-catechol and bis-catecholamide ligands have shown no evidence for the formation of a $[Ga_{2n}L_{3n}]^{6n-}$ complex where $n \neq 1$[9–11, 13–15] and prompts examination of the factors enhancing the stability of the larger $[M_4L_6]$ complex of $^{SS}L_{et}^{Me,Me}$. Conceptual modification of the known $[Ga_2(L_{et}^{H,H})^3]^{6-}$ structure[24] allows a simple conformational analysis of the hypothetical 2:3 complex $[Ga_2(^{SS}L_{et}^{Me,Me})_3]^{6-}$, since $L_{et}^{H,H}$ and $^{SS}L_{et}^{Me,Me}$ both have a two-carbon bridge between the catecholamide groups. This analysis predicts unfavorable steric interactions that are not present in the observed structure of $[Ga_4(^{SS}L_{et}^{Me,Me})_6]^{12-}$. Within the parent $[Ga_2(L_{et}^{H,H})_3]^{6-}$ complex, rotational freedom about the bonds of the ligand backbone is severely restricted.[11] As a result, the torsional angles observed in the ligand backbone of $[Ga_2(L_{et}^{H,H})_3]^{6-}$ are expected to be essentially unchanged in the hypothetical $[Ga_2(^{SS}L_{et}^{Me,Me})_3]^{6-}$. These torsional angles are 180° (N–C^1–C^2–N, Figure 3a), 120° (C–N–C^1–C^2, Figure 3b), 240° (C–N–C^1–H^1, Figure 3b), and 0° (C–N–C^1–H^2, Figure 3b).

Given such constraints, the hypothetical helical complex $[Ga_2(^{SS}L_{et}^{Me,Me})_3]^{6-}$ is readily visualized by substituting two methyl groups for both H^1 atoms or both H^2 atoms. The substitution of both H^1 atoms (Figure 3c) generates the conformation that is sterically the most favorable for the N–C^1 bond, whereas substituting methyl groups in the H^2

 © WILEY-VCH Verlag GmbH, D-69451 Weinheim, 1998 1433-7851/98/3707-0933 $ 17.50+.50/0

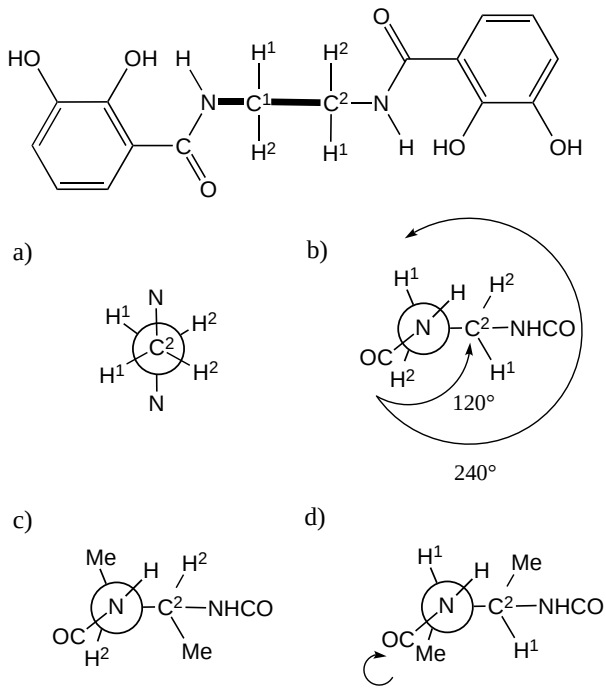


Figure 3. Newman projections of the ligand backbone (structure at the top) a) along the C^1–C^2 bond (highlighted in bold) and b), c), and d) along the N–C^1 bond (also highlighted). a, b) Representation of the ligand fragments in the $[Ga_2(L_{et}^{H,H})_3]^{6-}$ crystal structure. c, d) Modification of $[Ga_2(L_{et}^{H,H})_3]^{6-}$ to generate the hypothetical $[Ga_2(^{SS}L_{et}^{Me,Me})_3]^{6-}$ complex. In c) H^1 has been substituted by Me to yield the lowest energy conformation, whereas in d) H^2 has been substitued to yield the highest energy conformation.

positions (Figure 3d) generates the highest energy conformation for this bond. The stability of each conformation correlates with the distances between the amide carbonyl oxygen group and C^2 and the methyl group. Calculations indicate that the difference in energy between the two conformations is 2.7 kcal mol^{-1}.[34] Because $[Ga_2L_3]^{6-}$ complexes contain six such N – C^1 units, an energetic stabilization of 16 kcal mol^{-1} in favor of the H^1-substituted metal complexes over the H^2-substituted complexes is predicted, enough to favor the former complex quantitatively. However, within the hypothetical 2:3 complex, the H^1 substitution is not possible because the methyl groups of different ligands would come into contact in the interior of the complex. As a result, the less stable conformation (H^2 substitution) would be adopted, resulting in a strained conformation that has a C-N-C^1-Me torsional angle near zero degrees (Figure 3d).

The larger internal volume of a 4:6 complex is sufficient to allow inward projection of the methyl groups without interligand contact. As a result, a favorable N – C^1 conformation is possible (two conformations were observed crystallographically with torsional angles of 250° and 300°). Projection of the methyl groups towards the interior provides additional stabilization for the $[Ga_4L_6]^{12-}$ complex over the hypothetical $[Ga_2L_3]^{6-}$ complex. In a 4:6 complex the hydrophobic methyl groups are all located within the cavity of the metal complex, whereas a 2:3 complex would direct these hydrophobic groups into the aqueous solvent. This simple analysis illustrates two important factors, namely, a favorable torsional conformation and good packing of the hydrophobic methyl groups of $L_{et}^{Me,Me}$, which result in the formation of a $[M_4L_6]$ complex rather than the $[M_2L_3]$ type of complex formed by $L_{et}^{H,H}$ that lacks methyl substituents.

An interesting difference between $\Lambda,\Lambda,\Lambda,\Lambda$-$[Ga_4(^{SS}L_{et}^{Me,Me})_6]^{12-}$ and the previously characterized Λ,Λ-$[Ga_2(^{RR}L_{pr}^{Me,Me})_3]^{6-}$ is that the correlation between the ligand configuration and the metal configuration is reversed ($S-\Lambda$ versus $R-\Lambda$). This reversal correlates with a reversal in the preferred projection of the methyl groups in the two compounds. The inward projection in the 4:6 complex contrasts with the external projection in the 2:3 helical complex[35] which results in opposite metal configurations.

Experimental Section

$^{SS}L_{et}^{Me,Me}$ and $^{rac}L_{et}^{Me,Me}$: The ligands were synthesized as previously described,[36] from a reaction of an activated 2,3-dimethoxybenzoic acid derivative with diamine (0.5 equiv), followed by deprotection with BBr_3. The racemic and enantiomerically pure diamines used in the synthesis of $^{rac}L_{et}^{Me,Me}$ and $^{SS}L_{et}^{Me,Me}$ were prepared and resolved according to literature procedures.[26] ^{1}H NMR (400 MHz, [D$_6$]DMSO): $\delta = 12.48$ (s, 2 H; O*H*), 9.17 (s, 2 H; O*H*), 8.50 (d, $J = 8.1$ Hz, 2 H; N*H*), 7.28 (pseudo d, $J = 8.1$ Hz, 2 H; H_a), 6.90 (pseudo d, $J = 7.7$ Hz; H_c), 6.68 (pseudo t, $J = 7.9$ Hz, 2 H; H_b), 4.27 (m, 2 H; C*H*Me), 1.20 (d, $J = 6.3$ Hz, 6 H; CH*Me*). FABMS (FAB = fast-atom-bombardment): $m/z = 361.1$ calcd; 361.2 found.

$K_{12}[Ga_4(^{SS}L_{et}^{Me,Me})_6]$ and $K_{12}[Ga_4(^{rac}L_{et}^{Me,Me})_6]$: The metal complexes were synthesized by reaction of the ligand (6 equiv) with $[Ga(acac)_3]$ (4 equiv) and a base (KOH or $(R_4N)OH$, 12 equiv), followed by removal of the solvent and the resulting acacH under vacuum. The crude solid was dissolved in H_2O and equilibrated at 85 °C until a highly symmetric ^{1}H NMR spectrum was attained (≤ 3 hours). ^{1}H NMR (400 MHz, D_2O): $\delta =$ 6.87 (pseudo d, $J = 8.2$ Hz, 2 H; H_a), 6.44 (pseudo d, $J = 7.4$ Hz; H_c), 6.30 (pseudo t, $J = 7.8$ Hz, 2 H; H_b), 3.53 (m, 2 H; C*H*Me), 0.91 (d, $J = 6.2$ Hz, 6 H; CH*Me*).

Crystal data for $(Me_4N)_{12}[Ga_4(^{SS}L_{et}^{Me,Me})_6]\cdot 42.5\,H_2O$: the complex crystallized by diffusion of acetone into an acetonitrile/water solution in the F-centered cubic space group *F*23 (no. 196) or *F*432 (no. 209) with cell constants based on 8192 reflections ($3^\circ < 2\theta < 46.5^\circ$): $a = 35.3133(3)$ Å, $V =$ 44036.80 Å^3, $Z = 8$. A total of 51272 reflections ($3^\circ < 2\theta < 46.5^\circ$) was collected at 117 K with ω scans on an Siemens SMART diffractometer with graphite-monochromated $Mo_{K\alpha}$ radiation ($\lambda = 0.71069$ Å) of which 5275 were unique to space group *F*23 (no. 196). The structure was solved by direct methods (SHELXS-86). Many of the atoms were disordered, and the structure was considered a 50:50 orthogonal twin in the space group *F*23, which was most conveniently modeled as space group *F*432 with disorder. This disorder was modeled with the aid of rigid groups at reduced occupancies. The gallium centers, coordinated oxygen atoms, amide nitrogen atoms, and bridging carbon atoms were refined anisotropically. The amide oxygen atoms and well-ordered solvent water atoms were also refined anisotropically. All other solvent atoms were refined isotropically, and rigid groups were each refined with a single isotropic parameter. Full matrix refinement of 137 variables based on all data unique to *F*23 ($3^\circ < 2\theta < 46.5^\circ$, 5275 reflections) converged with final residuals of $R_1 =$ 0.088 ($I > 4\sigma(I)$), 1470 reflections, 912 unique to *F*432), $wR_2 = 0.213$. The absolute configuration of the space group was assigned by the chirality of the ligand (*S,S*).[26, 27] All calculations were performed with the teXsan crystallographic software package of Molecular Structure Corporation. Further details on the crystal structure investigation may be obtained from the Fachinformationszentrum Karlsruhe, D-76344 Eggenstein-Leopoldshafen, Germany (fax: (+49) 7247-808-666; e-mail: crysdata@fiz-karlsruhe.de), on quoting the depository number CSD-407 967.

Received: September 29, 1997 [Z 10982 IE]
German version: *Angew. Chem.* **1998**, *110*, 977 – 981

 © WILEY-VCH Verlag GmbH, D-69451 Weinheim, 1998 1433-7851/98/3707-0934 $ 17.50+.50/0

Keywords: chirality · gallium · self-assembly · supramolecular chemistry



[1] R. Krämer, J.-M. Lehn, A. De Cian, J. Fischer, *Angew. Chem.* **1993**, *105*, 764 – 768; *Angew. Chem. Int. Ed. Engl.* **1993**, *32*, 703 – 706.

[2] B. Hasenknopf, J.-M. Lehn, B. O. Kneisel, G. Baum, D. Fenske, *Angew. Chem.* **1996**, *108*, 1987 – 1990; *Angew. Chem. Int. Ed. Engl.* **1996**, *35*, 1838 – 1840.

[3] P. N. W. Baxter, J.-M. Lehn, K. Rissanen, *Chem. Commun.* **1997**, 1323 – 1324.

[4] F. M. Romero, R. Ziessel, A. Dupont-Gervais, A. Van Dorsselaer, *Chem. Commun.* **1996**, 551 – 553.

[5] C. Provent, S. Hewage, G. Brand, G. Bernardinelli, L. J. Charbonnière, A. F. Williams, *Angew. Chem.* **1997**, *109*, 1346 – 1348; *Angew. Chem. Int. Ed. Engl.* **1997**, *36*, 1287 – 1289.

[6] R. C. Scarrow, D. L. White, K. N. Raymond, *J. Am. Chem. Soc.* **1985**, *107*, 6540 – 6546.

[7] A. F. Williams, C. Piguet, G. Bernardinelli, *Angew. Chem.* **1991**, *103*, 1530 – 1533; *Angew. Chem. Int. Ed. Engl.* **1991**, *30*, 1490 – 1492.

[8] D. Zurita, P. Baret, J.-L. Pierre, *New J. Chem.* **1994**, *18*, 1143 – 1146.

[9] E. J. Enemark, T. D. P. Stack, *Angew. Chem.* **1995**, *107*, 1082 – 1084; *Angew. Chem. Int. Ed. Engl.* **1995**, *34*, 996 – 998.

[10] M. Albrecht, S. Kotila, *Angew. Chem.* **1995**, *107*, 2285 – 2287; *Angew. Chem. Int. Ed. Engl.* **1995**, *34*, 2134 – 2137.

[11] E. J. Enemark, T. D. P. Stack, *Inorg. Chem.* **1996**, *35*, 2719 – 2720.

[12] B. Kersting, M. Meyer, R. E. Powers, K. N. Raymond, *J. Am. Chem. Soc.* **1996**, *118*, 7221 – 7222.

[13] M. Albrecht, *Synlett* **1996**, 565 – 567.

[14] M. Albrecht, H. Röttele, P. Burger, *Chem. Eur. J.* **1996**, *2*, 1264 – 1268.

[15] M. Albrecht, S. Kotila, *Angew. Chem.* **1996**, *108*, 1299 – 1300; *Angew. Chem. Int. Ed. Engl.* **1996**, *35*, 1208 – 1210.

[16] V. A. Grillo, E. J. Seddon, C. M. Grant, G. Aromí, J. C. Bollinger, K. Folting, G. Christou, *Chem. Commun.* **1997**, 1561 – 1562.

[17] A. Williams, *Chem. Eur. J.* **1997**, *3*, 15 – 19.

[18] R. W. Saalfrank, A. Stark, K. Peters, H. G. von Schnering, *Angew. Chem.* **1988**, *100*, 878 – 880; *Angew. Chem. Int. Ed. Engl.* **1988**, *27*, 851 – 853.

[19] R. W. Saalfrank, A. Stark, M. Bremer, H.-U. Hummel, *Angew. Chem.* **1990**, *102*, 292 – 294; *Angew. Chem. Int. Ed. Engl.* **1990**, *29*, 311 – 314.

[20] R. W. Saalfrank, B. Hörner, D. Stalke, J. Salbeck, *Angew. Chem.* **1993**, *105*, 1223 – 1225; *Angew. Chem. Int. Ed. Engl.* **1993**, *32*, 1179 – 1182.

[21] R. W. Saalfrank, R. Burak, A. Breit, D. Stalke, R. Herbst-Irmer, J. Daub, M. Porsch, E. Bill, M. Müther, A. X. Trautwein, *Angew. Chem.* **1994**, *106*, 1697 – 1699; *Angew. Chem. Int. Ed. Engl.* **1994**, *33*, 1621 – 1623.

[22] T. Beissel, R. E. Powers, K. N. Raymond, *Angew. Chem.* **1996**, *108*, 1166 – 1168; *Angew. Chem. Int. Ed. Engl.* **1996**, *35*, 1084 – 1086.

[23] P. L. Jones, K. J. Byrom, J. C. Jeffery, J. A. McCleverty, M. D. Ward, *Chem. Commun.* **1997**, 1361 – 1362. A reviewer has pointed out that the reported 8:12 complex is a two-dimensional ring and that a three-dimensional 8:12 "molecular cube" is also possible.

[24] The crystal structure presented[11] is the structure of $(Et_4N)_6[Fe_2(L_{et}^{H,H})_3]\cdot 10H_2O$. The gallium structure is isomorphic. Crystal data for $(Et_4N)_6[Ga_2(L_{et}^{H,H})_3]\cdot 10H_2O$: $P3_221$ (no. 154) or $P3_121$ (no. 152), $a = 16.441(4)$, $c = 35.512(7)$ Å, $V = 8400(4)$ Å^3, $Z = 3$, $R(R_w) = 0.073(0.069)$.

[25] Since our initial report of this complex,[9] a crystal structure has been determined. Crystal data for $(TMI)_3[Ga_2(L_{pr}^{H,H})_3]\cdot 14H_2O$: $R\bar{3}c$ (no. 167), $a = 20.047(6)$, $c = 36.527(3)$ Å, $V = 12721(5)$ Å^3, $Z = 6$, $R(R_w) = 0.061(0.056)$. TMI = tetramethyldihydroimidazolinium.

[26] F. H. Dickey, W. Fickett, H. J. Lucas, *J. Am. Chem. Soc.* **1952**, *74*, 944 – 951.

[27] R. D. Gillard, *Tetrahedron* **1965**, *21*, 503 – 506.

[28] A single set of resonances is also consistent with a fluxional species or with a less symmetric species that has coinciding resonances. Fluxional behavior is highly unlikely given the lengthy equilibration time required to generate the complex and also the lack of fluxional behavior in $[Ga_2(L_{et}^{H,H})_3]^{6-}$ and $[Ga_2(L_{pr}^{H,H})_3]^{6-}$. This is demonstrated by diastereotopic signals in the ^{1}H NMR spectra of these complexes. Diastereotopic protons are not observed in $[Ga_4(^{SS}L_{et}^{Me,Me})_6]^{12-}$ or in $[Ga_2(^{RR}L_{pr}^{Me,Me})_3]^{6-}$, but none are anticipated for these complexes. A less symmetric species is also unlikely as it would be expected that the various methyl and methylene protons of the ligand backbone would have very different chemical environments.

[29] J. Libman, Y. Tor, A. Shanzer, *J. Am. Chem. Soc.* **1987**, *109*, 5880 – 5881.

[30] W. Zarges, J. Hall, J.-M. Lehn, C. Bolm, *Helv. Chim. Acta* **1991**, *74*, 1843 – 1852.

[31] R. W. Saalfrank, M. Decker, F. Hampel, K. Peters, H. G. von Schnering, *Chem. Ber.* **1997**, *130*, 1309 – 1313.

[32] Several combinations of the two ligand enantiomers are possible: $[Ga_4(^{SS}L_{et}^{Me,Me})_a(^{RR}L_{et}^{Me,Me})_{6-a}]^{12-}$ $(0 \le a \le 6)$. If more than one of each enantiomer is present in a metal complex $(2 \le a \le 4)$, these ligands can be arranged in multiple orientations relative to each other. A list of all possible isomers is given in the supporting information on the WWW.

[33] Other examples of self-selectivity in self-assembly: R. Krämer, J.-M. Lehn, A. Marquis-Rigault, *Proc. Natl. Acad. Sci. USA* **1993**, *90*, 5394 – 5398; D. L. Caulder, K. N. Raymond, *Angew. Chem.* **1997**, *109*, 1508 – 1510; *Angew. Chem. Int. Ed. Engl.* **1997**, *36*, 1439 – 1442; M. A. Masood, E. J. Enemark, T. D. P. Stack, *ibid.* **1998**, *110*, 973 – 977 and **1998**, *37*, 928 – 932.

[34] AM1 calculations were performed with an idealized isopropylformamide unit.

[35] The additional carbon atom in the bridge of $^{RR}L_{pr}^{Me,Me}$ versus $^{SS}L_{et}^{Me,Me}$ provides one additional degree of rotational freedom in the ligand backbone. This degree of freedom allows an external projection of methyl groups while maintaining a favorable torsional conformation for C-N-C^1-Me. This degree of freedom is also likely to play an important role in the lack of selectivity in racemic $L_{pr}^{Me,Me}$.

[36] T. B. Karpishin, T. D. P. Stack, K. N. Raymond, *J. Am. Chem. Soc.* **1993**, *115*, 6115 – 6125.

B_4 Tetrahedra for Aluminum Atoms—A Surprising Substitution in τ-Borides $Ni_{20}Al_3B_6$ and $Ni_{20}AlB_{14}$**

Harald Hillebrecht* and Martin Ade

The solid-state chemistry of boron is remarakably diverse, which is attributed to the tendency of boron to form homonuclear interactions and numerous clusters.[1] Isolated boron atoms are usually observed for metal-rich borides with a ratio M:B > 2. Among this class of compounds, "τ-borides" of the cubic $Cr_{23}C_6$-type ($Fm3m$, $cF112$[2]) represent the largest group with about 80 examples.[3] Usually ternary

[*] Prof. Dr. H. Hillebrecht,[+] Dr. M. Ade
Institut für Anorganische und Analytische Chemie
Albertstrasse 21, D-79104 Freiburg (Germany)

[+] New address:
Institut für Anorganische Chemie
Gerhard-Domagk-Strasse 1, 53121 Bonn (Germany)
Fax: (+49) 228 735-660
E-mail: hille@snchemie2.chemie.uni-bonn.de

[**] This work was supported by the Deutsche Forschungsgemeinschaft (DFG). We thank Prof Dr. G. Thiele (Freiburg) for his generous support of our work.

compounds of compositions $M_{20}M'_3B_6$ or $M_{21}M'_2B_6$ are observed, in which the major component M is frequently Ni or Co, and in some cases Cr, Mn, Fe, Ru, Re, or Ir. The minor component M′ can be either a main group metal (Li, Mg, Al, Ga, In, Ge, Sn, Sb), a rare earth metal (Er, Lu, Tm), or a transition metal. Several carbides, silicides,[4] germanides,[4] phosphides,[5] and binary borides ($Fe_{23}B_6$,[6] $Co_{23}B_6$[7]) can also be assigned this structure type. The τ-borides are characterized predominantly by X-ray crystallography with powder methods. Only in the cases of $Ni_{20}Li_3B_6$ and $Co_{21}Ta_2B_6$ are structures based on single-crystal data.

Among these τ-phases the Ni/Al/B system is a special case. Firstly, the lattice constants vary between 10.484 Å and 10.552 Å (800°C) and between 10.48 Å and 10.62 Å (1000°C) depending on the temperature of the synthesis. Secondly these variations of the lattice constants are connected to a remarkably large field of nonstoichiometry with respect to the boron content (10.48 Å: $Ni_{20}Al_3B_6$; 10.62 Å: $Ni_{20}Al_3B_{12}$). Stadelmaier et al. proposed that the enlargement of the unit cell with higher boron content might be attributed to the substitution of isolated boron atoms with a square-antiprismatical coordination by B_2 pairs. This would be very unusual for the structural chemistry of transition metal borides. In order to clarify the structure–chemical reasons for the variation of the boron content structure analyses based on single-crystal data were carried out across the whole range of existence of the τ phase.[12] Table 1 shows some of the results. Compositions were deduced from the refinement of site occupation factors and are in accordance with the corresponding conditions of formation (see Experimental Section).

Table 1. Results of structure analyses of τ-borides in the system Ni/Al/B: $Ni_{20+x}Al_{3-x-2y}B_{6+8y}$ (compositions from refinement of occupation factors).

Composition	Lattice constant	x	y
$Ni_{20.51(2)}Al_{2.49(2)}B_6$	10.4859(2)	0.51(2)	0[a]
$Ni_{20}Al_3B_6$	10.5110(4)	0[a]	0[a]
$Ni_{20}Al_{2.73(2)}B_{7.08(8)}$	10.5193(6)	0[a]	0.13(2)
$Ni_{20}Al_{2.40(4)}B_{8.4(2)}$	10.5689(2)	0[a]	0.30(2))
$Ni_{20}Al_{1.12(3)}B_{13.5(1)}$	10.5895(3)	0[a]	0.94(2)
$Ni_{20}Al_{1.19(3)}B_{13.2(1)}$	10.5922(6)	0[a]	0.91(2)
$Ni_{20}AlB_{14}$	10.6167(3)	0[a]	1[a]

[a] Value fixed.

With respect to the $Cr_{23}C_6$-type, $Ni_{20}Al_3B_6$ represents a ternary ordering variant (Figure 1). The two Ni sites form a NaCl-like pattern of Ni_8 cubes (site 32 f) and Ni_{12} cuboctahedra (48 h). The Al positions are inside the cuboctahedra (4a) and inside the fourfold capped truncated tetrahedra ("Friauf"-polyhedra, Figure 2 a), which are formed by four triangular faces of the cuboctahedra and four corners of the cubes (site 8c). The boron atoms reside in a square antiprism built up by the square planes of one cuboctahedron and one cube. Starting from $Ni_{20}Al_3B_6$ the variation of the compositon can be explained by two different ways of substituting the Al atoms.

With increasing Ni content, some of the Al atoms on site 4a are replaced by Ni atoms: $Ni_{20+x}Al_{3-x}B_6$. This kind of

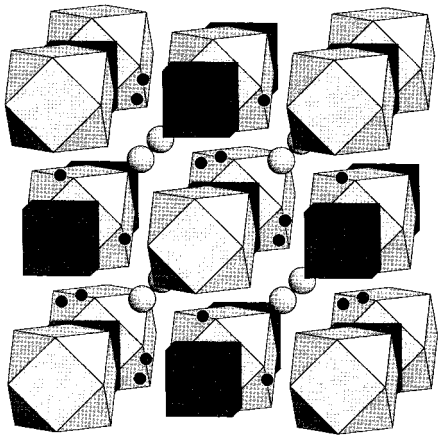


Figure 1. Crystal structure of the τ-boride $Ni_{20}Al_3B_6$ with Ni_{12} cuboctahedra (Ni2, 48h), Ni_8 cubes (Ni1, 32f), Al1 in the center of the cuboctahedra (4a), Al2: light spheres (8c), B: dark spheres (24e).

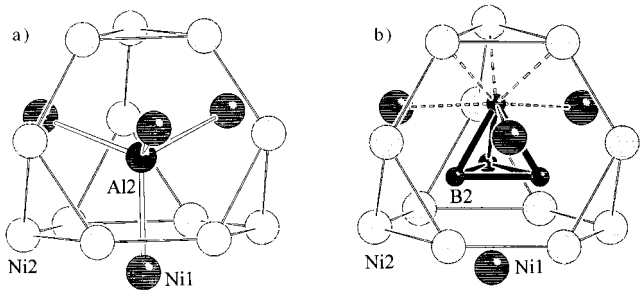


Figure 2. Coordination about a) Al2 in $Ni_{20}Al_3B_6$ [Al–Ni: $4 \times 2.411(1)$ Å, $12 \times 2.887(1)$ Å], and about b) B_4 tetrahedron in $Ni_{20}AlB_{14}$ [B–B: $3 \times 1.681(15)$ Å, B–Ni: $3 \times 2.093(8)$ Å, $3 \times 2.269(6)$ Å].

substitution is well known for τ-borides and τ-carbides.[3] Since Ni (1.246 Å) has a smaller atomic radius than Al (1.32 Å), this leads to a smaller lattice constant. For the single crystal with the highest Ni content (51(2)%) we found a lattice constant of 10.4859(2) Å. The complete replacement would result in the composition $Ni_{21}Al_2B_6$, but the minimum value of the lattice constant discounts the possibility of full substitution.

The variation of the boron content is achieved by a mechanism of substitution that is unique in solid-state chemistry. In the course of the structure analyses based on single-crystal data it became clear that the Al atoms on site 8c that are coordinated in a $4+12$-way are replaced by B_4 tetrahedra (Figure 2 b). This substitution takes place in a continuous way; that is, the electron density on site 8c decreases as the lattice constant and boron content increase. At the same time an additional maximum of electron density arises on a site 32 f with $x \approx 0.194$. If boron is located on this 32 f position, the resulting occupation factor and the deficit of aluminum at the 8c site are in a ratio of nearly 4:1. At the highest value of the lattice constant (10.6167(3) Å) the electron density on the 8c position is completely vanished. By placing boron on the 32 f site the refinement leads to full occupation. Therefore the composition $Ni_{20}AlB_{14}$ results as the end member of the series $Ni_{20}Al_{3-2y}B_{6+8y}$ with $y = 1$. The two ways of replacement are shown in Table 2. The changes of lattice constants caused by the substitution of Al by Ni and B_4

 © WILEY-VCH Verlag GmbH, D-69451 Weinheim, 1998 1433-7851/98/3707-0936 $ 17.50+.50/0

tetrahedra can be derived from the volume increments for the elements proposed by W. Biltz. [14] These patterns of substitutions are also supported by the experimental results, because by-products containing boron are observed if the ratio Ni:B is lower than 20:14.

Table 2. Representation of the two different ways of substitution in $Ni_{20+x}Al_{3-x-2y}B_{6+8y}$.

Composition	48h	32f	4a	8c	24e
$Ni_{21}Al_2B_6$	Ni_{12}	Ni_8	**Ni** ↑ **x**	Al_2	B_6
$Ni_{20}Al_3B_6$	Ni_{12}	Ni_8	**Al**	**Al_2** ↓ **y**	B_6
$Ni_{20}AlB_{14}$	Ni_{12}	Ni_8	Al	**$(B_4)_2$**	B_6

At first sight, the existence of B_4 tetrahedra in the τ-boride $Ni_{20}AlB_{14}$ seems to be very unusual; however, it is in accord with the geometrical situation, because B_4 tetrahedron and capped Friauf-polyhedron fit perfectly to each other. The B–B distances of 1.681(15) Å in the B_4 tetrahedron are comparable to those in B_4Cl_4 (1.65) Å[15] and $(t\mathrm{Bu})_4B_4$ (1.71 Å),[16] the only compounds in which B_4 tetrahedra have been proven by a structure analysis. Ni–B distances of 2.09 Å and 2.27 Å are similar to the values found for binary borides of nickel (Ni_4B_3,[17] NiB[18]). In addition, in this way the quite short distances between the Al atom in the center of the Friauf-polyhedron and the capping Ni atoms (2.411(1) Å) are avoided (Figure 2).

Solid-state compounds with tetrahedra of Group 14 elements and the heavier ones of Group 13 are well known and characterized (i.e. Zintl phases[19] with Al, Ga, In, Tl, Si, Ge, Sn, Pb). In contrast, B_4 tetrahedra have only been confirmed by structural analysis for the molecular compounds B_4Cl_4 and $(t\mathrm{Bu})_4B_4$. The formation of B_4 tetrahedra confirms the pronounced tendency of boron to form homonuclear bonds in solid-state compounds. Furthermore the example of B_4 tetrahedra in $Ni_{20}AlB_{14}$ shows that unusual structural units may be stabilized not only by special ligands as in molecular chemistry but also in a crystal structure if the structure–chemical conditions are fulfilled.

Finally investigations on the patterns of substitution of τ-phases are of great importance for technical applications, because τ-borides play an important role in the course of hardening processes of metallic materials by boriding[20] and in composites of ductile alloys and the extremely hard transition metal borides.[21]

Experimental Section

τ-phases of the system Ni/Al/B were synthesized by heating the elements to 1200–1300°C (Ar inert gas, corundum crucibles), slow cooling to 1000°C and quenching to room temperature. The phases were analyzed by X-ray diffraction on powdered samples. NiAl, Ni_4B_3, Ni_2B, and NiB were estabilished as border phases. The highest boron content obtained depends significantly on the temperature. Annealing at 900°C transforms a boron-rich sample ($a = 10.62$ Å) to a τ-boride with lower boron content ($a = 10.56$ Å), NiB, and a still unknown phase (probably ternary). (This might explain the different findings of Kuz'ma et al. and Stadelmaier et al.). Single crystals suitable for structure analyses were only obtained when a small excess of aluminum was used; the latter evidently serves as a flux. Irregularly shaped and air-stable single crystals with metallic luster were isolated from the solidified melt.

Received: June 26, 1997
Revised version: November 19, 1997 [Z10602IE]
German version: *Angew. Chem.* **1998**, *110*, 981–983

Keywords: aluminum · borides · boron · nickel · structure elucidation

[1] a) "Borides: Solid State Chemistry": T. Lundström in *Encyclopedia of Inorganic Chemistry*, (Ed.: R. B. King), Wiley, Chichester, UK, **1994**; b) *Boron and Refractory Borides*, (Ed.: V. I. Matkovich), Springer, Berlin, **1977**.
[2] A. Westgren, *Nature* **1933**, *132*, 480–481.
[3] P. Villars, L. D. Calvert, *Pearson's Handbook of Crystallographic Data for Intermetallic Phases*, ASM, Metals Park, Ohio, **1985**.
[4] A. V. Gribanov, Yu. D. Seropegin, *J. Alloys Compd.* **1994**, *204*, L9–11.
[5] a) M. Andersson-Söderberg, Y. Andersson, *J. Solid State Chem.* **1990**, *85*, 315–317; b) V. Keimes, A. Mewis, *Z. anorg. allg. Chem.* **1992**, *618*, 35–38.
[6] Y. Khan, H. Wibbeke, *Z. Metallkde.* **1991**, *82*, 703–706.
[7] M. Ade, Dissertation, Universität Freiburg, **1997**.
[8] W. Jung, *Z. Kristallogr.* **1980**, *151*, 113–120.
[9] H. H. Stadelmaier, H. H. Davis, H. K. Manaktala, E.-T. Henig, *Z. Metallkde.* **1989**, *80*, 370–373.
[10] a) H. H. Stadelmaier, A. C. Fraker, *Metall* **1962**, *16*, 212–215; b) H. H. Stadelmaier, R. A. Draughan, G. Hofer, *Z. Metallkde.* **1963**, *54*, 640–644.
[11] N. F. Chaban, Y. B. Kuz′ma, *Inorg. Mater.* **1973**, *9*, 1886–1888.
[12] Structure analyses of τ-phases in the system Ni/Al/B: irregular polyhedra with metallic luster $0.04 \times 0.04 \times 0.04$ mm; cubic, space group *Fm*3*m* (no. 225), $Mo_{K\alpha}$ radiation; Nonius-CAD4 diffractometer, graphite monochromator, $\omega/2\theta$-scan, $T = 293$ K, full-matrix least squares refinement, $Cr_{23}C_6$-type as a starting model [program SHELXL-93, G. Sheldrick, Universität Göttingen], all atoms were refined anisotropically except B atoms in $Ni_{20}AlB_{14}$; Lorentz- and polarization correction; empirical absorption correction using psi-scans. $Ni_{20.51(2)}Al_{2.49(2)}B_6$: $a = 10.4859(2)$ Å, $V = 1153.0$ Å^3, $2° < \theta < 35°$, 717 reflections measured, 160 independent reflections with $I > 0$, $\mu = 32.71$ mm^{-1}, $0.529 > t > 0.414$; 15 free parameters, $R1(F) = 0.014$ (157 reflections with $I > 2\sigma(I)$), $wR2(I) = 0.032$; $+0.64/-0.90$ e Å^{-3}, Ni1: $x = 0.38254(2)$, Ni2: 0.116938(2), B1: $x = 0.2733(3)$. $Ni_{20}Al_3B_6$: $a = 10.5110(4)$ Å, $V = 161.3$ Å^3; $2° < \theta < 40°$; 882 reflections measured; 217 independent reflections with $I > 0$; $\mu = 31.37$ mm^{-1}, $0.653 > t > 0.478$; 14 free parameters; $R1(F) = 0.073$ (193 reflections with $I > 2\sigma(I)$), $wR2(I) = 0.033$; $+1.90/-0.90$ e Å^{-3}, Ni1: $x = 0.38241(4)$, Ni2: $x = 0.16950(4)$, B1: $x = 0.2739(6)$. $Ni_{20}AlB_{14}$: $a = 10.6167(3)$ Å, $V = 1176.2$ Å^3; $2° < \theta < 40°$; 1040 reflections measured; 208 independent reflections with $I > 0$; $\mu = 30.73$ mm^{-1}, $0.746 > t > 0.546$; 16 free parameters; $R1(F) = 0.024$ (176 reflections with $I > 2\sigma(I)$) $wR2(I) = 0.065$; $+3.30$*$/-1.43$ e Å^{-3} (* site 4b, probably an artefact as a result of crystal quality (broad reflection profiles), no atom could be refined on this site), Ni1: $x = 0.37978(4)$, Ni2: $x = 0.16903(3)$, B1: $x = 0.2758(7)$, B2: $x = 0.1940(5)$. Further details on the crystal structure investigations may be obtained from the Fachinformationszentrum Karlsruhe, D-76344 Eggenstein-Leopoldshafen, Germany (fax: (+49) 7247-808-666 (Frau S. Höhler-Schlimm); e-mail: crysdata@fiz-karlsruhe.de), on quoting the depository numbers CSD-408417, -408418, and -408419.
[13] W. P. Pearson *The Chemistry and Physics of Metals and Alloys*, Wiley Interscience, New York, **1972**.
[14] W. Biltz *Raumchemie der festen Stoffe*, Verlag Leopold Voss, Leipzig, **1934**.
[15] D. Thierry, Dissertation, Max-Planck-Institut für Festkörperforschung, Stuttgart, **1992**.
[16] T. Menneke, P. Paetzold, R. Boese, D. Blaser, *Angew. Chem* **1991**, *103*, 199–201; *Angew. Chem. Int. Ed. Engl.* **1991**, *30*, 172–174.
[17] S. Rundquist, S. Pramatus, *Acta Chem. Scand* **1967**, *21*, 191–194.

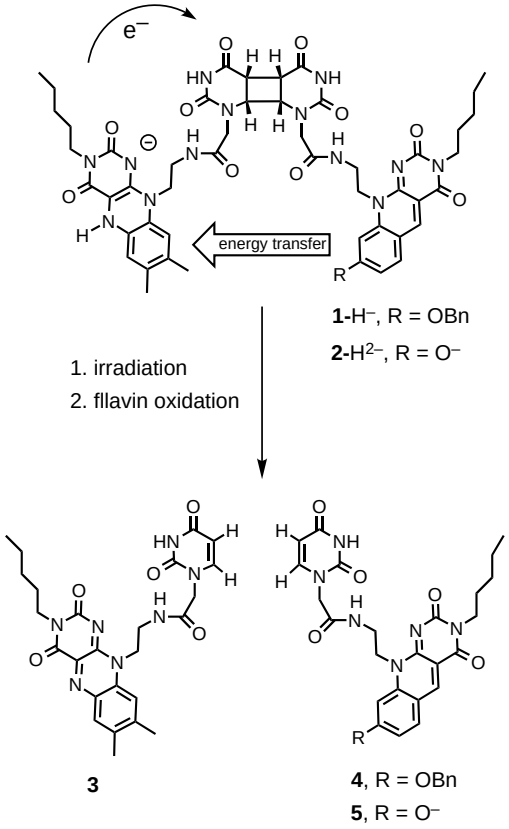
[18] S. Rundquist, *Acta Chem. Scand.* **1959**, *13*, 1193 – 1208.
[19] a) M. L. Fornasini, *Acta Crystallogr.* **1983**, *C39*, 943 – 946; b) C. Dohmeier, D. Loos, H. Schnöckel, *Angew. Chem.* **1996**, *108*, 141 – 161; *Angew. Chem. Int. Ed. Engl.* **1996**, *35*, 135 – 154; c) S. M. Kauzlarich, *Chemistry, Structure, and Bonding of Zintl Phases and Ions* VCH Publishers, New York, **1996**; d) H. Schäfer, B. Eisenmann, W. Müller, *Angew. Chem.* **1973**, *85*, 742 – 760; *Angew. Chem. Int. Ed. Engl.* **1973**, *12*, 725 – 743.
[20] a) R. Telle, *Chem. Unserer Zeit* **1988**, *22*, 93 – 99; b) E. Lugscheider, H. Reimann, R. Pankert, *Metall* **1982**, *36*, 247 – 251.
[21] C. B. Finch, P. F. Becher, M. K. Ferber, V. J. Tennery, C. S. Yust, *J. Cryst. Growth* **1982**, *58*, 647 – 655.

Flavin- and Deazaflavin-Containing Model Compounds Mimic the Energy Transfer Step in Type-II DNA-Photolyases

Robert Epple and Thomas Carell*

DNA-photolyases are DNA-repair enzymes, which remove pyrimidine dimer lesions (which are cyclobutane derivatives) from the genome. These lesions are formed upon irradiation of cells with UV light.[1, 2] The basis of the repair reaction is a light-driven electron transfer from the enzyme to the dimer to form the radical anion, which subsequently monomerizes.[3] For the repair reaction DNA-photolyases need a reduced and deprotonated riboflavin cofactor as the electron donor, and they require a methenyltetrahydrofolate (MTHF) or an 8-hydroxy-5-deazaflavin as the second cofactor.[4] Model investigations show that deazaflavins are able to initiate the electron-transfer-driven repair as well, but with a very low quantum yield.[4, 5] Detailed enzymatic studies indicate, however, that the deazaflavin functions within the enzyme entirely as a photoantenna.[6] It transfers excitation energy to the reduced flavin. This energy transfer was shown to accelerate the repair rate and to shift the wavelength of maximal activity from 370 nm to 430 nm.[7]

Although such studies indicate that an efficient interaction of the reduced, deprotonated flavin and the oxidized deazaflavin, and therefore their close juxtaposition, would be desirable, time-resolved fluorescence data[8] and the X-ray crystal structures[9] of the *E. coli* photolyase and the *A. nidulans* photolyase revealed a surprisingly large cofactor separation of 16.8 Å and 17.5 Å (center-to-center distance), respectively. This unexpected finding raised speculation that the energy transfer is not rate-limiting and has never been optimized during evolution.[9, 10] In the photosynthetic apparatus, however, the large distance between the final antenna pigment and the electron donor is explained by the need to suppress a competing electron transfer from the electron donor to the antenna.[11] In order to study energy transfer processes between deazaflavins and flavins, to clarify the influence of the protonation state of the deazaflavin on the energy transfer, and to investigate electron transfer possibilities between both cofactors, we prepared a series of flavin- and deazaflavin-containing model compounds like **1** and **2** (Scheme 1).[12] The analysis of these model compounds provides insight into the interactions of both cofactors depending on their redox and protonation states.



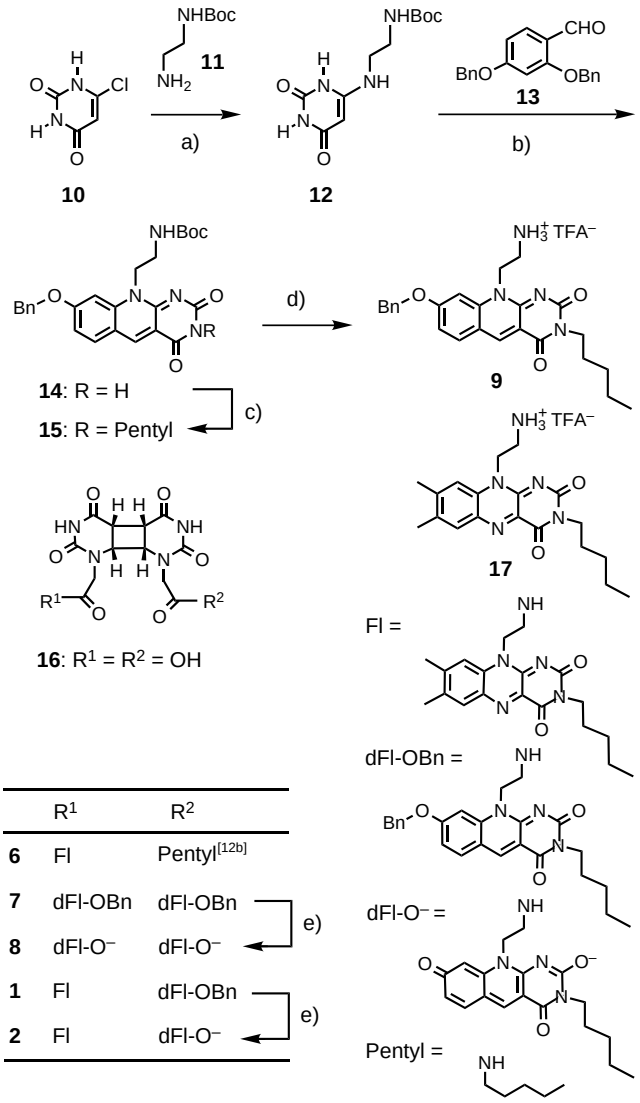
Scheme 1. The flavin- and deazaflavin-containing model compounds **1**-H$^-$ and **2**-H^{2-} and its investigated photoinduced cleavage reaction to **3** – **5**.

The synthesis of the deazaflavin- and flavin/deazaflavin-containing model compounds **1**, **2**, and **6** – **8** is depicted in Scheme 2. For the preparation of the aminoethyl-substituted deazaflavin **9**, 6-chlorouracil **10** was treated with the Boc-protected ethylene diamine **11**.[13] Subsequent treatment of the product **12** with the bis-benzyl-protected 2,4-dihydroxybenzaldehyde **13**[14] afforded the deazaflavin **14**, which was alkylated to **15** with pentyl bromide to increase the solubility of the model compounds. Cleavage of the Boc group to yield **9** and reaction with the bis-carboxymethyl-substituted cyclobutane derivative, uracil dimer **16**,[12] afforded the bis-deazaflavin model compound **7**. Reaction of **16** with one equivalent of **9** and of the aminoethyl flavin **17**[12b,c] furnished the mixed flavin/deazaflavin-containing model compound **1**. In the model compounds **1** and **7** the 8-OH group of the deazaflavin moiety is benzylated, which prevents its deprotonation and therefore maintains the deazaflavin chromophore in the protonated "OH-form". Hydrogenolytic cleavage of the

[*] Dr. T. Carell, Dipl.-Natw. R. Epple
Laboratorium für Organische Chemie, ETH-Zentrum
Universitätstrasse 16, CH-8092 Zürich (Switzerland)
Fax: (+41) 1-632-1109
E-mail: tcarell@org.chem.ethz.ch

[**] This work was supported by the Swiss National Science Foundation and by the ETH Zurich. We thank J. Wytko-Weiss for a careful inspection of the manuscript and Prof. F. Diederich for his generous support.

 © WILEY-VCH Verlag GmbH, D-69451 Weinheim, 1998 1433-7851/98/3707-0938 $ 17.50+.50/0



Scheme 2. Synthesis of the model compounds **1**, **2**, **6**–**8**. a) BnOH, 120°C, 4 h, 70%; b) DMF, 120°C, 12 h, 65%; c) pentyl bromide, DMF, $CsCO_3$, 1 d, 80%; d) conc. trifluoroacetic acid (TFA), room temperature, 1 h, quant.; e) AcOH, Pd/$BaSO_4$, H_2, 1 h, 90%. TFA^- = trifluoroacetate.

benzyl group in **1** and **7** with Pd/$BaSO_4$ catalyst in acetic acid and the adjustment of the pH to above 7 ($pKa_{8\text{-}OH} = 6$) yielded the model compounds **2** and **8**, which contain the deazaflavin cofactor in the deprotonated "8-(O^-) form".[4]

Initial measurements were performed to clarify whether or not deazaflavins are able to initiate the electron-transfer-based repair in the absence of a flavin chromophore. To this end, the bis-deazaflavin model compounds **7** and **8** were dissolved in ethylene glycol, acetonitrile, or DMF, and triethylamine was added to ensure basic conditions. The cleavage rate of the model compounds **7** and **8** to **4** and **5** (Scheme 1) was investigated with a recently described assay:[12] The solutions were purged with N_2 and irradiated at a given wavelength. After certain time intervals, small aliquots were removed and analyzed by reverse phase HPLC. For the determination of the quantum yields ϕ (ϕ = number of reacted molecules/number of absorbed photons), the photon flux of the monochromatic light beam was measured with ferrioxalate actinometry.[15] In the case of the model compounds **7** and **8**, however, even intense irradiation for more than 60 min yielded no photoconversion. In particular, none of the expected photoproducts **4** and **5** ($\phi < 10^{-4}$) were detected. Reduction of the deazaflavin in **7** to **7**-H_4 and subsequent irradiation ($\lambda > 350$ nm)[16] also gave no photoproduct **4**. In contrast, the reduced flavin-containing model compound **6**-H^-[12b] cleaved under comparable conditions within minutes ($\tau_{1/2} \approx 15$ min) to the expected photoproduct **3**. These experiments show that oxidized and reduced deazaflavins are unable to initiate the cleavage reaction with a substantial quantum yield.[4, 5]

In order to clarify the effect of the protonation status of the deazaflavin on the energy transfer, a variety of methods were explored to reduce the flavin-moiety to **1**-H^- or **2**-H^{2-} selectively in the presence of the protonated (benzylated) and the deprotonated deazaflavin species. In model compound **1** photoreduction finally proved to be successful. Anaerobic solutions of the model compound **1** were irradiated at $\lambda = 480$ nm, and a small amount of triethylamine was added as the $H^\bullet$ donor and to ensure deprotonation of the reduced flavin. Reduction of the flavin unit in the model compound **2** to **2**-H^{2-} was achieved with sodium dithionite/triethylamine.[17] UV spectra of the semireduced model compounds **1**-H^- and **2**-H^{2-} (Figure 1) prove that the flavin moiety was

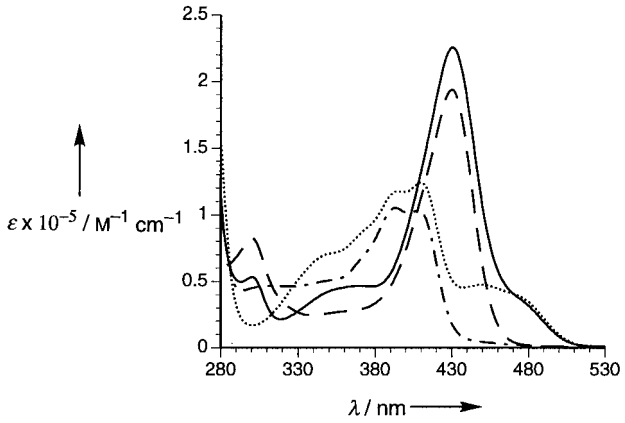


Figure 1. UV spectra of the model compounds **1** and **2** in their oxidized and semireduced forms (10^{-5} M in ethylene glycol). —— **1** (oxidized), – – – – **1**-H^- (semireduced), ···· **2** (oxidized), ·–·–·–· **2**-H^{2-} (semireduced).

successfully reduced. They show the disappearance of the oxidized flavin absorption at 340–360 nm and 450–520 nm and the intact absorption of the oxidized deazaflavin moieties at 390–410 nm (**1**-H^-) and 430 nm (**2**-H^{2-}).

The fluorescence spectra of bis-deazaflavin model compounds **7** and **8** showed strong fluorescence at 430 nm (**7**) and 470 nm (**8**) (Figure 2) corresponding to the protonated (benzylated) and the deprotonated oxidized deazaflavin, respectively.[18] Within the mixed cofactor model compounds **1** and **2**, however, the fluorescence of both deazaflavin moieties is quenched and stays significantly quenched even upon reduction of the flavins to **1**-H^- and **2**-H^{2-}. The experiments indicate the presence of an efficient energy transfer from both types of deazaflavins to the oxidized and the reduced flavin species in our model compounds. In

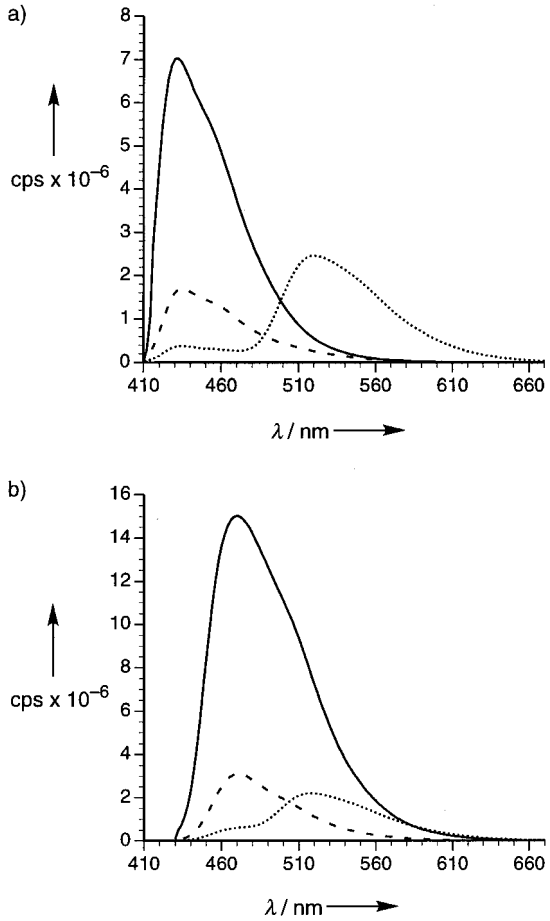


Figure 2. Comparison of the fluorescence spectra of the model compounds **1** and **2** in their oxidized and semireduced states and the bis-deazaflavin model compounds **7** and **8** (cps = counts per second). a) Protonated (benzylated) deazaflavin species (10^{-6} M in ethylene glycol, excitation wavelength 410 nm,) – **7** (5×10^{-7} M), – – – – **1**-H$^-$ (semireduced), ···· **1** (oxidized). b) Deprotonated deazaflavin species (10^{-6} M, excitation wavelength 430 nm, ethylene glycol) —— **8** (5×10^{-7} M), – – – – **2**-H^{2-} (semireduced), ···· **2** (oxidized). Flavin fluorescence is observed at 520 nm.

agreement with enzymatic studies, reduction of the flavin caused an increase of the fluorescence intensity. This can be explained by the lowered extinction coefficient of the reduced flavin, which results in a smaller spectral overlap between the deazaflavin fluorescence and the flavin absorption and consequently yields a less efficient energy transfer.[19]

Finally, action spectra were measured for both semireduced model compounds **1**-H$^-$ and **2**-H^{2-} for comparison with the reduced flavin-only model compound **6**-H$^-$ to quantify the effect of the deazaflavin–flavin interaction in both model compounds **1**-H$^-$ and **2**-H^{2-} on the photoinduced cyclobutane ring cleavage (Figure 3). The reference compound **6**-H$^-$ shows, as expected, maximal cleavage at 370 nm. In the presence of an oxidized and protonated (benzylated) deazaflavin (model compound **1**-H$^-$), this maximal cleavage wavelength is shifted from 370 nm to 390/410 nm. These are the wavelengths at which the benzylated deazaflavin features maximal absorption. Investigation of the model compound **2**-H^{2-} reveals maximal cleavage at 430 nm (a 60 nm shift!), where the deprotonated deazaflavin species possesses its absorption maximum. The latter result (430 nm) is in full

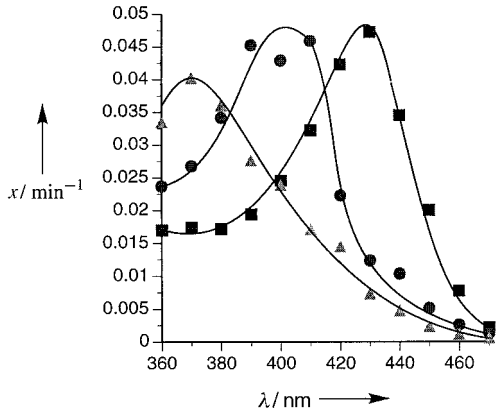


Figure 3. Action spectra of **1**, **2**, and **6** measured in ethylene glycol (5×10^{-5} M; 400 W xenon lamp, double grating monochromator, 3.4 nm bandwith, photon flux 5×10^{-7} Einstein min^{-1} ± 20%. x = relative conversion; ■ = **2**-H^{2-}, ● = **1**-H$^-$, ▲ = **6**-H$^-$.

agreement with studies at the *A. nidulans* photolyase[6] and confirms the presence of the deprotonated deazaflavin cofactor in these enzymes. These results, together with the finding that oxidized deazaflavins alone are unable to initiate the cleavage, support the view that the deazaflavin cofactor functions entirely as a photoantenna. The experiments reveal that both types of deazaflavins (protonated and deprotonated) would be able to perform the antenna function, and further measurements are now required to clarify why photolyases prefer to deprotonate the deazaflavin.

Table 1 summarizes the quantum yields for the cleavage reactions measured under our conditions. The best yield (ϕ = 0.031) was obtained for the flavin-containing compound **6**-H$^-$;

Table 1. Wavelength of maximal activity (λ_{max}) and averaged quantum yield ϕ (±25%, 5×10^{-5} M solutions) of the cleavage reaction, measured in ethylene glycol.[23]

Cmpd.	R^1	R^2	$\lambda_{max.}$ [nm]	ϕ
1-H$^-$	FlH$^-$	dFl-OBn	400	0.014
1-H$_3^-$	FlH$^-$	dFlH$_2$-OBn	370	0.030
2-H^{2-}	FlH$^-$	dFl-O$^-$	430	0.012
6-H$^-$	FlH$^-$	Pentyl	370	0.031
7	dFl-OBn	dFl-OBn	–	$< 10^{-4}$
8	dFl-O$^-$	dFl-O$^-$	–	$< 10^{-4}$

in this system absorbed photons are most efficiently used for the dimer cleavage. Despite the observation that in deazaflavin-dependent photolyases the quantum yield remains high in the presence of the deazaflavin cofactor, the quantum yields of the deazaflavin-containing models compound **1**-H$^-$ and **2**-H^{2-} are significantly decreased to ϕ = 0.012 (**2**-H^{2-}) and ϕ = 0.014 (**1**-H$^-$). Particularly interesting is the finding that the maximal cleavage rates are very similar for all three model compounds **1**-H$^-$, **2**-H^{2-} and **6**-H$^-$, which shows that the deazaflavins are unable to improve the reaction rates in our model compounds. In order to clarify how the oxidation state of the deazaflavin influences the cleavage rate, we reduced the deazaflavin unit in **1**-H$^-$ to **1**-H$_3^-$ during an irradiation experiment at 370 nm by addition of a dithionite solution. This reduction yielded an immediate improvement of the

 © WILEY-VCH Verlag GmbH, D-69451 Weinheim, 1998 1433-7851/98/3707-0940 $ 17.50+.50/0

cleavage rate ($\phi = 0.014$ jumps to $\phi = 0.03$), which shows that the nonabsorbing, reduced deazaflavin does not influence the flavin-driven cleavage rate. We currently have no explanation why the oxidized deazaflavins cause no cleavage rate increase. One reason clearly is that in the presence of a light-absorbing deazaflavin fewer photons are directly absorbed by the reduced flavin unit. Based on our cleavage results at 400 nm and 430 nm, however, we suspect that we also have to consider an alternative intercofactor electron transfer process from the reduced, photoexcited flavin to the oxidized deazaflavin, which would lower the cleavage efficiency. Such an electron transfer would be not entirely unexpected. The redox potentials show that an electron transfer from the photoexcited reduced flavin ($E^{*}_{ox} = -2.8$ V)[20] at least to the deazaflavin unit ($E_{red} \approx -0.9$ V)[21, 22] is more favorable then to the dimer unit ($E_{red} = -2.2$ V).[20]

With the help of the first flavin- and deazaflavin-containing model compounds and with selective reduction procedures for the corresponding flavin units in these compounds, it was possible to show that deazaflavins alone are unable to initiate the cleavage of cyclobutane-linked pyrimidine dimers at wavelengths above $\lambda = 350$ nm. Both the protonated (benzylated) and the deprotonated deazaflavins are able to transfer excitation energy to an oxidized and to a reduced flavin unit. The energy transfer process causes a shift of the maximal repair wavelength from 370 nm to 400 nm and 430 nm for the protonated and deprotonated deazaflavins, respectively. The observation that the presence of the deazaflavins does not improve the cleavage rate could mean that an alternative electron transfer between the reduced flavin and the oxidized deazaflavin interferes with the cleavage reaction in our model compounds. Within the enzyme such an electron transfer would jeopardize the DNA-repair function, and maybe, DNA-photolyases prefer a large separation between cofactors to suppress this process.

Received: October 8, 1997 [Z11016IE]
German version: *Angew. Chem.* **1998**, *110*, 986 – 989

Keywords: DNA repair · electron transfer · flavins · photolyases · UV lesions

[1] E. C. Friedberg, G. C. Walker, W. Siede, *DNA Repair and Mutagenesis*, ASM Press, Washington DC, **1995**.
[2] E. Fahr, *Angew. Chem.* **1969**, *81*, 581 – 632, *Angew. Chem. Int. Ed. Engl.* **1969**, *8*, 578 – 593 and references therein. See also G. M. Blackburn, R. J. H. Davies, *J. Chem Soc. C* **1966**, 2239 – 2244; R. B. Setlow, *Photochem. Photobiol.* **1968**, *7*, 643 – 649.
[3] Recent reviews: A. Sancar, *Biochemistry* **1994**, *33*, 1 – 9; S.-T. Kim, A. Sancar, *Photochem. Photobiol.* **1993**, *57*, 895 – 904; P. F. Heelis, S.-T. Kim, T. Okamura, A. Sancar, *J. Photochem. Photobiol. B. Biol.* **1993**, *17*, 219 – 228; P. F. Heelis, R. F. Hartman, S. D. Rose, *Chem. Soc. Rev.* **1995**, 289 – 297; T. Carell, *Angew. Chem.* **1995**, *107*, 2697 – 1700, *Angew. Chem. Int. Ed. Engl.* **1995**, *34*, 2491 – 2495.
[4] C. Walsh, *Acc. Chem. Res.* **1986**, *19*, 216 – 221.
[5] M. S. Jorn, *J. Am. Chem. Soc.* **1987**, *109*, 3133 – 3136; S. E. Rokita, C. T. Walsh, *ibid.* **1984**, *106*, 4589 – 4595.
[6] K. Malhotra, S.-T. Kim, C. Walsh, A. Sancar, *J. Biol. Chem.* **1992**, *267*, 15406 – 15411; G. Payne, M. Wills, C. Walsh, A. Sancar, *Biochemistry* **1990**, *29*, 5706-5711.
[7] A. P. M. Eker, R. H. Dekker, W. Berends, *Photochem. Photobiol.* **1981**, *33*, 65 – 72; Y. Yasui, M. Takao, A. Oikawa, A. Kiener, C. T. Walsh, A. P. M. Eker, *Nucleic Acids Res.* **1988**, *16*, 4447 – 4463.
[8] S.-T. Kim, P. F. Heelis, A. Sancar, *Biochemistry* **1992**, *31*, 11244 – 11248.
[9] *E. coli* structure: H. W. Park, S.-T. Kim, A. Sancar, J. Deisenhofer, *Science* **1995**, *268*, 1866 – 1872; *A. nidulans* structure: T. Tamada, K. Kitadokoro, Y. Higuchi, K. Inaka, A. Yasui, P. E. de Ruiter, A. P. M. Eker, K. Miki, *Nature Struct. Biol.* **1997**, *11*, 887 – 891.
[10] P. F. Heelis, *J. Photochem. Photobiol. B* **1997**, *38*, 31 – 34.
[11] G. R. Fleming, *Chimia* **1997**, *7*, 365; N. Krauss, W.-D. Schubert, O. Klukas, P. Fromme, H. T. Witt, W. Saenger, *Nature Struct. Biol.* **1996**, *3*, 965 – 973; recent review: R. van Grondelle, J. P. Dekker, T. Gillbro, V. Sundstrom, *Biochim. Biophys. Acta* **1994**, *1187*, 1 – 65.
[12] a) T. Carell, R. Epple, V. Gramlich, *Angew. Chem.* **1996**, *108*, 676 – 679; *Angew. Chem. Int. Ed. Engl.* **1996**, *35*, 620 – 623; b) R. Epple, E. U. Wallenborn, T. Carell, *J. Am. Chem. Soc.* **1997**, *119*, 7440-7451; c) T. Carell, R. Epple, V. Gramlich, *Helv. Chim. Acta* **1997**, *80*, 2191 – 2203.
[13] W. Pfleiderer, G. Nübel, *Justus Liebigs Ann. Chem.* **1959**, *631*, 168 – 174.
[14] T. Kimachi, K. Tanaka, F. Yoneda, *J. Heterocycl. Chem.* **1991**, *28*, 439 – 443.
[15] C. G. Hatchard, C. A. Parker, *Proc. R. Soc. A* **1956**, *235*, 518 – 536; A. M. Braun, M. T. Maurette, E. Oliveros, in *Photochemical Technology*, Wiley, Chichester, **1991**, pp. 77 – 81; S. L. Murov in *Handbook of Photochemistry*, Marcel Dekker, New York, **1973**, pp. 119-123.
[16] At 300 nm irradiation, a deazaflavin-dependent photocleavage was observed in photolyases in which FAD was replaced by a 5′-deaza-FAD (dFAD): A. J. Ramsey, M. S. Jorns, *Biochemistry* **1992**, *31*, 8437 – 8441.
[17] The dithionite reduction causes not only the reduction of the flavin unit but can also give rise to a small portion of a SO_3 adduct. Very similar results were obtained on repeating experiments with differents amounts of dithionite, which indicates that in our case adduct formation does not interfere with the experimental results. Photoreduction of the flavin in the presence of a deprotonated deazaflavin was unexpectedly unsuccessful.
[18] E. Purwantini, B. Mukhopadhyay, R. W. Spencer, L. Daniels, *Anal. Biochem.* **1992**, *205*, 342 – 350.
[19] M. Julliard, M. Chanon, *Chem. Rev.* **1983**, *83*, 425 – 506, or any text book of photochemistry, for example H. G. O. Becker *Einführung in die Photochemie*, Deutscher Verlag der Wissenschaften, Berlin, **1991**.
[20] M. P. Scannell, D. J. Fenick, S.-R. Yeh, D. E. Falvey *J. Am. Chem. Soc.* **1997**, *119*, 1971 – 1977.
[21] P. A. J. Link, H. C. van der Plas, *J. Org. Chem.* **1986**, *51*, 1602 – 1604.
[22] For deazaflavin radicals and photochemistry, see for example: H. Fenner, H. H. Roessler, P. Hemmerich in *Flavins and Flavoproteins* (Ed.: T. P. Singer), Elsevier, Amsterdam, **1976**, Chapter 36: "Structure and Reactivity of 5-Deazaflavins"; H.-J. Duchstein, H. Fenner, P. Hemmerich, W.-R. Knappe, *Eur. J. Biochem.* **1979**, *95*, 167 – 181; M. Goldberg, I. Pecht, H. E. A. Kramer, R. Traber, P. Hemmerich, *Biochim. Biophys. Acta* **1981**, *673*, 570 – 593.
[23] The presented quantum yields are preliminary due to the rather high concentrations (5×10^{-5} M), which were required for the measurements. All quantum yield measurements were performed under identical conditions within a short period of time to ensure maximal comparability of the data. We observed a very strong solvent dependence of the cleavage reaction in deazaflavin-containing model compounds. Best data were obtained in ethylene glycol (5×10^{-5} M)).

 © WILEY-VCH Verlag GmbH, D-69451 Weinheim, 1998 1433-7851/98/3707-0941 $ 17.50+.50/0

Extended Thienylenevinylene Oligomers as Highly Efficient Molecular Wires**

Isabelle Jestin, Pierre Frère, Philippe Blanchard, and Jean Roncali*

Linear π-conjugated oligomers with a well-defined chemical structure have been intensively investigated to simulate the electronic and electrochemical properties of the corresponding polydisperse polymers.[1] More recently, their possible use as molecular wires in molecular electronics or nanoscopic systems has attracted particular attention.[2] Although most of the work in these two areas has involved oligomers of intermediate chain length ($n = 2-10$),[1, 2] the synthesis of highly extended π-conjugated oligomers is of crucial importance for several reasons. On one hand, the use of π-conjugated oligomers as molecular wires in nanoscopic systems requires dimensions approaching the *present limit of nanopatterning techniques (namely the 100 Å gap regime).*[2c] *On the other hand, as the oligomeric model postulates that the properties of an oligomer series would approach those of the polymer as chain length increases, the analysis of the ultimate electronic properties of highly extended systems should permit assessment of the relevance of the oligomeric model and/or give evidence of novel properties.*

The recently synthesized hexadecamers of the oligothiophenes,[3] oligo(phenylenethynylene)s [4] and oligo(thiophenethynylene)s[5] series are the longest clearly characterized linear π-conjugated systems. Although the size of these molecules (65–120 Å) make them potentially interesting as molecular wires, these various classes of oligomers show a rapid saturation of effective conjugation with chain extension. In other words, the ultimate values of the oxidation potential and HOMO–LUMO gap are attained far before the maximum chain length (at $n = 10-12$ for oligothiophenes[1, 3] and $n = 8$ for oligo(phenylenethynylene)s and oligo(thienylenethynylene)s).[4, 5] As this saturation originates from π-electron confinement related to structural factors such as rotational disorder or resonance stabilization energy of the aromatic ring,[6] oligomeric systems in which such effects are minimized may even surpass the present limit.

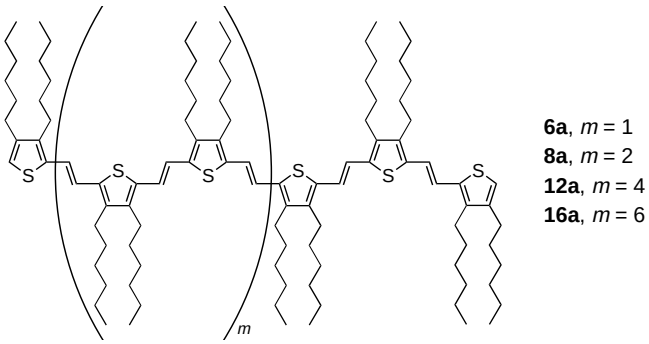
Although the excellent electron transmission efficiency of oligo(thienylenevinylene)s (nTVs) has been demonstrated in nonlinear optical chromophores[7] or extended tetrathiafulvalene analogues,[8] this class of conjugated oligomers has been scarcely considered until now. nTVs up to $n = 7$ were first synthesized by Kossmehl et al. by a succession of formylation reactions and Wittig olefinations.[9] More recently a slightly different approach was reported by Nakayama et al.; however, the insolubility of nTVs did not allow the $n = 7$ limit to be surpassed.[10]

[*] Prof. J. Roncali, Dr. I. Jestin, Dr. P. Frère, Dr. P. Blanchard
Ingénierie Moléculaire et Matériaux Organiques
CNRS UMR 6501, Université d'Angers
2 Bd Lavoisier, F-49045 Angers (France)
Fax: (+33) 02-4173-5405
E-mail: jean.roncali@univ-angers.fr

[**] We thank Dr. B. Illien (IMMO) for geometry optimization and Dr. J. C. Blais (LCSOB), University Paris VI, for recording the MALDI-TOF spectra.

We recently described the synthesis of alkyl-substituted soluble nTVs.[11] The chain length dependence of the electrochemical and electronic properties gave no evidence of saturation up to the decamer ($n = 10$), but further chain extension was hampered by solubility problems.

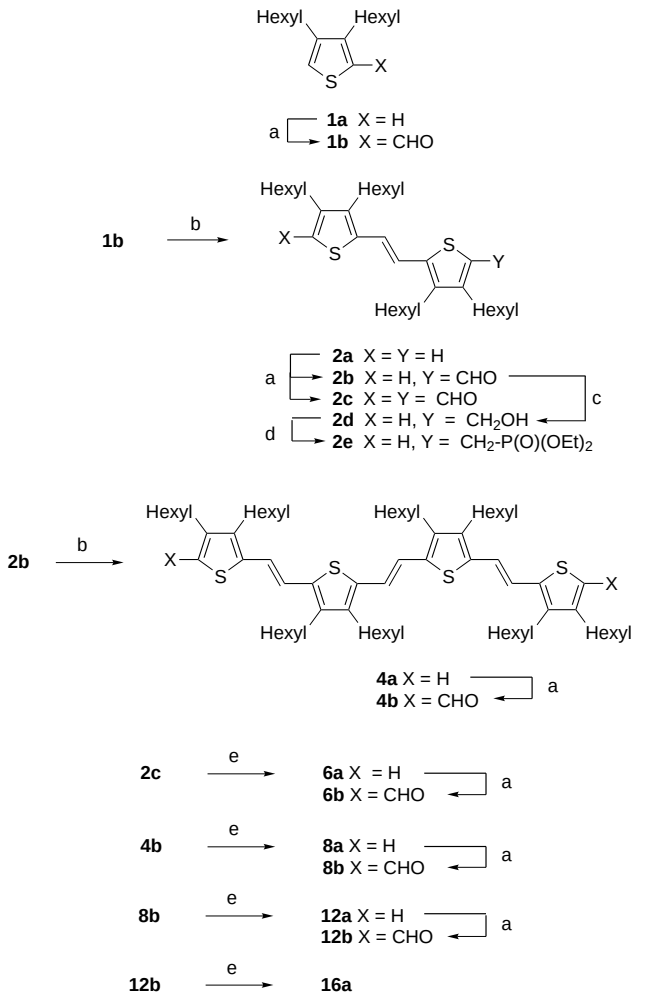
We report here on the synthesis and characterization of novel soluble nTVs based on 3,4-dihexylthiophene (**2a**, **4a**, **6a**, **8a**, **12a**, and **16a**) and on the analysis of the chain length dependence of their electrochemical and electronic properties. Except for the dimer (**2a**) and tetramer (**4a**), all longer nTVs have been synthesized by twofold Wittig–Horner olefination of dicarbaldehydes with phosphonate **2e** (Scheme 1). Although McMurry dimerization[12] leads to doubling of the chain length at each iterative step,[10,11] we finally opted for the double Wittig–Horner route because of the increasing difficulty to achieve monoformylation selectively as the chain length increases.



Dithienylethylene **2a** was prepared by McMurry coupling of 3,4-dihexylthiophene carbaldehyde (**1b**). Mono- and dialdehydes **2b** and **2c** were prepared by Vilsmeier formylation of **2a** with appropriate amounts of reagents. McMurry coupling of **2b** yielded the tetramer **4a**, while the hexamer **6a** was prepared by double Wittig–Horner olefination of **2c** with **2e**. Vilsmeier bisformylation of **4a** and twofold Wittig–Horner olefination of the resulting dialdehyde (**4b**) gave the octamer **8a**. Repetition of this procedure yielded the dodecamer **12a** and hexadecamer **16a** (Table 1), which are the longest ever reported nTVs (70 and 94 sp^2 carbon atoms). Optimization of the geometry of **16a** by the MM+ method (Hyperchem 5.0) gave a chain length of 95 Å, in good agreement with the value estimated from the X-ray structure of the tetramer.[13]

Table 2 lists the main cyclic voltammetry (CV) data for nTVs. As expected, chain extension leads to a negative shift of the redox potentials and to an increase in the number of accessible redox states. Whereas the CV of **2a** shows a first anodic peak indicative of an irreversible process (the subsequent polymerization),[14] that of **4a** exhibits two well-defined reversible one-electron oxidation waves corresponding to the successive generation of the cation radical and dication ($E_{pa}1$ and $E_{pa}2$). Chain extension produces a decrease in the difference $E_{pa}2 - E_{pa}1$, indicative of a reduction of Coulombic repulsion between positive charges in the dication. Thus, for **6a** the two oxidation peaks are almost merged into a single wave, and a third peak corresponding to the generation

 © WILEY-VCH Verlag GmbH, D-69451 Weinheim, 1998 1433-7851/98/3707-0942 $ 17.50+.50/0



Scheme 1. a) $POCl_3$, DMF/1,2-dichloroethane, reflux; b) $TiCl_4$, Zn, THF, reflux; c) $NaBH_4$, CH_2Cl_2/methanol, room temperature; d) PBr_3, toluene/benzene, $-10^\circ C$, then NaH, $HPO(OEt)_2$, THF, $-10^\circ C$, then reflux; e) *t*BuOK, THF, 3 equiv **2e**, room temperature.

Table 1. Selected spectroscopic data for **4a**, **6a**, **8a**, **12a** and **16a**.

4a: Yield 86%, m.p. 76°C (decomp.), ^1H NMR (500 MHz, $CDCl_3$): $\delta = 6.99$ (s, 4H, outer C*H*=C*H*), 6.98 (s, 2H, central C*H*=C*H*), 6.76 (s, 2H, thioph.), 2.64–2.56 (m, 12H), 2.49 (t, 4H, $^3J = 7.7$ Hz), 1.63 (q, 4H, $^3J = 7.7$ Hz), 1.56–1.51 (m, 12H), 1.41–1.35 (m, 48H), 0.93–0.90 (m, 24H, CH_3). ^{13}C NMR (67.5 MHz, $CDCl_3$): $\delta = 143.41, 141.48, 141.42, 139.99, 137.11, 134.99, 119.84, 119.37, 119.23, 117.90, 31.73, 31.58, 31.22, 31.18, 30.92, 29.63, 29.50, 29.36, 29.27, 29.02, 27.01, 26.88, 22.60, 14.14–14.07$. MS(FAB): m/z (%) = 1081 (100) [M^+](calcd for $C_{70}H_{112}S_4$) = 1080.76. C,H,S analysis (calcd): C 77.40 (77.71), H 10.69 (10.43); S 11.21 (11.85).

6a: Yield 84%, m.p. 134°C (decomp.), ^1H NMR (500 MHz, $CDCl_3$): $\delta =$ 7.00 (s 10H), 6.77 (s, 2H), 2.65–2.57 (m, 20H), 2.50 (t, 4H, $^3J = 7.7$ Hz), 1.63 (q, 4H, $^3J = 7.7$ Hz), 1.56–1.52 (m, 20H), 1.43–1.34 (m, 72H), 0.95–0.91 (m, 36H). MS(FAB): m/z (%) = 1634 (100) [M+H^+] (calcd for $C_{106}H_{168}S_6$) = 1633.14.

8a: Yield 64%, m.p. 171°C (decomp.), ^1H NMR (500 MHz, $CDCl_3$): $\delta =$ 6.99 (s, 14H), 6.76 (s, 2H), 2.61 (s, 28H) 2.50 (t, 4H, $^3J = 7.6$ Hz), 1.65–1.37 (m, 128H), 0.94–0.92 (m, 48H). MS(FAB): m/z(%) = 2186 (100) [M+H^+] (calcd for $C_{142}H_{224}S_8$) = 2185.53. C,H,S analysis (calcd): C 77.69 (77.96), H 10.25 (10.32), S 11.77 (11.72).

12a: Yield 55%, m.p. 224°C (decomp.), ^1H NMR (270 MHz, $CDCl_3$): $\delta =$ 7.03 (s, 22H), 6.79 (s, 2H), 2.64 (s, 44H), 2.52 (t, 4H, $^3J = 7.6$ Hz), 1.66–1.29 (m, 192H) 1.00–0.92 (m, 72H). MS(MALDI-TOF): m/z(%) = 3295.37 (100) [M^+] (calcd for $C_{214}H_{336}S_{12}$) = 3293.74. C,H,S analysis (calcd): C 77.79 (78.04), H 10.30(10.28), S 11.64 (11.68).

16a: Yield 30%, m.p. 250°C (decomp.), ^1H NMR (500 MHz, $CDCl_3$): $\delta =$ 7.00 (s, 30H), 6.77 (s, 2H), 2.62 (s, 60H), 2.50 (t, 4H, $^3J = 7.4$ Hz), 1.64–1.38 (m, 256H), 0.95 (s, 96H). MS(MALDI-TOF): m/z (%) = 4402.4 (100) [M^+] (calcd for $C_{286}H_{448}S_{16}$) = 4399.66. C,H,S analysis (calcd): C 77.58 (78.08), H 10.19 (10.26), S 11.42 (11.66).

Table 2. Cyclic voltammetry data for nTVs.[a]

Compd	$E_{pa}1$ [V]	$E_{pa}2$ [V]	$E_{pa}3$ [V]	$E_{pa}4$ [V]	$E_{pa}5$ [V]	$E_{pa}6$ [V]
2a	0.96	1.30				
4a	0.59	0.79				
6a	0.50	0.56	1.10			
8a	0.46		0.80	0.92		
12a	0.42		0.59		0.97	
16a	0.40		0.47		0.70	0.99

[a] 10^{-4} M substrate in 2×10^{-1} M Bu_4NPF_6/CH_2Cl_2; Pt electrodes; reference electrode: saturated calomel electrode (SCE); scan rate 100 mV s^{-1}.

of the trication radical appears at 1.10 V ($E_{pa}3$) (Figure 1). Coalescence of the two peaks occurs for **8a**, and the dication is formed directly through a two-electron transfer (as confirmed by the 30 mV difference between $E_{pa}1$ and the potential of the corresponding cathodic peak). This two-electron wave is followed by two one-electron peaks assigned to the formation of the trication radical and tetracation ($E_{pa}3$ and $E_{pa}4$). Further chain extension to **12a** leads to the coalescence of $E_{pa}3$ and $E_{pa}4$ and a new peak corresponding to the pentacation radical at 0.97 V ($E_{pa}5$). For **16a**, the CV shows two very close two-electron waves, a negative shift of $E_{pa}5$ to 0.70 V, and formation of the hexacation at 0.99 V ($E_{pa}6$). This general behavior is reminiscent of that reported by Heinze et al. for the reduction of oligo(phenylenevinylene)s.[15]

These results are summarized by the diagram in Figure 2 in which the potential of formation of the various cationic states are plotted against the number of carbons in the conjugated chain (n). The two first convergence points at $n = 46$ and $n =$ 70 correspond to the first and second bielectronic transfers $E_{pa}1$ and $E_{pa}2$ (**8a**) and $E_{pa}3$ and $E_{pa}4$ (**12a**). Extrapolation of this series of lines suggests a common convergence limit beyond $n = 120-130$. This hypothetical convergence point should correspond to the single-step multi-electron oxidation of the whole conjugated chain through a process ressembling the p-doping of the parent polythienylenevinylene (PTV).[16b]

The main optical data listed in Table 3 show that chain extension leads to an increase of the molecular extinction coefficient (ε), to a red shift of λ_{max}, and to a narrowing of the HOMO–LUMO gap as reflected by the long-wavelength absorption edge (λ_{edge}).[17] Comparison of the optical data for **16a** with those for hexadecamers with the same n value and similar or even larger dimensions such as hexadeca-1,4-phenylenethynylene (128 Å, $\lambda_{max} = 376$ nm)[4] and hexadecathiophenethynylene (100 Å, $\lambda_{max} = 442$ nm, $\varepsilon = 210000$)[5] clearly shows that **16a** exhibits the largest effective conjugation.

Although the band gap of solution-processed films of the octamer derived from 3-octylthiophene (1.70 eV)[11] is already slightly smaller than that of PTV (1.70–1.80 eV),[16] the optical data for **12a** and **16a** suggests that they should exhibit

 © WILEY-VCH Verlag GmbH, D-69451 Weinheim, 1998 1433-7851/98/3707-0943 $ 17.50+.50/0

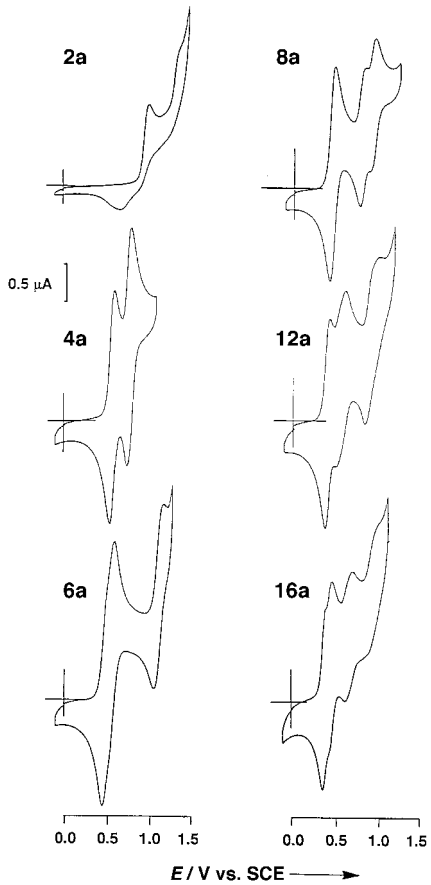


Figure 1. Cyclic voltammograms of *n*TVs. For experimental conditions see footnote [a] of Table 2.

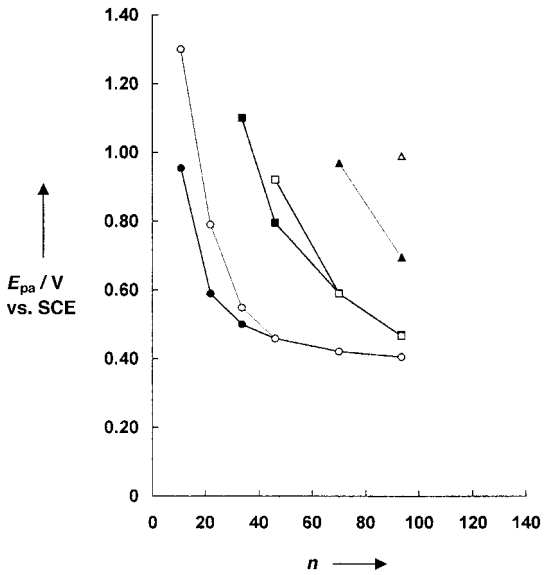


Figure 2. Anodic peak potential of the various oxidation steps for *n*TVs plotted against the number *n* of carbon atoms in the conjugated system. ●: radical cation; ○: dication; ■: radical trication; □: tetracation; ▲: radical pentacation; △: hexacation.

even smaller band gaps. This is confirmed by the solid-state optical spectra of solution-cast films of **12a** and **16a** (Figure 3). Whereas the persistence of the vibronic fine structure is consistent with a well-ordered material, the low-energy

Table 3. UV/Vis absorption data for *n*TVs in CH_2Cl_2.

Compd	λ_{max} [nm]	λ_{edge} [nm]	ε_{max} [$L\,mol^{-1}\,cm^{-1}$]
2a	360	399	18000
4a	489	552	69500
6a	548	624	109000
8a	574	657	156000
12a	595	679	206000
16a	601	685	319000

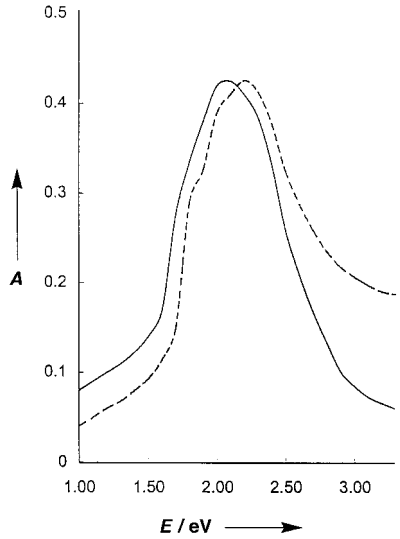


Figure 3. UV/Vis absorption spectra of films of **12a** (dashed line) and **16a** (solid line) cast on glass from a CH_2Cl_2 solution.

absorption edge leads to estimated band gaps of 1.65 and 1.55 eV for **12a** and **16a**, respectively. The 0.10 eV red shift of the absorption edge between **12a** and **16a** seems to indicate that in the solid state, saturation of the effective conjugation has not yet been reached for **16a.** This suggests possible further band gap reduction for longer oligomers.

As already discussed, all series of π-conjugated oligomers investigated so far exhibit saturation of effective conjugation for a certain chain length, which depends on the structure.[1, 3–6] The *n* value of the limit of the HOMO–LUMO gap and the band gap thus represents a measure of the relative efficiency of a given oligomeric system for use as molecular wires. Since nTVs exhibit the highest increase of effective conjugation per incremental carbon and the smallest gap among known π-conjugated oligomers, they are at present the most efficient extended molecular wires.

The trends in electrochemical and optical data on extension of the chain length and the indication that the saturation limit has not been reached yet provide a strong inducement to pursue chain extension: the synthesis of the higher oligomers up to the 20- to 25-mers is an urgent and exciting goal.

Received: October 24, 1997 [Z11078IE]
German version: *Angew. Chem.* **1998**, *110*, 990–993

Keywords: conducting materials · conjugation · nanostructures · oligomers · thienylenevinylene

 © WILEY-VCH Verlag GmbH, D-69451 Weinheim, 1998 1433-7851/98/3707-0944 $ 17.50+.50/0

[1] a) D. Jones, M. Guerra, L. Favaretto, A. Modelli, M. Fabrizio, G. Distefano, *J. Phys. Chem.* **1990**, *94*, 5761; b) P. Bäuerle, *Adv. Mater.* **1992**, *4*, 102; c) J. Guay, P. Kasai, A. Diaz, R. Wu, J. M. Tour, L. H. Dao, *Chem. Mater.* **1992**, *4*, 1097; d) E. E. Havinga, E. W. Meijer, W. ten Hoeve, H. Wynberg, *Synth. Met.* **1991**, *41–43*, 473; e) J. C. Horne, G. J. Blanchard, E. LeGoff, *J. Am. Chem. Soc.* **1995**, *117*, 9551.
[2] a) A. Aviram, *J. Am. Chem. Soc.* **1988**, *110*, 5687; b) F. Effenberger, H. Schlosser, P. Bäuerle, S. Maier, H. Port, H. C. Wolf, *Angew. Chem.* **1988**, *100*, 274; *Angew. Chem. Int. Ed. Engl.* **1988**, *27*, 281; c) J. Bonvoisin, J. P. Launay, C. Rovira, J. Veciana, *ibid.* **1994**, *106*, 2190 and **1994**, *33*, 2106; d) M. Beley, S. Chodorowski-Kimmes, J. P. Collin, P. Lainé, J. P. Launay, J. P. Sauvage, *ibid.* **1994**, *106*, 1854 and **1994**, *33*, 1775; e) F. Würthner, M. S. Vollmer, F. Effenberger, P. Emele, D. U. Meyer, H. Port, H. C. Wolf, *J. Am. Chem. Soc.* **1995**, *117*, 8090.
[3] P. Bäuerle, T. Fisher, B. Bidlingmeier, A. Stabel, J. Rabe, *Angew. Chem.* **1995**, *107*, 335; *Angew. Chem. Int. Ed. Engl.* **1995**, *34*, 303.
[4] J. S. Schumm, D. L. Pearson, J. M. Tour, *Angew. Chem.* **1994**, *106*, 1445; *Angew. Chem. Int. Ed. Engl.* **1994**, *33*, 1360.
[5] D. L. Pearson, J. M. Tour, *J. Org. Chem.* **1997**, *62*, 1376.
[6] J. Roncali, *Chem. Rev.* **1997**, *97*, 173.
[7] a) V. P. Rao, A. K.-Y. Jen, K. Y. Wong, K. J. Drost, *Tetrahedron Lett.* **1993**, *34*, 1747; b) V. P. Rao, Y. M. Cai, A.K-Y. Jen, *J. Chem. Soc. Chem. Commun.* **1994**, 1689.
[8] a) E. Elandaloussi, P. Frère, J. Roncali, P. Richomme, M. Jubault, A. Gorgues, *Adv. Mater.* **1995**, *7*, 390; b) E. Elandaloussi, P. Frère, J. Roncali, *Tetrahedron Lett.* **1996**, *37*, 6121.
[9] G. Kossmehl, M. Härtel, G. Manecke, *Makromol. Chem.* **1970**, *131*, 15.
[10] J. Nakayama, T. Fujimori, *Heterocycles* **1991**, *32*, 991.
[11] E. Elandaloussi, P. Frère, J. Roncali, *Chem. Commun.* **1997**, 301. E. Elandaloussi, P. Frère, P. Richomme, J. Orduna, J. Garin, J. Roncali, *J. Am. Chem. Soc.* **1997**, *119*, 10774.
[12] J. E. McMurry, *Chem. Rev.* **1989**, *89*, 1513.
[13] I. Jestin, P. Frère, N. Mercier, E. Levillain, J. Roncali, *J. Am. Chem. Soc.*, submitted.
[14] M. Catellani, S. Luzzati, A. Musco, F. Speroni, *Synth. Met.* **1994**, *62*, 223. P. Blanchard, H. Brisset, B. Illien, A. Riou, J. Roncali, *J. Org. Chem.* **1997**, *62*, 2401.
[15] J. Heinze, J. Mortensen, K. Müllen, R. Schenk, *J. Chem. Soc. Chem. Commun.* **1987**, 701; R. Schenk, H. Gregorius, K. Meerholz, J. Heinze, K. Müllen, *J. Am. Chem. Soc.* **1991**, *113*, 2634.
[16] a) S. Yamada, S. Tokito, T. Tsuisui, S. Saito, *J. Chem. Soc. Chem. Commun.* **1987**, 1448; b) J. Barker, *Synth. Met.* **1989**, *32*, 43.
[17] In several works including our previous communication[11] the gap was determined from the very onset of absorption (see R. D. McCullough, R. D. Lowe, M. Jayaraman, D. L. Anderson, *J. Org. Chem.* **1993**, *58*, 904; T. A. Chen, R. Rieke, *Synth. Met.* **1993**, *60*, 175). Since this procedure leads to rather large uncertainties, extrapolation of the absorption edge to zero was used here, although this procedure leads to larger values.

Deprotonated 2,3:5,6-Dibenzo-7-aza bicyclo[2.2.1]hepta-2,5-diene as a Nitrido Nitrogen Source by Anthracene Elimination: Synthesis of an Iodide(nitride)chromium(VI) Complex**

Daniel J. Mindiola and Christopher C. Cummins*

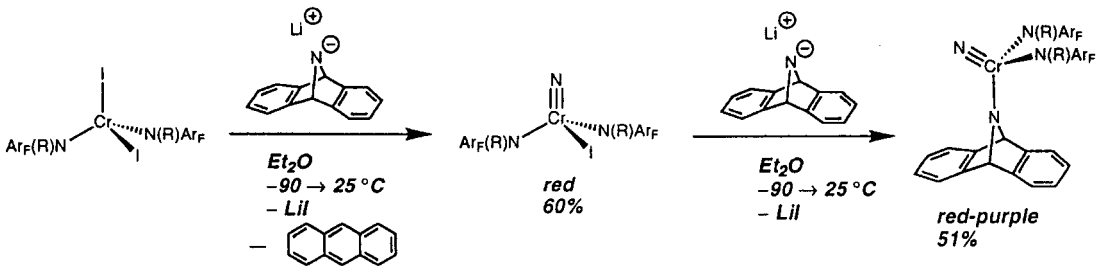
Nitrides constitute an important class of compounds in both solid-state[1, 2] and solution chemistries.[3] A common synthon for the six valence electron N^- ion, which is isoelectronic to an oxygen atom, is the ubiquitous azide ion.[3] Typifying the formation of a nitride from an azide is the classic synthesis of $[Mo(N)(Cl)_3(bpy)]$.[4] Generation of the nitrido functionality from an azide requires a source of two electrons. Therefore, successful syntheses are typically encountered when a d^n ($n \geq 2$) metal center is employed, and the nitride product has a d^{n-2} configuration. Oxidation of the metal center occurs concomitant with dinitrogen expulsion. However, azide is not always optimal for nitride introduction due to a) the explosive nature of many of its compounds, b) the low solubility in nonpolar solvents of salts such as sodium azide, or c) the lack of steric protection which can lead to multiple or unselective substitutions.

In connection with recent investigations of chromium(VI) organometallic chemistry[5, 6] we required the iodide–nitride complex $[Cr(I)(N)(NRAr_F)_2]$ ($R = C(CD_3)_2CH_3$, $Ar_F = 2,5\text{-}C_6H_3FMe$). Attempts to synthesize the compound from the corresponding azide were unsuccessful. Although the corresponding nitrosyl derivative $[Cr(I)(NO)(NRAr_F)_2]$ has been prepared,[7] attempts to deoxygenate it with vanadium(III)[5] have been unsuccessful, a circumstance attributable to the presence of a reactive iodide functionality. Here we describe the successful synthesis of $[Cr(I)(N)(NRAr_F)_2]$ by the reaction of d^2-$[Cr(I)_2(NRAr_F)_2]$ with $[Li(dbabh)(OEt_2)]$, where Hdbabh is 2,3:5,6-dibenzo-7-azabicyclo[2.2.1]hepta-2,5-diene).[8] This chemistry shows that Hdbabh can be considered an organic analogue of hydrazoic acid in the context of transition metal nitride chemistry.

The amine Hdbabh was prepared by the literature method,[8] and treated with *n*-butyllithium to form $[Li(dbabh)(OEt_2)]$. The chromium(IV) precursor $[Cr(I)_2(NRAr_F)_2]$ was obtained in 82% yield as a black solid following treatment of $[Cr(NRAr_F)_3]$[5] with iodine. Treatment of $[Cr(I)_2(NRAr_F)_2]$ with of $[Li(dbabh)(OEt_2)]$ in ether elicited a color change to redbrown and ultimately produced diamagnetic [Cr(I)(N)-

[*] Prof. Dr. C. C. Cummins, D. J. Mindiola
Department of Chemistry, room 2–227
Massachusetts Institute of Technology
77 Massachusetts Ave.
Cambridge, MA 02139-4307 (USA)
Fax: (+1) 617-253-7030
E-mail: ccummins@mit.edu

[**] C. C. C. grateful for funding from a Packard Foundation Fellowship (1995–2000), an Alfred P. Sloan Foundation Fellowship (1997–2000), a National Science Foundation CAREER Award (CHE-9501992), a 3M Innovation Fund Award (1996–1997), einen DuPont Young Professor Award (1995–1998) and a Union Carbide Innovation Recognition Award (1996–1997). Dr. A. L. Odom and Dr. W. M. Davis are acknowledged for their assistance with X-ray diffraction studies. R. Baumann's assistance is also acknowledged.



Scheme 1. $R = C(CD_3)_2CH_3$, $Ar_F = 2,5\text{-}C_6H_3FMe$.

$(NRAr_F)_2]$ along with anthracene in essentially quantitative yields, according to ^1H NMR spectra of crude reaction mixtures (Scheme 1). Following removal of anthracene, $[Cr(I)(N)(NRAr_F)_2]$ was isolated in about 60% yield. A ^2H NMR signal at $\delta = 14.8$ ($\Delta\nu_{1/2} = 28$ Hz) attributable to the presumed intermediate chromium(IV) compound $[Cr(dbabh)\text{-}(I)(NRAr_F)_2]$ was observed to grow in and decay during the reaction of $[Cr(I)_2(NRAr_F)_2]$ with $[Li(dbabh)(OEt_2)]$.

$[Cr(I)(N)(NRAr_F)_2]$ was characterized by elemental analysis, and by ^1H, ^2H, ^{19}F, ^{13}C NMR, and UV/Vis spectroscopies. X-ray crystallography also confirmed the formulation of $[Cr(I)(N)(NRAr_F)_2]$ as a terminal nitride complex; the Cr–N bond length is 1.541(5) Å (Figure 1). The structure of

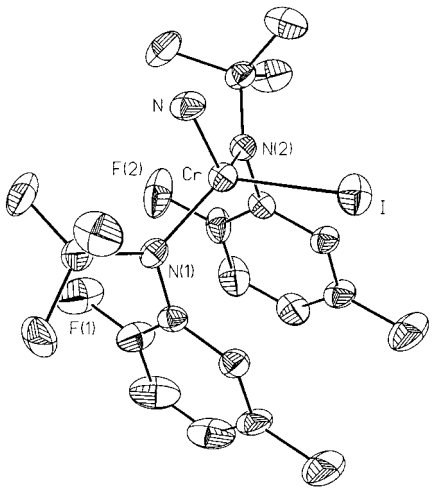


Figure 1. Structure of $[Cr(I)(N)(NRAr_F)_2]$ with thermal ellipsoids at the 35% probability level. Selected bond lengths [Å]: Cr–N 1.541(5), Cr–N(1) 1.823(5), Cr–N(2) 1.835(5), Cr–I 2.5995(11).

$[Cr(I)(N)(NRAr_F)_2]$ is characterized by coparallel stacking of the $2,5\text{-}C_6H_3FMe$ residues. The amido lone pairs are oriented perpendicular to the chromium nitrido functionality, which in turn is protected by the proximal *tert*-butyl groups. Such a conformation was seen previously for $[V(I)\text{-}(N_3Mes)(NRAr_F)_2]$;[9] in the present case a pseudo mirror plane renders the complex pseudo-C_s-symmetric and relates two parallel, π-stacked aryl rings.

Owing to the stability of $[Li(dbabh)(OEt_2)]$ at 25 °C, it was presaged that a d^0 complex of dbabh would be resistant to anthracene elimination. Accordingly, treatment of the precursor $[Cr(I)_2(NRAr_F)_2]$ with two equivalents of $[Li(dbabh)\text{-}(OEt_2)]$ led to formation of one equivalent of anthracene along with the new nitrido complex $[Cr(N)(dbabh)(NRAr_F)_2]$ (Scheme 1). The yield of isolated dark red $[Cr(N)(dbabh)\text{-}(NRAr_F)_2]$ subsequent to separation from antracene was 51%. $[Cr(N)(dbabh)(NRAr_F)_2]$ was characterized by X-ray crystallography in addition to elemental analysis and a battery of spectroscopies. The $Cr-N_{nitrido}$ bond length is 1.536(3) Å, and the appreciable steric crowding in the molecule is evident upon inspection of Figure 2. An interesting aspect of the

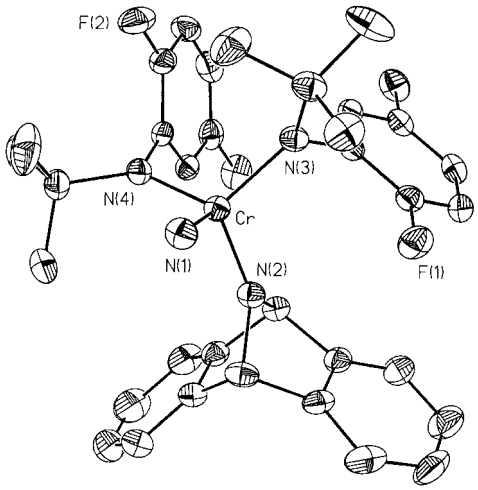


Figure 2. Structure of $[Cr(N)(dbabh)(NRAr_F)_2]$ with thermal ellipsoids at the 35% probability level. Selected bond lengths [Å]: Cr–N(1) 1.536(3), Cr–N(2) 1.814(3), Cr–N(3) 1.863(3), Cr–N(4) 1.856(3).

structure of $[Cr(N)(dbabh)(NRAr_F)_2]$ is the near planarity at the nitrogen atom in the complexed dbabh ligand; planarity at this nitrogen atom is disfavored by virtue of strain.[8] In addition, the $Cr-N_{dbabh}$ bond length of 1.814(3) Å compares well with the distances between chromium and the $NRAr_F$ nitrogen atoms. (1.856(3) and 1.863(3) Å). Extended Hückel calculations[10] performed on $[Cr(N)(dbabh)\text{-}(NRAr_F)_2]$ indicate dbabh to be similar to $NRAr_F$ in terms of π-donor ability, inasmuch as the three amide lone pairs all contribute substantially to the HOMO. In fact, examination of the Cr–N overlap populations (o.p.) indicates the dbabh nitrogen atom to interact with the chromium atom more strongly (o.p. 0.74) than the two $NRAr_F$ nitrogen atoms (o.p. 0.65, 0.66); the $Cr-N_{nitrido}$ o.p. is 1.18. Two isomers of $[Cr(N)(dbabh)$ $(NRAr_F)_2]$ are observed by solution ^{19}F and ^1H NMR spectroscopies. The major isomer exhibits inequivalent $NRAr_F$ ligands, which is consistent with the solid-state structure (Figure 2). The observed quivalence of the $NRAr_F$

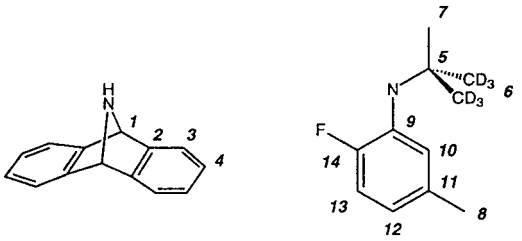
 © WILEY-VCH Verlag GmbH, D-69451 Weinheim, 1998 1433-7851/98/3707-0946 $ 17.50+.50/0

ligands for the minor isomer is indicative of a pseudo mirror symmetry, as observed for $[Cr(I)(N)(NRAr_F)_2]$.

In summary, the anion derived from deprotonation of Hdbabh has been demonstrated to serve as an organic analogue of azide ion in the context of nitride chemistry. Further applications of this approach to other molecular and solid-state nitrides will be described in due course.

Experimental Section

All manipulations were carried out under an atmosphere of purified nitrogen using standard glovebox or Schlenk techniques, unless stated otherwise. All solvents were dried and deoxygenated prior to use. NMR assignments are with reference to the numbering shown in Scheme 2.



Scheme 2. Numbering for the assignments for the NMR signals.

Lithiation of Hdbabh: To a thawing solution of Hdbabh[8] (5.88 g, 30.42 mmol) in ether (90 mL) was added *n*-butyllithium (32.0 mmol, 20 mL of a 1.6 M) drowpise with a pipet. On warming to room temperature the lithium amide (light salmonpink in color) began to precipitate. After partial removal of solvent the colorless solid was collected by filtration, washed with cold pentane, and dried (6.24 g, 22.8 mmol, 75.1%). Integration of the compound's ^{1}H NMR spectrum indicated one molecule of ether per lithium atom. ^{1}H NMR ([D$_8$]THF): $\delta = 4.99\,(1), 6.46-6.87\,(3, 4)$; ^{13}C NMR ([D$_8$]THF): $\delta = 71.24\,(1), 158.22\,(2), 115.81, 120.00\,(3, 4)$.

$[Cr(I)_2(NRAr_F)_2]$: To a solution of $[Cr(NRAr_F)_3]$[5] (1.1805 g, 1.97 mmol) in benzene (30 mL) was added dropwise iodine (0.505 g, 1.99 mmol) as a solution in benzene (10 mL). ^{2}H NMR spectroscopic monitoring indicated complete consumption of $[Cr(NRAr_F)_3]$ after 2 h at 28 °C. Subsequent to removal of benzene, $[Cr(I)_2(NRAr_F)_2]$ was obtained as black needles (1.096 g, 82%) by recrystallization (ether, − 35 °C); m.p. 146 – 147 °C. ^{2}H NMR (C_6D_6): $\delta = 16.6$ ($\delta\nu_{1/2}$, 14.5 Hz); magnetic susceptibility (benzene, 25 °C): 2.83 μ_B; EI-MS: $m/z = 678$ (M^+); elemental analysis calcd for $C_{22}H_{18}D_{12}CrF_2I_2N_2$: C 43.00, H 5.41, N 4.18; found: C 42.55, H 5.25, N 4.01.

$[Cr(I)(N)(NRAr_F)_2]$: To a thawing solution of $[Cr(I)_2(NRAr_F)_2]$ (1.002 g, 1.477 mmol) in ether (75 mL) was added dropwise a cold solution of $[Li(dbabh)(OEt_2)]$ (0.388 g, 1.420 mmol) in ether (15 mL). The mixture was stirred and allowed to warm to 25 °C. The mixture was stirred for 16 h, during which time the color changed from brown-black to red-brown. Subsequent to removal of solvent in vacuo the residue was extracted with pentane, and the extract was filtered through celite. Solvent was removed from the extract in vacuo. The residue was extracted with THF and the extract was filtered through activated charcoal to remove anthracene. Removal of and lyophilization from benzene afforded a red-brown powder (0.505 g, 0.894 mmol, 60.54%). Recrystallization from CH_3CN gave red crystals (0.301 g, 0.532 mmol, 36%); m.p. 188 – 190 °C. ^{1}H NMR (C_6D_6): $\delta = 7.504\,(10), 6.314-6.222\,(12,13), 1.873\,(8), 1.721\,(7)$. ^{13}C NMR ($C_6D_6$): $\delta = 19.96\,(8), 33.14\,(6), 33.88\,(7), 72.03\,(5), 116.5, 130.5, 132.9, 134.1, 148.7\,(9-13), 150.7\,(14)$; ^{19}F NMR ($C_6D_6$): $\delta = -113.7$ (major), − 109.7, − 115.1 (minor); UV/Vis (CH_3CN): 365 nm (ε 1951), 283 nm (ε 2699); elemental analysis calcd for $C_{22}H_{18}D_{12}CrF_2IN_3$: C 46.73, H 4.95, N 7.43; found: C 46.73, H 5.35, N 7.23.

X-ray structure analysis: Crystals were grown from at − 30 °C. A red plate of approximate dimensions $0.79 \times 0.35 \times 0.09$ mm was selected. Data collection was carried out on a Siemens platform goniometer equipped with a CCD detector. The structure was solved by direct methods in conjunction with difference Fourier techniques. All non-hydrogen atoms were refined anisotropically.[11] Crystal and refinement data: $C_{22}H_{30}CrF_2IN_3$, space group $P2_1/n$, $\alpha = 9.269\,(2)$, $b = 28.634\,(8)$, $c = 9.443\,(2)$ Å, $\alpha = 90$, $\beta = 97.09\,(3)$, $\gamma = 90°$, $Z = 4$, $V = 2487.2\,(11)$ Å^3, $\varrho_{calcd} = 1.478$ g cm^{-3}, $T = 183\,(2)$ K, $Mo_{K\alpha}$ radiation ($\lambda = 0.71073$ Å), $\mu(MO_{K\alpha}) = 1.728$ mm^{-1}, $F(000) = 1112$, total reflections = 9945, independent reflections = 3578, data/parameter ratio = 3574/263, $R_1 = 0.0474$, $wR_2 = 0.0980$, GOF = 1.062, residuals based on $I > 2\sigma(I)$.

$[Cr(N)(dbabh)(NRAr_F)_2]$: To a thawing solution of $[Cr(I)_2(NRAr_F)_2]$ (0.200 g, 0.295 mmol) in ether (20 mL) was added dropwise a cold solution of $[Li(dbabh)(OEt_2)]$ (0.164 g, 0.600 mmol) in ether (15 mL). After the mixture was warmed to 25 °C and stirred for 12 h, solvent was removed in vacuo. The residue was extracted with pentane, the extract was filtered through celite, and the solvent was removed in vacuo from the extract. The residue was dissolved in THF, and the solution filtered through activated charcoal and concentrated in vacuo. Recrystallization from CH_3CN gave $[Cr(N)(dbabh)(NRAr_F)_2]$ as a beet-red solid (0.094 g, 0.149 mmol, 51%); m.p. 170 °C (decomp.). ^{1}H NMR (C_6D_6): $\delta = 1.48-1.57\,(7, 8), 1.98-2.09\,(7, 8), 5.70-5.86\,(1), 6.51-7.00\,(3, 4, 9-14)$; ^{13}C NMR ($C_6D_6$): $\delta = 21.0, 32.91\,(6, 7), 64-66\,(1), 81.13\,(5), 116.5, 121.9, 126.2, 133.1, (9-13, 3, 4)\,140.7, 150.0\,14)$; ^{19}F NMR ($C_6D_6$): $\delta = -110.5, 117.7$ (major), − 113.5 (minor); UV/Vis (CH_3CN): 249 nm (ε 15, 146), 353 nm (ε 9709), 505 nm (ε 8932); elemental analysis calcd for $C_{36}H_{28}D_{12}CrF_2N_4$: C 68.55, H 6.39, N 8.88; found: C 68.55, H 6.08, N 7.85.

X-ray structure of $[Cr(N)(dbabh)(NRAr_F)_2] \cdot 0.5$ MeCN: Crystals were gronw from CH_3CN at − 30 °C. A red plate of approximate dimensions $0.70 \times 0.41 \times 0.22$ mm was selected. Data collection was carried out on a Siemens platform goniometer equipped with a CCD detector. The structure was solved by direct methods in conjunction with difference Fourier techniques. All non-hydrogen atoms were refined anisotropically.[11] Crystal and refinement data: $C_{37}H_{40}CrF_2N_{4.5}$, space group $P\bar{1}$, $a = 9.5207\,(3)$, $b = 11.0757\,(3)$, $c = 17.9577\,(5)$ Å, $\alpha = 83.3100\,(10)$, $\beta = 89.8710\,(10)$, $\gamma = 71.4340\,(10)°$, $Z = 2$, $V = 1781.62\,(9)$ Å^3, $\delta = _{calcd} = 1.189$ g cm^{-3}, 188 (2) K, $Mo_{K\alpha}$ radiation, ($\lambda = 0.71073$ Å), $\mu(Mo_{K\alpha}) = 0.362$ mm^{-1}, $F(000) = 671$, total reflections = 7324, independent reflections = 5002, data/parameter ratio = 4992/405, $R_1 = 0.0611$, $wR_2 = 0.1757$, GOF = 1.084, residuals based on $I > 2\sigma(I)$.

Received: October 30, 1997 [Z 11104IE]
German version: *Angew. Chem.* **1998**, *110*, 983 – 986

Keywords: azides · chromium · nitrides · nitrogen · N ligands

[1] D. S. Bem, C. M. Lampeonnerud, H. P. Olsen, H. C. zur Loye, *Inorg. Chem.* **1996**, *35*, 581.
[2] F. J. DiSalvo, S. J. Clarke, *Curr. Opinion Solid State Mater. Sci.* **1996**, *1*, 241.
[3] K. Dehnicke, J. Strähle, *Angew. Chem.* **1992**, *104*, 978; *Angew. Chem. Int. Ed. Engl.* **1992**, *31*, 955; K. Dehnicke, J. Strähle, *ibid.* **1981**, *93*, 451 bzw. **1981**, *20*, 413.
[4] J. Chatt, J. R. Dilworth, *J. Chem. Soc. Chem. Commun.* **1974**, 517.
[5] A. L. Odom, C. C. Cummins, J. D. Protasiewicz, *J. Am. Chem. Soc.* **1995**, *117*, 6613.
[6] A. L. Odom, C. C. Cummins, *Organometallics* **1996**, *15*, 898.
[7] A. L. Odom, C. C. Cummins, unpublished results.
[8] L. A. Carpino, R. E. Padykula, D. E. Barr, F. H. Hall, J. G. Krause, R. F. Dufresne, C. J. Thoman, *J. Org. Chem.* **1988**, *53*, 2565.
[9] M. G. Fickes, W. M. Davis, C. C. Cummins, *J. Am. Chem. Soc.* **1995**, *117*, 6384.
[10] G. A. Landrum, YAeHMOP: Yet Another extended Hückel Molecular Orbital Package. YAeHMOP is freely available on the World Wide Web at http://overlap.chem.cornell.edu:8080/yeahmop.html.
[11] Further details on the crystal structure investigations may be obtained from the Fachinformationszentrum Karlsruhe, D-76344 Eggenstein-Leopoldshafen, Germany (fax: (+ 49) 72 47-8 08-6 66 (Frau S. Höhler-Schlimm); e-mail: crysdata@fiz-karlsruhe.de), on quoting the depository numbers CSD-407 951 and -407 952.

 © WILEY-VCH Verlag GmbH, D-69451 Weinheim, 1998 1433-7851/98/3707-0947 $ 17.50+.50/0

In Situ NMR Investigations of Heterogeneous Catalysis with Samples Prepared under Standard Reaction Conditions**

James F. Haw*, Patrick W. Goguen, Teng Xu, Timothy W. Skloss, Weiguo Song, and Zhike Wang

In situ study of reaction mechanisms is a very high priority in heterogeneous catalysis.[1] One of the most successful methods has been magic angle spinning (MAS) solid-state NMR spectroscopy.[2, 3] Unfortunately, standard in situ NMR experiments use reaction conditions that differ in important aspects from those of actual catalysis. Catalytic reactors operate under flow conditions with addition of reactants and removal of volatile products.[4] Contact times between reactants and catalysts typically range from several tenths of a second to several seconds. In most in situ NMR experiments a sealed sample is used, and acquisition of a single ^{13}C NMR spectrum typically requires several hundred seconds. To partly compensate for the discrepancy in time scales, in situ NMR experiments are commonly performed at temperatures 100–150 K below those used for corresponding studies in flow reactors. Although there have been various attempts to make the reaction conditions used with in situ MAS NMR more like those in flow reactors,[5-9] such experiments have not yet been extended to probe irreversible reactions on time scales of a few seconds or less.

Here we report a novel approach to NMR studies of heterogeneous catalysis that provides information on short time scales and under actual reaction conditions. The inspiration for these experiments is the quenching of reactions in solution, which is extensively applied in spectroscopic studies of enzymatic catalysis.[10] Our pulse–quench catalytic reactor (Figure 1) has all of the characteristics of a standard research microreactor including provision for continuous and/or pulse introduction of reactants and gas chromatography (GC) for analysis of volatile products that exit the reactor. The most significant feature of the pulse–quench reactor is the provision for rapidly switching the gas stream that flows over the catalyst bed to cryogenically cooled nitrogen; the catalyst temperature can therefore be reduced very rapidly. Instrumentally, this is achieved through the use of high-speed, pneumatically actuated valves and computer control. The temperature of the catalyst bed is measured by a fast-response thermocouple that is in contact with zeolite pellets on the downstream end of the catalyst bed. The catalyst is cooled by 150 K in the first 170 ms of a quench, and reaches ambient temperature or lower in less than one second. Our experience indicates that the time resolution of in situ experiments with the pulse–quench reactor is 200 ms or less.

[*] Prof. J. F. Haw, P. W. Goguen, Dr. T. Xu, Dr. T. W. Skloss, W. Song, Z. Wang
The Laboratory for Magnetic Resonance and Molecular Science
Department of Chemistry
Texas A&M University
College Station, TX 77843 (USA)
Fax: (+1) 409-845-7638
E-mail: haw@chemvx.tamu.edu

[**] This work was supported by the National Science Foundation (CHE-9528959).

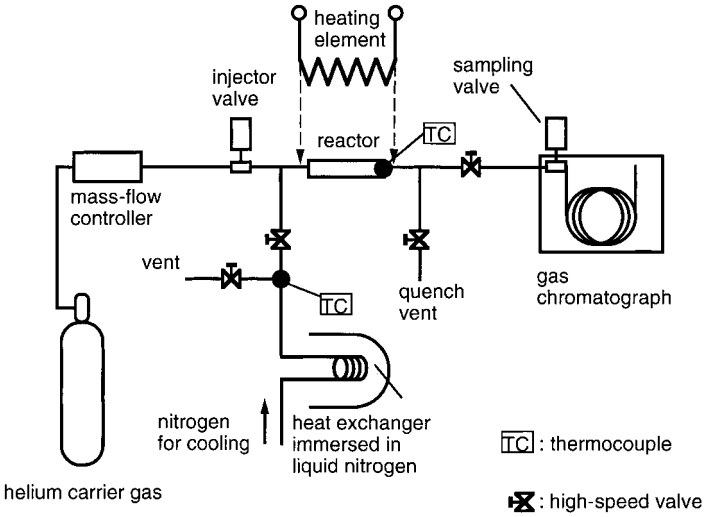


Figure 1. Schematic representation of the pulse–quench reactor used to prepare samples under standard flow-reactor conditions for study by NMR spectroscopy. The gray region indicates the catalyst bed. All valves and the heating element are under computer control.

Figure 2 shows results for the reactions of acetone on the acidic catalyst zeolite HZSM-5 (Figure 2), which we previously studied by conventional in situ NMR techniques in sealed rotors at lower temperatures.[11] We used the pulse–quench reactor to introduce (2-^{13}C)acetone (20.6 μL, two molecules per acid site) onto activated HZSM-5 pellets at 623 K with continuous removal of volatile products in a He flow. Samples were prepared (see Experimental Section) prior to quenching with reaction times ranging from 500 ms to

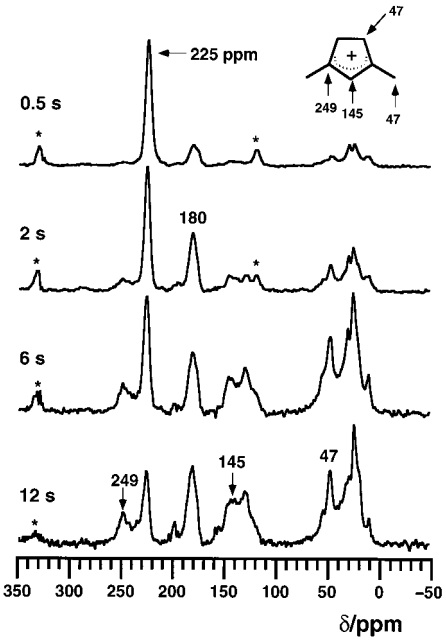


Figure 2. ^{13}C MAS NMR spectra for the reactions of (2-^{13}C)acetone on zeolite HZSM-5 under a flow of He carrier gas. Each spectrum is of a sample prepared by injecting acetone onto a freshly activated catalyst, allowing the reaction to occur for the time indicated at 623 K, and then thermally quenching the catalyst bed to 298 K. The spectra were measured at 77 K. The asterisks denote spinning sidebands.

 © WILEY-VCH Verlag GmbH, D-69451 Weinheim, 1998 1433-7851/98/3707-0948 $ 17.50+.50/0

12 s. Acetone ($\delta = 225$, CO) undergoes aldol condensation to 4-hydroxy-4-methylpentan-2-one (observed by gas chromatography (GC) in the product stream), which is dehydrated to 4-methylpent-3-en-2-one on the zeolite. Cracking of acetone dimers produces acetic acid ($\delta = 180$, COOH) and isobutylene (observed by GC). Oligomerization, isomerization, and cracking of hydrocarbons formed from isobutene result in many products that show other signals in the ^{13}C NMR spectra (Figure 2) and the gas chromatogram. Comparison of the spectra in Figure 2 with those from conventional in situ studies of this reaction suggests that there is no loss of acetone or other volatile species during transfer from the reactor to the MAS-NMR rotor.

Figure 2 also shows the development of strong ^{13}C NMR signals at $\delta = 249$, 145 (partially overlapped), and 47 after 2 to 12 s. This unique cluster of chemical shifts is the signature of alkyl-substituted cyclopentenylcarbenium ions; the 1,3-dimethylcylopentenyl cation shown in Figure 2 is a simple example of such a species. This very stable class of carbenium ion was previously observed in an early in situ NMR study of propene oligomerization,[12] but not in conventional in situ studies of acetone chemistry.

We have demonstrated a powerful experimental tool for studying reaction mechanisms of heterogeneous catalysis. The pulse–quench reactor can be used to prepare samples for NMR study under conditions identical to those for microreactor studies. In particular, in situ NMR spectrscopy can now be applied to probe reactions at appreciably higher temperatures and with continuous removal of volatile products from the catalyst. For the first time, NMR studies of irreversible reactions on zeolites have been carried out on time scales shorter than typical catalyst contact times.

Experimental Section

The catalyst was prepared from zeolite powder (Si/Al = 19) mixed with a minimum amount of alumina binder (typically 30 wt%) and extruded into pellets with a diameter of 1 mm. The catalyst (0.25 g, dry weight) was packed into a stainless steel tube (inner diameter 7.5 mm, outer diameter 10 mm) to form a bed that is 8 mm long. The entire length of the tube (5.5 cm) was heated to a controlled temperature with heating tape, and the catalyst was activated in the pulse–quench reactor under a flow of He immediately prior to reaction. The catalyst bed was isolated immediately following the quench and transferred to a MAS rotor, which was sealed in a glovebox at room temperature. The sample was at no time exposed to the atmosphere. Solid-state ^{13}C MAS NMR spectra were measured at 75.4 MHz with cross polarization on a Chemagnetics CMX-300 spectrometer.

Received: October 28, 1997 [Z11090IE]
German version: *Angew. Chem.* **1998**, *110*, 993–995

Keywords: carbocations · heterogeneous catalysis · microreactors · NMR spectroscopy · zeolites

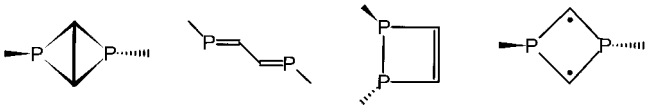
[1] National Research Council, *Catalysis Looks to the Future*, National Academy Press, Washington, DC, **1992**.
[2] J. F. Haw in *NMR Techniques in Catalysis* (Eds.: A. Bell, A. Pines), Marcel Dekker, New York, **1994**.
[3] J. F. Haw, J. B. Nicholas, T. Xu, L. W. Beck, D. B. Ferguson, *Acc. Chem. Res.* **1996**, *29*, 259–267.
[4] B. C. Gates, *Catalytic Chemistry*, Wiley, New York, **1992**.
[5] P. W. Goguen, J. F. Haw, *J. Catal.* **1996**, *161*, 870–872.
[6] M. Hunger, T. Horvath, *J. Chem. Soc. Chem. Commun.* **1995**, 1423–1424.
[7] H. Ernst, T. Freude, T. Mildner, *Chem. Phys. Lett.* **1994**, *229*, 291–296.
[8] D. B. Ferguson, J. F. Haw, *Anal. Chem.* **1995**, *67*, 3342–3348.
[9] T. Mildner, H. Ernst, D. Freude, W. F. Holderich, *J. Am. Chem. Soc.* **1997**, *119*, 4258–4262.
[10] R. C. Bray, *Biochem. J.* **1961**, *81*, 189–193.
[11] T. Xu, E. J. Munson, J. F. Haw, *J. Am. Chem. Soc.* **1994**, *116*, 1962–1972.
[12] J. F. Haw, B. R. Richardson, I. S. Oshiro, N. L. Lazo, J. A. Speed, *J. Am. Chem. Soc.* **1989**, *111*, 2052–2058.

Valence Isomerization in the Solid State: From 1,3-Diphosphacyclobutane-2,4-diyl to 1,2-Dihydro-1,2-diphosphete**

Olaf Schmidt, André Fuchs, Dietrich Gudat, Martin Nieger, Wilfried Hoffbauer, Edgar Niecke,* and Wolfgang W. Schoeller*

Dedicated to Professor Achim Müller on the occasion of his 60th birthday

Four-membered heterocycles of the type $P_2C_2R_4$ have attracted a great deal of interest as building blocks in organophosphorus and organometallic chemistry.[1] Within the series 2,4-diphosphabicyclobutane (**I**), 1,4-diphosphabutadiene (**II**), and 1,2-dihydro-1,2-diphosphete (**III**), the bicyclic system is the least and the 1,2-diphosphete the most stable valence isomer.[2] Hence, it appears logical that the most important synthetic route to **III** involves the valence isomerization of 1,4-diphosphabutadienes.[3]



I **II** **III** **IV**

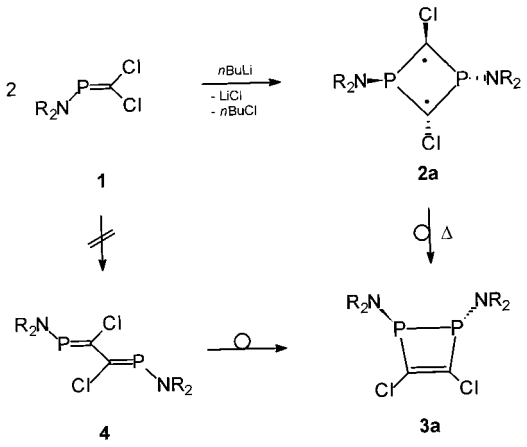
Recently we proved the existence of another valence isomer of **I**–**III**, the biradicaloid 1,3-diphosphacyclobutane-2,4-diyl (**IV**).[4] Although compounds of type **IV** are even less stable than those of type **I**, isolable derivatives do exist owing to the fact that isomerization to **I** by formation of a transannular C–C bond is forbidden according to the Woodward–Hoffmann rules. To gain more insight into the chemistry of

[*] Prof. Dr. E. Niecke, Dipl.-Chem. O. Schmidt, Dr. A. Fuchs, Priv.-Doz. Dr. D. Gudat, Dr. M. Nieger, Dr. W. Hoffbauer
Institut für Anorganische Chemie der Universität
D-53121 Bonn (Germany)
Fax: (+49) 228-735-327
Prof. Dr. W. W. Schoeller
Fakultät für Chemie der Universität
D-33501 Bielefeld (Germany)

[**] We thank the Deutsche Forschungsgemeinschaft (SFB 334) and the Fonds der Chemischen Industrie for financal support, and Dr. W. Hoffbauer for recording the solid-state NMR spectra.

such biradicaloid compounds, we investigated the effect of introducing amino substituents at the phosphorus positions. This was expected to increase the barrier to inversion at phosphorus and inhibit the delocalization of electron density in the P_2C_2 cycle, and thus bring the biradical character to the fore. Here we report on the synthesis of a 1,3-diamino-1,3-diphosphacyclobutane-2,4-diyl and its valence isomerization to a 1,2-dihydro-1,2-diphosphete in the solid state, as well as a likely mechanism involving an intermediate phosphanylcarbene.

Treatment of the amino(dichloromethylene)phosphane $R_2NP{=}CCl_2$ (**1**, $R_2 = 2,2,6,6\text{-}Me_4C_5H_6N$)[5] with *t*BuLi (0.5 equiv) under conditions similar to those employed for the synthesis of $[(2,4,6\text{-}t\text{Bu}_3C_6H_2)PC(Cl)]_2$ (**2b**)[4] ($-110\,^\circ$C, THF, stirring at $-80\,^\circ$C for 4 h) resulted in the precipitation of a deep purple solid, which was isolated in 70% yield after filtration at $-80\,^\circ$C (Scheme 1).[6] Recrystallization of the



Scheme 1. Synthesis of **3a**.

crude product from toluene at $-30\,^\circ$C afforded colorless crystals, whose solution MS (*m*/*z*: 436, $C_{20}H_{36}Cl_2N_2P_2$) and ^{31}P NMR data ($\delta = 17.4$ (s)) are in agreement with the expected constitution of 1,3-diamino-1,3-diphosphacyclobutane-2,4-diyl **2a**. However, according to the ^{13}C NMR spectra, the ring carbon atom is strongly deshielded with respect to that of **2b** (δ(**2a**) = 129.3, δ(**2b**) = 98.8[4]), and the deviations from an ideal 1:2:1 triplet pattern suggest the presence of an AA′X ($\Sigma J_{CP} = 13.4$ Hz) rather than an A_2X spin system.[7] A spectrum of this type is in agreement with the presence of 1,2-dihydro-1,2-diphosphete[21] **3a** rather than biradicaloid **2a**.

This constitution was confirmed by an X-ray crystal structure determination,[8] which revealed the presence of a folded four-membered P_2C_2 ring. The phosphorus atoms are located in the 1,2-positions, and there is a slightly twisted C–C double bond, as indicated by the P1-C1-C2-P2 dihedral angle of $-24.4(3)^\circ$ (Figure 1). The degree of pyramidalization at the phosphorus atoms (the sums of valence angles at P1 and P2 are 302 and 303°, respectively) is typical for saturated phosphorus(III) centers, and the *trans* orientation of the bulky amino substituents minimizes steric hindrance. Quite

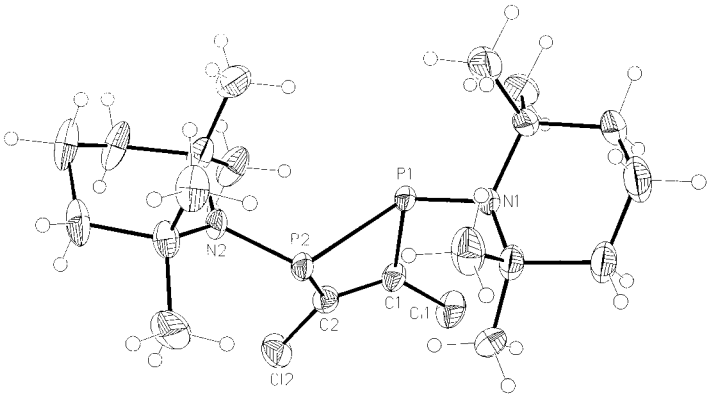


Figure 1. Molecular structure of **3a**; hydrogen atoms have been omitted for clarity. Important bond lengths [pm], bond angles [°], and torsion angles [°]: P1–P2 232.5(1), P1–C1 179.7(4), P2–C2 180.7(4), C1–C2 134.4(5), P1–N1 169.6(3), P2–N2 168.8(3), C1–Cl1 171.9(3), C2–Cl2 171.0(4); P2-P1-C1 73.1(1), P1-P2-C2 73.1(1), P1-C1-C2 104.2(2), C1-C2-P2 103.4(3), P2-P1-N1 118.0(1), C1-P1-N1 111.2(2), P1-P2-N2 118.7(1), C2-P2-N2 111.3(2), P1-C1-Cl1 128.6(2), C2-C1-Cl1 127.1(3), P2-C2-Cl2 128.9(2), C1-C2-Cl2 127.5(3); P1-C1-C2-P2 −24.4(3), Cl1-C1-C2-Cl2 −15.1(5), C1-P1-P2-C2 −14.3(2), N1-P1-P2-N2 134.9(2), P2-P1-C1-C2 19.1(2), P1-P2-C2-C1 18.9(2)

remarkably,the P1–P2 bond (232.5(1) pm) is substantially larger than known P–P single bonds in 1,2-dihydro-1,2-diphosphetes (219[10] to 225 pm[11]). The remaining bond distances and angles reveal no peculiarities.

Knowing that 1,2-dihydro-1,2-diphosphetes may arise from electrocyclic ring closure of 1,4-diphosphabutadienes,[12] we undertook a closer investigation of the initially formed purple precipitate to probe the occurrence of diene **4** (which might result from reductive coupling[13] of two molecules of **1**) as a possible intermediate. While analysis by X-ray powder diffraction gave no observable reflections, which is indicative of a very low degree of crystallinity of the sample, solid-state UV/Vis and CP/MAS NMR studies revealed that the precipitate is not composed of **3a**, but rather a new species, which must therefore be considered as an isolable intermediate of the overall reaction. However, even if a high-resolution mass spectrum (*m*/*z*: 436.732, calcd for $C_{20}H_{36}Cl_2N_2P_2$: 435.731) shows the product to be an isomer of **3a**, the appearance of a characteristic UV/Vis absorption band ($\lambda_{max} = 567$ nm, cf. $\lambda_{max} = 356$ nm for **2b**[4]) and the similarity of the isotropic ^{31}P and ^{13}C chemical shifts of the ring atoms ($\delta_{iso} = 18.9$ (^{31}P), 99.0 (^{13}C)) with those of **2b**[4] ($\delta_{iso} = 26.1$ (^{31}P), 100(^{13}C)) suggest a formulation as biradicaloid **2a** rather than a 1,4-diphosphadiene.

This assignment is further supported by the fact that the spinning sidebands in the solid-state ^{31}P MAS NMR spectra of **2a** (Figure 2) and **2b**[4] appear as singlets. This suggests a parallel alignment of all three principal axes of the two shielding tensors and implies that both tensors are related by a center of symmetry.[13] This condition can be fulfilled by biradicaloids of type **IV**, which, according to crystallographic and theoretical investigations,[4] possess molecular C_i symmetry, but not by a diphosphete of the type **II**, which may exhibit either C_2 or C_s symmetry (crystalline **3a** approximately displays noncrystallographic C_2 symmetry). Consequently, and in contrast to the case of **2a**, the spinning sidebands in the

 © WILEY-VCH Verlag GmbH, D-69451 Weinheim, 1998 1433-7851/98/3707-0950 $ 17.50+.50/0

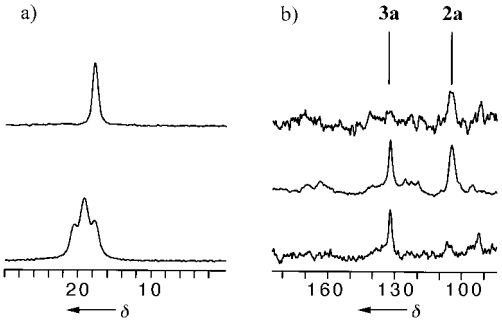
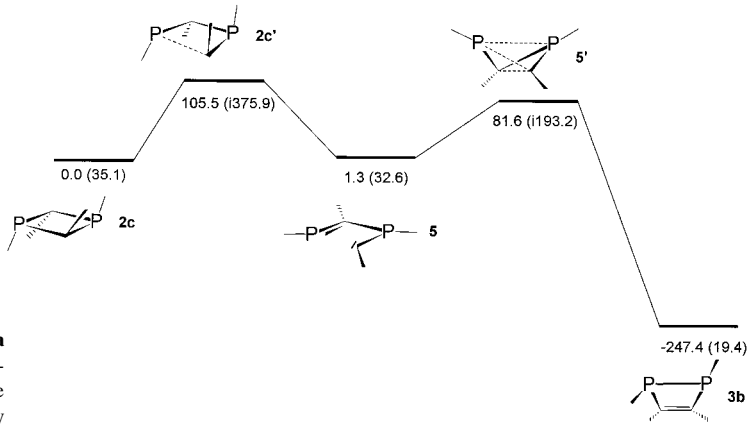


Figure 2. a) Section (centerband) of the ^{31}P MAS NMR spectra of solid **2a** (161.9 MHz, 40 transients, MAS frequency 7.044 kHz, top) and **3a** (recrystallized sample, 40 transients, MAS frequency 10.07 kHz, bottom). b) The olefinic region of the ^{13}C CP/MAS spectrum (100 MHz) of a freshly prepared sample of **2a** at ambient temperature. Top: 60 transients recorded immediately after sample preparation (measurement time 12 min); middle: 4000 transients (total measurement time 13.33 h); bottom: 80 transients (measurement time 16 min) immediately after the long-time acquisition. Signals without labels represent spinning sidebands of the resonances (not shown) of the tetramethylpiperidinyl substituents. The change in intensities of the labeled signals indicates the almost complete conversion **2a** → **3a** within the duration of the experiment.



Scheme 2. Schematic representation of the calculated stationary points and transition states on the electronic hypersurface for the reaction of **2c** to **3b** at the MCSCF(10,10) level. The relative energies are given in kJ mol^{-1}, and the values in parentheses indicate the lowest vibrational frequencies. The structures **2c′** and **5′** represent transition states and exhibit one imaginary vibrational frequency.

^{31}P MAS spectrum of **3a** consist of multiplets (Figure 2a) whose splittings vary with changing rotational speed. The ^{31}P spin pairs can thus be classified as an AB spin system, and the observed splitting represents a superposition of scalar and residual dipolar coupling contributions.[14]

Further investigations revealed that the conversion **2a** → **3a** is not only promoted by treatment of solid **2a** with a variety of solvents, but occurs also in the solid state. The isomerization can be monitored by the decay of the long-wave UV/Vis absorption band of **2a** as well as by ^{31}P and ^{13}C CP/MAS NMR spectroscopy (Figure 2b). Compared to the case in solution, where complete conversion of **3a** is achieved spontaneously, the rearrangement proceeds at a lower rate and takes days to complete at ambient temperature. The samples isomerize faster upon gentle heating or storing under MAS conditions for a prolonged period (more than 90% conversion in less than 20 h, Figure 2b).

The structural findings for **3a** are in accordance with the results of ab initio calculations at the MP2/6-31g(d,p) level on the model compound *cyclo*-[-(H$_2$N)P–C(Cl)=C(Cl)–P-(NH$_2$)-],[15] which gave the following bond lengths: P–P 230.9, C–P 180.8, C=C 136.2 pm. The lengthening of the P–P bond with respect to the parent compound *cyclo*-[-(H)P–C(H)=C(H)–P(H)-] (**3b**, P–P 222 pm) results, according to a population analysis, from a slightly higher p character in the bond and is accompanied by a shortening of the adjacent P–C bonds.

To gain further insight into the solid-state valence isomerization of **2a** to **3a**, we performed ab initio calculations on the parent compounds **2c** and **3b**, and further characterized the transition between these states on the electronic hypersurface. All calculations were performed at the MCSCF(10,10)/6-31g(d) level to ensure a proper treatment of the biradical and other open-shell structures.[16] According to the results, the isomerization of **2c** (^1A_g, C_i symmetry) to **3b** is a two-step process through an additional stationary point on the hypersurface, which was identified as the singlet phosphanylcarbene **5** (Scheme 2).[17] The rate-determining step ($\Delta E =$ 105.5 kJ mol^{-1}) is the ring opening of biradicaloid **2c** to give **5**, which is only 1.3 kJ mol^{-1} higher in energy than **2c**. The transition state for this reaction step (**2c′**, Scheme 2) is reached from **2c** by partial rupture of one P–C bond (244.2 pm) and a conrotatory twist of the hydrogen atoms at C(P). In **5** this P–C bond is completely broken (355.7 pm), and the other parameters (e.g. P–C bond distances 164.3, 181.3, 171.6 pm) indicate the formation of a planar, butadiene-like structure. Further conrotatory movement of the hydrogen atoms at P(C) leads to a second transition state **5′** (C_1 symmetry, ^{1}A) with a tetrahedrane-like structure in which the new P–P (321.6 pm) and C–C (245.8 pm) bonds are already partially formed. The final product, the 1,2-dihydro-1,2-diphosphete **3b**,[4] marks the lowest point on the electronic hypersurface (–247.0 kJ mol^{-1} with respect to **2c**).

The MCSCF calculations suggest a novel reaction pathway for the 1,3-diphosphacyclobutane-2,4-diyl ⇌ 1,2-dihydro-1,2-diphosphete rearrangement, which proceeds via an intermediate phosphanylcarbene[18] and requires only relatively small changes in the ring bonds throughout the entire reaction. Investigations of further aspects of the thermally induced rearrangement in solution,[20] as well as of the corresponding photochemically induced reaction, are in progress.

Received: October 23, 1997 [Z11071IE]
German version: *Angew. Chem.* **1998**, *110*, 995–998

Keywords: ab initio calculations · diradicals · NMR spectroscopy · phosphorus heterocycles · valence isomerization

[1] C. Charrier, N. Maigrot, F. Mathey, F. Robert, Y. Jeannin, *Organometallics* **1986**, *5*, 623.
[2] W. W. Schoeller, U. Tubbesing, *Chem. Ber.* **1996**, *129*, 419.
[3] R. Appel, V. Barth, *Tetrahedron Lett.* **1980**, *21*, 1923.
[4] E. Niecke, A. Fuchs, M. Nieger, W. W. Schoeller, *Angew. Chem.* **1995**, *107*, 640; *Angew. Chem. Int. Ed. Engl.* **1995**, *34*, 555.
[5] A. P. Marchenko, G. N. Koydan, V. A. Oleynik, A. M. Pinchuk, *Zh. Obshch. Khim.* **1988**, *58*, 1923.
[6] **2a**: A solution of *t*BuLi (4.7 mmol, 2.8 mL of a 1.7 M solution in hexane) was added dropwise to a solution of **1** (2.4 g, 9.4 mmol) in

 © WILEY-VCH Verlag GmbH, D-69451 Weinheim, 1998 1433-7851/98/3707-0951 $ 17.50+.50/0

THF (100 mL) at −105 °C. The reaction mixture was slowly warmed to −80 °C and stirred for 4 h. The resulting purple solid was separated by filtration at −80 °C to afford **2a** (1.44 g, 70 %). **3a**: A solution of *t*BuLi (4.7 mmol, 2.8 mL of a 1.7 M solution in hexane) was added dropwise to a solution of **1** (2.4 g, 9.4 mmol) in THF (100 mL) at −105 °C. The reaction mixture was slowly warmed to room temperature under stirring, and the solvents were removed in vacuo. The residue was washed with *n*-pentane (50 mL), and precipitated LiCl was separated by filtration. Removal of the solvent in vacuo afforded **3a** as beige crystals (1.93 g, 93 %; m.p. 148–149 °C).

[7] **3a**: ^{31}P NMR (121 MHz, THF, 303 K): $\delta = 18.9$; ^{1}H NMR (300 MHz, C_6D_6): $\delta = 1.5$ (m, 36H; CH_2, CH_3); ^{13}C NMR (75.47 MHz, C_6D_6, 303 K): $\delta = 129.3$ (pseudo t, $\Sigma J = 13.4$ Hz; *C*=*C*), 58.9 (s; *C*NP), 42.1 (s; *C*CN), 31.6 (pseudo t, $\Sigma J = 6.3$ Hz; C_2CNP), 17.7 (s, *C*CCN); UV/Vis (1 % $BaSO_4$ solution): $\lambda_{max} = 567$ nm; MS (40 eV, EI): *m*/*z* (%): 436 (22) [M^+], 421 (20) [$M^+ - CH_3$], 401 (4) [$M^+ - Cl$], 296 (13) [$M^+ - C_9H_{18}N$), 230 (20) [$C_{11}H_{18}ClNP^+$], 126 (37) [$C_9H_{18}N^+ - CH_2$], 69 (100) [$C_4H_7N^+$]; correct elemental analysis.

[8] Crystal data for **3a**: $C_{20}H_{36}Cl_2N_2P_2$, $M_r = 437.4$, orthorhombic, space group $P2_12_12_1$ (no. 19), colorless crystals, dimensions $0.50 \times 0.18 \times 0.13$ mm^3, $a = 11.078(1)$, $b = 14.570(2)$, $c = 14.596(1)$ Å, $V = 2355.9(4)$ Å^3, $\rho_{calcd} = 1.233$ Mg m^{-3}, $Z = 4$, $\mu(Cu_{K\alpha}) = 3.81$ mm^{-1}, $T = 200(2)$ K; of 5327 reflections collected, 3833 were symmetry-independent and used for the structure solution (direct methods)[9a] and refinement (full-matrix least squares on F^2, 236 parameters).[9b] Non-hydrogen atoms were refined anisotropically, and H atoms localized by difference electron density and refined with a riding model ($wR2 = 0.136$, $R1 = 0.051$, for $I > 2\sigma(I)$). An empirical absorption correction on the basis of ψ scans was applied; the absolute structure could not be determined reliably. Crystallographic data (excluding structure factors) for the structure reported in this paper have been deposited with the Cambridge Crystallographic Data Centre as supplementary publication no. CCDC-100757. Copies of the data can be obtained free of charge on application to CCDC, 12 Union Road, Cambridge CB2 1EZ, UK (fax: (+44) 1223-336-033; e-mail: deposit@ccdc.cam.ac.uk).

[9] a) G. M. Sheldrick, SHELXL-86, Universität Göttingen, **1986**; b) SHELXL-93, Universität Göttingen, **1993**.

[10] a) P. Binger, T. Wettling, R. Schneider, F. Zurmühlen, U. Bergsträsser, J. Hoffmann, G. Maas, M. Regitz, *Angew. Chem.* **1991**, *103*, 207; *Angew. Chem. Int. Ed. Engl.* **1991**, *30*, 207; b) F. Knoch, S. Kramer, U. Zenneck, *Synthesis*, **1996**, *2*, 265.

[11] a) R. Appel, V. Barth, F. Knoch, *Chem. Ber.* **1983**, *116*, 938; b) A. M. Arif, A. R. Barron, A. H. Cowley, S. W. Hall, *J. Chem. Soc. Chem. Commun.* **1988**, 171.

[12] C. Charrier, J. Guilhelm, F. Mathey, *J. Org. Chem.* **1981**, *46*, 3.

[13] S. Ito, K. Toyota, M. Yoshifuji, *Chem. Lett.* **1995**, 747.

[14] See also a) G. Wu, R. E. Wasylishen, R. D. Curtis, *Can. J. Chem.* **1992**, *70*, 863; b) K. Eichele, G. Wu, R. E. Wasylishen, *J. Magn. Reson. A* **1993**, *101*, 157, and references therein. Under consideration of the limitations outlined in ref. [13a], the following principal values of the phosphorus shielding tensors were obtained from the MAS spectra: **2a**: $\delta_{11} = 150$, $\delta_{22} = 85$, $\delta_{33} = -181$; **3a**: $\delta_{11} = 170$, $\delta_{22} = 72$, $\delta_{33} = -185$.

[15] The energy optimation at the MP2 level was performed with the Gaussian set of programs: Gaussian 94 (Revision D4), M. J. Frisch, G. W. Trucks, H. B. Schlegel, P. M. W. Gill, B. G. Johnson, M. A. Robb, J. R. Cioslowski, B. B. Stefanov, A. Nanayakkara, M. Challacombe, C. Y. Peng, P. Y. Ayala, W. Chen, M. W. Wong, J. L. Andres, E. S. Replogle, R. Gomperts, R. L. Martin, D. J. Fox, J. S. Binkley, D. J. Defrees, J. Baker, J. P. Stewart, M. Head-Gordon, C. Gonzalez, J. A. Pople, Gaussian Inc., Pittsburgh, PA, **1995**.

[16] The MCSCF calculations were conducted with the GAMESS set of programs: M. W.Schmidt, K. K. Baldridge, J. A. Boatz, J. H. Jensen, S. Koseki, M. S. Gordon, K. A. Nyugen, T. L. Windus, S. T. Elbert, *QCPE Bull.* **1990**, *10*, 52; M. W. Schmidt, K. K. Baldridge, J. A. Boatz, M. S. Gordon, J. H. Jensen, S. Koseki, N. Matsunaga, K. A. Nyugen, S. Su, T. I. Windus, *J. Comput. Chem.* **1993**, *14*, 1347. The active space in the MCSCF treatment included the HOMO, the LUMO, and the four ring orbitals of the P_2C_2 moiety, resulting in five occupied and five antibonding molecular orbitals.

[17] All stationary points on the electronic hypersurface were characterized by vibrational analysis based on the method of numerical differentiation of the first-order gradients. Consequently, energy minima possess overall positive vibrational frequencies, and the two transition states display one imaginary vibration. Energy values were obtained from the MCSCF energies after zero-point vibrational correction.

[18] A stable phosphanylcarbene is known;[19] intermediates of this type are also supposed to appear in the thermal rearrangement of 1,3-diphosphacyclobutane-2,4-diyl **2b** to an isomeric 1,3-diphosphapropene.[4]

[19] A. Igau, H. Grützmacher, A. Baceiredo, G. Bertrand, *J. Am. Chem. Soc.* **1988**, *110*, 6463.

[20] E. Niecke, O. Schmidt, W. W. Schoeller, G. Bertrand, unpublished results

[21] An alternative synthesis of **3a** was recently reported: N. Cēnac, A. Chrostowska, J.-M. Sotiropoulos, B. Bonnadieu, A. Igau, G. Pfister-Guillouzo, J.-P. Majoral, *Organometallics* **1997**, *16*, 4551.

Intense Dyes through Chromophore–Chromophore Interactions: Bi- and Trichromophoric Perylene-3,4:9,10-bis(dicarboximide)s**

Heinz Langhals* and Wolfgang Jona

Dedicated to Professor Heinrich Nöth on the occasion of his 70th birthday

The UV/Vis spectra of dyes have commonly been controlled by introducing suitable substituents or by altering the chromophore. An interesting alternative is allowing two or more identical chromophores to interact directly, which might be expected to give pronounced effects in color. Perylene-3,4:9,10-bis(dicarboximide)s **1** were chosen as the basic chromophore because of their unusually high chemical and photochemical persistency and their high fluorescent quantum yields.[1] Moreover, the absorption of **1** in the visible region is caused by only one electronic transition,[2] and there are orbital nodes[3] at the nitrogen atoms in the HOMO and LUMO, which make these atoms ideal positions for linking. The thus "closed chromophore" is only negligibly influenced by substituents. The linking of two chromophores of **1** through a longer spacer did not result in a considerable alteration of the UV/Vis spectra.[4–6] Only an appreciable overlap of the chromophors induced a strong exciton absorption at longer wavelengths.[7, 8]

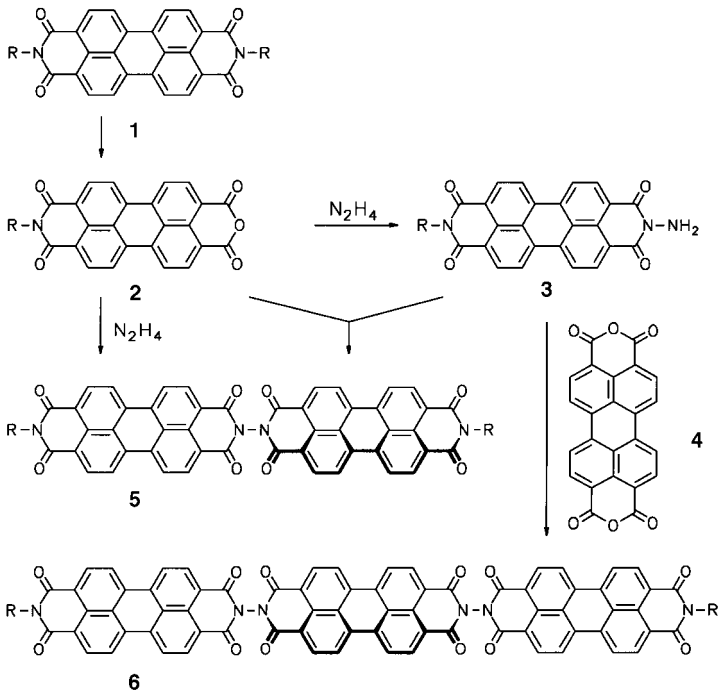
Here we try to adjust the chromophore–chromophore interaction to just an exciton coupling by reducing the separation between two chromophores to the distance of a single bond. Undesired interaction between the chromophores through conjugation is excluded by their orthogonal orientation and linkage at the nitrogen atoms (orbital nodes).

The starting material for the synthesis of such polychromophores are the peryleneimides **3**, which are readily soluble and have a free amino group at one nitrogen atom. Compounds **3**-

[*] Prof. Dr. H. Langhals, Dr. W. Jona
Institut für Organische Chemie der Universität
Karlstrasse 23, D-80333 München (Germany)
Fax: (+49) 89-5902-483
E-mail: langhals@lrz.uni-muenchen.de

[**] This work was supported by the Deutsche Forschungsgemeinschaft and the Fonds der Chemischen Industrie.

 © WILEY-VCH Verlag GmbH, D-69451 Weinheim, 1998 1433-7851/98/3707-0952 $ 17.50+.50/0



1-3,5,6	R
a	$CH(C_6H_{13})_2$
b	$CH(C_4H_9)_2$
c	$CH(C_7H_{15})_2$
d	$CH(C_8H_{17})_2$
e	$CH(C_9H_{19})_2$
f	2-CH_3-5-*t*-C_4H_9-C_6H_3

Scheme 1. Synthesis of bi- and trichromophoric perylene dyes.

are prepared from perylene anhydride imides **2** and hydrazine or hydrazinium salts under mild reaction conditions (100–130 °C, 0.5–1 h) in molten imidazole (Scheme 1). Aminoimides **3** are condensed with **2** to form bichromophoric perylenes **5**, which can even be directly prepared from **2** and hydrazine if the exact stoichiometry of 2:1 is guaranteed. This requires special care because of the low quantities of hydrazine to be added. An excess of **2** results in a decrease in yield, and an excess of hydrazine provides essentially **3**. Hydrazinium sulfate has been proven to be a source for hydrazine that can be easily dosed.

The expected low solubility of bichromophoric perylenes is a problem for synthesis, purification, and spectroscopic investigation. A notable improvement is brought about by the introducing solubilizing groups such as *sec*-alkyl groups[9] ("swallow-tail substituents") or aryl groups with *tert*-butyl substituents[10] which are linked to the terminal nitrogen atoms of the dyes. The solubility of the dyes so prepared is high enough for all investigations.

Trichromophoric perylene dyes **6** can be prepared in the same manner, in that amino derivative **3** is condensed with perylene-3,4:9,10-tetracarboxylic dianhydride (**4**). This reaction also proceeds under mild conditions in imidazole, and it too requires an exact stoichiometry.

The formamide of **3** (prepared from **3** and anhydrous formic acid, at least 99% at 70 °C) was also used for the condensation, because formamides are more reactive than free amines. This method has no advantages with respect to the yields and purity of **5** or **6**, but is to be favored if the absolute absence of heavy metals in the reaction products is required because no catalyst such as zinc acetate is necessary.

We tried to convert[4] one of the terminal imide groups of **5** into an anhydride group to obtain a building block for dyes with an even larger number of chromophores. However, this concept failed because saponification of the connection of two imides is the easier process. This bond can also be cleaved with hydrazine. Apparently the increase in reactivity of the carbonyl groups through the electron-withdrawing effect of the second imide unit dominates over the sterical shielding.

The bi- and trichromophoric dyes **5** and **6** are lightfast and exhibit structured UV/Vis spectra and a pronounced fluorescence in solution (Figure 1, Table 1). The absorption maxima are more and more bathochomically shifted as the number of chromophores increases. The extinction coefficients of most absorption bands are about two or three times higher than for the monochromophoric dyes. An notable deviation from this rule is observed for the most bathochromic vibration band of the bi- and trichromophoric dyes: An

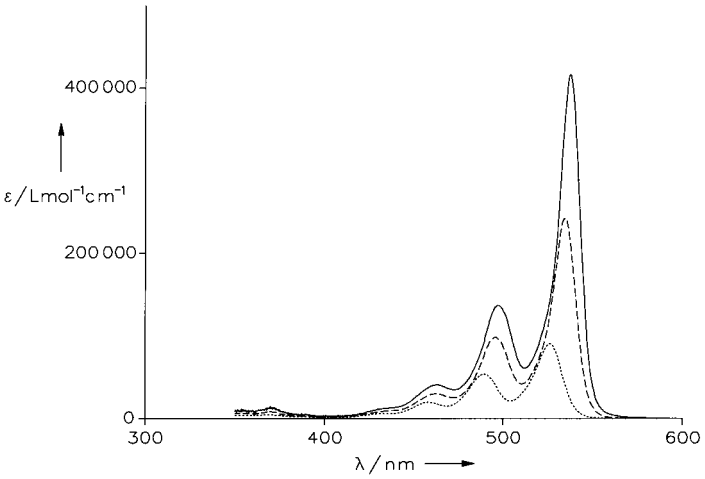


Figure 1. UV/Vis absorption spectra of **1a** (···; color coordinates:[14] $x = 0.3622$, $y = 0.3151$, $Y = 78.29$, 2°, normlight C, $T_{min} = 0.1$), **5a** (– – –; color coordinates: $x = 0.3467$, $y = 0.2940$, $Y = 77.46$), and **6a** (—; color coordinates: $x = 0.3409$, $y = 0.2901$, $Y = 78.47$) in $CHCl_3$.

Table 1. Yields, electron spectroscopic data, and R_f values for the perylene dyes **5** and **6**.

Entry	Yield [%][a]	UV/Vis[b] λ_{max} [nm] (ε [L mol^{-1} cm^{-1}])	Fluoresc.[b, c] λ_{max} [nm]	Solid[d] λ_{max} [nm]	R_f[e]
5a	39	535 (241 800), 496 (97 700)	540	530	0.33
5b	41	534 (230 100), 496 (94 700)	539	623	0.11
5c	29	535 (241 700), 496 (97 800)	539	534	0.40
5d	56	535 (242 000), 496 (98 300)	539	–	0.42
5e	31	534 (239 200), 496 (97 000)	538	534	0.21
5f	38	535 (250 200), 495 (100 600)	540	–	0.84[f]
6a	15	538 (416 900), 497 (135 000)	543	–	0.34
6c	8	537 (407 000), 497 (134 000)	544	–	–
6e	57	538 (422 100), 497 (139 500)	544	–	0.37

[a] Yield of isolated, analytically pure substance. [b] In $CHCl_3$. [c] Fluorescence spectrum. [d] Solid-state fluorescence. [e] Silica gel, $CHCl_3$/1-butanol (40/1). [f] $CHCl_3$/ethanol (10/1).

 © WILEY-VCH Verlag GmbH, D-69451 Weinheim, 1998 1433-7851/98/3707-0953 $ 17.50+.50/0

additional sharp band seems to be "sitting on" the normal vibration band, and a higher extinction coefficient is observed. This effect is even more pronounced for the trichromophoric perylene dyes (Figure 1). If one takes extinction coefficients of 85000 to 95000 $L\,mol^{-1}\,cm^{-1}$ as being "normal" for **1**, the value for bichromophoric dyes ($\varepsilon =$ 240000 $L\,mol^{-1}\,cm^{-1}$) is much more than twice that for **1**, and an extinction coefficient of 420000 $L\,mol^{-1}\,cm^{-1}$ for the trichromophoric dyes **6** is more than 135000 $L\,mol^{-1}\,cm^{-1}$ higher than three times the value for **1**. Such high extinction coefficients have not yet been reached by simple perylene dyes, and the multichromophoric dyes can therefore be considered as "intense dyes". The spectral characteristics of the bi- and trichromophoric dyes can be explained on the basis of an exciton interaction. Although the Davydov splitting becomes vanishingly low because of the relatively weak coupling between the chromophores, the exciton band[11] persists and falls in the same spectral region as the normal absorption of the individual chromophores. It is of interest that the absorption band at longest wavelengths is much sharper than the other absorption bands of the perylene dye. The low half-width value is useful for obtaining very brilliant shades of color, and the new principle may also be of interest for practical applications.

All bi- and trifluorophoric dyes are highly fluorescent; fluorescent quantum yields of 98, 89, 97, and 100 % have been measured for **5a**, **6a**, **6c**, and **6e**, respectively.[12] The fluorescence bands are also shifted to increasingly longer wavelengths with an increasing number of linked chromophores and exhibit the vibration structure which is typical for perylene dyes. The bathochromically shifted fluorescence is also of interest for practical applications.

Perylene dyes **1** tend to aggregate at high concentration.[13] This tendency is enhanced from bichromophoric to trichromophoric dyes and is very pronounced for the latter. However, spectra of nonaggregated dyes are obtained for concentrations below $5 \times 10^{-6}\,mol\,L^{-1}$ (see Figure 1). A further bathochromic shift along with a pink coloration is obtained for the aggregates; this is typical for J aggregates. An indicator for J aggregates is their pronounced fluorescence ($\lambda_{max} = 630$ nm), which is not observed for H aggregates.[14] Because of their long wavelengths J aggregates are of technical interest. On the other hand, the chain length of the N-terminal substituents can be made sufficiently long for the exclusion of aggregation in homogeneous solution (see also the increasing quantum yields from **6a** to **6e** as a result of a decreasing tendency to aggregate).

The principle of color strengthening through exciton interactions described here can certainly be generalized. It is therefore also of interest for other dyes.[15]

Experimental Section

3a: Compound **2a** (2.0 g, 3.5 mmol), hydrazine hydrate (350 mg, 6.9 mmol), and imidazole (7 g) were heated (130 °C, 60 min) and then treated with ethanol/2 N HCl (50 mL, 1/1). The solid precipitate was washed with methanol/water, dried (100 °C), and purified by column chromatography (neutral Al_2O_3, $CHCl_3$/ethanol (20/1) and then silica gel, $CHCl_3$/ethanol (20/1)) to give **3a** (830 mg, 40 %). M.p. 332 – 334 °C; R_f (silica gel, $CHCl_3$/ethanol (10/1)) = 0.80; R_f (silica gel, $CHCl_3$/ethanol 20/1) = 0.61; IR (KBr): $\tilde{\nu} = 2956$ (m), 2927 (s), 2857 (m), 1699 (s), 1658 (s), 1595 (s), 1578 (m), 1404 (s), 1350 (s), 1255 (s) 805 (s), 739 cm^{-1} (m); ^1H NMR ($CDCl_3$): $\delta = 0.81$ (t, 6H, $2CH_3$), 1.28 (m_c, 16H, $8CH_2$), 1.88 (m_c, 2H, 2α-CH_2), 2.24 (m_c, 2H, 2α-CH_2), 5.16 (m_c, 1H, NCH), 5.48 (s, 2H, NH_2), 8.33 (d, $^3J =$ 8.2 Hz, 2H, perylene), 8.41 (d, $^3J = 8.2$ Hz, 2H, perylene), 8.45 (d, $^3J =$ 8.0 Hz, 2H, perylene), 8.57 (br d, $^3J = 7.6$ Hz, 2H, perylene); ^{13}C NMR ($CDCl_3$): $\delta = 14.03$, 22.58, 26.97, 29.23, 31.76, 32.38, 54.91, 122.07, 122.80, 123.26, 125.90, 126.21, 127.78, 129.32, 131.40, 133.74, 134.91, 159.83; UV/Vis ($CHCl_3$): λ_{max} (ε) = 527 (80000), 491 (48600), 460 nm (17800); MS (70 eV): *m/z* (%): 588 (10), 587 (25) [M^+], 407 (14), 406 (53), 405 (100), 376 (22); elemental analysis calcd for $C_{37}H_{37}N_3O_4$ (587.7): C 75.61, H 6.35, N 7.15; found: C 75.32, H 6.24, N 7.01.

5a: Compound **2a** (110 mg, 0.19 mmol), **3a** (100 mg, 0.17 mmol), and imidazole (1 g) were heated under reflux with stirring (140 °C, 60 min). The reaction mixture was worked up as described for **3a** and purified by column separation (neutral Al_2O_3, $CHCl_3$/1-butanol (40/1) and then silica gel, $CHCl_3$/1-butanol (40/1)) to give **5a** (80 mg, 39 %). R_f (silica gel, $CHCl_3$/1-butanol (40/1)) = 0.33; IR (KBr): $\tilde{\nu} = 2954$ (m), 2927 (s), 2856 (m), 1735 (w), 1717 (s), 1698 (s), 1660 (s), 1594 (s), 1579 (s), 1457 (m), 1430 (m), 1404 (s), 1354 (m), 1334 (s), 1252 (s), 1204 (m), 1174 (m), 810 (s), 800 (m), 741 cm^{-1} (m); ^1H NMR ($CDCl_3$): $\delta = 0.80$ (t, 12H, $4CH_3$), 1.28 (m_c, 32H, $16CH_2$), 1.90 (m_c, 4H, 4α-CH_2), 2.27 (m_c, 4H, 4α-CH_2), 5.18 (m_c, 2H, 2NCH), 8.22 (d, $^3J = 7.9$ Hz, 4H, perylene), 8.38 (d, $^3J = 7.9$ Hz, 4H, perylene), 8.45 (d, $^3J = 7.9$ Hz, 4H, perylene), 8.61 (br s, 4H, perylene); ^{13}C NMR ($CDCl_3$): $\delta = 14.02$, 22.58, 27.02, 29.21, 31.76, 32.36, 54.88, 122.21, 122.55, 123.56, 124.24 (br), 125.82, 126.09, 129.03, 129.40, 131.01 (br), 131.73 (br), 132.10, 133.43, 135.15, 159.98, 163.21 (br), 164.31 (br); UV/Vis ($CHCl_3$): λ_{max} (ε) = 535 (241800), 496 (97700), 462 nm (29600); fluorescence ($CHCl_3$): $\lambda_{max} =$ 540, 581 nm; solid-state fluorescence: $\lambda_{max} = 530$, 637 nm; MS (70 eV): *m/z* (%): 1143 (0.8), 1142 (1.3) [M^+], 962 (1.3), 961 (2.7), 960 (1.2), 780 (1.7), 779 (5.4), 778 (6.3), 572 (0.9), 392 (1.8), 391 (8), 390 (14), 373 (2), 345 (1), 182 (52); elemental analysis calcd for $C_{74}H_{70}N_4O_8$ (1143.4): C 77.73, H 6.17, N 4.90; found: C 77.61, H 6.20, N 4.89.

6a: Compound **3a** (300 mg, 0.51 mol), **4** (100 mg, 0.26 mmol), zinc acetate dihydrate (60 mg, 0.26 mmol), and imidazole (2 g) were heated under reflux with stirring (150 °C, 3.5 h). The reaction mixture was worked up as described for **3a** and purified by column separation (neutral Al_2O_3, $CHCl_3$/ethanol (10/1) and then silica gel, toluene/acetic acid (15/1)). By-products were eluated first, and **6a** (60 mg, 15 %) was collected by elution with $CHCl_3$/1-butanol (40/1); R_f (silica gel, $CHCl_3$/1-butanol (40/1)) = 0.34; IR (KBr): $\tilde{\nu} = 3065$ (w), 2952 (m), 2927 (m), 2856 (m), 1738 (w), 1716 (br s), 1698 (br s), 1660 (s), 1593 (s), 1580 (m), 1428 (m), 1403 (m), 1353 (m), 1329 (s), 1252 (m), 1202 (m), 1126 (m), 965 (m), 852 (m), 810 (s), 796 (m), 738 (m), 725 (m), 663 cm^{-1} (m); ^1H NMR ($C_2D_2Cl_4$, 90 °C): $\delta = 0.87$ (t, 12H, $4CH_3$), 1.29 (m_c, 32H, $16CH_2$), 1.95 (m_c, 4H, 4α-CH_2), 2.27 (m_c, 4H, 4α-CH_2) 5.16 (m_c, 2H, 2NCH), 8.50 (m_c, 12H, perylene), 8.61 (d, $^3J = 7.8$ Hz, 4H, perylene), 8.66 (d, $^3J = 7.5$ Hz, 4H, perylene), 8.78 (d, $^3J = 8.0$ Hz, 4H, perylene); UV/Vis ($CHCl_3$): λ_{max} (ε) = 538 (416900), 497 (135000), 463 nm (38500); fluorescence ($CHCl_3$): $\lambda_{max} = 543$, 583 nm; MS (FAB, 3-nitrobenzyl alcohol matrix): *m/z* (%): 1532 (0.1), 1531 (0.1), 1530 (0.1) [M^+], 1350 (0.6), 1349 (0.6), 1168 (0.4), 1167 (0.5), 1166 (0.2), 961 (0.4), 779 (3), 391 (24), 390 (14), 373 (18), 345 (14); the molecular mass of **6a** was verified by gel chromatography;[5] elemental analysis calcd for $C_{98}H_{78}N_6O_{12}$ (1531.7): C 76.85, H 5.13, N 5.49; found: C 75.91, H 5.04, N 5.67.

Received: August 8, 1997 [Z10789IE]
German version: *Angew. Chem.* **1998**, *110*, 998 – 1001

Keywords: dyes · fluorescence spectroscopy · perylenes

[1] Review: H. Langhals, *Heterocycles* **1995**, *40*, 477 – 500.
[2] P. Edman, L. B.-Å. Johansson, H. Langhals, *J. Phys. Chem.* **1995**, *99*, 8504 – 8509.
[3] H. Langhals, S. Demmig, H. Huber, *Spectrochim. Acta Part A* **1988**, *44*, 1189 – 1193.
[4] H. Kaiser, J. Lindner, H. Langhals, *Chem. Ber.* **1991**, *124*, 529 – 535.
[5] H. Langhals, R. Kollefrath, J. Lindner, *Macromol. Rep.* **1995**, *A32*, 415 – 423.
[6] H. Langhals, J. Gold, *J. Prakt. Chem.* **1996**, *338*, 654 – 659.

 © WILEY-VCH Verlag GmbH, D-69451 Weinheim, 1998 1433-7851/98/3707-0954 $ 17.50+.50/0

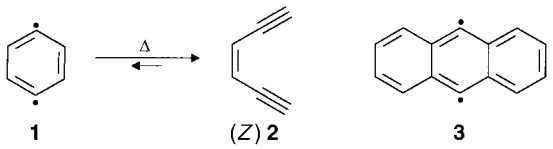
[7] H. Langhals, J. Gold, *Liebigs Ann.* **1997**, 1151 – 1153.
[8] See also A. Osuka, H. Shimidzu, *Angew. Chem.* **1997**, *109*, 93 – 95; *Angew. Chem. Int. Ed. Engl.* **1997**, *36*, 135 – 137.
[9] H. Langhals, S. Demmig, T. Potrawa, *J. Prakt. Chem.* **1991**, *333*, 733 – 748.
[10] H. Langhals, *Nachr. Chem. Tech. Lab.* **1980**, *28*, 716 – 718 [*Chem. Abstr.* **1981**, *95*, R9816q].
[11] M. Klessinger, J. Michl, *Lichtabsorption und Photochemie organischer Moleküle*, VCH, Weinheim, **1989**.
[12] The concentrations of **5a**, **6a**, **6c**, and **6e** in $CHCl_3$ were 4.12×10^{-7}, 2.33×10^{-7}, 2.57×10^{-7}, and 2.66×10^{-7} mol L^{-1}, respectively. The quantum yields Φ are quoted with respect to that of the reference compound **1a** ($\Phi = 100\,\%$).
[13] W. E. Ford, *J. Photochem.* **1987**, *37*, 189 – 204.
[14] T. Förster, *Naturwissenschaften* **1946**, 166 – 175.
[15] H. Zollinger, *Color Chemistry*, 2nd ed., VCH, Weinheim **1991**.

p-Benzyne**

Ralph Marquardt, Andreas Balster, Wolfram Sander,* Elfi Kraka, Dieter Cremer,* and J. George Radziszewski*

Dedicated to Professor Dr. Günther Maier on the occasion of his 66th birthday

Since the discovery of the enediyne antibiotics there has been great interest in *p*-benzyne (1,4-didehydrobenzene, **1**) and its derivatives.[1–3] Compound **1** is formed as a reactive intermediate at very low stationary concentrations in the rearrangement of (*Z*)-3-hexene-1,5-diyne [(*Z*)-**2**],[4–6] and can be trapped in the gas phase with O_2 or NO.[7] Roth et al. determined the heat of formation of **1** from the kinetics of these trapping reactions to be 138.0 ± 1 kcal mol^{-1} (which means it is 8.5 kcal mol^{-1} less stable than (*Z*)-**2**), and the barrier toward ring opening to be 19.8 kcal mol^{-1}.[7]

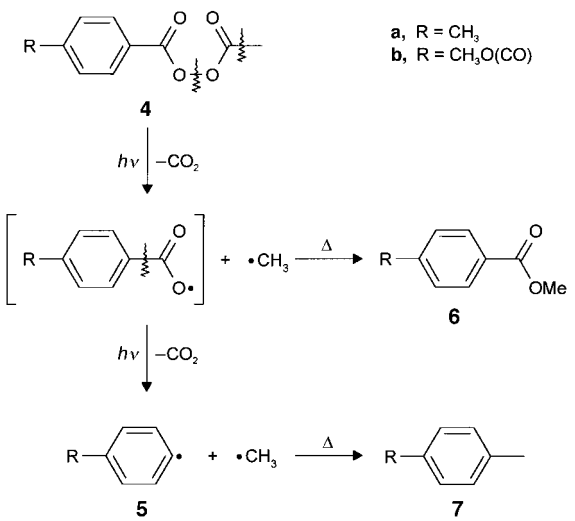


[*] Prof. Dr. W. Sander, Dr. R. Marquardt, A. Balster
Lehrstuhl für Organische Chemie II der Universität
D-44780 Bochum (Germany)
Fax: (+49) 234-709-4353
E-mail: sander@neon.orch.ruhr-uni-bochum.de
Prof. Dr. D. Cremer, Prof. Dr. E. Kraka
Department of Theoretical Chemistry
University of Göteborg
Kemigården 3, S-41296 Göteborg (Sweden)
Fax: (+46) 31-772-2933
E-mail: cremer@theoc.chalmers.se
Dr. J. G. Radziszewski
National Renewable Energy Laboratory (NREL, 1613)
1617 Cole Boulevard, Golden, CO 80401 (USA)
Fax: (+1) 303-275-2905
E-mail: jradzisz@nrel.nrel.gov

[**] This work was supported financially by the Deutschen Forschungsgemeinschaft, the Fonds der Chemischen Industrie, and the Swedish Natural Science Research Council. Calculations were carried out on a CRAY YMP/464 and a CRAY C90 of the Nationellt Superdatorcentrum (NSC), Linköping, Sweden, whose generous support we gratefully acknowledge. J. G. R. acknowledges support from the NREL FIRST program.

Although several attempts at the synthesis of **1** from *p*-substituted benzene derivatives are reported in the literature,[8, 9] the only derivative of **1** so far characterized spectroscopically, at low temperature, is 9,10-didehydroanthracene (**3**).[10] Squires et al. determined thermochemical data for **1** through collision-induced dissociation of the *p*-chlorophenyl anion in the gas phase in a quadrupole mass spectrometer.[11, 12] These data ($\Delta H_f^\circ = 137\pm3$ kcal mol^{-1}) are in excellent agreement with the values reported by Roth et al.[7] and with theoretical data from ab initio calculations at the CCSD(T)[13, 14] and CASSCF/CASPT2[15] levels of theory. Thus, both experiment and theory predict **1** to lie in an energy well sufficiently deep to permit, in principle, its isolation at low temperature. Here we report a matrix isolation and IR spectroscopic characterization of *p*-benzyne (**1**).

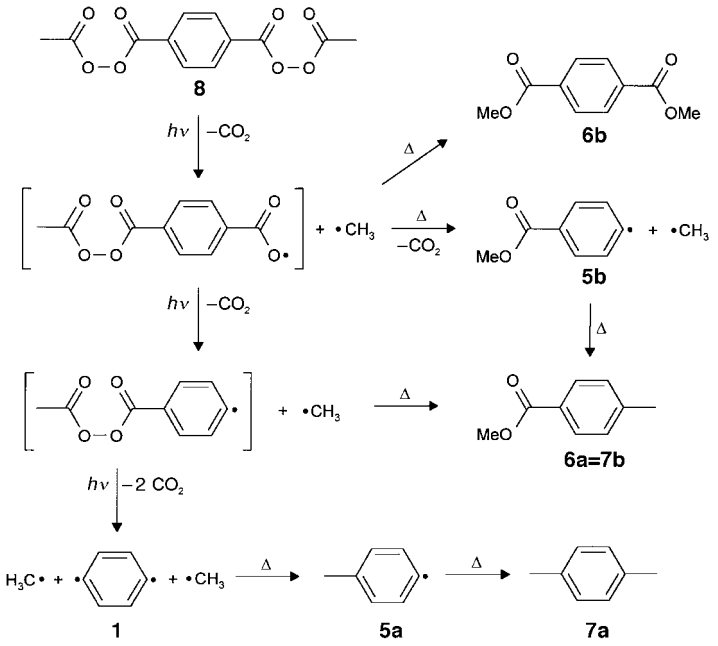
Acyl peroxides of type **4** were first used by Pacansky et al.[16, 17] for the matrix isolation of radicals, and were recently utilized for the generation of the phenyl radical[18] and the synthesis of *m*-benzyne.[17] Upon irradiation, **4** decomposes to an aryl radical **5**, CO_2, and a second radical, which in the case of acetyl peroxides is a methyl radical (Scheme 1). As long as the temperature of the matrix is kept low enough to prevent the diffusion of small molecules, the two radical fragments are separated by two CO_2 molecules, but at higher temperatures the radicals react rapidly to give **6** and **7**.



Scheme 1. Photolysis of **4a**, **b** in argon at 10 K.

Similarly, diacetylterephthaloyl diperoxide (**8**)[19] should yield **1**, CO_2, and methyl radicals (Scheme 2). Vacuum flash pyrolysis of **8** at temperatures between 300 and 600 °C and trapping of the products in argon at 10 K resulted in the formation of *Z* enediyne **2** and CO_2 as the main products, together with a small amount of dimethyl terephthalate (**6b**).

 © WILEY-VCH Verlag GmbH, D-69451 Weinheim, 1998 1433-7851/98/3707-0955 $ 17.50+.50/0



Scheme 2. Photolysis of **8** in argon at 10 K.

At higher pyrolysis temperatures (*Z*)-**2** is partially isomerized to (*E*)-**2**. No other products were observed, nor were IR absorption bands that could be attributed to **1**. This suggests that **1** is formed during pyrolysis of **8** but is not stable toward ring opening at the temperatures necessary for fragmentation of the peroxide. The fact that the Bergman rearrangement[4] is rapid under these conditions was readily demonstrated by vacuum flash pyrolysis of (*Z*)-[1,6-D_2]hex-3-en-1,5-diine at 300 – 500 °C, which resulted in an equilibrium mixture of the [1,6-D_2] and [3,4-D_2] isotopomers. Again, the *E* isomer was a secondary product formed only at temperatures above 800 °C.

The radicals expected to be formed upon photolysis of **8** are *p*-benzyne (**1**), the methyl radical, the *p*-tolyl radical (**5a**), and the 4-(methoxycarbonyl)phenyl radical (**5b**, Scheme 2). To obtain reference spectra of **5a**, **b** the photochemistry of acyl peroxides **4a**, **b**[19] was first investigated under matrix conditions.

Photolysis ($\lambda = 254$ nm, Scheme 1) of matrix-isolated acetyl 4-methylbenzoyl peroxide (**4a**) yielded CO_2, methyl *p*-toluate (**6a**), methyl radical, and a new species with strong IR absorption bands at 1450, 1029, 767, and 452 cm^{-1}. The two latter species disappeared when the matrix was annealed at 30 K, and *p*-xylene (**7a**) was formed. This thermal reaction and the similarity of the observed IR absorption bands to those of the phenyl radical[17] strongly suggest that the new species is the *p*-tolyl radical (**5a**).

Photolysis ($\lambda = 248$ nm) of acetyl 4-(methoxycarbonyl)benzoyl peroxide (**4b**) produced CO_2, dimethyl terephthalate (**6b**), methyl radical, and the 4-(methoxycarbonyl)phenyl radical (**5b**) with strong bands at 1438, 1372, and 739 cm^{-1}. Because of the strong carbonyl absorption of ester **6b** at 1740 cm^{-1} the carbonyl absorption of **5b** could not be clearly observed. When the matrix was annealed at 40 K the methyl radicals reacted with **5b** to produce methyl *p*-toluate (**7b** = **6a**).

The main products of photolysis ($\lambda = 254$ nm) of **8** were dimethyl terephthalate (**6b**) and CO_2 (Scheme 2). Other products were the methyl radical, radical **5b**, and small amounts of the *p*-tolyl radical (**5a**). Annealing of the matrix at 40 K reduced the number of these radicals. IR absorption bands of medium to low intensity at 1445, 980, 814, 725, and 691 cm^{-1} also disappeared when the matrix was warmed; however, it was not possible to assign these to any of the known compounds (Figure 1).

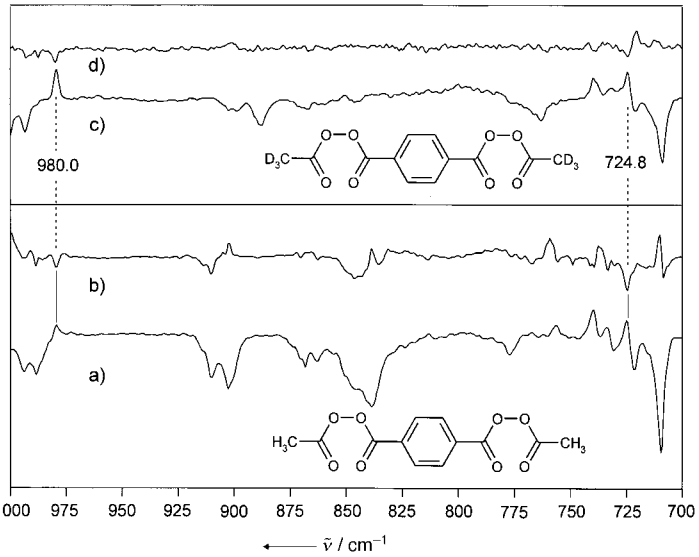
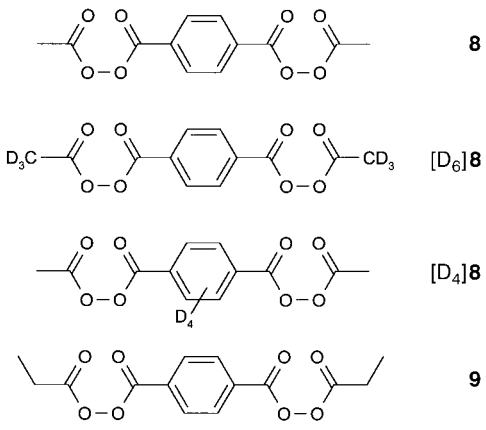


Figure 1. Difference IR absorption spectra after photolysis (254 nm, 10 K) of **8** (a) and [D_6]**8** (c) as well as spectra after subsequent annealing at 40 °C (b and d). After irradiation, no bands remain for the starting material, only those of the photolysis products are observed. Upon disappearance of the bands for the radicals and **1**, bands for unknown products appear.

Irradiation of matrix-isolated [D_6]**8** (with perdeuterated acetyl groups) again resulted in formation of a set of IR absorption bands for a thermolabile species. The bands at 980 and 725 cm^{-1} were the only ones that did not exhibit isotopic shifts (Figure 1) and therefore cannot be associated with a compound that contains methyl groups. It is tempting to assign these vibrations to *p*-benzyne (**1**). To obtain a third



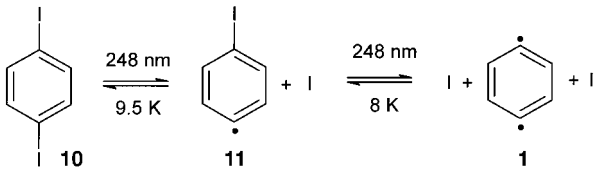
isotopomer of **8** the benzene ring was perdeuterated to give [D_4]**8**. Photolysis of [D_4]**8** under the same conditions did not result in absorption bands at 980 and 725 cm^{-1}. Instead, a very weak absorption appeared at 767 cm^{-1}, which was tentatively assigned to [D_4]**1**.

 © WILEY-VCH Verlag GmbH, D-69451 Weinheim, 1998 1433-7851/98/3707-0956 $ 17.50+.50/0

Irradiation ($\lambda = 254$ nm) of matrix-isolated dipropionyl terephthaloyl peroxide (**9**) produced CO_2, diethyl terephthalate, ethyl radicals,[20] and small amounts of the 4-(ethoxycarbonyl)phenyl radical, identified by the similarity of its IR spectrum to that of the methyl derivative **5b**. When the matrix was annealed, all the absorption bands assigned to the radicals decreased in intensity. Again, the bands at 980 and 725 cm^{-1} assigned to **1** became apparent during photolysis and disappeared after the matrix was annealed; therefore, the photochemistry of **9** is completely analogous to that of **8**.

Iodobenzenes are independent precursors of radicals and didehydrobenzenes. Indeed, irradiation of matrix-isolated 1,2-diiodobenzene produces *o*-benzyne.[21] Since the C–I bond energy is about 65 kcal mol^{-1} and aromatic iodides begin to absorb UV light at 270 nm, 248- or 254-nm irradiation provides direct energetic access to radicals.[22] From our earlier work with the phenyl radical we concluded on the basis of photoorientation and polarization measurements that partial in-plane rotation of the ring is necessary to permit the formation from iodobenzene of radical pairs that do not immediately recombine.

Neon matrices (at 6 K) provide unique viscosity conditions that allow rupture of the first C–I bond and subsequent partial rotation of the ring, which in the photolysis of 1,4-diiodobenzene (**10**) leads to radical **11**.[23] A small fraction of **11** is



converted into **1** by the subsequent absorption of photons. The observed set of IR absorption bands is exceedingly weak ($A \approx 10^{-3}$) but reproducible, and it corresponds well with results obtained from the photolysis of peroxides. These bands disappear from the spectra after annealing at about 8 K, while facile recombination of monoradical **11** with iodine atoms to form **10** is observed at 9.5 K. It is impossible to decide whether a small fraction of **10** originates from recombination of iodine atoms with **1**. The frequencies of the observed bands are very probably affected by the proximity of heavy iodine atoms, whereas the intensities may be distorted by nonlinearity in the detector response to such extremely weak signals.

To provide further support for this assignment, the vibrational spectrum of **1** was calculated at different levels of theory ranging from MP2 through MP4 to GVB, CCSD, CCSD(T), and density functional theory (DFT) with the B3LYP functional. Most of these descriptions turned out to be insufficient because of the multireference character of **1** and the necessity of providing a reasonable description of both static and dynamic electron correlation in **1**. Useful descriptions were obtained only at the CCSD(T)[24] and B3LYP[25, 26] levels of theory. Basis sets ranging from 6-31G(d,p) to 6-311 + G(3df,3pd)[27] were utilized; in the first case the size of the basis set was limited by the available computer capacity. All calculations were carried out with the programs ACES[28] and GAUSSIAN 94.[29]

In Table 1, scaled B3LYP vibrational frequencies and corresponding IR intensities calculated for the harmonic approximation are compared with the observed IR bands.

Table 1. Calculated IR frequencies $\tilde{\nu}$ [cm^{-1}] and intensities I [km mol^{-1}] for **1** and [D_4]**1** at the UB3LYP/6-311 + G(3d1f,3p1d) level.[a]

Entry	Sym.	**1**			$\tilde{\nu}_{exp.}$	[D_4]**1**		
		$\tilde{\nu}$	I	$\tilde{\nu}_{scaled}$[b]	for **10**/**8**	$\tilde{\nu}$	I	$\tilde{\nu}_{scaled}$[b]
1	a_u	414	0	396	–/–	360	0	345
2	b_{3u}	445	20	427	435 (w)/–	392	26	376
3	b_{3g}	577	0	554	–/–	557	0	535
4	b_{2g}	614	0	589	–/–	544	0	523
5	a_g	625	0	600	–/–	603	0	579
6	b_{1g}	731	0	702	–/–	568	0	546
7	b_{3u}	758	76	728	721 (s)/725 (s)	625	24	600
8	b_{2g}	915	0	876	–/–	760	0	729
9	b_{1u}	923	18	886	918 (w)/–	806	20	774 (767)
10	a_u	947	0	909	–/–	772	0	741
11	a_g	1021	0	980	–/–	849	0	815
12	b_{1u}	1047	17	1005	976 (w)/980 (s)	911	6	875
13	b_{2u}	1050	3	1008	–/–	798	0	766
14	a_g	1151	0	1105	–/–	990	0	950
15	b_{2u}	1231	5	1182	1207 (w)/–	1149	1	1103
16	b_{3g}	1279	0	1228	–/–	977	0	938
17	b_{2u}	1391	5	1335	1331 (w)/–	1361	< 1	1306
18	a_g	1394	0	1338	–/–	1369	0	1315
19	b_{1u}	1442	2	1384	1403 (w)/–	1320	1	1267
20	b_{3g}	1633	0	1568	–/–	1614	0	1549
21	b_{1u}	3173	1	3046	–/–	2340	1	2246
22	b_{3g}	3175	0	3048	–/–	2339	0	2245
23	b_{2u}	3189	3	3061	–/–	2357	2	2263
24	a_g	3190	0	3062	–/–	2360	0	2266

[a] The experimentally determined values were obtained by irradiation of **10** (first value) and **8** (second value). Relative intensities are indicated in parentheses, as is the only detected band for [D_4]**1**. UB3LYP/6-311+G (3d1f, 3p1d) geometry: $R(\cdot CC) = 1.366$, $R(CC) = 1.419$, $R(\cdot C \cdot C) = 2.664$, $R(CH) = 1.082$ Å; $\sphericalangle(C \cdot CC) = 125.8$, $\sphericalangle(\cdot CCC) = 117.2$, $\sphericalangle(\cdot CCH) = 123.4°$. [b] Scaling factor 0.96.

Calculations predict that the IR spectrum of **1** should be characterized by four relatively strong bands: the b_{3u}-symmetric ring torsion mode (boat conformation, out-of-plane) at 427 (entry 2), the b_{3u}-symmetric CH wagging mode at 728 (entry 7), the b_{1u}-symmetric ring deformation mode at 886 (entry 9), and the b_{1u}-symmetric C–C stretching and C-C-H bending mode at 1005 cm^{-1} (entry 12). In addition, four rather weak bands should appear at 1008 (entry 13, probably masked by entry 12), 1182 (entry 15), 1335 (entry 17), and 1384 cm^{-1} (entry 19). Of these bands, all but the weak bands 13 and 17 could be identified in the recorded IR spectra, with differences from the calculated frequencies of only 3 to at most 30 cm^{-1}. The agreement for the intense bands 12 and 7 is particularly satisfying.

Upon perdeuteration of **1** the IR spectrum changes significantly (Table 1). Of the six bands calculated for [D_4]**1** in the region 700 to 1500 cm^{-1} with weak (entries 15, 17, and 19), strong (entries 9 and 12), or very strong intensity (entry 7), all but band 9 are considerably weaker than in the non-deuterated case. According to our calculations, it should be nearly impossible to observe modes 12, 15, 17 (also not observed for **1**), or 19. The band corresponding to the b_{3u}-symmetric motion (entry 7) should have a reduced intensity of 24 km mol^{-1}, but its frequency is shifted to 600 cm^{-1} (into a

region in which the IR spectrum could not be recorded). The only detectable IR band of [D_4]**1** in the region 700 – 1500 cm^{-1} is predicted to fall at 774 cm^{-1} and should belong to the b_{1u}-symmetric mode 9 (masked in the case of **1** by IR absorption of other compounds, Table 1). This is in agreement with the fact that the only IR band observed for [D_4]**1** in the region 700 – 1500 cm^{-1} is at 767 cm^{-1}.

We were thus able to prepare in a matrix from two precursors a thermolabile species with IR absorption at 435, 721/725, 976/980, 1207, and 1403 cm^{-1}. These IR bands are in agreement with calculated frequencies for *p*-benzyne (**1**). The IR spectrum of [D_4]**1** is characterized by a single intense IR absorption (767 cm^{-1}) between 700 and 1500 cm^{-1}. The Bergman rearrangement is very rapid in the gas phase, and for this reason **1** is converted completely into ring-opened enediyne (*Z*)-**2**.

Experimental Section

General procedure for the synthesis of acyl peroxides: a solution of the acyl chloride (5 mmol for the synthesis of **4**, 10 mmol for **8**) in $CHCl_3$ (20 mL) and pyridine (12 mmol in 20 mL of $CHCl_3$) was added within one hour at – 10 °C to a suspension of the corresponding peroxy- or diperoxyacid (5 mmol) in $CHCl_3$ (100 mL) and stirred at this temperature for 2 h. The cold solution was filtered and washed with water (30 mL), 10 % HCl (30 mL), and a saturated solution of $NaHCO_3$ (2 × 30 mL). The $CHCl_3$ solution was dried over Na_2SO_4, and solvent was removed in vacuo at 15 °C. The peroxides were obtained in 40 – 80 % yield as crystalline material of generally high purity and, if necessary, purified by preparative HPLC (SiO_2, CH_2Cl_2/$CHCl_3$). Compounds **4a**,[30] **8**,[31] and **11**[31] were identified by comparison with literature data.

4b: M.p. 95 °C; IR (KBr): $\tilde{\nu}$ = 3106 (vw), 2961 (vw), 1814 (w), 1814 (m), 1771 (vs), 1723 (vs), 1578 (w), 1503 (vw), 1440 (m), 1408 (m), 1368 (w), 1288 (vs), 1229 (s), 1154 (m), 1110 (s), 1034 (vs), 1010 (vs), 958 (vw), 894 (w), 870 (w), 836 (w), 823 (w), 787 (vw), 720 (vs), 668 (m), 643 (w), 584 cm^- (vw); UV/Vis (EtOH): λ_{max} (lgε) = 208 (3.45), 244 (4.12), 286 nm (3.16); ^{1}H NMR (400 MHz, $CDCl_3$): δ = 8.09 (dd, *J* = 27.2, 8.4 Hz, 4 H), 3.93 (s, 3 H), 2.26 (s, 3 H); ^{13}C NMR (400 MHz, $CDCl_3$): δ = 166.0 (s, C=O), 165.8 (s, C=O), 162.2 (s, C=O), 135.1 (s), 129.9 (d), 129.7 (d), 129.3 (s), 52.6 (q), 16.6 (q); MS (70 eV): *m*/*z* (%): 238 (3) [M^+], 207 (4), 180 (13), 164 (10), 163 (100), 149 (36), 135 (13), 121 (8), 104 (14), 103 (10), 77 (9), 76 (17), 75 (9), 65 (11), 50 (15), 45 (7), 44 (11), 43 (27), 39 (6), 28 (6); HR-MS: calcd for $C_{11}H_{10}O_6$ 238.0477, found 238.0472.

8: ^{1}H NMR (200 MHz, $CDCl_3$): δ = 8.11 (s, 4 H), 2.27 (s, 6 H); ^{13}C NMR (200 MHz, $CDCl_3$): δ = 164.9, 160.8, 129.6, 129.0, 15.6; MS (70 eV): *m*/*z* (%): 282 (2) [M^+], 207 (87), 191 (5), 166 (15), 149 (100), 135 (9), 121 (16), 104 (53), 76 (31), 65 (20), 60 (17), 50 (32), 44 (60), 43 (95).

[D_6]8: ^{1}H NMR (200 MHz, $CDCl_3$): δ = 8.11 (s); ^{13}C NMR (200MHz, $CDCl_3$): δ = 164.9, 160.8, 129.6, 129.0, 15.6; MS (70 eV): *m*/*z* (%): 288 (1) [M^+], 210 (61), 194 (16), 166 (15), 149 (100), 138 (7), 121 (12), 104 (39), 76 (22), 65 (17), 63 (12), 50 (24), 46 (85), 44 (57).

[D_4]8: ^{1}H NMR (200 MHz, $CDCl_3$): δ = 2.27 (s); ^{13}C NMR (200 MHz, $CDCl_3$): δ = 164.9, 160.8, 129.6, 129.0, 15.6; MS (70 eV) *m*/*z* (%): 286 (3) [M^+], 211 (100), 170 (16), 153 (58), 139 (11), 125 (13), 108 (54), 80 (28), 69 (17), 60 (16), 52 (27), 44 (57), 43 (66).

Received: February 13, 1997
Revised version September 23, 1997 [Z10107IE]
German version: *Angew. Chem.* **1998**, *110*, 1001–1005

Keywords: ab initio calculations · density functional calculations · matrix isolation · photochemistry · radicals

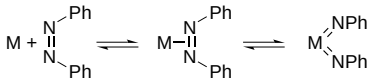
[1] K. C. Nicolaou, W. M. Dai, *Angew. Chem.* **1991**, *103*, 1453 – 1481; *Angew. Chem. Int. Ed. Engl.* **1991**, *30*, 1387 – 1416.
[2] K. C. Nicolaou, *Angew. Chem.* **1993**, *105*, 1462 – 1471; *Angew. Chem. Int. Ed. Engl.* **1993**, *32*, 1377 – 1385.
[3] P. Chen, *Angew. Chem.* **1996**, *108*, 1584 – 1586; *Angew. Chem. Int. Ed. Engl.* **1996**, *35*, 1478 – 1480.
[4] R. R. Jones, R. G. Bergman, *J. Am. Chem. Soc.* **1972**, *94*, 660 – 661.
[5] R. G. Bergman, *Acc. Chem. Res.* **1973**, *6*, 25 – 31.
[6] T. P. Lockhart, P. B. Comita, R. G. Bergman, *J. Am. Chem. Soc.* **1981**, *103*, 4082 – 4090.
[7] W. R. Roth, H. Hopf, C. Horn, *Chem. Ber.* **1994**, *127*, 1765 – 1779.
[8] R. S. Berry, J. Clardy, M. E. Schafer, *Tetrahedron Lett.* **1965**, *15*, 1003 – 1010.
[9] I. P. Fisher, F. P. Lossing, *J. Am. Chem. Soc.* **1963**, *85*, 1018 – 1019.
[10] O. L. Chapman, C. C. Chang, J. Kolc, *J. Am. Chem. Soc.* **1976**, *98*, 5703 – 5705.
[11] P. G. Wenthold, J. A. Paulino, R. R. Squires, *J. Am. Chem. Soc.* **1991**, *113*, 7414 – 7415.
[12] P. G. Wenthold, R. R. Squires, *J. Am. Chem. Soc.* **1994**, *116*, 6401 – 6412.
[13] E. Kraka, D. Cremer, *Chem. Phys. Lett.* **1993**, *216*, 333 – 340.
[14] E. Kraka, D. Cremer, *J. Am. Chem. Soc.* **1994**, *116*, 4929 – 4936.
[15] J. Cramer, J. J. Nash, R. R. Squires, *Chem. Phys. Lett.*, **1997**, *277*, 311 – 320.
[16] a) J. Pacansky, J. Bargon, *J. Am. Chem. Soc.* **1975**, *97*, 6896 – 6897; b) J. Pacansky, W. Koch, M. D. Miller, *ibid.* **1991**, *113*, 317 – 328.
[17] a) J. Pacansky, G. P. Gardini, J. Bargon, *Ber. Bunsen-Ges. Phys. Chem.* **1978**, *82*, 19 – 20; b) J. Pacansky, J. S. Chang, D. W. Brown, *Tetrahedron* **1982**, *38*, 257 – 260.
[18] J. G. Radziszewski, M. R. Nimlos, P. R. Winter, G. B. Ellison, *J. Am. Chem. Soc.* **1996**, *118*, 7400 – 7401.
[19] R. Marquardt, W. Sander, E. Kraka, *Angew. Chem.* **1996**, *108*, 825 – 827; *Angew. Chem. Int. Ed. Engl.* **1996**, *35*, 746 – 748.
[20] J. Pacansky, M. Dupuis, *J. Am. Chem. Soc.* **1982**, *104*, 415 – 421.
[21] J. G. Radziszewski, unpublished results.
[22] "Vibrational and Electronic Energy Levels of Polyatomic Transient Molecules": M. E. Jacox, *J. Phys. Chem. Ref. Data Monogr.* **1994**, *3*.
[23] Recorded ESR, UV/Vis, and IR absorption spectra are compatible with expectations for the 4-iodophenyl radical. In addition, the experimental IR spectrum is nicely reproduced by calculations at the B3LYP level of theory. A full account of this work will be presented elsewhere.
[24] K. Raghavachari, G. W. Trucks, J. A. Pople, M. Head-Gordon, *Chem. Phys. Lett.* **1989**, *157*, 479 – 483.
[25] A. Becke, *J. Chem. Phys.* **1993**, *98*, 5648 – 5652.
[26] P. J. Stephens, F. J. Devlin, C. F. Chabalowski, M. J. Frisch, *J. Phys. Chem.* **1993**, *98*, 11623 – 11627.
[27] a) P. C. Hariharan, J. A. Pople, *Chem. Phys. Lett.* **1972**, *16*, 217 – 219; b) R. Krishnan, M. Frisch, J. A. Pople, *J. Chem. Phys.* **1980**, *72*, 4244 – 4245.
[28] J. F. Stanton, J. Gauss, J. D. Watts, W. J. Lauderdale, R. J. Bartlett, *ACES II, Quantum Theory Project*, University of Florida, Gainesville, FL (USA), **1992**.
[29] M. J. Frisch, M. Head-Gordon, G. W. Trucks, J. B. Foresman, H. B. Schlegel, K. Raghavachari, M. A. Robb, J. S. Binkley, C. Gonzales, D. J. Defrees, D. J. Fox, R. A. Whiteside, R. Seeger, C. F. Melius, J. Baker, R. L. Martin, L. R. Kahn, J. J. P. Stewart, S. Topiol, J. A. Pople, *Gaussian 94*, Gaussian Inc., Pittsburgh PA (USA), **1994**.
[30] K. Rübsamen, W. P. Neumann, R. Sommer, U. Frommer, *Chem. Ber.* **1969**, *102*, 1290 – 1298.
[31] Y. A. Ol'dekop, G. S. Belina, M. S. Matveentseva, *Zh. Org. Khim.* **1986**, *4*, 585 – 587.

 © WILEY-VCH Verlag GmbH, D-69451 Weinheim, 1998 1433-7851/98/3707-0958 $ 17.50+.50/0

A Simple Preparative Route to Bis(imido)-uranium(VI) Complexes by the Direct Reductions of Diazenes and Azides**

Benjamin P. Warner, Brian L. Scott, and Carol J. Burns*

The four-electron reductive cleavage of a double bond is rarely observed on a single metal center (Scheme 1).[1] It has been suggested that this reaction is symmetry-forbidden for

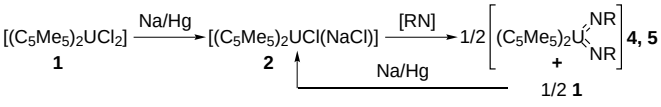


Scheme 1. Reaction of azobenzene to form bis(phenylimido) complexes.

most metal d-electron counts in the absence of strongly π-accepting ligands.[2] Metallocene complexes are not expected to effect this reaction, as they possess only three metal-based valence orbitals available to accommodate the four metal–ligand bonds formed. These orbital constraints do not exist for actinide metallocenes, however, if f orbitals are capable of participating in the metal–nitrogen bonding. This is illustrated by our previous report of the two-electron cleavage of hydrazines by uranium(IV) to yield stable uranium(VI) bis(organoimido) complexes.[3]

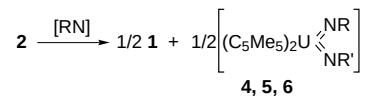
We are investigating high valent uranium compounds to elucidate the role of f orbitals in chemical bonding. This requires the development of simple synthetic routes to a broad spectrum of organouranium(VI) imido compounds. Previously reported preparations of these compounds involved multistep syntheses starting from **1**.[3] We now report two one-pot procedures for this transformation.

The uranium(III) complex **2** is known to act as a uranium(II) synthetic equivalent.[4] We report here that compound **2** also reacts with either organic azo or azido compounds to yield bis(imido)uranium(VI) compounds in high yields in a one-pot procedure (Scheme 2). Compound **2** is generated in situ by



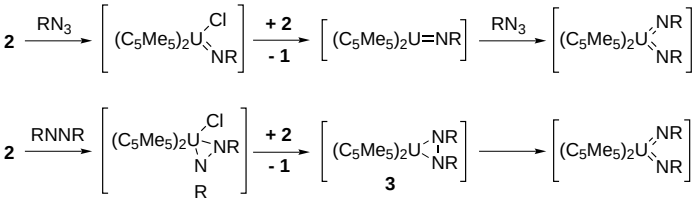
Scheme 2. One-pot synthesis of $[(C_5Me_5)_2U(NR)_2]$ (**4** and **5**) from **1**. **4** (R = Ph): [RN] = PhNNPh, 92%; [RN] = PhN_3, 84%; **5** (R = 1-Ad): [RN] = 1-AdN_3, 71%.

the Na/Hg reduction of **1**. The organic oxidant is then added, and the additional **1** that is produced in the course of the reaction is reduced by the second equivalent of Na present, so that all of the uranium is converted into the desired product (Scheme 2). These reactions have also been carried out with independently prepared **2**[5] in the absence of added Na, demonstrating that **2** is able to perform the four-electron reduction of the azo or azido functional groups, with the formation of one half equivalent of **1** (Scheme 3).



Scheme 3. Synthesis of $[(C_5Me_5)_2U(NR)_2]$ (**4**–**6**) from **2**. **4** (R = R′ = Ph): [RN] = PhNNPh, 94%; **5** (R = R′ = 1-Ad): [RN] = 1-AdN_3, 95%; **6** (R = Ph; R′ = $SiMe_3$): [RN] = $PhNNSiMe_3$,[16] 70%.

Although **2** acts as a uranium(II) synthetic equivalent,[4] there is no evidence that any uranium(II) species is ever produced.[6] By analogy to known reactions, it may be suggested that this reaction occurs as depicted in Scheme 4.



Scheme 4. Proposed mechanisms.

Compound **2** can react with an azide to generate a chloroimidouranium(V) species.[7] This species can comproportionate with a second equivalent of **2** to generate **1** and a imidouranium(IV) compound[8] which is known to react with azides to form bis(imido)uranium(VI) complexes.[3] Azo compounds can react similarly via the intermediacy of a chlorohydrazineuranium(V)[9] complex and an azouranium complex (**3**).

These reactions provide a source of high-valent organoimido complexes with a wider range of N-substitution, including saturated alkylimido analogues. The reaction of **2** with two equivalents of adamantylazide generates the bis (adamantylimido) complex **5** in high yield (Figure 1[10]). As in other organoimidouranium complexes,[11] the complex displays short uranium–nitrogen bonds (U–N(1):1.94(2) Å, U–N(2):1.96(2) Å), and nearly linear U-N-C angles (U-N(1)-C(1): 177(2)°, U-N(2)-C(11): 172(2)°), indicative of metal–ligand multiple bonding.[12] The N-U-N angle (96.6(8)°) is similar to that observed in **4**.[3a]

The oxidation of **2** with diazenes illustrates some differences between the transition metals and the f-block elements and suggests the possible involvement of the f orbitals in metal–ligand multiple bonding. As stated earlier, the four-electron reduction of unsaturated ligands does not often occur on a single transition metal center.[1] In contrast to proposed intermediate **3**, the analogous η^2-azobenzene- (or η^2-hydrazido-) molybdocene complex is stable.[13] There are both thermodynamic and kinetic factors that might explain these differences in reactivity. The analogous Group 6 bis(imido) metallocene complexes would be unstable as 20-electron species (assuming metal–nitrogen double bonds and η^5-Cp ligands). Further, the concerted cleavage of an E–E bond at a

[*] Dr. C. J. Burns, B. P. Warner, B. L. Scott
Los Alamos National Laboratory, MS J514
Los Alamos, NM 87545 (USA)
Fax: (+1) 505-667-9905
E-mail: cjb@lanl.gov

[**] We thank the US Department of Energy, Office of Basic Energy Sciences, Chemical Sciences Division for support of this work.

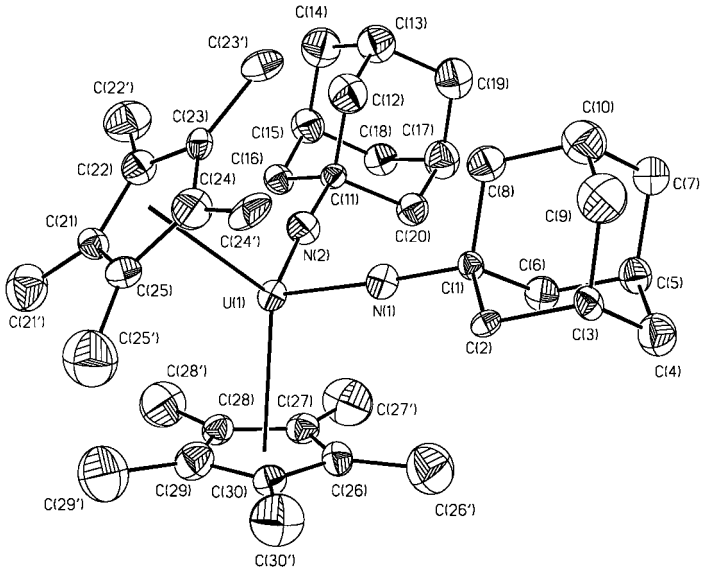


Figure 1. ORTEP depiction of **5**.

single metal center is generally symmetry-forbidden, based on a forbidden level crossing involving stabilization of the high-lying b_2-symmetric E–E σ* orbital.[2b] In contrast to the d^2 Cp_2Mo fragment, the d^2f^2 uranium center in **3** has low-lying f orbitals of the appropriate symmetry[14b] to assist both in making the cleavage symmetry allowed and in stabilizing the resulting organoimido ligands.

In conclusion, we have developed new one-pot syntheses of bis(imido)uranium(VI) compounds, based on the four-electron reduction of an azo or two azido functionalities. This azo–imido conversion is rare in the transition metals and has not been previously observed in either an actinide complex or a metallocene. That these reactions readily occur in our simple system illustrates one role of f-orbital participation in reactions of uranium. This synthetic methodology permits the preparation of a wide variety of organoimidouranium(VI) complexes. Preliminary experiments indicate that the alkylimido complexes display enhanced reactivity with respect to their arylimido analogues; we are currently investigating this reactivity.

Experimental Section

All operations were conducted in a He-filled drybox.

4: A vial was charged with **1**[15] (0.290 g, 0.5 mmol), Na (0.023 g, 1.0 mmol), THF (5 mL), and Hg (1 mL) and stirred for 1 h. Azobenzene (0.091 g, 0.5 mmol) was then added and the solution was stirred 16 h. The THF was removed in vacuo, and the residue was extracted with toluene (15 mL), filtered, and dried in vacuo to leave **4** (0.320 g, 0.46 mmol, 92 %).

5: A vial was charged with **1** (1.74 g, 3.0 mmol), Na (0.138 g, 6.0 mmol), THF (25 mL), and Hg (1 mL). The solution was stirred for 1 h, then 1-azidoadamantane (1.063 g, 6.0 mmol) was added, and the solution was stirred 16 h. The THF was removed in vacuo, and the residue was extracted with toluene (15 mL), filtered, and crystallized at −30 °C to yield **5** (1.720 g, 2.13 mmol, 71 %) as black crystals. ^{1}H NMR (300 MHz, C_6D_6) $\delta = 4.07$ (s, 30H), 3.18 (s, 6H), 1.46 (d, $J = 11$ Hz, 6H), 1.36 (d, $J = 11$ Hz, 6H), 1.16 (s, 12H); ^{13}C NMR (75 MHz, C_6D_6) $\delta = 137.2$, 84.4, 60.6, 36.6, 34.4, 10.6; IR (Kbr): $\tilde{\nu} = 748$ (w), 787 (w), 1095 (w), 1132 (m), 1298 (m), 1341 (w), 1376 (m), 1437 (w), 1449 (m), 2847 (s), 2900 (s), 2977 (w). Analysis calcd. for $C_{40}H_{60}N_2U$: C 59.54, H 7.49, N 3.47; found: C 59.26, H 7.48, N 3.40.

Received: August 29, 1997 [Z 10871 IE]
German version: *Angew. Chem.* **1998**, *110*, 1005–1007

Keywords: actinides · azo compounds · f orbitals · imido compounds · uranium

[1] a) J. C. Bryan, J. M. Mayer, *J. Am. Chem. Soc.* **1987**, *109*, 7213–7214; b) J. C. Bryan, S. J. Geib, A. Rheingold, J. M. Mayer, *ibid*. **1987**, *109*, 2826–2828; c) J. C. Bryan, J. M. Mayer, *ibid*. **1990**, *112*, 2298–2308; d) M. A. Lockwood, P. E. Fanwick, O. Eisenstein, I. P. Rothwell, *ibid*. **1996**, *118*, 2762–2763.

[2] a) S. N. Brown, J. M. Mayer, *Inorg. Chem.* **1992**, *31*, 4091–4100; b) R. Hoffmann, C. N. Wilker, O. Eisenstein, *J. Am. Chem. Soc.* **1982**, *104*, 632–634.

[3] a) D. S. J. Arney, C. J. Burns, D. C. Smith, *J. Am. Chem. Soc.* **1992**, *114*, 10068–10069; b) D. S. J. Arney, C. J. Burns, *ibid*. **1995**, *117*, 9448–9460.

[4] a) P. J. Fagan, Ph.D. Thesis, Northwestern University, Evanston, IL, **1981**, Chap. 2; b) P. J. Fagan, J. M. Manriquez, T. J. Marks, C. S. Day, S. H. Vollmer, V. W. Day, *Organometallics* **1982**, *1*, 170–180; c) J. M. Manriquez, P. J. Fagan, T. J. Marks, S. H. Vollmer, C. S. Day, V. W. Day, *J. Am. Chem. Soc.* **1979**, *101*, 5075–5078.

[5] According to ^{1}H NMR spectroscopy, this species is an adduct with 0.5 equiv THF.[4]

[6] R. G. Finke, G. Gaughan, R. Voegeli, *J. Organomet. Chem.* **1982**, *229*, 179–184.

[7] a) D. S. J. Arney, C. J. Burns, *J. Am. Chem. Soc.* **1993**, *115*, 9840–9841; b) P. C. Blake, M. F. Lappert, R. G. Taylor, J. L. Atwood, H. Zhang, *Inorg. Chim. Acta* **1987**, *139*, 13–20.

[8] J. G. Brennan, R. A. Andersen, A. Zalkin, *J. Am. Chem. Soc.* **1989**, *110*, 4554–4558.

[9] J. G. Brennan, Ph.D. Thesis, University of California, Berkeley, **1986**, pp. 154–157.

[10] Further details on the crystal structure investigation may be obtained from the Fachinformationszentrum Karlsruhe, D-76344 Eggenstein-Leopoldshafen, Germany (fax: (+49) 7247-808-666 (Frau S. Höhler-Schlimm); e-mail: crysdata§fiz-karlsruhe.de), on quoting the depository number CSD-406970.

[11] a) C. J. Burns, W. H. Smith, J. C. Huffman, A. P. Sattelberger, *J. Am. Chem. Soc.* **1990**, *112*, 3237–3238; b) J. G. Brennan, R. A. Andersen *ibid*. **1985**, *107*, 514–516; c) A. Zalkin, J. G. Brennan, R. A. Andersen, *Acta Crystallogr. Sect. C* **1988**, *44*, 1553–1554.

[12] G. A. Bowmaker, A. Goerling, O. Häberlen, N. Rösch, G. L. Goodman, D. E. Ellis, *Inorg. Chem*. **1992**, *32*, 577–581.

[13] A. Nakamura, M. Aotake, S. Otsuka, *J. Am. Chem. Soc.* **1974**, *96*, 3456–3462.

[14] a) J. W. Lauher, R. Hoffmann, *J. Am. Chem. Soc.* **1976**, *98*, 1729–1742; b) B. E. Bursten, A. Fang, *ibid.* **1983**, *105*, 6495–6496.

[15] J. M. Manriquez, P. J. Fagan, T. J. Marks, *J. Am. Chem. Soc.* **1978**, *100*, 3939–3941.

[16] J. C. Bottaro, *J. Chem. Soc. Chem. Commun.* **1978**, 990.

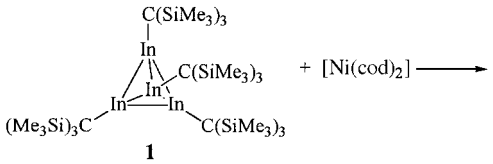
 © WILEY-VCH Verlag GmbH, D-69451 Weinheim, 1998 1433-7851/98/3707-0960 $ 17.50+.50/0

$Ni[In\{C(SiMe_3)_3\}_4]$: An Organometallic Nickel–Indium Compound Analogous to $[Ni(CO)_4]$**

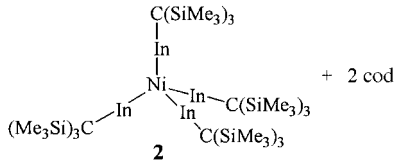
Werner Uhl*, Michael Pohlmann, and Rudolf Wartchow

The monomeric alkyl–element(I) compounds E–R containing the bulky alkyl substituent $C(SiMe_3)_3$ and the monovalent, coordinatively and electronically unsaturated elements Ga, In, and Tl have recently been identified unambiguously as degradation products of the tetrahedral clusters $E_4[C(SiMe_3)_3]_4$.[1–3] The molecular structure of the most stable compound, $GaC(SiMe_3)_3$, was determined by electron diffraction in the gas phase above 200 °C.[4] The tetrathallium compound is only weakly associated in the solid state and dissociates completely to the monomer on dissolution in benzene,[3] while the tetragallium cluster shows complete dissociation into the monomers only at high dilution in benzene.[1] The most stable of the clusters is $In_4[C(SiMe_3)_3]_4$ (**1**).[2] Owing to its low thermal stability the monomeric fragment could not be characterized by electron diffraction,[4] and dissociation was not observed even in highly diluted solutions in benzene.[2] However, InR was detected as a reactive intermediate by trapping reactions with benzil derivatives in boiling *n*-hexane.[5] The monomeric fragments have two empty p orbitals perpendicular to the element–carbon bond axis and an electron lone pair at the Ga, In, or Tl atoms; hence, their frontier orbitals are similar to those of carbon monoxide. Indeed, CO ligands are substituted by InR groups when transition metal carbonyl complexes are treated with the indium cluster **1**.[6] These reactions opened a new route to organometallic compounds of the transition metals with elements of Group 13 and led to novel compounds with unusual structures, for example, an Fe_2In_3 cluster.[7] Similar reactions have been reported by Schnöckel et al., who synthesized carbonyl analogous complexes with the ligand aluminum(I) pentamethylcyclopentadienide AlCp*.[8] In contrast to CO, the ER fragments almost exclusively occupy bridging positions between two metal atoms in the known derivatives. A single case of terminal coordination was recently reported by Fischer et al. in $[(CO)_4Fe(AlCp^*)]$,[9] for which significant π backbonding from the metal atom to the ligand was calculated. Up to now, analogues of mononuclear, binary carbonyl complexes with exclusively terminal ER groups were unknown. Such compounds would be proof of the isolobal relationship between CO and ER and would extend the class of carbonyl-analogous compounds by a remarkable new example.

For the synthesis of a nickel complex exclusively coordinated by four indanediyl ligands (InR) we did not use $[Ni(CO)_4]$ but bis(cyclooctadiene)nickel $[Ni(cod)_2]$, because of the facile substitution of the alkene ligands. In accordance with our experience of the chemical reactivity of **1**, solutions of the starting materials could be kept at room temperature for several days without any observable reaction. At 50 °C the reaction was complete after 2 h [Eq. (a)]. Dark red crystals of



1 (a)



2

the product **2** were isolated by recrystallization from cyclopentane in 75% yield. Compound **2** is extremely moisture-sensitive; reaction with water forms $[In_4O(OH)_6R_4]$,[10] which was identified by NMR spectroscopy and could not be removed by recrystallization. Therefore, all manipulations were performed with strict exclusion of water, and all solvents were additionally dried by treatment with *n*-butyllithium and freshly distilled before use. Elemental analysis of **2** is in agreement with the formula $[Ni\{InC(SiMe_3)_3\}_4]$, and determination of the relative molecular mass by cryoscopy in benzene gave the value expected for the undissociated molecule. The absorption of longest wavelength in the UV/Vis spectrum of **2** is at 395 nm, and the characteristic band of the In_4 cluster at 490 nm is no longer present.[2] The signal of the α-carbon atom in the ^{13}C NMR spectrum of **2** is at $\delta = 61.6$: It is shifted downfield by more than 30 ppm relative to the signals of indium(III) compounds ($\delta < 30$).[11] The corresponding signals of bridging InR groups in transition metal complexes occur in the range of $\delta = 48-52$,[6] and the signal of the tetraindium compound **1** is shifted even further to low field ($\delta = 72.0$)[2] owing to the the delocalized electron system in the central In_4 cluster. Compound **2** has surprisingly high thermal stability and decomposes above 285 °C; however, attempts to sublime it in vacuo were unsuccessful.

Compound **2** (Figure 1) crystallizes in the cubic space group $Fd\bar{3}m$[12] with the center of the molecule on a special crystallographic position ($\bar{4}3m$), that is, the Ni atoms are coordinated in an undistorted tetrahedral manner by four $InC(SiMe_3)_3$ ligands (In-Ni-In 109.5°), and the Ni-In-C units with two-coordinate In atoms are exactly linear (Ni-In-C 180.0°). Hence, **2** is isostructural with $[Ni(CO)_4]$ and analogous compounds with σ-donor/π-acceptor ligands such as $[Ni(PF_3)_4]$ and $[Ni(CNR)_4]$.[13] The complex $Ni[SnR_2]_4$ is also similar,[14] although the frontier orbitals of the SnR_2 groups do not correspond exactly to those of InR. The Ni–In bond lengths of **2** (231.0(1) pm) are considerably shorter than all Ni–In bond lengths reported to date, in spite of the high steric

[*] Prof. Dr. W. Uhl, Dipl. Chem. M. Pohlmann
Fachbereich Chemie der Universität
Postfach 2503, D-26111 Oldenburg (Germany)
Fax: (+49) 441-798-3352
Dr. R. Wartchow
Institut für Anorganische Chemie der Universität Hannover (Germany)

[**] We are grateful to the Deutsche Forschungsgemeinschaft and the Fonds der Chemischen Industrie for generous financial support.

 © WILEY-VCH Verlag GmbH, D-69451 Weinheim, 1998 1433-7851/98/3707-0961 $ 17.50+.50/0

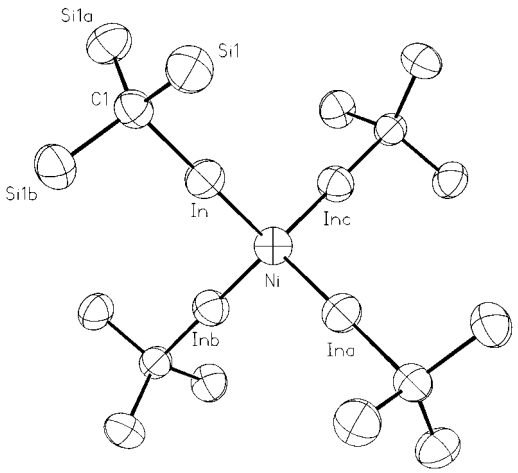


Figure 1. Molecular structure of **2**; methyl groups are omitted for clarity. Selected bond lengths [pm] and angles [°]: In – Ni 231.0(1), In – C1 219.5(13), C1 – Si1 187.2(4); In-Ni-In 109.5, Ni-In-C1 180.0, In-C1-Si1 105.3(4).

stress in the molecule caused by the four bulky substituents. Organometallic coordination compounds show Ni – In distances longer than 244.6 pm (av. 269.2 pm[15–17]), and distances of 262 pm[18] are observed in some alloys. The sum of the covalent radii can be estimated to be about 260 pm. The short Ni – In bond lengths in complexes such as $[Cp(Ph_3P)Ni-InBr_2(OPPh_3)]$ (244.6 pm)[16] and $[Cp(CO)Ni-InBr_2(NC_7H_{13})]$ (246.2 pm)[17] have been explained in terms of Ni(dπ) – ligand(σ*) interactions. The intramolecular In – In distances of 377 pm in **2** lie in the range of twice the van der Waals radius of indium (380 pm) and indicate no significant bonding interaction between the In atoms. The extent of the π backbonding in **2**, indicated by the very short Ni – In bonds, is uncertain. Theoretical investigations confirm such interactions in $[Fe(CO)_4(AlCp^*)]$,[9] in which, however, the contributing orbitals on the aluminum atoms are partially occupied by the cyclopentadienyl ligands.

Experimental Section

All procedures were carried out under purified argon. The solvents were dried by standard methods (toluene over Na/benzophenone, cyclopentane over $LiAlH_4$) and subsequently with solvent-free *n*-butyllithium, distilled in vacuo at room temperature, and used immediately or stored over molecular sieve. **1** (300 mg, 0.217 mmol) and $[Ni(cod)_2]$ (65 mg, 0.237 mmol) were dissolved in toluene (25 mL) and stirred at 50 °C for 2 h. The solvent was completely removed in vacuo, and the residue was recrystallized from cyclopentane at −30 °C. Yield of **2**: 240 mg (0.166 mmol, 76 %), dark red crystals. **2** crystallizes with varying amounts of cyclopentane, which can be removed by vacuum treatment of powdered samples. Decomposition (argon, sealed capillary): 285 °C. ^{1}H NMR (300 MHz, C_6D_6): $\delta = 0.427$ (s, $SiMe_3$). ^{13}C NMR (75 MHz, C_6D_6): $\delta = 6.50$ ($SiMe_3$), 61.6 (InC). IR (Nujol, CsBr plates): $\tilde{\nu} = 1263$ m, 1250 m ($\delta(CH_3)$); 1169 vw, 1155 vw, 1044 w, 1020 w; 864 vs, 837 vs, 774 w, 721 w ($\rho(CH_3(Si))$; 669 w (ν_{as}SiC); 644 w, 613 vw (ν_sSiC); 577 m; 521 vw, 465 cm^{-1} vw (νInC). UV/Vis (*n*-hexane): λ_{max} ($\lg\varepsilon$) = 250 (5.0), 280 (5.0), 395 nm (4.5). Relative molecular mass (cryoscopy in benzene): found 1475; calcd 1444.3.

Received: October 15, 1997 [Z11028IE]
German version: *Angew. Chem.* **1998**, *110*, 1007 – 1009

Keywords: clusters · electron deficiency · indium · isolobal relationship · nickel

[1] W. Uhl, W. Hiller, M. Layh, W. Schwarz, *Angew. Chem.* **1992**, *104*, 1378; *Angew. Chem. Int. Ed. Engl.* **1992**, *31*, 1364.
[2] W. Uhl, R. Graupner, M. Layh, U. Schüz, *J. Organomet. Chem.* **1995**, *493*, C1; see also: R. D. Schluter, A. H. Cowley, D. A. Atwood, R. A. Jones, J. L. Atwood, *J. Coord. Chem.* **1993**, *30*, 25.
[3] W. Uhl, S. U. Keimling, K. W. Klinkhammer, W. Schwarz, *Angew. Chem.* **1997**, *109*, 64; *Angew. Chem. Int. Ed. Engl.* **1997**, *36*, 64.
[4] A. Haaland, K.-G. Martinsen, H. V. Volden, W. Kaim, E. Waldhör, W. Uhl, U. Schütz, *Organometallics* **1996**, *15*, 1146.
[5] W. Uhl, S. U. Keimling, S. Pohl, W. Saak, R. Wartchow, *Chem. Ber.* **1997** *130*, 1269.
[6] W. Uhl, S. U. Keimling, W. Hiller, M. Neumayer, *Chem. Ber.* **1995**, *128*, 1137; W. Uhl, S. U. Keimling, W. Hiller, M. Neumayer, *ibid.* **1996**, *129*, 397.
[7] W. Uhl, M. Pohlmann, *Organometallics* **1997**, *16*, 2478.
[8] C. Dohmeier, C. Robl, M. Tacke, H. Schnöckel, *Angew. Chem.* **1991**, *103*, 594; *Angew. Chem. Int. Ed. Engl.* **1991**, *30*, 564; C. Dohmeier, H. Krautscheid, H. Schnöckel, *ibid.* **1994**, *106*, 2570; **1994**, *33*, 2482; Review: C. Dohmeier, D. Loos, H. Schnöckel, *ibid.* **1996**, *108*, 141; **1996**, *35*, 129.
[9] J. Weiss, D. Stetzkamp, B. Nuber, R. A. Fischer, C. Boehme, G. Frenking, *Angew. Chem* **1997**, *109*, 95; *Angew. Chem. Int. Ed. Engl.* **1997**, *36*, 70; the terminal coordination of a GaMe fragment, which is, however, further coordinated by TMEDA, is described in: M. M. Schulte, E. Herdtweck, G. Raudaschl-Sieber, R. A. Fischer, *ibid.* **1996**, *108*, 489; **1996**, *35*, 424.
[10] S. S. Al-Juaid, N. H. Buttrus, C. Eaborn, P. B. Hitchcock, A. T. L. Roberts, J. D. Smith, A. C. Sullivan, *J. Chem. Soc. Chem. Commun.* **1986**, 908.
[11] W. Uhl, M. Layh, W. Hiller, *J. Organomet. Chem.* **1989**, *368*, 139; W. Uhl, R. Graupner, H. Reuter, *ibid.* **1996**, *523*, 227; B. Neumüller, F. Gahlmann, M. Schäfer, S. Magull, *ibid.* **1992**, *440*, 263; A. J. Carty, M. J. S. Gynane, M. F. Lappert, S. J. Miles, A. Singh, N. J. Taylor, *Inorg. Chem.* **1980**, *19*, 3637.
[12] Crystal structure analysis of **2**: Single crystals of **2** were obtained from cyclopentane at 0 °C and were not dried in vacuo; $C_{40}H_{108}In_4NiSi_{12} \cdot 2.7C_5H_{10}$, cubic, space group $Fd\bar{3}m$, $a = 2608.7(3)$ pm, $V = 17753(4)$ Å^3, $Z = 8$, $\rho_{calcd} = 1.204$ g cm^{-3}, crystal dimensions $0.5 \times 0.5 \times 0.3$ mm, Stoe IPDS diffractometer, $Mo_{K\alpha}$ radiation, 300 K, measurement range: $4.4 < 2\theta < 47.8°$, 200 exposures, $\Delta\varphi = 1.1°$, 704 independent reflections, 332 reflections with $F > 4\sigma(F)$, $\mu = 1.419$ mm^{-1}, programs SHELXTL PLUS REL 4.1 and SHELXL-93, 54 parameters, $R1 = 0.037$ and $wR2$ (all data) = 0.085, max./min. residual electron density: $0.30/-0.50 \times 10^{30}$ e m^{-3}. Owing to the crystallographic position (*b*, $\bar{4}3m$) the $C(SiMe_3)_3$ groups are rotationally disordered, and six positions are observed for the three Si atoms with occupancy factors of 0.5. Two methyl groups lie on a mirror plane with bonds to two Si atoms, and the third methyl group occupies two positions above and below this plane. The cyclopentane molecules are strongly disordered over crystallographic symmetry elements; positions of the hydrogen atoms were not calculated. Crystallographic data (excluding structure factors) for the structure reported in this paper have been deposited with the Cambridge Crystallographic Data Centre as supplementary publication no. CCDC-100776. Copies of the data can be obtained free of charge on application to CCDC, 12 Union Road, Cambridge CB2 1EZ, UK (fax: (+44) 1223-336-033; e-mail: deposit@ccdc.cam.ac.uk).
[13] D. Braga, F. Grepioni, A. G. Orpen, *Organometallics* **1993**, *12*, 1481; J. C. Marriott, J. A. Salthouse, M. J. Ware, J. M. Freeman, *J. Chem. Soc. Chem. Commun.* **1970**, 595; C. Elschenbroich, M. Nowotny, A. Behrendt, W. Massa, S. Wocadlo, *Angew. Chem.* **1992**, *104*, 1388; *Angew. Chem. Int. Ed. Engl.* **1992**, *31*, 1343; M. B. Hursthouse, K. J. Izod, M. Motevalli, P. Thornton, *Polyhedron* **1994**, *13*, 151; E. Singleton, H. E. Oosthuizen, *Adv. Organomet. Chem.* **1983**, *22*, 209, and references therein.
[14] M. Veith, L. Stahl, V. Huch, *J. Chem. Soc. Chem. Commun.* **1990**, 359.
[15] F. Demartin, M. C. Iapalucci, G. Longoni, *Inorg. Chem.* **1993**, *32*, 5536; R. E. Marsh, I. Bernal, *Acta Crystallogr. Sect. B* **1995**, *51*, 300; R. A. Fischer, W. Scherer, M. Kleine, *Angew. Chem.* **1993**, *105*, 778; *Angew. Chem. Int. Ed. Engl.* **1993**, *32*, 748; R. A. Fischer, E. Herdtweck, T. Priermeier, *Inorg. Chem.* **1994**, *33*, 934; R. A. Fischer, S. Nlate, H. Hoffmann, E. Herdtweck, J. Blümel, *Organometallics* **1996**, *15*, 5746;

 © WILEY-VCH Verlag GmbH, D-69451 Weinheim, 1998 1433-7851/98/3707-0962 $ 17.50+.50/0

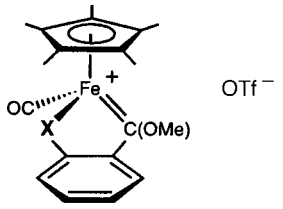
J. J. Schneider, U. Denninger, J. Hagen, C. Krüger, D. Bläser, R. Boese, *Chem. Ber.* **1997**, *130*, 1433.
[16] J. Weiss, T. Priermeier, R. A. Fischer, *Inorg. Chem.* **1996**, *35*, 71.
[17] J. Weiss, A. Frank, E. Herdtweck, S. Nlate, M. Mattner, R. A. Fischer, *Chem. Ber.* **1996**, *129*, 297.
[18] R. A. Fischer, M. Kleine, O. Lehmann, M. Stuke, *Chem. Mat.* **1995**, *7*, 1863.

Selective Activation of Ar–Cl and Ar–C Bonds with Iron(II) Complexes**

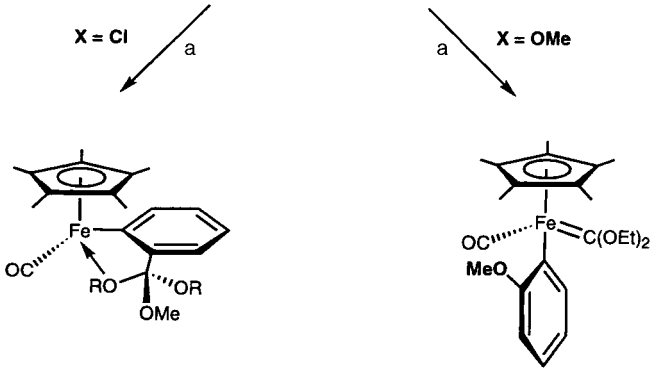
Géraldine Poignant, Sourisak Sinbandhit, Loïc Toupet, and Véronique Guerchais*

Selective bond-activation reactions mediated by transition metals are currently the focus of synthetic and mechanistic interest. These fundamental processes are particularly important in carbene and arene chemistry.[1, 2] In this context, the electrophilic arylcarbene chelate complexes **1** (X = Cl) and **2** (X = OMe) are good candidates for promoting new reactions within the coordination sphere, since the chelating group X can be activated by the Lewis acidic organo-iron fragment[3, 4] or dissociate to provide a vacant coordination site.[5, 6] Here we report on the reactivity of **1** and **2**[5] towards alkoxides. The outcome of the reaction depends on the nature of the chelate group; selective activation of Ar–Cl and Ar–C bonds was achieved.

Complex **1** reacts cleanly with alkoxides RONa to give the unexpected neutral chelate complexes **3a** (R = Me) and **3b** (R = Et), which were isolated as stable black crystals in 83–89% yield from pentane (Scheme 1). Both contain two additional alkoxy groups. The ^{1}H NMR spectrum (C_6D_6, 25 °C) of **3a** exhibits three broad signals for the methoxy substituents, one of which corresponds to the coordinated OMe group, while the other two methoxy groups are diastereotopic. The coalescence of these signals on warming (T_C(300 MHz) = 42 °C) to give a singlet at $\delta = 2.90$, indicates free exchange on the NMR time scale. For **3b**, the ^{1}H and ^{13}C NMR spectra each exhibit two well-resolved pairs of signals



1 (X = Cl), **2** (X = OMe)



3 (**a**, R = Me; **b**, R = Et) **8**

Scheme 1. a) RONa (3 equiv)/ROH, THF, −80 °C → room temperature. TfO = trifluoromethanesulfonate.

for the methyl and methylene groups, which indicates the presence of two different ethoxy groups. Moreover, in the ^{1}H NMR spectrum (25 °C) one of the methylene groups gives rise to an AB system at $\delta = 3.00$ and 2.78 ($^2J_{H,H} = 10$ Hz) when the corresponding methyl signal at $\delta = 0.98$ is selectively ^{1}H-decoupled.

As expected the OMe ligand is labile, and treatment of **3a** with PMe_3 quantitatively yields orange crystals of **4**. In this

$[Fe(C_5Me_5)(CO)(PMe_3)\{\eta^1\text{-}C_6H_4\text{-}o\text{-}C(OMe)_3\}]$ **4**

case, the three OMe groups are magnetically equivalent in the ^{1}H ($\delta = 3.29$) and ^{13}C ($\delta = 49.9$) NMR spectra (25 °C). An X-ray structure analysis confirms the proposed structure (Figure 1).[7] The FeC≡O unit deviates from the expected linear geometry (Fe-C-O 171.0(3)°). The bond angles at C_{ipso} of the aryl group are quite different owing to the presence of the bulky tris(methoxy)methyl substituent.

The formation of complexes **3a–b** involves cleavage of the Ar–Cl bond. This cleavage is promoted by coordination of the chlorine atom, as shown by the following experiment. Treatment of the nonchelated complex **5**$^+$OTf$^-$[5] under the same conditions led to formation of the acetal complexes **6a** (R = Me) and **6b** (R = Et) by addition of RO^- to the electrophilic carbene carbon atom. Although stable in the

$[Fe(C_5Me_5)(CO)_2\{\eta^1\text{-}C(OMe)C_6H_4\text{-}o\text{-}Cl\}]OTf$ **5**$^+$OTf$^-$

$[Fe(C_5Me_5)(CO)_2\{\eta^1\text{-}C(OMe)(OR)C_6H_4\text{-}o\text{-}Cl\}]$ **6a**, **b**

solid state as a yellow powder, these species undergo thermal decomposition in solution at 0 °C. Addition of $HBF_4 \cdot OEt_2$ to a crude solution of **6a** led quantitatively to the carbene

[*] Dr. V. Guerchais, G. Poignant
UMR 6509 CNRS-Université de Rennes 1
"Organométalliques et Catalyse: Chimie et Electrochimie Moléculaires"
Beaulieu, Université de Rennes 1
F-35042 Rennes Cedex (France)
Fax: (+33) 299-281646
E-mail: guerchai@univ-rennes1.fr
Dr. S. Sinbandhit
Centre Régional de Mesures Physiques de l'Ouest (C.R.M.P.O.)
Beaulieu, Université de Rennes 1
F-35042 Rennes Cedex (France)
Dr. L. Toupet
UMR 6626 Groupe Matière Condensée et Matériaux
Beaulieu, Université de Rennes 1
F-35042 Rennes Cedex (France)

[**] This work was supported by the CNRS and HCM program (contract number 940501). We thank the "Région Bretagne" for a grant to G.P. and Dr. P. Guénot for mass spectrometric measurements.

 © WILEY-VCH Verlag GmbH, D-69451 Weinheim, 1998 1433-7851/98/3707-0963 $ 17.50+.50/0

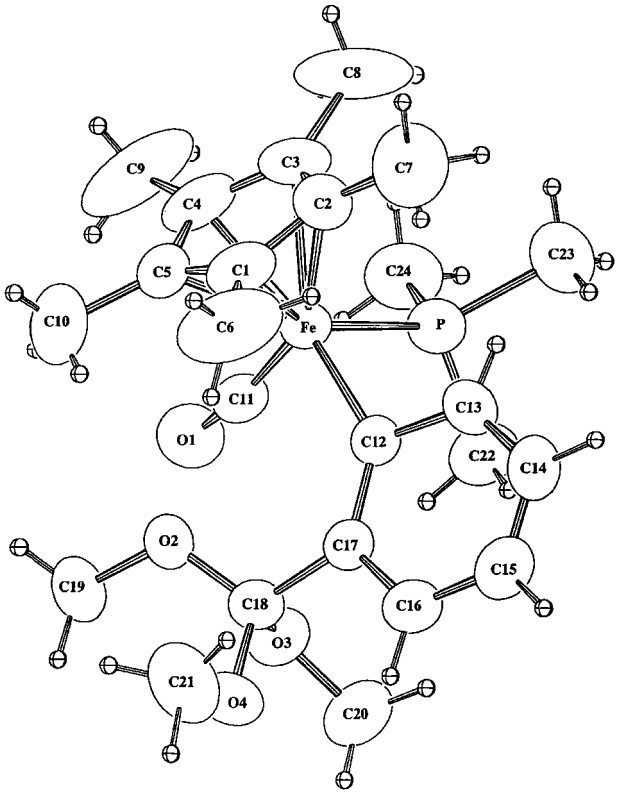


Figure 1. Crystal structure of **4**. Selected bond lengths [Å] and angles [°]: C17 – C18 1.519(6), O2 – C18 1.382(4), O3 – C18 1.411(4), O4 – C18 1.413(5), Fe – C12 2.033(3), Fe – P 2.187(1), Fe – C11 1.699(4), O2 – C19 1.426(6), O3 – C20 1.420(4), O4 – C21 1.421(5); Fe-C11-O1 171.0(3), C11-Fe-C12 99.6, P-Fe-C11 85.9(1), P-Fe-C12 89.2(1), Fe-C12-C17 133.3(3), Fe-C12-C13 112.6(2).

complex $\mathbf{5}^{+}BF_4^{-}$, which still contains the chlorine atom, as confirmed by mass spectrometry.

Activation of an Ar – F bond by an iron complex with formation of an Ar – Fe bond has been previously postulated, but no spectroscopic evidence for an Fe – F interaction was obtained.[8] Halohydrocarbon complexes [M(η^1-XR)] (X = halogen; R = alkyl, aryl) undergo nucleophilic attack at the C_α atom.[3] However, similar activation is not observed for the chlorobenzene complex **7** on addition of Lewis bases.[9] In our

$[Re(C_5Me_5)(NO)(PPh_3)(\eta^1\text{-}ClC_6H_5)]BF_4$ **7**

case, the intermediate formation of an Ar – OMe bond by nucleophilic substitution[10] was ruled out by the investigation of the anisyl derivative **2**. The formation of the Fe – aryl bond and the subsequent rearrangement processes are not yet understood.

In contrast, the reaction of **2** with EtONa takes a completely different course: the new carbene – aryl complex **8** was isolated as a yellow solid in 80 % yield (Scheme 1). The presence of the carbene ligand is indicated by the downfield signal at $\delta = 263.8$ in the ^{13}C NMR spectrum. The crystal structure (Figure 2) clearly shows that the geometry of the carbene ligand is distorted. There are two different Fe-C-O bond angles due to the presence of the anisyl ligand.[7]

We assume that the ethoxide ion initially adds to the carbene center and that the intermediate complex **9** then

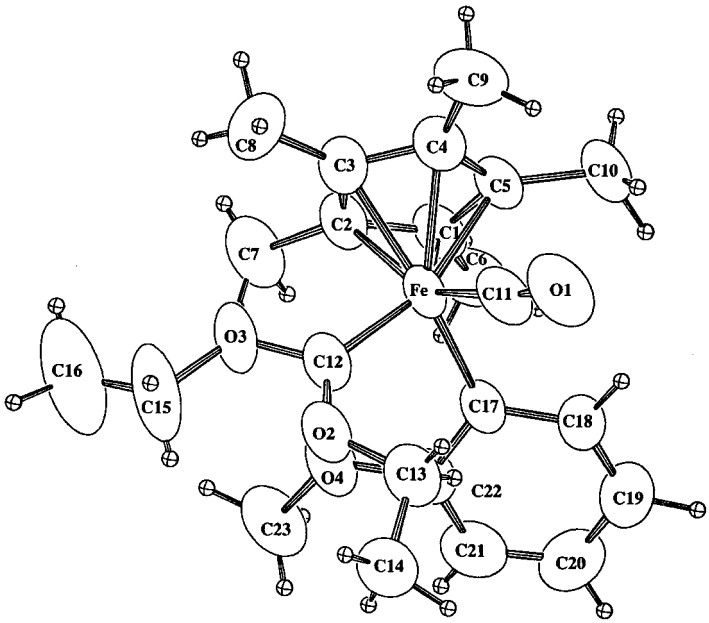


Figure 2. Crystal structure of **8**. Selected bond lengths [Å] and angles [°]: Fe – C17 1.990(6), Fe – C12 1.881(5), O2 – C12 1.305(7), O3 – C12 1.335(7), O4 – C23 1.423(7); Fe-C11-O1 173.2(6), O2-C12-O3 108.8(4), Fe-C12-O2 133.4(4), Fe-C12-O3 117.8(4).

$(\eta^2\text{-}C,O)[\overline{Fe(C_5Me_5)(CO)\{\eta^2\text{-}C(OR)_2C_6H_4\text{-}o\text{-}OMe\}}]$ **9**

rearranges by Ar – C_α bond cleavage, that is, α-aryl elimination. Examples of hydride, alkyl, and aryl migration to a carbene ligand are known;[11, 12] the reverse reaction is probably induced by the presence of the labile ligand[13] and/or the instability of the acetal complex (see above). Exchange of the alkyl group of the carbene ligand occurs in the presence of an excess of EtO^-/EtOH, a behavior already observed for vinyl ether complexes.[14]

This study illustrates the dichotomy of reactivity of iron complexes: exclusive Ar – Cl bond cleavage is promoted by the Lewis acid – base interaction, whereas the presence of a labile chelate ligand activates the Ar – C bond.

Experimental Section

A solution of **1**, **2**, or **5** (1 mmol) in THF was treated at $-80\,^\circ C$ with a freshly prepared solution of RONa (3 equiv) in ROH (R = Me, Et). After stirring for 1 h, the solution was evaporated to dryness. The products were extracted with pentane and crystallized.

3a (89 % yield, dark brown crystals): ^1H NMR (300 MHz, C_6D_6): $\delta = 7.84$ (dd, $^3J(H,H) = 7.5$, $^4J(H,H) = 0.8$ Hz, 1 H, Ar), 7.35 (td, $^3J(H,H) = 7.4$, $^4J(H,H) = 1.6$ Hz, 1 H, Ar), 7.10 (td, $^3J(H,H) = 7.4$, $^4J(H,H) = 1$ Hz, 1 H, Ar), 6.99 (dd, $^3J(H,H) = 7.5$, $^4J(H,H) = 1.5$ Hz, 1 H, Ar), 3.02 (brs, 3 H, OMe), 2.88 (brs, 3 H, OMe), 2.73 (brs, 3 H, OMe), 1.42 (s, 15 H, C_5Me_5); $^{13}C\{^1H\}$ NMR (50.3 MHz, $CDCl_3$): $\delta = 221.7$ (CO), 174.6 (FeAr), 140.2 (Ar), 136.5 (Ar_C), 127.9 (Ar), 126.8 ($C(OMe)_3$), 123.9 (Ar), 121.9 (Ar), 89.6 (C_5Me_5), 56.3 (OMe), 52.7 (OMe), 52.5 (OMe), 10.8 (C_5Me_5); IR (pentane): $\tilde{\nu} = 1917\ cm^{-1}$ (CO); C,H analysis calcd for $C_{21}H_{28}O_4Fe$: C 63.01, H 7.05; found: C 62.78, H 7.12.

3b (83 % yield, dark brown crystals): ^1H NMR (300 MHz, $CDCl_3$): $\delta = 7.57$ (d, $^3J(H,H) = 7.5$ Hz, 1 H, Ar), 7.17 (t, $^3J(H,H) = 6.7$ Hz, 1 H, Ar), 6.96 (t, $^3J(H,H) = 7$ Hz, 1 H, Ar), 6.84 (d, $^3J(H,H) = 7$ Hz, 1 H, Ar), 3.31 (q, $^3J(H,H) = 7$ Hz, 2 H, OCH_2CH_3), 3.15 (s, 3 H, OMe), 3.00 (m, 1 H, OCH_2CH_3), 2.79 (m, 1 H, OCH_2CH_3), 1.60 (s, 15 H, C_5Me_5), 1.14 (t,

 © WILEY-VCH Verlag GmbH, D-69451 Weinheim, 1998 1433-7851/98/3707-0964 $ 17.50+.50/0

^3J(H,H) = 7 Hz, 3H, OCH_2CH_3), 0.98 (t, ^3J(H,H) = 7 Hz, 3H, OCH_2CH_3); $^{13}C\{^1H\}$ NMR (75.47 MHz, $CDCl_3$): δ = 221.4 (CO), 173.5 (FeAr), 139.7 (Ar), 137.4 (Ar_C), 127.4 (Ar), 125.8 (C(OMe)(OEt)$_2$), 123.4 (Ar), 121.5 (Ar), 89.2 (C_5Me_5), 60.2 (OCH_2CH_3), 59.8 (OCH_2CH_3), 55.8 (OMe), 15.3 (OCH_2CH_3), 14.8 (OCH_2CH_3), 10.1 (C_5Me_5); IR (pentane): $\tilde{\nu}$ = 1914 cm^{-1} (CO); C,H analysis calcd for $C_{23}H_{32}O_4Fe$: C 64.49, H 7.53; found: C 64.82, H 7.47; HRMS (70 eV): *m/z*: 428.1641 [M^+], calcd for $C_{23}H_{32}O_4Fe$: 428.1649.

4 (65% yield): ^1H NMR (200 MHz, $CDCl_3$): δ = 7.84 (d, ^3J(H,H) = 7.6 Hz, 1H, Ar), 7.38 (dd ^3J(H,H) = 7.8, ^4J(H,H) = 1.7 Hz, 1H, Ar), 6.85 (td, ^3J(H,H) = 7.3, ^4J(H,H) = 1.4 Hz, 1H, Ar), 6.69 (td,^3J(H,H) = 7.3, ^4J(H,H) = 1.8 Hz, 1H, Ar), 3.29 (s, 9H, OMe), 1.65 (s, 15H, C_5Me_5), 1.12 (d, ^2J(P,H) = 8.4 Hz, 9H, PMe_3); $^{31}P\{^1H\}$ NMR (81 MHz, $CDCl_3$): δ = 36.51 (s, PMe_3); $^{13}C\{^1H\}$ NMR (75.47 MHz, $CDCl_3$): δ = 222.6 (d, ^2J(P,C) = 38 Hz, CO), 170.4 (d, ^2J(P,C) = 26 Hz, FeAr), 146.1 (d, ^2J(P,C) = 12 Hz, Ar), 145.8 (Ar_C), 129.2 (Ar), 122.6 (Ar), 119.3 (Ar), 117.7 (C(OMe)$_3$), 92.1 (C_5Me_5), 49.9 (OMe), 17.6 (d, ^1J(P,C) = 26 Hz, PMe_3), 10.2 (C_5Me_5); IR (CH_2Cl_2): $\tilde{\nu}$ = 1898 cm^{-1} (CO); C,H analysis calcd for $C_{24}H_{37}O_4FeP$: C 60.51, H 7.83; found: C 60.78, H 7.75.

6b (80% yield, isolated at $-40\,^\circ$C, yellow powder): ^1H NMR (300 MHz, $CDCl_3$, $-30\,^\circ$C): δ = 7.58 , 7.47, 7.17, 6.98 (Ar), 3.55, 3.40 (brm, OCH_2CH_3), 3.31 (s, OMe), 3.25, 3.05 (brm, OCH_2CH_3), 2.98 (s, OMe), 1.73, 1.64 (s, C_5Me_5), 1.35, 1.17 (brm, OCH_2CH_3); $^{13}C\{^1H\}$ NMR (75.47 MHz, $CDCl_3$, $-30\,^\circ$C): δ = 219.1, 218.8, 218.2 (CO), 149.6, 147.9.(Ar_C), 131.3, 130.9 (Ar), 129.8, 129.2 (Ar_{Cl}), 128.0, 126.9, 126.5, 125.9, 125.6 (Ar), 116.5, 114.9 (C_α), 97.9, 96.6 (C_5Me_5), 58.9, 57.1 (OCH_2CH_3), 51.5, 50.8 (OMe), 15.5, 15.0 (OCH_2CH_3), 10.0, 9.8 (C_5Me_5); IR (pentane): $\tilde{\nu}$ = 1997 (CO), 1947 cm^{-1} (CO). Two isomers were observed at $-30\,^\circ$C owing to hindered C^*_α–Ar rotation at low temperature. No coalescence was observed up to the decomposition temperature of O °C.

8 (80% yield, yellow crystals): ^1H NMR (300 MHz, C_6D_6): δ = 7.75 (d, ^3J(H,H) = 6.6 Hz, 1H, Ar), 7.11 (t, ^3J(H,H) = 7.5 Hz, 1H, Ar), 6.96 (t, ^3J(H,H) = 7 Hz, 1H, Ar), 6.59 (d,^3J(H,H) = 6.6 Hz, 1H, Ar), 4.05 (brm, 2H, OCH_2CH_3), 3.92 (brm, 2H, OCH_2CH_3), 3.48 (s, 3H, OMe), 1.61 (s, 15H, C_5Me_5), 0.92 (brm, 6H, OCH_2CH_3); $^{13}C\{^1H\}$ NMR (75.47 MHz, CD_2Cl_2): δ = 263.8 (=C_α), 226.6 (CO), 166.7 (FeAr), 154.3 (Ar_{OMe}), 143.9 (Ar), 122.5 (Ar), 119.8 (Ar), 108.2 (Ar), 95.5 (C_5Me_5), 66.7 (brs, OCH_2CH_3), 55.1 (OMe), 14.6 (OCH_2CH_3), 9.7 (C_5Me_5); IR (pentane): $\tilde{\nu}$ = 1936 cm^{-1} (CO); HRMS (70 eV): *m/z*: 383.1314 [M^+ – OEt], calcd for $C_{21}H_{27}O_3Fe$: 383.1310; 355.1355 [M^+ – OEt – CO], calcd for $C_{20}H_{27}O_2Fe$: 355.1361.

Received: October 21, 1997 [Z11021IE]
German version: *Angew. Chem.* **1998**, *110*, 1009 – 1012

Keywords: carbene complexes · C–C activation · C–Cl activation · iron

[1] V. V. Grushin, H. Alper, *Chem. Rev.* **1994**, *94*, 1047 – 1062, and references therein.
[2] Selective bond activation controlled by the choice of metal complex was recently described: M. E. van der Boom, S.-Y. Liou, Y. Ben-David, A. Vigalok, D. Milstein, *Angew. Chem.* **1997**, *109*, 636 – 637; *Angew. Chem. Int. Ed. Engl.* **1997**, *36*, 625 – 626; M. Gandelman, A. Vigalok, L. J. W. Shimon, D. Milstein, *Organometallics* **1997**, *16*, 3981 – 3986.
[3] R. J. Kulawiec, R. H. Crabtree, *Coord. Chem. Rev.* **1990**, *99*, 89 – 115, and references therein.
[4] M. D. Butts, B. L. Scott, G. J. Kubas, *J. Am. Chem. Soc.* **1996**, *118* 11831 – 11843.
[5] G. Poignant, S. Nlate, V. Guerchais, A. J. Edwards, P. R. Raithby, *Organometallics* **1997**, *16*, 124 – 132.
[6] S. Nlate, P. Guénot, S. Sinbandhit, L. Toupet, C. Lapinte, V. Guerchais, *Angew. Chem.* **1994**, *106*, 2294—2296; *Angew. Chem. Int. Ed. Engl.* **1994**, *33*, 2218 – 2219.
[7] Crystal structure of **4**: Enraf-Nonius CAD4 diffractometer, $Mo_{K\alpha}$ radiation, μ = 6.91 cm^{-1}, $F(000)$ = 508, T = 294 K, triclinic, space group $P\bar{1}$, a = 9.601(5), b = 10.711(5), c = 13.600(6) Å, α = 75.55(4), β = 84.46(4), γ = 67.88(3)°, V = 1246(1) Å^{-3}, Z = 2, ρ = 1.270 g cm^{-3}. Of 4402 reflections, 3524 with $I > 2\sigma(I)$ were observed ($\omega/2\theta$ = 1, *hkl*: 0.11, –12.12, –16.16). Lorentzian and polarization corrections (DEFLT 1990), R = 0.046, R_w = 0.047, $w = 1/\sigma(F_o)^2 = [\sigma^2(I) + (0.04F_o^2)^2]^{-1/2}$, S_w = 0.890 (residual $\Delta\rho < 0.44$ e Å^{-3}). Crystal structure of **8**: Enraf-Nonius CAD4 diffractometer, $Mo_{K\alpha}$ radiation, μ = 7.086 cm^{-1}, $F(000)$ = 456, T = 294 K, triclinic, space group $P\bar{1}$, a = 8.773(6), b = 9.185(9), c = 14.572(9) Å, α = 99.64(5), β = 89.89(2), γ = 108.34(5)°, V = 1097(1) Å^{-3}, Z = 2, ρ = 1.296 g cm^{-3}. Of 4133 reflections, 2364 observed with $I > 4\sigma(I)$ ($\omega/2\theta$ = 1, *hkl*: 0.10, –10.10, –17.17), Lorentzian and polarization corrections (DEFLT 1990), R = 0.056, R_w = 0.051, $w = 1/\sigma(F_o)^2 = [\sigma^2(I) + (0.04F_o^2)^2]^{-1/2}$, S_w = 1.13 (residual $\Delta\rho < 0.46$ e Å^{-3}). Crystallographic data (excluding structure factors) for the structures reported in this paper have been deposited with the Cambridge Crystallographic Data Centre as supplementary publication no. CCDC-100931. Copies of the data can be obtained free of charge on application to CCDC, 12 Union Road, Cambridge CB2 1EZ, UK (fax: (+44) 1223-336-033; e-mail: deposit@ccdc.cam.ac.uk).
[8] M. L. H. Green, J. Haggitt, C. P. Mehnert, *J. Chem. Soc. Chem. Commun.* **1995**, 1853 – 1854; A. N. Chernega, A. J. Graham, M. L. H. Green, J. Haggitt, J. Lloyd, C. P. Mehnert, N. Metzler, J. Souter, *J. Chem. Soc. Dalton Trans.* **1997**, 2293 – 2303.
[9] T.-S. Peng, C. H. Winter, J. A. Gladysz, *Inorg. Chem.* **1994**, *33*, 2534 – 2542.
[10] For a review, see L. Balas, D. Jurrhy, L. Latxague, S. Grelier, Y. Morel, M. Hamdani, N. Ardoin, D. Astruc, *Bull. Soc. Chim. Fr.* **1990**, *127*, 401 – 426.
[11] T. Braun, O. Gevert, H. Werner, *J. Am. Chem. Soc.* **1995**, *117*, 7291 – 7292.
[12] J. Yang, W. M. Jones, J. K. Dixon, N. T. Allison, *J. Am. Chem. Soc.* **1995**, *117*, 9776 – 9777.
[13] Y. Strentom, W. M. Jones, *Inorg. Chem.* **1986**, 5, 178 – 180; J. Yang, J. Yin, K. A. Abboud, J. W. Jones, *Organometallics* **1994**, *13*, 971-978, and references therein.
[14] A. Davison, D. L. Reger, *J. Am. Chem. Soc.* **1972**, *94*, 9237 – 9238. M. Rosenblum, *J. Organomet. Chem.* **1986**, *300*, 191 – 218.

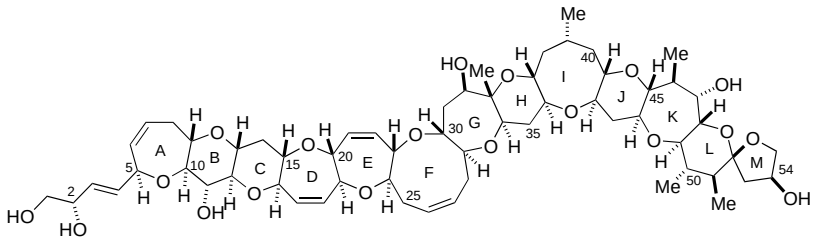
Synthetic Studies on Ciguatoxin: A Convergent Strategy for Construction of the F – M Ring Framework**

Masayuki Inoue, Makoto Sasaki,* and Kazuo Tachibana*

Ciguatoxin (CTX1B, **1**) and its congeners, naturally occurring polycyclic ethers found in marine unicellular algae, are the principal toxins associated with ciguatera fish poisoning.[1, 2] These potent neurotoxins reportedly bind to the same sites on voltage-sensitive sodium channels (VSSC) as brevetoxins, another class of structurally related marine toxins.[3] An important structural characteristic is the fact that the hexahydrooxonin ring (the F ring) in **1** and its congeners

[*] Dr. M. Sasaki, Prof. Dr. K. Tachibana, M. Inoue
Department of Chemistry, School of Science
The University of Tokyo
Hongo, Bunkyo-ku, Tokyo 113-0033 (Japan)
Fax: (+81) 3-5800-6898
E-mail: msasaki@chem. s.u-tokyo.ac.jp
ktachi@chem.s.u-tokyo.ac.jp

[**] This work was supported by the Japanese Ministry of Education, Science, Sports, and Culture (grant-in-aid no. 08245103) and the Japan Society for the Promotion of Science for Young Scientists through a fellowship for M.I. We thank Dr. Keiichi Konoki and Professor Michio Murata from our Department for binding assays and valuable discussions and advice.



1

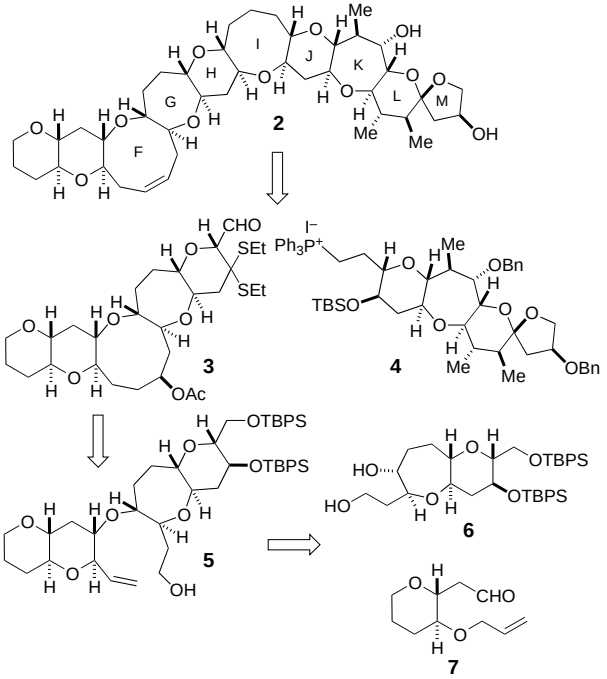
undergoes a slow conformational change in solution, which is thought to play a role in high-affinity binding to VSSC and/or VSSC activation.[1g] The structural complexity of the ciguatoxins and their exceptionally potent neurotoxicity together with their scarcity in natural sources make them prime targets for a total synthesis.[4, 5] In particular, construction of the hexahydrooxonin ring system represents a challenging synthetic problem. Despite recent advances in the synthesis of cyclic ethers,[6] there is still no general and convergent method for the assembly of a fused nine-membered ether ring system.[7]

We recently reported for the first time a convergent approach to the fused hexahydrooxonin ring system, one that features both an intramolecular reaction of a γ-alkoxyallylsilane with an acetal group to form an O-linked oxacycle and an SmI_2-mediated intramolecular Reformatsky reaction that leads to an oxonane ring.[5d] As part of our continuing investigation into the structural requirements for high-affinity binding of ciguatoxin to VSSC, we describe here the application of this strategy to a convergent synthesis of the decacyclic ciguatoxin mimic **2**, which contains the F – M ring framework but with the DE ring system of ciguatoxin replaced by a dioxadecalin unit.

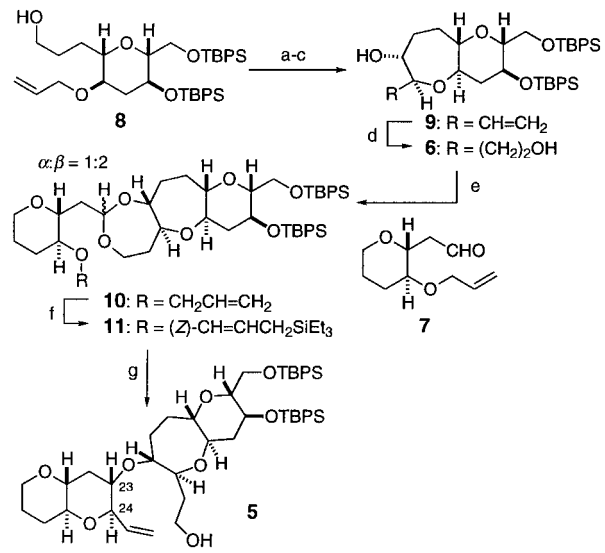
Based on a retrosynthetic analysis we anticipated that the target molecule **2**[8] could be prepared from aldehyde **3** and phosphonium salt **4** through a Wittig reaction followed by cyclization of the resulting hydroxy dithio acetal[9] (Scheme 1). The oxonane ring in **3** should be accessible from **5**, which in turn could be prepared from diol **6** and aldehyde **7** with the aid of our previously reported strategy.[5d]

Synthesis of the O-linked tetracycle **5** began with alcohol **8**,[10] which was converted into bicyclic compound **9** by the method of Yamamoto et al.[11] (Scheme 2). Formation of the corresponding alkoxy-substituted allylic anion followed by a trapping reaction with tributyltin chloride afforded the γ-alkoxyallylstannane in 88% yield. Oxidation of the primary hydroxyl group to a formyl group and subsequent treatment with boron trifluoride etherate provided **9** as a single stereoisomer in high yield. Hydroboration of **9** with 9-borabicyclononane (9-BBN) followed by oxidative work-up led to diol **6** (86% yield over three steps). Reaction of **6** with aldehyde **7** was carried out in the presence of 0.1 equivalents of scandium trifluoromethanesulfonate[12] to give an epimeric mixture of seven-membered acetals **10** in an approximately 2:1 ratio, with the β-H isomer predominating (82% combined yield).[13]

Metalation of **10** with *sec*-butyllithium followed by treatment with chlorotriethylsilane gave a mixture of γ-alkoxyallylsilanes **11** in 87% yield accompanied by recovered pure α-H isomer of **10** (12%). Use of the triethylsilyl group instead of the more common trimethylsilyl moiety in this reaction resulted in a higher yield and greater reproducibility.[14] Treatment of **11** with titanium(IV) chloride and triphenylphosphane[15] gave O-linked **5** with the desired stereochemistry as the major product, albeit in modest yield (36%), together with the (23*R*,24*R*) diastereoisomer (16%) and trace amounts of two other stereoisomers.[16]



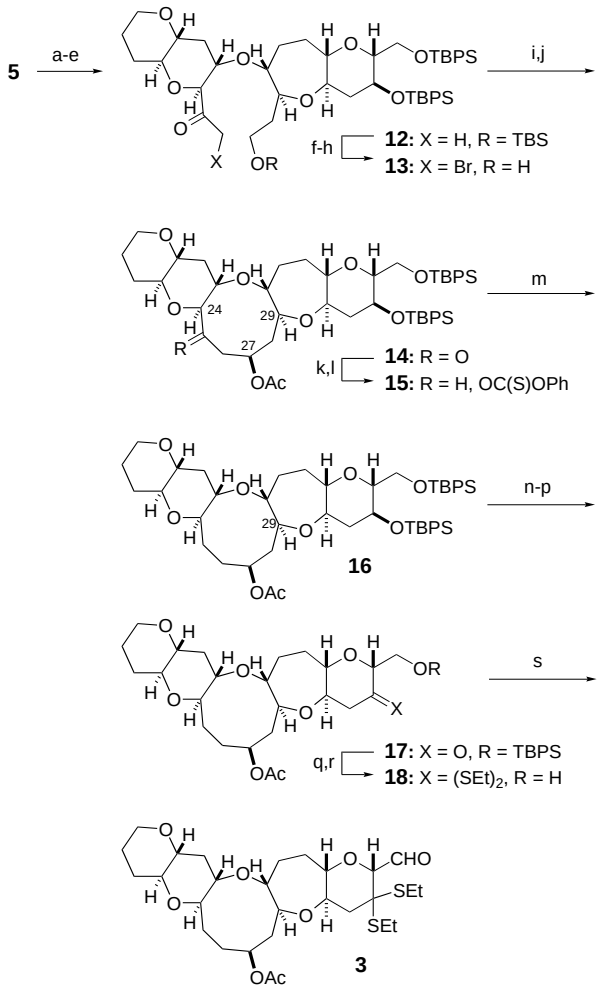
Scheme 1. Retrosynthesis of the decacyclic polyether **2**. Bn = benzyl, TBPS = *tert*-butyldiphenylsilyl.



Scheme 2. Synthesis of the O-linked tetracycle **5**. a) *s*BuLi, nBu$_3$SnCl, THF, $-78\,^{\circ}C$, 88%; b) $SO_3\cdot$pyridine, Et_3N, DMSO, CH_2Cl_2, RT, 92%; c) $BF_3\cdot OEt_2$, CH_2Cl_2, $-90\,^{\circ}C$; d) 9-BBN, THF, RT, then H_2O_2, $NaHCO_3$, RT, 94% (2 steps); e) $Sc(OTf)_3$ (cat.), benzene, RT, 82%; f) *s*BuLi, Et_3SiCl, THF, $-78\,^{\circ}C$, 87%; g) $TiCl_4$, PPh_3, CH_2Cl_2, $-78\rightarrow0\,^{\circ}C$, 36%. DMSO = dimethyl sulfoxide, 9-BBN = 9-borabicyclononane, OTf = trifluoromethanesulfonate.

 © WILEY-VCH Verlag GmbH, D-69451 Weinheim, 1998 1433-7851/98/3707-0966 $ 17.50+.50/0

The elaboration of **5** to aldehyde **3** is outlined in Scheme 3. Protection of **5** as the *tert*-butyldimethylsilyl ether and oxidative cleavage of the double bond led to an aldehyde



Scheme 3. Synthesis of pentacyclic aldehyde **3**. a) TBSOTf, 2,6-lutidine, CH_2Cl_2, 0 °C, 95 %; b) OsO_4, NMO, *t*BuOH/H_2O, RT; c) $Pb(OAc)_4$, benzene, RT, d) MeMgBr, THF, −78 → 0 °C, 91 % (3 steps); e) $(COCl)_2$, DMSO, Et_3N, CH_2Cl_2, −78 °C → RT, 94 %; f) LDA, Me_3SiCl, THF, −78 °C; g) NBS, THF, 0 °C; h) CSA (cat.), MeOH, RT, 83 % (3 steps); i) $SO_3 \cdot$ pyridine, Et_3N, DMSO, CH_2Cl_2, 0 °C; j) SmI_2 (5 equiv), THF, −78 °C, then Ac_2O, 4-DMAP, 0 °C; k) $NaBH_4$, CH_2Cl_2/MeOH, 0 °C; l) PhOC(S)Cl, 4-DMAP, CH_3CN, RT, 66 % (5 steps); m) $n$$Bu_3SnH$ (20 equiv), Et_3B (cat.), benzene, RT, 80 %; n) $n$$Bu_4NF$, THF, RT; o) TBPSCl, imidazole, DMF, 0 °C, 82 % (2 steps); p) $(COCl)_2$, DMSO, Et_3N, CH_2Cl_2, −78 °C → RT, 94 %; q) EtSH, $TiCl_4$, CH_2Cl_2, −78 °C; r) $n$$Bu_4NF$, THF, RT, 97 % (2 steps); s) $SO_3 \cdot$ pyridine, Et_3N, DMSO, CH_2Cl_2, 0 °C. TBS = *tert*-butyldimethylsilyl, NMO = *N*-methylmorpholine *N*-oxide, DMF = dimethylformamide, LDA = lithium diisopropylamide, NBS = *N*-bromosuccinimide, CSA = 10-camphorsulfonic acid, 4-DMAP = 4-dimethylaminopyridine.

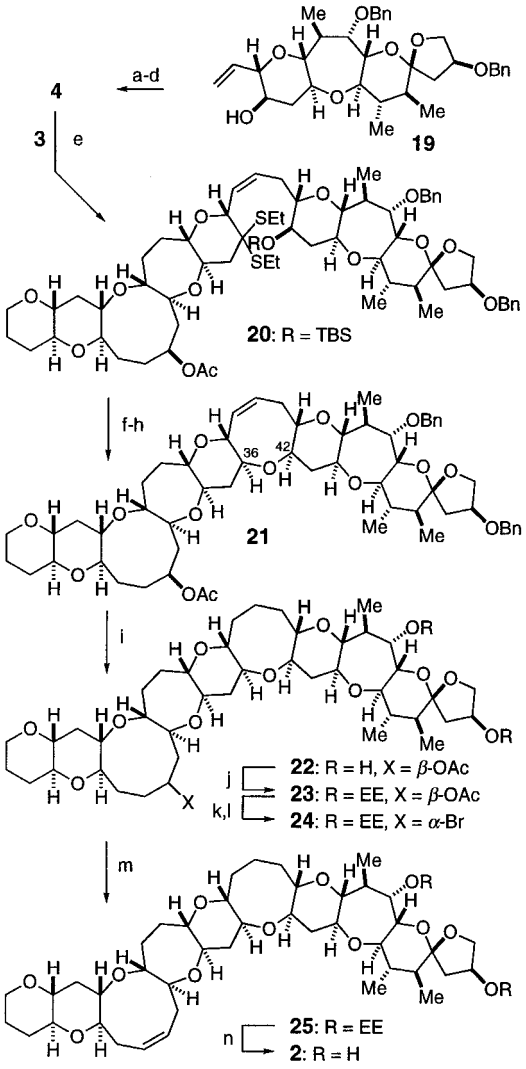
that reacted with methylmagnesium bromide. The resulting alcohol was oxidized under Swern conditions to afford methyl ketone **12** in an overall yield of 81 %. Formation of the silyl enol ether, treatment with NBS, and desilylation under acidic conditions gave alcohol **13** in 83 % yield over three steps. This was followed by oxidation of **13** with $SO_3 \cdot$ pyridine to the aldehyde, which was subjected to an SmI_2-mediated intramolecular Reformatsky reaction under the previously reported conditions.[5d] Thus, treatment of the aldehyde with five equivalents of SmI_2 in THF at −78 °C gave, after in situ acetylation, β-acetoxy ketone **14** in high yield as a single diastereomer,[17] which was immediately reduced with sodium borohydride.[18] The resulting alcohol was converted into phenyl thiocarbonate **15** (66 % overall yield based on **13**). A subsequent radical reduction of **15** proved to be problematic. When the reduction was carried out with $n$$Bu_3SnH$ and AIBN under thermal conditions (benzene, 80 °C), formation of the undesired C29 isomer of **16** predominated, presumably due to transannular hydrogen abstraction. After considerable experimentation, an optimal result was achieved with a large excess of $n$$Bu_3SnH$ in the presence of triethylborane[19] at room temperature; acetate **16** was obtained in 80 % yield. Removal of two silyl groups in **16** and selective reprotection of the primary hydroxyl group followed by oxidation of the secondary alcohol provided ketone **17** in an overall yield of 77 %. Formation of the thio acetal from **17** and desilylation gave alcohol **18** in 97 % yield. This was oxidized to the requisite aldehyde **3**, which was thereby available for coupling with **4**.

Phosphonium salt **4** was prepared from the previously reported JKLM ring fragment **19**[5b, c] by a four-step sequence of routine synthetic reactions (Scheme 4). Wittig reaction of the ylide generated from **4** with aldehyde **3** produced exclusively *Z* olefin **20** in 63 % yield. Desilylation of **20** followed by AgOTf-induced cyclization of the resulting hydroxy dithio acetal[9] and radical desulfurization[9] provided tetrahydrooxocin **21** and thus the desired decacyclic system.[20] Hydrogenation of the double bond in **21** and simultaneous hydrogenolysis of the benzyl groups gave diol **22**. Preliminary studies revealed that protection was required for the seriously hindered hydroxyl group at C47 to permit introduction of a *Z* double bond into the oxonane ring. Accordingly, **22** was protected as the bis(ethoxyethyl) ether **23** in quantitative yield. After deacetylation of **23** with diisobutylaluminum hydride, the alcohol product was treated with methanesulfonic anhydride in the presence of lithium bromide and Hünig base to give bromide **24** as a single stereoisomer, which upon exposure to potassium *tert*-butoxide in dimethyl sulfoxide[21] afforded the desired hexahydrooxonin **25** in a yield of 52 % based on **23**. Finally, removal of the ethoxy ethyl groups in **25** with pyridinium *p*-toluenesulfonate furnished the target compound **2**[22] in quantitative yield.

^1H and ^{13}C NMR signals due to the hexahydrooxonin ring of **2** were severely broadened at room temperature, which is consistent with the behavior of ring F in ciguatoxin. Dynamic NMR studies revealed that **2** exists as an approximately 1:1 equilibrium of two conformational states at the hexahydrooxonin ring. Preliminary investigation of the binding affinity of **2** to VSSC was conducted through a competitive inhibition assay.[3b] Synthetic **2** did not inhibit the binding of tritium-labeled dihydrobrevetoxin B (PbTx-3) to rat-brain synaptosomes at micromolar concentrations. Assay at higher levels proved impractical owing to low solubility of the compound in aqueous media. The possibility of noncompetitive binding is currently under investigation.

We have thus demonstrated that the SmI_2-mediated intramolecular Reformatsky reaction provides a general and powerful method for the construction of the *trans*-fused

 © WILEY-VCH Verlag GmbH, D-69451 Weinheim, 1998 1433-7851/98/3707-0967 $ 17.50+.50/0



Scheme 4. Synthesis of decacyclic polyether **2**. a) TBSOTf, 2,6-lutidine, CH_2Cl_2, 0 °C, 87%; b) 9-BBN, THF, RT, then H_2O_2, $NaHCO_3$, RT, 85%; c) I_2, PPh_3, imidazole, benzene, RT, 97%; d) PPh_3, CH_3CN, 70 °C, 97%; e) *n*BuLi, THF/HMPA, −78 °C→RT, 63%; f) nBu_4NF, THF, RT, 90%; g) AgOTf, $NaHCO_3$, 4-Å molecular sieves, silica gel, CH_3NO_2, RT, 76% based on 70% conversion; h) Ph_3SnH (10 equiv), AIBN (cat.), toluene, 110 °C, 82%; i) H_2, $Pd(OH)_2$/C, EtOAc/MeOH/AcOH, RT; j) ethyl vinyl ether, PPTS, CH_2Cl_2, RT, 99% (2 steps); k) DIBAL-H, CH_2Cl_2, −78 °C; l) Ms_2O, LiBr, *i*Pr_2NEt, CH_2Cl_2, 0 °C→RT; m) *t*BuOK, DMSO, RT, 52% (3 steps); n) PPTS (cat.), MeOH, RT, quant. HMPA = hexamethyl phosphoramide, AIBN = 2,2′-azobisisobutyronitrile, PPTS = pyridinium *p*-toluenesulfonate, EE = ethoxyethyl, DIBAL-H = diisobutylaluminum hydride, Ms_2O = methanesulfonic anhydride.

hexahydrooxonin ring system found in ciguatoxins. Studies directed toward the total synthesis of ciguatoxin and its simplified analogues are currently underway.

Received: October 14, 1997 [Z11034IE]
German version: *Angew. Chem.* **1998**, *110*, 1012 – 1015

Keywords: ciguatoxin · cyclizations · natural products · polyethers · synthetic methods

[1] a) M. Murata, A.-M. Legrand, Y. Ishibashi, T. Yasumoto, *J. Am. Chem. Soc.* **1989**, *111*, 8929 – 8931; b) M. Murata, A.-M. Legrand, Y. Ishibashi, M. Fukui, T. Yasumoto, *ibid*. **1990**, *112*, 4380 – 4386; c) R. J. Lewis, M. Sellin, M. A. Poli, R. S. Norton, J. K. MacLeod, M. M. Sheil, *Toxicon* **1991**, *29*, 1115 – 1127; d) M. Murata, A.-M. Legrand, P. J. Scheuer, T. Yasumoto, *Tetrahedron Lett.* **1992**, *33*, 525 – 526; e) M. Satake, M. Murata, T. Yasumoto, *ibid*. **1993**, *34*, 1975 – 1978; f) R. J. Lewis, R. S. Norton, I. M. Brereton, C. D. Eccles, *Toxicon* **1993**, *31*, 637 – 643; g) T. Yasumoto, M. Murata, *Chem. Rev.* **1993**, *93*, 1897 – 1909; h) P. J. Scheuer, *Tetrahedron* **1994**, *50*, 3 – 18; i) M. Satake, Y. Ishibashi, A.-M. Legrand, T. Yasumoto, *Biosci. Biochem. Biotech.* **1996**, *60*, 2103 – 2105.

[2] The absolute stereochemistry of ciguatoxin was determined to be that represented by structure **1**; see a) H. Oguri, S. Hishiyama, O. Sato, T. Oishi, M. Hirama, M. Murata, T. Yasumoto, N. Harada, *Tetrahedron* **1997**, *53*, 3057 – 3072; b) M. Satake, A. Morohashi, H. Oguri, T. Oishi, M. Hirama, N. Harada, T. Yasumoto, *J. Am. Chem. Soc.* **1997**, *119*, 11325 – 11326.

[3] a) J.-N. Bidard, H. P. M. Vijverberg, C. Frelin, E. Chungue, A.-M. Legrand, R. Bagnis, M. Lazdunski, *J. Biol. Chem*. **1984**, *259*, 8353 – 8357; b) A. Lambet, J. N. Bidard, M. Lazdunski, *FEBS Lett.* **1987**, *219*, 355 – 359.

[4] a) E. Alvarez, M. T. Díaz, L. Hanxing, J. D. Martín, *J. Am. Chem. Soc.* **1995**, *117*, 1437 – 1438; b) S. Hosokawa, M. Isobe, *Synlett* **1995**, 1179 – 1180; c) H. Oguri, S. Hishiyama, T. Oishi, M. Hirama, *ibid*. **1995**, 1252 – 1254; d) T. Oka, K. Fujiwara, A. Murai, *Tetrahedron*, **1996**, *52*, 12091 – 12110; e) T. Oishi, M. Shoji, K. Maeda, N. Kumahara, M. Hirama, *Synlett* **1996**, 1165 – 1167; f) E. Alvarez, M. Delgado, M. T. Díaz, L. Hanxing, R. Pérez, J. D. Martín, *Tetrahedron Lett.* **1996**, *37*, 2865 – 2868; g) M. Isobe, S. Hosokawa, K. Kira, *Chem. Lett*. **1996**, 473 – 474; h) H. Atsuta, K. Fujiwara, A. Murai, *Synlett* **1997**, 307 – 309; i) T. Oishi, K. Maeda, M. Hirama, *Chem. Commun.* **1997**, 1289 – 1290; j) T. Oishi, M. Shoji, N. Kumahara, M. Hirama, *Chem. Lett.* **1997**, 845 – 846; k) T. Oka, K. Fujiwara, A. Murai, *Tetrahedron Lett*. **1997**, *38*, 8053 – 8056.

[5] a) M. Sasaki, A. Hasegawa, K. Tachibana, *Tetrahedron Lett*. **1993**, *34*, 8489 – 8492; b) M. Sasaki, M. Inoue, K. Tachibana, *J. Org. Chem.* **1994**, *59*, 715 – 717; c) M. Sasaki, M. Inoue, M. Murata, K. Tachibana in *Proceedings of the International Symposium on Ciguatera and Marine Natural Products* (Eds.: Y. Hokama, P. J. Scheuer, T. Yasumoto), Asian-Pacific Research Foundation, Honolulu, **1995**, pp. 229 – 237; d) M. Inoue, M. Sasaki, K. Tachibana, *Tetrahedron Lett*. **1997**, *38*, 1611 – 1614.

[6] Recent reviews: a) E. Alvarez, M.-L. Candenas, R. Pérez, J. L. Ravelo, J. D. Martín, *Chem. Rev.* **1995**, *95*, 1953 – 1980; b) Y. Mori, *Chem. Eur. J.* **1997**, *3*, 849 – 852.

[7] Recently, a new synthetic method was reported for the construction of the nine-membered ether ring, together with an application of the method to synthesis of the EFGH ring skeleton of brevetoxin A: K. C. Nicolaou, Z. Yang, M. Ouellette, G.-Q. Shi, P. Gärtner, J. L. Gunzner, K. A. Agrios, R. Huber, R. Chadha, D. H. Huang, *J. Am. Chem. Soc.* **1997**, *119*, 8105 – 8106.

[8] The numbering of carbon atoms in all compounds in this communication corresponds to that of ciguatoxin.

[9] K. C. Nicolaou, C. V. C. Prasad, C.-K. Hwang, M. E. Duggan, C. A. Veale, *J. Am. Chem. Soc*. **1989**, *111*, 5321 – 5330.

[10] Compound **8** was prepared from the known 3-(2′,4′,6′-tri-*O*-benzyl-3′-deoxy-β-D-glucopyranosyl)-1-propanol by the following seven-step sequence of reactions (W. Zheng, J. A. DeMattei, J.-P. Wu, J. J.-W. Duran, L. R. Cook, H. Oinuma, Y. Kishi, *J. Am. Chem. Soc.* **1996**, *118*, 7946 – 7968): a) Ac_2O, 4-DMAP, Et_3N, CH_2Cl_2, RT; b) H_2, $Pd(OH)_2$/C, EtOAc/MeOH, RT; c) $Me_2C(OMe)_2$, PPTS (cat.), CH_2Cl_2/DMF, RT, 98% over three steps; d) $CH_2{=}CHCH_2OCO_2Me$, $[Pd_2(dibenzylideneacetone)_3]\cdot CHCl_3$, 1,4-bis(diphenylphosphanyl)butane, THF, 65 °C; e) CSA (cat.), MeOH, RT; f) *t*$BuPh_2SiCl$, imidazole, DMF, 60 °C; g) NaOMe, MeOH, RT, 69% over four steps.

[11] a) Y. Yamamoto, J. Yamada, I. Kadota, *Tetrahedron Lett*. **1991**, *32*, 7069 – 7072; b) V. Gevorgyan, I. Kadota, Y. Yamamoto, *ibid.* **1993**, *34*, 1313 – 1316; c) I. Kadota, Y. Yamamoto, *Main Group Met. Chem.* **1994**, *17*, 269 – 289.

[12] S. Fukuzawa, T. Tsuchimoto, T. Hotaka, T. Hiyama, *Synlett* **1995**, 1077 – 1078.

[13] Use of 10-camphorsulfonic acid as an acid catalyst in this acetalization gave a 1:1 mixture of acetals **10**.

 © WILEY-VCH Verlag GmbH, D-69451 Weinheim, 1998 1433-7851/98/3707-0968 $ 17.50+.50/0

[14] When chlorotrimethylsilane was used as silylating agent, a significant amount (10–20% yield) of α-alkoxyallylsilane was formed as a by-product.
[15] I. Kadota, V. Gevorgyan, J. Yamada, Y. Yamamoto, *Synlett* **1991**, 823–824.
[16] From the corresponding γ-alkoxyallyltrimethylsilane, cyclization of the β-H isomer gave the desired (23*S*,24*R*)-**5** in 42% yield as the major product together with its (23*R*,24*R*) diastereoisomer (30%), whereas cyclization of the α-H isomer produced **5** in only 29% yield together with three other stereoisomers for C23 and C24 in yields of 28, 27, and 13%.
[17] The configuration at C27 of **14** was assigned on the basis of strong NOEs between 24-H/27-H and 27-H/29-H. The *syn* relationship between 23-H and 30-H was also confirmed by NOE experiments.
[18] β-Acetoxy ketone **14** underwent partial β-elimination during chromatography over silica gel to yield the α,β-unsaturated ketone.
[19] K. Nozaki, K. Oshima, K. Utimoto, *Bull. Chem. Soc. Jpn.* **1990**, *63*, 2578–2583.
[20] The *syn* relationship between 36-H and 42-H in compound **21** was unambiguously established by NOE experiments.
[21] R. A. Bartsch, T. A. Shelley, *J. Org. Chem.* **1973**, *38*, 2911–2912.
[22] Selected spectroscopic data for **2**: IR (film): $\tilde{\nu}$ = 3446, 2929, 2863, 1455, 1375, 1338, 1280, 1080, 939 cm^{-1}; ^{1}H NMR (500 MHz, $CDCl_3$): δ = 5.74–5.61 (br, 2H; 26-H, 27-H), 4.48 (m, 1H; 54-H), 3.86 (dd, J = 10.1, 4.3 Hz, 1H; 55-H), 3.85 (m, 1H; 17-H), 3.77 (d, J = 10.1 Hz, 1H; 55-H), 3.67 (dd, J = 3.7, 1.5 Hz, 1H; 47-H), 3.66 (m, 1H; 44-H), 3.61 (dd, J = 9.8, 1.5 Hz, 1H; 48-H), 3.55 (br, 1H; 29-H), 3.43 (m, 1H; 30-H), 3.31 (m, 1H; 17-H), 3.22 (dd, J = 9.8, 9.8 Hz, 1H; 49-H), 3.19–3.13 (m, 3H; 34-H, 36-H, 42-H), 3.07 (m, 2H; 23-H, 24-H), 3.01 (m, 1H; 37-H), 2.94–2.89 (m, 4H; 20-H, 21-H, 33-H, 41-H), 2.83 (dd, J = 10.1, 5.2 Hz, 1H; 45-H), 2.80–2.56 (br, 2H; 25-H, 28-H), 2.34–1.35 (m, 27H; 18-H_2, 19-H_2, 22-H_2, 25-H, 28-H, 31-H_2, 32-H_2, 35-H_2, 38-H_2, 39-H_2, 40-H_2, 43-H_2, 46-H, 50-H, 51-H, 53-H_2), 1.11 (d, J = 7.6 Hz, 3H; 46-Me), 1.02 (d, J = 6.4 Hz, 3H; 50-Me), 0.98 (d, J = 6.7 Hz, 3H; 51-Me); HR-MS (FAB) calcd for $C_{42}H_{64}O_{12}Na$ [M+Na$^+$]: 783.4295, found: 783.4285.

Solution pH: A Selectivity Switch in Aqueous Organometallic Catalysis—Hydrogenation of Unsaturated Aldehydes Catalyzed by Sulfonatophenylphosphane–Ru Complexes**

Ferenc Joó,* József Kovács, Attila Cs. Bényei, and Ágnes Kathó

Organometallic catalysis in aqueous medium offers an important possibility for avoiding the greatest problem of homogeneous catalysis: having to separate the catalyst from the product. In two-phase mixtures with an aqueous and an organic phase, soluble catalysts can be recovered by phase separation.[1] In many cases, water-soluble transition metal catalysts are prepared with sulfonated phosphane ligands such as (3-sulfonatophenyl)diphenylphosphane (TPPMS, **1**) and tris(3-sulfonatophenyl)phosphane (TPPTS, **2**); in general, both are used as their sodium salts.

Selective hydrogenation of α,β-unsaturated aldehydes to the corresponding allylic alcohols gives valuable products for fragrance, flavor, and vitamin chemistry. The most successful two-phase processes use ruthenium(II) complexes with sulfonated phosphane ligands as (pre)catalysts. Complex **3a** can be used for the reduction of citronellal to citronellol by hydrogen transfer from aqueous sodium formate,[2] and for the hydrogenation of cinnamaldehyde.[3] $RuCl_3$ and **2** form an in situ catalyst for the hydrogenation of 3-methyl-2-butenal (prenal).[4] Of the complexes **3b**, **4b**, and **5b**, the most active and durable catalyst precursor for the hydrogenation of cinnamaldehyde was **5b**.[5] In all these reactions the selectivity towards the unsaturated alcohol was at least 95%. As an apparent contradiction, in the hydrogenation of prenal with **4b** the C=C bond also became extensively hydrogenated.[5]

[{$RuCl_2$(tppms)$_2$}$_2$] **3a** [{$RuCl_2$(tppts)$_2$}$_2$] **3b**

[HRuCl(tppms)$_3$] **4a** [HRuCl(tppts)$_3$] **4b**

[{H_2Ru(tppms)$_2$}$_2$] **5a** [{H_2Ru(tppts)$_2$}$_2$] **5b**

We are currently performing potentiometric studies on the formation and protic equilibria of water-soluble rhodium(I),[6] iridium(I),[7] and ruthenium(II) hydrides as a function of pH value to learn about the specific influence of water as solvent on the mechanism of catalyzed aqueous organometallic reactions. In several cases, such as with reactions (a) and (b), the equilibrium distribution of hydride complexes was strongly dependent on the pH of the solution.

$$\underset{\mathbf{3a}}{1/2[\{RuCl_2(tppms)_2\}_2]} + H_2 + TPPMS \rightleftharpoons \underset{\mathbf{4a}}{[HRuCl(tppms)_3]} + H^+ + Cl^- \quad (a)$$

$$\underset{\mathbf{4a}}{[HRuCl(tppms)_3]} + H_2 + TPPMS \rightleftharpoons \underset{\mathbf{5a}}{[H_2Ru(tppms)_4]} + H^+ + Cl^- \quad (b)$$

The amount of proton liberated during hydrogenation of **3a** (in the presence of three equivalents of **1**) was measured in solutions with different but constant pH values between 1 and 12 (static-pH hydrogenations). The major species in acidic solutions is **4a**, while in neutral and basic media **5a** can be found almost exclusively. This was confirmed by ^{1}H and ^{31}P NMR spectroscopy (Figure 1).[8] It is noteworthy that the shift in the hydride distribution occurs between pH 5 and 7.

Cinnamaldehyde was hydrogenated under the same experimental conditions used for the NMR measurements, except that the reactions were run at 80°C instead of 50°C. At pH values greater than 6, where the dominant ruthenium species is **5a**, exclusive hydrogenation of the aldehyde functionality occurred to yield cinnamyl alcohol. Conversely, **4a**, which forms below pH 5, was unreactive towards the aldehyde group but catalyzed a slow reduction of the C=C bond to furnish 3-phenylpropanal selectively.

The influence of the pH value on the selectivity of reactions catalyzed by [Ru(tppms)] complexes is demonstrated in

[*] Prof. F. Joó, J. Kovács, Dr. A. C. Bényei, Dr. Á. Kathó
Research Group on Homogeneous Catalysis
Hungarian Academy of Sciences and Institute of Physical Chemistry
Lajos Kossuth University
P. O. Box 7, H-4010 Debrecen (Hungary)
Fax: (+36) 52-310936
E-mail: jooferenc@tigris.klte.hu

[**] This work was supported by the European Comission (PECO ERBCIPDCT940617) and by the Hungarian Research Council (OTKA T016697). We thank Dr. S. Sinbandhit (University of Rennes, France) for his help in the initial phase of the NMR measurements. Johnson-Matthey p.l.c. is thanked for a loan of $RuCl_3 \cdot x H_2O$.

 © WILEY-VCH Verlag GmbH, D-69451 Weinheim, 1998 1433-7851/98/3707-0969 $ 17.50+.50/0

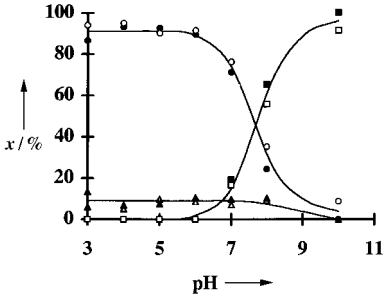


Figure 1. Distribution of water-soluble ruthenium(II) hydrides as a function of pH value based on the integrated intensities of ^{1}H (filled symbols) and ^{31}P NMR signals (empty symbols) of [HRuCl(tppms)$_3$] (●, ○, [H$_2$Ru(tppms)$_4$] (■, □), and [{HRuCl(tppms)$_2$}$_2$] (▲, △). [Ru] = 2.4 × 10^{-2} M, [TPPMS] = 7.2 × 10^{-2} M, 0.2 M KCl, 50 °C, H$_2$, p_{total} = 1 bar.

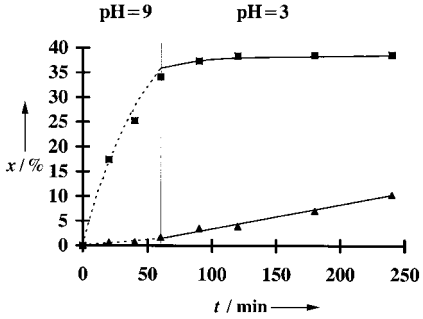


Figure 2. Selectivity of the hydrogenation of cinnamaldehyde to cinnamyl alcohol (■) and dihydrocinnamaldehyde (▲) as a function of pH value. For further details, see the Experimental Section.

Figure 2. The reaction was run for one hour at pH 9, and there was high selectivity towards formation of the unsaturated alcohol. Afterwards the pH value was lowered with HCl to 3, which halted the reduction of the aldehyde. Instead, hydrogenation of the C=C bond was observed. There was a complete inversion of selectivity.

Our results clearly show the effect that the pH value has on the rate and selectivity of the catalyzed reactions. Providing static-pH conditions is a must for performing meaningful mechanistic studies and for obtaining selective reactions.

Experimental Section

The pH of a solution of 0.2 M KCl (10 mL) kept at 60 °C was adjusted to the desired value (2–12) with HCl or KOH. Complex **3a** (40 mg) and **1** (50 mg) were dissolved in this solution under Ar. After equilibration, the Ar atmosphere was replaced by a H_2 atmosphere. During the dissolution and the hydrogenation of the complex the pH value was kept constant by delivering 0.2 M KOH with a Radiometer ABU 91 autoburette, and the extent of proton production in reaction (a) and (b) was calculated from the volume of added base. For recording the ^{1}H and ^{31}P NMR spectra of the final solutions (Bruker WP 360 SY, 50 °C), the solvent contained 20 % D_2O.

In a three-necked flask equipped with a reflux condenser a mixture of chlorobenzene (5 mL) and 0.2 M KCl (3 mL) buffered with Na_2HPO_4/NaH_2PO_4/HCl was purged for 15 min with H_2 at room temperature. Complex **3a** (10 mg) and **1** (12 mg) were added, and the mixture was heated to 80 °C under H_2. Following the appearance of the characteristic purple (**4a**) or yellow color (**5a**), cinnamaldehyde (50 μL) was added, and the mixture stirred vigorously. Samples of the organic phase were analyzed by gas chromatography (Chrom 5, Carbowax 20 M, 2-m packed column, 200 °C).

Received: August 13, 1997 [Z10810IE]
German version: *Angew. Chem.* **1998**, *110*, 1024–1026

Keywords: aldehydes · biphasic catalysis · homogeneous catalysis · hydrogenations · ruthenium · two-phase catalysis

[1] a) F. Joó, Á. Kathó, *J. Mol. Catal. A.* **1997**, *116*, 3–26; b) W. A. Herrmann, C. W. Kohlpaintner, *Angew. Chem.* **1993**, *105*, 1588–1609; *Angew. Chem. Int. Ed. Engl.* **1993**, *32*, 1524–1544; c) W. A. Herrmann in *Applied Homogeneous Catalysis with Organometallic Compounds* (Eds: B. Cornils, W. A. Herrmann), VCH, Weinheim, **1996**, pp. 575–601; d) *Aqueous Organometallic Chemistry and Catalysis* (Eds.: I. T. Horváth, F. Joó), Kluwer, Dordrecht, The Netherlands, **1995** (*NATO ASI Ser. 3/5*).

[2] a) A. Bényei, F. Joó, *J. Mol. Catal.* **1990**, *58*, 151–163; b) F.Joó, A. Bényei, *J. Organometal. Chem.* **1989**, *363*, C19–C21.

[3] a) R. A. Sánchez-Delgado, M. Medina, F. López-Linares, A. Fuentes, *J. Mol. Catal. A* **1997**, *116*, 167–177; b) A. Andriollo, J. Carrasquel, J. Mariño, F. A. López, D. E. Páez, I. Rojas, N. Valencia, *ibid.* **1997**, *116*, 157–165.

[4] J. M. Grosselin, C. Mercier, *J. Mol. Catal.* **1990**, *63*, L25–L27; J. M. Grosselin, C. Mercier, G. Allmang, F. Grass, *Organometallics* **1991**, *10*, 2126–2133.

[5] M. Hernandez, P. Kalck, *J. Mol. Catal. A* **1997**, *116*, 131–146.

[6] F. Joó, P. Csiba, A. Bényei, *J. Chem. Soc. Chem. Commun.* **1993**, 1602–1604

[7] H. Sertchook, D. Avnir, J. Blum, F. Joó, Á. Kathó, H. Schumann, R. Weimann, S. Wernik, *J. Mol. Catal. A* **1996**, *108*, 153–160

[8] [{HRuCl(tppms)$_2$}$_2$]: ^{1}H NMR: $\delta = -8.9$ (td, J(P,H) = 36 Hz, J(H,H) = 8 Hz); ^{31}P NMR: $\delta = 51.6$ (br s). **4a**: ^{1}H NMR: $\delta = -18.0$ (q, J(P,H) = 21 Hz); ^{31}P NMR: $\delta = 59.0$ (br s). **5a**: ^{1}H NMR: $\delta = -10.3$ (pseudo q, J(P,H) = 34 Hz); ^{31}P NMR: $\delta = 42.5$ (s), 53.2 (s). These data are in agreement with those in ref. [3a] and with those for analogous tppts complexes.[5, 9] The ^{1}H and ^{31}P NMR chemical shifts did not show a systematic change within pH 3 and 10.

[9] E. Fache, C. Santini, F. Senocq, J. M. Basset, *J. Mol. Catal.* **1992**, *72*, 337–350

Hemicarceplexes That Release Guests upon Irradiation**

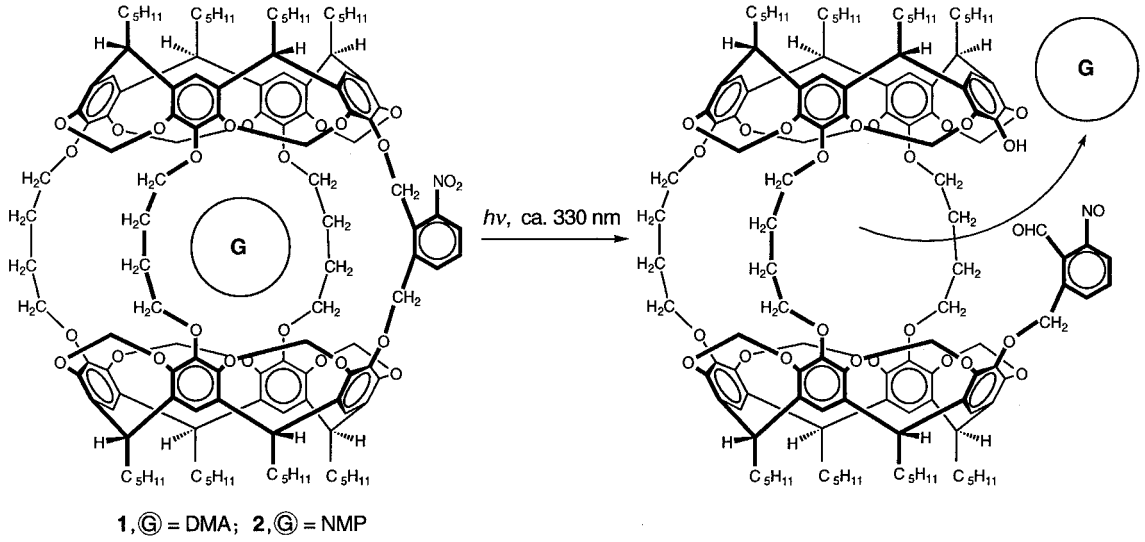
Evgueni L. Piatnitski and Kurt D. Deshayes*

In the last decade methodology has been developed primarily by Cram and Sherman to trap ("incarcerate") organic molecules within closed-shell organic molecules.[1, 2] The general term hemicarceplex was coined to describe a host for which it is possible to exchange encapsulated guests. When the kinetic barrier for guest entrance and egress is sufficiently high, hemicarceplexes are created which are stable indefinitely at room temperature, and extreme conditions are required to free the encapsulated guest.[3] However, useful systems for the delivery of chemical reagents or therapeutic agents should bind neutral species tightly, be chemically inactive with respect to the bound species, and release the

[*] Prof. Dr. K. D. Deshayes, E. L. Piatnitski
Department of Chemistry and Center for Photochemical Sciences
Bowling Green State University
Bowling Green, OH 43403 (USA)
Fax: (+1) 419-372-2460
E-mail: kdeshay@opie.bgsu.edu

[**] This work was supported by the donors to the Petroleum Research Foundation. E.L.P. would like to thank the McMaster foundation for a fellowship.

 © WILEY-VCH Verlag GmbH, D-69451 Weinheim, 1998 1433-7851/98/3707-0970 $ 17.50+.50/0



Scheme 1. Schematic representation of the photoinduced release of a guest molecule Ⓖ from a photoactive hemicarceplex.

bound species under definite, easily controlled conditions. We report here new photoactive complexes which are indefinitely stable at room temperature in the dark, but release guests upon irradiation.

Many examples are known where the hydrogen-abstraction reaction of the 2-nitrobenzyl group initiates bond cleavage that releases the substituent attached at the benzyl position.[4] Important applications of this chemistry range from photochemical release of adenosine triphosphate (ATP)[5] to the work of Grell and Warmuth,[6] in which a cryptand incorporating a 2-nitrobenzyl group releases alkali and alkaline earth cations upon irradiation. The concept of a photoactive carcerand is illustrated in Scheme 1. Irradiation leads to cleavage of one phenol ether bond with formation of a large gap in the host shell, through which the incarcerated guest can egress.[7]

The methodology of Cram[8] for creating hosts with mixed bridging units was used to synthesize complexes **1**, which contains a dimethyl acetamide (DMA) guest, and **2**, which contains a *N*-methyl-2-pyrrolidinone (NMP) guest. The position of the guest can easily be monitored by ^{1}H NMR spectroscopy: Upon encapsulation, the signals for the guest's protons (Table 1) are shifted upfield by over 2 ppm compared to the spectrum in chloroform solution. Although hemicarceplexes **1** and **2** are stable indefinitely at ambient temperature, the precursor, which contains only three butylene bridging units, does not retain a detectable amount of either DMA or NMP within its interior. It was believed that the photocleavage products of **1** and **2** would behave similarly.

From NMR spectroscopic studies, it is clear that the amount of released guest increases linearly with time until approximately 60 % of **1** or **2** are emptied. The results for **2** are shown in Figure 1. Once irradiation is stopped, guest release and photocleavage terminate in all cases. The cleavage reaction is independently monitored by the appearance of the proton signal for the photoproduct aldehyde at $\delta = 11.5$; the rate of appearance of the photoproduct corresponds to the rate of guest release. The rates of guest release for both hemicarceplexes show a linear dependence on light intensity, indicating that decomplexation is a single-photon process. This evidence supports a model in which excitation of the nitroxylyl group leads to bond cleavage, which removes the kinetic barrier to guest egress. The rate of DMA and NMP release are the same within experimental error, indicating that the portal formed is too large to retain guests containing six or seven heavy atoms.

A second class of photoactive hemicarceplexes with analogous thermal stability was constructed[9] in which all

Table 1. Selected data for compounds **1**–**3**.

1: ^{1}H NMR (400 MHz, $CDCl_3$): $\delta = 7.69$ (d, 1H; CH (nitroxylyl group)), 7.52 (d, 1H; CH (nitroxylyl group)), 7.40 (t, 1H; CH (nitroxylyl group)), 6.80 (m, 8H; CH (cage)), 5.74 (2d, 4H; H_{outer}), 5.68 (d, 2H; H_{outer}), 5.58 (d, 2H; H_{outer}), 5.28 (s, 2H; CH_2 (nitroxylyl group)), 5.14 (s, 2H; CH_2 (nitroxylyl group)), 4.66 (m, 8H; CH (methine)), 4.29 (d, 2H; H_{inner}), 4.22 (d, 2H; H_{inner}), 4.11 (d, 4H; H_{inner}), 3.85 (brs, 12H; α-CH_2 (tetrymethylene bridge)), 2.17 (brs, 16H; CH_2 (pentyl) and CH_3 (DMA)), 1.92 (m, 12H; β-CH_2 (tetrymethylene bridge)), 1.39 (m, 48H; $(CH_2)_3$ (pentyl)), 0.93 (q, 24H; CH_3 (pentyl)), −0.79 (s, 3H; CH_3 (DMA)), −1.89 (s, 3H; CH_3 (DMA)); FAB$^+$-MS for $[M^+]$: calcd 2157.121, found 2157.122; UV/Vis ($CHCl_3$): $\lambda_{max}(\varepsilon) = 276$ (5500)

2: ^{1}H NMR (400 MHz, $CDCl_3$): $\delta = 7.73$ (t, 2H; CH (nitroxylyl group)), 7.45 (t, 1H; CH (nitroxylyl group)), 6.80 (4s, 8H; CH (cage)), 5.74 (d, 4H; H_{outer}), 5,72 (d, 2H; H_{outer}), 5.50 (d, 2H; H_{outer}), 5.30 (s, 2H; CH_2 (nitroxylyl group)), 5.18 (s, 2H; CH_2 (nitroxylyl group)), 4.65 (m, 8H; CH (methine)), 4.26 (d, 2H; H_{inner}), 4.22 (2d, 4H; H_{inner}), 4.09 (d, 2H; H_{inner}), 3.85 (m, 12H; α-CH_2 (tetrymethylene bridge)), 2.16 (brs, 16H; CH_2 (pentyl)), 1.95 (brs, 12H; β-CH_2 (tetrymethylene bridge)), 1.80 (t, 2H; CH_2 (NMP)), 1.38 (m, 48H; 3CH_2 (pentyl)), 0.93 (q, 24H; CH_3 (pentyl)), −0.87 (t, 2H; CH_2 (NMP)), −1.10 (m, 5H; CH_2 and CH_3 (NMP)); FAB$^+$-MS for $[M^+]$: calcd 2169.121, found 2169.123; UV/Vis ($CHCl_3$): $\lambda_{max}(\varepsilon) = 276$ (5500)

3: ^{1}H NMR (400 MHz, $CDCl_3$): $\delta = 7.76$ (brd, 4H; CH (nitroxylyl group)), 7.50 (m, 8H; CH (nitroxylyl group)), 6.80 (2s, 8H; CH (cage)), 5.46 (d, 4H; H_{outer}), 5.30 (m, 14H; CH_2 (nitroxylyl group) and H_{outer}), 5.09 (m, 8H; CH_2 (nitroxylyl group)), 4.59 (m, 8H; CH (methine)), 4.00 (m, 8H; H_{inner}), 2.16 (brs, 16H; CH_2 (pentyl) and CH_3 (DMA)), 1.38 (m, 48H; 3CH_2 (pentyl)), 0.93 (q, 24H; CH_3 (pentyl)), −1.30 (m, 3H; CH_3 (DMA)), −1.26 (m, 3H; CH_3 (DMA)); FAB$^+$-MS for $[M^+ + H]$: calcd 2437.084, found 2437.084; UV/Vis ($CHCl_3$): $\lambda_{max}(\varepsilon) = 276$ (11900)

 © WILEY-VCH Verlag GmbH, D-69451 Weinheim, 1998 1433-7851/98/3707-0971 $ 17.50+.50/0

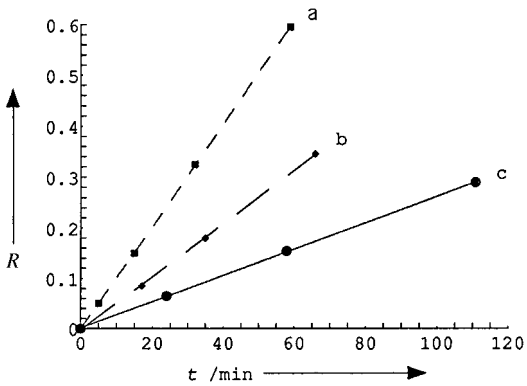
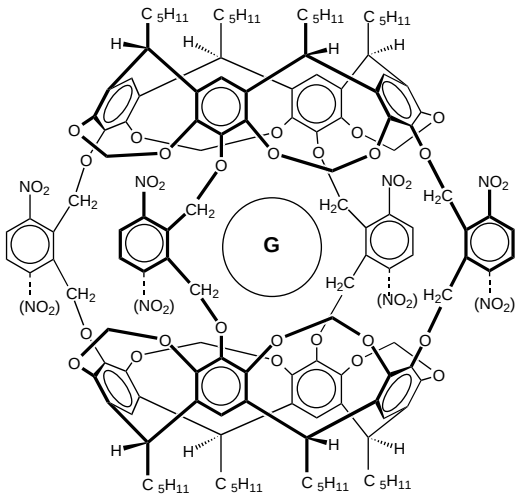


Figure 1. Ratio R of NMP released from **2** to total NMP plotted as a function of irradiation time at various light intensities: a) 2.6, b) 1.3, c) 0.65 W.

four bridging units incorporate the 3-nitro-*ortho*-xylyl functionality. Complex **3** exists as a mixture of inseparable isomers, as indicated by the complexity of the ^{1}H NMR spectrum (Table 1). The isomers differentiate themselves by the relative positions of the nitro groups around the middle of



3, G = DMA

the host (this is symbolized in the drawing by a dashed line between the benzene ring and the NO_2 group in parentheses). The photochemical properties of the four possible isomers are expected to be the same since the number of photoactive groups is equivalent in each case, and each 3-nitro-ortho-xylyl group is believed to react independently.

The absorption of the cage partially masks the absorption of the nitroxylyl groups in the region of the spectrum that was irradiated.[7] However, in the region of maximum light filter transmittance, at approximately 330 nm, the contribution of the nitroxylyl absorption is greater than that of the rest of the host and shows a significant increase when the number of nitroxylyl groups is increased. For example, the extinction coefficient ε in chloroform at 330 nm is $1055\,\text{M}^{-1}\text{cm}^{-1}$ for **1** and **2**, and $2950\,\text{M}^{-1}\text{cm}^{-1}$ for **3**. When solutions with equal concentrations of **1**, **2**, and **3** in chloroform were irradiated, the rate of guest release for **3** is 3.2 times faster than for **1** and **2**. It appears that the introduction of additional nitroxylyl groups increases the probability of a photochemical reaction leading to guest egress. The rate of guest release from **3** also increases linearly with light intensity, showing that guest release is a single-photon process and strongly suggesting that guest release occurs upon a single bond cleavage. In summary, all the photoactive hosts described here release guests into chloroform solution upon irradiation, and the rate of guest release can be controlled by modifying either host absorption or light intensity.

All hemicarceplexes discussed here undergo slow decomplexation when exposed to ambient light over long periods of time, but are stable indefinitely when kept in the dark. Hosts **1**, **2**, and **3** have broad absorption spectra ranging from 240 to 460 nm. A slow photochemical reaction may result from absorption of near-UV and visible light, even if that of the latter is very small. The thermal stability and photoactivity of these hemicarceplexes indicate that incarceration is potentially useful for the controlled delivery of chemical agents. An extension of this work to other hosts, including those which are soluble in aqueous solutions, is currently underway in our laboratory.

Received: September 8, 1997
Revised version: November 10, 1997 [Z10904IE]
German version: *Angew. Chem.* **1998**, *110*, 1022 – 1024

Keywords: cage compounds · drug delivery · host – guest chemistry · photochemistry

[1] D. J. Cram, J. M. Cram, *Container Molecules and Their Guests*, Royal Society of Chemistry, Cambridge, **1994**.
[2] R. G. Chapman, N. Chopra, E. D. Cochien, J. C. Sherman, *J. Am. Chem. Soc.* **1994**, *116*, 369.
[3] T. A. Robbins, C. B. Knobler, D. R. Bellew, D. J. Cram, *J. Am. Chem. Soc.* **1994**, *116*, 111.
[4] V. N. R. Pillai in *Organic Photochemistry, Vol. 9* (Ed.: A. Padwa), Marcel Decker, New York, **1987**, pp. 225.
[5] J. A. McGray, D. R. Trentham, *Annu. Rev. Biophys. Chem.* **1989**, *18*, 239.
[6] E. Grell, R. Warmuth, *Pure Appl. Chem.* **1993**, *65*, 373.
[7] All irradiation experiments were carried out with a xenon lamp and a light filter having transmittance between 280 and 390 nm with a maximum at 330 nm.
[8] S. K. Kurdistani, R. C. Helgeson, D. J. Cram, *J. Am. Chem. Soc.* **1995**, *117*, 1659.
[9] D. J. Cram, M. T. Blanda, K. Paek, C. B. Knobler, *J. Am. Chem. Soc.* **1992**, *114*, 7765.

 © WILEY-VCH Verlag GmbH, D-69451 Weinheim, 1998 1433-7851/98/3707-0972 $ 17.50+.50/0

Total Synthesis of Terprenin, a Highly Potent and Novel Immunoglobulin E Antibody Suppressant**

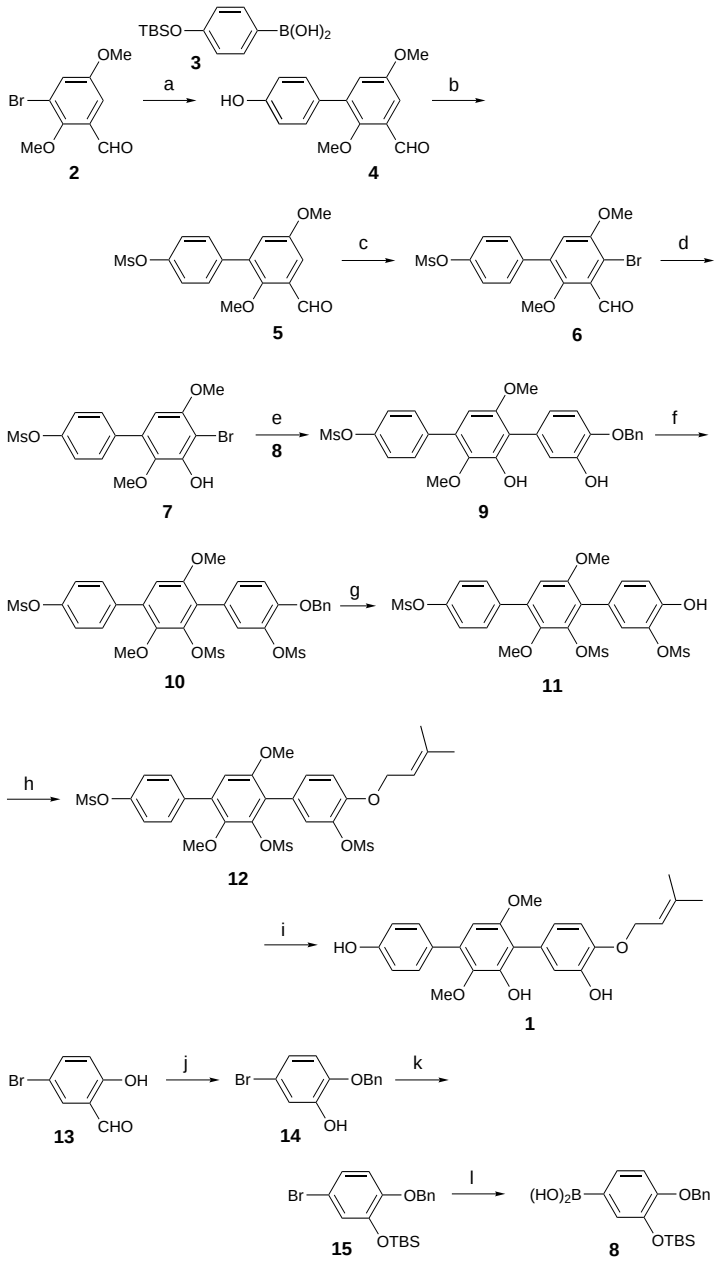
Kenji Kawada,* Akinori Arimura, Tatsuo Tsuri, Masahiro Fuji, Tadafumi Komurasaki, Shuji Yonezawa, Akira Kugimiya, Nobuhiro Haga, Susumu Mitsumori, Masanao Inagaki, Takuji Nakatani, Yoshinori Tamura, Shozo Takechi, Teruhiko Taishi, Junji Kishino, and Mitsuaki Ohtani*

Immunoglobulin E (IgE) antibody is known to play a central role in allergic diseases such as atopic dermatitis, bronchial asthma, allergic rhinitis, allergic conjunctivitis, and anaphylaxis; these disorders are caused by the binding of antigens to specific IgE on mast cells and/or basophiles.[1] Thus, an effective orally active IgE suppressant would be of considerable therapeutic value. FK506 and cyclosporin A are known to be strong immunosuppressants, but they potentiate IgE production in mice.[2] At present, no potent clinically useful IgE suppressant is available.[3]

In the course of our screening program aimed at new immunosuppressants from natural products, terprenin (**1**, see Scheme 1), a highly oxygenated terphenyl compound with a prenyloxy side chain, was discovered in the fermentation broth of *Aspergillus candidus*. The structure of terprenin was established on the basis of spectral data and an X-ray crystallographic analysis.[4]

Terprenin exhibits a remarkable suppressive effect on the in vitro IgE production of human lymphocytes stimulated with anti-CD40 and IL-4 (IC_{50} value of 0.18 nM). In contrast, FK506 shows little or no inhibition even at the high concentration of 1000 nM. The effects of terprenin on in vivo IgE synthesis were examined by immunization of mice by an intraperitoneal injection of ovalbumin (OVA) with alum. Antiserum was collected, and the anti-OVA IgE antibody titer was determined by passive cutaneous anaphylaxis on rats for 24 h. Terprenin was found to suppress antigen-specific IgE production in mice by oral administration in a dose-dependent manner. Even after immunization with OVA, when the IgE value had reached a high level, terprenin exhibited a significant suppressive effect at 20 and 40 mg kg^{-1} without any toxicological signs. FK506, unlike terprenin, enhanced the IgE level at low doses (0.1 – 3 mg kg^{-1}) and showed toxicity at 10 mg kg^{-1} in the form of decrease in body weight and thymus weight.

We describe here the first two total syntheses of terprenin, which permit highly efficient and practical production of this important natural product. The strategy for constructing the terphenyl skeleton was based on two Suzuki reactions,[5] in one case stepwise (first synthesis, see Scheme 1) and in the other as a one-pot reaction (second synthesis, see Scheme 2). Regioselective functionalization of the aromatic ring in the starting material 3-bromo-2,5-dimethoxybenzaldehyde (**2**)[6] was considered to be the crucial step. Because of the characteristic palladium-catalyzed elimination reaction of allylic phenyl ethers[7] as well as the instability of the prenyloxy group under acidic and hydrogenous conditions,[8]



Scheme 1. First synthesis of terprenin (**1**). a) [$Pd(PPh_3)_4$], 2 M Na_2CO_3, DME, EtOH (100 %); b) MsCl, Et_3N, CH_2Cl_2 (94 %); c) Br_2, NaOAc, HOAc (81 %); d) MCPBA, CH_2Cl_2 followed by 4 N HCl, dioxane (85 %); e) [$Pd(PPh_3)_4$], 2 M Na_2CO_3, DME, EtOH; f) MsCl, Et_3N, CH_2Cl_2 (68 % for steps e and f); g) H_2, $Pd(OH)_2$/C, dioxane (92 %); h) prenyl bromide, K_2CO_3, DMF (99 %); i) 3 N KOH, dioxane, MeOH (97 %); j) ref. [11]; k) TBSCl, imidazole, DMF (90 %); l) *n*BuLi, $B(OiPr)_3$, THF followed by H_2O (64 %). DME = dimethoxyethane, DMF = dimethylformamide, MCPBA = 3-chloroperoxybenzoic acid, Ms = mesyl, TBS = *tert*-butyldimethylsilyl.

[*] Dr. K. Kawada, Dr. M. Ohtani, Dr. A. Arimura, Dr. T. Tsuri, Dr. M. Fuji, T. Komurasaki, S. Yonezawa, A. Kugimiya, Dr. N. Haga, S. Mitsumori, M. Inagaki, Dr. T. Nakatani, Y. Tamura, Dr. S. Takechi, T. Taishi, Dr. J. Kishino
Shionogi Research Laboratories, Shionogi & Co., Ltd.
Fukushima-ku, Osaka 553 (Japan)
Fax: (+81) 6-458-0987

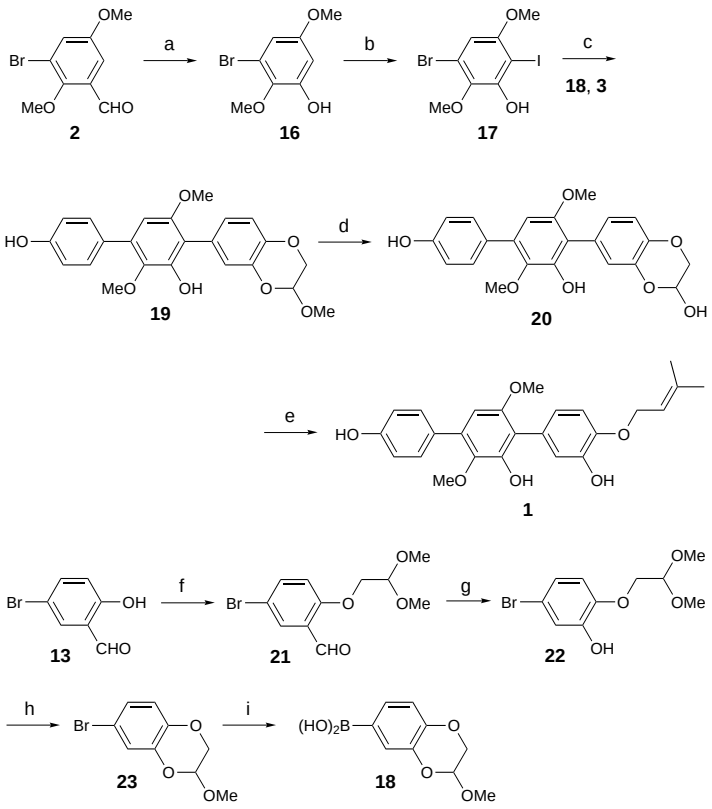
[**] We wish to thank Dr. H. Arita for his encouragement and valuable advice, Dr. R. Suzuki for biological discussions, and Dr. T. Konoike for large-scale preparations.

we decided that construction of the side-chain moiety should be the last step in the synthetic sequence. It was also necessary for us to be able to discriminate between six oxygen functionalities with the aid of appropriate protecting groups.

In the first synthesis (Scheme 1), bromobenzaldehyde **2** underwent a Suzuki reaction with boronic acid **3**[9] to give the biphenyl product almost quantitatively. The TBS-protected phenol was cleaved in the presence of water to produce phenol derivative **4**.[10] After protection of **4** as mesylate **5**, bromination with molecular bromine led exclusively to regioselective functionalization and the desired bromide **6**. Next, the formyl group of **6** was converted into a hydroxy group by Baeyer–Villiger oxidation. Suzuki reaction of the sterically hindered bromide **7** with boronic acid **8**, readily prepared from 5-bromosalicylaldehyde (**13**),[11] proceeded smoothly to afford the expected terphenyl compound **9**. After completion of the terphenyl skeleton, the free hydroxy groups of **9** were protected as mesylates **10**, chosen because they would be susceptible to removal under basic conditions. Other protecting groups such as acetyl or silyl groups were considered impractical because they would have migrated to the free hydroxy groups produced in the subsequent hydrogenolysis step. After cleavage of the benzyl ether functionality of **10** by hydrogenolysis, a prenyl group was introduced at the desired position in terphenyl compound **11** by reaction with prenyl bromide. Finally, removal of the mesyl groups of **12** with potassium hydroxide completed the first total synthesis of terprenin. The synthetic material was identical in all respects to the natural product from *Aspergillus candidus*, including biological activity.

The advantage of this synthesis is its applicability to large-scale production. The overall yield from **2** was 40%, and no chromatographic steps were required because of the high yield at each step; each product was purified by simple crystallization.

The second total synthesis (Scheme 2) was based on a one-pot process involving two successive Suzuki reactions. To ensure the desired regioselectivity, a functionality other than bromine was required in the *para* position of the starting material, bromobenzaldehyde **2**. Because iodination of **2** did not proceed selectively, the aldehyde was converted into phenol **16**. Treatment of **16** with iodine in the presence of *tert*-butylamine led to regioselective iodination and the desired iodide **17** in 92% yield.[12] Although the iodine atom in **17** is located at a more sterically hindered position than the bromine atom, boronic acid **18**, conveniently prepared from **13**, reacted preferentially at the iodine-substituted position with $[Pd_2(dba)_3]$ as catalyst. The Suzuki reaction in this case proceeded rather sluggishly and unselectively with $[Pd(PPh_3)_4]$ as catalyst. Without isolation of the biphenyl compound, boronic acid **3** and $[Pd(PPh_3)_4]$ were added to the reaction mixture, and the expected terphenyl compound **19** was obtained in 70% yield. Hydrolysis of the protected hemiacetal in **19** with *p*-toluenesulfonic acid in aqueous acetone followed by a Wittig reaction of **20** with excess isopropyltriphenylphosphonium iodide afforded terprenin (**1**) in 87% yield. Since this second synthesis does not require protection–deprotection of phenol groups, the synthetic sequence is sufficiently short for efficient production of terprenin by this route as well.



Scheme 2. Second synthesis of terprenin (**1**). a) MCPBA, CH_2Cl_2 followed by 1N KOH, MeOH (81%); b) I_2, tBuNH$_2$, toluene (92%); c) $[Pd_2(dba)_3]$, 2M Na_2CO_3, DME, EtOH followed by $[Pd(PPh_3)_4]$ (70%); d) *p*-TsOH, H_2O, acetone (83%); e) $[Ph_3PCHMe_2]I$, nBuLi, THF (87%); f) 2-bromo-1,1-dimethoxyethane, K_2CO_3, DMF (92%); g) MCPBA, EtOAc followed by 1N NaOH; h) *p*-TsOH, CH_2Cl_2, MeOH (70% for steps g and h); i) nBuLi, B(OiPr)$_3$, THF followed by H_2O (60%). dba = dibenzylideneacetone, Ts = 4-methylphenylsulfonyl (tosyl).

We have thus developed two practical syntheses of terprenin (**1**), a potent IgE antibody suppressant. Sufficient supplies of this important natural product should now become available to aid in the development of a new type of antiallergic drug as well as in the clarification of its interesting mechanism of action.

Received: December 8, 1997 [Z11235IE]
German version: *Angew. Chem.* **1998**, *110*, 1015–1017

Keywords: cross-coupling · immunosuppressants · natural products · terprenin · total synthesis

[1] General review: M. Plant, E. M. Zimmerman in *Fundamental Immunology* (Ed.: W. E. Pawl), 3rd ed., Raven, New York, **1993**, pp. 1399–1425.
[2] H. Nagai, H. Hiyama, A. Matsuo, Y. Ueda, N. Inagaki, K. Kawada, *J. Pharmacol. Exp. Ther.* **1997**, *283*, 321–327.
[3] Although splatast has been approved recently in Japan as an antiallergic drug with a suppressive effect on IgE production, its clinical effect remains obscure.
[4] Fermentation, isolation, and structure determination: T. Kamigauchi, R. Sakazaki, K. Nagashima, Y. Kawamura, Y. Yasuda, K. Matsushima, H. Tani, Y. Takahashi, K. Ishii, R. Suzuki, K. Koizumi, H. Nakai, Y. Ikenishi, Y. Terui, *J. Antibiot.*, submitted.
[5] Comprehensive review: N. Miyaura, A. Suzuki, *Chem. Rev.* **1995**, *95*, 2457–2483.
[6] L. Rubenstein, *J. Chem. Soc.* **1925**, 1998–2004.

 © WILEY-VCH Verlag GmbH, D-69451 Weinheim, 1998 1433-7851/98/3707-0974 $ 17.50+.50/0

[7] Palladium-catalyzed hydrogenolysis of allylic compounds: J. Tsuji, T. Mandai, *Synthesis* **1996**, 1–24.
[8] About 50% of the prenyl groups in terprenin were cleaved upon treatment with 3% trifluoroacetic acid in MeOH/H_2O for 1 h at 25 °C.
[9] A. W. Oxford, J. W. Clitherow (Glaxo), GB-B 2276162 A, **1994** [*Chem. Abstr.* **1994**, *121*, 300771z].
[10] A similar reaction has been reported recently; see N. S. Wilson, B. A. Keay, *Tetrahedron Lett.* **1996**, *37*, 153–156.
[11] Synthesis of **14**: a) U. Schmidt, R. Meyer, V. Leitenberger, H. Griesser, A. Lieberknecht, *Synthesis* **1992**, 1025–1030; b) K. Suzuki, N. Satake, A. Sugiura, T. Fujii (Kanto Kagaku), JP-B 5-213930, **1993** [*Chem. Abstr.* **1994**, *120*, 134493t].
[12] For related *ortho*-bromination of phenols, see a) D. E. Pearson, R. D. Wysong, C. V. Breder, *J. Org. Chem.* **1967**, *32*, 2358-2360; b) S. Fujisaki, H. Eguchi, A. Omura, A. Okamoto, A. Nishida, *Bull. Chem. Soc. Jpn.* **1993**, *66*, 1576–1579.

A Molecular Chameleon: Chromophoric Sensing by a Self-Complexing Molecular Assembly**

Reinhard Wolf, Masumi Asakawa, Peter R. Ashton, Marcos Gómez-López, Christoph Hamers, Stephan Menzer, Ian W. Parsons, Neil Spencer, J. Fraser Stoddart,* Malcolm S. Tolley, and David J. Williams*

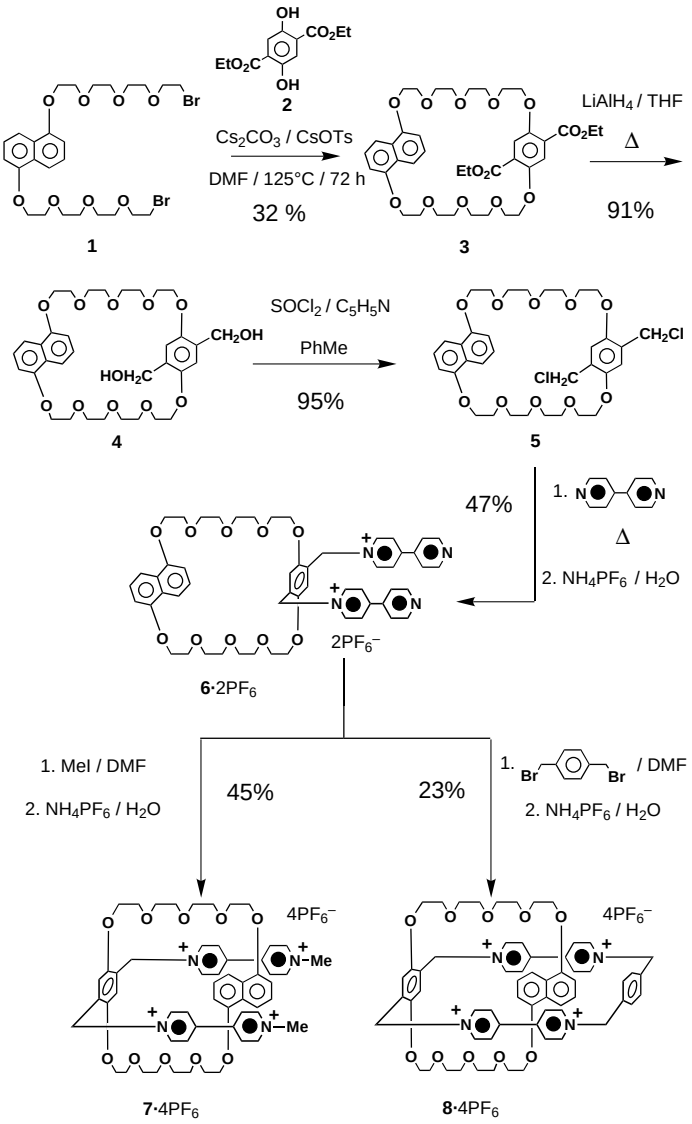
In supramolecular chemistry[1]—the domain of chemistry where noncovalent bonding interactions[2] become important—the concept of self-assembly[3] is being increasingly exploited to create molecular-based architectures at the nanoscale level. Over the last decade, numerous researchers have harnessed the power of the noncovalent bond to produce aesthetically pleasing molecular assemblies[4] as well as supramolecular arrays. In recent years, we have employed the molecular recognition[2] that exists between π electron rich aromatic rings (e.g. hydroquinone, 1,5-dioxynaphthalene) and π electron deficient aromatic units (e.g. bipyridinium, diazapyrenium) coupled with C–H···O and O–H···π interactions to assist in the self-assembly of catenanes,[5] rotaxanes,[6] and pseudorotaxanes.[7]

[*] Prof. J. F. Stoddart,[+] Dr. R. Wolf, Dr. M. Asakawa, P. R. Ashton, Dr. M. Gómez-López, Dr. C. Hamers, Dr. I. W. Parsons, Dr. N. Spencer, M. S. Tolley
School of Chemistry
University of Birmingham
Edgbaston, Birmingham B15 2TT (UK)
Prof. D. J. Williams, Dr. S. Menzer
Chemical Crystallography Laboratory
Department of Chemistry, Imperial College
South Kensington, London SW7 2AY (UK)
Fax: (+44) 171-594-5804
[+] Current address:
Department of Chemistry and Biochemistry
University of California at Los Angeles
405 Hilgard Avenue, Los Angeles, CA 90095 (USA)
Fax: (+1) 310-206 1843
E-mail: stoddart@chem.ucla.edu

[**] We thank the Eusko Jaurlaritza Unibersitate, Hizkuntza, eta Ikerketa Saila in the Basque Country (Spain) for the award of a predoctoral fellowship (to M.G.-L). The research was funded in the UK by the Engineering and Physical Sciences Research Council.

Here we report the four-step synthesis of an intermediate dicationic salt $\mathbf{6}\cdot 2PF_6$ (see Scheme 1), and the potential of the AB_2-type[8] monomeric tetracation $\mathbf{7}^{4+}$ possessing complementary recognition sites, which is easily obtained from $\mathbf{6}\cdot 2PF_6$, to self-assemble in the shape of a polysupramolecular dendritic wedge (see Scheme 2a).[9] Furthermore, we report on a related attempt to construct from $\mathbf{6}\cdot 2PF_6$ a polycatenane that is reminiscent of an anchor chain; however, the fascinating macrobicyclic tetracation $\mathbf{8}^{4+}$ is formed instead. It is composed of two complementary macrocycles linked together by a common aromatic ring in a manner that allows it to display an intriguing kind of self-complexation,[10] as demonstrated in solution by ^1H NMR spectroscopy and in the solid state by X-ray crystallography. We also describe how $\mathbf{8}^{4+}$ can act in a novel fashion as a chromophoric receptor[11] for tetrathiafulvalene (TTF; see Scheme 3), giving the macrobicyclic tetracation molecular switching[12] properties.

Scheme 1 outlines the synthesis of the key intermediate $\mathbf{6}\cdot 2PF_6$.[13] Reaction of the dibromide **1**[7] with the diester **2**



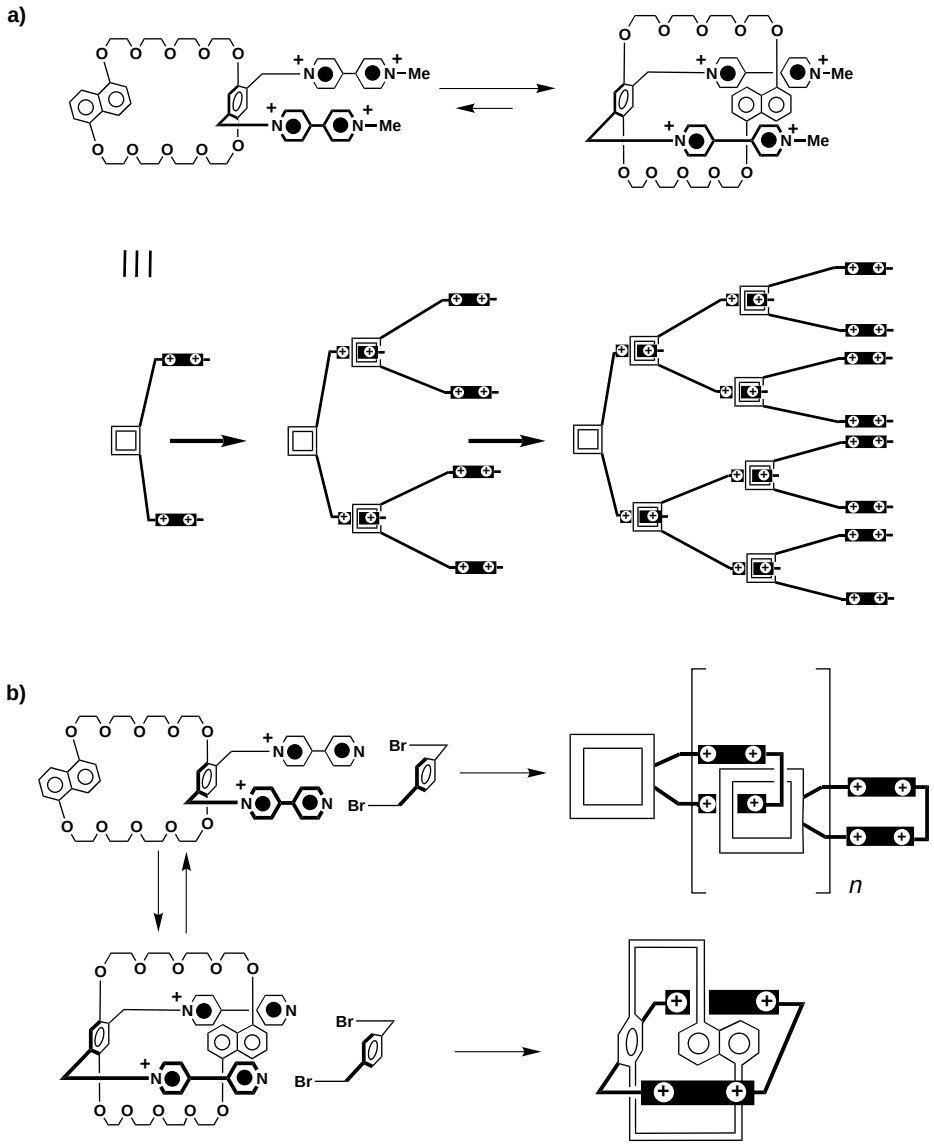
Scheme 1. The synthesis of the crown ether derivative $\mathbf{7}\cdot 4PF_6$ and the self-assembly of the self-complexing macrobicycle $\mathbf{8}\cdot 4PF_6$. Ts = toluenesulfonyl.

 © WILEY-VCH Verlag GmbH, D-69451 Weinheim, 1998 1433-7851/98/3707-0975 $ 17.50+.50/0

afforded the crown ether **3**. The ester groups in **3** were reduced to give the bis(hydroxymethyl) derivative **4**, which was converted into the corresponding dichloride **5**. Reaction of **5** with 4,4′-bipyridine yielded $\mathbf{6}\cdot 2PF_6$ after counterion exchange. Reaction of this salt with an excess of MeI afforded $\mathbf{7}\cdot 4PF_6$. The template-directed synthesis of $\mathbf{8}\cdot 4PF_6$ was achieved in 23% yield by the reaction of $\mathbf{6}\cdot 2PF_6$ with 1,4-bis(bromomethyl)benzene followed by counterion exchange.

Since the signals in the ^{1}H NMR spectra of $\mathbf{7}\cdot 4PF_6$ recorded in CD_3CN at 304 K show only marginal concentration dependences in a range from 2.76×10^{-2} to 6.10×10^{-4} M, it seems unlikely that dendritic supramolecular arrays, such as those shown in Scheme 2a, are being formed to any significant extent. Comparison of the ^{1}H NMR chemical shifts of $\mathbf{7}\cdot 4PF_6$ with those of model compounds suggests very strongly that $\mathbf{7}^{4+}$ adopts a conformation[13] in CD_3CN in which its 1,5-dioxynaphthalene ring system is sandwiched by its own bipyridinium units (Scheme 2a). Given this situation, it is perhaps hardly surprising that $\mathbf{6}^{2+}$ reacts with 1,4-bis(bromomethyl)benzene to give $\mathbf{8}^{4+}$ as the exclusive catenated product. In fact, no oligocatenanes in the series of the anchor-chain-like polycatenane (see Scheme 2b) appeared to be formed during this reaction. Nonetheless, the macrobicyclic tetracation is a fascinating self-complexing species in its own right. In this communication we report its structure and demonstrate its chameleonlike[14] properties.

The X-ray analysis[15] of a crystal obtained by vapor diffusion of iPr$_2$O into a solution of $\mathbf{8}\cdot 4PF_6$ in acetone revealed that the salt crystallized in a space group that imposes a crystallographic inversion center in the middle of the 1,5-dioxynaphthalene ring, thus requiring the structure to be disordered (Figure 1). However, two alternative orientations for the polyether linkages were clearly resolved, thereby permitting a straightforward analysis of the crystal structure.



Scheme 2. Schematic representation of a) a supramolecular dendrimer derived from $\mathbf{7}^{4+}$ and b) a polycatenane or macrobicycle derived from $\mathbf{6}^{2+}$ and 1,4-bis(bromomethyl)benzene.

 © WILEY-VCH Verlag GmbH, D-69451 Weinheim, 1998 1433-7851/98/3707-0976 $ 17.50+.50/0

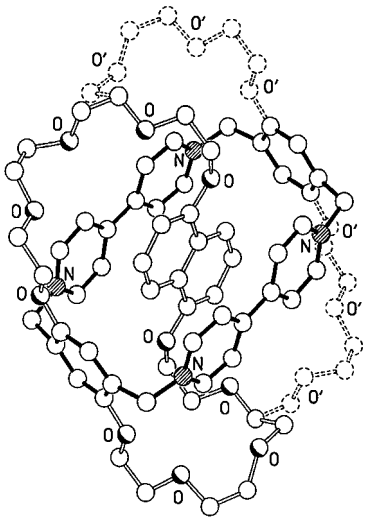
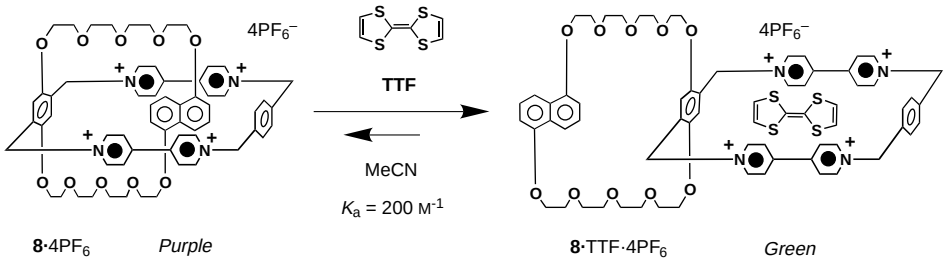


Figure 1. The solid-state structure of $\mathbf{8}^{4+}$. The broken bonds and atoms indicate alternative symmetry-imposed orientations for the polyether linkages.

The 1,5-dioxynaphthalene ring is sandwiched in a conventional manner between the two bipyridinium units[16] (mean interplanar separation 3.35 Å). The O-$C_{10}H_6$-O vector is inclined by 52° to the mean plane of the cyclophane component (as defined by the four methylene carbon atoms). The overall conformation is stabilized by π–π stacking interactions and by C–H···O hydrogen bonds involving the α- and β-bipyridinium hydrogen atoms of one of the pyridinium rings and the second and third oxygen atoms of one of the polyether linkages. The associated C···O and H···O distances are 3.25 and 2.38 Å, respectively, for the α-bipyridinium hydrogen atom and 3.28 and 2.38 Å, respectively for the β-bipyridinium hydrogen atom; the corresponding C–H···O angles are 150° and 157°. In addition, there are C–H···π interactions between the naphthalene hydrogen atoms on C-4 and C-8 and their proximal *p*-xylyl rings (the distance between the H atom and the π electron plane is 2.56 Å, and the C–H···π angle 150°). There are no intermolecular stacking interactions.

Although the resonances in the ^{1}H NMR spectrum of $\mathbf{8}\cdot 4PF_6$ recorded in CD_3CN at 304 K are very broad, they become sharp on cooling the sample down to 233 K. All the protons which are nonequivalent in the tetracation have been assigned with the aid of two-dimensional COSY and NOESY techniques. For example, eight signals[17] can be observed for the α- and β-bipyridinium protons, and the chemical shifts for the H-4 and H-8 protons on the 1,5-dioxynaphthalene ring system resonate at very high field ($\delta = 2.14$, 2.67). This indicates that the ring system is located inside the tetracationic cyclophane, as in the solid-state structure. The resonances for these protons coalesce at 309 K (T_c) as a result of a site-exchange process in which the 1,5-dioxynaphthalene ring system leaves the cavity of the tetracationic cyclophane by a process that involves rotation about the -$CH_2C_6H_2R_2CH_2$- axis of the disubstituted *p*-xylyl residue, undergoes a reorientation as a result of a pedalling motion about the axis defined by the naphthalene ring junction, and reenters the cavity of the tetracationic cyclophane. The free energy of activation $\Delta G_c^{\neq}$ for this process[18] was calculated[19] from the k_c value of 490 s^{-1} to be 14.3 ± 0.1 kcal mol^{-1}.

Addition of one molar equivalent of TTF to the solution of $\mathbf{8}\cdot 4PF_6$ in CD_3CN (Scheme 3) results in a dramatic change in the color of the solution from purple to green. This reflects a shift in the absorbance maximum, corresponding to the charge-transfer band associated with donor–acceptor interactions, from $\lambda_{max} = 537$ nm (when the 1,5-dioxynaphthalene ring system is the donor) to $\lambda_{max} = 846$ nm (when TTF is the donor). Spectrophotometric titration[20] of TTF with $\mathbf{8}\cdot 4PF_6$ in acetonitrile afforded a K_a value[21] of $200 \pm 10\ M^{-1}$ for the 1:1 complex $[\mathbf{8}\cdot TTF]\cdot 4PF_6$. The ^{1}H NMR spectrum of this complex recorded in CD_3CN displays signals at $\delta = 6.57$, 7.25, and 7.53 for the naphthalene ring protons, indicating that the



Scheme 3. The formation of the intermolecular 1:1 complex between $\mathbf{8}\cdot 4PF_6$ and tetrathiafulvalene (TTF) illustrates how the self-complexing macrobicycle acts as a chromophoric receptor.

1,5-dioxynaphthalene ring system has been expelled from the cavity and is rotating freely about the naphthalene ring junction axis. By contrast, the TTF ring protons resonate in the spectrum as a singlet at $\delta = 5.68$, which reflects their being shielded within the cavity of the tetracationic cyclophane. The switching action[22] between a molecular state and a supramolecular one is characterized by its efficiency and simplicity.

It is clear from the results reported here that the principle of maximum site occupancy[1] along with unfavorable entropy factors[3, 23] will always conspire, in the case of compounds like $\mathbf{7}\cdot 4PF_6$ and $\mathbf{8}\cdot 4PF_6$, against the formation of extended supramolecular arrays and large molecular assemblies. To favor their formation, self-complexation[24] has to be avoided at all costs.

Experimental Section

$\mathbf{6}\cdot 2PF_6$: The crown ether **5** (200 mg, 0.29 mmol) was added to a solution of 4,4′-bipyridine (940 mg, 6.0 mmol) in dry MeCN (120 mL). The reaction mixture was heated under reflux for 14 h. After evaporation of the solvent the mixture was purified by column chromatography (SiO_2, MeOH/$MeNO_2$/2 M NH_4Cl aq 7/1/2). Counterion exchange (NH_4PF_6/H_2O) produced a yellow solid precipitate, which was dried in vacuo to afford $\mathbf{6}\cdot 2PF_6$ as a yellow powder (165 mg, 47 %). M.p. > 270 °C (decomp); FAB-MS: *m*/*z* (%) = 1214 (5) [M^+], 1069 (100) [$M - PF_6$]$^+$; ^{1}H NMR (400 MHz, CD_3CN, 25 °C): $\delta = 8.90$ (d, $J = 7$ Hz, 4H), 8.78 (br s, 4H), 8.08 (d, $J = 7$ Hz, 4H), 7.66 (br s, 4H), 7.53 (d, $J = 8$ Hz, 2H), 7.06 (t, $J = 8$ Hz, 2H), 6.61 (d, $J = 8$ Hz, 2H), 6.56 (s, 2H), 5.65 (d, $J = 14$ Hz, 2H), 5.19 (d, $J = 14$ Hz, 2H),

 © WILEY-VCH Verlag GmbH, D-69451 Weinheim, 1998 1433-7851/98/3707-0977 $ 17.50+.50/0

3.60 – 4.17 (m, 32H); ^{13}C NMR (100.6 MHz, CD_3CN, 25 °C): $\delta = 150.5$, 147.5, 147.2, 147.8, 143.7, 139.1, 133.1, 132.7, 132.6, 129.7, 129.6, 127.6, 127.3, 126.2, 115.5, 114.9, 106.1, 77.1, 70.8, 70.6, 70.2, 70.1, 69.4, 69.1, 68.6, 52.5; HR-MS (LSI-MS) calcd for $C_{54}H_{60}N_4O_{10}PF_6$ $[M - PF_6]^+$: 1069.3951, found: 1069.3988.

7·4PF$_6$: The salt **6**·2PF$_6$ (35 mg, 0.029 mmol) was dissolved in MeCN (20 mL). MeI (100 mg, 0.70 mmol) was added, and the mixture heated under reflux for 14 h. The solvent of the dark red solution was evaporated in vacuo. The reaction mixture was purified by column chromatography (SiO_2; MeOH/$MeNO_2$/2 M NH_4Cl aq 7/1/2 and then original eluent/DMF 3/1). Counterion exchange (NH_4PF_6/H_2O) yielded a red solid, which was isolated by filtration and washed with H_2O. The solid was dried in vacuo to afford **7**·4PF$_6$ as a brown powder (20 mg, 45 %). M.p. > 270 °C (decomp); FAB-MS: $m/z = 1557$ $[M+Na]^+$, 1534 $[M^+]$, 1389 $[M - PF_6]^+$, 1245 $[M - 2PF_6]^+$, 1100 $[M - 3PF_6]^+$; ^{1}H NMR (400 MHz, CD_3CN, 25 °C): $\delta = 9.07$ (d, $J = 7$ Hz, 4H), 8.73 (d, $J = 7$ Hz, 4H), 8.20 (d, $J = 7$ Hz, 4H), 8.14 (d, $J = 7$ Hz, 4H), 7.40 (d, $J = 8$ Hz, 2H), 6.97 (s, 2H), 6.86 (t, $J = 8$ Hz, 2H), 6.50 (d, $J = 8$ Hz, 2H), 5.70 (d, $J = 14$ Hz, 2H), 5.30 (d, $J = 14$ Hz, 2H), 4.35 (s, 6H), 3.60 – 4.17 (m, 32H;); ^{13}C NMR (100.6 MHz, CD_3CN, 25 °C): $\delta =$ 158.8, 154.7, 151.8, 150.2, 147.5, 147.1, 127.6, 127.2, 126.8, 126.1, 124.3, 115.8, 114.9, 106.1, 70.9, 70.6, 70.4, 70.0, 69.9, 69.2, 68.9, 68.6, 61.7, 49.5, 30.9; HR-MS (LSI-MS) calcd for $C_{56}H_{66}N_4O_{10}P_1F_6$ $[M - 3PF_6]^+$: 1099.4421, found: 1099.4449.

8·4PF$_6$: The salt **6**·2PF$_6$ (81 mg, 0.067 mmol) was dissolved in MeCN (10 mL). 1,4-Bis(bromomethyl)benzene (19 mg, 0.072 mmol) was added, and the reaction mixture stirred at room temperature for 26 d. The dark purple solution was concentrated in vacuo, and the reaction mixture purified by column chromatography (SiO_2; MeOH/$MeNO_2$/2 M NH_4Cl aq 7/1/2 and then original eluent/DMF 2/1). Counterion exchange (NH_4PF_6/H_2O) produced a dark purple solid, which was isolated by filtration and washed with H_2O. The solid was dried in vacuo to afford **8**·4PF$_6$ as a purple powder (25 mg, 23 %). M.p. > 270 °C (decomp); FAB-MS: $m/z = 1632$ $[M+Na]^+$, 1609 $[M]^+$, 1463 $[M - PF_6]^+$, 1318 $[M - 2PF_6]^+$, 1173 $[M - 3PF_6]^+$; ^{1}H NMR (400 MHz, CD_3CN, −40 °C): $\delta = 9.19$ (d, $J = 7$ Hz, 1H), 9.14 (d, $J = 7$ Hz, 1H), 8.80 (d, $J = 7$ Hz, 1H), 8.77 (d, $J = 7$ Hz, 1H), 8.76 (d, $J = 7$ Hz, 1H), 8.68 (d, $J = 7$ Hz, 1H), 8.63 (d, $J = 7$ Hz, 1H), 8.50 (d, $J = 7$ Hz, 1H), 7.98 (s, 2H), 7.92 (s, 2H), 7.91 (s, 1H), 7.48 (dd, $J = 7$, 2 Hz, 1H), 7.40 (dd, $J = 7$, 2 Hz, 1H), 7.34 (dd, $J = 7$, 2 Hz, 1H), 7.33 (s, 1H), 7.32 (dd, $J = 7$, 2 Hz, 1H), 7.27 (dd, $J = 7$, 2 Hz, 1H), 7.23 (dd, $J = 7$, 2 Hz, 1H), 7.06 (dd, $J = 7$, 2 Hz, 1H), 7.02 (dd, $J = 7$, 2 Hz, 1H), 6.39 (d, $J = 8$ Hz, 1H), 6.36 (d, $J = 8$ Hz, 1H), 6.12 (t, $J = 8$ Hz, 1H), 6.09 (d, $J = 13$ Hz, 1H), 5.99 (d, $J = 13$ Hz, 1H), 5.75 (d, $J = 13$ Hz, 1H), 5.67 (d, $J = 13$ Hz, 1H), 5.65 (d, $J = 13$ Hz, 1H), 5.47 (t, $J = 8$ Hz, 1H), 5.28 (d, $J = 13$ Hz, 1H), 5.26 (d, $J = 13$ Hz, 1H), 3.45 – 4.55 (m, 32H), 2.67 (d, $J = 8$ Hz, 1H), 2.14 (d, $J = 8$ Hz, 1H); ^{13}C NMR (100.6 MHz, $(CD_3)_2CO$, −40 °C): $\delta = 153.0$, 152.3, 151.8, 150.8, 147.6, 146.0, 145.9, 145.8, 145.4, 145.0, 144.3, 143.9, 138.0, 137.5, 131.9, 131.7, 131.5, 131.3, 129.6, 127.9, 126.5, 126.2, 125.8, 125.1, 125.0, 124.9, 124.8, 124.6, 124.0, 114.0, 109.2, 108.3, 105.9, 105.4, 72.8, 72.6, 71.0, 70.2, 69.9, 69.7, 69.1, 68.8, 68.3, 68.1, 67.9, 65.4, 65.0, 60.2, 60.0; HR-MS (LSI-MS) calcd for $C_{62}H_{68}N_4O_{10}P_3F_{18}$ $[M - PF_6]^+$: 1463.3861, found: 1463.3912.

Received: September 29, 1997 [Z 10979 IE]
German version: *Angew. Chem.* **1998**, *110*, 1018 – 1022

Keywords: chromophores · molecular devices · nanostructures · receptors · supramolecular chemistry

[1] J.-M. Lehn, *Supramolecular Chemistry – – Concepts and Perspectives*, VCH, Weinheim, **1995**.

[2] a) C. A. Hunter, J. K. M. Sanders, *J. Am. Chem. Soc.* **1990**, *112*, 5525 – 5534; b) M. Nishio, Y. Umezawa, M. Hiroyta, Y. Takeuchi, *Tetrahedron* **1995**, *51*, 8665 – 8701; c) G. R. Desiraju, *Chem. Commun.* **1997**, 1475 – 1482.

[3] a) G. M. Whitesides, E. E. Simanek, J. P. Mathias, C. T. Seto, D. N. Chin, M. Mammen, D. M. Gordon, *Acc. Chem. Res.* **1995**, *28*, 37 – 44; b) D. S. Lawrence, T. Jiang, M. Levett, *Chem. Rev.* **1995**, *95*, 2229 – 2260; c) D. Philp, J. F. Stoddart, *Angew. Chem.* **1996**, *108*, 1242 – 1286; *Angew. Chem. Int. Ed. Engl.* **1996**, *35*, 1154 – 1196.

[4] a) J.-C. Chambron, C. O. Dietrich-Buchecker, J.-P. Sauvage, *Top. Curr. Chem.* **1993**, *165*, 131 – 162; d) D. B. Amabilino, J. F. Stoddart, *Chem. Rev.* **1995**, *95*, 2725 – 2828.

[5] a) P.-L. Anelli, P. R. Ashton, R. Ballardini, V. Balzani, M. Delgado, M. T. Gandolfi, T. T. Goodnow, A. E. Kaifer, D. Philp, M. Pietraszkiewicz, L. Prodi, M. V. Reddington, A. M. Z. Slawin, N. Spencer, J. F. Stoddart, C. Vicent, D. J. Williams, *J. Am. Chem. Soc.* **1992**, *114*, 193 – 218; b) D. B. Amabilino, P. R. Ashton, S. E. Boyd, J. Y. Lee, S. Menzer, J. F. Stoddart, D. J. Williams, *Angew. Chem.* **1997**, *109*, 2160 – 2162; *Angew. Chem. Int. Ed. Engl.* **1997**, *36*, 2070 – 2072.

[6] a) P.-L. Anelli, N. Spencer, J. F. Stoddart, *J. Am. Chem. Soc.* **1991**, *113*, 569 – 572; b) R. A. Bissell, E. Córdova, A. E. Kaifer, J. F. Stoddart, *Nature (London)* **1994**, *369*, 133 – 137; c) M. V. Martínez-Díaz, N. Spencer, J. F. Stoddart, *Angew. Chem.* **1997**, *109*, 1991 – 1994; *Angew. Chem. Int. Ed. Engl.* **1997**, *36*, 1904 – 1907.

[7] D. B. Amabilino, P.-L. Anelli, P. R. Ashton, G. R. Brown, E. Córdova, L. A. Godínez, W. Hayes, A. E. Kaifer, D. Philp, A. M. Z. Slawin, N. Spencer, J. F. Stoddart, M. S. Tolley, D. J. Williams, *J. Am. Chem. Soc.* **1995**, *117*, 11142 – 11170.

[8] a) K. L. Wooley, C. J. Hawker, J. M. J. Fréchet, *J. Am. Chem. Soc.* **1991**, *113*, 4252 – 4261; b) I. Gitsov, K. L. Wooley, J. M. J. Fréchet, *Angew. Chem.* **1992**, *104*, 1282 – 1285; *Angew. Chem. Int. Ed. Engl.* **1992**, *31*, 1200 – 1201; c) I. Gitsov, K. L. Wooley, C. J. Hawker, P. T. Ivanona, J. M. J. Fréchet, *Macromolecules* **1993**, *26*, 5621 – 5627; d) J. M. J. Fréchet, I. Gitsov, *Macromol. Symp.* **1995**, *98*, 441 – 465.

[9] a) S. C. Zimmerman, F. Zeng, D. E. C. Reichert, S. V. Kolotuchin, *Science (Washington)* **1996**, *271*, 1095 – 19098; b) F. Zeng, S. C. Zimmerman, *Chem. Rev.* **1997**, *97*, 1681 – 1712.

[10] a) A. Ueno, T. Kuwabara, A. Nakamura, F. Toda, *Nature (London)* **1992**, *356*, 136 – 137; b) A. Ueno, *Adv. Mater.* **1993**, 132 – 134; c) K. Hamashaki, H. Ikeda, A. Nakamura, A. Ueno, F. Toda, I. Suziki, T. Osa, *J. Am. Chem. Soc.* **1993**, *115*, 5035 – 5040; d) R. Corradini, A. Dossena, R. Marchelli, A. Panagia, G. Sartor, M. Saviano, A. Lombardi, V. Pavone, *Chem. Eur. J.* **1996**, *2*, 373 – 381; e) P. R. Ashton, V. Balzani, S. E. Boyd, M. Gómez-López, S. Iqbal, D. Philp, J. A. Preece, H. G. Ricketts, J. F. Stoddart, M. S. Tolley, A. J. P. White, D. J. Williams, *ibid. 997*, *3*, 146 – 164

[11] P. R. Ashton, M. Gómez-López, S. Iqbal, J. A. Preece, J. F. Stoddart, *Tetrahedron Lett.* **1997**, *38*, 3635 – 3638.

[12] a) B. L. Feringa, W. F. Jager, B. de Lange, *Tetrahedron* **1990**, 37, 8267 – 8310; b) M. Gómez-López, J. A. Preece, J. F. Stoddart, *Nanotechnology*, **1996**, *7*, 183 – 192.

[13] Both **6**·2PF$_6$ and **7**·4PF$_6$ exhibit planar chirality; the ring inversions between their enantiomers are slow on the ^{1}H NMR time scale at room temperature. In the case of **6**·2PF$_6$, the ^{1}H NMR spectrum (400 MHz) recorded in CD_3CN at 304 K exhibits an AB system ($J_{AB} =$ 14 Hz) with δ values of 5.22 and 5.62 for the diastereotopic benzylic methylene protons. Upon increasing the temperature of the solution in CD_3CN, the AB system broadens and finally coalesces ($T_c = 369$ K) to a singlet centered on $\delta = 5.47$. A rate constant k_c of 372 s^{-1} was calculated at T_c with the approximation $k_c = \pi[(\upsilon_a - \upsilon_b)^2 + 6J_{ab}^2]^{1/2}/2^{1/2}$ where $\upsilon_a - \upsilon_b = 164$ Hz. The Eyring equation was then used with k_c and T_c to obtain a value of 17.4 ± 0.2 kcal mol^{-1} for $\Delta G_c^{\neq}$. Although **3** – **5** also possess planes of chirality, their enantiomers are inverting quickly on the ^{1}H NMR time scale at room temperature.

[14] The macrobicyclic tetracationic host **8**$^{4+}$ not only has the capacity to turn itself inside out but, in the presence of an appropiate guest (e.g. TTF), it also changes color. Since **8**$^{4+}$ is a changeable entity, both in terms of its conformation and color, we like to refer to it as a "molecular chameleon". The term "catenane chameleons" has already been used: D. A. Leigh, K. Moody, J. P. Smart, K. J. Watson, A. M. Z. Slawin, *Angew. Chem.* **1996**, *108*, 326-331; *Angew. Chem. Int. Ed. Engl.* **1996**, *35*, 306 – 310.

[15] Crystal data for **8**·4PF$_6$ ($C_{62}H_{68}N_4O_{10}P_4F_{24} \cdot Me_2CO$): $M_r = 1667.2$, monoclinic, space group $P2_1/n$, $a = 14.218(2)$, $b = 21.164(2)$, $c =$ 14.890(2) Å, $\beta = 112.59(1)°$, $V = 4136.8(9)$ Å^3, $T = 203$ K, $Z = 2$ (the "molecule" has crystallographically imposed C_i symmetry), $\rho_{calcd} =$ 1.338 g cm^{-3}, $\mu(Cu_{K\alpha}) = 18.1$ cm^{-1}, $F(000) = 1712$. Data for the crystal of dimensions $0.13 \times 0.23 \times 0.60$ mm were collected on a Siemens P4/RA diffractometer ($2\theta \leq 110°$), ω scans, graphite-monochromated $Cu_{K\alpha}$ radiation. Of 5190 independent reflections measured, 3205 with $I > 2\sigma(I)$ were considered to be observed. The data were corrected for Lorentzian and polarization effects, but not for absorption. The structure was solved by direct methods, and the non-hydrogen atoms refined anisotropically. Because the space group requires the molecule

 © WILEY-VCH Verlag GmbH, D-69451 Weinheim, 1998 1433-7851/98/3707-0978 $ 17.50+.50/0

to possess an inversion center, the structure has to be disordered. Two alternate orientations for eight of the atoms in each polyether linkage were identified. These atoms were refined with occupancies of 0.5. A ΔF map revealed the inclusion of one molecule of Me_2CO for each "molecule" of $\mathbf{8}\cdot 4PF_6$. The non-hydrogen atoms of this solvent were refined isotropically. Hydrogen atoms were placed in calculated positions, assigned isotropic thermal parameters $U(H) = 1.2\,U_{eq}(C)$ [$U(H) = 1.5\,U_{eq}(CMe)$], and allowed to ride on their parent carbon atoms. The structure was refined by full-matrix least squares based on F^2 to give $R_1 = 0.148$ and $wR_2 = 0.395$ for 557 parameters. The maximum and minimum residual electron densities in the final ΔF map were 1.11 and $-0.48\,e\,Å^{-3}$. Crystallographic data (excluding structure factors) for the structure reported in this paper have been deposited with the Cambridge Crystallographic Data Centre as supplementary publication no. CCDC-100741. Copies of the data can be obtained free of charge on application to CCDC, 12 Union Road, Cambridge CB2 1EZ, UK (fax: (+44) 1223-336-033; e-mail: deposit@ccdc.cam.ac.uk).

[16] The angles of twist and bowing associated with the bipyridinium units[5a] are 5 and 22°, respectively.

[17] ^{1}H NMR: $\delta(\alpha$-bipyridinium-H) = 8.50, 8.63, 8.68, 8.76.8.77, 8.80, 9.14, 9.19; $\delta(\beta$-bipyridinium-H) = 7.02, 7.06, 7.23, 7.27, 7.32, 7.34, 7.40, 7.48.

[18] For a discussion of a very similar process in [2]catenanes, see M. Asakawa, P. R. Ashton, S. E. Boyd, C. L. Brown, R. E. Gillard, O. Kocian, F. M. Raymo, J. F. Stoddart, M. S. Tolley, A. J. P, White, D. J. Williams, *J. Org. Chem*. **1997**, *62*, 877 – 893.

[19] The temperature-dependent ^{1}H NMR spectra were analyzed with the coalescence method; values of k_c at T_c were obtained from the approximation $k_c = \pi\Delta\nu/2^{1/2}$, where $\Delta\nu$ is the limiting value for the difference [Hz] in chemical shifts for the exchanging protons. The Eyring equation was then used to calculate $\Delta G_c^{\neq}$ from k_c at T_c.

[20] The results of spectrophotometric titration were evaluated by a computer-assisted nonlinear least-square curve-fitting program (Ultrafit, Biosoft, Cambridge, **1992**).

[21] The binding constant K_a for the complex formed between TTF and the parent cyclophane cyclobis(paraquat-*p*-phenylene) in MeCN is $7190 \pm 970\,M^{-1}$ ($-\Delta G^\circ = 5.26 \pm 0.07$ kcal mol^{-1}): P.-L. Anelli, M. Asakawa, P. R. Ashton, R. A. Bissell, G. Clavier, R. Gorski, A. E. Kaifer, S. J. Langford, G. Mattersteig, S. Menzer, D. Philp, A. M. Z. Slawin, N. Spencer, J. F. Stoddart, M. S. Tolley, D. J. Williams, *Chem. Eur. J.* **1997**, *3*, 1113 – 1135. In the case of the [$\mathbf{8}^{4+}\cdot$ TTF] complex $K_a = 200 \pm 10\,M^{-1}$ ($-\Delta G^\circ = 3.14 \pm 0.02$ kcal mol^{-1}). It follows that $\Delta\Delta G^\circ = 2.12$ kcal mol^{-1}; this can be interpreted as the difference in free energy between the two extreme gross conformations of $\mathbf{8}^{4+}$, the self-complexed conformation and the "opened-up" conformation in which the two macrocycles incorporated into $\mathbf{8}^{4+}$ are free to associate with complementary guests.

[22] a) For an excellent review on current developments in molecular switches, see M. D. Ward, *Chem. Ind*. **1997**, 640 – 645. b) for our most recent publication on molecular switches, see M. Asakawa, P. R. Ashton, V. Balzani, A. Credi, C. Hamers, G. Mattersteig, M. Montalti, A. N. Shipway, N. Spencer, J. F. Stoddart, M. S. Tolley, M. Venturi, A. J. P. White, D. J. Williams, *Angew. Chem*. **1998**, *110*, 357 – 361; *Angew. Chem. Int. Ed.* **1998**, *37*, 333 – 337.

[23] a) P. R. Ashton, A. Collins, M. C. T. Fyfe, P. T. Glink, S. Menzer, J. F. Stoddart, D. J. Williams, *Angew. Chem*. **1997**, *109*, 59 – 62; *Angew. Chem. Int. Ed. Engl*. **1997**, *36*, 59 – 62; b) M. C. T. Fyfe, J. F. Stoddart, *Acc. Chem. Res*. **1997**, *30*, 393 – 401.

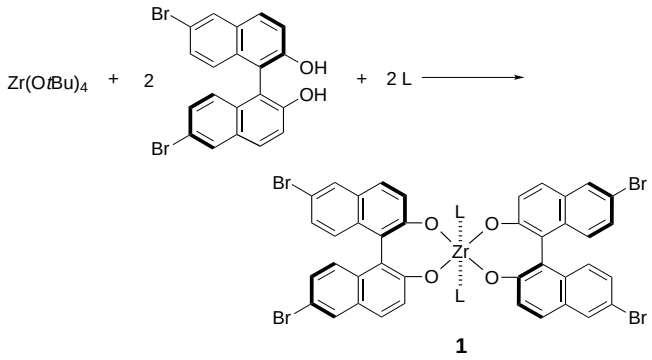
[24] Note added in proof (March 16, 1998): A self-complexing TTF macrocyle that can be switched has just appeared in the literature: see M. B. Nielsen, S. B. Nielsen, J. Becher, *Chem. Commun.* **1998**, 475 – 476.

The First Enantioselective Aza-Diels – Alder Reactions of Imino Dienophiles on Use of a Chiral Zirconium Catalyst**

Shū Kobayashi,* Susumu Komiyama, and Haruro Ishitani

Asymmetric aza-Diels – Alder reactions provide a useful route to optically active heterocycles such as piperidines and tetrahydroquinolines.[1] Although successful examples of diastereoselective approaches have been reported,[2] there have been few accounts of enantioselective reactions. Yamamoto et al. described elegant enantioselective aza-Diels – Alder reactions of aldimines with Danishefsky's diene on using chiral boron compounds; however, stoichiometric amounts of chiral sources were needed.[3] Quite recently, we reported the first example of a catalytic, enantioselective aza-Diels – Alder reaction of azadienes on using a chiral lanthanide catalyst.[4] While high diastereo- and enantioselectivities were attained in the reaction of azadienes with dienophiles, the products obtained were limited to 8-hydroxytetrahydroquinoline derivatives. Here we report the catalytic, enantioselective aza-Diels – Alder reactions of aldimines (imino dienophiles) with Danishefsky's diene for the synthesis of a wide variety of chiral piperidine derivatives; a chiral zirconium compound was used as catalyst.

The chiral zirconium compound **1**[5] was prepared from $Zr(OtBu)_4$, (*R*)-6,6′-dibromo-1,1′-binaphthol [(*R*)-Br-BINOL, 2 equiv],[6] and the ligand L (2 – 3 equiv; Scheme 1). The



1

Scheme 1. Synthesis of **1**. L = ligand.

reaction of aldimine **2**, which is obtained from 1-naphthaldehyde and 2-aminophenol (Nap = naphthyl), with Danishefsky's diene **3**[7] was investigated as the model reaction. The ligand and the solvent influenced the yields and enantiose-

[*] Prof. Dr. S. Kobayashi, S. Komiyama, H. Ishitani
Department of Applied Chemistry, Faculty of Science
Science University of Tokyo (SUT)
and
CREST, Japan Science and Technology Corporation (JST)
Kagurazaka, Shinjuku-ku, Tokyo 162 (Japan)
Fax: (+81) 3-3260-4726
E-mail: skobayas@ch.kagu.sut.ac.jp

[**] This work was partially supported by a Grant-in-Aid for Scientific Research from the Ministry of Education, Science, Sports, and Culture, Japan, and a SUT Special Grant for Research Promotion. H.I. thanks the JSPS fellowship for Japanese Junior Scientists.

lectivities strongly (Table 1).[8] 1-Methylimidazole as ligand gave the best results. When the chiral catalyst (10 mol%) was prepared in dichloromethane, the desired aza-Diels–Alder

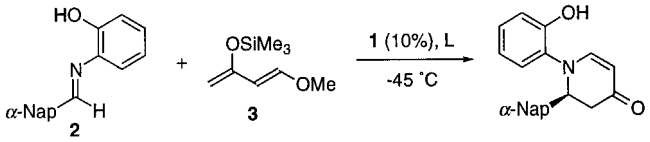
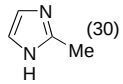
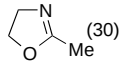


Table 1. Influence of the ligand and the solvent in the reaction of **2** with **3**.

Ligand[a]	Solvent	Yield[%]	*ee*[%]
NMI[b]	CH_2Cl_2	74	40
NMI	1. benzene 2. CH_2Cl_2[c]	81	61
NMI	1. benzene 2. CH_2Cl_2[c]	83[d]	41[d]
NMI	1. toluene 2. CH_2Cl_2[c]	81	71
NMI	toluene	86	82
DMI[e]	toluene	76	59
 (30)	toluene	28	24
 (30)	toluene	86	50
 (30)	toluene	81	46
–	toluene	65	10[f]

[a] 30 mol%, unless noted otherwise. [b] NMI = 1-Methylimidazole. [c] See text. [d] Reaction with 4-*tert*-butoxy-2-trimethylsilyloxy-1,3-butadiene as diene component. [e] DMI = 1,2-dimethylimidazole (20 mol%). [f] Reverse enantioselectivity.

reaction of **2** with **3** proceeded smoothly, but the enantiomeric excess of the adduct was only 40%. On the other hand, the enantioselectivity was improved to 61% *ee* when the catalyst was prepared in benzene by stirring for 1 h at room temperature, the mixture evaporated to remove benzene and *t*BuOH under reduced pressure, and the reaction then carried out in dichloromethane. While use of the bulky diene 4-*tert*-butoxy-2-trimethylsiloxy-1,3-butadiene[9] decreased the selectivity in this case, a higher enantiomeric excess was obtained when the catalyst was prepared in toluene. The best result was finally obtained when the catalyst was prepared and the successive reaction carried out in toluene.[10]

We then examined the influence of the metal (Table 2). Preliminary screening proved that zirconium compounds gave excellent catalytic abilities for the activation of aldimines.[11] Compounds of other Group 4 metals, titanium and hafnium, were screened. A chiral hafnium catalyst gave high yields and enantioselectivities in the model reaction of **2** with diene **3**, whereas lower yields and enantiomeric excesses were obtained with a chiral titanium catalyst.[12]

Several examples of the catalytic aza-Diels–Alder reactions with the chiral zirconium catalyst are shown in Table 3. In most cases, high chemical yields and good to high enantioselectivities were obtained in the presence of 5–20 mol% of the chiral catalyst.[13] 4-Methoxyl-3-methyl-2-

Table 2. Influence of the metal on the reaction of **2** with **3**.[a]

M	Mol%	Yield[%]	*ee*[%]
Zr	10	86	82
Zr	20	96	88
Hf	10	89	73
Hf	20	96	84
Ti	10	68	39
Ti	20	70	62

[a] Reaction at −45 °C in toluene, catalyst prepared from $M(OtBu)_4$, (*R*)-Br-BINOL (2 equiv), and NMI (3 equiv).

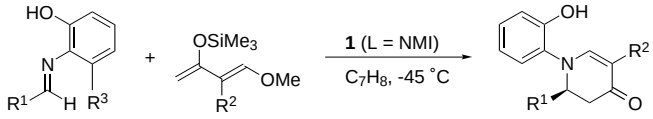
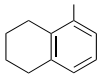
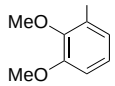
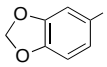


Table 3. Catalytic aza-Diels–Alder reactions.[a, b]

R^1	R^2	Cat.[mol%]	Yield[%]	*ee*[%]
α-Nap	H (**3**)	5	72	67
α-Nap	H (**3**)	10	86	82
α-Nap	H (**3**)	20	96	88
α-Nap	H (**3**)	30	98	89
α-Nap	H (**3**)	50	88	90
α-Nap	Me (**4**)	10	79	89
α-Nap	Me (**4**)	20	93	93
	H (**3**)	10	92	80
o-MeC_6H_4	H (**3**)	10	81	76
o-MeC_6H_4	H (**3**)	20	83	82
o-MeC_6H_4	Me (**4**)	20	97	77
Ph	Me (**4**)	20	83	65
	Me (**4**)	20	95	74
	Me(**4**)	10	80	67
2-thienyl	H (**3**)	10	86	64
c-C_6H_{11}[c]	Me (**4**)	10	47	78
c-C_6H_{11}[c]	Me (**4**)	20	51	86

[a] The absolute configuration was tentatively determined based on the results shown in reference [5]. [b] R^3 = H, unless noted otherwise. [c] R^3 = Me (see text).

trimethylsiloxy-1,3-butadiene (**4**)[14] also worked well under standard conditions, and the desired 2,3-dihydro-4-pyridone derivatives were obtained in high yields with high enantioselectivities. As for the R^1 group, *ortho*-subsubstituted arenes gave higher selectivities. For example, while the aldimine derived from benzaldehyde (R^1 = Ph) reacted with **4** to afford the corresponding adduct with 65% *ee*, an enantiomeric excess of 74% was obtained in the reaction of the aldimine derived from *o*-tolualdehyde with **4** under the same reaction conditions. The 2-thienyl-substituted aldimine reacted with **3** smoothly to give the corresponding pyridone derivative in a high yield with a good enantiomeric excess.

In the reaction of the cyclohexyl-substituted aldimine with **4**, a low enantiomeric excess of the adduct was observed under standard reaction conditions; the low selectivity was ascribed

 © WILEY-VCH Verlag GmbH, D-69451 Weinheim, 1998 1433-7851/98/3707-0980 $ 17.50+.50/0

to the isomerization of the *cis* and *trans* forms of the aldimine. To prevent the isomerization, the aldimine derived from cyclohexanecarbaldehyde and 2-amino-3-methylphenol was used. It was exciting to find that the enantiomeric excess of the corresponding pyridone derivative improved to 86%.

In summary, the first catalytic, enantioselective aza-Diels–Alder reactions of imino dienophiles with Danishefsky's dienes have been achieved on using our original chiral zirconium catalyst. Optically active 2,3-dihydro-4-pyridone derivatives were prepared in high yields with good to high enantiomeric excesses. Further investigations to use the zirconium catalyst in other enantioselective reactions as well as to apply the present enantioselective reactions for the synthesis of biologically active compounds are now in progress.

Experimental Section

A typical experimental procedure is described for the reaction of the aldimine obtained from *o*-tolualdehyde and 2-aminophenol with **3**: 6,6′-Dibromo-1,1′-bi-2-naphthol (0.088 mmol) in toluene (0.5 mL) and *N*-methylimidazole (0.12 mmol) in toluene (0.25 mL) were added to $Zr(OtBu)_4$ (0.04 mmol) in toluene (0.25 mL) at room temperature. The mixture was stirred for 1 h at the same temperature, and then cooled to −45 °C. Solutions of the aldimine (0.4 mmol) and **3** (0.6 mmol) in toluene (0.75 mL each) were successively added. The mixture was stirred for 35 h at the same temperature, and saturated $NaHCO_3$ was added to quench the reaction. The aqueous layer was extracted with CH_2Cl_2, and the crude adduct treated with THF/1N HCl (20/1) at 0 °C for 30 min. After a usual work-up, the crude product was purified by chromatography on silica gel to give the desired adduct (83%). ^{1}H NMR ($CDCl_3$): $\delta = 2.10$ (s, 3H), 2.68 (dd, 1H, $J = 7.6$, 16.6 Hz), 3.06 (dd, 1H, $J = 7.6$, 16.6 Hz), 5.15 (d, 1H, $J = 7.5$ Hz), 5.52 (t, 1H, $J = 7.5$ Hz), 6.57 (t, 1H, $J = 7.0$ Hz), 6.76–7.00 (m, 6H), 7.38–7.43 (m, 2H), 9.57 (br s, 1H); ^{13}C NMR ($CDCl_3$): $\delta = 19.0$, 42.7, 58.6, 98.2, 117.1, 119.6, 126.1, 126.2, 126.6, 127.7, 128.3, 130.9, 131.5, 134.8, 136.6, 151.8, 156.8, 192.0; HR-MS calcd for $C_{18}H_{17}NO_2$ [M^+]: 279.1259, found: 279.1271. The optical purity was determined to be 82% *ee* after methylation (MeI, K_2CO_3/acetone) by HPLC analysis with a chiral column. HPLC (Daicel Chiralcel OD, hexane/*i*PrOH (24/1), flow rate 1.0 mL min^{-1}): $t_R =$ 44.2 (major enantiomer), $t_R = 50.6$ min (minor enantiomer).

Received: September 19, 1997 [Z10947IE]
German version: *Angew. Chem.* **1998**, *110*, 1026–1028

Keywords: asymmetric catalysis · cycloadditions · homogeneous catalysis · Lewis acids · zirconium

[1] a) H. Waldmann, *Synthesis* **1994**, 535–551; b) *Organic Synthesis Highlights II* (Ed.: H. Waldmann), VCH, Weinheim, **1995**, pp. 37–48; c) L. F. Tietze, G. Kettschau, *Top. Curr. Chem.* **1997**, *189*, 1–20; d) S. M. Weinreb in *Comprehensive Organic Synthesis*, *Vol. 5* (Eds.: B. M. Trost, I. Fleming, M. F. Semmelhock), Pergamon, Oxford, **1991**, p. 401–449; e) D. L. Boger, S. M. Weinreb, *Hetero Diels-Alder Methodology in Organic Synthesis*, Academic Press, San Diego, **1987**, chap. 2, 9.

[2] For example, a) E. Borrione, M. Prato, G. Scorrano, M. Stiranello, *J. Chem. Soc. Perkin Trans. 1* **1989**, 2245–2250; b) H. Waldmann, M. Braun, M. Dräger, *Angew. Chem.* **1990**, *102*, 1455–1457; *Angew. Chem. Int. Ed. Engl.* **1990**, *29*, 1468–1471; c) P. D. Bailey, D. J. Londesbrough, T. C. Hancox, J. D. Heffernan, A. B. Holmes, *J. Chem. Soc. Chem. Commun.* **1994**, 2543–2544; d) A. K. McFarlane, G. Thomas, A. Whiting, *J. Chem. Soc. Perkin Trans. 1* **1995**, 2803–2808; e) E. P. Kündig, L. H. Xu, P. Romanens, G. Bernardinelli, *Synlett* **1996**, 270–272.

[3] a) K. Hattori, H. Yamamoto, *J. Org. Chem.* **1992**, *57*, 3264–3265; b) *Tetrahedron* **1993**, *49*, 1749–1760; c) K. Ishihara, M. Miyata, K. Hattori, T. Tada, H. Yamamoto, *J. Am. Chem. Soc.* **1994**, *116*, 10520–10524.

[4] H. Ishitani, S. Kobayashi, *Tetrahedron Lett.* **1996**, *37*, 7357–7360.

[5] H. Ishitani, M. Ueno, S. Kobayashi, *J. Am. Chem. Soc.* **1997**, *119*, 6984–6985.

[6] For the use of 6,6′-dibromo-1,1′-bi-2-naphthol, see a) M. Terada, Y. Motoyama, K. Mikami, *Tetrahedron Lett.* **1994**, *35*, 6693–6696; b) H. Sasai, T. Tokunaga, S. Watanabe, T. Suzuki, N. Itoh, M. Shibasaki, *J. Org. Chem.* **1995**, *60*, 7388–7389.

[7] a) S. Danishefsky, T. Kitahara, *J. Am. Chem. Soc.* **1974**, *96*, 7807–7809; b) J. F. Kerwin, Jr., S. Danishefsky, *Tetrahedron Lett.* **1982**, *23*, 3739–3742.

[8] We have already determined the importance of the free hydroxyl group of the aldimine for the selectivity.[4, 5] When the aldimine prepared from aniline or 2-methoxyaniline was used under the same reaction conditions, the corresponding pyridone derivatives were obtained in good yields but low enantiomeric excesses (aniline: 68% yield, 4% *ee*; 2-methoxyaniline: 74% yield, 25% *ee*).

[9] S. Danishefsky, M. Bednarski, T. Izawa, C. Maring, *J. Org. Chem.* **1984**, *49*, 2290–2292.

[10] The solvents influence the structure of the catalyst; details of the structure are now under investigation. See also L. F. Tietz, P. Saling, *Chirality* **1993**, *5*, 329–333.

[11] S. Kobayashi, S. Komiyama, H. Ishitani, unpublished results.

[12] Titanium(IV)-1,1′-bi-2-naphthol complexes were used in some asymmetric reactions: a) M. T. Reetz, S.-H. Kyung, C. Bolm, T. Zierke, *Chem. Ind.* **1986**, 824; b) S. Aoki, K. Mikami, M. Terada, T. Nakai, *Tetrahedron* **1993**, *49*, 1783–1792; c) A. L. Costa, M. G. Piazza, E. Tagliavini, C. Trombini, A. Umani-Ronchi, *J. Am. Chem. Soc.* **1993**, *115*, 7001–7002; d) G. E. Keck, K. H. Tarbet, L. S. Geraci, *ibid.* **1993**, *115*, 8467–8468; e) G. E. Keck, D. Krishnamurthy, M. C. Grier, *J. Org. Chem.* **1993**, *58*, 6543–6544; f) S. Matsukawa, K. Mikami, *Tetrahedron: Asymmetry* **1995**, *6*, 2571–2574; g) D. R. Gauthier, Jr, E. M. Carreira, *Angew. Chem.* **1996**, *108*, 2521–2523; *Angew. Chem. Int. Ed. Engl.* **1996**, *35*, 2363–2365; h) C.-M. Yu, H.-S. Choi, W.-H. Jung, S.-S. Lee, *Tetrahedron Lett.* **1996**, *37*, 7095–7098.

[13] For deprotection of the N-substituent of the products, see ref. [5].

[14] a) D. L. J. Clive, R. J. Bergstra, *J. Org. Chem.* **1991**, *56*, 4976–4977; b) S. Sugawara, S.-I. Yamada, M. Narahashi, *J. Pharm. Soc. Jpn.* **1951**, *71*, 1345–1355.

C_{60} and C_{70} Compounds in the Pincerlike Jaws of Calix[6]arene**

Jerry L. Atwood,* Leonard J. Barbour, Colin L. Raston, and Ida B. N. Sudria

Construction of supramolecular architectures involving electron-deficient fullerenes is of interest in crystal engineering, the synthesis of novel nanostructures, and the development of host–guest chemistry for use in the purification of fullerenes.[1–17] Host molecules that form discrete, albeit inherently weak, complexes with C_{60} and/or C_{70} include

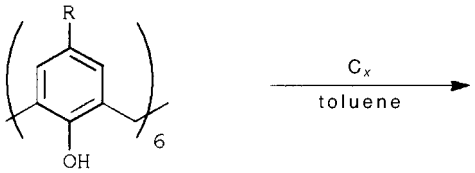
[*] Prof. J. L. Atwood, Dr. L. J. Barbour
Department of Chemistry
University of Missouri-Columbia
Columbia, MO 65211 (USA)
Fax: (+1) 573-884-9606
E-mail : chemja@showme.missouri.edu
Prof. C. L. Raston, I. B. N. Sudria
Department of Chemistry, Monash University (Australia)

[**] This work was supported by the Australian Research Council, the Department of Industry, Science and Tourism (Australia), and the National Science Foundation (USA). We also wish to thank Dr. Charles L. Barnes for assistance with initial solution of the crystal structure of the C_{60} complex.

 © WILEY-VCH Verlag GmbH, D-69451 Weinheim, 1998 1433-7851/98/3707-0981 $ 17.50+.50/0

calix[5]-, calix[6]-, and calix[8]arenes,[5–11] cyclotriveratrylene (CTV),[14, 15] γ-cyclodextrin,[16] and azacrown ethers.[17] Two complexes based on the rigid cup-shaped CTV with C_{60} have been structurally authenticated, and both contain "ball and socket" local host–guest structures dominated by fullerene–fullerene interactions. For calix[6]- and calix[8]arenes the nature of the local structures is difficult to predict[11] because of possible preorganization of the calixarene molecules through torsion along the C_{Ar}-CH_2-C_{Ar} bonds prior to complexation.

The calix[6]arenes **1** (R = H, *t*Bu) form fullerene-rich complexes with C_{60} and C_{70}, all of which were isolated as 1:2 complexes (Scheme 1). The synthesis of two of these compounds has been reported;[6] the two new compounds [(*p*-*t*Bu-calix[6]arene)$(C_{60})_2$] and [(calix[6]arene)$(C_{70})_2$] were prepared analytically pure in a similar way, but in more concentrated solutions in toluene. Of the four complexes, crystals suitable for X-ray diffraction studies were obtained only for [(calix[6]arene)$(C_{60})_2$] and [(calix[6]arene)$(C_{70})_2$].[18a] These were grown by controlled slow evaporation of a 1:1 mixture of toluene and dichloromethane containing 5 mg each of the fullerene and the calixarene. Large black crystals deposited over the course of several days as the mixtures became depleted in the chlorinated solvent. Dichloromethane itself blocks the complexation of calixarenes with C_{60} and C_{70}, possibly due to the formation of symmetrical nonclassical hydrogen bonds between hydrogen atoms of the solvent and the π electron clouds of the calixarene aromatic rings.[6, 7] There is little or no discrimination in complexation of C_{60} relative to C_{70} for calix[6]arene, but C_{70} binds preferentially with *p*-*t*Bu-calix[6]arene. Subsequent decomplexation with dichloromethane leads to C_{70} with a purity as great as 95%.



1 [(calix[6]arene)$(C_x)_2$], R = H

[(*p*-*t*Bu-calix[6]arene)$(C_x)_2$], R = *t*Bu

x = 60, 70

Scheme 1. Reaction of calixarenes with C_{60} and C_{70}.

The complexes [(calix[6]arene)$(C_{60})_2$] and [(calix[6]arene)$(C_{70})_2$] are isostructural despite the anisotropic shape of C_{70}, and both crystallize in the space group $P4_12_12$. The calixarenes are in the double-cone conformation, and each of the associated shallow cavities is occupied by a fullerene. The overall arrangement resembles the jaws of a pincer acting on two adjacent spheres/ellipsoids (Figure 1).

In both structures, the fullerene molecules are positioned unsymmetrically above their associated calixarene cavities. The C_{60} molecule is situated with its center at distances of 7.06(7), 6.91(7), and 6.65(8) Å from the closest ring centroids. In the C_{70} complex the principal axis of the ellipsoidal C_{70} molecule is not directed toward the calixarene cavity. Its center is positioned at distances of 6.85(6), 7.23(7), and 7.46(7) Å from the closest ring centroids.

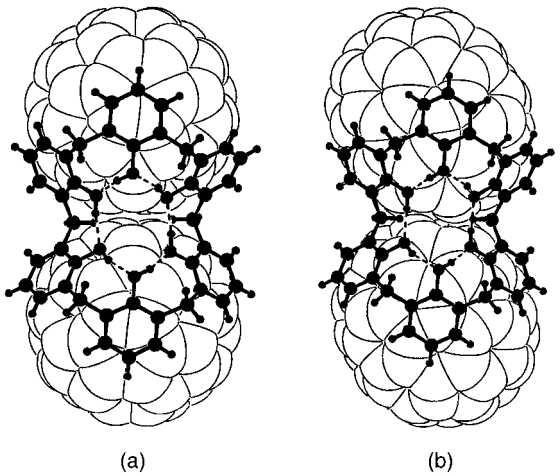


Figure 1. Projection of the structures of [(calix[6]arene)$(C_{60})_2$] (a) and [(calix[6]arene)$(C_{70})_2$] (b) as viewed from below the calixarene double cone. Atoms and bonds of the calixarene molecules are shown in shaded ball-and-stick representation, whereas fullerene molecules are shown as van der Waals surfaces. Hydrogen bonds are indicated by dashed lines.

Each fullerene molecule is in close proximity to six other fullerene molecules and is situated at the common vertex of two fullerene tetrahedra; individual fullerene molecules are less than 11 Å apart. These vertex-sharing tetrahedra form a three-dimensional array interspersed with molecules of calix[6]arene and solvent. Distances between independent centers are 10.04(7), 10.11(7), 10.21(8), and 10.76(7) Å for C_{60} and 10.53(7), 10.56(8), 10.60(7), and 10.66(8) Å for C_{70}. The distances between calixarene and fullerene molecules are somewhat greater than typical van der Waals distances, as are the distances between fullerene molecules in the supermolecules and between fullerenes in the gross structure. All hydroxyl groups of the calixarene units are situated on one side of the molecule and peripherally about the double cone. This is a similar arrangement to that found in solid-state structures of *p*-*t*Bu-calix[6]arene.[19] The OH stretching bands for both of the calix[6]arene complexes are shifted from about 3260 to 3080 cm^{-1}, which indicates a significant increase in the number of hydrogen bonds between hydroxyl groups. In contrast, *p*-*t*Bu-calix[6]arene complexes of the two fullerenes show no significant change in OH stretching bands relative to uncomplexed calixarene.

In solution, dimerization of fullerenes through the pincer/polarizing influence of calix[6]arene and *p*-*t*Bu-calix[6]arene may lead to higher order fullerene aggregates that are perhaps similar in structure to a portion of the solid-state structures described here. Another possibility is a micelle-like species with a central core of fullerene molecules surrounded by a sheath of calixarenes. Solutions in toluene of C_{60} and these calixarenes mobilized in the 5.4-nm pores of a mesoporous silica display a new absorption band at 450 nm, which is assigned to interfullerene electronic transitions.[13] No analogous bands have been identified for the C_{70} system, although spectral evidence suggests that aggregation of C_{70} molecules occurs in acetonitrile/toluene mixtures.[20]

 © WILEY-VCH Verlag GmbH, D-69451 Weinheim, 1998 1433-7851/98/3707-0982 $ 17.50+.50/0

For both calix[6]arene and *p*-*t*Bu-calix[6]arene it appears that fullerene dimerization is favored over a single fullerene residing in a single calixarene cavity. An interaction of this type would disrupt some of the H bonds. This is not the case for calix[5]arene complexes of C_{60} and C_{70}, for which a cone conformation is generally favored.[21, 22]

Our findings represent a major step forward in the construction of supramolecular assemblies based on calixarene-mediated interlocking of fullerenes. Furthermore, the results have implications in the rational design of host molecules for fullerenes and other large clusters such as icosahedral carboranes, for which the first host–guest species was recently established.[23]

Received: October 23, 1997 [Z11073IE]
German version: *Angew. Chem.* **1998**, *110*, 1029–1031

Keywords: calixarenes · fullerenes · supramolecular chemistry

[1] M. M. Olmstead, A. S. Ginwalla, B. C. Noll, D. S. Tinti, A. L. Balch, *J. Am. Chem. Soc.* **1996**, *118*, 7737–7745, and references therein.
[2] a) D. M. Eichhorn, S. Yang, W. Jarrell, T. F. Baumann, L. S. Beall, A. J. P. White, D. J. Williams, G. M. Barrett, B. M. Hoffman, *J. Chem. Soc. Chem. Commun.* **1995**, 1703–1704; b) L. Y. Chaing, J. W. Swirczewski, K. Liang, J. Millar, *Chem. Lett.* **1994**, 981–984.
[3] C. L. Raston in *Comprehensive Supramolecular Chemistry*, *Vol. 1* (Eds.: J. L. Atwood, J. E. D. Davies, D. D. MacNicol, F. Vögtle, K. S. Suslick), Pergamon, Oxford, **1996**, pp. 777–787.
[4] a) O. Ermer, *Helv. Chim. Acta* **1991**, *74*, 1339–1351; b) O. Ermer, C. A. Robke, *J. Am. Chem. Soc.* **1993**, *115*, 10077–10082.
[5] T. Haino, M. Yanase, Y. Fukazawa, *Angew. Chem.* **1997**, *109*, 288–290; *Angew. Chem. Int. Ed. Engl.* **1997**, *36*, 259–260.
[6] J. L. Atwood, G. A. Koutsantonis, C. L. Raston, *Nature* **1994**, *368*, 229–232.
[7] T. Suzuki, K. Nakashima, S. Shinkai, *Chem. Lett.* **1994**, 699–702.
[8] R. M. Williams, J. M. Zwier, J. W. Verhoeven, G. H. Nachtegaal, A. P. M. Kentgens, *J. Am. Chem. Soc.* **1994**, *116*, 6965–6966.
[9] T. Suzuki, K. Nakashima, S. Shinkai, *Tetrahedron Lett.* **1995**, *36*, 249–252.
[10] W. M. Williams, J. W. Verhoeven, *Recl. Trav. Chim. Pays-Bas* **1992**, *111*, 531–532.
[11] C. L. Raston, J. L. Atwood, P. J. Nichols, I. B. N. Sudria, *Chem. Commun.* **1996**, 2615–2616.
[12] K. Araki, K. Akao, A. Ikeda, T. Suzuki, S. Shinkai, *Tetrahedron Lett.* **1996**, *37*, 73–76.
[13] A. Drljaca, C. Kepert, C. L. Raston, C. A. Sandoval, T. D. Smith, L. Spiccia, *Chem. Commun.* **1997**, 195–196.
[14] J. W. Steed, P. C. Junk, J. L. Atwood, M. J. Barnes, C. L. Raston, R. S. Burkhalter, *J. Am. Chem. Soc.* **1994**, *116*, 10346-10347.
[15] J. L. Atwood, M. J. Barnes, M. G. Gardiner, C. L. Raston, *Chem. Commun.* **1996**, 1449–1450.
[16] a) T. Andersson, G. Westman, G. Stenhagen, M. Sundahi, O. Wennerstrom, *Tetrahedron Lett.* **1995**, *36*, 597–600; b) Z. Yoshida, H. Takekuma, S. Takekuma, Y. Matsubara, *Angew. Chem.* **1994**, *106*, 1658–1660; *Angew. Chem. Int. Ed. Engl.* **1994**, *33*, 1597–1599.
[17] F. Diederich, J. Effing, U. Jonas, L. Jullien, T. Plesnivy, H. Ringsdorf, C. Thilgen, D. Weinstein *Angew. Chem.* **1992**, *104*, 1683–1686; *Angew. Chem. Int. Ed. Engl.* **1992**, *31*, 1599–1602.
[18] a) Crystal data for $[(\text{calix[6]arene})(C_{60})_2]\cdot C_7H_8$: crystal dimensions $0.20\times0.20\times0.15\ mm^3$, tetragonal, space group $P4_12_12$, $a=b=18.8262(6)$, $c=25.6416(12)$ Å, $V=9088.0(6)$ Å^3, $\rho_{calcd}=1.586\ g\,cm^{-3}$, $\lambda(Mo_{K\alpha})=0.71070$ Å, $T=173$ K; of 49124 reflections, 9311 were independent and used in the refinement. Final refinement against F^2 converged with $R_1=0.1193$ ($wR_2=0.2821$) for 6309 unique reflections ($I>2\sigma(I)$, $1.34\le\theta\le26.40^\circ$), 788 parameters and 90 restraints. Maximum residual electron density was $0.49\ e^-$ Å^{-3}. Crystal data for $[(\text{calix[6]arene})(C_{70})_2]\cdot C_7H_8$: dimensions $0.50\times0.40\times0.30\ mm^3$, tetragonal, space group $P4_12_12$, $a=b=19.5897(7)$, $c=26.1122(14)$ Å, $V=10020.7(7)$ Å^3, $\rho_{calcd}=1.598\ g\,cm^{-3}$, $\lambda(Mo_{K\alpha})=0.71070$ Å, $T=173$ K; of 58301 reflections collected, 11096 were independent and used in the refinement. Final refinement against F^2 converged with $R_1=0.1260$ ($wR_2=0.3911$) for 8628 unique reflections ($I>2\sigma(I)$, $1.30\le\theta\le27.16^\circ$), 884 parameters and 105 restraints. Maximum residual electron density was $0.61\ e^-$ Å^{-3}. The structures were solved and refined with the Siemens SHELX-TL package. All non-hydrogen atoms were refined anisotropically, while hydrogen atoms were placed in calculated positions with their thermal parameters fixed at values 1.2 times those of the atoms to which they were bound. Difference electron density maps revealed the positions of all fullerene atoms included in the final model, and these were refined with full site occupancy. However, during all stages of refinement, relatively weak peaks of electron density were observed dispersed over the surfaces of the fullerene molecules. This is indicative of a small amount of disorder that was not modeled. As a further indication of possible fullerene disorder, the anisotropic thermal parameters of several of the fullerene atoms were negative. All fullerene bond lengths were constrained to values of 1.45(1) Å for the 6:5 ring fusions and 1.38(1) Å for the 6:6 ring fusions.[18b] A toluene molecule situated on a twofold rotation axis was located in each structure. Owing to disorder, the toluene methyl group was not located in the structure of the C_{60} complex, and hydrogen atoms were therefore not generated for this molecule. Crystallographic data (excluding structure factors) for the structures described in this paper have been deposited with the Cambridge Crystallographic Data Centre as supplementary publication no. CCDC-100886. Copies of the data can be obtained free of charge on application to CCDC, 12 Union Road, Cambridge CB2 1EZ, UK (fax: (+44) 1223-336-033; e-mail: deposit@ccdc.cam.ac.uk). b) M. Fedurco, M. Olmstead, W. R. Fawcett, *Inorg. Chem.* **1995**, *34*, 390–392.
[19] a) M. Halit, D. Oehler, M. Perrin, A. Thozet, R. Perrin, J. Vicens, M. Bourakhouadar, *J. Inclusion Phenom.* **1988**, *6*, 613–623; b) G. D. Andreetti, F. Ugozzoli, A. Casnati, E. Ghidini, A. Pochini, R. Ungaro, *Gazz. Chim. Ital.* **1989**, *119*, 47–50; c) P. Thuery, N. Keller, M. Lance, J.-D. Vigner, M. Nierlich, *J. Inclusion Phenom.* **1995**, *20*, 373–397.
[20] Y. P. Sun, C. E. Bunker, *Nature* **1993**, *365*, 398.
[21] T. Harada, S. Shinkai, *J. Chem. Soc. Perkin Trans. 2*, **1995**, 2231–2242.
[22] J. W. Steed, C. P. Johnson, C. L. Barnes, R. K. Juneja, J. L. Atwood, S. R. Reily, R. L. Hollis, P. H. Smith, D. L. Clark, *J. Am. Chem. Soc.* **1995**, *117*, 11426–11433.
[23] R. J. Blanch, M. Williams, G. D. Fallon, M. G. Gardiner, R. Kaddour, C. L. Raston, *Angew. Chem.* **1997**, *109*, 520–522; *Angew. Chem. Int. Ed. Engl.* **1997**, *36*, 504–506.

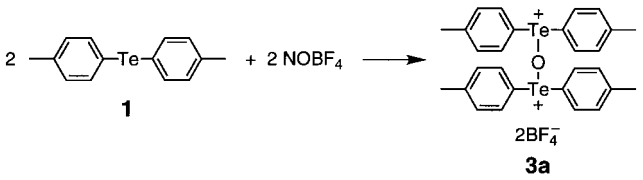
 © WILEY-VCH Verlag GmbH, D-69451 Weinheim, 1998 1433-7851/98/3707-0983 $ 17.50+.50/0

Insertion of an Oxygen Atom between Tellurium Atoms upon Oxidation of a Diaryl Telluride with $NOBF_4$ or $(CF_3SO_2)_2O/O_2$: Dicationic Bis[diaryltellurium(IV)] Oxide**

Kenji Kobayashi, Nobuo Deguchi, Ernst Horn, and Naomichi Furukawa*

Despite the large body of information on σ-bonded dichalcogen dications formed by intramolecular reactions through transannular effects,[1] bond formation by intermolecular reactions has received much less attention. Musker et al. pointed out that the radical cation prepared from 1,5-dithiacyclooctane and one equivalent of nitrosyl tetrafluoroborate ($NOBF_4$) would be dimerized in the solid state to form an intermolecular dithia dication.[2] As part of our aim to synthesize an intermolecularly formed ditellurium dication and multitellurium dications,[3] we report here on the preparation, crystal structure, and properties of the bis[diaryltellurium(IV)] oxide dication in **3**,[4, 5] which was apparently produced for the first time by insertion of the oxygen atom of nitrogen monoxide or an O_2 molecule between two tellurium atoms by various chemical oxidations of diaryl telluride.

Treatment of bis(4-methylphenyl) telluride (**1**) with one equivalent of $NOBF_4$ in dry CH_2Cl_2/CH_3CN at $-40\,^\circ C$ under an Ar atmosphere for 30 min afforded bis[bis(4-methylphenyl)tellurium(IV)] oxide bis(tetrafluoroborate) (**3a**) in quantitative yield (Scheme 1). The ^{125}Te NMR spectrum of **3a** in



Scheme 1. Synthesis of **3a** from **1** and $NOBF_4$.

CD_3CN shows a peak at $\delta = 1301.3$, that is, shifted downfield by 646 ppm relative to the signal for **1**. This remarkable downfield shift is characteristic of a cationic species. The FAB-MS spectrum of **3a** exhibits a parent peak at $m/z = 655$ for M^+ [$M^+ = (M - 2BF_4^- + F^-)^+$]. Compound **3a** reacted with four equivalents of thiophenol under an Ar atmosphere to give **1** and diphenyl disulfide in quantitative yields. Treatment of **3a** with aqueous NaOH quantitatively afforded bis(4-methylphenyl) telluroxide (**2**). These results undoubtedly support the formation of **3a** with the dicationic Te-O-Te bond, in which the Te atoms are threefold coordinated (Scheme 1).

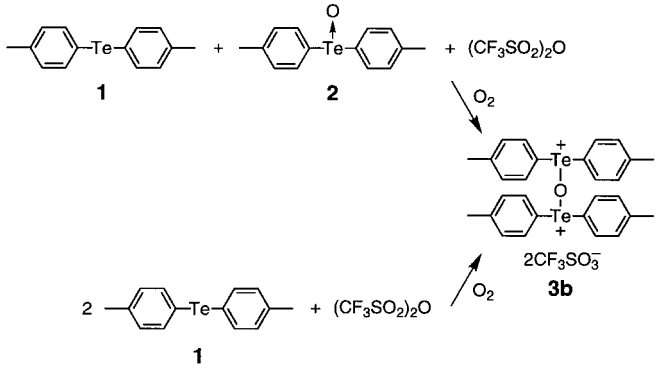
[*] Prof. Dr. N. Furukawa, Dr. K. Kobayashi, N. Deguchi, Dr. E. Horn
Department of Chemistry and Tsukuba Advanced Research Alliance Center
University of Tsukuba
Tsukuba, Ibaraki 305 (Japan)
Fax: (+81) 298-53-4313
E-mail: furukawa@staff.chem.tsukuba.ac.jp

[**] This work was supported in part by grants-in-aid from the Ministry of Education, Science, Sports, and Culture, Japan (no. 07404035) and University of Tsukuba (TARA project fund).

Bis[(halo)diaryltellurium(IV)] oxides having tetracoordinate Te atoms are generally prepared by the thermal dehydration of diaryltellurium hydroxy halides and their derivatives.[4–6] The present reaction is not of this type. It proceeds instantaneously at $-40\,^\circ C$ under anhydrous and anaerobic conditions. In the presence of two equivalents of $H_2{}^{18}O$, the reaction gave **3a**, whose FAB-MS spectrum showed no incorporation of an ^{18}O atom. These results suggest that nitrogen monoxide (NO), which is generated from the redox reaction of **1** with $NOBF_4$, would be a source of the oxygen atom in **3a**. Thus, a radical cation of **1** or the corresponding ditellurium dication formed by dimerization would react with NO to give **3a**.[7, 8]

The hypothesis that NO is the oxygen source was partly confirmed by the reaction of **1** with one equivalent of ethyl nitrite (10 wt% in ethanol) as a synthetic equivalent of NO in the presence of one equivalent of $Cu(ClO_4)_2 \cdot 6H_2O$ as an oxidizing agent in CH_3CN under an Ar atmosphere. A similar dicationic Te-O-Te bonded species was formed in quantitative yield.

The similar dicationic bis[diaryltellurium(IV)] oxide ditriflate (**3b**) was quantitatively obtained by the reaction of a 1:1 mixture of **1** and **2** with one equivalent of triflic anhydride (Tf_2O) in dry CH_3CN between $-40\,^\circ C$ and room temperature under an O_2 atmosphere for 1 h (Scheme 2).[9] Treatment of **1**



Scheme 2. Synthesis of **3b**.

with 0.5 equivalents of Tf_2O under the same conditions also afforded **3b** in quantitative yield. In solution, the triflate as a counterion is not expected to be coordinated to the Te atoms, because the chemical shift of **3b** in the ^{125}Te NMR spectrum ($\delta = 1288.4$) is almost the same as that of **3a**. Under an Ar atmosphere neither of the reactions shown in Scheme 2 afforded **3b**; hence, molecular oxygen is essential for the formation of **3b**.[10] The following mechanism seems to be plausible. The reaction of **2** with Tf_2O may lead to a diaryl(trifluoromethanesulfonyloxy)telluronium salt[11] or diaryltellurium ditriflate,[12] which reacts with **1** to afford an intermolecular ditellurium dication and two molecules of triflate. Insertion of O_2 into the resulting ditellurium dication would produce **3b**. In the other case, the reaction of **1** with Tf_2O leading to a diaryl(trifluoromethanesulfonyl)telluronium salt[13] and the subsequent reaction with the second molecule of **1** may afford the ditellurium dication and trifluoromethanesulfinate, both of which would be oxidized by O_2 to produce **3b**.

 © WILEY-VCH Verlag GmbH, D-69451 Weinheim, 1998 1433-7851/98/3707-0984 $ 17.50+.50/0

The crystal structure of **3b** was determined by X-ray diffraction analysis (Figure 1).[14] An inspection reveals several important points: 1) Molecules of **3b** associate in pairs

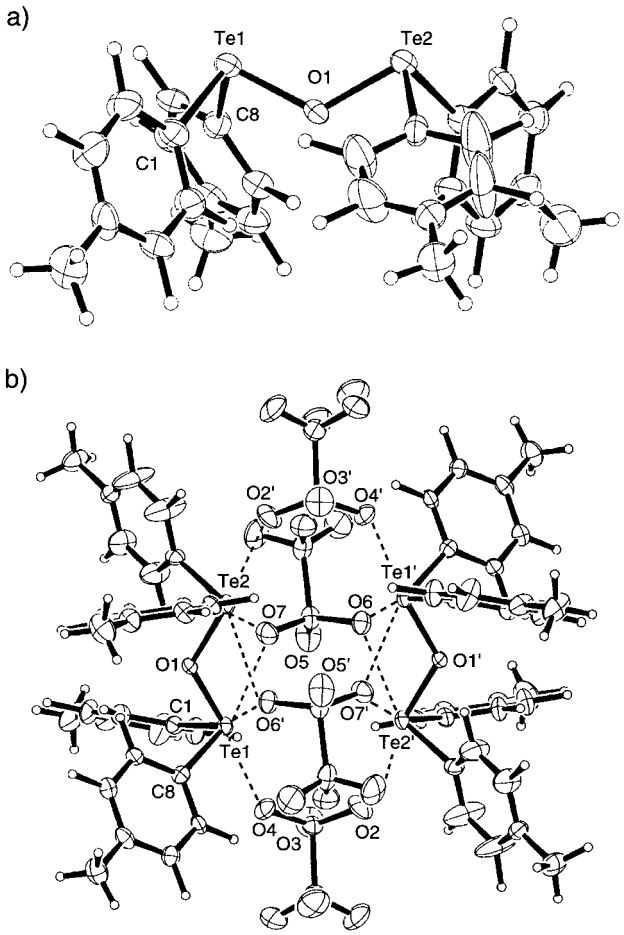


Figure 1. a) ORTEP drawing of the structure of **3b** (thermal ellipsoids represent the 30% probability level); for clarity the counterions have been removed. b) A pair of **3b** molecules with counterions. Selected bond lengths [Å] and angles [°]: Te1–O1 1.937(6), Te1 ··· O4 2.639(7), Te1 ··· O6′ 2.901(7), Te1 ··· O7 2.898(7), Te2–O1 1.957(6), Te2 ··· O2′ 2.680(7), Te2 ··· O6′ 2.977(7), Te2 ··· O7 2.922(8); Te1-O1-Te2 123.8(3), O1-Te1-C1 90.0(3), O1-Te1-C8 90.9(3), C1-Te1-C8 98.3(4), O4 ··· Te1-O1 174.4(2), O7 ··· Te1-C8 161.4(2), O6′ ··· Te1-C1 160.2(2).

across a center of symmetry located between the atoms O1 and O1′ (Figure 1b; the primed atoms refer to the respective symmetry-related atoms at $1-x, -y, -z$). Each of the four counterions interacts with the Te atoms of the paired dications through their O atoms in the range of 2.64–2.98 Å. These contacts are considerably shorter than the sum of the van der Waals radii (3.60 Å) of the two elements. 2) Each Te atom has a pseudo-octahedral geometry. 3) The pairs of bis[diaryltellurium(IV)] oxide dications are stacked in columns that run approximately parallel to the *a* axis. The resulting channels created by the dications are occupied by two columns of the triflate counterions.

In the present study we have demonstrated that NO and O_2 molecules can be the oxygen source to afford the dicationic Te-O-Te bonded species by chemical oxidations of diaryl telluride.[15]

Experimental Section

3a: To a solution of **1** (0.56 mmol) in dry CH_2Cl_2 (2 mL) at $-40\,^{\circ}C$ under an Ar atmosphere was added a solution of $NOBF_4$ (0.67 mmol) in dry CH_3CN (4 mL). The resulting deep red solution was stirred for 30 min at the same temperature, during which time it became pale yellow. The reaction mixture was evaporated in vacuo to give **3a** as a white powder in quantitative yield. Recrystallization of **3a** from CH_3CN/benzene gave colorless crystals. M.p. 155–160 °C (decomp); ^{1}H NMR (400 MHz, CD_3CN, 25 °C): $\delta = 2.42$ (s, 6H), 7.45, 7.65 (AB q, $J = 7.9$ Hz, 8H); ^{13}C NMR (100 MHz, CD_3CN, 25 °C): $\delta = 21.5$, 131.0, 131.9, 133.7, 145.0; ^{19}F NMR (254 MHz, CD_3CN, 25 °C): $\delta = -150.7$; ^{125}Te NMR (126 MHz, CD_3CN, 25 °C): $\delta = 1301.3$; FAB-MS (2-nitrophenyl octyl ether matrix): *m*/*z*: 655 [M^+] ($M^+ = (M - 2BF_4^- + F^-)^+$); elemental analysis calcd for $C_{28}H_{28}OTe_2 \cdot 2BF_4$: C 41.55, H 3.49; found: C 41.53, H 4.08.

3b: To a suspension of **1** (0.12 mmol) and **2** (0.12 mmol) in dry CH_3CN (2 mL) at $-40\,^{\circ}C$ under an O_2 atmosphere was added triflic anhydride (0.12 mmol). The resulting homogeneous deep red solution was stirred at room temperature for 1 h, during which time it became pale orange. The reaction mixture was evaporated in vacuo to give **3b** as a white powder in quantitative yield. Recrystallization of **3b** from CH_3CN at $-20\,^{\circ}C$ gave colorless single crystals that were suitable for an X-ray analysis. M.p. 273–274 °C (decomp); ^{1}H NMR (400 MHz, CD_3CN, 25 °C): $\delta = 2.42$ (s, 6H), 7.45, 7.66 (AB q, $J = 7.9$ Hz, 8H); ^{13}C NMR (100 MHz, CD_3CN, 25 °C): $\delta =$ 21.4, 121.2 ($^1J_{C,F} = 317.3$ Hz), 131.0, 131.6, 133.6, 144.8; ^{19}F NMR (254 MHz, CD_3CN, 25 °C): $\delta = -79.7$; ^{125}Te NMR (126 MHz, CD_3CN, 25 °C): $\delta =$ 1288.4; elemental analysis calcd for $C_{28}H_{28}OTe_2 \cdot 2CF_3SO_3$: C 38.59, H 3.02; found: C 38.40, H 2.93.

Received: September 3, 1997 [Z10886IE]
German version: *Angew. Chem.* **1998**, *110*, 1031–1033

Keywords: insertions · nitrogen monoxide · oxidations · tellurium

[1] a) W. K. Musker, *Acc. Chem. Res.* **1980**, *13*, 200–206; b) H. Fujihara, R. Akaishi, N. Furukawa, *Tetrahedron* **1993**, *49*, 1605–1618.
[2] a) W. K. Musker, T. L. Wolford, P. B. Roush, *J. Am. Chem. Soc.* **1978**, *100*, 6416–6421; b) M. Tamaoki, M. Serita, Y. Shiratori, K. Itoh, *J. Phys. Chem.* **1989**, *93*, 6052–6058.
[3] H. Fujihara, Y. Takaguchi, T. Ninoi, T. Erata, N. Furukawa, *J. Chem. Soc. Perkin Trans. 1* **1992**, 2583–2584.
[4] K. L. Irgolic, *The Organic Chemistry of Tellurium*, Gordon & Breach, New York, **1974**, pp. 187–188.
[5] a) C. S. Mancinelli, D. D. Titus, R. F. Ziolo, *J. Organomet. Chem.* **1977**, *140*, 113–125; b) V. I. Naddaka, K. V. Avenesyan, M. L. Cherkinskaya, V. I. Minkin, *Zh. Org. Khim.* **1987**, *23*, 885–886; c) I. D. Sadekov, A. A. Maksimento, B. B. Rivkin, V. I. Minkin, *Zh. Obsch. Khim.* **1989**, *59*, 2015–2021; d) P. Magnus, M. B. Roe, V. Lynch, C. Hulme, *J. Chem. Soc. Chem. Commun.* **1995**, 1609–1610.
[6] The only exception is reported by E. A. Meyers et al. The reaction of phenoxatellurine with its dinitrate in CH_2Cl_2 at room temperature gives bis(phenoxatelluronium) dinitrate: M. M. Mangion, M. R. Smith, E. A. Meyers, *J. Heterocycl. Chem.* **1973**, *10*, 543–549.
[7] The fate of the N atom of NO remains uncertain at this stage. The ESR spectrum of the reaction mixture under the same conditions did not show any signals probably owing to instability of a radical cation of **1** or a very fast reaction. For the related isolable Te^{III} radical cation of $Te[N(SiMe_3)_2]_2$, see M. Björgvinsson, T. Heinze, H. W. Roesky, F. Pauer, D. Stalke, G. M. Sheldrick, *Angew. Chem.* **1991**, *103*, 1671–1672; *Angew. Chem. Int. Ed. Engl.* **1991**, *30*, 1677–1678.
[8] We reported that 1,5-ditelluracyclooctane, in which the two Te atoms are juxtapositioned, reacts with two equivalents of $NOBF_4$ to give the stable ditellurium dication (H. Fujihara, T. Ninoi, R. Akaishi, T. Erata, N. Furukawa, *Tetrahedron Lett.* **1991**, *32*, 4537–4540). By dimerization of two radical cations of **1**, the present reaction may also form an intermolecular ditellurium dication which, in marked contrast, would be very unstable owing to a flexible conformation and may therefore react with NO to give **3a**.
[9] The reaction of **2** with 0.5 equivalents of Tf_2O gave **3b** in very low yield (ca. 16%). This difference may be partly explained by the

 © WILEY-VCH Verlag GmbH, D-69451 Weinheim, 1998 1433-7851/98/3707-0985 $ 17.50+.50/0

possibility that the reactivity of **2** with respect to a diaryl(trifluoromethanesulfonyloxy)telluronium salt which could be initially formed is lower than that of **1**.

[10] Both reactions in the absence of O_2 in CH_3CN were monitored by ESR spectroscopy. However, no ESR signals were detected. Even if a radical cation is formed, its concentration would be quite low.

[11] Diphenyl sulfoxide reacts with Tf_2O to form a diphenyl(trifluoromethanesulfonyloxy)sulfonium salt: B. A. Garcia, J. L. Poole, D. Y. Gin, *J. Am. Chem. Soc.* **1997**, *119*, 7597 – 7598.

[12] For diaryltellurium bis(trifluoroacetate), see Y. Takaguchi, H. Fujihara, N. Furukawa, *J. Organomet. Chem.* **1995**, *498*, 49 – 52.

[13] Dimethyl sulfide reacts with Tf_2O to produce a dimethyl(trifluoromethanesulfonyl)sulfonium salt: V. G. Nenajdenko, P. V. Vertelezkij, A. B. Koldobskij, I. V. Alabugin, E. S. Balenkova, *J. Org. Chem.* **1997**, *62*, 2483 – 2486.

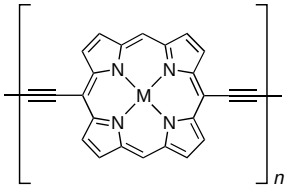
[14] Crystal structure analysis of **3b**: crystal dimensions $0.15 \times 0.25 \times 0.30$ mm, monoclinic, space group $P2_1/n$, $a = 13.318(4)$, $b = 18.319(7)$, $c = 14.871(4)$ Å, $\beta = 104.01(2)^\circ$, $V = 3520(1)$ Å^3, $Z = 4$, $\rho_{calcd} = 1.76$ g cm^{-3}, $2\theta_{max} = 51.9^\circ$. Rigaku AFC-7R four-circle diffractometer, $Mo_{K\alpha}$ radiation, $\lambda = 0.71069$ Å, $\omega/2\theta$ scan mode, $T = 253$ K, 5330 measured reflections, Lorentzian and polarization corrections, absorption coefficient 18.5 cm^{-1}, semi-empirical absorption correction (Ψ scans; transmission factors 0.60 – 1.00), structure solution with direct methods (SIR92), package teXsan (1992), full-matrix least-squares refinement based on F, 2893 observed reflections ($I > 3.0\sigma(I)$), 424 parameters, hydrogen atoms included but not refined, $R = 0.036$, $R_w = 0.039$, residual electron density 0.51 e Å^{-3}. Crystallographic data (excluding structure factors) for the structure reported in this paper have been deposited with the Cambridge Crystallographic Data Centre as supplementary publication no. CCDC-100642. Copies of the data can be obtained free of charge on application to CCDC, 12 Union Road, Cambridge CB2 1EZ, UK (fax: (+44) 1223-336-033; e-mail: deposit@ccdc.cam.ac.uk).

[15] For elements of Group 15 (E = Sb, Bi), insertion of O_2 molecules into E–E bonds occurs: a) F. Calderazzo, R. Poli, G. Pelizzi, *J. Chem. Soc. Dalton Trans.* **1984**, 2365 – 2369; b) H. J. Breunig, T. Krüger, E. Lork, *Angew. Chem.* **1997**, *109*, 654 – 655; *Angew. Chem. Int. Ed. Engl.* **1997**, *36*, 615 – 617.

Enhanced Electronic Conjugation in Anthracene-Linked Porphyrins

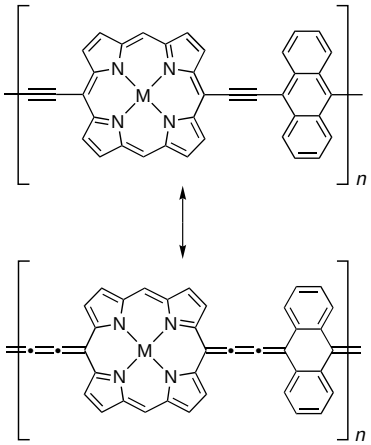
Peter N. Taylor, Andrew P. Wylie, Juhani Huuskonen, and Harry L. Anderson*

Porphyrin polymers such as **1** (side chains omitted for clarity) exhibit exceptionally strong third-order nonlinear optical (NLO) behavior[1] because of their extensive electronic conjugation. This is potentially useful for fabricating electro-optic modulators for telecommunications. However even in **1** the NLO coefficient $\chi^{(3)}$ is not high enough for practical devices, so we are exploring routes to more conjugated porphyrin polymers. Müllen et al. have shown



1

that the incorporation of 9,10-anthrylene units in conjugated polymers reduces the band-gap by reducing the energy difference between the aromatic and quinoidal resonance structures.[2] Thus the anthracene/porphyrin polymer **2** might be expected to be more conjugated than **1** because the



2 ↔ **3**

anthrylene units stabilize the quinoidal/cumulenic resonance structure **3**. 9,10-Diethynylanthracene units are also interesting because of their intense fluorescence and potential electroluminescence; several conjugated polymers containing these units have been synthesized.[3] Here we demonstrate, using model oligomers, that 9,10-diethynylanthracene spacers enhance the conjugation between *meso*-linked porphyrins better than butadiyne, 1,4-diethynylbenzene or 1,4-diethynylthiophene bridges.

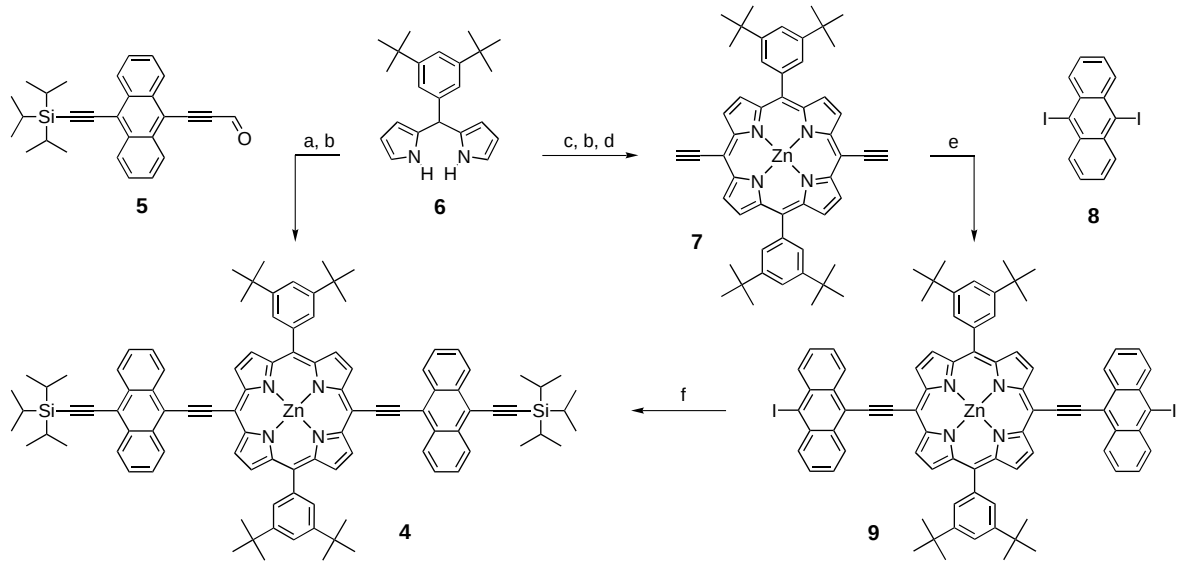
There are numerous examples of molecules containing porphyrins and anthracenes linked either directly[4] or through saturated bridges,[5] polyenes,[6] and aromatic linkages.[7] Few of these exhibit much porphyrin – anthracene conjugation, because most unsaturated bridges twist out of plane with the porphyrin to avoid steric clashes. Alkynyl substituents are the only effective way of making conjugated connections to the *meso* position of a porphyrin. Marx and Breitmaier[8] have reported a porphyrin connected through alkynyl substituents to the 1-position of anthracene, but this does not allow resonance of the type postulated for **2** ↔ **3**.

To develop a synthetic route to conjugated anthracene/porphyrin oligomers we first synthesized **4** by the two routes shown in Scheme 1. Condensation of aldehyde **5**[9] with 3,5-

[*] Dr. H. L. Anderson, Dr. P. N. Taylor, A. P. Wylie, Dr. J. Huuskonen
Dyson Perrins Laboratory, University of Oxford
South Parks Road, Oxford OX1 3QY (UK)
Fax: (+44) 1865-275674.
E-mail: harry.anderson@chem.ox.ac.uk

[**] We thank the Engineering and Physical Sciences Research Council (UK), the Finnish Academy, and Emil Aaltonen Foundation for support, and the EPSRC Mass Spectrometry Service in Swansea for FAB mass spectra. The crystallographic work was done at Chemical Crystallography, at the University of Oxford, with generous assistance from Dr. D. J. Watkin. We are grateful to Dr. Garry Rumbles for valuable discussion and for providing facilities for fluorescence measurements at the Department of Chemistry, Imperial College, London. We thank Micromass UK Ltd. for MALDI-TOF MS instrument time and Dr. R. T. Aplin for running these mass spectra.

 © WILEY-VCH Verlag GmbH, D-69451 Weinheim, 1998 1433-7851/98/3707-0986 $ 17.50+.50/0



Scheme 1. a) **5**, $BF_3 \cdot OEt_2$, CH_2Cl_2 then 2,3-dichloro-5,6-dicyano-*para*-benzoquinone (DDQ), 9%; b) $Zn(OAc)_2$, 90%; c) Me_3SiC_2CHO, $BF_3 \cdot OEt_2$, CH_2Cl_2, then DDQ, 30%; d) Bu_4NF, CH_2Cl_2, 95%; e) $LiN(SiMe_3)_2$, THF then $ZnCl_2$ then **8**, $[Pd_2(dba)_3]$ (dba = 1,3-dibenzylideneacetone), $AsPh_3$, 13%; f) $i Pr_3SiC_2ZnCl$, $[Pd_2(dba)_3]$, $AsPh_3$, 39%.

di(*tert*-butylphenyl)dipyrromethane (**6**)[10] and subsequent oxidation and metalation gave **4** (8% yield from **6**). Short reaction times (3 mins) are needed to avoid forming mixtures of porphyrins because the porphyrinogen intermediate is prone to acid-catalyzed scrambling. In the second route, **4** is produced by palladium-catalyzed coupling. The 5,15-diethynylporphyrin **7** (prepared in 26% yield from **6** using established methodology[10]) was treated with excess 9,10-diiodoanthracene (**8**)[11] under modified Heck conditions to give **9**, which was coupled to triisopropylsilylacetylene under similar conditions to give **4** (5% overall yield from **7**).

The UV/Vis absorption spectrum of **4** is compared to those of reference compounds **10** and **11** in Figure 1. In contrast to other anthracene-containing porphyrin dyads the absorption

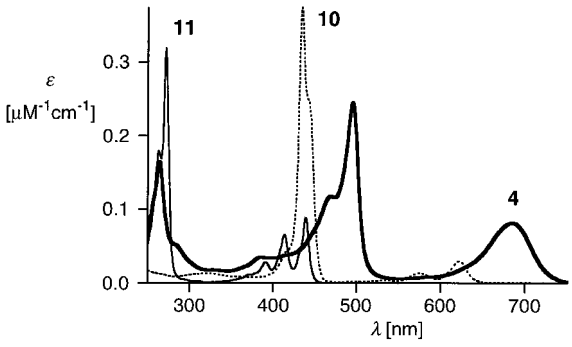


Figure 1. Absorption spectra of **4** (bold), **10** (dashed) and **11** (plain) in CH_2Cl_2. The spectrum of **11** is scaled up by a factor of 2 for better comparison with **4**.

spectrum of **4** is very different from those of both its components. The anthracene S_0-S_3 transition at 264 nm is abnormally weak in **4**, whereas the porphyrin S_0-S_2 B band (Soret) and S_0-S_1 Q band are unusually intense, as shown by oscillator strengths[12] f_B and f_Q in Table 1. The general increase in oscillator strength can be attributed to the

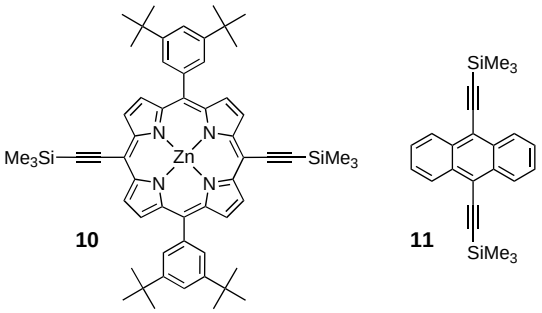


Table 1. Summary of electronic spectra.[a]

Porphyrin	λ_B [nm]	λ_Q [nm]	λ_f [nm]	Φ_f	f_B	f_Q
10	436	578, 625	629	0.025	1.2	0.12
4	469, 496	685	710	0.048	1.9	0.40
13	441, 531	706	764	0.052	1.2	0.35
14	458, 494	675, 741	749	0.055	1.2	0.23
15	455	686	693	0.043	1.4	0.25
16	456, 496	704	719	0.053	1.4	0.23

[a] All spectra were recorded in 1% C_5H_5N/CH_2Cl_2, except those of **4** and **10** which are in CH_2Cl_2. λ_B and λ_Q are the absorption λ_{max}, and f_B and f_Q are the oscillator strengths[12] per porphyrin, for the B and Q bands; Φ_f is the fluorescence quantum yield.[13]

extension of the porphyrin chromophore, while the intensification of the Q band is probably due to reduced a_{1u}-a_{2u} degeneracy.[1] Excitation of **4** at both 264 and 496 nm produces emission at 710 nm and there is close agreement between the excitation and absorption spectra showing that anthracene-to-porphyrin energy transfer is quantitative.

The crystal structure[14] of $\mathbf{4} \cdot 2(C_5H_5N)$ is shown in Figure 2. The bond lengths are normal[15] and show no manifestations of the distorted electronic structures of the porphyrin and anthracene chromophores. Interestingly, the plane of the anthracene units is at an angle of 40.90(7)° to that of the porphyrin. Molecular mechanics calculations indicate that

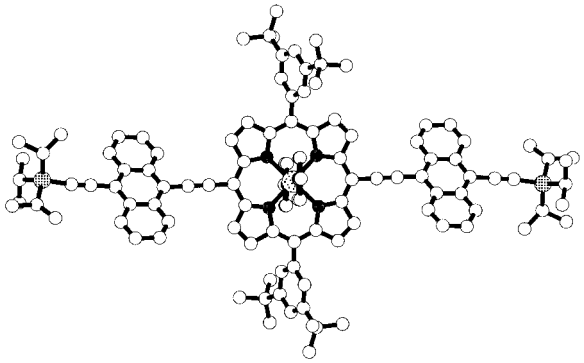
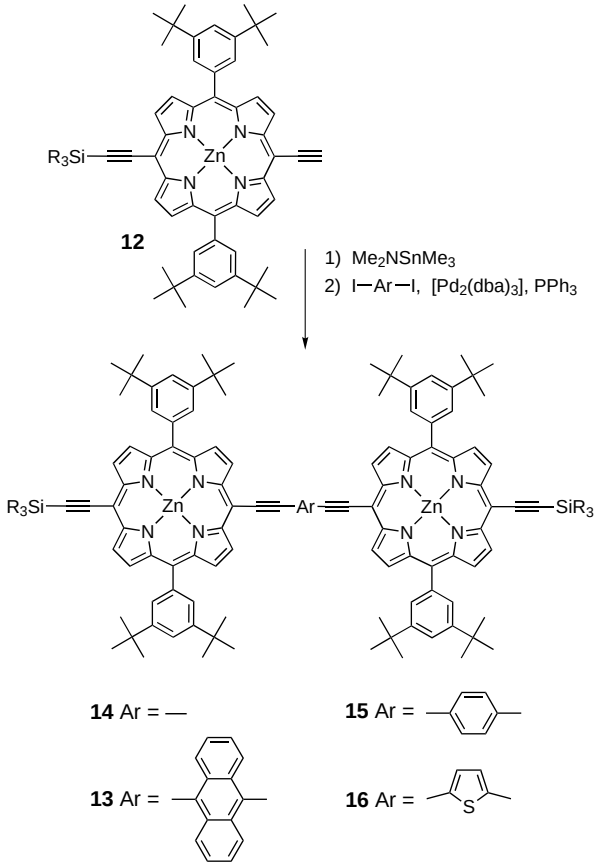


Figure 2. Crystal structure of porphyrin $\mathbf{4}\cdot(C_5H_5N)_2$.

there is no steric barrier to planarity, so the conformation is probably influenced by crystal packing.

Conjugated porphyrin dimers were synthesized as shown in Scheme 2. The terminal acetylene **12**[9] was stannylated, then Stille coupled with **8** to give the anthracene-linked dimer **13** in



Scheme 2. Synthesis of porphyrin dimers (R = *n*-hexyl).

46% yield and a small amount (ca. 5%) of the butadiyne-linked dimer **14**, which was also prepared by oxidative coupling of the terminal acetylene.[9] Similar conditions were used to prepare the 1,4-phenylene- and 2,5-thienylene-linked dimers **15** and **16** in 61 and 52% yield, respectively. Similar butadiyne-, benzene- and thiophene-linked dimers have been reported previously.[16] Selected spectroscopic data for **13**–**16** are listed in Tables 1 and 2.

Table 2. Selected spectroscopic data for porphyrin dimers **13**, **14**, and **15**.[a]

13: ^{1}H NMR: $\delta = 10.06$ (d, $J = 5$ Hz, 4H), 9.68 (d, $J = 5$ Hz, 4H), 9.52 (dd, $J = 7$ and 3 Hz, 4H), 9.02 (d, $J = 5$ Hz, 4H), 8.89 (d, $J = 5$ Hz, 4H), 8.08 (d, $J = 2$ Hz, 8H), 7.94 (dd, $J = 7$ and 3 Hz, 4H), 7.86 (t, $J = 2$ Hz, 4H), 1.82 (m, 12H), 1.60 (s, 72H), 1.58 (m, 12H), 1.43 (m, 24H), 1.08 (m, 12H), 0.92 (t, $J = 7$ Hz, 18H); ^{13}C NMR: $\delta = 152.76, 152.34, 150.96, 150.70, 148.92, 142.20, 133.59, 133.29, 132.93, 131.15, 130.84, 129.89, 128.43, 127.39, 124.56, 121.17, 120.03, 110.05, 107.64, 101.47, 101.27, 99.87, 94.44, 35.31, 33.54, 32.03, 31.94, 24.66, 22.87, 14.37, 14.27$; IR (KBr): $\tilde{\nu}_{max} = 2135$ cm^{-1}; UV/Vis: $\lambda_{max}(\log\varepsilon) = 706$ (4.96), 531 (4.91), 441 nm (5.18); TOF LD-MS: $m/z = 2335.1$ [M+H$^+$], correct for $C_{154}H_{186}N_8Si_2Zn_2$.

14: ^{1}H NMR: $\delta = 9.90$ (d, $J = 5$ Hz, 4H), 9.67 (d, $J = 5$ Hz, 4H), 8.99 (d, $J = 5$ Hz, 4H), 8.89 (d, $J = 5$ Hz, 4H), 8.06 (d, $J = 2$ Hz, 8H), 7.83 (t, $J = 2$ Hz, 4H), 1.79 (m, 12H), 1.58 (s, 72H), 1.56 (m, 12H), 1.40 (m, 24H), 1.04 (m, 12H), 0.91 (t, $J = 7$ Hz, 18H); ^{13}C NMR: $\delta = 153.11, 152.37, 150.89, 150.44, 148.76, 141.89, 133.37, 132.88, 131.09, 130.73, 130.11, 124.55, 121.04, 109.78, 101.73, 99.83, 99.46, 88.83, 82.56, 35.25, 33.57, 31.98, 31.90, 24.60, 22.89, 14.37, 14.14$; IR (KBr): $\tilde{\nu}_{max} = 2135$ cm^{-1}; UV/Vis: $\lambda_{max}(\log\varepsilon) = 741$ (5.11), 675 (4.91), 494 (5.34), 458 nm (5.62); TOF LD-MS: $m/z = 2159.3$ [M+H$^+$], correct for $C_{140}H_{178}N_8Si_2Zn_2$.

15: ^{1}H NMR: $\delta = 9.81$ (d, $J = 5$ Hz, 4H), 9.68 (d, $J = 5$ Hz, 4H), 8.96 (d, $J = 5$ Hz, 4H), 8.89 (d, $J = 5$ Hz, 4H), 8.20 (s, 4H), 8.07 (d, $J = 2$ Hz, 8H), 7.86 (t, $J = 2$ Hz, 4H), 1.83 (m, 12H), 1.61 (s, 72H), 1.59 (m, 12H), 1.44 (m, 24H), 1.06 (m, 12H), 0.93 (t, $J = 7$ Hz, 18H); ^{13}C NMR: $\delta = 152.50, 152.02, 150.73, 150.57, 148.75, 141.99, 133.04, 132.92, 131.91, 131.03, 130.63, 130.12, 124.40, 124.30, 121.01, 109.88, 101.14, 100.64, 99.55, 96.56, 96.29, 35.27, 33.59, 32.01, 31.92, 24.62, 22.90, 14.39, 14.18$; IR (KBr): $\tilde{\nu}_{max} = 2137$ cm^{-1}; UV/Vis: $\lambda_{max}(\log\varepsilon) = 686$ (5.18), 455 nm (5.65); TOF LD-MS: $m/z = 2235.1$ [M+H$^+$], correct for $C_{146}H_{182}N_8Si_2Zn_2$.

[a] ^{1}H (500 MHz) and ^{13}C (125 MHz) NMR spectra were recorded in 1% $C_5D_5N/CDCl_3$ and UV/Vis spectra in 1% C_5H_5N/CH_2Cl_2.

The absorption and emission spectra of three of the dimers, **13**, **14**, and **15** are shown in Figures 3 and 4. The effect of the anthracene unit on porphyrin–porphyrin electronic coupling is best seen by comparing the emission spectra of **13** and **15**. The distance between the porphyrins is the same in these two dimers, yet the emission from **13** is red-shifted by 71 nm

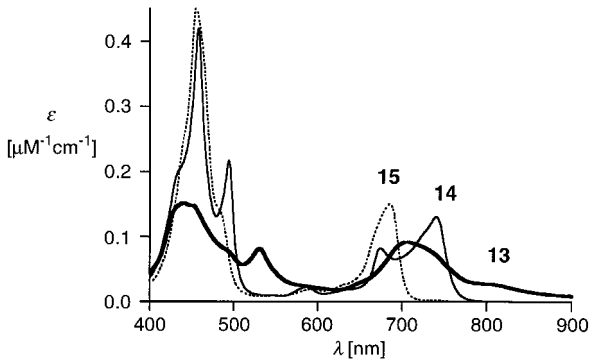


Figure 3. Absorption spectra of dimers **13** (bold), **14** (plain), and **15** (dashed) in 1% C_5H_5N/CH_2Cl_2.

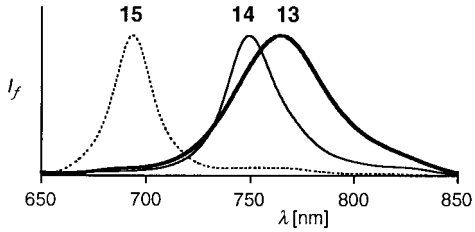


Figure 4. Emission spectra of dimers **13** (bold), **14**, (plain), and **15** (dashed) in 1% C_5H_5N/CH_2Cl_2.

 © WILEY-VCH Verlag GmbH, D-69451 Weinheim, 1998 1433-7851/98/3707-0988 $ 17.50+.50/0

indicating strong porphyrin–porphyrin conjugation. Comparing **13**, **15** and **16** shows that the thiophene unit leads to more conjugation than phenylene, but less than anthracene. It is remarkable that the 9,10-diethynylanthracene bridge allows even more electronic communication than the simple butadiyne link in **14**. This implies that longer oligomers of type **2**/**3** should have strong third-order NLO behavior.

Experimental Section

13: A solution of **12**[9] (54 mg, 50 μmol) in THF (8 mL) and pyridine (80 μL) was treated with dimethylaminotrimethyltin (41 μL, 250 μmol) at 50 °C for 2 h, then evaporated. To the resulting waxy residue was added THF (8 mL), **8**[11] (11 mg, 25 μmol), tris(dibenzylideneacetone)dipalladium(0) (2.7 mg, 3 μmol), and triphenylphosphane (3.1 mg, 12 μmol) under argon. The mixture was stirred at 50 °C for 24 h. Purification by chromatography on silica (eluting with 50/2/1 petroleum ether (60–80 °C)/ethyl acetate/pyridine) and recrystallization from CH_2Cl_2/methanol yielded **13** as a brown solid (27 mg, 46 %).

Received: September 5, 1997
Revised version: December 15, 1997 [Z10894IE]
German version: *Angew. Chem.* **1998**, *110*, 1033–1037

Keywords: alkynes · anthracene · conjugation · nonlinear optics · porphyrinoids

[1] H. L. Anderson, S. J. Martin, D. D. C. Bradley, *Angew. Chem.* **1994**, *106*, 711–713; *Angew. Chem. Int. Ed. Engl.* **1994**, *33*, 655–657; *Adv. Mater. Opt. Electron.* **1994**, *4*, 277–283; D. Beljonne, G. E. O'Keefe, P. J. Hamer, R. H. Friend, H. L. Anderson, J. L. Brédas, *J. Chem. Phys.* **1997**, *106*, 9439–9460. Second-order NLO materials with this type of structure have also been developed: S. M. LeCours, H.-W. Guan, S. G. DiMagno, C. H. Wang, M. J. Therien, *J. Am. Chem. Soc.* **1996**, *118*, 1497–1503; S. Priyadarshy, M. J. Therien, D. N. Beratan, *ibid*. **1996**, *118*, 1504–1510.

[2] R. O. Garay, H. Naarmann, K. Müllen, *Macromolecules* **1994**, *27*, 1922–1927; U. Scherf, K. Müllen, *Synthesis* **1992**, 23-38.

[3] T. M. Swager, C. J. Gil, M. S. Wrighton, *J. Phys. Chem.* **1995**, *99*, 4886–4893; D. Ofer, T. M. Swager, M. S. Wrighton, *Chem. Mater.* **1995**, *7*, 418–425; M. S. Khan, A. K. Kakkar, N. J. Long, J. Lewis, P. Raithby, P. Nguyen, T. B. Marder, F. Wittmann, R. H. Friend, *J. Mater. Chem.* **1994**, *4*, 1227–1232; K. Sonogashira, K. Asami, N. Takeuchi, *J. Mat. Sci. Lett.* **1985**, *4*, 737–740; K. Sanechika, T. Yamamoto, A. Yamamoto, *Bull. Chem. Soc. Jpn.* **1984**, *57*, 752–755.

[4] J.-M. Cense, R.-M. Le Quan, *Tetrahedron Lett.* **1979**, 3725–3728; S. Nakajima, A. Osuka, *ibid.* **1995**, *36*, 8457–8460.

[5] M. Sirish, R. Kache, B. G. Maiya, *J. Photochem. Photobiol. A* **1996**, *93*, 129–136.

[6] F. Effenberger, H. Schlosser, P. Bäuerle, S. Maier, H. Port, H. C. Wolf, *Angew. Chem.* **1988**, *100*, 274–277; *Angew. Chem. Int. Ed. Engl.* **1988**, *27*, 281–284.

[7] F. Würthner, M. S. Vollmer, F. Effenberger, P. Emele, D. U. Meyer, H. Port, H. C. Wolf, *J. Am. Chem. Soc.* **1995**, *117*, 8090–8099; S. Kawabata, I. Yamazaki, Y. Nishimura, *Bull. Chem. Soc. Jpn.* **1997**, *70*, 1125–1133.

[8] T. Marx, E. Breitmaier, *Liebigs Ann. Chem.* **1994**, 857–858.

[9] The synthesis of **5**, **12,** and **14** will be detailed elsewhere.

[10] G. S. Wilson, H. L. Anderson, *Synlett* **1996**, 1039–1040; H. L. Anderson, *Tetrahedron Lett.* **1992**, *33*, 1101–1104.

[11] B. F. Duerr, Y.-S. Chung, A. W. Czarnik, *J. Org. Chem.* **1988**, *53*, 2120–2122.

[12] The oscillator strength f is defined as: $f = (4.319 \times 10^{-9} n^{-1}) \int \varepsilon \, d\tilde{\nu}$, where n is the refractive index (1.42 for CH_2Cl_2), ε is the extinction coefficient ($M^{-1}\,cm^{-1}$) and $\tilde{\nu}$ is the frequency in wavenumbers (cm^{-1}).

[13] Fluorescence quantum yields were measured relative to 9,10-bis(phenylethynyl)anthracene ($\Phi_f = 0.58$); S. Nakatsuji, K. Matsuda, Y. Uesugi, K. Nakashima, S. Akiyama, W. Fabian, *J. Chem. Soc. Perkin Trans. 1* **1992**, 755–758.

[14] Crystals were grown by slow diffusion of *n*-pentane into a solution of **4** in 1 % $C_5H_5N/CHCl_3$, over two weeks. Crystal structure analysis for **4**·$2C_5H_5N$: $M_r = 1667.66$, triclinic, space group $P\bar{1}$, $a = 11.052(2)$, $b = 13.110(2)$, $c = 16.970(4)$ Å, $\alpha = 81.88(2)$, $\beta = 89.68(2)$, $\gamma = 77.20(2)°$, $V = 2372.9(8)$ Å^3, $Z = 1$, $T = 293$; $\rho_{calc} = 1.167$ g cm^{-3}; $\mu = 0.987$ mm^{-1}, crystal dimensions $0.25 \times 0.35 \times 0.45$ mm; diffractometer: Enraf-Nonius MACH3; radiation $Cu_{K\alpha}$ ($\lambda = 1.54184$ Å); scan mode: $\omega/2\theta$; range: $3.5 < \theta < 74.6$; measured reflections: 10156; independent reflections: 9712 ($R_{int} = 0.0186$); corrections applied: Lorentz polarization and experimental absorption correction (psi-scans, A. C. T. North, D. C. Phillips, F. S. Mathews, *Acta Crystallogr. A* **1968**, *24*, 351–359) T_{min}/T_{max} 0.7302/0.7839; R values ($I > 2\sigma I$): $R1 = 0.0847$, $wR2 = 0.2492$, all data: $R1 = 0.1344$, $wR2 = 0.2784$. Structure solution with direct methods (SHELXS-86, G. Sheldrick, 1990). Structure refinement (SHELXL-93, G. Sheldrick, 1993): Full-matrix least squares methods against F^2; 548 parameters, 28 constraints, max/min residual electron density 0.662/ – 0.825 e Å^{-3}. All non-hydrogen atoms were refined anisotropically and hydrogen atoms were placed in calculated positions. Crystallographic data (excluding structure factors) for the structure reported in this paper have been deposited with the Cambridge Crystallographic Data Center as supplementary publication no. CCDC-100671. Copies of the data can be obtained free of charge on application to CCDC, 12 Union Road, Cambridge CB2 1EZ, UK (fax: (+44) 1223-336-033; e-mail: deposit@ccdc.cam.ac.uk).

[15] Crystal structures of other 5,15-dialkynyl porphyrins have been reported: S. M. LeCours, S. G. DiMagno, M. J. Therien, *J. Am. Chem. Soc.* **1996**, *118*, 11854–11864; S.-P. J. Huuskonen, G. S. Wilson, H. L. Anderson, *Acta Crystallogr.*, in press.

[16] D. P. Arnold, D. A. James, *J. Org. Chem.* **1997**, *62*, 3460–3469; P. J. Angiolillo, V. S.-Y. Lin, J. M. Vanderkooi, M. J. Therien, *J. Am. Chem. Soc.* **1995**, *117*, 12514–12527; V. S.-Y. Lin, M. J. Therien, *Chem. Eur. J.* **1995**, *1*, 645–651; V. S.-Y. Lin, S. G. DiMagno, M. J. Therien, *Science* **1994**, *264*, 1105–1111; H. L. Anderson, *Inorg. Chem.* **1994**, *33*, 972–981; D. P. Arnold, D. A. James, C. H. L. Kennard, G. Smith, *J. Chem. Soc. Chem. Commun.* **1994**, 2131–2132; D. P. Arnold, L. J. Nitschinsk, *Tetrahedron Lett.* **1993**, *34*, 693–696.

The Azide-Nitrilimine Analogy in Aluminum Chemistry**

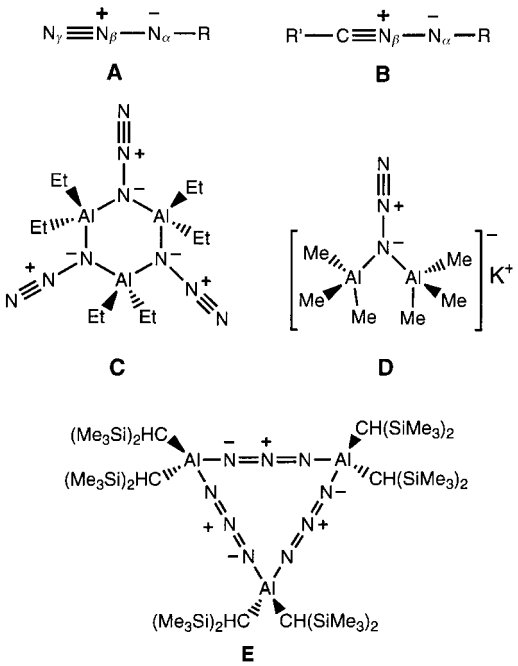
Norbert Emig, François P. Gabbaï, Harald Krautscheid, Régis Réau, and Guy Bertrand*

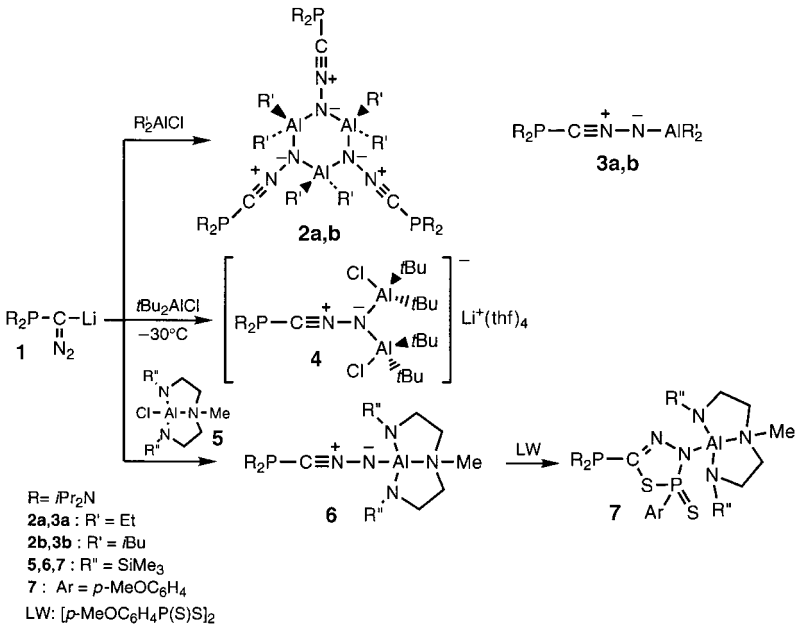
Covalent azides of type **A** are well-known 1,3-dipoles that have found widespread application in organic synthesis,[1] and that are also of increasing importance in inorganic chemistry.[2] Aluminum azides possess a rich structural diversity (derivatives **C**–**G**[3]) and constitute valuable single-source

[*] Dr. G. Bertrand, Dr. N. Emig, Dr. R. Réau
Laboratoire de Chimie de Coordination du CNRS
205, route de Narbonne, 31077 Toulouse Cédex (France)
Fax: (+33) 561553003
E-mail: gbertran@lcctoul.lcc-toulouse.fr
Dr. F. P. Gabbaï
Anorganisch-chemisches Institut
der Technischen Universität München
Lichtenbergstrasse 4, D-85747 Garching (Germany)
Fax: (+49) 89-289-13125
Dr. H. Krautscheid
Institut für Anorganische Chemie der Universität
Engesserstrasse, Geb. 30.45, D-76138 Karlsruhe (Germany)
Fax: (+49) 721-661-921

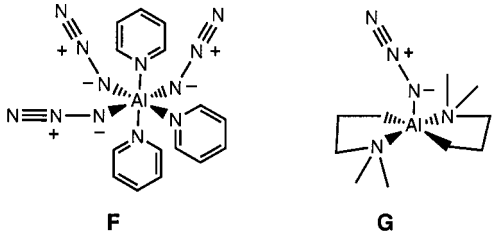
[**] We thank the CNRS for financial support of this work, and the Gottlieb Daimler- and Karl Benz-Foundation for a grant to N. E.

 © WILEY-VCH Verlag GmbH, D-69451 Weinheim, 1998 1433-7851/98/3707-0989 $ 17.50+.50/0





Scheme 1. Reactions of the lithium salt **1** with various aluminum chlorides.



precursors to AlN semiconducting phases.[4] For many years, the development of the chemistry of the isolobal nitrilimines of type **B** was hampered because of their potential instability and the lack of suitable preparative methods. In recent years, efficient routes have been established for preparing stable nitrilimines[5] and, just as for the azides, the $N_\alpha - N_\beta$ bond can be cleaved.[6] Here we report the synthesis of various aluminum–nitrogen derivatives featuring the nitrilimine skeleton.

The lithium salt of the [bis(diisopropylamino)phosphanyl]-diazomethane **1**[7] was allowed to react in THF, at $-78\,^\circ C$, with one equivalent of $ClAlEt_2$ and $ClAl(iBu)_2$. After workup at room temperature, compound **2a** and **2b** were isolated in 85 and 90% yield,[8] respectively (Scheme 1). The IR absorption at 2140 cm^{-1}, the ^{14}N chemical shift of the N_β center (**2a**: -203 ($\nu_{1/2} = 147$ Hz); **2b**: -203 ($\nu_{1/2} = 118$ Hz)), and the observation of doublet for the PC carbon atom (**2a**: 62.89 ($J_{P,C} = 74.3$ Hz); **2b**:63.21 ($J_{P,C} = 62.5$ Hz)) in the ^{13}C NMR spectrum were consistent with nitrilimine structures **3a**, **b**. However, derivatives **2a**, **b** are inert toward the Lawesson's reagent, one of the most effective 1,3-dipolarophiles.[9] Single crystals of **2b** suitable for an X-ray analysis[10] were grown from a solution in pentane at $-30\,^\circ C$ (Figure 1). Compound **2b** is a trimer of nitrilimine **3b**, and is the first structurally characterized six-membered Al–N heterocycle in which the nitrogen and aluminum atoms possess different coordination numbers[11] (an X-ray diffraction study performed of poor quality crystals

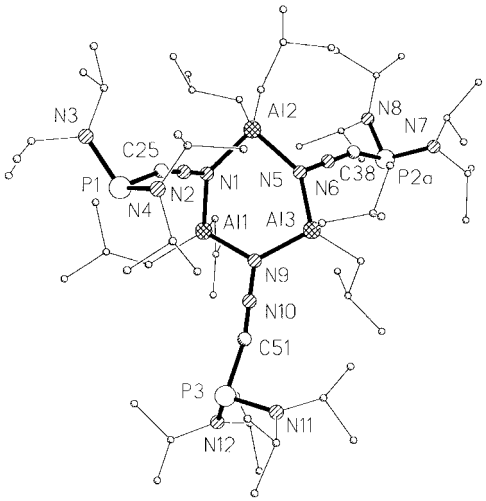
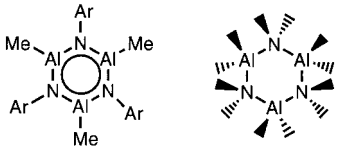


Figure 1. Molecular structure of **2b** in the solid state. Hydrogen atoms have been omitted for clarity. Selected bond lengths [Å] and angles [°]: P1–C25 1.804(7), C25–N2 1.144(7), N2–N1 1.287(6), N1–Al1 1.918(5), N1–Al2 1.893(5); P1-C25-N2 163.1(6), C25-N2-N1 177.9(6), N2-N1-Al1 114.5(4), N2-N1-Al2 119.2(4), Al1-N1-Al2 123.6(3), N1-Al1-N9 98.2(2).

of **2a** also reveals a six-membered Al–N core). The central six-membered $(AlN_\alpha)_3$ heterocycle features a twisted conformation, in contrast to the planar geometry postulated from IR and Raman data for the analogous azide derivative **C**.[3a] The mean endocyclic ring angles at the N_α (119.6°) and Al (109.6°) atoms reflect the sp^2 and sp^3 hybridization, respectively. The $Al-N_\alpha$ bond lengths (1.89–1.93 Å) are much longer than those observed for the only known aromatic alumazene **H** (1.78 Å),[11] which contains three-coordinate Al and N centers, but are comparable to those of tris(aminoalanes) **I** (1.95 Å),[12] which contain four-coordinate Al and N centers. The N-N-C fragments are almost linear (177.5–179.7°), as are the P-C-N angles (163.1–169.1°), reflecting the sp hybridization of the C and N_β atoms. The $N_\alpha - N_\beta$ bond

 © WILEY-VCH Verlag GmbH, D-69451 Weinheim, 1998 1433-7851/98/3707-0990 $ 17.50+.50/0



H

I

lengths (1.26 – 1.29 Å) are half way between those for a double and a single N – N bond, and the N_β – C bond lengths (1.14 – 1.16 Å) are typical for a C – N triple bond. Taken together, these data support a heteropropargylic canonical structure for the C-N-N fragment, in contrast to most of the known nitrilimines, which feature a cumulenic structure.[13]

The same reaction was carried out with the more sterically hindered $ClAl(tBu)_2$ in the hope of stabilizing a monomeric nitrilimine. After workup at below $-30\,^\circ C$, highly air- and moisture-sensitive crystals of **4** (Scheme 1) suitable for an X-ray crystallographic study were obtained from the pentane solution at $-30\,^\circ C$ (Scheme 1; Figure 2).[10] Compound **4** is a

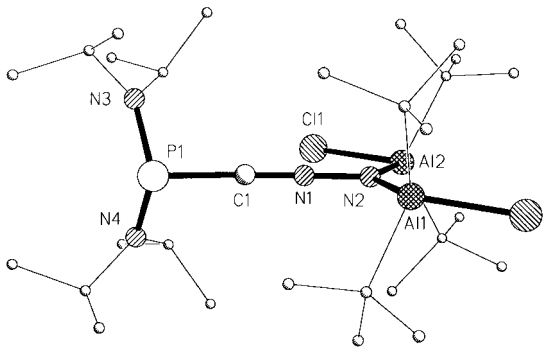


Figure 2. Molecular structure of the anion of **4** in the solid state. Hydrogen atoms have been omitted for clarity. Selected bond lengths [Å] and angles [°]: P1 – C1 1.800(3), C1 – N1 1.161(3), N1 – N2 1.293(3), N2 – Al1 1.954(3), N2 – Al2 1.958(3); P1-C1-N1 168.9(3), C1-N1-N2 178.9(3), N1-N2-Al1 107.8(2), N1-N2-Al2 114.5(2), Al1-N2-Al2 137.7(1).

nitrilimine analogue of the azido complex **D**,[3b] featuring a 1,1-μ-N_α bridging mode. In both cases, the Al_2N_2E (E = C or N) fragment is planar (maximum deviation: **4**: 0.006 Å; **C**: 0.01 Å), indicating an sp^2 hybridization for the bridging N_α nitrogen, while the N_β atom is sp-hybridized (**4:** C-N-N: 178.9°; **C**: N-N-N: 178°). The Al – N distances lie in the same range (**4**: 1.96 and 1.95 Å; **C**: 2.03 Å], the N – N bond length (1.29 Å) lies between the values for a double and a single bond, and the C – N bond length (1.16 Å) is typical for a C – N triple bond. The P-C-N fragment is almost linear (168.9°). Again these data as a whole support a heteropropargylic canonical structure for the C-N-N fragment. Compound **4** is one of the very rare examples of a lithium salt featuring an Al – Cl bond;[14] at temperatures above $-20\,^\circ C$, it decomposes rapidly leading to a complicated mixture of products.

We have recently shown that the tridentate diamidoamine ligand $[(Me_3SiNCH_2CH_2)_2NR]^{2-}$ allows the preparation of a variety of monomeric aluminum(III) derivatives.[15] Therefore, the lithium salt of **1** was allowed to react with the aluminum chloride **5**. After workup at room temperature, nitrilimine **6**[8] was isolated as an orange oil in 91 % yield (Scheme 1). The ^{31}P (48.51) and ^{13}C (61.17 (d, $J_{PC} = 83.5$ Hz)) NMR signals for the P-C-N-N skeleton are comparable to those observed for compounds **2a**, **b**, but the IR absorption is shifted to lower frequency ($\tilde{\nu} = 2076\ cm^{-1}$; $\Delta\tilde{\nu} = 64\ cm^{-1}$/**2a**, **b**). The simplicity of the NMR spectra for the diamidoamine part is in agreement with a monomeric structure.[15] Interestingly, in contrast to derivatives **2**, compound **6** reacted with the Lawesson's reagent,[9] affording the expected [3+2] adduct **6** as an orange oil in 63 % yield.

The only example of four-coordinate "monomeric" aluminum azide features intermolecular hydrogen bonding involving the N_α and N_γ atoms in the solid state.[3d] In contrast, the azide **8**,[8] which is analogous to nitrilimine **6**, prepared in 85 % yield by treatment of the aluminum chloride **5** with NaN_3, is monomeric as proved by a single-crystal X-ray diffraction study[10] (Figure 3). These results clearly show that nitrilimines of type **B** can indeed exhibit a comparable coordination behavior to that of covalent azides **A**.

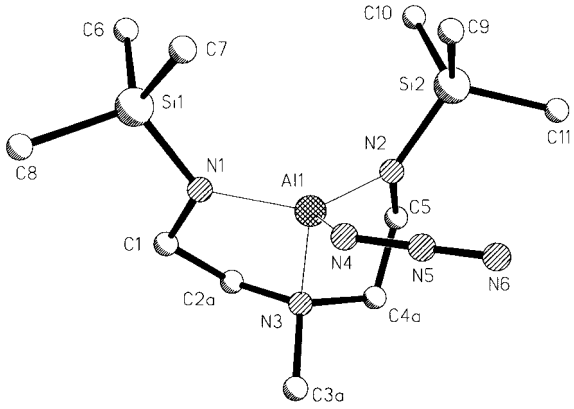


Figure 3. Molecular structure of **8** in the solid state. Hydrogen atoms have been omitted for clarity. Selected bond lengths [Å] and angles [°] Al1 – N1 1.805(4), Al1 – N2 1.807(4), Al1 – N3 1.970(4), Al1 – N4 1.837(5), N4 – N5 1.212(6), N5 – N6 1.137(6); Al1-N4-N5 129.9(4), N4-N5-N6 176.6(5).

Experimental Section

In a typical experiment a solution of Et_2AlCl (1M, 1.9 mL) in hexane was added dropwise at $-78\,^\circ C$ to a solution (10 mL) of **1** (prepared by addition at $-78\,^\circ C$ of a solution of BuLi (1.9 mmol) in hexane to the bis(diisopropylamino)phosphanyldiazomethane (0.52 g, 1.9 mmol)) in THF. The solution was allowed to warm to room temperature, stirred for 1 h, and the solvent was removed under vacuum. The residue was treated with pentane and filtered (10 mL). Compound **2a** was obtained from a pentane solution at $-30\,^\circ C$ as colorless crystals (0.64 g).

Received: October 17, 1997 [Z11045IE]
German version: *Angew. Chem.* **1998**, *110*, 1037 – 1040

Keywords: aluminum · azides · diazo compounds · heterocycles · lithium · nitrilimines

[1] Reviews: a) R. Huisgen, *Angew. Chem.* **1963**, *75*, 604; *Angew. Chem. Int. Ed. Engl.* **1963**, *2*, 565; *ibid.* **1963**, *75*, 741 and **1963**, *2*, 633; b) P. Caramella, P. Grünanger in *1,3-Dipolar Cycloaddition Chemistry* (Ed.: A. Padwa), Wiley, New York, **1984**, p. 559.

[2] a) I. C. Tornieporth-Oetting, T. M. Klapötke, *Angew. Chem.* **1995**, *107*, 559; *Angew. Chem. Int. Ed. Engl.* **1995**, *34*, 511; b) T. M. Klapötke, *Chem. Ber.* **1997**, *130*, 443; representative recent contributions: c) H. Hennig, K. Hofbauer, K. Handke, R. Stich, *Angew. Chem.* **1997**, *109*,

 © WILEY-VCH Verlag GmbH, D-69451 Weinheim, 1998 1433-7851/98/3707-0991 $ 17.50+.50/0

373; *Angew. Chem. Int. Ed. Engl.* **1997**, *36*, 408; d) G. De Munno, T. Poerio, G. Viau, M. Julve, F. Lloret, *ibid.* **1997**, *109*, 1531 and **1997**, *36*, 1459; e) C. J. Carmalt, A. H. Cowley, R. D. Culp, R. A. Jones, Y.-M. Sun, B. Fitts, S. Whaley, H. W. Roesky, *Inorg. Chem.* **1997**, *36*, 3108.

[3] a) J. Müller, K. Dehnicke, *J. Organomet. Chem.* **1968**, *12*, 37; b) J. L. Atwood, W. R. Newberry, *ibid.* **1974**, *65*, 145; c) W. Uhl, R. Gerding, S. Pohl, W. Saak, *Chem. Ber.* **1995**, *128*, 81; d) R. A. Fischer, A. Miehr, H. Sussek, H. Pritzkow, E. Herdtweck, J. Müller, O. Ambacher, T. Metzger, *Chem. Commun.* **1996**, 2685.

[4] a) D. C. Boyd, R. T. Haasch, D. R. Mantell, R. K. Schulze, J. F. Evans, W. L. Gladfelter, *Chem. Mater.* **1989**, *1*, 119; see also: b) A. Miehr, M. R. Mattner, R. A. Fischer, *Organometallics* **1996**, *15*, 2053; c) A. Miehr, O. Ambacher, T. Metzger, E. Born, R. A. Fischer, *Chem. Vap. Deposition* **1996**, *2*, 51; d) R. A. Fischer, A. Miehr, E. Herdtweck, M. R. Mattner, O. Ambacher, T. Metzger, E. Born, S. Weinkauf, C. R. Pulham, S. Parsons, *Chem. Eur. J.* **1996**, *2*, 101; e) C. J. Carmalt, A. H. Cowley, R. D. Culp, R. A. Jones, *Chem. Commun.* **1996**, 1453.

[5] G. Bertrand, C. Wentrup, *Angew. Chem.* **1994**, *106*, 549; *Angew. Chem. Int. Ed. Engl.* **1994**, *33*, 527.

[6] M. Granier, A. Bacereido, Y. Dartiguenave, M. Dartiguenave, M. J. Menu, G. Bertrand, *J. Am. Chem. Soc.* **1990**, *112*, 6277.

[7] G. Sicard, A. Baceiredo, G. Bertrand, *J. Am. Chem. Soc.* **1988**, *110*, 2663.

[8] Selected spectroscopic data: **2a**: M.p. 98 °C; ^{31}P NMR (C_6D_6): $\delta =$ 43.2(s); **2b**: M.p. 142 °C; ^{31}P NMR (C_6D_6): $\delta = 44.4$ (s); **6**: ^{1}H NMR (C_6D_6): $\delta = 0.37$ (s; $SiMe_3$), 1.16 (d, $J = 6.7$ Hz; $CHCH_3$), 1.29 (d, $J =$ 6.7 Hz; $CHCH_3$), 1.87 (dt, $J = 11.5$, 5.6 Hz; CH_2), 1.94 (s; NCH_3), 2.20 (dt, $J = 11.5$, 5.8 Hz; CH_2), 2.79 (dd, $J = 5.6$, 5.8 Hz; $2\,CH_2$), 3.46 (septd, $J = 6.7$, 6.7 Hz; $CHCH_3$), 3.52 (septd, $J = 6.7$, 6.7 Hz; $CHCH_3$); **7**: ^{31}P NMR (C_6D_6): $\delta = 49.1$ (d, $J = 4.3$ Hz), 104.7 (d, $J = 4.3$ Hz); ^{13}C{^{1}H} NMR (C_6D_6): $\delta = 134.5$ (dd, $J = 59.4$, 13.4 Hz; PCSP); IR (pentane): $\tilde{\nu} = 1594$ cm^{-1}; **8**: ^{1}H NMR (C_6D_6): $\delta = 0.48$ (s; $SiCH_3$), 1.96 (s; NCH_3), 1.99 (dt, $J = 11.7$, 5.8 Hz; CH_2), 2.34 (dt, $J = 11.7$, 5.7 Hz; CH_2), 2.91 (dd, $J = 5.7$, 5.8 Hz; $2\,CH_2$); ^{27}Al NMR (C_6D_6): $\delta = +118$ ($\nu_{1/2} = 3800$ Hz); ^{14}N NMR (C_6D_6): $\delta = -138.9$ ($\nu_{1/2} = 70$ Hz), -202.9 ($\nu_{1/2} = 15$ Hz), -224.5 ($\nu_{1/2} = 25$ Hz); IR (THF): $\tilde{\nu} = 2125$ cm^{-1}.

[9] N. Dubau-Assibat, A. Baceiredo, G. Bertrand, *J. Org. Chem.* **1995**, *60*, 3904.

[10] Crystal data: **2b**: $C_{63}H_{138}Al_3N_{12}P_3$, orthorhombic, $P2_12_12_1$, $a =$ 13.701(7), $b = 14.354(7)$, $c = 41.008(15)$ Å, $V = 8065(6)$ Å^3, $Z = 4$, with 665 parameters refined on 11282 reflections with $F > 2\sigma(F_o)$], $R1 =$ 0.063 and $wR2 = 0.196$; **4**: $C_{45}H_{87}Al_2Cl_2LiN_4O_4P$, monoclinic, $P2_1/c$, $a = 17.490(5)$, $b = 11.458(2)$, $c = 28.904(7)$ Å, $\beta = 92.67(2)°$, $V =$ 5786.1(24) Å^3, $Z = 4$, with 584 parameters refined on 9514 reflections with $F > 2\sigma(F_o)$], $R1 = 0.065$ and $wR2 = 0.200$; **8**: $C_{11}H_{29}AlN_6Si_2$, monoclinic, $P2_1/n$, $a = 9.366(1)$, $b = 8.123(1)$, $c = 25.794(3)$ Å, $\beta =$ 93.76(1)°, $V = 1958.1(4)$ Å^3, $Z = 4$, with 217 parameters refined on 2490 reflections with $F > 2\sigma(F_o)$], $R1 = 0.078$ and $wR2 = 0.185$. The structures were solved by direct methods[16a] and refined by full-matrix least squares on F^2 [16b].Crystallographic data (excluding structure factors) for the structures reported in this paper have been deposited with the Cambridge Crystallographic Data Centre as supplementary publication no. CCDC-100758. Copies of the data can be obtained free of charge on application to CCDC, 12 Union Road, Cambridge CB2 1EZ, UK (fax: (+44) 1223-336-033; e-mail: deposit@ccdc.cam.ac.uk).

[11] K. M. Waggoner, H. Hope, P. P. Power, *Angew. Chem.* **1988**, *100*, 1765; *Angew. Chem. Int. Ed. Engl.* **1988**, *27*, 1699.

[12] L. V. Interrante, G. A. Sigel, M. Garbauskas, C. Hejna, G. A. Slack, *Inorg. Chem.* **1989**, *28*, 252.

[13] a) J. L. Faure, R. Réau, M. W. Wong, R. Koch, C. Wentrup, G. Bertrand, *J. Am. Chem. Soc.* **1997**, *119*, 2819; b) M. W. Wong, C. Wentrup, *ibid.* **1993**, *115*, 7743; c) G. Maier, J. Eckwert, H. P. Reisenauer, A. Bothur, C. Schmidt, *Liebigs Ann.* **1996**, 1041.

[14] a) A. Heine, D. Stalke, *Angew. Chem.* **1993**, *105*, 90; *Angew. Chem. Int. Ed. Engl.* **1993**, *32*, 121; b) M. T. Reetz, B. M. Johnson, K. Harms, *Tetrahedron Lett.* **1994**, *35*, 2525.

[15] a) N. Emig, R. Réau, H. Krautscheid, D. Fenske, G. Bertrand, *J. Am. Chem. Soc.* **1996**, *118*, 5822; b) N. Emig, H. Nguyen, H. Krautscheid, R. Réau, G. Bertrand, unpublished results.

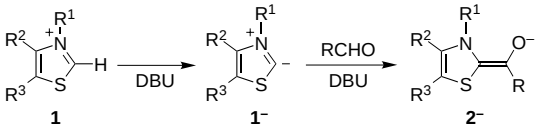
[16] a) G. M. Sheldrick, *Acta Crystallogr. Sect. A* **1990**, *46*, 467; b) SHELXL-97, Program crystal structure refinement, Universität Göttingen, **1997**.

Direct Observation of Radical Intermediates While Investigating the Redox Behavior of Thiamin Coenzyme Models**

Ikuo Nakanishi, Shinobu Itoh, Tomoyoshi Suenobu, and Shunichi Fukuzumi*

Thiamin diphosphate (ThDP) is the coenzyme for a number of important biochemical reactions, including the decarboxylation of pyruvic acid to acetaldehyde. The conjugate base of 2-hydroxyethyl-ThDP, which is an acyl carbanion equivalent and called an "active aldehyde", plays a key role in the catalysis of ThDP-dependent enzymes.[1] The active aldehyde is able to reduce various physiological electron acceptors, for example the lipoamide in the pyruvate dehydrogenase multienzyme complex,[2] the flavin adenine dinucleotide (FAD) in pyruvate oxidase,[3] and the Fe_4S_4 cluster in pyruvate-ferredoxin oxidoreductase.[4] Simple thiazolium ions have been studied extensively as models of the thiamin coenzyme, and valuable information about the elementary step of ThDP-dependent enzymatic reactions was provided.[5–10] The active aldehyde, however, readily undergoes acyloin-type condensation with a second pyruvate or aldehyde molecule in the absence of oxidizing agents.[1, 11] Such instability of the active aldehydes has precluded the direct determination of the most fundamental properties of the intermediates, such as oxidation potentials.[12] Therefore, no direct observation of the radical intermediates derived from thiamin coenzyme models has been described so far. Here we report the direct observation of radical intermediates of active aldehydes $\mathbf{2}^-$ with low-temperature cyclic voltammetry and EPR spectroscopy. Active aldehydes $\mathbf{2}^-$ are derived from 3-benzylthiazolium salts **1** and simple aldehydes such as acetaldehyde and benzaldehyde in the presence of 1,8-diazabicylco[5.4.0]undec-7-ene (DBU).

A cyclic voltammogram (CV) of the active aldehyde $\mathbf{2a}^-$—which is prepared in situ by adding neat DBU (1.0×10^{-2} M) to a deaerated solution of 3-benzylthiazolium ion **1a** ($5.0 \times$



1 **1**$^-$ **2**$^-$

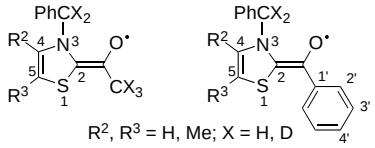
a $R^1 = PhCH_2$, $R^2 = Me$, $R^3 = H$, R = Me
b $R^1 = PhCH_2$, $R^2 = R^3 = Me$, R = Me
c $R^1 = PhCH_2$, $R^2 = R^3 = H$, R = Me
d $R^1 = PhCH_2$, $R^2 = Me$, $R^3 = H$, R = Ph
e $R^1 = PhCH_2$, $R^2 = R^3 = Me$, R = Ph
f $R^1 = PhCH_2$, $R^2 = R^3 = H$, R = Ph
g $R^1 = PhCD_2$, $R^2 = Me$, $R^3 = H$, R = Me
h $R^1 = PhCH_2$, $R^2 = Me$, $R^3 = H$, $R = CD_3$
i $R^1 = PhCD_2$, $R^2 = Me$, $R^3 = H$, R = Ph

[*] Prof. Dr. S. Fukuzumi, I. Nakanishi, Dr. S. Itoh, Dr. T. Suenobu
Department of Applied Chemistry, Faculty of Engineering
Osaka University
2-1 Yamada-oka Suita Osaka 565-0871 (Japan)
Fax: (+81) 6-879-7370
E-mail: fukuzumi@chem.eng.osaka-u.ac.jp

[**] This work was partially supported by a Grant-in-Aid from the Ministry of Education, Science, Sports, and Culture, Japan.

 © WILEY-VCH Verlag GmbH, D-69451 Weinheim, 1998 1433-7851/98/3707-0992 $ 17.50+.50/0

10^{-3} M), acetaldehyde (0.25 M), and 0.10 M tetrabutylammonium perchlorate (TBAP) in acetonitrile (MeCN) at 233 K—shows two reversible one-electron oxidations at $E^0_{ox} = -0.95$ and -0.74 V versus the saturated calomel electrode (SCE).[13] No reversible peaks can be observed at 298 K because of the fast acyloin condensation of $\mathbf{2a}^-$ with a second aldehyde molecule. Such a reversible CV at 233 K can be observed only in the presence of all the components (i.e., **1a**, DBU, and the aldehyde). This indicates that it is not the parent compound but the active aldehyde $\mathbf{2a}^-$ that undergoes the electrochemical redox reactions. The two one-electron oxidation potentials ($E^0_{ox(1)}$ and $E^0_{ox(2)}$) of various active aldehydes were also determined (Table 1). The $E^0_{ox(1)}$ and $E^0_{ox(2)}$ values of $\mathbf{2a}^- - \mathbf{2c}^-$, which are derived from acetaldehyde, are 200–300 mV more negative than those of active aldehydes $\mathbf{2d}^- - \mathbf{2f}^-$, which are derived from benzaldehyde. Substituents on the thiazolium rings have only minor effects on the oxidation potentials. The $E^0_{ox(1)}$ values in Table 1 support the proposal by Jordan et al. that the one-electron oxidation potential of the active aldehyde, which can reduce a flavin analogue, must be more negative than -0.67 V vs. SCE.[5e]



The observation of the well-defined one-electron redox couples indicates that a radical intermediate is formed in the first one-electron oxidation of the active aldehyde. Therefore, the EPR spectrum of a radical intermediate ($\mathbf{2}^\bullet$) generated by controlled-potential electrolysis was measured in deaerated MeCN (0.10 M TBAP) at 233 K. When the solution containing $\mathbf{2c}^-$ was electrolyzed at -1.20 or -0.50 V vs. SCE, there was no EPR signal. When the solution was electrolyzed at -0.80 V vs. SCE, however, a radical species with a g value of 2.0055 was detected at 233 K (Figure 1a). The observed spectrum can be simulated with the EPR parameters listed in Table 1 (Figure 1b).

The hyperfine splitting (hfs) constants of other active aldehyde radical species can also be determined in a similar manner (Table 1). The assignment of the hfs values indicates

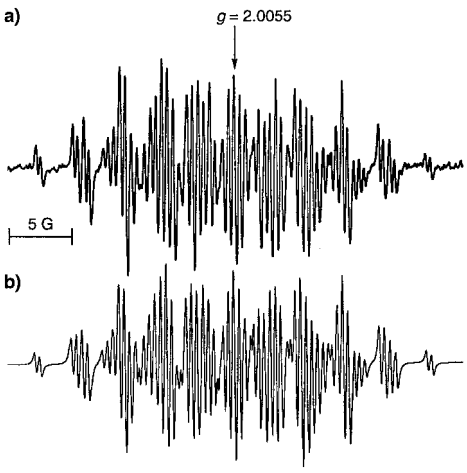


Figure 1. a) EPR spectum of $\mathbf{2c}^\bullet$ in MeCN at 233 K. b) The spectrum from a computer simulation; the hfs values used for the simulation are listed in Table 1.

that the detected radicals are neutral species ($\mathbf{2}^\bullet$). In the presence of a strong base such as DBU, the active aldehyde exists as an anion $\mathbf{2}^-$, since deprotonation of the OH group occurs. The first one-electron oxidation of $\mathbf{2}^-$ leads to the corresponding neutral radical species $\mathbf{2}^\bullet$, whose structure is similar to that suggested for the oxidized active aldehyde in pyruvate-ferredoxin oxidoreductase by Kerscher and Oesterhelt.[4b] The radical $\mathbf{2}^\bullet$ loses one more electron in the second oxidation step to form the 2-acylthiazolium ion $\mathbf{2}^+$. The assignments of $\mathbf{2}^\bullet$ in Table 1 are ensured by deuterium substitution at appropriate positions of the molecule. For example, deuterium substitution of the two hydrogen atoms at the benzylic positions of **1a** as well as that of the three hydrogen atoms of the acetyl moiety of $\mathbf{2a}^\bullet$ resulted in a drastic change in the splitting pattern. The hfs values of 2.34 and 3.46 G due to $PhCH_2$ and CH_3CO protons of $\mathbf{2a}^\bullet$ are decreased by a factor of 0.143, the magnetogyric ratio of proton to deuterium, to 0.33 and 0.51 G for $PhCD_2$ and CD_3CO deuterons of the corresponding deuterated radicals $\mathbf{2g}^\bullet$ and $\mathbf{2h}^\bullet$, respectively, when the other hfs values remain unchanged.[14]

Judging from the observed hfs values, the unpaired electron is highly delocalized in the active aldehyde moiety; the spin density is low only on C4. No appreciable change in the spin distribution is observed upon changing the substituents on the

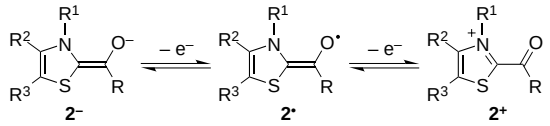
Table 1. One-electron oxidation potentials $E^0_{ox(1)}$ and $E^0_{ox(2)}$ vs. SCE of active aldehydes $\mathbf{2}^-$,[a] g values, and hyperfine splitting (hfs) values of $\mathbf{2}^\bullet$.

	$E^0_{ox(1)}$ [V][b]	$E^0_{ox(2)}$ [V][b]	g [G]	hfs [G]						
				a_N(N)	a_H($PhCH_2$)	a_H(C-4)	a_H(C-5)	a_H(CH_3CO)	a_H(C-2′)	a_H(C-4′)
a	−0.98	−0.74	2.0052	4.74	2.34	0.64	3.12	3.46	–	–
b	−0.96	−0.73	2.0052	5.02	2.24	0.50	2.85	3.54	–	–
c	−0.93	−0.73	2.0055	4.87	2.65	0.38	3.00	3.45	–	–
d	−0.78	−0.44	2.0057	4.53	2.40	0.42	3.10	–	0.24	0.48
e	−0.79	−0.45	2.0051	4.70	2.20	0.45	2.64	–	0.24	0.48
f	−0.77	−0.42	2.0057	4.66	2.48	0.42	2.83	–	0.21	0.43
g	−0.95	−0.74	2.0052	4.74	0.33[c]	0.64	3.12	3.46	–	–
h	−0.95	−0.74	2.0052	4.74	2.34	0.64	3.12	0.51[c]	–	–
i	−0.78	−0.44	2.0057	4.53	0.34[c]	0.42	3.10	–	0.24	0.48

[a] Active aldehydes $\mathbf{2}^-$ were prepared from **1** (5.0×10^{-3} M), RCHO (0.25 M), and DBU (1.0×10^{-2} M) in deaerated MeCN containing 0.10 M TBAP at 233 K. [b] Working electrode: Pt, sweep rate: 0.10 V s^{-1}. [c] Deuterium splitting value.

 © WILEY-VCH Verlag GmbH, D-69451 Weinheim, 1998 1433-7851/98/3707-0993 $ 17.50+.50/0

thiazolium ring. Therefore, the oxidative electron transfer processes of the active aldehyde can be described as shown in Scheme 1. The highly negative oxidation potentials of active



Scheme 1. Oxidation of active aldehydes $\mathbf{2}^-$ by two electron transfer steps.

aldehydes and the spin distribution of the intermediate radicals determined for the first time in this study provide the energetic basis for the ThDP-dependent electron transport systems as well as valuable mechanistic insight into the enzymatic reactions.

Experimental Section

Thiazoles, benzyl bromide, acetaldehyde, and benzaldehyde were purchased from Tokyo Chemical Industry and used as received. MeCN was purified and dried with CaH_2 by the standard procedure.[15] TBAP was recrystallized from ethanol and dried in vacuum at 40 °C prior to use. 3-Benzylthiazolium bromide was prepared by the reaction of the corresponding thiazole with benzyl bromide at 80 °C, and purified by recrystallization from acetone. Cyclic voltammetry measurements were performed on a BAS 100B electrochemical analyzer with solutions in deaerated MeCN containing 0.10 M TBAP as supporting electrolyte. The Pt working electrode (BAS) was polished with a BAS polishing alumina suspension and rinsed with acetone before use. The counter electrode was a platinum wire. The measured potentials were recorded with respect to the Ag/$AgNO_3$ (0.01 M) reference electrode and converted into values versus SCE by adding 0.29 V.[16] All electrochemical measurements were carried out under an atmospheric pressure of argon. EPR spectra were recorded on a JEOL JES-RE1XE instrument under nonsaturating microwave power conditions. The magnitude of the modulation was chosen to optimize the resolution and the signal-to-noise (S/N) ratio of the observed spectra. The *g* values and hyperfine splitting (hfs) constants were calibrated with a Mn^{2+} marker. Computer simulations of the EPR spectra were carried out with the program Calleo ESR Version 1.2 (Calleo Scientific) on a Macintosh personal computer.

Received: September 18, 1997 [Z 10944 IE]
German version: *Angew. Chem.* **1998**, *110*, 1040 – 1042

Keywords: coenzymes · cyclic voltammetry · EPR spectroscopy · radicals · thiamin

[1] a) R. Breslow, *J. Am. Chem. Soc.* **1958**, *80*, 3719 – 3726; b) L. O. Krampitz, *Annu. Rev. Biochem.* **1969**, *38*, 213 – 240; c) R. Kluger, *Chem. Rev.* **1987**, *87*, 863 – 876.
[2] L. J. Reed, *Acc. Chem. Res.* **1974**, *7*, 40 – 46.
[3] a) L. P. Hager, *J. Biol. Chem.* **1957**, *229*, 251 – 263; b) G. E. Schulz, Y. A. Müller, *Science* **1993**, *259*, 965 – 967.
[4] a) K. Uyeda, J. C. Rabinowitz, *J. Biol. Chem.* **1971**, *246*, 3120 – 3125; b) L. Kerscher, D. Oesterhelt, *Eur. J. Biochem.* **1981**, *116*, 595 – 600.
[5] a) F. Jordan, Z. H. Kudzin, C. B. Rios, *J. Am. Chem. Soc.* **1987**, *109*, 4415 – 4416; b) F. G. Bordwell, A. Y. Satish, F. Jordan, C. B. Rios, A. C. Chung, *ibid.* **1990**, *112*, 792 – 797; c) X. Zeng, A. Chung, M. Haran, F. Jordan, *ibid.* **1991**, *113*, 5842 – 5849; d) G. Barletta, W. P. Huskey, F. Jordan, *ibid.* **1992**, *114*, 7607 – 7608; e) C. C. Chiu, K. Pan, F. Jordan, *ibid.* **1995**, *117*, 7027 – 7028; f) C. C. Chiu, A. Chung, G. Barletta, F. Jordan, *ibid.* **1996**, *118*, 11 026 – 11 029; g) G. L. Barletta, Y. Zou, W. P. Huskey, F. Jordan, *ibid.* **1997**, *119*, 2356 – 2369.
[6] D. Hilvert, R. Breslow, *Bioorg. Chem.* **1984**, *12*, 206 – 220.
[7] a) S. Shinkai, T. Yamashita, T. Kusano, O. Manabe, *Tetrahedron Lett.* **1980**, 2543 – 2546; b) *J. Org. Chem.* **1980**, *45*, 4947 – 4952; c) *J. Am. Chem. Soc.* **1982**, *104*, 563 – 568.
[8] a) S. Ohshima, N. Tamura, T. Nabeshima, Y. Yano, *J. Chem. Soc. Chem. Commun.* **1993**, 712 – 713; b) A. Takaki, K. Utsumi, T. Kajiki, T. Kuroi, T. Nabeshima, Y. Yano, *Chem. Lett.* **1997**, 75 – 76.
[9] a) H. Inoue, K. Higashiura, *J. Chem. Soc. Chem. Commun.* **1980**, 549 – 550; b) H. Inoue, S. Tamura, *ibid.* **1985**, 141 – 142; c) *ibid.* **1986**, 858 – 859.
[10] a) S.-W. Tam-Chang, L. Jimenez, F. Diederich, *Helv. Chim. Acta* **1993**, *76*, 2616 – 2639; b) P. Mattei, F. Diederich, *Angew. Chem.* **1996**, *108*, 1434 – 1437; *Angew. Chem. Int. Ed. Engl.* **1996**, *35*, 1341 – 1344; c) *Helv. Chim. Acta* **1997**, *80*, 1555 – 1588.
[11] a) T. Ugai, S. Tanaka, S. Dokawa, *J. Pharm. Soc. Jpn.* **1943**, *63*, 296 – 300; b) W. Tagaki, H. Hara, *J. Chem. Soc. Chem. Commun.* **1973**, 891; c) J. A. Zoltewicz, J. K. O'Halloran, *J. Org. Chem.* **1978**, *43*, 1713 – 1718; d) R. Breslow, E. Kool, *Tetrahedron Lett.* **1988**, *29*, 1635 – 1638; e) F. Diederich, H.-D. Lutter, *J. Am. Chem. Soc.* **1989**, *111*, 8438 – 8446; f) Y. -T. Chen, G. L. Barletta, K. Haghjoo, J. T. Cheng, F. Jordan, *J. Org. Chem.* **1994**, *59*, 7714 – 7722.
[12] The more positive oxidation potentials of O-methylated analogues of active aldehydes have been reported. The formation of a radical cation intermediate upon electrochemical oxidation is suggested based on the chemical demonstration of the formation of a dimer at the C2α atom: G. Barletta, A. C. Chung, C. B. Rios, F. Jordan, J. M. Schlegel, *J. Am. Chem. Soc.* **1990**, *112*, 8144 – 8149.
[13] The generation of active aldehydes derived from *o*-tolualdehyde ($\lambda_{max} = 380$ nm) was confirmed by UV/Vis spectroscopy.[5e]
[14] S. Fukuzumi, Y. Tokuda, T. Kitano, T. Okamoto, J. Otera, *J. Am. Chem. Soc.* **1993**, *115*, 8960 – 8968; J. E. Wertz, J. R. Bolton, *Electron Spin Resonance Elementary Theory and Practical Applications*, McGraw-Hill, New York, **1972**.
[15] D. D. Perrin, W. L. F. Armarego, D. R. Perrin, *Purification of Laboratory Chemicals*, Pergamon, Elmsford, **1966**.
[16] C. K. Mann, K. K. Barnes, *Electrochemical Reactions in Non-aqueous Systems*, Marcel Deker, New York, **1990**.

Generation of "Naked" Fluoride Ions in Unprecedentedly High Concentrations from a Fluoropalladium Complex**

Vladimir V. Grushin*

Since the discovery of the first reliable sources of weakly solvated ("naked") fluoride ions,[1, 2] a number of intriguing reactivity patterns and applications of the F^- ion in synthesis have been reported which clearly indicate its extraordinarily strong basicity and nucleophilicity in media of low polarity.[1–8] However, the number of sources for "genuinely naked" F^-

[*] Prof. Dr. V. V. Grushin[+]
Department of Chemistry
Wilfrid Laurier University
Waterloo, Ontario N2L 3C5 (Canada)
[+] Current address:
DuPont CR&D, E328/306
Experimental Station
Wilmington, DE 19880-0328 (USA)
Fax: (+1) 302-695-8281
E-mail: vlad.grushin-1@usa.dupont.com

[**] This work was supported by DuPont and Wilfrid Laurier University. Dr. V. A. Petrov (DuPont) is thankfully acknowledged for many fruitful discussions.

 © WILEY-VCH Verlag GmbH, D-69451 Weinheim, 1998 1433-7851/98/3707-0994 $ 17.50+.50/0

ions known to date is limited to five "onium" compounds which contain no β-hydrogens as to avoid Hofmann elimination.[1, 2, 6–8] All of these salts are highly hygroscopic, and some are only sparingly soluble. Here we describe a totally different, novel approach to the generation of highly reactive naked fluoride ions in unprecedentedly high concentrations. An easily accessible, robust, air- and moisture-stable, non-hygroscopic organometallic fluoro complex can be efficiently used as the carrier of a naked fluoride ion that is easily displaced by a chloride ion.

Our recent study demonstrated that the preference of the metal center in $[(Ph_3P)_2Pd(X)Ph]$ for halide anions in anhydrous CH_2Cl_2 [Eq. (1)] follows the order $F^- > Cl^- > Br^- > I^-$.[9]

Once the equilibrium shown in Equation (1) had been established within the time of mixing at room temperature, the system remained unchanged in all cases except for X = F.

$$[(Ph_3P)_2Pd(X)Ph] + X'^- \rightleftharpoons [(Ph_3P)_2Pd(X')Ph] + X^- \quad (1)$$

X = I, Br, Cl, F; X' = I, Br, Cl

When $[(Ph_3P)_2Pd(F)Ph]$[10] and $[Et_3NCH_2Ph]Cl$ were dissolved in CH_2Cl_2, the equilibrium in Equation (1) was unstable and drifted slowly (within 5–8 h at 20 °C) toward $[(Ph_3P)_2Pd(Cl)Ph]$. This observation suggested that naked F^- ions are generated and cause Hofmann elimination of the ammonium cation. Indeed, NMR spectroscopic analysis of the reaction mixture confirmed the presence of the chloro complex (^{31}P NMR: $\delta = 24.1$ (s)) and HF_2^- (^{19}F NMR: $\delta = -150$ (d), $J(H,F) = 121$ Hz).[11] Benzyltriethylammonium bromide and iodide reacted similarly.[12]

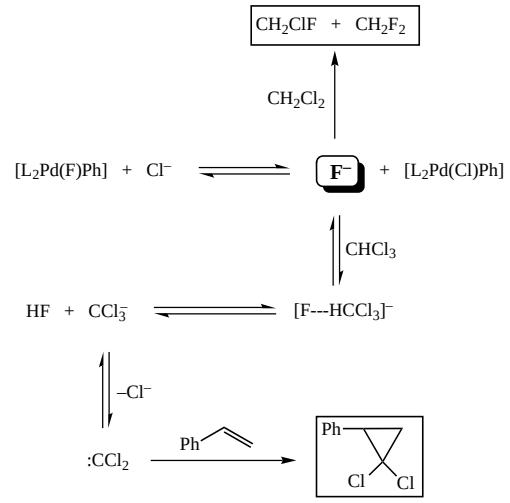
To avoid Hofmann eliminations, $[Ph_3P{=}N{=}PPh_3]Cl$ ([PPN]Cl) was employed instead of the benzyltriethylammonium salts. A typical run was monitored by ^{19}F NMR spectrscopy (Table 1). The reaction between

Table 1. Fluorination of CH_2Cl_2 (0.7 mL) with $[(Ph_3P)_2Pd(F)Ph]$ (0.065 mmol) and [PPN]Cl (0.093 mmol), as monitored by ^{19}F NMR spectroscopy.

t [min]	Product distribution [mol %]				
	$[(Ph_3P)_2Pd(F)Ph]$	F^-	HF_2^-	CH_2ClF	CH_2F_2
10	75	18	4	3	–
35	62	10	5	16	7
90	46	7	5	27	15
180	25	traces	6	38	31
420	traces	–	7	52	41

$[(Ph_3P)_2Pd(F)Ph]$ and [PPN]Cl in CH_2Cl_2 gave rise to CH_2ClF ($\delta = -170$(t), $J(H,F) = 48$ Hz) and CH_2F_2 ($\delta = -143$ (t), $J(H,F) = 52$ Hz) as main products. At early stages the F^- ion was present in considerable quantities ($\delta = -109$ (s), $\Delta\nu_{1/2} = 30-45$ Hz), and only small amounts of HF_2^- were formed. Resonances from both the F^- ion and the fluoropalladium complex rapidly diminished in intensity as the selective fluorination of the solvent readily occurred under *exceedingly mild conditions*. Nucleophilic substitution reactions of CH_2Cl_2 are rare,[13] and the fluorination of CH_2Cl_2 with metal fluorides, a process of potential industrial importance,[14] normally requires very high temperatures (180–300 °C) and pressures.[15, 16] As anticipated, no fluoromethanes were formed when the fluoropalladium complex and [PPN]Cl were allowed to react in CH_2Cl_2 saturated with water (ca. 0.2 %; H_2O:F molar ratio = 2:1).

A totally different reactivity pattern was observed when chloroform was used instead of dichloromethane (Scheme 1). The ^{19}F NMR spectrum measured five minutes after



Scheme 1. L = PPh_3.

$[(Ph_3P)_2Pd(F)Ph]$ (0.067 mmol) and [PPN]Cl (0.096 mmol) were dissolved in dry $CHCl_3$ (0.7 mL) revealed the presence of the starting fluoro complex ($\delta = -276$ (br t), $J(F,P) = 13$ Hz, 37 %), HF_2^- ($\delta = -164$ (d), $J(H,F) = 126.6$ Hz, 3 %), and F^- ($\delta = -141$ (s), $\Delta\nu_{1/2} = 9$ Hz, 60 %). No significant changes were observed in this pattern within the next 2–3 h; one day later minute amounts (ca. 1 %) of CHF_3 ($\delta = -79$ (d), $J(H,F) = 79.2$ Hz) and $CHCl_2F$ ($\delta = -81$ (d), $J(H,F) = 53.3$ Hz)[11] were detected. The increase in bifluoride content to about 15 % occurred concomitant to the proportional slight decrease in intensity of the Pd–F and F^- resonances. When complete conversion of the fluoropalladium complex was achieved in five days, only sharp singlets from $[(Ph_3P)_2Pd(Cl)Ph]$ ($\delta = 24.1$) and $[PPN]^+$ ($\delta = 21.5$) were observed in the ^{31}P NMR spectrum of the pale yellow, clear solution.

In a similar experiment styrene (threefold excess) was added to the sample after the equilibrium between the fluoropalladium complex, HF_2^-, and F^- in $CHCl_3$ was reached (< 10 min; [PPN]Cl:$[(Ph_3P)_2Pd(F)Ph] = 3.3:1$) and the system exhibited no significant changes for the following hour. As a result, the F^- and Pd–F resonances immediately started to diminish in intensity, while the HF_2^- doublet resonance became stronger.[17] The reaction was complete in about 8 h and furnished 1,1-dichloro-2-phenylcyclopropane, which was identified and quantified by ^{1}H NMR spectrscopy (ca. 40 % yield). It is clear that dichlorocarbene was produced in the reaction.

These results are summarized in Scheme 1. As can be concluded from the molar ratio of $[(Ph_3P)_2Pd(F)Ph]$ to

 © WILEY-VCH Verlag GmbH, D-69451 Weinheim, 1998 1433-7851/98/3707-0995 $ 17.50+.50/0

CH_2Cl_2 (ca. 6×10^{-4}) employed and the data in Table 1, CH_2ClF was at least three orders of magnitude more reactive toward the F^- ion than CH_2Cl_2. In comparison with CH_2Cl_2, $CHCl_3$ is much more acidic while being insufficiently electrophilic to undergo efficacious nucleophilic displacement by F^-.[18] Our system is somewhat similar to the phase transfer catalyzed generation of $:CCl_2$ from $CHCl_3$ and alkali metal.[19] Adding styrene to the reaction mixture shifts all equilibria toward the formation of $:CCl_2$, which is irreversibly trapped by the olefin present to furnish the cyclopropane derivative.

According to ^{31}P NMR spectra, in all reactions the corresponding organopalladium halide $[(Ph_3P)_2Pd(X)Ph]$ (X = Cl, Br, or I) was the only product that contained phosphorus and palladium. Remarkably, the Pd–C bond remained intact in the presence of such reactive species as naked F^-, HF, HF_2^-, CCl_3^-, and $:CCl_2$. The role of palladium in our system seems to be limited to the carrier of the F^- ion, which upon release may react as a strong nucleophile or base. Uncommonly high concentrations of the fluoride ion can be easily generated by simply dissolving the two *nonhygroscopic* reagents in a dry solvent of low polarity. Moreover, the fluoride concentration can be finely tuned by simply varying the ratio of the fluoropalladium complex to [PPN]Cl.

Significant conclusions may be drawn: 1) A novel strategy has been developed for the generation of highly reactive naked F^- ions. 2) Care should be exercised when conducting anion-metathesis studies with fluorometal complexes in chlorinated aliphatic solvents. 3) The reactivity of naked fluoride depends on the nature of its counterion. Thus, anhydrous $[Me_4N]F$ readily fluorinates $CHCl_3$, but reacts with CH_2Cl_2 more slowly to give CH_2ClF.[11] The HF_2^- ion is the only species detectable by ^{19}F NMR spectroscopy in solutions of methylurotropinium fluoride in CH_2Cl_2 or $CHCl_3$.[8] Our Pd–F/[PPN]Cl system readily fluorinates CH_2Cl_2 to a mixture of CH_2ClF and CH_2F_2, whereas only minor amounts of fluorinated methanes are formed in the sluggish reaction with $CHCl_3$.

Experimental Section

Chlorinated solvents were transferred under vacuum from P_2O_5 to a 5-mm glass NMR tube charged with the fluoropalladium complex and [PPN]Cl. The tube was sealed under nitrogen and placed into the probe of a Varian VXR-200 NMR spectrometer. In one of the experiments, after complete conversion of the fluoropalladium complex had been achieved, the pure chloro complex $[(Ph_3P)_2Pd(Cl)Ph]$ was isolated from the mixture in 96% yield and found to be identical with an authentic sample (^1H and ^{31}P NMR).

Received: October 13, 1997 [Z11030IE]
German version: *Angew. Chem.* **1998**, *110*, 1042 – 1044

Keywords: fluorinations · fluorine · fluoride ion · palladium

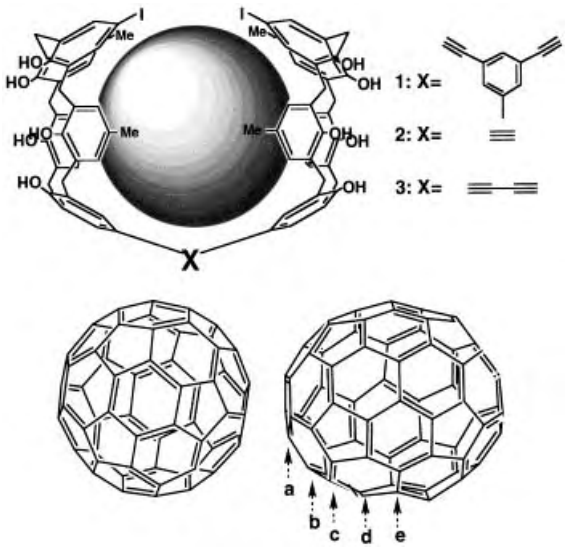
[1] K. O. Christe, W. W. Wilson, R. D. Wilson, R. Bau, J. Feng, *J. Am. Chem. Soc.* **1990**, *112*, 7619.
[2] R. Schwesinger, R. Link, G. Thiele, H. Rotter, D. Honert, H.-H. Limbach, F. Männle, *Angew. Chem.* **1991**, *103,* 1376; *Angew. Chem. Int. Ed. Engl.* **1991**, *30*, 1372.
[3] K. Seppelt, *Angew. Chem.* **1992**, *104,* 299; *Angew. Chem. Int. Ed. Engl.* **1992**, *31*, 292.
[4] K. O. Christe, D. A. Dixon, H. P. A. Mercier, J. C. P. Sanders, G. J. Schrobilgen, W. W. Wilson, *J. Am. Chem. Soc.* **1994**, *116*, 2850, and references therein.
[5] K. O. Christe, E. C. Kurtis, D. A. Dixon, H. P. A. Mercier, J. C. P. Sanders, G. J. Schrobilgen, W. W. Wilson in *Inorganic Fluorine Chemistry Toward the 21st Century* (Eds.: J. S. Thrasher, S. H. Strauss), ACS Symp. Ser. 555, American Chemical Society, Washington, DC, **1994**.
[6] K. M. Harmon, B. A. Southworth, K. E. Wilson, P. K. Keefer, *J. Org. Chem.* **1993**, *58*, 7294.
[7] A. R. Mahjoub, X. Zhang, K. Seppelt, *Chem. Eur. J.* **1995**, *1*, 261.
[8] R. Z. Gnann, R. I. Wagner, K. O. Christe, R. Bau, G. A. Olah, W. W. Wilson, *J. Am. Chem. Soc.* **1997**, *119*, 112.
[9] J. P. Flemming, V. V. Grushin, **1997**, unpublished results.
[10] S. L. Fraser, M. Yu. Antipin, V. N. Khroustalyov, V. V. Grushin, *J. Am. Chem. Soc.* **1997**, *119*, 4769.
[11] K. O. Christe, W. W. Wilson, *J. Fluorine Chem.* **1990**, *47*, 117.
[12] Because of the lower affinity of Br^- and especially I^- for the Pd center, concentrations of F^- in these experiments were also lower. This resulted in sluggish reactions (1 – 3 days).
[13] For an example of S_N2-type reactions of CH_2Cl_2, see S. Bekkevol, I. Svorstoel, H. Hoeiland, J. Songstad, *Acta Chem. Scand. Ser. B* **1983**, *37*, 935.
[14] *Chemistry of Organic Fluorine Compounds II: a Critical Review* (Eds.: M. Hudlicky, A. E. Pavlath), American Chemical Society, Washington, DC, **1995**; b) *Organofluorine Chemistry. Principles and Applications* (Eds.: R. E. Banks, B. E. Smart, J. C. Tatlow), Plenum, New York, **1994**; c) K. Wiessermel, H.-J. Arpe, *Industrial Organic Chemistry*, VCH, Weinheim, **1993**.
[15] a) The fluorination of CH_2Cl_2 with MF has been known for over 100 years: C. Chabrie, *Compt. Rend.* **1890**, *110*, 1202. The reaction between KF and CH_2Cl_2 in ethylene glycol furnishes CH_2ClF (19%) and CH_2F_2 (17%); for a table summarizing this and related reactions, see R. D. Chambers, *Fluorine Organic Chemistry*, Wiley, New York, **1973**, p. 22. All these processes require very drastic conditions.
[16] a) The fluorination of CH_2Cl_2 with *highest oxidation state* transition metal fluorides (W. W. Dukat, J. H. Holloway, E. G. Hope, M. R. Rieland, P. J. Townson, R. L. Powell, *J. Chem. Soc. Chem. Commun.* **1993**, 1429) and oxo fluorides (J. H. Holloway, E. G. Hope, P. J. Townson, R. L. Powell, *J. Fluorine Chem.* **1996**, *76*, 105) occurs under mild conditions.
[17] A triplet at $\delta = -163$ with $J(D,F) = 18.8$ Hz[11] from DF_2^- was observed when $CDCl_3$ was used instead of $CHCl_3$.
[18] The reactivity of CH_mCl_n in S_N2-type reactions decreases and in halophilic processes increases in the order CH_3Cl, CH_2Cl_2, $CHCl_3$, CCl_4; see N. S. Zefirov, D. A. Makhon'kov, *Chem. Rev.* **1982**, *82*, 615.
[19] E. V. Dehmlow, S. S. Dehmlow, *Phase Transfer Catalysis*, VCH, Weinheim, **1983**.

 © WILEY-VCH Verlag GmbH, D-69451 Weinheim, 1998 1433-7851/98/3707-0996 $ 17.50+.50/0

Fullerenes Enclosed in Bridged Calix[5]arenes

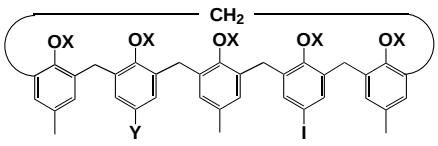
Takeharu Haino, Manabu Yanase, and Yoshimasa Fukazawa*

The development of host molecules for the inclusion of fullerenes is of interest in the direct purification of fullerenes,[1] although they can be separated and purified by chromatography.[2] The selective formation of a clathrate of *p-tert*-butylcalix[8]arene with C_{60} was used successfully to isolate C_{60}.[1a, 1b] The clathrate has a micellelike structure, and the host bound both C_{60} and C_{70} with a C_{60}/C_{70} selectivity of around 5/1.[1c] Thus, the design and synthesis of host molecules with reverse selectivity is of particular interest. We have reported that calix[5]arene receptors can strongly bind C_{60} in organic solvents[3] to give crystalline complexes with 1/1 and 2/1 host/guest ratios.[4] The structure of the crystalline 2/1 complex gave us a good suggestion of how two calix[5]arene units should be linked to give shape-selective receptors with well-defined cavity sizes. Thus, we synthesized host molecules for fullerenes that bind C_{70} preferentially to C_{60}. Here we report the synthesis of the host molecules **1**–**3** and their binding behavior towards C_{60} and C_{70} (Scheme 1).

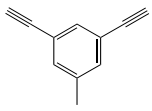


Scheme 1.

The starting material for the synthesis of the receptors was the readily available calix[5]arene derivative **4**,[3] which was converted into the pentaacetate **5**. A coupling reaction between **5** and **7** followed by removal of the acetyl groups furnished the desired receptor **1** in high yield. The palladium-catalyzed coupling of **5** with trimethylsilylacetylene followed by removal of the trimethylsilyl group afforded **6**.



4: X = H, Y = I
5: = Ac, = I
6: = Ac, = C≡CH



7

The receptor **2** was prepared by the coupling of **5** and **6** with palladium(0) as catalyst followed by deprotection. Oxidative coupling of two molecules of **6** with cupric acetate and removal of the acetyl groups afforded the receptor **3**.

To the best of our knowledge, the association constant of the complex of C_{60} with the host **1** of $(76 \pm 5) \times 10^3$ dm^3 mol^{-1} in toluene is the largest yet reported in organic solvents (Table 1). It is more than 36 times larger than the corresponding value of C_{60} and **4** in the same solvent ($(2.1 \pm 0.1) \times 10^3$ dm^3 mol^{-1}),[3] and this clearly indicates an effective cooperation between the two calix[5]arene cavities. The association constants of the host/C_{60} complexes are solvent dependent and decrease in the order toluene $\geq$ benzene $>$ CS_2 $>$ 1,2-dichlorobenzene.

Table 1. Association constants [dm^3 mol^{-1}] of the complexes of **1**–**3** with fullerenes.

Solvent	Fullerene	**1**	**2**	**3**
toluene	C_{60}	$(76 \pm 5) \times 10^3$	$(83 \pm 2) \times 10^2$	$(27 \pm 1) \times 10^2$
	C_{70}	$(163 \pm 16) \times 10^3$	$(85 \pm 13) \times 10^3$	$(55 \pm 2) \times 10^2$
benzene	C_{60}	$(47 \pm 2) \times 10^3$	$(57 \pm 2) \times 10^2$	$(30 \pm 1) \times 10^2$
	C_{70}	$(72 \pm 7) \times 10^3$	$(49 \pm 1) \times 10^3$	$(41 \pm 5) \times 10^2$
CS_2	C_{60}	$(54 \pm 8) \times 10^2$	$(15 \pm 1) \times 10^2$	$(67 \pm 1) \times 10$
	C_{70}	$(96 \pm 3) \times 10^2$	$(66 \pm 2) \times 10^2$	$(103 \pm 4) \times 10$
o-dichloro-	C_{60}	$(30 \pm 2) \times 10^2$	$(12 \pm 1) \times 10^2$	$(44 \pm 5) \times 10$
benzene	C_{70}	$(41 \pm 1) \times 10^2$	$(190 \pm 2) \times 10$	$(49 \pm 2) \times 10$

All the bridged hosts bind C_{70} preferentially to C_{60}. The association constant of the complex of **1** with C_{70} has its largest value of $(163 \pm 16) \times 10^3$ dm^3 mol^{-1} in toluene. The binding selectivity of **2** for C_{70}/C_{60} is highest in toluene with a value of 10.2, but is lower in other solvents (benzene: 8.6, CS_2: 3.6, 1,2-dichlorobenzene: 1.6). The same trend was observed for the other hosts (**1** and **3**), although their selectivity ratios were smaller than those of **2**.

To obtain information on the orientation of the bound guests with respect to the host cavity, ^{13}C NMR spectra of C_{70} were measured in the presence and absence of **1**. Complexation induced shift (CIS) values of the five sets of nonequivalent carbons of the guest were obtained from the differences between these chemical shifts ($\Delta\delta$). The up-field shift is largest for the carbon atoms at the poles of C_{70} (Scheme 1, a, $\Delta\delta = 1.77$) and decreases towards the equator [$\Delta\delta = 1.55$ (b), 1.16 (c), 0.81 (d) 0.69 (e)]. This indicates that the carbon atoms at the poles reside the deepest within the cavity. The CIS of each set of nonequivalent carbons depends on the orientation of the guest within the host cavity. They were estimated by molecular-mechanical calculations with the Amber* force-field model,[5] with summation of the local anisotropic magnetic contribution of the 11 aromatic rings of

[*] Prof. Dr. Y. Fukazawa, Dr. T. Haino, M. Yanase
Department of Chemistry, Faculty of Science
Hiroshima University
1-3-1 Kagamiyama Higashi-Hiroshima City 739 (Japan)
Fax: (+81) 824-24-0724
E-mail: fukazawa@sci.hiroshima-u.ac.jp

[**] This work was supported by Grant-in-Aid for Scientific Research on Priority Area (09238239) from the Ministry of Education, Science and Culture, Japan.

 © WILEY-VCH Verlag GmbH, D-69451 Weinheim, 1998 1433-7851/98/3707-0997 $ 17.50+.50/0

the host, by using our ring-current program.[6] In the calculated structure of lowest energy (Figure 1A), the estimated induced shift of the equatorial carbons is the smallest.

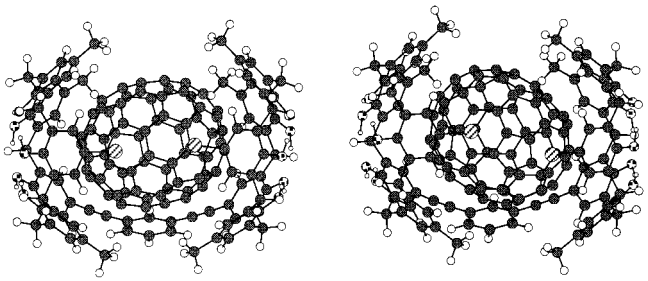


Figure 1. Assumed structures of supramolecular complex of **1** and C_{70} used in the calculation of chemical shifts.

However, in the structure with the second lowest energy (B), the corresponding value for the equatorial carbon atoms ($\Delta\delta = 1.202$) is larger than the induced shifts of the carbon atoms in positions d ($\Delta\delta = 1.119$) and c ($\Delta\delta = 1.185$). Apparently, structure B cannot reproduce the observed chemical-shift trend. Since molecular-mechanics calculations give "frozen" structures, the effect of thermal motion must be included. To take into account the dynamic movement of the host and guest molecules, a molecular dynamics simulation was carried out with a stochastic dynamic treatment at 300 K.[5] The calculation of a 2000 ps simulation revealed rapid movement of the guest within the host cavity. The average induced shifts of the guest carbon atoms were estimated from 500 structures monitored at 4 ps intervals during the simulation period. The calculated induced shifts[7] [$\Delta\delta = 1.651$ (a), 1.376 (b), 1.159 (c), 0.920 (d), 0.834(e)] showed good agreement with the experimental values (correlation coefficient $R^2 = 0.984$). Thus, molecular dynamics simulation analysis is efficient in reproducing the structure and the movement of the supramolecular complex with apolar guests such as fullerenes.

Received: October 28, 1997 [Z11096IE]
German version: *Angew. Chem.* **1998**, *110*, 1044 – 1046

Keywords: calixarenes · fullerenes · host – guest chemistry · molecular dynamics · ring-current method

[1] a) J. L. Atwood, G. A. Koutsantonis, C. L. Raston, *Nature* **1994**, *368*, 229 – 231; b) T. Suzuki, K. Nakashima, S. Shinkai, *Chem. Lett.* **1994**, 699 – 702; c) C. L. Raston, J. L. Atwood, P. J. Nichols, I. B. N. Sudria, *Chem. Commun.* **1996**, 2615 – 2616; d) A. Ikeda, M. Yoshimura, S. Shinkai, *Tetrahedron Lett.* **1997**, *38*, 2107 – 2110; e) K. Araki, A. Akao, A. Ikeda, T. Suzuki, S. Shinkai, *ibid.* **1996**, *37*, 73 – 76; f) R. M. Williams, J. W. Verhoeven, *Recl. Trav. Chim. Pays-Bas* **1992**, *111*, 531 – 532; g) T. Andersson, K. Nilsson, M. Sundahl, G. Westman, O. Wennerström *J. Chem. Soc. Chem. Commun.* **1992**, 604 – 606; h) Z. Yoshida, H. Takekuma, S. Takekuma, Y. Matsubara, *Angew. Chem.* **1994**, *106*, 1658 – 1660; *Angew. Chem. Int. Ed. Engl.* **1994**, *33*, 1597 – 1660; i) T. Suzuki, K. Nakashima, S. Shinkai, *Tetrahedron Lett.* **1995**, *36*, 249 – 252; j) A. L. Balch, V. J. Catalano, J. W. Lee, M. M. Olmstead, *J. Am. Chem. Soc*. **1992**, *114*, 5455 – 5457; k) T. Andersson, G. Westman, G. Stenhagen, M. Sundahl, O. Wennerström, *Tetrahedron Lett.* **1995**, *36*, 597 – 600; l) F. Diederich, J. Effing, U. Jonas, L. Jullien, T. Plesnivy, H. Ringsdorf, C. Thilgen, D. Weinstein, *Angew. Chem.* **1997**, *104*, 1683; *Angew. Chem. Int. Ed. Engl.* **1992**, *31*, 1599 – 1602; m) A. Izuoka, T. Tachikawa, T. Sugawara, Y. Saito, H. Shinohara, *Chem. Lett.* **1992**, 1049 – 1052; n) J. W. Steed, P. C. Junk, J. L. Atwood, *J. Am. Chem. Soc.* **1994**, *116*, 10346 – 10347; o) J. L. Atwood, M. J. Barnes, M. G. Gardiner, C. L. Raston, *Chem. Commun.* **1996**, 1449 – 1450.

[2] a) R. Taylor, J. P. Hare, A. K. Abdul-Sada, H. W. Kroto, *Chem. Commun.* **1990**, 1423 – 1425; b) J. M. Hawkins, T. A. Lewis, S. D. Loren, A. Meyer, J. R. Heath, Y. Shibato, R. J. Saykally, *J. Org. Chem.* **1990**, *55*, 6250 – 6252; c) K. Jinno, T. Uemura, H. Ohta, H. Nagashima, K. Itoh, *Anal. Chem.* **1993**, *65*, 2650 – 2654; d) H. Nagashima, H. Terasaki, Y. Saito, K. Jinno, K. Itoh, *J. Org. Chem.* **1995**, *60* 4966 – 4967.

[3] T. Haino, M. Yanase, Y. Fukazawa, *Angew. Chem.* **1997**, *109*, 288 – 290; *Angew. Chem. Int. Ed. Engl.* **1997**, *36*, 259 – 260.

[4] T. Haino, M. Yanase, Y. Fukazawa, *Tetrahedron Lett.* **1997**, *38*, 3739 – 3743.

[5] AMBER* was implemented in MacroModel V.5.5: F. Mohamadi, N. G. J. Richards, W. C. Guida, R. Liskamp, M. Lipton, C. Caufield, G. Chang, T. Hendrickson, W. C. Still, *J. Comp. Chem.* **1990**, *11*, 440 – 467.

[6] a) Y. Fukazawa, K. Ogata, S. Usui, *J. Am. Chem. Soc.* **1988**, *110*, 8692 – 8693; b) Y. Fukazawa, K. Deyama, S. Usui, *Tetrahedron Lett.* **1992**, *33*, 5803 – 5806; c) Y. Fukazawa, S. Usui, K. Tanimoto, Y. Hirai, *J. Am. Chem. Soc.* **1994**, *116*, 8169 – 8175; d) Y. Fukazawa, T. Hayashibara, Y. Yang, S. Usui, *Tetrahedron Lett.* **1995**, *36*, 3349 – 3352.

[7] Our ring-current program was developed for calculating the induced shift of protons $\Delta\delta(^1H)$. We estimated the induced shift of all the carbon atoms of the guest by assuming that they are protons. By comparing the calculated and experimental values for benzene, we found that the induced shift for ^{13}C can be estimated by multiplying $\Delta\delta(^1H)$ by 0.6 [$\Delta\delta(^{13}C) = 0.6\,\Delta\delta(^1H)$]. The $\Delta\delta(^{13}C)$ values are lower because the paramagnetic term, which can be neglected for the chemical shift of ^1H, contributes significantly to the chemical shift of ^{13}C.[8] The uncorrected $\Delta\delta$ values of the five groups of equivalent carbon atoms in C_{70} (standard deviation) are 2.74(26) (a), 2.29(21) (b), 1.93(11) (c), 1.53(16) (d), 1.39 (26) (e).

[8] a) N. F. Ramsey *Phys. Rev.* **1950**, *78*, 699 – 703; b) F. A. Bovey, *Nuclear Magnetic Resonance Spectroscopy*, Academic Press, New York, **1988**, pp. 88 – 93.

 © WILEY-VCH Verlag GmbH, D-69451 Weinheim, 1998 1433-7851/98/3707-0998 $ 17.50+.50/0